With a Foreword by **Professor Jean-Pierre Sauvage**, Université de Strasbourg, Strasbourg, France
and **Professor Makoto Fujita**, The University of Tokyo, Tokyo, Japan

CARSON J. BRUNS
J. FRASER STODDART



THE NATURE OF THE MECHANICAL BOND

From Molecules to Machines

WILEY

The Nature of the Mechanical Bond

Dedicated to the memory of
Linus Pauling and Ernest Eliel
whose 20th century classics on
The Nature of the Chemical Bond
and
The Stereochemistry of Carbon Compounds
changed the way chemists think about
chemistry for all times

The Nature of the Mechanical Bond

From Molecules to Machines

Carson J. Bruns
J. Fraser Stoddart

WILEY

Copyright © 2017 by John Wiley & Sons, Inc. All rights reserved

Published by John Wiley & Sons, Inc., Hoboken, New Jersey
Published simultaneously in Canada

No part of this publication may be reproduced, stored in a retrieval system, or transmitted in any form or by any means, electronic, mechanical, photocopying, recording, scanning, or otherwise, except as permitted under Section 107 or 108 of the 1976 United States Copyright Act, without either the prior written permission of the Publisher, or authorization through payment of the appropriate per-copy fee to the Copyright Clearance Center, Inc., 222 Rosewood Drive, Danvers, MA 01923, (978) 750-8400, fax (978) 750-4470, or on the web at www.copyright.com. Requests to the Publisher for permission should be addressed to the Permissions Department, John Wiley & Sons, Inc., 111 River Street, Hoboken, NJ 07030, (201) 748-6011, fax (201) 748-6008, or online at http://www.wiley.com/go/permissions.

Limit of Liability/Disclaimer of Warranty: While the publisher and author have used their best efforts in preparing this book, they make no representations or warranties with respect to the accuracy or completeness of the contents of this book and specifically disclaim any implied warranties of merchantability or fitness for a particular purpose. No warranty may be created or extended by sales representatives or written sales materials. The advice and strategies contained herein may not be suitable for your situation. You should consult with a professional where appropriate. Neither the publisher nor author shall be liable for any loss of profit or any other commercial damages, including but not limited to special, incidental, consequential, or other damages.

For general information on our other products and services or for technical support, please contact our Customer Care Department within the United States at (800) 762-2974, outside the United States at (317) 572-3993 or fax (317) 572-4002.

Wiley also publishes its books in a variety of electronic formats. Some content that appears in print may not be available in electronic formats. For more information about Wiley products, visit our web site at www.wiley.com.

Library of Congress Cataloging-in-Publication data has been applied for.

ISBN: 9781119044000

Printed in the United States of America

10 9 8 7 6 5 4 3 2 1

Contents

Foreword ix
Preface xi
Acknowledgments xiii
About the Authors xiv
Abbreviations, Acronyms, and Symbols xv

Part 1 Introducing Mechanical Bonds 1

1 An Introduction to the Mechanical Bond 3
Conspectus 3
Introduction 4
1.1 The Ubiquity of the Mechanical Bond 7
1.1.1 Mechanical Bonds in Nature 8
1.1.2 Mechanical Bonds in Art 10
1.1.3 Mechanical Bonds in Everyday Life 11
1.2 Representing Molecular Mechanical Bonds 13
1.2.1 A Historical Perspective 13
1.2.2 Perspective Stereoformulas 16
1.2.3 Depictions in Color 16
1.2.4 Solid-State Portrayals 17
1.2.5 Graphical Representations 18
1.2.6 Technomorphs 20
1.3 Aesthetics of Mechanical Bonds 21
1.3.1 Beauty in Diversity 21
1.3.2 Topological Beauty 21
1.3.3 Architectural Beauty 24
1.3.4 Simplicity and Elegance 28
1.3.5 Complexity and Emergence 30
1.3.6 Beautiful Machines with Mechanical Bonds 32
1.3.7 The Art of the Mechanical Bond 37
1.4 Evolution of Mechanostereochemistry 38
References 42

Part 2 Making Mechanical Bonds 55

2 The Fundamentals of Making Mechanical Bonds 57
Conspectus 57
Introduction 59
2.1 Statistical Synthesis 62
2.2 Directed Synthesis 65
2.2.1 Covalent Templates 65
2.2.2 Covalent-Directed Capture 69
2.2.3 The Möbius Approach 71
2.3 Template-Directed Synthesis 73
2.3.1 Solvophobic Forces 74
2.3.2 Transition Metals Templates 88
2.3.3 π-Donor/π-Acceptor Templates 102
2.3.4 Hydrogen-Bonded Templates 138
2.3.5 Halogen-Bonded Templates 173
2.3.6 Anion-Binding Templates 174
2.3.7 Ion-Pair Templates 191
2.3.8 Other Cationic Templates 195

2.3.9 Macrocyclic Arenes and Heteroarenes 199
2.3.10 Radical-Pair Templates 207
2.3.11 Homophilic Templates 210
2.3.12 Biomolecular Templates 211
2.4 Active Template Synthesis 218
2.4.1 Active Copper Templates 219
2.4.2 Active Zinc Templates 225
2.4.3 Active Palladium Templates 226
2.4.4 Active Nickel Templates 227
Conclusions and Outlook 229
References 230

3 Making Mechanical Bonds Under Thermodynamic Control 269
Conspectus 269
Introduction 271
3.1 Slippage 271
3.1.1 Pseudorotaxane or Rotaxane? 273
3.1.2 Slippage of π-Donor/π-Acceptor Rotaxanes 275
3.1.3 Slippage of Hydrogen-Bonded Rotaxanes 278
3.1.4 Slippage Driven by Hydrophobic Interactions 283
3.1.5 Slippage of Anion-Binding Rotaxanes 284
3.1.6 Triumphs and Tribulations of Slippage 285
3.2 Self-Assembling Metallo-Organic MIMs 285
3.2.1 MIMs Possessing Group 10 Elements 285
3.2.2 MIMs Possessing Group 11 Elements 292
3.2.3 MIMs Possessing Group 12 Elements 297
3.2.4 MIMs Possessing Elements of Groups 7–9 298
3.2.5 MIMs Possessing Alkaline Earth Elements 302
3.3 Mechanical Bond Formation by Condensation 303
3.3.1 Imines 303
3.3.2 Hydrazones 310
3.3.3 Boronic Esters and Boroxines 312
3.4 Mechanical Bond Formation by Olefin Metathesis 313
3.4.1 Ring-Closing Metathesis (RCM) 314
3.4.2 Cross Metathesis (CM) 323
3.5 Mechanical Bond Formation by Reversible Nucleophilic Reactions 324
3.5.1 Disulfide Exchange 324
3.5.2 Reversible Nucleophilic Substitutions 328
3.5.3 Michael Additions 330
3.6 Surface-Mounted MIMs 330
Conclusions and Outlook 333
References 333

Part 3 Cultivating Mechanical Bonds 347

4 Molecular Topologies and Architectures with Mechanical Bonds 349
Conspectus 349
Introduction 351
4.1 Catenane Topologies 352
4.1.1 Prime Links 352
4.1.2 Composite Links 361
4.1.3 Multi-Annulated Catenanes 369
4.1.4 Covalently Bridged Catenanes 386
4.2 Rotaxane Architectures 392
4.2.1 [*n*]Rotaxanes 392
4.2.2 Dendritic Rotaxanes 416
4.2.3 Covalently Bridged Rotaxanes 424

4.3 Other Architectures with Mechanical Bonds **441**
4.3.1 Catenarotaxanes 441
4.3.2 Rotamacrocycles 442
4.3.3 Ring-in-Ring Mechanomolecules 442
4.3.4 Self-Threaded Macropolycyclics 443
4.3.5 Suitanes 444
4.3.6 Foldaxanes 444
4.3.7 Braided and Interwoven Polymer Entanglements 444
Conclusions and Outlook **444**
References **445**

5 The Stereochemistry of the Mechanical Bond **471**
Conspectus **471**
Introduction **472**
5.1 Dynamic Mechanostereoisomerism **473**
5.1.1 Translation and Circumrotation 474
5.1.2 Pirouetting 502
5.1.3 Rocking 512
5.1.4 Robust Dynamics 513
5.2 Static Mechanostereoisomerism **515**
5.2.1 Orientational Mechanostereoisomers 515
5.2.2 Sequence Mechanostereoisomers 520
5.2.3 Mechanically Chiral Mechanostereoisomers 522
5.2.4 Topological Stereoisomerism 531
Concluding Remarks **540**
References **541**

6 Molecular Switches and Machines with Mechanical Bonds **555**
Conspectus **555**
Introduction **558**
6.1 Redox-Driven Switches **560**
6.1.1 Redox-Switchable Donor-Acceptor (D-A) MIMs 560
6.1.2 Redox Switching of Metallo-Mechanomolecules 566
6.1.3 Redox Switching of Hydrogen-Bonded MIMs 572
6.1.4 Aqueous Redox Switching 573
6.2 Photo-Driven Switches **574**
6.2.1 Switching Driven by Photoinduced Electron Transfer 574
6.2.2 Switching Driven by Photoisomerization 577
6.2.3 Switching in a Dissociative Excited State 580
6.2.4 Switching Driven by Photochemical Reactions 580
6.3 Acid/Base-Driven Switches **581**
6.3.1 pH Switching Driven by Hydrophobic Effects 581
6.3.2 pH Switching Driven by Electrostatic Repulsion 583
6.3.3 pH Switching Driven by Hydrogen Bonding 584
6.3.4 pH Switching Driven by Metal Chelation 588
6.4 Cation-Triggered Switches **591**
6.4.1 Switching with Transition Metal Cations 591
6.4.2 Switching with Alkali Metal Cations 594
6.4.3 Switching with Alkaline Earth Metal Cations 597
6.5 Anion-Triggered Switches **598**
6.5.1 Switches Driven by Anion Solvation Effects 598
6.5.2 Switching Through Second-Sphere Interactions 600
6.5.3 Switches Driven by Anion Binding 600
6.6 Switches Driven by Molecular Recognition **604**
6.6.1 Switches Driven by Neutral Small Molecules 604
6.6.2 Switches Driven by DNA Strand Displacement 606

6.7 Switches Driven by Covalent Reactions **607**
6.7.1 Switches Driven by Acylations of Amines 607
6.7.2 Switches Driven by Reactions of Pyridines 609
6.7.3 Switches Driven by Protection of Aldehydes 610
6.7.4 Switches Driven by Diels-Alder Reactions 610
6.7.5 Switches Driven by (De)Hydrogenation 610
6.7.6 Switches Driven by the Mitsunobu Reaction 610
6.8 Solvent-Driven Switches **611**
6.8.1 Switching Driven by Hydrogen Bond Disruption 612
6.8.2 Switching Driven by Solvation Effects 615
6.9 Thermally Driven Switches **616**
6.9.1 Switching Driven by Entropic Effects 616
6.9.2 Switching Driven by Thermal Decomposition 621
6.10 Pressure-Driven Switches **622**
6.11 Switches Driven by Electric Fields **623**
6.12 Switches Driven by Mechanical Force **624**
6.13 Beyond Translation and Circumrotation **627**
6.13.1 Expansion and Contraction: Molecular Muscles with Mechanical Bonds 627
6.13.2 Ultramacrocyclic Constriction/Dilation 639
6.13.3 Motions of Branched Rotaxanes 643
6.13.4 The Gemini Co-Conformation 645
6.13.5 Rotaxane Flapping 646
6.13.6 Collapsing Mechanomolecules 647
6.13.7 Mechanically Constrained Inflation/Deflation 647
6.13.8 Folding/Unfolding in Mechanomolecules 647
6.13.9 Stepwise Motion in Pseudocatenanes 649
6.13.10 Molecular Pulleys 649
6.13.11 Multicomponent Pirouetting and Translation 649
6.13.12 Molecular Conveyor Belts 652
6.14 Condensed-Phase Switching **652**
6.14.1 Condensed-Phase Redox Switches 652
6.14.2 Condensed-Phase Photoswitches 666
6.14.3 Condensed-Phase Chemical Switches 667
6.15 Mechanomolecular Motors and Machines **669**
6.15.1 Systems-Coupled Functional Switches 670
6.15.2 Brownian Ratchets with Mechanical Bonds 694
6.15.3 Mechanically Bonded Molecular Assemblers 706
Conclusions and Outlook **708**
References **709**

Appendix A: Glossary of Terminology **734**
Appendix B: Cover Art Gallery **742**
Index **753**

Foreword

The field of catenanes, rotaxanes and knots started many decades ago, mostly with intellectually stimulating discussions and even a few attempts at making interlocking ring systems. This research area cannot be disconnected from that of chemical topology with, in particular, the challenging problem of preparing molecules whose graphs are non-planar, i.e. which cannot be drawn on a sheet of paper without crossing points regardless of the hypothetical deformation that the bonds and angles may undergo. The concept of "Chemical Topology" was introduced to the chemical community by Frisch and Wasserman. They published a purely theoretical discussion on this field in 1961 which was much noticed at the time and which is still considered as a highly influential paper. From an experimental point of view the seminal work of Schill and Lüttringhaus with the first directed synthesis of a [2]catenane can certainly be regarded as a foundation stone. This communication, published in 1964, presents a fully convincing strategy for making a [2]catenane. Although the synthetic approach reported in this communication is far from being trivial, it made catenanes appear as real species rather than hypothetical objects for discussion. Unfortunately, Schill's work appeared perhaps too difficult for chemists whose expertise in organic chemistry was limited. As a consequence, research teams who were interested in interlocking molecules were probably discouraged by potential synthetic difficulties. The field, therefore, lay more or less dormant for about 20 years. The 1980s witnessed a new era thanks to a complete change of strategy for preparing catenanes and, later on, rotaxanes. Template strategies were introduced and, fortunately, they turned out to be particularly efficient while at the same time they made interlocking molecules accessible to non-experts in organic synthesis. This period can be regarded as a new birth for molecules which seemed to be either hypothetical species or very exotic compounds.

Since the 1980s, the field has undergone a remarkable development, to a large extent on account of the contributions of Stoddart and his co-workers as well as those of a few other groups, including our own. Chemical topology, the historical area to which research on catenanes belongs, underwent a complete revolution with the synthesis of more and more topologically complex molecules such as the trefoil knot and also the Solomon and Borromean links, to cite just a few examples. In addition, catenanes and rotaxanes were to a large extent at the origin of a rapidly expanding field related to molecular switches and machines, although beautiful work in this area has also been carried out with non-interlocking compounds. There is no doubt that topology, combined with switches and machines based on interlocking ring compounds, is nowadays a mature field for which an exhaustive book was impatiently expected by a large fraction of the molecular sciences community. The present treatise meets exactly this expectation. It is monumental, in agreement with the breadth of the field with its multiple developments and it is at the same time clearly written for a broad audience as well as being very attractive as a result of its many illustrations.

The six-chapter book, co-authored by Carson Bruns and Fraser Stoddart, is fashioned to feature the chemistry of the "Mechanical Bond". The authors define mechanical bonds as a type of bond found in chemically unbound yet mechanically interlocked molecules such as catenanes and rotaxanes. The book covers all aspects of the mechanical bond from its fascinating historical roots to their applications in the fabrication of molecular electronic devices and the construction of artificial molecular machines. A wide range of readers, including both experts and non-experts in the field of chemistry, will value and enjoy this book as if it were a bible.

In Chapter 1, a general introduction is given by the authors in the form of a broad and comprehensive overview of mechanical bonds in such a manner that even general readers will be drawn into their web of influence. They will be filled with wonder on finding many interesting stories, some of them full of surprises, in the history surrounding catenanes and the ubiquity of topologies encompassing mechanical bonds in ancient cultures and modern arts as well as in nature. Chapter 2 details the many different methodologies for the making of mechanical bonds in a molecular context. Templated synthesis, particularly the use of transition metal and π-donor/π-acceptor templates, are emphasized because of the fact that they have revealed remarkable generality and the potential to produce mechanically interlocked molecules, specifically catenanes and rotaxanes, in surprisingly efficient ways. Molecules with highly complex topologies, some – including Olympiadane and the molecular Borromean links – synthesized by the Stoddart group, fascinate the scientific community beyond reason, establishing them to be passed on from generation to generation. The templation strategy is enhanced by combining the preorganization of precursors with subsequent chemical transformations in order to furnish topological links and mechanical bonds. Chapter 3 classifies and provides a discussion of the variations available for chemical transformations leading to these links and bonds. By utilizing reversible bond-forming/breaking chemistry – for example, coordination bonds, Schiff base formation, olefin metathesis – it is demonstrated how catenanes and rotaxanes can be formed in very high yields under equilibrium control.

Catenanes and other molecules with prime link topologies, together with rotaxane architectures, are highlighted

in Chapter 4. Both polycatenanes and polyrotaxanes are featured in the context of linear and branched polymers as well as in networks that extend out into two- and three-dimensional space. These topologies and architectures hold considerable promise for chemists focussed on creating new materials with unique properties. Chapter 5 introduces the tenets of stereochemistry into mechanically interlocked molecules. Mechanostereoisomers are defined as isomers that possess identical mechanically interlocked component parts but which differ in their arrangement of component parts in space. It is particularly significant to note that when the isomers can be interconverted by dynamic processes that mechanostereoisomerism can become the basis for designing and constructing molecular switches and machines, challenges which are discussed in detail in Chapter 6. The dynamic motions of bistable catenanes and rotaxanes can be driven by a variety of external stimuli including redox, light and acid/base triggers. Molecular recognition, including small cation/anion binding, can also be used to initiate the internal movements of the component parts of bistable catenanes and rotaxanes.

Reflecting back in time to the 1960s when catenanes and rotaxanes were classes of chemical compounds that existed only in the imaginations of chemists, how times have changed in half-a-century. Dreams have turned into realities.

Makoto Fujita, The University of Tokyo, Japan
Jean-Pierre Sauvage, Université de Strasbourg,
Strasbourg, France

Preface

Chemists are often trained to think about bonding as a feature governed by *attractive* forces, such as those associated with electron sharing between atoms or electrostatic attractions between ions. If we look up the word “bond” in a dictionary, however, we find atop the list of many definitions, “something that binds or restrains”. It is this kind of non-chemical bond, which is governed in the final resort by *repulsive* forces that prevent chemical bonds from intersecting, that is known in chemistry as the mechanical bond. As a topic of research, the mechanical bond has received much less attention than chemical bonds, to the point of being all but anonymous until the 1960s, when chemistry was already a relatively mature discipline. Even more surprising is the fact that a comprehensive book on the mechanical bond has not, to the best of our knowledge, been written. Of course, we do not mean to diminish the momentous importance of influential monographs, such as Gottfried Schill’s 1971 *Catenanes, Rotaxanes, and Knots*, or the 1999 *Molecular Catenanes, Rotaxanes, and Knots* volume, edited by Jean-Pierre Sauvage and Christiane Dietrich-Buchecker, which pay considerable attention to mechanical bonding in mechanically interlocked molecules (MIMs). In our chronicle of the birth and life of molecules with mechanical bonds, such as catenanes and rotaxanes, we summarize the strategies for synthesizing them, the supramolecular/host-guest motifs utilized in their templation, their various molecular topologies and architectures, their chiralities, isomerism, and dynamics in solution and in condensed phases, not forgetting their switching properties under the influence of external stimuli and their many current and potential applications in science and technology. Taken as a whole, we hope that this book will illuminate the nature of the mechanical bond in chemistry and beyond.

When charged with the opportunity to write a book on the mechanical bond, we asked ourselves what we would like to see in a book. What would be useful to us and hopefully the readers? With a rapidly growing body of reviews in the chemical literature that cover almost every nook and cranny of contemporary research, a book ought to offer something more than a collection of reviews. Naturally, a book should be educational so as to allow students and newcomers to familiarize themselves with the field. It should consolidate and organize the seminal contributions and key fundamental topics that define the field. A book should look backwards as well as forwards, offering a perspective on the history and evolution of the field, as well as where it appears to be heading in the future. We have tried to go beyond these bare minimum requirements by paying a considerable amount of attention to presentation, with the goal of minimizing the time and effort required by a reader to learn almost anything about the mechanical bond. Because chemistry is blessed with a visual repertoire of symbolic language that enables us to communicate molecular structures and even their dynamics in a highly concise and effective manner, we have made every effort to compile an image-driven manuscript. *The Nature of the Mechanical Bond* commands 82 Tables, 382 Schemes, 426 Figures, and >4000 citations contained in an excess of a quarter of a million words (not counting captions or references) in six chapters. Not to feel discouraged, we suspect that a reader can assimilate 80% or more of the book’s information from viewing the images and reading the captions alone.

How to Read this Book

We have written this book with the contemporary formats of the digital age in mind. Readers of the electronic version of the book are privy to several advantages. Explained below are a handful of features to help readers make the most of the experience.

Compound Numbers. The systematic notation adopted in this book for compound numbers involves a letter to denote the type of structure (M for macrocycle, C for catenane, R for rotaxane, and L for ‘linear’ or ‘ligand’, which encompass everything else), followed by a number corresponding to the Chapter (1–6), followed by a number which is assigned sequentially in order of appearance. Compound numbers appear in bold text, whereas complexes, such as pseudorotaxanes, are italicized. We employ the mathematical notation of subsets ($\subset$) to denote the inclusion of a guest within a host—e.g., *guest*$\subset$*host*.

Color. We have made extensive use of color to aid in the representation of MIMs. In some cases, the colors have significance—π-donors are typically shaded in warmer colors such as red, orange, and green, for example, whereas π-acceptors embody cool shades such as blue and purple. In other cases, the colors are meant to reflect the actual color of the corresponding compound in solution, as in the case of π-associated radicals and several of the transition metal templates. Homocatenanes, which are composed of identical interlocking rings, have been shaded with differentiated ring colors (e.g., black and green) to help readers identify the component parts.

Hyperlinks. We have introduced a highly interconnected web of hyperlinks that enhance the navigability of the book in the digital version, with the goal of establishing a seamless connection between themes and concepts, as well as the primary literature. In the main text, a click on a reference number will redirect the reader to the reference section. By clicking on the chapter numbers in the top corners of any page, readers will be redirected back to

the chapter's Table of Contents (ToC). The ToC and cross-references embedded within the main text navigate to their respective Section headings.

References. At a total count of 3400 unique references, this book is a repository for many of the most important references related to the mechanical bond, dating to early 2016. Each Chapter of the book is intended to stand on its own as a useful compendium on the featured topic. References are therefore compiled at the end of each Chapter to sustain the modularity of the book. A click on a reference number within the reference section redirects the reader back to the first appearance of the citation in the main text. A click on a journal name in the reference section opens a weblink, which leads to the landing page of the primary article on the internet.

In writing this book, we decided to grasp the opportunity to tighten up, unify, and consolidate the language associated with the chemistry of mechanical bonds. We have attempted to create a resource that defines clearly the vocabulary and terminology by including a Glossary (Appendix A). In some cases, we felt it was necessary to introduce new terms for which an appropriate word or phrase was unavailable, or to emphasize distinctions that are often overlooked. For example, catenanes and rotaxanes possess mechanical bonds whereas molecular knots do not, yet all are grouped under the umbrella of MIMs. We have introduced the word 'mechanomolecule' as a way to describe molecules with mechanical bonds explicitly. In other cases, there was a need to describe unnamed phenomena that are related conceptually to phenomena with literature precedence. For example, we have introduced the term 'co-configuration' to describe the assignment of chirality that arises from mechanical bonds—a term inspired by the descriptor, 'co-conformation', which has been adopted widely in discussions of isomerism that arises from dynamic motions constrained by the mechanical bond. A similar scenario arose in the cases of 'mechanically axial chirality' and 'mechanical helicity', which we have coined in solidarity with the precedent for use of the term 'mechanically planar chirality'. Still other terms that are employed frequently in the literature are either misleading or have not been clearly defined until now. For example, the molecular entities engaged in mechanical bonding in catenanes and rotaxanes have been given many names, which include hoops, loops, rings, wheels, rods, axles, dumbbells, and components, among many others. We have chosen to define some of these terms in the context of *mechanostereochemistry*, our word of choice for the stereochemistry of mechanomolecules. We have also selected the term 'component part' as a generic phrase for describing these entities because 'component' has its own unrelated definition in chemistry.

Despite our own involvement in research on the mechanical bond, neither one of us appreciated fully the breadth and diversity of the field at the outset of writing this book. We have discovered that it has flourished in little more than 20 years into one of the most vibrant and interdisciplinary themes in chemistry, after a long induction period in the esoteric backwaters of unnatural product synthetic organic chemistry. For one of us (CJB), the intimate engagement with the mechanical bond rapidly became addictive, leading to many 16-hour sessions of reading, illustrating, and writing during a period of 30 months, whereas for the other (JFS), the commitment and dedication to unveiling the secrets behind the mechanical bond—an odyssey that began 30 years ago—continues unabated with no end in sight. Although we have been at considerable pains to present a comprehensive and unbiased account of the mechanical bond, we apologize in advance to any of our colleagues in the field whose work we may have oversimplified or overlooked, and invite readers to notify us of errors and omissions. We have indulged ourselves in celebrating the mechanical bond by emphasizing its beauty, as we perceive it, especially in Chapter 1 and the cover-art gallery in Appendix B. We trust that readers will embrace forgivingly this unconventional approach to introducing the chemistry of the mechanical bond.

Carson J. Bruns / J. Fraser Stoddart
June 2016

Acknowledgments

The proposal to write a book on mechanostereochemistry was first mounted by Anita Lekhwani, formerly Senior Editor of Chemistry Books with John Wiley and Sons, at the International Union of Pure and Applied Chemistry (IUPAC) World Congress in San Juan, Puerto Rico in August 2011. The idea lay dormant for three years, after which—following positive reviews of a proposal by us to write a book on *The Nature of the Mechanical Bond*—we met with Anita at the 248th American Chemical Society (ACS) National Meeting in San Francisco in August 2014. A contract changed hands and a journey that was to take another two years began. In the beginning, the journey was far from being a smooth one. Our hopes and aspirations in relation to the mode of production of the book were not aligned with those of the publishers who were looking to us for the delivery of a complete manuscript, followed by a 9-month period of reviewing, copy-editing and production on their part. Feeling in need of advice, we turned to Mark Ratner who advocated appealing to the publishers through one of their senior executives to have our case heard for a chapter-by-chapter production of the manuscript that would leave Wiley in a position to publish a book as close to the current state of research activity in the field as possible. An approach to Peter Gölitz, the long-standing Editor-in-Chief of *Angewandte Chemie* and Vice President and Publishing Director at Wiley, led to him introducing us to Jon Walmsley, formerly Managing Director and Senior Vice President, Professional Practice and Learning at Wiley. By August 2015, Jon had implemented a fast-to-market production process and introduced us to Rosie Hayden, UK Production Manager, Book Content Management, Global Research at Wiley. From this time onwards, it was plain sailing. We put on record our heartfelt thanks to Anita, Mark, Peter, Jon and Rosie.

There are no firsts in science. In the immortal words of Isaac Newton, “If I have seen further, it is by standing on the shoulders of giants.” We are indebted to a legion of scientists who forged the path to the modern frontier on which we tread today. In particular, we recognize the fundamental discoveries that led to the birth of modern structural chemistry by Linus Pauling, the ground-breaking leap taken beyond the molecule by Friedrich Cramer, Charles Pedersen, Donald Cram and Jean-Marie Lehn in establishing what has become known consecutively and progressively as inclusion complex, crown ether, host-guest and supramolecular chemistry, and the introduction to template-directed synthesis by Neil Curtis and Daryle Busch. Couple these major paradigm shifts with the progress made during more than a century in stereochemistry in the hands and minds of Louis Pasteur, Jacobus van ‘t Hoff, Josef Le Bel, Emil Fischer, Norman Haworth, Odd Hassel, Derek Barton, Vladimir Prelog, John Cornforth, Raymond (Ray) Lemieux, Kurt Mislow and Ernest Eliel and you have the bedrock for the emergence of the tenets of mechanostereochemistry with the advent of the mechanical bond. We pay homage to these giants of chemistry.

We take much pleasure in thanking two of the masters of chemical topology, Jean-Pierre Sauvage and Makoto Fujita, for expressing their support for the publication of our book on *The Nature of the Mechanical Bond* in a Foreword. As a part of the fast-to-market approach to publication, we enlisted the help of many colleagues to act as reviewers of selected sections of the book. In this regard, we are indebted to the following roster: Josef Michl, Jonathan Sessler, Stephen Goldup, Bruce Gibb, Jacobs Jordan, Ivan Aprahamian, Jeremy Sanders, David Amabilino, Paul Beer, Sheng-Hsien Chiu, Reed Izatt, Mark Ratner, Leonard (Len) Lindoy, Jehn-Marie Lehn, Alberto Credi, Frédéric Coutrot, Sébastien Vidal, Gautam Desiraju, A.P. de Silva, Roald Hoffmann, Amar Flood, Paul McGonigal, Haibo Yang, and Omar Farha. We thank all of them most warmly for agreeing to review sections of the manuscript and providing us with their critical feedback and helpful suggestions. We assume full responsibility, nevertheless, for the contents of the book from beginning to end.

We thank Aleksandr (Alex) Bosoy for providing images and taking the lead in designing the front and back covers of the book. We also thank Karel Hartlieb, Andrew Sue, and Haibo Yang for each contributing an image for the manuscript. Much of the heavy lifting in relation to the editing of manuscripts and proofs, and to the production of the index, was taken on board more than willingly by Margaret (Peggy) Schott and Xirui Gong with a relentless quest for quality control that knew no limits as they checked text line-by-line, word-by-word, letter-by-letter and number-by-number against information gathered in the illustrations (Schemes and Figures) and References.

Chemistry most likely welcomes into its fold thousands of new compounds every day and dozens of new reactions every week. By contrast, the entry of new bonds into chemistry is relatively few and far between. Only once in a blue moon does a bond, which is so fundamentally different from all the other bonds, enter chemistry’s pantheon with the potential to be scientifically and technologically disruptive. The mechanical bond is such a bond. We express our gratitude to all those chemists who have participated in its launch these past few decades: they have made it possible for us to put on record our commentary on *The Nature of the Mechanical Bond*.

Carson J. Bruns / J. Fraser Stoddart
June 2016

About the Authors



Carson Bruns, presently a Miller Research Fellow in the College of Chemistry at the University of California, Berkeley, was born in 1985 in the foothills of the Rocky Mountains in the United States, and raised and educated in the city of Loveland, on the front range of Colorado's eastern slopes. He attended Luther College in the rolling bluffs of Decorah, Iowa (2004–2008) where he earned undergraduate degrees in chemistry, religion, and mathematics. His international chemistry background includes former research appointments at Coe College in Cedar Rapids, Iowa, Chulabhorn Research Institute in Bangkok, Thailand, the University of Tokyo in Japan, and the Korea Advanced Institute of Science and Technology (KAIST) in Daejeon, South Korea. He received a PhD in organic chemistry from Northwestern University (2008–2013), where he was awarded research fellowships from the National Science Foundation (NSF) Graduate Research Fellowship Program (GRFP) and the East Asia and Pacific Summer Institutes (EAPSI), as well as the Japan Society for Promotion of Science (JSPS) Summer Program, the Global Center of Excellence at the University of Tokyo, and the World Class University Project at KAIST. Unified by the theme of unnatural product synthesis, his research has covered self-assembling materials for organic and inorganic/organic hybrid solution-processed solar cells, as well as therapeutic and diagnostic compounds, and molecular nanomachines. His mechanostereochemical research to date has taken advantage of mechanical bonds in (pseudo)rotaxanes for the development of spring-like foldamers, molecular muscles, gated self-assembled molecular flasks, fluorescent security inks, protein bioconjugates, and stimulus-responsive contrast agents.



Fraser Stoddart was born in the capital of Scotland on Victoria Day (May 24) in 1942. His academic career can be traced from the Athens of the North (Edinburgh University) to the Windy City beside Lake Michigan (Northwestern University) with interludes on the edge of the Canadian Shield beside Lake Ontario (Queen's University), in the Socialist Republic of South Yorkshire (Sheffield University), on the Plains of Cheshire beside the Wirral (ICI Corporate Laboratory), in the Midlands in the Heartland of Albion (Birmingham University) and in the City of Angels alongside the Peaceful Sea (University of California, Los Angeles). By contributing to the introduction of the mechanical bond into molecules, he has become one of the few chemists to have opened up an entirely new field of chemistry. More specifically, he has pioneered the development of the template-directed protocols for the synthesis of two-state mechanically interlocked molecules (MIMs) including bistable catenanes and rotaxanes which have found their way into molecular electronic devices and drug delivery systems. He was made a Knight Bachelor by Her Majesty Queen Elizabeth II in her 2007 New Year's Honours List for his services to chemistry and molecular nanotechnology. He is a Fellow of the Royal Society of London, the German Academy (Leopoldina) of Natural Sciences, and the Royal Netherlands Academy of Arts and Sciences, as well as an Honorary Fellow of the Royal Society of Edinburgh and the Royal Society of Chemistry. His numerous awards include the King Faisal International Prize in Science, the Albert Einstein World Prize in Science, the Feynman Prize in Nanotechnology, the Cope Award from the American Chemical Society and the Royal Medal of the Royal Society of Edinburgh presented to him by His Royal Highness Prince Philip, Duke of Edinburgh, in 2010. He is a Fellow of the American Academy of Arts and Sciences and a Member of the National Academy of Sciences. He has trained and served as an inspiration to more than 400 graduate and postdoctoral students of which close on 100 have subsequently embarked on successful independent academic careers. His current research interests include the design and synthesis of emergent systems and artificial molecular machines that operate away-from-equilibrium. Radical chemistry is playing a key role in this latest contribution to the chemistry of the mechanical bond.

Abbreviations, Acronyms, and Symbols

°C	degrees Celsius
16NP	1,6-dioxynaphthalene
1D	one-dimension(al)
20C6	[20]crown-6
21C7	[21]crown-7
24C8	[24]crown-8
26NP	2,6-dioxynaphthalene
27NP	2,7-dioxynaphthalene
2D	two-dimension(al)
2EG	diethylene glycol
2T	bithiophene
30C10	[30]crown-10
36C12	[36]crown-12
3D	three-dimension(al)
3EG	triethylene glycol
3T	terthiophene
42C14	[42]crown-14
48C16	[48]crown-16
4EG	tetraethylene glycol
4EGBA	tetraethylene glycol bis(*o*-aniline) ether
5EG	pentaethylene glycol
60C30	[60]crown-30
A	acceptor; adenine
A	surface area
Å	angstroms
A^-	anion
A18C6	aza[18]crown-6
$A_2$30C10$_2$	anthracene-bridged macrotricyclic [30]crown-10 dimer
AA	acetamide
ABTZ	acridanebis(*N*-methyltriazolium)
Ac	acetyl
Ad	adamantane
ADN35C8	allyldinaphtho[35]crown-8
AFM	atomic force microscopy
Aib6	aminoisobutyric acid hexamer
Am	amyl
AMM	artificial molecular machine
AMS	artificial molecular switch
APT	(3-amidophenyl)-*N*-methyltriazolium
Ar	aryl
ATO292PC	azatetroxa[2.9.2]paracyclophane
ATP	adenosine triphosphate
ATRP	atom transfer radical polymerization
AuNP	gold nanoparticle
B21C7	benzo[21]crown-7
BADA18C6	benzylic amide diaza[18]crown-6
$BArF^-$	tetrakis(pentafluorophenyl)borate
BBB	4,4´-bis(bromomethyl)-1,1´-biphenyl
BBE^{2+}	1,2-bis(benzimidazolium)ethane
BBN26C8	benzo-2,2´-binaphtho[26]crown-8
$BBPP^{2+}$	bitolyl-bis(4-pyridyl)pyridinium
BBPP37C7	2,2´-bipyridyl-4,4´-dicarboxamido-bis-*para*-phenylene[37]crown-7
bdnb	1,1´-binaphthyl-4,4´-dibenzoate
BET	back electron transfer
$BHCP^+$	3,5-bis(hexacarbamoyl)-*N*-methylpyridinium
BIB	4,4´-bis(iodomethyl)-1,1´-biphenyl
$BIMD^+$	benzimidazolium
bip	2,6-bis(*N*-alkylbenzimidazolyl)pyridine
BIPP33C9	bis(iodotriazole)-*para*-phenylene [33]crown-9
bipy	4,4´-bipyridine
$BIPY^{2+}$	4,4´-bipyridinium
BLA	bond length alternation
BM26C8	bis-*meta*-phenylene[26]crown-8
BMAT	1,4-bis(*meta*-anisole)-1*H*-1,2,3-triazole
BMP20C6	bis-*meta*-phenylene[20]crown-6
BMP24C6	bis-meta-phenylene[24]crown-6
BMP25C6SO_2	bis-meta-phenylene[25]crown-6 sulfone
BMP25C8	benzo-*meta*-phenylene[25]crown-8
BMP32C10	bis-*meta*-phenylene[32]crown-10
BMP443C	bis-meta-phenylene[4.4.3]cryptand
BMP444C	bis-*meta*-phenylene[4.4.4]cryptand
BMP553C	bis-*meta*-phenylene[5.5.3]cryptand
BMP555C	bis-*meta*-phenylene[5.5.5]cryptand
Bn	benzyl
BN24C8	benzonaphtho[24]crown-8
$BnPY^+$	benzylpyridinium
Boc	*tert*-butoxycarbonyl
BOM	benzyloxymethoxy
BOP443C	bis-*ortho*-phenylene[4.4.3]cryptand
BP	4,4´-biphenol
bp	base pairs
BPDMI	*N*,*N*´-bis-(propyl)-4,5-dimethylimidazolium
BPE^{2+}	1,2-bis(pyridinium)ethane
$BPIC^{2+}$	3,3´-dimethyl-4,4´-bipyridinium (bipicolinium)
BPMI	*N*,*N*´-bis(propyl)-1-methylimidazolium
BPP26C8	benzo-*para*-phenylene[26]crown-8
BPP34C10	bis-*para*-phenylene[34]crown-10
bpsa	bathophenanthrolinedisulfonic acid
BPTL	bispyridyl tetralactam macrocycle
BPTTF	bispyrrolotetrathiafulvalene
bpy	2,2´-bipyridine
BPY^{2+}	2,2´-bipyridinium
BQ	benzoquinone
BRs	Borromean rings
BS28C6	benzosalophen[28]crown-6
Bu	butyl

BX26C6	bis-*para*-xylylene[26]crown-6
$BX26S_2C6$	bis-*para*-xylylene[26]dithiacrown-6
BX29C7	bis-*para*-xylylene[29]crown-7
BZ	benzidine
Bz	benzoate
C	cytosine
^{c} or *c*-	cyclo-
C4DQ	calix[4]diquinone
$C4N3^{2+}$	*N*,*N*´-bis(3-pyridylmethyl)-1,4-butanediammonium
$C4N4^{2+}$	*N*,*N*´-bis(4-pyridylmethyl)-1,4-butanediammonium
$C5N2^{2+}$	*N*,*N*´-bis(2-pyridylmethyl)-1,6-hexanediammonium
$C5N3^{2+}$	*N*,*N*´-bis(3-pyridylmethyl)-1,5-pentanediammonium
$C5N4^{2+}$	*N*,*N*´-bis(4-pyridylmethyl)-1,5-pentanediammonium
$C6N3^{2+}$	*N*,*N*´-bis(3-pyridylmethyl)-1,6-hexanediammonium
$C6N4^{2+}$	*N*,*N*´-bis(4-pyridylmethyl)-1,6-hexanediammonium
CA4	calix[4]arene
CA5	calix[5]arene
CA6	calix[6]arene
CA7	calix[7]arene
CA8	calix[8]arene
CAA6	cyclo[6]aramide
CAC	critical aggregation concentration
CA*n*	calix[*n*]arene
CB5	cucurbit[5]uril
CB6	cucurbit[6]uril
CB6AAC	cucurbit[6]uril-catalyzed azide-alkyne cycloaddition
CB7	cucurbit[7]uril
CB8	cucurbit[8]uril
CB10	cucurbit[10]uril
$CBDAP^{4+}$	cyclobis(2,7-diazapyrenium-*p*-phenylene)
CBITZ	*N*-propylcarbazole bis(*N*-methyl-5-iodotriazolium)
CB*n*	cucurbit[*n*]uril
$CBPC7^{4+}$	cyclobis(paraquat-heptamethylene)
CBPDC8	cyclobis(pyromellitic diimide-octamethylene)
$CBPQB^{4+}$	cyclobis(paraquat-4,4´-biphenylene)
$CBPQT^{4+}$	cyclobis(paraquat-*p*-phenylene); blue box
CBTAM	cyclobis(tetraazamacrocycle)
CBXPDP	cyclo[2,6-bis(xylyloxymethyl) pyridine-2,6-diamidopyridine]
CD	cyclodextrin
CD/CB6AAC	cyclodextrin-assisted cucurbit[6]uril catalyzed azide-alkyne cycloaddition
CE2C6U	cyclobis(oxydiethylene hexamethyleneurethane)
CEE	carboxyethyl ester
CHLPA5	pillar[5]arene cyclic host liquid
CIDAPH	cyclo(isophthalobis(2,6-diamidopyridine-hexadecamethylene)
CIN	cinnamide
CITP	*N*-carboxamidomethyl-3-(5-iodotriazolyl) pyridinium
CLSM	confocal laser scanning microscopy
ClyA	Cytolysin A
CM	cross metathesis
cm	centimeters
CMC	critical micelle concentration
CN	coordination number
COSY	NMR correlation spectroscopy
Cp	cyclopentadienyl
CS	penta-*tert*-butylpentacyanopentabenzo[25] annulene (cyanostar)
CSD	Cambridge Structural Database
CT	charge transfer
CTAB	cetyl trimethylammonium bromide
CuAAC	copper(I)-catalyzed azide-alkyne cycloaddition
CV	cyclic voltammetry
Cy	cyclohexyl
CyDA	cyclohexane-1,2-diamine
D	donor
D-A	donor-acceptor
Da	unified atomic mass units (Daltons)
DAAP	di(acylamino)pyridine
DAB	4,4´-diaminomethyl-*p*-phenyleneoxy-2,2´-bipyridine
DABCO	1,4-diazabicyclo[2.2.2]octane
dach	1,2-cyclohexanediamine
DAN	1,5-diaminonaphthalene
DAP^{2+}	2,7-diazapyrenium
$DAPP^{2+}$	2,9-diazaperopyrenium
DB24C8	dibenzo[24]crown-8
DB30C10	dibenzo[30]crown-10
DB45C15	dibenzo[45]crown-15
DB57C19	dibenzo[57]crown-19
DBB	dibenzobicyclo[2.2.2]octane
$DBB_2$18$C6_2$	dibenzobicyclo[2.2.2]octane-bridged macrotricyclic [18]crown-6 dimer
$DBB_2$24$C8_2$	dibenzobicyclo[2.2.2]octane-bridged macrotricyclic [24]crown-8 dimer
DBU	1,8-diazabicyclo[5.4.0]undec-7-ene
DCAMP	3,5-dicarboxamido-*N*-methylpyridinium
DCC	dynamic combinatorial chemistry; dicyclohexylcarbodiimide
DCE	dichloroethane
DCL	dynamic combinatorial library
DCy24C8	dicyclohexyl[24]crown-8
DEF	*N*,*N*-diethylformamide
DFA	difluoroacetic acid
DFB	1,3-diformylbenzene (isophthalaldehyde)
DFF	2,5-diformylfuran
DFP	2,6-diformylpyridine
DFT	density functional theory
$DHFR_{ST}$	dihydrofolate reductase
DIEA	diisopropylethylamine

dien	diethylenetriamine
dist	distal
DM-β-CD	heptakis(2,6-di-*O*-methyl)-β-cyclodextrin
DMAE	*N*,*N*-dimethylaminoethyl
DMAP	*N*,*N*-dimethyl-4-aminopyridine
DMF	*N*,*N*-dimethylformamide
DMPA	dimyristoylphosphatidic acid
DMTMM	4-(4,6-dimethoxy-1,3,5-triazin-2-yl)-4-methylmorpholinium chloride
DN38C10	1,5-dinaphtho[38]crown-10
DNA	deoxyribonucleic acid
DNP	1,5-dioxynaphthalene
DOX	doxorubicin
DP	degree of polymerization
DP24C8	dipyrido[24]crown-8
dpbiq	8,8′-diphenyl-3,3′-biisoquinoline
dpp	1,10-diphenylphenanthroline
dppp	1,3-bis(diphenylphosphino)propane
DPSC	double potential step chromoamperometry
DSC	differential scanning calorimetry
dsDNA	double-stranded DNA
DTNP	1,5-dithianaphthalene
DTT	dithiothreitol
DX	double crossover DNA motif
E	energy; Young's modulus
E_A	activation energy
EDC	1-ethyl-3-(3-dimethylaminopropyl) carbodiimide hydrochloride
EDOT	3,4-ethylenedioxythiophene
EDTA	ethylenediaminetetraacetic acid
EET	excitation energy transfer
en	ethylenediamine
EPR	electron paramagnetic resonance
ET	electron transfer
Et	ethyl
$ExBox^{4+}$	extended viologen molecular box
FA	fumaramide
Fc	ferrocene
Fc^+	ferrocenium
FET	field-effect transistor
Fo8	figure-of-eight
FRET	Förster resonance energy transfer
g	grams
G	guanine
G1	first-generation
G2	second-generation
G3	third-generation
G4	fourth-generation
G*n*	generation number
GNI	*N*-glycylnaphthalimide
GPC	gel permeation chromatography
GSCC	ground state co-conformation
GSH	glutathione
h	Planck constant
h	hours
HFP	hexafluoro-2-propanol
HK60C18	hexaketo[60]crown-18
HMSNPs	hollow mesoporous silica nanoparticles
HO2122PC	hexoxa[2.12.2]paracyclophane
HOMO	highest occupied molecular orbital
HOPG	highly ordered pyrolytic graphite
HP-β-CD	2-hydroxypropyl-β-cyclodextrin
HPE	hydroxypropyl ether
HPLC	high-performance liquid chromatography
hppb	hexakis[4-(4-pyridyl)phenyl]benzene
HQ	hydroquinone
HQA	hydroquinone diacetate
HREELS	high-resolution electron energy loss spectroscopy
HRP	horseradish peroxidase
Hx	hexyl
hyperCEST	hyperpolarized chemical exchange saturation transfer
Hz	Hertz (cycles per second)
$h\nu$	photon energy
I	current; moment of inertia
i or *i*-	*iso*-
i-DB24C8	*iso*-dibenzo[24]crown-8
IBPDB18C6	isophthalamide-bis-*para*-phenylene-dibenzo[18]crown-6
IBPP31C6	isophthalamide-bis-*para*-phenylene[31]-crown-6
IBPP33C6	isophthalamide-bis-*para*-phenylene[33]-crown-6
IBPP34C7	isophthalamide-bis-*para*-phenylene[34]-crown-7
IBPP37C8	isophthalamide-bis-*para*-phenylene[37]-crown-8
IBPPC4DQ	isophthalamide-bis-*para*-phenylene/calix[4]diquinone receptor
$IBPQT^{4+}$	isophthalamide-bis-paraquat-*para*-phenylene
ICD	induced circular dichroism
ICZ	indolocarbazole
IMD^+	imidazolium
IMW	insulated molecular wire
*i*NCTG	(±)-tris(isonicotinyl)cyclotriguaiacylene
IR	infrared
ITC	isothermal titration calorimetry
IUPAC	International Union of Pure and Applied Chemistry
J	Joules
K	degrees Kelvin
K	equilibrium constant
k	rate constant
kbar	kilobar
kcal	kilocalories
kDa	kilodaltons
kg	kilograms
kHz	kilohertz
L	ligand; liter
l	length
LB	Langmuir-Blodgett
L_c	contour length

LC	liquid crystal
LCST	lower critical solution temperature
LED	light-emitting diode
LG	leaving group
LUMO	lowest unoccupied molecular orbital
M	molar; metal
m-	*meta*-
$M(dpp)_3$	macrobicyclic tris-dpp ligand
MA	maleamide
MALDI	matrix-assisted laser desorption ionization
MC	merocyanine
*m*CPBA	*meta*-chloroperoxybenzoic acid
MD	molecular dynamics
Mdpbiq37	37-membered macrocyclic dpbiq ligand
Mdpp30	30-membered macrocyclic dpp ligand
Mdpp32	32-membered macrocyclic dpp ligand
Mdpp39	39-membered macrocyclic dpp ligand
Mdpp46	46-membered macrocyclic dpp ligand
ME	2-mercaptoethanol
Me	methyl
MED	molecular electronic device
MIM	mechanically interlocked molecule
min	minutes
MLCT	metal-to-ligand charge transfer
mM	millimolar
MM	molecular mechanics
M_n	number average molecular weight
mN	millinewtons
MN	molecular necklace
MOF	metal-organic framework
mol	moles
MOPS	3-(*N*-morpholino)propanesulfonic acid
MORF	metal-organic rotaxane framework
Mphen34	34-membered macrocyclic phen ligand
MPTL	monopyridyl tetralactam macrocycle
MPTTF	monopyrrolotetrathiafulvalene
MRI	magnetic resonance imaging
MS	mass spectrometry/mass spectrum
ms	milliseconds
MSCC	metastable state co-conformation
MSNP	mesoporous silica nanoparticle
MSTJ	molecular switch tunnel junction
mV	millivolts
M_w	weight average molecular weight
N	number of molecules
n	number
n.r.	no reaction
N24C8	naphtho[24]crown-8
nA	nanoamps
NBS	*N*-bromosuccinimide
NDI	naphthalene diimide
NDOS	normalized density of states
NHS	*N*-hydroxysuccinimide
NI	1,8-naphthalimide
NIR	near-infrared
NITZ	naphthalimide-triazolium
nm	nanometers
NMR	nuclear magnetic resonance
nN	nanonewtons
NOE	nuclear Overhauser effect
NOESY	nuclear Overhauser effect NMR spectroscopy
NP	naphthalene
NPTTF40C10	naphthotetrathiafulvalene[40]crown-10
ns	nanoseconds
Nu^-	nucleophile
o-	*ortho*-
O_4C2T2N	tetraoxacalix[2]triptycene[2]naphthyridine
OCAPC6	oxacalix[2]arene[2]pyrazine
OMe	methoxyl
opba	*o*-phenylenebis(oxamato)
OTf^-	triflate
p-	*para*-
P21C7	pyrido[21]crown-7
P24C8	pyrido[24]crown-8
P3MO	poly(trimethylene oxide)
P3MT	poly(3-methylthiophene)
P4VP	poly(4-vinylpyridine)
pA	picoamps
PA5	pillar[5]arene
PA5/CB6AAC	pillar[5]arene-assisted cucurbit[6]uril-catalyzed azide-alkyne cycloaddition
PA6	pillar[6]arene
PAH	polycyclic aromatic hydrocarbon
PAMAM	polyaminoamide dendrimer
PA*n*	pillar[*n*]arene
PAN	poly(acrylonitrile)
PANI	polyaniline
PB	porphyrin basket
PBA26C6	pyrido-benzylic-amide[26]crown-6
PBA32C8	pyrido-benzylic-amide[32]crown-8
PBP24C8	*para*-bromophenol[24]crown-8
PBPPC4DQ	pyridine-3,5-dicarboxamide-bis-*para*-phenylene/calix[4]diquinone receptor
PBS	phosphate buffered saline
PBV	poly(*para*-biphenylene vinylene)
PBX26C6	pyridobis-*para*-xylyl[26]crown-6
PBX29C7	pyridobis-*para*-xylyl[29]crown-7
PC10S	polydecamethylene sebacate
$PC10V^{2n+}$	poly(decamethylene viologen)
PC4S	polytetramethylene sebacate
PC6S	polyhexamethylene sebacate
PDI	polydispersity index; perylene diimide
PDMS	poly(dimethylsiloxane)
pDNA	plasmid DNA
PE2C6U	poly(oxydiethylene hexamethylenediurethane)
PE2HQA	poly(diglycol hydroquinone-*O*,*O*´-diacetate)
PE2HQG	poly(*p*-phenylene diglycol diglycolate)

PE2HQO	poly(*p*-phenylene diglycol oxalate)
PE3DU	poly(tri(oxyethylene) diphenylmethylenediurethane)
PE3HQ	poly(*p*-phenylene trigycol ether)
PE3HQA	poly(triglycol hydroquinone-*O*,*O*´-diacetate)
PE3NP	poly(1,5-naphthylene triglycol ether)
PE3R	poly(*m*-phenylene triglycol ether)
PE3S	poly(triethylene glycol sebacate)
PE4DU	poly(tetra(oxyethylene) diphenylmethylenediurethane)
PE4HQ	poly(*p*-phenylene tetraglycol ether)
PE4HQNP	poly(*p*-phenylene tetraglycol-*alt*-1,5-naphthylene tetraglycol ether)
PE4NP	poly(1,5-naphthylene tetraglycol ether)
PEC6U	poly(ethylene hexamethylenediurethane)
PEG	poly(ethylene glycol)
PEI	poly(ethylene imine)
PELDOR	pulsed electron double resonance
PET	photoinduced electron transfer
PF	polyfluorene
PFBP	poly(dicarboxyethylfluorene-*alt*-biphenylene)
PFVP	poly(fluorene-*alt*-divinylphenylene)
Ph	phenyl
phen	phenanthroline
PIB	poly(isobutylene)
PIH	poly(iminohexamethylene)
PIODA	poly(isophthalic oxydianiline)
PM-α-CD	permethylated α-cyclodextrin
PM-β-CD	permethylated β-cyclodextrin
PMA	poly(methacrylate)
PMAN	poly(methylacrylonitrile)
PMDI	pyromellitic diimide
PMITZ	propyl-*N*-methyl-5-iodotriazolium
PMMA	poly(methyl methacrylate)
PMTZ	propyl-*N*-methyltriazolium
PMVE	poly(methyl vinyl ether)
pN	piconewtons
PNP24C8	*para*-nitrophenol[24]crown-8
PO292PC	pentoxa[2.9.2]paracyclophane
PP-β-CD	perpropyl-β-cyclodextrin
PPG	poly(propylene glycol)
pphen	2-(2-pyridyl)-1,10-phenanthroline
PPI	poly(propyleneimine)
ppm	parts per million
PPP	poly(*para*-phenylene)
PPV	poly(*para*-phenylene vinylene)
$PPYV^{n+}$	poly(pyridinium vinylene)
Pr	propyl
prox	proximal
ps	picoseconds
PS	polystyrene
PT	polythiophene
PTHF	poly(tetrahydrofuran)
PTP	*para*-tritylphenol
PTTF	pyrrolotetrathiafulvalene
PTTFS	pyrrolotetrathiafulvalene thioether
ptz	phenothiazine
PX25C7	pyrido-*para*-xylyl[25]crown-7
py	pyridine
PY^{+}	pyridinium
pybox	pyridine-2,6-bisoxazoline
pydc	pyridine-2,6-dicarboxamide
pytpy	2,4,6-tris(4-pyridyl)pyridine
QCM	quartz crystal microbalance
R	organic functional group; resistance
RCM	ring-closing metathesis
RCSR	Reticular Chemistry Structure Database
Re	Reynolds number
ref.	reference
RNA	ribonucleic acid
ROMP	ring-opening metathesis polymerization
RORCM	ring-opening ring-closing metathesis
RSCC	radical-state co-conformation
RT	room temperature
s	seconds
S	siemens
S/N	signal-to-noise
SA	succinamide
SAE	succinic amide ester
salen	salicylaldehyde–ethylenediamine condensate ligand
SALI	solvent-assisted ligand incorporation
salophen	salicylaldehyde–*o*-phenylenediamine condensate ligand
SAM	self-assembled monolayer
SBP	sulfate binding protein
SBU	secondary building unit
SCE	saturated calomel electrode
SEC	size exclusion chromatography
SEM	scanning electron microscopy
SERS	surface-enhanced Raman scattering
S_N1	unimolecular nucleophilic substitution
S_N2	bimolecular nucleophilic substitution
S_NAr	nucleophilic aromatic substitution
SP	spiropyran
ssDNA	single-stranded DNA
STTFS	tetrathiafulvalene dithioether
SWNT	single-walled carbon nanotube
T	temperature
t	time
T	thymine
^{t} or *t*-	*tert*-
$T_2$18C6$_2$	triptycene-bridged macrotricyclic [18]crown-6 dimer
$T_2$24C8$_2$	triptycene-bridged macrotricyclic [24]crown-8 dimer
$T_2$30C10$_2$	triptycene-bridged macrotricyclic [30]crown-10 dimer
TA24C8$_2$	triptycene/anthracene-bridged macrotricyclic [24]crown-8 dimer
TB24C8	tetraebenzo[24]crown-8
TB27C9	tribenzo[27]crown-9

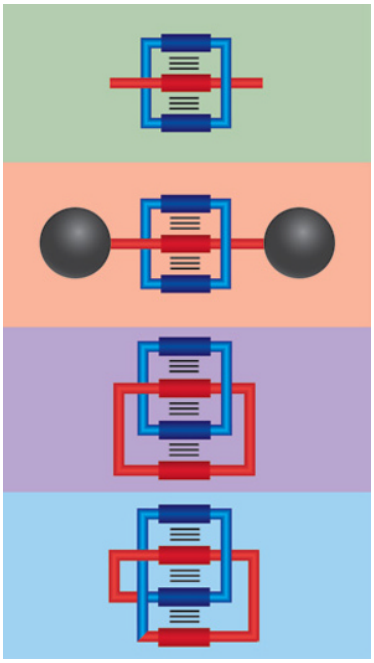
$TBPA^{\bullet+}$	tris(4-bromophenyl)aminium
TBTA	tris[(1-benzyl-1*H*-1,2,3-triazol-4-yl)methyl] amine
T_C	coalescence temperature
tcba	tris(4-carboxybenzyl)amine
TCBD	tetracyanobutadiene
TEM	transmission electron microscopy
TEMPO	(2,2,6,6-tetramethylpiperidin-1-yl)oxidanyl
TEOA	triethanolamine
terpy	2,2´:6´,2´´-terpyridine
$TexasBox^{4+}$	“Texas-sized” molecular box
TFA	trifluoroacetic acid
$TFPB^-$	tetrakis(3,5-trifluoromethylphenyl)borate
THF	tetrahydrofuran
THS-β-CD	pertrihexylsilyl-β-cyclodextrin
THYME	tetrahydroxymethylethylene
TIPS	triisopropylsilyl
TK30C9	triketo[30]crown-9
TL	tetralactam
TLC	thin layer chromatography
TMEDA	*N*,*N*,*N*´,*N*´-tetramethylethylenediamine
TMPD	tetramethylphenylenediamine
TMS	trimethylsilyl
TN57C15	trinaphtho[57]crown15
tnme	tris(isonicotinoxymethyl)ethane
TO*n*1*n*1PC	tetraoxa[*n*.1.*n*.1]paracyclophane
TPE	tetraphenylethene
TPP	tetraphenylporphyrin
TPP51C15	tris-*para*-phenylene[51]crown-15
TPP68C20	tetrakis-*para*-phenylene[68]crown-20
tpt	tris(4-pyridyl)-1,3,5-triazine
TPUCA6	triphenylureidocalix[6]arene
tpvb	1,3,5-tris((*E*)-2-(pyridin-3-yl)vinyl)benzene
Tr	trityl
trien	triethylenetetraamine
$TRIPY^{3+}$	benzene-1,3,5-tripyridin-4-ium
$TRISPHAT^-$	tris(tetrachlorobenzenediolato)phosphate(V)
trz^-	1,2,4-triazolide
Ts	tosyl
TTF	tetrathiafulvalene
TTL	triptycene tetralactam
TUC6	tetraphenylureido-calix[6]arene
TX	triple crossover DNA motif
TZ^+	triazolium
UHV	ultra high vacuum
UV	ultraviolet
V	volts
v/v; $^v/_v$	volume ratio
V24C8	vinylene[24]crown-8
Vis	visible
VT	variable temperature
W	Watts
w/w; $^w/_w$	weight ratio
wt. %	weight percent
X	linker
XAS	X-ray absorption spectroscopy
$XBPP^{2+}$	*para*-xylylene-bis(4-(4-pyridyl)pyridinium
XPS	X-ray photoelectron spectroscopy
XR	X-ray reflectometry
Xy	xylene
$XyBr_2$	α,α′-dibromo-*para*-xylene
$XyN3^{2+}$	*N*,*N*´-bis(3-pyridylmethyl)-*para*-xylylenediammonium
α-CD	α-cyclodextrin
α-HL	α-hemolysin
β-CD	β-cyclodextrin
β-gal	β-galactosidase
γ-CD	γ-cyclodextrin
Δ	thermal energy
Δ*G*	change in Gibbs free energy
Δ*H*	change in enthalpy
Δ*S*	change in entropy
δ	chemical shift
δ-VL	δ-valerolactone
ε	extinction coefficient
θ	angle
λ	wavelength; persistence length
μ	micro
μM	micromolar
μm	micrometers
π	π bond; surface pressure
ν	frequency
σ	grafting density
$\tau_{1/2}$	half-life
φ	quantum yield
ω	excluded volume
Ω	resistance (ohms)

Part 1

Introducing Mechanical Bonds

Chapter 1 An Introduction to the Mechanical Bond

Conspectus



Mechanical bonds are omnipresent and all pervasive. They occupy every nook and cranny of human experience in both static and dynamic settings that range from being close to infinitesimally small to those which can be described as large by comparison. In the domain of the molecular world, the mechanical bond emerges as an additional expression of the nature of the chemical bond in all its manifestations. This emergent phenomenon takes place in the lower reaches of the nanometer length scale as a special architectural feature. It emerges just as soon as it becomes spatially possible to entangle the *component parts* of molecules, the sizes of which are governed in part by the subnanometer distances between their constituent atoms.

The production of chemical compounds composed of *mechanically interlocked molecules* (MIMs) by acts of *templation*, be they passive or active in their origins, are hand-me-downs from the science of (supramolecular) chemistry beyond the molecule, which affords *molecular recognition* free rein to exercise its special powers of organization in marshaling the component parts of the MIMs prior to their being transported back into the molecular world by the formation of chemical bonds. This relatively recent extension of bonding in molecules opens the door on a yet little explored field of chemistry—namely that of *chemical topology*, which leads to the concept of *topological isomerism*, where two or more molecular ensembles may contain the same atoms and chemical bonds, yet cannot be interconverted by any deformations that do not involve the breaking and making of chemical bonds.

Intersecting the fields of *supramolecular chemistry* and *chemical topology* is the discipline of *mechanostereochemistry*. Just as stereochemistry is the study of the relative spatial arrangements of atoms in molecules, mechanostereochemistry is the stereochemistry of molecules with mechanical bonds. Catenanes and rotaxanes are a subset of MIMs that possess mechanical bonds. A *catenane* is a molecule with two or more interlocking ring-shaped component parts. The simplest of catenanes with two interlocked rings is a *topological isomer* of the two rings separated from each other. A *rotaxane* comprises (a) ring(s) threaded by (a) dumbbell(s) possessing stoppers that are too bulky for the ring(s) to transgress. The simplest of the rotaxanes with one ring and one dumbbell is not a topological isomer of the ring and dumbbell separated from one another since expansion of the ring or compression of the stoppers (without the breaking of chemical bonds) can lead to the separation of the component parts by a process known as *slippage*.

A *mechanical bond* is an entanglement in space between two or more component parts, such that they cannot be separated without breaking or distorting chemical bonds between atoms. It follows that a mechanical bond is as strong as the weakest participating chemical bond. Hence, catenanes and rotaxanes are most appropriately described as molecules, or more precisely, as *mechanomolecules*. Since entanglements are possible in molecules—for example, knots—that lack component parts, not all MIMs possess mechanical bonds. While catenanes and knots fall under the aegis of chemical topology, rotaxanes are considered to be topologically trivial because their component parts may be separated by the continuous deformation of chemical bonds. It is this dichotomy that exists between catenanes and knots on the one hand and rotaxanes on the other that has led to the adoption of the term mechanical bond when describing catenanes and rotaxanes in preference to topological bonds, which are present in catenanes and knots, but *not* in rotaxanes. One of the endearing charms of chemistry is that it defies repeatedly attempts at clear-cut descriptions of phenomena under its guard. In this particular instance, the much higher promise of wider applicability on the part of rotaxanes makes the case for promoting the chemistry of the mechanical bond.

Although the mechanical bond has been exploited and revered in society, art and Nature from time immemorial, it has proved to be immensely challenging to introduce synthetically into molecules and hence chemistry. Nothing of much significance had been recorded in the scientific literature up until the 1960s. This decade and the succeeding one witnessed simultaneously the advent of a painstaking classical approach, under the guidance of covalent-directed synthesis alongside statistical forays based on little more than the chance events of the threading of large-sized rings by suitably long molecular chains. With the emergence of host-guest and supramolecular chemistry in the 1970s, however, the stage was set for molecular recognition to lead to the *directed synthesis* of mechanomolecules through the acts of templation with coordinative, followed by noncovalent, bonds of many different persuasions. The result has been an exponential growth these past 35 years in *molecular nanotechnology*, coupled to a paradigm shift in molecular structure and function. While mechanomolecules have found their way, both singly and collectively, into switches and motors, the molecules themselves have led to a renaissance in *molecular aesthetics*. Introducing mechanical bonds into molecules can only assist in garnering support for the growing initiative to widen aesthetic considerations in chemistry.

The Nature of the Mechanical Bond: From Molecules to Machines, First Edition. Carson J. Bruns and J. Fraser Stoddart.
© 2017 John Wiley & Sons, Inc. Published 2017 by John Wiley & Sons, Inc.

Introduction 4
1.1 The Ubiquity of the Mechanical Bond 7
1.1.1 Mechanical Bonds in Nature 8
1.1.2 Mechanical Bonds in Art 10
1.1.3 Mechanical Bonds in Everyday Life 11
1.2 Representing Molecular Mechanical Bonds 13
1.2.1 A Historical Perspective 13
1.2.2 Perspective Stereoformulas 16
1.2.3 Depictions in Color 16
1.2.4 Solid-State Portrayals 17
1.2.5 Graphical Representations 18
1.2.6 Technomorphs 20
1.3 Aesthetics of Mechanical Bonds 21
1.3.1 Beauty in Diversity 21
1.3.2 Topological Beauty 21
1.3.3 Architectural Beauty 24
1.3.4 Simplicity and Elegance 28
1.3.5 Complexity and Emergence 30
1.3.6 Beautiful Machines with Mechanical Bonds 32
1.3.7 The Art of the Mechanical Bond 37
1.4 Evolution of Mechanostereochemistry 38
References 42

Introduction

A scientist wakes up in the morning, rubs her eyes, draws back the curtains and pulls up the window blinds. She goes through her morning ablutions and gets dressed; she buttons up her blouse, puts on her earrings, and ties her shoes. She plaits her hair into a braid before opening her door and hopping on a bicycle for her morning commute. As she rides in to work, she barely notices the other bicycles, cars, buses, and trains that carry the other morning commuters on their ways, or the swinging French doors, chain-link fences, and flagpole pulleys that decorate various home fronts on her route. On reaching work, she locks up her bicycle on a rack and takes an elevator up a few floors to her laboratory, where she opens up her computer and begins to think about something that has already pervaded her morning without even entering her consciousness. The window blinds, the blouse and buttons, the braids and earrings, the bicycles and automobiles, the fences and flagpoles, the bike lock and the elevator, not to mention the computer sitting in front of her, all share at least one thing in common—namely, the mechanical bond.

Although chemistry[1] has often been hailed[2–6] as "the central science", we must remember that chemists do not have a monopoly on the definition of a bond. In finance, a bond is an instrument of indebtedness. Biologists speak of pair bonding as a strong affinity between two individuals—often a breeding male and female—of a species. Social scientists speak of maternal bonds, paternal bonds, affectional bonds, male bonding, female bonding, and so on. Anthropologists classify acephalous societies, which lack political leaders and hierarchies, as land-bonded, village-bonded, or lineage-bonded societies. Indeed, bonds describe relationships, associations, and connectivity. A mechanical bond can therefore be understood as the connection between two objects that are held together by mechanical forces, meaning physical forces or contact forces, as a result of their entanglement in space. The mechanical bond is not at all exclusive to chemistry. In fact, the mechanical bond appears to be far more prevalent in our everyday lives—in art, technology, and nature, for example—than it is in synthetic molecules. Nevertheless, the study of the molecular mechanical bond has transitioned in little more than 50 years from being (i) a mere curiosity in the minds of a few forward-thinking intellectuals in the first half of the 20th century, to becoming (ii) a rather esoteric subfield of synthetic organic chemistry, practiced only by a handful of academic and industrial researchers in the 1950s, 60s, and 70s, to (iii) entering a phase of rapid and steady growth near the end of the 1980s on the back of new synthetic protocols which made the synthesis of molecules with mechanical bonds much more facile, to (iv) flourishing into the increasingly diverse and interdisciplinary field of chemistry that it is today.

Defining the Mechanical Bond

Arguably the most influential chemistry book ever to have been written—one which shaped profoundly our modern understanding of bonding in molecules—is Linus Pauling's 1939 monograph[1] on *The Nature of the Chemical Bond*. This classic treatise summarizes the pioneering work

carried out by himself and others during the 1920s and 1930s. Pauling classifies chemical bonding into three categories—electrostatic, covalent, and metallic bonds—representing extremes between which many intermediate types of bonds (e.g., hydrogen and halogen bonding) may exist. According to Pauling –

> *…there is a chemical bond between two atoms or groups of atoms in case that the forces acting between them are such as to lead to the formation of an aggregate with sufficient stability to make it convenient for the chemist to consider it as an independent molecular species.*[1]

It was not until more than two decades later that the newest bond in chemistry—namely, the mechanical bond—emerged on the scene. In Pauling-inspired prose, we might say that there is a mechanical bond between two objects in case that their ability to be separated is obstructed by an entanglement in three-dimensional space. This definition encompasses mechanical bonds at all scales, not only the molecular one. In chemistry, the mechanical bond is an emergent[A] type of bond that arises only when groups of atoms become large enough to permit the formation of entanglements in space. Whereas chemical bonds are typically shared between atoms, mechanical bonds are shared between groups of atoms, or molecular entities, which we will call component parts. In this volume we will refer to molecules with mechanical bonds as mechanomolecules.

Mechanical bond – An entanglement in space between two or more molecular entities (component parts) such that they cannot be separated without breaking or distorting chemical bonds between atoms.

Component part – A group of atoms, or 'molecular entity', comprised of chemical bonds, which is mutually engaged in mechanical bonding with another molecular entity.

Mechanomolecule – A molecule possessing one or more mechanical bonds.

The two quintessential types of mechanomolecules (**Figure 1.1**) are catenanes and rotaxanes. A catenane—its name derived from the Latin word *catena*, meaning 'chain'—is a molecule with two or more interlocking ring-shaped component parts. A rotaxane—derived from the Latin words *rota* (wheel) and *axis* (axle)—comprises a ring threaded by an axle-like molecular entity, or 'dumbbell', with endgroups (stoppers) that are too bulky for the ring to transgress. Some mechanomolecules, such as rotacatenanes,[7] suitanes,[8] double-lassos,[9] helix-rod assemblies,[10] mechanically self-locked ring-in-ring assemblies,[11] and Gemini catenanes[12] do not fit cleanly into either category—see **Section 4.3**.

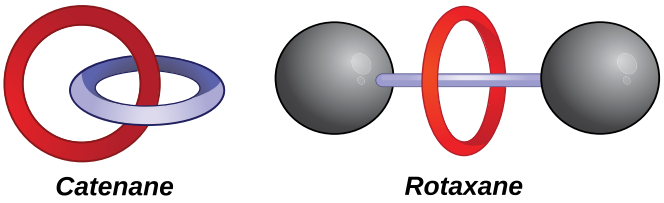


Figure 1.1 Graphical representations of a catenane (left) and a rotaxane (right), which comprise the two main classes of mechanomolecules.

Mechanomolecules belong to several intersecting fields (**Figure 1.2**) of chemical research. Catenanes and rotaxanes are a subset of a family of molecules known[13–17] as Mechanically Interlocked Molecules, or MIMs, for short. Not all MIMs necessarily possess mechanical bonds because entanglements are possible in molecules that lack distinguishable component parts, such as molecular knots. Another intersecting field of research is chemical topology,[18–25] which deals with the aspects of structure that are preserved throughout any process of continuous deformation—i.e., stretching, compressing, or bending of bonds without allowing them to cross or break. Discussions of chemical topology are featured in **Sections 1.2.1** and **1.3.2**, as well as the **Chapter 2** Introduction, **Section 4.1**, and **Section 5.2.4**. Some MIMs, such as knots and catenanes, fall under the umbrella of chemical topology, while other MIMs, such as rotaxanes and suitanes, are considered topologically trivial because their component parts may be separated by continuous deformation. The identification of rotaxanes as molecules with topological bonds is a common misnomer in the literature. Another common misnomer identifies catenanes and rotaxanes as supramolecular entities, or supermolecules. We do not consider most mechanomolecules to be supermolecules, at least when

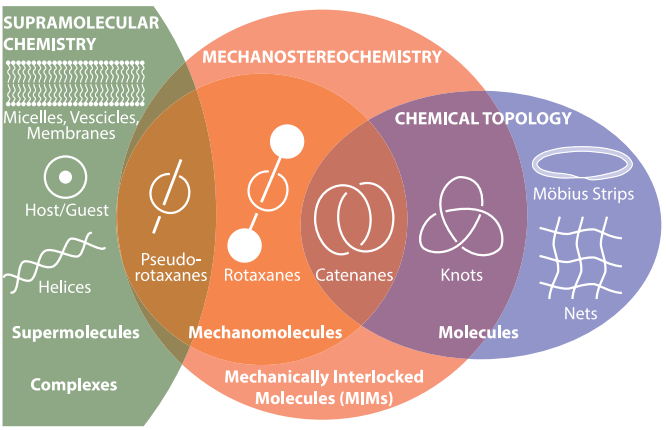


Figure 1.2 A Venn diagram illustrating how different types of molecular species fit into the intersecting fields of supramolecular chemistry, mechanostereochemistry, and chemical topology.

[A] The term 'emergent' is muddled with ambiguity in the literature. In our view, new properties that arise as a result of an increase in the complexity of a system may be considered emergent. See **Section 1.3.5**.

the mechanical bond is sealed by strong covalent bonds, because the component parts cannot dissociate and exchange as supramolecular complexes do. In the case of complexes known[26] as pseudorotaxanes, which lack stoppers that are sufficiently bulky to prevent the dissociation of component parts, the boundary between mechanomolecules and supermolecules is blurred. This grey area in between the supramolecular and the 'mechanomolecular' is discussed in **Section 3.1.1**.

It is clear to us that the boundaries and relationships between mechanical and chemical bonds are not always straightforward. Is the mechanical bond a chemical bond? Yes and no.

Yes, because…	**No**, because…
…mechanically interlocked molecular entities are engaged in a situation that fully satisfies Pauling's definition (also the IUPAC Gold Book definition[27]) of a chemical bond.	…the mechanical bond can exist between many types of objects other than discrete molecular entities – it is much more than a chemical bond!
…the mechanical bond can be identified in molecules.	…a mechanical bond cannot exist between atoms.
…like chemical bonds, mechanical bonds carry an entropic penalty[B].	…unlike chemical bonds, there is no enthalpy of a mechanical bond[B].

Mechanical bonds seem to be in a grey area when it comes to chemical bonding, arising from the fact that they are indeed stable bonds in molecules, yet maintained only by the physical forces that prevent bonds from passing through one another. A mechanical bond is therefore approximately as strong as the weakest participating chemical bond (**Table 1.1**) in the constitution of its component parts. A 'participating' chemical bond is one that is critical to maintaining a mechanical bond—i.e., cleavage of a participating chemical bond would cause the mechanical bond to break. The vast majority of synthetic mechanical bonds in the molecular world are sealed by covalent or coordinate (dative) bonds, owing to their high thermodynamic and kinetic stabilities. We reiterate that most rotaxanes and catenanes are better described as *molecules*, rather than *supermolecules*, when their molecular pieces cannot be separated without breaking strong chemical bonds. There are examples of mechanical bonds, however, that rely on weaker interactions, such as hydrogen bonding in biomolecular (**Section 2.3.12**) assemblies.

Table 1.1 Different types of bonds and typical ranges for their associated energies.

Bond Type	**Energy Range[a] / kcal·mol^{-1}**
'Weak' Chemical Bonds – Intermolecular & van der Waals	
Dispersion Forces	≤1
Dipole–Dipole Interactions	0.5–2
Hydrogen Bonds	1–10
Halogen Bonds	1–40
Ion-Pairing[b]	2–50
Strong Chemical Bonds – Covalent and Ionic	
Coordinate/Dative Bonds (M–X)	10–100
Organic Covalent Bonds (C–X)	60–100
Ionic Lattice[b]	250–4000
Mechanical Bond	≈ weakest participating chemical bond[c]

[a] Energy ranges are estimated on an atom-to-atom basis. Many van der Waals interactions, especially dispersion forces, are typically multivalent, increasing in strength with increasing molecular size.
[b] Ionic lattice energies reflect crystallization from the gas phase, while ion-pairing reflects the formation of contact, solvent-shared, or solvent-separated ion pairs in solution. The much weaker ion-pair interaction depends heavily on the dielectric constant, according to Debye-Hückel theory.
[c] The strength of a mechanical bond is approximately equal to, or greater than, the weakest chemical bond that 'participates' such that its cleavage would allow component parts to dissociate.

One can understand a lot about the chemistry of mechanical bonds by means of analogy with the chemistry of covalent bonds. In order to facilitate our discussion of molecules with mechanical bonds, it will be convenient to introduce terminology as a matter of comparison with counterpart terms involving chemical bonds—these definitions come either from our Glossary or the IUPAC Gold Book.[27] For example, since stereochemistry encompasses chemical bonding at all levels of structure in both dynamic and static contexts, we advocate the term 'mechanostereochemistry' for describing all aspects of mechanical bonding in molecules.[16]

Stereochemistry[27] – the study of the relative spatial arrangements of atoms that form the structure of molecules and their manipulation.

Mechanostereochemistry[16] – the stereochemistry of molecules with mechanical bonds.

Generalizing beyond chemistry the concept of the mechanical bond as a situation in which the physical separation of two objects is obstructed by an entanglement in space, it becomes apparent that life as we know it is deeply

[B] Any enthalpic gains or losses associated with breaking or making mechanical bonds are attributable to covalent, dative, and/or noncovalent (electrostatic) interactions between atoms that are gained or lost as a consequence of mechanical bonding, rather than to the mechanical bond itself. Since the mechanical bond limits the translational and conformational freedom of its component parts, however, the corresponding entropic penalty can be attributed directly to the mechanical bond.

entrenched in mechanical bonds. The prototypical mechanical bond is that of a chain link: two rings interlocked such that they cannot be separated, each of them able to move independently within the constraints of the other. This (constrained) freedom of motion is one of the enduring attributes of the mechanical bond. The ability of mechanically linked objects to move relative to one another serves as the basis for most machinery—take the spinning wheels of a bicycle as an archetypal example. Note, however, that objects can share a mechanical bond without freedom of motion as well. For example, the mechanically bonded bolt that constrains a street sign to a post is intended to prevent motion. The advantage of a mechanical bond in this context is modularity, since it is easier to change a sign that is screwed into a post than one that is welded onto it. Thus, the mechanical bond is conceptually different from a seal involving welding or glue, for example, or from containment,[28–31] where one object is encased completely within another.[C]

It is clear to us that the mechanical bond is everywhere and its role in our everyday lives is indispensable. Therefore, this book begins with an examination (**Section 1.1**) of the mechanical bond in contexts other than chemistry. Later, we survey how molecules with mechanical bonds, which cannot be seen by the naked eye, are represented (**Section 1.2**) in the scientific literature in the form of images. We give pride of place in this Chapter to a topic that is rarely covered in formal chemical literature—namely, beauty. There is a deep connection between chemistry and art, rendering both disciplines fair game for a branch of philosophy known as aesthetics—a field that deals with art, beauty, and taste. We are committed to the notion that the mechanical bond is a thing of immense beauty in addition to its all-pervasive functional diversity. Following an introduction to the mechanical bond across a variety of different settings, communities, and length scales, we will preview the range of this book's contents in the context of molecular aesthetics (**Section 1.3**), before finally offering a perspective (**Section 1.4**) on the evolution of mechanostereochemistry. The discussion in **Sections 1.1–1.3**, which is driven by the concept of beauty in chemistry,[32] is expanded upon and borrowed from, in part, our review[33] of mechanical bonds in the context of beauty, with permission from the publisher (copyright 2012 Springer-Verlag).

1.1 The Ubiquity of the Mechanical Bond

The unique connection between chemistry and art has been recognized since at least 1860, when French chemist Marcellin Berthelot wrote, "*La Chimie crée son objet. Cette faculté créatrice semblable à celle de l'art lui-même, la distingue essentiellement des sciences naturelles et historiques,*" which translates in English to:

> *"Chemistry creates its own object. This creative quality, resembling that of art itself, distinguishes it essentially from natural and historical sciences."*

Berthelot recognized that the creative component of chemistry is not only unlike other sciences, but also similar to that of art. But what is art? To attempt to define it is to enter a realm that chemists, naïve as we are in these matters, had best avoid. We note, nevertheless, that the former Wikipedia[34] definition, "the process or product of deliberately arranging elements in a way to affect the senses or emotions," can be truncated into a reasonably suitable definition for (synthetic) chemistry—the process or product of deliberately arranging elements. The essence of creativity is indeed inherent to both disciplines.

The similarities and differences between art and science have been long deliberated.[35] Foremost among these deliberations is the issue of beauty. Rather than attempting to summarize or evaluate the numerous angles on the relationship between science and art, let us simply draw attention to the philosophy that has profoundly shaped modern perceptions on the subject of beauty in science, which stems from the notion that science and art are different forms of symbolic activities. Werner Heisenberg, a Nobel Prize winner in Physics and proponent of this perspective, defined[36] beauty as "the proper conformity of the parts to one another and to the whole." He crowned mathematical beauty—unification through abstraction—as the prevailing flavor of beauty in science. This ideal is noble but it is unfortunate that it has reigned so exclusively; others have noted[37] the irony that chemistry, for all its sensory content—its colors, odors, textures—is much less associated with beauty than mathematical physics. Whence the beauty of empirical science? As Roald Hoffman and Pierre Laszlo[38] have commented, "*our discipline is a curious mix of empirical observation and abstract reasoning. This is not unlike music—but it parts chemistry from the pure rigor of mathematics.*" We hope this Chapter will garner support for the growing initiative[39–44] to widen aesthetic considerations in chemistry, even as a basis for research.[45]

A discussion of beauty in chemistry might consider the beauty of materials[46]—the color and texture of a pigment, or the shape and clarity of a crystal, for example—or refer to the molecules themselves. Both have an obvious connection with the visual arts; chemistry is largely responsible for the ever-growing diversity of materials artists manipulate, but there is beauty in the structures of molecules as well. In this Chapter, we will leave materials aside and focus on the beauty of molecular structures, or more accurately their representations in which chemists engage with pride and prejudice. The topic of molecular beauty is largely eschewed from the literature, residing instead primarily in the informal discussions, meetings, and conferences between colleagues. Nobel laureate Roald Hoffman,[47] who

[C] Examples of containment in the molecular world include carceplexes,[28] endohedral fullerenes[29] and molecular peapods,[30] and many kinds of self-assembled 'molecular flasks' and cages.[31] Our perspective is that these types of molecules and assemblies are fundamentally different than MIMs because they involve complete enclosure rather than entanglement.

recognized that chemistry's rich and visual symbolic language is an important contributor to beauty in science, spearheaded[48–51] a more formal discussion in 1988.

The roots of molecular beauty can be traced back to the Platonic tradition. To Plato, "the most beautiful bodies in the whole realm of bodies" were the tiny polyhedra, now deemed the Platonic solids, which he proposed comprise the universe: the four elements—earth (cube), fire (tetrahedron), air (octahedron), water (icosahedron)—and the ether (dodecahedron) (**Figure 1.3**). Joachim Schummer, who has written[41] extensively on chemical aesthetics, reflects:

> *"Modern chemistry is exactly the art that provides creative access to what Plato considered the realm of the most beautiful bodies. Therefore, it is no surprise that chemists put their creative activity also in the service of beauty."*

Of course, the 'realm of the most beautiful bodies' is too small to see, but there is something charming about the way a molecule is physically crafted, like sculpture, through diligent labor, yet is only perceived mentally, like poetical imagery, with the aid of symbols. Here, we engage these symbols—our imperfect and incomplete representations of molecules—as artwork. We will not hazard straying into the complex territory of contention on this issue, which has been discussed[41] superbly elsewhere, for we understand beauty as that which provides one with a sense of personal pleasure more than in the context of rigorous aesthetic formalisms. We take for granted that beauty has a place in chemistry because we know, as such, that chemists are passionate in their vocation and take great pleasure in their work. The same may be said of people in countless other occupations, from farmers to cyber hackers, who also undoubtedly find beauty in their work. Moreover, despite a lack of formal aesthetic training among most chemists—and the longstanding stigma associated with discussing beauty in the scientific literature—at least 2% of chemistry papers mention[52] aesthetic values as a justification for studying a molecule. Classic examples include a variety of synthetic Platonic and Archimedean objects[53] such as cubane,[54] dodecahedrane,[55,56] buckminsterfullerene,[57] and many metal-ligand coordination complexes and cages[58,59] that have been lauded[42] for their symmetry, simplicity, uniformity, and harmony—"simply beautiful and beautifully simple." On the other hand, natural products and their corresponding organic transformations have been admired[60–62] for the beauty in their elegance, complexity, and sophistication. Woodward, arguably the most preeminent organic chemist of the 20th century, recognized the art of organic synthesis—an art acknowledged even by the Nobel Prize committee—as an act of beauty.[63]

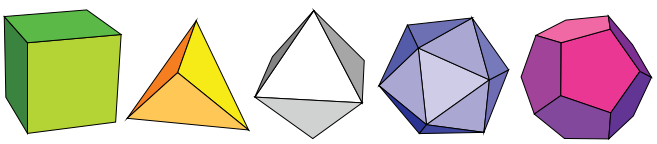


Figure 1.3 The Platonic solids were the most beautiful bodies according to Plato. Like molecules, these imperceptibly small objects were thought to compose the physical world.

Molecular nanotechnology has uncovered yet another way to address beauty in chemistry: miniaturization. Chemists now frequently "miniaturize" everyday objects by constructing them, to varying and sometimes quite liberal degrees of approximation, using molecules as their building blocks. Our affinity for miniaturization is a consequence of (i) the development of supramolecular chemistry,[64] which has made this kind of miniaturization possible, and (ii) the emergence of a paradigm shift in molecular representations, in which molecules are portrayed more ambiguously so as to resemble their macroscopic analogues. In other words, the vision of a miniaturized world has been catalyzed in part by the beautiful new ways of representing molecules, which deliberately blur the lines between the molecular world and the macroscopic one. We have referred to these graphical representations as cartoons, as well as illustrations, and—in this Chapter—art. In this regard, mechanically interlocked molecules are of particular interest because they have played a central role in molecular nanotechnology and the aforementioned paradigm shift to more artistically disposed figures and schemes in the literature. Moreover, the mechanical bond is ubiquitous in the macroscopic world, but has been, until relatively recently, challenging to introduce into molecules.

There is no question that beauty is subjective—even if chemistry is not *about* beauty, few who practice it would argue that it is devoid of beauty. In this Section, we will use images to highlight, support, and substantiate claims on the beauty of mechanostereochemistry. Insofar as beauty is derived from our surroundings, the mechanical bond cannot be ignored. It is applied and admired in society, art, and Nature alike, and its beauty is held as both an ancient and modern sentiment. The ubiquity of the mechanical bond is apparent in everyday life (**Section 1.1.3**) because of modern tools and machinery, many of which we consider beautiful—think of a sporty car or a delicate Rube Goldberg (Heath Robinson) machine. Likewise, interlocked rings can be found in thousands of works of art (**Section 1.1.2**) dating through antiquity. Perhaps most surprising to the casual reader will be the predominance of mechanical bonds in Nature (**Section 1.1.1**), even within the cells of our own bodies.

1.1.1 Mechanical Bonds in Nature

Perhaps the most incontrovertible source from which we derive beauty is Nature. In terms of molecular beauty, Nature has perfected its brand of chemistry over billions of years and is an endless source of inspiration for chemists. For all our efforts, the number of chemicals and reactions we have discovered and created seem diminished by the bewildering complexity and sheer abundance of those present in Nature. In particular, the diversity and intricacy of

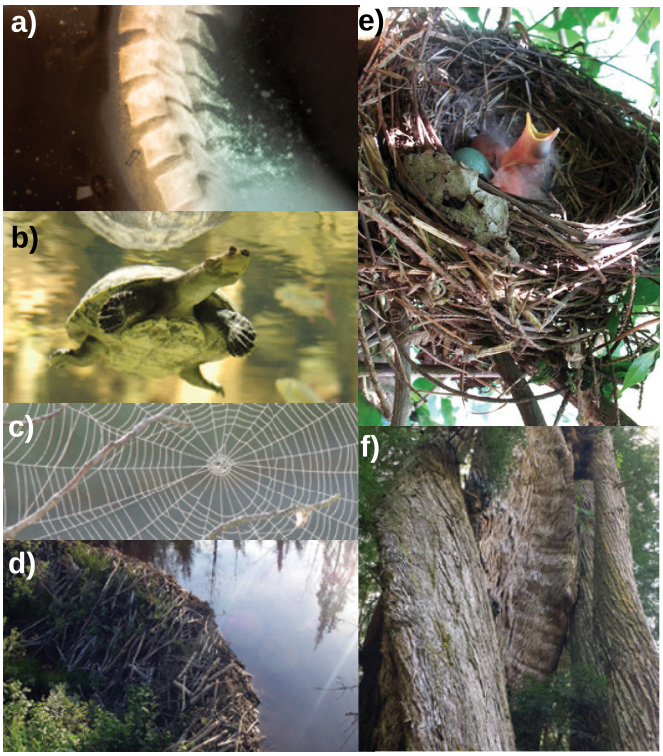


Figure 1.4 Examples of mechanical bonds in Nature. (a) X-Ray image of human vertebrae, which protect the spinal cord with rotaxane-like mechanical bonds. (b) A turtle forms a type of mechanical bond with its protective shell that is known in the molecular world as a suitane. (c) The mechanically criss-crossed network of a spider's web is what traps the spider's prey. (d) The structural integrity of a beaver dam is attributable, in large part, to a mechanically interlocked network of branches and logs. Photo: Lars Lindahl. (e) The mechanically bonded twigs which support the structure of a bird's nest provide a safe space for eggs and hatchlings. (f) If one of the entangled trunks of California Red-wood National Park's corkscrew trees were to be uprooted, the mechanical bond would prevent it from falling. Photo: Paul Herrig

systems and cycles in the chemistry of life processes are still far beyond our total comprehension. Even so, in a world where structure and function are so intrinsically linked, it should come as no surprise that Nature started dabbling with mechanical bonds long before humans came onto the scene. Our very bones form mechanical bonds with other tissues and organs, such as the rotaxane-like mammalian spine (**Figure 1.4a**). Just as the vertebrae offer protection for the fragile spinal cord, the suitane-like[8] mechanical bond of a turtle's shell (**Figure 1.4b**) helps protect the turtle's body. A number of animals rely on mechanical bonds for survival—spiders (**Figure 1.4c**) employ mechanical bonds to capture prey, while beavers (**Figure 1.4d**) and birds (**Figure 1.4e**) use them to build homes. Even trees (**Figure 1.4f**) occasionally tangle themselves into mechanically interlocked situations.

Although mechanical bonds can be identified in Nature across the macroscale, mechanical bonds are being made and broken incessantly within the microscopic world of cells. Contrary to modern industry, where technology utilizes the mechanical bond far more ubiquitously on the macroscale than on the nanoscale, Nature depends more vitally on mechanical interlocking at the molecular level. DNA is foremost among the players in biological MIMs. DNA catenanes[65] and knots[66] are intermediate structures in basic biological processes such as DNA recombination and replication, as mediated by various enzymes.[67] Many natural topological DNA structures have now been imaged[68] quite beautifully by electron microscopy (**Figure 1.5a**).

Not only does DNA form itself into catenated and knotted structures, it also rotaxanates itself with pseudo-macrocyclic enzymes.[69,70] λ-Exonuclease is an enzyme that participates (**Figure 1.5b**) in DNA replication and repair by encircling DNA fully as it sequentially hydrolyzes nucleotides—a biomolecular rotaxane! T4 DNA Polymerase holoenzyme[71] is an analogous example; its protein subunits clamp around a DNA strand to form a toroid in what chemists of the mechanical bond would call a 'clipping' process. It should be noted that chemists have been able to mimic this concept of a mechanically linked catalyst on a polymer[72–74] using traditional organic catalytic reactions. See **Section 6.15.3.1**.

DNA is not the only entity that can serve as component of biological MIMs—a continually growing number of mechanically interlocked protein structures have also been discovered –

- The extraordinary interlocked structure[75] of the bacteriophage HK97 capsid involves an icosahedral shell of topologically linked protein macrocycles (**Figure 1.5c**) which resemble the netting of chainmail. The 420 isopeptide crosslinks of this topological net strengthen[76] the mechanical properties of the capsid and may prevent it from bursting prematurely under the very high internal pressure (up to 40 atm) of its densely packed DNA cargo.
- *E. coli* Class Ia ribonuclease reductase[77] is another enzyme which forms a ring assembly that was found to be concatenated in the crystal.
- An enzyme known as CS_2 hydrolase, which converts carbon disulfide rapidly into carbon dioxide and hydrogen sulfide, has evolved in extremophilic life-forms—namely, acid-loving (acidophilic) and heat-loving (thermophilic) archaea living in harsh volcanic areas. The protein monomers of CS_2 hydrolase assemble into two different forms—one of them (**Figure 1.5d**) is a hexadecamer in which two octameric protein macrorings are catenated, while the other form is a non-catenated square-shaped octameric ring.[78,79] Measurements of the enzyme kinetics suggest that the hexadecameric catenane is more active than the octameric ring, most likely because it can accommodate a higher density of active sites per assembly.[80]
- The crystal structure (**Figure 1.5e**) of a C168S mutant of a typical Cys-2 peroxiredoxin III enzyme from bovine mitochondria was discovered[81] to be a [2]catenane comprising two interlocked dodecameric protein toroids. The protein-protein contacts within each ring are driven by

hydrophobic forces, while the ring-ring protein contacts arise from dipolar interactions.

- RecR, a protein involved in DNA repair in prokaryotes, assembles into a tetrameric protein complex with a central hole of over 3 nm in diameter. Two of these tetramers are concatenated in the crystal,[82] which implies that the tetramer can be easily opened and closed in the cell, since DNA occupies this cavity during repair.[83]
- Extremophiles that are adapted to survive in harsh conditions such as highly acidic environments and temperatures exceeding 100 °C must have evolved special strategies to prevent their cellular proteins from denaturation. Another thermophilic archaeon known as Pyrobaculum aerophilum relies on topologically linked proteins (**Figure 1.5f**) to stabilize its citrate synthase enzyme. The enzyme exists as a homodimer in which intramolecular disulfide bonds create a topological link—i.e., a catenane—which renders the monomers inseparable, imparting the protein with extra thermal stability.[84]
- During gene replication, the separation of sister chromatids (two identical copies of a chromosome) is regulated by the protein cohesin, which has been found[85] to entrap circular DNA loops in topologically catenated structures using chemical crosslinks, which influence the kinetics of cell division processes.
- Various proteins are recruited to the surface of mitochondria to form a nanotube around the entire organelle. The mechanical bond between this nanotube and the mitochondria is responsible for mitochondrial replication because it provides the contractile force for membrane scission.[86,87] The phenomenon of a ring contracting as it encircles a rod in order to sever it is not unlike certain digestive processes or a common method of bovine castration! It is intriguing that this mechanical pinching process happens at the scale of intracellular processes as well.

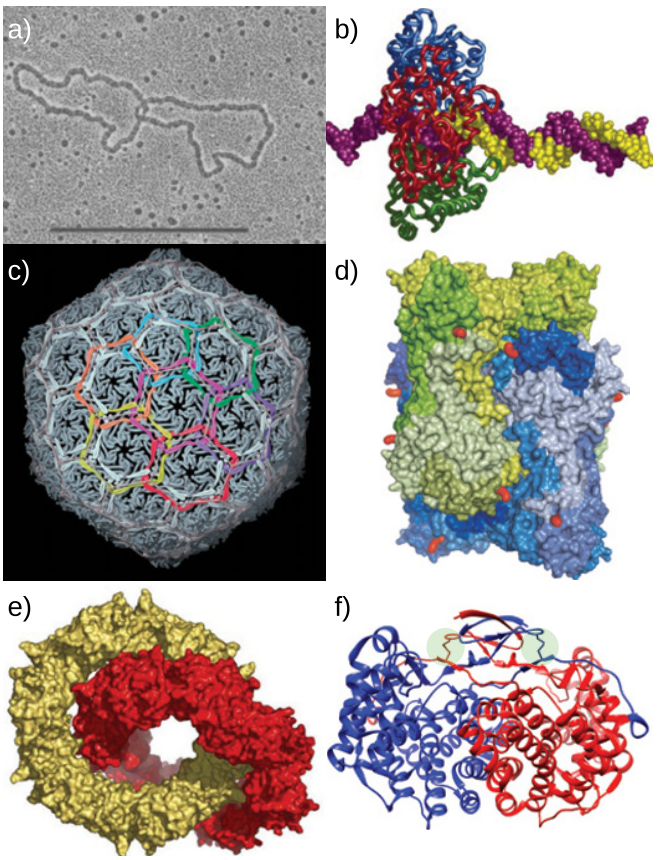


Figure 1.5 Examples of mechanical bonds in molecular biology. (a) Electron micrograph of a DNA catenane.[68] Scale bar: 1 μm. (b) The crystal structure of λ-exonuclease, paired with a model depicting how it encircles DNA while catalyzing its hydrolysis.[69] (c) 'Protein chainmail': The crystal structure of the bacteriophage HK97 capsid, highlighting catenated protein macrocycles.[75] (d) The crystal structure of the catenated enzyme CS_2 hydrolase.[80] (e) The crystal structure of the catenated peroxiredoxin III enzyme C168S mutant.[81] (f) Disulfide crosslinks (green circles) stabilize the citrate synthase enzyme of Pyrobaculum aerophilum.[84] (a)–(e) reproduced with permission from refs. 68 (copyright 1980 Elsevier), 69 (copyright 2003 Oxford Univesity Press), 75 (copyright 2000 AAAS), 80 (copyright 2014 Royal Society of Chemistry), 81 (Copyright 2005 Elsevier)

Although we feel that the beauty of this biomolecular machinery speaks for itself, Nature does not create art deliberately—the mechanical bond plays a vital functional role in these systems, which ranges from added stability to precise spatial organization of proteins and nucleic acids. It is apparent that our achievements as chemists in harnessing the chemistry of mechanical bonds have been surpassed as usual by Nature, who executes her particular brand of chemistry with a level of elegance, complexity, and beauty that we can only hold in awe, yet will surely use as a source of inspiration for many years to come.

1.1.2 Mechanical Bonds in Art

If anything can speak to the aesthetics of the mechanical bond, it is the art that portrays it. Nowhere is the beauty of the mechanical bond more validated than in the world of art—indeed, artists have been drawing, painting, carving, and sculpting mechanical bonds for thousands of years!

The mechanical bond may be celebrated (**Figure 1.6–1.7**) with many art forms, including (but not limited to) prints and carvings (**Figure 1.6c–d, 1.7a**), sculpture (**Figure 1.7b–c**), textiles (**Figure 1.7d–e**), stained glass (**Figure 1.7f**), origami (**Figure 1.7g**), body art (**Figure 1.7h**), mosaics (**Figure 1.7i**), architecture (**Figure 1.7j**), and even performance art (**Figure 1.7k**).

Borromean rings, such as those portrayed in **Figure 1.6** and **Figure 1.7e-f**, are a class of mechanically interlocked objects that deserve special attention in this Section on account of their prevalence in art, spanning across many cultures and thousands of years.[88] Their name originates from the aristocratic Borromeo family of what is now northern Italy, on whose crest (**Figure 1.6b**) and estate edifices the rings appear frequently. They have been associated with the Borromeo family from at least the 15th century, though recorded use of the symbols date back to at least the 13th century in Christian iconography (**Figure 1.6c**), the 12th century in Japanese emblems, and the 9th century in

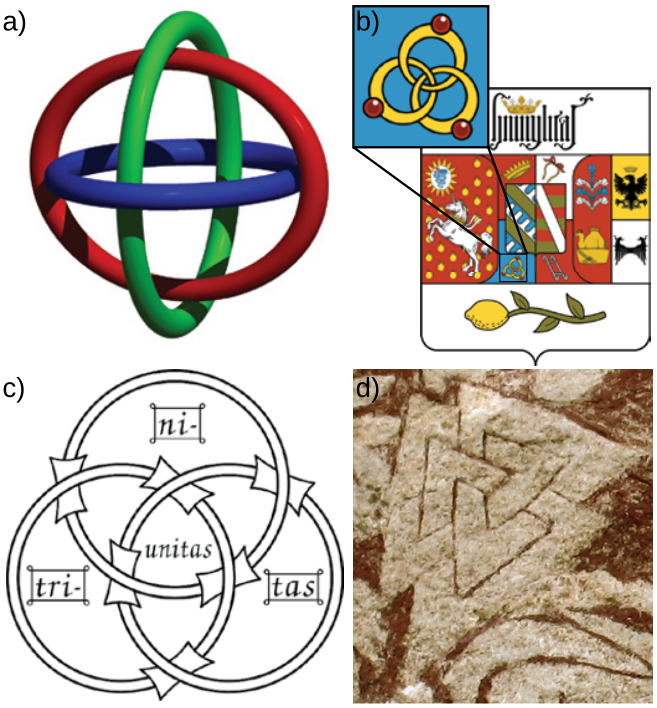


Figure 1.6 The Borromean Rings (BRs). (a) An orthogonal perspective of BRs visualizes the three inseparable rings, where breaking any one ring unlinks the other rings. (b) BRs as they appear on the Borromeo family crest. (c) The use of BRs to symbolize the Holy Trinity date back to the 13th century. (d) The Valknot is a Borromean Viking symbol found on ancient stone carvings from as early as the 9th century.

Viking symbols (**Figure 1.6d**), making them a remarkably universal icon.[D] Topologically speaking, the three rings are interlocked in such a way that breaking any one ring results in the dissociation of the other two intact rings (**Figure 1.6a**). This mutual dependence is what has made the rings such a powerful symbol for threefold unification, having been adopted to symbolize triads including Christianity's Holy Trinity (father, son, and holy spirit), Shintoism's three realms (heaven, earth, underworld), and even an advertising campaign (purity, body, flavor) for Ballantine Brewery's beer. The richness of symbolism, as well as the accompanying centuries of artwork associated with Borromean Rings, leaves little question as to their beauty. Molecular Borromean rings[89] are discussed in **Section 4.1.1.3**.

Solomon Knots have a similar history of predominance in art and history. The Solomon Knot is more accurately described as a link, since it consists of two rings that are doubly interlocked. The structure of the link, which has no obvious beginning or end, has made it a remarkably adaptable icon. It has been an important symbol in many cultures throughout history, including parts of Judaism, Christianity, and Islam, as well as with the Yoruba, Akan, and Kuba people of Africa.[90] The mosaic (**Figure 1.7i**) from the Byzantine Basilica beneath the Church of the Nativity in Bethlehem, Israel contains several examples of ancient artwork portraying the Solomon Knot. As the seal of the Biblical King Solomon, this symbol has represented wisdom and knowledge. In other contexts, it has signified eternity, beauty, and royalty. From ancient Roman mosaics to Celtic carvings to African headdresses to Middle Eastern relics and stained glass church windows, the Solomon Knot is a powerful symbol of beauty in art, religion, and culture. Seeing Solomon's Knot by Lois Rose Rose[91] is a recent and well-crafted exploration of the artwork of Solomon's Knot across time and cultures. Molecular Solomon Knots are discussed in **Section 4.1.1.1**.

Many artists employ links as symbols of unification, since their mechanical bonds bring together two or more otherwise unconnected objects. Particularly classic examples are the *Bonds of Friendship* statues (**Figure 1.7c**) by John Robinson in the sister cities of Sydney, Australia and Portsmouth, England depicting two linked rings,[92] as well as Ryoji Goto's 1978 *Intersecting Space Construction* (**Figure 1.7b**) symbolizing the beauty of human connections. One of the most famous artists to glorify the mechanical bond was M.C. Escher, whose math and science-based art has long encouraged discourse on the topic of beauty in science. His final print, *Snakes* (**Figure 1.7a**), portrays an array of interlocking rings that extends infinitely inwards, inhabited by a few mechanically interlocked serpents. We find this piece beautiful, not only for its rotational symmetry and mechanical bonds, but also because it points to the concept of infinitesimal smallness—foreshadowing the days when networks of interlocked rings almost too small to imagine are a reality—see **Section 4.1.3.5**. Minsuk Cho's Ring Dome Pavilion (**Figure 1.7j**) marks what must be one of the largest (and perhaps only) architectural structures comprising exclusively mechanically interlocked rings, while the attractive structure of Daniel Kwan's *Ten Interlocking Triangular Prisms* (**Figure 1.7g**) highlights the challenging complexity that can be attained among objects with mechanical bonds.

The mechanical bond is a focal point for human expression. With all sorts of different art forms celebrating the mechanical bond and the corresponding meaningful concepts and feelings which it symbolizes, it is not difficult to engender an eagerness to celebrate the beauty of the mechanical bond at the molecular level too.

1.1.3 Mechanical Bonds in Everyday Life

One cannot navigate the modern world without regularly encountering the mechanical bond. We typically take it for granted. So pervasive are interlocked structures in all things man-made, if we acknowledged consciously every mechanical bond we encountered, we might scarcely be able to accommodate any other mental processes! Here, we simply point (**Figure 1.8**) to fashion and technology as illustrative reminders of its omnipresence in society.

We all wear the mechanical bond day in and day out; those with body piercings even use it as a permanent

[D] For many more images of Borromean artwork, see ref. 88.



Figure 1.7 Examples of mechanical bonds in art. (a) In M.C. Escher's woodblock print, *Snakes*, a net of multiply interlocked rings extends infinitely inwards. © 2015 The M.C. Escher Company, The Netherlands. All rights reserved. www.mcescher.com (b) The *Intersecting Space Construction* statue at Hakone Open-Air Museum, Japan by Ryoji Goto presents an interlocked network of connected bodies. (c) Two copies of the *Bonds of Friendship* sculpture by John Robinson are located in Portsmouth, England and Sydney, Australia, commemorating a centuries-old relationship between these two sister cities. (d) Weaving is an art form that depends on mechanical bonds between enmeshed threads or reeds. (e) Borromean rings are portrayed in the textile artwork of Kirsten Griffiths. (f) Three interlocking rings are portrayed in the stained glass artwork within the Catedral de São Pedro de Alcântra in Petrópolis, Rio de Janeiro, Brazil. (g) Ten Interlocking Prisms origami design by Daniel Kwan (photo: Jakub Solovsk). (h) Permanent and semi-permanent mechanical bonds with the flesh represent a form of body art known as piercing. The earring ornament in this photo also contains hundreds of mechanical bonds comprising interlocked chains and beads. (i) Ancient mosaic of catenated objects and Solomon Knots in the Byzantine Basilica, Israel. (j) The Ring Dome Pavilion by architect Minsuk Cho is composed entirely of mechanically interlocked plastic rings—1500 hula hoops and 12000 zip-ties. Photo: Rory Hyde. (k) Performance arts such as trapeze also rely on mechanical bonds, such as transient ones between bodies in motion, as well as those which comprise the swing and its supporting structure.

decoration. This practice is not exclusive to Western society; note the mechanically bound objects around the headdress, ears, mouth, and neck of the Mursi woman of southern Ethiopia in **Figure 1.8a**, and the neck-extending rings of Northern Thailand's Kayan Lahwi woman (**Figure 1.8b**). These are perhaps extreme examples, but we all use the mechanical bond to a tremendous extent in the decoration of our bodies and clothing, from both a practical standpoint and an aesthetic one. Rings, necklaces, bracelets, belts, and even our shirts and trousers all form mechanical bonds with our bodies and with themselves. For example, compare a necklace with a rotaxane; the

necklace is the ring, while the head, neck, and shoulders comprise the dumbbell. Meanwhile, the necklace itself is composed of mechanical bonds if it is beaded or has a clasp. Consider getting dressed in the morning—if you tie your shoes, strap a belt around your waist, button up your shirt, and clasp on a watch or some jewelry, you have already formed dozens of mechanical bonds around your body before breakfast!

The mechanical bond and technology have gone hand-in-hand since the advent of machinery. Indeed, many of the world's simplest and oldest machines, a wheel-and-axle or a pulley (**Figure 1.8j**), for example, are based on the mechanical bond. Interlocking parts have been especially important in transportation—imagine trying to sail without knots and pulleys or drive without wheels! The mechanical bond also appeared as early as 2700 BCE in the world's first calculator—the abacus (**Figure 1.8f**). Just as we find it near the beginning of human history, most of us meet the mechanical bond near the beginning of our lives, since it is essential to many toys such as rattles or the bead maze in **Figure 1.8g**.

It is obvious by now that few modern machines would be capable of existing without some kind of mechanical bond, whether it is the washer around a screw or the disc in a hard drive. Even more examples are given in **Figure 1.8**. Indeed, with every draw of a curtain (**Figure 1.8c**), turn of a doorknob (**Figure 1.8d**), or flip of a switch, the mechanical bond is at our service. Between fashion and technology, societies are irrevocably dependent on the mechanical bond. With mechanical bonds being such a necessary component in machinery, it is only fitting that they also represent a cornerstone of molecular machines—see **Sections 1.3.6** and **6.15**.

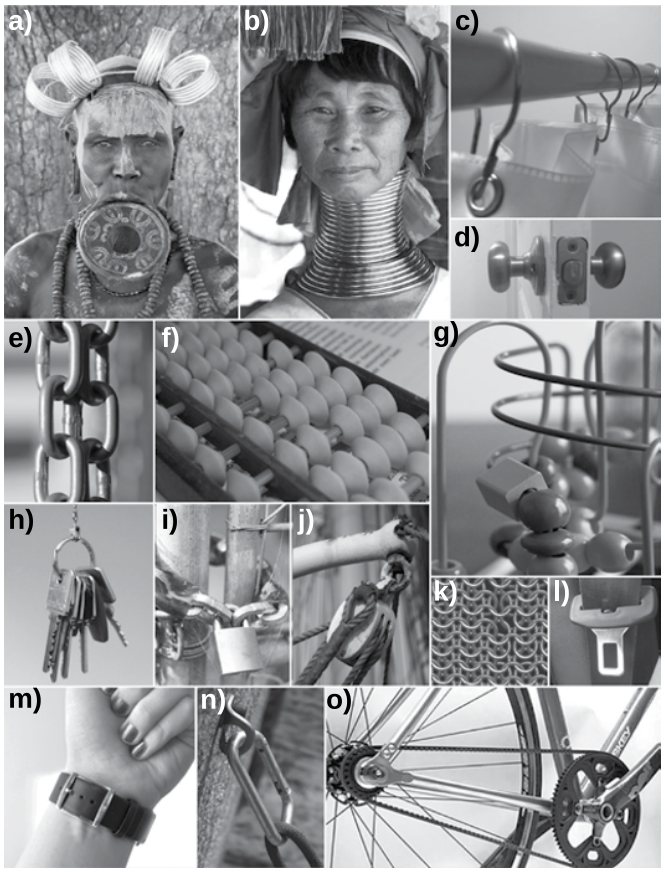


Figure 1.8 Examples of mechanical bonds in everyday life. (a) Decorative mechanical bonds of a Mursi woman. (b) A Khayan Lahwi woman with mechanically interlocked neck extenders. (c) A shower curtain. (d) A doorknob has the essence of the 'dumbbell' portion of a rotaxane, where the door is the ring! (e) A chain link. (f) Mechanically interlocked beads underpin the function of an abacus, as well as (g) a children's bead maze. (h) Keys catenated with a keychain ring. (i) A lock. (j) A pulley on a sailship. (k) Chainmail. (l) A seatbelt buckle. (m) A wristwatch makes a rotaxane with the hand and body as stoppers, while its clasp also relies on a mechanical bond to keep it fastened. (n) The mechanical bond of a carabiner helps climbers cling to rock faces. (o) Hundreds of mechanical bonds exist in the chain, crank, and wheels of a bicycle.

1.2 Representing Molecular Mechanical Bonds

Having established a background of beauty for the mechanical bond in art, nature, and society, we now consider beauty as the mechanical bond is miniaturized beyond our ability to perceive it directly. Since mechanomolecules are not available to our senses, their beauty is more associated with the wide variety of modes we use to represent them—e.g., symbols, drawings, models, and cartoons. Just as chemical signs and symbols have evolved over the centuries from primitive beginnings in alchemy,[93–95] the portrayal of MIMs have also evolved, even playing a vital role in modern notions of molecular representation in chemistry as a whole. In particular, as molecular structures have grown larger and more complex, it has become useful to represent them in ways that eliminate finer details, such as the bond order, atomic composition, and so on, especially when trying to convey a message that has more to do with self-assembly, intra- and intermolecular interactions, or secondary structure. Because it represents chemistry "beyond the molecule," supramolecular chemistry[64] has played a major role in this transition, but so has the chemistry of the mechanical bond, or as we call it, mechanostereochemistry.[16]

All sorts of everyday objects have been reconstructed as molecules by virtue of template-directed synthesis, from switches and buttons to rotors and elevators. The likeness of MIMs to macroscopic objects and machines has done much to advance molecular nanotechnology and is, as we shall see, another important aspect of their beauty.

1.2.1 A Historical Perspective

It is believed[18] that mechanical bonds were discussed hypothetically prior to 1912 by Wilstätter at a seminar in Zürich, but the idea did not appear in the chemical literature[96] until 1953. A significant publication by Frisch and Wasserman[18] in 1961 was the first to articulate the connection between

stereochemistry and topology. In chemistry, topology is concerned with the properties of a molecule that are independent of any spatial rearrangements and bond distortions that can be performed without allowing covalent bonds to break or pass through one another. Topologically speaking, catenanes and rotaxanes are very different. The linked rings of a [2]catenane (the bracketed term represents the number of component parts in a MIM) are topologically distinct from two rings that are not interlocked, i.e., they are topological isomers. On the other hand, a [2]rotaxane is topologically identical to its component parts because the ring can be separated from the dumbbell by stretching or compressing the appropriate bonds. The concept of chemical topology,[25] which has been expounded masterfully by David Walba[20] and Christopher Hunter,[97] among others, is also highly relevant to the study of molecular knots.[98,99] See **Section 1.3.2** for a discussion of topological beauty.

Following a noteworthy attempt[100] in 1958, the first claim to a successful MIM synthesis (**Figure 1.9a**) came in 1960, when Wasserman[101] reported that cyclization of a long polymethylene C_{32}-chain esterified at both ends in the presence of a large C_{34}-cycloalkane gave very low yields of a catenane, which was isolated by chromatography two years later.[102] Small improvements in the use of this statistical method were made—most notably, Harrison and Harrison's 6% yield of a rotaxane by repeating a statistical threading reaction on a resin-bound macrocycle 70 times,[103] and Zilkha's[104,105] two-step catenane synthesis that converted a statistical [2]rotaxane directly into a [2]catenane in 3% overall yield. Meanwhile, however, Schill was developing an important approach he called directed synthesis,[106] in which macrocycles are built up around an aromatic core such that severing a few bonds at the core in the final steps affords a catenane (**Figure 1.9b**). This approach was also applied to the directed synthesis of [3]catenanes,[107–110] and [2]rotaxanes.[111–114] Schill's 1971 monograph,[115] *Catenanes, Rotaxanes, and Knots*, is an indispensable reference on the early work in the chemistry of mechanical bonds.

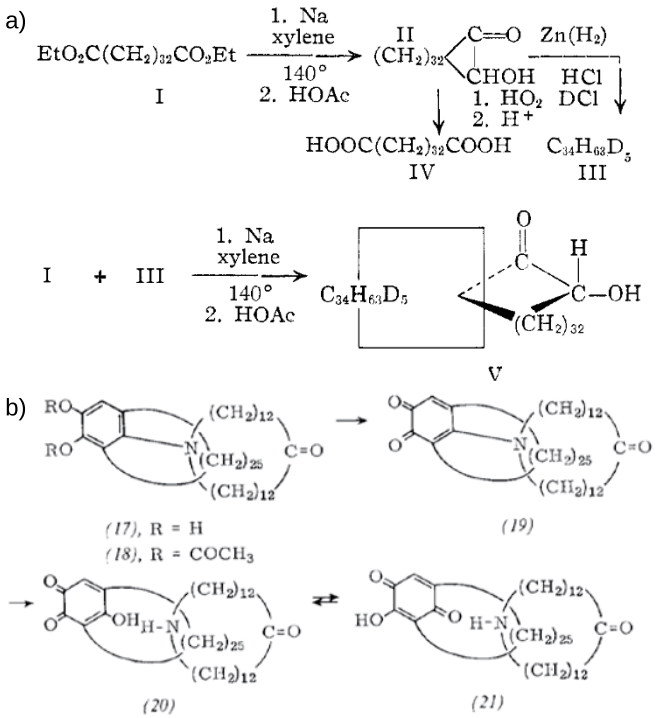


Figure 1.9 Historically significant synthetic schemes exemplifying the two applied approaches to catenane synthesis prior to 1983. (a) Wasserman's first statistical synthesis[101] relied on the macrocyclization of a linear compound (I) in the presence of a deuterated cycloalkane (III) to produce small amounts of the catenane V. (b) Schill's first example[106] of directed synthesis by covalent templation was a catenane that formed after cleaving the covalent bonds around the aromatic core in compound 16. Reproduced with permission from refs 101 (copyright 1960 American Chemical Society) and 106 (copyright 1964 Wiley-VCH)

Although the statistical and directed approaches were the only known routes to catenanes for decades, a Möbius strip approach (**Figure 1.10**) was proposed in the late 1950s independently by Frisch / Wasserman[18] and van Gulick.[116] These founders of molecular topology realized that molecules resembling Möbius strips could be cut (**Figure 1.10a**) into catenated and knotted structures, depending on the location of the cut and the number of half-twists in the strip. Walba[117–119] made this approach look more realistic in the early 1980s when he began synthesizing wreath-like macrocycles from tetrahydroxy-methylethylene (THYME) polyethers resembling a three-rung ladder. If the wreath with two half-twists could be isolated and its ladder rung crosslinks severed in half (**Figure 1.10b**), a [2]catenane would be the result. Walba synthesized[117] the zero-twist cylinder and subsequently also isolated[118] the molecular Möbius strip with one half-twist. He verified experimentally that two macrocycles are obtained by cutting the cylinder in half by ozonolysis of the THYME double bonds, while the same action on the Möbius strip leaves it in one piece as a larger macrocycle.[119] No double half-twist Möbius strip that would lead to the [2]catenane has been reported, however. See **Sections 2.1–2.2** for a more detailed discussion of these historical landmarks in mechanostereochemistry.

Sauvage's seminal publication[120] in 1983, which used a copper(I) ion to template the formation of mechanically interlocked ligands (catenates / catenands), breathed new life into the field of MIMs in relation to their accessibility, applicability, and even their structural portrayals. The early catenanes were portrayed (**Figure 1.9**) in condensed line formulas and represented for conceptual purposes by basic line drawings like those in **Figure 1.10**. The result was a picture that sufficiently communicated atomic and topological content, but bore little resemblance to what the actual structure might look like if we could set eyes on it. When Sauvage illustrated a structural diagram of his first

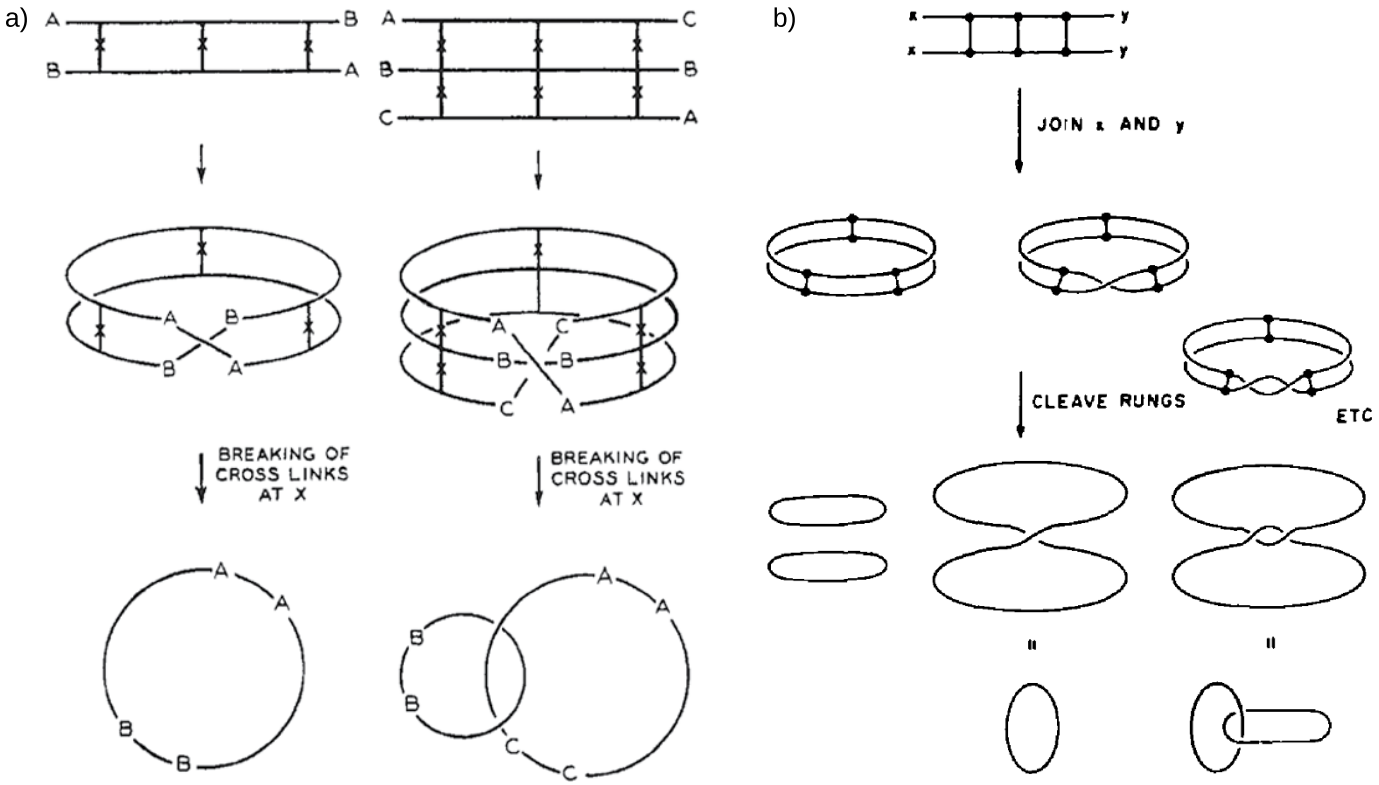


Figure 1.10 Historical strategies for synthesizing catenanes from Möbius strips. (a) Frisch and Wasserman[18] illustrated the results of cutting Möbius strips comprising grid-like bands. (b) Walba[20] outlined a strategy to produce three-rung molecules with different numbers of half-twists, where bisecting the one with two half-twists would afford a [2]catenane. Reproduced with permission from ref. 18 (copyright 1961 American Chemical Society) and ref. 20 (copyright 1985 Elsevier)

[2]catenate (**Figure 1.11**), the result was an image that was rich in beauty as well as topological and molecular information. This diagram—hand-drawn in India ink—expressed most elegantly the right information, while still hinting at the three-dimensional nature of the molecule. It has appeared[121] many times over the years in the literature from Sauvage's group and is a milestone in chemical representation. It is the gold standard of a MIM drawing, saturated with information and easy to interpret.

Sauvage's metal coordination template marked the beginning of the modern era for making mechanical bonds—namely, template-directed synthesis. Advances in this modern era have been associated with discovering new supramolecular template motifs (**Section 1.3.1**, **Section 2.3**) building new interlocked topologies and architectures (**Sections 1.3.2–1.3.3**, **Chapter 4**), discovering elegant protocols (**Section 1.3.4**, **Chapter 3**) and emergent properties (**Section 1.3.5**), crafting artificial molecular switches, machines, and motors (**Section 1.3.6**, **Chapter 6**), as well as featuring applications relying specifically on the mechanical bond. In **Sections 1.2.2–1.2.6**, we now examine how depictions of MIMs have changed alongside these many new developments of an evolutionary nature. With simple two- and three-component MIMs, it was possible to achieve Sauvage's gold standard of drawings, but as complexity and diversity grew in the field, it quickly became useful to turn to new tools that aided and abetted the depiction of MIMs in an eye-catching, easily discernable way—namely,

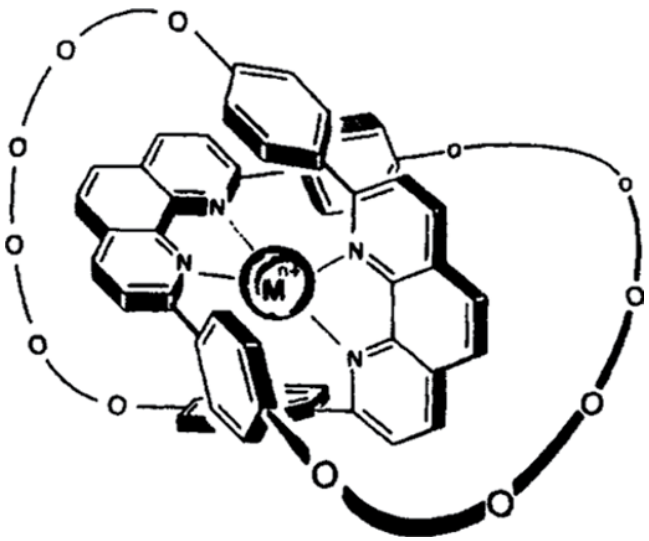


Figure 1.11 Sauvage's structural diagram of a catenand, a major breakthrough in 1983.[120] Reprinted with permission from ref. 121 (copyright 1986 American Chemical Society)

with the use of perspective stereoformulas (**Section 1.2.2**), depictions in color (**Section 1.2.3**), solid-state portrayals (**Section 1.2.4**), graphical representations (**Section 1.2.5**), and technomorphs (**Section 1.2.6**).

1.2.2 Perspective Stereoformulas

A stereoformula, also known as a projection formula, is defined in the IUPAC gold book[27] as a three-dimensional view of a molecule, either as such or in a projection. Examples of these projections include (i) Fischer, (ii) Newman, (iii) sawhorse, (iv) wedge, and (v) zig-zag projections. Sauvage's beautiful diagram (**Figure 1.11**) of his seminal [2]catenate is probably best classified as a type of projection known[27] as a perspective formula, which portrays the geometrical features of a molecule as a view from an appropriate direction. The perspective stereoformula will be our projection of choice for the majority of structural representation in this book.

In our perspective stereoformulas, we employ (**Figure 1.12**) 'full moons' to denote aromaticity in π-conjugated ring systems. This style of representation should not be mistaken for open circles, which are traditionally used to denote ring systems with precisely six π-electrons according to Clar's π-sextet rule.[122] Considering the example of anthracene, only one of Clar's π-sextets exists in any of its three major Kekulé resonance structures, meaning that the Clar structure of anthracene should be illustrated with only one open circle. By contrast, our full moons are placed in all three rings of anthracene to denote a fully unsaturated ring system without specifying a specific resonance structure. We feel that this slightly less detailed style of representation is not inappropriate in most cases involving mechanical bonds because the interactions of interest are between component parts rather than between atoms.

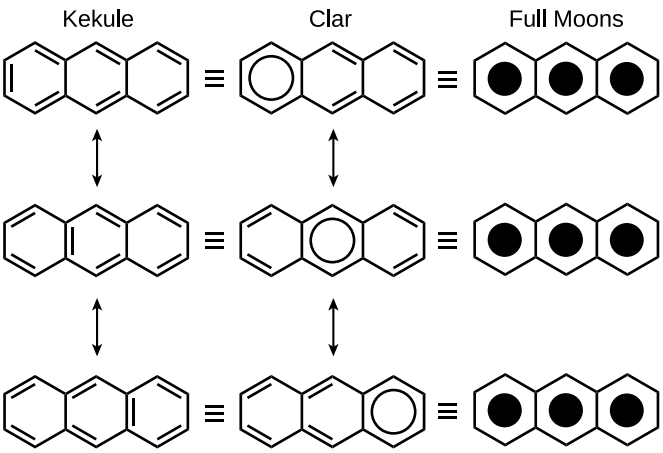


Figure 1.12 Three different representation styles for the structural formulas of aromatic molecules, exemplified by anthracene. When illustrated according to the conventions of Kekulé and Clar, the various resonance structures can be denoted unambiguously. The 'full moons' we employ in our structural formulas denote unsaturated ring systems more generally and do not offer an option for specifying resonance structures.

1.2.3 Depictions in Color

Color and MIMs go together like bread and butter. When journals began printing color in the mid-1980s, the mechanical bond made the perfect poster child because color dramatically clarified the portrayal of mechanically interlocked structures, which cannot be drawn without bonds crossing over and under one another. The first example in a primary publication[123] came in the form of the crystal structure (**Figure 1.13**) of a [3]catenate synthesized in the Sauvage laboratory. The carbon atoms in each macrocycle were uniquely colored, making each of the three component parts immediately and effortlessly discernable. This creative act represented a veritable leap forward in MIM portrayal and heralded the changes in structural depiction that would continue to evolve.



Figure 1.13 The solid-state structure of Sauvage's [3]catenate. The colors give unprecedented clarity (and beauty) to the image. Reprinted with permission from ref. 123 (copyright 1987 Wiley-VCH)

Gradually, color made its way past crystal structures and into different kinds of structural representation. Following the two initial communications[124,125] in 1988 describing in colorful detail the structure and host-guest properties of the tetracationic receptor, cyclobis(paraquat-*p*-phenylene) ($CBPQT^{4+}$), the donor-acceptor mechanomolecules based on $CBPQT^{4+}$ were among the earliest compounds to be depicted[126] in the form of colored stereoformulas (e.g., **Figure 1.14a**) and graphical representations. The π-donors were shaded in pillar-box red and the π-acceptors were shaded in royal blue, which is part of the reason[E] that $CBPQT^{4+}$ is known (**Section 2.3.3.8**) as the "little blue box".[127] This color palette has remained in use for more

[E] Another reason for the 'little blue box' nickname is that the compound is obtained on occasion as a blue-tinted solid. The blue color arises when a population of the viologen subunits becomes reduced to a radical cation.

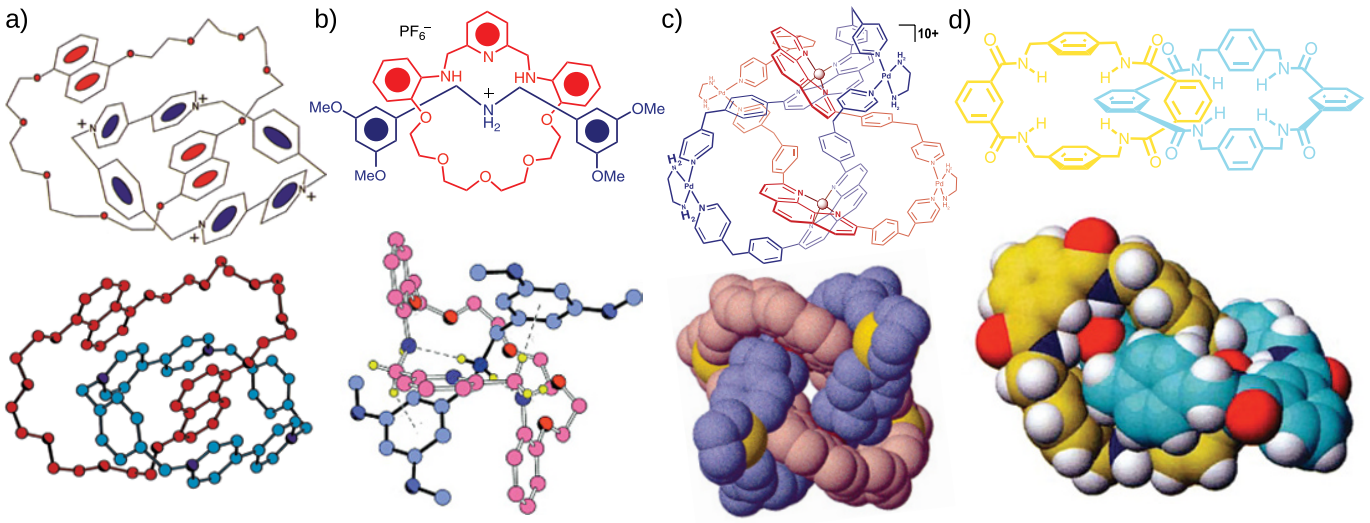


Figure 1.14 Examples of the use of color in depictions of various MIMs. Note how the colors and positions of component parts in the space-filling structures reflect those in the stereoformulas to unify different representations of (a) a donor-acceptor [2]catenane,[128] (b) a strong hydrogen-bonded [2]rotaxane,[129] (c) a transition metal-templated Solomon Knot,[130] and (d) a benzylic amide [2]catenane.[131] Reproduced with permission from refs 128 (copyright 1991 Royal Society of Chemistry), 129 (copyright 2000 Wiley-VCH), 130 (copyright 1999 Royal Society of Chemistry), and 131 (copyright 1995 Wiley-VCH)

than 25 years to the present day. Nowadays, the use of color has been embraced by many research groups and spread well beyond mechanostereochemistry—indeed, scientists in most fields of chemistry use color very effectively for the sake of bringing clarity to their representations.

Several examples of colored MIMs are shown in **Figure 1.14**. In particular these examples[128–131] illustrate how color-coding the constituents of a MIM can form a cohesive link between its various representations—two-dimensional, three-dimensional, graphical, or otherwise. The coherence and readability of these figures is what makes them beautiful, in addition to our natural proclivity for color. We will discuss shortly the use of graphical representations (cartoons) to represent MIMs, a context in which color can be employed to considerable advantage. To the scientifically minded person, the beauty that color gives to an image might have less to do with its aesthetic appeal than with the augmented intelligibility it imparts. We conclude that colors communicate molecular information more clearly, precisely, consistently, and in our minds, more beautifully as well.

1.2.4 Solid-State Portrayals

In the immortal words of John Keats, "beauty is truth, and truth beauty." We understand truth as that which is in accordance with fact or reality. Crystal structures are arguably among the most beautiful ways to represent molecules because of their high content of truth. X-ray crystallography provides some measure of truth about structure because it provides information about the real positions of atoms in the crystal, albeit in a form that is averaged over time and space. Thus, nothing can be more accurate about the way a molecule "looks"—in the solid state at least—than an X-ray crystal structure, save perhaps for some very recent advances in single molecule imaging provided by atomic-resolution microscopy.[132] When it comes to visualizing mechanical bonds, a solid-state structure gives unique insight into how the component parts in a mechanomolecule are oriented relative to each other, whilst also revealing the presence of any noncovalent bonding interactions between them. The ability to rotate and examine the structure of a MIM from any angle in three dimensions supplies an immensely satisfying sense of connection with the molecular world.

Likewise, three-dimensional renderings of MIMs remind us instantly of some of the ordinary objects we encounter in our everyday lives (see **Section 1.1**). Take Olympiadane,[133] for example (**Figure 1.15**), with its five interlocked rings unmistakably sharing the same topology as that of the Olympic logo. Most catenanes bear resemblance at least to the links of a chain, as their name implies. Regardless of their resemblance to familiar objects, hundreds of crystal structures of MIMs have been produced since their debut in 1985, when Sauvage[134] published the first solid-state structure (**Figure 1.16a**) of a [2]catenane. It is impossible to do

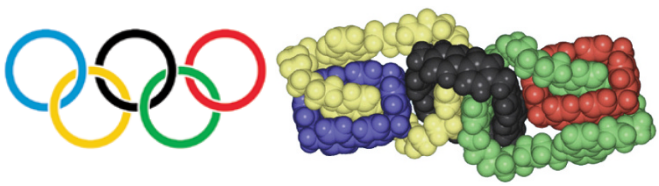


Figure 1.15 The solid-state structure of Olympiadane,[133] which shares its topology with the logo of the Olympic games.

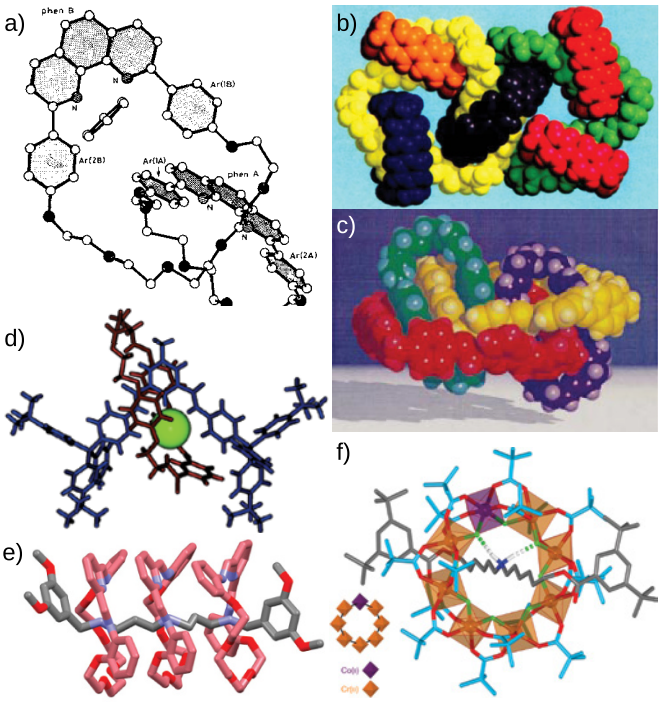


Figure 1.16 Examples of beautiful X-ray crystal structures of MIMs. (a) The first crystal structure of a MIM – Sauvage's [2]catenane.[134] (b) A branched heptacatenane[135] has a large number of interlocked rings for a discrete molecule. (c) Two identical catenanes embraced in a self-complexing dimeric assembly.[136] (d) Beer's first anion-binding rotaxane with its chloride template.[137] (e) A dynamically-assembled [4]rotaxane adopts a rigid rod shape by π–π stacking interactions.[138] (f) A simple and elegant inorganic-organic hybrid [2]rotaxane.[139] Reproduced with permission from refs. 134 (copyright 1985 Royal Society of Chemistry), 135 (copyright 1997 Wiley-VCH), 136 (copyright 2000 Wiley-VCH), 137 (copyright 2002 American Chemical Society), 138 (copyright 2010 Wiley-VCH), 139 (copyright 2009 Nature Publishing Group)

justice to all of the beauty contained in the databank of solid-state mechanically interlocked structures. In **Figure 1.16,** we simply present a few examples that we find noteworthy.[134–139] In **Section 1.3**, see **Figures 1.25**, **1.27**, and **1.29**, as well as **Scheme 1.3** to find more beautiful mechanically interlocked crystal structures.

It is convenient here to discuss a different kind of mechanically interlocked solid-state architecture made possible through the development of metal-organic frameworks[140–143] (MOFs) and coordination polymers. MOFs are infinite, robust, crystalline networks composed of organic struts coordinated to metals or metal clusters as secondary building units (SBUs) and have very high porosities on account of their rigid reticular architectures. The massive amount of void space in some kinds of MOFs oftentimes coaxes them into forming two or more interpenetrated networks in the same crystal, i.e., polyrotaxane[144] and catenated frameworks.[145–147] While researchers interested in high surface areas and porosities want to avoid catenated MOFs as much as possible, they are marvelous structures from the perspective of topology: these infinite catenated networks are the molecular cousins of the sculpture in **Figure 1.6b**. MIMs have also been introduced[148] into coordination polymers and MOFs as linkers by Kim,[149,150] Loeb,[151–159] our group in collaboration with Yaghi,[160,161] Sauvage,[162] and Hupp,[163,164] as well as Sessler,[165–167] Winpenny,[168] and Wang and Su.[169] The example illustrated in **Figure 1.17**, resulting from a collaboration with Yaghi,[160] incorporates a molecular catenane into a catenated MOF. The beauty of this framework lies in its unprecedented complexity, linker size, and topology—it is difficult to imagine a crystal any more jam-packed with mechanical bonds. The cartoon of the MOF in **Figure 1.17d**, which offers a more palatable depiction of its topology, testifies to the importance of the transition to graphical representations. Coordination networks with mechanical bonds are discussed in **Sections 4.1.3.5** and **4.2.3.8**.

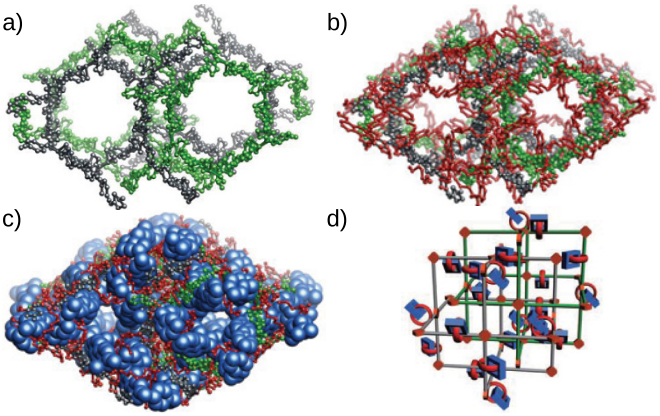


Figure 1.17 A catenated MOF with catenated linkers.[160] (a) A ball-and-stick representation of the X-ray crystal structure of the MOF with the pendent catenanes omitted in order to aid in the visualization of the interpenetrated networks, colored in green and grey. (b) The same MOF with pendant crown-10 macrocycles included in red – only the $CBPQT^{4+}$ rings are omitted. (c) A complete view of the MOF structure, in which the $CBPQT^{4+}$ cyclophanes are assigned space-filling representations in blue. (d) A graphical illustration of the catenated MOF topology. Adapted with permission from ref. 160 (copyright 2010 Wiley)

1.2.5 Graphical Representations

It will be recalled from **Section 1.2.1** that first-generation MIMs were represented primarily by primitive line drawings and line formulas. Although Sauvage took a refreshing step forward into stereoformulas and structural diagrams, there was still a need to find a compromise between the simple line drawings that convey only topology and the detailed structural formulas that detail every atom and bond. Again Sauvage was among the first to pioneer the next evolutionary step: graphical representations/cartoons. His 1985 report of a [3]catenate[170] included a graphically simplified reaction scheme with shading (**Figure 1.18a**) intended apparently for aesthetic purposes. Few, if any,

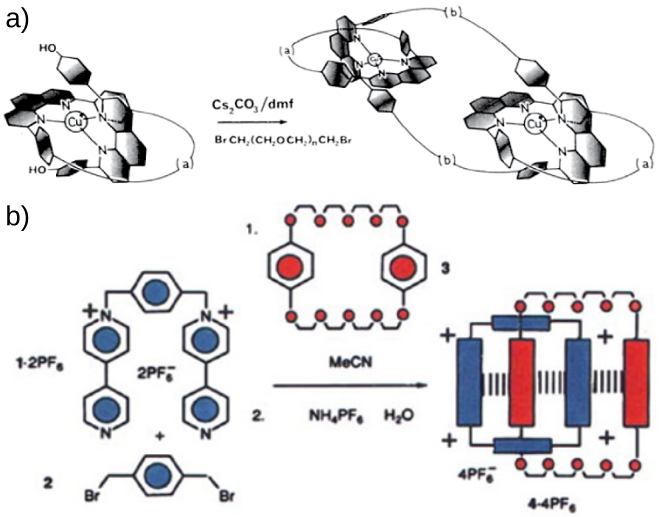


Figure 1.18 Early examples of MIM cartoons. (a) Sauvage's cartoon of a [3]catenate.[170] (b) A synthetic scheme depicting the synthesis of a donor-acceptor [2]catenane relies on abstraction, color, and hash marks in order to emphasize topology, noncovalent bonding interactions, and electronic properties.[171] Reproduced with permission from refs. 170 (copyright 1985 American Chemical Society) and 171 (copyright 1991 Wiley-VCH)

other cartoons existed in the literature until the first donor-acceptor [2]catenane was introduced[126] in 1989. The importance of this contribution is in the way the information about noncovalent bonding interactions is communicated through the use of simplified graphics.[171] Coloring in the rectangles, etc. with felt-tipped pens helped to clarify aspects of the molecular structure (**Figure 1.18b**) such as its topology, the electron density of its component parts (π-donor or π-acceptor), and the noncovalent bonds (thick hashed lines) involved in its formation.

Although graphical representations are an effective means of communication, they were met initially with a fair share of criticism. As the years passed by, we and others began taking the time to make them more aesthetically appealing, paying attention to details like size, shading, and readability. The result is that our cartoons—and graphical representations more generally—have gone through an evolutionary process of their own, represented chronologically in **Figure 1.19**, which was more or less at the point it is today by the year 2000. Two-dimensional cartoons were displaced progressively by three-dimensional ones, which inherently aid in the visualization of mechanostereochemistry by their portrayal of perspective. Our first 3D cartoon was a branched heptacatenane (**Figure 1.19**), which was illustrated directly below the space-filling representation of the solid-state structure (**Figure 1.16b**) in the original paper[135] in 1997. A comparison between the two modes of depiction makes it obvious why there is utility in such cartoons; they do justice to the topology as well as the Euclidean shape of the molecule.

Figure 1.20 presents a number of the different ways that have been employed to represent the same catenane. It is apparent that venturing into cartoons has opened space for much more freedom and creativity in the representation of molecules. Note that every type of cartoon in

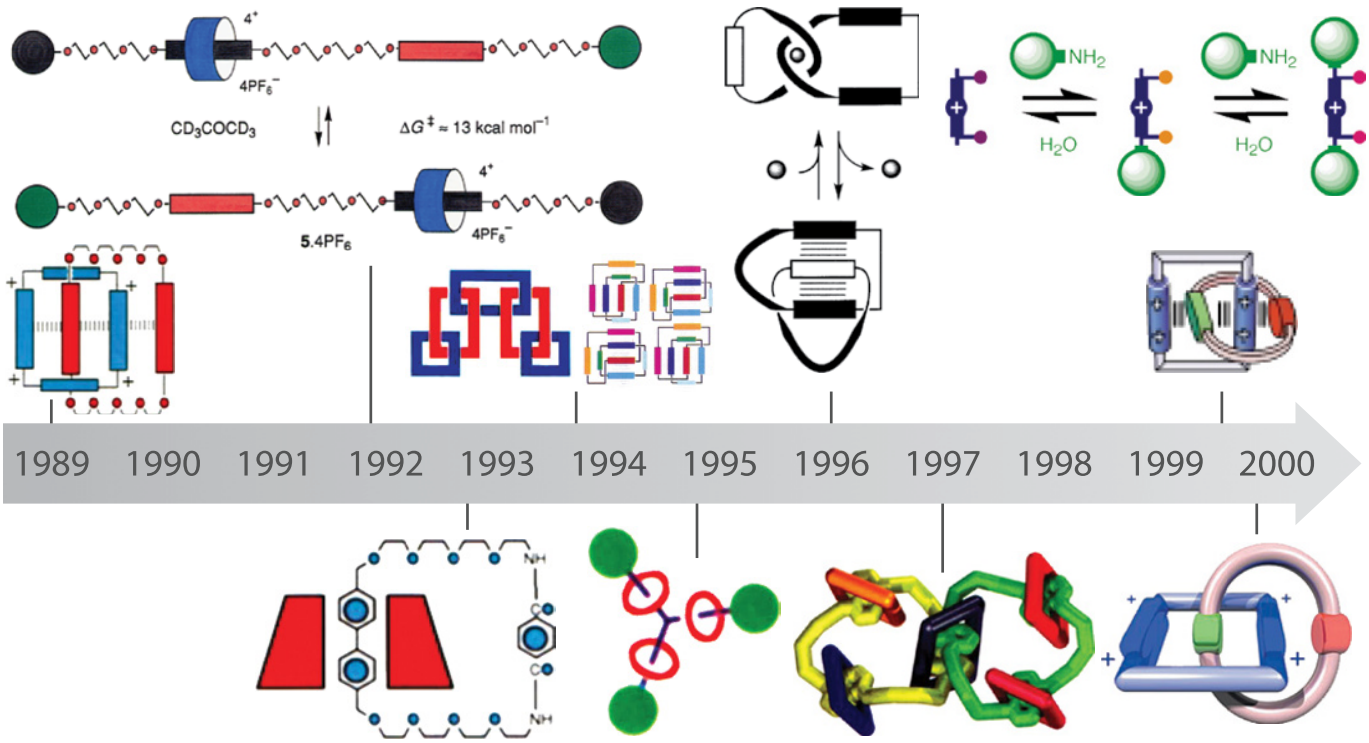


Figure 1.19 A timeline of selected MIM cartoons from our laboratory.

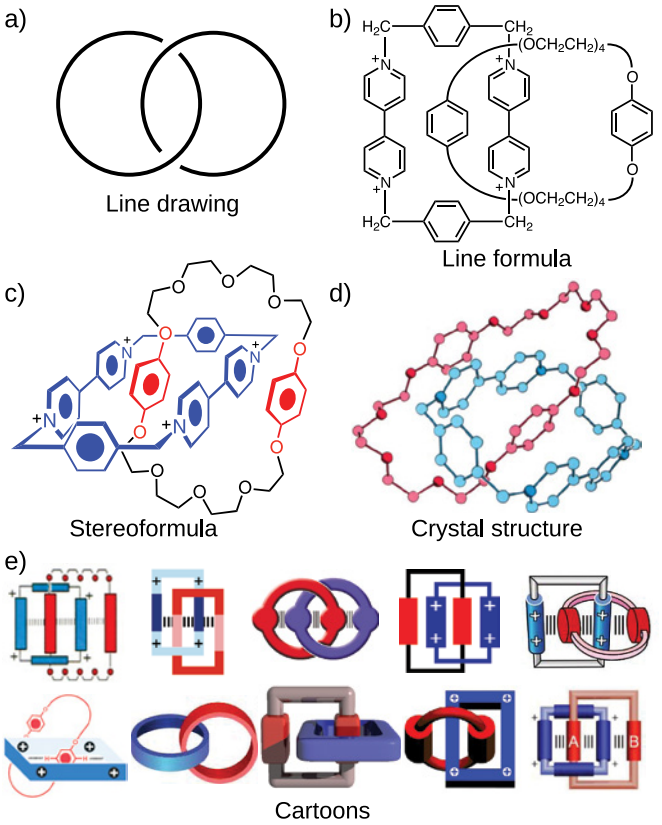


Figure 1.20 Different representations of the same donor–acceptor [2]catenane: (a) line drawings and (b) line formulas were the order of the day until the modern era of MIMs gave way to (c) perspective stereoformulas and (d) crystal structures, as well as (e) graphical representations. These cartoons (e) can be a helpful compromise between these representations when attempting to emphasize the topology, noncovalent bonding interactions, shape, beauty, or function of a MIM. Adapted with permission from ref 33 (copyright 2012 Springer)

Figure 1.20e has been published in the chemical literature. We conclude that the transition to cartoons has been a boon in the field simply because they (i) highlight topology by de-emphasizing atom and bond details, (ii) allow for the denotation of features that structural formulas lack—e.g., noncovalent bonding interactions, (iii) provide a more focused picture of a molecule's Euclidean shape, (iv) declutter and beautify figures and schemes, and (v) elicit creativity and inspire ideas for future research. The fifth and last point is related to the subject of **Section 1.2.6** on how MIMs have influenced the growth of molecular nanotechnology.

1.2.6 Technomorphs

In some cartoons, a MIM can look less like a molecule and more like a classical object, like a toy or LEGO set. Take the MIMs in **Figure 1.21** for example; these representations were drawn intentionally to look as though they were built from pipes, nuts, and bolts. Though they bear the same topology as the molecules they represent, they look more like the handiwork of a plumber than that of a synthetic chemist—chemically meaningless unless placed in the proper context. The objects in the figure hang in tension between the molecular world and the ordinary world, belonging ambiguously to both. The way in which these images refer at once to molecular and classical objects has been described by Joachim Schummer[172] as a "Gestalt Switch in Molecular Image Perception." Schummer's important thesis about "*an aesthetic phenomenon that symbolically linked the world of molecules and the world of ordinary objects, and…prompted the creation of a new sign language*" is embodied by images like those in **Figure 1.21**, for which he coined the term 'technomorphs.' Note that some cartoons in **Figure 1.20** are also technomorphs.

The technomorphic representations of supermolecules and mechanomolecules are truly valuable from both a practical and an aesthetic standpoint. Practically speaking, they played a role in inspiring chemists to think about molecules as classical objects and push back the frontiers of molecular nanotechnology. Because of technomorphism, suddenly a molecule that looks like a car should be driven as though it were a car,[173] those that look like cages should trap things inside,[31] and so on. This mode of thinking applies immensely to MIMs, where a frenzy of creative research accompanies imaginative project titles. Over the years, our own group has fabricated molecular shuttles,[174] switches,[175] push-buttons,[176] trains,[177] elevators,[178] pistons,[179] muscles,[180] abacuses,[181] motors,[182] and valves.[183] Other groups have reported MIMs as molecular necklaces,[184–186] locks,[187] rotors,[188] chameleons,[189] and charm bracelets[190]—the list goes on and on. These types of molecular nanostructures, whose names and representations are deliberately evocative, are known[191,192] also as technomimetic molecules. It is apparent that the visionary dream of nanotechnology is aided and abetted by the new symbols borne out of supramolecular chemistry[64,193] and mechanostereochemistry.[16]

Though we allow ourselves to talk freely about the beauty of molecular structures, technomorphic representations are among the few products of chemistry that can currently withstand a formal aesthetic philosophy. Schummer, a philosopher of science, has undertaken a systematic investigation[41] of chemical representations in the context of

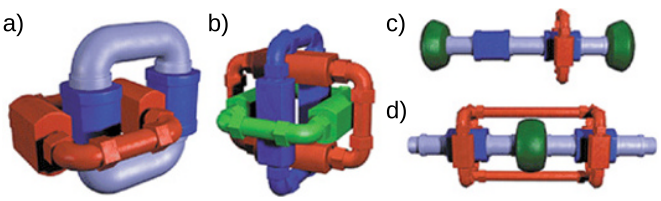


Figure 1.21 Technomorphic representations of (a) a [2]catenane, (b) Borromean rings, (c) a [2]rotaxane, and (d) a suit[2]ane. Adapted with permission from ref. 33 (copyright 2012 Springer)

idealistic aesthetics (Plato, Kant),[194] aesthetics of symbols (Goodman),[195] and Eco's semiotic theory,[196] concluding in the negative on all but Eco's theory. In brief, Umberto Eco's modern semiotic theory would recognize that technomorph symbols are rich in aesthetic content because they (i) can be interpreted ambiguously, (ii) challenge the interpreter to develop new interpretations, and (iii) redirect the interpreter's attention to the symbol itself. In other words, an individual's reflection on and interpretation of a technomorph is a *bona fide* aesthetic experience as well as a new, powerful driving force for ongoing research.

It is good news that cartoons, particularly the subset referred to as technomorphs, have been accepted by the chemical community as a new symbolic language. The result has been the formation of a symbolic link between molecular and classical objects, images that appeal to a broader audience—no background in chemistry is necessary!

1.3 Aesthetics of Mechanical Bonds

The various ways to represent MIMs on paper comprise, more often than not, a portrayal of beauty in their own right. In the previous Section, we have tried to engage you, the reader, in the beauty of printed molecular representations. There remain many other ways to perceive the beauty of molecular objects, some of them particularly unique to MIMs, but the situation becomes less well-defined when we depart from concrete illustrations and images and venture into even more subjective territory. Roald Hoffman,[197] a pioneer of molecular aesthetics, has approached beauty in chemistry from the perspective that "*beauty is built out of individual pleasure around an object or idea*." The aesthetic experience of molecular structures is therefore inexorably tied up with our subjective biases. Synthetically derived molecules are retroactively beautified out of a psychological need to associate pleasure with hard work. We find reasons to label a molecule beautiful and experiments elegant, because we experienced much work, time, and failure in order to achieve them. Nevertheless, these notions of beauty are common to the experiences of most, if not all, chemists, and are therefore very relevant to a more complete understanding of the discipline of chemistry. The words of Nobel Laureate Charles Pedersen,[198] whose serendipitous discovery of crown ethers eventually spawned the fields of host-guest chemistry,[199] supramolecular chemistry,[193] and mechanostereochemistry[16]—are a case in point:

> *"One of my first actions was motivated by esthetics more than science. I derived great esthetic pleasure from the three-dimensional structure of [the first crown ether]."* [198]

Pedersen's account demonstrates that molecular beauty is not just an interesting topic for discussion; it can also have a profound impact on scientific research. Here, we discuss aspects of beauty in MIMs that can be independent of their printed representations. In other words, this Section is about where chemists of the mechanical bond find pleasure in their research.

1.3.1 Beauty in Diversity

Molecular recognition motifs (**Section 2.3**) that are reported in the literature as templates for MIMs are continually growing more and more diverse. They include (**Figure 1.22**) molecules associating by dint of hydrophobic forces (**Section 2.3.1**), molecules assembling around cationic templates, such as transition metal (**Section 2.3.2**) and alkali, alkaline earth, and lanthanide metal ions (**Section 2.3.8**), π-associated donor-acceptor templates (**Section 2.3.3**), hydrogen (**Section 2.3.4**) and halogen (**Section 2.3.5**) bonding, anion binding (**Section 2.3.6**) and ion-pairing (**Section 2.3.7**) templates. Cyclophanes (**Section 2.3.9**), which often rely on a combination of these different types of noncovalent bonding interactions to encapsulate guests, radical pairs (**Section 2.3.10**), homophilic interactions (**Section 2.3.11**), and biomolecular self-assembly (**Section 2.3.12**) provide yet more territory for producing templation. The MIMs illustrated in **Figure 1.22** represent some of the seminal examples[120,126,137,139,200–230] of these motifs. The remarkable diversity of these interlocked structures is a source of beauty. To quote Donald Hicks,[231] "*there is no time of year when the trees are more beautiful than when they are different colors. Diversity adds beauty to our world.*" Although we can classify all of the supramolecular recognition motifs involved in mechanostereochemistry into only a handful of categories, there is ample diversity to create a potentially endless variety of beautiful molecules with mechanical bonds—an attitude captured by the ancient writings of Sun Tzu in The Art of War –

> *"There are not more than five musical notes, yet the combinations of these five give rise to more melodies than can ever be heard.*
> *There are not more than five primary colors, yet in combination they produce more hues than can ever be seen."*

1.3.2 Topological Beauty

Let us take a moment to clarify the difference between topography and topology. The aspects of a molecule relating to its geometry (tetrahedral, square planar, etc.), symmetry, size, and shape, are characterized by its topography. By contrast, the topology of a molecule relates to geometric properties and spatial relationships that remain invariant throughout continuous deformation, i.e., stretching, bending, and compressing bonds without breaking them). It is well accepted that the beauty of a molecular structure is often associated with its shape in Euclidean geometry (topography), but here we recognize that beauty can be associated with topology as well.

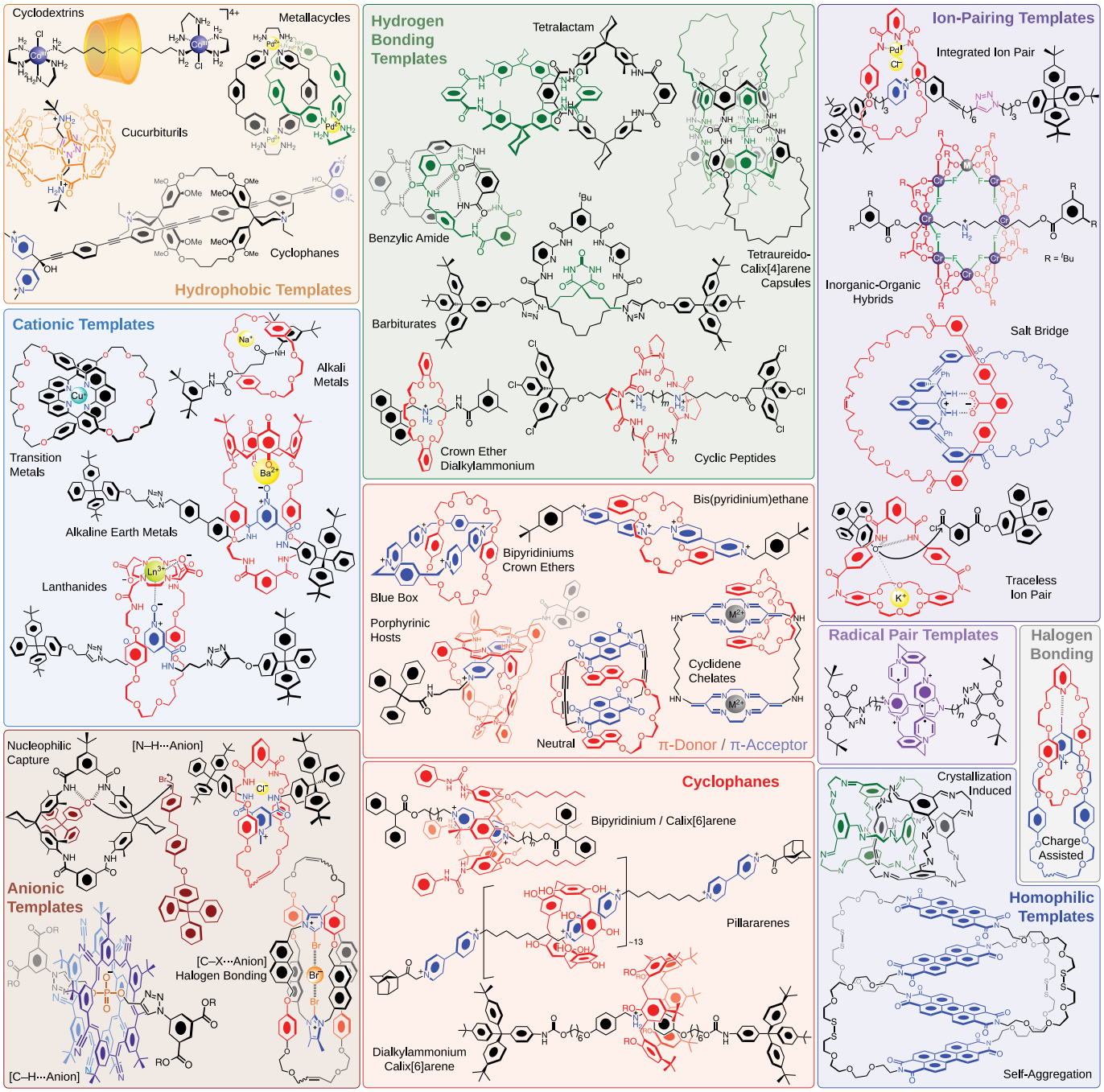


Figure 1.22 Beauty in diversity. Seminal examples of MIMs employing various types of supramolecular templates. Hydrophobic templates: cyclodextrins,[200] cucurbiturils,[201] metallacycles,[202] and other charged cyclophanes.[203] Cationic templates: transition metals,[120] alkali metals,[204] alkaline earth metals,[205] lanthanides.[206] π-Donor/π-Acceptor templates: bipyridinium derivatives (e.g., 'blue box') and crown ethers,[126] bis(pyridinium)ethane,[207] porphyrinic hosts,[208] neutral π-acceptors,[209] cyclidene chelates.[210] Hydrogen bonding: tetralactam rings,[211] benzylic amide rings,[212] tetraureidocalix[4]arene capsules,[213] barbiturates,[214] dialkylammonium⊂crown,[215] cyclic peptides.[216] Halogen Bonding: charge-assisted.[217] Anionic templates: nucleophilic capture,[218] [N–H···Anion] hydrogen bonding,[137] [C–H···Anion] interactions,[219] [C–X···Anion] halogen bonding.[220] Ion-pairing templates: integrated ion pairs,[221] inorganic-organic hybrids,[139] salt bridges,[222] traceless ion pairs.[223] Other cyclophanes: calix[6]arenes,[224,225] pillararenes.[226] Radical-pair templates.[227,228] Homophilic templates: self-aggregation,[229] crystallization-induced assembly.[230] See **Section 2.3**.

David Walba[20] in 1985 was among the first to discuss topological beauty in the primary literature, noting that "*topological stereochemistry is a unique field, esthetically and intellectually pleasing in the extreme.*" Two years later, Jean-Pierre Sauvage's first major review[232] of MIMs paid tribute to the aesthetic value of catenanes and catenands. He proposed that "*the beauty of some molecules might be independent of shape and rest only in [their] topological*

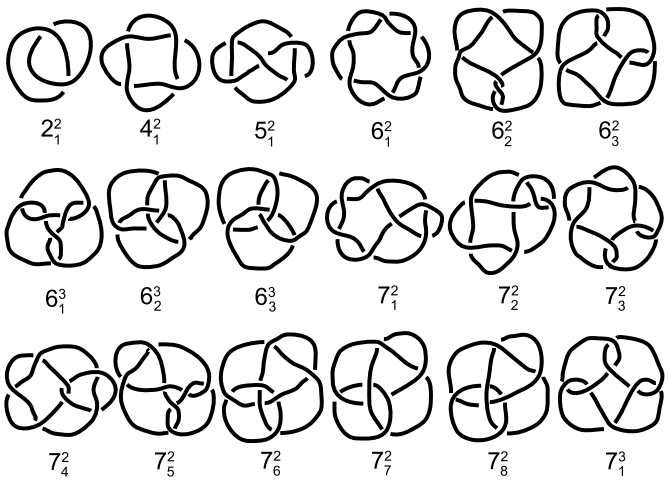


Figure 1.23 Projections of the 18 prime links with <8 crossings. Reprinted with permission from ref. 33 (copyright 2012 Springer)

properties." A review by Amabilino and Pérez-García[24] constitutes a delightful look at topological molecules in the context of how chemists represent them. Sauvage and Amabilino[233] have also engaged the beauty of molecular knots in a chapter in a monograph[32] on *Beauty in Chemistry*. We refer the reader to these articles for further discussion on topological beauty.

In the field of mathematical topology, all closed loops are called knots. Three-dimensional knots are often characterized by the minimal number of crossing points in their two-dimensional projections. In Alexander-Briggs[234] notation, prime knots are catalogued by their crossing number, with subscripts denoting an arbitrary order amongst other knots with equal crossing numbers. A circle with no entanglement is known as the unknot (crossing number 0), while the simplest non-trivial knot is the trefoil knot (crossing number 3).

Two or more knots interlocked in space are known in mathematics as links. Links can be described[234] by an extension of the Alexander-Briggs notation, where each link is characterized by its crossing number, with a superscript denoting the number of component knots and a subscript denoting an (arbitrary) rank order. **Figure 1.23** shows the 18 prime links with less than eight crossings. Only 2^2_1 (a [2]catenane or 'Hopf link'),[101] 4^2_1 (a doubly interlocked [2]catenane or 'Solomon Link'),[235] 6^2_1 (a triply interlocked [2]catenane or 'Star of David' catenane),[236] 6^3_2 (Borromean Rings),[237] and 6^3_3 (cyclic [3]catenane)[238] have been reproduced (**Figure 1.24**) in the form of synthetic molecules—see **Section 4.1.1**.

Although unlinked knots lack any formal mechanical bonds because they lack component parts, they are nevertheless topologically non-trivial mechanically interlocked objects. The challenge of synthesizing knots in molecular form has been met (**Figure 1.25**) with considerable success. Importantly, molecular knots have also paved a pathway for chemists to follow, inspiring molecular designs that incorporate other types of mechanical bonds. For example, Sauvage's seminal synthesis of a trefoil knot[239,240] from a dinuclear metallohelicate was the conceptual progenitor of his Solomon Link synthesis[235] from a trinuclear metallohelicate. Likewise, Leigh's seminal pentafoil knot synthesis[241,242] from a cyclopentameric double helicate set the stage for the construction[236] of his Star of David catenane from a cyclohexameric double helicate. Other topologically non-trivial structures lacking mechanical bonds, such as composite knots[243] and ravels,[244,245] provide further inspiration for the rational design of mechanically interlocked molecular topologies.

Other types of catenane topologies include composite (**Section 4.1.2**), multi-annulated (**Section 4.1.3**), and covalently bridged (**Section 4.1.4**) links. Selected seminal examples (**Figure 1.26**) of several of these topologies

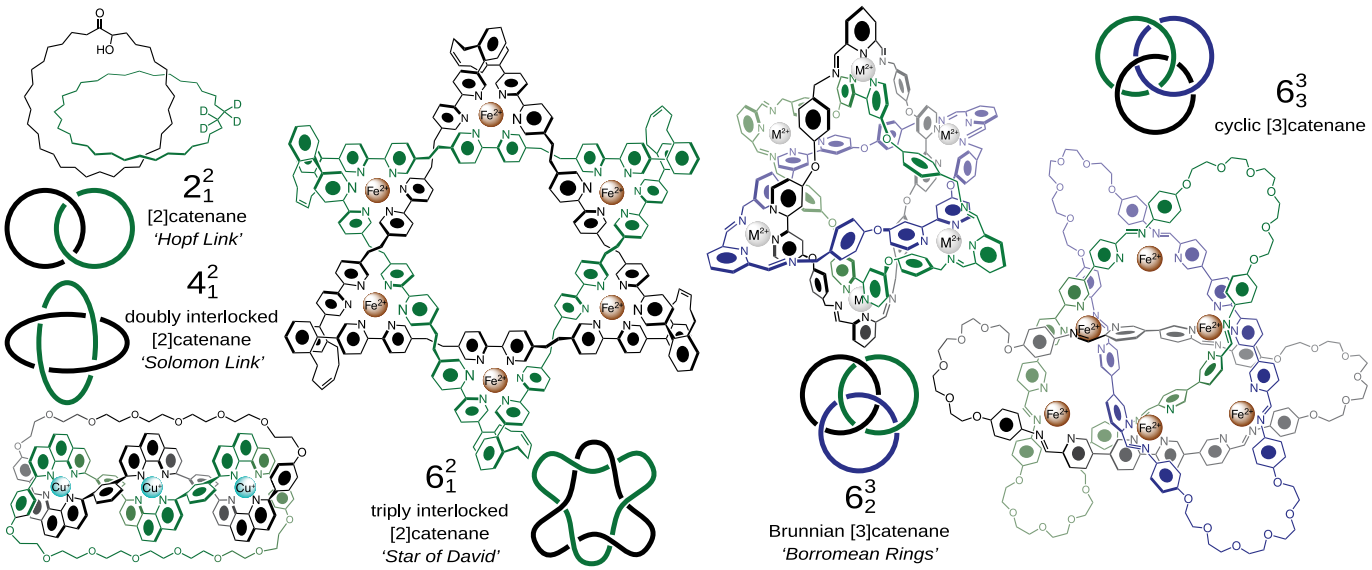


Figure 1.24 Seminal examples of synthetic prime links: 2^2_1 [2]catenane / Hopf link,[101] 4^2_1 doubly interlocked [2]catenane[235] / Solomon Link,[325] 6^2_1 triply interlocked [2]catenane / Star of David,[236] 6^2_2 Brunnian link / Borromean Rings,[237] 6^3_2 cyclic [3]catenane.[238]

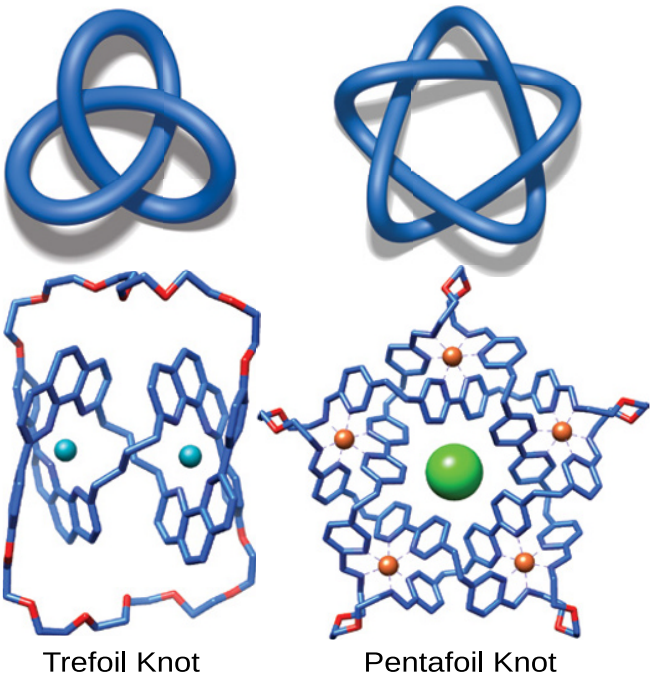


Figure 1.25 Knots, such as the seminal trefoil knot reported by Sauvage[239] and the pentafoil knot reported by Leigh,[241] are topologically non-trivial molecules which lack mechanical bonds, yet have laid the foundation for the synthesis of MIMs with exotic topologies and architectures.

include (i) Sauvage's radial [*n*]catenanes,[246] topologies also championed by Kimoon Kim[184,186,247] under the banner of 'molecular necklaces', (ii) Fujita's macrobicyclic homo[2]-catenane of triply interlocked cages,[248] (iii) Kuroda's macrotricyclic homo[2]catenane of quadruply interlocked cages,[249] (iv) a macrobicyclic [3]catenane, also known as a bis[2]catenane,[250] (v) a branched [6]catenane,[135] (vi) a side-chain poly[2]catenane,[251] (vii) a main-chain poly[2]catenane, which was originally introduced by Geerts,[252] (viii) a macrotricyclic hetero[2]catenane, introduced by Becher[253] (ix) a macrobicyclic hetero[4]catenane resulting from a collaboration between Vögtle and Sauvage,[254] (x) covalently bridged [2]catenanes, which originated[106] as precatenanes in Schill's directed syntheses, but later became known[255–257] as pretzelanes or [2]pseudocatenanes (xi) a doubly threaded macrobicyclic [2]catenane introduced by Becher[258] under the title of a [3]pseudocatenane, a topology also known[259–261] as a 'handcuff' catenane, (xii) a [4]pseudocatenane introduced by Chen,[262] (xiii) a macrotricyclic hetero[7]catenane arising from a Nitschke-Sanders collaboration,[263] (xiv) Vögtle's cyclic bis[2]-catenane,[264] and (xv) Chiu's cyclic tetrakis[2]catenane.[265]

The structures of many beautiful MIMs have also been elucidated in the solid state by X-ray crystallography. Space-filling representations of several of these novel topologies are presented in **Figure 1.27**. The collection includes examples of all of the synthetic prime links,[134,236–238,266] composite links such as a [3]catenane,[123] [5]catenanes—namely, Olympiadane[133] and Kimoon Kim's[186] appropriately titled 'molecular necklace'[184] radial [5]catenane—as well as a branched [7]catenane,[135] a pretzelane,[267] [3]- and [4] pseudocatenanes,[260,262] acyclic[268] and cyclic[265] bis[2]catenanes, and other topologies based on multi-annulated component parts[269] or molecular cages.[248,249,270] A more complete discussion of molecular topology is available **Section 5.2.4**, while the diversity of topologically linked molecules are summarized more comprehensively in **Section 4.1**. Topologically trivial architectures with mechanical bonds have also been prepared, and will be described in **Section 1.3.3** and **Sections 4.2–4.3**.

1.3.3 Architectural Beauty

A synthetic chemist has the opportunity to experience the same thrill that architects and artisans encounter when designing and building something new. We use the term 'architecture' to describe MIMs as we widen our scope from mathematical topology to include topologically trivial species such as rotaxanes. Mechanostereochemistry is full of opportunities to create new and exotic architectures. In **Figures 1.28–1.29** we feature the stereoformulas and solid-state structures, respectively, of a handful of MIMs with beautiful architectures.

A number of rotaxane-based architectures involve the installation of covalent bridges between mechanically bonded component parts. Recalling that covalently bridging the topological linkage of a [2]catenane results in a pretzelane (**Section 4.1.4.1**) and bridging two rings of a [3]catenane results in a handcuff catenane / pseudocatenane (**Section 4.2.3.4**), opportunities abound for linking various rotaxane component parts with covalent bonds, giving rise to a more diverse set of architectures—[1]rotaxanes, figures-of-eight, daisy chains, Bonnanes, bundles, elevators, suitanes, and others—depending on the nature of the covalent bridge(s). A [1]rotaxane[271,272] (**Figures 1.28b**, **1.29e**, **Section 4.2.3.1**) is the result of covalently linking the ring of a [2]rotaxane to its dumbbell. This architecture is also known as a molecular ouroboros,[273,274] a molecular lasso,[275–277] or a [*c*1]daisy chain.[278] A 'molecular 8'[279] or figure-of-eight[280,281] (**Figure 1.29j**, **Section 4.3.4**) arises from connecting the ring to the axle on both sides. Daisy chains[282] (**Section 4.2.3.2**) also comprise conjoined ring-rod component parts, yet they are cross threaded into acyclic or cyclic oligomers and polymers known[283] as [*an*]daisy chains or [*cn*]daisy chains, respectively, where *n* is the number of ring-rod monomers in the assembly. Examples of [*c*2]daisy chains[284,285] (**Figures 1.28d**, **1.29f**) and [*c*3]daisy chains[286] (**Figure 1.28h**) are presented. Coutrot[9,287] has described macrocyclized [*c*2]daisy chains and nicknamed them 'rotamacrocycle' architectures (**Section 4.3.2**). Bistable daisy chains can express[180,288–291] muscle-like actuation properties—see **Section 6.13.1.1**.

Other covalently bridged rotaxane-like architectures involve bis-, tris-, or tetra-macrocyclic species. Linear rotaxanes with covalently bridged rings (**Section 4.2.3**) have been dubbed 'bonnanes' by Vögtle,[292] after the city of Bonn, Germany's former 'bridge capital'. Rotaxanes possessing a

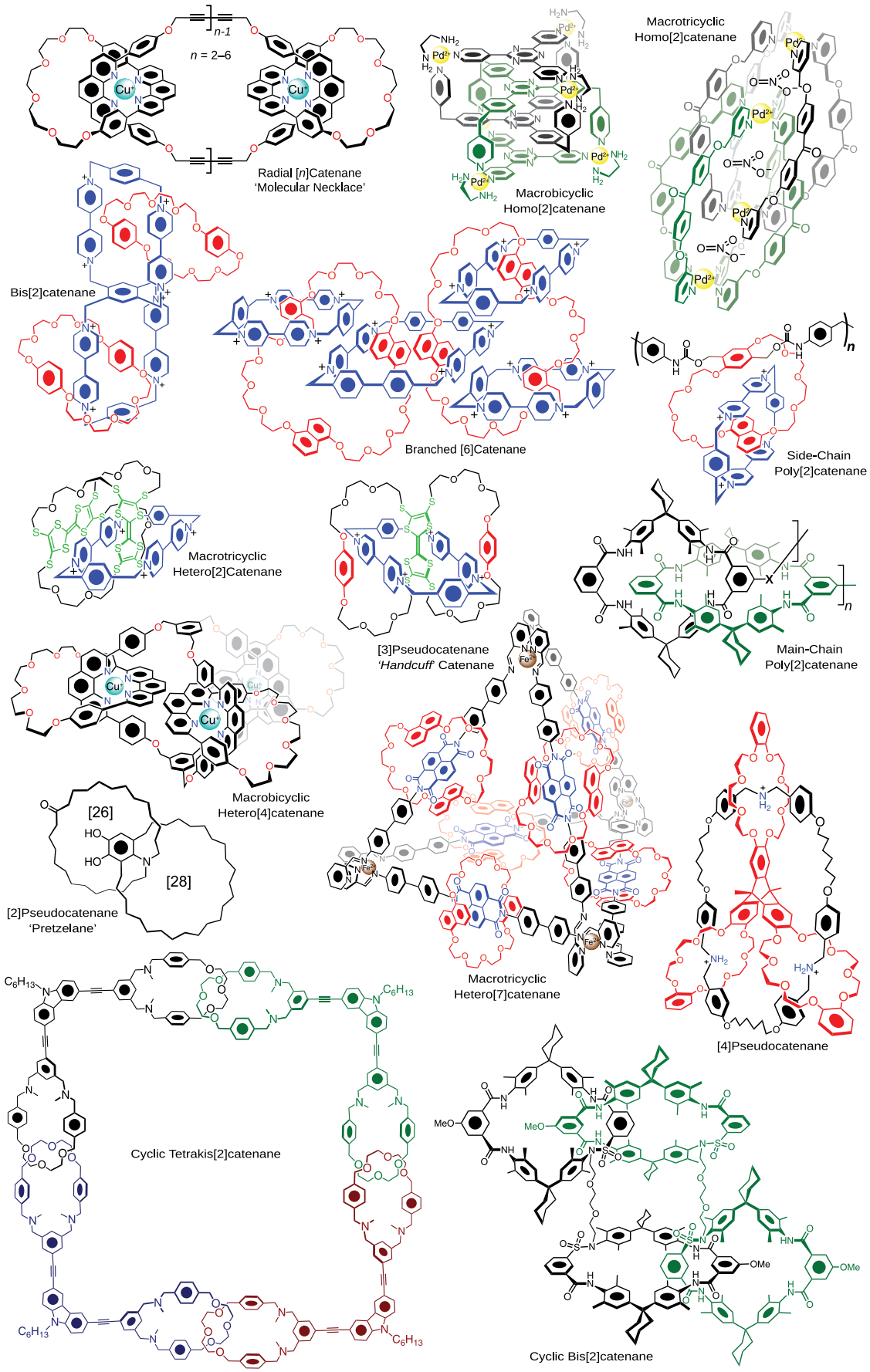


Figure 1.26 Seminal examples of selected molecular link topologies: Sauvage's radial [*n*]catenanes / 'molecular necklaces',[246] Fujita's macrobicyclic homo[2]catenane of triply interlocked cages,[248] Kuroda's macrotricyclic homo[2]catenane of quadruply interlocked cages,[249] bis[2]catenane,[250] branched [6]catenane,[135] side-chain poly[2]catenane,[251] main-chain poly[2]catenane,[252] macrotricyclic hetero[2]catenane,[253] macrobicyclic hetero[4]catenane,[254] [2]pseudocatenane / 'pretzelane',[106] [3]pseudocatenane / handcuff catenane,[258] [4]pseudocatenane,[262] macrotricyclic hetero[7]catenane,[263] cyclic bis[2]catenane,[264] cyclic tetrakis[2]catenane.[265]

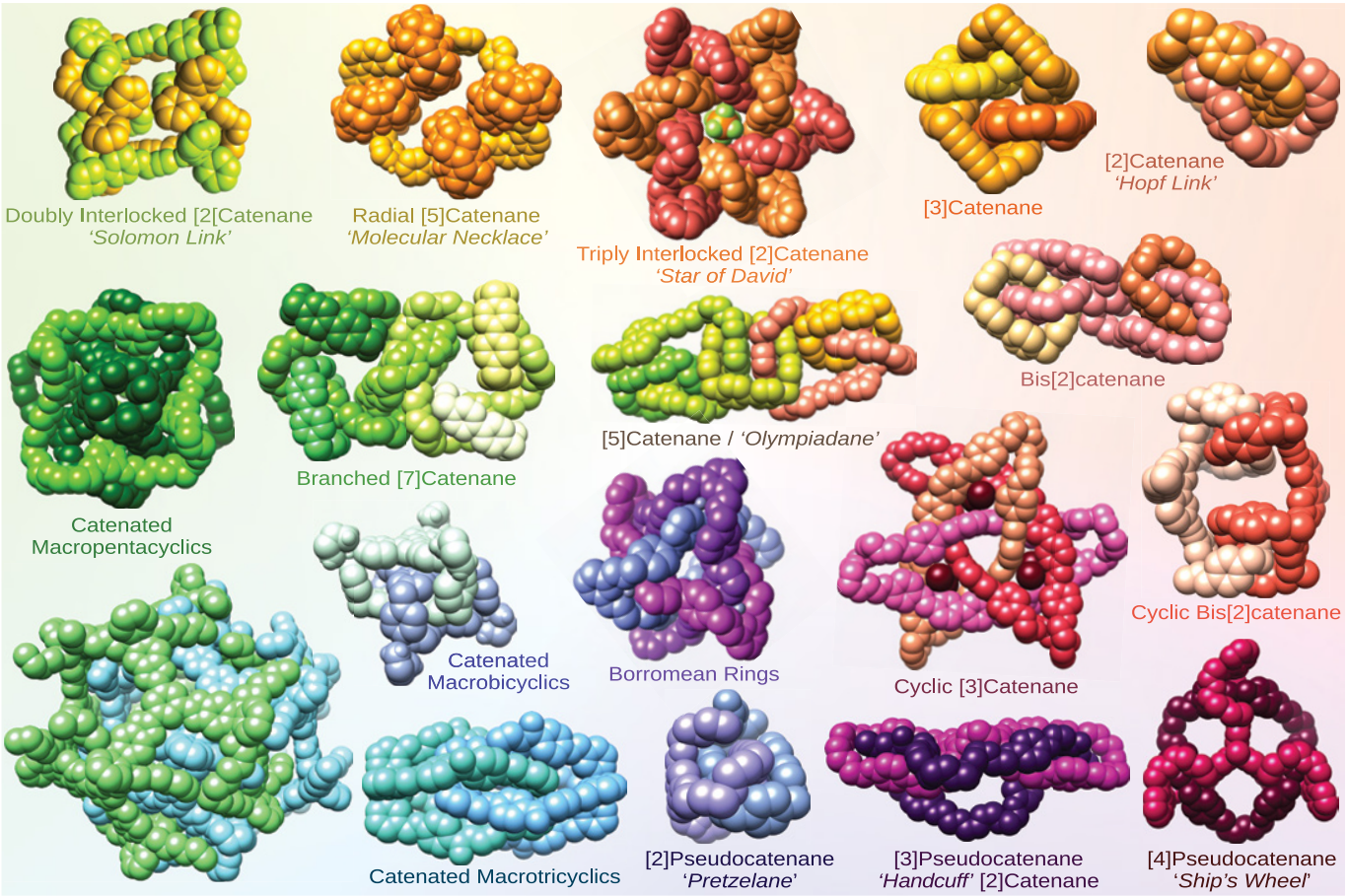


Figure 1.27 Space-filling representations of the solid-state structures of some beautiful MIM topologies: [2]catenane,[134] [3]catenane,[123] [5]catenane (Olympiadane),[133] [5]catenane 'molecular necklace',[184] branched [7]catenane,[135] eightfold interlocked multicatenane,[269] triply interlocked coordination cages,[248] quadruply interlocked coordination cages,[249,270] Solomon link,[266] Borromean Rings,[237] triply interlocked 'Star of David' [2]catenane,[236] cyclic [3]catenane,[238] pretzelane,[267] doubly threaded 'handcuff' [2]catenane or [3]pseudocatenane,[260] 'ship's wheel' [4]pseudocatenane,[262] bis[2]catenane,[268] cyclic bis[2]catenane.[265] Solvent molecules, counterions, and protons are omitted for the sake of clarity.

single bridge between two rings have also been called[293] handcuff rotaxanes, by analogy with handcuff catenanes. Cyclic [4]rotaxanes (**Figure 1.28c**) have been introduced[294] in which two bis-macrocycles are threaded by two dumbbells to give a ladder-like geometry. Sauvage[295] has obtained a crystal structure (**Figure 1.29i**) of a cyclic [4]rotaxane based on transition metal templates. Tris- and tetra-macrocyclic 'platforms', which are triply or quadruply interlocked with tripodal or tetrapodal 'rigs', respectively, have been described as mechanically interlocked 'bundles',[296] and 'molecular elevators',[178] the latter case pertaining to situations where a platform can be translocated under the influence of external stimuli—see **Section 6.13.1.3**. A triply interlocked bundle[296] is illustrated in **Figure 1.28g**, while the solid-state structure of a fourfold interlocked molecular elevator[297,298] is represented in **Figure 1.29d**. A suitane (**Section 4.3.5**) is a molecule that has been named[8,299] to reflect a molecular 'suit' which mechanically envelops a multi-limbed molecular 'body' (a suit[*n*]ane has *n* 'limbs'). A suit[2]ane (**Figure 1.29g**) thus involves a bulky molecular core bearing two appendages, all of which are encircled by a unibody macrotricyclic 'suit'.

There remain many architectures with mechanical bonds beyond simple two- or three-component rotaxanes that do not involve covalently bridged component parts. Polyrotaxanes, for example, are relatively commonplace in the literature—see **Section 4.2.1.1**. Recently, it has proven to be possible to control the secondary structure of oligorotaxanes, creating large, well-defined rigid-rods[138,300] (**Figure 1.28i**) and foldamers[301–303] (**Figure 1.28j**) based on the mechanical bond. Another type of multicomponent architecture is that of the rotacatenane (**Figure 1.28a**, **Section 4.3.1**), first introduced[7] in 1999, which comprises a [2]catenane threaded by a molecular dumbbell. More recently, the term rotacatenane has been expanded to describe[304] larger architectures possessing both rotaxane and catenane moieties. A similar concept involves two dumbbells encircled by a single ring—an architecture (**Figure 1.28e**, **Section 4.2.1.2**) first created by Anderson.[305] Sauvage[306] and Leigh[307] have also created examples of these doubly threaded architectures, the latter case, which was nicknamed a 'molecular sheaf', includes a crystal structure (**Figure 1.29c**) of the architecture. A larger

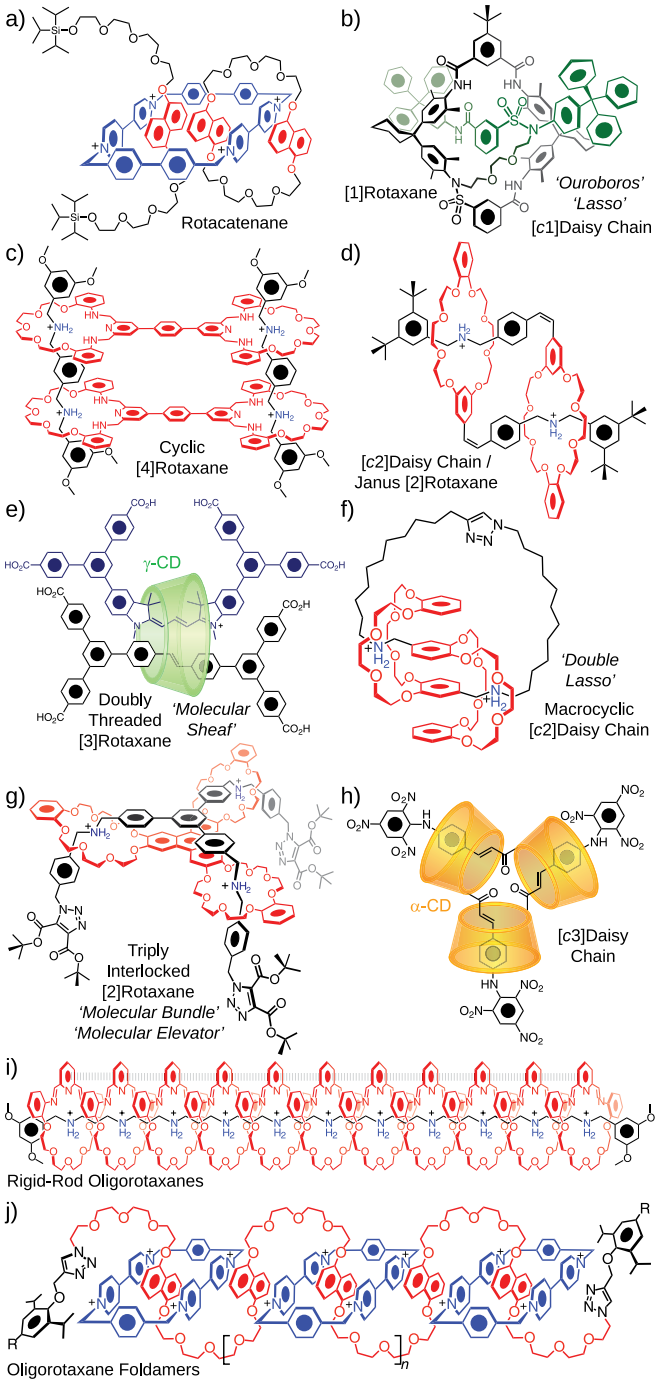


Figure 1.28 Seminal examples of MIM architectures. (a) Rotacatenane.[7] (b) [1]Rotaxane,[271] (c) Cyclic [4]rotaxane.[294] (d) [*c*2]-Daisy chain,[284] (e) Doubly threaded [3]rotaxane,[305] (f) Macrocyclic [*c*2]daisy chain double-lasso.[287] (g) Triply interlocked [2]rotaxane.[296] (h) [*c*3]Daisy chain.[286] (i) Rigid-rod oligorotaxanes.[138,300] (j) Oligorotaxane foldamers.[301,302]

molecular sheaf (**Figure 1.29h**) comprising two dumbbells, each encircled by two inorganic rings, has also been described by Leigh and Winpenny.[139]

The solid-state structures of two particularly unusual architectures are depicted in **Figure 1.29a–b**. Jiang and Huc[10] have produced a number of 'helix-rod' host-guest complexes, which resemble [2]rotaxanes wrapped (**Figure 1.29a**) in molecular helices instead of rings. The mechanical bond in this case lies in a grey area (see **Section 3.1.1**) since the rod and helix can dissociate, although the timescale of exchange is relatively slow, on the order of days, when the stoppers are sufficiently bulky. Stang and Chi[11] have reported the self-assembly of a rotaxane-like ring-in-ring architecture (**Figure 1.29b**) in which two bulky metallacycles are mechanically interlocked, yet not catenated.

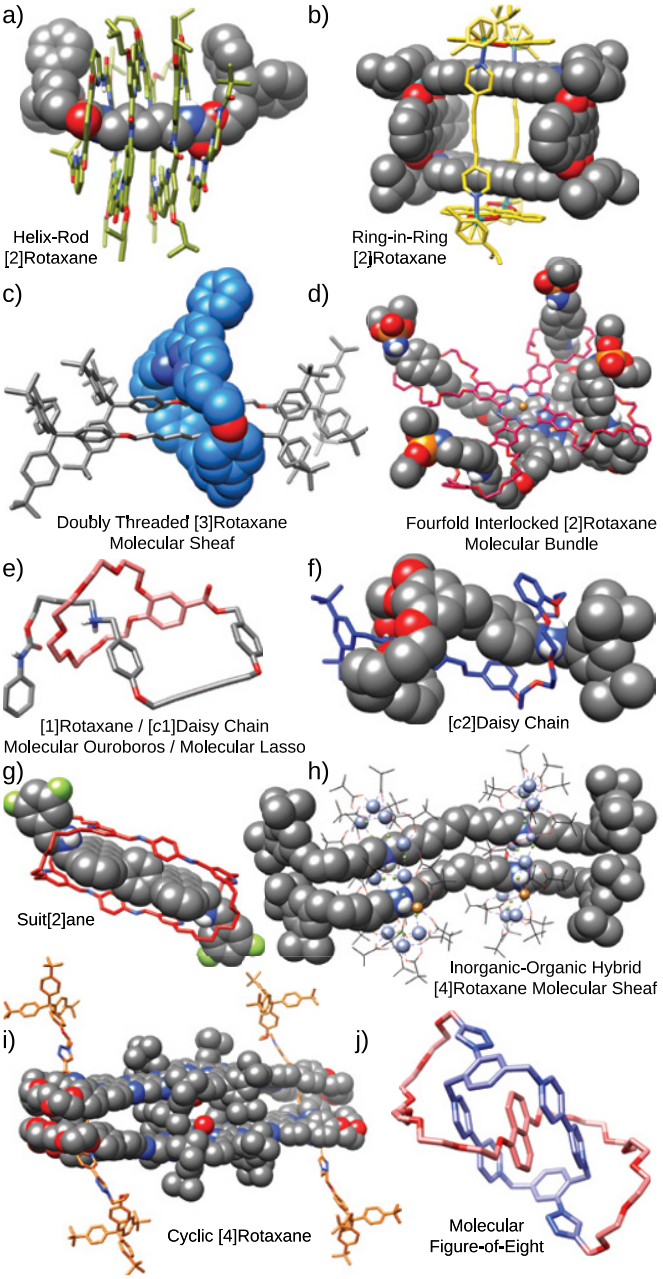


Figure 1.29 Solid-state structures of some beautiful MIM architectures. (a) Helix-rod rotaxane.[10] (b) Ring-in-ring rotaxane.[11] (c) Doubly-threaded [3]rotaxane.[307] (d) Fourfold interlocked [2]rotaxane.[298] (e) [1]Rotaxane.[272] (f) [*c*2]Daisy chain.[285] (g) Suit[2]ane.[8] (h) Organic-inorganic hybrid doubly threaded doubly encircled [4]rotaxane.[139] (i) Cyclic [4]rotaxane.[295] (j) Figure-of-eight.[281] Solvent/matrix molecules, counterions, and C–H protons are omitted for the sake of clarity.

Given all of the pleasure and beauty derived from creating new interlocked architectures, we have only scratched at the surface of what is possible. Many of the molecules shown in this Section were already framed in the context of beauty in the primary literature, and we expect that aesthetic considerations will continue to motivate new architectural developments.

1.3.4 Simplicity and Elegance

Simplicity is probably the least controversial trait that a molecule needs to be beautified in the minds of chemists, who have always been drawn to Platonic notions of beauty. Who could blame chemists for this kind of thinking? Simplicity is tied to the pleasing virtues of balance, symmetry, wholeness, and harmony. It is also tied to clarity and comprehension, which is tied to truth (**Section 1.2.4**), which is tied to beauty. When a chemist examines a simple molecule, a network of these related concepts inevitably leaves him or her with a sense of pleasure and satisfaction.

There is no lack of beautifully simple MIMs. The quintessential example is the all-hydrocarbon [2]catenane (**Figure 1.30**) prepared by Schill,[308] in which the simplest non-trivial topology is constituted only by methylene units. Other beautifully simple MIMs comprise highly symmetrical structures that make them "easy on the brain", such as many of the compounds in **Sections 1.3.2** and **1.3.3**. Although these molecules look relatively simple, it is clear that an IUPAC name would be far from simple, a testament to the growing importance of images and graphical representation in chemistry.

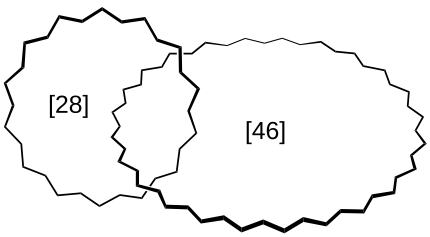


Figure 1.30 Stereoformula of an all-hydrocarbon [2]catenane introduced by Schill.[307] Bracketed numbers denote the number of carbon atoms constituting each ring.

Although we are, no doubt, aesthetically drawn to simple molecules—recall the Platonic solids from the introduction—experiments are where the beauty of simplicity truly shines. While we have chosen the word 'beauty' to describe the aesthetic value of structural representations, 'elegance' is a term that has been employed[61] to describe the aesthetic value of experiments. Here, we present some selected examples of experimental milestones that embody elegance in mechanostereochemistry. This case is our only foray into experimental beauty and the list is by no means exhaustive.

1. Templated Synthesis: Sauvage[120] revived an all but forsaken discipline by introducing (**Figure 1.31**) transition metal templates for synthesizing MIMs. His raison d'être for using coordination chemistry to position organic precursors appropriately to interlock them in subsequent reactions, which dramatically reduces the number of steps and increases the yield by orders of magnitude over those obtained for previous MIMs, was supremely elegant. **Figure 1.31** portrays his shorthand drawing of the original template strategies[120] for catenane synthesis. Sauvage's templated synthesis set the stage for the plethora of novel molecular recognition motifs (see **Figure 1.22** and **Section 2.3**) employed today in the making of mechanical bonds.

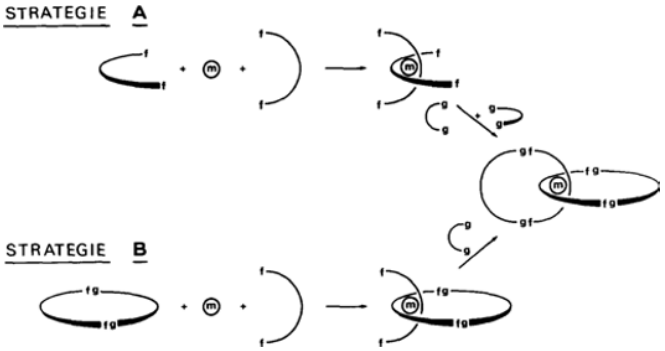


Figure 1.31 Sauvage's scheme depicting his seminal template-directed strategies for synthesizing MIMs. A tetrahedral center orients U-shaped species appropriately for subsequent ring-closure, resulting in a catenate. Reprinted with permission from ref. 120 (copyright 1983 Elsevier).

2. Thermodynamic Control: MIMs can now be synthesized routinely in near-quantitative yields—a convenience that can be attributed in large part to the advent of thermodynamically controlled protocols, although a number kinetically controlled reactions are also high yielding. See **Chapter 3** for a review of MIM synthesis under thermodynamic control. Seminal examples[129,202,309–314] of elegant thermodynamically controlled protocols for making mechanical bonds are illustrated in **Figure 1.32**. They include (in order of appearance) (i) slippage[309] (**Section 3.1**), which involves the passage of a ring over a size-complementary stopper that is sufficiently bulky to prevent deslipping, (ii) olefin metathesis[310] (**Section 3.4**), which involves a catalyst—typically Grubbs' Ru alkylidene catalysts—scrambling the constituents of double bonds, (iii) disulfide exchange (**Section 3.5.1**), which involves the oxidative coupling of thiols and reductive cleavage of disulfides, (iv) kinetically labile metal-ligand bonds (**Section 3.2**)—a revolution led by Makoto Fujita,[202] (v) reversible nucleophilic substitutions (**Section 3.5.2**), such competing S_N2 processes[312] in dynamic equilibrium, (vi) imine bonds[129,315] (**Section 3.3.1**) whose reversible nature facilitates the self-assembly of MIMs, (vii) boronic esters[313] (**Section 3.3.3**) formed reversibly from boronic acids and diols, and (viii) self-assembled monolayers[314] (SAMs) (**Section 3.6**).

We emphasize here that thermodynamically controlled reactions—especially olefin metathesis, metal coordination, and imine bonding—have been indispensible in orchestrating the self-assembly of many of the most exotic,

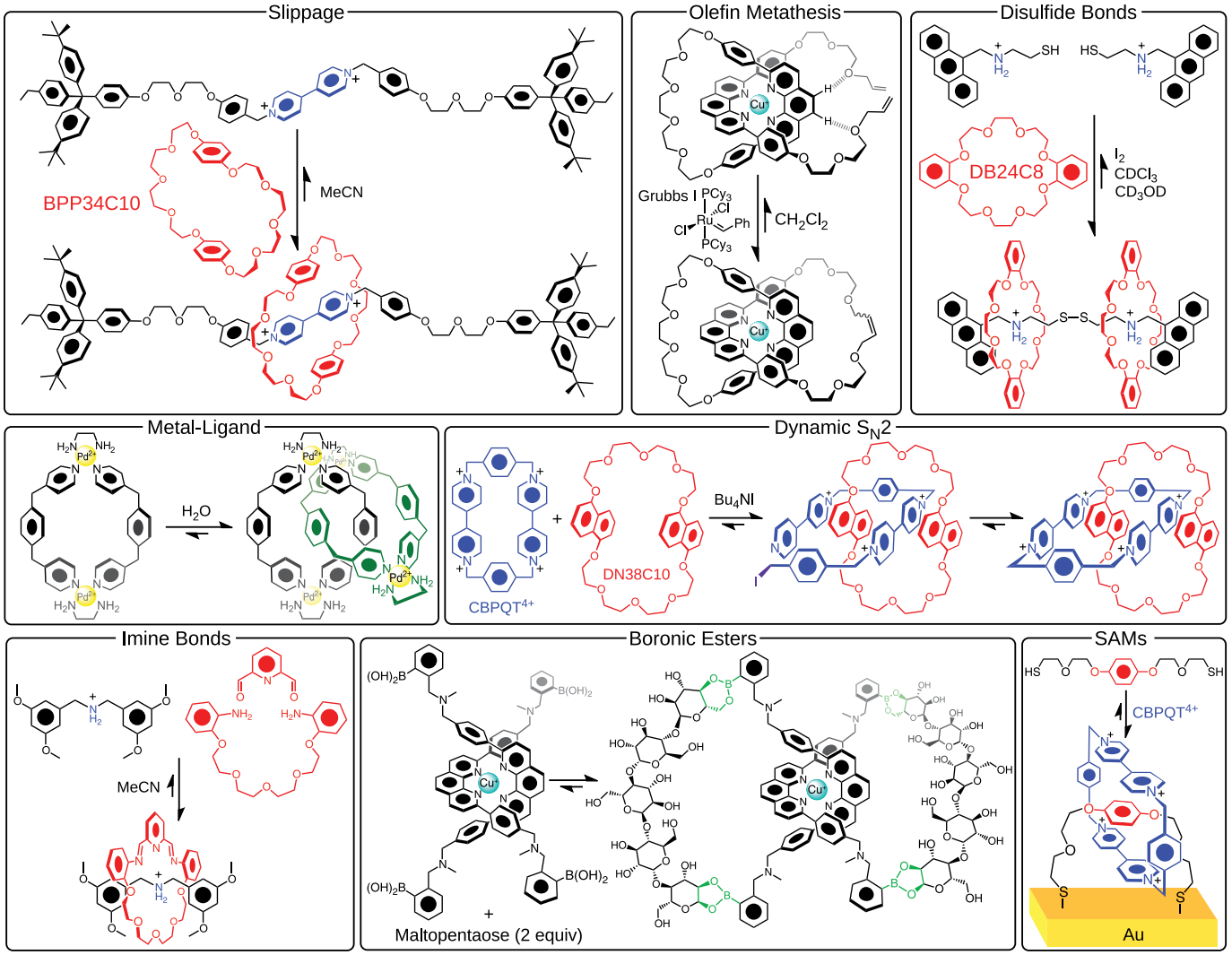
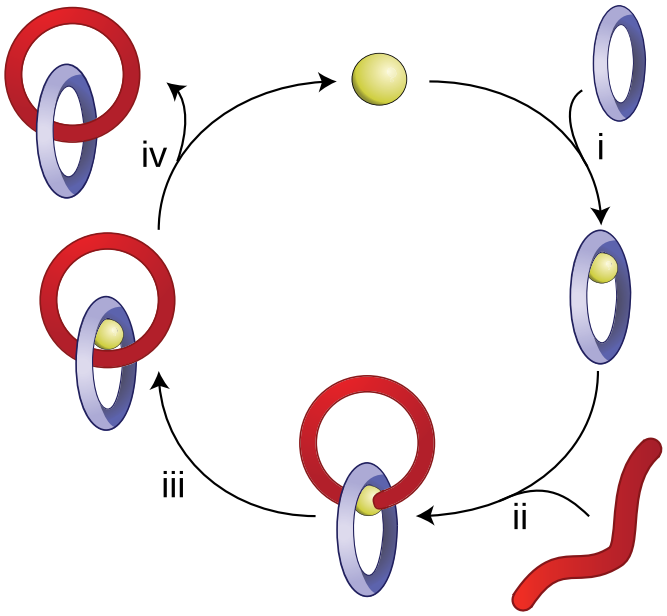


Figure 1.32 Examples of elegant thermodynamically-controlled reactions employed in the near-quantitative synthesis of MIMs. Slippage[309] involves the passage of a ring over a size-complimentary stopper that is sufficiently bulky to prevent deslipping. Grubbs' catalysts impart olefin-containing MIMs with dynamic properties by scrambling the constituents of double bonds via olefin metathesis.[310] Reversible disulfide bonds establish thermodynamic control by disulfide exchange.[311] Labile coordinative bonds are employed in the self-assembly of MIMs.[202] A weakly nucleophilic leaving group (I^-) competes with a nucleophilic macrocylization/catenation event in a reversible S_N2 reaction.[312] Reversible imine bonds facilitate the selection of MIMs from dynamic combinatorial libraries.[129] MIMs can be self-assembled from boronic acids and diols via the reversible formation of boronic esters.[313] Self-assembled monolayers (SAMs) provide a means to mount rotaxanes on surfaces under thermodynamic control.[314] See **Chapter 3**.

beautiful, and challenging topologies and architectures including molecular necklaces,[184,186,190,247,316,317] handcuff catenanes,[259,260,318] mechanically interlocked cages,[230,248,249,270,319] molecular trefoil knots,[320–323] pentafoil knots,[241,242] Solomon knots,[324–326] Borromean rings,[89,237,327,328] the Star of David catenane,[236] the cyclic [3]catenane,[238] daisy chains,[329,330] molecular bundles,[331] and very large discrete rigid-rod oligorotaxanes.[138,300]

3. Active Template Synthesis: A step beyond the template is the 'active template,' introduced in 2006 independently by the groups of Saito[332] and Leigh.[333] An active template is a moiety acting simultaneously as a template and a catalyst. It relies on the use of a macrocycle that is capable of immobilizing a template/catalyst within its cavity, such that it promotes an endotopic ring-closing reaction (for catenanes) or coupling (for rotaxanes), resulting in a mechanical bond. A cartoon depicting the concept of an active metal template is shown in **Scheme 1.1**. The elegant dual role of the template means that the metal ion can be used in sub-stoichiometric amounts without compromising yield, and permanent coordination sites need not be built into every component part of the corresponding MIM. Although they are relatively new to the scene, active templates have already been employed[334] in the synthesis of rotaxanes, catenanes, trefoil knots, shuttles, and switches, making use of copper-catalyzed Huisgen terminal azide-alkyne 1,3-cycloadditions,[333] Glaser terminal alkyne homo-couplings,[332] Ullmann-type



Scheme 1.1 Generalized mechanism of active template synthesis,[334] exemplified by the case of a [2]catenane. (i) A metal catalyst (gold) is bound within the cavity of a macrocycle (blue). (ii) A reagent (red) coordinates the metal within the macrocycle. (iii) A covalent bond is formed catalytically, resulting also in the topological and mechanical bond of a catenane. (iv) The catalyst is regenerated and the catenane is expelled. See **Section 2.4**.

C–S couplings,[332] Cadiot-Chodkiewicz alkyne heterocouplings,[335] as well as Pd- and Ni-mediated homocouplings,[336,337] Ni-catalyzed sp^3–sp^3 homocoupling of unactivated alkyl bromides,[307,338] oxidative Heck cross-couplings,[339] Michael additions,[340] Diels-Alder reactions,[341] and Goldberg amidations.[342] See **Section 2.4** for a review of active template strategies. This new method of making mechanical bonds is undeniably versatile and elegant.

1.3.5 Complexity and Emergence

Opposite the pleasure of comprehension, harmony, and tidiness that goes with the topics of simplicity and elegance is the pleasure of surprise and learning that accompanies the related concepts of complexity[343,344] and emergence.[345–348] Since complex systems are inherently difficult to understand, beauty must be sought in tension and challenge rather than simplicity and harmony. Emergence, however, is immediately pleasing when we encounter it: the 'Eureka' moment, the recognition that the whole is greater than the sum of its parts, that the output could not be predicted by inspection of the input. Emergence arises out of complexity—it is the diamond at the bottom of a dark mine.

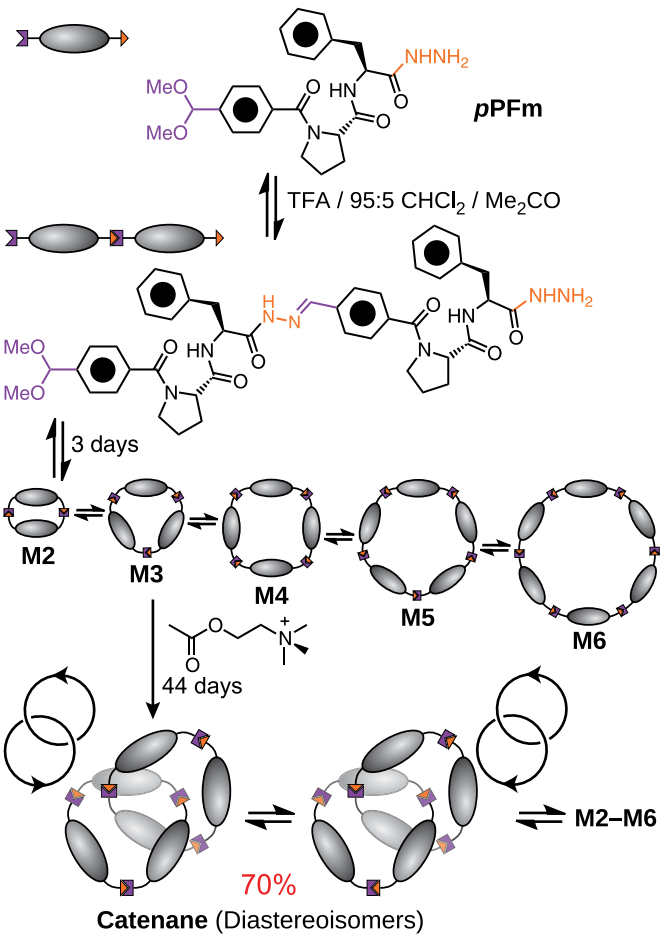
We are in danger of conflating 'complex' with 'complicated'. While there is undoubtedly beauty to be found in both, in science they have different meanings. Complexity is related to chaos—dynamic, non-equilibrium, and practically unpredictable phenomena. Chaos theory was borne out of meteorology and mathematics and is conceptually (and hypothetically) demonstrated by the famous "butterfly effect," a metaphor coined by Lorenz[349] which questioned if the flap of a butterfly's wings could trigger catastrophic weather weeks later and many miles away. Complexity and chaos is a growing and highly multidisciplinary field of research, characterized by systems that are highly sensitive to variations in initial conditions. By contrast, 'complicated' only refers to things that are, well…complicated—something with many parts or intricacies, perhaps. Again we find ourselves in muddy waters, where we must admit that there is a prominent subjective air to this business of complexity and emergence. What is complex to one person might seem only complicated to another, wiser person. What is emergent now will not be emergent in 100 years when it is more deeply understood. For example, the literature is sprinkled with tales of serendipity—unexpected discoveries of mechanical bonds in reactions that were intended for other purposes. Among the most famous of these allegories are the fortuitous discoveries of hydrogen-bonded catenanes of the neutral variety—see **Figure 1.22** and **Section 2.3.4.1**. Hunter's seminal synthesis[211] of a tetralactam [2]catenane was an unexpected result of an attempt to make a simple macrocycle. Likewise, Leigh's first benzylic amide catenane was isolated[131] serendipitously as the unexpected product of a reaction intended to prepare a macrocyclic host for CO_2. These stories reflect the subjective and temporal dependence of discovery and knowledge—although they were unexpected at the time of their discovery, these hydrogen-bonded molecular recognition systems are now well understood and employed with high frequency and success in mechanostereochemistry. Today, few would argue that they are extraordinary in terms of emergence and complexity. On the other hand, Whitesides[343] has noted that even the simplest organic reactions are complex when considered rigorously—substrates can adopt an unlimited number of conformations and reactants have an enormous variety of interactions with solvent molecules, ions, other reactants, and so on. Hence, chemistry is an empirical science. We understand these truly complex reactions by correlating structure and reactivity in the light of lots of data. In this sense, emergence might be an area of chemistry where our data is too incomplete to give us a reliable understanding of structure-response relationships. With this disclaimer, we share a few examples that we find of emergence in mechanostereochemistry.

A promising arena for observing emergent phenomena is dynamic combinatorial chemistry[350] (DCC), which involves a pool of molecules interacting through reversible covalent bonds. Often, preferred species in the dynamic combinatorial library (DCL) of these reactants can be selected and/or amplified under certain experimental conditions, such as the addition of a template or a change in solvent polarity or temperature. It can take days or weeks for a DCL to reach equilibrium and pass through an array of complex and emergent structures. Even at equilibrium, DCLs can easily be complicated, even complex or chaotic when they are highly sensitive to

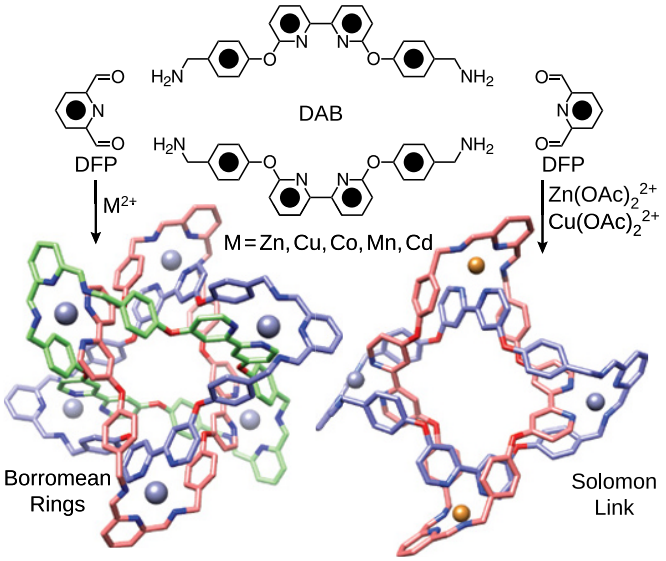
initial conditions. Sanders[351] demonstrated (**Scheme 1.2**) this idea beautifully in 2005, when he reported a DCL composed of a peptide (*p*PFm) that equilibrates over three days into a variety of macrocyclic oligomers ranging in size from a dimer (**M2**) up to a hexamer (**M6**), yet a more elaborate [2]catenane comprising two 42-membered **M3** rings is formed as the dominant species in the presence an acetylcholine additive, if given enough time to equilibrate—see **Section 3.3.2**.

Another possible case[325] of emergence (**Scheme 1.3**) is the fortuitous isolation of a Solomon Knot from the same pool of precursors employed in the self-assembly of the molecular Borromean Rings. Whereas a dynamic combinatorial library (DCL) of 2,6-diformylpyridine (DFP) and 2,2´-bipyridine derived diamine (DAB) ligands leads to the self-assembly[237,328] of molecular Borromean Rings in the presence of several metal templates, including Zn^{II} or Cu^{II}, the unexpected emergence[325] of a doubly-interlocked [2]catenane (Solomon Knot) is observed[325] upon crystallization of a DCL containing an equimolar mixture of Zn^{II} and Cu^{II} templates. The outcome's high sensitivity to subtle changes in initial conditions, with solvent, counterions, and templates all playing an important role in the (not yet well understood) crystallization process indicates a complex interplay of interactions. The crystallization of the Solomon Knot is most likely a kinetically controlled process, since the Borromean rings are the dominant species in solution, and indeed crystals of a Solomon knot possessing only Zn^{II} templates can be hand-separated from the crystals of Borromean rings under different crystallization conditions.[328] More recently, a subtle structural modification to the DAB ligand involving the addition of methylene spacers in between the amino and bipyridine moieties was found to lead to the simultaneous self-assembly[352] of a [2]catenane, trefoil knot, and Solomon knot in one pot, providing further evidence for the complexity of the equilibrium governing the formation of these molecular topologies.

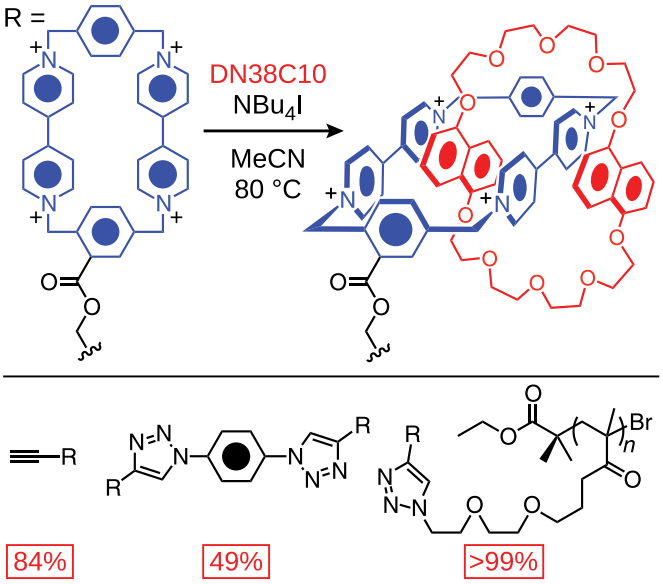
It has been discovered[353] that a polymer can demonstrate emergent phenomena when catenated under thermodynamic control. The previously-developed[312] iodide-catalyzed self-assembly of donor-acceptor [2]catenanes has been applied to a polymerizable monomer containing a derivative of cyclobis(paraquat-*p*-phenylene) ($CBPQT^{4+}$) in 84% yield. When dimerized, the catenation proceeds in an unsurprising 49% yield. However, when the catenation is performed on the poly-$CBPQT^{4+}$ compound, the reaction unexpectedly proceeds (**Scheme 1.4**) to >99% completion. This result[353] has been rationalized by postulating a cooperative,



Scheme 1.2 Sanders' dynamic combinatorial library based on the reversible imine bonds of the dipeptide building block *p*PFm, which yields mainly oligomeric macrocycles (**M2–M6**) until an acetylcholine template is added, which selects and amplifies an exquisite hexameric [2]catenane.[351]



Scheme 1.3 The self-assembly of molecular Borromean Rings[237,328] from a dynamic combinatorial library (DCL) containing DFP and DAB ligands with divalent metal combinatorial library (DCL) of 2,6-diformylpyridine (DFP) and 2,2´-bipyridine derived diamine (DAB) ligands leads to the self-assembly[237,328] of templates, as well as the unexpected emergence of a Solomon Knot[325] upon crystallization of a DCL containing a 1:1 mixture of Zn^{II} and Cu^{II} templates. Tubular representations of solid-state structures are illustrated with protons, counterions, and solvent molecules omitted for the sake of clarity.



Scheme 1.4 A polymerized derivative of the tetracationic cyclophane CBPQT^{4+} displays the emergent property of quantitative thermodynamic catenation by iodide-catalyzed self-assembly with the DN38C10 crown ether macrocycle. The analogous monomeric and dimeric species do not react quantitatively.[353]

synergistic templating effect by nearby tetracationic cyclophanes on the backbone of the polymer that are not present in the monomeric and dimeric compounds.

Owing to the ambiguous meanings of complexity and emergence, spectacular examples of emergent phenomena in mechanostereochemisty may abound, or they may be exceedingly rare, depending heavily on one's opinion. Nevertheless, the chemistry of complexity is sure to become a busier and ever more pleasing avenue that chemists will continue to traverse.

1.3.6 Beautiful Machines with Mechanical Bonds

Humanity has beautified machines since at least the time of the European Renaissance—as exemplified by the fusion of art and natural philosophy (the forerunner to modern science) in the manuscripts of the one and only Leonardo da Vinci—and probably for almost as long as machines have existed. Countless modern marketing campaigns are aimed at portraying the beauty of machines—automobiles, timepieces, electronic devices, and so on—in order to gain business. Molecular machines, such as the protein-based enzymes and assemblies that carry out life-sustaining nanoscopic work inside of cells, are perhaps the most beautiful machines of all because they were crafted by Nature over billions of years of evolution to express astonishing feats of mechanical work and motion against the enormous chaotic thermal fluctuations that dominate objects on the nanoscale, embodied by the "wiggles and jiggles" known as Brownian motion.[354,355] One of the most compelling aspects of MIMs is that their architectures are well suited for designing artificial molecular switches and machines. See **Chapter 6**. The motion of one component part relative to another can often be controlled by an external stimulus in bistable and multistable MIMs. The fact that MIMs can express these mechanical motions in response to an influx of energy is the reason why they are often referred to as "molecular machines" or "motor molecules", though it would be more accurate to call most of them switches unless the motions are harnessed to do work.

The ring of a catenane or rotaxane can be shuttled (**Figure 1.33**) from one site to another under the influence of a wide variety of stimuli, including redox, light, pH, cations, anions, solvents, covalent reactions, temperature, molecular recognition, pressure, and mechanical force. Seminal examples[175,356–365] of molecular switches employing these stimuli are illustrated in **Figure 1.33**, representing another case of beauty in diversity. In more recent years, a number of important examples[188,366–369] of mechanically interlocked systems expressing biased, mechanostereoselective, or "unidirectional" motion have been described, as well as a number of molecular ratchets that exhibit[369–376] energetically demanding and entropically unfavorable transport—see **Section 6.15.2**. These molecules are setting the foundation for artificial molecular machines that can perform complex tasks more akin to biological molecular machines. Reviews and monographs on the subject of mechanically interlocked molecular machines, such as switches and motors, are abundant in the literature.[377–396]

A car that doesn't start or a computer that doesn't boot up are machines that many people would more likely describe as 'useless' rather than 'beautiful'. Likewise, molecular switches that simply bump around and tumble randomly in solution aren't very useful—they must carry out a functional task to be considered machines in the true sense of the word. Thus, the most beautiful molecular machines are those that we put to work for us. One of most promising strategies for garnering function from artificial molecular machines is to organize them at interfaces or in bulk.[397–400] See **Sections 6.14** and **Section 6.15.1**. Here we highlight several noteworthy examples of molecular machines that go beyond being simple switches.

Wouldn't it be amazing if the tiny nanomotions of artificial molecular machines could be cooperatively scaled up to do work on macroscopic objects? Nature has implemented this strategy in muscle tissue, where the chemically driven mechanical motions of molecular machines known as myosin are scaled over many orders of magnitude, courtesy of their integration within a hierarchically organized material comprising bundles of aligned filaments. Rotaxanes have been recognized[180,288–291] for their ability to express muscle-like extensile and contractile motions. Furthermore, some single-molecule investigations[401,402] of switchable rotaxanes by force spectroscopy have shown unequivocally that they are capable of generating force, even against an external load, an observation which bodes well for the future of artificial molecular machines.

An enticing demonstration[403–405] of the possibility of doing macroscopic work with mechanically interlocked artificial

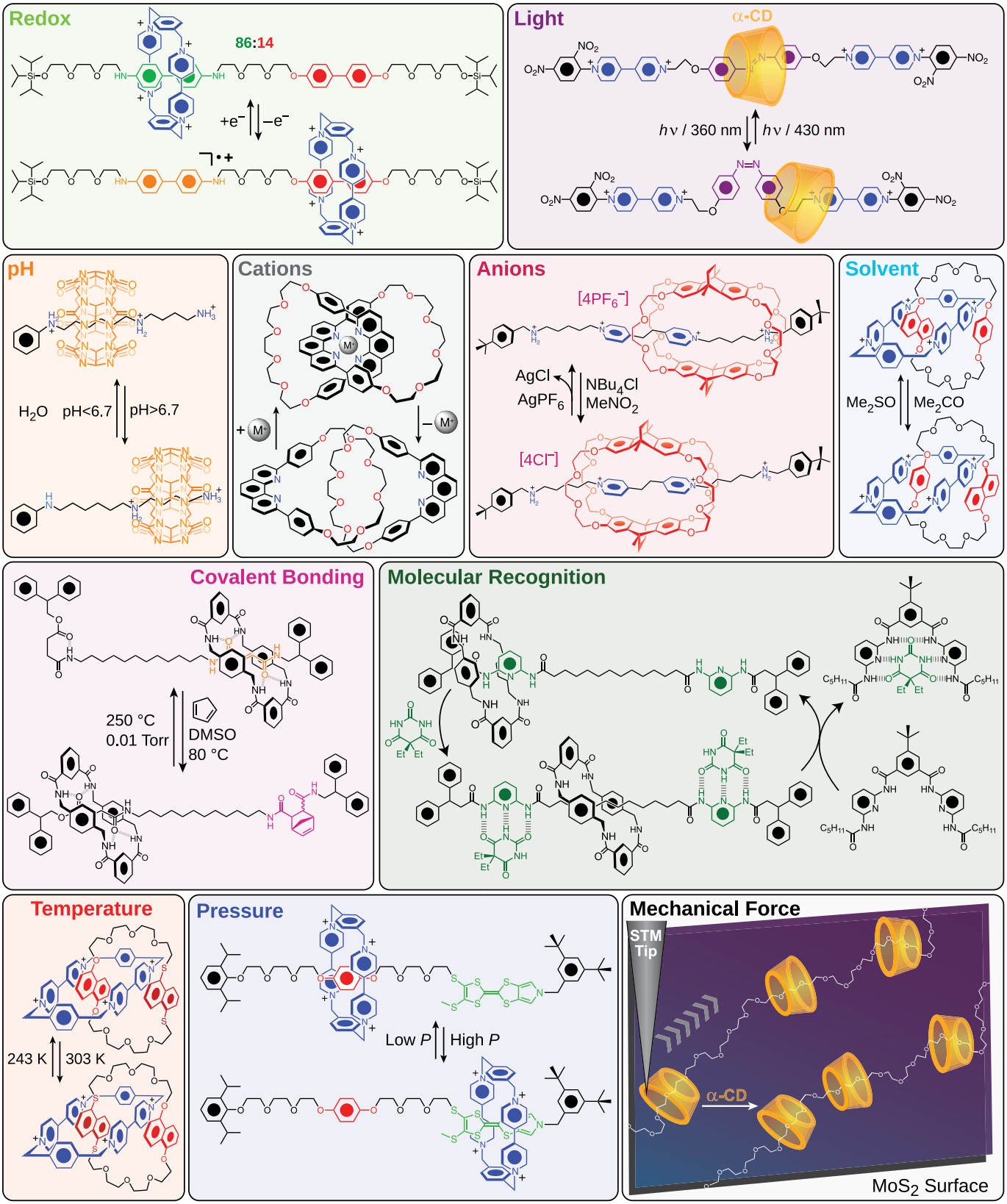


Figure 1.33 Beauty in diversity. Different types of stimuli that drive mechanically interlocked molecular switches include redox,[175] light,[356] pH,[357] cations,[358] anions,[359] solvent,[360] covalent bonding,[361] molecular recognition,[362] temperature,[363] pressure,[364] and mechanical force.[365]

molecular machines been devised by immobilizing zillions of redox-switchable, palindromic bistable [3]rotaxane 'molecular muscles' on the surface of a thin gold-coated microcantilever. Remarkably, the chemical or electrochemical redox actuation (**Figure 1.34**) of these anchored molecules bends the cantilever up and down, a movement that can be detected with a laser beam focused on its surface. Although it remains below the macroscopic scale, this experiment demonstrates that energy can be transduced and work can be done by molecular switches organized at an interface. More recently, Giuseppone[406,407] has demonstrated that the concerted acid/base actuation of bistable [*c*2]daisy chain monomers embedded in a long metallosupramolecular polymer can change its countour length by several microns—orders of magnitude greater in scale than the individual switches embedded in the backbone, and that aggregates of hydrogen-bonded [*c*2]daisy chain supramolecular polymers exhibit very different morphologies when the monomers are in the contracted and extended states. These experiments provide a strong proof-of-concept that rotaxanes are capable of serving as artificial muscles—see **Section 6.15.1.2**.

Leigh[408] described an experiment in 2005 that also utilizes molecular switches to transport (**Figure 1.35**) a macroscopic droplet across a surface. Bistable rotaxanes were physisorbed onto a surface and irradiated with UV light, which led to the photoisomerization of an olefin in a

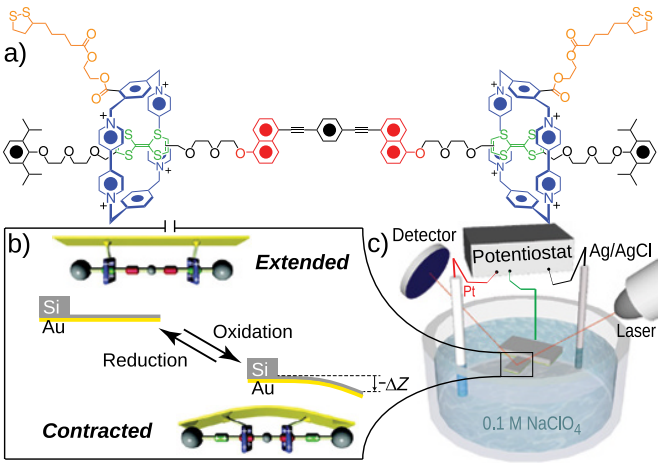


Figure 1.34 Electrochemically driven mechanical actuation of a gold-coated microcantilever by bistable [3]rotaxane 'molecular muscles.'[405] (a) Structural formula of a palindromic bistable [3]rotaxane with gold-binding dithiolanes attached to the rings. (b) Graphical representation of the reversible bending of a cantilever by actuation of a self-assembled monolayer (~8 billion molecules) of the rotaxanes on its surface. The rotaxanes 'contract' when stereoelectronic changes induced by redox stimuli cause them to glide in opposite directions. (c) Diagram of the electrochemical cell (Ag/AgCl, Pt, and the cantilever are the reference, counter, and working electrodes, respectively) and combined AFM device used to measure the bending by detecting a laser beam reflected off of the cantilever's surface. Adapted with permission from ref. 33 (copyright 2012 Springer)

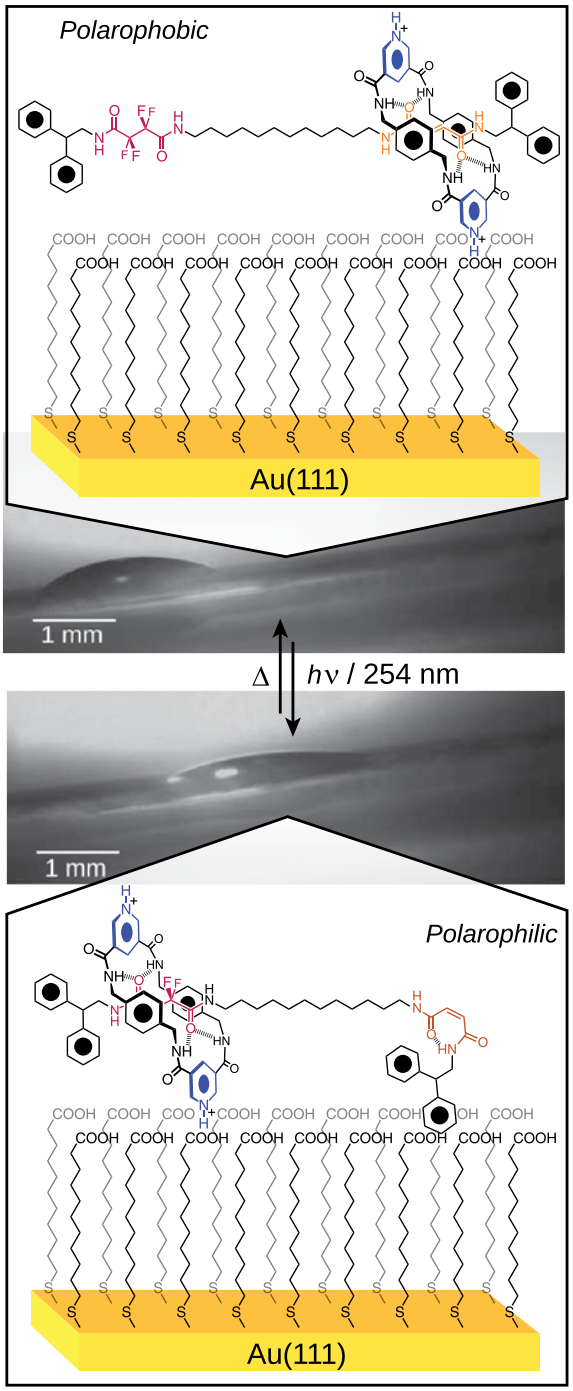


Figure 1.35 Light-driven transport of a diiodomethane droplet up a 12° incline on a Au(111) surface coated with a SAM of 11-mercaptoundecanoic acid and physisorbed, photoswitchable bistable [2]rotaxanes.[408] In the ground state (top), the ring preferentially encircles an unfluorinated fumaramide recognition site and the exposed tetrafluorosuccinamide recognition site contributes to the polarophobicity of the surface. When a light beam focused on one side of the droplet causes some of the fumaramide (*trans*-olefin) units to isomerize to maleamide (*cis*-olefin), the ring within this population of the photostationary state shuttles to encircle the fluorinated recognition unit (bottom), which decreases the surface polarophobicity and causes the droplet to move several millimeters uphill. Photographs reprinted with permission from ref. 408 (copyright 2005 Nature Publishing Group)

population of the rotaxanes and caused the ring to shuttle over to a fluorinated recognition site, which in turn changed the polarophobicity of the surface. Photoswitching the surface in this manner underneath one side of a diiodomethane droplet causes it to move several millimeters up a 12° incline.

Now for a bit of science fiction: what if single molecules could be utilized to perform logic operations or store information, like transistors? A joint effort toward this end between ourselves and Heath,[409–416] which addressed the organization and electrochemical actuation of bistable donor-acceptor MIMs as molecular monolayers within crossbar interfaces known as molecular switch tunnel junctions (MSTJs), culminated[416] after a decade in a high density memory device (**Figure 1.36**) in 2007. The monolayer of bistable rotaxanes was incorporated into a crossbar logic architecture (**Figure 1.36c**) in a size regime corresponding to little more than 100 molecules per junction. Actuation of the bistable switches in these MSTJs

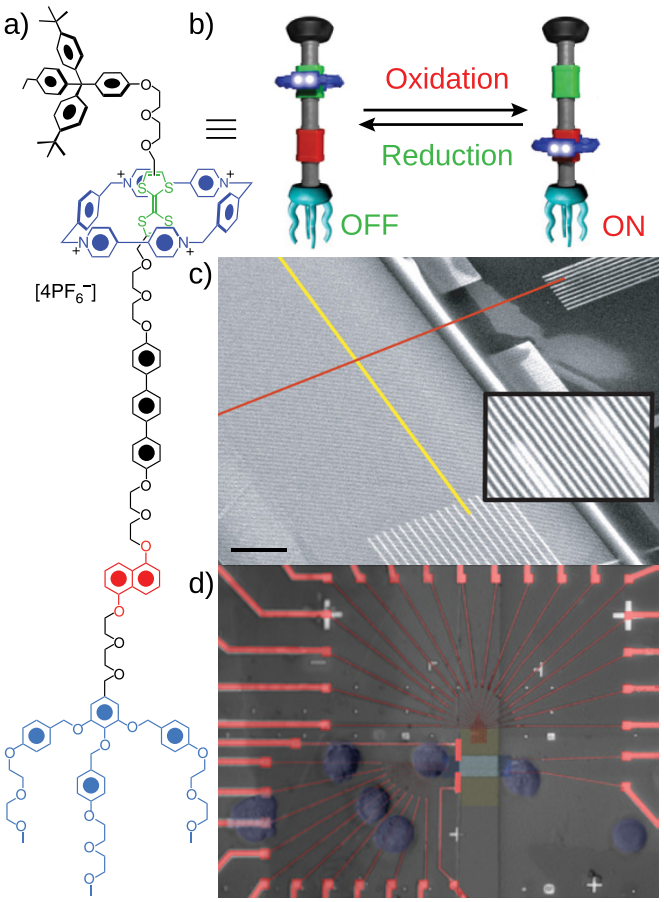


Figure 1.36 A 160-kbit molecular electronic memory device.[416] (a) Structural formula of the molecular switches used in the device. (b) Technomorph representations depicting how the molecular switches can be electrochemically toggled "on" and "off" in the device into co-conformational states with different conductivities. (c) SEM image of the intersection between top (red) and bottom (yellow) electrodes for the MSTJs. (d) Microscopic image of the memory device (blue area) and its electrical contacts (red) with white blood cells (green) as a reference of scale. Reprinted with permission from ref. 33 (copyright 2012 Springer)

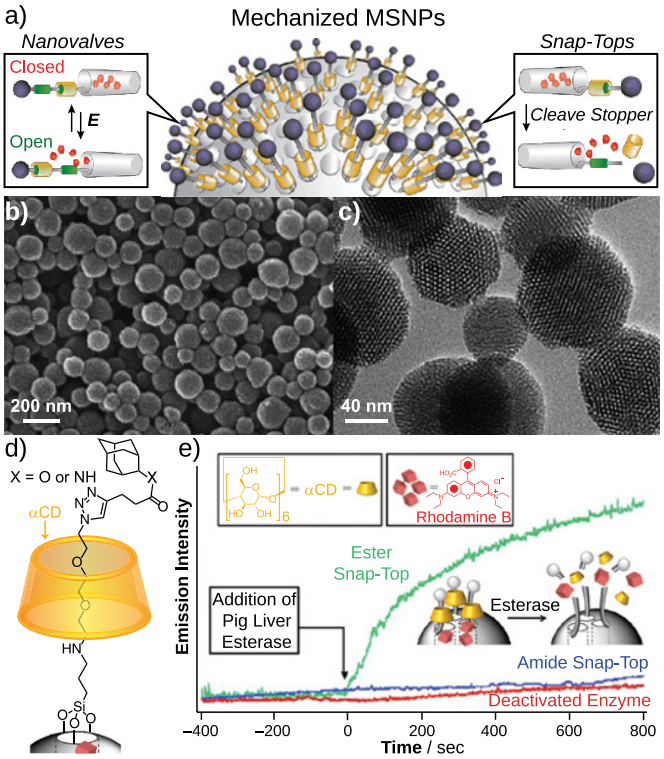
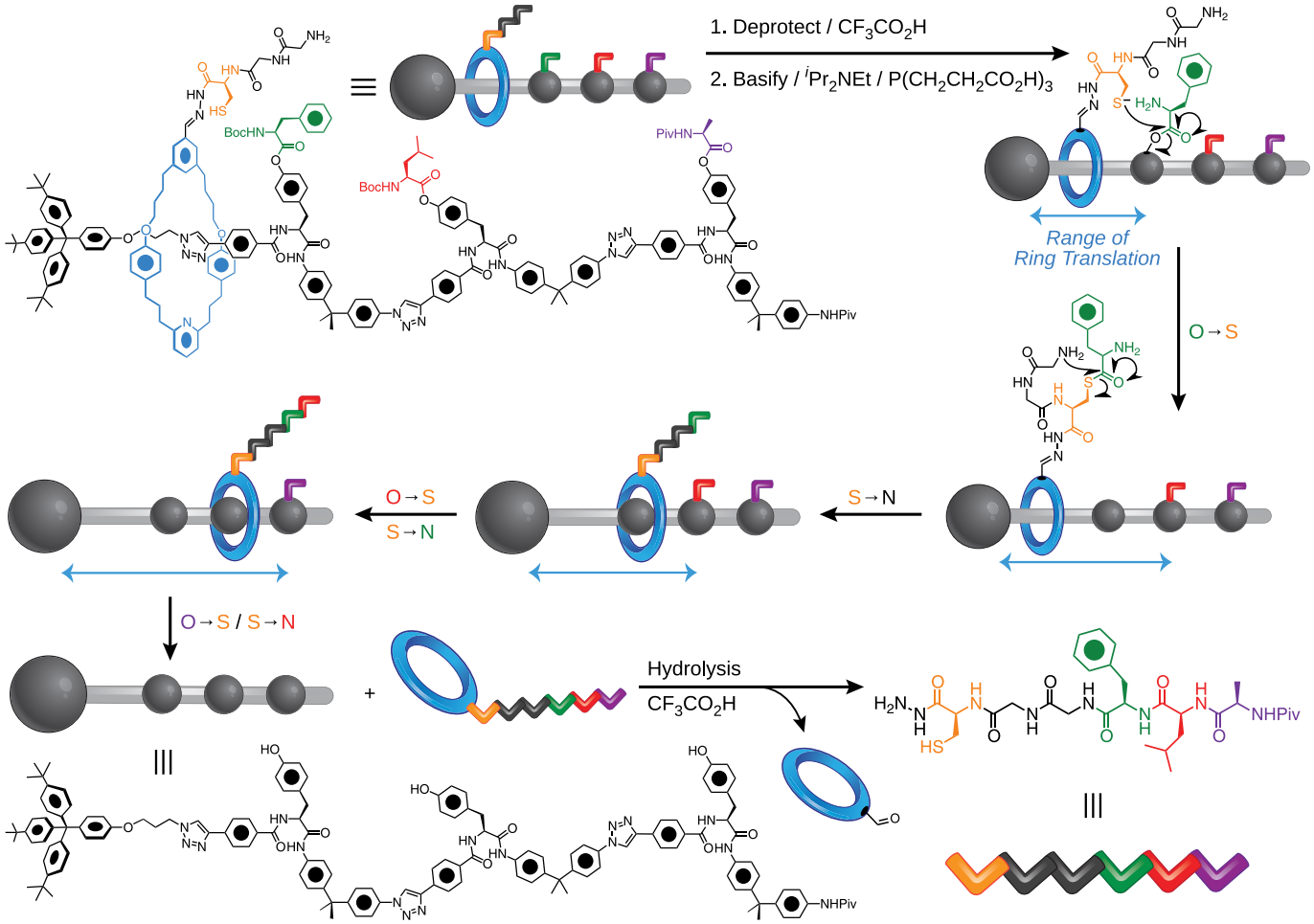


Figure 1.37 Examples of mechanized mesoporous silica nanoparticles (MSNPs).[418–420] (a) Illustrations of the functions of rotaxane nanovalve and snap-top mechanisms for controlled release of cargo.[394] (b) SEM image of MSNPs. (c) TEM image of MSNPs.[418] (d) Structural formula of an α-cyclodextrin (αCD)-based snap-top rotaxane blocking the pores of a MSNP. The stopper is connected to the axle by an amide bond or an enzyme-cleavable ester bond. (e) Release profile of rhodamine B from the snap-top MSNPs.[449] The addition of pig liver esterase decomposes the mechanical bond by cleavage of the ester-linked stopper, which releases αCD and hence the cargo from the nanoparticles, an outcome which is monitored by the fluorescence intensity of rhodamine B. Controls employing an amide bonded snap-top or deactivated enzyme do not release significant amounts of cargo from the MSNPs. SEM and TEM images reprinted with permission from ref. 418 (copyright 2009 Royal Society of Chemistry), release profile adapted with permission from ref. 449 (copyright 2008 American Chemical Society)

validated them as storage elements; about 25% of the bits had sufficient on/off ratios to be configured into a device. The resulting 160-kilobit memory circuit had a density of 10^{11} bits·cm^{-2}, for a total memory cell size of 0.0011 mm^2, which is approximately the cross-sectional area of a white blood cell (**Figure 1.36d**). A memory circuit of these dimensions is roughly on par with that of a storage density projected[417] to be available in 2020 if Moore's Law continues to be obeyed.

The question inevitably arises: can we build artificial molecular machines that are "smart" enough to respond to signals within our bodies, releasing therapeutic drugs or diagnostic contrast agents, for example, only at a localized and desired site? Once again, reality is not so far from the dream. A number of research groups are developing a variety of "mechanized nanoparticles"[418–420] (**Figure 1.37**)



Scheme 1.5 Sequence-specific peptide synthesis by a rotaxane artificial molecular machine.[454] The ring adds monomers to the end of its peptide sidechain by a series of native chemical ligation reactions, the sequence of which is defined by the sequence of monomers confining the ring to the rotaxane's dumbbell.

with these applications in mind. Efforts thus far have been associated chiefly with the covalent functionalization of supramolecular and molecular switches on the surfaces of mesoporous silica nanoparticles[421] (MSNPs, **Figure 1.37b–c**) that can act as stimulus-responsive (**Figure 1.37a**) gates to the nanopores.[422,423] Since 2004, bistable rotaxanes and pseudorotaxanes at the surface of these nanoparticles have been demonstrated over and over again to release cargo selectively from MSNPs in response to changes in pH,[179,424–434] light,[435–442] redox stimuli,[183,443–446] and salt concentration,[447] as well as in oscillating magnetic fields[448] and as a result of the introduction of specific enzymes[449,450] or small molecules.[451–453] **Figure 1.37d–e** provides one example[449] of how these mechanized nanoparticles operate, depicting the release profile of 'snap-top' rotaxane-gated MSNPs that are activated with an enzyme to release their internal cargo. One of the pH-responsive systems has been shown to work autonomously to release cargo *in vitro*,[429] making these materials highly promising candidates as drug delivery vehicles. The large number of examples produced in a relatively short time span signifies these nanocarriers as useful, beautiful applications of artificial molecular machinery. See **Section 6.15.1.1**.

With the exception of muscles, most of Nature's machines do their work on the nanoscale. A particularly important apparatus is the ribosome—the large, complex protein assembly responsible for reading the information encoded in messenger RNA and synthesizing the corresponding polypeptide chains that fold into proteins. Leigh[454] has constructed an artificial molecular machine that relies intimately on the mechanical bond to perform the ribosome-like task (**Scheme 1.5**) of synthesizing an oligopeptide chain in a sequence-specific manner. The machine is constructed by a combination of active template synthesis and Cu^I-catalyzed azide-alkyne cycloaddition (CuAAC) click chemistry to display a short cystine–glycine–glycine peptide sequence appended by a hydrazone linkage to a ring, which encircles a dumbbell possessing a pre-defined sequence of protected, phenolic ester-linked monomers, each separated by a rigid spacer. Once assembled, the machine is set into action by acidic deprotection of these reactive monomers, as well as by the addition of a non-nucleophilic base, which facilitates

a reaction known as native chemical ligation[455] (NCL), wherein (i) the dumbbell's peptide monomer in closest proximity to the ring is captured by trans-acylation to the thiolate site of the ring's reactive cystine residue, resulting in a thioester, which (ii) undergoes S→N shift, transferring the peptide monomer to the *N*-terminal residue, or "elongation site", at the end of the ring's peptide chain. Sequence specificity arises from the fact that each monomer displayed by the dumbbell acts as a stopper, forbidding the passage of the ring until it is cleaved, thus preventing any amino acids from being transferred to the elongation site out-of-turn. After the ring has picked up all three of the dumbbell's monomers by this sequential O→S / S→N acyl transfer process, it is no longer constrained by a mechanical bond and is therefore free to diffuse away from the dumbbell. The oligopeptide chain can then be isolated by hydrolysis of the hydrazone bond. Several limitations prevent this machine from competing with solid-phase peptide synthesis or the ribosome—long timescales (~12 h / peptide), short sequences limited to only a few amino acids, and loss of sequence information after it is "read" and "written". Despite these limitations, this ingenious piece of exquisite chemistry, which has been praised for its likeness to a Turing machine,[456] an automated peptide synthesizer,[456,457] and indeed the ribosome,[457,458] represents a major landmark for molecular machines and the mechanical bond.

The beauty of employing controlled molecular mechanical motions to do work and perform technologically important functions is similar to that of technomorphic representations (**Section 1.2.6**) in the sense that it draws a connection between the molecular and macroscopic worlds. Artificial molecular machines remind us of the classical machines we know and use every day, although they operate under completely different principles on account of the enormous thermal fluctuations that lead to Brownian motion on the molecular size scale. The tension between these two worlds presents a challenge that has led chemists to respond with creative, often bio-inspired solutions to operating machines at low Reynolds number. At the same time, the awesome molecular machinery of the cell has provided inspiration for the first artificial molecular machines that can perform complex tasks on the nanoscale, building a beautiful bridge between the synthetic and natural worlds.

1.3.7 The Art of the Mechanical Bond

We consider many of the figures and schemes of MIMs in the primary literature to be artwork in and of themselves, yet even more deliberate artwork inspired by MIMs has been created for journal covers and graphical abstracts over the years, along with the occasional work of art for arts' sake. We have curated a collection of over 100 cover art images in **Appendix A** paying tribute to publications that have been featured on journal covers on topics related to the mechanical bond. The large number and diversity of these titles reflects the interdisciplinary nature of the field and the highly creative and immensely productive attributes of its practitioners. Paintings (**Figure 1.38**) by Mike Thompson, which decorate the walls of the Evanston laboratory, are inspired directly by the topological beauty of mechanomolecules.

We do not need any convincing that the mechanical bond is indeed "a work of art". Although it is framed mostly outside the bounds of any formal aesthetic framework, molecular beauty is very much a part of chemists' experience. At the end of the day, MIMs are beautiful because they are researched by hard-working, passionate people who cannot help but to take pleasure in their work. We find beauty in many aspects of the mechanical bond, from its prevalence in nature (**Section 1.1.1**), art (**Section 1.1.2**), and daily life (**Section 1.1.3**), to the pleasure of building new supramolecular (**Section 1.3.1**) and molecular topologies (**Section 1.3.2**) and architectures (**Section 1.3.3**), to the appeal of elegant new protocols (**Section 1.3.4**), the prospect of uncovering complex and emergent phenomena (**Section 1.3.5**), not to mention the remarkable potential and functional utility of molecular switches and



Figure 1.38 MIM-inspired paintings by Mike Thompson.

machines (**Section 1.3.6**). At the same time, many chemists are surely artists at heart, sculpting molecules instead of clay, synthesizing masterpieces instead of painting them, even demonstrating a knack for visual presentation as evidenced by the development of new graphical modes (**Section 1.2**) of communication, such as the cartoons and technomorphs that simultaneously aid in communication and stimulate innovation. Roald Hoffman[197] has commented, "*It never ceases to amaze me how a community of people who are not talented at drawing, nor trained to do so, manages to communicate faultlessly so much three-dimensional information.*" We add to this comment our amazement at the beauty such images can bear, and their ability to draw connections between molecules and classical objects. Whether we speak of images, topologies and architectures, experimental elegance, or functional novelty, the research associated with mechanical bonds is indeed a pleasing, beautiful, and rewarding line of work.

1.4 Evolution of Mechanostereochemistry

We close this introductory Chapter with a perspective and brief assessment of the growth and development of the field of chemistry that deals with mechanical bonds—or, as we call it—mechanostereochemistry.[16,17] Without a doubt, the mechanical bond will continue to evolve. We believe that the publication of this book is timely because the evolution of MIMs appears to be approaching a turning point. The evolutionary tree is no longer a sapling as it enters a new stage of life. Soon it will not be possible to consolidate the diverse aspects of the mechanical bond in chemistry into a single volume. Consider the degree to which the field is growing (**Figure 1.39**)—the histograms tracking the approximate number of publications[F] (**Figure 1.39a**) and literature citations (**Figure 1.39b–c**) on the topic of catenanes and rotaxanes on a year-by-year basis reveals that the number of articles published in this field each year has undergone steady and linear growth for over two decades, beginning around 1990. At the close of 2015, there were well over 3000 publications and almost 100,000 citations related to catenanes and rotaxanes in chemistry. The journals with 10 or more publications indexed under the keywords 'catenane' or 'rotaxane' at the close of 2015 are ranked in **Figure 1.40**, with general chemistry journals such as the *Journal of the American Chemocal Society*, *Angewandte Chemie*, and *Chemical Communications* dominating the spread, in a testament to the interdisciplinarity of the field. Geographically, the publications on mechanical bonds originate (**Figure 1.41**) from all around the world: Japan and the United States are in close contention to be the most active countries in this particular field of research, with the UK and China not far behind. In spite of this evidence for a remarkable world-

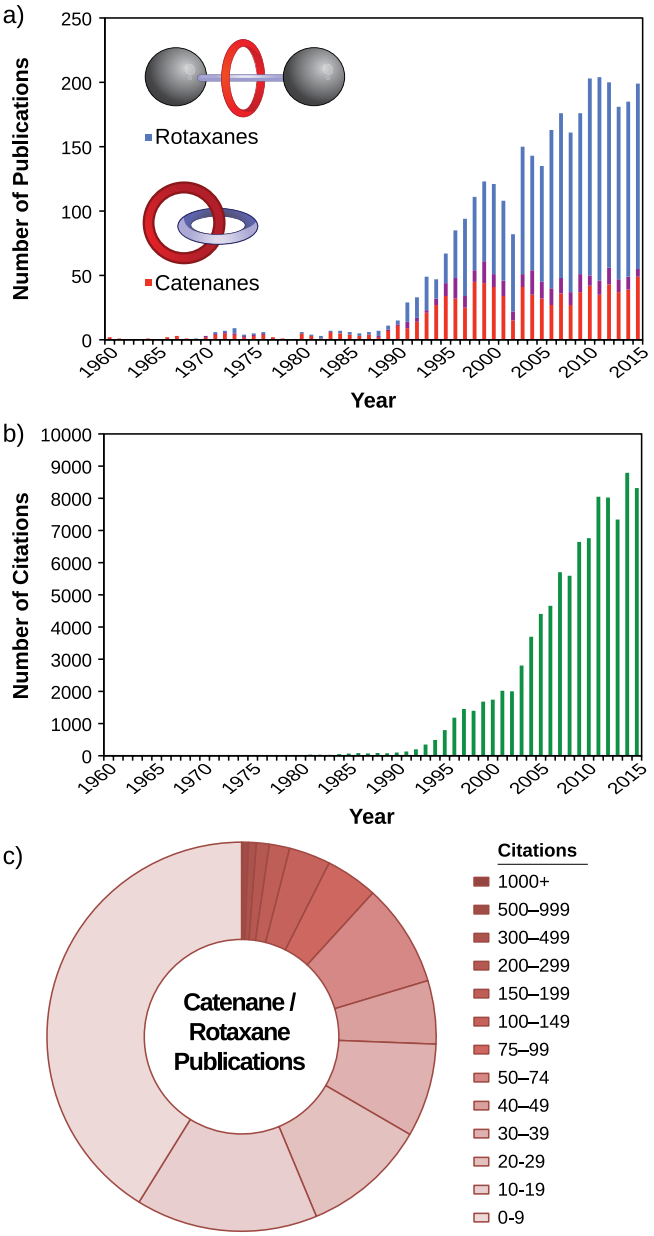


Figure 1.39 Statistics on journal publications indexed under the keywords, catenane or rotaxane. Histograms indicate the approximate number of (a) publications (total >3000) and (b) citations (total ~100,000) per year, from 1960 to 2015. Purple regions correspond to articles indexed under both keywords. The distribution of citations among these articles at the close of 2015 is represented by (c) a donut chart visualizing the proportionation of publications garnering different citation ranges. Citation counts are taken from Thomson Reuters Web of Science on 3 Jan 2016.

wide interest in mechanical bonds at the molecular level, we note that the whole of mechanostereochemistry is underrepresented in our statistics, since mechanical bonds are prevalent in many synthetic compounds (**Section 4.3**) and biomolecules that lie beyond the scope of catenanes and rotaxanes.

Another way to put perspective on the field is to look at the rhetoric of the literature in a time-resolved manner. The

[F] Publications were tabulated in Scifinder (www.scifinder.com) using the keywords 'catenane' and 'rotaxane'

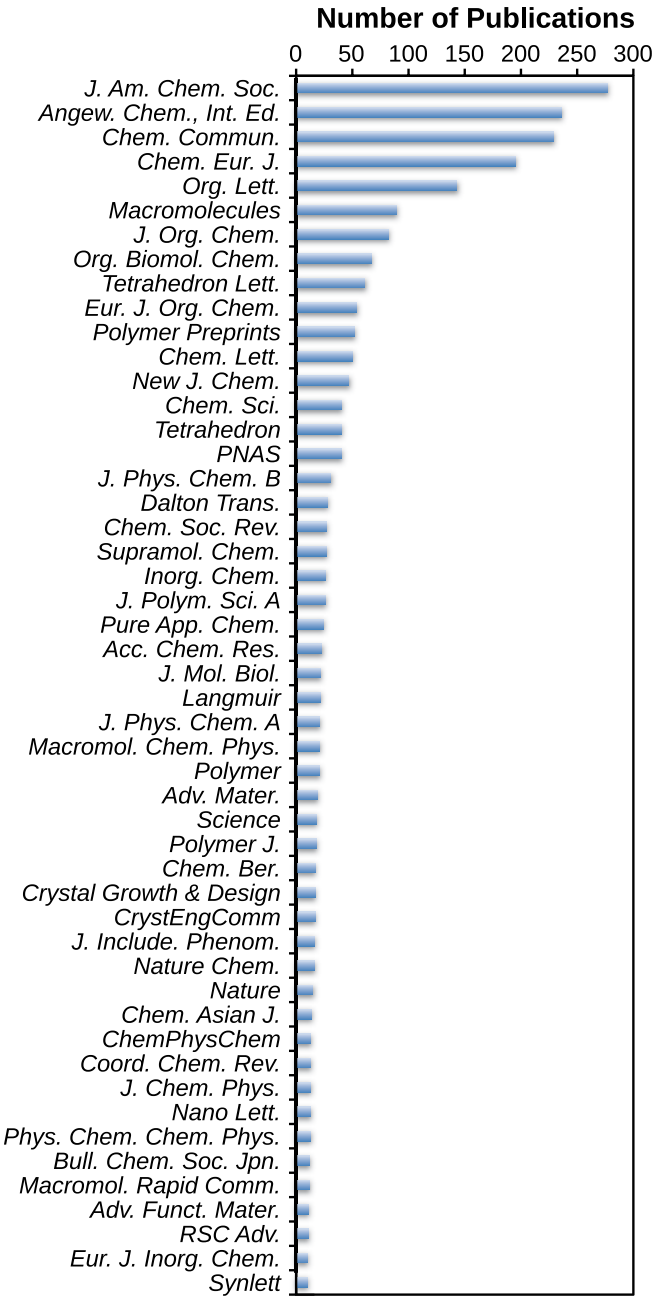


Figure 1.40 A comparison of international journals with 10 or more publications indexed under the keywords, catenane or rotaxane, at the end of 2015.

artwork[G] in **Figure 1.42** portrays words that are scaled according to their frequency of appearance in the abstracts of the most highly cited papers from different eras of the mechanical bond. These eras are divided into four time periods: Pre-1990, 1990–1999, 2000–2010, and 2010–2015. Some trends can be identified by careful inspection of the most frequently used words during these eras. Prior to 1990,

[G] These word art images are based on the first ~10,000 words to appear in abstracts, ranked in order of citation frequency for papers matching the keywords *rotaxane* or *catenane*.

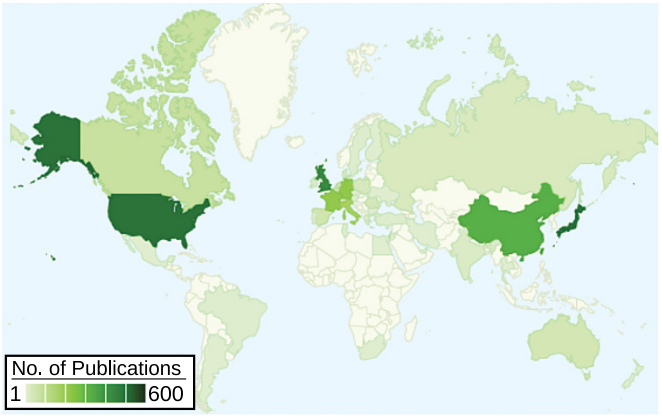


Figure 1.41 The distribution of publications indexed under the keywords, catenane or rotaxane, color-scaled on a world map according to country of origin.

the prominence of words such as copper, catenate, catenand, and ligand reveal that the early literature prior to the boom of research beginning in 1990 was dominated by Sauvage's work on metallo-catenanes and rotaxanes. In the 1990s, words such as assemble, self-assembly, complex, and supramolecular become much more visible, reflecting the novel template-directed synthetic methods based on supramolecular chemistry which became a high priority. In the 2000s, we can see words such as systems, control, machine, device, movement, and switch come into the limelight, suggesting

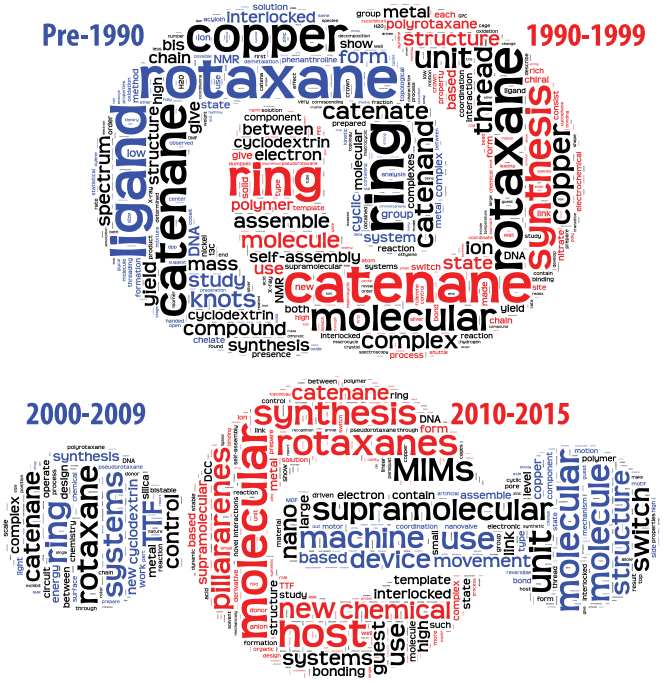


Figure 1.42 Word art based on abstracts from the most highly cited papers from various eras in the life of the mechanical bond. Each catenane or rotaxane component part is color-coded with respect to labels designating to which era the set of words belongs. Words are scaled according to the frequency with which they appear in the highly cited literature.

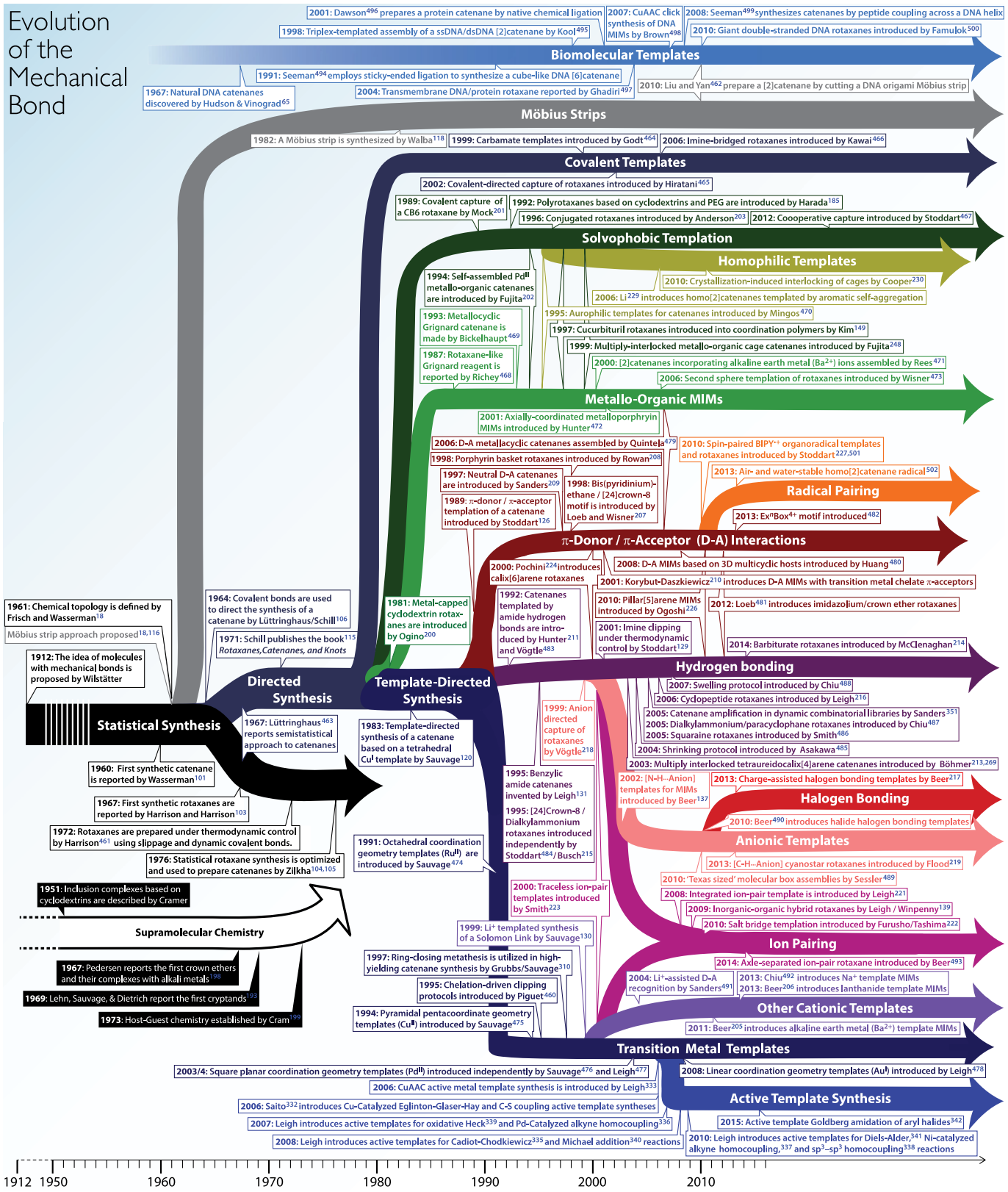


Figure 1.43 A time-resolved evolutionary tree, highlighting milestones and differentiation events in the synthesis of molecules with mechanical bonds and entanglements. See **Chapters 2–3**. A magnifying glass is prerequisite for readers who wish to explore the intricacies of the evolution of the mechanical bond in the molecular world.

that molecular switches were a heavy focus of this time period. Finally, a remarkable spike in research activity has placed pillararenes among the most frequent words in the highly cited abstracts of the current era, though we must wait at least another five years to find out which concepts will truly represent the hot topics of the present decade. An astute observer will notice from the information in the publication histogram (**Figure 1.39a**) and word art (**Figure 1.42**) that rotaxanes have been outcompeting catenanes in terms of research attention. Although much of the seminal work on mechanical bonds was done on catenanes, most of the growth of the field has been driven by rotaxane research. Catenane research, on the other hand, appears to have reached a plateau, at least for the time being. This inequality among the two main types of mechanically bonded molecules may be related to superior synthetic accessibility and potential applications of rotaxanes.

The evolution of the mechanical bond is not unlike Darwinian evolution by natural selection[459]—for example, events of differentiation can be identified in an evolutionary tree (**Figure 1.43**) describing milestones (see refs. 18,65, 101,103–106,115,116,118,120,126,129,131, 137,139,149,185,200–211,213–215,218,219,221–224, 226,227,229,230,248,269,307,310,324,332,333,335, 336,338–342,351,460–502) in the synthesis of mechanical bonds, where new strategies and template motifs have been introduced. An analogy to Darwin's 'survival of the fittest' mechanism for natural selection is also at play in mechanostereochemistry, since the majority of publications related to MIMs are attributable to only a handful of the 'fittest' types of recognition motifs: (i) hydrophobic forces (**Section 2.3.1**), especially those underpinning the supramolecular chemistry of the cyclodextrins and cucurbiturils, (ii) transition metal templates (**Section 2.3.2**), especially those based on copper, (iii) π-donor/π-acceptor templates (**Section 2.3.3**), especially those based on viologens, and (iv) hydrogen-bonded templates (**Section 2.3.4**), especially those based on macrocyclic lactams and crown ethers—which represent approximately 75% of the literature on mechanical bonds. See **Figure 2.87** in the conclusion of **Chapter 2** for a breakdown of the literature by template classification. Some of the newcomers to the field, such as anion binding (**Section 2.3.6**), active template synthesis (**Section 2.4**) and the host-guest chemistry of the pillararenes (**Section 2.3.9.2**), are proliferating rapidly.

The evolution of the mechanical bond is also captured in a timeline (**Figure 1.44**) showing how molecules with mechanical bonds have 'grown up' from a foundation of synthetic reactions and protocols, through to contemporary devices and applications. In the beginning, synthetic reactions and protocols for making mechanical bonds represented the only kind of research in mechanostereochemistry. As synthetic techniques (**Chapters 2–3**) became more highly developed—the most significant of which was the advent of template-directed synthesis—making mechanical bonds became more and more routine. As MIM synthesis was being mastered, more time and resources became

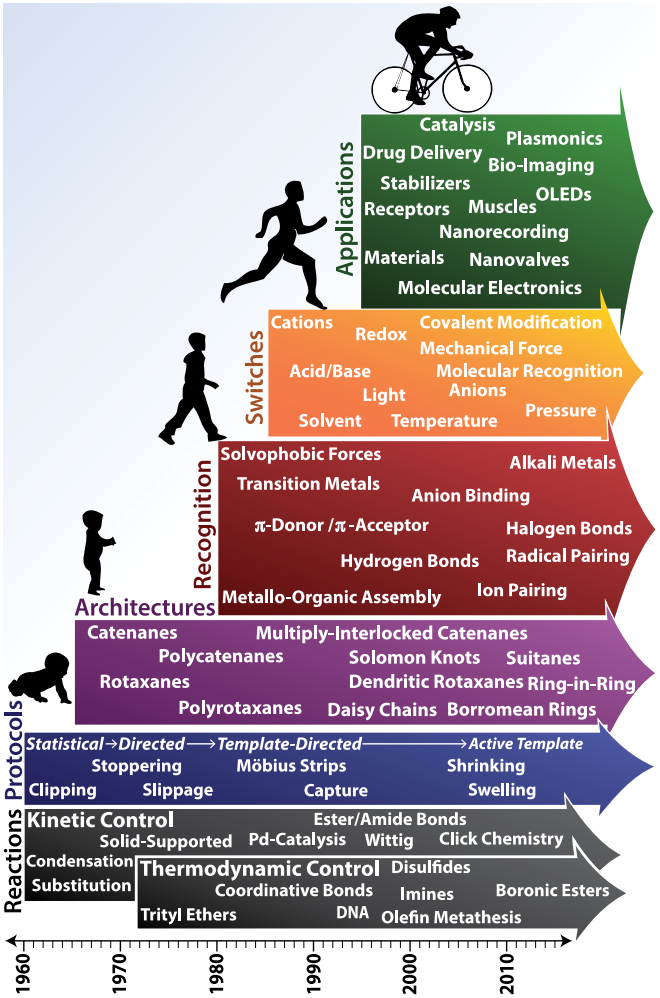


Figure 1.44 Timeline of research on the mechanical bond.

available for the development of new mechanically interlocked architectures (**Chapter 4**), novel types of dynamics, isomerism, and chirality (**Chapter 5**), as well as molecular switches (**Chapter 6**). This stage of research is also reaching maturity, clearing a path for the next stage, which will be associated with artificial molecular machines (**Chapter 6**) and practical applications for mechanical bonds in science and technology. Although progress will continue on all of these fronts, the time is now upon us to cast aside our complacency, forsake our muddling along in solution, and press on to new frontiers—e.g., integrated systems, materials, solid-state chemistry, genuine molecular machinery, non-equilibrium self-organization and dynamics, applications in energy and medicine, complexity and emergence, and so on. We expect that, as the field pushes back these frontiers and others, a compilation of the important discoveries of the past will help to set the stage for this next act.

It is clear to us that the mechanical bond represents a flourishing field of chemistry, to the extent that a completely comprehensive review of the entire body of literature would be next to impossible. We have tried to strike a balance between being as comprehensive as possible in our coverage

of topics related to MIMs, with the goal of summarizing synthetic protocols, molecular design motifs, techniques, dynamics, applications, significance, and future directions for the field, yet we have been forced in many cases to select only what we consider to be the most influential research. In this regard, we would be the first to admit that we might have been blind to or ignorant of some pieces of research that will give momentum to the mechanical bond's rise to prominence in chemistry.

References

(1) Pauling, L. *The Nature of the Chemical Bond: An Introduction to Modern Structural Chemistry*; Cornell University Press: Ithaca, **1939**.

(2) Brown, T. E.; LeMay, H. E.; Bursten, B. E.; Murphy, C.; Woodward, P.; Stoltzfus, M. E. *Chemistry - The Central Science*; 13th Ed.; Prentice Hall: Upper Saddle River, NJ, **2014**.

(3) Balaban, A. T.; Klein, D. J. Is Chemistry "the Central Science?" How Are Different Sciences Related? Co-Citations, Reductionism, Emergence, and Posets. *Scientometrics* **2006**, *69*, 615–637.

(4) Venturi, M.; Marchi, E.; Balzani, V. The Beauty of Chemistry in the Words of Writers and in the Hands of Scientists. *Top. Curr. Chem.* **2012**, *323*, 73–106.

(5) Bertozzi, C. R. The Centrality of Chemistry. *ACS Cent. Sci.* **2015**, *1*, 1–2.

(6) Desiraju, G. R. Chemistry: The Middle Kingdom. Resonance **2007**, *12*, 44–60.

(7) Amabilino, D. B.; Ashton, P. R.; Bravo, J. A.; Raymo, F. M.; Stoddart, J. F.; White, A. J. P.; Williams, D. J. Molecular Meccano 52. Template-Directed Synthesis of a Rotacatenane. *Eur. J. Org. Chem.* **1999**, 1295–1302.

(8) Williams, A. R.; Northrop, B. H.; Chang, T.; Stoddart, J. F.; White, A. J. P.; Williams, D. J. Suitanes. *Angew. Chem., Int. Ed.* **2006**, *45*, 6665–6669.

(9) Romuald, C.; Arda, A.; Clavel, C.; Jimenez-Barbero, J.; Coutrot, F. Tightening or Loosening a pH-Sensitive Double-Lasso Molecular Machine Readily Synthesized From an Ends-Activated [*c*2]Daisy Chain. *Chem. Sci.* **2012**, *3*, 1851–1857.

(10) Gan, Q.; Ferrand, Y.; Bao, C.; Kauffmann, B.; Grélard, A.; Jiang, H.; Huc, I. Helix-Rod Host-Guest Complexes with Shuttling Rates Much Faster Than Disassembly. *Science* **2011**, *331*, 1172–1175.

(11) Vajpayee, V.; Song, Y. H.; Cook, T. R.; Kim, H.; Lee, Y.; Stang, P. J.; Chi, K. W. A Unique Non-Catenane Interlocked Self-Assembled Supramolecular Architecture and Its Photophysical Properties. *J. Am. Chem. Soc.* **2011**, *133*, 19646–19649.

(12) Li, S.-H.; Zhang, H. Y.; Xu, X.; Liu, Y. Mechanically Selflocked Chiral Gemini-Catenanes. *Nature Commun*. **2015**, *6*: 7590.

(13) Anelli, P. L.; Ashton, P. R.; Ballardini, R.; Balzani, V.; Delgado, M.; Gandolfi, M. T.; Goodnow, T. T.; Kaifer, A. E.; Philp, D.; Pietraszkiewicz, M.; Prodi, L.; Reddington, M. V.; Slawin, A. M. Z.; Spencer, N.; Stoddart, J. F.; Vicent, C.; Williams, D. J. Molecular Meccano 1. [2]Rotaxanes and a [2]Catenane Made to Order. *J. Am. Chem. Soc*. **1992**, *114*, 193–218.

(14) Amabilino, D. B.; Stoddart, J. F. Interlocked and Intertwined Structures and Superstructures. *Chem. Rev.* **1995**, *95*, 2725–2828.

(15) Stoddart, J. F. The Chemistry of the Mechanical Bond. *Chem. Soc. Rev.* **2009**, *38*, 1802–1820.

(16) Olson, M. A.; Botros, Y. Y.; Stoddart, J. F. Mechanostereochemistry. *Pure Appl. Chem*. **2010**, *82*, 1569–1574.

(17) Barin, G.; Forgan, R. S.; Stoddart, J. F. Mechanostereochemistry and the Mechanical Bond. *Proc. R. Soc. A* **2012**, *468*, 2849–2880.

(18) Frisch, H. L.; Wasserman, E. Chemical Topology. *J. Am. Chem. Soc.* **1961**, *83*, 3789–3795.

(19) Sokolov, V. I. Topological Ideas in Stereochemistry. *Russian Chem. Rev.* **1973**, *42*, 452–463.

(20) Walba, D. M. Topological Stereochemistry. *Tetrahedron* **1985**, *41*, 3161–3212.

(21) Dodziuk, H.; Nowiński, K. S. Topological Isomerism: Should Rotaxanes, Endohedral Fullerene Complexes and In-Out Isomers of Hydrogenated Fullerenes Be Considered as Such? *Tetrahedron* **1998**, *54*, 2917–2930.

(22) Siegel, J. S. Chemical Topology and Interlocking Molecules. *Science* **2004**, *304*, 1256–1258.

(23) Fenlon, E. E. Open Problems in Chemical Topology. *Eur. J. Org. Chem.* **2008**, 5023–5035.

(24) Amabilino, D. B.; Pérez-García, L. Topology in Molecules Inspired, Seen and Represented. *Chem. Soc. Rev*. **2009**, *38*, 1562–1571.

(25) Forgan, R. S.; Sauvage, J.-P.; Stoddart, J. F. Chemical Topology: Complex Molecular Knots, Links, and Entanglements. *Chem. Rev.* **2011**, *111*, 5434–5464.

(26) Ashton, P. R.; Philp, D.; Spencer, N.; Stoddart, J. F. The Self-Assembly of [*n*]Pseudorotaxanes. *J. Chem. Soc., Chem. Commun.* **1991**, 1677–1679.

(27) IUPAC. *Compendium of Chemical Terminology;* 2nd Ed. (the "Gold Book"); Compiled by A. D. McNaught and A. Wilkinson. Blackwell Scientific Publications: Oxford, **1997**. XML Online Corrected Version: http://Goldbook.Iupac.org Created by M. Nic, J. Jirat, B. Kosata; Updates Compiled by A. Jenkins. ISBN 0-9678550-9-8.DOI:10.1351/Goldbook.

(28) Jasat, A.; Sherman, J. C. Carceplexes and Hemicarceplexes. *Chem. Rev.* **1999**, *99*, 931–968.

(29) Popov, A. A.; Yang, S.; Dunsch, L. Endohedral Fullerenes. *Chem. Rev.* **2013**, *113*, 5989–6113.

(30) Vostrowsky, O.; Hirsch, A. Molecular Peapods as Supramolecular Carbon Allotropes. *Angew. Chem., Int. Ed*. **2004**, *43*, 2326–2329.

(31) Yoshizawa, M.; Klosterman, J. K.; Fujita, M. Functional Molecular Flasks: New Properties and Reactions Within Discrete, Self-Assembled Hosts. *Angew. Chem., Int. Ed*. **2009**, *48*, 3418–3438.

(32) *Topics in Current Chemistry: Beauty in Chemistry*; Fabbrizzi, L., Ed.; Springer: Berlin Heidelberg, **2012**; Vol. *323*.

(33) Bruns, C. J.; Stoddart, J. F. The Mechanical Bond: A Work of Art. *Top. Curr. Chem.* **2012**, *323*, 19–72.

(34) Wikipedia. *Art*. http://en.wikipedia.org/art (Accessed Dec **2010**).

(35) Pfenninger, K. H.; Shubik, V. R. *The Origins of Creativity*; Oxford University Press: New York, **2001**.

(36) Heisenberg, W. *The Meaning of Beauty in the Exact Sciences*; Anshen, R. N., Ed.; Harper & Row: New York, **1974**.

(37) Spector, T. I.; Schummer, J. Aesthetics and Visualization in Chemistry. *HYLE* **2003**, *9*, 3–6.

(38) Hoffmann, R.; Laszlo, P. Representation in Chemistry. *Angew. Chem., Int. Ed. Engl*. **1991**, *30*, 1–16.

(39) Kretzenbacher, H. L. The Aesthetics and Heuristics of Analogy: Model and Metaphor in Chemical Communication. *HYLE* **2003**, *9*, 191–218.

(40) Laszlo, P. Foundations of Chemical Aesthetics. *HYLE* **2003**, *9*, 11–32.

(41) Schummer, J. Aesthetics of Chemical Products: Materials, Molecules, and Molecular Models. *HYLE* **2003**, *9*, 73–104.

(42) Hoffmann, R. Molecular Beauty. *J. Aesthet. Art Critic.* **1990**, *48*, 191–204.

(43) University of Science and Technology of China; Tsinghua University Press. Beautiful Chemistry http://beautifulchemistry.net (Accessed May 2015).

(44) Jogalekar, A. Truth and Beauty in Chemistry http://blogs.scientificamerican.com/the-curious-wavefunction/2013/01/24/truth-and-beauty-in-chemistry/ (Accessed May 2015).

(45) Root-Bernstein, R. Sensual Chemistry: Aesthetics as a Motivation for Research. *HYLE* **2003**, *9*, 33–50.

(46) Miodownik, M. A. Toward Designing New Sensoaesthetic Materials. *Pure Appl. Chem*. **2007**, *79*, 1635–1641.

(47) Hoffmann, R. *Roald Hoffman on the Philosophy, Art, and Science of Chemistry*; Kovac, J.; Weisberg, M., Eds.; Oxford University Press: New York, **2012**.
(48) Hoffmann, R. Molecular Beauty. *Am. Sci.* **1988**, *76*, 389–391.
(49) Hoffmann, R. Molecular Beauty II: Frogs About to Be Kissed. *Am. Sci.* **1988**, *76*, 604–605.
(50) Hoffmann, R. Molecular Beauty III: As Rich as Need Be. *Am. Sci.* **1989**, *77*, 177–178.
(51) Hoffmann, R. Molecular Beauty IV: Toward an Aesthetic Theory of Six-Coordinate Carbon. *Am. Sci.* **1989**, *77*, 330–332.
(52) Schummer, J. Scientometric Studies on Chemistry II: Aims and Methods of Producing New Chemical Substances. *Scientometrics* **1997**, *39*, 125–140.
(53) MacGillivray, L. R.; Atwood, J. L. Structural Classification and General Principles for the Design of Spherical Molecular Hosts. *Angew. Chem., Int. Ed*. **1999**, *38*, 1018–1033.
(54) Eaton, P. E.; Cole, T. W. Cubane. *J. Am. Chem. Soc.* **1964**, *86*, 3157–3158.
(55) Ternansky, R. J.; Balogh, D. W.; Paquette, L. A. Dodecahedrane. *J. Am. Chem. Soc.* **1982**, *104*, 4503–4504.
(56) Paquette, L. A.; Ternansky, R. J.; Balogh, D. W.; Kentgen, G. Total Synthesis of Dodecahedrane. *J. Am. Chem. Soc.* **1983**, *105*, 5446–5450.
(57) Kroto, H. W.; Heath, J. R.; O'Brien, S. C.; Curl, R. F.; Smalley, R. E. C_{60}: Buckminsterfullerene. *Nature* **1985**, *318*, 162–163.
(58) Seidel, S. R.; Stang, P. J. High-Symmetry Coordination Cages via Self-Assembly. *Acc. Chem. Res.* **2002**, *35*, 972–983.
(59) Harris, K.; Fujita, D.; Fujita, M. Giant Hollow M_nL_{2n} Spherical Complexes: Structure, Functionalisation and Applications. *Chem. Commun.* **2013**, *49*, 6703–6712.
(60) Nicolaou, K. C. Inspirations, Discoveries, and Future Perspectives in Total Synthesis. *J. Org. Chem.* **2009**, *74*, 951–972.
(61) Ball, P. *Elegant Solutions: Ten Beautiful Experiments in Chemistry*; The Royal Society of Chemistry: Cambridge, **2005**.
(62) Hall, N. Creating Complexity – the Beauty and Logic of Synthesis. *Chem. Commun.* **2003**, 661–664.
(63) Woodward, C. E. Art and Elegance in the Synthesis of Organic Compounds: Robert Burns Woodward. In *Creative People at Work: Twelve Cognitive Case Studies*; Wallace, D. B.; Gruber, H. E., Eds.; Oxford University Press: New York, **1989**; pp. 227–254.
(64) Lehn, J.-M. *Supramolecular Chemistry: Concepts and Perspectives*; Wiley-VCH: Weinheim, **1995**.
(65) Hudson, B.; Vinograd, J. Catenated Circular DNA Molecules in HeLa Cell Mitochondria. *Nature* **1967**, *216*, 647–652.
(66) Krasnow, M. A.; Stasiak, A.; Spengler, S. J.; Dean, F.; Koller, T.; Cozzarelli, N. R. Determination of the Absolute Handedness of Knots and Catenanes of DNA. *Nature* **1983**, *304*, 559–560.
(67) Wasserman, S. A.; Cozzarelli, N. R. Biochemical Topology: Applications to DNA Recombination and Replication. *Science* **1986**, *232*, 951–960.
(68) Kreuzer, K. N.; Cozzarelli, N. R. Formation and Resolution of DNA Catenanes by DNA Gyrase. *Cell* **1980**, *20*, 245–254.
(69) Subramanian, K.; Rutvisuttinunt, W.; Scott, W.; Myers, R. S. The Enzymatic Basis of Processivity in λ-Exonuclease. *Nucleic Acids Res.* **2003**, *31*, 1585–1596.
(70) Kovall, R.; Matthews, B. W. Toroidal Structure of λ-Exonuclease. *Science* **1997**, *277*, 1824–1827.
(71) Trakselis, M. A.; Alley, S. C.; Abel-Santos, E.; Benkovic, S. J. Creating a Dynamic Picture of the Sliding Clamp During T4 DNA Polymerase Holoenzyme Assembly by Using Fluorescence Resonance Energy Transfer. *Proc. Natl. Acad. Sci. U.S.A.* **2001**, *98*, 8368–8375.
(72) Thordarson, P.; Bijsterveld, E. J. A.; Rowan, A. E.; Nolte, R. J. M. Epoxidation of Polybutadiene by a Topologically Linked Catalyst. *Nature* **2003**, *424*, 915–918.
(73) Coumans, R. G. E.; Elemans, J. A. A. W.; Nolte, R. J. M.; Rowan, A. E. Processive Enzyme Mimic: Kinetics and Thermodynamics of the Threading and Sliding Process. *Proc. Natl. Acad. Sci. U.S.A.* **2006**, *103*, 19647–19651.
(74) Monnereau, C.; Ramos, P. H.; Deutman, A. B. C.; Elemans, J. A. A. W.; Nolte, R. J. M.; Rowan, A. E. Porphyrin Macrocyclic Catalysts for the Processive Oxidation of Polymer Substrates. *J. Am. Chem. Soc.* **2010**, *132*, 1529–1531.
(75) Wikoff, W. R.; Liljas, L.; Duda, R. L.; Tsuruta, H.; Hendrix, R. W.; Johnson, J. E. Topologically Linked Protein Rings in the Bacteriophage HK97 Capsid. *Science* **2000**, *289*, 2129–2133.
(76) Roos, W. H.; Gertsman, I.; May, E. R.; Brooks, C. L., III; Johnson, J. E.; Wuite, G. J. L. Mechanics of Bacteriophage Maturation. *Proc. Natl. Acad. Sci. U.S.A.* **2012**, *109*, 2342–2347.
(77) Zimanyi, C. M.; Ando, N.; Brignole, E. J.; Asturias, F. J.; Stubbe, J.; Drennan, C. L. Tangled Up in Knots: Structures of Inactivated Forms of *E.coli* Class Ia Ribonucleotide Reductase. *Structure* **2012**, *20*, 1374–1383.
(78) Smeulders, M. J.; Barends, T. R. M.; Pol, A.; Scherer, A.; Zandvoort, M. H.; Udvarhelyi, A.; Khadem, A. F.; Menzel, A.; Hermans, J.; Shoeman, R. L.; Wessels, H. J. C. T.; van den Heuvel, L. P.; Russ, L.; Schlichting, I.; Jetten, M. S. M.; Op den Camp, H. J. M. Evolution of a New Enzyme for Carbon Disulphide Conversion by an Acidothermophilic Archaeon. *Nature* **2011**, *478*, 412–416.
(79) van Eldijk, M. B.; van Leeuwen, I.; Mikhailov, V. A.; Neijenhuis, L.; Harhangi, H. R.; van Hest, J. C. M.; Jetten, M. S. M.; Op den Camp, H. J. M.; Robinson, C. V.; Mecinović, J. Evidence That the Catenane Form of CS_2 Hydrolase Is Not an Artefact. *Chem. Commun*. **2013**, *49*, 7770–7772.
(80) van Eldijk, M. B.; Pieters, B. J.; Mikhailov, V. A.; Robinson, C. V.; van Hest, J. C. M.; Mecinović, J. Catenane Versus Ring: Do Both Assemblies of CS_2 Hydrolase Exhibit the Same Stability and Catalytic Activity? *Chem. Sci.* **2014**, *5*, 2879–2884.
(81) Cao, Z.; Roszak, A. W.; Gourlay, L. J.; Lindsay, J. G.; Isaacs, N. W. Bovine Mitochondrial Peroxiredoxin III Forms a Two-Ring Catenane. *Structure* **2005**, *13*, 1661–1664.
(82) Lee, B. I.; Kim, K. H.; Park, S. J.; Eom, S. H.; Song, H. K.; Suh, S. W. Ring-Shaped Architecture of RecR: Implications for Its Role in Homologous Recombinational DNA Repair. *EMBO J*. **2004**, *23*, 2029–2038.
(83) Honda, M.; Fujisawa, T.; Shibata, T.; Mikawa, T. RecR Forms a Ring-Like Tetramer That Encircles dsDNA by Forming a Complex with RecF. *Nucleic Acids Res*. **2008**, *36*, 5013–5020.
(84) Boutz, D. R.; Cascio, D.; Whitelegge, J.; Perry, L. J.; Yeates, T. O. Discovery of a Thermophilic Protein Complex Stabilized by Topologically Interlinked Chains. *J. Mol. Biol*. **2007**, *368*, 1332–1344.
(85) Farcas, A.-M.; Uluocak, P.; Helmhart, W.; Nasmyth, K. Cohesin's Concatenation of Sister DNAs Maintains Their Intertwining. *Molecular Cell* **2011**, *44*, 97–107.
(86) Youle, R. J.; Karbowski, M. Mitochondrial Fission in Apoptosis. *Nature Rev. Mol. Cell Bio*. **2005**, *6*, 657–663.
(87) Mears, J. A.; Lackner, L. L.; Fang, S.; Ingerman, E.; Nunnari, J.; Hinshaw, J. E. Conformational Changes in Dnm1 Support a Contractile Mechanism for Mitochondrial Fission. *Nature Struct. Mol. Biol*. **2011**, *18*, 20–26.
(88) Cromwell, P. R. The Borromean Rings http://www.liv.ac.uk/~spmr02/rings/index.html (Accessed Apr **2011**).
(89) Cantrill, S. J.; Chichak, K. S.; Peters, A. J.; Stoddart, J. F. Nanoscale Borromean Rings. *Acc. Chem. Res*. **2005**, *38*, 1–9.
(90) *African Art and Leadership*; Fraser, D.; Cole, H. M., Eds.; University of Wisconsin Press: Madison, **1972**.
(91) Rose, L. R. *Seeing Solomon's Knot*; Lois Rose Rose: Los Angeles, **2005**.
(92) Stoddart, J. F. Whither and Thither Molecular Machines. *Chem. Aust*. **1992**, *59*, 576–577.
(93) Greenberg, A. *The Art of Chemistry: Myths, Medicines, and Materials*; Wiley: Hoboken, **2003**.
(94) Obrist, B. Visualization in Medieval Alchemy. *HYLE* **2003**, *9*, 131–170.
(95) Weininger, S. J. Contemplating the Finger - Visuality and the Semiotics of Chemistry. *HYLE* **1998**, *4*, 3–27.

(96) Frisch, H.; Martin, I.; Mark, H. Zur Struktur der Polysiloxene. *I. Monatsh. Chem*. **1953**, *84*, 250–256.

(97) Breault, G. A.; Hunter, C. A.; Mayers, P. C. Supramolecular Topology. *Tetrahedron* **1999**, *55*, 5265–5293.

(98) Dietrich-Buchecker, C.; Colasson, B. X.; Sauvage, J.-P. Molecular Knots. *Top. Curr. Chem*. **2005**, *249*, 261–283.

(99) Lukin, O.; Vögtle, F. Knotting and Threading of Molecules: Chemistry and Chirality of Molecular Knots and Their Assemblies. *Angew. Chem., Int. Ed*. **2005**, *44*, 1456–1477.

(100) Lüttringhaus, A.; Cramer, F.; Prinzbach, H.; Henglein, F. M. Cyclisationen von Langkettigen Dithiolen. Versuche zur Darstellung sich umfassender Ringe mit Hilfe von Einschlußverbindungen. *Liebigs Ann. Chem*. **1958**, *613*, 185–198.

(101) Wasserman, E. The Preparation of Interlocking Rings: a Catenane. *J. Am. Chem. Soc*. **1960**, *82*, 4433–4434.

(102) Wasserman, E. Chemical Topology. *Sci. Am*. **1962**, *207*, 94–102.

(103) Harrison, I. T.; Harrison, S. The Synthesis of a Stable Complex of a Macrocycle and a Threaded Chain. *J. Am. Chem. Soc*. **1967**, *89*, 5723–5724.

(104) Agam, G.; Graiver, D.; Zilkha, A. Studies on the Formation of Topological Isomers by Statistical Methods. *J. Am. Chem. Soc*. **1976**, *98*, 5206–5214.

(105) Agam, G.; Zilkha, A. Synthesis of a Catenane by a Statistical Double-Stage Method. *J. Am. Chem. Soc*. **1976**, *98*, 5214–5216.

(106) Schill, G.; Lüttringhaus, A. Preparation of Catena Compounds by Directed Synthesis. *Angew. Chem., Int. Ed. Engl*. **1964**, *3*, 546–547.

(107) Schill, G.; Zürcher, C. [3]-Catenanes. *Angew. Chem., Int. Ed. Engl*. **1969**, *8*, 988.

(108) Schill, G.; Zürcher, C. [3]-Catenane durch gezeiete Synthese. *Chem. Ber*. **1977**, *110*, 2046–2066.

(109) Schill, G.; Rissler, K.; Fritz, H.; Vetter, W. Synthesis, Isolation, and Identification of Translationally Isomeric [3] Catenanes. *Angew. Chem., Int. Ed. Engl*. **1981**, *20*, 187–189.

(110) Riβler, K.; Schill, G.; Fritz, H.; Vetter, W. Gezielte Synthese von translationsisomeren [3]-Catenanen. *Chem. Ber*. **1986**, *119*, 1374–1399.

(111) Schill, G.; Zollenkopf, H. Rotaxane. *Nachr. Chem. Techn*. **1967**, *15*, 149–150.

(112) Schill, G.; Zollenkopf, H. Rotaxan-Verbindungen, I. *Liebigs Ann. Chem*. **1969**, *721*, 53–74.

(113) Schill, G.; Henschel, R. Rotaxan-Verbindungen , II. Eine Diansa-Verbindung des 5-Amino-6-methoxy-4.7-dimethyl-benzodioxols als Modell zur Synthese von Catenanen und Rotaxanen. *Liebigs Ann. Chem*. **1970**, *731*, 113–119.

(114) Schill, G.; Zürcher, C.; Vetter, W. Rotaxan-Verbindungen, III. Synthese eines Rotaxans mit Triphenylmethyl-Sperrgruppen und massenspextrometrische Untersuchungen. *Chem. Ber*. **1973**, *106*, 228–235.

(115) Schill, G. *Catenanes, Rotaxanes, and Knots*; Academic Press: New York, **1971**.

(116) van Gulick, N. Theoretical Aspects of the Linked Ring Problem. *New J. Chem*. **1993**, *17*, 619–625.

(117) Walba, D. M.; Richards, R. M.; Sherwood, S. P.; Haltiwanger, R. C. Strategy for the Synthesis of Cylindrical Macropolycyclic Hosts with Hydrophilic Interior Surfaces: Crown Ether Rings Fused by the Tetrahydroxymethylethylene (THYME) Unit. *J. Am. Chem. Soc*. **1981**, *103*, 6213–6215.

(118) Walba, D. M.; Richards, R. M.; Haltiwanger, R. C. Total Synthesis of the First Molecular Möbius Strip. *J. Am. Chem. Soc*. **1982**, *104*, 3219–3221.

(119) Walba, D. M.; Armstrong, J. D., III; Perry, A. E.; Richards, R. M.; Homan, T. C.; Haltiwanger, R. C. The Thyme Polyethers: An Approach to the Synthesis of a Molecular Knotted Ring. *Tetrahedron* **1986**, *42*, 1883–1894.

(120) Dietrich-Buchecker, C. O.; Sauvage, J. P.; Kintzinger, J. P. Une Nouvelle Famille de Molecules: Les Metallo-Catenanes. *Tetrahedron Lett*. **1983**, *24*, 5095–5098.

(121) Cesario, M.; Dietrich, C. O.; Edel, A.; Guilhem, J.; Kintzinger, J.-P.; Pascard, C.; Sauvage, J.-P. Topological Enhancement of Basicity: Molecular Structure and Solution Study of a Monoprotonated Catenand. *J. Am. Chem. Soc*. **1986**, *108*, 6250–6254.

(122) Solà, M. Forty Years of Clar's Aromatic π-Sextet Rule. *Front. Chem*. **2013**, *1*, Article 22.

(123) Dietrich-Buchecker, C. O.; Guilhem, J.; Khemiss, A. K.; Kintzinger, J.-P.; Pascard, C.; Sauvage, J.-P. Molecular Structure of a [3]-Catenate: Curling up of the Interlocked System by Interaction between the Two Copper Complex Subunits. *Angew. Chem., Int. Ed. Engl*. **1987**, *26*, 661–663.

(124) Odell, B.; Reddington, M. V.; Slawin, A. M. Z.; Spencer, N.; Stoddart, J. F.; Williams, D. J. Cyclobis(paraquat-*p*-phenylene). A Tetracationic Multipurpose Receptor. *Angew. Chem., Int. Ed. Engl*. **1988**, *27*, 1547–1550.

(125) Ashton, P. R.; Odell, B.; Reddington, M. V.; Slawin, A. M. Z.; Stoddart, J. F.; Williams, D. J. Isostructural, Alternately-Charged Receptor Stacks. The Inclusion Complexes of Hydroquinone and Catechol Dimethyl Ethers with Cyclobis(paraquat-*p*-phenylene). *Angew. Chem., Int. Ed. Engl*. **1988**, *27*, 1550–1553.

(126) Ashton, P. R.; Goodnow, T. T.; Kaifer, A. E.; Reddington, M. V.; Slawin, A. M. Z.; Spencer, N.; Stoddart, J. F.; Vicent, C.; Williams, D. J. A [2]Catenane Made to Order. *Angew. Chem., Int. Ed. Engl*. **1989**, *28*, 1396–1399.

(127) Frasconi, M.; Fernando, I. R.; Wu, Y.; Liu, Z.; Liu, W.-G.; Dyar, S. M.; Barin, G.; Wasielewski, M. R.; Goddard, W. A., III; Stoddart, J. F. Redox Control of the Binding Modes of an Organic Receptor. *J. Am. Chem. Soc*. **2015**, *137*, 11057–11068.

(128) Ashton, P. R.; Brown, C. L.; Chrystal, E. J. T.; Goodnow, T. T.; Kaifer, A. E.; Parry, K. P.; Philp, D.; Slawin, A. M. Z.; Spencer, N.; Stoddart, J. F.; Williams, D. J. The Self-Assembly of a Highly Ordered [2]Catenane. *J. Chem. Soc., Chem. Commun.* **1991**, 634–639.

(129) Glink, P. T.; Oliva, A. I.; Stoddart, J. F.; White, A. J. P.; Williams, D. J. Template-Directed Synthesis of a [2]Rotaxane by the Clipping under Thermodynamic Control of a Crown Ether Like Macrocycle Around a Dialkylammonium Ion. *Angew. Chem., Int. Ed*. **2001**, *40*, 1870–1875.

(130) Ibukuro, F.; Fujita, M.; Yamaguchi, K.; Sauvage, J.-P. Quantitative and Spontaneous Formation of a Doubly Interlocking [2]Catenane Using Copper(I) and Palladium(II) as Templating and Assembling Centers. *J. Am. Chem. Soc*. **1999**, *121*, 11014–11015.

(131) Johnston, A. G.; Leigh, D. A.; Pritchard, R. J.; Deegan, M. D. Facile Synthesis and Solid-State Structure of a Benzylic Amide [2]Catenane. *Angew. Chem., Int. Ed. Engl*. **1995**, *34*, 1209–1212.

(132) Gross, L.; Mohn, F.; Moll, N.; Meyer, G.; Ebel, R.; Abdel-Mageed, W. M.; Jaspars, M. Organic Structure Determination Using Atomic-Resolution Scanning Probe Microscopy. *Nature Chem*. **2010**, *2*, 821–825.

(133) Amabilino, D. B.; Ashton, P. R.; Reder, A. S.; Spencer, N.; Stoddart, J. F. Olympiadane. *Angew. Chem., Int. Ed. Engl*. **1994**, *33*, 1286–1290.

(134) Cesario, M.; Dietrich-Buchecker, C. O.; Guilhem, J.; Pascard, C.; Sauvage, J.-P. Molecular Structure of a Catenand and Its Copper(I) Catenate: Complete Rearrangement of the Interlocked Macrocyclic Ligands by Complexation. *J. Chem. Soc., Chem. Commun*. **1985**, 244–247.

(135) Amabilino, D. B.; Ashton, P. R.; Boyd, S. E.; Lee, J. Y.; Menzer, S.; Stoddart, J. F.; Williams, D. J. The Five-Stage Self-Assembly of a Branched Heptacatenane. *Angew. Chem., Int. Ed. Engl*. **1997**, *36*, 2070–2072.

(136) Cabezon, B.; Cao, J.; Raymo, F. M.; Stoddart, J. F.; White, A. J. P.; Williams, D. J. A Self-Complexing [2]Catenane. *Angew. Chem., Int. Ed*. **2000**, *39*, 148–151.

(137) Wisner, J. A.; Beer, P. D.; Drew, M. G. B.; Sambrook, M. R. Anion-Templated Rotaxane Formation. *J. Am. Chem. Soc*. **2002**, *124*, 12469–12476.

(138) Belowich, M. E.; Valente, C.; Stoddart, J. F. Template-Directed Syntheses of Rigid Oligorotaxanes under Thermodynamic Control. *Angew. Chem., Int. Ed*. **2010**, *49*, 7208–7212.

(139) Lee, C. F.; Leigh, D. A.; Pritchard, R. G.; Schultz, D.; Teat, S. J.; Timco, G. A.; Winpenny, R. E. Hybrid Organic-Inorganic Rotaxanes and Molecular Shuttles. *Nature* **2009**, *458*, 314–318.

(140) Li, H.; Eddaoudi, M.; O'Keeffe, M.; Yaghi, O. M. Design and Synthesis of an Exceptionally Stable and Highly Porous Metal-Organic Framework. *Nature* **1999**, *402*, 276–279.

(141) Eddaoudi, M.; Kim, J.; Rosi, N.; Vodak, D.; Wachter, J.; O'Keeffe, M.; Yaghi, O. M. Systematic Design of Pore Size and Functionality in Isoreticular MOFs and Their Application in Methane Storage. *Science* **2002**, *295*, 469–472.

(142) Yaghi, O. M.; O'Keeffe, M.; Ockwig, N. W.; Chae, H. K.; Eddaoudi, M.; Kim, J. Reticular Synthesis and the Design of New Materials. *Nature* **2003**, *423*, 705–714.

(143) Chae, H. K.; Siberio-Pérez, D. Y.; Kim, J.; Go, Y.; Eddaoudi, M.; Matzger, A. J.; O'Keeffe, M.; Yaghi, O. M. A Route to High Surface Area, Porosity and Inclusion of Large Molecules in Crystals. *Nature* **2004**, *427*, 523–527.

(144) Yang, J.; Ma, J.-F.; Batten, S. R. Polyrotaxane Metal–Organic Frameworks (PMOFs). *Chem. Commun*. **2012**, *48*, 7899–7912.

(145) Batten, S. R.; Robson, R. Interpenetrating Nets: Ordered, Periodic Entanglement. *Angew. Chem., Int. Ed*. **1998**, *37*, 1460–1494.

(146) Reineke, T. M.; Eddaoudi, M.; Moler, D.; O'Keeffe, M.; Yaghi, O. M. Large Free Volume in Maximally Interpenetrating Networks: The Role of Secondary Building Units Exemplified by $Tb_2(ADB)_3[(CH_3)_2SO]_4$•$16[(CH_3)_2SO]$. *J. Am. Chem. Soc*. **2000**, *122*, 4843–4844.

(147) Chen, B.; Eddaoudi, M.; Hyde, S. T.; O'Keeffe, M.; Yaghi, O. M. Interwoven Metal-Organic Framework on a Periodic Minimal Surface with Extra-Large Pores. *Science* **2001**, *291*, 1021–1023.

(148) Loeb, S. J. Rotaxanes as Ligands: From Molecules to Materials. *Chem. Soc. Rev*. **2007**, *36*, 226–235.

(149) Whang, D.; Kim, K. Polycatenated Two-Dimensional Polyrotaxane Net. *J. Am. Chem. Soc*. **1997**, *119*, 451–452.

(150) Lee, E.; Kim, J.; Heo, J.; Whang, D.; Kim, K. A Two-Dimensional Polyrotaxane with Large Cavities and Channels: A Novel Approach to Metal–Organic Open-Frameworks by Using Supramolecular Building Blocks. *Angew. Chem., Int. Ed*. **2001**, *40*, 399–402.

(151) Hoffart, D. J.; Loeb, S. J. Metal-Organic Rotaxane Frameworks: Three-Dimensional Polyrotaxanes From Lanthanide-Ion Nodes, Pyridinium *N*-Oxide Axles, and Crown-Ether Wheels. *Angew. Chem., Int. Ed*. **2005**, *44*, 901–904.

(152) Loeb, S. J. Metal-Organic Rotaxane Frameworks; MORFs. *Chem. Commun.* **2005**, 1511–1518.

(153) Mercer, D. J.; Vukotic, V. N.; Loeb, S. J. Linking [2]Rotaxane Wheels to Create a New Type of Metal Organic Rotaxane Framework. *Chem. Commun*. **2010**, *47*, 896–898.

(154) Vukotic, V. N.; Loeb, S. J. One-, Two- and Three-Periodic Metal-Organic Rotaxane Frameworks (MORFs): Linking Cationic Transition-Metal Nodes with an Anionic Rotaxane Ligand. *Chem. Eur. J*. **2011**, *16*, 13630–13637.

(155) Mercer, D. J.; Yacoub, J.; Zhu, K.; Loeb, S. K. [2]Pseudorotaxanes, [2]Rotaxanes and Metal–Organic Rotaxane Frameworks Containing Tetra-Substituted Dibenzo[24]crown-8 Wheels. *Org. Biomol. Chem*. **2012**, *10*, 6094–6104.

(156) Vukotic, V. N.; Harris, K. J.; Zhu, K.; Schurko, R. W.; Loeb, S. J. Metal–Organic Frameworks with Dynamic Interlocked Components. *Nature Chem*. **2012**, *4*, 456–460.

(157) Frank, N. C.; Mercer, D. J.; Loeb, S. J. An Interwoven Metal-Organic Framework Combining Mechanically Interlocked Linkers and Interpenetrated Networks. *Chem. Eur. J*. **2013**, *19*, 14076–14080.

(158) Zhu, K.; Vukotic, V. N.; O'Keefe, C. A.; Schurko, R. W.; Loeb, S. J. Metal–Organic Frameworks with Mechanically Interlocked Pillars: Controlling Ring Dynamics in the Solid-State via a Reversible Phase Change. *J. Am. Chem. Soc*. **2014**, *136*, 7403–7409.

(159) Zhu, K.; O'Keefe, C. A.; Vukotic, V. N.; Schurko, R. W.; Loeb, S. J. A Molecular Shuttle That Operates Inside a Metal–Organic Framework. *Nature Chem*. **2015**, *7*, 514–519.

(160) Li, Q.; Sue, C.-H.; Basu, S.; Shveyd, A. K.; Zhang, W.; Barin, G.; Fang, L.; Sarjeant, A. A.; Stoddart, J. F.; Yaghi, O. M. A Catenated Strut in a Catenated Metal-Organic Framework. *Angew. Chem., Int. Ed*. **2010**, *49*, 6751–6755.

(161) Li, Q.; Zhang, W.; Miljanić, O. Š.; Knobler, C. B.; Stoddart, J. F.; Yaghi, O. M. A Metal–Organic Framework Replete with Ordered Donor–Acceptor Catenanes. *Chem. Commun*. **2010**, *46*, 380–382.

(162) Coskun, A.; Hmadeh, M.; Barin, G.; Gándara, F.; Li, Q.; Choi, E.; Strutt, N. L.; Cordes, D. B.; Slawin, A. M. Z.; Stoddart, J. F.; Sauvage, J.-P.; Yaghi, O. M. Metal-Organic Frameworks Incorporating Copper-Complexed Rotaxanes. *Angew. Chem., Int. Ed*. **2012**, *51*, 2160–2163.

(163) Cao, D.; Juríček, M.; Brown, Z. J.; Sue, A. C.-H.; Liu, Z.; Lei, J.; Blackburn, A. K.; Grunder, S.; Sarjeant, A. A.; Coskun, A.; Wang, C.; Farha, O. K.; Hupp, J. T.; Stoddart, J. F. Three-Dimensional Architectures Incorporating Stereoregular Donor-Acceptor Stacks. *Chem. Eur. J*. **2013**, *19*, 8457–8465.

(164) McGonigal, P. R.; Deria, P.; Hod, I.; Moghadam, P. Z.; Avestro, A.-J.; Horwitz, N. E.; Gibbs-Hall, I. C.; Blackburn, A. K.; Chen, D.; Botros, Y. Y.; Wasielewski, M. R.; Snurr, R. Q.; Hupp, J. T.; Farha, O. K.; Stoddart, J. F. Electrochemically Addressable Trisradical Rotaxanes Organized Within a Metal–Organic Framework. *Proc. Natl. Acad. Sci. U.S.A*. **2015**, *112*, 11161–11168.

(165) Gong, H.-Y.; Rambo, B. M.; Cho, W.; Lynch, V. M.; Oh, M.; Sessler, J. L. Anion-Directed Assembly of a Three-Dimensional Metal–Organic Rotaxane Framework. *Chem. Commun*. **2011**, *47*, 5973–5975.

(166) Gong, H.-Y.; Rambo, B. M.; Nelson, C. A.; Cho, W.; Lynch, V. M.; Zhu, X.; Oh, M.; Sessler, J. L. Multi Component Self-Assembly: Supramolecular Organic Frameworks Containing Metal–Rotaxane Subunits (RSOFs). *Dalton Trans*. **2012**, *41*, 1134–1137.

(167) Gong, H.-Y.; Rambo, B. M.; Nelson, C. A.; Lynch, V. M.; Zhu, X.; Sessler, J. L. Rare-Earth Cation Effects on Three-Dimensional Metal–Organic Rotaxane Framework (MORF) Self Assembly. *Chem. Commun*. **2012**, *48*, 10186–10188.

(168) Whitehead, G. F. S.; Cross, B.; Carthy, L.; Milway, V. A.; Rath, H.; Fernandez, A.; Heath, S. L.; Muryn, C. A.; Pritchard, R. G.; Teat, S. J.; Timco, G. A.; Winpenny, R. E. P. Rings and Threads as Linkers in Metal–Organic Frameworks and Poly-Rotaxanes. *Chem. Commun*. **2013**, *49*, 7195–7197.

(169) Liang, J.; Wang, X.-L.; Jiao, Y.-Q.; Qin, C.; Shao, K.-Z.; Su, Z.-M.; Wu, Q.-Y. Metal Ion Directed Metal–Organic Rotaxane Frameworks with Intrinsic Features of Self-Penetration and Interpenetration. *Chem. Commun*. **2013**, *49*, 8555–8557.

(170) Sauvage, J.-P.; Weiss, J. Synthesis of Dicopper(I) [3]Catenates: Multiring Interlocked Coordinating Systems. *J. Am. Chem. Soc*. **1985**, *107*, 6108–6110.

(171) Ashton, P. R.; Brown, C. L.; Chrystal, E. J. T.; Goodnow, T. T.; Kaifer, A. E.; Parry, K. P.; Slawin, A. M. Z.; Spencer, N.; Stoddart, J. F.; Williams, D. J. Self-Assembling [3]Catenanes. *Angew. Chem., Int. Ed. Engl*. **1991**, *30*, 1039–1042.

(172) Schummer, J. Gestalt Switch in Molecular Image Perception: The Aesthetic Origin of Molecular Nanotechnology in Supramolecular Chemistry. *Found. Chem*. **2006**, *8*, 53–72.

(173) Shirai, Y.; Osgood, A. J.; Zhao, Y.; Kelly, K. F.; Tour, J. M. Directional Control in Thermally Driven Single-Molecule Nanocars. *Nano Lett*. **2005**, *5*, 2330–2334.

(174) Anelli, P. L.; Spencer, N.; Stoddart, J. F. A Molecular Shuttle. *J. Am. Chem. Soc*. **1991**, *113*, 5131–5133.

(175) Bissell, R. A.; Córdova, E.; Kaifer, A. E.; Stoddart, J. F. A Chemically and Electrochemically Switchable Molecular Shuttle. *Nature* **1994**, *369*, 133–137.

(176) Spruell, J. M.; Paxton, W. F.; Olsen, J. C.; Benítez, D.; Tkatchouk, E.; Stern, C. L.; Trabolsi, A.; Friedman, D. C.; Goddard, W. A., III; Stoddart, J. F. A Push-Button Molecular Switch. *J. Am. Chem. Soc*. **2009**, *131*, 11571–11580.
(177) Ashton, P. R.; Brown, C. L.; Chrystal, E. J. T.; Parry, K. P.; Pietraszkiewicz, M.; Spencer, N.; Stoddart, J. F. Molecular Trains: Self Association and Dynamic Properties of Two New Catenanes. *Angew. Chem., Int. Ed. Engl*. **1991**, *30*, 1042–1045.
(178) Badjić, J. D.; Balzani, V.; Credi, A.; Silvi, S.; Stoddart, J. F. A Molecular Elevator. *Science* **2004**, *303*, 1845–1849.
(179) Zhao, Y.-L.; Li, Z.; Kabehie, S.; Botros, Y. Y.; Stoddart, J. F.; Zink, J. I. pH-Operated Nanopistons on the Surfaces of Mesoporous Silica Nanoparticles. *J. Am. Chem. Soc*. **2010**, *132*, 13016–13025.
(180) Bruns, C. J.; Stoddart, J. F. Rotaxane-Based Molecular Muscles. *Acc. Chem. Res*. **2014**, *47*, 2186–2199.
(181) Ashton, P. R.; Ballardini, R.; Balzani, V.; Credi, A.; Dress, K. R.; Ishow, E.; Kleverlaan, C. J.; Kocian, O.; Preece, J. A.; Spencer, N.; Stoddart, J. F.; Venturi, M.; Wenger, S. Molecular Meccano 61. A Photochemically Driven Molecular-Level Abacus. *Chem. Eur. J*. **2000**, *6*, 3558–3574.
(182) Balzani, V.; Clemente-León, M.; Credi, A.; Ferrer, B.; Venturi, M.; Flood, A. H.; Stoddart, J. F. Autonomous Artificial Nanomotor Powered by Sunlight. *Proc. Natl. Acad. Sci. U.S.A*. **2006**, *103*, 1178–1183.
(183) Saha, S.; Leung, K. C.-F.; Nguyen, T. D.; Stoddart, J. F.; Zink, J. I. Nanovalves. *Adv. Funct. Mater*. **2007**, *17*, 685–693.
(184) Roh, S.-G.; Park, K.-M.; Park, G.-J.; Sakamoto, S.; Yamaguchi, K.; Kim, K. Synthesis of a Five-Membered Molecular Necklace: A 2+2 Approach. *Angew. Chem., Int. Ed*. **1999**, *38*, 637–641.
(185) Harada, A.; Li, J.; Kamachi, M. The Molecular Necklace: A Rotaxane Containing Many Threaded α-Cyclodextrins. *Nature* **1992**, *356*, 325–327.
(186) Whang, D.; Park, K.-M.; Heo, J.; Ashton, P.; Kim, K. Molecular Necklace: Quantitative Self-Assembly of a Cyclic Oligorotaxane From Nine Molecules. *J. Am. Chem. Soc*. **1998**, *120*, 4899–4900.
(187) Fujita, M.; Ibukuro, F.; Yamaguchi, K.; Ogura, K. A Molecular Lock. *J. Am. Chem. Soc*. **1995**, *117*, 4175–4176.
(188) Leigh, D. A.; Wong, J. K. Y.; Dehez, F.; Zerbetto, F. Unidirectional Rotation in a Mechanically Interlocked Molecular Rotor. *Nature* **2003**, *424*, 174–179.
(189) Leigh, D. A.; Moody, K.; Smart, J. P.; Watson, K. J.; Slawin, A. M. Z. Catenane Chameleons: Environment-Sensitive Translational Isomerism in Amphiphilic Benzylic Amide [2]Catenanes. *Angew. Chem., Int. Ed. Engl*. **1996**, *35*, 306–310.
(190) Clark, P. G.; Guidry, E. N.; Chan, W. Y.; Steinmetz, W. E.; Grubbs, R. H. Synthesis of a Molecular Charm Bracelet via Click Cyclization and Olefin Metathesis Clipping. *J. Am. Chem. Soc*. **2010**, *132*, 3405–3412.
(191) Jimenez-Bueno, G.; Rapenne, G. Technomimetic Molecules: Synthesis of a Molecular Wheelbarrow. *Tetrahedron Lett*. **2003**, *44*, 6261–6263.
(192) Rapenne, G. Synthesis of Technomimetic Molecules: Towards Rotation Control in Single-Molecular Machines and Motors. *Org. Biomol. Chem*. **2005**, *3*, 1165–1169.
(193) Lehn, J.-M. Supramolecular Chemistry—Scope and Perspectives Molecules, Supermolecules, and Molecular Devices (Nobel Lecture). *Angew. Chem., Int. Ed. Engl*. **1988**, *27*, 89–112.
(194) Kant, I. *Critique of Judgement*; Macmillan: London, **1892**.
(195) Goodman, N. *Languages of Art: an Approach to a Theory of Symbols*; Bobbs-Merrill: Indianapolis, **1968**.
(196) Eco, U. *A Theory of Semiotics*; Indiana University Press: Bloomington, **1976**.
(197) Hoffmann, R. Thoughts on Aesthetics and Visualization in Chemistry. *HYLE* **2003**, *9*, 7–10.
(198) Pedersen, C. J. The Discovery of Crown Ethers (Nobel Lecture). *Angew. Chem., Int. Ed. Engl*. **1988**, *27*, 1021–1027.
(199) Cram, D. J. The Design of Molecular Hosts, Guests, and Their Complexes (Nobel Lecture). *Angew. Chem., Int. Ed. Engl*. **1988**, *27*, 1009–1020.
(200) Ogino, H. Relatively High-Yield Synthesis of Rotaxanes. Synthesis and Properties of Compounds Consisting of Cyclodextrins Threaded by α,ω-Diaminoalkanes Coordinated to Cobalt(III) Complexes. *J. Am. Chem. Soc*. **1981**, *103*, 1303–1304.
(201) Mock, W. L.; Irra, T. A.; Wepsiec, J. P.; Adhya, M. Catalysis by Cucurbituril. The Significance of Bound-Substrate Destabilization for Induced Triazole Formation. *J. Org. Chem*. **1989**, *54*, 5302–5308.
(202) Fujita, M.; Ibukuro, F.; Hagihara, H.; Ogura, K. Quantitative Self-Assembly of a [2]Catenane From Two Preformed Molecular Rings. *Nature* **1994**, *367*, 720–723.
(203) Anderson, S.; Anderson, H. L. Synthesis of a Water-Soluble Conjugated [3]Rotaxane. *Angew. Chem., Int. Ed. Engl*. **1996**, *35*, 1956–1959.
(204) Lin, Y.-H.; Lai, C.-C.; Liu, Y.-H.; Peng, S.-M.; Chiu, S.-H. Sodium Ions Template the Formation of Rotaxanes From BPX26C6 and Nonconjugated Amide and Urea Functionalities. *Angew. Chem., Int. Ed*. **2013**, *52*, 10231–10236.
(205) Hancock, L. M.; Beer, P. D. Sodium and Barium Cation-Templated Synthesis and Cation-Induced Molecular Pirouetting of a Pyridine *N*-Oxide Containing [2]Rotaxane. *Chem. Commun*. **2011**, *47*, 6012–6014.
(206) Zapata, F.; Blackburn, O. A.; Langton, M. J.; Faulkner, S.; Beer, P. D. Lanthanide Cation-Templated Synthesis of Rotaxanes. *Chem. Commun*. **2013**, *49*, 8157–8159.
(207) Loeb, S. J.; Wisner, J. A. 1,2-Bis(4,4′-dipyridinium)ethane: A Versatile Dication for the Formation of [2]Rotaxanes with Dibenzo-24-Crown-8 Ether. *Chem. Commun*. **1998**, *2757–2758*.
(208) Rowan, A. E.; Aarts, P. P. M.; Koutstaal, K. W. M. Novel Porphyrin–Viologen Rotaxanes. *Chem. Commun*. **1998**, *611–612*.
(209) Hamilton, D. G.; Sanders, J. K. M.; Davies, J. E.; Clegg, W.; Teat, S. J. Neutral [2]Catenanes From Oxidative Coupling of π-Stacked Components. *Chem. Commun*. **1997**, *897–898*.
(210) Korybut-Daszkiewicz, B.; Więckowska, A.; Bilewicz, R.; Domagala, S.; Wozniak, K. Novel [2]Catenane Structures Introducing Communication Between Transition Metal Centers via π···π Interactions. *J. Am. Chem. Soc*. **2001**, *123*, 9356–9366.
(211) Hunter, C. A. Synthesis and Structure Elucidation of a New [2]-Catenane. *J. Am. Chem. Soc*. **1992**, *114*, 5303–5311.
(212) Johnston, A. G.; Leigh, D. A.; Nezhat, L.; Smart, J. P.; Deegan, M. D. Structurally Diverse and Dynamically Versatile Benzylic Amide [2]Catenanes Assembled Directly From Commercially Available Precursors. *Angew. Chem., Int. Ed. Engl*. **1995**, *34*, 1212–1216.
(213) Vysotsky, M. O.; Bolte, M.; Thondorf, I.; Böhmer, V. New Molecular Topologies by Fourfold Metathesis Reactions Within a Hydrogen-Bonded Calix[4]arene Dimer. *Chem. Eur. J*. **2003**, *9*, 3375–3382.
(214) Tron, A.; Thornton, P. J.; Rocher, M.; Jacquot de Rouville, H. P.; Desvergne, J. P.; Kauffmann, B.; Buffeteau, T.; Cavagnat, D.; Tucker, J. H.; McClenaghan, N. D. Formation of a Hydrogen-Bonded Barbiturate [2]-Rotaxane. *Org. Lett*. **2014**, *16*, 1358–1361.
(215) Kolchinski, A. G.; Busch, D. H.; Alcock, N. W. Gaining Control Over Molecular Threading: Benefits of Second Coordination Sites and Aqueous-Organic Interfaces in Rotaxane Synthesis. *J. Chem. Soc., Chem. Commun.* **1995**, 1289–1291.
(216) Aucagne, V.; Leigh, D. A.; Lock, J. S.; Thomson, A. R. Rotaxanes of Cyclic Peptides. *J. Am. Chem. Soc*. **2006**, *128*, 1784–1785.
(217) Gilday, L. C.; Lang, T.; Caballero, A.; Costa, P. J.; Félix, V.; Beer, P. D. A Catenane Assembled Through a Single

Charge-Assisted Halogen Bond. *Angew. Chem., Int. Ed*. **2013**, *52*, 4356–4360.
(218) Hübner, G. M.; Gläser, J.; Seel, C.; Vögtle, F. High-Yielding Rotaxane Synthesis with an Anion Template. *Angew. Chem., Int. Ed*. **1999**, *38*, 383–386.
(219) Lee, S.; Chen, C.-H.; Flood, A. H. A Pentagonal Cyanostar Macrocycle with Cyanostilbene CH Donors Binds Anions and Forms Dialkylphosphate [3]Rotaxanes. *Nature Chem*. **2013**, *5*, 704–710.
(220) Caballero, A.; Zapata, F.; White, N. G.; Costa, P. J.; Félix, V.; Beer, P. D. A Halogen-Bonding Catenane for Anion Recognition and Sensing. *Angew. Chem., Int. Ed*. **2012**, *51*, 1876–1880.
(221) Barrell, M. J.; Leigh, D. A.; Lusby, P. J.; Slawin, A. M. Z. An Ion-Pair Template for Rotaxane Formation and Its Exploitation in an Orthogonal Interaction Anion-Switchable Molecular Shuttle. *Angew. Chem., Int. Ed*. **2008**, *47*, 8036–8039.
(222) Nakatani, Y.; Furusho, Y.; Yashima, E. Amidinium Carboxylate Salt Bridges as a Recognition Motif for Mechanically Interlocked Molecules: Synthesis of an Optically Active [2]Catenane and Control of Its Structure. *Angew. Chem., Int. Ed*. **2010**, *49*, 5463–5467.
(223) Shukla, R.; Deetz, M. J.; Smith, B. D. [2]Rotaxane with a Cation-Binding Wheel. *Chem. Commun.* **2000**, 2397–2398.
(224) Arduini, A.; Ferdani, R.; Pochini, A.; Secchi, A.; Ugozzoli, F. Calix[6]arene as a Wheel for Rotaxane Synthesis. *Angew. Chem., Int. Ed*. **2000**, *39*, 3453–3456.
(225) Pierro, T.; Gaeta, C.; Talotta, C.; Casapullo, A.; Neri, P. Fixed or Invertible Calixarene-Based Directional Shuttles. *Org. Lett*. **2011**, *13*, 2650–2653.
(226) Ogoshi, T.; Nishida, Y.; Yamagishi, T.-A.; Nakamoto, Y. High Yield Synthesis of Polyrotaxane Constructed From Pillar[5]arene and Viologen Polymer and Stabilization of Its Radical Cation. *Macromolecules* **2010**, *43*, 7068–7072.
(227) Li, H.; Fahrenbach, A. C.; Dey, S. K.; Basu, S.; Trabolsi, A.; Zhu, Z.; Botros, Y. Y.; Stoddart, J. F. Mechanical Bond Formation by Radical Templation. *Angew. Chem., Int. Ed*. **2010**, *49*, 8260–8265.
(228) Li, H.; Zhu, Z.; Fahrenbach, A. C.; Savoie, B. M.; Ke, C.; Barnes, J. C.; Lei, J.; Zhao, Y.-L.; Lilley, L. M.; Marks, T. J.; Ratner, M. A.; Stoddart, J. F. Mechanical Bond-Induced Radical Stabilization. *J. Am. Chem. Soc*. **2013**, *135*, 456–467.
(229) Wang, W.; Wang, L.; Palmer, B. J.; Exarhos, G. J.; Li, A. D. Cyclization and Catenation Directed by Molecular Self-Assembly. *J. Am. Chem. Soc*. **2006**, *128*, 11150–11159.
(230) Hasell, T.; Wu, X.; Jones, J. T. A.; Bacsa, J.; Steiner, A.; Mitra, T.; Trewin, A.; Adams, D. J.; Cooper, A. I. Triply Interlocked Covalent Organic Cages. *Nature Chem*. **2010**, *2*, 750–755.
(231) Hicks, D. *Look Into the Stillness: A Spiritual Journey through Inspirational Quotes*. Nature's Path: Amelia Court House, Virginia, **2015**.
(232) Dietrich-Buchecker, C. O.; Sauvage, J.-P. Interlocking of Molecular Threads: From the Statistical Approach to the Templated Synthesis of Catenands. *Chem. Rev*. **1987**, *87*, 795–810.
(233) Sauvage, J.-P.; Amabilino, D. B. The Beauty of Knots at the Molecular Level. *Top. Curr. Chem.* **2012**, *323*, 107–125.
(234) Rolfsen, D. *Knots and Links*; Publish or Perish: Berkeley, **1976**.
(235) Nierengarten, J.-F.; Dietrich-Buchecker, C. O.; Sauvage, J.-P. Synthesis of a Doubly Interlocked [2]-Catenane. *J. Am. Chem. Soc*. **1994**, *116*, 375–376.
(236) Leigh, D. A.; Pritchard, R. G.; Stephens, A. J. A Star of David Catenane. *Nature Chem*. **2014**, *6*, 978–982.
(237) Chichak, K. S.; Cantrill, S. J.; Pease, A. R.; Chiu, S. H.; Cave, G. W. V.; Atwood, J. L.; Stoddart, J. F. Molecular Borromean Rings. *Science* **2004**, *304*, 1308–1312.
(238) Wood, C. S.; Ronson, T. K.; Belenguer, A. M.; Holstein, J. J.; Nitschke, J. R. Two-Stage Directed Self-Assembly of a Cyclic [3]Catenane. *Nature Chem*. **2015**, *7*, 354–358.
(239) Dietrich-Buchecker, C. O.; Sauvage, J.-P. A Synthetic Molecular Trefoil Knot. *Angew. Chem., Int. Ed. Engl*. **1989**, *28*, 189–192.
(240) Dietrich-Buchecker, C. O.; Guilhem, J.; Pascard, C.; Sauvage, J.-P. Structure of a Synthetic Trefoil Knot Coordinated to Two Copper(I) Centers. *Angew. Chem., Int. Ed. Engl*. **1990**, *29*, 1154–1156.
(241) Ayme, J.-F.; Beves, J. E.; Leigh, D. A.; McBurney, R. T.; Rissanen, K.; Schultz, D. A Synthetic Molecular Pentafoil Knot. *Nature Chem*. **2012**, *4*, 15–20.
(242) Ayme, J.-F.; Beves, J. E.; Leigh, D. A.; McBurney, R. T.; Rissanen, K.; Schultz, D. Pentameric Circular Iron(II) Double Helicates and a Molecular Pentafoil Knot. *J. Am. Chem. Soc*. **2012**, 9488–9497.
(243) Carina, R. F.; Dietrich-Buchecker, C.; Sauvage, J.-P. Molecular Composite Knots. *J. Am. Chem. Soc*. **1996**, *118*, 9110–9116.
(244) Castle, T.; Evans, M. E.; Hyde, S. T. Ravels: Knot-Free but Not Free. Novel Entanglements of Graphs in 3-Space. *New J. Chem*. **2008**, *32*, 1484–1492.
(245) Li, F.; Clegg, J. K.; Lindoy, L. F.; Macquart, R. B.; Meehan, G. V. Metallosupramolecular Self-Assembly of a Universal 3-Ravel. *Nature Commun*. **2011**, *2*: 205.
(246) Bitsch, F.; Dietrich-Buchecker, C. O.; Khemiss, A. K.; Sauvage, J.-P.; Van Dorsselaer, A. Multiring Interlocked Systems: Structure Elucidation by Electrospray Mass Spectrometry. *J. Am. Chem. Soc*. **1991**, *113*, 4023–4025.
(247) Park, K.-M.; Kim, S.-Y.; Heo, J.; Whang, D.; Sakamoto, S.; Yamaguchi, K.; Kim, K. Designed Self-Assembly of Molecular Necklaces. *J. Am. Chem. Soc*. **2002**, *124*, 2140–2147.
(248) Fujita, M.; Fujita, N.; Ogura, K.; Yamaguchi, K. Spontaneous Assembly of Ten Components Into Two Interlocked, Identical Coordination Cages. *Nature* **1999**, *400*, 52–55.
(249) Fukuda, M.; Sekiya, R.; Kuroda, R. A Quadruply Stranded Metallohelicate and Its Spontaneous Dimerization Into an Interlocked Metallohelicate. *Angew. Chem., Int. Ed*. **2008**, *47*, 706–710.
(250) Ashton, P. R.; Reder, A. S.; Spencer, N.; Stoddart, J. F. Self-Assembly of a Chiral Bis[2]catenane. *J. Am. Chem. Soc*. **1993**, *115*, 5286–5287.
(251) Hamers, C.; Raymo, F. M.; Stoddart, J. F. Molecular Meccano 42. Main-Chain and Pendant Poly([2]catenane)s Incorporating Complementary π-Electron-Rich and -Deficient Components. *Eur. J. Org. Chem.* **1998**, 2109–2117.
(252) Geerts, Y.; Muscat, D.; Müllen, K. Synthesis of Oligo[2]catenanes. *Macromol. Chem. Phys*. **1995**, *196*, 3425–3435.
(253) Nielsen, M. B.; Thorup, N.; Becher, J. Synthesis of a Criss-Cross Overlapped Tetrathiafulvalenophane and a Topologically New [2]Catenane. *J. Chem. Soc., Perkin Trans. 1* **1998**, 1305–1308.
(254) Dietrich-Buchecker, C.; Frommberger, B.; Lüer, I.; Sauvage, J.-P.; Vögtle, F. Multiring Catenanes with a Macrobicyclic Core. *Angew. Chem., Int. Ed. Engl*. **1993**, *32*, 1434–1437.
(255) Vogtle, F.; Safarowsky, O.; Heim, C.; Affeld, A.; Braun, O.; Mohry, A. Catenanes, Rotaxanes and Pretzelanes-Template Synthesis and Chirality. *Pure Appl. Chem*. **1999**, *71*, 247–251.
(256) Safarowsky, O.; Windisch, B.; Mohry, A.; Vögtle, F. Nomenclature for Catenanes, Rotaxanes, Molecular Knots, and Assemblies Derived From These Structural Elements. *J. Prakt. Chem*. **2000**, *342*, 437–444.
(257) Reuter, C.; Mohry, A.; Sobanski, A.; Vögtle, F. [1]Rotaxanes and Pretzelanes: Synthesis, Chirality, and Absolute Configuration. *Chem. Eur. J*. **2000**, *6*, 1674–1682.
(258) Li, Z.-T.; Stein, P. C.; Svenstrup, N.; Lund, K. H.; Becher, J. Synthesis of Novel Tetrathiafulvalene-Based [3]Pseudocatenanes by Self-Assembly; Prevention of *Trans*/*Cis* Isomerization. *Angew. Chem., Int. Ed. Engl*. **1995**, *34*, 2524–2528.
(259) Frey, J.; Kraus, T.; Heitz, V.; Sauvage, J.-P. A Catenane Consisting of a Large Ring Threaded Through Both Cyclic Units of a Handcuff-Like Compound. *Chem. Commun.* **2005**, 5310–5312.
(260) Evans, N. H.; Serpell, C. J.; Beer, P. D. Chloride Anion Templated Synthesis and Crystal Structure of a Handcuff Catenane. *Angew. Chem., Int. Ed*. **2011**, *50*, 2507–2510.

(261) Hartlieb, K. J.; Blackburn, A. K.; Schneebeli, S. T.; Forgan, R. S.; Sarjeant, A. A.; Stern, C. L.; Cao, D.; Stoddart, J. F. Topological Isomerism in a Chiral Handcuff Catenane. *Chem. Sci*. **2014**, *5*, 90–100.

(262) Zhu, X.-Z.; Chen, C.-F. A Highly Efficient Approach to [4]Pseudocatenanes by Threefold Metathesis Reactions of a Triptycene-Based Tris[2]pseudorotaxane. *J. Am. Chem. Soc*. **2005**, *127*, 13158–13159.

(263) Black, S. P.; Stefankiewicz, A. R.; Smulders, M. M. J.; Sattler, D.; Schalley, C. A.; Nitschke, J. R.; Sanders, J. K. M. Generation of a Dynamic System of Three-Dimensional Tetrahedral Polycatenanes. *Angew. Chem., Int. Ed*. **2013**, *52*, 5749–5752.

(264) Jäger, R.; Schmidt, T.; Karbach, D.; Vögtle, F. The First Pretzel-Shaped Molecules. via Catenane Precursors. *Synlett* **1996**, 723–725.

(265) Wu, Y.-W.; Tung, S.-T.; Lai, C.-C.; Liu, Y.-H.; Peng, S.-M.; Chiu, S.-H. Cyclic [2]Catenane Dimers, Trimers, and Tetramers. *Angew. Chem., Int. Ed*. **2015**, *54*, 11745–11749.

(266) McArdle, C. P.; Vittal, J. J.; Puddephatt, R. J. Molecular Topology: Easy Self-Assembly of an Organometallic Doubly Braided [2]Catenane. *Angew. Chem., Int. Ed*. **2000**, *39*, 3819–3822.

(267) Liu, Y.; Bonvallet, P. A.; Vignon, S. A.; Khan, S. I.; Stoddart, J. F. Donor-Acceptor Pretzelanes and a Cyclic Bis[2]catenane Homologue. *Angew. Chem., Int. Ed*. **2005**, *44*, 3050–3055.

(268) Ashton, P. R.; Horn, T.; Menzer, S.; Preece, J. A.; Spencer, N.; Stoddart, J. F.; Williams, D. J. Towards a Molecular Anchor Chain. Synthesis and Catenations of Spiro Crown Ethers. *Synthesis* **1997**, 480–488.

(269) Wang, L.; Vysotsky, M. O.; Bogdan, A.; Bolte, M.; Böhmer, V. Multiple Catenanes Derived From Calix[4]arenes. *Science* **2004**, *304*, 1312–1314.

(270) Zhang, G.; Presly, O.; White, F.; Oppel, I. M.; Mastalerz, M. A Shape-Persistent Quadruply Interlocked Giant Cage Catenane with Two Distinct Pores in the Solid State. *Angew. Chem., Int. Ed*. **2014**, *53*, 5126–5130.

(271) Jäger, R.; Händel, M.; Harren, J.; Rissanen, K.; Vögtle, F.; Rissanen, K. Chemistry with Rotaxanes: Intra- and Intermolecularly Covalently Linked Rotaxanes. *Liebigs Ann*. **1996**, 1201–1207.

(272) Zhou, Q.; Wei, P.; Zhang, Y.; Yu, Y.; Yan, X. Benzo-21-crown-7-Based [1]Rotaxanes: Syntheses, X-Ray Crystal Structures, and Dynamic Characteristics. *Org. Lett*. **2013**, *15*, 5350–5353.

(273) Nygaard, S.; Liu, Y.; Stein, P C; Flood, A. H.; Jeppesen, J. O. Using Molecular Force to Overcome Steric Barriers in a Springlike Molecular Ouroboros. *Adv. Funct. Mater*. **2007**, *17*, 751–762.

(274) Nielsen, K. A.; Bähring, S.; Jeppesen, J. O. Acid/Base Controllable Molecular Recognition. *Chem. Eur. J*. **2011**, *17*, 11001–11007.

(275) Rosengren, K. J.; Clark, R. J.; Daly, N. L.; Göransson, U.; Jones, A.; Craik, D. J. Microcin J25 Has a Threaded Sidechain-to-Backbone Ring Structure and Not a Head-to-Tail Cyclized Backbone. *J. Am. Chem. Soc*. **2003**, *125*, 12464–12474.

(276) Wilson, K.-A.; Kalkum, M.; Ottesen, J.; Yuzenkova, J.; Chait, B. T.; Landick, R.; Muir, T.; Severinov, K.; Darst, S. A. Structure of Microcin J25, a Peptide Inhibitor of Bacterial RNA Polymerase, is a Lassoed Tail. *J. Am. Chem. Soc*. **2003**, *125*, 12475–12483.

(277) Clavel, C.; Romuald, C.; Brabet, E.; Coutrot, F. A pH-Sensitive Lasso-Based Rotaxane Molecular Switch. *Chem. Eur. J*. **2013**, *19*, 2982–2989.

(278) Bruns, C. J.; Frasconi, M.; Iehl, J.; Hartlieb, K. J.; Schneebeli, S. T.; Cheng, C.; Stupp, S. I.; Stoddart, J. F. Redox Switchable Daisy Chain Rotaxanes Driven by Radical–Radical Interactions. *J. Am. Chem. Soc*. **2014**, *136*, 4714–4723.

(279) Reuter, C.; Wienand, W.; Schmuck, C.; Vögtle, F. A Self-Threaded "Molecular 8." *Chem. Eur. J*. **2001**, *7*, 1728–1733.

(280) Boyle, M. M.; Forgan, R. S.; Friedman, D. C.; Gassensmith, J. J.; Smaldone, R. A.; Stoddart, J. F.; Sauvage, J.-P. Donor–Acceptor Molecular Figures-of-Eight. *Chem. Commun*. **2011**, *47*, 11870–11872.

(281) Boyle, M. M.; Gassensmith, J. J.; Whalley, A. C.; Forgan, R. S.; Smaldone, R. A.; Hartlieb, K. J.; Blackburn, A. K.; Sauvage, J.-P.; Stoddart, J. F. Stereochemistry of Molecular Figures-of-Eight. *Chem. Eur. J*. **2012**, *18*, 10312–10323.

(282) Rotzler, J.; Mayor, M. Molecular Daisy Chains. *Chem. Soc. Rev*. **2013**, *42*, 44–62.

(283) Ashton, P. R.; Parsons, I. W.; Raymo, F. M.; Stoddart, J. F.; White, A. J. P.; Williams, D. J.; Wolf, R. Self-Assembling Supramolecular Daisy Chains. *Angew. Chem., Int. Ed*. **1998**, *37*, 1913–1916.

(284) Rowan, S. J.; Cantrill, S. J.; Stoddart, J. F.; White, A. J. P.; Williams, D. J. Toward Daisy Chain Polymers: "Wittig Exchange" of Stoppers in [2]Rotaxane Monomers. *Org. Lett*. **2000**, *2*, 759–762.

(285) Chiu, S.-H.; Rowan, S. J.; Cantrill, S. J.; Stoddart, J. F.; White, A. J. P.; Williams, D. J. An Hermaphroditic [*c*2]Daisy Chain. *Chem. Commun*. **2002**, *2948–2949*.

(286) Hoshino, T.; Miyauchi, M.; Kawaguchi, Y.; Yamaguchi, H.; Harada, A. Daisy Chain Necklace: Tri[2]rotaxane Containing Cyclodextrins. *J. Am. Chem. Soc*. **2000**, *122*, 9876–9877.

(287) Romuald, C.; Cazals, G.; Enjalbal, C.; Coutrot, F. Straightforward Synthesis of a Double-Lasso Macrocycle From a Nonsymmetrical [*c*2]Daisy Chain. *Org. Lett*. **2013**, *15*, 184–187.

(288) Jiménez, M. C.; Dietrich-Buchecker, C.; Sauvage, J.-P. Towards Synthetic Molecular Muscles: Contraction and Stretching of a Linear Rotaxane Dimer. *Angew. Chem., Int. Ed*. **2000**, *39*, 3284–3287.

(289) Collin, J.-P.; Dietrich-Buchecker, C.; Gaviña, P.; Jimenez-Molero, M. C.; Sauvage, J.-P. Shuttles and Muscles: Linear Molecular Machines Based on Transition Metals. *Acc. Chem. Res*. **2001**, *34*, 477–487.

(290) Jimenez-Molero, M. C.; Dietrich-Buchecker, C.; Sauvage, J.-P. Towards Artificial Muscles at the Nanometric Level. *Chem. Commun.* **2003**, 1613–1616.

(291) Niess, F.; Duplan, V.; Sauvage, J.-P. Molecular Muscles: From Species in Solution to Materials and Devices. *Chem. Lett*. **2014**, *43*, 964–974.

(292) Kishan, M. R.; Parham, A.; Schelhase, F.; Yoneva, A.; Silva, G.; Chen, X.; Okamoto, Y.; Vögtle, F. Bridging Rotaxanes' Wheels—Cyclochiral Bonnanes. *Angew. Chem., Int. Ed*. **2006**, *45*, 7296–7299.

(293) Ciao, R.; Talotta, C.; Gaeta, C.; Margarucci, L.; Casapullo, A.; Neri, P. An Oriented Handcuff Rotaxane. *Org. Lett*. **2013**, *15*, 5694–5697.

(294) Aricó, F.; Chang, T.; Cantrill, S. J.; Khan, S. I.; Stoddart, J. F. Template-Directed Synthesis of Multiply Mechanically Interlocked Molecules Under Thermodynamic Control. *Chem. Eur. J*. **2005**, *11*, 4655–4666.

(295) Collin, J.-P.; Durola, F.; Frey, J.; Heitz, V.; Reviriego, F.; Sauvage, J.-P.; Trolez, Y.; Rissanen, K. Templated Synthesis of Cyclic [4]Rotaxanes Consisting of Two Stiff Rods Threaded Through Two Bis-Macrocycles with a Large and Rigid Central Plate as Spacer. *J. Am. Chem. Soc*. **2010**, *132*, 6840–6850.

(296) Badjić, J. D.; Balzani, V.; Credi, A.; Lowe, J. N.; Silvi, S.; Stoddart, J. F. A Mechanically Interlocked Bundle. *Chem. Eur. J*. **2004**, *10*, 1926–1935.

(297) Yamada, Y.; Okamoto, M.; Furukawa, K.; Kato, T.; Tanaka, K. Switchable Intermolecular Communication in a Four-Fold Rotaxane. *Angew. Chem., Int. Ed*. **2012**, *51*, 709–713.

(298) Yamada, Y.; Mihara, N.; Shibano, S.; Sugimoto, K.; Tanaka, K. Triply Stacked Heterogeneous Array of Porphyrins and Phthalocyanine Through Stepwise Formation of a Fourfold Rotaxane and an Ionic Complex. *J. Am. Chem. Soc*. **2013**, *135*, 11505–11508.

(299) Northrop, B. H.; Aricó, F.; Tangchiavang, N.; Badjić, J. D.; Stoddart, J. F. Template-Directed Synthesis of Mechanically Interlocked Molecular Bundles Using Dynamic Covalent Chemistry. *Org. Lett*. **2006**, *8*, 3899–3902.
(300) Belowich, M. E.; Valente, C.; Smaldone, R. A.; Friedman, D. C.; Thiel, J.; Cronin, L.; Stoddart, J. F. Positive Cooperativity in the Template-Directed Synthesis of Monodisperse Macromolecules. *J. Am. Chem. Soc*. **2012**, *134*, 5243–5261.
(301) Basu, S.; Coskun, A.; Friedman, D. C.; Olson, M. A.; Benítez, D.; Tkatchouk, E.; Barin, G.; Yang, J.; Fahrenbach, A. C.; Goddard, W. A. III; Stoddart, J. F. Donor-Acceptor Oligorotaxanes Made to Order. *Chem. Eur. J*. **2011**, *17*, 2107–2119.
(302) Zhu, Z.; Bruns, C. J.; Li, H.; Lei, J.; Ke, C.; Liu, Z.; Shafaie, S.; Colquhoun, H. M.; Stoddart, J. F. Synthesis and Solution-State Dynamics of Donor–Acceptor Oligorotaxane Foldamers. *Chem. Sci*. **2013**, *4*, 1470–1483.
(303) Bruns, C. J.; Stoddart, J. F. Mechanically Interlaced and Interlocked Donor–Acceptor Foldamers. *Adv. Polym. Sci*. **2013**, *261*, 271–294.
(304) Xue, W.; Li, Z.; Liu, G.; Chen, X.; Li, T.; Liu, S. H.; Yin, J. Construction of Rotacatenanes Using Rotaxane and Catenane Frameworks. *Org. Biomol. Chem*. **2014**, *12*, 4862–4871.
(305) Klotz, E. J. F.; Claridge, T. D. W.; Anderson, H. L. Homo- and Hetero-[3]Rotaxanes with Two π-Systems Clasped in a Single Macrocycle. *J. Am. Chem. Soc*. **2006**, *128*, 15374–15375.
(306) Prikhod'ko, A.; Sauvage, J.-P. Passing Two Strings Through the Same Ring Using an Octahedral Metal Center as Template: A New Synthesis of [3]Rotaxanes. *J. Am. Chem. Soc*. **2009**, *131*, 6794–6807.
(307) Chean, H. M.; Leigh, D. A.; Maffei, F.; McGonigal, P. R.; Slawin, A. M. Z.; Wu, J. En Route to a Molecular Sheaf: Active Metal Template Synthesis of a [3]Rotaxane with Two Axles Threaded Through One Ring. *J. Am. Chem. Soc*. **2011**, *133*, 12298–12303.
(308) Schill, G.; Schweickert, N.; Fritz, H.; Vetter, W. [2]-[Cyclohexatetraoctane][cyclooctacosane]catenane, the First Hydrocarbon Catenane. *Angew. Chem., Int. Ed. Engl*. **1983**, *22*, 889–891.
(309) Ashton, P. R.; Philp, D.; Spencer, N.; Stoddart, J. F. A New Design Strategy for the Self-Assembly of Molecular Shuttles. *J. Chem. Soc., Chem. Commun*. **1992**, 1124–1128.
(310) Mohr, B.; Sauvage, J.-P.; Grubbs, R. H.; Weck, M. High-Yield Synthesis of [2]Catenanes by Intramolecular Ring-Closing Metathesis. *Angew. Chem., Int. Ed. Engl*. **1997**, *36*, 1308–1310.
(311) Kolchinski, A. G.; Alcock, N. W.; Roesner, R. A.; Busch, D. H. Molecular Riveting: High Yield Preparation of a [3]-Rotaxane. *Chem. Commun.* **1998**, 1437–1438.
(312) Miljanić, O. Š.; Stoddart, J. F. Dynamic Donor-Acceptor [2]Catenanes. *Proc. Natl. Acad. Sci. U.S.A*. **2007**, *104*, 12966–12970.
(313) Yamamoto, M.; Takeuchi, M.; Shinkai, S. Oligosaccharide Binding to a Boronic-Acid-Appended Phenanthroline-Cu(I) Complex Which Creates Superstructural Helicates and Catenates. *Tetrahedron* **2002**, *58*, 7251–7258.
(314) Lu, T.; Zhang, L.; Gokel, G. W.; Kaifer, A. E. The First Surface-Attached Catenane: Self-Assembly of a Two-Component Monolayer. *J. Am. Chem. Soc*. **1993**, *115*, 2542–2543.
(315) Rowan, S. J.; Stoddart, J. F. Thermodynamic Synthesis of Rotaxanes by Imine Exchange. *Org. Lett*. **1999**, *1*, 1913–1916.
(316) Ko, Y. H.; Kim, K.; Kang, J.-K.; Chun, H.; Lee, J. W.; Sakamoto, S.; Yamaguchi, K.; Fettinger, J. C.; Kim, K. Designed Self-Assembly of Molecular Necklaces Using Host-Stabilized Charge-Transfer Interactions. *J. Am. Chem. Soc*. **2004**, *126*, 1932–1933.
(317) Dasgupta, S.; Wu, J. Template-Directed Synthesis of Kinetically and Thermodynamically Stable Molecular Necklace Using Ring Closing Metathesis. *Org. Biomol. Chem*. **2011**, *9*, 3504–3515.
(318) Frey, J.; Kraus, T.; Heitz, V.; Sauvage, J.-P. Synthesis of a Bis-Macrocycle Containing Two Back-to-Back Rigidly Connected 1,10-Phenanthroline Units as a Central Core and Its Incorporation in a Handcuff-Like Catenane. *Chem. Eur. J*. **2007**, *13*, 7584–7594.
(319) Henkelis, J. J.; Ronson, T. K.; Harding, L. P.; Hardie, M. J. M_3L_2 Metallo-Cryptophanes: [2]Catenane and Simple Cages. *Chem. Commun*. **2011**, *47*, 6560–6562.
(320) Rapenne, G.; Dietrich-Buchecker, C.; Sauvage, J.-P. Copper(I)- or Iron(II)-Templated Synthesis of Molecular Knots Containing Two Tetrahedral or Octahedral Coordination Sites. *J. Am. Chem. Soc*. **1999**, *121*, 994–1001.
(321) Dietrich-Buchecker, C.; Rapenne, G.; Sauvage, J.-P. Synthesis of Catenanes and Molecular Knots by Copper(I)-Directed Formation of the Precursors Followed by Ruthenium(II)-Catalyzed Ring-Closing Metathesis. *Coord. Chem. Rev*. **1999**, *185-186*, 167–176.
(322) Guo, J.; Mayers, P. C.; Breault, G. A.; Hunter, C. A. Synthesis of a Molecular Trefoil Knot by Folding and Closing on an Octahedral Coordination Template. *Nature Chem*. **2010**, *2*, 218–222.
(323) Ayme, J.-F.; Gil-Ramírez, G.; Leigh, D. A.; Lemonnier, J.-F.; Markevicius, A.; Muryn, C. A.; Zhang, G. Lanthanide Template Synthesis of a Molecular Trefoil Knot. *J. Am. Chem. Soc*. **2014**, *136*, 13142–13145.
(324) Dietrich-Buchecker, C.; Sauvage, J.-P. Lithium Templated Synthesis of Catenanes: Efficient Synthesis of Doubly Interlocked [2]-Catenanes. *Chem. Commun.* **1999**, 615–616.
(325) Pentecost, C. D.; Chichak, K. S.; Peters, A. J.; Cave, G. W. V.; Cantrill, S. J.; Stoddart, J. F. A Molecular Solomon Link. *Angew. Chem., Int. Ed*. **2007**, *46*, 218–222.
(326) Peinador, C.; Blanco, V.; Quintela, J. M. A New Doubly Interlocked [2]Catenane. *J. Am. Chem. Soc*. **2009**, *131*, 920–921.
(327) Chichak, K. S.; Cantrill, S. J.; Stoddart, J. F. Dynamic Nanoscale Borromean Links. *Chem. Commun.* **2005**, 3391–3393.
(328) Meyer, C. D.; Forgan, R. S.; Chichak, K. S.; Peters, A. J.; Tangchaivang, N.; Cave, G. W. V.; Khan, S. I.; Cantrill, S. J.; Stoddart, J. F. The Dynamic Chemistry of Molecular Borromean Rings and Solomon Knots. *Chem. Eur. J*. **2010**, *16*, 12570–12581.
(329) Evans, N. H.; Beer, P. D. A Janus [2]Rotaxane Synthesized by Using an Anion-Templated Clipping Methodology. *Chem. Eur. J*. **2011**, *17*, 10542–10546.
(330) Bozdemir, O. A.; Barin, G.; Belowich, M. E.; Basuray, A. N.; Beuerle, F.; Stoddart, J. F. Dynamic Covalent Templated-Synthesis of [c2]Daisy Chains. *Chem. Commun*. **2012**, *48*, 10401–10403.
(331) Badjić, J. D.; Cantrill, S. J.; Grubbs, R. H.; Guidry, E. N.; Orenes, R.; Stoddart, J. F. The Exclusivity of Multivalency in Dynamic Covalent Processes. *Angew. Chem., Int. Ed*. **2004**, *43*, 3273–3278.
(332) Saito, S.; Takahashi, E.; Nakazono, K. Synthesis of [2]Rotaxanes by the Catalytic Reactions of a Macrocyclic Copper Complex. *Org. Lett*. **2006**, *8*, 5133–5136.
(333) Aucagne, V.; Hänni, K. D.; Leigh, D. A.; Lusby, P. J.; Walker, D. Catalytic "Click" Rotaxanes: A Substoichiometric Metal-Template Pathway to Mechanically Interlocked Architectures. *J. Am. Chem. Soc*. **2006**, *128*, 2186–2187.
(334) Crowley, J. D.; Goldup, S. M.; Lee, A.-L.; Leigh, D. A.; McBurney, R. T. Active Metal Template Synthesis of Rotaxanes, Catenanes and Molecular Shuttles. *Chem. Soc. Rev*. **2009**, *38*, 1530–1541.
(335) Berná, J.; Goldup, S. M.; Lee, A.-L.; Leigh, D. A.; Symes, M. D.; Teobaldi, G.; Zerbetto, F. Cadiot-Chodkiewicz Active Template Synthesis of Rotaxanes and Switchable Molecular Shuttles with Weak Intercomponent Interactions. *Angew. Chem., Int. Ed*. **2008**, *47*, 4392–4396.
(336) Berná, J.; Crowley, J. D.; Goldup, S. M.; Hänni, K. D.; Lee, A.-L.; Leigh, D. A. A Catalytic Palladium Active-Metal Template

Pathway to [2]Rotaxanes. *Angew. Chem., Int. Ed*. **2007**, *46*, 5709–5713.
(337) Crowley, J. D.; Goldup, S. M.; Gowans, N. D.; Leigh, D. A.; Ronaldson, V. E.; Slawin, A. M. Z. An Unusual Nickel-Copper-Mediated Alkyne Homocoupling Reaction for the Active-Template Synthesis of [2]Rotaxanes. *J. Am. Chem. Soc*. **2010**, *132*, 6243–6248.
(338) Goldup, S. M.; Leigh, D. A.; McBurney, R. T.; McGonigal, P. R.; Plant, A. Ligand-Assisted Nickel-Catalysed sp^3–sp^3 Homocoupling of Unactivated Alkyl Bromides and Its Application to the Active Template Synthesis of Rotaxanes. *Chem. Sci*. **2010**, *1*, 383–386.
(339) Crowley, J. D.; Hänni, K. D.; Lee, A.-L.; Leigh, D. A. [2]Rotaxanes Through Palladium Active-Template Oxidative Heck Cross-Couplings. *J. Am. Chem. Soc*. **2007**, *129*, 12092–12093.
(340) Goldup, S. M.; Leigh, D. A.; Lusby, P. J.; McBurney, R. T.; Slawin, A. M. Z. Active Template Synthesis of Rotaxanes and Molecular Shuttles with Switchable Dynamics by Four-Component Pd^{II}-Promoted Michael Additions. *Angew. Chem., Int. Ed*. **2008**, *47*, 3381–3384.
(341) Crowley, J. D.; Hänni, K. D.; Leigh, D. A.; Slawin, A. M. Z. Diels-Alder Active-Template Synthesis of Rotaxanes and Metal-Ion-Switchable Molecular Shuttles. *J. Am. Chem. Soc*. **2010**, *132*, 5309–5314.
(342) Hoekman, S.; Kitching, M. O.; Leigh, D. A.; Papmeyer, M.; Roke, D. Goldberg Active Template Synthesis of a [2]Rotaxane Ligand for Asymmetric Transition-Metal Catalysis. *J. Am. Chem. Soc*. **2015**, *137*, 7656–7659.
(343) Whitesides, G. M.; Ismagilov, R. F. Complexity in Chemistry. *Science* **1999**, *284*, 89–92.
(344) Whitesides, G. M. Reinventing Chemistry. *Angew. Chem., Int. Ed*. **2015**, *54*, 3196–3209.
(345) Balazs, A. C.; Epstein, I. R. Emergent or Just Complex? *Science* **2009**, *325*, 1632–1633.
(346) Gibb, B. C. The Emergence of Emergence. *Nature Chem*. **2011**, *3*, 3–4.
(347) Taylor, E. An Explication of Emergence. *Philos. Stud*. **2015**, *172*, 653–669.
(348) Stoddart, J. F. A Platform for Change. *Supramol. Chem*. **2015**, *27*, 567–570.
(349) Lorenz, E. N. *The Essence of Chaos*; University of Washington Press: Seattle, **1995**.
(350) Corbett, P. T.; Leclaire, J.; Vial, L.; West, K. R.; Wietor, J.-L.; Sanders, J. K. M.; Otto, S. Dynamic Combinatorial Chemistry. *Chem. Rev*. **2006**, *106*, 3652–3711.
(351) Lam, R. T. S.; Belenguer, A.; Roberts, S. L.; Naumann, C.; Jarrosson, T.; Otto, S.; Sanders, J. K. M. Amplification of Acetylcholine-Binding Catenanes From Dynamic Combinatorial Libraries. *Science* **2005**, *308*, 667–669.
(352) Prakasam, T.; Lusi, M.; Elhabiri, M.; Platas-Iglesias, C.; Olsen, J.-C.; Asfari, Z.; Cianférani-Sanglier, S.; Debaene, F.; Charbonnière, L. J.; Trabolsi, A. Simultaneous Self-Assembly of a [2]Catenane, a Trefoil Knot, and a Solomon Link From a Simple Pair of Ligands. *Angew. Chem., Int. Ed*. **2013**, *52*, 9956–9960.
(353) Olson, M. A.; Coskun, A.; Fang, L.; Basuray, A. N.; Stoddart, J. F. Polycatenation under Thermodynamic Control. *Angew. Chem., Int. Ed*. **2010**, *49*, 3151–3156.
(354) Astumian, R. D. Thermodynamics and Kinetics of a Brownian Motor. *Science* **1997**, *276*, 917–922.
(355) Astumian, R. D.; Hänggi, P. Brownian Motors. *Phys. Today* **2002**, *55*, 33–39.
(356) Murakami, H.; Kawabuchi, A.; Kotoo, K.; Kunitake, M.; Nakashima, N. A Light-Driven Molecular Shuttle Based on a Rotaxane. *J. Am. Chem. Soc*. **1997**, *119*, 7605–7606.
(357) Mock, W. L.; Pierpont, J. A Cucurbituril-Based Molecular Switch. *J. Chem. Soc., Chem. Commun.* **1990**, 1509–1511.
(358) Dietrich-Buchecker, C. O.; Sauvage, J.-P.; Kern, J.-M. Templated Synthesis of Interlocked Macrocyclic Ligands: The Catenands. *J. Am. Chem. Soc*. **1984**, *106*, 3043–3045.
(359) Lin, C.-F.; Lai, C.-C.; Liu, Y.-H.; Peng, S.-M.; Chiu, S.-H. Use of Anions to Allow Translational Isomerism of a [2]Rotaxane. *Chem. Eur. J*. **2007**, *13*, 4350–4355.
(360) Ashton, P. R.; Blower, M. A.; Philp, D.; Spencer, N.; Stoddart, J. F.; Tolley, M. S.; Ballardini, R.; Ciano, M.; Balzani, V.; Gandolfi, M. T.; Prodi, L.; McLean, C. H. The Control of Translational Isomerism in Catenated Structures. *New J. Chem*. **1993**, *17*, 689–695.
(361) Leigh, D. A.; Pérez, E. M. Shuttling Through Reversible Covalent Chemistry. *Chem. Commun.* **2004**, 2262–2263.
(362) Martinez-Cuezva, A.; Berná, J.; Orenes, R.-A.; Pastor, A.; Alajarín, M. Small-Molecule Recognition for Controlling Molecular Motion in Hydrogen-Bond-Assembled Rotaxanes. *Angew. Chem., Int. Ed*. **2014**, *53*, 6762–6767.
(363) Asakawa, M.; Ashton, P. R.; Dehaen, W.; L'abbé, G.; Menzer, S.; Nouwen, J.; Raymo, F. M.; Stoddart, J. F.; Tolley, M. S.; Toppet, S.; White, A. J. P.; Williams, D. J. Molecular Meccano 19. Self-Assembly of Novel [2]Catenanes and [2]Pseudorotaxanes Incorporating Thiacrown Ethers or Their Acyclic Analogs. *Chem. Eur. J*. **1997**, *3*, 772–787.
(364) Sørensen, A.; Andersen, S. S.; Flood, A. H.; Jeppesen, J. O. Pressure Effects in the Synthesis of Isomeric Rotaxanes. *Chem. Commun*. **2013**, *49*, 5936–5938.
(365) Shigekawa, H.; Miyake, K.; Sumaoka, J.; Harada, A.; Komiyama, M. The Molecular Abacus: STM Manipulation of Cyclodextrin Necklace. *J. Am. Chem. Soc*. **2000**, *122*, 5411–5412.
(366) Hernandez, J. V.; Kay, E. R.; Leigh, D. A. A Reversible Synthetic Rotary Molecular Motor. *Science* **2004**, *306*, 1532–1537.
(367) Arduini, A.; Bussolati, R.; Credi, A.; Monaco, S.; Secchi, A.; Silvi, S.; Venturi, M. Solvent- and Light-Controlled Unidirectional Transit of a Nonsymmetric Molecular Axle Through a Nonsymmetric Molecular Wheel. *Chem. Eur. J*. **2012**, *18*, 16203–16213.
(368) Li, H.; Cheng, C.; McGonigal, P. R.; Fahrenbach, A. C.; Frasconi, M.; Liu, W.-G.; Zhu, Z.; Zhao, Y.; Ke, C.; Lei, J.; Young, R. Y.; Dyar, S. M.; Co, D. T.; Yang, Y.-W.; Botros, Y. Y.; Goddard, W. A. III; Wasielewski, M. R.; Astumian, R. D.; Stoddart, J. F. Relative Unidirectional Translation in an Artificial Molecular Assembly Fueled by Light. *J. Am. Chem. Soc*. **2013**, *135*, 18609–18620.
(369) Ragazzon, G.; Baroncini, M.; Silvi, S.; Venturi, M.; Credi, A. Light-Powered Autonomous and Directional Molecular Motion of a Dissipative Self-Assembling System. *Nature Nanotechnol*. **2015**, *10*, 70–75.
(370) Chatterjee, M. N.; Kay, E. R.; Leigh, D. A. Beyond Switches: Ratcheting a Particle Energetically Uphill with a Compartmentalized Molecular Machine. *J. Am. Chem. Soc*. **2006**, *128*, 4058–4073.
(371) Serreli, V.; Lee, C.-F.; Kay, E. R.; Leigh, D. A. A Molecular Information Ratchet. *Nature* **2007**, *445*, 523–527.
(372) Alvarez-Pérez, M.; Goldup, S. M.; Leigh, D. A.; Slawin, A. M. Z. A Chemically-Driven Molecular Information Ratchet. *J. Am. Chem. Soc*. **2008**, *130*, 1836–1838.
(373) Carlone, A.; Goldup, S. M.; Lebrasseur, N.; Leigh, D. A.; Wilson, A. A Three-Compartment Chemically-Driven Molecular Information Ratchet. *J. Am. Chem. Soc*. **2012**, *134*, 8321–8323.
(374) Cheng, C.; McGonigal, P. R.; Liu, W.-G.; Li, H.; Vermeulen, N. A.; Ke, C.; Frasconi, M.; Stern, C. L.; Goddard, W. A., III; Stoddart, J. F. Energetically Demanding Transport in a Supramolecular Assembly. *J. Am. Chem. Soc*. **2014**, *136*, 14702–14705.
(375) Cheng, C.; McGonigal, P. R.; Schneebeli, S. T.; Li, H.; Vermeulen, N. A.; Ke, C.; Stoddart, J. F. An Artificial Molecular Pump. *Nature Nanotechnol*. **2015**, *10*, 547–553.
(376) Sevick, E. Nanomachines: A Light-Driven Molecular Pump. *Nature Nanotechnol*. **2015**, *10*, 18–19.
(377) Balzani, V.; Gómez-López, M.; Stoddart, J. F. Molecular Machines. *Acc. Chem. Res*. **1998**, *31*, 405–414.

(378) Sauvage, J.-P. Transition Metal-Containing Rotaxanes and Catenanes in Motion: Toward Molecular Machines and Motors. *Acc. Chem. Res*. **1998**, *31*, 611–619.

(379) Balzani, V.; Credi, A.; Raymo, F. M.; Stoddart, J. F. Artificial Molecular Machines. *Angew. Chem., Int. Ed*. **2000**, *39*, 3348–3391.

(380) Dietrich-Buchecker, C.; Jimenez-Molero, M. C.; Sartor, V.; Sauvage, J.-P. Rotaxanes and Catenanes as Prototypes of Molecular Machines and Motors. *Pure Appl. Chem*. **2003**, *75*, 1383–1393.

(381) Balzani, V.; Venturi, M.; Credi, A. *Molecular Devices and Machines: A Journey Into the Nanoworld*; 2nd ed.; Wiley-VCH: Weinheim, **2008**.

(382) Flood, A. H.; Ramirez, R. J. A.; Deng, W.-Q.; Muller, R. P.; Goddard, W. A., III; Stoddart, J. F. Meccano on the Nanoscale - A Blueprint for Making Some of the World's Tiniest Machines. *Aust. J. Chem*. **2004**, *57*, 301–322.

(383) Collin, J.-P.; Heitz, V.; Sauvage, J.-P. Transition-Metal-Complexed Catenanes and Rotaxanes in Motion: Towards Molecular Machines. *Top. Curr. Chem*. **2005**, *262*, 29–62.

(384) Balzani, V.; Credi, A.; Silvi, S.; Venturi, M. Artificial Nanomachines Based on Interlocked Molecular Species: Recent Advances. *Chem. Soc. Rev*. **2006**, *35*, 1135–1149.

(385) Credi, A. Artificial Nanomachines Based on Interlocked Molecules. *J. Phys.: Condens. Matter* **2006**, *18*, S1779–S1795.

(386) Kay, E. R.; Leigh, D. A.; Zerbetto, F. Synthetic Molecular Motors and Mechanical Machines. *Angew. Chem., Int. Ed*. **2007**, *46*, 72–191.

(387) Kay, E. R.; Leigh, D. A. Beyond Switches: Rotaxane- and Catenane-Based Synthetic Molecular Motors. *Pure Appl. Chem*. **2008**, *80*, 17–29.

(388) Fahrenbach, A. C.; Bruns, C. J.; Cao, D.; Stoddart, J. F. Ground-State Thermodynamics of Bistable Redox-Active Donor–Acceptor Mechanically Interlocked Molecules. *Acc. Chem. Res*. **2012**, *45*, 1581–1592.

(389) Yang, W.; Li, Y.; Liu, H.; Chi, L.; Li, Y. Design and Assembly of Rotaxane-Based Molecular Switches and Machines. *Small* **2012**, *8*, 504–516.

(390) Neal, E. A.; Goldup, S. M. Chemical Consequences of Mechanical Bonding in Catenanes and Rotaxanes: Isomerism, Modification, Catalysis and Molecular Machines for Synthesis. *Chem. Commun*. **2014**, *50*, 5128–5142.

(391) Fahrenbach, A. C.; Bruns, C. J.; Li, H.; Trabolsi, A.; Coskun, A.; Stoddart, J. F. Ground-State Kinetics of Bistable Redox-Active Donor–Acceptor Mechanically Interlocked Molecules. *Acc. Chem. Res*. **2014**, *47*, 482–493.

(392) Coskun, A.; Banaszak, M.; Astumian, R. D.; Stoddart, J. F.; Grzybowski, B. A. Great Expectations: Can Artificial Molecular Machines Deliver on Their Promise? *Chem. Soc. Rev*. **2012**, *41*, 19–30.

(393) Abendroth, J. M.; Bushuyev, O. S.; Weiss, P. S.; Barrett, C. J. Controlling Motion at the Nanoscale: Rise of the Molecular Machines. *ACS Nano* **2015**, *9*, 7746–7768.

(394) Cheng, C.; McGonigal, P. R.; Stoddart, J. F.; Astumian, R. D. Design and Synthesis of Nonequilibrium Systems. *ACS Nano* **2015**, *9*, 8672–8688.

(395) Kay, E. R.; Leigh, D. A. Rise of the Molecular Machines. *Angew. Chem., Int. Ed*. **2015**, *54*, 10080–10088.

(396) Erbas-Cakmak, S.; Leigh, D. A.; McTernan, C. T.; Nussbaumer, A. L. Artificial Molecular Machines. *Chem. Rev*. **2015**, *115*, 10081–10206.

(397) Browne, W. R.; Feringa, B. L. Making Molecular Machines Work. *Nature Nanotechnol*. **2006**, *1*, 25–35.

(398) Stoddart, J. F. Thither Supramolecular Chemistry? *Nature Chem*. **2009**, *1*, 14–15.

(399) Deng, H.; Olson, M. A.; Stoddart, J. F.; Yaghi, O. M. Robust Dynamics. *Nature Chem*. **2010**, *2*, 439–443.

(400) Boyle, M. M.; Smaldone, R. A.; Whalley, A. C.; Ambrogio, M. W.; Botros, Y. Y.; Stoddart, J. F. Mechanised Materials. *Chem. Sci*. **2011**, *2*, 204–210.

(401) Brough, B.; Northrop, B. H.; Schmidt, J. J.; Tseng, H.-R.; Houk, K. N.; Stoddart, J. F.; Ho, C.-M. Evaluation of Synthetic Linear Motor-Molecule Actuation Energetics. *Proc. Natl. Acad. Sci. U.S.A*. **2006**, *103*, 8583–8588.

(402) Lussis, P.; Svaldo-Lanero, T.; Bertocco, A.; Fustin, C.-A.; Leigh, D. A.; Duwez, A.-S. A Single Synthetic Small Molecule That Generates Force Against a Load. *Nature Nanotechnol*. **2011**, *6*, 553–557.

(403) Huang, T. J.; Brough, B.; Ho, C.-M.; Liu, Y.; Flood, A. H.; Bonvallet, P. A.; Tseng, H.-R.; Stoddart, J. F.; Baller, M.; Magonov, S. A Nanomechanical Device Based on Linear Molecular Motors. *Appl. Phys. Lett*. **2004**, *85*, 5391–5393.

(404) Liu, Y.; Flood, A. H.; Bonvallet, P. A.; Vignon, S. A.; Northrop, B. H.; Tseng, H.-R.; Jeppesen, J. O.; Huang, T. J.; Brough, B.; Baller, M.; Magonov, S.; Solares, S. D.; Goddard, W. A. III; Ho, C.-M.; Stoddart, J. F. Linear Artificial Molecular Muscles. *J. Am. Chem. Soc*. **2005**, *127*, 9745–9759.

(405) Juluri, B. K.; Kumar, A. S.; Liu, Y.; Ye, T.; Yang, Y.-W.; Flood, A. H.; Fang, L.; Stoddart, J. F.; Weiss, P. S.; Huang, T. J. A Mechanical Actuator Driven Electrochemically by Artificial Molecular Muscles. *ACS Nano* **2009**, *3*, 291–300.

(406) Du, G.; Moulin, E.; Jouault, N.; Buhler, E.; Giuseppone, N. Muscle-Like Supramolecular Polymers: Integrated Motion From Thousands of Molecular Machines. *Angew. Chem., Int. Ed*. **2012**, *51*, 12504–12508.

(407) Goujon, A.; Du, G.; Moulin, E.; Fuks, G.; Maaloum, M.; Buhler, E.; Giuseppone, N. Hierarchical Self-Assembly of Supramolecular Muscle-Like Fibers. *Angew. Chem., Int. Ed*. **2016**, *55*, 703–707.

(408) Berná, J.; Leigh, D. A.; Lubomska, M.; Mendoza, S. M.; Pérez, E. M.; Rudolf, P.; Teobaldi, G.; Zerbetto, F. Macroscopic Transport by Synthetic Molecular Machines. *Nature Mater*. **2005**, *4*, 704–710.

(409) Collier, C. P.; Wong, E. W.; Behloradský, M.; Raymo, F. M.; Stoddart, J. F.; Kuekes, P. J.; Williams, R. S.; Heath, J. R. Electronically Configurable Molecular-Based Logic Gates. *Science* **1999**, *285*, 391–394.

(410) Wong, E. W.; Collier, C. P.; Behloradský, M.; Raymo, F. M.; Stoddart, J. F.; Heath, J. R. Fabrication and Transport Properties of Single-Molecule-Thick Electrochemical Junctions. *J. Am. Chem. Soc*. **2000**, *122*, 5831–5840.

(411) Collier, C. P.; Mattersteig, G.; Wong, E. W.; Luo, Y.; Beverly, K.; Sampaio, J.; Raymo, F. M.; Stoddart, J. F.; Heath, J. R. A [2]Catenane-Based Solid State Electronically Reconfigurable Switch. *Science* **2000**, *289*, 1172–1175.

(412) Collier, C. P.; Jeppesen, J. O.; Luo, Y.; Perkins, J.; Wong, E. W.; Heath, J. R.; Stoddart, J. F. Molecular-Based Electronically Switchable Tunnel Junction Devices. *J. Am. Chem. Soc*. **2001**, *123*, 12632–12641.

(413) Luo, Y.; Collier, C. P.; Jeppesen, J. O.; Nielsen, K. A.; DeIonno, E.; Ho, G.; Perkins, J.; Tseng, H.-R.; Yamamoto, T.; Stoddart, J. F.; Heath, J. R. Two-Dimensional Molecular Electronics Circuits. *ChemPhysChem* **2002**, *3*, 519–525.

(414) DeIonno, E.; Tseng, H.-R.; Harvey, D. D.; Stoddart, J. F.; Heath, J. R. Infrared Spectroscopic Characterization of [2]Rotaxane Molecular Switch Tunnel Junction Devices. *J. Phys. Chem. B* **2006**, *110*, 7609–7612.

(415) Choi, J. W.; Flood, A. H.; Steuerman, D. W.; Nygaard, S.; Braunschweig, A. B.; Moonen, N. N. P.; Laursen, B. W.; Luo, Y.; DeIonno, E.; Peters, A. J.; Jeppesen, J. O.; Xu, K.; Stoddart, J. F.; Heath, J. R. Ground-State Equilibrium Thermodynamics and Switching Kinetics of Bistable [2]Rotaxanes Switched in Solution, Polymer Gels, and Molecular Electronic Devices. *Chem. Eur. J*. **2006**, *12*, 261–279.

(416) Green, J. E.; Choi, J. W.; Boukai, A.; Bunimovich, Y.; Johnston-Halperin, E.; DeIonno, E.; Luo, Y.; Sheriff, B. A.; Xu, K.; Shin, Y. S.; Tseng, H.-R.; Stoddart, J. F.; Heath, J. R. A 160-Kilobit Molecular Electronic Memory Patterned at 10^{11} Bits Per Square Centimetre. *Nature* **2007**, *445*, 414–417.

(417) Semiconductor Industry Association. The International Technology Roadmap for Semiconductors: Process Integration, Devices, and Structures. SIA, Washington D.C., **2005**. http://www.itrs2.net/itrs-reports.html. (Accessed 24 May 2016).
(418) Cotí, K. K.; Belowich, M. E.; Liong, M.; Ambrogio, M. W.; Lau, Y. A.; Khatib, H. A.; Zink, J. I.; Khashab, N. M.; Stoddart, J. F. Mechanised Nanoparticles for Drug Delivery. *Nanoscale* **2009**, *1*, 16–39.
(419) Ambrogio, M. W.; Thomas, C. R.; Zhao, Y.-L.; Zink, J. I.; Stoddart, J. F. Mechanized Silica Nanoparticles: A New Frontier in Theranostic Nanomedicine. *Acc. Chem. Res*. **2011**, *44*, 903–913.
(420) Li, Z.; Barnes, J. C.; Bosoy, A.; Stoddart, J. F.; Zink, J. I. Mesoporous Silica Nanoparticles in Biomedical Applications. *Chem. Soc. Rev*. **2012**, *41*, 2590–2605.
(421) Klichko, Y.; Liong, M.; Choi, E.; Angelos, S.; Nel, A. E.; Stoddart, J. F.; Tamanoi, F.; Zink, J. I. Mesostructured Silica for Optical Functionality, Nanomachines, and Drug Delivery. *J. Am. Ceram. Soc*. **2009**, *92*, S2–S10.
(422) Angelos, S.; Johansson, E.; Stoddart, J. F.; Zink, J. I. Mesostructured Silica Supports for Functional Materials and Molecular Machines. *Adv. Funct. Mater*. **2007**, *17*, 2261–2271.
(423) Liong, M.; Angelos, S.; Choi, E.; Patel, K.; Stoddart, J. F.; Zink, J. I. Mesostructured Multifunctional Nanoparticles for Imaging and Drug Delivery. *J. Mater. Chem*. **2009**, *19*, 6251–6257.
(424) Angelos, S.; Yang, Y.-W.; Patel, K.; Stoddart, J. F.; Zink, J. I. pH-Responsive Supramolecular Nanovalves Based on Cucurbit[6]uril Pseudorotaxanes. *Angew. Chem., Int. Ed*. **2008**, *47*, 2222–2226.
(425) Angelos, S.; Khashab, N. M.; Yang, Y.-W.; Trabolsi, A.; Khatib, H. A.; Stoddart, J. F.; Zink, J. I. pH Clock-Operated Mechanized Nanoparticles. *J. Am. Chem. Soc.* **2009**, *131*, 12912–12914.
(426) Du, L.; Liao, S.; Khatib, H. A.; Stoddart, J. F.; Zink, J. I. Controlled-Access Hollow Mechanized Silica Nanocontainers. *J. Am. Chem. Soc*. **2009**, *131*, 15136–15142.
(427) Khashab, N. M.; Belowich, M. E.; Trabolsi, A.; Friedman, D. C.; Valente, C.; Lau, Y.; Khatib, H. A.; Zink, J. I.; Stoddart, J. F. pH-Responsive Mechanised Nanoparticles Gated by Semirotaxanes. *Chem. Commun*. **2009**, 5371–5373.
(428) Park, C.; Oh, K.; Lee, S. C.; Kim, C. Controlled Release of Guest Molecules From Mesoporous Silica Particles Based on a pH-Responsive Polypseudorotaxane Motif. *Angew. Chem., Int. Ed*. **2007**, *46*, 1455–1457.
(429) Meng, H.; Xue, M.; Xia, T.; Zhao, Y.-L.; Tamanoi, F.; Stoddart, J. F.; Zink, J. I.; Nel, A. E. Autonomous in Vitro Anticancer Drug Release From Mesoporous Silica Nanoparticles by pH-Sensitive Nanovalves. *J. Am. Chem. Soc*. **2010**, *132*, 12690–12697.
(430) Wang, C.; Li, Z.; Cao, D.; Zhao, Y.-L.; Gaines, J. W.; Bozdemir, O. A.; Ambrogio, M. W.; Frasconi, M.; Botros, Y. Y.; Zink, J. I.; Stoddart, J. F. Stimulated Release of Size-Selected Cargos in Succession From Mesoporous Silica Nanoparticles. *Angew. Chem., Int. Ed*. **2012**, *51*, 5460–5465.
(431) Xue, M.; Cao, D.; Stoddart, J. F.; Zink, J. I. Size-Selective pH-Operated Megagates on Mesoporous Silica Materials. *Nanoscale* **2012**, *4*, 7569–7574.
(432) Chen, T.; Yang, N.; Fu, J. Controlled Release of Cargo Molecules From Hollow Mesoporous Silica Nanoparticles Based on Acid and Base Dual-Responsive Cucurbit[7]uril Pseudorotaxanes. *Chem. Commun*. **2013**, *49*, 6555–6557.
(433) Fu, J.; Chen, T.; Wang, M.; Yang, N.; Li, S.; Wang, Y.; Liu, X. Acid and Alkaline Dual Stimuli-Responsive Mechanized Hollow Mesoporous Silica Nanoparticles as Smart Nanocontainers for Intelligent Anticorrosion Coatings. *ACS Nano* **2013**, *7*, 11397–11408.
(434) Wang, M.; Chen, T.; Ding, C.; Fu, J. Mechanized Silica Nanoparticles Based on Reversible Bistable [2]Pseudorotaxanes as Supramolecular Nanovalves for Multistage pH-Controlled Release. *Chem. Commun*. **2014**, *50*, 5068–5071.
(435) Hernandez, R.; Tseng, H.-R.; Wong, J. W.; Stoddart, J. F.; Zink, J. I. An Operational Supramolecular Nanovalve. *J. Am. Chem. Soc*. **2004**, *126*, 3370–3371.
(436) Ferris, D. P.; Zhao, Y.-L.; Khashab, N. M.; Khatib, H.; Stoddart, J. F.; Zink, J. I. Light-Operated Mechanized Nanoparticles. *J. Am. Chem. Soc*. **2009**, *131*, 1686–1688.
(437) Park, C.; Lee, K.; Kim, C. Photoresponsive Cyclodextrin-Covered Nanocontainers and Their Sol-Gel Transition Induced by Molecular Recognition. *Angew. Chem., Int. Ed*. **2009**, *48*, 1275–1278.
(438) Yan, H.; Teh, C.; Sreejith, S.; Zhu, L.; Kwok, A.; Fang, W.; Ma, X.; Nguyen, K. T.; Korzh, V.; Zhao, Y. Functional Mesoporous Silica Nanoparticles for Photothermal-Controlled Drug Delivery In Vivo. *Angew. Chem., Int. Ed*. **2012**, *51*, 8373–8377.
(439) Sun, Y.-L.; Yang, B.-J.; Zhang, S. X.-A.; Yang, Y.-W. Cucurbit[7]uril Pseudorotaxane-Based Photoresponsive Supramolecular Nanovalve. *Chem. Eur. J*. **2012**, *18*, 9212–9216.
(440) Tarn, D.; Ferris, D. P.; Barnes, J. C.; Ambrogio, M. W.; Stoddart, J. F.; Zink, J. I. A Reversible Light-Operated Nanovalve on Mesoporous Silica Nanoparticles. *Nanoscale* **2014**, *6*, 3335–3343.
(441) Li, M.; Yan, H.; Teh, C.; Korzh, V.; Zhao, Y. NIR-Triggered Drug Release From Switchable Rotaxane-Functionalized Silica-Covered Au Nanorods. *Chem. Commun*. **2014**, *50*, 9745–9748.
(442) Wang, W.; Wen, Y.; Xu, L.; Du, H.; Zhou, Y.; Zhang, X. A Selective Release System Based on Dual-Drug-Loaded Mesoporous Silica for Nanoparticle-Assisted Combination Therapy. *Chem. Eur. J*. **2014**, *20*, 7796–7802.
(443) Nguyen, T. D.; Tseng, H.-R.; Celestre, P. C.; Flood, A. H.; Liu, Y.; Stoddart, J. F.; Zink, J. I. A Reversible Molecular Valve. *Proc. Natl. Acad. Sci. U.S.A*. **2005**, *102*, 10029–10034.
(444) Khashab, N. M.; Trabolsi, A.; Lau, Y. A.; Ambrogio, M. W.; Friedman, D. C.; Khatib, H. A.; Zink, J. I.; Stoddart, J. F. Redox- and pH-Controlled Mechanized Nanoparticles. *Eur. J. Org. Chem.* **2009**, 1669–1673.
(445) Luo, Z.; Ding, X.; Hu, Y.; Wu, S.; Xiang, Y.; Zeng, Y.; Zhang, B.; Yan, H.; Zhang, H.; Zhu, L.; Liu, J.; Li, J.; Cai, K.; Zhao, Y. Engineering a Hollow Nanocontainer Platform with Multifunctional Molecular Machines for Tumor-Targeted Therapy *in Vitro* and *in Vivo*. *ACS Nano* **2013**, *7*, 10271–10284.
(446) Gayam, S. R.; Wu, S.-P. Redox Responsive Pd(II) Templated Rotaxane Nanovalve Capped Mesoporous Silica Nanoparticles: A Folic Acid Mediated Biocompatible Cancer-Targeted Drug Delivery System. *J. Mater. Chem. B* **2014**, *2*, 7009–7016.
(447) Nguyen, T. D.; Leung, K. C.-F.; Liong, M.; Pentecost, C. D.; Stoddart, J. F.; Zink, J. I. Construction of a pH-Driven Supramolecular Nanovalve. *Org. Lett*. **2006**, *8*, 3363–3366.
(448) Thomas, C. R.; Ferris, D. P.; Lee, J.-H.; Choi, E.; Cho, M. H.; Kim, E. S.; Stoddart, J. F.; Shin, J.-S.; Cheon, J.; Zink, J. I. Noninvasive Remote-Controlled Release of Drug Molecules in Vitro Using Magnetic Actuation of Mechanized Nanoparticles. *J. Am. Chem. Soc*. **2010**, *132*, 10623–10625.
(449) Patel, K.; Angelos, S.; Dichtel, W. R.; Coskun, A.; Yang, Y.-W.; Zink, J. I.; Stoddart, J. F. Enzyme-Responsive Snap-Top Covered Silica Nanocontainers. *J. Am. Chem. Soc*. **2008**, *130*, 2382–2383.
(450) Liu, J.; Du, X.; Zhang, X. Enzyme-Inspired Controlled Release of Cucurbit[7]uril Nanovalves by Using Magnetic Mesoporous Silica. *Chem. Eur. J*. **2011**, *17*, 810–815.
(451) Ambrogio, M. W.; Pecorelli, T. A.; Patel, K.; Khashab, N. M.; Trabolsi, A.; Khatib, H. A.; Botros, Y. Y.; Zink, J. I.; Stoddart, J. F. Snap-Top Nanocarriers. *Org. Lett*. **2010**, *12*, 3304–3307.

(452) Liu, J.; Du, X. pH- and Competitor-Driven Nanovalves of Cucurbit[7]uril Pseudorotaxanes Based on Mesoporous Silica Supports for Controlled Release. *J. Mater. Chem*. **2010**, *20*, 3642–3649.

(453) Raju, M. V. R.; Lin, H.-C. A Cyanide-Responsive Supramolecular Nanovalve Based on Pd(II)-Templated Pseudo-Rotaxane. *J. Mater. Chem. A* **2015**, *3*, 6414–6422.

(454) Lewandowski, B.; De Bo, G.; Ward, J. W.; Papmeyer, M.; Kuschel, S.; Aldegunde, M. J.; Gramlich, P. M. E.; Heckmann, D.; Goldup, S. M.; D'Souza, D. M.; Fernandes, A. E.; Leigh, D. A. Sequence-Specific Peptide Synthesis by an Artificial Small-Molecule Machine. *Science* **2013**, *339*, 189–193.

(455) Dawson, P. E.; Muir, T. W.; Clark-Lewis, I.; Kent, S. B. Synthesis of Proteins by Native Chemical Ligation. *Science* **1994**, *266*, 776–779.

(456) Wilson, C. M.; Gualandi, A.; Cozzi, P. G. A Rotaxane Turing Machine for Peptides. *ChemBioChem* **2013**, *14*, 1185–1187.

(457) Bertran-Vicente, J.; Hackenberger, C. P. R. A Supramolecular Peptide Synthesizer. *Angew. Chem., Int. Ed*. **2013**, *52*, 6140–6142.

(458) McGonigal, P. R.; Stoddart, J. F. Interlocked Molecules: A Molecular Production Line. *Nature Chem*. **2013**, *5*, 260–262.

(459) Darwin, C. R. *On the Origin of Species by Means of Natural Selection, or the Preservation of Favoured Races in the Struggle for Life*; John Murray: London, **1859**.

(460) Piguet, C.; Bernardinelli, G.; Williams, A. F.; Bocquet, B. Formation of the First Isomeric [2]Catenates by Self-Assembly About Two Different Metal Ions. *Angew. Chem., Int. Ed*. **1995**, *34*, 582–584.

(461) Harrison, I. T. The Effect of Ring Size on Threading Reactions of Macrocycles. *J. Chem. Soc., Chem. Commun.* **1972**, 231–232.

(462) Han, D.; Pal, S.; Liu, Y.; Yan, H. Folding and Cutting DNA Into Reconfigurable Topological Nanostructures. *Nature Nanotechnol*. **2010**, *5*, 712–717.

(463) Lüttringhaus, A.; Isele, G. Synthesis of a Catena Compound by the Semistatistical Principle. *Angew. Chem., Int. Ed. Engl*. **1967**, *6*, 956–957.

(464) Ünsal, Ö.; Godt, A. Synthesis of a [2] Catenane with Functionalities and 87-Membered Rings. *Chem. Eur. J*. **1999**, *5*, 1728–1733.

(465) Hiratani, K.; Suga, J.-I.; Nagawa, Y.; Houjou, H.; Tokuhisa, H.; Numata, M.; Watanabe, K. A New Synthetic Method for Rotaxanes via Tandem Claisen Rearrangement, Diesterification, and Aminolysis. *Tetrahedron Lett*. **2002**, *43*, 5747–5750.

(466) Kawai, H.; Umehara, T.; Fujiwara, K.; Tsuji, T.; Suzuki, T. Dynamic Covalently Bonded Rotaxanes Cross-Linked by Imine Bonds Between the Axle and Ring: Inverse Temperature Dependence of Subunit Mobility. *Angew. Chem., Int. Ed*. **2006**, *45*, 4281–4286.

(467) Ke, C.; Smaldone, R. A.; Kikuchi, T.; Li, H.; Davis, A. P.; Stoddart, J. F. Quantitative Emergence of Hetero[4]rotaxanes by Template-Directed Click Chemistry. *Angew. Chem., Int. Ed*. **2012**, *52*, 381–387.

(468) Richey, H. G., Jr; Kushlan, D. M. Interactions of a Diarylmagnesium Compound with Cryptands and Crown Ethers: Formation of Ar_3Mg^-, $ArMg(cryptand)^+$, and Threaded Ar_2Mg(crown ether). *J. Am. Chem. Soc*. **1987**, *109*, 2510–2512.

(469) Gruter, G.-J. M.; de Kanter, F. J. J.; Markies, P. R.; Nomoto, T.; Akkerman, O. S.; Bickelhaupt, F. Formation of the First Organometallic Catenane. *J. Am. Chem. Soc*. **1993**, *115*, 12179–12180.

(470) Mingos, D. M. P.; Yau, J.; Menzer, S.; Williams, D. J. A Gold(I) [2]Catenane. *Angew. Chem., Int. Ed. Engl*. **1995**, *34*, 1894–1895.

(471) Castro, S. L.; Just, O.; Rees, W. S., Jr. A Quadruply Stranded, Alkaline Earth Metal Containing Helical Catenate: A Charge-Neutral Heterotopic Homodinuclear [2] Catenane. *Angew. Chem., Int. Ed*. **2000**, *39*, 933–935.

(472) Hunter, C. A.; Low, C. M. R.; Packer, M. J.; Spey, S. E.; Vinter, J. G.; Vysotsky, M. O.; Zonta, C. Noncovalent Assembly of [2]Rotaxane Architectures. *Angew. Chem., Int. Ed*. **2001**, *40*, 2678–2682.

(473) Blight, B. A.; Wisner, J. A.; Jennings, M. C. Synthesis of a [2]Rotaxane Through First- and Second-Sphere Coordination. *Chem. Commun.* **2006**, 4593–4595.

(474) Sauvage, J.-P.; Ward, M. A Bis(rerpyridine)ruthenium(II) Catenate. *Inorg. Chem*. **1991**, *30*, 3869–3874.

(475) Livoreil, A.; Dietrich-Buchecker, C. O.; Sauvage, J.-P. Electrochemically Triggered Swinging of a [2]-Catenate. *J. Am. Chem. Soc*. **1994**, *116*, 9399–9400.

(476) Hamann, C.; Kern, J.-M.; Sauvage, J.-P. Palladium(II)-Directed Formation of Pseudo-Rotaxanes: The 3 + 1 Approach to Threaded Species Using Square-Planar Geometries. *Dalton Trans.* **2003**, 3770–3775.

(477) Fuller, A.-M.; Leigh, D. A.; Lusby, P. J.; Oswald, I. D. H.; Parsons, S.; Walker, D. B. A 3D Interlocked Structure From a 2D Template: Structural Requirements for the Assembly of a Square-Planar Metal-Coordinated [2]Rotaxane. *Angew. Chem., Int. Ed*. **2004**, *43*, 3914–3918.

(478) Goldup, S. M.; Leigh, D. A.; Lusby, P. J.; McBurney, R. T.; Slawin, A. M. Z. Gold(I)-Template Catenane and Rotaxane Synthesis. *Angew. Chem., Int. Ed*. **2008**, *47*, 6999–7003.

(479) Chas, M.; Blanco, V.; Peinador, C.; Quintela, J. M. Synthesis of [3]Catenanes Based on Metal-Directed Self-Assembly and π-Donor/π-Acceptor Interactions. *Org. Lett*. **2007**, *9*, 675–678.

(480) Li, S.; Liu, M.; Zhang, J.; Zheng, B.; Zhang, C.; Wen, X.; Li, N.; Huang, F. High-Yield Preparation of [2]Rotaxanes Based on the Bis(*m*-phenylene)-32-crown-10-Based Cryptand/Paraquat Derivative Recognition Motif. *Org. Biomol. Chem*. **2008**, *6*, 2103.

(481) Zhu, K.; Vukotic, V. N.; Loeb, S. J. Molecular Shuttling of a Compact and Rigid H-Shaped [2]Rotaxane. *Angew. Chem., Int. Ed*. **2012**, *51*, 2168–2172.

(482) Barnes, J. C.; Juríček, M.; Strutt, N. L.; Frasconi, M.; Sampath, S.; Giesener, M. A.; McGrier, P. L.; Bruns, C. J.; Stern, C. L.; Sarjeant, A. A.; Stoddart, J. F. ExBox: A Polycyclic Aromatic Hydrocarbon Scavenger. *J. Am. Chem. Soc*. **2013**, *135*, 183–192.

(483) Vögtle, F.; Meier, S.; Hoss, R. One-Step Synthesis of a Fourfold Functionalized Catenane. *Angew. Chem., Int. Ed. Engl*. **1992**, *31*, 1619–1622.

(484) Ashton, P. R.; Campbell, P. J.; Chrystal, E. J. T.; Glink, P. T.; Menzer, S.; Philp, D.; Spencer, N.; Stoddart, J. F.; Tasker, P. A.; Williams, D. J. Dialkylammonium Ion/Crown Ether Complexes: The Forerunners of a New Family of Interlocked Molecules. *Angew. Chem., Int. Ed. Engl*. **1995**, *34*, 1865–1869.

(485) Yoon, I.; Narita, M.; Shimizu, T.; Asakawa, M. Threading-Followed-by-Shrinking Protocol for the Synthesis of a [2]Rotaxane Incorporating a Pd(II)–Salophen Moiety. *J. Am. Chem. Soc*. **2004**, *126*, 16740–16741.

(486) Arunkumar, E.; Forbes, C. C.; Noll, B. C.; Smith, B. D. Squaraine-Derived Rotaxanes: Sterically Protected Fluorescent Near-IR Dyes. *J. Am. Chem. Soc*. **2005**, *127*, 3288–3289.

(487) Cheng, P.-N.; Hung, W.-C.; Chiu, S.-H. A New Macrocycle That Forms Pseudorotaxane-Like Complexes with Dibenzylammonium Ions. *Tetrahedron Lett*. **2005**, *46*, 4239–4242.

(488) Chiu, C.-W.; Lai, C.-C.; Chiu, S.-H. "Threading-Followed-by-Swelling": A New Protocol for Rotaxane Synthesis. *J. Am. Chem. Soc*. **2007**, *129*, 3500–3501.

(489) Gong, H.-Y.; Rambo, B. M.; Karnas, E.; Lynch, V. M.; Sessler, J. L. A "Texas-Sized" Molecular Box That Forms an Anion-Induced Supramolecular Necklace. *Nature Chem*. **2010**, *2*, 406–409.

(490) Serpell, C. J.; Kilah, N. L.; Costa, P. J.; Félix, V.; Beer, P. D. Halogen Bond Anion Templated Assembly of an Imidazolium

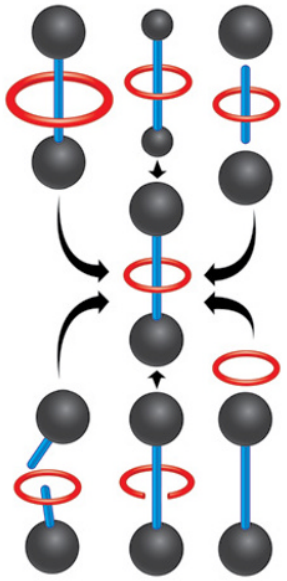
Pseudorotaxane. *Angew. Chem., Int. Ed*. **2010**, *49*, 5322–5326.
(491) Kaiser, G.; Jarrosson, T.; Otto, S.; Ng, Y.-F.; Bond, A. D.; Sanders, J. K. M. Lithium-Templated Synthesis of a Donor-Acceptor Pseudorotaxane and Catenane. *Angew. Chem., Int. Ed*. **2004**, *43*, 1959–1962.
(492) Tung, S.-T.; Lai, C.-C.; Liu, Y.-H.; Peng, S.-M.; Chiu, S.-H. Synthesis of a [2]Catenane From the Sodium Ion Templated Orthogonal Arrangement of Two Diethylene Glycol Chains. *Angew. Chem., Int. Ed*. **2013**, *52*, 13269–13272.
(493) Knighton, R. C.; Beer, P. D. Axle Component Separated Ion-Pair Recognition by a Neutral Heteroditopic [2]Rotaxane. *Chem. Commun*. **2014**, *50*, 1540–1542.
(494) Chen, J.; Seeman, N. C. Synthesis From DNA of a Molecule with the Connectivity of a Cube. *Nature* **1991**, *350*, 631–633.
(495) Ryan, K.; Kool, E. T. Triplex-Directed Self-Assembly of an Artificial Sliding Clamp on Duplex DNA. *Chem. Biol*. **1998**, *5*, 59–67.
(496) Yan, L. Z.; Dawson, P. E. Design and Synthesis of a Protein Catenane. *Angew. Chem., Int. Ed*. **2001**, *40*, 3625–3627.
(497) Sánchez-Quesada, J.; Saghatelian, A.; Cheley, S.; Bayley, H.; Ghadiri, M. R. Single DNA Rotaxanes of a Transmembrane Pore Protein. *Angew. Chem., Int. Ed*. **2004**, *43*, 3063–3067.
(498) Kumar, R.; El-Sagheer, A.; Tumpane, J.; Lincoln, P.; Wilhelmsson, L. M.; Brown, T. Template-Directed Oligonucleotide Strand Ligation, Covalent Intramolecular DNA Circularization and Catenation Using Click Chemistry. *J. Am. Chem. Soc*. **2007**, *129*, 6859–6864.
(499) Liu, Y.; Kuzuya, A.; Sha, R.; Guillaume, J.; Wang, R.; Canary, J. W.; Seeman, N. C. Coupling Across a DNA Helical Turn Yields a Hybrid DNA/Organic Catenane Doubly Tailed with Functional Termini. *J. Am. Chem. Soc*. **2008**, *130*, 10882–10883.
(500) Ackermann, D.; Schmidt, T. L.; Hannam, J. S.; Purohit, C. S.; Heckel, A.; Famulok, M. A Double-Stranded DNA Rotaxane. *Nature Nanotechnol*. **2010**, *5*, 436–442.
(501) Trabolsi, A.; Khashab, N.; Fahrenbach, A. C.; Friedman, D. C.; Colvin, M. T.; Cotí, K. K.; Benítez, D.; Tkatchouk, E.; Olsen, J.-C.; Belowich, M. E.; Carmielli, R.; Khatib, H. A.; Goddard, W. A. III; Wasielewski, M. R.; Stoddart, J. F. Radically Enhanced Molecular Recognition. *Nature Chem*. **2010**, *2*, 42–49.
(502) Barnes, J. C.; Fahrenbach, A. C.; Cao, D.; Dyar, S. M.; Frasconi, M.; Giesener, M. A.; Benitez, D.; Tkatchouk, E.; Chernyashevskyy, O.; Shin, W. H.; Li, H.; Sampath, S.; Stern, C. L.; Sarjeant, A. A.; Hartlieb, K. J.; Liu, Z.; Carmieli, R.; Botros, Y. Y.; Choi, J. W.; Slawin, A. M. Z.; Ketterson, J. B.; Wasielewski, M. R.; Goddard, W. A. III; Stoddart, J. F. A Radically Configurable Six-State Compound. *Science* **2013**, *339*, 429–433.

Part 2

Making Mechanical Bonds

Chapter 2 The Fundamentals of Making Mechanical Bonds

Conspectus



The advent of the mechanical bond has played a major role in orchestrating the dramatic growth in *unnatural product synthesis* during the past quarter of a century. Inventing strategies to make *mechanically interlocked molecules* (MIMs), such as rotaxanes and catenanes, has sparked the fertile imaginations, instigated the flow of creative juices, and challenged the practical ingenuity of synthetic chemists across the length and breadth of the discipline, uniting disparate factions in its wake. From strategizing to implementing synthetic protocols, making mechanical bonds relies heavily on synthetic chemists having, not only a command of the nature of the chemical bond in all its intricate manifestations, but also a fundamental knowledge and in-depth appreciation of molecular recognition as it is expressed at the levels of coordinative, noncovalent and electrostatic bonding. In essence, the mechanical bond has led to the redefining of chemical synthesis in its broadest sense.

While rotaxanes and catenanes are molecules, a common precursor is often a *pseudorotaxane*, that is essentially a complex in which, for example, a large-ring molecule, containing at least 20 atoms, and generally considerably more, is penetrated by a threadlike molecule. In the beginning, *rotaxanes* were obtained from pseudorotaxanes by a *threading-followed-by-stoppering* strategy or from a preformed dumbbell-shaped molecule by a *ring-clipping* approach. Subsequently, other approaches involving *slippage* of a *ring* onto a *dumbbell* or the *swelling* of *stoppers* or the *shrinking* of rings have been devised for the making of rotaxanes. Historically, the main focus was on the making of *catenanes* using a *threading-followed-by-clipping* strategy from preformed large-ring molecules. Subsequently, *ring-capture* and *dumbbell-capture* procedures have been invented to make catenanes and rotaxanes, respectively. The earliest of all approaches to the making of MIMs relied on (i) a *statistical threading* of rings by long linear molecules and (ii) a *directed synthesis* approach which relies on the formation of covalent bonds between rings and dumbbells that are cleaved subsequently following multiple (>20) reaction steps to afford component parts with little more than van der Waals interactions at best between the parts. The initial synthetic protocols, leading to the first generation of MIMs, were conducted under *kinetic control* for the most part and some were discovered serendipitously while others, such as the Möbius strip approach, await implementation.

In mechanostereochemistry, a template is an ion, a molecule or a radical that acts as a recognition platform for the assembly of another ion, molecule or radical such that both the original template and the assembled entity become the component parts of a MIM during transformations where ‘old’ molecules ‘disappear’ and ‘new’ molecules ‘appear.’ It was the rise of chemistry beyond the molecule—*supramolecular chemistry*—joining forces with *molecular recognition* and *templation* that transported MIMs from being esoteric curiosities to becoming one of the contemporary drivers of *molecular nanotechnology* and the nascent discipline of *chemical topology*. Aside from (i) the statistical threading and (ii) directed synthetic approaches, in addition to (iii) a much more recent and promising *active template* strategy for MIM production, by far the most successful methodology to date has been *template-directed synthesis*, which has evolved in a manner where usually one source of molecular recognition is dominant, yet never does that source act alone: more often it is in combination with other recognition motifs. A growing number of templates have lent their support to the making of MIMs, starting in the 1980s, while gaining momentum in the 1990s through into the 21st century. The frequency with which the range of templates have been used, as reflected by the number of reports relating to them in the literature, lends itself to the following identification of the top 10 recognition motifs—(i) *solvophobic/hydrophobic*, (ii) *hydrogen-bonding*, (iii) *donor-acceptor*, (iv) *metallo-organic*, (v) *biomolecular*, (vi) *macrocyclic (hetero)arenes*, (vii) *anionic*, (viii) *radical pair*, (ix) *ion-pair* and (x) *alkali-metal ion*. Hydrophobic templation is dominated by cyclodextrins, followed by cucurbiturils, while hydrogen-bonding comes with both neutral and charged variations. Donor-acceptor templates generally involve the stacking of aromatic rings, yet π–π interactions are usually foreshadowed energy-wise by the additional presence of stabilizing C–H···O hydrogen bonds. Metallo-organic templates, i.e., *linear*, *square*, *tetrahedral*, *trigonal bipyramidal* and *octahedral*, introduce rigidity and are ideal for defining geometries. A popular means of *covalent capture*, such as in the final steps of producing catenanes and rotaxanes in excellent yields with high atom efficiencies, is the use of the ubiquitous copper(I)-catalyzed azide-alkyne cycloaddition, an efficient type of "click" reaction. Employing this reaction, along with many other kinetically controlled reactions, has populated chemical laboratories with an enormously wide variety of MIMs, some of which can be easily rendered *bistable* so that, by appealing to acid-base or redox chemistry, *molecular switches* emerge as prototypes for the design and synthesis of *artificial molecular machines*. It could be argued that the mechanical bond has given unnatural product synthesis a new lease of life: much has been achieved in a short period of time, yet much remains to be accomplished by creative makers of molecules and materials.

The Nature of the Mechanical Bond: From Molecules to Machines, First Edition. Carson J. Bruns and J. Fraser Stoddart.
© 2017 John Wiley & Sons, Inc. Published 2017 by John Wiley & Sons, Inc.

Introduction **59**
2.1 Statistical Synthesis **62**
2.2 Directed Synthesis **65**
2.2.1 Covalent Templates 65
2.2.2 Covalent-Directed Capture 69
2.2.3 The Möbius Approach 71
2.3 Template-Directed Synthesis **73**
2.3.1 Solvophobic Forces 74
2.3.1.1 Cyclodextrins 74
2.3.1.2 Cucurbiturils 81
2.3.1.3 Cooperative Capture 85
2.3.1.4 Ionic Cyclophanes 87
2.3.1.5 Metallosupramolecular MIMs 88
2.3.2 Transition Metal Templates 88
2.3.2.1 Tetrahedral Templates 89
2.3.2.2 Trigonal Bipyramidal Templates 95
2.3.2.3 Octahedral Templates 96
2.3.2.4 Square Planar Templates 99
2.3.2.5 Linear Templates 101
2.3.3 π-Donor/π-Acceptor Templates 102
2.3.3.1 The Nature of Donor-Acceptor π–π Interactions 102
2.3.3.2 π-Donating Crown-10 Template Motifs 104
2.3.3.3 π-Donating Crown-8 Template Motifs 113
2.3.3.4 Bis-p-xylyl[26]crown-6 (BX26C6) 117
2.3.3.5 Crown/Cyclophane Hybrids 119
2.3.3.6 Porphyrinic π-Donating Hosts 119
2.3.3.7 Three-Dimensional π-Donor Motifs 120
2.3.3.8 The Little Blue Box: $CBPQT^{4+}$ 125
2.3.3.9 Other π-Accepting Molecular Boxes 131
2.3.4 Hydrogen-Bonded Templates 138
2.3.4.1 Tetralactam Hosts 139
2.3.4.2 Benzylic Amide Hosts 143
2.3.4.3 Cyclic Peptides 154
2.3.4.4 Bis-2,6-diamidopyridine/Barbiturate Templates 155
2.3.4.5 Tetraureido Calixarene Capsule Templates 156
2.3.4.6 Sec-Ammonium / Crown Ether Templates 157
2.3.5 Halogen-Bonded Templates 173
2.3.6 Anion-Binding Templates 174
2.3.6.1 Nucleophilic Rotaxane Capture 175
2.3.6.2 N–H···Anion Hydrogen-Bonded Templates 176
2.3.6.3 C–X···Halide Halogen-Bonded Templates 185
2.3.6.4 C–H···Anion Hydrogen-Bonded Templates 188
2.3.7 Ion-Pair Templates 191
2.3.7.1 Integrated Ion-Pair Templates 191
2.3.7.2 Separated Ion-Pair Templates 193
2.3.7.3 Traceless Ion-Pair Templates 194
2.3.8 Other Cationic Templates 195
2.3.8.1 Alkali Metals 195
2.3.8.2 Alkaline Earth Metals 198
2.3.8.3 Lanthanides 199
2.3.9 Macrocyclic Arenes and Heteroarenes 199
2.3.9.1 Calixarenes 200
2.3.9.2 Pillararenes 204
2.3.10 Radical-Pair Templates 207

2.3.11 Homophilic Templates 210
2.3.11.1 Aromatic Self-Aggregation 210
2.3.11.2 Lipophilic Self-Aggregation 210
2.3.11.3 Aurophilic Interactions 210
2.3.11.4 Crystallization-Induced Interlocking 210
2.3.12 Biomolecular Templates 211
2.3.12.1 Nucleic Acids with Mechanical Bonds 211
2.3.12.2 Proteins with Mechanical Bonds 217
2.4 Active Template Synthesis 218
2.4.1 Active Copper Templates 219
2.4.1.1 CuAAC Active Template Synthesis 219
2.4.1.2 Eglinton-Glaser-Hay Active Template Synthesis 222
2.4.1.3 Ullmann-Type Active Template Synthesis 222
2.4.1.4 Sonogashira-Type Active Template Synthesis 223
2.4.1.5 Cadiot-Chodkiewicz Active Template Synthesis 223
2.4.1.6 Goldberg Active Template Synthesis 224
2.4.1.7 Diels-Alder Active Template Synthesis 225
2.4.2 Active Zinc Templates 225
2.4.3 Active Palladium Templates 226
2.4.3.1 Michael Addition Active Template Synthesis 226
2.4.3.2 Oxidative Heck Active Template Synthesis 226
2.4.3.3 Active Palladium Alkyne Homocoupling 227
2.4.4 Active Nickel Templates 227
2.4.4.1 Active Nickel Alkyne Homocoupling 227
2.4.4.2 Active Nickel sp^3–sp^3 Homocoupling 228
Conclusions and Outlook 229
References 230

Introduction

Over 50 years passed between the first recorded discussion of the idea that molecules could be mechanically interlocked—which, according to Prelog, could be attributed[1] to Wilstätter at a seminar in Zürich sometime between 1906 and 1912—and the first known published suggestion of the same idea by Frisch[2] in 1953, in which the term 'mechanical bond' was coined. The 1950s were marked by failed attempts to create mechanically linked rings on the part of several groups,[3] including those of Lüttringhaus, Cramer, Kohler and Dietrich, Wasserman, and van Gulick, although only the attempt by Lüttringhaus[4] was published at the time. The first successful synthesis was claimed by Wasserman[5] in 1960. Shortly thereafter, Frisch and Wasserman[1] published a seminal article which pointed out that the sequence of atoms, their bond types, and the spatial arrangement of bonds around atoms are not sufficient by themselves to describe a molecular structure with a non-trivial *topology*. Topology is a field of mathematics concerned with the properties of space that are preserved under continuous deformation. With respect to molecular structure, topology is a characteristic that remains unchanged throughout any arbitrary distortion of a molecule—stretching, bending, and rotating of bonds—without allowing bonds to break or pass through one another. Thus, two compounds are topological isomers if they are identical in their constitution, yet different in their topology. A knotted ring, such as a trefoil knot, for example, is a topological isomer of the corresponding unknotted ring. Likewise, two non-interlocked rings are topologically isomeric with a [2]catenane comprising the same two rings. By introducing this further dimension into stereochemistry, Frisch and Wasserman[1] established the field[3,6–9] of chemical topology. A more detailed discussion of topology is undertaken in **Section 5.2.4**.

Frisch and Wasserman[1] also noted that a molecule comprising a ring interlocked with a dumbbell—later to become known[10] as a rotaxane—is topologically trivial because the ring can be separated from the dumbbell through continuous deformation—i.e., stretching the ring over the stoppers or compressing the stoppers through the ring—without breaking or crossing bonds. Although rotaxanes are topologically trivial, their covalently disconnected components may nevertheless be impossible to separate (in a practical sense) without breaking covalent bonds, and hence the component parts still share a mechanical bond. On the other hand, knots are rich in topological content, but are only mechanically entangled—i.e., they do not formally possess mechanical bonds because they lack distinguishable molecular component parts. Molecules with non-trivial topologies and molecules

with mechanical bonds can therefore be grouped (**Figure 2.1**) into two overlapping but non-identical categories. Chemical topology deals with molecular structures that withstand the formalisms of mathematical topology, whereas mechanostereochemistry[11] encompasses all molecules with mechanical bonds. Many topological structures such as Möbius strips and nets fall exclusively under the umbrella of chemical topology, whereas topologically trivial molecules with mechanical bonds such as rotaxanes are exclusively mechanostereochemical in nature. One can envision other types of mechanical bonds—for example, those found in braids and zippers—which may also enter the realm of mechanostereochemistry if they are realized in molecular form. Catenanes and other multicomponent links occupy the region of overlap where non-trivial topologies and mechanical bonds are both expressed.

Owing to the intimate connection between chemical topology and mechanostereochemistry, certain topologically rich molecules without mechanical bonds, such as knots and Möbius strips, cannot simply be ignored. Möbius strips are important, for example, in one of the general approaches (**Figure 2.2**) to catenane synthesis. Frisch and Wasserman[1] and van Gulick[12] both realized in the early 1960s that a molecule resembling a Möbius strip (**Section 2.2.3**) with two twists could be converted into a [2]catenane if it could be parted in the middle all along its length. The second and most common route to catenane synthesis is the 'clipping' protocol, which proceeds by cyclization of a threadlike molecule penetrating through the cavity of a ring. This type of host-guest complex resembling a rotaxane without stoppers has been defined[13] as a pseudorotaxane—the prefix *pseudo* indicates that the ring is free to dissociate from the axle and is therefore held chiefly by noncovalent bonds rather than mechanical bonds. A third strategy, which we call the 'ring capture' method, involves the trapping of a ring within another by virtue of one ring's ability to promote a coupling reaction within its cavity.

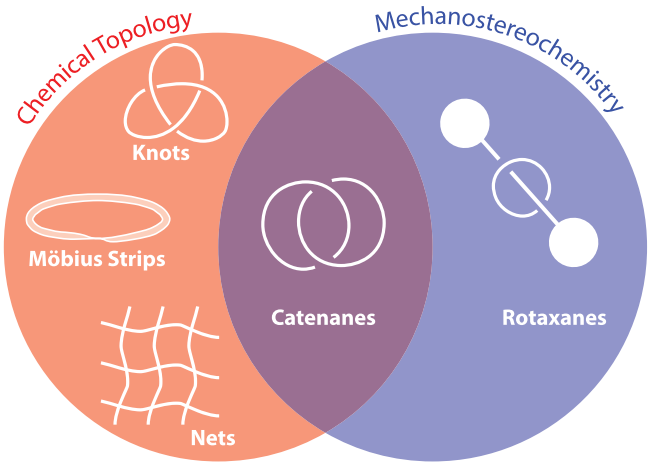


Figure 2.1 Venn diagram showing the relationship between chemical topology and mechanostereochemistry.

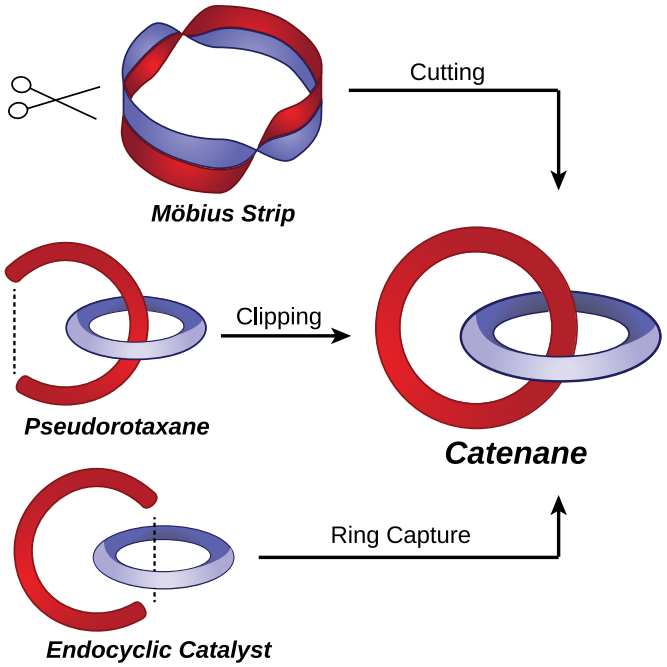


Figure 2.2 General strategies that can be employed in the formation of catenanes.

A wider set of strategies (**Figure 2.3**) are available for the formation of rotaxanes. Half of these strategies start from pseudorotaxane precursors, while the other half rely on other approaches. 'Stoppering', which involves attaching bulky groups to both ends of the axle of a pseudorotaxane in order to prevent the ring from deslipping, was the first[14] and remains the most commonly employed strategy. In a conceptually similar approach introduced by Chiu,[15,16] the 'dumbbell' component already has stoppers, but they are too small to prevent the ring from deslipping until a 'swelling' reaction increases their effective size. Alternatively, the same effect can be achieved by executing a 'shrinking' reaction that reduces the effective size of the ring's cavity—a strategy introduced by Asakawa.[17] The routes that do not proceed through pseudorotaxane precursors involve 'slippage', 'clipping', and 'dumbbell capture.' 'Slippage' is an approach introduced by Harrison[18] that relies on finely tuned size complementarity between the ring and stoppers, such that the ring can only bypass the stoppers when enough energy is applied—heat or pressure, for example—furnishing a kinetically stable rotaxane under ambient conditions. 'Clipping' utilizes the same principle as the clipping approach to catenane synthesis, except that an acyclic molecule is induced to cyclize around a dumbbell-shaped molecule instead of another ring. The dumbbell capture strategy in rotaxane synthesis is conceptually equivalent to the ring capture strategy in catenane synthesis, where two half-dumbbells are

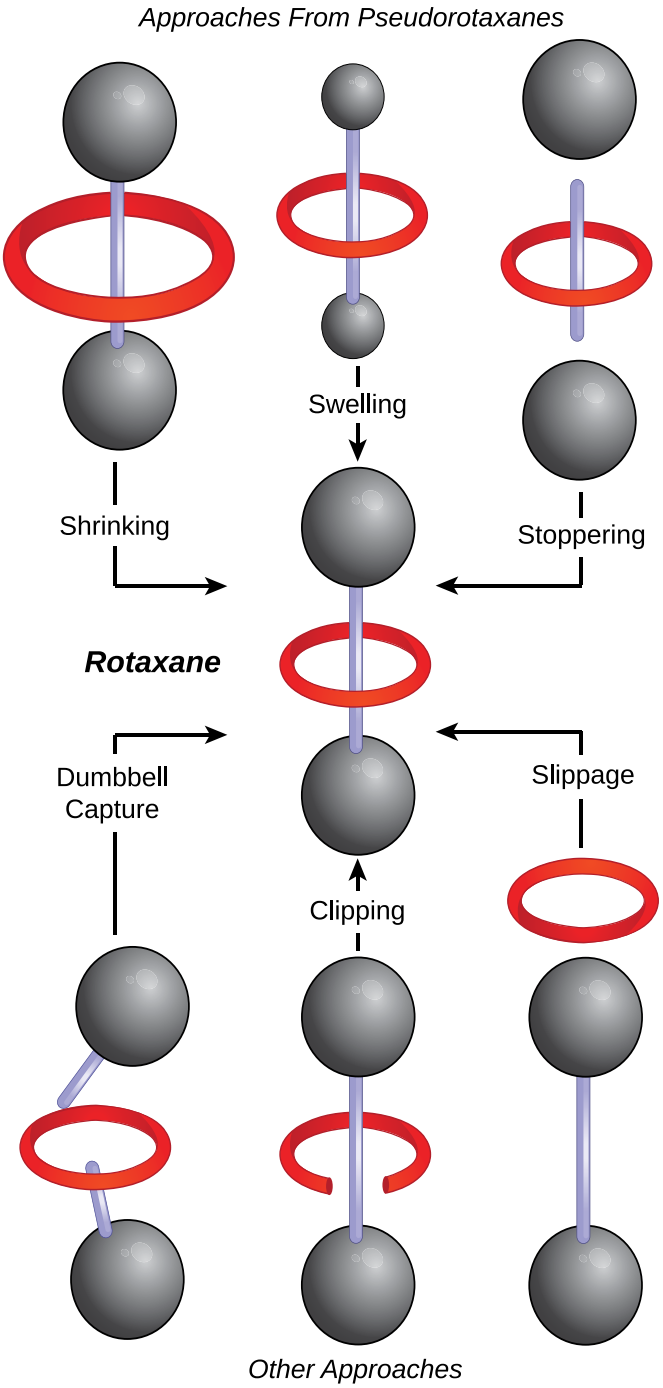


Figure 2.3 General strategies that can be employed in the formation of rotaxanes.

coupled within the cavity of a reaction-promoting ring. The earliest example of a capture strategy was reported by Mock.[19] Dumbbell capture and ring capture should not be mistaken for covalent capture,[20] a more general term used to describe the use of covalent bonds in the kinetic stabilization of noncovalent bonding interactions, i.e., the covalent linkage of components in any type of supramolecular species.

We can identify at least four types of general approaches (**Figure 2.4**) to the formation of mechanical bonds. The first synthetic MIMs were created[5] by statistical methods (**Section 2.1**) using no templates whatsoever. This strategy, which relies (**Figure 2.4a**) solely on the low statistical probability of cyclic and acyclic molecules occasionally becoming entangled in solution by random chance, is plagued by difficulty in the separation of products from starting materials and, inevitably, very low yields. These shortcomings were first addressed (**Figure 2.4b**) by pre-construction of mechanically interlocked components around a covalent template that could be cleaved subsequently, an approach (**Section 2.2**) known[21] as directed synthesis. Directed synthesis improves efficiencies but is still demanding because typically it requires numerous synthetic steps. Today the most widely used protocols (**Section 2.3**) fall under the umbrella of template-directed synthesis, in which noncovalent bonding interactions serve (**Figure 2.4c**) as templates instead of covalent bonds. Although the templated-directed synthesis (**Section 2.3**) of catenanes and rotaxanes most commonly employ clipping and stoppering reactions, the recent advent[22] of active template synthesis (**Section 2.4**) has made the ring capture and dumbbell capture strategies much more practical. Active template synthesis (**Figure 2.4d**) is a manifestation of these capture strategies that is mediated by an endocyclic

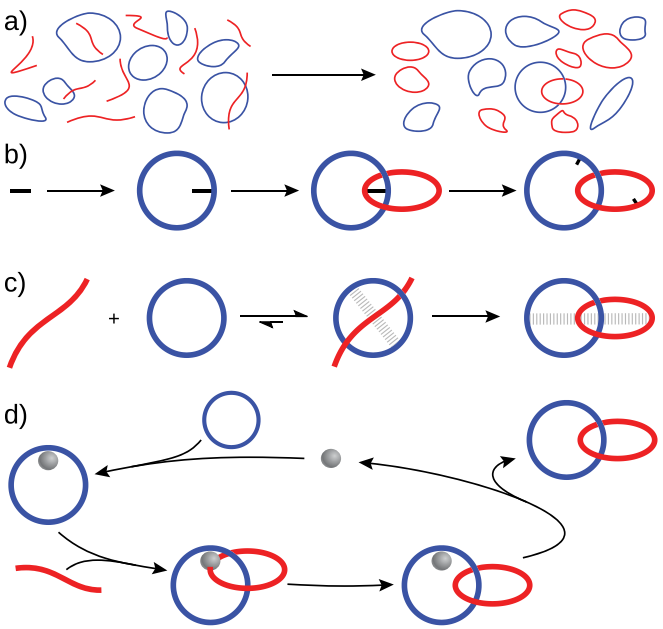


Figure 2.4 Four different ways of making mechanical bonds. (a) Statistical Synthesis. (b) Directed Synthesis (black line represents a covalent template). (c) Template-Directed Synthesis (hashed lines represent noncovalent bonding interactions). (d) Active Template Synthesis (grey ball represents a kinetically labile catalyst).

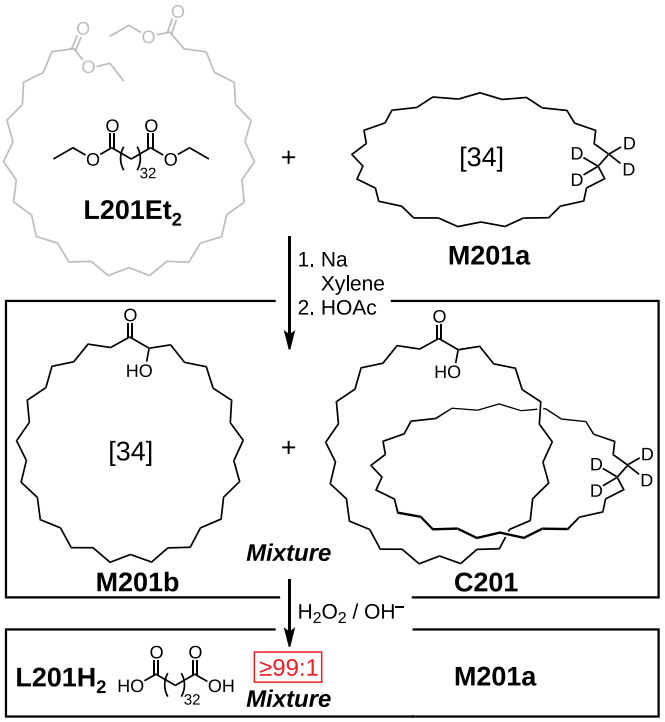
species—typically, a transition metal center—serving in the dual role of template and catalyst.

In the beginning, MIMs were produced using kinetically controlled reactions. The diversity of these reactions and their compatibilities, along with the various strategies and templation motifs, are vast. Although we have attempted to be as comprehensive as possible in our coverage of the types of kinetically controlled reactions that have been employed in the synthesis of mechanomolecules, we will be the first to admit that some of them may have been overlooked. For a review of thermodynamically controlled approaches to making mechanical bonds, see **Chapter 3**.

The strategies and molecular recognition processes involved in making mechanical bonds covered in **Chapters 2–3** are, in many ways, the foundation of mechanostereochemistry.[11] Many of the major milestones are depicted on the timeline in **Section 1.4**, **Figure 1.43**. Since it contains links to the content it describes, this timeline can also serve as a navigational map for most of **Chapters 2–3**.

2.1 Statistical Synthesis

The statistical approach to making mechanical bonds (**Figure 2.4a**) does not rely on any associative interactions[A] between components, but only on the (low) probability of having acyclic and cyclic molecules of sufficient size interpenetrate for fleeting moments as they tumble and dart around randomly in solution. The scalable synthesis of acyloin macrocycles with large enough cavities for interpenetration had been worked out in the 1940s by chemists such as Hansley[23] in the United States, as well as Prelog[24] in Switzerland and Stoll[25] in Germany. In actual fact, the first synthetic catenane had most likely been prepared statistically by these chemists long before Wasserman's seminal publication[5] in which he coined the term 'catenane' in 1960. The challenge at this time was one of detection on a very small analytical scale. Therefore Wasserman's achievement was, more accurately, providing evidence for the first time of the presence of a mechanically interlocked compound in admixture with macrocycles. His detection of the [2]catenane **C201** in a mixture is summarized in **Scheme 2.1**. Following acyloin condensation of diethyltetratriacontane (**L201Et$_2$**) in the presence of a deuterated 34-membered cycloalkane **M201a**, the cyclic acyloin product **M201b** was separated chromatographically from **M201a**. IR Spectroscopy indicated that carbon–deuterium

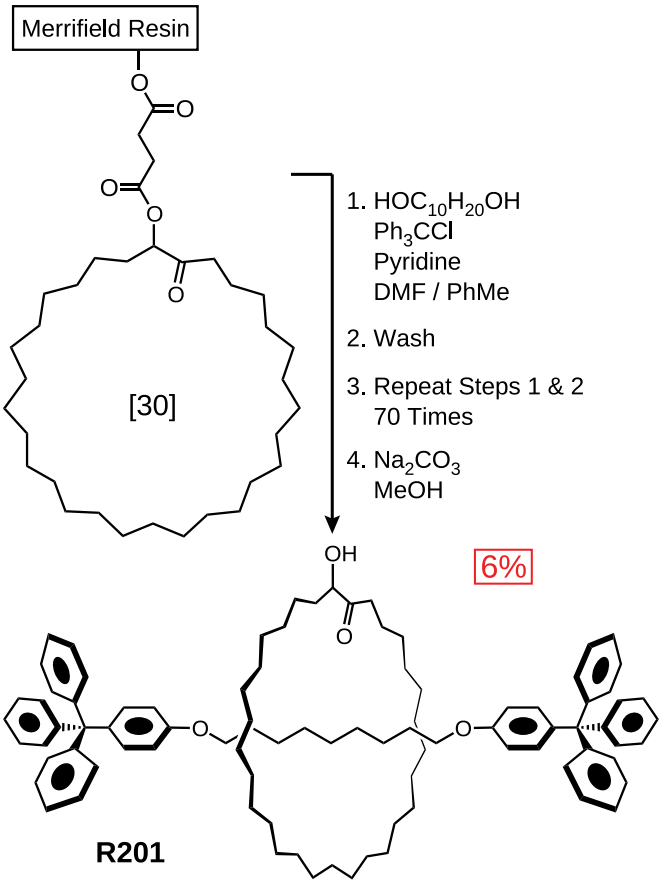


Scheme 2.1 Wasserman's 'synthesis' of the first [2]catenane[5] by statistical clipping of the diester **L201Et$_2$** with the deuterated cycloalkane **M201a** by acyloin condensation. Catenation was inferred by detecting the presence of the deuterated macrocycle **M201a** in admixture with the chromatographically isolated fraction of the product **M201b**, as well as in admixture with diacid **L201H$_2$** upon cleaving this fraction with alkaline H_2O_2. Ring sizes, given as a number of atoms, are denoted in square brackets. Wasserman reported[26] subsequently that several milligrams of **C201** were isolated as a pure compound in 0.0001% yield.

bonds were still present in the chromatographic fractions containing predominantly **M201b**, suggesting that some of them may have been catenated with **M201a**. Indeed, oxidative cleavage of this product afforded a small amount (≤1%) of the deuterated ring **M201a**, in addition to the expected diacid **L201H$_2$**, implying that catenane **C201** had been present as a minor species in the product mixture. Two years later, Wasserman reported[26] in *Scientific American* that a few milligrams of **C201** had been isolated chromatographically as a pure compound in 0.0001% yield.

Although the higher-yielding directed synthesis (**Section 2.2**) of catenanes also began to appear in the literature in the early 1960s, a number of researchers continued to develop and optimize the statistical synthesis of MIMs through into the 1980s, when template-directed synthesis (**Section 2.3**) began to revolutionize the field. One of the most important steps forward in statistical synthesis was made with the introduction of the first rotaxanes, which were prepared in 1967 independently by Ian and Shuyen Harrison[14] as well as by Schill and Zollenkopf.[27] The Harrisons' approach (**Scheme 2.2**) involved the immobilization of an acyloin macrocycle on a Merrifield resin as a

[A] One could argue that associative van der Waals interactions will exist between the components of any MIM, even although they may be very weak. The van der Waals interactions in a truly statistical synthesis are therefore non-directional and non-specific, i.e., equal in strength for entangled and non-entangled intermediates.

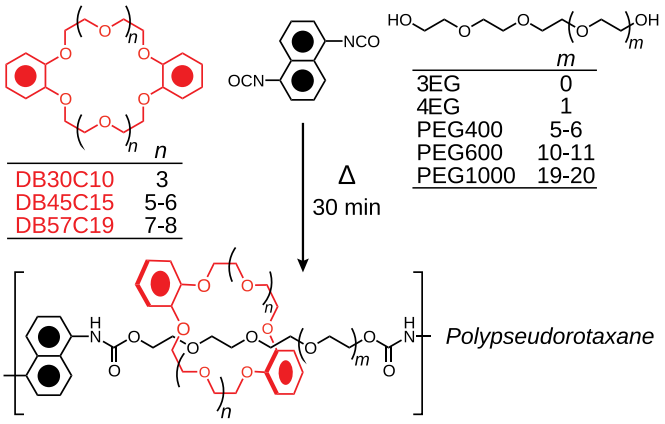


Scheme 2.2 The Harrisons' rotaxane synthesis on solid support.[14] The bracketed [30] denotes the number of atoms constituting the ring.

solid support in order to perform a statistical stoppering reaction between 1,10-decanediol and trityl chloride with 70 repetitions of the reaction. The [2]rotaxane **R201** was isolated in 6% yield after the release by hydrolysis from the resin, followed by column chromatography. Schill's first rotaxane was accessed[10,27] by the directed approach, involving a covalent template—see **Section 2.2**. Although the Harrisons proposed calling this type of compound a 'hooplane', Schill's suggestion[10] of the term 'rotaxane' ultimately prevailed, perhaps as a result of the visibility of his celebrated 1971 monograph published[28] under the title of *Catenanes, Rotaxanes, and Knots*. Later on, both Harrison[18,29] and Schill[30] improved rotaxane yields further through the use of thermodynamically controlled stoppering reactions—see **Chapter 3.6.1**.

Another significant advance in statistical synthesis was made in 1976 by Zilkha,[31] who conducted detailed investigations (**Table 2.1**) on the effects of molar ratios, ring size, chain length, dilution, and temperature on the extent of threading in polyether-based pseudorotaxanes. The study included three different sets of rings: (i) a monodisperse batch of dibenzo[30]crown-10 (DB30C10), and two polydisperse mixtures of crown ethers with mean formulas of

Table 2.1 Zilkha's statistical threading of polyether pseudorotaxanes[31]



Ring	Thread	*T* °C	[Ring] / [Thread]	Dilution Ratio[a]	Thread Rings[b] %
DB30C10[c]	3EG	120	1	0	2 ± 2
	4EG	120	1	0	9 ± 3
	PEG400	120	1	0	12 ± 8
	PEG600	120	0.4	0	15
			0.8		14
			1		11 ± 10
			1.6		11
	PEG1000	120	1	0	12 ± 8
DB45C15	3EG	120	1	0	30 ± 9
	4EG	120	1	0	22 ± 17
	PEG400	120	1	0	34 ± 14
	PEG600	120	0.5	0	60
			1		41 ± 18
			2		26
			4		11
	PEG1000	120	1	0	30 ± 13
DB57C19	3EG	120	1	0	10 ± 14
	4EG	120	1	0	32 ± 10
	PEG400	120	1	0	52 ± 13
	PEG600	120	0.4	0	50
			1		63 ± 11
			2		26
			4		19
		120	1	1	58 ± 10
				2	43 ± 17
				4	37 ± 17
				8	34 ± 5
				16	28 ± 9
		100	1	0	65 ± 19
		150	1	0	58 ± 15
		207	1	0	69 ± 20
	PEG1000	120	1	0	48 ± 10

[a]Dilution Ratio = $[C_2Cl_6]$/[Reactants]. 0 indicates a solvent-free reaction.
[b]Percentage of the total rings that encircle the polymer.
[c]Approximately one-third of the DB30C10 sample was benzo[15]crown-5.

(ii) dibenzo[44.1]crown-14.7 and (iii) dibenzo[58.2]crown-19.4. Here, we represent these polydisperse ring mixtures by their corresponding median ring constitutions of dibenzo[45]crown-15 (DB45C15), and dibenzo[57]crown-19 (DB57C19) for the sake of clarity. The poly(ethylene glycol) (PEG) thread lengths ranged from discrete triethylene glycol (3EG, n = 3) and tetraethylene glycol (4EG, n = 4) to compounds up to PEG1000 (average n = 22.3). These ring and thread components were mixed and heated under different experimental conditions and the PEG chains were subjected to further polymerization with naphthalene bis(isocyanate) to create high molecular weight polyurethane pseudorotaxanes. The percentage of rings that found their way onto the PEG polyurethanes was determined indirectly by adsorbing the product mixture onto silica gel and eluting the free macrocycles selectively with alcohol. The authors inferred that any ring not extracted from the silica had been threaded onto the polymer. The fraction of threaded rings reaches as high as ~70% in an equimolar mixture of PEG600 and DB57C19. Note that the average number of rings on the polypseudorotaxane itself is not reported in the Table. Although the ratio of threaded rings to starting rings decreases with an increasing excess of the rings, the number of rings on the polypseudorotaxane should always increase with a larger excess of rings. Indeed, the highest observed ring:thread molar ratio in the polypseudorotaxane was 0.76, a value which was obtained from the condition in which the DB57C19 ring was used in the largest excess—namely, 4 molar equivalents.

The general lessons that can be taken from Zilkha's study on statistical threading can be summarized as follows:

1. Large rings have a higher probability of becoming threaded than smaller ones. The implication for statistical rotaxane synthesis is that yields can be maximized by selecting the largest possible ring that is compatible with a given stopper. Just like threading the eye of a needle, the larger the eye, the easier it is to thread!

2. In general, long threads are better at collecting rings than short ones. The benefit of extending the thread length reaches a limit, however, since rings can only enter at the endpoints of a chain. Increasingly long polymers dilute the relative number of ring entry sites with respect to the volume of the reaction, causing the ring uptake to fall off for excessively long polymers.

3. Dilution of the reactants reduces the probability of threading. This rather intuitive point means that the statistical synthesis of rotaxanes should be carried out in neat mixtures or the minimum possible amount of solvent.

4. Temperature does not appear to affect the threading ratio significantly, provided that the reactants are in the liquid state.

Zilkha[31] also proposed a mathematical model to account for these effects and derived an equation (Eq. 2.1) which predicts the number of threadings (N) in a system of PEG chains and crown polyethers –

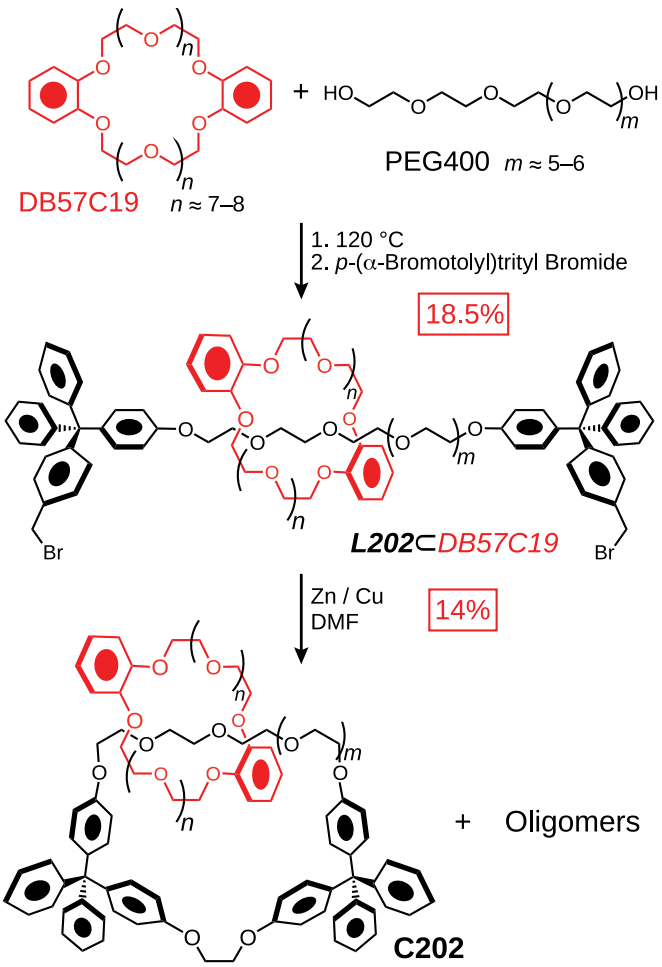
$$N = k\frac{m_e m_g\left(1 - e^{-n_e/n_g\pi}\right)n_e n_g{}^{\beta}\theta}{V} \qquad (2.1)$$

where k is a constant incorporating the values used to calculate (i) the volume of a sphere (the 'threading space' of a ring), (ii) the diameter of a PEG terminus, as well as (iii) a scalar accounting for incorrect thread orientations within the threading space, m_e and m_g are the moles of rings and chains, respectively, n_e and n_g are the average number of atoms in each ring and chain, respectively, β is a scaling factor ($1 < \beta < 2$) that accounts for two situations—(i) threaded rings inhibit the ability of a chain to adopt a random coil conformation, thus increasing its effective length, and (ii) threaded rings near the end of a chain hinder the inner rings' ability to dethread, θ is the 'threading angle', which is calculated based on molecular models and varies depending on ring size (θ = 0.92, 1.23, and 1.32 for DB30C10, DB45C15, and DB57C19, respectively), and V is the volume of the system. The observed threading number was in good agreement with those predicted from this model, indicating that the statistical threading of rings and threads can be rationalized rather well by the mathematical model.

Finally, Zilkha[31] used the insights from these studies to prepare a rotaxane with trityl stoppers by adding trityl chloride to a heated mixture of PEG400 and DB57C19. Although the authors provided circumstantial evidence for the isolation of a [2]rotaxane in 15% yield by this method using partition chromatography on silica gel, later work[32] on rotaxanes obtained by slippage (**Chapter 3.1**) indicates that the trityl stopper is far too small to trap a macrocycle as large as DB57C19 on a thread. Nevertheless, a bromomethyltrityl-functionalized pseudorotaxane ***L202⊂DB57C19*** has been utilized as a precursor for the synthesis (**Scheme 2.3**) of the [2]catenane **C202** in a subsequent publication.[33] **C202** was obtained in 14% yield by connecting the stoppers' bromomethyl groups together with a Zn/Cu couple. This approach to catenane synthesis has been called the "statistical double-stage method". Although the use of polydisperse components is not ideal for characterization purposes, Zilkha's work still managed (i) to reveal the important underlying principles of statistical synthesis, (ii) to push pseudorotaxane threading efficiency to the very limit, and (iii) to prepare a catenane with relatively high efficiency in a minimal number of steps.

Several attempts have been made to interlock even larger macromolecules by statistical approaches. Semlyen[34] attempted to prepare catenated polymers as early as 1994 by cyclizing linear polymer-supported polyesters in the presence of cyclic polyesters, and provided weak evidence of success on the basis of gel permeation chromatographic analysis. Hogen-Esch[35] has claimed to

synthesize a polystyrene-poly(2-vinylpyridine) hetero[2]-catenane copolymer by cyclizing a poly(2-vinylpyridine) thread in the presence of high concentrations of macrocyclic polystyrene. The catenated copolymer was isolated (0.5% yield) by precipitation-extraction procedures and characterized by size exclusion chromatography (SEC) and ^{1}H NMR spectroscopy. Takano[36] has made similar claims to a polystyrene-polyisoprene hetero[2]catenane in 0.8% yield. Endo[37] has reported on the catenation of poly(1,2-dithiane) and poly(oxyethylene) cyclic polymers—see **Section 4.1.2.3**. Finding evidence for catenation of high molecular weight macromolecules is not straightforward, however, since the ^{1}H NMR spectra and SEC chromatograms provide little more than molecular weight and functional group information. Deffieux[38,39] has devised a method of 'magnifying' the width of macrocyclic poly(chloroethyl vinyl ether) chains by grafting polystyrene sidechains onto their backbones, enabling the facile visualization of the macrorings by atomic force microscopy (AFM). This imaging trick has allowed him to observe[39] directly the [2]catenanes (**Figure 2.5**), trefoil knots, and other statistical byproducts of a polymer macrocyclization reaction.



Scheme 2.3 Zilkha's [2]catenane synthesis from a statistically threaded (pseudo)rotaxane.[33]

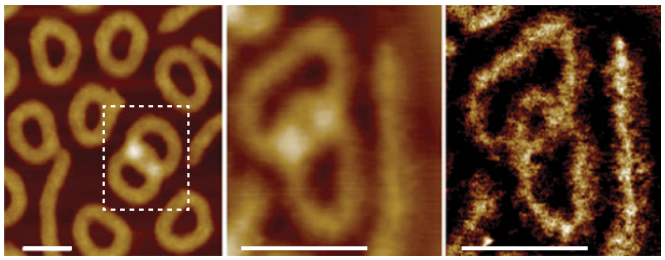


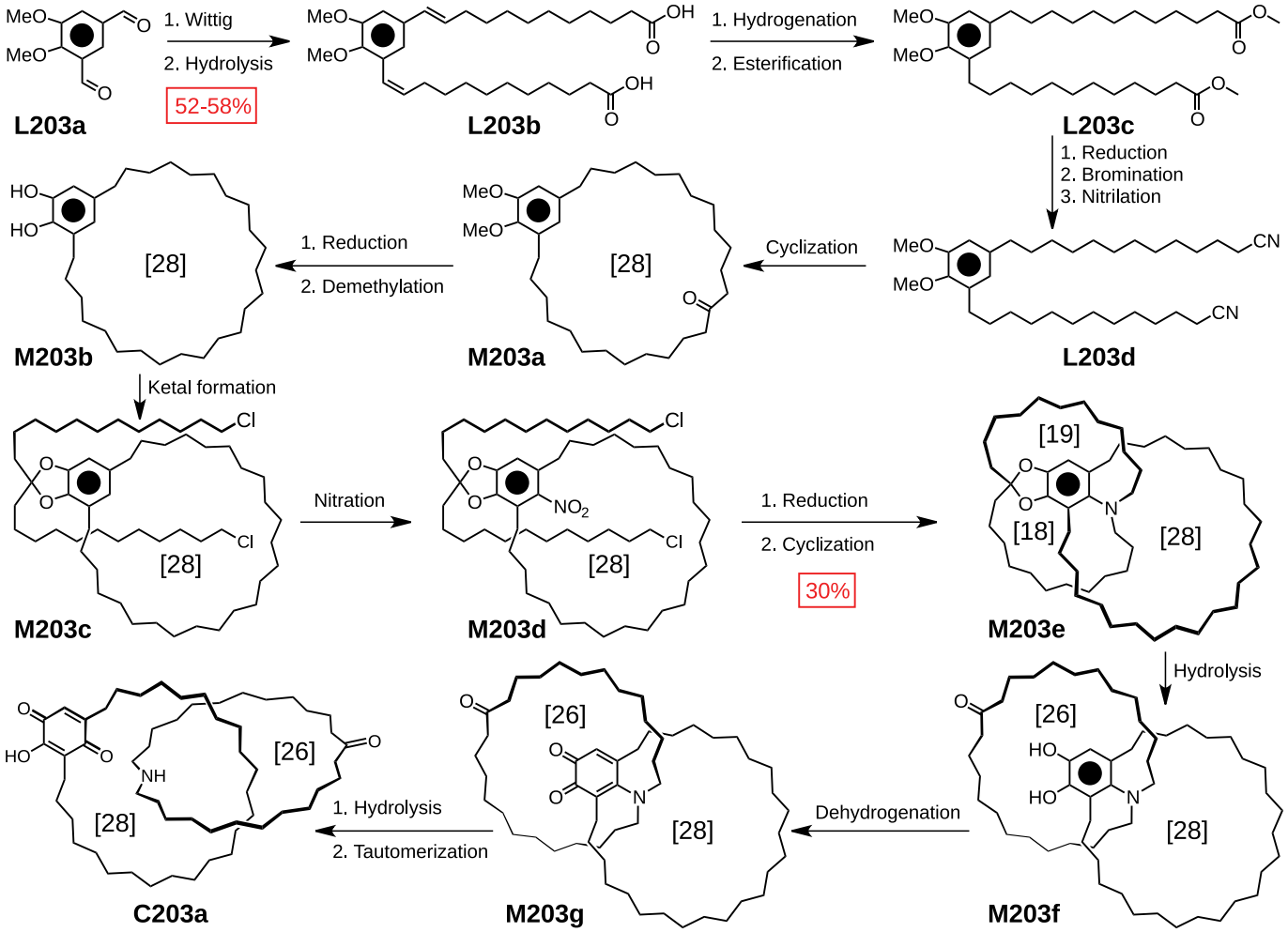
Figure 2.5 AFM images (scale bars: 100 nm) of brush polymer homo[2]catenanes generated[39] as statistical byproducts in the cyclization of a poly(chloroethyl vinyl ether) polymer with reactive endgroups, followed by grafting polystyrene chains onto the backbone in order to aid in visualization. Reprinted with permission from ref 39 (copyright 2009 Wiley)

2.2 Directed Synthesis

Directed synthesis (**Figure 2.4b**) is characterized by the preorganization of components around a covalent template that can be cleaved subsequently to afford a mechanically interlocked product. Although it was reported by Wasserman[26] that David Lemal at the University of Wisconsin and Lester Friedman at what is now Case Western Reserve University were working on this kind of approach in the early 1960s, it was Schill and Lüttringhaus[40] at the University of Freiburg who claimed the first success in the literature.

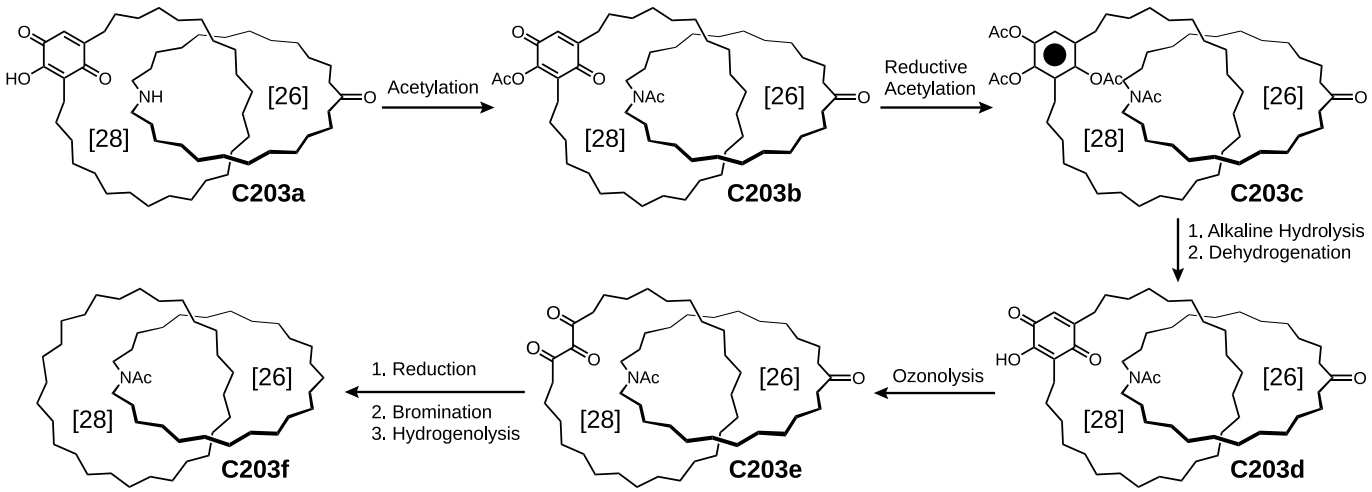
2.2.1 Covalent Templates

Gottfried Schill's 1959 Doctoral Thesis, under the supervision of Prof. Dr. Lüttringhaus, describes efforts toward the first directed synthesis of catenated compounds. The goal was not finally achieved[40] until 1964. Here we have condensed the entire synthetic sequence (**Scheme 2.4**) for the first catenane made by this method into a single scheme in order to showcase the remarkable effort that must have been required to carry it through from start to finish. Schill and Lüttringhaus[40] performed no less that 18 linear steps to reach the [2]catenane **C203**. The rings of the catenane were gradually constructed around an aromatic nucleus as the covalent template, using 4,5-dimethoxyisophthaldehyde (**L203a**) as the starting material. The sequence proceeds through several linear (**L203a-d**) and macrocyclic **(M203a-g**) compounds, key intermediates of which include the 28-membered macrocycle **M203b**, with its catechol unit that condenses with a long aliphatic dichloroketone—not shown, but which also had to be synthesized—as one of the cleavable linkers that connects the second ring to the template. A second cleavable linker is installed after several steps by double substitution of an amine site created within the first ring (by nitration and hydrolysis) to afford the multicyclic precatenane **M203e**. Yields for most of the synthetic steps were not reported, but those that were reported are noted in **Scheme 2.4**. Breaking sequentially the cleavable bonds around the aromatic template of **M203e** over a few steps leads to the [2]catenane **C203a** in near-quantitative



Scheme 2.4 The covalent directed synthesis of a catenane by Schill and Lüttringhaus[40] Ring sizes, given as a number of atoms, are denoted in square brackets.

yields. More details on the synthesis and characterization of these so-called diansa compounds, their relatives, and their corresponding catenanes appeared in a number of subsequent publications by Schill in a series[41–55] entitled *Die gezielte Synthese von Catena-Verbindungen* (Directed Synthesis of Catena Compounds) from 1964–1972, as well as a number of publications[56–59] in subsequent years. One notable finding from these investigations is that the C_{Aryl}–N bond cannot be cleaved if the surrounding macrocycle contains <20 methylene units.[51,59]



Scheme 2.5 Post-synthetic modifications[60] of the [2]catenane **C203**.

Post-synthetic modifications (**Scheme 2.5**) of the [2]catenane **C203a** have produced a number of related compounds. On account of instability issues, Schill and Lüttringhaus[40] describe in their seminal 1964 publication derivatives of **C203** in which the quinone unit has been acetylated (**C203b**) and re-aromatized (**C203c**). The first mass spectrum of the catenane **C203c**, which was published[48] in 1967, silenced any remaining skeptics that catenated molecular rings could indeed be synthesized. Eight years later, Schill reported[60] that the quinone can also be removed through hydrolysis and dehydrogenation of **C203c** to afford **C203d**, and (ii) ozonolytic degradation of **C203d** to afford the triketone catenane **C203e**. The carbonyl groups were stripped away subsequently by reducing them to the corresponding alcohols, which were subjected to bromination and catalytic hydrogenolysis to give an all-hydrocarbon ring catenated with a macrocyclic *sec*-amine in the [2]catenane **C203f**.

Schill continued pursuing these research themes independently for many years, creating a number of novel MIMs (**Figure 2.6**) along the way. He generalized the directed approach illustrated in **Scheme 2.4** and used it to prepare new architectures, including the first [3]catenanes[49,61–63]—e.g., **C204**—and [2]rotaxanes[10,27,64,65] such as **R202** as early as 1967. Apparently still dissatisfied with that pesky nitrogen atom in catenane **C203f**, Schill reported[66] in 1983 the first all-hydrocarbon catenane **C205** by post-synthesis modification of a different catenane structure, which he synthesized using a statistical double-stage method reminiscent of Zilkha's approach[33] described in **Section 2.1**. The road was not always an easy one for Schill in spite of some remarkable successes. This reality can be appreciated from a careful perusal of his publications, which reveal a number of near-misses. In 1965, he attempted[41] to make directed synthesis more facile by targeting the simpler multicyclic precatenane **M204**, but was unable to cleave its aryl C–N bonds to afford the corresponding catenane. Another diligent but ultimately unsuccessful effort[67,68] was focused towards obtaining molecular trefoil knots by directed synthesis. On the bright side, these attempts still yielded interesting interlocked structures such as **M205**. Even a pre-knot with the correct topology was most likely isolated but could not be confirmed unambiguously.[68] It has been a privilege to pry into the decades of labor by this forward-thinking, highly creative scientist, whose meticulous investigations on the mechanical bond were performed long before MIMs rose to popularity. Schill was decades ahead of his time![21]

Inspired by the directed approach, Lüttringhaus[69] also developed a 'semistatistical' method (**Scheme 2.6**) of catenane synthesis requiring fewer synthetic steps. Ziegler cyclization[70] of the nitrile threads attached endotopically to the macrocyclic precursor **M206a** leads to a mixture comprising the precatenane **M206b** and the bis-macrocycle **M206c** in 57% combined yield, in a ratio **M206b**:**M206c** of approximately 94:6. Cleavage of the aryl–nitrogen bond in these compounds and re-aromatization through reductive acetylation allows for the isolation of topological isomers—namely, the catenane **C206** and the corresponding rings **M206d** and **M206e**. Schill[71] has employed a similar semi-statistical strategy in the synthesis of a [2]rotaxane.

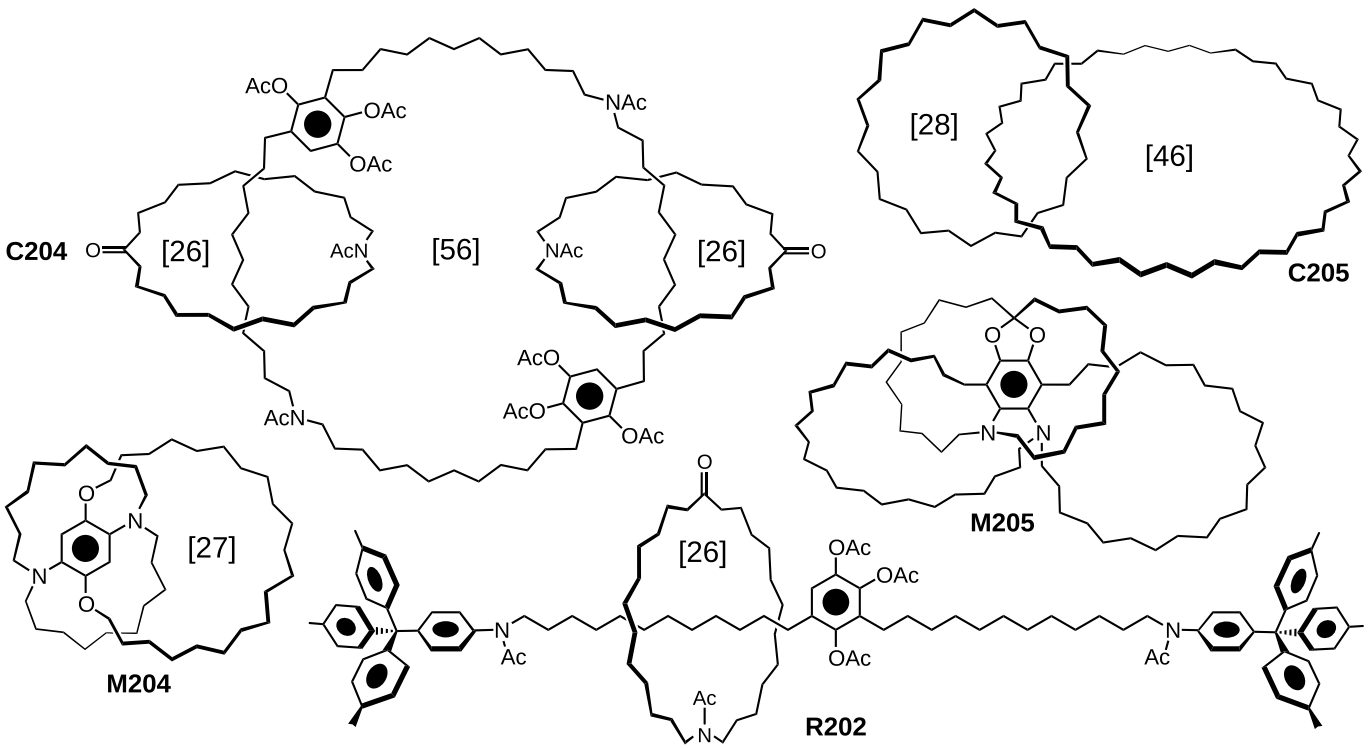
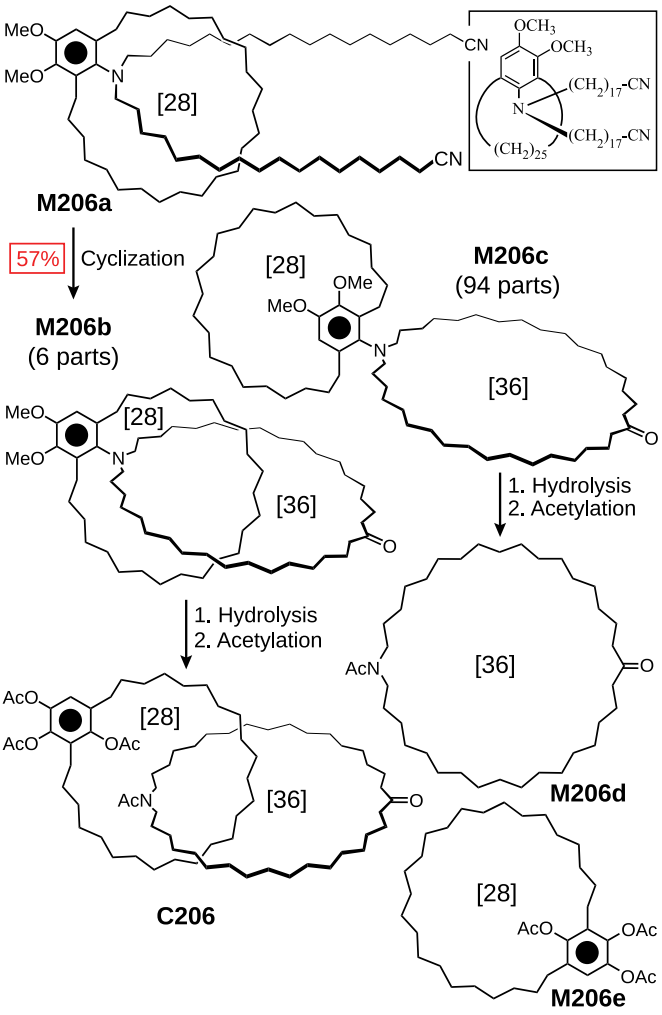


Figure 2.6 Other interlocked structures prepared by Schill.[10,41,49,66–68]

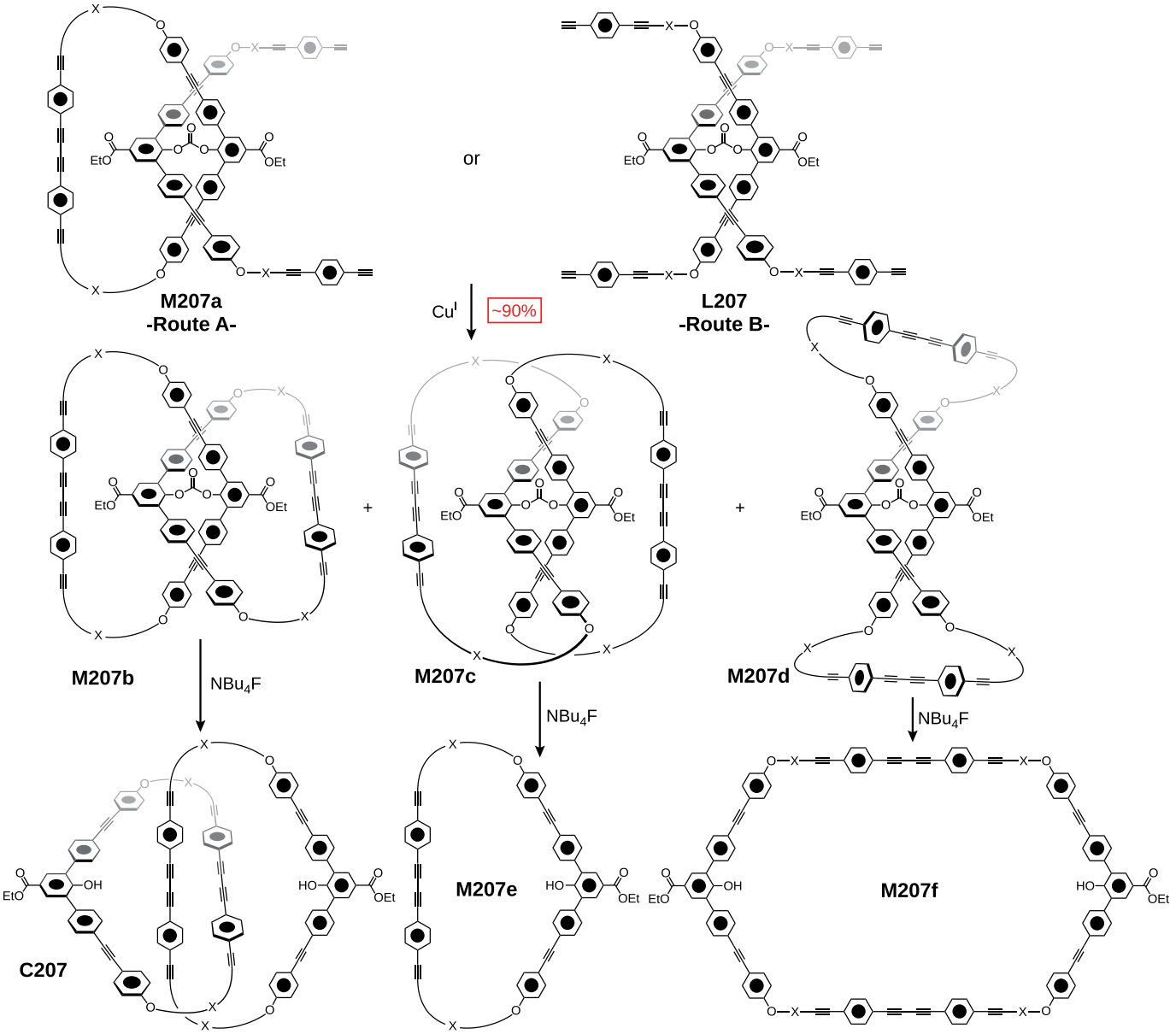


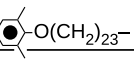
Scheme 2.6 Lüttringhaus' simplification of a directed catenane synthesis by a semistatistical approach, leading to the isolation of the topological isomers, **C206** and [**M206d**+**M206e**]. The Inset shows a depiction of starting material **M206a** in the style of the day.[69]

Directed synthesis was not altogether abandoned following Schill's retirement. Another German chemist, Adelheid Godt,[72] took up this line of work in the late 1990s. She was able to prepare[73–75] (**Scheme 2.7**) [2]catenanes by carrying out ring closures with rigid bent phenylacetylene linkers surrounding simple endotopic diphenylcarbonate templates. The catenanes can be accessed (**Scheme 2.7**) by one of two routes (A and B) which are conceptually equivalent to the two routes outlined by Sauvage[76] a decade earlier in his original template-directed synthesis of metallo[2]catenanes—see **Section 2.3.2.1**—which would later become known as "threading" (Route A) and "entwining" (Route B). Route A[73,74] proceeds from the macrocyclic precursor **M207a**, which is linked by the carbonate template to a threaded bis(alkyne), whereas Route B proceeds from the acyclic precursor **L207**, which comprises a pair of bis(alkynes) entwined around the same covalent template. These precursors come in three different sizes, defined by the length of the oligomethylene chain X denoted in each of their stereoformulas. These giant rings (up to 147 atoms) are large enough to observe[77] directly on surfaces by scanning tunneling microscopy (STM). The bis(alkyne) fragments of **L207** and **M207a** are converted efficiently (up to 90%) to macrocycles by an oxidative Cu^{I}-catalyzed Eglinton-Glaser-Hay homocoupling to afford a mixture of the precatenanes **M207b**, the bis-macrocycle **M207c**, as well as a constitutionally isomeric bis-macrocycle **M207d**, which is formed only in the case[75] of Route B. Since compounds **M207b–d** proved to be difficult to separate, they were employed in admixture for the final step of the reaction sequence. The fluoride-mediated cleavage of the carbonate templates affords a mixture of the [2]catenane **C207** and its non-interlocked component macrocycle **M207e**, as well as the very large ultramacrocyclic **M207f** derived from **M207d** in the case of Route B. The distribution (table inset in **Scheme 2.7**) of the products **C207**, **M207e**, and **M207f** depends on both the size of the rings and on the choice of route. The [2]catenanes (**C207**) dominate the product distribution by Route A, whereas the ultramacrocycle (**M207f**) is the dominant product of Route B. In general, smaller ring sizes correspond to greater bias in the product distributions. Godt[72] has described the [2]catenanes as 'non-rusty' because they lack any significant ring–ring interactions,[B] and therefore sample all of the available co-conformations rapidly (sub-microsecond timescale) in chloroform. This expectation has been proven[78,79] by electron paramagnetic resonance (EPR) spectroscopy on spin-labeled analogues of **C207**, which were accessed by post-synthetic modifications involving ester exchange. Although Godt[72] also experimented with polymerizing these compounds by several methods, she has so far been able to obtain only relatively low molecular weight polyesters, with degrees of polymerization (DP) in the range of 5–12.

Imine bonds have been introduced by Kawai[80] in the covalent directed synthesis (**Scheme 2.8**) of rotaxanes. Imine condensation between the two endotopic amino functions of macrocycle **M208a** and the pair of formyl groups on the hydrindacene[81] moiety of axle **L208** affords the macrobicyclic compound **M208b**. Deprotection of the phenolic endgroups of **M208b** and subsequent alkylation with a bulky stopper precursor derived from benzyl bromide affords **M208c**, which may also be called a prerotaxane or a [1]rotaxane. On account of the reversible hydrolysis and condensation of imine bonds in the presence of trace amounts of water, **M208c** exists in a temperature-dependent dynamic equilibrium with its corresponding [2]rotaxane **R203-O_2** in solution—see **Section 6.7**. The equilibrating mixture of **M208c** and **R203-O_2** can be converted to the "permanent" or non-equilibrating [2]rotaxane **R203-$C_4H_8S_4$** by dithioacetylization of the hydrindacene formyl groups with 1,2-ethanedithiol and TFA in wet $CHCl_3$. The ring of

[B] A very weak associative interaction has been observed between the phenylacetylene units of each ring, giving a slight preference for co-conformations involving rings that overlap at these sites.



–X–	Ratio **C207:M207e:M207f** (Route A)	Ratio **C207:M207e:M207f** (Route B)
–$(CH_2)_{11}$–	6.0 : 1 : 0	**C207** + **M207e** << **M207f**
–$(CH_2)_{23}$–	2.7 : 1 : 0	1 : 1 : 14
–$(CH_2)_{23}$–  –$O(CH_2)_{23}$–	1.6 : 1 : 0	1 : 1 : 4

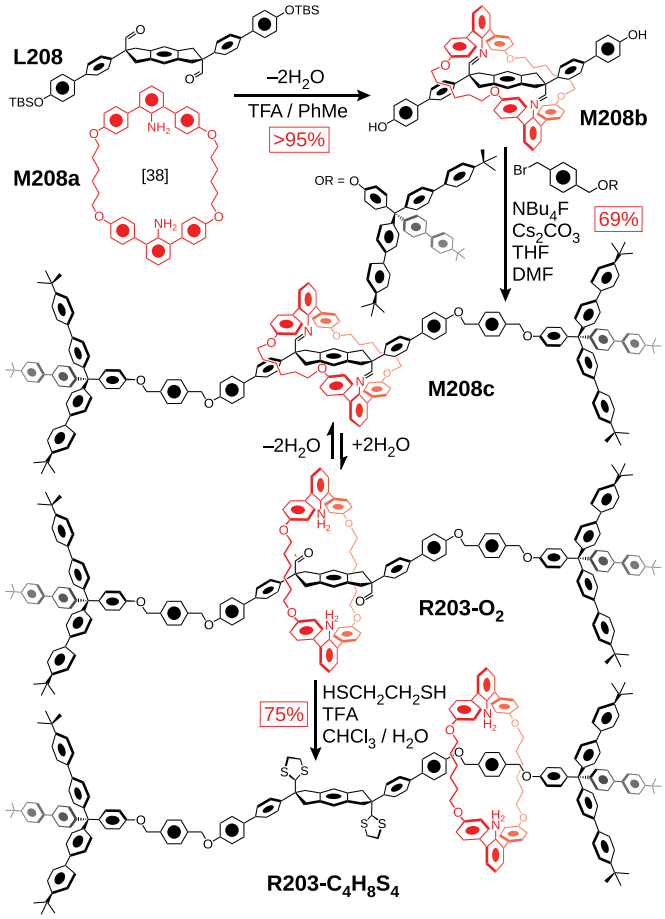
Scheme 2.7 Godt's directed synthesis[72–75] of the giant 'non-rusty' [2]catenane **C207**.

R203-$C_4H_8S_4$ preferentially encircles either of the dumbbell's two xylylene units, passing over the hydrindacene-derived speedbump as it shuttles back and forth.

The isomerism and dynamics of molecules with mechanical bonds are discussed in more detail in **Chapter 5**. Nevertheless, it is clear from these examples that the use of covalent templates constitutes a fruitful way to create MIMs that lack strong intercomponent interactions. It is becoming clear that such compounds—particularly when they are polymeric in nature—can display useful properties. See **Chapter 4**.

2.2.2 Covalent-Directed Capture

A manifestation of the dumbbell capture strategy for making rotaxanes (see **Figure 2.3**) has been implemented in the context of directed synthesis. The basic premise of this strategy is to immobilize part of a dumbbell within the cavity of a sufficiently large macrocycle with a covalent bond that can be displaced subsequently using a new bond-forming reaction. This approach (**Scheme 2.9**) was introduced by Hiratani[82] in 2002 using aminolysis of esters as the mechanical bond-forming reaction. The key building block in his strategy is the

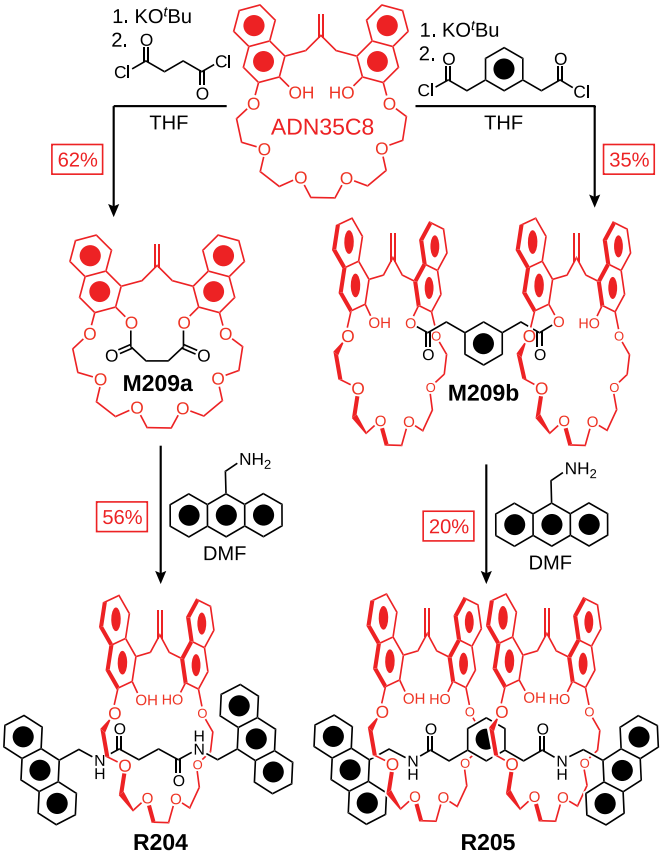


Scheme 2.8 Kawai's directed synthesis of a [2]rotaxane using a reversible imine bond template.[80]

crownophane allyldinaphtho[35]crown-8 (ADN35C8) on account of its endotopic naphthol groups. Dumbbell fragments can be localized at these naphthol sites by acylation before being exchanged for stoppers. If the nucleophilic dumbbell precursors approach the dumbbell fragment from opposite sides of the ring, a rotaxane will be formed. Thus, aminolysis of the ADN35C8 succinic ester **M209a** with 9-(aminomethyl)anthracene gives[82] the corresponding [2]rotaxane **R204** in 56% yield. It has also proven to be possible[83] to accomplish the stepwise displacement of these succinic esters to afford rotaxanes with constitutionally unsymmetric dumbbells. The [3]rotaxane **R205** has been accessed by aminolysis of the bis-macrocyclic ester **M209b** derived from ADN35C8 and 1,3-phenylenediacetic acid.[84] Yields are not outstanding because the approach of the nucleophilic amine is statistical in nature, giving dissociated rings and dumbbells as byproducts. This covalent-directed capture strategy appears to be quite general. Hiratani[85] has also extended it to the synthesis of chiral [2]rotaxanes.[86,87] and [1]rotaxanes,[88] an architecture also known as a molecular ouroboros or [*c*1]daisy chain—see **Section 4.2.3**.

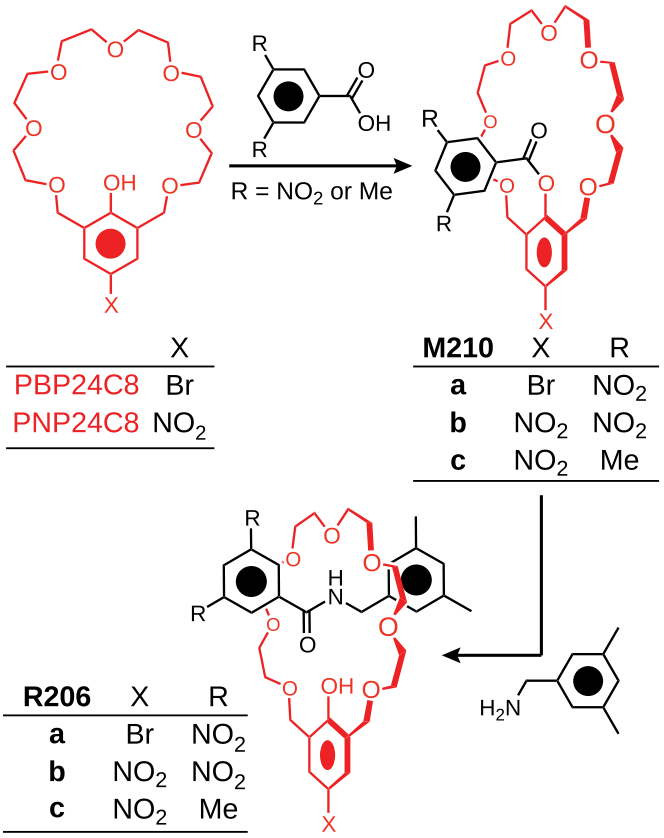
Hirose[89] has also developed a high-yielding synthesis (**Table 2.2**) of rotaxanes by optimizing a similar type of aminolysis capture reaction. The endotopic hydroxyl group of the crown ethers *para*-bromophenol[24]crown-8 (PBP24C8) and *para*-nitrophenol[24]crown-8 (PNP24C8) have been acylated to the corresponding 3,5-substituted benzoates **M210a–c**. Aminolysis of these prerotaxanes with 3,5-dimethylbenzylamine affords the corresponding [2]rotaxanes **R206a–c**. The conditions summarized in the table show that the selectivity of the reaction for the target rotaxane **R206** (versus dissociated dumbbell and ring components) is sensitive to solvent composition and substitution on the benzoate moiety of **M210a–c**, but insensitive to substitution on the phenolic ring of the crown ether. The effect of ring size was also tested by adding and subtracting ethylene glycol units from the rings, but neither option afforded rotaxanes as products. In general, lower polarity solvents promote rotaxane selectivity, as do the electron-withdrawing nitro groups on stopper. Under the best conditions, **R206a** was formed with 100% selectivity in near-quantitative yield (82% isolated) in benzene.

Recently, an unsuccessful attempt to construct rotaxanes and polyrotaxanes from phenylacetylene macrocycles by means of a covalent-directed dumbbell capture approach has been reported by Morin,[90] suggesting that the design of these systems can be none too easy to accomplish in some cases, even after careful optimization.



Scheme 2.9 Hiratani's capture of rotaxanes, directed by aminolysis of endotopically acylated crownophanes.[82,84]

Table 2.2 Effect of substitution and solvent on Hirose's covalent-directed capture[a] of rotaxanes[89]



Rotaxane	Solvent	Time	Yield[b]	Rotaxane Selectivity[c]
R206a	C_6D_6	28	82	100
R206a	$CDCl_3$	244	[d]	96
R206a	CD_3CN	24	[d]	95
R206a	DMF-d_7	36	[d]	67
R206b	C_6D_6	0.7	81	89
R206b	$CDCl_3$	2	[d]	85
R206c	C_6D_6	60	[d]	40
R206c	$CDCl_3$	160	[d]	12
R206c	C_6H_{12}	240	52	68

[a]Concentrations of reactants: **M210a** (7 mM), **M210b–c** (5 mM), 3,5-dimethylbenzylamine (10 mM) for all reactions.
[b]Isolated yield.
[c]Selectivity reflects the percent conversion of **M210** to **R206** over an unassociated dumbbell/ring mixture.
[d]Not isolated.

2.2.3 The Möbius Approach

The Möbius strip is an iconic object. The German mathematicians Johann Benedict Listing[91] and August Ferdinand Möbius[92] first described Möbius strips independently in 1858 and published their work in the 1860s. In three-dimensional space, a Möbius strip is a chiral closed band with only one surface and one edge. This curious property is beautifully demonstrated (**Figure 2.7**) by the ants marching along the continuous path of a Möbius strip's singular surface in M.C. Escher's famous woodcut, *Möbius Strip II*. Möbius strips can be constructed (**Figure 2.8a**) from a narrow band by twisting it 180° (known as a half-twist) before connecting its ends together. Möbius-like objects can be differentiated by the number, *n*, of half-twists, which influence the outcome of cutting them (**Figure 2.8b–e**) parallel to their edge(s). If *n* is an odd number, then bisecting the Möbius strip gives a strip of half the width and twice the length possessing (2*n*+2) half-twists, the loop of which assumes the topology of the unknot (**Figure 2.8b**) for *n* = 1 or a trefoil knot (**Figure 2.8e**) for *n* = 3. If *n* is an even number, then bisection yields (**Figure 2.8d**) a link with two rings of equal length, each having *n* half-twists. The rules are different for even and odd values of *n* because only odd values correspond to the unusual single-surface, single-edge topology. The bands with an even number of half-twists have the more intuitive two-surface situation common to ribbonlike objects, and are known rather as paradromic rings. Another interesting property, exclusive to the Möbius strips (*n* = odd), is that an off-center cut parallel to the edge will afford (**Figure 2.8c**) a link comprising a large ring with (2*n*+2) half-twists and a smaller ring with *n* half-twists.

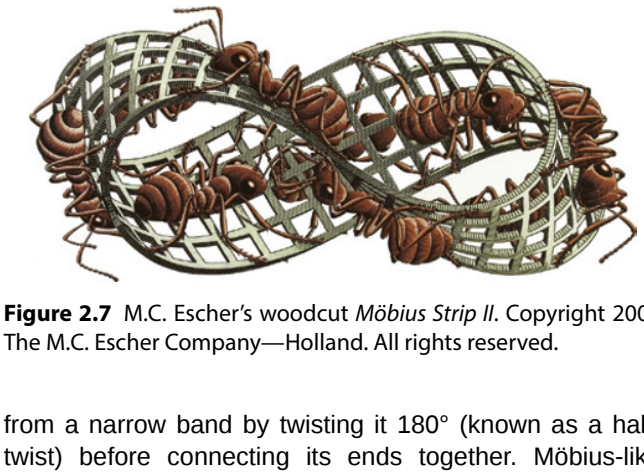


Figure 2.7 M.C. Escher's woodcut *Möbius Strip II*. Copyright 2006 The M.C. Escher Company—Holland. All rights reserved.

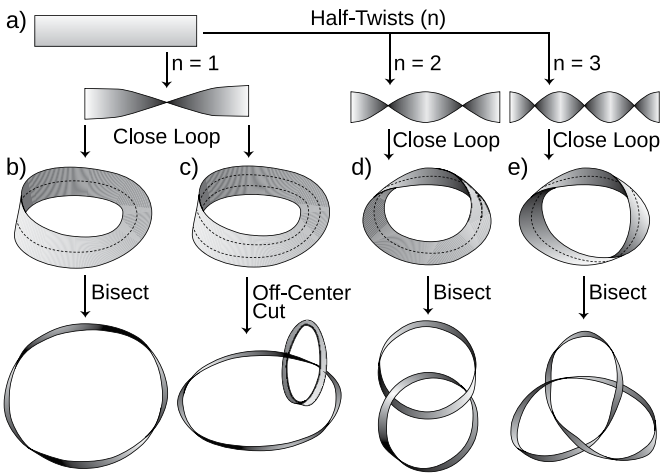
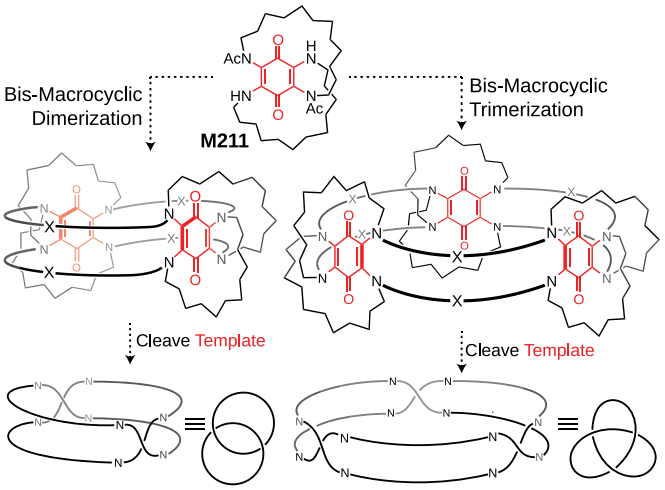


Figure 2.8 The Möbius approach to making mechanical entanglements. (a) The construction of Möbius strips with various numbers, *n*, of half-twists. (b) Bisecting a half-twist Möbius strip affords a larger, quadruply half-twisted ring. (c) An off-center cut on a Möbius strip (*n* = 1) affords two linked rings of unequal size. (d) A link is formed from a center cut on a full-twist (*n* = 2) paradromic ring. (e) The triple half-twist Möbius strip is converted to a trefoil knot upon bisection.

Bisecting more highly twisted surfaces or performing extra edge-parallel cuts give increasingly entangled products.[93]

The synthesis and cleavage of molecular Möbius strips was envisioned as a strategy for creating molecular entanglements by Frisch and Wasserman[1] as well as by van Gulick[12,94] ever since the birth of chemical topology.[c] Recall that Möbius strips are *surfaces*. Although molecules with Möbius surfaces such as twisted cyclic annulenes have been envisioned,[95] such compounds would surely be extraordinarily difficult to bisect for the purposes of making mechanical bonds. A more practical solution, which stems from the fact that molecules are composed of atoms and one-dimensional bonds, is based on the mathematical representation of a molecule's connectivity as a graph of vertices and edges, rather than a surface. A class of graphs that resemble Möbius strips, which are known as Möbius ladders, have been defined[96] in the mathematical literature. A Möbius ladder can be constructed from a ladder or grid in the same way that a Möbius strip is constructed (see **Figure 2.8a**) from a surface, i.e., by performing an odd number *n* of half-twists before joining the ends together to make a loop. An analogous graph with an even number *n* is known as a prism. In this scenario, removing or severing the 'rungs' of the Möbius ladder would deliver the same general topology as that of the corresponding Möbius strip. Unlike surfaces, however, the knots (*n* = odd) or links (*n* = even) generated by cutting the rungs of these ladder graphs are simply curves that inherently lack half-twists or an ability to be bisected along their length. The seminal work of Guy and Harary[96] stated that the graph of any Möbius ladder is minimally non-planar, which means that it cannot be projected onto a plane without its edges having at least one crossing point. Since at least five vertices are required for a graph to be non-planar, it follows that a Möbius ladder must have at least three rungs, corresponding to six nodes or vertices in its graph.

In spite of its early recognition, the Möbius approach has proved challenging to realize in practice. Schill[28,97] worked on a strategy to use directed synthesis to template twists in macrocyclic ladders. The goal was to pre-install (**Scheme 2.10**) entanglements in cyclic oligomers derived from compounds such as the doubly-strapped quinone **M211**, so that cleavage of the quinone template's C–N bonds would afford entangled products. The topology of the product would depend on that of the prism or Möbius ladder comprising a cyclic oligomer of **M211** from which it was obtained. For example, an appropriately connected cyclic dimer would possess two half-twists and therefore become a [2]catenane upon removal of the template, whereas the homologous cyclic trimer would yield a molecular trefoil knot. Schill[97] was successful in preparing the macrobicyclic quinone **M211**, but never reported any



Scheme 2.10 An envisioned Möbius synthesis of mechanically interlocked molecules using Schill's double-bridged quinone **M211** as a covalent template for half-twists in the corresponding bis-macrocyclic ladder oligomers.[28,97] Removal of the covalent template (red) would afford a catenane from the cyclic dimer, or a trefoil knot from the cyclic trimer.

oligomers thereof, most likely because of insurmountable synthetic challenges associated with maintaining proper connectivity in the bis-macrocyclic oligomerization. Some evidence[98,99] for the emergence of Möbius structures during olefin metathesis have also surfaced, but appear to have been discredited[100] ultimately upon revision of the mechanism[101–103] of olefin metathesis.

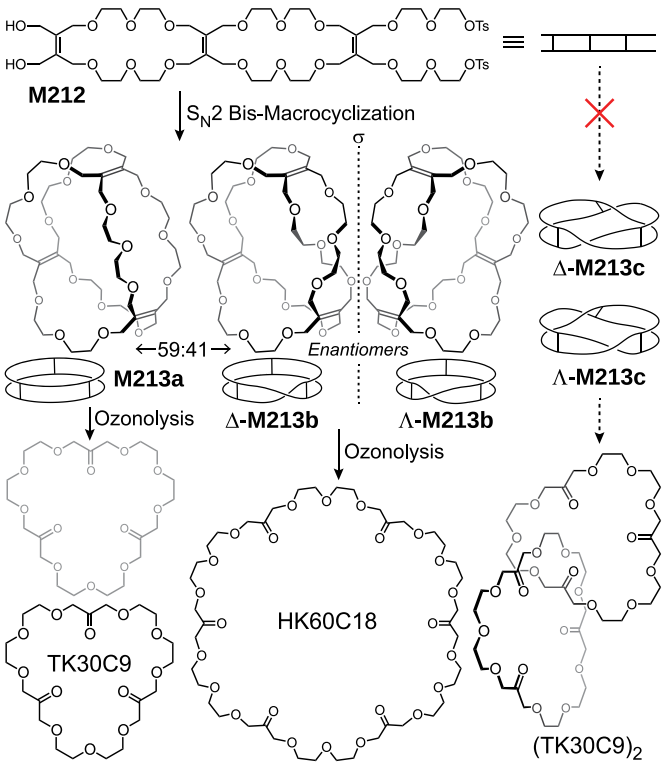
The synthesis and cleavage of the first molecular Möbius ladder was ultimately achieved[104] in 1982 by Walba[105] at the University of Colorado. The rungs of Walba's Möbius ladder are the double bonds of its tetrahydroxymethylethylene (THYME) units,[106–108] while the 'rails' of the ladders comprise simple polyether strands. The bis-macrocyclization of the THYME ladder **M212** under high dilution leads (**Scheme 2.11**) to a statistical mixture (59:41, ±3%) of the three-rung prism **M213a** and half-twist Möbius ladder **M213b** in up to 70% combined yield. The topological chirality (see **Section 5.2.4.1**) of Möbius strips leads to the expectation that **M213b** exists as a racemate of Δ and Λ enantiomers. The deceptively simple ^{1}H and ^{13}C NMR spectra containing only two and four resonances, respectively, indicate that the signals are averaged by rapid propagation of the Möbius ladder's twist throughout the whole structure on the NMR timescale, implying rapid through-the-annulus rotation of the ladder's rails. Furthermore, two sets of signals can be resolved in the NMR spectra in the presence of a chiral shift agent, confirming that **Δ-M213b** and **Λ-M213b** are present in equal proportions.

Although it was already known that the chirality of a half-twist Möbius *strip* is an extrinsic property of embedding it in three-dimensional space, there was no mathematical treatment in 1982 that could describe the chirality of a Möbius *ladder* in three-dimensional space. Remarkably, Walba's work stimulated the interest of mathematicians such as Jonathan Simon,[109] Erica Flapan,[110] and others[111]

[c] van Gulick's 1960 paper about 'the theoretical aspects of the linked ring problem' was rejected by *Tetrahedron* for 'not being chemistry' and was not published until 1993 in the *New Journal of Chemistry* in a special issue on molecular topology edited by Sauvage. During the intervening 33 years, copies of the manuscript were circulated between a small community of aficionados.

the low-dimensional topology of Möbius ladders, and ultimately helped catalyze the popularization of the mathematical field of extrinsic graph theory.[105] The mathematicians have found that the graphs of Walba's Möbius ladders **Δ-M213b** and **Λ-M213b** possess a very deep kind of topological chirality. Specifically, Flapan[110] found that *every* embedding of these graphs are topologically chiral, and so the graph is said to be intrinsically chiral. Even trefoil knots, which are topologically chiral in three-dimensional space, do not satisfy this condition!

The olefinic rungs of the THYME polyethers can be cleaved (**Scheme 2.11**) by ozonolysis. The bisection of prism **M213a** gives two equivalents of the triketone crown ether, triketo[30]crown-9 (TK30C9). In contrast, the rungs of the Möbius ladder **M213b** are broken only to have it remain in one piece as the larger hexaketo[60]crown-18 (HK60C18). The corresponding full-twist prism **M213c**, the cleavage of which would lead to catenated TK30C9 rings, has not yet been accessed. Walba[112] also investigated the possibility of using a 'hook-and-ladder' approach to building knotted structures, a strategy which is essentially a hybridization of Sauvage's metal-ligand templates (**Section 2.3.2**) and Walba's Möbius ladders. The envisioned protocol, which involves the bis-macrocyclization of a THYME precursor with a pair of ligands entwined around a Cu^{I} template, delivers only a hook-and-ladder without the requisite half-twist to be a figure-of-eight knot. The untwisted hook-and-ladder, which possesses a novel self-catenated macrotricyclic topology, is described in **Section 4.1.3.2**.



Scheme 2.11 Walba's synthesis of a pair of topological isomers comprising a prism (**M213a**) and a Möbius ladder (**Δ/Λ-M213b**), obtained by bis-macrocyclization of the THYME polyether ladder compound **M212**.[104,105] Upon ozonolytic cleavage of double bonds, the prism splits into two equivalents of triketo[30]crown-9 (TK30C9), whereas the Möbius ladder remains in one piece as hexaketo[60]crown-18 (HK60C18). The cyclic ladder with two half-twists (**M213c**) was not obtained, but its bisection would in principle afford a catenated homodimer of TK30C9.

Recently, DNA origami-based Möbius strips have been assembled and cleaved to form links,[113] but the world is still waiting for the first catenanes and knots to be synthesized from a unimolecular Möbius ladder. If a facile synthesis leading to a vast range of accessible molecular compounds could be identified, then perhaps a newly appointed assistant professor might be foolhardy enough to rush in where others have so far feared to tread.

2.3 Template-Directed Synthesis

Mechanostereochemistry, as we have chosen[11] to call it nowadays, started as a rather esoteric discipline, discussed only casually if at all by most chemists and practiced by only a select few individuals, most of whom have been named in the preceeding sections. It was not until the advent of template-directed[114–124] synthesis—a concept being developed throughout the 1950s, 60s, and 70s—was finally applied to MIM synthesis in the 1980s that mechanical bonds entered the mainstream of chemical research, largely as a result[8] of the research carried out by Jean-Pierre Sauvage (see **Section 2.3.2.1**) amongst others. In the broadest sense, a template is anything that can orient and direct reactants, although we focus here on templates acting through noncovalent bonding interactions. The template-directed synthesis of mechanically interlocked compounds has been reviewed many times in the literature.[118,121,125–139] over the past few decades.

The 1987 Nobel Prize in Chemistry was awarded to Cram,[140] Lehn,[141] and Pedersen,[142] 'for their development and use of molecules with structure-specific interactions of high selectivity', which we recognize today as host-guest or supramolecular chemistry. The majority of molecules with mechanical bonds have a foundation in these fields of research because they involve the self-assembly of molecules, guided by local noncovalent bonding interactions, into superstructures and complexes that become crucial templates in the art of mechanical bond formation. This Section therefore covers the types of supramolecular and host-guest recognition motifs that are used to template the formation of mechanical bonds. It also draws attention to some examples of synthetic methods employed in their conversion to MIMs. We have highlighted in each Section a number of the host-guest complexes and association constants for many of the most important supramolecular motifs in mechanostereochemistry to aid readers in the design of future MIMs. These interactions include solvophobic forces (**Section 2.3.1**), coordination to transtion metals (**Section 2.3.2**) or other cations (**Section 2.3.8**), π-associated donor-acceptor charge-transfer interactions (**Section 2.3.3**), hydrogen bonding (**Section 2.3.4**), halogen bonding

(**Section 2.3.5**), anion binding (**Section 2.3.6**), ion pairing (**Section 2.3.7**), and cyclophanes (**Section 2.3.9**) that rely on a combination of these forces, as well as radical pairing (**Section 2.3.10**), homophilic interactions (**Section 2.3.11**), and biomolecular self-assembly (**Section 2.3.12**).

2.3.1 Solvophobic Forces

The most characteristic noncovalent bonding interactions underpinning the self-assembly of the cyclodextrins (CDs), cucurbiturils (CBs), and other macrocyclic hosts described here are solvophobic forces, with an emphasis on the special case in water known as the hydrophobic effect.[143] Solvophobicity and hydrophobicity describe the interactions between polar and non-polar molecules. Polar solvents such as water have strong cohesive forces including dipole-dipole, ion-dipole, and/or hydrogen-bonding interactions. These intermolecular forces become disrupted when the solvent comes into contact with a non-polar or low-polarity solute. Water molecules, each of which participate in three or more hydrogen bonds on average in the liquid state, must rearrange themselves around a non-polar solute to avoid losing the enthalpic stabilization of their hydrogen bonds. Since this more highly 'structured' state of water in the solvation shell of the solute is entropically costly, it is energetically favorable for the structured water molecules to be liberated, perhaps by another molecule with low polarity or amphiphilicity. These entropic effects are important drivers (dispersion forces also play a role) for hydrophobic and other solvophobic interactions, including the separation of oil from water, the formation of micelles, lipid membranes, etc., and the inclusion phenomena of the host-guest systems outlined in this Section. In many cases, solvophobic and hydrophobic effects are also enthalpically driven because the release of 'high energy' solvent molecules from a cavity or surface allows them to regain stabilizing dipolar and/or hydrogen-bonding interactions in bulk solution.

A historical point[144] that often gets neglected is that a body of research from the community of carbohydrate chemists working with the cyclomalto-oligosaccharides or cyclodextrins (**Section 2.3.1**) preceeded the Nobel Prize-winning discoveries of Pedersen, Cram, and Lehn in what we recognize today as supramolecular and host-guest chemistry. Cramer's conjecture 'that cyclodextrins form inclusion compounds even in solution' was met with both fierce opposition and support for many years before gaining general acceptance by the chemical community at large.[145] Cramer's research[146–150] throughout the 1950s describing the promiscuity of the cyclodextrins in forming inclusion complexes with a wide range of substrates predated the rapid development of supramolecular and host-guest chemistry on the back of Pedersen's discovery[151,152] of the crown ethers by more than a decade!

2.3.1.1 Cyclodextrins

Cyclodextrins (CDs) are a family of natural products, first isolated from starch-fermenting bacteria cultures as mysterious crystalline substances by Villiers[153] in 1891, with structures that constitute macrocyclic arrays of sugars. The three major naturally occurring CDs (**Figure 2.9**) are α-CD, β-CD, and γ-CD, corresponding to six, seven, and eight glucose monomers, respectively. Although larger CDs (following the Greek alphabet, δ, ε, ζ, η, etc.) are more rare, they have also been known[154] for some time and have been characterized structurally up to at least the 26-mer, φ-CD.[155] Although the history[156,157] of the cyclodextrins records that the α- and β-CD compounds were isolated and purified by Schardinger in the early 1900s, their structures were not elucidated until the second half of the 1930s by Freudenberg, who also introduced[158] γ-CD with Cramer in 1948. The physical properties of the CDs were investigated extensively in the first half of the 1900s, notably by Pringsheim[159] in Germany and French[156] in the United States. Credit has to be given to Cramer,[146,147] however, for pioneering the study of inclusion phenomena in his work with the CDs in the early 1950s. His discoveries opened the door, not only to the development of supramolecular chemistry, but also to the emergence of organocatalytic chemistry pioneered by Bender,[160,161] Breslow,[162] and many others, not to mention breakthroughs in analytical chemistry,[163] separations,[164] medicine,[165,166] food science,[167] and other industrial applications.[168]

CDs are among the most widely used hosts in chemistry because of their low cost, wide availability, high stability, water solubility, biocompatibility, biodegradability, and, of course, their capacity to ensconce an enormous variety of guests with a vast range of association strengths. The three main CDs are slightly bowl-shaped (**Figure 2.9**), where the

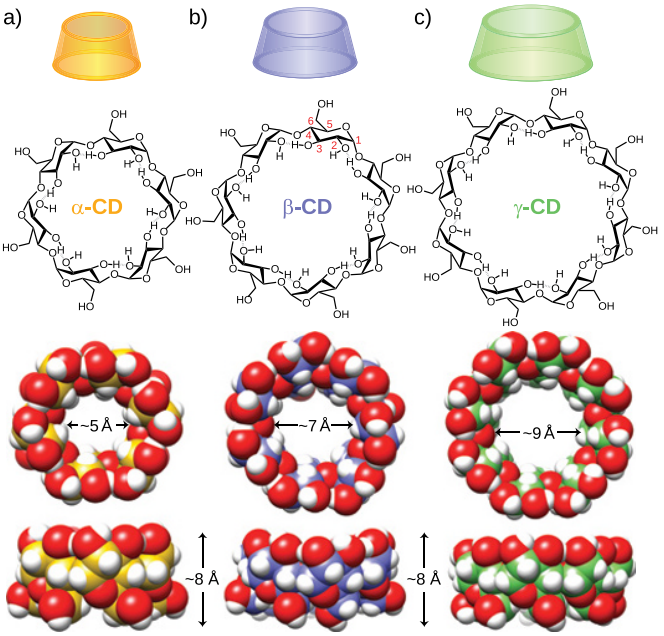


Figure 2.9 Graphical representations and structural formulas (top) and space-filling representations (bottom) of the three most well-known cyclodextrins: (a) α-CD. (b) β-CD. (c) γ-CD. The D-glucopyranosyl residues are linked together just as they are in amylose (starch) from whence the CDs are derived microbiologically.

wider '2,3-rim' (secondary face) is stiffened by hydrogen bonds between the secondary 2-OH and 3-OH groups, while the slightly smaller '6-rim' (primary face) is lined with all of the primary CH_2OH groups at the 6-position of the glucopyranose units. The CD cavities (**Figure 2.9**) are almost 8 Å in depth, while their diameters are in the ~5 to ~9 Å range (α<β<γ). Their interior surfaces are somewhat hydrophobic, allowing them to interact with lypophilic guests in water. The number of guests that are known to associate with the CDs in water number in the thousands. We offer a sample of their guests in **Table 2.3** and refer readers to more comprehensive sources[169,170] for obtaining information on CD host-guest complexes. Here, we focus mainly on the CD motifs that have been employed in the making of mechanical bonds. Several reviews[171–175] summarizing this research are also available in the literature.

One of the most common host-guest motifs for making CD rotaxanes is based on simple hydrocarbon chains. **Table 2.4** summarizes the K_a values for α-CD complexes comprising hydrocarbon chains of various lengths with charged endgroups.[176,177] In general, the association constants increase as chain length increases, provided the guests are sufficiently soluble in water.

Table 2.3 Thermodynamic parameters[a] of inclusion complexes based on the cyclodextrins and various guests near room temperature in water.

			Δ*G*	Δ*H*	*T*Δ*S*
CD	**Guest**	**log *K***	**– kcal·mol^{-1} –**		
α-CD	acetonitrile	0.75	–1.0	–2.4	–1.4
α-CD	hydroquinone	1.38	–1.9	–2.4	–0.5
α-CD	anthracene	1.87	–2.6	–18.9	–16.3
α-CD	1-adamantanecarboxylate	2.16	–2.9	–5.5	–2.6
α-CD	*trans*-4-methylcinnamate	2.55	–3.5	–9.6	–6.0
α-CD	(*E*)-stilbene-$(NHMe)_2$	3.10	–4.2	–6.4	–2.1
α-CD	1-pentylammonium	1.97	–2.7	–3.3	–0.6
α-CD	1-hexylammonium	2.58	–3.5	–4.2	–0.7
α-CD	1-heptylammonium	3.03	–4.1	–4.8	–0.6
α-CD	1-octylammonium	3.37	–4.6	–5.3	–0.7
α-CD	1,10-decanediol	3.85	–5.2	–5.9	–0.6
α-CD	1,12-diaminododecane	3.85	–5.2		
α-CD	methyl orange (anion)	3.96	–5.4	8.6	3.3
α-CD	indole	7.8	–11	–0.8	10
β-CD	1-hexylammonium	1.81	–2.5	0.6	3.1
β-CD	1-octylammonium	2.62	–3.6	–0.5	3.1
β-CD	hydroquinone	2.05	–2.8	–4.1	–1.3
β-CD	*trans*-4-methylcinnamate	2.67	–3.6	–4.2	–0.5
β-CD	pyrene	2.69	–3.7	–7.0	–3.3
β-CD	(*E*)-stilbene-$(NHMe)_2$	2.85	–3.9	–2.7	1.2
β-CD	anthracene	3.31	–4.5	–4.2	0.3
β-CD	1,10-decanediol	3.35	–4.6	–6.2	–1.7
β-CD	methyl orange (anion)	3.65	–5.0	–4.7	0.4
β-CD	4,4′-bipyridine	3.86	–5.3		
β-CD	1-adamantanecarboxylate	4.51	–6.1	–5.1	–1.0
γ-CD	anthracene	2.35	–3.2	–5.5	–2.3
γ-CD	pyrene	3.05	–4.2	–10.2	–6.0
γ-CD	1-adamantanecarboxylate	3.53	–4.8	1.2	6.0
γ-CD	methyl orange (anion)	7.08	–9.6	–12.0	–2.4

[a]See refs. 169,170 and references therein.

Table 2.4 Association constants (K_a) for pseudorotaxanes formed between α-CD and polymethylene chains with pyridinium and carboxylate endgroups.[176,177]

	K_a (M^{-1}) / no. of carbon atoms				
Endgroups	**8**	**9**	**10**	**11**	**12**
Pyridinium	110	640	2200	-	4800
Carboxylate	310	630	1400	1500	5400

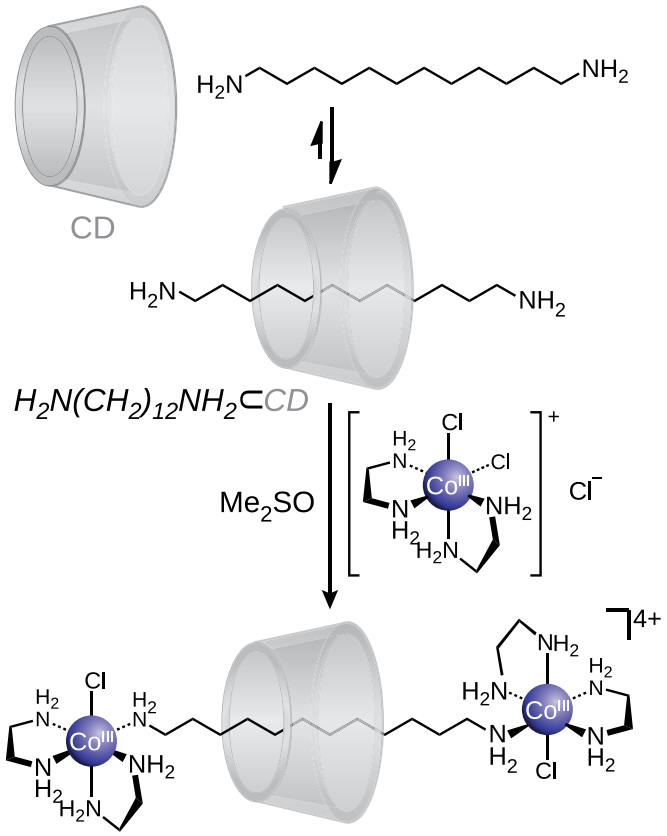
Since water is the best solvent for host-guest binding in CDs, the requirement for aqueous chemistry in the synthesis of CD-based MIMs limits the scope of usable reactions. One way to circumvent this limitation is to solubilize CDs in organic solvents by protection of some or all of the hydroxyl groups.[178] One of the most common modifications is partial methylation or permethylation. Curiously, in spite of the increased hydrophobicity of their surfaces, permethylated α-CDs are also more soluble in water than their native counterparts, suggesting that hydrogen bonding among the OH groups is responsible for the relatively low aqueous solubility of the CDs themselves.

CD Rotaxanes

The first successful (noncovalent) template-directed synthesis of a rotaxane can be attributed to Ogino,[179] who used metal-ligand complexation to stopper (**Scheme 2.12**) a 1,12-diaminododecane / CD pseudorotaxane. Mixing the $H_2NC_{12}H_{24}NH_2$⊂*CD* pseudorotaxane (CD = α-CD or β-CD) with *cis*-dichlorobis(ethylenediamine)cobalt(III) chloride $[CoCl_2(en)_2]Cl$ in Me_2SO at 75 °C generates a dumbbell in which each of the primary amine termini have displaced a chloride ion coordinated to the Co^{III} centers. The population of diaminoalkanes that are threaded by a CD ring during this coordination-driven stoppering reaction become either **α-R207^{4+}** or **β-R207^{4+}**, which are isolated by precipitation from Me_2CO following size exclusion chromatography in 19 and 7% yields, respectively. The higher yield (19%) for the rotaxane **α-R207^{4+}** versus **β-R207^{4+}** reflects the higher affinity for alkanes (**Table 2.3**) exhibited by α-CD. These yields were high for rotaxane synthesis in 1981, but low by today's standards because of the formation of cobalt-containing side-products and a relatively low association constant between components in Me_2SO. Shimura[180,181] has produced similar Co^{III}-stoppered CD rotaxanes.

The Harada[182] group found that electrostatic endgroups on a hydrocarbon thread can increase significantly the activation barrier for threading. For example, a dodecylene chain terminated with tricationic (2-ammonioethyl)-4,4′-bipyridinium barriers requires more than six hours to reach equilibrium. These 'electrostatic stoppers' can be considered as a basis for the synthesis of α-CD rotaxanes by the so-called slippage protocol—see **Section 3.1**.

CD Rotaxanes that are stoppered by covalent bonds did not begin to appear until the early 1990s. A noteworthy example is the zwitterionic [2]rotaxane **R208** prepared by Kaifer[183] in 1991. This rotaxane is synthesized (**Scheme 2.13**) by an amide bond-forming reaction between a ferrocene-terminated

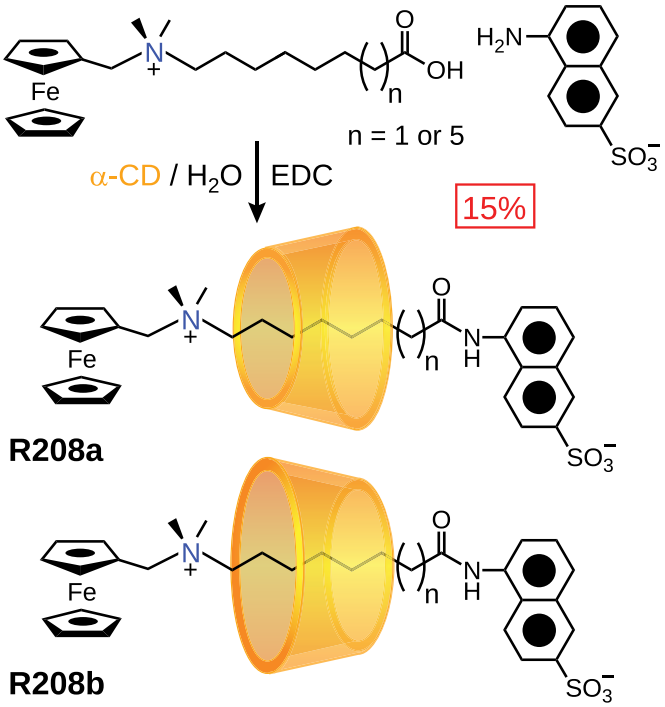


Rotaxane	CD	Yield (%)
α-R207^{4+}	α-CD	19
β-R207^{4+}	β-CD	7

Scheme 2.12 Ogino's seminal template-directed synthesis[179] of [2]rotaxanes comprising cyclodextrins threaded by 1,12-diaminododecane and capped with $Co^{III}(en)_2Cl$ coordination complexes.

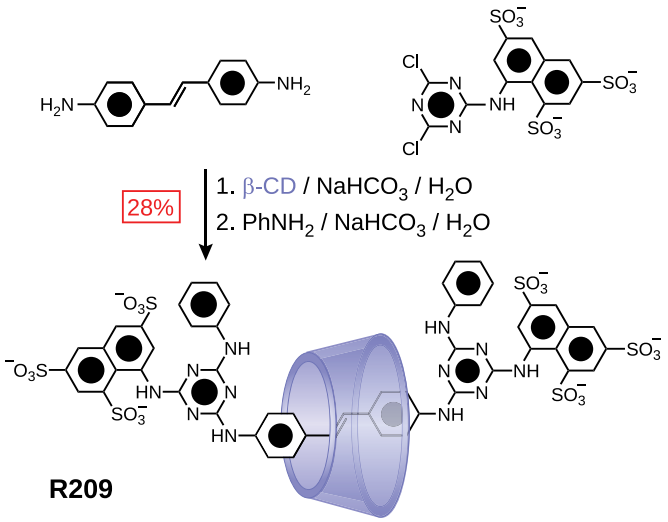
polymethylene half-dumbbell carrying a quaternary ammonium center and a 5-amino-2-naphthalene stopper in the presence of α-CD. The coupling reaction, which is mediated by the water-soluble reagent 1-ethyl-3-(3-diethylaminopropyl)carbodiimide (EDC), affords the rotaxane in 15% yield as a mixture of orientational isomers **R208a** and **R208b.** The efficiency of the reaction is identical for polymethylene chains with both 7 and 11 carbon atoms, and the α-CD ring does not exhibit any selectivity for which direction it faces with respect to the constitutionally unsymmetrical dumbbell. The orientational isomers have been separated by preparative thin-layer chromatography (TLC) and characterized. Surprisingly, a slow deslipping of the α-CD ring takes place in a solvent-dependent manner in **R208a**, yet the ring does not exit the dumbbell under any conditions in the case of **R208b**. This kind of discriminatory dethreading may serve as the basis for molecular motors and machines for which directionally biased motion is prerequisite—see **Section 6.12**.

Nakashima[184] introduced the concept of insulating chromophores using mechanically bonded CD rings by preparing the [2]rotaxane **R209**. The synthesis (**Scheme 2.14**)



Scheme 2.13 Synthesis of an asymmetric α-CD-based zwitterionic [2]rotaxane as a mixture of orientational isomers by EDC coupling in water.[183]

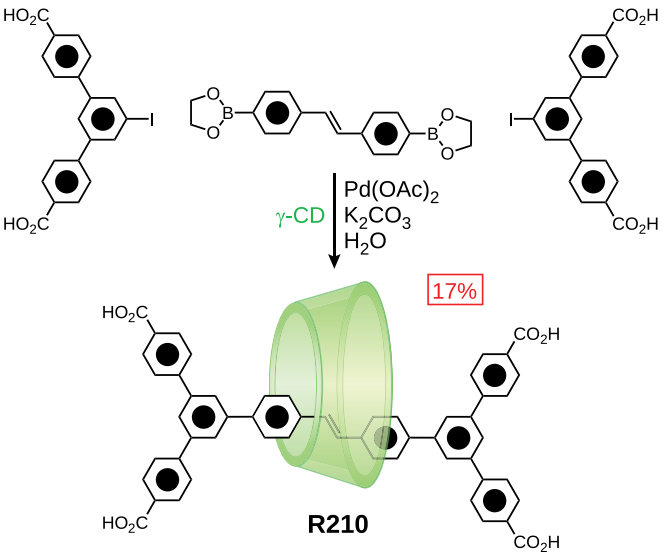
involves trapping kinetically a *4,4′-diaminostilbene⊂β-CD* pseudorotaxane with a triply sulfonated naphthalene stopper via a reactive dichlorotriazinyl linker under basic conditions ($NaHCO_3$) in water. The nucleophilicity of the amines is sufficient to displace the chloride leaving groups of the linker under these conditions. An aniline capping group is installed in a second step to passivate these reactive sites on the linker, affording **R209** in 28% yield over two steps. Nucleophilic aromatic substitution has also been utilized by Harada[185] to prepare CD rotaxanes. Beyond



Scheme 2.14 Nakashima's synthesis of a chromophoric β-CD [2]rotaxane using nucleophilic aromatic substitution.[184]

stilbenes, other types of conjugated templates for CD rotaxanes include azobenzenes,[186–190] cyanines,[191,192] tolan,[193] biphenyl,[193–195] tetrathiafulvalene,[196] oligothiophenes,[197–200] oligophenylene-ethynylenes,[174,201–203] and oligocarbynes.[204,205]

[2]Rotaxanes employing γ-CD as the ring component are relatively uncommon in comparison with those based on α-CD and β-CD. Anderson[206] prepared (**Scheme 2.15**) the chromophoric γ-CD [2]rotaxane **R210** by performing a Suzuki coupling between a boronic ester-terminated stilbene and an iodinated *meta*-terphenyl stopper in water. Anderson had already introduced the aqueous Suzuki coupling method for preparing α-CD and β-CD rotaxanes in the early 2000s.[193,207] Rotaxane **R210** possesses enough room inside of the γ-CD cavity to accommodate a second guest, which qualifies it as an excellent receptor for small hydrophobic molecules. This property has also enabled Anderson to synthesize[206] the first [3]rotaxane comprising two dumbbells threaded through a single ring—see **Section 4.2.1.2**.



Scheme 2.15 Synthesis of a γ-CD [2]rotaxane by Suzuki coupling.[206]

CD Polyrotaxanes

Although the cyclodextrins do not readily host small polyethers such as di- and triethylene glycol, Harada discovered[208] in 1990 that α-CD forms complexes with longer poly(ethylene glycol) (PEG) compounds with molecular weights exceeding ~400 Da (PEG400) in water. Aqueous mixtures of α-CD and PEG produce the corresponding polypseudorotaxanes as crystalline, nearly insoluble precipitates. The complexation is more efficient (**Figure 2.10**) as the molecular weight of the PEG backbone increases.[209] The different CDs recognize various polymer backbones with vastly different affinities—a fact which is illustrated by the selected examples summarized[210–215] in **Table 2.5**, which include poly(propylene glycol) (PPG),

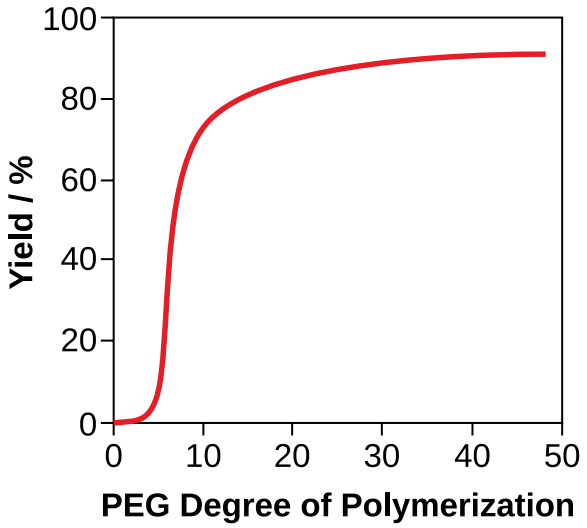
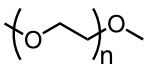
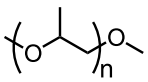
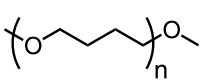
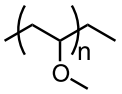
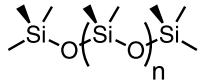


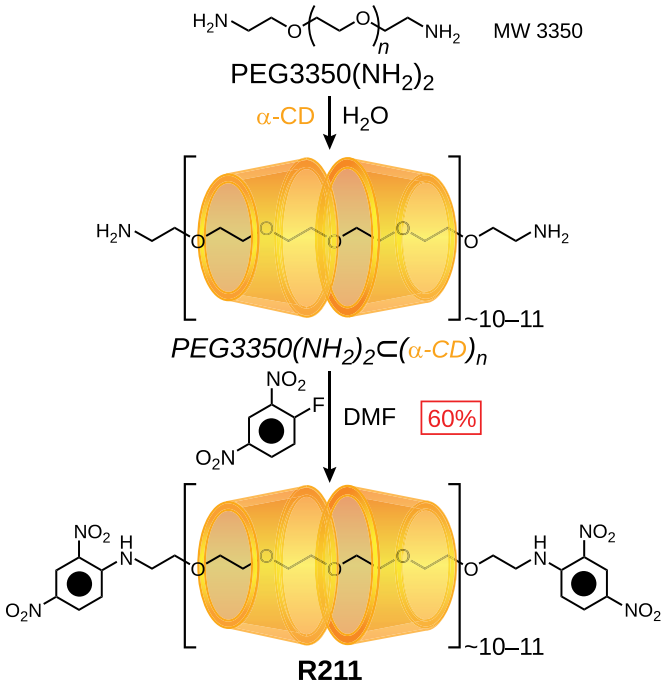
Figure 2.10 The yield of the *PEG⊂(α-CD)*$_n$ complexes as a function of the length of the PEG chain, based on data from ref. 209.

poly(tetrahydrofuran) (PTHF), poly(methyl vinyl ether) (PMVE), poly(isobutylene) (PIB), and poly(dimethylsiloxane) (PDMS). Harada's extensive work on characterizing many CD polypseudorotaxanes, which began with a number of seminal papers[208,209,211,214,216–218] in the 1990s, has not lost any steam in more recent years.[173,219–221]

The efficient self-assembly of CD polypseudorotaxanes has been a stepping-stone for the production of many CD polyrotaxanes. Since a comprehensive review of these polymers is beyond the scope of this monograph, readers are directed to the excellent review by Harada[173] on the

Table 2.5 The yields and threading ratios of polypseudorotaxanes formed between the CDs and various selected polymers.

Polymer		M_w (Da)	Yield Stoichiometry (monomer : CD) α-CD	β-CD	γ-CD	Ref
PEG		1000	91% 2:1	0%	trace	210
PPG		1000	0%	96% 2:1	80% 2:1	211
PTHF		250 (α-CD) 1000 (γ-CD)	82% 1.5:1		100% 2.8:1	212
PMVE		20,000	0%	0%	67% 3:1	213
PIB		500 (β-CD) 1350 (γ-CD)	0%	67%	96% 3:1	214
PDMS		760	0%	5%	91% 2:3	215



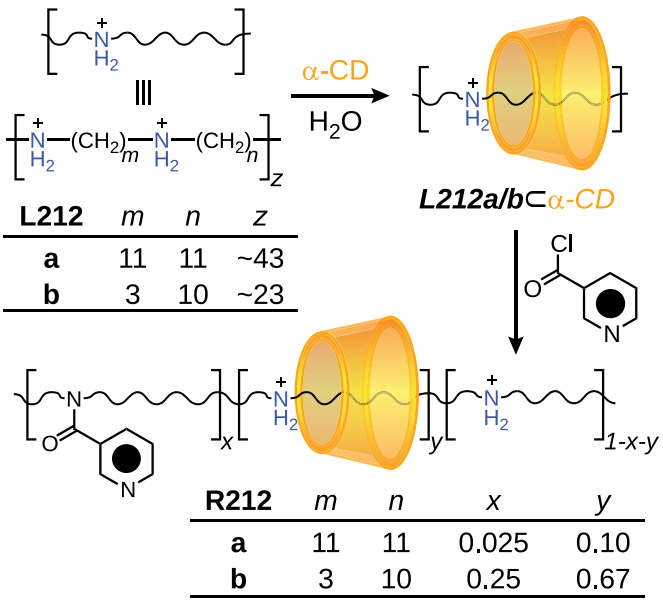
Scheme 2.16 Harada's seminal synthesis of an α-CD/PEG polyrotaxane.[216]

subject. Harada[216] laid claim to the first synthesis (**Scheme 2.16**) of a CD polyrotaxane in 1992. An amine-terminated polyether, PEG3350(NH_2)$_2$, was mixed with *α-CD* in water to generate the polypseudorotaxane *PEG3350(NH_2)$_2$⊂(α-CD)$_n$* as a crystalline precipitate. In a stoppering protocol, the complex was exposed overnight to an excess (46 equiv) of 2,4-dinitrofluorobenzene at room temperature in DMF, affording the polyrotaxane **R211** in 60% yield. The dinitrophenyl stoppers are bulky enough to prevent the rings from deslipping. The polyrotaxane, which is insoluble in water and DMF, yet soluble in Me_2SO and 0.1 M NaOH, contains an average of 20–23 α-CD rings per polymer chain. The rings predominantly self-organize into a 'channel-type' structure resembling a hydrogen bonded nanotube, in which neighboring rings orient themselves in a head-to-head / tail-to-tail packing arrangement.[210]

In addition to the low cost and wide availability of CD and polyether compounds, another convenience of this recognition system is that it does not necessarily require solvent. In 2005, Balik[222] and Harada[223] independently found that crystalline α-CD undergoes a crystal-to-crystal phase transition from a cage-like packing to the channel-type packing motif of the *PEG⊂(α-CD)$_n$* polypseudorotaxane upon mixing with a liquid sample of neat low molecular weight PEG. Takata[224,225] has devised a strategy for stoppering *PTHF⊂(α-CD)$_n$* polypseudorotaxanes in the solid state by simply grinding them in the presence of reactive stopper precursors. Isocyanate-functionalized stopper precursors have been successfully coupled[224,225] to hydroxyl-terminated PEG chains threaded by permethylated α-CD rings, while dinitroaryl stoppers with acid chloride or fluoride leaving groups have been coupled[226] to amine-terminated PEG chains threaded by natural α-CD rings under solvent-free conditions. Takata[227] has also relied on a cycloaddition between nitrile *N*-oxides and alkenes to stopper allyl-terminated *PEG⊂(α-CD)$_n$* pseudorotaxanes under solvent-free conditions by grinding at 70 °C for 1 h. Other solvent-free stoppering reactions are discussed in **Sections 2.3.3.2** and **2.3.4.6**.

The large cavity of γ-CD often accommodates two guests. Another one of Harada's[228] discoveries was the formation of double-stranded inclusion complexes involving γ-CD and PEG. Bulkier polymers such as PDMS, on the other hand, form[215] stable single-stranded pseudorotaxanes with γ-CD. The entries in **Table 2.5** show that the different CDs often exhibit remarkably different affinities for polymeric substrates, revealing that even modest changes to the size of a host cavity can result in dramatic changes in its recognition properties. Nevertheless, 'loose-fitting' single-stranded γ-CD polyrotaxanes have also been prepared, albeit in low yields, by Yui.[229]

Concurrently with Harada's efforts on the self assembly of CDs and neutral polymers, Wenz[230] was independently investigating CDs as hosts for polyelectrolytes. His first communication on the subject in 1992 employed (**Scheme 2.17**) poly(iminoundecamethylene) (**L212a**) and poly(iminotrimethylene-iminodecamethylene) (**L212b**) as the polyelectrolyte guests for CD rings. Wenz found that both α-CD and β-CD serve as hosts for these macromolecules. In contrast with Harada's polymers, these polyelectrolytes and their corresponding pseudorotaxanes are both fully soluble in water below neutral pH. The α-CD-based polypseudorotaxanes require a long time to reach equilibrium, while the β-CD homologues do not. The dialkylammonium units apparently serve as blocking groups, since ***L212b*⊂*α-CD*** requires much longer (170 h) than does ***L212a*⊂*α-CD*** (1.5



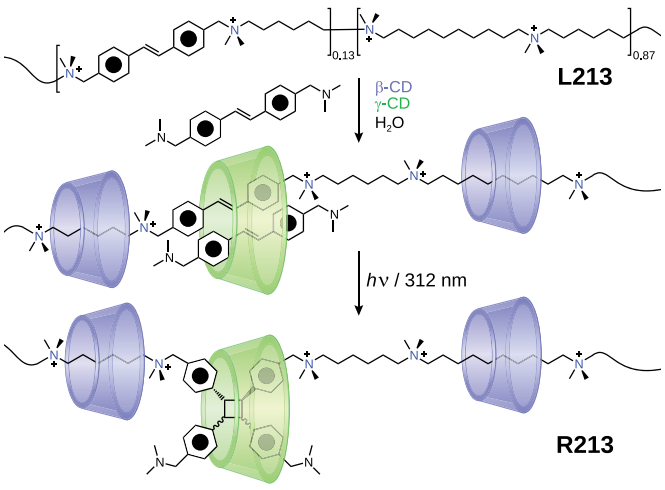
L212	*m*	*n*	*z*
a	11	11	~43
b	3	10	~23

R212	*m*	*n*	*x*	*y*
a	11	11	0.025	0.10
b	3	10	0.25	0.67

Scheme 2.17 Wenz's first synthesis of an α-CD polyrotaxane based on a polyelectrolyte backbone.[230]

h) to equilibrate after mixing. During equilibration, the threading of each new ring onto the end of the polymer chain requires that the ring before it moves inward toward the center of the polymer in order to open up a vacant binding site. These results indicate that the trimethylene units present a much larger barrier for the ring to pass over than the undecamethylene units, which may arise from the trimethylene chains being too short for the CD rings to bind effectively. This situation forces the CD rings to pass over two dialkylammonium centers between each binding site in **L212b**, as opposed to only one dialkylammonium center in the case of **L212a**. In order to stopper the pseudorotaxanes, some of the ammonium centers were allowed to react with nicotinyl chloride, which is bulky enough to prevent the passage of α-CD rings. The ratios of the CD-threaded, nicotinyl-stoppered, and unmodified repeating units in the polyrotaxane products **R212a/b** are summarized in **Scheme 2.17**.

Wenz[231] was also one of the first researchers to prepare (**Scheme 2.18**) polyrotaxanes employing γ-CD as the ring component. The γ-CD rings in the polyrotaxane **R213** promote its photochemical synthesis. Upon mixing the stilbene-containing polyelectrolyte copolymer **L213** with β-CD, γ-CD, and 4,4′-bis(dimethylamino)methylstilbene, the components self-assemble into the mixed-ring polypseudorotaxane in which the β-CD rings are thought to occupy primarily the quaternary ammonium-flanked polymethylene chains, while the γ-CD rings encircle the heterodimeric stilbene units. Photodimerization of two stilbene units—one in the polymer backbone and one as an additive in solution—is accomplished as a result of a [2+2] cycloaddition within the cavity of γ-CD under UV irradiation. Before photodimerization, both types of CD rings can be removed from the polymer by ultrafiltration. After photodimerization, ~20% of the included CDs remain associated with the polymer as a result of the blocking effect of the stilbene photodimers of **R213**.



Scheme 2.18 Photochemical synthesis of the mixed β-CD/γ-CD polyrotaxane **R213**, employing a [2+2]cycloaddition promoted by γ-CD in order to introduce stoppers on the polymer backbone.[231]

Although cyclodextrins larger than γ-CD are not commonly investigated in the context of rotaxane formation, it is also possible to make mechanical bonds with larger rings. Dodziuk[232] has reported a procedure for solubilizing single-walled carbon nanotubes (SWNTs) in water by sonicating them in the presence of the giant 12-membered η-CD ring, which is believed to encircle the SWNTs, forming a polypseudorotaxane. ^{1}H and ^{13}C NMR spectroscopic evidence, as well as molecular mechanics (MM) models, support the formation of polypseudorotaxanes in favor of those involving the η-CD rings associating with the SWNTs in some kind of side-on fashion. The MM simulations reveal (**Figure 2.11**) a tendency of the η-CD rings to move in pairs of hydrogen bonded head-to-head dimers analogous to those that constitute Harada's α-CD polyrotaxanes. Since only SWNTs with narrow diameters (≤1.22 nm) can fit within the η-CD cavity, these assemblies also effectively separate the smallest SWNTs from the larger ones by dispersing them selectively in water.

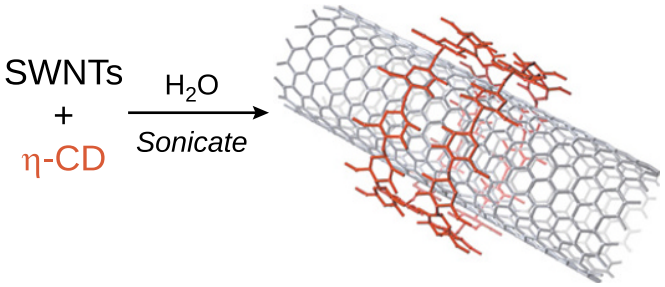
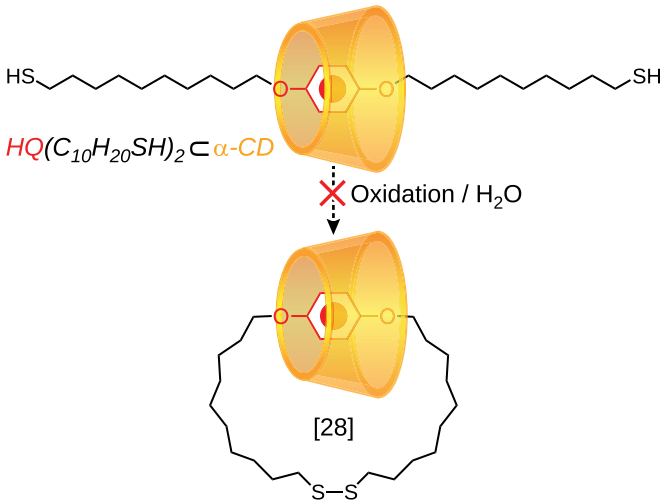


Figure 2.11 The large cavity of η-CD, which contains 12 glucose repeating units, threads onto ~1.2 nm diameter single-walled carbon nanotubes (SWNTs) and renders them water soluble. The simulation image on the right hand side is reproduced with permission from ref. 232 (copyright 2003 Royal Society of Chemistry).

CD Catenanes

Although the use of CD inclusion compounds as templates for forming mechanical bonds was not practiced until the 1980s, a 1958 publication[4] by Lüttringhaus, Cramer, Prinzbach, and Henglein reveals that a template-directed catenane synthesis was attempted even before the first statistical synthesis[5] had been reported. In a 'near miss' attempt (**Scheme 2.19**) at forming a [2]catenane derived from α-CD and $HQ(C_{10}H_{20}SH)_2$, the dimercaptodecyl ether of hydroquinone, only starting material was recovered after exposing the thiol-terminated pseudorotaxane *$HQ(C_{10}H_{20}SH)_2$⊂α-CD* to aqueous oxidative coupling conditions. It is not unlikely that the formation of the desired [2]catenane was inhibited by (i) the relatively small ring size (28) of the proposed macrocyclic disulfide, not to mention (ii) the increase in energy that will ensue on introducing gauche conformations all along the two decamethylene chains.

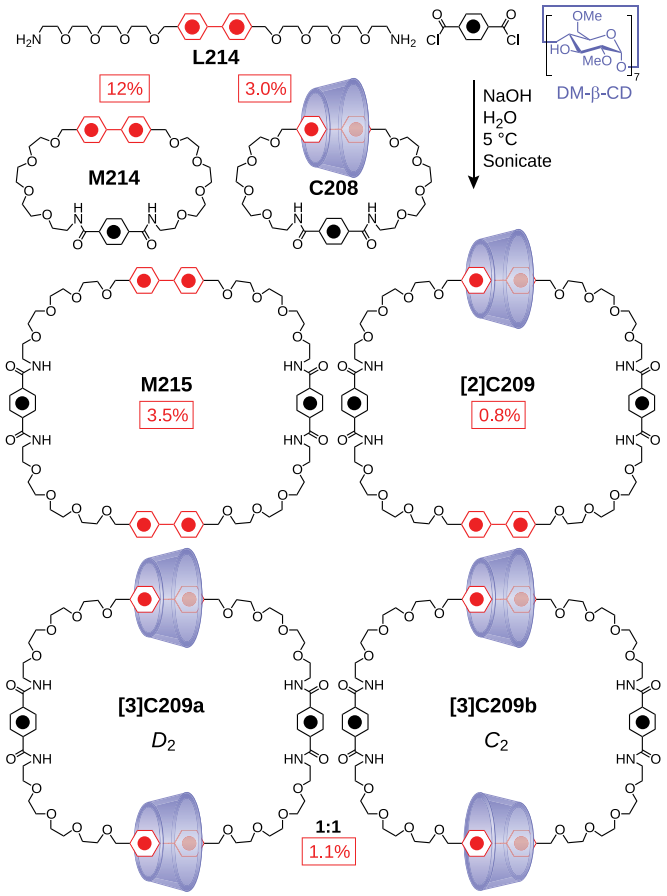
The first successful synthesis (**Scheme 2.20**) of catenated cyclodextrins was reported[233] in 1993. The methylated CD ring heptakis(2,6-di-*O*-methyl)-β-cyclodextrin



Scheme 2.19 The first reported attempt to prepare a [2]catenane.[4]

(DM-β-CD) was employed as the ring in order to improve solubility in organic solvents and thereby assist in purification of the catenated products. The deeper, more hydrophobic cavity of DM-β-CD relative to β-CD enhances its affinity for aromatic guests. In this case, an amine-terminated polyether of 4.4′-bitolyl (**L214**) comprises the axle of the corresponding pseudorotaxane ($K_a \approx 4 \times 10^4$ M^{-1} in D_2O) with DM-β-CD. A clipping reaction involving the coupling of **L214** with terephthaloyl chloride in water with 0.01 M aqueous NaOH (a Schotten-Baumann reaction) affords a mixture of cyclized products—two macrocycles **M214** and **M215**, the corresponding [2]catenanes **C208** and **[2]C209**, as well as a 1:1 mixture of the [3]catenane orientational isomers, **[3]C209a** and **[3]C209b**. These products were obtained from the $CHCl_3$ extracts of the crude reaction and separated by ordinary column chromatography. In the [3]catenane fraction, the presence of both orientational isomers, **[3]C209a** and **[3]C209b**, was confirmed unambiguously by the number of signals in the ^{13}C NMR spectra, since their different time-averaged molecular symmetries (C_2 and D_2) lead to different spectroscopic profiles. The relatively low yields (see **Scheme 2.20**) of these products indicates that the macrocyclization is inhibited by the presence of DM-β-CD. The solid-state structure of **C208** reveals (**Figure 2.12**) that the β-CD ring encircles the bitolyl unit, while the terephthalamide unit resides on the exterior. The oxygen atoms of the polyether chains do not engage in hydrogen-bonding interactions with the hydroxyl groups of the DM-β-CD ring, suggesting that the associative interactions are almost exclusively hydrophobic in nature. This protocol for making catenated CDs has been extended[234] to the synthesis of similar catenanes with topological chirality—see **Section 5.2.4.1**.

Another class of CD catenanes (**Scheme 2.21**) relies upon the self-assembly of trianglimines and their conversion to trianglamines. Trianglimines[235] are hexaimine macrocycles prepared by the [3+3] cyclocondensation of *trans*-1,2-diaminocyclohexane and aromatic dialdehydes. They



Scheme 2.20 One-pot synthesis[233] of [2]- and [3]catenanes based on the inclusion of bitolyl derivatives in β-CD. The [3]catenanes are obtained as an equimolar mixture of two orientational isomers.

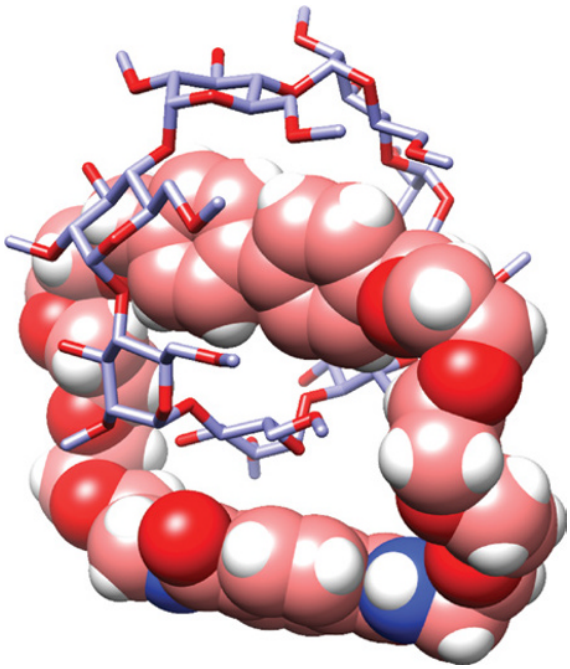
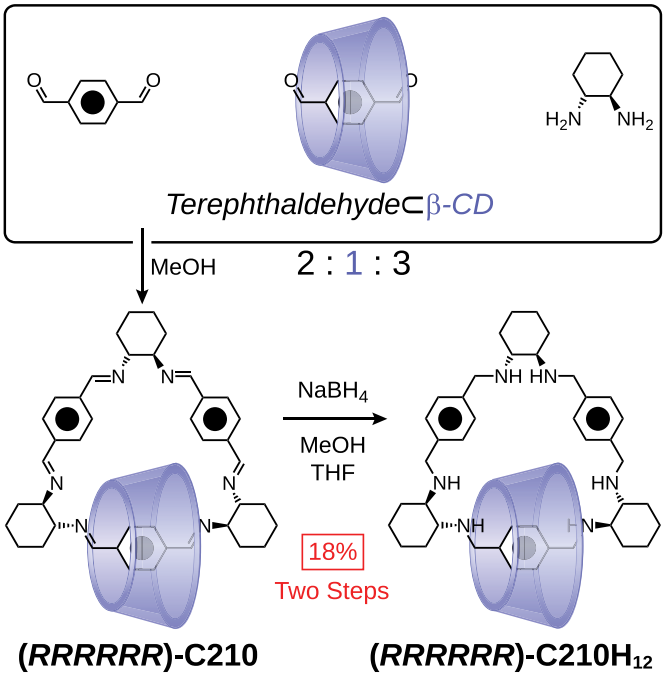


Figure 2.12 Solid-state structure of the [2]catenane **C208**,[233] with the β-CD ring and the synthetic macrocycle portrayed as tubular and space-filling representations, respectively. β-CD protons are omitted for the sake of clarity.

can be converted to trianglamines by reduction of the six imine bonds.[236] Kuhnert[237] has synthesized diastereoisomeric β-CD [2]catenanes with enantiopure trianglamines as the second ring component. The β-CD hexaimine catenanes **(*RRRRRR*)-C210** and **(*SSSSSS*)-C210** were first of all self-assembled from mixing 1.0 equiv of a *terephthaldehyde⊂β-CD* inclusion complex, 2.0 equiv terephthaldehyde, and 3.0 equiv of either (1*R*,2*R*)- or (1*S*,2*S*)-cyclohexanediamine, respectively, in MeOH for two days at room temperature. The crude product of this reaction constitutes approximately 75% trianglimine and 25% catenane. Reduction of the imine bonds *in situ* with $NaBH_4$ affords the corresponding trianglamine catenanes, either **(*RRRRRR*)-C210H$_{12}$** or **(*SSSSSS*)-C210H$_{12}$**, in 18% isolated yield after preparative thin layer chromatography. Only the synthesis of **(*RRRRRR*)-C210H$_{12}$** is depicted in **Scheme 2.21**. This



Scheme 2.21 Synthesis[237] of a trianglamine [2]catenane derived from terephthaldehyde, (*RR*)-1,2-diaminocyclohexane, and β-CD.

simple approach to making catenated CDs is noteworthy because it employs reversible bond forming chemistry to prepare catenanes under thermodynamic control—see **Chapter 3**—and because it relies exclusively on inexpensive, off-the-shelf starting materials and reagents.

2.3.1.2 Cucurbiturils

The cucurbit[*n*]urils (CB*n*) are a family[238] of cyclic methylene-bridged glycoluril oligomers, where *n* represents the number of repeating glycoluril units in the ring. CB6 (**Figure 2.13**), which is the most common and thermodynamically stable member of the CB*n* family, was first isolated in 1905 by Behrend[239] when he carried out the condensation of glycoluril and formaldehyde in concentrated HCl, affording an insoluble precipitate known as Behrend's polymer. It was not until over 75 years later, in 1981, when Behrend's

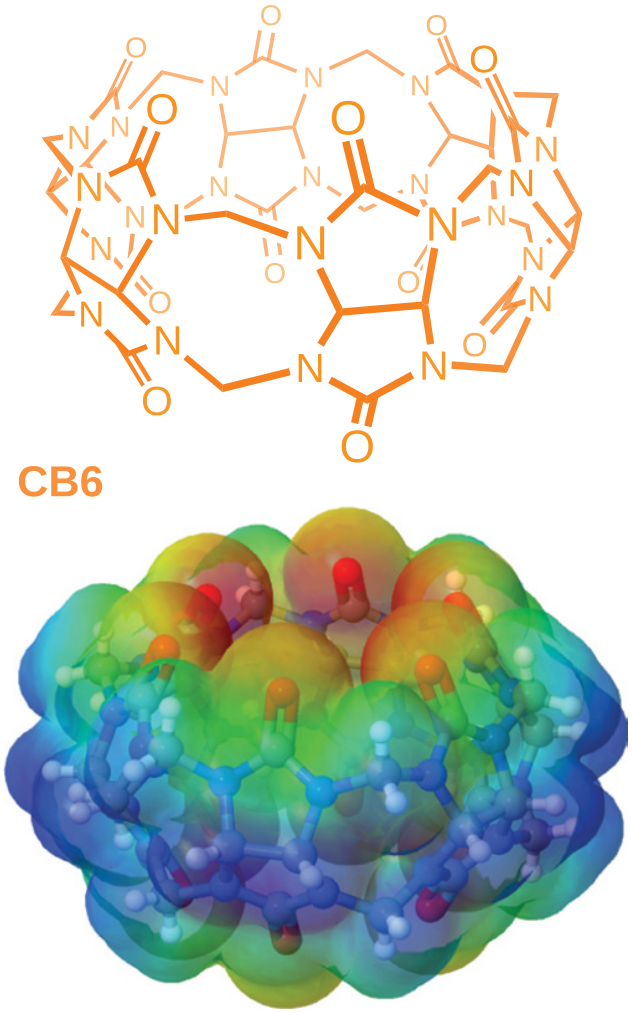


Figure 2.13 The structural formula and electrostatic potential map of cucurbit[6]uril[240] (CB6). Warmer colors (red, orange) represent negative electrostatic potential and cooler colors (blue) represent positive potential.

polymer was revisited by Mock[240] and shown crystallographically to be a cyclic hexamer, that the structure and name[D] of the cucurbiturils were established. CB6 was the only known member of this family of receptors until the turn of the millennium, when CB5, CB7, CB8, and CB10 were synthesized under milder, kinetically controlled conditions in the laboratories of Kim[241] and Day.[242,243] The structures and dimensions of CB5–CB8 are shown in **Figure 2.14**. Although the cucurbiturils were discovered contemporaneously with the cyclodextrins, investigations into their properties as hosts in supramolecular chemistry by leaders such as Mock,[244] Kim,[245,246] Buschmann,[247] Nau,[248] Kaifer,[249] Isaacs,[250,251] Scherman,[252] Masson,[253] and others began several decades after inclusion phenomena in CDs were first described by Cramer.[146–150]

The cucurbiturils possess a number of desirable properties that have made them useful components in supramolecular

[D] Mock named cucurbiturils after the gourd plant family *cucurbitaceae* because their structures resemble the shape of a pumpkin.

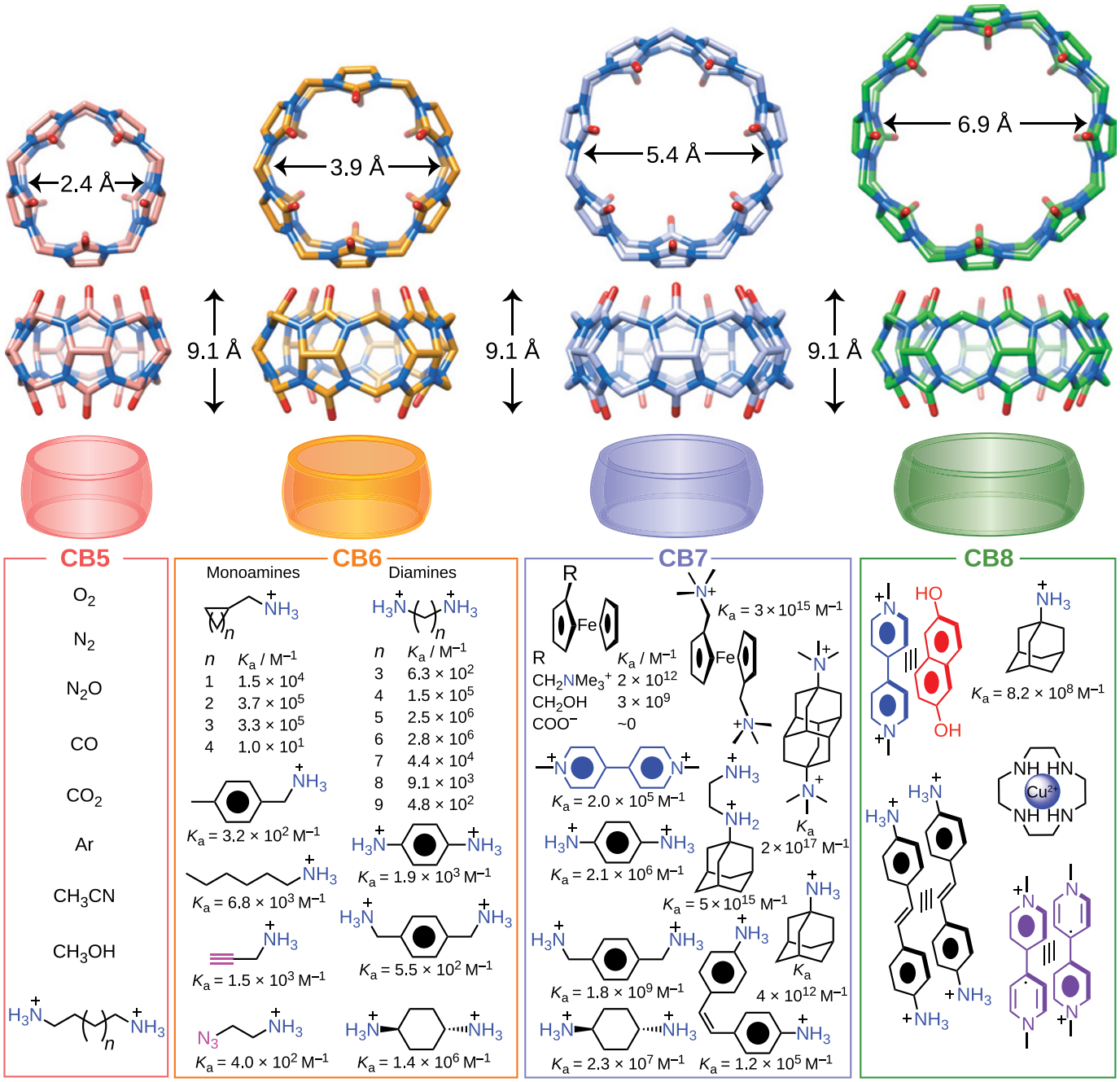


Figure 2.14 Single crystal X-ray structures,[240,241] dimensions, graphical representations, and selected examples of guests for the cucurbit[*n*]-urils CB5,[256,257] CB6,[238,262–265] CB7,[238,241,245,267,269,271,273,274] and CB8.[238,276,277,280,283] K_a values are reported for complexes in water.

and mechanically bonded systems, including (i) commercial availability in four sizes (CB5–CB8), (ii) structural stability, (iii) amenability to synthetic modifications, (iv) solubility in aqueous and organic solvents, (v) high symmetry, (vi) a promiscuity for a wide range of guests with (vii) a highly tunable energetic landscape governing the thermodynamics and kinetics of complexation, and (viii) an ability to promote (*vide infra*) the 1,3-dipolar azide-alkyne cycloaddition without a Cu^I catalyst. CB6 and CB8 are essentially insoluble in water, while CB5 and CB7 are sparingly soluble (20–30 mM) in water. The conjugate acids of the CBs have pK_a values of approximately 3, typically giving them high solubility (>60 mM) in acidic media,[254] such as 1:1 HOAc:H_2O or 3 M HCl. The negative electrostatic potential around the portals of the CB*n* annulus (see **Figure 2.13**) makes them predisposed to hosting cationic guests.

Figure 2.14 summarizes the association constants for a number of host-guest complexes involving CBs in water. On account of their different cavity sizes, each member of the CB family is prone to hosting differently sized guests. CB5 and its decamethylated homologue Me_{10}CB5[255] bind some small lipophilic gases[256] (N_2, O_2, Ar, N_2O, CO, CO_2)

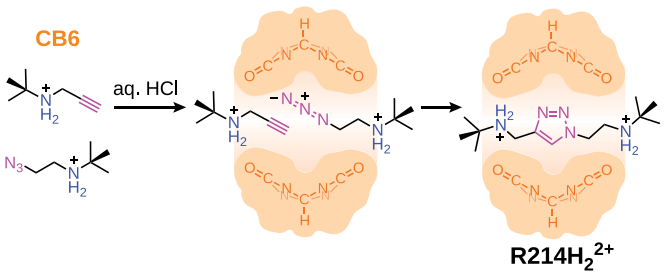
and solvents such as MeCN and MeOH.[257] CB5 can also bind alkylamines weakly, whereas the slightly more rigid Me_{10}CB5 cannot.[258,259] Cations such as Pb^{2+} and NH_4^+ also associate[260,261] with CB5 by capping the portals rather than entering the cavity. CB6 is an especially good host for diaminoalkanes,[262,263] with K_a values exceeding 10^6 M^{-1} in the case of 1,6-diaminohexane. CB6 can also host methylamine functionalized cycloalkanes[264,265] and a number of *para*-substituted aromatic rings. The tightest binding synthetic host-guest complexes that have been observed in aqueous solutions are based on CB7 and CB8, which can host a number of aromatic guests[249]—most notably naphthalenes,[241,266] viologens,[267,268] and bulky groups such as ferrocenes,[269] adamantanes and bicyclic compounds,[270,271] and carboranes,[272] especially when these guests are appended with cationic moieties. 1-Adamantylamine hydrochloride and (ferrocenylmethyl)trimethylammonium, for example, both bind CB7 with association constants of $>10^{12}$ M^{-1} in water. Even more remarkably, CB7 binds bis(trimethylammoniomethyl)ferrocene[273] and *N*-(adamantyl)ethane-1,2-diammonium[271] with K_a values exceeding 10^{15} M^{-1} in water, as well as bis(trimethylammonium)diadamantane[274] with attomolar ($K_a > 10^{17}$ M^{-1}) affinity. These stability constants are among the very highest for non-polyvalent host-guest complexes, exceeding even the biological biotin–avidin complex, which has become a cornerstone of analytical biochemistry.[275] An anionic ferrocenecarboxylate guest exhibits essentially no affinity for the CB7 host,[269] highlighting the sensitivity of CB recognition properties to electrostatic forces. CB8 binds many of the same guests as CB7, yet with its larger cavity it is also capable of accommodating two guests, including (i) naphthalene[241] and stilbene[276] homodimers, (ii) viologen[277,278] and tetrathiafulvalene[279] radical dimers, (iii) donor-acceptor charge-transfer heterodimers,[280–282] and (iv) metal-crown complexes such as *Cu^{II}⊂aza[12]crown-4*.[283]

In general, the self-assembly of inclusion complexes based on the CB*n* family of synthetic receptors is driven enthalpically by electrostatic, ion-dipole, and/or hydrogen-bonding interactions involving the carbonyl-lined rims of the hosts, as well as being driven entropically by the release[284] of high-energy water molecules from the CB*n* cavities. The promiscuity of the CB*n* hosts for various dyes, toxins, substrates, and drugs renders them promising compounds, not only for making mechanically interlocked molecules,[285] but also for participating in a range of medical and industrial applications.[238,286]

Dumbbell Capture of CB6 Rotaxanes

Mock[287] discovered in 1983 that CB6 is capable of promoting the 1,3-dipolar azide-alkyne cycloaddition within its cavity, even in the absence of a Cu^I catalyst, which is often employed nowadays in 'click chemistry'.[288] A ~10^5-fold rate enhancement is observed when both the alkyne and azide substrates are designed appropriately with ammonium groups to bind the CB6 portals. Mock investigated the binding affinities (**Figure 2.14**) of propargylammonium and 2-azidoethanammonium as guests and determined that their pairwise binding exceeds the volume capacity of the CB6 host to a greater extent than the transition state of their corresponding cycloadduct. This catalytic effect of the CB6 cavity is explained by the Pauling principle,[289] which states that an enzyme's active site binds the transition state of a catalytic reaction more strongly than it binds the reactants.

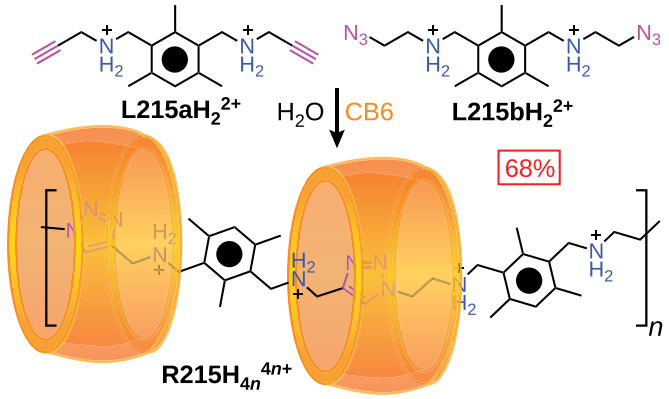
Mock's discovery of the CB6-catalyzed 1,3-dipolar azide-alkyne cycloaddition (CB6AAC) led him to the first synthesis (**Scheme 2.22**) of a CB6 rotaxane[19] using what can be referred to as the 'dumbbell capture' strategy. When the secondary dialkylammonium sites of the propargylammonium and 2-azidoethanammonium substrates are functionalized with *tert*-butyl groups, the cycloadduct which is formed within the CB6 cavity during the CB6AAC reaction cannot be expelled subsequently on account of the bulky ^{t}Bu stoppers at the periphery of the newly formed dumbbell. Although this [2]rotaxane, **R214H$_2^{2+}$**, was not isolated and fully characterized, Tuncel and Steinke[290] repeated Mock's synthesis in 1999 and obtained the rotaxane in 76% yield. The space-filling representation illustrates (**Scheme 2.22**) the conjectured fit of the reactants and cycloadduct within the CB6 cavity. Mock's approach represents a milestone in the synthesis of mechanical bonds because he simultaneously accomplished two 'firsts'—(i) synthesizing the first rotaxane employing a cucurbituril ring and (ii) the first rotaxane synthesis by dumbbell capture.



Scheme 2.22 Mock's synthesis of the first CB6 rotaxane by dumbbell capture, employing the CB6AAC reaction.[19]

Tuncel and Steinke[290] adapted Mock's procedure to prepare (**Scheme 2.23**) 'catalytically self-threading polyrotaxanes'.[E] They prepared two monomers, **L215aH$_2^{2+}$** and **L215bH$_2^{2+}$**—each of them possessing a mesitylene central core flanked by methylene linkers to propargylammonium and 2-azidoethylammonium moieties, respectively. Since each precursor possesses two reactive groups, subjecting these monomers to the CB6AAC reaction leads to ABAB polymerization rather than AB dimerization. The polyrotaxane **R215H$_{4n}^{4n+}$** (MW ≈ 10 kDa) was obtained in 68% yield upon mixing equal ratios of **L215aH$_2^{2+}$** and **L215bH$_2^{2+}$** at room temperature in the presence

[E] 'Catalytic' is, technically speaking, not the most appropriate term to describe the CB6AAC reaction when the product is a rotaxane, since the mechanical bond prevents catalytic turnover from taking place by forbidding the 'catalyst'—i.e., the ring—from dissociating with the product—i.e., the dumbbell.



Scheme 2.23 CB6-Promoted capture polymerization of a polyrotaxane.[290]

of 2 equiv of CB6 for 24 h. Since the azide-alkyne cycloaddition is prohibitively slow in the absence of CB6, the rotaxanation protocol is essentially error-proof—i.e., a mechanical bond is always formed concomitantly with a triazole unit. Tuncel has gone on to prepare a number of multicomponent rotaxanes and polyrotaxanes using similar capture protocols.[291–294]

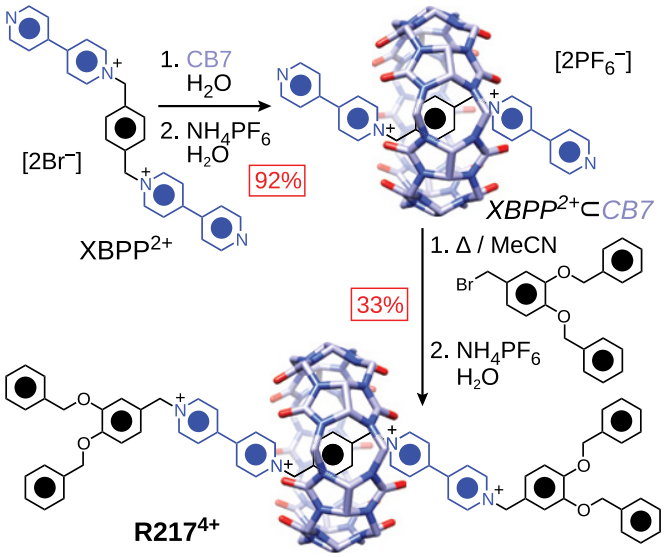
Lucarini[295,296] has used Mock's dumbbell capture reaction to prepare [3]rotaxanes with spin-labeled stoppers comprising the stable nitroxide radical (2,2,6,6-tetramethylpiperidin-1-yl)oxidanyl (TEMPO) in order to determine the end-to-end distance by pulsed electron double-resonance (PELDOR) spectroscopy, which confirmed that rotaxanes prepared by CB6AAC behave as rigid rods in solution.

The CB-promoted capture of rotaxanes has also been expanded upon in recent years to the facile preparation of hetero[*n*]rotaxanes. See **Section 2.3.1.3**.

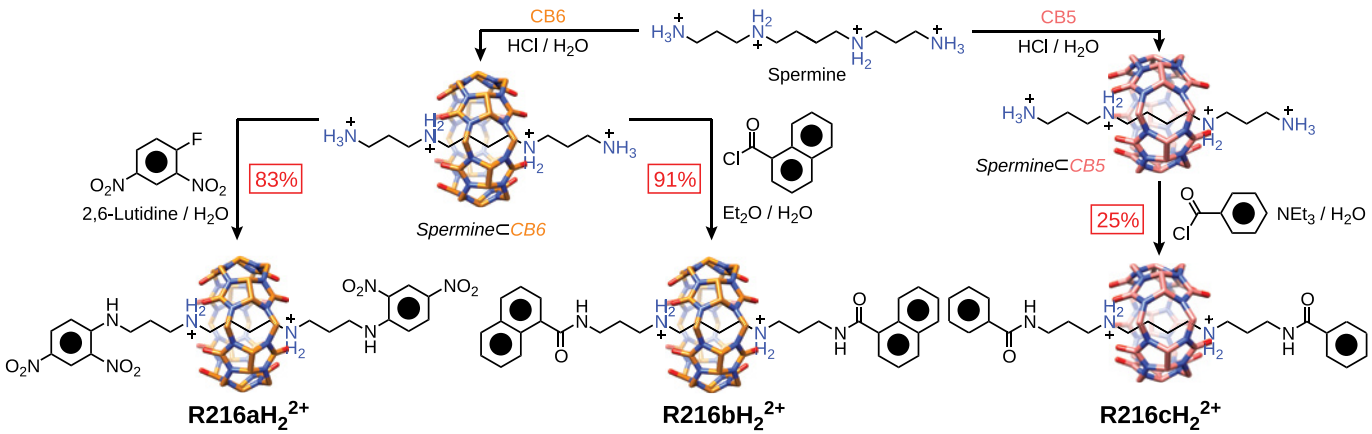
Other CBn Mechanomolecules

Kimoon Kim[297] introduced the first example of a stoppering protocol (**Scheme 2.24**) for making CB*n* rotaxanes in 1996. Realizing that spermine binds CB6 in water with high affinity ($K_a \approx 10^7$ M^{-1}) while possessing easily modifiable amines on each end, he capped a *spermine⊂CB6* pseudorotaxane with bulky dinitrophenyl groups using the same procedure developed by Harada[216] for his polyrotaxanes in 1992—see **Scheme 2.16**. Kim's protocol affords the [2]rotaxane **R216aH$_2^{2+}$** from off-the-shelf materials in high (83%) yield. Buschmann[298] has also prepared (**Scheme 2.24**) *spermine⊂CB6* rotaxanes such as **R216bH$_2^{2+}$** in up to 91% yield by reacting acid chloride stopper precursors with the spermine termini. The same approach was applied to the synthesis of oligo- and polyrotaxanes with diaminoalkane dumbbells,[299] as well as to the synthesis[259] of the CB5/spermine [2]rotaxane **R216cH$_2^{2+}$**.

CB7 is capable of adopting different binding modes with viologen derivatives. Whereas the CB7 ring is centered over the central BIPY^{2+} unit in dimethyl- or diethylviologen guests, it encircles the aliphatic side chains when they possess more than three carbon atoms.[300] In this knowledge, Kaifer[301] employed *para*-xylylene-bis(4-(4-pyridyl)pyridinium (XBPP^{2+}) as a guest for CB7 and precursor for the synthesis (**Scheme 2.25**) of the first CB7 rotaxane. The pseudorotaxane *XBPP·2Br⊂CB7* self-assembles in water within 1 h and can be isolated by precipitation with aqueous NH_4PF_6. The soft



Scheme 2.25 Kaifer's synthesis[301] of the first CB7 [2]rotaxane.

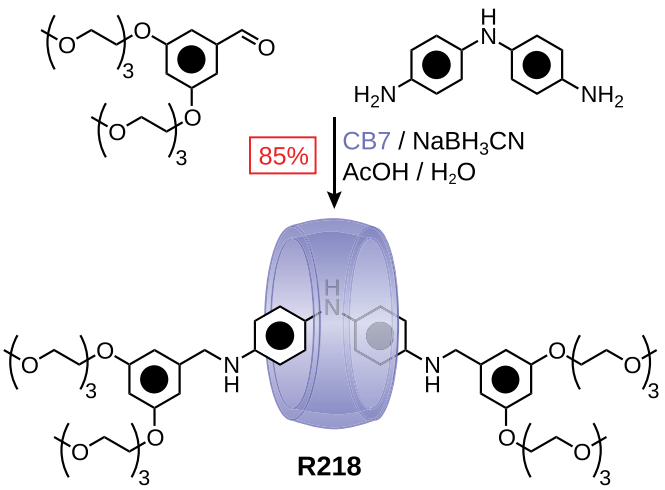


Scheme 2.24 Facile synthesis of [2]rotaxanes derived from spermine axles and CB5 or CB6 rings using aqueous stoppering protocols.[259,297,298]

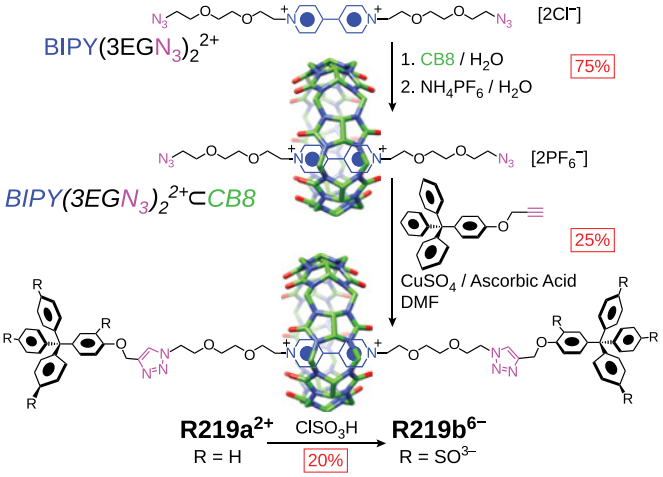
hexafluorophosphate counterions of the *XBPP·2PF$_6$⊂CB7* complex render it soluble in polar organic solvents. Exposing *XBPP^{2+}⊂CB7* to 3,4-bis(benzyloxy)benzyl chloride in refluxing MeCN affords the [2]rotaxane **R217^{4+}**, which was isolated in 33% yield after precipitation from hot water as its PF_6^- salt. More recently, Kaifer[302] has prepared a CB7 [2]rotaxane based on a single viologen unit as the template using a slippage mechanism—see **Section 3.1**.

A CB7 rotaxane has been prepared (**Scheme 2.26**) by Anderson[303] using aqueous reductive amination. His approach relies on the inclusion (K_a > 2.2 × 10^6 M^{-1}) of a short oligoaniline within a CB7 ring and the ability of $NaBH_3CN$ to reduce imines to amines selectively without reducing aldehydes, a feature which allows the aldehyde stopper precursor to be attached efficiently to the oligoaniline guest despite the high frequency of imine bond hydrolysis in water. The [2]rotaxane **R218** was obtained in up to 85% yield when the aldehyde stopper precursor was used in excess. The mechanical bond of this rotaxane also stabilizes an oligoaniline radical cation in the dumbbell.

Exploiting the ability of CB8 to bind either one guest or two guests of a heteroternary complex sequentially, Urbach[304] produced (**Scheme 2.27**) the first example of a CB8 rotaxane in 2011. The 4,4′-bipyridinium (BIPY^{2+}) guest, BIPY(3EGN$_3$)$_2^{2+}$, which possesses two azide-terminated triethylene glycol linkers, was encapsulated by CB8 in water as the Cl^- salt and subsequently precipitated from water as the PF_6^- salt with aqueous NH_4PF_6. Employing the Cu^I-catalyzed azide-alkyne 1,3-dipolar cycloaddition (CuAAC) to stopper the organic-soluble pseudorotaxane *BIPY(3EGN$_3$)$_2^{2+}$⊂CB8* with propargyloxy-tetraphenylmethane, the [2]rotaxane **R219a^{2+}** was obtained in 25% yield. The rotaxane **R219a^{2+}** and its ability to host electron-rich guests in the CB8 ring's open site can be investigated in polar organic solvents, or it can be converted to the water-soluble octasulfonated homologue **R219b^{6-}** after treatment with chlorosulfonic acid. It has been verified that the dumbbell of



Scheme 2.26 Anderson's synthesis of a CB7 [2]rotaxane by reductive amination.[303]



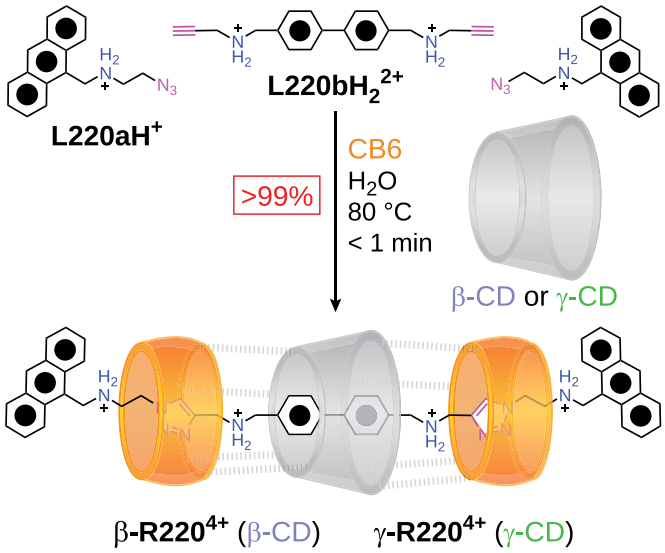
Scheme 2.27 Urbach's click synthesis[304] of the organic-soluble CB8 [2]rotaxane **R219a^{2+}** and sulfonated water-soluble analogue **R219b^{6-}**.

R219b^{6-} does not interfere with the ability of the CB8 ring to encapsulate a second guest such as 3,7-dihydroxynaphthalene, making this rotaxane an example of a mechanically interlocked receptor.

Kim[285] has made extensive use of CB*n* hosts in the synthesis of more challenging catenated architectures by appending metal ligating moieties to the termini of diaminoalkane guests. See **Sections 4.1.2.2**, **4.2.1.1**, and **4.2.3.8** for CB-based MIMs that have been prepared using his approach, including multicatenanes known as 'molecular necklaces' and a number of one-, two-, and three-dimensional catenated coordination polymers. Related macrocyclic oligomers based on methylene bridged urils, such as hemicucurb[*n*]iturils[305] and babus[*n*]urils,[306] appear to be potentially suitable for novel interlaced recognition motifs.

2.3.1.3 Cooperative Capture

A 'cooperative capture' strategy[307] for the efficient synthesis of mechanical bonds has been described recently.[165,308,309] It takes advantage of (i) the ability of CB6 to promote the azide-alkyne cycloaddition—i.e., the CB6AAC capture reaction, and (ii) cooperative binding interactions[310–314] between CB6 and hydrogen bond donating macrocycles, such as cyclodextrins and pillararenes, in the presence of a suitable template. The cooperative capture strategy was introduced[165] in the synthesis (**Scheme 2.28**) of the hetero[4]rotaxanes **β-R220^{4+}** and **γ-R220^{4+}**. These rotaxanes are obtained in >99% yield in <1 min at 80 °C in water upon mixing (i) *N*-(anthracen-9-ylmethyl)-2-azidoethanammonium chloride (**L220aH$^+$**), (ii) bis(propargylammonium)bitolyl dichloride (**L220bH$_2^{2+}$**), (iii) either β-CD or γ-CD, and (iv) CB6 in a 1:2:1:2 molar ratio, respectively. Isothermal titration calorimetry (ITC) experiments reveal that the ***L220bH$_2^{2+}$⊂CD*** pseudorotaxane stabilities are enhanced up to 20-fold in the presence of CB6, most likely as a result of multiple hydrogen-bonding interactions between the two kinds of hosts.

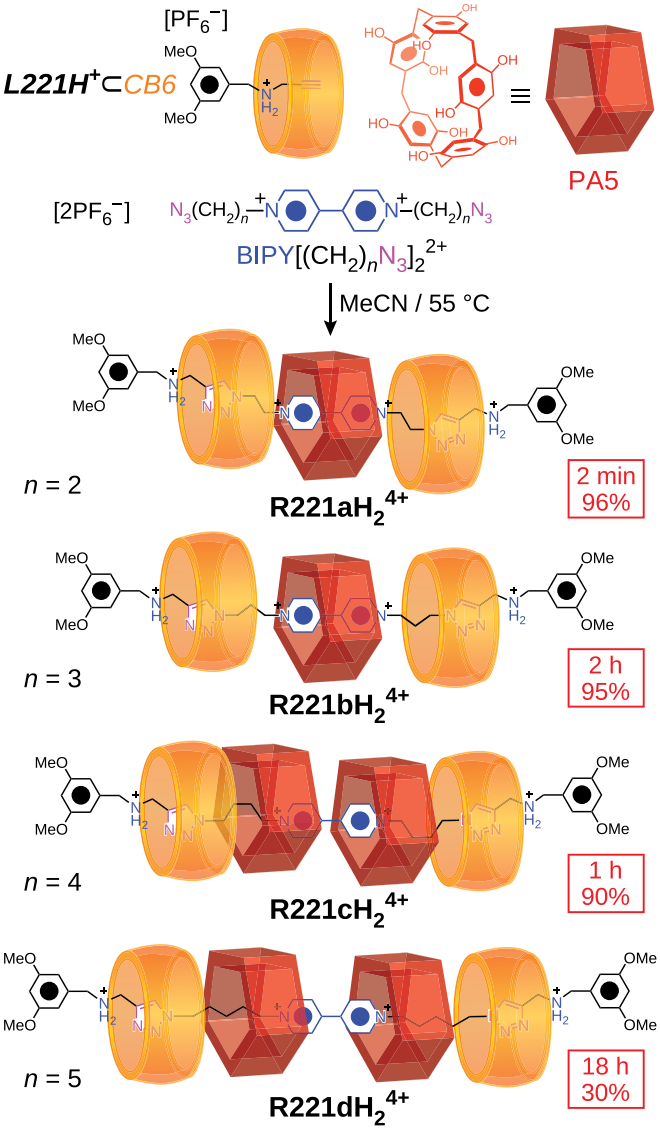


Scheme 2.28 Efficient synthesis of cyclodextrin / CB6 hetero[4]-rotaxanes by cooperative capture.[165]

Positive cooperativity among the rings is also evident from control experiments in which it was shown that the CB6AAC reaction proceeds much more slowly and does not reach completion in the absence of β-CD or γ-CD. This procedure has been adapted[165] to prepare a polyrotaxane with over 64 rings and a molecular weight of approximately 86 kDa. See **Section 4.2.1.1**.

The role of the CD rings in the cooperative capture reaction—call it the CD/CB6AAC reaction—can be compared to that of a coenzyme in biology, which participates in the binding of a substrate to the active site of another enzyme. Another class of 'cofactors' that have been found[308,309] to facilitate the CB6AAC cooperative capture reaction are the pillar[*n*]arenes[315,316] (PA*n*)—see **Section 2.3.9.2**—which are macrocycles comprising *n* hydroquinone rings, each connected through *para*-methylene bridges. Like the cyclodextrins, pillar[*n*]arenes can donate hydrogen bonds by virtue of having *n* hydroxyl groups surrounding each rim of the ring. It transpires that employing pillar[*5*]arene (PA5) as a co-factor in the cooperative capture reaction (**Scheme 2.29**) renders the reaction more tolerant of cationic substrates.[308] Since no solvent could be identified which dissolves both CB6 and PA5 simultaneously, the capped propargylammonium inclusion complex ***L221H*⁺⊂*CB6*** was pre-assembled[F] in water and precipitated as the PF_6^- salt in order to dissolve it in polar organic solvents. This complex was then mixed with PA5 and any of a series of azidoalkyl viologen templates, $BIPY[(CH_2)_nN_3]_2^{2+}$ (*n* = 2–5) at 55 °C in MeCN to produce hetero[*n*]rotaxanes. The outcome of the reaction depends on the length of this linker, affording the [4]rotaxanes **R221aH$_2^{4+}$** (*n* = 2, 96%) and **R221bH$_2^{4+}$** (*n* = 3, 95%) in the case of the shorter linkers, and the [5]rotaxanes **R221cH$_2^{4+}$** (*n* = 4, 90%) and **R221dH$_2^{4+}$** (*n* = 5, 30%) in the case of the longer linkers. Thus, whereas the CB6AAC and the CD/CB6AAC reactions only tolerate azide substrates separated by two methylene units from a cationic center, the PA5/CB6AAC reaction tolerates azide linkers with up to five methylene groups.

The PA5 ring encircling the $BIPY[(CH_2)_nN_3]_2^{2+}$ template apparently stabilizes an otherwise unfavorable binding



Scheme 2.29 The cooperative capture reactions employing pillar[5]arene as a co-factor expand the scope of CB6AAC-compatible substrates, providing access to [4]- and [5]heterorotaxanes with varying dumbbell lengths derived from azidoalkyl viologen axles and propargylammonium-derived stoppers.[308]

[F] It is preferable to use the binary complex ***L221H*⁺⊂*CB6*** rather than the more thermodynamically stable ternary complex ***[L221H⁺]$_2$*⊂CB6** because the second cationic substrate in the ternary complex competes with the viologen template for the CB6 cavity and reduces the efficiency of the PA5/CB6AAC reaction. The binary complex disproportionates into the ternary complex and free CB6 overnight at room temperature in MeCN, an event which can be avoided at elevated temperatures. Starting from an equimolar aqueous mixture of **L221H⁺** and CB6, precipitation with KPF_6 affords the binary complex, whereas precipitation with NH_4PF_6 affords the ternary complex.

geometry for the preorganized ***L221H***$^{+}$⊂*CB6* complex, allowing the azide moiety to enter the CB6 cavity where it can form a cycloadduct. It has been suggested that this process is facilitated by the mobility of the PA5 ring. For the short bi- and trimethylene linkers, the PA5 ring most likely moves along the vector of the viologen template after installing the first triazole unit in order to facilitate the binding and cycloaddition of the second stopper. The longer tetra- and pentamethylene linkers provide sufficient space for two PA5 rings to occupy as they interact, both with each other and with the CB6 portals of the preorganized stopper complexes, giving rise to hetero[5]rotaxanes instead of hetero[4]rotaxanes. The PA5 cofactors therefore serve as "molecular gaskets" in the efficient formation of these novel architectures. Recently, a pillar[6]arene (PA6) has been employed[309] as a co-factor in the cooperative capture of an oligo-hetero[4]rotaxane using an extended viologen template. The solid-state structure of this compound is portrayed in **Section 4.2.1**, **Figure 4.43**. The cooperative capture reaction has also enabled the construction[317] of a fluorescent rotaxane dye which is a key component in a novel type of encrypted aqueous security ink. See **Section 4.2.1.1**.

2.3.1.4 Ionic Cyclophanes

In the early 1980s, Diederich[318–321] introduced a new family[322] of tetraoxa[*n*.1.*n*.1]paracyclophanes[G] (TO*n*1*n*1PC) as aqueous macrocyclic receptors and described their ability to host neutral hydrophobic guests. The generalized structure of this family of macrocycles, which comprise two dialkoxyphenylmethane units and two oligomethylene chains, is illustrated in **Figure 2.15**. The diphenylmethane units are often substituted with ionic R groups to impart

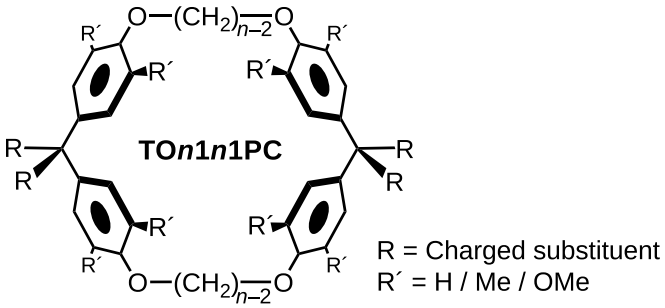
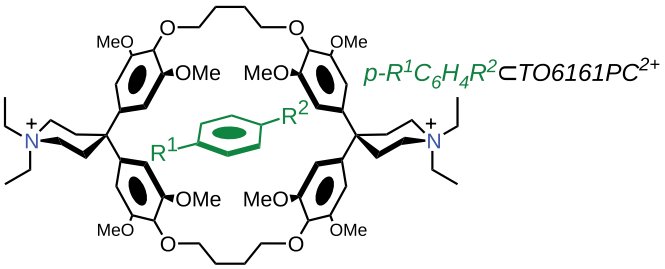


Figure 2.15 Generalized structural formula of Diederich's tetraoxa[*n*.1.*n*.1]paracyclophanes.[322]

[G] In cyclophane nomenclature, the bracketed term denotes the number of atoms in the linkers which connect each of the phenylene subunits together. For example, [2.2]paracyclophane consists of two *para*-substituted benzene rings, each connected by two-atom spacers. It is implied that the atoms are carbon, i.e., methylene units, unless heteroatoms are denoted by prefixes such as 'oxa' for oxygen, 'aza' for nitrogen, 'thia' for sulfur, and so on. Each heteroatom is assigned a number corresponding to its position in the macrocycle, where phenylene rings are 'superatoms' representing only one position.

Table 2.6 Association constants[323] of the 1:1 host-guest complexes of *para*-substituted phenylenes and the TO6161PC^{2+} host at 293 K.

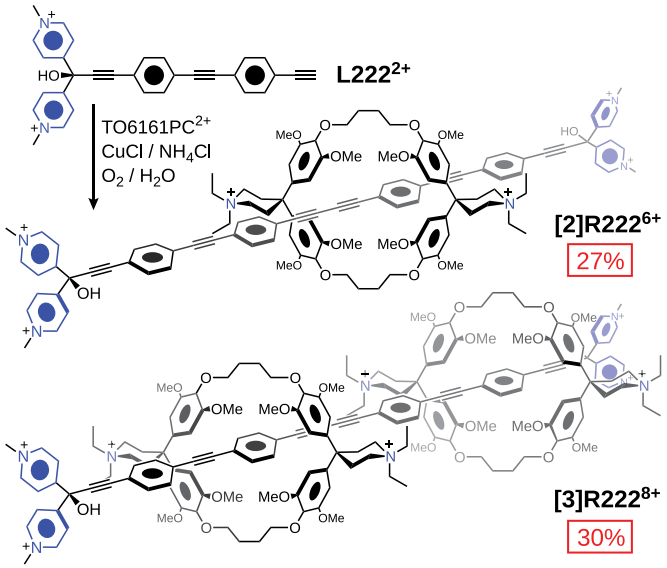


R^1	R^2	Solvent	K_a M^{-1}	$\Delta G°$	$\Delta H°$	$-T\Delta S°$
				– kcal·mol^{-1} –		
CO_2Me	CO_2Me	D_2O	1.17×10^5	–6.81	–10.7	4.0
NO_2	Me	D_2O	3.00×10^4	–6.01	–9.6	3.6
CN	Me	D_2O	2.99×10^4	–6.01	–9.8	3.8
NO_2	OH	D_2O	2.31×10^4	–5.86	–11.7	5.8
OMe	OMe	D_2O	1.02×10^4	–5.38	–10.2	4.8
Me	Me	D_2O	9.33×10^3	–5.33	–7.4	2.1
CN	CN	D_2O	7.83×10^3	–5.23	–9.5	4.3
NO_2	NO_2	D_2O	7.76×10^3	–5.22	–9.5	4.3
OH	OH	D_2O	3.21×10^3	–4.71	–9.1	4.4
NH_2	NH_2	D_2O	3.58×10^2	–3.43	–7.1	3.7
CN	CN	CD_3OD	2.4×10^1	–1.86	–4.2	2.4
OMe	OMe	CD_3OD	8×10^0	–1.20	–4.4	3.2

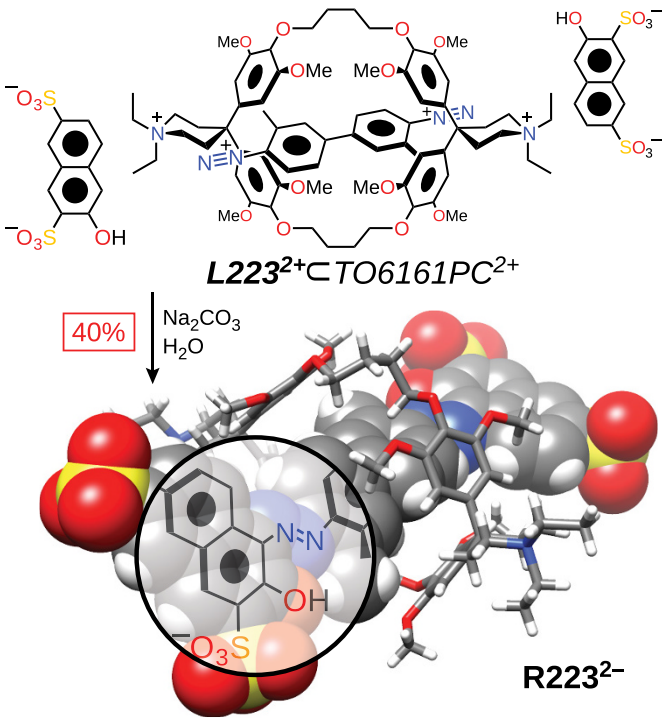
water solubility. Substitutions (Me or OMe) on the phenyl rings (R′) typically enhance its affinity for aromatic guests by deepening the cavity of the host and making its interior surface more polarizable.[323] The paracyclophane TO6161PC^{2+} has been optimized for binding benzene derivatives (**Table 2.6**) in water.

The high affinity of the TO6161PC^{2+} host for *para*-substituted benzene rings has been exploited by Anderson[324–326] in the synthesis of rotaxanes with π-conjugated dumbbells. The first examples of MIMs based on Diederich's host are the oligo(phenylene ethynylene) [2]rotaxane **[2]R222**$^{6+}$ and the corresponding [3]rotaxane **[3]R222**$^{8+}$. These compounds were synthesized (**Scheme 2.30**) in one pot by Glaser homocoupling of a pair of pyridinium-stoppered oligo(phenylene ethynylene) half-dumbbells **L222**$^{2+}$ in the presence of TO6161PC^{2+}, affording the [2]- and [3]rotaxanes in 27 and 30% yield, respectively. Since they represent the first examples of MIMs with fully conjugated backbones, these rotaxanes opened the door to a number of π-conjugated polymers in which mechanically bound rings act as insulators that prevent degradation, enhancing fluorescence emission.

In addition to oligo(phenylene ethynylene) rotaxanes, Anderson[327,328] has employed the TO6161PC^{2+} host in the synthesis of so-called azo-dye rotaxanes, so named because they are formed during an azo dye-forming stoppering reaction in water. One example of the azo-stoppering protocol (**Scheme 2.31**) involves the coupling of β-naphthol-3,6-disulfonate stopper precursors to the diazotolidine-derived axle of the pseudorotaxane



Scheme 2.30 Aqueous synthesis of [2]- and [3]rotaxanes with π-conjugated backbones.[324]



Scheme 2.31 Synthesis[327,328] and solid-state structure[327,328] of the azo rotaxane **R223**$^{2-}$. The TO6161PC^{2+} ring is portrayed in a tubular representation, while the tetrasulfonated azo dye dumbbell is portrayed in a space-filling representation. Solvent molecules and Na^+ counterions are omitted for the sake of clarity.

L223^{2+}⊂*TO6161PC*$^{2+}$ by dediazotization, affording the [2]rotaxane **R223**$^{2-}$ in 40% yield. The solid-state structure[328] of **R223**$^{2-}$ is depicted in the scheme. This protocol is general enough to accommodate[327,329] alternative diazo reactants, such as azobenzene, as well as other water-soluble rings, including α-CD and β-CD.

Recently, Yoshizawa[329] introduced a new dicationic cyclophane with a tube-like geometry of approximately 1 nm in both diameter and depth. This cyclophane binds long hydrocarbon guests within its cavity in water, rendering it an ideal condidate for designing new aqueous templates in the synthesis of mechanomolecules.

We note that several of the π-accepting cyclophanes that are most commonly employed in the synthesis of MIMs based on donor-acceptor templates are tetracationic, and these too have been employed occasionally in the aqueous synthesis of MIMs—see **Section 2.3.3.8**.

2.3.1.5 Metallosupramolecular MIMs

Many MIMs have been assembled under thermodynamic control by exploiting the reversibility of various metal-ligand bonds in polar media, especially water. This area of research was pioneered by Makoto Fujita,[330–332] who has specialized in, among others, the self-assembly of MIMs comprising interlocked metallacycles and metallacages, especially those involving Pd^{II} or Pt^{II} square planar coordination geometries.[333] Since they are typically assembled under thermodynamic control, this class of MIMs is discussed in depth in **Section 3.2**.

2.3.2 Transition Metals Templates

According to Frisch and Wasserman,[1] the idea of utilizing the geometry of ligands around a metal ion as a template for installing mechanical bonds was suggested as early as 1961 by W. Closson. In 1973, Sokolov[6] also suggested that "*coordination compounds of metals can be used as 'scaffolding' for building up catenoid structures*" in a review that was focused primarily on potential strategies for making molecular knots. Contemporaneously, the metal template effect was being investigated and developed in the context of macrocycles and other organic building blocks, especially in the pioneering work of Neil Curtis[334–337] in New Zealand and Daryle Busch[114,338–340] in the United States in the 1960s. It is worth noting, however, that the template-directed synthesis of macrocycles by metal cations can be traced to much earlier dates, such as that[341] of the phthalocyanines in 1927. It was not until the early 1980s, when Ogino[179] stoppered the first (supramolecular) template-directed rotaxanes with coordination complexes (*vide supra*) and Sauvage[76] introduced the first metallo-catenanes templated by tetrahedral copper(I) complexes (*vide infra*) that the idea of employing metal templates to make mechanical bonds was finally realized. The coordination geometry around transition metal ions has since become one of the most powerful tools for gathering and orienting the appropriate component parts and precursors during the formation of mechanical bonds.

The most thermodynamically stable state of a coordination complex is one in which the highest possible number of available binding sites are occupied on both the ligand and the metal—a powerful guiding principle introduced by Lehn[342] known as *maximal site occupancy*, which is often

invoked in metal-templated MIM syntheses in order to assemble ligands into predictable coordination complexes, which orientate them such that they possess the requisite crossing points or entanglements for making mechanical bonds. The transition metals most often employed in the templated synthesis of MIMs—e.g., Cu, Zn, Pd, Pt, Fe, Co, Ru, Ag, Au—typically form complexes with a coordination number (CN) of six or less. All of the most common coordination geometries[343] for ligands surrounding these metals have been employed in the template synthesis of MIMs. This Section is therefore organized according to the coordination geometries (**Figure 2.16**) of metal templates involved in MIM synthesis—namely, tetrahedral, trigonal bipyramidal, octahedral, square planar, and linear. This versatile toolbox of metals and geometries allows one to orient ligands in three-dimensional space in a wide variety of different ways. The heteroleptic '1+3', '2+3', and '2+4' coordination modes of square planar, trigonal bipyramidal, and octahedral complexes, respectively, are suited for rotaxanes and hetero[2]catenanes which require constitutionally different component parts. On the other hand, the homoleptic '1+1', '2+2', and '3+3' coordination modes of linear, tetrahedral, and octahedral complexes, respectively, can accommodate pairs of identical donor ligands. We note that metals surrounded by more than two ligands[344–346] or lanthanides[346–348] with CN>6 have also been employed as templates in a few instances.

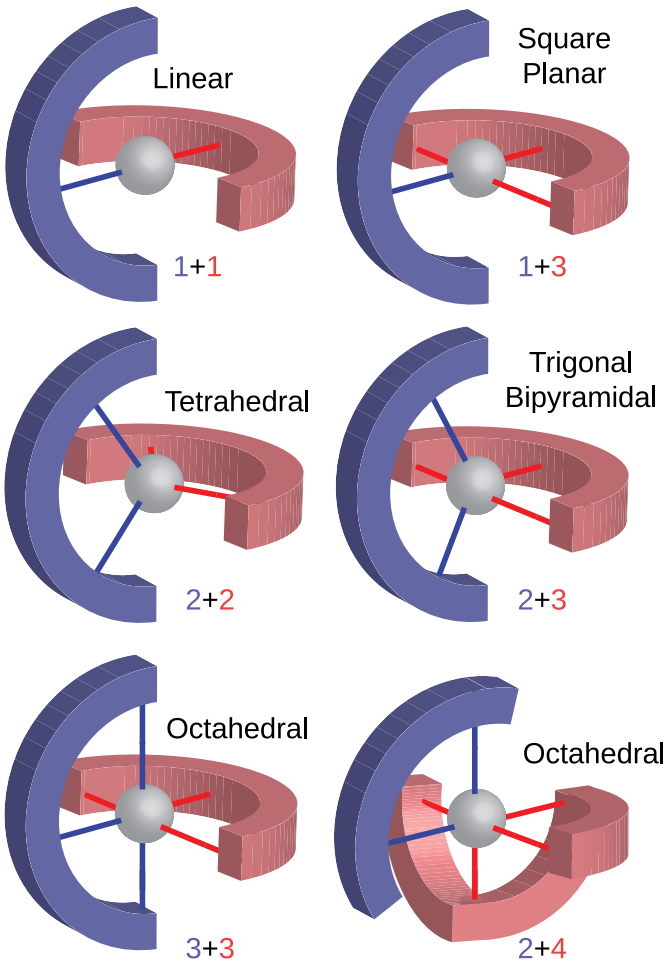


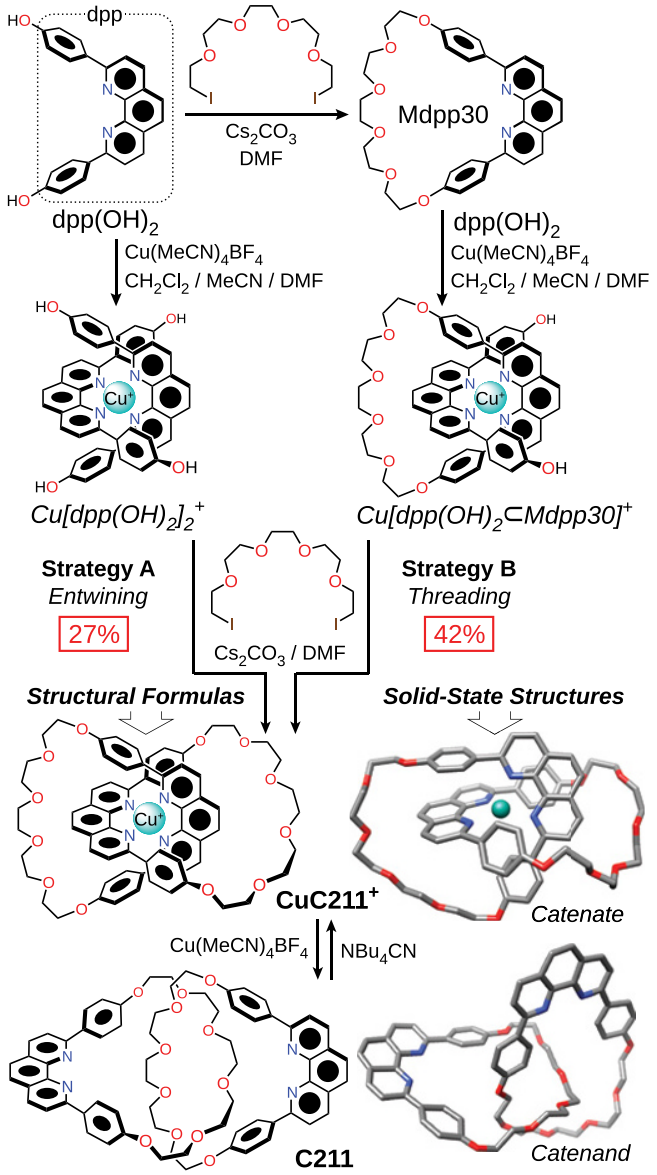
Figure 2.16 Coordination geometries (CN≤6) utilized to gather and pre-organize two ligands (illustrated in red and blue) around a metal (illustrated in grey) in the template synthesis of MIMs.

Since the synthesis of MIMs based on transition metal templates often relies on endocyclic chelates, we will employ in this work a systematic naming convention for macrocyclic ligands. Macrocycles will be denoted by the letter M, which will be followed by an abbreviation representing the ligating moiety—e.g., pyridine (py), 2,2′-bipyridine (bpy), pyridine-2,6-dicarboxamide (pydc), 2,2′:6′,2″-terpyridine (terpy), phenanthroline (phen), 1,10-diphenylphenanthroline (dpp)—followed finally by a number denoting the minimal amount of atoms in the loop of the macrocycle.

As a supplement to the research discussed in this Section, readers are directed to a comprehensive review on metal-directed synthesis of MIMs dating through 2011 by Leigh,[349] as well as a number of earlier reviews by Sauvage.[350–355] A number of MIMs incorporating cyclometalated rings or dumbbells with metalated backbones are described in **Section 3.2**. Metal-templated MIMs assembled under thermodynamic control using reversible covalent bonds are described in **Sections 3.2.1.1** and **3.4.1**. Active metal templates are discussed in **Section 2.4**.

2.3.2.1 Tetrahedral Templates

In the early 1980s, Sauvage[356,357] was experimenting in Strasbourg with 1,10-diphenylphenanthroline (dpp) ligands in order to prepare sterically protected Cu^{I} complexes with enhanced excited state lifetimes. Realizing that the entwined geometry of the ligands in a $Cu(dpp)_2^+$ complex are appropriately oriented for them to become concatenated upon macrocyclization, Sauvage and his long time collaborator Dietrich-Buchecker pioneered the first metal templated catenane synthesis, which they described in their native tongue (French) in a communication published[76] in *Tetrahedron Letters* in 1983. This seminal publication outlined two approaches (**Scheme 2.32**) to catenating dpp ligands around a Cu^{I} center, named originally 'Strategy A' and 'Strategy B', but later rebranded[353,358] under the titles of (A) entwining and (B) threading. Entwining involves macrocyclization of both ligands in one pot, whereas the threading approach involves catenating an acyclic ligand around a macrocyclic one. The latter approach is less prone to error because it requires fewer bond-forming steps while avoiding the possibility of ligand cross-reactions around the same metal. The first metal-templated catenane **CuC211$^+$** was therefore accessed[76] by the threading approach. This route relies on the formation of the metallo-pseudorotaxane *Cu[dpp(OH)$_2$⊂Mdpp30]*$^+$ from linear and macrocyclic dpp-based precursors $dpp(OH)_2$ and Mdpp30, respectively. Cyclization of the second ring is carried out by simple S_N2 substitution (Williamson ether synthesis) between the phenolic endgroups of the Cu-coordinated ligand $dpp(OH)_2$ and an iodinated hexaethylene glycol linker, affording **CuC211$^+$** in 42% yield. Sauvage's synthetic protocol was miles ahead



Scheme 2.32 Sauvage's entwining[76] and threading[359] approaches to the copper(I)-templated synthesis of the first catenate **CuC211**$^+$ and the corresponding catenand **C211**. Tubular representations of the solid-state structures of the catenate and catenand are portrayed alongside their structural formulas.

of any other catenation method known at the time on account of its relatively high yield and low number of reaction steps. The entwining approach (Strategy A) was realized[359] subsequently from the precursor *Cu[dpp(OH)$_2$]$_2^+$* and affords the same catenane in 27% yield.

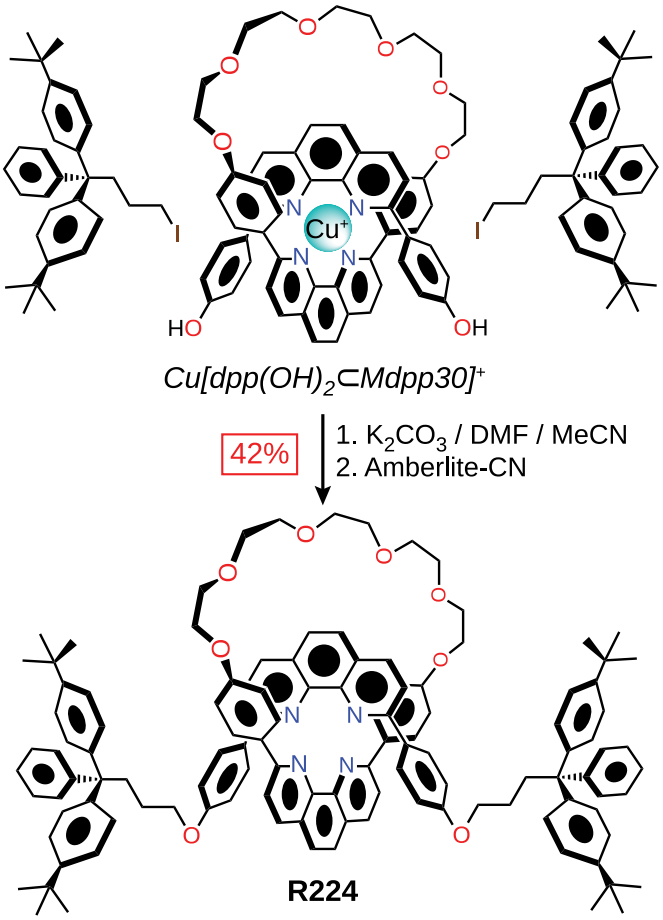
In 1984 Sauvage[359] reported that the Cu^I center can be removed (**Scheme 2.32**) from **CuC211**$^+$ to afford the neutral [2]catenane **C211** using CN^- ions in excess as competitive ligands. Borrowing from the nomenclature of cryptands and cryptates—a Nobel prize winning field of chemistry he pioneered during his doctoral research together with his supervisor Jean-Marie Lehn[360–362]—Sauvage[359] coined the terms 'catenand' and 'catenate' to describe catenated ligands and their corresponding coordination complexes, respectively. He also defined[363] the term 'catenand effect' as a phenomenon of enhanced stability in metals coordinated to topologically linked ligands. The synthesis[364] and solid-state structures[365] of the catenate **CuC211**$^+$ and the corresponding catenand **C211** are depicted (**Scheme 2.32**) alongside their structural formulas. The rings of the catenand are much more mobile than they are in the catenate, since the dpp ligand moieties are no longer tied up in coordinative bonds in the case of the catenand. In other words, removal of the Cu^I template eliminates almost all of the intercomponent noncovalent bonding interactions, resulting in a time-averaged co-conformation that is much less well-defined in solution. The catenand **C211** has been investigated extensively and is known[366–368] to bind many transition metal ions[H] in a tetrahedral geometry, including Cu^I , Ni^{II}, Cd^{II}, Zn^{II}, Co^{II}, and Ag^I.

Although topologically linked ligands and their complexes are known as catenands and catenates, respectively, mechanically interlocked ring/dumbbell ligands and their complexes have curiously not often been described as 'rotaxanates' and 'rotaxanands'. Metal template strategies of the kind pioneered by Sauvage are nevertheless equally appropriate for making rotaxanes. It was Gibson[369] who prepared (**Scheme 2.33**) the first [2]rotaxane by a metal template route. He employed the same pseudorotaxane precursor *Cu[dpp(OH)$_2$⊂Mdpp30]*$^+$ as the one introduced by Sauvage in his seminal work. The trityl-derived stopper precursor I(CH$_2$)$_3$C(*p*-^{t}BuPh)$_2$Ph is attached to the phenolic handles of this metallo-pseudorotaxane under Williamson ether synthesis conditions and the Cu^I template is stripped away subsequently by solid-supported cyanide (Amberlite-CN resin) to afford the [2]rotaxane **R224** in 42% yield over two steps.

The synthesis (**Scheme 2.34**) of the first rotaxanes in Strasbourg relied upon porphyrin-forming condensations.[370] The standard Cu(dpp)$_2^+$ template motif is employed to thread the Mdpp30 ring around the dpp-based Au^{III}-porphyrin stoppered semidumbbell **L225**$^+$ bearing a terminal aldehyde group to give *Cu(**L225**$^+$⊂Mdpp30)*$^+$, a key precursor that condenses with bis(3-ethyl-4-methyl-1*H*-pyrrol-2-yl) methane and 3,5-di-*tert*-butylbenzaldehyde in order to generate[I] the second porphyrin[371–373] stopper. The one-pot condensation affords the [2]rotaxane **CuR225a**$^{2+}$ and the [3]rotaxane **Cu$_2$R225b**$^{4+}$ in 25 and 32% yield, respectively, as well as a simple bis(3,5-di-*tert*-butylbenzene)-capped porphryin as a byproduct. The newly formed freebase

[H] The catenand **C211** is also capable of surrounding H$^+$ and Li$^+$ ions in a tetrahedral geometry with respect to the ligand moieties.

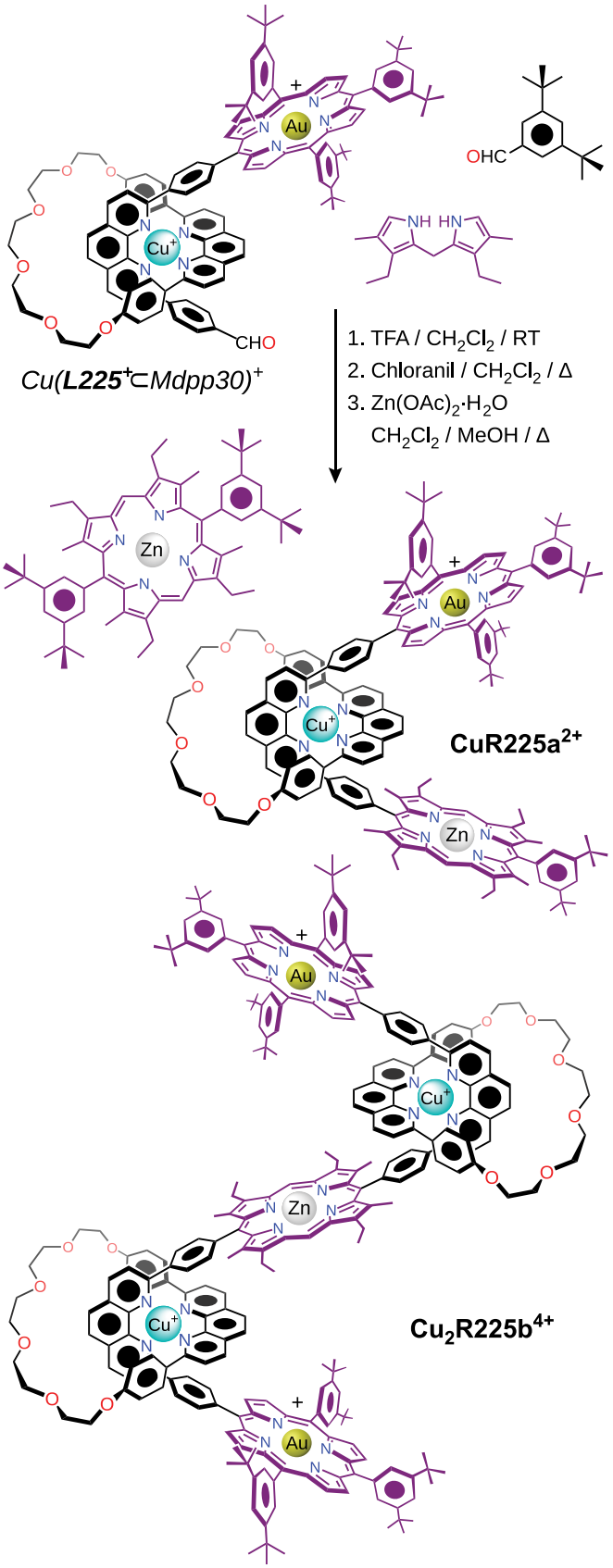
[I] Sauvage's method was enabled by the timely discovery of suitably mild conditions for porphyrin formation by Lindsey,[371] who revisited the Rothemund[372] / Adler-Longo[373] porphyrin synthesis in 1987. Lindsey found that pyrroles and benzaldehydes react reversibly with trace acid catalysis to form porphyrinogens at thermal equilibrium, which can be oxidized irreversibly (with chloranil, for example) to give porphyrins.



Scheme 2.33 Gibson's synthesis of the first metal-templated [2]rotaxane.[369]

porphyrin units were metallated with Zn^{II} in order to enhance their stability and photophysical properties. The positively charged Au^{III}-porphyrin stoppers readily accept electrons from the Zn^{II}-porphryins upon photoexcitation, making these rotaxanes attractive platforms for investigating photoinduced electron transfer phenomena.[374–377] A similar synthetic approach has been followed[378,379] to prepare porphyrinic oligorotaxanes with up to four rings. See **Section 4.2.1.1**. In one case,[380] an amine-functionalized porphyrin stopper was attached to a metallo-pseudorotaxane by way of amide bond formation at its terminal carboxylic acid sites activated by EDC.

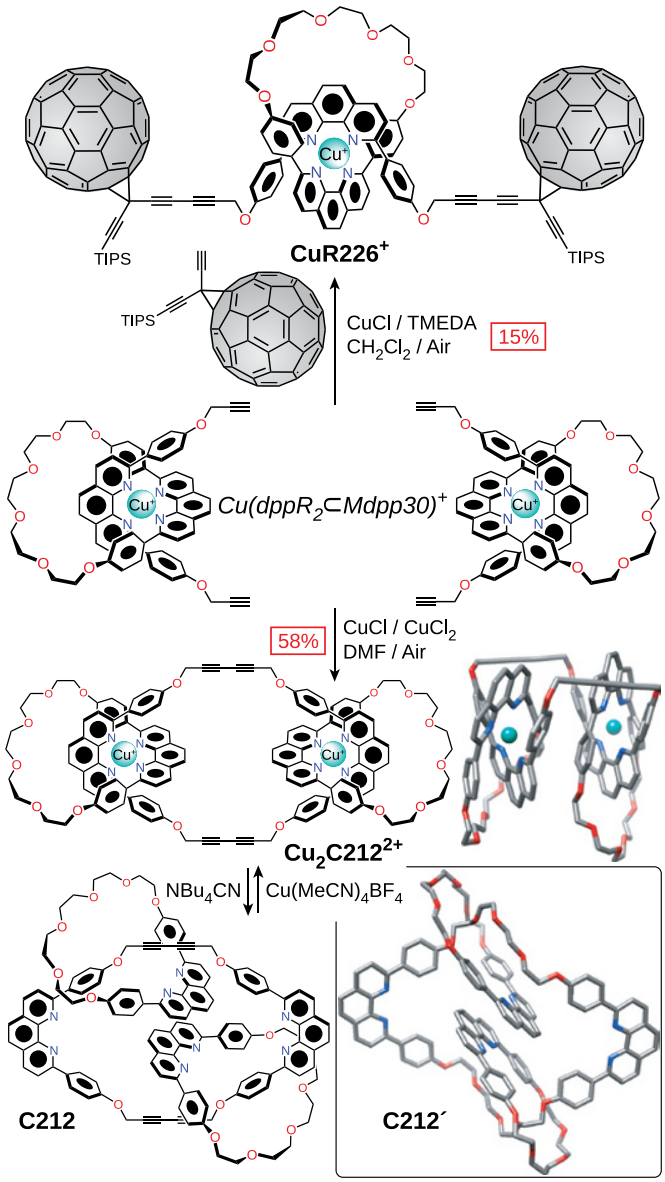
Although Sauvage's first rotaxanes involved the condensation of porphyrinic building blocks, we note that many of the rotaxanes[381–388] prepared by the Strasbourg group have also been constructed using the reliable Williamson ether synthesis originally employed in the synthesis of catenates. The alternative reactions that have served Sauvage most effectively during a stellar career[9,351,352,389–392] in designing, synthesizing, and characterizing MIMs lasting over 30 years are metal-catalyzed coupling reactions, most notably (i) olefin metathesis (**Section 3.4**), (ii) Eglinton-Glaser-Hay alkyne homocoupling, and (iii) the copper(I) mediated



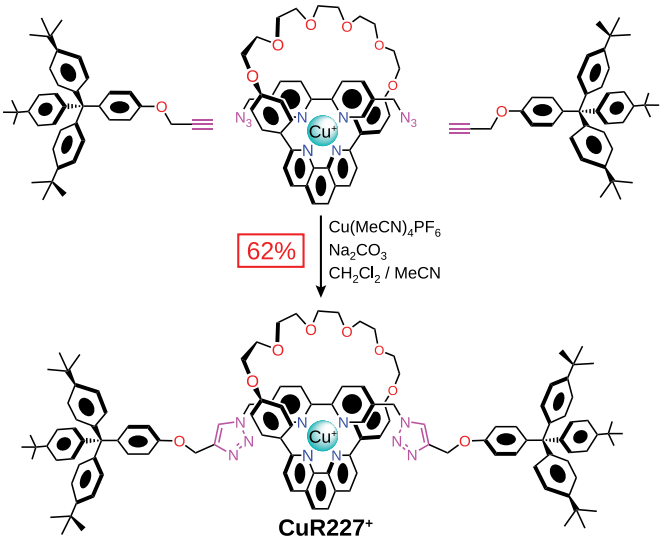
Scheme 2.34 Sauvage's first transition metal template-directed synthesis of rotaxanes, which relies upon the condensation of porphyrin precursors to form mechanical bonds.[370]

azide-alkyne cycloaddition (CuAAC) version of click chemistry. The MIMs that have been constructed using this simple chemical toolbox are scattered throughout every Chapter of this book. Here, we highlight a couple of representative examples of these protocols in action.

Two examples[393–396] of Sauvage's judicious usage of the Eglinton-Glaser-Hay coupling in the synthesis of catenanes and rotaxanes are illustrated in **Scheme 2.35**. The [3]catenate[393,394] **Cu_2C212^{2+}** and the corresponding [3]catenand **C212**—as well as the [2]rotaxane[395,396] **$CuR226^{+}$**—are accessible from a *$Cu(dppR_2{\subset}Mdpp30)^{+}$* pseudorotaxane, where R = propargyl. Remarkably, the major product (58%) of the acetylenic coupling reaction is a cyclic dimer, namely



Scheme 2.35 The synthesis[393,394] and tubular representations of the solid-state structures[397,398] of Sauvage's [3]catenates and [3]catenands, which are accessed by copper-catalyzed oxidative acetylinic coupling of two cupropseudorotaxane precursors. Fullerene stoppered rotaxanes have been prepared using the same protocol in the presence of an acetylated C_{60} stopper precursor.[395,396]



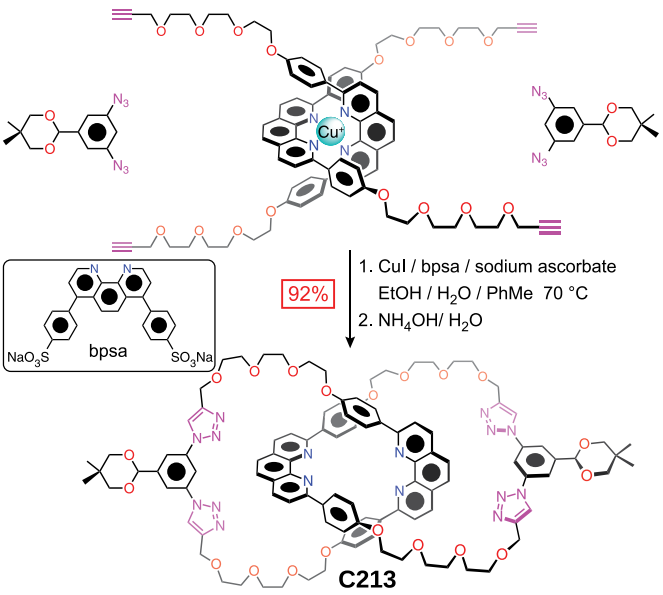
Scheme 2.36 Click synthesis of a metallo[2]rotaxane.[406]

the [3]catenate **Cu_2C212^{2+}**. This yield is substantially more efficient than the Williamson ether synthesis employed in the preparation of the first [2]catenate. The solid-state structures of the [3]catenate[397] and a structurally similar [3]catenand[398] **C212′** are portrayed alongside their structural formulas in **Scheme 2.35**. The [3]catenate adopts a 'curled up' secondary structure with the large central ring having a saddle-like geometry in the solid state, while the [3]catenand adopts a more outstretched geometry in which the two peripheral rings associate inside the central ring by way of π–π stacking interactions. Diederich and Sauvage[395,396] found that exposing the alkyne-terminated metallo-pseudorotaxane to the Hay catalyst (CuCl/TMEDA/O_2) in the presence of 5 equiv of an alkyne-terminated derivative of C_{60} as a stopper precursor in CH_2Cl_2 leads to the formation of the [2]rotaxane **$CuR226^{+}$** in 15% yield. In contrast with the [3]catenate, demetalation of the rotaxane **$CuR226^{+}$** with an excess of KCN is not a clean reaction, so much so that the generation of decomposition products prevents the isolation of the corresponding copper-free rotaxane as a pure compound.

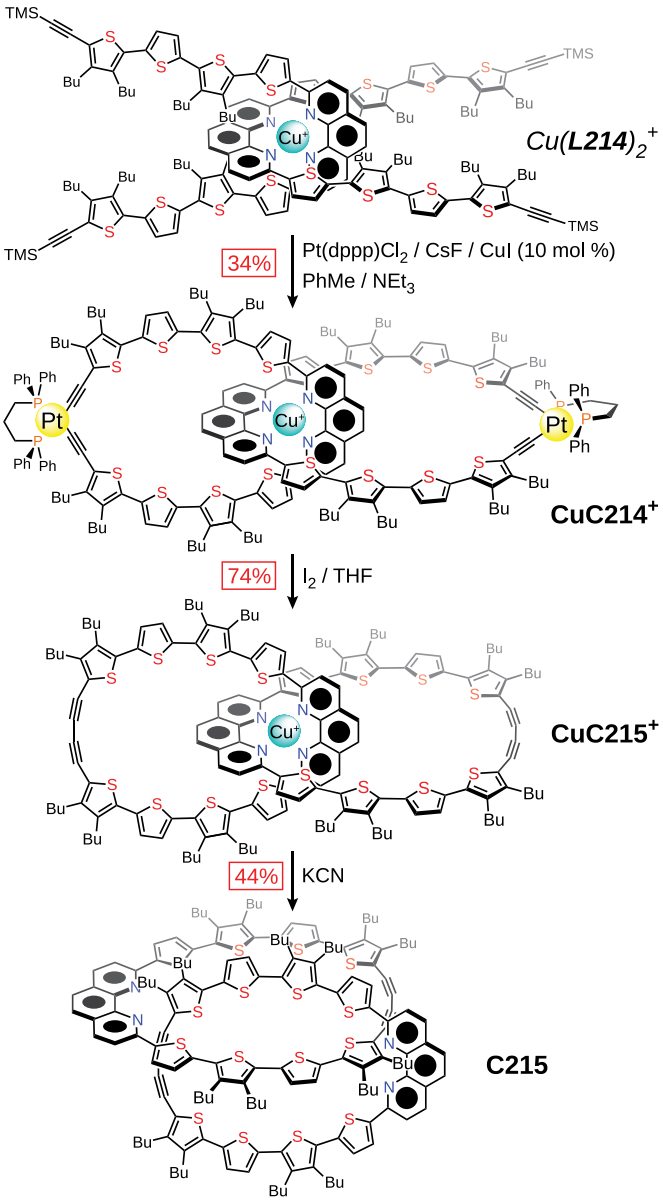
The azide-alkyne 1,3-dipolar cycloaddition has been an important tool for making MIMs because it proceeds from chemically stable components, requiring no transient or air- and water-sensitive reagents. The Cu^{I}-catalyzed version (CuAAC) of this reaction generally proceeds with high yields and regioselectivities, while tolerating a diverse set of functional groups and experimental conditions. Nearly all of the most common recognition motifs employed in MIM synthesis have been adapted to rely on click chemistry for forming mechanical bonds. Click syntheses of MIMs are summarized in a number of reviews[399–402] in the literature. The first reports[403–406] of CuAAC-clicked mechanical bonds were introduced independently in 2006—they involved active templates[403] (**Section 2.4**), π-associated donor-acceptor templates[404,405] (**Section 2.3.3**), and metal templates.[406] In Sauvage's click synthesis (**Scheme 2.36**) of a

metal-templated rotaxane, he and his long-time collaborator Collin obtained[406] the [2]rotaxane **CuR227**$^+$ in 62% yield from the metallo-pseudorotaxane *Cu(5,5′-bis(azidomethyl)-2,2′-bipyridine⊂Mdpp30)*$^+$, a propargylated tetraphenylmethane stopper precursor, and Na_2CO_3 in the presence of a $Cu(MeCN)_4PF_6$ catalyst at room temperature in CH_2Cl_2/MeCN. The protocol is remarkably facile, requiring only simple, easy-to-prepare precursors and no workup—the crude reaction can be loaded directly onto a TLC plate for purification. Although the 2,2′-bipyridine (bpy) ligand moiety of the dumbbell provides much less steric protection for the Cu^I template than the standard dpp ligand and consequently renders a much more labile Cu^I coordination complex, replacement of the bpy ligand with dpp results[407] in only a modest increase (67%) in yield. The CuAAC reaction has provided access to many novel rotaxanes[345,407–414] in Strasbourg, most of which are discussed in subsequent Chapters. The presence of a triazole group in a mechanomolecule often indicates that it has been prepared using the CuAAC reaction, with a few exceptions such as the ring capture, dumbbell capture, and cooperative capture strategies described throughout **Section 2.3.1**.

An even more efficient 'click' methodology for catenane synthesis has been developed by Megiatto and Schuster.[415–419] In their approach (**Scheme 2.37**), a total of four local CuAAC reactions are required to close both rings of the entwined *Cu(dpp)*$_2^+$ derivative possessing propargyl endgroups, which couple with a protected 3,5-diazidobenzaldehyde linker. The key ingredient in the efficient 'click' catenation of this system is a bathophenanthrolinedisulfonic acid (bpsa) auxiliary ligand, which is known[420] to accelerate the CuAAC reaction and probably also helps to prevent the Cu^I catalyst from being sequestered by the dpp ligands of the entwined reactants. Combining all of these reactants and reagents with copper(I) iodide and sodium ascorbate at



Scheme 2.37 An efficient click synthesis of a Cu^I-templated [2]catenane by Megiatto and Schuster.[415]



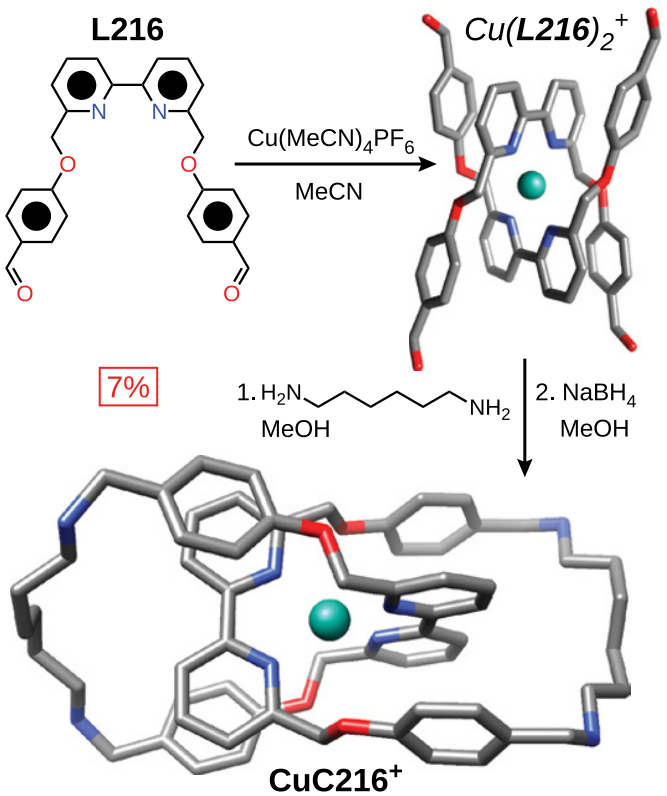
Scheme 2.38 Cu^I template synthesis[422] of the conjugated [2]catenane **C215**.

70 °C in 7:3:1 EtOH:H_2O:PhMe, the [2]catenane **C213** is isolated in 92% yield after an aqueous workup with NH_4OH, which removes the Cu^I template. An attractive feature of this protocol is the fact that the protected aldehyde in each of the catenane's rings can be deprotected and converted into another desired functional group. For example, a mechanically-bonded porphyrin–C_{60} donor-acceptor dyad has been constructed[419] recently by this kind of post-synthetic modification.

Bäuerle[421–423] has employed the tetrahedral Cu^I template in the synthesis (**Scheme 2.38**) of the first [2]catenanes comprising fully conjugated rings. His approach relies on the acetylenic coupling of oligothiophenes appended to a phenathroline core. The key starting material[422] is the homoleptic complex *Cu(**L214**)*$_2^+$, the ligands of which

constitute bis(quaterthienyl)phenanthroline units terminated with TMS-protected alkynes. After deprotection with CsF, attempts to close the rings under typical Eglinton-Glaser-Hay conditions returned only uncatenated macrocycles, suggesting that the closure of one ring forces the other ligand out of its cavity. When, however, the desilylated acetylene units are coordinated to Pt^{II} centers by displacing the chloride counterions of a *cis*-Pt(dppp)Cl_2 reagent, the cyclometalated [2]catenate **CuC214**$^+$ is obtained in 34% yield. This compound can then be converted to the diacetylenic [2]catenate **CuC215**$^+$ upon reductive elimination of the Pt^{II} corners with I_2 in THF (74%), followed by demetalation with KCN to afford the [2]catenane **C215** in 44% yield. This final demetalation step is not possible with bis(terthienyl) phenanthroline ligands, owing to steric constraints imposed by the smallness (28 atoms) of the corresponding rings.[421]

Lindoy[424] has shown that ordinary bipyridyl ligands can be employed in place of phenanthroline ligands when constructing catenanes around a copper(I) template by synthesizing (**Scheme 2.39**) the [2]catenate **CuC216**$^+$ from simple precursors—namely, $Cu(MeCN)_4PF_6$, 1,6-diaminohexane, and the benzaldehyde-functionalized bipyridyl ligand **L216**. Mixing $Cu(MeCN)_4PF_6$ and **L216** in MeCN affords the complex *Cu(**L216**)*$_2^+$, in which the ligands are appropriately entwined around the Cu^I center by virtue of the benzaldehyde appendages engaging in π–π stacking interactions

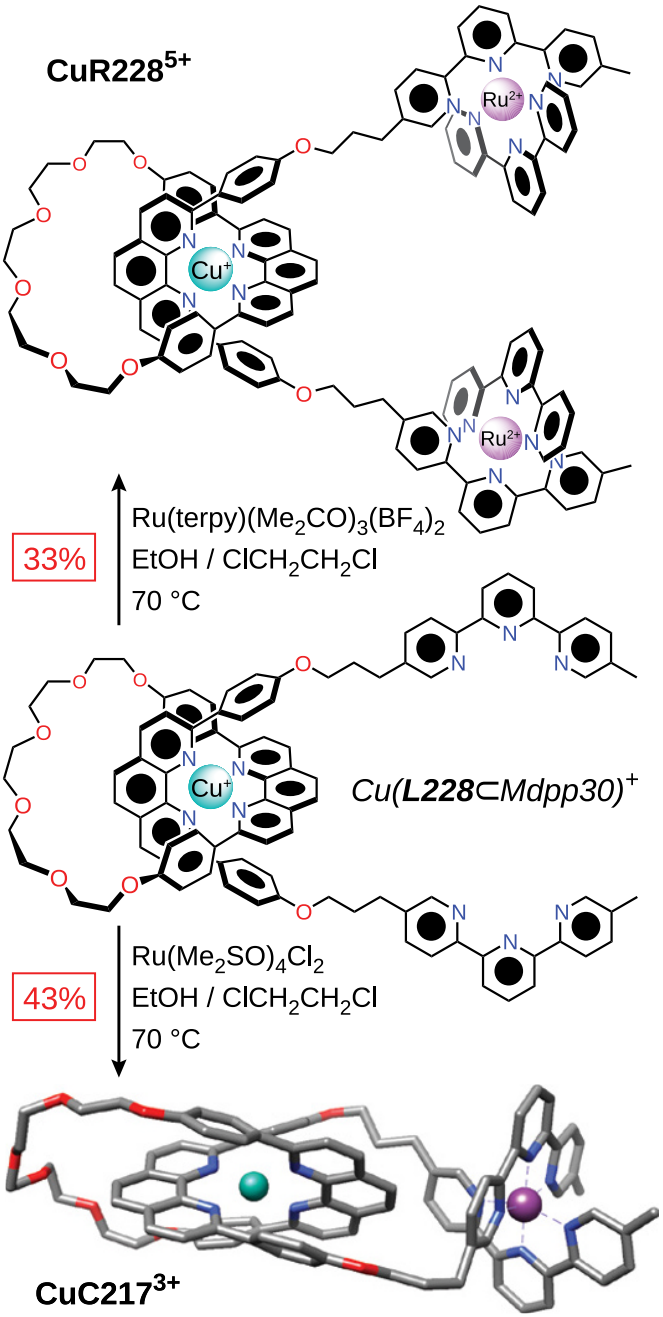


Scheme 2.39 Lindoy's synthesis of a copper(I) [2]catenate by reductive amination.[424] Tubular representations of **CuC216**$^+$ and its precursor *Cu(**L216**)*$_2^+$ are single crystal X-ray structures with protons, counterions, and solvents omitted for clarity.

with the bipyridyl units—a geometry which was predicted by molecular modeling *in silico* and confirmed by X-ray crystallography. Addition of the 1,6-diaminohexane linker under high dilution in MeOH leads to an imine-bridged [2]catenate in apparently quantitative yield, according to NMR spectroscopic data. Unfortunately, however, this catenate could not be isolated on account of the susceptibility of the imine bonds to hydrolysis. The catenated structure was therefore locked by reductive amination with $NaBH_4$, resulting in the precipitation of an orange microcrystalline powder, which was recrystallized to obtain the [2]catenate **CuC216**$^+$ in 7% yield. Imine bonds have been important motifs in the synthesis of MIMs under thermodynamic control—see **Section 3.3**.

One can also exploit kinetically stable coordinative bonds instead of covalent bonds in the interlocking of molecular components surrounding metal templates. This concept, which was first introduced by Piguet[425]—see **Section 3.2.2**—has been adopted by Sauvage to prepare (**Scheme 2.40**) [2]rotaxanes[426] and [2]catenanes[427,428] incorporating terpy ligands coordinated to Ru^{II} ions. The [2]rotaxane **CuR228**$^{5+}$ and the [2]catenane **CuC217**$^{3+}$ are both accessed from the same metallo-pseudorotaxane precursor *Cu(**L228**⊂Mdpp30)*$^+$, which is bis-functionalized with terpy ligands. The source and stoichiometry of Ru^{II} in the reaction is the main factor determining its outcome. The addition of 2 equiv of Ru(terpy)$(Me_2CO)_3(BF_4)_2$ at 70 °C in an EtOH/DCE solution affords the [2]rotaxane in 33% yield, while 1 equiv of a simpler $Ru(Me_2SO)_4Cl_2$ source delivers the [2]catenate in 43% yield. A Ru^{II}-bridged [2]catenate enclosed by means of the entwining strategy has been assembled[429] using a similar protocol. The high kinetic stability of Ru(terpy)$_2$ complexes is maintained in the MIMs, making them only marginally less robust than covalently stoppered or linked MIMs of the same genre. The high stability of the Ru(terpy)$_2$ complex also makes it possible to demetalate the Cu^I template selectively from the metallorotaxane and catenate with 59 and 83% efficiency, respectively.

Advincula,[430–433] now at Case Western Reserve University, has focused on the use of tetrahedral Cu^I phenanthroline complexes as templates for interlocking (**Figure 2.17**) macrocyclic polymers, which include the polymer [2]catenanes **CuC218a-e**$^+$. One strategy,[430,433] which involves a $Cu(dpp)_2^+$ core appended with linear polymers, relies on a ring-closing atom transfer radical coupling to afford the polystyrene-based catenates, **CuC218a**$^+$ and **CuC218b**$^+$. An alternative route involves preparing[431,432] the dpp-based Cu^I-catenate **CuC218c**$^+$, the rings of which contain organotin dialkoxide loops amenable to the insertion of cyclic ester monomers. Thus, ring expansion protocols involving the insertion of lactide and caprolactone into this compound generate the catenated poly(ε-caprolactone) **CuC218d**$^+$ and the catenated poly(L-lactide) **CuC218e**$^+$, respectively. Depending on the experimental conditions, catenated polymers of up to 43 kDa in size and polydispersity indices (PDIs) as low as 1.2 can be accessed by this method.



Scheme 2.40 The assembly of kinetically stable Ru(terpy)$_2$ complexes at the termini of the metallo-pseudorotaxane **Cu(*L228*⊂Mdpp30)**$^+$ leads to the formation of either the [2]rotaxane[426] **CuR228**$^{5+}$ or the [2]catenate[427,428] **CuC217**$^{3+}$, depending on the source and stoichiometry of the Ru^{II} reagent. A tubular representation of the solid-state structure of **CuC217**$^{3+}$ is portrayed with solvent, counterions, and protons are omitted for the sake of clarity.

2.3.2.2 Trigonal Bipyramidal Templates

Any trigonal bipyramidal complex with two ligands must necessarily be heteroleptic because this geometry involves an odd coordination number (CN) of 5. Sauvage[434] introduced this motif to MIM synthesis in 2003 when he described the [2]catenand **C219**. The key precursors in the synthesis (**Scheme 2.41**) of this compound are (i) Zn(OTf)$_2$ as the source of a cationic Zn^{II} template which can adopt pentacoordinate geometries, (ii) the 34-membered ring Mterpy34, which incorporates a tridentate terpyridine (terpy) ligand, and (iii) the olefinic polyether-terminated bidentate dpp ligand **L219**. Mixing these three components in CH_2Cl_2 in a stepwise fashion generates quantitatively the pentacoordinate metallo-pseudorotaxane *Zn(**L219**⊂Mterpy34)*$^{2+}$, which is subsequently subjected to ring-closing metathesis (RCM) with Grubbs' first generation ruthenium alkylidene catalyst to afford the corresponding [2]catenate **ZnC225**$^{2+}$. Olefin metathesis, which is typically a thermodynamically controlled reaction, is discussed in the context of MIM synthesis in **Section 3.4**. The metathesized double bonds of the product catenate are hydrogenated with H_2 on Pd/C and the Zn^{II} template is extracted subsequently in a biphasic mixture of CH_2Cl_2 and alkaline H_2O to afford the [2]catenand **C219** in 40% yield over the three steps. In addition to Zn^{II}, **C219** is capable of sequestering Cu^{II} and Fe^{II} in pentacoordinate complexes which are both highly stabilized by the catenand effect.[434] This [3+2]

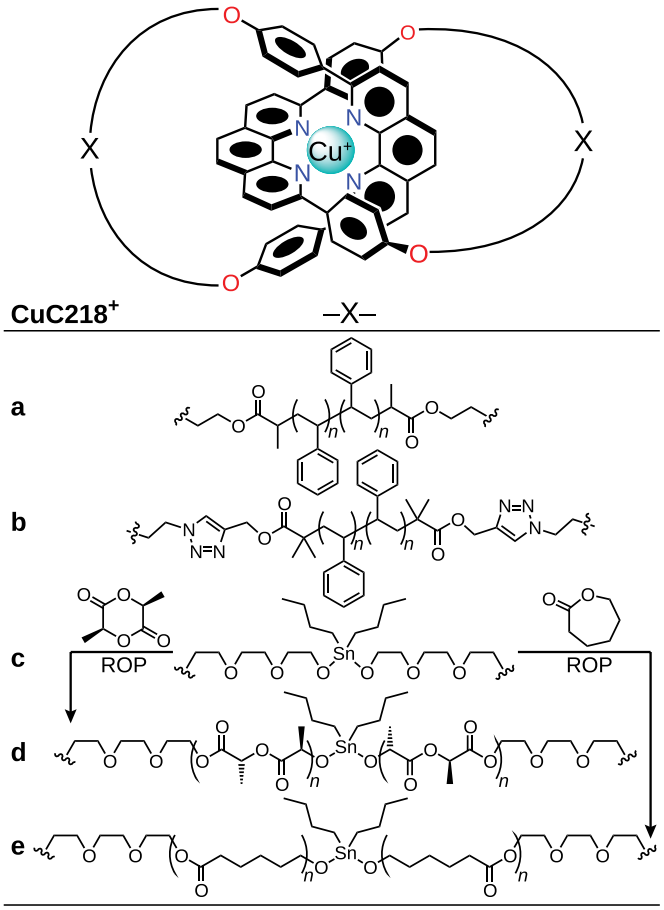
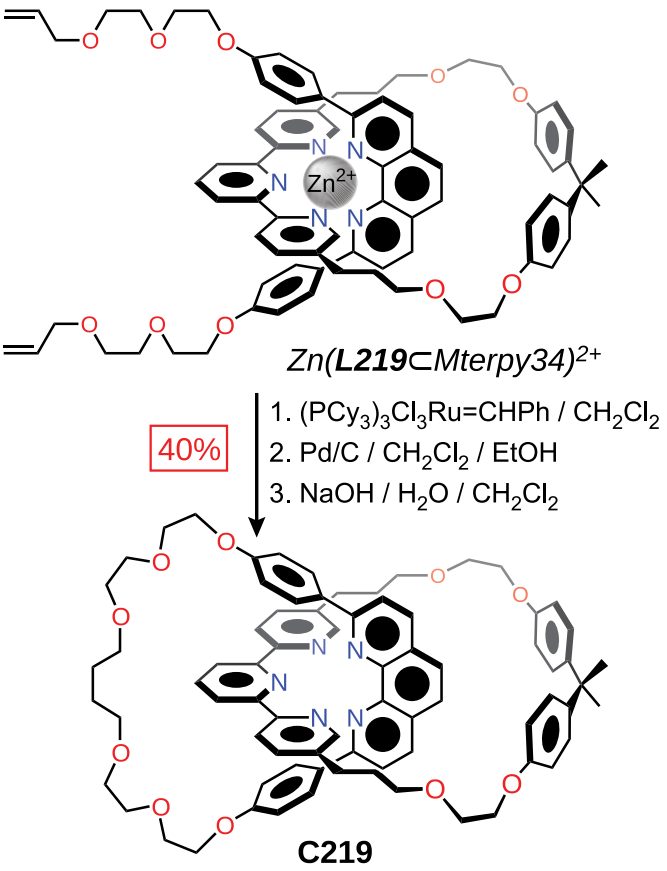


Figure 2.17 Advincula's metallo[2]catenanes comprising macrocyclic polymers.[430–432] **CuC218a-b**$^+$ are prepared by atom transfer radical coupling of entwined polystyrenes, while **CuC218d-e**$^+$ are prepared by ring expansion strategies involving the insertion of L-lactide and caprolactone monomers into the organotin [2]catenate **CuC218c**$^+$ via ring opening polymerization (ROP).

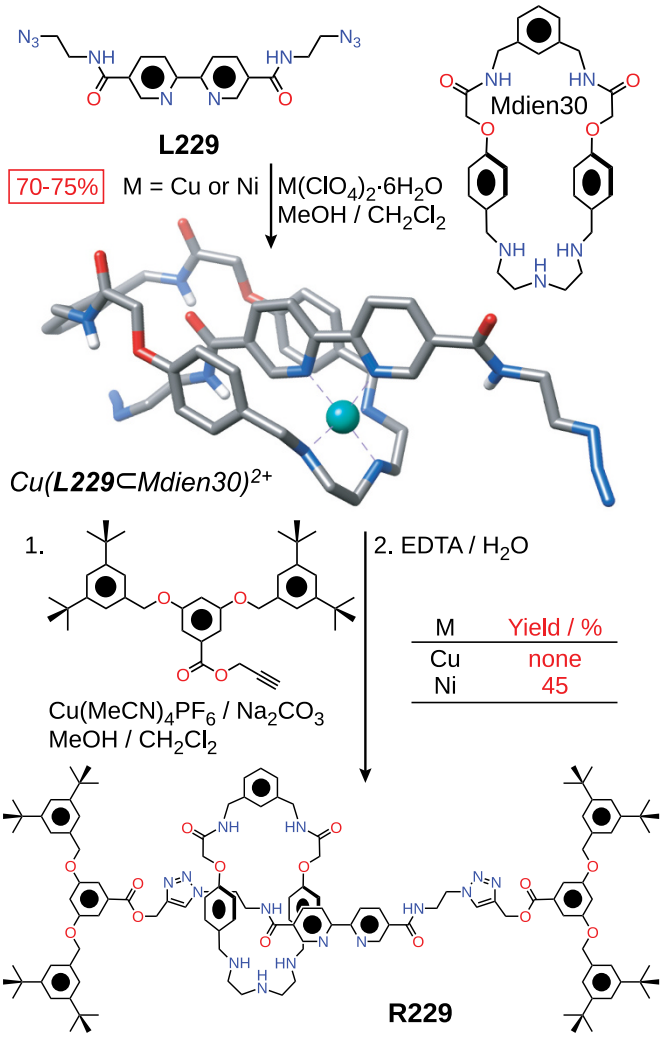
template motif has also been applied[413] to the click synthesis of a [5]rotaxane—see **Section 4.2.1.1**.

Ghosh[435] has recently introduced a novel macrocyclic ligand (Mdien30) derived from diethylenetriamine (dien) and employed it in the synthesis (**Scheme 2.42**) of a pseudorotaxane and [2]rotaxane templated by pentacoordinate Cu^{II} and Ni^{II} complexes, respectively, with the 2,2′-bipyridine-based ligand **L229**. The addition of $M(ClO_4)_2{\cdot}6H_2O$ (M = Ni^{II} or Cu^{II}) to an equimolar mixture of Mdien30 and **L229** in 1:1 MeOH / CH_2Cl_2 leads to the formation of a pentacoordinated metallo-pseudorotaxane in 70–75% yield after evaporation of the solvent and washing. The solid-state structure (**Scheme 2.42**) of *Cu(**L229**⊂Mdien30)*$^{2+}$ confirms the interpenetrated geometry of the complex. Although this Cu^{II}-based pseudorotaxane could not be converted to a [2]rotaxane by a CuAAC-mediated stoppering protocol, the Ni^{II}-based homologue *Ni(**L229**⊂Mdien30)*$^{2+}$ was converted into the neutral [2]rotaxane **R229** in 45% yield upon reacting it with an appropriate alkyne-terminated stopper precursor in the presence of Cu^{I} and subsequent demetalation with EDTA.

Although the trigonal bipyramidal geometry is not often employed in the templated syntheses of MIMs, it is often vital to the function of mechanically interlocked molecular switches which rely on changes in coordination geometry—often starting from tetrahedral geometries—triggered by chemical, photochemical, and electrochemical stimuli. See **Chapter 6**.



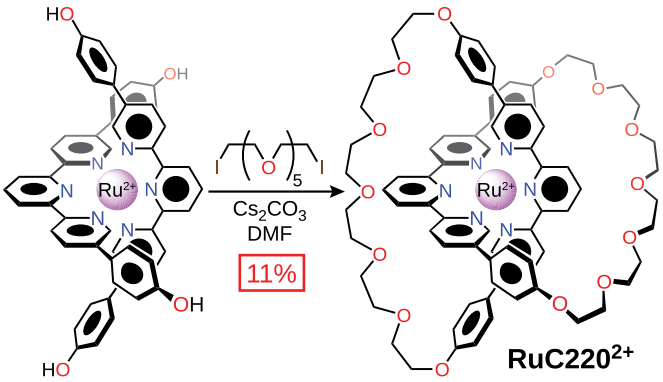
Scheme 2.41 Synthesis[434] of the [2]catenane **C219** from the trigonal bipyramidal metallo-pseudorotaxane *Zn(**L219**⊂Mterpy34)*$^{2+}$ by ring closing metathesis, hydrogenation, and demetalation. A strong catenand effect has been observed when **C219** binds Zn^{II}, Cu^{II}, and Fe^{II}.



Scheme 2.42 The self-assembly of a pentacoordinate complex between the bidentate ligand **L229** and the tris(amine)-containing macrocycle BATAM with Cu^{II} or Ni^{II} ions serves as a basis for the synthesis of the neutral [2]rotaxane **R229** by click chemistry and subsequent demetalation.[435] Counterions and protons are omitted from the tubular representation of the solid-state structure of *Cu(**L229**⊂BATAM)*$^{2+}$ for the sake of clarity.

2.3.2.3 Octahedral Templates

Sauvage[436] introduced octahedral templates[437] into mechanomolecules when he synthesized (**Scheme 2.43**) the first Ru^{II} [2]catenate in 1991. Yet again, the Williamson ether synthesis served as an effective ring-closing reaction, furnishing compound **RuC220**$^{2+}$ from an entwined phenol-derivatized bis(terpy)Ru^{II} complex in 11% yield. The orthogonal placement of terpy ligands around the Ru^{II} center mimics that of dpp ligands fixed around a Cu^{I} template. Sauvage was unable to demetalate the [2]catenate on account of the very high stability of its Ru(terpy)$_2^{2+}$ core.



Scheme 2.43 Sauvage's synthesis[436] of the bis(terpyridine) Ru^{II} catenate **RuC220**$^{2+}$.

More recently, Sauvage[438] has designed a bis-2,6-(phenylisoquinolinyl)pyridine coordinating unit in the interest of preparing catenates comprising less sterically hindered metal complexes. This ligand has been incorporated into the homo[2]catenate **FeC221**$^{2+}$, obtained from ring-closing metathesis and subsequent hydrogenation of the corresponding entwined template complex. The X-ray crystal structure (**Figure 2.18**) reveals an open structure with no significant steric constraints. After demetalation, Ru^{II} and Co^{II} can also be taken up by the catenand **C221**. In the context of molecular machines (**Chapter 6**), such as switches and motors, the extent of crowding around a metal center is a major factor in the kinetics and dynamics of induced mechanical motion, which motivates the design of these endocyclic, sterically non-hindering chelates.[439]

Siegel[440] has prepared a number of octahedral terpy-based Ru^{II} and Fe^{II} catenates. Compound **RuC222**$^{2+}$, which is one member of a series of chiral and achiral homologues

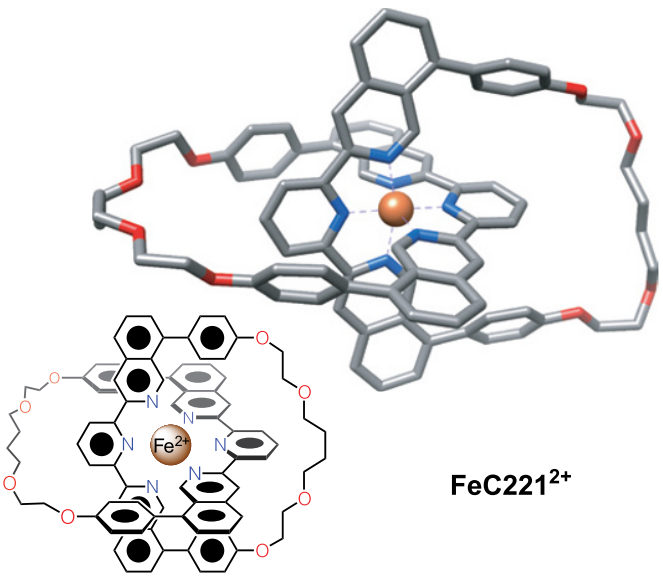


Figure 2.18 The structural formula and tubular representation of the solid-state structure of the ferrous [2]catenate[438] **FeC221**$^{2+}$. Solvent, counterions, and protons are omitted for the sake of clarity.

of different ring constitutions, was crystallized and characterized in the solid state (**Figure 2.19**) by X-ray crystallography. All of the homologues incorporate 2,6-dimethylphenyl rings appended directly to each end of the tridentate ligand. These disubstituted phenyl rings impart solubility, while extending the entwined arms outward to increase the likelihood of catenation. Although the ring-closing reaction involved in the synthesis of **RuC222**$^{2+}$ is an Eglinton-Glaser-Hay alkyne homocoupling, ring-closing metathesis has been employed in the synthesis of other homologues. In some cases, ligand cross reactions lead to a figure-of-eight macrocycle instead of a catenate. The formation of a figure-of-eight macrocycle is suppressed when Fe^{II} serves as a template instead of Ru^{II}, most likely because the increased pinching of ligands around Fe^{II} leads to a more favorable orientation of the reactive termini. The Fe^{II} catenates such as **FeC222**$^{2+}$ (not illustrated) can be demetalated easily by treatment with hydrogen peroxide. The use of 2-(2-pyridyl)-1,10-phenanthroline (pphen) instead of terpy as the ligating moiety in these catenates and catenanes affords topologically chiral species—see **Section 5.2.4.1**.

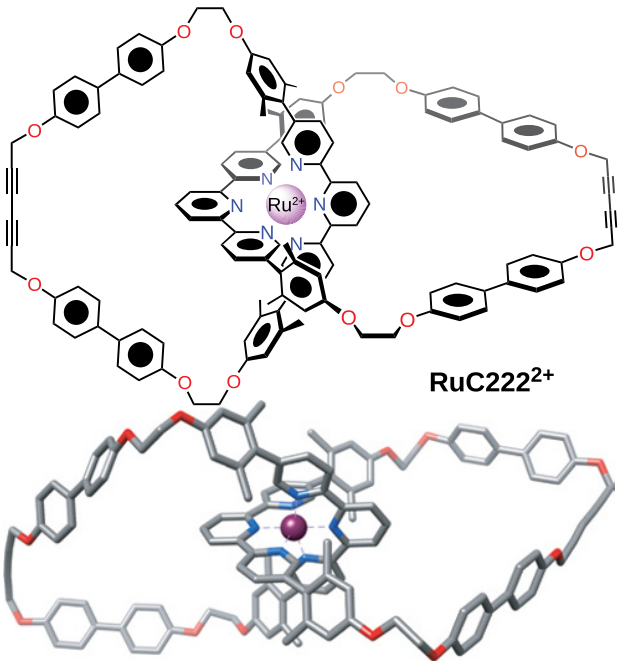


Figure 2.19 The structural formula and tubular representation of the solid-state structure of Siegel's octahedral Ru^{II} [2]catenate.[440] Solvent, counterions, and protons are omitted for the sake of clarity.

A homoleptic [3+3] ligand motif is common to all of the prior examples in the templated synthesis of catenates. Piguet's[425] metallocyclic homo[2]catenate is also based on a [3+3] assembly around an iron template—see **Section 3.2.4.2**. Rotaxanes and hetero[2]catenates, on the other hand, can be accessed more easily from octahedral templates by employing the heteroleptic binding geometry of a [4+2] ligand motif. Sauvage[441–445] was once again the pioneer—one example[445] of the manifestation (**Figure 2.20**)

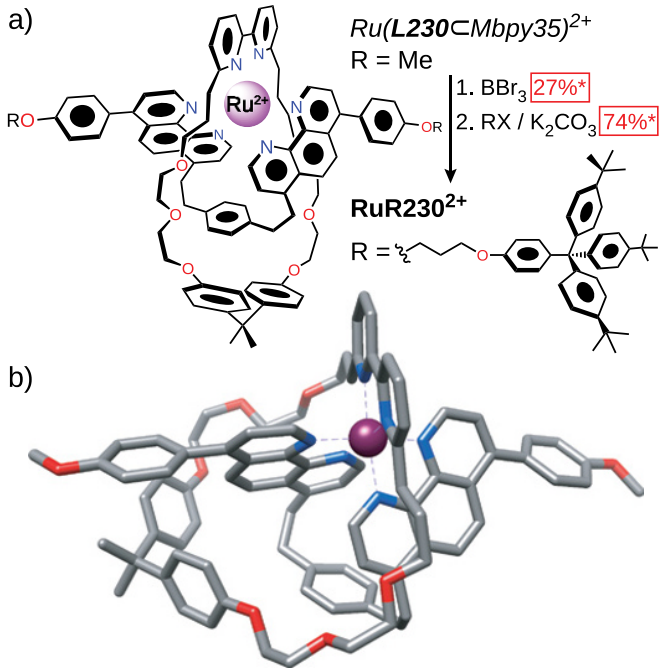


Figure 2.20 Sauvage's octahedral [4+2] ligand motif.[445] (a) Williamson ether synthesis of the metallo[2]rotaxane **RuR230**$^{2+}$. *Yields reflect a mixture of endocyclic and exocyclic homologues. (b) Tubular representation of the solid-state structure of *Ru(**L230**⊂Mbpy35)*$^{2+}$ with solvent, counterions, and protons omitted for the sake of clarity.

of this motif in a MIM is the rotaxane **RuR230**$^{2+}$. It is synthesized (**Figure 2.20a**) from the tetradentate ligand **L230**, which interpenetrates the bidentate macrocyclic ligand Mbpy35 about a Ru^{II} center. The solid-state structure (**Figure 2.20b**) of *Ru(**L230**⊂Mbpy35)*$^{2+}$ reveals the prerequisite endocyclic chelation of a pseudorotaxane assembly, with minimal distortion to the octahedral geometry of the ligand field. In solution, however, the endocyclic chelate could not be separated from the exocyclic one on a preparative scale. A steric barrier for the ring's passage over the thread is evident from the solid-state structure (**Figure 2.20b**) where the loop folds away from the bulky xylylene linker, bridging the two phen moieties of the tetradentate ligand. This steric interaction may explain the modest yield when obtaining the metallo[2]rotaxane **RuR230**$^{2+}$, which is isolated in admixture with the corresponding non-interlocked mechanostereoisomer. This [4+2] ligand motif was originally applied to the construction of [2]catenanes around octahedral Ru^{II} and Rh^{III} centers by ring-closing metathesis.[441–444] The structural formulas of these catenates are illustrated in **Figure 3.28** in **Section 3.4.1.1**. A more detailed account of Sauvage's research on Ru^{II}-based hetero[2]catenanes is provided in his review[437] on MIMs comprising octahedral transition metals.

Leigh[446,447] has employed (**Figure 2.21**) coordinative imine bonds in the self-assembly of MIMs with octahedral templates. The ligand design was inspired by the benzylic isophthalamide linkers of his signature hydrogen-bonded MIMs—see **Section 2.3.4.1**. This class of macrocycles has been adapted for metal chelation simply by replacing the isophthalamide groups with 2,6-diiminopyridine units. The reversibility of coordinative imine bonds facilitates the self-assembly of a number of catenates, **M(C223)**$^{2+}$ under thermodynamic control. A remarkable feature of this system is its tolerance for a wide range of metal dications (M = Mn, Fe, Co, Ni, Cu, Zn, Cd, or Hg) as templates. The solid-state structure of **Zn(C223)**$^{2+}$ is included as an example in **Figure 2.21a**. The catenates are also remarkably stable, resisting decomposition in the solid state up to temperatures exceeding 350 °C. Moreover, demetalation of the benzylic imine catenates does not occur even in the presence of a

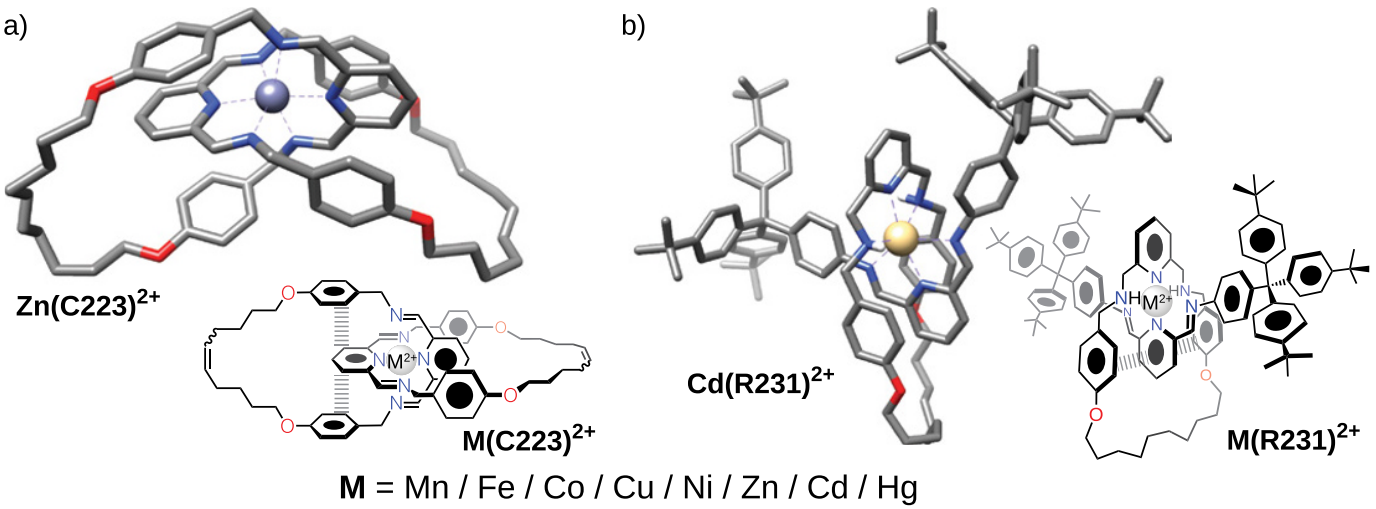


Figure 2.21 Leigh's benzylic imine mechanomolecules,[446,447] which accommodate a range of octahedral transition metal templates, M^{2+}. (a) Generalized structural formula of the catenates **M(C223)**$^{2+}$, with tubular representations of the X-ray crystal structure of **Zn(C223)**$^{2+}$. (b) Generalized structural formula of the metallorotaxanes **M(R231)**$^{2+}$, with a tubular representation of the X-ray crystal structure of **Cd(R231)**$^{2+}$. Dashed lines depict π–π stacking interactions, which stabilize the interlocked structures. Solvent, counterions, and protons are omitted for the sake of clarity.

100-fold excess of EDTA, whereas the corresponding benzylic amine catenates—generated by reduction of the imine bonds—are clearly more kinetically labile since their metal centers can be extracted with EDTA. The requisite heteroleptic binding of metallorotaxanes presents a challenge which requires an adjustment to the ligand motif (**Figure 2.21b**) for the self-assembly of the metallorotaxanes **M(R231)**$^{2+}$, which would otherwise compete with the corresponding homoleptic ring-ring and dumbbell-dumbbell complexes. This challenge has been overcome by (i) employing a macrocyclic chelate lacking any reversible bonds in order to avoid the possibility of catenation, while (ii) employing aniline-functionalized stoppers, as opposed to amines, in order to destabilize the dumbbell-dumbbell complex relative to the ring-dumbbell (rotaxane) 'complex'. Since the amino groups on the ring are more effective at stabilizing the octahedral metal templates than the anilinic imines of the dumbbell, the heteroleptic rotaxanes are formed in up to 99% yield (M = Co). The metallo[2]rotaxane **Cd(R231)**$^{2+}$ has been characterized in the solid state by X-ray crystallography. The synthetic pathways to both varieties of these mechanomolecules are discussed in **Section 3.3.1.1**.

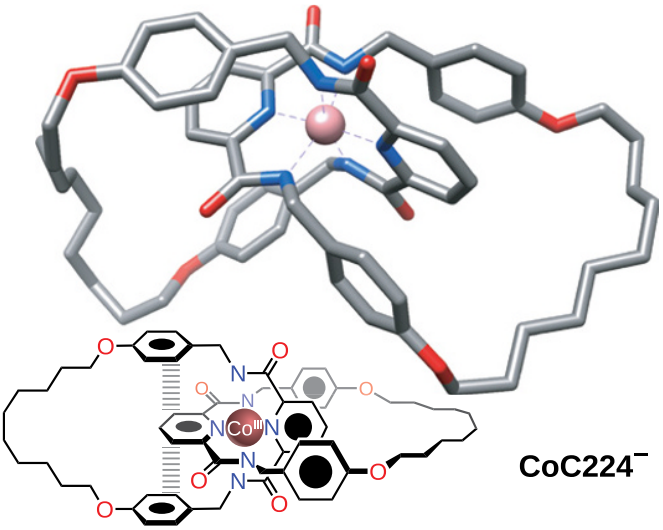


Figure 2.22 The structural formula and a tubular representation of the solid-state structure of Leigh's carboxamide Co^{III} [2]catenate[448] **CoC224**$^{-}$. Solvent, counterions, and protons are omitted for the sake of clarity.

The ligand motif of the benzylic imine MIMs is suitable for relatively soft transition metal ions. In the interest of expanding further the scope of metal templates available for synthesizing MIMs, Leigh[448] turned his attention to deprotonated carboxamide groups, which are known to be good ligands for hard ions such as Fe^{III} and Co^{III}. The structure of the Co^{III} [2]catenate **CoC224**$^{-}$ is represented in **Figure 2.22**. This catenate has been synthesized by a multi-step process involving (i) the assembly of a carboxamido metallo-pseudorotaxane around a softer cobalt(II) template under thermodynamic control, since ligand exchange around cobalt(III) is generally slow, followed by (ii) spontaneous oxidation to Co^{III} in air, a particularly favorable event in the presence of the ligands' four anionic charges, leading to a kinetically stable complex, and (iii) ring-closing metathesis on the acyclic ligand. **CoC224**$^{-}$ as shown is a post-synthetically modified homologue in which the olefinic ring closure has been hydrogenated. It is important to employ a threading strategy in this case, since attempting the entwining route from a pair of acyclic bis-olefin-terminated 2,6-carboxamidopyridine (pydc) ligands leads exclusively to a figure-of-eight macrocycle on account of ligand cross-reactions. The net negative charge on **CoC224**$^{-}$ afforded by the tetra-anionic catenated ligands is unusual, considering the fact that transition metal-based MIMs are typically cationic. The catenate can be demetalated and reprotonated with activated Zn dust in AcOH/MeOH to afford a simple benzylic amide MIM not unlike those which are templated by hydrogen-bonding interactions (**Section 2.3.4.1**), and it can also be re-metalated with a source of Co^{II}, base, and oxygen. Bis-carboxamido Co^{III} [2]rotaxanes have been prepared by an analogous strategy.[448,449]

2.3.2.4 Square Planar Templates

Sauvage and Schröder[450] prepared a square planar [2]catenate inadvertently in 1989 by insertion of Pd^{II} into Sauvage's original [2]catenand **C211**. Having hypothesized that the catenand effect of **C211** could impose a distorted tetrahedral geometry around an ordinarily square planar Pd^{II} center, they found instead that C–H activation occurs over a four-day period of refluxing in CH_2Cl_2, leading to the [2]catenate **Pd(C211–H)**$^{+}$. One of the expected N–Pd bonds has been forsaken for a C–Pd bond, concomitant with the loss of a proton, in compound **Pd(C211–H)**$^{+}$. The solid-state structure (**Figure 2.23**) of this organometallic catenate was determined by X-ray crystallography, revealing a distorted square planar geometry around the metal center and a

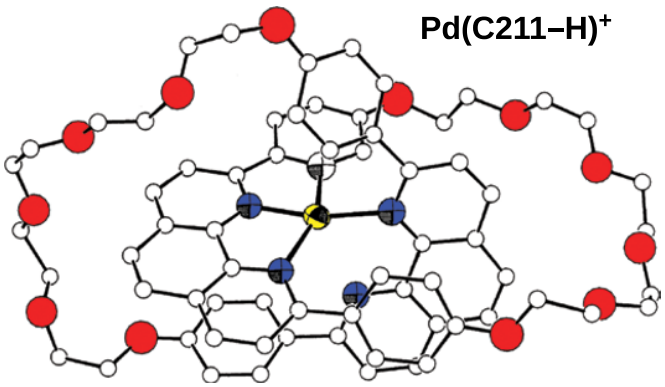


Figure 2.23 A ball-and-stick representation of the solid-state structure (C = white, O = red, N = blue, Pd = yellow) of Sauvage's distorted square planar [2]catenate **Pd(C211–H)**$^{+}$. Solvent, counterion, and protons are omitted for the sake of clarity. Adapted with permission from ref. 450 (copyright 1989 Royal Society of Chemistry).

vacancy—an uncoordinated nitrogen atom—in one of the dpp ligands. Apparently, C–H activation offers a compromise between the steric constraints of the catenated ligands, which favor the formation of tetrahedral complexes, and the electronic constraints of the Pd^{II} center, which favor the formation of square planar complexes. The fact that a heteroleptic [3+1] ligand motif arises from a pair of identical topologically linked bidentate ligands is a striking feature about this system.

A more deliberate strategy for constructing MIMs around square planar transition metals with a [3+1] ligand motif has been outlined independently by Sauvage[451] and Leigh.[452–455] Their [3+1] ligand motifs, both of which rely on Pd^{II} to gather components, are illustrated in **Figure 2.24**. Sauvage designed the endocyclic chelate *Pd(Mterpy34)(MeCN)*$^{2+}$ as a host for small monodentate ligands, such as 2,6-lutidine and diethylamine, which displace MeCN as they coordinate the Pd^{II} ion endotopically. The corresponding metallopseudorotaxanes would appear to be viable forerunners to rotaxanes and catenanes, although MIMs based on this motif have not yet been reported. Leigh's motif is based on benzylic pydc units, identical to those which coordinate the hard Co^{III} ion of the [2]catenate **CoC224**$^{-}$ described in the previous Section. His endocyclic chelate *Pd(Mpydc29)(MeCN)* functions analogously to that of Sauvage's, i.e., by ligand exchange of the endohedral MeCN ligand. In this case, the negatively charged carboxamide groups balance out the positive charges of the Pd^{II} dication, rendering a neutral compound that is capable of hosting monodentate ligands.

Leigh has gained a lot of mileage out of his square planar macrocyclic chelate in MIM synthesis. Endocyclic chelates of the type *Pd(Mpydc29)(L)*, where L is a ligand comprising a ring or dumbbell, are components of a number of

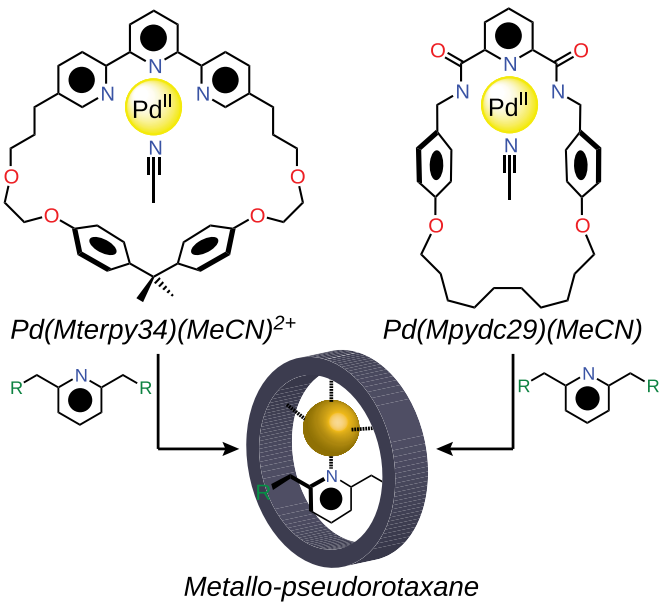
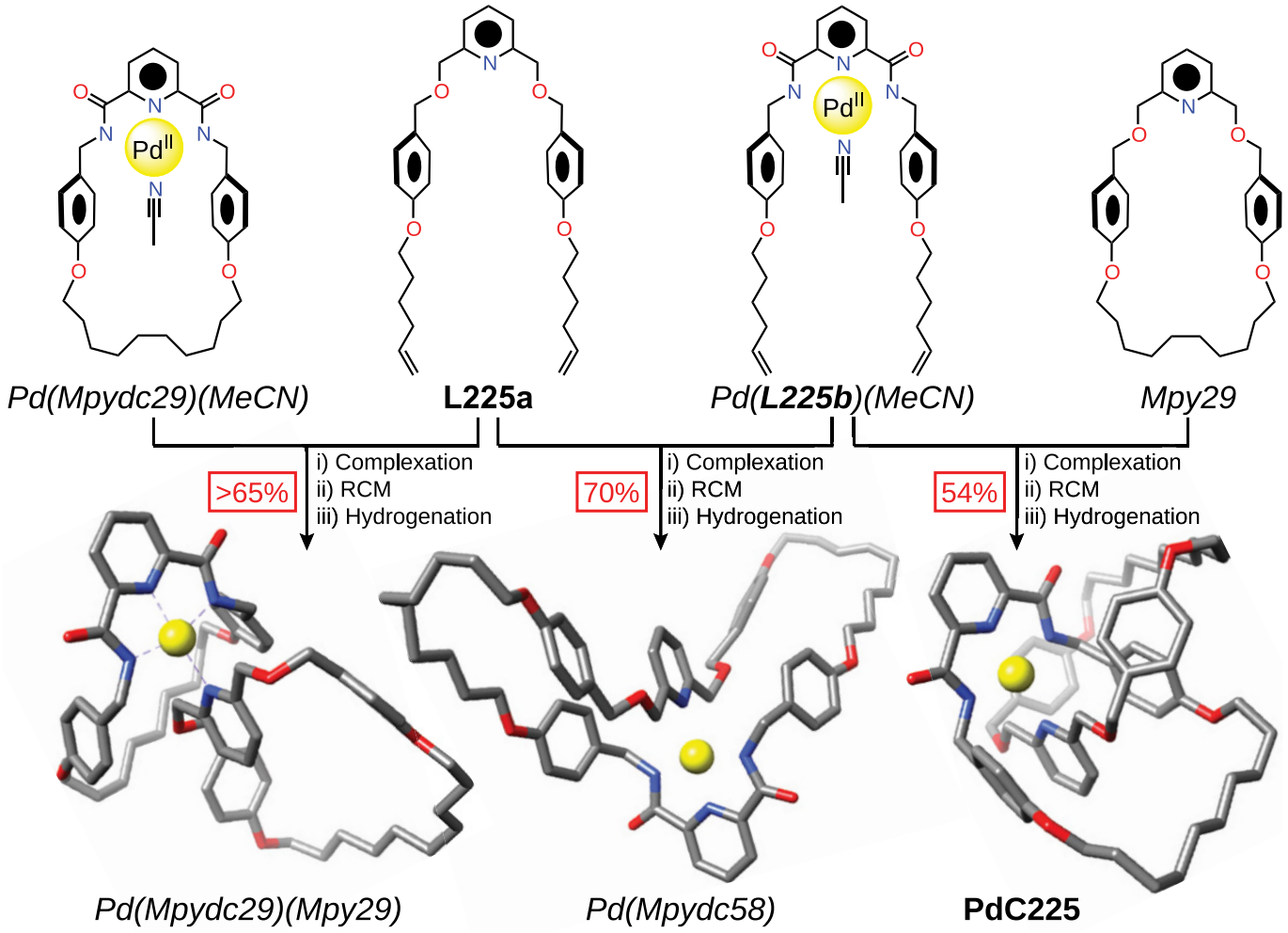


Figure 2.24 Structural formulas of the Pd^{II} endocyclic chelates introduced by Sauvage[451] and Leigh,[453] respectively. Both chelates self-assemble with 2,6-lutidine derivatives into metallo-pseudorotaxanes by displacement of an endotopic MeCN ligand.

rotaxanes[452,454,455] which embody novel templation strategies[454] (**Section 3.2.1.3**) and types of isomerism[455] (**Section 5.2.2**) in mechanostereochemistry. The endocyclic chelate has also been investigated[453] in the context of catenanes and their topological isomers. The synthesis and X-ray crystal structures of three topological isomers based on this motif are represented in **Scheme 2.44**—namely, the bis-macrocycle *Pd(Mpydc29)(Mpy29)*, the figure-of-eight macrocycle *Pd(Mpydc58)*, and the [2]catenate **PdC225**. These topological isomers can be 'selected' based on the initial conditions of a ring-closing metathesis (RCM) reaction involving components from a small toolbox of four precursors. The toolbox comprises two monodentate ligands derived from 2,6-lutidine[J]—namely, the macrocycle Mpy29 and its corresponding acyclic precursor **L225a**—as well as the endocyclic and acyclic benzylic amide chelates, *Pd(Mpydc29)(MeCN)* and *Pd(**L225b**)(MeCN)*, respectively. When the macrocyclic chelate *Pd(Mpydc29)(MeCN)* is combined with the olefin-terminated ligand **L225a**, the assembly of a *Pd(**L225a**⊂Mpydc29)* metallo-pseudorotaxane is accompanied by that of a nonthreaded isomer, *Pd(Mpydc29)(**L225a**)*. These threaded and non-threaded isomers (not shown) do not interconvert at room temperature in CH_2Cl_2, a solvent in which they exist in a 2:3 ratio. Heating in MeCN, however, enables the isomers to interconvert by ligand exchange and shifts their ratio to 8:1 at equilibrium. RCM and hydrogenation of the metallo-pseudorotaxane *Pd(**L225a**⊂Mpydc29)* leads to the [2]catenate **PdC225**, while the same procedure affords the bis-macrocyclic chelate *Pd(Mpydc29)(Mpy29)* from the non-threaded isomer, *Pd(Mpydc29)(**L225a**)*. Presumably, this bis-macrocyclic chelate could be accessed exclusively by simply mixing both of the macrocyclic precursors *Pd(Mpydc29)(MeCN)* and Mpy29 in solution. Employing the inverted recognition system comprising the macrocyclic ligand Mpy29 and the acyclic chelate *Pd(**L225b**)(MeCN)* in the RCM/hydrogenation protocol leads exclusively to the formation of the [2]catenate **PdC225**. This topological selectivity can be explained by differences in stability between the metallo-pseudorotaxane intermediates *Pd(**L225a**⊂Mpydc29)* and *Pd(**L2325b**⊂Mpy29)*, since the latter assembles exclusively into an interpenetrated complex. The larger figure-of-eight tetradentate macrocyclic chelate *Pd(Mpydc58)* is the dominant product when RCM is attempted on the entwined complex *Pd(**L225a**)(**L225b**)* as a result of ligand cross-reactivity. All three topological isomers can be demetallated in near-quantitative yields with KCN in CH_2Cl_2/MeOH and re-metallated by heating with $Pd(OAc)_2$ in MeCN. The syntheses of rotaxanes based on the same ligand motif are described in **Sections 3.4.1.1** and **5.2.2**.

[J] It is worth noting that, whereas 2,6-lutidine can serve as a subcomponent of MIMs based on these square planar Pd^{II} endocyclic chelates, ligands based on 3,5-lutidine fail to deliver mechanically interlocked products after ring closing metathesis, at least in the case of metallo-rotaxanes.[452]



Scheme 2.44 Selecting topology through metal-directed cyclization.[453] A toolbox of precursors comprises the cyclic and acyclic monodentate ligands Mpy29 and **L225a**, along with the complementary acyclic and cyclic chelates, *Pd(**L225b**)(MeCN)* and *Pd(Mpydc29)(MeCN)*, respectively. Different pairwise combinations of these compounds favor the formation of different topological isomers during ring-closing metathesis—namely, the bis-macrocyclic chelate *Pd(Mpydc29)(Mpy29)*, the figure-of-eight macrocyclic chelate *Pd(Mpydc58)*, and the [2]catenate **PdC225**. Tubular representations of the solid-state structures of these topological isomers are depicted with hydrogen atoms omitted for the sake of clarity.

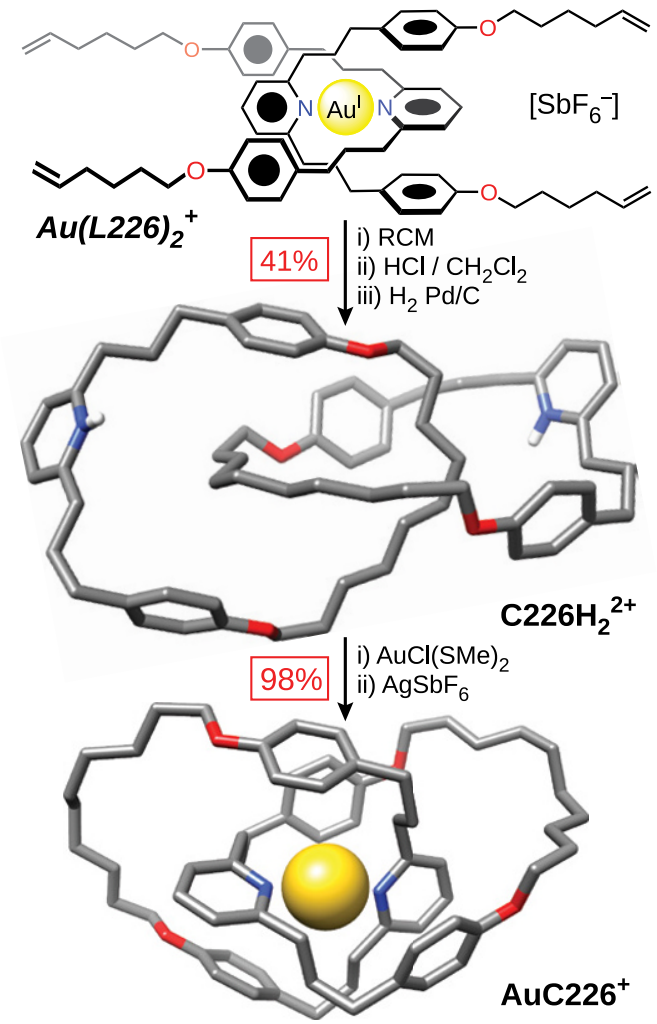
Recently, templates related to Leigh's palladium 2,6-dicarboxamides have been utilized by other groups in the synthesis of MIMs, including Sheng-Hsien Chiu[456] and Hong-Cheu Lin,[457] both of whom are located in Taiwan.

2.3.2.5 Linear Templates

All of the coordination motifs discussed up to now require at least one multidentate ligand because the corresponding geometries, regardless of whether they constitute homoleptic or heteroleptic donor sets, involve a coordination number of at least four. The most conceivable way to organize only two monodentate ligands around a metal center is to employ a linear coordination geometry, where CN = 2. Leigh[458] introduced the first catenates and catenands to be synthesized (**Scheme 2.45**) from linear templates in 2008 by employing Au^{I} as the transition metal center. The ligand design for this system can be described as being derived conceptually from the Pd^{II} catenates in the previous section, where the carboxamide groups adjacent to the central pyridine unit have been replaced by a methylene units. Thus, the 2,6-disubstituted monodentate pyridine ligand **L226** assembles with $AuCl(SMe)_2$ into the linear homoleptic precursor ***Au(L226)*$_2^+$**, a compound which is soluble in organic solvents such as CH_2Cl_2 after counterion exchange to the SbF_6^- salt. The entwined ***Au(L226)*$_2^+$** complex can be metathesized directly to the olefinic precursor of the [2]catenate **AuC226$^+$**, although for purification purposes this species is demetallated first of all with aqueous HCl in CH_2Cl_2 and hydrogenated over Pd/C in an atmosphere of H_2 in order to afford the [2]catenand **C226H$_2^{2+}$** intermediate, which is protonated at each of its two pyridinium sites. Although this transformation occurs in only modest yield (41%), the uncatenated macrocycles and a larger macrocycle derived from cross-reacted ligands are isolated as side products in 20 and 18% yields, respectively, indicating a high reaction efficiency with only moderate topological

selectivity. Remetalation of this catenand with a source of Au^{I} leads to the [2]catenate **AuC226**$^{+}$ in near-quantitative yield. The catenate and catenand have both been characterized in the single crystal by X-ray crystallography—their solid state structures are represented in **Scheme 2.45**. Whereas the pyridinium units reside on the outside of the [2]catenand, they are buried in the center of the [2]catenate, with a bend angle of 175° for the pyridine-Au-pyridine bonds. Protection from the phenylene rings around the Au^{I} center prevents the formation of aurophilic Au-Au interactions in the crystal superstructure. This Au^{I} template synthesis has been extended[458] to rotaxanes by cyclizing **L226** around a 2,6-lutidine-derived dumbbell.

Leigh's templated synthesis of catenanes and rotaxanes from linear complexes is the final addition to the family of common coordination geometries employed in mechanostereochemistry. The high compatibility between MIMs and all of the common geometries for donors surrounding transition metals bodes well for many potential applications that combine the structures and dynamics of mechanical bonds with the special catalytic and optoelectronic properties of coordination complexes.



Scheme 2.45 Leigh's synthesis of the [2]catenand **C226H$_2$**$^{2+}$ and [2]catenate **AuC226**$^{+}$ from a linear Au^{I} template by ring-closing olefin metathesis.[458] Tubular representations of the solid-state structures of the catenand and catenate are portrayed with solvent, counterions, and protons omitted for the sake of clarity.

2.3.3 π-Donor/π-Acceptor Templates

Catenanes and rotaxanes based on π-associated donor-acceptor (D-A) interactions constitute an important family of MIMs, if only because they have played a pivotal role in virtually every arena pertaining to the mechanical bond, including (i) the development of efficient self-assembly strategies for templating mechanical bonds (**Chapters 2–3**), (ii) constructing new interlocked architectures (**Chapter 4**), (iii) probing and understanding the dynamics, isomerism, and chirality of MIMs (**Chapter 5**), (iv) the development of molecular switches and machines that rely on mechanical bonds (**Chapter 6**), and a plethora of applications that motivate further research and give rise to new technologies. Many of these topics have been addressed in reviews[459–472] on π-donor/π-acceptor MIMs. In this Section we (i) explain the nature of π-associated donor-acceptor interactions, (ii) introduce the most common recognition motifs involved in the templation of π-donor/π-acceptor MIMs, and (iii) summarize a number of strategies for synthesizing donor-acceptor mechanomolecules using clipping and stoppering protocols. Slippage protocols leading to D-A rotaxanes are described in **Section 3.1.2**.

2.3.3.1 The Nature of Donor-Acceptor π–π Interactions

Associative interactions between aromatic compounds, which are governed in large part by the properties of π-electrons, are all-pervasive at the molecular level. In nature, π–π interactions are implicated in stabilizing, for example, the folded tertiary structures of proteins through associations between aromatic amino acid side chains,[473] as well as the double helical superstructure of DNA through stacking of Watson-Crick base pairs.[474] In synthetic systems, π–π interactions are among the most powerful forces for directing the self-assembly of numerous compounds comprising aromatic building blocks,[475] and are also responsible for electrical conductivity in organic conductors and semiconductors.[476]

Despite their ubiquity, the nature of π–π interactions continues to be the subject[477–479] of much debate as a result of an incomplete fundamental understanding of the parameters which define the geometries and strengths of the interactions, as well as the other forces (electrostatic, solvophobic, etc.) which act as convoluting factors. A seminal paper by Hunter and Sanders,[480] which proposed a simple model for predicting geometry on the basis of electrostatic interactions among π-orbitals, has been central to our thinking about π–π interactions for nearly a quarter of a century. The model takes into account the fact that π-electron density creates a quadrupole moment around most aromatic rings with partial positive charge above the faces and partial negative charge around the edges. Ordinary aromatic rings such as benzene therefore

engage (**Figure 2.25a**) more favorably in edge-to-face (T-shaped) or off-centered stacking (parallel displaced) interactions than aligned cofacial (face-centered) stacked geometries in order to maximize Coulombic attractions and minimize their repulsions. The situation changes completely (**Figure 2.25b**) when one of the aromatic units contains electron-withdrawing functional groups, which polarize π-electrons away from the aromatic core. The electron-deficient faces of this π-acceptor (A) will engage readily with the electron-rich surfaces of a π-donor (D) in a face-centered geometry. The mixing of π-orbitals and partial transfer of electronic charge from D to A in the ground state constitutes an associative interaction known[481] as a charge transfer (CT) complex (DA) which exists in equilibrium with its constituent molecules D and A:

$$D + A \rightleftharpoons DA$$

where DA is a resonance between a nonbonding state (D, A) and a dative state ($D^{+}\cdots A^{-}$). While ground-state[κ] D-A

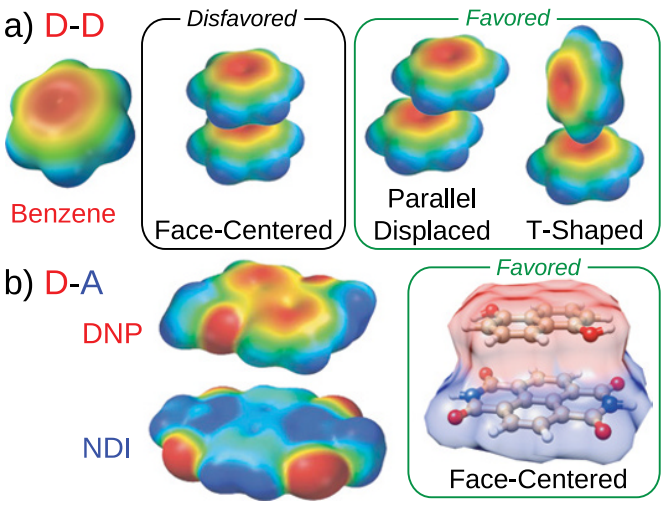


Figure 2.25 Examples of π–π interactions, rationalized in part by the distribution of electrostatic potential on an aromatic molecule's surface. (a) Benzene rings, which generally serve as π-donors (D) by virtue of their electron-rich faces, dimerize more favorably in parallel displaced and T-shaped geometries to avoid electrostatic repulsive forces that transpire in a face-centered stacking arrangement. (b) The withdrawal of π-electron density to the edges of a π-acceptor (A) such as in the case of naphthalenediimide (NDI) enables it to favor π-stacking interactions with a donor such as 1,5-dioxynaphthalene (DNP) in a π-associated D-A charge-transfer (CT) complex.[480]

[κ] The excitation of an electron from the HOMO of D to the LUMO of A is an electronic transition that often gives rise to optical absorption bands in the UV/Vis/NIR regions of the electromagnetic spectrum, and can therefore often be detected with the naked eye. Although ground-state interactions are the basis for the D-A recognition chemistry employed in MIMs synthesis, excited-state CT interactions can also enhance association between molecules. Excited-state CT complexes also play an important role in organic photovoltaics, for example, which may be relevant to potential applications for D-A MIMs.

CT complexes have been exploited in the context of ferromagnetic[482] and ferroelectric[483,484] materials, they also underpin the recognition chemistry[475] of the MIMs described in this Section.

It is now clear that the Hunter/Sanders model[480] is surprisingly reliable as a qualitative tool, despite being highly oversimplified in light of more recent computational research recognizing[477–479] the important, sometimes dominant, effects of solvation and other types of electrostatic forces, including through-space interactions between polarized atoms. At the center of the ongoing controversy is the (over)use of the term "π–π stacking", which is often interpreted as a "special" interaction transcending ordinary electrostatic, solvation, and van der Waals forces. It transpires that such kinds of "special" qualities arise only in large polycyclic systems.[478] The term "π–π stacking" should therefore be defined by authors who employ it because there is no unanimous consensus on its meaning. Throughout this monograph, we interpret π–π stacking as simply denoting any associative face-to-face interactions between aromatic molecules for historical, practical, and literal reasons, regardless of the actual sources of the interactions and their relative strengths.

Donor-acceptor charge transfer interactions have served[485] as the basis of many supramolecular assemblies and materials. A number of π-donor and π-acceptor recognition units and corresponding hosts that are most relevant in mechanostereochemistry are illustrated in **Figure 2.26**. Planar dications are commonly employed as acceptor units—they include derivatives of 4,4′-bipyridinium ($BIPY^{2+}$), also known as viologens, and homologues thereof possessing larger π-systems such as diazapyrenium (DAP^{2+}) and diazaperopyrenium ($DAPP^{2+}$), as well 1,2-bis(pyridinium)ethane (BPE^{2+}) and a number of tetraimine macrocycles with cationic metal centers. Aromatic diimides such as pyromellitic diimide (PMDI), naphthalene diimide (NDI), and perylene diimide (PDI) are often employed as neutral π-acceptors. Common donor units are derived routinely from small aromatic hydrocarbons such as benzene and naphthalane. Hydroquinone (HQ), 1,5-dioxynaphthalene (DNP), and 1,5-diaminonaphthalene (DAN) are particularly well-explored in this arena, as are 4,4′-biphenol (BP) and benzidine (BZ). Derivatives of tetrathiafulvalene (TTF) such as pyrrolotetrathiafulvalene (PTTF) and bispyrrolotetrathiafulvalene (BPTTF) are frequently employed because of their well-understood and highly reversible redox processes. Porphyrins and oligothiophenes (*n*T, where *n* equals the number of repeating thiophene units) have also been implicated in D-A MIM synthesis to a lesser extent. By our estimation, the vast majority of mechanomolecules templated by donor-acceptor π-stacking interactions incorporate the above components. In the figures and schemes, π-donors are warm-colored (reds, greens) while π-acceptors are cool-colored (blues, violets) as a way to signify their role in

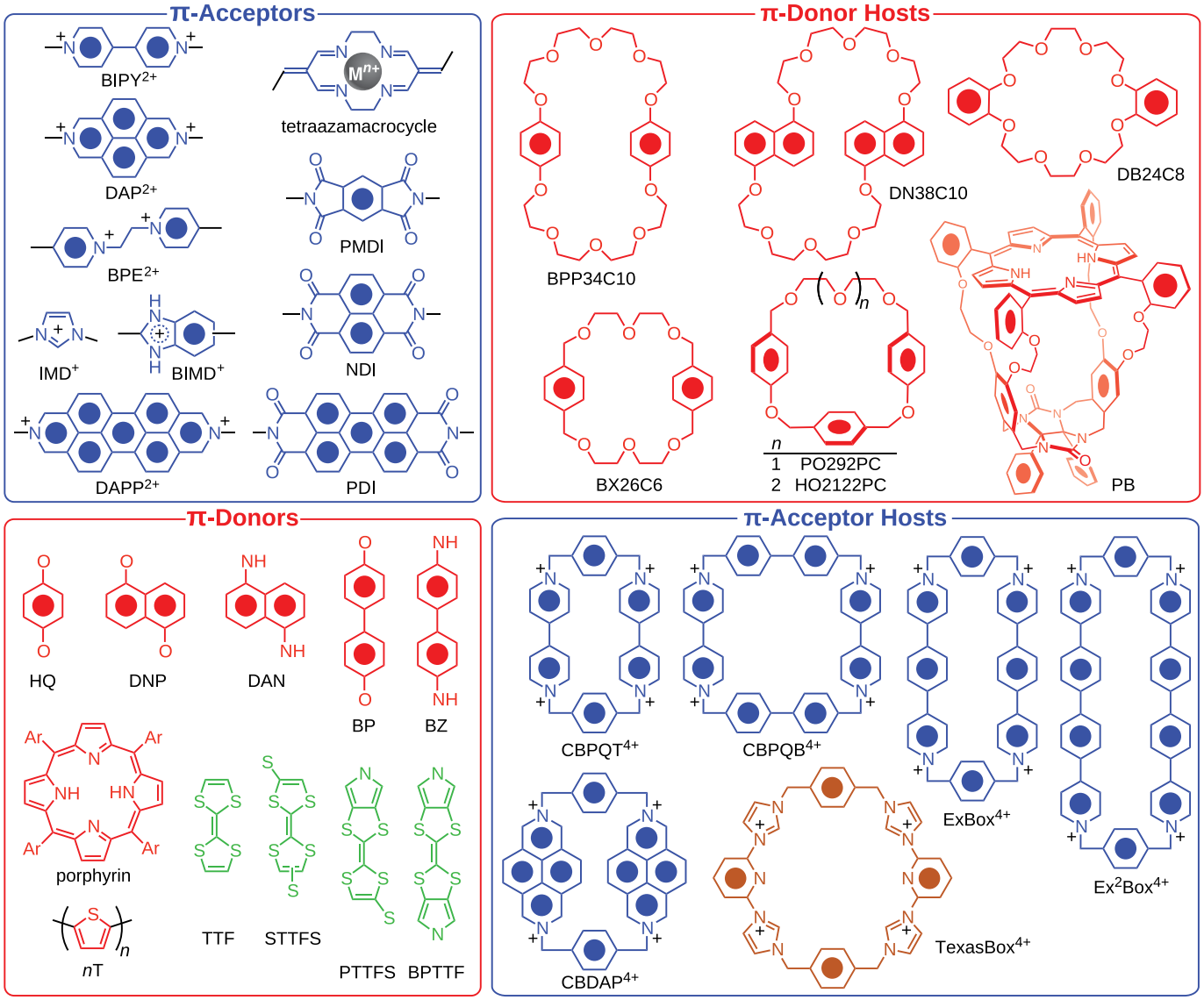


Figure 2.26 Examples of recognition units and hosts commonly employed in the synthesis of donor-acceptor MIMs.

D-A CT interactions. The color choices for the π-donors reflect the actual colors observed in solution when they are hosted by the tetracationic cyclophane $CBPQT^{4+}$ (**Section 2.3.3.8**), while the blue-colored π-acceptors reflect the intense blue-colored solutions produced by redox-active viologen derivatives when they are reduced to radical cations. The construction of D-A MIMs typically proceeds from a pseudorotaxane precursor or intermediate comprising a ring of two π-donor or π-acceptor recognition units, with a guest of the opposite recognition type sandwiched in between them.

Common hosts of both the π-donating and π-accepting varieties are also illustrated in **Figure 2.26**. The remainder of **Section 2.3.3** is organized according to host type and structure. We begin firstly with template motifs and mechanical bonds based on π-donating (**Sections 2.3.3.2–2.3.3.7)** hosts, followed by those based on π-accepting (**Sections 2.3.3.8–2.3.3.9)** hosts.

2.3.3.2 π-Donating Crown-10 Template Motifs

The template-directed synthesis of supermolecules and mechanomolecules based on π-associated donor-acceptor interactions began in the mid-1980s when it was recognized[486–491] that macrocyclic polyethers with π-electron rich aromatic units can serve as suitable hosts for π-electron poor bipyridinium herbicides such as diquat and paraquat. Pseudorotaxanes comprising π-donating macrocyclic polyethers and bipyridinium compounds—in particular the family of $BIPY^{2+}$ derivatives known as viologens[492]—are prominent donor-acceptor templates in mechanostereochemistry. Two of the most high-profile components in this context are the bis-*para*-phenylene[34]crown-10[491,493] (BPP34C10) and bis-1,5-dioxynaphtho[38]crown-10[490,494] (DN38C10) rings.

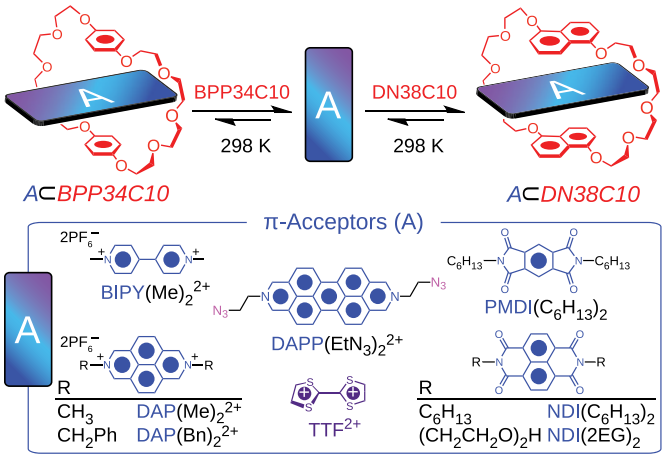
BPP34C10 and DN38C10 Pseudorotaxanes

The association constants, K_a, for pseudorotaxanes comprising either BPP34C10 or DN38C10 and a number

of π-accepting guests are summarized[495–502] in **Table 2.7**. The methods employed in the determination of K_a values are noted in the Table because there is some variation in the observed K_a values depending on the techniques[503] used to measure them. We observe some trends upon comparing the data: (i) K_a values increase as solvent polarity decreases, (ii) neutral guests, such as PMDI and NDI, tend to associate with the crown ethers more weakly than do planar dications, such as $BIPY^{2+}$ and DAP^{2+}, and (iii) increasing the size of the π-system usually results in an increase in K_a values, a trend which applies to the aromatic recognition units of both host and guest. The latter trend results in DN38C10-based pseudorotaxanes outperforming the BPP34C10 homologues in terms of binding strengths. Likewise, the larger DAP^{2+} and NDI derivatives bind to the crown ethers more strongly than do their smaller $BIPY^{2+}$ and PMDI relatives, respectively. One noteworthy case[502] is that of the oxidized TTF dication TTF^{2+}. Whereas TTF is an electron-rich compound with essentially no affinity for the DN38C10 ring, the TTF^{2+} dication binds to it in MeCN with a K_a value on the order of 10^3 M^{-1}, highlighting the importance of electrostatic forces in these systems.

The solid-state superstructures[489,490] of pseudorotaxanes comprising DN38C10 and a number of common π-acceptors, namely (a) methyl viologen,[489] (b) *N*,*N*′-dimethyldiazapyrenium,[495] (c) hexyl-functionalized PMDI,[504] and (d) bis-propargylated NDI,[505] are portrayed in **Figure 2.27.** These complexes are stabilized, not only by D-A CT and π–π stacking interactions, but also by [C–H···O] hydrogen bonding[506,507] interactions[L] between acidic protons of the recognition units and the oxygen atoms of the ring's polyether loops. These [C–H···O] interactions are represented by hatched lines in the FIgure. A comparison (**Figure 2.27a–b**) of the two dicationic complexes reveals a similar binding geometry for the guests. In each case, [C–H···O] hydrogen bonds are observed extending from the α protons of the $BIPY^{2+}$ and DAP^{2+} units, as well as from the adjacent methyl protons. The specific assignments of these interactions, however, are not identical in each complex. The $BIPY^{2+}$-based pseudorotaxane possesses a crystallographic center of symmetry which is coincident for both host and guest, meaning that the [C–H···O] interactions are identical on both sides of the complex. The binding geometry of DAP^{2+} within DN38C10 lacks symmetry—one of the crown's polyether loops engages only methyl protons while the other loop engages only α protons of DAP^{2+} in [C–H···O] hydrogen-bonding interactions. Although we speak of this recognition chemistry with a focus on π-donor/π-acceptor CT interactions, in actual fact the [C–H···O] interactions can be more than four times stronger than the D-A π–π stacking interactions.[508]

Table 2.7 Association constants, K_a, and the derived free energies (ΔG) of complexation for pseudorotaxanes formed between BPP34C10 or DN38C10 donors and various π-acceptors.



Guest	Solvent	K_a M^{-1}	ΔG kcal·mol^{-1}	Method[a]	Ref
		Guest⊂BPP34C10			
$BIPY(Me)_2 \cdot 2PF_6$	CD_3CN	2.4×10^2	–3.3	NMRD	495
$BIPY(Me)_2 \cdot 2PF_6$	Me_2CO	7.3×10^2	–3.9	ST	500
$DAP(Me)_2 \cdot 2PF_6$	CD_3CN	5.9×10^3	–5.1	NMRD	495
$DAP(Bn)_2 \cdot 2PF_6$	CD_3CN	2.9×10^4	–6.1	ST	495
		Guest⊂DN38C10			
$BIPY(Me)_2 \cdot 2PF_6$	CD_3CN	1.19×10^3	–4.2	ST	496
$BIPY(Me)_2 \cdot 2PF_6$	CD_3CN	6.7×10^2	–3.8	ST	495
$BIPY(Me)_2 \cdot 2PF_6$	DMF	33	–2.0	ST	497
$DAP(Me)_2 \cdot 2PF_6$	CD_3CN	1.1×10^4	–5.5	NMRD	495
$DAP(Bn)_2 \cdot 2PF_6$	MeCN	2.2×10^5	–7.3	FT	501
$DAP(Bn)_2 \cdot 2PF_6$	CD_3CN	2.9×10^5	–7.4	ST	495
$DAPP(EtN_3)_2 \cdot 2PF_6$	MeCN	1.05×10^6	–5.5	ITC	571
$TTF \cdot 2ClO_4$	MeCN	4.1×10^3	–4.9	ST/FT	502
$TTF \cdot 2ClO_4$	MeCN	2.6×10^3	–4.7	NMRT	502
$PMDI(C_6H_{13})_2$	$CHCl_3$[b]	21	–1.8	ITC	499
$NDI(C_6H_{13})_2$	$CHCl_3$[b]	100	–2.7	ITC	498
$NDI(CH_2CH_2O)_2H$	DMF	33	–2.1	ST	497

[a]Methods of K_a Determination: Isothermal Titration Calorimetry (ITC), NMR Dilution Method (NMRD), NMR Titration Method (NMRT), NMR Continuous Variation Method (NMRCV), Spectrophotometric Titration (ST).
[b]$CHCl_3$ solution containing 2% $^v/_v$ MeOH.

[L] The question as to whether these types of [C–H···O] interactions constitute hydrogen bonds is grounds for debate. In 2011 an IUPAC Task Group recommended[507] the following evidence-based definition for the hydrogen bond: 'an attractive interaction between a hydrogen atom from a molecule or molecular fragment X–H in which X is more electronegative than H, and an atom or group of atoms in the same or different molecule, in which there is evidence of bond formation.' The IUPAC provides a list of six criteria[506] that can be used as evidence for a hydrogen bond. The criteria encompass the physical forces, geometries, spectroscopic features, and energies which characterize the [X–H···Y] interaction of a hydrogen bond, where Y is the hydrogen bond acceptor. The [C–H···O] interactions underpinning π-associated donor-acceptor pseudorotaxanes satisfy all six of the criteria, and therefore constitute hydrogen bonds in our view.

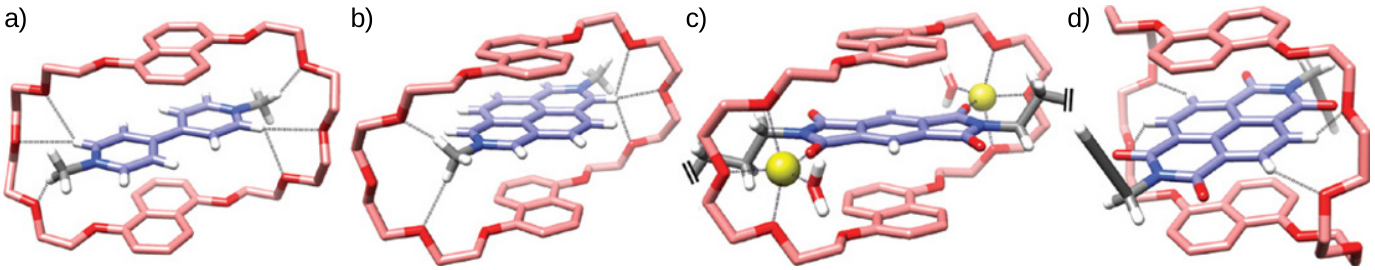


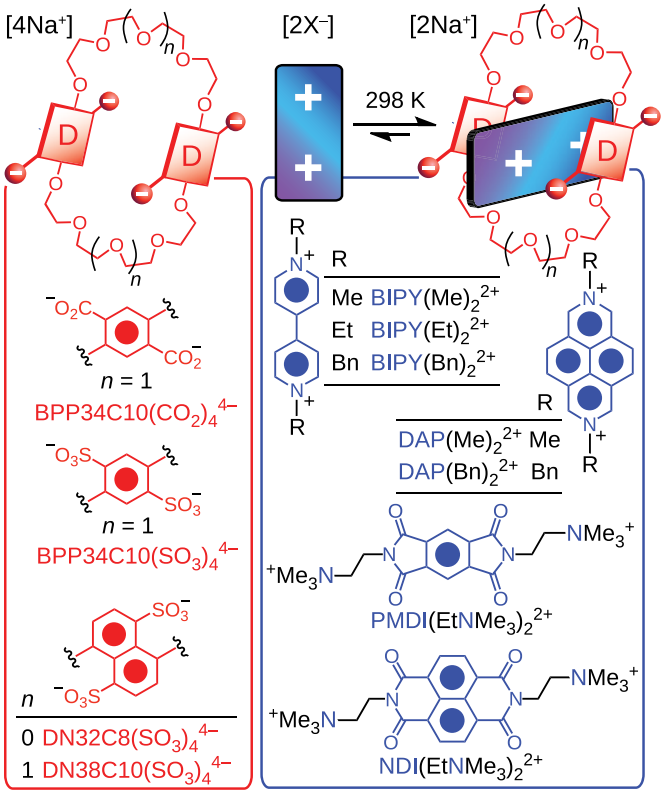
Figure 2.27 Tubular representations of the solid-state superstructures of pseudorotaxanes comprising the π-electron rich DN38C10 ring and guests derived from (a) $BIPY^{2+}$,[489] (b) DAP^{2+},[495] (c) PMDI (with two Li^+ ions and two water molecules),[504] and (d) NDI π-acceptors.[505] Solvent molecules, counterions, protons of the DN38C10 ring, and sections of the PMDI hexyl chains are omitted for the sake of clarity.

Investigations of host-guest complexes and MIMs based on crown ethers and the neutral PMDI and NDI guests were spearheaded by Sanders[505,509] in 1997. The *PMDI⊂DN38C10* complex represents a unique recognition system, since it requires[504] Li^+ or Na^+ cations as cofactors in the stabilization of the pseudorotaxane in solution. A 1:1 mixture of bis-hexyl-PMDI and DN38C10 in 98:2 $CHCl_3$:MeOH allows 2 equiv of lithium iodide to become soluble over a period of hours. The solid-state superstructure (**Figure 2.27c**) of the complex reveals that each Li^+ ion adopts a pentacoordinate geometry in which it accepts electron density from one of the PMDI unit's carbonyl oxygen atoms, as well as from three oxygen atoms of the crown's polyether loops and a water molecule. Thus, the typical [C–H···O] contacts are replaced by [Li···O] contacts in this particular system. The ion-promoted binding is also highly cooperative, since the *PMDI⊂DN38C10* assembly always takes up two Li^+ ions at once rather than one Li^+ ion at a time. This mechanistic insight is revealed by the observation that adding 1 equiv of Li^+ to a 1:1 mixture of PMDI and DN38C10 results in 50% of the molecular population forming the *PMDI⊂DN38C10* pseudorotaxane. The self-assembly is not complete until at least 2 equiv of Li^+ are added. NDI derivatives, on the other hand, bind DN38C10 more effectively without the need for Li^+ ions. In the solid state, the pseudorotaxane based on a bis-propargylated NDI unit also possesses (**Figure 2.27d**) a crystallographic center of symmetry coincident with both host and guest, such that each of the four hydrogen atoms of the NDI core participate in identical, singular [C–H···O] hydrogen bonds with unique oxygen atoms in the ring. A hexyl-functionalized NDI unit crystallizes[498] with DN38C10 as a pseudorotaxane with a different geometry involving the hydrogen bond network, suggesting the possibility of multiple, nearly isoenergetic (co)conformations for this class of pseudorotaxanes.

BPP34C10 and DN38C10 are soluble only in mid- to high-polarity organic solvents. Association constants, K_a, increase as solvent polarity decreases because nonbonding electrons in polar solvents tend to disrupt the relatively weak interactions holding these complexes together. By installing negative charges around the π-donating crown ethers, it should be possible to increase their affinities for π-acceptors in polar solvents by enhancing the contributions of solvophobic and/or ion-pairing interactions. Fitzmaurice[510] began to explore this possibility in 2008, when he reported that the tetracarboxylated and tetrasulfonated rings $BPP34C10(CO_2)_4^{4-}$ and $BPP34C10(SO_3)_4^{4-}$ bind (**Table 2.8**) ethyl viologen, $BIPY(Et)_2^{2+}$, more tightly than do their neutral precursors by over three orders of magnitude in MeCN and MeOH, whereas K_a values on the order of 10^2 M^{-1} reflect relatively weak interactions in water. The investigation revealed that sulfonated crowns bind the $BIPY^{2+}$ guests more tightly than carboxylated ones, and also that the strength of the interaction is influenced by counterions, since the PF_6^- salt of ethyl viologen associates with the tetra-anionic crowns more strongly than do the corresponding Br^- salts by about an order of magnitude. The viologen/$BPP34C10(SO_3)_2^{2-}$ recognition pair has been employed[510] in the synthesis of [2]rotaxanes. Yu Liu[511] and Feihe Huang[512] have found that a sulfonated bismetaphenylene[26]crown-8 also binds planar aromatic dications in water.

Yu Liu[513–515] has recently described the outstanding host-guest properties (**Table 2.8**) of a tetrasulfonated DN38C10 ring—call it $DN38C10(SO_3)_4^{4-}$—as well as a smaller homologue $DN32C8(SO_3)_4^{4-}$ possessing shorter polyether loops. These crown ethers bind planar π-acceptors in aqueous solutions with substantially higher affinities than do their neutral counterparts in organic solvents. Viologen derivatives are taken up by the smaller $DN32C8(SO_3)_4^{4-}$ derivative with higher K_a values (~10^7 M^{-1}) than that (~10^5 M^{-1}) of the larger $DN38C10(SO_3)_4^{4-}$ derivative, while both crown ethers exhibit similar affinities (~10^5–10^6 M^{-1}) for the neutral PMDI and NDI recognition units appended with quaternary ammonium ions, namely $PMDI(EtNMe_3)_2^{2+}$ and $NDI(EtNMe_3)_2^{2+}$, respectively. The most strongly associating guests, which are based on diazapyrenium (DAP^{2+}) units, reach up to 10^8 M^{-1} in the case of $DAP(Me)_2^{2+}⊂DN38C10(SO_3)_4^{4-}$. Solid-state superstructures of these pseudorotaxanes reveal binding geometries similar to those of the unsulfonated parent pseudorotaxanes. Carbonyl groups in the PMDI and NDI guests participate in coordinating to the Na^+ counterions of the sulfonate groups as an additional stabilizing interaction, not unlike the *PMDI⊂DN38C10*

Table 2.8 Association constants, K_a, and derived free energies (ΔG) of complexation for pseudorotaxanes[510,513–515] comprising tetra-anionic π-donating crown ethers and aromatic dications at 298 K.



Guest	[X⁻]	Solvent	K_a[a] M^{-1}	ΔG kcal·mol^{-1}	Ref
Guest⊂BPP34C10(CO$_2$)$_4^{4-}$					
BIPY(Et)$_2^{2+}$	Br⁻	H_2O	6.0×10^2	–3.8	510
	Br⁻	MeOH	7.8×10^5	–8.0	510
	Br⁻	MeCN	3.6×10^6	–8.9	510
	PF_6^-	MeCN	1.2×10^7	–9.6	510
Guest⊂BPP34C10(SO$_3$)$_4^{4-}$					
BIPY(Et)$_2^{2+}$	Br⁻	MeOH	4×10^6	–9	510
	PF_6^-	MeOH	4×10^7	–10	510
Guest⊂DN32C8(SO$_3$)$_4^{4-}$					
BIPY(Me)$_2^{2+}$	Br⁻	H_2O	4.04×10^7	–10.4	513
BIPY(Et)$_2^{2+}$	Br⁻	H_2O	5.25×10^7	–10.5	513
PMDI(EtNMe$_3$)$_2^{2+}$	Br⁻	H_2O	5.82×10^5	–7.86	514
NDI(E tNMe$_3$)$_2^{2+}$	Br⁻	H_2O	9.81×10^5	–8.16	514
Guest⊂DN38C10(SO$_3$)$_4^{4-}$					
BIPY(Me)$_2^{2+}$	Br⁻	H_2O	3.25×10^5	–7.51	513
BIPY(Et)$_2^{2+}$	Br⁻	H_2O	1.85×10^5	–7.18	513
BIPY(Bn)$_2^{2+}$	Br⁻	H_2O	7.12×10^5	–7.97	515
DAP(Me)$_2^{2+}$	Br⁻	H_2O	1.12×10^8	–11.0	515
DAP(Bn)$_2^{2+}$	Br⁻	H_2O	2.25×10^7	–10.0	515
PMDI(EtNMe$_3$)$_2^{2+}$	Br⁻	H_2O	8.08×10^4	–6.69	514
NDI(EtNMe$_3$)$_2^{2+}$	Br⁻	H_2O	2.33×10^6	–8.68	514

[a]Methods of K_a Determination: NMR Dilution (Ref 510), Isothermal Titration Calorimetry (Refs. 513–515)

pseudorotoxane in **Figure 2.27c**. In summary, introducing anionic charges around the π-electron-rich crown ethers can enhance their affinities substantially for π-accepting dications in polar solvents.

Other π-Donating Crown-10 Ether Derivatives

The donor-acceptor molecular recognition properties of a number of different aromatic crown-10 derivatives have been investigated in detail—both in the context of host-guest chemistry and mechanostereochemistry. The majority of these derivatives were introduced in a 67-part[M] "Molecular Meccano" series of publications, which appeared in the literature between 1992 and 2003. The "meccano set"[462] of recognition units and linkers that have been fabricated for this class of electron-rich rings are summarized in **Figure 2.28**. Alternative recognition units to DNP (1/5-dioxynaphthalene) include 1/6, 2/6, and 2/7 substituted dioxynaphthalene units,[496] none of which bind methyl viologen guests with greater affinity than DN38C10 when incorporated into crown-10 macrocyclic polyethers. In a family of fluorinated BPP34C10 analogues,[516,517] each

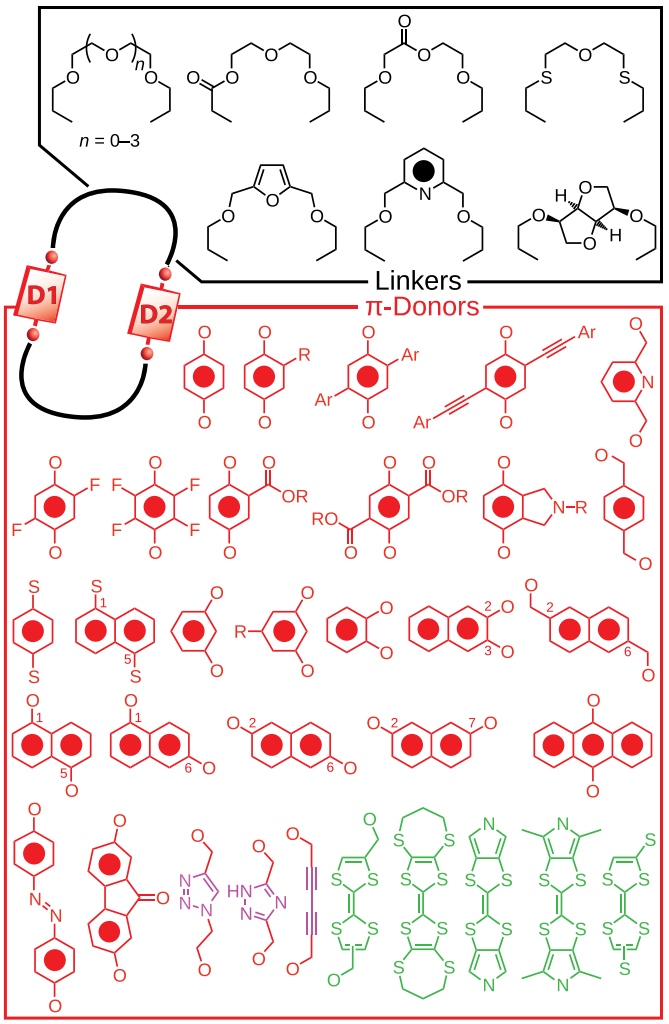


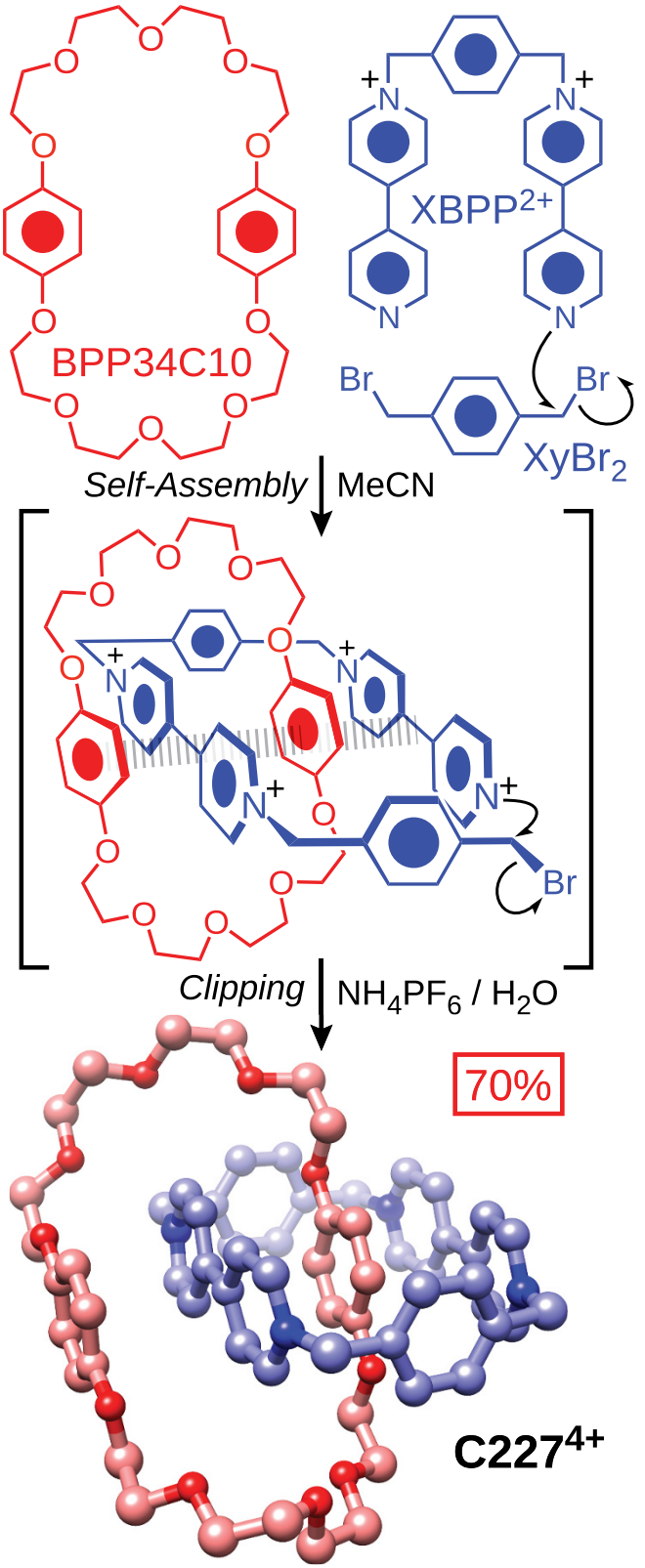
Figure 2.28 A 'meccano set' of π-donating units and linkers employed in the construction of π-electron-rich hosts.

[M] Although the Molecular Meccano series are only numbered up to Molecular Meccano 66, two publications were mistakenly attributed to Molecular Meccano 26.[462,973]

electronegative fluorine atom, which withdraws electrons from the phenylene core, further decreases the crown ether's affinity for π-acceptors, to the extent that the octafluorinated ring exhibits essentially no recognition for $BIPY^{2+}$ dications. Although ester groups are also electron-withdrawing, BPP34C10 derivatives bearing ester substituents bind methyl viologen slightly better than the parent crown ether because their carbonyl groups engage[518] in [C–H···O] interactions with the acidic α protons on the viologen guest. An amine-bearing five-membered ring fused to one of the *para*-phenylene units offers a high-symmetry functional handle from which further modifications can be accomplished synthetically.[519] Extending the conjugation of the *para*-phenylene ring with *para*-substituted alkynes or azides has allowed researchers to incorporate[520–522] these crown ethers and their derived catenanes into metal-organic frameworks (MOFs). Other alternative recognition sites include resorcinol derivatives,[523–526] catechols,[526,527] 2,3-dioxynaphthalene,[526] 9,10-dioxyanthracene,[528] benzylic groups,[529] dithiaarenes,[530,531] 2,6-dimethylpyridines,[532] fluorenones,[533,534] azobenzenes,[534,535] and triazoles.[405,536] Several crown-10 ethers incorporating TTF derivatives as π-donors have also been constructed[537–543] and employed as components of redox-switchable catenanes—see **Section 6.1**. Modifications to the polyether loops, which range from triethylene glycol[491] to hexaethylene glycol[544] in size, include ester[545] or thioether[530] bonds, as well as furan,[546] pyridine,[547] and D-mannitol-derived[548] connectors.

Crown-10 Based D-A Catenanes

D-A MIMs entered the scene in 1989 when the recognition chemistry of the BPP34C10 ring for viologen guests was exploited in the context of a clipping protocol for catenane synthesis. The mechanism (**Scheme 2.46**) for the synthesis[549] of the first D-A [2]catenane **C227**$^{4+}$ involves the self-assembly of a pseudorotaxane intermediate, which forms upon mixing (i) *para*-xylylene-bis(4-(4-pyridyl)pyridinium ($XBPP^{2+}$) and (ii) α,α′-dibromo-*para*-xylene ($XyBr_2$), with (iii) BPP34C10 at room temperature in MeCN. The first reaction between $XBPP^{2+}$ and $XyBr_2$ generates *in situ* a tricationic intermediate possessing a $BIPY^{2+}$ recognition unit, which becomes encircled by BPP34C10 before a second ring-closing nucleophilic substitution takes place to afford the [2]catenane **C227**$^{4+}$ as a precipitate that crashes out of MeCN solution over the course of two days. After counterion exchange with aqueous NH_4PF_6 and recrystallization of the corresponding PF_6^- salt from H_2O/MeCN, the pure compound **C227**$^{4+}$ is obtained in 70% yield. The X-ray crystal structure of **C227**$^{4+}$, a ball-and-stick representation of which is illustrated at the bottom of **Scheme 2.46**, reveals that the HQ units of BPP34C10 participate in 'inside' and 'alongside' π–π stacking interactions with one of the $BIPY^{2+}$ units of the clipped $CBPQT^{4+}$ cyclophane, in a geometry that is typical[500,550–552] for $CBPQT^{4+}$



Scheme 2.46 The mechanism of the clipping reaction that leads[549] to the donor-acceptor [2]catenane **C227**$^{4+}$. A ball-and-stick representation of the solid-state structure of **C227**$^{4+}$ is portrayed with solvent molecules, counterions, and protons omitted for the sake of clarity.

(sub)complexes.[N] Likewise, the two $BIPY^{2+}$ units of the $CBPQT^{4+}$ ring participate in inside/alongside π-stacking interactions with the ensconced DNP unit of the crown ether.

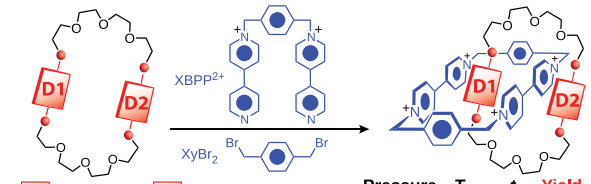
A number of reactions involving the clipping of $CBPQT^{4+}$ rings around crown-10 ethers to afford D-A catenanes are summarized (see refs. 496, 516, 525, 528–530, 533, 535–537, 541, 543, 549, 550, 553–558) in **Table 2.9**. The outcome of the clipping reaction is influenced by a number of factors, including (i) the reactant stoichiometry, where an excess of either π-donating (red) or π-accepting (blue) precursors typically leads to a yield enhancement, (ii) the solvent—e.g., reactions are typically higher yielding in MeCN than in DMF, most likely because D-A pseudorotaxanes exhibit higher association constants in MeCN, (iii) pressure—high (~10^4 bar) pressures at room temperature in DMF lead to yield enhancements, a feature which is common[559] to reactions involving the conversion of tertiary amines to quaternary ammonium salts, i.e., the Menschutkin reaction, (iv) temperature—although association constants decrease with increasing temperature, it was found[554] recently that heat can accelerate the catenation and improve yields in some cases, (v) reaction time—the clipping reaction is sluggish at room temperature in DMF, often requiring a week or more, yet it is accelerated to days or hours at elevated pressures[560] and temperatures,[554] respectively.

Intuitively, one might expect that the size and/or π-donating ability of the crown ether's recognition units would correlate with the yield of the clipping reaction, yet in practice there is not a strong correlation between recognition unit binding strengths and yield outcomes. In some cases, yields are enhanced by the better recognition units, e.g., DNP in comparison with HQ units in catenanes possessing 1,2,4-triazole rings as the second recognition site.[561] In other cases, the outcome is less predictable. For example, the clipping of a $CBPQT^{4+}$ ring to afford a catenane is higher yielding for the $BPP34C10$[549] ring (70%) than the $DN38C10$[556] ring (51%) in MeCN at RT, despite of the fact that DN38C10 exhibits higher association constants for $BIPY^{2+}$ derivatives, yet DN38C10 becomes catenated much more efficiently (88%) than does BPP34C10 (34%) at 80 °C in DMF.[554] Catenanes possessing bis(pyrrolo)tetrathiafulvalene (BPTTF) units as the alongside recognition site also exhibit an inverse relationship, where the catenation yield for a HQ-based crown ether is higher (31%) than that (7%) for a homologous DNP-based crown ether.[541]

Several examples of catenations involving less common π-donors are also summarized in **Table 2.9**. Fluorination of one of the HQ units of BPP34C10 results[516] in only a modest decrease in the catenation yield from 70% to 60%, whereas even a partial fluorination of both HQ units leads[517] to a near-zero yield. Although anthracene is a larger, stronger π-donor than benzene or naphthalene, the yield of

[N] We introduce[552] the term 'subcomplex' to describe a local host-guest interaction, e.g., *HQ⊂CBPQT⁴⁺*, within a larger assembly or MIM.

Table 2.9 Summary of the conditions and yields for the clipping of $CBPQT^{4+}$ rings around π-donating crown ethers.



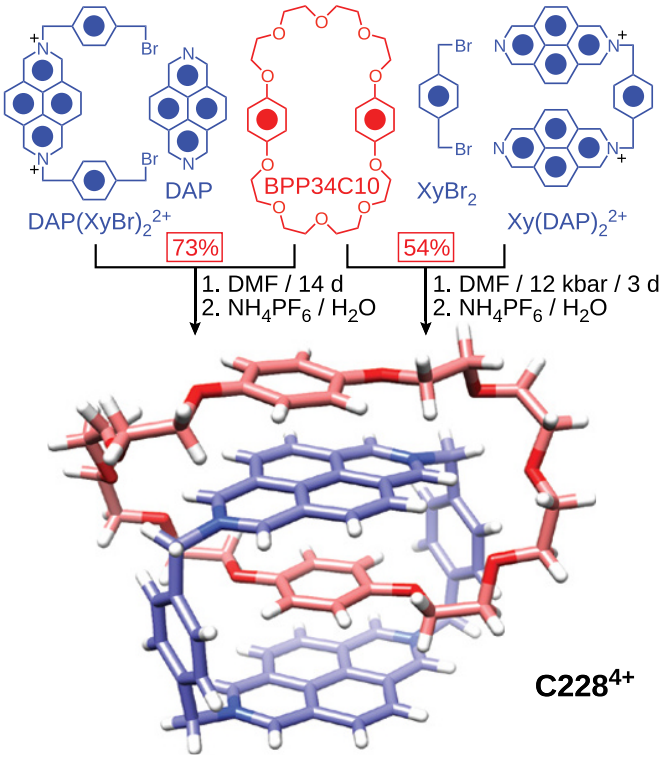
D1	D2	Equiv	Solvent	Pressure bar	T °C	t h	Yield %	Ref
		1	DMF	10^4	RT	72	34	536
		2.5	MeCN	1	RT	48	70	549
		3	DMF	10^4	RT	72	74	550
		5	DMF	1	80	1	34	554
		2.5	MeCN	1	RT	120	57	517
		2.5	MeCN	1	RT	120	60	516
		6	DMF	1	RT	96	53	530
		2.5	MeCN	1	RT	120	11	529
		2	MeCN	1	RT	144	47	529
		3	DMF	1	RT	432	15	550
		2.5	DMF	1	RT	96	50	530
		6	DMF	1	RT	96	65	530
		2	DMF	1	RT	240	82	496
		2	DMF	1	RT	240	89	496
		2	DMF	1	RT	240	74	496
		2	MeCN	1	RT	120	45	496
		3	MeCN	1	RT	96	59	528
		3	DMF	10^4	RT	96	31	541
		2	MeCN	1	RT	336	35	535
		3	DMF	10^4	RT	20	15	530
		6	DMF	1	RT	96	0	530
		1-2	DMF	10^4	RT	72	23	517
		2	MeCN	1	RT	120	38	529
		2.3	DMF	1	RT	168	17	550
		2	DMF	1	RT	96	48	557
		1	DMF	10^4	RT	72	65	536
			MeCN	1	RT		50	555
		2	DMF	1	RT	336	34	558
		6	DMF	1	RT	96	86	530
		2.5	MeCN	1	RT	120	52	529
		2	DMF	1	RT	336	34	525
		2	DMF	1	RT	336	23	525
		1	MeCN	1	RT	48	51	556
		5	DMF	1	80	1	88	554
		2.5	DMF	1	RT	96	60	530
		6	DMF	1	RT	96	77	530
		2	DMF	1	RT	240	64	496
		2	DMF	1	RT	240	74	496
		2	DMF	1	RT	240	84	496
		3	DMF	10^4	RT	96	7	541
		2	MeCN	1	RT	336	37	535
		2	MeCN	1	RT	48	91	533
		1.7	DMF	1	RT	144	43	539
		1	DMF	1	20	120	23	537
		5	DMF	1	80	1	63	554
		4	MeCN	1	RT	72	35	543
		2	DMF	1	RT	480	8	534
		2.5	DMF	1	RT	96	47	530
		6	DMF	1	RT	96	70	530
		2.5	MeCN	1	RT	120	41	529
		2	DMF	1	RT	240	35	496
		2.5	MeCN	1	RT	120	42	529
		2	DMF	10^4	40	120	16	496
		2	DMF	1	RT	240	25	496
		2.5	MeCN	1	RT	120	28	529
		2	DMF	10^4	40	120	27	496

the clipping reaction involving 9,10-dioxyanthracene as an alongside recognition unit is decreased relative to that of the BPP34C10- and DN38C10-based catenanes.[528] This detrimental effect of 9,10-dioxyanthracene may be explained by a subtle stereoelectronic effect. Although it possesses a larger π-system, the π-donating ability of 9,10-dialkoxyanthracene is lessened by steric interference from the protons at positions 1, 4, 5, and 8—their presence adjacent to the 9,10-alkoxy groups causes the latter to rotate out-of-plane with respect to the π-surface, which leaves the lone pairs of oxygen less engaged in the π-system. HQ and DNP donors, by contrast, are not sterically forced to make this accommodation. Employing a *meta*-substituted phenylene ring as one of the recognition sites in the crown ether decreases the catenation yield, which is also sensitive to appended functional groups with different constitutions and substitution patterns. Counterintuitively, yields are higher when the *meta*-phenylene unit is functionalized with an electron-withdrawing carboxylic acid group than with a slightly electron-donating hydroxymethyl group.[525]

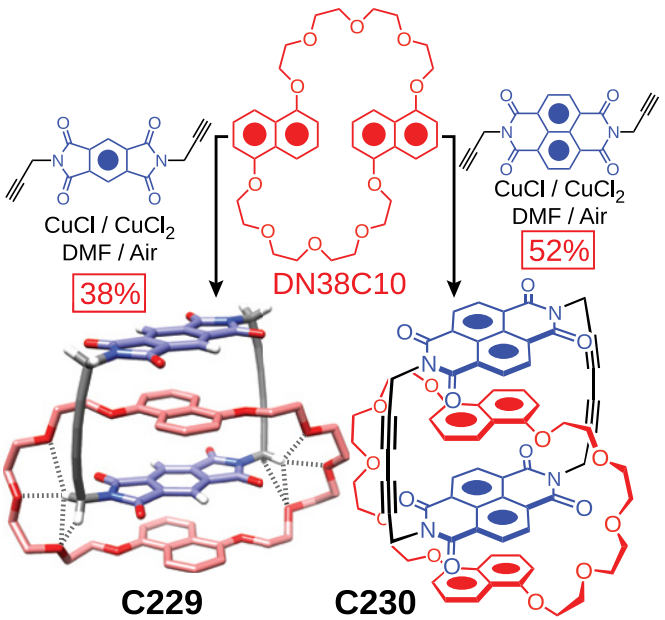
A number of catenanes based on HQ and DNP recognition sites with thioether bonds have also been prepared.[530] Although catenanes in which sulfur atoms flank both recognition units of the crown ether are obtained in low (0–15%) yields, reaction efficiencies as high as 86% are reached when thioether sulfur atoms flank only the alongside recognition units. Lukyanenko[533] has observed a surprisingly high yield of 91% employing fluorenone as the alongside recognition unit in a DNP-containing macrocycle, albeit with a crown-8 constitution rather than a crown-10 one. On the other hand, an azobenzene/fluorenone crown ether is catenated in low (8%) yield.[534] Clipping yields are relatively low (35–37%) in general for catenanes containing azobenzene, even as the alongside recognition unit.

Tetracationic cyclophanes may also be clipped around a crown ether template using a bis(bromoxylyl)bipyridinium dication, BIPY(XyBr)$_2^{2+}$, as the precursor.[495] In the case of the CBDAP^{4+}/BPP34C10 [2]catenane **C228^{4+}**, it transpires that this route (**Scheme 2.47**) is more efficient than the more traditional route involving $XyBr_2$ as the dibromide reactant, even when the latter reaction is carried out under high pressure. The solid-state structure of **C228^{4+}**, which is illustrated in **Scheme 2.47**, reveals the presence of D-A π–π stacking and [C–H···O] interactions in a similar geometry to that of its homologous CBPQT^{4+}-based predecessor **C227^{4+}**.

Sanders[505,509] introduced the genre of neutral D-A MIMs back in 1997 when he described the synthesis (**Scheme 2.48**) and characterization of the PMDI- and NDI-based [2]catenanes **C229** and **C230**, respectively. The catenanes are prepared by copper-catalyzed oxidative acetylenic coupling of propargyl-functionalized PMDI or NDI units in the presence of DN38C10 in DMF, affording the respective neutral catenanes in up to 38% and 52% yields, respectively. The X-ray crystal structure of **C229** shows that the oxygen atoms of the DN38C10 ring's polyether loops engage in [C–H···O] interactions with the acidic protons of



Scheme 2.47 Two clipping reactions[495] that lead to the CBDAP^{4+}/BPP34C10 [2]catenane **C228^{4+}**. A tubular representation of the solid-state structure is portrayed with solvent molecules and PF_6^- counterions omitted for the sake of clarity.

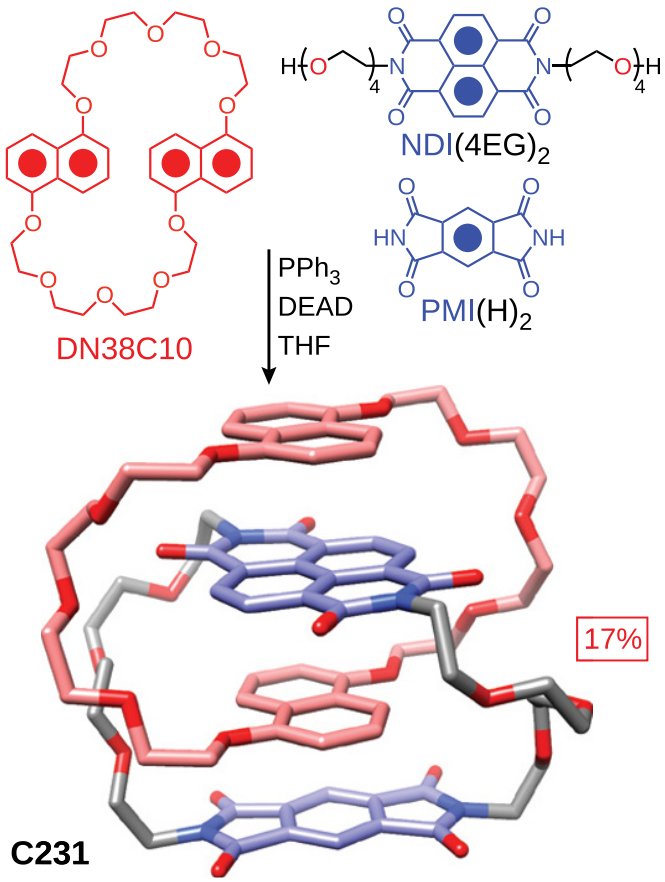


Scheme 2.48 Sanders' synthesis of the first neutral π-associated D-A [2]catenanes.[505,509] Solvent and hydrogen atoms of DN38C10 are omitted from the tubular representation of the X-ray crystal structure of **C229** for the sake of clarity.

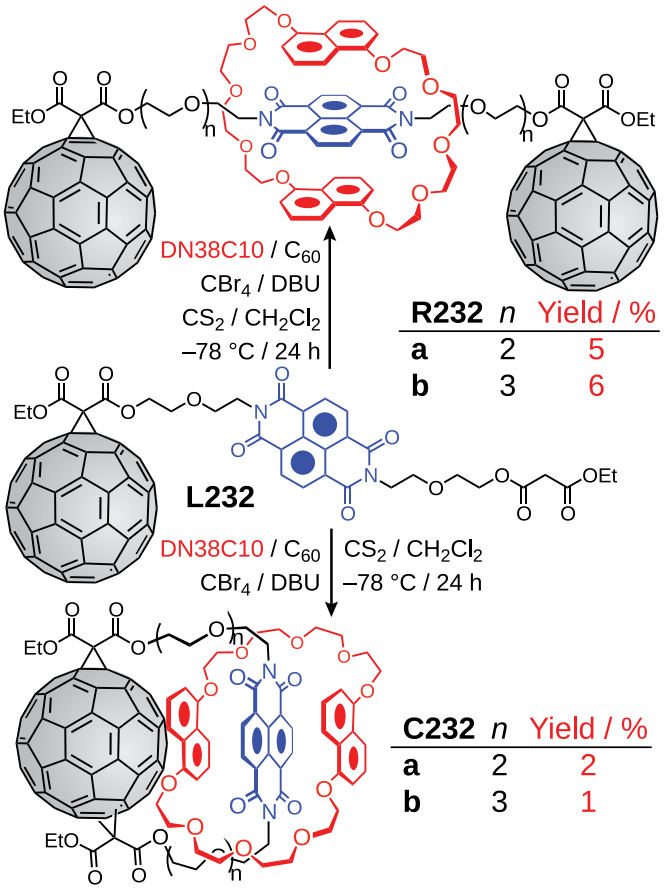
the adjacent methylene units, since these diimides do not possess acidic α-protons as do their $BIPY^{2+}$ counterparts.

Reversal of the polyether and acetylenic linkers in Sander's catenanes is detrimental to their synthesis, since the Eglinton-Glaser-Hay coupling of a propargylated DNP unit in the presence of a PMDI- or NDI-based macrocyclic polyether does not lead[449] to the formation of any mechanical bonds at all. This dependence on linker/recognition site pairing is attributed to the importance of [C–H···O] interactions between the propargylic protons of the diimide macrocycles and the polyether loops in the original catenanes. Sanders[449] has, however, prepared (**Scheme 2.49**) a neutral D-A [2]catenane in which both rings are constituted by polyether loops. Ring closure of a tetraethylene glycol-appended NDI unit with a PMDI unit in the presence of the DN38C10 ring under Mitsunobu alkylation conditions leads to the [2]catenane **C231** in 17% yield. The X-ray crystal structure reveals a familiar looking D-A-D-A stack, with the cavity of the DN38C10 ring being occupied by the larger NDI π-acceptor.

Nishimura[562] has employed C_{60} derivatives as the reactive groups for either stoppering or catenating (**Scheme 2.50**) pseudorotaxanes derived from NDI and DN38C10.



Scheme 2.49 Sanders' synthesis of a neutral D-A [2]catenane **C237** by Mitsunobu alkylation.[449] The product is portrayed as a tubular representation of the X-ray crystal structure of **C231**, with protons omitted for the sake of clarity.



Scheme 2.50 Nishimura's synthesis of neutral D-A [2]rotaxanes and [2]catenanes as C_{60} adducts employing the Bingel reaction.[562]

His synthetic strategy relies on the cyclopropylation of fullerenes by Michael addition of a malonic ester carbanion—i.e., the Bingel[563] reaction. Thus, a C_{60}/NDI polyether monoadduct in the presence of DN38C10 is reacted, either with an unfunctionalized C_{60} compound or with itself, affording the [2]rotaxanes **R232a–b** or the [2]catenane **C232a–b**, respectively, albeit in low (≤6%) yield.

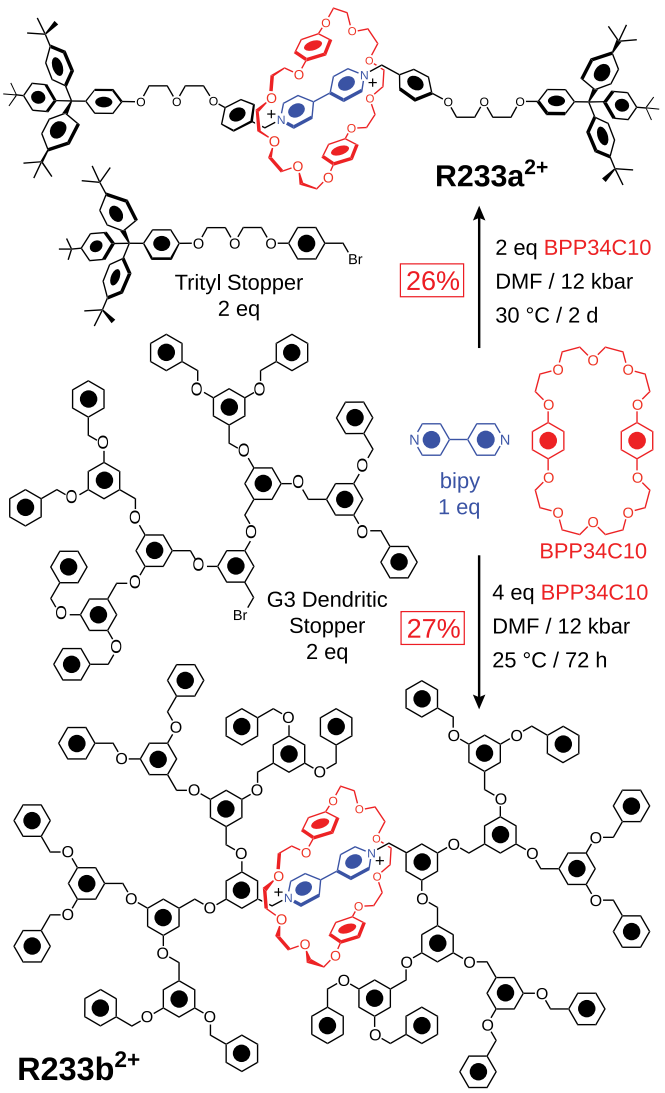
We note that D-A catenanes and rotaxanes can also be assembled in good yields under thermodynamic control. Examples of charged D-A mechanomolecules of this type have been made by protocols employing slippage (**Sections 3.1.2**), kinetically labile coordinative bonds (**Section 3.2.1.4**), imine exchange (**Section 3.3.1**), and dynamic S_N2 chemistry (**Section 3.5.2.2**), while examples based on Sanders' neutral D-A recognition motif have also employed olefin metathesis (**Section 3.4.1.2**), labile coordinative bonds (**Section 3.2**), disulfide bond formation (**Section 3.5.1**), and boronic esters (**Section 3.3.3**).

Crown-10 D-A Rotaxanes

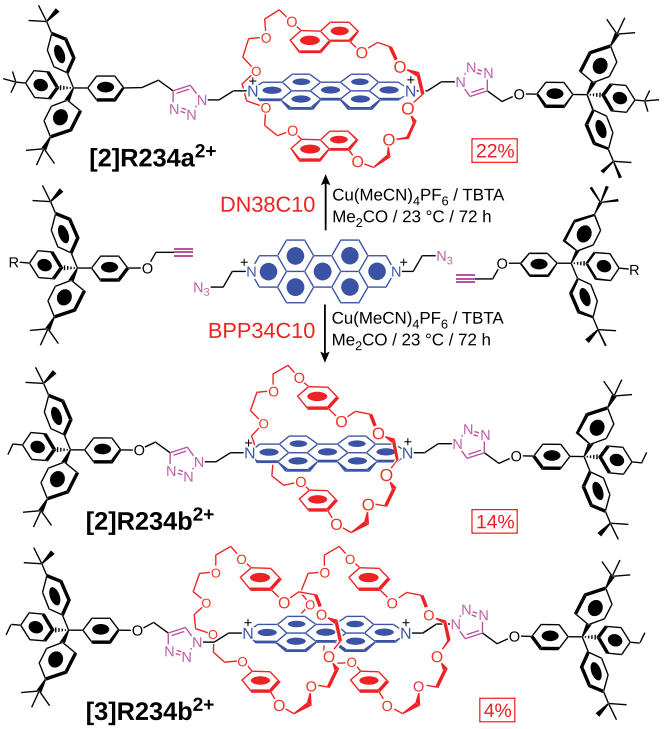
The first rotaxanes possessing the BPP34C10 and DN38C10 rings were prepared[564,565] by a protocol known as slippage, which is a process whereby the ring's cavity and 'diameter' of the dumbbell's stoppers are similar in size, such that the ring can pass over the stoppers to reach a recognition

site under certain conditions, while being unable to make its departure over the stoppers under a different set of milder conditions. Slippage is therefore a thermodynamically controlled reaction. See **Section 3.1** for a detailed account of the slippage approach to synthesizing rotaxanes.

Since S_N2-based (Menschutkin) clipping reactions have been a workhorse for preparing D-A catenanes, it should come as no surprise that S_N2 reactions have also been employed in the synthesis of D-A rotaxanes. Early examples[566,567] of S_N2-mediated stoppering reactions are illustrated in **Scheme 2.51**. When 4,4′-bipyridine (bipy) is mixed in DMF with 2 equiv of a benzyl bromide stopper precursor comprising either a trityl derivative or a 3rd generation benzylic ether dendrimer in the presence of an excess of BPP34C10, the [2]rotaxanes **R233a**$^{2+}$ and **R233b**$^{2+}$ are obtained in 26 and 27% yields, respectively, after a few days at 12 kbar of pressure. The most plausible mechanism for this rotaxanation involves the *in situ* self-assembly of a pseudorotaxane between the BPP34C10 ring and a



Scheme 2.51 Synthesis of D-A [2]rotaxanes from neutral precursors by stoppering.[566,567]



Scheme 2.52 Click synthesis of diazaperopyrenium [2]- and [3]rotaxanes based on DN38C10 and BPP34C10, respectively.[571]

half-dumbbell (or semidumbbell) intermediate—a threaded species known[568] as a semirotaxane—before the final stoppering event occurs. Since the BIPY^{2+} recognition site of the [2]rotaxanes **R233a/b**$^{2+}$ are not formed until after the final stoppering step has already taken place, it follows that BPP34C10 is capable of recognizing monopyridinium cations. Examples of [3]- and [4]rotaxanes have been prepared[567] by adapting the same stoppering protocol in the presence of oligomeric BIPY^{2+} precursors. A similar type of S_N2-mediated stoppering protocol has been employed by Fitzmaurice[510] to assemble donor-acceptor rotaxanes based on anionic BPP34C10 derivatives. Otera[569,570] has investigated the efficiency of this type of stoppering reaction in the solid state, obtaining BPP34C10-based [2]rotaxanes in yields as high as 85% under solvent-free conditions after a solution-state pre-mixing step and evaporation to a thin film.

The CuAAC click reaction is another convenient transformation for stoppering D-A pseudorotaxanes. For example, the click synthesis[571] of rotaxanes comprising DN38C10 or BPP34C10 and DAPP^{2+} templates are illustrated in **Scheme 2.52**. More evidence for the ability of BPP34C10 to encircle aromatic monocations is given by the formation of the [3]rotaxane **[3]R234b**$^{2+}$ (4%) along with the expected [2]rotaxane **[2]R234b**$^{2+}$ (14%) when the stoppers are clicked onto a *DAPP*$(C_2H_4N_3)_2^{2+}$⊂*BPP34C10* pseudorotaxane template in Me_2CO. The formation of the [3]rotaxane **[3]R234b**$^{2+}$ is enabled by the extended length of the DAPP^{2+} dication in comparison with BIPY^{2+}-based templates. On the contrary, no [3]rotaxane is isolated when the bulkier DN38C10 ring is

employed in the same protocol, although the corresponding [2]rotaxane **R234a**$^{2+}$ is obtained (22%) in a slightly higher yield.

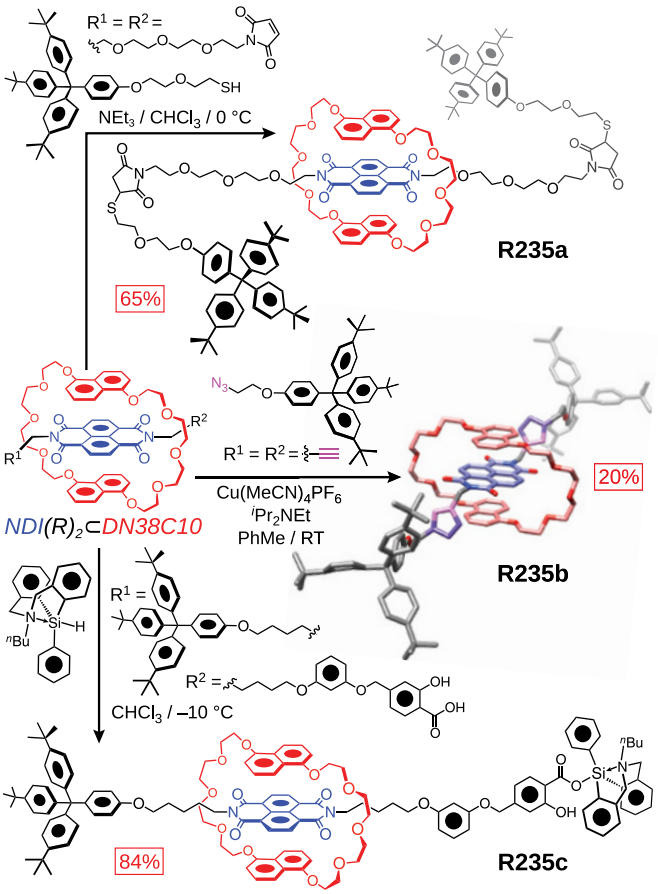
A few click reactions that typically proceed with high efficiency under kinetic control have been leveraged in the syntheses (**Scheme 2.53**) of the neutral D-A [2]rotaxanes **R235a-c** based on *NDI⊂DN38C10* templates**.** The stoppering reactions that rely on (i) the thiol–maleimide Michael addition, (ii) the Cu^{I}-catalyzed azide-alkyne cycloaddition (CuAAC), and (iii) silyl ester formation between salicylic acids and pentacoordinated hydrosilanes, afford the [2]rotaxanes **R235a**, **R235b**, and **R235c**, respectively, from the corresponding *NDI(R)$_2$⊂DN38C10* pseudorotaxanes, where the NDI-appended R groups contain the reactive functionalities.

Although the click reaction involving a Michael addition between an activated alkene such as maleimide and a nucleophile such as a thiol is used extensively in bioconjugation reactions, its application[572,573] in MIM synthesis is not widespread. Northrop[573] employed this reaction in $CHCl_3$ in order to obtain (**Scheme 2.53**) the neutral D-A [2]rotaxane **R235a** in 65% yield by simply mixing a maleimide-terminated NDI bis(tetraethylene glycol) thread with a thiol-terminated triarylmethyl stopper in the presence of DN38C10 and a catalytic amount of base (NEt_3) in $CHCl_3$ at 0 °C. This proof of concept that MIM synthesis is compatible with a common bioconjugation reaction opens the door for the preparation of MIM/protein bioconjugates, which could become targets for biological appications.

The CuAAC reaction has also been applied[574,575] to the synthesis of neutral D-A rotaxanes. One such rotaxane based on NDI and DN38C10 is **R235b**, which comprises a short NDI-based dumbbell and a DN38C10 ring. The very short axle length of **R235b**, which may be responsible in large part for its relatively low yielding (20%) synthesis, proved to facilitate the ease with which single crystals of the compounds could be grown. A stick representation of the solid-state structure of **R235b** is illustrated in **Scheme 2.53**. A similar protocol was described earlier by Gunter for preparing neutral D-A [2]rotaxanes based on strapped porphyrins—see **Section 2.3.3.6**.

Another efficient type of click stoppering protocol, which was originally developed by Kawashima[576] for the catalyst-free synthesis of crown ether / dialkylammonoium rotaxanes, involves the spontaneous coupling a salicylic acid derivative with a pentacoordinated hydrosilane. This protocol has recently been adapted by Goto[577] in order to stopper the NDI/DN38C10 [2]rotaxane **R235c** in high isolated yield of up to 84%, the highest reported for this class of rotaxanes. See row q of **Table 2.27** in **Section 2.3.4.6** for examples of this efficient capping reaction's involvement in the synthesis of hydrogen-bonded rotaxanes. This protocol is highly advantageous from an atom economy perspective—in addition to high efficiency, no additives are required and the only byproduct is H_2 gas derived from the displaced hydrogen atoms of the salicylic acid and hydrosilane precursors.

Other reactions that have been employed in the synthesis of NDI/DN38C10 MIMs include condensations[578] affording porphyrin-stoppered rotaxanes, immobilization[579] on gel-phase supports via esterification, and a number of thermodynamically controlled approaches, including those based on olefin metathesis (**Section 3.4.1.2**), labile coordinative bonds (**Section 3.2.3.1** and **3.2.4.1**), disulfide bonds (**Section 3.5.1**), and boronic esters (**Section 3.3.3**).



Scheme 2.53 Three click protocols[573,575,577] for the synthesis of neutral D-A [2]rotaxanes based on *NDI(R)$_2$⊂DN38C10* templates: (top) Northrop's click synthesis[573] of the [2]rotaxane **R235a** by thiol-maleimide Michael addition; (middle) CuAAC synthesis[575] and tubular representation of the solid-state structure of the [2]rotaxane **R235b**, with hydrogen atoms omitted for the sake of clarity; (bottom) Goto's formation[577] of a silyl ester-capped [2]rotaxane **R235c** by efficient coupling of a pentacoordinate hydrosilane stopper precursor and a salicylic acid endgroup.

2.3.3.3 π-Donating Crown-8 Template Motifs

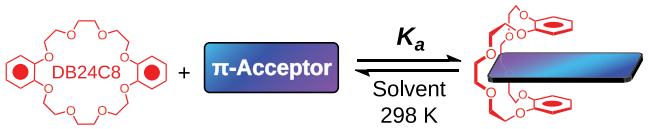
From among the meccano set of components illustrated in **Figure 2.28**, those incorporating catechol (1,2-dihydroxybenzene) and 2,3-dioxynaphthalene units are often connected by triethylene glycol linkers, thus constituting crown-8 rings. Dibenzo[24]crown-8 (DB24C8) has turned out to be a workhorse for the construction of both donor-acceptor (*vide infra*) and hydrogen bonded (**Section 2.3.4**) MIMs.

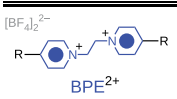
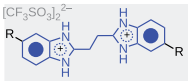
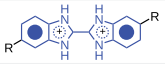
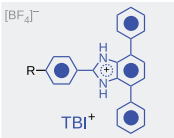
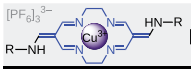
Dibenzo[24]crown-8 (DB24C8) and dinaphtho[24]crown-8 (DN24C8) Pseudorotaxanes

In the context of D-A interactions, DB24C8 and its homologues such as dinaphtho[24]crown-8 (DN24C8) are suitable receptors for $BIPY^{2+}$ and DAP^{2+} derivatives.[566] The association constants, K_a, for D-A pseudorotaxanes comprising DB24C8 and various π-acceptors are summarized in **Table 2.10**. The $BIPY^{2+}$ and DAP^{2+} dications are known[532,580–583] to engage in both 1:1 and 1:2 guest:host binding modes with DB24C8. The 1:1 complex is stabilized by D-A π–π stacking interactions and [C–H···O] interactions. The π–π stacking interactions prevent the benzo units of the second DB24C8 ring of the 1:2 complex from engaging with the π-acceptor on account of steric crowding which weakens the binding of the second ring by about an order of magnitude. Although the major species in solution is the 1:1 complex, the pseudorotaxane crystallizes (**Figure 2.29**) out of solution as the 1:2 complex *DAP^{2+}⊂(DN38C10)$_2$*.

Stephen Loeb[527,584] at the University of Windsor made the discovery in 1998 that DB24C8 and DN24C8 are excellent 1:1

Table 2.10 Association constants, K_a, and derived free energies (ΔG) of complexation for 1:1 pseudorotaxane complexes between DB24C8 and various π-acceptors at 298 K.



π-Acceptor	R	Solvent	K_a M^{-1}	$-\Delta G_a$ kcal·mol^{-1}	Method[a]	Ref
 BPE^{2+}	H	MeCN	180	3.1	ST	527
	Me		230	3.2		
	Ph		320	3.4		
	CO_2Et		1200	4.2		
 BBE^{2+}	H	CD_3CN	400	3.1	NMRSP	587
	Me		250	3.2		
	CO_2Et		540	4.2		
	Me	CD_3NO_3	3050	4.0	NMRSP	590
	Me	CD_3CN	140[b]	2.9[b]	NMRSP	593
 TBI^+	CO_2Et	CD_3OD	90	4.2	NMRD	596
		CD_3COCD_3	400	4.2		
		CD_3CN	1780	4.2		
		CD_3NO_2	3900	4.2		
		CD_2Cl_2	75200	4.2		
 $BIPY^{2+}$	Bn	MeCN	82	2.6	ITC	532
	Me	CD_3COCD_3	1300	4.2	NMRD	582
 DAP^{2+}	Me	CD_3CN	840	4.0	NMRD	566
	Bu	CD_3CN	714	3.9	NMRT	585
	Bu	MeCN[c]	311	3.9	DPV	585
	Bu	MeCN[c]	15300	5.7	DPV	585

[a]Methods: spectrophotometric titration (ST), NMR single-point method (NMRSP), isothermal titration calorimetry (ITC), NMR dilution method (NMRD), NMR titration (NMRT), differential pulse voltammetry (DPV).
[b]Measured at a temperature of 308 K.
[c]With 0.1 M NBu_4PF_6.

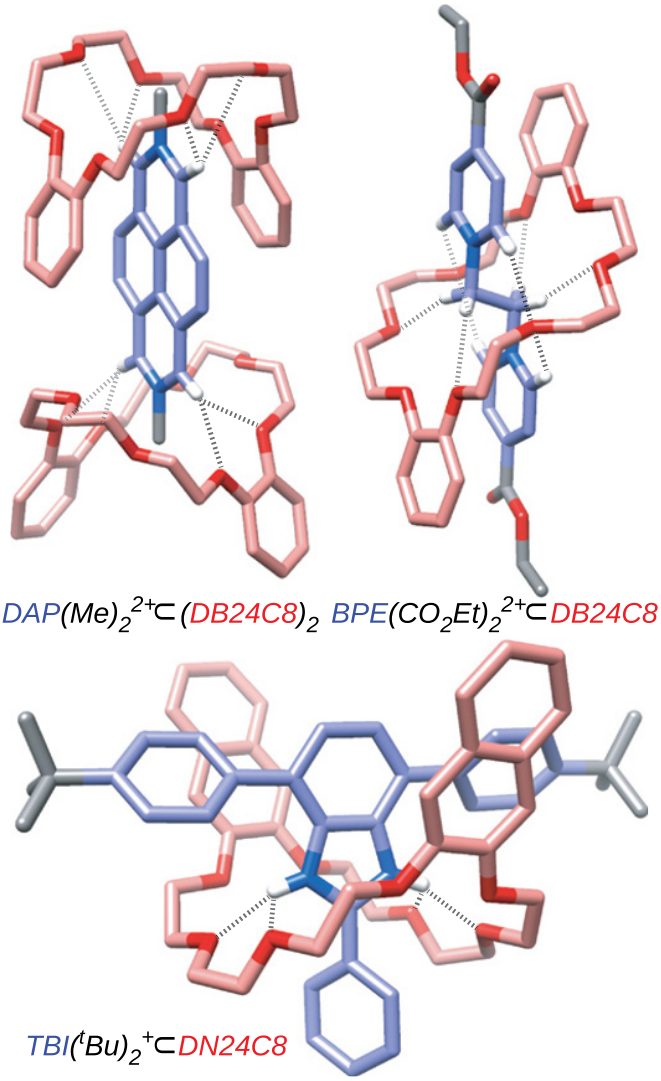


Figure 2.29 Comparison of 24C8-based D-A pseudorotaxanes involving DAP^{2+}, BPE^{2+}, and TBI^+ recognition units in the solid state, where the superstructures are represented in tubular forms. Two DB24C8 rings bind DAP^{2+} by adopting boat-like conformations in which only one engages in D-A π–π stacking interactions,[566] while the DB24C8 ring binds BPE^{2+} in a chair-like conformation with a 1:1 stoichiometry.[527] Solvent, counterions, and protons not engaged in hydrogen bonding are omitted for the sake of clarity.

receptors for 1,2-bis(pyridinium)ethane (BPE^{2+}). Whereas DB24C8 adopts a boat-like conformation when binding the periphery of a $BIPY^{2+}$ or DAP^{2+} guest, it adopts a chair-like conformation while spanning the entire length of a BPE^{2+} recognition unit. The solid-state superstructures of *$DAP(Me)_2^{2+}⊂(DB24C8)_2$* and *$BPE(CO_2Et)_2^{2+}⊂DB24C8$* are compared in **Figure 2.29**. Both structures are stabilized by D-A π–π stacking interactions between the benzo rings of DB24C8 and the aromatic units of the respective guests. The complexes are also significantly stabilized by hydrogen-bonding interactions. A total of eight [C–H···O] interactions can be identified in *$BPE(CO_2Et)_2^{2+}⊂DB24C8$*, for example, where each of the four pyridinium a protons and each of the four ethylene protons are located less than 2.7 Å away from

oxygen atoms of the polyether loops. On account of these interactions, even the parent [24]crown-8 (24C8) ring encircles BPE^{2+} in solution, albeit with less affinity in the absence of any π-associated D-A interactions—the K_a value for *24C8⊂BPE(CO$_2$Et)$_2^{2+}$* is 320 M^{-1} in MeCN, almost an order of magnitude lower than that (1200 M^{-1}) of DB24C8. The ester group appended to BPE^{2+} also enhances the association constant with DB24C8 considerably in comparison with other non-electron-withdrawing groups, in keeping with the expectation that D-A π–π stacking interactions stabilize the pseudorotaxane.

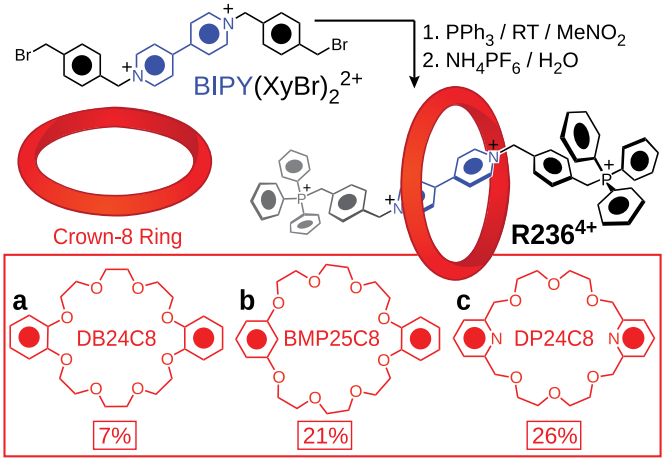
Korybut-Daszkiewicz and Bilewicz[585] have characterized (**Table 2.10**) the self-assembly of a pseudorotaxane, comprising copper-complexed tetraazamacrocyclic recognition units, and DB24C8. They found that a Cu^{III}-complexed tetraazamacrocycle binds the DB24C8 ring (K_a = 1.53 × 10^4 M^{-1}) much more effectively than a Cu^{II}-complexed one (K_a = 7.14 × 10^2 M^{-1}) in MeCN. The crystal structures[586] of catenanes (*vide infra*) templated by this recognition motif reveal a binding geometry analogous to that of DB24C8 pseudorotaxanes based on $BIPY^{2+}$ or DAP^{2+} derivatives, in which a boat-like conformation of DB24C8 orients its polyether loops around the periphery of the recognition unit while its benzo rings stack with the core.

Another class of guests (**Table 2.10**) for DB24C8 involving π-associated D-A interactions are imidazolium and benzimidazolium derivatives. Tiburcio[587–589] and Clarkson[590] have introduced independently benzimidazolium guests, namely 1,2-bis(benzimidazolium)ethane (BBE^{2+}), linked by alkyl chains in a manner analogous to BPE^{2+}, which complex DB24C8 with association constants of up to 3 × 10^3 M^{-1} in $MeNO_2$ at 298 K. Mukhopadhyay[591–593] has found that bis(benzimidazolium) guests connected by zero-, one-, and three-carbon methylene linkers also bind DB24C8 in CD_3CN with K_a values on the order of 10^2 M^{-1}, which is close to that of BBE^{2+}, indicating that these pseudorotaxanes have a high tolerance for different spacer lengths. Although the interactions between DB24C8 and imidazolium[594] (K_a = 8 M^{-1}) or phenylbenzimidazolium[595] (K_a = 54 M^{-1}) units are weak in MeCN, Loeb has shown that extended T-shaped[596] (TBI^+) and Y-shaped[597] benzimidazolium π-surfaces—afforded by adding extra phenyl substituents onto benzimidazolium—enhance the association constants up to as high as 1.78 × 10^3 M^{-1} in MeCN and 7.52 × 10^4 M^{-1} in CH_2Cl_2. There is some fluctuation in K_a values in all of these systems when the counterions are changed—in general, softer counterions (e.g., BF_4^-, PF_6^-) result in stronger complexes—although the variations are always less than an order of magnitude among soluble salts in identical solvent systems.

In similar fashion to the anionic BPP34C10 and DN38C10 crown ethers, Loeb[598] has developed a bisulfonated DB24C8 ring which likewise exhibits enhanced affinity for BPE^{2+}-derived guests in polar solvents. The most tightly bound complex is one in which DB24C8$(SO_3)_2^{2-}$ encircles a 1,2-bis(benzylbipyridinium)ethane guest. Although the association constant is reasonably high (2.3 × 10^3 M^{-1}) in water, a K_a value of >10^5 M^{-1} in methanol is at least two orders of magnitude greater than that of the parent complex without sulfonate appendages. Thus, It would appear that sulfonation of a π-donating crown ether is a very general strategy for enhancing the binding affinities toward appropriate guests, especially cationic ones, in polar solvents on account of additional ion-pairing and solvophobic interactions.

Crown-8 / $BIPY^{2+}$ Mechanomolecules

Although 1:2 guest:host ratios are possible for the complexes of $BIPY^{2+}$ and DAP^{2+} dications with DB24C8 hosts, rotaxanes based on this recognition motif have always been isolated in 1:1 stoichiometries, reflecting the weak association constant and unfavorable geometry when binding the second ring. The first rotaxanes of this type were **R236^{4+}a-c**, which were prepared[532] by capping (**Scheme 2.54**) the benzyl bromide termini of bis(α-bromoxylyl)-4,4′-bipyridinium, $BIPY(XyBr)_2^{2+}$, with triphenylphosphium groups. In addition to DB24C8, benzometaphenylene[25]crown-8 (BMP25C8) and dipyridyl[24]crown-8 (DP24C8) were also employed in the synthesis of rotaxanes. Curiously, stoppering the respective pseudorotaxane precursors with PPh_3 is accomplished more efficiently with BMP25C8 (21%) and DP24C8 (26%) rings than it is with DB24C8 (7%) at room temperature in $MeNO_2$, in spite of the higher affinity of DB24C8 for $BIPY^{2+}$ guests. In general, the low yields can be attributed to the low association constants (<100 M^{-1}) which characterize all three of the pseudorotaxane precursors.

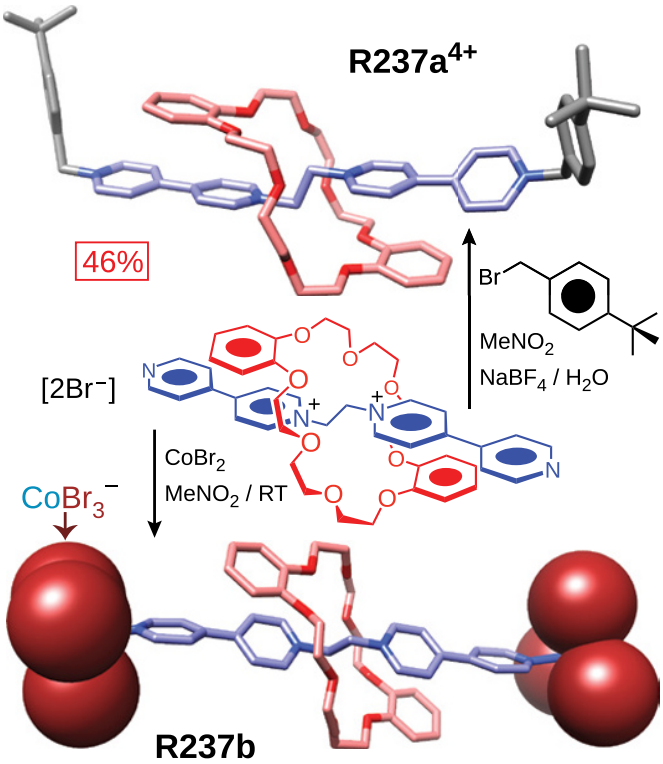


Scheme 2.54 The synthesis of triphenylphosphonium-stoppered [2]rotaxanes comprising $BIPY^{2+}$ recognition sites and crown-8 macrocyclic polyethers.[532]

Crown-8 / BPE^{2+} Mechanomolecules

Rotaxanes based on crown-8 ethers and BPE^{2+} are a workhorse in the Loeb laboratory. The first rotaxanes[584] of this variety were synthesized (**Scheme 2.55**) from a BPE^{2+}/DB24C8 pseudorotaxane terminated on each end with reactive 4-pyridyl groups. When an S_N2 substitution with

4-*tert*-butylbenzyl bromide is carried out at these nucleophilic sites in BPE^{2+} in a vigorously stirred biphasic mixture of aqueous NH_4BF_4 and $MeNO_2$, the tetracationic [2]rotaxane **R237a**$^{4+}$ is obtained in 46% yield. Loeb's BPE^{2+}/DB24C8 rotaxanes are more commonly stoppered by means of metal ligation.[599] The example[600] in **Scheme 2.55** is one in which $CoBr_3^-$ stoppers are installed to afford the neutral, zwitterionic [2]rotaxane **R237b**. The pseudorotaxane precursor is employed as the bromide salt in this case so that the counterions may become incorporated into the anionic stopper upon addition of a $CoBr_2$ reagent. The yield of this stoppering reaction is in the range of 30–40% and it is also compatible with Mn^{II} as the stoppers' metal core. The BPE^{2+} recognition unit is the basis for a number of rotaxanes that have emerged from the Windsor group from 2000 up to the present.[601–607] Credi[608] has also constructed rotaxanes based on this motif. See **Section 4.2.3.8** for a discussion of coordination polymers based on this system.



Scheme 2.55 The synthesis of [2]rotaxanes based on Loeb's BPE^{2+}/DB24C8 recognition motif.[584,600] Protons and counterions are omitted from the tubular representations of the solid-state structures of the rotaxanes for the sake of clarity.

Crown-8 / Tetrazamacrocycle Mechanomolecules

Korybut-Daszkiewicz[609] has developed the genre of planar tetraazamacrocyclic chelates which can serve as π-acceptors in pseudorotaxanes and MIMs (**Figure 2.30**) based on the DB24C8 ring. The first MIMs to be synthesized[586] employing this recognition motif were the dinuclear D-A [2]catenanes **M$_2$C233**$^{4+}$, where M represents either Ni^{II} or Cu^{II} metal centers. These [2]catenanes are obtained

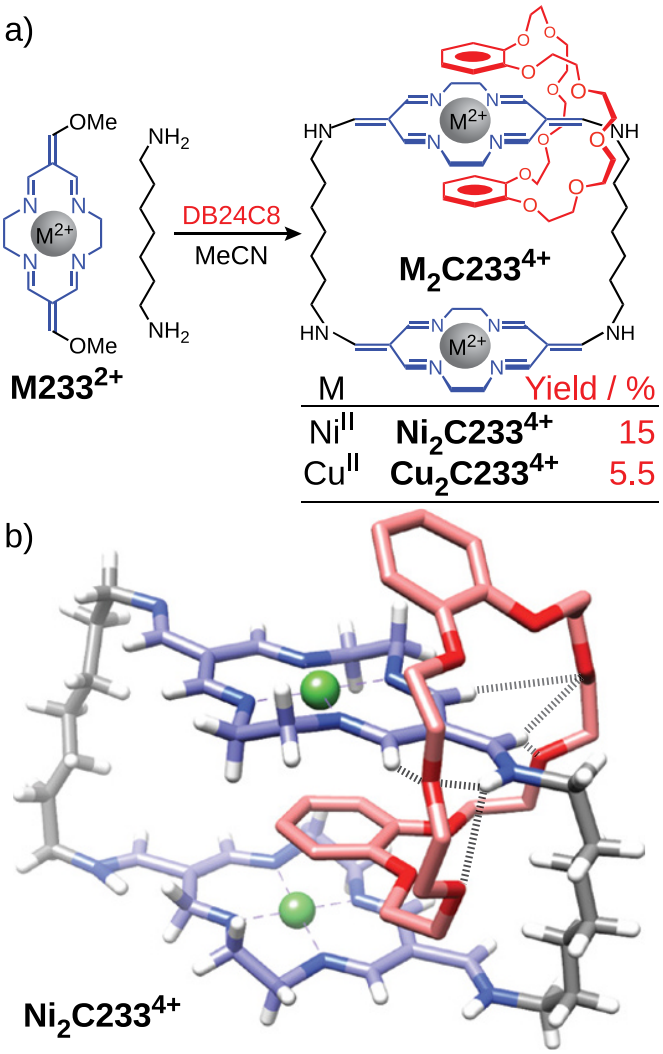


Figure 2.30 Korybut-Daszkiewicz's [2]catenanes based on DB24C8 ring and metallated tetraazamacrocyclic π-acceptor units.[586] (a) The synthesis of the D-A [2]catenanes **Ni$_2$C233**$^{4+}$ and **Cu$_2$C233**$^{4+}$ from tetraazamacrocycles **M233**$^{2+}$ and 1,7-diaminohexane. (b) Tubular representation of the X-ray crystal structure of **Ni$_2$C233**$^{4+}$. [C–H···O] hydrogen bonds are labeled with hatched lines. DB24C8 protons, solvent molecules, and PF_6^- counterions are omitted for the sake of clarity.

(**Figure 2.30a**) by employing a cyclization procedure pioneered by Busch[610] which involves simply mixing the methoxy-terminated tetraazamacrocycle **M233**$^{2+}$ with 1,7-diaminohexane under high dilution in MeCN in the presence of an excess of DB24C8. The X-ray crystal structure (**Figure 2.30b**) of **Ni$_2$C233**$^{4+}$ reveals that the ring adopts a boat-like conformation which is not uncommon for D-A pseudorotaxanes based on DB24C8, with one of the benzo rings residing within the cavity of the cyclidene ring in order to engage in D-A π–π stacking interactions with both of the tetraazamacrocyclic recognition sites. The structure is also stabilized by multiple [C–H···O] interactions between the DB24C8 ring's polyether loops and the olefinic and amine protons of the cyclidene ring. This recognition motif has been extended

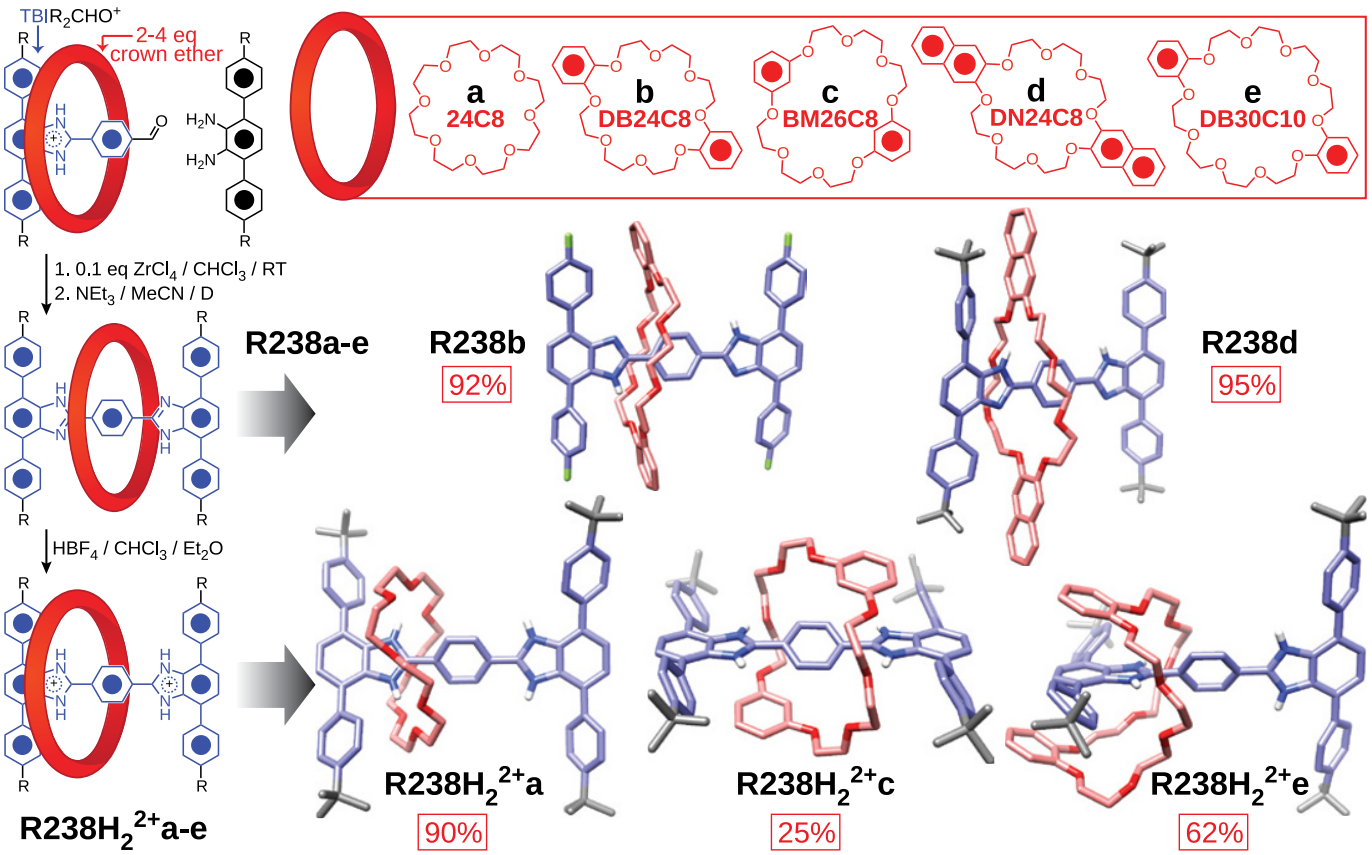
recently to include the synthesis of [2]rotaxanes.[611,612] Catenanes and rotaxanes based on this recognition motif undergo reversible redox processes at the metal centers which are useful in the development of novel electromechanical switches—see **Section 6.1.2** and **Section 6.13.8**.

Crown-8 / Benzimidazolium MIMs

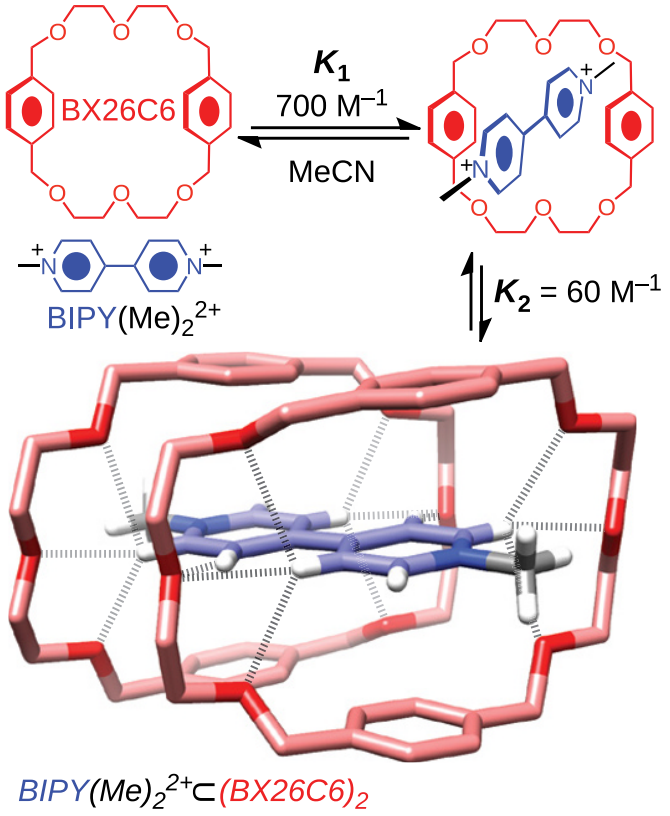
In the interest of preparing functionally rigid rotaxanes, Loeb[526] has described the synthesis (**Scheme 2.56**) of the H-shaped [2]rotaxanes **R238a-e** and **R238H$_2$$^{2+}$a-e** based on the recognition of various crown ethers for benzimidazolium π-acceptors. The stoppering protocol relies on the condensation of an aldehyde-terminated T-shaped benzimidazolium with a bulky *ortho*-phenylenediamine derivative, which forms a second imidazole linkage. Yields are remarkably high (up to 95%) for rotaxanes based on the crown-8 ethers, 24C8, DB24C8, and DN24C8, whereas they are lower (25–62%) when employing the larger bis-metaphenylene[26]crown-8 (BM26C8) and dibenzo[30]-crown-10 (DB30C10) rings. It is possible to toggle the two degenerate recognition sites between imidazolium and imidazole using acids and bases, respectively. Solution-state and X-ray crystallographic evidence confirm that the associative interactions between the crown ether rings and the imidazolium recognition units are greater than those involving neutral imidazole recognition units. The solid-state structures obtained for catenanes **R238b** and **R238d** reveal a lack of π–π interactions between the π-donor units of the rings and the imidazole units in the dumbbell. On the other hand, the rings of the rotaxanes **R238H$_2$$^{2+}$a**, **R238H$_2$$^{2+}$c**, and **R238H$_2$$^{2+}$e** are located much closer to the benzimidazolium units, with evidence of hydrogen bonding in all three cases and D-A π-stacking interactions in the latter two cases. The rate of the ring's shuttling between the two recognition sites is slower in **R238H$_2$$^{2+}$a-e** than it is in **R238a-e**, an observation which is consistent with the expectation that stronger noncovalent bonding interactions transpire in the cationic homologues.

2.3.3.4 Bis-p-xylyl[26]crown-6 (BX26C6)

The crown ether, bis-*para*-xylyl[26]crown-6 (BX26C6), is another ring that is compatible with both D-A and hydrogen-bonded template motifs. Whereas bipyridinium cations are among the most prevalent π-acceptors in mechanostereochemistry, reports[613] of receptors that bind monopyridinium cations are relatively uncommon, despite evidence (*vide supra*) that the BPP34C10 and DB24C8 can also bind monocationic π-acceptors. Chiu[614] discovered that the π-donating BX26C6 ring is also capable of monopyridinium cation recognition when he observed (**Scheme 2.57**) that it



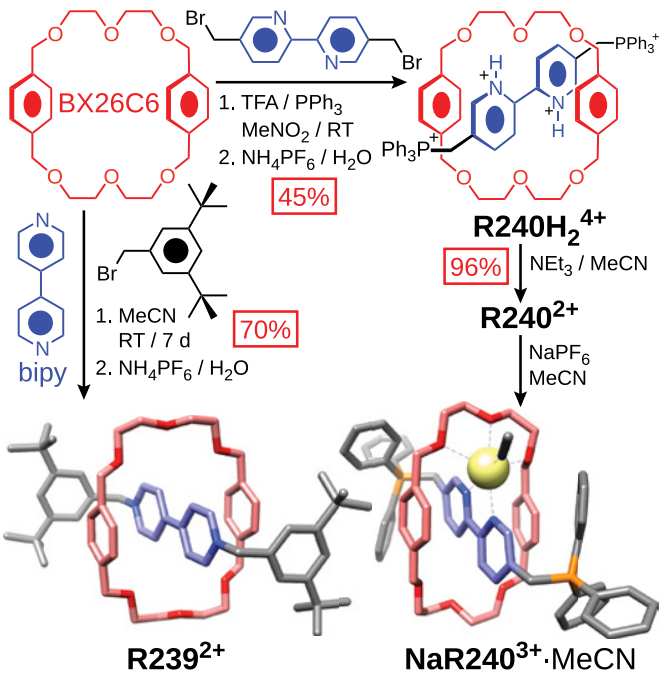
Scheme 2.56 Loeb's synthesis of functionally rigid H-shaped [2]rotaxanes from a T-shaped benzimidazolium (TBI$^+$) template and various crown ether rings.[526,595] The H-shaped rotaxanes can be accessed as either the neutral bis(imidazole) [2]rotaxanes **R238a-e** or the corresponding dicationic bis(imidazolium) [2]rotaxanes **R238H$_2$$^{2+}$a-e**. Tubular representations of the solid state structures of the rotaxanes are rendered with protons (except imidazole/imidazolium protons), solvent molecules, and counterions omitted for the sake of clarity.



Scheme 2.57 The self-assembly and a tubular representation of the solid-state superstructure of a [3]pseudorotaxane comprising methyl viologen and two BX26C6 rings.[614] Solvent molecules, PF_6^- counterions, and protons of the BX26C6 rings are omitted for the sake of clarity.

binds methyl viologen, $BIPY(Me)_2^{2+}$, in a 2:1 ratio, with one ring surrounding each pyridinium subunit of the $BIPY^{2+}$ recognition site. Using ^1H NMR spectroscopy as a tool for determining the ratios of complexed and uncomplexed components when mixed in different molar ratios at 298 K in CD_3CN, i.e., the continuous variation method, it was determined that the first ring binds methyl viologen with an association constant, K_1, of 700 M^{-1}, while the second ring binds with a K_2 value of only 60 M^{-1}. The ratio K_2/K_1 (0.09) is much lower than the value (0.25) expected for statistical complexation, indicating negative cooperativity which is most likely caused by sterically repulsive ring–ring interactions. This interpretation is further supported by the fact that the K_2/K_1 ratio is 0.25, indicating neither positive nor negative cooperativity, when the axle comprises an extended viologen guest with a phenylene spacer in between the two pyridinium units, although the K_1 value (72 M^{-1}) is considerably lower in the latter case. The interaction is even weaker (16 M^{-1}) for a monomeric pyridinium cation *N*-methyl-4-methylpyridinium, yet strong enough to template (*vide infra*) the formation of mechanical bonds.

Taking advantage of the fact that the BX26C6 ring is capable of binding pyridinium cations, Chiu[614,615] has synthesized (**Scheme 2.58**) the simple [2]rotaxanes **R239**$^{2+}$ and **R240H**$_2^{4+}$ from neutral precursors. In the case[614] of **R239**$^{2+}$, the reaction proceeds by (i) an S_N2 substitution on the 1-bromomethyl-3,5-di-*tert*-butylbenzene stopper precursor by 4,4′-bipyridine (bipy), leading to a cationic monopyridinium half-dumbbell, which is (ii) threaded by BX26C6 to form a semirotaxane, followed by (iii) a substitution by the second pyridine subunit with another stopper precursor as the final mechanical bond-forming step. This protocol is reminiscent of the self-assembly of the D-A [2]rotaxanes **R233a-b**$^{2+}$ based on BPP34C10—see **Scheme 2.51**. On the other hand, the template for the [2]rotaxane **R240H**$_2^{4+}$ is 2,2′-bipyridinium dihydrogen hexafluorophosphate ($BPYH_2^{2+}$), which binds BX26C6 with K_a values of 67, 131, and 257 M^{-1} in CD_3CN, CD_3NO_2, and 1:1 $CDCl_3$:CD_3CN, respectively. The synthesis[615] of **R240H**$_2^{4+}$ employs a neutral bis-(bromomethyl)-2,2′-bipyridine unit, which is protonated by TFA *in situ* and allowed to react with triphenylphosphine in the same pot, forming triphenylphosphonium groups as the stoppers. Following deprotonation of the 2,2′-bipyridinium template with NEt_3, the [2]rotaxane **R240**$^{2+}$ can bind to a number of alkali and alkaline earth metals, including Li^+, Na^+, K^+, Mg^{2+}, and Ca^{2+}, the complexes of which can all be detected by ^1H NMR spectroscopy. The solid-state structure of **NaR240**$^{3+}$·MeCN reveals that the 2,2′-bipyridine template and one of the diethylene glycol loops of BX26C6 cooperate with a single MeCN solvent molecule in the stabilization of the Na^+ ion. Sodium-templated MIMs, including those based on BX26C6, are discussed in **Section 2.3.7**.

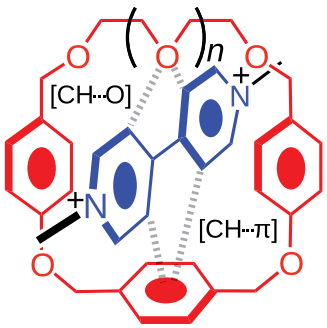


Scheme 2.58 Chiu's synthesis of the BX26C6-based D-A [2]rotaxanes **R239**$^{2+}$ and **R240H**$_2^{4+}$ from neutral starting materials, made possible by the recognition of the BX26C6 ring for pyridinium intermediates generated *in situ*.[614,615] A deprotonated **R240**$^{2+}$ binds cations such as Na^+. Tubular representations of solid-state structures of **R239**$^{2+}$ and **NaR240**$^{3+}$ are shown with protons, PF_6^- counterions, and non-coordinating solvent molecules omitted for the sake of clarity.

The BX26C6 ring is also a component of hydrogen-bonded MIMs (**Section 2.3.4.6**) and a couple of cation- and anion-driven (**Sections 6.4** and **6.5**) switchable molecular shuttles.

2.3.3.5 Crown/Cyclophane Hybrids

Chiu[616,617] has also introduced rings which are half crown ether, half paracyclophane, as hosts for dialkylammonium ions (**Section 2.3.4.2**) as well as for π-acceptors. The 'crown' half of these rings are benzylic polyether loops similar to those of BX26C6, while the 'phane' half constitutes a *para*-phenolic *para*-xylyl linker. The generalized structural formula of these rings, while hosting a methyl viologen guest, is depicted in **Figure 2.31**. According to cyclophane nomenclature, the ring with a diethylene glycol loop is pentoxa[2.9.2]paracyclophane (PO292PC), while the ring with a triethylene glycol loop is hexoxa[2.12.2]paracyclophane (HO2122PC). The larger HO2122PC ring binds methyl viologen in CD_3NO_2 with an association constant (K_a = 130 M^{-1}) which is about twice as high as that (K_a = 60 M^{-1}) involving the smaller PO292PC ring, most likely because it can engage more effectively in [C–H···O] hydrogen-bonding interactions with the $BIPY^{2+}$ unit by virtue of its longer polyether loop. An additional weak stabilizing effect arising from [C–H···π] interactions is provided to the methyl viologen guest by the *p*-xylyl linker. Although these paracyclophane/crown hybrids are similar in size to BX26C6, there has been no indication that these rings bind $BIPY^{2+}$ dications in a 2:1 fashion, as observed in the case of BX26C6.



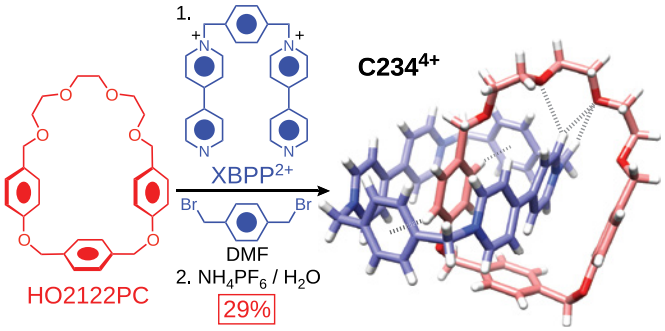
n	Host	K_a / M^{-1}
1	PO292PC	60
2	HO2122PC	130

Figure 2.31 Structural formulas and association constants, K_a, in $MeNO_2$ of $BIPY^{2+}$ pseudorotaxanes[617] based on Chiu's paracyclophane/crown hybrid hosts PO292PC and HO2122PC.

Chiu[617] has harnessed the recognition chemistry of his PO292PC and HO2122PC paracyclophanes for $BIPY^{2+}$ derivatives to prepare (**Scheme 2.59**) $CBPQT^{4+}$-based D-A [2]catenanes by clipping. Employing the larger HO2122PC as the ring results in a slightly higher yield (29%) than the yield (21%) obtained in the case of PO292PC, reflecting the higher affinity (**Section 2.3.3.2**) of $BIPY^{2+}$ units for the HO2122PC ring. The solid-state structure of the [2]catenane **C234^{4+}** based on the larger ring is also portrayed in **Scheme 2.59**.

2.3.3.6 Porphyrinic π-Donating Hosts

Since porphyrins are excellent π-donors on account of their electron-rich pyrrole subunits, they have been incorporated into hosts for D-A recognition motifs. Although many



Scheme 2.59 The self-assembly of a D-A [2]catenane by clipping a $CBPQT^{4+}$ ring around the HO2122PC crown ether/cyclophane ring.[617] A tubular representation of the X-ray crystal structure of the catenane **C234^{4+}** is portrayed with counterions omitted for the sake of clarity.

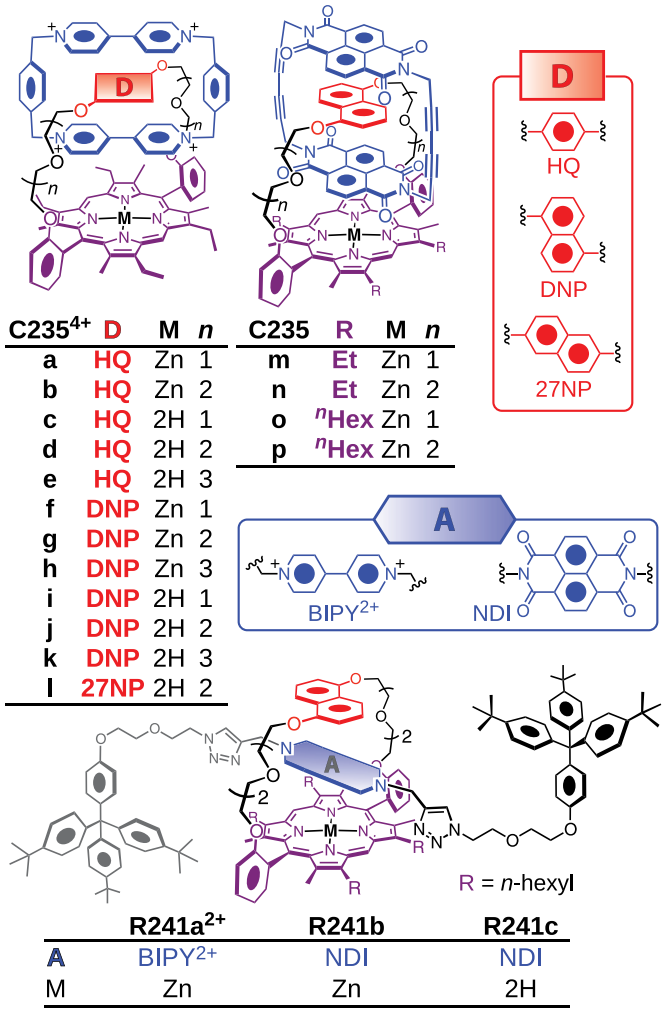
types of porphyrinic macrocycles and cages, such as 'capped',[618–620] 'strapped',[621,622] or 'basket'[623] porphyrins, have been known[619–627] for their host-guest[618,620,624,627] and catalytic[619,621–623,626] properties since the 1980s, only a few of them have been featured in the making of mechanical bonds.

Strapped Porphyrins

MIMs incorporating strapped porphyrin hosts[628] into their topologies and architectures (**Figure 2.32**) have been known since at least the early 1990s, when Gunter[628–632] at the University of New England in Australia described a series of [2]catenanes based on porphyrinic donor-acceptor recognition chemistry. These hosts bind[633] $BIPY^{2+}$ derivatives with K_a values on the order of 10^3–10^4 M^{-1} in MeCN, with shorter macrocyclic polyether chains generally leading to higher association constants. The strapped porphyrins have also been catenated with the tetracationic π-accepting cyclophane $CBPQT^{4+}$ by conventional clipping reactions akin to those summarized in **Table 2.9**, affording catenanes **C235a^{4+}–C235l^{4+}** in yields of up to 28%. In 2003, Gunter[634] expanded this family of porphyrinic catenanes to accommodate neutral rings based on NDI by an oxidative homocoupling clipping procedure akin to that employed (**Scheme 2.48**) by Sanders[505,509] in the synthesis of the first neutral D-A catenanes, which afforded the neutral porphyrinic D-A [2]catenanes **C235m–C235p** in up to 60% yield. More recently, Gunter[574] and Mullen[574,635] have also synthesized rotaxanes (**Figure 2.32**) based on strapped porphyrins possessing DNP π-donors, employing CuAAC click chemistry to access the dicationic [2]rotaxane **R241a^{2+}** or the neutral [2]rotaxanes **R241b-c**, possessing $BIPY^{2+}$ or NDI π-accepting units, respectively, in yields of approximately 20%. Spectroscopic evidence[629,632,634] suggests that the π-acceptors engage the porphyrin subunits in CT and photoinduced CT interactions, indicating that porphyrins make good π-donors for this type of physicochemical process.

Porphyrin Basket (PB)

In 1995, Nolte and Rowan[636] described a porphyrinic "basket-shaped" receptor possessing two tetraethylene



C235^{4+}	D	M	n
a	HQ	Zn	1
b	HQ	Zn	2
c	HQ	2H	1
d	HQ	2H	2
e	HQ	2H	3
f	DNP	Zn	1
g	DNP	Zn	2
h	DNP	Zn	3
i	DNP	2H	1
j	DNP	2H	2
k	DNP	2H	3
l	27NP	2H	2

C235	R	M	n
m	Et	Zn	1
n	Et	Zn	2
o	^{n}Hex	Zn	1
p	^{n}Hex	Zn	2

	R241a^{2+}	R241b	R241c
A	BIPY^{2+}	NDI	NDI
M	Zn	Zn	2H

Figure 2.32 Structural formulas of D-A catenanes and rotaxanes based on strapped porphyrin macrocycles prepared by Gunter[574,628–631] and Mullen.[574,635]

glycol linkers and a diphenylglycoluril bridging moiety, which exhibits high (K_a ~10^4 M^{-1}) affinity for methyl viologen in MeCN, Me_2CO, and $CHCl_3$/MeOH (1:1 v/v), albeit in a non-interpenetrated geometry. This receptor was the forerunner to the macrotricyclic basket-shaped porphyrinic receptor[637] depicted in **Scheme 2.60**, which we will refer to as the porphyrin basket (PB) for short. In contrast with its predecessor, the PB host accommodates BIPY^{2+} derivatives in the geometry of a pseudorotaxane. A high association constant of 6.0×10^5 M^{-1} was determined for a methyl viologen pseudorotaxane, *Me$_2$BIPY^{2+}⊂PB*, at 298 K in 1:1 MeCN:$CHCl_3$. Although solid-state superstructures of complexes of this ilk have not yet been reported in the literature, the presence of π-associated D-A interactions between the porphyrin donor and BIPY^{2+} acceptor are apparent from the appearance of CT absorption bands in the UV-Vis spectra. Mechanomolecules such as the [2]rotaxane **R242^{2+}** are easily prepared (**Scheme 2.60**, see also **Section 3.4.2**) from PB and BIPY^{2+} derivatives. The stoppering protocol in the case of **R242^{2+}** involves the amide bond-forming reaction of tritylacetic acid chloride and diaminopropyl viologen.

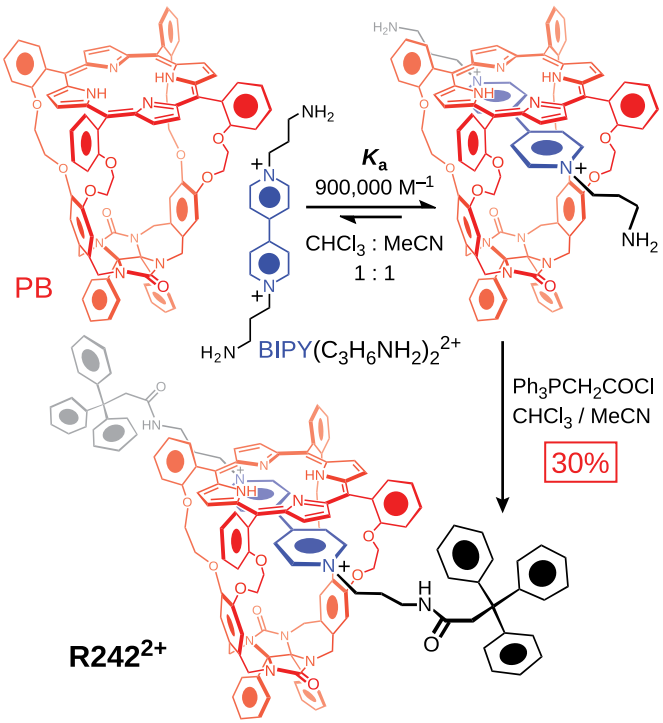
A noteworthy feature of the PB host is the fact that its porphyrin functional group can be exploted to impart the corresponding mechanomolecules with novel catalytic properties, allowing Rowan and Nolte[638–642] to embark on a quest to develop the chemistry of processive catalysis[638] constrained by the mechanical bond—see **Section 6.15.3.1**.

2.3.3.7 Three-Dimensional π-Donor Motifs

A vast array of cage-like macropolycyclic polyethers have mushroomed[643] in the literature on the back of Lehn's Nobel prize-winning research[141] on cryptands as supramolecular receptors. All of the 'red rings' featured so far in this Section, except for the porphyrin basket, are ordinary macrocycles: now, we will describe cage-like π-donating hosts, such as cryptands and other three-dimensional receptors, which have been employed in the construction of MIMs. A dedicated review of cryptand-based hosts for organic guests has been released recently by Chen.[644]

Macrobicyclic Polyether Cryptands

Although BPP34C10, DN38C10, and DB24C8 all encircle BIPY^{2+} guests to form pseudorotaxanes, the bis-*meta*-phenylene[32]crown-10 (BMP32C10) ring is an exception.[487] Instead, BMP32C10 adopts a boat-like conformation as it wraps around the side of a BIPY^{2+} guest, forming[645] a taco-like complex. This side-on binding geometry of *BIPY^{2+}⊂BMP32C10* complexes motivated Gibson[646] to close the BMP32C10 taco by adding a third polyether loop, which generates a macrobicyclic polyether host, or cryptand. In the



Scheme 2.60 Rowan's porphyrin basket[637] (PB) and its self-assembly into a pseudorotaxane-like complex with viologen derivatives, which may be stoppered to form mechanical bonds in rotaxanes such as **R242^{2+}**.

first instance, Gibson prepared the macrobicyclic host bis-*meta*-phenylene[5.5.5]cryptand (BMP555C), which is constitutionally similar to the BMP32C10 ring, but carries a third tetraethylene glycol loop linking the two phenylene units at the *meta* positions. A homologue possessing shorter triethylene glycol loops is bis-*meta*-phenylene[4.4.4]cryptand (BMP444C). BMP444C and BMP555C exhibit K_a values of 1.4×10^4 and 6.1×10^4 M^{-1}, respectively, in Me_2CO at 298 K for the assembly of pseudorotaxane-like complexes with methyl viologen, $BIPY(Me)_2^{2+}$. This binding constant is more than two orders of magnitude higher than that of BMP32C10 and one order of magnitude higher than that of DN38C10. The increase in affinity is not unexpected in view of the macrobicyclic effect, which is also known as the cryptate effect.[362] Macrobicyclic cation receptors often exhibit association constants that are several orders of magnitude higher than those of their monocyclic homologues on account of their additional donor atoms to help stabilize guests, as well as their more favorable preorganization,[647,648] a term introduced by Cram[647] denoting how the stabilities of supramolecular complexes are enhanced when hosts minimize the conformational changes involved in the binding of guests. Since the enthalpic contribution to free energy is identical in the BMP32C10 taco complex and the BMP555C receptor, the enhanced association of the cryptand can be attributed[646] entirely to preorganization in this case, as reflected by a reduced entropic term in the free energy relationship.

The K_a values for several of Gibson's pseudorotaxanes[649] of methyl viologen, hosted by BMP32C10-derived cryptands possessing different linkers as the third bridging moieties, are summarized in **Figure 2.33**. Whereas resorcinol- and hydroquinone-based linkers have a detrimental effect on the association constant, a 2,6-dicarboxypyridine linker—connected to the *m*-phenylene units by methylene ester bonds—leads to a nearly 100-fold enhancement ($K_a = 5.0 \times 10^6$ M^{-1}) in complex stability relative to BMP555C. Since this linker possesses three donor atoms—namely, the nitrogen atom of the pyridine unit and the weakly donating ester oxygen atoms—we will refer to this stronger-binding cryptand as the bis-*meta*-phenylene[5.5.3]cryptand (BMP553C). A comparison (**Figure 2.33**) of the crystallographically determined solid-state superstructures[646,649] of the *BIPY(Me)*$_2^{2+}$*⊂BMP555C* and *BIPY(Me)*$_2^{2+}$*⊂BMP553C* pseudorotaxanes suggests an explanation for the binding enhancement. In both complexes, two of the tetraethylene glycol bridges engage in multiple [C–H···O] interactions with protons that are located on one side of the $BIPY^{2+}$ dication, reflecting the same geometry as that of the BMP32C10 taco complex. While the oxygen atoms in the third polyether loop of BMP555C are too far away to engage in hydrogen bonding with protons on the other side of the $BIPY^{2+}$ unit, the shorter 2,6-dicarboxypyridine linker of the BMP553C receptor is able to incorporate several [C–H···O] and [C–H···N] hydrogen bonds with the β protons of methyl viologen without disturbing the side-on interactions involving polyether loops. These favorable interactions with the third bridging moiety are most likely responsible for the higher affinity exhibited by BMP553C

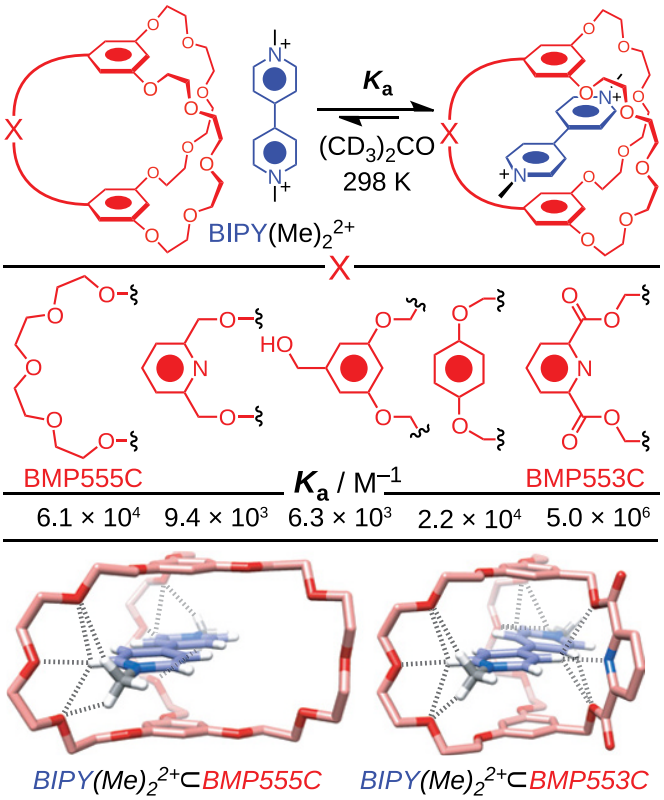
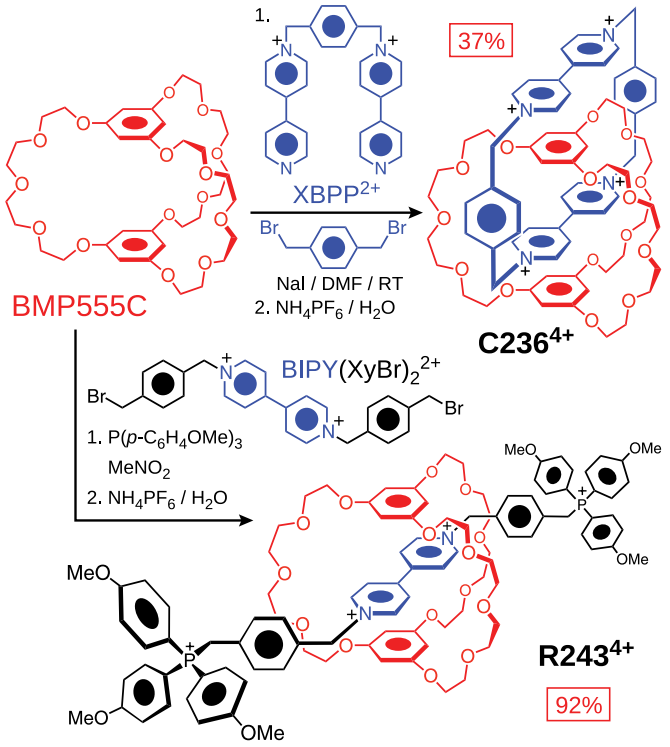


Figure 2.33 Stereoformulas and association constants, K_a, in Me_2CO for the formation of pseudorotaxanes comprising various π-donating cryptands and methyl viologen, $BIPY(Me)_2^{2+}$. Tubular representations of the solid-state superstructures[646] of *BIPY(Me)*$_2^{2+}$*⊂BMP555C* and *BIPY(Me)*$_2^{2+}$*⊂BMP553C* are illustrated with solvent molecules, counterions, and hydrogen atoms of the cryptands omitted for the sake of clarity.

for $BIPY^{2+}$-based guests. Although these pseudorotaxanes exist as 1:1 complexes in solution, Huang[650] has also characterized a 1:2 complex involving two BMP555C hosts in the solid state. Such 1:2 complexes also assemble[651,652] around BPE^{2+} derivatives with K_1 values of up to 224 M^{-1} in Me_2CO.

Mechanomolecules based on the BMP555C cryptand have been synthesized (**Scheme 2.61**) using similar protocols to those available for ordinary crown ethers. For example, the [2]catenane **C236**$^{4+}$ has been obtained[653] in 37% yield by a typical clipping protocol involving the xylyl-bridged bis(pyridine) dication $XBPP^{2+}$ and $XyBr_2$ at RT in DMF. An impressive 92% yield has been recorded[654] for the synthesis of the triphenylphosphonium-capped [2]rotaxane **R243**$^{4+}$ by an S_N2 stoppering protocol involving bis(α-bromoxylyl)bipyridinium, $BIPY(XyBr)_2^{2+}$, as the axle precursor. Stoppering with triphenylphosphine works equally well (91%) in the case of the slightly smaller *BIPY(XyBr)*$_2^{2+}$*⊂BMP553C* pseudorotaxane. The high yields for obtaining these rotaxanates are attributed to the high association constants of the corresponding cryptand pseudorotaxanes. The lower yield observed for the catenation of **C236**$^{4+}$ is therefore most likely dictated, not by the binding strength, but by the entropically demanding ring-closing step, which introduces a substantial amount of ring



Scheme 2.61 The synthesis of D-A MIMs based on the BMP555C cryptand employing S_N2 clipping and stoppering protocols.[653,654]

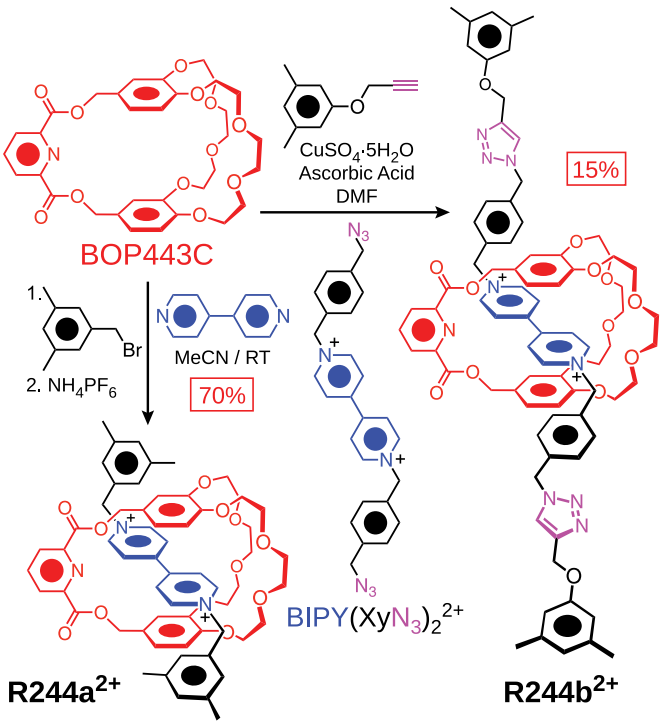
strain into the tetracationic cyclophane. These protocols have been applied to the syntheses of [3]catenanes[653] and [3]rotaxanes[655] with only modest decreases in yields. Cryptand-based MIMs have also been synthesized from taco complex templates under thermodynamic control using olefin metathesis (**Section 3.4**) and Schiff base (**Section 3.3.1**) clipping reactions.

Other related cryptands possessing *ortho* substitution at the phenylene bridgeheads and/or shorter polyether loops have also been described.[486,656–659] These homologues are capable of binding a number of other guests, including monopyridinium salts,[660,661] DAP^{2+} derivatives,[662] diquat,[486,656,658,663] 1,2-bis(*N*,*N*-alkylimidazolium)ethane,[664] tris-pyridinium derivatives,[665] and tropylium cations.[666] One such smaller cryptand possessing benzo-*ortho*-phenylene bridgeheads is BOP443C, which binds bipyridinium derivatives with K_a values on the order of 10^3 M^{-1} in Me_2CO. Cryptand BOP443C has been employed (**Scheme 2.62**) by Zhou[667] in the synthesis of a couple of [2]rotaxanes. The synthesis of the [2]rotaxane **R244a**$^{2+}$, which involves a double Menschutkin reaction between a 4,4′-bipyridyl template and 3,5-dimethylbenzyl bromide, proceeds in MeCN in 70% yield, whereas **R244b**$^{2+}$ is obtained in 15% yield by CuAAC click chemistry at room temperature in DMF. The lower yield in the latter case is most likely attributable to a small binding constant for the pseudorotaxane precursor, *BIPY(XyN$_3$)$_2^{2+}$⊂BOP443C*, in DMF. Much of the research on macrobicyclic polyethers in donor-acceptor assemblies has been carried out by Feihe Huang in the laboratory of Harry Gibson and independently in his own laboratory in Zhejiang University thereafter. These authors have covered progress in this area in a recent review.[668] More examples of catenated cryptands are discussed in **Section 4.1.3**.

Macrotricyclic Polyether Cryptands

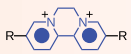
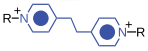
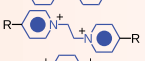
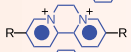
In 2006, Chen[669,670] at the Chinese Academy of Sciences and Chiu[671,672] at National Taiwan University independently introduced macrotricyclic polyethers with very similar constitutions, each involving a pair of [24]crown-8 rings which are doubly conjoined by either triptycene or dibenzobicyclo[2.2.2]-octane linkers, respectively. The triptycene-based host,[669,670] $T_2$24C8$_2$, and dibenzobicyclo host,[671,672] $DBB_2$24C8$_2$, spawned the development[644,673] of a number of macrotricyclic hosts as receptors for π-accepting templates. They include (i) smaller homologues ($T_2$18C6$_2$) based on [18]crown-6,[674] (ii) other 24C8-based hosts incorporating mixed triptycene/anthracene[675,676] (TA24C8$_2$) units, and (iii) larger homologues based on [30]crown-10 with triptycene[677–680] ($T_2$30C10$_2$) or anthracene[681] ($A_2$30C10$_2$) bridging units, amongst others. The structural formulas of these hosts and their affinities, obtained from refs. 669, 674–676, 678–684, for various π-acceptors in binary mixtures of $CDCl_3$ and CD_3CN are tabulated in **Table 2.11**. A representative collection of X-ray crystal structures based on these hosts is portrayed in **Figure 2.34**. We will refer to these data during discussions of some general features of the D-A macrotricyclic recognition systems.

The effects of polyether loop size on the stabilities of the corresponding host-guest complexes can be probed by comparing the binding constants for pseudorotaxanes comprising the triptycene-based hosts, $T_2$18C6$_2$, $T_2$24C8$_2$, and $T_2$30C10$_2$, and viologen derivatives. This comparison reveals



Scheme 2.62 S_N2 and click stoppering protocols[667] for the synthesis of D-A MIMs based on $BIPY^{2+}$ templates and the cryptand BMP443C.

Table 2.11 Association constants[a] (K_a) for pseudorotaxanes comprising macrotricyclic polyether hosts and π-accepting guests in $CDCl_3$:CD_3CN (1:1 v/v), at 298 K.

Host	Guest	R	Host:Guest Ratio	K_a M^{-1}	Ref
$T_2$18C6$_2$[b]		Me	1:1	4.0×10^2	674
		n-Pr	1:1	2.0×10^2	674
		allyl	1:1	9.0×10^2	674
		propargyl	1:1	3.0×10^2	674
		C_2H_4OH	1:1	4.0×10^2	674
		9-anthryl	1:1	1.4×10^3	674
$T_2$24C8$_2$		Me	1:1	4×10^5	669
		Et	1:1	4.0×10^3	682
		n-Pr	1:1	2×10^3	669
		n-Oct	1:1	2×10^3	669
		C_2H_4OH	1:2	4.2×10^3	682
		C_3H_6OH	1:2	3.6×10^3	682
		$C_5H_{10}OH$	1:1	2.6×10^3	682
		C_2H_4OMe	1:1	8.2×10^3	682
		$C_2H_4NHCOMe$	1:1	1.2×10^3	682
		$CH_2NHCOBn$	1:1	9.6×10^3	682
		9-anthryl	1:1	5.8×10^3	682
		H	1:1	3.5×10^3	683
		H	1:1	4.6×10^3	683
DBB$_2$24C8$_2$[c]		Me	1:1	1.1×10^7	684
		Et	1:1	1.9×10^4	684
		Me	1:1	1.8×10^8	684
		propargyl	1:1	1.7×10^6	684
		n-C_5H_{11}	1:1	2.9×10^5	684
TA24C8$_2$[d]		*n*-Pr	1:1	4.4×10^3	675
		H	1:1	1.06×10^5	676
		H	1:1	6.37×10^5	676
		*n*-Pr	1:1	1.51×10^6	676
$T_2$30C10$_2$		Me	1:1	5.3×10^3	680
		Et	1:2	1.0×10^3	678
		n-Pr	1:2	4.8×10^2	678
		C_2H_4OH	1:2	1.3×10^3	678
		C_2H_4OMe	1:2	6.8×10^2	678
		Bn	1:2	3.1×10^2	680
		p-(Me)ArCH_2	1:2	3.1×10^2	680
		p-(F)ArCH_2	1:2	3.8×10^2	680
		p-(Cl)ArCH_2	1:1	4.3×10^2	680
		p-(Br)ArCH_2	1:1	7.4×10^2	680
		9-anthryl	1:1	5.6×10^2	680
		H	1:2		680
		*n*-Pr	1:1	9.0×10^2	680
		C_3H_6OH	1:1	3.0×10^2	679
		C_3H_6OH	1:1	1.2×10^3	679
$A_2$30C10$_2$		Me	1:1	3.1×10^5	681
		Me	1:1	1.4×10^6	681
		Me	1:1	2.1×10^6	681

[a] K_a values were determined by ^{1}H NMR spectroscopic titrations except where noted. For ternary complexes, K_a values are reported as an average (K_{av}) of K_1 and K_2.
[b] In 3:2 $CDCl_3$:CD_3CN.
[c] Determined by ITC in 1:1 $CHCl_3$:MeCN.
[d] Values from ref. 676 were determined spectrophotometrically in 1:1 $CHCl_3$:MeCN.

(**Table 2.11**) that $T_2$24C8$_2$ exhibits higher affinities (~10^3 M^{-1}) for most viologen guests than does $T_2$18C$_6$ or $T_2$30C10$_2$ (~10^2 M^{-1}). The lower affinity of $T_2$18C6$_2$ may be attributable to the scarcity of aliphatic oxygen atoms available for

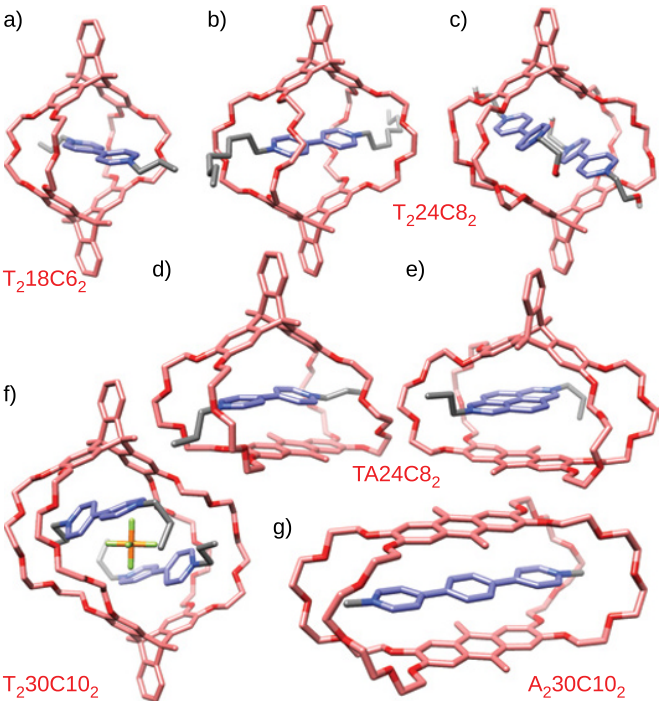


Figure 2.34 Solid-state superstructures of pseudorotaxanes based on macrotricyclic polyethers in various binding modes. (a) 1:1 complex of $T_2$18C6$_2$ and propyl viologen.[674] (b) 1:1 complex of $T_2$24C8$_2$ and octyl viologen.[669] (c) Ternary complex of $T_2$24C8$_2$ and a pair of hydroxyethyl viologen guests.[682] (d) 1:1 complex of TA24C8$_2$ and propyl viologen.[675] (e) 1:1 complex of TA24C8$_2$ and *n*-propyl-functionalized DAP^{2+}.[676] (f) The ternary complex of $T_2$30C10$_2$ and propyl viologen is stabilized by anion–π interactions involving a central PF_6^- counterion.[680] (g) 1:1 complex of the $A_2$30C10$_2$ host and an extended methyl viologen guest.[681] Protons, counterions, and solvent molecules are omitted for the sake of clarity.

[C–H···O] hydrogen bonding, as well as to the lateral [18]crown-6 cavities being prohibitively small to allow the encirclement of the R groups appended to the viologen guests. A comparison of the solid-state superstructures[669,674] of the 1:1 complexes based on $T_2$18C6$_2$ and $T_2$24C8$_2$ in **Figure 2.34a–b** reveals different binding modes for these two hosts. Whereas the $BIPY^{2+}$ guest within $T_2$18C6$_2$ is oriented such that its propyl groups are directed outward from each portal of the host's central cavity, the octyl groups of the $BIPY^{2+}$ guest ensconced by $T_2$24C8$_2$ penetrate through each of its [24]crown-8 cavities, which is more optimal for [C–H···O] interactions between the polyether loops and the acidic protons of the guest. On the other hand, the lower average affinities exhibited by the larger $T_2$30C10$_2$ host may be related to its cavity being too large for a complementary fit, since it tends to form ternary complexes (**Table 2.11**) with most $BIPY^{2+}$ derivatives. Sandwiched in between the two propyl viologen guests of the $T_2$30C10$_2$-hosted complex portrayed in **Figure 2.34f** is one PF_6^- counterion, which stabilizes the complex via anion–π interactions in the solid state.[678] Note that $T_2$24C8$_2$ is also capable of hosting two $BIPY^{2+}$ guests, yet these ternary complexes are only observed (**Table 2.11**) in the cases of hydroxypropyl viologen and hydroxyethyl

viologen.[682] In the solid state, the two hydroxyethyl viologen guests are staggered (**Figure 2.34c**) within the central cavity of the $T_2$24C8$_2$ host, each of them accepting hydrogen bonds from opposing 24C8 loops and engaging in π–π stacking and [C–H···π] interactions with opposing triptycene bridgeheads. $T_2$24C8$_2$ is also capable of accommodating[685] D-A pairs within its large cavity in heteroternary complexes.

The effect of employing different π-donating units as bridgeheads in these macrotricyclic polyethers can be probed by comparing K_a values (**Table 2.11**) for pseudorotaxanes comprising $T_2$24C8$_2$, DBB$_2$24C8$_2$, and TA24C8$_2$, as well as $T_2$30C10$_2$ and $A_2$30C10$_2$. From these data, it would appear that the dibenzobicyclooctane (DBB) bridgehead is more conducive to the binding of π-acceptors than is the nearly isostructural triptycene unit, since methyl viologen binds to DBB$_2$24C8$_2$ (K_a = 1.1 × 10^7 M^{-1}) with much higher affinity than it binds to $T_2$24C8$_2$ (K_a = 4 × 10^5 M^{-1}) in a 1:1 mixture of $CDCl_3$ and CD_3CN. This comparison should be made with caution, however, because the K_a values for DBB$_2$24C8$_2$ were obtained[684] by a different method (ITC) than that (^{1}H NMR titration) which was employed[669] in the case of $T_2$24C8$_2$. A more trustworthy comparison is that[675,676] of $T_2$24C8$_2$ versus TA24C8$_2$, as well as that[681] of $T_2$30C10$_2$ versus $A_2$30C10$_2$. The anthracene bridgehead is clearly a better π-donor than triptycene on account of its more planar structure and larger π-system, which enhances its affinity for π-acceptors. Accordingly, the K_a values (**Table 2.11**) for TA24C8$_2$ and $A_2$30C10$_2$ are among the highest (up to >10^6 M^{-1}) that have been recorded for this class of receptors. Representative solid-state superstructures for these complexes are illustrated in **Figure 2.34d–e**. Although methyl viologen and propyl-functionalized DAP^{2+} acceptors bind to TA24C8$_2$ in different geometries, both guests are clearly engaged in strong D-A π–π stacking interactions with the anthracene bridgeheads. The extended viologen guest encapsulated by $A_2$30C10$_2$ is engaged (**Figure 2.34g**) likewise in D-A π-stacking interactions with both anthracene-derived bridgeheads.

Among these macrotricyclic hosts, DBB$_2$24C8$_2$ and $T_2$24C8$_2$ have been the most widely used for making mechanical bonds, giving rise to a number of rotaxanes (**Section 4.2.1.3**) and switches (**Sections 6.5.1** and **6.13.1.4**) with novel kinds of architectures and stimulus-responsive motion, respectively. The stronger-binding triptycene/anthracene host TA24C8$_2$ has also been employed to make [2]rotaxanes and switchable molecular shuttles (**Section 6.4.2**). Chen[686] found that the binding mode of a viologen template can be controlled (**Figure 2.35**) by the steric bulk of its side chains. Whereas BIPY^{2+} derivatives with long unbranched alkyl chains penetrate both of the 24C8 cavities of the TA24C8$_2$ host (as in **Figure 2.34d**), a viologen derivative with benzylic pseudo-stoppers which are too bulky to pass through the 24C8 portals must direct its functionalities through each opening of the host's larger central cavity. This sterically controlled binding has allowed the synthesis[686] of the viologen/TA24C8$_2$ [2]rotaxanes **R245a^{2+}** and **R245b^{2+}**, the co-conformations (**Figure 2.35**) of which reflect those of their respective templates.

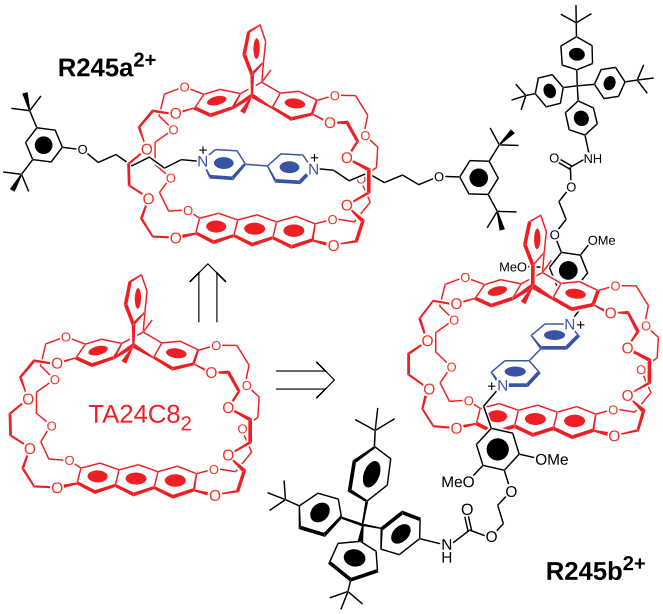
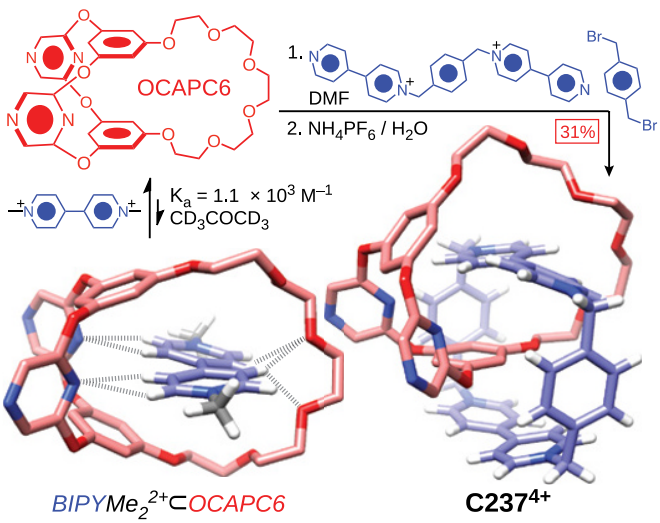


Figure 2.35 The steric bulk of the sidechains appended to a BIPY^{2+} template control its orientation with respect to the cavities of the macrotricyclic host TA24C8$_2$, leading to rotaxanes with different co-conformations, yet based on the same recognition motif.[686]

Huang[687] and Gibson[688] have described a couple of macrotricyclic cryptands derived from BMP32C10 which bind methyl viologen with K_a values of up to 2.5 × 10^4 M^{-1} at ambient temperature in 1:1 $CHCl_3$:MeCN. Recent and more comprehensive reviews[644,673] on macrotricyclic hosts are available in the literature. See **Section 2.3.4.6** for examples of pseudorotaxanes comprising macrotricyclic hosts and dialkylammonium cations. See **Section 2.3.8.1** for alkali metal templates involving these macrotricyclic hosts. Catenanes incorporating macrotricyclic component parts are discussed in **Section 4.1.3.2**.

Oxacalixcrowns

Li, Jiang, and Wen[689] at the Chinese Academy of Science in Shanghai have prepared a crown-6 host derived from oxacalix[2]arene[2]pyrazine (OCAPC6) which binds (**Scheme 2.63**) methyl viologen with an association constant of K_a = 1.1 × 10^3 M^{-1} in $(CD_3)_2CO$. The solid-state superstructure of this complex reveals the presence of (i) bifurcated [C–H···N] interactions between the OCAPC6 host's pyrazine units and the α and β protons of methyl viologen, (ii) [C–H···O] contacts between the viologen β protons and the crown-6 polyether loops, as well as (iii) D-A π–π stacking interactions between the oxacalixarene and viologen aromatic rings. This templation motif was employed successfully in the synthesis (**Scheme 2.63**) of the [2]catenane **C237^{4+}** by a clipping protocol. The solid-state structure of **C237^{4+}** reveals a similar set of noncovalent stabilizing interactions as those present in the pseudorotaxane progenitor. Hosts with larger (crown-7) and DNP-containing polyether loops have also been prepared and investigated as hosts for viologen derivatives with similar outcomes.[689]



Scheme 2.63 The self-assembly and synthesis of pseudorotaxanes and catenanes, respectively, arising from the recognition of an oxacalix[2]arene[2]pyrazine crown-6 (OCAPC6) host for viologen-derived guests.[689] PF_6^- counterions and protons of the OCAPC6 host are omitted for the sake of clarity.

2.3.3.8 The Little Blue Box: CBPQT^{4+}

The electron-deficient rings employed in mechanostereochemistry often take the form of tetracationic rectangular cyclophanes—see **Figure 2.25**. Foremost among these charged cyclophanes is cyclobis(paraquat-*p*-phenylene)[690,691] (CBPQT^{4+}), which is known[692–695] also as the 'little blue box'. The source of this nickname comes from the fact that the BIPY^{2+} recognition units of CBPQT^{4+} are easily reduced to the BIPY$^{\bullet+}$ radical cations, which appear blue in color because they absorb red wavelengths of light. Incidentally, spin-pairing interactions between BIPY$^{\bullet+}$ radical cations are the basis of one of the newest genres of molecular recognition in mechanostereochemistry—see **Section 2.3.10**. The little blue box is featured in over 500 publications in the chemical literature, as well as approximately 200 structures[o] that have been deposited in the Cambridge Crystallographic Data Centre—a testament to its versatility and applicability in both molecular and supramolecular systems.

Cyclobis(diazapyrenium-*p*-phenylene) (CBDAP^{4+}) is a homologue of the little blue box which tends to bind guests more tightly than CBPQT^{4+} on account of its deeper cavity and larger π-surface provided by the DAP^{2+} recognition units. A number of related box-shaped hosts are described in **Section 2.3.3.9**.

Cyclobis(paraquat-p-phenylene) (CBPQT^{4+})

The CBPQT^{4+} ring was introduced[690] in 1988 as a multipurpose receptor. It was recognized immediately that this tetracationic cyclophane is highly promiscuous when it comes to binding relatively small π-donors. Solid-state superstructures[691,696–699] of several pseudorotaxanes based on CBPQT^{4+} are portrayed as tubular representations in **Figure 2.36**. CBPQT^{4+} can be dissolved in polar organic solvents as its PF_6^- salt, or in aqueous solutions as its Cl^- salt. As its Cl^- salt, CBPQT^{4+} is capable of hosting a variety of guests in water, aided and abetted by the hydrophobic effect in addition to π–π interactions. Neurotransmitters such as dopamine, seratonin, and epinephrine bind[700] CBPQT^{4+} with affinities on the order of 10^3 M^{-1} in aqueous phosphate buffer, for example. The first compounds to be characterized as guests for CBPQT·4PF_6 were isomers of dimethoxybenzene, which exhibit K_a values on the order of

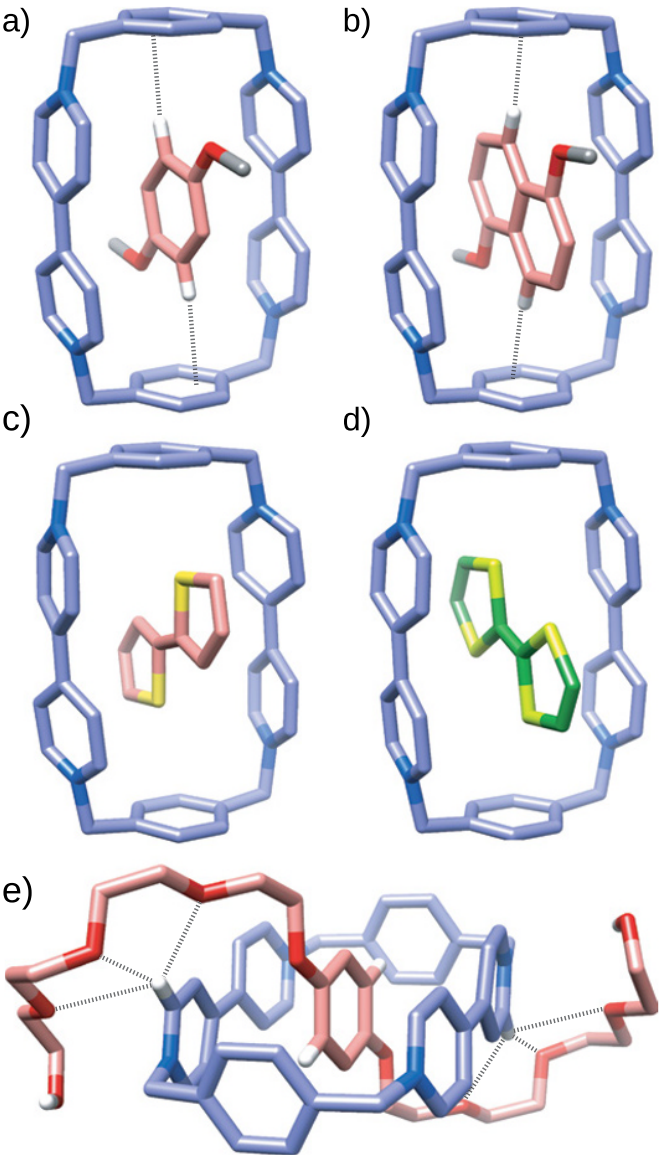


Figure 2.36 Tubular representations of the solid-state superstructures of selected pseudorotaxanes comprising CBPQT^{4+} hosts and guests with HQ[691,696] (a,e), DNP[697] (b), 2T[698] (c), and TTF[699] (d) recognition units. Solvent molecules, counterions, and hydrogen atoms not engaged in [C–H···π] or [C–H···O] interactions are omitted for the sake of clarity.

[o] The large number of CCDC depositions related to CBPQT^{4+} can be explained, not only by its prominent standing in mechanostereochemistry, but also by the fact that CBPQT^{4+} and its relatives are often easy to crystallize on account of their tetracationic nature and rectangular geometries.

10^1 M^{-1} in MeCN. The isomer with the highest K_a value (17 M^{-1}) is *para*-dimethoxybenzene or dimethylhydroquinone ($HQMe_2$), whose protons partake (**Figure 2.36a**) in stabilizing [C–H···π] interactions with the *para*-phenylene units of the $CBPQT^{4+}$ ring. Derivatives of 1,5-dioxynaphthalene (DNP), which have more π-electrons and a larger π-surface area than HQ derivatives, associate (**Figure 2.36b**) with $CBPQT^{4+}$ much more strongly, with K_a values of ~10^4 M^{-1} in MeCN and ~10^6 M^{-1} in H_2O. The [C–H···π] interaction is implicated once again in the *DNP⊂CBPQT*$^{4+}$ complexes. Owing to their richness of π-electrons, sulfur-containing conjugated heterocycles such as oligothiophenes[698] (**Figure 2.36c**), including bithiophene (2T), as well as tetrathiafulvalenes[699] (**Figure 2.36d**), are also highly stabilized within the π-electron poor cavity of the $CBPQT^{4+}$ receptor.

Appending (**Figure 2.36e**) oligoethylene glycol chains to guests for $CBPQT^{4+}$ usually leads to increases in K_a values because the polyether loops can engage in stabilizing [C–H···O] interactions with the acidic α-protons of the tetracationic cyclophane's $BIPY^{2+}$ recognition units. A series of systematic investigations[500,701,702] on the binding properties (**Table 2.12**) of pseudorotaxanes comprising the $CBPQT^{4+}$ ring and R_2HQ or R_2DNP guests underline the importance of [C–H···O] hydrogen bonds in these systems. Appending one or two ethylene glycol units onto HQ, for example, raises the corresponding K_a values by one or two orders of magnitude, respectively, while additional repeating units do not lead to further significant enhancements. A similar trend is observed for DNP and bis-2-(2-hydroxyethoxy)ethoxynaphthalene (BHEEN) guests, which bind to $CBPQT^{4+}$ with K_a values of 1 × 10^4 and 5.7 × 10^5 M^{-1}, respectively, in MeCN. The magic of the ethylene glycol linkers lies in the *gauche* effect, whereby the two vicinal oxygen atoms in each repeating unit of ethylene glycol are related by a torsion angle of ~60° without incurring a significant energy penalty. The *gauche* effect allows the loops to 'wrap around' the $BIPY^{2+}$ units and simultaneously direct multiple oxygen atoms toward the acidic guest protons. Other R substituents, which do not benefit from the *gauche* effect (e.g., hydroxyphenyl) or lack oxygen atoms (e.g., propyl, hexyl), do not enhance the K_a values of the *$R_2HQ⊂CBPQT^{4+}$* pseudorotaxanes nearly as effectively as do the polyether loops. A comparison (**Table 2.12**) of *$R_2DNP⊂CBPQT^{4+}$* pseudorotaxanes in MeCN and H_2O reveals that affinities are higher in water, in spite of its higher polarity, on account of the hydrophobic effect.

A collection of π-donating guests for $CBPQT^{4+}$ and their corresponding association constants in MeCN, collected from refs. 496, 500, 502, 517, 530, 535, 692, 701-708, are summarized in **Table 2.13**. The K_a values for guests derived from tetrathiafulvalene (TTF), pyrrolotetrathiafulvalene (PTTF), and bispyrrolotetrathiafulvalene (BPTTF) and their thioethers, collected from refs. 502, 538, 703, 707-714, are summarized in **Table 2.14**. One observation revealed by comparing guests is that the enhancing effect of polyether loops appended to the π-donor is not universal. The stabilities (**Table 2.13i–k**) of complexes based on disubstituted 1/6-, 2/7-, and 2/6-dioxynaphthalene derivatives (16NP, 27NP, and 26NP, respectively) are not as sensitive to the polyether loops as the 1/5-substituted DNP derivatives.[496] Longer guests such as biphenol[704] (**Table 2.13m–n**), benzidine[704,705] (BZ, **Table 2.13o–p**), difluorobenzidine (F_2BZ, **Table 2.13q–r**),[706] azobenzene[535] (**Table 2.13s**), and BPTTF (**Table 2.14n–p**),[703,711] are also relatively insensitive to the presence and length of appended polyether chains. These results suggest that the polyethers do not participate significantly in stabilizing the pseudorotaxanes comprising these guests, most likely because their longer dimensions extend the distance between the polyether loops and the rims of the $CBPQT^{4+}$ ring, such that establishing [C–H···O] hydrogen bonds becomes too costly from an energetic standpoint.

The data in **Tables 2.13–2.14** also indicate a high dependence of association strengths on the π-electron density of the guests. In general, guests with more π-electron rich aromatic surfaces are hosted by the $CBPQT^{4+}$ ring with greater affinities than guests of similar size with less electron density. This conclusion can be drawn by comparing, for example, BZ[704,705] versus F_2BZ[706] (**Table 2.13o–r**) derivatives , as well as HQ[500] versus difluorohydroquinone[517] and tetrafluorohydroquinone (**Table 2.13a–c**) derivatives.[516,517] A strong π-donating effect also explains the particularly high K_a values observed (**Table 2.14**) for many TTF derivatives. Guests are shaded so as to reflect the color generated in solution upon complexation with $CBPQT^{4+}$ on account of charge transfer interactions. Dioxyarenes are typically orange to red, while diaminoarenes and TTF derivatives are typically green. The difluorobenzidine unit produces[706] a blue color in solution, which is uncommon for this class of complexes. In the case of TTF derivatives (**Table 2.14**) the wide variability in thermodynamic

Table 2.12 Association constants, K_a, of *$HQ(R)_2⊂CBPQT^{4+}$* and *$DNP(R)_2⊂CBPQT^{4+}$* pseudorotaxanes, determined by spectrophotometric titrations in MeCN and H_2O.[500,701,702]

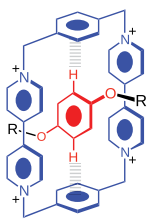
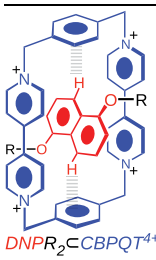
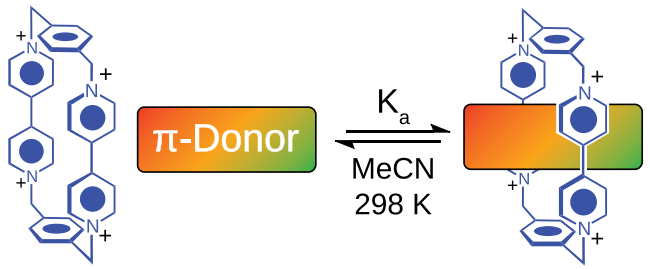
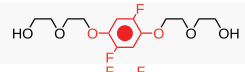
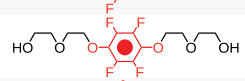
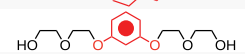
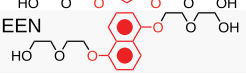
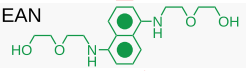
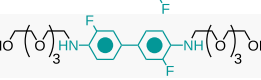
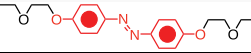
Pseudorotaxane	*T* / K	Solvent	—OR	K_a / M^{-1}
 *$HQR_2⊂CBPQT^{4+}$*	298	MeCN	—OH	1.8×10^1
	298	MeCN	—O	1.7×10^1
	298	MeCN	—O	2.8×10^1
	298	MeCN	—O	2.2×10^1
	298	MeCN	—O	5.4×10^1
	298	MeCN	—O	2.57×10^2
	298	MeCN	—O	2.90×10^2
	298	MeCN	—O	2.22×10^3
	298	MeCN	—O	2.24×10^3
	298	MeCN	—O	2.52×10^3
 *$DNPR_2⊂CBPQT^{4+}$*	293	MeCN	—OH	1×10^4
	293	MeCN	—O	4×10^4
	293	MeCN	—O	5.7×10^5
	293	MeCN	—O	4.0×10^5
	293	H_2O	—OH	9.0×10^5
	293	H_2O	—O	6.2×10^5
	293	H_2O	—O	1.4×10^6
	293	H_2O	—O	6.1×10^5

Table 2.13 K_a and ΔG values for the complexation of CBPQT^{4+} and various π-donors at 298 K in MeCN.



Entry	π-Donor	K_a M^{-1}	$-\Delta G_a$ kcal·mol^{-1}	Method[a]	Ref
a		2220	4.6	ST	500
b		15	1.6	NMRD	517
c		0	-	NMRD	517
d		1900	4.5	ST	529
e		1070	4.1	NMRT	550
f	BHEEN 	25400 36400	6.0 6.2	ST ITC	701 703
g		1010	4.1	ST	530
h	BHEAN 	58000	6.5	ITC	692
i		378	3.5	NMRT	496
j		177	3.1	NMRT	496
k		221	3.2	NMRT	496
l		796	4.0	ST	529
m		140	2.9	ST	704
n		104	2.7	ST	704
o	BZ 	1040	4.1	ST	704
p		1100	4.1	ST	705
q	F_2BZ 	68	2.5	ITC	706
r		312	3.4	ITC	706
s		437	3.6	NMRD	535

[a]Methods: spectrophotometric titration (ST), isothermal titration calorimetry (ITC), NMR titration (NMRT), NMR dilution method (NMRD).

stabilities between the different pseudorotaxanes indicates that they are highly sensitive[715] to TTF substituent effects,[P] which can be used to tune the energetics and dynamics of the corresponding MIMs—see **Section 5.1.1**.

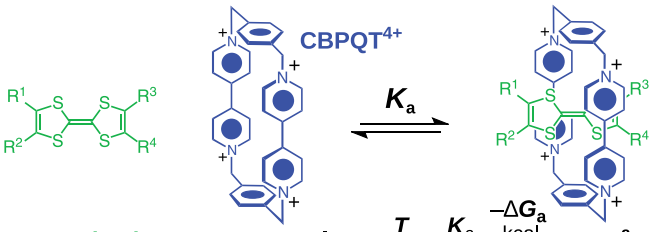
[P] Incidentally, substituents on the phenylene ring of CBPQT^{4+} have been found, universally, to decrease the binding affinities of guests, regardless of the electron donating or withdrawing character of the functional group. Although the penalties for substituting the phenylene rings typically amount to less than an order of magnitude of difference in K_a, it is much less significant than the effect of changing the constitution of the TTF unit.

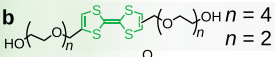
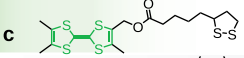
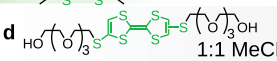
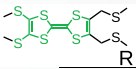
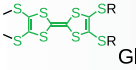
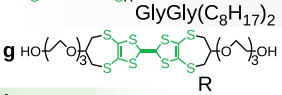
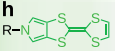
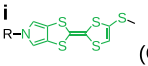
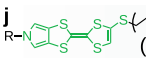
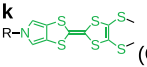
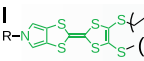
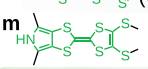
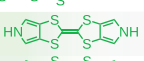
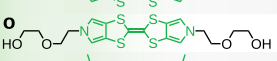
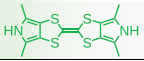
Dan Li[716] recently found that CBPQT^{4+} and the larger CBPQB^{4+} homologue can also host completely inorganic guests to form inorganic-organic hybrid pseudorotaxanes and rotaxanes. See **Section 4.2.3.6**.

CBPQT^{4+} Catenanes

Although D-A [2]catenanes are more often prepared (**Section 2.3.3.2** / **Table 2.9**) by clipping the CBPQT^{4+} ring

Table 2.14 Association constants (K_a) and corresponding free energies of association (ΔG_a) for pseudorotaxane complexes formed between the CBPQT·4PF$_6$ host and various TTF derivatives.



	TTF Derivative	Solvent	T K	K_a M^{-1}	$-\Delta G_a$ kcal mol	Method[a]	
TTF	a 	MeCN	298	6900	5.2	ITC	705
		MeCN	298	7200	5.3	NMRD	707
		MeCN	298	8000	5.3	ST	707
		MeCN	300	10000	5.5	NMRT	502
		Me_2CO	294	2600	4.7	SD	712
	b  n = 4	MeCN	298	50000	6.4	FQC	709
	n = 2	MeCN	298	380000	7.6	ITC	705
	c 	MeCN	298	45000	6.3	SD	710
TTF Thioethers	d 	MeCN	298	8580	5.4	ITC	708
		1:1 MeCN / H_2O	298	7600	5.3	ITC	708
	e  R	Me_2CO	303	490	3.7	NMRSP	711
	f  Me	MeCN	303	180	3.1	NMRSP	711
	Me	Me_2CO	303	40	2.2	NMRSP	711
	$GlyGly(C_8H_{17})_2$	MeCN	298	4400	5.0	NMRSP	713
	g  R	MeCN	298	10000	5.5	ST	538
PTTF	h  H	Me_2CO	296	5800	5.1	SD	714
	$(CH_2CH_2O)_3H$	Me_2CO	296	13000	5.6	SD	714
PTTF Thioethers	i  H	Me_2CO	296	3900	4.9	SD	714
	Me	Me_2CO	296	4100	4.9	SD	714
	$(CH_2CH_2O)_3H$	Me_2CO	296	11600	5.5	SD	714
	j  H	Me_2CO	296	4700	5.0	SD	714
	$(CH_2CH_2O)_3H$	Me_2CO	296	12000	5.5	SD	714
	k  H	Me_2CO	296	1300	4.2	SD	714
	Me	Me_2CO	296	1800	4.4	SD	714
	$(CH_2CH_2O)_3H$	Me_2CO	296	4200	4.9	SD	714
	l  H	Me_2CO	296	2100	4.5	SD	714
	$(CH_2CH_2O)_3H$	Me_2CO	296	5500	5.1	SD	714
	m 	Me_2CO	303	1000	4.2	NMRSP	711
BPTTF	n 	MeCN	298	70800	6.6	ITC	705
		Me_2CO	295	12000	5.5	SD	711
	o 	MeCN	298	168000	7.1	ITC	705
	p 	Me_2CO	295	18000	5.7	SD	711
		Me_2CO	298	7900	5.4	NMRSP	711

[a]Methods: isothermal titration calorimetry (ITC), NMR Dilution (NMRD), spectrophotometric titration (ST), fluorescence quenching competition (FQC), spectrophotometric dilution (SD), NMR single-point method (NMRSP).

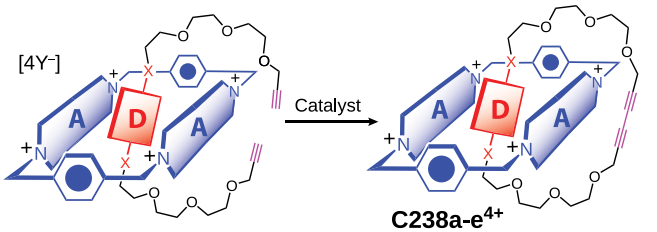
around a crown ether template, it is also possible to clip a crown ether around a CBPQT^{4+} template. This strategy has been realized using thermodynamically controlled approaches such as olefin metathesis (**Section 3.4.1.2**) and imine bond formation (**Section 3.3.1**), as well as by esterifications[545] and CuAAC click reactions[405] under kinetic control. Clipping reactions[405,717,718] that involve Eglinton-Glaser-Hay coupling of alkyne-terminated aromatic polyethers in the presence of CBPQT^{4+} to generate [2]catenanes are summarized in **Table 2.15**. The oxidative clipping reaction affords D-A [2]catenanes in modest (21%) to fair (64%) yields, with the variations in efficiency reflecting, to some extent, the differences in binding affinities (**Tables 2.12–14**) among the pseudorotaxane precursors. For example, the clipping reactions involving DNP π-donors proceed[718] more efficiently in water at RT than they do[405] in MeCN at 90 °C, where the pseudorotaxane precursors are less stable. The same clipping reaction[718] is also more efficient in the presence of the tighter-binding CBDAP^{4+} template than the smaller CBPQT^{4+} cyclophane. The reaction is most efficient when a polyether-appended TTF unit—the guest with the highest affinity[703] for CBPQT^{4+}—is employed[717] as the π-donor, while diaminonaphthalene-based catenanes are obtained[718] in yields that are slightly lower than expected, perhaps on account of oxidative damage to the π-donor recognition unit.

CBPQT^{4+} Rotaxanes

In a conceptual extension of the original D-A catenane synthesis, the first D-A [2]rotaxanes were prepared by clipping CBPQT^{4+} rings around π-donating dumbbells. The reaction conditions and yields associated with the syntheses of a collection of 18 [2]rotaxanes (**R246a^{4+}–R246r^{4+}**) are tabulated in **Table 2.16**. The same kind of clipping protocol has also been employed in the synthesis of many bistable[470,471] D-A [2]rotaxanes, such as those described in **Section 6.1**. The solid-state (super)structures of some of these compounds are illustrated in **Figure 2.37**. The reaction yields are sensitive to structural parameters, such as the donor unit, linker length, and stopper moiety, as well as the reaction conditions—i.e., stoichiometry, solvent, pressure, time, and temperature.

Donor Unit. The π-donors that have assumed the role of axle in these rotaxanes include the now-familiar HQ[719–723]

Table 2.15 Synthesis of the donor-acceptor [2]catenanes, **C238a^{4+}–C238e^{4+}**, by clipping via Eglinton-Glaser-Hay coupling.[405,717,718]



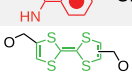
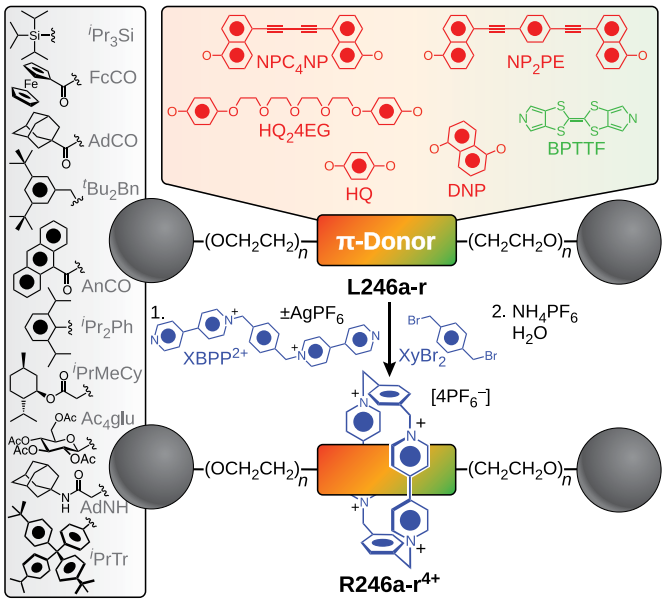
	A	D	Y⁻	Catalyst	Solvent	T °C	Yield %	Ref
a			PF_6^-	$Cu(OAc)_2$	MeCN	90	21	405
			$CF_3CO_2^-$	CuCl/TMEDA	H_2O	RT	51	718
b			$CF_3CO_2^-$	CuCl/TMEDA	H_2O	RT	40	718
c			PF_6^-	$Cu(OAc)_2{\cdot}5H_2O$	MeCN	23	64	717
d			$CF_3CO_2^-$	CuCl/TMEDA	H_2O	RT	63	718
e			$CF_3CO_2^-$	CuCl/TMEDA	H_2O	RT	34	718

Table 2.16 Summary of room-temperature clipping protocols for the synthesis of the D-A [2]rotaxanes **R246a^{4+}–R246r^{4+}** from CBPQT^{4+} precursors (XyR_2) and π-donating dumbbells **L246a-r**.



	π-Donor	*n*	Stopper	Equiv L246	Equiv XyR_2[a]	Solvent	*P* bar	*t* d	%	Ref
a	$HQ_2$4EG	3	$^iPr_3$Si	3	1[b]	MeCN	1	7	32	728
b	$HQ_2$4EG	3	FcCO	3	1[b]	MeCN	1	7	10	729
c	$HQ_2$4EG	3	AnCO	3	1[b]	MeCN	1	7	36	719
d	$HQ_2$4EQ	3	Ac_4glu	2	1[b]	MeCN	1	5	6	723
e	HQ	3	AdCO	1.5	1[b]	MeCN	1	7	10	719
f	HQ	3	FcCO	3	1[b]	MeCN	1	7	10	720
g	HQ	3	AnCO	3	1[b]	MeCN	1	7	25	721
h	HQ	2	AdNH	1	5	MeCN	1	10	6	722
i	HQ	3	Ac_4glu	2	1[b]	MeCN	1	5	2	723
j	DNP	2	$^iPr_3$Si	1	2.8	MeCN	1	10	32	724
k	DNP	3	$^iPr_3$Si	1	2.6	MeCN	1	10	72	724
l	DNP	2	^{i}PrMeCy	1	3	MeCN	1	10	55	725
m	DNP	2	$^iPr_2$Ph	1.7	1	DMF	10^4	3	62	726
n	DNP	2	^{t}PrTr	1.7	1	DMF	10^4	3	66	726
o	DNP	0	$^tBu_2$Bn	1	3	DMF	10^4	3	27	727
p	BPTTF	0	$^tBu_2$Bn	1	3	DMF	10^4	3	22	727
q	NPC_4NP	2	$^iPr_2$Ph	1	3	DMF	10^4	3	8	730
r	NP_2PE	2	$^iPr_2$Ph	1	10	DMF	10^4	3	10	731

[a] XyR_2 = $XBPP^{2+}$ and $XyBr_2$, each introduced in approximately equal molar ratios.
[b] $AgPF_6$ (2–3 equiv) was introduced to improve yields by sequestering Br^- anions, which are generated from $XyBr_2$ as it is consumed in reaction, since Br^- can cause the cationic intermediates and precursors to precipitate.

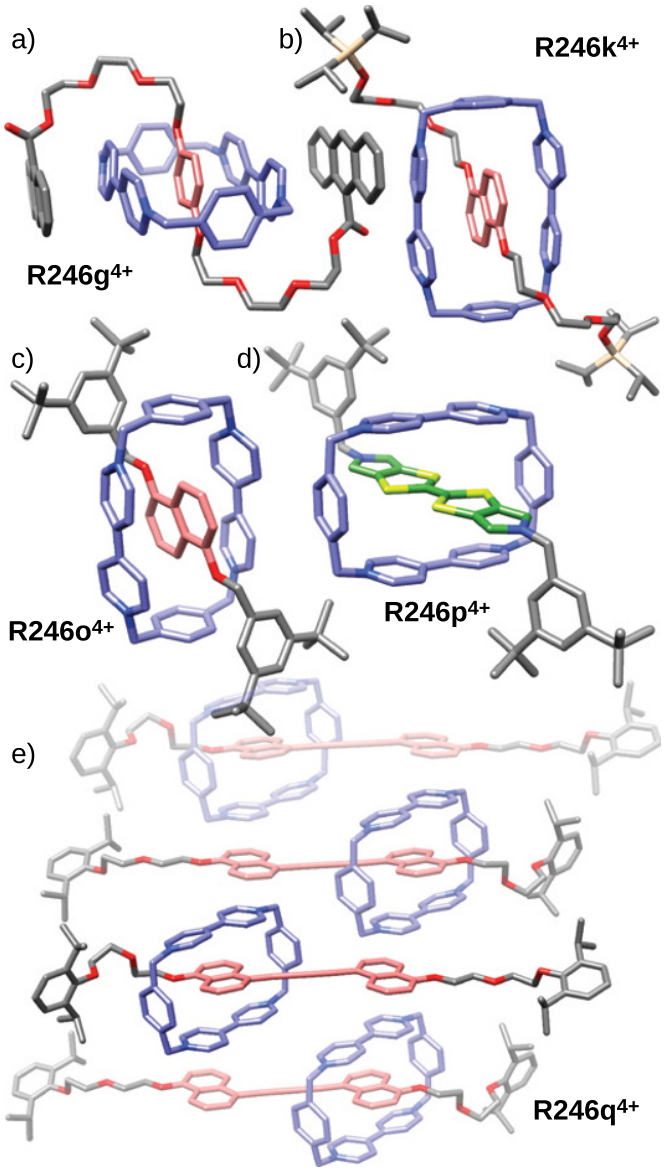


Figure 2.37 Solid-state (super)structures of selected D-A [2]rotaxanes possessing CBPQT^{4+} rings. (a) The dumbbell of **R246g^{4+}** adopts[729] a folded secondary structure as its anthracene stoppers engage in 'alongside' π–π stacking interactions with CBPQT^{4+}. (b) The structure[724] of homologue **R246k^{4+}** is less folded by comparison, since its $^{i}Pr_3Si$ stoppers do not interact favorably with the ring's π-acceptors. (c)–(d) Jeppesen's [2]rotaxanes[727] **R246o^{4+}** and **R246p^{4+}** possess no polyether linkers, and therefore none of the [C–H···O] hydrogen-bonding interactions that typically play a significant role in templation. (e) The functionally rigid [2]rotaxane[730] **R246q^{4+}**, which possesses two naphthyl π-donors, adopts[732] an interdigitated columnar superstructure that is stabilized by continuous D–A π–π stacking. The tubular representations are shown with hydrogen atoms, PF_6^- counterions, and solvent molecules omitted for the sake of clarity.

(**R246e^{4+}–R246i^{4+}**), DNP[724–727] (**R246j^{4+}–R246o^{4+}**), and BPTTF[727] (**R246p^{4+}**) units, as well as a few axles possessing a pair of degenerate π-donors—namely bis(hydroquinoyl) tetraethylene glycol[723,728,729] ($HQ_2$4EG), bis-5-(-1-oxynaphtho)butadiyne[730] (NPC_4NP), and bis-5-(1-oxynaphtho) phenylene ethynylene[731] (NP2PE). In general, the CBPQT^{4+} rings clip more efficiently around DNP donors than HQ, most likely because DNP is a better π-electron donor. This rule is not universal however, since **R246p^{4+}** is obtained in lower yield than **R246o^{4+}**, in spite of the fact that the former's BPTTF unit is a better π-donor than the latter's DNP unit. Rotaxanes containing the $HQ_2$4EG motif are obtained in higher yields than their counterparts based on a single HQ unit, an observation which suggests that both HQ units particpate favorably in templating interactions, most likely by way of the dumbbell adopting a folded conformation that allows *both* HQ units to engage in stabilizing D-A π–π interactions with the BIPY^{2+} dications present in the transition state.

Linker length. CBPQT^{4+} rings have been clipped successfully around dumbbells containing 0–3 ethylene glycol repeating units in between the stoppers and the π-donor unit(s). Comparing, for example, compounds **R246j^{4+}** and **R246k^{4+}**, which differ only in their linker length, the rotaxane possessing triethylene glycol (3EG) linkers is generated much more efficiently (72%) than is the one (32%) possessing diethylene glycol (2EG) linkers at ambient temperature and pressure. Likewise, the DNP-based [2]rotaxanes **R246m^{4+}** and **R246n^{4+}**, which contain 2EG linkers, are obtained in much higher yields (>60%) than is the linker-free [2]rotaxane **R246o^{4+}** (27%) under similar high-pressure conditions. These results can be rationalized by the fact that longer linkers engage more effectively in [C–H···O] interactions with the acidic BIPY^{2+} protons of CBPQT^{4+}, and also because longer linkers help relieve steric crowding on the part of the stoppers near the site of templation. Recalling from the beginning of **Section 2.3.3.2** that the stabilizing contributions from [C–H···O] interactions can outweigh[508] substantially those arising from D-A π–π stacking interactions in these systems, Jeppesen[727] proved that these interactions are not mandatory for preparing D-A MIMs. Since **R246o-p^{4+}** do not contain polyether linkers (**Figure 2.37c–d**), their synthesis must be templated almost entirely by π–π and D-A CT interactions.[727]

Stoppers. The dumbbell's stoppers can also command a major influence over the outcome of a clipping reaction, especially if they interact by way of π–π interactions. For example, the adamantyl-stoppered HQ/CBPQT^{4+} rotaxanes **R246e^{4+}** and **R246h^{4+}** are obtained[719,722] in 6–10% yield, whereas the anthracene-stoppered homologue **R246g^{4+}** is isolated[729] in 25% yield. A similar comparison underlies the the degenerately bistable [2]rotaxanes **R236a-d^{4+}** possessing the $HQ_2$4EG motif. [723,728,729] Evidence for the anthracene unit's ability to engage in these 'alongside' interactions can be found (**Figure 2.37a**) in the solid-state structure of **R246g^{4+}**. For the sake of comparison, the $^{i}Pr_3Si$ stoppers of **R246k^{4+}** do not interact[724] (**Figure 2.37b**) alongside of CBPQT^{4+}.

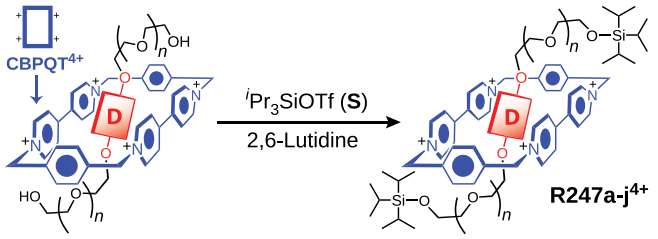
Conditions. Of course, experimental factors such as concentration and stoichiometry, as well as solvent, pressure, time, and temperature can influence the outcome of a reaction. These reactions are almost always carried out

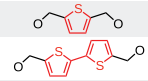
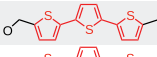
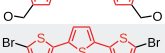
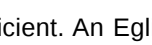
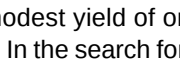
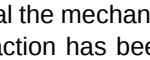
with an excess of either the CBPQT^{4+} precursors (XyR_2) or the dumbbell. In general, reaction times are slow (≥1 week), but the clipping rates can be accelerated and yields can be improved by operating at high pressure (10–12 kbar). Under ambient conditions, MeCN often makes a better choice of solvent than DMF because it has a lower propensity to interfere with templating interactions by donating nonbonding electrons. In some cases, $AgPF_6$ is introduced in MeCN in order to prevent the Br^- salts of BIPY^{2+} derivatives from precipitating, which also improves yields. For the most part, it is apparent that the CBPQT^{4+} clipping reaction is less efficient in the case of rotaxanes (**Table 2.16**) than it is in the case catenanes (**Table 2.9** in **Section 2.3.3.2**), highlighting the importance of the 'alongside' interactions. Although most clipping protocols are carried out under ambient conditions, the catenane advantage is particularly apparent at elevated temperatures. Whereas the catenation of crown ethers with CBPQT^{4+} can be accelerated to reach completion within an hour without sacrificing high yields at 80 °C, no rotaxanation of an elongated homologue of **L246m** was observed[554] under the same conditions.

Supermolecules and mechanomolecules incorporating CBPQT^{4+} rings are often relatively easy to crystallize on account of the presence of ions and counterions, as well as the cyclophane's high symmetry. In addition to the rotaxanes described already, the solid-state structure[732] of **R246q^{4+}** is noteworthy because it adopts (**Figure 2.37e**) an unusual interdigitated superstructure in the solid state, in which the rotaxanes are stacked and staggered in an antiparallel manner, such that continuous D-A-D-A π–π stacking can take place between the BIPY^{2+} units of the rings and the unencircled halves of the dumbbells' NPC_4NP units. The long-range ordering, which is attributable to a combination of bistability, mechanical bonds, and functional rigidity, indicates that the noncovalent interactions underpinning the templation of mechanical bonds can be harnessed, not only to design novel *intramolecular* interactions, but *intermolecular* self-assembly as well.

It was not until 1992 that stoppering reactions began[500] to be utilized in the transformation of D-A pseudorotaxanes into rotaxanes. Since the CBPQT^{4+} rings are fully formed at the outset, these template-directed stoppering protocols benefit from the full thermodynamic binding of the CBPQT^{4+} rings to their corresponding recognition units. In the beginning, the main stoppering protocol (**Table 2.17**) involved silylation of a pseudorotaxane's terminal OH functions with triisopropylsilyl groups in the presence of 2,6-lutidine, affording [2]rotaxanes such as **R247a^{4+}–R247j^{4+}**. This stoppering protocol has been applied to the synthesis of [2]rotaxanes with hydroquinone,[500] *para*-phenylenediamine,[705] benzidine,[704,705] and biphenol[704] recognition units. It should be added that Ikeda[706,733,734] has employed the silylation procedure in the synthesis of D-A [2]rotaxanes with oligothiophene recognition units, as well as a blue-colored difluorobenzidine (BZF_2)-based [2]rotaxane. With yields ranging from 5 to 43%, silylation as a stoppering protocol is not particularly

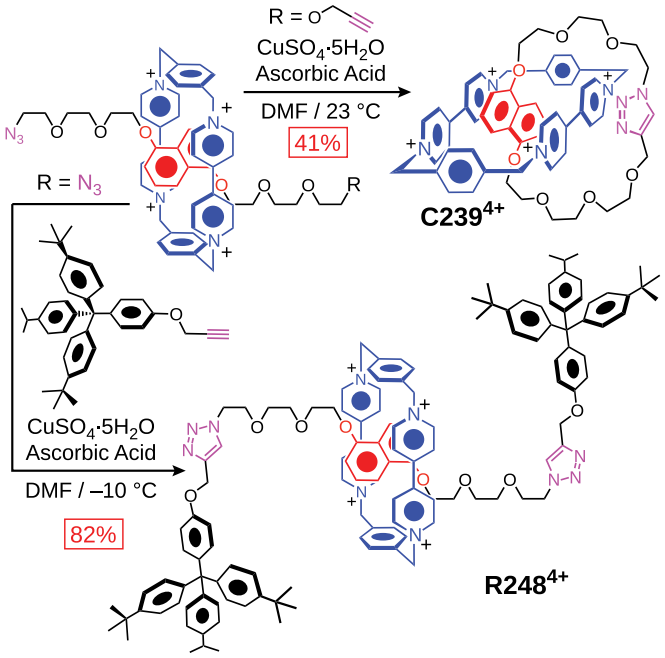
Table 2.17 Summary of stoppering protocols for making CBPQT^{4+}-based D-A rotaxane with triisopropylsilyl groups.



R247^{4+}		*n*	Solvent	Equiv [ring]	Equiv D	Equiv S	Equiv Lutidine	*T* °C	*t* h	Yield %	Ref
a		1	MeCN	1	3	7.5	7.5	RT	1	22	500
		2	MeCN	1	3	7.5	7.5	RT	1	22	500
b		2	MeCN	1	3	7	7	RT	48	43	705
c		2	MeCN	1	3	8	8	RT	12	39	704
d		3	DMF	1	2,8	25	56	RT	36	39	706
e		2	DMF	1	3	8	8	RT	12	5	704
f		1	MeCN	1	2	10	24	RT	1.5	12	733
g		1	MeCN	1	2	10	24	RT	1.5	15	733
h		1	MeCN	1	2	10	24	RT	1.5	17	733
i		1	MeCN	1	1.1	3.7	4.3	RT	1	26	734
j		1	MeCN	1.1	1	4.0	4.6	RT	1.5	11	734

efficient. An Eglinton-Glaser-Hay coupling has also been utilized[732] to stopper CBPQT^{4+} [2]rotaxane, but also in a modest yield of only 18%.

In the search for more efficient organic transformations to seal the mechanical bond, the now-ubiquitous CuAAC click reaction has been particularly transformative as a tool for synthesizing donor-acceptor rotaxanes.[399–402] The CuAAC reaction was introduced[404,405] into D-A MIM chemistry in 2006, contemporaneously with the first applications of CuAAC to MIMs prepared by transition metal[406] and active metal[403] templates. The seminal synthesis (**Scheme 2.64**) of the [2]rotaxane **R248^{4+}**, wherein the thread comprises a DNP recognition unit appended to azide-terminated triethylene glycol loops, proceeds[404] to near completion (82% yield) in the presence of a propargylated tetraphenylmethane stopper and $CuSO_4$/ascorbic acid in DMF at –10 °C. The seminal CuAAC click catenation (**Scheme 2.64**) was accomplished[405] in the same year by allowing the Cu^I-catalyzed triazole linkage to couple the two ends of a DNP-polyether axle. The yield of **C239^{4+}** is lower (41%) in this case, most likely because oligomerization of the thread competes with macrocyclization. This click stoppering protocol has been utilized in the preparation of branched[404,735,736] [3]- and [4]rotaxanes, many bistable molecular shuttles (**Section 5.1.1**) and switches (**Sections 6.1.1–6.1.2),** as well as a number of more sophisticated topologies (**Section 4.1**) and architectures (**Section 4.2**), including oligorotaxanes, mechanically bonded foldamers, and daisy chains.



Scheme 2.64 The seminal CuAAC click syntheses of the π-associated donor-acceptor [2]rotaxane[404] **R247**$^{4+}$ and the [2]catenane[405] **C239**$^{4+}$.

2.3.3.9 Other π-Accepting Molecular Boxes

The rectangular framework of the little blue box has been gradually expanded over the years into a large "meccano set" (**Figure 2.38**) of π-acceptors and linkers, which can be substituted for the BIPY^{2+} recognition units and *p*-xylylene linkers, respectively, of the CBPQT^{4+} ring. Alternative linkers include those based on *meta*-phenylenes,[525,550,737–740] biphenylenes,[741] naphthalenes,[725,737,742] binapthyl,[548,743–745] anthracenyl,[746] pyridyl,[747,748] bipyridyl,[749] thiophenes,[750] dibenzofurans,[751] 1,2,4-triazoles,[752] polyethers,[744,753] dibenzylammoniums,[754] various dialkoxy π-donors,[755–758] bipyridinium derivatives,[740,759] and oligomethylene chains.[760] The blue box framework has also been modified such that one or both of the *para*-phenylene linkers are functionalized with esters,[746,761–764] imides,[765–768] halides,[715] ethers,[715] azides,[769] and alkynes.[770] Although many of these functional groups provide useful synthetic handles for constructing new architectures or immobilizing MIMs on surfaces, in most cases the replacement or derivatization of the *para*-phenylene spacer reduces[715] the corresponding cyclophane's affinity for guests relative to that of CBPQT^{4+} itself.

Another option for creating π-accepting cyclophanes inspired by CBPQT^{4+} is to replace one or both of its BIPY^{2+} recognition units with a different π-acceptor. Alternative π-acceptors which have been incorporated into the CBPQT^{4+} framework include diazapyrenium,[495] bis(pyridinium) ethylene,[558,739,771,772] azopyridinium and hydrazopyridinium,[773] bipicolinium (BPIC^{2+}),[759] and a series (*vide infra*) of extended viologens,[774–779] the latter of which are known[778] as "ExBox" cyclophanes.

Neutral π-acceptors, such as PMDI and NDI, can also be incorporated[780,781] into the blue box framework. Liu[780–782] has developed a group of D-A [2]catenanes (**C240a**$^{2+}$**–C240e**$^{2+}$) with desymmetrized cyclophanes comprising one BIPY^{2+} unit and one neutral diimide (PMDI or NDI) unit as the π-acceptors. These catenanes are obtained (**Figure 2.39**) by a clipping protocol involving the cyclization of neutral bis(bromoxylyl)-functionalized PMDI or NDI precursors with

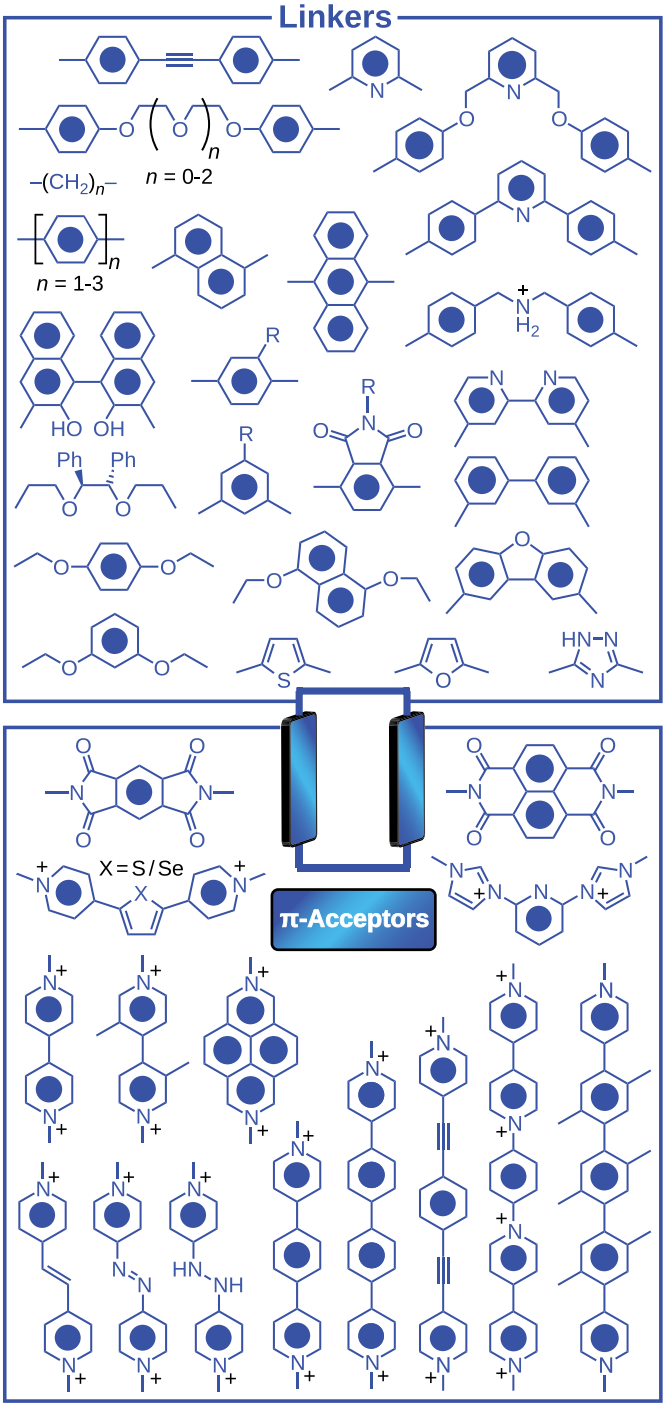
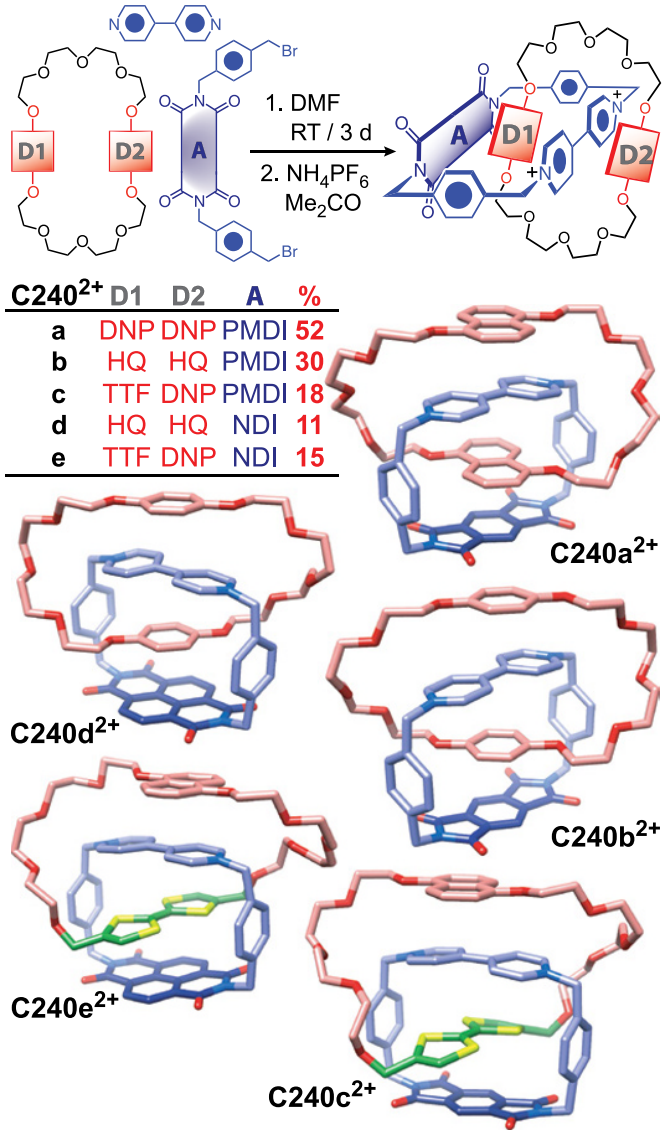


Figure 2.38 The molecular meccano set of π-acceptors and linkers employed in the construction of electron-poor receptors related to the "little blue box".



C240^{2+}	D1	D2	A	%
a	DNP	DNP	PMDI	52
b	HQ	HQ	PMDI	30
c	TTF	DNP	PMDI	18
d	HQ	HQ	NDI	11
e	TTF	DNP	NDI	15

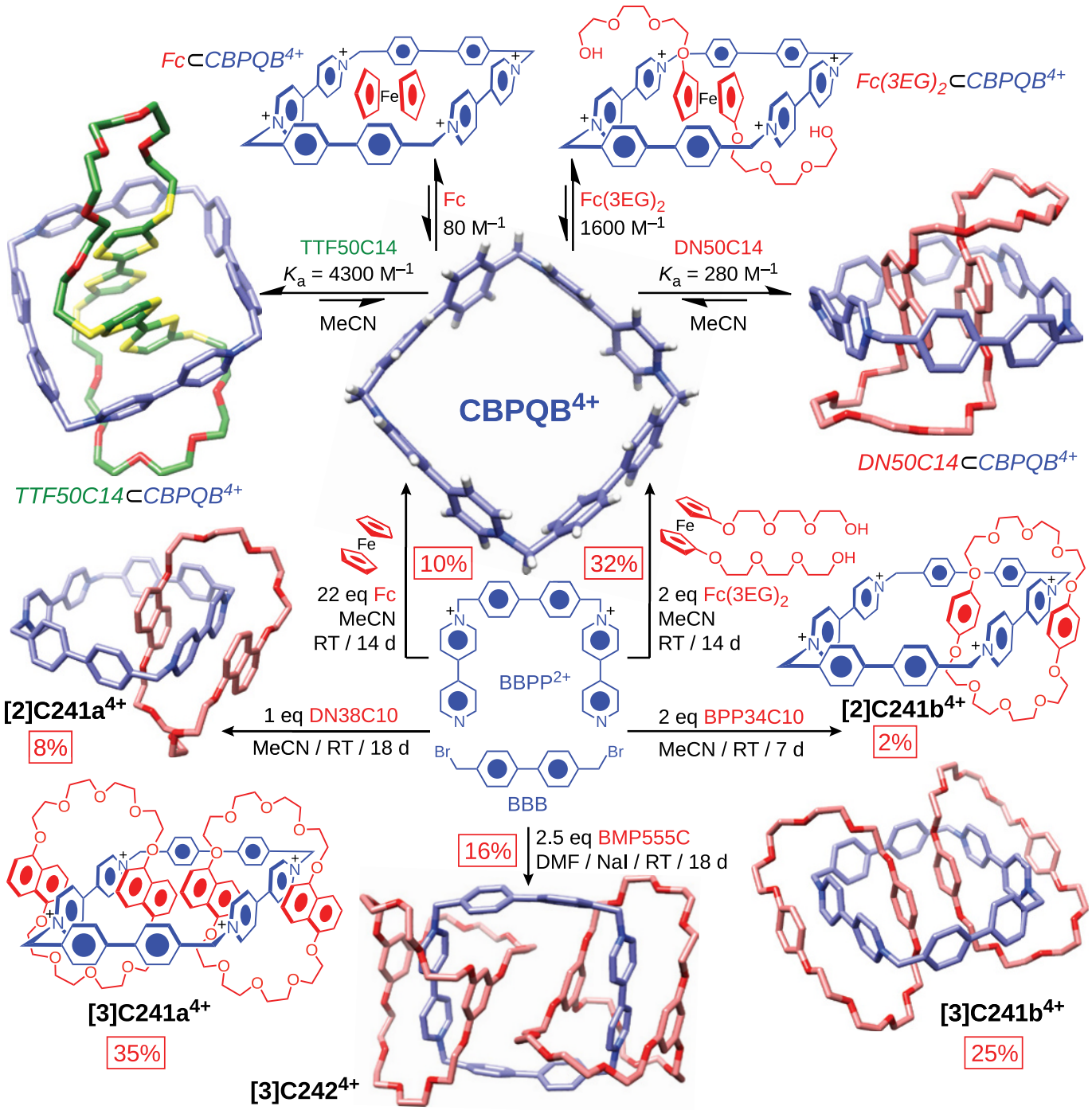
Figure 2.39 Synthesis and tubular representations of the solid-state structures of Liu's desymmetrized [2]catenanes[780,781] **C240a^{2+}–C240e^{2+}**.

bipyridine in the presence of an appropriate crown ether. In general, the yields (11–30%) are lower than those (43–53%) for the corresponding CBPQT^{4+} catenanes, except in the case (52%) of the [2]catenane **C240a^{2+}**, which comprises a DN38C10 π-donating ring and a π-accepting cyclophane with BIPY^{2+} and PMDI recognition units. The solid-state structures (**Figure 2.39**) of the catenanes are not dissimilar to their CBPQT^{4+}-based counterparts, with the expected D-A π–π stacking interactions and [C–H···O] interactions stabilizing each co-conformation. The neutral recognition sites reside outside the cavity of the crown ether in all cases.

The "Big Blue Box" CBPQB^{4+}—A Tetracationic Square

The tetracationic cyclophane cyclobis(paraquat-4,4′-biphenylene)[783] (CBPQB^{4+}) is a square-shaped host in which the two BIPY^{2+} recognition units are separated by 4,4′-bitolyl instead of *para*-xylyl spacers, leading to a doubling in width of the host's cavity from 3.5 to 7 Å (accounting for van der Waals radii) in comparison with CBPQT^{4+}. Consequently, CBPQB^{4+} is capable of hosting two π-donors within its cavity. The CBPQB^{4+} ring first appeared[741] in the literature in 1991 as the central π-accepting ring of a [3]catenane, the synthesis (**Scheme 2.65**) of which relied on the clipping of the CBPQB^{4+} precursors bitolyl-bis(4-pyridyl)pyridinium (BBPP^{2+}) and 4,4′-bis(bromomethyl)-1,1′-biphenyl (BBB) around either DN38C10 or BPP34C10, affording[784] the [3]catenanes **[3]C241a^{4+}** and **[3]C241b^{4+}** in up to 25 and 35% yield, respectively. It was not until 1996, five years after the [3]catenanes were introduced, that the CBPQB^{4+} ring was finally isolated[785] and characterized[783,786] on its own and in host-guest complexes. The HQ- or DNP-templated synthesis of CBPQB^{4} presents a challenge because it would require the formation of a ternary complex. This templating problem has been circumvented[785] by introducing (**Scheme 2.65**) ferrocene (Fc) and triethylene glycol-appended ferrocene, Fc(3EG)$_2$, as templates in the cyclization of CBPQB^{4+}. The cyclopentadienyl rings of Fc are separated by 3.3 Å, which is close to the 3.6 Å separation between HQ units in the solid-state structure (**Scheme 2.65**) of the [3]catenane **[3]C241b^{4+}**, rendering it a more suitable template. CBPQB^{4+} is obtained in yields of 10 and 32% from the BBPP^{4+} and BBB precursors in the presence of an excess of Fc and Fc(3EG)$_2$, respectively. Ferrocene compounds Fc and Fc3EG$_2$ also self-assemble (**Scheme 2.65**) with CBPQB^{4+} into pseudorotaxanes in a 1:1 stoichiometry, with association constants of 80 and 1600 M^{-1}, respectively, at 25 °C in CD$_3$CN. The only other compounds which are known[787] to bind (**Scheme 2.65**) CBPQB^{4+} in a 1:1 fashion are π-donating crown ethers with two recognition units such as bis-1,5-dioxynaphtho[50]crown-14 (DN50C14) and its TTF-based homologue bis-tetrathiafulvalene[50]crown-14 (TTF50C14), which form ring-in-ring complexes that exhibit K_a values of 280 and 4300 M^{-1}, respectively.

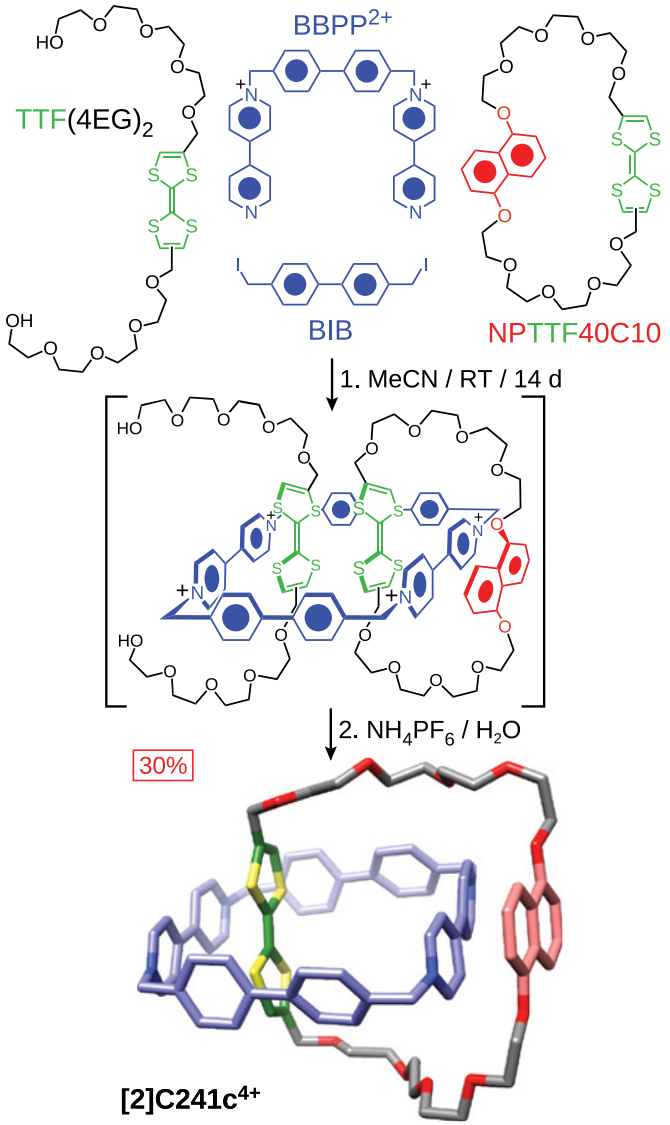
Owing to its proclivity for hosting two guests in the form of a ternary complex, the CBPQB^{4+} ring is not readily converted into [2]catenanes and [2]rotaxanes. The [2]catenane **[2]C241a^{4+}**, which comprises CBPQB^{4+} and DN38C10 rings, has been isolated[784,788] as a minor byproduct (up to 8% yield) of the clipping reaction (**Scheme 2.65**) that produces the [3]catenane **[3]C241a^{4+}** in 35% yield. Likewise, the BPP34C10/CBPQB^{4+} [2]catenane **[2]C241b^{4+}** is obtained (**Scheme 2.65**) in 2% yield, along with **[3]C241b^{4+}** as the major (25%) product. One exception[789] is the synthesis (**Scheme 2.66**) of the [2]catenane **[2]C241c^{4+}**, which is obtained in up to 30% yield after clipping the larger 4,4′-bis(iodomethyl)-1,1′-biphenyl (BIB) and BBPP^{2+} compounds around naphthotetrathiafulvalene[40]crown-10 (NPTTF40C10) as the template. Employing an additional TTF-based thread as an additive enhances the yield because it can occupy one of the binding pockets of CBPQB^{4+}, reducing the probability of a competing process in which two crown ether rings are



Scheme 2.65 Host-guest complexes[785,787] and catenanes[653,741,784,788] based on the $CBPQB^{4+}$ molecular square. Note that each reaction leading to $CBPQB^{4+}$ or $CBPQB^{4+}$ catenanes is followed by a counterion exchange with aqueous NH_4PF_6 (not shown). Tubular representations of solid-state structures are depicted with protons, solvent molecules, and counterions omitted for the sake of clarity.

captured to afford a [3]catenane. The yield of **[2]C241c^{4+}** is reduced to 17% in the absence of the surrogate acyclic TTF template. The solid-state structure of **[2]C241c^{4+}** reveals an empty binding pocket within the $CBPQB^{4+}$ cavity, which is capable of hosting an additional guest. See **Section 6.13.11** for a discussion of the redox-controlled binding properties of this topologically linked host. $CBPQB^{4+}$ can serve as a 'molecular flask' for stabilizing weak interactions such as spin-paired radical dimers and mixed-valence radical dimers.

The ability of the $CBPQB^{4+}$ ring to accommodate two other catenated rings has made it an important building block for the construction (**Section 4.1.2**) of higher order links and chains. Huang[653] has also taken advantage of this feature to prepare (**Scheme 2.65**) the cryptand-based [3]catenane **[3]C242^{4+}**.



Scheme 2.66 Optimization of the yield of a CBPQB^{4+} [2]catenane through the use of a surrogate template in combination with a crown ether ring during clipping.[789] The tubular representation of the solid-state structure of the [2]catenane **[2]C241c^{4+}** is shown with protons, solvent molecules, and counterions omitted for the sake of clarity.

Ex^{n}Box^{4+}

The recent advent[774–779] of extended viologen boxes, Ex^{n}Box^{4+}, has brought with it the opportunity to construct[777,790] mechanomolecules out of ever larger recognition units on account of the longer dimensions of their cavities. The cavity sizes of CBPQT^{4+}, ExBox^{4+}, and Ex^{2}Box^{4+}, are compared in **Figure 2.40**. Taking into account the van der Waals radii, the width of the cavity within each molecular box is approximately 3.5 Å, which is an ideal width for encapsulated aromatic guests to engage in π–π stacking interactions with both of the dicationic recognition units. The length of the cavity increases with each extension of the viologen recognition units, from 7.1 Å for CBPQT^{4+} to 11.3 Å for ExBox^{4+} and 15.5 Å for Ex^{2}Box^{4+}.

ExBox^{4+} has an extraordinary ability[774,791] to recognize polycyclic aromatic hydrocarbons (PAHs). Single crystals of 12 *PAH⊂ExBox^{4+}* host-guest complexes have been characterized (**Figure 2.41**) by X-ray crystallography. The crystals appear in a wide range of colors on account of different D-A charge-transfer interactions between ExBox^{4+} and various guests. PAHs ranging in size from azulene (10 π-electrons) to coronene (24 π-electrons) have been investigated as guests for ExBox^{4+}. The corresponding solid-state superstructures reveal that some of these PAHs—namely, tetracene, tetraphene, chrysene, and helicene—cannot fit within the ExBox^{4+} cavity along their longest axis, forcing them to tilt off-axis with respect to the extended viologen recognition units of the host. The PAH guests whose outer van der Waals surfaces span less than 11.3 Å along their longest axes can rotate 360° without needing to withdraw from the ExBox^{4+} cavity. Among these compounds—namely, azulene, anthracene, phenanthrene, pyrene, triphenylene, perylene, coronene—the K_a values increase (**Figure 2.42**) exponentially with the π-electron count of the PAH. On account of its promiscuous PAH binding, ExBox^{4+} as its Cl^{-} salt can extract many PAHs from crude oil into an aqueous phase for recovery and purification purposes.

In addition to PAHs, ExBox^{4+} can host porphyrins—see **Section 3.2.1.2** and **6.3.2** for a discussion of the synthesis and pH-switchability of a porphyrinic ExBox^{4+} [2]catenane.[790] Furthermore, Scherman[792] has discovered that the Cl^{-} salt of ExBox^{4+} can accommodate dicationic perylene diimide (PDI) derivatives with K_a values of up to 1.3 × 10^{6} M^{-1} in water—a surprisingly high value considering the fact that both host and guest are cationic π-acceptors, which suggests that the hydrophobic effect and dispersion forces drive self-assembly in this case.

In cases of longer extended viologen units—such as that[775] of the biphenylene extension in Ex^{2}Box^{4+}—regions of relatively high electron density exist (**Figure 2.43**) around

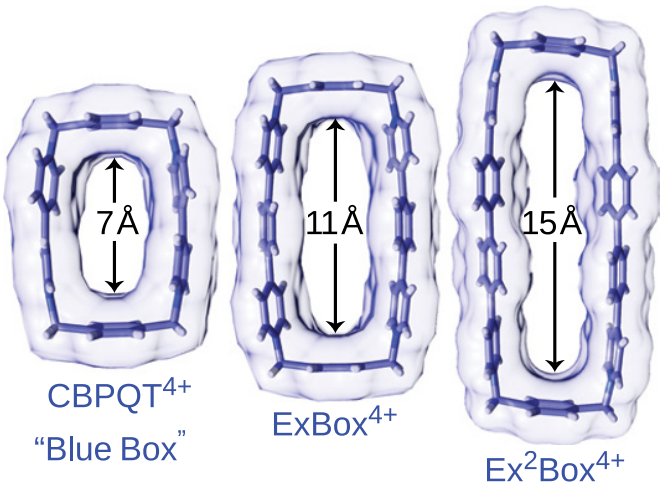


Figure 2.40 A comparison of the cavity sizes of the solid-state structures of CBPQT^{4+},[690] ExBox^{4+},[774] and Ex^{2}Box^{4+}.[775] All three cyclophanes share approximately the same inner width of 3.5 Å, accounting for the van der Waals radii.

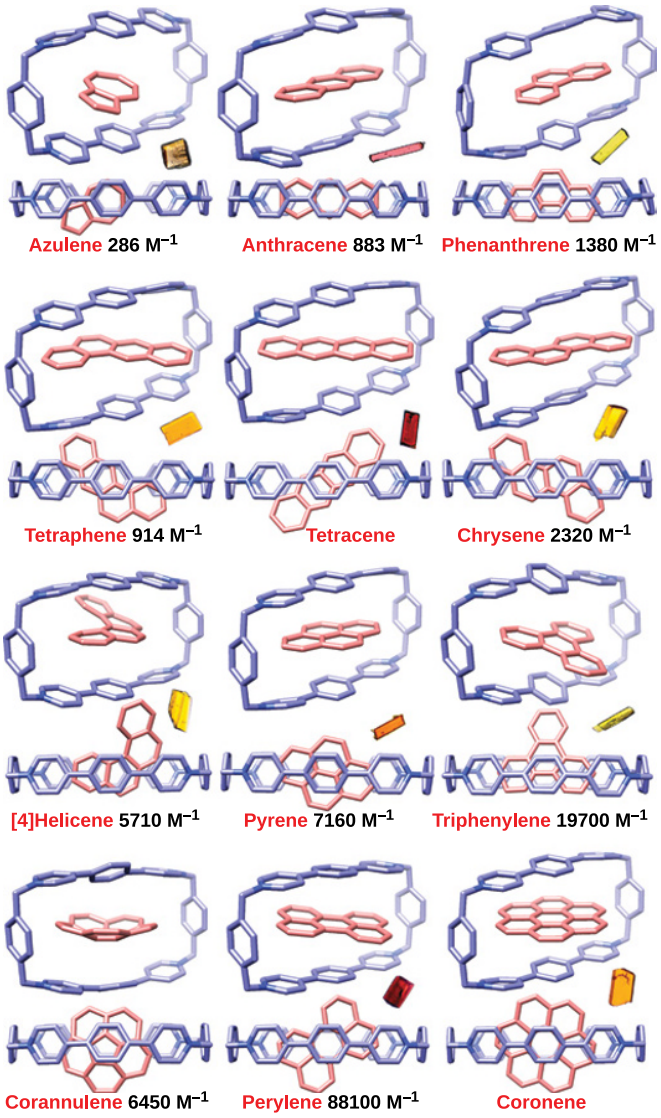


Figure 2.41 The promiscuity of ExBox^{4+} in the recognition of polycyclic aromatic hydrocarbons.[774,791] Tubular representations of the solid-state superstructures are depicted with protons, counterions, and solvent molecules omitted for the sake of clarity. Crystals are pictured to convey their colors, attributable to CT interactions. Association constants, K_a, are listed for these complexes in MeCN at 25 °C. ^{1}H NMR titrations were employed to determine K_a values for azulene, anthracene, chrysene, triphenylene and perylene, while isothermal titration calorimetry (ITC) was employed to determine K_a values for phenanthrene, pyrene, tetraphene, [4]helicene, and corannulene. K_a values for tetracene and coronene could not be measured on account of low solubility issues in MeCN.

the central spacers, where the inductive effects of the pyridinium cations are less significant than in the case of the *para*-phenylene spacer of ExBox^{4+}. This situation leads to an unusual type of A-D-A hybrid cavity in Ex^{2}Box^{4+} with multiple binding pockets that can be differentiated according to their recognition motifs. The electron-poor ends of the cavity interact with π-donors in a manner analogous to that of CBPQT^{4+}. Compounds such as anthracene and pyrene bind Ex^{2}Box^{4+} in a 1:1 stoichiometry, yet they remain

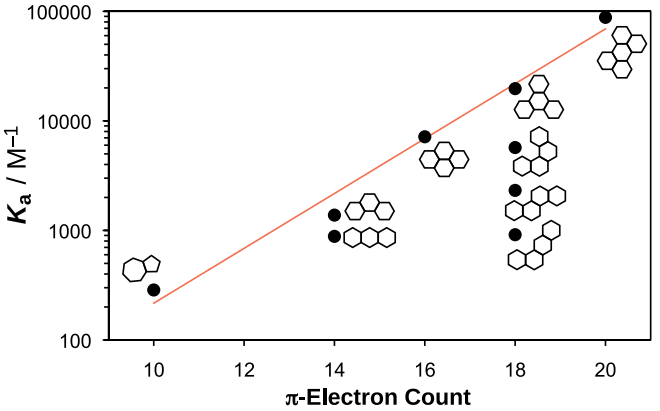


Figure 2.42 Logarithmic plot of the association constants, K_a, of *PAH⊂ExBox*$^{4+}$ host-guest complexes in MeCN as a function of the PAH π-electron count, revealing an exponential relationship, except in cases where the PAHs do not fit lengthwise inside the ExBox^{4+} cavity.[774]

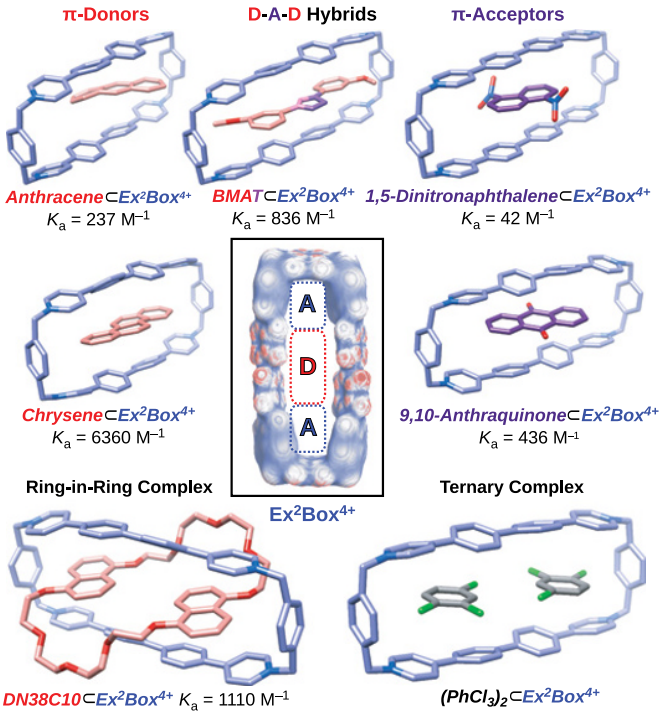


Figure 2.43 The diverse binding modes[775] of Ex^{2}Box^{4+}. An electron density map (inset) of the cyclophane reveals regions of relatively low electron density (blue) near each end of the cavity, while the *para*-phenylene spacers of the extended viologen units provide a region of higher electron density (red) in the center. The electron-poor binding pockets can be occupied by π-donors, while the central electron-rich pocket can accommodate π-acceptors. Other modes include ring-in-ring and ternary complexes, as well as D-A-D hybrid guests such as bis(*m*-anisole)triazole (BMAT), which engages all three binding pockets of the Ex^{2}Box^{4+} cavity. Tubular representations of the solid-state superstructures are shown with protons, solvent molecules, and counterions omitted for the sake of clarity.

localized on one end of the cavity in the solid state and exhibit lower K_a values (237 and 172 M^{-1}, respectively) in comparison to $ExBox^{4+}$ (883 and 7160 M^{-1} , respectively) at 25 °C in MeCN. On the other hand, PAHs that cannot fit lengthwise inside of $ExBox^{4+}$, such as chrysene, tetraphene, and tetracene, are easily accommodated in Ex^2Box^{4+}. Accordingly, the K_a values of *tetraphene⊂Ex²Box⁴⁺* (1460 M^{-1}) and *chrysene⊂Ex²Box⁴⁺* (6360 M^{-1}) are higher than those of *tetraphene⊂ExBox⁴⁺* (914 M^{-1}) and *chrysene⊂ExBox⁴⁺* (2320 M^{-1}) at 25 °C in MeCN. Like the $CBPQB^{4+}$ molecular square, the cavity of Ex^2Box^{4+} is also large enough to accommodate two π-donors—a ternary *(trichlorobenzene)₂⊂Ex²Box⁴⁺* complex, as well as a *DN38C10⊂Ex²Box⁴⁺* ring-in-ring complex (1110 M^{-1}) have been characterized in solution and in the solid state by X-ray crystallography. Most unusually, Ex^2Box^{4+} can bind π-acceptors such as 2,6-dinitrotoluene (22 M^{-1}), 1,5-dinitronaphthalene (42 M^{-1}), 9,10-anthraquinone (463 M^{-1}), and 1,4-anthraquinone (825 M^{-1}) within its central pocket of higher electron density. Whereas the π-donors are stabilized by CT interactions with pyridinium subunits of Ex^2Box^{4+}, the π-acceptors are stabilized mainly by van der Waals interactions, since there is no evidence for CT interactions with the biphenylene subunits of Ex^2Box^{4+}. In the knowledge of the hybrid A-D-A pattern of the binding pocket in Ex^2Box^{4+}, one can design complementary hybrid D-A-D guests such as 1,4-bis(*meta*-anisole)-1*H*-1,2,3-triazole (BMAT), which interacts with all three binding pockets, leading to a relatively high K_a value of 836 M^{-1}. This latter motif appears promising for the construction of Ex^2Box^{4+}-based MIMs—although none have yet been reported—on account of its amenability to click chemistry and pseudorotaxane-like geometry in which the two methoxy groups are directed out from opposite ends of the cyclophane's cavity.

It is possible to construct even larger Ex^nBoxes possessing viologen extensions (see **Figure 2.38**), such as *p*-terphenylene[776]—hexamethylated for sake of solubility, which dramatically lowers its affinity for guests—as well as bis-*p*-phenylene-ethynylene spacers, which lend themselves to a high-yielding preparation of the corresponding host, $Ex^{2.2}Box^{4+}$.[778] The structural formula of $Ex^{2.2}Box^{4+}$ is included among a collection of π-accepting receptors illustrated in **Figure 2.44**. These hosts currently have only limited involvement in MIM synthesis, yet appear promising on account of their ability to self-assemble with π-donors into host-guest complexes. Other members of the Ex^nBox^{4+} family of tetracationic cyclophanes include the heterocycle-extended $TExBox^{4+}$, $SeExBox^{4+}$, which possess (**Figure 2.44**) thiophene and selenophene viologen extension units, respectively. When hosting guests derived from perylene diimide, photoinduced energy transfer between the host and guest is ultrafast and quantitative.[777] Enlarging the Ex^nBox^{4+} framework in the orthogonal direction, $ExBox_2^{4+}$ is derived (**Figure 2.44**) from the same 4,4′-bitolyl linker as that of the big blue box, $CBPQB^{4+}$. The wide cavity of $ExBox_2^{4+}$ allows it to accommodate C_{60} as part of a 1:1 incusion complex,[779] which may be processed into

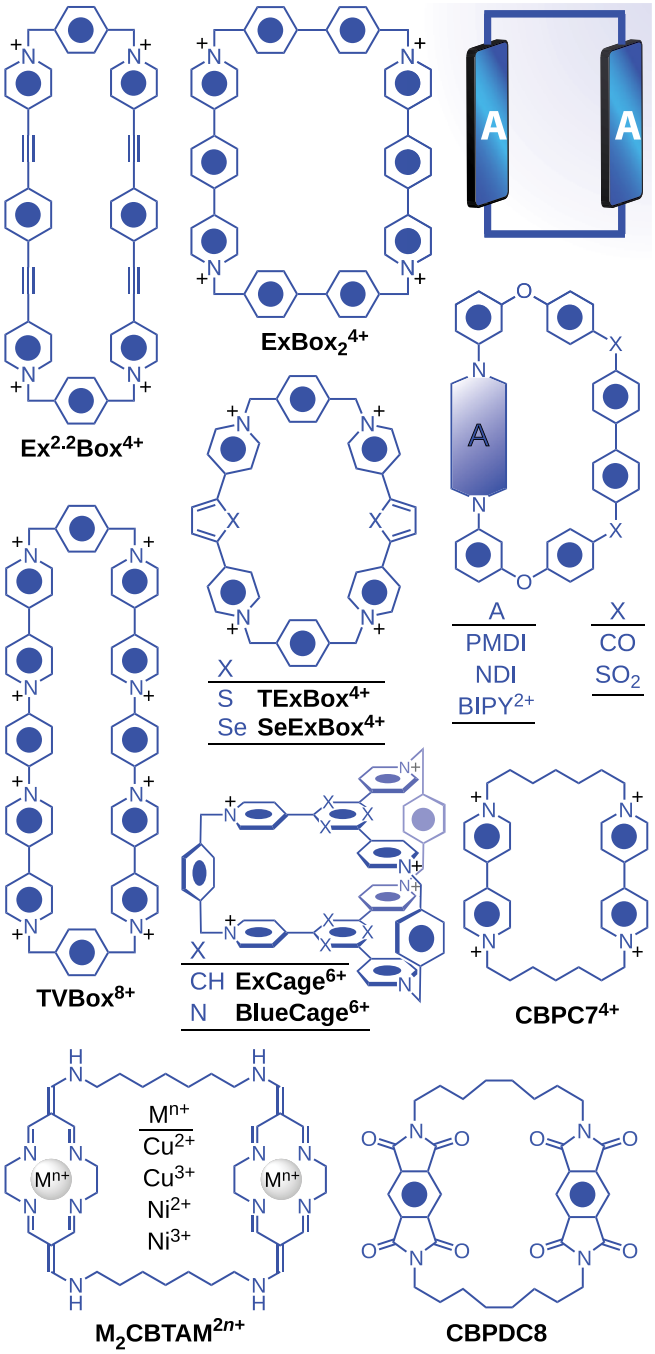


Figure 2.44 More π-accepting hosts that are suitable for the template-directed synthesis of D-A MIMs include the pyridinium-based hosts, $Ex^{2.2}Box^{4+}$, $ExBox_2^{4+}$, $TVBox^{8+}$,[793] $TExBox^{4+}$ / $SeExBox^{4+}$, $ExCage^{6+}$,[794] $BlueCage^{6+}$,[795] $CBPC7^{4+}$,[760] receptors (M_2CBTAM^{2n+}) based on π-accepting tetraazamacrocyclic chelates,[796–798] the neutral PMDI-based macrocycle CBPDC8,[782] as well as a number of macrocyclic ketones[803] and sulfones[800–802] possessing $BIPY^{2+}$, NDI, or PMDI recognition units.

semiconducting single crystals comprising columnar arrays of these host-guest assemblies.

Another recent addition[793] to the family (**Figure 2.44**) of extended viologen boxes is the octacationic tetraviologen box ($TVBox^{8+}$), which binds the π-donating crown ether

DN38C10 to form a ring-in-ring complex with K_a values on the order of 10^3 M^{-1} in MeCN—an observation that bodes well for the design of novel topologies and architectures.

Three-DImensional Boxes

A cryptand-like homologue of $ExBox^{4+}$, the so-called $ExCage^{6+}$ (**Figure 2.44**), was reported[794] recently. $ExCage^{6+}$ exhibits a much higher affinity for PAHs than does $ExBox^{4+}$, and some of the highest known association constants for D-A host-guest complexes in general—the K_a value of *coronene⊂ExCage*$^{6+}$, for example, has been estimated to be $>10^7$ M^{-1} in MeCN at 25 °C. The molecular recognition properties of $ExCage^{6+}$ confirm that the cryptand (macrobicyclic) effect,[360–362] which predicts that three-dimensional host geometries lead to increased binding strengths and selectivities, is valid not only for polyether hosts, but also for rigid multicationic ones. A related hexacationic host, known[795] as $BlueCage^{6+}$, which possesses (**Figure 2.44**) electron-poor triazine units as the central connectors, also exhibits high affinities for PAHs, yet the K_a value of 4.93×10^5 M^{-1} for *pyrene⊂BlueCage*$^{6+}$ is slightly lower than that (6.77×10^5 M^{-1}) of *pyrene⊂ExCage*$^{6+}$ because the PF_6^- counterions of $BlueCage^{6+}$ compete for the cage's cavity as a result of stabilizing anion–π interactions. On the other hand, the tetrakis(pentafluorophenyl)borate ($BArF^-$) counterions of BlueCage·6BArF are too bulky for this interaction, increasing its affinity for pyrene ($K_a = 3.95 \times 10^6$ M^{-1}) by one order of magnitude, which is substantially higher than the corresponding *pyrene⊂ExCage·6BArF* complex ($K_a = 6.0 \times 10^5$ M^{-1}) at 25 °C in MeCN.

Non-Viologen Cyclophane π-Accepting Hosts

Korybut-Daszkiewicz[796] and co-workers at Warsaw University have investigated the host-guest properties of cyclobis(tetraazamacrocycles) (CBTAM), the π-accepting recognition units of which comprise (**Figure 2.44**) copper or nickel chelates in various redox states, The macrocycle *$(Ni^{II})_2$⊂CBTAM*, can host[797] electron-rich guests such as HQ, DNP, and TTF with association constants on the order of 10^2 M^{-1} in CD_3CN, as well as a charge-neutral Ni^{2+}/tetraazamacrocycle^{2-} guest.[798] The inverse recognition system comprising receptors with neutral tetraazamacrocyclic complexes and cationic tetraazamacrocyclic guests has also been introduced by the Warsaw team.[799] These pseudorotaxanes are viable forerunners for rotaxanes and catenanes in the future.

Colquhoun[800–803] has developed a series (**Figure 2.44**) of macrocyclic sulfone and ketone π-acceptors which incorporate π-accepting units (PMDI, NDI, $BIPY^{2+}$) into their backbones. Although these rings assemble[802] into pseudorotaxane complexes with electron-rich guests such as pyrene and perylene with association constants of up to ~10^3 M^{-1} in 6:1 $CHCl_3$–HFP (HFP = hexafluoro-2-propanol), they have not yet been utilized in the making of mechanical bonds.

A macrocycle comprising two PMDI units linked by octamethylene chains—call it cyclobis(pyromellitic diimide-octamethylene) (CBPDC8)—has been synthesized[782] and characterized as a host with for diethylene glycol-appended DNP ($K_a = 5.8 \times 10^2$ M^{-1}) and TTF ($K_a = 6.3 \times 10^3$ M^{-1}) threads at 298 K in CH_2Cl_2. CBPDC8 has been employed in the synthesis[782] of a neutral, redox-switchable bistable [2]rotaxane—see **Section 6.1.1.1**. Wytko[760] has similarly prepared the oligomethylene-bridged viologen cyclophane cyclobis(paraquat-heptamethylene) ($CBPC7^{4+}$) and obtained single-crystal X-ray structures of the corresponding host-guest complex with TTF.

$TexasBox^{4+}$—The 'Texas-Sized' Molecular Box

The tetracationic cyclophane concept has been further generalized by Sessler[804–809] at the University of Texas (UT) at Austin. Sessler has incorporated 2,6-pyridyl-bis(imidazolium) cations into the 'blue box' framework. This Texas-sized[Q] box ($TexasBox^{4+}$) has been colored burnt orange in the literature in homage to the UT Austin colors. An advantage of $TexasBox^{4+}$ is that it can be synthesized in relatively high yield (58%) from 2,6-di(1H-imidazol-1-yl)pyridine and 1,4-bis(bromomethyl)benzene without the need for a template. The bent nature of the dicationic recognition units renders the burnt-orange box more conformationally flexible than the blue box family of cyclophanes—two single-crystal polymorphs of $TexasBox^{4+}$ have been characterized by X-ray crystallography, revealing (**Figure 2.45**) that it can adopt either a boat-like or a chair-like conformation.

Terephthalic acid and its corresponding anions have been investigated as guests for $TexasBox^{4+}$ in solution and in the solid state—a different response has been observed in each of its three protonation states. Whereas terephthalic acid exhibits no affinity for $TexasBox^{4+}$ in Me_2SO, the terephthalate dianion binds ($K_a = 3300$ M^{-1}) outside of the ring's cavity. The terephthalate mono-anion ($HO_2CC_6H_4CO_2^-$) is the only protonation state that assembles ($K_a = 2100$ M^{-1}) with $TexasBox^{4+}$ into a pseudorotaxane. The *$HO_2CC_6H_4CO_2^-$⊂TexasBox*$^{4+}$ pseudorotaxane further assembles (**Figure 2.45**) into dimers, trimers, and oligomers in Me_2SO. These pseudorotaxanes and their supramolecular polymers, which are increasingly favored at high concentrations and low temperatures, are held together by intermolecular hydrogen bonds, as well as by π–π stacking and anion–π interactions. The 2,6-naphthalenedicarboxylate dianion is another guest which assembles[805] with $TexasBox^{4+}$ into a pseudorotaxane. The concentration, temperature, and pH-sensitive behavior of these assemblies may render them useful for the design of molecular switches and machines. These pseudorotaxane carboxylates can also serve as ligands for the construction of coordination polymers and metal-organic frameworks (MOFs)—see **Section 4.2.3.8**. Some aromatic sulfonates also induce[809] pseudorotaxane formation with $TexasBox^{4+}$ with relatively high K_a values, namely 2,6-disulfonatonaphthalene ($K_a = 3.4 \times 10^5$ M^{-1}) and 4,4′-disulfonatobiphenyl ($K_a = 3.5 \times 10^4$ M^{-1}),

[Q] Texas, formerly the largest state in the US until Alaska was admitted as the 49th state in 1959, carries the reputation that 'everything is bigger in Texas'. The phrase 'Texas-sized' is used to describe an object, usually originating from Texas, which is large compared to other objects of its type.

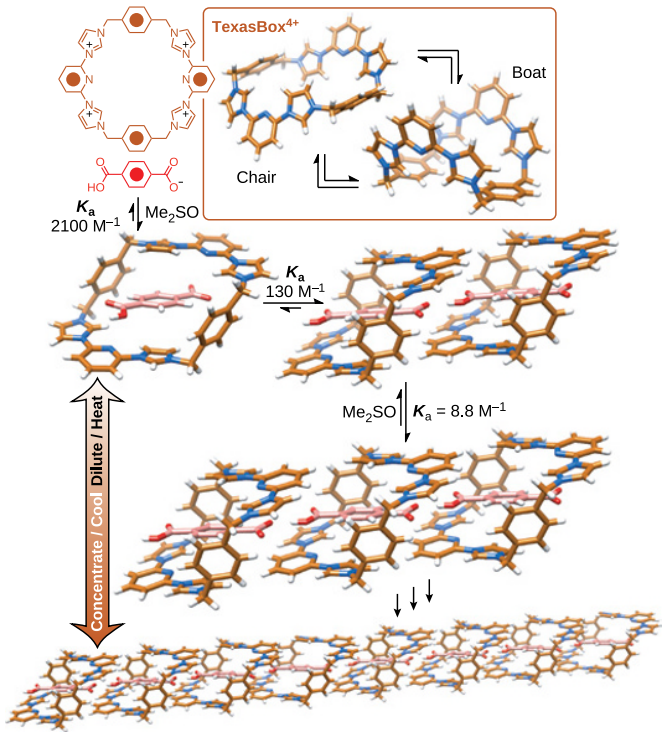


Figure 2.45 Pseudorotaxane assemblies of the Texas-sized burnt orange box,[804] TexasBox^{4+}. Tubular representations of the solid-state structures and superstructures of TexasBox^{4+} and $HO_2CPhCO_2^-$⊂*TexasBox*$^{4+}$, respectively, are depicted with solvent molecules and counterions omitted for the sake of clarity.

at room temperature in water. The co-crystallization of TexasBox^{4+} pseudorotaxanes and certain metal salts leads to the multicomponent self-assembly[805,810,811] of metal-organic rotaxane frameworks.

Concluding Remarks

The diversity of recognition motifs of both neutral and charged varieties, as summarized in **Section 2.3.3**, is a testament to the proclivity of π-electron-poor and π-electron-rich planar aromatic molecules to interact non-covalently in specific and directionally well-defined geometries. Although these recognition units typically engage π–π stacking, as well as ground-state and/or excited-state charge-transfer interactions which bolster their mutual attraction, it is important to remember that these interactions are weak and therefore do not typically occur in isolation—rather, most donor-acceptor templates in mechanostereochemistry rely on a combination of these interactions and others, such as ion-pairing, [C–H···π], and especially [C–H···O] hydrogen-bonding interactions.

Although the number of π-associated donor-acceptor recognition motifs are already vast, the continual discovery of new π-donating cyclophanes and crown ethers, and especially the recent introduction of a plethora of new π-accepting boxes, suggests that the field remains poised to continue in its expansion. Furthermore, the synthesis of mechanomolecules under the auspices of π-donor/π-acceptor templation have relied almost exclusively on host-guest chemistry (pseudorotaxanes) as the key precursors, yet a number of entwined / helical assemblies based on D-A interactions that have emerged on the scene also appear suitable to template the formation of mechanical bonds. For example, Colquhoun[812–816] has described a number of assemblies of folded sulfone oligomers containing π-accepting PMDI or NDI recognition units interdigitated with π-donating pyrene tweezer molecules, as well as an entwined "Roman Handshake" motif[817] driven chiefly by a combination of D-A and hydrogen-bonding interactions between the same set of recognition units. Iverson[818] has described heteroduplexes of oligo-DNP and oligo-NDI molecules whose intercalative folding in solution produces highly entangled, well-defined superstructures. Highly intertwined donor-acceptor constructs that could be suitable for the templation of mechanical bonds have also been described by Zhao and Li.[819] Indeed, it appears that there will be no shortage of promising new π-donor/π-acceptor motifs to harness as templates in the future of the mechanical bond in chemistry.

2.3.4 Hydrogen-Bonded Templates

The hydrogen bond is an attractive interaction between (i) a proton, which is bound covalently to a more electronegative atom X, and (ii) another electronegative atom or group of atoms Y. Although electrostatic (dipole-dipole) interactions are the principle ingredients in [X–H···Y] hydrogen bonds, a 2011 IUPAC committee charged with defining[506,507] the hydrogen bond has noted that "*today it is well accepted that hydrogen bonding has contributions from electrostatic interactions between permanent multipoles, polarization, or induction interactions between permanent and induced multipoles, dispersion arising from instantaneous multipoles-induced multipoles, charge transfer induced covalency, and exchange correlation effects from short-range repulsion due to overlap of the electron distribution*." Thus, the definition of the hydrogen bond, which was formerly reserved for FH, OH, and NH donors, has expanded considerably to include any example of [X–H···Y] for which there is evidence of an attractive interaction. The [C–H···O] interactions which stabilize many donor-acceptor MIMs (**Section 2.3.3**) constitute one such example. In this Section, we limit ourselves to the traditional types of hydrogen bonds involving primarily nitrogen- and oxygen-based donors and acceptors. Since polar solvent molecules compete for hydrogen bonds, host-guest complexes which associate by dint of these interactions are best preserved in low polarity solvents. Halogenated solvents such as CH_2Cl_2 and $CHCl_3$ are among the most commonly employed, although polar solvents are often required to solvate ionic recognition systems that rely on hydrogen bonding.

It could be argued that the hydrogen bond is the most ubiquitous noncovalent bonding interaction utilized[820,821] in the template-directed synthesis and self-assembly of organic molecules. This claim is especially true in the case of mechanical bonds, since hydrogen bonding underpins, not only the [C–H···O] interactions present in the vast majority of D-A MIMs (**Section 2.3.3**), but also the

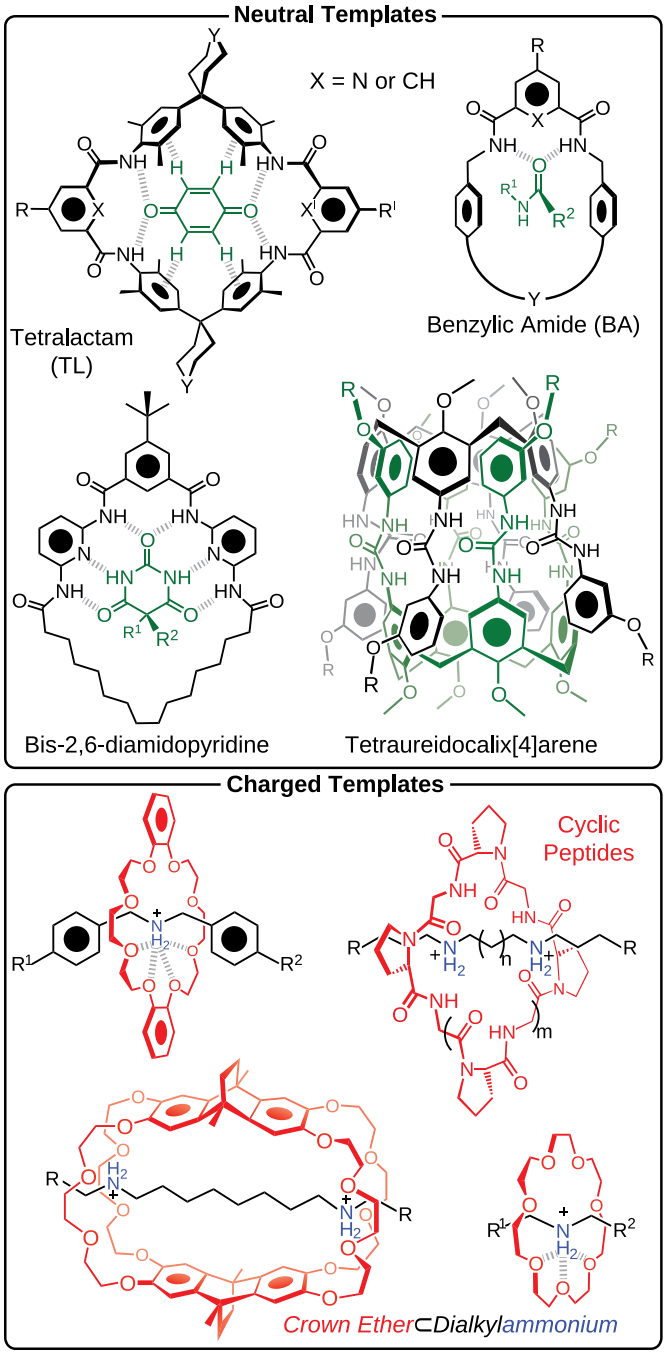
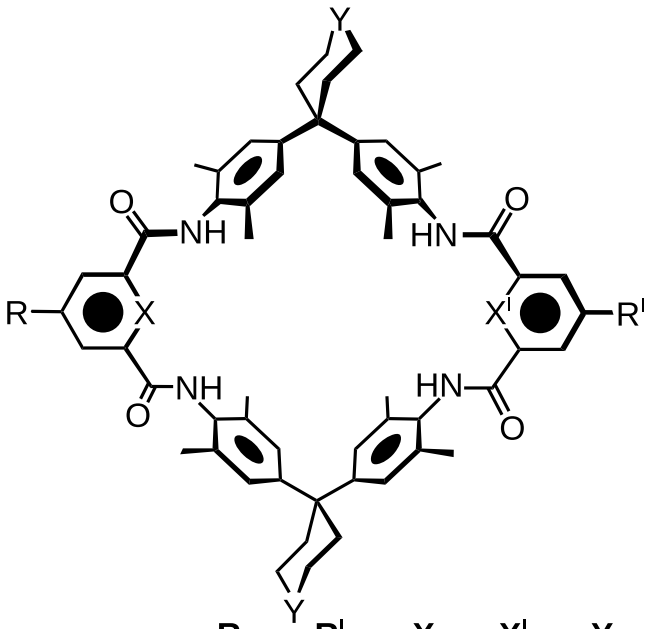


Figure 2.46 Examples of hydrogen-bonded template motifs.

more conventional [N–H···O] interactions that guide the templated synthesis of tetralactam (**Section 2.3.4.1**), benzylic amide (**Section 2.3.4.2**), cyclopeptide (**Section 2.3.4.3**), bis-2,6-diamidopyridine (**Section 2.3.4.4**), tetraureidocalixarene (**Section 2.3.4.5**), and crown ether / dialkylammonium (**Section 2.3.4.6**) mechanomolecules (**Figure 2.46**) described in this Section. This class of MIMs is also probably the most diverse in terms of the strategies and tactics that have been employed in their synthesis. The most comprehensive reviews[822,823] on the topic of hydrogen bond template-directed synthesis of MIMs are already more than 10 years old. We present here an updated review of the major hydrogen-bonded templates in mechanostereochemistry and corresponding strategies for making MIMs.

2.3.4.1 Tetralactam Hosts

In 1991, Hunter[824] introduced a macrocyclic host for *para*-benzoquinone comprising two isophthalamide units separated by cyclohexylidene-bisphenylene spacers. This first member of a new family of synthetic receptors, which we will refer to as the tetralactam (TL) macrocycles, stabilizes *para*-benzoquinone by donating two [N–H···O] hydrogen bonds to each of its carbonyl groups, while also engaging the benzoquinone protons in [C–H···π] interactions with its diphenylmethane linkers. The 1:1 host-guest complex forms with an association constant, K_a, of 1.2×10^3 M^{-1} at ambient temperature in $CDCl_3$. The utility of this host for encapsulating carbonyl-bearing compounds has spawned the development of a number of structurally related homologues (**Figure 2.47**) involving modifications to the isophthalamide or cyclohexylidene structural fragments. These homologues include (i) tetralactam rings with substituents[825] at the *meta*-position of the isophthaloyl units (TLR_2 when R = R′ ≠ H and TLRR′ when R ≠ R′ ≠ H), as well as (ii) monopyridyl- (MPTL) and bispyridyl-tetralactams (BPTL) in which the isophthalamide



	R	R^I	X	X^I	Y
TL	H	H	CH	CH	CH_2
TL^{t}Bu	H	^{t}Bu	CH	CH	CH_2
TL(OMe)$_2$	OMe	OMe	CH	CH	CH_2
MPTL	H	H	CH	N	CH_2
BPTL	H	H	N	N	CH_2
BPTL^{2+}	H	H	N	N	NMe_2^+

Figure 2.47 Structural formulas for some of the tetralactam hosts pioneered by Hunter[824] and Vögtle.[825,834,835]

units have been replaced by 2,6-pyridinecarboxamide ones, and (iii) dicationic tetralactams such as $BPTL^{2+}$ possessing quaternary ammonium ions in the cyclohexylidene appendages.

The structural variants of the TL rings are effective handles for tuning solubility and recognition properties. The K_a values of a number of host-guest complexes based on the tetralactam hosts are summarized in **Tables 2.18** and **2.19**. The entries in **Table 2.18** cover a range of different hosts and guests in different solvent systems. Hunter[826] found that $BPTL^{2+}$ can bind cyclic dipeptides in water, yet not as tightly as the neutral homologue BPTL binds the same cyclic dipeptides in chloroform. In general, the tetralactams based on 2,6-pyridinecarboxamide, such as MPTL and BPTL, exhibit higher K_a values for amide-based guests than the isophthalamide-based TL rings on account of the hydrogen bond accepting capacity of the pyridyl unit, whereas guests lacking hydrogen bond donors bind more efficiently to the TL rings. It is clear that NH groups contribute significantly to a guest's affinity for the BPTL-based hosts—amide-based guests exhibit K_a values that far exceed those of ester homologues, often by several orders of magnitude, reaching as high as 10^6 M^{-1} in the case of a cyclic diglycine. An investigation by Vögtle[827] on a series of amides, esters, and acid chlorides is in agreement with these trends. Jeong[828] has probed (**Table 2.19**) the effect of substitution on the pyridyl units of the BPTL ring and found that the K_a values are decreased by electron-donating OMe and NMe_2 groups, whereas they are increased by electron-withdrawing Cl and NO_2 groups. This stereoelectronic effect can be rationalized by the expectation that the withdrawal of electron density enhances the hydrogen bond donating ability of the appended amide groups, while also reducing electrostatic repulsion between the nitrogen atoms of the pyridyl unit and oxygen atoms of the guest's carbonyl groups.

Table 2.18 Association constants, K_a, for some tetralactam-based host-guest complexes.

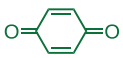
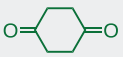
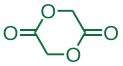
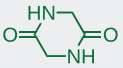
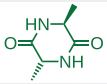
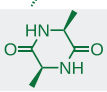
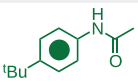
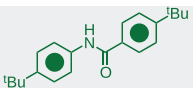
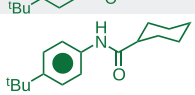
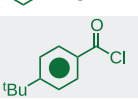
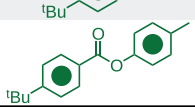
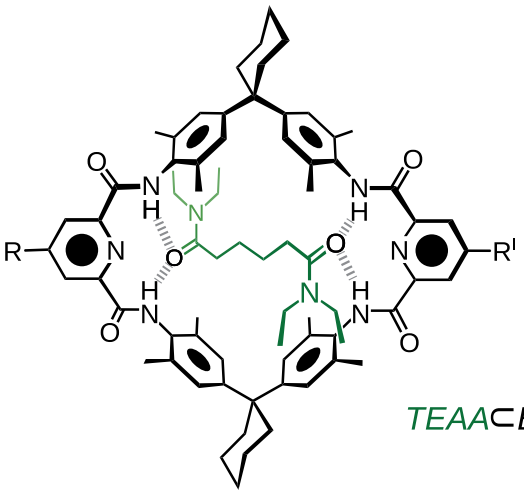
Guest	Host	Solvent	K_a / M^{-1}	Ref
	TL	$CDCl_3$	1200	824
	TL	9:1 $CDCl_3/CD_3OD$	100	824
	BPTL	$CDCl_3$	230	826
	$BPTL^{2+}$	D_2O	<5	826
	BPTL	$CDCl_3$	850	826
	$BPTL^{2+}$	D_2O	94	826
	BPTL	$CDCl_3$	340	826
	$BPTL^{2+}$	D_2O	< 5	826
	BPTL	$CDCl_3$	10^6	826
	$BPTL^{2+}$	D_2O	71	826
	$BPTL^{2+}$	D_2O	100	826
	$BPTL^{2+}$	D_2O	760	826
	TL^{t}Bu	CD_2Cl_2	50	827
	TL^{t}Bu	CD_2Cl_2	260	827
	TL^{t}Bu	CD_2Cl_2	360	827
	TL^{t}Bu	CD_2Cl_2	< 5	827
	TL^{t}Bu	CD_2Cl_2	< 5	827

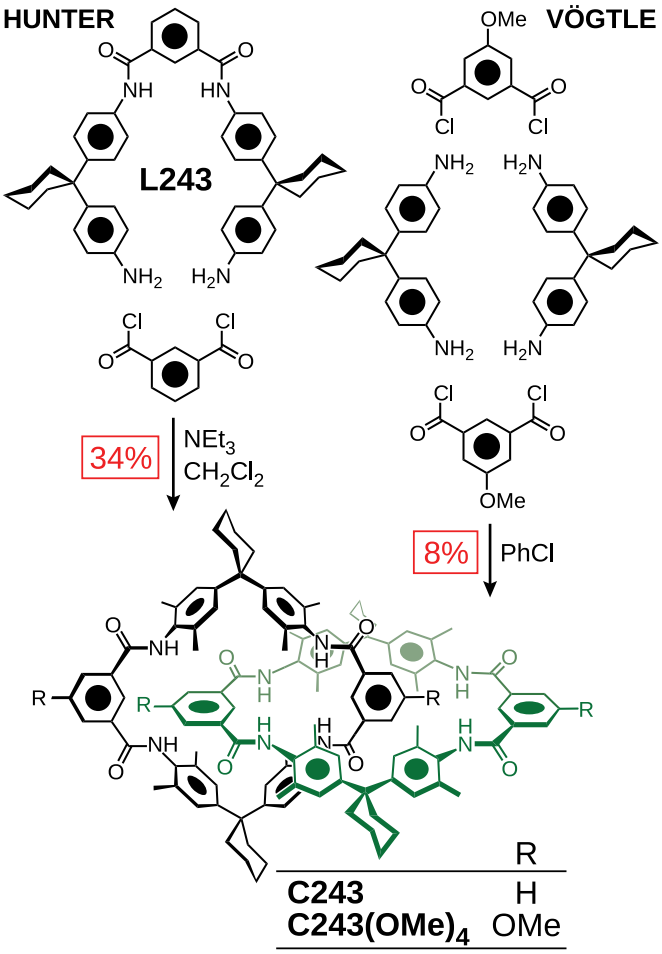
Table 2.19 The effects[828] of substituents on the association constants, K_a, of pseudorotaxanes comprising bispyridyl-tetralactam (BPTL) rings and a tetraethyladipamide (TEAA) guest at 23 °C in $CDCl_3$.



R	R′	K_a / M^{-1}	ΔG_a / kcal·mol^{-1}
H	H	780	–3.9
H	NMe_2	240	–3.2
H	OMe	550	–3.7
H	Cl	1360	–4.3
H	NO_2	4730	–5.0
NMe_2	NMe_2	70	–2.5
OMe	OMe	410	–3.6
Cl	Cl	2430	–4.6
NO_2	NO_2	24200	–6.0

Tetralactam Catenanes

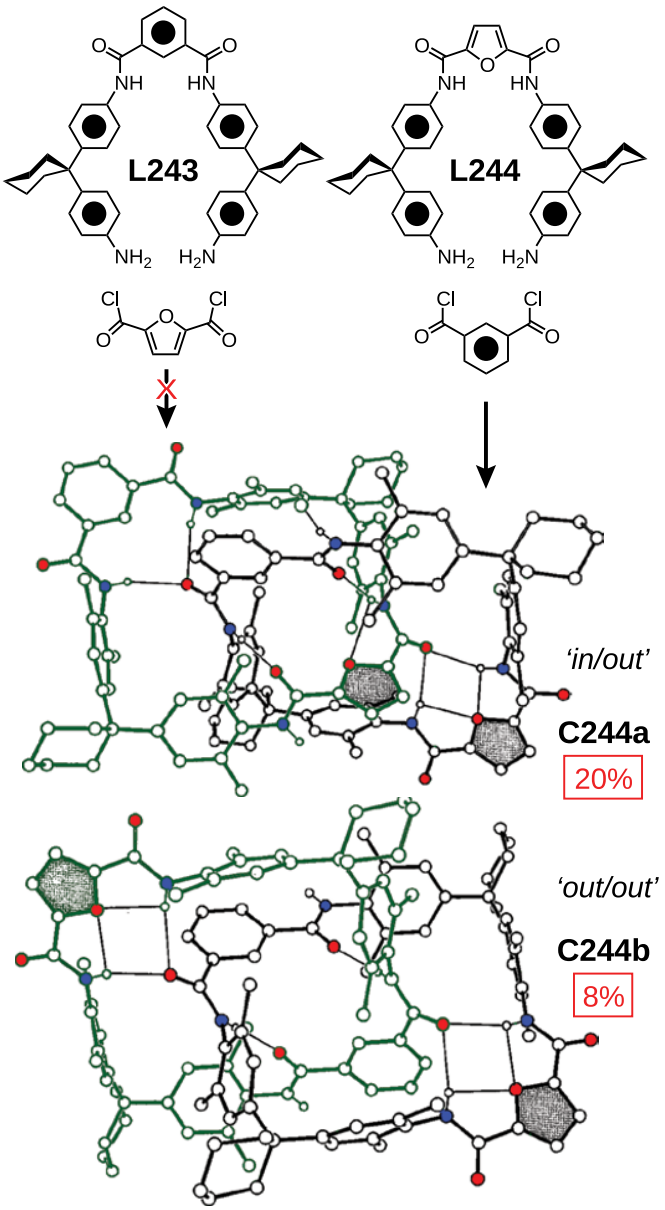
Shortly after Hunter introduced the TL host, he reported[829] the synthesis (**Scheme 2.67**) of the first tetralactam [2]catenane **C243**—a compound discovered serendipitously during a two-step protocol which was originally intended to optimize the yield of TL production. The [2]catenane **C243** is obtained in 34% yield along with the TL ring (51%) and a related cyclic tetramer (5%) upon mixing isophthaloyl chloride with isophthaloyl 4,4-cyclohexylidene-bisaniline (**L243**) in NEt_3-basified CH_2Cl_2. It was not long thereafter that Vögtle[825] reported a one-step synthesis of the homologous



Scheme 2.67 Synthesis of the first tetralactam-based [2]catenanes according to the protocols developed by Hunter[829] and Vögtle[825]

[2]catenane **C243(OMe)$_4$** comprising two TL(OMe)$_2$ rings directly from the corresponding isophthaloyl chloride and cyclohexylidene-bisaniline precursors in chlorobenzene (PhCl), albeit in lower yield (8%) than Hunter's two-step protocol. Although the rings possess some conformational mobility, the bulky cyclohexylidene groups prevent them from circumrotating freely, leading to relatively complicated NMR spectra. Following these seminal publications in 1992, it was Vögtle[830–833] who would go on to take the tetralactam design motif under his wing for a journey in mechanostereochemistry that was to continue for the rest of his career in academia.

Many of Vögtle's experiments were aimed at investigating[834,835] how structural modifications to the tetralactam framework lead to new kinds of architectures (**Chapter 4**)—i.e., knots, pretzelanes, bonnanes, [1]rotaxanes, figures-of-eight, etc.—as well as novel types of isomerism and chirality (**Chapter 5**) in MIMs. One such investigation[836] involved the synthesis (**Scheme 2.68**) of the furano[2]catenanes **C244a** and **C244b**—the first catenanes of this genre to be characterized in the solid-state by X-ray crystallography—following a two-step protocol from isophthaloyl chloride and a furan-derived homologue of the bis-amine precursor **L244** akin to that (**L243**) employed by Hunter in his seminal catenane synthesis. Curiously, no catenane is generated when attempting to catenate the same tetralactam rings when employing **L243** and furan-2,5-dicarbonyl chloride as the reactants. Catenanes **C244a** and **C244b** are circumrotational isomers that do not interconvert. **C244a** is the '*in/out*' isomer, signifying that one furan unit is buried within the cavity of its cognate ring while the other furan unit is situated on the periphery of the catenane, whereas **C244b** is the '*out/out*' isomer in which both furan units reside on the



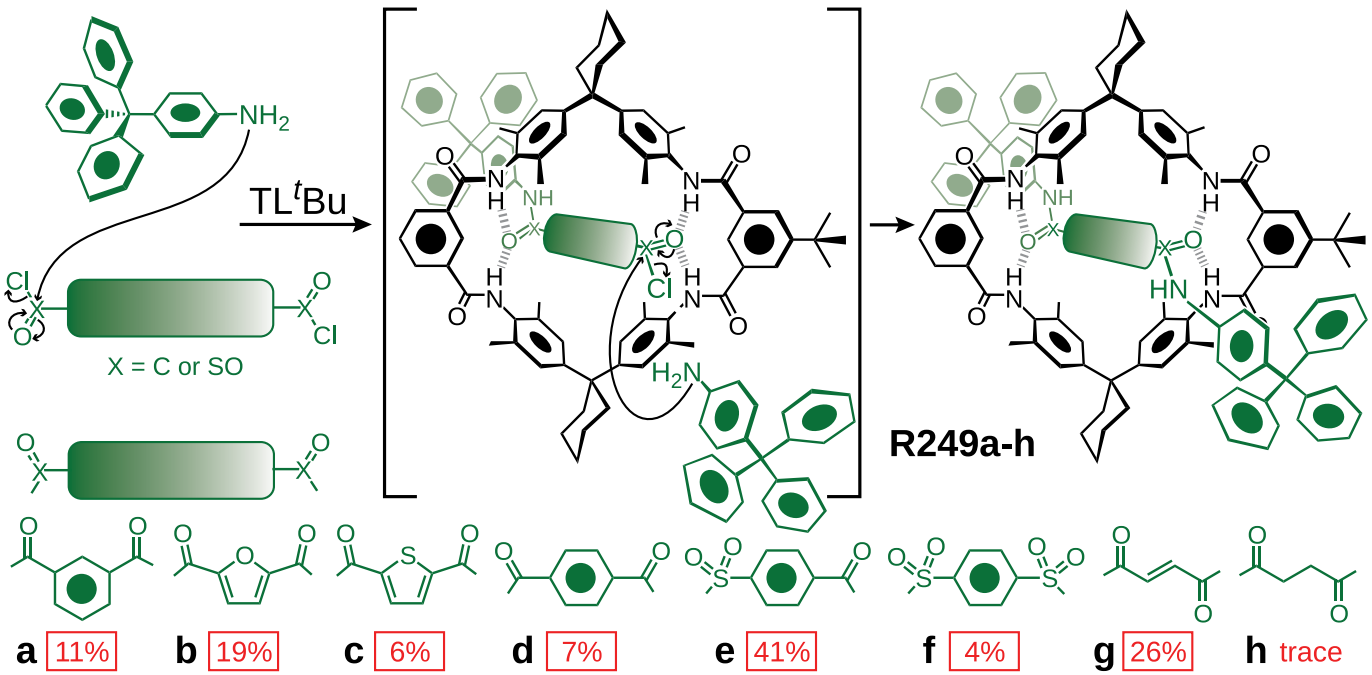
Scheme 2.68 Vögtle's synthesis of furano-tetralactam [2]catenanes, the outcome of which is sensitive to the choice of precursor clipping partners, affords a mixture of *in/out* and *out/out* isomers.[836] No *in/in* isomer has been detected. Ball-and-stick representations (O = red, N = blue, C/H = white) of the solid-state structures have been adapted with permission from ref 830. Protons not engaged in hydrogen bonding are omitted.

catenane's exterior. No '*in/in*' isomer was detected, indicating that the furan bis-amide units do not associate as readily with TL rings as do the isophthaloyl homologues. Other catenanes created by Vögtle incorporate rings with sulfonamide,[837] oligomethylene,[838] and acryloyl[839] moieties in their backbones. Larger [3] and [4]catenanes are made more accessible by switching from *meta*-substituted (isophthalamide) to *para*-substituted (terephthalamide) backbones, since this change helps promote the formation[840] of large octalactam macrocycles and the various concatenated compounds they spawn.

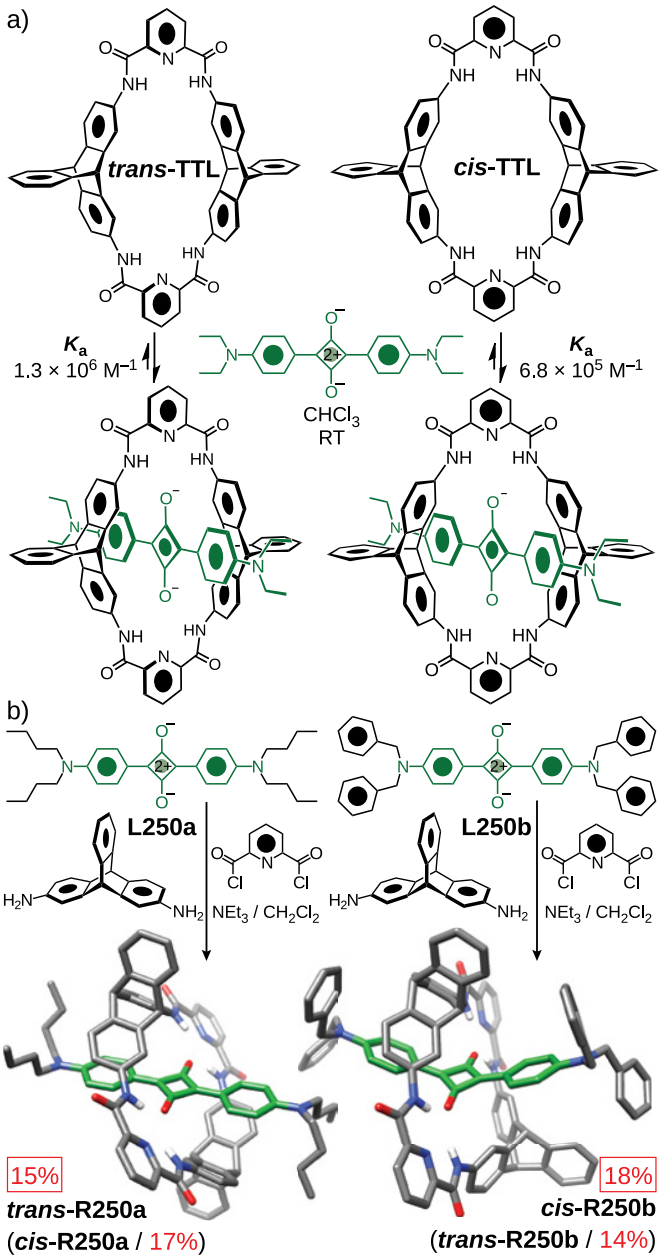
Tetralactam Rotaxanes

Subsequently, Vögtle[841–843] adapted the tetralactam recognition chemistry for the synthesis (**Scheme 2.69**) of rotaxanes by simply mixing an aromatic diacid dichloride axle precursor with a *p*-tritylaniline stopper precursor in the presence of the TL^{t}Bu host in a non-competing solvent such as CH_2Cl_2. The most likely mechanism (**Scheme 2.69**) for the self-assembly of these rotaxanes (**R249a-h**) involves the formation of an amide-linked half-dumbbell when the aniline-based stopper precursor reacts with the first acid chloride moiety of the template, generating a reactive semirotaxane *in situ* which can subsequently couple with the second stopper precursor. This stoppering protocol has also been applied to the synthesis of related porphyrin-stoppered rotaxanes[844] as well as [3]rotaxanes.[845] The protocol is likewise compatible with bis-isocyanate templates instead of diacid dichlorides.[846] Schalley[847] has applied the CuAAC click reaction to the synthesis of tritylphenyl-stoppered tetralactam rotaxanes with diketopiperazine recognition units, which can be prepared in up to 75% yield in CH_2Cl_2 with PPh_3CuBr as the catalyst.

Chen[848,849] has uncovered a couple of triptycene tetralactam (TTL) hosts which accommodate (**Scheme 2.70**) squaraine dyes as guests. These receptors can exist (**Scheme 2.70a**) as the *cis*-TTL or *trans*-TTL isomers, depending on how the 2,7-substituted triptycene linkers are connected to the 2,6-dicarboxamidopyridine joints. Bis(*N*,*N*-diethylanilino)squaraine binds with a high affinity to both the *trans*-TTL (1.3×10^6 M^{-1}) and *cis*-TTL (6.8×10^5 M–1) isomers at ambient temperature in $CHCl_3$. These values are higher than those recorded for TL(^{t}Bu)$_2$, which is known[850] to host squaraines with K_a values on the order of 10^3 M^{-1} in CH_2Cl_2 at 25 °C. The [2]rotaxanes ***cis/trans*-R250a** and ***cis/trans*-R250b** comprising these rings have been generated (**Scheme 2.70b**) by clipping 2,7-diaminotriptycene and 2,6-pyridinedicarbonyl chloride around bis(*N*,*N*-di-*n*-butylanilino)squaraine (**L250a**) and bis(*N*,*N*-dibenzylamino) squaraine (**L250b**) dumbbells, respectively. The X-ray crystal structures (**Scheme 2.70b**) of ***trans*-R250a** and ***cis*-R250b** reveal that the different macrocyclic isomers bind to the squaraine template in dramatically different ways. Although both squaraine cores accept bifurcated hydrogen bonds from each of the 2,6-dicarboxamidopyridine units, the ***trans*-R250a** isomer is stabilized by π–π stacking interactions between the aromatic rings of the triptycene and bis(anilino)squaraine subunits, yet these subunits are engaged in [C–H···π] interactions in the case of ***cis*-R250b**. Whereas the bis(anilino)squaraine template is planar in ***trans*-R250a**, this unit is distorted substantially into a curved surface in the case of ***cis*-R258**. See **Section 2.3.4.2** for more examples of squaraine-based rotaxanes.



Scheme 2.69 The mechanism of rotaxane formation upon mixing various diacid dichlorides with at least 2 equiv of a *p*-tritylaniline stopper precursor in the presence of the TL^{t}Bu ring.[841–843]



Scheme 2.70 Chen's triptycene tetralactam (TTL) hosts for squaraine dyes.[848,849] (a) The self-assembly of pseudorotaxanes comprising bis(*N*,*N*-diethylanilino)squaraine and *trans*-TTL or *cis*-TTL in $CHCl_3$.[848] (b) The synthesis of TTL-based rotaxanes by clipping.[849]

Tetralactam rotaxanes are also prepared readily by slippage (**Section 3.1.3**) protocols. See **Section 2.3.5.1** for mechanomolecules templated by anion-binding tetralactams.

We summarize a few key features of the tetralactam-based MIMs in the following bullet points.

- The reaction of bisanilines with diacid dichlorides—often based on isophthaloyl or 2,6-pyridyl frameworks—leads to the formation of [2+2] macrocycles and catenanes, larger [4+4] rings—[3+3] is rarely formed in more than trace amounts—and their corresponding catenanes, as well as acyclic oligomers and, in some cases, knots.[851,852] Rotaxanes are formed in the presence of appropriate hydrogen-bonded dumbbell templates.
- Catenated products are obtained only in low polarity solvents. Macrocycles and acyclic oligomers are the dominant products in polar solvents.
- Both clipping and stoppering reactions are tolerant of many different acid chlorides, yet they can have a dramatic influence on both the yields and product ratios.

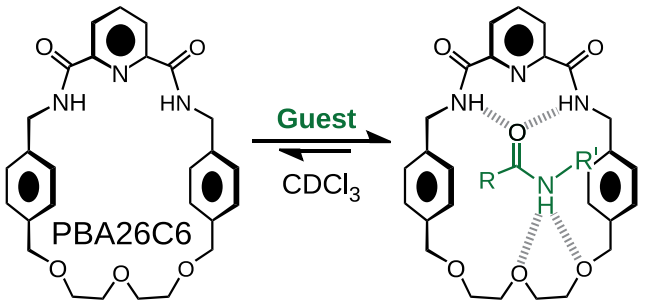
2.3.4.2 Benzylic Amide Hosts

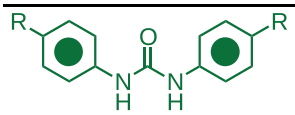
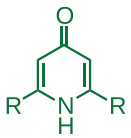
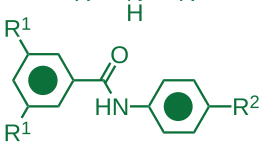
In common with the tetralactams, the benzylic amides[853] represent a recognition motif that relies on endotopic *meta*-substituted amide groups to intertwine components by way of hydrogen-bonding interactions. In this case, however, the amide groups are connected to benzylic linkers (*para*-xylylene) instead of cyclohexylidene bisphenylenes, and the hosts sometimes possess only one isophthalamide subunit instead of two of them. Many X-ray crystal structures of MIMs incorporating this motif reveal that the planes of the benzylic units are positioned relative to each other at a distance (7 Å) which is ideal for an intercalated guest to partake in π–π stacking interactions with both of the aromatic rings. MIMs based on the benzylic amide rings are therefore characterized typically by a combination of multiple hydrogen bonds not unlike those characterizing the tetralactam motif, as well as by π–π interactions in the form of triply (rotaxane) or quadruply (catenane) stacked aromatic rings.

Few benzylic amide pseudorotaxanes of the tetralactam type have been characterized because the most commonly employed benzylic amide ring, cyclobis(isophthalamide-*para*-xylylene), derived from the [2+2] cyclization of isophthaloyl chloride and *para*-xylylenediamine, has very low solubility in non-competing solvents.[854] Another type of benzylic amide ring is desymmetrized such that it possesses one dicarboxamide unit and a polyether loop. In 2006, Leigh[855] reported a pH-switchable bistable [2]rotaxane in which the loop of the benzylic amide ring is closed by a tetraethylene glycol chain—see **Section 6.3.3.2**. The hybrid nature of this ring allows it to associate with recognition sites that are common to both benzylic amide (i.e., dipeptides) as well as crown ether (i.e., secondary ammonium groups) receptors. In 2007, Chiu[856] introduced a benzylic amide ring with a shorter diethylene glycol loop, which resembles closely his BX26C6 ring in its constitution. Template motifs comprising this pyrido-benzylic-amide[26]-crown-6 (PBA26C6) ring have been characterized and employed independently by Chiu[856] and Philp.[857,858] Pseudorotaxanes comprising PBA26C6 and a variety of amide and urea derivatives exhibit (**Table 2.20**) association constants (K_a) of up to ~10^4 M^{-1} in $CDCl_3$, and have been utilized (*vide infra*) in the synthesis of [2]rotaxanes. Jiang[859] has reported a number of close relatives of the PBA26C6 host which bind pyridine *N*-oxide derivatives with K_a values of up to 5.5×10^3 M^{-1} in 3:1 $CDCl_3$:CD_3OD.

Here, we summarize the kinetically controlled synthesis of some simple benzylic amide MIMs. Thermodynamically

Table 2.20 Association constants, K_a, for pseudorotaxanes comprising a benzylic amide macrocycle with a diethylene glycol ring closure and various guests possessing carbonyl groups.[856–858]



Guest		T / K	K_a / M^{-1}
	R = OC_6H_{13}	298	180
	R = CO_2Me	298	11000
	R = H	298	500
	R = CCPh	298	1500
	R^1 = R^2 = H	298	160
	R^1 = Me	283	67
	R^2 = $EtPhN_3$	263	118

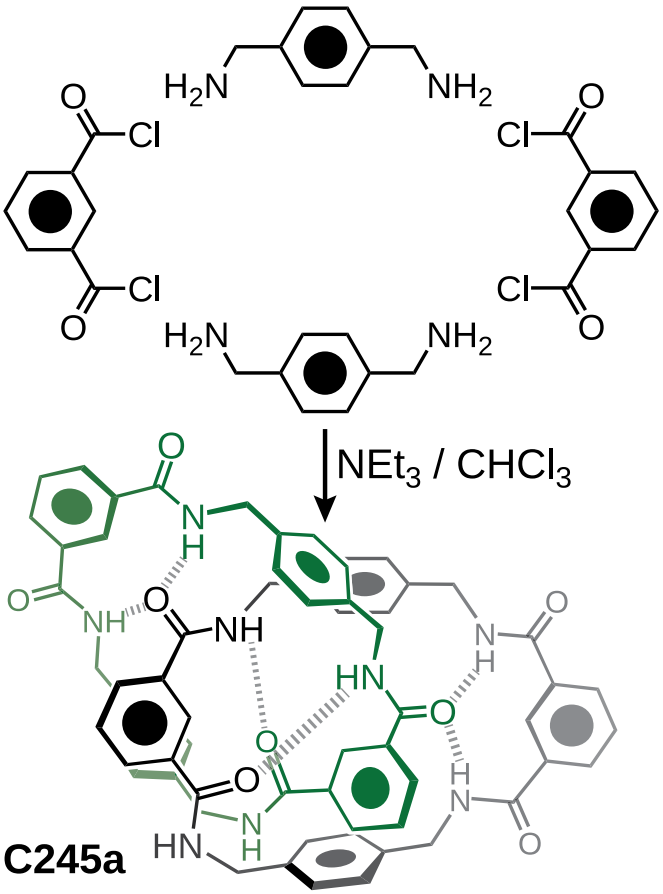
controlled reactions leading to MIMs of this genre are described in **Sections 3.1.3, 3.4.1.3**, and **3.4.2**.

Benzylic Amide Catenanes

Leigh's discovery[860] of the first benzylic amide homo[2]-catenane **C245a** was the serendipitous outcome (**Scheme 2.71**) of an attempt to prepare a benzylic tetralactam receptor for CO_2, in which a white solid precipitated gradually from a mixture of isophthaloyl chloride and *p*-xylylenediamine in a solution of NEt_3 and CH_2Cl_2. The precipitate proved to comprise the desired benzylic amide ring as a single compound, yet the rings are concatenated such that they cannot host CO_2 within their cavities. The solid-state structure of **C245a** is shown in **Figure 1.14d** in **Section 1.2.3**. Each of the rings adopt (**Scheme 2.71**) identical chair-like conformations in the solid state, with one [C=O] bond directed into the macrocyclic cavity and three of them directed outwards, i.e., one *endo* and three *exo* carbonyl groups. A network of six hydrogen bonds fixes the co-conformation of the two interlocked rings of the homo[2]-catenane. The *exo* carbonyl group belonging to the transoid isophthalamide units, which are buried in the center of the catenane, accept bifurcated hydrogen bonds from the two amide protons of the cisoid isophthalamide units on the exterior of the catenane. Computational investigations[861] on the mechanism of catenane formation indicate that these bifurcated hydrogen bonds, which are observed repeatedly in the solid-state structures of benzylic amide MIMs, are the hallmark of this templation motif, playing a much greater role in driving catenations than do singular hydrogen bonds or π–π stacking interactions. In contrast with the tetralactam-based catenanes (**Section 2.3.4.1**) of Hunter and Vögtle, the rings of catenane **C245a** can both circumrotate 360° on account of the relatively small profile of the benzylic linkers in terms of steric bulk.

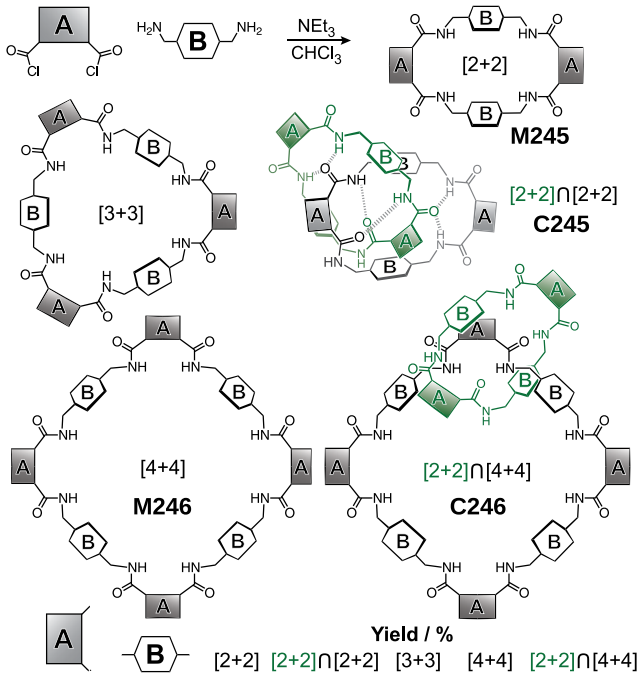
A great deal of physical chemistry has been carried out on the simplest benzylic amide [2]catenane **C253a**, allowing Leigh and co-workers to characterize (i) vibrational modes by infrared and Raman spectroscopy[862–864] and inelastic neutron scattering,[865,866] (ii) molecular ordering on surfaces and in thin films by high-resolution electron energy loss spectroscopy[867,868] (HREELS) and scanning tunneling microscopy[869] (STM), (iii) the mechanism of ring rotation (**Sections 5.1.1** and **5.1.2**) by computational methods,[870,871] (iv) the lowest electronically excited states by a combination of experimental and theoretical techniques, including transient absorption, fluorescence, and optoacoustic spectroscopies,[872] and (v) linear and second-order nonlinear optical properties.[873]

The benzylic amide catenane motif is also less sensitive to substituent effects than the Hunter/Vögtle cyclohexylidine-bisphenylene tetralactam catenanes. A series (**Table 2.21**) of catenations[874] involving different dicarboxylic acid chlorides—i.e., thiophenes, pyridines, and phenylenes with nitro, alkyl, alkene, ether, and halogen substitutions—as



Scheme 2.71 Leigh's seminal synthesis of a benzylic amide [2]catenane.[860]

Table 2.21 The effects of structural modifications to the diamide (A) and benzylic (B) linkers on the product distribution of a clipping reaction. [874]



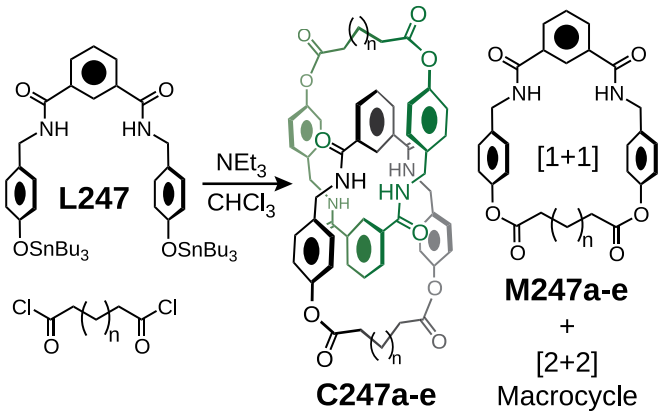
		[2+2]	[2+2]∩[2+2]	[3+3]	[4+4]	[2+2]∩[4+4]
a		*a*	20	*a*	*a*	*a*
b		22	20	3	10	5
c		25	18	trace	10	5
d		20	18	-	5	-
e	$C_6H_{13}O$	20	21	trace	3	trace
f	$C_8H_{17}O$	19	20	-	trace	-
g	$C_{18}H_{37}O$	22	15	-	5	-
h	Br	20	20	-	7	trace
i	O_2N, Br	22	18	-	5	-
j		25	15	-	5	-
k	S	25	25	trace	2	-
l	N	20	27	-	6	trace
m	N	21	20	-	5	trace
n	O	21	18	trace	6	-
o	O	19	19	-	5	-
p	F, F, F	20	-	-	5	-

[a]Products are too insoluble for analysis.

well as benzylic diamines with 2,6-naphthyl and 4,4′-bitolyl spacers, exhibit relatively small differences in product distributions. In general, [2+2] macrocycles and their corresponding [2]catenanes (**C245a-o**) are both obtained in yields of approximately 20% ± 5%. One exception is when perfluorinated isophthalic units are employed, which do not give rise to the [2]catenane **C245p**. Like the tetralactam system, [4+4] macrocycles (**M246a-p**) are also observed as minor side-products (~5%) whereas [3+3] rings are detected in only trace amounts at best. In a few cases, [2+2]∩[4+4] catenanes (**C246**) are also formed in low (≤5%) yields. Except in the case of **C245a**, which precipitates from solution, these products must be separated chromatographically, although the [2+2]∩[2+2] catenane is conveniently always the first product to elute on SiO_2 in $MeOH/CH_2Cl_2$ eluant.

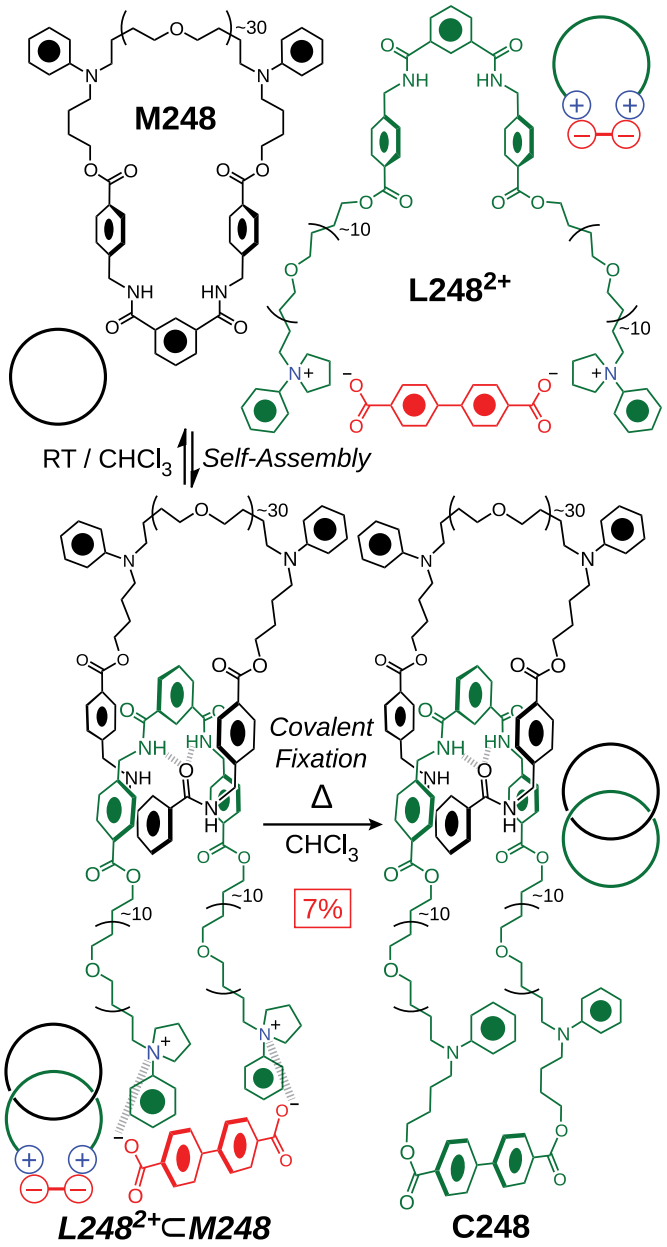
All of the benzylic amide catenanes in Leigh's initial investigations possessed symmetrical tetralactam rings. Leigh's next task[875] was the synthesis (**Scheme 2.72**) of the benzylic amide [2]catenanes **C247a-e** with desymmetrized rings possessing only one isophthalamide unit per ring. Different lengths of hydrocarbon linkers, which can be attached by ester bonds upon coupling the benzylic amide silyl ether precursor **L247** with appropriate dicarboxylic acid dichlorides, were investigated as closures for these rings. Linkers with longer, more flexible hydrocarbon chains increase the yields of the catenanes with respect to the [1+1] macrocycle **M247** and the [2+2] macrocycle. The solvent-induced switchability of the [2]catenane **C247d** is discussed in **Section 6.6.1**.

Tezuka[876] has reported a creative strategy for the synthesis (**Scheme 2.73**) of the [2]catenane polymer **C248** by combining the hydrogen bond-driven entwining of a benzylic amide template with a ring-closing reaction guided by ion-pair-driven self-assembly. The key to this approach is a process[877] referred to as 'electrostatic self-assembly and covalent fixation'. This process involves (i) the



		Yield / %		
	n	C247	M247	[2+2] Macrocycle
a	2	-	-	trace
b	4	-	10.5	trace
c	6	0.5	13	7
d	8	18	19	14
e	10	18	20	10

Scheme 2.72 The synthesis of benzylic amide catenanes and macrocycles with aliphatic ring closures.[875]



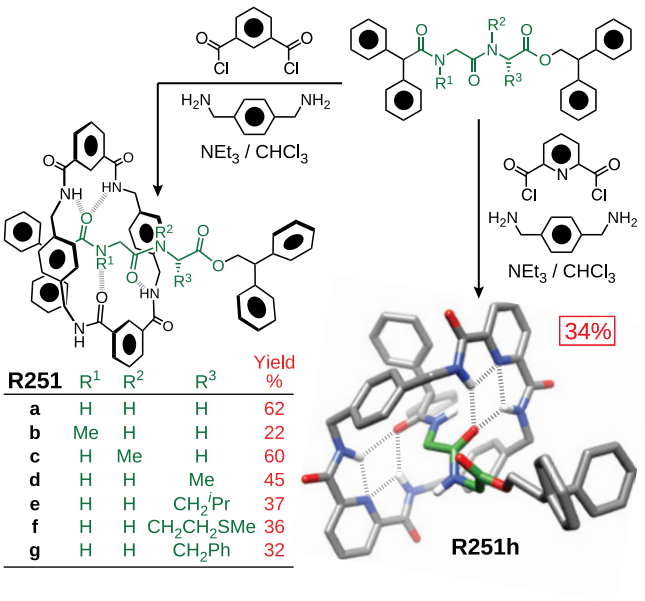
Scheme 2.73 The electrostatic self-assembly and covalent fixation approach to the synthesis of a benzylic amide [2]catenane polymer by Tezuka.[876]

self-assembly of a telechelic[R] poly(tetrahydrofuran) chain (**L248**$^{2+}$) containing cationic *N*-phenylpyrrolidinium endgroups which are charge-balanced by a biphenyldicarboxylate dianion, together forming a proposed [1+1] supramolecular macrocycle, followed by (ii) covalent fixation of the macrocycle as a result of ring-opening nucleophilic substitution of the cyclic ammonium endgroups by the ion-paired carboxylate anions at elevated temperatures. The benzylic amide / poly(THF) macrocycle **M248**, which is itself prepared by electrostatic self-assembly and covalent fixation, is thus converted to the hetero[2]catenane **C248**, by way of the intermediate pseudorotaxane ***L248***$^{2+}$***⊂M248***, in up to 7% yield after 3 h of heating in the presence of a slight excess of 4,4′-biphenyldicarboxylate. The non-interlocked parent macrocycles are recovered in 40–60% yield, and a homo[2]catenane arising from the double macrocyclization of an entwined ***(L248***$^{2+}$***)***$_2$ dimer is also obtained as a minor side product. At a molecular weight of more than 3000 Da, **C248** is one of the largest [2]catenanes ever to be synthesized.

[R] A polymer is described as telechelic if it is capable of undergoing further polymerizations or reactions at its reactive endgroups.

Benzylic Amide Rotaxanes

Rotaxanes of the benzylic amide variety are typically prepared by a five-component clipping protocol involving the [2+2] cyclization of diacid dichlorides and xylylenediamines around a hydrogen bond accepting dumbbell as the template, a procedure which is analogous conceptually to the eight-component dual-clipping reaction of Leigh's seminal [2]catenanes. An early example[878] of this protocol in action is the relatively high yielding (62%) synthesis (**Scheme 2.74**) of the peptido[2]rotaxane **R251a**, which possesses a glycylglycine (GlyGly) dipeptide recognition unit as the templating element in its axle. Leigh[879,880] has probed substituent effects in the dipeptide recognition motif systematically. The rotaxane **R251b** possessing an *N*-terminal sarcosine (Sar, or *N*-methylglycine) is obtained[879] in much lower yield (22%) than its constitutional isomer **R251c** (60%) possessing a C-terminal Sar residue. A likely explanation for the large disparity between the efficiency of clipping around SarGly versus GlySar is that the yields reflect the affinity of the benzylic amide macrocycle for the dipeptide; since the ring binds preferentially to the ketone of the *N*-terminal stopper, it loses a hydrogen bond donor in the former case and not the latter. Leigh[880] also found that replacing the



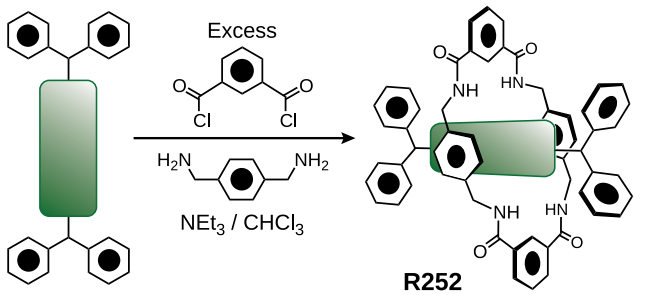
R251	R^1	R^2	R^3	Yield %
a	H	H	H	62
b	Me	H	H	22
c	H	Me	H	60
d	H	H	Me	45
e	H	H	$CH_2{}^iPr$	37
f	H	H	CH_2CH_2SMe	36
g	H	H	CH_2Ph	32

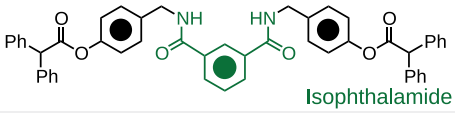
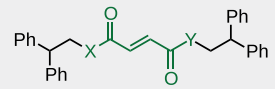
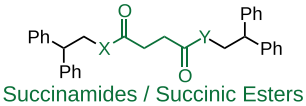
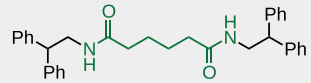
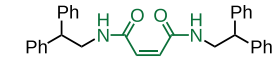
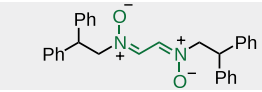
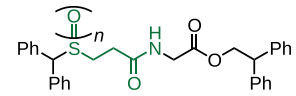
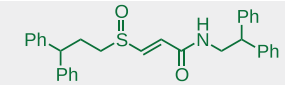
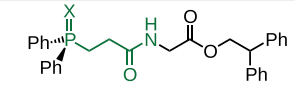
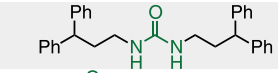
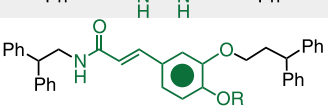
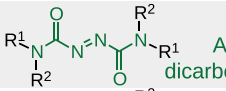
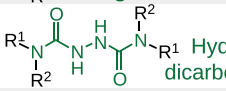
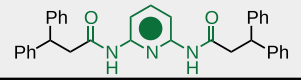
Scheme 2.74 The synthesis of glycylglycine [2]rotaxanes by clipping.[878–880]

rotaxane's C-terminal Gly unit with alanine (Ala), valine (Val), methionine (Met) or phenylalanine (Phe) reduces the product yields of the corresponding [2]rotaxanes **R251d** (45%), **R251e** (37%), **R251f** (36%), and **R251g** (32%), respectively, indicating that the steric bulk of amino acid side chains interferes with the clipping reaction. Although employing 2,6-diamidopyridine as an alternative recognition unit in the synthesis of **R251h** is also lower yielding, the hydrogen bond network is ultimately reinforced by the pyridine unit, leading to a strong preference for the *cisoid* conformation of the ring's amide donors, as reflected (**Scheme 2.74**) in the solid-state structure of **R251h**.

Beyond dipeptides, a vast range of hydrogen bond accepting recognition units have been utilized as templates for the clipping (**Table 2.22**) of benzylic amide tetralactam rings around the diphenylmethane-stoppered dumbbells **L252a-u** to afford the corresponding [2]rotaxanes **R252a-u**. The first benzylic amide rotaxane, **R252a**, was obtained[854] from an isophthalamide-based dumbbell in 26% yield. The most effective template for the synthesis of benzylic amide rotaxanes in terms of efficiency is the fumaramide (FA) unit. The FA dumbbell **L252b** gives rise to the [2]rotaxane **R252b** in a remarkable 97% yield when subjected[881] to standard clipping conditions with a five-fold excess of isophthaloyl dichloride and *p*-xylylenediamine in $NEt_3/CHCl_3$. Leigh[881] descrbes the FA template as "stiff, and sticky in the right places" because the template/ring interaction benefits from the preorganization of its "stiff" *trans*-olefinic bond, as well as the positioning of the fumaric "sticky" carbonyl groups at a distance well-matched to that of the ring's amide groups. This rationale is supported[882] by comparing clipping protocols involving (i) the succinamide (SA) unit in **L252e** and **R252e**, which is more flexible than FA, (ii) the maleamide (MA) unit in **L252h**, the *cis*-olefinic bond of which provides equal rigidity, yet very different distances and orientations for the carbonyl groups in comparison with FA, and (iii) the adipamide unit of **L252g** and **R252g**, which is both longer and more flexible than FA. In all cases, carbonyl positions and template backbones which deviate from FA in length or rigidity correspond to lower rotaxane yields. It is also clear from Leigh's investigations[881,882] that the NH atoms of the recognition units are important factors in the noncovalent bonding interactions that template rotaxane formation, since substituting the amide bonds for ester bonds, as in compounds **R252c**, **R252d**, and **R252f**, leads to significant reductions in yield. This effect can be attributed mainly to the fact that esters are poor hydrogen bond acceptors on account of the relatively weaker basicity of their carbonyl groups, and perhaps also to some extent on the hydrogen bond donating capability that is a feature of amides (and not esters), corresponding to an availability of extra "sticky" sites. A rich anthology of physical chemistry has assisted the detailed characterization of FA- and SA-based rotaxanes, including HREELS,[883] femtosecond 2D-IR spectroscopy,[884–886] three-pulse photon-echo peak shift spectroscopy,[887] surface-enhanced second harmonic generation,[888] electronic spectroscopy in the gas phase,[889,890]

Table 2.22 Summary of clipping protocols for the template-directed synthesis of diphenylmethyl-stoppered benzylic amide [2]rotaxanes **R252a-w**.



L252	Recognition Site			Yield / %	Ref
a				28	854
	Isophthalamide				
		X	Y		
b		NH	NH	97	881
c		NH	O	36	881
d	Fumaramides / Fumaric Esters	O	O	3	881
		X	Y		
e		NH	NH	52	882
f	Succinamides / Succinic Esters	NH	O	4	882
g		Adipamide		8	882
h		Maleamide		0	882
i		Dinitrone		70	882
			n		
j		Sulfide	0	12	897
k		Sulfoxide	1	43	897
l		Sulfone	2	10	897
m		Vinyl Sulfoxide		63	897
			X		
n		Phosphine	O	60	898
o		Thiophosphine	S	18	898
p		Selenophosphine	Se	20	898
q		Urea		*a*	899
r		Coumaric Amide R = $CH_2CH_2SiMe_3$		14	900
			R^1	R^2	
s		Azo-dicarboxamide	Ph_2CHCH_2	H	43	902
t			$PhCH_2$	$PhCH_2$	58	902
			R^1	R^2		
u		Hydrazo-dicarboxamide	Ph_2CHCH_2	H	6	902
v			$PhCH_2$	$PhCH_2$	11	902
w		Diacylaminopyridine		33	904

[a]Although neither a synthetic protocol nor a yield have been reported for **R252q**, a solid-state structure of this rotaxane has been deposited in the Cambridge Crystallographic Data Centre (CCDC).

microsolvated clusters,[891] and in helium nanodroplets,[892] as well as by computational models.[893,894]

Other recognition moieties (**Table 2.22**) that have been employed in the synthesis of benzylic amide [2]rotaxanes include dinitrones[895,896] (**R252i**), sulfur-containing[897] (sulfide, sulfoxide, sulfone) analogues of succinamide and fumaramide (**R252k–R252m**), phosphorus-based[898] (phosphinamide, thiophosphinamide, and selenophosphinamide) groups (**R252n–R252p**), urea (**R252q**),[899] coumaric amide (**R252r**),[900] and glycylnaphthalimide[901] derivatives as hydrogen bond acceptors. Berná[902] has investigated rotaxanes possessing azodicarboxamide (**R252s**, **R252t**) and hydrazodicarboxamide (**R252u**, **R252v**) recognition units, finding that the former is much more efficient than the latter as a template. The dinitrone, sulfoxide, and phosphine-based templates produce [2]rotaxanes in good yields, whereas yields are relatively low in the case of sulfides, sulfones, thiophosphines, and selenophosphines on account of steric and electronic misfits. The most effective templates are those—i.e., dinitrone, vinyl sulfoxide—which most closely mimic the geometry of the FA template. Berná[903] has also introduced rotaxanes (e.g., **R252w**) based on di(acylamino) pyridine templates that have been useful in the design[904] of novel types of molecular shuttles—see **Sections 6.7** and **6.10.1**. In general, it can be concluded that the template effect of benzylic amide rotaxanes is optimized by increasing the hydrogen bond basicity (amide>ester) of the binding sites, as well as by fixing their distances (succinic>adipic), rigidities (fumaric>succinic) and orientations (*trans*>*cis*) through preorganized molecular designs.

Takata[905–907] has developed (**Scheme 2.75**) the mechanostereochemistry of the macrocyclic benzylic amide **MBASO$_2$**, which contains a sulfolene functional group as a versatile synthetic handle for the post-synthesis modification of catenanes and rotaxanes. Employing the **MBASO$_2$** ring as a template during the coupling of isophthaloyl chloride and *p*-xylylenediamine in $CHCl_3$ affords[905] the hetero[2]-catenane **C249SO$_2$**, which comprises mechanically interlocked benzylic tetralactam and sulfolene bislactam rings, in 25% yield. This catenane can be converted to the catenated 1,3-diene **C249** as a result of the elimination of SO_2 from the sulfolene unit by thermolysis at 150 °C. Alternatively, the diene **C249** can be generated and reacted *in situ* with an appropriate dienophile such as methyl fumarate to afford the hetero[2]catenane **C250** in good (85%) yield. A four-atom ring expansion of the catenane's larger ring can also be accomplished[905] by ozonolysis of the double bond of this Diels-Alder adduct, affording the expanded [2]catenane **C251**. The hetero[2]catenane **C252SO$_2$**, which possesses the sulfolene unit in one ring and a fumaric ester in the other ring, was designed[907] to be polymerized. The *in situ* thermolysis and Diels-Alder condensation (**Scheme 2.75**) of the bifunctional **C252SO$_2$** is achieved with prolonged heating at 140 °C in the solid state, leading quantitatively to the poly[2]catenane **C253**, which has an average molecular weight (M_W) of ~8000 Da corresponding to approximately 6–7 repeating units, and a polydispersity index of 1.98.

Takata[906,908] has also employed the sulfolene macrocycle **MBASO$_2$** in the synthesis (**Scheme 2.75**) of rotaxanes such as the porphyrin-stoppered [2]rotaxane **R253SO$_2$** and subsequently carried out a Diels-Alder cycloaddition in order to attach buckminsterfullerene (C_{60}) to the ring and investigate the photoinduced electron transfer properties of the resulting mechanically-linked **R253C$_{60}$** donor-acceptor triad.

Graeme Cooke[909,910] has relied on the clipping of benzylic amide macrocycles around succinamide templates to prepare (**Figure 2.48**) rotaxanes[909] and catenanes[910] incorporating redox-active flavin moieties in their constitution. The [2]rotaxane **R254** and [2]catenane **C254** are prepared by the standard clipping protocol in yields of 67% and 26%, respectively.

The synthesis (**Scheme 2.76**) of rotaxanes derived from the PBA26C6 ring (see **Table 2.20**) have been carried out in the laboratories of Chiu[856,911] and Philp.[857,858] Chiu[856,911] has employed urea derivatives as templates in the synthesis of the [2]rotaxanes such as **R255**, which relies on a urethane-forming reaction between an phenylisocyanate-functionalized tetraphenylmethane stopper precursor and a hexanol-terminated semidumbbell in the presence of the PBA26C6 ring. Philp,[857,858] on the other hand, has employed diarylamides as recognition units in the synthesis of the [2]rotaxanes **R256–R258**. The protocol that generates **R257**, **R258**, and **R258H$_2$** involves 'capturing' a ring on a dumbbell at low temperature under thermodynamic control before

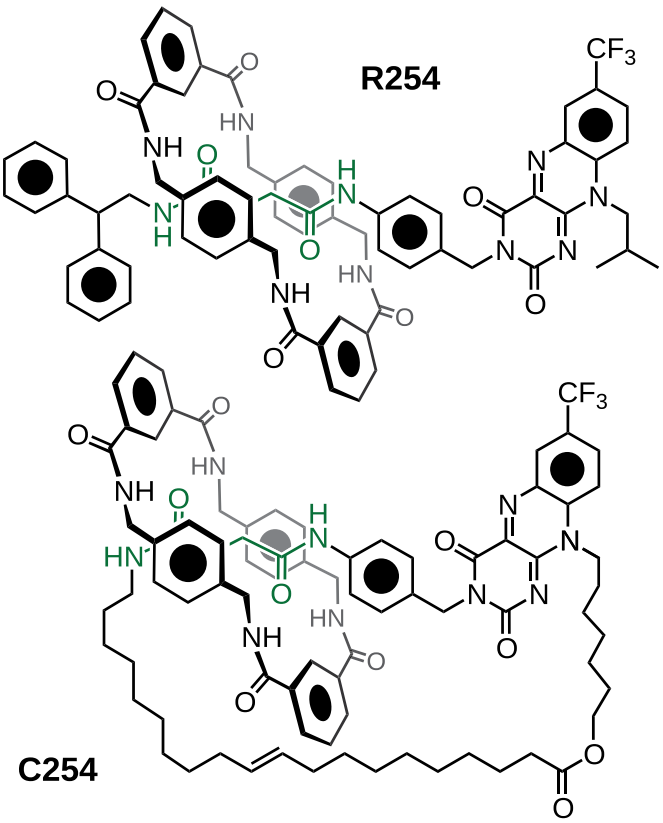
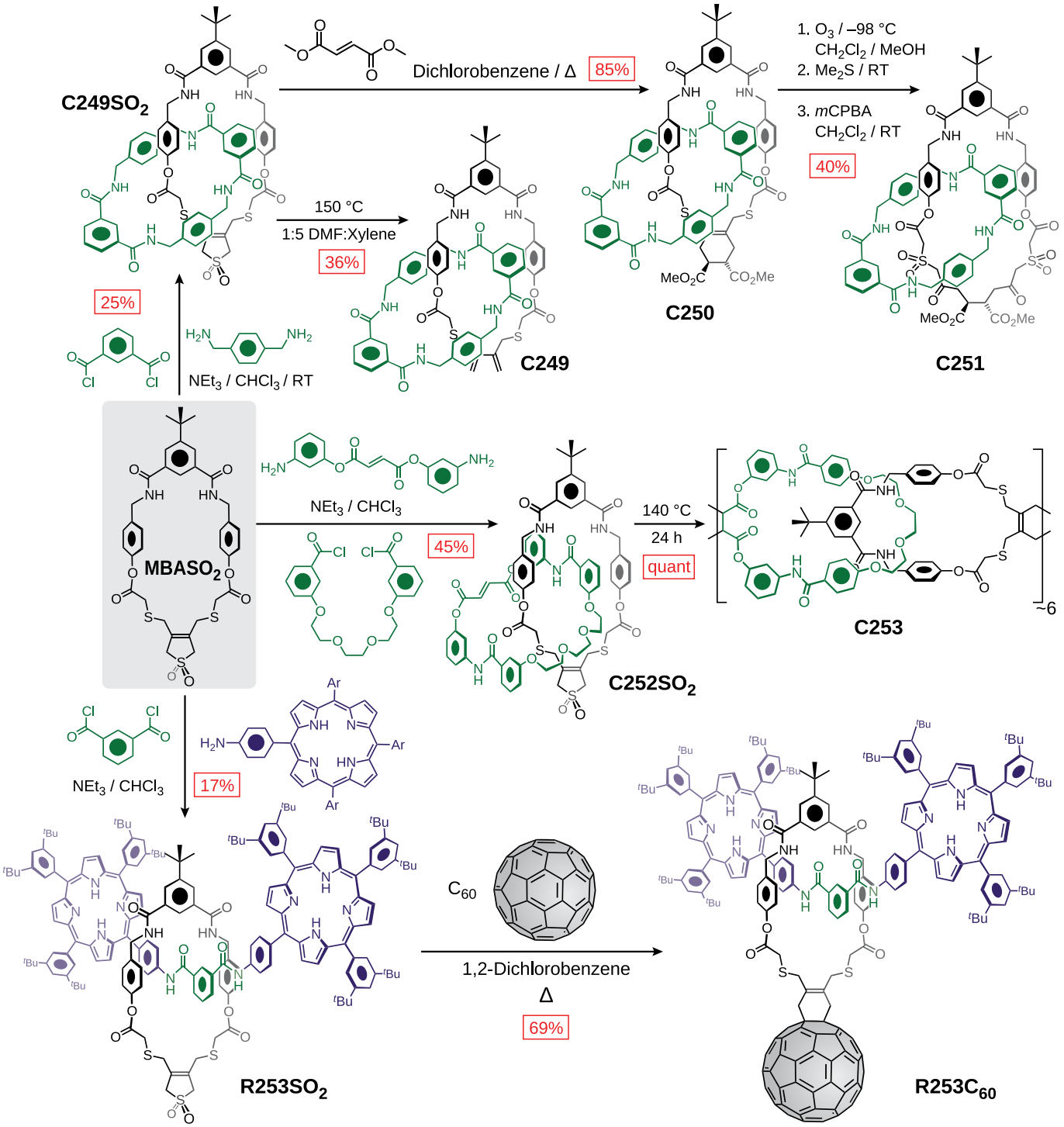
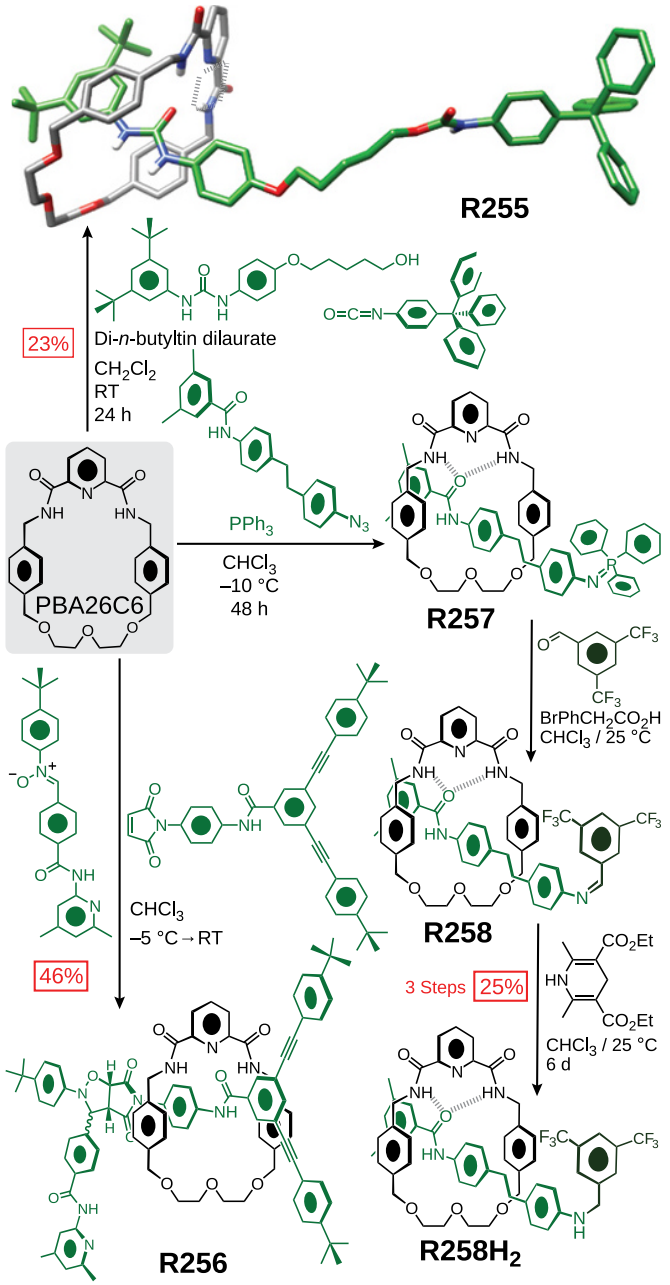


Figure 2.48 Cooke's flavin [2]rotaxane[909] **R254** and [2]catenane[910] **C254**



Scheme 2.75 Synthesis and post-synthetic Diels-Alder modifications of benzylic amide catenanes and rotaxanes based on Takata's sulfolene-containing macrocycle $MBASO_2$[905–908]

fixing it under kinetic control at higher temperature. Philp's approach[858] relies upon a stoppering reaction involving the rapid formation of an iminophosphorane (i.e., Staudinger ligation) from an azide-terminated half-dumbbell and triphenylphosphine in the presence of the benzylic amide macrocycle. This reaction proceeds rapidly even at low temperatures, where the association constant (**Table 2.20**) between the diarylamide recognition unit and the PBA26C6 ring is higher. The resulting rotaxane **R257** can be manipulated subsequently at elevated temperatures. Stopper exchange with 3,5-bis(trifluoromethyl)benzaldehyde affords the imine-stoppered rotaxane **R258**, and reduction of the corresponding imine bonds affords the kinetically stable rotaxane $\mathbf{R258H_2}$ in a 25% yield over the three steps from the macrocyclic and dumbbell precursors. This idea of trapping weakly associated components with labile mechanical



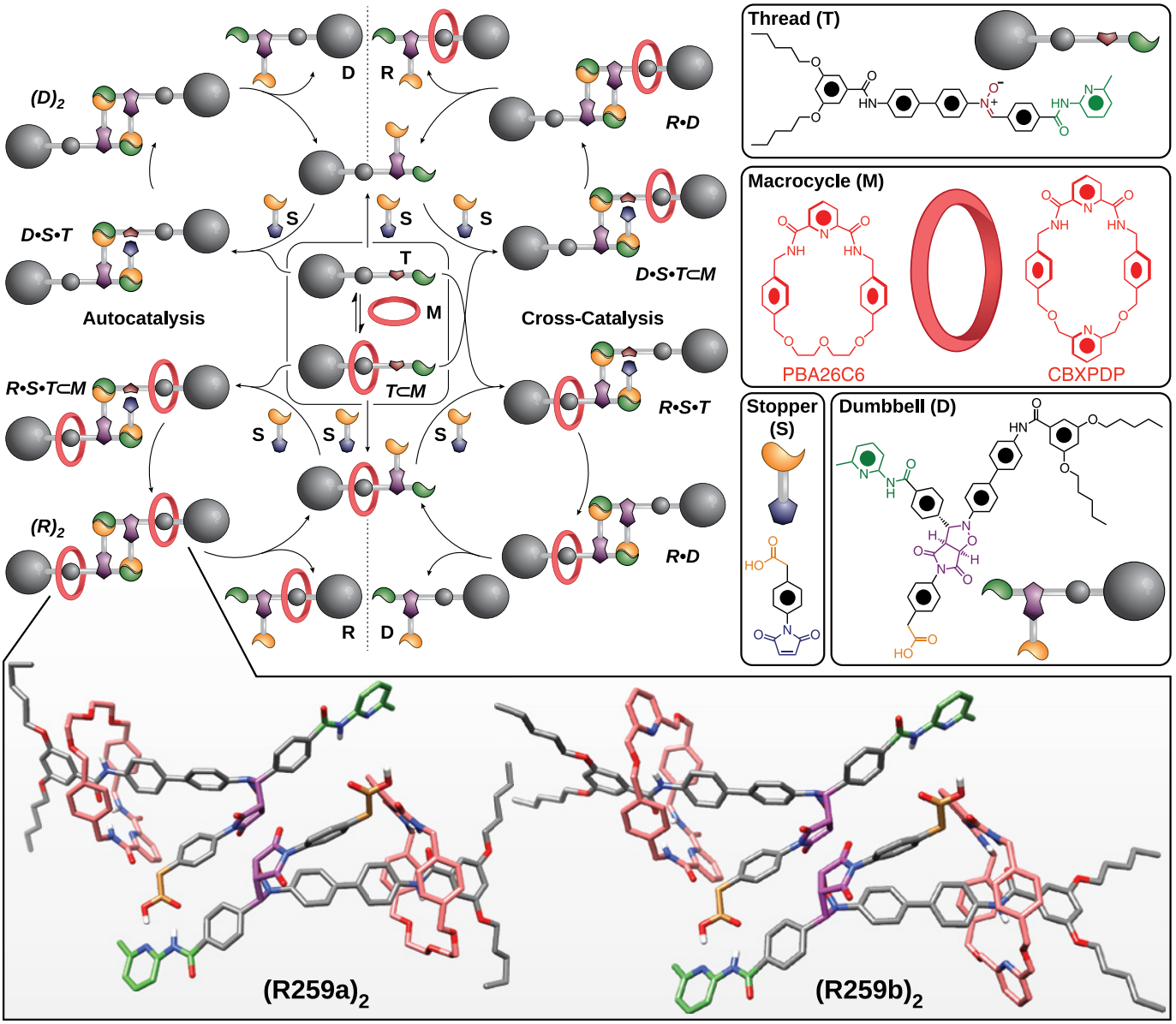
Scheme 2.76 Various synthetic routes[856–858] to rotaxanes based on a pyrido benzylic amide ring PBA26C6.

bonds at low temperature could be applied, in principle, to the synthesis of MIMs based on other host-guest and supramolecular systems.

R256 and a structurally similar homologue possessing a carboxylic acid moiety were designed initially to explore the possibility of self-replicating rotaxanes.[857] Although this goal was met with limited success in the beginning, Philp's latest iteration[912] of a self-replicating (**Scheme 2.77**) rotaxane design has produced more promising results. The reactants involved in this self-replicating system include a semidumbbell thread (T), a stopper precursor (S), and a macrocycle (M). Thread T possesses in its consitution (i) an amide recognition site for M to encircle, (ii) a 6-methyl-2-amidopyridine recognition site that hydrogen bonds with a complementary phenylacetic acid moiety in the constitution of the stopper, and (iii) a reactive nitrone group that readily undergoes a 1,3-dipolar cycloaddition with the maleimide unit of S. Semidumbbell T and the corresponding semirotaxane *T⊂M* ($K_a \approx 4–5 \times 10^3$ M^{-1} at 223 K in $CDCl_3$) generate a dumbbell (D) and a rotaxane (R), respectively, when they react with S. In turn, D and R both act as templates for the formation of themselves and each other in autocatalytic and cross-catalytic cycles (**Scheme 2.77**), respectively. Autocatalysis is promoted by the formation of the intermediate ternary complexes, [*D•S•T*] and [*R•S•T⊂M*], which template the formation of homodimers $(D)_2$ and $(R)_2$, respectively. Cross-catalysis is promoted by the formation of intermediates [*D•S•T⊂M*] and [*R•S•T*], both of which lead to the [*D•R*] heterodimer as S is consumed in the reaction. The production of D and R is accelerated as these heterodimers and homodimers dissociate, rendering more D and R templates available. The rotaxane self-replicators have incorporated either PBA26C6 or cyclo[2,6-bis(xylyloxymethyl)pyridine-2,6-diamidopyridine] (CBXPDP) rings as component M, giving rise to rotaxanes **R259a** and **R259b**, respectively. The crystallographically determined solid-state structures of the $\mathbf{(R259a)_2}$ and $\mathbf{(R259b)_2}$ homodimers are also illustrated in **Scheme 2.77**. An analysis of the reaction kinetics provides evidence that these autocatalytic and cross-catalytic cycles are indeed operative with approximately equal efficiency. In the absence of any added template, an initial lag period in product formation is followed by a rate acceleration, generating a sigmoidal curve that is characteristic of autocatalytic systems. When 10 mol % T, D, or R are introduced at the outset of the reaction as instructing templates, an initial rate enhancement is observed on account of the disappearance of this lag period. At initial reactant concentrations of 10 mM, the D:R ratios are 3:1 in the case of **R259a** and 2:1 in the case of **R259b** after 4 h at 278 K in $CHCl_3$, reflecting a slightly higher binding constant of CBXPDP compared to PBA26C6. Fitting of the kinetic data to an appropriate model reveals apparent K_a values for the *T⊂M* pseudorotaxanes that are an order of magnitude lower than the experimentally determined K_a values exceeding 10^3 M^{-1}. This result can be rationalized by the rings' ability to bind the thread's nitrone site, which inhibits reactivity, as well as its 6-methyl-2-amidopyridine unit, which interferes with the formation of the ternary intermediates. Thus, the D:R ratios can be improved to favor rotaxane formation by increasing the apparent K_a value of the semidumbbell complexes *T⊂M*.

Squaraine Rotaxanes

Smith[913] at the University of Notre Dame has developed a novel family of benzylic amide rotaxanes that are templated by the zwitterionic chromophores known as squaraines. His group's first communication[914] on this class of compounds showed that surrounding a bis(anilino)squaraine dye

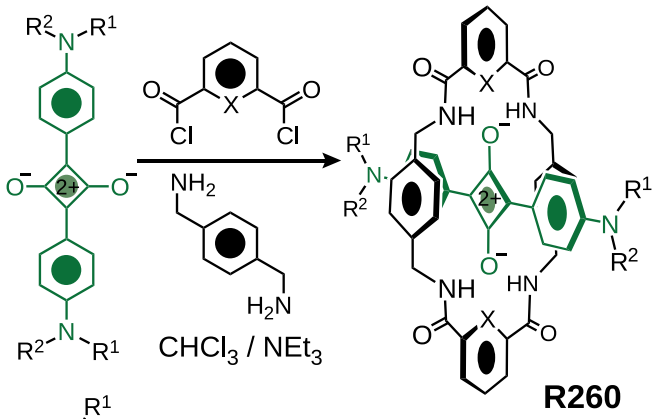


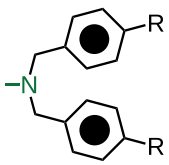
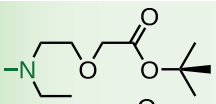
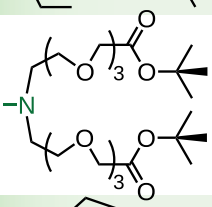
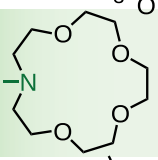
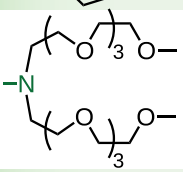
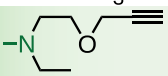
Scheme 2.77 The autocatalytic and cross-catalytic cycles associated with the synthesis of Philp's self-replicating rotaxanes, as well as solid-state structures of the product dimers in the crystal.[912] Hydrogen atoms and solvent molecules are omitted for the sake of clarity.

molecule with a benzylic amide macrocycle can enhance its chemical stability and improve its photophysical properties by preventing aggregation-induced broadening or quenching effects. The syntheses[914–918] of a number of squaraine rotaxanes with different stoppers are summarized in **Table 2.23**. The rotaxanes **R260a-g** have been prepared by the same clipping protocol employed by Leigh (*vide supra*) in the synthesis of benzylic amide MIMs, usually with yields (20–50%) ranging from average to relatively high for benzylic amide rotaxanes. All of these squaraine rotaxanes are stable at room temperature in low-polarity solvents.[917] Even in polar organic solvents, only **R260g**, which possesses a small propargylic stopper, allows the ring to deslip gradually on the laboratory timescale, with a half-life of 12 h in Me_2SO. The *tert*-butoxycarbonyl stoppers of rotaxanes such as **R260c** and **R260d** can be converted efficiently to the corresponding carboxylic acids and thus rendered water-soluble. Stability in water is also high, as revealed by an investigation[919] on a number of water-soluble homologues in which the most stable squaraine rotaxanes were those possessing the bulkiest stopper groups.

According to Smith,[913] the benzylic amide / squaraine rotaxanes are relatively easy to crystallize, allowing a number of them to be characterized (**Figure 2.49**) by X-ray crystallography. The solid-state structures[914,916,918] reveal that the tetralactam ring can adopt either a chair-like or boat-like conformation. Whereas isophthalamide-based rings adopt a chair-like conformation in both cases (**R260a** and **R260c**), 2,6-dicarboxamidopyridine-based rings can adopt either chair-like (**R260b**) or boat-like (**R260e-f**)

Table 2.23 Summary of the synthesis of some of Smith's benzylic amide / squaraine rotaxanes.



		R	X	Yield / %	Ref
a		H	CH	28	914
b		H	N	30	914
c		Me	CH	45	918
d		Me	N	31	918
e		Br	N	29	918
f		I	N	26	916
g			N	20	915
h			N	15	917
i			CH	29	917
j			N	20	917
k			N	22	917

conformations. In solution, the chair and boat conformations are rapidly equilibrating on the ^{1}H NMR timescale even at low temperatures, as the rings shuttle back and forth about the center of the zwitterionic C_4O_2 core of the squaraine dumbbell. The rings with pyridyl subunits wrap more tightly around the squaraine templates than their isophthalamide counterparts, since the centroid-to-centroid distance in much shorter in the case of the former (~6.6 Å) compared to the latter (~7.1 Å) in the solid state.

Other squaraine-based templates that have been employed in the synthesis (**Scheme 2.78**) of benzylic amide rotaxanes

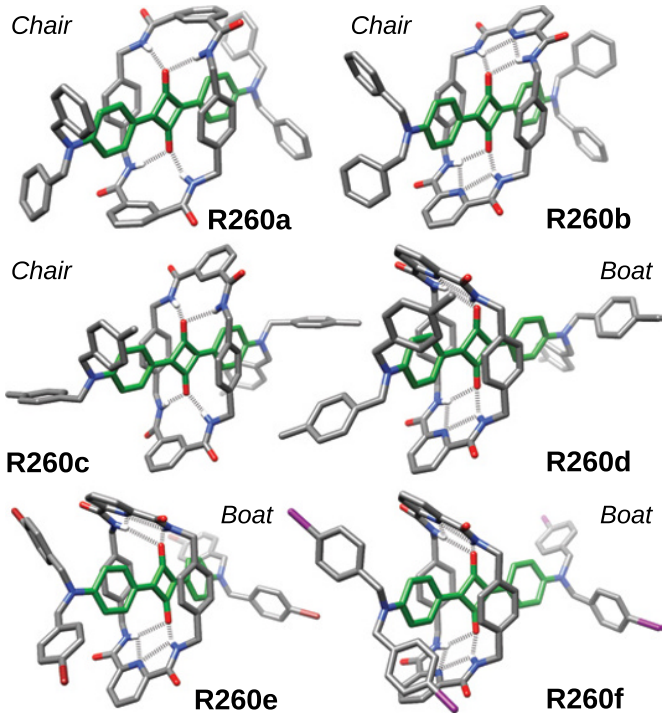
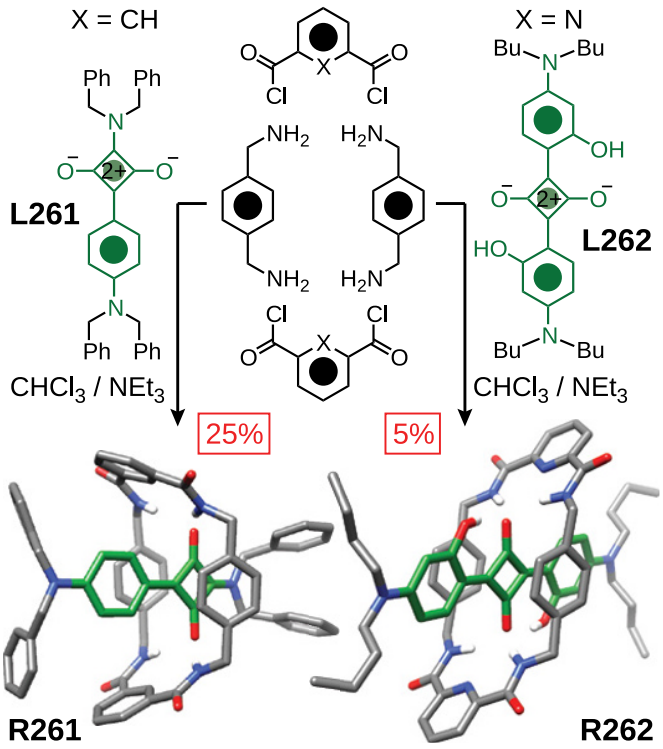


Figure 2.49 Single-crystal X-ray structures[914,918] of squaraine rotaxanes **R260a-f**—see **Table 2.23**. The tetralacatam ring adopts a chair-like conformation when the ring comprises isophthalamide linkers, whereas rings possessing 2,6-dicarboxamidopyridine units are more likely to adopt boat-like conformations.



Scheme 2.78 The synthesis[918,920] of squaraine rotaxanes **R261** and **R262**.

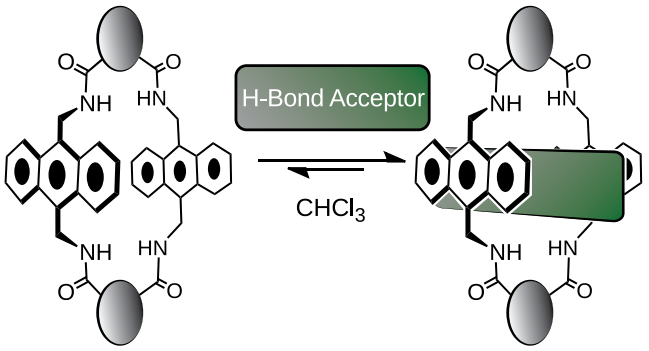
include (i) the 'truncated' mono(anilino)squaraine[918] **L261**, which is less electrophilic than the bis(anilino)squaraines as a result of having a tertiary amine connected directly to its C_4O_2 core, as well as (ii) the *o*-hydroxyphenyl-substituted squaraine[920] **L262**, which is rigidified by internal hydrogen bonds between the hydroxyl protons and the oxygen atoms of the C_4O_2 core, such that rotation of the phenylene and squaraine rings about the C–C bonds connecting them is inhibited. Whereas the **L261→R261** clipping reaction proceeds in 25% yield, the **L261→R261** clipping yield is only 5%, most likely because the internal hydrogen bond network of the squaraine template competes with the intermolecular hydrogen bonding network with the ring precursors that is required to promote rotaxane formation. **R261** represents a rare case of an isophthalamide-based ring adopting a boat conformation, most likely on account of steric constraints imposed by the truncated squaraine dumbbell.

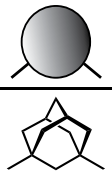
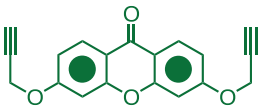
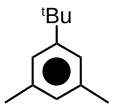
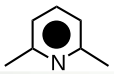
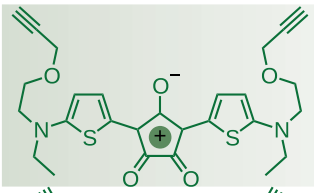
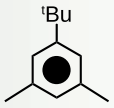
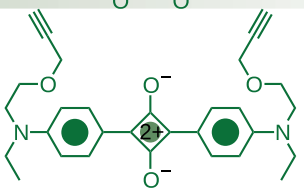
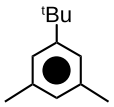
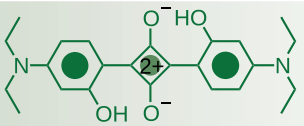
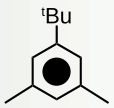
Anthrylic Amide Rings

Although the tetralactam benzylic amide rings are essentially insoluble, Smith[921] made the surprising discovery that the 9,10-anthrylic homologues are soluble in organic solvents. This increased solubility facilitates the self-assembly (**Table 2.24**) of pseudorotaxanes in solution, opening up the possibility of preparing anthrylic amide rotaxanes by stoppering protocols as an alternative to the conventional clipping routes. In addition to bis(anilino) squaraine derivatives,[921,922] xanthone[923] and croconaine[924,925] dyes have been encapsulated within anthrylic tetralactam macrocycles and characterized quantitatively in terms of their binding constants. Pseudorotaxanes comprising bis(propargyloxy)xanthone and anthrylic rings with different dicarboxamido linkers—namely, 1,3-adamantane, 2,6-pyridine, and 5-*tert*-butyl-isophthalic units—are highly sensitive to the linker, since the corresponding K_a values in $CHCl_3$ span more than an order of magnitude, with the adamantyl spacer being the least effective and the pyridyl spacer being the most effective at stabilizing the host-guest complex.

The syntheses (**Scheme 2.79**) of the two rotaxanes, **R264a** and **R264b**, employing squaraine[850] and thiosquaraine[926] templates, respectively, have been carried out by stoppering protocols involving CuAAC click chemistry. The squaraine rotaxane **R264a** is obtained[850] in 90% yield, reflecting the high association constant (>10^5 M^{-1}) of the squaraine template. The much lower yield (30%) obtained[926] when employing a thiosquaraine template suggests a lower K_a value, although no binding constant was measured in this case. NMR Spectroscopy and geometry optimization *in silico* both indicate that the thiosquaraine [2]rotaxane **R264b** adopts an unsymmetrical co-conformation, with the ring in a boat conformation centered in between the C_4S_2 core and one of the anilino appendages, on account of the larger atomic radius (1.8 Å) of sulfur compared to that (1.5 Å) of oxygen, which inhibits the passage of the ring over the thiosquaraine moiety. Translocation of the ring

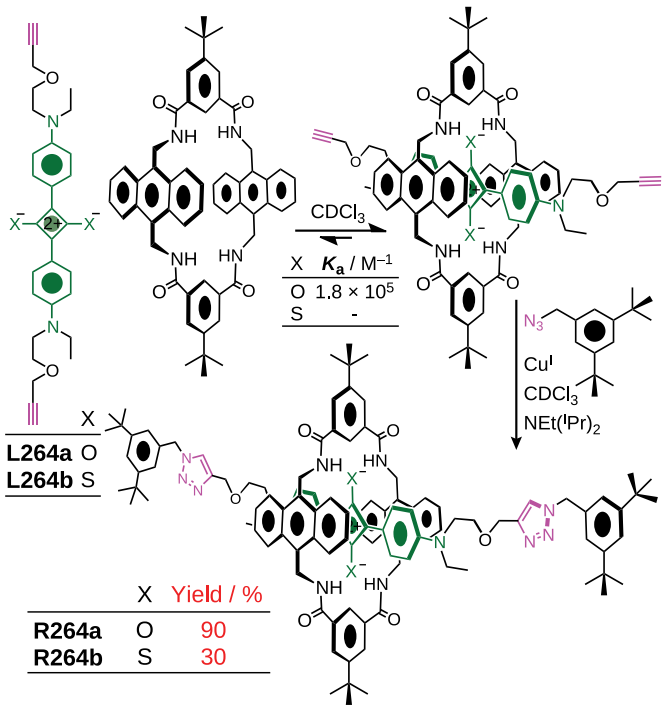
Table 2.24 Association constants, K_a, for pseudorotaxanes comprising 9,10-anthrylic amide tetralactam rings with different dicarboxamido linkers and various hydrogen bond accepting guests.



Acceptor	K_a / M^{-1}	Ref
	95	923
 	356	923
	1080	923
 	340,000	924
 	180,000	921
 	15,000	922

across the thiosquaraine barrier in **R264b** is slow on the ^1H NMR timescale even at elevated temperatures, in contrast with the oxygen-based homologue **R264a**.

Since the croconaine zwitterion also binds anthrylic tetralactams with high affinities (see **Table 2.24**), a corresponding thiophene-functionalized croconaine rotaxane **R265** has been prepared[927] (**Scheme 2.80**) by a CuAAC stoppering protocol in 84% yield. Perhaps even more remarkably, the standard clipping protocol, which typically proceeds in <50% yield for benzylic amide rotaxanes, delivers (**Scheme 2.80**) the croconaine / anthrylic amide [2]rotaxane **R266** in 81% yield. These croconaine rotaxane dyes appear to have photothermal properties which show some promise as prospects for a number of potential applications, including photothermal therapy.[925]

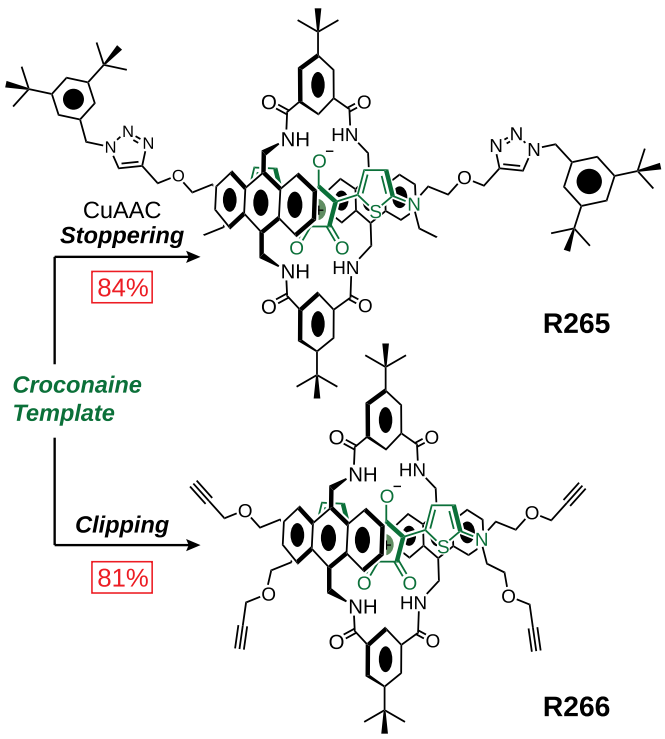


Scheme 2.79 Synthesis of squaraine and thiosquaraine rotaxanes from a soluble anthrylic amide macrocycle using CuAAC click chemistry[850,926]

Another important property of the anthrylic amide macrocycle is its ability to undergo a cycloaddition reaction with singlet molecular oxygen at the site of the anthracene sidewalls.[928] Photooxygenation[929] of the squaraine / anthrylic amide rotaxane **R264a** with red light in the presence of air produces the corresponding mono(endoperoxide) in quantitative yield. The anthrylic amide macrocyclic receptor still exhibits high affinity for squaraine guests as the endoperoxide, and binds them much more favorably than does the corresponding exoperoxide, which is the kinetic product of the cycloaddition.[930] Endoperoxide rotaxanes are storable indefinitely at low temperatures and undergo a clean thermal cycloreversion above room temperature, releasing singlet oxygen and emitting light.

Davis[931] has recently reported that 9,10-anthrylic tetralactams, when rendered water-soluble by the introduction of multiple negatively charged carboxylic acid sites on the isophthalamide units, bind glucose with remarkably high selectivities and association constants on the order of 10^2 M^{-1} in water. This 'synthetic lectin' has not yet been utilized, however, in the synthesis of carbohydrate-containing mechanomolecules. More recently, Davis[932] found that polysaccharides thread through the cavity of a three-dimensional, pyrene-based hexalactam analogue of this synthetic lectin with high affinities (up to 19,000 M^{-1}), leading to the formation of carbohydrate polypseudorotaxanes of cellulose and chitosan. See **Section 4.1.1.1**. These new results on π-extended benzylic amides suggests that they may be suitable component parts for the genesis of a new class of MIMs based on threaded carbohydrates.

A meccano set of building blocks employed in the construction of tetralactam hosts is presented in **Figure 2.50** as a partial summary of **Sections 2.3.4.2–2.3.4.3**. It is remarkable that such a diverse and functional set of molecules with mechanical bonds can arise from such a small set of readily available components.



Scheme 2.80 Croconaine rotaxanes[927] prepared by stoppering and clipping protocols.

2.3.4.3 Cyclic Peptides

The mechanical interlocking of peptide fragments in proteins is a known, albeit somewhat rare, phenomenon in biochemistry—see **Sections 1.1.1** and **2.3.11.2**. Little is known, however, about how to interlock oligo- and polypeptides in a wholly synthetic context. Leigh's dipeptide-templated benzylic amide MIMs (**Section 2.3.4.2**) are accompanied by very few other recognition motifs that rely on peptides as part of a templation strategy for making mechanical bonds. Interlocking peptide fragments is challenging in practice because intermolecular noncovalent bonding interactions are generally required to direct the templation of a mechanomolecule, yet the amide groups of a polypeptide chain are largely self-satisfied by intramolecular hydrogen-bonding interactions. One of the only other recognition motifs to accompany benzylic amides in the (partial) use of peptides as recognition elements in mechanostereochemistry has also been introduced by Leigh,[933] who has employed the octameric and decameric cyclic peptide hosts cyclo(ProGly)$_4$ and cyclo(ProGly)$_5$, respectively, in the synthesis (**Scheme 2.81**) of the [2]rotaxanes **R267a-d.** These stoppering reactions rely on the coupling

of acyl chloride-functionalized stopper precursors with hydroxylated termini of threads possessing (a) ethane-1,2-diammonium or (b) butane-1,4-diammonium units as templates in $CHCl_3$/MeCN (3:7 v/v) at room temperature for one week. These proline/glycine cyclic peptides and their complexes with alkylammonium guests were introduced in the 1970s by Blout.[934,935] Although the cyclopeptides exhibit high affinities (10^3–10^5 M^{-1}) for cationic guests in MeCN, monocationic dialkylammonium or pyridinium threads lead to rotaxanes in only trace amounts by this method. The dicationic templates of **R267a-d**, however, promote the formation of mechanical bonds in 56–63% yield. The forces involved in the templation of these rotaxanes include [N^+–H···O] hydrogen bonds between the dialkylammonium centers and the carbonyl groups of the cyclopeptides, which outcompete the internal hydrogen bond network of the hosts, as well as electrostatic [C=Oδ^-···N^+] interactions. The rings—especially the larger cyclo(ProGly)$_5$ one—are held relatively loosely on the dumbbell, allowing them access to both dialkylammonium sites by their rapid shuttling along its entire length.

Although they are not the canonical amino acids, polypseudorotaxanes based on cyclic hexamers of β-glucosamino acid and PEG chains have also been reported.[936]

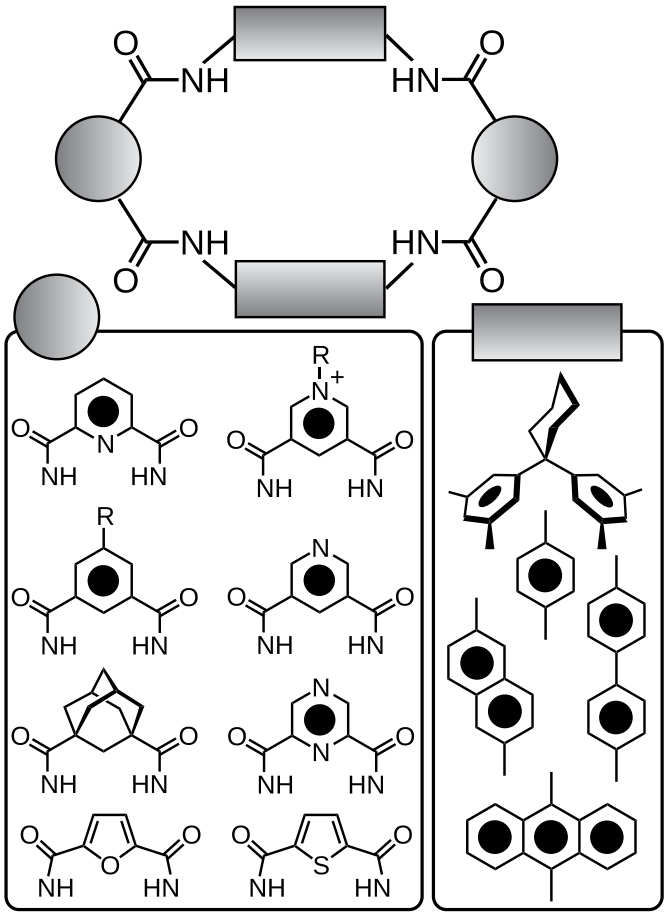
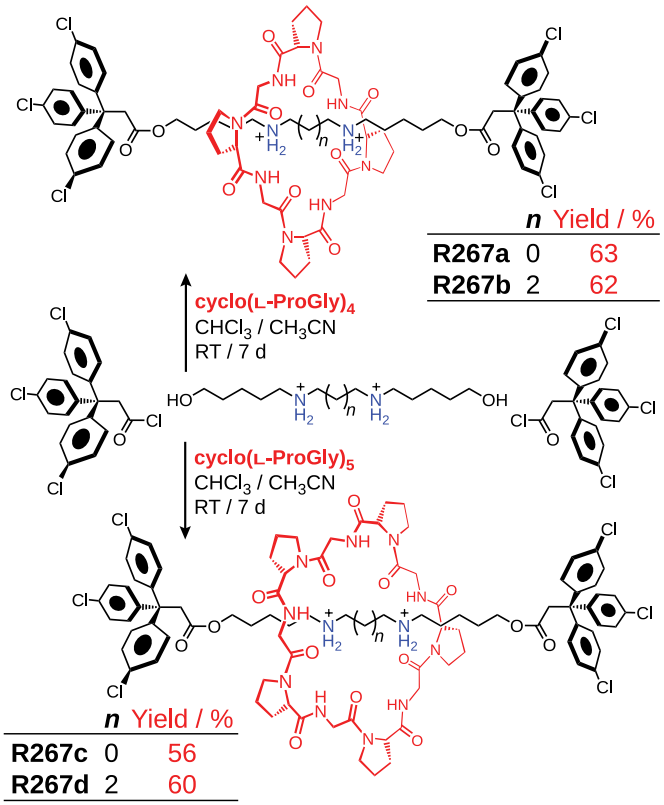


Figure 2.50 The meccano set of building blocks involved in the mechanostereochemistry of tetralactam macrocycles.

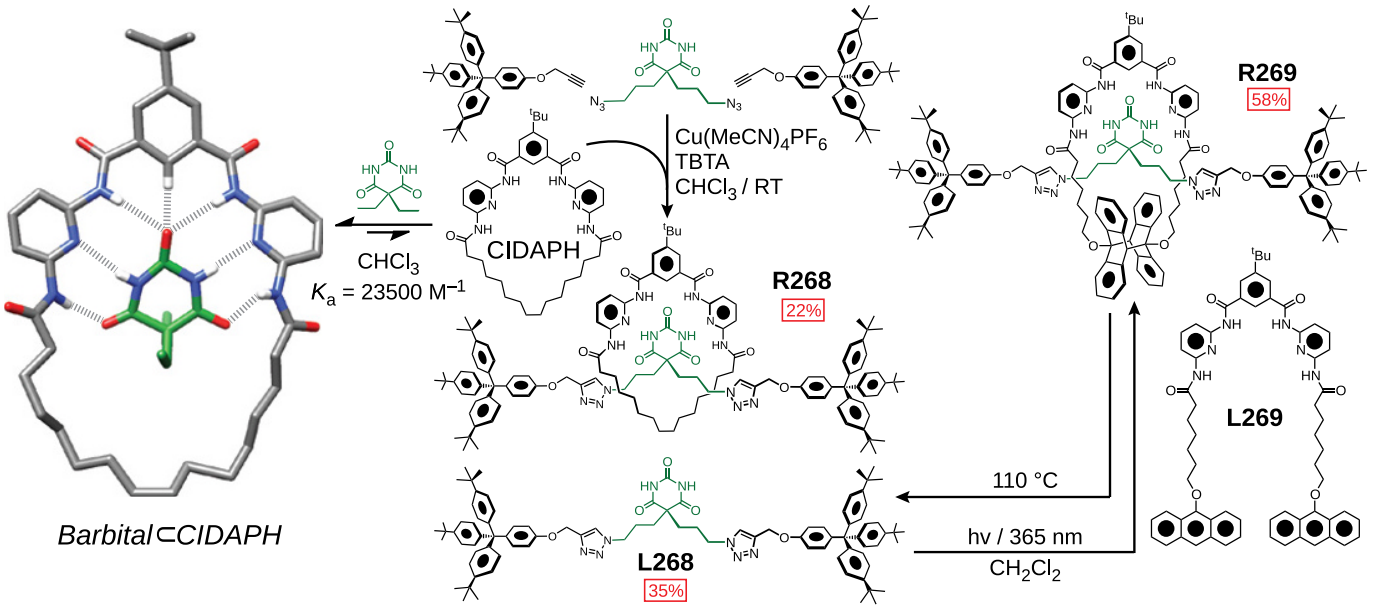


	n	Yield / %
R267a	0	63
R267b	2	62
R267c	0	56
R267d	2	60

Scheme 2.81 Leigh's synthesis of [2]rotaxanes from the cyclic peptides cyclo(L-ProGly)$_4$ and cyclo(L-ProGly)$_5$ and bis(dialkylammonium) templates with either ethylene or butylene bridging units by a stoppering protocol.[933]

2.3.4.4 Bis-2,6-diamidopyridine/Barbiturate Templates

Late in the 1980s, Hamilton[937,938] developed a series of receptors based on an isophthalic bis-2,6-diamidopyridine recognition motif with endotopic hydrogen bond donors (D) and acceptors (A) arranged in a pattern (DADDAD) that is fully complementary to that (ADAADA) of the double-imide motif of barbiturates. These bis-2,6-diamidopyridine receptors exhibit high selectivities and affinities for barbiturates in non-competing solvents on account of their ability to form up to six intermolecular hydrogen bonds—barbital, for example, binds[938] to some of these hosts with association constants of up to ~10^6 M^{-1} in CH_2Cl_2. Although this class of receptors has been applied to a number of different problems in the supramolecular community, it was only very recently that McClenaghan[939,940] employed this recognition motif in the synthesis (**Scheme 2.82**) of rotaxanes. The macrocyclic Hamilton-type receptor, cyclo(isophthalobis(2,6-diamidopyridine-hexadecamethylene) (CIDAPH) binds barbital with a high K_a value of 23500 M^{-1} in $CHCl_3$. The X-ray crystal structure (**Scheme 2.82**) of this host-guest complex reveals the presence of the expected six [N–H···O] hydrogen bonds, as well as a short-contact [C–H···O] interaction between the endotopic proton of the host's central phenylene bridge and the guest's central carbonyl group. The *barbital⊂CIDAPH* complex adopts a pseudorotaxane-like geometry, with each of the Et groups appended to the ring of barbital protruding



Scheme 2.82 Synthesis of bis-2,6-diamidopyridine / barbiturate rotaxanes by stoppering (left) and clipping (right) protocols, driven by CuAAC and anthracene photodimerization reactions,[939,940] respectively. The solid-state superstructure of *barbital⊂CIDAPH* is represented with protons not engaged in hydrogen-bonding interactions omitted for the sake of clarity.

from opposite ends of the CIDAPH cavity. McClenaghan[939] reasoned that appending reactive endgroups to the barbital template would make it possible to construct rotaxanes by a stoppering protocol. Indeed, the Cu^{I}-catalyzed click reaction (**Scheme 2.82**) between 5,5-diazidopropylbarbituric acid and bulky propargylated tetraphenylmethane stopper precursors in the presence of CIDAPH leads to the formation of the [2]rotaxane **R268** in 22% yield.

The major product (35%) of the click reaction is the unrotaxanated dumbbell **L268**, which can also be synthesized[939] in 80% yield in the absence of CIDAPH. **L268** has been employed[940] in the template-directed synthesis (**Scheme 2.82**) of the barbiturate [2]rotaxane **R269** by a clipping protocol involving anthracene photodimerization. In this case, an acyclic bis-2,6-diamidopyridine recognition unit appended with 9-anthracenyloxy groups, **L269**, serves as the reactive precursor. Irradiation of an equilibrated mixture of **L268** and **L269** (K_a of ***L268⊂L269*** = 55000 M^{-1}) in CH_2Cl_2 with UV light (365 nm cutoff) generates the [2]rotaxane **R269** in 58% yield. The length of the oligomethylene linkers connecting the reactive 9-alkoxyanthracene groups to the bis-2,6-diamidopyridine recognition unit was optimized at the hexamethylene size. Trimethylene linkers provide no interlocked products and nonamethylene linkers deliver a kinetically labile pseudorotaxane instead. The [4π+4π] photocyclization of the anthracene units was found to occur only in the antiparallel, or head-to-tail, geometry. The process can be also reversed by heating at 110 °C for 14 h, which leads to a retrodimerization of the anthracene units and restores the starting materials. The photodimerization and retrodimerization were repeated with some fatigue (37%) over four thermal cycles. This newly introduced class of bis-2,6-diamidopyridine / barbiturate rotaxanes appears to hold some promise for the development of bistable and multistable molecular shuttles and switches.

2.3.4.5 Tetraureido Calixarene Capsule Templates

Volker Böhmer[941] at the University of Mainz is a leading figure in the world of calixarenes. His group has employed calix[4]arenes with urea appendages on each of the arene subunits as templates in the synthesis of mechanical bonds. The ability of tetraureidocalix[4]arenes to self-assemble into dimeric capsules held together by a seam of intermolecular hydrogen bonds is now a well-known phenomenon, first reported by Rebek[942,943] late in 1995 and quickly followed independently by Böhmer[944,945] in 1996. The solid-state superstructure[945] of a dimeric capsule of the kind serving as a basis for Böhmer's MIMs is illustrated in **Figure 2.51**.

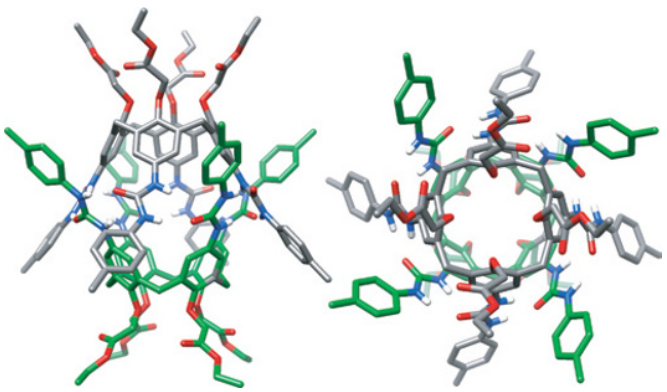
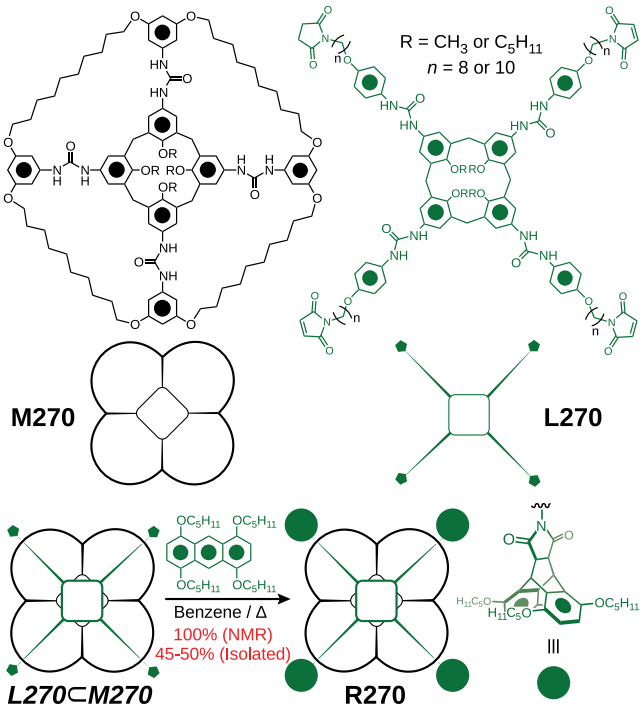


Figure 2.51 Two views of tubular representations of the solid-state structure of Böhmer's tetraureidocalix[4]arene homodimeric capsule, stabilized at the center by a seam of bifurcated [N–H···O] hydrogen bonds.[945] Solvent molecules and protons are omitted for the sake of clarity.

Böhmer[946] has outlined a strategy for preparing MIMs from the interdigitated capsules by crosslinking their urea appendages in various patterns in order to produce multi-annulated structures and multicatenanes. Olefin metathesis, a thermodynamically controlled reaction, has been the main workhorse for this chemistry (**Section 3.4**). There is, however, one example[947] of a fourfold interlocked [2]rotaxane, **R270**, which is based on this motif and prepared (**Scheme 2.83**) by a Diels-Alder cycloaddition.



Scheme 2.83 Böhmer's synthesis of a fourfold interlocked [2]rotaxane from a heterodimeric calix[4]arene capsule template via a Diels-Alder cycloaddition as the stoppering reaction.[947]

The stoppering protocol relies on the self-assembly of the heterodimeric capsule / pseudorotaxane ***L270⊂M270*** from the respective macropentacyclic calix[4]arene macrocycle **M270** and the imide-terminated calix[4]arene **L270** in benzene. The Diels-Alder cycloaddition between the imide dienophiles and 1,4,5,8-tetrapentyloxyanthracene as the diene creates a stopper, which is sufficiently bulky to prevent the capsule from dissociating. The yield appears to be quantitative when the reaction is carried out within an NMR tube, although isolated yields are only 45–50%. See **Section 4.1.3.4** for other multiply interlocked architectures templated by the tetraureidocalix[4]arene capsules.

2.3.4.6 Sec-Ammonium / Crown Ether Templates

The self-assembly of host-guest complexes comprising crown ethers and secondary dialkylammonium ions is among the most widespread motifs[948–950] in mechanostereochemistry, mainly on account of (i) the ready availability of starting materials, which are often sold commercially or accessible in only one or two synthetic steps, as well as (ii) their good solubility in many organic solvents. The complexes (pseudorotaxanes) are dissociated for the most part in high polarity solvents such as DMF and Me_2SO, and so these solvents have to be avoided when synthesizing MIMs of this kind.

Dialkylammonium/Crown Ether Pseudorotaxanes

Although the complexes formed between crown ethers and substituted primary alkylammonium cations are among the oldest[151,152] and most well studied entities in supramolecular chemistry, interpenetrated superstructures based on these components were relatively late to appear on the scene because chemists had focused their attention primarily on inorganic ammonium and primary alkylammonium cations with relatively small crown ethers such as [18]crown-6 (18C6), which are too small to be interpenetrated by these cations. Instead, primary ammonium groups interacting with crown ethers usually adopt (**Figure 2.52a**) 'perched' co-conformations with a 3-point binding geometry involving three [N^+–H···O] contacts between the ammonium protons and the oxygen atoms of ring. Prior to 1995, only a handful of complexes comprising secondary dialkylammonium salts and crown ethers were known,[951,952] the $–NH_2^+–$ centers of which adopt (**Figure 2.52b**) conceptually similar two-point geometries with crowns ranging from [12]crown-4 (12C4) to [18]crown-6 (18C6) in size. It was not until larger crown ethers, such as dibenzo[24]crown-8 (DB24C8), were introduced as hosts for dialkylammonium cations that pseudorotaxanes (**Figure 2.52c**) based on these components were realized in a discovery that was made independently in 1995 by our group[953] at Birmingham University and that of Daryle Busch[954] at the University of Kansas.

Owing to their commercial availability and status as the first components to be introduced[953,954] into dialkylammonium pseudorotaxanes, dibenzo[24]crown-8 (DB24C8) hosts and dialkylammonium guests are the most widely and frequently employed components in the meccano set (**Figure 2.53**) of components representing this recognition motif. Alkylanilinium guests have been employed[955,956] to a much lesser extent, as have a number of 20–30-membered

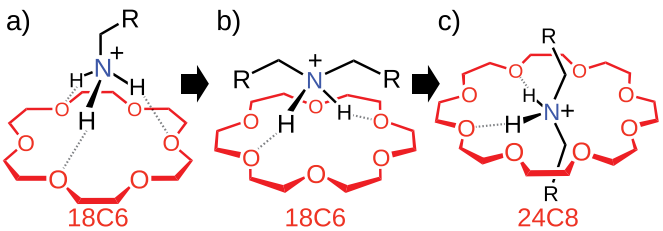


Figure 2.52 A conceptual journey from the three-point binding geometry of face-to-face (perched) complexes of primary ammonium groups and small crown ethers such as 18C6 (a), to analogous two-point complexes based on secondary ammonium salts (b), to pseudorotaxanes comprising secondary ammonium salts and larger crown ethers such as those based on 24C8 (c) which constitute a robust meccano set for constructing MIMs.

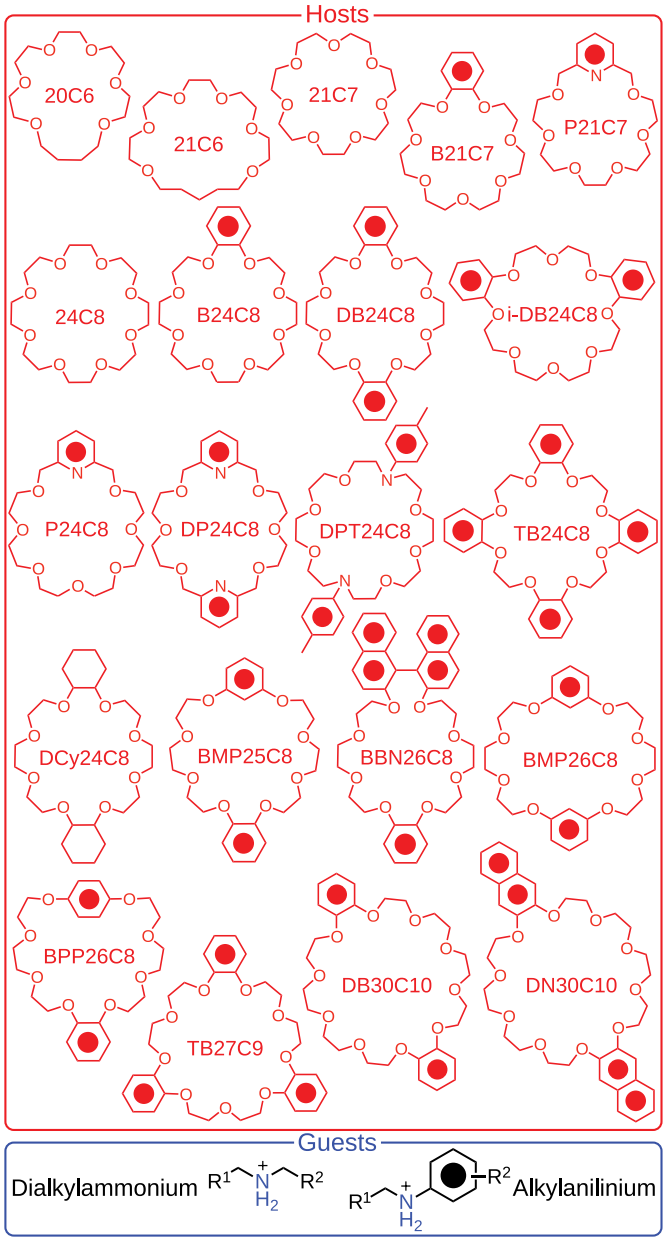


Figure 2.53 A meccano set of components for pseudorotaxanes and MIMs based on crown ethers and secondary ammonium ions.

crown ethers of various constitutions,[957] all of which bind secondary ammonium ions in a 1:1 ratio. The self-assembly of pseudorotaxanes and rotaxanes comprising various components in the meccano set are driven primarily by strong [N^+–H···O] hydrogen-bonding interactions. Their (super)structures in the solid state, a variety of which are sampled[953,958–967] in **Figure 2.54**, reveal the presence of two to four of these intercomponent hydrogen bonds with distances of ≤2.50 Å in each assembly. A statistical analysis[957] of 25 unique crystal structures based on this motif calculated a mean of approximately 3 for these close-contact hydrogen bonds per $R_2NH_2^+\subset crown$ interaction, with a mean [N^+–H···O] distance of 2.26 Å. The hydrogen-bonding modes, which vary with ring constitution and different substituents, include situations in which (i) both N^+–H protons donate bifurcated hydrogen bonds, either exclusively to aliphatic acceptors (**Figure 2.54a**), to a combination of aliphatic and phenolic acceptors (**Figure 2.54k**), or to all-phenolic acceptors (**Figure 2.54i**), (ii) a combination of bifurcated and non-bifurcated hydrogen bonds are donated to aliphatic (**Figure 2.54b,c,f**) mixed aliphatic/phenolic (**Figure 2.54e,j,k**), or mixed aliphatic/pyridyl (**Figure 2.54d**) acceptors, and (iii) both N^+–H protons donate single hydrogen bonds—one to an aliphatic oxygen atom and the other to either a phenolic (**Figure 2.54l**) or pyridyl (**Figure 2.54g,h**) acceptor. In the aforementioned analysis,[957] the mean length of hydrogen bonds to non-phenolic oxygen atoms is shorter (2.21 Å) than the mean distance (2.31 Å) to phenolic oxygen atoms, while the mean [N^+–H···O] angles are approximately 150° in both cases. Most superstructures also benefit from one to three [C–H···O] close contacts (≤2.50 Å) involving the methylene protons adjacent to the $–NH_2^+–$ center. Some assemblies with aryl rings appended to both host and guest are also stabilized by π–π stacking interactions (**Figure 2.54i–l**), especially in the cases of crowns larger than 24C8 in their constitution. If we assign numbers to each hydrogen bond acceptor in a crown ether sequentially, beginning with the atom in closest contact to the $–NH_2^+–$ center, the two shortest hydrogen bonds are directed toward acceptors 1 and 3 in all cases—i.e., the closest [N^+–H···X] contacts (where X is an acceptor O or N) are always separated by a [C–C–O–C–C] spacer. The preferred 1,3-arrangement of hydrogen bonds is one of the only features that are conserved throughout the entire meccano set of interpenetrated structures based on this molecular recognition motif.

Association constants for various pseudorotaxanes comprising dialkylammonium guests and the crown ethers of the meccano set illustrated in **Figure 2.53** in various solvent systems are tabulated[953,959–963,965,966,968–979] in **Table 2.25**. The vast majority of these K_a values have been estimated by ^{1}H NMR spectroscopy using the single point method. This method of determining K_a values requires that the complex of interest is in slow exchange with its dissociated components on the ^{1}H NMR timescale, allowing an experimentalist with a knowledge of the initial concentrations to determine the concentrations of all species in solution by simple integration of their ^{1}H signals and plugging them into the expression in Eq 2.2

$$G + H \underset{}{\overset{Ka}{\rightleftharpoons}} G \subset H.$$

$$K_a = \frac{[G \subset H]}{[G][H]} \qquad (2.2)$$

where *H* is the host, *G* is the guest, and *H*⊂*G* is the host-guest (pseudorotaxane) complex. We rely on the data in **Table 2.25** to summarize and point out some general trends regarding the stabilities of *dialkylammonium⊂crown ether* pseudorotaxanes in solution, which serve as templates for the making of

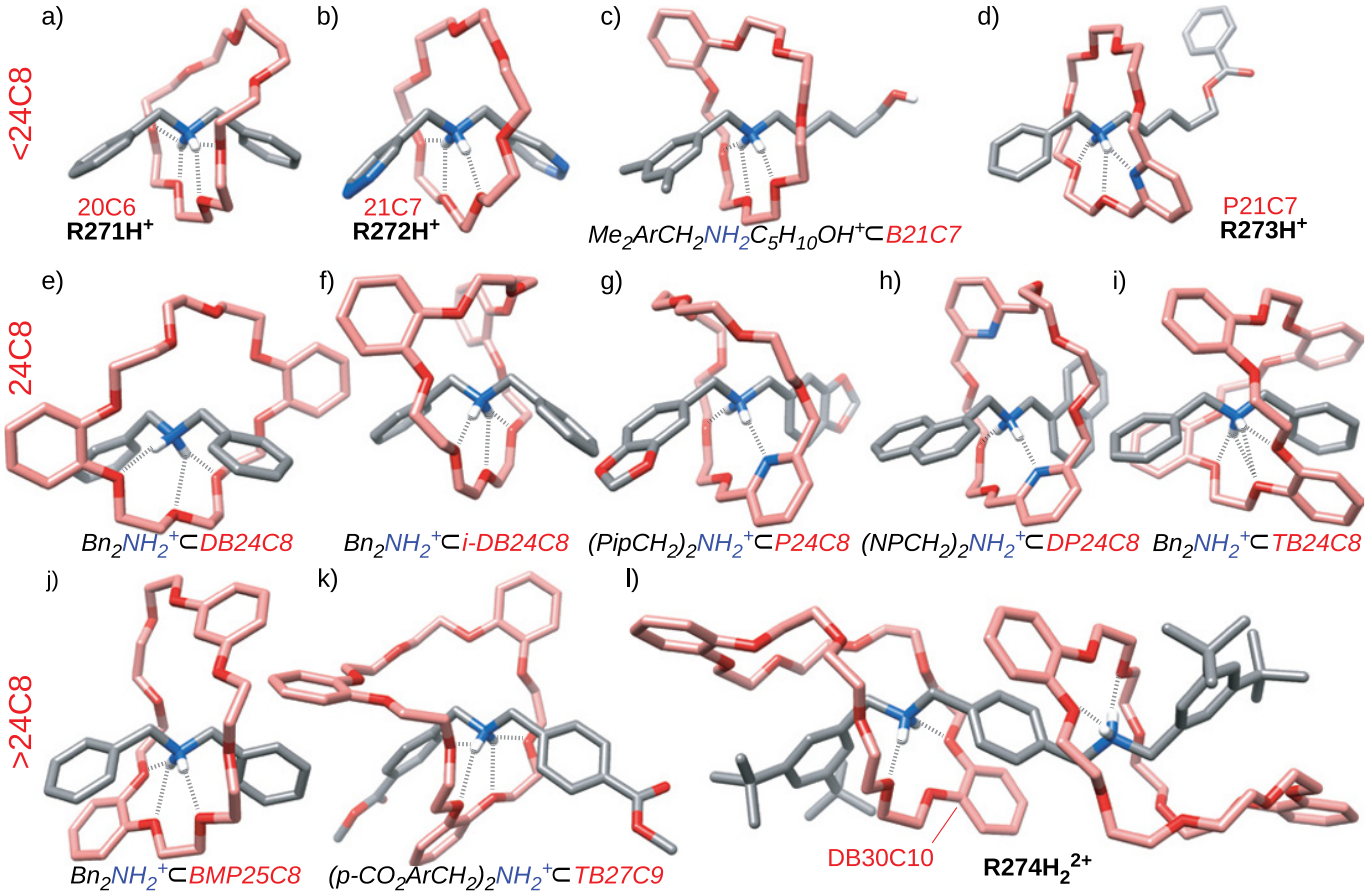


Figure 2.54 X-Ray crystal structures of pseudorotaxanes and rotaxanes comprising dialkylammonium cations and the following crown ethers: (a) 20C6,[958] (b) 21C7,[959] (c) B21C7,[960] (d) P21C7,[961] (e) DB24C8,[953] (f) *i*-DB24C8,[962] (g) P24C8,[963] (h) DP24C8,[963] (i) TB24C8,[964] (j) BMP25C8,[965] (k) TB27C9[966]. (l) DB30C10.[967] Hydrogen bonds <2.5 Å in length are depicted as hashed lines. Only NH/OH protons are shown and PF_6^- counterions and solvent molecules are omitted for the sake of clarity.

mechanical bonds. The kinetics of assembly and disassembly in these systems is related to these thermodynamic stabilities, as well as to the size complementarity between the cavity of the ring and the steric bulk of the guest—a topic which is discussed in more detail in **Section 3.1**.

Effect of Solvent Polarity

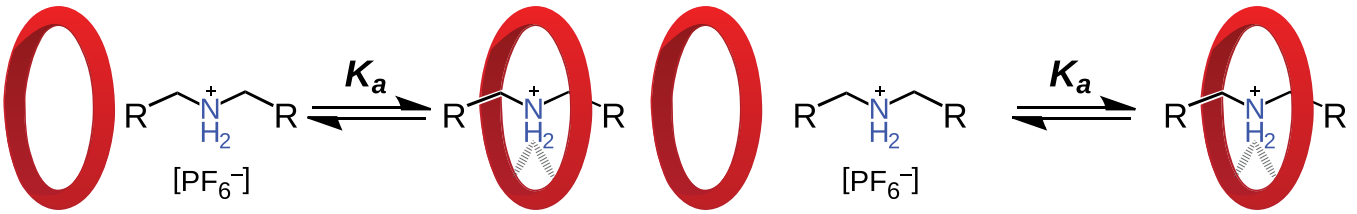
It comes as no surprise that association constants decrease in magnitude as solvent polarity increases,[953] since increasingly polar solvent molecules compete more effectively with the crown ethers in stabilizing the $-NH_2^+-$ centers of a dialkylammonium guest. The data in **Table 2.25** reveal a trend of $Me_2SO<Me_2CO<MeCN<MeNO_2<CH_2Cl_2\approx CHCl_3$ with respect to K_a values. This trend compares well with the Gutmann[980] donor numbers[S] of the solvents, where K_a values increase with decreasing donor numbers. Association constants are particularly high (up to 10^6 M^{-1}) in halogenated solvents such as CH_2Cl_2 and $CHCl_3$, although it is often difficult to determine accurate K_a values in these solvents because most dialkylammonium ions are not soluble in them in the absence of crown ethers. As a result, binary solvent systems such as CH_2Cl_2/MeCN and $CHCl_3$/MeCN are often employed in order to enhance solubility while maintaining high association constants.

Counterion Effects

Quantitative treatments of the stabilities of charged complexes in low-polarity organic media are laden with complications on account of ion-pairing effects. The most comprehensive and detailed investigations of the role of ion pairing in the dialkylammonium/crown ether recognition motif have been undertaken by Gibson[581,981,982] at Virginia Tech. Gibson has noted that the experimentally observed K_a values for pseudorotaxanes comprising dibenzylammonium and DB24C8 vary with concentration in a 3:2 $CDCl_3$:CD_3CN solvent system. In this case, the concentration-dependent variations in the apparent binding constants have been attributed to the fact that the uncomplexed $Bn_2NH_2^+$ cation is ion-paired with its counterion, whereas

[S] The Gutmann donor number provides[980] a semiquantitative measurement of a solvent's ability to donate electron density into noncovalent bonds. These numbers predict the relative association strengths of dialkylammonium⊂crown pseudorotaxanes in different solvent systems more reliably than do solvent dielectric constants.

Table 2.25 K_a values[a] for various pseudorotaxanes comprising crown ethers and dialkylammonium guests.



Ring	R	Solvent	T K	K_a M^{-1}	Ref	Ring	R	Solvent	T K	K_a M^{-1}	Ref
21C7	C≡CH	CH_3CN	298	14000[b]	959	DB24C8	*p*-(OMe)Ar	1:1 $CDCl_3$:CD_3CN	304	990	969
B21C7	*n*-Pr	CD_3COCD_3	295	527	960	DB24C8	*m*-(OMe)Ar	1:1 $CDCl_3$:CD_3CN	304	1350	969
B21C7	Ph[c]	CD_3COCD_3	295	615	960	DB24C8	*p*-(Me)Ar	1:1 $CDCl_3$:CD_3CN	304	960	969
B21C7	*p*-(CN)Ar[d]	CD_3COCD_3	295	1062	960	DB24C8	*m*-(Me)Ar	1:1 $CDCl_3$:CD_3CN	304	1100	969
P21C7	*n*-Pr	CD_3COCD_3	295	1625	961	DB24C8	*p*-(Cl)Ar	1:1 $CDCl_3$:CD_3CN	304	1890	969
P21C7	Ph[c]	CD_3COCD_3	295	6396	961	DB24C8	*m*-(Cl)Ar	1:1 $CDCl_3$:CD_3CN	304	2810	969
P21C7	*p*-(CN)Ar[d]	CD_3COCD_3	295	7479	961	DB24C8	*p*-(Br)Ar	1:1 $CDCl_3$:CD_3CN	304	2010	969
24C8	Ph	CD_3CN	300	1700	968	DB24C8	*m*-(Br)Ar	1:1 $CDCl_3$:CD_3CN	304	2760	969
24C8	*p*-(Br)Ar	CD_3CN	300	3500	968	DB24C8	*p*-(CO_2H)Ar	1:1 $CDCl_3$:CD_3CN	304	2520	969
24C8	*p*-(CO_2Me)Ar	CD_3CN	300	4500	968	DB24C8	*m*-(CO_2H)Ar	1:1 $CDCl_3$:CD_3CN	304	2850	969
B24C8	Ph	CD_3CN	300	420	968	DB24C8	*p*-(NO_2)Ar	1:1 $CDCl_3$:CD_3CN	304	5940	969
B24C8	Ph	3:1 $CDCl_3$:CD_3CN	298	12300	977	DB24C8	*m*-(NO_2)Ar	1:1 $CDCl_3$:CD_3CN	304	6460	969
B24C8	*p*-(Br)Ar	CD_3CN	300	720	968	DB24C8	*p*-(Me)Ar	3:1 $CDCl_3$:CD_3CN	300	1900	978
B24C8	*p*-(CO_2Me)Ar	CD_3CN	300	880	968	DB24C8	9-anthryl[e]	CH_2Cl_2	298	1.0×10^6	974
DB24C8	*n*-Pr	CD_3CN	298	50	962	*i*-DB24C8	Ph	CD_3COCD_3	298	310	962
DB24C8	*n*-Pr	$CDCl_3$	298	≥10^4	962	*i*-DB24C8	Ph	CD_3CN	298	360	962
DB24C8	*n*-Pr	CD_2Cl_2	298	≥10^4	962	*i*-DB24C8	Ph	$CDCl_3$	298	22000	962
DB24C8	Ph	CD_3SOCD_3	298	0	953	P24C8	1-naphthyl	CD_3CN	298	2230	963
DB24C8	Ph	CD_3COCD_3	298	360	953	P24C8	2-naphthyl	CD_3CN	298	2270	963
DB24C8	Ph	CD_3CN	298	420	953	P24C8	piperonyl	CD_3CN	298	1130	963
DB24C8	Ph	CD_3CN	304	200	969	DP24C8	1-naphthyl	CD_3CN	298	720	963
DB24C8	Ph	1:1 $CDCl_3$:CD_3CN	298	1700	953	DP24C8	2-naphthyl	CD_3CN	298	940	963
DB24C8	Ph	1:1 $CDCl_3$:CD_3CN	304	1100	969	DP24C8	piperonyl	CD_3CN	298	710	963
DB24C8	Ph	3:1 $CDCl_3$:CD_3CN	298	4500	977	DP24C8	Ph	CD_3CN	235	23000	971
DB24C8	Ph	$CDCl_3$	298	27000	953	DP24C8	*p*-($BrCH_2$)Ar	CD_3CN	298	1100	971
DB24C8	*p*-(OMe)Ar	CD_3CN	304	130	969	DP24C8	*p*-(CO_2Me)Ar	CD_3CN	298	1700	971
DB24C8	*m*-(OMe)Ar	CD_3CN	304	280	969	DCy24C8	Ph	CD_3CN	RT	20	975
DB24C8	*p*-(Me)Ar	CD_3CN	304	170	969	DPT24C8	Ph	1:1 $CDCl_3$:CD_3CN	298	<15	972
DB24C8	*m*-(Me)Ar	CD_3CN	304	180	969	DPT24C8	*p*-(F)Ar	2:1 $CDCl_3$:CD_3NO_2	298	15	976
DB24C8	*p*-($BrCH_2$)Ar	CD_3CN	300	352	970	TB24C8	Ph	CD_3COCD_3	300	0	968
DB24C8	*p*-(Cl)Ar	CD_3CN	304	470	969	TB24C8	2-furano	3:1 $CDCl_3$:CD_3CN	298	49	977
DB24C8	*m*-(Cl)Ar	CD_3CN	304	580	969	TB24C8	*p*-(Br)Ar	CD_3COCD_3	300	0	968
DB24C8	*p*-(Br)Ar	CD_3CN	300	800	968	TB24C8	*p*-(CO_2Me)Ar	CD_3COCD_3	300	0	968
DB24C8	*p*-(Br)Ar	CD_3CN	304	460	969	BMP25C8	*p*-(CO_2Me)Ar	CD_2Cl_2	300	50	965
DB24C8	*m*-(Br)Ar	CD_3CN	304	570	969	BMP25C8	*i*-Pr	1:1 $CDCl_3$:CD_3CN	298	57	973
DB24C8	*p*-(CO_2H)Ar	CD_3CN	304	510	969	BPP26C8	*i*-Pr	1:1 $CDCl_3$:CD_3CN	298	35	973
DB24C8	*m*-(CO_2H)Ar	CD_3CN	304	660	969	BBN26C8	*p*-(Me)Ar	3:1 $CDCl_3$:CD_3CN	300	960	978
DB24C8	*p*-(CO_2Me)Ar	CD_3CN	300	1100	968	BMP26C8	Ph	CD_3CN or $CDCl_3$	RT	0	979
DB24C8	*p*-(NO_2)Ar	CD_3CN	304	1300	969	TB27C9	Ph	3:1 $CDCl_3$:CD_3CN	300	270	966
DB24C8	*m*-(NO_2)Ar	CD_3CN	304	1350	969	TB27C9	*p*-(CO_2Et)Ar	3:1 $CDCl_3$:CD_3CN	300	710	966
DB24C8	1-naphthyl	CD_3CN	298	760	963	DB30C10	*t*-Bu	1:1 $CDCl_3$:CD_3CN	298	127	973
DB24C8	2-naphthyl	CD_3CN	298	900	963	DB30C10	9-anthryl[e]	CH_2Cl_2	298	2.0×10^5	974
DB24C8	piperonyl	CD_3CN	298	520	963	DN30C10	9-anthryl[e]	CH_2Cl_2	298	4.0×10^5	974

[a]Determined by ^{1}H NMR spectroscopy using the single-point method (Error ≤ ±15%) except where noted.
[b]Determined by isothermal titration calorimetry (ITC) as the BF_4^- salt.
[c]Asymmetric guest; R^1 = Ph, R^2 = *n*-Pr.
[d]Asymmetric guest; R^1 = *p*-(CN)Ar, R^2 = *n*-Pr.
[e]Asymmetric guest; R^1 = anthracene, R^2 = Ph. K_a values obtained spectrofluorimetrically.

the corresponding *$Bn_2NH_2^+$⊂DB24C8* pseudorotaxane is not ion-paired. A rigorous analysis of this system should therefore consider not only the association of the free $Bn_2NH_2^+$ cation with the DB24C8 host, but also the dissociation constant, K_{ipd}, for the ion-paired dibenzylammonium salt. Nearly all of the K_a values in the literature have been estimated, at different and sometimes unspecified concentrations, based on the model described by Eq. 2.2, which implicitly assumes that the guest *G* is in the same ion-pair state before and after complexation with host *H*. Gibson[982]

proposed a more appropriate pre-equilibrium model (Eq. 2.3) accounting for an ion-paired guest assuming that the corresponding host-guest complex is not ion-paired, which is derived as follows:

$$G^+X^- \underset{}{\overset{K_{ipd}}{\rightleftharpoons}} G^+ + X^-$$

$$G^+H \underset{}{\overset{K_a}{\rightleftharpoons}} G^+ \subset H$$

$$G^+X^- + H \underset{}{\overset{K_o}{\rightleftharpoons}} G^+ \subset H + X^-$$

$$K_o = K_a K_{ipd} = \frac{\left[G^+ \subset H\right]\left[X^-\right]}{\left[G^+X^-\right]\left(\left[H\right]_0 - \left[G^+ \subset H\right]\right)} \qquad (2.3)$$

Unfortunately, $[X^-]$ and $[G^+X^-]$ cannot be determined directly, nor is their estimation a straightforward task. Gibson set out to calculate activity coefficients (γ) empirically for solutions of $Bn_2NH_2^+X^-$ and DB24C8, where X^- = PF_6^-, BF_4^-, OTs^-, and TFA^-, only to find that γ is also highly sensitive to concentration, making it nigh impossible to predict accurately the experimentally observed binding constants for this system under arbitrarily chosen conditions in low polarity solvents. The risk of encountering this kind of unpredictability increases as solvent polarity decreases. In more polar Me_2CO solutions, for example, the concentration dependence is not observed. The bottom line is that researchers must exercise a great deal of caution when interpreting observed K_a values for charged systems in low-polarity organic solvents, and opt for qualitative rather than quantitative comparisons.

The scatter plot in **Figure 2.55** relies on Gibson's data[982] and the somewhat dubious, yet much more commonly employed, model (Eq. 2.2) for estimating K_a values in order to demonstrate a qualitative relationship describing the effect of different counterions on pseudorotaxane self-assembly. Although the observed K_a values do indeed vary with concentration, the counterions of four dibenzylammonium salts consistently follow the trend PF_6^->BF_4^->OTs^->TFA^- in terms of the extent to which they favor pseudorotaxane formation. Gibson has calculated that the dibenzylammonium ion pair by itself is dissociated to the following extents in 3:2 $CDCl_3$:CD_3CN (1 mM / 10 mM) as the salts of PF_6^- (90% / 55%), BF_4^- (82% / 46%), OTs^- (49% / 19%), and TFA^- (35% / 12%). Binding is strongest, therefore, when ion pairing is weakest. Recognizing that the formation of tight ion-pairs leads to dissociation of $R_2NH_2^+$⊂*crown* complexes, Prodi[983] has designed an anthracene-stoppered DB24C8-based semirotaxane which acts as a luminescent sensor for Cl^- ions. This kind of competitive ion pairing has also been exploited to drive switching in molecular shuttles—see **Section 6.5.3**.

In summary, dialkylammonium guests for crown ethers are employed most effectively as salts with weakly paired anions such as PF_6^- or BF_4^- in order to (i) enhance solubilities in low-polarity organic solvents, and (ii) weaken ion-pairing interactions between an $R_2NH_2^+$ cation and its counteranion, which allows stronger binding by the crown ether.

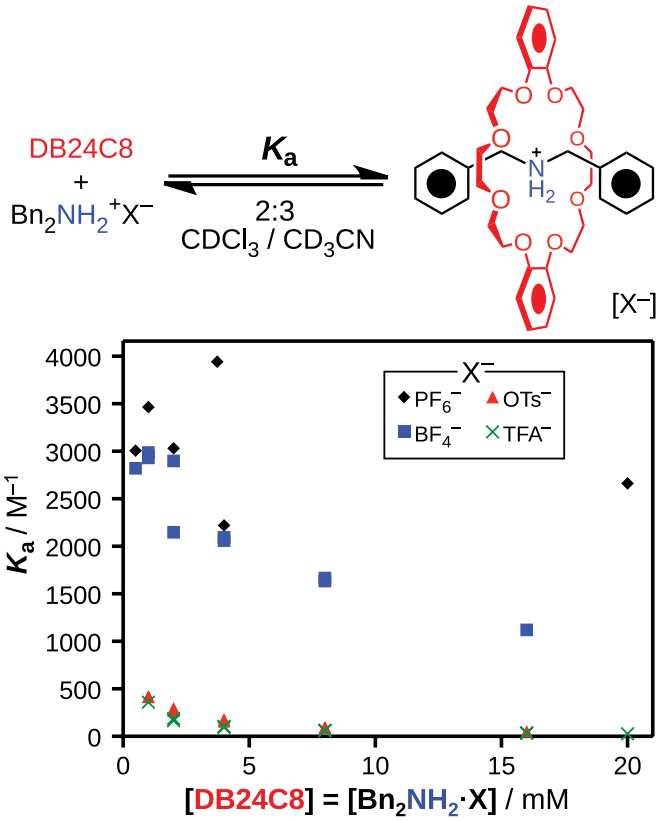


Figure 2.55 The effects of concentration and counterions on the single-point K_a values for pseudorotaxanes assembled in equimolar mixtures of DB24C8 and $Bn_2NH_2^+$ with PF_6^-, BF_4^-, OTs^-, or TFA^- counterions in 3:2 $CDCl_3$:CD_3CN. Data taken from ref. 982

Effects of Ring Size and Constitution

DB24C8 is accompanied by a number of 24-membered crown ethers in the meccano set (**Figure 2.53**), including the unsubstituted parent [24]crown-8 (24C8) and other benzo-24C8 derivatives such as benzo[24]crown-8,[968,977,984] and tetrabenzo[24]crown-8.[964,977] In his seminal work, Pedersen[151] reported an unsymmetrical isomer of dibenzo[24]crown-8 in which the benzo units are bridged by one diethylene glycol loop and one tetraethylene glycol loop—call it *iso*-dibenzo[24]crown-8 (*i*-DB24C8)—which has also been employed occasionally as a host for cations. Other 24C8 derivatives include the pyridocrowns pyrido[24]-crown-8[963] (P24C8), dipyrido[24]crown-8[963,971] (DP24C8), as well as dicyclohexyl[24]crown-8[975,985] (DCy24C8) and di(*p*-toluidine)[24]crown-8.[972,976]

Owing chiefly to the early work of Harrison,[18] it was widely believed until relatively recently that a ring must constitute at least 22 atoms in order to be threaded by a polymethylene chain, although Schill[30] reported a very low yield (0.35%) for a rotaxane comprising a 21-membered cycloalkane in 1986. Gibson[986] suggested in 2004 that the cavity of bis-*meta*-phenylene[20]crown-6 (BMP20C6) may also be threaded by polymethylene chains. It was not until 2007, however, that crown ethers smaller than 24C8 began to appear in pseudorotaxanes and rotaxanes possessing dialkylammonium centers. As part of a systematic study on the

effect of dibenzocrown ring size on pseudorotaxane formation, Tokunaga[973] found that crown ethers as small as [22]crown-7 could bind a furan-terminated dialkylammonium guest, albeit very weakly (6 M^{-1}) in a 1:1 $CDCl_3$:CD_3CN. One of the issues hampering the development of recognition systems based on smaller rings is that even unsubstituted aryl rings act as stoppers for [21]crown-7 (21C7)-derived macrocyclic polyethers. Feihe Huang[960] made the discovery that 21C7 derivatives can indeed encircle (**Figure 2.54b–d**) a dialkylammonium guest, provided that there are no aryl rings to block its trajectory onto the thread. Subsequently, Chiu[959] developed a solvent-free stoppering protocol leading (**Figure 2.54b**) to the [2]rotaxane **R272H**$^+$, which was the smallest [2]rotaxane to be reported until Wu[958] introduced (**Figure 2.54a**) in 2012 the even smaller [2]rotaxane **R271H**$^+$ based on the 20-membered [20]crown-6 (20C6) macrocycle, which was clipped around the dialkylammonium dumbbell by means of ring-closing olefin metathesis, followed by reduction of the resulting double bond. 20C6 and its slightly larger relatives, such as [21]crown-6 (21C6) and [22]crown-6 (22C6), can be incorporated into rotaxane architectures by this thermodynamically controlled clipping protocol—see **Section 3.2.1.3**. Rings with larger cavities than DB24C8, such as benzo-metaphenylene[25]crown-8[965,968,973] (BMP25C8; **Figure 2.54j**), benzoparaphenylene[26]crown-8[973,987] (BPP26C8), benzo-2,2′-binaphtho[26]crown-8[978] (BBN26C8), bismeta-phenylene[26]crown-6[965,979] (BMP26C6), tribenzo[27]crown-9[966] (TB27C9; **Figure 2.54k**), dibenzo[30]crown-10[967,973,974] (DB30C10; **Figure 2.54l**), and dinaphtho[30]crown-10[974] (DN30C10) are also capable of encircling a single dialkylammonium ion guest.

Any disruption to the cyclo(C–C–O)$_n$ constitution of the crown ether backbones by the introduction of extra carbon atoms has a profoundly detrimental effect[965,968,973] on their affinities (**Table 2.25**) for dialkylammonium guests—an observation that can be made by comparing pseudorotaxanes based on DB24C8 versus BMP25C8, BPP26C8, BBN26C8, and BMP26C8. Whereas DB24C8 binds dibenzylammonium-based guest ions with K_a values >10^4 M^{-1} in halogenated solvents, simply replacing one of the *ortho*-phenylene units of DB24C8 with *meta*-phenylene (BMP25C8) or *para*-phenylene (BPP26C8) reduces the K_a values by approximately two orders of magnitude. Correspondingly, an X-ray crystal structure[965] reveals (**Figure 2.54j**) that the *meta*-substituted aryl ring of BMP25C8 and its appended oxygen atoms are not engaged in hydrogen bonding with a dibenzylammonium guest in the solid state. In spite of the high penalty in K_a values, BMP25C8 is an attractive building block in mechanostereochemistry because its *meta*-phenylene ring can be substituted at the 5-position with R groups without reducing the symmetry of the crown ether. By contrast, substituted DB24C8 derivatives have lower symmetries, rendering the two faces of the macrocycle enantiotopic—a feature which can lead to different kinds of mechanostereoisomerism (see **Chapter 5**) in MIMs. The binaphthol-containing crown ether BBN26C8 exhibits[978] surprisingly high affinity (960 M^{-1} in 3:1 $CDCl_3$:CD_3CN) for a dibenzylammonium-derived guest ion. The K_a value is approximately half that (1900 M^{-1} under identical conditions) of DB24C8, indicating that 2,2′-binaphthol is better at simulating the O–C–C–O repeating unit of a typical crown ether than is *meta*- or *para*-phenylene. It has been reported[965,979] that BMP26C8, which possesses two *meta*-phenylene units, does not self-assemble with dialkylammonium guest ions in solution at all, although there is some evidence[979] that it can form 1:1 inclusion complexes in the solid state.

In general, there is an inverse relationship between ring size and K_a values—i.e., association constants increase as ring size decreases, provided that the repeating (C–C–O)$_n$ backbone of the crown ether is not disrupted. This trend can be recognized by comparing, for example, the K_a values for pseudorotaxanes based on 21C7 versus 24C8, B21C7 versus B24C8, P21C7 versus P24C8, or DB24C8 versus DB30C10. A comparison of the interpenetrated (super)structures based on these motifs in the solid state reveals (**Figure 2.54**) that smaller rings are interlocked around the –NH_2^+– centers more 'tightly', since they tend to exhibit shorter [N^+–H···O] hydrogen bond lengths on average. The smaller rings most likely contribute more preorganization relative to the larger ones by virtue of their smaller constitutions.

A comparison of the binding constants for pseudorotaxanes comprising different equally sized crowns makes it possible to understand how substituent effects influence the thermodynamic stabilities of these complexes. Since the average length of a single C–C bond (1.54 Å) is longer than that of benzene's C–C bond (1.40 Å), the replacement of an ethylene glycol segment of a crown ether with a catechol unit leads to a slight decrease in cavity size, which generally enhances K_a values. On the other hand, however, the phenolic oxygen atoms of benzo-substituted crowns are poor acceptors of hydrogen bonds compared to aliphatic oxygens, which generally decreases K_a values. Furthermore, aryl rings increase the rigidity of crown ethers and render them capable of engaging in π–π stacking and [C–H···π] interactions. The interplay of all these forces in different host-guest pairs can lead to large differences in K_a values ranging from 0 to >10^6 M^{-1}.

In general, benzo rings appended to crown ethers tend to decrease association constants. A comparison of pseudorotaxanes based on 21C7 versus B21C7, for example, reveals that 21C7 binds a dialkylammonium guest ion more tightly than does B21C7 by more than an order of magnitude. The same trend is observed for 24C8 derivatives—e.g., B24C8, DB24C8, and TB24C8. Tokunaga[977] has probed the effect of adding benzo substituents to a [24]crown-8 constitution systematically, finding that K_a values for pseudorotaxanes comprising dibenzylammonium guests decrease by about an order of magnitude with each additional benzo ring, from 12300 M^{-1} in the case of B24C8 to 49 M^{-1} in the case of TB24C8 in 3:1 $CDCl_3$:CD_3CN. TB24C8 does not associate[964,968] with dialkylammonium guests in solution, although *dibenzylammonium⊂TB24C8* pseudorotaxanes have been observed and characterized

crystallographically (**Figure 2.54i**) in the solid state as a result of a kinetically controlled crystallization process assisted by [C–H···F] hydrogen-bonding interactions involving the PF_6^- counterions. The detrimental effect of benzo rings can be attributed to the lower basicity of their phenolic oxygen atoms, which reduces the enthalpic favorability of the [N^+–H···O] hydrogen bonds relative to those involving aliphatic oxygen atoms at the unsubstituted sites of a crown ether. An entropic penalty associated with the increased rigidity of the benzo-functionalized crowns may also contribute to their relatively lower affinity for $R_2NH_2^+$ guests. Once complexed, however, the rigid TB24C8 ring is slow to dissociate from the dialkylammonium template, since the *$Bn_2NH_2^+$⊂TB24C8* pseudorotaxane disassembles,[988] upon dissolution of the crystals in CD_3COCD_3 at 25 °C, with a half-life of 15.5 days, corresponding to a high $\Delta G^{\ddagger}$ value of 26 kcal·mol^{-1} for the deslipping process.

A comparison of the dibenzocrown constitutional isomers, DB24C8 and *i*-DB24C8, reveals that the relative positions of aryl substituents can also influence the stability of the corresponding pseudorotaxanes. The tetraethylene glycol loop of *i*-DB24C8 allows both protons of the –NH_2^+– center to engage[962] in more enthalpically favorable [N^+–H···O] hydrogen bonds with aliphatic oxygen atoms. Although this more favorable hydrogen-bonding pattern is manifested[962] (**Figure 2.54f**) in the solid state, the K_a values (**Table 2.25**) in solution exhibit a 10–20% decrease with respect to those involving DB24C8. Apparently, this more favorable binding geometry is more than compensated for by less favorable geometries sampled by the complex in solution, in which the dialkylammonium ion would be required to engage two phenolic oxygen atoms simultaneously in its preferred 1,3 hydrogen-bonding mode.

2,6-Disubstituted pyridyl units can also be incorporated into crown ethers without interrupting the favorable constitution involving all hydrogen bond acceptors being separated by two carbon atoms. Owing to the enhanced basicity of the pyridyl nitrogen atom relative to that of oxygen, pyridocrown rings exhibit (**Table 2.25**) higher affinities for dialkylammonium ions than do benzo-derived crowns. Comparisons of P21C7 with B21C7, P24C8 with B24C8, and DP24C8 with DB24C8 reveal that the K_a values associated with pyridine-based hosts are often more than tripled with respect to those of the corresponding benzocrown hosts. In the solid state, the [N^+–H···N] distance (2.07 Å) of the pseudorotaxane comprising the dipyridocrown DP24C8 (**Figure 2.54h**) is shorter than the phenolic [N^+–H···O] distance (2.17 Å) of a pseudorotaxane (**Figure 2.54e**) based on DB24C8. In common with benzo rings, additional pyrido rings decrease the corresponding K_a values, as can be appreciated by comparing (**Table 2.25**) pseudorotaxanes based on P24C8 with those based on DP24C8.

Effects of Dialkylammonium Substituents

The R groups appended to the central –$CH_2NH_2^+CH_2$– core of a dialkylammonium guest can also influence the K_a values (**Table 2.25**) of a pseudorotaxane. An investigation[969] of a series of disubstituted dibenzylammonium cations serving as guests for DB24C8 has revealed that a linear free energy relationship exists[969] between the stability constants (K_a) and the Hammett substituent constants (σ) of the R group. For reactions involving aromatic reactants with R substituents, the Hammett[989] equation (Eq. 2.4) describes a linear free energy relationship between the equilibrium constant (K_R) for the reaction with substituent R, normalized to that of the same reaction when R = H (K_H), and an empirical constant, σ, which depends only on the constitution of the aromatic substituent R, modified by a reaction constant, ρ, which depends on the reaction type.

$$\log\frac{K_R}{K_H} = \sigma\rho \qquad (2.4)$$

It transpires that Hammett correlations hold true for supramolecular equilibria as well as covalent ones. The Hammett plots in **Figure 2.56** reveal that log[K_a(R)/K_a(H)]

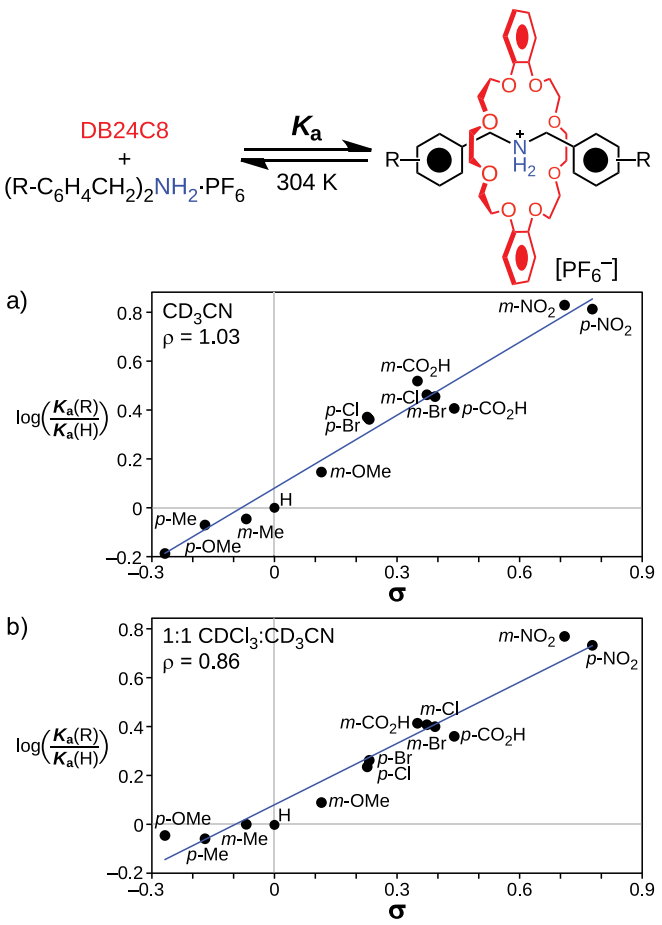


Figure 2.56 Hammett correlations[969] for pseudorotaxanes comprising disubstituted dibenzylammonium cations and DB24C8 in CD_3CN (a) and 1:1 $CDCl_3$:CD_3CN (b) at 304 K, which reveal a linear free energy relationship between log[K_a(R)/K_a(H)] and the Hammett constant σ. The supramolecular reaction constant ρ is calculated from the slope of the line.

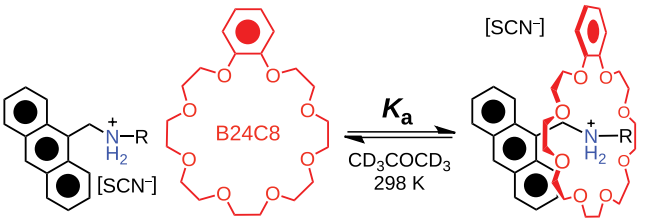
does indeed scale linearly with σ for dibenzylammonium/DB24C8 pseudorotaxanes in two different solvent systems. The slope of these plots represents the supramolecular reaction constant ρ for the equilibrium in each solvent system. These data suggest that the strength of the host-guest interaction in this motif can be controlled rather precisely and predictably by simple manipulation of the dibenzylammonium substituents. The positive ρ values (1.03 and 0.86, respectively) in CD_3CN and 1:1 $CDCl_3$:CD_3CN mean that the stabilities of *(R-$C_6H_4CH_2$)$_2NH_2^+$⊂DB24C8* pseudorotaxanes increase with with electron-withdrawing substituents (e.g., R = NO_2 or CO_2H) and decrease with electron-donating substituents, e.g., R = OMe or Me.

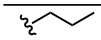
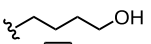
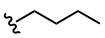
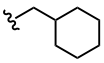
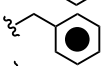
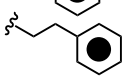
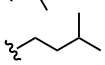
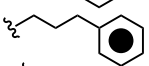
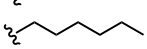
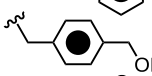
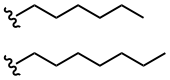
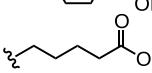
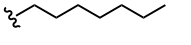
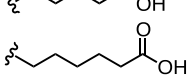
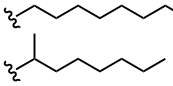
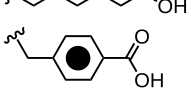
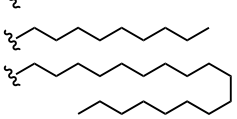
Busch[984] has undertaken a systematic investigation on the effects of a wider range of substituents on the observed K_a values for semirotaxanes comprising anthracen-9-ylmethyl-*N*-alkylammonium thiocyanate salts as guests for the B24C8 host. The K_a values for a wide range of aliphatic R groups have been recorded (**Table 2.26**, left-hand side) as well as a number of guests containing alcoholic, alicyclic, aromatic, and acidic moities (**Table 2.26**, right hand side) in acetone at 298 K. A comparison of the K_a values for unbranched aliphatic chains—i.e., *n*-propyl (149 M^{-1}), *n*-butyl (127 M^{-1}), *n*-hexyl (177 M^{-1}), *n*-heptyl (161 M^{-1}), *n*-octyl (151 M^{-1}), *n*-nonyl (120 M^{-1}), and *n*-octadecyl (178 M^{-1})—reveals no obvious correlations between the number of carbon atoms and K_a values, indicating that the thermodynamic stability is insensitive to odd/even effects and chain length. The kinetics of exchange, however, are affected by chain length, since components exchange rapidly for chains <5 carbons and slowly for chains >5 carbons in length on the ^{1}H NMR timescale. A more important factor affecting the thermodynamic landscape is the steric effect of branching points, which lower the K_a values as a function of their distance from the $–NH_2^+–$ center. Taking different butyl groups as an example, the observed trend of *iso*-butyl>*sec*-butyl>*tert*-butyl (43.5>12.9>0 M^{-1}) correlates well with the expected steric crowding near the adjacent $–NH_2^+–$ center, a situation which increases as *iso*<*sec*<*tert* for the different butyl isomers. The detrimental effect of branching points appears to apply only to the first two carbon atoms, since the K_a value observed in the case of an *iso*-pentyl group (163 M^{-1}) is in the same range as that (120–178 M^{-1}) of the unbranched alkyl chains. The importance of avoiding steric bulk around the first two atoms adjacent to the $–NH_2^+–$ center is also reflected in the phenyl-terminated guests with methylene (94 M^{-1}), ethylene (194 M^{-1}), and propylene (282 M^{-1}) spacers, as well as guests with cyclohexyl (16.9 M^{-1}) and cyclohexylmethyl (0 M^{-1}) R groups. In addition to these steric effects, the alcoholic and acidic guests reveal an electronic effect, in which electron-withdrawing groups, such as pentanoic acid (280 M^{-1}), hexanoic acid (223 M^{-1}), and benzoic acid (221 M^{-1}) enhance pseudorotaxane stabilities, while electron-donating groups, such as propanol (92 M^{-1}), butanol (82 M^{-1}), and benzylic methanol (100 M^{-1}), decrease K_a values relative to those of their aliphatic homologues. This electronic effect is consistent with the Hammett correlations (**Figure 2.56**) and can most likely be attributed to inductive effects which modulate the strength of the intermolecular [C–H···O] and [N^+–H···O] interactions. We note that there are also examples[974] of anthracene-functionalized pseudorotaxanes comprising different crown ethers in **Table 2.25**, which exhibit some of the highest K_a values that have been recorded for this recognition motif, most likely aided and abetted by D-A π–π stacking interactions between the anthracene stopper and the aryl rings of the crown ethers.

Let us summarize the important features affecting the stability of dialkylammonium / crown ether pseudorotaxanes with the following bullet points.

- The association between secondary dialkylammonium salts and crown ethers is maximized when temperatures and solvent polarities are low.
- Binding constants increase with decreasing ion-pairing interctions between the $–NH_2^+–$ center and its counterion.

Table 2.26 Stability constants (K_a) for pseudorotaxanes comprising[984] B24C8 and various anthracen-9-ylmethyl-*N*-alkylammonium thiocyanate guests in CD_3COCD_3 at 298 K.



Aliphatic Groups		*Alcohols, Alicyclics, Aromatics, Acids*	
R	K_a / M^{-1}	R	K_a / M^{-1}
	149		92
	17		82
	127		17
	44		0
	13		94
	0		194
	163		282
	177		100
	161		280
	151		223
	27		221
	120		
	178		

- Disrupting the repeating $(C–C–O)_n$ backbone of a crown ether with the addition of extra carbon atoms leads to dramatic reductions in K_a values relative to analogous crowns with uniform two-carbon linkers.
- Crowns with larger ring constitutions exhibit lower affinities for dialkylammonium cations than crowns with smaller ring constitutions, all else being equal.
- Crowns with more aryl rings exhibit lower affinities for dialkylammonium cations than analogous crowns with fewer aryl rings, unless compensated for by significant π–π interactions between the host and guest.
- Benzo-derived crowns exhibit lower affinities for dialkylammonium cations than do pyridyl-derived crowns of equal ring size.
- Dialkylammonium cationic guests exhibit higher affinities for crown ether hosts when steric crowding is minimized near the $–NH_2^+–$ centers, especially with respect to the first two adjacent carbon atoms.
- Electron-withdrawing substituents on the aromatic rings of dibenzylammonium cations increase K_a values, while electron-donating substitutents decrease K_a values.

Dialkylammonium / Paracyclophane Pseudorotaxanes

Several of the crown ether cyclophanes which serve as hosts for π-acceptors (**Section 2.3.3.4** and **2.3.3.5**) are equally capable of binding dialkylammonium cations. In 2006, Chiu[617] raised the provocative question "*is [N⁺–H···O] hydrogen bonding the most important in macrocycle-dibenzylammonium complexes?*" and challenged this question with examples (**Figure 2.57**) of tight-binding hosts for $Bn_2NH_2^+$, the stabilization of which may be dominated by [C–H···π], [N⁺–H···π], and cation–π interactions more than [N⁺–H···O] hydrogen bonding. The *para*-cyclophanes (see **Section 2.3.3.5**) PO292PC[616] (**Figure 2.57a**) HO2122PC[617] (**Figure 2.57b**), and azatetroxa[2.9.2]paracyclophane[990] (ATO292PC; **Figure 2.57c**), as well as the BX26C6[614] (**Figure 2.57d**) and PBA26C6[456] (**Figure 2.57e**) crown ethers, all act as hosts for the dibenzylammonium cation. Stability constants[T] in CD_3NO_2 increase from PBA26C6 (330 M^{-1}) to BX26C6 (340 M^{-1}) to ATO292PC (770 M^{-1}) to HO2122PC (2200 M^{-1}), with PO292PC (15000 M^{-1}) being the highest in the set. Counterintuitively, the rings with the fewest aliphatic oxygen atoms available to accept [N⁺–H···O] hydrogen bonds exhibit the highest affinities for the dibenzylammonium guest. The observation that the *$Bn_2NH_2^+$⊂PO292PC* complex is ~7-fold stronger than *$Bn_2NH_2^+$⊂HO2122PC* and ~44-fold stronger than *$Bn_2NH_2^+$⊂BX26C6*, in spite of the fact that the more weakly bound hosts carry more hydrogen bond accepting atoms, implicates the π-systems of these paracyclophane crowns as stabilizers of the $Bn_2NH_2^+$ cation. The results suggest that electron-rich π-surfaces can effectively replace oxygen atoms in the constitution of a crown ether, such that the loss of [N⁺–H···O] and [C–H···O] interactions are compensated for by [N⁺–H···π] and [C–H···π] interactions. Indeed, these

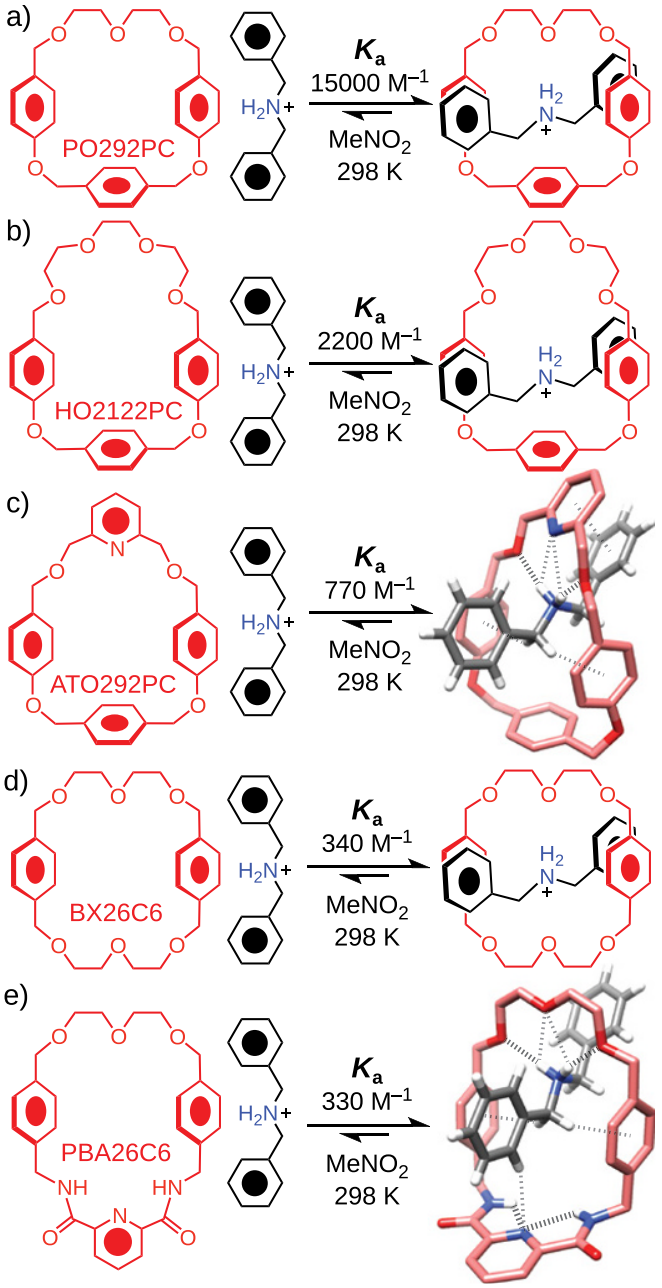


Figure 2.57 Stability constants and solid-state superstructures of pseudorotaxanes comprising.[456,617,990] the paracyclophane crown ethers PO292PC (a), HO2122PC (b), ATO292PC (c), BX26C6 (d), and PBA26C6 (e) with dibenzylammonium hexafluorophosphate guests in CD_3NO_2 at 298 K. The available solid-state superstructures[456,990] are portrayed with PF_6^- counterions and C–H protons of the host omitted for the sake of clarity. Noncovalent bonding interactions are represented as hashed lines and weighted according to their distances, where thicker lines represent shorter distances.

[T] The K_a values are dramatically lower in CD_3CN solutions—for example, *$Bn_2NH_2^+$⊂PO292PC* in 1:1 $CDCl_3$:CD_3CN (550 M^{-1}) and CD_3CN (200 M^{-1}), and $Bn_2NH_2^+$⊂ATO292PC in CD_3CN (40 M^{-1}).

interactions have been observed[617] in the calculated energy-minimized structures of the complexes. Solid-state superstructures have been obtained[456,990] in the cases of the $Bn_2NH_2^+ \subset ATO292PC$ and $Bn_2NH_2^+ \subset PBA26C6$ pseudorotaxanes, which also reveal (**Figure 2.57c**, **e**) the presence of [C–H···π] interactions between the methylene protons of the guest and the aromatic rings of the hosts, as well as weaker [N^+H···N], [C–H···N], and π–π stacking interactions. Given these insights, the high affinity of the PO292PC ring for $Bn_2NH_2^+$ can be explained by its superior preorganization, i.e., an enhanced macrocyclic effect. PO292PC has also been employed[616] in the synthesis of a [2]rotaxane—see **Table 2.27p**.

Multicomponent Dialkylammonium/Crown Assemblies

Macrocyclic polyethers larger than 30C10 in their constitution have the capacity to encapsulate more than one dialkylammonium cationic guest. Consider the macrocyclic polyethers comprising *para*-phenylene units linked by an equal number of tetra(ethylene glycol) (4EG) loops—bis-*para*-phenylene[34]crown-10 (BPP34C10), tris-*para*-phenylene[51]crown-15 (TPP51C15), and tetrakis-*para*-phenylene[68]crown-20 (TPP68C20). Dibenzyl ammonium cations can occupy the cavities of the crowns at a ratio of one $BnNH_2^+$ guest per 4EG loop. The solid-state superstructures portrayed in **Figure 2.58a–c** showcase ternary,[991] quaternary,[992,993] and quinary[992,993] host-guest complexes comprising BPP30C10, TPP51C15, and TPP68C20, respectively, and dibenzylammonium cationic guests. The PF_6^- counterions are not merely spectators in the assembly of these complexes. The quaternary and quinary complexes especially are stabilized in the solid-state by multiple [C–H···F] interactions between the fluorine atoms of a centralized PF_6^- counterion and the protons of the macroring's *para*-phenylene units, as well as the methylene protons of the $Bn_2NH_2^+$ guests. The PF_6^- core of the $(Bn_2NH_2^+)_4 \subset TPP68C10$ [5]pseudorotaxane is shown in **Figure 2.58c**, in which the anion-binding interactions appear to dictate and define the saddle-shaped (co)conformation of the assembly.

The two-site binding capacity of BPP34C10 has been further exploited to assemble a number of other interwoven superstructures,[948,974,994–997] including a ring-in-ring[998] complex with a macrocyclic bis(benzylammonium) guest (**Figure 2.58d**), a doubly threaded, doubly encircled pseudo[4]rotaxane[991] (**Figure 2.58e**), and doubly docked[999] pseudo[2]rotaxanes (**Figure 2.58f**). In the latter case, it was found[999] that a minimum distance amounting to six carbon-carbon bonds must separate the two $–NH_2^+–$ centers of a bis(dialkylammonium) ion template in order to achieve an interpenetrated, doubly docked complex with BPP34C10. Gibson[979] has found that ternary complexes also form in the case of BMP32C10 as the host with a K_a value of ~5 M^{-2} in CD_3CN. Gibson[979] has also estimated K_a values in the region of 10^3–10^4 M^{-1} for the binding of dibenzylammonium cationic guests within the loops of BPP34C10. Stability constants are most likely even higher in halogenated solvents, since the BPP24C10, TPP51C15, and TPP68C20 rings can extract[991–993] two, three, and four equiv, respectively, of the nearly insoluble $Bn_2NH_2 \cdot PF_6$ salts into a CD_2Cl_2 solution. In these multicomponent assemblies, the N^+–H protons of each dialkylammonium ion center can donate (**Figure 2.58**) up to four hydrogen bonds (<2.60 Å) to the oxygen atoms of a single 4EG loop. Even larger multicomponent assemblies based on the $R_2NH_2^+ \subset 4EG$ interaction have been reported, including [3+2] and [4+2] supramolecular bundles comprising BPP34C10 and tripodal[1000] or tetrapodal[1001] dialkylammonium cationic templates, respectively. These types of multicomponent assemblies can, in principle, serve as templates for a variety of exotic mechanically interlocked architectures, such as a hetero[7]rotaxane,[1002] the advent of which is discussed in **Section 4.2.1.2**.

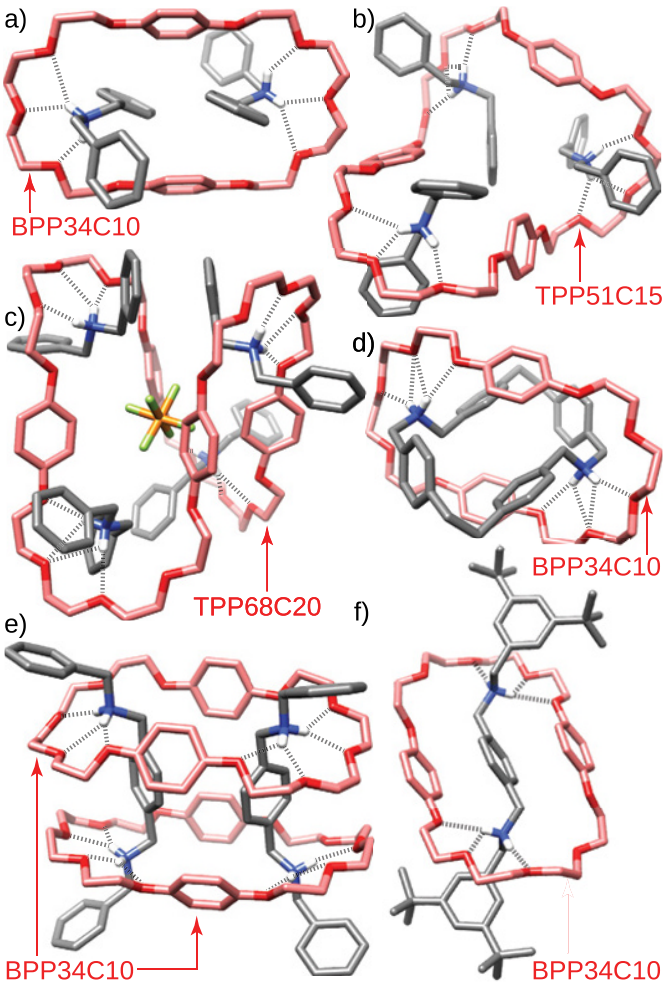


Figure 2.58 X-Ray crystal superstructures of selected examples of multicomponent assemblies driven by $R_2NH_2^{2+} \subset 4EG$ hydrogen-bonding interactions within *para*-phenylene-based macrocyclic polyethers. (a) Ternary $(Bn_2NH_2^+)2 \subset BPP34C10$ complex.[991] (b) Quaternary $(Bn_2NH_2^+)_3 \subset TPP51C15$ complex.[992,993] (c) Quinary $(Bn_2NH_2^+)_4 \subset TPP68C20$ complex.[992,993] (d) A ring-in-ring complex.[998] (e) Doubly stranded, doubly encircled pseudo[4]rotaxane.[991] (f) Doubly docked pseudo[2]rotaxane.[999] [N^+–H···O] hydrogen bonds (<2.60 Å) are represented as dashed lines. C–H protons, counterions, and solvent molecules are omitted for the sake of clarity.

Macrotricyclic Polyethers

The macrotricyclic hosts designed by Chen[669,670] and Chiu[671,672] as receptors for π-acceptors (see **Section 2.3.3.7**) are also capable of hosting[670,677,682] dialkylammonium cations within the loops of their peripheral crown ethers. Two solid-state superstructures are illustrated in **Figure 2.59** as representative examples of this recognition motif. Enabled by a slow exchange regime in ^{1}H NMR spectroscopy, the association constants for the first and second binding of $Bn_2NH_2^+$ guests within the crown-like cavities of $T_2$24C8$_2$ were determined[670] to be K_1 = 1.2 × 10^4 M^{-1} and K_2 = 2.4 × 10^3 M^{-1}, respectively, in a 10:1 mixture of $CDCl_3$:CD_3CN (10:1 v/v) using the single-point method. In addition to the typical 1,3-arrangement of [N$^+$–H···O] hydrogen bonds with respect to the crown ether moieties, the ternary *(Bn$_2$NH$_2^+$)$_2$⊂T$_2$24C8$_2$* complex is stabilized (**Figure 2.59a**) by weak π–π stacking interactions between the benzyl groups and the triptycene bridgeheads, as well as π–π stacking interactions between the two innermost phenyl rings of the two guests. A similar geometry has been observed[677] for a pair of anthrylbenzylammonium guests encapsulated by the larger $T_2$30C10$_2$ macrotricyclic polyether, in which the anthrylic groups engage in stronger π–π interactions within the central cavity of the host. By contrast, anthryl groups of the same guest reside outside of the cavity of the $T_2$24C8$_2$ host in the solid state on account of its smaller central pocket.

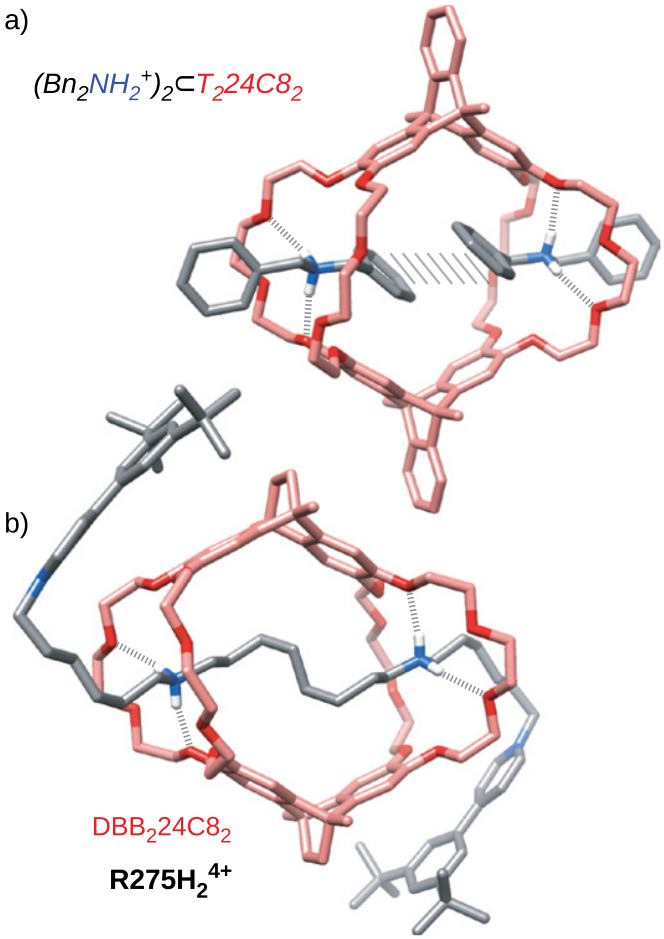


Figure 2.59 X-Ray crystal (super)structures of interpenetrated architectures based on macrotricyclic hosts and dialkylammonium ions. (a) A ternary complex in which each of the two outer 24C8 loops of the $T_2$24C8$_2$ host encircle dibenzylammonium guests.[670] (b) The [2]rotaxane **R275H$_2^{4+}$** employs[1003] a template motif involving a single thread with two –NH_2^+– centers which interact with both 24C8 loops of the DBB$_2$24C8$_2$ cage. CH protons and PF_6^- counterions are omitted for the sake of clarity.

Recognizing that the macrotricyclic polyethers possess two binding sites for dialkylammonium cations, Chiu[1003] designed a thread with two –NH_2^+– centers separated by an octamethylene chain and employed it as a template in the synthesis of the [2]rotaxane **R275H$_2^{4+}$**, in which a single thread passes (**Figure 2.59b**) through both of the 24C8 moieties of the DBB$_2$24C8$_2$ cage. The monopyridinium-derived endgroups of **R275H$_2^{4+}$**, which can also bind the 24C8 loops, enable muscle-like actuation of the rotaxane driven by anion exchange—see **Section 6.13.1.4**. Other rotaxanes comprising macrotricyclic polyethers and dialkylammonium ion recognition units are described in **Sections 4.1.2.2** and **6.5.1**.

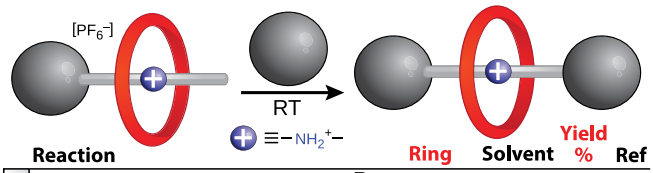
Secondary Ammonium / Crown Ether MIMs

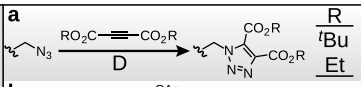
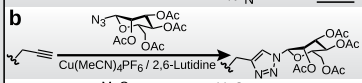
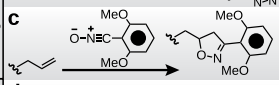
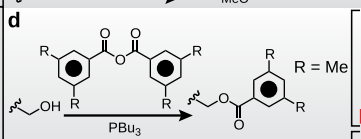
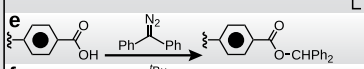
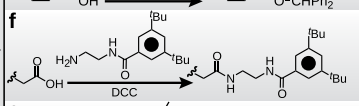
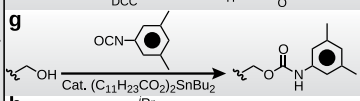
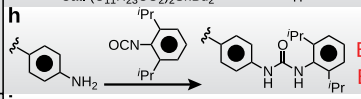
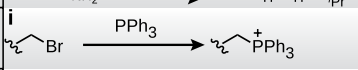
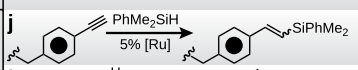
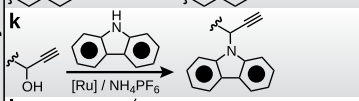
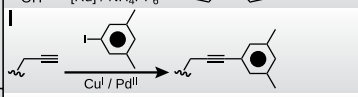
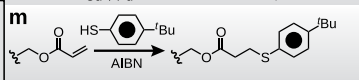
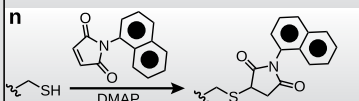
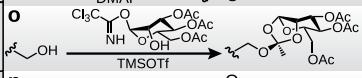
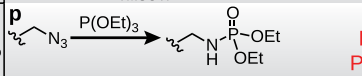
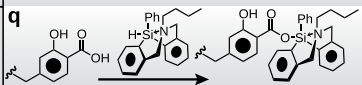
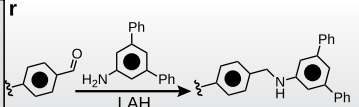
Reactions involving *R$_2$NH$_2^+$⊂crown* pseudorotaxanes must be relatively mild, since they are not typically compatible with (i) most bases and nucleophiles, which can deprotonate the ammonium center and cause them to dissociate, (ii) hard anions, which can outcompete crown ethers in binding the –NH_2^+– centers and thus lead to dissociation or precipitation when they serve as counterions, or (iii) high temperatures, which also favor dissociation. For these reasons, crown ethers and dialkylammonium ions represent an excellent test bed for researchers who are interested in the synthetic methodology of mechanostereochemistry. Indeed, this motif encompasses a relatively high number and diversity of stoppering reactions and other strategies (i.e., shrinking, swelling) that have been developed (*vide infra*) over the past 20 years in order to make molecular mechanical bonds, especially rotaxanes. See **Chapter 4** for many examples of novel rotaxane topologies and architectures based on this motif. Advances in the synthesis of ammonium-based MIMs has been reviewed[134,949] recently in the literature.

Dialkylammonium / Crown Ether Rotaxanes by Stoppering

The dialkylammonium / crown ether recognition systems comprise what has been arguably the most fertile ground for developing and testing the efficiency of new stoppering reactions for the synthesis of rotaxanes. Their status as such can be attributed to (i) the fact that they do not require very bulky stoppers, allowing researchers to select small, often commercially available stopper precursors, and (ii) successful stoppering protocols have a high likelihood of being adapted for other recognition systems, since dialkylammonium / crown ether complexes tolerate only mild reaction conditions, i.e., no bases and low temperatures. Many types of stoppering reactions (**Table 2.27**) have been

Table 2.27 Summary of *dialkylammonium⊂crown* stoppering reactions.



		Reaction		Ring	Solvent	Yield %	Ref
Cycloadditions	a		R = ^{t}Bu	DB24C8	$CHCl_3$	31	1008
			R = Et	DB24C8	CH_2Cl_2	77	1009
	b			DB24C8	CH_2Cl_2	72	1014
	c			DB24C8	CH_2Cl_2	98	1024
				DB24C8	CH_2Cl_2[a]	85	1024
Esters, Amides, Urethanes, Ureas	d		R = Me	DB24C8	CH_2Cl_2	90	1004
				DB24C8	Benzene	88	1004
				DB24C8	MeCN	90	1004
				DB24C8	Dioxane	74	1004
				DCy24C8	CH_2Cl_2	88	1015
			R = H	B21C7	CH_2Cl_2	74	960
				P21C7	CH_2Cl_2	62	961
	e			DB24C8	$CHCl_3$	97	1010
				1:1 $CHCl_3$ / MeCN		97	1010
	f			DB24C8	$CDCl_3$	73	1013
				DB24C8	CD_3CN	71	1013
	g			DB24C8	$CHCl_3$	87	1011
				DB24C8	PhCl	90	1011
				DB24C8	$MeNO_2$	83	1011
	h			DB24C8	CH_2Cl_2	64	965
				BMP25C8	CH_2Cl_2	36	965
				BBN26C8	CH_2Cl_2	42	978
S_N2	i			DB24C8	CH_2Cl_2	80	970
				DP24C8	CH_2Cl_2	39	971
Metal-Catalyzed	j			DB24C8	$CHCl_3$	84	1043
				DCy24C8	$CHCl_3$	80	1043
	k			DB24C8	DCE[b]	97	1012
				DB24C8	DCE[a]	90	1012
	l			DB24C8	MeCN	≤ 26	1006
Thiols	m			DB24C8	CH_2Cl_2	18	1005
				DB24C8	Benzene[b]	17	1005
				DB24C8	Dioxane[b]	25	1005
	n			DB24C8	PhMe	44	572
				DB24C8	$CHCl_3$	61	572
				DB24C8	$CHCl_3$[c]	71	572
Glycosylation	o			DB24C8	CH_2Cl_2[d]	74	955
Ligation	p			DB24C8	CH_2Cl_2	87	972
				DPT24C8	CH_2Cl_2	40	972
				PO292PC	CH_2Cl_2	57	617
Silylation	q			DB24C8	$CDCl_3$	75	576
Reductive Amination	r			24C8	DCE	77	987
				DB24C8	DCE	79	987
				DN24C8	DCE	49	987
				BPP26C8	DCE	51	987
				TN27C9	DCE	22	987
				DN30C10	DCE	31	987

[a] 40 °C. [b] 60 °C. [c] 0 °C. [d] –30° C.

employed to date, including cycloadditions, amide and ester bond-forming reactions, nucleophilic substitutions, metal-catalyzed cross-couplings, silylations, reductive aminations, and reactions involving thiols, azides, and sugars. These data have been tabulated from refs. 572, 576, 617, 955, 961, 965, 970–972, 978, 987, 1004–1015.

Cycloadditions

One of the early reactions to be employed[1008] in the synthesis (**Table 2.27a**) of dialkylammonium / crown ether rotaxanes was an uncatalyzed Huisgen[1016] 1,3-dipolar azide-alkyne cycloaddition. Although the rate of this reaction is typically very slow in the absence of a Cu^I catalyst, a sufficiently electrophilic[1017] or strained[1018,1019] alkyne can enhance the rate enough to render it practical for organic synthesis. This kind of copper-free click chemistry predates the Cu^I-catalyzed azide-alkyne click reactions pioneered by Sharpless[288] by several decades, although it is less versatile because of the constraints it imposes on the alkyne reactants. Nevertheless, sufficiently bulky electrophilic alkynes are commercially available, making it possible to design a facile stoppering protocol involving azide-terminated dibenzylammonium dumbbells, affording DB24C8-based [2]- and [3]rotaxanes in up to 77% yield. The electrophilic alkyne in this protocol is an ester of acetylenedicarboxylic acid, where ethyl esters react more efficiently (77% yield) than do *tert*-butyl esters (31% yield), most likely because of steric interference in the latter case.

The copper-catalyzed version (CuAAC) of the azide-alkyne cycloaddition, the quintessential click reaction, has also been utilized effectively in the synthesis of dialkylammonium rotaxanes, particularly bistable molecular shuttles—see **Chapter 6**. Coutrot[1014] has employed an acetylated mannosyl azide as the stopper precursor in a click reaction (**Table 2.27b**) with an alkyne-terminated pseudorotaxane in the presence of an excess of DB24C8 and catalytic amounts of $Cu(MeCN)_4PF_6$ and 2,6-lutidine, which proceeds in CH_2Cl_2 at room temperature in 72% yield. The CuAAC reaction has been employed[1020–1023] by several research groups in order to synthesize rotaxanes.

Takata[1024] has pioneered the click synthesis of rotaxanes involving the cycloaddition of nitrile *N*-oxide stopper precursors to alkene-, alkyne-, or nitrile-terminated pseudorotaxanes, affording isoxazole, isoxazoline, and oxadiazole linkages, respectively. The reaction (**Table 2.27c**) proceeds in CH_2Cl_2 or 1,2-dichloroethane (DCE) very efficiently (up to 97%) at room temperature without the need for a catalyst. The protocol is equally efficient with alkene and alkyne substrates, while nitriles lead to lower yields, most likely because the more basic oxadiazole product can deprotonate the ammonium center. Takata's novel protocol has also enabled[1025] the production of [2]catenanes (*vide infra*) by means of a double-click annulation of a pseudorotaxane's dumbbell.

Another type of cycloaddition employed by Takata[1026] in a stoppering protocol is the Diels-Alder cycloaddition

between a sultine derivative and C_{60} as the stopper precursor. This reaction is not unlike the one[906,908] involving a sulfolene-containing benzylic amide rotaxane and C_{60} as portrayed in **Scheme 2.75** in **Section 2.3.4.2**.

Esters, Amides, Urethanes, and Ureas

In 1999, Takata[1004] introduced tributylphosphine-catalyzed acylation reactions as a very efficient (up to 90% yield) stoppering technique. The reaction (**Table 2.27d**) involves capping the terminal –OH group of a dumbbell precursor with a dimethylphenyl stopper in the presence of an excess (1.05–3 equiv) of DB24C8, using 3,5-dimethylbenzoic anhydride as the acylation reagent with 0.1 equiv PBu_3 as catalyst, and is tolerant to a wide range of organic solvents. 2-Pyridylthioesters are also effective as capping agents employing this protocol.[954,1027] The same reaction is very low yielding, however, when employing acyl chlorides as the capping agent, most likely because the Cl^- leaving group causes a counterion exchange that reduces the ring's affinity for the $–NH_2^+–$ center. Takata's stoppering protocol has reappeared in a number of projects from his group[1015,1028–1032] and others.[960,1033–1035] An ester-forming capping methodology[1010] involving the reaction (**Table 2.27e**) of diazophenyl stopper precursors with carboxylic acid-terminated dumbbells in the presence of DB24C8 also proceeds in up to 97% (83% isolated) yield.

Owing to the hydrolytic instability of esters, it is useful to have stoppering reactions at one's disposal that create more stable bonds. Smithrud[1013] has shown that a conventional amide bond-forming condensation reaction involving *N*,*N*′-dicyclohexylcarbodiimide (DCC) can deliver (**Table 2.27f**) rotaxanes in up to 73% yield from a dialkylammonium / crown ether pseudorotaxane in CD_3CN. It is important in this case to have at least two methylene units in between the $–NH_2^+–$ center and the carboxylic acid terminus of the dumbbell precursor in order to avoid steric hindrance from the ring. It is also possible to isolate the DCC-[2]rotaxane intermediate species by liquid or column chromatography and store it at low temperatures for prolonged periods (>1 week) without showing signs of degradation.

Takata[1011] has developed a stoppering protocol that relies upon urethane formation (**Table 2.27g**) during the dibutyltin dilaurate-catalyzed reaction of terminal OH groups with dimethylphenyl isocyanates, which affords rotaxanes in >80% yield in a variety of medium-polarity solvents. This method has been employed by Takata[908,1036,1037] as well as Morin[1038,1039] to prepare a number of different photoactive crown ether / dialkylammonium rotaxanes.

Exposing isocyanates to anilines gives rise to urea derivatives—a reaction which has also been exploited (**Table 2.27h**) to synthesize rotaxanes on several occasions.[965,978,1040]

S_N2 Reactions

Another widely utilized reaction for synthesizing rotaxanes is nucleophilic substitution. Triphenylphosphonium-stoppered rotaxanes (**Table 2.27i**) are important in this area because (i) they can be prepared[970] in good yields of up to 80%, and (ii) the triphenylphosphonium stopper can act as a surrogate,[1041,1042] providing access to new rotaxanes by Wittig exchange. Hydrogen bonded triphenylphosphonium-stoppered rotaxanes have been prepared from both DB24C8[970] and DP24C8[971] crown ethers.

Transition Metal Catalyzed Reactions

Takata[1043] has employed a Ru-catalyzed hydrosilylation of alkynes as a means of stoppering (**Table 2.27j**) *dialkylammonium⊂crown* pseudorotaxanes. [2]Rotaxanes are obtained in yields as high as 88% under optimized conditions, which involve mixing a phenylacetylene-terminated 24C8-based semirotaxane with an excess of dimethylphenylsilane and 5 mol % $RuHCl(CO)(PPh_3)_3$ as catalyst in $CDCl_3$. A spacer is needed to avoid steric interference at the reactive site by the DB24C8 ring, since no rotaxane is obtained when the alkyne group is appended directly to a dibenzylammonium template. The hydrosilylation tolerates a number of different 24C8 derivatives and counterions, and proceeds with high regio- and stereoselectivity, affording a β-*trans* olefin product as >90% of the product population.

Tokunaga[1012] has described a ruthenium-catalyzed propargylic substitution for rotaxane synthesis, in which a $[(Cp^*)RuCl(SMe)]_2$ catalyst facilitates the exchange of a propargylic hydroxyl group with a nucleophile. The entry in **Table 2.27k** depicts a carbazole substitution, which is the most efficient stopper precursor that was uncovered, delivering a [2]rotaxane in 97% (83% isolated) yield. Other suitable nucleophiles include anilines, sulfonamides, thiols, phosphine oxides, and carbanions, all of which give rise to rotaxanes in >50% yield.

Note that olefin cross metathesis with Grubbs' ruthenium-alkylidene catalysts represents a powerful approach to creating mechanical bonds—these transformations are summarized in **Section 3.2**.

Palladium-catalyzed cross-coupling reactions have also been applied successfully to the synthesis of *dialkylammonium⊂crown* rotaxanes. Morin[1006] has employed the Sonogashira reaction, which couples aryl halides with alkynecuprates, in the synthesis (**Table 2.27l**) of [2] and [3]rotaxanes. The main drawback of this approach is that the Sonogashira reaction works best in polar solvents with an excess of base in order to facilitate the formation of the necessary alkynecuprate intermediates from terminal alkyne reactants, whereas the pseudorotaxane precursors have a low tolerance for bases and polar solvents. Under optimized conditions, [2]rotaxanes can be obtained by this approach in up to 26% yield.

Reactions of Thiols

In 1999 Takata[1005] introduced a conjugate addition (**Table 2.27m**) approach to stoppering pseudorotaxanes involving the addition of a 4-*tert*-butylthiophenol radical as a stopper precursor to a dumbbell precursor's α,β-unsaturated ester

group in the presence of an excess of DB24C8, affording aryl sulfide-capped rotaxanes in up to 25% yield.

Takata[572] has found that the 'base-free' requirement for stoppering dialkylammonium-based rotaxanes can be circumvented if the capping reaction is faster than the combined rate of deprotonation and dissociation of the pseudorotaxane precursor. The Michael addition (**Table 2.27n**) between a thiol and a maleimide proceeds very rapidly in polar solvents without the need for a base as a reaction accelerator, a feature underpinning its ubiquity as a bioconjugation reaction. In low polarity solvents, however, a base is needed to maintain high reaction rates. In $CDCl_3$ and PhMe, 1 equiv of DMAP as a base accelerates this reaction enough to produce [2]rotaxanes in up to 71% yield.

Disulfide bonds are formed reversibly via the oxidative coupling of thiols—the use of these bonds in the thermodynamically controlled synthesis of MIMs is discussed in **Section 3.5**.

Glycosylation

Coutrot[955] has prepared glycosidic [2]rotaxanes by reacting (**Table 2.27o**) an acetylated mannosyl trichloroacetimidate stopper precursor with a hydroxyl-terminated anilinium dumbbell in the presence of an excess of DB24C8 and a catalytic amount of trimethylsilyl triflate (TMSOTf) in CH_2Cl_2. The optimized reaction conditions, which employ 2.2 equiv DB24C8 and 0.2 equiv TMSOTf at –30 °C for 1 min, afford an orthoester-capped [2]rotaxane in 74% yield.

Staudinger Ligation

A particularly facile reaction (**Table 2.27p**) developed by Chiu[617,972] for the synthesis of rotaxanes relies on the first step of the Staudinger reaction followed by a spontaneous Arbuzov-type dealkylation, in which an organic azide is converted to a phosphoramidate by a phosphite reagent in low polarity solvents. The reaction is not only high yielding (up to 87%) at room temperature in CH_2Cl_2, but also relatively green and atom-economical, since it releases only nitrogen gas and ethanol in the case of triethyl phosphite as the capping agent for an azide-terminated pseudorotaxane precursor.

Silylation

Goto and Kawashima[576] have employed a pentacoordinated hydrosilane activated by an intramolecular [N→Si] bond as a stopper precursor for the synthesis (**Table 2.27q**) of dialkylammonium / crown ether [2]rotaxanes. The reaction is fast (<1 h) and efficient (75% yield) at room temperature in $CHCl_3$, as well as atom-economical since it requires no other additives and releases only H_2 gas as a byproduct. These conveniences come at the penalty of extra synthetic steps, however, since multiple steps are involved in the synthesis of the pentacoordinated hydrosilane precursor as well as the salicylic acid-terminated dumbbell. Pseudorotaxanes terminated with simple phenols are also converted to rotaxanes by this protocol, yet they require higher temperatures, longer reaction times, and give lower yields. The application[577] of this "click" methodology to the synthesis of a π-donor/π-acceptor [2]rotaxane is described in **Scheme 2.53** and the accompanying discussion in **Section 2.3.3.2**.

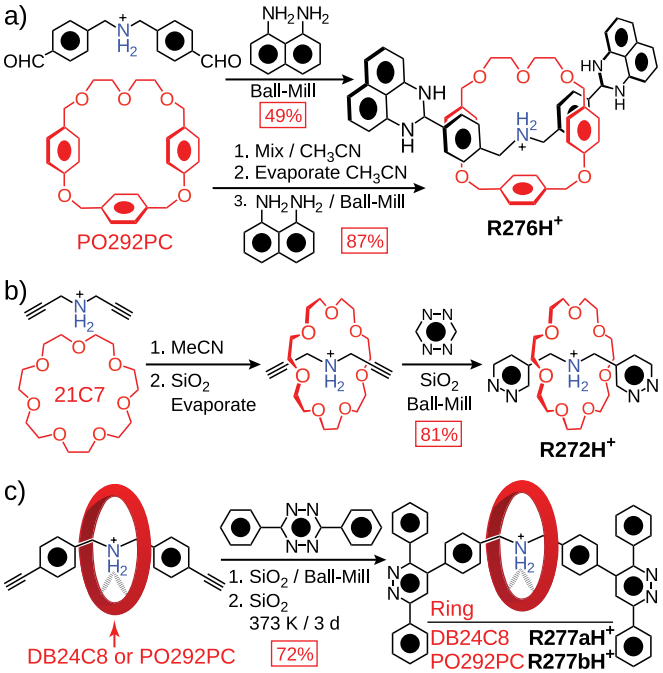
Reductive Amination

Tokunaga[987,1044] has relied on reductive aminations (**Table 2.27r**) to prepare a series of dialkylammonium [2]rotaxanes with different crown ethers. These reactions involve the formation of an imine bond between benzaldehyde-terminated pseudorotaxanes and 3,5-dimethylphenylamine stopper precursors, followed by reduction of the imine bond with LAH at room temperature in 1,2-dichloroethane. The yields span from 22 to 79% depending on the crown ether, with 24C8 and DB24C8 being the most effective.

Solid-State Stoppering Reactions

Solid-state reactions offer an attractive alternative to solution-phase organic synthesis, especially in cases of supramolecular and template-directed synthesis,[1045] since (i) the dissociation of a supramolecular template in solution as a result of competition with solvent molecules or chemical exchange can lead to errors that decrease efficiencies, whereas this problem is a non-issue in the solid state, (ii) the formation of side-products, which is typically more likely in solution than in the solid state, can also impact efficiency, (iii) insolubility is not a concern in the solid state, and (iv) solid-state reactions typically generate less waste and are more environmentally friendly than their solution-phase counterparts. Solid-to-solid transformations involving mechanical activation of covalent bonds, often by grinding or milling a well-mixed powder, fall under the umbrella of the field of mechanochemistry[1046]—not to be mistaken for mechanostereochemistry, the main topic of this monograph. Mechanochemical reactions are, however, more limited in scope[1047] than solution-phase chemistry, which presents a challenge in identifying appropriate solid-state stoppering or clipping protocols.

Solid-state stoppering reactions (**Scheme 2.84**) for dialkylammonium rotaxanes were introduced by Chiu[1007] in 2008. When 4-formylbenzylammonium hexafluorophosphate and PO292PC (1.2 equiv) are mixed in CD_3CN and concentrated to dryness—presumably as the corresponding pseudorotaxane—the naphthodihydropyrimidine-capped [2]rotaxane **R276H⁺** is produced (**Scheme 2.84a**) in 87% yield by ball-milling in the presence of 2 equiv of 1,8-diaminonaphthalene. Even more remarkably, **R276H⁺** can be obtained[1007] by ball-milling the unassembled mixture of the ring, thread, and stopper precursors in 49% yield. By contrast, performing the same reaction at a concentration of 20 mM in MeCN affords the [2]rotaxane in only 48% yield. The same protocol has been applied to the synthesis of a tripodal [4]rotaxane.[1007] The only examples of solid-state stoppering reactions to preceed Chiu's robust strategy were those of (i) Otera,[569,570] whose S_N2-mediated



Scheme 2.84 Chiu's syntheses of dialkylammonium rotaxanes under solvent-free conditions. (a) Pyrimidine formation.[1007] (b)–(c) Diels-Alder reactions.[959,1048]

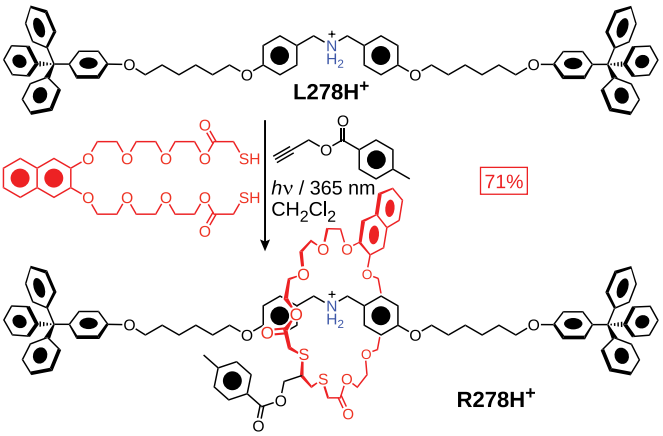
approach to capping D-A *BIPY*$^{2+}$⊂*BPP34C10* pseudorotaxanes in the solid state is inefficient (11%) unless a solution-state pre-mixing step is first performed (**Section 2.3.3.2**), and (ii) Takata,[224,225] whose approach involving grinding cyclodextrin-based polypseudorotaxanes with stopper precursors (**Section 2.3.1.1**) is modest yielding (<50%) when the polypseudorotaxanes are first assembled in solution and low-yielding[226] (<6%) under truly solvent-free conditions.

Another type of reaction employed by Chiu[959,1048,1049] in the solid-state synthesis of rotaxanes is a Diels-Alder reaction between terminal alkyne units and 1,2,4,5-tetrazine derivatives, which leads to pyridazine-derived stopper groups upon liberation of N_2 as the byproduct. This approach was first applied (**Scheme 2.84b**) to the synthesis[959] of the [2]rotaxane **R272H**$^+$. In this case, the reaction was performed on SiO_2 as a solid support because the pseudorotaxane comprising 21C7 and dipropargylammonium tetrafluoroborate is a sticky solid. The ring and thread components were mixed with silica gel in MeCN, dried, combined with 1,2,4,5-tetrazine (2.2 equiv), and ball-milled at ambient temperature for 9 h to afford **R272H**$^+$ in 81% yield. The solid-state structure of **R272H**$^+$, which was the smallest rotaxane ever prepared at the time of publication, is portrayed in **Figure 2.54b**. Expanding the scope of the reaction to be compatible with larger macrocycles, Chiu[1048] employed 3,6-diphenyl-1,2,3,4-tetrazine as a bulkier stopper precursor, which enables the solvent-free synthesis (**Scheme 2.84c**) of the DB24C8- and PO292PC-based rotaxanes **R277aH**$^+$ and **R277bH**$^+$ by ball-milling and prolonged heating at 373 K on a SiO_2 support with equal efficiencies of 72% yield. A self-sorting hetero[3]rotaxane has also been synthesized[1049] using this solid-state Diels-Alder methodology.

Crown Ether / Dialkylammonium Rotaxanes by Clipping

The thiol-ene and thiol-yne radical additions are click reactions which have been employed[1005,1050] only rarely in order to make mechanical bonds. In the case of the thiol-yne reaction, the addition of a thiol to an alkyne is followed by the addition of another thiol to the resulting alkene. Yongjun Li and Yuliang Li[1051] have exploited this double-click reaction to synthesize (**Scheme 2.85**) the [2]rotaxane **R278H**$^+$ by a clipping protocol, whereby the macrocyclic polyether precursor is terminated with two thiol groups which react with the alkyne terminus of propargyl *para*-toluate. The reaction proceeds in good yield (71%) under an atmosphere of air under ambient conditions in CH_2Cl_2.

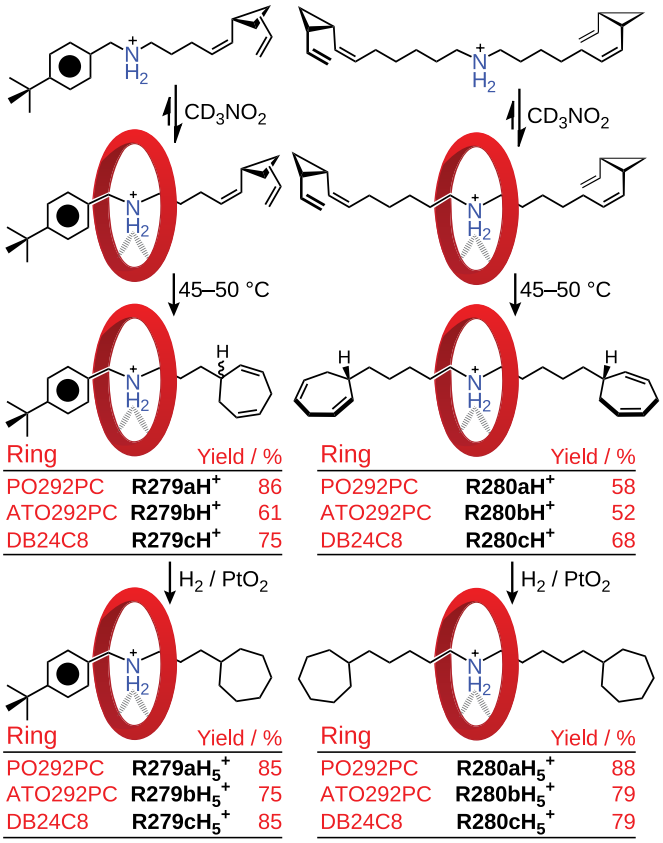
A very efficient thermodynamically controlled clipping protocol[1052] involving dialkylammonium templates and a macrocyclic polyether with dynamic imine bonds has been important in the design of a number of novel rotaxane architectures—see **Section 3.3.1.2**.



Scheme 2.85 Clipping a macrocyclic polyether around a dibenzylammonium-based dumbbell using a thiol–yne click reaction.[1051]

Threading Followed by Swelling

Chiu[15,16] introduced a creative alternative to the 'stoppering' reaction known as threading followed by 'swelling'. Swelling is distinguished from stoppering because it entails an intramolecular rearrangement that increases the steric bulk of a pseudorotaxane's endgroups without attaching any new atoms, rather than an intermolecular reaction that installs new stoppers. The swellable group of this novel protocol (**Scheme 2.86**) is cis-1-[(*Z*)-alk-1′-enyl]-2-vinylcyclopropane, which is small enough to allow the passage of an PO292PC ring until it spontaneously undergoes a pericyclic Cope rearrangement to a cycloheptadiene, the rate of which is slow at room temperature. Thus, the divinylcyclopropane-terminated pseudorotaxane



Ring		Yield / %
PO292PC	**R279aH$^+$**	86
ATO292PC	**R279bH$^+$**	61
DB24C8	**R279cH$^+$**	75

Ring		Yield / %
PO292PC	**R280aH$^+$**	58
ATO292PC	**R280bH$^+$**	52
DB24C8	**R280cH$^+$**	68

Ring		Yield / %
PO292PC	**R279aH$_5^+$**	85
ATO292PC	**R279bH$_5^+$**	75
DB24C8	**R279cH$_5^+$**	85

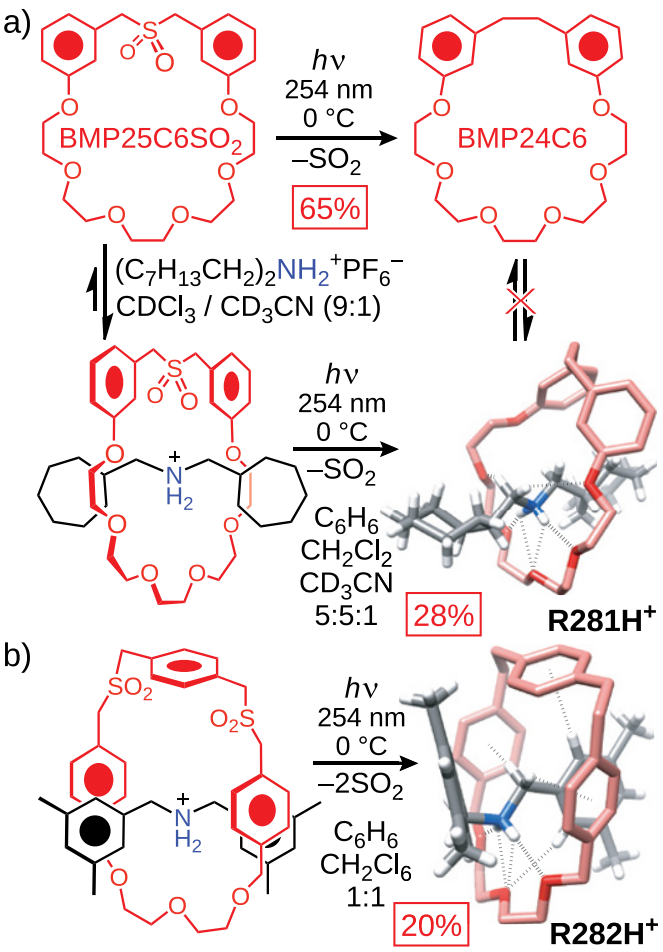
Ring		Yield / %
PO292PC	**R280aH$_5^+$**	88
ATO292PC	**R280bH$_5^+$**	79
DB24C8	**R280cH$_5^+$**	79

Scheme 2.86 Chiu's swelling protocol[15,16] for the synthesis of [2]rotaxanes, in which a pseudorotaxane's racemic (left) or optically pure (right) divinylcyclopropane endgroups undergo a pericyclic rearrangement to the bulkier cycloheptadiene groups, followed optionally by hydrogenation to cycloheptane.

precursor is isolated at room temperature before inducing the swelling process at an elevated temperature (45–50 °C) in CD_3NO_2 for 48 h, leading to the [2]rotaxane **R279aH$^+$** in 86% yield. Since the racemate of the chiral cycloheptadiene product gives rise to a complicated ^{1}H NMR spectrum, the enantiomeric mixture can be converted to the achiral [2]rotaxane **R279aH$_5^+$** by hydrogenation of the cycloheptadiene to cycloheptane over a PtO_2 catalyst. The same protocol has been applied[15,16] to the synthesis of rotaxanes **R279bH$^+$** and **R279cH$^+$** possessing ATO292PC and DB24C8 rings in yields of 61 and 75%, respectively, as well as the corresponding hydrogenated counterparts **R279bH$_5^+$** and **R279cH$_5^+$**. The swelling reactions also proceed under solvent-free conditions in moderately lower yields of 45–55%. Chiu[16] has also repeated the protocol using symmetrical dumbbells with optically pure divinylcyclopropane endgroups, affording the cycloheptadiene-stoppered rotaxanes **R280aH$^+$–R280cH$^+$** as single enantiomers in up to 68% yield, as well as the corresponding cycloheptane-stoppered rotaxanes **R280aH$_5^+$–R280cH$_5^+$**. The swelling reaction is not only efficient, but also highly atom-economical, since no atoms are added or lost in the process and no additional reagents are required.

Threading Followed by Shrinking

The 'shrinking' strategy, which converts a pseudorotaxane to a rotaxane by means of a reaction that reduces the size of a ring's cavity, was introduced in 2004 by Asakawa,[17] who employed reversible coordinative imine bonds to shrink a macrocyclic polyether around a dibenzylammonium-derived dumbbell—see **Section 3.4.1**. A couple of metal-free shrinking protocols (**Scheme 2.87**) were introduced subsequently by Chiu.[1053,1054] The key to this approach is the photoextrusion of SO_2 from the ring of a pseudorotaxane. The first example[1053] of a metal-free shrinking protocol (**Scheme 2.87a**) involves the macrocyclic polyether sulfone BMP25C6SO$_2$, which is converted to the smaller bis-*meta*-phenylene[24]crown-6 (BMP24C6) under 254 nm irradiation in 65% yield. Both rings were found to bind dialkylammonium derivatives with K_a values on the order of 10^2 M^{-1} in 9:1 $CDCl_3$:CD_3CN. It transpires that a cycloheptane group is small enough to allow the passage of BMP25C6SO$_2$, yet large enough to block the passage of BMP24C6. Thus,

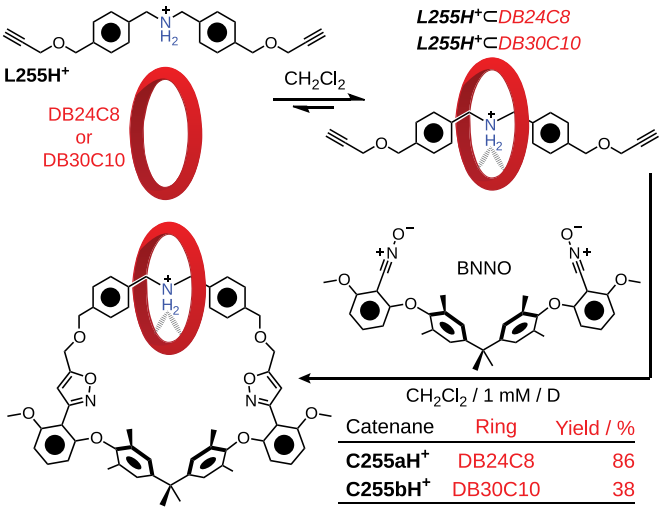


Scheme 2.87 Chiu's shrinking protocols[1053,1054] for the synthesis of rotaxanes **R281H$^+$** (a) and **R282H$^+$** (b) via the photoextrusion of SO_2 from the macrocycles encircling dialkylammonium dumbbells. Tubular representations of the solid-state structures of the rotaxanes are portrayed with counterions, solvent molecules, and protons of the hosts omitted for the sake of clarity, with noncovalent bonding interactions <2.8 Å depicted as dashed lines.

irradiation of a pseudorotaxane comprising BMP25C6SO$_2$ and a cycloheptane-terminated dialkylammonium template leads to the [2]rotaxane **R281H$^+$** upon photoextrusion of SO$_2$ gas. Chiu[1054] subsequently reported a shrinking protocol (**Scheme 2.87b**) involving the photoextrusion of two SO$_2$ groups from a cyclophane in the preparation of the dialkylammonium-based rotaxane **R282H$^+$**, which is generated in yields of up to 20% under optimized conditions involving the portionwise addition of a fourfold excess of dialkylammonium template. The solid-state structures of both rotaxanes are depicted in **Scheme 2.87**, which reveal a number of [C–H···O] contacts in the case of **R281H$^+$** as well as [C–H···π] contacts in the case of **R282H$^+$**, in addition to the expected 1,3-arranged [N$^+$–H···O] hydrogen-bonding pattern of the –NH$_2^+$– centers with respect to the polyether loops.

Dialkylammonium/Crown Ether Catenanes

Although the majority of MIMs relying on dialkylammonium ions as templates are rotaxanes, several catenanes based on this motif have also been reported. Most of these dialkylammonium/crown catenanes have been prepared under thermodynamic control—see **Sections 3.2.4.1**, **3.3.1.2**, **3.4.1.3**, **4.1.2.1**, **4.1.2.2**, **4.1.4.1**, and **4.1.4.3**. One kinetically controlled click reaction involving the cycloaddition of nitrile *N*-oxides to alkenes, alkynes, or nitriles, which has been championed by Takata[227,1024] for rotaxane synthesis (**Table 2.27c**), has also been applied[1025] to the synthesis (**Scheme 2.88**) of [2]catenanes. This approach relies on a bis-nitrile *N*-oxide (BNNO) compound as a homoditopic linker, which reacts with both termini of the pseudorotaxanes comprising the dibenzylammonium bis(propargyl ether) template **L255H$^+$** and either the DB24C8 or DB30C10 macrocyclic polyethers. Under optimized conditions (refluxing CH$_2$Cl$_2$ at a reactant concentration of 1 mM) the catalyst-free formation of two isoxazole linkages in one pot leads to the DB24C8-based rotaxane **C255aH$^+$** in 86% yield, whereas the DB30C10-based rotaxane **C255bH$^+$** is obtained in 38% yield.



Scheme 2.88 Takata's synthesis[1025] of [2]catenanes via double click annulation exploiting the cycloaddition of nitrile *N*-oxides to alkyne-terminated pseudorotaxanes based on DB24C8 and DB30C10 rings.

Concluding Remarks

Just as Nature relies heavily on hydrogen-bonding interactions to stabilize the functional self-assembled nanostructures which constitute the building blocks of life—i.e., DNA, RNA, proteins—so too do researchers rely on hydrogen-bonding interactions to template the formation of mechanical bonds in one of the most diverse recognition motifs of mechanostereochemistry. Not only do hydrogen bonds support a rich variety of structural motifs as templates, but these motifs have also served as the basis for some of the most innovative synthetic methodologies for making mechanical bonds, including the novel shrinking and swelling protocols for rotaxane synthesis, and a large array of mild and high-yielding reactions for efficiently trapping mechanically interlocked products under kinetic control. No less innovative are the thermodynamically controlled approaches to making hydrogen-bonded MIMs (**Chapter 3**) and the novel topologies and architectures (**Chapter 4**) that have arisen as a result of these templates.

2.3.5 Halogen-Bonded Templates

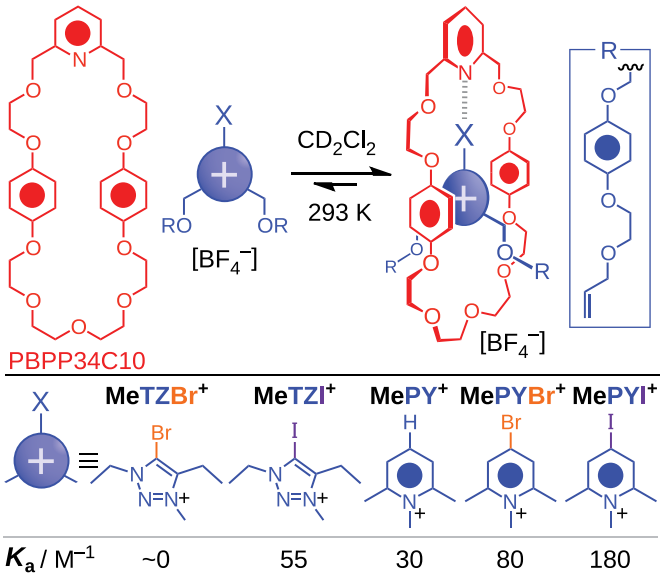
Halogen atoms are versatile in their ability to interact noncovalently. One type of halogen interaction arises from their high electronegativities—halogen atoms can become electron-rich/nucleophilic and attract electron-poor/electrophilic partners, such as polarized hydrogen atoms. This interaction is simply a hydrogen bond, however, or a conceptually equivalent dipole–dipole interaction. Another type of interaction, which is known[1055] as a 'halogen bond', involves halogen atoms as electron acceptors, i.e., an association between electron-poor halogen atoms and electron-rich partners. According to a 2013 IUPAC task committee[1055] charged with defining it, "*a halogen bond occurs when there is evidence of a net attraction between an electrophilic region associated with a halogen atom in a molecular entity and a nucleophilic region in another, or the same, molecular entity*." Halogen-bonding recognition processes[1056] most commonly involve at least one halogen atom that is covalently bonded to a cationic or other electron-withdrawing group, which polarizes the atom to expose a patch of positive electron density along the axis of the X–R bond surrounded by a belt of negative electron density. The larger, less electronegative halogens such as Br and I are more polarized by this effect than the smaller, more electronegative halogens such as F and Cl.

The halogen bond-directed template synthesis of mechanically interlocked and interpenetrated structures and superstructures has been pioneered by Beer[1057–1065] at the University of Oxford, whose discovery of halogen-bonding supramolecular templates arose out of his research

(**Sections 2.3.6.2–2.3.6.4**) on anion-binding templates. The majority of halogen bond templates involve halide anions and are therefore described in Section **Section 2.3.6.3** on anion-binding motifs.

Beer[1060] has also characterized the self-assembly (**Table 2.28**) of pseudorotaxanes which do not rely on anionic templates, but rather on a combination of halogen bonding and π-associated D-A stacking. The host of this recognition motif incorporates a Lewis base—namely, pyridine—into the framework of the π-donating BPP34C10 crown ether. The pyridine ring of pyrido-bis-*para*-phenylene[34]crown-10 (PBPP34C10) enables it to associate with electrophilic halogen atoms appended to cationic cores of guest molecules possessing various halogenated π-acceptors—namely, *N*–methyl-5-bromotriazolium (MeTZBr$^+$), *N*-methyl-5-iodotriazolium (MeTZI$^+$), or *N*-methyl-4-bromopyridinium (MePYBr$^+$), and *N*-methyl-4-iodopyridinium (MePYI$^+$) as their BF_4^- salts. A comparison of the K_a values (**Table 2.28**) recorded for these PBPP34C10-derived pseudorotaxanes in CD_2Cl_2 reveals that (i) consistent with expectations, iodine is a more effective halogen bond donor than bromide, since the iodinated templates bind more strongly than the corresponding brominated templates, and (ii) the pyridinium unit is more effective at bolstering the halogen bond than is the triazolium unit, since the MePYBr$^+$ and MePYI$^+$ guests bind PBPP34C10 more strongly (K_a = 80 and 180 M^{-1}, respectively) than do the MeTZBr$^+$ and MeTZI$^+$ (K_a = 0 and 55 M^{-1}, respectively) derivatives. A non-halogenated *N*-methylpyridinium (MePY^{2+}) derivative associates (K_a = 30 M^{-1}) with PBPP34C10 more weakly than its halogenated homologues, confirming that halogen bonds are involved in stabilizing these pseudorotaxanes. Beer has employed[1060] this recognition motif in the synthesis of the [2]catenane **C256**$^+$ (**Figure 2.60**), which is obtained, albeit in low yield (<7%), by ring-closing metathesis (**Section 3.4.1.4**) on a *MePYI*$^+$*R*$_2$*⊂PBPP34C10* pseudorotaxane. The self-assembly of **C256**$^+$ is therefore templated, not only by D-A charge-transfer and π–π stacking interactions, but also by a single charge-assisted [C–I···N] halogen bond. MD simulations confirm that this halogen bond defines the prevailing co-conformation (**Figure 2.60**) of the [2]catenane **C256**$^+$ in $CHCl_3$. The world still awaits the first neutral MIM to be templated exclusively by halogen-bonding interactions.

Table 2.28 Association constants for the self-assembly of pseudorotaxanes,[1060] guided by charge-assisted halogen-bonding and π-associated D-A interactions, in CD_2Cl_2 at 293 K.



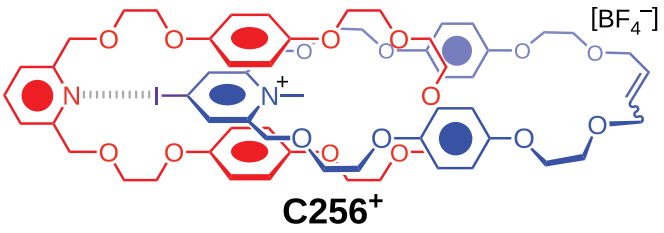


Figure 2.60 Stereoformula of the halogen-bonded [2]catenane[1060] **C256**$^+$.

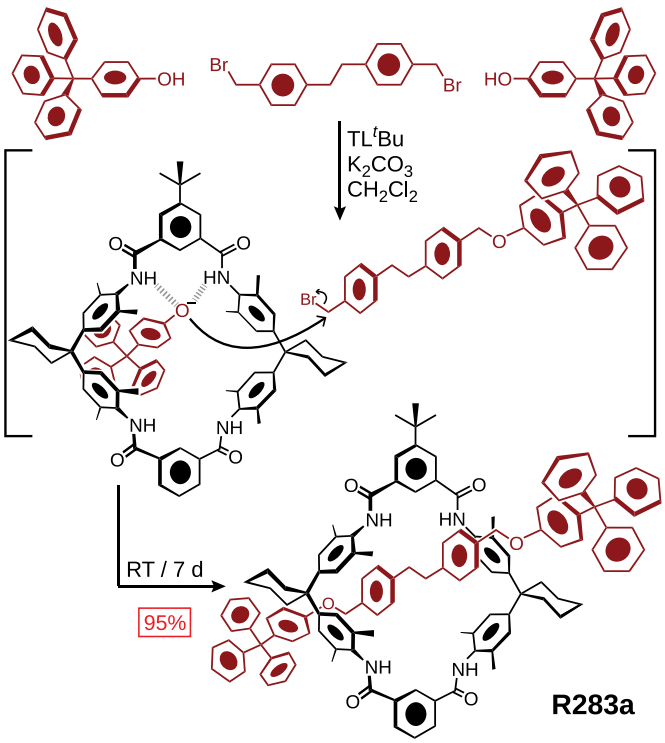
2.3.6 Anion-Binding Templates

The anion-templated synthesis of compounds with mechanical bonds has been enabled by the field[1066–1072] of supramolecular chemistry dealing with anion recognition and sensing. It would not be unfair to argue that anion-binding motifs are more challenging to design than cation binding ones, since anions have, in general, (i) larger radii and lower charge densities than cations, (ii) correspondingly higher energies of solvation which must be overcome before binding, (iii) a diverse set of geometries—i.e., spherical, linear, tetrahedral, octahedral, etc.—and shapes, not to mention (iv) the fact that the legacy of supramolecular chemistry and template-directed synthesis was built upon a foundation of cation binding, such as that of Pedersen's crown ethers[142] or the phthalocyanines,[341] to name some earlier examples. Early attempts at anion recognition involved ion-pairing with protonated azacrowns and other cationic ligands as hosts.[1066] Later, the anion binding properties of neutral receptors[1073–1076] possessing N–H hydrogen bond donors such as amides,[1077,1078] pyrroles[1079,1080] and ureas[1081] became a well-known phenomenon. The N–H hydrogen bond donors of these receptors approximate hydrogen bonding in the form of ion-dipole interactions, which support the synthesis of MIMs templated by anionic nucleophiles (**Section 2.3.6.1**) and halogens (**Section 2.3.6.2**). More recent additions to the anion binding motifs serving as templates for making mechanical bonds include halogen–halide bonding (**Section 2.3.6.3**) and C–H hydrogen bond donors (**Section 2.3.6.4**). The anion-directed synthesis of MIMs and their applications as hosts and sensors for anions has been the subject of a number of reviews in the chemical literature.[1082–1088]

2.3.6.1 Nucleophilic Rotaxane Capture

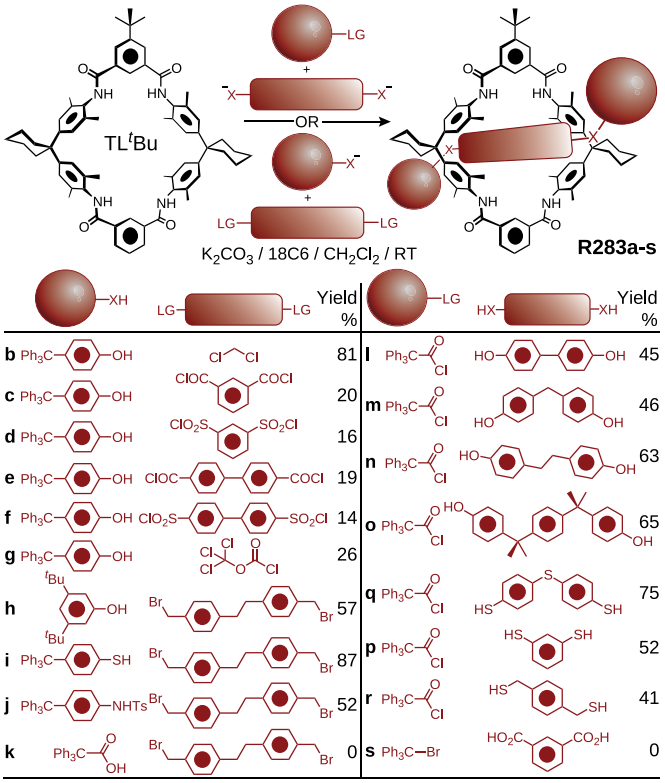
Some of the earliest examples of anion-templated MIMs were introduced by Vögtle,[1089–1092] who recognized that his tetralactam macrocycles (**Section 2.3.4.1**) such as TL^{t}Bu are capable of hosting anionic nucleophiles within their cavity by virtue of their four endotopic amides as hydrogen bond donors. Oxyanions in particular exhibit high affinities for the tetralactam macrocycles because they are strong hydrogen bond acceptors. The acetate anion, for example, was found[1089] to bind TL^{t}Bu with K_a values of 1.8×10^5 and 120 M^{-1} in CD_2Cl_2 and CD_2Cl_2/CD_3OD (4:1 $^v/_v$), respectively. This discovery led Vögtle to devise a procedure (**Scheme 2.89**) whereby a nucleophilic substitution between *p*-trityl-phenol and 1,2-bis(4-(bromomethyl)phenyl)ethane in the presence of a base (solid K_2CO_3) and the TL^{t}Bu host leads to the highly efficient capture of the [2]rotaxane **R283a** in CH_2Cl_2 in near-quantitative (95%) yield. Since the ether linkages of the dumbbell associate only very weakly with the tetralactam ring, the efficient formation of **R283a** can be attributed to the host's tendency to encircle the *p*-tritylphenolate anion as it attacks (**Scheme 2.89**) the bromomethyl endgroups of 1,2-bis(4-(bromomethyl)phenyl)ethane axle and its corresponding half-dumbbell intermediate.

In subsequent investigations, Vögtle[1090,1091] has employed the anion capture strategy in order to prepare (**Table 2.29**) the [2]rotaxane homologues **R283b-s**. A comparison of the yields for each compound illuminates how various structural parameters influence the efficiency of the nucleophilic capture. These parameters include:



Scheme 2.89 The proposed mechanism[1089] for the high-yielding synthesis of Vögtle's anion-templated tetralactam [2]rotaxane **R283a**.

Table 2.29 Summary[a] of yields for the anion-templated capture[1090,1091] of the [2]rotaxanes **R283a-s** during nucleophilic substitutions in the presence of the tetralactam macrocycle TL^{t}Bu.



[a]X = Nucleophile, LG = Leaving Group. **R283a**; see **Scheme 2.89**.

- The type of nucleophilic anion, which can take the form of phenolates (**R283a–R283g, R283l–R283o**), thiophenolates (**R283h, R283p, R283q**), thiolates (**R283r**), and amines (**R283j**). The protocol fails[1090] only in cases (**Table 2.29k,s**) involving carboxylates as the nucleophilic precursors. The most efficient (>60% yielding) reactions are those that employ phenolates and thiophenolates as the nucleophiles, such as **R283b**, **R283h**, **R283n–R283q**. The *N*-tosylaniline homologue **R283j** is obtained in lower yield (52%), most likely because it is capable of reacting without being deprotonated and therefore without being bound to the TL^{t}Bu host.
- The type of leaving group (LG), which may come from alkyl halide (**R283b**, **R283h–R283k**), acid chloride (**R283c**, **R283e**, **R283m**, **R283l–R283r**), or sulfonyl chloride (**R283d**, **R283f**) functionalities.
- The location of the nucleophilic anion to either the stopper (**R283a–R283k**) or the axle (**R283l–R283s**) stopper precursors, and *vice versa* for the leaving group. Both options seem more or less equally compatible, since high-yielding and low-yielding examples arise in both cases.
- Different axle moieties such as, *inter alia*, methylene, *meta*-phenylene, biphenyl, and diphenylmethane. Axle precursors of different lengths and flexibilities clearly influence the probability of rotaxanation, with yields ranging from as low as 14% in the case of **R283f** to as high as 95% in the case of **R283a.**

- Stoppering groups. A smaller 3,5-di-*tert*-butylphenol stopper precursor has a surprisingly detrimental effect[1089] on the yield (57%) of **R284h**, as compared to that (95%) of the *p*-trityltylphenol-stoppered homologue **R283a** possessing the same axle. This result has been corroborated by Schalley[1093] in an independent investigation. Schalley's computational modeling[1093] suggests that the sterics of the nucleophile modulate the geometry of the *nucleophile⊂TL^{t}Bu* intermediate host-guest complex and consequently the accessibility of the nucleophilic site, which in turn affects the probability that a substitution will occur through-the-annulus versus outside of the ring. The lowest energy co-conformations of *p-tritylphenol⊂TL^{t}Bu* involve geometries in which two lone pairs of the phenolate anion are engaged in hydrogen bonding with the N–H donors of the host, while the third lone pair is pointed into the cavity of the host, such that nucleophilic attack would most likely occur through-the-annulus. On the other hand, the phenolate anion of 3,5-di-*tert*-butylphenol directs its third lone pair preferentially away from the TL^{t}Bu ring's cavity, lending itself to substitutions that do not proceed through-the-annulus.

These results reveal that, although the efficiency of Vögtle's nucleophilic dumbbell capture reaction is rather sensitive to the geometric and stereoelectronic properties of the precursors, it remains tolerant to a wide range of different reactant types and structural motifs.

2.3.6.2 N–H···Anion Hydrogen-Bonded Templates

Beer[1082–1088,1094] has led the charge in the development of interlocked and interpenetrated structures and superstructures that depend on N–H···anion hydrogen bonds as templating forces, an enterprise which began[1095] in 2001 when he described the self-assembly (**Figure 2.61a**) of tight ion pairs comprising 3,5-bis(hexacarbamoyl)-*N*-methylpyridinium salts (BHCP·X), where counterion X^- = Cl^-, Br^-, I^-, or PF_6^-, and a hydrogen bond donating crown ether cyclophane—call it isophthalamide-bis-*para*-phenylene[34]-crown-7 (IBPP34C7)—in a pseudorotaxane-like geometry. The counterion X^- resides primarily in a cleft between the two lactam groups of $BHCP^+$ with its unsaturated coordination shell accessible to solvent. The encirclement of the BHCP·X tight ion-pair by IBPP34C7 creates a binding pocket for the anion, which is stabilized by multiple hydrogen bonds. The K_a values for *$BHCP^+$⊂IBPP34C7* pseudorotaxanes reach as high as 2400 M^{-1} in CH_2Cl_2 in the case of the chloride salt, which has also been characterized (**Figure 2.61b**) in the solid state by X-ray crystallography. The chloride ion is stabilized in its binding pocket by four [N–H···Cl^-] hydrogen bonds involving all four of the amide groups, as well as two [C–H···Cl^-] interactions involving the protons of the central aromatic rings. The pseudorotaxane is further stabilized by donor-acceptor π-stacking interactions, where the electron-poor pyridinium subunit of the guest is sandwiched between the electron-rich

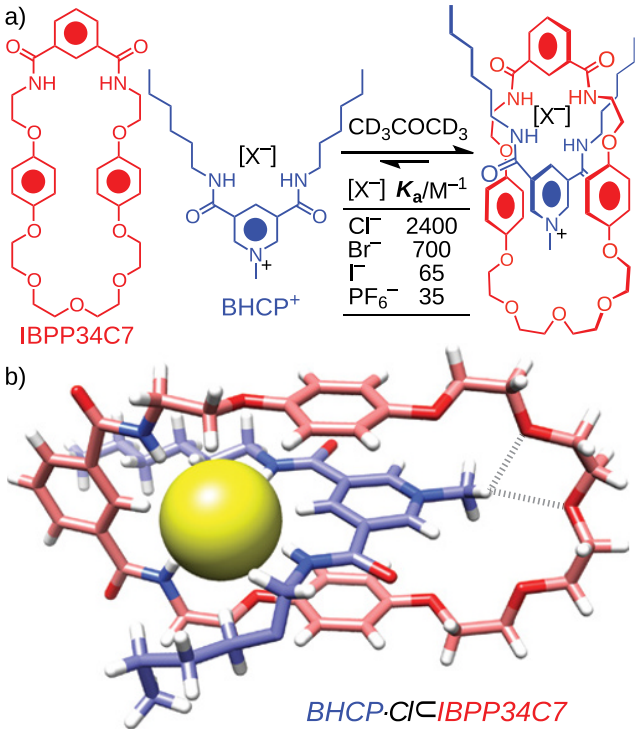


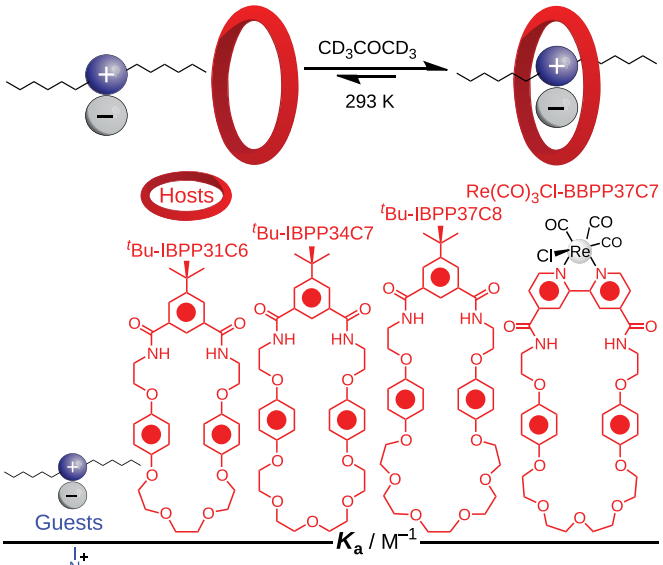
Figure 2.61 Beer's first interpenetrated anion recognition system.[1095] (a) The self-assembly of pseudorotaxanes comprising the isophthaloyl crown ether IBPP34C7 and the bis(carbamoyl) pyridinium guests $BHCP^+$ with different counterions, which is templated primarily by anion hydrogen-bonding interactions. (b) A tubular representation of the solid-state superstructure of the *BHCP·Cl⊂IBPP34C7* pseudorotaxane reveals [N–H···Cl^-], [C–H···Cl^-], D-A π–π stacking, and [C–H···O] stabilizing interactions.

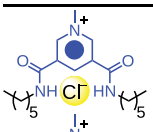
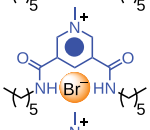
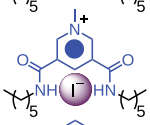
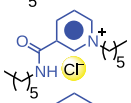
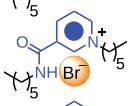
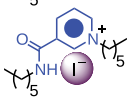
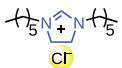
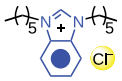
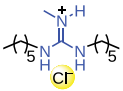
hydroquinone subunits of the host, as well as [C–H···O] interactions between the acidic methyl protons of the pyridinium core and the oxygen atoms of the host's polyether loop. Through a series of incremental changes to this original design motif, Beer has created a robust meccano set of components for templating the synthesis of molecules with mechanical bonds, which can be guided by halides or oxyanions.

Halide Templates

A number of halide-binding pseudorotaxane motifs developed by the Beer group are summarized in **Table 2.30**. In general, the self-assembly of these pseudorotaxanes is driven by electrostatic (ion-pairing) forces and charge-assisted hydrogen bonds. The halide ions are escorted by ion-paired organic cations—e.g., pyridinium carboxamide, imidazolium, and guanidinium derivatives—as the thread components, which provide stabilization to the anion, as well as a synthetic handle for tuning K_a values, anion selectivities, and preparing MIMs. The effects of changing the size and constitution of the cation, anion, and host molecules have been probed[1096,1097] systematically, as demonstrated by the K_a values (**Table 2.30**) that have been estimated for a number of pseudorotaxanes in CD_3COCD_3

Table 2.30 Stability constants (K_a) for pseudorotaxanes[1096,1097] comprising halide ion-pair guests and anion-binding hosts in CD_3COCD_3 at 293 K.

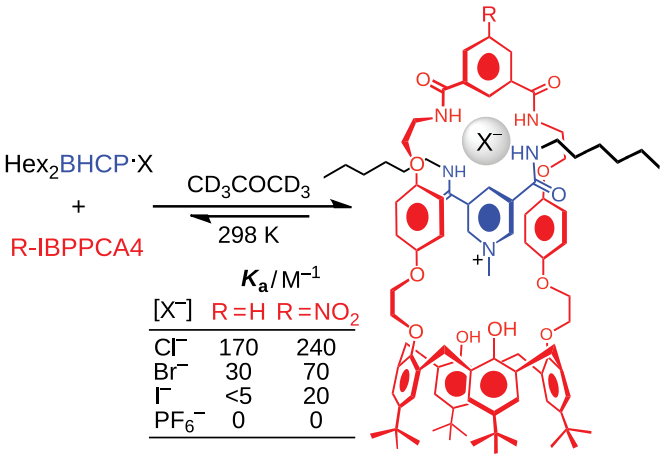


Guests	K_a / M^{-1}			
	9500	2400	980	1500
	610	700	120	1200
	<50	65	<50	140
	1900	950	320	6100
	200	240	180	-
	65	<50	50	-
	1340	1720	1690	-
	1630	2600	1200	>10^5
	390	340	400	1300

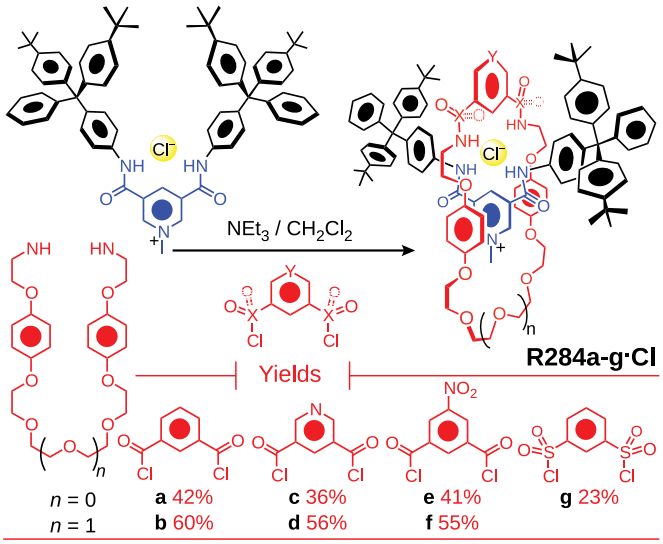
at 293 K. The *tert*-butyl isophthalamide crown ethers ^{t}Bu-IBPP31C6, ^{t}Bu-IBPP34C7, and ^{t}Bu-IBPP37C8 represent of series of structural homologues, which differ only in the size of their polyether loops connecting the *para*-phenylene units. A comparison of K_a values for the pseudorotaxanes comprising these three rings and various ion-pairs highlights the importance of size complementarity between host and guest, as no one ring universally outperforms the others as a host. Typically, the chloride salts are bound most strongly (up to 9500 M^{-1}) by the smallest ^{t}Bu-IBPP31C6 ring—with the exception of imidazolium chlorides—whereas bromide salts exhibit a slight preference for the larger ^{t}Bu-IBPP34C7 ring. Metallo-organic homologues of these anion-binding rings have also been described[1097–1100] such as $Re(CO)_3Cl$-BBPP37C7, which incorporates a Re^I complex ligated to a 2,2′-bipyridyl-4,4′-dicarboxamide unit as the hydrogen bond donor. This luminescent host exhibits[1097] very high affinity (>10^5 M^{-1}) for *N*,*N*′-dihexylbenzimidazolium chloride and binds almost every ion-paired guest more tightly than the *tert*-butyl isophthalamide homologues. In general, this recognition system is robust in the sense that any of the rings will bind a given guest with K_a values that vary in most cases by little more than an order of magnitude.

Other types of hosts from the Oxford laboratory contain calix[4]arene (CA4) wheels instead of polyether loops as ring closures for the isophthalamide-bis-*para*-phenylene anion recognition element.[1101,1102] The macrobicyclic hosts R-IBPPCA4 (R = H or NO_2) have been found[1101] to bind (**Scheme 2.90**) BHCP$^+$ halide salts in the form of a pseudorotaxane with K_a values of up to 240 M^{-1} in CD_3COCD_3. In common with the polyether loops of the R-IBPP31C6, R-IBPP34C7, and R-IBPP37C8 hosts, the oxygen atoms of the calixarene help stabilize these assemblies by engaging the acidic methyl protons of the pyridinium guest in [C–H···O] interactions. It is anticipated that "*modification of the highly adaptable calixarene framework will lead to increasingly sophisticated derivatives, the applicability of which appears to be limited only by the imagination.*"[1101]

Beer has developed a number of clipping protocols (**Schemes 2.91–2.94**) for the synthesis of halide-binding catenanes and rotaxanes. Firstly, Beer has made extensive use of olefin metathesis in anion-templated clipping reactions for the synthesis of rotaxanes[1103] and catenanes[1104] under thermodynamic control—see **Section 3.4.1.4**. Owing to the incompatibility of Grubbs' catalysts with certain ligating functional groups, Beer introduced[1105–1107] an alternative clipping protocol (**Schemes 2.91–2.92**) involving

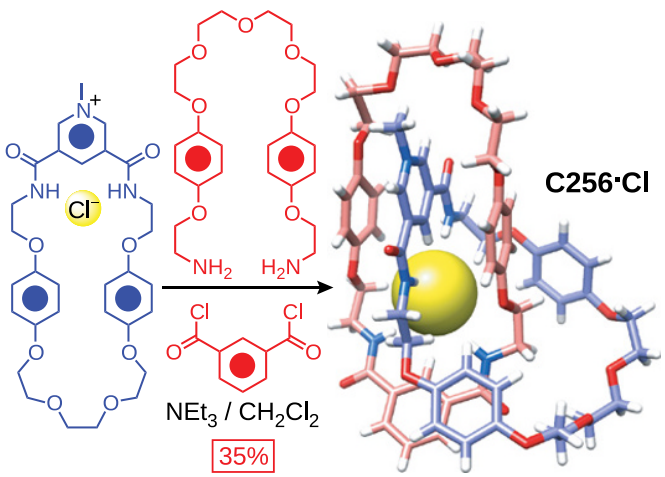


Scheme 2.90 The self-assembly[1101] of pseudorotaxanes comprising BHCP·X ion-pairs and the calix[4]arene-derived hosts H-IBPPCA4 and NO_2-IBPPCA4.



Scheme 2.91 The synthesis of rotaxanes **R284a-g** by clipping bis-*para*-phenylene polyethers and various diacid dichlorides around a trityl-capped *N*-methyl-3,5-dicarboxamidopyridinium chloride ion-pair.[1105,1106]

the macrocyclic coupling of amine-terminated bis-*para*-phenylene polyether loops and diacid dichlorides around ion-pair templates in NEt_3/CH_2Cl_2 under kinetic control. This protocol was investigated[1105,1106] initially as a way to synthesize (**Scheme 2.91**) the [2]rotaxanes **R284a·Cl–R284g·Cl**, all of which possess identical tritylphenylene-stoppered *N*-methyl-3,5-dicarboxamidopyridinium chloride dumbbells and differ only in the constitutions of the rings' N–H hydrogen bond donor units and the size of their polyether loops. The protocol is compatible with a number of dichloride linkers, including isophthaloyl dichloride (**R284a-b**), pyridine 3,5-dicarbonyl dichloride (**R284c-d**), 5-nitroisophthaloyl dichloride (**R284e-f**), and benzene-1,3-disulfonyl dichloride (**R284g**). Yields are uniformly higher (55–60%) when the polyether loop linking the two hydroquinone units constitutes the four repeating units of 4EG versus a smaller 3EG linker, which leads to **R284·Cl** derivatives in lower yields (23–42%) on account of more unfavorable steric interactions. Yields are optimized[1106] when the amount of NEt_3 is limited to 2.5 equiv, since the base is capable of degrading the pyridinium-derived axle component. The clipping protocol was applied[1107] later on to the synthesis (**Scheme 2.92**) of the [2]catenane **C256·Cl** in 35% yield by employing a macrocyclic dicarboxamidopyridinium chloride ion pair as the template. The solid-state structure of **C256·Cl** reflects the superstructure (**Figure 2.61**) of the analogous pseudorotaxane, with D-A π–π stacking and [C–H···O] stabilizing interactions in addition to the important [N–H···Cl^-] and [C–H···Cl^-] ion–dipole interactions.



Scheme 2.92 The clipping synthesis and tubular representation of the solid-state (super)structure of the [2]catenane **C256·Cl** with solvent molecules omitted for the sake of clarity.[1107]

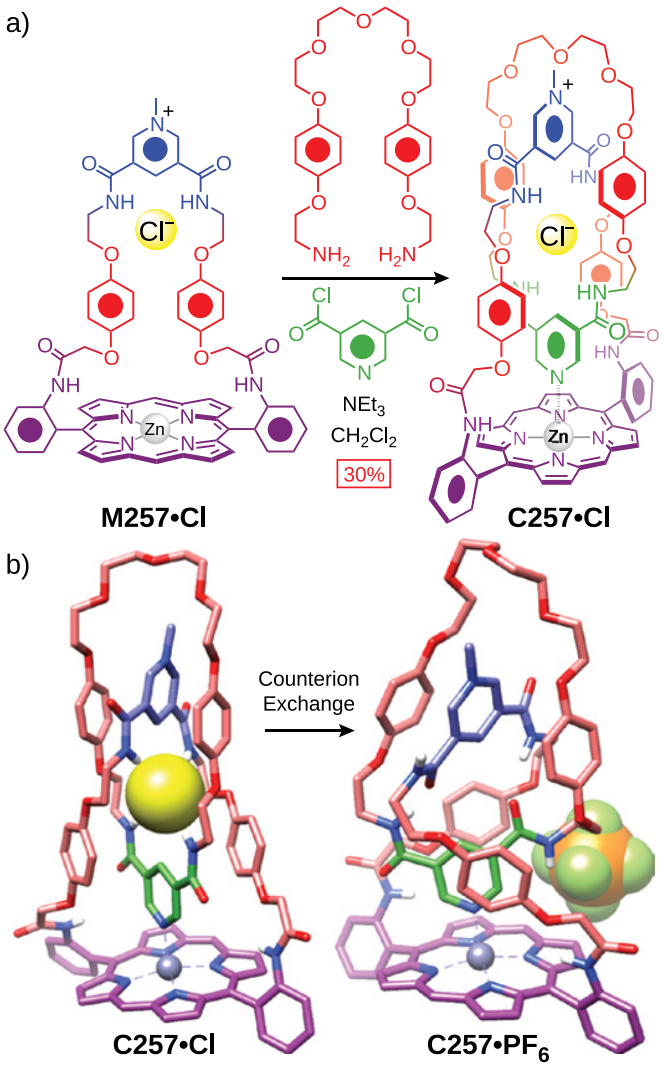
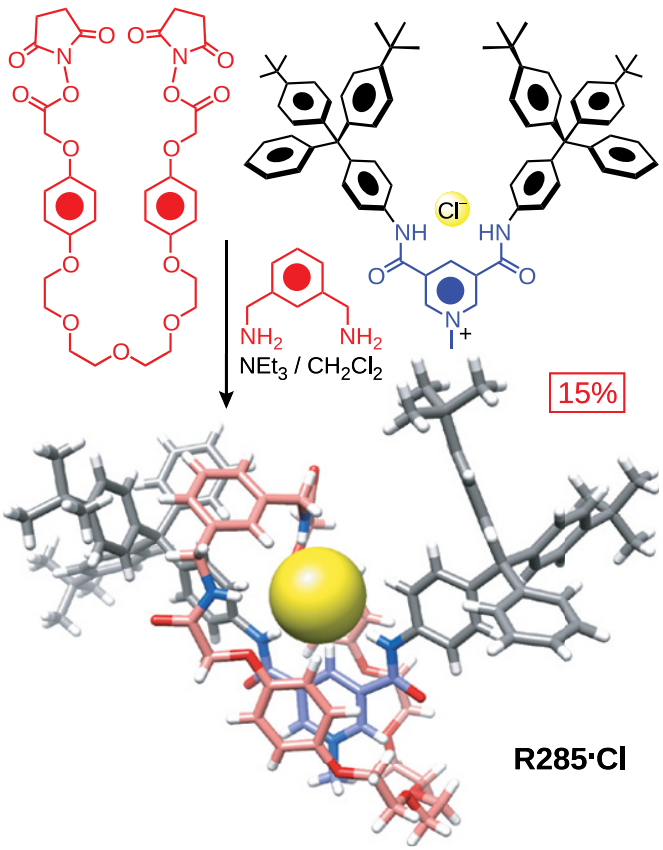


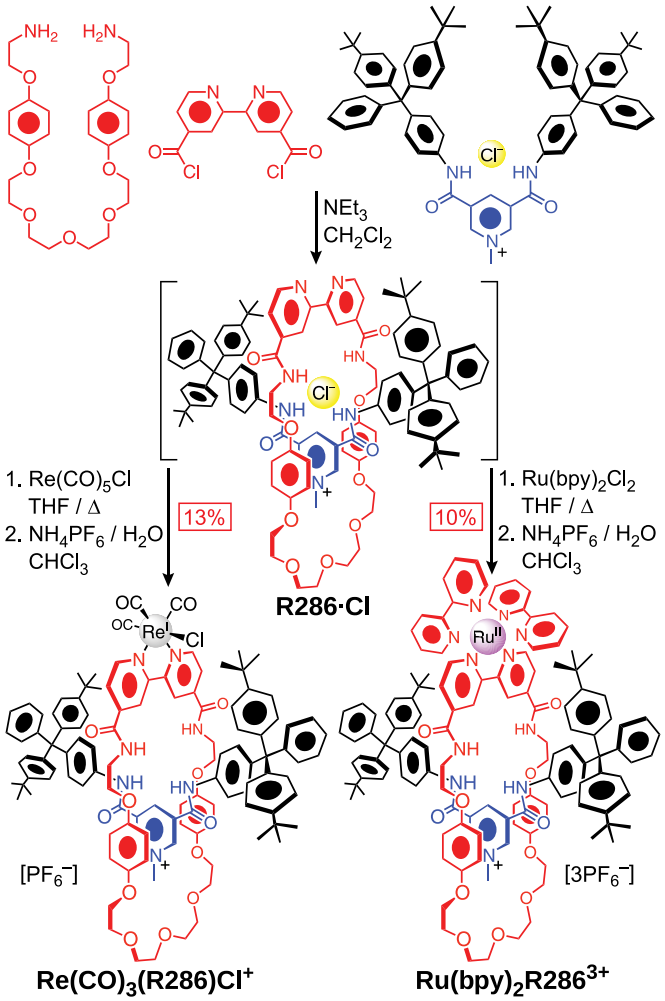
Figure 2.62 Beer's chloride-binding [2]catenanes based on the strapped porphyrin macrocycle **M257·Cl**.[1108] (a) The synthesis of **C257·Cl**. The clipping protocol relies on a combination of chloride anion templation and the docking of pyridine-derived reactants and intermediates within the strapped metalloporphyrin's cavity via axial coordination to the Zn^{II} center. (b) Tubular representations of the solid-state structures of **C257·Cl** and **C257·PF_6**. Hydrogen atoms and solvent molecules are omitted for the sake of clarity.

The chloride-templated synthesis[1108] of Beer's porphyrinic [2]catenane **C257·Cl** also relies on the clipping (**Figure 2.62a**) of bis(amines) and diacid dichlorides, yet templation is further aided and abetted in this case by the axial coordination of pyridine-derived reactants to an endotopic Zn^{II} center of the strapped porphyrin macrocyclic precursor **M257·Cl**. As illustrated by their solid-state structures (**Figure 2.62b**), the Cl^- anion occupies the central binding pocket of **C257·Cl**, whereas counterion exchange with $AgNO_3/NH_4PF_6$ affords crystals of **C257·PF$_6$** in which the PF_6^- counterions are excluded from the cavity and replaced by hydrogen bonds between the catenanes' component macrocycles. Both salts of **C257$^+$** adopt mechanically helical (**Section 5.2.3.3**) geometries in the crystal.

An alternative approach to the clipping of anion-binding rings around halide ion-pair templates relies[1106,1109] on *N*-hydroxysuccinimide (NHS) activated esters instead of acid chlorides as the reactive precursors. For example, the [2]rotaxane **R284b·Cl** can be obtained[1106] in 42% yield by reacting the bis(amine) oligoether with a bis-NHS ester of isophthalic acid in the presence of DCC as a coupling reagent. Another example is the synthesis (**Scheme 2.93**) of **R285·Cl**, which is a constitutional isomer of **R284b·Cl** in which the carbonyl groups have switched positions with the



Scheme 2.93 The synthesis and tubular representation of the solid-state (super)structure of the [2]rotaxane **R285·Cl**, which is generated by clipping *meta*-xylylenediamine and a bis-NHS ester-terminated polyether loop around an ion-paired chloride dumbbell.[1109]



Scheme 2.94 Beer's synthesis[1099] of transition metal-complexed anion-binding [2]rotaxanes.

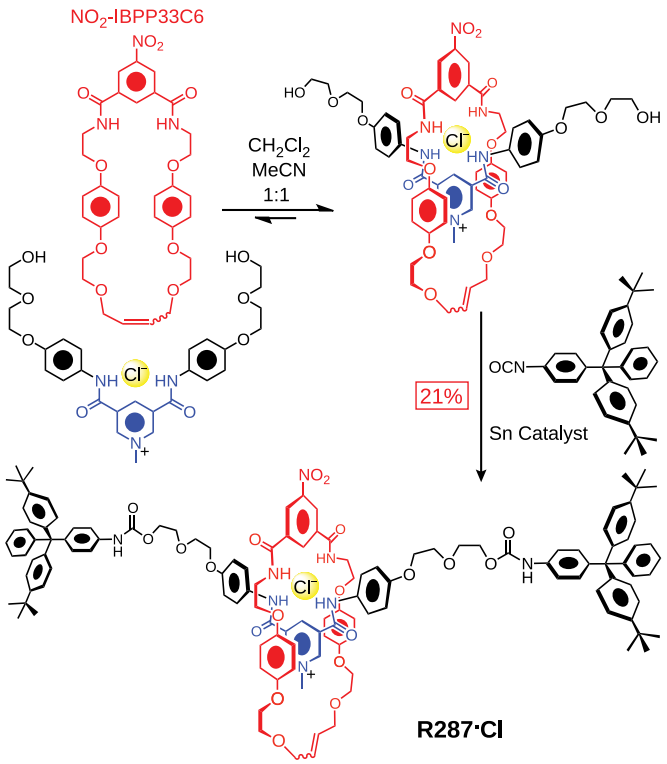
methylene groups that are also bound to the ring's N–H donors. In other words, instead of being conjugated to an aromatic ring, the amide carbonyl group of **R285·Cl** is adjacent to a methylene unit. **R285·Cl** is obtained by macrocyclic coupling of *meta*-xylylenediamine and a bis-NHS ester of the corresponding bis-*para*-phenylene polyether thread in the presence of DCC and the dicarboxamidopyridinium dumbbell, albeit in lower (15%) yield.[1109] The solid-state structure of **R285·Cl** reveals (**Scheme 2.93**) a similar set of noncovalent bonding interactions as its predecessors, with D-A π-stacking and [C–H···O] interactions lending support to the ion-dipole interactions that stabilize the mechanically interlocked assembly. The [N–H···Cl$^-$] bonds within **R285·Cl** are longer, however, than in the case[1106] of the isophthalamide-derived homologue **R284b·Cl**, an observation which explains the lower synthetic yield and reflects the relatively weaker hydrogen bond donating capacity of the amide protons in **R285·Cl** because they are not conjugated directly to an electron-withdrawing aromatic ring.

Beer's clipping protocols have further enabled the synthesis of [3]rotaxanes,[1110] redox-active ferrocene-derived rotaxanes serving as electrochemical sensors for chloride

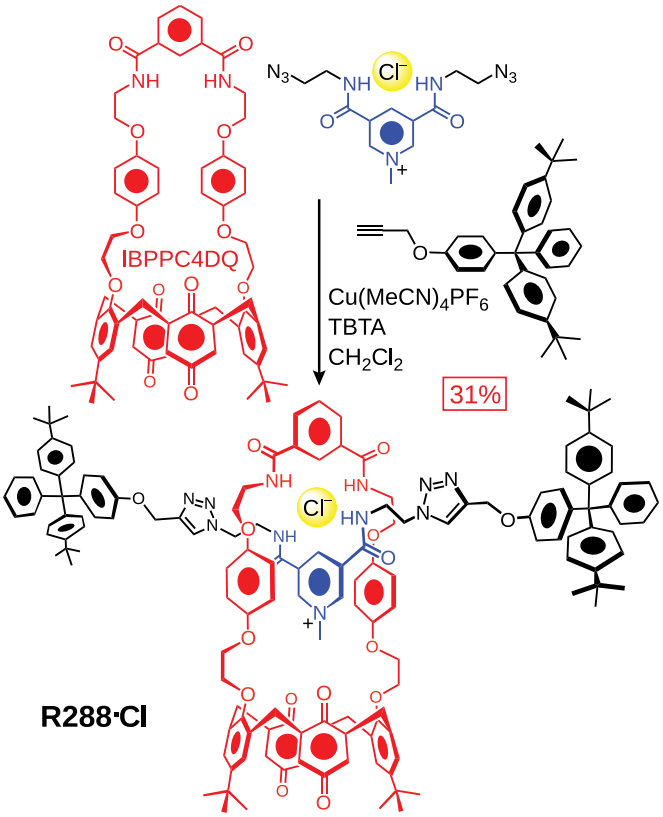
and sulfate anions,[1111] lanthanide-appended [2]rotaxanes,[1112] and photoactive [2]rotaxanes[1099] incorporating transition metal complexes. The latter examples have been synthesized (**Scheme 2.94**) using a typical clipping protocol involving a 4,4′-bis(chlorocarbonyl)-2,2′-bipyridine precursor, generating a chloride-templated rotaxane **R286·Cl** in admixture with the corresponding free macrocycle. The [2]rotaxane **R286·Cl** is converted into the transition metal-cooordination compounds, **$Re(CO)_3(R286)Cl^+$** and **$Ru(bpy)_2R286^{3+}$** by the addition of $[Re(CO)_5Cl]$ and $[Ru(bpy)_2Cl_2]$, respectively, followed by removal of the Cl^- templates and conversion to the PF_6^- salts by washing in $CHCl_3$ with aqueous NH_4PF_6. These rotaxanes can bind[1099] chloride selectively in 30% aqueous Me_2CO and exhibit enhanced luminescence with increasing concentrations of NBu_4Cl, a property which could provide a convenient readout for potential anion sensing applications.

In addition to these reliable clipping protocols, Beer has also prepared several rotaxanes by way of stoppering methods. One approach[1113] involves a di-*n*-butyltin dilaureate-catalyzed carbamate-forming reaction (**Scheme 2.95**) between an isocyanate-functionalized stopper precursor and a hydroxyl-terminated pseudorotaxane comprising a 3,5-dicarboxamidopyridinium chloride derivative and the metathesized macrocycle NO_2-IBPP33C6 in CH_2Cl_2/MeCN (1:1), which affords the [2]rotaxane **R287·Cl** in 21% yield.

Other stoppering reactions have relied upon CuAAC click chemistry to install the stoppers. For example, Beer has



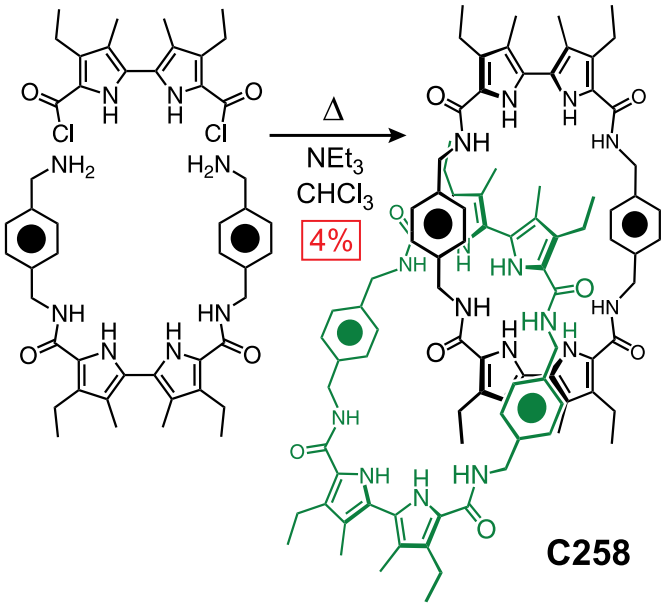
Scheme 2.95 The chloride-templated synthesis[1113] of the [2]rotaxane **R287·Cl** by capping with an isocyanate-functionalized stopper precursor.



Scheme 2.96 The chloride-templated CuAAC click synthesis[1118] of Beer's calix[4]diquinone-derived [2]rotaxane.

described[1114–1117] a number of heteroditopic macrobicyclic hosts possessing calix[4]diquinone (C4DQ) wheels for ion-pair recognition—one of them (IBPPC4DQ) incorporating the original isophthalamide/bis-*para*-phenylene (IBPP) anion recognition element has been employed[1118] in the click synthesis (**Scheme 2.96**) of the [2]rotaxane **R288·Cl**, which proceeds in 31% yield from an azide-terminated 3,5-dicarboxamidopyridinium chloride template and an alkyne-terminated trityl-derived stopper precursor in the presence of a Cu^I catalyst with tris[(1-benzyl-1*H*-1,2,3-triazol-4-yl)methyl]-amine (TBTA) ligand. The C4DQ unit equips the rotaxane **R288·Cl** with a binding pocket for cations (e.g., Na^+, K^+, NH_4^+) in addition to its tetragonal amide cavity for binding halides. This rotaxane is capable of expressing ion-driven shuttling motions—see **Section 6.4.3**.

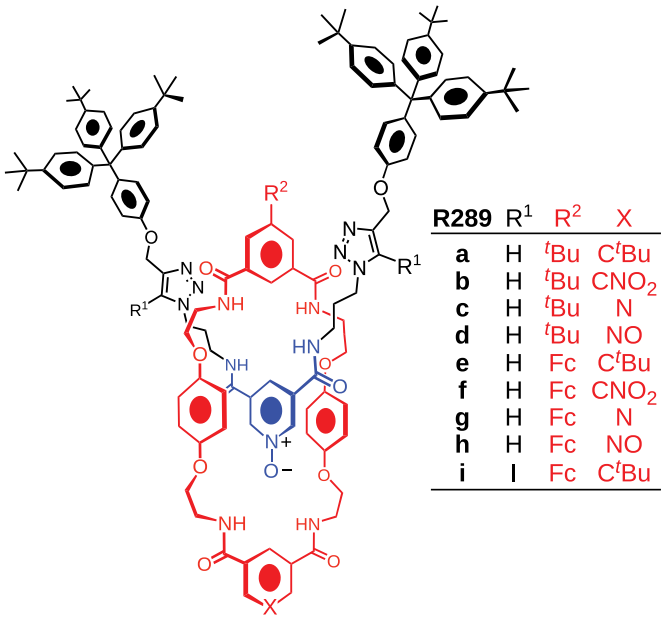
The earliest example of a halide-binding MIM, to our knowledge, was introduced in 1998 by Sessler and Vögtle,[1119] who synthesized (**Scheme 2.97**) the bipyrrole-derived benzylic amide [2]catenane **C258**. Although the relatively low-yielding (≤4%) catenation is templated primarily by hydrogen-bonding interactions in the same manner (**Section 2.3.4.2**) as Leigh's benzylic amide catenanes, the bipyrrole NH donors of **C258** widen its cavity enough to allow it to serve as a neutral receptor for fluoride (1.48×10^5 M^{-1}) and chloride (3.55×10^6 M^{-1}) ions as their tetrabutylammonium salts in tetrachloroethane. Bromide, by contrast, associates only very weakly



Scheme 2.97 The synthesis[1119] of Sessler's neutral anion-binding benzylic amide bipyrrole [2]catenane **C258**.

with **C258**, indicating that Br^- ions are too large for the catenane's NH donor-lined cavity. $H_2PO_4^-$ and OAc^- anions also associate strongly with **C258**, although their binding geometries have not been elucidated in detail and $H_2PO_4^-$ is involved in multiple equilibria with the catenane.

Another set of neutral mechanically interlocked receptors to accompany **C258** in the selective binding of halides are the [2]rotaxanes **R289a-i** (**Figure 2.63**) from Beer's



R289	R^1	R^2	X
a	H	^{t}Bu	C^{t}Bu
b	H	^{t}Bu	CNO_2
c	H	^{t}Bu	N
d	H	^{t}Bu	NO
e	H	Fc	C^{t}Bu
f	H	Fc	CNO_2
g	H	Fc	N
h	H	Fc	NO
i	I	Fc	C^{t}Bu

Figure 2.63 Beer's neutral anion-binding [2]rotaxanes **R289a-i**, possessing a 3,5-diamidopyridinium *N*-oxide axle units encircled by bis-isophthalamide-derived rings carrying various functional groups.[1120,1121]

group.[1120,1121] These rotaxanes possess two isophthalamide-derived units in each hemisphere of the ring component, which surrounds a dumbbell possessing a zwitterionic 3,5-dicarboxamidopyridine *N*-oxide recognition unit. The relatively minor structural differences between rotaxanes **R289a-i** involve different functional groups, such as *tert*-butyl, nitro, pyridine, or pyridine *N*-oxides, appended to the isophthalamide units (X, R^2) of the ring, as well as hydrogen or iodine atoms on the triazole sites (R^1) connecting the stopper to the axle. The rotaxanes **R289a-d** are obtained in up to 17% yield by CuAAC click chemistry in $CHCl_3$ from an azide-terminated 3,5-dicarboxamidopyridine *N*–oxide-derived axle, a propargylated tetraphenylmethane-derived stopper precursor, and various bis-isophthalamide rings in the presence of the $Cu(MeCN)_4PF_6$/TBTA catalyst system. The ferrocene-functionalized homologues **R289e-i**, which are designed[1121] for electrochemical halide sensing, are obtained by clipping protocols in up to 22% yield. All reactions were carried out in the presence of NBu_4Cl as a source of templating chloride anions. Rotaxanes **R289a-h** all exhibit similar halide selectivities ($Cl^- > Br^- > I^-$) and low sensitivities to the different functional groups appended to the isophthalamide units. In the case of **R289i**, the iodinated triazole units appear to be detrimental to halide binding constants. As for the dynamics of these rotaxanes, the pyridine *N*-oxide units of the axles rotate freely so as to engage both isophthalamide units of the corresponding rings in bifurcated hydrogen bonds, while also engaging the hydroquinone units of the ring in D-A π–π stacking interactions. The amide groups of the axle and one of the ring's isophthalamide units form a three-dimensional binding pocket for anions, which recognizes chloride and bromide selectively over dihydrogen phosphate. Halides bind either of the isophthalamide derived units of the ring with nearly equal preference.

The K_a values for a number of anion-binding MIMs are summarized in **Table 2.31**. When the cationic MIMs are converted into their PF_6^- salts, the interlocked structures possess an empty, buried cavity which is preorganized so as to bind halide ions selectively—especially Cl^- and Br^-—in organic and aqueous solvent mixtures. By contrast, bulkier $H_2PO_4^-$ and OAc^- anions bind these receptors outside of the binding pocket, an observation that has been confirmed[1106] by molecular dynamics simulations and explains their lower affinities for the mechanically bonded hosts. The chloride ion binding in particular can be modulated and enhanced by electron-withdrawing groups—i.e., pyridyl, pyridinium, nitro groups, or transition metal complexes—appended to the hydrogen bond donating isophthalamide units occupying the three-dimensional cavities of these catenanes and rotaxanes. The non-interlocked mechanical and topological isomers of these MIMs consistently bind halides with much weaker K_a values.[1096,1113,1119] The high affinities and selectivities can therefore be attributed to an anion-binding version of the catenand effect (see **Section 2.3.2.1**), wherein the topological/mechanical

geometry of the host enhances binding as it enables nearly complete encapsulation of the guest.

Feng and Yuan[1122] have described a different strategy (**Figure 2.64**) for assembling interpenetrated structures around halide templates by employing the heteroditopic cyclo[6]aramide CAA6 as a receptor. The cavity of CAA6 contains a dialkylammonium ion binding pocket comprising four endotopic amide carbonyl groups—rigidified in the conformation illustrated in **Figure 2.64** by exotopic hydrogen bonds—as well as a binding pocket for the accompanying anion, afforded by an isophthalamide unit presenting two endotopic N–H donors belonging to rotatable amide bonds. CAA6 binds (**Figure 2.64a**) dibutylammonium halide salts in chloroform with K_a values of up to ~10^5 M^{-1} in the case of the chloride salt, which decrease by about an order of magnitude as the size of the halide is increased to bromide and iodide. Dibenzylammonium salts exhibit similar stabilities under the same conditions. A solid-state superstructure (**Figure 2.64b**) of the *$Bu_2NH_2{\cdot}Cl{\subset}CAA6$* complex reveals that the dialkylammonium axle and the isophthalamide unit of CAA6 form cooperatively a buried cavity for the Cl^- anion, which accepts hydrogen bonds from the amide protons of the host and an N–H proton of $Bu_2NH_2^+$, as well as C–H protons from both host and guest. The $–NH_2^+–$ center and its adjacent methylene protons also engage the carbonyl groups of CAA6 in hydrogen-bonding interactions. This new anion-binding recognition motif is poised to be tapped for the template-directed synthesis of MIMs.

Table 2.31 Association constants[a] (K_a) for the encapsulation of anions[b] by mechanically interlocked anion receptors in organic and aqueous media. See refs. 1099, 1105–1107, 1109, 1113, 1118–1121

MIM	Solvent System	K_a / M^{-1} Cl^-	Br^-	I^-	$H_2PO_4^-$	OAc^-
R284a·PF_6[c]		860	-	-	110	120
R284b·PF_6[c]		1190	-	-	120	180
R284c·PF_6[c]		1450	-	-	120	250
R284d·PF_6[c]		1500	780	-	60	110
R284e·PF_6[c]		1175	-	-	150	200
R284f·PF_6[c]		1800	-	-	170	180
R287·PF_6[d]	$CDCl_3$	4610	1820	315	340	180
R289a[d]	CD_3OD	501	311	59	-	-
R289b[d]	D_2O	475	442	92	-	-
R289c[d]	45:45:10	552	466	139	-	-
R289d[d]		487	324	175	-	-
R289e[d]		546	373	138	~0	-
R289f[d]		423	259	120	~0	-
R289g[d]		569	346	124	~0	-
R289h[d]		542	376	149	~0	-
R289i[d]		152	133	81	~0	-
C256·PF_6[c]		1550	1030	-	350	180
R284d·PF_6[c]		>10^4	-	-	720	520
R298·PF_6[c]		810	1070	-	645	285
R285·PF_6[d]	$CDCl_3$	>10^4	>10^4	-	355	1040
R288·PF_6[c]	CD_3OD	5000	2570	-	890	500
R289a[c]	1:1	2720	1330	295	129	-
R289b[c]		2790	2050	667	152	-
R289c[c]		>10^4	>10^4	1700	112	-
R289d[c]		3010	2090	635	671	-
	Me_2CO / H_2O[c]					
Re(CO)$_3$R286Cl·PF_6	9:1	1.2 × 10^4	-	-	7.6 × 10^3	160
Ru(bpy)$_2$R286•3PF_6	9:1	1.2 × 10^6	-	-	7.6 × 10^5	-
Ru(bpy)$_2$R286•3PF_6	7:3	1500	-	-	130	-
C257·PF_6[d]	$(CD_3)_2SO$	2144	~0	~0	-	-
C258[e]	$C_2D_2Cl_4$	3.55 × 10^6	~0	-	>10^7	9.63 × 10^5

[a]Errors are estimated to be <15%.
[b]Anions were introduced as tetrabutylammonium salts.
[c]At 293 K.
[d]At 298 K.
[e]Temperature not reported.

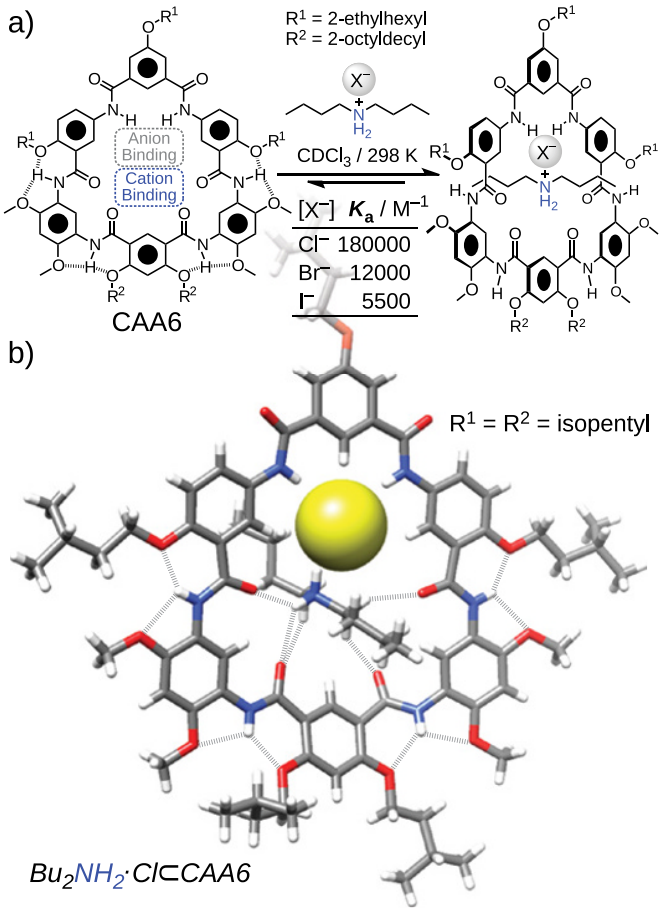


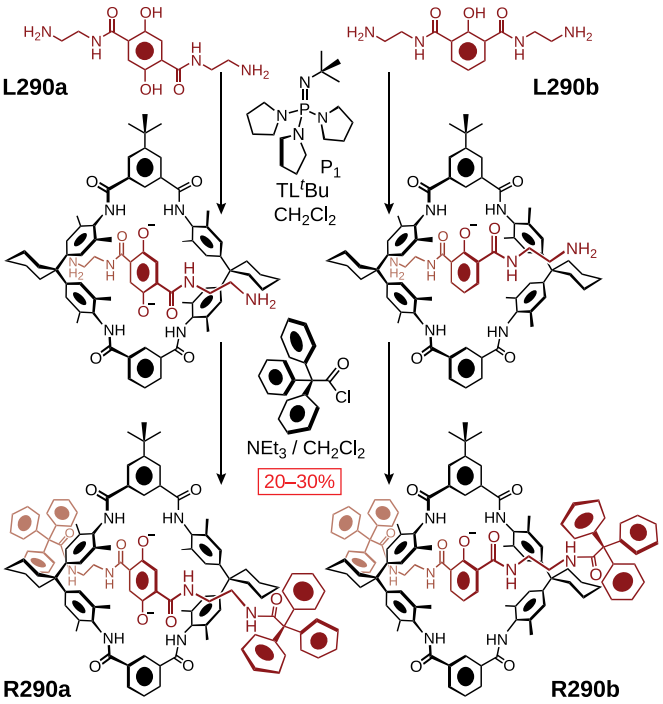
Figure 2.64 Pseudorotaxanes based on heteroditopic cyclo[6]-aramide (CAA6) hosts.[1122] (a) The self-assembly of *$Bu_2NH_2^+{\subset}CAA6$* pseudorotaxanes with chloride, bromide, or iodide templates. (b) Tubular representation of the solid-state superstructure of *$Bu_2NH_2{\cdot}Cl{\subset}CAA6$* with solvent molecules omitted for the sake of clarity.

Organic Oxyanion Templates

Inspired by Vögtle's oxyanion-directed capture motif (**Section 2.3.6.1**), Schalley[1123] has designed tetralactam-based templates in which the oxyanions of hydroquinone or phenol derivatives reside at the center of the axle precursors instead of near their termini. In principle, this design reduces the probability of error by ensuring that the axle is

fully threaded through-the-annulus of the TL^{t}Bu ring. Of necessity, however, this approach involves a stoppering reaction (**Scheme 2.98**), which is relatively low yielding (20–30%) in practice, as opposed to a dumbbell capture reaction. Templates comprising either hydroquinone or phenol centers with a pair of 2-aminoethylamide appendages (**L290a** and **L290b**, respectively) were deprotonated with P_1 base—a phosphazine which is sufficiently basic to deprotonate the hydroxyl groups while maintaining the solubility of the corresponding oxyanionic salts—and subsequently allowed to react with triphenylacetic acid chloride stopper precursors in the presence of NEt_3 to produce the [2]rotaxanes **R290a** and **R290b**. Although the K_a value of 2200 M^{-1} observed in the case of ***L290a***$\subset$*TL^{t}Bu* is sufficiently high, the low yields have been rationalized by inspection of molecular models which indicate that the phenolate ions engage primarily in intermolecular hydrogen bonding with their amide appendages as opposed to the intended intermolecular hydrogen bonds with the tetralactam ring. It follows that this stoppering protocol could most likely be improved by employing phenolate templates lacking any adjacent hydrogen bond donors.

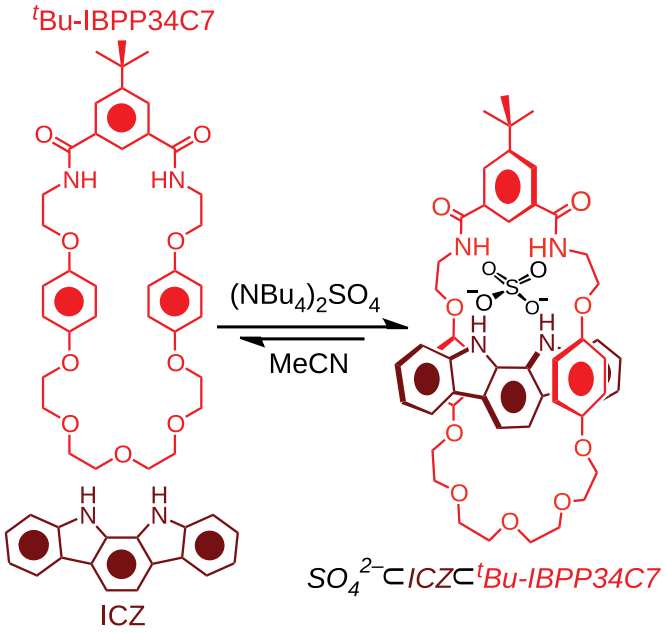
Leigh[1124] has described molecular switches which are driven by the binding of tetralactam macrocycles to phenolate anions—see **Section 6.3.3.2**.



Scheme 2.98 Schalley's stoppering protocol[1123] for the synthesis of phenolate/tetralactam rotaxanes.

Inorganic Oxyanion Templates

Nature has evolved proteins that bind inorganic oxyanions such as sulfates and phosphates with high affinities and selectivities in water. The sulfate-binding protein (SBP) is a remarkable example which relies[1125] only on dipolar and



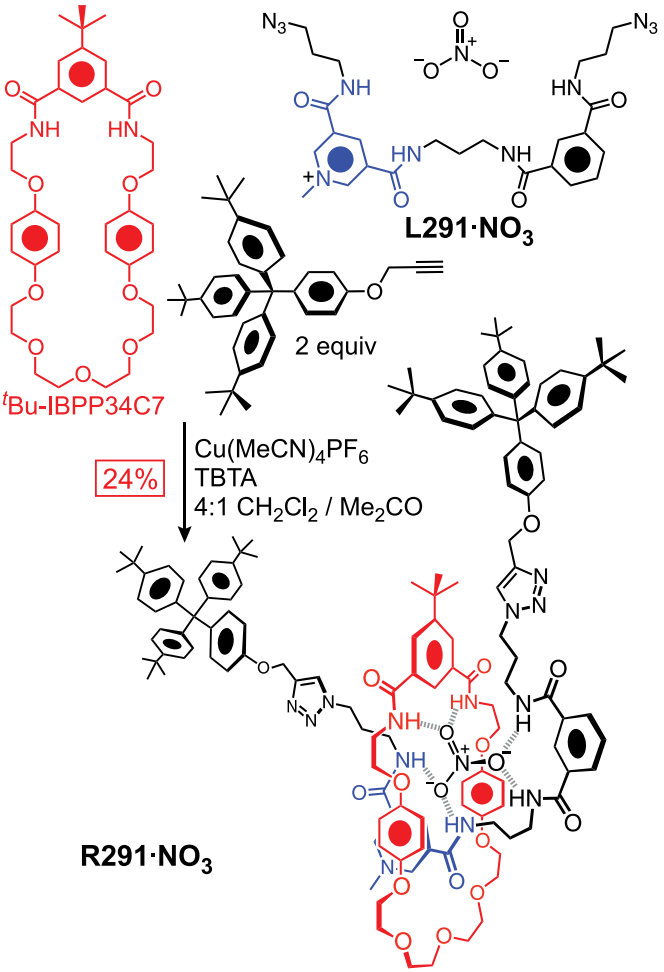
Scheme 2.99 The sulfate-directed self-assembly of a ternary pseudorotaxane comprising indolocarbazole (ICZ) and the ^{t}Bu-IBPP34C7 host.[1126]

steric interactions to stabilize the sulfate dianion, which is sequestered deep within a binding pocket containing seven residues engaged in seven hydrogen bonds with SO_4^{2-}. Proteins such as SBP serve as inspiration for the design of new anion-binding receptors, suggesting that deeply buried hydrogen bond donating pockets—even neutral ones—can accommodate anions with very high affinities and selectivities. Indeed, Beer's research (*vide supra*) has shown that the topological and mechanical bonds of catenanes and rotaxanes can emulate these types of three-dimensional anion-binding pockets. It comes as no surprise, therefore, that mechanically interlocked receptors are also compatible with inorganic oxyanions such as sulfate,[1085,1110,1111,1126,1127] bisulfate,[1101,1128] and nitrate.[1129]

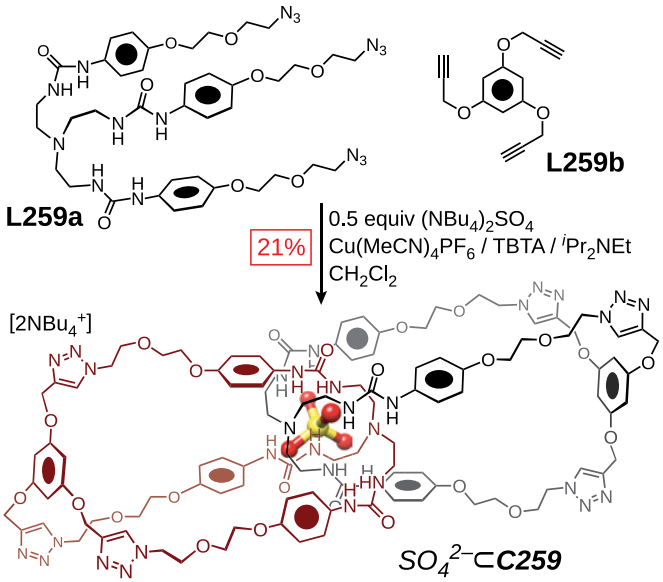
The indole group of tryptamine belongs to one of the seven residues that participate in the stabilization of the SO_4^{2-} dianion in the SBP via hydrogen bonding. Harnessing the utility of the indole group in recognizing sulfate, Beer[1126] has introduced the first example of a neutral pseudorotaxane to be assembled (**Scheme 2.99**) around an anionic template, which involves a sulfate dianion accepting hydrogen bonds from an indolocarbazole (ICZ) thread and the ^{t}Bu-IBPP34C7 host. The ternary *SO_4^{2-}*$\subset$*ICZ*$\subset$*^{t}Bu-IBPP34C7* pseudorotaxane is stable even in the relatively polar solvent, MeCN. ^{1}H NMR Spectroscopy and molecular dynamics simulations indicate that the SO_4^{2-} dianion resides at the center of the assembly, while accepting four hydrogen bonds from all four of the NH donors in the ring and axle. This recognition motif has been further employed to prepare surface-mounted rotaxanes—see **Section 3.6**. Jeong[1130] has employed indolocarbazole as an anion recognition unit in the synthesis of a chloride-templated [2]catenane by olefin metathesis—see **Section 3.4.1.4**.

Not long after introducing his neutral sulfonato-pseudorotaxane, Beer[1131] described the neutral, sulfate-binding triply interlocked [2]catenane or 'capsule' assembly **C259**, which is synthesized (**Scheme 2.100**) in 21% yield by the dimerization of an azide-terminated tris(urea) precursor around the SO_4^{2-} dianion, followed by capsule closure with a six-fold CuAAC click reaction. In the absense of an anionic template, the hydrogen bonding network of the tris(urea) precursors is sufficient to deliver the triply interlocked capsule in 9% yield. When employing Cl^- anions as a templates, however, only a non-interlocked macrobicyclic cryptand was isolated. Although an association constant was not obtained, the capsule appears to bind the SO_4^{2-} dianion tightly and selectively, since the untemplated capsule picks them up from the column during chromatographic purification, and also because the SO_4^{2-} dianion cannot be removed according to Beer's standard protocol of precipitation with a source of Ba^{2+}. The strong association of the SO_4^{2-}⊂***C259*** complex is explained by molecular dynamics simulations, which indicate that the SO_4^{2-} dianion engages all six of the urea groups in hydrogen-bonding interactions.

Recently, Beer[1129] has re-purposed the halide-binding recognition motif based on IBPP34C7 and 3,5-dicarboxamidopyridinium derivatives to accommodate nitrate anions by introducing an additional isophthalamide unit into the axle. This design allows the NO_3^- anion, in its trigonal planar geometry, to engage each of its three oxygen atoms in bifurcated hydrogen bonds with isophthalic hydrogen bond donors—two in the axle and one in the ring. An azide terminated axle **L291·NO$_3$** based on this design has been employed in the CuAAC click synthesis (**Scheme 2.101**) of the [2]rotaxane **R291·NO$_3$**, which proceeds at room temperature in CH_2Cl_2/MeCN (4:1) with the Cu^I/TBTA catalyst in 24% yield. Molecular recognition and template synthesis with NO_3^- is challenging because its low basicity and high hydration energy of the anion renders it a poor acceptor of hydrogen bonds. Another rare example of nitrate-directed assembly of a MIM has been contributed by Sekiya and Kuroda,[1132,1133] who described a [2]catenane comprising two quadruply interlocked metallacages templated in part by intercalated NO_3^- anions—see **Sections 3.2.1.1** and **4.1.3.2.**



Scheme 2.101 The nitrate-templated synthesis[1129] of the [2]rotaxane **R291·NO$_3$**.

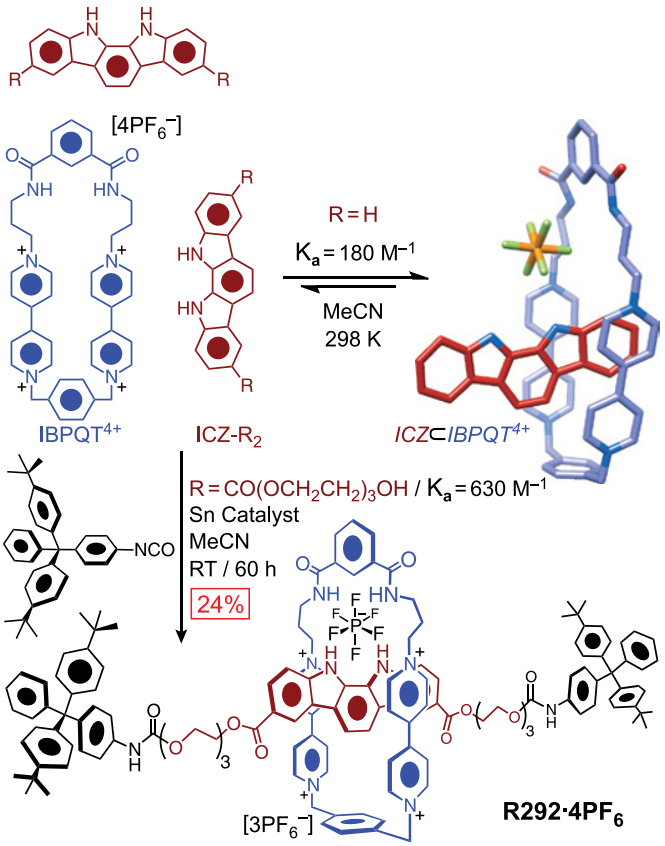


Scheme 2.100 Beer's sulfate-templated click synthesis[1131] of a triply interlocked [2]catenane.

Fluorinated Anions

Beer[1134] has designed a receptor constituting a hybridization of his isophthalamide-derived anion-binding hosts and the 'little blue box' tetracationic cyclophane which is widely employed (**Section 2.3.3.8**) in donor-acceptor template motifs—call it isophthalamide-bis-paraquat-*para*-phenylene ($IBPQT^{4+}$)—in order to prepare a rotaxane derived from the electron-rich, anion-binding indolocarbazole (ICZ) recognition unit. As its PF_6^- salt, $IBPQT^{4+}$ binds (**Scheme 2.102**) ICZ with a K_a value of 180 M^{-1} in MeCN. The solid-state superstructure of this complex reveals (**Scheme 2.102**) an off-centered docking geometry involving D-A π-stacking of the ICZ unit sandwiched in between the $BIPY^{2+}$ units of the host, resulting in a red-colored solution with a CT absorbtion band at a wavelength of 525 nm. Furthermore, one of the PF_6^- counterions of $IBPQT^{4+}$ is held within a cavity

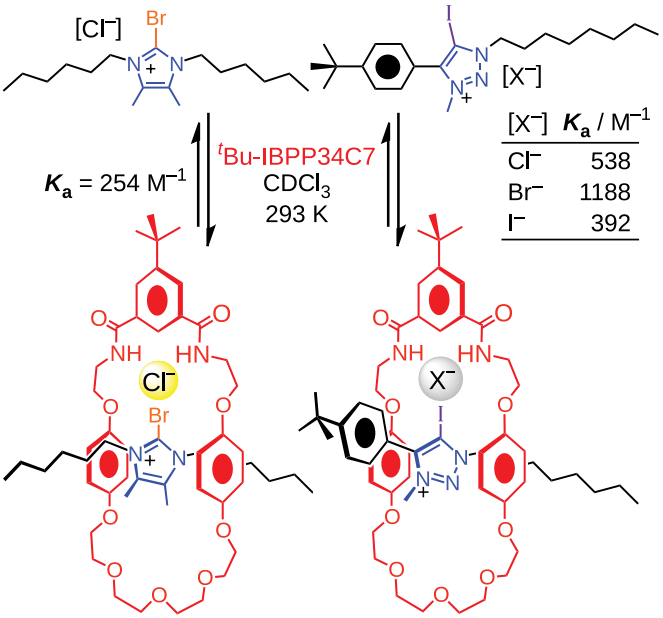
created by the isophthalamide and indole groups of the host and guest, respectively, stabilized by several [N–H···F] contacts. The $IBPQT^{4+}$ ring and an ICZ derivative with triethylene glycol appendages have been employed in the synthesis (**Scheme 2.102**) of the [2]rotaxane **R292·4PF$_6$** employing the carbamate-forming coupling of an isocyanate-functionalized stopper precursor catalyzed by di-*n*-butyltin dilaureate. The yield is nearly identical with and without NBu_4Cl (21 and 19% yield, respectively), indicating that the Cl^- anion is not involved in templation to a significant extent. The rotaxane does bind chloride, however, with a K_a value of 3000 M^{-1} in Me_2SO. D-A interactions most likely outweigh the contributions from anion-binding to the stability of this recognition motif. Although it has not been proven unequivocally that the PF_6^- anion actually contributes to templation, receptors[992,993] for the PF_6^- are uncommon on account of the anion's low basicity, low electron density, relatively large size and diffuse electron cloud, and octahedral geometry.



Scheme 2.102 The self-assembly and tubular representation of the solid-state superstructure of the pseudorotaxane *ICZ⊂IBPQT*$^{4+}$ with protons and matrix molecules omitted for the sake of clarity, as well as the synthesis[1134] of the donor-acceptor/anion-binding [2]rotaxane **R292·4PF$_6$** derived therefrom.

2.3.6.3 C–X···Halide Halogen-Bonded Templates

This Section covers templates in which halide ions serve as acceptors of halogen bonds. See **Section 2.3.5** for a discussion of halogen bonds and halogen-bonded templates that do not involve anions. Beer[1057,1058] began



Scheme 2.103 The self-assembly of pseudorotaxanes comprising the ^{t}Bu-IBPP34C7 host and bromoimidazolium (left) or iodotriazolium (right) derived guests, guided by halogen bonding with halide templates.[1057,1058]

investigating halogen bonding as a templation strategy circa 2010 when he described the self-assembly (**Scheme 2.103**) of pseudorotaxanes stabilized by [C–X···X$^-$] halogen bonds, where X is Cl, Br, or I, involving ^{t}Bu-IBPP34C7 hosts and guests derived from halogenated triazolium or imidazolium cations as their halide salts. Conceptually, the [C–X···X$^-$] halogen bonds replace the [N–H···X$^-$] hydrogen bonds supporting the assemblies and MIMs described in the previous Section. Beer has noted that halogen bonding is among the least exploited types of noncovalent bonding interactions in anion receptor chemistry, which is surprising given their similarity to hydrogen bonds. Halogen bonds are comparable to hydrogen bonds in strength, yet more strictly constrained to adopting linear geometries. In general, Beer has found that receptors employing [C–X···X$^-$] interactions in cationic halogen-bonded templates outperform structurally analogous receptors that rely instead on [C–H···X$^-$] interactions (**Section 2.3.6.4**) in binding halides with high affinities,[1057,1058,1063] with few[1064] exceptions.

More recently, Beer[1057,1059,1061–1065] has expanded the meccano set of halogen-bonding recognition motifs considerably. A selection of halide-templated halogen-bonded mechanomolecules are illustrated in **Figure 2.65**, all of which have been prepared by ring closing metathesis—see **Section 3.4.1.4**. The iodotriazolium-derived recognition motif has been further elaborated to create[1057,1061,1063,1064] [2]rotaxanes such as **R293·Br**, **Re(CO)$_3$R294·3Cl**, **R295·2Cl,** and **R296·Cl**, as well as bistable [2]rotaxane molecular shuttles which respond to anionic stimuli—see **Section 6.5.1**. The three-dimensional cavity designed for binding halide ions in the [2]rotaxane[1061] **Re(CO)$_3$R294·3Cl** is lined with up to four polarized iodine atoms—two from the

iodotriazolium units appended to the axle's central carbazole, and two from the iodotriazole units appended to the luminescent Re^{I} complex of the ring. Compound **Re(CO)$_3$R294·3Cl** is unique in the sense that its recognition properties rely almost exclusively on halogen bonding, since no built-in D-A, π–π stacking, or hydrogen-bonding interactions are present in this case, although electrostatic and ion-pairing effects are inevitably involved as well. By contrast, the [2]rotaxanes **R293·Br** and **R295·2Cl** combine[1057,1061] halogen-bonded axles based on iodotriazolium and carbazolebis(iodotriazolium) recognition sites, respectively, with a ring possessing hydrogen-bonded isophthalamide units that are more typical of Beer's mechanomolecules. In the case[1064] of the [2]rotaxane **R296$^+$**, which comprises an isophthalamide based macrocycle encircling an axle containing a 3-(5-iodo-1,2,3-triazole)pyridinium unit, the halide ion selectivity ($Br^- > I^- > Cl^-$) differs from that ($Cl^- > Br^- > I^-$) of a homologue based on a non-halogenated triazole unit, most likely on account of a difference in the size of the anion binding pocket.

Beer[1059,1062,1065] has also described a few [2]catenanes (**Figure 2.65**) incorporating halogen-bonding template motifs. The [2]catenanes **C260Br·Br** and **C260I·I** are halogen-bonding[1062] receptors based on halogenated *N*-methylpyridinium templates. The bromoimidazole recognition motif has been employed[1059] to make the [2]catenane **C261·BrPF$_6$**, in which the central bromide template is stabilized by two [C–Br···Br$^-$] halogen bonds. Other noncovalent bonding interactions within the catenated structure of **C261·BrPF$_6$** include D-A π–π stacking interactions between the hydroquinone and bromoimidazolium units in each ring, and possibly weak anion–π interactions involving the pendant naphthalene units. The [2]catenane **C262·X**, where X is an anion of Cl, Br, or I, binds[1065] all three halides with high affinity and high selectivity (*vide infra*) by virtue of its two halogen bond accepting iodotriazolium units. The bromo- and iodo-functionalized pyridinium groups bind IBPP34C7 with greater affinity than do their protonated counterparts, in common with halogenated triazolium and imidazolium recognition units.

The single-crystal X-ray structures of **R293·Br**, **Re(CO)$_3$R294·3Cl**, and **C262·Cl** are illustrated as tubular representations in **Figure 2.66**. Evidence for halogen bonding is found in the halogen–halide distances (3.0–3.1 Å), which are less than 85% of the sum of the van der Waals radii. The single halogen bond stabilizing the Br$^-$ anion of **R293·Br** is accompanied (**Figure 2.66a**) by two hydrogen bonds and a [C–H···O] interaction from the ring's isophthalamide unit, which tilts the halogen bond angle (165°) slightly away from linearity. In the solid state, one of the Cl$^-$ anions of **Re(CO)$_3$R294·3Cl** accepts (**Figure 2.66b**) three halogen bonds from the rotaxane framework, while the second accepts only one halogen bond, and the third is bound tightly to the Re^{I} center. Thus, none of the Cl$^-$ anions of **Re(CO)$_3$R294·3Cl** are located in a fully buried cavity in the solid state. In the case of **C262$^+$**, solid-state structures have been obtained for complexes of Cl$^-$, Br$^-$, and I$^-$. Although only

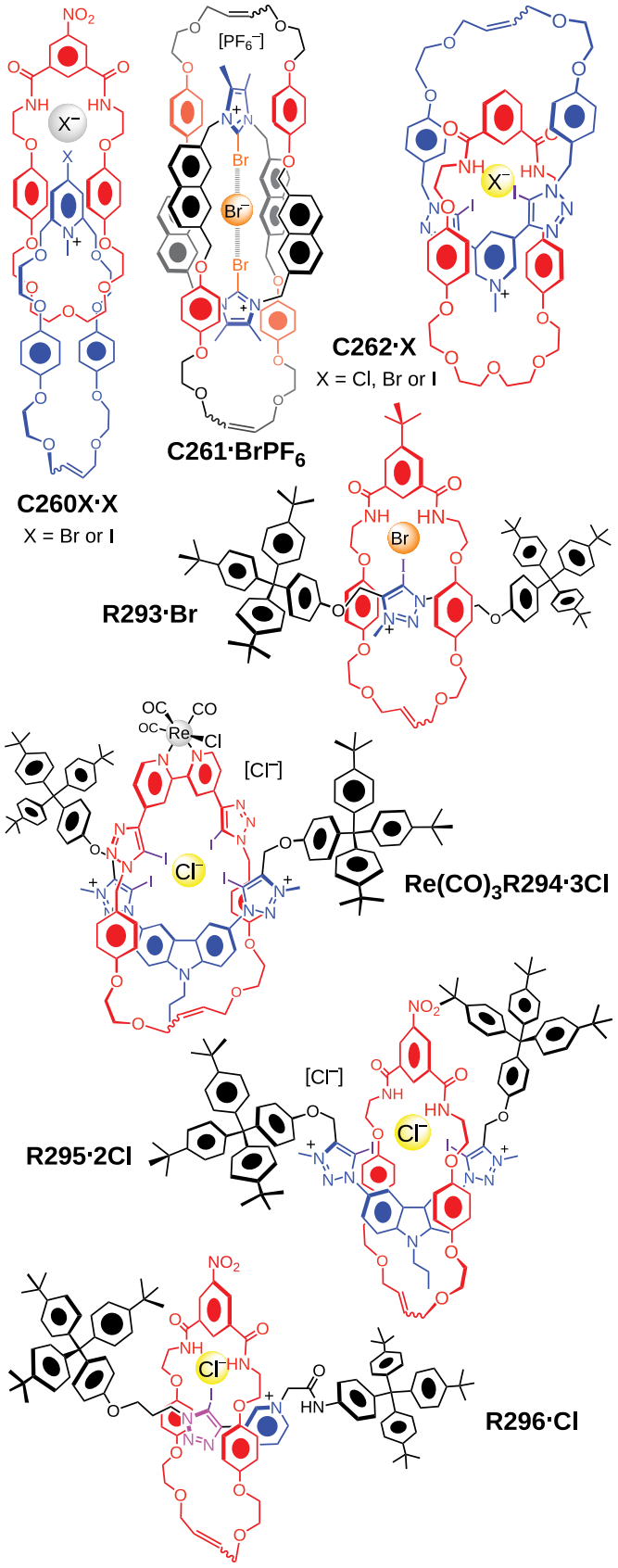


Figure 2.65 Structural formulas of some MIMs from the Beer group which rely on halogen-bonding interactions to bind halide anions. See refs. 1057, 1059, 1061, 1062, 1064, 1065

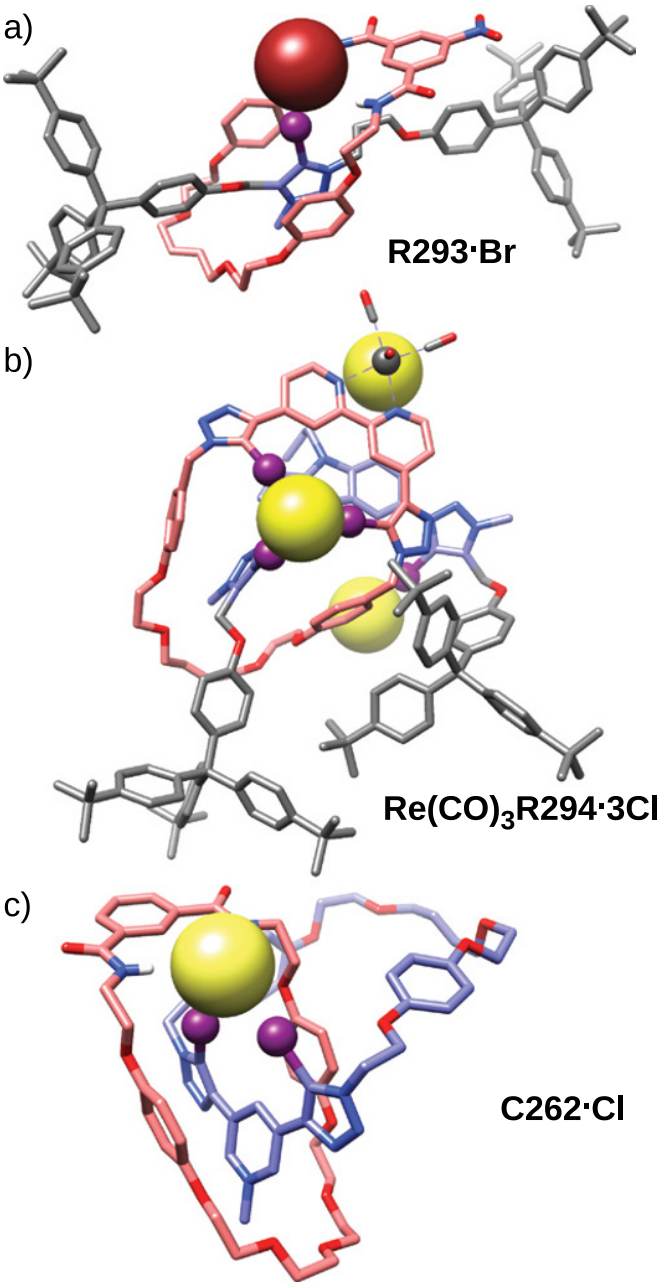


Figure 2.66 The solid-state (super)structures of anion-binding mechanomolecules that rely on halogen-bonding interactions. (a) The [2]rotaxane[1057] **R293·Br**. (b) The luminescent [2]rotaxane[1061] **Re(CO)$_3$R294·3Cl**. (c) The [2]catenane[1065] **C262·Cl**. Hydrogen atoms and solvent molecules omitted for the sake of clarity.

C268·Cl is shown in **Figure 2.66c**, all three structures adopt similar co-conformations in the solid state, with one ring engaging in hydrogen bonding and the other ring engaging in halogen bonding with the halide anion. X-Ray absorption spectroscopy (XAS) experiments on **C262·Cl** provided[1065] evidence for a degree of covalency in the halogen bonds that is comparable to that of transition metal halide complexes. This level of partial covalency is most likely preserved in the other halogen-bonding receptors as well.

The association constants quantifying the recognition of Beer's mechanically interlocked halogen-bonding receptors, as their PF_6^- salts, for halides are summarized in **Table 2.32**. In general, K_a values are comparable to those of the hydrogen-bonding receptors tabulated in **Table 2.31**. Compounds **C262^{2+}**, **Re(CO)$_3$R294Cl^{2+}**, and **R295^{2+}** are noteworthy for their ability to bind halides with high affinities (>10^4 M^{-1}) even in up to 50% aqueous mixtures. Compound **C261^{2+}** is noteworthy for its remarkable selectivity; it seems to bind *only* Br^- and Cl^-, since no binding interactions have been observed in the cases of F^-, I^-, OAc^-, $H_2PO_4^-$, NO_3^-, or HCO_3^- anions. These results verify, at an early stage in the development of these recognition motifs, that halogen bonds are excellent tools for designing strong and selective receptors for halides.

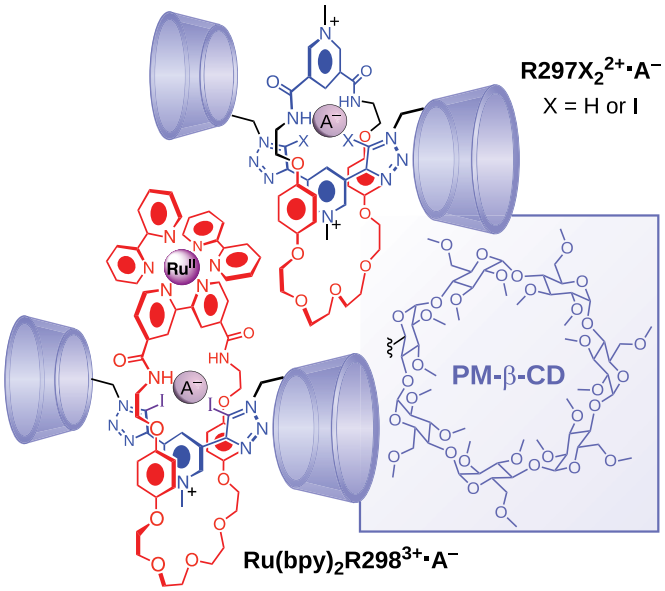
Anion recognition in water is[1135] "a key challenge in supramolecular chemistry". Arguably the most successful of Beer's anion-binding MIMs have been halogen-bonded [2]rotaxanes capped with permethylated β-cyclodextrin (PM-β-CD) stoppers because they bind (**Table 2.33**) halides with relatively high affinities even in pure water. The [2]rotaxane **R297I$_2$·2NO$_3$**, possessing dicarboxamidopyridinium and bis(iodotriazole)pyridinium recognition units in the ring and axle, respectively, binds[1136] halides with affinities of up to 2200 M^{-1} in the case of iodide. The homologous [2]rotaxane **R297H$_2^{2+}$**, in which the triazole units are not iodinated, binds iodide (≤50 M^{-1}) more weakly by several orders of magnitude, as does[1137] a hydrogen-bonded homologue (K_a = 10–35 M^{-1}) in which the triazole units have been replaced by amides. A van't Hoff analysis reveals that the formation of ***I*$^-$⊂R297I$_2^{2+}$** is entirely driven enthalpically, whereas the formation of ***I*$^-$⊂R297H$_2^{2+}$** is driven entropically. Beer's investigations of these two rotaxanes and their corresponding dumbbells constitutes the first systematic and quantitative comparision of hydrogen and halogen-bonding

Table 2.32 Association constants[a] (K_a) for the encapsulation of anions[b] by halogen-bonding mechanically interlocked anion receptors as their PF_6^- salts in organic and binary aqueous solvents.

MIM	T / K	Solvent System	K_a / M^{-1} Cl^-	Br^-	I^-	$H_2PO_4^-$
R293$^+$	293	$CDCl_3$ CD_3OD	457	1251	2228	-
C262^{2+}	293	D_2O	1850	>10^4	>10^4	49
R295^{2+}	298	45:45:10	2300	>10^4	750	~0
C261^{2+}	293	CH_3CN	0	3.71×10^6	1.48×10^5	~0
Re(CO)$_3$	293	10% H_2O	11000	1.05×10^5	1.38×10^5	~0
R294Cl^{2+}		20% H_2O	3090	3.09×10^4	8.91×10^4	~0
		50% H_2O	513	5750	2.40×10^4	~0
C260^{2+}	298	$CDCl_3$	130	200	220	-
C260I$^+$	298	CD_3OD	160	230	340	-
R296$^+$	298	1:1	381	532	466	211

[a]Data taken from refs. 1057, 1059, 1061, 1062, 1064. Errors are estimated to be ≤15%.
[b]Anions were Introduced as tetrabutylammonium salts.

Table 2.33 Anion binding affinities[1136,1138] (K_a) of β-CD-stoppered [2]rotaxanes as their nitrate salts at 298 K in D_2O.



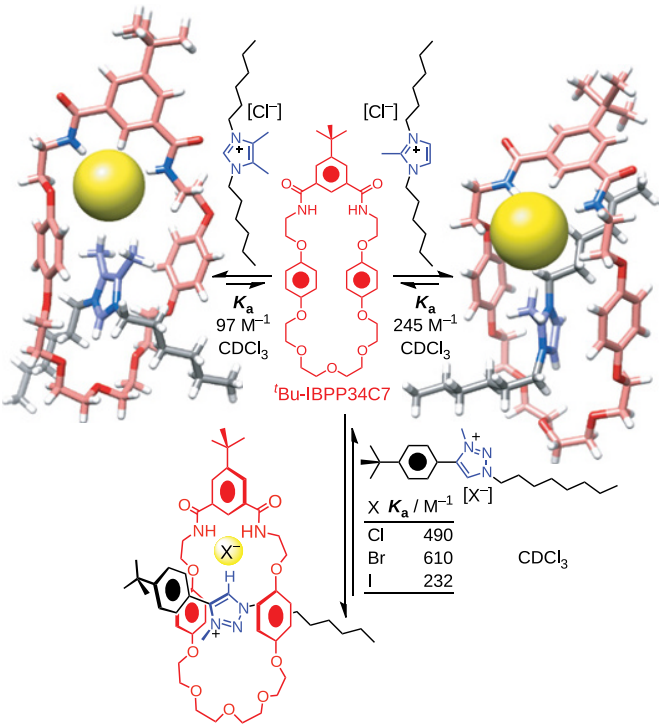
		Anion (A^-) K_a / M^{-1}			
Rotaxane	**X**	**Cl^-**	**Br^-**	**I^-**	**SO_4^-**
R297H$_2$·2NO$_3$	H	0	10	20	0
R297I$_2$·2NO$_3$	I	55	290	2200	30
Ru(bpy)$_2$R298·3NO$_3$		190	1020	6300	450

anion receptors in water. More recently, Beer[1138] reported a halogen-bonded homologue of **R297I$_2^{2+}$** with a Ru(bpy)$^{2+}$ bis(amide) unit instead of 3,5-dicarboxamidopyridinium as the ring's recognition unit. This [2]rotaxane, **Ru(bpy)$_2$R298^{3+}**, binds iodide (K_a = 6300 M^{-1}) even more tightly than does its predecessor at 298 K in D_2O. The observation that the halogen-bonding receptors outperform significantly the hydrogen-bonding receptors suggests that halogen bonding may be a powerful alternative to hydrogen bonding in the design of aqueous molecular recognition processes and templates.

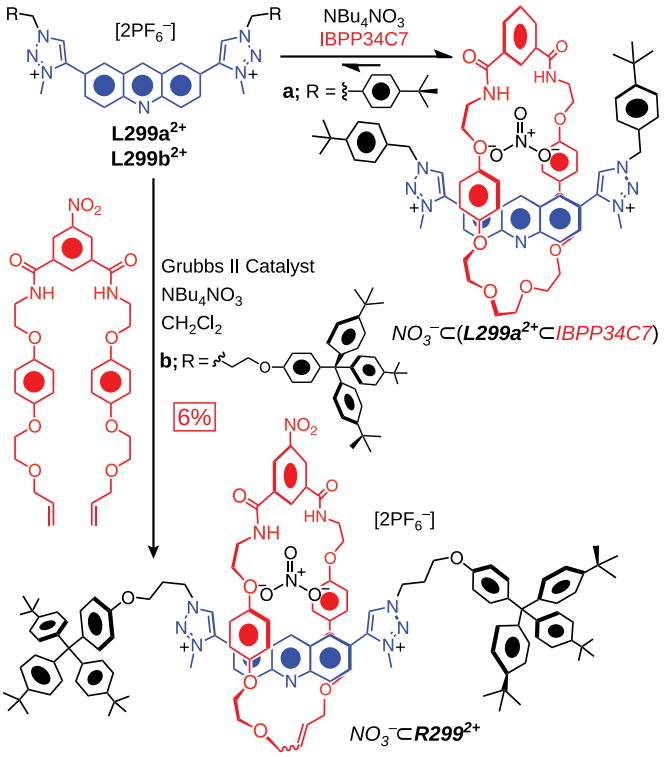
2.3.6.4 C–H···Anion Hydrogen-Bonded Templates

Electropositive C–H protons can engage with anions (A^-) in [C–H···A^-] hydrogen-bonding interactions that approach those of more conventional N–H hydrogen bond donors in terms of their strength, especially when the protons are conjugated to highly electron-deficient π-systems, such as imidazoles, triazoles, and cyano-olefins. Early evidence that [C–H···A^-] interactions could be employed to template the formation of mechanical bonds came when Beer[1057,1139,1140] described the self-assembly (**Scheme 2.104**) of pseudorotaxanes comprising the ^{t}Bu-IBPP34C7 host and guests derived from 4,5-dimethylimidazolium and 2-methylimidazolium as their chloride salts,[1139] as well as *N*-methyltriazolium derivatives as the chloride, bromide, or iodide salts.[1057,1140] The solid-state superstructures (**Scheme 2.104**) of the imidazolium-derived pseudorotaxanes confirm the presence of [C–H···Cl^-] interactions involving the acidic protons of the organocations. The K_a values for these pseudorotaxanes at 293 K in $CDCl_3$ are comparable to those of their halogen-bonded counterparts illustrated in **Scheme 2.103**, albeit uniformly lower, regardless of the anion. Anion-binding imidazolium motifs have also been employed[1141] in molecular switches driven by ion exchange—see **Section 6.5.3.1**.

Following on the successful nitrate-templated synthesis (**Scheme 2.101** in **Section 2.3.6.2**) of the [2]rotaxane **R291·NO$_3$**, which relies extensively on [NO_3^-···H–N] interactions, Beer[1142] designed a new nitrate recognition motif that is stabilized by a number of [NO_3^-···H–C] interactions involving the protons of a bis(triazolium)acridine recognition unit in the axle. The acridine linker provides an optimum distance between both triazolium units, allowing their acidic protons to donate hydrogen bonds to two of the nitrate anion's oxygen atoms simultaneously. The addition of a source of nitrate (NBu_4NO_3) to a mixture of the *para-tert*-butyl-phenylene-capped thread **L299a^{2+}** results in the self-assembly (**Scheme 2.105**) of the ternary [2]pseudorotaxane *NO_3^-⊂(**L299a**$^{2+}$⊂IBPP34C7)* by virtue of the components' organization around the NO_3^- template. Olefin metathesis (**Section 3.4**) with Grubbs II catalyst has been



Scheme 2.104 The self-assembly of pseudorotaxanes comprising the ^{t}Bu-IBPP34C7 ring and hexyl functionalized 4,5-dimethylimidazolium (left) or 2-methylimidazolium (right) guests as their chloride salts,[1139] as well as a triazolium derived guest (bottom) as the chloride, bromide, and iodide salts,[1057,1140] at 293 K in $CDCl_3$. Tubular representations of the solid-state superstructures the imidazolium-derived complexes are shown with solvent molecules omitted for the sake of clarity.



Scheme 2.105 The self-assembly and synthesis of pseudorotaxanes and rotaxanes, respectively, based on nitrate anion recognition involving a bis(triazolium)acridane axle and isophthalamide-based hydrogen-bonding macrocycles.[1142]

utilized to clip an isophthalamide-based macrocycle around the bis(triazolium)acridine dumbbell **L299b·2PF6** in the presence of an NO_3^- template, affording the [2]rotaxane **R299**$^{2+}$ in 6% yield. The yield can be raised to 15% by templation with Cl^-, which binds the cavity of **R299**$^{2+}$ with an affinity (K_a = 1070 M^{-1}) that is comparable to that (K_a = 1010 M^{-1}) that of NO_3^- in $CDCl_3$/MeOD/D_2O (45:45:10) at 298 K. **R299**$^{2+}$ also recognizes NO_3^- selectively over several more basic oxoanions, including OAc^-, HCO_3^-, and $H_2PO_4^-$, which bind with low affinities of ≤110 M^{-1} under the same conditions.

Flood[1143] at Indiana University specializes in molecular anion-binding systems that rely on "privileged" C–H hydrogen bond donors as the primary recognition elements, especially cyclophane receptors which present electropositive C–H protons endotopically. In one iteration of this concept, Flood[1144] has designed (**Figure 2.67**) the cyanostilbene-derived macrocycle penta-*tert*-butylpentacyanopentabenzo[25]annulene—nicknamed the cyanostar (CS)—the C_5-symmetric constitution of which displays 10 endotopic activated C–H donors. CS is available in high yield (81%) in multigram-scale quantities from a one-pot Knoevenagel condensation of a *tert*-butylarene precursor, *meta*-substituted with benzylic nitrile and formyl groups. In the solid state, $(CS)_2$ dimers populate the crystal lattice, adopting oppositely facing bowl-shaped geometries. The CS bowls can exist (**Figure 2.67a**) as either *M* or *P* stereoisomers, which represent 63 and 37% of the population in the crystal, respectively, and presumably interconvert rapidly in solution by bowl-to-bowl inversion. With a diameter of ~5 Å, the cavity of CS is capacious enough to accommodate relatively large anions. Indeed, a wide range of anions (Cl^-, Br^-, I^-, NO_3^-, SCN^-, ClO_4^-, ReO_4^-, IO_4^-, PF_6^-, SbF_6^-, $FeCl_4^-$, $PtCl_6^{2-}$) have been found to bind (**Figure 2.67b**) CS in 6:4 CH_2Cl_2/MeOH. At low anion concentrations, CS binds anions preferentially in the form of a 2:1 sandwich complex defined by the equilibrium constant β_2, while the 1:1 complex (K_{11}) becomes dominant when an excess of the anion is available. There is a strong correlation between the size of the anion and binding strength, except in the cases of $FeCl_4^-$ and $PtCl_6^{2-}$ which are too large for CS to encircle. In particular, the high affinities (K_{11} > 10^5 M^{-1}, β_2 > 10^{11} M^{-2}) of the weakly coordinating BF_4^-, ClO_4^-, and PF_6^- anions are unprecedented and they experience positive cooperativity in the case of the 2:1 sandwich complex.

Applying the cyanostar's recognition for anions to the synthesis of rotaxanes, Flood[1144] has devised a click reaction (**Scheme 2.106**) between a tetrabutylammonium dipropargylphosphate axle and dimethyl 5-azidoisophthalate stopper precursors in the presence of CS and a Cu^I

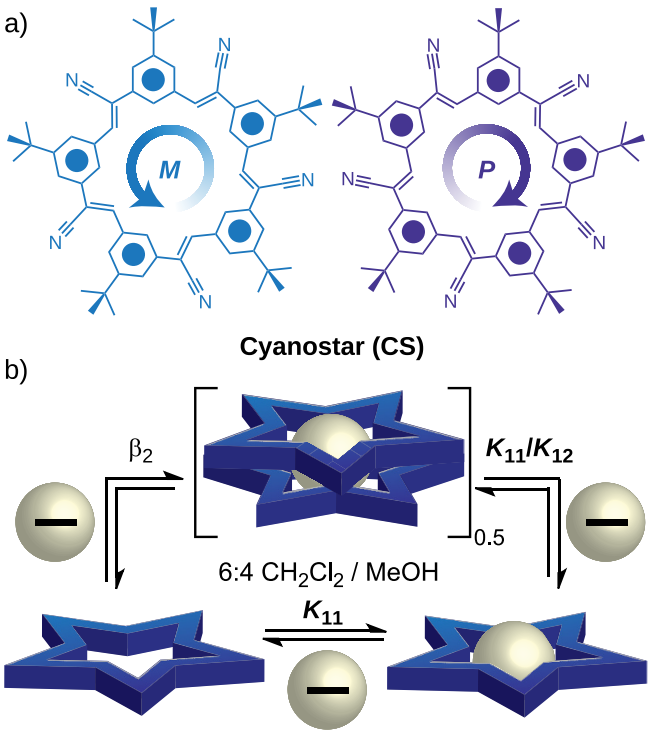
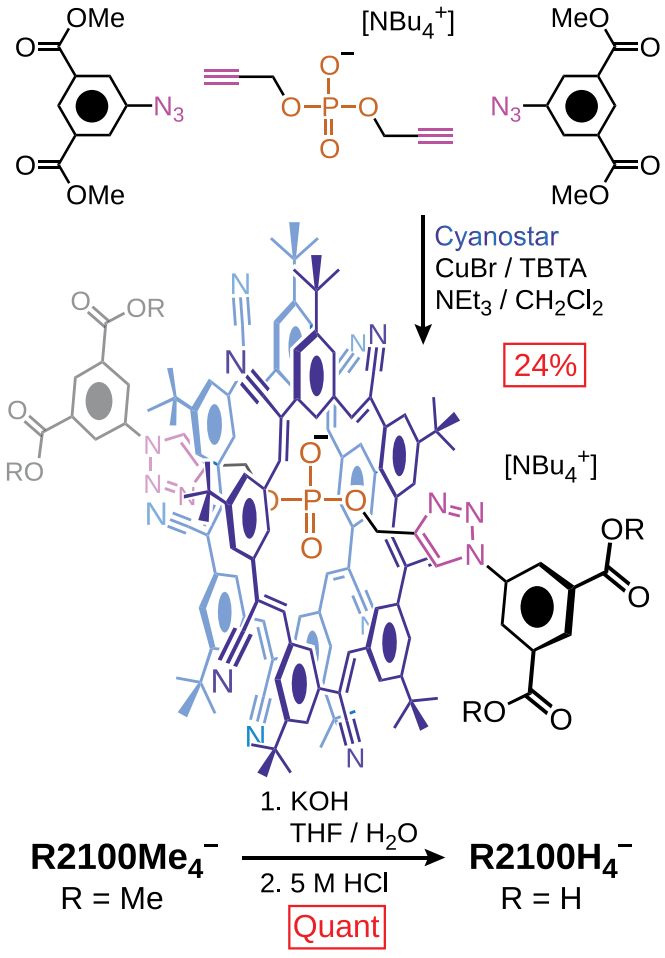


Figure 2.67 The pentagonal cyanostar (CS) macrocycle.[1144] (a) CS adopts a slightly bowl-shaped geometry. Viewed from the top side of the bowl, CS exists as either the *M* or *P* stereoisomers, which can interconvert by bowl-to-bowl inversion. (b) Generalized schematic of the anion binding modes for CS macrocycles.

catalyst, affording the [3]rotaxane **R2100Me$_4^-$** in 24% yield. The methyl esters can be hydrolyzed quantitatively to give the corresponding tetra-acid [3]rotaxane **R2100H$_4^-$**. The 2:1 sandwich complex that serves as a template for this reaction 'lives on' in the rotaxane, as revealed (**Figure 2.68**) by the solid-state structure of **R2100H$_4^-$** as its tetrabutylammonium salt. Since the CS rings exist as a mixture of *M* and *P* isomers, the rotaxane is isolated as a 4:1 mixture of *meso* and *chiral* diastereoisomers, which are configurationally stable at temperatures up to 433 K in CD_3SOCD_3, according to ^{1}H NMR spectroscopic analysis. The CS rings are π–π stacked at their inner seams with oppositely facing bowls (**Figure 2.68a–b**) and with the phosphate anion of the dumbbell centered squarely in between them. This co-conformation allows the oxygen atoms of the PO_4R_2 core to accept (**Figure 2.68c**) no less than 18 hydrogen bonds from the endotopic activated C–H donors of the CS rings. The facile multigram synthesis and promiscuous anion-binding properties of the cyanostar will no doubt make it an important new receptor in supramolecular and mechanostereochemistry.



Scheme 2.106 The click synthesis[1144] of Flood's [3]rotaxane **R2100Me$_4^-$**, which is templated by the binding of a $(CS)_2$ dimer and a dipropargylphosphate anion. Deprotection of the methyl esters affords the homologue **R2100H$_4^-$**.

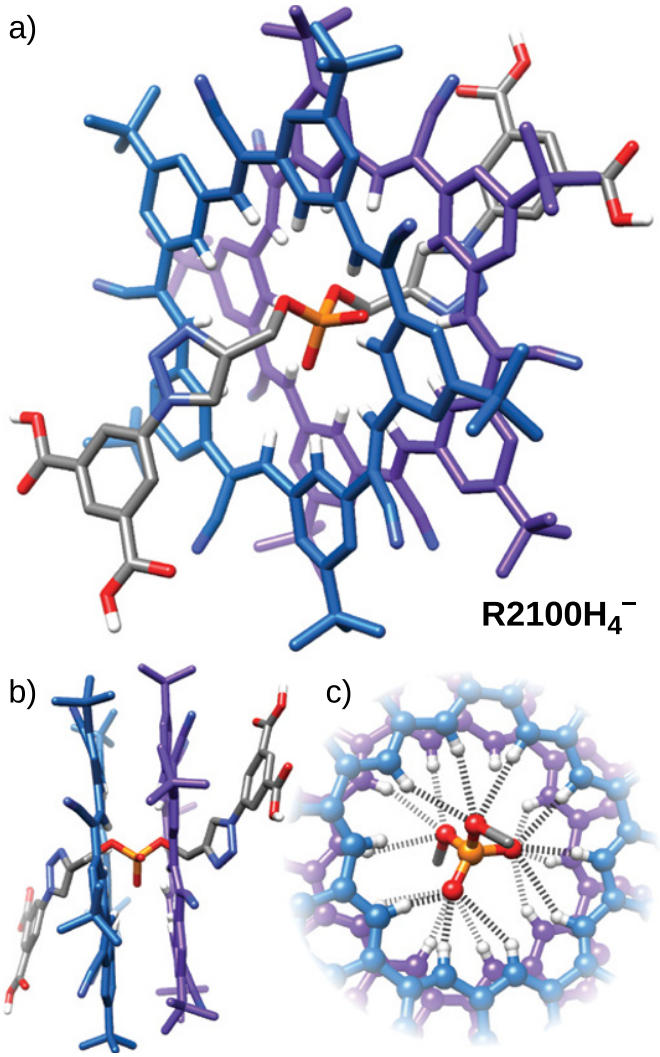


Figure 2.68 The solid-state structure[1144] of **R2100H$_4^-$**. Angled (a) and side-on (b) views of a tubular representation reveal the *phosphate⊂(CS)$_2$* sandwich subcomplex at the core of the molecule, in which the CS macrocycles meet at their inner seams with their bowls facing outward. An enlarged image of the *phosphate⊂(CS)$_2$* region (c) as a ball-and-stick representation shows all of the [C–H···O] interactions (<3 Å) as dashed lines. For the sake of clarity, NBu_4^+ counterions are omitted and only endotopic C–H protons are shown.

Concluding Remarks

The research summarized in **Section 2.3.6** demonstrates that anions constitute a powerful set of templates for the construction of MIMs. The numerous subtly different motifs rely upon anion binding forces, which amount to a combination of electrostatic, hydrogen or halogen bonding, Lewis acid/base, and anion···π interactions, as well as additional types of forces such as D-A charge transfer, π–π stacking, and [C–H···O] interactions. The design of successful anion-binding pseudorotaxanes and MIMs hinges on an appropriate size- and shape-complementarity between a host's topologically and/or mechanically constrained cavity, which is lined with Lewis acidic atoms—either N–H, C–X, or C–H donors—often, but not necessarily, assisted by an

ion-paired organocation, which enhances binding through ion-pairing interactions and/or induction of electron density. Many more anion recognition motifs remain available,[1066–1069,1145] simply waiting to become templates for making mechanical bonds. We conclude in the words of Beer[1142] that "*the careful design of the interlocked host's three-dimensional binding cavity with the appropriate pre-organized recognition elements (in both the axle and the macrocycle components) can facilitate enhanced guest complexation strength and selectivity for a target complementary anion guest.*"

2.3.7 Ion-Pair Templates

The electrostatic attractive forces that lead to the pairing of cations and anions are involved in many of the template motifs described in previous Sections, such as (i) the ion-pairing of viologen guests with sulfonated π-donating macrocyclic polyethers[510,513–515] (**Table 2.8**), (ii) the recognition[804,805,809] of Sessler's TexasBox^{4+} for π-donating anions (**Figure 2.45**), (iii) the multicomponent assemblies[992,993] based on crown ethers and dialkylammonium cations with fluorinated counterions (e.g., **Figure 2.58c**), or (iv) the ion-paired anionic templates and cationic axles / rings of Beer's anion-binding molecular recognition motifs[1084,1088] (**Sections 2.3.6.2–2.3.6.4**). Here we describe several motifs that rely more deliberately on ion-pairing forces as templates for mechanical bonds. In addition to being involved in either cation- or anion-binding receptors, ion-pair template motifs can belong to any of three categories (**Figure 2.69**), which we describe as (i) integrated (**Section 2.3.7.1**), in which different components possess oppositely charged ions within their constitutions, (ii) separated (**Section 2.3.7.2**), which involve interpenetrated templates with separate binding pockets for both cations and anions, and (iii) traceless (**Section 2.3.7.3**) ion-pair templates, whereby an ion-pair is neutralized or discarded upon formation of a mechanical bond. Ion-pair template strategies for the synthesis of MIMs have been reviewed recently by Spence and Smith.[1146]

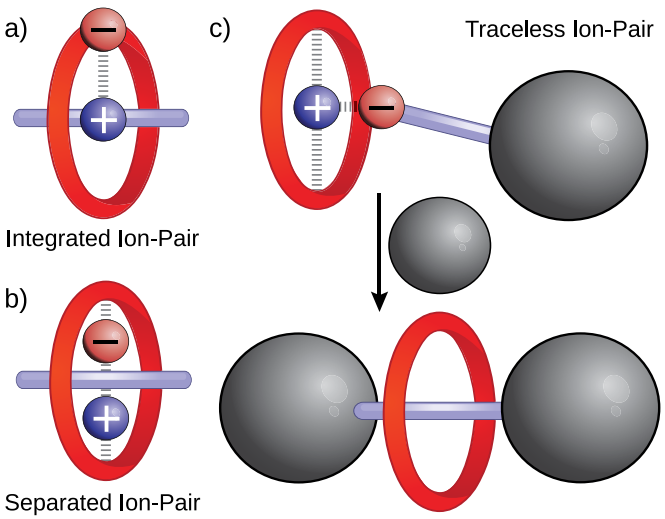


Figure 2.69 Graphical representations of examples of integrated (a), separated (b) and traceless (c) ion-pair templates.

2.3.7.1 Integrated Ion-Pair Templates

Recognition motifs that rely on ion-pairing as the primary driving force for molecular interpenetration include (i) amidinium carboxylate salt bridges, (ii) transition metal coordination compounds, and (iii) inorganic-organic hybrid structures.

Amidinium-Carboxylate Salt Bridges

Furusho and Yashima[1147,1148] at Nagoya University have developed a supramolecular recognition motif (**Figure 2.70**) involving ion-paired and hydrogen-bonded salt bridges as the primary driving force. In their seminal research[1149] in this area, the Nagoya team installed complementary diamidine and carboxylic acid moieties within the crescent-shaped centers of *meta*-terphenyl derivatives. The transfer of a proton from the carboxylic acid to the diamidine unit generates (**Figure 2.70a**) an amidinium carboxylate salt bridge. On account of their charge-assisted hydrogen-bonding interactions, the noncovalent bonding interactions of amidinium carboxylate salt bridges, which orient their substituents in a well-defined linear geometry, are maintained even in polar solvents. The helical chirality of the salt-bridged assembly can be controlled by the chirality of the R groups appended to the amidine precursor. Diacetylene-bridged covalent dimers of these recognition elements self-assemble (**Figure 2.70b**) into homochiral duplexes with double-helical superstructures. These assemblies exhibit high stabilities (>10^6 M^{-1}) in $CDCl_3$ at

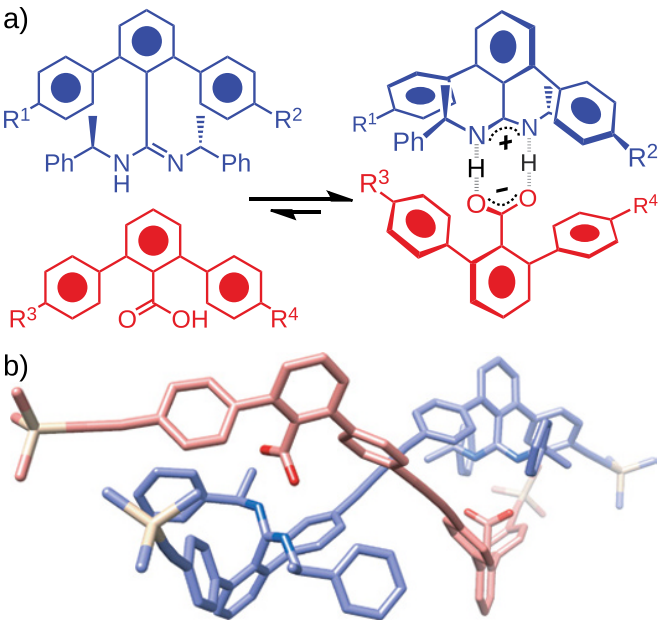
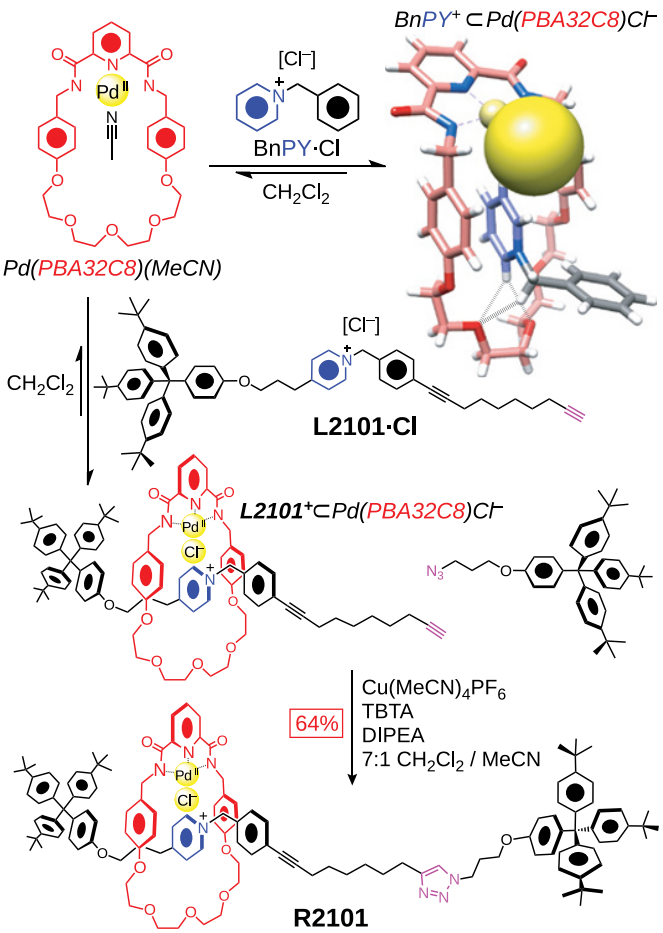


Figure 2.70 The amidinium carboxylate salt bridge as an ion-pair template motif for intertwined (super)structures.[1149] (a) The self-assembly of entwined *meta*-terphenylene backbones via the formation of an amidinium carboxylate salt bridge with chiral appendages. (b) The solid-state superstructure of a double-helical duplex comprising terphenylene-derived amidinium and carboxylate dimers, shown in a tubular representation with hydrogen atoms and solvent molecules omitted for the sake of clarity.

293 K and persist even in highly polar Me_2SO solutions. The construction[1150] of a [2]catenane based on this recognition motif, which relies on thermodynamically controlled ring-closing metathesis, is described in **Section 3.4.1.5**.

Transition Metal Ion-Pair Templates

In 2008, Leigh[1151] reported the serendipitous discovery of an ion-pair template motif (**Scheme 2.107**) involving an anionic macrocyclic transition metal complex and a cationic pyridinium axle. The Pd^{II} endocyclic chelate of the pyridobenzylic amide [32]crown-8 (PBA32C8) ring can adopt the neutral form *Pd(PBA32C8)(MeCN)* when its endotopic vacant site is coordinated by MeCN, or it can adopt the anionic form *Pd(PBA32C8)Cl*$^-$ in the presence of chloride. The chance observation in this case was that the anion of benzylpyridinium chloride (BnPY·Cl) displaces the endotopic MeCN ligand of *PdPBA32C8(MeCN)* and leads to the assembly (**Scheme 2.107**) of an integrated ion-pair pseudorotaxane, *BnPY*$^+$*⊂Pd(PBA32C8)Cl*$^-$. The solid-state structure of this rotaxane reveals that the tight ion-pair



Scheme 2.107 Leigh's transition metal ion-pair template motif,[1151] including the self-assembly and solid-state superstructure of a pseudorotaxane (top right) comprising the $BnPY^+$ cation and $Pd(PBA32C8)Cl^-$ anion, as well as the CuAAC click synthesis (bottom) of the [2]rotaxane **R2101** incorporating the same recognition elements.

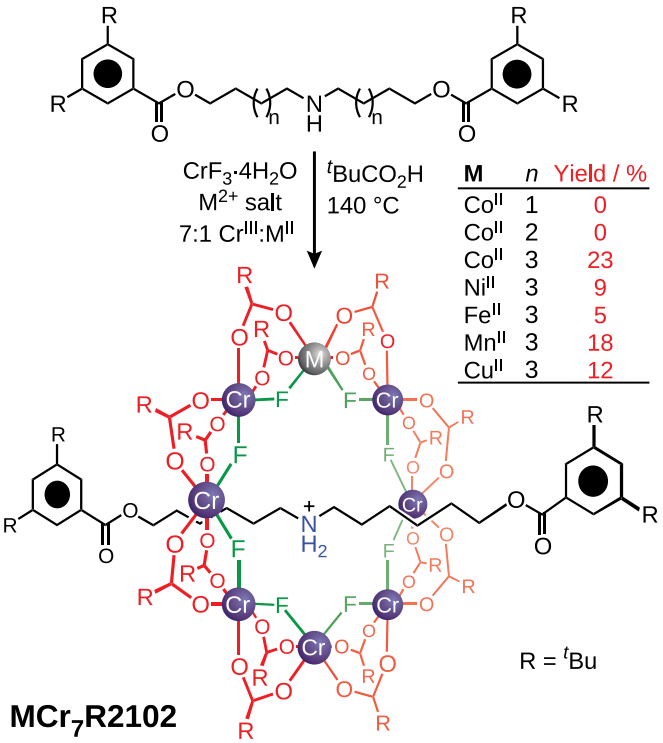
between $Pd(PBA32C8)Cl^-$ and $BnPY^+$ is assisted by D-A π–π stacking, [C–H···O], and second-sphere [C–H···Cl] interactions between the host and guest. Pseudorotaxane assembly does not take place in the absence of the chloride ion or in highly polar solvents such as Me_2SO. Using CuAAC click chemistry, the [2]rotaxane **R2101** was obtained in 64% yield by reacting semidumbell **L2101·Cl** with an azidoethyl-functionalized stopper precursor in the presence of *Pd(PBA32C8)(MeCN)* and Cu^I/TBTA in CH_2Cl_2/MeCN. The PBA32C8 ring can be shuttled back and forth along the axle of this rotaxane by addition and removal of the chloride anion—see **Section 6.5.2**.

Inorganic Organic Hybrids

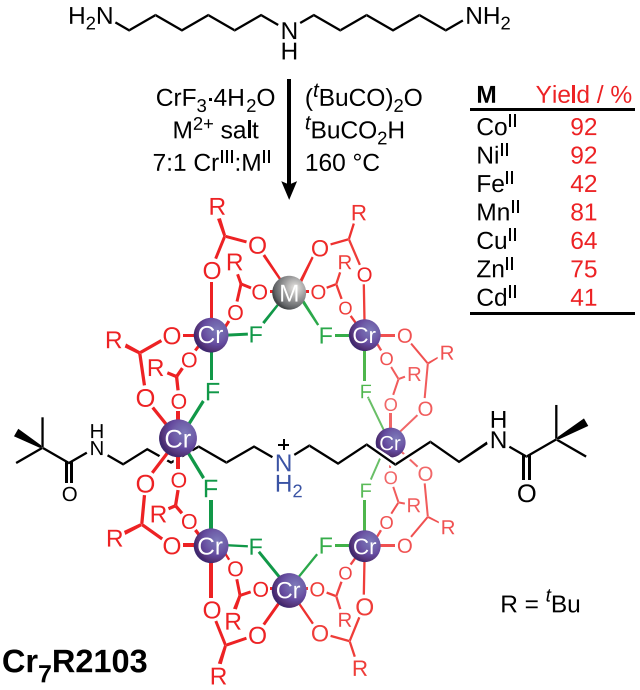
Leigh and Winpenny[1152,1153] have introduced a novel rotaxane motif involving organic axles and inorganic rings that was enabled by Timco and Winpenny's discovery[1154] and development[1155–1157] of a class[1158] of large anionic heterometallic wheels surrounding organocationic templates. These macrocyclic inorganic clusters comprise seven or more trivalent Cr^{III} ions and one or more divalent heteroatoms (M^{2+}) bridged by carboxylate and fluoride anions, while the organocationic templates are derived from imidazolium or (di)alkylammonium centers. Ion pairing drives the encapsulation of organocations by the inorganic wheels, since they possess an anionic charge for each divalent metal atom in their constitution. Leigh and Winpenny[1152] reasoned that assembling these inorganic wheels around dialkylammonium dumbbells with sufficiently bulky stoppers would lead to the genesis of inorganic-organic hybrid rotaxanes. Indeed, the reaction (**Scheme 2.108**) of a 7:1 molar ratio of Cr^{III} and Co^{II} ions in the form of the inorganic salts $\{CrF_3{\cdot}4H_2O\}$ and $\{Co_2(H_2O)(^tBuCO_2)_4(^tBuCO_2H)_4\}$ with a 3,5-di-*tert*-butylphenyl ester-stoppered dialkylammonium dumbbell at 140 °C in pivalic acid leads to the 33-component assembly of the [2]rotaxane **$CoCr_7$R2102** in 23% yield. The solid-state structure of **$CoCr_7$R2102**, which is shown in **Figure 1.16f** in **Section 1.2.4**, reveals that intercomponent [N–H···F] hydrogen bonds between the dumbbell and the inner walls of the ring act as additional stabilizing forces. It transpires that the oligomethylene spacer in between the $–NH_2^+–$ center and the stoppers must be at least six carbon atoms in length in order to generate the rotaxane. The stoppers presumably interfere sterically with the assembly of the ring around the dumbbell when the spacers are shorter. This protocol for inorganic-organic hybrid rotaxanes has been generalized[1153] to accommodate (**Scheme 2.108**) other divalent metal cations instead of Co^{II} in the wheel component of the rotaxanes **MCr_7R2102**, where M is Ni, Fe, Mn, or Cu.

Further investigations[1153] and optimizations of the multicomponent self-assembly of inorganic-organic hybrid rotaxanes have probed the effects of secondary, tertiary, and quaternary amines and ammonium salts as additives. The optimized yield for rotaxane **$CoCr_7$R2102** is increased to 58% in the presence of 5 mol% Et_2NH, 58% with 30 mol% Et_2NH_2Cl, up to 70% in the presence of Et_3N at a loading ratio of 5–100%, and 57% in the presence

of 75 mol% Et_4NCl. These additives are believed to enhance yields by acting as dynamic templates that promote ring formation. Since the ester bonds of **MCr$_7$R2102** are susceptible to hydrolytic cleavage, a revision of the stopper groups to *tert*-butyl amides leads to further yield enhancements.[1153] The synthesis (**Scheme 2.109**) of rotaxanes **MCr$_7$R2103**, where M is Co, Ni, Fe, Mn, Cu, Zn, or Cd, proceeds in up to 92% yield by a novel combined clipping/stoppering protocol. In this case, the *tert*-butyl amide stoppers are formed *in situ* by the coupling of an amine-terminated dihexylammonium template with pivalic anhydride, concomitantly with the assembly of the inorganic wheels around the $-NH_2^+-$ center in one pot. It is not clear if the high efficiencies of this clipping/stoppering protocol can be attributed solely to the higher stability of the stopper linkage or if the terminal amines of the dumbbell precursor play a supporting role in the template assembly of the rings. Although the inorganic wheels are dynamic and subject to exchange under the conditions of their syntheses at 140 °C, they have proved to be kinetically stable at 60 °C in $C_2D_2Cl_4$ since no ligand exchange is observed under these conditions. This ion-paired inorganic-organic hybrid motif has also been applied to the synthesis[1152] of multicomponent [3]- and [4]rotaxanes (**Section 4.2.1.1–4.2.1.2**), molecular shuttles (**Section 5.1.1.2**), and supramolecular daisy chains[1159] (**Section 4.2.3.2**).



Scheme 2.108 The 33-component self-assembly of the inorganic-organic hybrid [2]rotaxanes **MCr$_7$R2101** comprising dialkylammonium dumbbells and heterometallic {MCr_7} rings.[1152,1153] The divalent ions M^{2+} of the rings are introduced as the following salts: $Co_2(H_2O)(^tBuCO_2)_4(^tBuCO_2H)_4$, $2NiCO_3{\cdot}3Ni(OH)_2{\cdot}4H_2O$, $FeCl_2{\cdot}4H_2O$, $MnCl_2{\cdot}4H_2O$, and $CuCO_3{\cdot}Cu(OH)_2$.



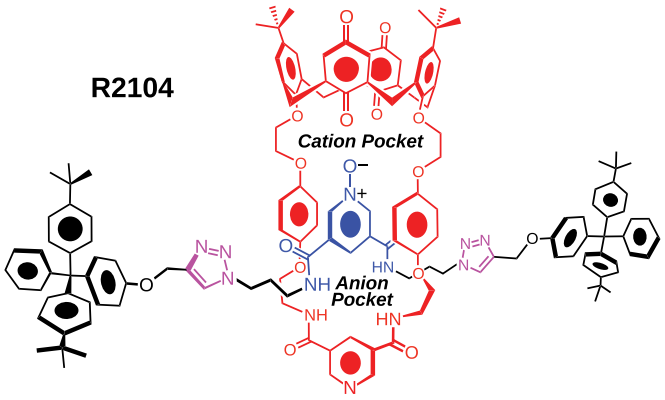
Scheme 2.109 The efficient synthesis of the *tert*-butylamide-stoppered [2]rotaxanes **MCr$_7$R2103** by a combined clipping/stoppering protocol.[1153] The divalent ions M^{2+} of the rings are introduced as the following salts: $Co(^tBuCO_2)_2$, $Ni(H_2O)(^tBuCO_2)_4(^tBuCO_2H)_4$, $Fe(MeCO_2)_2{\cdot}2H_2O$, $MnCO_3{\cdot}2H_2O$, $CuCO_3{\cdot}Cu(OH)_2$, $[ZnCO_3]_2{\cdot}[Zn(OH)_2]_3$, and $CdCO_3$.

2.3.7.2 Separated Ion-Pair Templates

Heteroditopic receptors for ion pairs can be differentiated according to whether the cation and anion are in contact or separated. Contact ion pairs within heteroditopic receptors serve as the basis for a number of anion-template MIMs, such as the halide-binding MIMs developed by Beer[1084,1088] and the cyclo[6]aramides of Feng and Yuan[1122]—see **Sections 2.3.6.2–2.3.6.4**—in which an anionic template is ion-paired with an organocation in the backbone of a ring or dumbbell. Separated ion-pair recognition, by contrast, involves a pair of anionic and cationic templates that are physically separated by a structural component.

One class of heteroditopic receptors from the Beer laboratory are the macrobicyclic hosts incorporating calix[4]-diquinone (C4DQ) and isophthalamide-derived recognition elements, such as the IBPPC4DQ ring of the anion-binding [2]rotaxane[1118] **R288**$^+$—see **Scheme 2.96** in **Section 2.3.6.2**. A pyridine-derived variant of this receptor, PBPPC4DQ, has been judiciously combined with the versatile 3,5-dicarboxamidopyridine *N*-oxide recognition unit, which is capable of recognizing both cations (see **Section 2.3.8**) and anions (see **Section 2.3.6.2**), to create the [2]rotaxane **R2104** exhibiting (**Table 2.34**) axle-separated ion-pair recognition.[1117] The mechanically interlocked receptor **R2104** is accessed by CuAAC click chemistry in 62% yield in the presence of NaOTf as a source of Na^+ templates, whereas the yield is <10% without added Na^+ ions. The Na^+ ion is an excellent template because it is stabilized by the electron-rich

Table 2.34 Association constants and cooperativity factors for the binding[1117] of axle-separated ion-pairs within the neutral [2]rotaxane receptor **R2104**.



Cation[a]	Anion[b]	K_a / M^{-1}	Cooperativity Factor[c]
NBu_4^+	Cl^-	71	-
	Br^-	88	-
	I^-	92	-
Li^+	Cl^-	80	1.1
	Br^-	166	1.9
Na^+	Cl^-	1079	15.1
	Br^-	930	10.6
K^+	Cl^-	676	9.5
	Br^-	633	7.2

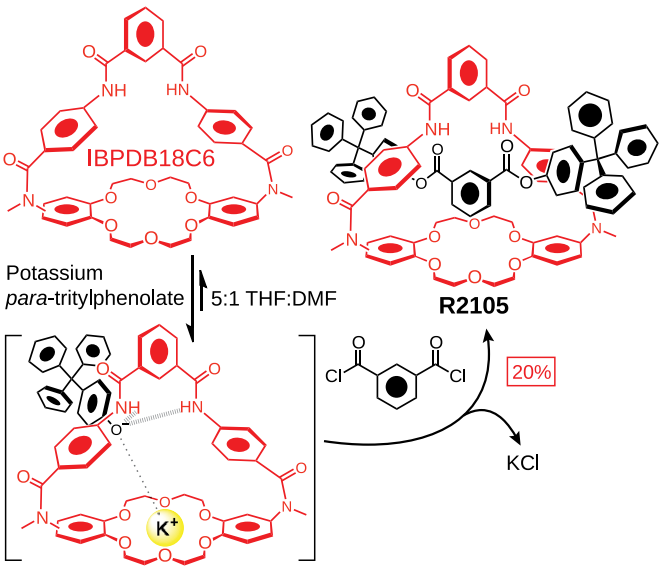
[a]Cations were introduced as salts with non-coordinating anions: $LiPF_6$, NaOTf, KPF_6.
[b]Anions were introduced as tetrabutylammonium salts.
[c]The cooperativity factor is the K_a of the guest (anion) in the presence of a cooperative binder—in this case, alkali metal cations—divided by the K_a of the guest in the absence of a partner that displays positive cooperativity—in this case, NBu_4^+.

oxygen atoms of the quinone and *N*-oxide groups of the wheel and axle, respectively. The opposing isophthalamide moieties of each component part provide a binding pocket for anions resembling that of Beer's halide binding MIMs.

The dual-pocket design of the PBPPC4DQ host allows **R2104** to accommodate ion-paired alkali metal cations and halide anions simultaneously. The halide anions, all introduced as salts of the non-coordinating organocation NBu_4^+, exhibit (**Table 2.34**) modest affinities (<10^3 M^{-1}) for **R2104** in 4:1 $CDCl_3$:CD_3OD. The anion-binding interactions are limited in this case by the enthalpic cost of disrupting the hydrogen-bonding interactions between the axle's *N*-oxide unit and the ring's 3,5-dicarboxamidopyridine unit. This cost can be paid for by the binding of Li^+, Na^+, and K^+ cations, introduced as the salts of non-coordinating PF_6^- anions. The presence of these alkali metal additives increases the affinity of the chloride and bromide anions substantially. Thus, the alkali metal cations and the halide anions, each introduced separately, exhibit positive cooperativity in the binding of **R2104**. Cooperativity factors, defined in this case as the K_a of the anion in the presence of an alkali metal cation divided by the K_a of the "free" anion (NBu_4^+ salt), are >1 for all combinations of Li^+, Na^+, K^+, Cl^-, and Br^-, reaching as high as 15 in the case of the NaCl ion pair. This uniformly positive cooperativity, combined with ^{1}H NMR spectroscopic evidence, confirms that both cations and anions are bound in an axle-separated manner within the **R2104** host, and explains why its yield increases by an order of magnitude in the presence of added Na^+ templates.

2.3.7.3 Traceless Ion-Pair Templates

Smith[1160–1162] has adapted Vögtle's nucleophilic rotaxane capture concept (**Section 2.3.5.1**) to rely on ion-pair recognition in a strategy he describes[1146] as a 'traceless' ion-pair template, since the neutral mechanically interlocked product retains niether the cationic nor anionic templates. The key to this strategy is the introduction of a macrobicyclic receptor constituting an [18]crown-6 polyether bridged by an isophthalamide unit, which is capable of recruiting cations to its 18C6 moiety and anions to its endotopic isophthalamide cavity by a combination of ion-pairing and hydrogen-bonding interactions. The first of these receptors to be described by Smith[1160,1161,1163] possesses a dibenzo[18]-crown-6 unit, which is connected by amide bonds to a *tert*-butyl isophthalamide unit via *para*-phenylene linkers—call it isophthalamide-bis-*p*-phenylene-dibenzo[18]crown-6 (IBPDB18C6)—binds[1163] alkali metal halide salts as a solvent-separated ion-pair with cooperativity factors of up to 7 in the case of KCl. Employing potassium tritylphenolate as the stopper precursor, the *K^+⊂IBPDB18C6* assembly captures (**Scheme 2.110**) the [2]rotaxane **R2105** in 20% yield by means of a double-esterification with isophthaloyl chloride, releasing KCl as a byproduct. Whereas Vögtle's

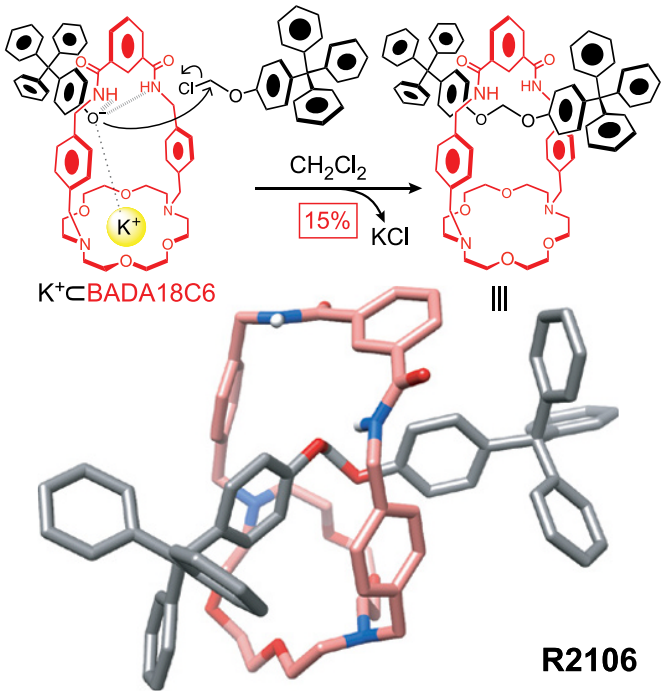


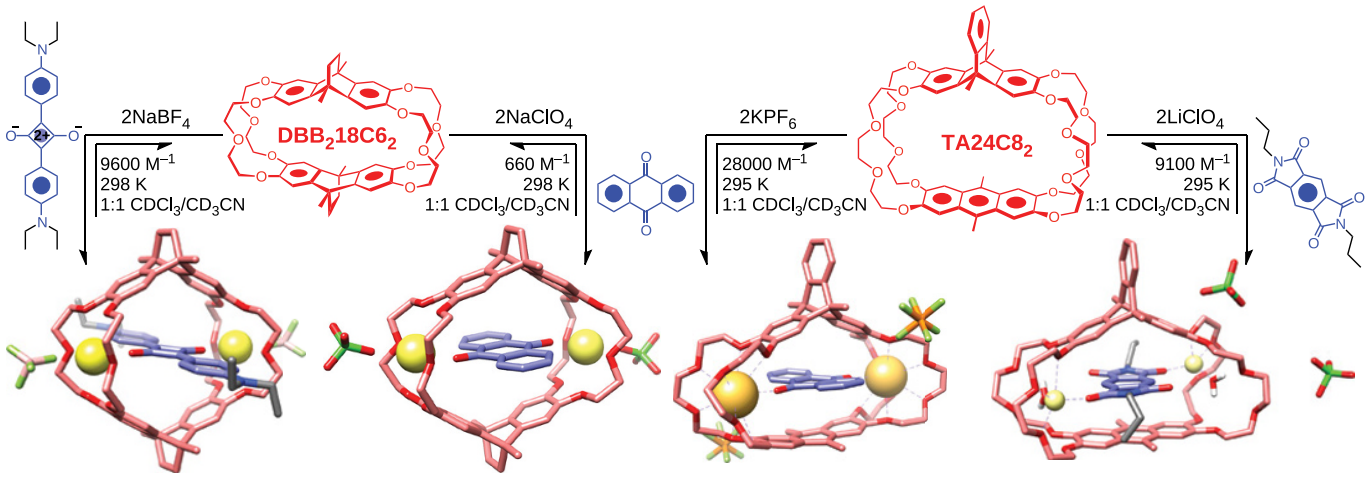
Scheme 2.110 Smith's 'traceless' ion-pair template method for rotaxane capture,[1160,1161] which is guided by the dual recognition of the macrobicyclic isophthalamide / [18]crown-6 host IBPDB18C6 for potassium *p*-tritylphenolate during nucleophilic esterification.

tetralactam rotaxanes are captured in CH_2Cl_2, the ion-pairing forces involved in this ion-pair-directed nucleophilic capture reaction allow it to proceed successfully in a much more polar THF/DMF (5:1 $^{v}/_{v}$) solvent system.

A second generation of Smith's macrobicyclic ion-pair receptors—call it benzylic amide diaza[18]crown-6 (BADA18C6)—has been employed[1162] in the traceless ion-pair template capture (**Scheme 2.111**) of the neutral [2]rotaxane **R2106** in 15% yield. In this case, the potassium tritylphenolate stopper precursors couple with CH_2Cl_2 in a nucleophilic substitution reaction, resulting in a dumbbell axle comprising a single methylene unit. Curiously, the capture reaction fails completely when a 2,6-dicarboxamidopyridine unit is employed as the bridgehead of the macrobicycle instead of isophthalamide. The solid-state structure of **R2106** is portrayed in **Scheme 2.111**, confirming the absence of ionic templates. Although the strong templating forces are no longer present, the component parts of the rotaxane engage in [N–H···O] and [C–H···O] hydrogen bonds involving the ether sites of the axle and the isophthalamide and crown moieties of the ring, as well as [C–H···π] and edge-to-face π–π interactions between the aryl rings of the ring and stoppers.

Although rotaxanes **R2105** and **R2106** are neutral, they retain, to some extent, their capability to bind[1161,1162] cations and anions in organic media, albeit more weakly than the parent macrobicyclic receptors. In the case of **R2105**, the introduction of K^+ ions freezes out a single co-conformation on the ^{1}H NMR timescale and restricts the dynamics of the relative motions of the ring and axle. The same effect is not observed in the case of **R2106**.


NH
HN
Cl
O
O
O



Scheme 2.112 The self-assembly and solid-state structures of macrotricyclic donor-acceptor pseudorotaxanes assisted by cationic alkali metal templates.[675,1166] From left to right: *bis(N,N-diethylanilino)squaraine⊂DBB$_2$18C6$_2$·2NaBF$_4$*, *9,10-anthraquinone⊂DBB$_2$18C6$_2$·2NaClO$_4$*, *9,10-anthraquinone⊂TA24C8$_2$·2KPF$_6$*, *dipropylpyromellitic diimide⊂TA24C8$_2$·2H$_2$O·2LiClO$_4$*. Solvent molecules and protons are omitted from the tubular representations of the solid-state structures for the sake of clarity.

cationic templates range from 10^3–10^5 M^{-1} in 1:1 $CDCl_3$/CD_3CN. These recognition motifs have further served[1167,1168] as templates in the synthesis of [2]rotaxanes by the slippage approach—see **Section 3.1.2**.

Recently, Chiu[1169–1172] has developed motifs (**Figure 2.71**) for the synthesis of MIMs that rely much more exclusively on cation binding as the principal templating interaction. In 2013 he discovered[1169] that the macrocyclic polyether BX26C6—a π-donating host employed in donor-acceptor MIMs (**Section 2.3.3.4**) which was already known[615,1173] to cooperate with interlocked 2,2′-bipyridine derived dumbbells in the binding (see **Scheme 2.58** in **Section 2.3.3.4**) of Na^+—also recognizes (**Figure 2.71a**) single amide or urea functionalities in the presence of Na^+ cations. Other rings incorporating diethylene glycol (2EG) loops as Na^+ recognition units are also suitable hosts. The Na^+ ion is stabilized in these pseudorotaxanes by ion-dipole interactions involving the electron-rich oxygen atoms of the ring's polyether loops and the guests' carbonyl groups. Entwined $Na(2EG)_2^+$ complexes (**Figure 2.72b**) have served likewise as templates for making mechanical bonds.

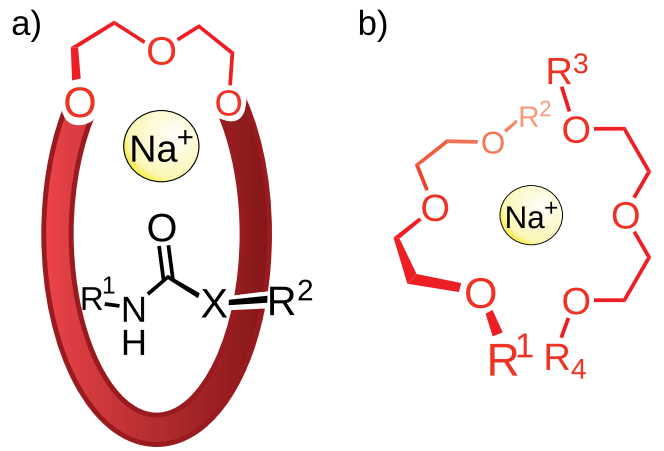


Figure 2.71 Chiu's sodium template motifs comprising functionalized diethylene glycol (2EG) components paired with (a) amide-[1169,1171] and (b) 2EG-[1171,1172] derived partners, threaded and entwined, respectively, around a central Na^+ template.

Chiu[1169,1171] has constructed (**Figure 2.72**) a meccano set of crown ether rings and amide- or urea-derived axles with nucleophilic endgroups, which can be mixed and matched to synthesize the [2]rotaxanes **R2107–R2115** when reacted with any of the stopper precursors **SP1–SP3** in the presence of Na^+ templates as their tetrakis(3,5-trifluoromethylphenyl) borate ($TFPB^-$) or ClO_4^- salts. Although the Na^+ ions are crucial for assembly, they are removed during the workup by aqueous extraction. In addition to BX26C6, Chiu[1171] has found that bis-*para*-xylyl[26]dithiacrown-6 (BX26S$_2$C6), pyridobis-*para*-xylyl[26]crown-6 (PBX26C6), pyrido-*para*-xylyl[25]crown-7 (PX25C7), pyridobis-*para*-xylyl[29]crown-7 (PBX29C7), and bis-*para*-xylyl[29]crown-7 (BX29C7), are all capable of being threaded by amides and ureas in the presence of Na^+ cations. Esters, by contrast, do not thread the cavities of these rings even in the presence of Na^+ cations, most likely on account of their weaker propensity for ion-dipole and hydrogen-bonding interactions. The 3,5-di-*tert*-butyl stoppers of **SP1** and **SP2** are sufficiently bulky to resist passage through the rings except for BX27C9, which requires the larger **SP3**-derived stopper in order to avoid deslipping. The results of the rotaxanations by the stoppering approach reveal that the recognition motif exhibits high structural flexibility, yet the efficiency is sensitive to the constitution of both the ring and the axle, since yields range from near-zero up to 73%. Among the many successfully threaded axles are the basic repeating units of ubiquitous macromolecules such as polypeptides (proteins) and nylon, which bodes well for the possibility of designing bulk materials with mechanical bonds using these protocols.

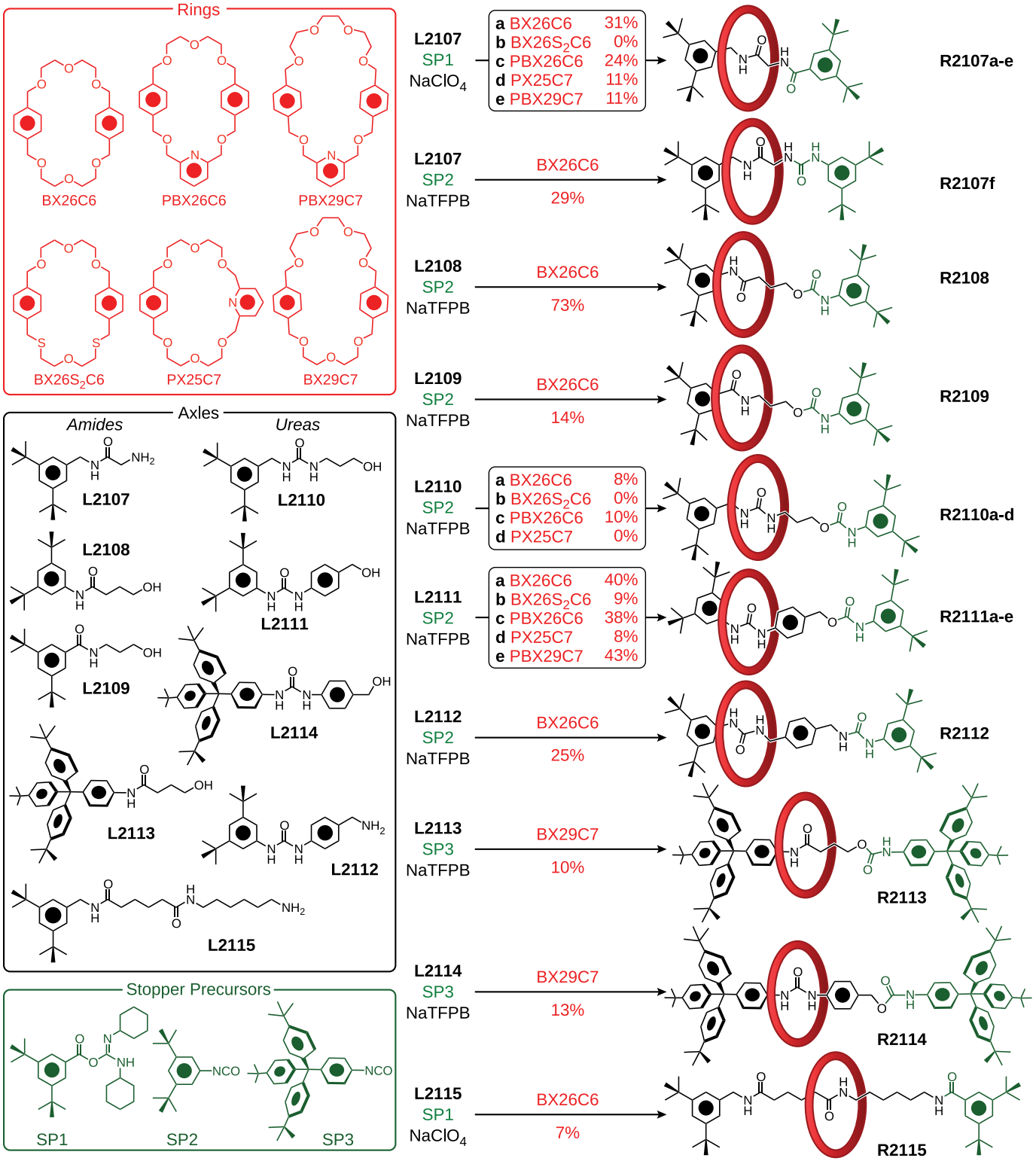
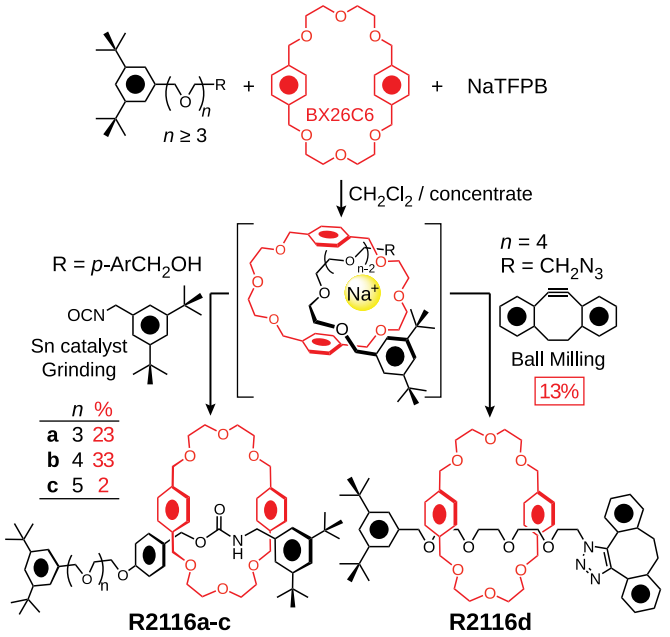


Figure 2.72 The sodium-templated syntheses[1169,1171] of rotaxanes **R2107–R2115** from a meccano set of crown ether rings, amide- and urea-derived axles, and reactive stopper precursors. All reactions are carried out in CH_2Cl_2 at ambient temperature and the Na^+ templates are removed during aqueous workup.

In 2013 Chiu[1170] prepared a [2]catenane templated solely by an entwined $Na(2EG)_2^+$ derived complex, which self-assembles in $CDCl_3$ with the assistance of reversible imine bonds—see **Section 3.3.1.2**. Chiu[1172] has also described the synthesis (**Scheme 2.113**) of a number of [2]rotaxanes based on the same motif. In this case, the Na^+ templates orchestrate the threading of oligo(ethylene glycol) (OEG) derived semidumbbells with reactive



Scheme 2.113 The solvent-free synthesis of Chiu's [2]rotaxanes **R2116a-d**, which is templated by the weak cooperative chelating interactions of polyether loops of the BX26C6 ring and the axle precursors with Na^+ ions.[1172]

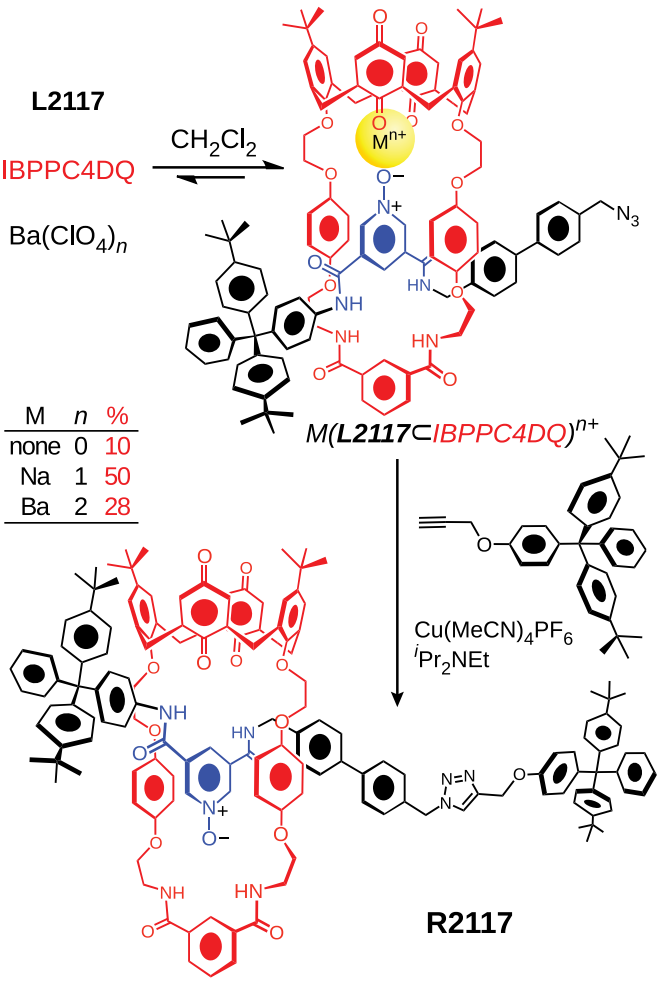
endgroups through the cavity of BX26C6 by virtue of its 2EG loops, which cooperate with the OEG threads in stabilizing the cation. This interaction is very weak, since no evidence was found for *Na(OEG⊂BX26C6)*$^+$ pseudorotaxanes even in low-polarity CH_2Cl_2 solvent. Under solvent-free conditions, however, [2]rotaxanes are obtained in yields of up to 33% by simply grinding a pre-mixed sample of the precursors which has been concentrated to dryness from CH_2Cl_2. This approach has been found to be compatible with carbamate-forming stoppering reactions involving isocyanate stopper precursors catalyzed by di-*n*-butyltin dilaureate, affording the [2]rotaxanes **R2116a-c**, as well as with strained alkyne stopper precursors for copper-free azide-alkyne cycloaddition click chemistry, leading to the [2]rotaxane **R2116d**. The reactions are sensitive to the length of the thread's OEG loops, with 3EG being optimal in the case of the rotaxanes **R2116a-c**. Since the BX26C6 ring of the rotaxanes **R2116a-c** encircles the carbamate linkage preferentially in the absence of a catiionic template, the rotaxane **R2116c** has been employed as a cation-driven molecular switch—see **Section 6.4.2**.

Retrospectively, it is somewhat surprising that the association of polyether loops for alkali metal cations has not been employed more widely and until very recently, since these interactions supported the very birth of supramolecular chemistry on the back of Pedersen's seminal research[151,152] on crown ethers. This recognition motif is likely to gain more traction in mechanostereochemistry in the future on account of its remarkable simplicity.

2.3.8.2 Alkaline Earth Metals

Alkaline earth metals have been employed even more rarely as templates in mechanostereochemistry, with Mg^{2+} and Ba^{2+} being the only examples[1174,1175] that have been reported to our knowledge. Early examples of MIMs based on alkaline earth metal templates were assembled under thermodynamic control. Richey[1176] and Bickelhaupt[1177] both described mechanically interlocked Grignard reagents possessing organomagnesium centers—see **Section 3.2.5.1**. Rees[1174] introduced a self-assembled [2]catenane in which a Ba^{2+} cation is part of the constitution of each ring component—see **Section 3.2.5.2**.

More recently, Beer[1175] has employed Ba^{2+} in the template-directed synthesis (**Scheme 2.114**) of the [2]rotaxane **R2117**. The key intermediate in this protocol is the pseudorotaxane *Ba(**L2117**⊂IBPPC4DQ)*$^{2+}$, which self-assembles in CH_2Cl_2 solution from a mixture of $Ba(ClO_4)_2$ salt, the IBPPC4DQ ring, and the azide-terminated semidumbbell **L2117** possessing a pyridinium *N*-oxide recognition unit. Ion-dipole interactions involving the carbonyl groups of the ring's C4DQ moiety and the *N*-oxide group of the thread

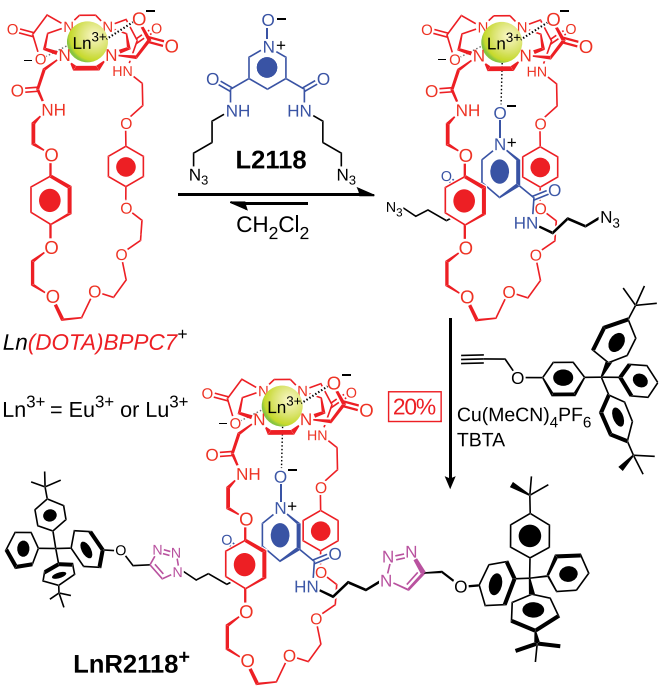


Scheme 2.114 Beer's click synthesis of the [2]rotaxane **R2117** employing either a Na^+ or Ba^{2+} template, which is coordinated by an *N*-oxide group in the axle and hydroquinone subunits in the ring.[1175]

stabilize the Ba^{2+} cation in a cooperative manner. Following a standard CuAAC stoppering protocol with a propargylated tetraphenylmethane-derived stopper precursor, the [2]rotaxane **R2117** is obtained from the pseudorotaxane precursor in 28% yield. The reaction is more efficient (50% yield) when employing Na^+ as the template, and less efficient (10% yield) in the absence of an alkali or alkaline earth metal cation. The cationic template is removed during purification by preparative TLC, which allows the *N*-oxide group to engage the isophthalamide unit of the IBPPC4DQ ring in hydrogen-bonding interactions. This pirouetting of the ring with respect to the axle can be reversed and actuated by the addition and removal of Ba^{2+} cations in solution. A related Ba^{2+}-driven molecular switch is discussed in **Section 6.4.3**.

2.3.8.3 *Lanthanides*

Beer has recently expanded the family of cationic templates even further to include lanthanides. In a 2013 communication,[348] he described how his cation-binding template motifs, such as the one reviewed in **Section 2.3.8.2**, was modified and adapted for lanthanide trications (Ln^{3+}), where Ln^{3+} = Eu^{3+} or Lu^{3+}. The synthetic strategy (**Scheme 2.115**) involves the installation of the well-known Ln^{3+}-chelator 1,4,7,10,tetraazacyclododecane-1,4,7,10-tetraacetic acid (DOTA) cyclen instead of C4DQ within the framework of a bis-*para*-phenylene crown ether—call it Ln(DOTA)BPPC7$^+$—with an open site in the La^{3+} coordination sphere. Although the La^{3+} ions are stabilized by solvent molecules in Ln(DOTA)BPPC7^{3+}, they can recruit pyridinium *N*-oxide units into the ring's cavity on account of the *N*-oxide's stronger electron-donating ability. Thus, the pyridinium *N*-oxide bis-azide thread **L2118** is combined with the Ln(DOTA)BPPC7^{3+} macrobicycle in order to form the pseudorotaxane ***L2118*⊂*Ln(DOTA)BPPC7***$^+$, which is then capped with bulky alkyne-bearing stopper precursors to afford either of the [2]rotaxanes **LuR2118**$^+$ and **EuR2118**$^+$ by CuAAC click chemistry in 20% yield. In addition to ^{1}H NMR spectroscopy, luminescence studies on **EuR2118**$^+$ verify that the inner coordination sphere of the Eu^{III} center is closed off to solvent on account of the interpenetrated *N*-oxide group.



Scheme 2.115 Beer's lanthanide-templated synthesis of the [2]rotaxanes **EuR2118**$^{3+}$ and **LuR2118**$^{3+}$ by CuAAC click chemistry.[348]

Beer[1178] has also employed the Ln(DOTA)BPPC7$^+$ ring in a nitrite anion-templated synthesis (**Figure 2.73**) of the [2]rotaxane **LnR2119·NO$_2$** using CuAAC click chemistry, in which the ion-paired nitrite template accepts hydrogen bonds from a 3,5-dicarboxamidopyridinium axle while coordinating the Ln^{3+} cation. More recently, Gunnlaugsson[346] has employed Eu^{III} templates in the synthesis of [2]- and [3]catenanes by ring closing metathesis—see **Sections 3.4.1.4** and **4.1.1.4**. Leigh[347] has devised a similar strategy for the lanthanide template-directed synthesis of a molecular trefoil knot. The favorable luminescent, paramagnetic, and catalytic properties of lanthanides may render lanthanide-templated MIMs attractive candidates for a range of potential applications, such as dyes and contrast agents for medical diagnostics.

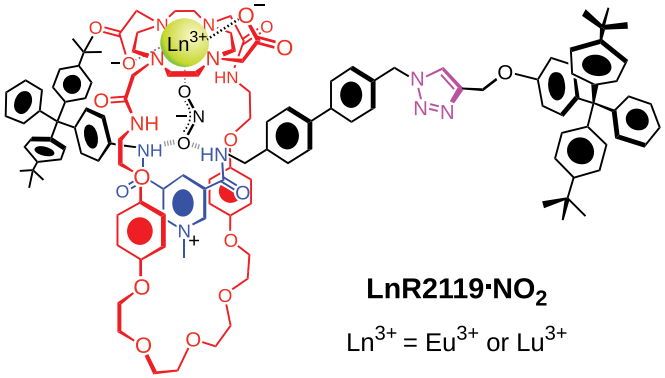


Figure 2.73 Structural formula of Beer's nitrite/lanthanide [2]rotaxane.[1178]

2.3.9 Macrocyclic Arenes and Heteroarenes

Cyclophanes—macrocycles comprising a combination of aromatic and aliphatic groups—represent a very broad class of hosts in supramolecular and mechanostereochemistry. The ionic hosts in **Section 2.3.1.4**, the macrocyclic ligands in **Section 2.3.2**, the π-donating crown ethers and π-accepting molecular boxes in **Section 2.3.3**, the majority of lactam and crown ether derived hosts in **Section 2.3.4**, as well as most of the cation- and anion-binding hosts in **Sections 2.3.5–2.3.8**, are cyclophanes. Cyclophanes are a subset of macrocyclic (hetero)arenes, which constitute any macrocycles possessing arene or heteroarene subunits in their constiutions. Macrocyclic arenes that do not qualify as cyclophanes include all sorts of fully π-conjugated

macrocycles, since they do not incorporate aliphatic chains into their loops—e.g., macrocyclic annulenes[1179] and other carbon nanorings such as cycloparaphenylenes[1180,1181] and cycloparaphenylene-ethynylenes,[1182,1183] as well as similar systems involving heteroarenes such as porphyrin nanorings,[1184–1189] cyclic oligothiophenes,[1190] and many others.[1191] Several of these macrocyclic arenes appear to be viable candidates for becoming the component parts of novel mechanomolecules.

In this Section, we focus on macrocyclic arene templates that defy categorization elsewhere because their molecular recognition processes rely on a diverse combination of multiple noncovalent forces, which may include any of those described in **Sections 2.3.1–2.3.8**. In particular, methylene-bridged macrocyclic oligomers of hydroxy- and alkoxy-substituted arenes, most notably calix[*n*]arenes[1192–1194] (**Section 2.3.9.1**) and pillar[*n*]arenes[1195] (**Section 2.3.9.2**) and their derivatives, have received much attention from researchers of the mechanical bond. The structural formulas of methylene-bridged orthocyclophanes, metacyclophanes, and paracyclophanes are compared in **Figure 2.74**. The

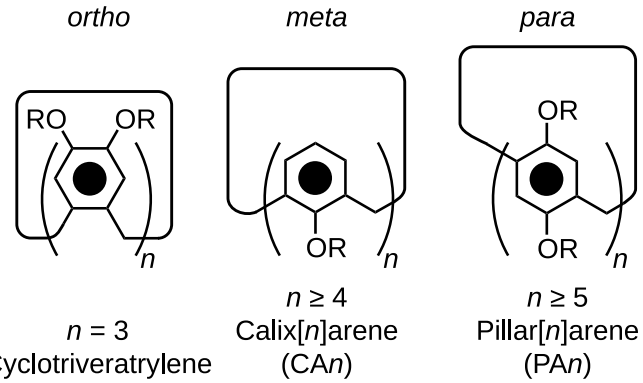


Figure 2.74 Structural formulas of methylene-bridged macrocyclic arenes with *ortho, meta,* and *para* substitution patterns.

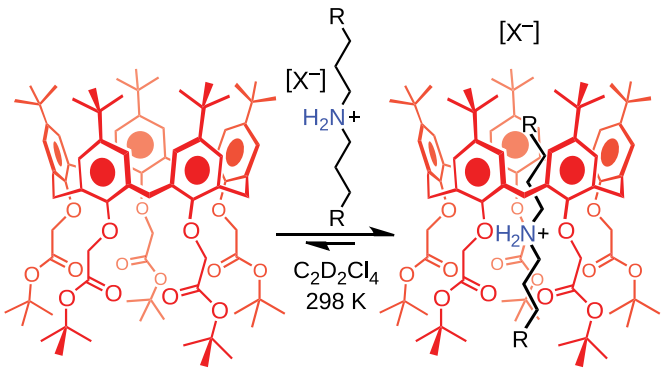
orthocyclophanes, cyclotriveratrylene[1196] (*n* = 3) and cyclotetraveratrylene (*n* = 4), as well as the metacyclophanes, known[1192,1193] as calix[*n*]arenes (CA*n*, *n* ≥ 4), belong to the class of receptors dubbed by Cram[1197,1198] as cavitands on account of their concave bowl-shaped geometries, which provide a cavity that interacts favorably with the convex surfaces of guest molecules. Indeed, the root 'calix' refers to a cuplike or chalice shape.[1194] Pillar[*n*]arenes[1195,1199–1201] (PA*n*), by contrast, adopt cylindrical or pillar-like conformations on account of their *para*-methylene substitution patterns. Any of these methylene-bridged macrocyclic arenes can be synthesized by acid-catalyzed electrophilic aromatic substitutions involving alkoxy- or hydroxy-substituted arenes and aldehydes. Although the thermodynamic products of the cyclooligomerizations of *ortho*, *meta*-, and *para*-cyclophanes are trimeric (cyclotriveratrylene), tetrameric (calix[4]arene), and pentameric (pillar[5]arene), respectively, it is possible to isolate a number of the larger cyclooligomers as kinetic products. The orthocyclophanes cyclotriveratrylene and cyclotetraveratrylene, as well as calix[4]arene (CA4), are too small to accommodate guests which interpenetrate through-the-annulus and, consequently, they are not employed as rings in pseudorotaxanes, rotaxanes, or catenanes. Mechanostereochemists are therefore limited mainly to the CA5, CA6, PA5, and PA6 frameworks, although it remains possible to thread the cavities of larger, more uncommon cyclooligomers such as PA7,[1202,1203] CA8,[1204] PA9,[1205] and PA10.[1205,1206]

2.3.9.1 Calixarenes

Calix[*n*]arenes[1192–1194] (CA*n*) and related macrocyclic arenes such as thiacalixarenes,[1207] oxacalixarenes,[1208] resorcinarenes,[1209] calixpyrroles,[1210] and others,[1211] represent a large and growing family of hosts in supramolecular chemistry with a diverse range of molecular recognition properties. Although there are a number of examples[1101,1102,1128,1212–1217] of MIMs posessing appended CA4 units in their constitution, the prohibitively small cavity of CA4 does not allow linear guests to fully interpenetrate through the annulus, limiting most supramolecular calixarene template motifs in mechanostereochemistry to CA5 and CA6, excepting for the multiply interlocked MIMs derived from entwined tetraureidocalix[4]arene capsules (**Section 2.3.4.5**). The calixarenes and their relatives can be easily derivatized at either the wide or narrow rim, imparting them with tunable recognition properties.[1194]

A team led by Parisi[1218] and Pappalardo[1219] provided experimental evidence[1219] that the CA5 annulus is sufficiently large for interpenetrative threading by dialkylammonium guests. The self-assembly (**Table 2.35**) of these pseudorotaxanes involves a CA5 ring functionalized with *tert*-butyl groups around the wide rim and *tert*-butyl acetate groups appended to phenolic sites of the narrow rim, as

Table 2.35 Association constants for pseudorotaxanes[1219] comprising a derivatized CA5 host and dialkylammonium guest ions as their hexafluorophosphate, picrate, and chloride salts in 1,1,2,2-tetrachloroethane at 298 K.

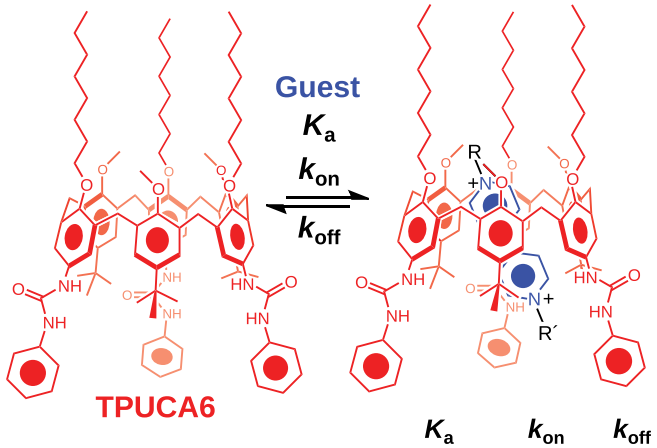


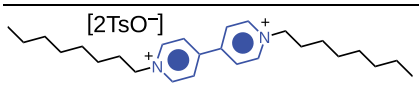
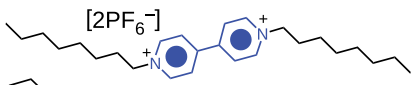
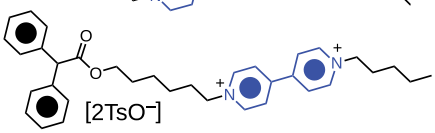
	K_a / M^{-1}	
[X$^-$]	R = Me	R = *n*-Pr
PF_6^-	12000	1400
$(NO_2)_3ArO^-$	610	210
Cl^-	<5	<5

well as di-*n*-butylammonium or di-*n*-hexylammonium guests as their hexafluorophosphate (PF_6^-), picrate ($(NO_2)_3ArO^-$), or chloride (Cl^-) salts. The association constants (K_a) for the host-guest complexes depend on the strength of the ion-pairing interactions between the guests and their counterions, where PF_6^- salts are the most weakly ion-paired and the Cl^- salts are the most strongly ion-paired guests in the series. ^1H NMR spectroscopy and molecular models suggest that the $–NH_2^+–$ centers of the dialkylammonium axles reside within the CA5 cavity in the plane of the phenolic oxygen atoms, facilitating the [N^+–H···O] hydrogen bond network which is reminiscent of the dialkylammonium/crown ether (**Section 2.3.4.6**) recognition motif. Pseudorotaxanes based on di-*n*-butylammonium exhibit higher stabilities (up to 1.2×10^4 M^{-1} in 1,1,2,2,-tetrachloroethane) than those based on di-*n*-hexylammonium (up to 1.2×10^3 M^{-1}), and the kinetics of assembly and disassembly are much faster in the case of the former. Whereas the self-assembly of the *di-n-hexylammonium⊂CA5* pseudorotaxane requires >24 h to reach completion, the *di-n-butylammonium⊂CA5* assembly is complete within minutes. The disassembly of the pseudorotaxanes can be triggered by counterion exchange with NBu_4Cl, deprotonation with NEt_3, or by introducing primary ammonium ions as competitive binding agents, making this host-guest system a suitable candidate for the design of molecular switches and machines.

A cohort of Italian researchers, the senior authors of which include Pochini,[1220] Arduini,[1221–1224] Credi,[1222,1223] Venturi,[1224] Ugozolli,[1223,1225] Silvi,[1226] and Secchi,[1226,1227] have focused on calix[6]arene (CA6) templates in the construction of mechanomolecules. Most of these investigations have employed a triphenylureidocalix[6]arene (TPUCA6) host, which displays three phenylurea appendages and three *tert*-butyl groups in alternating fashion around the wide rim, as well as various alkoxy substituents appended to the narrow phenolic rim of the calixarene. TPUCA6 derivatives recognize aromatic organocations—i.e., 4,4′-bipyridinium[1220–1222,1224,1227] ($BIPY^{2+}$), 2,7-diazapyrenium[1226] (DAP^{2+}), and 1,2-bis(4-pyridinium)ethene[1228] ($BIPYE^{2+}$)—in low-polarity organic solvents such as benzene, PhMe, and CH_2Cl_2. The K_a values, determined[1222] by spectrophotometric titrations, as well as the rate constants, determined[1222] by stopped-flow absorption experiments, for the threading (k_{on}) and dethreading (k_{off}) of pseudorotaxanes based on a 1,3,5-trimethoxy-2,4,6-trioctyloxy-functionalized TPUCA6 and $BIPY^{2+}$ derivatives as either their tosylate (TsO^-) or PF_6^- salts at 293 K in CH_2Cl_2 are summarized in **Table 2.36**. The results reveal that the thermodynamics and kinetics of association are sensitive to the nature of the $BIPY^{2+}$ counterion and well as to the sterics of its appended R groups. In spite of the fact that the tosylate salts of $BIPY^{2+}$ experience stonger ion-pairing forces than do the corresponding hexafluorophosphate salts, the tosylate salts exhibit higher affinites for the TPUCA6 ring and faster kinetics, indicating that the $BIPY^{2+}$ counterions can contribute to the stability of the pseudorotaxanes in solution. Since TsO^- is a better acceptor

Table 2.36 Binding constants (K_a) and threading/dethreading rate constants (k_{on}/k_{off}) for pseudorotaxanes[1222] based on the TPUCA6 calix ring in CH_2Cl_2 at 293 K.



Guest	K_a 10^6 M^{-1}	k_{on} 10^3 $M^{-1}s^{-1}$	k_{off} s^{-1}
 [2TsO⁻]	6	1700	0.3
 [2PF₆⁻]	0.8	6	0.008
 [2TsO⁻]	3	58000	19

of hydrogen bonds than is PF_6^-, the higher affinities of the tosylates can be attributed to hydrogen-bonding interactions involving the phenylurea appendages of the host. The faster threading/dethreading rates of the tosylates can also be attributed to these hydrogen-bonding interactions, since the phenylurea groups disengage the TsO^- counterions more effectively from the $BIPY^{2+}$ guests. The appearance of a new absorption band around 460 nm indicates that these pseudorotaxanes are stabilized by charge-transfer interactions, while the solid-state superstructure[1220,1225] of an *octylviologen⊂TPUCA6* pseudorotaxane as its iodide salt reveals (**Figure 2.75**) that [C–H···O], [C–H···π], π–π, and van der Waals (vdW) interactions also contribute to the stability of the complex.

The syntheses[1220,1221,1224] of a series of [2]rotaxanes (**R2120a-c**) derived from the $BIPY^{2+}$ axle precursors **L2120a-c** and the TPUCA6 ring are summarized in **Scheme 2.116**. Hydroxyl-terminated derivatives of the *$BIPY^{2+}$⊂TPUCA6* pseudorotaxanes are capped with diphenylmethane stoppers during a reaction with diphenylacetyl chloride in PhMe. The yields (10–20%) for these stoppering reactions appear to correlate inversely with the length of the $BIPY^{2+}$ hydrocarbon linkers.

Yet another Italian team, led in this case by Neri[1229–1234] and Gaeta[1229–1234] at the University of Salerno, have employed hexamethoxy-*para-tert*-butylcalix[6]arene ($^tBu_6OMe_6CA6$) and heptamethoxy-*para-tert*-butylcalix[7]arene ($^tBu_7OMe_7CA7$) rings as hosts for dialkylammonium cations. The key to their

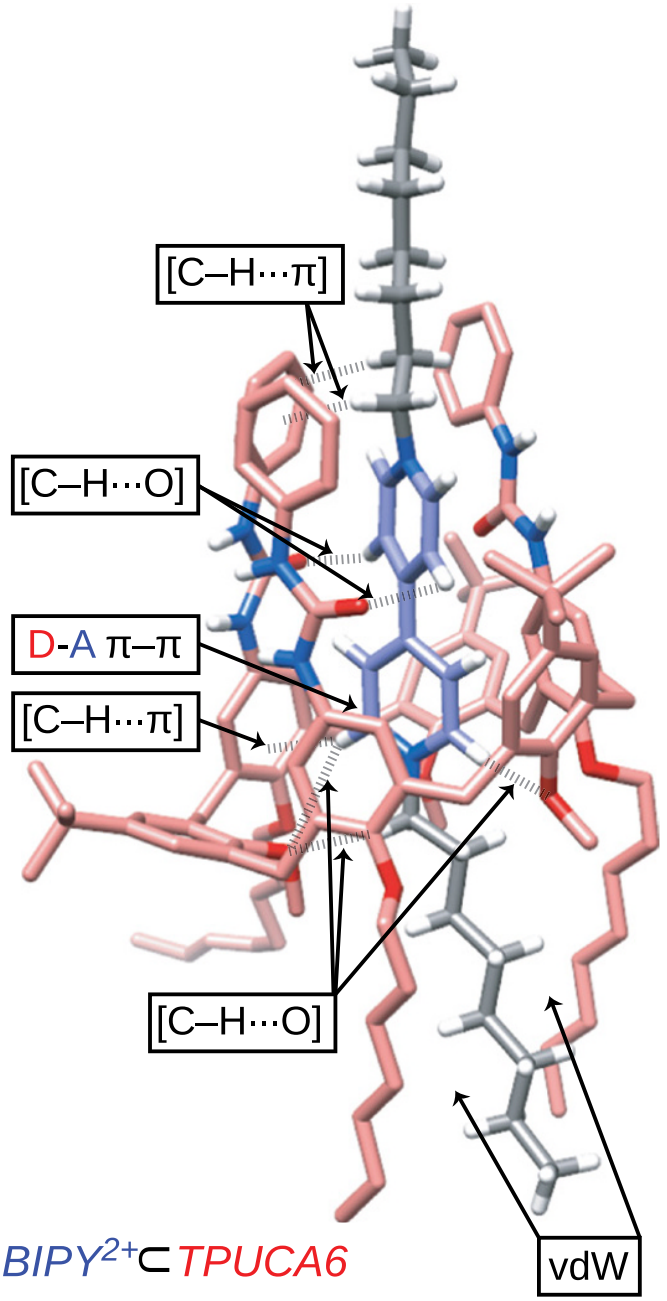
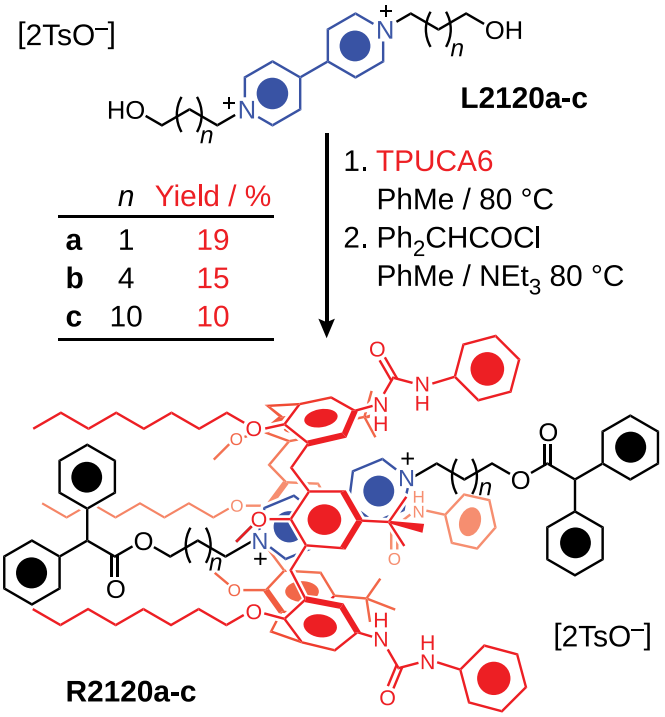


Figure 2.75 The solid-state superstructure of a pseudorotaxane comprising dioctylviologen diiodide and TPUCA6, which is stabilized by a variety of noncovalent bonding interactions.[1220] C–H protons of TPUCA6 and counterions are omitted for the sake of clarity.

2010 discovery[1229] of this recognition motif was to employ a 'superweak' tetrakis(3,5-trifluoromethylphenyl)borate ($TFPB^-$) anion as the counterion for the dialkylammonium guests, since the weak[u] $R_2NH_2^+ \subset calixarene$ interaction is not

[u] The difficulty in threading these large calixarene rings, which present hydrogen bond accepting oxygen atoms within their annulus in a manner similar to the crown ethers, is attributed in large part to their high conformational mobilities, which provide very little preorganization energy for complexation.

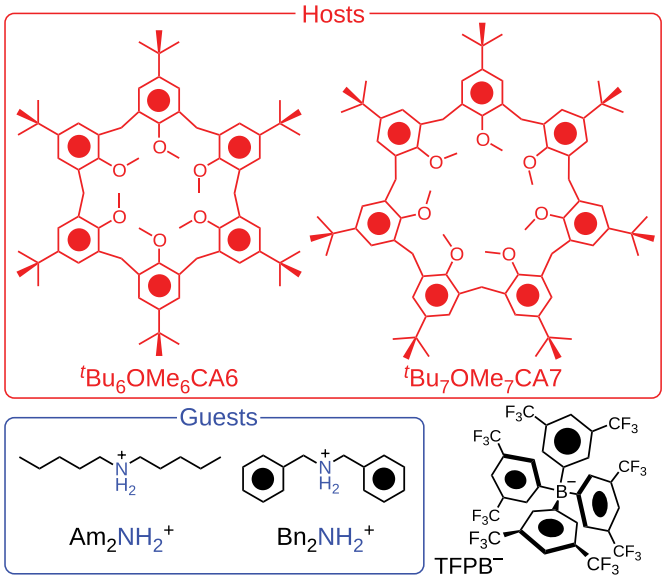


	n	Yield / %
a	1	19
b	4	15
c	10	10

Scheme 2.116 The synthesis of [2]rotaxanes from *BIPY*$^{2+}\subset$*TPUCA6* pseudorotaxane templates.[1220,1221,1224]

sufficient to overcome the ion-pairing energies of the dialkylammonium ions as their PF_6^- or BPh_4^- salts. Single-point construed association constants (**Table 2.37**) for pseudoro-

Table 2.37 Association constants[1229] for the self-assembly of pseudorotaxanes comprising dialkylammonium guests and CA6- or CA7-derived hosts at 293 K in $CDCl_3$.



Pseudorotaxane	K_a / M^{-1}
$Am_2NH_2 \cdot TFPB \subset {}^tBu_6OMe_6CA6$	440
$Am_2NH_2 \cdot TFPB \subset {}^tBu_7OMe_7CA7$	1500
$Bn_2NH_2 \cdot TFPB \subset {}^tBu_6OMe_6CA6$	2500
$Bn_2NH_2 \cdot TFPB \subset {}^tBu_7OMe_7CA7$	4500

taxanes comprising these rings and either diamylammonium ($Am_2NH_2^+$) or dibenzylammonium ($Bn_2NH_2^+$) ionic guests reveal that the CA7 ring binds dialkylammonium ions more tightly than does CA6, while $Bn_2NH_2^+$ binds calixarenes more strongly than do $Am_2NH_2^+$ cations—observations that can most likely be attributed to hydrogen bonding and steric considerations in the former case, and π–π and [C–H···π] interactions in the latter case. Recently, Talotta and Neri[1235] have shown that trialkylammonium cations can also be threaded through the annulus of CA6.

Neri and Gaeta[1230,1232,1233] have employed a simple OMe_6CA6 ring in the syntheses (**Figure 2.76**) of rotaxanes and catenanes which display stereospecific orientational isomerism. Having noticed[1229,1231] in their initial investigations that unsymmetrical *N*-alkyl-*N*-benzylammonium cations preferentially self-assemble with CA6 as *endo*-alkyl complexes over *endo*-benzyl ones—a biased directionality attributable to the asymmetry of the calixarenes' truncated cone-shaped geometries—the Salerno group has exploited[1232,1233] the orientational specificity of the *Bn–NH_2^+–R⊂CA6* motif to prepare [3]rotaxanes and [2]catenanes with stereoprogrammed isomerism by rational design of the axle-like precursors. The catenane **C263$^+$**, the *tail-to-tail* [3]rotaxane **R2122^{2+}**, and the *head-to-head* [3]rotaxane **R2123^{2+}** are prepared by clipping and stoppering, respectively, where hydroxyl termini of the corresponding *endo*-alkyl pseudorotaxane precursors couple with isocyanate derivatives in a carbamate-forming reaction catalyzed by di-*n*-butyltin dilaureate at ~60 °C in $CHCl_3$ for ≥60 h. These protocols lead to **C263$^+$**, **R2122^{2+}**, and **R2123^{2+}** in 23, 52, and 72% yields, respectively. Cone-to-cone inversion of the OMe_6CA6 rings would lead to alternative stereoisomers such as a *head-to-tail* sequence in the case of the [3]rotaxanes, for example. Interestingly, this cone-to-cone inversion is observed[1232] only when the ammonium centers are neutralized to the corresponding freebase amines. The well-defined *tail-to-tail* and *head-to-head* stereosequences of **R2122^{2+}** and **R2123^{2+}** are restored upon reprotonation of the ammonium centers under acidic conditions.

The calixarenes exhibit recognition for cationic π-acceptors and hydrogen bond donors in a manner similar to that of the crown ethers (**Sections 2.3.3.2–2.3.3.5** and **2.3.4.6**), yet they possess a conical geometry similar to that of the cyclodextrins (**Section 2.3.1.1**). This combination of properties makes them excellent candidates for the design of molecular shuttles, switches, and machines expressing biased, or mechanostereoselective (**Section 6.15.2.2**), motions in response to external stimuli, although they currently remain underexplored in this context.

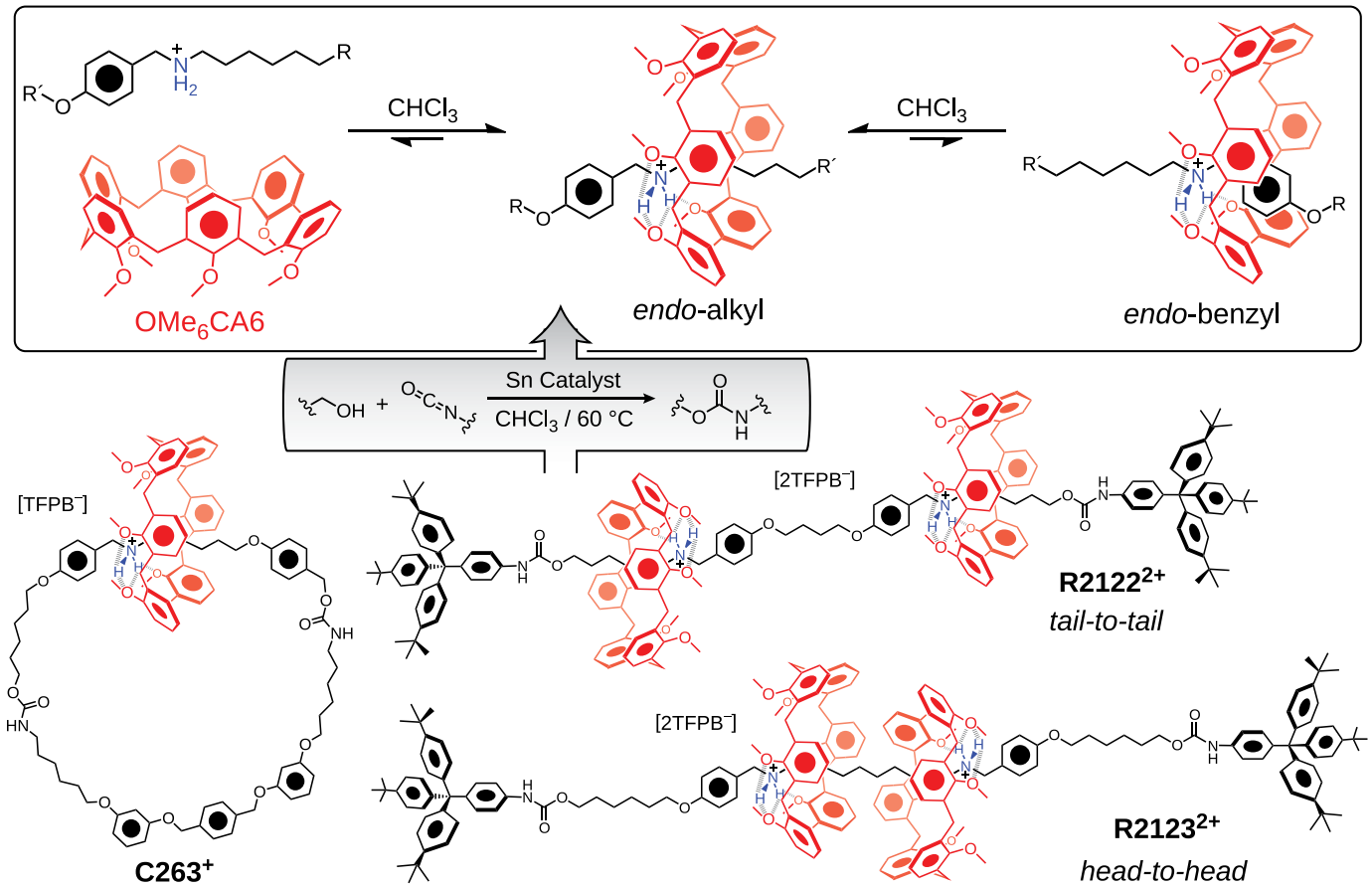
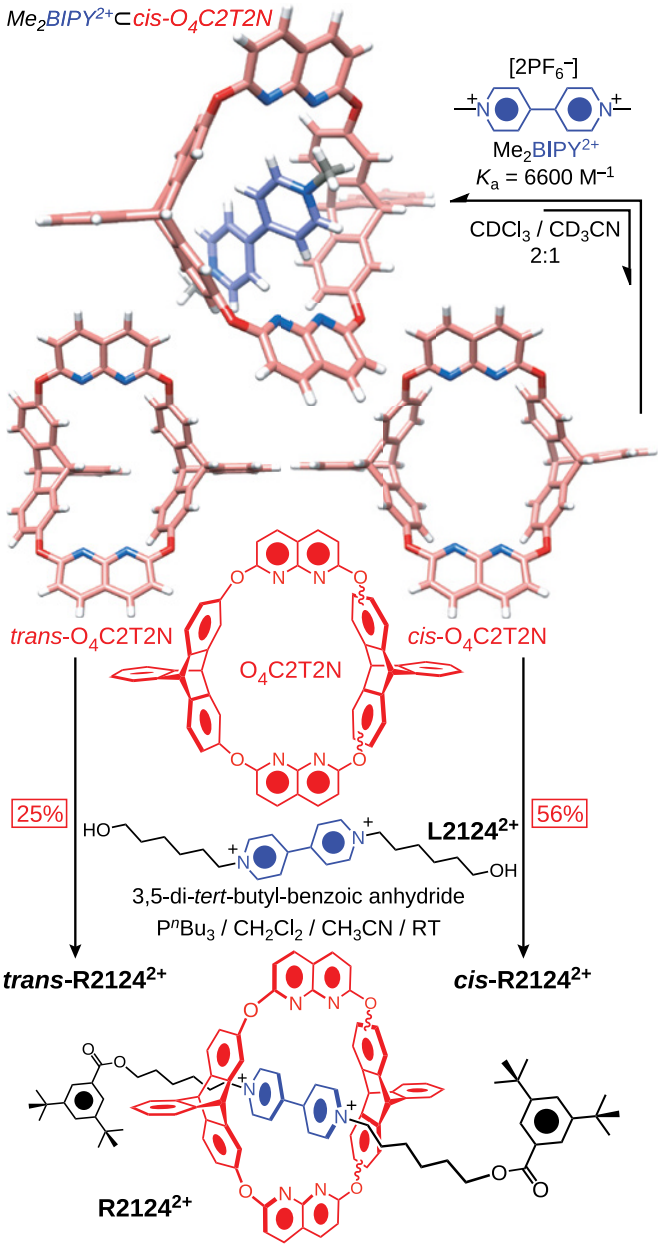


Figure 2.76 Catenanes and rotaxanes are accessed as mechanostereochemically pure orientational isomers from *endo*-alkyl pseudorotaxanes comprising OMe_6CA6 and *N*-benzyl-*N*-alkylammonium derived precursors.[1232,1233]

Hetero-oxacalixarenes

Macrocyclic hosts in which calixarene phenolic units have been replaced by heterocycles are called heterocalixarenes, whereas replacing the methylene linkers with oxygen atoms yields oxacalixarenes. Thus, hetero-oxacalixarenes are macrocyclic hosts containing heterocyclic repeating units and oxygen linkers. Chen[1236] has investigated the host-guest and mechanostereochemistry of tetraoxacalix[2]triptycene[2]naphthyridine[1237] (O_4C2T2N) hosts (**Scheme 2.117**), which may be obtained as either *cis* or *trans* isomers. It transpires that *cis*-O_4C2T2N binds viologen derivatives with K_a values (~10^4 M^{-1}) almost an order of magnitude higher than those (~10^3 M^{-1}) of *trans*-O_4C2T2N. For example, methyl viologen bonds the *cis* and *trans* isomers of O_4C2T2N with K_a values of 6600 and 960 M^{-1}, respectively, at 298 K in 2:1 $CDCl_3$/CD_3CN. A substantial difference the size and depth of the cavities of the *cis*-O_4C2T2N and *trans*-O_4C2T2N, as indicated by their solid-state structures illustrated in **Scheme 2.117**, may account for the large difference in the two isomers' affinities for viologens. Each of these hosts have also been employed[1236] in the synthesis (**Scheme 2.117**) of [2]rotaxanes by esterification-driven stoppering protocols, yielding ***cis*-R2124^{2+}** and ***trans*-R2124^{2+}** in 56 and 25% yields, respectively, reflecting the higher affinity of the viologen-derived axle **L2121^{2+}** for the *cis*-O_4C2T2N host. The asymmetry of *cis*-O_4C2T2N across the plane of its cavity renders it amenable to the construction of orientational isomers—see **Section 5.2.1**.



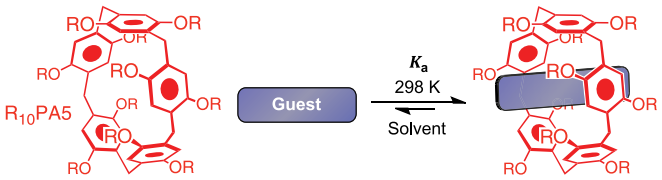
Scheme 2.117 The self-assembly and synthesis of the pseudorotaxane *Me$_2$BIPY^{2+}⊂cis-O$_4$C2T2N* and the [2]rotaxane **R2124^{2+}** based on the heterotetraoxacalixarene, *cis/trans*-O_4C2T2N, and a viologen-derived axle.[1236]

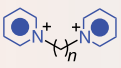
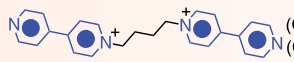
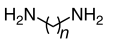
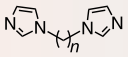
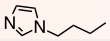
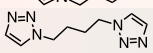
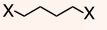
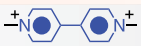
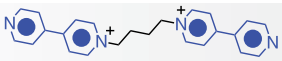
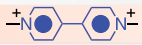
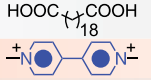
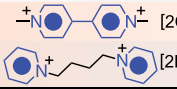
2.3.9.2 Pillararenes

The pillar[*n*]arenes (PA*n*)—see refs. 316, 1195, 1199-1201, 1238-1241—are a family of *para*-methylene bridged cyclooligomers of hydroquinone introduced in 2008 by Ogoshi.[315] These receptors have exploded onto the supramolecular and mechanostereochemistry scenes with a rich set of assemblies and applications in spite of their short history. The considerable interest they have drawn arises from their (i) facile synthesis by Lewis acid-catalyzed cyclocondensations, (ii) availability[1205,1206] in a wide range of sizes (PA5–PA15), (iii) amenability to site-selective derivatization[1240] around their rims in a variety of different configurations and constitutions with (iv) a diverse range of functional groups, which equip them with (v) highly tailorable solubilities in both organic and aqueous solvents and (vi) the promiscuous hosting of guests of all kinds. The π-electron rich aromatic surfaces of the rigid PA*n* cavities make them particularly suitable hosts for π-acceptors. Pillar[*n*]arenes also possess elements of planar chirality, which leads to novel types of isomerism (**Sections 5.2.1** and **5.2.4.1**) in MIMs.

The most well-explored host-guest chemistry among the pillararene family is that of PA5—the most thermodynamically stable and easily accessed pillararene. PA5 macrocycles have served (**Table 2.38**) as hosts for derivatives of pyridinium[315] and bis(pyridinium),[1242] bis(imidazolium) derivatives,[1243] viologens,[1244,1245] and extended viologens.[1246] These complexes are stabilized by donor-acceptor π–π stacking, charge transfer, [C–H···O], and cation–π interactions akin to other donor-acceptor motifs (**Section 2.3.3**) based on crown ethers and/or cyclophanes. The ~4.7 Å diameter cavity of PA5—taking into account the van der Waals radii—is also well matched with the size of oligomethylene chains. Indeed, PA5 derivatives also host (**Table 2.38**) a number of these derivatives, such as alkylammonium salts,[1247] alkanediamines,[1248–1250] dihaloalkanes,[1251] dinitriles,[1252] other bis-functionalized alkanes,[1251,1253–1255] and even unsubstituted alkanes.[1256–1258] In general, guests

Table 2.38 Association constants for the self-assembly of selected pseudo[2]rotaxanes comprising pillar[5]arene derivatives and various guests.



–OR	Guest[a]		Solvent[b]	K_a / M^{-1}	Method[c]	Ref
		n				
		2	$(CD_3)_2SO$	~0	SP	1242
		3	Me_2SO	88	ST	1242
		4	Me_2SO	450	ST	1242
		5	Me_2SO	370	ST	1242
		6	Me_2SO	120	ST	1242
			$(CD_3)_2SO$	740	SP	1242
–OH			$(CD_3)_2SO:CD_3OD$	2300	SP	1242
			$(CD_3)_2SO:CD_3CN$	4900	SP	1242
			$(CD_3)_2SO:(CD_3)_2CO$	5400	SP	1242
		R				
		Me	$(CD_3)_2SO$	140	NMRT	1243
		H	$(CD_3)_2SO$	55	NMRT	1243
		H	$(CD_3)_2CO$	460	NMRT	1243
		H	$(CD_3)_2CO:CDCl_3$	3100	NMRT	1243
		n				
		3	H_2O:MeCN	10000[d]	FT	1248
		4	H_2O:MeCN	16300[d]	FT	1248
		5	H_2O:MeCN	21200[d]	FT	1248
–OMe		6	H_2O:MeCN	11500[d]	FT	1248
		7	H_2O:MeCN	19100[d]	FT	1248
		8	H_2O:MeCN	36000[d]	FT	1248
		8	$CDCl_3$	70	NMRT	1248
		n				
		2	$CDCl_3$	320	SP	1253
		3	$CDCl_3$	20000	SP	1253
		4	$CDCl_3$	790	SP	1253
			$CDCl_3$	240	NMRT	1253
–OEt			$CDCl_3$	160000	SP	1254
		X				
		F	$CDCl_3$	86	NMRT	1251
		Cl	$CDCl_3$	1900	NMRT	1251
		Br	$CDCl_3$	4900	NMRT	1251
		I	$CDCl_3$	10000	NMRT	1251
		CN	$CDCl_3$[e]	15000	SP	1252
		OH	$CDCl_3$	540	NMRT	1251
		N_3	$CDCl_3$	350	NMRT	1251
			MeCN	33500	ITC	1245
–O⌒O–			MeCN	33300	FT	1246
			MeCN	50000	ST	1246
			MeCN	1920	FT	1246
			MeCN	1450	NMRT	1246
–O(CH2CH2O)n–			MeCN	1790	ITC	1245
–O⌒NH_2	HOOC(CH2)18COOH		D_2O	15000	NMRT	1257
–O⌒O⁻ $[NH_4^+]$		[2Cl⁻]	H_2O	82000	FT	1244
		[2Br⁻]	Phosphate Buffer pH 7.2	1.1×10^6	FT	1260

[a]Cationic guests were introduced as their PF_6^- salts except where noted.
[b]Binary solvent mixtures are 1:1 v/v unless noted otherwise.
[c]Method abbreviations: SP: NMR single-point method. ST: spectrophotometric titration. FT: fluorescence titration. NMRT: NMR titration.
[d]P5A host monofunctionalized with a fluorescent pyrene derivative.
[e]10% $(CD_3)_2SO$.

derived from butane give rise to the highest K_a values, most likely because the alkane is the best complementary fit within the rigid annulus of PA5. The K_a values of 1,4-dihalobutanes increase[1251] with the polarizability of the halogen atoms (F^-<Cl^-<Br^-<I^-), indicating that the *alkane⊂PA5* pseudorotaxanes are dominated by dispersion forces, although solid-state evidence reveals[1251,1252,1256] that [C–H···π] interactions are also at play. On the other hand, alkanes bis-functionalized with nitrogen-containing heterocycles are dominated by [C–H···N] interactions.[1254] Complexes based on water-soluble[1255,1257,1259–1261] PA5 derivatives are stabilized even more so by the hydrophobic effect. The solid-state structures of representative pseudorotaxanes showcasing the interaction of PA5 hosts with π-acceptors and alkanes are portrayed in **Figure 2.77**.

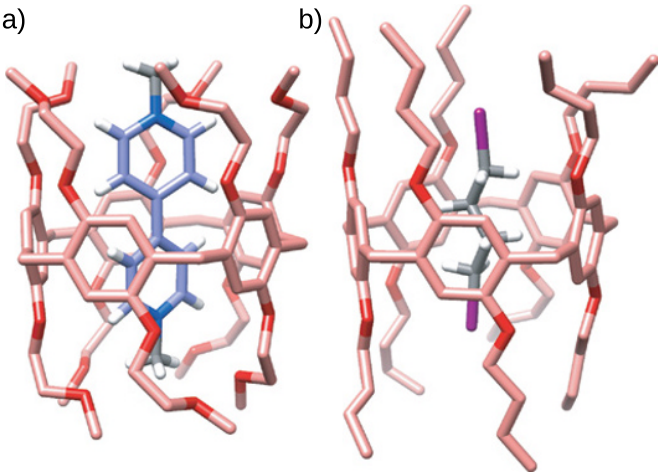
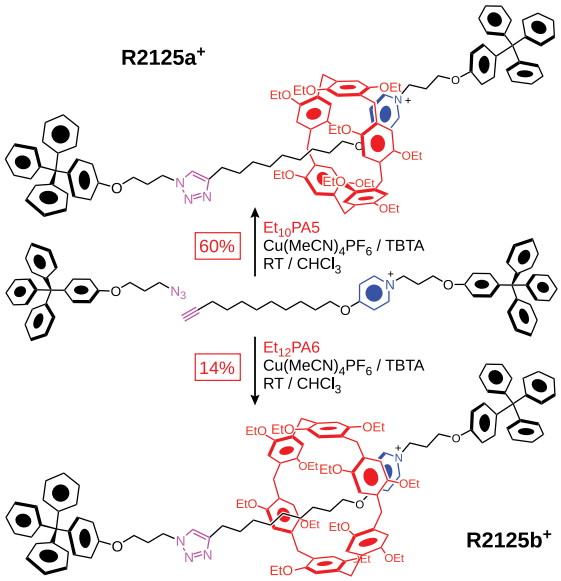


Figure 2.77 Tubular representations of the solid-state superstructures of pseudorotaxanes comprising PA5 hosts and π-acceptor and alkyl derived guests. (a) *Me_2BIPY^{2+}⊂$(MeOCH_2CH_2)_{10}$PA5* is stabilized by [C–H···O], [C–H···π], cation–π, π–π, and D-A charge transfer interactions.[1245] (b) *IC_4H_8I⊂Bu_{10}PA5* is stabilized by [C–H···π], [C–H···O], [C–H···I], and dispersion forces.[1251] Solvent molecules, counterions, and C–H protons of the hosts are omitted for the sake of clarity.

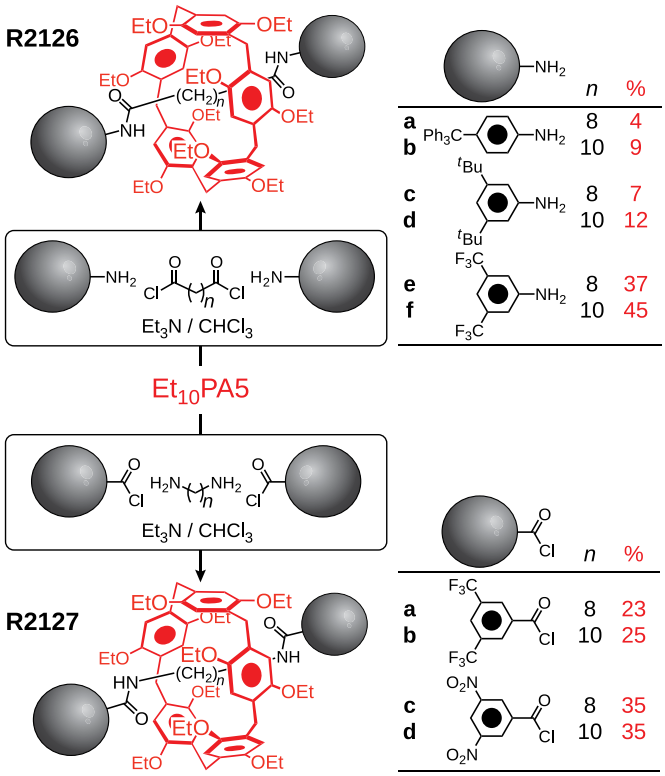
Although fewer guests for PA6 are known, its ~5.8 Å cavity—accounting for van der Waals radii—associates (**Table 2.39**) with cationic π-acceptors (e.g., pyridinium and viologen derivatives[1262]), albeit more weakly than in the case of PA5, as well as diquat,[1263] tropylium,[1264] ferrocenium/cobaltocenium,[1265] and cationic derivatives of adamantane,[1266,1267] DABCO,[1268] and azobenzene.[1269] Cationic PA6 derivatives also bind naphthalenesulfonates.[1270] In general, alkyl derivatives do not associate strongly with PA6, although diisobutylpillar[6]arene has been found[1271] to encapsulate *n*-octyltriethylammonium hexafluorophosphate, while the homologous PA5 ring does not form a complex with the same guest.

Ogoshi,[1272–1275] inventor of the pillararenes, has often relied on CuAAC click chemistry in order to synthesize pillararene-based rotaxanes. The [2]rotaxanes **R2125a**$^+$ and

R2125b$^+$, which comprise dumbbells derived from a 4-alkoxy-*N*-alkylpyridinium recognition unit encircled by perethylated PA5 (Et_{10}PA5) and perethylated PA6 (Et_{12}PA6), respectively, have been synthesized (**Scheme 2.118**) in 60 and 14% yields, respectively, by CuAAC protocols. The better yield in the case of PA5 most likely reflects its higher affinity for functionalized alkanes.

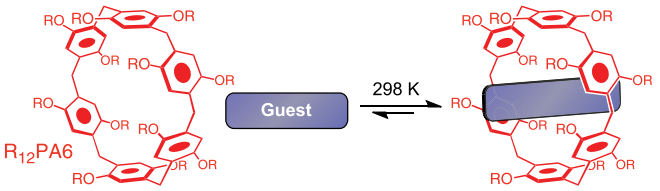


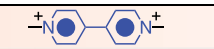
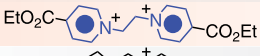
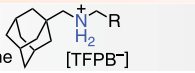
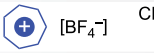
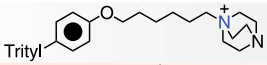
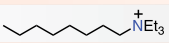
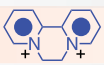
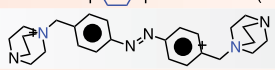
Scheme 2.118 Ogoshi's click synthesis of PA5- and PA6-derived [2]rotaxanes.[1273]



Scheme 2.119 The synthesis of PA5-based [2]rotaxanes by stoppering protocols[1276] involving reactions of amines with acid chlorides in the presence of a twofold excess of Et_{10}PA5 in $CHCl_3$.

Table 2.39 Association constants (K_a) for the self-assembly of selected pseudo[2]rotaxanes comprising pillar[6]arene derivatives and various guests.



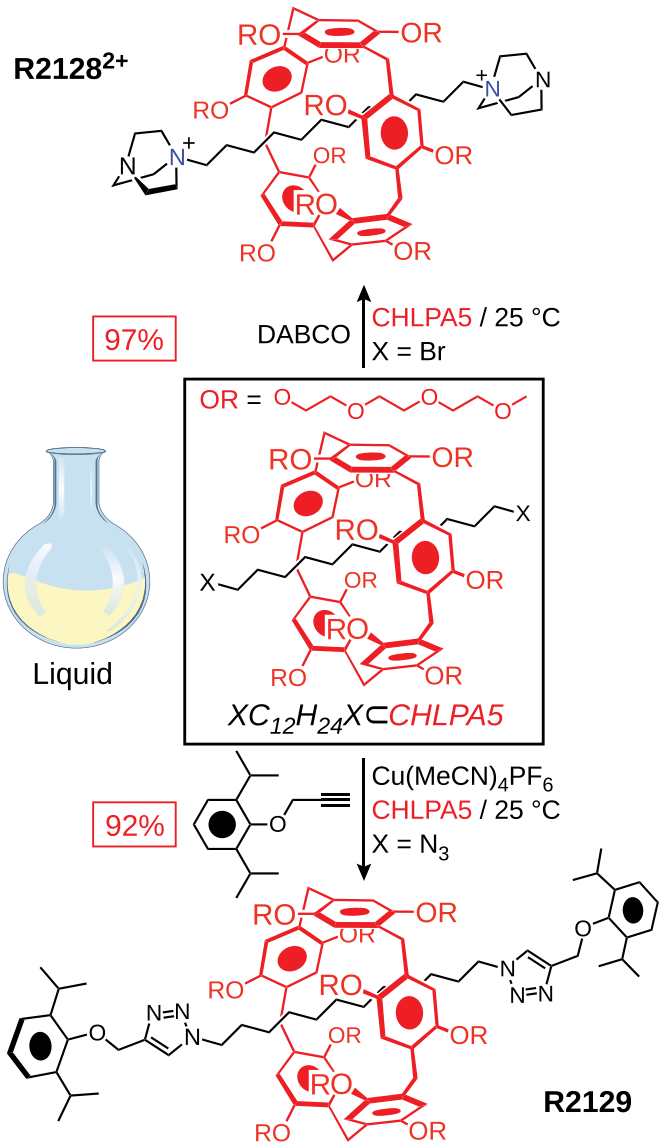
–OR	Guest[a]	Solvent[b]	K_a / M^{-1}	Method[c]	Ref
		$(CD_3)_2CO$	220	NMRT	1262
–OH		$(CD_3)_2CO$	<20	NMRT	1262
		$(CD_3)_2CO$	<20	NMRT	1262
	 R = anthracene [TFPB$^-$]	$CDCl_3$	3400	NMRT	1266
–OEt	 [BF_4^-]	$CDCl_3$:$(CD_3)_2CO$	1800	NMRT	1264
		$(CD_3)_2CO$	220	NMRT	1264
	 Trityl	$CDCl_3$	550	NMRT	1268
	 M = Fe^{III}	5:1 $CHCl_3$:CH_3CN	20000[d]	FT	1265
–O	M = Co^{III}	5:1 $CHCl_3$:CH_3CN	31000[d]	FT	1265
	M = Co^{III}	5:1 $CDCl_3$:$(CD_3)_2SO$	37000	SP	1265
–O		$CDCl_3$	334	NMRT	1271
–O		CD_3CN	2.5×10^5	SP	1263
		$(CD_3)_2CO$	3.9×10^5	SP	1263
–O(CH2)n		D_2O	1010	SP	1269
–O		Phosphate Buffer pH 7.2	2.1×10^5	FT	1270
		Phosphate Buffer pH 7.2	3.8×10^4	FT	1270

[a] Cationic guests were introduced as their PF_6^- salts except where noted.
[b] Binary solvent mixtures are 1:1 $^v/_v$ unless noted otherwise.
[c] Method abbreviations: SP: NMR single-point method. ST: spectrophotometric titration. FT: fluorescence titration. NMRT: NMR titration.
[d] PA6 monofunctionalized with a fluorescent carbazole derivative.

Deschenaux and Nierengarten[1276] have prepared (**Scheme 2.119**) a series of [2]rotaxanes which rely upon *alkane⊂PA5* pseudorotaxanes as a templating motif for stoppering protocols involving reactions of acid chlorides with amines. The [2]rotaxanes **R2126a-f** and **R2127a-d** have been synthesized in yields of up to 45 and 35%, respectively, from diacid dichloride and alkanediamine axles encircled by Et_{10}PA5 hosts present in a twofold molar excess. These reactions are most efficient in $CHCl_3$ because it does not compete with reactants in binding the PA5 cavity—although the rotaxanation fails in CH_2Cl_2 and $ClCH_2CH_2Cl$, the yields for rotaxane **R2126f** are 1% in pentane, 6% in THF, and 10% in PhMe. The yield in $CHCl_3$ can be boosted up to 63% by introducing the Et_{10}PA5 ring in threefold molar excess. In general, it can be appreciated by noting the yields of **R2126a-f** and **R2127a-d** that the efficiency of the protocol improves with increasingly electron-deficient stoppers and longer oligomethylene axle precursors on account of electronic and steric factors, respectively. Rotaxanes constructed from *alkanediamine⊂PA5*

pseudorotaxanes have also been accessed[1248] by reductive amination in modest (7%) yields.

Pillar[5]arenes perfunctionalized with oligo(ethylene glycol) (OEG) chains, which have been reported by Ogoshi[1277] to be nonvolatile liquids over wide temperature ranges, have been utilized[1278] in a very high-yielding synthesis (**Scheme 2.120**) of [2]rotaxanes under solvent-free conditions. A so-called cyclic host liquid (CHL) PA5 core, modified with triethylene glycol monomethyl ether (CHLPA5), has been used to dissolve 1,12-dibromododecane, which was reacted subsequently with DABCO (3 equiv) as a stopper precursor. Conversion to the [2]rotaxane **R2128**$^{2+}$ by nucleophilic substitution is 61% efficient in the presence of 1 molar equiv of CHLPA5 and 97% efficient with 5 equiv of CHLPA5. Isolation of the [2]rotaxane is remarkably facile, since the naked dumbbell can be separated from the liquid rotaxane by precipitation in Me_2CO



Scheme 2.120 The high-yield syntheses of [2]rotaxanes employing Ogoshi's cyclic host liquid pillar[5]arene CHLPA5 in the dual role of ring and solvent.[1278]

and the excess of CHLPA5 can be extracted selectively into Et_2O and recycled. The approach is also compatible with CuAAC click chemistry, affording the neutral [2]rotaxane **R2129** from 1,12-diazidododecane and 2-propargyloxy-1,3-diisopropylbenzene as the axle and stopper precursors, respectively, in 92% yield. Cyclic host liquids of the cyclodextrins can also be prepared[1277] by alkylation of the parent hosts with OEG chains.

The pillararenes are rising stars in supramolecular chemistry on account of their rich host-guest behavior and highly tunable physical properties, all of which have been discovered and developed in less than a decade, and their stake of the literature is increasing rapidly. This upward trajectory will make PA*n* assemblies increasingly important in the mechanostereochemical future. Looking forward, the imperative is to (i) continue improving the synthetic accessibility of functionalized and multifunctionalized pillararenes as well as the larger pillar[*n*]arenes ($n \geq 7$), (ii) identify and diversify high-affinity guests for PA*n* hosts, and (iii) to develop pillararene assemblies, materials, devices, etc. with practical applications.

2.3.10 Radical-Pair Templates

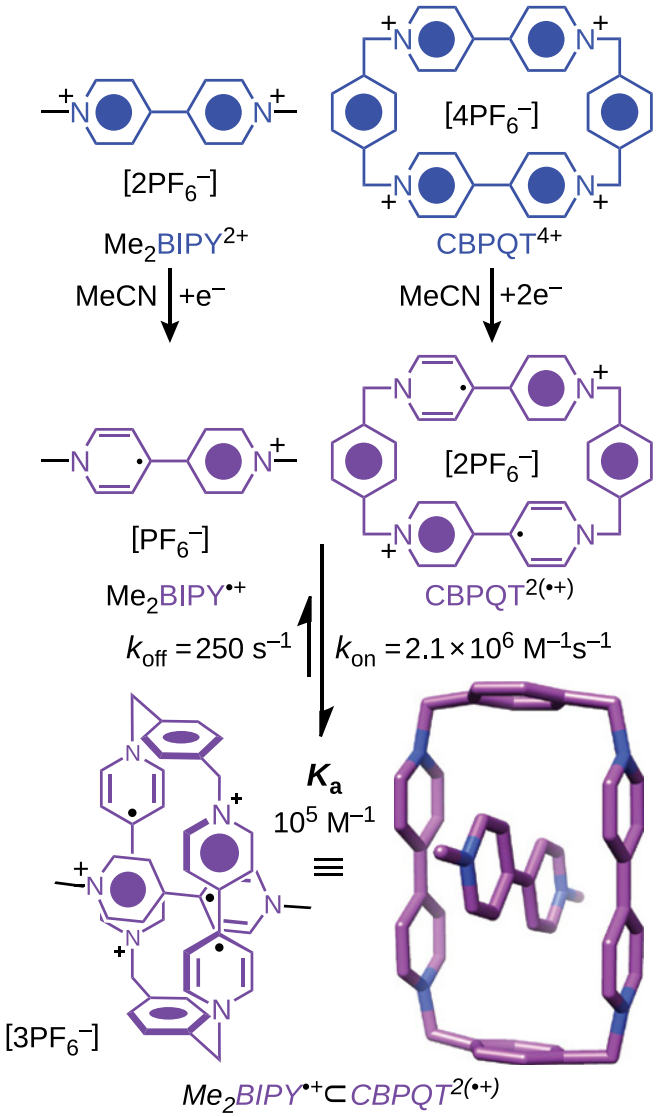
Free radicals are atoms or molecules possessing an open electron shell, i.e., unpaired valence electrons. Organic free radicals are typically relatively unstable compounds with a high reactivity towards other compounds and themselves—they tend to dimerize, polymerize, or oxidize rapidly in order to resolve their so-called 'dangling' covalent bonds constituting the unpaired valence electrons. A few decades after Gomberg's discovery[1279] of the triphenylmethyl radical in 1900, Michaelis[1280,1281] investigated the redox chemistry of *N*,*N*′-dialkyl-4,4′-bipyridinium (R_2BIPY^{2+}) compounds—also known as the viologens—and their singly-reduced radical cations ($R_2BIPY^{\bullet+}$) that produce deep blue and violet colors to which the viologen namesake is attributed. Schwarz[1282] and Kosower[1283] found in the 1960s that the violet colors find their origin in the near-IR absorption of $(BIPY^{\bullet+})_2$ dimers, which are sometimes reffered to as pimers[1284] on account of their spin-paired π-electrons. The $BIPY^{\bullet+}$ monomers, which become more dominant as the concentration is lowered, give rise to blue-colored solutions. Viologen radicals are among the most well understood organic free radicals on account of their widespread availability, synthetic accessibility, facile derivatization, and highly reversible redox properties. Tetrathiafulvalene (TTF) is another well-known compound with a capacity to "pimerize" into $(TTF^{\bullet+})_2$ dimers upon one-electron oxidation. Both $BIPY^{2+}$ and TTF have been widely employed in mechanostereochemistry as recognition units in donor-acceptor (**Section 2.3.3**) motifs on account of their π-accepting and π-donating characteristics, respectively.

Although organic free radicals have been known for over a century, it is only very recently that they have become components of host-guest assemblies and templates. $(BIPY^{\bullet+})_2$ and $(TTF^{\bullet+})_2$ radical dimers have been encapsulated within 'molecular flasks' such as (i) Kimoon Kim's

cucurbit[8]uril host,[278] (ii) Makoto Fujita's self-assembled metallacycles,[1285] and (iii) the cyclobis(paraquat-4,4′-biphenylene) (CBPQB^{4+}, see **Section 6.13.11**) molecular square.[1286,1287] In 2010, our group discovered[1288] that the BIPY$^{\bullet+}$ radical cation can be stabilized within the cavity of the doubly reduced 'blue box' diradical dication CBPQT$^{2(\bullet+)}$ in both pseudorotaxanes and rotaxanes, courtesy of the host's two BIPY$^{\bullet+}$ units which are positioned 7 Å apart—an ideal distance for intercalated planar aromatic guests to engage in π–π interactions with both recognition units. This trisradical tricationic inclusion complex has spawned a new generation of molecular recognition motifs for the template synthesis of MIMs (*vide infra*) and the actuation of molecular switches (**Section 6.1.1.2**) and machines (**Section 6.15**) under electrochemical control.

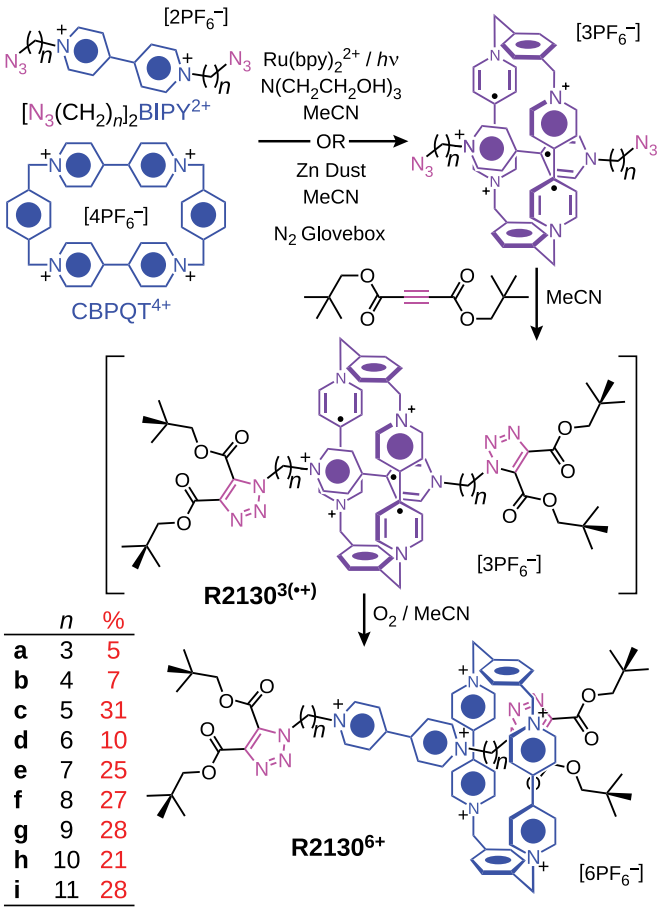
The self-assembly (**Scheme 2.121**) of a pseudorotaxane derived from methyl viologen (Me_2BIPY^{2+}) and CBPQT^{4+} occurs in MeCN upon reduction of both compounds to the $Me_2BIPY^{\bullet+}$ and CBPQT$^{2(\bullet+)}$ radicals, respectively, either by electrochemical[1288] means or with chemical reductants such as zinc dust.[1289] The association constant[v] for this inclusion complex 298 K is at least on the order of 10^5 M^{-1}, since it was estimated[1289] to be 5.05×10^4 M^{-1} by ITC and 7.9×10^4 M^{-1} by spectrophotometric titrations after reduction with Zn dust. The kinetics of association ($k_{on} = 2.1 \times 10^6$ $M^{-1}s^{-1}$) and dissociation—as measured[1289] by stopped-flow spectrophotometry—are rapid, indicating low steric and electrostatic barriers to self-assembly. The solid-state structure (**Scheme 2.121**) of *$Me_2BIPY^{\bullet+}$⊂CBPQT$^{2(\bullet+)}$* reveals that the BIPY$^{\bullet+}$ guest is oriented centrosymmetrically within the CBPQT$^{2(\bullet+)}$ cavity, with its long axis tilted 76° with respect to that of the cyclophane. This deviation from orthogonality is explained by the observation that it increases π-orbital overlap, thus increasing the stability of the complex. Another characteristic feature of the viologen radicals in the solid state is their nearly 0° torsional angles of the BIPY$^{\cdot+}$ units about their 4,4′ C–C bond. Crystalline needles of this pseudorotaxane are *p*-type semiconductors with hole mobilities[1290] of 0.05 $cm^2V^{-1}s^{-1}$.

What might happen if the *BIPY$^{\bullet+}$⊂CBPQT$^{2(\bullet+)}$* interaction is oxidized back to BIPY^{2+} and CBPQT^{4+} while being constrained by the mechanical bond? This question has led to the genesis[1291] of a series[1292–1294] of MIMs harboring BIPY^{2+} units in mechanically confined spaces. Fast on the heels of the discovery[1288] of the trisradical inclusion complex, a stoppering protocol (**Scheme 2.122**) was developed,[1291,1292] which captures the *BIPY$^{\bullet+}$⊂CBPQT$^{2(\bullet+)}$* template in a mechanical bond with a copper-free azide-alkyne cycloaddition. Subsequently, the mechanically constrained intermediate is oxidized in air to afford the hexacationic rotaxanes **R2130^{6+}a-i**, whose intercomponent interactions are dominated by repulsive electrostatic forces. The trisradical template can be assembled in degassed MeCN from CBPQT^{4+} and azide-terminated BIPY^{2+} derivatives by either (i) photoinduced charge transfer from the excited state of a $Ru(bpy)_3^{2+}$ catalyst under visible irradiation in the presence of an excess of triethanolamine as a sacrificial electron donor,[1291] or (ii) reduction with Zn dust.[1292] The azide-terminated pseudorotaxane trisradical trications react[1292] with di(*tert*-amyl)acetylenedicarboxate stopper precursors in MeCN to afford, after oxidation in ambient atmosphere, the hexacationic [2]rotaxanes **R2130^{6+}a-i** in yields of up to 31%. Coulombic repulsion between the



Scheme 2.121 Self-assembly[1289] of the trisradical trication pseudorotaxane *$Me_2BIPY^{\bullet+}$⊂CBPQT$^{2(\bullet+)}$* in MeCN. A tubular representation of the solid-state superstructure of the pseudorotaxane is illustrated with solvent molecules, counterions, and protons omitted for the sake of clarity.

[v] These K_a values are most likely underestimates because the excess Zn dust can cause a two-electron reduction for some of the BIPY^{2+} population, affording electron-rich neutral species, which would not be expected to participate in complexation. A K_a value of 10^{12} M^{-1} (–17 kcal·mol^{-1}) has been estimated by variable scan-rate cyclic voltammetry data, which agrees well with initial theoretical predictions based on DFT calculations of approximately –20 kcal·mol. See ref. 1288.

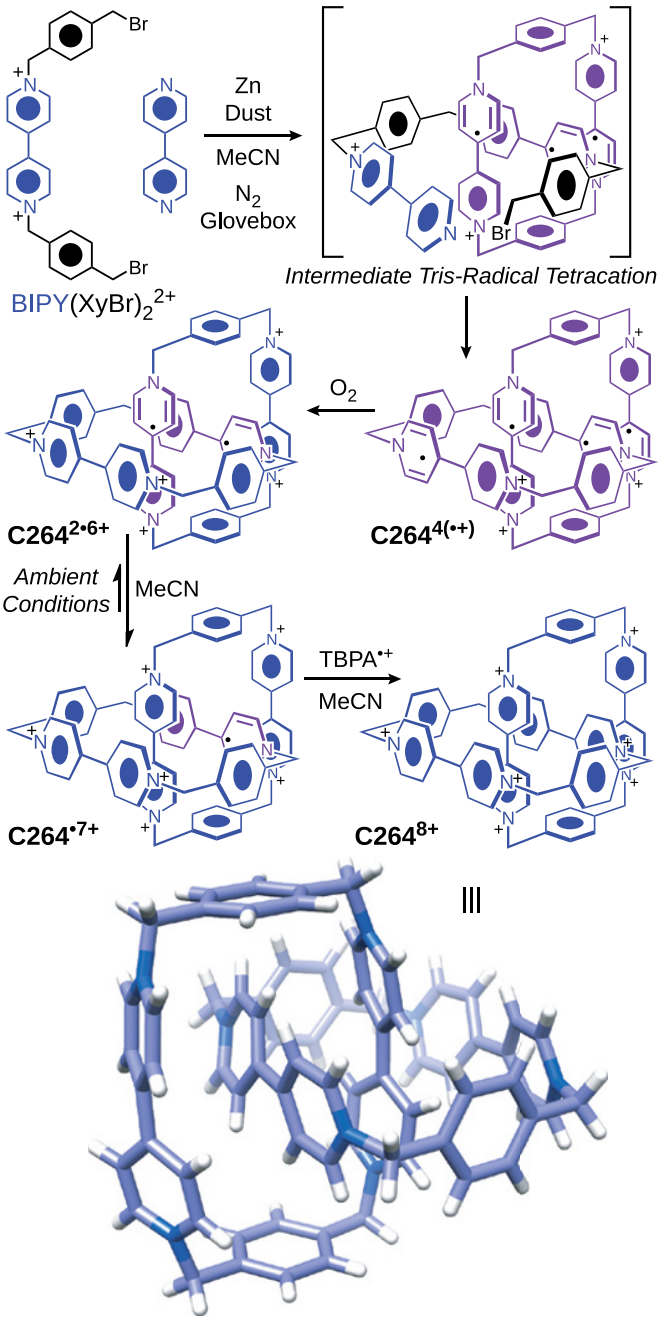


	n	%
a	3	5
b	4	7
c	5	31
d	6	10
e	7	25
f	8	27
g	9	28
h	10	21
i	11	28

Scheme 2.122 Radical template synthesis of the hexacationic [2]rotaxanes **R2130^{6+}a-i** whose intercomponent interactions are dominated by repulsive electrostatic forces.[1291,1292]

BIPY^{2+} units of the rings and axles forces the rings to encircle the oligomethylene chains adjacent to the BIPY^{2+} cores of the dumbbells. The rotaxanes with shorter dumbbells were found to persist longer in their radical states while being exposed to ambient oxygen and also to express lower activation barriers to the shuttling of the rings back and forth over the central BIPY^{2+} units. The mechanical bond thus imposes steric constraints, which raise the kinetic barriers to oxidation of the radical cations, while enhancing their thermodynamic stability via spin-pairing interactions. See **Section 6.13.11** for a discussion of the mechanical bond's ability to enhance the stability of free radicals.

An even more mechanically constrained and electrostatically frustrating environment for the BIPY^{2+} cation is provided by the topological bond of the (CBPQT^{4+})$_2$ homo[2]catenane **C264^{8+}**, which is so energetically demanding that it can only be accessed[1293,1294] by oxidation of the radical septacation **C264$^{•7+}$** with a strong oxidant. The synthesis (**Scheme 2.123**) of the homocatenane is remarkably simple—it involves mixing the bis(α-bromoxylyl)bipyridinium precursor BIPY(XyBr)$_2^{2+}$ with 4,4′-bipyridine and Zn dust in MeCN under an inert atmosphere. The nucleophilic substitution of the two reactants generates CBPQT^{4+} and other xylylene-bridged BIPY^{2+} oligomers, which become reduced *in situ* by the Zn dust as the reaction proceeds. The key intermediate in this process is a tetracationic tris-radical inclusion complex, which is transformed into the homo[2]catenane **C264$^{4(•+)}$** after a final ring-closing nucleophilic substitution and reduction. Exposure to ambient air



Scheme 2.123 Radical template synthesis[1293] of the CBPQT^{4+} homo[2]catenane **C264^{8+}**. Under ambient conditions, the catenane exists in equilibrium as a mixture of the diradical hexacation **C264$^{2•6+}$** and radical septacation **C264$^{•7+}$**. An excess of a strong oxidant, tris(4-bromophenyl)aminium hexachloroantimonate (TBPA$^{•+}$), is required to access the octacationic state. A tubular representation of the X-ray crystal structure[1294] of **C264^{8+}** is portrayed with solvent and SbF_6^- counterions omitted for the sake of clarity.

generates **C264**$^{\bullet 7+}$, which exists in equilibrium with the diradical hexacation **C264**$^{2\bullet 6+}$, a minor species containing a spin-paired $(BIPY^{\bullet +})_2$ radical dimer at its center. In other words, the constraints of a mechanical bond force the homo[2]catenane into such an energetically unfavorable situation under ambient conditions that it becomes a completely novel type of air- and water-stable organic radical! The homo[2]catenane also exhibits remarkable[1295,1296] electrochemical properties, passing through a total of six accessible redox states (**C264**$^{8+}$ → **C264**$^{\bullet 7+}$ → **C264**$^{2\bullet 6+}$ → **C264**$^{4(\bullet +)}$ → **C264**$^{6\bullet 2+}$ → **C264**) during a voltammetric scan, thus storing up to eight electons within its tiny volume of little more than a cubic nanometer.

Although radical pairs are among the newest noncovalent complexes and templates in supramolecular and mechanostereochemistry, respectively, they have already proven to be quite versatile. Their interactions can be leveraged, not only to control mechanical motions in electrochemically bistable and multistable MIMs with very high switching fidelity in solution (see **Section 6.1**), but also to access compounds with highly unlikely compositions and high-lying energy states that may be relevant to a number of applications, not least of which are energy storage technologies.[1296]

2.3.11 Homophilic Templates

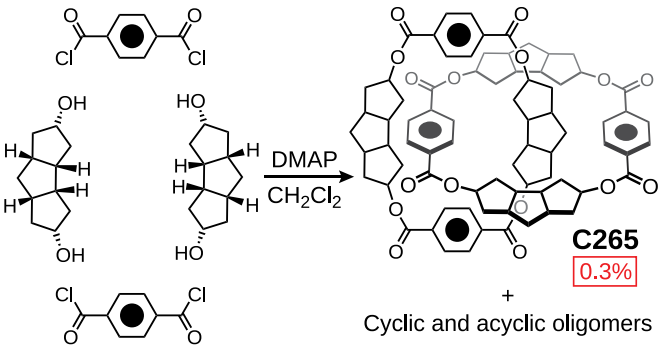
The radical pairs described in the previous Section represent a type of homophilic template, since self-assembly is driven by 'self-loving' radical cations. Many of the catenanes based on amides (**Sections 2.3.4.1–2.3.4.2**) are based on homophilic hydrogen-bonding interactions. Some of Fujita's self-assembled metallo-organic catenanes (**Section 3.3.1**) are driven by homophilic hydrophobic forces. Other types of self-aggregation include aromatic π–π stacking interactions (**Section 2.3.11.1**), lipophilic interactions (**Section 2.3.11.2**) driven by van der Waals interactions, and aurophilic interactions (**Section 2.3.11.3**). In some cases, it has been possible to observe homocatenation as a result of crystal packing effects—see **Section 2.3.11.4**. One can envision other types of self-aggregation, such as fluorous interactions,[1297] which remain to be introduced as motifs in mechanostereochemistry.

2.3.11.1 Aromatic Self-Aggregation

One class of molecules with homophilic recognition properties are the polycyclic aromatic hydrocarbons (PHCs) and their heterocyclic derivatives. Large PHCs have low solubilities owing to their tendency to self-aggregate—a process driven by weak homophilic π–π interactions[477–479,1298] and solvophobic interactions. Li[1299] has reported a homo[2]catenane synthesis driven by the self-assembly of thiol-terminated homophilic $(NDI)_4$ quadruple-stacks under oxidative coupling conditions—see **Section 3.5.1.2**. Like these NDI π-acceptors, the large π-surfaces of the diazaperopyrenium (DPP^{2+}) dication have been shown[571,1300] to possess both homophilic and heterophilic recognition properties, the former being attributable to aromatic self-aggregation.

2.3.11.2 Lipophilic Self-Aggregation

Another example of mechanical bond formation templated presumably by (weak) homophilic interactions is the triquinane lactone derived homo[2]catenane **C265** introduced in 1998 by Mehta.[1301] Although the synthesis (**Scheme 2.124**) of **C265** from *endo*,*endo*-triquinanediol and terephthaloyl dichloride in the presence of DMAP in CH_2Cl_2 is low yielding (0.3%), the yield is still higher than what would be expected (see **Section 2.1**) for a purely statistical synthesis, especially since the reaction is carried out under relatively dilute conditions of 15 mM with respect to the reactants. Since the triquinane moieties were determined to be too bulky to allow through-the-annulus pirouetting (see **Section 5.1.2.2**) to occur, it follows that the terephthalic ester groups serve as the recognition units within the cavity of the rings. We suspect that [C–H···π] interactions and nonspecific lipophilic interactions are the major noncovalent forces involved in the templation of this catenane.



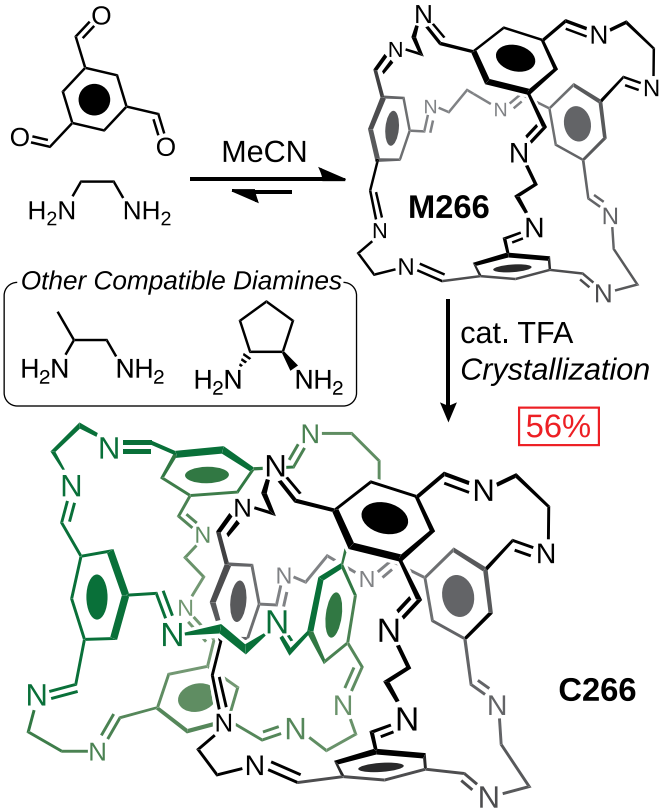
Scheme 2.124 Mehta's synthesis of a homo[2]catenane derived from *endo,endo*-triquinane diol and terephthaloyl dichloride.[1301]

2.3.11.3 Aurophilic Interactions

Aurophilic interactions are another type of weak noncovalent bonding interactions that have been leveraged in the self-assembly of molecules with mechanical bonds, especially "gold catenanes".[1302,1303] The catenated organometallic gold clusters described by Mingos,[1304] Puddephatt,[1305] and Che[1306] are exemplary—see **Section 3.2.2.1**.

2.3.11.4 Crystallization-Induced Interlocking

Although the concept of supramolecular templation has had an immensely transformative presence in the chemistry of mechanical bonds, Andrew Cooper[1307] has shown that MIMs can be self-assembled (**Scheme 2.125**) in reasonable yields (≤60%) 'without^{W} templates'[1308] by crystallization-induced catenation of covalent organic cages, a process enabled by a combination of reversible covalent bonds and *horror vacui*—the phenomenon first proposed by Aristotle, often simply stated as "Nature abhors a vacuum". Cooper's earlier work[1309] had shown that a [4+6] cyloimination reaction involving 1,3,5-triformylbenzene and 1,2-vicinal diamines generates tetrahedral covalent organic



Scheme 2.125 The crystallization-induced self-assembly of the triply interlocked tetrahedral covalent organic cages **C266** from an acid-catalyzed dynamic combinatorial library derived from 1,3,5-triformylbenzene and ethylenediamine.[1307]

cages (e.g., **M266**) which crystallize as stable microporous solids with high surface areas. The triply interlocked [2]catenane **C266** arises (**Scheme 2.125**) from the same dynamic mixture and comprises the same tetrahedral cages—the key difference leading to interpenetration in this case is the presence of TFA as an acid catalyst to accelerate the imine exchange process. Only monomeric, uncatenated cages of **M266** crystallize in the absence of TFA. The triply interlocked catenane derived from ethylenediamine crystallizes from MeCN as a mixture with **M266**, whereas the homologous catenanes derived from propane-1,2-diamine or (*R*,*R*)-1,2-diaminocyclopentane crystallize exclusively from MeCN and CH_2Cl_2, respectively, with slow diffusion of MeOH. The pure catenane **C266** can be crystallized from *p*-xylene with or without the TFA catalyst, although the latter process requires 50 days to complete. The assembly of the catenane is thus a solid-state phenomenon, which is less attributable to templation[w] than it is to crystal packing effects—namely, Nature's tendency to maximize van der Waals interactions while filling void space during crystallization. The solid-state structure of **C266** is shown in **Section 4.1.3.4**.

Crystallization-induced catenation is also responsible for a number of [*n*]catenane chain polymers (**Section 4.1.2.1**) comprising metallacycles[1310–1312] and metallacages[1313–1319] (**Section 4.1.3**) that exist only in the solid state, as well as an unusual infinite molecular chainmail network exhibiting elements of the Borromean link (**Section 4.1.1.3**) topology,[1320] not to mention countless coordination polymers and metal-organic frameworks that form interpenetrated nets (**Sections 4.1.3.5** and **4.2.3.8**) in the solid state.[1321–1330] These examples suggest that crystallization-induced catenation may be generalized to achieve many types of mechanical bonds in the solid state, although it is not yet clear if the approach can be harnessed to make mechanical bonds that remain stable in the liquid and gas phases.

2.3.12 Biomolecular Templates

In **Section 1.1.1** we described a number of examples of mechanical bonds employed by Nature to carry out the complex chemistry of life processes. Here, we summarize synthetic approaches to making artificial mechanical bonds in biomolecules.

2.3.12.1 Nucleic Acids with Mechanical Bonds

Although natural DNA catenanes and knots have been known[1331] since the 1960s, it was not until the early 1990s that synthetic DNA catenanes began to emerge. Indeed, the mechanical bond has had an influential role in structural DNA nanotechnology.[1332–1337] Seeman[1332,1338] at New York University was an early pioneer in the area of DNA nanotechnology, recognizing that "*DNA has the most predictable and readily programmed intermolecular interactions of any molecular species on its scale*"—a statement made[1332] in 1998 that remains true to the present day. In contrast with other macromolecules, DNA strands self-assemble (**Figure 2.78**) according to a simple set of Watson-Crick[474] base-pairing rules. The molecular recognition elements of DNA are called *nucleobases*—adenine (A), thymine (T) guanine (G) and cytosine (C). Nucleobases preferentially assemble into *base pairs* (bp) or *duplexes*—A with T, G with C—by sharing two or three hydrogen bonds, respectively. The repeating unit of DNA is the *nucleotide*, comprising one nucleobase connected to a deoxyribose unit, which is connected to a phosphate group. The backbone of DNA is constituted by phophodiester bonds at the 3 and 5 positions of deoxyribose. Complementary sequences of nucleotides typically combine to form a right-handed double helix superstructure (B-DNA, **Figure 2.78a**) in water which is both stable and stiff, with a pitch of ~10.5 base pairs (~3.4 nm) per 360° helical turn, a width of ~1 nm, and a persistence length of ~50 nm. Less common naturally occurring DNA superstructures (**Figure 2.78b**) include left-handed[1339] double helices (Z-DNA) possessing a zig-zag phosphate backbone, triple-stranded DNA triple

[w] The crystal structure of the triply interlocked cages reveal the presence of π–π stacking interactions, which might be interpreted as a templating interaction. The catenane is probably a minority species in solution, however, since these interactions are most likely too weak to overcome the entropic cost of catenation and the enthalpic cost of desolvation in solution.

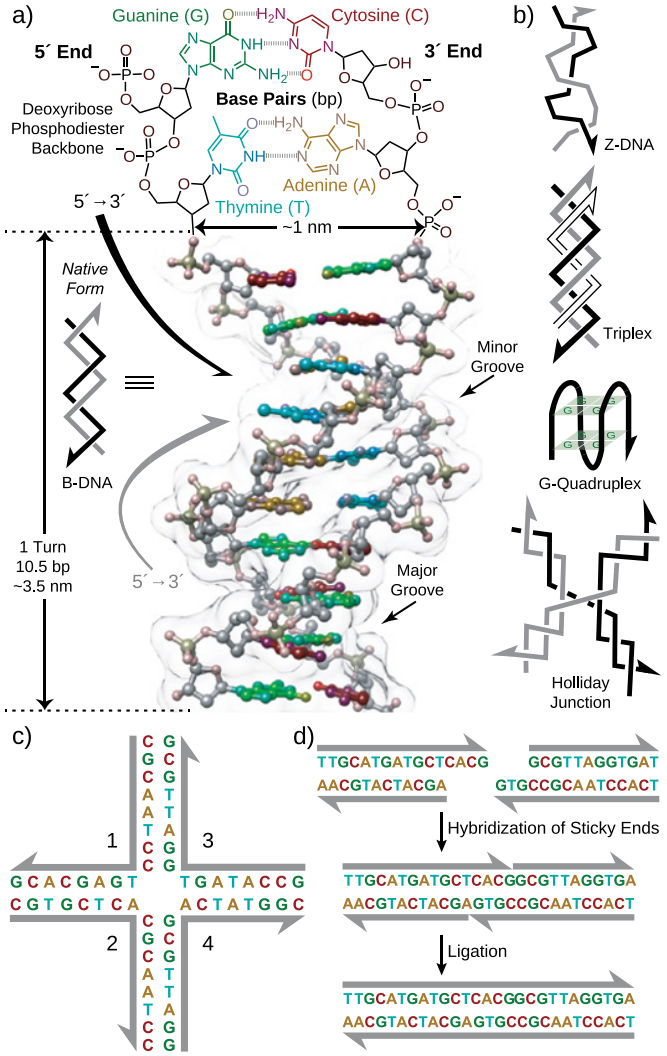


Figure 2.78 The structural chemistry of DNA. (a) Structural formulas of Watson-Crick[474] base pairs: guanine (G, green) cytosine (C, crimson / carmine), adenine (A, amber / auburn), thymine (T, teal / turquoise) with a ball-and-stick representation of the native right-handed (B-DNA) double helix superstructure. (b) Line drawings representing less common forms of natural DNA superstructures. (c) A fixed DNA branched junction can be designed by combining multiple unsymmetrical synthetic strands with bisected complementarity.[1347] (d) The process of fusing two duplexed DNA fragments by hybridization of their overhanging 'sticky ends' followed by enzymatic ligation.

helices or triplexes,[1340] square-shaped or columnar G-quadruplexes,[1341] and X-shaped Holliday junctions,[1342] the latter being intermediate, mobile branched structures undergoing a migration process along the DNA backbone during genetic recombination. Seeman proposed,[1343] developed,[1344–1346] and implemented[1347–1349] a strategy for assembling stable,[1350] immobile / fixed branched junctions (**Figure 2.78c**) with high predictability by combining synthetic single-stranded DNA (ssDNA) segments with appropriately designed sequences, based on the simple principle that the most stable structures will be those that maximize Watson-Crick base pairing. Synthetic DNA junctions comprising three,[1348] four,[1347] five,[1349] or six[1349] arms have been made and characterized.

The synthesis of molecular DNA catenanes often relies on subjecting multiple branched junctions to a ligation process (**Figure 2.78d**) involving two DNA double helices with complementary overhanging sequences, or 'sticky ends'. Hybridization of the sticky ends via hydrogen bond-driven duplex formation leads to a single double helix with 'knicks' along the backbone, which can be mended catalytically by a DNA ligase enzyme that promotes the formation of phosphodiester bonds. Many kinds of topological DNA structures can be constructed (**Figure 2.79**) by stitching branched junctions together using DNA ligation. The regularity of the DNA double helix has enormous implications for the topology of two-dimensional DNA networks, two hypothetical projections of which are illustrated in **Figure 2.79a–b**. When projected onto a plane, each half-turn in the DNA double helix leads to one crossing point or node in the projection. A network with an even number of nodes between branched junctions results in a 2D poly[*n*]catenane (**Figure 2.79a**), while a network with an odd number of nodes between junctions leads to a 2D 'warp and weave' (**Figure 2.79b**) network. Although this simple odd/even effect governs the *topology* of the network, branched junctions are not rigid but flexible,[1348] sampling a range of angles in real experiments, which can lead to variability in the *topography* or geometry of the assemblies. This handicap can be overcome, however, by programming a specific series of unique sticky ends, which can be ligated into a self-reinforcing structure such as a knot, link, or polyhedron. Seeman's first demonstration[1351] of this simple, yet powerful design principle was the synthesis (**Figure 2.79e**) of a multiply interlocked [6]catenane possessing eight three-way branched junctions representing the vertices of a cube. A ladder-like intermediate is first assembled from 10 unique strands and purified under denaturing conditions before being reconstituted and subjected to a final ligation. Simple [2]catenanes have been prepared (**Figure 2.79d**) from the same ladder-like motif by a 'topological protection'[1352] methodology employing non-sticky ended strands as structural templates which can be removed after the catenane-forming ligation step. Knotted topologies, such as trefoil knots[1353–1356] (**Figure 2.79c**) and figure-of-eight knots,[1355–1358] which express either invertible[1358] or predictably well-defined chirality[1356,1357] determined by the flexibility and chirality of the DNA superstructures selected as building blocks, have also been constructed by DNA ligation. The knotting of these circular ssDNA molecules also requires sections of unstructured deoxythymidine nucleotides to serve as flexible spacers in between the helices.

Other topological and mechanically bonded DNA nanostructures are showcased in **Figure 2.80**. Seeman[1359] has constructed Borromean rings (**Figure 2.80a**) by ligating the sticky ends of a right-handed (B-DNA) three-armed branched junction to a left-handed (Z-DNA) one, each possessing 1.5 turns per arm. He has also

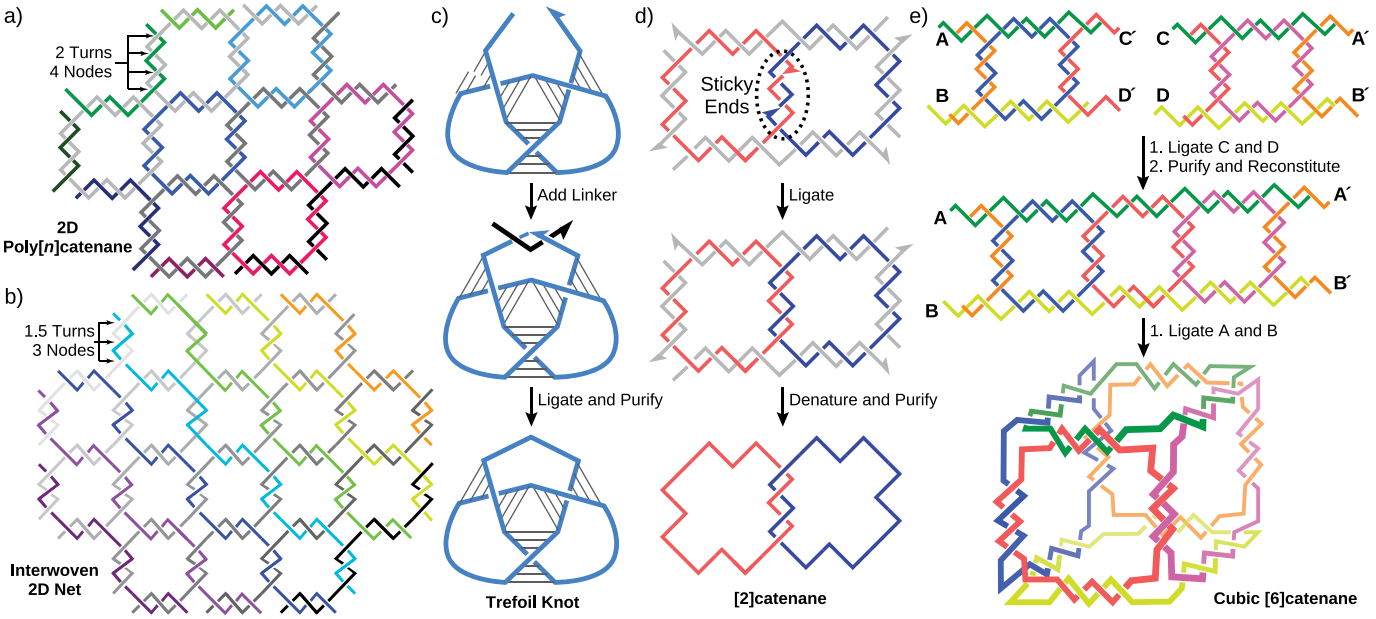


Figure 2.79 Topological consequences of sticky ended ligation with DNA branched junctions. (a–b) The odd/even effect: 2D networks possessing (a) an even number of half-turns between branched junctions give rise to polycatenated nets, whereas (b) an odd number of half-turns/nodes leads to a 'warp and weave' network topology.[1332] (c) The synthesis of a trefoil knot from a single-stranded three-arm junction (blue), which relies on unstructured deoxythymidine spacers (curved sections) and a complementary linker (black) to template the knot-closing ligation.[1354] (d) The synthesis of a DNA [2]catenane by 'topological protection'.[1352] (e) The synthesis of Seeman's seminal DNA hexacatenane, in which the sticky ends of flexible three-way branched junctions are ligated stepwise into the shape of a cube via a ladderlike intermediate.[1351]

devised[1360] a more facile preparation of DNA polyhedra by performing sticky-ended ligations on solid supports, a protocol which reduces the probability of erroneous ligations by isolating the DNA molecules from one another. Employing this methodology, Seeman has generated a square-shaped [2]catenane[1360] as well as a [14]catenane (**Figure 2.80b**) with the vertex connectivity of a truncated octahedron.[1361] Turberfield[1362] has constructed tetrahedra[1363] (**Figure 2.80c**) and bipyramids[1364] (**Figure 2.80d**) using high-yielding single-step protocols. Although these polyhedra retain knicks along their backbones because they were not ligated, ligation would lead in principle to [4]- and [6]catenanes from the tetrahedron and bipyramid, respectively.

Another type of DNA construct pioneered by Seeman[1365] is the DNA double crossover (DX) motif, in which two double helices are crosslinked by shared strands. Ligation[1366] and crystallization[1367] of DX molecules is efficient and facile as a result of their well-defined and rigid geometries reinforced by the crossover topology. A 'molecular chainmail' based on one type of DX topology (there are five isomeric DX motifs) is illustrated[1368] in **Figure 2.80e**. More double helices can be tangled together by employing conceptually similar designs, such as the triple-crossover[1369] (TX) DNA topology illustrated[1368] in **Figure 2.80f**. Segments of sticky-ended DX molecules can be commandeered as tiles[1367] in the self-assembly of even larger nanostructures comprising mechanically bonded DNA molecules. Yan and LaBean[1370] have employed cross-shaped four-arm DX branched junction tiles in the self-assembly of large two-dimensional DNA grids. Mao[1371,1372] has assembled tetrahedra, dodecahedra, buckyballs, and icosahedra of 40–500 nm in size by allowing multiple copies of identical three-arm or five-arm DX branched junction tiles to self-assemble into closed polyhedra. This assembly process, which is not unlike that of viral capsids, is controlled in large part by the length of the mechanically entangled DNA strands within the tiles. Seeman[1373] described a method of obtaining specific catenane and knot topologies by linking DNA tiles in the presence of *E. coli* topoisomerase 1, an enzyme that mediates DNA catenation and knotting processes during gene replication.

Another useful structural aspect of DNA is the curvature of the axis of the double helix. For example, the axis of native double-stranded DNA (dsDNA) commonly twists[1374] into more compact structures known as supercoils, which facilitate the tight packing of DNA inside of cell nuclei. Researchers began to understand[1375] the inherent curvature of DNA sequences in the 1980s. Different dinucleotides deflect the axis of the double helix at slightly different angles. The most pronounced deflections have been observed[1376] for tracts of all-adenine and all-thymine when positioned (**Figure 2.81a**) with regular periodicities matching the pitch (10.5 bp) of the double helix. These so-called AT tract motifs have enabled the synthesis[1376] of well-defined double-stranded DNA (dsDNA) 'minicircles' by sticky-ended ligation. Although they represent topological

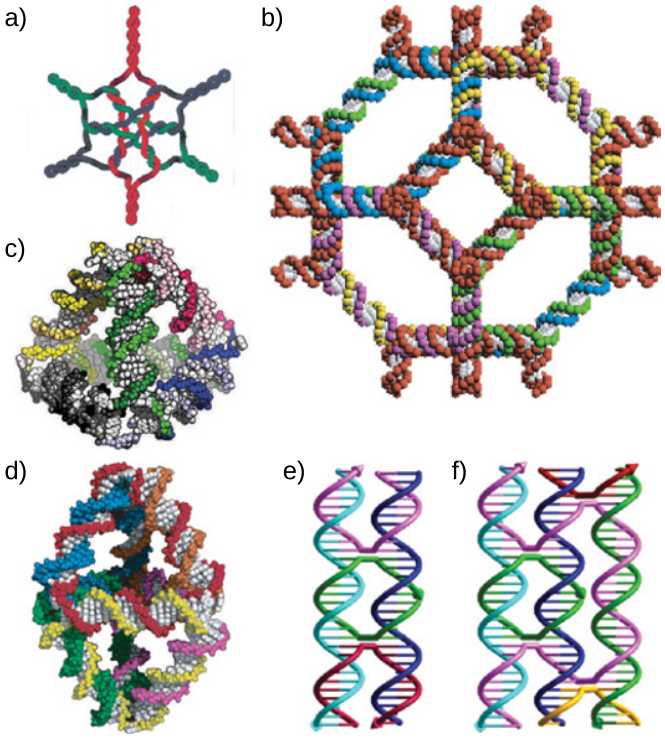


Figure 2.80 Examples of mechanically bonded DNA constructs. (a) Borromean rings[1359] constructed by ligating B-DNA and Z-DNA three-arm junctions. (b) A [14]catenane with the vertex connectivity of a truncated octahedron.[1361] (c) A tetrahedron.[1363] (d) A bipyramid.[1364] (e–f) 'Molecular chainmail' comprising (e) double crossover[1365] (DX) and (f) triple crossover[1369] (TX) DNA. Images reproduced with permission from refs. 1359 (copyright 1997 Nature Publishing Group), 1361 (copyright 1994 American Chemical Society) 1362 (copyright 2007 Nature Publishing group), 1364 (copyright 2007 American Chemical Society) and 1368 (copyright 2012 RM Zadegan, ML Norton).

marvels[x] in their own right, these shape-persistant DNA circles have also been employed (**Figure 2.81**) as components of even larger MIMs. Kool[1377] has orchestrated the catenation (**Figure 2.81b**) of ssDNA around a dsDNA minicircle. This protocol relies on a circular ssDNA strand with the unique capability to form a triplex with AT-rich sequences of dsDNA, which gives rise to a pseudorotaxane-like assembly that becomes a catenane upon circularization of the dsDNA axle during ligation. Escudé[1378,1379] has prepared a similar catenane by circularization of the triplexed ssDNA around a dsDNA minicircle. Famulok[1336,1380–1382] at the University of Bonn has assembled (**Figure 2.81c**) double-stranded DNA rotaxanes by designing[1383] DNA minicircles possessing a 13 bp single-stranded 'gap' that can accept complementary sequences of circular ssDNA, which serve as the rings of pseudorotaxanes with sticky-ended dsDNA axles that can be stoppered by ligation. Extending this design motif even further, Alexander Heckel[1384] at the University of Frankfurt has employed the shape-persistant DNA circles as components of even larger DNA-based MIMs. Famulok[1385] has also assembled a number of dsDNA catenanes.

Mechanically bonded DNA constructs are most commonly prepared by enzymatic ligation of a duplexed precursor. Yingfu Li[1386] has recently described a fundamentally different approach to linking ssDNA macrorings by *in vitro*

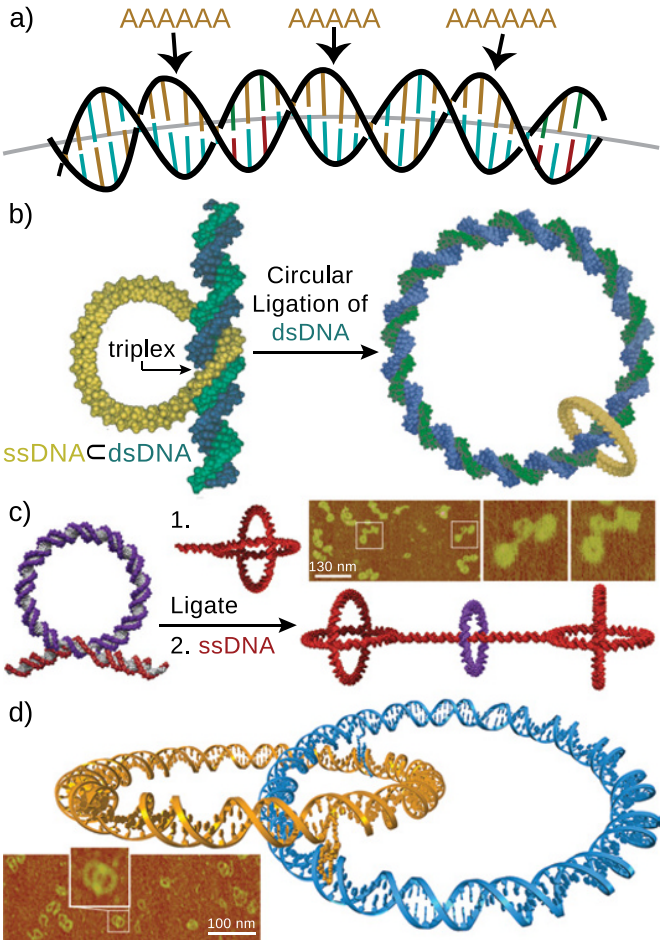


Figure 2.81 MIMs derived from double-stranded DNA (dsDNA) minicircles. (a) Tracts of A/T-rich oligonucleotides with periodicities matching the 10.5 bp pitch of dsDNA deflect the axis of the helix, providing sufficient curvature to prepare DNA minicircles by sticky-ended ligation of the AT tracts.[1376] (b) The assembly of a triplex comprising a circular ssDNA strand and an AT tract-bearing curved double helix leads to the formation of a ssDNA/dsDNA [2]catenane upon ring closure by sticky-ended ligation.[1377] (c) A 13-bp ssDNA 'gap' in a dsDNA minicircle (purple) is hybridized with a complementary gap in a sticky-ended dsDNA axle (red) and ligated to bulky dsDNA stoppers, affording a large (~100 nm) [2]rotaxane, which is visualizable[1380] by AFM. (d) Graphical representation and AFM images of catenated dsDNA minicircles, which rely on sequence-specific DNA-binding oligopeptides as templates for catenation.[1384] Images in (b)–(d) are reproduced with permission from refs. 1377 (copyright 1998 Elsevier), 1380 (copyright 2010 Nature Publishing Group), 1384 (copyright 2011 American Chemical Society)

[x] Circular dsDNA molecules are multiply interlocked [2]catenanes in which the linking number is equal to the number of turns in the double helix, i.e., one link unit per 10.5 base pairs.

selection of catenated DNA rings emerging from a randomized library of precursors. Ligation-induced catenation in this case is driven not by duplex formation, but by much weaker physical interactions between the cyclic and acyclic ssDNA precursors. This approach adds a new level of diversity to DNA-based catenanes because the rings can move and operate independently as a result of their weak intercomponent interactions.

Enzymatic ligation is not the only way to construct mechanical bonds with DNA—another possibility is to introduce artificial reactive moieties into the structure of synthetic DNA molecules that can be chemically crosslinked (**Figure 2.82**) in order to produce mechanical bonds. Brown[1387] has replaced enzymatic ligation with an aqueous CuAAC reaction by coupling 3′-azide and 5′-alkyne groups of artificial nucleic acids. This 'click ligation' (**Figure 2.82a**) of a 72-bp ssDNA strand, which is duplexed with a 70-bp circular ssDNA constituting six complementary 10-bp segments connected by flexible TT dinucleotide hinges, results in a 'pseudo-hexagonal' [2]catenane. Although the extent of interlocking in the catenated product(s) is unknown, molecular models suggest that catenanes with three-fold and six-fold interlocked topologies appear to be possible. Seeman[1388] has described an approach involving a peptide coupling reaction (**Figure 2.82b**) across the 3.5 nm gap comprising one helical turn of a duplexed DNA backbone, leading to a hybrid DNA/oligopeptide [2]catenane. The reaction involves two artificial uracil nucleotides with thioether appendages at the 2-position of deoxyribose, which carry long flexible polyether linkers terminating in carboxylic acid and amine endgroups. When these carboxylate- and amine-functionalized sites are separated by either 9 or 10 bp (close to the distance of a single helical turn) in the presence of a complementary circular ssDNA, the introduction of the peptide coupling agent DMTMM results in the near-quantitative formation of the [2]catenane **C267**, owing to the efficient formation of an amide bond. By bridging the double helix with this 'cross-turn' coupling reaction, both the 5′ and 3′ sticky ends of the hybrid DNA ring remain available as functional handles. More recently, Onizuka and Abe[1389] have cyclized ssDNA across a helical turn by inventing an 'automatic' Cu-free azide-alkyne cycloaddition in which nucleotides displaying strained alkynes and azides do not cross-react until hybridized with a complementary strand.

DNA catenanes need not necessarily rely on covalent chemistry to be instilled with mechanical bonds, since the multivalency of hydrogen bonding between nucleotides may be sufficient to stabilize a mechanical linkage for some purposes. For example, Sugiyama[1390] has employed G-quadruplex formation as the ring-closing step in the self-assembly (**Scheme 2.126**) of the noncovalent DNA [2]catenane **C268**, resulting in a mechanical bond that is sealed by the hydrogen bonding and cation-binding network of a single-stranded G-quadruplex assembly, rather than by covalent bonds. Although the catenane remains intact during gel electrophoresis, the catenation is a reversible process, since the rings can be separated by denaturation of DNA at elevated temperatures or by removal of the quadruplex-templating K^+ ions.

The extraordinary specificity of Watson-Crick base pairing is harnessed nowadays in the production of two-[1391] and three-dimensional[1392,1393] DNA nanostructures with exquisite control over size and shape using a DNA folding technology[1391] known as 'DNA origami',[1394] in which long ssDNA strands are folded (**Figure 2.83a**) into a chosen geometry

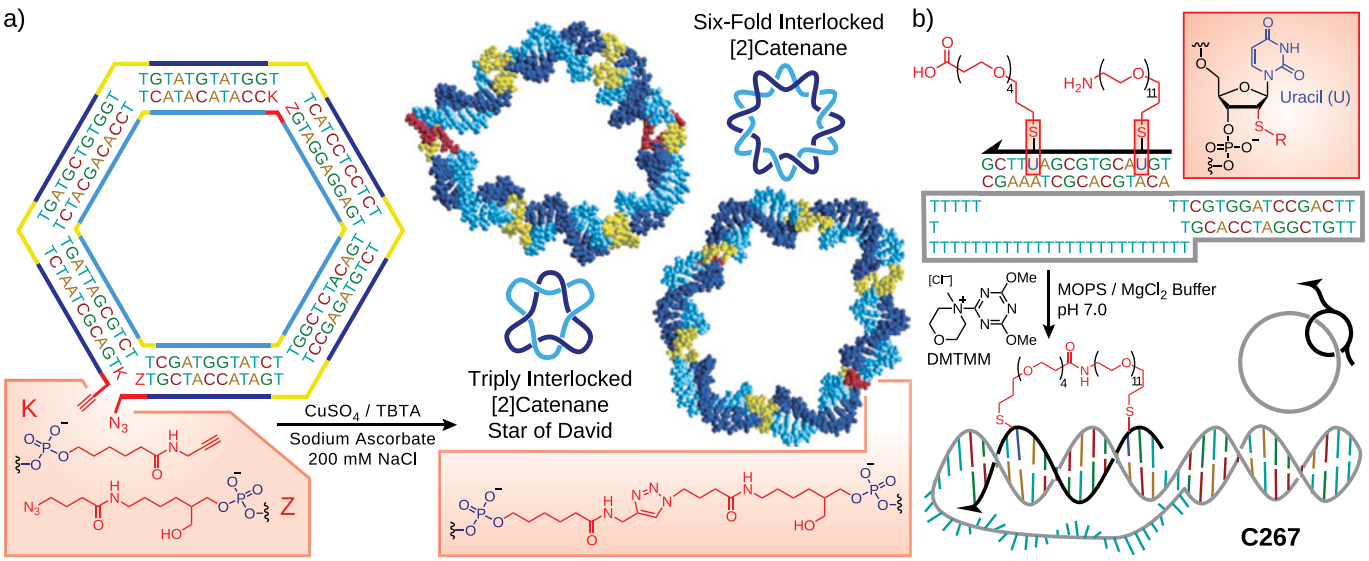
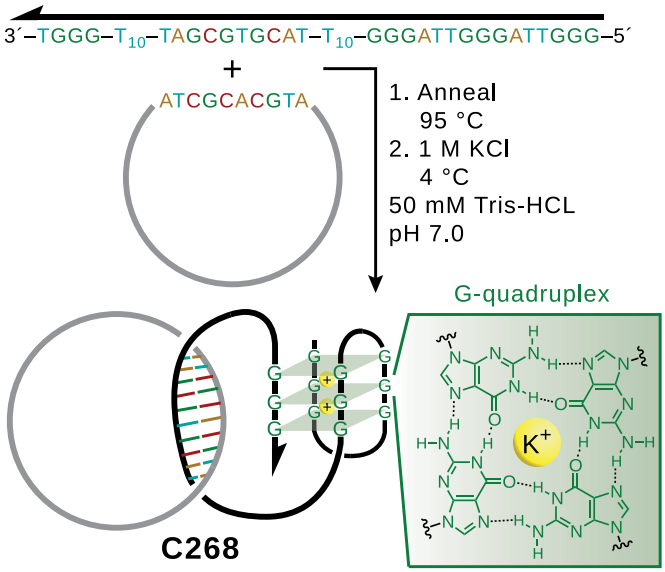


Figure 2.82 Non-enzymatic coupling reactions for synthesizing hybrid DNA catenanes. (a) Brown's CuAAC 'click ligation' of dsDNA [2]catenanes from a pseudo-hexagonal template comprising duplexed circular ssDNA (light blue) and a linear ssDNA (dark blue) strands of 70 and 72 bp in length, respectively, derived from artificial 5′-alkyne (K) and 3′-azide (Z) nucleic acid precursors.[1387] (b) Seeman's synthesis[1388] of a hybrid [2]catenane **C267** by peptide coupling across the DNA helical turn, which employs artificial 2-thioether-linked uracil nucleotides as anchor points for the reactants.



Scheme 2.126 The self-assembly of a noncovalent [2]catenane by clipping G-rich linear ssDNA around circular ssDNA via the K^+-promoted formation of a G-quadruplex.[1390]

and reinforced by a number of short oligonucleotide 'staple strands'. Two-dimensional (**Figure 2.83b**) and three-dimensional (**Figure 2.83c–f**) objects of arbitrary shape can now be constructed routinely from the bottom up. Thus, it is possible to construct mechanical bonds from DNA at two levels: (i) the molecular level, which involves mechanically linked circular DNA loops as already described, and (ii) the mesoscopic level, which involves interlocked DNA origami, the mechanical bonds of which are enforced by many hydrogen bonds. Examples of the latter kind are represented in **Figure 2.83c–f**.

Castro[1395] has constructed DNA origami 'mechanisms' exhibiting well-defined and programmable sliding motions constrained by the mechanical bond. One of these mechanisms is a DNA origami slider (**Figure 2.83c**), comprising a 30-helix bundle in the form of a nanotube, which is arranged concentrically around an axle of six bundled helices stoppered by a 42-helix bundle. The outer nanotube component is tethered to both ends of the axle by flexible ssDNA strands. TEM images reveal (**Figure 2.83c)** that this assembly constitutes a molecular shuttle of epic proportions, since the nanotube can translate >20 nm along the length of the shuttle. This sliding motion has also been coupled with bending joints in a so-called crank-slider (**Figure 2.83d**) mechanism. It is anticipated that these types of mechanical joints and mechanisms could be integrated with others into more sophisticated molecular machines and devices in the fullness of time.

A compelling demonstration of the power of DNA origami for making mechanical bonds has been reported by Yan,[113] who implemented the first successful Möbius strip approach (**Figure 2.83e–f**) to making catenanes. The Möbius strip is designed (**Figure 2.83e**) as a ribbonlike band of 11 double helices crosslinked by staple strands, the chirality of which

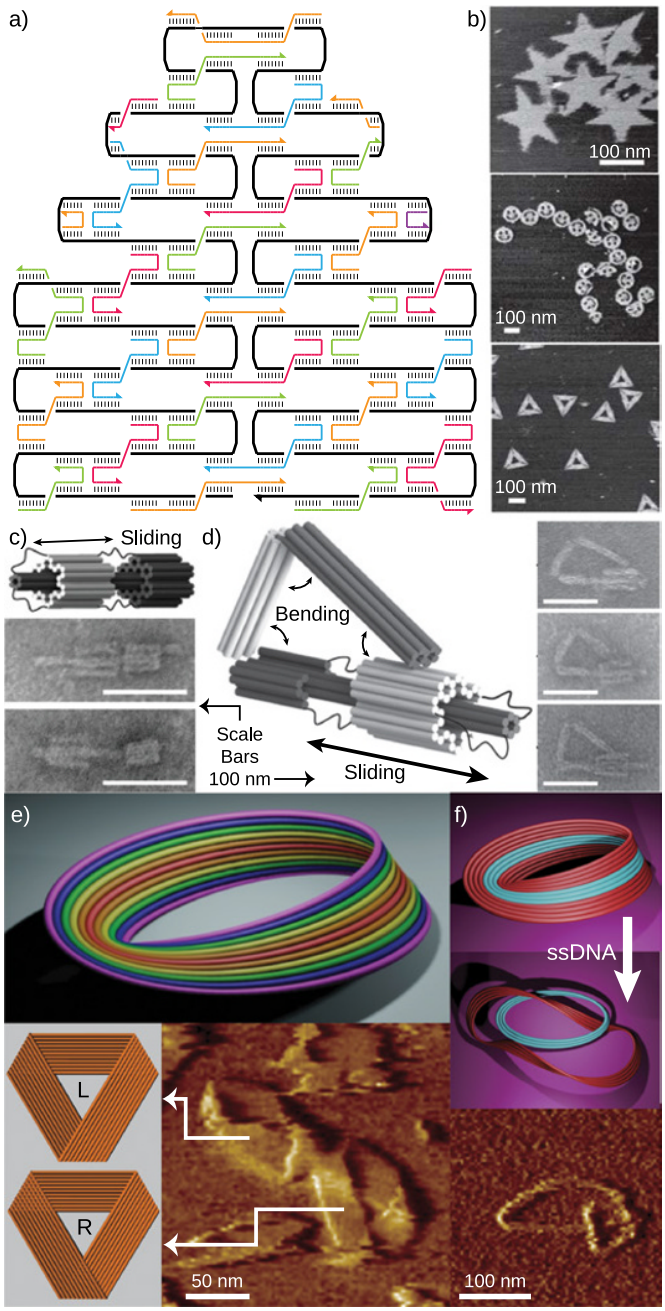


Figure 2.83 DNA origami and mechanical bonds. (a) Line drawing of a simple DNA origami design.[1391] The desired shape is raster-filled with a long ssDNA scaffold (black) and held by cross-linking 'staple strands' (colored). (b) AFM images of 2D DNA origami. (c) A DNA origami 'slider' tethered to an axle by ssDNA. TEM images visualize the rotaxane-like structure and verify the mobility of the slider. (d) Cartoon and TEM images of a 'crank-slider'.[1395] (e) Cartoon and AFM images of a DNA origami Möbius strip.[113] Each band represents a double helix. (f) An off-center 'cut' along the edge of the Möbius strip by staple strand displacement results in a catenane. Images reproduced with permission from refs 1391 (copyright 2006 Nature Publishing Group), 1395 (copyright 2015 National Academy of Sciences) 113 (copyright 2010 Nature Publishing Group)

leads to a mixture of left-handed (L) and right-handed (R) isomers. The Möbius strip was designed to be reconfigurable by strand displacement reactions involving externally added nucleic acids. Recall from **Section 2.2.3** (see **Figure 2.8**) that an off-center bisection of a Möbius strip along its single edge leads to a pair of concatenated rings, unequally sized. This kind of cut has been incised (**Figure 2.83f**) in the DNA origami Möbius strip by strand displacement of the ssDNA crosslinks in between the three innermost double helices and the surrounding rows of helices extending to the edge. AFM images confirm that the strip is reconfigured thusly into a link.

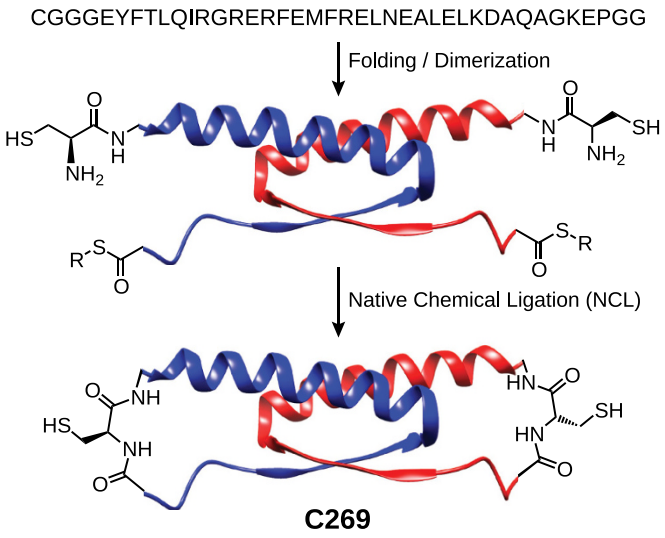
Clearly, mechanically bonded DNA molecules are accessible by a diverse array of strategies, but to what end? It transpires that researchers have found a number of promising target applications for DNA MIMs. Landegren,[1396] Demidov,[1397] Frank-Kamenetskii,[1397,1398] and Fujimoto[1399] have employed catenated ssDNA macrorings as topological labels, or 'padlock probes', for DNA detection and structural elucidation purposes. Itamar Willner[1400–1402] at the Hebrew University of Jerusalem has used DNA catenanes and rotaxanes as versatile scaffolds for assembling hierarchical nanostructures comprising proteins, nanoparticles, and small molecules. Willner[1337,1401,1403–1407] has also pioneered the use of DNA catenanes as molecular switches, producing a number of examples of DNA catenanes whose ring positions can be controlled by strand displacement—see **Section 6.6.2**.

2.3.12.2 Proteins with Mechanical Bonds

Catenated and knotted structures in proteins have been identified in a number of entries in the Protein Databank. Mislow[1408–1410] at Princeton University was one of the early pioneers to recognize the presence of topological pseudolinks and pseudoknots in native proteins, which arise from amino acid sidechains coordinating to metals or from disulfide bridges that form as a result of the oxidative coupling of a pair of cystine residues. One knotted motif, found in growth factors and inhibitors, is known as the cystine knot,[1411] in which disulfide bridges generate a polypeptide loop through which another disulfide bridge passes. These catenane-like and rotaxane-like subregions of proteins most likely contribute to stability by raising the activation barrier to unfolding/denaturation. A rotaxane-like motif comprising a proteinaceous 'lasso'—i.e., a self-threaded loop or [1]rotaxane (see **Section 4.2.3.1**)—has also been identified[1412,1413] in the natural antibacterial protein, Microcin J25. See **Section 1.1.1** for more examples of naturally occurring biomolecular MIMs.

Although examples of synthetic MIMs derived from proteins are much more sparse than in the case of DNA, proteins can adopt an even wider array of different superstructures and folding motifs than DNA in natural settings, albeit with a much lower degree of predictability. It stands to reason that there are many protein folds, among the thousands that have been observed by structural interrogation, which could serve as suitable structures for the fold-directed templation of mechanical bonds. One of the few examples (**Scheme 2.127**) of a *designed* protein catenane was reported by Dawson[1414,1415] at the Scripps Research Institute, who selected the tetramerization domain[1416] of the tumor suppressor protein p53 as an entwined template. Dawson's ring-closing step is an important bioconjugation protocol known[1417] as native chemical ligation (NCL), which involves the spontaneous formation of a native peptide bond between an *N*-terminal cysteine and a *C*-terminal thioester as a result of the rearrangement of a cross-reacted thioester intermediate. The mechanism underlying NCL is illustrated in **Scheme 1.5** in **Section 1.3.6**. Since the entwined p53 protein template is derived from a tetramer domain, the protein [2]catenane **C269** exists in water as a supramolecular dimer. Just as topological links have been found to stabilize the folded structures of some natural proteins (see **Section 1.1.1**), the mechanical bond also stabilizes[1414] the secondary structure of this artificially catenated protein. Whereas the linear p53 tetramer domain denatures at 83 °C, the catenane **C269** denatures at 98 °C. In the case[1415] of a p53 domain mutated to form a dimer instead of a tetramer, the mechanical bond raises the melting temperature by a remarkable 59 °C. The protein catenane also displays 30-fold enhanced resistance to hydrolysis in the presence of trypsin, a protease employed routinely in protein digestion. These results suggest that the mechanical bond could be a useful tool for engineering proteins with highly enhanced stabilities.

Ghadiri[1418] at the Scripps Research Institute has described a strategy for preparing noncovalent protein/DNA hybrid [2]rotaxanes by stoppering a single DNA strand threaded through the opening of a protein nanopore. α-Hemolysin[1419] (α-HL), a toxin secreted by *Staphylococcus aureus* bacteria, is monomeric in water, yet self-assembles at the surface of lipid membranes into a mushroom-shaped heptamer (**Figure 2.84a**) possessing a 10-nm water-filled



Scheme 2.127 Dawson's synthesis[1414] of a designed protein catenane by native chemical ligation.

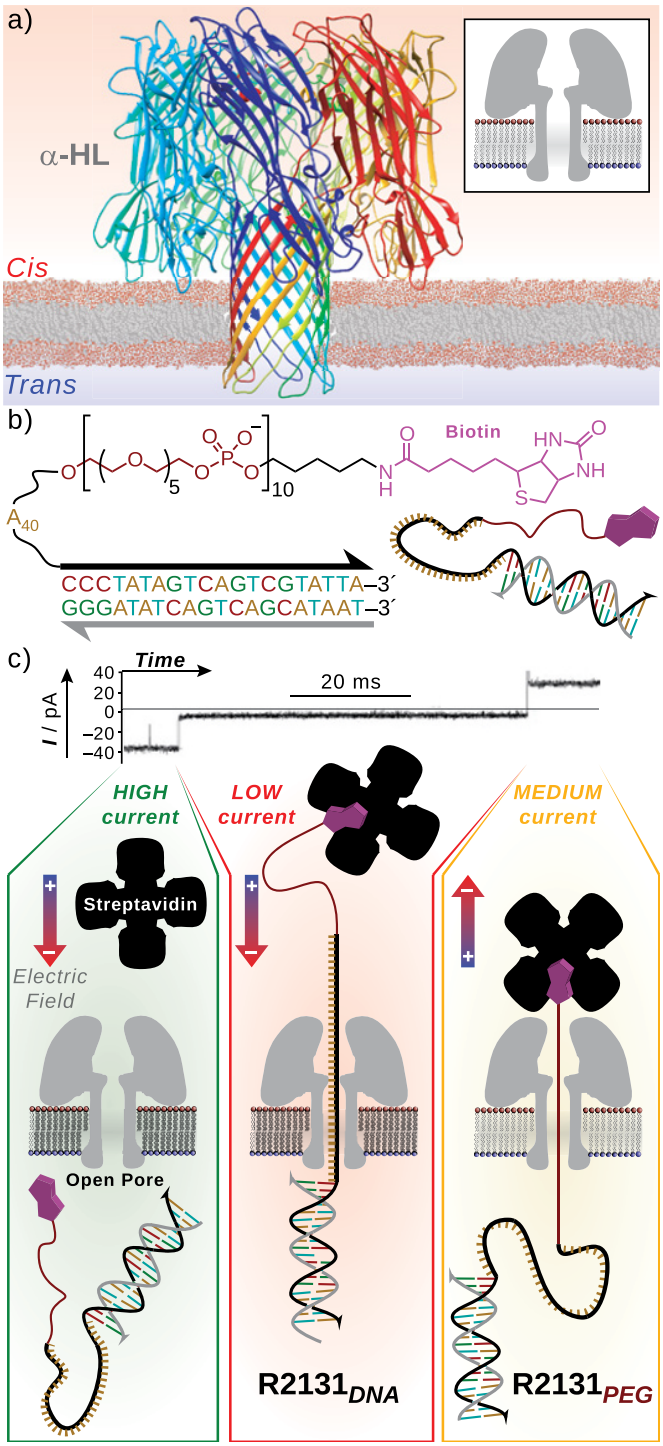
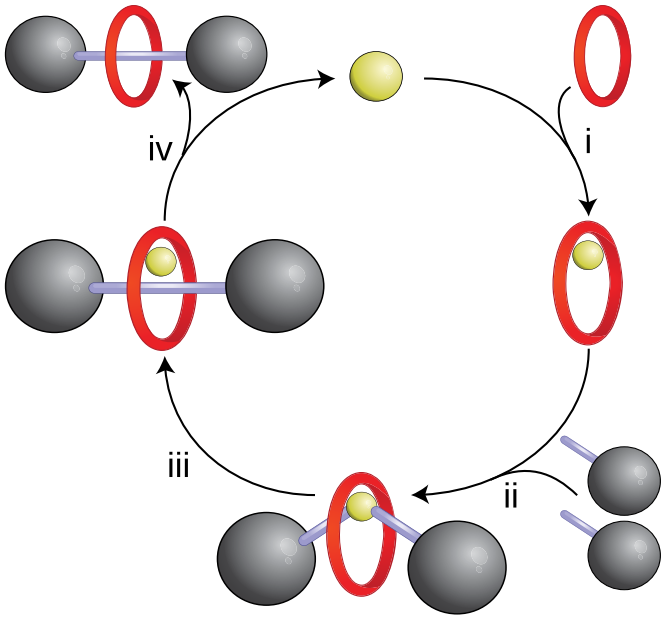


Figure 2.84 A transmembrane rotaxane.[1418] (a) Graphical representation and crystal structure[1419] of the nanopore protein α-HL, superimposed on a lipid bilayer separating the *cis* and *trans* aqueous compartments. (b) Structural formula of a biotin-labeled ssDNA/PEG block copolymer axle and its complementary stopper strand. (c) Electrophysiological assembly of rotaxane **R2142**, which can be switched between the states $\mathbf{R2142}_{DNA}$ and $\mathbf{R2142}_{PEG}$ by changing the direction of the electric field. The level of the transmembrane current (*I*) reports the axle's position in the nanopore.

channel with a diameter of 1.5 nm at its narrowest point. DNA and other polymers can be transported[1420] through the α-HL pore, driven by the potential of an electric field across the membrane. Since the ionic conductance of the channel is highly sensitive to the size of the nanopore, the current passing through it is modulated by the occupancy of different molecules. These protein nanopores are therefore being utilized in devices for single-molecule detection and even DNA sequencing.[1421,1422] Ghadiri's experiment[1418] relies on a ssDNA/PEG copolymer (**Figure 2.84b**) with a 20-bp sequence at the 3′ end designed for duplex formation with complementary ssDNA, which is connected by a 40-mer of A nucleotides to a 5′-functionalized poly(hexathylene glycol phosphate) extension terminated with a biotin moiety. Duplexed DNA at the 3′ end and *biotin⊂streptavidin* complexes at the 5′ end both act as noncovalent stoppers for the copolymer, since they are kinetically stable and sufficiently bulky to block transport through the lumen of α-HL. Thus, the α-HL/DNA [2]rotaxane **R2131** is assembled (**Figure 2.84c**) by introducing the duplex-stoppered ssDNA/PEG copolymer in solution on one side of the membrane (labeled the *trans* compartment) and threading the 3′ end through the nanopore under an applied potential into a compartment (*cis*) containing streptavidin, which binds biotin on the opposite side of the membrane. Since conductance is higher when the PEG block occupies the channel ($\mathbf{R2131}_{PEG}$) than when it is occupied by DNA ($\mathbf{R2131}_{DNA}$), the position of the DNA copolymer axle relative to the α-HL nanopore is reported by the transmembrane current. The rotaxane can be switched reversibly between the states $\mathbf{R2131}_{PEG}$ and $\mathbf{R2131}_{DNA}$ by changing the direction and magnitude of the transmembrane potential. The introduction of mechanical bonds by this kind of stoppering technique may reduce error rates in single-molecule DNA sequencing by enabling repeated passes through the nanopore. Devices employing protein-DNA hybrid rotaxanes have been devised, which can (i) monitor[1423,1424] the enzymatic activity of DNA polymerase in real-time, as well as (ii) control[1425] the translocation of proteins across a membrane.

2.4 Active Template Synthesis

Active template synthesis is an approach to forming mechanical bonds introduced independently by the Leigh[403] and Saito[1426] groups circa 2006. Leigh[22] and Saito[1427] have both authored reviews on active template approaches, which rely on catalytic centers to act as both templates and catalysts. Since the dual template/catalyst has been a transition metal ion in all cases reported to date, this approach is also known[22] as active metal template synthesis, although it should be possible to employ organocatalysts likewise in principle. A generalized catalytic cycle for the active template synthesis of a [2]rotaxane is illustrated in **Scheme 2.128**, while a similar scheme depicting catenane synthesis is presented in **Scheme 2.4d**. Active templates typically involve a transition metal catalyst bound endotopically within a macrocyclic ligand,



Scheme 2.128 Generalized mechanism of active template synthesis, exemplified by the case of a [2]rotaxane. (i) A catalyst (gold) is bound within the cavity of a macrocycle (red). (ii) Reagents (blue/black semidumbbells in this example) coordinate the catalyst within the macrocycle. (iii) A covalent bond is formed catalytically, resulting also in the mechanical bond of a rotaxane. (iv) The catalyst is regenerated and the rotaxane is expelled.

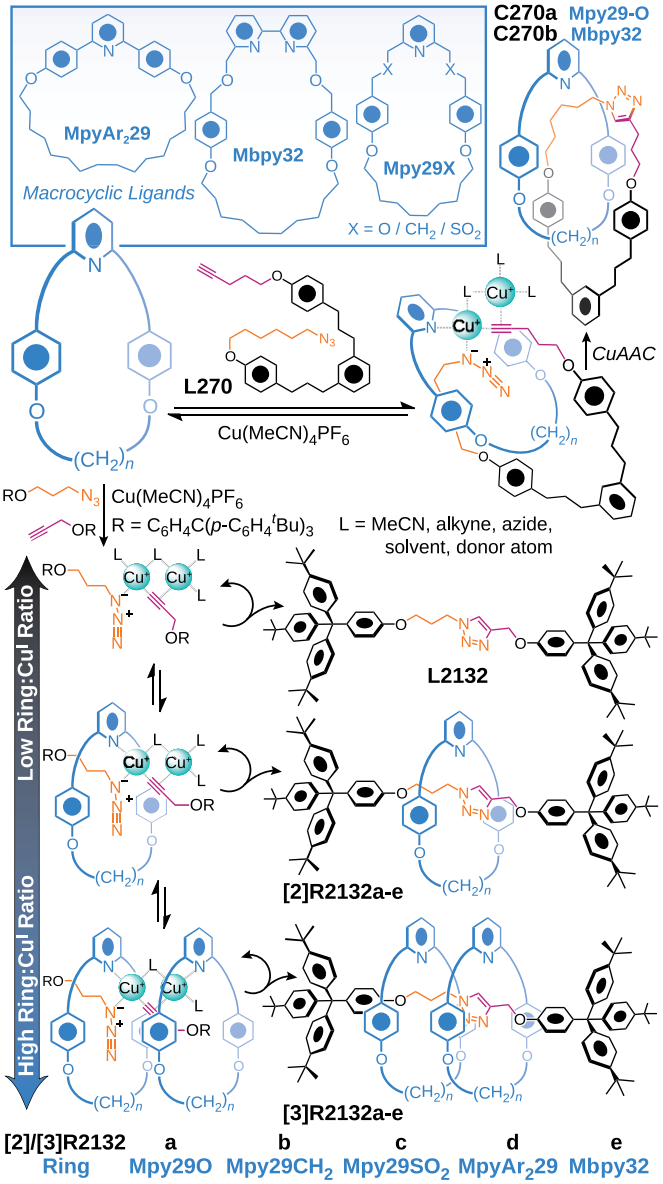
providing a situation which promotes the coupling of the ends of a macrocyclic precursor (for catenanes) or semidumbbells (for rotaxanes) within its cavity. Hence, active templates are a manifestation of the ring capture (see **Figure 2.2**) and dumbbell capture (see **Figure 2.3**) strategies for MIM synthesis in the context of catalysis. Transition metals that have been employed as active templates include copper (**Section 2.4.1**), zinc (**Section 2.4.2**), palladium (**Section 2.4.3**), and nickel (**Section 2.4.4**). The reaction parameters and yields for most of the active template syntheses described in **Section 2.4** are summarized in **Table 2.40**.

2.4.1 Active Copper Templates

As in the case of transition metal template-directed synthesis (**Section 2.3.3**), copper has been the most widely used metal for synthesizing mechanolecules by active template synthesis. Catalytic transformations that have relied on active copper templates to form mechanical bonds include the Cu^{I}-catalyzed azide-alkyne cycloaddition (CuAAC, **Section 2.4.1.1),** the Eglinton-Glaser-Hay homocoupling (**Section 2.4.1.2**) of terminal alkynes, the Ullmann-type C–S coupling (**Section 2.4.1.3**) of thiols and aryl halides, a Sonogashira-type C–C bond forming reaction of alkynes and aryl halides (**Section 2.4.1.4**), the Cadiot-Chodkiewicz cross-coupling (**Section 2.4.1.5**) between acetylenes and bromoacetylenes, the Goldberg reaction (**Section 2.4.1.6**) producing C_{Aryl}–N bonds, and the Lewis acid-catalyzed Diels-Alder (**Section 2.4.1.7**) cycloaddition.

2.4.1.1 CuAAC Active Template Synthesis

Leigh's introductory demonstration[403,1428] of active template synthesis (**Scheme 2.129**) employed the CuAAC click reaction in combination with a variety of macrocyclic ligands derived from 2,6-substituted pyridine (py) or 2,2′-bipyridine (bpy)—referred to here as compounds Mpy29-X (where X is O, CH_2, or S), $MpyAr_2$29, and Mbpy32—in order to prepare [2]- and [3]rotaxanes from alkyne- and azide-terminated semidumbbell substrates. Since the mechanism[1429] of the CuAAC reaction involves a dinuclear Cu^{I} intermediate, the outcome of the active template synthesis depends on whether this bimetallic catalyst is bound by zero, one, or two of the ligating rings, leading to the dumbbell **L2132**, the [2]rotaxanes



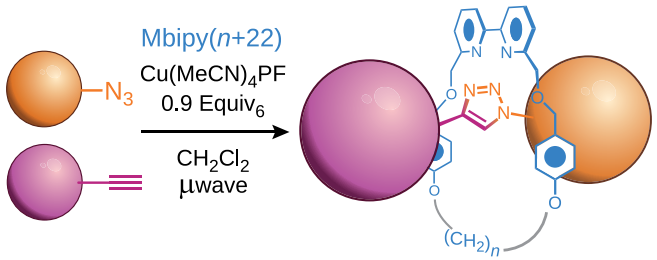
Scheme 2.129 Leigh's active metal template syntheses of [2]- and [3]rotaxanes,[403,1428] **[2]R2132a-e** and **[3]R2132a-e**, respectively, as well as the [2]catenanes[1430] **C270a-b**, by CuAAC click chemistry. In the case of the rotaxanes, the product distribution is affected by the catalyst loading ratio with respect to the endotopic chelates serving as rings.

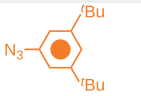
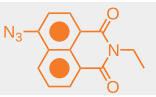
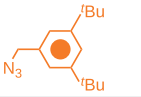
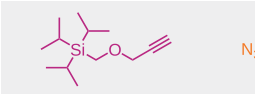
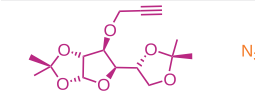
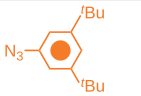
Table 2.40 Summary of the reaction conditions and yields for the active template synthesis of rotaxanes and catenanes.

Reaction	Ring	Catalyst	Solvent	T °C	Equivalents Ring	Cat.	Substrate	Product	Yield %	Ref
CuAAC	Mpy29-O	$Cu(MeCN)_4PF_6$	$H_2O/^tBuOH$	25	1	1	1	**[2]R2132a**	22	403
CuAAC	Mpy29-O	$Cu(MeCN)_4PF_6$	CH_2Cl_2	25	1	1	1	**[2]R2132a**	57	403
CuAAC	Mpy29-O	$Cu(MeCN)_4PF_6$	CH_2Cl_2	25	1	1	3	**[2]R2132a**	83	403
CuAAC	Mpy29-O	$Cu(MeCN)_4PF_6$	CH_2Cl_2	25	1	1	5	**[2]R2132a**	94	403
CuAAC	Mpy29-O	$Cu(MeCN)_4PF_6$[a]	CH_2Cl_2	25	1	0.2	5	**[2]R2132a**	59	403
CuAAC	Mpy29-O	$Cu(MeCN)_4PF_6$[a]	$ClCH_2CH_2Cl$	70	1	0.2	5	**[2]R2132a**	82	403
CuAAC	Mpy29-O	$Cu(MeCN)_4PF_6$	CH_2Cl_2	RT	10	1	1	**[2]R2132a**	90	1428
								[3]R2132a	5	1428
CuAAC	Mpy29-O	$Cu(MeCN)_4PF_6$	CH_2Cl_2	RT	1	1	1	**C270a**	<5	1430
CuAAC	Mpy29-O	$Cu(MeCN)_4PF_6$	$ClCH_2CH_2Cl$	80	1	1	1	**C270a**	16	1430
CuAAC	Mpy29-O	$Cu(MeCN)_4PF_6$	$ClCH_2CH_2Cl$	80	1	1	5	**C270a**	53	1430
CuAAC	$Mpy29\text{-}CH_2$	$Cu(MeCN)_4PF_6$	CH_2Cl_2	RT	1	1	1	**[2]R2132b**	60	1428
CuAAC	$Mpy29\text{-}SO_2$	$Cu(MeCN)_4PF_6$	CH_2Cl_2	RT	1	1	1	**[2]R2132c**	13	1428
CuAAC	$MpyAr_229$	$Cu(MeCN)_4PF_6$	CH_2Cl_2	RT	1	1	1	**[2]R2132d**	25	1428
CuAAC	$MpyAr_229$	$Cu(MeCN)_4PF_6$	CH_2Cl_2	RT	10	1	1	**[2]R2132d**	37	1428
								[3]R2132d	33	1428
CuAAC	Mbpy32	$Cu(MeCN)_4PF_6$	CH_2Cl_2	RT	1	1	1	**[2]R2132e**	45	1428
CuAAC	Mbpy32	$Cu(MeCN)_4PF_6$	CH_2Cl_2	RT	10	1	1	**[2]R2132e**	97	1428
								[3]R2132e	0	1428
CuAAC	Mbpy32	$Cu(MeCN)_4PF_6$	$ClCH_2CH_2Cl$	80	1	1	5	**C270b**	50	1430
CuAAC	BIPP33C9	$Cu(MeCN)_4PF_6$	CH_2Cl_2	RT	1	0.9	5	**R2133**	25	1438
CuAAC	CIDAPH	$Cu(MeCN)_4PF_6$	$CHCl_3$	RT	1	1	1.2	**R2134**	20	1439
Eglinton-Glaser-Hay	CIDAPH	CuI[b]	THF	60	1	1	2.5	**R2135**	9	939
Eglinton-Glaser-Hay	Mdpp33	CuI[c]	PhMe	110	1	1	2.5	**R2136**	72	1426
Eglinton-Glaser-Hay	Mdpp33	CuI[d]	Xylene	130	1	1	5	**C271**	64	1440
Ullmann C–S Coupling	Mdpp33	CuI[e]	PhMe	110	1	1	10	**R2137**	27	1426
Sonogashira-Type	Mdpp33	CuI[f]	Xylene	120	1	1	2.2	***o*-R2138**	52	1446
Sonogashira-Type	Mdpp33	CuI[f]	Xylene	120	1	1	2.2	***m*-R2138**	24	1446
Sonogashira-Type	Mdpp33	CuI[f]	Xylene	120	1	1	2.2	***p*-R2138**	24	1446
Cadiot-Chodkiewicz	Mbpy32	CuI[g]	THF	–78→RT	1	1	1	**R2139**	84	1447
Cadiot-Chodkiewicz	Mbpy32	CuI[g]	THF	–78→80	1	1	5	**C272**	21	1430
Goldberg Reaction	MCyDA32	$Cu(OAc)_2$[h]	PhMe	110	1	0.1	1/1.5	**R2140**	14	1448
Goldberg Reaction	MCyDA32	$Cu(OAc)_2$[h]	PhMe	110	1	0.5	1/1.5	**R2140**	21	1448
Goldberg Reaction	MCyDA32	$Cu(OAc)_2$[h]	PhMe	110	1	2	1/1.5	**R2140**	11	1448
Goldberg Reaction	MCyDA32	$Cu(OAc)_2$[h]	PhMe	110	1	0.5	4.5/4	**R2140**	51	1448
Goldberg Reaction	MCyDA32	$Cu(OAc)_2$[h]	PhMe	120	1	0.9	5/5.5	**R2140**	57	1448
Diels-Alder	Mbpy32	$Cu(OTf)_2$	CH_2Cl_2	–78→RT	1	1	2	**R2141a**	91	1451
Diels-Alder	Mpy29-O	$Cu(OTf)_2$	CH_2Cl_2	–78→RT	1	1	2	**R2141b**	83	1451
Diels-Alder	Mpy29-O	$Zn(OTf)_2$	CH_2Cl_2	–78→RT	1	1	2	**R2141b**	42	1451
Michael Addition	Mpydc33	Pd^{II}[i]	CH_2Cl_2	40	1	1	1	**R2142**	60	1464
Michael Addition	Mpydc33	Pd^{II}[i]	CH_2Cl_2	40	1	1	1.5	**R2142**	85	1464
Michael Addition	Mpydc33	Pd^{II}[i]	CH_2Cl_2	40	1	1	2.5	**R2142**	>99	1464
Oxidative Heck	Mbpy32	$Pd(OAc)_2$[j]	$CHCl_3/CH_2Cl_2$	RT	1	0.1	1-Feb	**R2143a**	73	1463
Oxidative Heck	Mbpy32	$Pd(OAc)_2$[j]	$CHCl_3/CH_2Cl_2$	RT	1	0.01	1-Feb	**R2143a**	66	1463
Alkyne homocoupling	Mpy29-O	$Pd(MeCN)Cl_2$[k]	$^iPr_2NH$	25	1	1	2.5	**R2144a**	43	1465
Alkyne homocoupling	Mpy29-O	$Pd(MeCN)Cl_2$[k]	$^iPr_2NH$	25	1	1	10	**R2144a**	61	1465
Alkyne homocoupling	Mpy29-O	$Pd(MeCN)Cl_2$[l]	Benzene	25	1	0.1	10	**R2144a**	35	1465
Alkyne homocoupling	Mpy29-O	$Pd(MeCN)Cl_2$[l]	Benzene	25	1	0.05	15	**R2144a**	81	1465
Alkyne homocoupling	Mpy29-O	$Pd(MeCN)Cl_2$[l]	Benzene	50	1	0.05	15	**R2144a**	47	1465
Alkyne homocoupling	Mpy29-O	$Pd(MeCN)Cl_2$[l]	Benzene	25	1	0.05	30	**R2144a**	90	1465
Alkyne homocoupling	$Mpy29\text{-}CH_2$	$Pd(MeCN)Cl_2$[k]	$^iPr_2NH$	25	1	1	2.5	**R2144b**	38	1465
Alkyne homocoupling	$Mpy29\text{-}CH_2$	$Pd(MeCN)Cl_2$[k]	$^iPr_2NH$	25	1	1	30	**R2144b**	14	1465
Alkyne homocoupling	Mbpy32	$PdCl_2$[k]	$^iPr_2NH$	25	1	1	2.5	**R2144c**	10	1465
Alkyne homocoupling	Mbpy32	$PdCl_2$[k]	$^iPr_2NH$	25	1	1	30	**R2144c**	76	1465
Alkyne homocoupling	Mbpy32	$NiCl_2/CuI$[m]	THF	–78→80	1	1	2	**R2144c**	32	1468
Alkyne homocoupling	Mbpy32	$NiCl_2/CuI$[n]	THF	–78→80	1	1	2	**R2144c**	67	1468
Alkyne homocoupling	Mbpy32	$NiCl_2/CuI$[m]	THF	–78→80	1	2	4	**R2144c**	95	1468
Haloalkane	Mpybox31	$NiCl_2{\cdot}DME$[o]	THF/DME	RT	1	1	2.2	**R2145**	46	1469
homocoupling	Mpybox31	$NiCl_2{\cdot}DME$[o]	THF/DME	80	1	1	2.2	**R2145**	24	1469

[a]With pyridine (3 equiv). [b]With K_2CO_3 (9.3 equiv) and I_2 (1 equiv). [c]With K_2CO_3 (3.75 equiv) and I_2 (1.25 equiv). [d]With K_2CO_3 (15 equiv) and I_2 (5 equiv). [e]With KO^tBu (15 equiv). [f]With K_2CO_3 (4 equiv). [g]Cu^I catalyst introduced as an aryl acetylide salt by pretreatment of the substrate with 1 equiv *n*-BuLi and transmetalation with CuI. [h]With Cs_2CO_3 (2 equiv). [i]With $^iPr_2NH$ (0.1 equiv). [j]With benzoquinone (1 equiv). [k]With 5 mol% CuI. [l]With 5 mol% CuI and *i*-Pr_2NH (5 equiv). [m]1:1 $NiCl_2$:CuI with *n*-BuLi (2 equiv). [n]1:2 $NiCl_2$:CuI with *n*-BuLi (2 equiv). [o]With 4 equiv Zn dust.

Table 2.41 The effect of ring size and stopper constitution on the CuAAC active metal template synthesis of [2]rotaxanes based on a macrocyclic bpy ligand.[1434]

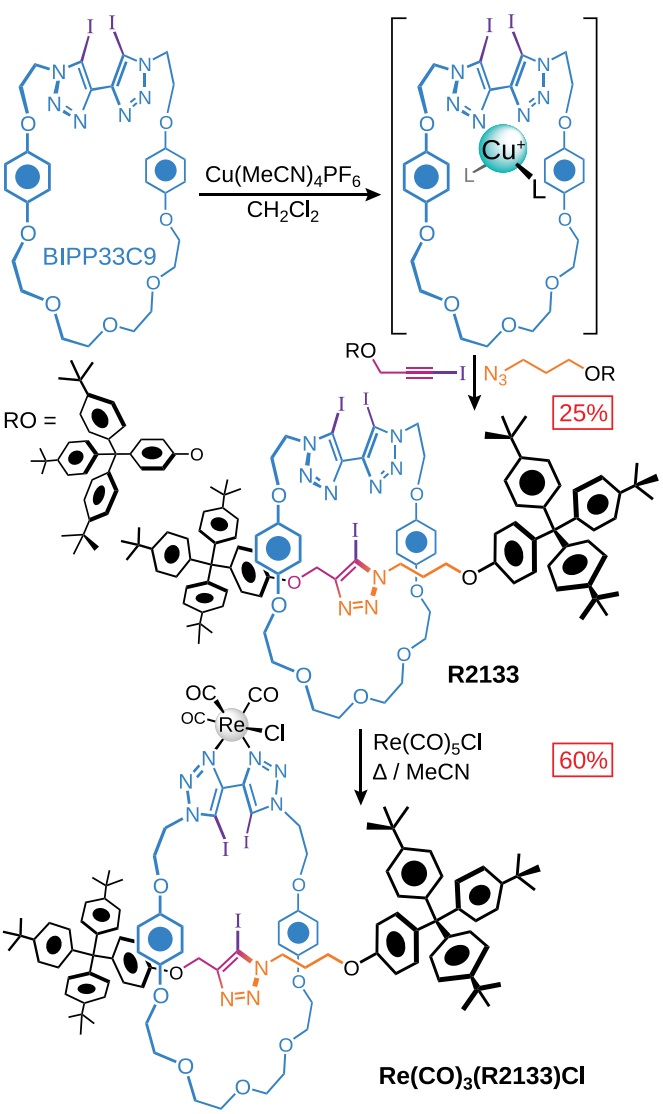


Alkyne	Azide	*n*	Equiv	T / °C	Yield / %
		2	1:1:1	80	100
		4	1:1:1	80	76
		6	1:1:1	80	34
		6	1:1:1	25	<5
		8	1:1:1	80	48
		8	1:1:1	25	85
		4	1:1:1	80	40
		4	1:5:5	80	99
		4	1:1:1	80	99
		4	1:1:1	80	40
		4	1:5:5	80	100
		4	1:1:1	80	40
		4	1:5:5	80	93
		4	1:1:1	80	40
		4	1:5:5	80	100
		4	1:1:1	80	40
		4	1:5:5	80	96

[2]R2132a-e, or the [3]rotaxane **[3]R2132a-e**, respectively. Governed by ligand exchange processes at equilibrium, the product distribution favors the [3]rotaxanes **[3]R2132a-e** at low catalyst loading ratios with respect to the ring, whereas an abundance of Cu^{I} ions facilitates the production of the **L2132** dumbbell. The reaction is highly sensitive to the constitution of the endocyclic chelates. For example, in the case of Mpy29-X, rotaxanes are produced successfully when X = O, CH_2, or SO_2, yet not when X = NH, NAc, or S, most likely because the latter, more strongly coordinating atoms reduce the Lewis acidity of the metal center. Other macrocyclic ligands such as Mpydc29 and Mdpp30 (see **Section 2.3.2**) also fail to capture dumbbells within their cavities. In the presence of 10 equiv of the macrocyclic ligand, it is possible to access the [3]rotaxanes in up to 33% yield, except in the case of the bidentate ring Mbpy32. This CuAAC active template strategy has also been applied[1430] to the synthesis of [2]catenanes (**C270a-b**) by both threading and entwining approaches, as well as to a [3]rotaxane from a homologous endobicyclic chelate,[1431] a [2]rotaxane molecular shuttle[1428] (see **Section 5.1.1.2**), a molecular trefoil knot,[1432] and a [2]rotaxane-based molecular machine[1433] (see **Scheme 1.5** in **Section 1.3.6**) designed for sequence-specific peptide synthesis.

Goldup[1434–1437] has carried the torch of CuAAC active template synthesis from Leigh's group into his independent career initially at Queen Mary University of London and subsequently at the University of Southampton. Goldup[1434] has probed the effect of ring size on the CuAAC active metal template synthesis (**Table 2.41**) of rotaxanes, finding that smaller rings lead to more efficient dumbbell capture processes. Emanating from this work, mechanically protected organometallic copper triazolides, stabilized by a mechanical bond, have been prepared,[1435] as well as rotaxanes possessing mechanically planar chirality (see **Section 5.2.3.1**) in high enantiopurity.[1436]

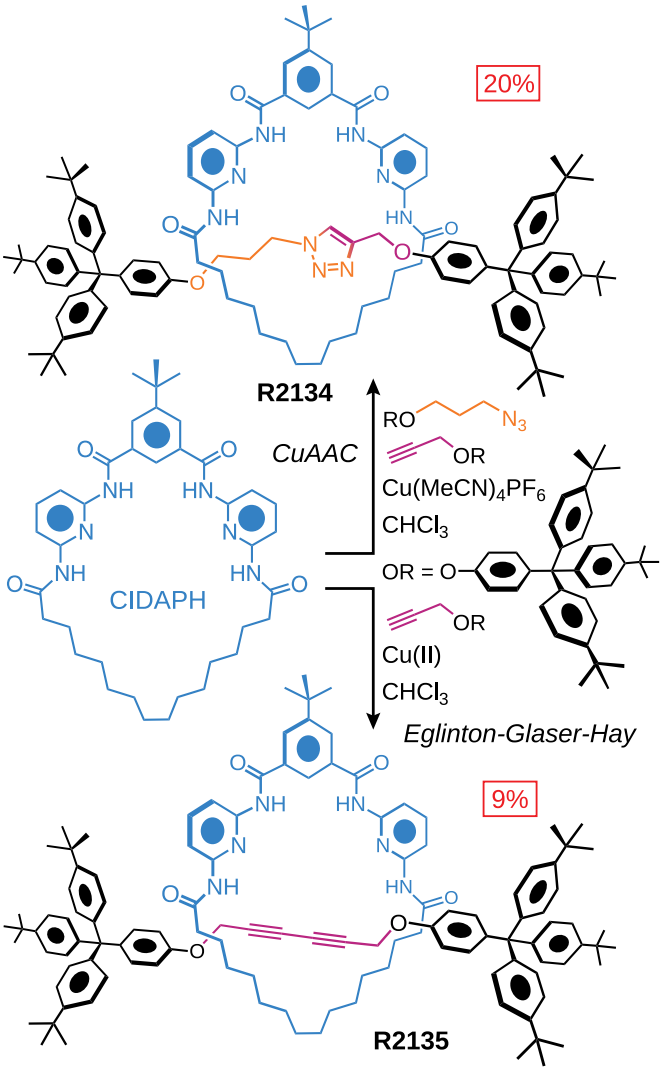
Beer[1438] has employed an active Cu^{I} template to synthesize (**Scheme 2.130**) a [2]rotaxane as a halogen-bonding anion



Scheme 2.130 Beer's active template CuAAC synthesis of an iodotriazole-containing [2]rotaxane and subsequent metalation with Re^{I} in order to enhance its capacity for halogen bonding.[1438]

receptor. The macrocyclic template/catalyst is generated by endotopic binding of Cu^{I} to the bis(iodotriazole) unit of bis(iodotriazole)-*para*-phenylene[33]crown-9 (BIPP33C9) upon addition of a stoichiometric amount of $Cu(MeCN)_4PF_6$ to a CH_2Cl_2 solution of the macrocycle, together with four equivalents of a pair of triarylmethyl-stoppered semidumbbells possessing reactive azide and iodoalkyne terminal groups. An endotopic CuAAC coupling of the azide and iodoalkyne substrates captures an iodotriazole-based dumbbell within the [2]rotaxane **R2133** in 25% yield, after removal of the Cu^{I} template in an aqueous solution of EDTA. Metalation of the bis(iodotriazole) with $Re(CO)_5Cl$ generates a sterically demanding exotopic coordination complex, which orientates the iodine atoms endotopically. Thus, the three iodotriazole units of **Re(CO)$_3$(R2133)Cl** constitute the binding pocket of a neutral mechanically interlocked all-halogen bonding receptor, which binds Cl^-, Br^-, and I^- with modest K_a values of 560, 120, and 80 M^{-1}, respectively, in $CHCl_3$. This active template protocol represents an unusual example of how cations may be employed to template the formation of anion receptors.

Recently, McClenaghan[1439] has re-purposed his hydrogen-bonding Hamilton receptor, CIDAPH—see **Scheme 2.82** and the accompanying discussion in **Section 2.3.4.4**—as a macrocyclic ligand for the active copper template synthesis (**Scheme 2.131**) of [2]rotaxanes, since CIDAPH was found to bind Cu^{I} with a K_a value of 60000 M^{-1} in $CHCl_3$. In the presence of Cu^{I}, this strong binding interaction allows CIDAPH to capture azide and alkyne semidumbbells in an endotopic CuAAC reaction, forming the triazole-containing [2]rotaxane **R2134** in 20% yield.



Scheme 2.131 McClenaghan's active copper template syntheses[1439] of the [2]rotaxanes **R2134** and **R2135** by CuAAC and Eglinton-Glaser-Hay coupling reactions, respectively, within the annulus of the hydrogen-bonding CIDAPH receptor.

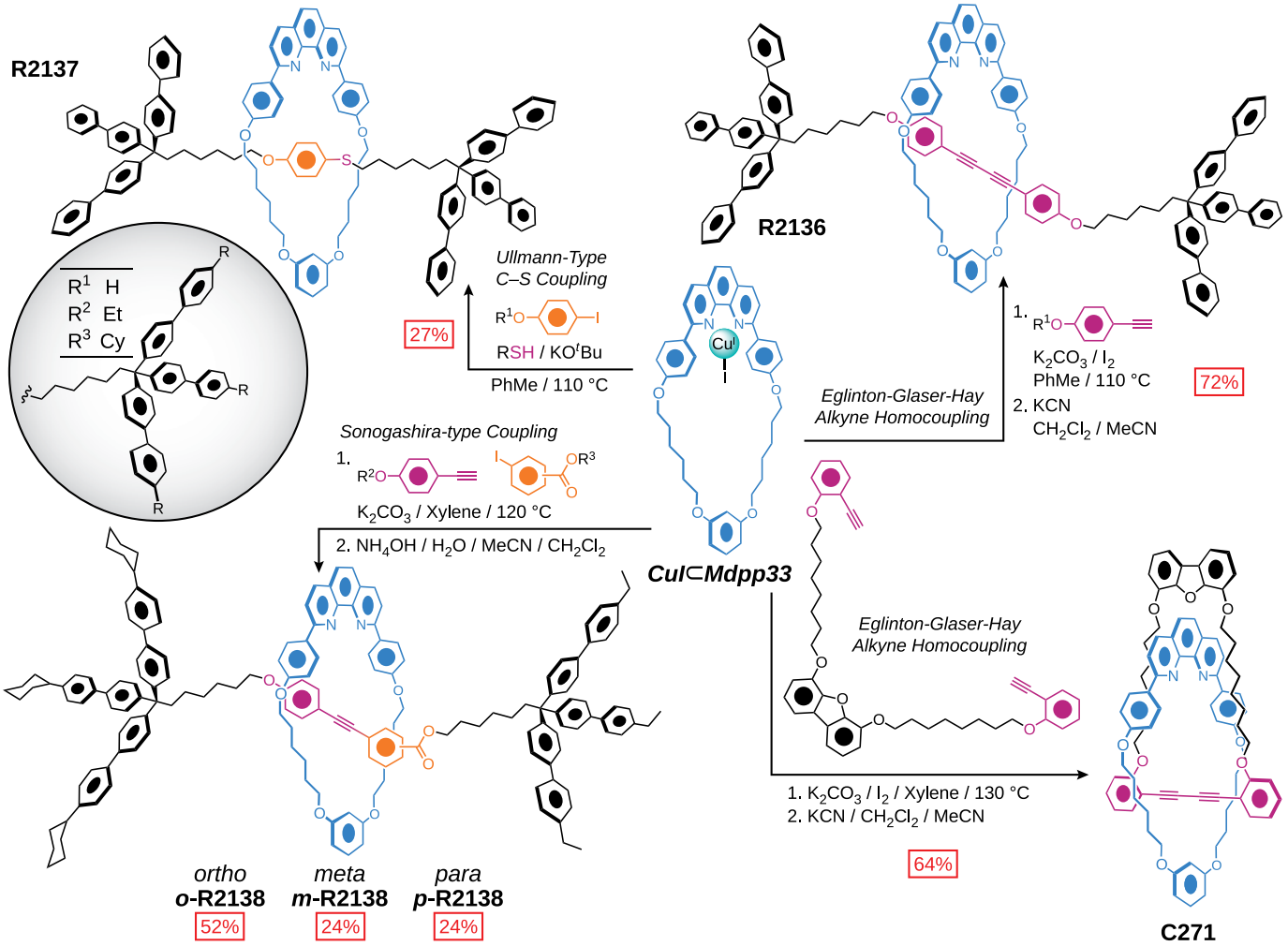
2.4.1.2 Eglinton-Glaser-Hay Active Template Synthesis

In the presence of a Cu^{II} active template, the endotopic Eglinton-Glaser-Hay homocoupling of a pair of propargylated semidumbbells within McClenaghan's CIDAPH receptor leads to the formation (**Scheme 2.131**) of the [2]rotaxane **R2135** in 9% yield. The presence of a mechanically bonded dumbbell reduces the Hamilton receptor's affinity for guests. Compared to *barbital⊂CIDAPH* (K_a = 23500 M^{-1}), **R2135** binds barbital with a K_a value of 8000 M^{-1} in $CHCl_3$, while an interaction between the triazole-based homologue **R2134** and barbital could not be detected. This difference in affinities for barbital may be accounted for, not only by the bulkier size of the triazole unit **R2134** compared to that of the butadiyne unit in **R2135**, but also by the triazole unit's capacity to compete with barbital for hydrogen bonds from the Hamilton receptor's NH donors.

When Saito[1426] co-introduced the first active template syntheses in 2006, one of several reactions (**Scheme 2.132**) he employed was the Eglinton-Glaser-Hay homocoupling of alkynes. The endocyclic chelate underpinning this seminal work is *CuI⊂Mdpp33*, comprising a dpp ligating moiety bound to copper(I) iodide. Since *CuI⊂Mdpp33* was isolated as a pure compound, the CuI catalyst was not introduced in sub-stoichiometric quantities. Upon reacting *CuI⊂Mdpp33* with 2.5 equiv of an alkyne-terminated semidumbbell in the presence of K_2CO_3 and I_2 in refluxing PhMe, the [2]rotaxane **R2136** is obtained in 72% yield after removal of the copper template with KCN in a CH_2Cl_2 / MeCN solution. Saito[1440] has employed a similar Eglinton-Glaser-Hay homocoupling protocol (**Scheme 2.132**) in the active template synthesis of [2]catenanes (e.g., **C271**) in up to 64% yield. Combining both of these dumbbell and ring capture methods, Saito[1441] has also constructed a rotacatenane comprising similar, yet larger, ring and dumbbell components.

2.4.1.3 Ullmann-Type Active Template Synthesis

Another one of Saito's intitial active template reactions (**Scheme 2.132**) was the Ullmann-type C–S coupling of aryl iodide and thiol-terminated semidumbbells. In this case,



Scheme 2.132 Active metal template syntheses developed by the Saito group, which employ the endocyclic chelate *CuI⊂Mdpp33* in dumbbell capture by Ulmann-type C–S coupling,[1426] dumbbell and ring capture by Eglinton-Glaser-Hay alkyne homocoupling,[1426,1440] and dumbbell capture by Sonogashira coupling.[1446]

CuI⊂Mdpp33 was combined with thiol- and *p*-iodophenyloxy-derived semidumbbells in refluxing toluene to afford the [2]rotaxane **R2137**. This endotopic C–S coupling is a less efficient (27%) capture reaction than the corresponding Eglinton-Glaser-Hay homocoupling (72%) leading to the [2]rotaxane **R2137**, in spite of the fact that it consumes a much larger excess (10 equiv) of substrates—see **Table 2.40**.

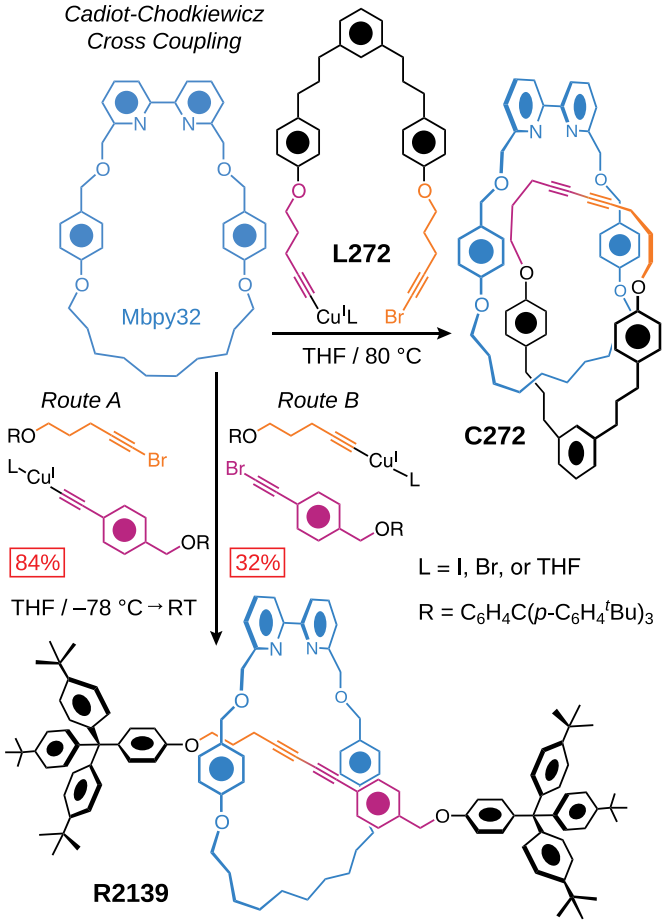
Anderson[1442–1444] has adopted Saito's oxidative homocoupling protocol in order to capture (i) long oligoyne dumbbells by acetylenic homocoupling via active template synthesis with *CuI⊂Mdpp33*,[1442] as well as (ii) an exotic [4]catenane 'molecular necklace' comprising Mdpp33 and a cyclohexameric porphyrin nanoring.[1443] Gladysz[1445] has also adopted the same strategy to prepare Pt-capped isulated molecular wires.

2.4.1.4 Sonogashira-Type Active Template Synthesis

Most recently, Saito[1446] has shown that the *CuI⊂Mdpp33* active template complex can capture (**Scheme 2.132**) the dumbbells of rotaxanes ***o*-R2138**, ***m*-R2138**, and ***p*-R2138** by promoting an endotopic Sonagashira-type heterocoupling between terminal aryl halide and alkyne semidumbbell substrates. These rotaxanes are obtained in yields ranging from 24% (*meta*, *para*) to 52% (*ortho*) under similar conditions to those employed in Saito's corresponding Eglinton-Glaser-Hay (**Section 2.4.1.2**) active template synthesis of **R2136**.

2.4.1.5 Cadiot-Chodkiewicz Active Template Synthesis

A Cu^{I}-catalyzed heterocoupling between copper acetylides, generated *in situ*, and bromoacetylenes (the Cadiot-Chodkiewicz reaction) has been applied to the active template synthesis[1447] (**Scheme 2.133**) of [2]rotaxanes such as **R2139.** Two routes (A and B) are depicted, in which the copper acetylide and bromoacetylide substrates derive from phenylacetylene and 1-pentyne, respectively (Route A) or *vice versa* (Route B). Mechanistically, both routes involve (i) the endotopic chelation of the copper acetylide substrate to the macrocyclic bidentate ligand Mbpy32, followed by (ii) oxidative addition of the bromoacetylene substrate, generating a copper diacetylide intermediate, which (iii) reductively



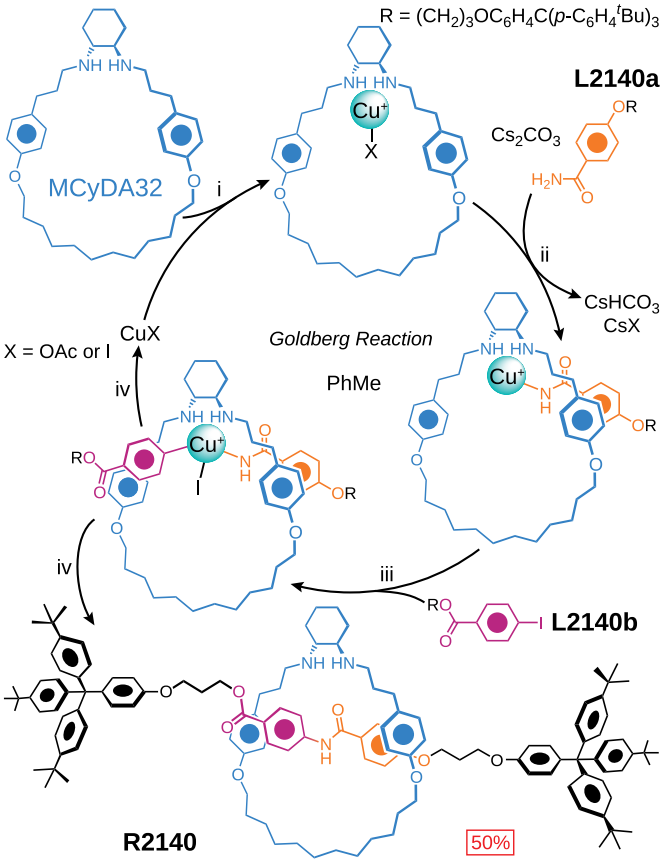
Scheme 2.133 Leigh's Cadiot-Chodkiewicz active template syntheses of mechanomolecules.[1447] The copper acetylide precursors are generated *in situ* prior to addition of the macrocyclic ligand Mbpy32 and the bromoacetylene coupling partner.

eliminates to produce the heterocoupled butadiyne dumbbell of the [2]rotaxane **R2139**. Route A is more efficient (84%) and proceeds with high selectivity (>98%) for the heterocoupled dumbbell, whereas Route B is less efficient (32%) on account of its lower selectivity, since it generates a homocoupled dumbbell derived from the bromoacetylene substrate as the major product. When both the bromoacetylene and copper acetylide semidumbbells derive from alkylacetylenes (not shown), the corresponding rotaxanes are also obtained in high yields (up to 85%) in high (>98%) selectivity. These results showcase the advantage of Cadiot-Chodkiewicz active templates in comparison to Eglinton-Glaser-Hay (**Section 2.4.1.2**) active templates—while both methods generate butadiyne-derived products, the Cadiot-Chodkiewicz method allows for the selective synthesis of constitutionally asymmetric, heterocoupled dumbbells, while the Eglinton-Glaser-Hay homocoupling does not.

Leigh[1430] has also adapted the Cadiot-Chodkiewicz active template protocol in the synthesis (**Scheme 2.133**) of the [2]catenane **C272** from an acyclic precursor (**L272**) possessing both bromoacetylene and copper acetylide terminal functional groups.

2.4.1.6 Goldberg Active Template Synthesis

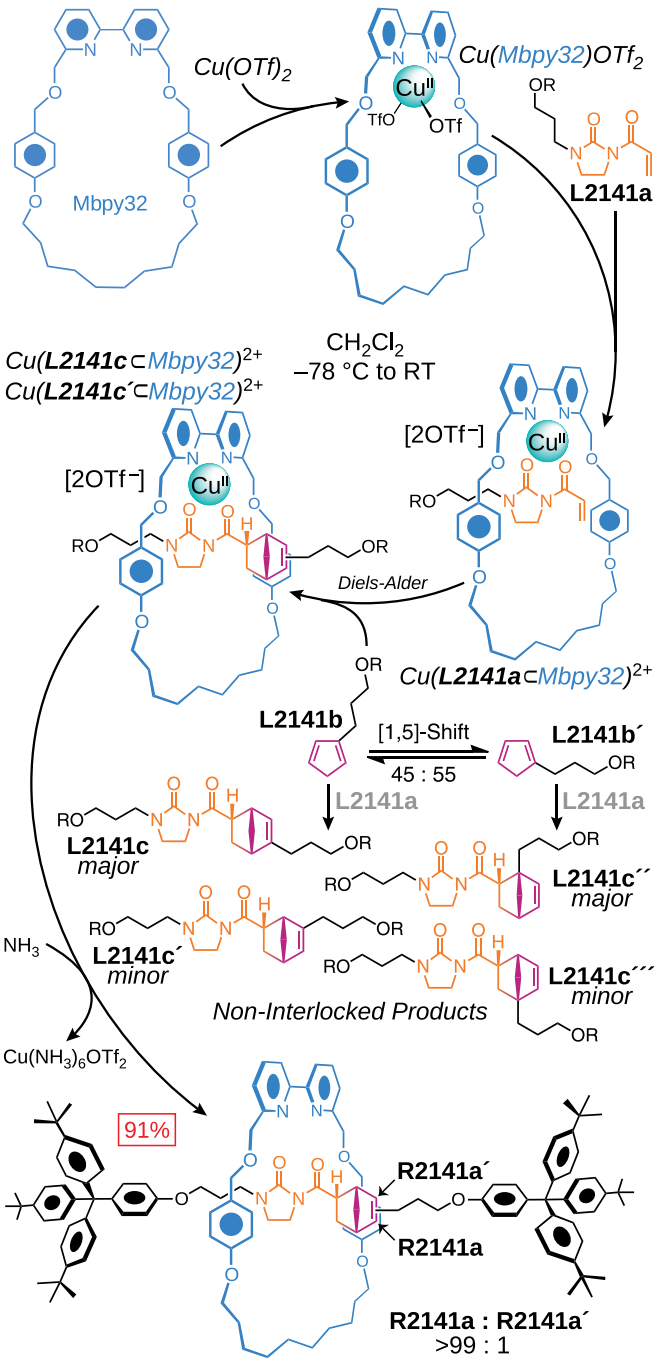
Recently, Leigh[1448] has introduced a new chiral macrocyclic chelate incorporating *R*,*R*-cyclohexane-1,2-diamine (CyDA) as the ligating moiety for active template synthesis and employed it to synthesize (**Scheme 2.134**) a [2]rotaxane. The reaction involves the Cu-catalyzed C_{Aryl}–N bond formation—the Goldberg reaction[1449]—between semidumbbells derived from aryl iodides and aryl amides. Under optimized conditions, the macrocycle MCyDA32 is combined with the substrates (≥5 equiv), CuOAc (0.5–0.9 equiv), and Cs_2CO_3 (10 equiv) in PhMe and heated at 120 °C for 15–48 h at concentrations near the solubility limit (150 mM) of the amide substrate to afford the [2]rotaxane **R2140** in ~50% yield. The proposed mechanism[1450] (**Scheme 2.134**) proceeds through (i) endocyclic coordination of Cu^I to MCyDA32, (ii) substitution of the Cu^I counterion by the depronated amide substrate, (iii) oxidative insertion of the C_{Aryl}–I bond of the second substrate to generate a Cu^{III} intermediate, which is (iv) converted to the [2]rotaxane **R2140** and the regenerated Cu^I catalyst by reductive elimination. Compound **R2140** has been employed[1448] subsequently as a ligand in asymmetric catalysis, promoting a Ni-catalyzed Michael addition with high enantioselectivity.



Scheme 2.134 Proposed mechanism of Leigh's active template synthesis of the [2]rotaxane **R2140** by a Goldberg copper-catalyzed C_{Aryl}–N bond forming reaction,[1448] which employs a chiral macrocyclic ligand MCyDA32 derived from cyclohexane-1,2-diamine.

2.4.1.7 Diels-Alder Active Template Synthesis

Leigh[1451] has introduced an active template dumbbell capture protocol (**Scheme 2.135**) in which an endocyclic chelate of a catalytic Lewis acid promotes a mechanical bond-forming Diels-Alder cycloaddition. The capture reaction couples semidumbbells derived from acryloyl imidazolidone (**L2141a**) and cyclopentadiene (**L2141b**) within the cavity of the macrocyclic chelate *Cu(Mbpy32)*$^{2+}$, releasing the [2]rotaxane **R2141a** as a product, upon removal of the Cu^{II} template with an excess of ammonia. The side-product that is produced when the Diels-Alder cycloaddition does not occur through the annulus is dumbbell **L2141c**. Since the precursor semidumbbell derived from cyclopentadiene equilibrates between the 2-substituted **L2141b** (55%) and 1-substituted **L2141b′** (45%) constitutional isomers, the corresponding cycloadduct exists as four isomers—**L2141c** (major isomer) and **L2141c′** (minor isomer) are adducts of 2-cyclopentadiene, while **L2141c″** (major isomer) and **L2141c‴** (minor isomer) are adducts of 1-cyclopentadiene. In the case of the [2]rotaxane, only the isomers **R2141a** and **R2141a′** arising from the 2-substituted cyclopentadiene (**L2141b**) are obtained, indicating that the 1-substituted cyclopentadiene (**L2141b′**) does not react through the annulus. Among these two rotaxanes, the cycloadduct with a 1,4-substitution pattern (**R2141a**) is formed >99:1 in favor over the other (**R2141a′**) isomer. This Diels-Alder active template protocol is also compatible with Mpy29-O as the macrocyclic ligand, but not with Mpy29-S or Mpy29-CH_2. In the case of the *Cu(Mpy29-0)*$^{+}$ active template, the analogous [2]rotaxane isomers **R2141b** and **R2141b′** are obtained (**Table 2.42**) in yields of up to 83% and selectivities as high as 9:1.

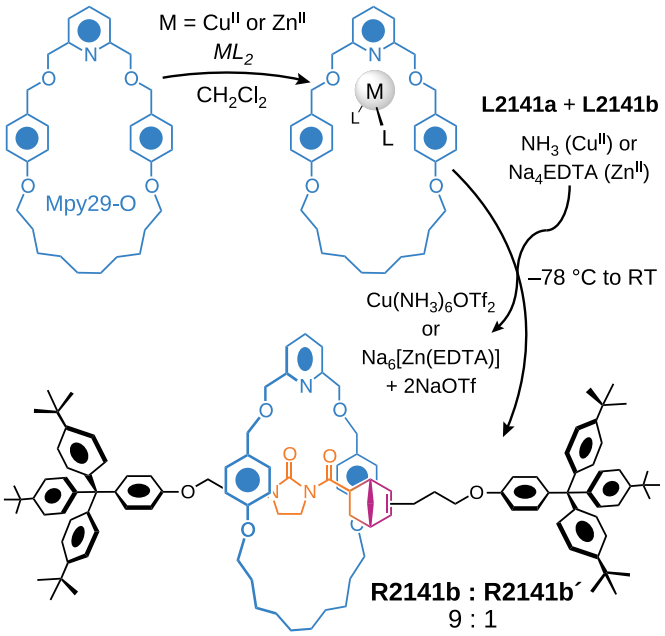


Scheme 2.135 Leigh's Diels-Alder active template synthesis of the [2]rotaxane **R2141**.

2.4.2 Active Zinc Templates

The Diels-Alder active template synthesis[1451] described in **Table 2.42** can also be catalyzed by Zn^{II} instead of Cu^{II}, affording **R2141b** in up to 42% yield. Although it is less

Table 2.42 The effects of metal ion (Zn^{II} or Cu^{II}), counterion (Cl^- or OTf^-), stoichiometry, and reaction time on the yield of Diels-Alder active template syntheses[1451] of the [2]rotaxane **R2141b**.



	Equivalents			
ML_2	L2141a	L2141b	*t* / h	Yield / %
$ZnCl_2$	1	1	24	0
$Zn(OTf)_2$	1	1	24	8
$Zn(OTf)_2$	1.2	2	96	42
$Cu(OTf)_2$	1	1	24	47
$Cu(OTf)_2$	1.2	2	96	83

efficient as an active template than copper in this case, this initial demonstration of a Zn^{II} active template opens the door to the possibility of desiging new active templates that rely on zinc catalysis,[1452] a field on the rise[1453] in organic synthesis on account of advantages including zinc's abundance, low cost, low toxicity, and capacity to promote the formation of C–C, C–N, and C–O bonds efficiently.[1454]

2.4.3 Active Palladium Templates

Palladium catalysis[1455–1457] has revolutionized the field of organic synthesis on account of its importance in C–C bond-forming reactions, a fact which was recognized[1458] with the award of the 2010 Nobel Prize in Chemistry to Heck,[1459,1460] Negishi,[1461] and Suzuki,[1462] "for palladium-catalyzed cross couplings in organic synthesis."

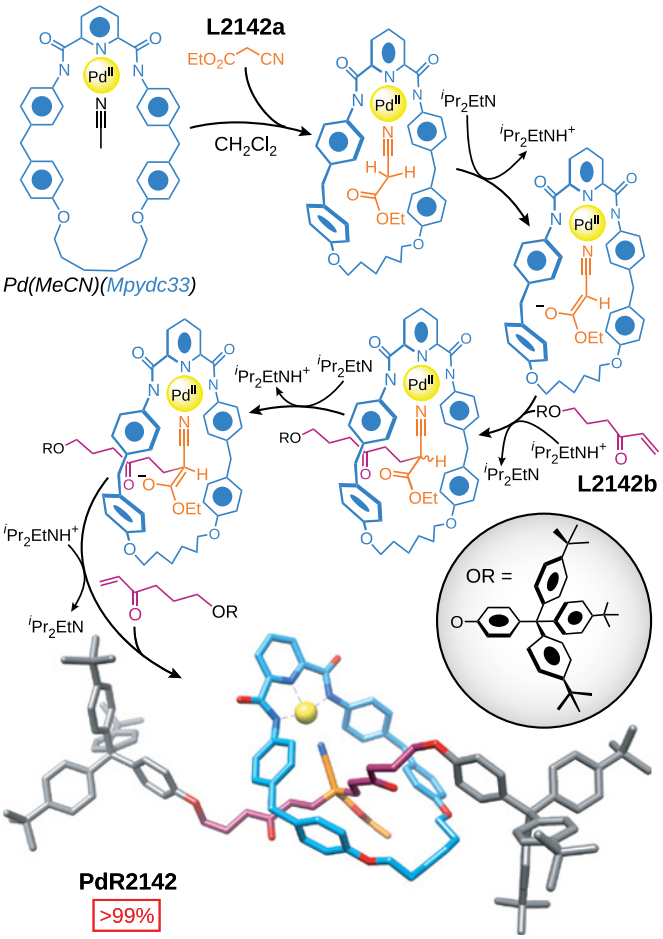
Leigh's initial attempts[1463] to utilize Pd^0-catalysed coupling reactions—i.e., the Heck reaction—in active template protocols failed to capture any dumbbells through the annulus, owing most likely to a highly labile or weak interaction between Pd^0 and the macrocylic ligands. Successful active Pd templates have relied instead on Pd^{II} catalysis, including (i) Pd-promoted Michael addition[1464] (**Section 2.4.3.1**), (ii) the Pd^{II}-catalyzed oxidative Heck reaction[1463] (**Section 2.4.3.2**), and (iii) Pd^{II}-catalyzed homocoupling[1465] (**Section 2.4.3.3**) of monosubstituted alkynes.

2.4.3.1 Michael Addition Active Template Synthesis

The case[1464] of the active template synthesis of rotaxanes by Michael addition (**Scheme 2.136**) stands apart from the others for a number of reasons: (i) the dumbbell is assembled from three components instead of a simple binary coupling, (ii) the active metal template is retained in the rotaxane upon completion of the reaction, and (iii) the yield (>99%) of the reaction is truly quantitative with only a modest excess (2.5 equiv) of substrates. The four-component self-assembly of the [2]rotaxane **PdR2142** relies on the open coordination site of the endocyclic chelate *Pd(MeCN)(Mpydc33)*, which is charge-neutral on account of its deprotonated carboxamide units coordinating the Pd^{II} center. The formation of a nitrile-Pd^{II} coordination bond positions α-cyanoesters within the cavity of the ring, while promoting the formation of C–C bonds by two successive 1,4-conjugate additions of the α-cyanoester substrate to vinyl ketone semidumbbells, a process catalyzed by a tertiary amine as a proton shuttle in solution. The enduring presence of the Pd^{II} center, which is apparent in the X-ray crystal structure (**Scheme 2.136**) of **PdR2142**, has allowed Leigh[1464] to construct a [2]rotaxane molecular shuttle (**Section 5.1.1.2**), which is driven by ligand exchange between two nitrile groups in a captured dumbbell.

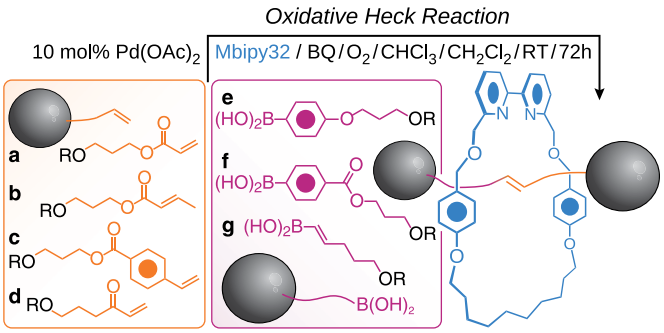
2.4.3.2 Oxidative Heck Active Template Synthesis

Leigh[1463] has employed the oxidative Heck reaction of aryl boronic acids and electron-poor alkenes in an active palladium template protocol, which affords (**Table 2.43**) the



Scheme 2.136 The quantitative four-component assembly[1464] of the [2]rotaxane **PdR2142** by Pd-promoted Michael addition at the open coordination site within the endocyclic chelate Pd(Mpydc33). Reaction conditions: 2.5 equiv α-cyanoester and vinyl ketone precursors (1:2 ratio), 0.1 equiv ^{i}PrEtN, CH_2Cl_2, 40 °C, 7 d. The tubular representation of the solid-state structure of the rotaxane is presented with protons and solvent molecules omitted for the sake of clarity.

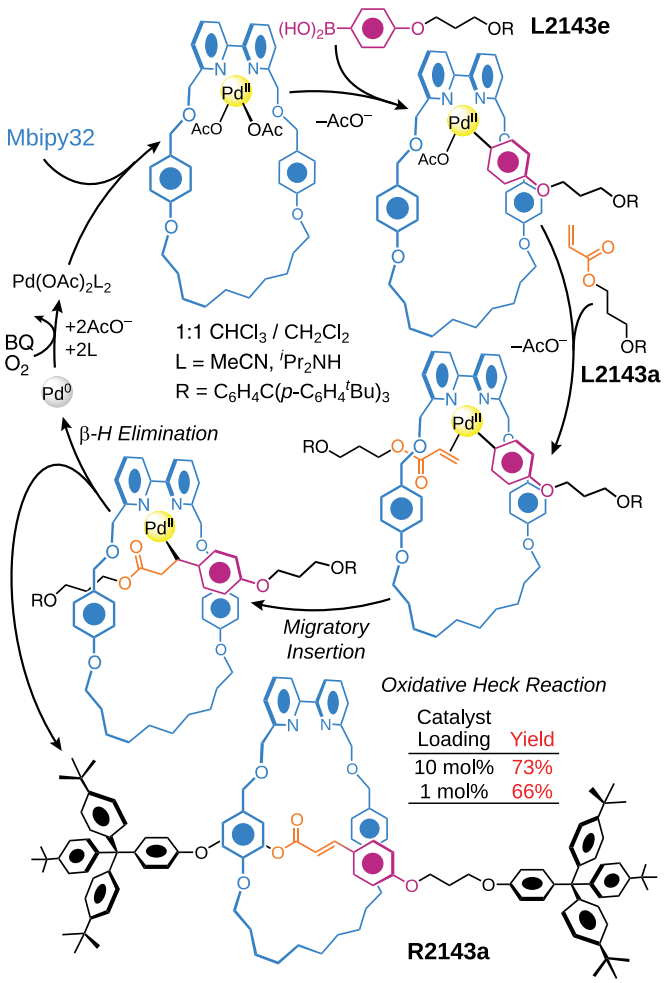
Table 2.43 Substrate scope of the oxidative Heck active template synthesis of [2]rotaxanes.[1463]



Alkene	L2143	Boronic Acid	Rotaxane	Yield / %
L2143a		L2143e	R2143a	73
L2143a		L2143f	R2143b	76
L2143a		L2143g	R2143c	30
L2143b		L2143e	R2143d	trace
L2143c		L2143e	R2143e	50
L2143d		L2143e	R2143f	70

[2]rotaxanes **R2143a-f**. The dumbbells of these rotaxanes are captured by combining the endotopic Pd^{II} chelate of Mbpy32 with different pairs of semidumbbell precursors derived from vinyl ketones/esters and aryl/vinyl boronic acids. The yield data indicate that the active template reaction tolerates both arylboronic (**L2143e-f**) and vinylboronic (**L2143g**) acids, as well as vinyl esters (**L2143a**), vinyl ketones (**L2143b**), and vinylphenylenes (**L2143d**), but not vinyl esters of disubstituted alkenes (**L2143b**), with optimal efficiency (up to 76%) in the cases of vinyl esters and arylboronic acids.

The mechanism (**Scheme 2.137**) of the oxidative Heck dumbbell capture is exemplified[1463] by the case of the [2]rotaxane **R2143a**. The endotopic chelation of $Pd(OAc)_2$ within the bidentate macrocycle Mbpy32 is followed by a transmetalation with the boronic acid-derived semidumbbell **L2143e**. The electron-deficient alkene of the acrylic ester semidumbbell **L2143a** displaces the second acetate counterion, leading to a square planar intermediate in which both semidumbbells and the macrocycle all surround the Pd^{II} center. A new C–C bond is formed through the annulus as a result of migratory insertion of an aryl–Pd bond, and



Scheme 2.137 The proposed mechanism of Leigh's active palladium template synthesis[1463] of the [2]rotaxane **R2143** based on the oxidative Heck reaction.

the rotaxane **R2131** is finally released upon β–hydride elimination, which generates a Pd^0 species with little to no affinity for the rotaxane. The Pd^{II} active template can be regenerated *in situ* by oxidation with benzoquinone (BQ) in O_2, allowing for truly catalytic turnover. Remarkably, **R2143a** is obtained in yields of up to 73% with 10 mol% Pd^{II}, and 66% yield with only 1 mol% Pd^{II}.

2.4.3.3 Active Palladium Alkyne Homocoupling

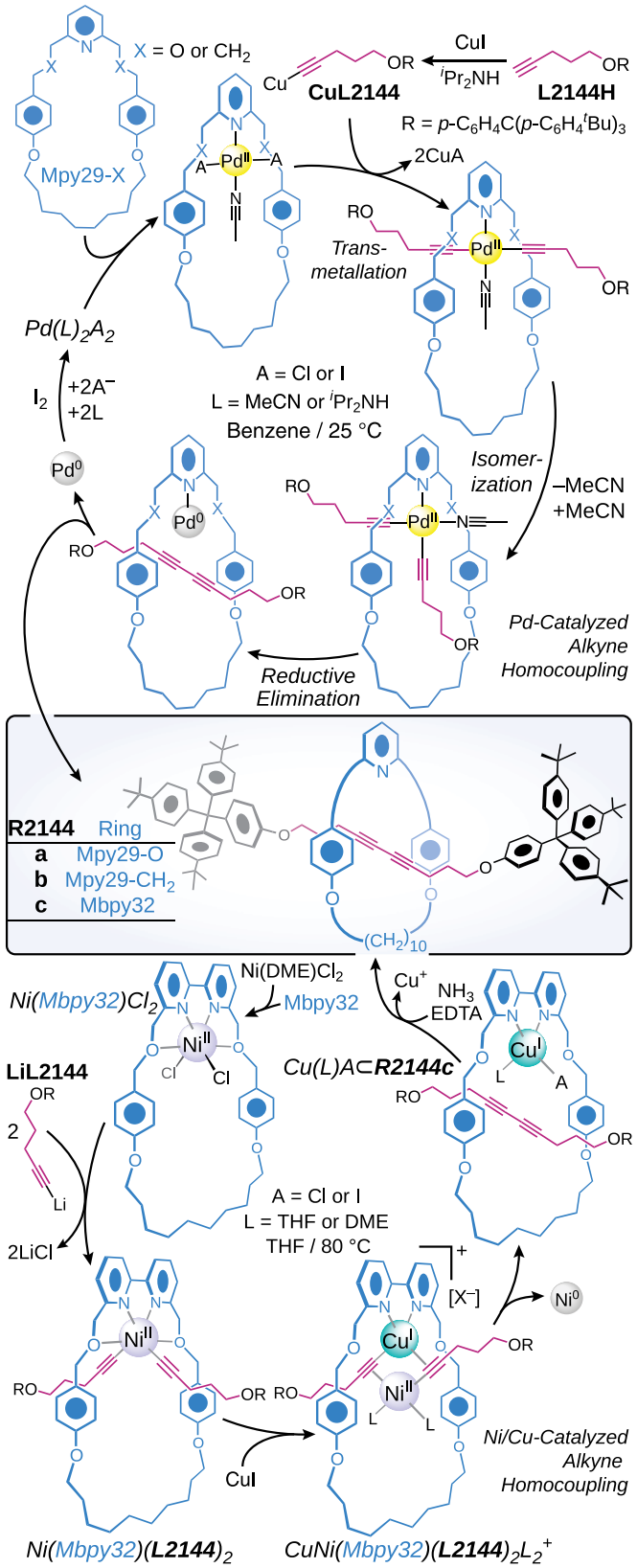
Leigh[1465] conceived of a Pd^{II}-catalyzed alkyne homocoupling active template synthesis (**Scheme 2.138**), which captures the rotaxanes **R2144a-c** derived from the Pd^{II} endocyclic chelates of Mpy29-O, Mpy29-CH_2, or Mbpy32. Mechanistically, the reaction begins when two Cu^{I} acetylide semidumbbells of **CuL2144**, generated *in situ*, displace each of the *trans*-coordinated anions of the active template complex, initially introduced by ligating the macrocyclic ligand to $PdCl_2$. The two Pd^{II}-coordinated acetylenes couple by reductive elimination after a *trans-cis* isomerization positions them adjacently. If the Pd^{II} source is introduced sub-stoichiometrically, catalytic turnover takes place when the Pd^0 center is oxidized back to a Pd^{II} active template by iodine. Under mild conditions in benzene at 298 K, the [2]rotaxanes **R2144a-c** are often produced in higher yields (**Table 2.40**) in a catalytic regime (5 mol% Pd^{II}) than in a stoichiometric one, most likely by avoiding the formation of side-products. The yields reach as high as 90, 38, and 76% when the rings comprise Mpy29-O (**R2144a**), Mpy29-CH_2 (**R2144b**), or Mbpy32 (**R2144c**), respectively.

2.4.4 Active Nickel Templates

Homogeneous nickel catalysis is a tool with widespread application in industrial chemical processes.[1466] The field has also undergone tremendous advances[1467] in recent years, marking nickel as a powerful catalytic metal for carrying out a wide variety of transformations in organic synthesis. The optimistic outlook for the future of Ni catalysis bodes well for the development of new active nickel template syntheses, which have thus far relied on alkyne homocoupling (**Section 2.4.4.1**) and sp^3–sp^3 homocoupling (**Section 2.4.4.2**) transformations in order to produce mechanical bonds by the capture of dumbbells.

2.4.4.1 Active Nickel Alkyne Homocoupling

The first active template protocol[1468] to employ a metal with an octahedral coordination geometry involved an unusual Ni^{II}-mediated alkyne homocoupling, leading to the [2]rotaxane **R2144c** by an alternative, more efficient route than that afforded[1465] by the original (**Section 2.4.3.3**) Pd^{II} active template. The proposed mechanism proceeds (**Scheme 2.138**) as follows: (i) the endotopic chelate *Ni(Mbpy32)*Cl_2, possessing an octahedral geometry which commandeers the ethereal oxygen atoms of the ring, forms upon mixing Ni(DME)Cl_2 (DME = dimethoxyethane) with ligand Mbpy32, (ii) the coordinated Cl groups are displaced



Scheme 2.138 Proposed mechanisms of the Pd-Catalyzed[1465] (top) and Ni/Cu-catalyzed[1468] (bottom) active metal template routes to the butadiyne [2]rotaxanes **R2144a-c**.

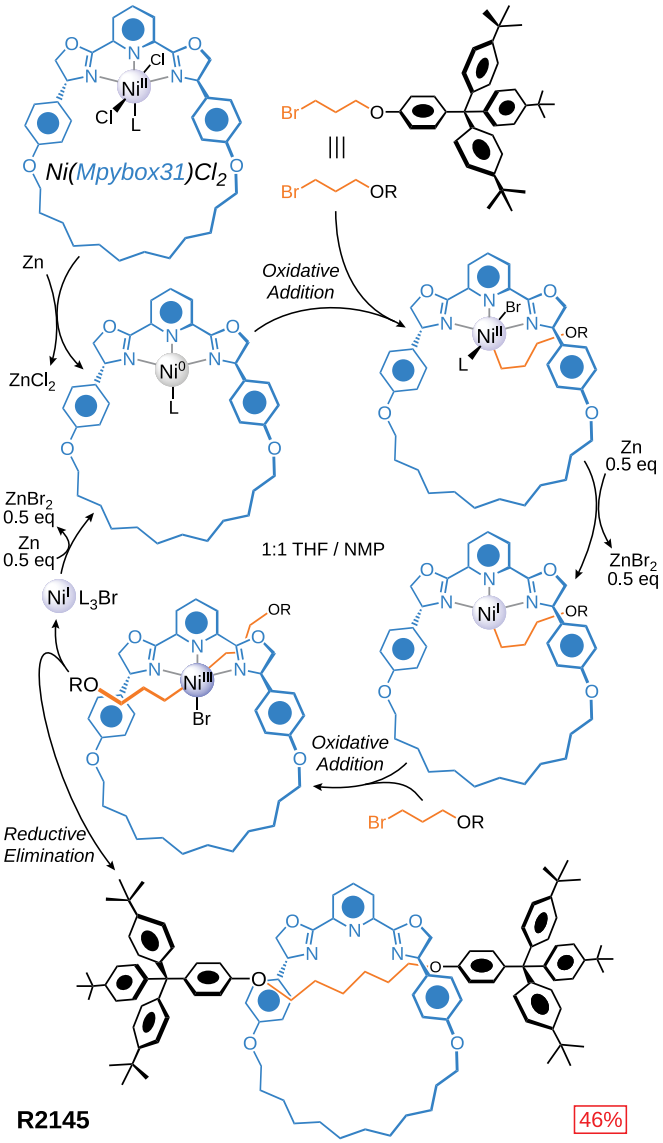
by the acetylide anions sourced from the organothium semidumbbell **LiR2144**, (iii) the nickel, which fails to eliminate from this diacetylide species in the absence of CuI, is displaced by Cu^{I}, generating a bimetallic, mixed-metal intermediate *CuNi(Mbpy32)*L_2^+, the π-activated, σ-bonded acetylides of which (iv) reductively eliminate to the Cu^{I}-metallated [2]rotaxane *Cu(**R2144c**)(L)A*, where L is a ligand (THF or OMe) and A is an anion (Cl or I), which is (v) removed by an excess of ammonia upon workup to generate **R2144c**. Under optimized conditions with 4 equiv **LiR2144** at 80 °C in THF, the [2]rotaxane is obtained in a remarkable 95% yield.

2.4.4.2 Active Nickel sp^3–sp^3 Homocoupling

Leigh[1431,1469] has also reported on the active nickel template synthesis (**Scheme 2.139**) of [2]rotaxanes via Ni-catalyzed sp^3–sp^3 homocoupling of bromoalkanes. The pyridine-2,6-bisoxazoline (pybox) ligand was incorporated[1469] into the endocyclic chelate Ni(Mpybox31)Cl_2, which reacts in 1:1 NMP-THF with two equivalents of a bromopropoxyphenyltrityl semidumbbell in the presence of four equiv of Zn dust to afford the [2]rotaxane **R2145** in up to 46% yield. The mechanism (**Scheme 2.139**) of the capture reaction involves the stepwise insertion of semidumbbells into a Ni^{II} center via Ni^{0} (first insertion) and Ni^{I} (second insertion) intermediates, followed by an endotopic reductive elimination, which generates the dumbbell. The Zn dust picks up the Cl^- and Br^- anions produced during the oxidative additions as it becomes oxidized to Zn^{II} during the reduction of the high oxidation state Ni centers throughout the catalytic cycle. Employing a larger tridentate chelate derived from terpyridine, the same reaction has been applied[1431] to the synthesis of a [3]rotaxane 'molecular sheaf' possessing one ring and two dumbbells—see **Section 4.2.1.2**.

Concluding Remarks

In summary, metal templates have evolved from being 'passive' directional scaffolds to being involved actively in covalent and mechanical bond-forming steps. Not surprisingly, the active template approach to MIM synthesis has attracted a lot of interest in only a short amount of time. Although it has been less than a decade since its introduction, active templation has already proven to be (i) compatible with a wide variety of catalytic reactions, which (ii) rely on a variety of different macrocyclic ligands and metal centers, as well as being (iii) amenable to the synthesis of the major types of MIMs (catenanes, rotaxanes, and knots) and (iv) applicable to the construction of challenging and exotic architectures, including molecular shuttles, switches, sheafs, necklaces, etc., and in particular, MIMs whose noncovalent bonding interactions do not 'live on' as they do in most cases of template-directed synthesis. As told by Leigh[22] and colleagues, "*the active template approach represents a change in philosophy for the synthesis of interlocked molecular architectures.*" Active template synthesis



Scheme 2.139 Proposed mechanism[1469] of the active template synthesis of the [2]rotaxane **R2145** by Ni-catalyzed homocoupling of inactivated bromoalkane semidumbbells.

will most likely become an increasingly important tool for chemists interested in making mechanical bonds.

Conclusions and Outlook

In summary, molecules with mechanical bonds can be obtained by statistical (**Section 2.1**), directed (**Section 2.2**), template-directed (**Section 2.3**), and active template (**Section 2.4**) strategies. The vast majority of mechanical bonds in chemistry have been made by template-directed protocols. We have sorted a random sample of 500 papers from the literature on catenanes and rotaxanes into these four categories, while sub-sorting the template-directed category into the different types of template motifs. This data, which is visualized as a pie chart in **Figure 2.85**, reveals that solvophobic/hydrophobic, metallo-organic, donor-acceptor, and hydrogen-bonded templates (**Sections 2.3.1–2.3.4**) claim the majority of the publications, representing approximately three-quarters of the chemical literature on mechanical bonds.

Each one of the major supramolecular genres possesses its own set of strengths and weaknesses, each lending itself to different niches in mechanostereochemistry. Owing to their water solubility, hydrophobic templates (**Section 2.3.1**) such as the CDs and CBs are the most suitable, in general, for biological applications—except, of course, for biomolecular (**Section 2.3.12**) templates. CDs also outcompete all the others in terms of low cost and widespread availability. Metallo-catenanes and rotaxanes (**Section 2.3.2**), such as those contained in the Sauvage, Fujita, and Leigh collections, exhibit well-defined and predictable geometries, with highly tailorable structural rigidity and dynamics—advantageous properties responsible for many of the 'firsts' in molecular topology, such as the interlocked cages, the trefoil and pentafoil knots, Solomon links, Borromean rings, Star of David, etc.—see **Section 4.1.1**. Donor-acceptor (D-A) templates (**Section 2.3.3**) come in a great many varieties, supported by an expansive 'meccano set' of π-donating and π-accepting building blocks, some of which have been central to many innovations in the realm of artificial molecular switches, machines, and motors. Hydrogen bonding (**Section 2.3.4**) is also characterized by diversity and abundance when it comes to design motifs, in addition to playing a role in most of the other recognition motifs, including hydrophobic, ionic, and D-A templates. Correspondingly, hydrogen-bonding

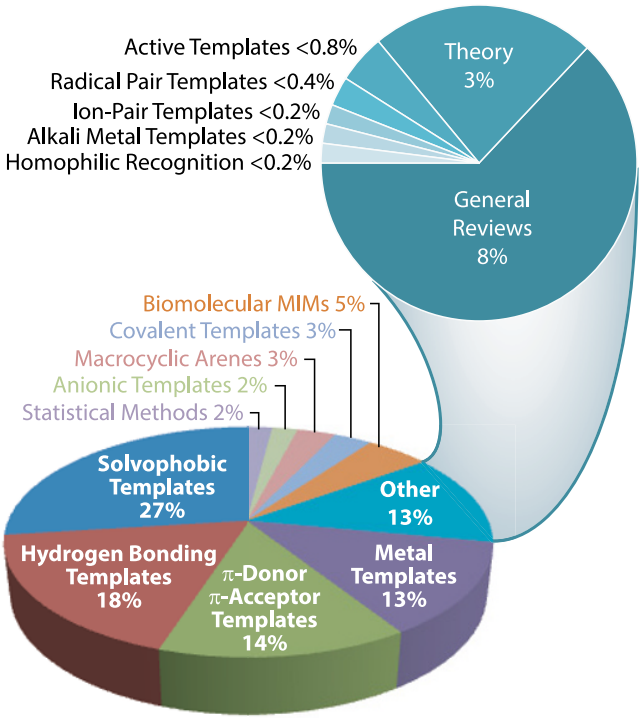


Figure 2.85 Breakdown of the literature on mechanical bonds by template classification. Data is based on a random sample of ~15% of the publications indexed in the SciFinder database under the keywords *catenane* and/or *rotaxane*.

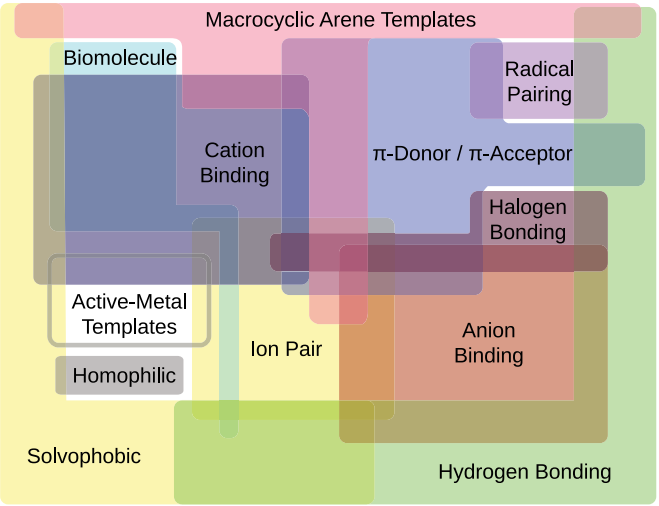


Figure 2.86 A Venn diagram illustrating how different molecular recognition motifs overlap in the template-directed synthesis of molecules with mechanical bonds.

motifs rival D-A motifs in their importance to artificial molecular switches and machines, as well as being currently the motif behind many synthetic milestones in the making of mechanical bonds, especially efficient ways to prepare rotaxanes under both kinetic and thermodynamic (**Chapter 3**) control. Up-and-comers such as halogen bonding (**Section 2.3.5**), anion binding (**Section 2.3.6**), ion-pairing (**Section 2.3.7**), cyclophanes (**Section 2.3.9**), radical-pairing (**Section 2.3.10**), and homophilic (**Section 2.3.11**) templates all promise to open new doors with their own unique properties and potential applications.

Although we have classified different recognition motifs into different categories, the lines between categories are not so clear in reality. Most of the MIMs constructed by template-directed synthesis rely on a combination of forces, as illustrated by the Venn diagram in **Figure 2.86**. Over 1300 references and 250 Figures, Schemes, and Tables presented in this Chapter say it loudly and clearly—there are lots of ways to make mechanical bonds!

References

(1) Frisch, H. L.; Wasserman, E. Chemical Topology. *J. Am. Chem. Soc*. **1961**, *83*, 3789–3795.
(2) Frisch, H.; Martin, I.; Mark, H. Zur Struktur der Polysiloxene. I. *Monatsh. Chem*. **1953**, *84*, 250–256.
(3) Walba, D. M. Topological Stereochemistry. *Tetrahedron* **1985**, *41*, 3161–3212.
(4) Lüttringhaus, A.; Cramer, F.; Prinzbach, H.; Henglein, F. M. Cyclisationen von Langkettigen Dithiolen. Versuche zur Darstellung sich umfassender Ringe mit Hilfe von Einschlußverbindungen. *Liebigs Ann. Chem*. **1958**, *613*, 185–198.
(5) Wasserman, E. The Preparation of Interlocking Rings: A Catenane. *J. Am. Chem. Soc.* **1960**, *82*, 4433–4434.
(6) Sokolov, V. I. Topological Ideas in Stereochemistry. *Russian Chem. Rev.* **1973**, *42*, 452–463.
(7) Breault, G. A.; Hunter, C. A.; Mayers, P. C. Supramolecular Topology. *Tetrahedron* **1999**, *55*, 5265–5293.
(8) Stoddart, J. F. The Master of Chemical Topology. *Chem. Soc. Rev.* **2009**, *38*, 1521–1529.
(9) Forgan, R. S.; Sauvage, J.-P.; Stoddart, J. F. Chemical Topology: Complex Molecular Knots, Links, and Entanglements. *Chem. Rev.* **2011**, *111*, 5434–5464.
(10) Schill, G.; Zollenkopf, H. Rotaxan-Verbindungen, I. *Liebigs Ann. Chem.* **1969**, *721*, 53–74.
(11) Olson, M. A.; Botros, Y. Y.; Stoddart, J. F. Mechanostereochemistry. *Pure Appl. Chem*. **2010**, *82*, 1569–1574.
(12) van Gulick, N. Theoretical Aspects of the Linked Ring Problem. *New J. Chem.* **1993**, *17*, 619–625.
(13) Ashton, P. R.; Philip, D.; Spencer, N.; Stoddart, J. F. The Self-Assembly of [*n*]Pseudorotaxanes. *J. Chem. Soc., Chem. Commun*. **1991**, 1677–1679.
(14) Harrison, I. T.; Harrison, S. The Synthesis of a Stable Complex of a Macrocycle and a Threaded Chain. *J. Am. Chem. Soc.* **1967**, *89*, 5723–5724.
(15) Chiu, C.-W.; Lai, C.-C.; Chiu, S.-H. "Threading-Followed-by-Swelling": A New Protocol for Rotaxane Synthesis. *J. Am. Chem. Soc.* **2007**, *129*, 3500–3501.
(16) Ko, J.-L.; Ueng, S.-H.; Chiu, C.-W.; Lai, C.-C.; Liu, Y.-H.; Peng, S.-M.; Chiu, S.-H. Using a Threading-Followed-by-Swelling Approach to Synthesize [2]Rotaxanes. *Chem. Eur. J.* **2010**, *16*, 6950–6960.
(17) Yoon, I.; Narita, M.; Shimizu, T.; Asakawa, M. Threading-Followed-by-Shrinking Protocol for the Synthesis of a [2]Rotaxane Incorporating a Pd(II)–Salophen Moiety. *J. Am. Chem. Soc.* **2004**, *126*, 16740–16741.
(18) Harrison, I. T. The Effect of Ring Size on Threading Reactions of Macrocycles. *J. Chem. Soc., Chem. Commun*. **1972**, 231–232.
(19) Mock, W. L.; Irra, T. A.; Wepsiec, J. P.; Adhya, M. Catalysis by Cucurbituril. The Significance of Bound-Substrate Destabilization for Induced Triazole Formation. *J. Org. Chem*. **1989**, *54*, 5302–5308.
(20) Prins, L. J.; Scrimin, P. Covalent Capture: Merging Covalent and Noncovalent Synthesis. *Angew. Chem., Int. Ed*. **2009**, *48*, 2288–2306.
(21) Stoddart, J. F. Putting Mechanically Interlocked Molecules (MIMs) to Work in Tomorrow's World. *Angew. Chem., Int. Ed*. **2014**, *53*, 11102–11104.
(22) Crowley, J. D.; Goldup, S. M.; Lee, A.-L.; Leigh, D. A.; McBurney, R. T. Active Metal Template Synthesis of Rotaxanes, Catenanes and Molecular Shuttles. *Chem. Soc. Rev.* **2009**, *38*, 1530–1541.
(23) Hansley, V. L. US Patent 2,228,268.
(24) Prelog, V.; Frenkiel, L.; Kobelt, M.; Barman, P. Zur Kenntnis des Kohlenstoffringes. Ein Herstellungsverfahren für vielgliedrige Cyclanone. *Helv. Chim. Acta* **1947**, *30*, 1741–1749.
(25) Stoll, M.; Hulstkamp, J. Synthèse de Produits Macrocycliques à Odeur Musquée. Sur Une Amélioration de la Préparation des Acyloïnes Cycliques. *Helv. Chim. Acta* **1947**, *30*, 1815–1821.
(26) Wasserman, E. Chemical Topology. *Sci. Am*. **1962**, *207*, 94–102.
(27) Schill, G.; Zollenkopf, H. Rotaxane. *Nachr. Chem. Techn*. **1967**, *15*, 149–150.
(28) Schill, G. *Catenanes, Rotaxanes, and Knots*; Academic Press: New York, 1971.
(29) Harrison, I. T. Preparation of Rotaxanes by the Statistical Method. *J. Chem. Soc., Perkin Trans*. *1* **1974**, 301–304.
(30) Schill, G.; Beckmann, W.; Schweickert, N.; Fritz, H. Untersuchungen zur Statistischen Synthese von Rotaxanen. *Chem. Ber.* **1986**, *119*, 2647–2655.
(31) Agam, G.; Graiver, D.; Zilkha, A. Studies on the Formation of Topological Isomers by Statistical Methods. *J. Am. Chem. Soc.* **1976**, *98*, 5206–5214.
(32) Raymo, F. M.; Stoddart, J. F. Slippage—A Simple and Efficient Way to Self-Assemble [*n*]Rotaxanes. *Pure Appl. Chem.* **1997**, *69*, 1987–1997.
(33) Agam, G.; Zilkha, A. Synthesis of a Catenane by a Statistical Double-Stage Method. *J. Am. Chem. Soc.* **1976**, *98*, 5214–5216.

(34) Wood, B. R.; Semlyen, J. A.; Hodge, P. Cyclic Polyesters 3. Attempts to Prepare Catenated Polymers Using Polymer-Supported Reagents. *Polymer* **1994**, *35*, 1542–1548.
(35) Gan, Y.; Dong, D.; Hogen-Esch, T. E. Synthesis and Characterization of a Catenated Polystyrene−Poly(2-Vinylpyridine) Block Copolymer. *Macromolecules* **2002**, *35*, 6799–6803.
(36) Ohta, Y.; Kushida, Y.; Kawaguchi, D.; Matsushita, Y.; Takano, A. Preparation, Characterization, and Nanophase-Separated Structure of Catenated Polystyrene−Polyisoprene. *Macromolecules* **2008**, *41*, 3957–3961.
(37) Endo, K.; Shiroi, T.; Murata, N.; Kojima, G.; Yamanaka, T. Synthesis and Characterization of Poly(1,2-Dithiane). *Macromolecules* **2004**, *37*, 3143–3150.
(38) Schappacher, M.; Deffieux, A. Atomic Force Microscopy Imaging and Dilute Solution Properties of Cyclic and Linear Polystyrene Combs. *J. Am. Chem. Soc.* **2008**, *130*, 14684–14689.
(39) Schappacher, M.; Deffieux, A. Imaging of Catenated, Figure-of-Eight, and Trefoil Knot Polymer Rings. *Angew. Chem., Int. Ed*. **2009**, *48*, 5930–5933.
(40) Schill, G.; Lüttringhaus, A. The Preparation of Catena Compounds by Directed Synthesis [1]. *Angew. Chem., Int. Ed. Engl*. **1964**, *3*, 546–547.
(41) Schill, G. Die gezielte Synthese von Catena-Verbindungen, II. *Chem. Ber*. **1965**, *98*, 2906–2915.
(42) Schill, G. Die gezielte Synthese von Catena-Verbindungen, III. Untersuchungen zur Synthese von Makrocyclen aus Doppelansaverbindungen durch Herausspalten des Aromatischen Ringes. *Chem. Ber*. **1965**, *98*, 3439–3445.
(43) Schill, G. Die gezielte Synthese von Catena-Verbindungen, IV. Einwirkung von Salpetersäure auf 2.5-Disubstituierte Hydrochinonäther. *Liebigs Ann. Chem*. **1966**, *691*, 79–87.
(44) Schill, G. Die gezielte Synthese von Catena-Verbindungen, V. Herstellung und Reaktionsfahigkeit von 2.5-Dialkyl-3.6-Dinitro-Benzochinonen. *Liebigs Ann. Chem*. **1966**, *693*, 182–186.
(45) Schill, G. Die gezielte Synthese von Catena-Verbindungen, VI. Doppelansa-Verbindungen von 5-Amino-Benzdioxol und seinen Dialkylderivaten. *Liebigs Ann. Chem*. **1966**, *695*, 65–76.
(46) Schill, G. Die gezielte Synthese von Catena-Verbindungen, VII. 3.5-Pentacosamethylen-Brenzcatechin. *Chem. Ber*. **1966**, *99*, 2689–2698.
(47) Schill, G. Die gezielte Synthese von Catena-Verbindungen, VIII. Urnwandlung einer Triansa-Verbindung in eine Catena-Verbindung. *Chem. Ber*. **1967**, *100*, 2021–2037.
(48) Vetter, W.; Schill, G. Die gezielte Synthese von Catena-Verbindungen, IX. Das Massenspektrum einer Catena-Verbindung. *Tetrahedron* **1967**, *23*, 3079–3093.
(49) Schill, G.; Zürcher, C. Die gezielte Synthese von Catena-Verbindungen, X. [3]-Catenanes. *Angew. Chem., Int. Ed. Engl*. **1969**, *8*, 988.
(50) Schill, G.; Murjahn, K.; Vetter, W. Die gezielte Synthese von Catena-Verbindungen, XI. Bis-diansa-Verbindungen des 5-Amino-Benzodioxols als Modelle fur die Synthese von [3]-Catenanen. *Liebigs Ann. Chem*. **1970**, *740*, 18–30.
(51) Schill, G.; Neubauer, H. Gezielte Synthese von Catena-Verbindungen, XII. Zweifach Uberbruckte 1.4-Diamino-2.5-Dimethoxy-3.6-Dialkyl-Benzol-Derivate als Modelle zur Gezielten Synthese von Catenanen und Rotaxanen. *Liebigs Ann. Chem*. **1971**, *750*, 76–90.
(52) Schill, G.; Vetter, W. Gezielte Synthese von Catena-Verbindungen, XIII. Zur Struktur von Bis-diansa-Verbindungen. *Chem. Ber*. **1971**, *104*, 3582–3586.
(53) Schill, G.; Murjahn, K. Gezielte Synthese von Catenanen, XIV. Alkylierung von Polyphenolderivaten, I. Derivate von α.ω-Bis-[5.6-Dihydroxy-3-Alkyl-Phenyl]-Alkanen und α.ω-Bis-[4.5-Dihydroxy-3-Alkyl-Phenyl]-Alkanen. *Chem. Ber*. **1971**, *104*, 3587–3593.
(54) Schill, G.; Neubauer, H. Gezielte Synthese von Catenanen, XV. 3,6-Dinitro-2,5-Dialkyl-Hydrochinon-Dimethylather. *Chem. Ber*. **1971**, *104*, 3810–3815.
(55) Schill, G.; Murjahn, K.; Beckmann, W. Gezielte Synthese von Catenanen, XVI. Untersuchungen zur Synthese Hohergliedriger Catenane und Rotaxane Bis-diansa-Verbindungen des 5-Aminobenzodioxols. *Chem. Ber*. **1972**, *105*, 3591–3599.
(56) Logemann, E.; Schill, G. Synthase von [2]-[Azacyclohaxacosan]-Cyclooctasan]-Catenan. *Chem. Ber.* **1978**, *111*, 2615–2629.
(57) Schill, G.; Doerjer, G.; Logemann, E.; Vetter, W. Reduktive Spaltung von 2,2-Dialkyl-1,3-benzodioxol-Derivaten mit Diisobutylaluminiumhydrid. Synthese eines [2]-Catenans mit einem 22-gliedrigen Makroheterocyclus. *Chem. Ber*. **1980**, *113*, 3697–3705.
(58) Logemann, E.; Riβler, K.; Schill, G.; Fritz, H. Synthese und Spektren von Zwei Neuen Catenanen. *Chem. Ber.* **1981**, *114*, 2245–2260.
(59) Schill, G.; Riβler, K.; Fritz, H. Über den Anwendungsbereich gezielter Catenansynthesen. Verbesserte Synthese von zweifachuberbruckten 1,4-Diamino-benzol-Derivaten. *Chem. Ber*. **1983**, *116*, 1866–1872.
(60) Schill, G.; Logemann, E.; Vetter, W. Ozonolytic Degradation of a Catenane. *Angew. Chem., Int. Ed. Engl*. **1972**, *11*, 1089–1090.
(61) Schill, G.; Zürcher, C. [3]-Catenane durch gezeilte Synthese. *Chem. Ber*. **1977**, *110*, 2046–2066.
(62) Schill, G.; Rissler, K.; Fritz, H.; Vetter, W. Synthesis, Isolation, and Identification of Translationally Isomeric [3]Catenanes. *Angew. Chem., Int. Ed. Engl*. **1981**, *20*, 187–189.
(63) Riβler, K.; Schill, G.; Fritz, H.; Vetter, W. Gezielte Synthese von translationsisomeren [3]-Catenanen. *Chem. Ber.* **1986**, *119*, 1374–1399.
(64) Schill, G.; Henschel, R. Rotaxan-Verbindungen, II. Eine Diansa-Verbindung des 5-Amino-6-methoxy-4.7-dimethyl-benzodioxols als Modell zur Synthese von Catenanen und Rotaxanen. *Liebigs Ann. Chem*. **1970**, *731*, 113–119.
(65) Schill, G.; Zürcher, C.; Vetter, W. Rotaxan-Verbindungen, III. Synthese eines Rotaxans mit Triphenylmethyl-Sperrgruppen und massenspextrometrische Untersuchungen. *Chem. Ber.* **1973**, *106*, 228–235.
(66) Schill, G.; Schweickert, N.; Fritz, H.; Vetter, W. [2]-[Cyclohexatetraoctane][cyclooctacosane]catenane, the First Hydrocarbon Catenane. *Angew. Chem., Int. Ed. Engl*. **1983**, *22*, 889–891.
(67) Schill, G.; Henschel, R.; Boeckmann, J. Untersuchungen zur Synthese eines Moleküls von der Gestalt eines dreiblättrigen Knotens.—Zweifach überbrückte 5,6-Diamino-1,3-benzodioxole. *Liebigs Ann. Chem*. **1974**, *1974*, 709–733.
(68) Schill, G.; Doerjer, G.; Logemann, E.; Fritz, H. Untersuchungen zur Synthese von Molekulen mit Knotenstruktur Vierfach überbrückte 5,6-Diamino-1,3-benzodioxol-Derivate. *Chem. Ber.* **1979**, *112*, 3603–3615.
(69) Lüttringhaus, A.; Isele, G. Synthesis of a Catena Compound by the Semistatistical Principle. *Angew. Chem., Int. Ed. Engl*. **1967**, *6*, 956–957.
(70) Ziegler, K.; Eberle, H.; Ohlinger, H. Über vielgliedrige Ringsysteme. I. Die Präparativ ergiebige Synthese der Polymethylenketone mit mehr als 6 Ringgliedern. *Liebigs Ann. Chem*. **1933**, *504*, 94–130.
(71) Schill, G.; Beckmann, W.; Vetter, W. Statistiche Synthesen von Rotaxanen. *Chem. Ber*. **1980**, *113*, 941–954.
(72) Godt, A. Non-Rusty [2]Catenanes with Huge Rings and Their Polymers. *Eur. J. Org. Chem.* **2004**, 1639–1654.
(73) Ünsal, Ö.; Godt, A. Synthesis of a [2]Catenane with Functionalities and 87-Membered Rings. *Chem. Eur. J.* **1999**, *5*, 1728–1733.
(74) Duda, S.; Godt, A. The Effect of Ring Size on Catenane Synthesis. *Eur. J. Org. Chem.* **2003**, 3412–3420.
(75) Shah, M. R.; Duda, S.; Müller, B.; Godt, A.; Malik, A. Facile Access to Monodisperse Ultralarge Rings. *J. Am. Chem. Soc.* **2003**, *125*, 5408–5414.
(76) Dietrich-Buchecker, C. O.; Sauvage, J.-P.; Kintzinger, J. P.. Une Nouvelle Famille de Molecules: les Metallo-Catenanes. *Tetrahedron Lett*. **1983**, *24*, 5095–5098.

(77) Samorì, P.; Jäckel, F.; Ünsal, Ö.; Godt, A.; Rabe, J. P. Ordered Nanostructures of a [2]Catenane Through Self-Assembly at Surfaces—An STM Study with Sub-Molecular Resolution. *ChemPhysChem* **2001**, *2*, 461–464.

(78) Jeschke, G.; Godt, A. Co-Conformational Distribution of Nanosized [2]Catenanes Determined by Pulse EPR Measurements. *ChemPhysChem* **2003**, *4*, 1328–1334.

(79) Godt, A.; Jeschke, G. Separation of Motional Processes in a [2]Catenane by Combining Synthetic, Dual-Frequency EPR and Molecular Modelling Approaches. *Magn. Reson. Chem.* **2005**, *43*, S110–S118.

(80) Kawai, H.; Umehara, T.; Fujiwara, K.; Tsuji, T.; Suzuki, T. Dynamic Covalently Bonded Rotaxanes Cross-Linked by Imine Bonds Between the Axle and Ring: Inverse Temperature Dependence of Subunit Mobility. *Angew. Chem., Int. Ed*. **2006**, *45*, 4281–4286.

(81) Kawai, H. Hydrindacenes as Versatile Supramolecular Scaffolds. *Bull. Chem. Soc. Jpn.* **2015**, *88*, 399–409.

(82) Hiratani, K.; Suga, J.-I.; Nagawa, Y.; Houjou, H.; Tokuhisa, H.; Numata, M.; Watanabe, K. A New Synthetic Method for Rotaxanes via Tandem Claisen Rearrangement, Diesterification, and Aminolysis. *Tetrahedron Lett.* **2002**, *43*, 5747–5750.

(83) Azehara, H.; Mizutani, W.; Suzuki, Y.; Ishida, T.; Nagawa, Y.; Tokumoto, H.; Hiratani, K. Fixation and Systematic Dilution of Rotaxane Molecules on Self-Assembled Monolayers. *Langmuir* **2003**, *19*, 2115–2123.

(84) Nagawa, Y.; Suga, J.-I.; Hiratani, K.; Koyama, E.; Kanesato, M. [3]Rotaxane Synthesized *via* Covalent Bond Formation Can Recognize Cations Forming a Sandwich Structure. *Chem. Commun*. **2005**, 749–751.

(85) Hiratani, K.; Albrecht, M. The Tandem Claisen Rearrangement in the Construction of Building Blocks for Supramolecular Chemistry. *Chem. Soc. Rev.* **2008**, *37*, 2413–2421.

(86) Kameta, N.; Hiratani, K.; Nagawa, Y. A Novel Synthesis of Chiral Rotaxanes *via* Covalent Bond Formation. *Chem. Commun*. **2004**, 466–467.

(87) Kameta, N.; Nagawa, Y.; Karikomi, M.; Hiratani, K. Chiral Sensing for Amino Acid Derivative Based on a [2]Rotaxane Composed of an Asymmetric Rotor and an Asymmetric Axle. *Chem. Commun*. **2006**, 3714–3716.

(88) Hiratani, K.; Kaneyama, M.; Nagawa, Y.; Koyama, E.; Kanesato, M. Synthesis of [1]Rotaxane via Covalent Bond Formation and its Unique Fluorescent Response by Energy Transfer in the Presence of Lithium Ion. *J. Am. Chem. Soc.* **2004**, *126*, 13568–13569.

(89) Hirose, K.; Nishihara, K.; Harada, N.; Nakamura, Y.; Masuda, D.; Araki, M.; Tobe, Y. Highly Selective and High-Yielding Rotaxane Synthesis via Aminolysis of Prerotaxanes Consisting of a Ring Component and a Stopper Unit. *Org. Lett.* **2007**, *9*, 2969–2972.

(90) Cantin, K.; Lafleur-Lambert, A.; Dufour, P.; Morin, J.-F. Studies Toward the Synthesis of Phenylacetylene Macrocycle Based Rotaxane Precursors as Building Blocks for Organic Nanotubes. *Eur. J. Org. Chem.* **2012**, 5335–5349.

(91) Listing, J. B. *Der Census Räumlicher Complexe: Der Verallgemeinerung des Euler'schen Satzes von den Polyedern*; Dieterich: Göttingen, 1862.

(92) Möbius, A. F. Über Die Bestimmung des Inhaltes eines Polyëders. *Reports of the Royal Saxon Society Sciences, Mathematics and Phsycial Class* **1865**, *17*, 31–68.

(93) *Möbius Strip*; Weisstein, E. W., Ed.; Wolfram MathWorld. (accessed online on January 22, 2016) http://mathworld.wolfram.com/MoebiusStrip.html

(94) Walba, D. M. Topology in Molecular Stereochemistry - Preface. *New J. Chem*. **1993**, *17*, 618.

(95) Herges, R. Topology in Chemistry: Designing Möbius Molecules. *Chem. Rev.* **2006**, *106*, 4820–4842.

(96) Guy, R. K.; Harary, F. On the Möbius Ladders. *Can. Math. Bull.* **1967**, *10*, 493–496.

(97) Schill, G.; Tafelmair, L. Untersuchungen zur Synthese von Catenanen und Knoten nach dem Prinzip des Möbius-Bandes Zweifach überbrückte Tetraamino-*p*-Benzochinone. *Synthesis* **1971**, 546–548.

(98) Wasserman, E.; Ben-Efraim, D. A.; Wolovsky, R. The Synthesis of Carbon Macrocycles to C_{120}. *J. Am. Chem. Soc.* **1968**, *90*, 3286–3287.

(99) Ben-Efraim, D. A.; Batich, C.; Wasserman, E. Mass Spectral Evidence for Catenanes Form via a "Möbius Strip" Approach. *J. Am. Chem. Soc.* **1970**, *92*, 2133–2135.

(100) Gruter, G.-J. M.; Akkerman, O. S.; Bickelhaupt, F. The Formation of Catenanes. The Möbius Strip Approach Revisited. *Tetrahedron* **1996**, *52*, 2565–2572.

(101) Hérisson, J.-L.; Chauvin, Y. Catalyse de Transformation des Oléfines par les Complexes du Tungstène. II. Télomérisation des Oléfines Cycliques en Présence d'Oléfines Acycliques. *Makromol. Chem*. **1971**, *141*, 161–176.

(102) Katz, T. J.; McGinnis, J. The Mechanism of the Olefin Metathesis Reaction. *J. Am. Chem. Soc.* **1975**, *97*, 1592–1594.

(103) Grubbs, R. H.; Carr, D. D.; Hoppin, C.; Burk, P. L. Consideration of the Mechanism of the Metal Catalyzed Olefin Metathesis Reaction. *J. Am. Chem. Soc.* **1976**, *98*, 3478–3483.

(104) Walba, D. M.; Richards, R. M.; Haltiwanger, R. C. Total Synthesis of the First Molecular Möbius Strip. *J. Am. Chem. Soc.* **1982**, *104*, 3219–3221.

(105) Walba, D. M.; Homan, T. C.; Richards, R. M.; Haltiwanger, R. C. Topological Stereochemistry. 9. Synthesis and Cutting "in Half" of a Molecular Möbius Strip. *New J. Chem*. **1993**, *17*, 661–681.

(106) Walba, D. M.; Richards, R. M.; Sherwood, S. P.; Haltiwanger, R. C. Strategy for the Synthesis of Cylindrical Macropolycyclic Hosts with Hydrophilic Interior Surfaces: Crown Ether Rings Fused by the Tetrahydroxymethylethylene (THYME) Unit. *J. Am. Chem. Soc.* **1981**, *103*, 6213–6215.

(107) Walba, D. M.; Armstrong, J. D., III; Perry, A. E.; Richards, R. M.; Homan, T. C.; Haltiwanger, R. C. The THYME Polyethers: An Approach to the Synthesis of a Molecular Knotted Ring. *Tetrahedron* **1986**, *42*, 1883–1894.

(108) Walba, D. M.; Richards, R. M.; Hermsmeier, M.; Haltiwanger, R. C. Conformational Properties of the THYME Polyethers. The Bis-THYME Cylinder: A Three-Dimensional Analog of 18-Crown-6. *J. Am. Chem. Soc*. **1987**, *109*, 7081–7087.

(109) Simon, J. Topological Chirality of Certain Molecules. *Topology* **1986**, *25*, 229–235.

(110) Flapan, E. Symmetries of Möbius Ladders. *Math. Ann*. **1989**, *283*, 271–283.

(111) Qui, W.-Y.; Xin, H.-W. Molecular Design and Topological Chirality of the T_q-Möbius Ladders. *J. Mol. Struc. Theochem* **1997**, *401*, 151–156.

(112) Walba, D. M.; Zheng, Q. Y.; Schilling, K. Experimental Studies on the Hook and Ladder Approach to Molecular Knots: Synthesis of a Topologically Chiral Cyclized Hook and Ladder. *J. Am. Chem. Soc.* **1992**, *114*, 6259–6260.

(113) Han, D.; Pal, S.; Liu, Y.; Yan, H. Folding and Cutting DNA Into Reconfigurable Topological Nanostructures. *Nature Nanotechnol.* **2010**, *5*, 712–717.

(114) Busch, D. H. Molecular Organization, Portal to Supramolecular Chemistry. Structural Analysis of the Factors Associated with Molecular Organization in Coordination and Inclusion Chemistry, Including the Coordination Template Effect. *Coord. Chem. Rev*. **1990**, *100*, 119–154.

(115) Philp, D.; Stoddart, J. F. Self-Assembly in Organic Synthesis. *Synlett* **1991**, 445–458.

(116) Anderson, S.; Anderson, H. L.; Sanders, J. K. M. Expanding Roles for Templates in Synthesis. *Acc. Chem. Res.* **1993**, *26*, 469–475.

(117) Cacciapaglia, R.; Mandolins, L. Catalysis by Metal Ions in Reactions of Crown Ether Substrates. *Chem. Soc. Rev.* **1993**, *22*, 221–231.

(118) Hoss, R.; Vögtle, F. Template Syntheses. *Angew. Chem., Int. Ed. Engl*. **1994**, *33*, 375–384.
(119) Chapman, R. G.; Sherman, J. C. Templation and Encapsulation in Supramolecular Chemistry. *Tetrahedron* **1997**, *53*, 15911–15945.
(120) *Templated Organic Synthesis*; Diederich, F.; Stang, P. J., Eds.; Wiley-VCH: Weinheim, 1999.
(121) Hubin, T. J.; Busch, D. H. Template Routes to Interlocked Molecular Structures and Orderly Molecular Entanglements. *Coord. Chem. Rev.* **2000**, *200*, 5–52.
(122) Laughrey, Z. R.; Gibb, B. C. Macrocycle Synthesis Through Templation. *Top. Curr. Chem.* **2005**, *249*, 67–125.
(123) Busch, D. H. First Considerations: Principles, Classification, and History. *Top. Curr. Chem.* **2005**, *249*, 1–65.
(124) Meyer, C. D.; Joiner, C. S.; Stoddart, J. F. Template-Directed Synthesis Employing Reversible Imine Bond Formation. *Chem. Soc. Rev.* **2007**, *36*, 1705–1723.
(125) Amabilino, D. B.; Stoddart, J. F. Interlocked and Intertwined Structures and Superstructures. *Chem. Rev.* **1995**, *95*, 2725–2829.
(126) Fyfe, M. C. T.; Stoddart, J. F. Synthetic Supramolecular Chemistry. *Acc. Chem. Res*. **1997**, *30*, 393–401.
(127) Aricó, F.; Badjić, J. D.; Cantrill, S. J.; Flood, A. H.; Leung, K. C.-F.; Liu, Y.; Stoddart, J. F. Templated Synthesis of Interlocked Molecules. *Top. Curr. Chem.* **2005**, *249*, 203–259.
(128) Barin, G.; Forgan, R. S.; Stoddart, J. F. Mechanostereochemistry and the Mechanical Bond. *Proc R. Soc. A* **2012**, *468*, 2849–2880.
(129) Evans, N. H.; Beer, P. D. Progress in the Synthesis and Exploitation of Catenanes Since the Millennium. *Chem. Soc. Rev.* **2014**, *43*, 4658–4683.
(130) Gil-Ramírez, G.; Leigh, D. A.; Stephens, A. J. Catenanes: Fifty Years of Molecular Links. *Angew. Chem., Int. Ed*. **2015**, *54*, 6110–6150.
(131) Gibson, H. W.; Bheda, M. C.; Engen, P. T. Rotaxanes, Catenanes, Polyrotaxanes, Polycatenanes and Related Materials. *Prog. Polym. Sci*. **1994**, *19*, 843–945.
(132) Raehm, L.; Hamilton, D. G.; Sanders, J. K. M. From Kinetic to Thermodynamic Assembly of Catenanes: Error Checking, Supramolecular Protection and Oligocatenanes. *Synlett* **2002**, 1743–1761.
(133) Stoddart, J. F. The Chemistry of the Mechanical Bond. *Chem. Soc. Rev.* **2009**, *38*, 1802–1820.
(134) Zhang, Z.-J.; Liu, Y. Construction and Function of Interpenetrated Molecules Based on the Positively Charged Axle Components. *Synlett* **2012**, *23*, 1733–1750.
(135) Xue, M.; Yang, Y.; Chi, X.; Yan, X.; Huang, F. Development of Pseudorotaxanes and Rotaxanes: From Synthesis to Stimuli-Responsive Motions to Applications. *Chem. Rev.* **2015**, *115*, 7398–7501.
(136) Belohradsky, M.; Raymo, F. M.; Stoddart, J. F. Template-Directed Syntheses of Catenanes. *Collect. Czech. Chem. Commun.* **1997**, *62*, 527–557.
(137) Agrawal, Y. K.; Pancholi, Y. A.; Menon, S. K.; Srivastava, P. Rotaxanes and Their Complexing Abilities. *Rev. Inorg. Chem.* **2001**, *21*, 43–91.
(138) Schalley, C. A. Elements for the Construction of Molecular Devices: Template Effects and Self-Assembly. *J. Phys. Org. Chem.* **2004**, *17*, 967–972.
(139) Gavina, P.; Tatay, S. Synthetic Strategies for the Construction of Threaded and Interlocked Molecules. *Curr. Org. Synth.* **2010**, *7*, 24–43.
(140) Cram, D. J. The Design of Molecular Hosts, Guests, and Their Complexes (Nobel Lecture). *Angew. Chem., Int. Ed. Engl*. **1988**, *27*, 1009–1020.
(141) Lehn, J.-M. Supramolecular Chemistry—Scope and Perspectives Molecules, Supermolecules, and Molecular Devices (Nobel Lecture). *Angew. Chem., Int. Ed. Engl*. **1988**, *27*, 89–112.
(142) Pedersen, C. J. The Discovery of Crown Ethers (Nobel Lecture). *Angew. Chem., Int. Ed. Engl*. **1988**, *27*, 1021–1027.
(143) Chandler, D. Interfaces and the Driving Force of Hydrophobic Assembly. *Nature* **2005**, *437*, 640–647.
(144) Stoddart, J. F. A Century of Cyclodextrins. *Carbohyd. Res*. **1989**, *192*, xii–xv.
(145) Cramer, F. *Cyclodextrins and Their Industrial Uses*; Duchêne, D., Ed.; Editions de Santé: Paris, 1987; pp. 11–20
(146) Cramer, F. Über Einschlußverbindungen, I. Mitteil. Additionsverbuindungen Der Cycloamylosen. *Chem. Ber*. **1951**, *84*, 851–854.
(147) Cramer, F. Über Einschlußverbindungen, II. Mitteil. Die Blauen Jodadditionsverbindungen Organischer Moleküle. *Chem. Ber*. **1951**, *84*, 855–859.
(148) Cramer, F. Einschlußverbindungen Der Cyclodextrine. *Angew. Chem*. **1952**, *64*, 136.
(149) Cramer, F. Einschlußverbindungen. *Angew. Chem*. **1952**, *64*, 437–447.
(150) Cramer, F.; Saenger, W.; Spatz, H.-C. Inclusion Compounds. XIX. The Formation of Inclusion Compounds of α-Cyclodextrin in Aqueous Solutions. Thermodynamics and Kinetics. *J. Am. Chem. Soc*. **1967**, *89*, 14–20.
(151) Pedersen, C. J. Cyclic Polyethers and Their Complexes with Metal Salts. *J. Am. Chem. Soc.* **1967**, *89*, 2495–2496.
(152) Pedersen, C. J. Cyclic Polyethers and Their Complexes with Metal Salts. *J. Am. Chem. Soc.* **1967**, *89*, 7017–7036.
(153) Villiers, A. Sur la Transformation de la Fécule en Dextrine par le Ferment Butyrique. *Compt. Rend. Fr. Acad. Sci.* **1891**, *112*, 435–438.
(154) French, D.; Pulley, A. O.; Effenberger, J. A.; Rougvie, M. A.; Abdullah, M. Studies on the Schardinger Dextrins. XII. The Molecular Size and Structure of the δ-, ε-, -ζ, and η-Dextrins. *Arch. Biochem. Biophys*. **1965**, *111*, 153–160.
(155) Gessler, K.; Usón, I.; Takaha, T.; Krauss, N.; Smith, S. M.; Okada, S.; Sheldrick, G. M.; Saenger, W. V-Amylose at Atomic Resolution: X-Ray Structure of a Cycloamylose with 26 Glucose Residues (Cyclomaltohexaicosaose). *Proc. Natl. Acad. Sci. U.S.A.* **1999**, *96*, 4246–4251.
(156) French, D. The Schardinger Dextrins. *Adv. Carbohydr. Chem*. **1957**, *12*, 189–260.
(157) Szejtli, J. Introduction and General Overview of Cyclodextrin Chemistry. *Chem. Rev.* **1998**, *98*, 1743–1754.
(158) Freudenberg, K.; Cramer, F. Die Konstitution der Schardinger-Dextrine α, β, und γ. *Zeitschrift für Naturforschung* **1948**, *3b*, 464.
(159) Pringsheim, H. Chemistry of the Polysaccharides. *Angew. Chem*. **1922**, *35*, 345–349.
(160) VanEtten, R. L.; Sebastian, J. F.; Clowes, G. A.; Bender, M. L. Acceleration of Phenyl Ester Cleavage by Cycloamyloses. A Model for Enzymic Specificity. *J. Am. Chem. Soc*. **1967**, *89*, 3242–3253.
(161) VanEtten, R. L.; Clowes, G. A.; Sebastian, J. F.; Bender, M. L. The Mechanism of the Cycloamylose-Accelerated Cleavage of Phenyl Esters. *J. Am. Chem. Soc.* **1967**, *89*, 3253–3262.
(162) Breslow, R. Biomimetic Chemistry and Artificial Enzymes: Catalysis by Design. *Acc. Chem. Res.* **1995**, *28*, 146–153.
(163) Li, S.; Purdy, W. C. Cyclodextrins and Their Applications in Analytical Chemistry. *Chem. Rev.* **1992**, *92*, 1457–1470.
(164) Schneiderman, E.; Stalcup, A. M. Cyclodextrins: A Versatile Tool in Separation Science. *J. Chromatogr. B Biomed. Sci. Appl.* **2000**, *745*, 83–102.
(165) Ke, C.; Smaldone, R. A.; Kikuchi, T.; Li, H.; Davis, A. P.; Stoddart, J. F. Quantitative Emergence of Hetero[4]rotaxanes by Template-Directed Click Chemistry. *Angew. Chem., Int. Ed*. **2012**, *52*, 381–387.
(166) Szejtli, J. Medicinal Applications of Cyclodextrins. *Med. Res. Rev.* **1994**, *14*, 353–386.
(167) Szente, L.; Szejtli, J. Cyclodextrins as Food Ingredients. *Trends Food Sci. Tech.* **2004**, *15*, 137–142.
(168) Hedges, A. R. Industrial Applications of Cyclodextrins. *Chem. Rev*. **1998**, *98*, 2035–2044.
(169) Connors, K. A. The Stability of Cyclodextrin Complexes in Solution. *Chem. Rev.* **1997**, *97*, 1325–1358.

(170) Rekharsky, M. V.; Inoue, Y. Complexation Thermodynamics of Cyclodextrins. *Chem. Rev*. **1998**, *98*, 1875–1918.

(171) Nepogodiev, S. A.; Stoddart, J. F. Cyclodextrin-Based Catenanes and Rotaxanes. *Chem. Rev*. **1998**, *98*, 1959–1976.

(172) Wenz, G.; Han, B.-H.; Müller, A. Cyclodextrin Rotaxanes and Polyrotaxanes. *Chem. Rev*. **2006**, *106*, 782–817.

(173) Harada, A.; Hashidzume, A.; Yamaguchi, H.; Takashima, Y. Polymeric Rotaxanes. *Chem. Rev*. **2009**, *109*, 5974–6023.

(174) Terao, J. π-Conjugated Molecules Covered by Permethylated Cyclodextrins. *Chem. Rec*. **2011**, *11*, 269–283.

(175) Girek, T. Cyclodextrin-Based Rotaxanes. *J. Incl. Phenom. Macrocycl. Chem.* **2012**, *74*, 1–21.

(176) Saito, H.; Yonemura, H.; Nakamura, H.; Matsuo, T. Stability and Exchange Properties of Through-Ring Cyclodextrin Complexes. Effects of Chain Length in Polymethylene Bis(1-pyridinium) as Guest Molecules. *Chem. Lett*. **1990**, *19*, 535–538.

(177) Watanabe, M.; Nakamura, H.; Matsuo, T. Formation of Through-Ring α-Cyclodextrin Complexes with α,ω-Alkanedicarboxylate Anion. Effects of the Aliphatic Chain Length and Electrostatic Factors on the Complexation Behavior. *Bull. Chem. Soc. Jpn*. **1992**, *65*, 164–169.

(178) Khan, A. R.; Forgo, P.; Stine, K. J.; D'Souza, V. T. Methods for Selective Modifications of Cyclodextrins. *Chem. Rev.* **1998**, *98*, 1977–1976.

(179) Ogino, H. Relatively High-Yield Synthesis of Rotaxanes. Synthesis and Properties of Compounds Consisting of Cyclodextrins Threaded by α,ω-Diaminoalkanes Coordinated to Cobalt(III) Complexes. *J. Am. Chem. Soc.* **1981**, *103*, 1303–1304.

(180) Yamanari, K.; Shimura, Y. Stereoselective Formation of Rotaxanes Composed of Polymethylene-bridged Dinuclear Cobalt(III) Complexes and α- or β-Cyclodextrin *Bull. Chem. Soc. Jpn.* **1983**, *56*, 2283–2289.

(181) Yamanari, K.; Shimura, Y. Stereoselective Formation of Rotaxanes Composed of Polymethylene-bridged Dinuclear Cobalt(III) Complexes and α-Cyclodextrin. II. *Bull. Chem. Soc. Jpn*. **1984**, *57*, 1596–1603.

(182) Kawaguchi, Y.; Harada, A. An Electric Trap: A New Method for Entrapping Cyclodextrin in a Rotaxane Structure. *J. Am. Chem. Soc.* **2000**, *122*, 3797–3798.

(183) Isnin, R.; Kaifer, A. E. Novel Class of Asymmetric Zwitterionic Rotaxanes Based on α-Cyclodextrin. *J. Am. Chem. Soc.* **1991**, *113*, 8188–8190.

(184) Kunitake, M.; Kotoo, K.; Manabe, O.; Muramatsu, T.; Nakashima, N. Synthesis and Spectral Characterization of a Rotaxane of β-Cyclodextrin Threaded by a 4,4′-Diaminostilbene. *Chem. Lett*. **1993**, 1033–1036.

(185) Harada, A.; Li, J.; Kamachi, M. Non-ionic [2]Rotaxanes Containing Methylated α-Cyclodextrins. *Chem. Commun*. **1997**, 1413–1414.

(186) Craig, M. R.; Claridge, T. D. W.; Anderson, H. L.; Hutchings, M. G. Synthesis of a Cyclodextrin Azo Dye [3]Rotaxane as a Single Isomer. *Chem. Commun*. **1999**, 1537–1538.

(187) Craig, M. R.; Hutchings, M. G.; Claridge, T. D. W.; Anderson, H. L. Rotaxane Encapsulation Enhances the Stability of an Azo Dye, in Solution and When Bonded to Cellulose. *Angew. Chem., Int. Ed.* **2001**, *40*, 1071–1074.

(188) Haque, S. A.; Park, J. S.; Srinivasarao, M.; Durrant, J. R. Molecular-Level Insulation: An Approach to Controlling Interfacial Charge Transfer. *Adv. Mater.* **2004**, *16*, 1177–1181.

(189) Cheetham, A. G.; Hutchings, M. G.; Claridge, T. D. W.; Anderson, H. L. Enzymatic Synthesis and Photoswitchable Enzymatic Cleavage of a Peptide-Linked Rotaxane. *Angew. Chem., Int. Ed.* **2006**, *45*, 1596–1599.

(190) Maniam, S.; Cieslinski, M. M.; Lincoln, S. F.; Onagi, H.; Steel, P. J.; Willis, A. C.; Easton, C. J. Molecular Fibers and Wires in Solid-State and Solution Self-Assemblies of Cyclodextrin [2]Rotaxanes. *Org. Lett.* **2008**, *10*, 1885–1888.

(191) Buston, J. E. H.; Young, J. R.; Anderson, H. L. Rotaxane-Encapsulated Cyanine Dyes: Enhanced Fluorescence Efficiency and Photostability. *Chem. Commun.* **2000**, 905–906.

(192) Yau, C. M. S.; Pascu, S. I.; Odom, S. A.; Warren, J. E.; Klotz, E. J. F.; Frampton, M. J.; Williams, C. C.; Coropceanu, V.; Kuimova, M. K.; Phillips, D.; Barlow, S.; Brédas, J.-L.; Marder, S. R.; Millar, V.; Anderson, H. L. Stabilisation of a Heptamethine Cyanine Dye by Rotaxane Encapsulation. *Chem. Commun*. **2008**, 2897–2899.

(193) Stanier, C. A.; O'Connell, M. J.; Clegg, W.; Anderson, H. L. Synthesis of Fluorescent Stilbene and Tolan Rotaxanes by Suzuki Coupling. *Chem. Commun*. **2001**, 493–494.

(194) Park, J. S.; Wilson, J. N.; Hardcastle, K. I.; Bunz, U. H. F.; Srinivasarao, M. Reduced Fluorescence Quenching of Cyclodextrin–Acetylene Dye Rotaxanes. *J. Am. Chem. Soc.* **2006**, *128*, 7714–7715.

(195) Zhao, Y.-L.; Chen, Y.; Wang, M.; Liu, Y. Multi[2]rotaxanes with Gold Nanoparticles as Centers. *Org. Lett.* **2006**, *8*, 1267–1270.

(196) Zhao, Y.-L.; Dichtel, W. R.; Trabolsi, A.; Saha, S.; Aprahamian, I.; Stoddart, J. F. A Redox-Switchable α-Cyclodextrin-Based [2]Rotaxane. *J. Am. Chem. Soc.* **2008**, *130*, 11294–11296.

(197) Sakamoto, K.; Takashima, Y.; Yamaguchi, H.; Harada, A. Preparation and Properties of Rotaxanes Formed by Dimethyl-β-cyclodextrin and Oligo(thiophene)s with β-Cyclodextrin Stoppers. *J. Org. Chem.* **2007**, *72*, 459–465.

(198) Sakamoto, K.; Takashima, Y.; Hamada, N.; Ichida, H.; Yamaguchi, H.; Yamamoto, H.; Harada, A. Selective Photoinduced Energy Transfer From a Thiophene Rotaxane to Acceptor. *Org. Lett.* **2011**, *13*, 672–675.

(199) Zalewski, L.; Wykes, M.; Brovelli, S.; Bonini, M.; Breiner, T.; Kastler, M.; Dötz, F.; Beljonne, D.; Anderson, H. L.; Cacialli, F.; Samorí, P. A Conjugated Thiophene-Based Rotaxane: Synthesis, Spectroscopy, and Modeling. *Chem. Eur. J.* **2010**, *16*, 3933–3941.

(200) Zalewski, L.; Mativetsky, J. M.; Brovelli, S.; Bonini, M.; Crivillers, N.; Breiner, T.; Anderson, H. L.; Cacialli, F.; Samorì, P. A Quaterthiophene-Based Rotaxane: Synthesis, Spectroscopy, and Self-Assembly at Surfaces. *Small* **2012**, *8*, 1835–1839.

(201) Daniell, H. W.; Klotz, E. J. F.; Odell, B.; Claridge, T. D. W.; Anderson, H. L. Solid-Phase Synthesis of Oligo(phenylene ethynylene) Rotaxanes. *Angew. Chem., Int. Ed.* **2007**, *46*, 6845–6848.

(202) Terao, J.; Tanaka, Y.; Tsuda, S.; Kambe, N.; Taniguchi, M.; Kawai, T.; Saeki, A.; Seki, S. Insulated Molecular Wire with Highly Conductive π-Conjugated Polymer Core. *J. Am. Chem. Soc.* **2009**, *131*, 18046–18047.

(203) Terao, J.; Wadahama, A.; Matono, A.; Tada, T.; Watanabe, S.; Seki, S.; Fujihara, T.; Tsuji, Y. Design Principle for Increasing Charge Mobility of π-Conjugated Polymers Using Regularly Localized Molecular Orbitals. *Nature Commun.* **2013**, *4*:1691.

(204) Sugiyama, J.; Tomita, I. Novel Approach to Stabilize Unstable Molecular Wires by Simultaneous Rotaxane Formation—Synthesis of Inclusion Complexes of Oligocarbynes with Cyclic Host Molecules. *Eur. J. Org. Chem*. **2007**, 4651–4653.

(205) Schrettl, S.; Contal, E.; Hoheisel, T. N.; Fritzsche, M.; Balog, S.; Szilluweit, R.; Frauenrath, H. Facile Synthesis of Oligoyne Amphiphiles and Their Rotaxanes. *Chem. Sci.* **2014**, *6*, 564–574.

(206) Klotz, E. J. F.; Claridge, T. D. W.; Anderson, H. L. Homo- and Hetero-[3]Rotaxanes with Two π-Systems Clasped in a Single Macrocycle. *J. Am. Chem. Soc.* **2006**, *128*, 15374–15375.

(207) Taylor, P. N.; O'Connell, M. J.; McNeill, L. A.; Hall, M. J.; Aplin, R. T.; Anderson, H. L. Insulated Molecular Wires: Synthesis of Conjugated Polyrotaxanes by Suzuki Coupling in Water. *Angew. Chem., Int. Ed.* **2000**, *39*, 3456–3460.

(208) Harada, A.; Kamachi, M. Complex Formation between Poly(ethylene glycol) and α-Cyclodextrin. *Macromolecules* **1990**, *23*, 2821–2823.

(209) Harada, A.; Li, J.; Kamachi, M. Formation of Inclusion Complexes of Monodisperse Oligo(ethylene glycol)s with α-Cyclodextrin. *Macromolecules* **1994**, *27*, 4538–4543.

(210) Harada, A.; Li, J.; Kamachi, M. Preparation and Properties of Inclusion Complexes of Poly(ethylene glycol) with α-Cyclodextrin. *Macromolecules* **1993**, *26*, 5698–5703.
(211) Harada, A.; Okada, M.; Li, J.; Kamachi, M. Preparation and Characterization of Inclusion Complexes of Poly(propylene glycol) with Cyclodextrins. *Macromolecules* **1995**, *28*, 8406–8411.
(212) Harada, A.; Suzuki, S.; Nakamitsu, T.; Okada, M.; Kamachi, M. Construction of Supramolecules Consisting of Cyclodextrins and Poly(tetrahydrofuran). *Kobunshi Ronbunshu* **1995**, *52*, 594–598.
(213) Harada, A.; Li, J.; Kamachi, M. Complex Formation between Poly(methyl vinyl ether) and γ-Cyclodextrin. *Chem. Lett*. **1993**, 237–240.
(214) Harada, A.; Li, J.; Suzuki, S.; Kamachi, M. Complex Formation Between Polyisobutylene and Cyclodextrins: Inversion of Chain-Length Selectivity Between. β-Cyclodextrin and γ-Cyclodextrin. *Macromolecules* **1993**, *26*, 5267–5268.
(215) Okumura, H.; Okada, M.; Kawaguchi, Y.; Harada, A. Complex Formation Between Poly(dimethylsiloxane) and Cyclodextrins: New *Pseudo*-Polyrotaxanes Containing Inorganic Polymers. *Macromolecules* **2000**, *33*, 4297– 4298.
(216) Harada, A.; Li, J.; Kamachi, M. The Molecular Necklace: A Rotaxane Containing Many Threaded α-Cyclodextrins. *Nature* **1992**, *356*, 325–327.
(217) Harada, A.; Kawaguchi, Y.; Nishiyama, T.; Kamachi, M. Complex Formation of Poly(ε-caprolactone) with Cyclodextrin. *Macromol. Rapid Comm.* **1997**, *18*, 535–539.
(218) Harada, A.; Nishiyama, T.; Kawaguchi, Y.; Okada, M.; Kamachi, M. Preparation and Characterization of Inclusion Complexes of Aliphatic Polyesters with Cyclodextrins. *Macromolecules* **1997**, *30*, 7115–7118.
(219) Harada, A.; Takashima, Y.; Yamaguchi, H. Cyclodextrin-Based Supramolecular Polymers. *Chem. Soc. Rev*. **2009**, *38*, 875–882.
(220) Harada, A.; Takashima, Y. Macromolecular Recognition and Macroscopic Interactions by Cyclodextrins. *Chem. Rec.* **2013**, *13*, 420–431.
(221) Harada, A.; Takashima, Y.; Nakahata, M. Supramolecular Polymeric Materials via Cyclodextrin–Guest Interactions. *Acc. Chem. Res.* **2014**, *47*, 2128–2140.
(222) Peet, J.; Rusa, C. C.; Hunt, M. A.; Tonelli, A. E.; Balik, C. M. Solid-State Complexation of Poly(Ethylene Glycol) with α-Cyclodextrin. *Macromolecules* **2005**, *38*, 537–541.
(223) Harada, A.; Okada, M.; Kawaguchi, Y. Formation of Self-Assembled Tubular Structures by Mixing Cyclodextrin and Polymers Without Solvents. *Chem. Lett.* **2005**, *34*, 542–543.
(224) Kihara, N.; Hinoue, K.; Takata, T. Solid-State End-Capping of Pseudopolyrotaxane Possessing Hydroxy- Terminated Axle to Polyrotaxane and Its Application to the Synthesis of a Functionalized Polyrotaxane Capable of Yielding a Polyrotaxane Network. *Macromolecules* **2005**, *38*, 223–226.
(225) Liu, R.; Maeda, T.; Kihara, N.; Harada, A.; Takata, T. Solvent-Free Synthesis of Pseudopolyrotaxane and Polyrotaxane: Efficient Threading Complexation of a Cyclodextrin Wheel and a Linear Polymer Axle to Yield Pseudopolyrotaxane and Its Fixation to Polyrotaxane by the Direct Grinding of a Solid Mixture. *J. Polym. Sci. Pol. Chem.* **2007**, *45*, 1571–1574.
(226) Liu, R.; Harada, A.; Takata, T. Solvent-Free Synthesis of Unmodified Cyclodextrin-Based Pseudopolyrotaxane and Polyrotaxane by Grinding. *Polym. J.* **2007**, *39*, 21–23.
(227) Jang, K.; Miura, K.; Koyama, Y.; Takata, T. Catalyst- and Solvent-Free Click Synthesis of Cyclodextrin-Based Polyrotaxanes Exploiting a Nitrile *N*-Oxide. *Org. Lett.* **2012**, *14*, 3088–3091.
(228) Harada, A.; Li, J.; Kamachi, M. Double-Stranded Inclusion Complexes of Cyclodextrin Threaded on Poly(Ethylene Glycol). *Nature* **1994**, *370*, 126–128.
(229) Takahashi, A.; Katoono, R.; Yui, N. Loose-Fit Polyrotaxane Composed of =-Cyclodextrin and Single Poly(Ethylene Glycol) Chain: Making Room in γ-CD Cavity for Additional Inclusion Complexation. *Macromolecules* **2009**, *42*, 8587–8589.
(230) Wenz, G.; Keller, B. Threading Cyclodextrin Rings on Polymer Chains. *Angew. Chem., Int. Ed*. **1992**, *31*, 197–199.
(231) Herrmann, W.; Schneider, M.; Wenz, G. Photochemical Synthesis of Polyrotaxanes From Stilbene Polymers and Cyclodextrins. *Angew. Chem., Int. Ed*. **1997**, *36*, 2511–2514.
(232) Dodziuk, H.; Ejchart, A.; Anczewski, W.; Ueda, H.; Krinichnaya, E.; Dolgonos, G.; Kutner, W. Water Solubilization, Determination of the Number of Different Types of Single-Wall Carbon Nanotubes and Their Partial Separation with Respect to Diameters by Complexation with ŋ-Cyclodextrin. *Chem. Commun*. **2003**, 986– 987.
(233) Armspach, D.; Ashton, P. R.; Moore, C. P.; Spencer, N.; Stoddart, J. F.; Wear, T. J.; Williams, D. J. Self-Assembly of Catenanes with Cyclodextrin Units. *Angew. Chem., Int. Ed. Engl*. **1993**, *32*, 854–858.
(234) Armspach, D.; Ashton, P. R.; Ballardini, R.; Balzani, V.; Godi, A.; Moore, C. P.; Prodi, L.; Spencer, N.; Stoddart, J. F.; Tolley, M. S.; Wear, T. J.; Williams, D. J. Catenated Cyclodextrins. *Chem. Eur. J*. **1995**, *1*, 33–55.
(235) Gawroński, J.; Kołbon, H.; Kwit, M.; Katrusiak, A. Designing Large Triangular Chiral Macrocycles: Efficient [3 + 3] Diamine–Dialdehyde Condensations Based on Conformational Bias. *J. Org. Chem.* **2000**, *65*, 5768–5773.
(236) Kuhnert, N.; Straßnig, C.; Lopez-Periago, A. M. Synthesis of Novel Enantiomerically Pure Trianglimine and Trianglamine Macrocycles. *Tetrahedron: Asymmetry* **2002**, *13*, 123–128.
(237) Kuhnert, N.; Tang, B. Synthesis of Diastereomeric Trianglamine-β-Cyclodextrin-[2]-Catenanes. *Tetrahedron Lett.* **2006**, *47*, 2985–2988.
(238) Lagona, J.; Mukhopadhyay, P.; Chakrabarti, S.; Isaacs, L. The Cucurbit[*n*]uril Family. *Angew. Chem., Int. Ed*. **2005**, *44*, 4844–4870.
(239) Behrend, R.; Meyer, E.; Rusche, F. Ueber Condensationsproducte aus Glycoluril und Formaldehyd. *Justus Liebigs Ann. Chem.* **1905**, *339*, 1–37.
(240) Freeman, W. A.; Mock, W. L.; Shih, N. Y. Cucurbituril. *J. Am. Chem. Soc*. **1981**, *103*, 7367–7368.
(241) Kim, J.; Jung, I.-S.; Kim, S.-Y.; Lee, E.; Kang, J.-K.; Sakamoto, S.; Yamaguchi, K.; Kim, K. New Cucurbituril Homologues: Syntheses, Isolation, Characterization, and X-ray Crystal Structures of Cucurbit[*n*]uril (*n* = 5, 7, and 8). *J. Am. Chem. Soc.* **2000**, *122*, 540–541.
(242) Day, A. I.; Arnold, A. P.; Blanch, R. J.; Snushall, B. Controlling Factors in the Synthesis of Cucurbituril and Its Homologues. *J. Org. Chem.* **2001**, *66*, 8094–8100.
(243) Day, A. I.; Blanch, R. J.; Arnold, A. P.; Lorenzo, S.; Lewis, G. R.; Dance, I. A Cucurbituril-Based Gyroscane: A New Supramolecular Form. *Angew. Chem., Int. Ed*. **2002**, *41*, 275–277.
(244) Mock, W. L. Cucurbituril. *Top. Curr. Chem*. **1995**, *175*, 1–24.
(245) Lee, J. W.; Samal, S.; Selvapalam, N.; Kim, H.-J.; Kim, K. Cucurbituril Homologues and Derivatives: New Opportunities in Supramolecular Chemistry. *Acc. Chem. Res.* **2003**, *36*, 621–630.
(246) Kim, K.; Selvapalam, N.; Ko, Y. H.; Park, K. M.; Kim, D.; Kim, J. Functionalized Cucurbiturils and Their Applications. *Chem. Soc. Rev.* **2007**, *36*, 267–279.
(247) Buschmann, H.-J.; Mutihac, L.; Jansen, K. Complexation of Some Amine Compounds by Macrocyclic Receptors. *J. Incl. Phenom. Macrocycl. Chem.* **2001**, *39*, 1–11.
(248) Nau, W. M.; Florea, M.; Assaf, K. I. Deep Inside Cucurbiturils: Physical Properties and Volumes of Their Inner Cavity Determine the Hydrophobic Driving Force for Host-Guest Complexation. *Isr. J. Chem.* **2011**, *51*, 559–577.
(249) Kaifer, A. E. Toward Reversible Control of Cucurbit[*n*]uril Complexes. *Acc. Chem. Res.* **2014**, *47*, 2160–2167.
(250) Isaacs, L. Cucurbit[*n*]urils: From Mechanism to Structure and Function. *Chem. Commun*. **2009**, 619–629.
(251) Isaacs, L. Stimuli Responsive Systems Constructed Using Cucurbit[*n*]uril-Type Molecular Containers. *Acc. Chem. Res.* **2014**, *47*, 2052–2062.

(252) Das, D.; Scherman, O. A. Cucurbituril: at the Interface of Small Molecule Host-Guest Chemistry and Dynamic Aggregates. *Isr. J. Chem.* **2011**, *51*, 537–550.

(253) Masson, E.; Ling, X.; Joseph, R.; Kyeremeh-Mensah, L.; Lu, X. Cucurbituril Chemistry: A Tale of Supramolecular Success. *RSC Adv.* **2012**, *2*, 1213–1247.

(254) Buschmann, H.-J.; Jansen, K.; Meschke, C.; Schollmeyer, E. Thermodynamic Data for Complex Formation between Cucurbituril and Alkali and Alkaline Earth Cations in aqueous Formic Acid Solution. *J. Solution Chem.* **1998**, *27*, 135– 140.

(255) Flinn, A.; Hough, G. C.; Stoddart, J. F.; Williams, D. J. Decamethylcucurbit[5]uril. *Angew. Chem., Int. Ed. Engl*. **1992**, *31*, 1475–1477.

(256) Miyahara, Y.; Abe, K.; Inazu, T. "Molecular" Molecular Sieves: Lid-Free Decamethylcucurbit[5]uril Absorbs and Desorbs Gases Selectively. *Angew. Chem., Int. Ed*. **2002**, *41*, 3020–3023.

(257) Kellersberger, K. A.; Anderson, J. D.; Ward, S. M.; Krakowiak, K. E.; Dearden, D. V. Encapsulation of N_2, O_2, Methanol, or Acetonitrile by Decamethylcucurbit[5]uril$(NH_4^+)_2$ Complexes in the Gas Phase: Influence of the Guest on "Lid" Tightness. *J. Am. Chem. Soc.* **2001**, *123*, 11316–11317.

(258) Jansen, K.; Buschmann, H.-J.; Wego, A.; Döpp, D.; Mayer, C.; Drexler, H.-J.; Holdt, H.-J.; Schollmeyer, E. Cucurbit[5]uril, Decamethylcucurbit[5]uril and Cucurbit[6]uril. Synthesis, Solubility and Amine Complex Formation. *J. Incl. Phenom. Macrocycl. Chem*. **2001**, *39*, 357–363.

(259) Wego, A.; Jansen, K.; Buschmann, H.; Schollmeyer, E.; Döpp, D. Synthesis of Cucurbit[5]uril-Spermine-[2]Rotaxanes. *J. Incl. Phenom. Macrocycl. Chem.* **2002**, *43*, 201–205.

(260) Zhang, X. X.; Krakowiak, K. E.; Xue, G.; Bradshaw, J. S.; Izatt, R. M. A Highly Selective Compound for Lead: Complexation Studies of Decamethylcucurbit[5]uril with Metal Ions. *Ind. Eng. Chem. Res.* **2000**, *39*, 3516–3520.

(261) Buschmann, H.-J.; Cleve, E.; Jansen, K.; Wego, A.; Schollmeyer, E. Complex Formation Between Cucurbit[*n*]urils and Alkali, Alkaline Earth and Ammonium Ions in Aqueous Solution. *J. Incl. Phenom. Macrocycl. Chem.* **2001**, *40*, 117–120.

(262) Mock, W. L.; Shih, N. Y. Structure and Selectivity in Host-Guest Complexes of Cucurbituril. *J. Org. Chem.* **1986**, *51*, 4440–4446.

(263) Meschke, C.; Buschmann, H.-J.; Schollmeyer, E. Complexes of Cucurbituril with Alkyl Mono- and Diammonium Ions in Aqueous Formic Acid Studied by Calorimetric Titrations. *Thermochimica Acta* **1997**, *297*, 43–48.

(264) Mock, W. L.; Shih, N. Y. Dynamics of Molecular Recognition Involving Cucurbituril. *J. Am. Chem. Soc.* **1989**, *111*, 2697–2699.

(265) Marquez, C.; Nau, W. M. Two Mechanisms of Slow Host–Guest Complexation Between Cucurbit[6]uril and Cyclohexylmethylamine: pH-Responsive Supramolecular Kinetics. *Angew. Chem., Int. Ed*. **2001**, *40*, 3155–3160.

(266) Wagner, B. D.; Stojanovic, N.; Day, A. I.; Blanch, R. J. Host Properties of Cucurbit[7]uril: Fluorescence Enhancement of Anilinonaphthalene Sulfonates. *J. Phys. Chem. B* **2003**, *107*, 10741–10746.

(267) Kim, H.-J.; Jeon, W. S.; Ko, Y. H.; Kim, K. Inclusion of Methylviologen in Cucurbit[7]uril. *Proc. Natl. Acad. Sci. U.S.A.* **2002**, *99*, 5007–5011.

(268) Ong, W.; Gómez-Kaifer, M.; Kaifer, A. E. Cucurbit[7]uril: A Very Effective Host for Viologens and Their Cation Radicals. *Org. Lett.* **2002**, *4*, 1791–1794.

(269) Jeon, W. S.; Moon, K.; Park, S. H.; Chun, H.; Ko, Y. H.; Lee, J. Y.; Lee, E. S.; Samal, S.; Selvapalam, N.; Rekharsky, M. V.; Sindelar, V.; Sobransingh, D.; Inoue, Y.; Kaifer, A. E.; Kim, K. Complexation of Ferrocene Derivatives by the Cucurbit[7]uril Host: A Comparative Study of the Cucurbituril and Cyclodextrin Host Families. *J. Am. Chem. Soc.* **2005**, *127*, 12984–12989.

(270) Marquez, C.; Nau, W. M. Polarizabilities Inside Molecular Containers. *Angew. Chem., Int. Ed*. **2001**, *40*, 4387–4390.

(271) Moghaddam, S.; Yang, C.; Rekharsky, M.; Ko, Y. H..; Kim, K.; Inoue, Y.; Gilson, M. K. New Ultrahigh Host–Guest Complexes of Cucurbit[7]uril with Bicyclo[2.2.2]octane and Adamantane Guests: Thermodynamic Analysis and Evaluation of M2 Affinity Calculations. *J. Am. Chem. Soc*. **2011**, *133*, 3570–3581.

(272) Blanch, R. J.; Sleeman, A. J.; White, T. J.; Arnold, A. P.; Day, A. I. Cucurbit[7]uril and *o*-Carborane Self-Assemble to Form a Molecular Ball Bearing. *Nano Lett.* **2002**, *2*, 147–149.

(273) Rekharsky, M. V.; Mori, T.; Yang, C.; Ko, Y. H.; Selvapalam, N.; Kim, H.; Sobransingh, D.; Kaifer, A. E.; Liu, S.; Isaacs, L.; Chen, W.; Moghaddam, S.; Gilson, M. K.; Kim, K.; Inoue, Y. A Synthetic Host-Guest System Achieves Avidin-Biotin Affinity by Overcoming Enthalpy–Entropy Compensation. *Proc. Natl. Acad. Sci. U.S.A.* **2007**, *104*, 20737–20742.

(274) Cao, L.; Šekutor, M.; Zavalij, P. Y.; Mlinarić-Majerski, K.; Glaser, R.; Isaacs, L. Cucurbit[7]uril•Guest Pair with an Attomolar Dissociation Constant. *Angew. Chem., Int. Ed*. **2014**, *53*, 988–993.

(275) Wilchek, M.; Bayer, E. A. The Avidin-Biotin Complex in Bioanalytical Applications. *Anal. Biochem.* **1988**, *171*, 1– 32.

(276) Jon, S. Y.; Ko, Y. H.; Park, S. H.; Kim, H.-J.; Kim, K. A Facile, Stereoselective [2 + 2] Photoreaction Mediated by Cucurbit[8]uril. *Chem. Commun*. **2001**, 1938–1939.

(277) Jeon, W. S.; Kim, H.-J.; Lee, C.; Kim, K. Control of the Stoichiometry in Host-Guest Complexation by Redox Chemistry of Guests: Inclusion of Methylviologen in Cucurbit[8]uril. *Chem. Commun*. **2002**, 1828–1829.

(278) Jeon, W. S.; Ziganshina, A. Y.; Lee, J. W.; Ko, Y. H.; Kang, J.-K.; Lee, C.; Kim, K. A [2]Pseudorotaxane-Based Molecular Machine: Reversible Formation of a Molecular Loop Driven by Electrochemical and Photochemical Stimuli. *Angew. Chem., Int. Ed*. **2003**, *42*, 4097–4100.

(279) Ziganshina, A. Y.; Ko, Y. H.; Jeon, W. S.; Kim, K. Stable π-Dimer of a Tetrathiafulvalene Cation Radical Encapsulated in the Cavity of Cucurbit[8]uril. *Chem. Commun*. **2004**, 806–807.

(280) Kim, H.-J.; Heo, J.; Jeon, W. S.; Lee, E.; Kim, J.; Sakamoto, S.; Yamaguchi, K.; Kim, K. Selective Inclusion of a Hetero-Guest Pair in a Molecular Host: Formation of Stable Charge-Transfer Complexes in Cucurbit[8]uril. *Angew. Chem., Int. Ed*. **2001**, *40*, 1526–1529.

(281) Jeon, W. S.; Kim, E.; Ko, Y. H.; Hwang, I.; Lee, J. W.; Kim, S.-Y.; Kim, H.-J.; Kim, K. Molecular Loop Lock: A Redox-Driven Molecular Machine Based on a Host-Stabilized Charge-Transfer Complex. *Angew. Chem., Int. Ed*. **2005**, *44*, 87–91.

(282) Trabolsi, A.; Hmadeh, M.; Khashab, N. M.; Friedman, D. C.; Belowich, M. E.; Humbert, N.; Elhabiri, M.; Khatib, H. A.; Albrecht-Gary, A.-M.; Stoddart, J. F. Redox-Driven Switching in Pseudorotaxanes. *New J. Chem.* **2009**, *33*, 254–263.

(283) Kim, S.-Y.; Jung, I.-S.; Lee, E.; Kim, J.; Sakamoto, S.; Yamaguchi, K.; Kim, K. Macrocycles Within Macrocycles: Cyclen, Cyclam, and Their Transition Metal Complexes Encapsulated in Cucurbit[8]uril. *Angew. Chem., Int. Ed*. **2001**, *40*, 2119–2121.

(284) Biedermann, F.; Uzunova, V. D.; Scherman, O. A.; Nau, W. M.; De Simone, A. Release of High-Energy Water as an Essential Driving Force for the High-Affinity Binding of Cucurbit[*n*]urils. *J. Am. Chem. Soc.* **2012**, *134*, 15318–15323.

(285) Kim, K. Mechanically Interlocked Molecules Incorporating Cucurbituril and Their Supramolecular Assemblies. *Chem. Soc. Rev.* **2002**, *31*, 96–107.

(286) Parvari, G.; Reany, O.; Keinan, E. Applicable Properties of Cucurbiturils. *Isr. J. Chem.* **2011**, *51*, 646–663.

(287) Mock, W. L.; Irra, T. A.; Wepsiec, J. P.; Manimaran, T. L. Cycloaddition Induced by Cucurbituril. A Case of Pauling Principle Catalysis. *J. Org. Chem.* **1983**, *48*, 3619–3620.

(288) Kolb, H. C.; Finn, M. G.; Sharpless, K. B. Click Chemistry: Diverse Chemical Function From a Few Good Reactions. *Angew. Chem., Int. Ed*. **2001**, *40*, 2004–2021.

(289) Pauling, L. Chemical Achievement and Hope for Future. *Am. Sci.* **1948**, *36*, 51–58.
(290) Tuncel, D.; Steinke, J. H. G. Catalytically Self-Threading Polyrotaxanes. *Chem. Commun*. **1999**, 1509–1510.
(291) Tuncel, D.; Steinke, J. H. G. The Synthesis of [2], [3] and [4]Rotaxanes and Semirotaxanes. *Chem. Commun*. **2002**, 496–497.
(292) Tuncel, D.; Steinke, J. H. G. Catalytic Self-Threading: A New Route for the Synthesis of Polyrotaxanes. *Macromolecules* **2004**, *37*, 288–302.
(293) Tuncel, D.; Cindir, N.; Koldemir, Ü. [5]Rotaxane and [5]Pseudorotaxane Based on Cucurbit[6]uril and Anchored to a Meso-Tetraphenyl Porphyrin. *J. Incl. Phenom. Macrocycl. Chem*. **2006**, *55*, 373–380.
(294) Tuncel, D.; Ünal, Ö.; Artar, M. Supramolecular Assemblies Constructed by Cucurbituril-Catalyzed Click Reaction. *Isr. J. Chem.* **2011**, *51*, 525–532.
(295) Mileo, E.; Casati, C.; Franchi, P.; Mezzina, E.; Lucarini, M. Nitroxide Biradicals as Thread Units in Paramagnetic Cucurbituril-Based Rotaxanes. *Org. Biomol. Chem.* **2011**, *9*, 2920–2924.
(296) Pievo, R.; Casati, C.; Franchi, P.; Mezzina, E.; Bennati, M.; Lucarini, M. End-to-End Distance Determination in a Cucurbit[6]uril-Based Rotaxane by PELDOR Spectroscopy. *ChemPhysChem* **2012**, *13*, 2659–2661.
(297) Jeon, Y.-M.; Whang, D.; Kim, J.; Kim, K. A Simple Construction of a Rotaxane and Pseudorotaxane: Syntheses and X-Ray Crystal Structures of Cucurbituril Threaded on Substituted Spermine. *Chem. Lett*. **1996**, *1996*, 503– 504.
(298) Buschmann, H.-J.; Wego, A.; Schollmeyer, E.; Döpp, D. Synthesis of Cucurbituril-Spermine-[2]Rotaxanes of the Amide-Type. *Supramol. Chem.* **2000**, *11*, 225–231.
(299) Meschke, C.; Buschmann, H.-J.; Schollmeyer, E. Synthesis of Mono-, Oligo- and Polyamide-Cucurbituril Rotaxanes. *Macromol. Rapid Comm.* **1998**, *19*, 59–63.
(300) Moon, K.; Kaifer, A. E. Modes of Binding Interaction Between Viologen Guests and the Cucurbit[7]uril Host. *Org. Lett.* **2004**, *6*, 185–188.
(301) Sindelar, V.; Moon, K.; Kaifer, A. E. Binding Selectivity of Cucurbit[7]uril: Bis(pyridinium)-1,4-xylylene Versus 4,4'-Bipyridinium Guest Sites. *Org. Lett.* **2004**, *6*, 2665–2668.
(302) Senler, S.; Cheng, B.; Kaifer, A. E. Rotaxane Formation by Cucurbit[7]uril in Water and DMSO Solutions. *Org. Lett.* **2014**, *16*, 5834–5837.
(303) Eelkema, R.; Maeda, K.; Odell, B.; Anderson, H. L. Radical Cation Stabilization in a Cucurbituril Oligoaniline Rotaxane. *J. Am. Chem. Soc.* **2007**, *129*, 12384–12385.
(304) Ramalingam, V.; Urbach, A. R. Cucurbit[8]uril Rotaxanes. *Org. Lett.* **2011**, *13*, 4898–4901.
(305) Miyahara, Y.; Goto, K.; Oka, M.; Inazu, T. Remarkably Facile Ring-Size Control in Macrocyclization: Synthesis of Hemicucurbit[6]uril and Hemicucurbit[12]uril. *Angew. Chem., Int. Ed*. **2004**, *43*, 5019–5022.
(306) Svec, J.; Necas, M.; Sindelar, V. Bambus[6]uril. *Angew. Chem., Int. Ed*. **2010**, *49*, 2378–2381.
(307) Hou, X.; Ke, C.; Stoddart, J. F. Cooperative Capture Synthesis: Yet Another Playground for Copper-Free Click Chemistry. *Chem. Soc. Rev*. **2016**, *45*, 3766–3780
(308) Ke, C.; Strutt, N. L.; Li, H.; Hou, X.; Hartlieb, K. J.; McGonigal, P. R.; Ma, Z.; Iehl, J.; Stern, C. L.; Cheng, C.; Zhu, Z.; Vermeulen, N. A.; Meade, T. J.; Botros, Y. Y.; Stoddart, J. F. Pillar[5]arene as a Co-Factor in Templating Rotaxane Formation. *J. Am. Chem. Soc.* **2013**, *135*, 17019–17030.
(309) Hou, X.; Ke, C.; Cheng, C.; Song, N.; Blackburn, A. K.; Sarjeant, A. A.; Botros, Y. Y.; Yang, Y.-W.; Stoddart, J. F. Efficient Syntheses of Pillar[6]arene-Based Hetero[4]rotaxanes Using a Cooperative Capture Strategy. *Chem. Commun.* **2014**, *50*, 6196–6199.
(310) Rekharsky, M. V.; Yamamura, H.; Kawai, M.; Osaka, I.; Arakawa, R.; Sato, A.; Ko, Y. H.; Selvapalam, N.; Kim, K.; Inoue, Y. Sequential Formation of a Ternary Complex Among Dihexylammonium, Cucurbit[6]uril, and Cyclodextrin with Positive Cooperativity. *Org. Lett.* **2006**, *8*, 815–818.
(311) Yang, C.; Ko, Y. H.; Selvapalam, N.; Origane, Y.; Mori, T.; Wada, T.; Kim, K.; Inoue, Y. Dynamic Switching Between Single- and Double-Axial Rotaxanes Manipulated by Charge and Bulkiness of Axle Termini. *Org. Lett.* **2007**, *9*, 4789–4792.
(312) Liu, Y.; Li, X.-Y.; Zhang, H.-Y.; Li, C.-J.; Ding, F. Cyclodextrin-Driven Movement of Cucurbit[7]uril. *J. Org. Chem.* **2007**, *72*, 3640–3645.
(313) Leclercq, L.; Noujeim, N.; H Sanon, S.; Schmitzer, A. R. Study of the Supramolecular Cooperativity in the Multirecognition Mechanism of Cyclodextrins/Cucurbituril/Disubstituted Diimidazolium Bromides. *J. Phys. Chem. B* **2008**, *112*, 14176–14184.
(314) Chen, Y.; Zhang, Y.-M.; Liu, Y. Molecular Selective Binding and Nanofabrication of Cucurbituril/Cyclodextrin Pairs. *Isr. J. Chem.* **2011**, *51*, 515–524.
(315) Ogoshi, T.; Kanai, S.; Fujinami, S.; Yamagishi, T.-A.; Nakamoto, Y. *para*-Bridged Symmetrical Pillar[5]arenes: Their Lewis Acid Catalyzed Synthesis and Host–Guest Property. *J. Am. Chem. Soc*. **2008**, *130*, 5022–5023.
(316) Ogoshi, T.; Yamagishi, T.-A. New Synthetic Host Pillararenes: Their Synthesis and Application to Supramolecular Materials. *Bull. Chem. Soc. Jpn.* **2013**, *86*, 312–332.
(317) Hou, X.; Ke, C.; Bruns, C. J.; McGonigal, P. R.; Pettman, R. B.; Stoddart, J. F. Tunable Solid-State Fluorescent Materials for Supramolecular Encryption. *Nature Commun.* **2015**, *6*:6884.
(318) Diederich, F.; Dick, K. New Water-Soluble Macrocycles of the Paracyclophane Type: Aggregation Behavior and Host-Guest-Interaction with Hydrophobic Substrates. *Tetrahedron Lett.* **1982**, *23*, 3167–3170.
(319) Diederich, F.; Dick, K. Inclusion Complexes Between a Macrocyclic Host Molecule and Aromatic Hydrocarbons in Aqueous Solution. *Angew. Chem., Int. Ed. Engl*. **1983**, *22*, 715–716.
(320) Diederich, F.; Dick, K. A New Water-Soluble Macrocyclic Host of the Cyclophane Type: Host-Guest Complexation with Aromatic Guests in Aqueous Solution and Acceleration of the Transport of Arenes Through an Aqueous Phase. *J. Am. Chem. Soc.* **1984**, *106*, 8024–8036.
(321) Diederich, F.; Dick, K.; Griebel, D. Water-Soluble Tetraoxa [*n*.1.*n*.1] Paracyclophanes: Synthesis and Host-Guest Interactions in Aqueous Solution. *Chem. Ber*. **1985**, *118*, 3588–3619.
(322) Diederich, F. Complexation of Neutral Molecules by Cyclophane Hosts. *Angew. Chem., Int. Ed. Engl*. **1988**, *27*, 362–386.
(323) Ferguson, S. B.; Seward, E. M.; Diederich, F.; Sanford, E. M.; Chou, A.; Inocencio-Szweda, P.; Knobler, C. B. Strong Enthalpically Driven Complexation of Neutral Benzene Guests in Aqueous Solution. *J. Org. Chem.* **1988**, *53*, 5593–5595.
(324) Anderson, S.; Anderson, H. L. Synthesis of a Water-Soluble Conjugated [3]Rotaxane. *Angew. Chem., Int. Ed. Engl*. **1996**, *35*, 1956–1959.
(325) Anderson, S.; Aplin, R. T.; Claridge, T. D. W.; Goodson, T., III; Maciel, A. C.; Rumbles, G.; Ryan, J. F.; Anderson, H. L. An Approach to Insulated Molecular Wires: Synthesis of Water-Soluble Conjugated Rotaxanes. *J. Chem. Soc., Perkin Trans*. *1* **1998**, 2383–2398.
(326) Taylor, P. N.; Hagan, A. J.; Anderson, H. L. Hindered Fluorescence Quenching in an Insulated Molecular Wire. *Org. Biomol. Chem.* **2003**, *1*, 3851.
(327) Anderson, S.; Claridge, T. D. W.; Anderson, H. L. Azo-Dye Rotaxanes. *Angew. Chem., Int. Ed. Engl*. **1997**, *36*, 1310–1313.
(328) Anderson, S.; Anderson, H. L.; Clegg, W. Crystal Structure of an Azo Dye Rotaxane. *Chem. Commun*. **1998**, 2379–2380.
(329) Yazaki, K.; Sei, Y.; Akita, M.; Yoshizawa, M. A Polyaromatic Molecular Tube That Binds Long Hydrocarbons with High Selectivity. *Nature Commun.* **2014**, *5*:5179.

(330) Fujita, M.; Ibukuro, F.; Hagihara, H.; Ogura, K. Quantitative Self-Assembly of a [2]Catenane From Two Preformed Molecular Rings. *Nature* **1994**, *367*, 720–723.
(331) Fujita, M.; Fujita, N.; Ogura, K.; Yamaguchi, K. Spontaneous Assembly of Ten Components Into Two Interlocked, Identical Coordination Cages. Nature **1999**, *400*, 52–55.
(332) Fujita, M. Self-Assembly of [2]Catenanes Containing Metals in Their Backbones. *Acc. Chem. Res.* **1999**, *32*, 53–61.
(333) Fujita, M.; Tominaga, M.; Hori, A.; Therrien, B. Coordination Assemblies From a Pd(II)-Cornered Square Complex. *Acc. Chem. Res.* **2005**, *38*, 369–378.
(334) Curtis, N. F. Transition-Metal Complexes with Aliphatic Schiff Bases. Part I. Nickel(II) Complexes with *N*-Isopropylidene-Ethylenediamine Schiff Bases. *J. Chem. Soc*. **1960**, 4409–4413.
(335) Curtis, N. F. Some Cyclic Tetra-Amines and Their Metal-Ion Complexes. Part I. Two Isomeric Hexamethyltetra-Azacyclotetradecanes and Their Copper(II) and Nickel(II) Complexes. *J. Chem. Soc*. **1964**, 2644–2650.
(336) Curtis, N. F.; Curtis, Y. M. Some Nitrato-Amine Nickel(II) Compounds with Monodentate and Bidentate Nitrate Ions. *Inorg. Chem.* **1965**, *4*, 804–809.
(337) Curtis, N. F. Macrocyclic Coordination Compounds Formed by Condensation of Metal-Amine Complexes with Aliphatic Carbonyl Compounds. *Coord. Chem. Rev.* **1968**, *3*, 3–47.
(338) Thompson, M. C.; Busch, D. H. Reactions of Coordinated Ligands. II. Nickel(II) Complexes of Some Novel Ligands. *J. Am. Chem. Soc*. **1962**, *84*, 1762–1763.
(339) Thompson, M. C.; Busch, D. H. Reactions of Coordinated Ligands. IX. Utilization of the Template Hypothesis to Synthesize Macrocyclic Ligands in Situ. *J. Am. Chem. Soc*. **1964**, *86*, 3651–3656.
(340) Busch, D. H. Metal Ion Control of Chemical Reactions. *Science* **1971**, *171*, 241–248.
(341) de Diesbach, H.; Weid, von der, E. Quelque Sels Complexes des *o*-Dinitriles avec le Cuivre et la Pyridine. *Helv. Chim. Acta* **1927**, *10*, 886–888.
(342) Kramer, R.; Lehn, J.-M.; Marquis-Rigault, A. Self-Recognition in Helicate Self-Assembly: Spontaneous Formation of Helical Metal Complexes From Mixtures of Ligands and Metal Ions. *Proc. Natl. Acad. Sci. U.S.A.* **1993**, *90*, 5394–5398.
(343) King, R. B. Atomic Orbitals, Symmetry, and Coordination Polyhedra. *Coord. Chem. Rev.* **2000**, *197*, 141–168.
(344) Prikhod'ko, A.; Durola, F.; Sauvage, J.-P. Iron(II)-Templated Synthesis of [3]Rotaxanes by Passing Two Threads through the Same Ring. *J. Am. Chem. Soc.* **2008**, *130*, 448–449.
(345) Prikhod'ko, A. L.; Sauvage, J.-P. Passing Two Strings through the Same Ring Using an Octahedral Metal Center as Template: A New Synthesis of [3]Rotaxanes. *J. Am. Chem. Soc.* **2009**, *131*, 6794–6807.
(346) Lincheneau, C.; Jean-Denis, B.; Gunnlaugsson, T. Self-Assembly Formation of Mechanically Interlocked [2]- and [3]Catenanes Using Lanthanide Ion [Eu(III)] Templation and Ring Closing Metathesis Reactions. *Chem. Commun.* **2014**, *50*, 2857–2860.
(347) Ayme, J.-F.; Gil-Ramírez, G.; Leigh, D. A.; Lemonnier, J.-F.; Markevicius, A.; Muryn, C. A.; Zhang, G. Lanthanide Template Synthesis of a Molecular Trefoil Knot. *J. Am. Chem. Soc.* **2014**, *136*, 13142–13145.
(348) Zapata, F.; Blackburn, O. A.; Langton, M. J.; Faulkner, S.; Beer, P. D. Lanthanide Cation-Templated Synthesis of Rotaxanes. *Chem. Commun.* **2013**, *49*, 8157–8159.
(349) Beves, J. E.; Blight, B. A.; Campbell, C. J.; Leigh, D. A.; McBurney, R. T. Strategies and Tactics for the Metal-Directed Synthesis of Rotaxanes, Knots, Catenanes, and Higher Order Links. *Angew. Chem., Int. Ed.* **2011**, *50*, 9260–9327.
(350) Dietrich-Buchecker, C. O.; Sauvage, J.-P. Interlocking of Molecular Threads: From the Statistical Approach to the Templated Synthesis of Catenands. *Chem. Rev.* **1987**, *87*, 795–810.
(351) Chambron, J.-C.; Dietrich-Buchecker, C. O.; Hemmert, C.; Khemiss, A.-K.; Mitchell, D.; Sauvage, J.-P.; Weiss, J. Interlacing Molecular Threads on Transition Metals. *Pure Appl. Chem.* **1990**, *62*, 1027–1034.
(352) Chambron, J.-C.; Dietrich-Buchecker, C. O.; Heitz, V.; Nierengarten, J.-F.; Sauvage, J.-P.; Pascard, C.; Guilhem, J. Transition Metals as Assembling and Templating Species: From Catenanes and Knots to Organized Multi-Porphyrins Arrays. *Pure Appl. Chem.* **1995**, *67*, 233–240.
(353) Dietrich-Buchecker, C.; Rapenne, G.; Sauvage, J.-P. Synthesis of Catenanes and Molecular Knots by Copper(I)-Directed Formation of the Precursors Followed by Ruthenium(II)-Catalyzed Ring-Closing Metathesis. *Coord. Chem. Rev.* **1999**, *185-186*, 167–176.
(354) Kern, J.-M.; Sauvage, J.-P.; Bidan, G.; Divisia-Blohorn, B. Transition-Metal-Templated Synthesis of Rotaxanes and Catenanes: From Small Molecules to Polymers. *J. Polym. Sci. Pol. Chem.* **2003**, *41*, 3470–3477.
(355) Blanco, M. J.; Chambron, J. C.; Jimenez, M. C.; Sauvage, J.-P. Transition-Metal-Templated Synthesis of Rotaxanes. *Top. Stereochem*. **2003**, *23*, 125–273.
(356) Dietrich-Buchecker, C. O.; Marnot, P. A.; Sauvage, J.-P. Direct Synthesis of Disubstituted Aromatic Polyimine Chelates. *Tetrahedron Lett.* **1982**, *23*, 5291–5294.
(357) Dietrich-Buchecker, C. O.; Sauvage, J.-P. Synthese de Composes Polyethers Macrocycliques Derives de la Phenanthroline-1,10 Diphenyl-2,9. *Tetrahedron Lett.* **1983**, *24*, 5091–5094.
(358) Dietrich-Buchecker, C.; Colasson, B.; Fujita, M.; Hori, A.; Geum, N.; Sakamoto, S.; Yamaguchi, K.; Sauvage, J.-P. Quantitative Formation of [2]Catenanes Using Copper(I) and Palladium(II) as Templating and Assembling Centers: The Entwining Route and the Threading Approach. *J. Am. Chem. Soc.* **2003**, *125*, 5717–5725.
(359) Dietrich-Buchecker, C. O.; Sauvage, J.-P.; Kern, J.-M. Templated Synthesis of Interlocked Macrocyclic Ligands: The Catenands. *J. Am. Chem. Soc.* **1984**, *106*, 3043–3045.
(360) Dietrich, B.; Lehn, J.-M.; Sauvage, J.-P. Diaza-Polyoxa-Macrocycles et Macrobicycles. *Tetrahedron Lett.* **1969**, *10*, 2885–2888.
(361) Dietrich, B.; Lehn, J.-M.; Sauvage, J.-P. Les Cryptates. *Tetrahedron Lett.* **1969**, *10*, 2889–2892.
(362) Lehn, J.-M.; Sauvage, J.-P. Cryptates. XVI. [2]-Cryptates. Stability and Selectivity of Alkali and Alkaline-Earth Macrobicyclic Complexes. *J. Am. Chem. Soc*. **1975**, *97*, 6700–6707.
(363) Albrecht-Gary, A.-M.; Saad, Z.; Dietrich-Buchecker, C. O.; Sauvage, J.-P. Interlocked Macrocyclic Ligands: A Kinetic Catenand Effect in Copper(I) Complexes. *J. Am. Chem. Soc.* **1985**, *107*, 3205–3209.
(364) Dietrich-Buchecker, C.; Sauvage, J.-P. Templated Synthesis of Interlocked Macrocyclic Ligands, the Catenands. Preparation and Characterization of the Prototypical bis-30 Membered Ring System. *Tetrahedron* **1990**, *46*, 503–512.
(365) Cesario, M.; Dietrich-Buchecker, C. O.; Guilhem, J.; Pascard, C.; Sauvage, J.-P. Molecular Structure of a Catenand and Its Copper(I) Catenate: Complete Rearrangement of the Interlocked Macrocyclic Ligands by Complexation. *J. Chem. Soc., Chem. Commun*. **1985**, 244–247.
(366) Dietrich-Buchecker, C.; Kern, J.-M.; Sauvage, J.-P. An Air-Stable d^9 Nickel(I) Catenate: Stabilization of Monovalent Nickel by Interlocked Macrocyclic Ligands. *J. Chem. Soc., Chem. Commun*. **1985**, 760–762.
(367) Albrecht-Gary, A.-M.; Dietrich-Buchecker, C.; Saad, Z.; Sauvage, J.-P. Topological Kinetic Effects: Complexation of Interlocked Macrocyclic Ligands by Cationic Species. *J. Am. Chem. Soc.* **1988**, *110*, 1467–1472.
(368) Albrecht-Gary, A.-M.; Dietrich-Buchecker, C.; Saad, Z.; Sauvage, J.-P. Formation of Li^+ and Cd^{2+} Catenates, a Reaction with a Negative Enthalpy of Activation. *J. Chem. Soc., Chem. Commun*. **1992**, 280–282.
(369) Wu, C.; Lecavalier, P. R.; Shen, Y. X.; Gibson, H. W. Synthesis of a Rotaxane via the Template Method. *Chem. Mater.* **1991**, *3*, 569–572.

(370) Chambron, J.-C.; Heitz, V.; Sauvage, J.-P. A Rotaxane with Two Rigidly Held Porphyrins as Stoppers. *J. Chem. Soc., Chem. Commun*. **1992**, 1131–1133.
(371) Lindsey, J. S.; Schreiman, I. C.; Hsu, H. C.; Kearney, P. C.; Marguerettaz, A. M. Rothemund and Adler-Longo Reactions Revisited: Synthesis of Tetraphenylporphyrins Under Equilibrium Conditions. *J. Org. Chem.* **1987**, *52*, 827–836.
(372) Rothemund, P. A New Porphyrin Synthesis. The Synthesis of Porphin. *J. Am. Chem. Soc*. **1936**, *58*, 625–627.
(373) Adler, A. D.; Longo, F. R.; Finarelli, J. D.; Goldmacher, J.; Assour, J.; Korsakoff, L. A Simplified Synthesis for Meso-Tetraphenylporphine. *J. Org. Chem.* **1967**, *32*, 476–476.
(374) Chambron, J.-C.; Collin, J.-P.; Dalbavie, J.-O.; Dietrich-Buchecker, C.; Heitz, V.; Odobel, F.; Solladie, N.; Sauvage, J.-P. Rotaxanes and Other Transition Metal-Assembled Porphyrin Arrays for Long-Range Photoinduced Charge Separation. *Coord. Chem. Rev.* **1998**, *178-180*, 1299–1312.
(375) Chambron, J.-C.; Sauvage, J.-P. Functional Rotaxanes: From Controlled Molecular Motions to Electron Transfer between Chemically Nonconnected Chromophores. *Chem. Eur. J.* **1998**, *4*, 1362–1366.
(376) Blanco, M.-J.; Jiménez, M. C.; Chambron, J.-C.; Heitz, V.; Linke, M.; Sauvage, J.-P. Rotaxanes as New Architectures for Photoinduced Electron Transfer and Molecular Motions. *Chem. Soc. Rev.* **1999**, *28*, 293–305.
(377) Flamigni, L.; Heitz, V.; Sauvage, J.-P. Porphyrin Rotaxanes and Catenanes: Copper(I)-Templated Synthesis and Photoinduced Processes. *Struct. Bond.* **2006**, *121*, 217–261.
(378) Solladié, N.; Chambron, J.-C.; Dietrich-Buchecker, C.; Sauvage, J.-P. Multicomponent Molecular Systems Incorporating Porphyrins and Copper(I) Complexes: Simultaneous Synthesis of [3]- and [5]Rotaxanes. *Angew. Chem., Int. Ed. Engl*. **1996**, *35*, 906–909.
(379) Solladié, N.; Chambron, J.-C.; Sauvage, J.-P. Porphyrin-Stoppered [3]- and [5]-Rotaxanes. *J. Am. Chem. Soc.* **1999**, *121*, 3684–3692.
(380) Blanco, M.-J.; Chambron, J.-C.; Heitz, V.; Sauvage, J.-P. A Linear Multiporphyrinic [2]-Rotaxane via Amide Bond Formation. *Org. Lett.* **2000**, *2*, 3051–3054.
(381) Gaviña, P.; Sauvage, J.-P. Transition-Metal Template Synthesis of a Rotaxane Incorporating Two Different Coordinating Units in its Thread. *Tetrahedron Lett.* **1997**, *38*, 3521–3524.
(382) Armaroli, N.; Balzani, V.; Collin, J.-P.; Gaviña, P.; Sauvage, J.-P; Ventura, B. Rotaxanes Incorporating Two Different Coordinating Units in Their Thread: Synthesis and Electrochemically and Photochemically Induced Molecular Motions. *J. Am. Chem. Soc.* **1999**, *121*, 4397–4408.
(383) Chambron, J.-C.; Sauvage, J.-P.; Mislow, K.; De Cian, A.; Fischer, J. A [2]Catenane and a [2]Rotaxane as Prototypes of Topological and Euclidean Molecular “Rubber Gloves.” *Chem. Eur. J.* **2001**, *7*, 4085–4096.
(384) Jimenez-Molero, M. C.; Dietrich-Buchecker, C.; Sauvage, J.-P. Chemically Induced Contraction and Stretching of a Linear Rotaxane Dimer. *Chem. Eur. J.* **2002**, *8*, 1456–1466.
(385) Poleschak, I.; Kern, J.-M.; Sauvage, J.-P. A Copper-Complexed Rotaxane in Motion: Pirouetting of the Ring on the Millisecond Timescale. *Chem. Commun*. **2004**, 474–476.
(386) Létinois-Halbes, U.; Hanss, D.; Sauvage, J.-P.; Beierle, J. M.; Collin, J.-P. A Fast-Moving [2]Rotaxane Whose Stoppers Are Remote From the Copper Complex Core. *Org. Lett.* **2005**, *7*, 5753–5756.
(387) Collin, J.-P.;Durola, F.; Lux, J.; Sauvage, J.-P. A Rapidly Shuttling Copper-Complexed [2]Rotaxane with Three Different Chelating Groups in its Axis. *Angew. Chem., Int. Ed*. **2009**, *48*, 8532–8535.
(388) Collin, J.-P.; Durola, F.; Lux, J.; Sauvage, J.-P. A Copper-Based Shuttling [2]Rotaxane with Two Bidentate Chelates in the Axis: Steric Control of the Motion. *New J. Chem.* **2010**, *34*, 34–43.
(389) Sauvage, J.-P. Interlacing Molecular Threads on Transition Metals: Catenands, Catenates, and Knots. *Acc. Chem. Res.* **1990**, *23*, 319–327.
(390) Sauvage, J.-P. Transition Metal-Containing Rotaxanes and Catenanes in Motion: Toward Molecular Machines and Motors. *Acc. Chem. Res.* **1998**, *31*, 611–619.
(391) Dietrich-Buchecker, C.; Jimenez-Molero, M. C.; Sartor, V.; Sauvage, J.-P. Rotaxanes and Catenanes as Prototypes of Molecular Machines and Motors. *Pure Appl. Chem.* **2003**, *75*, 1383–1393.
(392) Dietrich-Buchecker, C.; Colasson, B. X.; Sauvage, J.-P. Molecular Knots. *Top. Curr. Chem.* **2005**, *249*, 261–283.
(393) Dietrich-Buchecker, C. O.; Khemiss, A.; Sauvage, J.-P. High-Yield Synthesis of Multiring Copper(I) Catenates by Acetylenic Oxidative Coupling. *J. Chem. Soc., Chem. Commun*. **1986**, 1376–1378.
(394) Dietrich-Buchecker, C. O.; Hemmert, C.; Khemiss, A.-K.; Sauvage, J.-P. Synthesis of Dicopper [3]-Catenates and [3]-Catenands by Acetylenic Oxidative Coupling. Preparation and Study of Corresponding Homodimetallic [3]-Catenates [Silver(1+), Zinc(2+), Cobalt(2+), and Nickel(2+)]. *J. Am. Chem. Soc*. **1990**, *112*, 8002–8008.
(395) Diederich, F.; Dietrich-Buchecker, C.; Nierengarten, J.-F.; Sauvage, J.-P. A Copper(I)-Complexed Rotaxane with Two Fullerene Stoppers. *J. Chem. Soc., Chem. Commun*. **1995**, 781–782.
(396) Armaroli, N.; Diederich, F.; Dietrich-Buchecker, C. O.; Flamigni, L.; Marconi, G.; Nierengarten, J.-F.; Sauvage, J.-P. A Copper(I)-Complexed Rotaxane with Two Fullerene Stoppers: Synthesis, Electrochemistry, and Photoinduced Processes. *Chem. Eur. J.* **1998**, *4*, 406–416.
(397) Dietrich-Buchecker, C. O.; Guilhem, J.; Khemiss, A.-K.; Kintzinger, J.-P.; Pascard, C.; Sauvage, J.-P. Molecular Structure of a [3]-Catenate: Curling up of the Interlocked System by Interaction between the Two Copper Complex Subunits. *Angew. Chem., Int. Ed. Engl*. **1987**, *26*, 661–663.
(398) Guilhem, J.; Pascard, C.; Sauvage, J.-P.; Weiss, J. Solution Study and Molecular Structure of a [3]-Catenand. Intramolecular Interaction Between the Two Peripheral Rings. *J. Am. Chem. Soc*. **1988**, *110*, 8711–8713.
(399) Miljanić, O. Š.; Dichtel, W. R.; Aprahamian, I.; Rohde, R. D.; Agnew, H. D.; Heath, J. R.; Stoddart, J. F. Rotaxanes and Catenanes by Click Chemistry. *QSAR Comb. Sci.* **2007**, *26*, 1165–1174.
(400) Aprahamian, I.; Miljanić, O. Š.; Dichtel, W. R.; Isoda, K.; Yasuda, T.; Kato, T.; Stoddart, J. F. Clicked Interlocked Molecules. *Bull. Chem. Soc. Jpn.* **2007**, *80*, 1856–1869
(401) Hänni, K. D.; Leigh, D. A. The Application of CuAAC “Click” Chemistry to Catenane and Rotaxane Synthesis. *Chem. Soc. Rev.* **2010**, *39*, 1240–1251.
(402) Fahrenbach, A. C.; Stoddart, J. F. Reactions Under the Click Chemistry Philosophy Employed in Supramolecular and Mechanostereochemical Systems. *Chem. Asian J.* **2011**, *6*, 2660–2669.
(403) Aucagne, V.; Hänni, K. D.; Leigh, D. A.; Lusby, P. J.; Walker, D. B. Catalytic “Click” Rotaxanes: A Substoichiometric Metal-Template Pathway to Mechanically Interlocked Architectures. *J. Am. Chem. Soc.* **2006**, *128*, 2186–2187.
(404) Dichtel, W. R.; Miljanić, O. Š.; Spruell, J. M.; Heath, J. R.; Stoddart, J. F. Efficient Templated Synthesis of Donor–Acceptor Rotaxanes Using Click Chemistry. *J. Am. Chem. Soc.* **2006**, *128*, 10388–10390.
(405) Miljanić, O. Š.; Dichtel, W. R.; Mortezaei, S.; Stoddart, J. F. Cyclobis(paraquat-*p*-phenylene)-Based [2]Catenanes Prepared by Kinetically Controlled Reactions Involving Alkynes. *Org. Lett.* **2006**, *8*, 4835–4838.
(406) Mobian, P.; Collin, J.-P.; Sauvage, J.-P. Efficient Synthesis of a Labile Copper(I)-Rotaxane Complex Using Click Chemistry. *Tetrahedron Lett.* **2006**, *47*, 4907–4909.
(407) Durot, S.; Mobian, P.; Collin, J.-P.; Sauvage, J.-P. Synthesis of New Copper(I)-Complexed Rotaxanes via Click Chemistry. *Tetrahedron* **2008**, *64*, 8496–8503.

(408) Collin, J.-P.; Sauvage, J.-P.; Trolez, Y.; Rissanen, K. [3]Rotaxanes and [3]Pseudorotaxanes with a Rigid Two-bidentate Chelate Axle Threaded Through Two Coordinating Rings. *New J. Chem*. **2009**, *33*, 2148–2154.

(409) Collin, J.-P.; Frey, J.; Heitz, V.; Sauvage, J.-P.; Tock, C.; Allouche, L. Adjustable Receptor Based on a [3]Rotaxane Whose Two Threaded Rings Are Rigidly Attached to Two Porphyrinic Plates: Synthesis and Complexation Studies. *J. Am. Chem. Soc.* **2009**, *131*, 5609–5620.

(410) Collin, J.-P.; Durola, F.; Frey, J.; Heitz, V.; Reviriego, F.; Sauvage, J.-P.; Trolez, Y.; Rissanen, K. Templated Synthesis of Cyclic [4]Rotaxanes Consisting of Two Stiff Rods Threaded Through Two Bis-macrocycles with a Large and Rigid Central Plate as Spacer. *J. Am. Chem. Soc.* **2010**, *132*, 6840–6850.

(411) Collin, J.-P.; Durola, F.; Heitz, V.; Reviriego, F.; Sauvage, J.-P.; Trolez, Y. A Cyclic [4]Rotaxane that Behaves as a Switchable Molecular Receptor: Formation of a Rigid Scaffold from a Collapsed Structure by Complexation with Copper(I) Ions. *Angew. Chem., Int. Ed*. **2010**, *49*, 10172–10175.

(412) Roche, C.; Sauvage, J.-P.; Sour, A.; Strutt, N. L. A [3]Rotaxane Composed of a Zinc Porphyrin Tetra-substituted with Coordinating Macrocycles and of Two Short Rigid Axles. *New J. Chem.* **2011**, *35*, 2820–2825.

(413) Collin, J.-P.; Durot, S.; Keller, M.; Sauvage, J.-P.; Trolez, Y.; Cetina, M.; Rissanen, K. Synthesis of [5]Rotaxanes Containing Bi- and Tridentate Coordination Sites in the Axis. *Chem. Eur. J.* **2011**, *17*, 947–957.

(414) Roche, C.; Sour, A.; Sauvage, J.-P. A Flexible Copper(I)-Complexed [4]Rotaxane Containing Two Face-to-Face Porphyrinic Plates that Behaves as a Distensible Receptor. *Chem. Eur. J.* **2012**, *18*, 8366–8376.

(415) Megiatto, J. D.; Schuster, D. I. General Method for Synthesis of Functionalized Macrocycles and Catenanes Utilizing "Click" Chemistry. *J. Am. Chem. Soc.* **2008**, *130*, 12872–12873.

(416) Megiatto, J. D., Jr.; Schuster, D. I. "Click" Methodology for Synthesis of Functionalized [3]Catenanes: Toward Higher Interlocked Structures. *Chem. Eur. J.* **2009**, *15*, 5444–5448.

(417) Megiatto, J. D., Jr.; Schuster, D. I. Introduction of Useful Peripheral Functional Groups on [2]Catenanes by Combining Cu(I) Template Synthesis with "Click" Chemistry. *New J. Chem.* **2010**, *34*, 276–286.

(418) Megiatto, J. D., Jr.; Schuster, D. I.; Abwandner, S.; de Miguel, G.; Guldi, D. M. [2]Catenanes Decorated with Porphyrin and [60]Fullerene Groups: Design, Convergent Synthesis, and Photoinduced Processes. *J. Am. Chem. Soc*. **2010**, *132*, 3847–3861.

(419) Kirner, S. V.; Guldi, D. M.; Megiatto, J. D., Jr.; Schuster, D. I. Synthesis and Photophysical Properties of New Catenated Electron Donor–Acceptor Materials with Magnesium and Free Base Porphyrins as Donors and C_{60} as the Acceptor. *Nanoscale* **2015**, *7*, 1145–1160.

(420) Lewis, W. G.; Magallon, F. G.; Fokin, V. V.; Finn, M. G. Discovery and Characterization of Catalysts for Azide−Alkyne Cycloaddition by Fluorescence Quenching. *J. Am. Chem. Soc.* **2004**, *126*, 9152–9153.

(421) Ammann, M.; Rang, A.; Schalley, C. A.; Bäuerle, P. A Synthetic Approach Towards Interlocked π-Conjugated Macrocycles. *Eur. J. Org. Chem*. **2006**, 1940–1948.

(422) Bäuerle, P.; Ammann, M.; Wilde, M.; Götz, G.; Mena-Osteritz, E.; Rang, A.; Schalley, C. A. Oligothiophene-Based Catenanes: Synthesis and Electronic Properties of a Novel Conjugated Topological Structure. *Angew. Chem., Int. Ed*. **2007**, *46*, 363–368.

(423) Götz, G.; Zhu, X.; Mishra, A.; Segura, J.-L.; Mena-Osteritz, E.; Bäuerle, P. π-Conjugated [2]Catenanes Based on Oligothiophenes and Phenanthrolines: Efficient Synthesis and Electronic Properties. *Chem. Eur. J.* **2015**, *21*, 7193–7210.

(424) Price, J. R.; Clegg, J. K.; Fenton, R. R.; Lindoy, L. F.; McMurtrie, J. C.; Meehan, G. V.; Parkin, A.; Perkins, D.; Turner, P. Copper(I) Templated Synthesis of a 2,2′-Bipyridine Derived 2-Catenane: Synthetic, Modelling, and X-ray Studies. *Aust. J. Chem.* **2009**, *62*, 1014–1019.

(425) Piguet, C.; Bernardinelli, G.; Williams, A. F.; Bocquet, B. Formation of the First Isomeric [2]Catenates by Self-Assembly About Two Different Metal Ions. *Angew. Chem., Int. Ed. Engl*. **1995**, *34*, 582–584.

(426) Cárdenas, D. J.; Gaviña, P.; Sauvage, J.-P. A Rotaxane with Two Ru(terpy)$_2$ Derivatives as Stoppers. *Chem. Commun*. **1996**, 1915–1916.

(427) Cárdenas, D. J.; Gaviña, P.; Sauvage, J.-P. Construction of Interlocking and Threaded Rings Using Two Different Transition Metals as Templating and Connecting Centers: Catenanes and Rotaxanes Incorporating Ru(terpy)$_2$-Units in Their Framework. *J. Am. Chem. Soc.* **1997**, *119*, 2656–2664.

(428) Cárdenas, D. J.; Collin, J.-P.; Gaviña, P.; Sauvage, J. P.; De Cian, A.; Fischer, J.; Armaroli, N.; Flamigni, L.; Vicinelli, V.; Balzani, V. Synthesis, X-ray Structure, and Electrochemical and Excited-State Properties of Multicomponent Complexes Made of a $[Ru(Tpy)_2]^{2+}$ Unit Covalently Linked to a [2]-Catenate Moiety. Controlling the Energy-Transfer Direction by Changing the Catenate Metal Ion. *J. Am. Chem. Soc*. **1999**, *121*, 5481–5488.

(429) Cárdenas, D. J.; Sauvage, J.-P. Templating and Clipping Coordination Reactions Leading to Heteronuclear Trimetallic Complexes Containing Interlocking Rings. *Inorg. Chem.* **1997**, *36*, 2777–2783.

(430) Bunha, A.; Tria, M. C.; Advincula, R. C. Polymer Catenanes via a Supramolecularly Templated ATRP Initiator. *Chem. Commun.* **2011**, *47*, 9173.

(431) Cao, P.-F.; Bunha, A.; Mangadlao, J.; Felipe, M. J.; Mongcopa, K. I.; Advincula, R. C. A Supramolecularly Templated Catenane Initiator and a Controlled Ring Expansion Strategy. *Chem. Commun.* **2012**, *48*, 12094–12096.

(432) Cao, P.-F.; Mangadlao, J. D.; de Leon, A.; Su, Z.; Advincula, R. C. Catenated Poly(ε-caprolactone) and Poly(L-lactide) via Ring-Expansion Strategy. *Macromolecules* **2015**, *48*, 3825–3833.

(433) Bunha, A.; Cao, P.-F.; Mangadlao, J.; Shi, F.-M.; Foster, E.; Pangilinan, K.; Advincula, R. C. Polymeric Catenanes Synthesized *via* "Click" Chemistry and Atom Transfer Radical Coupling. *Chem. Commun.* **2015**, *51*, 7528–7531.

(434) Hamann, C.; Kern, J.-M.; Sauvage, J.-P. Zinc(II)-Templated Synthesis of a [2]-Catenane Consisting of a 2,2′,6′,2″-Terpyridine-Incorporating Cycle and a 1,10-Phenanthroline-Containing Ring. *Inorg. Chem.* **2003**, *42*, 1877–1883.

(435) Saha, S.; Santra, S.; Akhuli, B.; Ghosh, P. [2]Rotaxane with Multiple Functional Groups. *J. Org. Chem*. **2014**, *79*, 11170–11178.

(436) Sauvage, J.-P.; Ward, M. A Bis(terpyridine)ruthenium(II) Catenate. *Inorg. Chem.* **1991**, *30*, 3869–3874.

(437) Chambron, J.-C.; Collin, J.-P.; Heitz, V.; Jouvenot, D.; Kern, J.-M.; Mobian, P.; Pomeranc, D.; Sauvage, J.-P. Rotaxanes and Catenanes Built Around Octahedral Transition Metals. *Eur. J. Org. Chem*. **2004**, 1627–1638.

(438) Ayme, J.-F.; Lux, J.; Sauvage, J.-P.; Sour, A. [2]Catenanes Built around Octahedral Transition-Metal Complexes that Contain Two Intertwined Endocyclic but Non-Sterically Hindering Tridentate Ligands. *Chem. Eur. J*. **2012**, *18*, 5565–5573.

(439) Durola, F.; Sauvage, J.-P.; Wenger, O. S. The Magic Effect of Endocyclic but Non-Sterically Hindering Biisoquinoline Chelates: From Fast-Moving Molecular Shuttles to [3]Rotaxanes. *Coord. Chem. Rev.* **2010**, *254*, 1748–1759.

(440) Loren, J. C.; Gantzel, P.; Linden, A.; Siegel, J. S. Synthesis of Achiral and Racemic Catenanes Based on Terpyridine and a Directionalized Terpyridine Mimic, Pyridyl-Phenanthroline. *Org. Biomol. Chem*. **2005**, *3*, 3105–3116.

(441) Mobian, P.; Kern, J.-M.; Sauvage, J.-P. Building [2]Catenanes Around a Tris(diimine)ruthenium(2+)($[Ru(Diimine)_3]^{2+}$) Complex Core Used as Template. *Helv. Chim. Acta* **2003**, *86*, 4195–4213.

(442) Mobian, P.; Kern, J.-M.; Sauvage, J.-P. A [2]Catenane Constructed Around a Ru(diimine)$_3^{2+}$ Complex Used as a Template. *J. Am. Chem. Soc.* **2003**, *125*, 2016–2017.

(443) Mobian, P.; Kern, J.-M.; Sauvage, J.-P. A [2]Catenane Constructed Around a Rhodium(III) Center Used as a Template. *Inorg. Chem.* **2003**, *42*, 8633–8637.

(444) Mobian, P.; Kern, J.-M.; Sauvage, J.-P. Light-Driven Machine Prototypes Based on Dissociative Excited States: Photoinduced Decoordination and Thermal Recoordination of a Ring in a Ruthenium(II)-Containing [2]Catenane. *Angew. Chem., Int. Ed*. **2004**, *43*, 2392–2395.

(445) Pomeranc, D.; Jouvenot, D.; Chambron, J.-C.; Collin, J.P.; Heitz, V.; Sauvage, J.-P. Templated Synthesis of a Rotaxane with a [Ru(diimine)$_3$]$^{2+}$ Core. *Chem. Eur. J.* **2003**, *9*, 4247–4254.

(446) Leigh, D. A.; Lusby, P. J.; Teat, S. J.; Wilson, A. J.; Wong, J. K. Y. Benzylic Imine Catenates: Readily Accessible Octahedral Analogues of the Sauvage Catenates. *Angew. Chem., Int. Ed*. **2001**, *40*, 1538–1543.

(447) Hogg, L.; Leigh, D. A.; Lusby, P. J.; Morelli, A.; Parsons, S.; Wong, J. K. Y. A Simple General Ligand System for Assembling Octahedral Metal-Rotaxane Complexes. *Angew. Chem., Int. Ed*. **2004**, *43*, 1218–1221.

(448) Leigh, D. A.; Lusby, P. J.; McBurney, R. T.; Morelli, A.; Slawin, A. M. Z.; Thomson, A. R.; Walker, D. B. Getting Harder: Cobalt(III)-Template Synthesis of Catenanes and Rotaxanes. *J. Am. Chem. Soc*. **2009**, *131*, 3762–3771.

(449) Hansen, J. G.; Feeder, N.; Hamilton, D. G.; Gunter, M. J.; Becher, J.; Becher, J.; Sanders, J. K. M. Macrocyclization and Molecular Interlocking via Mitsunobu Alkylation: Highlighting the Role of C-H···O Interactions in Templating. *Org. Lett.* **2000**, *2*, 449–452.

(450) Blake, A. J.; Dietrich-Buchecker, C. O.; Hyde, T. I.; Sauvage, J.-P.; Schröder, M. C–H Activation in a Co-ordinated Catenand: *ortho*-Metallation of Cat30 by Palladium(II). *J. Chem. Soc., Chem. Commun*. **1989**, 1663–1665.

(451) Hamann, C.; Kern, J.-M.; Sauvage, J.-P. Palladium(II)-Directed Formation of Pseudo-Rotaxanes: The 3 + 1 Approach to Threaded Species using Square-Planar Geometries. *Dalton Trans*. **2003**, 3770–3775.

(452) Fuller, A.-M.; Leigh, D. A.; Lusby, P. J.; Oswald, I. D. H.; Parsons, S.; Walker, D. B. A 3D Interlocked Structure From a 2D Template: Structural Requirements for the Assembly of a Square-Planar Metal-Coordinated [2]Rotaxane. *Angew. Chem., Int. Ed*. **2004**, *43*, 3914–3918.

(453) Fuller, A.-M. L.; Leigh, D. A.; Lusby, P. J.; Slawin, A. M. Z.; Walker, D. B. Selecting Topology and Connectivity Through Metal-Directed Macrocyclization Reactions: A Square Planar Palladium [2]Catenate and Two Noninterlocked Isomers. *J. Am. Chem. Soc.* **2005**, *127*, 12612–12619.

(454) Fuller, A.-M. L.; Leigh, D. A.; Lusby, P. J. One Template, Multiple Rings: Controlled Iterative Addition of Macrocycles onto a Single Binding Site Rotaxane Thread. *Angew. Chem., Int. Ed*. **2007**, *46*, 5015–5019.

(455) Fuller, A.-M. L.; Leigh, D. A.; Lusby, P. J. Sequence Isomerism in [3]Rotaxanes. *J. Am. Chem. Soc.* **2010**, *132*, 4954–4959.

(456) Hung, W.-C.; Wang, L.-Y.; Lai, C.-C.; Liu, Y.-H.; Peng, S.-M.; Chiu, S.-H. Two [2]Pseudorotaxane-like Complexes and their Corresponding [2]Rotaxanes Stabilized via Interactions on Opposite Ends of the Same Macrocycle. *Tetrahedron Lett.* **2009**, *50*, 267–270.

(457) Ramakrishnam Raju, M. V.; Lin, H.-C. Self-Assembly of Tetraphenylethene-based [2]Catenane Driven by Acid–Base-Controllable Molecular Switching and its Enabled Aggregation-Induced Emission. *Org. Lett.* **2014**, *16*, 5564–5567.

(458) Goldup, S. M.; Leigh, D. A.; Lusby, P. J.; McBurney, R. T.; Slawin, A. M. Z. Gold(I)-Template Catenane and Rotaxane Synthesis. *Angew. Chem., Int. Ed*. **2008**, *47*, 6999–7003.

(459) Amabilino, D. B.; Stoddart, J. F.; Williams, D. J. From Solid-State Structures and Superstructures to Self-Assembly Processes. *Chem. Mater.* **1994**, *6*, 1159–1167.

(460) Langford, S. J.; Stoddart, J. F. Self-Assembly in Chemical Systems. *Pure Appl. Chem.* **1996**, *68*, 1255–1260.

(461) Gómez-López, M.; Preece, J. A.; Stoddart, J. F. The Art and Science of Self-Assembling Molecular Machines. *Nanotechnology* **1996**, *7*, 183–192.

(462) Gillard, R. E.; Raymo, F. M.; Stoddart, J. F. Molecular Meccano 26. Controlling Self-Assembly. *Chem. Eur. J*. **1997**, *3*, 1933–1940.

(463) Stoddart, J. F.; Tseng, H.-R. Chemical Synthesis Gets a Fillip From Molecular Recognition and Self-Assembly Processes. *Proc. Natl. Acad. Sci. U.S.A.* **2002**, *99*, 4797–4800.

(464) Flood, A. H.; Ramirez, R. J. A.; Deng, W.-Q.; Muller, R. P.; Goddard, W. A., III; Stoddart, J. F. Meccano on the Nanoscale: A Blueprint for Making Some of the World's Tiniest Machines. *Aust. J. Chem.* **2004**, *57*, 301–322.

(465) Moonen, N. N. P.; Flood, A. H.; Fernández, J. M.; Stoddart, J. F. Towards a Rational Design of Molecular Switches and Sensors From Their Basic Building Blocks. *Top. Curr. Chem.* **2005**, *262*, 99–132.

(466) Stoddart, J. F. From a Meccano Set to Nano Meccano. *Pure Appl. Chem.* **2005**, *77*, 1089–1106.

(467) Griffiths, K. E.; Stoddart, J. F. Template-Directed Synthesis of Donor/Acceptor [2]Catenanes and [2]Rotaxanes. *Pure Appl. Chem.* **2008**, *80*, 485–506.

(468) Stoddart, J. F.; Colquhoun, H. M. Big and little Meccano. *Tetrahedron* **2008**, *64*, 8231–8263.

(469) Barin, G.; Coskun, A.; Fouda, M. M. G.; Stoddart, J. F. Mechanically Interlocked Molecules Assembled by π–π Recognition. *ChemPlusChem* **2012**, *77*, 159–185.

(470) Fahrenbach, A. C.; Bruns, C. J.; Cao, D.; Stoddart, J. F. Ground-State Thermodynamics of Bistable Redox-Active Donor–Acceptor Mechanically Interlocked Molecules. *Acc. Chem. Res.* **2012**, *45*, 1581–1592.

(471) Fahrenbach, A. C.; Bruns, C. J.; Li, H.; Trabolsi, A.; Coskun, A.; Stoddart, J. F. Ground-State Kinetics of Bistable Redox-Active Donor–Acceptor Mechanically Interlocked Molecules. *Acc. Chem. Res.* **2014**, *47*, 482–493.

(472) Sliwa, W.; Bachowska, B. Rotaxanes Containing Quaternary Azaaromatic Moieties. *Heterocycles* **2004**, *63*, 2131–2158.

(473) Burley, S. K.; Petsko, G. A. Aromatic-Aromatic Interaction: a Mechanism of Protein Structure Stabilization. *Science* **1985**, *229*, 23–29.

(474) Watson, J. D.; Crick, F. Molecular Structure of Nucleic Acids; A Structure for Deoxyribose Nucleic Acid. *Nature* **1953**, *171*, 737–738.

(475) Claessens, C. G.; Stoddart, J. F. π–π Interactions in Self-Assembly. *J. Phys. Org. Chem*. **1997**, *10*, 254–272.

(476) Heeger, A. J. Semiconducting and Metallic Polymers: The Fourth Generation of Polymeric Materials (Nobel Lecture). *Angew. Chem., Int. Ed*. **2001**, *40*, 2591–2611.

(477) Sinnokrot, M. O.; Sherrill, C. D. High-Accuracy Quantum Mechanical Studies of π–π Interactions in Benzene Dimers. *J. Phys. Chem. A* **2006**, *110*, 10656–10668.

(478) Grimme, S. Do Special Noncovalent π–π Stacking Interactions Really Exist? *Angew. Chem., Int. Ed*. **2008**, *47*, 3430–3434.

(479) Martinez, C. R.; Iverson, B. L. Rethinking the Term "pi-stacking." *Chem. Sci.* **2012**, *3*, 2191–2201.

(480) Hunter, C. A.; Sanders, J. K. M. The Nature of π–π Interactions. *J. Am. Chem. Soc.* **1990**, *112*, 5525–5534.

(481) Foster, R. *Organic Charge-Transfer Complexes*; Academic Press: New York, 1969.

(482) Miller, J. S.; Epstein, A. J.; Reiff, W. M. Ferromagnetic Molecular Charge-Transfer Complexes. *Chem. Rev*. **1988**, *88*, 201–220.

(483) Horiuchi, S.; Tokura, Y. Organic Ferroelectrics. *Nature Mater*. **2008**, *7*, 357–366.

(484) Tayi, A. S.; Shveyd, A. K.; Sue, A. C. H.; Szarko, J. M.; Rolczynski, B. S.; Cao, D.; Kennedy, T. J.; Sarjeant, A. A.; Stern, C. L.; Paxton, W. F.; Wu, W.; Dey, S. K.; Fahrenbach, A. C.; Guest, J. R.; Mohseni, H.; Chen, L. X.; Wang, K. L.; Stoddart, J. F.; Stupp, S. I. Room-Temperature Ferroelectricity in Supramolecular Networks of Charge-Transfer Complexes. *Nature* **2013**, *488*, 485–489.

(485) Das, A.; Ghosh, S. Supramolecular Assemblies by Charge-Transfer Interactions Between Donor and Acceptor Chromophores. *Angew. Chem., Int. Ed*. **2014**, *53*, 2038–2054.

(486) Allwood, B. L.; Kohnke, F. H.; Slawin, A. M. Z.; Stoddart, J. F.; Williams, D. J. Complexation of Diquat by a Regiospecifically Synthesised Macrobicyclic Receptor Molecule. *J. Chem. Soc., Chem. Commun*. **1985**, 311–314.

(487) Allwood, B. L.; Shahriari-Zavareh, H.; Stoddart, J. F.; Williams, D. J. Complexation of Paraquat and Diquat by a Bismetaphenylene-32-Crown-10 Derivative. *J. Chem. Soc., Chem. Commun*. **1987**, 1058–1061.

(488) Allwood, B. L.; Shahriari-Zavareh, H.; Spencer, N.; Stoddart, J. F.; Williams, D. J. Complexation of Diquat by a Bisparaphenylene-34-Crown-10 Derivative. *J. Chem. Soc., Chem. Commun*. **1987**, 1061–1064.

(489) Allwood, B. L.; Shahriari-Zavareh, H.; Spencer, N.; Stoddart, J. F.; Williams, D. J. Complexation of Paraquat by a Bisparaphenylene-34-Crown-10 Derivative. *J. Chem. Soc., Chem. Commun*. **1987**, 1064–1066.

(490) Ashton, P. R.; Chrystal, E. J. T.; Mathias, J. P.; Parry, K. P.; Slawin, A. M. Z.; Spencer, N.; Stoddart, J. F.; Williams, D. J. Complexation of Diquat and Paraquat by Macrocyclic Polyethers Incorporating Two Dihydroxynaphthalene Residues. *Tetrahedron Lett.* **1987**, *28*, 6367–6370.

(491) Ashton, P. R.; Slawin, A. M. Z.; Spencer, N.; Stoddart, J. F.; Williams, D. J. Complex Formation Between Bisparaphenylene-(3*n* + 4)-crown-*n* Ethers and the Paraquat and Diquat Dications. *J. Chem. Soc., Chem. Commun*. **1987**, 1066–1069.

(492) Bird, C. L.; Kuhn, A. T. Electrochemistry of the Viologens. *Chem. Soc. Rev.* **1981**, *10*, 49–82.

(493) Slawin, A. M. Z.; Spencer, N.; Stoddart, J. F.; Williams, D. J. The Dependence of the Solid State Structures of Bisparaphenylene-(3*n* + 4)-crown-*n* Ethers upon Macrocyclic Ring Size. *J. Chem. Soc., Chem. Commun*. **1987**, 1070–1072.

(494) Bruns, C. J.; Basu, S.; Stoddart, J. F. Improved Synthesis of 1,5-Dinaphtho[38]crown-10. *Tetrahedron Lett.* **2010**, *51*, 983–986.

(495) Ashton, P. R.; Boyd, S. E.; Brindle, A.; Langford, S. J.; Menzer, S.; Pérez-García, L.; Preece, J. A.; Raymo, F. M.; Spencer, N.; Stoddart, J. F.; White, A. J. P.; Williams, D. J. Molecular Meccano 50. Diazapyrenium-Containing Catenanes and Rotaxanes. *New J. Chem*. **1999**, *23*, 587–602.

(496) Asakawa, M.; Ashton, P. R.; Boyd, S. E.; Brown, C. L.; Gillard, R. E.; Kocian, O.; Raymo, F. M.; Stoddart, J. F.; Tolley, M. S.; White, A. J. P.; Williams, D. J. Molecular Meccano 11. Recognition of Bipyridinium-Based Derivatives by Hydroquinone- and/or Dioxynaphthalene-Based Macrocyclic Polyethers: From Inclusion Complexes to the Self-Assembly of [2]Catenanes. *J. Org. Chem*. **1997**, *62*, 26–37.

(497) Dey, S. K.; Coskun, A.; Fahrenbach, A. C.; Barin, G.; Basuray, A. N.; Trabolsi, A.; Botros, Y. Y.; Stoddart, J. F. A Redox-Active Reverse Donor–Acceptor Bistable [2]Rotaxane. *Chem. Sci.* **2011**, *2*, 1046–1053.

(498) Pascu, S. I.; Naumann, C.; Kaiser, G.; Bond, A. D.; Sanders, J. K. M.; Jarrosson, T. Structures and Solution Dynamics of Pseudorotaxanes Mediated by Alkali-Metal Cations. *Dalton Trans*. **2007**, 3874–3884.

(499) Pascu, S. I.; Jarrosson, T.; Naumann, C.; Otto, S.; Kaiser, G.; Sanders, J. K. M. Cation-Reinforced Donor-Acceptor Pseudorotaxanes. *New J. Chem*. **2005**, *29*, 80–89.

(500) Anelli, P. L.; Ashton, P. R.; Ballardini, R.; Balzani, V.; Delgado, M.; Gandolfi, M. T.; Goodnow, T. T.; Kaifer, A. E.; Philp, D.; Pietraszkiewicz, M.; Prodi, L.; Reddington, M. V.; Slawin, A. M. Z.; Spencer, N.; Stoddart, J. F.; Vicent, C.; Williams, D. J. Molecular Meccano 1. [2]Rotaxanes and a [2]Catenane Made to Order. *J. Am. Chem. Soc*. **1992**, *114*, 193–218.

(501) Credi, A.; Prodi, L. From Observed to Corrected Luminescence Intensity of Solution Systems: An Easy-to-Apply Correction Method for Standard Spectrofluorimeters. *Spectrochim. Acta A* **1998**, *54*, 159–170.

(502) Ashton, P. R.; Balzani, V.; Becher, J.; Credi, A.; Fyfe, M. C. T.; Mattersteig, G.; Menzer, S.; Nielsen, M. B.; Raymo, F. M.; Stoddart, J. F. Venturi, M.; White, A. J. P.; Williams, D. J. Molecular Meccano 53. A Three-Pole Supramolecular Switch. *J. Am. Chem. Soc*. **1999**, *121*, 3951–3957.

(503) Connors, K. A. *Binding Constants*; Wiley: New York, 1987.

(504) Kaiser, G.; Jarrosson, T.; Otto, S.; Ng, Y.-F.; Bond, A. D.; Sanders, J. K. M. Lithium-Templated Synthesis of a Donor-Acceptor Pseudorotaxane and Catenane. *Angew. Chem., Int. Ed*. **2004**, *43*, 1959–1962.

(505) Hamilton, D. G.; Davies, J. E.; Prodi, L.; Sanders, J. K. M. Synthesis, Structure and Photophysics of Neutral π-Associated [2]Catenanes. *Chem. Eur. J.* **1998**, *4*, 608–620.

(506) Arunan, E.; Desiraju, G. R.; Klein, R. A.; Sadlej, J.; Scheiner, S.; Alkorta, I.; Clary, D. C.; Crabtree, R. H.; Dannenberg, J. J.; Hobza, P.; Kjaergaard, H. G.; Legon, A. C.; Mennucci, B.; Nesbitt, D. J. Defining the Hydrogen Bond: An Account (IUPAC Technical Report). *Pure Appl. Chem.* **2011**, *83*, 1619–1636.

(507) Arunan, E.; Desiraju, G. R.; Klein, R. A.; Sadlej, J.; Scheiner, S.; Alkorta, I.; Clary, D. C.; Crabtree, R. H.; Dannenberg, J. J.; Hobza, P.; Kjaergaard, H. G.; Legon, A. C.; Mennucci, B.; Nesbitt, D. J. Definition of the Hydrogen Bond (IUPAC Recommendations 2011). *Pure Appl. Chem*. **2011**, *83*, 1637–1641.

(508) Houk, K. N.; Menzer, S.; Newton, S. P.; Raymo, F. M.; Stoddart, J. F.; Williams, D. J. Molecular Meccano 47. [C–H···O] Interactions as a Control Element in Supramolecular Complexes: Experimental and Theoretical Evaluation of Receptor Affinities for the Binding of Bipyridinium-Based Guests by Catenated Hosts. *J. Am. Chem. Soc*. **1999**, *121*, 1479–1487.

(509) Hamilton, D. G.; Sanders, J. K. M.; Davies, J. E.; Clegg, W.; Teat, S. J. Neutral [2]Catenanes From Oxidative Coupling of π-Stacked Components. *Chem. Commun*. **1997**, 897–898.

(510) Lestini, E.; Nikitin, K.; Müller-Bunz, H.; Fitzmaurice, D. Introducing Negative Charges Into Bis-*p*-phenylene Crown Ethers: A Study of Bipyridinium-Based [2]Pseudorotaxanes and [2]Rotaxanes. *Chem. Eur. J.* **2008**, *14*, 1095–1106.

(511) Chen, L.; Zhang, Y.-M.; Liu, Y. Molecular Binding Behaviors Between Tetrasulfonated Bis(*m*-phenylene)-26-Crown-8 and Bispyridinium Guests in Aqueous Solution. *J. Phys. Chem. B* **2012**, *116*, 9500–9506.

(512) Ji, X.; Li, J.; Chen, J.; Chi, X.; Zhu, K.; Yan, X.; Zhang, M.; Huang, F. Supramolecular Micelles Constructed by Crown Ether-Based Molecular Recognition. *Macromolecules* **2012**, *45*, 6457–6463.

(513) Chen, L.; Zhang, H.-Y.; Liu, Y. High Affinity Crown Ether Complexes in Water: Thermodynamic Analysis, Evidence of Crystallography and Binding of NAD. *J. Org. Chem.* **2012**, *77*, 9766–9773.

(514) Chen, L.; Zhang, Y.-M.; Wang, L.-H.; Liu, Y. Molecular Binding Behaviors of Pyromellitic and Naphthalene Diimide Derivatives by Tetrasulfonated 1,5-Dinaphtho-(3*n*+8)-Crown-*n* (*n*= 8, 10) in Aqueous Solution. *J. Org. Chem.* **2013**, *78*, 5357–5363.

(515) Zhang, Y.-M.; Wang, Z.; Chen, L.; Song, H.-B.; Liu, Y. Thermodynamics and Structures of Complexation Between Tetrasulfonated 1,5-Dinaphtho-38-Crown-10 and Diquaternary Salts in Aqueous Solution. *J. Phys. Chem. B* **2014**, *118*, 2433–2441.

(516) Gillard, R. E.; Stoddart, J. F.; White, A. J. P.; Williams, B. J.; Williams, D. J. A Novel Fluorine-Containing [2]Catenane. *J. Org. Chem.* **1996**, *61*, 4504–4505.

(517) Ballardini, R.; Balzani, V.; Credi, A.; Brown, C. L.; Gillard, R. E.; Montalti, M.; Philp, D.; Stoddart, J. F.; Venturi, M.; White, A. J. P.; Williams, B. J.; Williams, D. J. Molecular Meccano 22. Controlling Catenations, Properties and Relative Ring-Component Movements in Catenanes with Aromatic Fluorine Substituents. *J. Am. Chem. Soc*. **1997**, *119*, 12503–12513.

(518) Pérez-Alvarez, M.; Raymo, F. M.; Rowan, S. J.; Schiraldi, D.; Stoddart, J. F.; Wang, Z.-H.; White, A. J. P.; Williams, D. J. The Balance Between Electronic and Steric Effects in the Template-Directed Syntheses of [2]Catenanes. *Tetrahedron* **2001**, *57*, 3799–3808.
(519) Ashton, P. R.; Huff, J.; Menzer, S.; Parsons, I. W.; Preece, J. A.; Stoddart, J. F.; Tolley, M. S.; White, A. J. P.; Williams, D. J. Molecular Meccano 5. Bis[2]catenanes and a Bis[2]rotaxane—Model Compounds for Polymers with Mechanically Interlocked Components. *Chem. Eur. J.* **1996**, *2*, 31–44.
(520) Li, Q.; Zhang, W.; Miljanic, O. S.; Sue, C.-H.; Zhao, Y.-L.; Liu, L.; Knobler, C. B.; Stoddart, J. F.; Yaghi, O. M. Docking in Metal-Organic Frameworks. *Science* **2009**, *325*, 855–859.
(521) Cao, D.; Juríček, M.; Brown, Z. J.; Sue, C.-H.; Liu, Z.; Lei, J.; Blackburn, A. K.; Grunder, S.; Sarjeant, A. A.; Coskun, A.; Wang, C.; Farha, O. K.; Hupp, J. T.; Stoddart, J. F. Three-Dimensional Architectures Incorporating Stereoregular Donor–Acceptor Stacks. *Chem. Eur. J.* **2013**, *19*, 8457–8465.
(522) Zhao, Y.-L.; Liu, L.; Zhang, W.; Sue, C.-H.; Li, Q.; Miljanić, O. Š.; Yaghi, O. M.; Stoddart, J. F. Rigid-Strut-Containing Crown Ethers and [2]Catenanes for Incorporation Into Metal-Organic Frameworks. *Chem. Eur. J.* **2009**, *15*, 13356–13380.
(523) Amabilino, D. B.; Ashton, P. R.; Boyd, S. E.; Gómez-López, M.; Hayes, W.; Stoddart, J. F. Molecular Meccano 17. Translational Isomerism in Some Two- and Three-Station [2]Rotaxanes. *J. Org. Chem*. **1997**, *62*, 3062–3075.
(524) Hamers, C.; Kocian, O.; Raymo, F. M.; Stoddart, J. F. A Poly(bis[2]catenane) Containing a Combination of Covalent, Mechanical, and Coordinative Bonds. *Adv. Mater.* **1998**, *10*, 1366–1369.
(525) Menzer, S.; White, A. J. P.; Williams, D. J.; Bělohradský, M.; Behloradsky, M.; Raymo, F. M.; Hamers, C.; Stoddart, J. F.; Shipway, A. N. Molecular Meccano 25. Self-Assembly of Functionalized [2]Catenanes Bearing a Reactive Functional Group on Either One or Both Macrocyclic Components: From Monomeric [2]Catenanes to Polycatenanes. *Macromolecules* **1998**, *31*, 295–307.
(526) Zhu, K.; Vukotic, V. N.; Noujeim, N.; Loeb, S. J. Bis(benzimidazolium) Axles and Crown Ether Wheels: A Versatile Templating Pair for the Formation of [2]Rotaxane Molecular Shuttles. *Chem. Sci.* **2012**, *3*, 3265–3271.
(527) Loeb, S. J.; Wisner, J. A. A New Motif for the Self-Assembly of [2]Pseudorotaxanes; 1,2-Bis(pyridinium)ethane ‘Axles’ and [24]Crown-8 Ether ‘Wheels’. *Angew. Chem., Int. Ed*. **1998**, *37*, 2838–2840.
(528) Ballardini, R.; Balzani, V.; Credi, A.; Gandolfi, M. T.; Marquis, D.; Pérez-García, L.; Stoddart, J. F. Molecular Meccano 29. The Synthesis and Spectroscopic Properties of a [2]Catenane Incorporating an Anthracene Chromophoric Unit. *Eur. J. Org. Chem*. **1998**, 81–89.
(529) Ballardini, R.; Balzani, V.; Gandolfi, M. T.; Gillard, R. E.; Stoddart, J. F.; Tabellini, E. Molecular Meccano 31. The Synthesis and Spectroscopic Properties of Macrocyclic Polyethers Containing Two Different Aromatic Moieties and Their [2]Catenanes Incorporating Cyclobis(paraquat-*p*-Phenylene). *Chem. Eur. J*. **1998**, *4*, 449–459.
(530) Asakawa, M.; Ashton, P. R.; Dehaen, W.; L’abbé, G.; Menzer, S.; Nouwen, J.; Raymo, F. M.; Stoddart, J. F.; Tolley, M. S.; Toppet, S.; White, A. J. P.; Williams, D. J. Molecular Meccano 19. Self-Assembly of Novel [2]Catenanes and [2]Pseudorotaxanes Incorporating Thiacrown Ethers or Their Acyclic Analogs. *Chem. Eur. J*. **1997**, *3*, 772–787.
(531) Raymo, F. M.; Houk, K. N.; Stoddart, J. F. Molecular Meccano 28. Origins of Selectivity in Molecular and Supramolecular Entities: Solvent and Electrostatic Control of the Translational Isomerism in [2]Catenanes. *J. Org. Chem*. **1998**, *63*, 6523–6528.
(532) Braunschweig, A. B.; Ronconi, C. M.; Han, J.-Y.; Aricó, F.; Cantrill, S. J.; Stoddart, J. F.; Khan, S. I.; White, A. J. P.; Williams, D. J. Pseudorotaxanes and Rotaxanes Formed by Viologen Derivatives. *Eur. J. Org. Chem*. **2006**, 1857–1866.
(533) Lukyanenko, N. G.; Lyapunov, A. Y.; Kirichenko, T. I.; Botoshansky, M. M.; Simonov, Y. A.; Fonari, M. S. A High Yielding Template-Directed Synthesis of the First Fluorenone-Containing [2]Catenane. *Tetrahedron Lett.* **2005**, *46*, 2109–2112.
(534) Lukyanenko, N. G.; Lyapunov, A. Y.; Kirichenko, T. I.; Zubatyuk, R. I.; Shishkin, O. V. Self-Assembly of a [2]Catenane Incorporating a Fluorenonophane-Containing Azobenzene Moiety. *Mendeleev Commun.* **2006**, *16*, 143–145.
(535) Asakawa, M.; Ashton, P. R.; Balzani, V.; Brown, C. L.; Credi, A.; Matthews, O. A.; Newton, S. P.; Raymo, F. M.; Shipway, A. N.; Spencer, N.; Quick, A.; Stoddart, J. F.; White, A. J. P.; Williams, D. J. Molecular Meccano 44. Photoactive Azobenzene-Containing Supramolecular Complexes and Related Interlocked Molecular Compounds. *Chem. Eur. J*. **1999**, *5*, 860–875.
(536) Alcalde, E.; Pérez-García, L.; Ramos, S.; Stoddart, J. F.; Vignon, S. A.; White, A. J. P.; Williams, D. J. Spontaneous Resolution of a Non-Degenerate Donor–Acceptor [2]Catenane. *Mendeleev Commun.* **2003**, *13*, 100–102.
(537) Asakawa, M.; Ashton, P. R.; Balzani, V.; Credi, A.; Hamers, C.; Mattersteig, G.; Montalti, M.; Shipway, A. N.; Spencer, N.; Stoddart, J. F.; Tolley, M. S.; Venturi, M.; White, A. J. P.; Williams, D. J. A Chemically and Electrochemically Switchable [2]Catenane Incorporating a Tetrathiafulvalene Unit. *Angew. Chem., Int. Ed*. **1998**, *37*, 333–337.
(538) Asakawa, M.; Ashton, P. R.; Balzani, V.; Boyd, S. E.; Credi, A.; Mattersteig, G.; Menzer, S.; Montalti, M.; Raymo, F. M.; Ruffilli, C.; Stoddart, J. F.; Venturi, M.; Williams, D. J. Molecular Meccano 49. Pseudorotaxanes and Catenanes Containing a Redox-Active Unit Derived From Tetrathiafulvalene. *Eur. J. Org. Chem*. **1999**, 985–994.
(539) Balzani, V.; Credi, A.; Mattersteig, G.; Matthews, O. A.; Raymo, F. M.; Stoddart, J. F.; Venturi, M.; White, A. J. P.; Williams, D. J. Molecular Meccano 54. Switching of Pseudorotaxanes and Catenanes Incorporating a Tetrathiafulvalene Unit by Redox and Chemical Inputs. *J. Org. Chem*. **2000**, *65*, 1924–1936.
(540) Ballardini, R.; Balzani, V.; Di Fabio, A.; Gandolfi, M. T.; Becher, J.; Lau, J.; Nielsen, M. B.; Stoddart, J. F. Macrocycles, Pseudorotaxanes and Catenanes Containing a Pyrrolo-Tetrathiafulvalene Unit: Absorption Spectra, Luminescence Properties and Redox Behavior. *New J. Chem.* **2001**, *25*, 293–298.
(541) Tomcsi, M. R.; Stoddart, J. F. Bispyrrolotetrathiafulvalene-Containing [2]Catenanes. *J. Org. Chem.* **2007**, *72*, 9335–9338.
(542) Wang, C.; Olson, M. A.; Fang, L.; Benítez, D.; Tkatchouk, E.; Basu, S.; Basuray, A. N.; Zhang, D.; Zhu, D.; Goddard, W. A., III; Stoddart, J. F. Isolation by Crystallization of Translational Isomers of a Bistable Donor-Acceptor [2]Catenane. *Proc. Natl. Acad. Sci. U.S.A.* **2010**, *107*, 13991–13996.
(543) Wang, C.; Dyar, S. M.; Cao, D.; Fahrenbach, A. C.; Horwitz, N.; Colvin, M. T.; Carmieli, R.; Stern, C. L.; Dey, S. K.; Wasielewski, M. R.; Stoddart, J. F. Tetrathiafulvalene Hetero Radical Cation Dimerization in a Redox-Active [2]Catenane. *J. Am. Chem. Soc.* **2012**, *134*, 19136–19145.
(544) Forgan, R. S.; Friedman, D. C.; Stern, C. L.; Bruns, C. J.; Stoddart, J. F. Directed Self-Assembly of a Ring-in-Ring Complex. *Chem. Commun.* **2010**, *46*, 5861–5863.
(545) Asakawa, M.; Brown, C. L.; Menzer, S.; Raymo, F. M.; Stoddart, J. F.; Williams, D. J. Molecular Meccano 15. Structure–Reactivity Relationship in Interlocked Molecular Compounds and in Their Supramolecular Model Complexes. *J. Am. Chem. Soc*. **1997**, *119*, 2614–2627.
(546) Ashton, P. R.; Blower, M. A.; Iqbal, S.; McLean, C. H.; Stoddart, J. F.; Tolley, M. S.; Williams, D. J. The Design and Self-Assembly of a Furan-Containing [2]Catenane. *Synlett* **1994**, 1059–1062.
(547) Ashton, P. R.; Blower, M. A.; McLean, C. H.; Stoddart, J. F.; Tolley, M. S. The Design and Self-Assembly of a Pyridine-Containing [2]Catenane. *Synlett* **1994**, 1063–1066.

(548) Ashton, P. R.; Heiss, A. M.; Pasini, D.; Raymo, F. M.; Shipway, A. N.; Stoddart, J. F.; Spencer, N. Molecular Meccano 51. Diastereoselective Self-Assembly of [2]Catenanes. *Eur. J. Org. Chem*. **1999**, 995–1004.
(549) Ashton, P. R.; Goodnow, T. T.; Kaifer, A. E.; Reddington, M. V.; Slawin, A. M. Z.; Spencer, N.; Stoddart, J. F.; Vicent, C.; Williams, D. J. A [2]Catenane Made to Order. *Angew. Chem., Int. Ed. Engl*. **1989**, *28*, 1396–1399.
(550) Amabilino, D. B.; Anelli, P.-L.; Ashton, P. R.; Brown, G. R.; Córdova, E.; Godínez, L. A.; Hayes, W.; Kaifer, A. E.; Philp, D.; Slawin, A. M. Z.; Spencer, N.; Stoddart, J. F.; Tolley, M. S.; Williams, D. J. Molecular Meccano 3. Constitutional and Translational Isomerism in [2]Catenanes and [*n*]Pseudorotaxanes. *J. Am. Chem. Soc*. **1995**, *117*, 11142–11170.
(551) Forgan, R. S.; Gassensmith, J. J.; Cordes, D. B.; Boyle, M. M.; Hartlieb, K. J.; Friedman, D. C.; Slawin, A. M. Z.; Stoddart, J. F. Self-Assembly of a [2]Pseudorota[3]catenane in Water. *J. Am. Chem. Soc.* **2012**, *134*, 17007–17010.
(552) Zhu, Z.; Bruns, C. J.; Li, H.; Lei, J.; Ke, C.; Liu, Z.; Shafaie, S.; Colquhoun, H. M.; Stoddart, J. F. Synthesis and Solution-State Dynamics of Donor–Acceptor Oligorotaxane Foldamers. *Chem. Sci.* **2013**, *4*, 1470–1483.
(553) Brown C. L.; Philp D.; Spencer, N.; Stoddart, J. F. The Mechanisms of Making Molecules to Order. *Isr. J. Chem.* **1992**, *32*, 61–67.
(554) Fahrenbach, A. C.; Hartlieb, K. J.; Sue, C.-H.; Bruns, C. J.; Barin, G.; Basu, S.; Olson, M. A.; Botros, Y. Y.; Bagabas, A.; Khdary, N. H.; Stoddart, J. F. Rapid Thermally Assisted Donor–Acceptor Catenation. *Chem. Commun.* **2012**, *48*, 9141–9143.
(555) Ashton, P. R.; Blower, M. A.; Philp, D.; Spencer, N.; Stoddart, J. F.; Tolley, M. S.; Ballardini, R.; Ciano, M.; Balzani, V.; Gandolfi, M. T.; Prodi, L.; McLean, C. H. The Control of Translational Isomerism in Catenated Structures. *New J. Chem.* **1993**, *17*, 689–695.
(556) Ashton, P. R.; Brown, C. L.; Chrystal, E. J. T.; Goodnow, T. T.; Kaifer, A. E.; Parry, K. P.; Philp, D.; Slawin, A. M. Z.; Spencer, N.; Stoddart, J. F.; Williams, D. J. The Self-Assembly of a Highly Ordered [2]Catenane. *J. Chem. Soc., Chem. Commun*. **1991**, 634–639.
(557) Grunder, S.; McGrier, P. L.; Whalley, A. C.; Boyle, M. M.; Stern, C.; Stoddart, J. F. A Water-Soluble pH-Triggered Molecular Switch. *J. Am. Chem. Soc.* **2013**, *135*, 17691–17694.
(558) Ashton, P. R.; Ballardini, R.; Balzani, V.; Credi, A.; Gandolfi, M. T.; Menzer, S.; Pérez-García, L.; Prodi, L.; Stoddart, J. F.; Venturi, M.; White, A. J. P.; Williams, D. J. Molecular Meccano 4. The Self-Assembly of [2]Catenanes Incorporating Photoactive and Electroactive π-Extended Systems. *J. Am. Chem. Soc*. **1995**, *117*, 11171–11197.
(559) Klärner, F.-G.; Wurche, F. The Effect of Pressure on Organic Reactions. *J. Prakt. Chem.* **2000**, *342*, 609–636.
(560) Brown, C. L.; Stoddart, J. F.; Philp, D. The Self-Assembly of a [2]Catenane. *Synlett* **1991**, *19*, 459–461.
(561) Alcalde, E.; Pérez-García, L.; Ramos, S.; Stoddart, J. F.; White, A. J. P.; Williams, D. J. Nondegenerate π-Donor/π-Acceptor [2]Catenanes Containing Proton-Ionizable 1*H*-1,2,4-Triazole Subunits: Synthesis and Spontaneous Resolution. *Chem. Eur. J.* **2007**, *13*, 3964–3979.
(562) Nakamura, Y.; Minami, S.; Iizuka, K.; Nishimura, J. Preparation of Neutral [60]Fullerene-Based [2]Catenanes and [2]Rotaxanes Bearing an Electron-Deficient Aromatic Diimide Moiety. *Angew. Chem., Int. Ed*. **2003**, *42*, 3158–3162.
(563) Bingel, C. Cyclopropanierung von Fullerenen. *Chem. Ber.* **1993**, *126*, 1957–1959.
(564) Ashton, P. R.; Bělohradský, M.; Philp, D.; Stoddart, J. F. Slippage—An Alternative Method for Assembling [2]Rotaxanes. *J. Chem. Soc., Chem. Commun*. **1993**, 1269–1274.
(565) Ashton, P. R.; Bělohradský, M.; Philp, D.; Spencer, N.; Stoddart, J. F. The Self Assembly of [2]- and [3]-Rotaxanes by Slippage. *J. Chem. Soc., Chem. Commun*. **1993**, 1274–1277.
(566) Ashton, P. R.; Langford, S. J.; Spencer, N.; Stoddart, J. F.; White, A. J. P.; Williams, D. J. The Self-Assembly of a Complex with a [3]Pseudorotaxane Superstructure. *Chem. Commun.* **1996**, 1387–1388.
(567) Amabilino, D. B.; Ashton, P. R.; Balzani, V.; Brown, C. L.; Credi, A.; Fréchet, J. M. J.; Leon, J. W.; Raymo, F. M.; Spencer, N.; Stoddart, J. F.; Venturi, M. Molecular Meccano 13. Self-Assembly of [*n*]Rotaxanes Bearing Dendritic Stoppers. *J. Am. Chem. Soc*. **1996**, *118*, 12012–12020.
(568) Collin, J.-P.; Gaviña, P.; Sauvage, J.-P. Electrochemically Induced Molecular Motions in Copper-Complexed Threaded Systems: From the Unstoppered Compound to the Semi-Rotaxane and the Fully Blocked Rotaxane. *New J. Chem.* **1997**, *21*, 525–528.
(569) Orita, A.; Okano, J.; Tawa, Y.; Jiang, L.; Otera, J. Rate Acceleration of the Reaction Between Solid Reactants by Premixing in Solution: Application to the Efficient Synthesis of a [2]Rotaxane. *Angew. Chem., Int. Ed*. **2004**, *43*, 3724–3728.
(570) Orita, A.; Okano, J.; Uehara, G.; Jiang, L.; Otera, J. Importance of Molecular-Level Contacts Under Solventless Conditions for Chemical Reactions and Self-Assembly. *Bull. Chem. Soc. Jpn.* **2007**, *80*, 1617–1623.
(571) Basuray, A. N.; Jacquot de Rouville, H.-P.; Hartlieb, K. J.; Kikuchi, T.; Strutt, N. L.; Bruns, C. J.; Ambrogio, M. W.; Avestro, A.-J.; Schneebeli, S. T.; Fahrenbach, A. C.; Stoddart, J. F. Chameleonic Nature of Diazaperopyrenium Recognition Processes. *Angew. Chem., Int. Ed*. **2012**, *51*, 11872–11877.
(572) Nakazono, K.; Oku, T.; Takata, T. Synthesis of Rotaxanes Consisting of Crown Ether Wheel and *sec*-Ammonium Axle Under Basic Condition. *Tetrahedron Lett*. **2007**, *48*, 3409–3411.
(573) Choudhary, U.; Northrop, B. H. Rotaxanes and Biofunctionalized Pseudorotaxanes via Thiol-Maleimide Click Chemistry. *Org. Lett.* **2012**, *14*, 2082–2085.
(574) Mullen, K. M.; Gunter, M. J. Toward Multistation Rotaxanes Using Metalloporphyrin Coordination Templating. *J. Org. Chem.* **2008**, *73*, 3336–3350.
(575) Jacquot de Rouville, H.-P.; Iehl, J.; Bruns, C. J.; McGrier, P. L.; Frasconi, M.; Sarjeant, A. A.; Stoddart, J. F. A Neutral Naphthalene Diimide [2]Rotaxane. *Org. Lett*. **2012**, *14*, 5188–5191.
(576) Domoto, Y.; Fukushima, A.; Kasuga, Y.; Sase, S.; Goto, K.; Kawashima, T. Catalyst-Free Syntheses of [2]Rotaxanes Utilizing a Pentacoordinated Hydrosilane as an End-Capping Agent. *Org. Lett.* **2010**, *12*, 2586–2589.
(577) Domoto, Y.; Sase, S.; Goto, K. Efficient End-Capping Synthesis of Neutral Donor–Acceptor [2]Rotaxanes Under Additive-Free and Mild Conditions. *Chem. Eur. J.* **2014**, *20*, 15998–16005.
(578) Gunter, M.; Merican, Z. Neutral Donor-Acceptor Porphyrin-Stoppered [2]Rotaxanes. *Supramol. Chem.* **2005**, *17*, 521–528.
(579) Johnstone, K. D.; Bampos, N.; Sanders, J. K. M.; Gunter, M. J. Gel-Phase HR-MAS ^{1}H NMR Spectroscopy as a Probe for Solid-Tethered Diimide Rotaxanes and Catenanes. *New J. Chem.* **2006**, *30*, 861–867.
(580) Huang, F.; Jones, J. W.; Slebodnick, C.; Gibson, H. W. Ion Pairing in Fast-Exchange Host−Guest Systems: Concentration Dependence of Apparent Association Constants for Complexes of Neutral Hosts and Divalent Guest Salts with Monovalent Counterions. *J. Am. Chem. Soc.* **2003**, *125*, 14458–14464.
(581) Huang, F.; Jones, J. W.; Gibson, H. W. Competitive Interactions of Two Ion-Paired Salts with a Neutral Host to Form Two Non-Ion-Paired Complexes. *J. Org. Chem.* **2007**, *72*, 6573–6576.
(582) Gasa, T. B.; Spruell, J. M.; Dichtel, W. R.; Sørensen, T. J.; Philp, D.; Stoddart, J. F.; Kuzmič, P. Complexation Between

Methyl Viologen (Paraquat) Bis(Hexafluorophosphate) and Dibenzo[24]Crown-8 Revisited. *Chem. Eur. J.* **2009**, *15*, 106–116.
(583) Nikitin, K.; Müller-Bunz, H. Encapsulation of 4,4′-Bipyridinium Cations by Two Crown Ether Molecules: Formation and Structure of [3]Pseudorotaxanes. *New J. Chem.* **2009**, *33*, 2472–2478.
(584) Loeb, S. J.; Wisner, J. A. 1,2-Bis(4,4′-dipyridinium)ethane: A Versatile Dication for the Formation of [2]Rotaxanes with Dibenzo-24-Crown-8 Ether. *Chem. Commun*. **1998**, 2757–2758.
(585) Małecka, J.; Mames, I.; Woźny, M.; Korybut-Daszkiewicz, B.; Bilewicz, R. Pseudorotaxane Based on Tetraazamacrocyclic Copper Complex and Dibenzocrown Ether. *Dalton Trans.* **2012**, *41*, 12452–12456.
(586) Korybut-Daszkiewicz, B.; Wieckowska, A.; Bilewicz, R.; Domagała, S.; Woźniak, K. Novel [2]Catenane Structures Introducing Communication Between Transition Metal Centers via π···π Interactions. *J. Am. Chem. Soc.* **2001**, *123*, 9356–9366.
(587) Castillo, D.; Astudillo, P.; Mares, J.; González, F. J.; Vela, A.; Tiburcio, J. Chemically Controlled Self-Assembly of [2]Pseudorotaxanes Based on 1,2-Bis(benzimidazolium) ethane Cations and 24-Crown-8 Macrocycles. *Org. Biomol. Chem.* **2007**, *5*, 2252–2256.
(588) Moreno-Olivares, S. I.; Cervantes, R.; Tiburcio, J. Complexation of Imidazopyridine-Based Cations with a 24-Crown-8 Ether Host: [2]Pseudorotaxane and Partially Threaded Structures. *J. Org. Chem.* **2013**, *78*, 10724–10731.
(589) Castillo, D.; Cervantes, R.; Frontana, C.; Gonzalez, F. J.; Tiburcio, J. Self-Assembly of a [2]Pseudorotaxane Complex by the Threading of a Nitrobenzimidazol-Based Guest on Dibenzo-24-Crown Ether Host. *J. Phys. Org. Chem.* **2014**, *27*, 701–706.
(590) Li, L.; Clarkson, G. J. New Bis(benzimidazole) Cations for Threading Through Dibenzo-24-Crown-8. *Org. Lett.* **2007**, *9*, 497–500.
(591) Mukhopadhyay, C.; Ghosh, S.; Schmiedekamp, A. M. Unraveling the Molecular Recognition of “Three Methylene Spacer” Bis(benzimidazolium) Moiety by Dibenzo-24-Crown-8: Pseudorotaxanes Under Study. *Org. Biomol. Chem.* **2012**, *10*, 1434–1439.
(592) Ghosh, S.; Schmiedekamp, A. M.; Mukhopadhyay, C. Bis(benzimidazolium)methane salts: A Potential Guest for Dibenzi-24-Crown-8 towards [2]Pseudorotaxanes. *Tetrahedron* **2012**, *68*, 9826–9835.
(593) Ghosh, S.; Chaudhuri, T.; Schmiedekamp, A. M.; Padmanaban, E.; Mukhopadhyay, C. A 2,2′-Bis(benzimidazolium)-dibenzo[24]Crown[8] Rigid Pseudorotaxane System. *Tetrahedron* **2014**, *70*, 6885–6893.
(594) Kiviniemi, S.; Nissinen, M.; Lämsä, M. T.; Jalonen, J.; Rissanen, K.; Pursiainen, J. Complexation of Planar, Organic, Five-Membered Cations with Crown Ethers. *New J. Chem.* **2000**, *24*, 47–52.
(595) Zhu, K.; Vukotic, V. N.; Loeb, S. J. Molecular Shuttling of a Compact and Rigid H-Shaped [2]Rotaxane. *Angew. Chem., Int. Ed*. **2012**, *51*, 2168–2172.
(596) Noujeim, N.; Zhu, K.; Vukotic, V. N.; Loeb, S. J. [2]Pseudorotaxanes From T-Shaped Benzimidazolium Axles and [24]Crown-8 Wheels. *Org. Lett*. **2012**, *14*, 2484–2487.
(597) Farahani, N.; Zhu, K.; Noujeim, N.; Loeb, S. J. [2]Pseudorotaxane Formation Between Rigid Y-Shaped 2,4,5-Triphenylimidazolium Axles and [24]Crown-8 Ether Wheels. *Org. Biomol. Chem*. **2014**, *12*, 4824–4827.
(598) Hoffart, D. J.; Tiburcio, J.; La Torre, De, A.; Knight, L. K.; Loeb, S. J. Cooperative Ion–Ion Interactions in the Formation of Interpenetrated Molecules. *Angew. Chem., Int. Ed*. **2008**, *47*, 97–101.
(599) Loeb, S. J. Rotaxanes as Ligands: From Molecules to Materials. *Chem. Soc. Rev.* **2007**, *36*, 226–235.
(600) Davidson, G. J. E.; Loeb, S. J.; Parekh, N. A.; Wisner, J. A. Zwitterionic [2]Rotaxanes Utilising Anionic Transition Metal Stoppers. *J. Chem. Soc., Dalton Trans*. **2001**, 3135–3136.
(601) Loeb, S. J.; Wisner, J. A. [3]Rotaxanes Employing Multiple 1,2-Bis(pyridinium) Ethane Binding Sites and Dibenzo-24-Crown-8 Ethers. *Chem. Commun*. **2000**, 845–846.
(602) Loeb, S. J.; Wisner, J. A. [2]Rotaxane Molecular Shuttles Employing 1,2-Bis(pyridinium) Ethane Binding Sites and Dibenzo-24-Crown-8 Ethers. *Chem. Commun*. **2000**, 1939–1940.
(603) Davidson, G. J. E.; Loeb, S. J. Iron(II) Complexes Utilising Terpyridine Containing [2]Rotaxanes as Ligands. *Dalton Trans*. **2003**, 4319–4323.
(604) Vella, S. J.; Tiburcio, J.; Loeb, S. J. Optically Sensed, Molecular Shuttles Driven by Acid–Base Chemistry. *Chem. Commun*. **2007**, 4752–4754.
(605) Bolla, M. A.; Tiburcio, J.; Loeb, S. J. Characterization of a Slippage Stopper for the 1,2-Bis(pyridinium)ethane-[24]crown-8 Ether [2]Pseudorotaxane Motif. *Tetrahedron* **2008**, *64*, 8423–8427.
(606) Davidson, G. J. E.; Sharma, S.; Loeb, S. J. A [2]Rotaxane Flip Switch Driven by Coordination Geometry. *Angew. Chem., Int. Ed*. **2010**, *49*, 4938–4942.
(607) Suhan, N. D.; Loeb, S. J.; Eichhorn, S. H. Mesomorphic [2]Rotaxanes: Sheltering Ionic Cores with Interlocking Components. *J. Am. Chem. Soc.* **2013**, *135*, 400–408.
(608) Davidson, G. J. E.; Loeb, S. J.; Passaniti, P.; Silvi, S.; Credi, A. Wire-Type Ruthenium(II) Complexes with Terpyridine-Containing [2]Rotaxanes as Ligands: Synthesis, Characterization, and Photophysical Properties. *Chem. Eur. J.* **2006**, *12*, 3233–3242.
(609) Korybut-Daszkiewicz, B.; Bilewicz, R.; Woźniak, K. Tetraimine Macrocyclic Transition Metal Complexes as Building Blocks for Molecular Devices. *Coord. Chem. Rev.* **2010**, *254*, 1637–1660.
(610) Hoshino, N.; Goldsby, K. A.; Busch, D. H. Structure and Dynamic Behavior in Solution of Binuclear Nickel(II) Face-to-Face Complexes with Bis(cyclidene) Ligands. *Inorg. Chem.* **1986**, *25*, 3000–3006.
(611) Woźny, M.; Pawłowska, J.; Osior, A.; Świder, P.; Bilewicz, R.; Korybut-Daszkiewicz, B. An Electrochemically Switchable Foldamer—A Surprising Feature of a Rotaxane with Equivalent Stations. *Chem. Sci.* **2014**, *5*, 2836–2842.
(612) Woźny, M.; Pawłowska, J.; Tomczyk, K. M.; Bilewicz, R.; Bilewicz, R.; Korybut-Daszkiewicz, B. Potential-Controlled Rotaxane Molecular Shuttles Based on Electron-Deficient Macrocyclic Complexes. *Chem. Commun.* **2014**, *50*, 13718–13721.
(613) Huang, F.; Slebodnick, C.; Ratliff, A. E.; Gibson, H. W. Bis(*m*-phenylene)-32-crown-10/Monopyridinium [2]Pseudorotaxanes. *Tetrahedron Lett.* **2005**, *46*, 6019–6022.
(614) Cheng, P.-N.; Lin, C.-F.; Liu, Y.-H.; Lai, C.-C.; Peng, S.-M.; Chiu, S.-H. [3]Pseudorotaxane-Like Complexes Formed Between Bipyridinium Dications and Bis-*p*-xylyl[26]crown-6. *Org. Lett*. **2006**, *8*, 435–438.
(615) Chen, N.-C.; Huang, P.-Y.; Lai, C.-C.; Liu, Y.-H.; Wang, Y.; Peng, S.-M.; Chiu, S.-H. A [2] Rotaxane-Based ^{1}H NMR Spectroscopic Probe for the Simultaneous Identification of Physiologically Important Metal Ions in Solution. *Chem. Commun*. **2007**, 4122–4124.
(616) Cheng, P.-N.; Hung, W.-C.; Chiu, S.-H. A New Macrocycle that Forms Pseudorotaxane-Like Complexes with Dibenzylammonium Ions. *Tetrahedron Lett.* **2005**, *46*, 4239–4242.
(617) Cheng, P.-N.; Huang, P.-Y.; Li, W.-S.; Ueng, S.-H.; Hung, W.-C.; Liu, Y.-H.; Lai, C.-C.; Wang, Y.; Peng, S.-M.; Chao, I.; Chiu, S-H. [N^{+}–H···O] Hydrogen Bonding the Most Important Noncovalent Interaction in Macrocycle-Dibenzylammonium Ion Complexes? *J. Org. Chem*. **2006**, *71*, 2373–2383.
(618) Baldwin, J. E.; Perlmutter, P. Bridged, Capped and Fenced Porphyrins. *Top. Curr. Chem.* **1984**, *121*, 181–220.
(619) Blasko, A.; Garcia, B.; Bruice, T. C. Pendant-Capped Porphyrins. 2. Structural Analysis and Dynamics of the Biphenyl Pendant-Capped Porphyrin Model of Catalase and

Its Iron(III) Complex by One- and Two-Dimensional Proton NMR Spectroscopy and Distance Geometry/Molecular Modeling Refinement. *J. Org. Chem*. **1993**, *58*, 5738–5747.
(620) Bonar-Law, R. P.; Sanders, J. K. M. Polyol Recognition by a Steroid-Capped Porphyrin. Enhancement and Modulation of Misfit Guest Binding by Added Water or Methanol. *J. Am. Chem. Soc*. **1995**, *117*, 259–271.
(621) Konishi, K.; Oda, K.; Nishida, K.; Aida, T.; Inoue, S. Asymmetric Epoxidation of Olefins Catalyzed by Manganese Complexes of Chiral “Strapped” Porphyrins with Diastereotopic Faces. A Novel Strategy for Stereochemical Modeling of the Active Site of Cytochrome P-450. *J. Am. Chem. Soc.* **1992**, *114*, 1313–1317.
(622) Collman, J. P.; Lee, V. J.; Zhang, X.; Ibers, J. A.; Brauman, J. I. Enantioselective Epoxidation of Unfunctionalized Olefins Catalyzed by Threitol-Strapped Manganese Porphyrins. *J. Am. Chem. Soc.* **1993**, *115*, 3834–3835.
(623) Collman, J. P.; Zhang, X.; Hembre, R. T.; Brauman, J. I. Shape-Selective Olefin Epoxidation Catalyzed by Manganese Picnic Basket Porphyrins. *J. Am. Chem. Soc.* **1990**, *112*, 5356–5357.
(624) Traylor, T. G.; Tsuchiya, S.; Campbell, D.; Mitchell, M.; Stynes, D.; Koga, N. Anthracene Heme Cyclophanes. Steric Effects in Carbon Monoxide, Molecular Oxygen, and RNC Binding. *J. Am. Chem. Soc*. **1985**, *107*, 604–614.
(625) Momenteau, M. Synthesis and Coordination Properties of Superstructured Iron-Porphyrins. *Pure Appl. Chem*. **1986**, 1493–1502.
(626) Benson, D. R.; Valentekovich, R.; Diederich, F. Catalytic Cyclophanes: A Porphyrin-Bridged Cyclophane as a Model for Cytochrome P-450 Enzymes. *Angew. Chem., Int. Ed. Engl*. **1990**, *29*, 191–193.
(627) Tashiro, K.; Aida, T. Metalloporphyrin Hosts for Supramolecular Chemistry of Fullerenes. *Chem. Soc. Rev.* **2007**, *36*, 189–197.
(628) Gunter, M. J. Superstructured Porphyrins as Effectors in Dynamic Supramolecular Assemblies: Receptors, Rotaxanes and Catenanes. *Eur. J. Org. Chem.* **2004**, 1655–1673.
(629) Gunter, M. J.; Johnston, M. R. Towards Molecular Scale Mechano-Electronic Devices: Porphyrin Catenanes. *J. Chem. Soc., Chem. Commun*. **1992**, 1163–1165.
(630) Gunter, M. J.; Johnston, M. R. Porphyrin [2]Catenanes—Dynamic Control Through Protonation. *J. Chem. Soc., Chem. Commun*. **1994**, 829–830.
(631) Gunter, M. J.; Hockless, D. C. R.; Johnston, M. R.; Skelton, B. W.; White, A. H. Self-Assembling Porphyrin [2]-Catenanes. *J. Am. Chem. Soc.* **1994**, *116*, 4810–4823.
(632) Flamigni, L.; Talarico, A. M.; Serroni, S.; Puntoriero, F.; Gunter, M. J.; Johnston, M. R.; Jeynes, T. P. Photoinduced Electron Transfer Between the Interlocked Components of Porphyrin Catenanes: Effect of the Presence of Nonequivalent Reduction Sites on the Charge Recombination Rate. *Chem. Eur. J.* **2003**, *9*, 2649–2659.
(633) Flamigni, L.; Maria Talarico, A.; Gunter, M. J.; Johnston, M. R.; Jeynes, T. P. Photoinduced Electron Transfer in Paraquat Inclusion Complexes of Porphyrin-Based Receptors. *New J. Chem.* **2003**, *27*, 551–559.
(634) Gunter, M. J.; Farquhar, S. M. Neutral π-Associated Porphyrin [2]Catenanes. *Org. Biomol. Chem.* **2003**, *1*, 3450–3457.
(635) Raymont, V.; Wilson, H.; Pfrunder, M.; McMurtrie, J. C.; Mullen, K. M. New Approaches to the Synthesis of Strapped Porphyrin Containing Bipyridinium [2]Rotaxanes. *New J. Chem.* **2013**, *37*, 893–900.
(636) Schenning, A. P. H. J.; de Bruin, B.; Rowan, A. E.; Kooijman, H.; Spek, A. L.; Nolte, R. J. Strong Binding of Paraquat and Polymeric Paraquat Derivatives by Basket-Shaped Hosts. *Angew. Chem., Int. Ed. Engl*. **1995**, *34*, 2132–2134.
(637) Rowan, A. E.; Aarts, P. P. M.; Koutstaal, K. W. M. Novel Porphyrin–Viologen Rotaxanes. *Chem. Commun*. **1998**, 611–612.
(638) Thordarson, P.; Bijsterveld, E. J. A.; Rowan, A. E.; Nolte, R. J. M. Epoxidation of Polybutadiene by a Topologically Linked Catalyst. *Nature* **2003**, *424*, 915–918.
(639) Coumans, R. G. E.; Elemans, J. A. A. W.; Nolte, R. J.; Rowan, A. E. Processive Enzyme Mimic: Kinetics and Thermodynamics of the Threading and Sliding Process. *Proc. Natl. Acad. Sci. U.S.A.* **2006**, *103*, 19647–19651.
(640) Ramos, P. H.; Coumans, R. G. E.; Deutman, A. B. C.; Smits, J. M. M.; de Gelder, R.; Elemans, J. A. A. W.; Nolte, R. J. M.; Rowan, A. E. Processive Rotaxane Systems. Studies on the Mechanism and Control of the Threading Process. *J. Am. Chem. Soc.* **2007**, *129*, 5699–5702.
(641) Monnereau, C.; Ramos, P. H.; Deutman, A. B. C.; Elemans, J. A. A. W.; Nolte, R. J. M.; Rowan, A. E. Porphyrin Macrocyclic Catalysts for the Processive Oxidation of Polymer Substrates. *J. Am. Chem. Soc.* **2010**, *132*, 1529–1531.
(642) Deutman, A. B. C.; Cantekin, S.; Elemans, J. A. A. W.; Rowan, A. E.; Nolte, R. J. M. Designing Processive Catalytic Systems. Threading Polymers Through a Flexible Macrocycle Ring. *J. Am. Chem. Soc*. **2014**, *136*, 9165–9172.
(643) An, H.; Bradshaw, J. S.; Izatt, R. M. Macropolycyclic Polyethers (Cages) and Related Compounds. *Chem. Rev.* **1992**, *92*, 543–572.
(644) Han, Y.; Jiang, Y.; Chen, C.-F. Cryptand-Based Hosts for Organic Guests. *Tetrahedron* **2015**, *71*, 503–522.
(645) Jones, J. W.; Zakharov, L. N.; Rheingold, A. L.; Gibson, H. W. Cooperative Host/Guest Interactions via Counterion Assisted Chelation: Pseudorotaxanes From Supramolecular Cryptands. *J. Am. Chem. Soc.* **2002**, *124*, 13378–13379.
(646) Bryant, W. S.; Jones, J. W.; Mason, P. E.; Guzei, I.; Rheingold, A. L.; Fronczek, F. R.; Nagvekar, D. S.; Gibson, H. W. A New Cryptand: Synthesis and Complexation with Paraquat. *Org. Lett.* **1999**, *1*, 1001–1004.
(647) Cram, D. J. Preorganization—From Solvents to Spherands. *Angew. Chem., Int. Ed. Engl*. **1986**, *25*, 1039–1057.
(648) Reindhoudt, D. N.; Dijkstra, P. J. Role of Preorganization in Host-Guest-Chemistry. *Pure Appl. Chem*. **1988**, *60*, 477–482.
(649) Huang, F.; Switek, K. A.; Zakharov, L. N.; Fronczek, F. R.; Slebodnick, C.; Lam, M.; Golen, J. A.; Bryant, W. S.; Mason, P. E.; Rheingold, A. L.;Ashraf-Khorassani, M.; Gibson, H. W. Bis(*m*-phenylene)-32-crown-10-Based Cryptands, Powerful Hosts for Paraquat Derivatives. *J. Org. Chem.* **2005**, *70*, 3231–3241.
(650) Huang, F.; Gibson, H. W.; Bryant, W. S.; Nagvekar, D. S.; Fronczek, F. R. First Pseudorotaxane-Like [3]Complexes Based on Cryptands and Paraquat: Self-Assembly and Crystal Structures. *J. Am. Chem. Soc.* **2003**, *125*, 9367–9371.
(651) Yan, X.; Wei, P.; Xia, B.; Huang, F.; Zhou, Q. Pseudorotaxanes From Self-Assembly of Two Crown Ether-Based Cryptands and a 1,2-Bis(pyridinium) Ethane Derivative. *Chem. Commun.* **2012**, *48*, 4968–4970.
(652) Yan, X.; Chi, X.; Wei, P.; Zhang, M.; Huang, F. [*n*]Pseudorotaxanes (*n* = 2, 3) From Self-Assembly of Two Cryptands and a 1,2-Bis(4-pyridinium)ethane Derivative. *Eur. J. Org. Chem*. **2012**, 6351–6356.
(653) Liu, M.; Li, S.; Zhang, M.; Zhou, Q.; Wang, F.; Hu, M.; Fronczek, F. R.; Li, N.; Huang, F. Three-Dimensional Bis(*m*-phenylene)-32-Crown-10-Based Cryptand/Paraquat Catenanes. *Org. Biomol. Chem.* **2009**, *7*, 1288–1291.
(654) Li, S.; Liu, M.; Zhang, J.; Zheng, B.; Zhang, C.; Xue, W.; Li, N.; Huang, F. High-Yield Preparation of [2]Rotaxanes Based on the Bis(*m*-phenylene)-32-Crown-10-Based Cryptand/Paraquat Derivative Recognition Motif. *Org. Biomol. Chem.* **2008**, 2103–2107.
(655) Li, S.; Liu, M.; Zhang, J.; Zheng, B.; Wen X.; Xue, W.; Li, N.; Huang, F. Preparation of Bis(*m*-phenylene)-32-Crown-10-Based Cryptand/Bisparaquat [3]Rotaxanes with High Efficiency. *Eur. J. Org. Chem.* **2008**, 6128–6133.
(656) Kohnke, F. H.; Stoddart, J. F. An Investigation of the Kinetic and Thermodynamic Stability of a Tribenzomacrobicyclic

Polyether Complex with Diquat in Acetone Solution. *J. Chem. Soc., Chem. Commun*. **1985**, 314–317.
(657) Zhang, J.; Huang, F.; Li, N.; Wang, H.; Gibson, H. W.; Gantzel, P.; Rheingold, A. L. Paraquat Substituent Effect on Complexation with a Dibenzo-24-Crown-8-Based Cryptand. *J. Org. Chem.* **2007**, *72*, 8935–8938.
(658) Pederson, A. M. P.; Ward, E. M.; Schoonover, D. V.; Slebodnick, C.; Gibson, H. W. High-Yielding, Regiospecific Synthesis of *cis*(4,4′)-Di(carbomethoxybenzo)-30-crown-10, Its Conversion to a Pyridyl Cryptand and Strong Complexation of 2,2′- and 4,4′-Bipyridinium Derivatives. *J. Org. Chem.* **2008**, *73*, 9094–9101.
(659) Gibson, H. W.; Wang, H.; Slebodnick, C.; Merola, J.; Kassel, W. S.; Rheingold, A. L. Isomeric 2,6-Pyridino-Cryptands Based on Dibenzo-24-Crown-8. *J. Org. Chem.* **2007**, *72*, 3381–3393.
(660) Huang, F.; Rheingold, A. L.; Slebodnick, C.; Ohs, A.; Switek, K. A.; Gibson, H. W. [2]Pseudorotaxanes Based on the Cryptand/Monopyridinium Recognition Motif. *Tetrahedron* **2005**, *61*, 10242–10253.
(661) Huang, F.; Slebodnick, C.; Mahan, E. J.; Gibson, H. W. [3]Pseudorotaxanes Based on the Cryptand/Monopyridinium Salt Recognition Motif. *Tetrahedron* **2007**, *63*, 2875–2881.
(662) Zhang, X.; Zhai, C.; Li, N.; Liu, M.; Li, S.; Zhu, K.; Zhang, J.; Huang, F.; Gibson, H. W. Host Size Effect in the Complexation of Two Bis(*m*-phenylene)-32-Crown-10-Based Cryptands with a Diazapyrenium Salt. *Tetrahedron Lett.* **2007**, *48*, 7537–7541.
(663) Huang, F.; Slebodnick, C.; Switek, K. A.; Gibson, H. W. Inclusion [2]Complexes Based on the Cryptand/Diquat Recognition Motif. *Tetrahedron* **2007**, *63*, 2829–2839.
(664) Lee, M.; Niu, Z.; Schoonover, D. V.; Slebodnick, C.; Gibson, H. W. 1,2-Bis[*N*-(*N*′-alkylimidazolium)]ethane Salts as New Guests for Crown Ethers and Cryptands. *Tetrahedron* **2010**, *66*, 7077–7082.
(665) Huang, F.; Fronczek, F. R.; Ashraf-Khorassani, M.; Gibson, H. W. Slow-Exchange C_3-Symmetric Cryptand/Trispyridinium Inclusion Complexes Containing Non-Linear Guests: A New Type of Threaded Structure. *Tetrahedron Lett.* **2005**, *46*, 6765–6769.
(666) Wu, X.; Li, J.; Yan, X.; Zhou, Q. Crown Ether-Based Cryptand/Tropylium Cation Inclusion Complexes. *Tetrahedron* **2013**, *69*, 9573–9579.
(667) Wu, X.; Xue, M.; Li, J.; Yan, X.; Zhou, Q. Two Protocols for the Preparation of [2]Rotaxanes Based on the Dibenzo-24-Crown-8-Based Cryptand/Paraquat Recognition Motif. *Tetrahedron Lett.* **2013**, *54*, 6640–6643.
(668) Zhang, M.; Yan, X.; Huang, F.; Niu, Z.; Gibson, H. W. Stimuli-Responsive Host–Guest Systems Based on the Recognition of Cryptands by Organic Guests. *Acc. Chem. Res.* **2014**, *47*, 1995–2005.
(669) Zong, Q.-S.; Chen, C.-F. Novel Triptycene-Based Cylindrical Macrotricyclic Host: Synthesis and Complexation with Paraquat Derivatives. *Org. Lett.* **2006**, *8*, 211–214.
(670) Zong, Q.-S.; Zhang, C.; Chen, C.-F. Self-Assembly of Triptycene-Based Cylindrical Macrotricyclic Host with Dibenzylammonium Ions: Construction of Dendritic [3]Pseudorotaxanes. *Org. Lett.* **2006**, *8*, 1859–1862.
(671) Lin, C.-F.; Liu, Y.-H.; Lai, C.-C.; Peng, S.-M.; Chiu, S.-H. Precise Facial Control in Threading Guests into a Molecular Cage and the Formation of a Turtlelike Supramolecular Complex. *Angew. Chem., Int. Ed*. **2006**, *45*, 3176–3181.
(672) Lin, C.-F.; Liu, Y.-H.; Lai, C.-C.; Peng, S.-M.; Chiu, S.-H. An Extremely Stable Host–Guest Complex that Functions as a Fluorescence Probe for Calcium Ions. *Chem. Eur. J.* **2006**, *12*, 4594–4599.
(673) Chen, C.-F. Novel Triptycene-Derived Hosts: Synthesis and Their Applications in Supramolecular Chemistry. *Chem. Commun.* **2011**, *47*, 1674–1688.
(674) Han, Y.; Lu, H.-Y.; Zong, Q.-S.; Guo, J.-B.; Chen, C.-F. Synthesis of Triptycene-Derived Macrotricyclic Host Containing Two Dibenzo-[18]-Crown-6 Moieties and Its Complexation with Paraquat Derivatives: Li^+-Ion-Controlled Binding and Release of the Guests in the Complexes. *J. Org. Chem.* **2012**, *77*, 2422–2430.
(675) Han, T.; Chen, C.-F. Selective Templated Complexation of a Cylindrical Macrotricyclic Host with Neutral Guests: Three Cation-Controlled Switchable Processes. *J. Org. Chem.* **2007**, *72*, 7287–7293.
(676) Gu, Y.-K.; Zeng, F.; Meng, Z.; Chen, C.-F. Triptycene-Derived Macrotricyclic Polyether Containing an Anthracene Unit as a Powerful Host for 1,2-Bis(pyridium)ethane, Diquat and 2,7-Diazapyrenium Salt. *Org. Biomol. Chem.* **2014**, *12*, 2850–2853.
(677) Zhao, J.-M.; Zong, Q.-S.; Chen, C.-F. Complexation of Triptycene-Based Macrotricyclic Host Toward (9-Anthracylmethyl)benzylammonium Salt: A Ba^{2+} Selective Fluorescence Probe. *J. Org. Chem.* **2010**, *75*, 5092–5098.
(678) Guo, J.-B.; Han, Y.; Cao, J.; Chen, C.-F. Formation of 1:2 Host–Guest Complexes Based on Triptycene-Derived Macrotricycle and Paraquat Derivatives: Anion−π Interactions Between PF_6^- and Bipyridinium Rings in the Solid State. *Org. Lett*. **2011**, *13*, 5688–5691.
(679) Han, Y.; Gu, Y.-K.; Xiang, J.-F.; Chen, C.-F. Complexation Between Triptycene-Based Macrotricyclic Host and π-Extended Viologens: Formation of Supramolecular Poly[3]-Pseudorotaxanes. *Chem. Commun.* **2012**, *48*, 11076–11078.
(680) Han, Y.; Cao, J.; Li, P.-F.; Zong, Q.-S.; Zhao, J.-M.; Guo, J.-B.; Xiang, J.-F.; Chen, C.-F. Complexation of Triptycene-Derived Macrotricyclic Polyether with Paraquat Derivatives, Diquat, and a 2,7-Diazapyrenium Salt: Guest-Induced Conformational Changes of the Host. *J. Org. Chem.* **2013**, *78*, 3235–3242.
(681) Su, Y.-S.; Chen, C.-F. Novel Anthracene-Based Cylindrical Macrotricyclic Polyether: Powerful Host for Bispyridinium Dications. *Org. Lett.* **2010**, *12*, 1888–1891.
(682) Zhao, J.-M.; Zong, Q.-S.; Han, T.; Xiang, J.-F.; Chen, C.-F. Guest-Dependent Complexation of Triptycene-Based Macrotricyclic Host with Paraquat Derivatives and Secondary Ammonium Salts: A Chemically Controlled Complexation Process. *J. Org. Chem.* **2008**, *73*, 6800–6806.
(683) Han, T.; Zong, Q.-S.; Chen, C.-F. Complexation of Triptycene-Based Cylindrical Macrotricyclic Polyether Toward Diquaternary Salts: Ion-Controlled Binding and Release of the Guests. *J. Org. Chem.* **2007**, *72*, 3108–3111.
(684) Yen, M.-L.; Chen, N.-C.; Lai, C.-C.; Liu, Y.-H.; Peng, S.-M.; Chiu, S.-H. A Molecular Cage That Selectively Complexes Three Different Guests in Solution. *Org. Lett.* **2009**, *11*, 4604–4607.
(685) Han, T.; Chen, C.-F. Formation of Ternary Complexes Between a Macrotricyclic Host and Hetero-Guest Pairs: An Acid−Base Controlled Selective Complexation Process. *Org. Lett.* **2007**, *9*, 4207–4210.
(686) Gu, Y.-K.; Han, Y.; Chen, C.-F. Guest-Dependent Complexation of Triptycene-Derived Macrotricyclic Host Containing One Anthracene Moiety with Paraquat Derivatives: Construction of [2]Rotaxanes. *Supramol. Chem.* **2014**, *27*, 357–363.
(687) Zhang, M.; Zheng, B.; Huang, F. Synthesis of a Four-Armed Cage Molecule and Its pH-Controlled Complexation with Paraquat. *Chem. Commun.* **2011**, *47*, 10103–10105.
(688) Huang, F.; Zakharov, L. N.; Rheingold, A. L.; Ashraf-Khorassani, M.; Gibson, H. W. Synthesis of a Symmetric Cylindrical Bis(crown ether) Host and Its Complexation with Paraquat. *J. Org. Chem.* **2005**, *70*, 809–813.
(689) Liu, H.; Li, X.-Y.; Zhao, X.-L.; Liu, Y. A.; Li, J.-S.; Jiang, B.; Wen, K. [2]Pseudorotaxanes and [2]Catenanes Constructed by Oxacalixcrowns/Viologen Molecular Recognition Motifs. *Org. Lett*. **2014**, *16*, 5894–5897.
(690) Odell, B.; Reddington, M. V.; Slawin, A. M. Z.; Spencer, N.; Stoddart, J. F.; Williams, D. J. Cyclobis(paraquat-*p*-phenylene). A Tetracationic Multipurpose Receptor. *Angew. Chem., Int. Ed. Engl*. **1988**, *27*, 1547–1550.

(691) Ashton, P. R.; Odell, B.; Reddington, M. V.; Slawin, A. M. Z.; Stoddart, J. F.; Williams, D. J. Isostructural, Alternately-Charged Receptor Stacks. The Inclusion Complexes of Hydroquinone and Catechol Dimethyl Ethers with Cyclobis(paraquat-*p*-phenylene). *Angew. Chem., Int. Ed. Engl*. **1988**, *27*, 1550–1553.
(692) Sue, C.-H.; Basu, S.; Fahrenbach, A. C.; Shveyd, A. K.; Dey, S. K.; Botros, Y. Y.; Stoddart, J. F. Enabling Tetracationic Cyclophane Production by Trading Templates. *Chem. Sci.* **2010**, *1*, 119–125.
(693) Tejerina, B.; Gothard, C. M.; Grzybowski, B. A. Molecular Tethering or Aggregation: Is the Existence of Charge-Transfer Bands Indicative of the Formation of Blue-Box/Tetrathiafulvalene Inclusion Complexes? *Chem. Eur. J.* **2012**, *18*, 5606–5611.
(694) Steed, J. W.; Atwood, J. L. *Supramolecular Chemistry*; John Wiley & Sons: West Sussex, 2012.
(695) Biedermann, F.; Vendruscolo, M.; Scherman, O. A.; De Simone, A.; Nau, W. M. Cucurbit[8]uril and Blue-Box: High-Energy Water Release Overwhelms Electrostatic Interactions. *J. Am. Chem. Soc.* **2013**, *135*, 14879–14888.
(696) Anelli, P.-L.; Ashton, P. R.; Spencer, N.; Slawin, A. M. Z.; Stoddart, J. F.; Williams, D. J. Self-Assembling [2]Pseudorotaxanes. *Angew. Chem., Int. Ed. Engl*. **1991**, *30*, 1036–1039.
(697) Reddington, M. V.; Slawin, A. M. Z.; Spencer, N.; Stoddart, J. F.; Vicent, C.; Williams, D. J. Towards a Molecular Abacus. *J. Chem. Soc., Chem. Commun*. **1991**, 630–634.
(698) Ikeda, T.; Higuchi, M.; Kurth, D. G. Inclusion Complexation of Cyclobis(paraquat-*p*-phenylene) with Thiophene, Bithiophene and Terthiophene. *J. Incl. Phenom. Macrocycl. Chem.* **2009**, *64*, 299–303.
(699) Philp, D.; Slawin, A. M. Z.; Spencer, N.; Stoddart, J. F.; Williams, D. J. The Complexation of Tetrathiafulvalene by Cyclobis(paraquat-*p*-phenylene). *J. Chem. Soc., Chem. Commun*. **1991**, 1584–1586.
(700) Bernardo, A. R.; Stoddart, J. F.; Kaifer, A. E. Cyclobis(paraquat-*p*-phenylene) as a Synthetic Receptor for Electron-Rich Aromatic Compounds: Electrochemical and Spectroscopic Studies of Neurotransmitter Binding. *J. Am. Chem. Soc.* **1992**, *114*, 10624–10631.
(701) Castro, R.; Nixon, K. R.; Evanseck, J. D.; Kaifer, A. E. Effects of Side Arm Length and Structure of *para*-Substituted Phenyl Derivatives on Their Binding to the Host Cyclobis(paraquat-*p*-phenylene). *J. Org. Chem.* **1996**, *61*, 7298–7303.
(702) Venturi, M.; Dumas, S.; Balzani, V.; Cao, J.; Stoddart, J. F. Threading/Dethreading Processes in Pseudorotaxanes. A Thermodynamic and Kinetic Study. *New J. Chem*. **2004**, *28*, 1032.
(703) Choi, J. W.; Flood, A. H.; Steuerman, D. W.; Nygaard, S.; Braunschweig, A. B.; Moonen, N. N. P.; Laursen, B. W.; Luo, Y.; DeIonno, E.; Peters, A. J.; Jeppesen, J. O.; Xu K.; Stoddart, J. F.; Heath, J. R. Ground-State Equilibrium Thermodynamics and Switching Kinetics of Bistable [2]Rotaxanes Switched in Solution, Polymer Gels, and Molecular Electronic Devices. *Chem. Eur. J.* **2006**, *12*, 261–279.
(704) Córdova, E.; Bissell, R. A.; Spencer, N.; Ashton, P. R.; Stoddart, J. F.; Kaifer, A. Novel Rotaxanes Based on the Inclusion Complexation of Biphenyl Guests by Cyclobis(paraquat-*p*-phenylene). *J. Org. Chem.* **1993**, *58*, 6550–6552.
(705) Córdova, E.; Bissell, R. A.; Kaifer, A. E. Synthesis and Electrochemical Properties of Redox-Active [2]Rotaxanes Based on the Inclusion Complexation of 1,4-Phenylenediamine and Benzidine by Cyclobis(paraquat-*p*-phenylene). *J. Org. Chem.* **1995**, *60*, 1033–1038.
(706) Ikeda, T.; Aprahamian, I.; Stoddart, J. F. Blue-Colored Donor-Acceptor [2]Rotaxane. *Org. Lett.* **2007**, *9*, 1481–1484.
(707) Anelli, P.-L.; Asakawa, M.; Ashton, P. R.; Bissell, R. A.; Clavier, G.; Górski, R.; Kaifer, A. E.; Langford, S. J.; Mattersteig, G.; Menzer, S.; Philp, D.; Slawin, A. M. Z.; Spencer, N.; Stoddart, J. F.; Tolley, M. S.; Williams, D. J. Molecular Meccano 10. Toward Controllable Molecular Shuttles. *Chem. Eur. J.* **1997**, *3*, 1113–1135.
(708) Wang, C.; Cao, D.; Fahrenbach, A. C.; Fang, L.; Olson, M. A.; Friedman, D. C.; Basu, S.; Dey, S. K.; Botros, Y. Y.; Stoddart, J. F. Solvent-Dependent Ground-State Distributions in a Donor–Acceptor Redox-Active Bistable [2]Catenane. *J. Phys. Org. Chem.* **2012**, *25*, 544–552.
(709) Asakawa, M.; Ashton, P. R.; Balzani, V.; Credi, A.; Mattersteig, G.; Matthews, O. A.; Montalti, M.; Spencer, N.; Stoddart, J. F.; Venturi, M. Electrochemically Induced Molecular Motions in Pseudorotaxanes: A Case of Dual-Mode (Oxidative and Reductive) Dethreading. *Chem. Eur. J.* **1997**, *3*, 1992–1996.
(710) Bryce, M. R.; Cooke, G.; Duclairoir, F. M. A.; John, P.; Perepichka, D. F.; Polwart, N.; Rotello, V. M.; Stoddart, J. F.; Tseng, H.-R. Surface Confined Pseudorotaxanes with Electrochemically Controllable Complexation Properties. *J. Mater. Chem.* **2003**, *13*, 2111–2117.
(711) Nielsen, M. B.; Jeppesen, J. O.; Lau, J.; Lomholt, C.; Damgaard, D.; Jacobsen, J. P.; Becher, J.; Stoddart, J. F. Binding Studies Between Tetrathiafulvalene Derivatives and Cyclobis(paraquat-*p*-phenylene). *J. Org. Chem.* **2001**, *66*, 3559–3563.
(712) Devonport, W.; Blower, M. A.; Bryce, M. R.; Goldenberg, L. M. A Redox-Active Tetrathiafulvalene [2] Pseudorotaxane: Spectroelectrochemical and Cyclic Voltammetric Studies of the Highly Reversible Complexation/Decomplexation Process. *J. Org. Chem.* **1997**, *62*, 885–887.
(713) Zhang, K.-D.; Wang, G.-T.; Zhao, X.; Jiang, X.-K.; Li, Z.-T. Vesicle Self-Assembly by Tetrathiafulvalene Derivatives in Both Polar and Nonpolar Solvents and Pseudo-Rotaxane Mediated Vesicle-to-Microtube Transformation. *Langmuir* **2010**, *26*, 6878–6882.
(714) Nygaard, S.; Hansen, C. N.; Jeppesen, J. O. Binding Studies Between Triethylene Glycol-Substituted Monopyrrolotetrathiafulvalene Derivatives and Cyclobis(paraquat-*p*-phenylene). *J. Org. Chem.* **2007**, *72*, 1617–1626.
(715) Olson, M. A.; Braunschweig, A. B.; Ikeda, T.; Fang, L.; Trabolsi, A.; Slawin, A. M. Z.; Khan, S. I.; Stoddart, J. F. Thermodynamic Forecasting of Mechanically Interlocked Switches. *Org. Biomol. Chem.* **2009**, *7*, 4391–4405.
(716) Yu, L.; Li, M.; Zhou, X.-P.; Li, D. Hybrid Inorganic–Organic Polyrotaxane, Pseudorotaxane, and Sandwich. *Inorg. Chem.* **2013**, *52*, 10232–10234.
(717) Spruell, J. M.; Paxton, W. F.; Olsen, J.-C.; Benítez, D.; Tkatchouk, E.; Stern, C. L.; Trabolsi, A.; Friedman, D. C.; Goddard, W. A., III; Stoddart, J. F. A Push-Button Molecular Switch. *J. Am. Chem. Soc.* **2009**, *131*, 11571–11580.
(718) Fang, L.; Basu, S.; Sue, C.-H.; Fahrenbach, A. C.; Stoddart, J. F. Syntheses and Dynamics of Donor–Acceptor [2]Catenanes in Water. *J. Am. Chem. Soc.* **2011**, *133*, 396–399.
(719) Ashton, P. R.; Grognuz, M.; Slawin, A. M. Z.; Stoddart, J. F.; Williams, D. J. The Template-Directed Synthesis of a [2]Rotaxane. *Tetrahedron Lett.* **1991**, *32*, 6235–6238.
(720) Benniston, A. C.; Harriman, A. A Light-Induced Molecular Shuttle Based on a [2]Rotaxane-Derived Triad. *Angew. Chem., Int. Ed. Engl*. **1993**, *32*, 1459–1461.
(721) Benniston, A. C.; Harriman, A.; Lynch, V. M. Photoactive [2]Rotaxanes Formed by Multiple π-Stacking. *Tetrahedron Lett.* **1994**, *35*, 1473–1476.
(722) Asakawa, M.; Ashton, P. R.; Iqbal, S.; Quick, A.; Stoddart, J. F.; Tinker, N. D.; White, A. J. P.; Williams, D. J. Functionalized [2]Rotaxanes. *Isr. J. Chem.* **1996**, *36*, 329–340.
(723) Archut, A.; Müller, W. M.; Baumann, S.; Habel, M.; Vögtle, F. Rotaxanes with Chiral Stoppers and Complexation of Cations by Podand Axles with Sugar Terminal Groups. *Liebigs Ann./Recueil* **1997**, 495–499.
(724) Bravo, J. A.; Raymo, F. M.; Stoddart, J. F.; White, A. J. P.; Williams, D. J. Molecular Meccano 45. High Yielding

Template-Directed Syntheses of [2]Rotaxanes. *Eur. J. Org. Chem*. **1998**, 2565–2571.
(725) Ashton, P. R.; Bravo, J. A.; Raymo, F. M.; Stoddart, J. F.; White, A. J. P.; Williams, D. J. Molecular Meccano 48. Probing Co-Conformational Changes in Chiral [2]Rotaxanes by ^{1}H-NMR Spectroscopy. *Eur. J. Org. Chem*. **1999**, 899–908.
(726) Zhao, Y.-L.; Shveyd, A. K.; Stoddart, J. F. Solid-State Structures and Superstructures of Two Charged Donor–Acceptor Rotaxanes. *Tetrahedron Lett.* **2011**, *52*, 2044–2047.
(727) Nygaard, S.; Laursen, B. W.; Hansen, T. S.; Bond, A. D.; Flood, A. H.; Jeppesen, J. O. Preparation of Cyclobis(paraquat-*p*-phenylene)-Based [2]Rotaxanes Without Flexible Glycol Chains. *Angew. Chem., Int. Ed*. **2007**, *46*, 6093–6097.
(728) Anelli, P.-L.; Spencer, N.; Stoddart, J. F. A Molecular Shuttle. *J. Am. Chem. Soc.* **1991**, *113*, 5131–5133.
(729) Benniston, A. C.; Harriman, A.; Lynch, V. M. Photoactive [2]Rotaxanes: Structure and Photophysical Properties of Anthracene- and Ferrocene-Stoppered [2]Rotaxanes. *J. Am. Chem. Soc.* **1995**, *117*, 5275–5291.
(730) Nygaard, S.; Leung, K. C.-F.; Aprahamian, I.; Ikeda, T.; Saha, S.; Laursen, B. W.; Kim, S.-Y.; Hansen, S. W.; Stein, P. C.; Flood, A. H.; Stoddart, J. F.; Jeppesen, J. O. Functionally Rigid Bistable [2]Rotaxanes. *J. Am. Chem. Soc.* **2007**, *129*, 960–970.
(731) Yoon, I. L.; Benítez, D.; Zhao, Y.-L.; Miljanić, O. Š.; Kim, S.-Y.; Tkatchouk, E.; Leung, K. C. F.; Khan, S. I.; Goddard, W. A., III; Stoddart, J. F. Functionally Rigid and Degenerate Molecular Shuttles. *Chem. Eur. J.* **2009**, *15*, 1115–1122.
(732) Yoon, I. L.; Miljanić, O. Š.; Benítez, D.; Khan, S. I.; Stoddart, J. F. An Interdigitated Functionally Rigid [2]Rotaxane. *Chem. Commun*. **2008**, 4561–4563.
(733) Ikeda, T.; Higuchi, M.; Sato, A.; Kurth, D. G. Thiophene Donor-Acceptor [2]Rotaxanes. *Org. Lett.* **2008**, *10*, 2215–2218.
(734) Ikeda, T.; Higuchi, M.; Kurth, D. G. β-Substituted Terthiophene [2]Rotaxanes. *Chem. Eur. J*. **2009**, *15*, 4906–4913.
(735) Braunschweig, A. B.; Dichtel, W. R.; Miljanić, O. Š.; Olson, M. A.; Spruell, J. M.; Khan, S. I.; Heath, J. R.; Stoddart, J. F. Modular Synthesis and Dynamics of a Variety of Donor–Acceptor Interlocked Compounds Prepared by Click Chemistry. *Chem. Asian J.* **2007**, *2*, 634–647.
(736) Spruell, J. M.; Dichtel, W. R.; Heath, J. R.; Stoddart, J. F. A One-Pot Synthesis of Constitutionally Unsymmetrical Rotaxanes Using Sequential Cu^{I}-Catalyzed Azide–Alkyne Cycloadditions. *Chem. Eur. J.* **2008**, *14*, 4168–4177.
(737) Bühner, M.; Geuder, W.; Gries, W. K.; Hünig, S.; Koch, M.; Poll, T. A Novel Type of Cationic Host Molecules with π-Acceptor Properties. *Angew. Chem., Int. Ed. Engl*. **1988**, *27*, 1553–1556.
(738) Amabilino, D. B.; Ashton, P. R.; Tolley, M. S.; Stoddart, J. F.; Williams, D. J. Isomeric Self-Assembling [2]Catenanes. *Angew. Chem., Int. Ed. Engl*. **1993**, *32*, 1297–1301.
(739) Amabilino, D. B.; Ashton, P. R.; Pérez-García, L.; Stoddart, J. F. Kinetic Selection in the Template-Directed Self-Assembly of [2]Catenanes. *Angew. Chem., Int. Ed. Engl*. **1995**, *34*, 2378–2380.
(740) Amabilino, D. B.; Ashton, P. R.; Stoddart, J. F.; White, A. J. P.; Williams, D. J. Molecular Meccano 32. Kinetic and Thermodynamic Effects in the Self-Assembly of [3]Catenanes in the Solution and Solid States. *Chem. Eur. J*. **1998**, *4*, 460–468.
(741) Ashton, P. R.; Brown, C. L.; Chrystal, E. J. T.; Goodnow, T. T.; Kaifer, A. E.; Parry, K. P.; Slawin, A. M. Z.; Spencer, N.; Stoddart, J. F.; Williams, D. J. Self-Assembling [3]Catenanes. *Angew. Chem., Int. Ed. Engl*. **1991**, *30*, 1039–1042.
(742) Ashton, P. R.; Boyd, S. E.; Boyd, S. E.; Menzer, S.; Pasini, D.; Raymo, F. M.; Spencer, N.; Stoddart, J. F.; White, A. J. P.; Wyatt, P. G.; Williams, D. J.; Wyatt, P. G. Molecular Meccano 23. Self-Assembling Cyclophanes and Catenanes Possessing Elements of Planar Chirality. *Chem. Eur. J*. **1998**, *4*, 299–310.
(743) Asakawa, M.; Brown, C. L.; Pasini, D.; Stoddart, J. F.; Wyatt, P. G. Enantioselective Recognition of Amino Acids by Axially-Chiral π-Electron-Deficient Receptors. *J. Org. Chem.* **1996**, *61*, 7234–7235.
(744) Asakawa, M.; Ashton, P. R.; Boyd, S. E.; Brown, C. L.; Menzer, S.; Pasini, D.; Stoddart, J. F.; Tolley, M. S.; White, A. J. P; Williams, D. J.; Wyatt, P. G. Molecular Meccano 16. Axially Chiral Catenanes and π-Electron-Deficient Receptors. *Chem. Eur. J*. **1997**, *3*, 463–481.
(745) Asakawa, M.; Janssen, H. M.; Meijer, E. W.; Pasini, D.; Stoddart, J. F. Molecular Meccano 38. Enantioselective Discrimination in the Self-Assembly of [2]Pseudorotaxanes. *Eur. J. Org. Chem*. **1998**, 983–986.
(746) Ashton, P. R.; Ballardini, R.; Balzani, V.; Boyd, S. E.; Credi, A.; Gandolfi, M. T.; Gómez-López, M.; Iqbal, S.; Philp, D.; Preece, J. A.; Prodi, L.; Ricketts, H. G.; Stoddart, J. F.; Tolley, M. S.; Venturi, M.; White, A. J. P.; Williams, D. J. Molecular Meccano 14. Simple Mechanical Molecular and Supramolecular Machines: Photochemical and Electrochemical Control of Switching Processes. *Chem. Eur. J*. **1997**, *3*, 152–170.
(747) Cabezon, B.; Cao, J.; Raymo, F. M.; Stoddart, J. F.; White, A. J. P.; Williams, D. J. Molecular Meccano 59. Self-Complementary [2]Catenanes and Their Related [3]Catenanes. *Chem. Eur. J*. **2000**, *6*, 2262–2273.
(748) Cabezon, B.; Cao, J.; Cao, J.; Raymo, F. M.; Stoddart, J. F.; White, A. J. P.; Williams, D. J. A Self-Complexing [2]Catenane. *Angew. Chem., Int. Ed*. **2000**, *39*, 148–151.
(749) Ashton, P. R.; Balzani, V.; Credi, A.; Kocian, O.; Pasini, D.; Prodi, L.; Spencer, N.; Stoddart, J. F.; Tolley, M. S.; Venturi, M.; White, A. J. P.; Williams, D. J. Molecular Meccano 35. Cyclophanes and [2]Catenanes as Ligands for Transition Metal Complexes: Synthesis, Structure, Absorption Spectra, and Excited State and Electrochemical Properties. *Chem. Eur. J*. **1998**, *4*, 590–607.
(750) Ashton, P. R.; Preece, J. A.; Stoddart, J. F.; Tolley, M. S.; White, A. J. P.; Williams, D. J. The Self-Assembly and Dynamic Properties of Thiophene-Containing [2]Catenanes. *Synthesis* **1994**, 1344–1352.
(751) Asakawa, M.; Ashton, P. R.; Brown C. L.; Fyfe, M. C. T.; Menzer, S.; Pasini, D.; Scheuer, C.; Spencer, N.; Stoddart, J. F.; White, A. J. P.; Williams, D. J. Molecular Meccano 18. Molecular and Supramolecular Synthesis with Dibenzofuran-Containing Systems. *Chem. Eur. J*. **1997**, *3*, 1136–1150.
(752) Ramos, S.; Alcalde, E.; Stoddart, J. F.; White, A. J. P.; Williams, D. J.; Pérez-García, L. Proton Ionizable 1*H*-1,2,4-Triazole π-Electron Deficient Cyclophanes as Hosts and in [2]Catenanes. *New J. Chem.* **2009**, *33*, 300–317.
(753) Ashton, P. R.; Iriepa, I.; Reddington, M. V.; Spencer, N.; Slawin, A. M. Z.; Stoddart, J. F.; Williams, D. J. An Optically-Active [2]Catenane Made to Order. *Tetrahedron Lett.* **1994**, *35*, 4835–4838.
(754) Ashton, P. R.; Baldoni, V.; Balzani, V.; Credi, A.; Hoffmann, H. D. A.; Martínez-Díaz, M.-V.; Raymo, F. M.; Stoddart, J. F.; Venturi, M. Molecular Meccano 63. Dual-Mode "Co-Conformational" Switching in Catenanes Incorporating Bipyridinium and Dialkylammonium Recognition Sites. *Chem. Eur. J*. **2001**, *7*, 3482–3493.
(755) Ashton, P. R.; Claessens, C. G.; Hayes, W.; Menzer, S.; Stoddart, J. F.; White, A. J. P.; Williams, D. J. Molecular Mosaics Formed by a Square Cyclophane and Its Inclusion Complex with Ferrocene. *Angew. Chem., Int. Ed. Engl*. **1995**, *34*, 1862–1865.
(756) Ashton, P. R.; Boyd, S. E.; Boyd, S. E.; Claessens, C. G.; Gillard, R. E.; Menzer, S.; Stoddart, J. F.; Tolley, M. S.; White, A. J. P.; Williams, D. J. Molecular Meccano 20. A Novel Type of Isomerism in [3]Catenanes. *Chem. Eur. J*. **1997**, *3*, 788–798.
(757) Ashton, P. R.; Chemin, A.; Claessens, C. G.; Menzer, S.; Stoddart, J. F.; White, A. J. P.; Williams, D. J. Molecular

Meccano 37. Self-Assembly and Self-Organization of Self-Recognizing Cyclophanes. *Eur. J. Org. Chem*. **1998**, 969–981.

(758) Ashton, P. R.; Baldoni, V.; Balzani, V.; Claessens, C. G.; Credi, A.; Hoffmann, H. D. A.; Raymo, F. M.; Stoddart, J. F.; Venturi, M.; White, A. J. P.; Willliams, D. J. Molecular Meccano 57. Template-Directed Syntheses, Spectroscopic Properties, and Electrochemical Behavior of [*n*]Catenanes. *Eur. J. Org. Chem*. **2000**, 1121–1130.

(759) Tseng, H.-R.; Vignon, S. A.; Celestre, P. C.; Stoddart, J. F.; White, A. J. P.; Williams, D. J. Molecular Meccano 66. Dynamic Chirality: Keen Selection in the Face of Stereochemical Diversity in Mechanically Bonded Compounds. *Chem. Eur. J.* **2003**, *9*, 543–556.

(760) Weiss, J.; Wytko, J.; Berville, M.; Karmazin, L. Viologen Cyclophanes: Redox Controlled Host-Guest Interactions. *Chem*. *Commun*. **2015**, *51*, 15772–15775.

(761) Ashton, P. R.; Reder, A. S.; Spencer, N.; Stoddart, J. F. Self-Assembly of a Chiral Bis[2]catenane. *J. Am. Chem. Soc.* **1993**, *115*, 5286–5287.

(762) Ashton, P. R.; Preece, J. A.; Stoddart, J. F.; Tolley, M. S. Template-Directed Syntheses of a Bis[2]catenane and a Bis[2]Rotaxane—Towards Self-Assembling Polymers. *Synlett* **1994**, 789–792.

(763) Ashton, P. R.; Gómez-López, M.; Iqbal, S.; Preece, J. A.; Stoddart, J. F. A Self-Complexing Macrocycle Acting as a Chromophoric Receptor. *Tetrahedron Lett.* **1997**, *38*, 3635–3638.

(764) Wolf, R.; Asakawa, M.; Ashton, P. R.; Gómez-López, M.; Hamers, C.; Menzer, S.; Parsons, I. W.; Spencer, N.; Stoddart, J. F.; Tolley, M. S.; Williams, D. J. Molecular Chameleon: Chromophoric Sensing by a Self-Complexing Molecular Assembly. *Angew. Chem., Int. Ed*. **1998**, *37*, 975–979.

(765) Liu, Y.; Flood, A. H.; Stoddart, J. F. Thermally and Electrochemically Controllable Self-Complexing Molecular Switches. *J. Am. Chem. Soc.* **2004**, *126*, 9150–9151.

(766) Liu, Y.; Saha, S.; Vignon, S. A.; Flood, A. H.; Stoddart, J. F. Template-Directed Syntheses of Configurable and Reconfigurable Molecular Switches. *Synthesis* **2005**, 3437–3445.

(767) Liu, Y.; Flood, A. H.; Moskowitz, R. M.; Stoddart, J. F. Versatile Self-Complexing Compounds Based on Covalently Linked Donor–Acceptor Cyclophanes. *Chem. Eur. J.* **2005**, *11*, 369–385.

(768) Cao, D.; Wang, C.; Giesener, M. A.; Liu, Z.; Stoddart, J. F. A Rigid Donor–Acceptor Daisy Chain Dimer. *Chem. Commun.* **2012**, *48*, 6791–6793.

(769) Boyle, M. M.; Forgan, R. S.; Friedman, D. C.; Gassensmith, J. J.; Smaldone, R. A.; Stoddart, J. F.; Sauvage, J.-P. Donor–Acceptor Molecular Figures-of-Eight. *Chem*. *Commun*. **2011**, *47*, 11870–11872.

(770) Boyle, M. M.; Gassensmith, J. J.; Whalley, A. C.; Forgan, R. S.; Smaldone, R. A.; Hartlieb, K. J.; Blackburn, A. K.; Sauvage, J.-P.; Stoddart, J. F. Stereochemistry of Molecular Figures-of-Eight. *Chem. Eur. J.* **2012**, *18*, 10312–10323.

(771) Ashton, P. R.; Ballardini, R.; Balzani, V.; Gandolfi, M. T.; Marquis, D. J.-F.; Pérez-García, L.; Prodi, L.; Stoddart, J. F.; Venturi, M. The Self Assembly of Controllable [2]Catenanes. *J. Chem. Soc., Chem. Commun*. **1994**, *19*, 177–180.

(772) Ashton, P. R.; Pérez-García, L.; Stoddart, J. F.; White, A. J. P.; Williams, D. J. Controlling Translational Isomerism in [2]Catenanes. *Angew. Chem., Int. Ed. Engl*. **1995**, *34*, 571–574.

(773) Ashton, P. R.; Brown, C. L.; Cao, J.; Lee, J.-Y.; Newton, S. P.; White, A. J. P.; Raymo, F. M.; Stoddart, J. F.; Williams, D. J. Molecular Meccano 62. Azopyridinium-Containing [2]Pseudorotaxanes and Hydrazopyridinium-Containing [2]Catenanes. *Eur. J. Org. Chem*. **2001**, 957–965.

(774) Barnes, J. C.; Juríček, M.; Strutt, N. L.; Frasconi, M.; Sampath, S.; Giesener, M. A.; McGrier, P. L.; Bruns, C. J.; Stern, C. L.; Sarjeant, A. A.; Stoddart, J. F. ExBox: A Polycyclic Aromatic Hydrocarbon Scavenger. *J. Am. Chem. Soc.* **2013**, *135*, 183–192.

(775) Juríček, M.; Barnes, J. C.; Dale, E. J.; Liu, W.-G.; Strutt, N. L.; Bruns, C. J.; Vermeulen, N. A.; Ghooray, K. C.; Sarjeant, A. A.; Stern, C. L.; Botros, Y. Y.; Goddard, W. A., III; Stoddart, J. F. Ex^2Box: Interdependent Modes of Binding in a Two-Nanometer-Long Synthetic Receptor. *J. Am. Chem. Soc.* **2013**, *135*, 12736–12746.

(776) Barnes, J. C.; Juríček, M.; Vermeulen, N. A.; Dale, E. J.; Stoddart, J. F. Synthesis of Ex^nBox Cyclophanes. *J. Org. Chem.* **2013**, *78*, 11962–11969.

(777) Ryan, S. T. J.; Young, R. M.; Henkelis, J. J.; Hafezi, N.; Vermeulen, N. A.; Hennig, A.; Dale, E. J.; Wu, Y.; Krzyaniak, M. D.; Fox, A.; Nau, W. M.; Wasielewski, M. R.; Stoddart, J. F.; Scherman, O. A. Energy and Electron Transfer Dynamics Within a Series of Perylene Diimide/Cyclophane Systems. *J. Am. Chem. Soc.* **2015**, *137*, 15299–15307.

(778) Dale, E. J.; Vermeulen, N. A.; Juríček, M.; Barnes, J. C.; Young, R. M.; Wasielewski, M. R.; Stoddart, J. F. Supramolecular Explorations: Exhibiting the Extent of Extended Cationic Cyclophanes. *Acc. Chem. Res*. **2016**, *49*, 262–273.

(779) Barnes, J. C.; Dale, E. J.; Prokofjevs, A.; Narayanan, A.; Gibbs-Hall, I. C.; Juríček, M.; Stern, C. L.; Sarjeant, A. A.; Botros, Y. Y.; Stupp, S. I.; Stoddart, J. F. Semiconducting Single Crystals Comprising Segregated Arrays of Complexes of C_{60}. *J. Am. Chem. Soc.* **2015**, *137*, 2392–2399.

(780) Liu, Y.; Klivansky, L. M.; Khan, S. I.; Zhang, X. Templated Synthesis of Desymmetrized [2]Catenanes with Excellent Translational Selectivity. *Org. Lett.* **2007**, *9*, 2577–2580.

(781) Cao, D.; Amelia, M.; Klivansky, L. M.; Koshkakaryan, G.; Khan, S. I.; Semeraro, M.; Silvi, S.; Venturi, M.; Credi, A.; Liu, Y. Probing Donor−Acceptor Interactions and Co-Conformational Changes in Redox Active Desymmetrized [2]Catenanes. *J. Am. Chem. Soc.* **2010**, *132*, 1110–1122.

(782) Olsen, J.-C.; Fahrenbach, A. C.; Trabolsi, A.; Friedman, D. C.; Dey, S. K.; Gothard, C. M.; Shveyd, A. K.; Gasa, T. B.; Spruell, J. M.; Olson, M. A.; Wang, C.; Jacquot de Rouville, H.-P.; Botros, Y. Y.; Stoddart, J. F. A Neutral Redox-Switchable [2]Rotaxane. *Org. Biomol. Chem.* **2011**, *9*, 7126–7133.

(783) Raymo, F. M.; Stoddart, J. F. Self-Assembling Cyclobis(paraquat-4,4′-biphenylene). *Pure Appl. Chem.* **1996**, *68*, 313–322.

(784) Amabilino, D. B.; Ashton, P. R.; Brown, C. L.; Córdova, E.; Godinez, L. A.; Goodnow, T. T.; Kaifer, A. E.; Newton, S. P.; Pietraszkiewicz, M.; Philp, D.; Raymo, F. M.; Reder, A. S.; Slawin, A. M. Z.; Spencer, N.;Stoddart, J. F.; Williams, D. J. Molecular Meccano 2. Self-Assembly of [*n*]Catenanes. *J. Am. Chem. Soc*. **1995**, *117*, 1271–1293.

(785) Ashton, P. R.; Menzer, S.; Raymo, F. M.; Shimizu, G. K. H.; Stoddart, J. F.; Williams, D. J. The Template-Directed Synthesis of Cyclobis(paraquat-4,4′-biphenylene). *Chem. Commun.* **1996**, 487–490.

(786) Asakawa, M.; Ashton, P. R.; Menzer, S.; Raymo, F. M.; Stoddart, J. F.; White, A. J. P.; Williams, D. J. Molecular Meccano 8. Cyclobis(paraquat-4,4′-biphenylene)—An Organic Molecular Square. *Chem. Eur. J.* **1996**, *2*, 877–893.

(787) Forgan, R. S.; Wang, C.; Friedman, D. C.; Spruell, J. M.; Stern, C. L.; Sarjeant, A. A.; Cao, D.; Stoddart, J. F. Donor-Acceptor Ring-in-Ring Complexes. *Chem. Eur. J*. **2012**, *18*, 202–212.

(788) Amabilino, D. B.; Ashton, P. R.; Bravo, J. A.; Raymo, F. M.; Stoddart, J. F.; White, A. J. P.; Williams, D. J. Molecular Meccano 52. Template-Directed Synthesis of a Rotacatenane. *Eur. J. Org. Chem*. **1999**, 1295–1302.

(789) Barin, G.; Coskun, A.; Friedman, D. C.; Olson, M. A.; Colvin, M. T.; Carmielli, R.; Dey, S. K.; Bozdemir, O. A.; Wasielewski, M. R.; Stoddart, J. F. A Multistate Switchable [3]Rotacatenane. *Chem. Eur. J.* **2011**, *17*, 213–222.

(790) Juríček, M.; Barnes, J. C.; Strutt, N. L.; Vermeulen, N. A.; Ghooray, K. C.; Dale, E. J.; McGonigal, P. R.; Blackburn, A. K.;

Avestro, A.-J.; Stoddart, J. F. An ExBox [2]Catenane. *Chem. Sci.* **2014**, *5*, 2724–2731.
(791) Juríček, M.; Strutt, N. L.; Barnes, J. C.; Butterfield, A. M.; Dale, E. J.; Baldridge, K. K.; Stoddart, J. F.; Siegel, J. S. Induced-Fit Catalysis of Corannulene Bowl-to-Bowl Inversion. *Nature Chem.* **2014**, *6*, 222–228.
(792) Ryan, S. T. J.; del Barrio, J.; Ghosh, I.; Biedermann, F.; Lazar, A. I.; Lan, Y.; Coulston, R. J.; Nau, W. M.; Scherman, O. A. Efficient Host–Guest Energy Transfer in Polycationic Cyclophane–Perylene Diimide Complexes in Water. *J. Am. Chem. Soc.* **2014**, *136*, 9053–9060.
(793) Sun, J.; Frasconi, M.; Liu, Z.; Barnes, J. C.; Wang, Y.; Chen, D.; Stern, C. L.; Stoddart, J. F. Formation of Ring-in-Ring Complexes Between Crown Ethers and Rigid $TVBox^{8+}$. *Chem. Commun.* **2015**, *51*, 1432–1435.
(794) Dale, E. J.; Vermeulen, N. A.; Thomas, A. A.; Barnes, J. C.; Juríček, M.; Blackburn, A. K.; Strutt, N. L.; Sarjeant, A. A.; Stern, C. L.; Denmark, S. E.; Stoddart, J. F. ExCage. *J. Am. Chem. Soc*. **2014**, *136*, 10669–10682.
(795) Hafezi, N.; Holcroft, J. M.; Hartlieb, K. J.; Dale, E. J.; Vermeulen, N. A.; Stern, C. L.; Sarjeant, A. A.; Stoddart, J. F. Modulating the Binding of Polycyclic Aromatic Hydrocarbons Inside a Hexacationic Cage by Anion–π Interactions. *Angew. Chem., Int. Ed*. **2015**, *54*, 456–461.
(796) Małecka, J.; Lewandowska, U.; Kamiński, R.; Mames, I.; Więckowska, A.; Bilewicz, R.; Korybut-Daszkiewicz, B.; Woźniak, K. Macrocyclic Multicenter Complexes of Nickel and Copper of Increasing Complexity. *Chem. Eur. J.* **2011**, *17*, 12385–12395.
(797) Domagała, S.; Więckowska, A.; Kowalski, J.; Rogowska, A.; Szydłowska, J.; Korybut-Daszkiewicz, B.; Bilewicz, R.; Woźniak, K. Fine-Tuning of Properties of Bismacrocyclic Dinuclear Cyclidene Receptors by *N*-Methylation. *Chem. Eur. J.* **2006**, *12*, 2967–2981.
(798) Więckowska, A.; Wiśniewska, M.; Chrzanowski, M.; Kowalski, J.; Korybut-Daszkiewicz, B.; Bilewicz, R. Self-Assembly of a Nickel(II) Pseudorotaxane Nanostructure on a Gold Surface. *Pure Appl. Chem.* **2007**, *79*, 1077–1085.
(799) Mames, I.; Wawrzyniak, U. E.; Woźny, M.; Bilewicz, R.; Korybut-Daszkiewicz, B. Neutral Bis-macrocyclic Nickel(II) and Copper(II) Complexes as π-Donor Receptors. *Dalton Trans.* **2013**, *42*, 2382–2391.
(800) Colquhoun, H. M.; Williams, D. J.; Zhu, Z. Macrocyclic Aromatic Ether-Imide-Sulfones: Versatile Supramolecular Receptors with Extreme Thermochemical and Oxidative Stability. *J. Am. Chem. Soc.* **2002**, *124*, 13346–13347.
(801) Colquhoun, H. M.; Greenland, B. W.; Zhu, Z.; Shaw, J. S.; Cardin, C. J.; Burattini, S.; Elliott, J. M.; Basu, S.; Gasa, T. B.; Stoddart, J. F. A General Synthesis of Macrocyclic π-Electron-Acceptor Systems. *Org. Lett.* **2009**, *11*, 5238–5241.
(802) Colquhoun, H. M.; Zhu, Z.; Williams, D. J.; Drew, M. G. B.; Cardin, C. J.; Gan, Y.; Crawford, A. G.; Marder, T. B. Induced-Fit Binding of π-Electron-Donor Substrates to Macrocyclic Aromatic Ether Imide Sulfones: A Versatile Approach to Molecular Assembly. *Chem. Eur. J.* **2009**, *16*, 907–918.
(803) Zhu, Z.; Cardin, C. J.; Gan, Y.; Murray, C. A.; White, A. J. P.; Williams, D. J.; Colquhoun, H. M. Conformational Modulation of Sequence Recognition in Synthetic Macromolecules. *J. Am. Chem. Soc.* **2011**, *133*, 19442–19447.
(804) Gong, H.-Y.; Rambo, B. M.; Karnas, E.; Lynch, V. M.; Sessler, J. L. A "Texas-Sized" Molecular Box That Forms an Anion-Induced Supramolecular Necklace. *Nature Chem.* **2010**, *2*, 406–409.
(805) Gong, H.-Y.; Rambo, B. M.; Cho, W.; Lynch, V. M.; Oh, M.; Sessler, J. L. Anion-Directed Assembly of a Three-Dimensional Metal–Organic Rotaxane Framework. *Chem. Commun.* **2011**, *47*, 5973–5975.
(806) Gong, H.-Y.; Rambo, B. M.; Karnas, E.; Lynch, V. M.; Keller, K. M.; Sessler, J. L. Environmentally Responsive Threading, Dethreading, and Fixation of Anion-Induced Pseudorotaxanes. *J. Am. Chem. Soc.* **2011**, *133*, 1526–1533.
(807) Gong, H.-Y.; Rambo, B. M.; Lynch, V. M.; Keller, K. M.; Sessler, J. L. Neutral and Anionic Guests and Their Effect on the Formation of Pseudorotaxanes by Using a Flexible Tetracationic Imidazolium Macrocycle. *Chem. Eur. J.* **2012**, *18*, 7803–7809.
(808) Rambo, B. M.; Gong, H.-Y.; Oh, M.; Sessler, J. L. The "Texas-Sized" Molecular Box: A Versatile Building Block for the Construction of Anion-Directed Mechanically Interlocked Structures. *Acc. Chem. Res.* **2012**, *45*, 1390–1401.
(809) Gong, H.-Y.; Tang, F.; Rambo, B. M.; Cao, R.; Xiang, J.-F.; Sessler, J. L. Aromatic Sulfonate Anion-Induced Pseudorotaxanes: Environmentally Benign Synthesis, Selectivity, and Structural Characterization. *Chem. Commun.* **2015**, *51*, 1975–1978.
(810) Gong, H.-Y.; Rambo, B. M.; Nelson, C. A.; Lynch, V. M.; Zhu, X.; Sessler, J. L. Rare-Earth Cation Effects on Three-Dimensional Metal–Organic Rotaxane Framework (MORF) Self Assembly. *Chem. Commun.* **2012**, *48*, 10186–10188.
(811) Gong, H.-Y.; Rambo, B. M.; Nelson, C. A.; Cho, W.; Lynch, V. M.; Zhu, X.; Oh, M.; Sessler, J. L. Multi Component Self-Assembly: Supramolecular Organic Frameworks Containing Metal–Rotaxane Subunits (RSOFs). *Dalton Trans.* **2012**, *41*, 1134–1137.
(812) Colquhoun, H. M.; Zhu, Z.; Cardin, C. J.; Gan, Y. Principles of Sequence-Recognition in Aromatic Polyimides. *Chem. Commun*. **2004**, 2650–2652..
(813) Colquhoun, H. M.; Zhu, Z. Recognition of Polyimide Sequence Information by a Molecular Tweezer. *Angew. Chem., Int. Ed*. **2004**, *43*, 5040–5045.
(814) Colquhoun, H. M.; Zhu, Z.; Cardin, C. J.; Gan, Y.; Drew, M. G. B. Sterically Controlled Recognition of Macromolecular Sequence Information by Molecular Tweezers. *J. Am. Chem. Soc.* **2007**, *129*, 16163–16174.
(815) Colquhoun, H. M.; Zhu, Z.; Cardin, C. J.; Drew, M. G. B.; Gan, Y. Recognition of Sequence-Information in Synthetic Copolymer Chains by a Conformationally-Constrained Tweezer Molecule. *Faraday Discuss.* **2009**, *143*, 205–220.
(816) Zhu, Z.; Cardin, C. J.; Gan, Y.; Colquhoun, H. M. Sequence-Selective Assembly of Tweezer Molecules on Linear Templates Enables Frameshift-Reading of Sequence Information. *Nature Chem.* **2010**, *2*, 653–660.
(817) Greenland, B. W.; Bird, M. B.; Burattini, S.; Cramer, R.; O'Reilly, R. K.; Patterson, J. P.; Hayes, W.; Cardin, C. J.; Colquhoun, H. M. Mutual Binding of Polymer End-Groups by Complementary π–π-Stacking: A Molecular "Roman Handshake." *Chem. Commun.* **2013**, *49*, 454–456.
(818) Gabriel, G. J.; Iverson, B. L. Aromatic Oligomers That Form Hetero Duplexes in Aqueous Solution. *J. Am. Chem. Soc.* **2002**, *124*, 15174–15175.
(819) Zhan, T.-G.; Lu, B.-Y.; Lin, F.; Zhou, T.-Y.; Zhao, X.; Li, Z.-T. Donor–Acceptor Interaction-Driven Folding of Linear Naphthalene–Glycol Oligomers Templated by a Rigid Bipyridinium Rod. *Org. Chem. Front.* **2015**, *2*, 1578–1583.
(820) Prins, L. J.; Reinhoudt, D. N.; Timmerman, P. Noncovalent Synthesis Using Hydrogen Bonding. *Angew. Chem., Int. Ed*. **2001**, *40*, 2382–2426.
(821) Archer, E. A.; Gong, H.; Krische, M. J. Hydrogen Bonding in Noncovalent Synthesis: Selectivity and the Directed Organization of Molecular Strands. *Tetrahedron* **2001**, *57*, 1139–1159.
(822) Schalley, C. A.; Weilandt, T.; Brüggemann, J.; Vögtle, F. Hydrogen-Bond-Mediated Template Synthesis of Rotaxanes, Catenanes, and Knotanes. *Top. Curr. Chem.* **2004**, *248*, 141–200.
(823) Vilar, R. Hydrogen-Bonding Templated Assemblies. *Top. Curr. Chem*. **2004**, *111*, 85–137.
(824) Hunter, C. A. Molecular Recognition of *p*-Benzoquinone by a Macrocyclic Host. *J. Chem. Soc., Chem. Commun.* **1991**, 749–751.
(825) Vögtle, F.; Meier, S.; Hoss, R. One-Step Synthesis of a Fourfold Functionalized Catenane. *Angew. Chem., Int. Ed. Engl*. **1992**, *31*, 1619–1622.

(826) Allott, C.; Adams, H.; Hunter, C. A.; Thomas, J. A.; Bernad, P. L., Jr; Rotger, C. Hydrogen-Bond Recognition of Cyclic Dipeptides in Water. *Chem*. *Commun*. **1998**, 2449–2450.

(827) Seel, C.; Parham, A. H.; Safarowsky, O.; Hubner, G.; Vögtle, F. How Selective Threading of Amides Through Macrocylic Lactam Wheels Leads to Rotaxane Synthesis. *J. Org. Chem.* **1999**, *64*, 7236–7242.

(828) Chang, S.-Y.; Kim, H. S.; Chang, K.-J.; Jeong, K.-S. Efficient Modulation of Hydrogen-Bonding Interactions by Remote Substituents. *Org. Lett.* **2004**, *6*, 181–184.

(829) Hunter, C. A. Synthesis and Structure Elucidation of a New [2]-Catenane. *J. Am. Chem. Soc.* **1992**, *114*, 5303–5311.

(830) Vögtle, F.; Jaeger R.; Haendel M.; Ottens-Hildebrandt, S. Catenanes and Rotaxanes of the Amide Type. *Pure Appl. Chem.* **1996**, *68*, 225–232.

(831) Jäger, R.; Vögtle, F. A New Synthetic Strategy Towards Molecules with Mechanical Bonds: Nonionic Template Synthesis of Amide-Linked Catenanes and Rotaxanes. *Angew. Chem., Int. Ed. Engl*. **1997**, *36*, 930–944.

(832) Vögtle, F.; Safarowsky, O.; Heim, C.; Affeld, A.; Braun, O.; Mohry, A. Catenanes, Rotaxanes and Pretzelanes—Template Synthesis and Chirality. *Pure Appl. Chem.* **1999**, *71*, 247–251.

(833) Reuter, C.; Schmieder, R.; Vögtle, F. From Rotaxanes to Knots. Templating, Hydrogen Bond Patterns, and Cyclochirality. *Pure Appl. Chem*. **2000**, *72*, 2233–2241.

(834) Ottens-Hildebrandt, S.; Meier, S.; Schmidt, W.; Vögtle, F. Isomeric Catenanes of Lactam Type and Their Formation Mechanism. *Angew. Chem., Int. Ed. Engl*. **1994**, *33*, 1767–1770.

(835) Schalley, C. A.; Reckien, W.; Peyerimhoff, S.; Baytekin, B.; Vögtle, F. Theory and Experiment in Concert: Templated Synthesis of Amide Rotaxanes, Catenanes, and Knots. *Chem. Eur. J.* **2004**, *10*, 4777–4789.

(836) Ottens-Hildebrandt, S.; Nieger, M.; Rissanen, K.; Rouvinen, J.; Meier, S.; Harder, G.; Vögtle, F. Amide-Based Furano-Catenanes: Regioselective Template Synthesis and Crystal Structure. *J. Chem. Soc., Chem. Commun*. **1995**, 777–778.

(837) Ottens-Hildebrandt, S.; Schmidt, T.; Harren, J.; Vögtle, F. Sulfonamide-Based Catenanes—Regioselective Template Synthesis. *Liebigs Ann*. **1995**, 1855–1860.

(838) Safarowsky, O.; Vogel, E.; Vögtle, F. Amide-Based [3]Catenanes and [2]Catenanes with Aliphatic Chains. *Eur. J. Org. Chem*. **2000**, 499–505.

(839) Li, Q. V.; Vogel, E.; Parham, A. H.; Nieger, M.; Bolte, M.; Fröhlich, R.; Saarenketo, P.; Rissanen, K.; Vögtle, F. Synthesis and X-Ray Structure of Amide-Based Macrocycles, Catenanes and Pretzelane. *Eur. J. Org. Chem*. **2001**, 4041–4049.

(840) Schwanke F.; Heim C.; Safarowsky, O.; Silva, G.; Vögtle, F. Amide-Based Oligocatenanes by an Iterative Template Strategy. *Helv. Chim. Acta* **2000**, *83*, 3279–3290.

(841) Vögtle, F.; Händel, M.; Meier, S.; Ottens-Hildebrandt, S.; Ott, F.; Schmidt, T. Template Synthesis of the First Amide-Based Rotaxanes. *Liebigs Ann*. **1995**, 739–743.

(842) Vögtle, F.; Jäger, R.; Händel, M.; Ottens-Hildebrandt, S.; Schmidt, W. Amide-Based Rotaxanes with Terephthal, Furan, Thiophene, and Sulfonamide Subunits. *Synthesis* **1996**, 353–356.

(843) Jäger, R.; Baumann, S.; Fischer, M.; Safarowsky, O.; Nieger, M.; Vögtle, F. Non-Ionic Template Synthesis of Amide-Linked Rotaxanes: Olefinic and Aliphatic Axle Building Blocks. *Eur. J. Org. Chem.* **1997**, 2269–2273.

(844) Vögtle, F.; Ahuis, F.; Baumann, S.; Sessler, J. L. Porphyrin Blocking Groups in Amide-Based Rotaxanes. *Liebigs Ann*. **1996**, 921–926.

(845) Vögtle, F.; Dünnwald, T.; Händel, M.; Jäger, R.; Meier, S.; Harder, G. A [3]Rotaxane of the Amide Type. *Chem. Eur. J.* **1996**, *2*, 640–643.

(846) Braun O.; Vögtle, F. A Threading Method Yielding Non-Polymeric Rotaxanes Containing Urea and Carbamate Units. *Synlett* **1997**, 1184–1186.

(847) Dzyuba, E. V.; Kaufmann, L.; Löw, N. L.; Meyer, A. K.; Winkler, H. D. F.; Rissanen, K.; Schalley, C. A. C–H···O Hydrogen Bonds in "Clicked" Diketopiperazine-Based Amide Rotaxanes. *Org. Lett.* **2011**, *13*, 4838–4841.

(848) Xue, M.; Chen, C.-F. Triptycene-Based Tetralactam Macrocycles: Synthesis, Structure and Complexation with Squaraine. *Chem*. *Commun*. **2008**, 6128–6130.

(849) Xue, M.; Su, Y.-S.; Chen, C.-F. Isomeric Squaraine-Based [2]Pseudorotaxanes and [2]Rotaxanes: Synthesis, Optical Properties, and Their Tubular Structures in the Solid State. *Chem. Eur. J.* **2010**, *16*, 8537–8544.

(850) Gassensmith, J. J.; Barr, L.; Baumes, J. M.; Paek, A.; Nguyen, A.; Smith, B. D. Synthesis and Photophysical Investigation of Squaraine Rotaxanes by "Clicked Capping." *Org. Lett.* **2008**, *10*, 3343–3346.

(851) Safarowsky, O.; Nieger, M.; Fröhlich, R.; Vögtle, F. A Molecular Knot with Twelve Amide Groups: One-Step Synthesis, Crystal Structure, Chirality. *Angew*. *Chem., Int. Ed*. **2000**, *39*, 1616–1618.

(852) Brueggemann, J.; Bitter, S.; Mueller, S.; Mueller, W. M.; Mueller, U.; Maier, N. M.; Lindner, W.; Vögtle, F. Spontaneous Knotting—From Oligoamide Threads to Trefoil Knots. *Angew. Chem., Int. Ed*. **2007**, *46*, 254–259.

(853) Fioravanti, G. Benzylic Amide Rotaxanes: a Versatile Architecture. *Curr. Org. Synth.* **2012**, *9*, 199–214.

(854) Johnston, A. G.; Leigh, D. A.; Murphy, A.; Smart, J. P.; Deegan, M. D. The Synthesis and Solubilization of Amide Macrocycles via Rotaxane Formation. *J. Am. Chem. Soc.* **1996**, *118*, 10662–10663.

(855) Leigh, D. A.; Thomson, A. R. Switchable Dual Binding Mode Molecular Shuttle. *Org. Lett.* **2006**, *8*, 5377–5379.

(856) Huang, Y.-L.; Hung, W.-C.; Lai, C.-C.; Liu, Y.-H.; Peng, S.-M.; Chiu, S.-H. Using Acetate Anions to Induce Translational Isomerization in a Neutral Urea-Based Molecular Switch. *Angew. Chem., Int. Ed.* **2007**, *46*, 6629–6633.

(857) Vidonne, A.; Philp, D. Integrating Replication Processes with Mechanically Interlocked Molecular Architectures. *Tetrahedron* **2008**, *64*, 8464–8475.

(858) Hassan, N. I.; del Amo, V.; Calder, E.; Philp, D. Low Temperature Capture of Pseudorotaxanes. *Org. Lett.* **2011**, *13*, 458–461.

(859) Chen, M.; Han, S.; Jiang, L.; Zhou, S.; Jiang, F.; Xu, Z.; Liang, J.; Zhang, S. New Switchable [2]Pseudorotaxanes Formed by Pyridine *N*-Oxide Derivatives with Diamide-Based Macrocycles. *Chem. Commun.* **2010**, *46*, 3932–3934.

(860) Johnston, A. G.; Leigh, D. A.; Pritchard, R. J.; Deegan, M. D. Facile Synthesis and Solid-State Structure of a Benzylic Amide [2]Catenane. *Angew. Chem., Int. Ed. Engl*. **1995**, *34*, 1209–1212.

(861) Leigh, D. A.; Venturini, A.; Wilson A. J.; Wong, J. K. Y.; Zerbetto, F. The Mechanism of Formation of Amide-Based Interlocked Compounds: Prediction of a New Rotaxane-Forming Motif. *Chem. Eur. J.* **2004**, *10*, 4960–4969.

(862) Fanti, M.; Fustin, C.-A.; Leigh, D. A.; Murphy, A.; Rudolf, P.; Caudano, R.; Zamboni, R.; Zerbetto, F. High-Frequency Vibrations of the Simplest Benzylic Amide [2]Catenane. *J. Phys. Chem. A* **1998**, *102*, 5782–5788.

(863) Zamboni, R.; Muccini, M.; Gebauer, W.; Biscarini, F.; Murgia, M.; Ruani, G.; Leigh, D. A.; Murphy, A.; Tetard, D. Raman and Far Infrared Characterization of the Simplest Benzylic Amide [2]Catenane. *Synth. Met.* **1999**, *102*, 1556–1557.

(864) Fustin, C.-A.; Leigh, D. A.; Rudolf, P.; Timpel, D.; Zerbetto, F. Physical Consequences of a Mechanically Interlocked Architecture: Benzylic Amide Catenane NH Stretching Vibrations as Sensitive Probes for Weakly Hydrogen-Bonding Environments. *ChemPhysChem* **2000**, *1*, 97–100.

(865) Caciuffo, R.; Esposti, A. D.; Deleuze, M. S.; Leigh, D. A.; Murphy, A.; Paci, B.; Parker, S. F.; Zerbetto, F. Inelastic Neutron Scattering of Large Molecular Systems: The Case of the Original Benzylic Amide [2]Catenane. *J. Chem. Phys.* **1998**, *109*, 11094–11100.

(866) Leigh, D. A.; Parker, S. F.; Timpel, D.; Zerbetto, F. The Inelastic Neutron Scattering of Two Benzylic Amide [2]Catenanes. *J. Chem. Phys.* **2001**, *114*, 5006–5011.
(867) Fustin, C.-A.; Rudolf, P.; Taminiaux, A. F.; Zerbetto, F.; Leigh D. A.; Caudano, R. Growth and Characterization of Benzylic Amide [2]Catenane Thin Films. *Thin Solid Films* **1998**, *327*, 321–325.
(868) De Nadaï, C.; Whelan, C. M.; Perollier, C.; Clarkson, G.; Leigh, D. A.; Caudano, R.; Rudolf, P. Self-Assembly of Mechanically Interlocked and Threaded Rings: A HREELS and XPS Study of Thiol-Functionalised Catenane and Rotaxane Molecules on Au(111). *Surf. Sci.* **2000**, *454*, 112–117.
(869) Biscarini, F.; Gebauer, W.; Di Domenico, D.; Zamboni, R.; Pascual, J.-I.; Leigh, D. A.; Murphy, A.; Tetard, D. STM Investigation of Flexible Supramolecules: Benzylic Amide [2] Catenanes. *Synth. Met.* **1999**, *102*, 1466–1467.
(870) Deleuze, M. S.; Leigh, D. A.; Zerbetto, F. How Do Benzylic Amide [2]Catenane Rings Rotate? *J. Am. Chem. Soc.* **1999**, *121*, 2364–2379.
(871) Leigh, D. A.; Troisi, A.; Zerbetto, F. A Quantum-Mechanical Description of Macrocyclic Ring Rotation in Benzylic Amide [2]Catenanes. *Chem. Eur. J.* **2001**, *7*, 1450–1454.
(872) Brouwer, A. M.; Buma, W. J.; Caudano, R.; Fanti, M.; Fustin, C.-A.; Leigh, D. A.; Murphy, A.; Rudolf, P.; Zerbetto, F.; Zwier, J. M. Experimental and Theoretical Studies of the Low-Lying Electronic States of the Simplest Benzylic Amide [2]Catenane. *Chem. Phys.* **1998**, *238*, 421–428.
(873) Gase, T.; Grando, D.; Chollet, P.-A.; Kajzar, F.; Murphy, A.; Leigh, D. A. Linear and Unanticipated Second-Order Nonlinear Optical Properties of Benzylic Amide [2]Catenane Thin Films. Evidence of Partial Rotation of the Interlocked Molecular Rings in the Solid State. *Adv. Mater*. **1999**, *11*, 1303–1306.
(874) Johnston, A. G.; Leigh, D. A.; Nezhat, L.; Smart, J. P.; Deegan, M. D. Structurally Diverse and Dynamically Versatile Benzylic Amide [2]Catenanes Assembled Directly From Commercially Available Precursors. *Angew. Chem., Int. Ed. Engl*. **1995**, *34*, 1212–1216.
(875) Leigh, D. A.; Moody, K.; Smart, J. P.; Watson, K. J.; Slawin, A. M. Z. Catenane Chameleons: Environment-Sensitive Translational Isomerism in Amphiphilic Benzylic Amide [2]Catenanes. *Angew. Chem., Int. Ed. Engl*. **1996**, *35*, 306–310.
(876) Ishikawa, K.; Yamamoto, T.; Asakawa, M.; Tezuka, Y. Effective Synthesis of Polymer Catenanes by Cooperative Electrostatic/Hydrogen-Bonding Self-Assembly and Covalent Fixation. *Macromolecules* **2010**, *43*, 168–176.
(877) Oike, H.; Imaizumi, H.; Mouri, T.; Yoshioka, Y.; Uchibori, A.; Tezuka, Y. Designing Unusual Polymer Topologies by Electrostatic Self-Assembly and Covalent Fixation. *J. Am. Chem. Soc.* **2000**, *122*, 9592–9599.
(878) Leigh, D. A.; Murphy, A.; Smart, J. P.; Slawin, A. M. Z. Glycylglycine Rotaxanes—The Hydrogen Bond Directed Assembly of Synthetic Peptide Rotaxanes. *Angew. Chem., Int. Ed. Engl*. **1997**, *36*, 728–732.
(879) Clegg, W.; Gimenez-Saiz, C.; Leigh, D. A.; Murphy, A.; Slawin, A. M. Z.; Teat, S. J. "Smart" Rotaxanes: Shape Memory and Control in Tertiary Amide Peptido[2]rotaxanes. *J. Am. Chem. Soc.* **1999**, *121*, 4124–4129.
(880) Brancato G.; Coutrot, F.; Leigh, D. A.; Murphy, A.; Wong, J. K. Y.; Zerbetto, F. From Reactants to Products via Simple Hydrogen-Bonding Networks: Information Transmission in Chemical Reactions. *Proc. Natl. Acad. Sci. U.S.A.* **2002**, *99*, 4967–4971.
(881) Gatti, F. G.; Leigh, D. A.; Nepogodiev, S. A.; Slawin, A. M. Z.; Teat, S. J.; Wong, J. K. Y. Stiff, and Sticky in the Right Places: The Dramatic Influence of Preorganizing Guest Binding Sites on the Hydrogen Bond-Directed Assembly of Rotaxanes. *J. Am. Chem. Soc.* **2001**, *123*, 5983–5989.
(882) Altieri, A.; Bottari, G.; Dehez, F.; Leigh, D. A.; Wong, J. K. Y.; Zerbetto, F. Remarkable Positional Discrimination in Bistable Light- and Heat-Switchable Hydrogen-Bonded Molecular Shuttles. *Angew. Chem., Int. Ed*. **2003**, *42*, 2296–2300.
(883) Whelan, C.; Gatti, F.; Leigh, D. A.; Rapino, S.; Zerbetto, F.; Rudolf, P. Adsorption of Fumaramide [2]Rotaxane and Its Components on a Solid Substrate: A Coverage-Dependent Study. *J. Phys. Chem. B* **2006**, *110*, 17076–17081.
(884) Larsen, O. F. A.; Bodis, P.; Buma, W. J.; Hannam, J. S.; Leigh, D. A.; Woutersen, S. Probing the Structure of a Rotaxane with Two-Dimensional Infrared Spectroscopy. *Proc. Natl. Acad. Sci. U.S.A.* **2005**, *102*, 13378–13382.
(885) Bodis, P.; Timmer, R.; Yeremenko, S.; Buma, W. J.; Buma, W.; Hannam, J. S.; Leigh, D. A.; Woutersen, S. Heterovibrational Interactions, Cooperative Hydrogen Bonding, and Vibrational Energy Relaxation Pathways in a Rotaxane. *J. Phys. Chem. C* **2007**, *111*, 6798–6804.
(886) Bodis, P.; Panman, M. R.; Bakker, B. H.; Mateo-Alonso, A.; Prato, M.; Buma, W. J.; Brouwer, A. M.; Kay, E. R; Leigh, D. A.; Woutersen, S. Two-Dimensional Vibrational Spectroscopy of Rotaxane-Based Molecular Machines. *Acc. Chem. Res.* **2009**, *42*, 1462–1469.
(887) Bodis, P.; Yeremenko, S.; Berná, J.; Buma, W. J.;Leigh, D. A.; Woutersen, S. Bimodal Dynamics of Mechanically Constrained Hydrogen Bonds Revealed by Vibrational Photon Echoes. *J. Chem. Phys.* **2011**, *134*, 134504.
(888) Arfaoui, I.; Bermúdez, V.; Bottari, G.; De Nadai, C.; Jalkanen, J.-P.; Kajzar, F.; Leigh, D. A.; Lubomska, M.; Mendoza, S. M.; Niziol, J.; Rudolf, P.; Zerbetto, F. Surface Enhanced Second Harmonic Generation From Macrocycle, Catenane, and Rotaxane Thin Films: Experiments and Theory. *J. Phys. Chem. B* **2006**, *110*, 7648–7652.
(889) Rijs, A. M.; Crews, B. O.; de Vries, M. S.; Hannam, J. S.; Leigh, D. A.; Fanti, M.; Zerbetto, F.; Buma, W. J. Shaping of a Conformationally Flexible Molecular Structure for Spectroscopy. *Angew. Chem., Int. Ed*. **2008**, *47*, 3174–3179.
(890) Rijs, A. M.; Compagnon, I.; Oomens, J.; Hannam, J. S.; Leigh, D. A.; Buma, W. J. Stiff, and Sticky in the Right Places: Binding Interactions in Isolated Mechanically Interlocked Molecules Probed by Mid-Infrared Spectroscopy. *J. Am. Chem. Soc.* **2009**, *131*, 2428–2429.
(891) Rijs, A. M.; Sändig, N.; Blom, M. N.; Oomens, J.; Hannam, J. S.; Leigh, D. A.; Zerbetto, F.; Buma, W. J. Controlled Hydrogen-Bond Breaking in a Rotaxane by Discrete Solvation. *Angew. Chem., Int. Ed*. **2010**, *49*, 3896–3900.
(892) Smolarek, S.; Rijs, A. M.; Hannam, J. S.; Leigh, D. A.; Drabbels, M.; Buma, W. J. Conformational Flexibility of a Rotaxane Thread Probed by Electronic Spectroscopy in Helium Nanodroplets. *J. Am. Chem. Soc.* **2009**, *131*, 12902–12903.
(893) Altoè, P.; Haraszkiewicz, N.; Gatti, F. G.; Wiering, P. G.; Frochot, C.; Brouwer, A. M.; Balkowski, G.; Shaw, D.; Woutersen, S.; Buma, W. J.; Zerbetto, F.; Orlandi, G.; Leigh, D. A.; Garavelli, M. Multistate Photo-Induced Relaxation and Photoisomerization Ability of Fumaramide Threads: A Computational and Experimental Study. *J. Am. Chem. Soc.* **2009**, *131*, 104–117.
(894) Mancini, G.; Zazza, C.; Aschi, M.; Sanna, N. Conformational Analysis and UV/Vis Spectroscopic Properties of a Rotaxane-Based Molecular Machine in Acetonitrile Dilute Solution: When Simulations Meet Experiments. *Phys. Chem. Chem. Phys.* **2011**, *13*, 2342.
(895) Bermudez, V.; Capron, N.; Gase, T.; Gatti, F. G.; Kajzar, F.; Leigh, D. A.; Zerbetto, F.; Zhang, S. Influencing Intramolecular Motion with an Alternating Electric Field. *Nature* **2000**, *406*, 608–611.
(896) D'Souza, D. M.; Leigh, D. A.; Mottier, L.; Mullen, K. M.; Paolucci, F.; Teat, S. J.; Zhang, S. Nitrone [2]Rotaxanes: Simultaneous Chemical Protection and Electrochemical Activation of a Functional Group. *J. Am. Chem. Soc.* **2010**, *132*, 9465–9470.
(897) Altieri, A.; Aucagne, V.; Carrillo, R.; Clarkson, G. J.; D'Souza, D. M.; Dunnett, J. A.; Leigh, D. A.; Mullen, K. M. Sulfur-

Containing Amide-Based [2]Rotaxanes and Molecular Shuttles. *Chem. Sci.* **2011**, *2*, 1922–1928.
(898) Ahmed, R.; Altieri, A.; D'Souza, D. M.; Leigh, D. A.; Mullen, K. M.; Papmeyer, M.; Slawin, A. M. Z.; Wong, J. K. Y.; Woollins, J. D. Phosphorus-Based Functional Groups as Hydrogen Bonding Templates for Rotaxane Formation. *J. Am. Chem. Soc.* **2011**, *133*, 12304–12310.
(899) Biscarini, F.; Cavallini, M.; Leigh, D. A.; León, S.; Teat, S. J.; Wong, J. K. Y.; Zerbetto, F. The Effect of Mechanical Interlocking on Crystal Packing: Predictions and Testing. *J. Am. Chem. Soc.* **2002**, *124*, 225–233.
(900) Berná, J.; Brouwer, A. M.; Fazio, S. M.; Haraszkiewicz, N.; Leigh, D. A.; Lennon, C. M. A Rotaxane Mimic of the Photoactive Yellow Protein Chromophore Environment: Effects of Hydrogen Bonding and Mechanical Interlocking on a Coumaric Amide Derivative. *Chem. Commun.* **2007**, 1910–1912.
(901) Günbaş, D. D.; Zalewski, L.; Brouwer, A. M. Energy Landscape of a Hydrogen-Bonded Non-Degenerate Molecular Shuttle. *Chem. Commun.* **2010**, *46*, 2061–2063.
(902) Berná, J.; Alajarín, M.; Orenes, R.-A. Azodicarboxamides as Template Binding Motifs for the Building of Hydrogen-Bonded Molecular Shuttles. *J. Am. Chem. Soc.* **2010**, *132*, 10741–10747.
(903) Martinez-Cuezva, A.; Pastor, A.; Cioncoloni, G.; Orenes, R.-A.; Alajarín, M.; Symes, M. D.; Berná, J. Versatile Control of the Submolecular Motion of Di(acylamino)pyridine-Based [2]Rotaxanes. *Chem. Sci.* **2015**, *6*, 3087–3094.
(904) Martinez-Cuezva, A.; Berná, J.; Orenes, R.-A.; Pastor, A.; Alajarín, M. Small-Molecule Recognition for Controlling Molecular Motion in Hydrogen-Bond-Assembled Rotaxanes. *Angew. Chem., Int. Ed*. **2014**, *53*, 6762–6767.
(905) Watanabe, N.; Kihara, N.; Takata, T. Change of Connectivity on Catenane Ring: Ring Expansion by Annulation-Ring Scission Sequence. *Org. Lett.* **2001**, *3*, 3519–3522.
(906) Watanabe, N.; Kihara, N.; Furusho, Y.; Takata, T.; Araki, Y.; Ito, O. Photoinduced Intrarotaxane Electron Transfer Between Zinc Porphyrin and [60] Fullerene in Benzonitrile. *Angew. Chem.Int. Ed.* **2003**, *42*, 681–683.
(907) Watanabe, N.; Ikari, Y.; Kihara, N.; Takata, T. Bridged Polycatenane. *Macromolecules* **2004**, *37*, 6663–6666.
(908) Sasabe, H.; Ikeshita, K.-i; Rajkumar, G. A.; Watanabe, N.; Kihara, N.; Furusho, Y.; Mizuno, K.; Ogawa, A.; Takata, T. Synthesis of [60]Fullerene-Functionalized Rotaxanes. *Tetrahedron* **2006**, *62*, 1988–1997.
(909) Cooke, G.; Garety, J. F.; Jordan, B.; Kryvokhyzha, N.; Parkin, A.; Rabani, G.; Rotello, V. M. Flavin-Based [2]Rotaxanes. *Org. Lett.* **2006**, *8*, 2297–2300.
(910) Caldwell, S. T.; Cooke, G.; Fitzpatrick, B.; Long, D.-L.; Rabani, G.; Rotello, V. M. A Flavin-Based [2]Catenane. *Chem. Commun*. **2008**, 5912–5914.
(911) Hsueh, S.-Y.; Kuo, C.-T.; Lu, T.-W.; Lai, C.-C.; Liu, Y.-H.; Hsu, H.-F.; Peng, S.-M.; Chen, C.-H.; Chiu, S.-H. Acid/Base- and Anion-Controllable Organogels Formed From a Urea-Based Molecular Switch. *Angew. Chem., Int. Ed*. **2010**, *49*, 9170–9173.
(912) Kosikova, T.; Hassan, N. I.; Cordes, D. B.; Slawin, A. M. Z.; Philp, D. Orthogonal Recognition Processes Drive the Assembly and Replication of a [2]Rotaxane. *J. Am. Chem. Soc.* **2015**, *137*, 16074–16083.
(913) Gassensmith, J. J.; Baumes, J. M.; Smith, B. D. Discovery and Early Development of Squaraine Rotaxanes. *Chem. Commun*. **2009**, 6329–6338.
(914) Arunkumar, E.; Forbes, C. C.; Noll, B. C.; Smith, B. D. Squaraine-Derived Rotaxanes: Sterically Protected Fluorescent Near-IR Dyes. *J. Am. Chem. Soc.* **2005**, *127*, 3288–3289.
(915) Johnson, J. R.; Fu, N.; Arunkumar, E.; Leevy, W. M.; Gammon, S. T.; Piwnica-Worms, D.; Smith, B. D. Squaraine Rotaxanes: Superior Substitutes for Cy-5 in Molecular Probes for Near-Infrared Fluorescence Cell Imaging. *Angew. Chem., Int. Ed*. **2007**, *46*, 5528–5531.
(916) Arunkumar, E.; Sudeep, P. K.; Kamat, P. V.; Noll, B. C.; Smith, B. D. Singlet Oxygen Generation Using Iodinated Squaraine and Squaraine-Rotaxane Dyes. *New J. Chem.* **2007**, *31*, 677.
(917) Fu, N.; Gassensmith, J. J.; Smith, B. D. Effect of Stopper Size on Squaraine Rotaxane Stability. *Supramol. Chem.* **2009**, *21*, 118–124.
(918) Fu, N.; Baumes, J. M.; Arunkumar, E.; Noll, B. C.; Smith, B. D. Squaraine Rotaxanes with Boat Conformation Macrocycles. *J. Org. Chem.* **2009**, *74*, 6462–6468.
(919) Cole, E. L.; Arunkumar, E.; Xiao, S.; Smith, B. A.; Smith, B. D. Water-Soluble, Deep-Red Fluorescent Squaraine Rotaxanes. *Org. Biomol. Chem.* **2012**, *10*, 5769–5773.
(920) Fu, N.; Gassensmith, J. J.; Smith, B. D. A New Class of Hydroxy-Substituted Squaraine Rotaxane. *Aust. J. Chem.* **2010**, *63*, 792–796.
(921) Gassensmith, J. J.; Arunkumar, E.; Barr, L.; Baumes, J. M.; DiVittorio, K. M.; Johnson, J. R.; Noll, B. C.; Smith, B. D. Self-Assembly of Fluorescent Inclusion Complexes in Competitive Media Including the Interior of Living Cells. *J. Am. Chem. Soc.* **2007**, *129*, 15054–15059.
(922) Collins, C. G.; Peck, E. M.; Kramer, P. J.; Smith, B. D. Squaraine Rotaxane Shuttle as a Ratiometric Deep-Red Optical Chloride Sensor. *Chem. Sci.* **2013**, *4*, 2557–2563.
(923) Collins, C. G.; Johnson, A. T.; Connell, R. D.; Nelson, R. A.; Murgu, I.; Oliver, A. G.; Smith, B. D. Effect of 1,3-Adamantane Bridging Units Within the Surrounding Macrocycle of Squaraine Rotaxanes. *New J. Chem.* **2014**, *38*, 3992–3998.
(924) Spence, G. T.; Hartland, G. V.; Smith, B. D. Activated Photothermal Heating Using Croconaine Dyes. *Chem. Sci.* **2013**, *4*, 4240–4244.
(925) Guha, S.; Shaw, G. K.; Mitcham, T. M.; Bouchard, R. R.; Smith, B. D. Croconaine Rotaxane for Acid Activated Photothermal Heating and Ratiometric Photoacoustic Imaging of Acidic pH. *Chem. Commun.* **2015**, *52*, 120–123.
(926) Peck, E. M.; Collins, C. G.; Smith, B. D. Thiosquaraine Rotaxanes: Synthesis, Dynamic Structure, and Oxygen Photosensitization. *Org. Lett.* **2013**, *15*, 2762–2765.
(927) Spence, G. T.; Lo, S. S.; Ke, C.; Destecroix, H.; Davis, A. P.; Hartland, G. V.; Smith, B. D. Near-Infrared Croconaine Rotaxanes and Doped Nanoparticles for Enhanced Aqueous Photothermal Heating. *Chem*. *Eur*. *J*. **2014**, 12628–12635.
(928) Gassensmith, J. J.; Baumes, J. M.; Eberhard, J.; Smith, B. D. Cycloaddition to an Anthracene-Derived Macrocyclic Receptor with Supramolecular Control of Regioselectivity. *Chem*. *Commun*. **2009**, 2517–2519.
(929) Baumes, J. M.; Gassensmith, J. J.; Giblin, J.; Lee, J.-J.; White, A. G.; Culligan, W. J.; Leevy, W. M.; Kuno, M.; Smith, B. D. Storable, Thermally Activated, Near-Infrared Chemiluminescent Dyes and Dye-Stained Microparticles for Optical Imaging. *Nature Chem.* **2010**, *2*, 1025–1030.
(930) Collins, C. G.; Lee, J. M.; Oliver, A. G.; Wiest, O.; Smith, B. D. Internal and External Stereoisomers of Squaraine Rotaxane Endoperoxide: Synthesis, Chemical Differences, and Structural Revision. *J. Org. Chem.* **2014**, *79*, 1120–1130.
(931) Ke, C.; Destecroix, H.; Crump, M. P.; Davis, A. P. A Simple and Accessible Synthetic Lectin for Glucose Recognition and Sensing. *Nature Chem.* **2012**, *4*, 718–723.
(932) Mooibroek, T. J.; Casas-Solvas, J. M.; Harniman, R. L.; Renney, C. M.; Carter, T. S.; Crump, M. P.; Davis, A. P. A Threading Receptor for Polysaccharides. *Nature Chem.* **2016**, *8*, 69–74.
(933) Aucagne, V.; Leigh, D. A.; Lock, J. S.; Thomson, A. R. Rotaxanes of Cyclic Peptides. *J. Am. Chem. Soc.* **2006**, *128*, 1784–1785.
(934) Deber, C. M.; Blout, E. R. Cyclic Peptides. Amino Acid–Cyclic Peptides Complexes. *J. Am. Chem. Soc*. **1974**, *96*, 7566–7568.
(935) Madison, V.; Deber, C. M.; Blout, E. R. Cyclic Peptides. 17. Metal and Amino Acid Complexes of Cyclo(Pro-Gly)$_4$ and Analogues Studied by Nuclear Magnetic Resonance and Circular Dichroism. *J. Am. Chem. Soc*. **1977**, *99*, 4788–4798.

(936) Hirata, T.; Fujimura, F.; Kimura, S. A Novel Polypseudorotaxane Composed of Cyclic β-Peptide as Bead Component. *Chem*. *Commun*. **2007**, 1023–1025.
(937) Chang, S. K.; Hamilton, A. D. Molecular Recognition of Biologically Interesting Substrates: Synthesis of an Artificial Receptor for Barbiturates Employing Six Hydrogen Bonds. *J. Am. Chem. Soc.* **1988**, *110*, 1318–1319.
(938) Chang, S. K.; Van Engen, D.; Fan, E.; Hamilton, A. D. Hydrogen Bonding and Molecular Recognition: Synthetic, Complexation, and Structural Studies on Barbiturate Binding to an Artificial Receptor. *J. Am. Chem. Soc.* **1991**, *113*, 7640–7645.
(939) Tron, A.; Thornton, P. J.; Rocher, M.; Jacquot de Rouville, H.-P.; Desvergne, J.-P.; Kauffmann, B.; Buffeteau, T.; Cavagnat, D.; Tucker, J. H. R.; McClenaghan, N. D. Formation of a Hydrogen-Bonded Barbiturate [2]-Rotaxane. *Org. Lett*. **2014**, *16*, 1358–1361.
(940) Tron, A.; Thornton, P. J.; Lincheneau, C.; Desvergne, J.-P.; Spencer, N.; Tucker, J. H. R.; McClenaghan, N. D. Reversible Photocapture of a [2]Rotaxane Harnessing a Barbiturate Template. *J. Org. Chem.* **2015**, *80*, 988–996.
(941) Böhmer, V. Calixarenes, Macrocycles with (Almost) Unlimited Possibilities. *Angew. Chem., Int. Ed. Engl*. **1995**, *34*, 713–745.
(942) Shimizu, K. D.; Rebek, J. Synthesis and Assembly of Self-Complementary Calix[4]arenes. *Proc. Natl. Acad. Sci. U.S.A.* **1995**, *92*, 12403–12407.
(943) Rebek, J., Jr. Host–Guest Chemistry of Calixarene Capsules. *Chem*. *Commun*. **2000**, 637–643.
(944) Mogck, O.; Böhmer, V.; Vogt, W. Hydrogen Bonded Homo- and Heterodimers of Tetra Urea Derivatives of Calix[4]arenes. *Tetrahedron* **1996**, *52*, 8489–8496.
(945) Mogck, O.; Paulus, E. F.; Böhmer, V.; Thondorf, I.; Vogt, W. Hydrogen-Bonded Dimers of Tetraurea Calix[4]arenes: Unambiguous Proof by Single Crystal X-ray Analysis. *Chem*. *Commun*. **1996**, 2533–2534.
(946) Böhmer, V.; Rudzevich, Y.; Rudzevich, V. Rotaxanes and Catenanes Derived From Tetra-Urea Calix[4]arenes. **2010**, *287*, 42–50.
(947) Gaeta, C.; Vysotsky, M. O.; Bogdan, A.; Böhmer, V. Fourfold [2]Rotaxanes Based on Calix[4]arenes. *J. Am. Chem. Soc.* **2005**, *127*, 13136–13137.
(948) Glink, P. T.; Schiavo, C.; Stoddart, J. F.; Williams, D. J. The Genesis of a New Range of Interlocked Molecules. *Chem. Commun.* **1996**, *19*, 1483–1490.
(949) Thibeault, D.; Morin, J.-F. Recent Advances in the Synthesis of Ammonium-Based Rotaxanes. *Molecules* **2010**, *15*, 3709–3730.
(950) Späth, A.; König, B. Molecular Recognition of Organic Ammonium-Ions in Solution Using Synthetic Receptors. *Beilstein J. Org. Chem*. **2010**, *6*:32.
(951) Metcalfe, J. C.; Stoddart, J. F.; Jones, G. Complexation of Primary Alkylammonium Salts and Secondary Dialkylammonium Salts by *N,N*-Dimethyl-1,7-diaza-4,10-dioxacyclododecane. *J. Am. Chem. Soc.* **1977**, *99*, 8317–8319.
(952) Izatt, R. M.; Lamb, J. D.; Izatt, N. E.; Rossiter, B. E., Jr; Christensen, J. J.; Haymore, B. L. A Calorimetric Titration Study of the Reaction of Several Organic Ammonium Cations with 18-Crown-6 in Methanol. *J. Am. Chem. Soc.* **1979**, *101*, 6273–6276.
(953) Ashton, P. R.; Campbell, P. J.; Chrystal, E. J. T.; Glink, P. T.; Menzer, S.; Philp, D.; Spencer, N.; Stoddart, J. F.; Tasker, P. A.; Williams, D. J. Dialkylammonium Ion/Crown Ether Complexes: The Forerunners of a New Family of Interlocked Molecules. *Angew. Chem., Int. Ed. Engl*. **1995**, *34*, 1865–1869.
(954) Kolchinski, A. G.; Busch, D. H.; Alcock, N. W. Gaining Control Over Molecular Threading: Benefits of Second Coordination Sites and Aqueous-Organic Interfaces in Rotaxane Synthesis. *J. Chem*. *Soc., Chem*. *Commun*. **1995**, 1289–1291.
(955) Coutrot, F.; Busseron, E.; Montero, J.-L. A Very Efficient Synthesis of a Mannosyl Orthoester [2]Rotaxane and Mannosidic [2]Rotaxanes. *Org. Lett.* **2008**, *10*, 753–756.
(956) Vukotic, V. N.; Harris, K. J.; Zhu, K.; Schurko, R. W.; Loeb, S. J. Metal–Organic Frameworks with Dynamic Interlocked Components. *Nature Chem.* **2012**, *4*, 456–460.
(957) Cantrill, S. J.; Pease, A. R.; Stoddart, J. F. A Molecular Meccano Kit. *J. Chem*. *Soc., Dalton Trans*. **2000**, 3715–3734.
(958) Dasgupta, S.; Wu, J. Formation of [2]Rotaxanes by Encircling [20], [21] and [22]Crown Ethers Onto the Dibenzylammonium Dumbbell. *Chem. Sci.* **2012**, *3*, 425–432.
(959) Hsu, C.-C.; Chen, N.-C.; Lai, C.-C.; Liu, Y.-H.; Peng, S.-M.; Chiu, S.-H. Solvent-Free Synthesis of the Smallest Rotaxane Prepared to Date. *Angew. Chem., Int. Ed*. **2008**, *47*, 7475–7478.
(960) Zhang, C.; Li, S.; Zhang, J.; Zhu, K.; Li, N.; Huang, F. Benzo-21-Crown-7/Secondary Dialkylammonium Salt [2]Pseudorotaxane- and [2]Rotaxane-Type Threaded Structures. *Org. Lett.* **2007**, *9*, 5553–5556.
(961) Zhang, C.; Zhu, K.; Li, S.; Zhang, J.; Wang, F.; Liu, M.; Li, N.; Huang, F. Binding of Secondary Dialkylammonium Salts by Pyrido-21-Crown-7. *Tetrahedron Lett.* **2008**, *49*, 6917–6920.
(962) Ashton, P. R.; Chrystal, E. J. T.; Glink, P. T.; Menzer, S.; Schiavo, C.; Spencer, N.; Stoddart, J. F.; Tasker, P. A.; White, A. J. P.; Williams, D. J. Molecular Meccano 6. Pseudorotaxanes Formed Between Secondary Dialkylammonium Salts and Crown Ethers. *Chem. Eur. J*. **1996**, *2*, 709–728.
(963) Williams, A. R.; Northrop, B. H.; Houk, K. N.; Stoddart, J. F; Williams, D. J. The Influence of Constitutional Isomerism and Change on Molecular Recognition Processes. *Chem. Eur. J.* **2004**, *10*, 5406–5421.
(964) Ashton, P. R.; Cantrill, S. J.; Preece, J. A.; Stoddart, J. F.; Wang, Z.-H.; White, A. J. P.; Williams, D. J. Anion-Orchestrated Formation in the Crystalline State of [2]Pseudorotaxane Arrays. *Org. Lett.* **1999**, *1*, 1917–1920.
(965) Cantrill, S. J.; Fulton, D. A.; Heiss, A. M.; Pease, A. R.; Stoddart, J. F.; White, A. J. P.; Williams, D. J. Molecular Meccano 60. The Influence of Macrocyclic Polyether Constitution Upon Ammonium Ion/Crown Ether Recognition Processes. *Chem. Eur. J*. **2000**, *6*, 2274–2287.
(966) Cantrill, S. J.; Fyfe, M. C. T.; Heiss, A. M.; Stoddart, J. F.; White, A. J. P.; Williams, D. J. Tribenzo[27]Crown-9: A New Ring for Dibenzylammonium Rods. *Org. Lett.* **2000**, *2*, 61–64.
(967) Ashton, P. R.; Fyfe, M. C. T.; Schiavo, C.; Stoddart, J. F.; White, A. J. P.; Williams, D. J. A New Slippage Synthesis. *Tetrahedron Lett*. **1998**, *39*, 5455–5458.
(968) Ashton, P. R.; Bartsch, R. A.; Cantrill, S. J.; Hanes, R. E., Jr.; Hickingbottom, S. K.; Lowe, J. N.; Preece, J. A.; Stoddart, J. F.; Talanov, V. S.; Wang, Z.-H. Secondary Dibenzylammonium Ion Binding by [24]Crown-8 and [25]Crown-8 Macrocycles. *Tetrahedron Lett.* **1999**, *40*, 3661–3664.
(969) Ashton, P. R.; Fyfe, M. C. T.; Hickingbottom, S. K.; Stoddart, J. F.; White, A. J. P.; Williams, D. J. Molecular Meccano 43. Hammett Correlations “Beyond the Molecule.” *J. Chem*. *Soc., Perkin Trans*. *2* **1998**, 2117–2128.
(970) Rowan, S. J.; Cantrill, S. J.; Stoddart, J. F. Triphenylphosphonium-Stoppered [2]Rotaxanes. *Org. Lett.* **1999**, *1*, 129–132.
(971) Chang, T.; Heiss, A. M.; Fyfe, M. C. T.; Cantrill, S. J.; Stoddart, J. F.; Pease, A. R.; White, A. J. P.; Rowan, S. J.; Williams, D. J. Ammonium Ion Binding with Pyridine-Containing Crown Ethers. *Org. Lett.* **2000**, *2*, 2947–2950.
(972) Hung, W.-C.; Liao, K.-S.; Liu, Y.-H.; Peng, S.-M.; Chiu, S.-H. Mild and High-Yielding Syntheses of Diethyl Phosphoramidate-Stoppered [2]Rotaxanes. *Org. Lett.* **2004**, *6*, 4183–4186.
(973) Tokunaga, Y.; Yoshioka, M.; Nakamura, T.; Goda, T.; Nakata, R.; Kakuchi, S.; Shimomura, Y. Do Dibenzo[22–30]Crown Ethers Bind Secondary Ammonium Ions to Form Pseudorotaxanes? *Bull. Chem. Soc. Jpn.* **2007**, *80*, 1377–1382.

(974) Ashton, P. R.; Ballardini, R.; Balzani, V.; Gómez-López, M.; Lawrence, S. E.; Martínez-Díaz, M.-V.; Montalti, M.; Piersanti, A.; Prodi, L.; Stoddart, J. F.; Williams, D. J. Molecular Meccano 26. Hydrogen-Bonded Complexes of Aromatic Crown Ethers with (9-Anthracenyl)methylammonium Derivatives. Supramolecular Photochemistry and Photophysics. pH-Controllable Supramolecular Switching. *J. Am. Chem. Soc*. **1997**, *119*, 10641–10651.

(975) Suzaki, Y.; Osakada, K. Formation, Dynamic Behavior, and Chemical Transformation of Pt Complexes with a Rotaxane-Like Structure. *Chem. Asian J.* **2006**, *1*, 331–343.

(976) Chiu, S.-H.; Liao, K.-S.; Su, J.-K. Substituent Effects in the Binding of Bis(4-fluorobenzyl)ammonium Ions by Dianilino[24]Crown-8. *Tetrahedron Lett.* **2004**, *45*, 213–216.

(977) Tokunaga, Y.; Goda, T.; Wakamatsu, N.; Nakata, R.; Shimomura, Y. Effects of Small Structural Changing on the Kinetic and Thermodynamic Stabilities of Pseudorotaxanes. *Heterocycles* **2006**, *68*, 5–10.

(978) Cantrill, S. J.; Fyfe, M. C. T.; Heiss, A. M.; White, A. J. P.; Williams, D. J.; Stoddart, J. F. Rotaxane Construction with a Binaphthol-Derived Crown Ether. *Chem. Commun*. **1999**, 1251–1252.

(979) Bryant, W. S.; Guzei, I. A.; Rheingold, A. L.; Merola, J. S.; Gibson, H. W. A Study of the Complexation of Bis(*m*-phenylene) Crown Ethers and Secondary Ammonium Ions. *J. Org. Chem.* **1998**, *63*, 7634–7639.

(980) Gutmann, V.; Wychera, E. Coordination Reactions in Non Aqueous Solutions—The Role of the Donor Strength. *Inorg. Nucl. Chem. Lett.* **1966**, *2*, 257–260.

(981) Jones, J. W.; Gibson, H. W. Ion Pairing and Host−Guest Complexation in Low Dielectric Constant Solvents. *J. Am. Chem. Soc.* **2003**, *125*, 7001–7004.

(982) Gibson, H. W.; Jones, J. W.; Zakharov, L. N.; Rheingold, A. L.; Slebodnick, C. Complexation Equilibria Involving Salts in Non-Aqueous Solvents: Ion Pairing and Activity Considerations. *Chem. Eur. J.* **2011**, *17*, 3192–3206.

(983) Montalti, M.; Prodi, L. A Supramolecular Assembly Controlled by Anions: Threading and Unthreading of a Pseudorotaxane. *Chem. Commun*. **1998**, 1461–1462.

(984) Clifford, T.; Abushamleh, A.; Busch, D. H. Factors Affecting the Threading of Axle Molecules Through Macrocycles: Binding Constants for Semirotaxane Formation. *Proc. Natl. Acad. Sci. U.S.A.* **2002**, *99*, 4830–4836.

(985) Ashton, P. R.; Ballardini, R.; Balzani, V.; Fyfe, M. C. T.; Gandolfi, M. T.; Martínez-Díaz, M.-V.; Morosini, M.; Schiavo, C.; Shibata, K.; Stoddart, J. F; White, A. J. P.; Williams, D. J. M Meccano 41. Selective Self-Assembly and Acid-Base Controlled De/Rethreading of Pseudorotaxanes Constructed Using Multiple Recognition Motifs. *Chem. Eur. J*. **1998**, *4*, 2332–2341.

(986) Gibson, H. W.; Nagvekar, D. S.; Yamaguchi, N.; Bhattacharjee, S.; Wang, H.; Vergne, M. J.; Hercules, D. M. Polyamide Pseudorotaxanes, Rotaxanes, and Catenanes Based on Bis(5-carboxy-1,3-phenylene)-(3*x*+2)-crown-*x* Ethers. *Macromolecules* **2004**, *37*, 7514–7529.

(987) Tokunaga, Y.; Iwamoto, T.; Nakashima, S.; Shoji, E.; Nakata, R. Electrochemical Properties of 3,5-Diphenylaniline Units Encapsulated Within a Crown Ether. Effects of the Macrocycle's Aromatic Functionality and Ring Size. *Tetrahedron Lett*. **2011**, *52*, 240–243.

(988) Northrop, B. H.; Khan, S. J.; Stoddart, J. F. Kinetically Controlled Self-Assembly of Pseudorotaxanes on Crystallization. *Org. Lett.* **2006**, *8*, 2159–2162.

(989) Hammett, L. P. The Effect of Structure Upon the Reactions of Organic Compounds. Benzene Derivatives. *J. Am. Chem. Soc.* **1937**, *59*, 96–103.

(990) Ueng, S.-H.; Hsueh, S.-Y.; Lai, C.-C.; Liu, Y.-H.; Peng, S.-M.; Chiu, S.-H. Capturing a [*c*2]Daisy Chain Using the Threading-Followed-by-Swelling Approach. *Chem*. *Commun*. **2008**, 817–819.

(991) Ashton, P. R.; Chrystal, E. J. T.; Glink, P. T.; Menzer, S.; Schiavo, C.; Stoddart, J. F.; Tasker, P. A.; Williams, D. J. Doubly Encircled and Double-Stranded Pseudorotaxanes. *Angew. Chem., Int. Ed. Engl*. **1995**, *34*, 1869–1871.

(992) Fyfe, M. C. T.; Glink, P. T.; Menzer, S.; Stoddart, J. F.; White, A. J. P.; Williams, D. J. Anion-Assisted Self-Assembly. *Angew. Chem., Int. Ed. Engl*. **1997**, *36*, 2068–2070.

(993) Ashton, P. R.; Fyfe, M. C. T.; Glink, P. T.; Menzer, S.; Stoddart, J. F.; White, A. J. P.; Williams, D. J. Molecular Meccano 24. Multiply Stranded and Multiply Encircled Pseudorotaxanes. *J. Am. Chem. Soc.* **1997**, *119*, 12514–12524.

(994) Ashton, P. R.; Collins, A. N.; Fyfe, M. C. T.; Menzer, S.; Stoddart, J. F.; Williams, D. J. Supramolecular Weaving. *Angew. Chem., Int. Ed. Engl*. **1997**, *36*, 735–739.

(995) Ashton, P. R.; Fyfe, M. C. T.; Hickingbottom, S. K.; Menzer, S.; Stoddart, J. F.; White, A. J. P.; Williams, D. J. Molecular Meccano 34. Combining Different Hydrogen-Bonding Motifs to Self-Assemble Interwoven Superstructures. *Chem. Eur. J.* **1998**, *4*, 577–589.

(996) Fyfe, M. C. T.; Stoddart, J. F.; Williams, D. J. X-ray Crystallographic Studies on the Noncovalent Syntheses of Supermolecules. *Struct. Chem.* **1999**, *10*, 243–259.

(997) Fyfe, M. C. T.; Stoddart, J. F. Interwoven Supramolecular Arrays via the Noncovalent Polymerization of Pseudorotaxanes. *Coord. Chem. Rev.* **1999**, *183*, 139–155.

(998) Chiu, S.-H.; Pease A. R.; Stoddart, J. F.; White, A. J. P.; Williams, D. J. A Ring-in-Ring Complex. *Angew. Chem., Int. Ed*. **2002**, *41*, 270–274.

(999) Ashton, P. R.; Fyfe, M. C. T.; Martínez-Díaz, M.-V.; Menzer, S.; Schiavo, C.; Stoddart, J. F.; White, A. J. P.; Williams, D. J. Molecular Meccano 39. Doubly Docked Pseudorotaxanes. *Chem. Eur. J*. **1998**, *4*, 1523–1534.

(1000) Ashton, P. R.; Collins, A. N.; Fyfe, M. C. T.; Glink, P. T.; Menzer, S.; Stoddart, J. F.; Williams, D. J. An Interwoven Supramolecular Cage. *Angew. Chem., Int. Ed. Engl*. **1997**, *36*, 59–62.

(1001) Feiters, M. C.; Fyfe, M. C. T.; Martínez-Díaz, M.-V.; Menzer, S.; Nolte, R. J. M.; Stoddart, J. F.; van Kan, P. J. M.; Williams, D. J. A Supramolecular Analog of the Photosynthetic Special Pair. *J. Am. Chem. Soc.* **1997**, *119*, 8119–8120

(1002) Zhang, Z.-J.; Zhang, H.-Y.; Wang, H.; Liu, Y. A Twin-Axial Hetero[7]rotaxane. *Angew. Chem., Int. Ed*. **2011**, *50*, 10834–10838.

(1003) Chuang, C.-J.; Li, W.-S.; Lai, C.-C.; Liu, Y.-H.; Peng, S.-M.; Chao, I.; Chiu, S.-H. A Molecular Cage-Based [2]Rotaxane That Behaves as a Molecular Muscle. *Org. Lett.* **2009**, *11*, 385–388.

(1004) Kawasaki, H.; Kihara, N.; Takata, T. High Yielding and Practical Synthesis of Rotaxanes by Acylative End-Capping Catalyzed by Tributylphosphine. *Chem. Lett*. **1999**, 1015–1016.

(1005) Takata, T.; Kawasaki, H.; Asai, S.; Furusho, Y.; Kihara, N. Conjugate Addition-Approach to End-Capping Pseudorotaxanes for Rotaxane Synthesis. *Chem. Lett*. **1999**, 223–224.

(1006) Giguère, J.-B.; Thibeault, D.; Cronier, F.; Marois, J.-S.; Auger, M.; Morin, J.-F. Synthesis of [2]- and [3]Rotaxanes Through Sonogashira Coupling. *Tetrahedron Lett.* **2009**, *50*, 5497–5500.

(1007) Hsueh, S.-Y.; Cheng, K.-W.; Lai, C.-C.; Chiu, S.-H. Efficient Solvent-Free Syntheses of [2]- and [4]Rotaxanes. *Angew. Chem., Int. Ed*. **2008**, *47*, 4436–4439.

(1008) Ashton, P. R.; Glink, P. T.; Stoddart, J. F.; Tasker, P. A.; White, A. J. P.; Williams, D. J. Molecular Meccano 7. Self-Assembling [2]- and [3]Rotaxanes From Secondary Dialkylammonium Salts and Crown Ethers. *Chem. Eur. J*. **1996**, *2*, 729–736.

(1009) Cao, J.; Fyfe, M. C. T.; Stoddart, J. F.; Cousins, G. R. L.; Glink, P. T. Molecular Meccano 55. Molecular Shuttles by the

Protecting Group Approach. *J. Org. Chem*. **2000**, *65*, 1937–1946.
(1010) Tokunaga, Y.; Kakuchi, S.; Akasaka, K.; Nishikawa, N.; Shimomura, Y.; Isa, K.; Seo, T. A High-Yielding and Convenient Synthesis of Rotaxane Based on an Ester Forming Capping Methodology. *Chem. Lett.* **2002**, 810–811.
(1011) Furusho, Y.; Sasabe, H.; Natsui, D.; Murakawa, K.-I.; Takata, T.; Harada, T. Synthesis of [2]- and [3]Rotaxanes by an End-Capping Approach Utilizing Urethane Formation. *Bull. Chem. Soc. Jpn.* **2004**, *77*, 179–185.
(1012) Tokunaga, Y.; Kawai, N.; Shimomura, Y. Using Ruthenium-Catalysed Propargylic Substitutions for the Efficient Syntheses of Rotaxanes. *Tetrahedron Lett.* **2007**, *48*, 4995–4998.
(1013) Zehnder, D. W.; Smithrud, D. B. Facile Synthesis of Rotaxanes Through Condensation Reactions of DCC-[2]Rotaxanes. *Org. Lett.* **2001**, *3*, 2485–2487.
(1014) Coutrot, F.; Busseron, E. A New Glycorotaxane Molecular Machine Based on an Anilinium and a Triazolium Station. *Chem. Eur. J.* **2008**, *14*, 4784–4787.
(1015) Tachibana, Y.; Kawasaki, H.; Kihara, N.; Takata, T. Sequential *O*- and *N*-Acylation Protocol for High-Yield Preparation and Modification of Rotaxanes: Synthesis, Functionalization, Structure, and Intercomponent Interaction of Rotaxanes. *J. Org. Chem.* **2006**, *71*, 5093–5104.
(1016) Huisgen, R. 1,3-Dipolar Cycloadditions. Past and Future. *Angew. Chem., Int. Ed. Engl*. **1963**, *2*, 565–598.
(1017) Huisgen, R. Kinetics and Mechanism of 1,3-Dipolar Cycloadditions. *Angew. Chem., Int. Ed. Engl*. **1963**, *2*, 633–696.
(1018) Wittig, G.; Krebs, A. Zur Existenz Niedergliedriger Cycloalkine, I. *Chem*. *Ber*. **1961**, *94*, 3360–3275.
(1019) Agard, N. J.; Prescher, J. A.; Bertozzi, C. R. A Strain-Promoted [3 + 2] Azide−Alkyne Cycloaddition for Covalent Modification of Biomolecules in Living Systems. *J. Am. Chem. Soc.* **2004**, *126*, 15046–15047.
(1020) Wang, X.-Y.; Han, J.-M.; Pei, J. Energy Transfer and Concentration-Dependent Conformational Modulation: A Porphyrin-Containing [3]Rotaxane. *Chem. Asian J.* **2012**, *7*, 2429–2437.
(1021) Zheng, H.; Zhou, W.; Lv, J.; Yin, X.; Li, Y.; Liu, H.; Li, Y. A Dual-Response [2]Rotaxane Based on a 1,2,3-Triazole Ring as a Novel Recognition Station. *Chem. Eur. J.* **2009**, *15*, 13253–13262.
(1022) Jiang, Y.; Guo, J.-B.; Chen, C.-F. A New [3]Rotaxane Molecular Machine Based on a Dibenzylammonium Ion and a Triazolium Station. *Org. Lett.* **2010**, *12*, 4248–4251.
(1023) Yu, G.; Suzaki, Y.; Abe, T.; Osakada, K. Organometallic Rotaxanes with a Triazole Group in the Axle Component and Their Behavior as Ligands of Pt^{II} Complexes. *Chem. Asian J.* **2012**, *7*, 207–213.
(1024) Matsumura, T.; Ishiwari, F.; Koyama, Y.; Takata, T. C−C Bond-Forming Click Synthesis of Rotaxanes Exploiting Nitrile *N*-Oxide. *Org. Lett.* **2010**, *12*, 3828–3831.
(1025) Yuki, T.; Koyama, Y.; Matsumura, T.; Takata, T. Click Annulation of Pseudo[2]rotaxane to [2]Catenane Exploiting Homoditopic Nitrile *N*-Oxide. *Org. Lett.* **2013**, *15*, 4438–4441.
(1026) Sasabe, H.; Kihara, N.; Furusho, Y.; Mizuno, K.; Ogawa, A.; Takata, T. End-Capping of a Pseudorotaxane via Diels-Alder Reaction for the Construction of C_{60}-Terminated [2]Rotaxanes. *Org. Lett.* **2004**, *6*, 3957–3960.
(1027) Kihara, N.; Nakakoji, N.; Takata, T. Tributylphosphine-Catalyzed Acylation of Alcohol by Active Ester Directed Toward Effective End-Capping of Pseudorotaxane Consisting of Ammonium Group and Crown Ether. *Chem*. *Lett*. **2002**, 924–925.
(1028) Watanabe, N.; Yagi, T.; Kihara, N.; Takata, T. Highly Efficient Synthesis of [3]- and [5]-Rotaxanes Consisting of Crown Ether and a Sec-Ammonium Salt. *Chem*. *Commun*. **2002**, 2720–2721.
(1029) Tachibana, Y.; Kihara, N.; Furusho, Y.; Takata, T. Is the *tert*-Butyl Group Bulky Enough to End-Cap a Pseudorotaxane with a 24-Crown-8-Ether Wheel? *Org. Lett.* **2004**, *6*, 4507–4509.
(1030) Kihara, N.; Hashimoto, M.; Takata, T. Redox Behavior of Ferrocene-Containing Rotaxane: Transposition of the Rotaxane Wheel by Redox Reaction of a Ferrocene Moiety Tethered at the End of the Axle. *Org. Lett.* **2004**, *6*, 1693–1696.
(1031) Sato, T.; Takata, T. Rotaxane Axle as an Effective Scaffold: Synthesis of Functionalized [3]Rotaxane and Connection of the Wheel Components Arranged on the Axle. *Tetrahedron Lett.* **2007**, *48*, 2797–2801.
(1032) Nakazono, K.; Kuwata, S.; Takata, T. Crown Ether–*tert*-Ammonium Salt Complex Fixed as Rotaxane and Its Derivation to Nonionic Rotaxane. *Tetrahedron Lett.* **2008**, *49*, 2397–2401.
(1033) Jiang, W.; Winkler, H. D. F.; Schalley, C. A. Integrative Self-Sorting: Construction of a Cascade-Stoppered Hetero[3]rotaxane. *J. Am. Chem. Soc.* **2008**, *130*, 13852–13853.
(1034) Zheng, B.; Zhang, M.; Yan, X.; Huang, F. Threaded Structures Based on the Benzo-21-Crown-7/Secondary Ammonium Salt Recognition Motif Using Esters as End Groups. *Org. Biomol. Chem.* **2013**, *11*, 3880–3885.
(1035) Zheng, B.; Zhang, M.; Dong, S.; Yan, X.; Xue, M. Benzo-21-Crown-7/Secondary Ammonium Salt [2]Rotaxanes with Fluoro/Chlorocarbon Blocking Groups. *Org. Lett.* **2013**, *15*, 3538–3541.
(1036) Sandanayaka, A. S. D.; Sasabe, H.; Araki, Y.; Furusho, Y.; Ito, O.; Takata, T. Photoinduced Electron-Transfer Processes Between [C60]Fullerene and Triphenylamine Moieties Tethered by Rotaxane Structures. Through-Space Electron Transfer via Excited Triplet States of [60]Fullerene. *J. Phys. Chem. A* **2004**, *108*, 5145–5155.
(1037) Rajkumar, G. A.; Sandanayaka, A. S. D.; Ikeshita, K.-I.; Araki, Y.; Furusho, Y.; Takata, T.; Ito, O. Prolongation of the Lifetime of the Charge-Separated State at Low Temperatures in a Photoinduced Electron-Transfer System of [60]Fullerene and Ferrocene Moieties Tethered by Rotaxane Structures. *J. Phys. Chem. B* **2006**, *110*, 6516–6525.
(1038) Marois, J.-S.; Cantin, K.; Desmarais, A.; Morin, J.-F. [3]Rotaxane−Porphyrin Conjugate as a Novel Supramolecular Host for Fullerenes. *Org. Lett*. **2008**, *10*, 33–36.
(1039) Marois, J.-S.; Morin, J.-F. Synthesis and Surface Self-Assembly of [3]Rotaxane−Porphyrin Conjugates: Toward the Development of a Supramolecular Surface Tweezer for C_{60}. *Langmuir* **2008**, *24*, 10865–10873.
(1040) Fulton, D. A.; Cantrill, S. J.; Fyfe, M. C. T.; Stoddart, J. F.; White, A. J. P.; Williams, D. J. A New Protocol for Rotaxane Synthesis. *Tetrahedron Lett.* **1999**, *40*, 3669–3672.
(1041) Rowan, S. J.; Stoddart, J. F. Precision Molecular Grafting: Exchanging Surrogate Stoppers in [2]Rotaxanes. *J. Am. Chem. Soc.* **2000**, *122*, 164–165.
(1042) Rowan, S. J.; Stoddart, J. F. Surrogate-Stoppered [2]Rotaxanes: A New Route to Larger Interlocked Architectures. *Polym. Advan. Technol.* **2002**, *13*, 777–787.
(1043) Sasabe, H.; Kihara, N.; Mizuno, K.; Ogawa, A.; Takata, T. Efficient Synthesis of [2]- and Higher Order Rotaxanes via the Transition Metal-Catalyzed Hydrosilylation of Alkyne. *Tetrahedron Lett.* **2005**, *46*, 3851–3853.
(1044) Tokunaga, Y.; Nakashima, S.; Iwamoto, T.; Gambayashi, K.; Hisada, K.; Hoshi, T. Preparation and Photochemical Properties of [2]Rotaxanes Containing an Aniline Moiety Encapsulated by Crown Ethers. *Heterocycles* **2010**, *80*, 819.
(1045) Friščić, T. Supramolecular Concepts and New Techniques in Mechanochemistry: Cocrystals, Cages, Rotaxanes, Open Metal–Organic Frameworks. *Chem. Soc. Rev*. **2012**, *41*, 3493–3510.
(1046) Beyer, M. K.; Clausen-Schaumann, H. Mechanochemistry: The Mechanical Activation of Covalent Bonds. *Chem. Rev.* **2005**, *105*, 2921–2948.

(1047) Wang, G.-W. Mechanochemical Organic Synthesis. *Chem. Soc. Rev.* **2013**, *42*, 7668–7700.
(1048) Hsu, C.-C.; Lai, C.-C.; Chiu, S.-H. Using Diels-Alder Reactions to Synthesize [2]Rotaxanes Under Solvent-Free Conditions. *Tetrahedron* **2009**, *65*, 2824–2829.
(1049) Chen, P.-N.; Lai, C.-C.; Chiu, S.-H. Self-Sorting Under Solvent-Free Conditions: One-Pot Synthesis of a Hetero[3]rotaxane. *Org. Lett.* **2011**, *13*, 4660–4663.
(1050) Zheng, H.; Li, Y.; Zhou, C.; Li, Y.; Yang, W.; Zhou, W.; Zuo, Z.; Liu, H. Synthesis of a [2]Rotaxane Incorporating a “Magic Sulfur Ring” by the Thiol-Ene Click Reaction. *Chem. Eur. J.* **2011**, *17*, 2160–2167.
(1051) Zhou, W.; Zheng, H.; Li, Y.; Liu, H.; Li, Y. Synthesis of Sulfuric Macrocycles and a Rotaxane Through Thiol-Yne Click and Dithiol Coupling Reactions. *Org. Lett.* **2010**, *12*, 4078–4081.
(1052) Glink, P. T.; Oliva, A. I.; Stoddart, J. F.; White, A. J. P.; Williams, D. J. Template-Directed Synthesis of a [2]Rotaxane by the Clipping Under Thermodynamic Control of a Crown Ether Like Macrocycle Around a Dialkylammonium Ion. *Angew. Chem., Int. Ed*. **2001**, *40*, 1870–1875.
(1053) Hsueh, S.-Y.; Ko, J.-L.; Lai, C.-C.; Liu, Y.-H.; Peng, S.-M.; Chiu, S.-H. A Metal-Free “Threading-Followed-by-Shrinking” Protocol for Rotaxane Synthesis. *Angew. Chem., Int. Ed*. **2011**, *50*, 6643–6646.
(1054) Wang, L.-Y.; Ko, J.-L.; Lai, C.-C.; Liu, Y.-H.; Peng, S.-M.; Chiu, S.-H. Using “Threading Followed by Shrinking” to Synthesize Highly Stable Dialkylammonium-Ion-Based Rotaxanes. *Chem. Eur. J.* **2013**, *19*, 8850–8860.
(1055) Desiraju, G. R.; Ho, P. S.; Kloo, L.; Legon, A. C.; Marquardt, R.; Metrangolo, P.; Politzer, P.; Resnati, G.; Rissanen, K. Definition of the Halogen Bond (IUPAC Recommendations 2013). *Pure Appl. Chem*. **2013**, *85*, 1711–1713.
(1056) Metrangolo, P.; Neukirch, H.; Pilati, T.; Resnati, G. Halogen Bonding Based Recognition Processes: A World Parallel to Hydrogen Bonding. *Acc. Chem. Res.* **2005**, *38*, 386–395.
(1057) Kilah, N. L.; Wise, M. D.; Serpell, C. J.; Thompson, A. L.; White, N. G.; Christensen, K. E.; Beer, P. D. Enhancement of Anion Recognition Exhibited by a Halogen-Bonding Rotaxane Host System. *J. Am. Chem. Soc.* **2010**, *132*, 11893–11895.
(1058) Serpell, C. J.; Kilah, N. L.; Costa, P. J.; Félix, V.; Beer, P. D. Halogen Bond Anion Templated Assembly of an Imidazolium Pseudorotaxane. *Angew. Chem., Int. Ed*. **2010**, *49*, 5322–5326.
(1059) Caballero, A.; Zapata, F.; White, N. G.; Costa, P. J.; Félix, V.; Beer, P. D. A Halogen-Bonding Catenane for Anion Recognition and Sensing. *Angew. Chem., Int. Ed*. **2012**, *51*, 1876–1880.
(1060) Gilday, L. C.; Lang, T.; Caballero, A.; Costa, P. J.; Félix, V.; Beer, P. D. A Catenane Assembled Through a Single Charge-Assisted Halogen Bond. *Angew. Chem., Int. Ed*. **2013**, *52*, 4356–4360.
(1061) Mullaney, B. R.; Thompson, A. L.; Beer, P. D. An All-Halogen Bonding Rotaxane for Selective Sensing of Halides in Aqueous Media. *Angew. Chem., Int. Ed*. **2014**, *53*, 11458–11462.
(1062) Gilday, L. C.; Beer, P. D. Halogen- and Hydrogen-Bonding Catenanes for Halide-Anion Recognition. *Chem. Eur. J.* **2014**, *20*, 8379–8385.
(1063) Caballero, A.; Swan, L.; Zapata, F.; Beer, P. D. Iodide-Induced Shuttling of a Halogen- and Hydrogen-Bonding Two-Station Rotaxane. *Angew. Chem., Int. Ed*. **2014**, *53*, 11854–11858.
(1064) Cornes, S. P.; Davies, C. H.; Blyghton, D.; Sambrook, M. R.; Beer, P. D. Contrasting Anion Recognition Behaviour Exhibited by Halogen and Hydrogen Bonding Rotaxane Hosts. *Org. Biomol. Chem.* **2015**, *13*, 2582–2587.
(1065) Robinson, S. W.; Mustoe, C. L.; White, N. G.; Brown, A.; Thompson, A. L.; Kennepohl, P.; Beer, P. D. Evidence for Halogen Bond Covalency in Acyclic and Interlocked Halogen-Bonding Receptor Anion Recognition. *J. Am. Chem. Soc.* **2015**, *137*, 499–507.
(1066) Dietrich, B. Design of Anion Receptors: Applications. *Pure Appl. Chem.* **1993**, *65*, 1457–1464.
(1067) Bianchi, A.; Bowman-James, K.; Garcia-Espana, E. *Supramolecular Chemistry of Anions*; Wiley-VCH: Weinheim, 1997.
(1068) Beer, P. D.; Gale, P. A. Anion Recognition and Sensing: The State of the Art and Future Perspectives. *Angew. Chem., Int. Ed*. **2001**, *40*, 486–516.
(1069) Sessler, J. L.; Gale, P. A.; Cho, W.-S. *Anion Receptor Chemistry*; RSC Publishing: Cambridge, 2006.
(1070) Vilar, R. Anion-Templated Synthesis. *Angew. Chem., Int. Ed*. **2003**, *42*, 1460–1477.
(1071) Gimeno, N.; Vilar, R. Anions as Templates in Coordination and Supramolecular Chemistry. *Coord. Chem. Rev.* **2006**, *250*, 3161–3189.
(1072) Gale, P. A. Anion Receptor Chemistry. *Chem. Commun.* **2011**, *47*, 82–86.
(1073) Antonisse, M. M. G.; Reinhoudt, D. N. Neutral Anion Receptors: Design and Application. *Chem*. *Commun*. **1998**, 443–448.
(1074) Dydio, P.; Lichosyt, D.; Jurczak, J. Amide- and Urea-Functionalized Pyrroles and Benzopyrroles as Synthetic, Neutral Anion Receptors. *Chem. Soc. Rev.* **2011**, *40*, 2971–2985.
(1075) Amendola, V.; Esteban-Gómez, D.; Fabbrizzi, L.; Licchelli, M. What Anions Do to N−H-Containing Receptors. *Acc. Chem. Res.* **2006**, *39*, 343–353.
(1076) Gale, P. A. Structural and Molecular Recognition Studies with Acyclic Anion Receptors. *Acc. Chem. Res.* **2006**, *39*, 465–475.
(1077) Kang, S. O.; Begum, R. A.; Bowman-James, K. Amide-Based Ligands for Anion Coordination. *Angew. Chem., Int. Ed*. **2006**, *45*, 7882–7894.
(1078) Kang, S. O.; Hossain, M. A.; Bowman-James, K. Influence of Dimensionality and Charge on Anion Binding in Amide-Based Macrocyclic Receptors. *Coord. Chem. Rev.* **2006**, *250*, 3038–3052.
(1079) Sessler, J. L.; Cyr, M.; Furuta, H.; Král, V.; Mody, T.; Morishima, T.; Shionoya, M.; Weghorn, S. Anion Binding: A New Direction in Porphyrin-Related Research. *Pure Appl. Chem.* **1993**, *65*, 393–398.
(1080) Sessler, J. L.; Camiolo, S.; Gale, P. A. Pyrrolic and Polypyrrolic Anion Binding Agents. *Coord. Chem. Rev.* **2003**, *240*, 17–55.
(1081) Amendola, V.; Fabbrizzi, L.; Mosca, L. Anion Recognition by Hydrogen Bonding: Urea-Based Receptors. *Chem. Soc. Rev.* **2010**, *39*, 3889–3915.
(1082) Beer, P. D.; Sambrook, M. R.; Curiel, D. Anion-Templated Assembly of Interpenetrated and Interlocked Structures. *Chem*. *Commun*. **2006**, 2105–2117.
(1083) Vickers, M. S.; Beer, P. D. Anion Templated Assembly of Mechanically Interlocked Structures. *Chem. Soc. Rev.* **2007**, *36*, 211–225.
(1084) Lankshear, M. D.; Beer, P. D. Interweaving Anion Templation. *Acc. Chem. Res.* **2007**, *40*, 657–668.
(1085) Mullen, K. M.; Beer, P. D. Sulfate Anion Templation of Macrocycles, Capsules, Interpenetrated and Interlocked Structures. *Chem. Soc. Rev.* **2009**, *38*, 1701–1713.
(1086) Chmielewski, M. J.; Davis, J. J.; Beer, P. D. Interlocked Host Rotaxane and Catenane Structures for Sensing Charged Guest Species via Optical and Electrochemical Methodologies. *Org. Biomol. Chem.* **2009**, *7*, 415–424.
(1087) Caballero, A.; Zapata, F.; Beer, P. D. Interlocked Host Molecules for Anion Recognition and Sensing. *Coord. Chem. Rev.* **2013**, *257*, 2434–2455.
(1088) Spence, G. T.; Beer, P. D. Expanding the Scope of the Anion Templated Synthesis of Interlocked Structures. *Acc. Chem. Res.* **2013**, *46*, 571–586.

(1089) Hubner, G.; Glaser, J.; Seel, C.; Vögtle, F. High-Yielding Rotaxane Synthesis with an Anion Template. *Angew. Chem., Int. Ed*. **1999**, *38*, 383–386.
(1090) Reuter, C.; Wienand, W.; Hübner, G. M.; Seel, C.; Vögtle, F. High-Yield Synthesis of Ester, Carbonate, and Acetal Rotaxanes by Anion Template Assistance and Their Hydrolytic Dethreading. *Chem. Eur. J.* **1999**, *5*, 2692–2697.
(1091) Hubner, G. M.; Reuter, C.; Seel, C.; Vögtle, F. Rotaxane Synthesis via Nucleophilic Substitution Reactions. The Trapping of Electrophilic Threads by Organic Anion-Wheel Complexes. *Synthesis* **2000**, 103–108.
(1092) Seel, C.; Vögtle, F. Templates, “Wheeled Reagents,” and a New Route to Rotaxanes by Anion Complexation: The Trapping Method. *Chem. Eur. J.* **2000**, *6*, 21–24.
(1093) Schalley, C. A.; Silva, G.; Nising, C. F.; Linnartz, P. Analysis and Improvement of an Anion-Templated Rotaxane Synthesis. *Helv. Chim. Acta* **2002**, *85*, 1578–1596.
(1094) Langton, M. J.; Beer, P. D. Rotaxane and Catenane Host Structures for Sensing Charged Guest Species. *Acc. Chem. Res.* **2014**, *47*, 1935–1949.
(1095) Wisner, J. A.; Beer, P. D.; Drew, M. G. B. A Demonstration of Anion Templation and Selectivity in Pseudorotaxane Formation. *Angew. Chem., Int. Ed*. **2001**, *40*, 3606–3609.
(1096) Sambrook, M. R.; Beer, P. D.; Wisner, J. A.; Paul, R. L.; Cowley, A. R.; Szemes, F.; Drew, M. G. B. Anion-Templated Assembly of Pseudorotaxanes: Importance of Anion Template, Strength of Ion-Pair Thread Association, and Macrocycle Ring Size. *J. Am. Chem. Soc.* **2005**, *127*, 2292–2302.
(1097) Curiel, D.; Beer, P. D.; Paul, R. L.; Cowley, A. R.; Sambrook, M. R.; Szemes, F. Halide Anion Directed Assembly of Luminescent Pseudorotaxanes. *Chem. Commun*. **2004**, 1162–1163.
(1098) Sambrook, M. R.; Curiel, D.; Hayes, E. J.; Beer, P. D.; Pope, S. J. A.; Faulkner, S. Sensitised Near Infrared Emission From Lanthanides via Anion-Templated Assembly of D-F Heteronuclear [2]Pseudorotaxanes. *New J. Chem.* **2006**, *30*, 1133–1136.
(1099) Hancock, L. M.; Marchi, E.; Ceroni, P.; Beer, P. D. Anion Sensing in Aqueous Media by Photo-Active Transition-Metal Bipyridyl Rotaxanes. *Chem. Eur. J.* **2012**, *18*, 11277–11283.
(1100) Lehr, J.; Lang, T.; Blackburn, O. A.; Barendt, T. A.; Faulkner, S.; Davis, J. J.; Beer, P. D. Anion Sensing by Solution- and Surface-Assembled Osmium(II) Bipyridyl Rotaxanes. *Chem. Eur. J.* **2013**, *19*, 15898–15906.
(1101) Lankshear, M. D.; Evans, N. H.; Bayly, S. R.; Beer, P. D. Anion-Templated Calix[4]arene-Based Pseudorotaxanes and Catenanes. *Chem. Eur. J.* **2007**, *13*, 3861–3870.
(1102) Phipps, D. E.; Beer, P. D. A [2]Catenane Containing an Upper-Rim Functionalized Calix[4]arene for Anion Recognition. *Tetrahedron Lett.* **2009**, *50*, 3454–3457.
(1103) Wisner, J. A.; Beer, P. D.; Drew, M. G. B.; Sambrook, M. R. Anion-Templated Rotaxane Formation. *J. Am. Chem. Soc.* **2002**, *124*, 12469–12476.
(1104) Sambrook, M. R.; Beer, P. D.; Wisner, J. A.; Paul, R. L.; Cowley, A. R. Anion-Templated Assembly of a [2]Catenane. *J. Am. Chem. Soc.* **2004**, *126*, 15364–15365.
(1105) Hancock, L. M.; Beer, P. D. Chloride Recognition in Aqueous Media by a Rotaxane Prepared via a New Synthetic Pathway. *Chem. Eur. J.* **2009**, *15*, 42–44.
(1106) Hancock, L. M.; Gilday, L. C.; Carvalho, S.; Costa, P. J.; Félix, V.; Serpell, C. J.; Kilah, N. L.; Beer, P. D. Rotaxanes Capable of Recognising Chloride in Aqueous Media. *Chem. Eur. J.* **2010**, *16*, 13082–13094.
(1107) Hancock, L. M.; Gilday, L. C.; Kilah, N. L.; Serpell, C. J.; Beer, P. D. A New Synthetic Route to Chloride Selective [2]Catenanes. *Chem. Commun.* **2011**, *47*, 1725–1727.
(1108) Brown, A.; Langton, M. J.; Kilah, N. L.; Thompson, A. L.; Beer, P. D. Chloride-Anion-Templated Synthesis of a Strapped-Porphyrin-Containing Catenane Host System. *Chem. Eur. J.* **2015**, *21*, 17664–17675.
(1109) Evans, N. H.; Serpell, C. J.; Beer, P. D. A Meta-Xylenediamide Macrocycle Containing Rotaxane Anion Host System Constructed by a New Synthetic Clipping Methodology. *New J. Chem.* **2011**, *35*, 2047–2053.
(1110) Langton, M. J.; Beer, P. D. Sulfate-Selective Binding and Sensing of a Fluorescent [3]Rotaxane Host System. *Chem. Eur. J.* **2012**, *18*, 14406–14412.
(1111) Evans, N. H.; Serpell, C. J.; Beer, P. D. A Redox-Active [3]Rotaxane Capable of Binding and Electrochemically Sensing Chloride and Sulfate Anions. *Chem. Commun.* **2011**, *47*, 8775–8777.
(1112) Allain, C.; Beer, P. D.; Faulkner, S.; Jones, M. W.; Kenwright, A. M.; Kilah, N. L.; Knighton, R. C.; Sørensen, T. J.; Tropiano, M. Lanthanide Appended Rotaxanes Respond to Changing Chloride Concentration. *Chem. Sci.* **2012**, *4*, 489–493.
(1113) Li, Y.; Mullen, K. M.; Sardinha, J.; Félix, V.; Beer, P. D. Clipping and Stoppering Anion Templated Synthesis of a [2]Rotaxane Host System. *Dalton Trans.* **2011**, *40*, 12180–12190.
(1114) Lankshear, M. D.; Cowley, A. R.; Beer, P. D. Cooperative and Receptor for Ion-Pairs. *Chem*. *Commun*. **2006**, 612–614.
(1115) Lankshear, M. D.; Dudley, I. M.; Chan, K.-M.; Beer, P. D. Tuning the Strength and Selectivity of Ion-Pair Recognition Using Heteroditopic Calix[4]arene-Based Receptors. *New J. Chem.* **2007**, *31*, 684–690.
(1116) Lankshear, M. D.; Dudley, I. M.; Chan, K.-M.; Cowley, A. R.; Santos, S. M.; Félix, V.; Beer, P. D. Cooperative and Ion-Pair Recognition by Heteroditopic Calix[4]diquinone Receptors. *Chem. Eur. J.* **2008**, *14*, 2248–2263.
(1117) Knighton, R. C.; Beer, P. D. Axle Component Separated Ion-Pair Recognition by a Neutral Heteroditopic [2]Rotaxane. *Chem. Commun.* **2014**, *50*, 1540–1542.
(1118) Leontiev, A. V.; Jemmett, C. A.; Beer, P. D. Anion Recognition and Cation-Induced Molecular Motion in a Heteroditopic [2]Rotaxane. *Chem. Eur. J.* **2010**, *17*, 816–825.
(1119) Andrievsky, A.; Ahuis, F.; Sessler, J. L.; Vögtle, F.; Gudat, D.; Moini, M. Bipyrrole-Based [2]Catenane: A New Type of Anion Receptor. *J. Am. Chem. Soc.* **1998**, *120*, 9712–9713.
(1120) Mercurio, J. M.; Tyrrell, F.; Cookson, J.; Beer, P. D. Neutral [2]Rotaxane Host Systems That Recognise Halide Anions in Aqueous Solvent Mixtures. *Chem. Commun.* **2013**, *49*, 10793–10795.
(1121) Lim, J. Y. C.; Cunningham, M. J.; Davis, J. J.; Beer, P. D. Neutral Redox-Active Hydrogen- and Halogen-Bonding [2]Rotaxanes for the Electrochemical Sensing of Chloride. *Dalton Trans.* **2014**, *43*, 17274–17282.
(1122) Hu, J.; Chen, L.; Shen, J.; Luo, J.; Deng, P.; Ren, Y.; Zeng, H.; Feng, W.; Yuan, L. Convergent Heteroditopic Cyclo[6]aramides as Macrocyclic Ion-Pair Receptors for Constructing [2]Pseudorotaxanes. *Chem. Commun.* **2014**, *50*, 8024.
(1123) Ghosh, P.; Mermagen, O.; Schalley, C. A. Novel Template Effect for the Preparation of [2]Rotaxanes with Functionalised Centre Pieces. *Chem*. *Commun*. **2002**, 2628–2629.
(1124) Keaveney, C. M.; Leigh, D. A. Shuttling Through Anion Recognition. *Angew. Chem., Int. Ed*. **2004**, *43*, 1222–1224.
(1125) He, J. J.; Quiocho, F. A. A Nonconservative Serine to Cysteine Mutation in the Sulfate-Binding Protein, a Transport Receptor. *Science* **1991**, *251*, 1479–1481.
(1126) Chmielewski, M. J.; Zhao, L.; Brown, A.; Curiel, D.; Sambrook, M. R.; Thompson, A. L.; Santos, S. M.; Félix, V.; Davis, J. J.; Beer, P. D. Sulfate Anion Templation of a Neutral Pseudorotaxane Assembly Using an Indolocarbazole Threading Component. *Chem*. *Commun*. **2008**, 3154–3156.
(1127) Huang, B.; Santos, S. M.; Félix, V.; Beer, P. D. Sulfate Anion-Templated Assembly of a [2]Catenane. *Chem*. *Commun*. **2008**, 4610–4612.
(1128) Curiel, D.; Beer, P. D. Anion Directed Synthesis of a Hydrogensulfate Selective Luminescent Rotaxane. *Chem*. *Commun*. **2005**, 1909–1911.

(1129) Langton, M. J.; Duckworth, L. C.; Beer, P. D. Nitrate Anion Templated Assembly of a [2]Rotaxane for Selective Nitrate Recognition in Aqueous Solvent Mixtures. *Chem. Commun.* **2013**, *49*, 8608–8610.
(1130) Chae, M. K.; Suk, J.-M.; Jeong, K.-S. A Catenated Anion Receptor Based on Indolocarbazole. *Tetrahedron Lett.* **2010**, *51*, 4240–4242.
(1131) Li, Y.; Mullen, K. M.; Claridge, T. D. W.; Costa, P. J.; Félix, V.; Beer, P. D. Sulfate Anion Templated Synthesis of a Triply Interlocked Capsule. *Chem*. *Commun*. **2009**, 7134–7136.
(1132) Fukuda, M.; Sekiya, R.; Kuroda, R. A Quadruply Stranded Metallohelicate and Its Spontaneous Dimerization Into an Interlocked Metallohelicate. *Angew. Chem., Int. Ed*. **2008**, *47*, 706–710.
(1133) Sekiya, R.; Fukuda, M.; Kuroda, R. Anion-Directed Formation and Degradation of an Interlocked Metallohelicate. *J. Am. Chem. Soc.* **2012**, *134*, 10987–10997.
(1134) Brown, A.; Mullen, K. M.; Ryu, J.; Chmielewski, M. J.; Santos, S. M.; Felix, V.; Thompson, A. L.; Warren, J. E.; Pascu, S. I.; Beer, P. D. Interlocked Host Anion Recognition by an Indolocarbazole-Containing [2]Rotaxane. *J. Am. Chem. Soc.* **2009**, *131*, 4937–4952.
(1135) Langton, M. J.; Serpell, C. J.; Beer, P. D. Anion Recognition in Water: Recent Advances From a Supramolecular and Macromolecular Perspective. *Angew. Chem., Int. Ed*. **2016**, *55*, 1974–1987.
(1136) Langton, M. J.; Robinson, S. W.; Marques, I.; Félix, V.; Beer, P. D. Halogen Bonding in Water Results in Enhanced Anion Recognition in Acyclic and Rotaxane Hosts. *Nature Chem.* **2014**, *6*, 1039–1043.
(1137) Rezanka, M.; Langton, M. J.; Beer, P. D. Anion Recognition in Water by a Rotaxane Containing a Secondary Rim Functionalised Cyclodextrin Stoppered Axle. *Chem. Commun.* **2015**, *51*, 4499–4502.
(1138) Langton, M. J.; Marques, I.; Robinson, S. W.; Félix, V.; Beer, P. D. Iodide Recognition and Sensing in Water by a Halogen-Bonding Ruthenium(II)-Based Rotaxane. *Chem. Eur. J.* **2016**, *22*, 185–192.
(1139) Spence, G. T.; Serpell, C. J.; Sardinha, J.; Costa, P. J.; Félix, V.; Beer, P. D. Investigating the Imidazolium-Anion Interaction Through the Anion-Templated Construction of Interpenetrated and Interlocked Assemblies. *Chem. Eur. J.* **2011**, *17*, 12955–12966.
(1140) Mullen, K. M.; Mercurio, J.; Serpell, C. J.; Beer, P. D. Exploiting the 1,2,3-Triazolium Motif in Anion-Templated Formation of a Bromide-Selective Rotaxane Host Assembly. *Angew. Chem., Int. Ed*. **2009**, *48*, 4781–4784.
(1141) Serpell, C. J.; Chall, R.; Thompson, A. L.; Beer, P. D. Chloride Anion Triggered Motion in a Bis-Imidazolium Rotaxane. *Dalton Trans.* **2011**, *40*, 12052–12055.
(1142) Martí-Centelles, V.; Beer, P. D. Nitrate Anion Recognition in Organic-Aqueous Solvent Mixtures by a Bis(Triazolium) Acridine-Containing [2]Rotaxane. *Chem. Eur. J.* **2015**, *21*, 9397–9404.
(1143) Hua, Y.; Flood, A. H. Click Chemistry Generates Privileged CH Hydrogen-Bonding Triazoles: The Latest Addition to Anion Supramolecular Chemistry. *Chem. Soc. Rev.* **2010**, *39*, 1262–1271.
(1144) Lee, S.; Chen, C.-H.; Flood, A. H. A Pentagonal Cyanostar Macrocycle with Cyanostilbene CH Donors Binds Anions and Forms Dialkylphosphate [3]Rotaxanes. *Nature Chem.* **2013**, *5*, 704–710.
(1145) Valderrey, V.; Escudero-Adán, E. C.; Ballester, P. Polyatomic Anion Assistance in the Assembly of [2]Pseudorotaxanes. *J. Am. Chem. Soc.* **2012**, *134*, 10733–10736.
(1146) Spence, G. T.; Smith, B. D. Ion Pair Templation Strategies for Synthesis of Interlocked Molecules. In *Synergy in Supramolecular Chemistry*; Nabeshima, T., Ed.; CRC Press, 2014; pp. 173–190.
(1147) Furusho, Y.; Yashima, E. Molecular Design and Synthesis of Artificial Double Helices. *Chem. Rec.* **2007**, *7*, 1–11.
(1148) Yashima, E.; Maeda, K.; Furusho, Y. Single- and Double-Stranded Helical Polymers: Synthesis, Structures, and Functions. *Acc. Chem. Res.* **2008**, *41*, 1166–1180.
(1149) Tanaka, Y.; Katagiri, H.; Furusho, Y.; Yashima, E. A Modular Strategy to Artificial Double Helices. *Angew. Chem., Int. Ed*. **2005**, *44*, 3867–3870.
(1150) Nakatani, Y.; Furusho, Y.; Yashima, E. Amidinium Carboxylate Salt Bridges as a Recognition Motif for Mechanically Interlocked Molecules: Synthesis of an Optically Active [2]Catenane and Control of Its Structure. *Angew. Chem., Int. Ed*. **2010**, *49*, 5463–5467.
(1151) Barrell, M. J.; Leigh, D. A.; Lusby, P. J.; Slawin, A. M. Z. An Ion-Pair Template for Rotaxane Formation and Its Exploitation in an Orthogonal Interaction Anion-Switchable Molecular Shuttle. *Angew. Chem., Int. Ed*. **2008**, *47*, 8036–8039.
(1152) Lee, C.-F.; Leigh, D. A.; Pritchard, R. G.; Schultz, D.; Teat, S. J.; Timco, G. A.; Winpenny, R. E. P. Hybrid Organic-Inorganic Rotaxanes and Molecular Shuttles. *Nature* **2009**, *458*, 314–318.
(1153) Ballesteros, B.; Faust, T. B.; Lee, C.-F.; Leigh, D. A.; Muryn, C. A.; Pritchard, R. G.; Schultz, D.; Teat, S. J.; Timco, G. A.; Winpenny, R. E. P. Synthesis, Structure, and Dynamic Properties of Hybrid Organic-Inorganic Rotaxanes. *J. Am. Chem. Soc.* **2010**, *132*, 15435–15444.
(1154) Larsen, F. K.; McInnes, E. J. L.; Mkami, H. E.; Overgaard, J.; Piligkos, S.; Rajaraman, G.; Rentschler, E.; Smith, A. A.; Smith, G. M.; Boote, V.; Jennings, M.; Timco, G. A.; Winpenny R. E. P. Synthesis and Characterization of Heterometallic $\{Cr_7M\}$ Wheels. *Angew. Chem., Int. Ed*. **2003**, *42*, 101–105.
(1155) Cador, O.; Gatteschi, D.; Sessoli, R.; Larsen, F. K.; Overgaard, J.; Barra, A.-L.; Teat, S. J.; Timco, G. A.; Winpenny, R. E. P. The Magnetic Möbius Strip: Synthesis, Structure, and Magnetic Studies of Odd-Numbered Antiferromagnetically Coupled Wheels. *Angew. Chem., Int. Ed*. **2004**, *43*, 5196–5200.
(1156) Timco, G. A.; Batsanov, A. S.; Larsen, F. K.; Muryn, C. A.; Overgaard, J.; Teat, S. J.; Winpenny, R. E. P. Influencing the Nuclearity and Constitution of Heterometallic Rings via Templates. *Chem*. *Commun*. **2005**, 3649–3651.
(1157) Affronte, M.; Carretta, S.; Timco, G. A.; Winpenny, R. E. P. A Ring Cycle: Studies of Heterometallic Wheels. *Chem*. *Commun*. **2007**, 1789–1797.
(1158) McInnes, E. J. L.; Timco, G. A.; Whitehead, G. F. S.; Winpenny, R. E. P. Heterometallic Rings: Their Physics and Use as Supramolecular Building Blocks. *Angew. Chem., Int. Ed*. **2015**, *54*, 14244–14269.
(1159) Fernandez, A.; Pineda, E. M.; Ferrando-Soria, J.; McInnes, E. J. L.; Timco, G. A.; Winpenny, R. E. P. A Hybrid Organic-Inorganic Molecular Daisy Chain. *Chem. Commun.* **2015**, *51*, 11126–11129.
(1160) Shukla, R.; Deetz, M. J.; Smith, B. D. [2]Rotaxane with a Cation-Binding Wheel. *Chem*. *Commun*. **2000**, 2397–2398.
(1161) Deetz, M. J.; Shukla, R.; Smith, B. D. Recognition-Directed Assembly of Salt-Binding [2]Rotaxanes. *Tetrahedron* **2002**, *58*, 799–805.
(1162) Mahoney, J. M.; Shukla, R.; Marshall, R. A.; Beatty, A. M.; Zajicek, J.; Smith, B. D. Templated Conversion of a Crown Ether-Containing Macrobicycle Into [2]Rotaxanes. *J. Org. Chem.* **2002**, *67*, 1436–1440.
(1163) Deetz, M. J.; Shang, M.; Smith, B. D. A Macrobicyclic Receptor with Versatile Recognition Properties: Simultaneous Binding of an Ion Pair and Selective Complexation of Dimethylsulfoxide. *J. Am. Chem. Soc.* **2000**, *122*, 6201–6207.
(1164) Dietrich-Buchecker, C.; Sauvage, J.-P. Lithium Templated Synthesis of Catenanes: Efficient Synthesis of Doubly Interlocked [2]-Catenanes. *Chem*. *Commun*. **1999**, 615–616.

(1165) Divisia-Blohorn, B.; Genoud, F.; Borel, C.; Bidan, G.; Kern, J.-M.; Sauvage, J.-P. Conjugated Polymetallorotaxanes: in-Situ ESR and Conductivity Investigations of Metal-Backbone Interactions. *J. Phys. Chem. B* **2003**, *107*, 5126–5132.
(1166) Hsueh, S.-Y.; Lai, C.-C.; Liu, Y.-H.; Peng, S.-M.; Chiu, S.-H. Highly Selective Na^+-Templated Formation of [2]Pseudorotaxanes Exhibiting Significant Optical Outputs. *Angew. Chem., Int. Ed*. **2007**, *46*, 2013–2017.
(1167) Hsueh, S.-Y.; Lai, C.-C.; Liu, Y.-H.; Wang, Y.; Peng, S.-M.; Chiu, S.-H. Protecting a Squaraine Near-IR Dye Through Its Incorporation in a Slippage-Derived [2]Rotaxane. *Org. Lett.* **2007**, *9*, 4523–4526.
(1168) Han, T.; Chen, C.-F. Efficient Potassium-Ion-Templated Synthesis and Controlled Destruction of [2]Rotaxanes Based on Cascade Complexes. *J. Org. Chem.* **2008**, *73*, 7735–7742.
(1169) Lin, Y.-H.; Lai, C.-C.; Liu, Y.-H.; Peng, S.-M.; Chiu, S.-H. Sodium Ions Template the Formation of Rotaxanes From BPX26C6 and Nonconjugated Amide and Urea Functionalities. *Angew. Chem., Int. Ed*. **2013**, *52*, 10231–10236.
(1170) Tung, S.-T.; Lai, C.-C.; Liu, Y.-H.; Peng, S.-M.; Chiu, S.-H. Synthesis of a [2]Catenane From the Sodium Ion Templated Orthogonal Arrangement of Two Diethylene Glycol Chains. *Angew. Chem., Int. Ed*. **2013**, *52*, 13269–13272.
(1171) Lin, Y.-H.; Lai, C.-C.; Chiu, S.-H. Five Additional Macrocycles That Allow Na^+ Ion-Templated Threading of Guest Units Featuring a Single Urea or Amide Functionality. *Org. Biomol. Chem.* **2014**, *12*, 2907–2917.
(1172) Wu, K.-D.; Lin, Y.-H.; Lai, C.-C.; Chiu, S.-H. Na^+ Ion Templated Threading of Oligo(Ethylene Glycol) Chains Through BPX26C6 Allows Synthesis of [2]Rotaxanes Under Solvent-Free Conditions. *Org. Lett.* **2014**, *16*, 1068–1071.
(1173) You, Y.-C.; Tzeng, M.-C.; Lai, C.-C.; Chiu, S.-H. Using Oppositely Charged Ions to Operate a Three-Station [2]Rotaxane in Two Different Switching Modes. *Org. Lett.* **2012**, *14*, 1046–1049.
(1174) Castro, S. L.; Just, O.; Rees, W. S., Jr. A Quadruply Stranded, Alkaline Earth Metal Containing Helical Catenate: A Charge-Neutral Heterotopic Homodinuclear [2]Catenane. *Angew. Chem., Int. Ed*. **2000**, *39*, 933–935.
(1175) Hancock, L. M.; Beer, P. D. Sodium and Barium Cation-Templated Synthesis and Cation-Induced Molecular Pirouetting of a Pyridine N-Oxide Containing [2]Rotaxane. *Chem. Commun.* **2011**, *47*, 6012–6014.
(1176) Richey, H. G., Jr; Kushlan, D. M. Interactions of a Diarylmagnesium Compound with Cryptands and Crown Ethers: Formation of Ar_3Mg^-, $ArMg(Cryptand)^+$, and Threaded Ar_2Mg(Crown Ether). *J. Am. Chem. Soc.* **1987**, *109*, 2510–2512.
(1177) Gruter, G.-J. M.; de Kanter, F. J. J.; Markies, P. R.; Nomoto, T.; Akkerman, O. S.; Bickelhaupt, F. Formation of the First Organometallic Catenane. *J. Am. Chem. Soc.* **1993**, *115*, 12179–12180.
(1178) Langton, M. J.; Blackburn, O. A.; Lang, T.; Faulkner, S.; Beer, P. D. Nitrite-Templated Synthesis of Lanthanide-Containing [2]Rotaxanes for Anion Sensing. *Angew. Chem., Int. Ed*. **2014**, *53*, 11463–11466.
(1179) Spitler, E. L.; Johnson, C. A.; Haley, M. M. Renaissance of Annulene Chemistry. *Chem. Rev*. **2006**, *106*, 5344–5386.
(1180) Iwamoto, T.; Watanabe, Y.; Sadahiro, T.; Haino, T.; Yamago, S. Size-Selective Encapsulation of C_{60} by [10]Cycloparaphenylene: Formation of the Shortest Fullerene-Peapod. *Angew. Chem., Int. Ed*. **2011**, *50*, 8342–8344.
(1181) Iwamoto, T.; Watanabe, Y.; Takaya, H.; Haino, T.; Yasuda, N.; Yamago, S. Size- and Orientation-Selective Encapsulation of C_{70} by Cycloparaphenylenes. *Chem. Eur. J.* **2013**, *19*, 14061–14068.
(1182) Kawase, T.; Tanaka, K.; Fujiwara, N.; Darabi, H. R.; Oda, M. Complexation of a Carbon Nanoring with Fullerenes. *Angew. Chem., Int. Ed*. **2003**, *42*, 1624–1628.
(1183) Miki, K.; Matsushita, T.; Inoue, Y.; Senda, Y.; Kowada, T.; Ohe, K. Electron-Rich Carbon Nanorings as Macrocyclic Hosts for Fullerenes. *Chem. Commun.* **2013**, *49*, 9092–9094.
(1184) Hoffmann, M.; Kärnbratt, J.; Chang, M.-H.; Herz, L. M.; Albinsson, B.; Anderson, H. L. Enhanced π Conjugation Around a Porphyrin[6] Nanoring. *Angew. Chem., Int. Ed*. **2008**, *47*, 4993–4996.
(1185) Aratani, N.; Kim, D.; Osuka, A. Discrete Cyclic Porphyrin Arrays as Artificial Light-Harvesting Antenna. *Acc. Chem. Res.* **2009**, *42*, 1922–1934.
(1186) Kleij, A. W. Vernier Templating of Nanoscopic Porphyrin Rings. *Angew. Chem., Int. Ed*. **2011**, *50*, 10770–10771.
(1187) O'Sullivan, M. C.; Sprafke, J. K.; Kondratuk, D. V.; Rinfray, C.; Claridge, T. D. W.; Saywell, A.; Blunt, M. O.; O'Shea, J. N.; Beton, P. H.; Malfois, M.; Anderson, H. L. Vernier Templating and Synthesis of a 12-Porphyrin Nano-Ring. *Nature* **2012**, *469*, 72–75.
(1188) Pawlicki, M.; Latos-Grażyński, L. A Dynamic Library of Porphyrinic True Nanorings. *Angew. Chem., Int. Ed*. **2012**, *51*, 11205–11207.
(1189) Rousseaux, S. A. L.; Gong, J. Q.; Haver, R.; Odell, B.; Claridge, T. D. W.; Herz, L. M.; Anderson, H. L. Self-Assembly of Russian Doll Concentric Porphyrin Nanorings. *J. Am. Chem. Soc.* **2015**, *137*, 12713–12718.
(1190) Nakao, K.; Nishimura, M.; Tamachi, T.; Kuwatani, Y.; Miyasaka, H.; Nishinaga, T.; Iyoda, M. Giant Macrocycles Composed of Thiophene, Acetylene, and Ethylene Building Blocks. *J. Am. Chem. Soc.* **2006**, *128*, 16740–16747.
(1191) Iyoda, M.; Yamakawa, J.; Rahman, M. J. Conjugated Macrocycles: Concepts and Applications. *Angew. Chem., Int. Ed*. **2011**, *50*, 10522–10553.
(1192) Ikeda, A.; Shinkai, S. Novel Cavity Design Using Calix[*n*]arene Skeletons: Toward Molecular Recognition and Metal Binding. *Chem. Rev.* **1997**, *97*, 1713–1734.
(1193) Sliwa, W.; Kozlowski, C. *Calixarenes and Resorcinarenes*; Wiley-VCH: Weinheim, 1999.
(1194) Gutsche, C. D. *Calixarenes: An Introduction*; 2nd ed.; The Royal Society of Chemistry: Cambridge, 2008.
(1195) Xue, M.; Yang, Y.; Chi, X.; Zhang, Z.; Huang, F. Pillararenes, A New Class of Macrocycles for Supramolecular Chemistry. *Acc. Chem. Res.* **2012**, *45*, 1294–1308.
(1196) Hardie, M. J. Recent Advances in the Chemistry of Cyclotriveratrylene. *Chem. Soc. Rev.* **2010**, *39*, 516–527.
(1197) Moran, J. R.; Karbach, S.; Cram, D. J. Cavitands: Synthetic Molecular Vessels. *J. Am. Chem. Soc.* **1982**, *104*, 5826–5828.
(1198) Cram, D. J. Cavitands: Organic Hosts with Enforced Cavities. *Science* **1983**, *219*, 1177–1183.
(1199) Cragg, P. J.; Sharma, K. Pillar[5]arenes: Fascinating Cyclophanes with a Bright Future. *Chem. Soc. Rev.* **2012**, *41*, 597–607.
(1200) Tan, L.-L.; Yang, Y.-W. Molecular Recognition and Self-Assembly of Pillarenes. *J. Incl. Phenom. Macrocycl. Chem.* **2014**, *81*, 13–33.
(1201) Ogoshi, T.; Yamagishi, T. Pillar[5]- and Pillar[6]arene-Based Supramolecular Assemblies Built by Using Their Cavity-Size-Dependent Host–Guest Interactions. *Chem. Commun.* **2014**, *50*, 4776–4787.
(1202) Fan, J.; Chen, Y.; Cao, D.; Yang, Y.-W.; Jia, X.; Li, C. Host–Guest Properties of Pillar[7]arene Towards Substituted Adamantane Ammonium Cations. *RSC Adv.* **2014**, *4*, 4330–4333.
(1203) Li, Z.; Yang, J.; Yu, G.; He, J.; Abliz, Z.; Huang, F. Water-Soluble Pillar[7]arene: Synthesis, pH-Controlled Complexation with Paraquat, and Application in Constructing Supramolecular Vesicles. *Org. Lett.* **2014**, *16*, 2066–2069.

(1204) Gaeta, C.; Talotta, C.; Margarucci, L.; Casapullo, A.; Neri, P. Through-the-Annulus Threading of the Larger Calix[8]arene Macrocycle. *J. Org. Chem.* **2013**, *78*, 7627–7638.
(1205) Hu, X.-B.; Chen, Z.; Chen, L.; Zhang, L.; Hou, J.-L.; Li, Z.-T. Pillar[*n*]arenes (*n* = 8–10) with Two Cavities: Synthesis, Structures and Complexing Properties. *Chem. Commun*. **2012**, *48*, 10999–11001.
(1206) Ogoshi, T.; Ueshima, N.; Sakakibara, F.; Yamagishi, T.-A.; Haino, T. Conversion From Pillar[5]arene to Pillar[6–15] arenes by Ring Expansion and Encapsulation of C_{60} by Pillar[*n*]arenes with Nanosize Cavities. *Org. Lett.* **2014**, *16*, 2896–2899.
(1207) Morohashi, N.; Narumi, F.; Iki, N.; Hattori, T.; Miyano, S. Thiacalixarenes. *Chem. Rev*. **2006**, *106*, 5291–5316.
(1208) Maes, W.; Dehaen, W. Oxacalix[*n*](het)arenes. *Chem. Soc. Rev.* **2008**, *37*, 2393–2402.
(1209) Timmerman, P.; Verboom, W.; Reinhoudt, D. N. Resorcinarenes. *Tetrahedron* **1996**, *52*, 2663–2704.
(1210) Gale, P. A.; Anzenbacher, P., Jr.; Sessler, J. L. Calixpyrroles II. *Coord. Chem. Rev*. **2001**, *222*, 57–102.
(1211) Wang, M.-X. Nitrogen and Oxygen Bridged Calixaromatics: Synthesis, Structure, Functionalization, and Molecular Recognition. *Acc. Chem. Res.* **2012**, *45*, 182–195.
(1212) Fischer, C.; Nieger, M.; Mogck, O.; Böhmer, V.; Ungaro, R.; Vögtle, F. Calixarenes as Stoppers in Rotaxanes. *Eur. J. Org. Chem.* **1998**, 155–161.
(1213) Li, Z.-T.; Ji, G.-Z.; Yuan, S.-D.; Du, A.-L.; Ding, H.; Wei, M. The Self-Assembly of Catenated Calix[4]arenes. *Tetrahedron Lett.* **1998**, *39*, 6517–6520.
(1214) Li, Z.-T.; Ji, G.-Z.; Zhao, C.-X.; Yuan, S.-D.; Ding, H.; Huang, C.; Du, A.-L.; Wei, M. Self-Assembling Calix[4]arene [2]Catenanes. Preorganization, Conformation, Selectivity, and Efficiency. *J. Org. Chem*. **1999**, *64*, 3572–3584.
(1215) Li, Z.-T.; Zhang, X.-L.; Lian, X.-D.; Yu, Y.-H.; Xia, Y.; Zhao, C.-X.; Chen, Z.; Lin, Z.-P.; Chen, H. [2]Catenane Assembly From Calix[4]arene Crown Ethers. *J. Org. Chem*. **2000**, *65*, 5136–5142.
(1216) Lu, L.-G.; Li, G.-K.; Peng, X.-X.; Chen, C.-F.; Huang, Z.-T. Synthesis and Self-Assembly of Novel Calix[4]arenocrowns: Formation of Calix[4]areno[2]catenanes. *Tetrahedron Lett.* **2006**, *47*, 6021–6025.
(1217) Li, J.; Li, Y.; Guo, Y.; Xu, J.; Lv, J.; Li, Y.; Liu, H.; Wang, S.; Zhu, D. A Novel Supramolecular System: Combination of Two Switchable Processes in a [2]Rotaxane. *Chem. Asian J.* **2008**, *3*, 2091–2096.
(1218) Gattuso, G.; Notti, A.; Pappalardo, S.; Parisi, M. F.; Pilati, T.; Resnati, G.; Terraneo, G. Ion-Pair Separation via Selective Inclusion/Segregation Processes. *CrystEngComm* **2009**, *11*, 1204–1206.
(1219) Gattuso, G.; Notti, A.; Parisi, M. F.; Pisagatti, I.; Amato, M. E.; Pappalardo, A.; Pappalardo, S. Threading the Calix[5]arene Annulus. *Chem. Eur. J.* **2010**, *16*, 2381–2385.
(1220) Arduini, A.; Ferdani, R.; Pochini, A.; Secchi, A.; Ugozzoli, F. Calix[6]arene as a Wheel for Rotaxane Synthesis. *Angew. Chem., Int. Ed*. **2000**, *39*, 3453–3456.
(1221) Arduini, A.; Calzavacca, F.; Pochini, A.; Secchi, A. Unidirectional Threading of Triphenylureidocalix[6]arene-Based Wheels: Oriented Pseudorotaxane Synthesis. *Chem. Eur. J.* **2003**, *9*, 793–799.
(1222) Credi, A.; Dumas, S.; Silvi, S.; Venturi, M.; Arduini, A.; Pochini, A.; Secchi, A. Viologen-Calix[6]arene Pseudorotaxanes. Ion-Pair Recognition and Threading/Dethreading Molecular Motions. *J. Org. Chem*. **2004**, *69*, 5881–5887.
(1223) Arduini, A.; Credi, A.; Faimani, G.; Massera, C.; Pochini, A.; Secchi, A.; Semeraro, M.; Silvi, S.; Ugozzoli, F. Self-Assembly of a Double Calix[6]arene Pseudorotaxane in Oriented Channels. *Chem. Eur. J.* **2008**, *14*, 98–106.
(1224) Arduini, A.; Bussolati, R.; Credi, A.; Pochini, A.; Secchi, A.; Silvi, S.; Venturi, M. Rotaxanes with a Calix[6]arene Wheel and Axles of Different Length. Synthesis, Characterization, and Photophysical and Electrochemical Properties. *Tetrahedron* **2008**, *64*, 8279–8286.
(1225) Ugozzoli, F.; Massera, C.; Arduini, A.; Pochini, A.; Secchi, A. Calix[6]arene-Based Pseudorotaxanes: A Solid State Structural Investigation. *CrystEngComm* **2004**, *6*, 227.
(1226) Semeraro, M.; Arduini, A.; Baroncini, M.; Battelli, R.; Credi, A.; Venturi, M.; Pochini, A.; Secchi, A.; Silvi, S. Self-Assembly of Calix[6]arene-Diazapyrenium Pseudorotaxanes: Interplay of Molecular Recognition and Ion-Pairing Effects. *Chem. Eur. J.* **2010**, *16*, 3467–3475.
(1227) Boccia, A.; Lanzilotto, V.; Di Castro, V.; Zanoni, R.; Pescatori, L.; Arduini, A.; Secchi, A. Preparation, Reactivity and Controlled Release of SAMs of Calix[4,6]arenes and Calix[6]arene-Based Rotaxanes and Pseudorotaxanes Formed on Polycrystalline Cu. *Phys. Chem. Chem. Phys.* **2011**, *13*, 4452–4462.
(1228) Wu, S.-F.; Ma, X. Vinylbipyridinium Dication-Triphenylureidocalix[6]arene Pseudorotaxane. *Tetrahedron Lett.* **2011**, *52*, 5960–5962.
(1229) Gaeta, C.; Troisi, F.; Neri, P. Endo-Cavity Complexation and Through-the-Annulus Threading of Large Calixarenes Induced by Very Loose Alkylammonium Ion Pairs. *Org. Lett.* **2010**, *12*, 2092–2095.
(1230) Pierro, T.; Gaeta, C.; Talotta, C.; Casapullo, A.; Neri, P. Fixed or Invertible Calixarene-Based Directional Shuttles. *Org. Lett.* **2011**, *13*, 2650–2653.
(1231) Talotta, C.; Gaeta, C.; Pierro, T.; Neri, P. Sequence Stereoisomerism in Calixarene-Based Pseudo[3]rotaxanes. *Org. Lett.* **2011**, *13*, 2098–2101.
(1232) Talotta, C.; Gaeta, C.; Neri, P. Stereoprogrammed Direct Synthesis of Calixarene-Based [3]Rotaxanes. *Org. Lett.* **2012**, *14*, 3104–3107.
(1233) Gaeta, C.; Talotta, C.; Mirra, S.; Margarucci, L.; Casapullo, A.; Neri, P. Catenation of Calixarene Annulus. *Org. Lett.* **2013**, *15*, 116–119.
(1234) Gaeta, C.; Talotta, C.; Neri, P. Pseudorotaxane Orientational Stereoisomerism Driven by π-Electron Density. *Chem. Commun.* **2014**, *50*, 9917–9920.
(1235) Talotta, C.; De Simone, N. A.; Gaeta, C.; Neri, P. Calix[6]arene Threading with Weakly Interacting Tertiary Ammonium Axles: Generation of Chiral Pseudorotaxane Architectures. *Org. Lett.* **2015**, *17*, 1006–1009.
(1236) Hu, S.-Z.; Chen, C.-F. Triptycene-Derived Oxacalixarenes as New Wheels for the Synthesis of [2]Rotaxanes: Acid-Base- and Metal-Ion-Switchable Complexation Processes. *Chem. Eur. J.* **2011**, *17*, 5424–5431.
(1237) Hu, S.-Z.; Chen, C.-F. Triptycene-Derived Oxacalixarene with Expanded Cavity: Synthesis, Structure and Its Complexation with Fullerenes C_{60} and C_{70}. *Chem. Commun.* **2010**, *46*, 4199–4201.
(1238) Ogoshi, T.; Yamagishi, T.-A. Pillararenes: Versatile Synthetic Receptors for Supramolecular Chemistry. *Eur. J. Org. Chem.* **2013**, 2961–2975.
(1239) Cao, D.; Meier, H. Pillar[*n*]arenes—a Novel, Highly Promising Class of Macrocyclic Host Molecules. *Asian J. Org. Chem.* **2014**, *3*, 244–262.
(1240) Strutt, N. L.; Zhang, H.; Schneebeli, S. T.; Stoddart, J. F. Functionalizing Pillar[*n*]arenes. *Acc. Chem. Res.* **2014**, *47*, 2631–2642.
(1241) *Pillararenes*; Ogoshi, T.; Gale, P. A.; Steed, J. W., Eds.; Royal Society of Chemistry: London, 2015.
(1242) Li, C.; Xu, Q.; Li, J.; Yao, F.; Jia, X. Complex Interactions of Pillar[5]arene with Paraquats and Bis(pyridinium) Derivatives. *Org. Biomol. Chem.* **2010**, *8*, 1568–1576.
(1243) Li, C.; Zhao, L.; Li, J.; Ding, X.; Chen, S.; Zhang, Q.; Yu, Y.; Jia, X. Self-Assembly of [2]Pseudorotaxanes Based on Pillar[5]arene and Bis(imidazolium) Cations. *Chem. Commun.* **2010**, *46*, 9016–9018.
(1244) Ogoshi, T.; Hashizume, M.; Yamagishi, T.-A.; Nakamoto, Y. Synthesis, Conformational and Host–Guest Properties of

Water-Soluble Pillar[5]arene. *Chem. Commun.* **2010**, *46*, 3708–3710.
(1245) Chi, X.; Xue, M.; Yao, Y.; Huang, F. Redox-Responsive Complexation Between a Pillar[5]arene with Mono(Ethylene Oxide) Substituents and Paraquat. *Org. Lett.* **2013**, *15*, 4722–4725.
(1246) Zhou, Y.; Li, Z.; Chi, X.; Thompson, C.; Yao, Y. Formation of a [2]Pseudorotaxane Based on a Pillar[5]arene and a Rigid Guest in Solution and in the Solid State. *Chem. Commun.* **2014**, *50*, 10482–10484.
(1247) Zhang, Z.; Luo, Y.; Xia, B.; Han, C.; Yu, Y.; Chen, X.; Huang, F. Four Constitutional Isomers of BMpillar[5]arene: Synthesis, Crystal Structures and Complexation with *N*-Octyltrimethyl Ammonium Hexafluorophosphate. *Chem. Commun.* **2011**, *47*, 2417–2419.
(1248) Strutt, N. L.; Forgan, R. S.; Spruell, J. M.; Botros, Y. Y.; Stoddart, J. F. Monofunctionalized Pillar[5]arene as a Host for Alkanediamines. *J. Am. Chem. Soc.* **2011**, *133*, 5668–5671.
(1249) Deng, H.; Shu, X.; Hu, X.; Li, J.; Jia, X.; Li, C. Synthesis of a Fully Functionalized Pillar[5]arene by “Click Chemistry” and Its Effective Binding Toward Neutral Alkanediamines. *Tetrahedron Lett.* **2012**, *53*, 4609–4612.
(1250) Yu, G.; Hua, B.; Han, C. Proton Transfer in Host–Guest Complexation Between a Difunctional Pillar[5]arene and Alkyldiamines. *Org. Lett.* **2014**, *16*, 2486–2489.
(1251) Shu, X.; Fan, J.; Li, J.; Wang, X.; Chen, W.; Jia, X.; Li, C. Complexation of Neutral 1,4-Dihalobutanes with Simple Pillar[5]arenes That Is Dominated by Dispersion Forces. *Org. Biomol. Chem.* **2012**, *10*, 3393–3397.
(1252) Shu, X.; Chen, S.; Li, J.; Chen, Z.; Weng, L.; Jia, X.; Li, C. Highly Effective Binding of Neutral Dinitriles by Simple Pillar[5]arenes. *Chem. Commun.* **2012**, *48*, 2967–2969.
(1253) Li, C.; Chen, S.; Li, J.; Han, K.; Xu, M.; Hu, B.; Yu, Y.; Jia, X. Novel Neutral Guest Recognition and Interpenetrated Complex Formation From Pillar[5]arenes. *Chem. Commun.* **2011**, *47*, 11294–11296.
(1254) Han, K.; Zhang, Y.; Li, J.; Yu, Y.; Jia, X.; Li, C. Binding Mechanisms and Driving Forces for the Selective Complexation Between Pillar[5]arenes and Neutral Nitrogen Heterocyclic Compounds. *Eur. J. Org. Chem.* **2013**, 2057–2060.
(1255) Wei, P.; Yan, X.; Li, J.; Ma, Y.; Huang, F. Two 2:3 Copillar[5]arene Constitutional Isomers: Syntheses, Crystal Structures and Host–Guest Complexation of Their Derivatives with Dicarboxylic Acid Sodium Salts in Water. *Chem. Commun.* **2013**, *49*, 1070–1072.
(1256) Zhang, Z.; Xia, B.; Han, C.; Yu, Y.; Huang, F. Syntheses of Copillar[5]arenes by Co-Oligomerization of Different Monomers. *Org. Lett.* **2010**, *12*, 3285–3287.
(1257) Hu, X.-B.; Chen, L.; Si, W.; Yu, Y.; Hou, J.-L. Pillar[5]arene Decaamine: Synthesis, Encapsulation of Very Long Linear Diacids and Formation of Ion Pair-Stopped [2]Rotaxanes. *Chem. Commun.* **2011**, *47*, 4694–4696.
(1258) Hu, X.-S.; Deng, H.-M.; Li, J.; Jia, X.-S.; Li, C.-J. Selective Binding of Unsaturated Aliphatic Hydrocarbons by a Pillar[5]arene. *Chin. Chem. Lett.* **2013**, *24*, 707–709.
(1259) Ma, Y.; Ji, X.; Xiang, F.; Chi, X.; Han, C.; He, J.; Abliz, Z.; Chen, W.; Huang, F. A Cationic Water-Soluble Pillar[5]arene: Synthesis and Host–Guest Complexation with Sodium 1-Octanesulfonate. *Chem. Commun.* **2011**, *47*, 12340–12342.
(1260) Li, C.; Shu, X.; Li, J.; Chen, S.; Han, K.; Xu, M.; Hu, B.; Yu, Y.; Jia, X. Complexation of 1,4-Bis(pyridinium)butanes by Negatively Charged Carboxylatopillar[5]arene. *J. Org. Chem.* **2011**, *76*, 8458–8465.
(1261) Ma, Y.; Xue, M.; Zhang, Z.; Chi, X.; Huang, F. Neutral Guest Capture by a Cationic Water-Soluble Pillar[5]arene in Water. *Tetrahedron* **2013**, *69*, 4532–4535.
(1262) Ma, Y.; Chi, X.; Yan, X.; Liu, J.; Yao, Y.; Chen, W.; Huang, F.; Hou, J.-L. Per-Hydroxylated Pillar[6]arene: Synthesis, X-Ray Crystal Structure, and Host–Guest Complexation. *Org. Lett.* **2012**, *14*, 1532–1535.
(1263) Chi, X.; Xue, M.; Ma, Y.; Yan, X.; Huang, F. A Pillar[6]arene with Mono(Ethylene Oxide) Substituents: Synthesis and Complexation with Diquat. *Chem. Commun.* **2013**, *49*, 8175–8177.
(1264) Fan, J.; Deng, H.; Li, J.; Jia, X.; Li, C. Charge-Transfer Inclusion Complex Formation of Tropylium Cation with Pillar[6]arenes. *Chem. Commun.* **2013**, *49*, 6343–6345.
(1265) Xia, W.; Hu, X.-Y.; Chen, Y.; Lin, C.; Wang, L. A Novel Redox-Responsive Pillar[6]arene-Based Inclusion Complex with a Ferrocenium Guest. *Chem. Commun.* **2013**, *49*, 5085–5087.
(1266) Li, C.; Shu, X.; Li, J.; Fan, J.; Chen, Z.; Weng, L.; Jia, X. Selective and Effective Binding of Pillar[5,6]arenes Toward Secondary Ammonium Salts with a Weakly Coordinating Counteranion. *Org. Lett.* **2012**, *14*, 4126–4129.
(1267) Han, C.; Gao, L.; Yu, G.; Zhang, Z.; Dong, S.; Huang, F. Synthesis of a Difunctionalized Pillar[6]arene and Its Complexation with an Ammonium Salt Coupled to a Weakly Coordinating Counteranion. *Eur. J. Org. Chem.* **2013**, 2529–2532.
(1268) Ogoshi, T.; Kayama, H.; Yamafuji, D.; Aoki, T.; Yamagishi, T.-A. Supramolecular Polymers with Alternating Pillar[5]arene and Pillar[6]arene Units From a Highly Selective Multiple Host–Guest Complexation System and Monofunctionalized Pillar[6]arene. *Chem. Sci.* **2012**, *3*, 3221–3226.
(1269) Ogoshi, T.; Kida, K.; Yamagishi, T.-A. Photoreversible Switching of the Lower Critical Solution Temperature in a Photoresponsive Host–Guest System of Pillar[6]arene with Triethylene Oxide Substituents and an Azobenzene Derivative. *J. Am. Chem. Soc.* **2012**, *134*, 20146–20150.
(1270) Chen, W.; Zhang, Y.; Li, J.; Lou, X.; Yu, Y.; Jia, X.; Li, C. Synthesis of a Cationic Water-Soluble Pillar[6]arene and Its Effective Complexation Towards Naphthalenesulfonate Guests. *Chem. Commun.* **2013**, *49*, 7956–7958.
(1271) Han, C.; Ma, F.; Zhang, Z.; Xia, B.; Yu, Y.; Huang, F. DIBPillar[*n*]arenes (*n* = 5, 6): Syntheses, X-Ray Crystal Structures, and Complexation with *N*-Octyltriethyl Ammonium Hexafluorophosphate. *Org. Lett.* **2010**, *12*, 4360–4363.
(1272) Ogoshi, T.; Yamafuji, D.; Aoki, T.; Kitajima, K.; Yamagishi, T.-A.; Hayashi, Y.; Kawauchi, S. High-Yield Diastereoselective Synthesis of Planar Chiral [2]- and [3]Rotaxanes Constructed From Per-Ethylated Pillar[5]arene and Pyridinium Derivatives. *Chem. Eur. J.* **2012**, *18*, 7493–7500.
(1273) Ogoshi, T.; Yamafuji, D.; Aoki, T.; Yamagishi, T.-A. Thermally Responsive Shuttling Behavior of a Pillar[6]arene-Based [2]Rotaxane. *Chem. Commun.* **2012**, *48*, 6842–6844.
(1274) Ogoshi, T.; Yamafuji, D.; Yamagishi, T.-A.; Brouwer, A. M. Förster Resonance Energy Transfer by Formation of a Mechanically Interlocked [2]Rotaxane. *Chem. Commun.* **2013**, *49*, 5468–5470.
(1275) Ogoshi, T.; Iizuka, R.; Kotera, D.; Yamagishi, T.-A. Synthesis of a Pillar[5]arene-Based [2]Rotaxane with Two Equivalent Stations via Copper(I)-Catalyzed Alkyne–Azide Cycloaddition. *Org. Lett.* **2015**, *17*, 350–353.
(1276) Milev, R.; Lopez-Pacheco, A.; Nierengarten, I.; Trinh, T. M. N.; Holler, M.; Deschenaux, R.; Nierengarten, J.-F. Preparation of Pillar[5]arene-Based [2]Rotaxanes From Acyl Chlorides and Amines. *Eur. J. Org. Chem.* **2014**, 479–485.
(1277) Ogoshi, T.; Shiga, R.; Yamagishi, T.-A. Reversibly Tunable Lower Critical Solution Temperature Utilizing Host–Guest Complexation of Pillar[5]arene with Triethylene Oxide Substituents. *J. Am. Chem. Soc.* **2012**, *134*, 4577–4580.
(1278) Ogoshi, T.; Aoki, T.; Shiga, R.; Iizuka, R.; Ueda, S.; Demachi, K.; Yamafuji, D.; Kayama, H.; Yamagishi, T.-A. Cyclic Host

Liquids for Facile and High-Yield Synthesis of [2]Rotaxanes. *J. Am. Chem. Soc.* **2012**, *134*, 20322–20325.
(1279) Gomberg, M. An Instance of Trivalent Carbon: Triphenylmethyl. *J. Am. Chem. Soc.* **1900**, *22*, 757–771.
(1280) Michaelis, L.; Hill, E. S. Potentiometric Studies on Semiquinones. *J. Am. Chem. Soc.* **1933**, *55*, 1481–1494.
(1281) Michaelis, L. Semiquinones, the Intermediate Steps of Reversible Organic Oxidation-Reduction. *Chem. Rev.* **1935**, *16*, 243–286.
(1282) Schwarz, W. M., Jr. PhD Thesis. The University of Wisconsin, Madison, 1961.
(1283) Kosower, E. M.; Cotter, J. L. Stable Free Radicals. II. the Reduction of 1-Methyl-4-cyanopyridinium Ion to Methylviologen Cation Radical. *J. Am. Chem. Soc*. **1964**, *86*, 5524–5527.
(1284) Kosower, E. M.; Hajdu, J. Pyridinyl Diradical. π-Mer. Magnesium Iodide Complexes. *J. Am. Chem. Soc*. **1971**, *93*, 2534–2535.
(1285) Yoshizawa, M.; Kumazawa, K.; Fujita, M. Room-Temperature and Solution-State Observation of the Mixed-Valence Cation Radical Dimer of Tetrathiafulvalene, $[(TTF)_2]^{+\bullet}$, Within a Self-Assembled Cage. *J. Am. Chem. Soc.* **2005**, *127*, 13456–13457.
(1286) Spruell, J. M.; Coskun, A.; Friedman, D. C.; Forgan, R. S.; Sarjeant, A. A.; Trabolsi, A.; Fahrenbach, A. C.; Barin, G.; Paxton, W. F.; Dey, S. K.; Olson, M. A.; Benítez, D.; Tkatchouk, E.; Colvin, M. T.; Carmielli, R.; Caldwell, S. T.; Rosair, G. M.; Hewage, S. G.; Duclairoir, F.; Seymour, J. L.; Slawin, A. M. Z.; Goddard, W. A., III; Wasielewski, M. R.; Cooke, G.; Stoddart, J. F. Highly Stable Tetrathiafulvalene Radical Dimers in [3]Catenanes. *Nature Chem.* **2010**, *2*, 870–879.
(1287) Coskun, A.; Spruell, J. M.; Barin, G.; Fahrenbach, A. C.; Forgan, R. S.; Colvin, M. T.; Carmieli, R.; Benítez, D.; Tkatchouk, E.; Friedman, D. C.; Sarjeant, A. A.; Wasielewski, M. R.; Goddard, W. A., III; Stoddart, J. F. Mechanically Stabilized Tetrathiafulvalene Radical Dimers. *J. Am. Chem. Soc.* **2011**, *133*, 4538–4547.
(1288) Trabolsi, A.; Khashab, N.; Fahrenbach, A. C.; Friedman, D. C.; Colvin, M. T.; Cotí, K. K.; Benítez, D.; Tkatchouk, E.; Olsen, J.-C.; Belowich, M. E.; Carmielli, R.; Khatib, H. A.; Goddard, W. A., III; Wasielewski, M. R.; Stoddart, J. F. Radically Enhanced Molecular Recognition. *Nature Chem.* **2010**, *2*, 42–49.
(1289) Fahrenbach, A. C.; Barnes, J. C.; Lanfranchi, D. A.; Li, H.; Coskun, A.; Gassensmith, J. J.; Liu, Z.; Benítez, D.; Trabolsi, A.; Goddard, W. A., III; Elhabiri, M.; Stoddart, J. F. Solution-Phase Mechanistic Study and Solid-State Structure of a Tris(Bipyridinium Radical Cation) Inclusion Complex. *J. Am. Chem. Soc.* **2012**, *134*, 3061–3072.
(1290) Fahrenbach, A. C.; Sampath, S.; Late, D. J.; Barnes, J. C.; Kleinman, S. L.; Valley, N.; Hartlieb, K. J.; Liu, Z.; Dravid, V. P.; Schatz, G. C.; Van Duyne, R. P.; Stoddart, J. F. A Semiconducting Organic Radical Cationic Host–Guest Complex. *ACS Nano* **2012**, *6*, 9964–9971.
(1291) Li, H.; Fahrenbach, A. C.; Dey, S. K.; Basu, S.; Trabolsi, A.; Zhu, Z.; Botros, Y. Y.; Stoddart, J. F. Mechanical Bond Formation by Radical Templation. *Angew. Chem., Int. Ed*. **2010**, *49*, 8260–8265.
(1292) Li, H.; Zhu, Z.; Fahrenbach, A. C.; Savoie, B. M.; Ke, C.; Barnes, J. C.; Lei, J.; Zhao, Y.-L.; Lilley, L. M.; Marks, T. J.; Ratner, M. A.; Stoddart, J. F. Mechanical Bond-Induced Radical Stabilization. *J. Am. Chem. Soc.* **2013**, *135*, 456–467.
(1293) Barnes, J. C.; Fahrenbach, A. C.; Cao, D.; Dyar, S. M.; Frasconi, M.; Giesener, M. A.; Benitez, D.; Tkatchouk, E.; Chernyashevskyy, O.; Shin, W. H.; Li, H.; Sampath, S.; Stern, C. L.; Sarjeant, A. A.; Hartlieb, K. J.; Liu, Z.; Carmieli, R.; Botros, Y. Y.; Choi, J. W.; Slawin, A. M. Z.; Ketterson, J. B.; Wasielewski, M. R.; Goddard, W. A., III; Stoddart, J. F. A Radically Configurable Six-State Compound. *Science* **2013**, *339*, 429–433.
(1294) Barnes, J. C.; Frasconi, M.; Young, R. M.; Khdary, N. H.; Liu, W.-G.; Dyar, S. M.; McGonigal, P. R.; Gibbs-Hall, I. C.; Diercks, C. S.; Sarjeant, A. A.; Stern, C. L.; Goddard, W. A., III; Wasielewski, M. R.; Stoddart, J. F. Solid-State Characterization and Photoinduced Intramolecular Electron Transfer in a Nanoconfined Octacationic Homo[2]catenane. *J. Am. Chem. Soc.* **2014**, *136*, 10569–10572.
(1295) Amabilino, D. B. Highly Charged. *Nature Chem.* **2013**, *5*, 365–366.
(1296) Benniston, A. Corralling Positively Charged Molecular Radicals. *Science* **2013**, *339*, 404–405.
(1297) Gladysz, J. A.; Curran, D. P. Fluorous Chemistry: From Biphasic Catalysis to a Parallel Chemical Universe and Beyond. *Tetrahedron* **2002**, *58*, 3823–3825.
(1298) Tewari, A. K.; Dubey, R. Emerging Trends in Molecular Recognition: Utility of Weak Aromatic Interactions. *Bioorg. Med. Chem.* **2008**, *16*, 126–143.
(1299) Wang, W.; Wang, L.; Palmer, B. J.; Exarhos, G. J.; Li, A. D. Q. Cyclization and Catenation Directed by Molecular Self-Assembly. *J. Am. Chem. Soc.* **2006**, *128*, 11150–11159.
(1300) Basuray, A. N.; de Rouville, H.-P. J.; Hartlieb, K. J.; Fahrenbach, A. C.; Stoddart, J. F. Beyond Perylene Diimides-Diazaperopyrenium Dications as Chameleonic Nanoscale Building Blocks. *Chem. Asian J.* **2012**, *8*, 524–532.
(1301) Mehta, G.; Srinivas, K.; Vidya, R.; Uma, R.; Kunwar, A. C.; Kumar, K. R.; Vairamani, M. Triquinane-Derived Macrocyclic Lactones and a [2]-Catenane: Synthesis and Characterization. *Tetrahedron* **1998**, *54*, 10879–10890.
(1302) Puddephatt, R. J. Macrocycles, Catenanes, Oligomers and Polymers in Gold Chemistry. *Chem. Soc. Rev*. **2008**, *37*, 2012.
(1303) Puddephatt, R. J. Gold Catenanes. *J. Organomet. Chem.* **2015**, *792*, 13–24.
(1304) Mingos, D. M. P.; Yau, J.; Menzer, S.; Williams, D. J. A Gold(I) [2]Catenane. *Angew. Chem., Int. Ed. Engl*. **1995**, *34*, 1894–1895.
(1305) McArdle, C. P.; Irwin, M. J.; Jennings, M. C.; Puddephatt, R. J. Controlled Self-Assembly of Cyclic Gold (I) Complexes: the First Family of Organometallic Catenanes. *Angew. Chem., Int. Ed*. **1999**, *38*, 3376–3378.
(1306) Chui, S. S.-Y.; Chen, R.; Che, C.-M. A Chiral [2]Catenane Precursor of the Antiarthritic Gold(I) Drug Auranofin. *Angew. Chem., Int. Ed*. **2006**, *45*, 1621–1624.
(1307) Hasell, T.; Wu, X.; Jones, J. T. A.; Bacsa, J.; Steiner, A.; Mitra, T.; Trewin, A.; Adams, D. J.; Cooper, A. I. Triply Interlocked Covalent Organic Cages. *Nature Chem.* **2010**, *2*, 750–755.
(1308) Beves, J. E.; Leigh, D. A. Linking Rings Without Templates. *Nature Chem*. **2010**, *2*, 708–710.
(1309) Tozawa, T.; Jones, J. T. A.; Swamy, S. I.; Jiang, S.; Adams, D. J.; Shakespeare, S.; Clowes, R.; Bradshaw, D.; Hasell, T.; Chong, S. Y.; Tang, C.; Thompson, S.; Parker, J.; Trewin, A.; Bacsa, J.; Slawin, A. M. Z.; Steiner, A.; Cooper, A. I. Porous Organic Cages. *Nature Mater.* **2009**, *8*, 973–978.
(1310) Jin, C.-M.; Lu, H.; Wu, L.-Y.; Huang, J. A New Infinite Inorganic [*n*]Catenane From Silver and Bis(2-methylimidazolyl)methane Ligand. *Chem. Commun*. **2006**, 5039–5041.
(1311) Yin, Z.; Zhang, Y.; He, J.; Cheng, J.-P. Hydrogen Bond Assisted Helical Self-Assembly Into [*n*]Catenane. *Chem. Commun*. **2007**, 2599–2601.
(1312) Loots, L.; Barbour, L. J. An Infinite Catenane Self-Assembled by π···π Interactions. *Chem. Commun.* **2013**, *49*, 671–673.
(1313) Heine, J.; Schmedt auf der Günne, J.; Dehnen, S. Formation of a Strandlike Polycatenane of Icosahedral Cages for Reversible One-Dimensional Encapsulation of Guests. *J. Am. Chem. Soc.* **2011**, *133*, 10018–10021.

(1314) Chen, Q.; Jiang, F.; Yuan, D.; Lyu, G.; Chen, L.; Hong, M. A Controllable and Dynamic Assembly System Based on Discrete Metallocages. *Chem. Sci.* **2014**, *5*, 483–488.
(1315) Chen, Q.; Chen, L.; Jiang, F.; Hong, M. Controllable Coordination Self-Assembly Based on Flexible Tripodal Ligands: From Finite Metallocages to Infinite Polycatenanes Step by Step. *Chem. Rec*. **2015**, 711–727.
(1316) Kuang, X.; Wu, X.; Yu, R.; Donahue, J. P.; Huang, J.; Lu, C.-Z. Assembly of a Metal-Organic Framework by Sextuple Intercatenation of Discrete Adamantane-Like Cages. *Nature Chem.* **2010**, *2*, 461–465.
(1317) Jiang, L.; Ju, P.; Meng, X.-R.; Kuang, X.-J.; Lu, T.-B. Constructions of Two Polycatenanes and One Polypseudo-Rotaxane by Discrete Tetrahedral Cages and Stool-Like Building Units. *Sci. Rep.* **2012**, *2*:668
(1318) Chen, Q.; Jiang, F.; Yuan, D.; Chen, L.; Lyu, G.; Hong, M. Anion-Driven Self-Assembly: From Discrete Cages to Infinite Polycatenanes Step by Step. *Chem. Commun.* **2013**, *49*, 719–721.
(1319) Guo, H.; Yan, Y.; Wang, N.; Guo, X.; Zheng, G.; Qi, Y. A Series of Entangled Coordination Polymers Assembled by a V-Shaped Bisimidazole Ligand and Various Dicarboxylic Acids: Synthesis, Characterization and Luminescence Properties. *CrystEngComm* **2015**, *17*, 6512–6526.
(1320) Thorp-Greenwood, F. L.; Kulak, A. N.; Hardie, M. J. An Infinite Chainmail of M_6L_6 Metallacycles Featuring Multiple Borromean Links. *Nature Chem.* **2015**, *7*, 526–531.
(1321) Batten, S. R.; Robson, R. Interpenetrating Nets: Ordered, Periodic Entanglement. *Angew. Chem., Int. Ed*. **1998**, *37*, 1460–1494.
(1322) Carlucci, L.; Ciani, G.; Proserpio, D. M. Borromean Links and Other Non-Conventional Links in “Polycatenated” Coordination Polymers: Re-Examination of Some Puzzling Networks Publication. *CrystEngComm* **2003**, *5*, 269–279.
(1323) Carlucci, L.; Ciani, G.; Proserpio, D. M. Polycatenation, Polythreading and Polyknotting in Coordination Network Chemistry. *Coord. Chem. Rev.* **2003**, *246*, 247–289.
(1324) Ke, X.-J.; Li, D.-S.; Du, M. Design and Construction of Self-Penetrating Coordination Frameworks. *Inorg. Chem. Commun.* **2011**, *14*, 788–803.
(1325) Furukawa, S.; Sakata, Y.; Kitagawa, S. Control Over Flexibility of Entangled Porous Coordination Frameworks by Molecular and Mesoscopic Chemistries. *Chem. Lett.* **2013**, *42*, 570–576.
(1326) Yang, G.-P.; Hou, L.; Ma, L.-F.; Wang, Y.-Y. Investigation on the Prime Factors Influencing the Formation of Entangled Metal–Organic Frameworks. *CrystEngComm* **2013**, *15*, 2561–2578.
(1327) Jiang, H.-L.; Makal, T. A.; Zhou, H.-C. Interpenetration Control in Metal–Organic Frameworks for Functional Applications. *Coord. Chem. Rev.* **2013**, *257*, 2232–2249.
(1328) Zhang, S.-Y.; Zhang, Z.; Zaworotko, M. J. Topology, Chirality and Interpenetration in Coordination Polymers. *Chem. Commun.* **2013**, *49*, 9700–9703.
(1329) He, W.-W.; Li, S.-L.; Zang, H.-Y.; Yang, G.-S.; Zhang, S.-R.; Su, Z.-M.; Lan, Y.-Q. Entangled Structures in Polyoxometalate-Based Coordination Polymers. *Coord. Chem. Rev.* **2014**, *279*, 141–160.
(1330) Carlucci, L.; Ciani, G.; Proserpio, D. M.; Mitina, T. G.; Blatov, V. A. Entangled Two-Dimensional Coordination Networks: A General Survey. *Chem. Rev.* **2014**, *114*, 7557–7580.
(1331) Hudson, B.; Vinograd, J. Catenated Circular DNA Molecules in HeLa Cell Mitochondria. *Nature* **1967**, *216*, 647–652.
(1332) Seeman, N. C. Nucleic Acid Nanostructures and Topology. *Angew. Chem., Int. Ed*. **1998**, *37*, 3220–3238.
(1333) Seeman, N. C. An Overview of Structural DNA Nanotechnology. *Mol. Biotechnol.* **2007**, *37*, 246–257.
(1334) Aldaye, F. A.; Sleiman, H. F. Supramolecular DNA Nanotechnology. *Pure Appl. Chem*. **2009**, *81*, 2157–2181.
(1335) Endo, M.; Sugiyama, H. Chemical Approaches to DNA Nanotechnology. *ChemBioChem* **2009**, *10*, 2420–2443.
(1336) Jester, S.-S.; Famulok, M. Mechanically Interlocked DNA Nanostructures for Functional Devices. *Acc. Chem. Res.* **2014**, *47*, 1700–1709.
(1337) Liu, X.; Lu, C.-H.; Willner, I. Switchable Reconfiguration of Nucleic Acid Nanostructures by Stimuli-Responsive DNA Machines. *Acc. Chem. Res.* **2014**, *47*, 1673–1680.
(1338) Seeman, N. C.; Chen, J.; Du, S. M.; Mueller, J. E.; Zhang, Y.; Fu, T. J.; Wang, Y.; Wang, H.; Zhang, S. Synthetic DNA Knots and Catenanes. *New J. Chem*. **1993**, 739–755.
(1339) Mitsui, Y.; Langridge, R.; Shortle, B. E.; Cantor, C. R.; Grant, R. C.; Kodama, M.; Wells, R. D. Physical and Enzymatic Studies on Poly d(I–C). Poly d(I–C), an Unusual Double-Helical DNA. *Nature* **1970**, *228*, 1166–1169.
(1340) Soyfer, V. N.; Potaman, V. N. *Triple Helical Nucleic Acids*; Springer: New York, 1995.
(1341) Burge, S.; Parkinson, G. N.; Hazel, P.; Todd, A. K.; Neidle, S. Quadruplex DNA: Sequence, Topology and Structure. *Nucleic Acids Res.* **2006**, *34*, 5402–5415.
(1342) Holliday, R. A Mechanism for Gene Conversion in Fungi. *Genet. Res.* **1964**, *5*, 282–304.
(1343) Seeman, N. C. Nucleic Acid Junctions and Lattices. *J. Theor. Biol.* **1982**, *99*, 237–247.
(1344) Seeman, N. C.; Kallenbach, N. R. Design of Immobile Nucleic Acid Junctions. *Biophys. J.* **1983**, *44*, 201–209.
(1345) Seeman, N. C. Interactive Design and Manipulation of Macro-Molecular Architecture Utilizing Nucleic Acid Junctions. *J. Mol. Graphics* **1985**, *3*, 34–39.
(1346) Seeman, N. C. De Novo Design of Sequences for Nucleic Acid Structural Engineering. *J. Biomol. Struct. Dynam.* **1990**, *8*, 573–581.
(1347) Kallenbach, N. R.; Ma, R.-I.; Seeman, N. C. An Immobile Nucleic Acid Junction Constructed From Oligonucleotides. *Nature* **1983**, *305*, 829–831.
(1348) Ma, R.-I.; Kallenbach, N. R.; Sheardy, R. D.; Petrillo, M. L.; Seeman, N. C. Three-Arm Nucleic Acid Junctions Are Flexible. *Nucleic Acids Res.* **1986**, *14*, 9745–9753.
(1349) Wang, Y.; Mueller, J. E.; Kemper, B.; Seeman, N. C. Assembly and Characterization of Five-Arm and Six-Arm DNA Branched Junctions. *Biochemistry* **1991**, *30*, 5667–5674.
(1350) Lu, M.; Guo, Q.; Marky, L. A.; Seeman, N. C.; Kallenbach, N. R. Thermodynamics of DNA Branching. *J. Mol. Biol.* **1992**, *223*, 781–789.
(1351) Chen, J.; Seeman, N. C. Synthesis From DNA of a Molecule with the Connectivity of a Cube. *Nature* **1991**, *350*, 631–633.
(1352) Fu, T. J.; Tse-Dinh, Y.-C.; Seeman, N. C. Holliday Junction Crossover Topology. *J. Mol. Biol.* **1994**, *236*, 91–105.
(1353) Mueller, J. E.; Du, S. M.; Seeman, N. C. Design and Synthesis of a Knot From Single-Stranded DNA. *J. Am. Chem. Soc.* **1991**, *113*, 6306–6308.
(1354) Du, S. M.; Seeman, N. C. The Construction of a Trefoil Knot From a DNA Branched Junction Motif. *Biopolymers* **1994**, *34*, 31–37.
(1355) Du, S. M.; Stollar, B. D.; Seeman, N. C. A Synthetic DNA Molecule in Three Knotted Topologies. *J. Am. Chem. Soc.* **1995**, *117*, 1194–1200.
(1356) Du, S. M.; Wang, H.; Tse-Dinh, Y.-C.; Seeman, N. C. Topological Transformations of Synthetic DNA Knots. *Biochemistry* **1995**, *34*, 673–682.
(1357) Du, S. M.; Seeman, N. C. Synthesis of a DNA Knot Containing Both Positive and Negative Nodes. *J. Am. Chem. Soc.* **1992**, *114*, 9652–9655.
(1358) Flapan, E.; Seeman, N. C. A Topological Rubber Glove Obtained From a Synthetic Single-Stranded DNA Molecule. *J. Chem. Soc., Chem. Commun*. **1995**, 2249–2250.
(1359) Mao, C.; Sun, W.; Seeman, N. C. Assembly of Borromean Rings From DNA. *Nature* **1997**, *386*, 137–138.
(1360) Zhang, Y.; Seeman, N. C. A Solid-Support Methodology for the Construction of Geometrical Objects From DNA. *J. Am. Chem. Soc.* **1992**, *114*, 2656–2663.
(1361) Zhang, Y.; Seeman, N. C. Construction of a DNA-Truncated Octahedron. *J. Am. Chem. Soc.* **1994**, *116*, 1661–1669.

(1362) Bath, J.; Turberfield, A. J. DNA Nanomachines. *Nature Nanotechnol.* **2007**, *2*, 275–284.
(1363) Goodman, R. P.; Schaap, I. A.; Tardin, C. F.; Erben, C. M.; Berry, R. M.; Schmidt, C. F.; Turberfield, A. J. Rapid Chiral Assembly of Rigid DNA Building Blocks for Molecular Nanofabrication. *Science* **2005**, *310*, 1661–1665.
(1364) Erben, C. M.; Goodman, R. P.; Turberfield, A. J. A Self-Assembled DNA Bipyramid. *J. Am. Chem. Soc.* **2007**, *129*, 6992–6993.
(1365) Fu, T. J.; Seeman, N. C. DNA Double-Crossover Molecules. *Biochemistry* **1993**, *32*, 3211–3220.
(1366) Li, X.; Yang, X.; Qi, J.; Seeman, N. C. Antiparallel DNA Double Crossover Molecules as Components for Nanoconstruction. *J. Am. Chem. Soc.* **1996**, *118*, 6131–6140.
(1367) Winfree, E.; Liu, F.; Wenzler, L. A.; Seeman, N. C. Design and Self-Assembly of Two-Dimensional DNA Crystals. *Nature* **1998**, *394*, 539–544.
(1368) Zadegan, R. M.; Norton, M. L. Structural DNA Nanotechnology: From Design to Applications. *Int. J. Mol. Sci.* **2012**, *13*, 7149–7162.
(1369) LaBean, T. H.; Yan, H.; Kopatsch, J.; Liu, F.; Winfree, E.; Reif, J. H.; Seeman, N. C. Construction, Analysis, Ligation, and Self-Assembly of DNA Triple Crossover Complexes. *J. Am. Chem. Soc.* **2000**, *122*, 1848–1860.
(1370) Yan, H.; Park, S. H.; Finkelstein, G.; Reif, J. H.; LaBean, T. H. DNA-Templated Self-Assembly of Protein Arrays and Highly Conductive Nanowires. *Science* **2003**, *301*, 1882–1884.
(1371) He, Y.; Ye, T.; Su, M.; Zhang, C.; Ribbe, A. E.; Jiang, W.; Mao, C. Hierarchical Self-Assembly of DNA Into Symmetric Supramolecular Polyhedra. *Nature* **2008**, *452*, 198–201.
(1372) Zhang, C.; Su, M.; He, Y.; Zhao, X.; Fang, P.-A.; Ribbe, A. E.; Jiang, W.; Mao, C. Conformational Flexibility Facilitates Self-Assembly of Complex DNA Nanostructures. *Proc. Natl. Acad. Sci. U.S.A.* **2008**, *105*, 10665–10669.
(1373) Ohayon, Y. P.; Sha, R.; Flint, O.; Chandrasekaran, A. R.; Abdallah, H. O.; Wang, T.; Wang, X.; Zhang, X.; Seeman, N. C. Topological Linkage of DNA Tiles Bonded by Paranemic Cohesion. *ACS Nano* **2015**, *9*, 10296–10303.
(1374) Vinograd, J.; Lebowitz, J.; Radloff, R.; Watson, R.; Laipis, P. The Twisted Circular Form of Polyoma Viral DNA. *Proc. Natl. Acad. Sci. U.S.A.* **1965**, *53*, 1104–1111.
(1375) Trifonov, E. N.; Sussman, J. L. The Pitch of Chromatin DNA Is Reflected in Its Nucleotide Sequence. *Proc. Natl. Acad. Sci. U.S.A.* **1980**, *77*, 3816–3820.
(1376) Ulanovsky, L.; Bodner, M.; Trifonov, E. N.; Choder, M. Curved DNA: Design, Synthesis, and Circularization. *Proc. Natl. Acad. Sci. U.S.A.* **1986**, *83*, 862–866.
(1377) Ryan, K.; Kool, E. T. Triplex-Directed Self-Assembly of an Artificial Sliding Clamp on Duplex DNA. *Chem. Biol.* **1998**, *5*, 59–67.
(1378) Escudé, C.; Garestier, T.; Hélène, C. Padlock Oligonucleotides for Duplex DNA Based on Sequence-Specific Triple Helix Formation. *Proc. Natl. Acad. Sci. U.S.A.* **1999**, *96*, 10603–10607.
(1379) Roulon, T.; Hélène, C.; Escudé, C. Coupling of a Targeting Peptide to Plasmid DNA Using a New Type of Padlock Oligonucleotide. *Bioconjugate Chem.* **2002**, *13*, 1134–1139.
(1380) Ackermann, D.; Schmidt, T. L.; Hannam, J. S.; Purohit, C. S.; Heckel, A.; Famulok, M. A Double-Stranded DNA Rotaxane. *Nature Nanotechnol.* **2010**, *5*, 436–442.
(1381) Ackermann, D.; Jester, S.-S.; Famulok, M. Design Strategy for DNA Rotaxanes with a Mechanically Reinforced PX100 Axle. *Angew. Chem., Int. Ed.* **2012**, *51*, 6771–6775.
(1382) Ackermann, D.; Famulok, M. Pseudo-Complementary PNA Actuators as Reversible Switches in Dynamic DNA Nanotechnology. *Nucleic Acids Res.* **2013**, *41*, 4729–4739.
(1383) Rasched, G.; Ackermann, D.; Schmidt, T. L.; Broekmann, P.; Heckel, A.; Famulok, M. DNA Minicircles with Gaps for Versatile Functionalization. *Angew. Chem., Int. Ed*. **2008**, *47*, 967–970.
(1384) Schmidt, T. L.; Heckel, A. Construction of a Structurally Defined Double-Stranded DNA Catenane. *Nano Lett.* **2011**, *11*, 1739–1742.
(1385) Lohmann, F.; Valero, J.; Famulok, M. A Novel Family of Structurally Stable Double Stranded DNA Catenanes. *Chem. Commun.* **2014**, *50*, 6091–6093.
(1386) Wu, Z.-S.; Shen, Z.; Tram, K.; Li, Y. Engineering Interlocking DNA Rings with Weak Physical Interactions. *Nature Commun.* **2014**, *5*:4279.
(1387) Kumar, R.; El-Sagheer, A.; Tumpane, J.; Lincoln, P.; Wilhelmsson, L. M.; Brown, T. Template-Directed Oligonucleotide Strand Ligation, Covalent Intramolecular DNA Circularization and Catenation Using Click Chemistry. *J. Am. Chem. Soc.* **2007**, *129*, 6859–6864.
(1388) Liu, Y.; Kuzuya, A.; Sha, R.; Guillaume, J.; Wang, R.; Canary, J. W.; Seeman, N. C. Coupling Across a DNA Helical Turn Yields a Hybrid DNA/Organic Catenane Doubly Tailed with Functional Termini. *J. Am. Chem. Soc.* **2008**, *130*, 10882–10883.
(1389) Onizuka, K.; Nagatsugi, F.; Ito, Y.; Abe, H. Automatic Pseudorotaxane Formation Targeting on Nucleic Acids Using a Pair of Reactive Oligodeoxynucleotides. *J. Am. Chem. Soc.* **2014**, *136*, 7201–7204.
(1390) Sannohe, Y.; Sugiyama, H. Single Strand DNA Catenane Synthesis Using the Formation of G-Quadruplex Structure. *Bioorg. Med. Chem.* **2012**, *20*, 2030–2034.
(1391) Rothemund, P. W. K. Folding DNA to Create Nanoscale Shapes and Patterns. *Nature* **2006**, *440*, 297–302.
(1392) Andersen, E. S.; Dong, M.; Nielsen, M. M.; Jahn, K.; Subramani, R.; Mamdouh, W.; Golas, M. M.; Sander, B.; Stark, H.; Oliveira, C. L. P.; Pedersen, J. S.; Birkedal, V.; Besenbacher, F.; Gothelf, K. V.; Kjems, J. Self-Assembly of a Nanoscale DNA Box with a Controllable Lid. *Nature* **2009**, *459*, 73–76.
(1393) Han, D.; Pal, S.; Nangreave, J.; Deng, Z.; Liu, Y.; Yan, H. DNA Origami with Complex Curvatures in Three-Dimensional Space. *Science* **2011**, *332*, 342–346.
(1394) Castro, C. E.; Kilchherr, F.; Kim, D.-N.; Shiao, E. L.; Wauer, T.; Wortmann, P.; Bathe, M.; Dietz, H. A Primer to Scaffolded DNA Origami. *Nature Meth.* **2011**, *8*, 221–229.
(1395) Marras, A. E.; Zhou, L.; Su, H.-J.; Castro, C. E. Programmable Motion of DNA Origami Mechanisms. *Proc. Natl. Acad. Sci. U.S.A.* **2015**, *112*, 712–718.
(1396) Nilsson, M.; Malmgren, H.; Samiotaki, M.; Kwiatkowski, M.; Chowdhary, B. P.; Landegren, U. Padlock Probes: Circularizing Oligonucleotides for Localized DNA Detection. *Science* **1994**, *265*, 2085–2088.
(1397) Demidov, V. V.; Kuhn, H.; Lavrentieva-Smolina, I. V.; Frank-Kamenetskii, M. D. Peptide Nucleic Acid-Assisted Topological Labeling of Duplex DNA. *Methods* **2001**, *23*, 123–131.
(1398) Liang, X.; Kuhn, H.; Frank-Kamenetskii, M. D. Monitoring Single-Stranded DNA Secondary Structure Formation by Determining the Topological State of DNA Catenanes. *Biophys. J.* **2006**, *90*, 2877–2889.
(1399) Fujimoto, K.; Matsuda, S.; Yoshimura, Y.; Ami, T.; Saito, I. Reversible Photopadlocking on Double-Stranded DNA. *Chem. Commun*. **2007**, 2968–2970.
(1400) Weizmann, Y.; Braunschweig, A. B.; Wilner, O. I.; Cheglakov, Z.; Willner, I. A Polycatenated DNA Scaffold for the One-Step Assembly of Hierarchical Nanostructures. *Proc. Natl. Acad. Sci. U.S.A.* **2008**, *105*, 5289–5294.
(1401) Elbaz, J.; Cecconello, A.; Fan, Z.; Govorov, A. O.; Willner, I. Powering the Programmed Nanostructure and Function of Gold Nanoparticles with Catenated DNA Machines. *Nature Commun.* **2013**, *4*:2000.
(1402) Cecconello, A.; Lu, C.-H.; Elbaz, J.; Willner, I. Au Nanoparticle/DNA Rotaxane Hybrid Nanostructures Exhibiting Switchable Fluorescence Properties. *Nano Lett.* **2013**, *13*, 6275–6280.

(1403) Elbaz, J.; Wang, Z.-G.; Wang, F.; Willner, I. Programmed Dynamic Topologies in DNA Catenanes. *Angew. Chem., Int. Ed*. **2012**, *51*, 2349–2353.
(1404) Lu, C.-H.; Cecconello, A.; Elbaz, J.; Credi, A.; Willner, I. A Three-Station DNA Catenane Rotary Motor with Controlled Directionality. *Nano Lett.* **2013**, *13*, 2303–2308.
(1405) Qi, X.-J.; Lu, C.-H.; Cecconello, A.; Yang, H.-H.; Willner, I. A Two-Ring Interlocked DNA Catenane Rotor Undergoing Switchable Transitions Across Three States. *Chem. Commun.* **2014**, *50*, 4717–4720.
(1406) Lu, C.-H.; Qi, X.-J.; Cecconello, A.; Jester, S.-S.; Famulok, M.; Willner, I. Switchable Reconfiguration of an Interlocked DNA Olympiadane Nanostructure. *Angew. Chem., Int. Ed*. **2014**, *53*, 7499–7503.
(1407) Hu, L.; Lu, C.-H.; Willner, I. Switchable Catalytic DNA Catenanes. *Nano Lett.* **2015**, *15*, 2099–2103.
(1408) Liang, C.; Mislow, K. Topological Chirality of Proteins. *J. Am. Chem. Soc.* **1994**, *116*, 3588–3592.
(1409) Liang, C.; Mislow, K. Knots in Proteins. *J. Am. Chem. Soc.* **1994**, *116*, 11189–11190.
(1410) Liang, C.; Mislow, K. Topological Features of Protein Structures: Knots and Links. *J. Am. Chem. Soc.* **1995**, *117*, 4201–4213.
(1411) McDonald, N. Q.; Hendrickson, W. A. A Structural Superfamily of Growth Factors Containing a Cystine Knot Motif. *Cell* **1993**, *73*, 421–424.
(1412) Bayro, M. J.; Mukhopadhyay, J.; Swapna, G. V. T.; Huang, J. Y.; Ma, L.-C.; Sineva, E.; Dawson, P. E.; Montelione, G. T.; Ebright, R. H. Structure of Antibacterial Peptide Microcin J25: A 21-Residue Lariat Protoknot. *J. Am. Chem. Soc.* **2003**, *125*, 12382–12383.
(1413) Rosengren, K. J.; Clark, R. J.; Daly, N. L.; Göransson, U.; Jones, A.; Craik, D. J. Microcin J25 Has a Threaded Sidechain-to-Backbone Ring Structure and Not a Head-to-Tail Cyclized Backbone. *J. Am. Chem. Soc.* **2003**, *125*, 12464–12474.
(1414) Yan, L. Z.; Dawson, P. E. Design and Synthesis of a Protein Catenane. *Angew. Chem., Int. Ed*. **2001**, *40*, 3625–3627.
(1415) Blankenship, J. W.; Dawson, P. E. Thermodynamics of a Designed Protein Catenane. *J. Mol. Biol.* **2003**, *327*, 537–548.
(1416) Jeffrey, P. D.; Gorina, S.; Pavletich, N. P. Crystal Structure of the Tetramerization Domain of the p53 Tumor Suppressor at 1.7 Ångstroms. *Science* **1995**, *267*, 1498–1502.
(1417) Dawson, P. E.; Muir, T. W.; Clark-Lewis, I.; Kent, S. B. Synthesis of Proteins by Native Chemical Ligation. *Science* **1994**, *266*, 776–779.
(1418) Sánchez-Quesada, J.; Saghatelian, A.; Cheley, S.; Bayley, H.; Ghadiri, M. R. Single DNA Rotaxanes of a Transmembrane Pore Protein. *Angew. Chem., Int. Ed*. **2004**, *43*, 3063–3067.
(1419) Song, L.; Hobaugh, M. R.; Shustak, C.; Cheley, S.; Bayley, H.; Gouaux, J. E. Structure of Staphylococcal α-Hemolysin, a Heptameric Transmembrane Pore. *Science* **1996**, *274*, 1859–1865.
(1420) Kasianowicz, J. J.; Brandin, E.; Branton, D.; Deamer, D. W. Characterization of Individual Polynucleotide Molecules Using a Membrane Channel. *Proc. Natl. Acad. Sci. U.S.A.* **1996**, *93*, 13770–13773.
(1421) Branton, D.; Deamer, D. W.; Marziali, A.; Bayley, H.; Benner, S. A.; Butler, T.; Di Ventra, M.; Garaj, S.; Hibbs, A.; Huang, X.; B'Jovanovich, S.; Krstic, P. S.; Lindsay, S.; Ling, X. S.; Mastrangelo, C. H.; Meller, A.; Oliver, J. S.; Pershin, Y. V.; Ramsey, J. M.; Riehn, R.; Soni, G. V.; Tabard-Cossa, V.; Wanunu, M.; Wiggin, M.; Schloss, J. A. The Potential and Challenges of Nanopore Sequencing. *Nat. Biotechnol.* **2008**, *26*, 1146–1153.
(1422) Schneider, G. F.; Dekker, C. DNA Sequencing with Nanopores. *Nature Biotechnol.* **2012**, *30*, 326–328.
(1423) Cockroft, S. L.; Chu, J.; Amorin, M.; Ghadiri, M. R. A Single-Molecule Nanopore Device Detects DNA Polymerase Activity with Single-Nucleotide Resolution. *J. Am. Chem. Soc.* **2008**, *130*, 818–820.
(1424) Chu, J.; González-López, M.; Cockroft, S. L.; Amorin, M.; Ghadiri, M. R. Real-Time Monitoring of DNA Polymerase Function and Stepwise Single-Nucleotide DNA Strand Translocation Through a Protein Nanopore. *Angew. Chem., Int. Ed*. **2010**, *49*, 10106–10109.
(1425) Biesemans, A.; Soskine, M.; Maglia, G. A Protein Rotaxane Controls the Translocation of Proteins Across a ClyA Nanopore. *Nano Lett.* **2015**, *15*, 6076–6081.
(1426) Saito, S.; Takahashi, E.; Nakazono, K. Synthesis of [2]Rotaxanes by the Catalytic Reactions of a Macrocyclic Copper Complex. *Org. Lett.* **2006**, *8*, 5133–5136.
(1427) Saito, S. Synthesis of Interlocked Compounds Utilizing the Catalytic Activity of Macrocyclic Phenanthroline–Cu Complexes. *J. Incl. Phenom. Macrocycl. Chem.* **2015**, *82*, 437–451.
(1428) Aucagne, V.; Berná, J.; Crowley, J. D.; Goldup, S. M.; Hänni, K. D.; Leigh, D. A.; Lusby, P.; Ronaldson, V. E.; Slawin, A. M. Z.; Viterisi, A.; Walker, D. B. Catalytic "Active-Metal" Template Synthesis of [2]Rotaxanes, [3]Rotaxanes, and Molecular Shuttles, and Some Observations on the Mechanism of the Cu(I)-Catalyzed Azide-Alkyne 1,3-Cycloaddition. *J. Am. Chem. Soc.* **2007**, *129*, 11950–11963.
(1429) Worrell, B. T.; Malik, J. A.; Fokin, V. V. Direct Evidence of a Dinuclear Copper Intermediate in Cu(I)-Catalyzed Azide-Alkyne Cycloadditions. *Science* **2013**, *340*, 457–460.
(1430) Goldup, S. M.; Leigh, D. A.; Long, T.; McGonigal, P.; Symes, M.; Wu, J. Active Metal Template Synthesis of [2]Catenanes. *J. Am. Chem. Soc.* **2009**, *131*, 15924–15929.
(1431) Chean, H. M.; Leigh, D. A.; Maffei, F.; McGonigal, P. R.; Slawin, A. M. Z.; Wu, J. En Route to a Molecular Sheaf: Active Metal Template Synthesis of a [3]Rotaxane with Two Axles Threaded Through One Ring. *J. Am. Chem. Soc.* **2011**, *133*, 12298–12303.
(1432) Barran, P. E.; Cole, H. L.; Goldup, S. M.; Leigh, D. A.; McGonigal, P. R.; Symes, M. D.; Wu, J.; Zengerle, M. Active-Metal Template Synthesis of a Molecular Trefoil Knot. *Angew. Chem., Int. Ed*. **2011**, *50*, 12280–12284.
(1433) Lewandowski, B.; De Bo, G.; Ward, J. W.; Papmeyer, M.; Kuschel, S.; Aldegunde, M. J.; Gramlich, P. M. E.; Heckmann, D.; Goldup, S. M.; D'Souza, D. M.; Fernandez, A. E.; Leigh, D. A. Sequence-Specific Peptide Synthesis by an Artificial Small-Molecule Machine. *Science* **2013**, *339*, 189–193.
(1434) Lahlali, H.; Jobe, K.; Watkinson, M.; Goldup, S. M. Macrocycle Size Matters: "Small" Functionalized Rotaxanes in Excellent Yield Using the CuAAC Active Template Approach. *Angew. Chem., Int. Ed*. **2011**, *50*, 4151–4155.
(1435) Winn, J.; Pinczewska, A.; Goldup, S. M. Synthesis of a Rotaxane Cu^{I} Triazolide Under Aqueous Conditions. *J. Am. Chem. Soc.* **2013**, *135*, 13318–13321.
(1436) Bordoli, R. J.; Goldup, S. M. An Efficient Approach to Mechanically Planar Chiral Rotaxanes. *J. Am. Chem. Soc.* **2014**, *136*, 4817–4820.
(1437) Neal, E. A.; Goldup, S. M. Chemical Consequences of Mechanical Bonding in Catenanes and Rotaxanes: Isomerism, Modification, Catalysis and Molecular Machines for Synthesis. *Chem. Commun.* **2014**, *50*, 5128–5142.
(1438) Langton, M. J.; Xiong, Y.; Beer, P. D. Active-Metal Template Synthesis of a Halogen-Bonding Rotaxane for Anion Recognition. *Chem. Eur. J.* **2015**, *21*, 18910–18914.
(1439) Tron, A.; Thornton, P. J.; Kauffmann, B.; Tucker, J. H. R.; McClenaghan, N. D. [2]Rotaxanes Comprising a Macrocylic Hamilton Receptor Obtained Using Active Template Synthesis: Synthesis and Guest Complexation. *Supramol. Chem*. **2016**, *28*, 1–9.
(1440) Sato, Y.; Yamasaki, R.; Saito, S. Synthesis of [2]Catenanes by Oxidative Intramolecular Diyne Coupling Mediated by

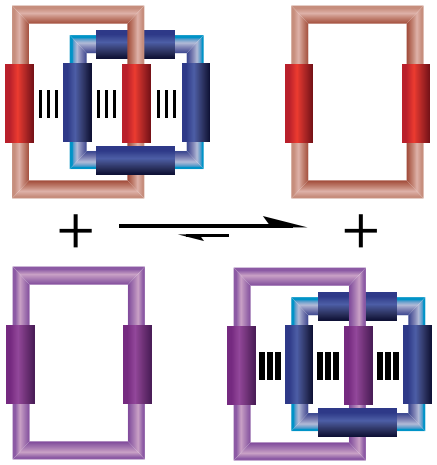
Macrocyclic Copper(I) Complexes. *Angew. Chem., Int. Ed*. **2009**, *48*, 504–507.
(1441) Hayashi, R.; Wakatsuki, K.; Yamasaki, R.; Mutoh, Y.; Kasama, T.; Saito, S. Synthesis of Rotacatenanes by the Combination of Cu-Mediated Threading Reaction and the Template Method: The Dual Role of One Ligand. *Chem. Commun.* **2013**, *50*, 204–206.
(1442) Movsisyan, L. D.; Kondratuk, D. V.; Franz, M.; Thompson, A. L.; Tykwinski, R. R.; Anderson, H. L. Synthesis of Polyyne Rotaxanes. *Org. Lett*. **2012**, *14*, 3424–3426.
(1443) Langton, M. J.; Matichak, J. D.; Thompson, A. L.; Anderson, H. L. Template-Directed Synthesis of π-Conjugated Porphyrin [2]Rotaxanes and a [4]Catenane Based on a Six-Porphyrin Nanoring. *Chem. Sci.* **2011**, *2*, 1897–1901.
(1444) Franz, M.; Januszewski, J. A.; Wendinger, D.; Neiss, C.; Movsisyan, L. D.; Hampel, F.; Anderson, H. L.; Görling, A.; Tykwinski, R. R. Cumulene Rotaxanes: Stabilization and Study of [9]Cumulenes. *Angew. Chem., Int. Ed.* **2015**, *54*, 6645–6649.
(1445) Weisbach, N.; Baranová, Z.; Gauthier, S.; Reibenspies, J. H.; Gladysz, J. A. A New Type of Insulated Molecular Wire: A Rotaxane Derived From a Metal-Capped Conjugated Tetrayne. *Chem. Commun.* **2012**, *48*, 7562–7564.
(1446) Ugajin, K.; Takahashi, E.; Yamasaki, R.; Mutoh, Y.; Kasama, T.; Saito, S. Synthesis of [2]Rotaxanes by the Copper-Mediated Threading Reactions of Aryl Iodides with Alkynes. *Org. Lett.* **2013**, *15*, 2684–2687.
(1447) Berná, J.; Goldup, S. M.; Lee, A.-L.; Leigh, D. A.; Symes, M. D.; Teobaldi, G.; Zerbetto, F. Cadiot-Chodkiewicz Active Template Synthesis of Rotaxanes and Switchable Molecular Shuttles with Weak Intercomponent Interactions. *Angew. Chem., Int. Ed*. **2008**, *47*, 4392–4396.
(1448) Hoekman, S.; Kitching, M. O.; Leigh, D. A.; Papmeyer, M.; Roke, D. Goldberg Active Template Synthesis of a [2]Rotaxane Ligand for Asymmetric Transition-Metal Catalysis. *J. Am. Chem. Soc.* **2015**, *137*, 7656–7659.
(1449) Goldberg, I. Ueber Phenylirungen bei Gegenwart von Kupfer als Katalysator. *Ber. Dtsch. Chem. Ges.* **1906**, *39*, 1691–1692.
(1450) Strieter, E. R.; Bhayana, B.; Buchwald, S. L. Mechanistic Studies on the Copper-Catalyzed *N*-Arylation of Amides. *J. Am. Chem. Soc.* **2009**, *131*, 78–88.
(1451) Crowley, J. D.; Hänni, K. D.; Leigh, D. A.; Slawin, A. M. Z. Diels-Alder Active-Template Synthesis of Rotaxanes and Metal-Ion-Switchable Molecular Shuttles. *J. Am. Chem. Soc.* **2010**, *132*, 5309–5314.
(1452) *Zinc Catalysis : Applications in Organic Synthesis*; Enthaler, S.; Wu, X.-F., Eds.; Wiley-VCH: Weinheim, 2016.
(1453) Enthaler, S. Rise of the Zinc Age in Homogeneous Catalysis? *ACS Catal.* **2013**, *3*, 150–158.
(1454) Wu, X.-F.; Neumann, H. Zinc-Catalyzed Organic Synthesis: C-C, C-N, C-O Bond Formation Reactions. *Adv. Synth. Catal.* **2012**, *354*, 3141–3160.
(1455) Miyaura, N.; Suzuki, A. Palladium-Catalyzed Cross-Coupling Reactions of Organoboron Compounds. *Chem. Rev.* **1995**, *95*, 2457–2483.
(1456) Beletskaya, I. P.; Cheprakov, A. V. The Heck Reaction as a Sharpening Stone of Palladium Catalysis. *Chem. Rev.* **2000**, *100*, 3009–3066.
(1457) Negishi, E.-I.; Anastasia, L. Palladium-Catalyzed Alkynylation. *Chem. Rev*. **2003**, *103*, 1979–2018.
(1458) Johansson Seechurn, C. C. C.; Kitching, M. O.; Colacot, T. J.; Snieckus, V. Palladium-Catalyzed Cross-Coupling: A Historical Contextual Perspective to the 2010 Nobel Prize. *Angew. Chem., Int. Ed*. **2012**, *51*, 5062–5085.
(1459) Heck, R. F.; Nolley, J. P., Jr. Palladium-Catalyzed Vinylic Hydrogen Substitution Reactions with Aryl, Benzyl, and Styryl Halides. *J. Org. Chem.* **1972**, *37*, 2320–2322.
(1460) Heck, R. F. Palladium-Catalyzed Reactions of Organic Halides with Olefins. *Acc. Chem. Res.* **1979**, *12*, 146–151.
(1461) Negishi, E.-I. Magical Power of Transition Metals: Past, Present, and Future (Nobel Lecture). *Angew. Chem., Int. Ed*. **2011**, *50*, 6738–6764.
(1462) Suzuki, A. Cross-Coupling Reactions of Organoboranes: An Easy Way to Construct C-C Bonds (Nobel Lecture). *Angew. Chem., Int. Ed*. **2011**, *50*, 6722–6737.
(1463) Crowley, J. D.; Hänni, K. D.; Lee, A.-L.; Leigh, D. A. [2]Rotaxanes Through Palladium Active-Template Oxidative Heck Cross-Couplings. *J. Am. Chem. Soc*. **2007**, *129*, 12092–12093.
(1464) Goldup, S. M.; Leigh, D. A.; Lusby, P. J.; McBurney, R. T.; Slawin, A. M. Z. Active Template Synthesis of Rotaxanes and Molecular Shuttles with Switchable Dynamics by Four-Component Pd^{II}-Promoted Michael Additions. *Angew. Chem., Int. Ed*. **2008**, *47*, 3381–3384.
(1465) Berná, J.; Crowley, J. D.; Goldup, S. M.; Hänni, K. D.; Lee, A.-L.; Leigh, D. A. A Catalytic Palladium Active-Metal Template Pathway to [2]Rotaxanes. *Angew. Chem., Int. Ed*. **2007**, *46*, 5709–5713.
(1466) Keim, W. Nickel: an Element with Wide Application in Industrial Homogeneous Catalysis. *Angew. Chem., Int. Ed*. **1990**, *29*, 235–244.
(1467) Tasker, S. Z.; Standley, E. A.; Jamison, T. F. Recent Advances in Homogeneous Nickel Catalysis. *Nature* **2014**, *509*, 299–309.
(1468) Crowley, J. D.; Goldup, S. M.; Gowans, N. D.; Leigh, D. A.; Ronaldson, V. E.; Slawin, A. M. Z. An Unusual Nickel-Copper-Mediated Alkyne Homocoupling Reaction for the Active-Template Synthesis of [2]Rotaxanes. *J. Am. Chem. Soc.* **2010**, *132*, 6243–6248.
(1469) Goldup, S. M.; Leigh, D. A.; McBurney, R. T.; McGonigal, P. R.; Plant, A. Ligand-Assisted Nickel-Catalysed sp^3–sp^3 Homocoupling of Unactivated Alkyl Bromides and Its Application to the Active Template Synthesis of Rotaxanes. *Chem. Sci.* **2010**, *1*, 383–386.

Chapter 3 Making Mechanical Bonds Under Thermodynamic Control

Conspectus

Making mechanical bonds employing concepts and protocols where finely balanced and environmentally sensitive equilibria in solution or in melts are in the order of minutes or hours or days or weeks or even months and patience is a virtue, has opened doors to the production of mechanically interlocked molecules (MIMs) that have so far remained out of reach using more conventional 'billiard-ball' chemistry—that is, the time-honored approach to chemical synthesis where, given reactant substrate molecules, ions or radicals, there is no going back: the desired products and undesired byproducts are what they are when the reaction is terminated. Replacing 'one-way' reactions under kinetic control with 'two-way', and ultimately 'multiple-way', processes under thermodynamic control not only engenders the need for out-of-the-box retrosynthetic analysis but it also calls for a mindset change on the part of synthetic chemists purveying their practice in the laboratory.

The concept of slippage offers a unique opportunity to synthesize rotaxanes without making or breaking any strong covalent or coordinative bonds and with one hundred percent atom efficiency: it can be looked upon as a physical synthesis as opposed to a chemical one. The conceptual framework wherein slippage lies relates to the logic of fuzzy sets that define the relationship between pseudorotaxanes (complexes) and rotaxanes (molecules). There is no fine dividing line between pseudorotaxanes and rotaxanes, where the former may be regarded (i) as being high in rotaxane character if its component parts exhibit slow exchange kinetics and high association constants and (ii) as being low in rotaxane character if it associates more weakly and exchanges more rapidly. Slippage is a manifestation of rotaxanes not sharing topological links along with their mechanical bonds and therefore being able to overcome either steric or electrostatic barriers that discourage them from dissociating. Since both slippage and deslipping are highly condition-dependent, with solvent and temperature playing decisive roles, finding stereoelectronic matches between stoppers—both neutral and charged—in addition to controlling the templation arising from molecular recognition between the dumbbells and the rings that is dictated by noncovalent bonding interactions, that are (i) hydrophobic, (ii) hydrogen-bonded, (iii) donor-acceptor, (iv) radical etc. in nature, is a chance event. If only computational chemistry could make the leap from providing rationalizations after the chance event to being predictive ahead of the practice, then the synthetic utility of slippage would be enhanced beyond being simply a hit or miss activity in the laboratory. The importance of gaining a good fundamental understanding of slippage and deslipping is taking on more urgency as the design and synthesis of molecular machines that work away from equilibrium gathers momentum.



Although kinetically controlled reactions account for the lion's share of the production of chemical compounds, there are a relatively small, yet significant, number of reactions that proceed under thermodynamic control which means that at the same time as chemical bonds—covalent and coordinative ones for the most part—are being made, they are also being broken. This brand of chemistry in which combinatorial libraries of molecules are engaged in dynamic equilibrium processes involving reversible reactions is often referred to as dynamic covalent chemistry or DCC for short. Not only is the time it takes for reactions to reach equilibrium dependent on conditions such as solvent, temperature and concentration, but also the outcome of the reactions with special reference to the product composition can be swayed by the presence of templates and other additives. It is also not uncommon to be able to isolate products that are trapped in kinetic energy wells. The ability to be able to control the free energy landscape means that the thermodynamic parameters can often be amplified by the presence of a template or simply by a subtle change in solvent composition. Such was the case during the application of DCC to the synthesis of the first wholly synthetic molecular Borromean rings (BRs)—three rings linked in such a manner that should one be cleaved, the other two rings will fall apart. When the BR crystallization solvents were changed from methanol/diethyl ether to a 3:1 mixture of *n*-propyl ether and methanol/diethyl ether, a Solomon link, or doubly interlocked [2]catenane, crystallizes as a racemic mixture of topological enantiomers. A similar outcome can be achieved when the metal templates constitute a 1:1 mixture of zinc(II) and copper(II), whereas either metal template on its own affords only the Borromean rings! Aside from these two transition metal ions, (i) metal-ligand pairs that are kinetically labile under mild conditions, yet thermodynamically stable, have embraced much of the Periodic Table in the pursuit of MIMs, while the (ii) condensation and exchange of (coordinative) imine, hydrazone, and boronic ester bonds, along with (iii) the range of thermodynamically controllable olefin metathesis under the spell of the right catalysts, (iv) the redox reversibility associated with disulfide bond formation and cleavage, (v) reversible nucleophilic substitutions and additions, and (vi) reversible surface bonds, especially those involving the formation of self-assembled monolayers on gold, have all occupied pride of place in the promotion of DCC when it comes to producing MIMs with the greatest of ease. So far, a relatively small collection of reactions that are subject to equilibrium control has provided ready access to mechanically interlocked architectures and topologies, some of which can only be described as exotic in the extreme.

The Nature of the Mechanical Bond: From Molecules to Machines, First Edition. Carson J. Bruns and J. Fraser Stoddart.
© 2017 John Wiley & Sons, Inc. Published 2017 by John Wiley & Sons, Inc.

Introduction **271**
3.1 Slippage **271**
3.1.1 Pseudorotaxane or Rotaxane? 273
3.1.2 Slippage of π-Donor/π-Acceptor Rotaxanes 275
3.1.3 Slippage of Hydrogen-Bonded Rotaxanes 278
3.1.4 Slippage Driven by Hydrophobic Interactions 283
3.1.5 Slippage of Anion-Binding Rotaxanes 284
3.1.6 Triumphs and Tribulations of Slippage 285
3.2 Self-Assembling Metallo-Organic MIMs **285**
3.2.1 MIMs Possessing Group 10 Elements 285
3.2.1.1 Homophilic Catenation of Pd^{II}/Pt^{II} Assemblies 285
3.2.1.2 Pd^{II} Metallacyclic Catenates 288
3.2.1.3 Aqueous Catenation of Pd^{II}/Pt^{II} Metallacycles 289
3.2.1.4 Donor-Acceptor Metallacyclic Catenanes 289
3.2.1.5 Pd^{II} and Pt^{II} Stoppered Rotaxanes 290
3.2.2 MIMs Possessing Group 11 Elements 292
3.2.2.1 Gold MIMs 292
3.2.2.2 Silver MIMs 293
3.2.2.3 Copper MIMs 295
3.2.3 MIMs Possessing Group 12 Elements 297
3.2.3.1 Zinc MIMs 297
3.2.3.2 Mercury MIMs 297
3.2.4 MIMs Possessing Elements of Groups 7–9 298
3.2.4.1 Self-Assembled Metalloporphyrin MIMs 298
3.2.4.2 Iron MIMs 300
3.2.4.3 Ruthenium and Rhodium MIMs 300
3.2.4.4 Osmium MIMs 301
3.2.4.5 Cobalt MIMs 301
3.2.5 MIMs Possessing Alkaline Earth Elements 302
3.2.5.1 Mechanically Interlocked Grignard Reagents 302
3.2.5.2 Barium Catenanes 302
3.3 Mechanical Bond Formation by Condensation **303**
3.3.1 Imines 303
3.3.1.1 Coordinative Imine Bonding 303
3.3.1.2 Clipping With Imine Exchange 305
3.3.1.3 Stoppering With Imine Exchange 309
3.3.2 Hydrazones 310
3.3.3 Boronic Esters and Boroxines 312
3.4 Mechanical Bond Formation by Olefin Metathesis **313**
3.4.1 Ring-Closing Metathesis (RCM) 314
3.4.1.1 RCM in Metal-Templated MIMs 314
3.4.1.2 RCM in Donor-Acceptor MIMs 316
3.4.1.3 RCM in Hydrogen-Bonded MIMs 319
3.4.1.4 RCM in Anion-Binding MIMs 320
3.4.1.5 RCM in Ion-Paired MIMs 322
3.4.2 Cross Metathesis (CM) 323
3.5 Mechanical Bond Formation by Reversible Nucleophilic Reactions **324**
3.5.1 Disulfide Exchange 324
3.5.1.1 Rotaxanes Obtained by Disulfide Exchange 325
3.5.1.2 Catenanes Obtained by Disulfide Exchange 326

3.5.2 Reversible Nucleophilic Substitutions 328
3.5.2.1 Dynamic S_N1 329
3.5.2.2 Dynamic S_N2 329
3.5.3 Michael Additions 330
3.6 Surface-Mounted MIMs 330
Conclusions and Outlook 333
References 333

Introduction

Although the world of MIMs was built in the beginning around kinetically controlled reactions (**Chapter 2**), thermodynamically controlled approaches—i.e., those that employ reversible bond-forming and bond-breaking reactions and processes—have made considerable inroads during the past couple of decades, rendering the synthesis of MIMs even easier and more efficient, with yields approaching unity from starting materials that are all but commercially available in many cases. In more than a few instances, these equilibrium-orchestrated approaches have resulted in new molecular topologies and architectures (**Chapter 4**) becoming available. Indeed, the gateway to the strict self-assembly[1] of MIMs at thermodynamic equilibrium constitutes the growing collection of dynamic reactions summarized in this Chapter. A particular stronghold in this respect is the concept of dynamic covalent chemistry[2–9] (DCC)[A] in which combinatorial libraries of molecules in dynamic equilibrium, undergoing reversible reactions, respond to templates or other additives according to their free energies of binding, such that certain compounds, including interlocked species on occasion, can be selected and amplified under appropriate conditions. Many of the recognition motifs discussed in **Chapter 2** will reappear here in a thermodynamically controlled regime. Thermodynamic approaches to the self-assembly of MIMs have been addressed[10–13] in a number of reviews. We will focus in this Chapter on discrete molecules, rather than macromolecules,[14,15] with mechanical bonds, although the two categories often overlap and many of the same dynamic reactions are relevant to both topics.

The strategies outlined here for making mechanical bonds, which include slippage (**Section 3.1**), metallosupramolecular self-assembly (**Section 3.2**), condensation (**Section 3.3**), olefin metathesis (**Section 3.4**), dynamic nucleophilic reactions (**Section 3.5**), and the formation of surface monolayers (**Section 3.6**), can be combined with those discussed in **Chapter 2** to provide a comprehensive picture of how mechanical bonds are made, setting the stage for understanding (i) the construction of more sophisticated mechanically interlocked topologies and architectures (**Chapter 4**), (ii) the chirality, isomerism, and dynamics of molecules incorporating mechanical bonds (**Chapter 5**), and (iii) their use as stimulus-responsive mechanical switches and machines (**Chapter 6**).

[A] Dynamic covalent chemistry is also known as dynamic combinatorial chemistry.

3.1 Slippage

Since the mechanical bond in any rotaxane is not a topological link, the ring(s) and dumbbell(s) can be separated, in principle, by applying enough energy to overcome the steric and/or electrostatic barriers that discourage them from dissociating. The difference between a rotaxane and a pseudorotaxane is therefore superficial, in a sense, since the only distinction between them is the height of the activation barrier, $\Delta G^{\ddagger}$, and the corresponding kinetics that govern the timescale over which this 'deslipping' process occurs. Deslipping is the reverse of slippage,[16] in which a ring passes over a dumbbell's stopper to generate a (pseudo)rotaxane. Slippage (**Figure 3.1**) is one of the earliest and most fundamental examples of thermodynamic control in mechanical bond-forming reactions. Since it relies on size complementarity between rings and stoppers, slippage applies only to rotaxanes and rotaxane-like assemblies. The key to any slippage protocol lies in matching the magnitude of the repulsive steric and electronic interactions between rings and stoppers with the amount of available thermal energy. An appropriately designed slippage protocol is characterized by an activation barrier that is insurmountable at a particular temperature, over a practical timescale (of minutes, hours, or days), in a given solvent,

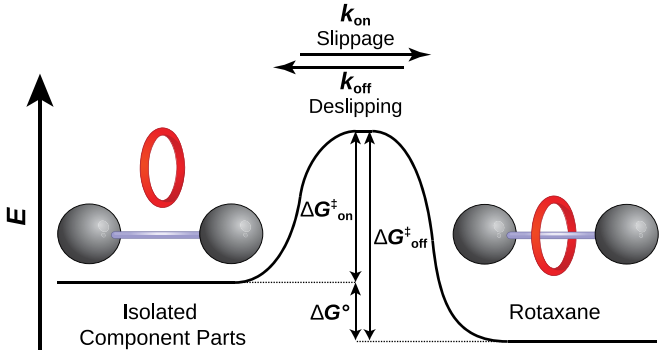


Figure 3.1 Reaction coordinate diagram of rotaxane synthesis relying on slippage.

yet becomes surmountable at higher temperatures, over longer timescales, and/or in different solvents. **Figure 3.1** illustrates diagrammatically the reaction coordinates for the slippage mechanism. Experimentally, the ring and dumbbell are each prepared separately before being heated together in solution or in a melt and cooled back down to yield a kinetically stable rotaxane.

Although the term 'slippage' was coined[17] in the early 1990s, the protocol had been introduced some two decades earlier in the pioneering work of Harrison.[18,19] He prepared 27 different cycloalkanes containing between 14 and 40 methylene groups in their macrorings, and heated them together with approximately equimolar amounts of trityl-stoppered dumbbells in a melt. Analyses of the products revealed that the magic number of carbon atoms required for an all-hydrocarbon macrocycle to slip over a trityl stopper at 120 °C is 29. Products containing more than 29 atoms are kinetically unstable, with both slippage and deslipping occurring rapidly at room temperature, while the barriers to slippage are simply too high for rings with less than 29 carbon atoms. In 1986, Schill[20] revisited Harrison's work and resubjected only the 29-membered ring compound to slippage conditions over the trityl stoppers of dumbbells with varying chain lengths. He found that the yields of rotaxanes rose considerably with increasing chain lengths, reaching a relatively high yield of 11.3% in the case of the longest (38-carbon) chain. See **Section 3.5.2.1** for a more in-depth discussion of these systems.

Recalling that the relationship between the rate constant (k), temperature (T), and the free energy of activation ($\Delta G^{\ddagger}$) of a reaction is given by the Eyring equation (3.1):

$$k = \frac{k_B T}{h} e^{-\Delta G^{\ddagger}/RT} \qquad (3.1)$$

where k_B, h, and R represent the Boltzmann, Planck, and universal gas constants, respectively. The Eyring equation provides a context (**Figure 3.2**) for designing an appropriate slippage motif for a chosen set of experimental conditions. Suppose we want to design a (pseudo)rotaxane in which the rate of deslipping (k_{off}) is slow on the laboratory timescale—let us define 'slow' arbitrarily as having a half-life ($\tau_{1/2}$) of one day (86400 s). Assuming the system obeys first order kinetics, then $\tau_{1/2}$ is given by $\ln(2) \cdot k_{off}^{-1}$. A rotaxane meeting this requirement at room temperature (298 K) would require a deslipping activation barrier $\Delta G^{\ddagger}_{off}$ of $\geq 24.4\ \text{kcal} \cdot \text{mol}^{-1}$. At the temperature (195 K) of an acetone/dry ice bath, however, the same timescale is realized at a very much lower barrier of only $\geq 15.8\ \text{kcal} \cdot \text{mol}^{-1}$. On the other hand, if the magnitude of $\Delta G^{\ddagger}_{on}$ is too great, then the rate of slippage (k_{on}) may be forbidden, to all intents and purposes, even at elevated temperatures. At the boiling point of water (373 K), for example, a half-life of less than one day would require $\Delta G^{\ddagger}_{on} < 30.7\ \text{kcal} \cdot \text{mol}^{-1}$. The relationships between $\Delta G^{\ddagger}$ and $\tau_{1/2}$ at various temperatures are plotted logarithmically in **Figure 3.2**.

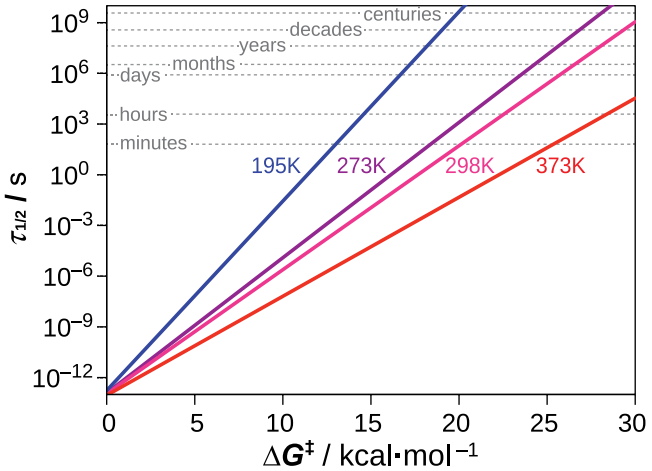


Figure 3.2 Logarithmic plot of the half-life ($\tau_{1/2}$) of a first-order reaction against the activation barriers ($\Delta G^{\ddagger}$) at 195, 273, 298, and 373 K. The dashed lines indicate relevant timescales.

Practically speaking, many shades of grey (**Section 3.1.1**) span the spectrum between what constitutes a rotaxane on the one hand and a pseudorotaxane on the other hand (**Figure 3.3**). To our knowledge, no formal rules are available which describe when it is acceptable to use one term or the other. The most appropriate terminology should therefore depend entirely on context. The same chemical entity might be considered a rotaxane in one environment, i.e., at low temperatures or over short timescales, and a pseudorotaxane in a different context, i.e., at high temperatures or over

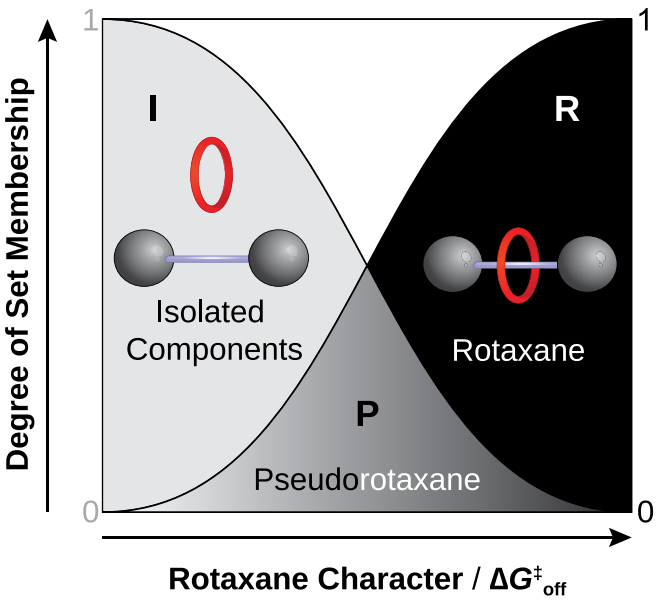


Figure 3.3 Illustration of the fuzzy logic behind pseudorotaxanes, indicating that pseudorotaxanes **P** are a fuzzy set at the intersection of the sets of isolated components **I** and rotaxanes **R**, according to the relationship $\mathbf{P} = [\mathbf{I} \cap \mathbf{R}]$. If the number 0 represents no set membership and the number 1 represents complete set membership, then pseudorotaxanes have characteristics ($0 < \mathbf{P} < 1$) of both sets **I** and **R**.

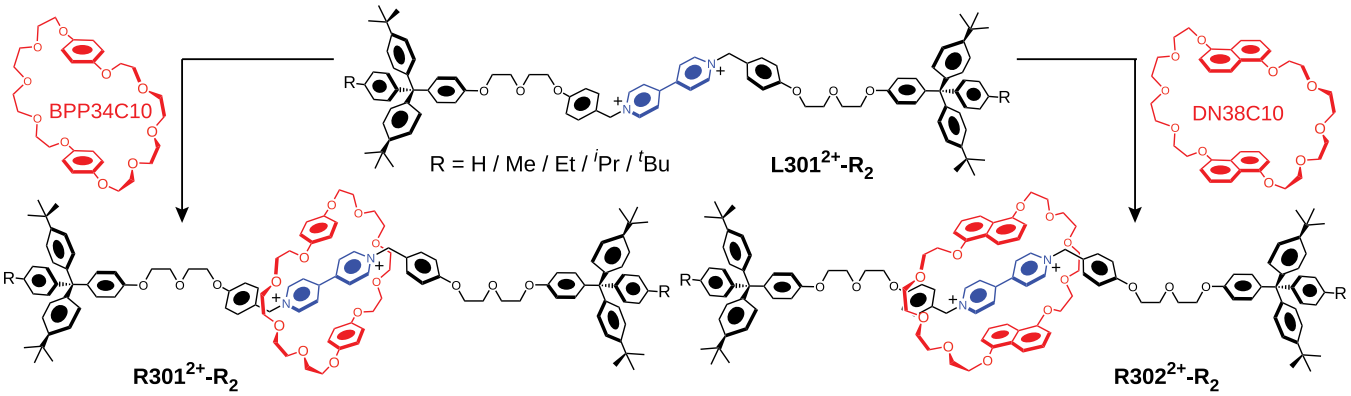
long timescales. This grey area has been explored for a wide variety of different (pseudo)rotaxanes, including those based on π-donor/π-acceptor (**Section 3.1.2**), hydrogen-bonded (**Section 3.1.3**), anion binding (**Section 3.1.4**), and hydrophobic (**Section 3.1.5**) interactions.

3.1.1 Pseudorotaxane or Rotaxane?

The phenomenon of slippage innately draws attention to the differences between a pseudorotaxane and a rotaxane. A rotaxane is generally assumed to be a kinetically stable molecule in which the components never dissociate, while a pseudorotaxane is a kinetically labile complex in which the components exchange freely. Interpreting this definition strictly, one could point out (tongue-in-cheek) that pseudorotaxanes cannot exist in the solid state, since component exchange does not generally occur in highly condensed phases. Even in solution, how do we describe (pseudo)rotaxanes in which dissociation is highly condition-dependent? Since exchange rates are sensitive to temperature—see Equation 3.1 and **Figure 3.2**—this question applies to all pseudorotaxanes and rotaxanes, in principle.

We advocate[21] the logic of fuzzy sets[22] as a conceptual framework for describing chemical entities in the grey area of (pseudo)rotaxanes. Although we refer rather crudely to rotaxanes and pseudorotaxanes in a context-dependent manner, one can invoke fuzzy logic to describe the 'rotaxane character' of a complex. Pseudorotaxanes can thus be understood as a set that lies in between, and possesses characteristics of, both the set of kinetically stable rotaxanes as well as the set of the corresponding isolated components. According to this logic, the transition [isolated molecules → pseudorotaxane → rotaxane] is a gradual one. Pseudorotaxanes that are high in rotaxane character have high association constants and slow exchange kinetics, while pseudorotaxanes that are low in rotaxane character associate more weakly and exchange more rapidly. Fuzzy logic confers a more realistic description (**Figure 3.3**) of these systems, where the pseudorotaxane set (**P**) belongs, to some extent, both to the set of rotaxanes (**R**) and also to the set of isolated molecules (**I**) according to the relationship **P** = [**R** ∩ **I**]. Although our discussion of pseudorotaxanes and rotaxanes remains context-dependent, this logic can be applied to any of the assemblies reviewed in this Section, which are summarized in **Figure 3.4**. We will employ the prefix *pseudo-* parenthetically—i.e., (pseudo) rotaxane—in cases that are in the middle of this fuzzy grey area.

Table 3.1 Summary of slippage conditions for donor-acceptor rotaxanes based on crown ethers (BPP34C10 and DN38C10) and $BIPY^{2+}$ dumbbells with stoppers of various steric bulk.[17,23]



Rotaxane	R	Solvent	*T* / *K*	*P* / atm	Yield / %	$\Delta G^{\ddagger}_{on}$ / kcal·mol^{-1}
R301^{2+}-H$_2$	H	MeCN	333	1	52[a]	↓[a]
		DMF	298	12000	-[a]	↓[a]
R301^{2+}-Me$_2$	Me	MeCN	333	1	45[a]	↓[a]
		DMF	298	12000	-[a]	↓[a]
R301^{2+}-Et$_2$	Et	MeCN	333	1	47	24.5
		DMF	298	12000	-[a]	↓[a]
R301^{2+}-^{i}Pr$_2$	^{i}Pr	MeCN	333	1	0	↑[b]
		DMF	298	12000	19	-
R301^{2+}-^{t}Bu$_2$	^{t}Bu	MeCN	333	1	0	↑[b]
		DMF	298	12000	25	-
R302^{2+}-H$_2$	H	MeCN	308	1	-[a]	↓[a]
R302^{2+}-Me$_2$	Me	MeCN	308	1	-[a]	↓[a]
R302^{2+}-Et$_2$	Et	MeCN	308	1	-[a]	21.3[a]
R302^{2+}-^{i}Pr$_2$	^{i}Pr	MeCN	308	1	57	23.9
R302^{2+}-^{t}Bu$_2$	^{t}Bu	MeCN	313	1	0	↑[b]

[a]Kinetically labile pseudorotaxane. Downward arrow indicates a low activation barrier.
[b]Slippage is forbidden. Upward arrow indicates a high activation barrier.

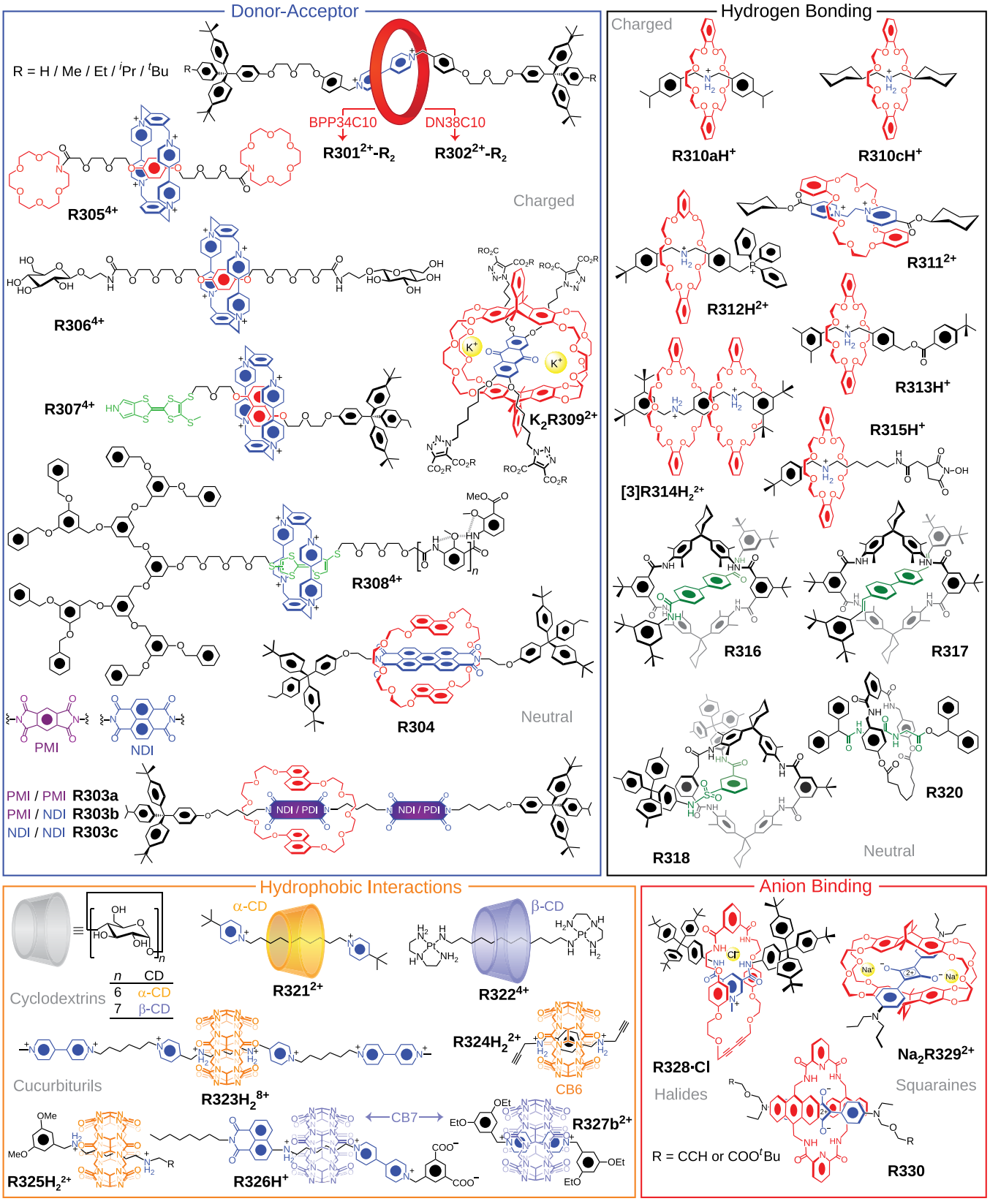


Figure 3.4 A selection of some different types of rotaxanes prepared by slippage.[21,33,46,65,66,70,71,75,77,80,81,83]

3.1.2 Slippage of π-Donor/π-Acceptor Rotaxanes

One of the original template-directed approaches[17] to slippage relied upon the favorable noncovalent bonding interactions—namely, hydrogen bonding, donor-acceptor charge transfer, and π–π stacking—between 4,4′-bipyridinium ($BIPY^{2+}$) dications and electron-rich crown ethers such as bisparaphenylene[34]crown-10 (BPP34C10) and bis-1,5-dinaphtho[38]crown-10 (DN38C10) in order to prepare trityl-capped (pseudo)rotaxanes **R301²⁺-R$_2$** and **R302²⁺-R$_2$**, respectively. **Table 3.1** summarizes the results[23] of varying the steric bulk of the stoppers on the dumbbells **L301²⁺-R$_2$** of these (pseudo)rotaxanes under different experimental conditions. The trityl stoppers comprise two 4-*tert*-butylphenyl (^{t}BuPh) rings and a third ring with a variable functional group R. The stopper that affords the most kinetically stable (pseudo)rotaxane depends on ring size, solvent, temperature, and pressure. The BPP34C10 ring can pass over a stopper no larger than that of **R301²⁺-Et$_2$** (R = Et) at 60 °C in MeCN under atmospheric pressure, whereas it can pass over even the largest stopper (R = ^{t}Bu) to afford **R301²⁺-^{t}Bu$_2$** at 12 kbar of pressure and ambient temperature in DMF. The slightly larger DN38C10 ring slips over a correspondingly larger stopper (R = ^{i}Pr) in MeCN to afford **R302²⁺-^{i}Pr$_2$** as the most kinetically stable derivative in 57% yield. These results indicate that systems falling near the pseudorotaxane/rotaxane borderline are highly sensitive to subtle steric modifications to the stoppers, which result in relatively large differences in the kinetics of the slipping and deslipping processes.

Computational work by Houk[24] has revealed (**Figure 3.5**) a proposed mechanism to explain the origin of the 'all-or-nothing' substituent effect in **R301²⁺-R$_2$**. Focusing on the case of slippage in MeCN, the all-or-nothing effect refers to the fact that yields are reasonable when R = H/Me/Et but drop suddenly to zero when R = ^{i}Pr. It transpires that two main energy barriers are in place as the BPP34C10 ring passes over the stopper and onto the **L301²⁺R$_2$** dumbbell. When R is H or Me, the rate-determining step is the passage of the ring over one of the ^{t}Bu-C_6H_4 units of the stopper. By contrast, when R is Et or ^{i}Pr, passage over the R-C_6H_4 unit becomes the rate-limiting step. The energy barrier increases rapidly as the size of R is increased in this regime—the barrier to pass over the ^{i}Pr group under these conditions was calculated to be at least 21 kcal · mol^{-1} greater than those for any of the smaller stoppers, in good agreement with the experimental results.

Slippage has provided access to a handful of higher-component $BIPY^{2+}$/crown ether MIMs inspired by **R301²⁺-R$_2$** and **R302²⁺-R$_2$**, including linear,[23,25,26] branched,[27,28] and dendritic[29] rotaxanes—see **Sections 4.2.1–4.2.2**—as well as bistable[30] and autonomously[31] photoswitchable [2]rotaxanes—see **Section 6.2.1**. Slippage of the DN38C10 ring has also been utilized[32,33] to prepare neutral π-associated donor-acceptor rotaxanes **R303a**–**R303c** (**Figure 3.4**), which are based on pyromellitic diimide (PMDI) and naphthalene diimide (NDI) recognition units,

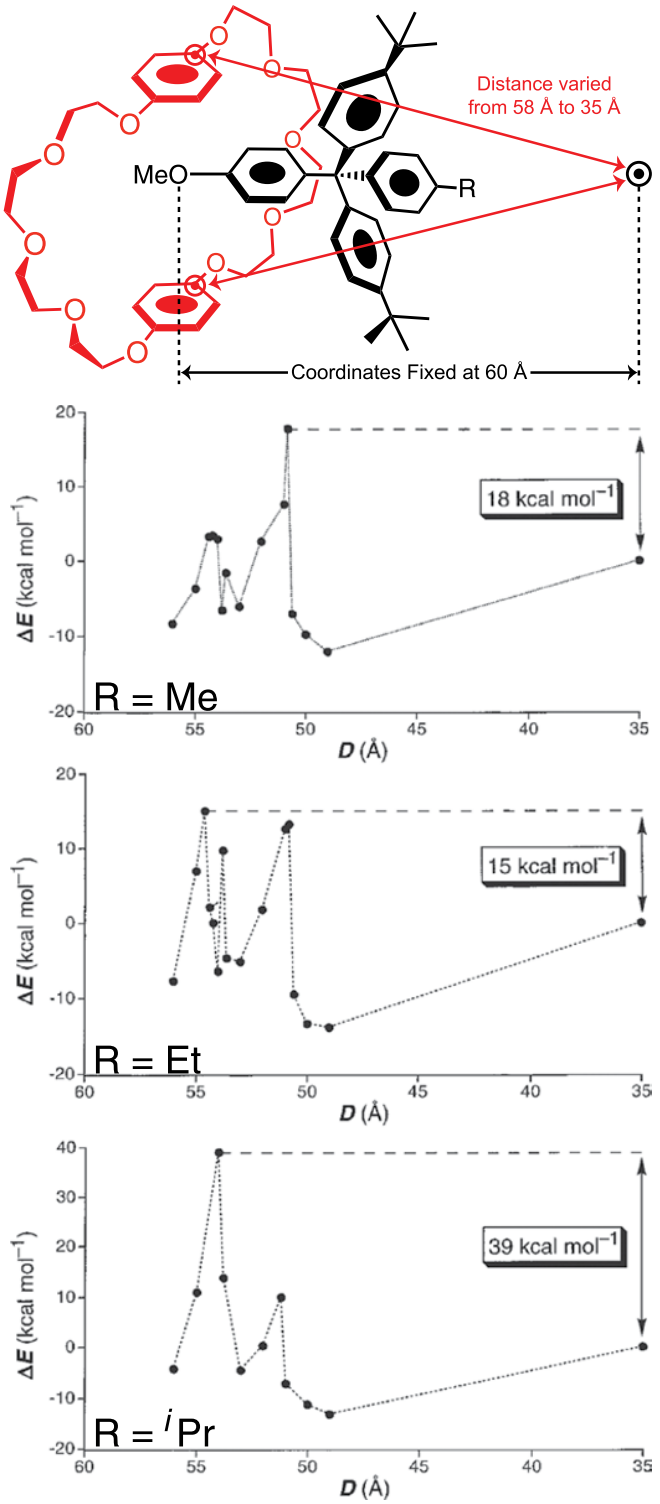
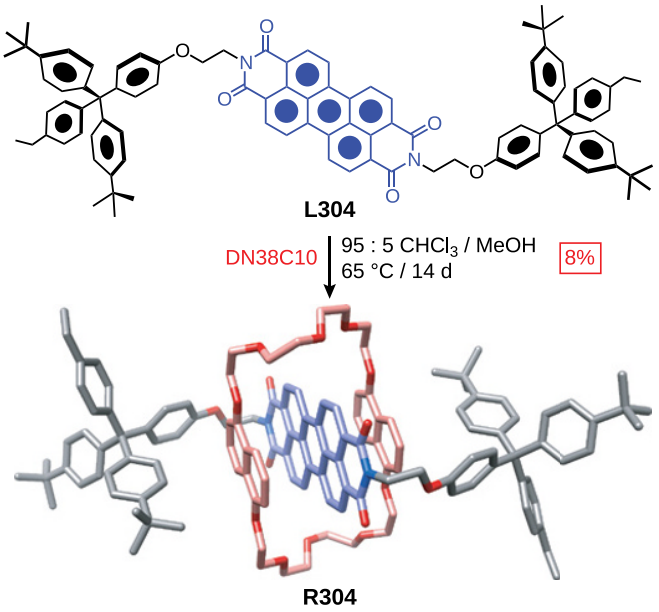


Figure 3.5 Computational evidence for the all-or-nothing substituent effect for the slippage of a BPP34C10 ring over tetraphenyl stoppers.[24] The diagram (top) portrays the geometry and constraints for the ring's passage. The relative energies, determined by energy minimization followed by molecular dynamics, are plotted as a function of the ring's position for different functional groups (R) on the stopper. Data reproduced with permission from ref. 24 (copyright 1998 American Chemical Society)



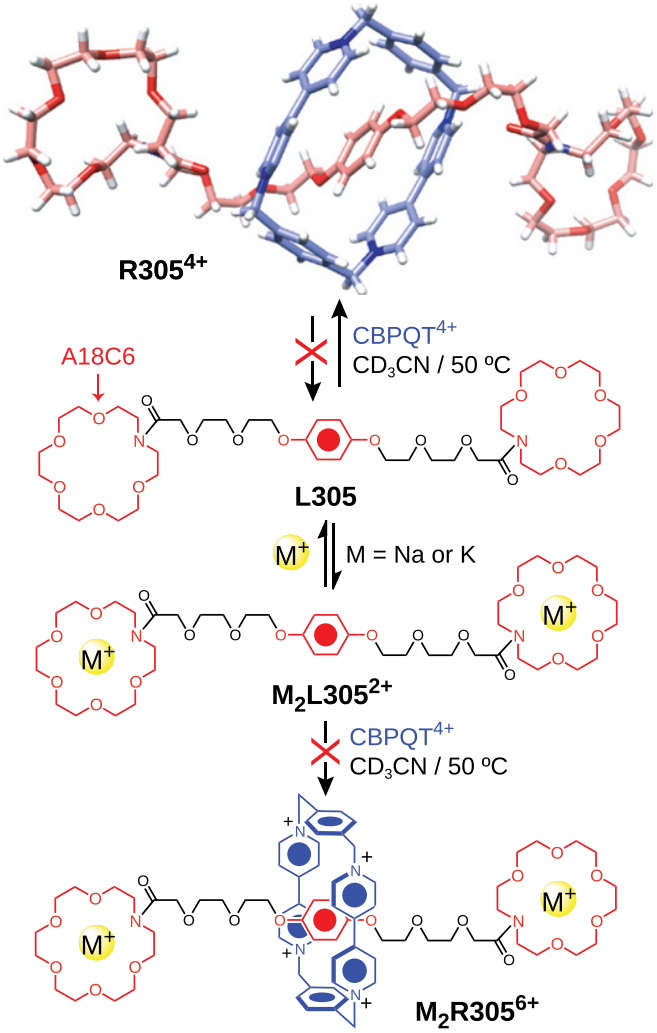
Scheme 3.1 The slippage synthesis of the PDI [2]rotaxane **R304** from **L304** and DN38C10 by Champness.[34] A tubular representation of the rotaxane's solid-state structure is illustrated with hydrogen atoms omitted for the sake of clarity.

as popularized by Sanders—see **Section 2.3.3.2**. Champness[34] has assembled (**Scheme 3.1**) the neutral [2]rotaxane **R304**, possessing a perylene diimide (PDI) recognition unit, by slippage of the DN38C10 ring over its size-matched stopper in the dumbbell **L304**. **R304** was also found to dissociate partially under reducing conditions, since DN38C10 is less attracted to the $PDI^{\bullet-}$ radical anion.

The inverted donor-acceptor recognition motif based on the tetracationic cyclophane, cyclobis(paraquat-*p*-phenylene) ($CBPQT^{4+}$) has also been investigated extensively in the context of slippage. Several examples are illustrated in **Figure 3.4**. These examples all constitute discrete and monodisperse assemblies. One case of a polymeric slippage protocol investigated by Gibson[35] allowed him to elucidate the kinetics associated with the threading of $CBPQT^{4+}$ rings onto polyurethane-based polymers with methylenebis(*p*-phenylisocyanate) recognition units and bisphenol A blocking groups. Without bisphenol A blocking groups, the $CBPQT^{4+}$ rings equilibrate with the polymer in less than one day, whereas a polymer with a 12.5% mass fraction of the blocking groups requires over six months to reach equilibrium!

Aza[18]crown-6 (A18C6) hosts have been investigated[36] (**Scheme 3.2**) as stimulus-responsive slippage stoppers for the $CBPQT^{4+}$ ring of rotaxane $\mathbf{R305^{4+}}$. The ring passes over the A18C6 stoppers of the HQ dumbbell **L305** at 50 °C in CD_3CN. No evidence for deslipping was found, however, even at 80 °C in MeCN. When Na^+ or K^+ ions are taken up by the crown ethers, however, the increased steric and electrostatic interactions between these complexes and the $CBPQT^{4+}$ ring prevent slippage completely. When smaller aza[12]crown-4 endcaps are employed[37] in an analogous system, slipping and deslipping take place rapidly on the ^1H NMR timescale at room temperature.

The slippage synthesis[38] of the donor-acceptor [2]rotaxane $\mathbf{R306^{4+}}$—see **Figure 3.4** for a stereoformula—occurs when the $CBPQT^{4+}$ ring passes over the β-D-glucopyranose stoppers and onto a hydroquinone (HQ) recognition unit over the course of one week at room temperature in aqueous solution. Since the hydrophobic HQ recognition unit is protected from water within the cavity of the $CBPQT^{4+}$ ring, hydrophobic interactions (**Section 3.1.4**) most likely play an important role in this situation.



Scheme 3.2 The cation-binding stoppers of dumbbell **L305** afford[36] a stimulus-responsive slippage regime for the $CBPQT^{4+}$-based rotaxane $\mathbf{R305^{4+}}$. Slippage is allowed over the A18C6 stoppers of **L305**, yet forbidden over $\mathbf{M_2L305^{2+}}$ in the presence of alkali metal cations ($M^+ = Na^+$ or K^+) on account of increased steric and electrostatics of the cation-complexed stoppers. The solid-state structure of $\mathbf{R305^{4+}}$ is illustrated with the PF_6^- counterions omitted for the sake of clarity.

A CBPQT^{4+}-based (pseudo)rotaxane rooted[39,40] firmly in the fuzzy grey area is the half-dumbbell **L307**, which possesses a thiomethyl group as a steric barrier appended to its monopyrrolotetrathiafulvalene (MPTTF) recognition unit. A mixture of **L307** and CBPQT^{4+} rapidly populates the pseudorotaxane **L307**⊂CBPQT^{4+}, in which the CBPQT^{4+} ring encircles the terminal MPTTF unit, but converts (**Figure 3.6**) overnight into the more rotaxane-like species **R307**$^{4+}$ in Me_2CO at 295 K. Exchange occurs over a slow enough timescale to separate the mixture by flash column chromatography at ambient temperature and isolate compound **R307**$^{4+}$ in 20% yield.

A creative use of a synthetic arylamide foldamer as a slippage stopper for CBPQT^{4+} has been realized (**Table 3.2**) by Li[41,42] in the rotaxane **R308**$^{4+}$. In this assembly, a 2-methoxy-1,3-benzamide-based oligomer, which adopts a folded conformation by virtue of hydrogen bonds between neighboring repeating units, serves as a hurdle for the CBPQT^{4+} ring to pass over as it departs from the dumbbell possessing a tetrathiafulvalene dithioether (STTFS) recognition unit. The effect of solvent polarity and the length of this terminal arylamide foldamer has been investigated systematically. Since the strength of hydrogen-bonding interactions are sensitive to the polarity of the medium, the foldamer hurdle should be more difficult to overcome in low polarity solvents, where it adopts a more rigid and well-defined folded structure. Indeed, the deslipping rates slow down by several orders of magnitude as the medium is changed from highly polar solvents (e.g., Me_2SO and DMF) to low-polarity solvents, e.g., $CHCl_3$ and PhMe. Since this effect could also be attributed to a more highly stabilized STTFS⊂CBPQT^{4+}

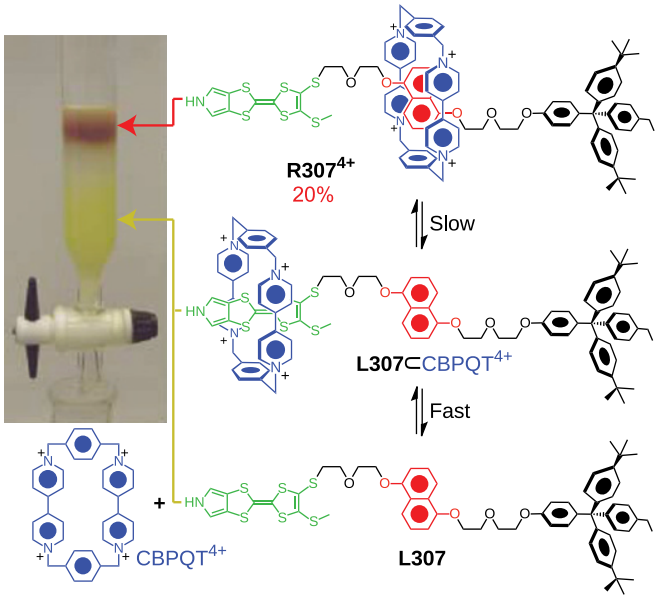
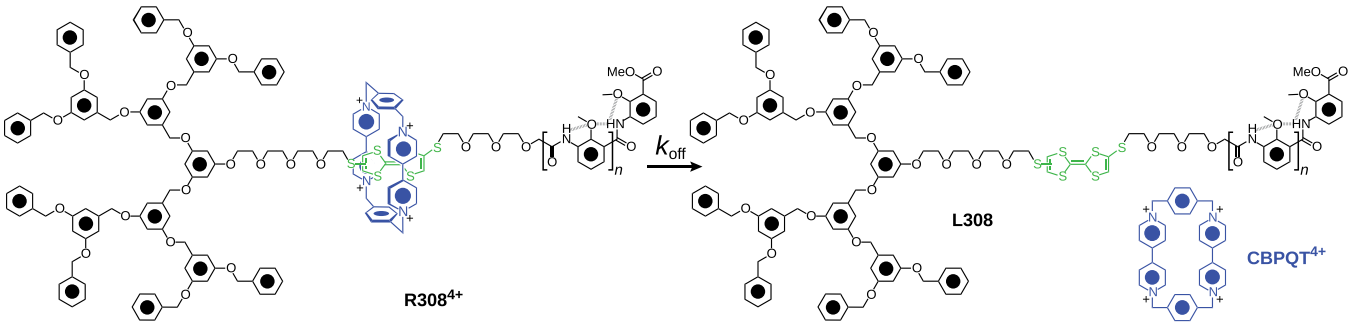
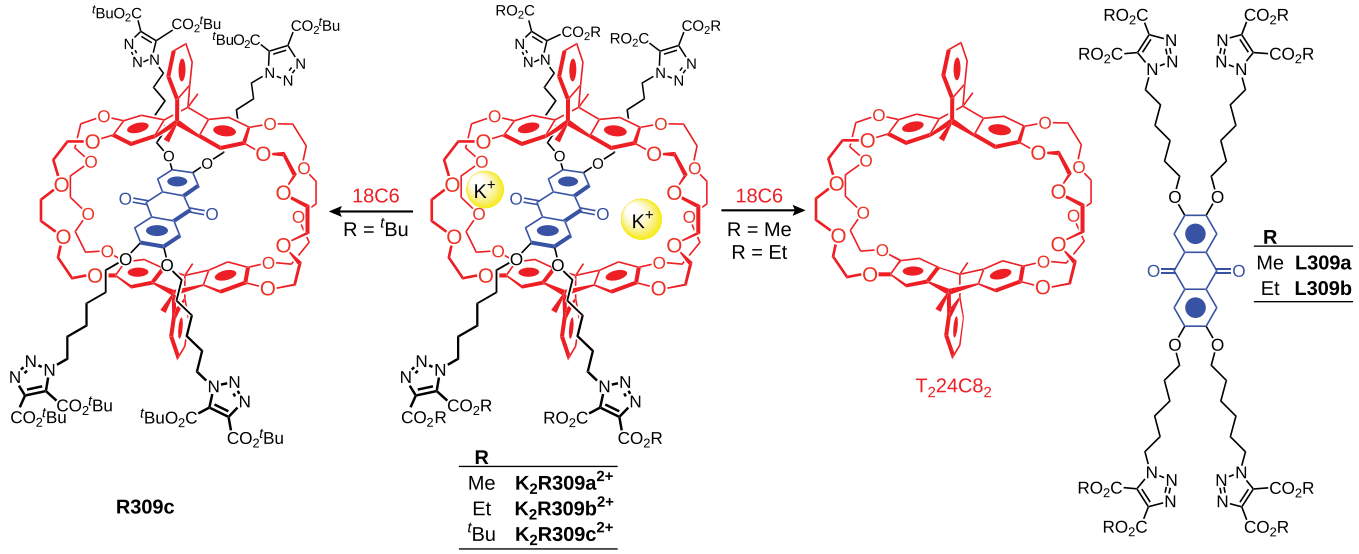


Figure 3.6 The donor-acceptor (pseudo)rotaxane **R307**$^{4+}$ is on the verge of being a rotaxane at 295 K in Me_2CO, since it can be separated from **L307**⊂CBPQT^{4+} on the timescale of a flash column on silica gel. Photograph reprinted with permission from ref. 40 (copyright 2003 Wiley-VCH)

Table 3.2 Deslipping kinetics[42] in foldamer-stoppered (pseudo)rotaxanes **R308**$^{4+}$.



	$n=1$			$n=2$			$n=3$		
Solvent	k_{off} / s^{-1}	$-\Delta G^{\ddagger}_{off}$ / kcal·mol^{-1}	$t_{1/2}$ / s	k_{off} / s^{-1}	$-\Delta G^{\ddagger}_{off}$ / kcal·mol^{-1}	$t_{1/2}$ / s	k_{off} / s^{-1}	$-\Delta G^{\ddagger}_{off}$ / kcal·mol^{-1}	$t_{1/2}$ / s
$CHCl_3$	1.9×10^{-6}	25.2	3.6×10^{5}	1.2×10^{-7}	27.0	5.8×10^{6}	3.6×10^{-7}	27.7	1.9×10^{6}
$ClCH_2CH_2Cl$	7.5×10^{-6}	24.4	9.2×10^{4}	2.0×10^{-7}	26.5	3.5×10^{6}	5.1×10^{-7}	27.5	1.4×10^{6}
THF	2.6×10^{-4}	22.3	2.7×10^{3}	8.3×10^{-6}	24.4	8.5×10^{4}	2.1×10^{-6}	25.1	3.3×10^{5}
$ClCH_2CO_2Et$	1.0×10^{-4}	22.9	6.9×10^{3}	6.7×10^{-6}	24.6	1.0×10^{5}	2.6×10^{-6}	25.1	2.7×10^{5}
C_5H_9CO	7.5×10^{-4}	21.7	9.2×10^{2}	6.0×10^{-5}	23.2	1.2×10^{4}	3.0×10^{-5}	23.9	2.3×10^{4}
$C_6H_{11}CO$	7.8×10^{-4}	21.7	8.8×10^{2}	6.0×10^{-5}	23.2	1.2×10^{4}	2.0×10^{-5}	23.9	3.5×10^{4}
MeCOEt	6.6×10^{-4}	21.8	1.0×10^{3}	6.0×10^{-5}	23.2	1.2×10^{4}	3.0×10^{-5}	23.7	2.3×10^{4}
Me_2CO	8.4×10^{-4}	21.6	8.2×10^{2}	1.3×10^{-4}	22.7	5.3×10^{3}	2.5×10^{-5}	23.7	2.8×10^{4}
PhCN	2.8×10^{-4}	22.3	2.5×10^{3}	2.0×10^{-5}	23.9	3.5×10^{4}	8.9×10^{-6}	24.4	7.8×10^{4}
MeCN	5.2×10^{-4}	21.9	5.5×10^{4}	4.0×10^{-5}	23.4	1.7×10^{4}	9.7×10^{-6}	24.4	7.1×10^{4}
DMF	2.3×10^{-3}	21.0	3.0×10^{2}	4.7×10^{-4}	22.0	1.7×10^{3}	1.0×10^{-4}	22.9	6.9×10^{3}
Me_2SO	1.0×10^{-3}	21.4	6.9×10^{2}	1.1×10^{-4}	22.9	6.3×10^{3}	4.0×10^{-5}	23.4	1.7×10^{4}



Scheme 3.3 When the potassium ions are removed from the donor-acceptor [2]rotaxanes **K_2R309a^{2+}**–**K_2R309c^{2+}**, their macrotricyclic $T_2$24C8$_2$ crown ethers are subject to deslipping if the triazole diester stoppers are sufficiently small (R = Me, Et), owing to the expansion of the ring and loss of complex stability in the absence of K^+ templates.[43]

interaction in low polarity media, the effect of foldamer length is another important piece of evidence for the claim that the dynamic structure of the foldamer influences deslipping kinetics. The results in **Table 3.2** show that deslipping rates slow down as the foldamer is lengthened. Since folded conformations are better stabilized in the longer sequences, it follows that the folding of the benzamide oligomer is responsible for slowing down the deslipping rates of the CBPQT^{4+} ring. This system can be used to tune the deslipping kinetics across a wide range of timescales, since the deslipping half-lives span from as low as 300 seconds (n = 1 in DMF) to as high as 67 days (n = 2 in $CHCl_3$) and everywhere in between.

Chen[43] has investigated the ion-sensitive slipping and deslipping (**Scheme 3.3**) of the triptycene-based macrotricyclic polyether $T_2$24C8$_2$—see **Section 2.3.3.7**—with respect to anthraquinone dumbbells possessing triazole diester stoppers of varying size. In the presence of K^+ templates, the [2]rotaxanes **K_2R309a^{2+}**–**K_2R309c^{2+}** are all kinetically stable. The removal of the K^+ ions from these assemblies with [18]crown-6 (18C6) results in deslipping when the dumbbell stoppers carry methyl (**L309a**) or ethyl (**L309b**) esters, whereas the ^{t}Bu esters of **R309c** are bulky enough to prevent deslipping.

3.1.3 Slippage of Hydrogen-Bonded Rotaxanes

Slippage of hydrogen-bonded rotaxanes can be subdivided into charged and neutral motifs.

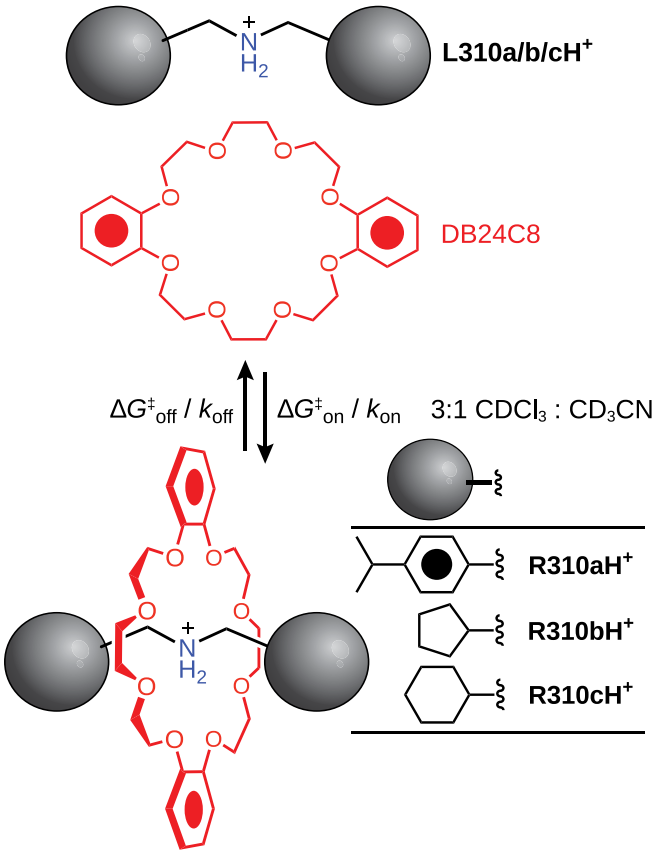
Slippage of Charged Hydrogen-Bonded Rotaxanes

The fuzzy grey area becomes[21] most apparent under conditions where it is difficult to distinguish between a rotaxane and pseudorotaxane. This situation first came to our attention while studying[21] the slippage of hydrogen-bonded *dialkylammonium⊂DB24C8* complexes. The slippage (**Table 3.3**) of a DB24C8 ring over the *p*-isopropylphenyl (^{i}PrC$_6$H$_4$), cyclopentyl (*c*-C$_5$H$_9$), and cyclohexyl (*c*-C$_6$H$_{11}$) stoppers of the dialkylammonium dumbbells of rotaxanes **R310aH$^+$**, **R310bH$^+$**, and **R310cH$^+$**, respectively, occurs over relatively long timescales. Using ^{1}H NMR spectroscopy to monitor the molecular distribution in a 3:1 mixture of $CDCl_3$ and CD_3CN, it was found that equilibrium is reached in 9.5 days for **R310aH$^+$** and 90 min for **R310bH$^+$** at 20 °C, while **R310cH$^+$** requires several weeks at 40 °C. Although the [2]rotaxane **R310cH$^+$** is kinetically stable in this low polarity medium, the DB24C8 ring dissociates from its cyclohexyl-stoppered dumbbell with a half-life of 100 min in Me_2SO. Tokunaga[44] has found that the rate of slippage in the synthesis of **R310cH$^+$** is sensitive to pressure,[B] proceeding 20 times faster at 5000 kg·cm^{-2} than at 1 kg·cm^{-2}. The cyclopentyl stopper has recently been utilized[45] in the context of molecular machines for designing a pseudorotaxane prototype that exhibits one-way motion—see **Section 6.12.2.2**.

The substituent effects for deslipping in crown ether/dialkylammonium rotaxanes have been investigated (**Figure 3.7**) in computational methods[21] similar to those carried out by Houk[24]—see **Figure 3.5** in the previous Section. The position of the –NH_2^+– center is fixed with respect to an arbitrary site 6 nm away, and the distance between one of the atoms of the DB24C8 ring and the fixed reference point is decreased stepwise from 56.5 to 38 Å. These constraints

[B] In the same investigation, Tokunaga found that the slippage of tetrabenzo[24]crown-8 over a dibenzylammonium dumbbell is also a pressure-sensitive process with even more negative activation volumes, indicating a more beneficial effect of pressure on the reaction.

Table 3.3 Summary[21] of the activation barriers and rate constants for slippage and deslipping of DB24C8 over the dialkylammonium dumbbells of (pseudo)rotaxanes **R310aH⁺–R310cH⁺**.



	T °C	k_{on} $M^{-1}\cdot s^{-1}$	k_{off} s^{-1}	$\Delta G^{\ddagger}_{on}$	$\Delta G^{\ddagger}_{off}$	$\Delta G°$
				kcal·mol⁻¹		
R310aH⁺	20	1.1×10^{-3}	3.9×10^{-7}	–21.1	–25.7	–4.7
	40	3.2×10^{-3}	1.3×10^{-6}	–21.9	–26.8	–4.9
R310bH⁺	20	8.2×10^{-2}	2.8×10^{-4}	–18.6	–21.9	–3.3
	40	1.4×10^{-1}	1.3×10^{-3}	–19.6	–22.5	–2.9
R310cH⁺	40	2.9×10^{-5}	2.6×10^{-7}	–24.9	–27.8	–2.9

force the ring to move along the dumbbell and eventually pass over the stopper as an energy-minimizing geometry optimization is performed at each step. The plots in **Figure 3.7** reveal that a significant energy barrier must be overcome for isopropyl- and *tert*-butyl functionalized benzyl stoppers, but not for a simple benzyl stopper. Likewise, cycloheptyl and cyclohexyl stoppers constitute a significant steric barrier for the ring to overcome, yet a cyclopentyl stopper presents only a small obstacle for the ring's passage.

The size complementarity between cyclohexyl stoppers and DB24C8 for rings has been adapted by Loeb[46] to assemble a 1,2-bis(pyridinium)ethane (BPE^{2+})-based rotaxane **$R311^{2+}$**. The kinetics of slippage and deslipping over the dumbbell **$L311^{2+}$** in four solvent systems are summarized in **Table 3.4**. **$R311^{2+}$** is high in rotaxane character in CD_3CN and binary $CDCl_3$:CD_3CN solvents, with half-lives for deslipping on the order of days to months—e.g., 287 days in MeCN—whereas deslipping is complete in only a few minutes in $(CD_3)_2SO$. Note that this rotaxane contains donor-acceptor interactions (**Section 3.1.2**) between the benzo rings in DB24C8 and the BPE^{2+} unit, in addition to significant [C–H···O] hydrogen-bonding interactions between the polyether loops and α-pyridinium protons. These interactions clearly contribute to the kinetic stability

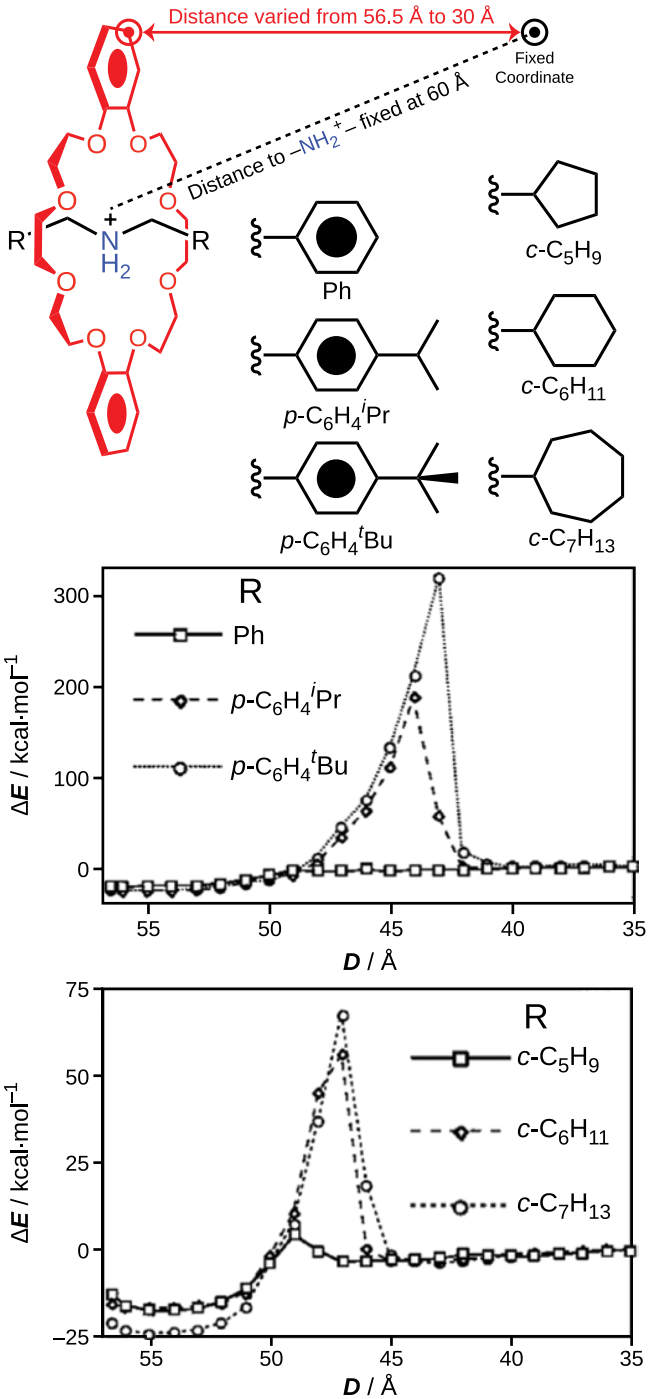
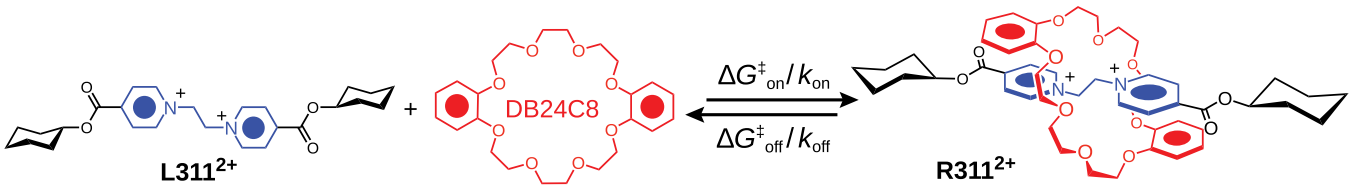


Figure 3.7 Computational evidence for the all-or-nothing substituent effect for the slippage of the DB24C8 ring over *para*-substituted benzyl stoppers and cycloalkane stoppers.[21] The diagram (top) portrays the geometry and constraints for the ring's passage. The relative energies, determined by energy minimization, are plotted as a function of the ring's position for different stoppers. Data reproduced with permission from ref. 21 (copyright 1998 American Chemical Society)

Table 3.4 The solvent-dependent parameters[46] for slippage in the BPE^{2+}/DB24C8 (pseudo)rotaxane **R311**$^{2+}$.



Solvent	T K	k_{off} s^{-1}	$\Delta G^{\ddagger}_{off}$ kcal·mol^{-1}	$\tau_{1/2}$ h	k_{on} s^{-1}	$\Delta G^{\ddagger}_{on}$ kcal·mol^{-1}	$\tau_{1/2}$ s	$\Delta G°$ kcal·mol^{-1}
CD_3CN	298	1.68×10^{-6}	–25.32	115	4.33×10^{-3}	–20.67	161	–4.66
CD_3CN : $CDCl_3$ (1:1)	298	2.10×10^{-6}	–25.19	92	2.81×10^{-3}	–20.92	245	–4.25
CD_3CN : $CDCl_3$ (2:1)	298	3.02×10^{-6}	–24.97	64	1.59×10^{-3}	–21.27	436	–3.70
$(CD_3)_2SO$	298	4.19×10^{-3}	–20.69	0.046	- [a]	- [a]	- [a]	- [a]

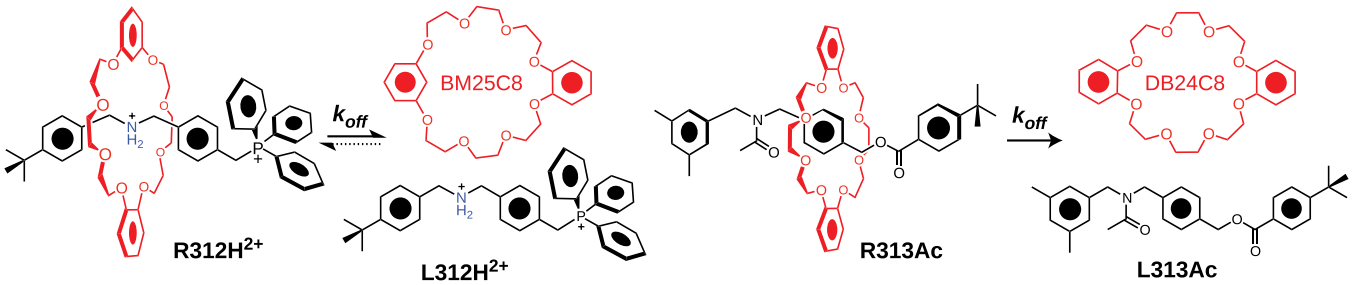
[a]A rate could not be measured because the association constant is negligibly small.

of the mechanical bond in this system, since deslipping is much faster when the interactions are all but erased in the high polarity medium of $(CD_3)_2SO$.

Although the investigation[21] summarized in **Table 3.5** found a 4-*tert*-butylphenyl ($^tBuC_6H_4$) stopper to be too bulky for the DB24C8 ring to overcome, $^tBuC_6H_4$ can be utilized as a slippage stopper with slightly larger rings or in more polar media. Increasing the ring size by only one atom with the use of benzometaphenylene[25]crown-8 (BM25C8) affords[47] a (pseudo)rotaxane **R312H**$^{2+}$ with controlled release characteristics. By changing either the temperature or the solvent polarity (**Table 3.5**), the half-life of deslipping over the $^tBuC_6H_4$ hurdle in the BM25C8-based rotaxane **R312H**$^{2+}$ can be varied from minutes to months. The dogma that $^tBuC_6H_4$ is too bulky for the smaller DB24C8 ring to pass over made it one of the most commonly used[48–60] dumbbell stoppers until Takata[61] demonstrated that the $^tBuC_6H_4$-stoppered DB24C8 rotaxane **R313Ac** also falls into the grey area. The dialkylammonium precursor to this rotaxane, namely **R313H**$^+$ (not illustrated), is kinetically stable, showing no dissociation after one month even at 100 °C in Me_2SO. Only after deactivation of the hydrogen-bonded recognition site through acylation of the nitrogen atom can the DB24C8 ring dissociate from the neutral dumbbell. This deslipping process (**Table 3.5**) is also temperature- and solvent-dependent. A homologous control rotaxane with two 3,5-dimethylphenyl stoppers did not dissociate under the same conditions, confirming that the $^tBuC_6H_4$ stopper is small enough to squeeze through the cavity of the DB24C8 ring.

Another complementary ring-stopper pair for slippage of dialkylammonium rotaxanes is that[62] of the larger dibenzo[30]crown-10 (DB30C10) ring and the 3,5-di-*tert*-butylphenyl stopper of the [2]rotaxane **[2]R314H**$_2^{2+}$ and

Table 3.5 Solvent- and temperature-dependent deslipping rates of crown ethers in 4-*tert*-butylphenyl-stoppered dialkylammonium (pseudo)rotaxanes.[47]



Rotaxane	Solvent	T K	k_{off} s^{-1}	$\tau_{1/2}$ h	$-\Delta G^{\ddagger}_{off}$ kcal·mol^{-1}	$\Delta H^{\ddagger}$ kcal·mol^{-1}	$\Delta S^{\ddagger}$ cal·mol^{-1}K^{-1}
R312H^{2+}	CD_2Cl_2	298	1.3×10^{-7}	1500	26.9	35.5	29.2
R312H^{2+}	CD_3CN	298	5.3×10^{-7}	360	26.0	15.7	–34.8
R312H^{2+}	CD_3OD	298	5.4×10^{-6}	36	24.7	14.4	–34.5
R312H^{2+}	CD_2Cl_2 : $(CD_3)_2SO$ (3:1)	298	9.2×10^{-5}	2.0	23.0	-	-
R312H^{2+}	CD_2Cl_2 : $(CD_3)_2SO$ (1:1)	298	1.0×10^{-3}	0.18	21.5	-	-
R313Ac	$(CD_3)_2SO$	313	4.6×10^{-6}	42	26.0	20.1	19
R313Ac	$CDCl_3$	313	2.0×10^{-6}	97	26.6	20.7	18
R313Ac	C_6D_6	313	1.4×10^{-6}	143	26.8	20.2	18

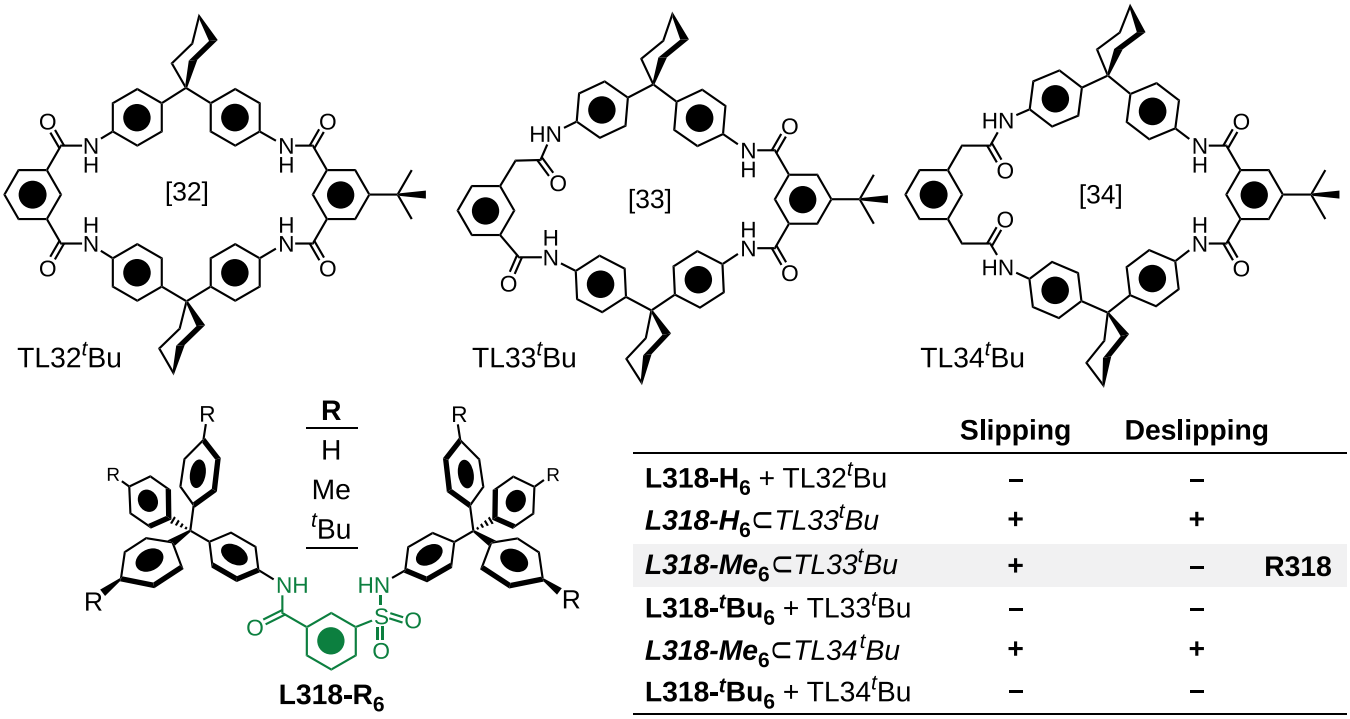
corresponding [3]rotaxane **[3]R314H$_2^{2+}$**. The structural formula of **[3]R314H$_2^{2+}$** is illustrated in **Figure 3.4**. This rotaxane is stable on the laboratory timescale, having been isolated by flash column chromatography at room temperature as a 1:5 mixture of the [2]- and [3]rotaxanes. This 1:5 mixture is gradually converted to a 1:3 mixture over the course of 7 days in CH_2Cl_2 at room temperature as a result of one of the DB30C10 rings deslipping slowly over the stopper.

A recent report by Coutrot[63] has described the slippage characteristics of an *N*-hydroxysuccinimide (NHS) unit as a hurdle terminating the (pseudo)rotaxane **R315H$^+$**, the stereoformula of which is illustrated in **Figure 3.4**. In MeCN at room temperature, it takes about two days for the slippage reaction to reach equilbrium by allowing the ring to pass over the NHS hurdle in 83% yield. The half-lives of deslipping in CD_3CN and $(CD_3)_2SO$ are 160 and 6.5 hours, respectively. This (pseudo)rotaxane has also been employed[64] as a recyclable auxiliary or 'transporter' molecular machine for preparing a different [2]rotaxane possessing only a very weakly associating recognition site for the DB24C8 ring—see **Section 6.15.3.3**.

Slippage of Neutral Hydrogen-Bonded Rotaxanes

Neutral amide-based hydrogen-bonded rotaxanes have also proven to be amenable to slippage protocols. Vögtle[65] has reported a simple technique for accessing some of his tetralactam (TL)-based rotaxanes (see **Figure 3.4**) such as **R316** by briefly melting a neat mixture of the ring and dumbbell components at 350 °C for one minute. The rotaxane **R316** was isolated in 3% yield by this protocol and is kinetically stable in both DMF and THF at ambient temperature. By contrast, a homologous rotaxane **R317** with no hydrogen-bonded recognition units is able to dissociate,[66] with deslipping half-lives of 26 and 20 h in DMF and THF, respectively. A more systematic investigation[66] employing this melting technique has uncovered (**Figure 3.8**) the size complementarity relationships between differently sized TL rings (TL32^{t}Bu, TL33^{t}Bu, and TL34^{t}Bu) and the trityl-stoppered hydrogen-bonded dumbbell **L318-R$_6$** with variable R groups (H/Me/^{t}Bu) at the *para* positions of the trityl stoppers' rings. **Figure 3.8** summarizes when slippage and deslipping processes are allowed or forbidden for different combinations of these components. Although ***L318-H$_6$*⊂*TL33^{t}Bu*** exhibits slow deslipping kinetics ($\tau_{1/2}$ = 13.6 h in DMF and 115 h in THF), the most ideally matched pair is ***L318-Me$_6$*⊂*TL33^{t}Bu***. Slippage happens in the melt for this system, yet deslipping does not occur in solution. Thus, ***L318-Me$_6$*⊂*TL33^{t}Bu*** is a rotaxane (**R318**) for all intents and purposes. The stereoformula of **R318** is illustrated in **Figure 3.4**.

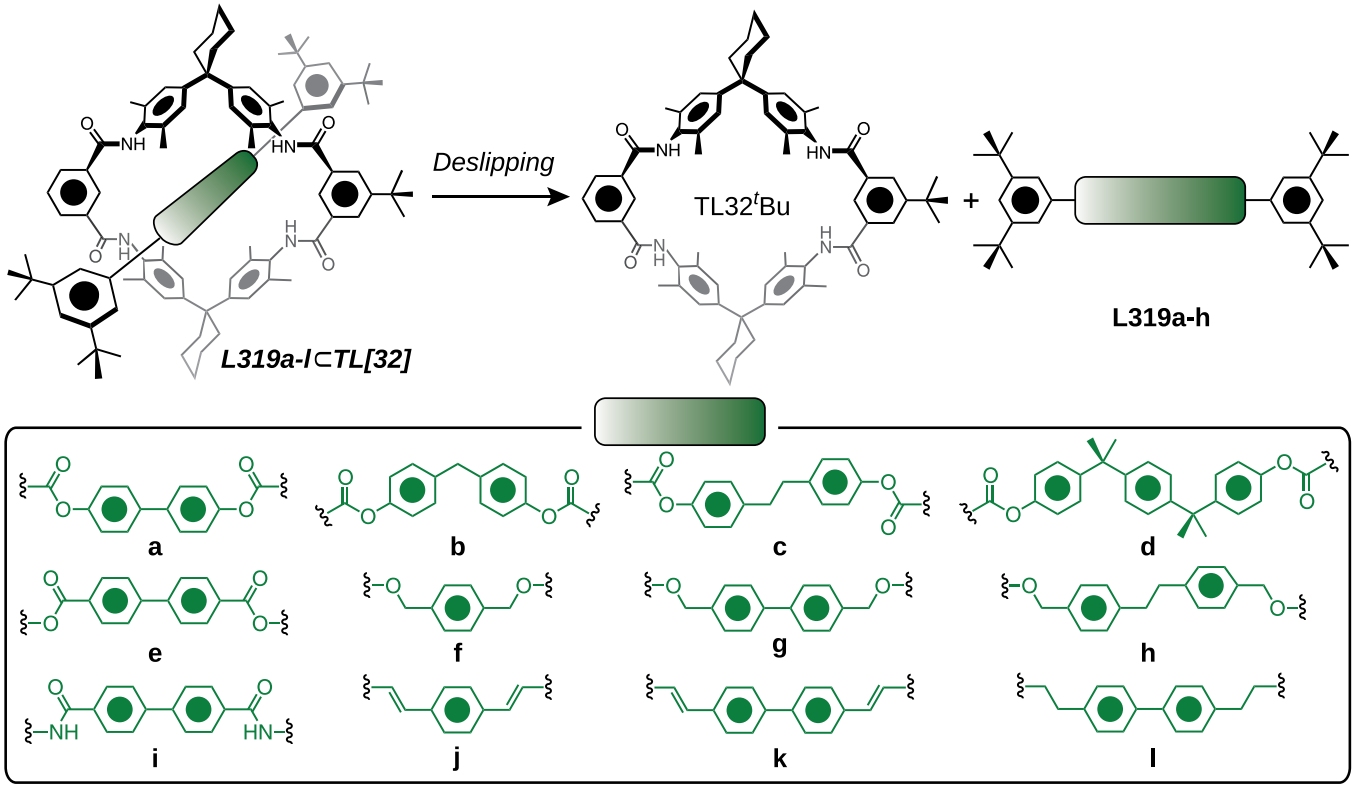
A detailed study on the deslipping kinetics (**Table 3.6**) of a family of tetralactam-based (pseudo)rotaxanes ***L319a*⊂*TL32^{t}Bu*–*L319h*⊂*TL32^{t}Bu*** has been undertaken by Schalley.[67] The deslipping rates were investigated in several different solvent systems at temperatures of either 333 or 373 K. The results in **Table 3.6** show that relatively subtle modifications to the constitution of the dumbbells, all



	Slipping	Deslipping	
L318-H$_6$ + TL32^{t}Bu	–	–	
L318-H$_6$*⊂*TL33^{t}Bu	+	+	
L318-Me$_6$*⊂*TL33^{t}Bu	+	–	**R318**
L318-^{t}Bu$_6$ + TL33^{t}Bu	–	–	
L318-Me$_6$*⊂*TL34^{t}Bu	+	+	
L318-^{t}Bu$_6$ + TL34^{t}Bu	–	–	

Figure 3.8 Vögtle's investigation of ring-stopper complementarity in tetralactam-based (pseudo)rotaxanes.[66] Plus signs (+) indicate that a slipping or dislipping process is allowed, while minus signs (–) indicate that a process is forbidden, at ambient temperature in THF. The shaded entry (***L318-Me$_6$*⊂*TL33^{t}Bu***) is equivalent to being a rotaxane (**R318**) since slippage is allowed and deslipping is forbidden.

Table 3.6 The solvent-, temperature-, and structure-dependent deslipping rates (k_{off}) and corresponding activation energies (E_A), half-lives ($\tau_{1/2}$), and thermodynamic parameters ($\Delta G_{298}^{\ddagger}$, $\Delta H^{\ddagger}$, $\Delta S^{\ddagger}$) in Schalley's pseudorotaxanes ***L319a-l*⊂*TL[32]*** at 333 K.[67,68]



Dumbbell	Solvent	T K	E_A kcal·mol^{-1}	k_{off} s^{-1}	$\tau_{1/2}$ h	$\Delta G_{298}^{\ddagger}$ kcal·mol^{-1}	$\Delta H^{\ddagger}$ kcal·mol^{-1}	$\Delta S^{\ddagger}$ cal·mol^{-1}K^{-1}
L319a	$(CD_3)_2SO$	373	20.8	1×10^{6}	560	30.6	20.1	–34.9
L319a	$C_2D_2Cl_4$	373	-	-	>25000	-	-	-
L319b	$(CD_3)_2SO$	373	24.1	4.1×10^{7}	650	31.1	23.2	–26.3
L319c	$(CD_3)_2SO$	373	23.4	4.7×10^{7}	220	30.1	22.5	–26.1
L319d	$(CD_3)_2SO$	373	25.3	3.28×10^{8}	410	31.1	24.4	–22.2
L319e	$(CD_3)_2SO$	373	21.7	7.8×10^{7}	14	28.2	21.0	–24.9
L319e	$C_2D_2Cl_4$	373	20.3	1.6×10^{7}	10	27.7	19.6	–28.0
L319f	$C_2D_2Cl_4$	333	24.9	4.83×10^{10}	82	22.9	24.1	4.3
L319g	$C_2D_2Cl_4$	333	23.4	1.21×10^{10}	38	22.2	22.7	1.7
L319h	$C_2D_2Cl_4$	333	21.0	1.53×10^{9}	16	21.0	20.3	–2.4
L319h	$CDCl_3$	333	20.3	8.48×10^{8}	16	19.6	20.8	–3.6
L319i	DMF-d_7	333	19.4	1.6×10^{7}	61	22.2	18.6	–11.7
L319j	DMF-d_7	333	19.8	4.2×10^{7}	48	22.0	19.4	–9.3
L319k	DMF-d_7	333	18.4	4×10^{6}	58	22.0	16,3	–19.1
L319k	THF-d_8	333	15.1	1×10^{5}	23	21.0	14.3	–22.2
L319l	DMF-d_7	333	20.1	2.6×10^{7}	111	22.5	19.4	–10.8

of which are terminated by 3,5-di-*tert*-butylphenyl stoppers, have a non-negligible effect on the deslipping kinetics. It would appear that the (i) length, (ii) flexibility, and (iii) steric bulk of the dumbbells, as well as (iv) the nature of the functional groups, all influence the deslipping kinetics. Comparing **L319f** with **L319g** and **L319j** with **L319k**, it seems that deslipping occurs more slowly in the case of the shorter dumbbells, all else being equal. Comparing **L319a–d** reveals that conformational flexibility also tends to slow down the deslipping kinetics. The constitutional isomers **L319a** and **L319e**, which differ only in the orientation of their ester bonds, exhibit[68] surprisingly different deslipping rates, revealing that the system is sensitive to subtle orientational differences among the functional groups. Schalley[67] has also probed (**Figure 3.9**) the effect of hydrogen bonding by experimenting with different ring components possessing endotopic hydrogen-bond accepting pyridyl moieties to complement the amide-based dumbbell **L319i**. Intercomponent hydrogen bonding has a much greater effect on the kinetics of deslipping than the more subtle dumbbell modifications summarized in **Table 3.6**. When the ring is able to accept two hydrogen bonds from

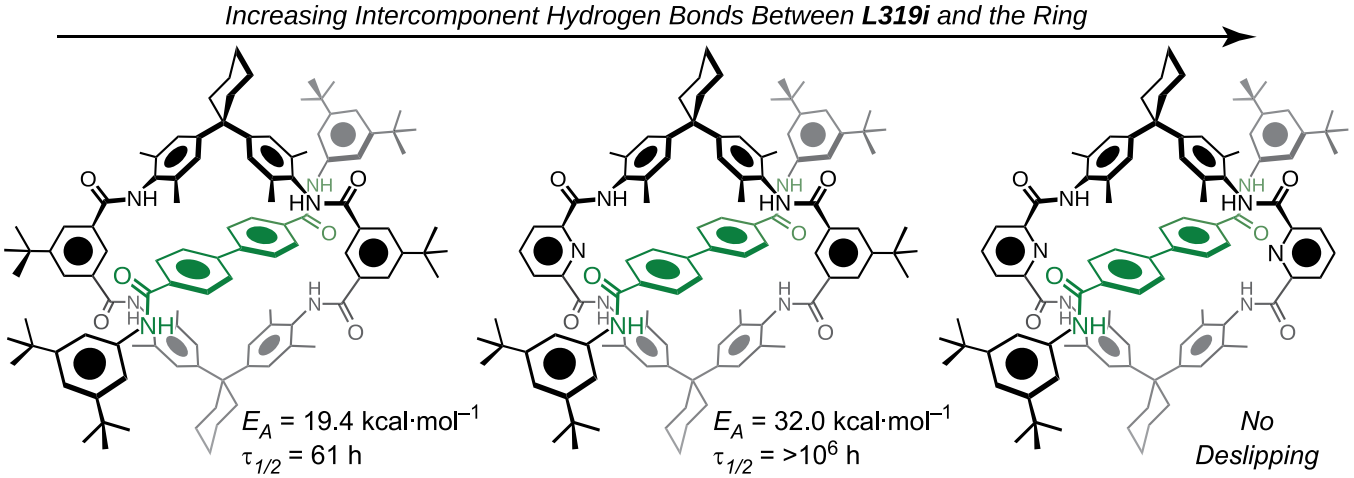


Figure 3.9 Increasing the hydrogen bond accepting character of the tetralactam ring encircling dumbbell **L319i** by introducing endotopic pyridine-based hydrogen bond acceptors leads to a stabilization that dramatically slows down the kinetics of deslipping.[67]

L319i, no deslipping is observed even under relatively harsh conditions. Schalley[69] has found that the deslipping kinetics of **L319f** and **L319g** are slower than their corresponding isotopologues possessing deuterated ^{t}Bu groups in their stoppers, which are slightly smaller because the C–D bond is 0.005 Å shorter than the C–H bond.

Leigh[70] has also described an example of slippage in the benzylic amide rotaxane **R320**—see **Figure 3.4**. A mixture of the ring and dumbbell requires approximately one day to reach equilibrium in $CDCl_3$, a solvent in which the association constant of the (pseudo)rotaxane is 470 M^{-1}.

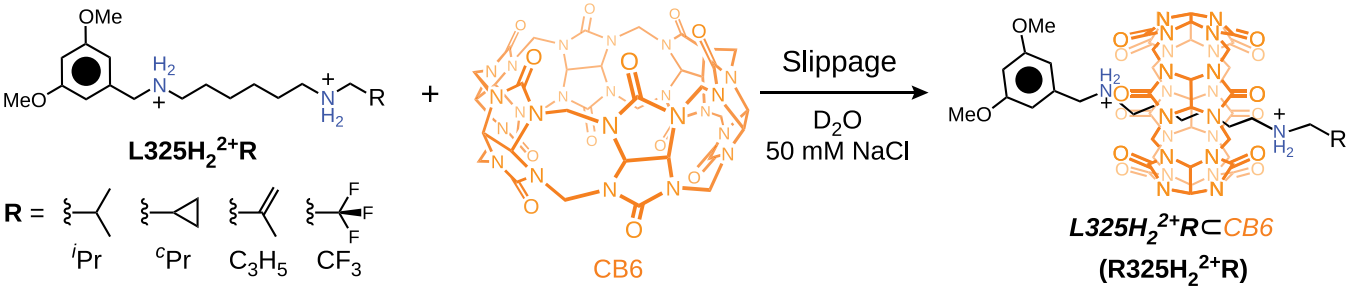
3.1.4 Slippage Driven by Hydrophobic Interactions

Cyclodextrins have been utilized (**Figure 3.4**) in a slippage synthesis by Macartney,[71] who passed an α-cyclodextrin (α-CD) ring over the 4-substituted *tert*-butyl groups on the pyridinium stoppers of rotaxane **R321**$^{2+}$. Several slippage systems, which involve the passage of the α-CD ring over various quaternary ammonium and phosphonium hurdles, have also been described by Macartney.[72] More recently, he has extended[73] the slippage synthesis of α-CD and β-CD (pseudo)rotaxanes to dumbbells stoppered with Pt^{II} complexes. In the latter case (**R322**$^{4+}$ in **Figure 3.4**) rate constants for slippage ($k_{on} = 1.05 \times 10^{-2}$ s^{-1}, $\tau_{1/2} = 11$ min) and deslipping ($k_{off} = 2.14 \times 10^{-5}$ s^{-1}, $\tau_{1/2} = 9$ h) and the activation enthalpy ($\Delta H^{\ddagger} = 22$ kcal · mol^{-1}) and entropy ($\Delta S^{\ddagger} = -5.5$ cal · mol^{-1} · K^{-1}) have been measured in D_2O with 50 mM NaCl present.

The other main class of aqueous MIMs to be investigated (**Figure 3.4**) in the context of slippage are based on cucurbiturils. Kimoon Kim[74] has suggested implicitly that an electrostatic stopper can be used in lieu of a steric one in his slippage synthesis of the BIPY^{2+}-terminated cucurbit[6]uril (CB6)-based [2]rotaxane **R323H$_2$**$^{8+}$, in which the CB6 ring does not dissociate from the dumbbell on the laboratory timescale. The notion of cucurbituril-based rotaxanes without steric stoppers has also been proposed by Reany and Keinan,[75] who measured a high free energy of activation barrier, $\Delta G^{\ddagger}$, of 24.4 kcal for the threading of a CB6 ring over propargylammonium groups onto the *para*-xylylene axle of the (pseudo)rotaxane **R324H$_2$**$^{2+}$.

Masson[76] has carried out detailed investigations on the slippage of CB6 rings over various functional groups. He has suggested, on the basis of computer simulations, that the CB6 ring is much more likely to slip over a secondary dialkylamine than over a secondary dialkylammonium center, since the former is calculated to be more stable within the CB6 cavity by 40–50 kcal · mol^{-1}. The experimental results summarized in **Table 3.7** probe how the stereoelectronics of different pseudo-stoppers influence the thermodynamics and kinetics of slippage in assembling (pseudo)rotaxanes ***L325H$_2$***$^{2+}$***R*** ⊂ *CB6* (or **R325H$_2$**$^{2+}$**R**) comprising CB6 and 1,6-diaminohexane-based semidumbbells in D_2O at room temperature. These assemblies are high in rotaxane character. A large free energy of activation ($\Delta G^{\ddagger}$) of up to 28.9 kcal · mol^{-1} for slippage was recorded in the presence of an isopropyl pseudo-stopper—the bulkiest of the series. The smaller cyclopropyl and propenyl hurdles are nearly isovolumetric, yet they differ by over 3 kcal · mol^{-1} in their free energies of activation for slippage at room temperature, and by more than an order of magnitude in their corresponding half-lives for deslipping (**Table 3.7**) at 100 °C. Furthermore, a trifluoromethyl hurdle—by far the smallest pseudo-stopper in the series—hinders the passage of the CB6 ring more effectively than does the much larger cyclopropyl hurdle. These results indicate that the electronic interactions between the carbonyl-decorated rims of CB6 and the stopper have a significant influence on the energy landscape of the system, in addition to the steric effects associated with their bulk. This hypothesis explains the unexpectedly high activation barrier for slippage over the small CF_3 hurdle, owing to electrostatic repulsion between many lone pairs of electrons in each species.

Table 3.7 Thermodynamic and kinetic parameters for the slippage-based self-assembly of CB6 (pseudo)rotaxanes ***L325H$_2^{2+}$R*⊂*CB6*** with various stoppers.[76]



Hurdle	V[a] Å^3	(Pseudo)rotaxane	K_a M^{-1}	$\Delta G^{\ddagger}$ kcal·mol^{-1}	$\Delta H^{\ddagger}$ kcal·mol^{-1}	$\Delta S^{\ddagger}$ cal·mol^{-1}K^{-1}	$\tau_{1/2}$[b]
^{i}Pr	70	**L325H^{2+}-^{i}Pr**⊂CB6	5.4×10^5	28.9±1.6	27.9±1.3	–3±3	3.2 h
^{c}Pr	63	**L325H^{2+}-^{c}Pr**⊂CB6	1.1×10^6	23.7±0.5	21.1±0.4	–9±1	2.4 s
C_3H_5	66	**L325H^{2+}-C_3H_5**⊂CB6	1.8×10^5	26.8±0.9	24.7±0.4	–7±2	4.0 min
CF_3	47	**L325H^{2+}-CF_3**⊂CB6	1.1×10^5	24.0±1.4	23.2±1.1	–3±3	19 s

[a]Calculated pseudo-stopper volume.
[b]$\tau_{1/2}$ is given for the deslipping of CB6 from **L325H$_2^{2+}$** derivatives at 100 °C.

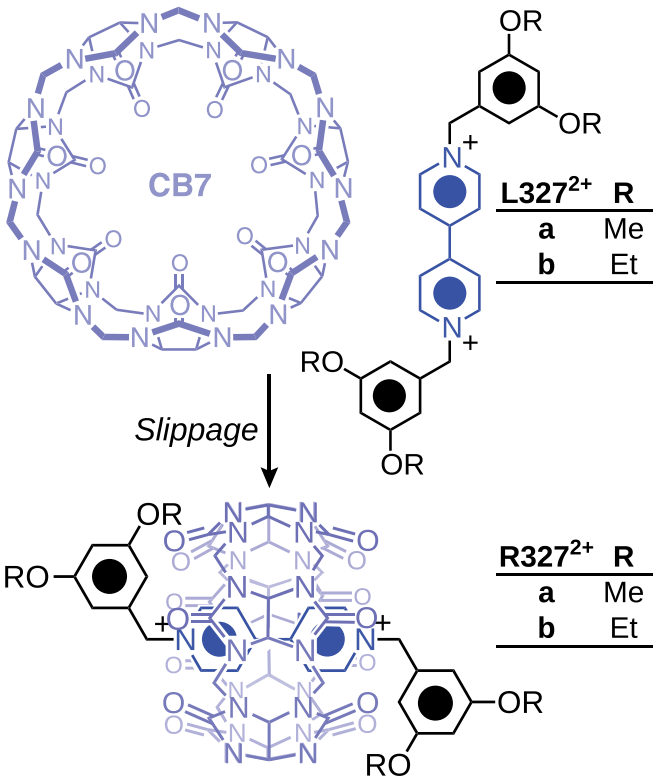
Cucurbit[7]uril (CB7) has also been employed in slippage protocols. For example, the CB7-based rotaxane **R326H$^+$** introduced (**Figure 3.4**) by Wang,[77] which employs a BIPY^{2+} unit with its associated isophthalate counterions as a pseudo-stopper, over which a high activation barrier of 26 kcal·mol^{-1} must be surmounted in order to slip the ring onto the dumbbell. Masson[78] has investigated deslipping in a CB7-based pseudorotaxane with benzo[15]crown-6 hurdles, finding that inorganic and organic cations can act as 'lubricants' that accelerate the rate of dethreading driven by a competitive binder.

Kaifer[79] has assembled (**Table 3.8**) the [2]rotaxanes **R327a^{2+}** and **R327b^{2+}**, comprising CB7-encircled bis(3,5-dimethoxybenzyl)bipyridinium or bis(3,5-diethoxybenzyl) bipyridinium dumbbells, respectively, in D_2O and Me_2SO. The kinetics of slippage (k_{on}) are faster in the case of **R327a^{2+}** than they are for **R327b^{2+}**, on account of its less bulky stoppers. Slippage of **R327a^{2+}** is faster and more thermodynamically favorable in D_2O than in $(CD_3)_2SO$, while **R327b^{2+}** manifests itself in D_2O only.

3.1.5 Slippage of Anion-Binding Rotaxanes

Beer[80] has applied a slippage protocol (**Figure 3.4**) to the self-assembly of the anion-binding rotaxane **R328** in the presence of various templates—namely PF_6^-, I^-, Br^-, and Cl^-. The association constants are on the order of 10^2 M^{-1} for all four anions. Predictably, the slippage and deslipping rates depend on the composition of the anionic template as well as on the solvent. In $CDCl_3$, slippage and deslipping processes in **R328·Cl** are too slow to measure at 298 K. Under the same conditions, the half-lives for MeOH-driven deslipping in **R328·PF$_6$**, **R328·I**, and **R328·Br** are 14, 16, and 41 h, respectively.

Table 3.8 The slippage[79] of *BIPY^{2+}⊂CB7* (pseudo)rotaxanes at 25 °C.



	Solvent	K_a	k_{on}/M^{-1}s^{-1}	k_{off}/s^{-1}
R327a^{2+}	D_2O	≥8×10^5	Fast	
	$(CD_3)_2SO$	3.4×10^3	0.3	8×10^{-5}
R327b^{2+}	D_2O	≥8×10^5	0.9	1×10^{-6}
	$(CD_3)_2SO$	[a]	[a]	[a]

[a]No binding.

Squaraine recognition units have been employed (**Figure 3.4**) in the slippage synthesis of rotaxanes **Na_2R329^{2+}** and **R330** by Chiu[81] and Smith,[82,83] respectively. These two squaraine-based rotaxanes employ different ring components. The cage of **Na_2R329^{2+}** recruits two Na^+ ions to assist[81] in stabilizing the squaraine dumbbell. The bulky anthracene groups of the benzylic amide-derived ring are crucial to the microwave-assisted slippage assembly[83] of **$R330R_2$**, where the stoppers (R) can be as bulky as a butoxycarbonyl (Boc) group. Although detailed kinetic data on the slippage of these assemblies are not available, the 'all-or-nothing' substituent effect was observed in the case of **$R330R_2$**.

3.1.6 Triumphs and Tribulations of Slippage

A more or less intuitive point that has been confirmed[21] experimentally is that smaller, more rigid macrocycles (such as DB24C8) are more sensitive to steric effects than larger, more flexible macrocycles (such as DN38C10), which are slightly more forgiving with respect to stopper size. In general, deslipping rates are sensitive to solvent composition when the mechanical bond is stabilized by significant noncovalent bonding interactions, as in most cases of rotaxanes prepared by template-directed synthesis. Correspondingly, deslipping is relatively less sensitive to solvent composition when the mechanical bond is stabilized only by steric constraints. The experimental evidence for this rationale is demonstrated by comparing the solvent sensitivity of constitutionally related rotaxanes with and without internal noncovalent bonding interactions. Note the substantial differences (**Table 3.5**) in solvent sensitivity between **$R312H^{2+}$** and **R313Ac**, for example, or between (**Figure 3.4**) Vögtle's tetralactam rotaxanes **R316** and **R317**.

The challenges and limitations of slippage are at least twofold. They are (i) the 'all-or-nothing' substituent effect[24]: slippage systems are highly sensitive to substituent effects on the stoppers and therefore require careful design of size complementarity between components—merely one carbon atom can mean all the difference between a reasonable yield and no yield at all, and (ii) the fact that the various noncovalent bonding interactions often employed in the templation of mechanical bonds are typically weakened at the elevated temperatures required to overcome the activation barriers to slippage: the correspondingly diminished binding constants are reflected in the moderate yields. Thermodynamic control involving slippage is often employed at high cost in terms of yields. Alternative routes can circumvent these issues by employing reversible coordinative (**Section 3.2**), covalent (**Sections 3.3–3.5**), or surface (**Section 3.6**) bonds to enable self-correcting behavior.

3.2 Self-Assembling Metallo-Organic MIMs

The rich tradition of coordination chemistry[84] developed by inorganic and organometallic chemists over many decades has left supramolecular chemists and mechanostereochemists with a wealth of potential motifs to choose from in the construction of new metallo-supramolecular architectures,[85,86] an enterprise revitalized in large part by Lehn's first deliberate synthesis[87] of a trinuclear helicate in 1987, as well as the pioneering early work of Sauvage—see **Section 2.3.2**. In the context of thermodynamically controlled MIM synthesis, any metal-ligand pairs that are *kinetically* labile under mild, or at least controllable, reaction conditions, but *thermodynamically* stable, are fit for recruitment. The mechanomolecules reviewed in this Section are not necessarily templated by coordination bonds—rather, metal-ligand interactions act as the reversible bonds that eliminate kinetic traps as the system approaches thermodynamic equilibrium. All of the mechanomolecules in this Section possess metals somewhere in the backbones of their co-constitutions. The roots of this approach can be traced back to the seminal template-directed synthesis of a [2]rotaxane by Ogino,[88] who employed Co^{III} complexes to stopper an alkanediamine threaded through the annulus of β-CD—see **Scheme 2.12** in **Section 2.3.1.1**.

Among the available metals which engage in kinetically labile coordination bonds, palladium(II) casts the largest beam of light over mechanostereochemistry, but the list is growing continually. When using metals to design MIMs, we recall the importance of the stereochemical preference (topography) of the metal ions as well as the maximal site occupancy principle,[89,90] which dictates that it is thermodynamically favorable for a metallosupramolecular complex $[M_nL_m]$ to adopt a configuration that maximizes the number of occupied binding sites on both the metal M and the ligand L.

While we focus in this Section on discrete mechanically interlocked assemblies, metallosupramolecular polymers based on the self-assembly of interpenetrated ligands and metals can also be assembled under thermodynamic control. For example, Kimoon Kim[91] has pioneered a metallosupramolecular approach to the synthesis of one-, two-, and three-dimensional polyrotaxanes based on the cucurbituril hosts. See **Sections 4.1.3.5** and **4.2.3.8** for discussions of mechanically interlocked coordination polymers and metal-organic frameworks.

3.2.1 MIMs Possessing Group 10 Elements

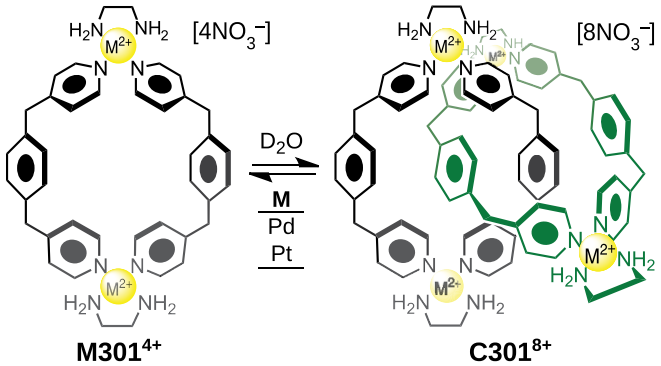
Since it has been used to great effect from an early stage in the development of the mechanical bond to create MIMs under thermodynamic control, palladium occupies a special place in mechanostereochemistry. Palladium(II) forms kinetically labile bonds with pyridyl ligands, a feature which has facilitated the assembly of unprecedented mechanically interlocked architectures in high efficiencies. Platinum, one of palladium's heavier cousins in the Group 10 transition metal elements, behaves just like palladium, but forms more kinetically stable bonds in general.

3.2.1.1 Homophilic Catenation of Pd^{II}/Pt^{II} Assemblies

Fujita,[92,93] who is in the vanguard when it comes to the launch of metallosupramolecular-based mechanostereochemistry, demonstrated a "magic ring" catenation[94] of aqueous metallacycles in 1994. The appearance and growth

of a new compound was noticed at increasingly higher concentrations of the Pd^{II}-based metallacycle **M301**$^{4+}$, which self-assembles from two simple xylyl-bridged divalent pyridine ligands and two (en)$Pd(NO_3)_2$ ions (en = ethylenediamine) in D_2O. This new compound proved to be the homo[2]catenane **C301**$^{8+}$, comprising two interlocked copies of the same metallacycle. The self-complexation (**Scheme 3.4**) of the macrocycle to afford the homo[2]catenane at high concentrations is mediated by hydrophobic interactions between the aromatic rings at the catenane's core and, of course, the labile Pd-pyridine bonds which allow for rapid equilibration of the reactants. Fujita confirmed this conclusion by preparing a control in the form of an analogous Pt^{II} homo[2]catenane, which is kinetically inert at room temperature, since the kinetic distribution of products does not change when the concentration is increased or decreased subsequently. The extent of conversion of the precursors into the Pd^{II} homo[2]catenane was pushed all the way to unity at 1 M concentration in highly polar media. It was reported[95] shortly thereafter that the Pt^{II}-based homo[2]catenane can be assembled quantitatively at elevated temperatures (100 °C) and subsequently 'locked' kinetically by returning the reaction mixture to ambient temperature. Proton exchange and ligand scrambling investigations have revealed[96] that the free macrocycle and corresponding catenane exchange so rapidly that the transfer cannot be observed. Careful consideration of the data also led to the conclusion that an intermediate between the macrocycle and catenated compounds must exist—possibly a larger macrocycle—suggesting that the catenation proceeds not by the intuitive ring-opening, threading, ring-closing mechanism but instead[96] by 'two sequential ligand exchanges between two rings concomitant with a twisting of the rings around each other,' which has also been dubbed a ring slippage or Möbius strip mechanism.

Fujita's discovery of the labile metal-ligand bond as an arbiter of catenane self-assembly inaugurated a new generation of mechanomolecules. In the beginning, the Fujita group designed ligands to make new, albeit quite similar, catenanes to those constituting the original discovery. This activity generalized[97] their approach such that a variety of self-assembled transition metal boxes with *cis*-protected



Scheme 3.4 Fujita's self-assembly of Pd- or Pt-bridged [2]catenanes in water.[94] Interlocking is increasingly favored at higher concentrations.

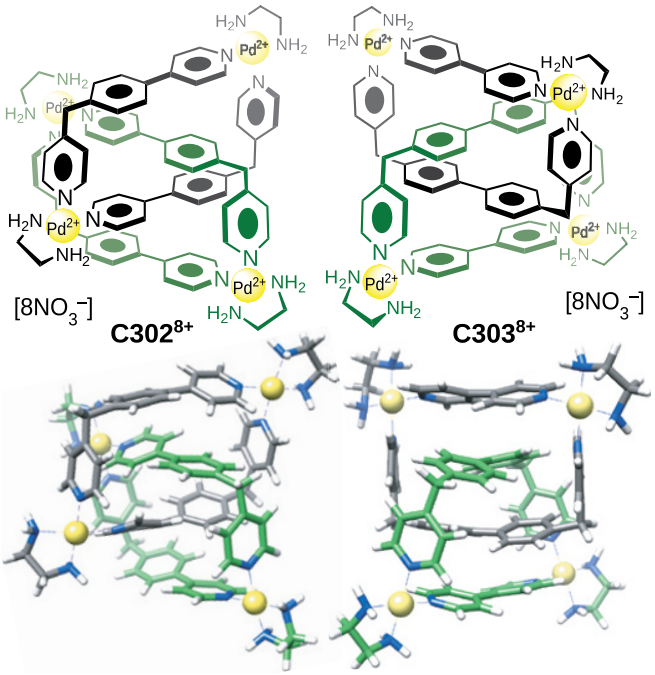
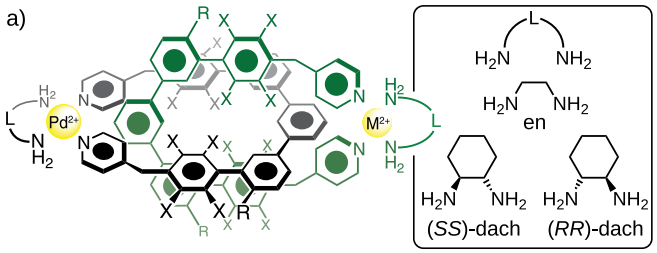


Figure 3.10 Stereoformulas and tubular representations of the solid-state structures of self-assembled [2]catenanes based on labile Pd-pyridine bonds and hydrophobic interactions in water.[97] Counterions are omitted from the solid-state structures for the sake of clarity.

Pd^{II} 'corners' and ~3.5 Å interplane distances could be conceived, prepared, and catenated rationally, affording MIMs such as **C302**$^{8+}$ and **C303**$^{8+}$ portrayed in **Figure 3.10**.

Another workhorse emanating from the Fujita laboratory has been a catenane motif (**Figure 3.11**) with only one bridging metal instead of two corner pieces. These catenanes are assembled[98,99] through double-helical stacking of divalent pentakis(*m*-phenylene) ligands. Catenanes **C304a**$^{4+}$**–C304f**$^{4+}$, bearing either Pd^{2+} or Pt^{2+} metal centers, self-assemble (**Figure 3.11a**) in a 2:1 H_2O:DMF solvent mixture. Nearly quantitative yields are reached when the oligo-*m*-phenylene ligands are fluorinated (**C304b**$^{4+}$–**C304f**$^{4+}$), while the uncatenated metallacycles are more favored in the case (**C304a**$^{4+}$) of the non-fluorinated ligands. The uncatenated metallacycles are also more favored in neat DMF, confirming that assembly is driven by the hydrophobic effect. The Pd^{II} or Pt^{II} bridgeheads are stabilized by en or chiral 1,2-cyclohexanediamine (dach) ligands—employing enantiomerically pure (*SS*)-dach or (*RR*)-dach ligands during assembly induces homochiral helical stacking of ligands within the [2]catenanes **C304e**$^{4+}$ and **C304f**$^{4+}$, respectively. This induced chirality can be monitored by circular dichroism measurements, which show a strong signal only for the catenane and not for the corresponding uncatenated chiral metallacycle. The structure of the oligoether-functionalized [2]catenane **C304c**$^{4+}$ has been characterized (**Figure 3.11b**) in the solid state by X-ray crystallography. Furthermore, by taking advantage of the kinetically inert Pt^{II} linkage, the rings of **C304d**$^{4+}$ can be cross-catenated[100]

a)



C304^{4+}	X	R	M	L
a	H	H	Pd	en
b	F	H	Pd	en
c	F	OCH_2CH_2OMe	Pd	en
d	F	H	Pt	en
e	F	H	Pd	(*SS*)-dach
f	F	H	Pd	(*RR*)-dach

b)

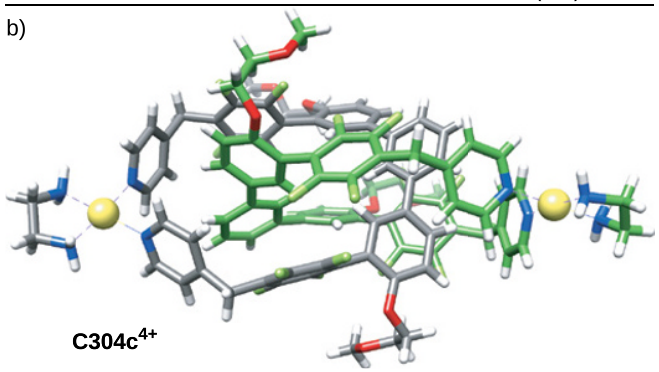
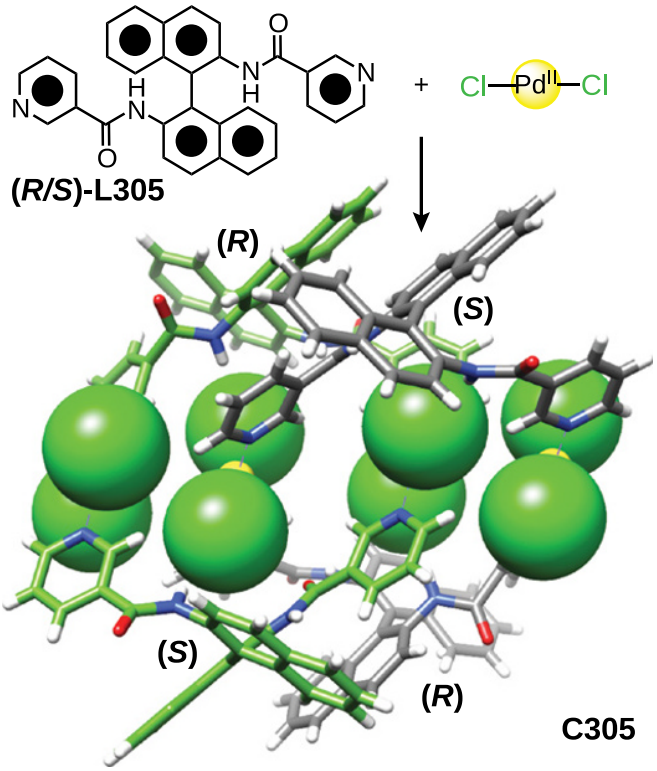


Figure 3.11 Cross-catenated structures based on helical stacking of metal-bridged *m*-phenylene ligands.[98–100] (a) Stereoformulas of self-assembled [2]catenanes based on this motif. (b) A tubular representation of the solid-state structure of **C304c^{4+}**, with solvent and counterions omitted for the sake of clarity.

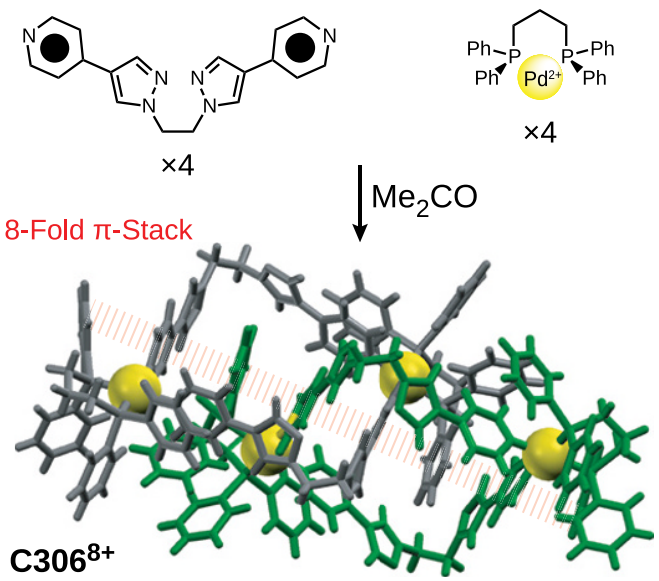


Scheme 3.5 The self-assembly[104] of Puddephatt's [2]catenane **C305** from a racemic mixture of chiral bis(pyridine) ligands derived from binaphthyl units. A tubular representation of the solid-state structure is illustrated with solvent molecules omitted for the sake of clarity.

selectively into a Pd^{II}/Pt^{II} heterocatenane. This cross-catenation has been applied subsequently to the preparation[101] of bis- and tris[2]catenanes—see **Section 4.1.4.5**—by using a naked bridging Pd^{II} ion that yields oligo-*m*-phenylene bismetallacycles. The quantitative assembly of these catenanes has also been used to access some remarkable new mechanomolecular architectures, such as a cyclic tris[2]catenane and an ultramacrocyclic[102,103] bis[2]catenane, which are illustrated and discussed in **Section 4.1.4.4**.

Puddephatt[104] has assembled (**Scheme 3.5**) the homo[2]catenane **C305** in 90% yield from a mixture of the racemic binaphthyl bis(pyridine) ligand **(*R/S*)-L305** and $PdCl_2$ in CH_2Cl_2. The crystals obtained by slow diffusion of hexane into a solution of the catenane contain only the *meso*-metallacycles—i.e., the (*R*) and (*S*) enantiomers of the ligands are both represented equally in each ring of the catenane. The catenane itself also displays helical chirality in the solid state—see **Section 5.2.3.3**. It is believed that the catenane exists also in solution, since it is stabilized by intercomponent second-sphere [N–H···Cl] anion-binding interactions involving the ligands' amide groups, although the solution-state assembly has not been characterized in detail.

A Pd^{II} catenane driven by π-stacking—an eightfold stack in this case—has been described by Batten.[105] The metallo[2]catenane **C306^{8+}** is assembled (**Scheme 3.6**)



Scheme 3.6 Batten's self-assembly of a metallo[2]catenane from four ditopic bis(4-pyridylpyrazolyl) ligands and four Pd^{II} ions. The assembly is driven[105] by 'octapi' interactions, in which a stack of eight π-associated rings are observed in the solid state. The X-ray crystal structure of **C306^{8+}** is shown with the BF_4^- counterions omitted for the sake of clarity.

from four identical ditopic bis(4-pyridylpyrazolyl) ligands and four Pd(dppp)OTf_2 ions in Me_2CO in 73% isolated yield after precipitation in Et_2O. The crystal structure of the product reveals that the catenation of the metallacycles is driven by an eightfold π-stack of aromatic units involving both the pyrazolyl and dppp (dppp = 1,3-bis(diphenylphosphino) propane) ligands. These subtle interactions dictate that the assembly is highly sensitive to the constitution of the ligands: indeed, adding only one extra carbon atom to the linker of the ditopic 4-pyridylpyrazolyl ligands results in a non-catenated macrocycle.

Catenation of Pd^{II}/Pt^{II} Metallacages

Mechanically interlocked assemblies based on multicyclic Pd^{II} metallacages have been reported by Kuroda,[106,107] Shionoya,[108] and Clever.[109–111] The seminal examples from Fujita[112] and Kuroda[106] are illustrated in **Figures 3.12**. See **Sections 4.1.3.2** and **4.2.3.2**. In a natural extension of his research on catenanes, Fujita[112] utilized the kinetically labile enPd^{II} corner pieces to interlock (**Figure 3.12a**) coordination cages with C_3 symmetry in the triply interlocked macrobicyclic homo[2]catenane **C307^{12+}** in 1999. This discovery was important because it laid the foundation for subsequent investigations in which planar organic molecules could be intercalated, encapsulated, and stacked within analogous cages—either isolated or interlocked—in a discrete and well-defined manner.[93] See **Section 4.1.3**. One application of these assemblies has allowed Fujita to engineer discrete stacks of seven, eight, or nine aromatic compounds in "towers" organized by these topologically linked cages of increasingly larger sizes.[113]

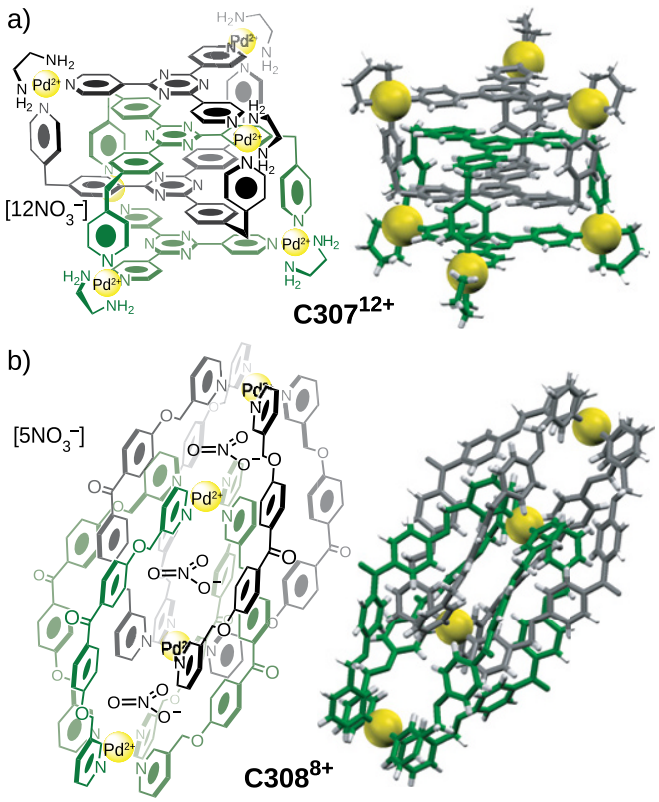
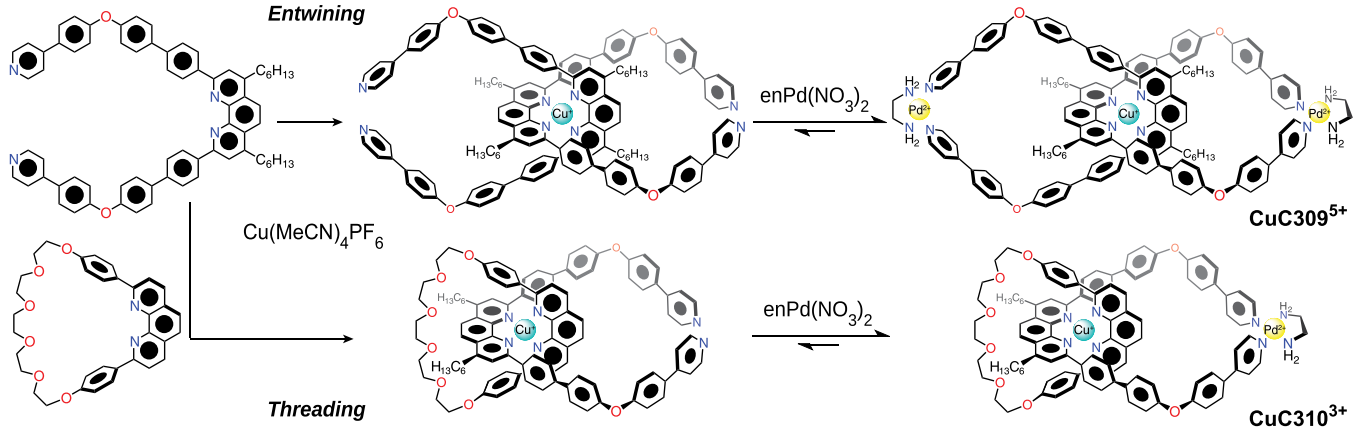


Figure 3.12 Mechanically interlocked Pd^{II}-based metallacage assemblies. (a) Structural formula and X-ray crystal structure of Fujita's[112] triply interlocked [2]catenane **C307^{12+}**. (b) Structural formula and X-ray crystal structure of Sekiya and Kuroda's[106] quadruply interlocked [2]catenane **C308^{8+}**. Solvent and counterions have been omitted for the sake of clarity.

A quadruply interlocked metallacage dimer has been investigated by Sekiya and Kuroda.[106,107] The self-assembly (**Figure 3.12b**) of **C308^{8+}** in Me_2SO involves the square planar coordination of crescent-shaped divalent pyridine ligands to naked Pd^{II} centers, producing the M_4L_8 macrotricyclic cages which comprise the catenane. The non-interlocked M_2L_4 cage is formed initially as the kinetic product,[106] but time and heat eventually convert these free cages into the thermodynamically favored catenated ones. The counterions play an important role in the stabilization of the mechanically interlocked structure.[107] Three anions can occupy each of the three cavities intercalated between the catenane's four Pd^{II} centers. The NO_3^- counterions bind these sites intercalatively with high affinity, so as to promote and stabilize the catenated structure efficiently. The $3NO_3^- \subset$ **C308^{8+}** complex is the most thermodynamically favored product, to the extent that the catenane will take up nitrate anions selectively from a pool of mixed anions, including OTf^-, BF_4^-, and PF_6^-. In contrast with nitrate, larger anions such as BF_4^- and PF_6^- cannot intercalate efficiently and so shift the equilibrium in favor of the non-catenated monomeric cages.

3.2.1.2 Pd^{II} Metallacyclic Catenates

Sauvage and Fujita[114] have teamed up to create self-assembled Cu^{I}-templated catenanes with labile Pd^{II} bonds. They unexpectedly instigated the self-assembly of the relatively exotic doubly interlocked [2]catenane, also known as the Solomon Link—see **Section 4.1.1.1**—in 1999, two years before producing their first joint example[115] of an ordinary [2]catenane. By exploiting labile Pd^{II}-pyridine bonds at two ends of a U-shaped phenanthroline derivative preorganized appropriately around the classical Cu^{I} template, [2]catenate **CuC309^{5+}** can be generated (**Scheme 3.7**) by the so-called 'entwining' approach. The two groups subsequently defined[116] a 'threading' approach which uses the same principle of ring-closing Pd^{II} ligation to produce the [2]catenate **CuC310^{3+}**, a species in which one of the rings is pre-formed so that only one ring closure is required. The two approaches, which are summarized in **Scheme 3.7**, represent the thermodynamically controlled counterpart to the original strategies described by Sauvage in his seminal communication[117] on transition metal-templated catenane synthesis—see **Sections 1.2.1** and **2.3.2.1**. The strength of this approach is rooted in the combined use of a kinetically stable template (Cu^{I}) with a kinetically labile (Pd^{II}) bond that facilitates the quantitative assembly of the desired catenane in both cases.



Scheme 3.7 The thermodynamically controlled entwining and threading strategies for quantitative Cu^{I}-templated catenane synthesis, mediated by labile Pd^{II}-pyridine bonds.[114]

3.2.1.3 Aqueous Catenation of Pd^{II}/Pt^{II} Metallacycles

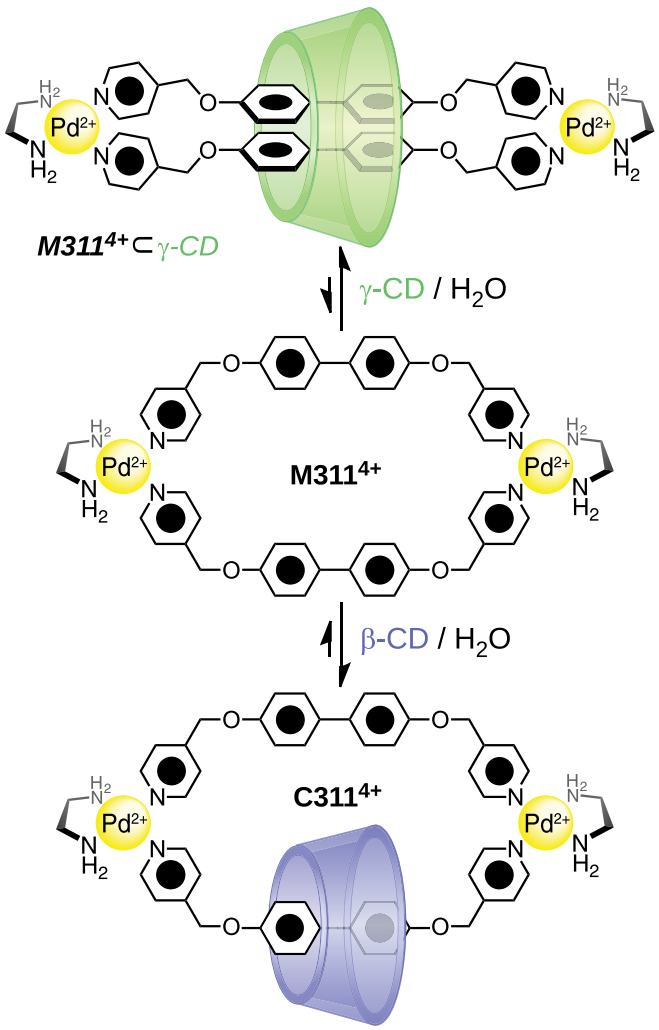
Since Fujita's catenanes are self-assembled in water, the synthesis of other MIMs, driven by hydrophobic interactions (**Section 2.3.1**), are also compatible with his approach. Kimoon Kim has combined his well-established cucurbituril chemistry with Fujita's protocol in order to self-assemble so-called[118–120] 'molecular necklaces'—defined[118] as a catenane in which one large ring is threaded by a number of smaller 'beads'—simply by refluxing pyridyl-terminated CB[6]/diaminoalkane [2]- or [3]pseudorotaxanes with (en)Pt^{II} in water, to yield [4]-component[118,120] and [5]-component[119,120] molecular necklaces, respectively. See **Section 4.1.2.2**.

The reversible nature of Pd^{II} metallacycles has also been exploited in the synthesis (**Scheme 3.8**) of catenated cyclodextrins. Hong[121] discovered that the macrocycle **M311^{4+}**, which constitutes two biphenyl-based ligands doubly bridged by (en)$Pd(NO_3)_2$ ions, becomes catenated in the presence of β-CD, whereas it assembles with γ-CD. **M311^{4+}** is the predominant species in D_2O at concentrations below 1 mM at ambient temperature. Addition of an excess (≥2 equiv) of β-CD to a 0.5 mM solution aqueous solution of **M311^{4+}** leads to the quantitative formation of the [2]catenane **C311^{4+}**. Since the γ-CD ring is large enough to accommodate two face-to-face aromatic guests within its cavity, the addition of 1.2 or more equiv of γ-CD to the **M311^{4+}** assembly at 0.3 mM leads to the quantitative formation of the ring-in-ring complex ***M311^{4+}⊂γ-CD***. The γ-CD ring can also be used to influence the distribution of metallo-organic assemblies—at higher concentrations (2 mM) the addition of γ-CD causes the mixture of various oligomeric assemblies to equilibrate back to the macrocyclic dimer as a result of the stability of the ***M311^{4+}⊂γ-CD*** complex.

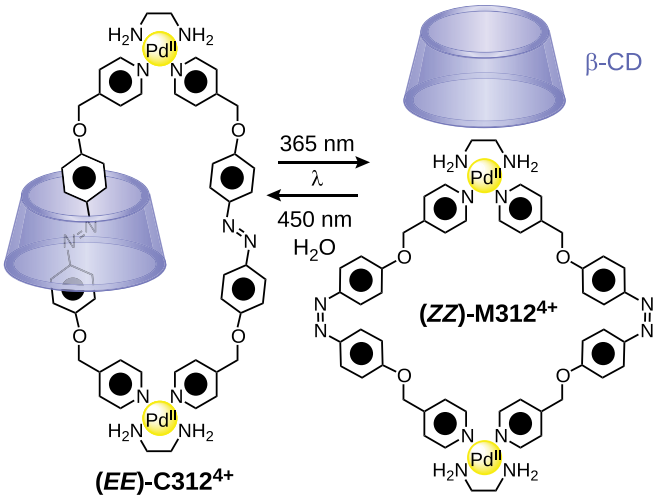
Stang[122] has found that the self-assembly (**Scheme 3.9**) of the [2]catenane **(*EE*)-C312^{4+}**, comprising an azobenzene-based Pd_2L_2 metallacycle interlocked with a β-CD ring, is reversed by the *trans*-to-*cis* photoisomerization of its azobenzene units. The β-CD ring dissociates from the **(*ZZ*)-M312^{4+}**, which is the dominant configuration of the metallacyclic component part in the photostationary state.

3.2.1.4 Donor-Acceptor Metallacyclic Catenanes

Quintela and Peinador have adopted Fujita's strategy for mechanical interlocking mediated by labile Pd^{II} and



Scheme 3.8 The Pd^{II} metallacycle **M311^{4+}** self-assembles with β-CD into the [2]catenane **C311^{4+}**, whereas it self-assembles into a ring-in-ring complex in the presence of γ-CD.[121]



Scheme 3.9 The photoreversible capture and release of Stang's metallacyclic β-CD [2]catenane.[122]

Pt^{II} complexes in the self-assembly (**Figure 3.13**) of π-associated donor-acceptor MIMs. The seminal research[123] on this motif involved the interlocking of BPP34C10 crown ethers with self-assembled Pd^{II}- or Pt^{II}-cornered metallacycles derived from **L313^{3+}**, leading to the [2]catenanes **C313a^{5+}** and **C313b^{5+}**, respectively, in near-quantitative yields in water. While the metallacycle derived from **L313^{3+}** is highly reminiscent of the all-organic $CBPQT^{4+}$ ring, the combination of *para*-xylylene-bis(4-(4-pyridyl)pyridinium ($XBPP^{2+}$/**L314^{2+}**) and $PdCl_2$ leads[124] to a self-assembled metallacycle reminiscent of the Ex^nBox^{4n+} and $TVBox^{8+}$ receptors—see **Section 2.3.3.9**—which intersects a pair of BPP34C10 rings to form the [3]catenane **C314^{4+}**. Similar catenanes have been assembled[124] from diazapyrenium-based π-acceptors and DN38C10 crown ethers. The diazapyrene-based ligands **L315^{+}** and **L316^{+}** combine pairwise with $enPd^{II}$ cornerpieces in the presence of BPP34C10 and DN38C10 to form[125,126] the [2]catenanes **C315^{6+}** and **C316^{6+}**, respectively. The methylene-bridged divalent ligands **L317^{2+}** and **L318^{2+}**, based on 2,7-diazapyrene and 4,4´-bipyridine, respectively, self-assemble with $enPd^{II}$ or $enPt^{II}$ into square-shaped receptors reminiscent of cyclobis(paraquat-4,4´-biphenylene)[127] ($CBPQB^{4+}$)—see **Section 2.3.3.9**. The Solomon link **C317^{8+}** emerges[128] from a combination of **L317^{2+}**, tetrakis-*para*-phenylene[68]crown-20 (TPP68C20), and $enPd(OTf)_2$ in CD_3NO_2, while similar Solomon links arise from mixtures of TPP68C20 and **L318^{2+}** with either $enPd^{II}$ or $enPt^{II}$ cornerpieces. **L318^{2+}** has also been employed[129] in the self-assembly of the [3]catenanes **C318a–c^{8+}**, which possess BPP34C10 or DN38C10 rings and either $enPd^{II}$ or $enPt^{II}$ corners. In the cases of aqueous synthesis, the hydrophobic effect is probably at least as important, if not more so, than the π-associated donor-acceptor interactions in directing the self-assembly of these mechanomolecules. The regioselective catenation of BPP34C10 and DN38C10 with molecular squares based on monocationic ligands similar to the **L318^{2+}** dication has also been described.[130]

Other groups who have relied on metallosupramolecular chemistry to construct donor-acceptor catenanes include those of Liu[131,132] and Stang.[133–135] Liu[131,132] has also assembled donor-acceptor [2]catenanes based on π-donating crown ethers and π-accepting metallacycles using $enPd^{II}$ cornerpieces not unlike those employed by Quintela and Peinador. Stang[133–135] has orchestrated the self-assembly of [3]catenanes and molecular necklaces—see **Section 4.1.2.2**—by relying on kinetically labile Pt–N and Pt–O bonds to achieve thermodynamic control.

3.2.1.5 Pd^{II} and Pt^{II} Stoppered Rotaxanes

The widely utilized donor-acceptor/hydrogen-bonded recognition motifs based on dibenzo[24]crown-8 (DB24C8) and 1,2-bis(pyridinium)ethane (BPE^{2+}) and popularized by Loeb have been combined with labile coordination bonds (**Figure 3.14**), especially at the points of connection between the axle and the stopper. Loeb[48] himself has stoppered a rendition of his $BPE^{2+} \subset DB24C8$ pseudorotaxanes by terminating them with pyridyl ligands, which coordinate to a bulky Pd^{II} organometallic complex in rotaxane **R328^{6+}**. Shinoda[136] has also employed a bulky Pd^{II} complex, possessing a pyridine-2,6-bis(oxazoline) ligand, as a capping agent for a pyridine-terminated *dialkylammonium* ⊂ *DB24C8* semirotaxane to afford the [2]rotaxane **R329H^{3+}** in high (>90%) yield. In a departure from the more ubiquitous pyridine-metal bond, Osakada[137] has stoppered a threaded dibenzylammonium semidumbbell under thermodynamic control using the even more labile Pt–O bond of **R330H^{+}**.

Wisner[138] has invented a particularly novel use of Pd^{II} in the self-assembly (**Figure 3.15**) of MIMs—namely, the dual use of first- and second-sphere coordination at the rotaxane's core. In the convergent 4-component self-assembly of this rotaxane, first-sphere coordination of two pyridine stoppers to $PdCl_2$ is accompanied by second-sphere coordination of the chlorides to a tetralactam macrocycle by way of hydrogen–halogen bonding. The resulting rotaxane, **R331**, was obtained in 89% isolated yield by crystallization: it is an unusual case in which the metal acts as both a template and as the kinetically labile site which is crucial for thermodynamic control. By rearranging the elements of the rotaxane **R331**, Wisner[139] has also designed and prepared the [2]catenane **C319** based on the same recognition processes. By terminating a tetralactam thread with pyridyl groups, the ditopic C-shaped ligands of **C319** 'pinches' the $PdCl_2$ complex while interlocking itself with an identical copy to form the homo[2]catenane, in which the link topology maximizes the number of possible hydrogen–halide noncovalent bonding interactions.

Pd^{II} and Pd^{II} capping reactions have also been employed in the synthesis of higher-order oligorotaxanes. Osakada[140] has connected a pair of α-CD-based [3]pseudorotaxane ligands together with *cis*-protected Pd^{II} or Pt^{II} ions to generate L-shaped [5]rotaxanes—see **Section 4.2.1.1**—while Yang[141,142] has created a modular approach to building

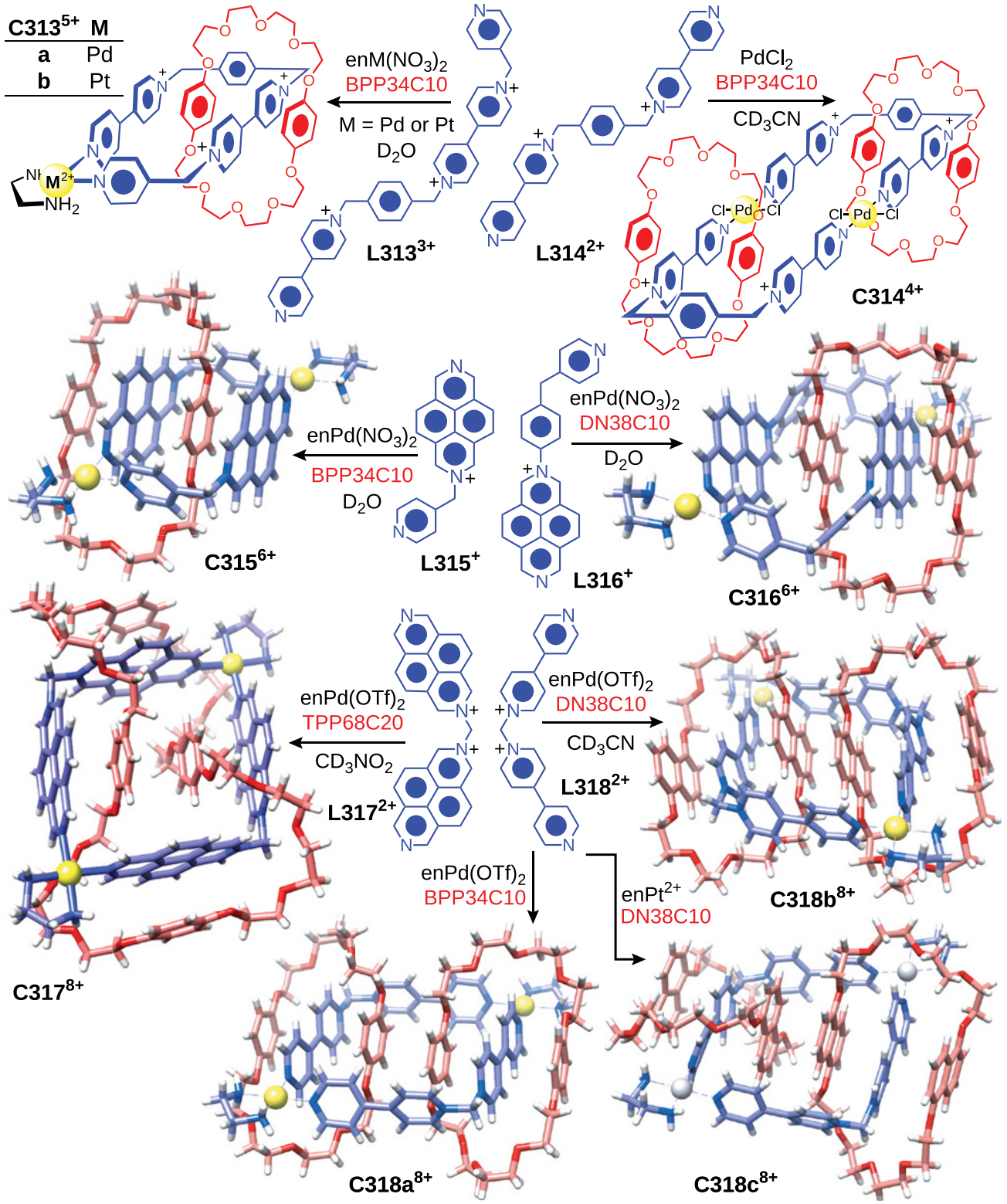


Figure 3.13 Examples of self-assembled donor-acceptor catenanes introduced by Peinador and Quintela.[123–126,128,129] Tubular representations of the X-ray crystal structures are illustrated with solvent molecules and counterions omitted for the sake of clarity.

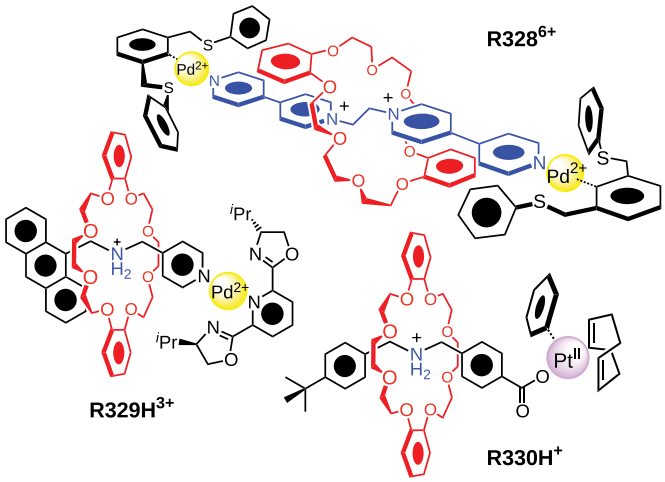


Figure 3.14 Self-assembled rotaxanes that combine dialkylammonium/DB24C8 recognition motifs with labile metal-ligand stoppers.[48,136,137]

organometallic rotaxane dendrimers based on pillar[5]arene recognition—see **Section 4.2.2.3**.

3.2.2. MIMs Possessing Group 11 Elements

Kinetically labile complexes of gold (**Section 3.2.2.1**), silver (**Section 3.2.2.2**), and copper (**Section 3.2.2.3**) have all been utilized as linkers in the self-assembly of mechanomolecules based on Group 11 transition metal elements.

3.2.2.1 Gold MIMs

The self-assembly of a variety of gold catenanes[143–145] have relied upon the reversibility of [Au–Au] and [Au–C] bonds. The original gold [2]catenane (**C320**) introduced by Mingos[146] comprises (**Figure 3.16**) rings of acetylenic gold–carbon bonds, the homocatenation of which is driven by aurophilic (**Section 2.3.11.3**) interactions. The Au^{I} [2]catenane **C320** assembles from a mixture of $[Au(NH_3)_2]^+$ and *tert*-butylacetylene (C≡C^{t}Bu) in MeCN. The labile[147] ammonia ligands are lost in the self-assembly process to afford a catenated cluster having the formula

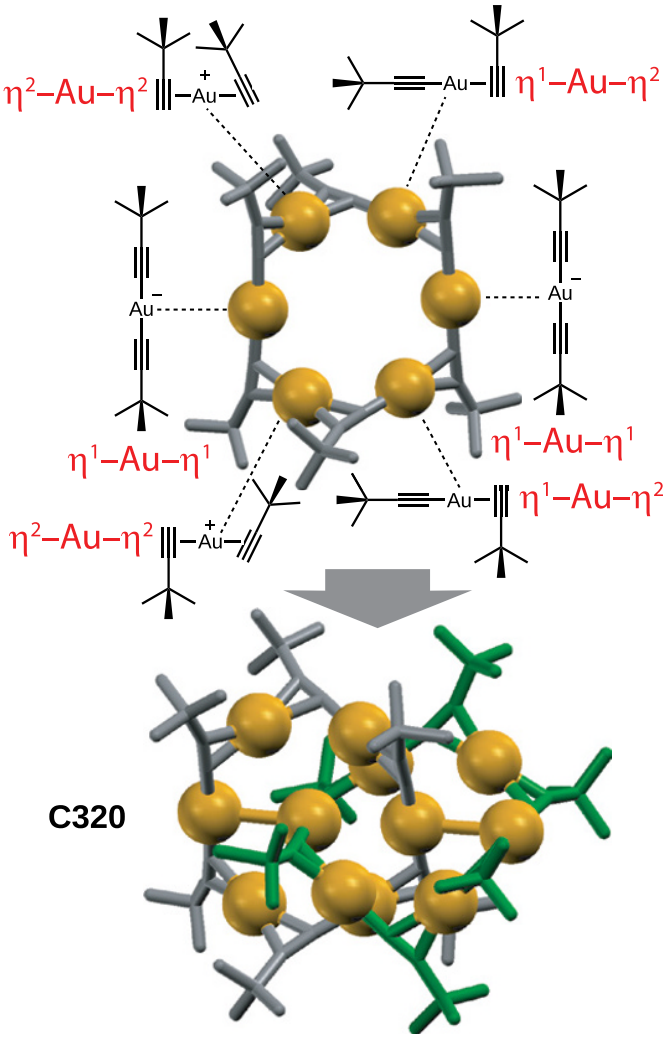


Figure 3.16 A self-assembled [2]catenane based on three different types (η^1–Au–η^1, η^1–Au–η^2, η^2–Au–η^2) of Au^{I}—C≡C coordination modes. Bonds between Au^{I} atoms (shaded gold) indicate aurophilic interactions.[146]

[{Au(C≡C^{t}Bu)}$_6$]$_2$. Each ring of the catenane comprises six Au^{I} atoms and six C≡C^{t}Bu ligands. The C≡C^{t}Bu ligands can adopt either the η^1 or η^2 coordination modes, giving rise to three distinct arrangements, namely [η^1–Au–η^1]$^-$,

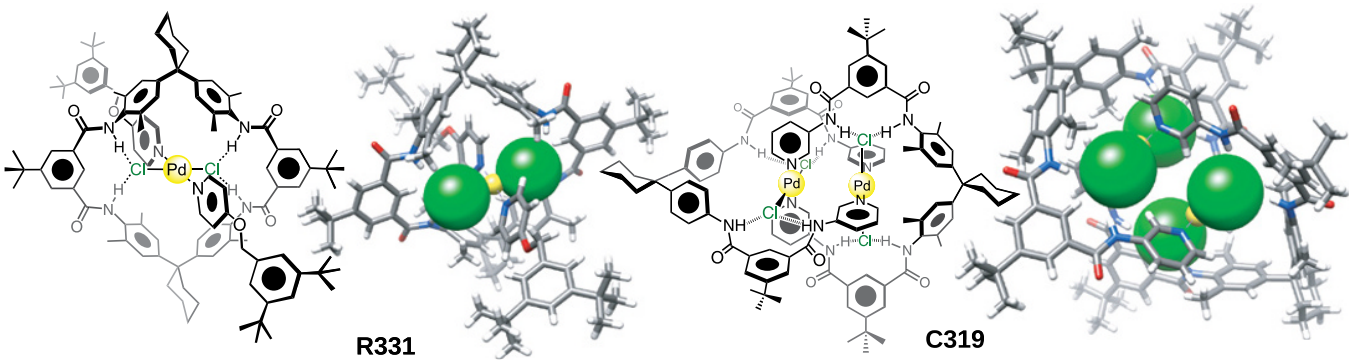


Figure 3.15 Structural formulas and X-ray crystal structures of the self-assembled MIMs templated by a synergy of first- and second-sphere coordination around $PdCl_2$ by Wisner.[138,139]

[η^1–Au–η^2], and [η^2–Au–η^2]$^+$, each of which exist in pairs that are distributed on opposite ends of the catenane's rings. Each ring therefore possesses C_2 symmetry when considered individually. The templating aurophilic interactions can be identified between four pairs of gold atoms, each of which forms a noncovalent bridge between rings. A similar set of gold clusters comprising catenated Au^I acetylide pentamers, instead of hexamers, has been prepared by Chou.[148]

A number of gold catenanes possessing thiolate ligands instead of acetylides have also been described. Brisdon[149] introduced the [2]catenanes **C321** and **C322**, each of which self-assembles (**Figure 3.17**) in >90% yield from biphasic mixtures of aqueous AuCl($C_2H_5SC_2H_4OH$) and *tert*-butylthiophenol in xylenes. Whereas **C321** comprises two rings, each with five Au^I atoms and five bridging ligands, the two rings of **C322** comprise six Au^I atoms and six bridging ligands. The only differences between the bridging ligands in these two assemblies are the positions of the *tert*-butyl groups, which are located at the *para* positions in **C321** and the *ortho* positions in **C322**. Che[150] has discovered the catenation of pentameric Au^I metallacycles with hexameric Au^I metallacycles in a cluster possessing glycosylated thiolate ligands, which serve as precursors for the antiarthritic drug Auranofin. In addition to these examples, Zeng[151] has predicted, based on computational models, that an $Au_{20}(SR)_{24}$ gold-thiolate cluster adopts a catenane-like geometry as its lowest energy structure, indicating that gold clusters with mechanical bonds may be important intermediates during the growth of thiolate-capped gold nanoparticles.

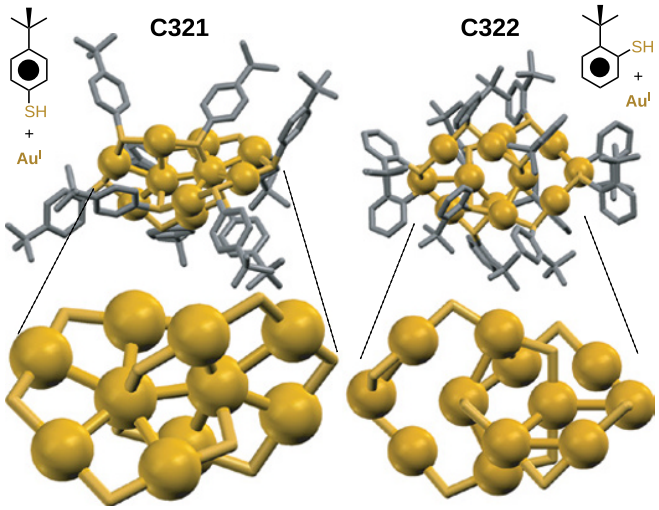


Figure 3.17 Thiolate-bridged gold catenanes assembled by Brisdon.[149] The number of Au^I atoms per ring in these catenanes is determined by the location of the ^{t}Bu substitution on the thiophenolate bridges, where *para* substitution affords the catenane **C321** with five Au^I atoms per ring, while *ortho* substitution affords the catenane **C322** with six Au^I atoms per ring. Portrayals of the solid-state structures of the catenanes (bottom) with all carbon atoms omitted show the gold–thiolate and aurophilic gold–gold interactions more clearly.

Puddephatt[152–159] has constructed a collection of phosphine-bridged Au^I catenanes via the self-assembly (**Figure 3.18**) of bis(diphenylphosphino)alkanes (**L323a–c**) with digold(I) diacetylide precursors derived from the propargyloxy-functionalized diphenyl compounds **L324a–g** possessing different hinge groups, –X–, as central linkers. The outcome of the self-assembly of these ligands at room temperature in CH_2Cl_2 in the presence of Au^I is sensitive to subtle differences in their constitutions. For example, digold diacetylides based on the isopropylene-hinged ligand **L324a** combine with 1,2-bis(diphenylphosphino)ethane (**L323a**) to form a metallacycle (**M323a**), whereas the catenated metallacycles **C323b** and **C323c** are formed[152] if the diphenylphosphino ligands possess propylene (**L323b**) or butylene (**L323c**) linkers, respectively. Employing the cyclohexylene-hinged **L324b** instead of **L324a** as the source of Au^I diacetylide, the doubly interlocked [2]catenane **C324**, also known as a Solomon link, is produced.[153] Gold [2]catenanes based on on the 4-bromophenylmethylene-hinged[156] ligand **L324c**, the bromomethyl acetal-hinged[157] ligand **L324d**, and the pyridylmethylene-hinged[158] ligands **L324e–g** have also been assembled, giving rise to catenanes that exhibit a novel form of topological chirality, which we refer to as mechanically axial chirality—see **Section 5.2.3.2**. Puddephatt's strategy for the assembly of Au^I metallacyclic [2]catenanes is also general enough to accommodate[160] many other hinge groups –X– not illustrated in **Figure 3.18**.

Beer[161] has employed kinetically inert Au^{III} dithiocarbamate metallacycles in the self-assembly of several mixed-metal catenanes that interlock with kinetically labile Cu^{II}-based metallacycles—see **Section 3.2.2.3**.

3.2.2.2 Silver MIMs

The transition metal template synthesis of catenates possessing metallacyclic component parts was originally introduced by Piguet.[162] The complexation of Ag^I ions has been employed as the ring-closing reaction for entwined templates surrounding an Fe^{II} center in the self-assembly (**Scheme 3.10**) of the [2]catenate **FeC325^{4+}**. The catenane is obtained in a stepwise manner from the multivalent ligand **L325**, possessing both tridentate and bidentate imidazolylpyridine units, the central tridentate portions of which combine with $Fe(ClO_4)_2 \cdot 6H_2O$ in $MeCN/CH_2Cl_2$ to form the entwined octahedral coordination complex **Fe(L325)$_2^{2+}$**. The subsequent introduction of $AgClO_4 \cdot H_2O$ causes the rings to close as a result of the pairwise tetrahedral coordination of the bidentate units to the Ag^I centers, producing **FeC325^{4+}** in 87% isolated yield. The pseudotetrahedral Ag^I linkers impart each metallacycle in the assembly with either *M* or *P* helicity, allowing for up to three co-configurational isomers of **Fe(L325)$_2^{2+}$**—namely, two homochiral enantiomers and a heterochiral *meso* diastereoisomer. The homochiral enantiomers crystallize separately from the *meso* diastereoisomer to form a conglomerate in the solid state. In **Scheme 3.10**, only the heterochiral *meso*

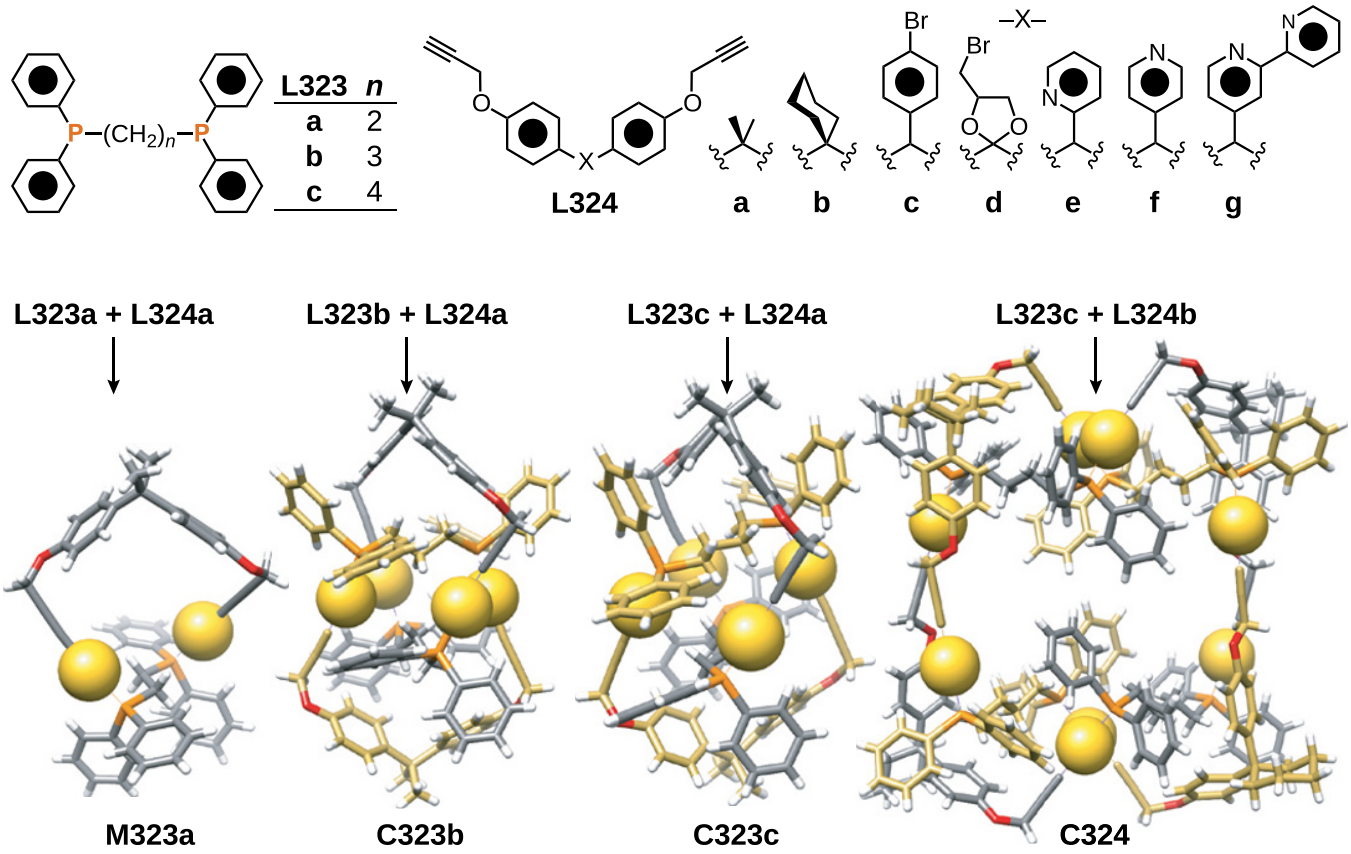
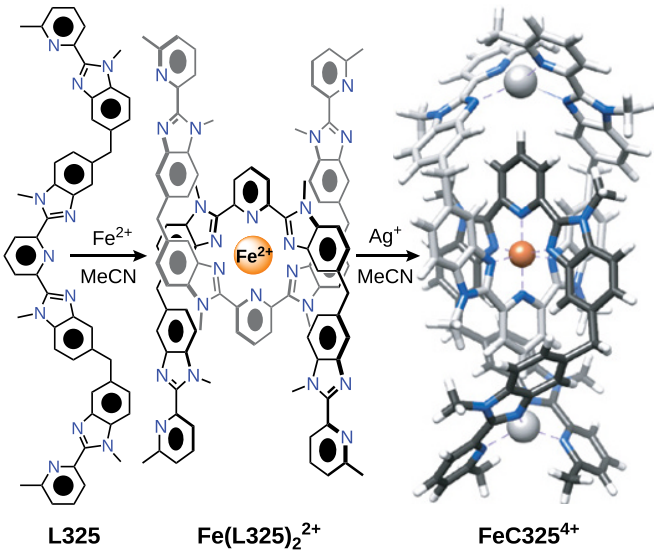


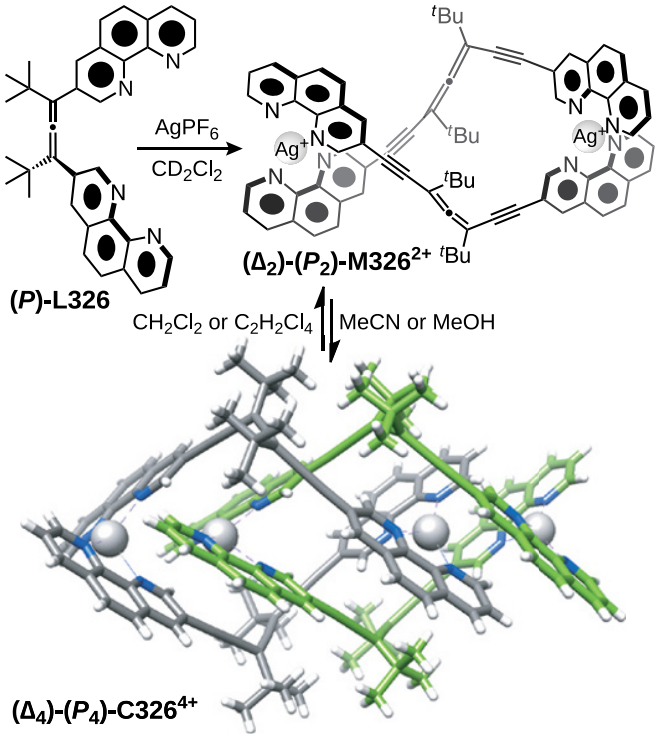
Figure 3.18 The self-assembly and solid-state structures of selected examples of Puddephatt's Au^{I} [2]catenanes templated by space-filling and aurophilic interactions. Tubular representations of the solid-state structures are illustrated with solvent molecules omitted for the sake of clarity.



Scheme 3.10 The self-assembly of Piguet's metallacyclic [2]catenate possessing an octahedral Fe^{II} template and dynamic linkers based on tetrahedral AgI complexes.[162] A tubular representation of the solid-state structure of **FeC325**$^{4+}$ is illustrated with PF_6^- counterions and solvent molecules omitted for the sake of clarity.

[2]catenate is illustrated. See **Section 5.2.3.3** for a discussion of molecular helicity associated with mechanical bonds.

Another class of Ag^{I}-bridged helical catenanes has been introduced recently by Diederich.[163] The enantiomerically pure [2]catenane **(Δ$_4$)-(*P*$_4$)-C326**$^{4+}$ possesses only right-handed helicity on account of the homochiral ligands, **(*P*)-L326**, from which it is assembled (**Scheme 3.11**) in organic solvents via the reversible catenation of the corresponding metallacycle **(Δ$_2$)-(*P*$_2$)-M326**$^{2+}$. The formation of this homochiral macrocyclic helicate is driven by the pairwise coordination of phenanthroline (phen) units, which terminate the axially chiral alleno-acetylenic backbone of the ligand, while catenation of the metallacycles is driven by space-filling and solvophobic stacking interactions in polar solvents such as MeCN and MeOH. The non-catenated metallacycle can be accessed cleanly in halogenated solvents, such as CH_2Cl_2 and $C_2H_2Cl_4$. An enhancement in the chiroptical properties is observed upon catenation, owing most likely to the increase in rigidity afforded by the tight-fitting intercalation of the two helical rings. A longer bis(alleno-acetylene) ligand possessing three phen groups self-assembles likewise into a bis[2]catenane with homochiral mechanical helicity. These assemblies also exhibit "narcissistic self-sorting", since mixed-ligand assemblies



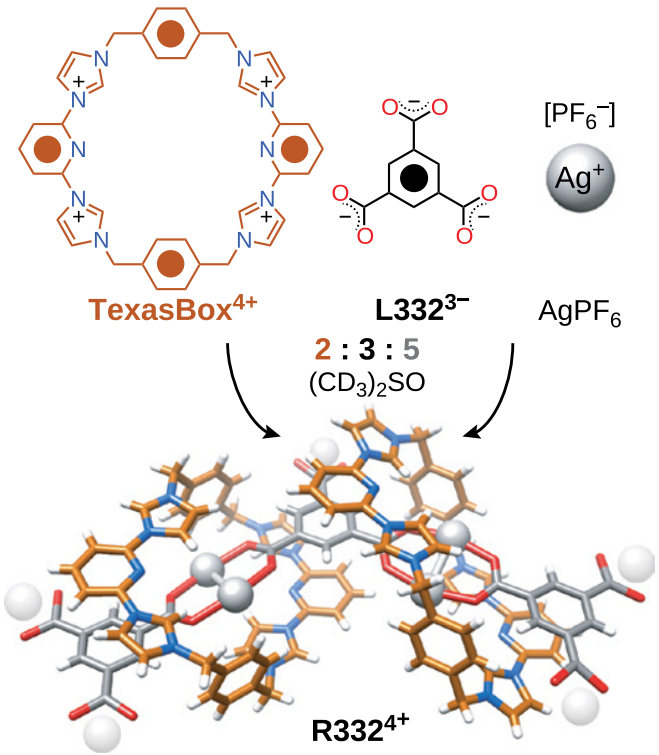
Scheme 3.11 Diederich's [2]catenane **(*Δ*$_4$)-(*P*$_4$)-C326**$^{4+}$ self-assembles in polar organic solvents, driven by helical π-associated stacking of its Ag^{I}-bridged homochiral alleno-acetylenic phenanthroline ligands, **(*P*)-L326**.[163] A tubular representation of the solid-state structure is illustrated with PF_6^- counterions omitted for the sake of clarity.

derived from precursors of different lengths and/or chiralities are never observed, even when they are present in the same solution.

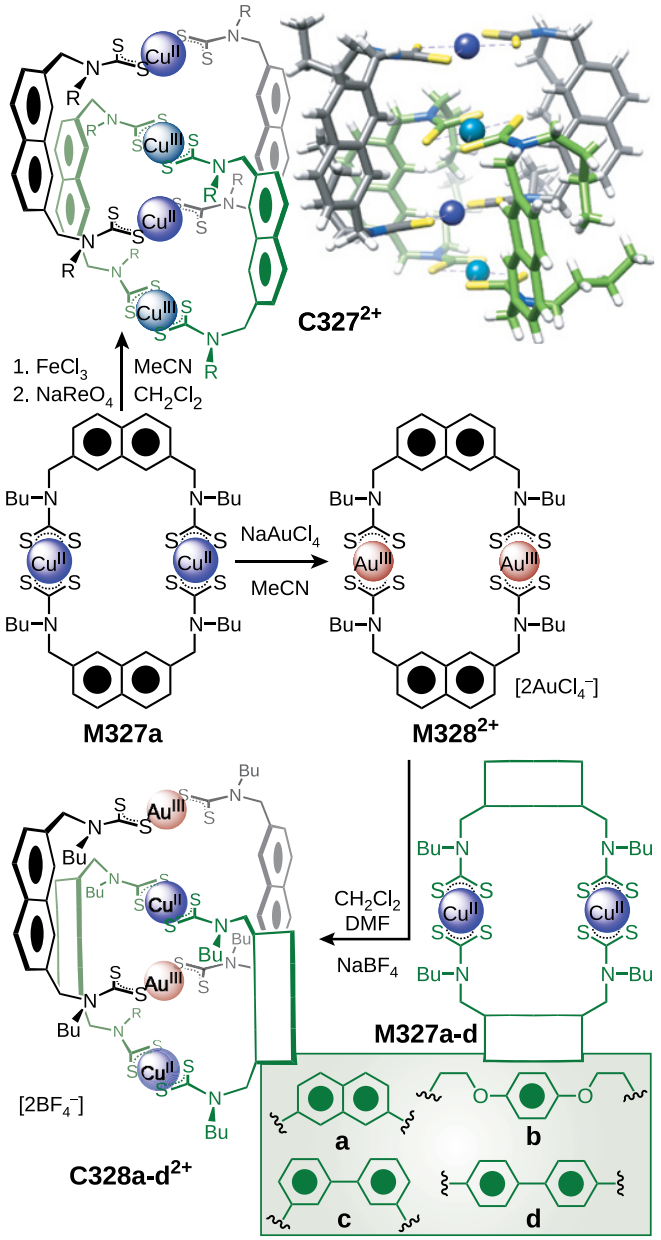
Sessler[164] has recently described the metallosupramolecular self-assembly (**Scheme 3.12**) of the [3]rotaxane **R332**$^{4+}$ by combining the TexasBox^{4+} receptor (**Section 2.3.3.9**) with Ag^{I} and trimesic acid in $(CD_3)_2SO$ solution. The co-constitution of the [3]rotaxane contains two TexasBox^{4+} rings, each encircling a dumbbell assembly comprising three deprotonated trimesic acid units (**L332**$^{3-}$) and five Ag^{I} ions. Since it represents approximately two-thirds of the molecular population in $(CD_3)_2SO$, **R332**$^{4+}$ is assumed to be the thermodynamic product, since the outcome of the reaction is relatively invariant to differences in stoichiometry and order of addition, when provided with at least 2.5 equiv of Ag^{I} relative to TexasBox^{4+}. In contrast with the typical stoppering and clipping protocols for rotaxane synthesis, the preparation of **R332**$^{4+}$ more closely resembles a dumbbell capture protocol—see **Sections 2.3.1.3** and **2.4**—since all of the pieces self-assemble directly in one step to give the [3]rotaxane. Since it is held together by dynamic coordinative bonds, the assembly also responds to various stimuli. **R332**$^{4+}$ can be fully or partially dissociated by the introduction of iodide as a competitive counterion for Ag^+, a process that can be reversed cleanly by adding more $AgPF_6$. The dynamics underlying the conformational chair-to-chair flip of the TexasBox^{4+} are also sensitive to stimuli, such as changes in temperature and solvent composition. The two-dimensional nature of the trimesic acid template enables the formation of extended networks when employing alternative templating ions such as Cd^{2+}.

3.2.2.3 Copper MIMs

A particularly unique example (**Scheme 3.13**) of coordination-driven self-assembly of mechanomolecules has been described by Beer,[165] who found serendipitously that the Cu^{II} dithiocarbamate metallacycle **M327a** self-interlocks spontaneously upon chemical oxidation to give the mixed-valence Cu^{II}/Cu^{III} [2]catenane **C327**$^{2+}$. The topology of the catenane provides the optimal stabilization by virtue of donor-acceptor charge transfer interactions between the mixed-valence Cu$^{II/III}$ ions for the kinetically labile Cu^{II} oxidation state. In other words, a redox stimulus initiates the thermodynamically controlled catenation event. In a subsequent investigation, Beer[161] found that the Au^{III}-transmetallated macrocycle **M328**$^{2+}$, which is derived from **M327a**, can be interlocked with a variety of homologues



Scheme 3.12 Sessler's self-assembled TexasBox^{4+} [3]rotaxane.[164] The tubular representation of **R332**$^{4+}$ is a model of a mechanically interlocked $(Ag^+)_5$(TexasBox^{4+})$_2$(**L332**$^{3-}$)$_3$ cluster (Ag^{I} ions illustrated translucently indicate possible sites for the fifth Ag^{I} center), based on the crystallographic structure of a smaller $(Ag^+)_2$(TexasBox^{4+})(**L332**$^{3-}$)$_3$ [2]rotaxane.



Scheme 3.13 Beer's self-assembled [2]catenanes based on dynamic Cu^{II} dithiocarbamate metallosupramolecular rings.[161,165] Oxidation of half of the Cu^{II} centers of **M327a** induces the catenation (top) of the mixed-valence Cu^{II}/Cu^{III} species, **C327**$^{2+}$. The tubular representation of the solid-state structure of **C327**$^{2+}$ is illustrated with BF_4^- counterions omitted for the sake of clarity. Alternatively, **M327a** can be transmetallated to the Au^{III} macrocycle **M328**$^{2+}$, which interlocks (bottom) with macrocycles **M327a**–**M327d** to form the corresponding [2]catenanes **C328a**$^{2+}$–**C328d**$^{2+}$.

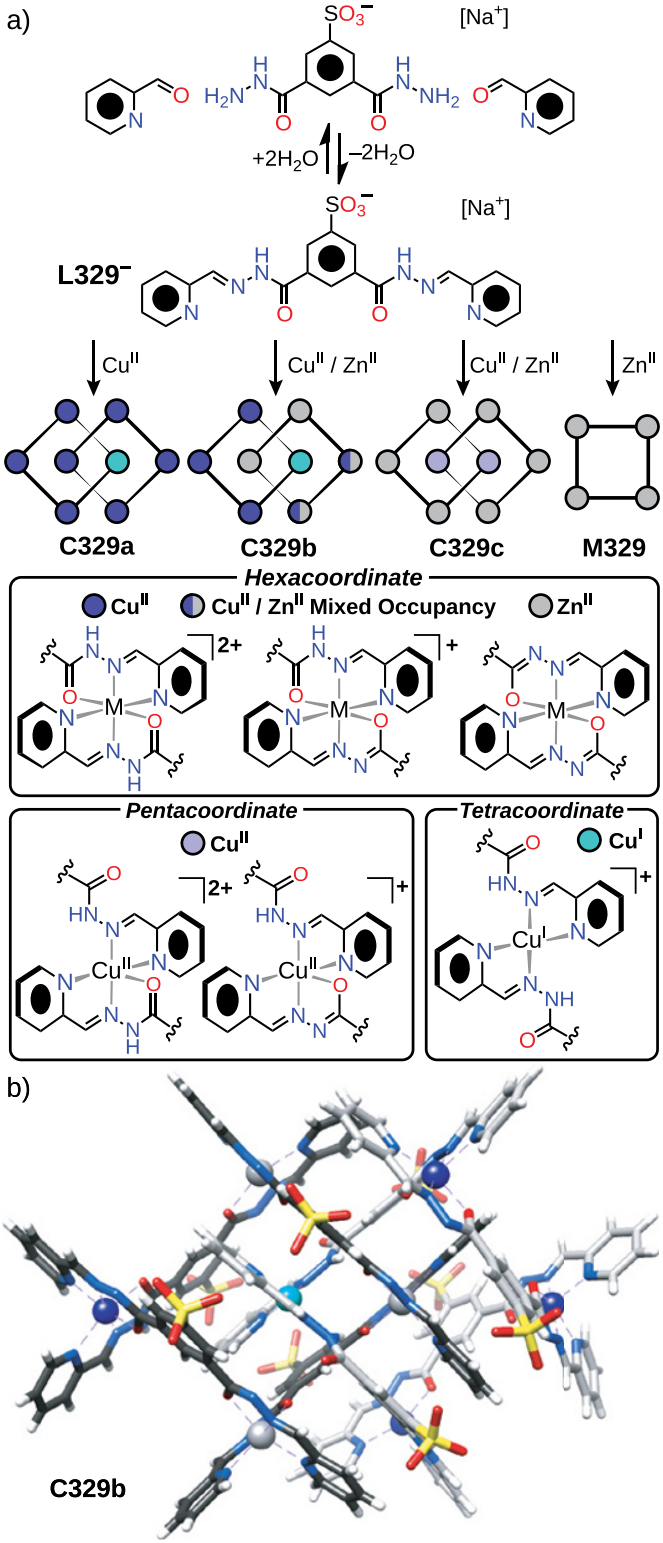


Figure 3.19 Metallogrid [2]catenanes introduced by Cametti and Rissanen.[166] (a) The self-assembly of mixed-metal [2]catenanes **C329a**–**C329c** and the uncatenated Zn^{II} metallogrid **M329**. The external nodes of the metallogrids adopt hexacoordinate geometries, while the internal heterometallic sites possess at least one pentacoordinate or tetracoordinate center. (b) A tubular representation of the solid-state structure of **C329b** with Na^+ ions and solvent molecules omitted for the sake of clarity.

(**M327a–d**) under thermodynamic control to give the corresponding mixed-metal [2]catenanes **C328a**$^{2+}$–**C328d**$^{2+}$. The mixed-valence redox states of these catenated assemblies have been confirmed[161,165] by EPR spectroscopy.

Cametti and Rissanen[166] have also discovered Zn^{II}/Cu^{II} and Cu^{I}/Cu^{II} mixed-valence metal-ligand motifs for the self-assembly (**Figure 3.19**) of the [2]catenanes **C329a**–**C329c**.

Their motif involves the 32-component self-assembly of ligands and transition metal ions into interpenetrated molecular grids. The condensation (**Figure 3.19a**) of 3,5-di(hydrazinecarbonyl)benzenesulfonate with two equivalents of 2-pyridinecarboxaldehyde gives rise to the ligand **L329**$^-$, establishing reversible hydrazone bonds that can coordinate to Cu^I, Cu^{II}, or Zn^{II} in tetra-, penta-, or hexacoordinate geometries. Four ligands and four metals co-assemble into square-shaped "metallogrids", which interpenetrate to form [2]catenanes possessing eight metal-ligand complexes—six located externally and two located internally—serving as the nodes for the macrocycles. The hexacoordinate and pentacoordinate nodes may be either neutral or cationic, depending on the local protonation state of the ligands, which could not be determined crystallographically. The metallogrids only concatenate in a mixed-valence setting, since (i) the [2]catenane **C329a** derived from Cu^{II} contains a tetrahedral Cu^I complex, presumably as a result of an *in situ* reduction of Cu^{II}, and (ii) a non-catenated metallogrid **M329** is isolated when Zn^{II} is the only template available. The solid-state structure (**Figure 3.19b**) of the [2]catenane **C329b**, as well that of the other [2]catenanes (not illustrated), reveals that the coordination modes of the internally located heterometallic centers allow the hydrazone NH protons to engage in intercomponent hydrogen-bonding interactions, which are responsible for stabilizing the catenanes as opposed to the corresponding isolated macrocycles.

3.2.3 MIMs Possessing Group 12 Elements

Zinc (**Section 3.2.3.1**) and mercury (**Section 3.2.3.2**) are two group 12 metals that have been employed in thermodynamically controlled syntheses of mechanomolecules.

3.2.3.1 Zinc MIMs

The labile coordination bonds between Zn^{II} ions and 2,2´-bipyridine (bpy) ligands have been put to good use (**Figure 3.20**) in MIM synthesis. Sanders[167] has reported the quantitative preparation of the [2]catenane **C330**$^{4+}$ under thermodynamic control by equilibrating a labile Zn^{II}/bipyridine-based [M_2L_2] metallacycle with NDI recognition units in the presence of DN38C10 in CD_3CN. The catenane is kinetically stable on the ^{1}H NMR timescale up to a temperature of 350 K. More recently, a collaborative effort between Schalley, Sanders, and Nitschke[168] has produced tetrahedral cages possessing Zn^{II} complexed corners, the π-accepting ligands of which can be threaded by up to two DN38C10 macrocycles to form the [3]catenane **C331**$^{8+}$. See **Section 4.1.3.2** for a discussion of even larger catenated metallosupramolecular tetrahedra. Using a similar ligand motif, Hardie[169] has prepared the triply interlocked chiral coordination cage assembly **C332**$^{12+}$. This M_6L_4 catenane comprises four tripodal cyclotriveratrylene units, each terminated with three bpy ligands on each of their arms. The tripodal ligands assemble pairwise into trigonal bipyramidal cages in the presence of Zn^{II} or Co^{II} ions, with the metal centers bridging the ligands in form of distorted octahedral coordination complexes involving two bpy ligands and one nitrate counterion. The catenane is isolated in up to 64% yield from a mixture of the ligands and metals in DMSO. The solid-state structures of **C332**$^{12+}$ and other catenated macrobicyclic compounds are illustrated in **Section 4.1.3.1**.

3.2.3.2 Mercury MIMs

Ward,[170] while investigating the metallosupramolecular chemistry of coordination compounds based on pyrazolylpyridine ligand motifs, has found a case (**Scheme 3.14**) of a self-assembled M_3L_2 [2]catenate. The multivalent ligand,

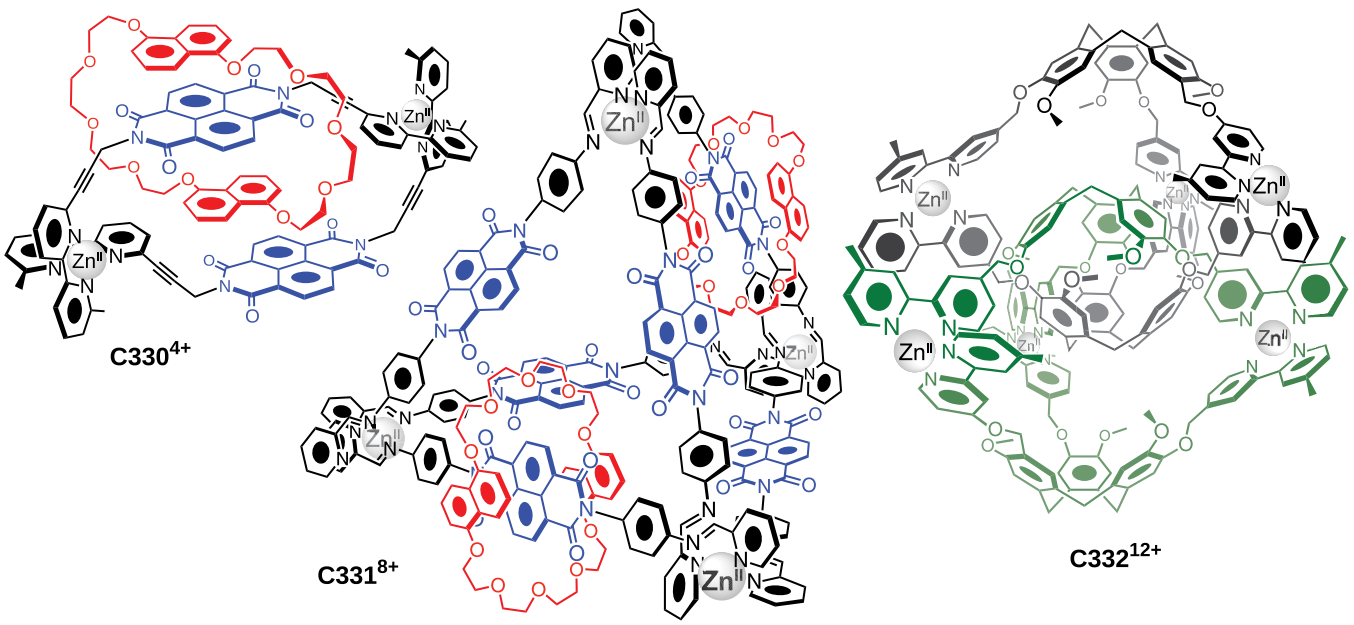
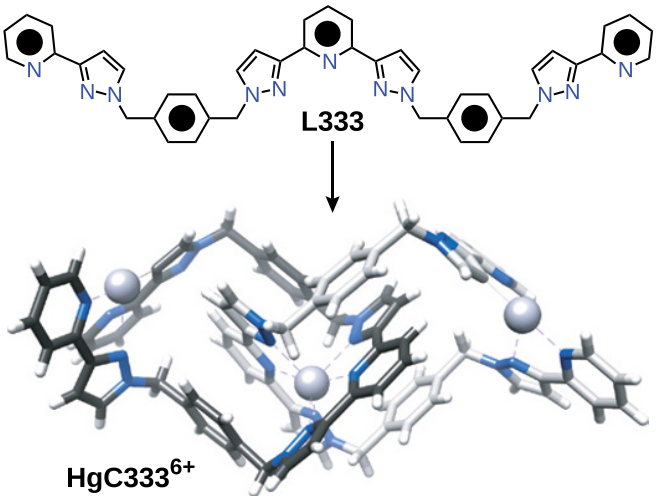


Figure 3.20 Stereoformulas of self-assembled catenanes based on labile Zn-bipyridine bonding motifs.[167,169]



Scheme 3.14 The self-assembly[170] of Ward's [2]catenane **Hg333^{6+}**, which is both templated and sealed by Hg^{II} coordination complexes. A tubular representation of the solid-state structure of **HgC333^{6+}** is illustrated with ClO_4^- counterions and solvent molecules omitted for the sake of clarity.

namely **L333**, contains a central tridentate and two terminal bidentate units—a design reminiscent of Piguet's seminal [2]catenate **FeC325^{4+}** (**Scheme 3.10**), the Ag^I-containing rings of which surround a Fe^{II} template. In contrast with Piguet's motif, however, Ward's ligand **L333** forms[171] trinuclear double helicates when mixed with Ag^I and Fe^{II}. Mercury(II), on the other hand, gives rise to two products—a trinuclear helicate (major) and a [2]catenate (minor)—the crystals of which can be separated by hand from the conglomerate. The Hg^{II} ions serve as both the template and the ring-closing linkers in the formation of the [2]catenate **HgC333^{6+}**. The central Hg^{II} center adopts a hexacoordinated octahedral geometry, while each of the peripheral Hg^{II}-based ring closures engage the bidentate ligands in a four-coordinate geometry that includes a cyclometallating organometallic C–Hg bond, revealing that the ligand **L333** becomes mono-deprotonated during the assembly of **HgC333^{6+}**. The [2]catenate is further stabilized by π-stacking interactions among the ligands' *para*-phenylene and pyrazolylpyridine aromatic units.

3.2.4 MIMs Possessing Elements of Groups 7–9

The transition metals in groups 7–9 on the periodic table have been involved in the thermodynamically controlled synthesis of MIMs possessing metalloporphyrin (**Section 3.2.4.1**) stoppers and linkers, as well as a number of coordination complexes of iron (**Section 3.2.4.2**), ruthenium (**Section 3.2.4.3**), osmium (**Section 3.2.4.4**), and cobalt (**Section 3.2.4.5**).

3.2.4.1 Self-Assembled Metalloporphyrin MIMs

Metalloporphyrins[172] serve as excellent building blocks for supramolecular chemists because the equatorial ligation of the porphyrin's pyrrole units leave vacant sites at the axial positions open for relatively weak and labile metal-ligand bonding to take place.

Self-Assembling Porphyrin Rotaxanes

A number of research groups have utilized axially coordinated metalloporphyrin stoppers (**Figure 3.21**) to access a thermodynamically controlled regime in the synthesis of MIMs templated by donor-acceptor and hydrogen-bonding interactions. Branda[173] was amongst the first to demonstrate this approach by using a Ru(CO) metallated porphyrin to stopper a pyridine-terminated Loeb-type *BPE^{2+}⊂DB24C8* pseudorotaxane, yielding **R333^{2+}**. Gunter[174–178] has reported several instances involving the axial coordination of pyridine ligands at the termini of *NDI⊂DN38C10* pseudorotaxanes to vacant sites of Zn-, Ru-, or Rh-metalloporphyrins in thermodynamically-controlled stoppering protocols. The [2]rotaxane **R334** is a representative example[174] of Gunter's donor-acceptor designs, which have also been immobilized[175] on resins using the same chemistry. Hunter[179] has created the neutral, hydrogen-bonded, porphyrin-stoppered [2]rotaxane **R335**, in which the ring is a self-assembled cyclic homodimer of noncovalently associated porphyrin/pyridine ligands, while Gunter[180] has also employed axially coordinated porphyrin stoppers in the self-assembly of the neutral [2]rotaxane **R336** templated by isophthalamide hydrogen-bonding interactions. Shimizu[57,58,181] has utilized the open axial site of a few different Rh^{III} metalloporphyrins to stopper derivatives of dialkylammonium/DB24C8 rotaxanes, e.g., **R337aH$^+$–R337cH$^+$** and **R338aH$^+$–R338cH$^+$**, while Shinoda[136] has employed a similar motif in the construction of the Ru^{III} metalloporphyrin-stoppered [2]rotaxane **R339H$^+$**.

Self-Assembling Porphyrin Catenanes

A number of self-assembling [2]catenanes based on the axial coordination of porphyrin units are also illustrated in **Figure 3.21**. Bampos[182] has orchestrated the four-component self-assembly of the donor-acceptor [2]catenanes **C334a^{2+}** and **C334b^{2+}** by interlocking DN38C10 around the NDI unit of a self-assembled metallacycle possessing dynamic $Fe(terpy)_2^{2+}$ and axially coordinated porphyrin linkers metallated with Ru(CO) and Zn centers, respectively. Dialkylammonium/crown ether recognition motifs have also been employed to guide the self-assembly of the [2]catenanes. Liu[183] has assembled the [2]catenane **C335H$^+$** under thermodynamic control by allowing phenolic endgroups of a *dialkylammonium⊂crown* pseudorotaxane to coordinate to both axial sites of a Sn-based metalloporphyrin linker, while Li and Yu[184] have prepared the [2]catenane **C336H$^+$** by co-assembling a bis(pyridyl) pseudorotaxane with a divalent porphyrinic tweezer compound.

Sauvage[185–187] has prepared porphyrinic catenanes under thermodynamic control using a clever adaptation of his so-called entwining strategy. A divalent ligand (**L337** or **L338**) bridges the two porphyrin termini of **L339**—

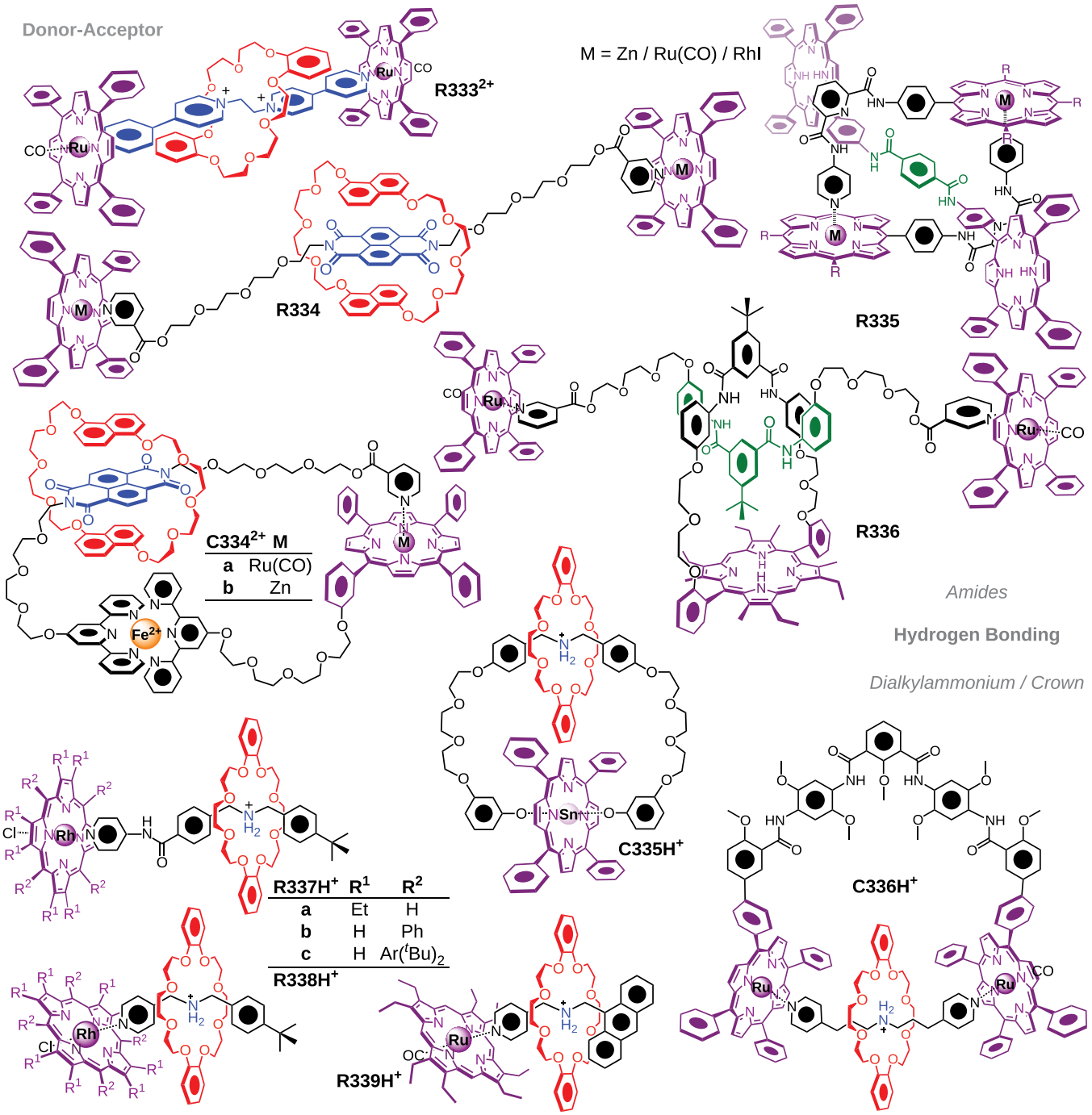
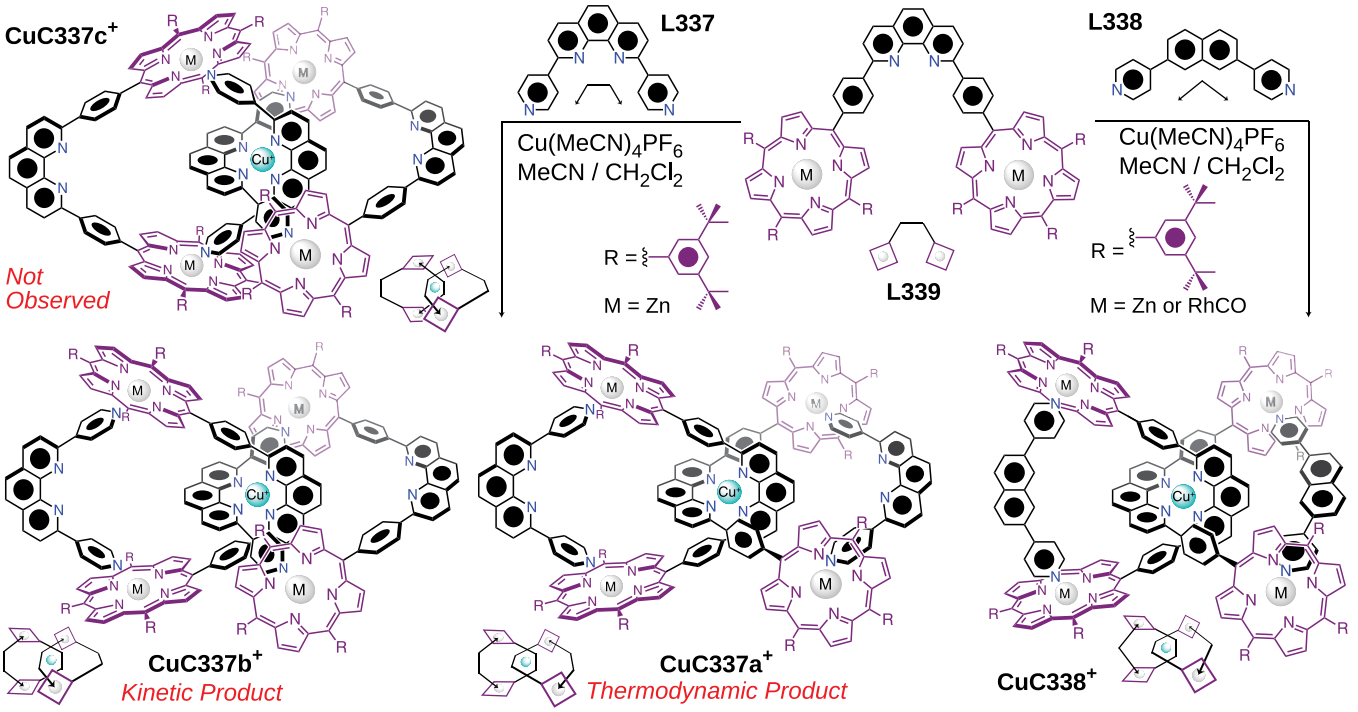


Figure 3.21 Examples of self-assembled rotaxanes[57,58,136,173,174,179–181] and catenanes[182–184] based on the reversible axial coordination of metalloporphyrin stoppers and linkers, respectively.

preorganized around the traditional Cu^{I}–phenanthroline template motif—in a ring-closing self-assembly event according to **Scheme 3.15**. The resulting [2]catenanes rely on axial coordination of the ligating pyridine units to Zn or Rh metal centers in **L339**. Since the phenanthroline moiety of **L337** can compete with **L339** for Cu^{I}, a mixture of translationally isomeric catenanes is obtained when thermodynamic equilibrium is reached. The ratio of the thermodynamic and kinetic products, **CuC337a**$^{+}$ and **CuC337b**$^{+}$, is sensitive to initial conditions and reaction time, while **CuC337c**$^{+}$ is not observed on account of steric constraints. The higher stability of **Cu337a**$^{+}$ is rationalized by the expectation that its axial Zn–N bonds are stronger than those of **CuC337b**$^{+}$, since its porphyrinic Zn centers are weaker Lewis acids when the phenanthroline center is not occupied by a Cu^{I} ion. On the contrary, the [2]catenate **CuC338**$^{+}$ is obtained as the sole product, since the ligand **L338** from which it derives possesses no Lewis basic coordination sites to compete for the Cu^{I} template.



Scheme 3.15 An entwining strategy from the Sauvage group, in which axially-coordinating ligands bridge metalloporphyrinic sites organized around Cu^{I} to form [2]catenanes under thermodynamic control.[186]

3.2.4.2 Iron MIMs

Macartney[188] has employed ligand exchange reactions involving Fe^{II} clusters as thermodynamically controlled α-CD rotaxane capping mechanisms, similar to those exhibited by the porphyrin stoppers in **Section 3.2.4.1**. The [2]rotaxanes **R340a**$^{4-}$–**R340e**$^{4-}$, each of which possesses (**Figure 3.22**) a pair of inorganic $[Fe(CN)_5]^{3-}$ stoppers coordinated by their axles' terminal pyridine moieties, self-assemble quantitatively in water. The same types of pentacyanoferrate endcaps have been employed to assemble cyclodextrin rotaxanes possessing a variety of different threading moieties.[189–192]

A relatively new topology introduced recently into the chemical record books is the universal 3-ravel,[193] which was obtained in a crystalline form by Lindoy[194] from an oxybisphenylene-linked 1,3-dione ligand and $FeCl_3$ in basic

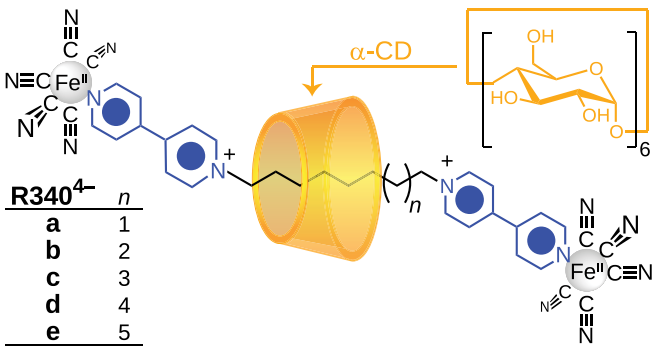


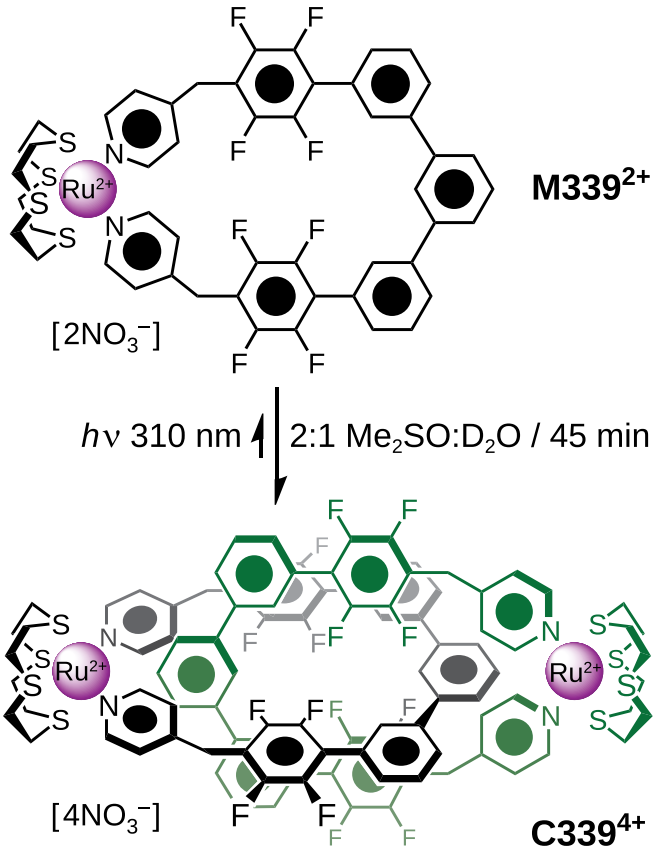
Figure 3.22 A series of α-cyclodextrin rotaxanes stoppered with an inorganic coordination complex from the Macartney group.[188]

THF solution over three months in 97% yield. The near-quantitative yield and long duration of assembly indicate that the 3-ravel is the thermodynamic product.

3.2.4.3 Ruthenium and Rhodium MIMs

Since Ru^{II} complexes have well-known[195] ligand photodissociation[196] properties, MIMs incorporating Ru^{II} can be assembled thermodynamically under UV irradiation. The principle of using photolabile Pd^{II} or Pt^{II} coordination as the ring-closing bond in various catenanes has been championed by Fujita,[197] who extended his style of catenane assembly to Ru^{II} metallacycles. The [2]catenane **C339**$^{4+}$ is a 'photoswitchable molecular lock'[197] (**Scheme 3.16**) based on Fujita's pentakis(*m*-phenylene) ditopic ligand, with its proclivity for helical stacking among its *m*-phenylene units. Macrocycle **M339**$^{2+}$ comprises this ligand when it is bridged by $([12]aneS_4)Ru^{II}$ in 1:2 $Me_2SO{:}D_2O$. The catenation of the **M339**$^{2+}$ rings to afford **C339**$^{4+}$ is accomplished by irradiating for 45 minutes, during which time the photolabilization of the ligands allows ring scission and re-forming to take place. The photolabilization process works for Pt^{II} metallacycles as well.

A number of shape-persistent self-assembled metallarectangles based on kinetically labile Rh^{II} or Ru^{II}-corners have been utilized in the construction of mechanically interlocked metallosupramolecular assemblies, including Borromean rings[198,199] (**Section 4.1.1.3**) and ring-in-ring rotaxanes[200] (**Section 4.3.3**). Chi[201] has assembled (**Scheme 3.17**) the homo[2]catenane **C340**$^{8+}$, which comprises an interlocked pair of Ru^{II}-cornered M_2L_2 metallarectangles,



Scheme 3.16 A photolabile Ru^{II} [2]catenane 'molecular lock' from the Fujita group.[197]

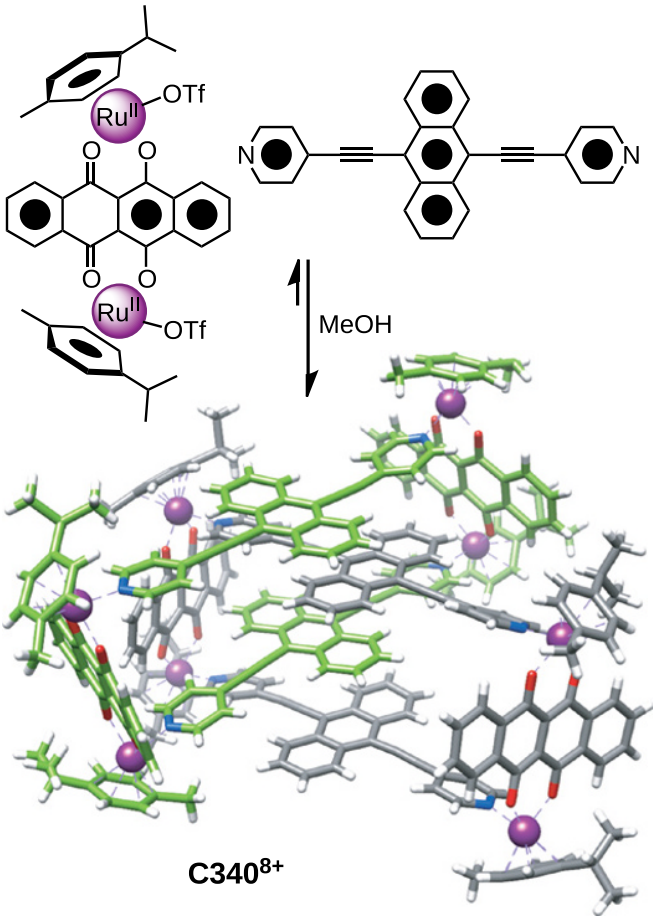
by combining 9,10-bis(4-pyridylethynyl)anthracene with a tetracenedione bisruthenium linker in MeOH. Polarophobic π–π stacking interactions are important contributors to the stability of the catenane, since uncatenated metallarectangles are obtained in the less polar solvent, $MeNO_2$, as well as in the presence of pyrene as a competitive π-donating guest.

3.2.4.4 Osmium MIMs

Jeong[202] was amongst the first to incorporate a kinetically labile metallacycle into the synthesis of rotaxanes (**Figure 3.23**) rather than catenanes. A labile transition metal is shared between pyridine groups and osmium tetroxide, while the ring is a close relative of the tetralactam hydrogen-bonded MIMs pioneered by Vögtle[203] and Hunter.[204] Rotaxane **R341a** self-assembles from this metallocycle and an adipamide-based dumbbell with an association constant K_a of 560 M^{-1} in $CDCl_3$ at 23 °C. Since the product distribution is in dynamic equilibrium, the ratio of the rotaxane to the dissociated components is concentration-dependent; at room temperature in $CDCl_3$, the rotaxane represents up to 65% of the distribution at a concentration of 10 mM. When a strongly electron-withdrawing NO_2 group is added to the pyridine dicarboxamide sites of the ring in order to improve its ability to accept hydrogen bonds from the dumbbell in **R341b**, the association constant is increased to a K_a value of 10^4 M^{-1}, and only 0.5 mM concentration in $CDCl_3$ is required to reach a 65% population of rotaxanes. This motif has also been employed[205] in the synthesis of [3]rotaxanes.

3.2.4.5 Cobalt MIMs

A few examples of self-assembled mechanomolecules possessing reversible coordinative bonds to cobalt are illustrated in **Figure 3.24**. Chen[206] has stoppered (**Figure 3.24a**)



Scheme 3.17 The self-assembly of Chi's homo[2]catenane comprising Ru^{II}-cornered metallarectangles.[201]

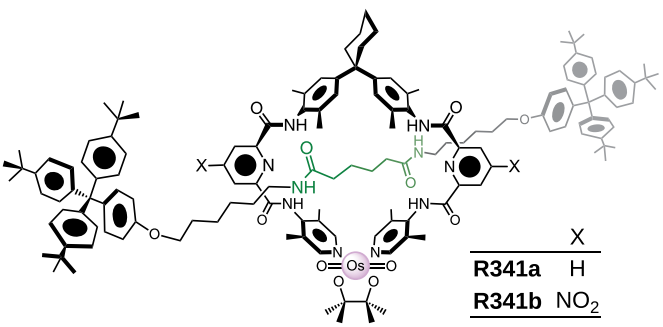


Figure 3.23 Stereoformulas of labile osmium metallacycle-based rotaxanes introduced by Jeong.[202]

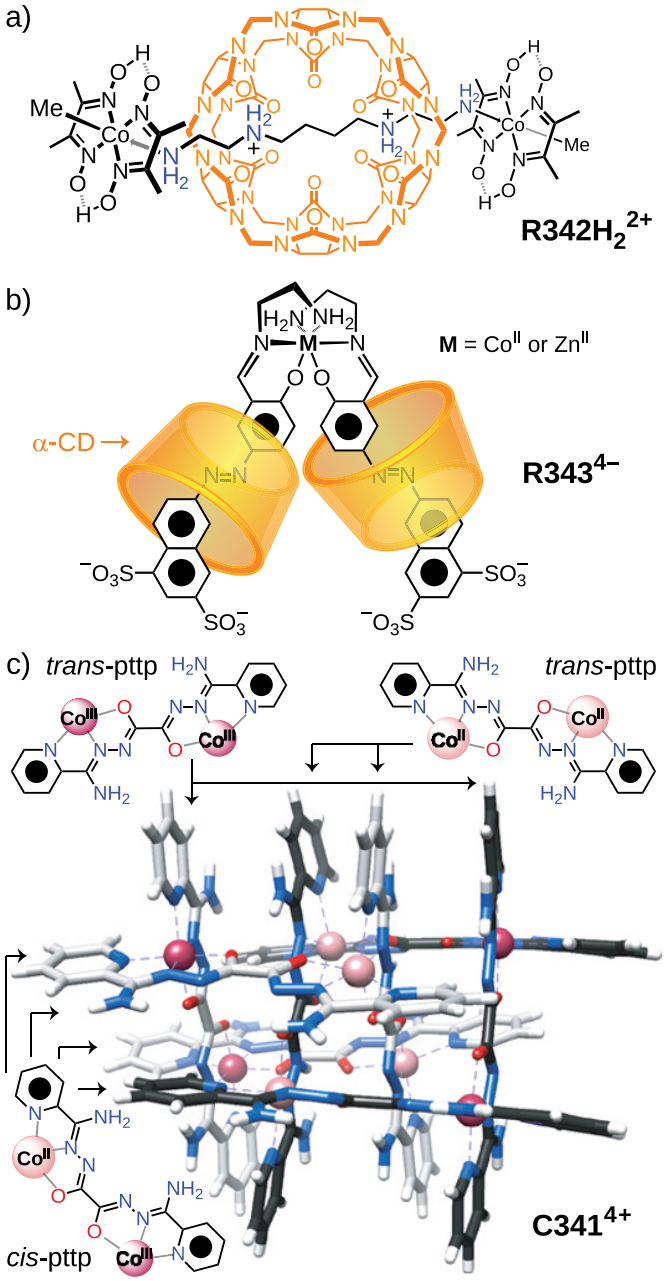


Figure 3.24 Mechanomolecules possessing dynamic coordinative bonds to cobalt. The CB6-based [2]rotaxane[206] **R342H$_2$**$^{2+}$ (a) and the α-CD-based [3]rotaxane[207] **R343**$^{4-}$ (b) self-assemble in water, courtesy of reversible coordinative bonds to cobaloxime stoppers and octahedral cobalt(II) salicylideneimine (salen) linkers, respectively. (c) Thompson's homo[2]catenane **C341**$^{4+}$ arises[208] from the catenation of mixed-valence M_4L_4 metallogrids comprising Co^{II}/Co^{III} nodes connected by oxalic bisamidrazone ligands. A tubular representation of the solid-state structure of **C341**$^{4+}$ is illustrated with NCS^- counterions and solvent molecules omitted for the sake of clarity.

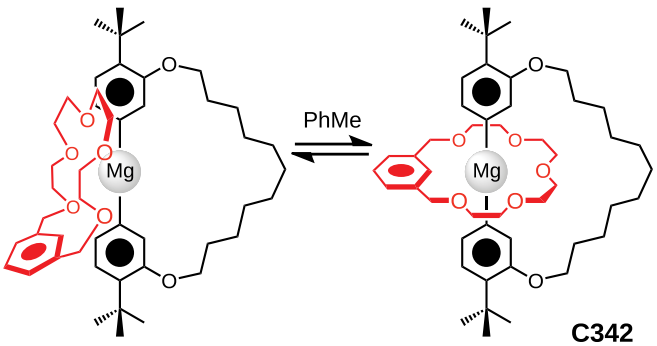
a *spermine⊂CB6* pseudorotaxane via the coordination of its primary amines to the axial positions of aqua(methyl) cobaloxime to afford the self-assembled [2]rotaxane **R342H$_2$**$^{2+}$. The [3]rotaxane **R343**$^{4-}$, which was introduced by Anderson,[207] self-assembles (**Figure 3.24b**) when two *azo⊂α-CD* semirotaxanes form salicylideneimine coordinative bonds surrounding a central Co^{II} linker. Thompson[208] assembled the homo[2]catenane **C341**$^{4+}$ from mixed-valence M_4L_4 metallogrids—each comprising Co^{II}, Co^{III}, and oxalic bis(2-pyridyl)amidrazone (pttp) ligands in both *cis* (heterometallic) and *trans* (homometallic) configurations—by allowing them to concatenate (**Figure 3.24c**) in MeOH in the presence of NH_4NCS, which helps to maintain reversibility by labilizing competitively the metal-ligand bonds. The catenane is stabilized in the solid state by space-filling, π–π stacking, and intercomponent [N–H···O] hydrogen-bonding interactions.

3.2.5 MIMs Possessing Alkaline Earth Elements

Mechanical bonds sealed by coordinative bonds to alkaline earth elements include those that involve catenated Grignard reagents (**Section 3.2.5.1**) and barium complexes (**Section 3.2.5.2**).

3.2.5.1 Mechanically Interlocked Grignard Reagents

To our knowledge, the first example of an organometallic catenane, and one of the earliest examples of a mechanomolecule possessing kinetically labile metal-ligand component parts in general, was a Grignard reagent [2]catenane prepared by Bickelhaupt[209] in 1993. He took advantage of the well-known stabilizing interactions of crown ethers with cations so as to thread

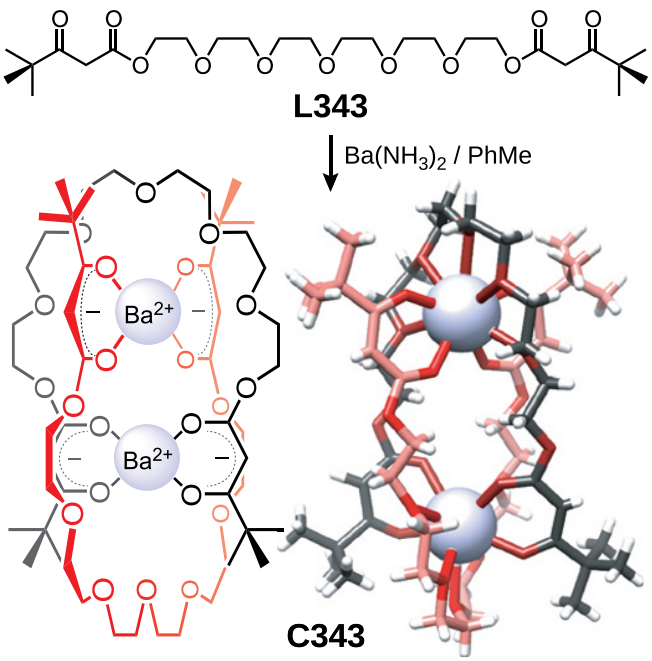


Scheme 3.18 Equilibration of a crown ether and a cyclic Grignard reagent between a side-on complex and a [2]catenane.[209]

(**Scheme 3.18**) a small crown ether around the Mg center of a macrocyclic Grignard reagent. The side-on complex and the [2]catenane **C342** exist in equlibrium in PhMe, with the interlocked species being more favored at lower temperatures.

3.2.5.2 Barium Catenanes

Rees[210] has described the self-assembly of catenated (**Scheme 3.19**) metallacycles comprising heavy alkaline earth metals, namely Ba^{2+}, instead of the more conventional transition metal templates. The ligand **L343** consists of a hexaethylene glycol chain terminated by β-ketoester



Scheme 3.19 Structural formula and X-ray crystal structure of a dinuclear Ba^{2+} [2]catenane by Rees.[210]

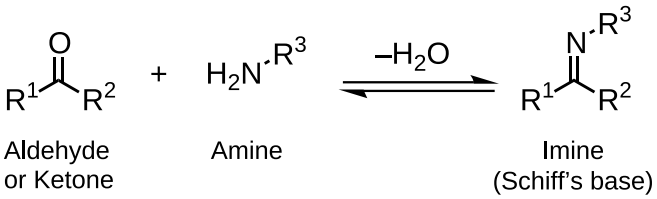
moieties. The dinuclear [2]catenane **C343** is assembled from a slurry of 1:1 $Ba(NH_3)_2$ and **L343** in PhMe. Once assembled, the [2]catenane comprises two entwined ligands, each conjoined by a single Ba^{2+} cation that is doubly coordinated by the deprotonated β-ketoesters, while being further stabilized by the hexaethylene chains wrapping around their periphery. Since each of the β-ketoesters are anionic and the barium atoms are doubly cationic, the catenane **C343** is charge-neutral overall. The catenane has also been described as a quadruply stranded helicate on account of the left-handed helical twist of the ligands in the solid state.

3.3 Mechanical Bond Formation by Condensation

Reversible condensation reactions—especially those involving the loss of water, such as the formation of imines (**Section 3.3.1**), hydrazones (**Section 3.3.2**), and boronic esters or boroxines (**Section 3.3.3**)—are powerful tools for establishing mechanical bonds in interpenetrated assemblies under thermodynamic control.

3.3.1 Imines

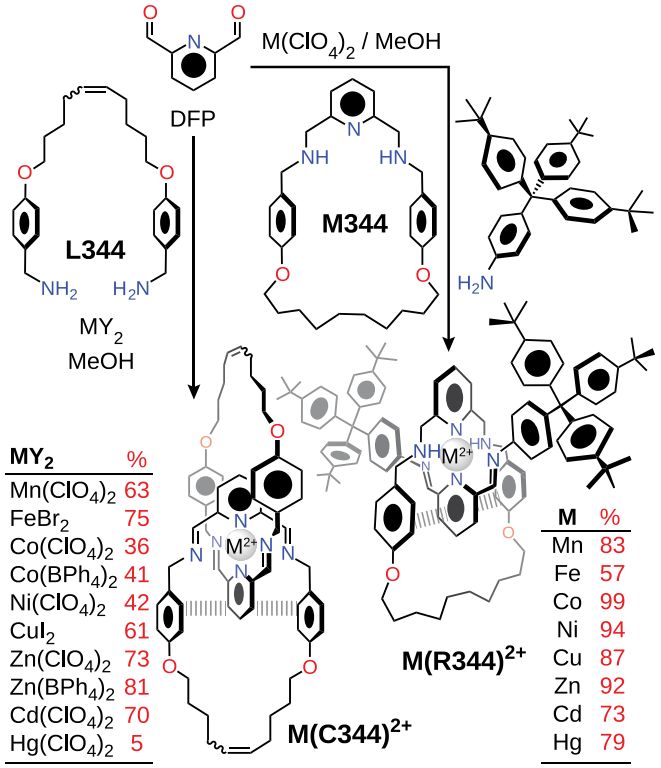
Although the use of labile metal-ligand bonds is widespread, the imine bond is another one of the most important reversible bonds when it comes to the self-assembly of MIMs under thermodynamic control. The imine bond was discovered in 1868 by Hugo Schiff, who is immortalized by the bond's nickname, 'Schiff's base.' This German chemist who moved to Italy as a young man discovered that aryl aldehydes R^1CHO and amines R^2NH_2 condense reversibly, by the extrusion of water, to form species of the type $R^1HC{=}NR^2$. The C=N bond is hydrolyzed by water to achieve the reversibility that has become indispensable to the construction of MIMs.



3.3.1.1 Coordinative Imine Bonding

The coordination of imines around a metal center is one of the most powerful ways to build mechanically interlocked structures because of the combined advantages of (i) predictable, well-understood coordination geometries and (ii) the thermodynamic control of strict self-assembly. Since imines make better ligands than aldehydes, molecules can be easily designed to organize themselves around metal centers such that they satisfy the maximal site occupancy principle[89,90] only when all of the aldehydes and have been converted to the corresponding Schiff bases. Some of the most sought-after, exotic, beautiful, and challenging topologies,[211,212] such as Borromean rings and pentafoil knots, have been accessed only as a consequence of this powerhouse of a strategy.

Leigh[213,214] has developed a coordinative imine bonding strategy (**Scheme 3.20**) for producing MIMs, which is notably general in its compatibility with a wide variety of metals. In his first application[213] of this strategy, the bis-benzylamine linker **L344**, which is prepared using olefin cross metathesis, co-assembles with 2,6-diformylpyridine (DFP) around octahedral metals to produce the [2]catenanes **M(C344)²⁺**, where M represents a transition metal with a proclivity to form octahedral coordination complexes. Yields noted in **Scheme 3.20** are underestimates—they represent the outcome of the catenation reaction using olefin metathesis. Yields are always higher when employing **L344**, a diamine ligand which has already been metathesized. Simply mixing DFP and **L344** with an octahedral metal template in MeOH constitutes the superior synthetic route, forming **M(C344)²⁺** in up to 81% yield. In other words, imine coordinative bonding is a more effective catenation strategy than olefin metathesis for this particular design motif. Leigh[214] has extended the protocol to rotaxanes by co-assembling the tridentate ring **M344** with a dumbbell comprising the imine condensation product of DFP and an aniline-based stopper, delivering the [2]rotaxane **M(R344)²⁺** in high (up to 99%) yields. The dashed lines in **Scheme 3.20** depict π–π stacking interactions between components which most likely stabilize the MIMs and promote their self-assembly. These MIMs are attractive from a synthetic standpoint because they can be isolated as pure, stable compounds without chromatographic purification by simply washing or precipitating them with an appropriate solvent such as diethyl ether.



MY_2	%
$Mn(ClO_4)_2$	63
$FeBr_2$	75
$Co(ClO_4)_2$	36
$Co(BPh_4)_2$	41
$Ni(ClO_4)_2$	42
CuI_2	61
$Zn(ClO_4)_2$	73
$Zn(BPh_4)_2$	81
$Cd(ClO_4)_2$	70
$Hg(ClO_4)_2$	5

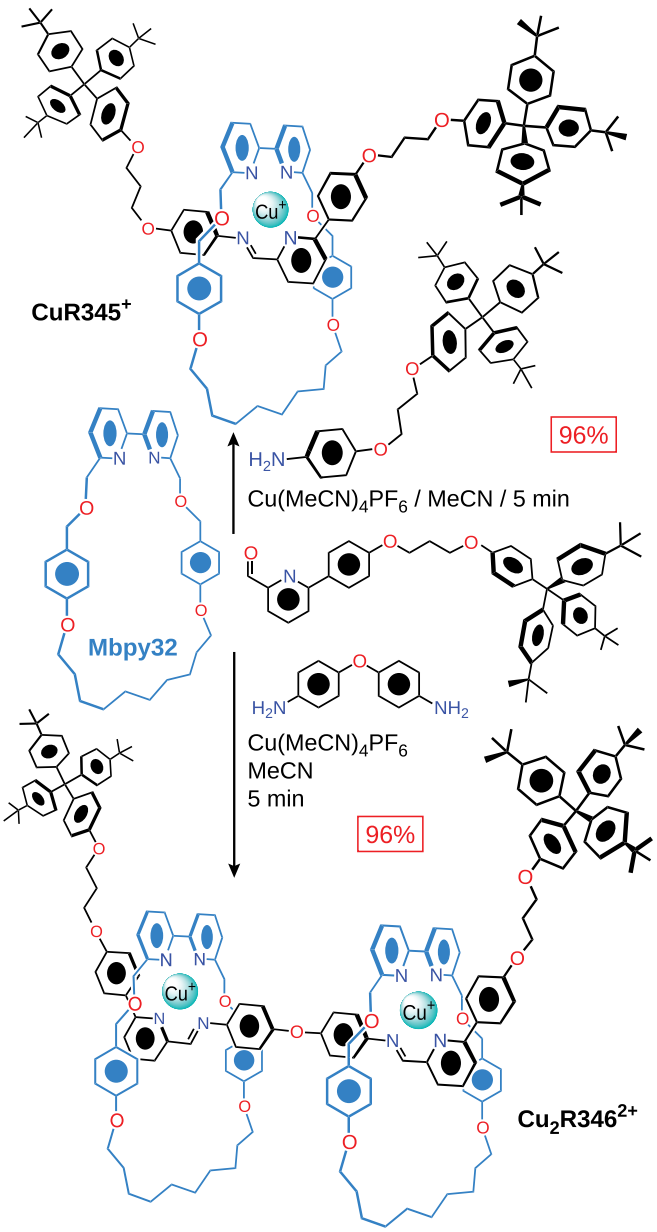
M	%
Mn	83
Fe	57
Co	99
Ni	94
Cu	87
Zn	92
Cd	73
Hg	79

Scheme 3.20 Leigh's imine condensation-driven synthesis of catenanes and rotaxanes from 2,6-diformylpyridine (DFP).[213,214] The condensation of the bis-amine ligand **L344** with DFP in the presence of various octahedral metals affords the [2]catenane **M(C344)**$^{2+}$, where M can take the form of a number of transition metals. Condensation between DFP and a sufficiently bulky amine-functionalized stopper in the presence of the ring **M344** affords the [2]rotaxane **M(R344)**$^{2+}$ in good yields by virtue of coordinative imine bonding around octahedral transition metal templates.

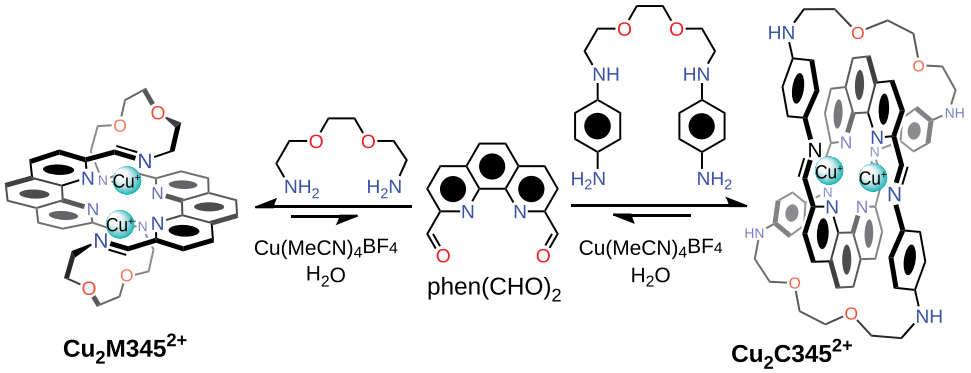
Leigh[215] has developed "a simple and highly effective ligand system" for the self-assembly (**Scheme 3.21**) of rotaxanes. The [2]rotaxanes **CuR345**$^{+}$ and the [3]rotaxane **Cu$_2$R346**$^{2+}$ form via the bidentate coordinative imine bonding of aniline and picolinaldehyde semidumbbells to Cu^{I} templates immobilized within the endotopic bipyridyl ligands of Mdpp30 macrocycles. The assembly is almost quantitative (96%) within only a few minutes in MeCN, while also being high-yielding (>80%) in other solvents including CH_2Cl_2, $CHCl_3$, DMF, MeOH, and THF. The success of this protocol relates to the fact that the rotaxane is the only assembly product that satisfies the maximal site occupancy principle.

Nitschke[216] has used an imine-based copper(I) helicate platform to self-assemble (**Scheme 3.22**) the [2]catenane **Cu$_2$C345**$^{2+}$. The length, basicity, and rigidity of the diamine ligand—either 2,2´-(ethylenedioxy)bis(ethylamine) or 2,2´-(ethylenedioxy)bis(ethylene-*para*-phenylenediamine)—has a dramatic effect on the product outcome when it is mixed with Cu^{I} and 1,10-phenanthroline-2,9-dialdehyde (phen(CHO)$_2$) in aqueous solution. Whereas the shorter 2,2´-(ethylenedioxy)bis(ethylamine) ligand gives rise to the helicate macrocycle **Cu$_2$M345**$^{2+}$ as the thermodynamic product in water, the longer and more rigid bis(aniline) affords the [2]catenate **Cu$_2$C345**$^{2+}$ as the sole product in quantitative yield. A diamine of intermediate length (not shown) gives rise to a mixture of products rather than one dominant species. A kinetically stable [2]catenane can also be prepared from the dynamic [2]catenate **Cu$_2$C345**$^{2+}$ by reduction of the imine bonds with $NaBH_4$ and subsequent demetalation with EDTA in >50% yield.

Asakawa[217] has laid claim to the first report of a 'shrinking' approach (**Scheme 3.23**) to rotaxane synthesis. When benzosalophen[28]crown-6 (BS28C6) is combined with the *tert*-butyl-stoppered dibenzylammonium dumbbell **L347H**$^{+}$,



Scheme 3.21 The near-quantitative self-assembly of [2]- and [3]rotaxanes by a dumbbell capture strategy involving reversible coordinative imine bonding to Cu^{I} templates.[215]



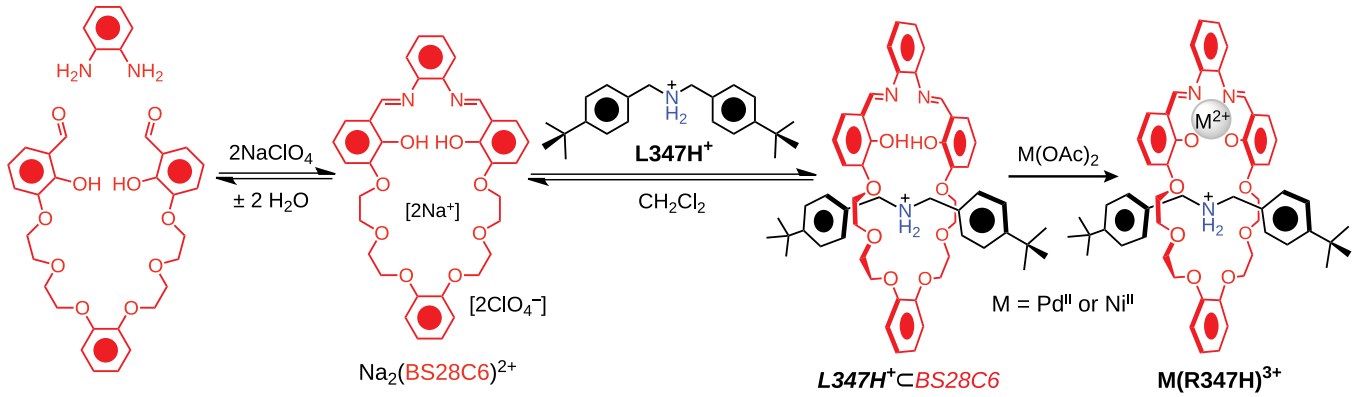
Scheme 3.22 Nitschke's aqueous Cu^{I}-helicate assemblies.[216] Short and flexible bis(amine) ligands yield the macrocycle $\mathbf{Cu_2M345^{2+}}$ as the thermodynamic product when mixed with Cu^{I} and phen(CHO)$_2$, whereas the [2]catenane $\mathbf{Cu_2C345^{2+}}$ is formed exclusively when the linker is sufficiently long and rigid.

the corresponding pseudorotaxane ***L347H*$^+$⊂*BS28C6*** forms as a result of the familiar stabilizing polyether-ammonium hydrogen-bonding interactions. BS28C6 is equipped with an endotopic salophen moiety, which is capable of capturing metal templates (M^{2+}) in square planar coordination geometries. Thus, the addition of M^{2+} (M = Pd or Ni) to a solution of ***L347H*$^+$⊂*BS28C6*** causes the macrocyclic cavity to shrink, which prevents the ring of the corresponding [2]rotaxane $\mathbf{M(R347H)^{3+}}$ from deslipping. The dynamic imine bonds in BS28C6 enable a more traditional clipping mechanism to proceed as well, since it was demonstrated that BS28C6 can be interlocked with a dumbbell possessing triphenylphosphonium stoppers too bulky for slippage.[218] Asakawa[219] has also prepared bis[2]-rotaxanes—see **Section 4.2.2.1**—from these shrinking rings.

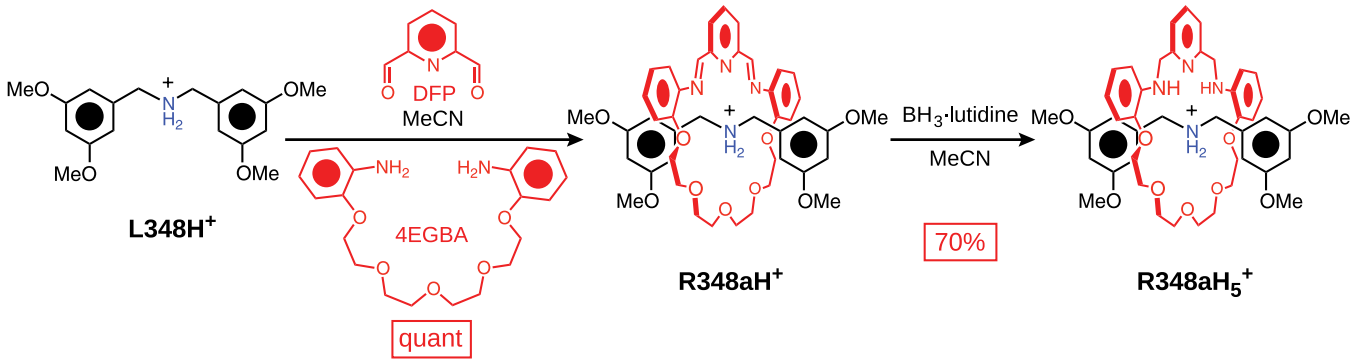
Some of the most exotic and challenging mechanically interlocked topologies and architectures (**Chapter 4**) have been accessed by the coordinative imine bonding approach to molecular self-assembly—some examples include molecular Solomon links[220,221] (**Section 4.1.1.1**), Borromean rings[222–229] (**Section 4.1.1.3**), cyclic [3]catenanes[230] (**Section 4.1.1.4**), pentafoil knots,[231,232] and three-dimensional tetrahedral oligocatenanes[233] (**Section 4.1.3.2**). Charboniere and Trabolsi[234,235] have also prepared [2]catenanes and knots of various topologies by relying on coordinative imine bonding. See **Section 4.1.1.1** and **Section 5.2.4.1** for a glimpse of a Solomon Link and a dynamically chiral [2]catenane, respectively, based on their metallosupramolecular motifs.

3.3.1.2 *Clipping With Imine Exchange*

A remarkably fruitful discovery[236] for using reversible imine bonds in the synthesis of MIMs has been that of a dynamic clipping protocol for wrapping macrocyclic polyethers around dialkylammonium templates. An important imine-based clipping reaction was introduced (**Scheme 3.24**) in 2001 for the dialkylammonium/crown ether recognition motif. DFP and tetraethylene glycol bis-*ortho*-aniline ether (4EGBA) were found to self-assemble with the dibenzylammonium template $\mathbf{L348H^+}$ rapidly and quantitatively (by ^{1}H NMR spectroscopy) to give the [2]rotaxane $\mathbf{R348aH^+}$ simply by mixing the three components in a 1:1:1 molar ratio in MeCN. The simplicity of a protocol like this is a theme that is common to most if not all of the imine clipping reactions; mix A, B, and C at ambient temperature in an appropriate solvent, and *voilà*! Bob's your uncle. It has also been demonstrated that the ring can be 'fixed' by reduction of the imine bonds with BH_3 to give the kinetically stable rotaxane $\mathbf{R348aH_5^+}$.



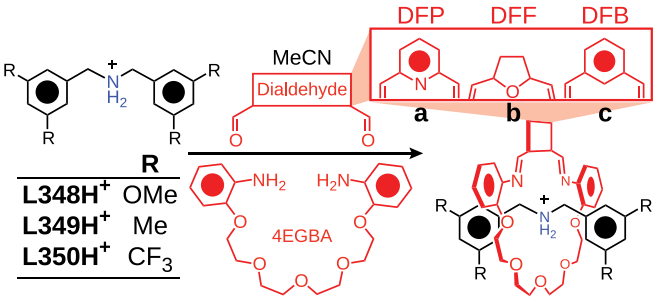
Scheme 3.23 Asakawa[217] introduces the 'threading-followed-by-shrinking' approach to rotaxane synthesis. The reversible imine bonds of the BS28C8 ring's salophen unit allow the component parts to equilibrate and respond dynamically to the addition of metal templates such as Pd^{II} or Ni^{II}. The endotopic coordination of a metal ion causes the effective cavity size of the ring to shrink, generating a stable mechanical bond in the process.



Scheme 3.24 A thermodynamically controlled clipping reaction between DFP and 4EGBA around the dibenzylammonium-based dumbbell **L348H**$^+$ leads to a dynamic [2]rotaxane **R348aH**$^+$, which is fixed to yield the kinetically stable rotaxane **R348aH$_5$**$^+$ by reduction of the imine bonds.[236]

The dynamic clipping reaction tolerates a range of functionalities on the dumbbell and the dialdehyde. Further investigations[237] have revealed (**Table 3.9**) that while DFP and the 3,5-dimethoxy-substituted dumbbell **L348H**$^+$ exhibit the fastest kinetics, 2,5-diformylfuran (DFF) and 3,5-bistrifluoromethyl-substituted dumbbell **L350H**$^+$ claim the highest stability constants (K_{eff}) and free energies (ΔG_{eff}) of complexation. The most likely causes for the enhanced stability in these cases are the stronger hydrogen bond accepting ability of DFF and the more electron-poor character of the **L350H**$^+$ dumbbell, respectively. These explanations are further supported by the fact that a 1,3-diformylbenzene (DFB) compound, which cannot accept a hydrogen bond in between its aldehyde substituents, leads to the most weakly associated dynamic rotaxanes. Furthermore, the tetramethyl-substituted dumbbell **L349H**$^+$, which is essentially identical to **L350H**$^+$ in its size but not in its electron density profile, exhibits similar behavior to the methoxy-substituted **L348H**$^+$, indicating that the enhancement by the CF_3 groups of **L350H**$^+$ is an electronic effect. The clear trend that emerges in this system is that the strength of the noncovalent bonding interactions are maximized by having more oxygen atoms in the crown ether and stronger electron-withdrawing groups in the dumbbell.

Table 3.9 Effective stability constants (K_a), free energies of complexation ($\Delta G°$), and times (t) required to reach equilibrium for the thermodynamically controlled assembly of rotaxanes based on various dibenzylammonium dumbbells and dialdehydes.[237]

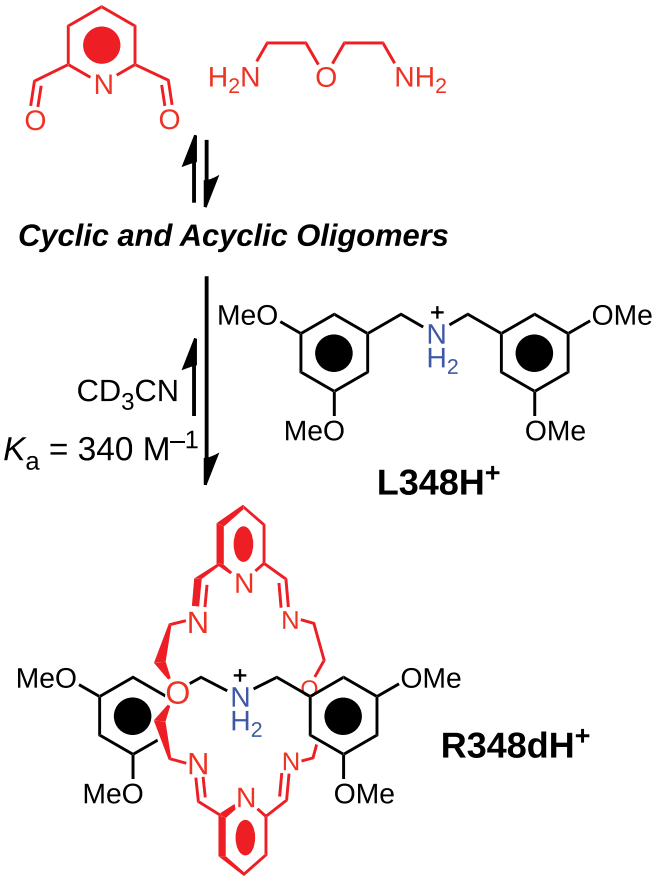


	R	Dialdehyde	K M^{-1}	$\Delta G°$ kcal·mol^{-1}	t h
R348aH$^+$	OMe	DFP	480 ± 190	–3.6 ± 0.3	0.1
R348bH$^+$	OMe	DFF	390 ± 160	–3.5 ± 0.3	48
R348cH$^+$	OMe	DFB	100 ± 40	–2.7 ± 0.3	20
R349aH$^+$	Me	DFP	340 ± 140	–3.4 ± 0.3	0.5
R349bH$^+$	Me	DFF	530 ± 210	–3.7 ± 0.3	72
R349cH$^+$	Me	DFB	90 ± 36	–2.7 ± 0.3	20
R350aH$^+$	CF_3	DFP	2900 ± 1200	–4.7 ± 0.3	3
R350bH$^+$	CF_3	DFF	7900 ± 3200	–5.3 ± 0.3	4
R350cH$^+$	CF_3	DFB	86 ± 34	–2.6 ± 0.3	3

DFP = 2,6-diformylpyridine. DFF = 2,5-diformylfuran. DFB = 1,3-diformylbenzene.

[2]Rotaxanes can also be assembled[238] around dialkylammonium templates from two 2-(2-aminoethoxy)ethylamine and two DFP precursors. The five-component self-assembly (**Scheme 3.25**) of the [2]rotaxane **R348dH**$^+$ occurs in mere minutes upon the addition of the dibenzylammonium dumbbell **L348H**$^+$ to an equilibrated mixture of DFP and this simple diamine. Based on ^{1}H NMR spectroscopic analysis in CD_3CN, the ring and dumbbell are associated with a binding constant K_a of 340 M^{-1}, which is consistent with the similar systems described above. The enthalpy (ΔH = –5.5 kcal·mol^{-1}) and entropy (ΔS = +6.9 cal·mol^{-1}·K^{-1}) of binding indicate that the self-assembly of the rotaxane is an enthalpically driven process. Surprisingly, crystallization of the dynamic mixture results only in the crown-8-like macrocycle, indicating that a kinetic selection process occurs during the phase transition from solution to the solid state.

The imine-based clipping reaction has been extended (**Scheme 3.26**) to a range of interlocked species, including bis[2]rotaxanes[239] (**R351H$_2$**$^{2+}$), [3]rotaxanes,[239,240] cyclic [4]rotaxanes[239] (**R352H$_4$**$^{4+}$), branched [4]rotaxanes[239,241,242] (**R353aH$_3$**$^{3+}$ and **R353bH$_3$**$^{3+}$), [*c*2]daisy chains[243] (**R354H$_2$**$^{2+}$), and a handful of larger linear oligorotaxanes,[244–247] such as **R355H$_{n+2}$**$^{(n+2)+}$ and **R356H$_{n+2}$**$^{(n+2)+}$. Jishan Wu,[244] who synthesized the latter oligorotaxanes possessing up to 10 rings in all but quantitative yields, has continued exploring this system independently, reporting[248] a rectangular [4]rotaxane composed of two dumbbells and two bis-macrocycles, for example, as well as the linear hetero[4]rotaxane[249] **R357H$_4$**$^{4+}$ in which the two outer macrocycles are clipped reversibly and the inner one is a CB[6] encircling a diaminoalkane portion of the thread. See



Scheme 3.25 The five-component dynamic clipping reaction[238] of DFP and 2-(2-aminoethoxy)ethylamine around a dibenzylammonium template to afford the [2]rotaxane **R348dH**$^+$.

Section 4.2.1.1 for a more detailed discussion of oligorotaxane architectures. Yin[250–255] has also constructed a number of catenanes (e.g., **C346H**$^+$),[250,254] rotacatenanes[252] (**Section 4.3.1**), and oligo-and hetero[*n*]rotaxanes[251,253–255] Recently, the imine-based clipping reaction has also been adapted to create hetero[3]rotaxanes from a combination of two different homo[3]-rotaxanes in a dynamic component-swapping process.[240] Yet another novel architecture to be forged in the fire of imine chemistry is the class of molecules known as suitanes[256–258]—two-component MIMs in which a molecular 'body' with some number of protruding 'limbs' has its central 'torso' encompassed by an all-in-one molecular 'suit.' See **Section 4.3.5**.

Yi Liu[259] has invented a similarly inspired motif to form (**Figure 3.25**) mechanical bonds around pyridinium-based templates. A bipyridinium (BIPY^{2+}) dumbbell templates the self-assembly of a cryptand-like host constituting six imine bonds and five components—three diamines and two tris-aldehydes—to form the macrobicyclic [2]rotaxane **R358**$^{2+}$. The same macrobicyclic clipping reaction has been applied[260] to a C_3-symmetric tripyridinium (TRIPY^{3+}) template to afford the triply interpenetrated rotaxane bundle **R359**$^{3+}$. Recently, Liu[261] described how solvent composition can drive the selective assembly of one rotaxane or the other when both BIPY^{2+} and TRIPY^{3+} templates are present in solution. Since clipping around BIPY^{2+} is driven more by electrostatic donor-acceptor interactions between π-surfaces, whereas clipping around TRIPY^{3+} is driven more by solvophobic effects, BIPY^{2+} wins the competition in low-polarity solvents such as $CDCl_3$ and TRIPY^{3+} wins out in more polar media such as CD_3CN. This clipping protocol has also been applied[262] to catenane synthesis—two diamines and two different dialdehydes

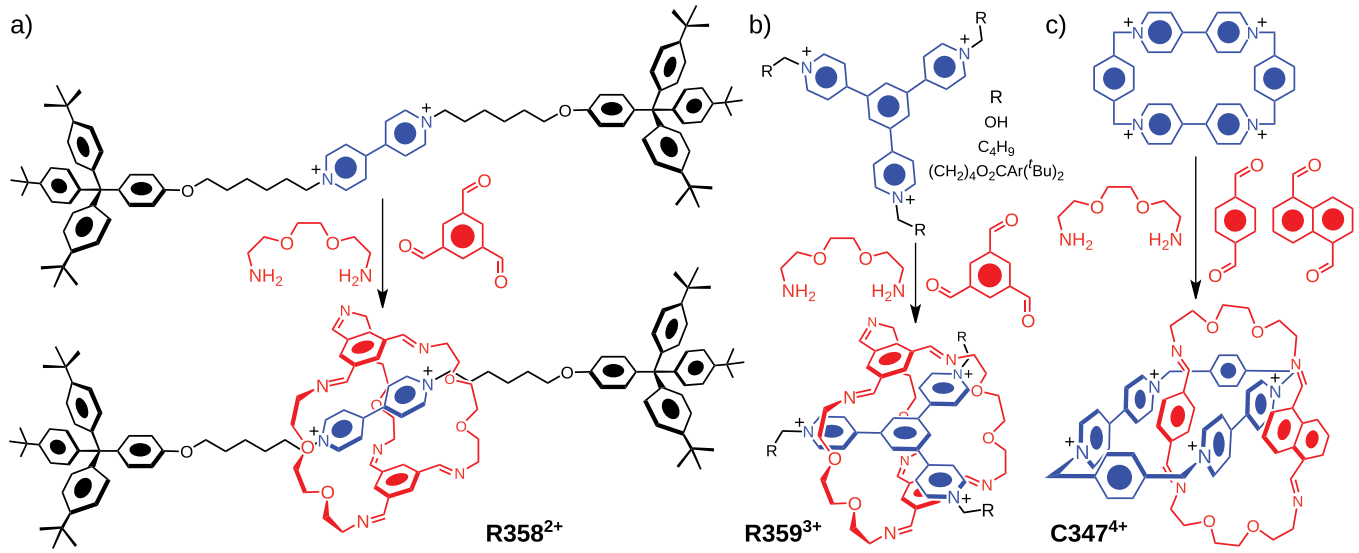
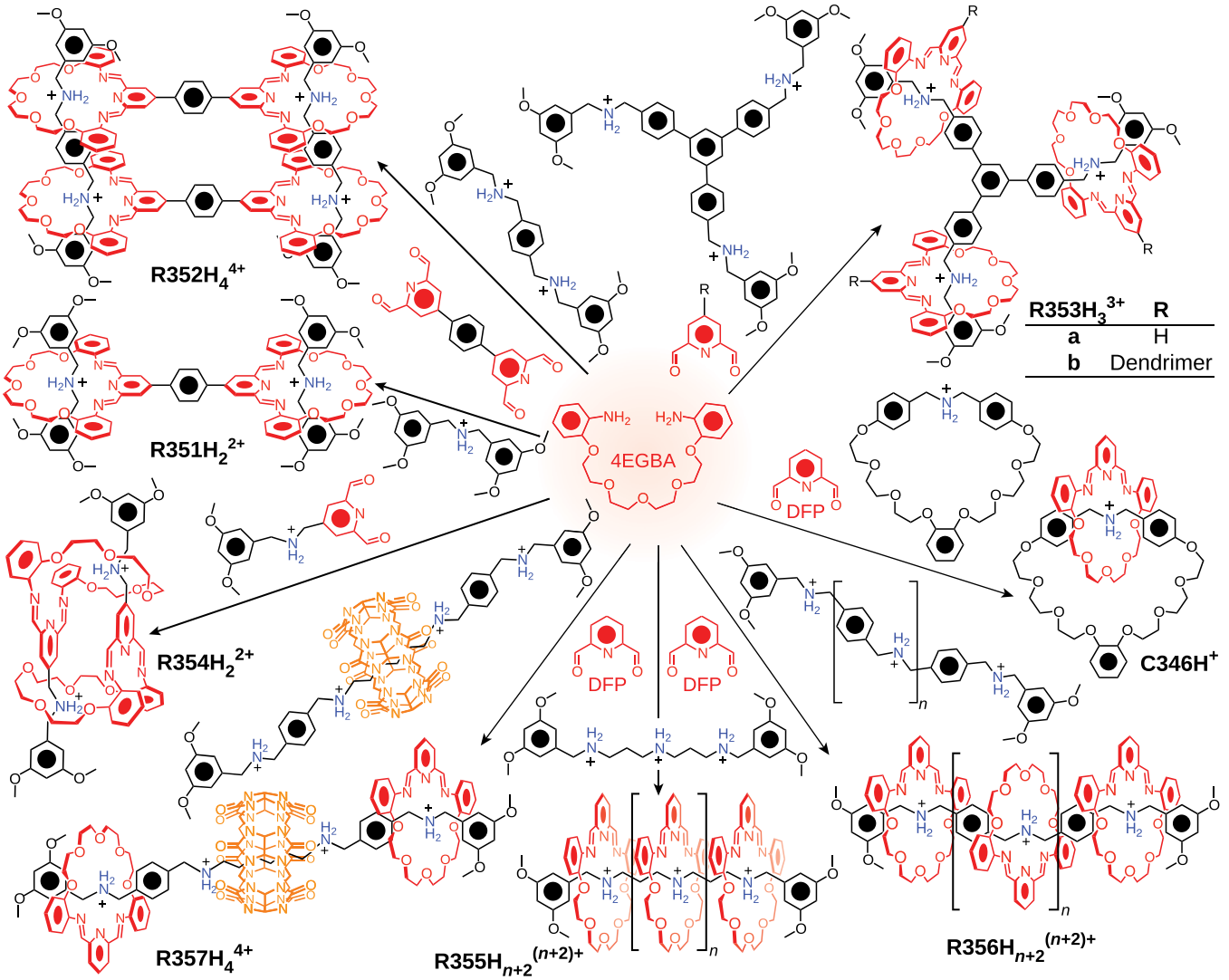


Figure 3.25 π-Donor/π-acceptor-directed thermodynamically controlled clipping protocols developed by Liu, which involve the condensation of aromatic aldehydes and 2,2′-(ethylenedioxy)diethylamine in order to self-assemble mechanically interlocked architectures around pyridinium-based templates. (a) [3 + 2 + 1] clipping self-assembly of the macrobicyclic [2]rotaxane **R358**$^{2+}$ around a BIPY^{2+}-based dumbbell.[259] (b) The same [3 + 2 + 1] clipping protocol, applied to TRIPY^{3+} template to form the C_3-symmetric rotaxane **R359**$^{3+}$. (c) [2 + 2 + 1] clipping self-assembly of the CBPQT^{4+}-based donor-acceptor [2]catenane **C347**$^{4+}$, in which one of two possible translational isomers is generated with >97% translational selectivity.[262]

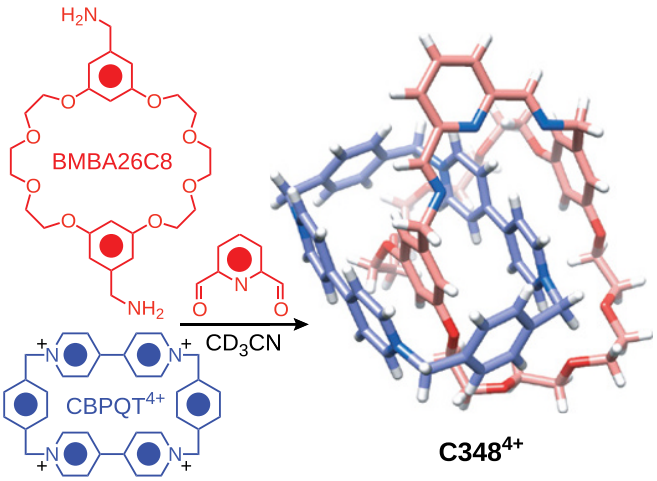


Scheme 3.26 Various mechanomolecules that have been synthesized using the reversible imine-mediated clipping protocol.[239,241–246,249] See **Section 4.2**.

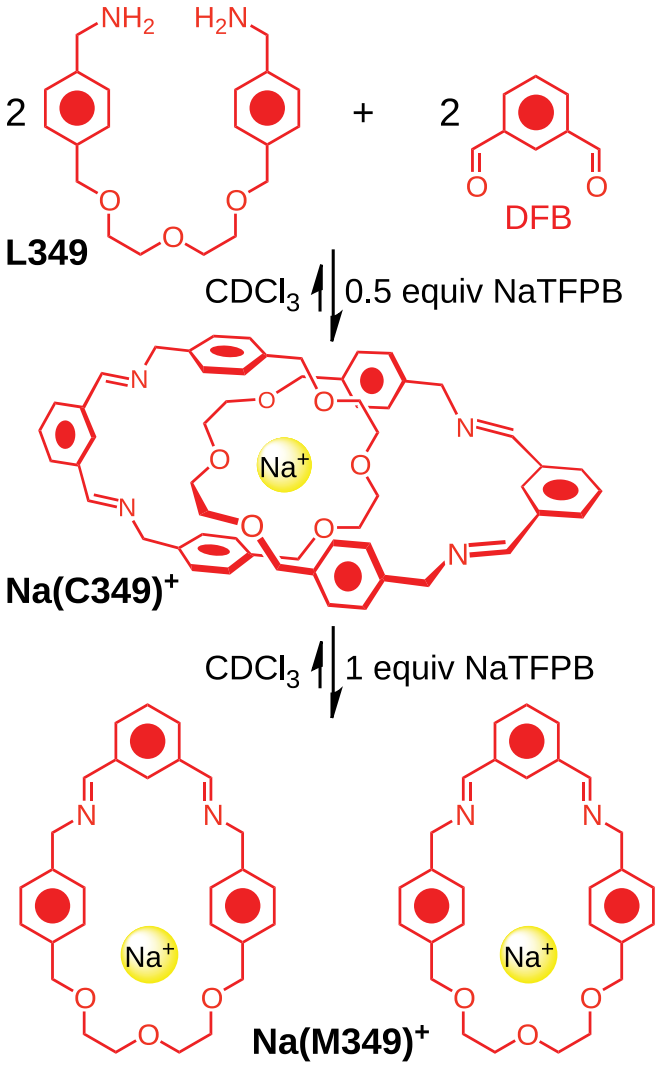
appended to benzene and naphthalene cores self-assemble in the presence of a $CBPQT^{4+}$ ring into the [2]catenane **C347**$^{4+}$. The [2]catenane is formed in greater >90% yield in CD_3CN with >97% selectivity for the translational isomer in which the benzene unit occupies the cavity of the ring rather than the naphthalene unit.

Yan and Zhou[263] have also established a donor-acceptor design motif involving the formation of multi-annulated mechanical bonds by the dynamic imine clipping of cryptand polyethers templated by "taco complexes" based on $BIPY^{2+}$ and $CBPQT^{4+}$ templates. The synthesis and solid-state structure of the [2]catenane **C348**$^{4+}$, which self-assembles from bis-*meta*-benzylamine[26]crown-8 (BMBA26C8), $CBPQT^{4+}$, and DFP in MeCN, is summarized in **Scheme 3.27**. Similar taco complexes based on olefin-functionalized crown ethers have been stitched into rotaxanes and catenanes using olefin metathesis—see **Section 3.4.1.2**.

Chiu[264] has relied upon reversible imine bonds to orchestrate the self-assembly of the [2]catenane **Na(C349)**$^{+}$, which is templated only by the ion-dipole interactions underpinning



Scheme 3.27 The clipping synthesis of a donor-acceptor [2]catenane possessing a macrobicyclic crown ether derived from a $CBPQT^{4+}$ "taco complex" introduced by Yan and Zhou.[263] A tubular representation of the solid-state structure of **C348**$^{4+}$ is illustrated with PF_6^- counterions omitted for the sake of clarity.



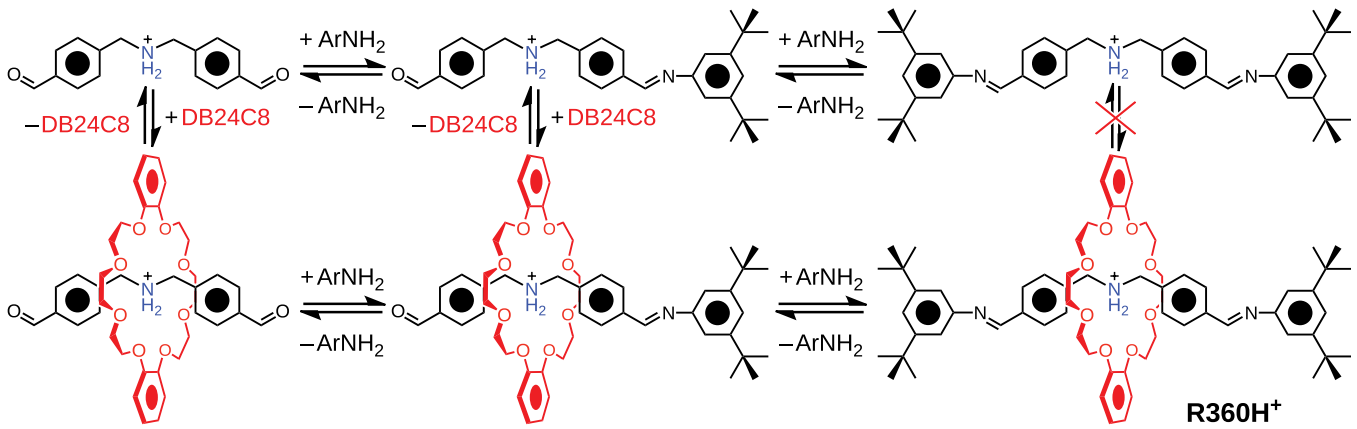
Scheme 3.28 The self-assembly of a [2]catenane templated only by ion-dipole interactions between 2EG loops and Na^+ cations.[264]

(**Section 2.3.8.1**) the association of polyether loops and sodium cations. A 1:1 mixture of DFB and the diamine **L349**, which incorporates a diethylene glycol (2EG) loop at its center, equilibrates (**Scheme 3.28**) with 0.5 equiv of Na^+ as its tetrakis(3,5-trifluoromethylphenyl)borate (TFPB) salt in $CDCl_3$ to generate the dynamic [2]catenane **Na(C349)$^+$**, a process which is accelerated to completion at 323 K in 20 min. The imine bonds can be fixed with PhSeH to afford a kinetically stable [2]catenane in 17% yield. The addition of more Na^+ ions results in the formation of non-interlocked macrocycles **Na(M349)$^+$** upon re-establishment of equilibrium. More recently, Chiu[265] has also applied his Na^+ template clipping protocol to the synthesis of [2]rotaxanes possessing oligoether axles.

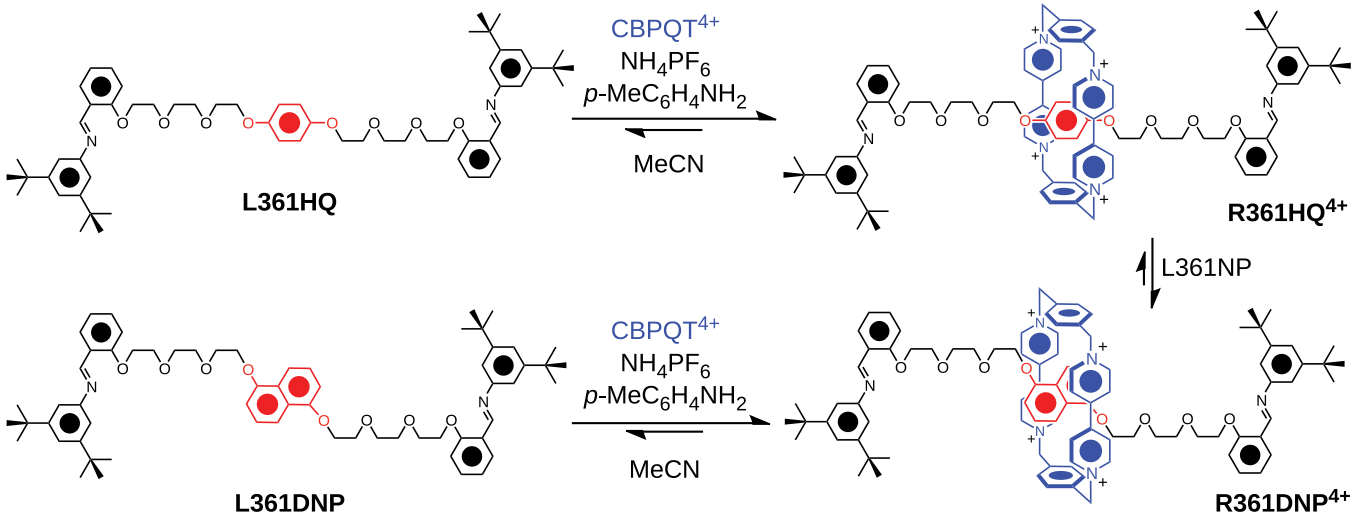
3.3.1.3 Stoppering With Imine Exchange

One of the earliest forays of Schiff's bases into mechanosterochemistry was the demonstration of a stoppering protocol for rotaxanes. The dialkylammonium/crown ether recognition motif was among the first to be employed[266] in a stoppering protocol (**Scheme 3.29**) by imine formation and exchange. A dumbbell was prepared in which imine bonds connect a bulky aniline stopper to a dibenzylammonium unit terminated with formyl groups. This dumbbell represents 73% of the molecular population at equilibrium in MeCN. Following the addition of DB24C8 rings to the mixture, the [2]rotaxane **R360H$^+$** is generated gradually, reaching up to 47% of the equilibrium population over a 4.5-day period. Since only 27% of the dibenzylammonium units are unstoppered at the outset of the experiment, it follows that the rings become threaded onto the dumbbells during a dynamic process involving the dissociation and re-attachment of the imine-linked stoppers.

The same protocol was subsequently applied (**Scheme 3.30**) to $CBPQT^{4+}$-based rotaxanes with formyl-terminated π-electron rich polyether chains.[267] Mixing the stoppered dumbbells **L361HQ** or **L361DNP** with $CBPQT^{4+}$ in MeCN at a concentration of 10 mM in the presence of a drying agent such as $MgSO_4$ or 4 Å molecular sieves results in the formation of the rotaxanes **R361HQ^{4+}** (65%) and **R361DNP^{4+}** (90%), respectively, the yields of which reflect the weaker affinity of $CBPQT \cdot 4PF_6$ for the HQ ($1.8 \pm 0.4 \times 10^3\ M^{-1}$) dumbbell over the DNP ($1.7 \pm 0.4 \times 10^4\ M^{-1}$) dumbbell. Equilibrium is reached after a two-week period, yet it can be reduced to less than 2 h by the addition of a weak acid (NH_4PF_6) and a non-stoppering amine (*p*-$MeC_6H_4NH_2$) as



Scheme 3.29 Stoppering a dibenzylammonium/DB24C8 pseudorotaxane dynamically using imine exchange.[266] The [2]rotaxane **R360H$^+$** represents 47% of the population at thermodynamic equilibrium at a concentration of 20 mM in CD_3CN.



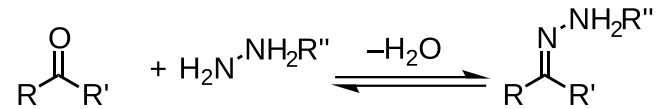
Scheme 3.30 The self-assembly of donor-acceptor rotaxanes **R361HQ**$^{4+}$ and **R361DNP**$^{4+}$ from dumbbells stoppered with dynamic imine bonds.[267]

catalysts, which act to accelerate the reaction by facilitating imine exchange. In the absence of the acidic NH_4PF_6 catalyst, *p*-$MeC_6H_4NH_2$ acts as a catalyst and accelerates the reaction, resulting in an equilibration time of 2 days. The **R361HQ**$^{4+}$ rotaxane can even be converted to **R361DNP**$^{4+}$ by simply introducing the **L361DNP** dumbbell into a solution of **R361HQ**$^{4+}$ in MeCN—the HQ and NP rotaxanes are populated in 1:6 ratio at equilibrium, which is reached in 14 h in MeCN in the presence of the NH_4PF_6 and *p*-$MeC_6H_4NH_2$ catalysts. This strategy qualifies as another example of a 'magic rod' rotaxane synthesis, although the rotaxanes can be assembled likewise from the aldehyde- and amine-based precursors to **L361HQ** and **L361DNP**.

The dynamic exchange of stoppers in these rotaxanes can be avoided by 'fixing' them as secondary amines upon reduction of the imine bonds. **R360H**$^{+}$ was fixed with PhSeH in 18% yield and **R361DNP**$^{4+}$ was fixed with $BH_3 \cdot$2,6-lutidine in 40% yield with MeCN as the solvent in both cases.

3.3.2 Hydrazones

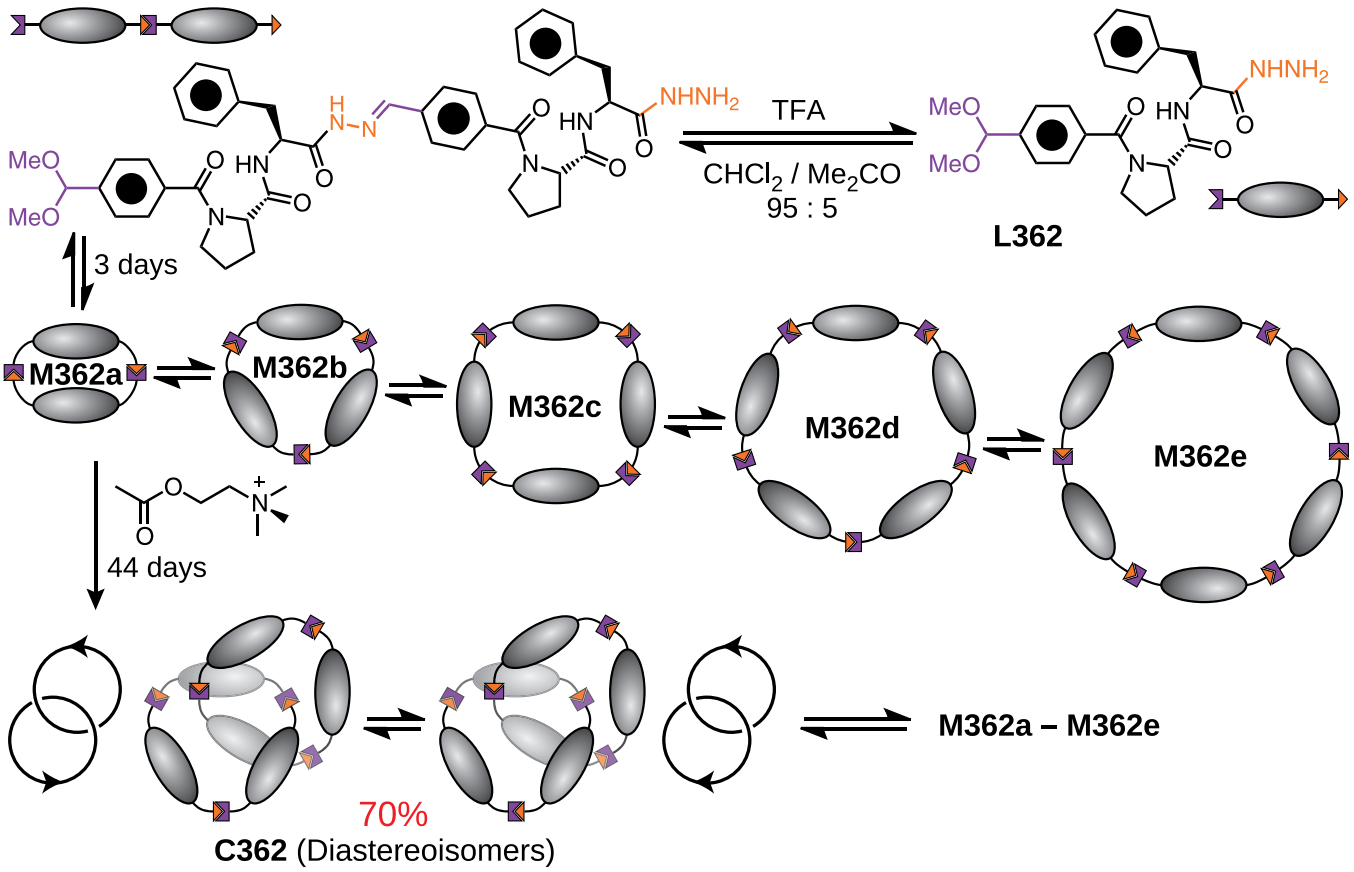
The hydrazone bond is another reversible bond formed by the condensation of carbonyls and $–NH_2–$ groups. In contrast with imines, however, the $–NH_2–$ groups that condense with aldehydes or ketones to form hydrazine bonds derive from substituted hydrazines.



Aldehyde or Ketone — Hydrazine — Hydrazone

One approach to the clipping of rings around a template using dynamic covalent chemisty is the selection of interlocked species from a dynamic combinatorial library (DCL) upon the introduction of a template. This idea has been pioneered in large part by Sanders,[268] who has reported on the emergence (**Scheme 3.31**) of a [2]catenane in a DCL of cyclic oligomers when the cationic neurotransmitter acetylcholine is added as a template. The hydrazone dipeptide **L362** assembles into the macrocyclic oligomers **M362a**–**M362e** ($n = 2–6$, where n is the number of dipeptide repeating units) in a 95:5 solution of $CHCl_3/Me_2SO$ in the presence of 43 equiv of TFA. After a three-day equilibration period, the cyclic dimer, trimer, and tetramer are the major products, with small amounts of the pentamer and hexamer also present in the mixture. Subsequently, on adding 10 equiv of the acetylcholine template, the DCL requires 44 days to reach equilibrium as it slowly amplifies the [2]catenane **C362** as the dominant species in the library, reaching as high as 70% of the population. The slow kinetics of equilibration indicate that catenation is an improbable process, yet the catenane is the most thermodynamically favorable receptor for the template. The catenated receptor **C362** has been isolated in 67% yield on a preparative scale and its high binding affinity for acetylcholine ($K_a = 1.4 \times 10^7\ M^{-1}$; $\Delta H = –5.47\ kcal \cdot mol^{-1}$; $T\Delta S = +4.25\ kcal \cdot mol^{-1}$) has been quantified.

Gagné[269–271] has undertaken a more in-depth investigation (**Figure 3.26**) into the catenation of dipeptide compounds similar to those in Sanders' DCL. Gagne's initial discovery[269] was that a combination of the dipeptide **L363a** and any of the related dipeptides **L363b-f** assemble (**Figure 3.26a**) into octamers comprising two interlocked tetrameric rings, in addition to macrocyclic dimers, trimers, tetramers, pentamers, and hexamers. Although there are many possible combinations for arranging two different monomers into a catenated octamer, only two of these possibilities have been observed experimentally—namely, those with a 6:2 or 5:3 ratio of **L363a**:**L363b-f** monomers. The 6:2 octamers



Scheme 3.31 The introduction of an acetylcholine template to a dynamic combinatorial library (DCL) of cyclic oligomers based on the Schiff base chemistry of the dipeptide hydrazone **L362** leads unexpectedly to the amplification of the hexameric [2]catenane **C362** as the major species in solution.[268]

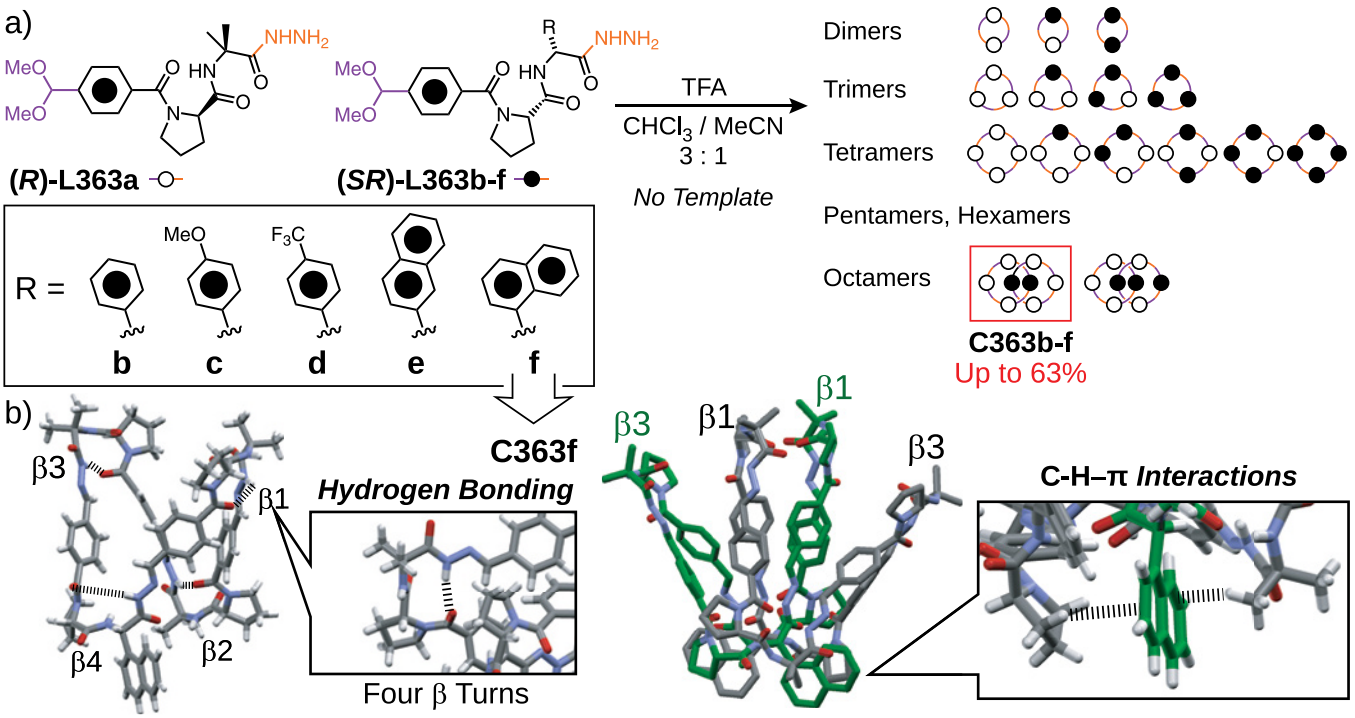
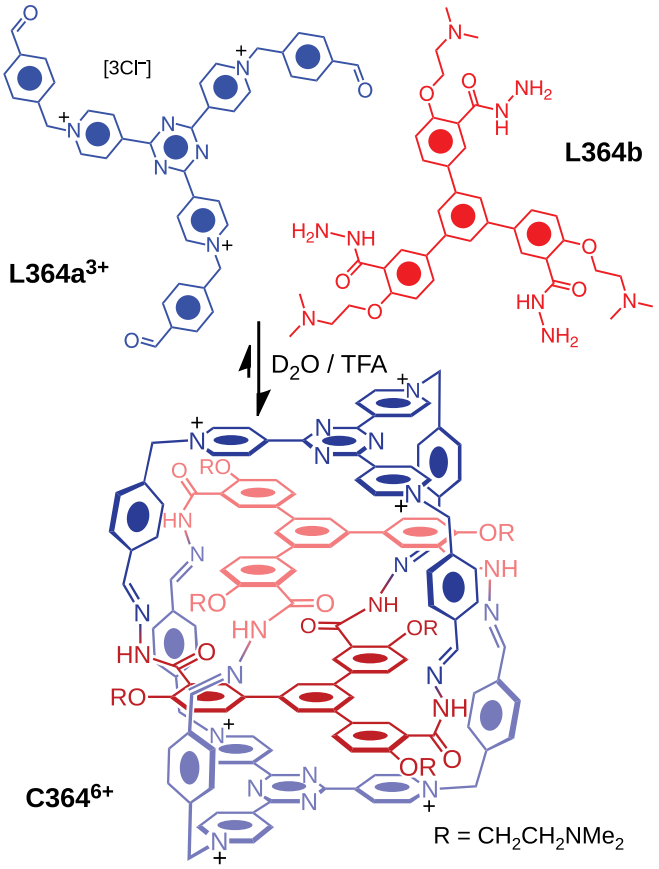


Figure 3.26 The co-assembly and solid-state structure of an octameric [2]catenane (**C363**) based on combinations of dipeptide monomers **L363a-f**.[269] (a) A mixture of catenated and non-catenated cyclic oligomers results from combining ligand **(*R*)-L363a** with any of ligands **(*SR*)-L363b-f**. The reaction is selective for [2]catenanes **C363b-f**, which possess two interlocked [$\mathbf{a}_3$(**b-f**)$_1$] rings. (b) In the crystal, the two identical rings of **C363f** adopt saddle geometries which are related by a C_2 axis. The insets show magnified views of the intra-component hydrogen-bonding interactions in one of the four β-turns (left hand side) of the rings, and the stabilizing inter-component CH–π interactions involving the naphtho side-groups.

C363b-f, which comprise exclusively the $[a_3(b\text{-}f)_1]_2$ species involving two identical rings, each with a 3:1 ratio of the **L363a** and **L363b-f** monomers, is formed in a highly selective manner. Without the addition of any template, these catenanes are often populated as the main component of the DCL after about 10 days of equilibration, reaching isolated yields as high as 64% in the case of **C363f** when the corresponding **L363a** and **L363f** precursors are combined in a 3:1 ratio. Examination of the X-ray crystal structure (**Figure 3.26b**) of the $[a_3f_1]_2$ octamer **C363f** reveals that the catenated structure is stabilized by a number intra- and inter-component hydrogen bonds and [C–H···π] interactions. Each of the two identical interlocked tetramers, which are related by a C_2 axis, adopt a saddle-shaped geometry enabled by four peptide β-turns in the secondary structure of the rings. The chirality of the **(*R*)-L363a** and **(*SR*)-L363b-f** monomers is important—different combinations of stereocenters, with the exception of the mirror image combination, do not lead to catenated octamers. Two more recent reports[270,271] describe the structural characteristics of other homologues based on this motif, in which the side chains of both dipeptide monomers are modified systematically and characterized with respect to the stabilities and solid-state packing of the corresponding catenanes.

The remarkable aspect of the DCL systems investigated by Sanders and Gagné is the emergence of relatively complex structures from relatively simple building blocks. Protein folding, which involves a subtle interplay of many weak interactions, is a phenomenon that exemplifies nature's ability to build complex structures from simple building blocks. These dynamic catenanes would appear to be bridging the gap between the simplicity of small-molecule model systems and the complexity of biomolecular systems such as proteins.

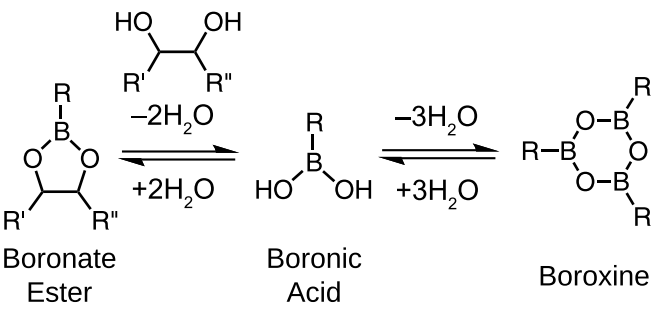
Recently, Sessler[272] has reported on the quantitative self-assembly (**Scheme 3.32**) of the homo[2]catenane **C364^{6+}** in water. A benzaldehyde-terminated trication (**L364a^{3+}**) derived from tris(4-pyridyl)triazine and its hydrazine-terminated partner (**L364b**) derived from triphenylbenzene are cross-coupled via reversible hydrazone linkages in acidic aqueous media to give the catenated organic cages **C364^{6+}** in quantitative yield. The same combination of reactants yields only the uncatenated cages in Me_2SO, suggesting that the high-yielding aqueous catenation is driven by a combination of solvophobic and π-associated donor-acceptor interactions, which are enhanced in water compared to Me_2SO. The catenane has been characterized by NMR spectroscopy, mass spectrometry, and X-ray crystallography. The solid-state structure of the compound is illustrated in **Section 4.1.3.1**. Conveniently, the reversible hydrazone bonds may be 'locked' by raising the pH of the solution so as to impart the catenane with greater kinetic stability.



Scheme 3.32 The quantitative aqueous self-assembly of Sessler's triply interlocked homo[2]catenane is enabled by reversible hydrazone bonds.[272]

3.3.3 Boronic Esters and Boroxines

Boronic acids have have been a boon to the field of supramolecular chemistry because they condense efficiently and reversibly with diols to form boronate esters, and also self-condense into boroxines.[273] Their use is especially widespread in the self-assembly[274,275] of organic macrocycles and cages,[276,277] as well as covalent organic frameworks.[278]



Cases in which the reversible bonding of boron has been employed in the synthesis of MIMs remains relatively uncommon. Three examples are given in **Figure 3.27**.

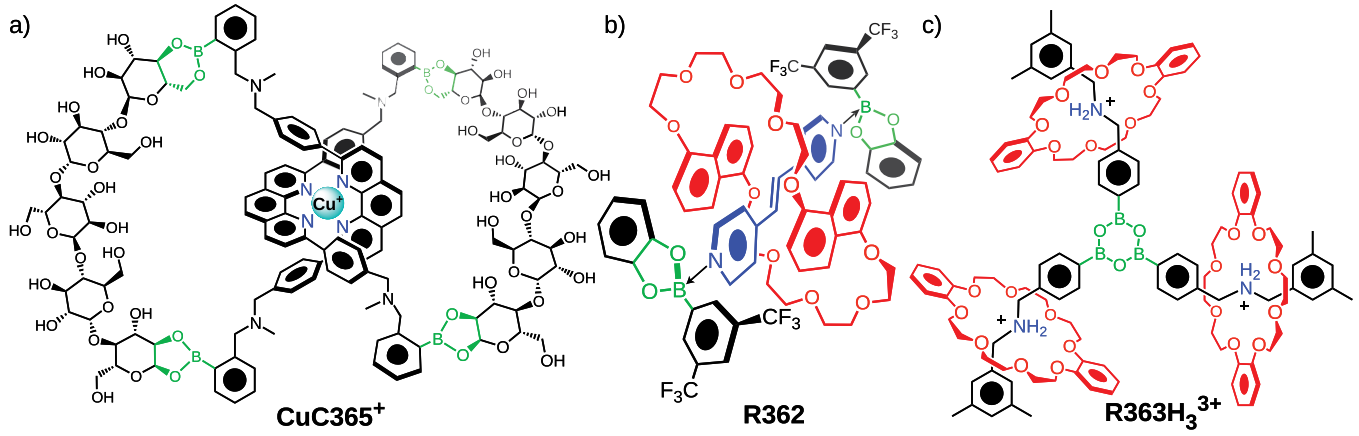


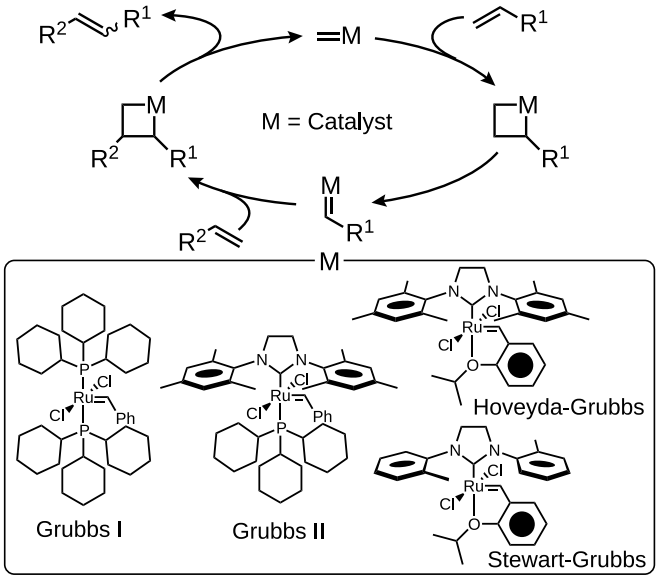
Figure 3.27 Self-assembled MIMs based on reversible boronic acid condensations. (a) The oligosaccharide-bridged [2]catenate **CuC365**$^{+}$ introduced by Shinkai.[279] (b) The boronic ester-stoppered [2]rotaxane **R362** introduced by Severin.[280] (c) The branched [4]catenane **R363H$_3$**$^{3+}$, accessed through boroxine formation by Tokunaga.[281]

The earliest one (**Figure 3.27a**), to our knowledge, was a clever design by Shinkai[279] involving the condensation of an oligosaccharide bridge with a pre-organized Sauvage-type tetrahedral (phen)$_2$Cu^{I} complex in order to form the [2]catenate **CuC365**$^{+}$. Shinkai showed that molecular topology in this system is sensitive to the length of the oligosaccharide—shorter oligosaccharides (D-glucose and maltose) yield helicates while longer ones (maltopentaose and maltohexaose) afford the catenate. The directionality of the glycosidic bonds in each ring of **CuC365**$^{+}$ enable it to express a form of topological chirality, a topic which is discussed in **Section 5.2.4.1**. Severin[280] prepared the noncovalently-stoppered [2]rotaxane **R362** (**Figure 3.27b**) by orchestrating the six-component self-assembly of a DN38C10 macrocycle encircling a stilbene-like bidentate pyridine ligand, which coordinates axially to dioxaborole stoppers, which are themselves assembled from a catechol/boronic acid pair. Tokunaga[281] took advantage of the threefold symmetry of boroxines in order to assemble the C_3-symmetric branched [4]rotaxane **R363H$_3$**$^{3+}$ (**Figure 3.27c**) based on the hydrogen-bonded dibenzylammonium/crown ether motif.

Although there are still few examples of MIMs interlocked through boronic acid self-assembly, the relatively large and growing library of boronate ester cycles and cages is an indication that this category of MIMs will continue to grow.

3.4 Mechanical Bond Formation by Olefin Metathesis

Olefin metathesis[282] is a reaction which redistributes the alkene substituents of carbon-carbon double bonds. Ring-opening metathesis polymerization (ROMP), ring closing metathesis (RCM), and olefin cross-metathesis (CM) are three major types of metathesis reactions. Since the formation of mechanical bonds almost always involves the closure of a loop or ring at some stage of synthesis, RCM (**Section 3.4.1**) is of particular interest for our purposes, while CM (**Section 3.4.2**) has also played an important role in MIM synthesis.



A noteworthy, if slightly digressive, point is that several claims[283–285] have been made for the production of catenated cycloalkanes employing olefin metathesis in the 1960s and 1970s by the so-called Möbius strip mechanism—see **Section 2.2.3**—with only mass spectrometric evidence to support them. These claims were disproven[286] after the mechanism[287,288] of olefin metathesis had been established definitively. Further evidence for these metathesis-mediated cycloalkane catenanes remains to be demonstrated. If catenanes are indeed produced during the olefin metathesis of cycloalkanes, they must be formed by a statistical threading process—see **Section 2.1**.

3.4.1 Ring-Closing Metathesis (RCM)

A distinction is made between ring-closing metathesis (RCM) and ring-opening ring-closing metathesis (RORCM). RCM, which is driven entropically by the generation of two product molecules per substrate, is often irreversible in practice because volatile ethene gas is released upon ring closure. RORCM, by contrast, starts from pre-closed rings such that the metathesis catalyst continuously scrambles the double bonds, rendering it a fully reversible system. We note, however, that although RCM is irreversible, it still offers the promise of thermodynamic control once the ring is closed, since it can move into the RORCM regime in the presence of an appropriate catalyst such as one of the Grubbs ruthenium-alkylidine catalysts. Among the most widely employed of Grubbs' catalysts are the first generation[289] (Grubbs I), second generation[290] (Grubbs II), and the phosphine-free second generation Hoveyda-Grubbs[291] (Hoyveda-Grubbs II) catalysts. These catalysts scramble olefins so efficiently that they can be utilized to make MIMs with the excellent error-checking and proof-reading capabilities that are characteristic of thermodynamically controlled reactions.

3.4.1.1 RCM in Metal-Templated MIMs

Olefin metathesis began to take root in MIM synthesis as early as 1997 as a result of a collaboration[292,293] between Sauvage and Grubbs. The catenates **Cu(C366a)**$^+$ and **Cu(C366b)**$^+$ are both prepared (**Scheme 3.33**) through RCM with Grubbs' first generation Ru^{IV} benzylidene catalyst (Grubbs I) in CH_2Cl_2. Both catenates can be obtained from coordination complexes involving olefin-terminated 1,10-diphenylphenanthroline (dpp)-based ligands—as well as the corresponding macrocyclic ligand (Mdpp30) possessing a pentaethylene glycol loop—which pair up tetrahedrally around Cu^I templates. While **Cu(C366a)**$^+$ is obtained from RCM of a pseudorotaxane template *Cu(**L366**⊂Mdpp30)*$^+$, **Cu(C366b)**$^+$ is obtained from a double-RCM of the entwined template Cu(***L366***)$_2^+$. The different synthetic routes apparently have little affect on the outcome of obtaining a catenated topology, since both compounds are obtained in high (≥90%) yields. This catenation is more efficient than cyclization of the free ligand, indicating that [C–H···O] hydrogen-bonding interactions between the acidic protons of the dpp ligand and the oxygen atoms of the polyether loops most likely assist and stabilize the ring-closing reaction. The Grubbs I catalyst does not produce the *trans* isomers of the product olefins exclusively: the *cis* olefins are present in very low (2–3%) proportions in the catenates. The diastereoisomeric mixture of olefins can also be nullified[293] easily and quantitatively by reductive hydrogenation.

RCM is widely applicable (**Figure 3.28**) to Sauvage-type MIMs.[294] It should be noted, however, that the ring-closing reaction is sensitive to coordination geometry and ligand constitution. For example, an attempt[295] to catenate terpyridine (terpy)-based ligands surrounding a Ru^{II} template by RCM of their olefin-terminated polyether chains resulted surprisingly in only the large figure-of-eight macrocycle *Ru(Mterpy$_2$58)*$^{2+}$. Later on, RCM was applied[296,297]

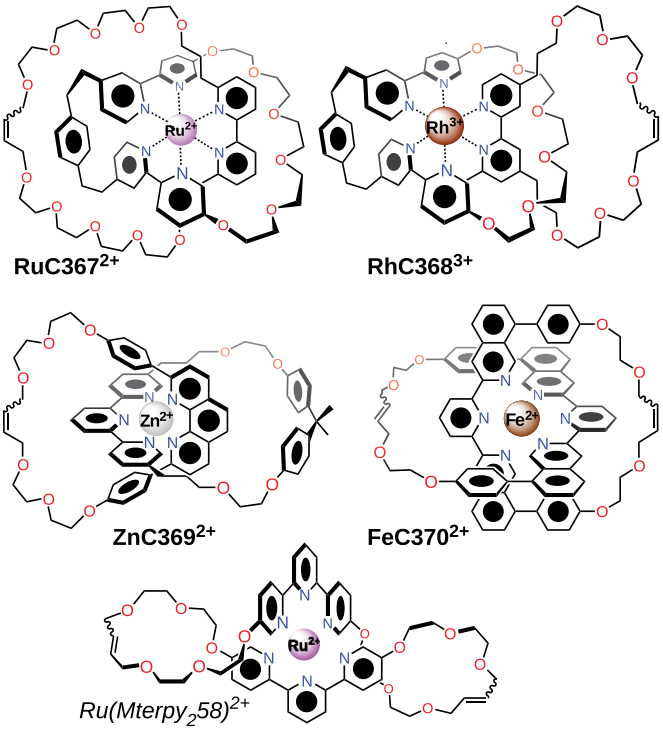
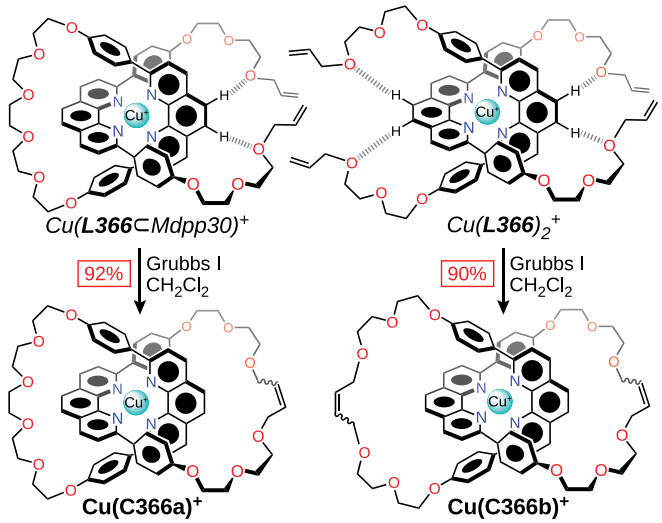


Figure 3.28 Various iterations of a metal-templated RCM catenate synthesis by Sauvage. Catenates **RuC367**$^{2+}$ and **RhC368**$^{3+}$ involve a combination of bidentate and bis-bidentate chelates around Ru^{II} and Rh^{III} templates, respectively.[296–298] Catenate **ZnC369**$^{2+}$ is based on a five-coordinate Zn^{II} complex,[299] while **FeC370**$^{2+}$ relies on endocyclic yet sterically non-hindered octahedral Fe^{II} chelates.[300] The figure-of-eight-shaped macrocycle *Ru(Mterpy$_2$58)*$^{2+}$ is the unexpected outcome of a failed attempt to make a catenate with two terpy ligands.[295]

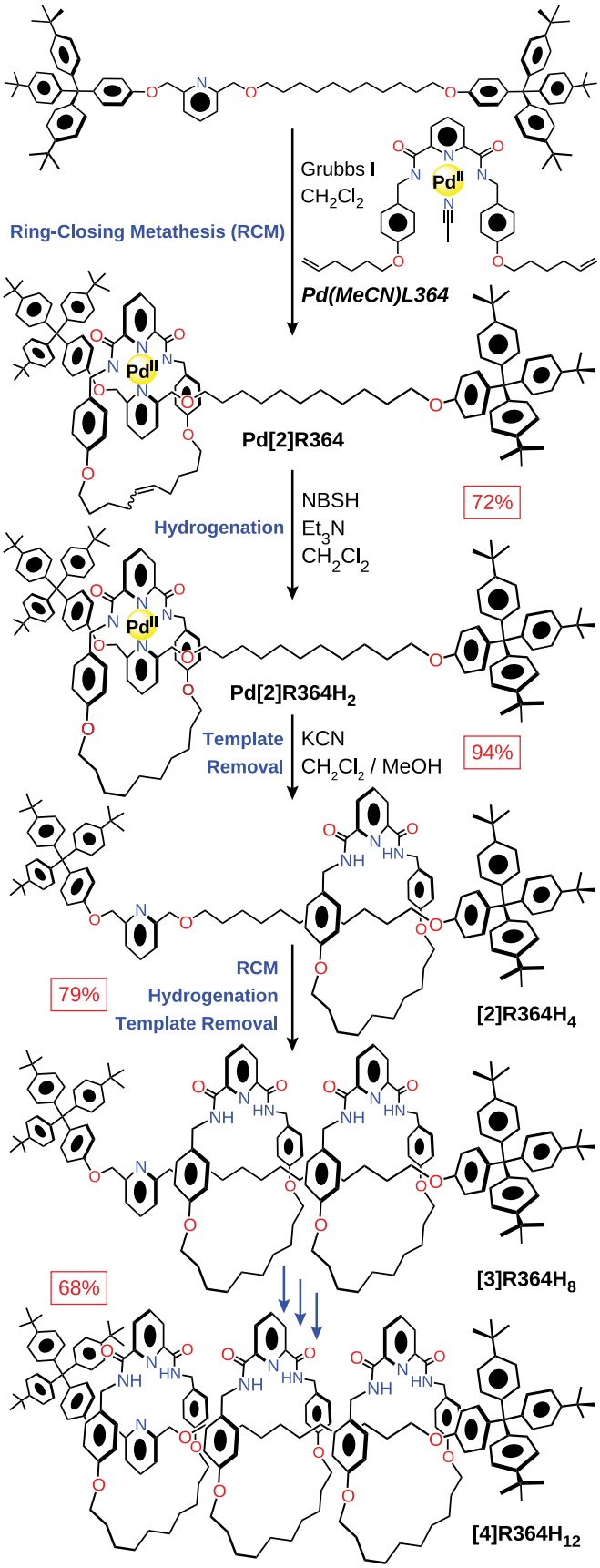


Scheme 3.33 The first RCM-mediated catenane syntheses by Sauvage and Grubbs.[292] Dashed lines depict [C–H···O] interactions that most likely assist in the efficient ring-closing reaction.

successfully to the preparation of the Ru^{II}-based catenate **RuC367**$^{2+}$, which is obtained from a unique tris-bidentate pre-organized coordination complex in 68% yield. See **Section 6.2.3** for a discussion of this catenane's photo-driven circumrotation. A similar structure was fashioned around the Rh^{III} template of catenate **RhC368**$^{3+}$.[298] Five-coordinate Zn^{II} complexes are also amenable to RCM catenation, as demonstrated[299] by the formation of the catenate **ZnC369**$^{2+}$, while a bis-tridentate chelate involving octahedral Fe^{II} complexes has been metathesized[300] into the [2]catenane **FeC370**$^{2+}$. The Strasbourg group has tapped RCM to access a number of more sophisticated molecular topologies, including trefoil knots,[294,301–304] Solomon links[303] (**Section 4.1.1.1**), and 'handcuff' catenanes[305,306] (**Section 4.1.4.2**).

Another pioneer of metal-templated mechanomolecules is Leigh.[307] He has utilized RCM extensively in the synthesis of a number of MIMs based on octahedral,[213,308] square planar,[309–313] and linear[314] templates—see **Sections 2.3.2.3**–**2.3.2.5**. One particularly clever rotaxanation strategy[312] has enabled the clipping (**Scheme 3.34**) of multiple rings around a dumbbell possessing only one templating recognition unit in its axle. After the neutral bis-olefinic chelate ***Pd(MeCN)L364*** is clipped around a dumbbell's pyridine-2,6-dimethylene template, the corresponding metallo[2]rotaxane intermediate **Pd[2]R364** is hydrogenated to afford **Pd[2]R364H$_2$** in 72% yield over two steps. The Pd^{II} template is removed efficiently (94%) with KCN to give the [2]rotaxane **[2]R364H$_4$**. Since the ***Pd(MeCN)L364*** chelate outcompetes the non-metallated benzylic amide ring for the pyridine template, the sequence of RCM, hydrogenation, and template removal can be repeated a second time to afford the [3]rotaxane **[3]R364H$_8$**, while a third cycle provides the [4]rotaxane **[4]R364H$_{12}$**, with no significant losses in the efficiency (68–79%) of the three-step rotaxanation. Leigh has also prepared challenging topological molecules, including a trefoil knot,[315] Solomon link[316] (**Section 4.1.1.1**) and a Star of David[317] [2]catenane (**Section 4.1.2.2**), by ring-closing metathesis of ligands surrounding metal templates. This iterative clipping strategy has enabled the genesis[313] of [3]rotaxanes displaying sequence isomerism—see **Section 5.2.2**—as well as [2]catenane switches[311,318] driven by interconvertible Pd^{II} coordination modes—see **Sections 6.3.4** and **6.4.1.2**.

Metal-templated RCM-mediated synthesis of MIMs has also found application outside the realms of Strasbourg (Sauvage) and Edinburgh/Manchester (Leigh). Mayer[319,320] has used RCM, for example, in high-yielding syntheses of Sauvage-type Cu^{I}/phenanthroline [3]catenates and a self-entangled [1]metallorotaxane—see **Section 6.13.2**. Gunnlaugson[321] claims to have synthesized Hopf links and cyclic [3]catenanes—see **Section 4.1.1.4**—by RCM of olefin-polyether-functionalized 2,6-pyridinedicarboxamides organized around a Eu^{III} template. Hunter[322] has employed RCM to close an 'open knot' structure[323] into a trefoil knot (**Figure 3.29**) comprising a chain of three bipyridine ligands wrapped around a single Zn^{II} center—a molecular knotting strategy



Scheme 3.34 Leigh's oligorotaxane synthesis by iterative metal-ligand template-directed clipping of multiple macrocycles around a single-template dumbbell by RCM.[312]

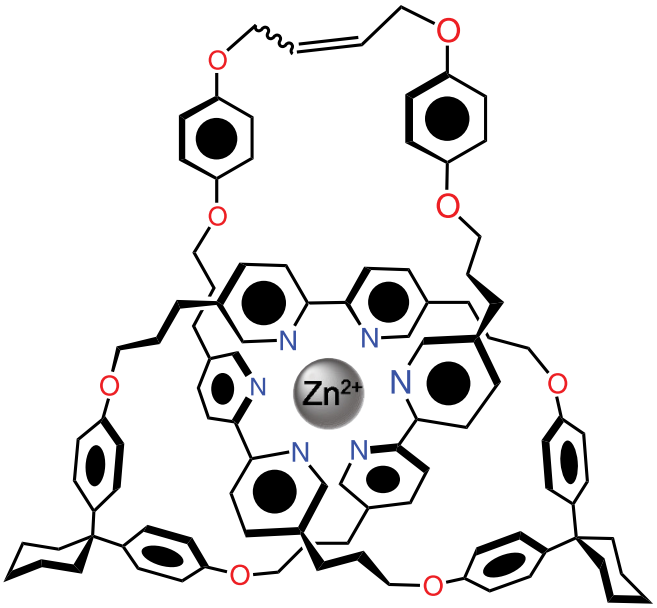


Figure 3.29 Stereoformula of Hunter's trefoil knot, accessed by RCM of a bis-olefinic thread entwined around a single Zn^{II} template.[322]

that had been anticipated[324] without becoming realized for nearly four decades!

Stuart Rowan[325] employed a 2,6-bis(*N*-alkylbenzimidazolyl)pyridine (bip) ligand motif in the metal-templated RCM-mediated synthesis (**Scheme 3.35**) of [3]catenates and [3]catenands. The [3]catenates are generated in a RCM reaction on a pseudo[3]rotaxane, promoted by the Hoveyda-Grubbs II catalyst. The structure of the ligands were optimized empirically because yields are sensitive to conformational flexibility, a property which influences the pre-organization of the necessary [3]metallopseudorotaxane precursor. The reaction proceeds more efficiently when the central ring of the catenane contains a bent xanthene linker ($\mathbf{Zn_2C372}_{Hx}^{4+}$) in comparison with a straight biphenyl one ($\mathbf{Zn_2C371}_{Hx}^{4+}$), the evidence for which is the fact that these targets comprise 83 and 63% of the RORCM product mixtures, respectively. By replacing the hexyl solubilizing groups for ethyl groups on the peripheral rings of the catenate, the sterically less encumbered catenate $\mathbf{Zn_2C372}_{Et}^{4+}$ is generated as the dominant (95%) species in the reaction mixture. A scaled-up synthesis of the Fe^{II}–templated xanthene homologues, followed by demetalation with 1M NaOH under sonication, affords the catenands $\mathbf{C372}_{Et}$ and $\mathbf{C372}_{Hx}$ in 38 and 45% isolated yields, respectively. These isolated yields are substantially lower than the crude estimates for the Zn^{II} homologues, a fact that has been attributed to unoptimized metal removal and purification protocols.

3.4.1.2. RCM in Donor-Acceptor MIMs

In the π-donor/π-acceptor genre, the early pioneer in RCM-mediated MIM synthesis was Sanders,[326] who employed the Grubbs I catalyst to obtain (**Scheme 3.36**) the neutral π-associated [2]catenanes **C373** and **C374**, which are based on the recognition of the electron-rich 1,5-dinaphtho[38]crown-10 (DN38C10) ring for the olefin-terminated guests **L373** and **L374** based on electron-deficient PMDI and NDI recognition units, respectively. Poor solubility in $CHCl_3$ limited the rate of the RCM reaction, however, leading to only modest yields of 25 and 50%, respectively, for the [2]catenanes. Importantly, it was also demonstrated that the pre-formed **C373** could be converted to the more stable **C374** by RORCM in the presence of the NDI-bisalkene **L374** and Grubbs I catalyst, demonstrating the reversibility of the system.

Huang[327] has employed RCM to close olefin-modified *meta*-phenylene[32]crown-8 (MP32C8) 'taco' complexes around linear and cyclic bipyridinium ($BIPY^{2+}$) derivatives in order to prepare (**Figure 3.30**) the corresponding macrobicyclic [2]catenane $\mathbf{C375}^{4+}$ and [2]rotaxane $\mathbf{R365}^{4+}$. These MIMs have been isolated in 85 and 90% yields, respectively, in Me_2CO using the Grubbs II catalyst.

Recently, an extended tetracationic cyclophane related to $CBPQT^{4+}$, known[328] as $ExBox^{4+}$ (**Section 2.3.3.9**), has been employed[329] in the synthesis (**Scheme 3.37**) by RCM of the porphyrinic [2]catenane $\mathbf{C376}^{4+}$. Although the bis-olefin **L376** possesses a tetraphenylporphyrin (TPP) recognition unit that binds strongly ($K_a = 5.5 \times 10^3\ M^{-1}$) to $ExBox^{4+}$ in Me_2CO, $\mathbf{C376}^{4+}$ is obtained in relatively low yield (17%) after 3 days of reacting the precursors in the presence of the Grubbs II catalyst at 40 °C in Me_2CO. See **Section 6.3.2** for a demonstration of this catenane functioning as a pH-driven molecular switch.

Perez[330,331] has employed RCM to interlock (**Figure 3.31**) molecular rings mechanically around single-walled carbon nanotubes (SWNTs). The π-electron rich macrocyclic host **M366** (**Figure 3.31a**), which is based on extended tetrathiafulvalene recognition units and their known[332] affinity for SWNTs, has been cyclized with the Grubbs II catalyst

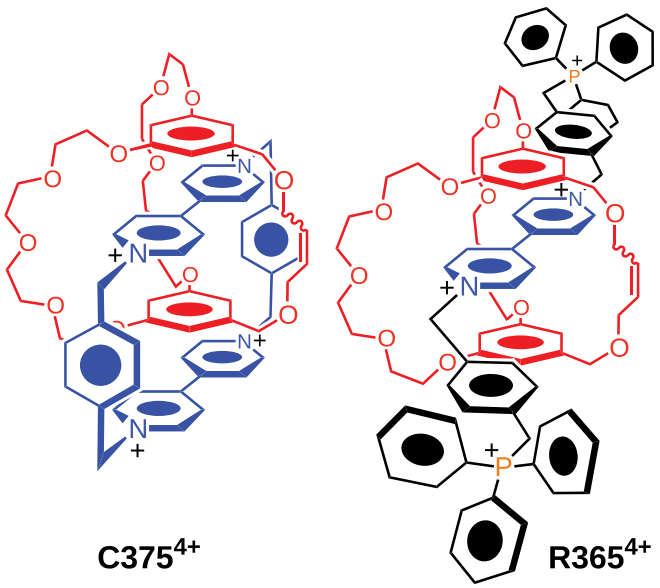
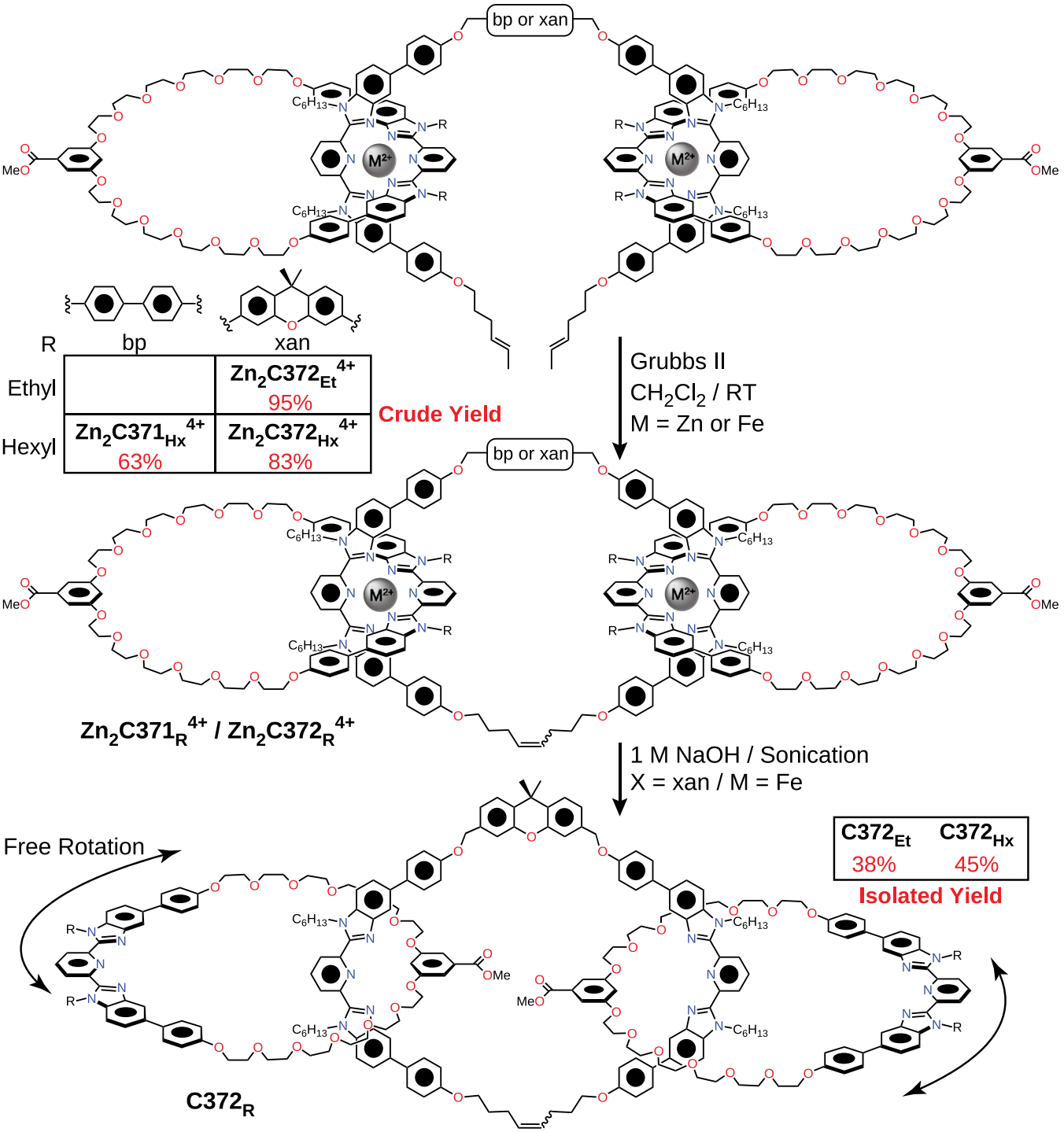
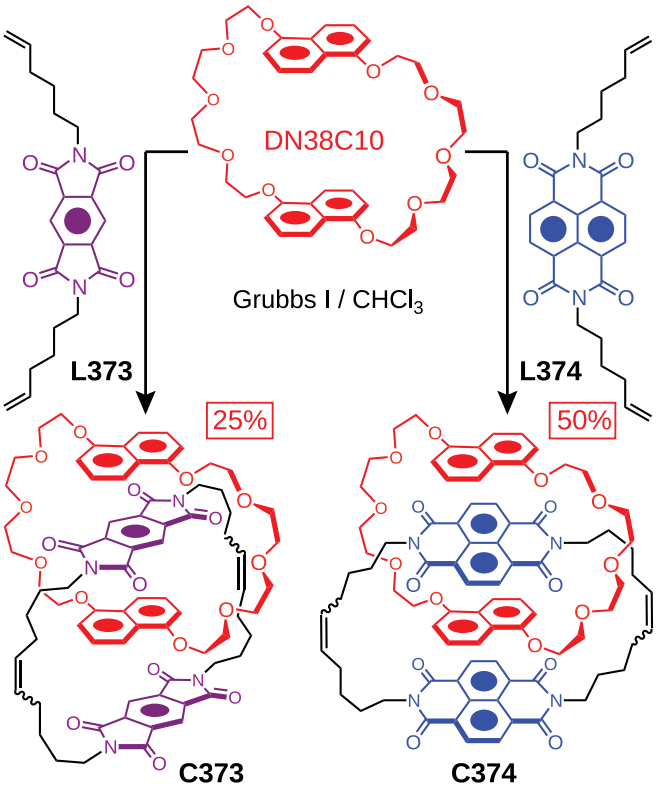


Figure 3.30 MIMs accessed by RCM on crown ether/bipyridinium "taco complexes".[327]



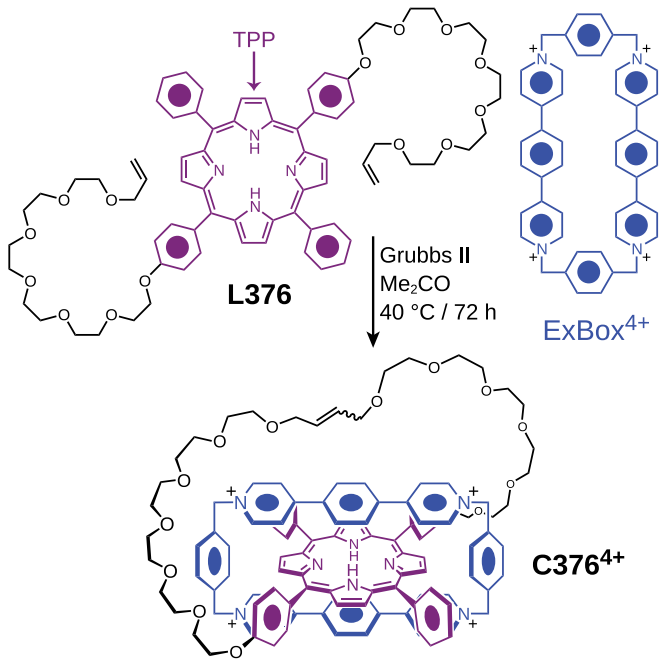
Scheme 3.35 The RCM-mediated synthesis of [3]catenates and catenands, based on the preorganization of 2,6-bis(*N*-alkyl-benzimidazolyl)pyridine (Bip) ligands around metal (Zn^{II} or Fe^{II}) templates.[325]

in a suspension of SWNTs (0.7–1.1 nm in diameter) in tetrachloroethane, affording (**Figure 3.31b**) rotaxane-like *SWNT⊂**M366*** assemblies (**R366**) as the main products of the reaction. Thermogravimetric analysis indicates that the rings comprise up to 40 wt % of the isolated mechanically interlocked SWNT materials. The Spanish team performed a large number of experiments in support of their claim that the rings encircle the SWNTs. Repeated cycles of washing, sonicating, and filtering did not reduce significantly the number of rings in the sample, suggesting that they are bound mechanically. Solid-state ^{13}C NMR, Raman, and UV/Vis/NIR spectroscopies, in addition to photoluminescence excitation intensity mapping, all reveal changes before and after the RCM-mediated rotaxanation protocol that also point to mechanical encirclement. Perhaps the most convincing evidence, however, are AFM and SEM images



Scheme 3.36 Sanders' RCM-mediated synthesis of neutral π-associated donor-acceptor [2]catenanes.[326]

(**Figure 3.31c–d**) that provide a visualization of the rings around the SWNTs. Similarly rotaxanated SWNTs have recently been prepared[331] using pyrene instead of TTF-based recognition units.



Scheme 3.37 RCM-mediated synthesis of the [2]catenane **C376**$^{4+}$ from the porphyrinic bis-olefin **L376** and ExBox^{4+}.[329]

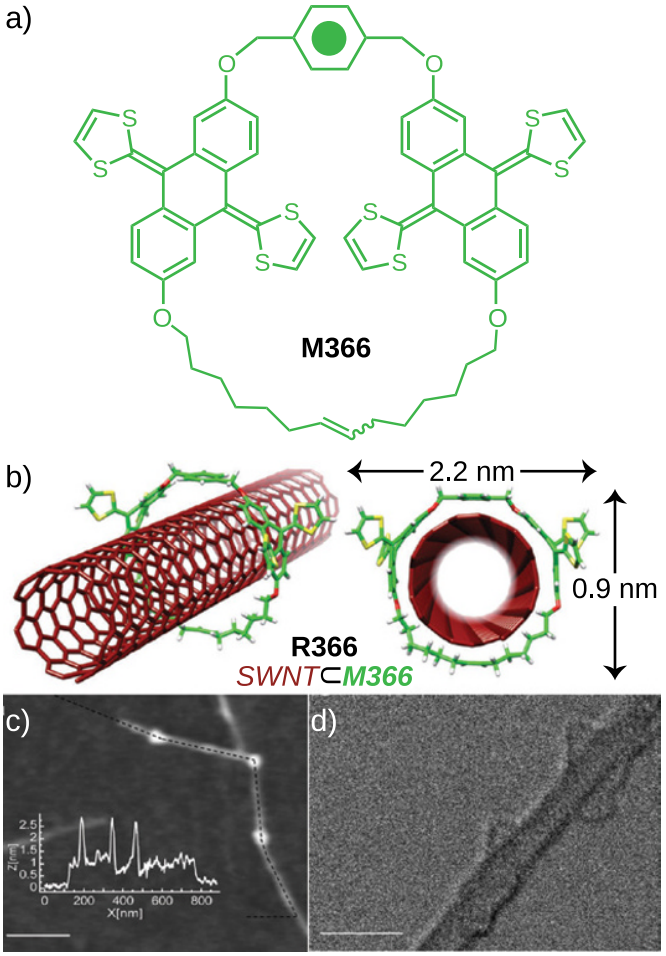


Figure 3.31 Single-walled carbon nanotubes (SWNTs) with mechanical bonds.[330] (a) Structural formula of a π-electron rich macrocycle **M366**. The extended tetrathiafulvalene- and anthracene-based units recognize the π-surface of SWNTs. (b) Models of the rotaxane-like structures afforded by ring-closing metathesis of **M366** in the presence of SWNTs. (c) AFM image of SWNTs rotaxanated by **M366**. The dashed line traces the path along which the height profile (inset) is recorded. (d) SEM image of two **M366** rings interlocked around a SWNT. (b)–(d) Reproduced with permission from ref. 330 (copyright 2014 Wiley).

Catenanes based on macrocyclic arenes (**Section 2.3.9**) have also been prepared (**Figure 3.32**) by ring-closing metathesis. Ogoshi[333] has employed a donor-acceptor pseudorotaxane, based on a pyridinium guest and the planar chiral pillar[5]arene (PA5) host, in the synthesis of the [2]catenane **C377**$^{+}$, which displays a novel kind of topological chirality—see **Section 5.2.4.1**. Recently, Arduini and Silvi[334] utilized their viologen/calix[6]arene (CA6) threading motif (**Section 2.3.9.1**) in the RCM-mediated synthesis of the [2]catenane **C378**$^{2+}$. It is envisioned that the conical shape of the CA6 ring may enable the design of switchable catenanes that exhibit directionally biased, or "mechanostereoselective"—see **Section 6.15.2.2**—motion.

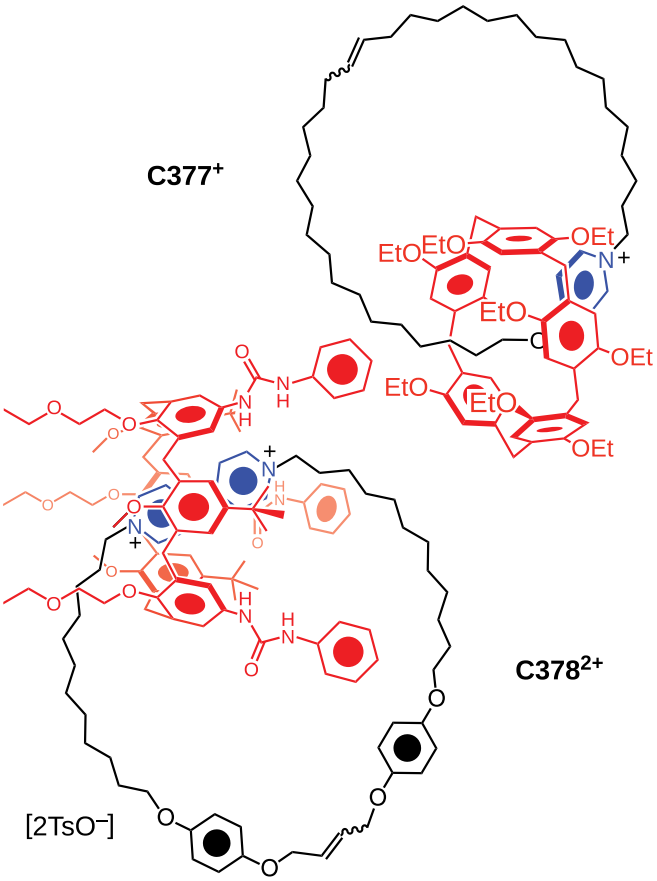


Figure 3.32 Stereoformulas of [2]catenanes based on macrocyclic arene templates, obtained by ring-closing metathesis.

3.4.1.3 RCM in Hydrogen-Bonded MIMs

RCM has been applied to the synthesis of hydrogen-bonded MIMs that rely on both neutral and charged templates.

RCM in Neutral Hydrogen-Bonded MIMs

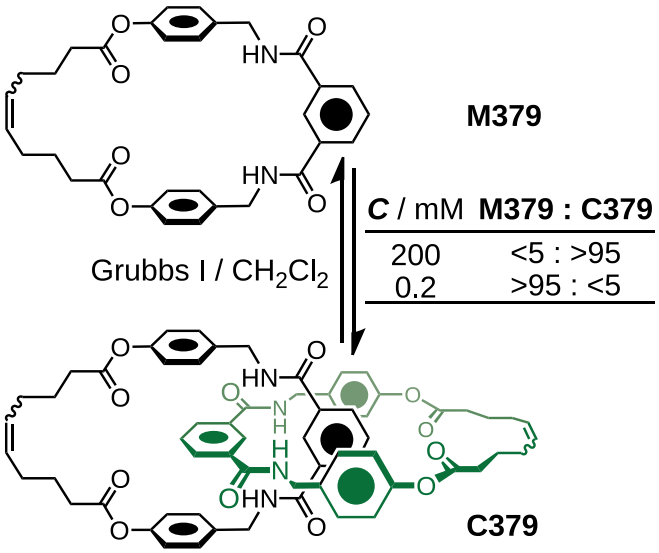
Leigh[335] charted new territory in RCM-promoted MIM synthesis by introducing a 'magic ring' approach to catenation. Subjecting the olefin-containing benzylic amide macrocycle **M379** to RORCM conditions with the Grubbs I catalyst produces (**Scheme 3.38**) the corresponding homo[2]catenane **C379**. The product distribution of the reaction exhibits a high sensitivity to reactant concentrations and solvent polarity. Under the optimized conditions of a high concentration (200 mM) in a low polarity solvent (CH_2Cl_2), the catenated product is obtained in excess of 95% yield. This phenomenon has been likened to the famous illusion known as the Chinese linking rings or 'magic rings', in which two apparently closed rings are made by conjurers to interlock with one another like magic before the audience's very eyes.

Other classes of hydrogen-bonded MIMs that have benefited from RCM include those introduced by (i) Böhmer,[336–340] whose tetraureido-calixarenes template the formation of multi-annulated catenanes—see **Sections 4.1.3** and **6.12**, and (ii) Smith,[341] who has employed RCM to prepare squaraine macrocycles, which have been used as templates for the formation of anthrylic amide (**Section 2.3.4.2**) [2]catenanes by clipping.

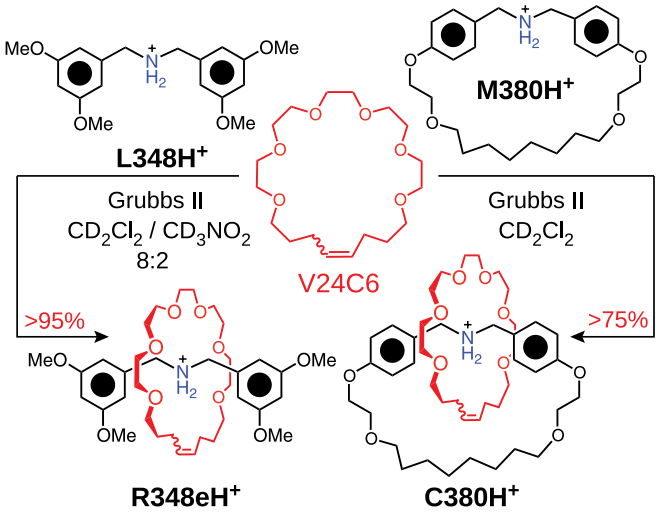
RCM on Charged Hydrogen-Bonding MIMs

Rotaxanes and catenanes of the dialkylammonium/crown ether type have also been accessed under RORCM conditions. The ring component of these systems has often been an olefinic macrocyclic polyether that resembles a conventional crown ether upon closure with RCM. A strategy for thermodynamically controlled RCM-mediated synthesis (**Scheme 3.39**) of dialkylammonium MIMs was introduced in 2003 by Grubbs.[342,343] A mixture of a dibenzylammonium-based dumbbell (**L348H⁺**) or ring (**M380H⁺**) and vinylene[24]-crown-6 (V24C6) equilibrates to the corresponding [2]rotaxane **R348eH⁺** and [2]catenane **C380H⁺** in yields of 73 and 95%, respectively, in heated CH_2Cl_2 solutions in the presence of the Grubbs II catalyst. A noteworthy aspect of this particular motif is that it has been employed in the synthesis of more exotic interlocked topologies and architectures, including daisy chains[344] (**Section 4.2.3.2**), triply interlocked rotaxane superbundles[345] (**Section 4.2.3.5**), and molecular necklaces[346,347] (**Section 4.1.2.2**).

Fukazawa[348] has described a cyclic dimerization driven by olefin metathesis, which generates (**Table 3.10**) the [2]- and [3]catenanes **[2]C381H⁺** and **[3]C381H$_2$²⁺** in a ratio that depends on the length of the olefinic linkers appended to the dibenzylammonium ($Bn_2NH_2^+$) recognition sites of the pseudorotaxane precursors. When the linker between $Bn_2NH_2^+$ and the terminal olefin is relatively short ($n = 3$), the [2]catenane is not observed and the only isolated catenane is the [3]catenane **C381H$_2$²⁺**, while higher concentrations lead to better (up to 35%) yields. For a longer linker length



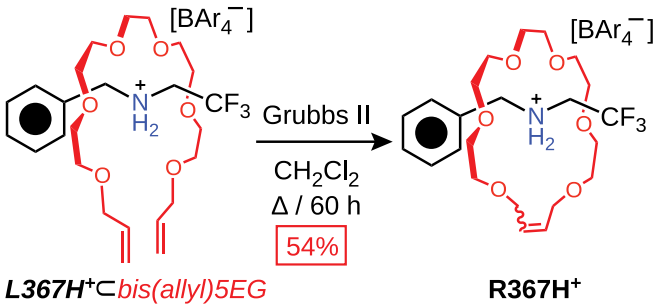
Scheme 3.38 Leigh's 'magic ring' synthesis under RORCM conditions on **M379** affords the [2]catenane **C379** in near-quantitative yield at high concentrations in low-polarity solvents such as CH_2Cl_2.[335]



Scheme 3.39 Dialkylammonium–crown ether MIMs accessed by RCM.[342,343]

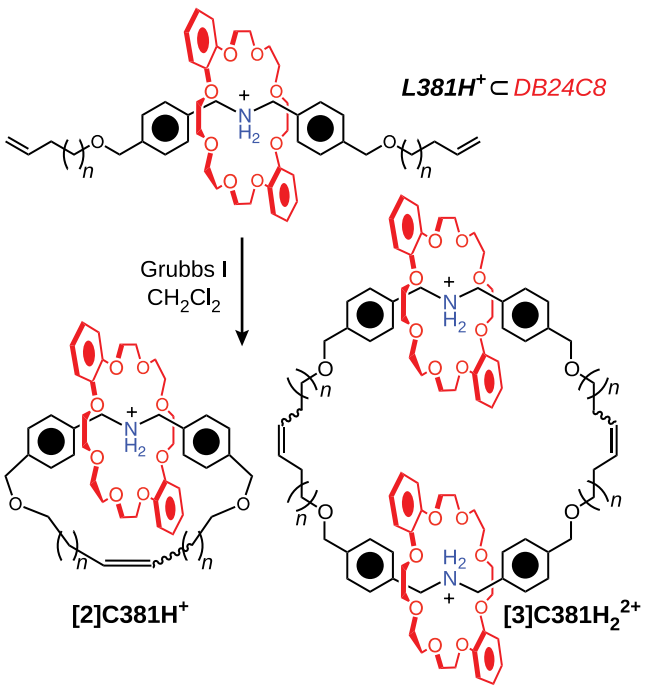
($n = 7$), the [2]- and [3]catenanes are both formed in a concentration-dependent manner, with higher concentrations enriching the [3]catenane content of the product mixture. Iwamoto[349,350] has continued this work as an independent researcher, employed the RCM clipping protocol to access larger oligorotaxanes (up to a [5]catenane) by employing crown ethers large enough to accommodate two dibenzylammonium guests—see **Section 4.1.2.1**.

Jishan Wu[351] has accessed (**Scheme 3.40**) one of the world's smallest rotaxanes by utilizing RCM to close a 20-membered macrocyclic polyether around a dialkylammonium dumbbell, in which a small trifluoromethyl group serves as a sufficient stopper. The rotaxane **R367H⁺** is obtained in 54% isolated yield after subjecting the dialkylammonium ion **L367H⁺** and bis(allyl)-functionalized pentaethylene glycol (5EG) to RORCM conditions for 3 days in refluxing CH_2Cl_2 with the Grubbs II catalyst. The solid-state structure of **R367H⁺** is shown in **Figure 2.55a** in **Section 2.3.4.6**.



Scheme 3.40 The smallest ring to become a component of a MIM is the 20-membered crown ether-like ring of Wu's [2]rotaxane **R367H⁺**, for which even a small trifluoromethyl stopper is sufficient to prevent deslipping.[351]

Table 3.10 The concentration- and length-dependent distribution of [2]- and [3]catenanes **[2]C381H⁺** and **[3]C381H$_2^{2+}$** in the product mixture of a metathesis-driven ring closure of DB24C8/dibenzylammonium pseudorotaxane precursors.[348]



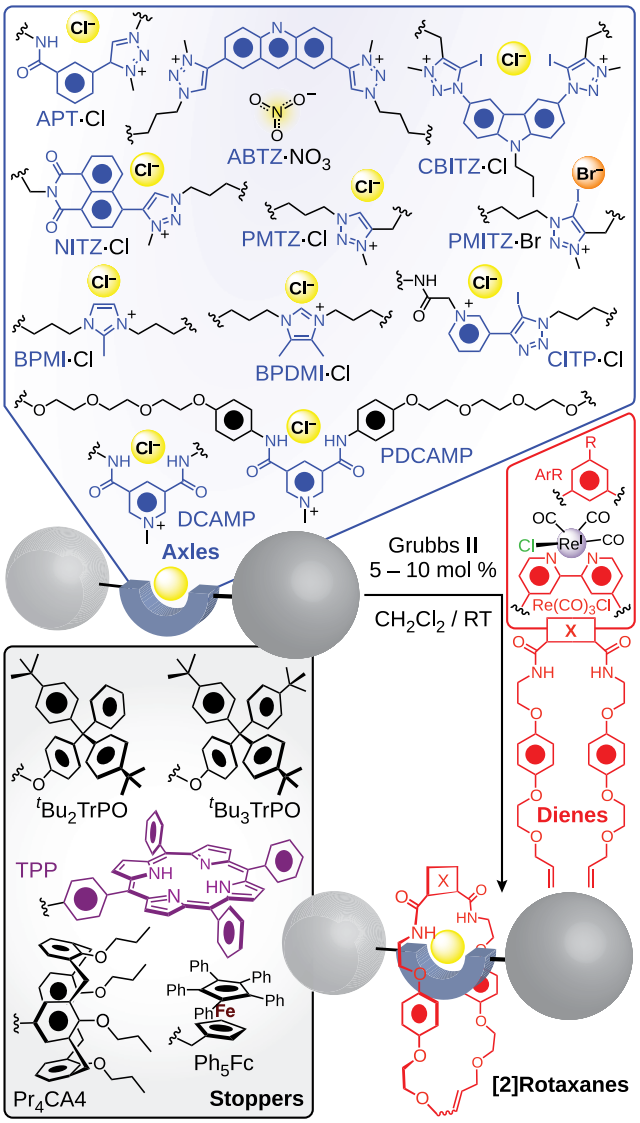
n	Concentration mM	[2]C315H⁺ % Yield	[3]C315H$_2^{2+}$ % Yield
3	2	0	25
3	20	0	35
7	2	56	2
7	10	41	16
7	20	31	20

A novel type of catenated architecture called a [4]pseudocatenane has been crafted by Chen[352–354] from pseudorotaxane templates comprising olefin-functionalized dialkylammonium guests and tris(crown ether) hosts in the presence of the Grubbs II catalyst—see **Section 4.1.4.3**. Loeb[355–357] has employed RCM to prepare dialkylammonium/crown rotaxanes as struts for metal-organic frameworks possessing mechanically interlocked dynamic rings—see **Section 5.1.4**. Loeb and Stephan have employed[358] a similar RCM motif to prepare rotaxanes as frustrated Lewis bases for heterolytic activation of H_2.

3.4.1.4 RCM in Anion-Binding MIMs

Beer has employed RCM extensively in the synthesis of anion-template[359,360]—see **Section 2.3.6**—rotaxanes[361–376] and catenanes.[377–391] A typical RCM clipping procedure[377] involves stirring the olefin-terminated precursor(s) at room temperature in CH_2Cl_2 in the presence of 1–2 equiv of an appropriate template and 5–10 mol % Grubbs II catalyst. Beer and his collaborators have devised a number of reactions (**Table 3.11**) that clip dienes—all of which possess diamide recognition units derived from aryl linkers modified with a functional group R (ArR) or (bpy)$Re(CO)_3Cl$—around ion-paired dumbbells possessing anionic templates to afford [2]rotaxanes by RCM. The rotaxanes' axles incorporate ion-pair templates based on the halide salts of hydrogen bond-donating organocations,

Table 3.11 Summary of Beer's anion-templated RCM clipping protocols for the synthesis of [2]rotaxanes.



	Axle	Stopper	X[a]	Diene Equiv	Yield %	Ref
R368·Cl	DCAMP	^{t}Bu$_2$TrPO	ArH	1.8[b]	47	361
R369·Cl	DCAMP	^{t}Bu$_2$TrPO	Ar^{t}Bu$_6$TPP	1.0	52	365
R370·Cl	DCAMP	^{t}Bu$_2$TrPO	ArFc	1.0	25	366
R371·Cl	DCAMP	Ph$_5$Fc	ArH	1.0	52	367
R372·Cl	DCAMP	TPP	ArNO$_2$	1.0	30	365
R373·Cl	DCAMP	Pr$_4$CA4	Re(CO)$_3$Cl[b]		21	362
R374·Cl	PDCAMP	^{t}Bu$_2$TrPO	ArNO$_2$	1.0	55	370
R375·Cl	BPMI	^{t}Bu$_3$TrPO	ArNO$_2$	1.0	19	369
R376·Cl	BPDMI	^{t}Bu$_3$TrPO	ArNO$_2$	1.0	30	369
R377·Cl	APT	^{t}Bu$_3$TrPO	ArNO$_2$	1.5	47	372
R378·Cl	NITZ	^{t}Bu$_3$TrPO	ArNO$_2$	1.5	47	371
R379·Cl	PMTZ	^{t}Bu$_3$TrPO	ArNO$_2$	1.5[c]	21	363
R380·Br	PMITZ	^{t}Bu$_3$TrPO	ArNO$_2$	1	15	364
R381$^+$·Cl	CBITZ	^{t}Bu$_3$TrPO	Re(CO)$_3$Cl	1.4[c,d]	7	392
R382·Cl	CITP	^{t}Bu$_3$TrPO	ArNO$_2$	1.0	22	374
R383$^+$·Cl	ABTZ	^{t}Bu$_3$TrPO	ArNO$_2$	1.0[c]	13	375
R383$^+$·NO$_3$	ABTZ	^{t}Bu$_3$TrPO	ArNO$_2$	1.0[c]	6	375

[a]Functional Group Abbreviations: Fc = Ferrocene. ^{t}Bu$_6$TPP = *meso*-tris(3,5-di-*tert*-butylphenyl)porphyrin. [b]With 20 mol% Grubbs I catalyst. [c]With 1 equiv NBu_4^+ as the BF_4^- or PF_6^- salt. [d]With 10 wt% Stewart-Grubbs catalyst.

including (i) 3,5-dicarboxamido-*N*-methylpyridinium[361] (DCAMP) and (ii) a homologue[370] (PDCAMP) possessing phenylene-triethyleneglycol linkers, (iii) the imidazolium-based[369] recognition units *N*,*N*′-bis(propyl)-1-methylimidazolium (BPMI) and (iv) *N*,*N*′-bis-(propyl)-4,5-dimethylimidazolium (BPDMI), (v) (3-amidophenyl)-*N*-methyltriazolium[372] (APT), (vi) naphthalimide-triazolium[371] (NITZ), (vii) propyl-*N*-methyltriazolium[363] (PMTZ), and (viii) propyl-*N*-methyl-5-iodotriazolium[364] (PMITZ), (ix) *N*-propylcarbazole bis(*N*-methyl-5-iodotriazolium)[392] (CBITZ), (x) *N*-carboxamidomethyl-3-(5-iodotriazolyl)pyridinium[374] (CITP), and (xi) acridanebis(*N*-methyltriazolium)[375] (ABTZ). Stoppers that have been employed include tritylphenylene oxide units functionalized with *tert*-butyl groups on either two (^{t}Bu$_2$TrPO) or three (^{t}Bu$_3$TrPO) aryl rings, as well as pentaphenylferrocenylmethyl (Ph$_5$Fc) tetrapropylcalix[4]arene (Pr$_4$CA4), and tetraphenylporphyrin (TPP). The [2]rotaxanes **R368·Cl**–**R383$^+$·NO$_3$** are obtained from different combinations of these molecular portions in moderate yields. This recognition system can therefore be generalized for a range of reliable mechanical bond-forming reactions by RCM, owing to the templating [N–H···anion] binding interactions established between the dienes and their ion-paired anionic templates. Beer's seminal anion-templated mechanomolecule in 2002 was the [2]rotaxane[361] **R368·Cl**.

In addition to the [2]rotaxanes in **Table 3.11**, a collection of Beer's anion-binding catenanes, which have been accessed by RCM protocols, are illustrated in **Figure 3.33**. The seminal [2]- and [3]catenanes[377] of this genre are compounds **C382·Cl** and **C383·2Cl**, which were prepared from isophthalamide-based dienes and DCAMP recognition units similar to those employed in the syntheses of the [2]rotaxanes **R368·Cl**–**R372·Cl**. The same template motif underlies (i) the [2]catenane[380] **C384·Cl**, in which the metathesized ring is enlarged and its isophthalamide unit carries a hydrogen-bond donating hydroxyl group, (ii) the homo[2]catenane **C385·2Cl**, obtained[378,383] by double-RCM of entwined DCAMP dienes, as well as (iii) the [2]catenane[379] **C386·Cl**, which possesses a calix[4]arene receptor instead of a polyether loop to close one of its rings. Beer[382,384] has employed calixarenes in portions of several other [2]catenanes (not illustrated) obtained by RCM. The homo[2]catenane[381] **C387·2SO$_4$** has a slightly larger cavity, courtesy of its pyridinium nicotinamided-derived recognition unit, in order to accommodate its sulfate anionic template. The [2]catenanes **C388·X**,[391] **C389X·X**[390] (where X is a halogen atom), and **C390·BrPF$_6$**,[388] which are templated by halogen-bonding interactions, are also discussed in **Section 2.3.6.3**. Although the [2]catenane[387] **C391$^+$** is not templated by anion-binding interactions, its charge-assisted halogen-bonding motif is reminiscent of the catenanes templated by halogen–halide interactions—see **Section 2.5**.

Anion-templated mechanomolecules obtained by RCM are featured elsewhere throughout this work, including:

- A collection[364,373,374,388,390,391] of catenanes and rotaxanes that have been accessed by RCM of templates involving halogen–halide interactions. See **Figure 2.65** in **Section 2.3.6.3**.

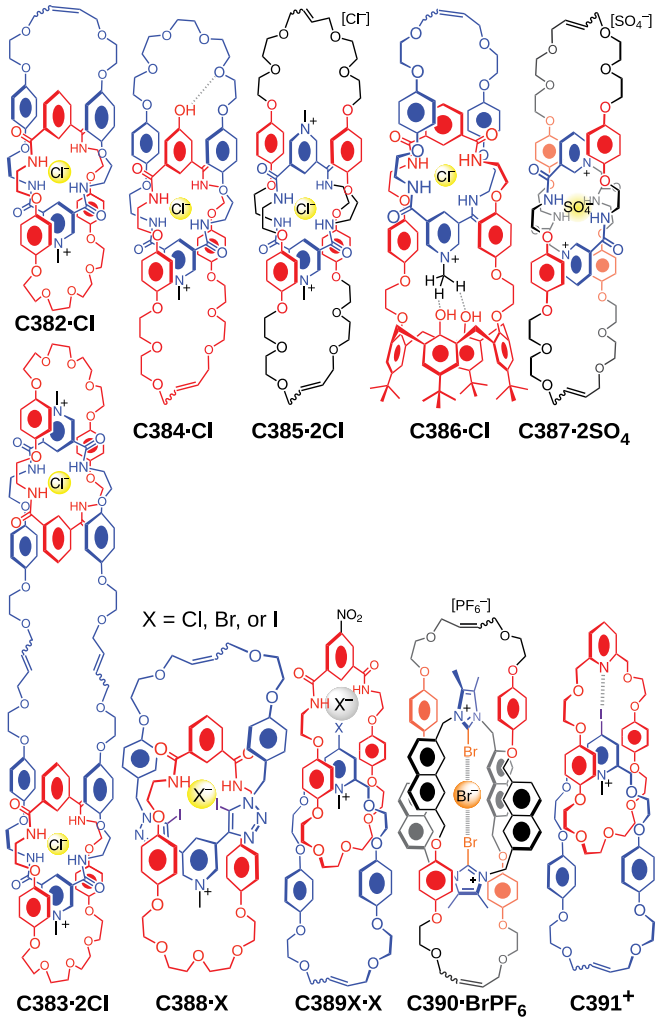
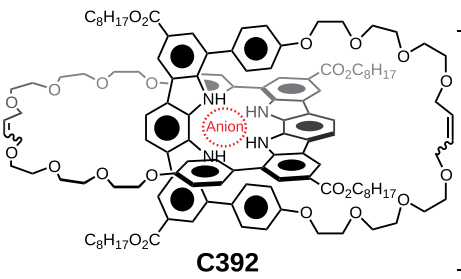


Figure 3.33 Stereoformulas of selected examples of Beer's catenanes obtained by RCM.[377–381,383,387,388,391]

- The [2]rotaxane[375] templated by nitrate, illustrated in **Scheme 2.105** in **Section 2.3.6.4**.
- A "handcuff" [2]catenane.[385] See **Figure 4.40c** in **Section 4.1.4.2**.
- A [*c*2]daisy chain [2]rotaxane.[368] See **Figure 4.81** in **Section 4.2.3.2**.
- Circumrotational [2]catenane molecular switches driven by acids and bases[380]—**Scheme 6.47** in **Section 6.3.4**—and by debenzylation[386]—see **Scheme 6.75** in **Section 6.7.2.1**.
- Anion-driven [2]rotaxane translational molecular switches.[371,393] See **Schemes 6.66** and **6.68** in **Section 6.5.3.1**.

Since Beer[361,383,394] has also shown that the mechanical bond improves the selectivity of the interlocked systems as anion receptors—see **Section 2.3.6**—RCM allows the design of sophisticated mechanically interlocked anion hosts and sensors.[362,366,387]

Jeong[395] has employed RCM in the preparation of a catenane with anion recognition properties enabled by hydrogen-bond donating indolocarbazole recognition units. The homo[2]catenane **C392** is an intermediate (**Figure 3.34**) in the synthesis of an anion-binding catenane which is identical to **C392** except that its olefin units have been hydrogenated. The chloride-templated synthesis of this catenane delivers the target compound in 25% yield after RCM and hydrogenation. The affinity of various anions for the indolocarbazole binding pocket in wet Me_2CO are summarized in **Figure 3.34**.



Anion	K_a (M^{-1})
Cl^-	140,000
Br^-	660
I^-	-
AcO^-	71,000
$H_2PO_4^-$	5700
N_3^-	30,000
HSO_4^-	130
NO_3^-	-

Figure 3.34 Structural formula of the indolocarbazole-based anion-binding [2]catenane **C392** and its affinity for various anions in 1% v/v H_2O/acetone at 24 °C. Although the olefins were hydrolyzed for the binding studies, they have been drawn in the structural formula to point out where the rings were closed during the thermodynamically controlled RCM-mediated synthesis of the catenane.[395]

3.4.1.5 RCM of Ion-Paired MIMs

In one of only a few novel templating motifs to be employed in the first instance under thermodynamic rather than kinetic control, Furusho and Yashima[396] pre-organized two ion-paired U-shaped components around an amidinium carboxylate salt bridge in order to access (**Figure 3.35**) the [2]catenane **C393** by RCM. The salt bridge motif,[397] which

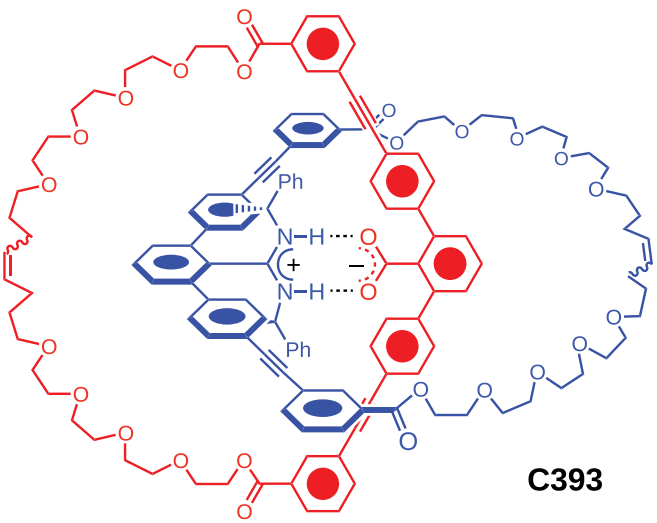


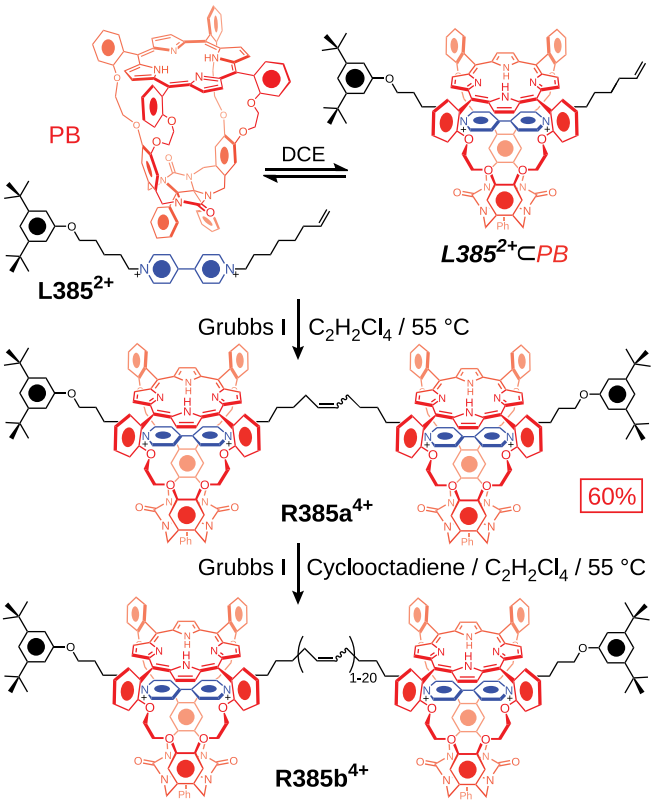
Figure 3.35 Structure of a salt-bridge templated [2]catenane formed by RCM.[396]

can be turned on and off with pH or metal coordination, promises[398] to be a productive new avenue for controlling dynamics (**Chapter 5**) and co-conformational states (**Chapter 6**) in MIMs.

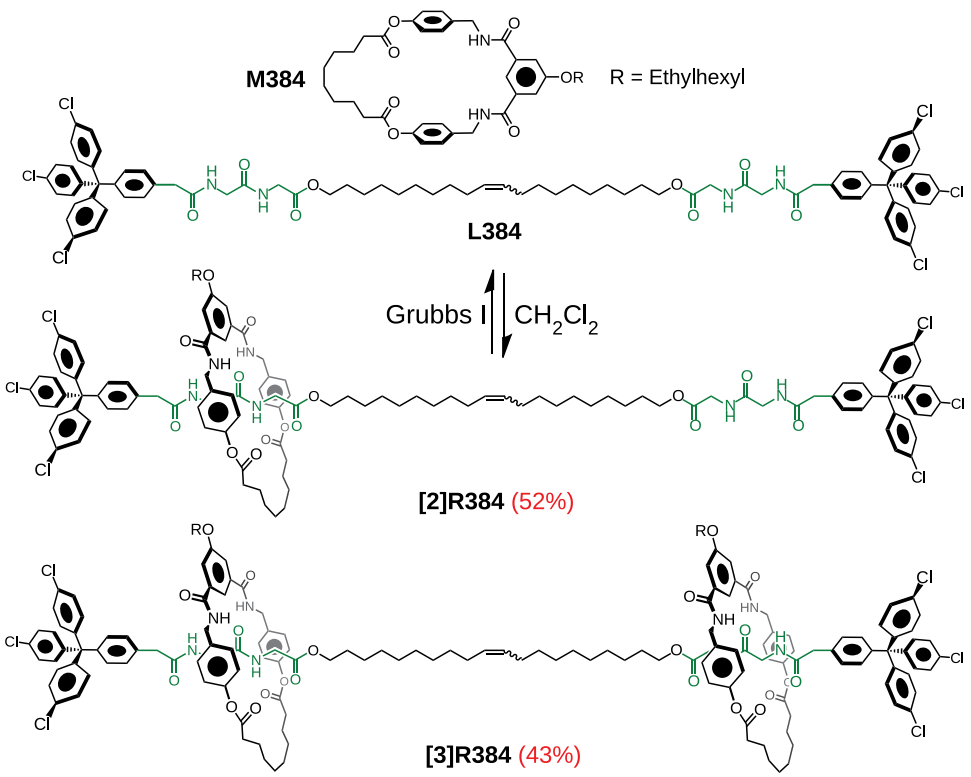
3.4.2 Cross Metathesis (CM)

Just as 'magic rings' are catenated by RCM, 'magic rods' can likewise be applied to rotaxane synthesis using CM. Leigh[70] followed his "magic ring" trick (**Scheme 3.38**) in 1999 with a "magic rod" trick in 2003. A symmetrical dumbbell **L384** with a 'magic olefin' at its center was mixed with a benzylic amide macrocycle **M384** in the presence of the Grubbs I catalyst to produce [2]- and [3] rotaxanes by a sequential mechanism where the rod was first broken, then threaded on one side through hydrogen-bonding interactions—the catalyst acts as a stopper that prevents threading onto the other half-dumbbell—then the dumbbell is reformed, and the process is repeated in the case of the [3]rotaxane. Optimized conditions produced (**Scheme 3.41**) roughly equal amounts of the [2]- and [3]rotaxanes **[2]R384** and **[3]R384**, respectively, in a combined yield of 95%. The 'magic rod' approach has also been referred[18] to much earlier as the 'insertion' strategy—see **Section 3.5.2.1**.

Rowan and Nolte[399] have taken advantage of olefin cross metathesis to prepare (**Scheme 3.42**) the [3]rotaxane **R385a**$^{4+}$, which is based on their porphyrin basket (PB)



Scheme 3.42 Synthesis and expansion of [3]rotaxanes based on the porphyrin basket (PB) by cross metathesis.[399]



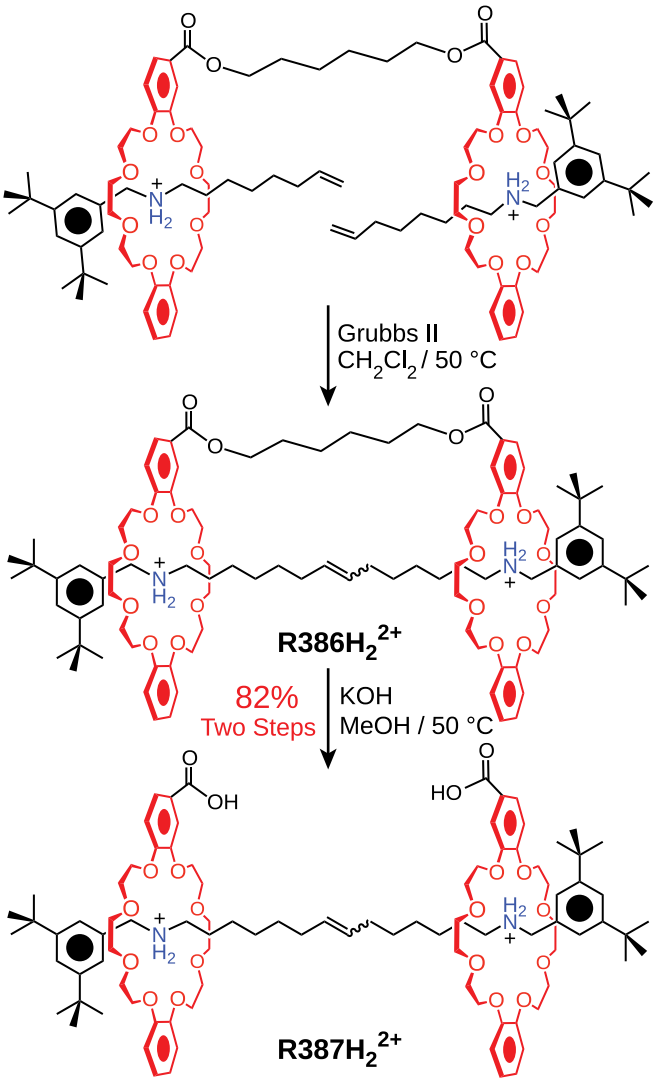
Scheme 3.41 Leigh's 'magic rod' synthesis of benzylic amide rotaxanes by cross metathesis on a bis(glycylglycine) dumbbell possessing an olefinic linker.[70]

hosts (**Section 2.3.3.6**) that encapsulate $BIPY^{2+}$ recognition units. The [3]rotaxane is prepared from two semi-dumbbells **L385**$^{2+}$ in the presence of the Grubbs I catalyst in dichloroethane (DCE). An unexpected [4]rotaxane byproduct was also observed, implying that the host can form a 1:2 complex with $BIPY^{2+}$, since there are only two recognition sites on the dumbbell. Post-metathesis olefinic bonds—located in this case at the dumbbell's center—are typically considered a nuisance because they exist as *cis* and *trans* isomers, a situation which complicates spectroscopic characterization. Although these olefins are commonly nullified by hydrogenation in a final synthetic step, the Nijmegen group cleverly harnessed the olefin functionality as a chain-transfer agent in the metathesis polymerization of cyclooctadiene. The resulting polyolefin [3]rotaxane **R385b**$^{4+}$ was a forerunner to some remarkable research[400,401] on processive catalysis, in which the porphyrin cage acts as a mechanically linked epoxidation catalyst. This seminal work is discussed in **Section 6.15.3.1**. When the viologen reactants are bis-functionalized with olefins, CM and RCM afford[402] multicomponent catenane molecular necklaces—see **Section 4.1.2.2**.

Bistable [2]rotaxanes incorporating neutral π-donor/π-acceptor recognition units have also been prepared[32] by CM protocols, enabling a DN38C10 ring to shuttle back and forth in a controllable manner in response to the addition and removal of Li^+ ions as a stimulus. See **Sections 6.1.1.2** and **6.4.2** for discussions of molecular switches based on this design.

Iwamoto[403,404] has introduced a so-called tether-assisted approach (**Scheme 3.43**) into the synthesis of rotaxanes. In this case, two dialkylammonium semi-dumbbells are conjoined by CM with the assistance of a bis-DB24C8 macrocyclic template under thermodynamic control. The product **R386H**$_2^{2+}$ is a [3]Bonn-1(1,2)ane according to Vögtle[405] nomenclature—see **Section 4.2.3.4**. The tether between macrocycles was subsequently cleaved to afford the [3]rotaxane **R387H**$_2^{2+}$. The [3]Bonnane **R386H**$_2^{2+}$ is the more novel architecture, since the role of the tether is not crucial to forming a [3]rotaxane, as Osakada[406] has demonstrated. The tether does appear to improve the rotaxane yield, however, most likely by reducing the entropic penalty for capturing the dumbbell.

These examples demonstrate the utility of RCM and CM as a method for the high-yielding synthesis of MIMs.



Scheme 3.43 Tether-assisted synthesis of a [3]rotaxane **R387H**$_2^{2+}$ via solvolysis of Bonnane **R386H**$_2^{2+}$, which was prepared by template-directed cross metathesis.[403,404]

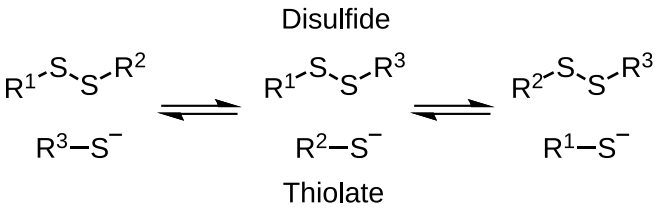
3.5 Mechanical Bond Formation by Reversible Nucleophilic Reactions

Reversible nucleophilic reactions that have been employed in the thermodynamically controlled syntheses of MIMs include disulfide exchange (**Section 3.5.1**), reversible nucleophilic substitutions (**Section 3.5.2**), and Michael additions (**Section 3.5.3**).

3.5.1 Disulfide Exchange

The reversibility of disulfide bond formation and cleavage is a key redox process in biological systems and its properties are well-known and understood.[407] The dynamic oxidative coupling and reductive scission of disulfides—at near-neutral pH in oxygenated water, or in organic solvents with a catalytic amount of free thiol, for example—is emerging as a very useful tool in the creation of dynamic combinatorial libraries.[8,408,409] Mechanistically, the disulfide exchange reaction occurs by nucleophilic attack of a thiolate anion on one of the sulfur atoms of a disulfide bridge, which severs one disulfide bond while creating another. Disulfides are particularly attractive for thermodynamically controlled MIM synthesis because they are stable to a wide range of functional groups and the dynamic disulfide exchange reaction can be easily

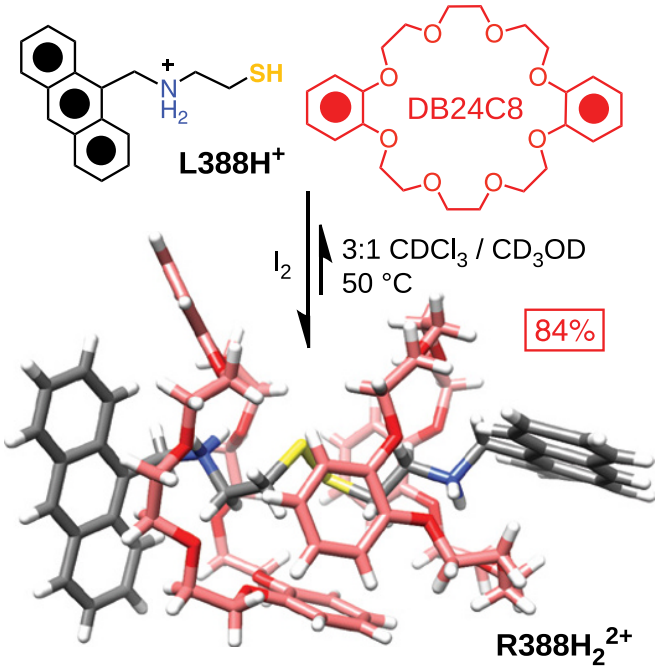
'switched off' at acidic pH, where the thiolate anion is relatively unpopulated relative to its protonated thiol counterpart.



3.5.1.1 Rotaxanes Obtained by Disulfide Exchange

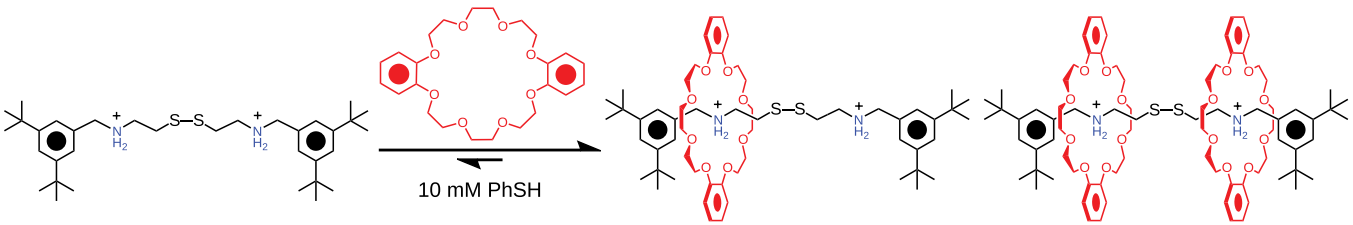
The use of disulfides in rotaxane synthesis was pioneered by Busch,[410] who "riveted" (**Scheme 3.44**) two thiol-terminated pseudorotaxanes in order to form the [3]rotaxane **R388H$_2^{2+}$**. Busch used I_2 in a 3:1 mixture of $CDCl_3$ and CD_3OD to promote the oxidative thiol-thiol coupling reaction of two anthracene-capped dialkylammonium half-dumbbells (**L388H$^+$**) in the presence of an excess (3 equiv) of DB24C8 to obtain **R388H$_2^{2+}$** in high (84%) yield.

Takata[59,411] has prepared (**Table 3.12**) the [3]rotaxane **[3]R389H$_2^{2+}$**, which is structurally similar to that of Busch, except that his approach can be described as yet another magic rod synthesis not unlike those involving olefin metathesis in **Section 3.4.2**. Employing a thiophenol catalyst as a 'key' to 'unlock' and 'lock' the dumbbell **L389H$_2^{2+}$** at the site of its disulfide linkage, a mixture of separated ring and dumbbell components equilibrates gradually at room temperature over a 30-day period to a mixture of the [2]- and [3]rotaxanes **[2]R389H$_2^{2+}$** and **[3]R389H$_2^{2+}$**. The equilibration process is reduced to about a day at 50 °C. A more detailed investigation (**Table 3.12**) of this



Scheme 3.44 Busch's riveting approach to the synthesis of the [3]rotaxane **R388H$_2^{2+}$** through oxidative thiol-thiol coupling.[410] The X-ray crystal structure of **R388H$_2^{2+}$** is portrayed with solvent and counterions omitted for the sake of clarity.

Table 3.12 The effect of solvent, temperature, and stoichiometry on the product yields in the 'magic-rod' synthesis of rotaxanes **[2]R389H$_2^{2+}$** and **[3]R389H$_2^{2+}$**.



L389H$_2^{2+}$ **[2]R389H$_2^{2+}$** **[3]R389H$_2^{2+}$**

Solvent	Concentration (mM)		*T*/°C	Yield[a]/%	
	L389H$_2^{2+}$	DB24C8		[2]R389H$_2^{2+}$	[3]R389H$_2^{2+}$
CD_3CN	100	200	20	15	81
			50	29	65
7:3 $CDCl_3/CD_3CN$	100	200	20	15	77
			50	24	64
1:1 $CDCl_3/CD_3CN$	100	100	50	65	10
		150		69	26
		200		29	65
		300		12	88
		400		10	82
	710	1420	20	10	89
1:1 $CDCl_3/CD_3OD$	100	200	50	37	60
CD_3NO_2	100	200	50	17	83
DMF-d_7	100	300	50	<10	0

[a]Yields are based on integration of the ^{1}H NMR signals in the crude product mixture.

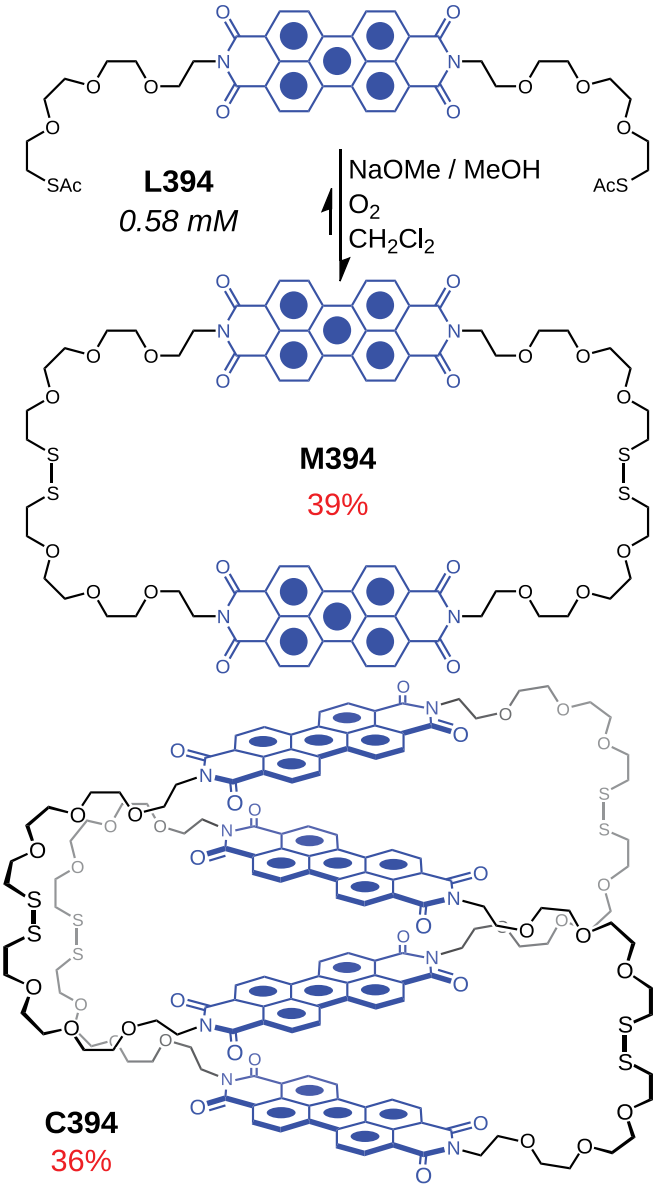
system probed[59] the relationship between various parameters such as solvent polarity, temperature, stoichiometry, etc. and the distribution of [2]- and [3]rotaxane products. The [2]- and [3]rotaxanes can be populated with up to 70 and 90% selectivity, respectively, under optimized conditions. A probable sequential mechanism to [3]rotaxane formation has been proposed, which involves 1) cleavage of the disulfide bond, (2) pseudorotaxane formation on a half-dumbbell, 3) formation of a [2]rotaxane intermediate (a-product at equilibrium) by reconstitution of the disulfide bond, and 4) the repetition of steps 1–3 with a second ring to access the [3]rotaxane. Amines and phosphines are also effective unlock-lock catalysts for this reaction sequence.

More recently, Takata[412] has extended his unlock-lock strategy to aromatic disulfide bonds instead of aliphatic ones, dramatically reducing the reaction time required to reach equilibrium at room temperature from weeks to hours, on account of a faster rate of aromatic disulfide cleavage by the thiol catalyst. Takata[413] has extended the disulfide-mediated approach to thermodynamically controlled MIM synthesis to the production of polymers.[414,415] Li[416] has also devised another 'magic ring' trick with the disulfide linkage in the familiar dibenzylammonium/crown ether recognition motif. In contrast with Takata's work, the disulfide linkage is labilized with a radical initiator and UV irradiation to obtain a [2]rotaxane.

3.5.1.2 Catenanes Obtained by Disulfide Exchange

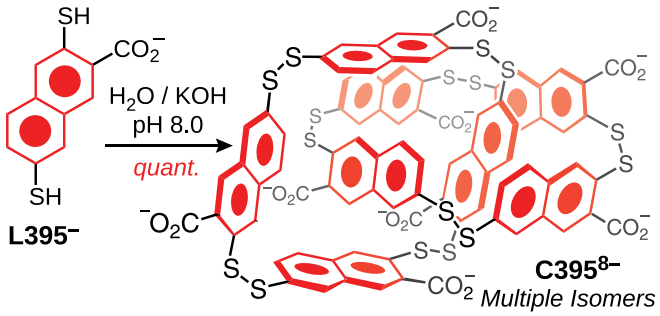
The thermodynamically controlled preparation (**Scheme 3.45**) of catenanes based on disulfide exchange mechanisms was introduced by Li[417] in 2006. The self-recognition of the acetyl thioester-teminated perylene diimide (PDI) monomer **L394**, with its large planar π-faces and tendency to self-stack above its critical aggregation concentration (CAC) of ~0.1 mM, provides a thermodynamic driving force for the catenation of PDI-based macrocyclic dimers. The self-templated homo[2]catenane **C394** is formed under basic deacetylation conditions (NaOMe/MeOH/CH_2Cl_2) in air as a result of oxidative thiol-thiol coupling and disulfide exchange reactions among the thiol-terminated polyether chains, which are generated *in situ*. The only other major product to accompany **C394** is the macrocyclic dimer **M394**. These two products are isolated in a combined yield of 75%, with a nearly equal distribution of **C394** (36%) and **M394** (39%) at a monomer concentration of 0.58 mM. A more diverse set of products has been observed at the higher monomer concentration of 2.58 mM as a result of the formation of multilayered aggregates. *Ab initio* calculations suggest that the neighboring PDI units in the catenane stack with a ~30° rotational offset.

One aspect of disulfide bonds that makes them popular tools for DCLs is the fact that disulfide exchange is easily accomplished in water at neutral pH in ambient air. Otto[418]



Scheme 3.45 Self-assembly of the PDI-based macrocyclic dimer **M394** and tetrameric homo[2]catenane **C394**, a process mediated by the coupling and exchange of thiols and disulfide bonds, respectively, under thermodynamic control.[417]

has described a DCL based on the water-soluble 3,7-dimercaptonaphthalene-2-carboxylate monomer **L395**$^-$, from which the octameric [2]catenane **C395**$^{8-}$ emerges (**Scheme 3.46**) quantitatively as a mixture of isomers. Many different constitutional isomers of **C395**$^{8-}$ are present in water at pH 8.0 on account of the many possible arrangements for the carboxylate groups, of which only one example is shown in **Scheme 3.46**. Although these isomers have not been separated, analytical HPLC analysis revealed that different isomers elute at different rates on a reversed-phase column. The unexpected assembly of this [2]catenane is driven by the hydrophobic effect, where each of the two tetrameric square-shaped macrocycles



Scheme 3.46 The quantitative self-assembly of the [2]catenane octamer **C395**$^{8-}$ in an aqueous DCL of 3,7-dimercaptonaphthalene-2-carboxylate (**L395**$^{-}$) monomers.[418]

possess hydrophobic interior cavities that host one of the naphthalene units. The hydrophobic driving force has been confirmed by re-equilibrating the DCL in the presence of a hydrophobic adamantyl ammonium guest, which de-catenates the assembly in favor of a tetrameric square which acts as a better host for adamantane. Otto and Li[419] have shown that the addition of a 1-adamantyl trimethylammonium template to the same DCL triggers the emergence of a non-interlocked, self-replicating tetramer that self-assembles into thin nanosheets. More recently, Otto[420] has reported on the catenation of disulfide-bridged azobenzenes and cyclodextrins in dynamic libraries.

Sanders has also developed a number of [2]catenanes (**Figure 3.36**) based on aqueous DCLs of cysteine-terminated π-donors and π-acceptors that form disulfide bonds, including compounds **C396**$^{8-}$,[421] **C397**$^{8-}$,[422] **C398a-b**$^{6-}$,[423] **C399**$^{8-}$,[424] **C3100**$^{8-}$,[425] **C3101**$^{8-}$,[422] **C3102**$^{8-}$,[422] **C3103**$^{8-}$.[423] The aqueous self-assembly of these catenanes typically involves the emergence of a mixture of cyclic oligomers and donor-acceptor [2]catenanes from a mixture of precursors derived from DNP or 2,6-dioxynaphthalene (26NP) π-donors and NDI-based π-acceptors

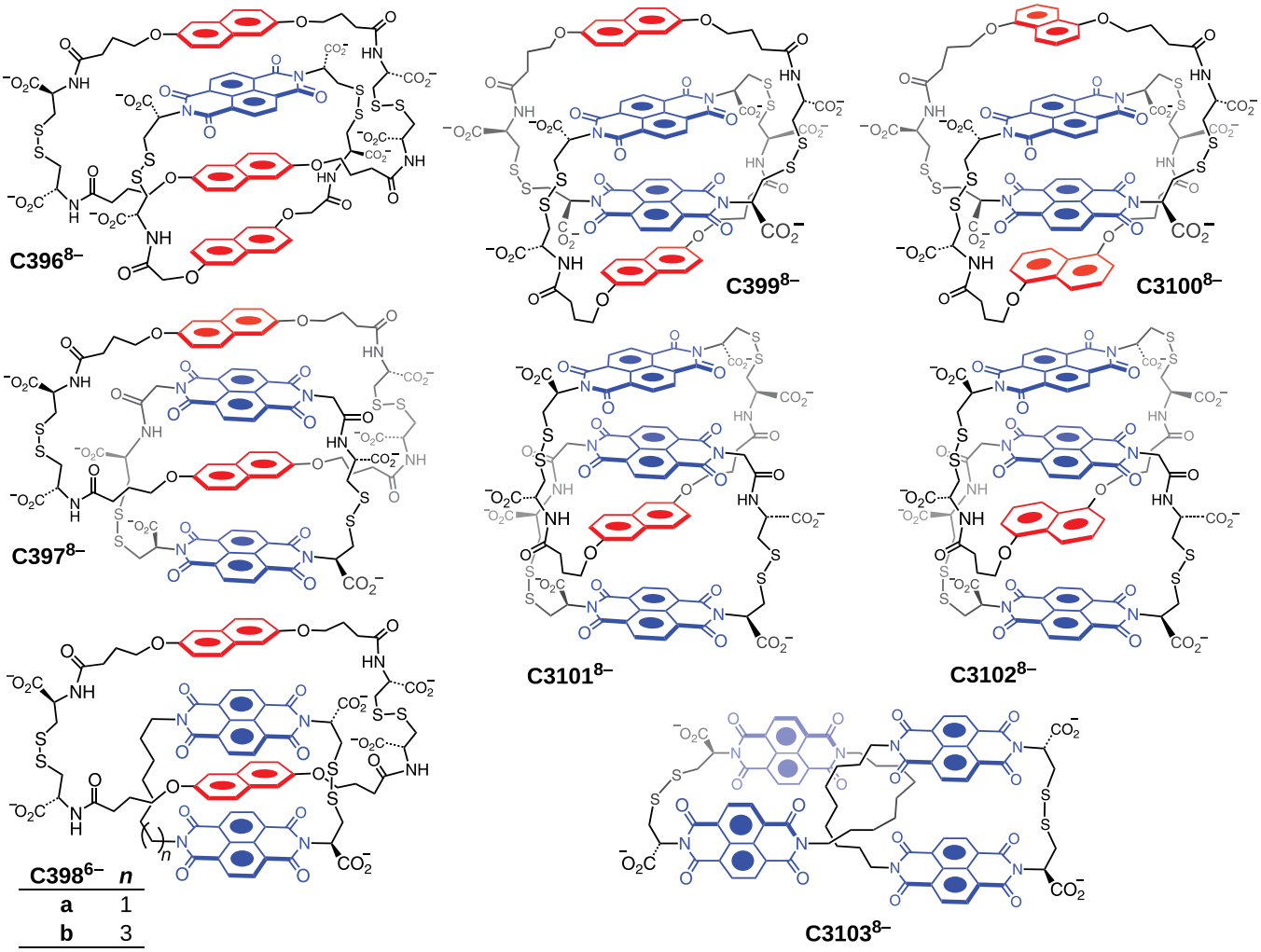
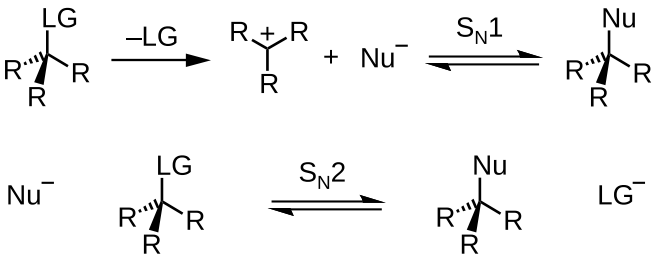


Figure 3.36 Stereoformulas of various self-assembled disulfide-based donor-acceptor catenanes prepared by Sanders: **C396**$^{8-}$,[421] **C397**$^{8-}$,[422] **C398a-b**$^{6-}$,[423] **C399**$^{8-}$,[424] **C3100**$^{8-}$,[425] **C3101**$^{8-}$,[422] **C3102**$^{8-}$,[422] **C3103**$^{8-}$.[423]

under oxidative coupling conditions around pH 8. The homo[2]catenanes, **C399**$^{8-}$ and **C3100**$^{8-}$, are unusual because each one of their rings possesses a combination of donors and acceptors—such rings are rarely catenated on account of their proclivity to self-associate as a result of intramolecular π-associated donor-acceptor charge transfer interactions. Intuitively, one would expect a catenane comprising four donor and acceptor monomers to arrange into a D-A-D-A stack, as in the cases of **C397**$^{8-}$ and **C398a-b**$^{6-}$. The favorability of the D-A-A-D stacking in the [2]catenanes **C399**$^{8-}$ and **C3100**$^{8-}$ is attributable to the observation[426,427] that the cavity of the macrocyclic $(NDI)_2$ homodimer is not large enough to be threaded by aromatic molecules. Hydrophobic interactions are also involved in the self-assembly of these catenanes, which is consistent with the stability of the hetero[2]catenanes **C396**$^{8-}$, **C3101**$^{8-}$, and **C3102**$^{8-}$, which exhibit unusual D-A-D-D, A-D-A-A, and A-D-A-A stacks, respectively, representing up to 50% of the population in DCLs containing unequal proportions of donors and acceptors. Furthermore, even in the absence of π-donating coupling partners, cysteine-functionalized NDI and bis(NDI) precursors can self-assemble into various entangled topologies in the DCL, including the A-A-A-A [2]catenane **C3103**$^{8-}$,[423] as well as a [3]catenane[428] and a nonameric trefoil knot,[429] a Solomon link,[430] and a figure-of-eight knot.[430] In a testament to the adaptability of these DCLs, the ratio of species can be changed by exposing the DCL to stimuli. For example, the interlocked species **C399**$^{8-}$ can be amplified[424] up to 6-fold by (i) introducing a positively charged donor template which stabilizes the internal NDI–NDI stack, (ii) adding salt in order to raise solvent polarity and thus augment the hydrophobic effect, or (iii) increasing the concentration of reactants. See **Section 6.13.4** for a discussion of this [2]catenane's unusual new type of co-conformational switching behavior. This body of work from the Cambridge group demonstrates that a wide range of supramolecular principles and noncovalent bonding interactions can be harnessed in DCC to select for a desired topological outcome. A similar motif involving $BIPY^{2+}$ acceptors instead of the NDI ones has been introduced recently by Stefankiewicz.[431] Mullen[432] has also employed thiol-terminated NDI and DNP units in various clipping protocols in order to obtain donor-acceptor rotaxanes and catenanes under thermodynamic control.

3.5.2 Reversible Nucleophilic Substitutions

Both S_N1 (**Section 3.5.2.1**) and S_N2 (**Section 3.5.2.2**) substitutions, in which a nucleophile (Nu^-) displaces a leaving group (LG) in a thermodynamically reversible regime, have been employed—albeit relatively rarely—in the synthesis of rotaxanes and catenanes.



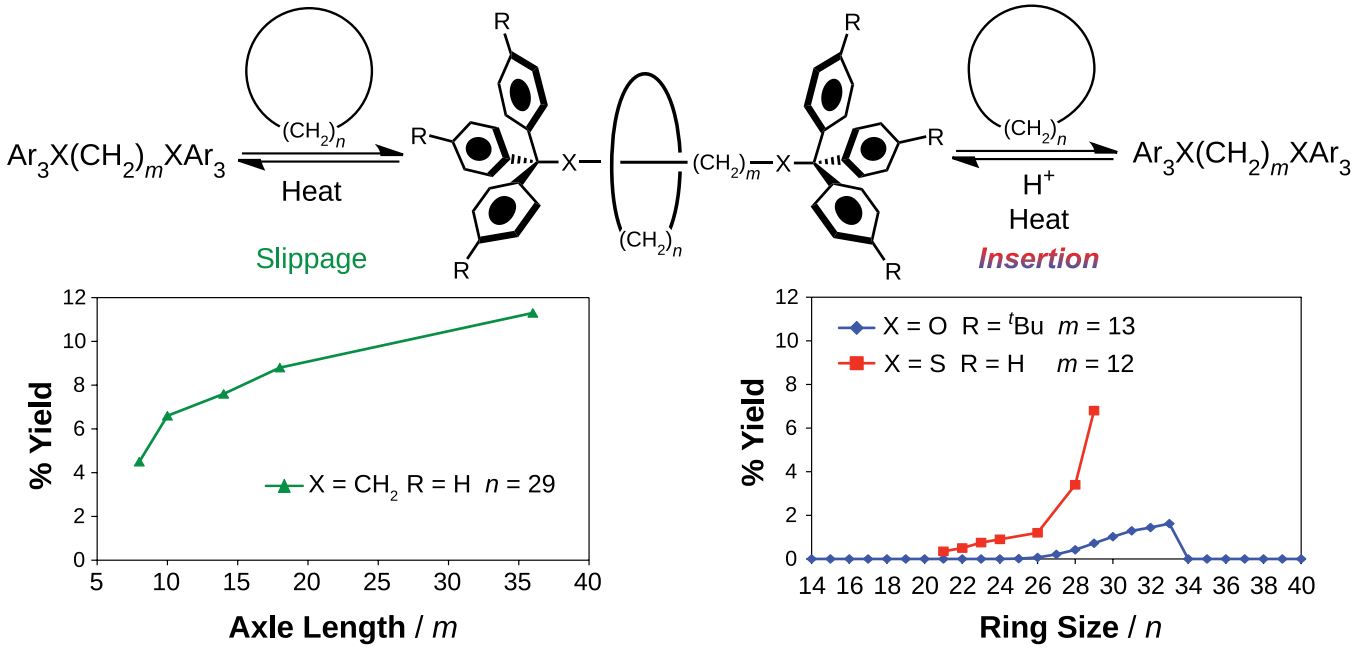


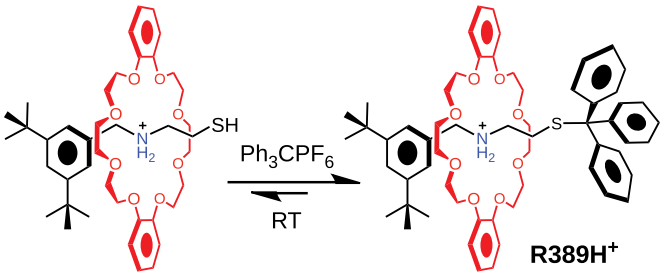
Figure 3.37 Summary of the statistical syntheses of rotaxanes by means of slippage and insertion strategies.[18–20]

3.5.2.1 Dynamic S_N1

Not only did Harrison forge the first path to slippage, as we discussed in **Section 3.1.1**, but in the same initial publication[18] he reported the first use of a reversible covalent bond in the synthesis (**Figure 3.37**) of MIMs—the trityl ether bond. Having already learned that fewer than 29 ring carbon atoms forbids slippage of a cycloalkane over the trityl stopper of a dumbbell even at 120 °C in a statistical synthesis, he found[19] that adding a catalytic amount of acid to the heated reaction mixture allows some smaller macrocycles (containing as few as 24 carbon atoms) to thread onto the dumbbell. Harrison postulated that the trityl ether bond is cleaved reversibly, presumably by an S_N1-type process, to realize this so-called 'insertion' event under thermodynamic control. He also added *tert*-butyl groups to the trityl stopper to allow even larger macrocycles to thread; as expected, the largest macrocycles had the highest-yielding rotaxanes. In a follow-up investigation many years later, Schill[20] reasoned that a more finely-tuned mixture of macrocycles should increase the rotaxane yield, since only a relatively small fraction of Harrison's 14–42-carbon cycloalkane mixture is properly sized for rotaxane incorporation, while the others are simply dilutants. Schill used only a seven-component mixture of cycloalkanes ranging from 21–29 carbon atoms and equilibrated it with a trityl thioether-stoppered dumbbell. He achieved significantly higher yields in general and also observed better rotaxanation efficiency for larger macrocycles. Schill also detected 21, 22, and 23-carbon cycloalkane rotaxanes that had not been observed by Harrison, probably because Harrisons's more polydisperse mixture results in a lower detection limit for these minor species. Both groups estimate their yields on the basis of gas chromatograms, in addition to conducting preparative-scale experiments. **Figure 3.37** presents a summary of their combined results for both slippage and insertion reactions. As noted in **Section 2.1**, these results definitively confirm that the yields of the rotaxanes increase with both increasing macrocycle size and thread length in a statistical regime.

Takata[433] revisited the trityl ether and thioether bonds in 2002, armed with the advantage of supramolecular templation. Using the dialkylammonium/crown motif, Takata stoppered ring-threaded half-dumbbells bearing thiol or hydroxyl functionalities with trityl hexafluorophosphate to generate (**Table 3.13**) the [2]rotaxane **R389H$^+$** in up to 98% (91% isolated) yield. The yield is sensitive to the solvents' ability to donate non-bonding electrons, a parameter known as the Gutmann donor number. The near-quantitative yields in Takata's tritylative end-capping reactions demonstrate the synthetic advantage that is created by employing reversible covalent chemistry in combination with supramolecular templation for the formation of mechanical bonds under thermodynamic control.

Table 3.13 The solvent dependence of yield in the formation of the [2]rotaxane **R389H$^+$** by tritylative stoppering.[433]

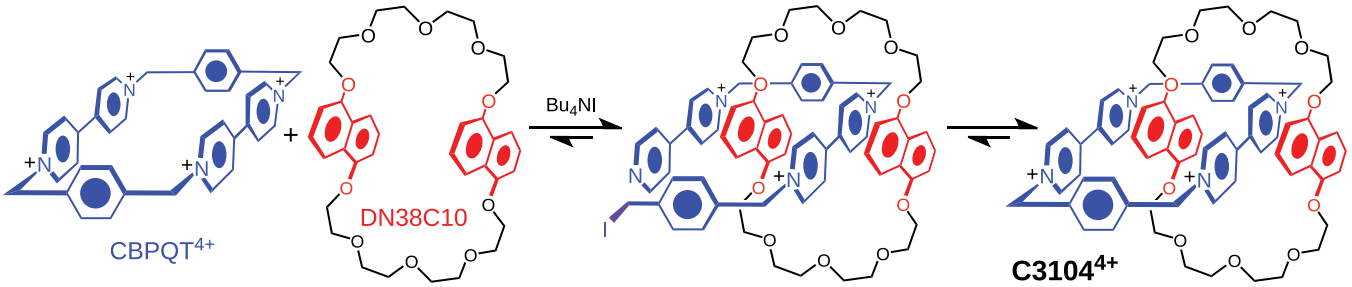


Solvent	D_N [a]	Yield/%
PhMe	0.1	80
CH_2Cl_2	1.0	93 (91)
CH_3NO_2	2.7	98
$CHCl_3$	4.0	88
CH_3CN	14.1	82 (77)
1,4-Dioxane	14.8	89

[a] A solvent's Guttman donor number reflects its ability to donate non-bonding electrons.

3.5.2.2 Dynamic S_N2

The S_N2 reaction is traditionally used as a kinetic approach because it is irreversible, unless the product of the S_N2 reaction is itself susceptible to nucleophilic attack, as in the Finkelstein reaction,[434] for example. Such is the case for the tetracationic cyclophane CBPQT^{4+}, whose strained methylene bonds compromise its stability under basic conditions. A nucleophile will readily attack any of the four methylene carbon atoms to 'open the box' and release the ring strain. Since the methylene sites in CBPQT^{4+} can be resubjected to substitution chemistry, it was reasoned that a suitably mild nucleophile that can also act as a leaving group could be used to make the S_N2 chemistry of CBPQT^{4+} at least semi-dynamic. A double S_N2-mediated equilibration in which a ring-closing S_N2 reaction competes with a different ring-opening one to open and close the box dynamically in the presence of a template was envisioned. As luck would have it, iodide ions serve[435] this purpose very well. On mixing the DN38C10 crown ether with CBPQT^{4+} and Bu_4NI (a source of I^-) in CD_3CN and heating for a few days in an NMR tube, the gradual conversion (**Scheme 3.47**) of the mixture to the corresponding [2]catenane **C3104^{4+}** appears to be quantitative by ^{1}H NMR spectroscopy. Isolated yields are lower than unity, however, most likely because of oligomerization and precipitation of bipyridinium side-products derived from the opened-up CBPQT^{4+} rings. Later, it was discovered[436] that quantitative yields can be achieved when this dynamic S_N2 chemistry is carried out on a polymer sidechain, where cooperative interactions from neighboring cyclophanes apparently avert the buildup of side-products. This dynamic S_N2 chemistry can be readily extended[437] to other catenated systems based on CBPQT^{4+}, although rotaxanes have not so far been generated efficiently using the same protocol.

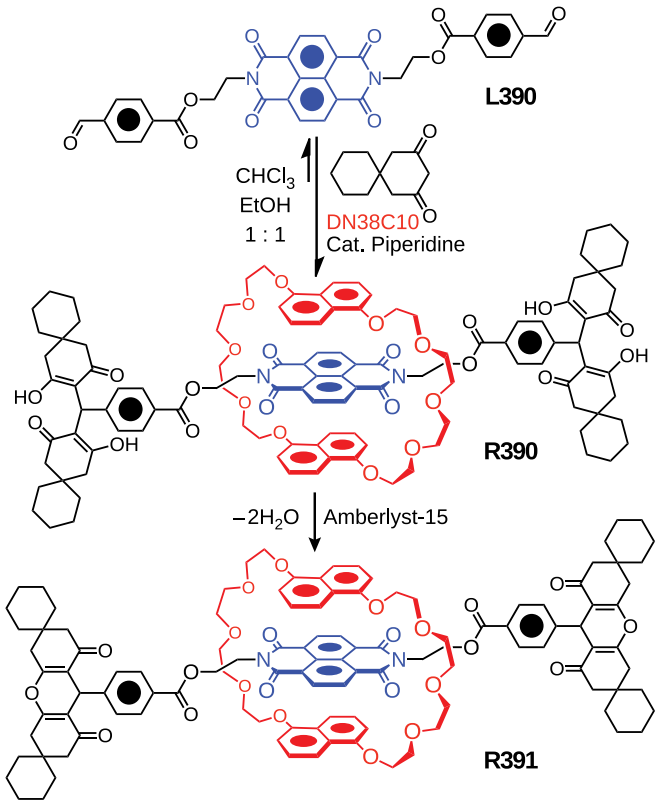


Scheme 3.47 The self-assembly of the donor-acceptor [2]catenane **C3104**$^{4+}$ under thermodynamic control by virtue of a dynamic double-S_N2 process mediated by iodide ions.[435]

3.5.3 Michael Additions

The Michael addition is a thermodynamically controlled conjugate addition[438] between activated methylene reaction donors (resonance-stabilized carbanions) and activated double bonds. Thermodynamic control becomes possible under conditions where the retro-Michael addition is also allowed to take place.

Hamilton[439] has invented a molecular "locking mechanism" (**Scheme 3.48**) enabled by the reversible base-catalyzed double-addition of 1,3-spirodiketones to benzaldehyde. The dynamic [2]rotaxane **R390** self-assembles in 1:1 $CHCl_3$/EtOH from a mixture of the NDI-based dialdehyde thread **L390**, an activated 1,3-spirodiketone, and the π-donating macrocycle DN38C10, in the presence of a catalytic amount of piperidine. At 10 mM reactant concentrations, **R390** represents about 60% of the molecular population. This [2]rotaxane is stable under neutral conditions, allowing for its isolation as a pure compound by column chromatography in 52% yield. The locking mechanism can be initiated by the addition of acid, which promotes the intramolecular dehydrative condensation of the stopper adducts. Thus, the addition of Amberlyst-15 to a solution of **R390** catalyzes the irreversible formation of the corresponding [2]rotaxane **R391** in near-quantitative yield.



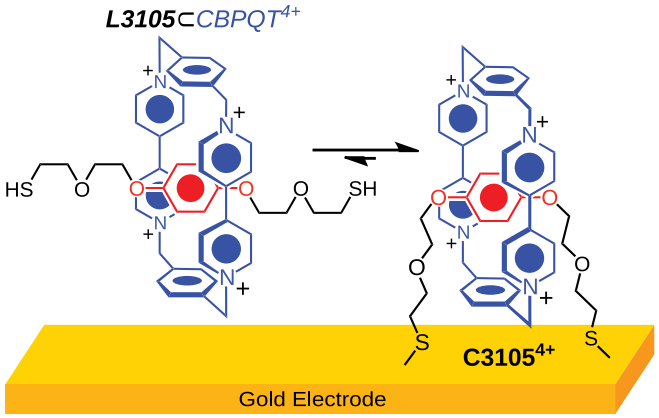
Scheme 3.48 The reversible double-addition of a 1,3-spirodiketone to the benzaldehyde termini of NDI derivative **L390**, in the presence of DN38C10 and piperidine, leads to the formation of Hamilton's [2]rotaxane **R390**, which can be converted irreversibly to the kinetically locked [2]rotaxane **R391** by intramolecular condensation of the stopper adducts.[439]

Leigh[440] has incorporated a Michael addition into his active template approach to MIM synthesis—see **Scheme 2.136** in **Section 2.4.3.1**. His near-quantitative rotaxane synthesis involves the coordination of an α-cyanoester to a Pd^{II} ion positioned within the cavity of a macrocycle, promoting a double Michael addition to two vinyl ketone half-dumbbells almost exclusively through the aperture of the macrocycle.

3.6 Surface-Mounted MIMs

In addition to the reversible mechanical bond-forming reactions that occur in solution (**Sections 3.1–3.5**), reversible surface bonds at interfaces, such as the gold-thiolate bonds underpinning the formation of self-assembled monlayers (SAMs), can be employed in the thermodynamically controlled synthesis of MIMs. While there are many examples[441–443] of mechanomolecules immobilized on gold and other surfaces, more often than not their mechanical bonds are either sealed prior to deposition, or by kinetically controlled reactions at the interface. In this Section, we review systems in which molecular mechanical bonds are formed concomitantly with surface attachment. A number of mechanomolecules that have been positioned at interfaces under kinetic control are described in **Sections 6.14.1** and **6.15.1**.

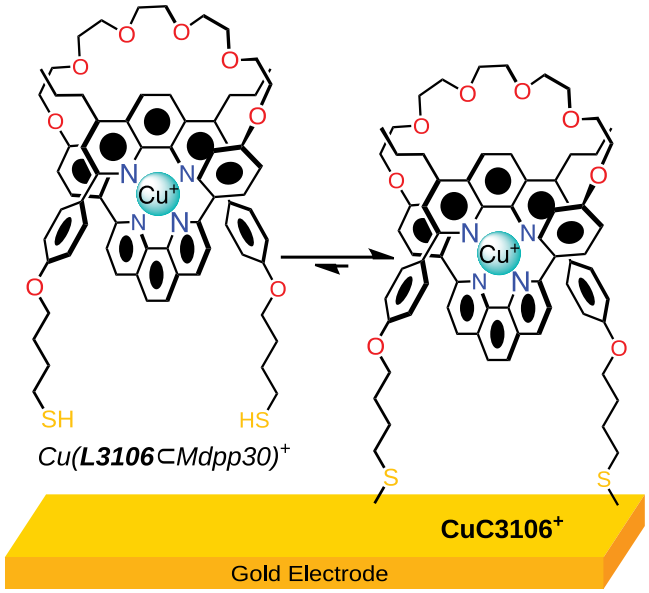
The idea of assembling surface-mounted mechanomolecules was introduced by Gokel and Kaifer[444] in 1993, when



Scheme 3.49 The self-assembly of a [2]catenane mounted on a gold electrode's surface, as claimed by Kaifer.[444]

they claimed[c] to observe the formation (**Scheme 3.49**) of a monolayer of [2]catenanes (**C3105^{4+}**) on gold surfaces from the thiol-terminated, HQ-threaded pseudorotaxane ***L3105*** $\subset$ *CBPQT*$^{4+}$. The presence of the BIPY^{2+} units of the mechanically bonded CBPQT^{4+} ring were detected on the electrode by cyclic voltammetry after treatment with a solution of ***L3105*** $\subset$ *CBPQT*$^{4+}$ (K_a = 253 M^{-1} at 25 °C) containing a 6-fold molar excess of CBPQT^{4+}. Donor-acceptor rotaxanes based on CBPQT^{4+} have also been assembled under thermodynamic control on gold electrodes by Willner[447–449]—see **Section 6.14.1.2**.

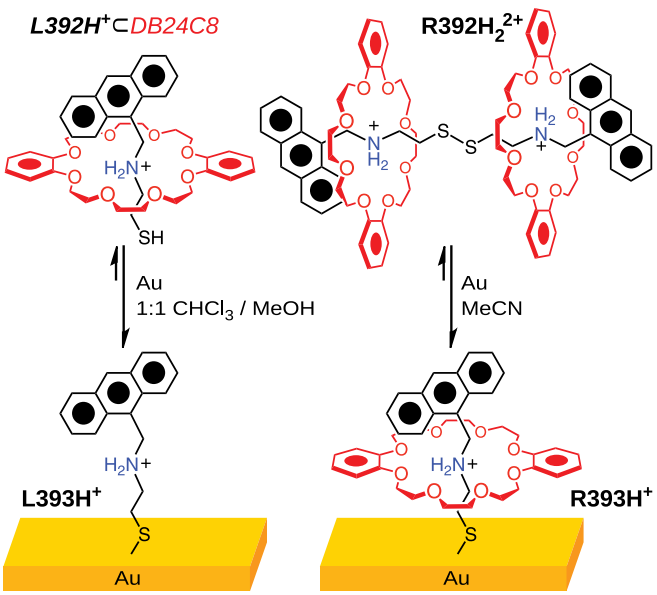
Sauvage[450–453] has assembled a number of Cu^{I}-template mechanomolecules on the surfaces of gold electrodes. In his seminal example[450] (**Scheme 3.50**), a solution of the thiol-terminated axle of the metallo-pseudorotaxane *Cu(**L3106** $\subset$ Mdpp30)*$^{+}$ is employed to deposit a SAM of the [2]catenane **CuC3106^{+}** on the surface of a gold electrode. The redox activity of the metallic cores can be detected readily by electrochemical means. Sauvage's other surface-mounted mechanomolecules have been



Scheme 3.50 Assembly of a surface-mounted [2]catenate by Sauvage.[450]

adsorbed[451–453] on gold surfaces by allowing solutions of disulfide-containing metallo-catenanes and rotaxanes to equilibrate in the presence of a gold surface, in a manner reminiscent of the disulfide exchange (**Section 3.5.1**) reaction. Waterland and Telfer[454] have employed entwined Cu(dpp)$_2^{+}$ templates as cross-linkers for gold nanoparticles (AuNPs), such that nanoparticle-bridging catenanes are formed as the thiolates chemisorb to the AuNP surfaces.

Vance[455] has also employed disulfide-bridged rotaxanes to deposit (**Scheme 3.51**) rotaxane monolayers under thermodynamic control, relying instead on the dialkylammonium/crown ether recognition motif to template the formation of mechanical bonds. The surface-anchored [2]rotaxane



Scheme 3.51 Unsuccessful (left) and successful (right) depositions of dialkylammonium/crown rotaxanes on gold by Vance.[455]

[c] Since the successful formation of the [2]catenane was inferred only by electrochemical means, the possibility of a pseudorotaxane assembly cannot be ruled out. In support of this counterargument, one could point out that only a single reduction wave was recorded in the CV of **C3105^{4+}**. The observation of a second redox wave would have provided stronger evidence for a mechanical bond, since the diradical dication CBPQT$^{2(\bullet+)}$ can dissociate from the pseudorotaxane, but not the catenane. More significantly, the electrode, which was prepared in MeCN, was rinsed and probed in aqueous solutions, yet the MeCN-soluble PF_6^- salt of CBPQT^{4+} is all but insoluble in water, which could have prevented it from deslipping even from a pseudorotaxane mounted on the surface. In a control electrode coated with a thread possessing only one thiol-terminated oligoether chain extending from its HQ unit, no CBPQT^{4+} reduction was detected, yet subsequent research by Kaifer[445,446] indicates that this thread would have had a far lower affinity for CBPQT^{4+}—low enough, perhaps, to compromise the successful formation of a pseudorotaxane monolayer. More control CV experiments or another line of evidence would be needed for more definitive proof of this catenane's successful self-assembly at the interface.

R393H^{+} is obtained only when deposited from the disulfide-bridged [3]rotaxane **R392H**$_2^{2+}$, whereas the corresponding thiol-terminated semirotaxane ***L392H***$^{+}$$\subset$*DB24C8* produces monolayers of only the dumbbell, **L393H**$^{+}$. X-ray absorption spectroscopy (XAS) and X-ray photoemission spectroscopy were employed to characterize the monolayers and confirm their compositions unambiguously.

Davis and Beer[456–459] have adapted a number of the interpenetrated anion-binding motifs to enable the assembly (**Figure 3.38**) of mechanomolecules on gold. The [2]rotaxanes **R394·Cl** and **R395·SO**$_4$, which employ [N–H···Anion] templates (**Section 2.3.6.2**), are self-assembled on gold surfaces from semirotaxanes displaying dithiolane anchoring groups derived from lipoic acid. The surface [2]catenane **C3107·Cl** is assembled from the corresponding bis-thiolated pseudorotaxane, in a similar manner as **C3105**$^{4+}$ and **CuC3106**$^{+}$—see **Schemes 3.49** and **3.50**, respectively. The co-consitutions of **C3107·Cl** and **R394·Cl** contain ferrocene groups as probes for electrochemical detection. Upon template removal, gold electrodes coated with monolayers of **R394**$^{+}$ serve as electrochemical anion sensors, which are sensitive to Cl^- and $H_2PO_4^-$ at micromolar concentrations. In

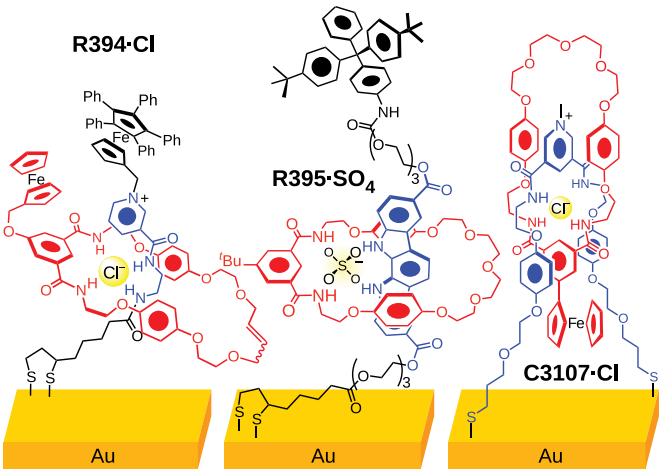


Figure 3.38 Stereoformulas of some of Beer's self-assembled surface-mounted rotaxanes.[454–456]

the case of **R395·SO**$_4$, the deposition of the rotaxane was confirmed by detecting the release of the macrocycle into solution by mass spectroscopy upon electrochemical stripping of the indolocarbazole-based axle from the surface at high reductive potential. Monolayers of this rotaxane, which can also be assembled by F^- templation, were also characterized by SPR and FTIR surface spectroscopic techniques.

Arduini[460] has assembled (**Figure 3.39**) a monolayer of the [2]rotaxanes **R396**$^{2+}$, based on the CA6 host and viologen guests, employing for the first time Cu instead of Au as the substrate. The films were assembled by immersion of polycrystalline Cu into a CH_2Cl_2 solution of the corresponding thiol-terminated *BIPY*$^{2+}$$\subset$*CA6* semirotaxane. The CA6 ring was detected in the monolayer by XPS measurements, confirming the formation of mechanical bonds at the surface. The breaking of Cu–S bonds at an applied potential of –1.7 V

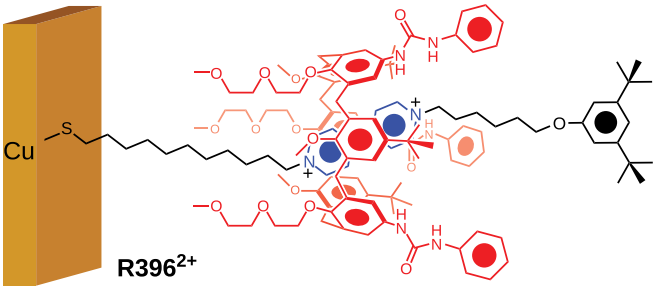
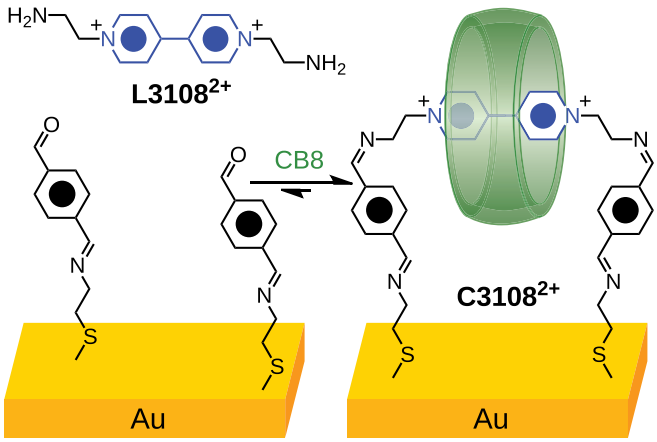


Figure 3.39 Arduini's CA6 [2]rotaxane monolayer.[460]

induced the release of the rotaxanes from the surface, in a process that could also be monitored by XPS.

Scherman[461] has employed dynamic imine bonds (**Section 3.3.1**) in the surface mounting (**Scheme 3.52**) of catenanes possessing viologen recognition units and cucurbit[8]uril (CB8) rings. The pseudorotaxane of CB8 and 2-aminoethyl viologen (**L3108**$^{2+}$) is deposited on the surface by dehydrative coupling of its amine termini with surface-bound benzaldehyde units, affording the surface [2]catenane **C3108**$^{2+}$ at a density of almost 5×10^{13} molecules per cm^2. The cavity of the *BIPY*$^{2+}$$\subset$*CB8* complex is large enough to accommodate a second guest, especially electron-rich guests that can engage the BIPY^{2+} unit in π-associated donor-acceptor interactions. Thus, the successful immobilization **C3108**$^{2+}$ was confirmed by direct imaging of its heteroternary complexes involving azobenzene-coated SiO_2 colloids and fluorescein-labeled dopamine by optical and fluorescence microscopy, respectively, as well as contact angle measurements. The films allow sensing of dopamine at concentrations as low as 50 nM, showing that self-assembled mechanomolecules on surfaces have promise for sensing applications.

Willner[462] has employed AuNPs to stopper the axles of DNA pseudorotaxanes, affording DNA/nanoparticle hybrid rotaxanes that can be imaged directly (**Figure 3.40**) by TEM on account of the contrast provided by the AuNPs. The mechanical bond of these rotaxanes has been



Scheme 3.52 The self-assembly of Scherman's CB8 rotaxane monolayers by dynamic imine bonding to a SAM of benzaldehydes.[461]

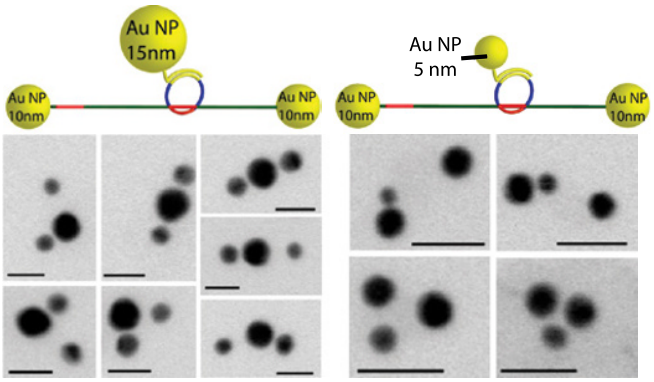


Figure 3.40 Graphical representations and TEM images of Willner's [2]rotaxanes comprising DNA axles, AuNP stoppers, and AuNP-labeled DNA macrorings. All scale bars are 20 nm. Images reproduced with permission from ref. 462 (copyright 2013 American Chemical Society)

confirmed by conjugating AuNPs of different sizes to the rings of the rotaxanes by hybridization of complimentary DNA strands displayed by the AuNPs. See **Section 2.3.12.1** for a more detailed discussion of DNA-based mechanical bonds.

Conclusions and Outlook

The MIMs that have been highlighted in this Chapter illuminate the diverse strategies, recognition chemistry, and reversible bonding motifs that have been invoked in order to create mechanical bonds. The synthesis of rotaxanes by slippage (**Section 3.1**) is unique among these approaches because it does not involve the making and breaking of any chemical bonds. Slippage occupies the grey area that lies in between the fuzzy domains of fully dissociated components and permanently interlocked ones. Slippage has helped us realize that the existence of a mechanical bond, at least when it comes to (pseudo)rotaxanes, is a matter of context. Since the components of a rotaxane do not share a topological link, deslipping is a possible outcome, in principle, for any rotaxane. It may be important in many applications to know under which conditions a rotaxane is kinetically stable and under which conditions it is kinetically labile. Much of the groundwork has been laid in the more common recognition systems to allow chemists to tune the kinetic barriers to slippage in order to meet their specific needs. One outstanding problem is that the size complementarity between rings and stoppers has often been determined empirically, which is a costly hit-or-miss process. The challenge now on the table is for computational and theoretical chemists to develop reliable, efficient ways of examining slippage systems *in silico* in order to save time and resources. This challenge is particularly important because slippage and deslipping processes, associated intimately as they are with the thermodynamic landscape of a MIM, are crucial factors in the successful operation of artificial molecular machines—see **Section 6.15**—which represent one of the next frontiers in mechanostereochemistry.

Reversible covalent bonds (**Sections 3.2–3.6**) have also enriched the field of mechanostereochemistry by allowing MIMs to be synthesized in up to near-quantitative yields from relatively simple and even commercially available building blocks. The design motifs have relied heavily thus far on olefin metathesis, kinetically labile metal-ligand bonds, and the making and breaking of imines and disulfides. We would be justified in believing that many more opportunities for introducing new types of dynamic reactions for high-yielding MIM syntheses are probably still on the horizon. One example is the reversible formation of acetals—another type of dynamic condensation which has been employed in the assembly[463] of pseudorotaxanes. More importantly, the efficiency with which MIMs can now be made, thanks to these dynamic reactions, allows researchers more time to focus on new challenges associated with (i) building ever more sophisticated architectures (**Chapter 4**), (ii) controlling and understanding the chirality and dynamics of molecular objects with mechanical bonds (**Chapter 5**), and (iii) designing and operating molecular switches and machines (**Chapter 6**). Thermodynamically controlled reactions are like the steel support beams that strengthen the concrete used in the construction of skyscrapers—they provide the support that is absolutely vital for making progress on the long journey upwards.

References

(1) Philp, D.; Stoddart, J. F. Self-Assembly in Natural and Unnatural Systems. *Angew. Chem., Int. Ed. Engl*. **1996**, *35*, 1155–1196.
(2) Lehn, J.-M. Dynamic Combinatorial Chemistry and Virtual Combinatorial Libraries. *Chem. Eur. J.* **1999**, *5*, 2455–2463.
(3) Lehn, J.-M; Eliseev, A. V. Dynamic Combinatorial Chemistry. *Science* **2001**, *291*, 2331–2332.
(4) Rowan, S. J.; Cantrill, S. J.; Cousins, G. R. L.; Sanders, J. K. M.; Stoddart, J. F. Dynamic Covalent Chemistry. *Angew. Chem., Int. Ed*. **2002**, *41*, 899–952.
(5) Corbett, P. T.; Leclaire, J.; Vial, L.; West, K. R.; Wietor, J.-L.; Sanders, J. K. M.; Otto, S. Dynamic Combinatorial Chemistry. *Chem. Rev*. **2006**, *106*, 3652–3711.
(6) Ludlow, R. F.; Otto, S. Systems Chemistry. *Chem*. *Soc. Rev*. **2008**, *37*, 101-108.
(7) Otto, S. Dynamic Molecular Networks: From Synthetic Receptors to Self-Replicators. *Acc. Chem. Res.* **2012**, *45*, 2200–2210.
(8) Cougnon, F. B. L.; Sanders, J. K. M. Evolution of Dynamic Combinatorial Chemistry. *Acc. Chem. Res.* **2012**, *45*, 2211–2221.
(9) Greig, L. M.; Philp, D. Applying Biological Principles to the Assembly and Selection of Synthetic Superstructures. *Chem. Soc. Rev.* **2001**, *30*, 287–302.
(10) Raehm, L.; Hamilton, D. G.; Sanders, J. K. M. From Kinetic to Thermodynamic Assembly of Catenanes: Error Checking, Supramolecular Protection and Oligocatenanes. *Synlett* **2002**, 1743–1761.
(11) Aricó, F.; Badjić, J. D.; Cantrill, S. J.; Flood, A. H.; Leung, K. C.-F.; Liu, Y.; Stoddart, J. F. Templated Synthesis of Interlocked Molecules. *Top. Curr. Chem.* **2005**, *249*, 203–259.
(12) Haussmann, P. C.; Stoddart, J. F. Synthesizing Interlocked Molecules Dynamically. *Chem. Rec*. **2009**, *9*, 136–154.
(13) Avestro, A.-J.; Belowich, M. E.; Stoddart, J. F. Cooperative Self-Assembly: Producing Synthetic Polymers with Precise and Concise Primary Structures. *Chem. Soc. Rev.* **2012**, *41*, 5881–5895.

(14) Harada, A.; Hashidzume, A.; Yamaguchi, H.; Takashima, Y. Polymeric Rotaxanes. *Chem. Rev*. **2009**, *109*, 5974–6023.

(15) Fang, L.; Olson, M. A.; Benítez, D.; Tkatchouk, E.; Goddard, W. A., III; Stoddart, J. F. Mechanically Bonded Macromolecules. *Chem. Soc. Rev.* **2010**, *39*, 17–29.

(16) Raymo, F. M.; Stoddart, J. F. Slippage-a Simple and Efficient Way to Self-Assemble [*n*]Rotaxanes. *Pure Appl. Chem.* **1997**, *69*, 1987–1997.

(17) Ashton, P. R.; Bělohradský, M.; Philp, D.; Stoddart, J. F. Slippage—An Alternative Method for Assembling [2]Rotaxanes. *J. Chem. Soc., Chem. Commun.* **1993**, 1269–1274.

(18) Harrison, I. T. The Effect of Ring Size on Threading Reactions of Macrocycles. *J. Chem. Soc., Chem. Commun.* **1972**, 231–232.

(19) Harrison, I. T. Preparation of Rotaxanes by the Statistical Method. *J. Chem. Soc., Perkin Trans*. *1*, **1974**, 301–304.

(20) Schill, G.; Beckmann, W.; Schweickert, N.; Fritz, H. Untersuchungen zur statistischen Synthese von Rotaxanen. *Chem. Ber.* **1986**, *119*, 2647–2655.

(21) Ashton, P. R.; Baxter, I.; Fyfe, M. C. T.; Raymo, F. M.; Spencer, N.; Stoddart, J. F.; White, A. J. P.; Williams, D. J. Rotaxane or Pseudorotaxane? That Is the Question! *J. Am. Chem. Soc.* **1998**, *120*, 2297–2307.

(22) *Fuzzy Logic in Chemistry*; Rouvray, D. H., Ed.; Academic Press: Waltham, Massachusettes, **1997**.

(23) Asakawa, M.; Ashton, P. R.; Ballardini, R.; Balzani, V.; Bělohradský, M.; Gandolfi, M. T.; Kocian, O.; Prodi, L.; Raymo, F. M.; Stoddart, J. F.; Venturi, M. Molecular Meccano 12. The Slipping Approach to Self-Assembling [*n*]Rotaxanes. *J. Am. Chem. Soc*. **1997**, *119*, 302–310.

(24) Raymo, F. M.; Houk, K. N.; Stoddart, J. F. Molecular Meccano 40. The Mechanism of the Slippage Approach to Rotaxanes. Origin of the “All-or-Nothing” Substituent Effect. *J. Am. Chem. Soc*. **1998**, *120*, 9318–9322.

(25) Ashton, P. R.; Bělohradský, M.; Philp, D.; Spencer, N.; Stoddart, J. F. The Self Assembly of [2]- and [3]-Rotaxanes by Slippage. *J. Chem. Soc., Chem. Commun.* **1993**, 1274–1277.

(26) Amabilino, D. B.; Ashton, P. R.; Bělohradský, M.; Raymo, F. M.; Stoddart, J. F. The Controlled Self-Assembly of a [3]Rotaxane Incorporating Three Constitutionally Different Components. *J. Chem. Soc., Chem. Commun.* **1995**, 747–750.

(27) Amabilino, D. B.; Ashton, P. R.; Bělohradský, M.; Raymo, F. M.; Stoddart, J. F. The Self-Assembly of Branched [*n*]Rotaxanes—The First Step Towards Dendritic Rotaxanes. *J. Chem. Soc., Chem. Commun.* **1995**, 751–754.

(28) Amabilino, D. B.; Asakawa, M.; Ashton, P. R.; Ballardini, R.; Balzani, V.; Bělohradský, M.; Credi, A.; Higuchi, M.; Raymo, F. M.; Shimizu, T.; Stoddart, J. F.; Venturi, M.; Yase, K. Molecular Meccano 36. Aggregation of Self-Assembling Branched [*n*]Rotaxanes. *New J. Chem*. **1998**, *22*, 959–972.

(29) Elizarov, A. M.; Chang, T.; Chiu, S.-H.; Stoddart, J. F. Self-Assembly of Dendrimers by Slippage. *Org. Lett.* **2002**, *4*, 3565–3568.

(30) Ashton, P. R.; Ballardini, R.; Balzani, V.; Credi, A.; Dress, K. R.; Ishow, E.; Kleverlaan, C. J.; Kocian, O.; Preece, J. A.; Spencer, N.; Stoddart, J. F.; Venturi, M.; Wenger, S. Molecular Meccano 61. A Photochemically Driven Molecular-Level Abacus. *Chem. Eur. J.* **2000**, *6*, 3558–3574.

(31) Balzani, V.; Clemente-León, M.; Credi, A.; Ferrer, B.; Venturi, M.; Flood, A. H.; Stoddart, J. F. Autonomous Artificial Nanomotor Powered by Sunlight. *Proc. Natl. Acad. Sci. U.S.A.* **2006**, *103*, 1178–1183.

(32) Vignon, S. A.; Jarrosson, T.; Iijima, T.; Tseng, H.-R.; Sanders, J. K. M.; Stoddart, J. F. Switchable Neutral Bistable Rotaxanes. *J. Am. Chem. Soc.* **2004**, *126*, 9884–9885.

(33) Iijima, T.; Vignon, S. A.; Tseng, H.-R.; Jarrosson, T.; Sanders, J. K. M.; Marchioni, F.; Venturi, M.; Apostoli, E.; Balzani, V.; Stoddart, J. F. Controllable Donor-Acceptor Neutral [2]Rotaxanes. *Chem. Eur. J.* **2004**, *10*, 6375–6392.

(34) Slater, B. J.; Davies, E. S.; Argent, S. P.; Nowell, H.; Lewis, W.; Blake, A. J.; Champness, N. R. A Perylene Diimide Rotaxane: Synthesis, Structure and Electrochemically Driven De-Threading. *Chem. Eur. J.* **2011**, *17*, 14746–14751.

(35) Mason, P. E.; Bryant, W. S.; Gibson, H. W. Threading/Dethreading Exchange Rates as Structural Probes in Polypseudorotaxanes. *Macromolecules* **1999**, *32*, 1559–1569.

(36) Asakawa, M.; Ashton, P. R.; Iqbal, S.; Stoddart, J. F.; Tinker, N. D.; White, A. J. P.; Williams, D. J. The Self-Assembly of Some Novel [2]Rotaxanes and Their Alkali Metal Cation Complexation. *Chem. Commun.* **1996**, 483–486.

(37) Ashton, P. R.; Iqbal, S.; Stoddart, J. F.; Tinker, N. D. The Self-Assembly and Metal-Mediated Disassembly of a Multi-Topic [2]Pseudorotaxane. *Chem. Commun.* **1996**, 479–481.

(38) Ashton, P. R.; Everitt, S. R. L.; Gómez-López, M.; Jayaraman, N.; Stoddart, J. F. Self-Assembly of a Water-Soluble [2]Rotaxane with Carbohydrate Stoppers. *Tetrahedron Lett.* **1997**, *38*, 5691–5694.

(39) Jeppesen, J. O.; Becher, J.; Stoddart, J. F. Poised on the Brink Between a Bistable Complex and a Compound. *Org. Lett.* **2002**, *4*, 557–560.

(40) Jeppesen, J. O.; Vignon, S. A.; Stoddart, J. F. In the Twilight Zone Between [2]Pseudorotaxanes and [2]Rotaxanes. *Chem. Eur. J.* **2003**, *9*, 4611–4625.

(41) Zhang, K.-D.; Zhao, X.; Wang, G.-T.; Liu, Y.; Zhang, Y.; Lu, H.-J.; Jiang, X.-K.; Li, Z.-T. Foldamer-Tuned Switching Kinetics and Metastability of [2]Rotaxanes. *Angew. Chem., Int. Ed*. **2011**, *50*, 9866–9870.

(42) Zhang, K.-D.; Zhao, X.; Wang, G.-T.; Liu, Y.; Zhang, Y.; Lu, H.-J.; Jiang, X.-K.; Li, Z.-T. Foldamers in Pseudo[2]Rotaxanes and [2]Rotaxanes: Tuning the Switching Kinetics and Metastability. *Tetrahedron* **2012**, *68*, 4517–4527.

(43) Han, T.; Chen, C.-F. Efficient Potassium-Ion-Templated Synthesis and Controlled Destruction of [2]Rotaxanes Based on Cascade Complexes. *J. Org. Chem.* **2008**, *73*, 7735–7742.

(44) Tokunaga, Y.; Wakamatsu, N.; Ohbayashi, A.; Akasaka, K.; Saeki, S.; Hisada, K.; Goda, T.; Shimomura, Y. The Effect of Pressure on Pseudorotaxane Formation by Using the Slipping Method. *Tetrahedron Lett.* **2006**, *47*, 2679–2682.

(45) Baroncini, M.; Silvi, S.; Venturi, M.; Credi, A. Photoactivated Directionally Controlled Transit of a Non-Symmetric Molecular Axle Through a Macrocycle. *Angew. Chem., Int. Ed*. **2012**, *51*, 4223–4226.

(46) Bolla, M. A.; Tiburcio, J.; Loeb, S. J. Characterization of a Slippage Stopper for the 1,2-Bis(pyridinium)ethane-[24]crown-8 Ether [2]Pseudorotaxane Motif. *Tetrahedron* **2008**, *64*, 8423–8427.

(47) Chiu, S.-H.; Rowan, S. J.; Cantrill, S. J.; Glink, P. T.; Garrell, R. L.; Stoddart, J. F. A Rotaxane-Like Complex with Controlled-Release Characteristics. *Org. Lett.* **2000**, *2*, 3631–3634.

(48) Loeb, S. J.; Wisner, J. A. 1,2-Bis(4,4′-dipyridinium)ethane: A Versatile Dication for the Formation of [2]Rotaxanes with Dibenzo-24-Crown-8 Ether. *Chem. Commun.* **1998**, 2757–2758.

(49) Rowan, S. J.; Cantrill, S. J.; Stoddart, J. F. Triphenylphosphonium-Stoppered [2]Rotaxanes. *Org. Lett.* **1999**, *1*, 129–132.

(50) Rowan, S. J.; Stoddart, J. F. Precision Molecular Grafting: Exchanging Surrogate Stoppers in [2]Rotaxanes. *J. Am. Chem. Soc.* **2000**, *122*, 164–165.

(51) Loeb, S. J.; Wisner, J. A. [3]Rotaxanes Employing Multiple 1,2-Bis(pyridinium) Ethane Binding Sites and Dibenzo-24-Crown-8 Ethers. *Chem. Commun.* **2000**, 845–846.

(52) Loeb, S. J.; Wisner, J. A. [2]Rotaxane Molecular Shuttles Employing 1,2-Bis(pyridinium)ethane Binding Sites and Dibenzo-24-Crown-8 Ethers. *Chem. Commun.* **2000**, 1939–1940.

(53) Chiu, S.-H.; Rowan, S. J.; Cantrill, S. J.; Stoddart, J. F.; White, A. J. P.; Williams, D. J. Molecular Meccano 65. Post-Assembly Processing of [2]Rotaxanes. *Chem. Eur. J*. **2002**, *8*, 5170–5183.

(54) Chiu, S.-H.; Elizarov, A. M.; Glink, P. T.; Stoddart, J. F. Translational Isomerism in a [3]Catenane and a [3]Rotaxane. *Org. Lett.* **2002**, *4*, 3561–3564.

(55) Tokunaga, Y.; Kakuchi, S.; Akasaka, K.; Nishikawa, N.; Shimomura, Y.; Isa, K.; Seo, T. A High-Yielding and Convenient Synthesis of Rotaxane Based on an Ester Forming Capping Methodology. *Chem. Lett.* **2002**, 31, 810–811.
(56) Tokunaga, Y.; Akasaka, K.; Hisada, K.; Shimomura, Y.; Kakuchi, S. A Rotaxane Synthesis Based on Stilbene Photoisomerization. A Photoswitchable Catch and Release Process. *Chem. Commun.* **2003**, 2250–2251.
(57) Asakawa, M.; Ikeda, T.; Yui, N.; Shimizu, T. Preparation of Porphyrin-Stoppered Rotaxane Aiming at Immobilization on Substrate. *Chem. Lett.* **2002**, 31, 174–175.
(58) Ikeda, T.; Asakawa, M.; Goto, M.; Nagawa, Y.; Shimizu, T. NMR and X-Ray Crystallographic Analysis of Thermodynamically Stable Tetraphenylporphyrin-Stoppered Rotaxanes. *Eur. J. Org. Chem.* **2003**, 3744–3751.
(59) Furusho, Y.; Oku, T.; Hasegawa, T.; Tsuboi, A.; Kihara, N.; Takata, T. Dynamic Covalent Approach to [2]- and [3]Rotaxanes by Utilizing a Reversible Thiol-Disulfide Interchange Reaction. *Chem. Eur. J.* **2003**, *9*, 2895–2903.
(60) Davidson, G. J. E.; Loeb, S. J. Iron(II) Complexes Utilising Terpyridine Containing [2]Rotaxanes as Ligands. *Dalton Trans.* **2003**, 4319–4323.
(61) Tachibana, Y.; Kihara, N.; Furusho, Y.; Takata, T. Is the Tert-Butyl Group Bulky Enough to End-Cap a Pseudorotaxane with a 24-Crown-8-Ether Wheel? *Org. Lett.* **2004**, *6*, 4507–4509.
(62) Ashton, P. R.; Fyfe, M. C. T.; Schiavo, C.; Stoddart, J. F.; White, A. J. P.; Williams, D. J. A New Slippage Synthesis. *Tetrahedron Lett*. **1998**, *39*, 5455–5458.
(63) Chao, S.; Romuald, C.; Fournel-Marotte, K.; Clavel, C.; Coutrot, F. A Strategy Utilizing a Recyclable Macrocycle Transporter for the Efficient Synthesis of a Triazolium-Based [2]Rotaxane. *Angew. Chem., Int. Ed*. **2014**, *53*, 6914–6919.
(64) Hannam, J. S.; Lacy, S. M.; Leigh, D. A.; Saiz, C. G.; Slawin, A. M. Z.; Stitchell, S. G. Controlled Submolecular Translational Motion in Synthesis: A Mechanically Interlocking Auxiliary. *Angew. Chem., Int. Ed*. **2004**, *43*, 3260–3264.
(65) Handel, M.; Plevoets, M.; Gestermann, S.; Vögtle, F. Synthesis of Rotaxanes by Brief Melting of Wheel and Axle Components. *Angew. Chem., Int. Ed. Engl*. **1997**, *36*, 1199–1201.
(66) Heim, C.; Affeld, A.; Nieger, M.; Vögtle, F. Size Complementarity of Macrocyclic Cavities and Stoppers in Amide-Rotaxanes. *Helv. Chim. Acta* **1999**, *82*, 746–759.
(67) Affeld, A.; Hübner, G. M.; Seel, C.; Schalley, C. A. Rotaxane or Pseudorotaxane? Effects of Small Structural Variations on the Deslipping Kinetics of Rotaxanes with Stopper Groups of Intermediate Size. *Eur. J. Org. Chem.* **2001**, 2877–2890.
(68) Linnartz, P.; Bitter, S.; Schalley, C. A. Deslipping of Ester Rotaxanes: A Cooperative Interplay of Hydrogen Bonding with Rotational Barriers. *Eur. J. Org. Chem.* **2003**, 4819–4829.
(69) Felder, T.; Schalley, C. A. Secondary Isotope Effects on the Deslipping Reaction of Rotaxanes: High-Precision Measurement of Steric Size. *Angew. Chem., Int. Ed*. **2003**, *42*, 2258–2260.
(70) Hannam, J. S.; Kidd, T. J.; Leigh, D. A.; Wilson, A. J. "Magic Rod" Rotaxanes: The Hydrogen Bond-Directed Synthesis of Molecular Shuttles under Thermodynamic Control. *Org. Lett*. **2003**, *5*, 1907–1910.
(71) Macartney, D. H. The Self-Assembly of a [2]Pseudorotaxane of α-Cyclodextrin by the Slippage Mechanism. *J. Chem. Soc., Perkin Trans*. *2* **1996**, 2775–2778.
(72) Lyon, A. P.; Banton, N. J.; Macartney, D. H. Kinetics of the Self-Assembly of Bold α-Cyclodextrin [2]Pseudorotaxanes with Polymethylene Threads Bearing Quaternary Ammonium and Phosphonium End Groups. *Can. J. Chem.* **1998**, *76*, 843–850.
(73) Jin, V. X.; Macartney, D. H.; Buncel, E. α- and β-Cyclodextrin [2]Rotaxanes with (Diethylenetriamine)Platinum(II) Stoppers. *Can. J. Chem*. **2005**, *83*, 2091–2097.
(74) Lee, J. W.; Kim, K.; Kim, K. A Kinetically Controlled Molecular Switch Based on Bistable [2]Rotaxane. *Chem. Commun.* **2001**, 1042–1043.
(75) Sinha, M. K.; Reany, O.; Yefet, M.; Botoshansky, M.; Keinan, E. Bistable Cucurbituril Rotaxanes Without Stoppers. *Chem. Eur. J.* **2012**, *18*, 5589–5605.
(76) Ling, X.; Samuel, E. L.; Patchell, D. L.; Masson, E. Cucurbituril Slippage: Translation Is a Complex Motion. *Org. Lett.* **2010**, *12*, 2730–2733.
(77) Huang, X.; Huang, S.; Zhai, B.; Zhang, Y.; Xu, Y.; Wang, Q. Slipping Synthesis of Cucurbit[7]uril-Based [2]Rotaxane in Organic Environment. *Tetrahedron Lett.* **2012**, *53*, 6414–6417.
(78) Ling, X.; Masson, E. Cucurbituril Slippage: Cations as Supramolecular Lubricants. *Org. Lett.* **2012**, *14*, 4866–4869.
(79) Senler, S.; Cheng, B.; Kaifer, A. E. Rotaxane Formation by Cucurbit[7]uril in Water and DMSO Solutions. *Org. Lett.* **2014**, *16*, 5834–5837.
(80) McConnell, A. J.; Beer, P. D. Kinetic Studies Exploring the Role of Anion Templation in the Slippage Formation of Rotaxane-Like Structures. *Chem. Eur. J.* **2011**, *17*, 2724–2733.
(81) Hsueh, S.-Y.; Lai, C.-C.; Liu, Y.-H.; Wang, Y.; Peng, S.-M.; Chiu, S.-H. Protecting a Squaraine Near-IR Dye Through Its Incorporation in a Slippage-Derived [2]Rotaxane. *Org. Lett.* **2007**, *9*, 4523–4526.
(82) Gassensmith, J. J.; Arunkumar, E.; Barr, L.; Baumes, J. M.; DiVittorio, K. M.; Johnson, J. R.; Noll, B. C.; Smith, B. D. Self-Assembly of Fluorescent Inclusion Complexes in Competitive Media Including the Interior of Living Cells. *J. Am. Chem. Soc.* **2007**, *129*, 15054–15059.
(83) Lee, J.-J.; White, A. G.; Baumes, J. M.; Smith, B. D. Microwave-Assisted Slipping Synthesis of Fluorescent Squaraine Rotaxane Probe for Bacterial Imaging. *Chem. Commun.* **2010**, *46*, 1068–1069.
(84) Lawrence, G. A. *Introduction to Coordination Chemistry*; Wiley: Weinheim, **2010**.
(85) Albrecht, M. From Molecular Diversity to Template-Directed Self-Assembly – New Trends in Metallo-Supramolecular Chemistry. *J. Incl. Phenom. Macrocycl. Chem.* **2000**, *36*, 127–151.
(86) Kumar, A.; Sun, S.-S.; Lees, A. J. Directed Assembly Metallocyclic Supramolecular Systems for Molecular Recognition and Chemical Sensing. *Coord. Chem. Rev.* **2008**, *252*, 922–939.
(87) Lehn, J.-M.; Rigault, A.; Siegel, J.; Harrowfield, J.; Chevrier, B.; Moras, D. Spontaneous Assembly of Double-Stranded Helicates From Oligobipyridine Ligands and Copper(I) Cations: Structure of an Inorganic Double Helix. *Proc. Natl. Acad. Sci. U.S.A.* **1987**, *84*, 2565–2569.
(88) Ogino, H. Relatively High-Yield Synthesis of Rotaxanes. Synthesis and Properties of Compounds Consisting of Cyclodextrins Threaded by α,ω-Diaminoalkanes Coordinated to Cobalt(III) Complexes. *J. Am. Chem. Soc.* **1981**, *103*, 1303–1304.
(89) Krämer, R.; Lehn, J.-M.; Marquis-Rigault, A. Self-Recognition in Helicate Self-Assembly: Spontaneous Formation of Helical Metal Complexes From Mixtures of Ligands and Metal Ions. *Proc. Natl. Acad. Sci. U.S.A.* **1993**, *90*, 5394–5398.
(90) Lehn, J.-M. *Supramolecular Chemistry: Concepts and Perspectives*; Wiley-VCH: Weinheim, 1995.
(91) Kim, K. Mechanically Interlocked Molecules Incorporating Cucurbituril and Their Supramolecular Assemblies. *Chem. Soc. Rev.* **2002**, *31*, 96–107.
(92) Fujita, M. Self-Assembly of [2]Catenanes Containing Metals in Their Backbones. *Acc. Chem. Res.* **1999**, *32*, 53–61.
(93) Klosterman, J. K.; Yamauchi, Y.; Fujita, M. Engineering Discrete Stacks of Aromatic Molecules. *Chem. Soc. Rev.* **2009**, *38*, 1714–1725.
(94) Fujita, M.; Ibukuro, F.; Hagihara, H.; Ogura, K. Quantitative Self-Assembly of a [2]Catenane From Two Preformed Molecular Rings. *Nature* **1994**, *367*, 720–723.
(95) Fujita, M.; Ibukuro, F.; Yamaguchi, K.; Ogura, K. A Molecular Lock. *J. Am. Chem. Soc.* **1995**, *117*, 4175–4176.
(96) Fujita, M.; Ibukuro, F.; Seki, H.; Kamo, O.; Imanari, M.; Ogura, K. Catenane Formation from Two Molecular Rings through Very Rapid Slippage. A Möbius Strip Mechanism. *J. Am. Chem. Soc*. **1996**, *118*, 899–900.

(97) Fujita, M.; Aoyagi, M.; Ibukuro, F.; Ogura, K.; Yamaguchi, K. Made-to-Order Assembling of [2]Catenanes From Palladium(II)-Linked Rectangular Molecular Boxes. *J. Am. Chem. Soc.* **1998**, *120*, 611–612.
(98) Hori, A.; Akasaka, A.; Biradha, K.; Sakamoto, S.; Yamaguchi, K.; Fujita, M. Chirality Induction Through the Reversible Catenation of Coordination Rings. *Angew. Chem., Int. Ed*. **2002**, *41*, 3269–3272.
(99) Hori, A.; Kataoka, H.; Akasaka, A.; Okano, T.; Fujita, M. Reversible Catenation of Coordination Rings with Pd(II) and/or Pt(II) Metal Centers: Chirality Induction Through Catenation. *J. Polym. Sci. Pol. Chem.* **2003**, *41*, 3478–3485.
(100) Hori, A.; Kataoka, H.; Okano, T.; Sakamoto, S.; Yamaguchi, K.; Fujita, M. Selective Cross-Catenation of Pd(II) and Pt(II) Coordination Rings. *Chem. Commun.* **2003**, 182–183.
(101) Yamashita, K.-I.; Hori, A.; Fujita, M. Formation of Bis- and Tris[2]Catenanes via the Cross-Catenation of Pd(II)- and Pt(II)-Linked Coordination Rings. *Tetrahedron* **2007**, *63*, 8435–8439.
(102) Hori, A.; Yamashita, K.-I.; Kusukawa, T.; Akasaka, A.; Biradha, K.; Fujita, M. A Circular Tris[2]Catenane From Molecular "Figure-of-Eight." *Chem. Commun.* **2004**, 1798–1799.
(103) Hori, A.; Sawada, T.; Yamashita, K.-I.; Fujita, M. Ultramacrocyclization Through Reversible Catenation. *Angew. Chem., Int. Ed*. **2005**, *44*, 4896–4899.
(104) Burchell, T. J.; Eisler, D. J.; Puddephatt, R. J. A Chiral [2]Catenane Self-Assembled from *meso*-Macrocycles of Palladium(II). *Dalton Trans.* **2005**, 268–272.
(105) Lu, J.; Turner, D. R.; Harding, L. P.; Byrne, L. T.; Baker, M. V.; Batten, S. R. Octapi Interactions: Self-Assembly of a Pd-Based [2]Catenane Driven by Eightfold π Interactions. *J. Am. Chem. Soc.* **2009**, *131*, 10372–10373.
(106) Fukuda, M.; Sekiya, R.; Kuroda, R. A Quadruply Stranded Metallohelicate and Its Spontaneous Dimerization into an Interlocked Metallohelicate. *Angew. Chem., Int. Ed*. **2008**, *47*, 706–710.
(107) Sekiya, R.; Fukuda, M.; Kuroda, R. Anion-Directed Formation and Degradation of an Interlocked Metallohelicate. *J. Am. Chem. Soc.* **2012**, *134*, 10987–10997.
(108) Clever, G. H.; Shionoya, M. A pH Switchable Pseudorotaxane Based on a Metal Cage and a Bis-Anionic Thread. *Chem. Eur. J.* **2010**, *16*, 11792–11796.
(109) Freye, S.; Hey, J.; Torras-Galán, A.; Stalke, D.; Herbst-Irmer, R.; John, M.; Clever, G. H. Allosteric Binding of Halide Anions by a New Dimeric Interpenetrated Coordination Cage. *Angew. Chem., Int. Ed*. **2012**, *51*, 2191–2194.
(110) Frank, M.; Hey, J.; Balcioglu, I.; Chen, Y.-S.; Stalke, D.; Suenobu, T.; Fukuzumi, S.; Frauendorf, H.; Clever, G. H. Assembly and Stepwise Oxidation of Interpenetrated Coordination Cages Based on Phenothiazine. *Angew. Chem., Int. Ed*. **2013**, *52*, 10102–10106.
(111) Zhu, R.; Lübben, J.; Dittrich, B.; Clever, G. H. Stepwise Halide-Triggered Double and Triple Catenation of Self-Assembled Coordination Cages. *Angew. Chem., Int. Ed*. **2015**, *54*, 2796–2800.
(112) Fujita, M.; Fujita, N.; Ogura, K.; Yamaguchi, K. Spontaneous Assembly of Ten Components into Two Interlocked, Identical Coordination Cages. *Nature* **1999**, *400*, 52–55.
(113) Yamauchi, Y.; Yoshizawa, M.; Fujita, M. Engineering Stacks of Aromatic Rings by the Interpenetration of Self-Assembled Coordination Cages. *J. Am. Chem. Soc.* **2008**, *130*, 5832–5833.
(114) Ibukuro, F.; Fujita, M.; Yamaguchi, K.; Sauvage, J.-P. Quantitative and Spontaneous Formation of a Doubly Interlocking [2]Catenane Using Copper(I) and Palladium(II) as Templating and Assembling Centers. *J. Am. Chem. Soc.* **1999**, *121*, 11014–11015.
(115) Dietrich-Buchecker, C.; Geum, N.; Hori, A.; Fujita, M.; Sakamoto, S.; Yamaguchi, K.; Sauvage, J.-P. A [2]Catenane Quantitatively Assembled via Copper(I) and Palladium(II) Coordination. *Chem. Commun.* **2001**, 1182–1183.
(116) Dietrich-Buchecker, C.; Colasson, B.; Fujita, M.; Hori, A.; Geum, N.; Sakamoto, S.; Yamaguchi, K.; Sauvage, J.-P. Quantitative Formation of [2]Catenanes Using Copper(I) and Palladium(II) as Templating and Assembling Centers: the Entwining Route and the Threading Approach. *J. Am. Chem. Soc.* **2003**, *125*, 5717–5725.
(117) Dietrich-Buchecker, C. O.; Sauvage, J.-P.; Kintzinger J. P. Une Nouvelle Famille de Molecules: Les Metallo-Catenanes. *Tetrahedron Lett.* **1983**, *24*, 5095–5098.
(118) Whang, D.; Park, K.-M.; Heo, J.; Ashton, P. R.; Kim, K. Molecular Necklace: Quantitative Self-Assembly of a Cyclic Oligorotaxane From Nine Molecules. *J. Am. Chem. Soc.* **1998**, *120*, 4899–4900.
(119) Roh, S.-G.; Park, K.-M.; Park, G.-J.; Sakamoto, S.; Yamaguchi, K.; Kim, K. Synthesis of a Five-Membered Molecular Necklace: A 2 + 2 Approach. *Angew. Chem., Int. Ed*. **1999**, *38*, 638–641.
(120) Park, K.-M.; Kim, S.-Y.; Heo, J.; Whang, D.; Sakamoto, S.; Yamaguchi, K.; Kim, K. Designed Self-Assembly of Molecular Necklaces. *J. Am. Chem. Soc.* **2002**, *124*, 2140–2147.
(121) Lim, C. W.; Sakamoto, S.; Yamaguchi, K.; Hong, J.-I. Versatile Formation of [2]Catenane and [2]Pseudorotaxane Structures; Threading and Noncovalent Stoppering by a Self-Assembled Macrocycle. *Org. Lett.* **2004**, *6*, 1079–1082.
(122) Zhang, D.; Nie, Y.; Saha, M. L.; He, Z.; Jiang, L.; Zhou, Z.; Stang, P. J. Photoreversible [2]Catenane via the Host–Guest Interactions Between a Palladium Metallacycle and β-Cyclodextrin. *Inorg. Chem.* **2015**, *54*, 11807–11812.
(123) Chas, M.; Pia, E.; Toba, R.; Peinador, C.; Quintela, J. M. New Hybrid [2]Catenanes Based on a 4,4 '-Bipyridinium Ligand. *Inorg. Chem.* **2006**, *45*, 6117–6119.
(124) Chas, M.; Blanco, V.; Peinador, C.; Quintela, J. M. Synthesis of [3]Catenanes Based on Metal-Directed Self-Assembly and π-Donor/π-Acceptor Interactions. *Org. Lett.* **2007**, *9*, 675–678.
(125) Alvariño, C.; Terenzi, A.; Blanco, V.; García, M. D.; Peinador, C.; Quintela, J. M. [2]Catenanes and Inclusion Complexes Derived From Self-Assembled Rectangular Pd(II) and Pt(II) Metallocycles. *Dalton Trans*. **2012**, *41*, 11992–11998.
(126) Rama, T.; López-Vidal, E. M.; García, M. D.; Peinador, C.; Quintela, J. M. Complexation and Catenation in Aqueous Media Using a Self-Assembled Pd^{II} Metallacyclic Receptor. *Chem. Eur. J.* **2015**, *21*, 9482–9487.
(127) Asakawa, M.; Ashton, P. R.; Menzer, S.; Raymo, F. M.; Stoddart, J. F.; White, A. J. P.; Williams, D. J. Molecular Meccano 8. Cyclobis(paraquat-4,4′-biphenylene) - An Organic Molecular Square. *Chem. Eur. J*. **1996**, *2*, 877–893.
(128) Peinador, C.; Blanco, V.; Quintela, J. M. A New Doubly Interlocked [2]Catenane. *J. Am. Chem. Soc.* **2009**, *131*, 920–921.
(129) Blanco, V.; Chas, M.; Abella, D.; Peinador, C.; Quintela, J. M. Molecular Catenation *via* Metal-Directed Self-Assembly and π-Donor/π-Acceptor Interactions: Efficient One-Pot Synthesis, Characterization, and Crystal Structures of [3]Catenanes Based on Pd or Pt Dinuclear Metallocycles. *J. Am. Chem. Soc.* **2007**, *129*, 13978–13986.
(130) Blanco, V.; Abella, D.; Pia, E.; Platas-Iglesias, C.; Peinador, C.; Quintela, J. M. Regioselective Catenation-of Dinuclear Palladium and Platinum Metallocycles Promoted by π…π Interactions. *Inorg. Chem.* **2009**, *48*, 4098–4107.
(131) Liu, Y.; Bruneau, A.; He, J.; Abliz, Z. Palladium(II)-Directed Self-Assembly of Dynamic Donor-Acceptor [2]Catenanes. *Org. Lett.* **2008**, *10*, 765–768.
(132) Koshkakaryan, G.; Parimal, K.; He, J.; Zhang, X.; Abliz, Z.; Flood, A. H.; Liu, Y. π-Stacking Enhanced Dynamic and Redox-Switchable Self-Assembly of Donor-Acceptor Metallo-[2]Catenanes From Diimide Derivatives and Crown Ethers. *Chem. Eur. J*. **2008**, *14*, 10211–10218.
(133) Li, S.; Huang, J.; Cook, T. R.; Pollock, J. B.; Kim, H.; Chi, K.-W.; Stang, P. J. Formation of [3]Catenanes From 10 Precursors via Multicomponent Coordination-Driven

Self-Assembly of Metallarectangles. *J. Am. Chem. Soc.* **2013**, *135*, 2084–2087.
(134) Li, S.; Huang, J.; Zhou, F.; Cook, T. R.; Yan, X.; Ye, Y.; Zhu, B.; Zheng, B.; Stang, P. J. Self-Assembly of Triangular and Hexagonal Molecular Necklaces. *J. Am. Chem. Soc.* **2014**, *136*, 5908–5911.
(135) Ye, Y.; Wang, S.-P.; Zhu, B.; Cook, T. R.; Wu, J.; Li, S.; Stang, P. J. Self-Assembly of [3]Catenanes and a [4]Molecular Necklace Based on a Cryptand/Paraquat Recognition Motif. *Org. Lett.* **2015**, *17*, 2804–2807.
(136) Shinoda, S.; Maeda, T.; Miyake, H.; Tsukube, H. Dynamically Capped Rotaxanes: Metal Coordination vs. Acid–Base Pairing in the Chiral End-Capping. *Supramol. Chem.* **2011**, *23*, 244–248.
(137) Suzaki, Y.; Osakada, K. Formation, Dynamic Behavior, and Chemical Transformation of Pt Complexes with a Rotaxane-Like Structure. *Chem. Asian J.* **2006**, *1*, 331–343.
(138) Blight, B. A.; Wisner, J. A.; Jennings, M. C. Synthesis of a [2]Rotaxane Through First- and Second-Sphere Coordination. *Chem. Commun.* **2006**, 4593–4595.
(139) Blight, B. A.; Wisner, J. A.; Jennings, M. C. Reversible Formation of a [2]Catenane Through First- and Second-Sphere Coordination. *Angew. Chem., Int. Ed*. **2007**, *46*, 2835–2838.
(140) Taira, T.; Suzaki, Y.; Osakada, K. Pd-II and Pt-III Complexes with Amphiphilic Ligands: Formation of Micelles and [5]Rotaxanes with α-Cyclodextrin in Aqueous Solution. *Chem. Asian J.* **2008**, *3*, 895–902.
(141) Wang, W.; Sun, B.; Wang, X.-Q.; Ren, Y.-Y.; Chen, L.-J.; Ma, J.; Zhang, Y.; Li, X.; Yu, Y.; Tan, H.; Yang, H. B. Discrete Stimuli-Responsive Multirotaxanes with Supramolecular Cores Constructed Through a Modular Approach. *Chem. Eur. J.* **2015**, 21, 6286–6294.
(142) Wang, W.; Chen, L.-J.; Wang, X.-Q.; Sun, B.; Li, X.; Zhang, Y.; Shi, J.; Yu, Y.; Zhang, L.; Liu, M.; Yang, H. B. Organometallic Rotaxane Dendrimers with Fourth-Generation Mechanically Interlocked Branches. *Proc. Natl. Acad. Sci. U.S.A.* **2015**, *112*, 5597–5601.
(143) Grohmann, A. Gold in Chains: Self-Assembly of a Gold(I) Catenane. *Angew. Chem., Int. Ed. Engl*. **1995**, *34*, 2107–2109.
(144) Puddephatt, R. J. Macrocycles, Catenanes, Oligomers and Polymers in Gold Chemistry. *Chem. Soc. Rev.* **2008**, *37*, 2012–2027.
(145) Puddephatt, R. J. Gold Catenanes. *J. Organomet. Chem*. **2015**, *792*, 13–24.
(146) Mingos, D. M. P.; Yau, J.; Menzer, S.; Williams, D. J. A Gold(I) [2]Catenane. *Angew. Chem., Int. Ed. Engl*. **1995**, *34*, 1894–1895.
(147) Mingos, D. M. P.; Yau, J. Synthesis and Applications of $[Au(NCPh)_2][BF_4]$. A Versatile Labile Intermediate for Gold(I) Chemistry. *J. Organomet. Chem*. **1994**, *479*, c16–c17.
(148) Koshevoy, I. O.; Chang, Y.-C.; Karttunen, A. J.; Selivanov, S. I.; Jänis, J.; Haukka, M.; Pakkanen, T.; Tunik, S. P.; Chou, P.-T. Intensely Luminescent Homoleptic Alkynyl Decanuclear Gold(I) Clusters and Their Cationic Octanuclear Phosphine Derivatives. *Inorg. Chem.* **2012**, *51*, 7392–7403.
(149) Wiseman, M. R.; Marsh, P. A.; Bishop, P. T.; Brisdon, B. J.; Mahon, M. F. Homoleptic Gold Thiolate Catenanes. *J. Am. Chem. Soc.* **2000**, *122*, 12598–12599.
(150) Chui, S. S.-Y.; Chen, R.; Che, C.-M. A Chiral [2]Catenane Precursor of the Antiarthritic Gold(I) Drug Auranofin. *Angew. Chem., Int. Ed*. **2006**, *45*, 1621–1624.
(151) Pei, Y.; Pal, R.; Liu, C.; Gao, Y.; Zhang, Z.; Zeng, X. C. Interlocked Catenane-Like Structure Predicted in $Au_{24}(SR)_{20}$: Implication to Structural Evolution of Thiolated Gold Clusters From Homoleptic Gold(I) Thiolates to Core-Stacked Nanoparticles. *J. Am. Chem. Soc.* **2012**, *134*, 3015–3024.
(152) McArdle, C. P.; Irwin, M. J.; Jennings, M. C.; Puddephatt, R. J. Controlled Self-Assembly of Cyclic Gold (I) Complexes: The First Family of Organometallic Catenanes. *Angew. Chem., Int. Ed.* **1999**, *38*, 3376–3378.
(153) McArdle, C. P.; Vittal, J. J.; Puddephatt, R. J. Molecular Topology: Easy Self-Assembly of an Organometallic Doubly Braided [2]Catenane. *Angew. Chem., Int. Ed*. **2000**, *39*, 3819–3822.
(154) McArdle, C. P.; Jennings, M. C.; Vittal, J. J.; Puddephatt, R. J. Self-Assembly of Rings, Catenanes, and a Doubly Braided Catenane Containing Gold(I):The Hinge-Group Effect in Diacetylide Ligands. *Chem. Eur. J.* **2001**, *7*, 3572–3583.
(155) McArdle, C. P.; Irwin, M. J.; Jennings, M. C.; Vittal, J. J.; Puddephatt, R. J. Self-Assembly of Gold(I) Rings and Reversible Formation of Organometallic [2]Catenanes. *Chem. Eur. J.* **2002**, *8*, 723–734.
(156) McArdle, C. P.; Van, S.; Jennings, M. C.; Puddephatt, R. J. Gold(I) Macrocycles and Topologically Chiral [2]Catenanes. *J. Am. Chem. Soc.* **2002**, *124*, 3959–3965.
(157) Mohr, F.; Eisler, D. J.; McArdle, C. P.; Atieh, K.; Jennings, M. C.; Puddephatt, R. J. Macrocyclic Gold(I) Complexes and [2]Catenanes Containing Carbonyl Functionalized Diacetylide Ligands. *J. Organomet. Chem.* **2003**, *670*, 27–36.
(158) Habermehl, N. C.; Mohr, F.; Eisler, D. J.; Jennings, M. C.; Puddephatt, R. J. Organogold(I) Macrocycles and [2]Catenanes Containing Pyridyl and Bipyridyl Substituents—Organometallic Catenanes as Ligands. *Can. J. Chem.* **2006**, *84*, 111–123.
(159) Habermehl, N. C.; Eisler, D. J.; Kirby, C. W.; Yue, N. L.-S.; Puddephatt, R. J. A Structural Probe for Organogold(I) Rings and [2]Catenanes. *Organometallics* **2006**, *25*, 2921–2928.
(160) Habermehl, N. C.; Jennings, M. C.; McArdle, C. P.; Mohr, F.; Puddephatt, R. J. Selectivity in the Self-Assembly of Organometallic Gold(I) Rings and [2]Catenanes. *Organometallics* **2005**, *24*, 5004–5014.
(161) Wong, W. W. H.; Cookson, J.; Evans, E. A. L.; McInnes, E. J. L.; Wolowska, J.; Maher, J. P.; Bishop, P.; Beer, P. D. Heteropolymetallic Copper(II)–Gold(III) Dithiocarbamate [2]Catenanes *via* Magic Ring Synthesis. *Chem. Commun.* **2005**, 2214–2216.
(162) Piguet, C.; Bocquet, B.; Hopfgartner, G. Syntheses of Segmental Heteroleptic Ligands for the Self-Assembly of Heteronuclear Helical Supramolecular Complexes. *Helv. Chim. Acta* **1994**, *77*, 931–942.
(163) Gidron, O.; Jirásek, M.; Trapp, N.; Ebert, M.-O.; Zhang, X.; Diederich, F. Homochiral [2]Catenane and Bis[2]Catenane From Alleno-Acetylenic Helicates - A Highly Selective Narcissistic Self-Sorting Process. *J. Am. Chem. Soc.* **2015**, *137*, 12502–12505.
(164) Yang, Y.-D.; Fan, C.-C.; Rambo, B. M.; Gong, H.-Y.; Xu, L.-J.; Xiang, J.-F.; Sessler, J. L. Multicomponent Self-Assembled Metal–Organic [3]Rotaxanes. *J. Am. Chem. Soc.* **2015**, *137*, 12966–12976.
(165) Padilla-Tosta, M. E.; Fox, O. D.; Drew, M. G. B.; Beer, P. D. Self-Assembly of a Mixed-Valence Copper(II)/Copper(III) Dithiocarbamate Catenane. *Angew. Chem., Int. Ed*. **2001**, *40*, 4235–4239.
(166) Giri, C.; Topić, F.; Cametti, M.; Rissanen, K. Mixed Valence Mono- and Hetero-Metallic Grid Catenanes. *Chem. Sci.* **2015**, *6*, 5712–5718.
(167) Try, A. C.; Harding, M. M.; Hamilton, D. G.; Sanders, J. K. M. Reversible Five-Component Assembly of a [2]Catenane from a Chiral Metallomacrocycle and a Dinaphtho-Crown Ether. *Chem. Commun.* **1998**, 723–724.
(168) Black, S. P.; Wood, D. M.; Schwarz, F. B.; Ronson, T. K.; Holstein, J. J.; Stefankiewicz, A. R.; Schalley, C. A.; Sanders, J. K. M.; Nitschke, J. R. Catenation and Encapsulation Induce Distinct Reconstitutions Within a Dynamic Library of Mixed-Ligand Zn_4L_6 Cages. *Chem. Sci.* **2016**, *7*, 2614–2620.
(169) Westcott, A.; Fisher, J.; Harding, L. P.; Rizkallah, P.; Hardie, M. J. Self-Assembly of a 3-D Triply Interlocked Chiral [2]Catenane. *J. Am. Chem. Soc.* **2008**, *130*, 2950–2951.
(170) Argent, S. P.; Adams, H.; Riis-Johannessen, T.; Jeffery, J. C.; Harding, L. P.; Clegg, W.; Harrington, R. W.; Ward, M. D. Complexes of Ag(I), Hg(I) and Hg(II) with Multidentate

Pyrazolyl-Pyridine Ligands: From Mononuclear Complexes to Coordination Polymers *via* Helicates, a Mesocate, a Cage and a Catenate. *Dalton Trans.* **2006**, 4996–5013.
(171) Argent, S. P.; Adams, H.; Harding, L. P.; Riis-Johannessen, T.; Jeffery, J. C.; Ward, M. D. Homo- and Heteropolynuclear Helicates with a ′2+3+2′-Dentate Compartmental Ligand. *New J. Chem.* **2005**, *29*, 904–908.
(172) Elemans, J. A. A. W.; van Hameren, R.; Nolte, R. J. M.; Rowan, A. E. Molecular Materials by Self-Assembly of Porphyrins, Phthalocyanines, and Perylenes. *Adv. Mater.* **2006**, *18*, 1251–1266.
(173) Chichak, K.; Walsh, M. C.; Branda, N. R. Axially Coordinated Porphyrins as New Rotaxane Stoppers. *Chem. Commun.* **2000**, 847–848.
(174) Gunter, M. J.; Bampos, N.; Johnstone, K. D.; Sanders, J. K. M. Thermodynamically Self-Assembling Porphyrin-Stoppered Rotaxanes. *New J. Chem.* **2001**, *25*, 166–173.
(175) Johnstone, K. D.; Bampos, N.; Sanders, J. K. M.; Gunter, M. J. A Self-Assembling Polymer-Bound Rotaxane under Thermodynamic Control. *Chem. Commun.* **2003**, 1396–1397.
(176) Johnstone, K. D.; Yamaguchi, K.; Gunter, M. J. Flexible Self-Assembling Porphyrin Supramolecules. *Org. Biomol. Chem.* **2005**, *3*, 3008–3017.
(177) Mullen, K. M.; Johnstone, K. D.; Webb, M.; Bampos, N.; Sanders, J. K. M.; Gunter, M. J. Monitoring the Thermodynamically-Controlled Formation of Diimide-Based Resin-Attached Rotaxanes by Gel-Phase HR MAS ^{1}H NMR Spectroscopy. *Org. Biomol. Chem.* **2008**, *6*, 278–286.
(178) Mullen, K. M.; Johnstone, K. D.; Nath, D.; Bampos, N.; Sanders, J. K. M.; Gunter, M. J. Crown-Ether- and Porphyrin-Attached Gel-Phase Resins in Thermodynamically Controlled Rotaxane Assembly. *Org. Biomol. Chem.* **2009**, *7*, 293–303.
(179) Hunter, C. A.; Low, C. M. R.; Packer, M. J.; Spey, S. E.; Vinter, J. G.; Vysotsky, M. O.; Zonta, C. Noncovalent Assembly of [2]Rotaxane Architectures. *Angew. Chem., Int. Ed*. **2001**, *40*, 2678–2682.
(180) Gunter, M. J.; Farquhar, S. M.; Mullen, K. M. Amide-Appended Porphyrins as Scaffolds for Catenanes, Rotaxanes and Anion Receptors. *New J. Chem*. **2004**, *28*, 1443–1449.
(181) Ikeda, T.; Asakawa, M.; Shimizu, T. ^{1}H NMR Analysis of Porphyrin-Stoppered Rotaxanes: Effect of the Porphyrin Substituents on the Macrocycle. *New J. Chem.* **2004**, *28*, 870–873.
(182) Alemán García, M. Á.; Bampos, N. Synthesis of a Four-Component [3]Catenane Using Three Distinct Noncovalent Interactions. *Org. Biomol. Chem.* **2013**, *11*, 27–30.
(183) Han, M.; Zhang, H.-Y.; Yang, L.-X.; Ding, Z.-J.; Zhuang, R.-J.; Liu, Y. A [2]Catenane and Pretzelane Based on Sn-Porphyrin and Crown Ether. *Eur. J. Org. Chem.* **2011**, 7271–7277.
(184) Wu, J.; Fang, F.; Lu, W.-Y.; Hou, J.-L.; Li, C.; Wu, Z.-Q.; Jiang, X.-K.; Li, Z.-T.; Yu, Y.-H. Dynamic [2]Catenanes Based on a Hydrogen Bonding-Mediated Bis-Zinc Porphyrin Foldamer Tweezer: A Case Study. *J. Org. Chem.* **2007**, *72*, 2897–2905.
(185) Beyler, M.; Heitz, V.; Sauvage, J.-P. Quantitative Formation of a Tetraporphyrin[2]Catenane *via* Copper and Zinc Coordination. *Chem. Commun.* **2008**, 5396–5398.
(186) Beyler, M.; Heitz, V.; Sauvage, J.-P. Coordination Chemistry-Assembled Porphyrinic Catenanes. *J. Am. Chem. Soc.* **2010**, *132*, 4409–4417.
(187) Beyler, M.; Heitz, V.; Sauvage, J.-P. The Dual Role of Cu(I) as a Protective Group and a Template in the Synthesis of a Tetra-Rhodium(III)Porphyrin [2]Catenane. *New J. Chem.* **2010**, *34*, 1825–1829.
(188) Wylie, R. S.; Macartney, D. H. Self-Assembling Metal Rotaxane Complexes of α-Cyclodextrin. *J. Am. Chem. Soc.* **1992**, *114*, 3136–3138.
(189) Wylie, R. S.; Macartney, D. H. The Self-Assembly of α-Cyclodextrin Rotaxanes of μ-(1,1″-(α,ω-alkanediyl) Bis-(4,4′-bipyridinium))bis[pentacyanoferrate-(II)] Complexes. *Supramol. Chem.* **1993**, *3*, 29–35.
(190) Macartney, D. H.; Waddling, C. A. Kinetic and Spectroscopic Studies on Pentacyano(*N*-Heterocycle)ferrate(II) Rotaxanes of α-Cyclodextrin with Symmetric and Asymmetric Threads. *Inorg. Chem.* **1994**, *33*, 5912–5919.
(191) Lyon, A. P.; Macartney, D. H. Kinetic and Spectroscopic Studies on α-Cyclodextrin Rotaxanes with Pentacyano(cyanopyridinium)ferrate(II) Stoppers. *Inorg. Chem.* **1997**, *36*, 729–736.
(192) Baer, A. J.; Macartney, D. H. α- and β-Cyclodextrin Rotaxanes of μ-Bis(4-pyridyl)bis[pentacyanoferrate(II)] Complexes. *Inorg. Chem*. **2000**, *39*, 1410–1417.
(193) Castle, T.; Evans, M. E.; Hyde, S. T. Ravels: Knot-Free but Not Free. Novel Entanglements of Graphs in 3-Space. *New J. Chem*. **2008**, *32*, 1484–1492.
(194) Li, F.; Clegg, J. K.; Lindoy, L. F.; Macquart, R. B.; Meehan, G. V. Metallosupramolecular Self-Assembly of a Universal 3-Ravel. *Nature Commun*. **2011**, *2*: 205.
(195) Durham, B.; Walsh, J. L.; Carter, C. L.; Meyer, T. J. Synthetic Applications of Photosubstitution Reactions of Poly(pyridyl) Complexes of Ruthenium(II). *Inorg. Chem.* **1980**, *19*, 860–865.
(196) Salassa, L.; Garino, C.; Salassa, G.; Gobetto, R.; Nervi, C. Mechanism of Ligand Photodissociation in Photoactivable $[Ru(bpy)_2L_2]^{2+}$ Complexes: A Density Functional Theory Study. *J. Am. Chem. Soc.* **2008**, *130*, 9590–9597.
(197) Yamashita, K.-I.; Kawano, M.; Fujita, M. Photoswitchable Molecular Lock. One-Way Catenation of a Pt(II)-Linked Coordination Ring *via* the Photolabilization of a Pt(II)-Pyridine Bond. *J. Am. Chem. Soc.* **2007**, *129*, 1850–1851.
(198) Huang, S.-L.; Lin, Y.-J.; Hor, T. S. A.; Jin, G.-X. Cp*Rh-Based Heterometallic Metallarectangles: Size-Dependent Borromean Link Structures and Catalytic Acyl Transfer. *J. Am. Chem. Soc.* **2013**, *135*, 8125–8128.
(199) Huang, S.-L.; Lin, Y.-J.; Li, Z.-H.; Jin, G.-X. Self-Assembly of Molecular Borromean Rings From Bimetallic Coordination Rectangles. *Angew. Chem., Int. Ed*. **2014**, *53*, 11218–11222.
(200) Vajpayee, V.; Song, Y. H.; Cook, T. R.; Kim, H.; Lee, Y.; Stang, P. J.; Chi, K.-W. A Unique Non-catenane Interlocked Self-Assembled Supramolecular Architecture and Its Photophysical Properties. *J. Am. Chem. Soc.* **2011**, *133*, 19646–19649.
(201) Lee, H.; Elumalai, P.; Singh, N.; Kim, H.; Lee, S. U.; Chi, K.-W. Selective Synthesis of Ruthenium(II) Metalla[2]-Catenane *via* Solvent and Guest-Dependent Self-Assembly. *J. Am. Chem. Soc.* **2015**, *137*, 4674–4677.
(202) Jeong, K.-S.; Choi, J.; Chang, S.-Y.; Chang, H.-Y. Self-Assembly of Rotaxane-Like Complexes with Macrocycles Containing Reversible Coordinate Bonds. *Angew. Chem., Int. Ed*. **2000**, *39*, 1692–1695.
(203) Vögtle, F.; Meier, S.; Hoss, R. One-Step Synthesis of a Fourfold Functionalized Catenane. *Angew. Chem., Int. Ed. Engl*. **1992**, *31*, 1619–1622.
(204) Hunter, C. A. Synthesis and Structure Elucidation of a New [2]-Catenane. *J. Am. Chem. Soc.* **1992**, *114*, 5303–5311.
(205) Chang, S.-Y.; Choi, J. S.; Jeong, K.-S. Self-Assembly and Dynamics of [2]- and [3]Rotaxanes with a Dinuclear Macrocycle Containing Reversible Os-N Coordinate Bonds. *Chem. Eur. J.* **2001**, *7*, 2687–2697.
(206) He, X.; Li, G.; Chen, H. A New Cucurbituril-Based Metallo-Rotaxane. *Inorg. Chem. Commun.* **2002**, *5*, 633–636.
(207) Cheetham, A. G.; Claridge, T. D. W.; Anderson, H. L. Metal-Driven Ligand Assembly in the Synthesis of Cyclodextrin [2] and [3]Rotaxanes. *Org. Biomol. Chem.* **2007**, *5*, 457–462.
(208) Abedin, T. S. M.; Thompson, L. K.; Miller, D. O. An Octanuclear $[Co(II)_2–Co(III)_2]_2$ Interlocked Grid—Example of an Inorganic [2]Catenane. *Chem. Commun.* **2005**, 5512–5514.
(209) Gruter, G.-J. M.; de Kanter, F. J. J.; Markies, P. R.; Nomoto, T.; Akkerman, O. S.; Bickelhaupt, F. Formation of the First

Organometallic Catenane. *J. Am. Chem. Soc.* **1993**, *115*, 12179–12180.
(210) Castro, S. L.; Just, O.; Rees, W. S., Jr. A Quadruply Stranded, Alkaline Earth Metal Containing Helical Catenate: A Charge-Neutral Heterotopic Homodinuclear [2]Catenane. *Angew. Chem., Int. Ed*. **2000**, *39*, 933–935.
(211) Sauvage, J.-P.; Amabilino, D. B. The Beauty of Knots at the Molecular Level. *Top. Curr. Chem.* **2012**, *323*, 107–125.
(212) Bruns, C. J.; Stoddart, J. F. The Mechanical Bond: A Work of Art. *Top. Curr. Chem.* **2012**, *323*, 19–72.
(213) Leigh, D. A.; Lusby, P. J.; Teat, S. J.; Wilson, A. J.; Wong, J. K. Y. Benzylic Imine Catenates: Readily Accessible Octahedral Analogues of the Sauvage Catenates. *Angew. Chem., Int. Ed*. **2001**, *40*, 1538–1543.
(214) Hogg, L.; Leigh, D. A.; Lusby, P. J.; Morelli, A.; Parsons, S.; Wong, J. K. Y. A Simple General Ligand System for Assembling Octahedral Metal-Rotaxane Complexes. *Angew. Chem., Int. Ed*. **2004**, *43*, 1218–1221.
(215) Campbell, C. J.; Leigh, D. A.; Vitorica-Yrezabal, I. J.; Woltering, S. L. A Simple and Highly Effective Ligand System for the Copper(I)-Mediated Assembly of Rotaxanes. *Angew. Chem., Int. Ed*. **2014**, *53*, 13771–13774.
(216) Hutin, M.; Schalley, C. A.; Bernardinelli, G.; Nitschke, J. R. Helicate, Macrocycle, or Catenate: Dynamic Topological Control Over Subcomponent Self-Assembly. *Chem. Eur. J.* **2006**, *12*, 4069–4076.
(217) Yoon, I.; Narita, M.; Shimizu, T.; Asakawa, M. Threading-Followed-by-Shrinking Protocol for the Synthesis of a [2]Rotaxane Incorporating a Pd(II)–Salophen Moiety. *J. Am. Chem. Soc.* **2004**, *126*, 16740–16741.
(218) Yoon, I.; Narita, M.; Goto, M.; Shimizu, T.; Asakawa, M. Synthesis of a [2]Rotaxane Incorporating a Ni(II)-Salen Moiety: Evidence of Ring-Opening-and-Closing Protocol. *Org. Lett.* **2006**, *8*, 2341–2344.
(219) Narita, M.; Yoon, I.; Aoyagi, M.; Goto, M.; Shimizu, T.; Asakawa, M. Transition Metal(II)–Salen and –Salophen Macrocyclic Complexes for Rotaxane Formation: Syntheses and Crystal Structures. *Eur. J. Inorg. Chem.* **2007**, 4229–4237.
(220) Pentecost, C. D.; Chichak, K. S.; Peters, A. J.; Cave, G. W. V.; Cantrill, S. J.; Stoddart, J. F. A Molecular Solomon Link. *Angew. Chem., Int. Ed*. **2007**, *46*, 218–222.
(221) Beves, J. E.; Campbell, C. J.; Leigh, D. A.; Pritchard, R. G. Tetrameric Cyclic Double Helicates as a Scaffold for a Molecular Solomon Link. *Angew. Chem., Int. Ed*. **2013**, *52*, 6464–6467.
(222) Chichak, K.; Cantrill, S. J.; Pease, A. R.; Chiu, S.-H.; Cave, G. W. V.; Atwood, J. L.; Stoddart, J. F. Molecular Borromean Rings. *Science* **2004**, *304*, 1308–1312.
(223) Chichak, K. S.; Cantrill, S. J.; Stoddart, J. F. Dynamic Nanoscale Borromean Links. *Chem. Commun.* **2005**, 3391–3393.
(224) Peters, A. J.; Chichak, K. S.; Cantrill, S. J.; Stoddart, J. F. Nanoscale Borromean Links for Real. *Chem. Commun.* **2005**, 3394–3396.
(225) Chichak, K. S.; Peters, A. J.; Cantrill, S. J.; Stoddart, J. F. Nanoscale Borromeates. *J. Org. Chem*. **2005**, *70*, 7956–7962.
(226) Cantrill, S. J.; Chichak, K. S.; Peters, A. J.; Stoddart, J. F. Nanoscale Borromean Rings. *Acc. Chem. Res*. **2005**, *38*, 1–9.
(227) Pentecost, C. D.; Peters, A. J.; Chichak, K. S.; Cave, G. W. V.; Cantrill, S. J.; Stoddart, J. F. Chiral Borromeates. *Angew. Chem., Int. Ed*. **2006**, *45*, 4099–4104.
(228) Pentecost, C. D.; Tangchaivang, N.; Cantrill, S. J.; Chichak, K. S.; Peters, A. J.; Stoddart, J. F. Making Molecular Borromean Rings. A Gram-Scale Synthetic Procedure for the Undergraduate Organic Lab. *J. Chem. Ed*. **2007**, *84*, 855–859.
(229) Meyer, C. D.; Forgan, R. S.; Chichak, K. S.; Peters, A. J.; Tangchaivang, N.; Cave, G. W. V.; Khan, S. I.; Cantrill, S. J.; Stoddart, J. F. The Dynamic Chemistry of Molecular Borromean Rings and Solomon Knots. *Chem. Eur. J.* **2010**, *16*, 12570–12581.
(230) Wood, C. S.; Ronson, T. K.; Belenguer, A. M.; Holstein, J. J.; Nitschke, J. R. Two-Stage Directed Self-Assembly of a Cyclic [3]Catenane. *Nature Chem.* **2015**, *7*, 354–358.
(231) Ayme, J.-F.; Beves, J. E.; Leigh, D. A.; McBurney, R. T.; Rissanen, K.; Schultz, D. A Synthetic Molecular Pentafoil Knot. *Nature Chem.* **2012**, *4*, 15–20.
(232) Ayme, J.-F.; Beves, J. E.; Leigh, D. A.; McBurney, R. T.; Rissanen, K.; Schultz, D. Pentameric Circular Iron(II) Double Helicates and a Molecular Pentafoil Knot. *J. Am. Chem. Soc.* **2012**, *134*, 9488–9497.
(233) Black, S. P.; Stefankiewicz, A. R.; Smulders, M. M. J.; Sattler, D.; Schalley, C. A.; Nitschke, J. R.; Sanders, J. K. M. Generation of a Dynamic System of Three-Dimensional Tetrahedral Polycatenanes. *Angew. Chem., Int. Ed*. **2013**, *52*, 5749–5752.
(234) Prakasam, T.; Lusi, M.; Elhabiri, M.; Platas-Iglesias, C.; Olsen, J.-C.; Asfari, Z.; Cianférani-Sanglier, S.; Debaene, F.; Charbonnière, L. J.; Trabolsi, A. Simultaneous Self-Assembly of a [2]Catenane, a Trefoil Knot, and a Solomon Link From a Simple Pair of Ligands. *Angew. Chem., Int. Ed*. **2013**, *52*, 9956–9960.
(235) Prakasam, T.; Lusi, M.; Nauha, E.; Olsen, J.-C.; Sy, M.; Platas-Iglesias, C.; Charbonnière, L. J.; Trabolsi, A. Dynamic Stereoisomerization in Inherently Chiral Bimetallic [2]Catenanes. *Chem. Commun.* **2015**, *51*, 5840–5843.
(236) Glink, P. T.; Oliva, A. I.; Stoddart, J. F.; White, A. J. P.; Williams, D. J. Template-Directed Synthesis of a [2]Rotaxane by the Clipping Under Thermodynamic Control of a Crown Ether Like Macrocycle Around a Dialkylammonium Ion. *Angew. Chem., Int. Ed*. **2001**, *40*, 1870–1875.
(237) Horn, M.; Ihringer, J.; Glink, P. T.; Stoddart, J. F. Kinetic versus Thermodynamic Control During the Formation of [2]Rotaxanes by a Dynamic Template-Directed Clipping Process. *Chem. Eur. J.* **2003**, *9*, 4046–4054.
(238) Haussmann, P. C.; Khan, S. I.; Stoddart, J. F. Equilibrating Dynamic [2]Rotaxanes. *J. Org. Chem.* **2007**, *72*, 6708–6713.
(239) Aricó, F.; Chang, T.; Cantrill, S. J.; Khan, S. I.; Stoddart, J. F. Template-Directed Synthesis of Multiply Mechanically Interlocked Molecules under Thermodynamic Control. *Chem. Eur. J.* **2005**, *11*, 4655–4666.
(240) Wilson, E. A.; Vermeulen, N. A.; McGonigal, P. R.; Avestro, A.-J.; Sarjeant, A. A.; Stern, C. L.; Stoddart, J. F. Formation of a Hetero[3]Rotaxane by a Dynamic Component-Swapping Strategy. *Chem. Commun.* **2014**, *50*, 9665–9668.
(241) Leung, K. C.-F.; Aricó, F.; Cantrill, S. J.; Stoddart, J. F. Template-Directed Dynamic Synthesis of Mechanically Interlocked Dendrimers. *J. Am. Chem. Soc.* **2005**, *127*, 5808–5810.
(242) Leung, K. C.-F.; Aricó, F.; Cantrill, S. J.; Stoddart, J. F. Dynamic Mechanically Interlocked Dendrimers: Amplification in Dendritic Dynamic Combinatorial Libraries. *Macromolecules* **2007**, *40*, 3951–3959.
(243) Bozdemir, O. A.; Barin, G.; Belowich, M. E.; Basuray, A. N.; Beuerle, F.; Stoddart, J. F. Dynamic Covalent Templated-Synthesis of [*c*2]Daisy Chains. *Chem. Commun.* **2012**, *48*, 10401–10403.
(244) Wu, J.; Leung, K. C.-F.; Stoddart, J. F. Efficient Production of [*n*]Rotaxanes by Using Template-Directed Clipping Reactions. *Proc. Natl. Acad. Sci. U.S.A.* **2007**, *104*, 17266–17271.
(245) Belowich, M. E.; Valente, C.; Stoddart, J. F. Template-Directed Syntheses of Rigid Oligorotaxanes under Thermodynamic Control. *Angew. Chem., Int. Ed*. **2010**, *49*, 7208–7212.
(246) Belowich, M. E.; Valente, C.; Smaldone, R. A.; Friedman, D. C.; Thiel, J.; Cronin, L.; Stoddart, J. F. Positive Cooperativity in the Template-Directed Synthesis of Monodisperse Macromolecules. *J. Am. Chem. Soc.* **2012**, *134*, 5243–5261.
(247) Avestro, A.-J.; Gardner, D. M.; Vermeulen, N. A.; Wilson, E. A.; Schneebeli, S. T.; Whalley, A. C.; Belowich, M. E.; Carmieli, R.; Wasielewski, M. R.; Stoddart, J. F. Gated

Electron Sharing Within Dynamic Naphthalene Diimide-Based Oligorotaxanes. *Angew. Chem., Int. Ed*. **2014**, *53*, 4442–4449.
(248) Yin, J.; Dasgupta, S.; Wu, J. Synthesis of [*n*]Rotaxanes by Template-Directed Clipping: The Role of the Dialkylammonium Recognition Sites. *Org. Lett.* **2010**, *12*, 1712–1715.
(249) Yin, J.; Chi, C.; Wu, J. Efficient Synthesis of a Hetero[4]-Rotaxane by a "Threading-Stoppering-Followed-by-Clipping" Approach. *Org. Biomol. Chem.* **2010**, *8*, 2594–2599.
(250) Li, Z.; Liu, W.; Wu, J.; Liu, S. H.; Yin, J. Synthesis of [2]Catenanes by Template-Directed Clipping Approach. *J. Org. Chem.* **2012**, *77*, 7129–7135.
(251) Li, Z.; Liu, G.; Xue, W.; Wu, D.; Yang, Y.-W.; Wu, J.; Liu, S. H.; Yoon, J.; Yin, J. Construction of Hetero[*n*]Rotaxanes by Use of Polyfunctional Rotaxane Frameworks. *J. Org. Chem.* **2013**, *78*, 11560–11570.
(252) Xue, W.; Li, Z.; Liu, G.; Chen, X.; Li, T.; Liu, S. H.; Yin, J. Construction of Rotacatenanes Using Rotaxane and Catenane Frameworks. *Org. Biomol. Chem.* **2014**, *12*, 4862–4871.
(253) Hu, F.; Huang, J.; Cao, M.; Chen, Z.; Yang, Y.-W.; Liu, S. H.; Yin, J. Dithienylethene-Based Rotaxanes: Synthesis, Characterization and Properties. *Org. Biomol. Chem*. **2014**, *12*, 7712–7720.
(254) Li, Z.; Han, X.; Chen, H.; Wu, D.; Hu, F.; Liu, S. H.; Yin, J. Construction of Photoswitchable Rotaxanes and Catenanes Containing Dithienylethene Fragments. *Org. Biomol. Chem.* **2015**, *13*, 7313–7322.
(255) Han, X.; Cao, M.; Xu, Z.; Wu, D.; Chen, Z.; Wu, A.; Liu, S. H.; Yin, J. Aggregation-Induced Emission Behavior of a pH-Controlled Molecular Shuttle Based on a Tetraphenylethene Moiety. *Org. Biomol. Chem.* **2015**, *13*, 9767–9774.
(256) Williams, A. R.; Northrop, B. H.; Chang, T.; Stoddart, J. F.; White, A. J. P.; Williams, D. J. Suitanes. *Angew. Chem., Int. Ed*. **2006**, *45*, 6665–6669.
(257) Northrop, B. H.; Aricó, F.; Tangchiavang, N.; Badjić, J. D.; Stoddart, J. F. Template-Directed Synthesis of Mechanically Interlocked Molecular Bundles Using Dynamic Covalent Chemistry. *Org. Lett.* **2006**, *8*, 3899–3902.
(258) Northrop, B. H.; Spruell, J. M.; Stoddart, J. F. Efficient Routes to Novel Molecular Architectures: Template-Directed Synthesis of Mechanically Interlocked Structures. *Chim. Oggi* **2007**, *25*, 4–7.
(259) Klivansky, L. M.; Koshkakaryan, G.; Cao, D.; Liu, Y. Linear π-Acceptor-Templated Dynamic Clipping to Macrobicycles and [2]Rotaxanes. *Angew. Chem., Int. Ed*. **2009**, *48*, 4185–4189.
(260) Pun, A.; Hanifi, D. A.; Kiel, G.; O'Brien, E.; Liu, Y. Facile Route to an All-Organic, Triply Threaded, Interlocked Structure by Templated Dynamic Clipping. *Angew. Chem., Int. Ed*. **2012**, *51*, 13119–13122.
(261) Pun, A. B.; Gagnon, K. J.; Klivansky, L. M.; Teat, S. J.; Li, Z.-T.; Liu, Y. Solvent-Driven Selective π-Cation Templating in Dynamic Assembly of Interlocked Molecules. *Org. Chem. Front.* **2014**, *1*, 167–175.
(262) Koshkakaryan, G.; Cao, D.; Klivansky, L. M.; Teat, S. J.; Tran, J. L.; Liu, Y. Dual Selectivity Expressed in [2+2+1] Dynamic Clipping of Unsymmetrical [2]Catenanes. *Org. Lett.* **2010**, *12*, 1528–1531.
(263) Li, J.; Wei, P.; Wu, X.; Xue, M.; Yan, X.; Zhou, Q. Taco Complex-Templated Dynamic Clipping to Cryptand-Based [2]Rotaxane- and [2]Catenane-Type Mechanically Interlocked Structures. *RSC Adv.* **2013**, *3*, 21289–21293.
(264) Tung, S.-T.; Lai, C.-C.; Liu, Y.-H.; Peng, S.-M.; Chiu, S.-H. Synthesis of a [2]Catenane From the Sodium Ion Templated Orthogonal Arrangement of Two Diethylene Glycol Chains. *Angew. Chem., Int. Ed*. **2013**, *52*, 13269–13272.
(265) Wu, Y.-W.; Chen, P.-N.; Chang, C.-F.; Lai, C.-C.; Chiu, S.-H. Synthesizing [2]Rotaxanes and [2]Catenanes Through Na^+-Templated Clipping of Macrocycles Around Oligo(ethylene glycol) Units. *Org. Lett.* **2015**, *17*, 2158–2161.
(266) Cantrill, S. J.; Rowan, S. J.; Stoddart, J. F. Rotaxane Formation under Thermodynamic Control. *Org. Lett.* **1999**, *1*, 1363–1366.
(267) Rowan, S. J.; Stoddart, J. F. Thermodynamic Synthesis of Rotaxanes by Imine Exchange. *Org. Lett.* **1999**, *1*, 1913–1916.
(268) Lam, R. T. S.; Belenguer, A.; Roberts, S. L.; Naumann, C.; Jarrosson, T.; Otto, S.; Sanders, J. K. M. Amplification of Acetylcholine-Binding Catenanes From Dynamic Combinatorial Libraries. *Science* **2005**, *308*, 667–669.
(269) Chung, M.-K.; White, P. S.; Lee, S. J.; Gagné, M. R. Synthesis of Interlocked 56-Membered Rings by Dynamic Self-Templating. *Angew. Chem., Int. Ed*. **2009**, *48*, 8683–8686.
(270) Chung, M.-K.; White, P. S.; Lee, S. J.; Waters, M. L.; Gagné, M. R. Self-Assembled Multi-Component Catenanes: Structural Insights Into an Adaptable Class of Molecular Receptors and [2]-Catenanes. *J. Am. Chem. Soc.* **2012**, *134*, 11415–11429.
(271) Chung, M.-K.; Lee, S. J.; Waters, M. L.; Gagné, M. R. Self-Assembled Multi-Component Catenanes: The Effect of Multivalency and Cooperativity on Structure and Stability. *J. Am. Chem. Soc.* **2012**, *134*, 11430–11443.
(272) Li, H.; Zhang, H.; Lammer, A. D.; Wang, M.; Li, X.; Lynch, V. M.; Sessler, J. L. Quantitative Self-Assembly of a Purely Organic Three-Dimensional Catenane in Water. *Nature Chem.* **2015**, *7*, 1003–1008.
(273) Korich, A. L.; Iovine, P. M. Boroxine Chemistry and Applications: A Perspective. *Dalton Trans.* **2010**, *39*, 1423–1431.
(274) Nishiyabu, R.; Kubo, Y.; James, T. D.; Fossey, J. S. Boronic Acid Building Blocks: Tools for Self Assembly. *Chem. Commun.* **2011**, *47*, 1124–1150.
(275) Fujita, N.; Shinkai, S.; James, T. D. Boronic Acids in Molecular Self-Assembly. *Chem. Asian J.* **2008**, *3*, 1076–1091.
(276) Christinat, N.; Scopelliti, R.; Severin, K. Multicomponent Assembly of Boronic Acid Based Macrocycles and Cages. *Angew. Chem., Int. Ed*. **2008**, *47*, 1848–1852.
(277) Severin, K. Boronic Acids as Building Blocks for Molecular Nanostructures and Polymeric Materials. *Dalton Trans.* **2009**, 5254–5264.
(278) Ding, S.-Y.; Wang, W. Covalent Organic Frameworks (COFs): From Design to Applications. *Chem. Soc. Rev.* **2012**, *42*, 548–568.
(279) Yamamoto, M.; Takeuchi, M.; Shinkai, S. Oligosaccharide Binding to a Boronic-Acid-Appended Phenanthroline-Cu(I) Complex Which Creates Superstructural Helicates and Catenates. *Tetrahedron* **2002**, *58*, 7251–7258.
(280) Christinat, N.; Scopelliti, R.; Severin, K. Boron-Based Rotaxanes by Multicomponent Self-Assembly. *Chem. Commun.* **2008**, 3660–3662.
(281) Tokunaga, Y.; Ito, T.; Sugawara, H.; Nakata, R. Dynamic Covalent Chemistry of a Boronylammonium Ion and a Crown Ether: Formation of a C_3-Symmetric [4]Rotaxane. *Tetrahedron Lett.* **2008**, *49*, 3449–3452.
(282) *Handbook of Metathesis*; Grubbs, R. H., Ed.; Wiley-VCH: Weinheim, 2003.
(283) Wasserman, E.; Ben-Efraim, D. A.; Wolovsky, R. The Synthesis of Carbon Macrocycles to C120. *J. Am. Chem. Soc.* **1968**, *90*, 3286–3287.
(284) Ben-Efraim, D. A.; Batich, C.; Wasserman, E. Mass Spectral Evidence for Catenanes Form *via* a "Möbius Strip" Approach. *J. Am. Chem. Soc.* **1970**, *92*, 2133–2135.
(285) Wolovsky, R. Interlocked Ring Systems Obtained by the Metathesis Reaction of Cyclododecane. Mass Spectral Evidence. *J. Am. Chem. Soc.* **1970**, *92*, 2132–2133.
(286) Gruter, G.-J. M.; Akkerman, O. S.; Bickelhaupt, F. The Formation of Catenanes. The Möbius Strip Approach Revisited. *Tetrahedron* **1996**, *52*, 2565–2572.
(287) Hérisson, J.-L.; Chauvin, Y. Catalyse de Transformation des Oléfines par les Complexes du Tungstène. II. Télomérisation des Oléfines Cycliques en Présence D'Oléfines Acycliques. *Makromol. Chem*. **1971**, *141*, 161–176.

(288) Grubbs, R. H.; Carr, D. D.; Hoppin, C.; Burk, P. L. Consideration of the Mechanism of the Metal Catalyzed Olefin Metathesis Reaction. *J. Am. Chem. Soc.* **1976**, *98*, 3478–3483.

(289) Schwab, P.; France, M. B.; Ziller, J. W.; Grubbs, R. H. A Series of Well-Defined Metathesis Catalysts–Synthesis of $[RuCl_2(=CHR')(PR_3)_2]$ and Its Reactions. *Angew. Chem., Int. Ed. Engl.* **1995**, *34*, 2039–2041.

(290) Trnka, T. M.; Grubbs, R. H. The Development of $L_2X_2Ru=CHR$ Olefin Metathesis Catalysts: An Organometallic Success Story. *Acc. Chem. Res.* **2001**, *34*, 18–29.

(291) Garber, S. B.; Kingsbury, J. S.; Gray, B. L.; Hoveyda, A. H. Efficient and Recyclable Monomeric and Dendritic Ru-Based Metathesis Catalysts. *J. Am. Chem. Soc.* **2000**, *122*, 8168–8179.

(292) Mohr, B.; Weck, M.; Sauvage, J.-P.; Grubbs, R. H. High-Yield Synthesis of [2]Catenanes by Intramolecular Ring-Closing Metathesis. *Angew. Chem., Int. Ed. Engl*. **1997**, *36*, 1308–1310.

(293) Weck, M.; Mohr, B.; Sauvage, J.-P.; Grubbs, R. H. Synthesis of Catenane Structures *via* Ring-Closing Metathesis. *J. Org. Chem.* **1999**, *64*. 5463–5471.

(294) Dietrich-Buchecker, C.; Rapenne, G.; Sauvage, J.-P. Synthesis of Catenanes and Molecular Knots by Copper(I)-Directed Formation of the Precursors Followed by Ruthenium(II)-Catalyzed Ring-Closing Metathesis. *Coord. Chem. Rev.* **1999**, *185–186*. 167–176.

(295) Belfrekh, N.; Dietrich-Buchecker, C.; Sauvage, J.-P. Unexpected Synthesis of an 8-Shaped Macrocycle Instead of an Interlocking-Ring System. *Inorg. Chem.* **2000**, *39*, 5169–5172.

(296) Mobian, P.; Kern, J.-M.; Sauvage, J.-P. A [2]Catenane Constructed Around a Ru(diimine)$_3^{2+}$ Complex Used as a Template. *J. Am. Chem. Soc.* **2003**, *125*, 2016–2017.

(297) Aricó, F.; Mobian, P.; Kern, J.-M.; Sauvage, J.-P. Synthesis of a [2]Catenane Around a Ru(diimine)$_3^{2+}$ Scaffold by Ring-Closing Metathesis of Olefins. *Org. Lett.* **2003**, *5*, 1887–1890.

(298) Mobian, P.; Kern, J.-M.; Sauvage, J.-P. A [2]Catenane Constructed Around a Rhodium(III) Center Used as a Template. *Inorg. Chem.* **2003**, *42*, 8633–8637.

(299) Hamann, C.; Kern, J.-M.; Sauvage, J.-P. Zinc(II)-Templated Synthesis of a [2]-Catenane Consisting of a 2,2′,6′,2"-Terpyridine-Incorporating Cycle and a 1,10-Phenanthroline-Containing Ring. *Inorg. Chem.* **2003**, *42*, 1877–1883.

(300) Ayme, J.-F.; Lux, J.; Sauvage, J.-P.; Sour, A. [2]Catenanes Built Around Octahedral Transition-Metal Complexes That Contain Two Intertwined Endocyclic but Non-Sterically Hindering Tridentate Ligands. *Chem. Eur. J.* **2012**, *18*, 5565–5573.

(301) Dietrich-Buchecker, C.; Rapenne, G.; Sauvage, J.-P. Efficient Synthesis of a Molecular Knot by Copper (I)-Induced Formation of the Precursor Followed by Ruthenium(II)-Catalysed Ring Closing Metathesis. *Chem. Commun.* **1997**, 2053–2054.

(302) Rapenne, G.; Dietrich-Buchecker, C.; Sauvage, J.-P. Copper(I)- or Iron(II)-Templated Synthesis of Molecular Knots Containing Two Tetrahedral or Octahedral Coordination Sites. *J. Am. Chem. Soc.* **1999**, *121*, 994–1001.

(303) Dietrich-Buchecker, C.; Sauvage, J.-P. Lithium Templated Synthesis of Catenanes: Efficient Synthesis of Doubly Interlocked [2]-Catenanes. *Chem. Commun.* **1999**, 615–616.

(304) Perret-Aebi, L.-E.; von Zelewsky, A.; Dietrich-Buchecker, C.; Sauvage, J.-P. Stereoselective Synthesis of a Topologically Chiral Molecule: The Trefoil Knot. *Angew. Chem., Int. Ed*. **2004**, *43*, 4482–4485.

(305) Frey, J.; Kraus, T.; Heitz, V.; Sauvage, J.-P. A Catenane Consisting of a Large Ring Threaded Through Both Cyclic Units of a Handcuff-Like Compound. *Chem. Commun.* **2005**, 5310–5312.

(306) Frey, J.; Kraus, T.; Heitz, V.; Sauvage, J.-P. Synthesis of a Bis-Macrocycle Containing Two Back-to-Back Rigidly Connected 1,10-Phenanthroline Units as a Central Core and Its Incorporation in a Handcuff-Like Catenane. *Chem. Eur. J.* **2007**, *13*, 7584–7594.

(307) Beves, J. E.; Blight, B. A.; Campbell, C. J.; Leigh, D. A.; McBurney, R. T. Strategies and Tactics for the Metal-Directed Synthesis of Rotaxanes, Knots, Catenanes, and Higher Order Links. *Angew. Chem., Int. Ed*. **2011**, *50*, 9260–9327.

(308) Leigh, D. A.; Lusby, P. J.; McBurney, R. T.; Morelli, A.; Slawin, A. M. Z.; Thomson, A. R.; Walker, D. B. Getting Harder: Cobalt(III)-Template Synthesis of Catenanes and Rotaxanes. *J. Am. Chem. Soc.* **2009**, *131*, 3762–3771.

(309) Fuller, A.-M.; Leigh, D. A.; Lusby, P. J.; Oswald, I. D. H.; Parsons, S.; Walker, D. B. A 3D Interlocked Structure From a 2D Template: Structural Requirements for the Assembly of a Square-Planar Metal-Coordinated [2]Rotaxane. *Angew. Chem., Int. Ed*. **2004**, *43*, 3914–3918.

(310) Fuller, A.-M. L.; Leigh, D. A.; Lusby, P. J.; Slawin, A. M. Z.; Walker, D. B. Selecting Topology and Connectivity Through Metal-Directed Macrocyclization Reactions: A Square Planar Palladium [2]Catenate and Two Noninterlocked Isomers. *J. Am. Chem. Soc.* **2005**, *127*, 12612–12619.

(311) Leigh, D. A.; Lusby, P. J.; Slawin, A. M. Z.; Walker, D. B. Half-Rotation in a [2]Catenane via Interconvertible Pd(II) Coordination Modes. *Chem. Commun.* **2005**, 4919–4921.

(312) Fuller, A.-M. L.; Leigh, D. A.; Lusby, P. J. One Template, Multiple Rings: Controlled Iterative Addition of Macrocycles onto a Single Binding Site Rotaxane Thread. *Angew. Chem., Int. Ed*. **2007**, *46*, 5015–5019.

(313) Fuller, A.-M. L.; Leigh, D. A.; Lusby, P. J. Sequence Isomerism in [3]Rotaxanes. *J. Am. Chem. Soc.* **2010**, *132*, 4954–4959.

(314) Goldup, S. M.; Leigh, D. A.; Lusby, P. J.; McBurney, R. T.; Slawin, A. M. Z. Gold(I)-Template Catenane and Rotaxane Synthesis. *Angew. Chem., Int. Ed*. **2008**, *47*, 6999–7003.

(315) Ayme, J.-F.; Gil-Ramírez, G.; Leigh, D. A.; Lemonnier, J.-F.; Markevicius, A.; Muryn, C. A.; Zhang, G. Lanthanide Template Synthesis of a Molecular Trefoil Knot. *J. Am. Chem. Soc.* **2014**, *136*, 13142–13145.

(316) Beves, J. E.; Danon, J. J.; Leigh, D. A.; Lemonnier, J.-F.; Vitorica-Yrezabal, I. J. A Solomon Link Through an Interwoven Molecular Grid. *Angew. Chem., Int. Ed*. **2015**, *54*, 7555–7559.

(317) Leigh, D. A.; Pritchard, R. G.; Stephens, A. J. A Star of David Catenane. *Nature Chem.* **2014**, *6*, 978–982.

(318) Leigh, D. A.; Lusby, P. J.; Slawin, A. M. Z.; Walker, D. B. Half-Rotation in a Kinetically Locked [2]Catenane Induced by Transition Metal Ion Substitution. *Chem. Commun.* **2012**, *48*, 5826–5828.

(319) Gupta, M.; Kang, S.; Mayer, M. F. A Double Ring-Closing Olefin Metathesis Approach to [3]Catenanes. *Tetrahedron Lett.* **2008**, *49*, 2946–2950.

(320) Xue, Z.; Mayer, M. F. Actuator Prototype: Capture and Release of a Self-Entangled [1]Rotaxane. *J. Am. Chem. Soc.* **2010**, *132*, 3274–3276.

(321) Lincheneau, C.; Jean-Denis, B.; Gunnlaugsson, T. Self-Assembly Formation of Mechanically Interlocked [2]- and [3]Catenanes Using Lanthanide Ion [Eu(III)] Templation and Ring Closing Metathesis Reactions. *Chem. Commun.* **2014**, *50*, 2857–2860.

(322) Guo, J.; Mayers, P. C.; Breault, G. A.; Hunter, C. A. Synthesis of a Molecular Trefoil Knot by Folding and Closing on an Octahedral Coordination Template. *Nature Chem.* **2010**, *2*, 218–222.

(323) Hunter, C. A.; Mayers, P. C. Knot Tied Around an Octahedral Metal Centre. *Nature* **2001**, *411*, 763.

(324) Sokolov, V. I. Topological Ideas in Stereochemistry. *Russian Chem. Rev.* **1973**, *42*, 452–463.

(325) Wojtecki, R. J.; Wu, Q.; Johnson, J. C.; Ray, D. G.; Korley, L. T. J.; Rowan, S. J. Optimizing the Formation of 2,6-Bis (*N*-alkyl-benzimidazolyl)pyridine-Containing [3]Catenates Through Component Design. *Chem. Sci.* **2013**, *4*, 4440–4448.

(326) Hamilton, D. G.; Feeder, N.; Teat, S. J.; Sanders, J. K. M. Reversible Synthesis of π-Associated [2]Catenanes by Ring-Closing Metathesis: Towards Dynamic Combinatorial Libraries of Catenanes. *New J. Chem.* **1998**, *22*, 1019–1021.

(327) Li, S.; Liu, M.; Zheng, B.; Zhu, K.; Wang, F.; Li, N.; Zhao, X.-L.; Huang, F. Taco Complex Templated Syntheses of a Cryptand/Paraquat [2]Rotaxane and a [2]Catenane by Olefin Metathesis. *Org. Lett.* **2009**, *11*, 3350–3353.

(328) Barnes, J. C.; Juríček, M.; Strutt, N. L.; Frasconi, M.; Sampath, S.; Giesener, M. A.; McGrier, P. L.; Bruns, C. J.; Stern, C. L.; Sarjeant, A. A.; Stoddart, J. F. ExBox: A Polycyclic Aromatic Hydrocarbon Scavenger. *J. Am. Chem. Soc.* **2013**, *135*, 183–192.

(329) Juríček, M.; Barnes, J. C.; Strutt, N. L.; Vermeulen, N. A.; Ghooray, K. C.; Dale, E. J.; McGonigal, P. R.; Blackburn, A. K.; Avestro, A.-J.; Stoddart, J. F. An ExBox [2]Catenane. *Chem. Sci.* **2014**, *5*, 2724–2731.

(330) de Juan, A.; Pouillon, Y.; Ruiz-González, L.; Torres-Pardo, A.; Casado, S.; Martín, N.; Rubio, Á.; Pérez, E. M. Mechanically Interlocked Single-Wall Carbon Nanotubes. *Angew. Chem., Int. Ed*. **2014**, *53*, 5394–5400.

(331) López-Moreno, A.; Pérez, E. M. Pyrene-Based Mechanically Interlocked SWNTs. *Chem. Commun*. **2015**, *51*, 5421–5424.

(332) Romero-Nieto, C.; García, R.; Herranz, M. Á.; Ehli, C.; Ruppert, M.; Hirsch, A.; Guldi, D. M.; Martín, N. Tetrathiafulvalene-Based Nanotweezers—Noncovalent Binding of Carbon Nanotubes in Aqueous Media with Charge Transfer Implications. *J. Am. Chem. Soc.* **2012**, *134*, 9183–9192.

(333) Kitajima, K.; Ogoshi, T.; Yamagishi, T.-A. Diastereoselective Synthesis of a [2]Catenane From a Pillar[5]arene and a Pyridinium Derivative. *Chem. Commun.* **2014**, *50*, 2925–2927.

(334) Orlandini, G.; Zanichelli, V.; Secchi, A.; Arduini, A.; Ragazzon, G.; Credi, A.; Venturi, M.; Silvi, S. Synthesis by Ring Closing Metathesis and Properties of an Electroactive Calix[6]arene [2]Catenane. *Supramol. Chem.* **2016**, *28*, 427–435.

(335) Kidd, T. J.; Leigh, D. A.; Wilson, A. J. Organic “Magic Rings”: The Hydrogen Bond-Directed Assembly of Catenanes under Thermodynamic Control. *J. Am. Chem. Soc.* **1999**, *121*, 1599–1600.

(336) Wang, L.; Vysotsky, M. O.; Bogdan, A.; Bolte, M.; Böhmer, V. Multiple Catenanes Derived From Calix[4]arenes. *Science* **2004**, *304*, 1312–1314.

(337) Molokanova, O.; Vysotsky, M. O.; Cao, Y.; Thondorf, I.; Böhmer, V. Fourfold [2]Rotaxanes of Calix[4]arenes by Ring Closure. *Angew. Chem., Int. Ed*. **2006**, *45*, 8051–8055.

(338) Molokanova, O.; Podoprygorina, G.; Bolte, M.; Böhmer, V. Multiple Catenanes Based on Tetraloop Derivatives of Calix[4]arenes. *Tetrahedron* **2009**, *65*, 7220–7233.

(339) Molokanova, O.; Bogdan, A.; Vysotsky, M. O.; Bolte, M.; Ikai, T.; Okamoto, Y.; Böhmer, V. Calix[4]arene-Based Bis[2]Catenanes: Synthesis and Chiral Resolution. *Chem. Eur. J.* **2007**, *13*, 6157–6170.

(340) Janke, M.; Rudzevich, Y.; Molokanova, O.; Metzroth, T.; Mey, I.; Diezemann, G.; Marszalek, P. E.; Gauss, J.; Böhmer, V.; Janshoff, A. Mechanically Interlocked Calix[4]arene Dimers Display Reversible Bond Breakage under Force. *Nature Nanotechnol.* **2009**, *4*, 225–229.

(341) Lee, J.-J.; Baumes, J. M.; Connell, R. D.; Oliver, A. G.; Smith, B. D. Squaraine [2]Catenanes: Synthesis, Structure and Molecular Dynamics. *Chem. Commun*. **2011**, *47*, 7188–7190.

(342) Kilbinger, A. F. M.; Cantrill, S. J.; Waltman, A. W.; Day, M. W.; Grubbs, R. H. Magic Ring Rotaxanes by Olefin Metathesis. *Angew. Chem., Int. Ed*. **2003**, *42*, 3281–3285.

(343) Guidry, E. N.; Cantrill, S. J.; Stoddart, J. F.; Grubbs, R. H. Magic Ring Catenation by Olefin Metathesis. *Org. Lett.* **2005**, *7*, 2129–2132.

(344) Guidry, E. N.; Li, J.; Stoddart, J. F.; Grubbs, R. H. Bifunctional [*c*2]Daisy-Chains and Their Incorporation Into Mechanically Interlocked Polymers. *J. Am. Chem. Soc.* **2007**, *129*, 8944–8945.

(345) Badjić, J. D.; Cantrill, S. J.; Grubbs, R. H.; Guidry, E. N.; Orenes, R.; Stoddart, J. F. The Exclusivity of Multivalency in Dynamic Covalent Processes. *Angew. Chem., Int. Ed*. **2004**, *43*, 3273–3278.

(346) Clark, P. G.; Guidry, E. N.; Chan, W. Y.; Steinmetz, W. E.; Grubbs, R. H. Synthesis of a Molecular Charm Bracelet *via* Click Cyclization and Olefin Metathesis Clipping. *J. Am. Chem. Soc.* **2010**, *132*, 3405–3412.

(347) Dasgupta, S.; Wu, J. Template-Directed Synthesis of Kinetically and Thermodynamically Stable Molecular Necklace Using Ring Closing Metathesis. *Org. Biomol. Chem.* **2011**, *9*, 3504–3515.

(348) Iwamoto, H.; Itoh, K.; Nagamiya, H.; Fukazawa, Y. Convenient Synthesis of [3]Catenane by Olefin Metathesis Dimerizations. *Tetrahedron Lett.* **2003**, *44*, 5773–5776.

(349) Iwamoto, H.; Takizawa, W.; Itoh, K.; Hagiwara, T.; Tayama, E.; Hasegawa, E.; Haino, T. Selective Synthesis of [2]- and [3]Catenane Tuned by Ring Size and Concentration. *J. Org. Chem.* **2013**, *78*, 5205–5217.

(350) Iwamoto, H.; Tafuku, S.; Sato, Y.; Takizawa, W.; Katagiri, W.; Tayama, E.; Hasegawa, E.; Fukazawa, Y.; Haino, T. Synthesis of Linear [5]Catenanes *via* Olefin Metathesis Dimerization of Pseudorotaxanes Composed of a [2]Catenane and a Secondary Ammonium Salt. *Chem. Commun.* **2016**, *52*, 319–322.

(351) Dasgupta, S.; Huang, K.-W.; Wu, J. Trifluoromethyl Acting as Stopper in [2]Rotaxane. *Chem. Commun.* **2012**, *48*, 4821–4823.

(352) Zhu, X.-Z.; Chen, C.-F. A Highly Efficient Approach to [4]Pseudocatenanes by Threefold Metathesis Reactions of a Triptycene-Based Tris[2]pseudorotaxane. *J. Am. Chem. Soc.* **2005**, *127*, 13158–13159.

(353) Zhu, X.-Z.; Chen, C.-F. Efficient Synthesis of a Chiral [4]Pseudocatenane and Its Derivatives: A Novel Ship’s Wheel-Like Interlocked Structure. *Chem. Eur. J.* **2006**, *12*, 5603–5609.

(354) Jiang, Y.; Zhu, X.-Z.; Chen, C.-F. Multivalency-Directed Magic-Ring [2](3)Catenane by Olefin Metathesis. *Chem. Eur. J.* **2010**, *16*, 14285–14289.

(355) Vukotic, V. N.; Harris, K. J.; Zhu, K.; Schurko, R. W.; Loeb, S. J. Metal–Organic Frameworks with Dynamic Interlocked Components. *Nature Chem.* **2012**, *4*, 456–460.

(356) Zhu, K.; Vukotic, V. N.; O’Keefe, C. A.; Schurko, R. W.; Loeb, S. J. Metal–Organic Frameworks with Mechanically Interlocked Pillars: Controlling Ring Dynamics in the Solid-State *via* a Reversible Phase Change. *J. Am. Chem. Soc.* **2014**, *136*, 7403–7409.

(357) Vukotic, V. N.; O’Keefe, C. A.; Zhu, K.; Harris, K. J.; To, C.; Schurko, R. W.; Loeb, S. J. Mechanically Interlocked Linkers Inside Metal–Organic Frameworks: Effect of Ring Size on Rotational Dynamics. *J. Am. Chem. Soc.* **2015**, *137*, 9643–9651.

(358) Caputo, C. B.; Zhu, K.; Vukotic, V. N.; Loeb, S. J.; Stephan, D. W. Heterolytic Activation of H_2 Using a Mechanically Interlocked Molecule as a Frustrated Lewis Base. *Angew. Chem., Int. Ed*. **2013**, *52*, 960–963.

(359) Vickers, M. S.; Beer, P. D. Anion Templated Assembly of Mechanically Interlocked Structures. *Chem. Soc. Rev.* **2007**, *36*, 211–225.

(360) Spence, G. T.; Beer, P. D. Expanding the Scope of the Anion Templated Synthesis of Interlocked Structures. *Acc. Chem. Res.* **2013**, *46*, 571–586.

(361) Wisner, J. A.; Beer, P. D.; Drew, M. G. B.; Sambrook, M. R. Anion-Templated Rotaxane Formation. *J. Am. Chem. Soc.* **2002**, *124*, 12469–12476.

(362) Curiel, D.; Beer, P. D. Anion Directed Synthesis of a Hydrogensulfate Selective Luminescent Rotaxane. *Chem. Commun.* **2005**, 1909–1911.

(363) Mullen, K. M.; Mercurio, J.; Serpell, C. J.; Beer, P. D. Exploiting the 1,2,3-Triazolium Motif in Anion-Templated Formation of a Bromide-Selective Rotaxane Host Assembly. *Angew. Chem., Int. Ed*. **2009**, *48*, 4781–4784.

(364) Kilah, N. L.; Wise, M. D.; Serpell, C. J.; Thompson, A. L.; White, N. G.; Christensen, K. E.; Beer, P. D. Enhancement of Anion Recognition Exhibited by a Halogen-Bonding Rotaxane Host System. *J. Am. Chem. Soc.* **2010**, *132*, 11893–11895.
(365) Brown, A.; Beer, P. D. Porphyrin-Functionalised Rotaxanes for Anion Recognition. *Dalton Trans.* **2011**, *41*, 118–129.
(366) Evans, N. H.; Beer, P. D. A Ferrocene Functionalized Rotaxane Host System Capable of the Electrochemical Recognition of Chloride. *Org. Biomol. Chem.* **2011**, *9*, 92–100.
(367) Evans, N. H.; Serpell, C. J.; White, N. G.; Beer, P. D. A 1,2,3,4,5-Pentaphenylferrocene-Stoppered Rotaxane Capable of Electrochemical Anion Recognition. *Chem. Eur. J.* **2011**, *17*, 12347–12354.
(368) Evans, N. H.; Beer, P. D. A Janus [2]Rotaxane Synthesized by Using an Anion-Templated Clipping Methodology. *Chem. Eur. J.* **2011**, *17*, 10542–10546.
(369) Spence, G. T.; Serpell, C. J.; Sardinha, J.; Costa, P. J.; Félix, V.; Beer, P. D. Investigating the Imidazolium-Anion Interaction Through the Anion-Templated Construction of Interpenetrated and Interlocked Assemblies. *Chem. Eur. J.* **2011**, *17*, 12955–12966.
(370) Li, Y.; Mullen, K. M.; Sardinha, J.; Félix, V.; Beer, P. D. Clipping and Stoppering Anion Templated Synthesis of a [2]Rotaxane Host System. *Dalton Trans.* **2011**, *40*, 12180–12190.
(371) Spence, G. T.; Pitak, M. B.; Beer, P. D. Anion-Induced Shuttling of a Naphthalimide Triazolium Rotaxane. *Chem. Eur. J.* **2012**, *18*, 7100–7108.
(372) White, N. G.; Colaço, A. R.; Marques, I.; Félix, V.; Beer, P. D. Halide Selective Anion Recognition by an Amide-Triazolium Axle Containing [2]Rotaxane. *Org. Biomol. Chem.* **2014**, *12*, 4924–4931.
(373) Mullaney, B. R.; Thompson, A. L.; Beer, P. D. An All-Halogen Bonding Rotaxane for Selective Sensing of Halides in Aqueous Media. *Angew. Chem., Int. Ed*. **2014**, *53*, 11458–11462.
(374) Cornes, S. P.; Davies, C. H.; Blyghton, D.; Sambrook, M. R.; Beer, P. D. Contrasting Anion Recognition Behaviour Exhibited by Halogen and Hydrogen Bonding Rotaxane Hosts. *Org. Biomol. Chem.* **2015**, *13*, 2582–2587.
(375) Martí-Centelles, V.; Beer, P. D. Nitrate Anion Recognition in Organic-Aqueous Solvent Mixtures by a Bis(triazolium) acridine-Containing [2]Rotaxane. *Chem. Eur. J.* **2015**, *21*, 9397–9404.
(376) Gilday, L. C.; White, N. G.; Beer, P. D. Shielded Alkyl-Functionalised Rotaxane Host Cavities for Improved Anion Recognition. *Supramol. Chem.* **2015**, *28*, 62–83.
(377) Sambrook, M. R.; Beer, P. D.; Wisner, J. A.; Paul, R. L.; Cowley, A. R. Anion-Templated Assembly of a [2]Catenane. *J. Am. Chem. Soc.* **2004**, *126*, 15364–15365.
(378) Ng, K.-Y.; Cowley, A. R.; Beer, P. D. Anion Templated Double Cyclization Assembly of a Chloride Selective [2]Catenane. *Chem. Commun.* **2006**, 3676–3678.
(379) Lankshear, M. D.; Evans, N. H.; Bayly, S. R.; Beer, P. D. Anion-Templated Calix[4]arene-Based Pseudorotaxanes and Catenanes. *Chem. Eur. J.* **2007**, *13*, 3861–3870.
(380) Ng, K.-Y.; Félix, V.; Santos, S. M.; Rees, N. H.; Beer, P. D. Anion Induced and Inhibited Circumrotation of a [2]Catenane. *Chem. Commun.* **2008**, 1281–1283.
(381) Huang, B.; Santos, S. M.; Félix, V.; Beer, P. D. Sulfate Anion-Templated Assembly of a [2]Catenane. *Chem. Commun.* **2008**, 4610–4612.
(382) Phipps, D. E.; Beer, P. D. A [2]Catenane Containing an Upper-Rim Functionalized Calix[4]arene for Anion Recognition. *Tetrahedron Lett.* **2009**, *50*, 3454–3457.
(383) Evans, N. H.; Allinson, E. S. H.; Lankshear, M. D.; Ng, K.-Y.; Cowley, A. R.; Serpell, C. J.; Santos, S. M.; Costa, P. J.; Félix, V.; Beer, P. D. Anion Templated Assembly of [2]Catenanes Capable of Chloride Anion Recognition in Aqueous Solvent Media. *RSC Adv.* **2011**, *1*, 995–1003.
(384) Leontiev, A. V.; Serpell, C. J.; White, N. G.; Beer, P. D. Cation-Induced Molecular Motion of Spring-Like [2]Catenanes. *Chem. Sci.* **2011**, *2*, 922–927.
(385) Evans, N. H.; Serpell, C. J.; Beer, P. D. Chloride Anion Templated Synthesis and Crystal Structure of a Handcuff Catenane. *Angew. Chem., Int. Ed*. **2011**, *50*, 2507–2510.
(386) Evans, N. H.; Serpell, C. J.; Beer, P. D. A [2]Catenane Displaying Pirouetting Motion Triggered by Debenzylation and Locked by Chloride Anion Recognition. *Chem. Eur. J.* **2011**, *17*, 7734–7738.
(387) White, N. G.; Beer, P. D. A Catenane Host System Containing Integrated Triazole C–H Hydrogen Bond Donors for Anion Recognition. *Chem. Commun.* **2012**, *48*, 8499–8501.
(388) Caballero, A.; Zapata, F.; White, N. G.; Costa, P. J.; Félix, V.; Beer, P. D. A Halogen-Bonding Catenane for Anion Recognition and Sensing. *Angew. Chem., Int. Ed*. **2012**, *51*, 1876–1880.
(389) Gilday, L. C.; Lang, T.; Caballero, A.; Costa, P. J.; Félix, V.; Beer, P. D. A Catenane Assembled Through a Single Charge-Assisted Halogen Bond. *Angew. Chem., Int. Ed*. **2013**, *52*, 4356–4360.
(390) Gilday, L. C.; Beer, P. D. Halogen- and Hydrogen-Bonding Catenanes for Halide-Anion Recognition. *Chem. Eur. J.* **2014**, *20*, 8379–8385.
(391) Robinson, S. W.; Mustoe, C. L.; White, N. G.; Brown, A.; Thompson, A. L.; Kennepohl, P.; Beer, P. D. Evidence for Halogen Bond Covalency in Acyclic and Interlocked Halogen-Bonding Receptor Anion Recognition. *J. Am. Chem. Soc.* **2015**, *137*, 499–507.
(392) Mullaney, B. R.; Partridge, B. E.; Beer, P. D. A Halogen-Bonding Bis-Triazolium Rotaxane for Halide-Selective Anion Recognition. *Chem. Eur. J.* **2014**, *21*, 1660–1665.
(393) Caballero, A.; Swan, L.; Zapata, F.; Beer, P. D. Iodide-Induced Shuttling of a Halogen- and Hydrogen-Bonding Two-Station Rotaxane. *Angew. Chem., Int. Ed*. **2014**, *53*, 11854–11858.
(394) Langton, M. J.; Beer, P. D. Rotaxane and Catenane Host Structures for Sensing Charged Guest Species. *Acc. Chem. Res.* **2014**, *47*, 1935–1949.
(395) Chae, M. K.; Suk, J.-M.; Jeong, K.-S. A Catenated Anion Receptor Based on Indolocarbazole. *Tetrahedron Lett.* **2010**, *51*, 4240–4242.
(396) Nakatani, Y.; Furusho, Y.; Yashima, E. Amidinium Carboxylate Salt Bridges as a Recognition Motif for Mechanically Interlocked Molecules: Synthesis of an Optically Active [2]Catenane and Control of Its Structure. *Angew. Chem., Int. Ed*. **2010**, *49*, 5463–5467.
(397) Yashima, E.; Maeda, K.; Furusho, Y. Single- and Double-Stranded Helical Polymers: Synthesis, Structures, and Functions. *Acc. Chem. Res.* **2008**, *41*, 1166–1180.
(398) Dixon, I. M.; Rapenne, G. Bridging the Gap: Making the Link in Mechanically Interlocked Chiral Molecules. *Angew. Chem., Int. Ed*. **2010**, *49*, 8792–8794.
(399) Coumans, R. G. E.; Elemans, J. A. A. W.; Thordarson, P.; Nolte, R. J. M.; Rowan, A. E. Synthesis of Porphyrin-Containing [3]Rotaxanes by Olefin Metathesis. *Angew. Chem., Int. Ed*. **2003**, *42*, 650–654.
(400) Thordarson, P.; Bijsterveld, E. J. A.; Rowan, A. E.; Nolte, R. J. M. Epoxidation of Polybutadiene by a Topologically Linked Catalyst. *Nature* **2003**, *424*, 915–918.
(401) Deutman, A. B. C.; Cantekin, S.; Elemans, J. A. A. W.; Rowan, A. E.; Nolte, R. J. M. Designing Processive Catalytic Systems. Threading Polymers Through a Flexible Macrocycle Ring. *J. Am. Chem. Soc*. **2014**, *136*, 9165–9172.
(402) Coumans, R. G. E.; Elemans, J. A. A. W.; Rowan, A. E.; Nolte, R. J. M. Interlocked Porphyrin Switches. *Chem. Eur. J*. **2013**, *19*, 7758–7770.
(403) Iwamoto, H.; Yawata, Y.; Fukazawa, Y.; Haino, T. Tether-Assisted Synthesis of [3]Rotaxane by Olefin Metathesis. *Chem. Lett.* **2010**, *39*, 24–25.
(404) Iwamoto, H.; Yawata, Y.; Fukazawa, Y.; Haino, T. Highly Efficient Synthesis of [3]Rotaxane Assisted by Preorganisation

of Pseudorotaxane Using Bis(crown ether)s. *Supramol. Chem.* **2010**, *22*, 815–826.
(405) Kishan, M. R.; Parham, A.-H.; Schelhase, F.; Yoneva, A.; Silva, G.; Chen, X.; Okamoto, Y.; Vögtle, F. Bridging Rotaxanes' Wheels-Cyclochiral Bonnanes. *Angew. Chem., Int. Ed*. **2006**, *45*, 7296–7299.
(406) Suzaki, Y.; Osakada, K. Ferrocene-Containing [2]- and [3]Rotaxanes. Preparation *via* an End-Capping Cross-Metathesis Reaction and Electrochemical Properties. *Dalton Trans.* **2007**, 2376–2383.
(407) Lees, W. J.; Whitesides, G. M. Equilibrium Constants for Thiol-Disulfide Interchange Reactions: A Coherent, Corrected Set. *J. Org. Chem*. **1993**, *58*, 642–647.
(408) Otto, S.; Furlan, R.; Sanders, J. K. M. Dynamic Combinatorial Libraries of Macrocyclic Disulfides in Water. *J. Am. Chem. Soc.* **2000**, *122*, 12063–12064.
(409) Black, S. P.; Sanders, J. K. M.; Stefankiewicz, A. R. Disulfide Exchange: Exposing Supramolecular Reactivity Through Dynamic Covalent Chemistry. *Chem. Soc. Rev.* **2014**, *43*, 1861–1872.
(410) Kolchinski, A. G.; Alcock, N. W.; Roesner, R. A.; Busch, D. H. Molecular Riveting: High Yield Preparation of a [3]-Rotaxane. *Chem. Commun.* **1998**, 1437–1438.
(411) Furusho, Y.; Hasegawa, T.; Tsuboi, A.; Kihara, N.; Takata, T. "Unlock-Lock" Approach to [2] and [3]Rotaxanes: Entering of a Ring Through Disulfide Linkage That is Unlocked by Thiol "Key". *Chem. Lett.* **2000**, *29*, 18–19.
(412) Yoshii, T.; Kohsaka, Y.; Moriyama, T.; Suzuki, T.; Koyama, Y.; Takata, T. An Efficient Synthetic Entry to Rotaxanes Utilising Reversible Cleavage of Aromatic Disulphide Bonds. *Supramol. Chem.* **2011**, *23*, 65–68.
(413) Oku, T.; Furusho, Y.; Takata, T. First Poly[3]Rotaxane Synthesized Through the Noncovalent Step-Growth Polymerization of a Homoditopic Dumbbell Compound and a Macrocycle with a Reversible Thiol-Disulfide Interchange Reaction. *J. Polym. Sci. Pol. Chem.* **2003**, *41*, 119–123.
(414) Oku, T.; Furusho, Y.; Takata, T. A Concept for Recyclable Cross-Linked Polymers: Topologically Networked Polyrotaxane Capable of Undergoing Reversible Assembly and Disassembly. *Angew. Chem., Int. Ed*. **2004**, *43*, 966–969.
(415) Bilig, T.; Oku, T.; Furusho, Y.; Koyama, Y.; Asai, S.; Takata, T. Polyrotaxane Networks Formed *via* Rotaxanation Utilizing Dynamic Covalent Chemistry of Disulfide. *Macromolecules* **2008**, *41*, 8496–8503.
(416) Zheng, H.; Li, Y.; Zhou, C.; Li, Y.; Yang, W.; Zhou, W.; Zuo, Z.; Liu, H. Synthesis of a [2]Rotaxane Incorporating a "Magic Sulfur Ring" by the Thiol-Ene Click Reaction. *Chem. Eur. J.* **2011**, *17*, 2160–2167.
(417) Wang, W.; Wang, L.; Palmer, B. J.; Exarhos, G. J.; Li, A. D. Q. Cyclization and Catenation Directed by Molecular Self-Assembly. *J. Am. Chem. Soc.* **2006**, *128*, 11150–11159.
(418) West, K. R.; Ludlow, R. F.; Corbett, P. T.; Besenius, P.; Mansfeld, F. M.; Cormack, P. A. G.; Sherrington, D. C.; Goodman, J. M.; Stuart, M. C. A.; Otto, S. Dynamic Combinatorial Discovery of a [2]-Catenane and its Guest-Induced Conversion into a Molecular Square Host. *J. Am. Chem. Soc.* **2008**, *130*, 10834–10835.
(419) Nowak, P.; Colomb-Delsuc, M.; Otto, S.; Li, J. Template-Triggered Emergence of a Self-Replicator From a Dynamic Combinatorial Library. *J. Am. Chem. Soc.* **2015**, *137*, 10965–10969.
(420) Li, J.; Nowak, P.; Fanlo-Virgós, H.; Otto, S. Catenanes from Catenanes: Quantitative Assessment of Cooperativity in Dynamic Combinatorial Catenation. *Chem. Sci.* **2014**, *5*, 4968–4974.
(421) Au-Yeung, H. Y.; Pantoş, G. D.; Sanders, J. K. M. Amplifying Different [2]Catenanes in an Aqueous Donor-Acceptor Dynamic Combinatorial Library. *J. Am. Chem. Soc.* **2009**, *131*, 16030–16032.
(422) Cougnon, F. B. L.; Au-Yeung, H. Y.; Pantoş, G. D.; Sanders, J. K. M. Exploring the Formation Pathways of Donor−Acceptor Catenanes in Aqueous Dynamic Combinatorial Libraries. *J. Am. Chem. Soc.* **2011**, *133*, 3198–3207.
(423) Cougnon, F. B. L.; Ponnuswamy, N.; Jenkins, N. A.; Pantoş, G. D.; Sanders, J. K. M. Structural Parameters Governing the Dynamic Combinatorial Synthesis of Catenanes in Water. *J. Am. Chem. Soc.* **2012**, *134*, 19129–19135.
(424) Au-Yeung, H. Y.; Pantoş, G. D.; Sanders, J. K. M. A Water Soluble Donor-Acceptor [2]Catenane that Can Switch between a Coplanar and a Gemini-Sign Conformation. *Angew. Chem., Int. Ed*. **2010**, *49*, 5331–5334.
(425) Au-Yeung, H. Y.; Pantoş, G. D.; Sanders, J. K. M. Dynamic Combinatorial Synthesis of a Catenane Based on Donor-Acceptor Interactions in Water. *Proc. Natl. Acad. Sci. U.S.A.* **2009**, *106*, 10466–10470.
(426) Au-Yeung, H. Y.; Pengo, P.; Pantoş, G. D.; Otto, S.; Sanders, J. K. M. Templated Amplification of a Naphthalenediimide-Based Receptor from a Donor–Acceptor Dynamic Combinatorial Library in Water. *Chem. Commun.* **2009**, 419–421.
(427) Au-Yeung, H. Y.; Cougnon, F. B. L.; Otto, S.; Pantoş, G. D.; Sanders, J. K. M. Exploiting Donor–Acceptor Interactions in Aqueous Dynamic Combinatorial Libraries: Exploratory Studies of Simple Systems. *Chem. Sci.* **2010**, *1*, 567–574.
(428) Cougnon, F. B. L.; Jenkins, N. A.; Pantoş, G. D.; Sanders, J. K. M. Templated Dynamic Synthesis of a [3]Catenane. *Angew. Chem., Int. Ed*. **2011**, *51*, 1443–1447.
(429) Ponnuswamy, N.; Cougnon, F. B. L.; Clough, J. M.; Pantoş, G. D.; Sanders, J. K. M. Discovery of an Organic Trefoil Knot. *Science* **2012**, *338*, 783–785.
(430) Ponnuswamy, N.; Cougnon, F. B. L.; Pantoş, G. D.; Sanders, J. K. M. Homochiral and Meso Figure Eight Knots and a Solomon Link. *J. Am. Chem. Soc.* **2014**, *136*, 8243–8251.
(431) Drożdż, W.; Kołodziejski, M.; Markiewicz, G.; Jenczak, A.; Stefankiewicz, A. Generation of a Multicomponent Library of Disulfide Donor-Acceptor Architectures Using Dynamic Combinatorial Chemistry. *Int. J. Mol. Sci.* **2015**, *16*, 16300–16312.
(432) Wilson, H.; Byrne, S.; Mullen, K. M. Dynamic Covalent Synthesis of Donor-Acceptor Interlocked Architectures in Solution and at the Solution: Surface Interface. *Chem. Asian J.* **2015**, *10*, 715–721.
(433) Furusho, Y.; Rajkumar, G. A.; Oku, T.; Takata, T. Synthesis of [2]Rotaxanes by Tritylative Endcapping of *in situ* Formed Pseudorotaxanes Having Thiol or Hydroxyl Functionality on the Axle Termini. *Tetrahedron* **2002**, *58*, 6609–6613.
(434) Finkelstein, H. Darstellung organischer Jodide aus den entsprechenden Bromiden und Chloriden. *Ber. Dtsch. Chem. Ges.* **1910**, *43*, 1528–1532.
(435) Miljanić, O. Š.; Stoddart, J. F. Dynamic Donor-Acceptor [2]Catenanes. *Proc. Natl. Acad. Sci. U.S.A.* **2007**, *104*, 12966–12970.
(436) Olson, M. A.; Coskun, A.; Fang, L.; Basuray, A. N.; Stoddart, J. F. Polycatenation under Thermodynamic Control. *Angew. Chem., Int. Ed*. **2010**, *49*, 3151–3156.
(437) Patel, K.; Miljanić, O. Š.; Stoddart, J. F. Iodide-Catalysed Self-Assembly of Donor-Acceptor [3]Catenanes. *Chem. Commun.* **2008**, 1853–1855.
(438) Reuter, C.; Vögtle, F. Rotaxanes *via* Michael Addition. *Org. Lett*. **2000**, *2*, 593–595.
(439) Cagulada, A. M.; Hamilton, D. G. An Approach to Thermodynamically Controlled Supramolecular Assembly Possessing an Integral Locking Mechanism. *J. Am. Chem. Soc.* **2009**, *131*, 902–903.
(440) Goldup, S. M.; Leigh, D. A.; Lusby, P. J.; McBurney, R. T.; Slawin, A. M. Z. Active Template Synthesis of Rotaxanes and Molecular Shuttles with Switchable Dynamics by Four-Component Pd^{II}-Promoted Michael Additions. *Angew. Chem., Int. Ed*. **2008**, *47*, 3381–3384.
(441) Willner, I.; Basnar, B.; Willner, B. From Molecular Machines to Microscale Motility of Objects: Application as "Smart

Materials," Sensors, and Nanodevices. *Adv. Funct. Mater.* **2007**, *17*, 702–717.
(442) Coronado, E.; Gaviña, P.; Tatay, S. Catenanes and Threaded Systems: From Solution to Surfaces. *Chem. Soc. Rev.* **2009**, *38*, 1674–1689.
(443) Davis, J. J.; Orlowski, G. A.; Rahman, H.; Beer, P. D. Mechanically Interlocked and Switchable Molecules at Surfaces. *Chem. Commun.* **2010**, *46*, 54–63.
(444) Lu, T.; Zhang, L.; Gokel, G. W.; Kaifer, A. E. The First Surface-Attached Catenane: Self-Assembly of a Two-Component Monolayer. *J. Am. Chem. Soc.* **1993**, *115*, 2542–2543.
(445) Castro, R.; Nixon, K. R.; Evanseck, J. D.; Kaifer, A. E. Effects of Side Arm Length and Structure of *Para*-Substituted Phenyl Derivatives on Their Binding to the Host Cyclobis(paraquat-*p*-phenylene). *J. Org. Chem.* **1996**, *61*, 7298–7303.
(446) Castro, R.; Davidov, P. D.; Kumar, K. A.; Marchand, A. P.; Evanseck, J. D.; Kaifer, A. E. Inclusion Complexation of Cyclobis(paraquat-*p*-phenylene) and Related Cyclophane Derivatives with Substituted Aromatics: Cooperative Non-Covalent Cavity and External Interactions. *J. Phys. Org. Chem.* **1997**, *10*, 369–382.
(447) Katz, E.; Sheeney-Haj-Ichia, L.; Willner, I. Electrical Contacting of Glucose Oxidase in a Redox-Active Rotaxane Configuration. *Angew. Chem., Int. Ed*. **2004**, *43*, 3292–3300.
(448) Katz, E.; Lioubashevsky, O.; Willner, I. Electromechanics of a Redox-Active Rotaxane in a Monolayer Assembly on an Electrode. *J. Am. Chem. Soc.* **2004**, *126*, 15520–15532.
(449) Katz, E.; Baron, R.; Willner, I.; Richke, N.; Levine, R. D. Temperature-Dependent and Friction-Controlled Electrochemically Induced Shuttling Along Molecular Strings Associated with Electrodes. *ChemPhysChem* **2005**, *6*, 2179–2189.
(450) Kern, J.-M.; Raehm, L.; Sauvage, J.-P. Formation of a Copper(I) Catenate on an Electrode Surface *via* S-Au Interactions. *C. R. Acad. Sci., Paris, IIc* **1999**, *2*, 41–47.
(451) Raehm, L.; Hamann, C.; Kern, J.-M.; Sauvage, J.-P. Synthesis of Copper(I) Catenanes Incorporating a Disulfide Bridge and Their Deposition on a Gold Surface. *Org. Lett.* **2000**, *2*, 1991–1994.
(452) Raehm, L.; Kern, J.-M.; Sauvage, J.-P.; Hamann, C.; Palacin, S.; Bourgoin, J.-P. Disulfide- and Thiol-Incorporating Copper Catenanes: Synthesis, Deposition onto Gold, and Surface Studies. *Chem. Eur. J.* **2002**, *8*, 2153–2162.
(453) Weber, N.; Hamann, C.; Kern, J.-M.; Sauvage, J.-P. Synthesis of a Copper [3]Rotaxane Able to Function as an Electrochemically Driven Oscillatory Machine in Solution, and to Form SAMs on a Metal Surface. *Inorg. Chem.* **2003**, *42*, 6780–6792.
(454) Otter, C. A.; Patty, P. J.; Williams, M. A. K.; Waterland, M. R.; Telfer, S. G. Mechanically Interlocked Gold and Silver Nanoparticles Using Metallosupramolecular Catenane Chemistry. *Nanoscale* **2011**, *3*, 941–944.
(455) Vance, A. L.; Willey, T. M.; van Buuren, T.; Nelson, A. J.; Bostedt, C.; Fox, G. A.; Terminello, L. J. XAS and XPS Characterization of a Surface-Attached Rotaxane. *Nano Lett.* **2003**, *3*, 81–84.
(456) Bayly, S. R.; Gray, T. M.; Chmielewski, M. J.; Davis, J. J.; Beer, P. D. Anion Templated Surface Assembly of a Redox-Active Sensory Rotaxane. *Chem. Commun.* **2007**, 2234–2236.
(457) Zhao, L.; Davis, J. J.; Mullen, K. M.; Chmielewski, M. J.; Jacobs, R. M. J.; Brown, A.; Beer, P. D. Anion Templated Formation of Pseudorotaxane and Rotaxane Monolayers on Gold From Neutral Components. *Langmuir* **2009**, *25*, 2935–2940.
(458) Evans, N. H.; Rahman, H.; Leontiev, A. V.; Greenham, N. D.; Orlowski, G. A.; Zeng, Q.; Jacobs, R. M. J.; Serpell, C. J.; Kilah, N. L.; Davis, J. J.; Beer, P. D. Solution and Surface-Confined Chloride Anion Templated Redox-Active Ferrocene Catenanes. *Chem. Sci.* **2012**, *3*, 1080–1089.
(459) Lehr, J.; Lang, T.; Blackburn, O. A.; Barendt, T. A.; Faulkner, S.; Davis, J. J.; Beer, P. D. Anion Sensing by Solution- and Surface-Assembled Osmium(II) Bipyridyl Rotaxanes. *Chem. Eur. J.* **2013**, *19*, 15898–15906.
(460) Arduini, A.; Ferdani, R.; Pochini, A.; Secchi, A.; Ugozzoli, F. Calix[6]arene as a Wheel for Rotaxane Synthesis. *Angew. Chem., Int. Ed. Engl*. **2000**, *39*, 3453–3456.
(461) Hu, C.; Lan, Y.; Tian, F.; West, K. R.; Scherman, O. A. Facile Method for Preparing Surface-Mounted Cucurbit[8]uril-Based Rotaxanes. *Langmuir* **2014**, *30*, 10926–10932.
(462) Cecconello, A.; Lu, C.-H.; Elbaz, J.; Willner, I. Au Nanoparticle/DNA Rotaxane Hybrid Nanostructures Exhibiting Switchable Fluorescence Properties. *Nano Lett.* **2013**, *13*, 6275–6280.
(463) Fuchs, B.; Nelson, A.; Star, A.; Stoddart, J. F.; Vidal, S. Amplification of Dynamic Chiral Crown Ether Complexes During Cyclic Acetal Formation. *Angew. Chem., Int. Ed*. **2003**, *42*, 4220–4224.

Part 3

Cultivating Mechanical Bonds

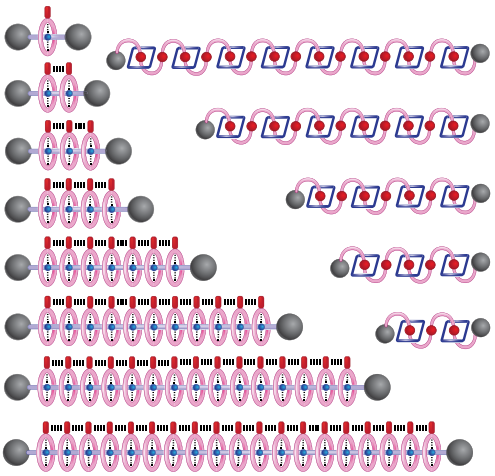
Chapter 4 Molecular Topologies and Architectures with Mechanical Bonds

Conspectus

Classically, the structure of a chemical compound can be described by three C's—its constitution, its configuration (relative and absolute), and its conformation. Introducing knotted and interlocked rings into the molecular potpourri leaves us confronted with also having to consider a molecule's *topology*, whilst recognizing that the three C's are obliged to come under serious scrutiny—given their classical roots and definitions—so much so that we find it convenient to advocate the use of the qualified descriptors—namely, *co-constitution*, *co-configuration* and *co-conformation*—to define the structures of mechanomolecules. In the realm of chemical topology, rotaxanes are positioned poles apart from catenanes—a dichotomy which has led us to refer in this Chapter to a catenane's *topology* and a rotaxane's *architecture* and, moreover, it is why this book as a whole cannot be an account of the nature of the *topological* bond, yet it can, catenanes willing, be a story about the nature of the *mechanical bond*.

Catenane topologies, be they based on prime links or composite ones, wherein mechanically interlocked rings displayed in linear, branched and radial (molecular necklaces) fashions, have been very much at the forefront—and ahead of rotaxanes at the outset—of the agendas of synthetic chemists targeting intellectually challenging unnatural products. Despite much effort and commitment, however, this community has still to uncover high molecular weight polycatenanes that can be produced on a commercial scale at the drop of a hat. They are a 'holy grail' in the field since there is every reason to believe that polycatenanes, with appropriate co-constitutions, will display unique thermal and viscoelastic properties, making them much sought after as plasticizers in everything from concrete to rocket fuel.

As time has progressed, catenanes have assumed ever more complex multi-annulated co-constitutions incorporating macrobi-, -tri-, -tetra-, and -pentacyclic component parts, not to mention covalently bridged ones known as pseudocatenanes. Hopf links have also intruded into the mesomolecular domain with cyclic oligo[2]catenanes, and main-chain/side-chain poly[2]catenanes. Lurking inside all this impressive array of complex co-constitutions are thousands of conventional polymer networks that become entangled in the solid state. These entangled networks emerge more commonly from the multi-annulated structures associated with cages and two- or three-dimensional polymer nets. Interpenetrated and polycatenated networks pervade the realm of coordination polymers, also known as metal-organic frameworks (MOFs), where more often than not the solid-state (super)structures tell us that the crystal is the (super)molecule and the (super)molecule is the crystal.



The sky is the limit when rotaxane architectures are brought into the picture. Simply limiting the component parts to dumbbells and rings alone opens up architectures involving (i) one dumbbell and many rings, (ii) one ring with many dumbbells (molecular sheafs), (iii) many rings and many dumbbells. While architectures finding their niche in categories (ii) and (iii) are not yet commonplace, coming out of category (i), main chain [*n*]rotaxane polymers are not only ubiquitous, they are also abundant. In particular, the promiscuous manner in which cyclodextrins (CDs) thread in aqueous solutions onto polymers—be they polyethers, -esters, -amides, -olefins, etc.—has been taken to the extremes for good reason. For example, the fact that CDs threaded onto π-conjugated polymers enhances their optical, electrical and luminescent properties drives research along in the direction of providing new electroluminescent display technologies, including light-emitting diodes (LEDs). Cucurbituril (CB) threaded polymers have commonly surfaced following either crystal growth of rotaxanated coordination polymers or from cucurbit[6]uril-promoted azide-alkyne cycloadditions (CB6AAC) where the introduction of CDs can lead to spectacular yields of high molecular weight polyrotaxanes by what has been dubbed *cooperative capture synthesis*. The hydrogen bonding between the CB and CD rings acts orthogonally and in concert with solvophobic templation to orchestrate high atom-efficient polymerizations. The theme of "the bigger, the better" when it comes to [*n*]rotaxanes carries over to the making of oligorotaxanes under thermodynamic control where strong hydrogen bonding conspires with stabilizing π–π interactions exercising positive cooperativity to produce disctrete mechanomolecules as large as a [20]rotaxane with dynamic covalent chemistry playing a helping hand with awesome aplomb. Not to be outdone, donor-acceptor templation between donating threads and accepting rings can produce foldamers, demonstrating that the mechanical bond can be deployed as a tool to install well-defined secondary structures into macromolecules.

Rotaxane architectures stretch far and wide embracing within their remit (Type 1) dendrimers with rotaxane cores, (Type II) dendrimers with (pseudo)rotaxane termini, and (Type III) dendrimers with rotaxane branches, not to mention covalently bridged rotaxanes, including [1]rotaxane (the molecular ouroboros), daisy chains, ladder rotaxanes, Bonnanes, handcuff rotaxanes, molecular bundles, slide-ring gels, rotacatenanes, ring-in-ring mechanomolecules, suitanes etc., etc., etc. The list will continue to grow at a high rate of knots!

The Nature of the Mechanical Bond: From Molecules to Machines, First Edition. Carson J. Bruns and J. Fraser Stoddart.
© 2017 John Wiley & Sons, Inc. Published 2017 by John Wiley & Sons, Inc.

Introduction **351**
4.1 Catenane Topologies **352**
4.1.1 Prime Links 352
4.1.1.1 Solomon Link 354
4.1.1.2 Star of David 356
4.1.1.3 Borromean Rings (BRs) 356
4.1.1.4 Cyclic [3]Catenane 359
4.1.1.5 Whitehead Link 360
4.1.1.6 12-Crossing [4]Catenane 360
4.1.2 Composite Links 361
4.1.2.1 Linear [n]Catenanes 361
4.1.2.2 Radial [n]Catenanes – Molecular Necklaces 364
4.1.2.3 Branched [n]Catenanes 368
4.1.3 Multi-Annulated Catenanes 369
4.1.3.1 Catenated Macrobicyclics 370
4.1.3.2 Catenated Macrotricyclics 375
4.1.3.3 Catenated Macrotetracyclics 378
4.1.3.4 Catenated Macropentacyclics 378
4.1.3.5 Topologically Entangled Networks 379
4.1.4 Covalently Bridged Catenanes 386
4.1.4.1 [2]Pseudocatenanes/Pretzelanes 386
4.1.4.2 [3]Pseudocatenanes/Handcuff Catenanes 386
4.1.4.3 [4]Pseudocatenanes 386
4.1.4.4 Cyclic Oligo[2]catenanes 387
4.1.4.5 Acyclic Oligo- and Poly[2]catenanes 388
4.2 Rotaxane Architectures **392**
4.2.1 [*n*]Rotaxanes 392
4.2.1.1 Single-Axle Oligo- and Polyrotaxanes 392
4.2.1.2 Multi-Axle Rotaxanes/Molecular Sheafs 411
4.2.1.3 Multi-Annulated [n]Rotaxanes 414
4.2.2 Dendritic Rotaxanes 416
4.2.2.1 Type I Rotaxane Dendrimers 417
4.2.2.2 Type II Rotaxane Dendrimers 419
4.2.2.3 Type III Rotaxane Dendrimers 420
4.2.3 Covalently Bridged Rotaxanes 424
4.2.3.1 [1]Rotaxanes 424
4.2.3.2 Daisy Chains 427
4.2.3.3 Ladder Rotaxanes 430
4.2.3.4 Bonnanes/Handcuff Rotaxanes 431
4.2.3.5 n*-Fold [2]Rotaxanes: Molecular Bundles* 433
4.2.3.6 One-Dimensional Oligo- and Poly[2]rotaxanes 434
4.2.3.7 One-Dimensional Poly[3]rotaxanes 437
4.2.3.8 Extended Polyrotaxane Networks 438
4.3 Other Architectures with Mechanical Bonds **441**
4.3.1 Catenarotaxanes 441
4.3.2 Rotamacrocycles 442
4.3.3 Ring-in-Ring Mechanomolecules 442
4.3.4 Self-Threaded Macropolycyclics 443
4.3.5 Suitanes 444
4.3.6 Foldaxanes 444
4.3.7 Braided and Interwoven Polymer Entanglements 444
Conclusions and Outlook **444**
References **445**

Introduction

In the wake of having featured the remarkably diverse set of strategies, templates, and reactions employed in the synthesis of mechanical bonds under both kinetic (**Chapter 2**) and thermodynamic (**Chapter 3**) control, we turn our attention now to illustrating the mechanically bonded topologies and architectures that have been built upon this foundation. Rather than revisiting the synthetic details, which are described in the previous two Chapters, this image-driven Chapter will serve as a gallery for showcasing many of the mechanically interlocked structures that have emerged during the evolution of the mechanical bond in chemistry. Mechanomolecules can be classified into catenane topologies (**Section 4.1**), rotaxane architectures (**Section 4.2**), or other (**Section 4.3**) categories. Before perusing the cornucopia of mechanomolecular structures, we pause to introduce the language that is employed to describe them.

The Vernacular of Mechanomolecules

Names like 'catenane' or 'rotaxane' convey a lot of ambiguity and do not represent any specific molecular composition—instead they only indicate the type of mechanical bond at a very general level. Moreover, it is extremely impractical, in most cases, to describe the exact co-constitution of a mechanomolecule exhaustively using only words. The mechanical bond has added such a high level of complexity to molecules that it forces IUPAC nomenclature[1,2] out of the picture from a practical standpoint, since all but the very simplest of catenanes and rotaxanes generate IUPAC names of debilitating length and convolution. Therefore, images must bear most of the weight in communicating mechanically interlocked molecule (MIM) structures. Images are indispensible to mechanostereochemistry because they disclose structural, topological, and compositional characteristics of molecules far more concisely and accurately than do words. As such, images in mechanostereochemistry have been on a trajectory of continuous evolution that has improved the efficiency and clarity with which they convey information—see **Section 1.2**. The nomenclature discussion is, nevertheless, important for the sake of maintaining clarity and consistency in the literature, as confusion would reign if every paper contained a different nickname for the same interlocked architecture.

The reality of naming conventions, for better or worse, is that some names receive widespread adoption in the literature, while others fail to garner support. It is clear that 'catenane' and 'rotaxane' are employed ubiquitously, as are the bracketed prefixes [*n*] to denote the number of mechanically bonded component parts, yet variations on the traditional architectures that seem to call for new naming conventions have typically been received with, at best, partial acceptance of the proposed name from the community, or at worst, a lack of any attempt to propose a naming convention at all. Take, for example, the simplest combination of a catenane and rotaxane—a link interlocked with a dumbbell. This catenane/rotaxane hybrid architecture (**Section 4.3.1**) has been called a 'rotacatenane' by some[3] and 'catrotaxane' by others,[4] while IUPAC[1] prefers 'catenarotaxane'. Another case-in-point is the growing number of multiply interlocked cryptands, cages, and other polycyclic molecules throughout **Section 4.1.3** and **4.2.1.3** that have not been distinguished from other types of catenanes with a concise terminology.

Attempts have been made, most notably by Vögtle,[4] to impose a systematic nomenclature for mechanomolecules that is suitable for widespread adoption, but as yet to no avail. Over a decade has passed and a widely adopted nomenclature is still nowhere in sight. The strength of Vögtle's nomenclature—the most systematic one to be advanced thus far—is its modularity. The rules are robust enough that more or less any interlocked architecture—even those with combined mechanical and covalent linkages between component parts—can be named unambiguously. Each interlocked component is assigned a sequential number, and its linkage with the other components is described using short abbreviations like "mec" for mechanical and "cov" for covalent. In other words, it is possible in principle to draw the graph of a MIM based only on its name. The same nomenclature suffers, however, from potentially long strings of numbers and letters within brackets. For example, a pair of [2]rotaxanes bridged by covalent linker connecting the rings can be called a bis[2]-rotaxane ambiguously, or it can be called a [2^{ax1meccy2}-(cy2covcy3)-2^{cy3mecax4}]rotaxane unambiguously.

We advocate the use of a 'vernacular nomenclature' that sacrifices rigorous naming accuracy for the sake of brevity and memorability. A nearly perfect analogy to this practice is already omnipresent in organic chemistry. Though an IUPAC name can be generated for almost any organic molecule, many compounds have a trivial name—also known as a common name or vernacular name—for the same reason that the systematized titles are too cumbersome. For example, caffeine and cholesterol are often more convenient names than 1,3,7-trimethyl-1*H*-purine-2,6(3*H*,7*H*)-dione and 10,13-dimethyl-17-(6-methylheptan-2-yl)-2,3,4,7,8,9,11,12,14,15,16,17-dodecahydro-1*H*-cyclopenta[a]phenanthren-3-ol, respectively. Caffeine and cholesterol also come with absolute stereogenic centers that are defined by the trivial name. When in comes to carbohydrates[A]—in common with cholesterol—the IUPAC names are almost never used. In addition to brevity, one of the most attractive roles of a vernacular nomenclature is the freedom and fun of naming a new type of MIM according to the discoverer's creative preferences, not unlike the inventors of synthetic elements such as Americium, Curium, Berkelium, Californium, Einsteinium, etc. Furthermore, just as IUPAC and trivial names coexist

[A] In carbohydrate chemistry, in the case of the hexoses, descriptors like, e.g., Glu, Gal, Man, etc. define the relative configurations of four stereogenic centers. The D and L descriptors then define the absolute configuration, while α and β define the relative configurations of a fifth stereogenic center at the anomeric carbon atom.

in organic chemistry, so can a vernacular nomenclature coexist with a more systematically robust one likened to that proposed[4] by Vögtle in mechanostereochemistry, if such a nomenclature ever comes to pass. Problems of naming incongruencies still persist, however, as we have alluded to in the case of rotacatenanes. We believe that a vernacular nomenclature that is both ubiquitous and systematic—to the fullest extent that a trivial nomenclature can be—is both desirable and achievable. Toward these ends, we proffer the following suggestions for a vernacular naming system in mechanostereochemistry:

1. *Pragmatic systematic*. If an all-encompassing systematic naming convention is either unattainable or widely ignored, then we can at least try to build systematic features into the vernacular nomenclature according to 'classes' of MIMs with analogous structural features. Take suit[*n*]anes (**Section 4.3.5**) as an example. A four-limbed molecular body encompassed by a 'molecular suit' has not been reported to our knowledge, but we know it will be named a suit[4]ane if it ever materializes.

2. *She who installs it, calls it*. The right to name a new class of interlocked compounds should belong to the first person(s) to synthesize it. This code of conduct would simplify the literature by eradicating 'naming competitions' in which different camps of researchers try to push their own brand name. It would also prevent the stigmatized practice of 'patenting' exotic compounds that do not yet exist.

3. *If it looks like a duck…*If images are the most important bits of information for conveying the structure of a MIM, then the best name is one that readily paints a mental picture. One of the most effective ways to instill a mental image of a structure is to compare it with an already familiar object. Catenanes and rotaxanes are based on this principle (recall the Latin roots: *catena* = chain, *rota* = wheel, *axis* = axle). In this regard, molecular Solomon links (**Section 4.1.1.1**), Stars of David (**Section 4.1.1.2**), Borromean rings (**Section 4.1.1.3**), Olympiadanes (**Section 4.1.2.1**), molecular necklaces (**Section 4.1.2.2**), pretzelanes (**Section 4.1.4.1**), handcuff catenanes (**Section 4.2.3.4**) daisy chains (**Section 4.2.3.2**), molecular sheafs (**Section 4.2.1.2**), and suitanes (**Section 4.3.5**) are exemplary.

4. *Try that in some Latin*. MIMs already have an established history of invoking Latin roots, and Latin is still commonly drawn from to create new words in English. Greek roots also have precedence in supramolecular chemistry (e.g., cryptands) when naming new classes of compounds. Thus, it may be appropriate to turn to Latin or Greek when English fails to yield an appropriate name for a MIM.

5. *Don't reinvent the wheel (and axle)*. Since most MIMs are derived from catenanes, rotaxanes, and knots, it might be preferable in some cases to add a simple prefix or suffix to the very familiar 'catenane' or 'rotaxane' roots in order to assist with mental imagery, as in the case of rotacatenanes (**Section 4.3.1**), pseudocatenanes (**Sections 4.1.4.1–4.1.4.3**), branched/dendritic rotaxanes (**Section 4.2.2**), and so on.

With these suggestions in mind, we have amassed in this Chapter a compilation of different known types of mechanically interlocked topologies and architectures, using (when possible) the vernacular names that were originally coined in the literature as the convention of choice for describing them. We conclude our introduction to the vernacular nomenclature with the acknowledgement that such a nomenclature is far from perfect. New species of mechanomolecules that do not fit cleanly into any category—see **Section 4.3**—will continue to emerge. It will be up to the inventors of these future MIMs to introduce their own vernacular, or else to suffer the inadequacies of a more general name such as [*n*]rotaxane with qualifying descriptors.

Line drawings depicting the simplified topologies and architectures of the mechanomolecules described in this Chapter are compiled in **Figure 4.0**. Images of each topology/architecture serve as hyperlinks to their corresponding Section headings in the digital version of the monograph.

4.1 Catenane Topologies

Catenanes and rotaxanes are readily distinguished on the basis of topological arguments.[5] Rotaxanes are said to be topologically trivial because their component parts may be dissociated through continuous deformation without allowing covalent bonds to break or pass through one another, in contrast with catenanes, which assume the non-trivial topologies of links. In other words, the mechanical bond of a catenane is also a topological bond, yet the mechanical bond of a rotaxane is not. These topological differences explain why it is more appropriate to refer to a rotaxane's *architecture* (**Section 4.2**) than to its *topology*. A discussion of chemical topology can be found in **Section 5.2.4**, as well as in **Section 1.3.2** and in the Introduction to **Chapter 2**. In this Section we survey many types of catenated molecular topologies (**Figure 4.0**), including prime links (**Section 4.1.1**) beyond the simplest [2]catenane Hopf links, as well as composite links constituting linear, radial, and branched [*n*]catenanes (**Section 4.1.2**), multi-annulated catenanes based on macrobicyclic, macrotricyclic, macrotetracyclic, and macropentacyclic component parts (**Section 4.1.3**), and covalently bridged catenanes (**Section 4.1.4**).

4.1.1 Prime Links

A prime link is defined[6] in mathematics as a link that cannot be represented as a knot sum of other links, while a link comprising combinations of other links is known as a composite link—see **Section 4.1.2**. Only a few prime link topologies (**Figure 4.1**) have been engendered in molecules. The simplest prime link, which is also known as the Hopf link, is catalogued in Alexander-Briggs[7] notation as the

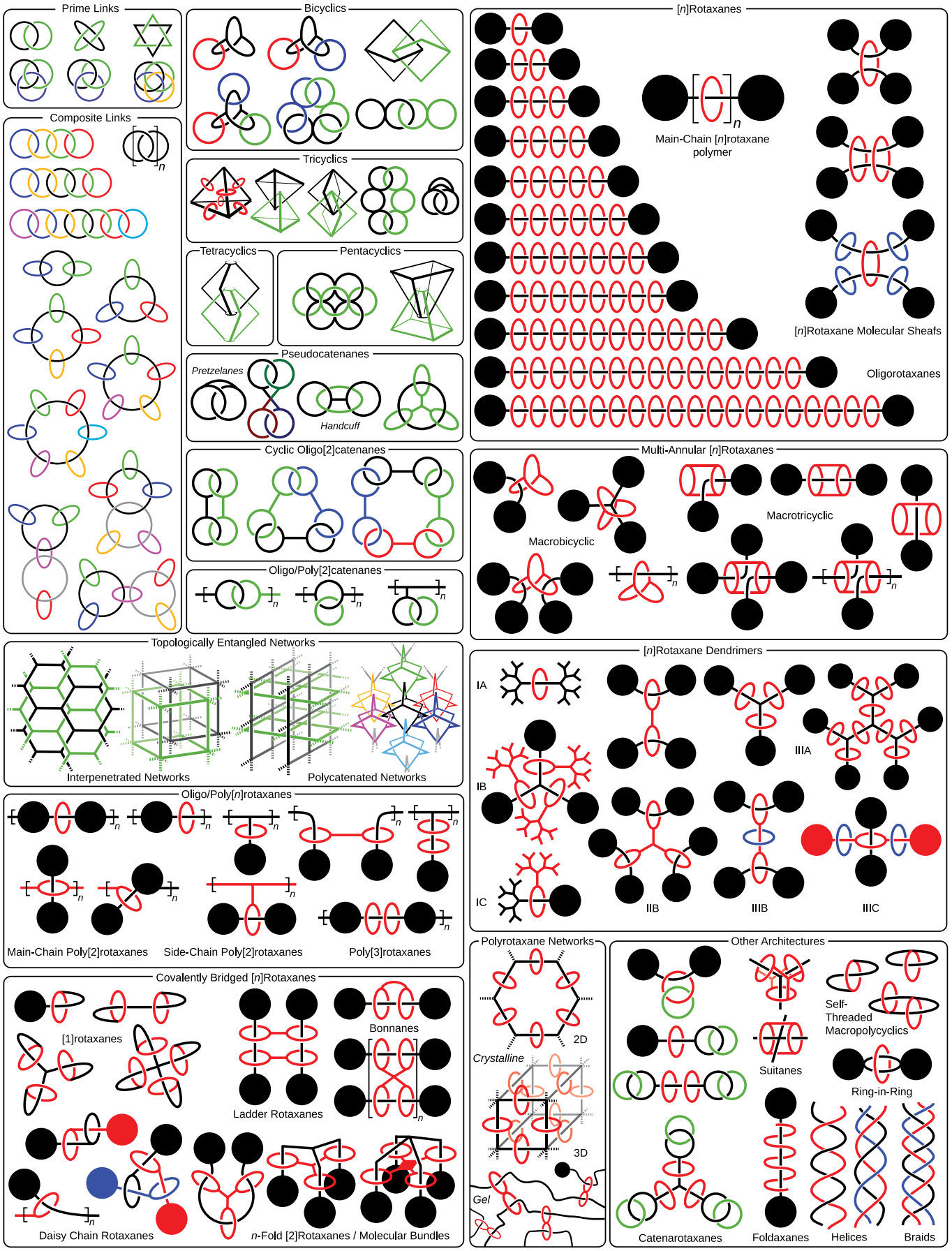


Figure 4.0 Line drawings of molecular catenane topologies and rotaxane architectures.

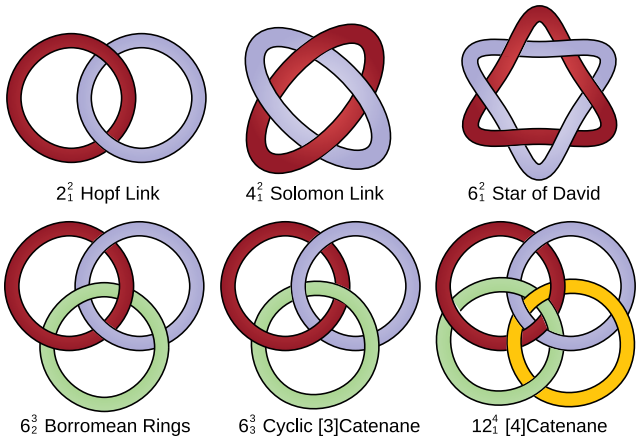


Figure 4.1 Graphical illustrations of the prime link topologies that have been realized synthetically in molecular forms.

2_1^2 link, signifying that its graph (i) possesses two crossings, (ii) two component parts (superscripted), and (iii) an assigned number (subscripted) which differentiates it from other links of equal crossing number. Since there is only one two-crossing prime link, the subscript is unnecessary in this case, yet it becomes important when differentiating between links possessing six or more crossings. A few of the simplest prime link topologies possess special names, such as the 6_2^3 Borromean rings (**Section 4.1.1.3**) and the 5_1^2 Whitehead link (**Section 4.1.1.5**). Some synthetic prime links have been nicknamed by chemists, such as the 4_1^2 Solomon link[8] (**Section 4.1.1.1**), the 6_1^2 Star of David link[9] (**Section 4.1.1.2**), and the 6_3^3 cyclic [3]catenane[10] (**Section 4.1.1.4**). Examples of molecules possessing these higher order prime link topologies remain exceedingly rare—a symptom of their synthetically challenging molecular structures. Many of the as-yet-unrealized molecular link topologies remain as potential targets for ambitious synthetic chemists to tackle in the future. The prime link topologies with less than eight crossings are illustrated in **Section 1.3.2**, **Figure 1.22**. The Whitehead link and the 6_1^3 link, which has been called[10] a closed three-link chain, appear to be the simplest prime link topologies that remain to be realized in molecular form at the beginning of 2016.

4.1.1.1 Solomon Link

The 4_1^2 link in Alexander-Briggs notation possesses the topology known as the Solomon Knot, named after the Biblical King Solomon. Since this topology is a link rather than a knot, it has also been called[8] a Solomon link. The Solomon link wears other hats in molecular chemistry as a doubly interlocked,[11] doubly braided,[12] or four-crossing[13] [2]catenane. See **Section 1.1.2** for more information on the history and cultural significance of Solomon links.

The vast majority of molecular Solomon links (**Figure 4.2**) rely on metal centers as templates and/or as kinetically labile hinges that promote self-assembly under thermodynamic control. Sauvage's original tricopper(I) Solomon link[11,13] **Cu_3C401^{3+}**, as well as one[14] (**Li_3C402^{3+}**) based on Li^+ templates and ring-closing olefin metathesis, rely on metals to template the formation of the necessary trinuclear double-stranded helicate precursors. In 1998, Sauvage and Fujita[15] reported the accidental discovery of the Solomon link **Cu_2C403^{10+}**, comprising Pd^{II}-bridged metallacycles and Cu^{I} templates. More recently, Severin[16] has assembled a much larger Solomon Link (**Cu_6C404^{30+}**) comprising a doubly interlocked pair of hexameric Pd^{II} metallacycles, coordinating six Cu^{I} templates. In 2000, Puddephatt[12,17] discovered the organometallic Solomon link **C405**, which relies on aurophilic interactions between phosphine-bridged Au^{I} acetylide metallacycles in order to generate its doubly interlocked structure. The Solomon link[8] **$Cu_2Zn_2C406^{8+}$**, which is derived from the same *exo*-bidentate bipyridyl and *endo*-tridentate diiminopyridyl ligands employed in the synthesis[18] of the molecular Borromean rings (**Section 4.1.1.3**), constitutes yet another unexpected discovery—see **Section 1.3.5**. **M_4C406^{8+}** homologues based on Zn^{II} and Cd^{II} templates were also found[19] to form alongside the Borromean rings under some circumstances.[B] A very similar set of ligands has been employed by Charbonnière and Trabolsi[20] in their assembly of the Solomon link **Zn_4C407^{8+}**, along with a Hopf link and a trefoil knot, all in a single one-pot reaction, while Leigh[21] has employed tetrameric Fe^{II} circular helicates in the self-assembly of the Solomon Link **Fe_4C408^{8+}**. An 'interwoven supramolecular grid' comprising a criss-crossed mesh of bis(benzimidazolepyridyl) benzthiazolo[4,5-d]thiazole ligands chelating four divalent metal cations has also served[22] as a template for the Solomon links **M_4C409^{8+}**, where M is Zn^{II}, Fe^{II}, or Co^{II}. The Solomon catenand **C409** can be isolated upon demetalation of the corresponding Solomon catenate.

Most of the Solomon links reported in the literature are homo[2]catenanes. By relying on π-associated donor-acceptor interactions between electron-rich crown ethers and kinetically labile electron-poor metallacyclic hosts inspired by Fujita's molecular squares,[23] Peinador and Quintela[24] succeeded in assembling the first hetero[2]catenanes (**$C410^{8+}$**) possessing the topology of a Solomon link. Tetrathiafulvalene (TTF) and 1,5-dioxynaphthalene (DNP) units have also been incorporated[25] into homologous Solomon links. The topology of the bistable Solomon link **$C410e^{8+}$** gives rise to a unique type of mechanical motion resembling that of a conveyor belt when the catenane is switched (**Section 6.13.12**) in response to redox stimuli.

Compounds **Cu_6C404^{30+}**, **C405**, **$Cu_2Zn_2C406^{8+}$**, **Fe_4C408^{8+}**, **Zn_4C409^{8+}**, and **$C410^{8+}c$** have been structurally characterized in the solid state by X-ray crystallography. These structures

[B] The all-Zn^{II} and all-Cd^{II} Solomon Links are minor side products found in the crude powders obtained in the assembly of the corresponding Borromean Rings. Crystals of the former were separated from the Borromean ones by hand. While the Cd^{II} Solomon Links were not obtained as high-quality single crystals, they represent the largest fraction of the dynamic combinatorial library among the metals investigated, since they are populated in up to a 10:9 ratio.

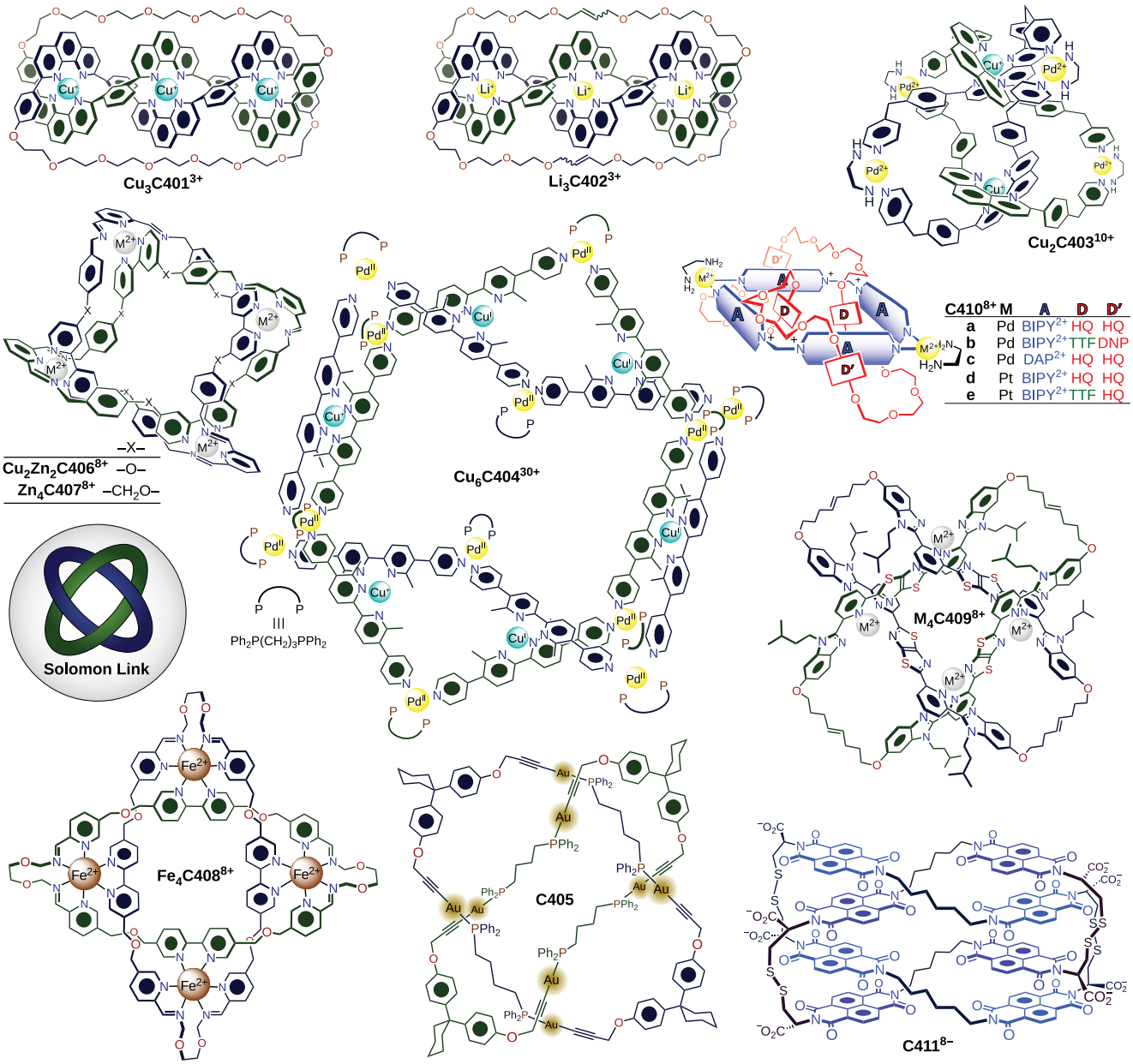


Figure 4.2 Stereoformulas of molecular Solomon links.[8,11–17,19–22,24–26]

are illustrated (**Figure 5.40**) in **Section 5.2.4.1**, which features a discussion of their topological chirality.

The only examples up to now of molecular Solomon links that do not rely on metals are anionic MIMs based on aqueous dynamic combinatorial libraries[26] (DCLs) or self-assembled DNA nanostructures.[27] Sanders[26] introduced the Solomon link **C411**$^{8-}$, which self-assembles in water as a member of a DCL derived from cystine-terminated naphthalenediimide (NDI) dimers bridged by hexamethylene linkers. The self-assembly of these dimers into catenated and knotted structures is driven mainly by the hydrophobic effect, suggesting that aggregation driven by hydrophobic collapse might be a more broadly applicable approach to synthetic chemical topology. The self-assembly of Seeman's DNA

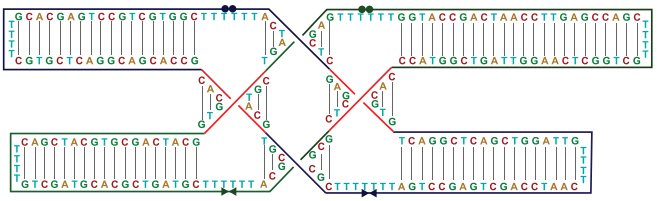


Figure 4.3 Diagram of Seeman's DNA Solomon link,[27] which relies on Watson-Crick base pairing (C = cytosine, G = guanine, A = adenine, T = thymine) to bring four single DNA strands together into a pair of doubly interlocked loops conjoined at the 5′–5′ (circles) and 3′–3′ (arrowheads) ends. Segments in red are L-nucleotides, which are employed instead of D-nucleotides in order to induce the opposite helicity at two of the nodes, which is required to template the Solomon link.

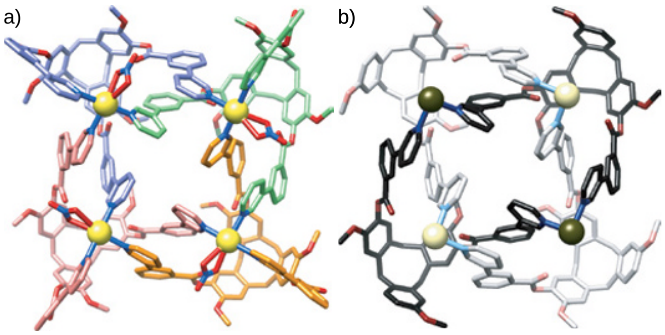


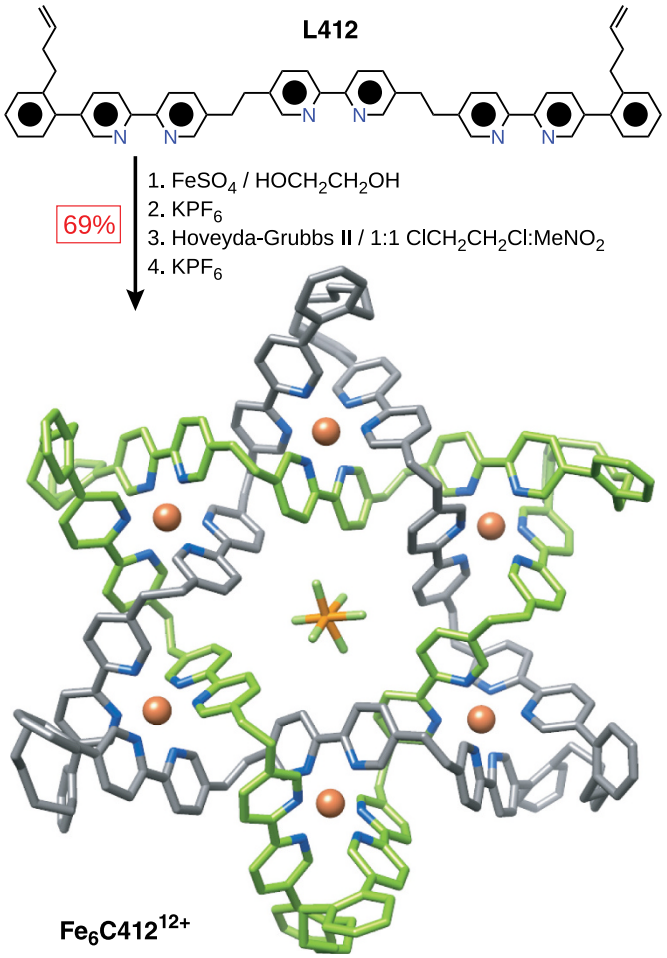
Figure 4.4 Hardie's metallosupramolecular 'Solomon's Cube'.[29] (a) The solid-state structure of the Pd_4L_4 Solomon's cube comprising four Pd^{II} ions (yellow) and four ligands L (red, blue, green, orange) with solvent molecules/hydrogen atoms omitted for the sake of clarity. (b) A cutaway of one arm from each ligand reveals an internal Solomon link topology, with the rings shaded in black and grey.

Solomon link (**Figure 4.3**) involves the duplexation of four single-stranded DNA molecules, each possessing small segments of complementary L-nucleotides, which generate the requisite positive nodes to accompany the negative nodes of the D-nucleotides in defining the 4_1^2 topology of the assembly. The rings of the DNA Solomon Link are closed by unusual 3′–3′ and 5′–5′ linkages developed for structures known[28] as 'bowtie' junctions, rather than the 3′–5′ linkages generated by ligase enzymes.

Hardie[29] has described the self-assembly and structure (**Figure 4.4a**) of a topologically complicated metallo-organic 'Solomon's cube' comprising four Pd^{II} ions and four tris(pyridine) ligands derived from cyclotriveratrylene. Although this Pd_4L_4 coordination compound is not a link, it possesses a remarkable self-interlocked topology in which each of the arms of the tridentate ligands coordinates to three separate and distinct Pd^{II} centers. A Solomon link can be discovered (**Figure 4.4b**) within the topology of this assembly by cutting away one arm from each of the ligands.

4.1.1.2 Star of David

The Star of David link (6_1^2 in Alexander-Briggs notation) is one of the most recent new additions to the collection of synthetic prime links, and it is considered[30] to be among the most sophisticated to have earned a molecular representative. Sauvage[31] attempted to prepare a Star of David using a pentacopper(I) double stranded helicate as the template according to his entwining strategy, yet the target could not be isolated, most likely on account of the long distance between reactive sites of the linear helical template. Leigh[9] overcame this obstacle by employing circular double-stranded helicates of the kind pioneered by Lehn.[32–34] The counterions play an important role in the templation of these circular helicates—Cl^- anions promote the assembly of pentameric circular helicates, while SO_4^{2-} anions promote the assembly of hexameric circular helicates. The Star of David **Fe_6C412^{12+}** is prepared (**Scheme 4.1**) in a one-pot



Scheme 4.1 The synthesis[9] and solid-state structure of Leigh's Star of David [2]catenane **Fe_6C412^{12+}** by ring-closing olefin metathesis of hexameric circular helicates based on ligand **L412**. Protons, solvent molecules, and PF_6^- counterions, except for one in the catenane's central anion-binding pocket, are omitted for the sake of clarity.

reaction involving the self-assembly of a heptameric circular helicate comprising six $FeSO_4$ templates and six ligands, each possessing three bidentate bipyridine units (**L412**), which become cross-linked into the 6_1^2 topology by olefin metathesis in the presence of the Hoveyda-Grubbs II catalyst. See **Section 3.4** for a summary of MIM syntheses by olefin metathesis. After counterion exchange to the corresponding PF_6^- salt, a PF_6^- anion occupies the central binding pocket, which was previously occupied by the anionic sulfate template, as evidenced in the solid-state structure of **Fe_6C412^{12+}**. Pentameric and tetrameric circular helicates have also been employed in order to assemble a pentafoil knot[35,36]—see **Section 1.3.2**, **Figure 1.24**—and a Solomon link[21] (**Fe_4C408^{8+}**, **Figure 4.2**), respectively.

4.1.1.3 Borromean Rings (BRs)

Brunnian links are topologies in which the rings interlock such that breaking any one of them will cause all of the other rings to unlink. Brunnian links comprising three rings are known as Borromean rings (BRs), owing to their

appearance on the crest of the aristocratic Borromeo family that rose to prominence during the European Renaissance in what is now northern Italy. See **Section 1.1.2** for more information on the history and significance of BRs. Molecular BRs[37] are [3]catenanes possessing the 6_2^3 topology. Although strategies to synthesize molecular BRs in a stepwise fashion had been proposed[38] and pursued[38–44] for many years from ring-in-ring complexes—see **Section 4.3.3**—the only approaches that have proved to be successful have involved the all-in-one self-assembly of either (i) DNA strands,[45] or (ii) metal-ligand coordination compounds, the latter of which have been realized by serendipitous discovery[46] as well as by rational design.[18]

The earliest example (**Figure 4.5**) of molecular Borromean rings was introduced by Seeman,[45] who conceived of an approach to assembling BRs that relies on the predictable self-assembly of nucleic acids (**Section 2.3.12.1**) by Watson-Crick base pairing. A combination of right-handed and left-handed DNA three-arm branch junctions are hybridized into a cyclohexameric array in order to template the requisite Brunnian topology that affords the DNA BRs upon enzymatic ligation. From the six unique strands that are cross-stitched into the DNA BRs, the three left-handed helical crosslinks of the hybridized Z-DNA strands represent the positive nodes, while the three right-handed helical crosslinks of the hybridized B-DNA strands represent the negative nodes. Each of three rings was designed to contain a unique site that is targeted by a different restriction enzyme, making it possible to prove the Brunnian topology of the DNA BRs by cleaving enzymatically only one ring and confirming the dissociation of the other two rings by gel electrophoresis.

The remaining examples (**Figure 4.6**) of molecular Borromean rings have relied on transition metal chelation to direct their self-assembly. Champness[46] discovered serendipitously that metallo-BR assemblies, such as the hexacationic Ag^{I} coordination compound **C413**·6SbF_6, form (**Figure 4.6a**) spontaneously upon mixing equimolar quantities of 6,6´-bis(4-ethynylpyridine)-2,2´-bipyridine ligands (**L413**) with Ag^{I} or Cu^{I} or ions as their BF_4^- or SbF_6^- salts, either in alcoholic solutions or in binary mixtures of CH_2Cl_2 and MeCN. The solid-state structure of **C413**$^{6+}$ reveals how the six ligands and six ions form a Brunnian link of identical tetrahedral Ag^{I} centers, with a single counterion in the center of the structure. Schmittel[47] has shown that homologous Borromean links of Cu^{I} metallacycles are also obtained when the ethynylene linker of **L413** is replaced by *para*-tetramethylphenylene.

The first molecular BRs to be assembled (**Figure 4.6b**) by rational design without relying on the predictability of Watson-Crick base pairing in DNA involved a one-pot reaction[18] that brings together 18 building blocks—six *exo*-bidentate bipyridine ligands (**L414**), six *endo*-tridentate diiminopyridine ligands derived from 2,6-diformylpyridine (dfp), and six Zn^{II} templates—by reversible coordinative imine bonding to afford **Zn_6C414**$^{12+}$ in near-quantitative yields. A more detailed reaction scheme is illustrated in

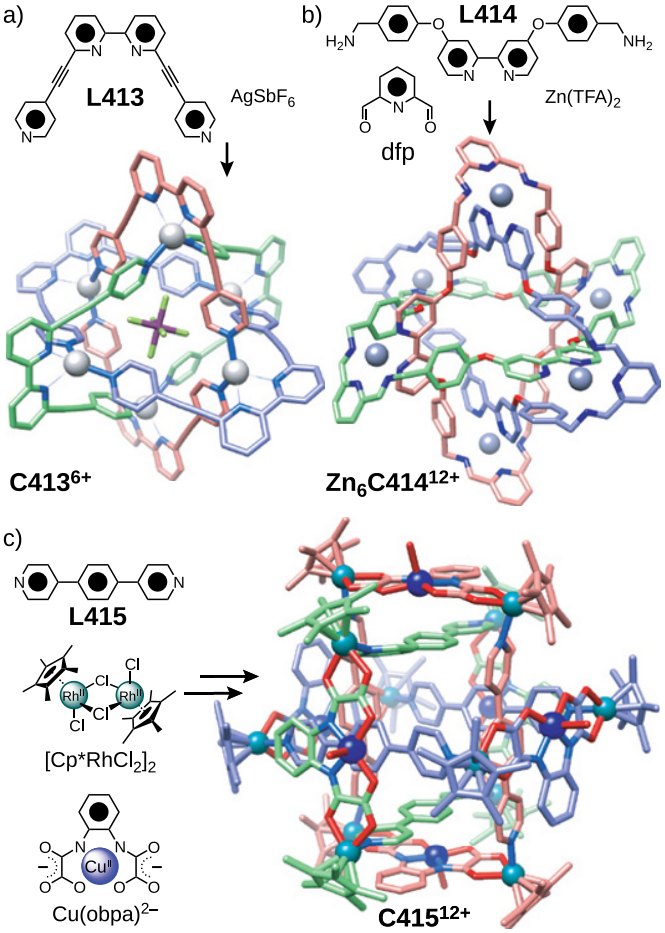


Figure 4.6 Molecular BRs and the compounds from which they are assembled. (a) The 12-component self-assembled BRs **C413**$^{6+}$ introduced by Champness.[46] (b) The 18-component self-assembled BRs[18] **Zn_6C414**$^{12+}$. (c) The 24-component self-assembled BRs **C415**$^{12+}$ introduced by Jin.[50,51]

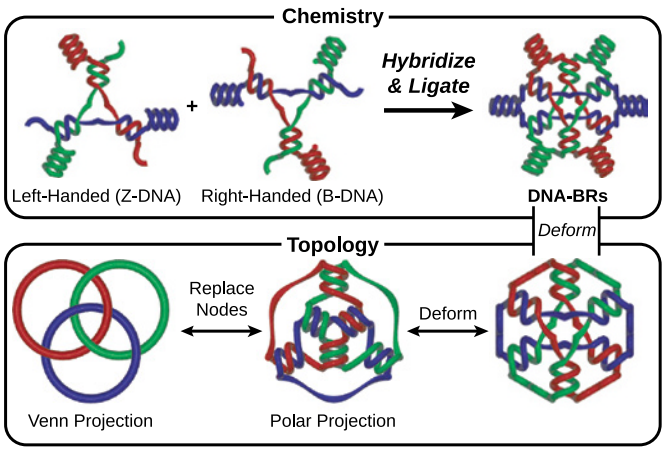
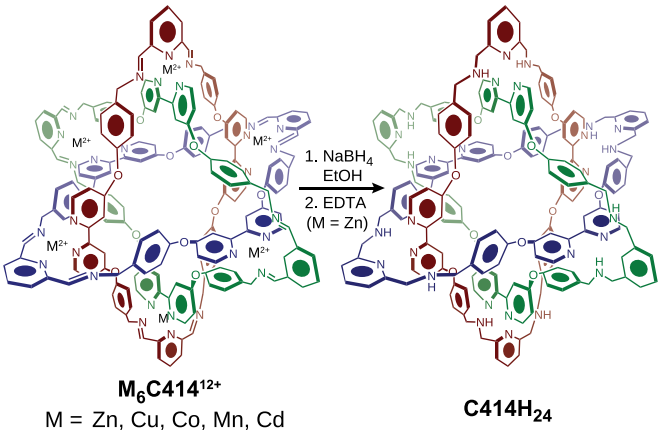


Figure 4.5 Graphical representation of Seeman's DNA Borromean Rings[45] (BRs). Hybridization and ligation of complementary left-handed (Z-DNA) and right-handed (B-DNA) three-arm junctions affords Brunnian links, which possess the topology of BRs if each of their 1.5-turn nodes are taken as crossing points in a topological projection. Images adapted with permission from ref. 37 (copyright 2005 American Chemical Society).



Scheme 4.2 Synthesis[49] of the all-organic, charge-neutral BRs **C414H$_{24}$** by reduction and demetalation of **Zn$_6$C414^{12+}**.

Section 1.3.4, **Scheme 1.3**, while MIM self-assembly driven by coordinative imine bonding is reviewed in **Section 3.4.1**. Although Zn^{II} served as templating ions initially, the **M$_6$C414^{12+}** BR assembly tolerates[19] several other divalent metals (M = Cu^{II}, Co^{II}, Mn^{II}, Cd^{II}) as well. Since the reversible coordinative imine bonds keep the BRs in dynamic equilibrium, new *exo* dfp-based ligands presenting different functional groups can be exchanged[48] statistically into their constitutions. It is also possible to convert[49] the **Zn$_6$C414^{12+}** assemblies into the neutral, kinetically stable BR catenane **C414H$_{24}$** by reducing (**Scheme 4.2**) the imine bonds with sodium borohydride in ethanol.

Jin[50,51] has employed bimetallic [Rh_4Cu_2] molecular rectangles in the self-assembly of Borromean ring compounds. For example, in the case (**Figure 4.6c**) of BR compound **C415^{12+}**, the edges of the three identical metallarectangles comprise two pairs of ligands—namely, 1,4-bis(4-pyridyl) benzene (**L415**) and metallaligand $Cu(opba)^{2-}$ [opba = *o*-phenylenebis(oxamato)]—while the corners comprise four 'half-sandwich' Cp^*Rh^{2+} centers. The stepwise 24-component self-assembly of **C415^{12+}** in MeOH involves capping the bis(pyridyl) linkers with two Cp^*RhCl_2 groups using $[Cp^*RhCl_2]_2$ as a reagent, followed by Cl^- abstraction with AgOTf in the presence of $Na_2Cu(opba)$ to close the metallacycles. These BRs have been characterized in the solid, liquid, and gas phases. Similar BRs are formed when the bis(4-pyridyl)benzene linkers are replaced by *N*,*N*′-4-pyridyloxalamide, which is essentially identical in length (11.4 Å), yet shorter bifunctional linkers such as pyrazine (2.7 Å), 4,4′-bipyridyl (7.1 Å), and 1,2-bis(4-pyridyl)ethylene (9.4 Å) afford only uncatenated metallarectangles. BRs also form when employing a longer (15.6 Å) *N*,*N*′-(1,4-phenylene)diisonicotinamide linkers, but not the very long (19.8 Å) *N*,*N*′-(4,4′-biphenylene)diisonicotinamide. The driving force for BR formation therefore depends critically on the linker length. X-Ray crystallographic studies on a series of BRs based on this motif and DFT investigations[51] suggest that (i) [Cu···O] interactions between metallarectangles and (ii) π–π stacking interactions between the electron-rich $Cu(obpa)^{2-}$ and electron-poor bis(4-pyridyl)benzene linkers are what drive and stabilize the 'Borromeation' of the metallacycles. The sensitivity to linker length is therefore related to how these interactions are promoted within only a narrow range of rectangular cavity sizes.

Borromean Networks

Hardie[52] has reported on the crystallization of a remarkable molecular chainmail **C416** comprising (**Figure 4.7**) an infinite network of giant metallacycles derived from the chiral cyclotriveratrylene-based ligand (±)-tris(*iso*-nicotinyl) cyclotriguaiacylene (^{i}NCTG) and $CuBr_2$, arranged such that no ring interpenetrates through the annulus of any of its six

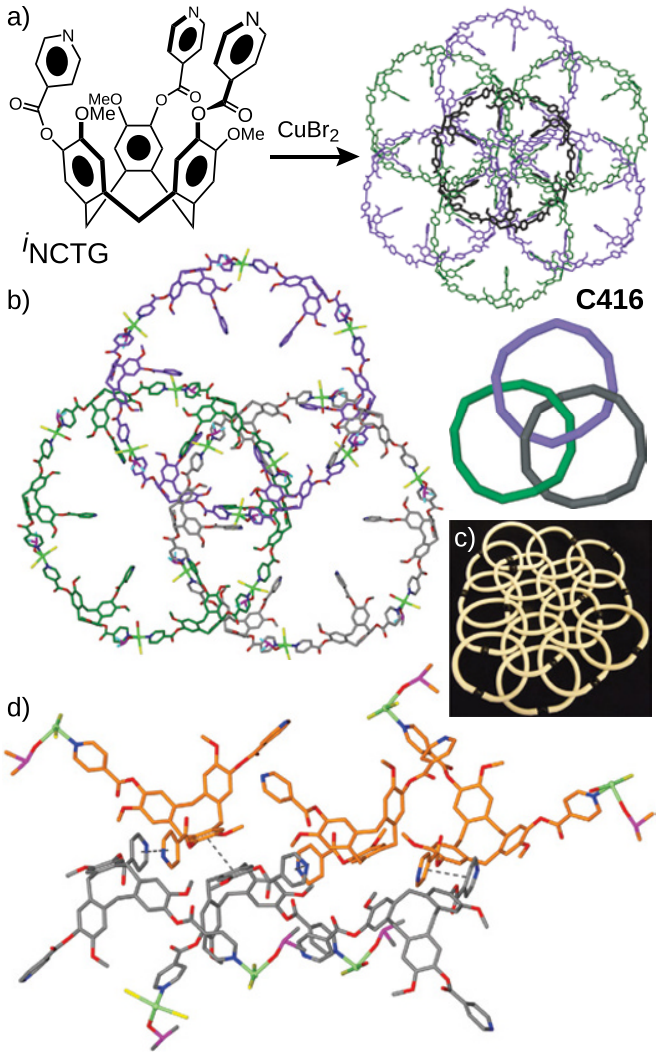


Figure 4.7 Hardie's infinite molecular chainmail, **C416**, possessing the Brunnian topological elements of Borromean rings.[52] (a) The infinite chainmail of M_6L_6 metallacycles forms in the crystal upon mixing $CuBr_2$ with ^{i}NCTG ligands. (b) A magnified view of three rings from the network, and graphical representation of their Borromean topology. (c) Photograph of a reconstructed model of the Brunnian chainmail. (d) A magnified view of the π–π stacking interactions between chainmail layers. Tubular representations are illustrated with hydrogen atoms omitted for the sake of clarity. Adapted with permission from ref. 52 (copyright 2015 Nature Publishing Group)

nearest neighbors. This Brunnian network topology is replete with local Borromean links. Their formation, which occurs only in the solid state, involves the coordination-driven self-assembly of M_6L_6 metallacycles in which each ^{i}NCTG ligand engages two of its three pyridyl groups in *trans*-coordination modes with the Cu^{II} joints. The M_6L_6 rings are achiral because they comprise alternating (+) and (−) enantiomers of the ^{i}NCTG ligand, all of them oriented with their bowls faced endotopically. Hardie claims that this crystal represents the first example of an infinite molecular chainmail motif, irrespective of the topological connectivity of the rings.

Another type of Borromean network can arise when three or more infinite two-dimensional nets are catenated such that no two networks would interpenetrate if the others were removed. These networks have been observed[53,54] in a number of crystalline coordination polymers, which are beyond the scope of this book.

4.1.1.4 Cyclic [3]Catenane

The 6^3_3 topology, which as been called[10] a cyclic [3]catenane, is a link in which in which each of three rings is catenated with both of the others. Although this molecular topology has been pursued from at least 2007, when Sauvage[55] began reporting his investigations on $M(biisoquinoline)_3^{n+}$ coordination compounds (M = octahedral transition metal), it was not until 2014 that this topology was finally realized. The case was cracked independently by Gunnlaugsson,[56] Clever,[57] and Nitschke[10] within a timeframe of less than a year. Gunnlaugsson[56] was the first to claim that he had synthesized a 6^3_3 link. His approach involved the 'triple clipping' by ring-closing olefin metathesis of a set of three identical pyridine-2,6-dicarboxamide ligands around a Eu^{III} center to afford the cyclic [3]catenate **C417^{3+}**, the stereoformula of which is illustrated in **Figure 4.8**. In the absence of an X-ray crystal structure or rigorous spectroscopic evidence, however, the successful isolation and characterization of **C417^{3+}**, as opposed to other knotted or macrocyclic topologies, may continue to be called into question.

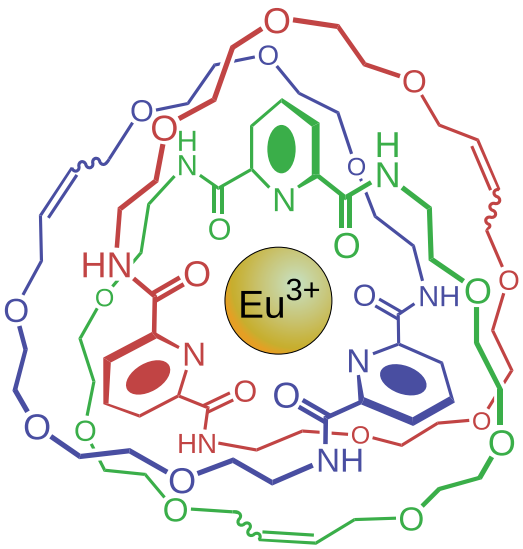
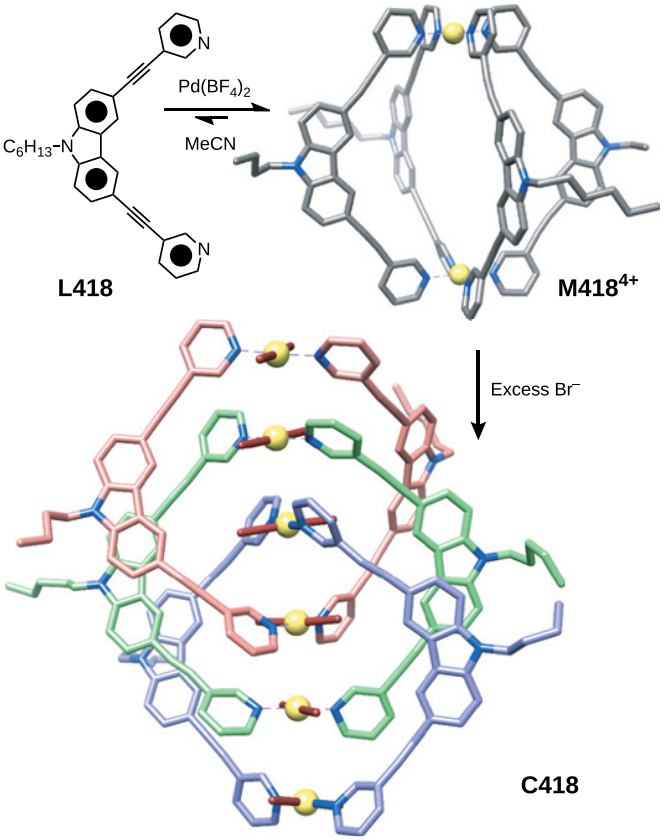
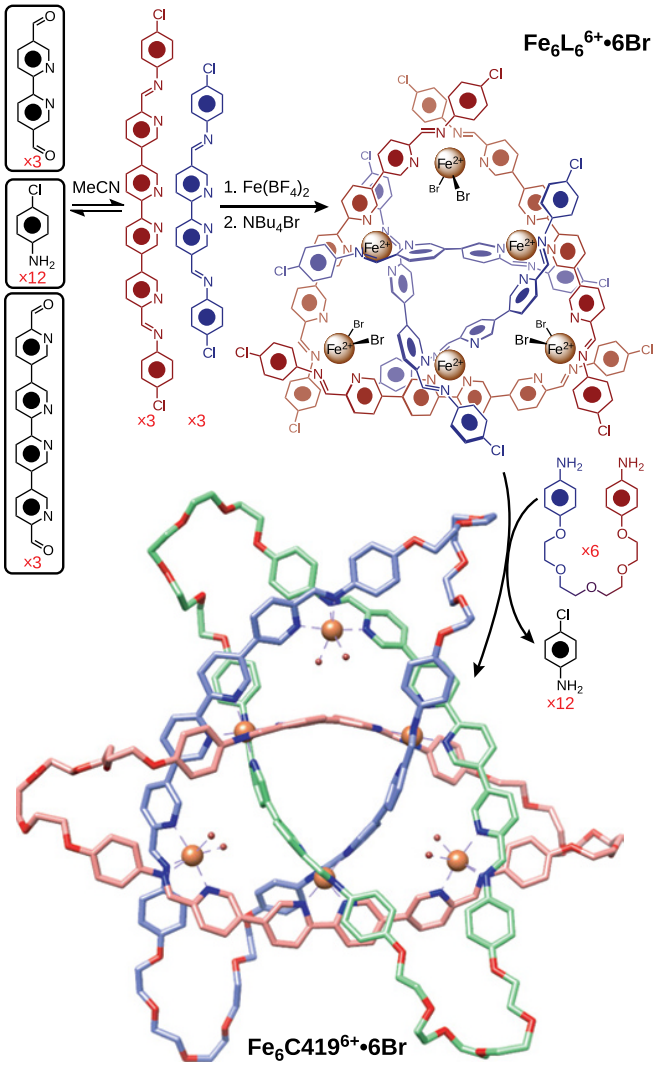


Figure 4.8 The stereoformula of the Eu^{III} cyclic [3]catenate **C417^{3+}**, which has been claimed by Gunnlaugsson[56] to form via ring-closing olefin metathesis.



Scheme 4.3 The synthesis and solid-state structure of the cyclic metallo[3]catenane **C418** assembled by Clever[57] from the coordination cage **M418^{4+}** in the presence of an excess of Br^- ions. Hydrogen atoms, and BF_4^- counterions in the case of **M418^{4+}**, are omitted from the tubular representations of the solid-state structures for the sake of clarity.

Clever[57] posted the first X-ray crystal structure of a 6^3_3 link shortly after Gunnlaugsson's initial attempt. His synthesis (**Scheme 4.3**) of the cyclic [3]catenane **C418** involves a dynamic equilibrium involving the carbazole-based bis(pyridyl) ligand **L418**, Pd^{II} ions, and halide salts. In the absence of salt, four **L418** ligands and two Pd^{II} ions assemble quantitatively into the Pd_2L_4 cage **M418^{4+}** in MeCN. The addition of a stoichiometric amount of halide (Cl^- or Br^-) ions induces the catenation of these cages to form a quadruply interlocked species akin to those discussed in **Section 4.1.3.3**, with the halide anions intercalated between the planes of the Pd^{II} centers. An excess of Cl^- or Br^- ions induces a second structural change in which the halide anions displace two pyridyl ligands from each Pd^{II} center, resulting in Pd_2L_2 metallacycles that were discovered by X-ray crystallography to interpenetrate in the form of the cyclic [3]catenane. **C418** carries no net charge because the Pd^{II} ions are each saturated with a pair of Br^- counterions. The appealing co-conformation of the [3]catenane, in which the Pd^{II} centers are neatly stacked (average



Scheme 4.4 The stepwise self-assembly of Nitschke's cyclic [3]catenane **$Fe_6C419^{6+}\cdot 6Br$** from five distinct starting materials.[10]

Pd–Pd distance = 4.36 Å) with their ligands in a helical arrangement, is most likely driven by π–π stacking interactions dominated by the ligands' carbazole units.

Nitschke's cyclic [3]catenane **$Fe_6C419^{6+}\cdot 6Br$** has been prepared[10] (**Scheme 4.4**) by a two-stage directed self-assembly relying on thermodynamically controlled imine coordinative bonds. In the first instance, a collection of five different compounds is assembled into a triangular Fe_6L_6 framework comprising a pair of crosslinked Fe_3L_3 circular helicates. The complicated Fe_6L_6 triangular framework is heteroleptic as a result of the mixed-component reactant pool—three hexadentate ligands conjoined by octahedral FeL_2Br_2 corners define the outer edges of the triangle, whereas the smaller tetradentate ligands crosslink each of the triangle's edges by virtue of three inset octahedral FeL_3^{2+} centers. The cornerpiece bromide ions are important ligands because they satisfy the octahedral ligand field of the otherwise tetra-coordinated Fe^{II} centers. In the second stage of assembly, the 12 chloroaniline moities engaged in coordinative imine bonding at the ligands' endcaps are displaced by six flexible tetra(ethylene glycol)bis(aniline) linkers, affording **$Fe_6C419^{6+}\cdot 6Br$**. This cyclic catenane has been characterized by X-ray crystallography in the solid state, as well as by NMR spectroscopic and mass spectrometric techniques. In a manner similar to the reduction and isolation (**Scheme 4.2**) of the all-organic BRs **$C414H_{24}$**, Nitschke also reduced the imine bonds of **Fe_6C419^{6+}** and stripped away the metal ions to afford the corresponding all-organic cyclic [3]catenane **$C419H_{24}$**, (not illustrated) albeit in low yield. The efficiency (79%) of the two-stage self-assembly process, despite its relatively high complexity, suggests that even more intricate topologies may be accessible by these thermodynamically controlled metallosupramolecular approaches.

4.1.1.5 Whitehead Link

The 5_1^2 link is named after the mathematician JHC Whitehead[58] who used the link in 1934 as a part of a counterexample to refute his own purported proof of the Poincaré conjecture, which was seen as one of the most important and difficult open problems in mathematical topology. Incidentally, almost 70 more years would pass until Perelman[59–61] finally proved the Poincaré conjecture in 2002/2003. The Whitehead link is now the simplest link topology that has not yet been realized in molecular form. It is only a matter of time before this topology is put to rest by chemists drawn to unnatural product synthesis. Indeed, we are aware of several (unsuccessful) attempts that have already been made to synthesize a Whitehead link. Fenlon[62] has listed the Whitehead link synthesis among his 'open problems in chemical topology' in his excellent exposition on the subject. As noted by Chambron and Sauvage,[63] strategies for synthesizing a particular knot or link in molecular form are determined by a rigid presentation of its topology, of which an infinite variety are accessible through continuous deformation. Three different presentations of the Whitehead link are illustrated in **Figure 4.9**, each of which may lend itself to different sorts of potential templation strategies. We predict that it won't be long before a molecular Whitehead link is recorded in the annals of chemistry.

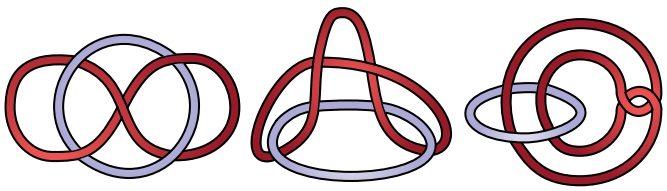
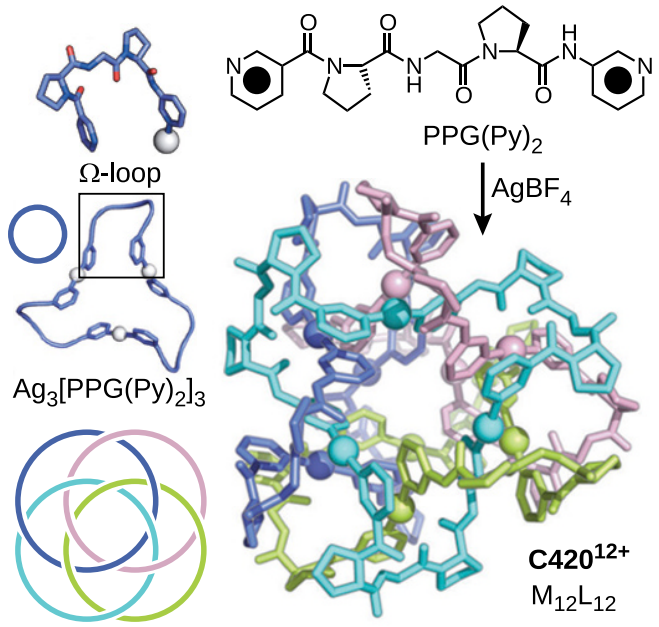


Figure 4.9 Three different presentations of the as-yet elusive 5^2_1 topology, known also as the Whitehead link.

4.1.1.6 12-Crossing [4]Catenane

Fujita[64] has recently introduced a self-assembled metallopeptide [4]catenane possessing a 12-crossing topology of unprecedented complexity. The self-assembly (**Scheme 4.5**) of this exotic catenane, **$C420^{12+}$**, involves 12 Ag^I ions and 12 peptidic ligands, which distribute into four concatenated M_3L_3 metallacycles. The peptidic ligands, $PGP(Py)_2$, comprise a *Pro–Gly–Pro* tripeptide sequence possessing 3-pyridyl ligands at the *C*- and *N*-termini. The metallacycles



Scheme 4.5 The self-assembly of Fujita's 12-crossing [4]catenane by simultaneous folding and assembly of 12 Ag^{I} ions and 12 pyridyl-functionalized tripeptide ligands,[64]

are unidirectional with respect to the $N \rightarrow C$ sequence. The short tripeptide fragments fold into the so-called Ω-looped geometry upon coordination to the Ag^{I} ions. The entwinement of the Ω-loops among the four M_3L_3 rings leads to the highest possible number of crossings, such that each individual ring intersects all three of the others. The [4]catenane persists in the solution state with dissolved in CD_3NO_2, yet ^1H NMR spectroscopic characterization suggests that the cubic lattice observed in the solid state distorts into a rhombohedral one in solution. This latest leap forward in molecular topology suggests that the simultaneous combination of orthogonal self-assembly processes—in this case, molecular folding and metallosupramolecular crosslinking—can provide access to complex molecular structures that are otherwise unobtainable by the individual assembly processes in isolation.

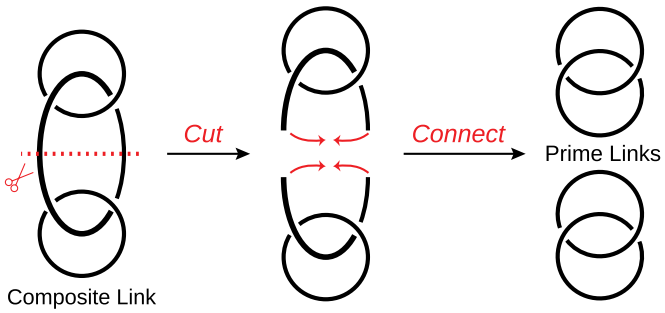


Figure 4.10 An example of how a composite link—in this case, a three-ring chain—can be 'factored' into a combination of prime links—in this case, two Hopf links—by cutting and reconnecting the component knots.

4.1.2 Composite Links

A link that can be represented as a sum of other (prime) links is a composite link. A three-link chain, or linear [3]catenane, is the most common example of a composite link. The diagram in **Figure 4.10** illustrates how the three-link chain can be 'factored' into two Hopf links by cutting the center ring in half and mending the endpoints of each half back together. We distinguish between three types (**Figure 4.11**) of molecular composite links—linear [*n*]catenanes (**Section 4.1.2.1**) representing the form of chain links, radial [*n*]catenanes (**Section 4.1.2.2**), also known as 'molecular necklaces', and branched [*n*]catenanes (**Section 4.1.2.3**), which combine linear and radial linking elements.

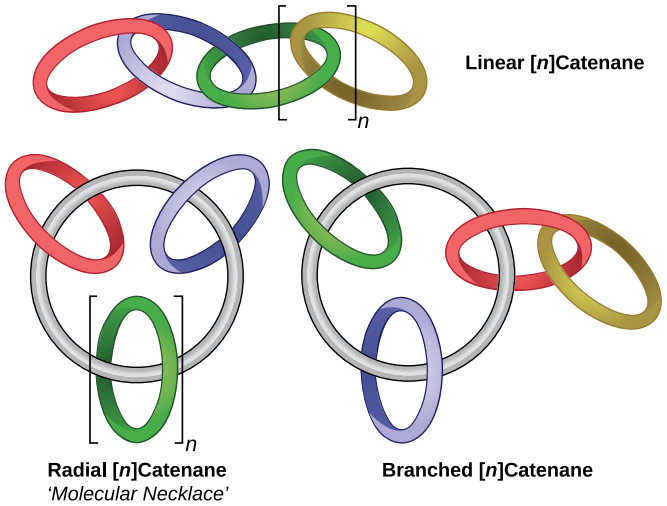


Figure 4.11 Graphical representations of linear, radial, and branched [*n*]catenane composite links.

4.1.2.1 Linear [n]Catenanes

The simplest form of a molecular composite link is that of a linear [3]catenane, of which there have been many examples[65–105] in the literature. For examples of [3]catenanes, see **Figure 1.13** in **Section 1.2.3**, **Figure 1.18a** in **Section 1.2.5**, **Figure 2.6** in **Section 2.2.1**, **Scheme 2.20** in **Section 2.3.1.1**, **Scheme 2.35** in **Section 2.3.2.1**, **Scheme 2.65** in **Section 2.3.3.9**, **Figure 3.13** in **Section 3.2.1.4**, **Scheme 3.35** in **Section 3.4.1.1**, and **Figure 3.33** in **Section 3.4.1.5**.

In contrast with [3]catenane composite links, linear [*n*]catenanes possessing four or more rings remain relatively rare. The majority of linear [$n \geq 4$]catenanes have relied[69,70,73,74,77] on π-associated donor-acceptor interactions to guide self-assembly during their template-directed synthesis by clipping protocols. They include (**Figure 4.12**) the [4]catenanes **C421**$^{8+}$ and **C422**$^{8+}$, the [5]catenanes **C423**$^{12+}$, **C424**$^{12+}$, and **C425**$^{8+}$—also known as 'Olympiadanes' owing to their topological identity with the logo of the Olympic games—as well as the [7]catenane[77] **C426**$^{12+}$.

Iwamoto[104] has exploited the ability of the BPP34C10 ring to accommodate two dialkylammonium guests—see **Figure 2.58a** in **Section 2.3.4.6**—in the construction of the [5]catenane **C427H**$_4^{4+}$. This linear [5]catenane is obtained by olefin metathesis (**Section 3.4**) of a pair of

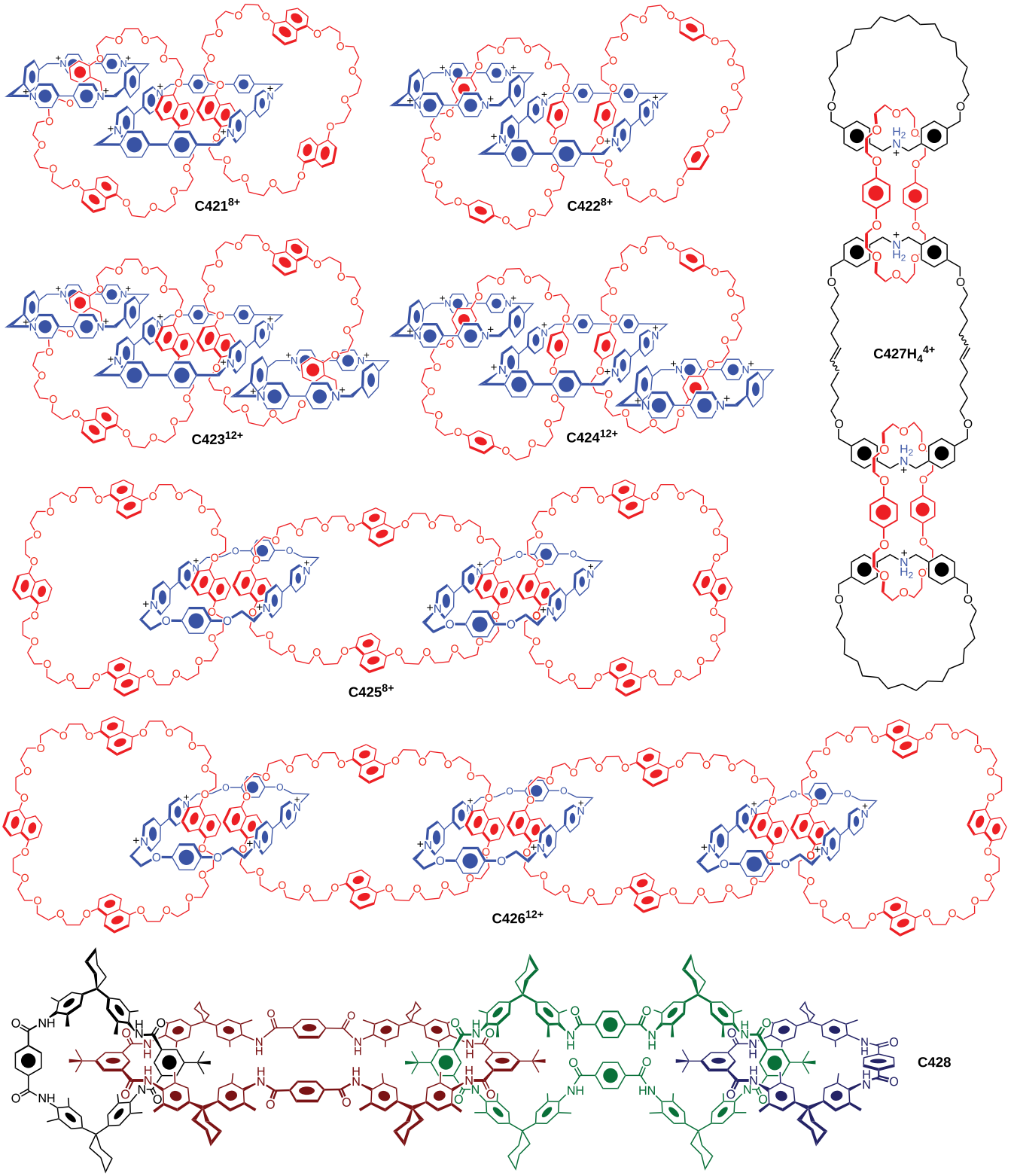


Figure 4.12 Stereoformulas of linear [*n*]catenanes possessing four or more rings in the chain.[69,70,73,74,77,106]

dialkylammonium⊂BPP34C10 [2]catenanes, each threaded by a second dialkylammonium axle displaying reactive terminal olefins. Thus, closure of the central bis(dialkylammonium) ring by ring-closing metathesis dimerization affords **C427H$_4^{4+}$** in up to 12% yield.

Vögtle[106] introduced a new class of oligo[*n*]catenanes based on hydrogen-bonded amide templates when he managed to isolate by HPLC the [4]catenane **C428** in <1% yield from a clipping reaction. The constitutions (**Figure 4.12**) of the two central octalactam macrocycles and the two peripheral

tetralactam macrocycles each comprise an alternating pattern of terephthalamide and *tert*-butyl-functionalized isophthalamide units bridged by cyclohexylidene-bisphenylene linkers. The corresponding diacid dichlorides and diamine precursors were optimized structurally for generating octalactam rather than tetralactam macrocycles. The synthesis of **C428** is an iterative template strategy involving a homo[2]catenane precursor comprising a pair of octalactam macrocycles. Although an octalactam homo[3]catenane is the major product (10%) aside from starting material, trace amounts of oligo[*n*]catenanes even longer than **C428** were also detected by mass spectrometry. In spite of the low yields, these results clearly demonstrate that the isophthalamide/terephthalamide octalactam rings possess cavities of sufficient size to accommodate two axles, including them among the candidates that are suitable for building [*n*]catenanes of arbitrary length.

Examples of [4]catenanes[107], Olympiadanes[108] and larger branched [*n*]catenanes[109] (**Section 4.1.2.3**) comprising circular DNA strands have also been described by Willner.

[n]Catenane Chain Polymers

A number of crystalline 'infinite' [*n*]catenanes (**Figure 4.13**) have been generated[110–114] in the solid state by crystallization-induced (**Section 2.3.11.4**) catenation of metallo-organic macrocycles. The [*n*]catenanes **C429^{n+}–C432** are formed by crystallization induced catenation (**Section 4.3.11.2**) of metallacycles assembled from various mixtures of divalent ligands and transition metal salts.

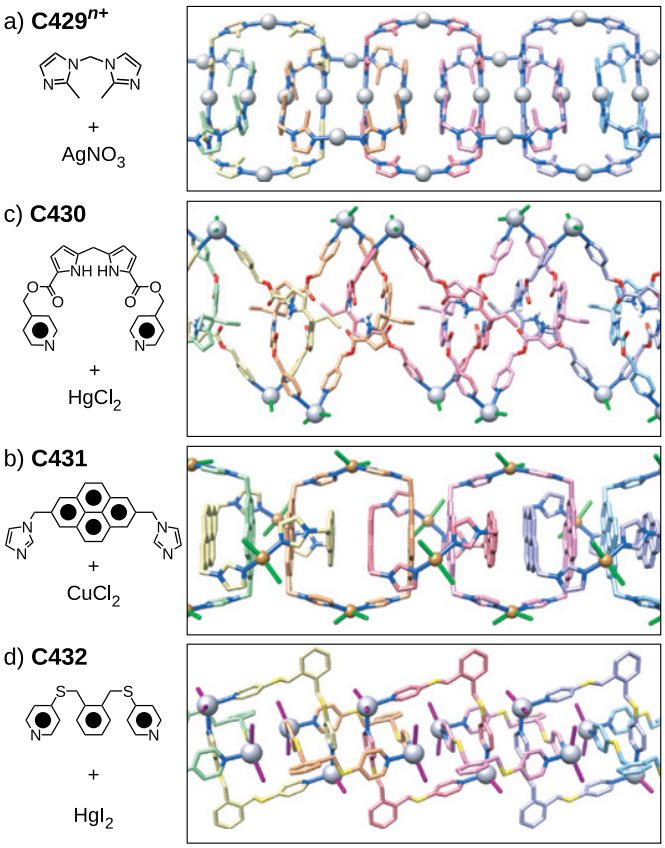


Figure 4.13 Solid-state structures of infinite [*n*]catenane chains grown by crystallization-induced catenation of metallacycles. (a) **C429^{n+}**, with NO_3^- counterions omitted for the sake of clarity.[110,112] (b) **C430**.[111] (c) **C431**.[113] (d) **C432**.[114] Hydrogen atoms are omitted from all tubular representations for the sake of clarity.

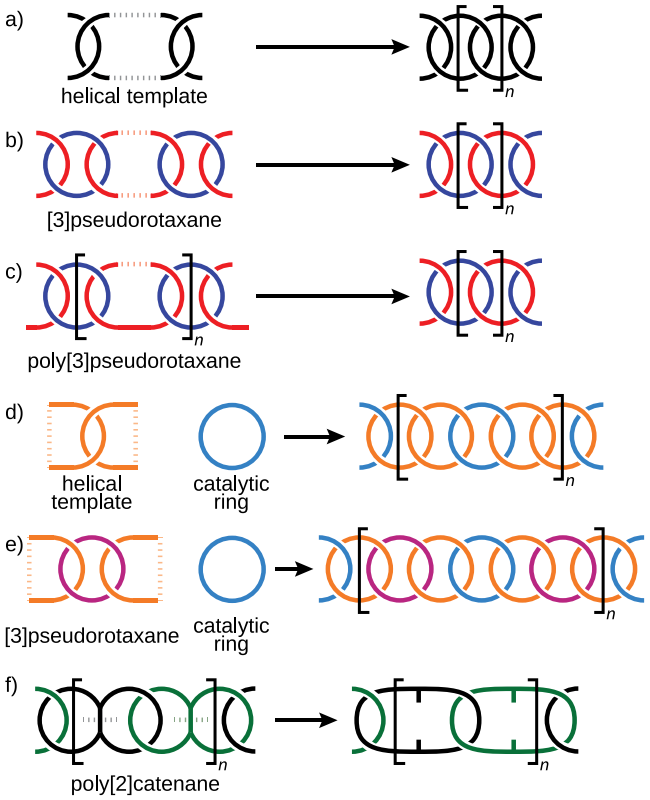


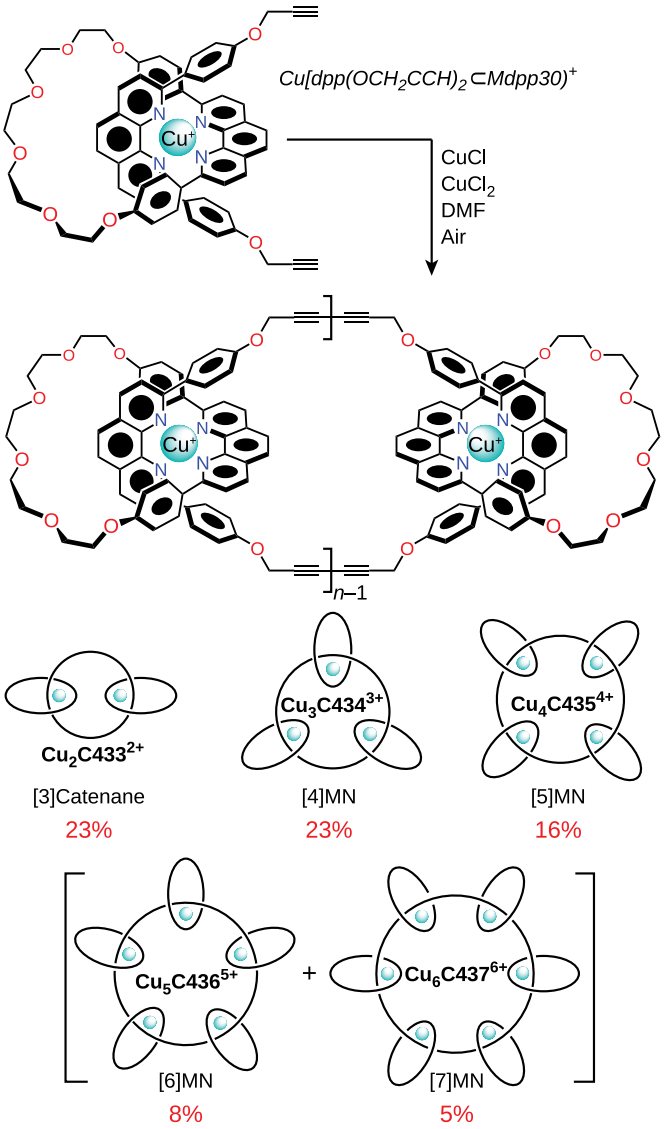
Figure 4.14 Some potential strategies for the synthesis of [*n*]catenane chain polymers: (a) entwining followed by clipping, (b) [3]pseudorotaxane threading followed by clipping, (c) poly[3]-pseudorotaxane threading followed by clipping, (d) ring capture of helical templates, (e) ring capture of threaded templates, (f) bridgehead cleavage of poly[2]catenanes. In the line drawings, dashed lines indicate where new bonds are formed (a–e) or broken (f) to afford the [*n*]catenanes.

When It comes to kinetically stable, solution-processable, all-covalent [*n*]catenanes—the molecular analogs of macroscopic chains—oligo[*n*]catenanes are rare sightings in the chemical literature, while long [*n*]catenane chains (e.g., $n > 10$) remain among the 'holy grails' in mechanostereochemistry. These compounds are inherently far from easy to synthesize, especially at high molecular weights, since they would require multicatenations that proceed with >99% efficiency. Several potential strategies (**Figure 4.14**) for constructing polycatenane chains may be envisioned, including (i) clipping[115,116] reactions involving either entwined (**Figure 4.14a**) or threaded (**Figure 4.14b–c**) templates, (ii) ring capture reactions, such as active metal template synthesis (**Section 2.4**), involving either entwined (**Figure 4.14d**) or threaded (**Figure 4.14e**) templates, and (iii) scission (**Figure 4.14f**) of bridgeheads in poly[2]catenanes—for example, by ozonolysis of olefins remaining after ladder polymerization of [2]catenanes by Diels-Alder cycloaddition.[117,118] The world is still anticipating long [*n*]catenane

polymers, the members of which are likely to exhibit unusual viscoelastic,[119–121] and thermal[122] properties arising[123] from their mechanical bonds.

4.1.2.2 Radial [n]Catenanes – Molecular Necklaces

The variety of ways to link the rings of catenanes with four or more component parts calls for new ways to distinguish them. One arrangement is that of a large macrocycle threaded by a number of smaller rings. These 'radial' [*n*]-catenanes, as described by Leigh,[124] have been appropriately dubbed 'molecular necklaces'[c] by Kimoon Kim.[125] An



Scheme 4.6 Sauvage's synthesis[126] of molecular necklaces by oxidative homocoupling of alkyne-terminate metallo-pseudorotaxane precursors.

[c] Although Harada had earlier described his seminal polyether-threaded cyclodextrins as 'molecular necklaces', they are more commonly described as polyrotaxanes. See **Scheme 2.16** and accompanying text in **Section 2.3.1.1**.

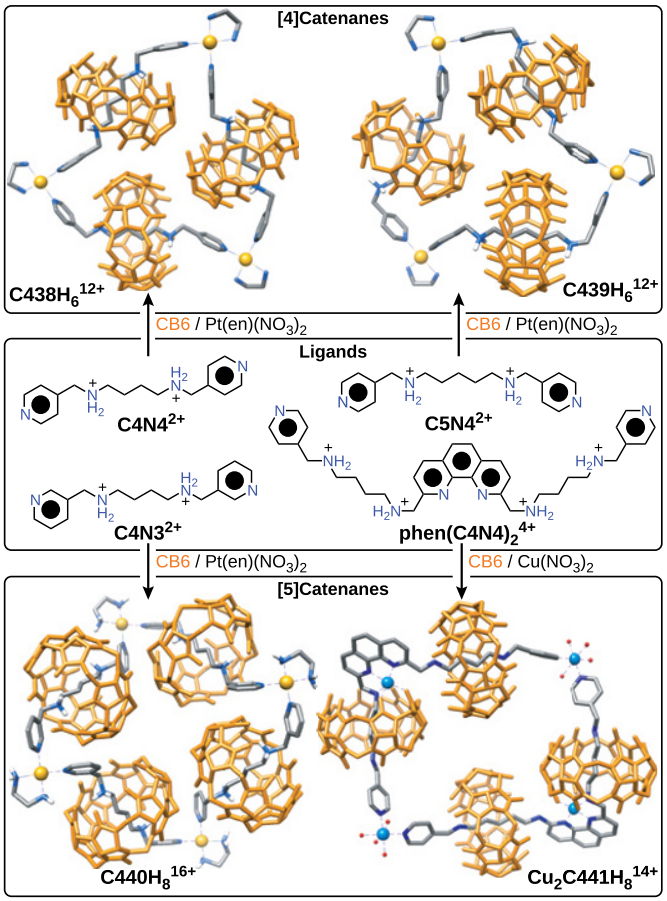


Figure 4.15 Kimoon Kim's metallosupramolecular molecular necklaces.[125,127,129] Tubular representations of the solid-state (super) structures are illustrated with hydrogen atoms, solvent molecules, and counterions omitted for the sake of clarity.

[*n*]molecular necklace (abbreviated [*n*]MN) is an *n*-component catenane consisting of one large macrocycle threaded by [*n*–1] rings. A number of [4]MNs and [5]MNs have been isolated,[70,72,75,125–130] while even larger ones have been detected[126] as side products or synthesized[131,132] intentionally from polypseudorotaxane precursors.

Molecular necklaces ($n \geq 4$) were first introduced (**Scheme 4.6**) circa 1991 by Dietrich-Buchecker, Sauvage, Van Dorsselaer, and co-corkers.[126] The oxidative homocoupling of the terminal alkynes of the bis(propargyl) metallo-pseudorotaxane *Cu[dpp(OCH$_2$CCH)$_2$⊂Mdpp30]$^+$* affords, not only the expected [3]catenate **Cu$_2$C433^{2+}** (23%), but also the [4]MN **Cu$_3$C434^{3+}** (23%), the [5]MN **Cu$_4$C435^{4+}** (16%), as well as the [6]MN **Cu$_5$C436^{5+}** (8%) and [7]MN **Cu$_6$C437^{6+}** (5%) in admixture, as determined by electrospray mass spectrometry. Appending alkyl chains to positions 4 and 7 of the phenanthroline ligands seems to reduce the probability of generating molecular necklaces, since a hexyl-functionalized [4]MN was obtained in only 6% yield using the same synthetic protocol.[72]

Kimoon Kim[125,127,129] described the first high-yielding thermodynamically controlled syntheses (**Figure 4.15**) of molecular necklaces by employing dialkylammonium-based

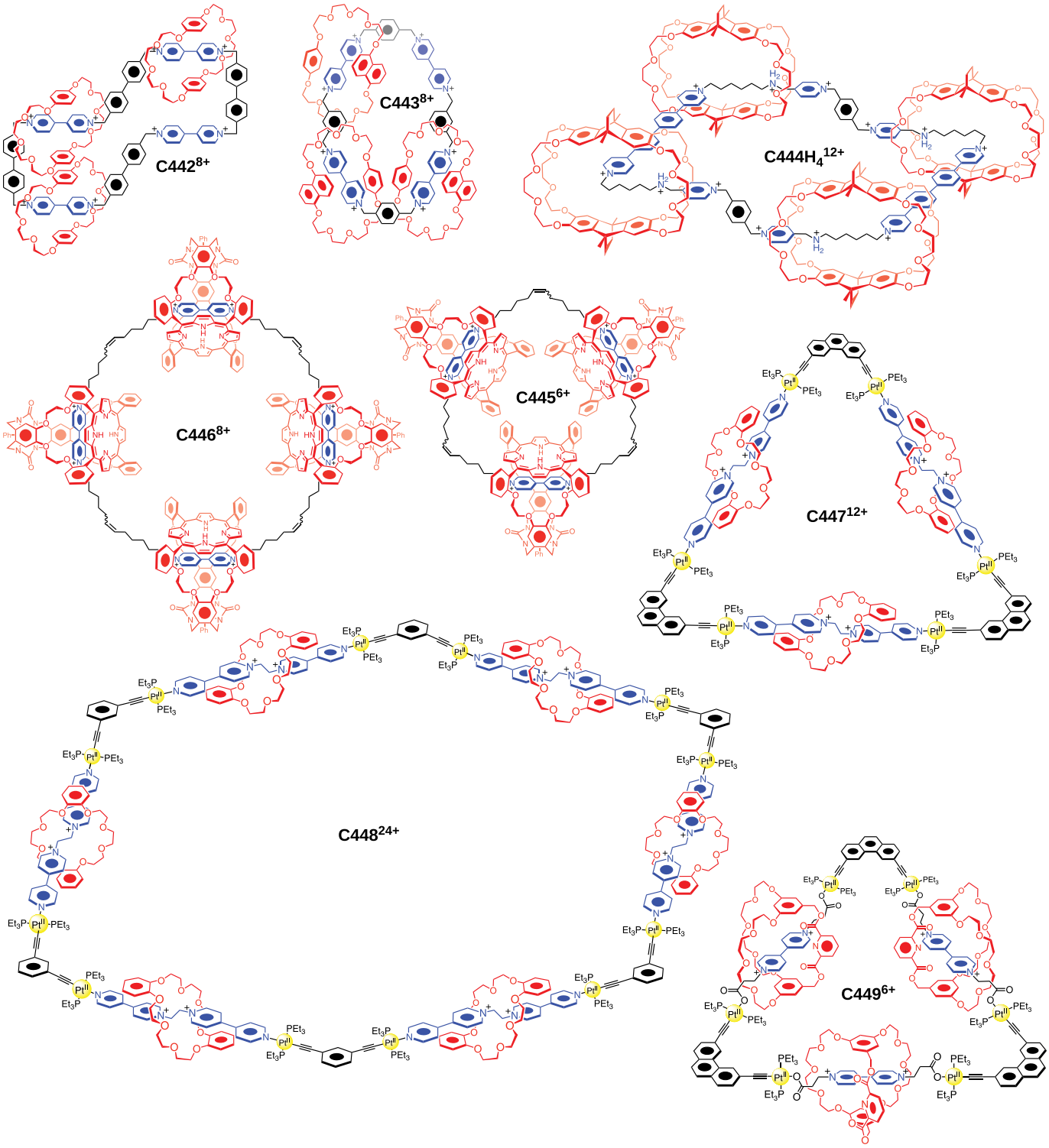


Figure 4.16 Stereoformulas of π-associated donor-acceptor molecular necklaces.[70,75,91,99,103,134]

cucurbit[6]uril (CB6) pseudorotaxanes possessing pyridyl endgroups as ligands for Pt^{II}- or Cu^{II}-based metallacycles. Four molecular necklaces, each deriving from a different ligand, have been characterized in the solid state by X-ray crystallography. The [4]MN **C438H$_6^{12+}$** and **C439H$_6^{12+}$**, each comprising triangular Pt^{II}-cornered assemblies which differ only in the length of the central hydrocarbon linkers in their corresponding ligands, *N*,*N*´-bis(4-pyridylmethyl)-1,4-butanediammonium (C4N4^{2+}) and *N*,*N*´-bis(4-pyridylmethyl)-1,4-pentanediammonium (C5N4^{2+}), respectively. The [5]MN **C440H$_8^{16+}$** derives from a constitutional isomer of C4N4^{2+}—namely, *N*,*N*´-bis(3-pyridylmethyl)-1,4-butanediammonium (C4N3^{2+}). It is noteworthy that this simple change from 4-pyridyl to 3-pyridyl ligating groups

results in the incorporation of an additional ring-and-thread in the metallacyclic self-assembly. Finally, the [5]MN **$Cu_2C441H_6^{14+}$** incorporates two copies of the ligand phen(C4N4)$_2^{4+}$, which comprises a central phenanthroline ligand flanked by a pair of (4-pyridylmethyl)-1,4-butanediammonium threads. The assembly of **$Cu_2C441H_6^{14+}$** involves the sequestration of two Cu^{II} bridgeheads and two Cu^{II} templates, the latter of which accept coordination bonds from the phenantholine and amine donors of the thread, as well as the carbonyl donors of the CB6 rings. The reactions typically proceed in 80–90% yield by simply refluxing the appropriate combination of ligands, CB6, and transition metal salts in water. Kim[133] has also assembled a pseudo[6]molecular necklace based on ternary cucurbit[8]uril inclusion complexes.

The π-donor/π-acceptor template motifs (**Section 2.3.3**) have also been utilized[70,75,91,99,103,134,135] to render (**Figure 4.16**) molecular necklaces. The earliest donor-acceptor molecular necklaces were obtained[70] by the clipping of tetracationic cyclophanes around crown ethers under kinetic control. The [4]MN **$C442^{8+}$** was isolated in 0.2% yield as a side product in the synthesis of [3]catenanes based on cyclobis(paraquat-4,4´-biphenylene) (CBPQB^{4+}) and BPP34C10 crown ethers. A similar [4]MN **$C443^{8+}$** was observed[75] subsequently in 2.7% yield during a template-directed clipping of *meta*- and *para*-xylylene bridged bipyridinium precursors in the presence of the 1,5-naphtho-*para*-phenylene[36]crown-10 (NPP36C10) macrocyclic polyether. Chiu[91] has employed the macrotricyclic host $DBB_2$24C8_2 (see **Table 2.11** in **Section 2.3.3.7**) in a clipping reaction that affords the [5]MN **$C444H_4^{12+}$** in 4% yield.

The remaining π-associated donor-acceptor molecular necklaces rely on thermodynamically controlled approaches—namely, ring closing olefin metathesis (**Section 3.4.1**) and coordination-driven self-assembly (**Section 3.2.1**)—to afford radial [*n*]catenanes in much higher yields. Elemans, Rowan, and Nolte[99] have utilized their π-electron rich 'porphyrin basket' receptor (see **Section 2.3.3.6**) in the one-pot synthesis of the [4]MN **$C445^{6+}$** and the [5]MN **$C446^{8+}$** by ring-closing olefin metathesis of di(octenyl)bipyridinium guests in 18 and 11% yields, respectively. Although these molecular necklaces are the dominant products, a smaller [3]catenane and larger [*n*]MNs are also generated in trace amounts. The product distribution is sensitive to the length of the bipyridinium units' alkene chains, since a longer 21-atom chain leads almost exclusively to smaller [2]- and [3]catenanes under the same conditions. Li and Stang[134] have combined the 1,2-bis(pyridinium) ethane (BPE^{2+})/dibenzo[24]crown-8 (DB24C8) pseudorotaxane ligand motif originally developed by Loeb[136] with reversible metallosupramolecular joints based on Stang's 60° and 120° bis(Pt^{II}-acetylide) acceptors[137,138] in order to orchestrate the nine-component coordination-driven self-assembly of the [4]MN **$C447^{12+}$**, as well as the 18-component self-assembly of the [7]MN **$C448^{24+}$** in near-quantitative yields. The same team has also described the coordination-driven, near-quantitative, nine-component self-assembly[103] of the [4]MN **$C449^{6+}$** by linking the same 60° bis(Pt^{II}) joints with 4,4´-bipyridinium bis(propionate) ligands threaded by π-donating cryptands. Loeb[135] has recently contributed a new [4]MN (not illustrated) derived from *N-benzylaniline⊂24C8* [2]rotaxane ligands and Pt^{II} corners.

Hydrogen-bonded *dialkylammonium⊂crown* ether recognition motifs (**Section 2.3.4.6**) have also been harnessed to assemble (**Figure 4.17**) molecular necklaces. These kinds of molecular necklaces were first observed[128] as side products in the polymerization of triphenylphosphonium-stoppered[139] dibenzylammonium/DB24C8-based [2]rotaxane monomers by Wittig exchange. The benzyloxymethoxy (BOM)-protected [4]MN **$C450H_3^{3+}$** was isolated[128] in 4% yield after hydrogenation of the double bonds, while trace amounts of a larger [5]MN were also detected by mass

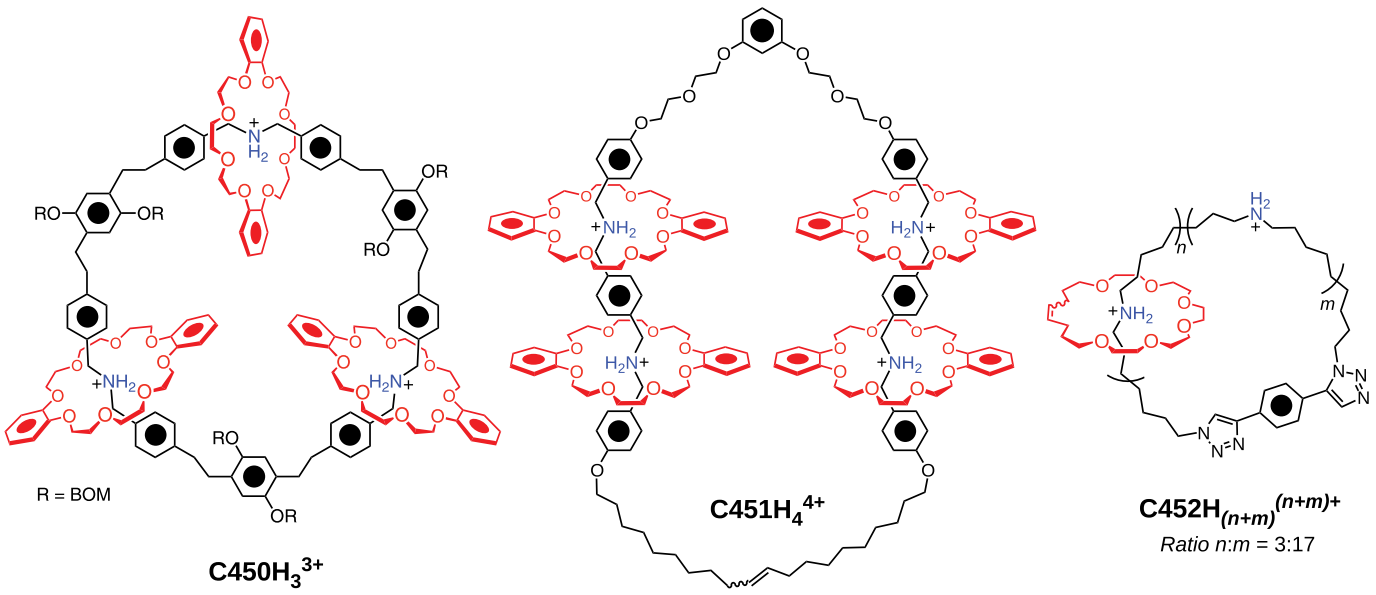
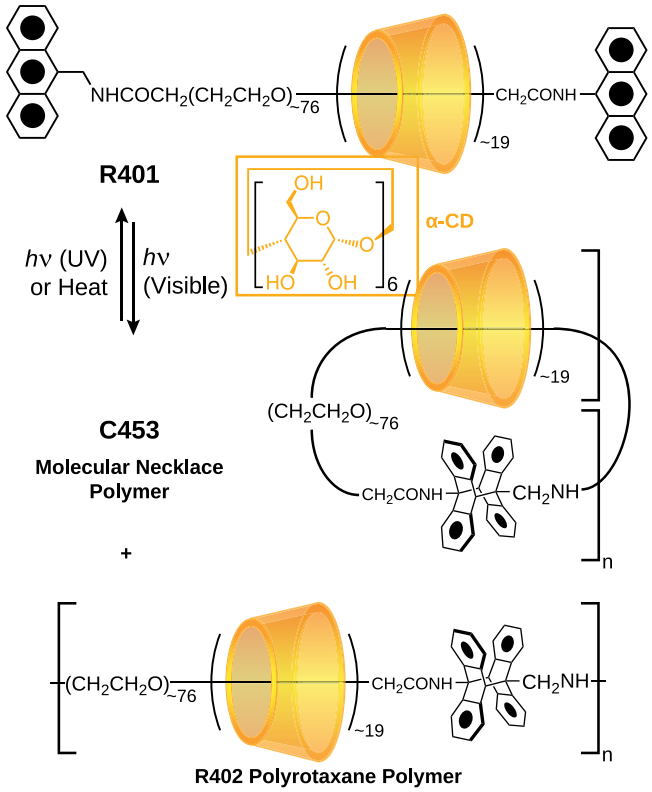


Figure 4.17 Stereoformulas of molecular necklaces[128,130,132] based on macrocyclic oligo- and poly(dialkylammonium) cations and crown ethers.

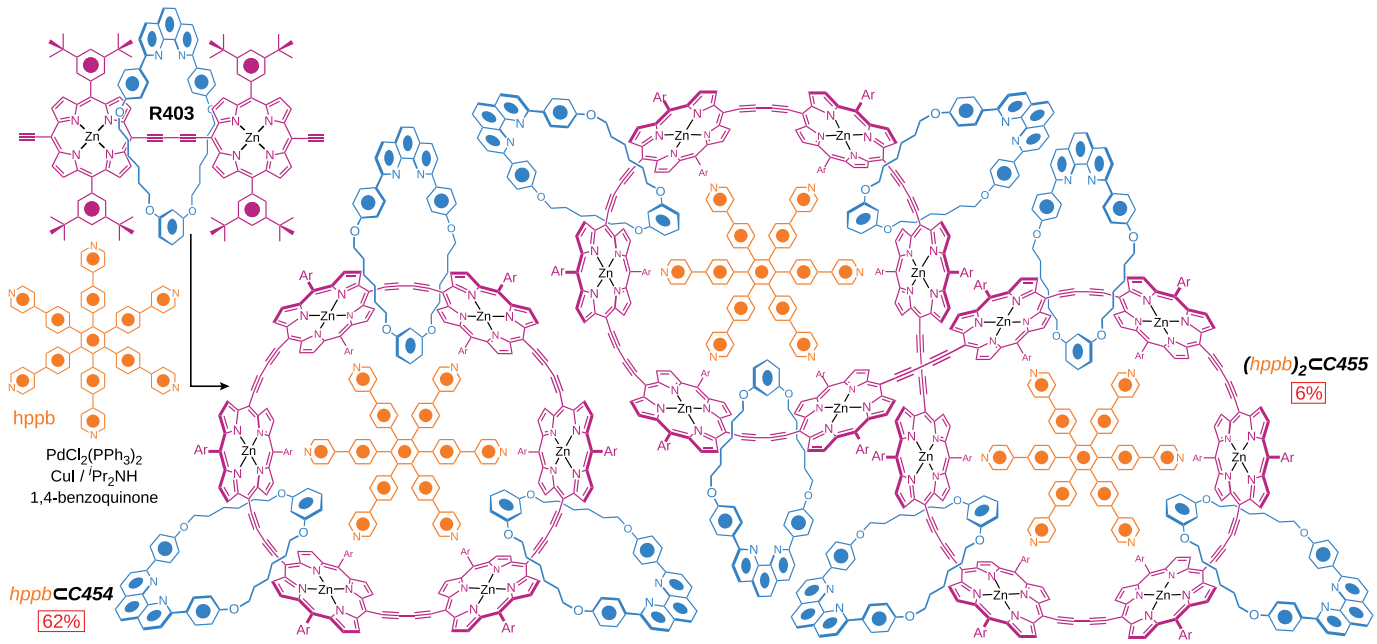


Scheme 4.7 Harada's synthesis[131] of molecular necklaces and polyrotaxane polymers via the reversible photodimerization of anthracene stoppers in *αCD⊂PEG*-based polyrotaxanes. The molecular necklaces are more favored under high-dilution conditions.

spectrometry. Jishan Wu[130] has isolated the [5]MN **C451H$_4^{4+}$** selectively in 20% yield by performing ring-closing olefin metathesis on a long and flexible pseudo[5]rotaxane precursor. Poor solubility prevented the successful synthesis of a [7]MN from the corresponding pseudo[7]rotaxane. Grubbs[132] employed ring-closing olefin metathesis to clip crown ethers around circular polymers possessing approximately 17–19 dialkylammonium groups (polydispersity index 1.49) in order to generate [*n*]MN 'charm bracelet' polymers **C452H$_{(n+m)}^{(n+m)+}$**, where *n* and *m* represent the number of encircled and unencircled $-NH_2^+-$ recognition sites, respectively. ^{1}H NMR spectroscopic analysis indicated that approximately 15% of the dialkylammonium sites were encircled by rings (*n*:*m* = 3:17), corresponding to mostly [3]catenane and [4]molecular neckace polymer topologies. The relatively low clipping yield was rationalized on the basis of solubility and secondary structure arguments.

Harada[131] has prepared (**Scheme 4.7**) anthracene-capped α-cyclodextrin/PEG polyrotaxanes **R401**, possessing an average of approximately 19 αCD rings per chain, and cyclized them into molecular necklaces (**C453**) under UV irradiation by virtue of the reversible photodimerization of the stoppers. The ratio of **C453** necklace polymers to acyclic polyrotaxanes **R402** is influenced by concentration, where the necklaces are favored at higher dilution ratios.

Harry Anderson[140] has combined Saito's active metal template approach[141] (**Section 2.4**) to making mechanical bonds with his own template synthesis[142] of porphyrin nanorings to prepare (**Scheme 4.8**) molecular necklaces. After an active metal template protocol, the [2]rotaxane **R403**, equipped with a pair of porphyrinic stoppers each displaying terminal alkyne groups, is exposed to oxidative coupling conditions in the presence of hexakis[4-(4-pyridyl) phenyl]benzene (hppb), a hexavalent ligand which coordinates the axial sites of the zinc porphyrin stoppers. The homocoupling reaction yields the [4]MN *hppb⊂**C454*** in



Scheme 4.8 Anderson's template synthesis of porphyrin nanoring molecular necklaces from porphyrin-stoppered [2]rotaxanes.[140]

high yield (62%) on account of the hppb template's preorganizing effect. The [7]MN (*hppb*)$_2$⊂***C455*** was also isolated (6%) as a minor product. By introducing into solution an excess of DABCO, which competes for the open coordination sites in the porphyrin nanoring, the hppb guest can be separated efficiently (89%) from the [4]catenane **C454**. Anderson has developed similar template protocols for making even larger[143,144] and more sophisticated[145,146] porphyrin nanoring structures, suggesting that even more challenging composite links may be accessible by this approach.

4.1.2.3 Branched [n]Catenanes

Examples of branched [*n*]catenanes, which possess a combination of linear and radial links, remain few and far between. Branched [6]- and [7]catenanes were introduced[73,74] via π-donor/π-acceptor templation by subjecting a [3]catenane based on CBPQB^{4+} and trinaphtho[57]crown-15 (TN57C15) to a high-pressure (12 kbar) reaction in DMF involving the clipping of CBPQT^{4+} around any of four vacant DNP recognition sites, yielding a mixture of linear [4]- and [5]catenanes (Olympiadane in the latter case—see **Section 4.1.2.1**) in 5 and 37% yields, as well as the branched [6]- and [7]catenanes **C456**$^{16+}$ and **C457**$^{20+}$ in yields of 30 and 12%, respectively. The stereoformula **C456**$^{16+}$ and the solid-state structure of **C457**$^{20+}$, as determined by single crystal X-ray diffraction, are illustrated in **Figure 4.18a** and **4.18b**, respectively.

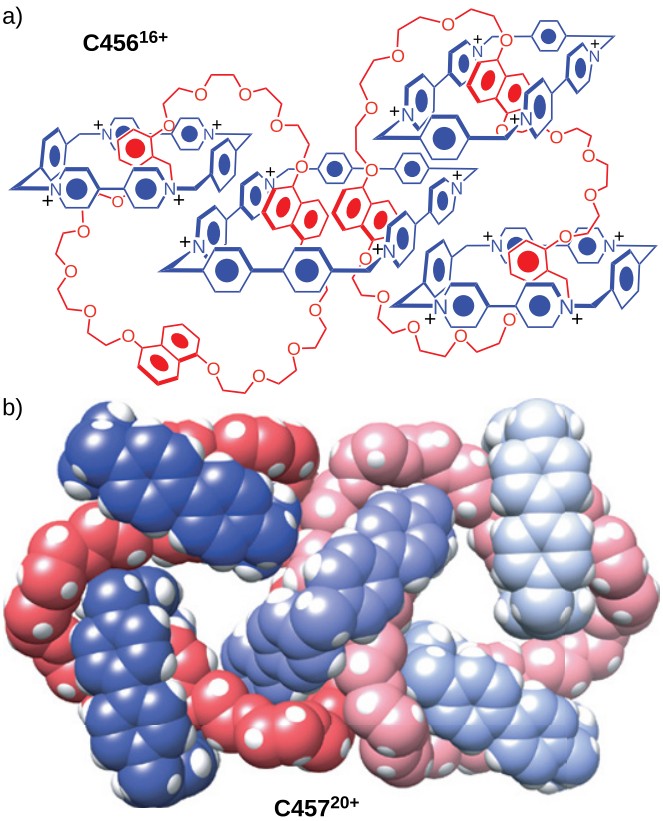
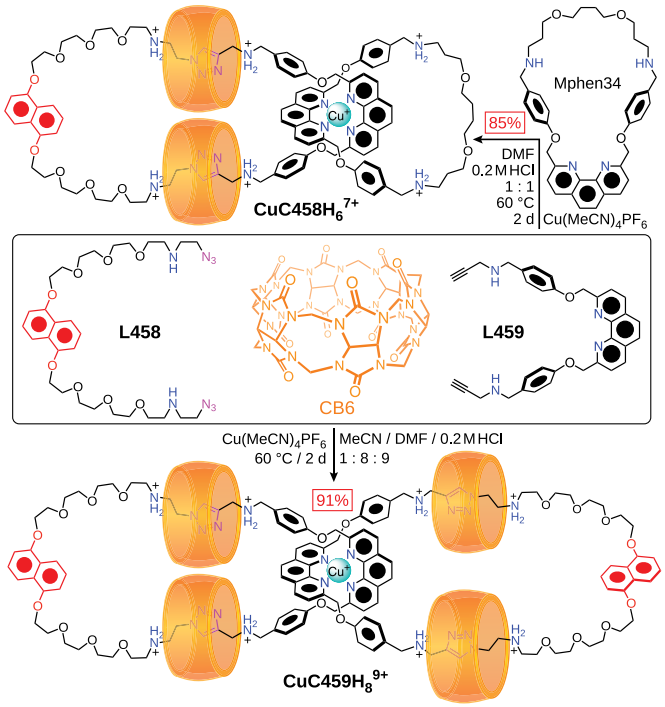


Figure 4.18 Donor-acceptor branched [*n*]catenanes.[73,74] (a) Stereoformula of the branched [6]catenane **C456**$^{16+}$. (b) Space-filling representation of the solid-state structure of the branched [7]catenane **C457**$^{20+}$, which is identical to **C456**$^{16+}$ in its constitution except that it possesses one more CBPQT^{4+} ring. Solvent molecules and PF_6^- counterions are omitted for the sake of clarity.

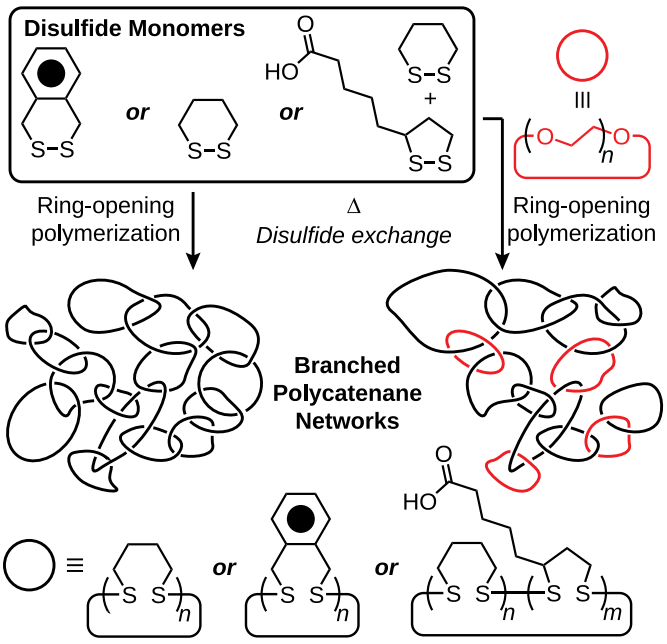


Scheme 4.9 Au-Yeung's syntheses of a radial [4]catenane molecular necklace (top) and a branched [6]catenane (bottom) by a combination of Cu^{I} templation and CB6AAC covalent capture strategies.[105]

Au-Yeung[105] has employed the cucubit[6]uril (CB6)-catalyzed azide-alkyne cycloaddition (CB6AAC) in the covalent capture—see **Sections 2.3.1.2–2.3.1.3**—of both radial and branched oligocatenanes. The synthesis (**Scheme 4.9**) of these catenanes involves the capture of catenated CB6 rings during the CB6AAC macrocyclization of entiwined templates derived from phenanthroline (phen) ligands surrounding Cu^{I} ions. The radial [4]catenane **CuC458H$_6^{7+}$** and the branched [6]catenane **CuC459H$_8^{9+}$** are obtained in yields of 85% (54% isolated) and 91% (69% isolated), respectively, from acidic aqueous DMF mixtures containing CB6, the bis(azide) **L458**, and the phen-based bis(propargylammonium) ligand **L459**, as well as the bidentate macrocycle Mphen34 in the case of **CuC458H$_6^{7+}$**. These results suggest that combining multiple types of molecular recognition motifs into a single system can be beneficial to the synthesis of sophisticated molecular topologies and the efficiencies with which they are made.

It is easy to imagine two- and three-dimensional polycatenated nets akin to chainmail, and macromolecular materials based on these branched topologies are expected[147] to exhibit different dynamics and mechanical

properties than ordinary linear polymers. Indeed, mechanical bonds have been invoked to explain anomalous physical properties in networks containing cyclic polysiloxanes,[148–150] polyphosphonitrilic chlorides,[151] and other polymers[152] from as early as the 1950s. More recently, Endo[153–157] has claimed that the ring-opening bulk polymerization of 1,2-dithiane or *o*-xylenedisulfide, as well as the co-polymerization of lipoic acid and 1,2-dithiane, are reactions that generate (**Scheme 4.10**) polycatenated networks via disulfide exchange. These claims have been supported by the observation of significant differences[D] in the thermal and physical properties of the alleged polycatenanes as compared to homologous linear polydisulfides, while further evidence is provided by the fact that cyclic polyethers cannot be removed from the polymer networks if they are present during the polymerization. In a possible contradiction of these results, Juskis[158] has observed the presence of only branched polymers when visualizing thermally polymerized poly(α-lipoic acid) by atomic force microscopy (AFM). Meijer and Di Stefano[159] have also prepared polydisperse branched [*n*]catenanes, along with linear [*n*]catenanes and molecular necklaces, by ring-opening metathesis polymerization



Scheme 4.10 Endo's syntheses[153,155,157] of branched polycatenane networks by ring-opening polymerization of cyclic disulfides in the absence (left-hand side) or presence (right-hand side) of cyclic polyethers.

[D] The catenated polydisulfides exhibited glass transition temperatures that were independent of polymer length, a plateau in storage modulus upon melting, and stress resistance behavior that remains reversible up to 3000% elongation—properties not observed in the case of the control polymers.

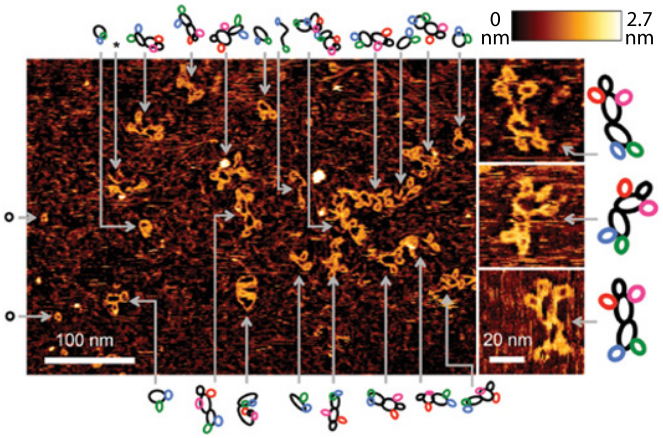


Figure 4.19 AFM images of Willner's DNA branched [7]catenane and other catenated DNA side-products, represented graphically in the colored line drawings. Adapted with permission from ref. 109 (copyright 2015 American Chemical Society).

of olefin-containing [2]catenanes based on Sauvage's $Cu(dpp)_2^+$ template motif. A mixture of cyclic compounds possessing between one and six of these monomers was isolated and confirmed to comprise mainly cyclic, rather than linear species. More controllable, versatile, and rational approaches to the synthesis 'macromolecular chainmail' like these preliminary examples are needed in order to understand how mechanical bonds can influence macroscopic properties—for example, in bulk plastic materials.

Recently, Willner[109] has reported the preparation and switchable reconfiguration of a branched [7]catenane composed entirely of circular single-stranded DNA. The successful formation of these heptacatenanes has been confirmed, not only by gel electrophoresis and mass spectrometry, but also by high-resolution imaging (**Figure 4.19**) using AFM. Four of the heptacatenane's rings—colored red, pink, blue, and green in the graphical representations—may be switched between two positions via strand displacement, resulting in a total of 16 possible co-conformational states. Thus, the [7]catenanes are not unlike 'stick figures' with arms and legs that move in response to DNA-based chemical fuels. More details on switching DNA-based catenanes are discussed in **Section 6.10.2**. The synthesis of DNA mechanomolecules by enzymatic ligation is discussed in **Section 2.3.12.1**.

4.1.3 Multi-Annulated Catenanes

Polycyclic, polyhedral, and cage-like compounds with multi-annulated component parts offer opportunities to construct new mechanically interlocked topologies that are not possible to construct using simple rings. The prime links and composite links described in **Sections 4.1.1–4.1.2** contain only two-order vertices in their molecular graphs; here, we consider link topologies whose molecular graphs

include vertices with three or more branches. We subdivide these catenanes according to the topologies of their polycyclic component parts, which may be characterized by the torus number, which amounts to the minimum number of 'holes' in a surface. For example, a macrobicyclic compound possesses the topology of a double torus, while macrotricyclic structures embody the triple torus, and so on. Multi-annulated catenanes that have been described in the literature include those incorporating macrobicyclic (**Section 4.1.3.1**), macrotricyclic (**Section 4.1.3.2**), macrotetracyclic (**Section 4.1.3.3**), and macropentacyclic (**Section 4.1.3.4**) component parts.

The types of compounds that have been important in the genesis of multi-annulated catenanes are cryptands, self-assembled cages/polyhedra, and fused rings. Cryptands are defined[160] as polycyclic assemblies of binding sites arranged into three-dimensional cavities that bind guests (typically cations) more strongly than the individual binding sites. Cryptand-based hosts,[161] such as macrobicyclic[162–165] and macrotricyclic[91,166] polyethers, have been incorporated into a variety of polycyclic [2]catenanes. Cryptands have also been incorporated into a number of [3]catenanes[91,99,162] and molecular necklaces[91,99,103]—e.g., **C444H$_4$$^{12+}$–C446^{8+}** and **C449^{6+}** in **Figure 4.16** in **Section 4.1.2.2**. Self-assembled molecular cages and polyhedra of both the metallo-organic[57,167–175] and all-organic[176–179] varieties also lend themselves to the production of multi-annulated catenanes. A tetrahedral cage, for example, possesses the same triple torus topology as macrotricyclic cryptands, despite their substantial differences in Euclidean shape. Multi-annulated catenanes are also based occasionally on fused[E] rings[180–187] that cannot be classified as cryptands, nor as cages.

4.1.3.1 Catenated Macrobicyclics

Macrobicyclic catenane topologies (**Figure 4.20**) may be subdivided into either heterocatenated or homocatenated categories. Heterocatenated macrobicyclic catenanes are those in which the macrobicyclic component(s) are not identical, while homocatenated macrobicyclic catenanes possess two or more identical component parts. One can envision many ways to interlock a double torus with one (**Figure 4.20a**), two (**Figure 4.20b**), or three (**Figure 4.20c**) rings. Different presentations of each of these topologies are illustrated in order to point out that, although there are no topological differences in three dimensions between the objects within each category, they may exhibit dramatic differences in Euclidean shape, corresponding to dramatically different chemical design motifs in practice. In the case of

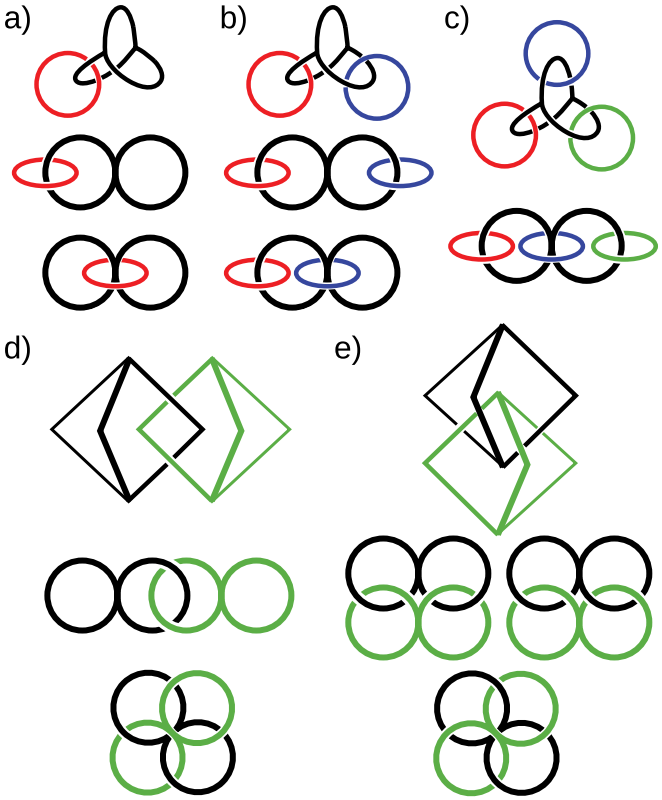


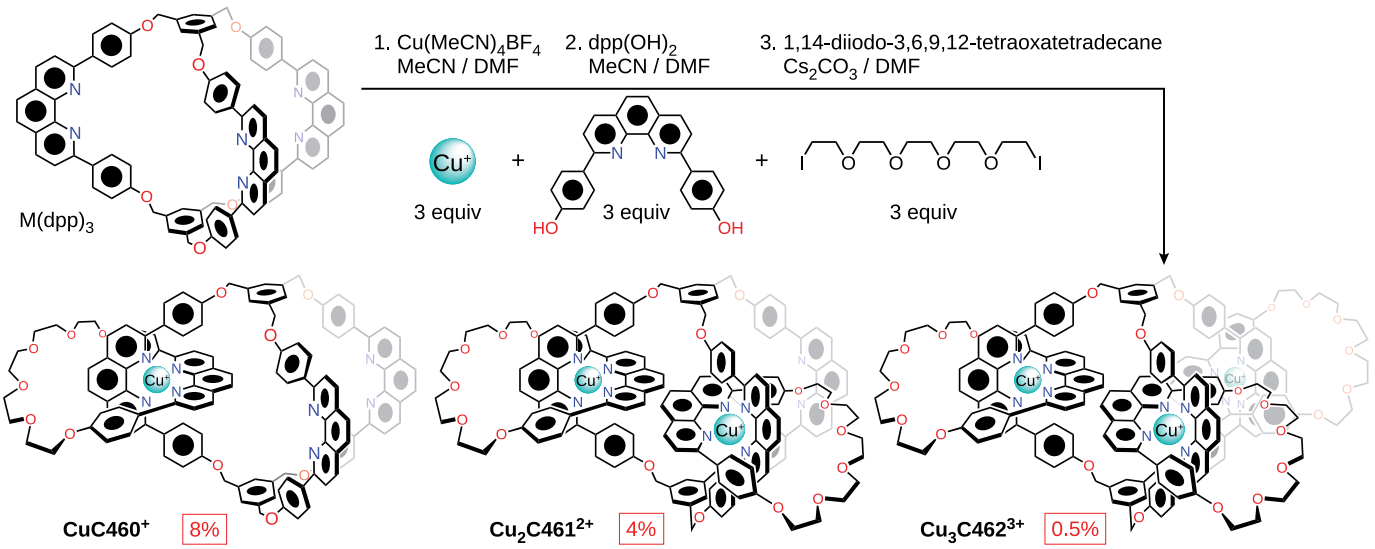
Figure 4.20 Simplified graphs of macrobicyclic catenanes. The heterocatenated macrobicyclic [2]catenane (a), [3]catenane (b), and [4]catenane (c) comprise a single macrobicyclic component part catenated by one, two, or three rings, respectively. Macrobicyclic homo[2]catenanes may take the form of singly (d) and doubly (e) interlocked topologies. In spite of their different two-dimensional presentations, the objects within each category are topologically equivalent (isotopic) in three-dimensional space, meaning that they can be interconverted by continuous deformation.

macrobicyclic homo[2]catenanes, the double tori may be singly (**Figure 4.20d**) or doubly (**Figure 4.20e**) interlocked. Different presentations are illustrated again in order to emphasize that different types of component parts, including cryptands, cages, and fused rings, may be employed to construct identical topologies in spite of their substantial Euclidean differences.

Heterocatenated Macrobicyclics

In 1991, Vögtle[176] described the synthesis and endotopic chelation properties of a macrobicyclic ligand M(dpp)$_3$ possessing three 2,7-diphenylphenanthroline (dpp) arms flanking a pair of mesitylene-derived bridgeheads. Two years later, in a collaboration with Sauvage,[188] M(dpp)$_3$ was employed in the synthesis (**Scheme 4.11**) of catenates based on Sauvage's revolutionary[189] Cu(dpp)$_2^+$ templation motif (**Section 2.3.3.1**). The Williamson ether synthesis of Mdpp30 macrocycles from dpp(OH)$_2$ and the corresponding iodine-terminated polyether derived from pentaethylene glycol (5EG) in the presence of M(dpp)$_3$ and Cu^{I} templates

[E] We distinguish fused rings from covalently linked ones on the basis of relatively subtle topological considerations. In the case of fused macrobicyclic topologies, for example, two rings are fused to a central core such that each ring shares part of its constitution with that of the other. By contrast, the rings of a bis-macrocycle share no constitutional overlap since they are connected by a covalent linker.



Scheme 4.11 The synthesis of [2]-, [3]-, and [4]catenanes with macrobicyclic cores introduced by Sauvage and Vögtle.[176]

affords a mixture of the [2]catenate **CuC460**$^{+}$, the [3]catenate **Cu$_2$C461**$^{2+}$, and the [4]catenate **Cu$_3$C462**$^{3+}$, in yields of 8, 4, and 0.5%, respectively. To the best of our knowledge, the macrobicyclic [4]catenate **Cu$_3$C462**$^{3+}$ is the first and only catenane exhibiting this particular topology, while the topologies of **CuC460**$^{+}$ and **Cu$_2$C461**$^{2+}$ have been replicated subsequently in several catenanes (*vide infra*) based on fused rings and cryptands.

A number of macrobicyclic [2]- and [3]catenanes have been constructed (**Figure 4.21**) by clipping protocols employing π-associated donor-acceptor template motifs. The earliest catenanes of this type were based on fused

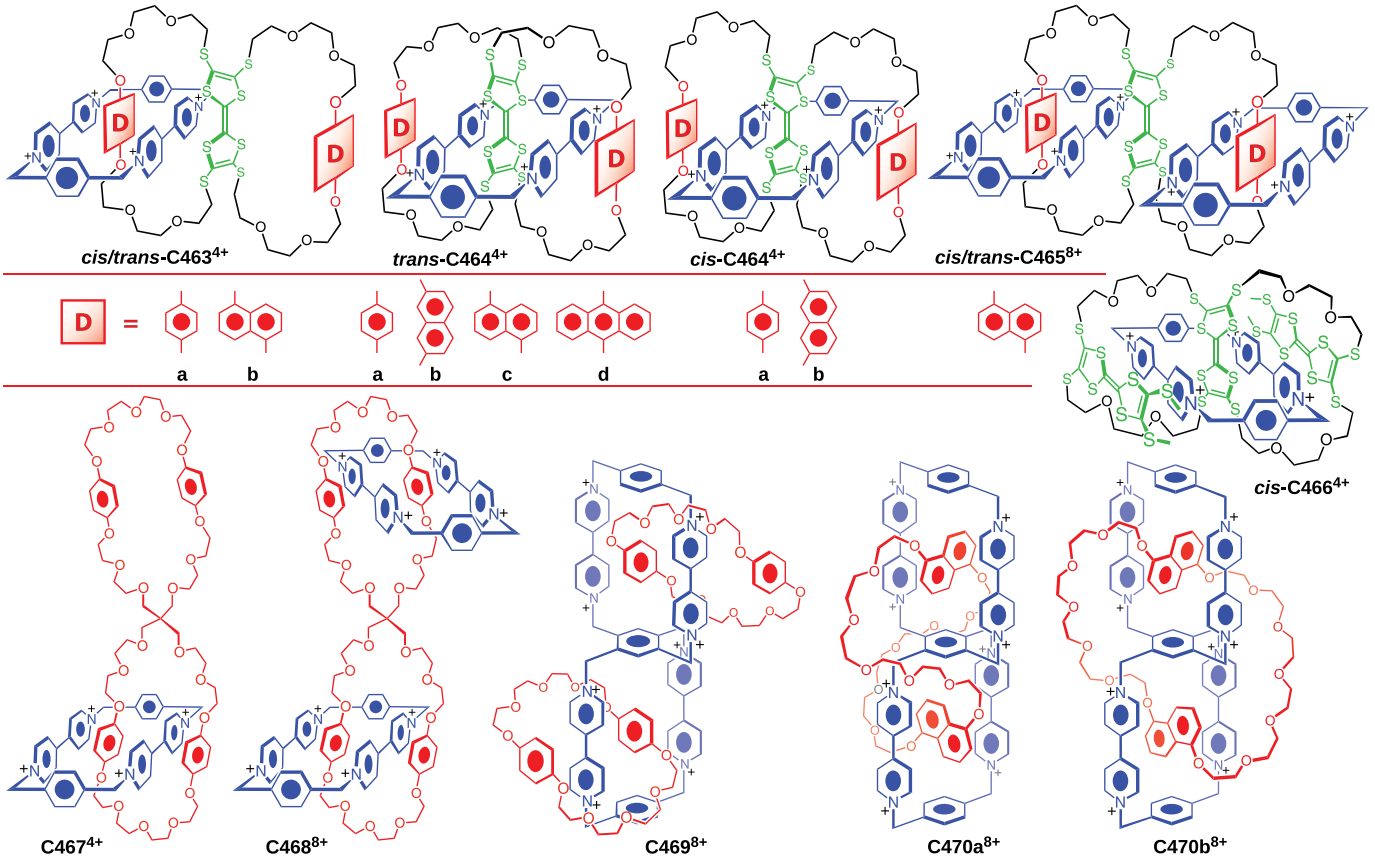


Figure 4.21 Stereoformulas of [2]- and [3]catenanes based on fused-ring macrobicyclic π-donors[180–182,184,191] (**C463^{4+}–C468^{8+}**) as well as fused-ring macrobicyclic π-acceptors[187,190] (**C469^{8+}–C470^{8+}**).

cyclophanes and $CBPQT^{4+}$ rings.[180,190] Becher[180–184] has employed various fused tetrathiafulvalenophanes as π-donating synthons for multi-annulated catenanes. The double torus component parts of compounds **C463^{4+}–C466^{4+}** all comprise π-donating macrocyclic polyethers fused to a central TTF core. Clipping reactions in the presence of these fused bicyclics can produce [3]catenanes/bis[2]catenanes (**Section 4.1.4.4**) such as **C465^{8+}**, as well as [2]catenanes in which the $CBPQT^{4+}$ ring encircles one of the peripheral π-donors (**C463^{4+}**) or the central TTF unit (**C464^{4+}** and **C466^{4+}**). These latter compounds have also been described as [3]pseudocatenanes[180] and 'handcuff'[185,187] catenanes—see **Section 4.1.4.2**. The isomerism of these catenanes is noteworthy, since the two rings of the macrobicyclic polyethers may be fused to the central TTF core exhibiting either a *cis* or *trans* configuration. In cases (e.g., **C463^{4+}** and **C465^{8+}**) where the TTF unit is not encircled by a $CBPQT^{4+}$ ring, the TTF unit undergoes rapid *cis*/*trans* isomerization, especially in the presence of a catalytic amount of acid. By contrast, the *cis* and *trans* isomers of the handcuff catenanes **C464^{4+}** do not interconvert. Furthermore, the selectivity for *cis* and *trans* isomers is influenced by the peripheral π-donors. In the cases of hydroquinone[180] (HQ) and 2,7-dioxynaphthalene[181] (**C464a^{4+}** and **C464b^{4+}**, respectively), both *cis* and *trans* isomers are obtained with low selectivity. On the contrary, only the *trans* isomer was observed in the cases of 1,5-dioxynaphthalene[181] (DNP) and hydroanthraquinone[180] (**C464c^{4+}** and **C464d^{4+}**, respectively). The all-TTF [2]catenane ***cis*-C466^{4+}** is also produced[182] with high configurational selectivities. While Becher's macrobicyclic [2]catenanes all possess π-donating polyethers fused to a central TTF core, the π-donating rings of the [2]catenane **C467^{4+}** and the macrobicyclic [3]catenane/bis[2]catenane **C468^{8+}** are fused to a single tetrahedral carbon atom at the center of each of their polyether loops.[191] The solid-state structure of **C468^{8+}** is illustrated in **Figure 4.22**. A planar chiral receptor comprising two $CBPQT^{4+}$ rings fused to a central phenylene unit has also been employed (**Figure 4.21**) in the synthesis of the bis[2]catenane[190] **C469^{8+}**, as well as a chiral handcuff catenane[187] comprising a mixture of the

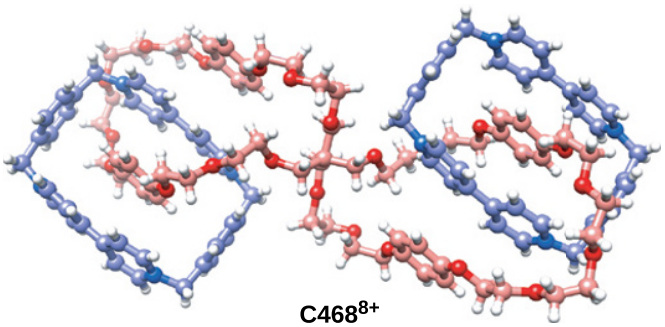


Figure 4.22 Ball-and-stick representation of the solid-state structure of **C468^{8+}**.[191] The PF_6^- counterions and MeCN solvent molecules are omitted for the sake of clarity.

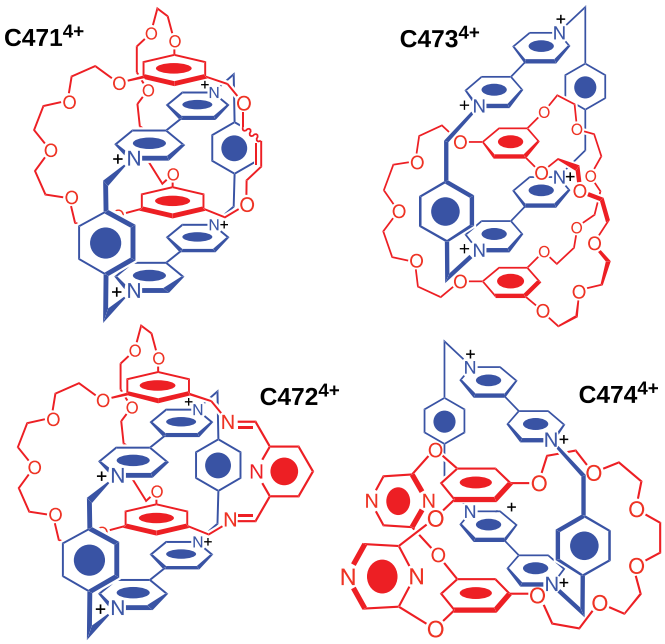


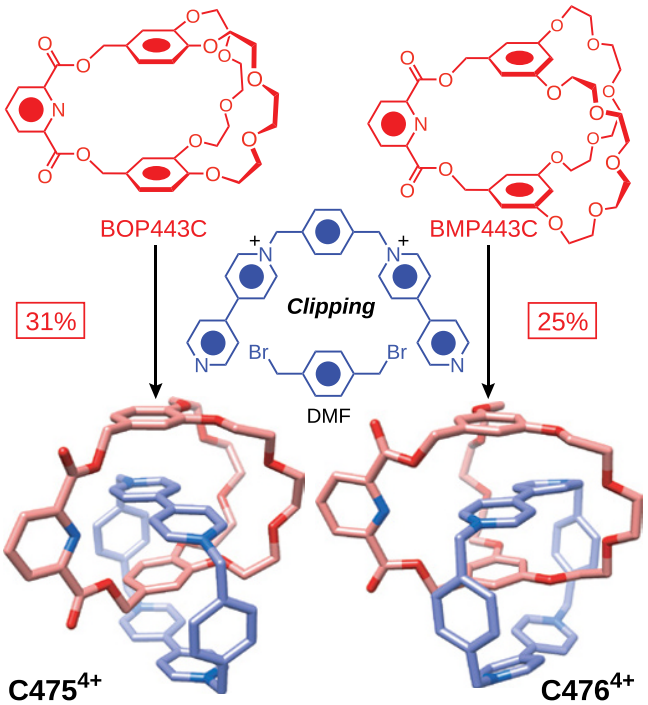
Figure 4.23 Stereoformulas of donor-acceptor [2]catenanes incorporating cryptand-like macrobicyclic polyethers.[162–165]

mechanostereoisomers **C470a^{8+}** and **C470b^{8+}**, which are discussed in **Section 5.2.4.1**.

Macrobicyclic cryptands have also been incorporated[162–165] into a number of [2]catenanes, including (**Figure 4.23**) **C471^{4+}–C474^{4+}**, which are described in the sections accompanying **Scheme 2.61**, **Scheme 2.63**, and **Figure 3.13** in previous Chapters. These macrobicyclic [2]catenanes can exhibit novel types of isomerism if the cryptand is desymmetrized such that its loops do not possess identical constitutions. For example, Huang[192] has described how a subtle change in the constitution of a macrobicyclic cryptand can lead to large differences in the co-conformations and solid-state packings in the corresponding catenanes. In a pair of clipping reactions (**Scheme 4.12**) with $CBPQT^{4+}$ precursors, the benzo-*ortho*-phenylene [4.4.3]cryptand BOP443C gives rise to a [2]catenane (**C475^{4+}**) with a completely different co-conformation than that of the [2]catenane (**C476^{4+}**) derived from its constitutional isomer based on benzo-*meta*-phenylene, BMP443C. Whereas the $CBPQT^{4+}$ ring passes through both of the [4.3] annuli[F] of BOP443C, it passes through the [4.4] annulus[F] and only one [4.3] annulus[F] of BMP443C. In both cases, the cyclophane avoids interlocking the smallest ring within the cryptand's macrobicyclic constitution.

Beer[193,194] has prepared macrobicyclic anion-binding receptors comprising strapped calix[4]arenes and employed them in the synthesis of [2]catenanes—see **Section 3.4.1.4**.

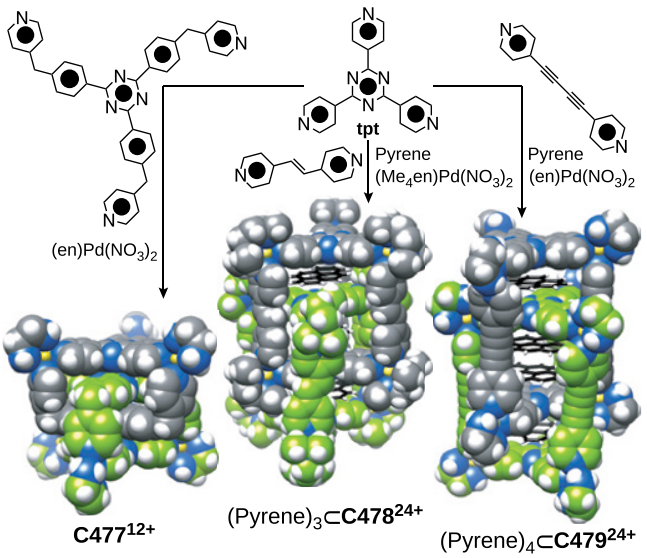
[F] The bracketed numbers denote the number of donor atoms, O or N, in each of the cryptands' three polyether loops.



Scheme 4.12 Clipping protocols involving Huang's constitutionally isomeric cryptands, BOP443C and BMP443C, produce [2]catenanes with different co-conformations defined by the relative orientations of the CBPQT^{4+} rings.[192] Solid-state structures of the [2]catenanes are portrayed with hydrogen atoms, PF_6^- counterions, and MeCN solvent molecules omitted for the sake of clarity.

Homocatenated Macrobicyclics

Makoto Fujita[167] pioneered the aqueous self-assembly (**Scheme 4.13**) of catenated coordination cages in 1999 when he reported the 10-component self-assembly of the



Scheme 4.13 The aqueous self-assembly of Fujita's mechanically interlocked molecular cages.[167,168] The interlocked extended cages **C478**$^{24+}$ and **C479**$^{24+}$ are supported by intercalated pyrene molecules. Space-filling representations of the solid-state (super)structures of the catenanes are illustrated with NO_3^- counterions omitted for the sake of clarity.

Pd_6L_4 homo[2]catenane **C477**$^{12+}$ comprising a pair of macrobicyclic Pd_3L_2 coordination cages. The metallosupramolecular strategies for making mechanical bonds on which its self-assembly is based are discussed in **Section 3.3**. Fujita[168] has utilized similar catenanes (e.g., **C478**$^{24+}$ and **C479**$^{24+}$) derived from tris(4-pyridyl)-1,3,5-triazine (tpt) and various bis(pyridyl) extension ligands in order to engineer discrete stacks of catenated Pd_6L_5 cages intercalated with pyrene molecules, the number of which depends on the length of the extension ligands, stabilized by hydrophobic effects and donor-acceptor π–π stacking interactions.

In addition to metallosupramolecular cages, cryptands are an equally viable class of synthons for catenating macrobicyclic compounds. Beer[195] has described an example (**Figure 4.24**) of a homo[2]catenane (**C480**) comprising catenated tris(urea)-derived cryptands surrounding a sulfate dianion, the synthesis of which is discussed in **Section 2.3.6.2**.

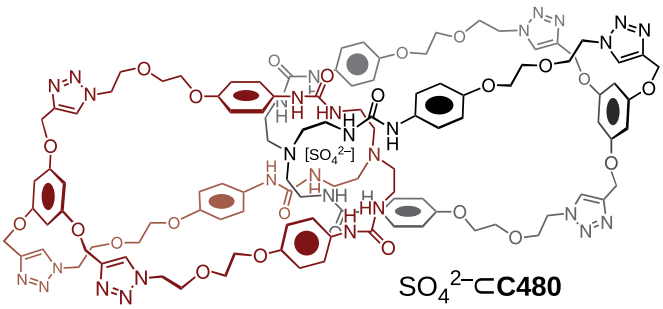


Figure 4.24 Stereoformula of Beer's catenated cryptands, which bind a sulfate dianion.[195]

Recently, Sessler[179] has reported on the quantitative self-assembly (**Figure 4.25**) of an all-organic homo[2]catenane **C481**$^{6+}$ in water—see **Section 3.3.2** for synthetic details. The [2]catenane, which is stabilized by a combination of hydrophobic, donor-acceptor π–π stacking, and hydrogen-bonding interactions, can be locked into a relatively kinetically stable molecule by increasing the pH of the solution, stabilizing the dynamic hydrazone bonds.

Nabeshima[196] has recently introduced (**Scheme 4.14**) homocatenated macrobicyclic assemblies based on the intercalative dimerization of organic cages derived from tripodal metallohelicates. The macrobicyclic [2]catenates **Ru$_4$C482**$^{8+}$ and **Fe$_4$C482**$^{8+}$ exist in equilibrium with the corresponding uncatenated cages, **Ru$_2$M482**$^{4+}$ and **Fe$_2$M482**$^{4+}$, with the catenates being favored at higher concentrations. Each macrobicyclic cage assembles from two tripodal metallohelicates—either **RuL482**$^{2+}$ or **FeL482**$^{2+}$—and three 1,3-diaminopropane molecules by way of reversible imine bond formation. The metal centers line up in linear arrays within the catenates and adopt homochiral (all-Λ or all-Δ) configurations. Other MIMs exhibiting helicity about their mechanical bonds, or "mechanical helicity", are discussed in **Section 5.2.3.3**.

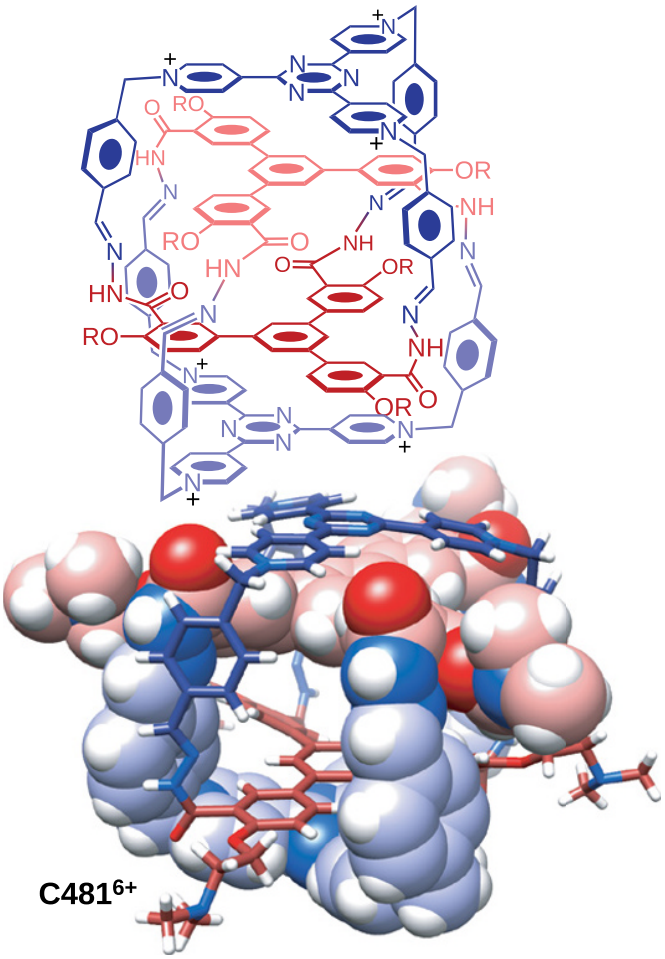
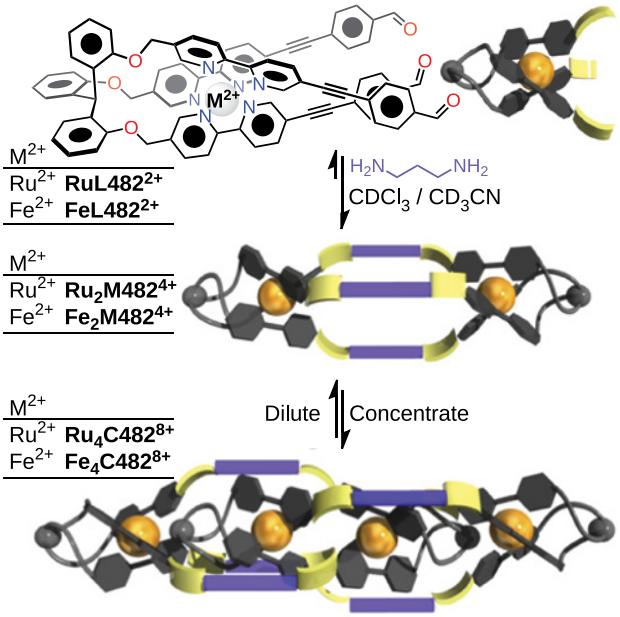


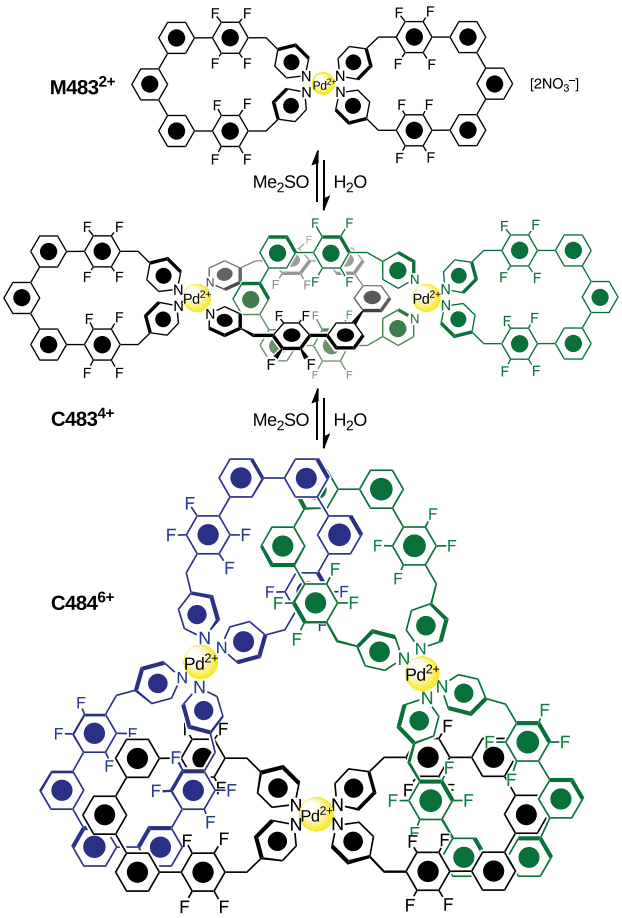
Figure 4.25 Sessler's self-assembled all-organic three-dimensional [2]catenane.[179] The space-filling/tubular representation of the solid-state structure of **C481^{6+}** is illustrated with solvent molecules and Cl^- counterions omitted for the sake of clarity.

Although it is exceedingly uncommon, it is also possible to construct catenanes comprising three or more macrobicyclic component parts. Fujita [197,198] has described the self-assembly (**Scheme 4.15**) of the circular tris[3]catenane **C483^{6+}** comprising three identical metallobicyclic assemblies fused to a central Pd^{II} core. The ratio of the uncatenated bis(macrocyclic) monomer **M483^{2+}** to the catenated dimer **C483^{4+}** and the ultramacrocyclic trimer **C484^{6+}** is controlled by the water content in a 0.5 mM Me_2SO solution: the dimer **C483^{4+}** comprises up to 60% of the population in a 2:3 Me_2SO:H_2O mixture and the trimer **C484^{6+}** reaches up to 50% of the population in a 10:9 Me_2SO:H_2O mixture. Although higher water ratios result in precipitation, both catenanes could be detected and characterized by ^1H NMR spectroscopy and mass spectrometry.

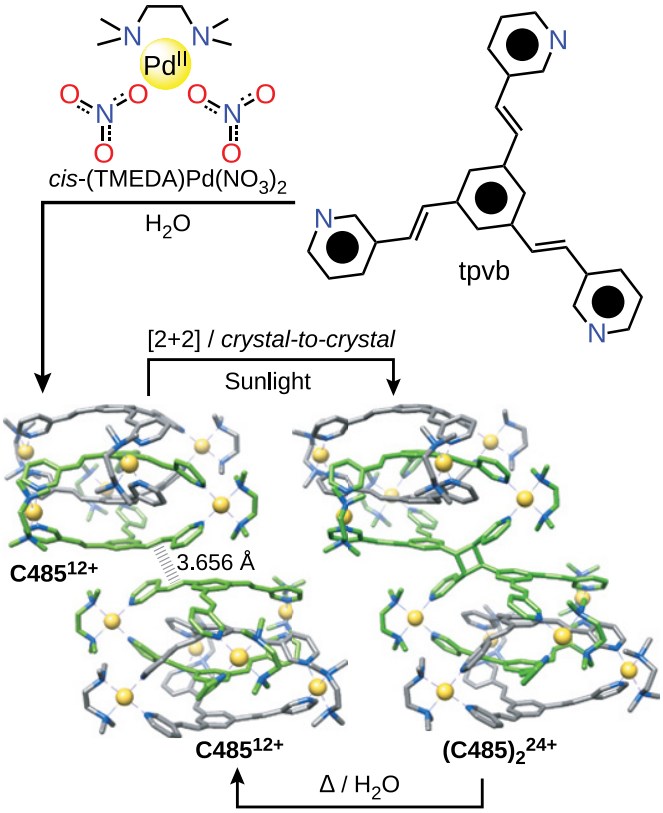
Another case (**Scheme 4.16**) of an unusual higher-order multi-annular catenane has been reported by Mukherjee.[199] The interpenetrated macrobicyclic M_6L_4 cages of the homo[2]catenane **C485^{12+}** self-assemble from *cis*-(TMEDA)$Pd(NO_3)_2$ (TMEDA=*N*,*N*,*N*′,*N*′-tetramethylethylenediamine) and 1,3,5-tris((*E*)-2-(pyridin-3-yl)vinyl)benzene (tpvb) in



Scheme 4.14 Nabeshima's self-assembly of a macrobicyclic homo[2]catenane from tripodal metallohelicates via imine bond formation. Graphical representations reprinted with permission from ref. 196 (copyright 2016 American Chemical Society)



Scheme 4.15 Fujita's penta-*meta*-phenylene fused metallacycles **M483^{2+}** self-assemble[197,198] in binary aqueous solvents into the [2]catenane **C483^{4+}** and the circular tris[2]catenane **C484^{6+}**.



Scheme 4.16 Mukherjee's self-assembly of the macrobicyclic homo[2]catenane **C485**$^{12+}$ and its photochemical crystal-to-crystal dimerization to the corresponding [2 + 2] cycloaddition adduct **(C485)**$_2^{24+}$ in sunlight, a coupling which is thermally reversible in solution.[199] Hydrogen atoms and nitrate counterions are omitted from the solid-state structures for the sake of clarity.

water. One pair of double bonds in the tpvb ligands of adjacent catenanes align *head-to-tail* in the crystal with only 3.656 Å separation, a distance suitable for photoreactivity. Thus irradiation of the crystal with UV light or simple exposure to sunlight results in a [2 + 2] cycloaddition that gives the dimer **(C485)**$_2^{24+}$ in a single-crystal-to-single-crystal transformation. The cycloaddition is thermally reversible, since the bis-macrobicyclo[2]catenane dissociates back to **C485**$^{12+}$ at 90 °C in water by cleavage of the cyclobutane crosslink.

4.1.3.2 Catenated Macrotricyclics

As in the case of macrobicyclic compounds, researchers have prepared macrotricyclic catenanes that fit into either heterocatenated or homocatenated categories.

Heterocatenated Macrotricyclics

The seminal examples (**Figure 4.26**) of catenanes based on macrotricyclic hosts were templated by π-associated donor-acceptor interactions.[166,191] They include the [2]catenane **C486**$^{4+}$ and the homologous [3]catenane **C487**$^{8+}$, which comprise[191] a fused triple-torus polyether catenated by one and two CBPQT^{4+} rings, respectively, around the hydroquinone recognition units of the outermost rings. Becher[166] introduced the heterocatenated macrotricyclic [2]catenane **C488**$^{4+}$ by clipping a CBPQT^{4+} ring around one of the tetrathiafulvalene (TTF) donor units of a so-called 'criss-cross overlapped tetrathiafulvalenophane' macrotricyclic polyether in DMF under high pressure (10 kbar) in 28% yield.

Schalley, Sanders, and Nitschke[172] have collaborated in orchestrating the self-assembly (**Scheme 4.17**) of tetrahedral (macrotricyclic) cages catenated with macrocycles. Each edge of the metallatetrahedral cage **M489**$^{8+}$ is derived from the divalent ligand **L489** containing a π-electron-accepting naphthalenediimide (NDI) recognition site with

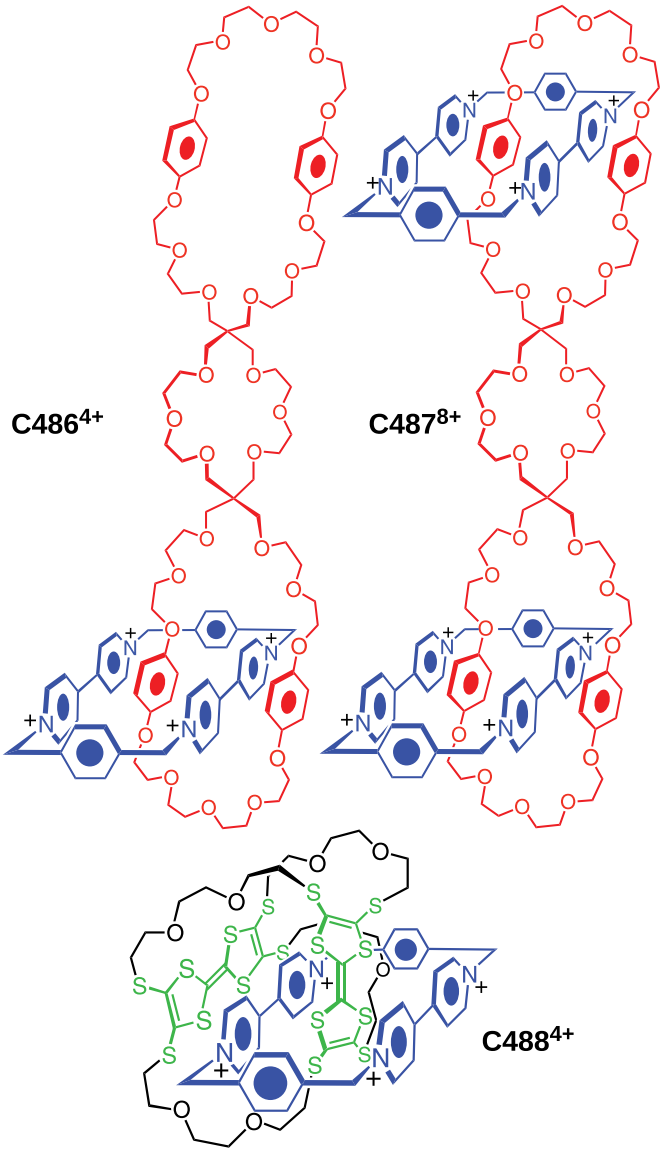
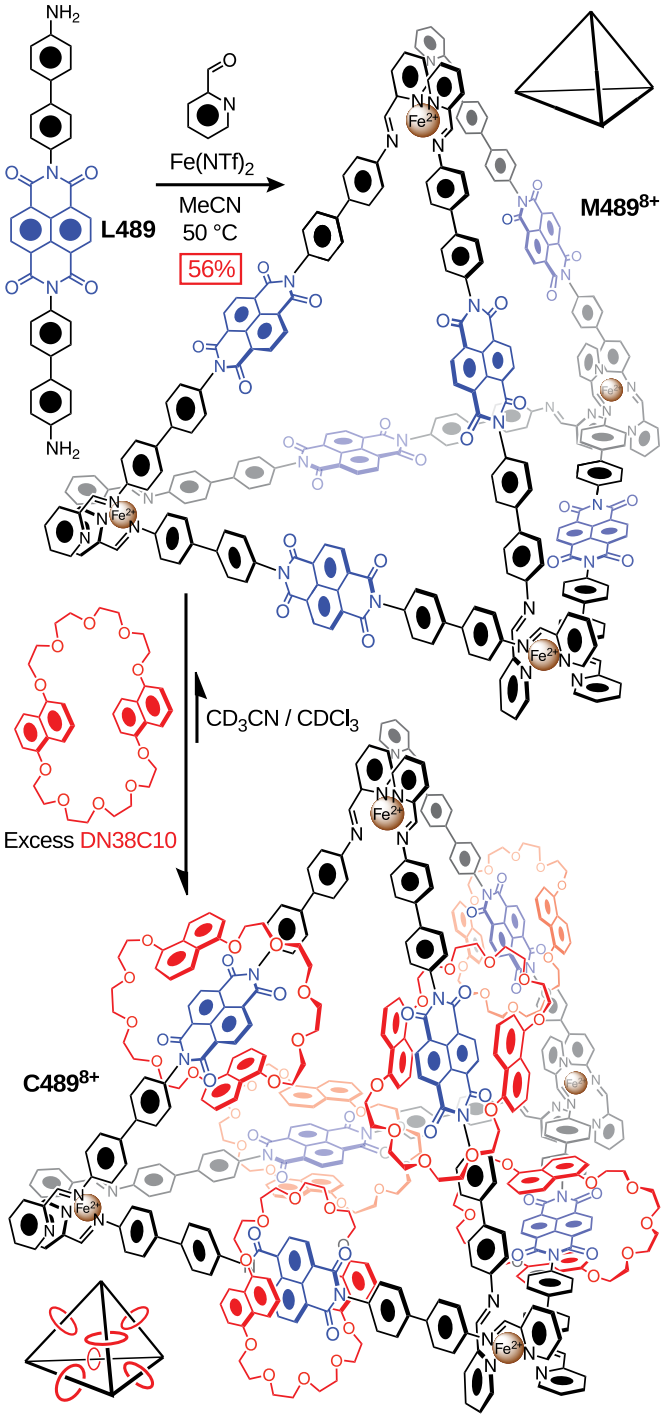


Figure 4.26 Stereoformulas of donor-acceptor catenanes comprising π-donating macrotricyclic polyethers and π-accepting CBPQT^{4+} cyclophanes. The [2]- and [3]catenanes **C486**$^{4+}$ and **C487**$^{8+}$ are based on a triple-torus fused polyether, while Becher's [2]catenane **C488**$^{4+}$ possesses a macrotricyclic tetrathiafulvalenophane.[166]



Scheme 4.17 The self-assembly of a tetrahedral [7]catenane.[172]

a relatively high affinity (see **Table 2.7** in **Section 2.3.3.2**) for the π-donating crown ether dinaphtho[38]crown-10 (DN38C10). The reversible coordinative imine bonds of the tetrahedral cage allow it to re-equillibrate in the presence of an excess of DN38C10 to the tetrahedral [7]catenane **C489**$^{8+}$, in which each edge of the cage is encircled by a ring. Since **C489**$^{8+}$ is held together by a number of reversible covalent, coordinative, and mechanical bonds, it exists in a dynamic equilibrium that can be controlled by the concentrations of the ligands, ions, and macrocycles, respectively. Thus, mixtures of the corresponding [2]–[6]catenanes, in which less than all six of the NDI recognition units are encircled by rings, are also populated and can be detected in the dynamic combinatorial library under appropriate conditions. More recently, the team has assembled[173] dynamic combinatorial libraries based on smaller Zn^{II} tetrahedral cages, finding that no more than two DN38C10 rings can intersect the metallacage at once—see **Figure 3.20** in **Section 3.2.3.1** for a stereoformula of the macrotricyclic hetero[3]catenane.

Homocatenated Macrotricyclics

In 1992, Walba[200] prepared the self-interlocked (**Figure 4.27**) macrotricyclic compounds **C490a-b**, which were isolated during experimental studies on a so-called 'hook-and-ladder' approach he conceived for the synthesis of molecular knots, especially the figure-of-eight knot which is a 'topological rubber glove'—see **Section 5.2.4.2**. The structures of **C490a-b** comprise a local [2]catenane moiety—the 'hook'—based on Sauvage's $Cu(dpp)_2^+$ template motif, with each ring connected covalently to the other via Walba's multicyclic THYME polyether motif[201–203] possessing a pair of olefin rungs—the 'ladder'—which are cleavable by ozonolysis. See **Section 2.2.3** for a discussion featuring the ozonolysis of THYME polyethers. Walba has described this novel self-catenated topology as a ¼-twist cyclized hook-and-ladder. It is believed to adopt two diastereotopic conformations which undergo relatively slow interconversion ($\Delta G^{\ddagger} \approx 20\,kcal \cdot mol^{-1}$) in a hot DMF solution.

Kuroda[169,204] and Clever[57,170,171] have adapted Fujita's Pd^{II} ligation strategy in order to assemble (**Scheme 4.18**) interlocked macrotricyclic homo[2]catenanes based on square planar Pd^{II} complexes as joints. The M_4L_8 catenanes **C491**$^{8+}$ and **C492**$^{8+}$ are self-assembled quantitatively from the crescent-shaped divalent ligands 4,4´-bis(3-pyridinemethoxy)benzophenone (**L491**) and 3,7-bis(4-pyridylethynyl) phenothiazine (**L492**), respectively, which combine with

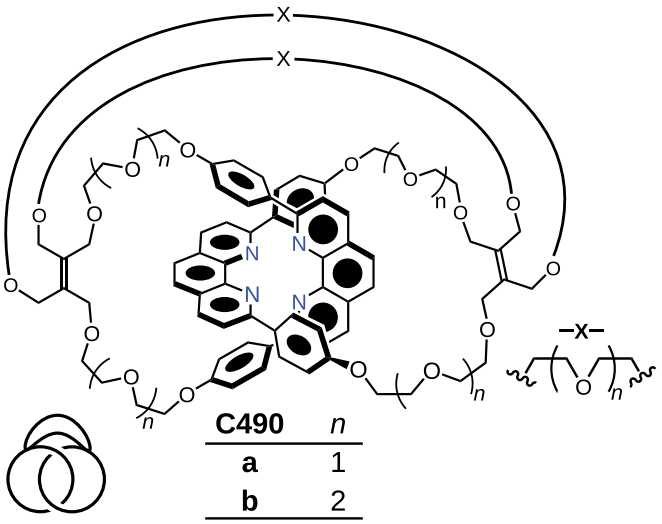
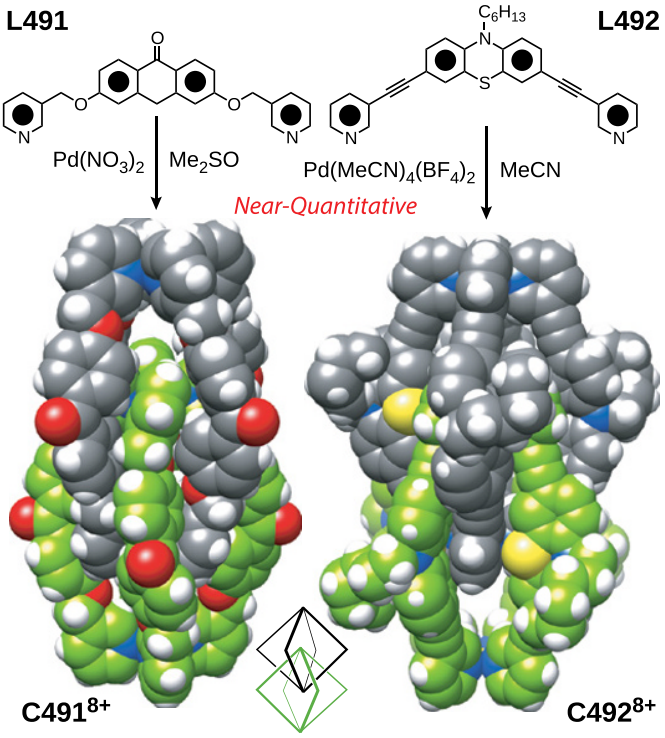


Figure 4.27 Stereoformulas of the self-catenated macrotricyclic 'hook and ladder' compounds introduced by Walba.[200]



Scheme 4.18 The self-assembly and space-filling representations of the solid-state structures of interlocked M_2L_4 coordination cages[169–171] based on crescent-shaped divalent ligands engaged in square planar Pd^{II} complexes. Intercalated and surrounding counterions are omitted for the sake of clarity.

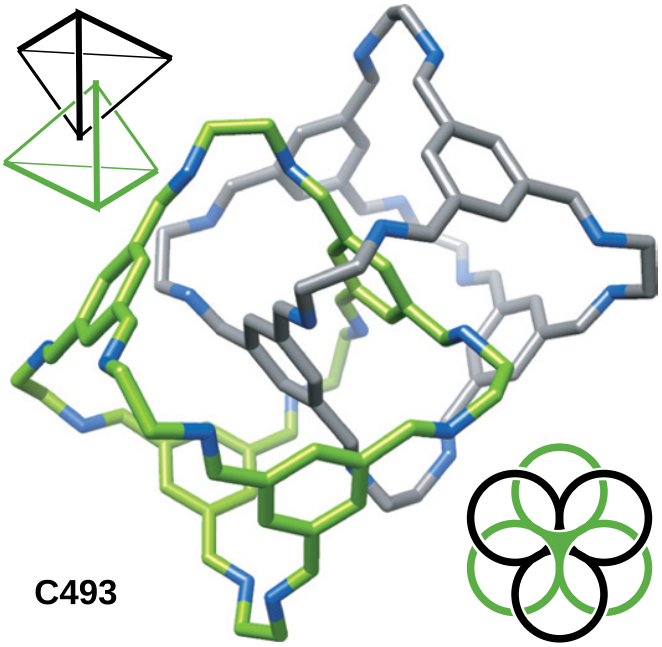
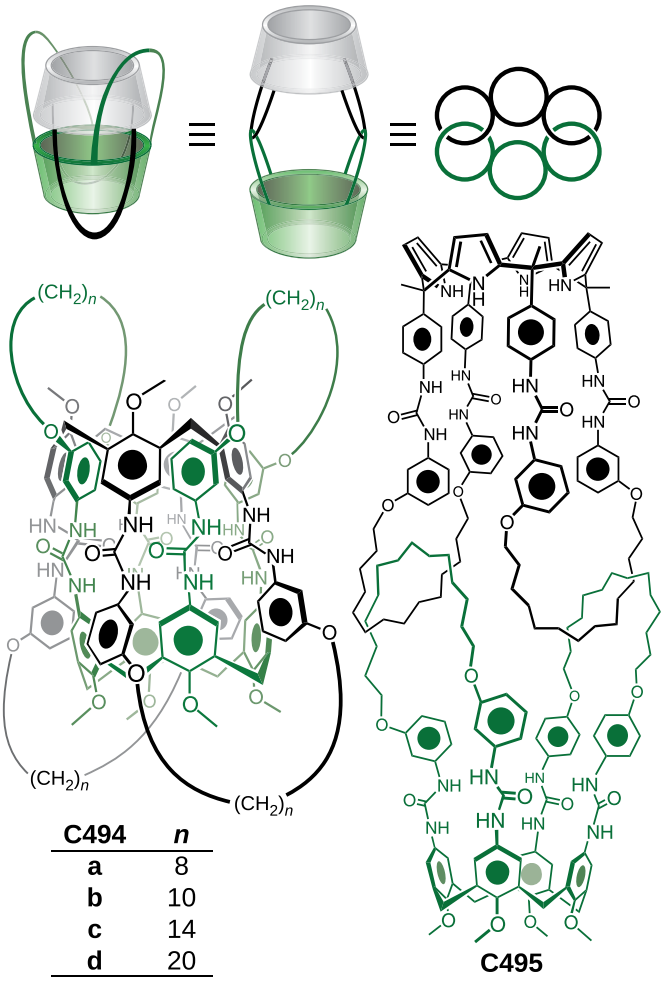


Figure 4.28 The solid-state structure and line drawings portraying the topology of Cooper's catenated macrotricyclic covalent organic cages.[177] The tubular representation is illustrated with hydrogen atoms omitted for the sake of clarity.

Pd^{II} ions in Me_2SO or MeCN to generate quadruply interpenetrated dimers of M_2L_4 metallacages.

Andrew Cooper[177] has assembled the catenane **C493** by crystallization-induced interlocking of macrotricyclic covalent organic cages held together by reversible imine bonds—see **Section 2.3.11.4**. The solid-state structure of **C493** and graphical representations of its topology are illustrated in **Figure 4.28**.



C494	*n*
a	8
b	10
c	14
d	20

Figure 4.29 Stereoformulas of doubly catenated macrotricyclic [2]catenanes[208–210,212] based on homodimeric (**C494a-d**) and heterodimeric (**C495**) tetraureidocalix[4]arene and tetraureidocalix[4]-pyrrole templates.

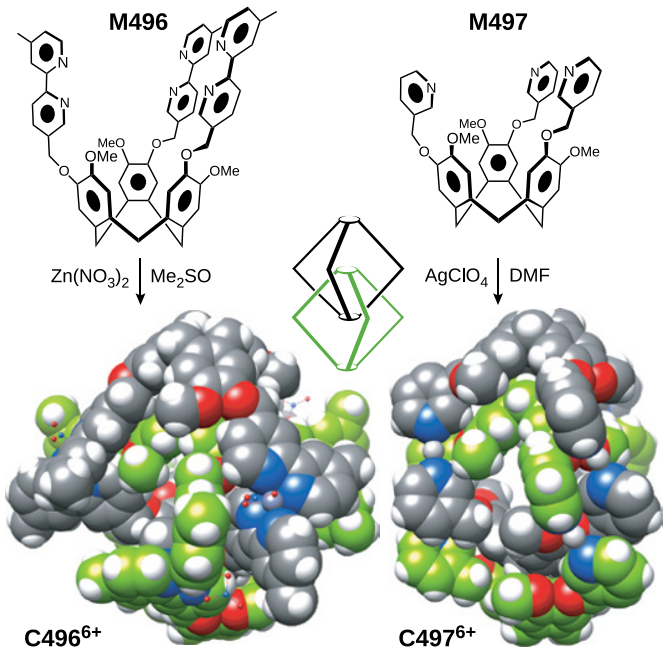
Böhmer's interpenetrated template motifs[205–207] (**Section 2.3.4.5**) based on dimeric tetraureidocalix[4]arene capsules have been utilized[208–211] to create a number of different catenanes (**Figure 4.29**) based on macrotricyclic component parts. Various 'bisloop' derivatives[G] of these calixarenes have been fashioned into the bis[2]catenanes **C494a–d** by ring-closing olefin metathesis (**Section 3.2.1.3**) protocols, followed by hydrogenation of the double bonds.

[G] Although the 'bisloop' nickname suggests a macrobicyclic structure, these compounds are macrotricyclic when considering the cavity of the calix[4]arene rings as part of their constitutions.

Similarly, Ballester[212] has synthesized the macrotricyclic bis[2]catenane **C495** from a heterodimeric capsule precursor in which one of the tetraurea compounds is derived from calix[4]arene, while the other is derived from calix[4]-pyrrole. For a discussion of the nature of the chirality in these compounds, see **Section 5.2.3.2**. For a discussion of their dynamics under the pulling force of an AFM cantilever,[211] see **Section 6.12**.

4.1.3.3 Catenated Macrotetracyclics

Hardie[174,175] has employed tripodal cyclotriveratrylene derivatives[213] as ligands for the self-assembly (**Scheme 4.19**) of metallosupramolecular cages, catenanes, and other topologically non-trivial structures. The solid-state structures of the triply interlocked cage-based [2]catenanes, **C496**$^{6+}$ and **C497**$^{6+}$, are illustrated in **Scheme 4.19**. The M_6L_4 [2]catenane **C496**$^{6+}$ comprises[174] a triply interlocked pair of identical M_3L_2 metallo-cryptophanes derived from 2,2´bipyridine-functionalized cyclotriveratrylene ligands (**M496**) and Zn^{II} metal centers. Each of the six Zn^{II} coordination sites help conjoin the two hemispheres of their respective cages by forming octahedral metal centers in which one NO_3^- counterion participates. Analogous catenanes are formed when employing Co^{II} instead of Zn^{II} as the transition metal joints. Similarly, the [2]catenane **C497**$^{6+}$ also comprises[175] two interlocked M_3L_2 metallo-cryptophanes, each containing a pair of 3-pyridyl-functionalized cyclotriveratrylene tripods (**M497**) engaged in linear coordination modes with Ag^{I} ions. The topologies of **C496**$^{6+}$ and **C497**$^{6+}$ closely resemble those of the catenated macrobicyclic cages described in **Section 4.1.3.2**, despite the fact that the cages in this case are macrotetracyclic when accounting for the cavities of the cyclotriveratrylene linkers.

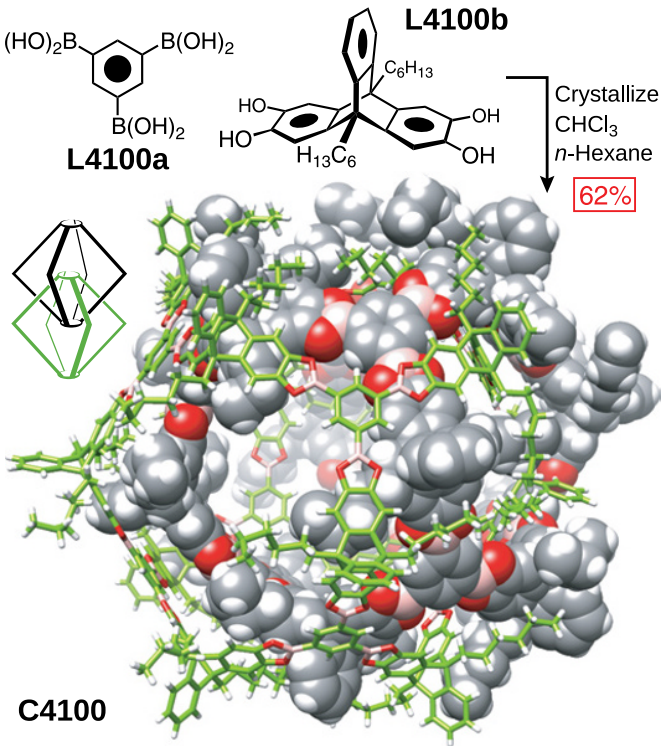


Scheme 4.19 The self-assembly[174,175] and space-filling representations of the solid-state structures of triply interlocked M_3L_2 coordination cages based on Hardie's tripodal cyclotriveratrylene-derived ligands engaged in octahedral (**C496**$^{6+}$) and linear (**C497**$^{6+}$) coordination modes with Zn^{II} and Ag^{I} ions, respectively. Counterions not coordinated to metal centers and solvent molecules are omitted for the sake of clarity.

4.1.3.4 Catenated Macropentacyclics

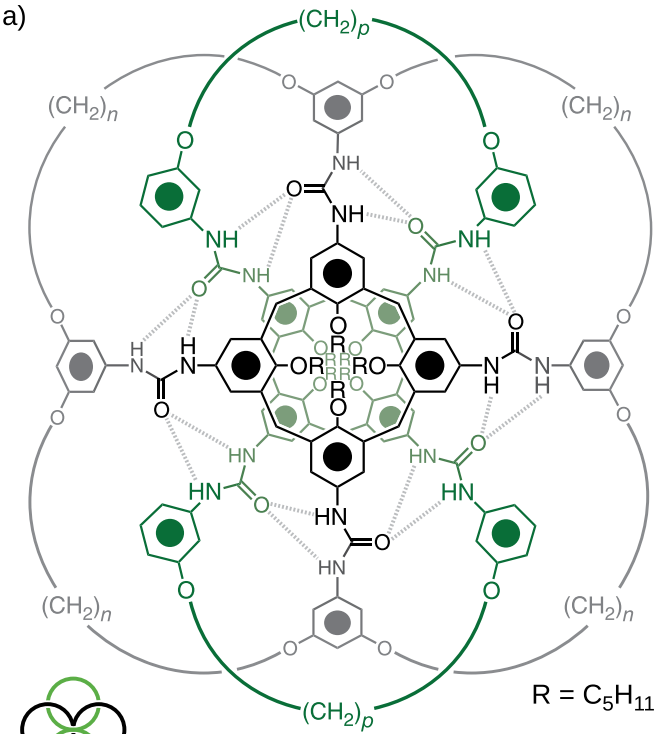
The so-called tetraloop derivatives of Böhmer's tetraureidocalix[4]arene motifs[205–207] are pentacyclic compounds, accounting for the unthreadable annulus of the calix[4]arenes. These pentacyclic 'tetraloops' have been employed[206,214,215] in the synthesis of both heterocatenanes (**Figure 4.30a**) and homocatenanes (**Figure 4.30b**). The olefinic precursors to the beautiful six- and eight-fold interlocked [2]catenanes **C498a-e** and **C499**, respectively, are all formed as exclusive products by virtue of thermodynamically controlled ring-closing metathesis protocols.

Michael Mastalerz[178] has reported on the crystallization-induced (see **Section 2.3.11.4**) catenation (**Scheme 4.20**) of giant covalent organic cages[216] derived from benzene-1,3,5-triylboronic acid joints (**L4100a**) and triptycene-based bis(catechol) (**L4100b**) linkers. Each one of the



Scheme 4.20 The self-assembly of catenated covalent organic cages via reversible boronic ester formation.[178] The mixed space-filling/tubular representation of the solid-state structure of **C4100** is illustrated with solvent molecules omitted for the sake of clarity.

a)



C498	a	b	c	d	e
n	8	10	14	20	8
p	8	10	14	20	10

b)

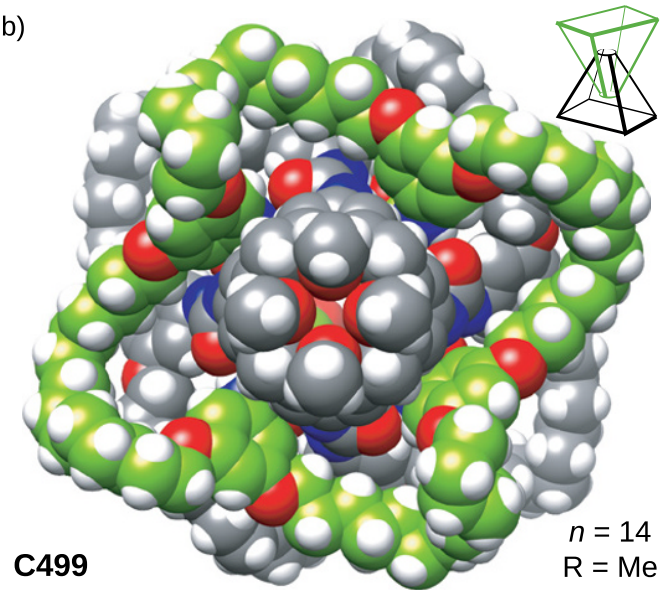


Figure 4.30 Böhmer's multicatenanes based on macropentacyclic 'tetraloop' tetraureidocalix[4]arenes. (a) Structural formulas of a series of six-fold interlocked hetero[2]catenanes **C498a-e** derived from a combination of tetraloop and bisloop component parts.[215] (b) Space-filling representation of the solid-state structure of an eight-fold interlocked homo[2]catenane **C499** derived from identical tetraloop component parts.[214]

cages is self-assembled in solution from 20 components (8 joints and 12 linkers) by way of 48 condensations. The reversible boronic ester linkages allow the cages to become catenated (**C4100**) upon crystallization from *n*-hexane in $CHCl_3$ in 62% yield. The system reverts to the unlinked cages upon dissolution of the crystal in tetrachloroethane.

4.1.3.5 Topologically Entangled Networks

The mechanical bond can be identified in thousands of polymer networks, especially coordination networks, which become entangled[217] in the solid state. In this Section, we focus our attention on topologies in which mechanical entanglements extend infinitely in at least one dimension. While extended chains and networks linked by mechanical bonds have been observed in a few cases involving macrocycles—see **Figure 4.7** in **Section 4.1.1.3** and **Figure 4.13** in **Section 4.1.2.1**—entangled networks emerge more commonly from multi-annulated structures, associated with cages and two- or three-dimensional polymer nets. Although topological links have been invoked to explain the properties of interpenetrating polymer networks,[218–226] including double-network hydrogels,[227–230] amphiphilic conetworks,[231] etc., the nature of the mechanical bonds in these materials is difficult to characterize on account of their polydisperse structures. In the case of coordination polymers, some of them can be obtained as crystalline networks, resulting in much more regular entanglements that are easier to characterize crystallographically in the solid state. Although we focus our attention on organic and metallo-organic chemistry, it is worth mentioning that entanglements have been observed in networks[232] of wholly inorganic materials as well—indeed, two-fold interpenetrated diamonoid networks, such as that of Cu_2O, were discovered[233,234] long before any interpenetrated coordination polymers were known, although the interpenetration in these materials may reflect the conventions of X-ray crystallographic structural analysis more than the actual bonding in the crystal.

Networked Cages

A number of solid-state infinite poly[*n*]catenanes[235–241] based on three-dimensional cage structures with topologies ranging from macrotricyclic to macroheptacyclic have been crystallized and characterized structurally in the solid state. Lu[235] introduced the first three-dimensional network of catenated discrete cages (**C4101**) in 2010 while reporting the topology (**Figure 4.31**) of networked $M_{24}L_{18}$ polyhedra, where M is Ag^+ and L is 1,2,4-triazolide (trz^-). These $[Ag_{24}trz_{18}]^{6+}$ nanocages assume a geometry resembling that of adamantane, although they are formally macroheptacyclic when accounting for the small triangular windows in each of their four panels derived from Ag_4trz_3 clusters. The mechanical bonds of the **C4101** network are arranged in an octahedral lattice, where each cage intersects six of its neighbors, one for each edge of its diamond-like framework. Two of these octahedrally linked lattices are interpenetrated in the solid-state structure. The voids of the interpenetrated network are filled by Keggin polyoxometallate $[PW_{12}O_{40}]^{3-}$ counter-anions, formed as a result of a

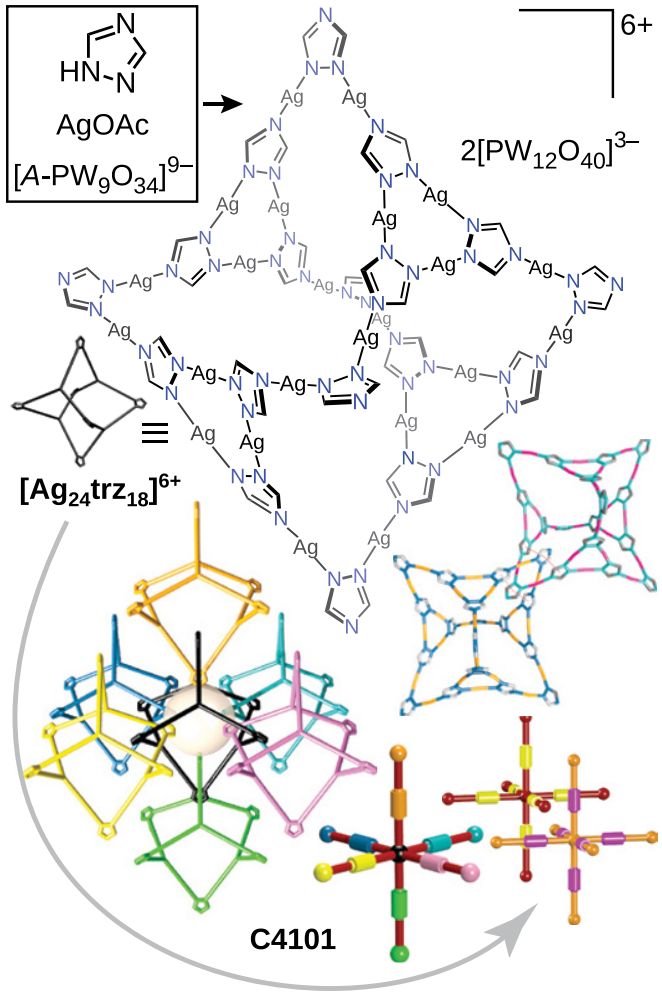


Figure 4.31 The first infinite three-dimensional network of catenated metallacages, represented at various levels of abstraction. The crystal of **C4101** is a self-interpenetrated, bicontinuous network of macroheptacyclic $[Ag_{24}trz_{18}]^{6+}$ cages, each linked in an octahedral array of mechanical bonds with its nearest neighbors. Images reproduced with permission from ref. 235 (copyright 2010 Nature Publishing Group)

phase transition from the $[A\text{-}PW_9O_{34}]^{9-}$ polyoxometallate anions introduced in the crystallization media. It is remarkable that such a sophisticated topological network can emerge from such a simple combination of chemical ingredients.

Dehnen[236] has assembled (**Figure 4.32**) catenated macropentacyclic $M_{12}L_8$ cages derived from 2,4,6-tris(4-pyridyl)pyridine (pytpy) ligands and $ZnCl_2$ metals. The $(ZnCl_2)_{12}(pytpy)_8$ cages interlock into infinite one-dimensional polycatenanes (**C4102**) with triple interlocking between each individual cage. The large void space (2700 Å^3) enclosed within the cavity of each discrete cage in the network can accommodate nanodroplets of guest molecules, including $CHCl_3$ and C_6H_5Br. The pytpy ligand is essential to the formation of the catenated network, since the equally sized tris(4-pyridyl)-1,3,5-triazine (tpt) ligand gives rise to only two-dimensional networks, instead of cages, when combined with Zn^{II} halogenides. This observation may be attributable to electronic differences between the pyridyl core of pytpy versus the triazine core of tpt, since pytpy engages more readily in face-to-face π–π stacking interactions, which are observed between pytpy panels in **C4102**, than does the more electron-deficient tpt homologue, which engages preferentially in offset stacking. The formation of polycatenanes instead of [2]catenanes akin to those originally introduced by Fujita[167] (**C477^{12+}**, **Scheme 4.13**) can be explained by the charge neutrality allowed by the Cl^- counterions of $ZnCl_2$, which reduces electrostatic repulsion between cages, as well as the large void volumes of the $M_{12}L_8$ cages that allow plenty of room for multiple entanglements.

Lu[237] has catenated (**Figure 4.33**) tetrahedral M_6L_4 cages derived from $Ni(trien)^{2+}$, (trien = triethylenetretramine) metals and tris(4-carboxylbenzyl)amine (tcba) ligands. Three different crystalline networks were isolated from mixtures of $Ni(trien)(PF_6)_2$ or $Ni(trien)(ClO_4)_2$ metal sources and the tcba ligands under different crystallization conditions. One of the isolated crystals, **C4103**, comprises an infinite three-dimensional network of catenated M_6L_4 tetrahedra,

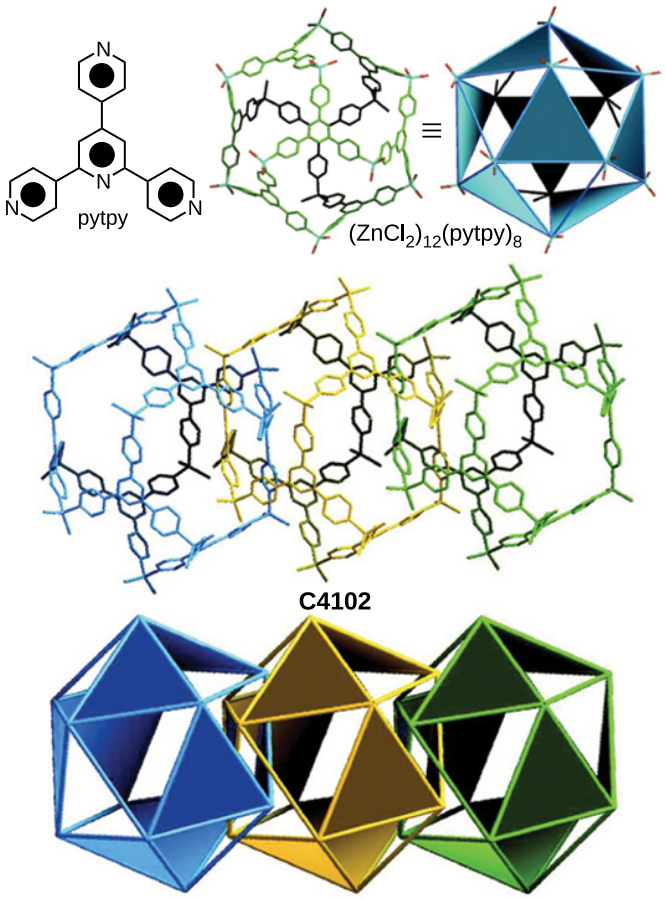


Figure 4.32 Infinite one-dimensional chains of catenated icosahedral $(ZnCl_2)_{12}(pytpy)_8$ metallacages comprise the crystal of compound **C4102** introduced by Dehnen. Images reproduced with permission from ref. 236 (copyright 2011 American Chemical Society)

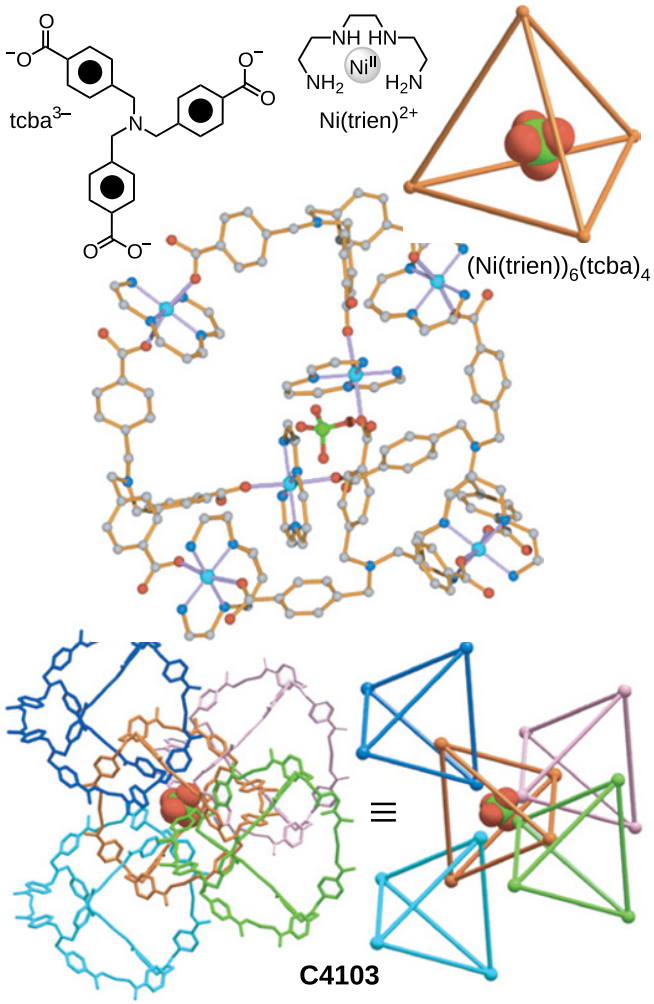
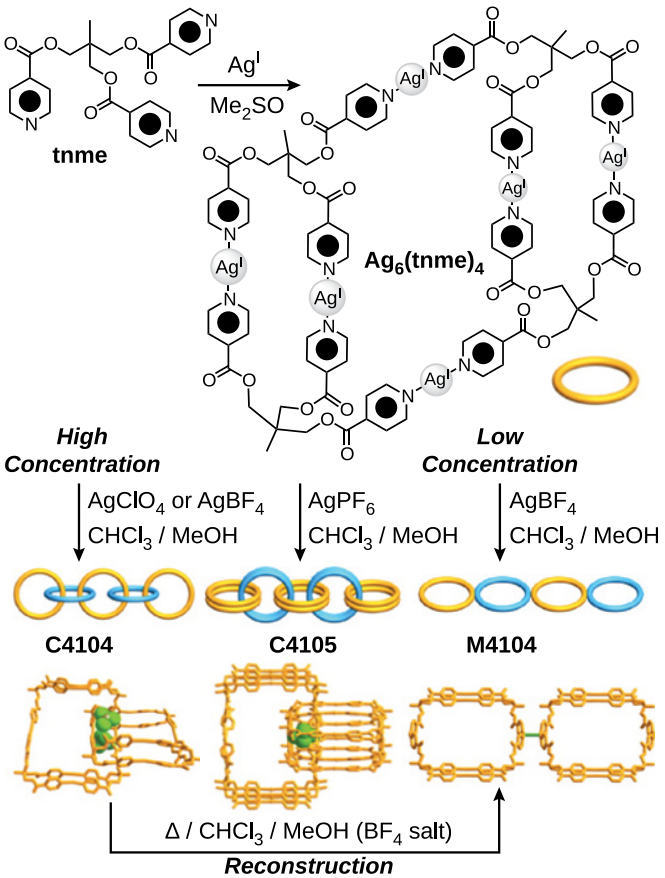


Figure 4.33 An inifinite three-dimensional network of catenated tetrahedral M_6L_4 metallacages encapsulating one ClO_4^- anion per cage. Images representing the crystallographic structure of **C4103** are reproduced with permission from ref. 237 (copyright 2012 Nature Publishing Group)

while the other two networks (not illustrated) are more pseudorotaxane-like in nature, on account of having certain pieces of their cages missing from the M_6L_4 tetrahedral framework. The Ni(trien)$^{2+}$ units act as the edges of the tetrahedron, while the trivalent tcba ligands coordinating the axial sites of the Ni^{II} centers serve as the vertices. Each tetrahedral cage is interlocked with four of its neighbors, one for each vertex. Each cage also encapsulates a single ClO_4^- anion and an accompanying proton that cannot be identified crystallographically, as it is located in a disordered manner either on the tcba ligands or on the water molecules in the crystal. The dynamic pores of the network enable the material to exhibit size-dependent absorption and desorption of alcohols.

Hong[238–241] has also prepared catenated M_6L_4 cages assembled from trivalent ligands coordinated to metals in a linear geometry. Different assemblies crystallize[238,239] (**Scheme 4.21**) from mixtures of the tris(isonicotinoxymethyl) ethane (tnme) ligand and Ag^I metals, depending on the counterion and the conditions of crystallization. **C4104** is a one-dimensional polycatenated chain of $Ag_6(tnme)_4$ cages stabilized by intercalated ClO_4^- anions, while **C4105** comprises a similar chain of $Ag_{12}(tnme)_8$ cages stabilized by intercalated PF_6^- anions. The $Ag_{12}(tnme)_8$ cages of **C4105** are essentially dimers of the $Ag_6(tnme)_4$ cages of **C4104**. Crystallization of these polycatenanes appears to be driven in large part by π–π stacking interactions between the isonicotinic moieties, as well as electrostatic interactions between the Ag^I centers and their counterions. An Ag_6L_4 intermediate is believed to be responsible for enabling the cages to interlock during crystallization. The **C4104** network can also be formed[239] from $AgBF_4$ salts at high concentrations, while low concentrations afford only the networked $Ag_6(tnme)_4$ cages **M4104**. These non-catenated $Ag_6(tnme)_4$ metallacages also self-assemble from Ag^I salts in Me_2SO. Compound **M4104** is the thermodynamic product, since the BF_4^- salt of **C4104** converts itself into that of **M4104** over time at 30 °C in $CHCl_3$/MeOH.



Scheme 4.21 The self-assembly[238,239] of Hong's M_6L_4 metallacages derived from various Ag^I salts and the tnme ligand gives rise to networked polycatenanes (**C4104** and **C4105**) and cages (**M4104**), depending on the counterion and the concentration of the $CHCl_3$/MeOH (1:1) crystallization bath. Graphical and tubular representations of the networks are reproduced with permission from ref. 241 (copyright 2015 American Chemical Society)

Entangled Coordination Nets

While the polycatenation of discrete cages into networks is becoming more prevalent in the literature, there is already a myriad of examples of entangled networks of coordination polymers,[217,242–245] resulting in large part from the remarkable increase in research on metal-organic frameworks[246–251] (MOFs) over the past decade or so, owing to their promising potential applications[252–256] in gas storage[257–260] and separations,[261,262] catalysis,[263–268] chemical sensing,[269,270] as well as luminescent,[270–272] magnetic,[273] ferroelectric,[274] non-linear optical,[275] biomedicinal[276–278] and composite[279] materials. The preparation of MOFs is based[247] on the modular combination of (i) ligands and (ii) secondary building units[280] (SBUs), comprising metallic or metallo-organic centers or clusters, which link the ligands into extended reticular networks. The properties[281] of these crystalline coordination polymers depend not only on their (co)constitutions, but also on the topologies[242,282–287] of their networks. When multiple topologically independent networks are entangled in space, they are often referred to as interpenetrated or polycatenated networks. The entanglement of coordination frameworks can often be controlled[244,288] by experimental parameters, such as solvent composition,[289,290] temperature,[291,292] concentration,[292] pH,[293] templates,[294,295] nuclearity of the metallic nodes,[296] counterions,[297] ligand exchange,[298] etc., during their synthesis, as well as by organic ligand design.[299,300]

It is convenient to characterize the mechanical bonds of networks according to their dimensionality. We will describe polycatenanes as one-, two-, or three-dimensional when the mechanical bonds of their networks extended infinitely in one, two, or three dimesions, respectively. Coordination nets are often described[301] by three-letter codes denoting their topologies, a nomenclature associated with the Reticular Chemistry Structure Resource (RCSR) Database.[282] Entangled two-dimensional[H] coordination polymers have recently been reviewed comprehensively by Carlucci, Proserpio, and Blatov.[245] who have identified (**Figure 4.34**) hundreds network topologies with mechanical bonds in the Cambridge Structural Database (CSD), using the crystallochemical analysis software package TOPOS.[287] Among the most common 2D topologies (**Figure 4.34a**) that have been observed to interpenetrate in coordination polymers are the square-lattice net **sql**, and the hexagonal-lattice net **hcb**, which underlie approximately 60 and 26%, respectively, of the 2D interpenetrated network structures deposited in the CSD.[245] The entanglement modes (**Figure 4.34b**) of 2D nets can be characterized by comparing the dimensionality[302] of the building blocks with that of the network. Systems are described as "polycatenated" when there

[H] A two-dimensional net is one that extends infinitely in two dimensions. Two or more interpenetrated 2D nets cannot be drawn without edge crossings—a clear sign of a topological linkage—yet they may still be considered two-dimensional if their average planes overlap, leading to a layered structure in the crystal.

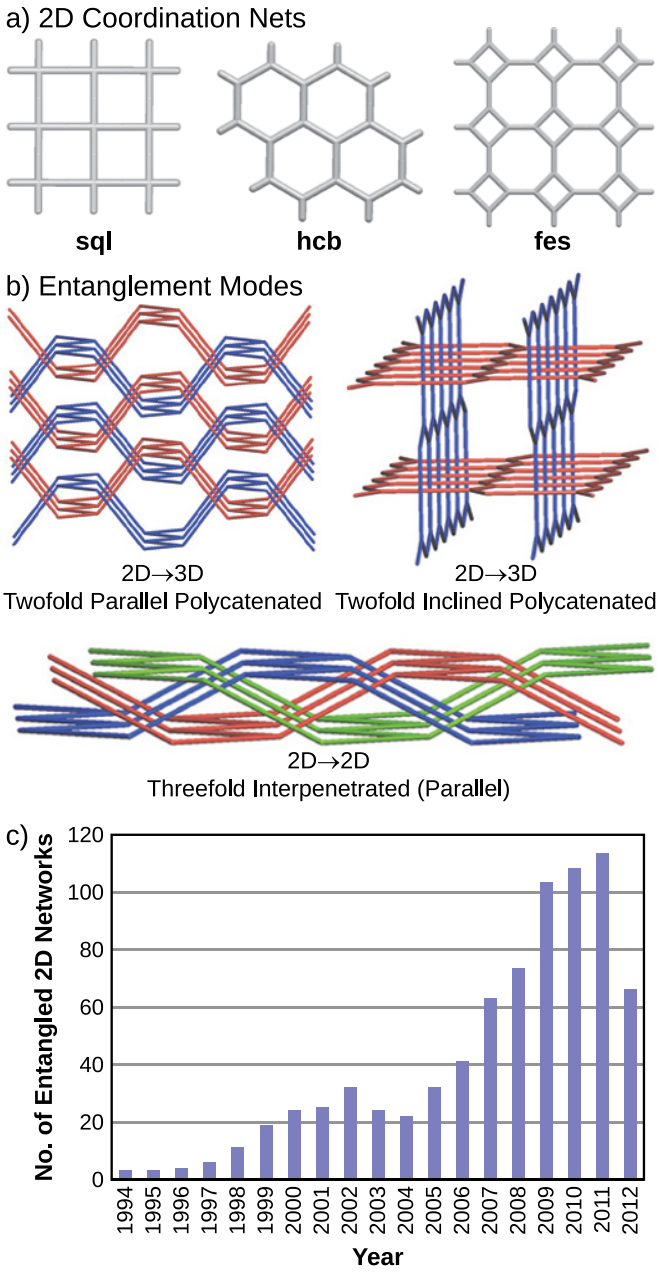


Figure 4.34 Entanglement in 2D networks. (a) Illustrations of a few of the most common 2D network topologies that have been observed to entangle in coordination chemistry. (b) Different modes of entanglement in polycatenated networks, illustrated in the form of *n*-fold entangled hcb nets as representative examples, where *n* is the number of component 2D nets. Polycatenated networks exhibit higher dimensionality than their component nets, while interpenetrated networks possess the same dimensionality as their component nets. The average planes of the entangled nets can be disposed in either parallel (offset or overlapping) or inclined geometries. (c) A histogram plotting the number of topologically entangled 2D coordination networks deposited in the crystallographic database from 1994 to 2012. Data and images reproduced with permission from refs. 284 and 245 (copyright 2013–2014 American Chemical Society)

has been an increase in dimensionality (e.g., 2D → 3D), or "interpenetrated" when the dimensionality is unchanged (e.g., 2D → 2D, 3D → 2D). In two-dimensional nets, polycatenation can be further characterized as either parallel or inclined, denoting that the average plane of the entangled nets are either parallel or intersecting, respectively. These planes are necessarily aligned in 2D networks and offset in 3D networks. The histogram in **Figure 4.34c** reveals how a remarkable increase in research activity has generated a rapidly growing library of polycatenated and interpenetrated 2D coordination networks. It is worth noting that mechanical bonds can also be formed in 2D networks upon entanglement with one-dimensional polymers.[303]

One of the earliest examples of an interpenetrated coordination network was described by Konnert and Britton[304] in 1966, when they found that the crystals of $AgC(CN)_3$ form (**Figure 4.35**) layers of catenated two-dimensional hexagonal nets. An earlier report by Higuchi and Saito[305] described a three-dimensional interpenetrated network of bis(adiponitrilo)copper(I) nitrate.

Three-dimensional coordination polymers are also capable of interpenetrating (**Figure 4.36**) in the solid state.

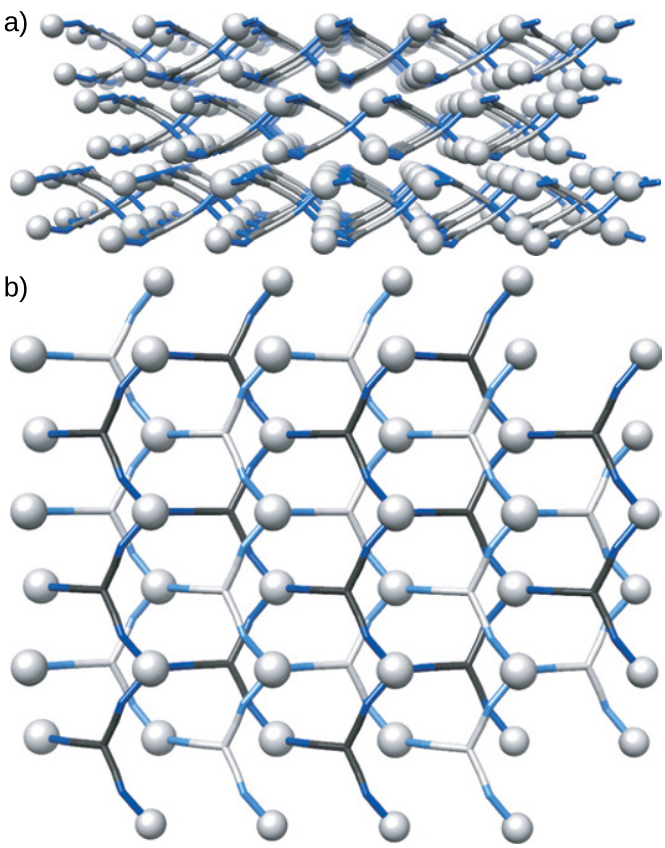


Figure 4.35 The solid-state structure of $AgC(CN)_3$, the first interpenetrated 2D coordination polymer.[304] (a) Side-on view illustrating how layers of the 2D $AgC(CN)_3$ coordination networks stack in the crystal. (b) A single layer of the $AgC(CN)_3$ crystal, revealing two interpenetrated hexagonal networks.

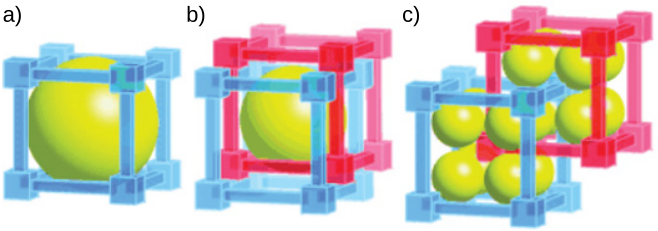


Figure 4.36 Graphical representations of the unit cells of three-dimensional cubic MOFs illustrating how the pores (yellow balls) of uncatenated frameworks (a) can differ from their catenated homologues, which can adopt either offset (b) or centered (c) catenation modes. Images reproduced with permission from ref. 257 (copyright 2005 Wiley-VCH)

Blatov and Proserpio[306] have investigated the topologies of interpenetrated three-dimensional networks, finding that interpenetration is most common in primitive diamondoid (**dia**), cubic (**pcu**), and the highest-symmetry three-connected nets of both chiral (**srs**) and achiral (**ths**) varieties—see **Figure 4.37**.

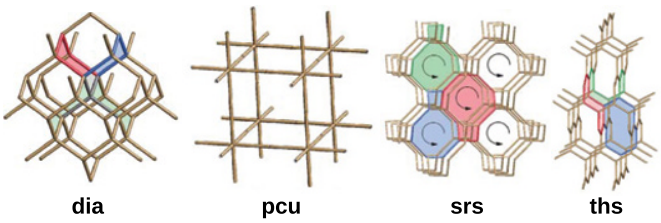


Figure 4.37 Illustrations of the 3D nets for which interpenetrated structures are most commonly observed in the CSD. Adapted with permission from ref. 306 (copyright 2004 Royal Society of Chemistry)

Interpenetration typically reduces the microporosity of the crystal relative to its non-interpenetrated isoform. More often than not, researchers interested in developing applications for MOFs hope to avoid finding mechanical bonds in their networks, simply because the reduced porosity of the crystal decreases its surface area. While a lower surface area, one might expect, should decrease the adsorption capacity of the framework, recent results are beginning to suggest that mechanical bonds can also improve the properties of porous materials for certain applications,[244,307] including their sorption properties. Several coordination polymers obtained as both single and interpenetrated frameworks (**Figure 4.38**) have been discovered in which the interpenetrated network has the more advantageous properties for an intended application.

One of the most important coordination polymers in porous materials research is **MOF-5**, a compound which revitalized the field when it was introduced by Yaghi[246] in 1999, on account of its ability to maintain stable porosity upon solvent evacuation and its excellent gas sorption

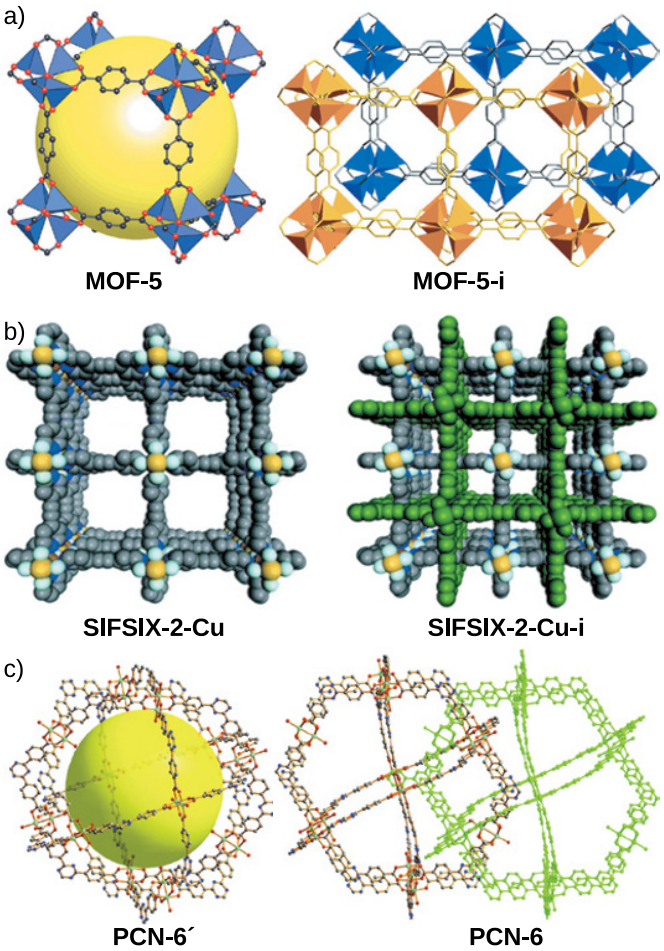


Figure 4.38 Examples of interpenetrated MOFs. (a) A comparison between **MOF-5**[246] and **MOF-5-i**,[289,308,309] its interpenetrated isoform. (b) A comparison of **SIFSIX-2-Cu** and **SIFSIX-2-Cu-i**.[310] (c) A comparison of **PCN-6´**[312] and its interpenetrated isoform, **PCN-6**.[311] Images reproduced from refs. 249 (copyright 2003 Nature Publishing Group), 309 (copyright 2011 American Chemical Society), 295 (copyright 2014 Royal Society of Chemistry)

properties enabled by its high surface area. **MOF-5** is a cubic network of Zn_4O clusters, coordinated and cross-linked in an octahedral geometry by 1,4-benzenedicarboxylate linkers. A crystalline polymorph of **MOF-5** is **MOF-5-i**, a structure (**Figure 4.38a**) wherein two **MOF-5** nets catenate into a bicontinuous interpenetrated network.[289,308,309] Despite the lower Langmuir surface area of **MOF-5-i** (1130 m^2g^{-1}) compared to **MOF-5** (4400 m^2g^{-1}), the catenated **MOF-5-i** exhibits[309] a much higher hydrogen capacity than does MOF-5 up to 100 bar of pressure at 298 K, owing presumably to having higher enthalpy (1.8 versus 1.2 $kcal \cdot mol^{-1}$) of adsorption, enabled perhaps by multivalent interactions between the H_2 molecules and the more crowded pores.

Eddaoudi and Zawarotko[310] have developed the porous crystalline materials **SIFSIX-2-Cu** and **SIFSIX-2-Cu-i** (**Figure 4.38b**), the latter of which is an interpenetrated isoform of the former. Although the surface area of **SIFSIX-2-Cu-i** (735 m^2g^{-1}) is much lower than that (3140 m^2g^{-1}) of **SIFSIX-2-Cu**, catenated **SIFSIX-2-Cu-i** nevertheless exhibits higher CO_2 uptake and better CO_2/CH_4 and CO_2/N_2 selectivity. The catenation is assumed to engender better overlap of electrostatic potential fields lining the narrower pores of **SIFSIX-2-Cu-i**, since the enhanced CO_2 uptake is attributable to its relatively higher heat of adsorption.

Zhou[311,312] was the first to compare the gas sorption properties of a MOF with an isomeric catenated MOF, by isolating the non-interpenetrated **PCN-6´** for comparison (**Figure 4.38c**) with the interpenetrated isomer **PCN-6**. Surprisingly, the catenated PCN-6 was found to possess a higher Langmuir surface area (3800 m^2g^{-1}) and 133% higher volumetric uptake of H_2 than non-catenated (2700 m^2g^{-1}) **PCN-6´**. This result has been rationalized by the hypothesis that the catenation creates smaller pores that enhance the *apparent* surface area by binding gas molecules more tightly through more multivalent interactions.

The idea of exploiting interpenetration in order to fine-tune the dimensions of the nanopores and enhance the properties of MOFs for application purposes has also been demonstrated in a number of instances by Lin.[297,313–315] Employing interpenetrated homochiral MOFs derived from a chiral 1,1´-binaphthyl-4,4´dibenzoate (bndb) ligands. For example, Lin demonstrated that strong MOF–H_2 interactions were made possible by a four-fold interpenetration of coordination networks of these ligands bridged by Zn^{II} nodes.[313] In another case,[297] two different interpenetrated MOFs—each comprising bndb linkers and Cd^{II}, nodes, yet adopting different catenation modes—exhibit dramatically different activities in asymmetric catalysis. The different catalytic activities are attributable to their different pore geometries, which are a result of in turn to their different topologies, which are maintained in essence by the mechanical bond. This strategy appears to be generalizable, since Lin[314] has shown more recently that Mn(salen) catalysts embedded in struts of different lengths residing in isoreticular networks adopting different catenation modes influence the efficiency of asymmetric alkene epoxidation. In some cases, increasing the catenation appears to increase enantioselectivity, although reaction efficiencies suffer more often in the interpenetrated cases, owing most likely to diffusional barriers. Lin[315] has also implicated the entanglement of multiply interlocked diamondoid networks in the facile crystal engineering of nonlinear optical materials.

Another potential advantage of the mechanical bond in coordination networks is the possibility of increasing the flexibility of the network, allowing the pores to adapt and change size in response to different guests, for example. A number of investigations have looked into the “breathing” of interpenetrated MOFs. Fujita[316] has described the expansion and contraction of an interpenetrated MOF derived from tpt and ZnI_2, triggered by guest adsorption and removal. Kitagawa[317] has reported interpenetrated MOFs that expand and contract upon the adsorption and removal of various supercritical gases. Atwood[318] has described a twofold interpenetrated MOF that contracts and expands

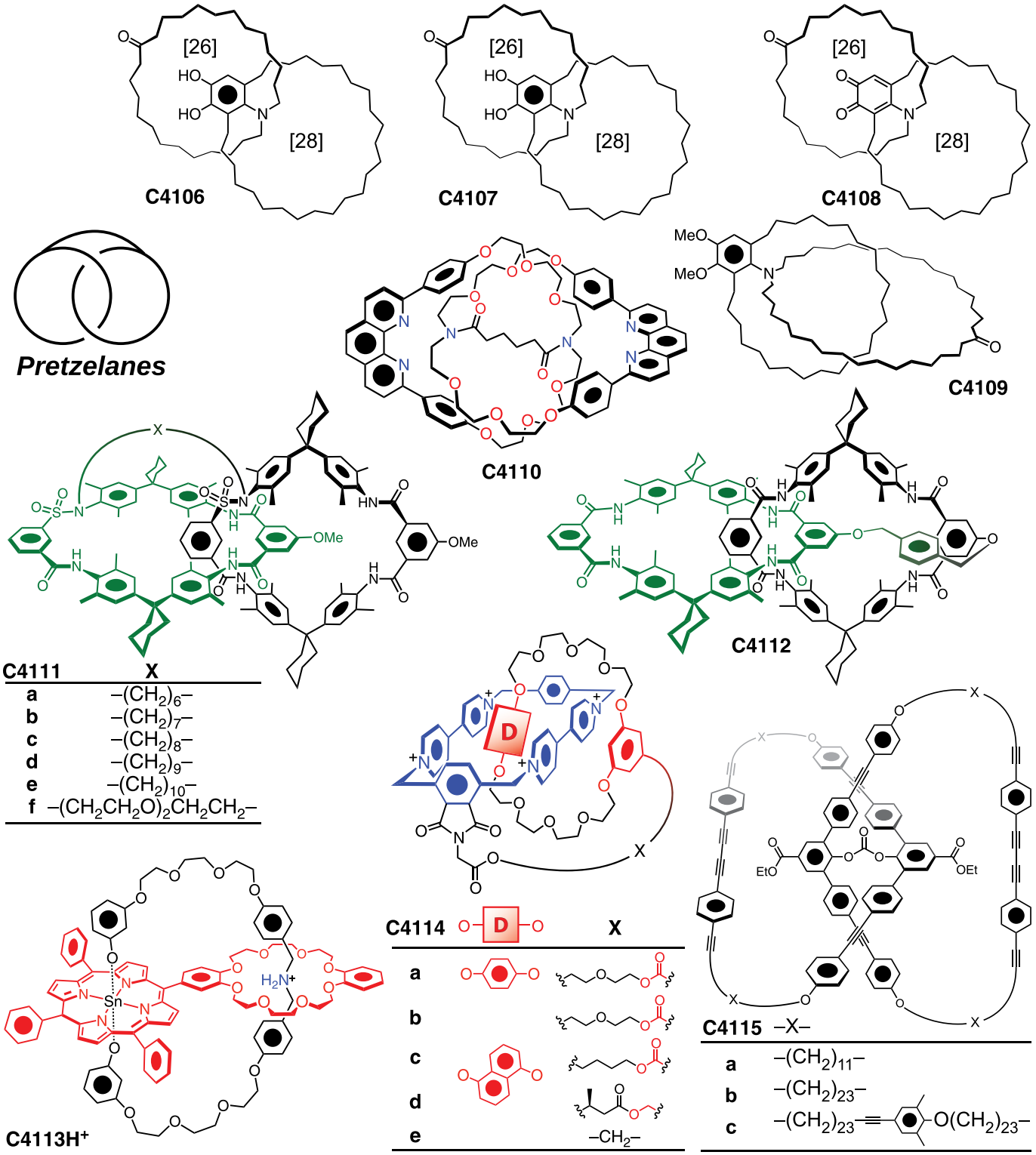


Figure 4.39 Stereoformulas of various pretzelanes.[208,321,323–340]

upon solvent evacuation and CO_2 inclusion, respectively. Recently, Maji[319] reported another twofold interpenetrated MOF with dynamic pores enabled by the mechanical bond, which adsorbs CO_2, as well as C2 and C3 hydrocarbons, with good selectivity in ambient conditions. Hupp[320] has also discovered an interpenetrated framework in which the nets move with respect to each other depending on the temperature and pressure.

In summary, entanglements (mechanical bonds) are a common feature in coordination networks. While interpenetration has often been considered as a negative feature, it is regaining traction as a strategy to increase network

stability, tailor pore dimensions, and engender desirable physical, mechanical, and dynamic properties. Mechanically entangled coordination polymers possessing polyrotaxane motifs are considered in **Section 4.2.3.8**, while entangled one-dimensional polymers are discussed in **Section 4.3.7**.

4.1.4 Covalently Bridged Catenanes

Linking together multiple component parts using covalent linkers enables the genesis of novel topologies. Becher[180] introduced the term 'pseudocatenane' to describe catenanes modified with covalent bridges. In the simplest case, for example, the two rings of a [2]catenane Hopf link can be connected by a covalent linker to afford a [2]pseudocatenane (**Section 4.1.4.1**), which is also known[321,322] as a pretzelane. Likewise, a linear chain of three rings with covalent bridges may be called a [3]pseudocatenane (**Section 4.1.4.2**), while [4]pseudocatenanes (**Section 4.1.4.3**) possess four rings with one or more covalent bridges, and so on. The polymerization of catenanes also relies on covalent bridges, either within the constitution of the main chain (**Section 4.1.4.4–4.1.4.5**) or as side chains (**Section 4.1.4.6**) extending from the oligomer/polymer backbone.

4.1.4.1 [2]Pseudocatenanes/Pretzelanes

A [2]pseudocatenane in which the mechanical bond of a Hopf link is trivialized by a covalent connection between the rings has also taken the vernacular name of 'pretzelane', since its graph resembles that of a pretzel. The pretzel-shaped topology of these pseudocatenanes (**Figure 4.39**) was first noted[321,323] by Vögtle, who also coined[322] the term 'pretzelane', although it should be noted that pretzelanes were intermediates (e.g., **C4106–C4109**) en route to catenanes prepared by Lüttringhaus and Schill[324–326] using directed synthesis many years earlier—see **Section 2.2**. To date, researchers have described pretzelanes based on transition metal[327] (e.g., **C4110**), hydrogen-bonded[208,321,323,328–331] (e.g., **C4111a-f**, **C4112**, **C4113H$^+$**), donor-acceptor[332–335] (e.g., **C4114a-e^{4+}**), and covalent[336–340] (e.g., **C4115a-c**) templates. One of the donor-acceptor pretzelanes, namely **C4114b^{4+}**, has been obtained as single crystals and its solid-state structure has been deciphered[334] by X-ray crystallography—see **Figure 1.26** in **Section 1.3.2** for a space-filling representation.

4.1.4.2 [3]Pseudocatenanes/Handcuff Catenanes

[3]Pseudocatenanes or 'handcuff' catenanes are the topological consequence of linking covalently two of the rings in a linear [3]catenane. The subtle topological difference between two rings connected by a covalent linker versus two rings fused to a common core—see **Section 4.1.3.1**—has been ignored in this naming convention. Thus, handcuff catenanes are partitioned between two different topologies (**Figure 4.40a**)—those[180,182,183,187] based on macrobicyclics (e.g., see **Figure 4.21**) and those based on covalently bridged bis-macrocycles. Two examples (**Figure 4.40b-c**) of the latter kind include the handcuff catenane **Cu$_2$C4116^{2+}** described by Sauvage[185,186] using templates derived from his Cu(dpp)$_2^+$ motif, as well as the handcuff catenane **C4117·2Cl** introduced by Beer[341] using one of his anion-binding template motifs. Both catenanes were prepared by olefin metathesis clipping protocols—see **Section 3.4**. **C4117·2Cl** was the first handcuff catenane for which a solid-state structure (**Figure 4.40c**) was solved by single-crystal X-ray diffraction techniques.

4.1.4.3 [4]Pseudocatenanes

Although several different topologies are possible in the case of [4]pseudocatenanes, the only such topology that has been described, to our knowledge, resembles a radial [4]catenane (**Section 4.1.2.2**) in which the three peripheral rings are linked covalently to a central core. Several compounds (**Figure 4.41a**) exhibiting this topology have been

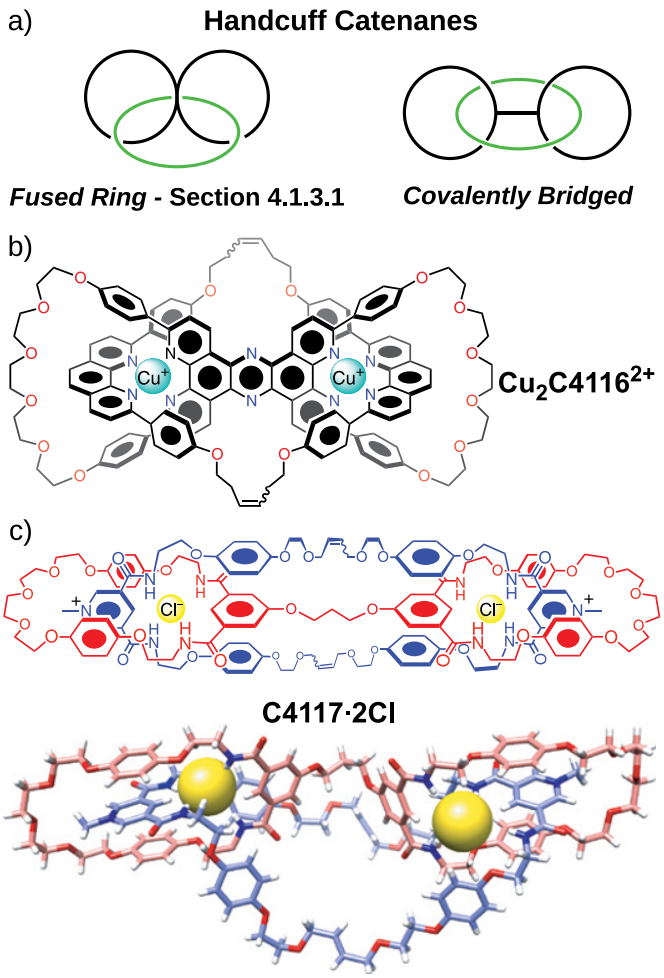


Figure 4.40 Handcuff catenanes. (a) Simplified graphs of handcuff catenanes based on fused macrobicyclics and covalently bridged bis-macrocycles. (b) Stereoformula of Sauvage's handcuff [2]catenane based on transition metal templates.[185,186] (c) Stereoformula and tubular representation of the solid-state structure of Beer's anion-binding handcuff catenane.[341]

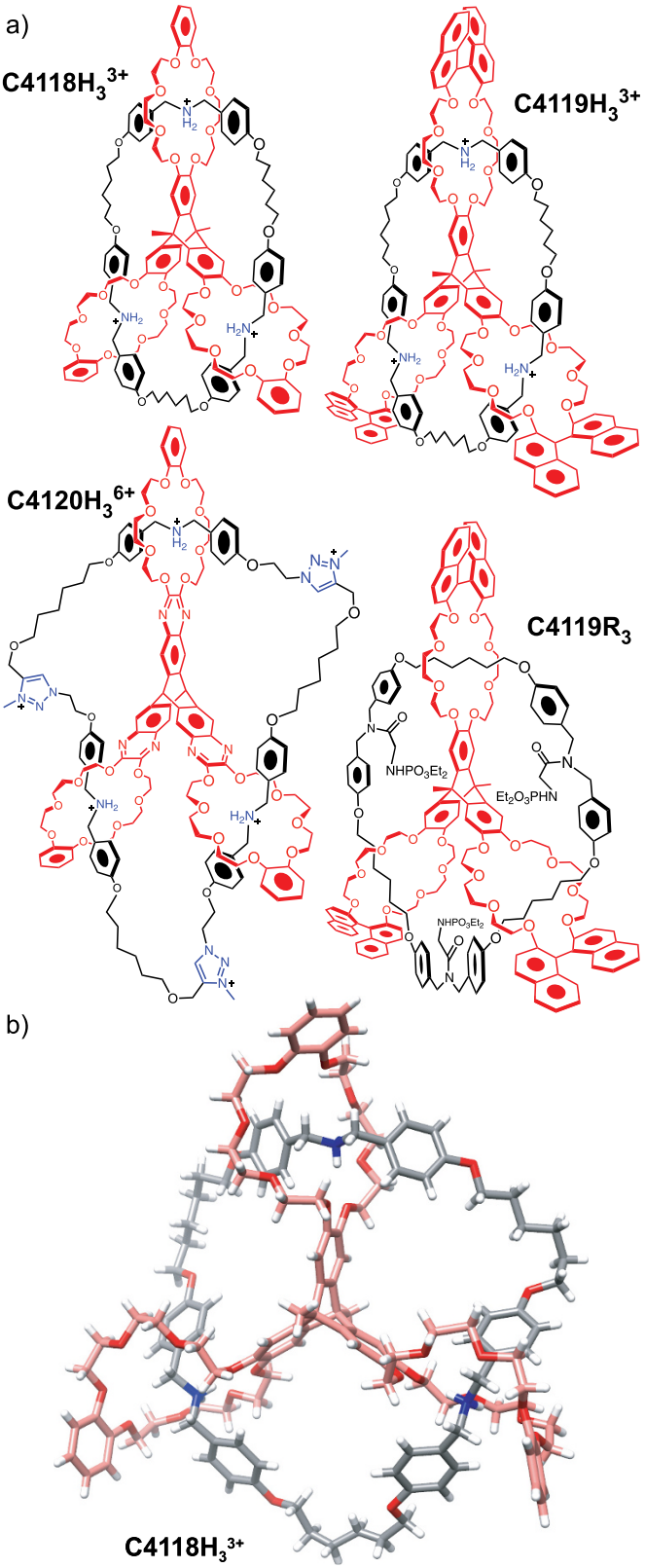


Figure 4.41 [4]Pseudocatenanes. (a) Stereoformulas of several [4]pseudocatenanes introduced by Chen.[342–345] (b) A tubular representation of the solid-state structure of the [4]pseudocatenane **C4118H$_3$**$^{3+}$. Solvent molecules and PF_6^- counterions are omitted for the sake of clarity.

designed and synthesized in the laboratories of Chuan-Feng Chen.[342–345] All of these catenanes are constituted by one large macroring derived from three dibenzylammonium recognition units threaded through each of the three crown ethers fused to a central trypticene core in the corresponding component part. Compound **C4118H$_3$**$^{3+}$ was the first in this class to be synthesized[342,344]—it has also been characterized[342] in the solid state (**Figure 4.41b**) by X-ray crystallography. The compound **C4119H$_3$**$^{3+}$ and its *N*-acylated derivative **C4119R$_3$**, which resembles a 'ship's wheel', possess homochiral binaphthyl subunits within the constitutions of its peripheral crown ethers. Circular dichroism suggests that the chirality of the binaphthyl-based tris(crown) component is transferred to the achiral macroring with which it is interlocked.[343] Most recently, Chen[345] has reported on the synthesis and pH-driven stepwise switching properties—see **Section 6.3.3.1**—of the [4]pseudocatenane **C4120H$_3$**$^{6+}$. All four of these compounds were obtained by olefin cross metathesis and ring-closing metathesis reactions—see **Section 3.2**—of alkene-terminated dibenzylammonium derivatives threaded through the crown ether subunits of the tris-macrocyclic component part in the presence of Grubbs' catalysts. Alternative [4]pseudocatenane topologies may surface in the future—either by rearranging the connectivity of covalent linkers in these radial [4]pseudocatenanes, or by bridging the rings of linear [4]catenanes. To the best of our knowledge, pseudocatenanes based on even larger oligomers such as Olympiadanes[69] or branched catenanes (**Section 4.1.2.3**) have not yet been reported.

4.1.4.4 Cyclic Oligo[2]catenanes

When connecting multiple [2]catenanes together by covalent linkers, the corresponding oligomers/polymers may take the form of cyclic or acyclic chains. Cyclic oligomers are relatively uncommon. We are aware of only a handful (**Figure 4.42**) of cyclic bis[2]catenanes, which have been prepared by various methods of templation, including (i) amide hydrogen bonding[321,346] (e.g, **C4121**, **C4124**), (ii) π-donor/π-acceptor[334] (**C4122**$^{8+}$), (iii) Fujita's brand of coordination-driven self-assembly[347] (**C4123**$^{8+}$), and (iv) Na^+ templated catenation[348] of cyclic polyethers.

Very few cases[348,349] of cyclic oligo[2]catenanes larger than dimers are known. The cyclic tris[2]catenane **C4125** was isolated (**Figure 4.43**) by Geerts[349] as a side-product in the polymerization of a bis-hydroxylated Hunter/Vögtle-type amide-based [2]catenane with terephthalate-derived comonomers. Chiu[348] has synthesized (**Scheme 4.22**) several cyclic [2]catenane oligomers in a one-pot reaction, which involves the thermodynamically controlled self-assembly of catenaned polyethers from bis(amine) (**L4126a**) and carbazole-bridged bis(isophthalamide) (**L4126b**) precursors via reversible imine bond formation in the presence of Na^+ templates. The cyclic dimer $(Na^+)_2 \subset$**C4126a**, trimer $(Na^+)_3 \subset$**C4126b**, tetramer $(Na^+)_4 \subset$**C4126c**, and pentamer $(Na^+)_5 \subset$**C4126d** were all detected in the dynamic combinatorial library by mass spectrometry, but not isolated on account of their incorporation of reversible bonds. The milieu was

converted to a mixture of kinetically stable compounds by reduction of the imine bonds, followed by methylation of the corresponding amines. Isolated from this mixture were the cyclic bis[2]catenane **C4127**, the cyclic tris[2]catenane **C4128**, and the cyclic tetrakis[2]catenane **C4129**. While the cyclic tetramer **C4129** represents an unprecedented molecular topology, compound **C4127** was the first of its kind for which a single crystal X-ray structure (**Figure 4.44**) has been solved.

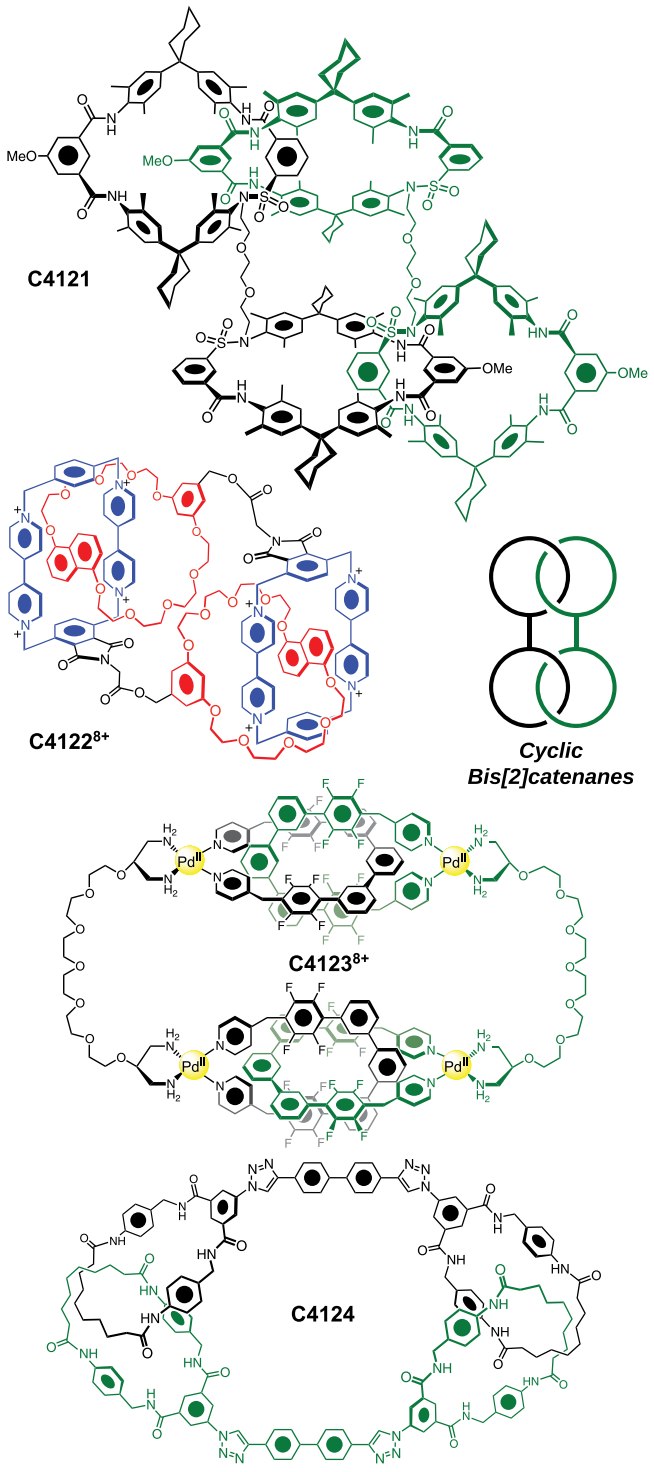


Figure 4.42 Stereoformulas of cyclic bis[2]catenanes.[321,334,346,347]

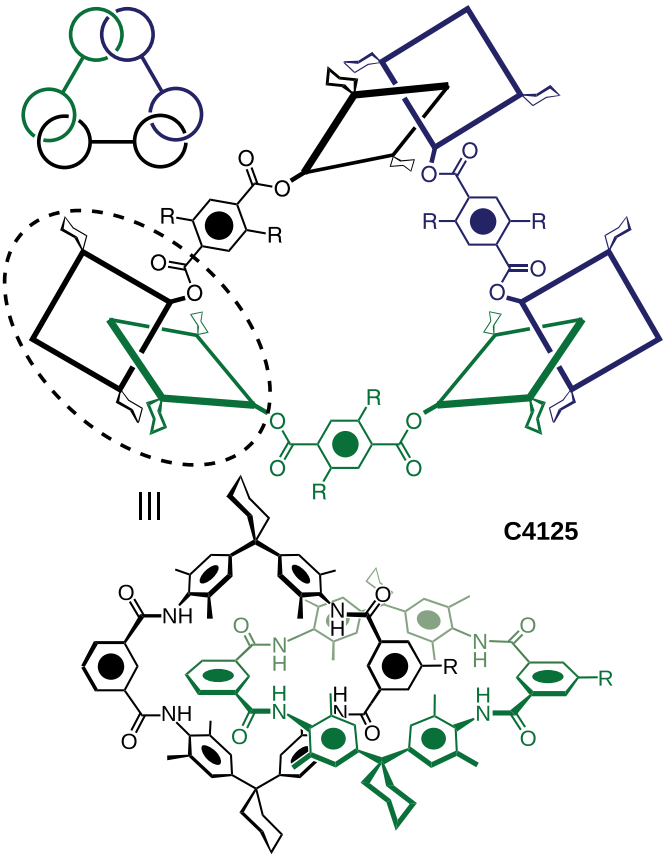


Figure 4.43 A cyclic tris[2]catenane.[349]

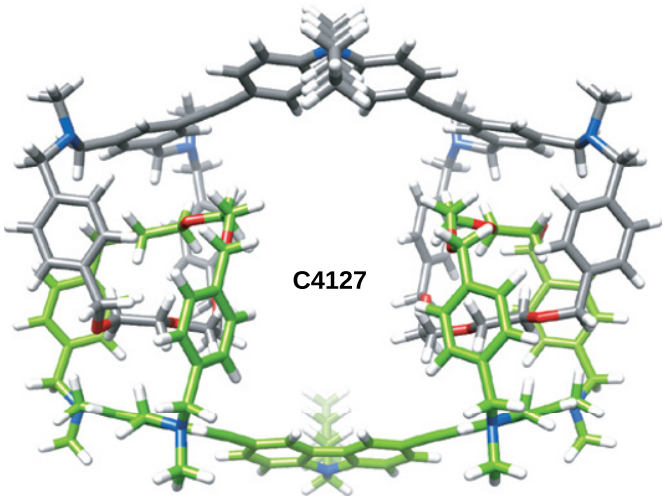


Figure 4.44 The single crystal X-ray structure[348] of Chiu's cyclic bis[2]catenane **C4127**.

4.1.4.5 Acyclic Oligo- and Poly[2]catenanes

Oligo- and poly[2]catenanes are much more common in the literature than their cyclic counterparts, and these materials have been discussed in a number of literature reviews.[116,118,243,350–354] Poly[2]catenanes may be subdivided into two main categories: main-chain and side-chain. Simple graphs exemplifying these two topologies are illustrated in **Figure 4.45**.

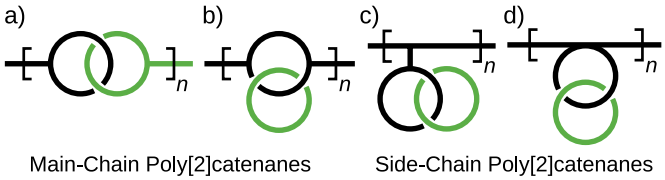
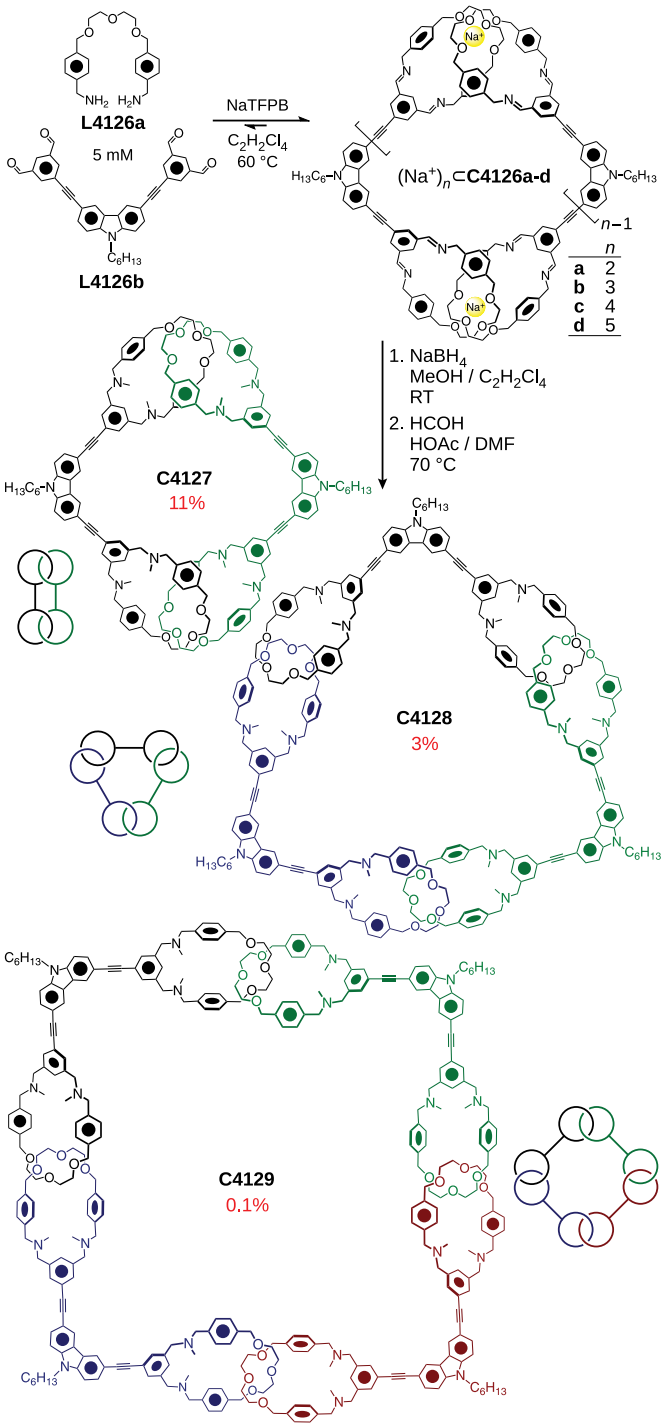


Figure 4.45 Graphs of main-chain (a,b) and side-chain (c,d) poly[2]catenane topologies.



Scheme 4.22 Chiu's Na^+ template synthesis of cyclic oligo[2]catenanes, including dimers, trimers, and tetramers.[348]

Bis[2]Catenanes

The shortest possible main-chain oligo[2]catenane is a dimer, or bis[2]catenane. Several donor-acceptor bis[2]-catenanes were among the earliest examples of any kind of covalently bridged catenanes to be described. Examples[355–358] include (**Figure 4.46**) the bis[2]catenanes **C4130**$^{8+}$, **C4131**$^{8+}$, **C4132a-b**$^{8+}$, and **C4133a-c**$^{8+}$. Bis[2]catenanes based on fused rings, as opposed to covalently bridged ones, are described in **Section 4.1.3.1**.

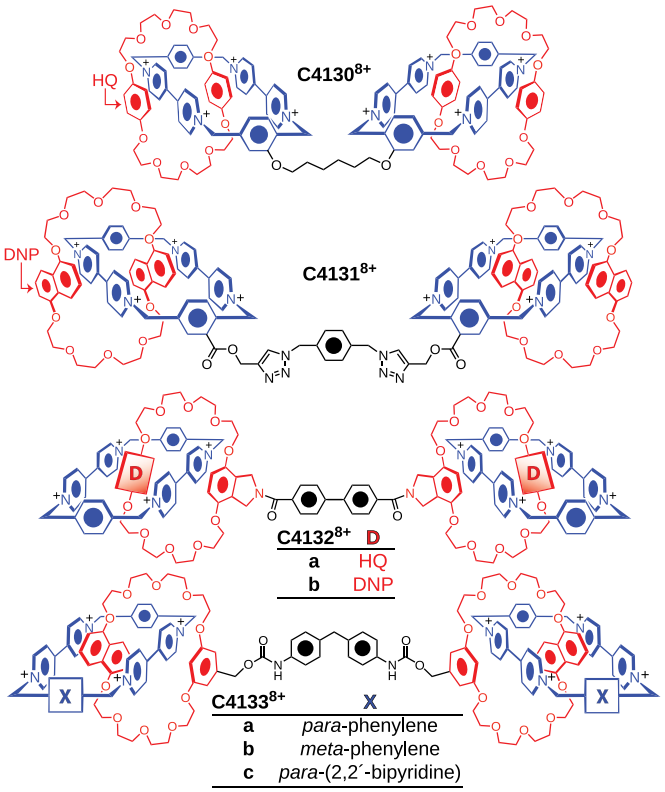


Figure 4.46 Stereoformulas of donor-acceptor bis[2]catenanes.[355–358]

Vögtle[328] has also described one case (**Figure 4.47**) of a bis[2]catenane in which a pair of tetralactam homo[2]catenanes is dimerized by a dendritic linker connecting all four of the sulfonamide subunits in the constitution of each ring. Since both of the rings within each [2]catenane are connected to each other by this xylylene-based linker, compound **C4134** may also be appropriately referred to as a bis(pretzelane).

Main-Chain Poly[2]Catenanes

A number of main-chain poly[2]catenanes are illustrated in **Figure 4.48**. Poly[2]catenanes were initially introduced in 1995 by Geerts,[359] who employed the Hunter/Vögtle-type tetralactam [2]catenanes (**Section 2.3.4.1**) as co-monomers in the polymerization of polycatenanes **C4135a-d**. The polymers were obtained by Pd-mediated cross coupling protocols, including the Sonogashira, Suzuki, and Stille reactions, involving catenated monomers with brominated

isophthalamide units[I] and co-monomers possessing reactive alkyne, boronic ester, and stannane functional groups, respectively. In the following year, Sauvage and Geerts[360,361] began investigating the polymerization of hydroxyl-terminated catenands and catenates by a polyesterification method[362] involving terephthalic acid derivatives as co-monomers. In the presence of the Cu^{I} template, the catenates are co-polymerized into the mechanically linked polyester **C4136** with a molecular weight corresponding to an average degree of polymerization (DP) of 8–9 repeating units. By contrast, the catenands give rise to cyclic molecules (mostly pretzelanes) under the same polymerization conditions, most likely as a result of their much more mobile rings. The same polyesterification method was applied[349,363] subsequently to the synthesis of the poly[2]catenane **C4135e**. Compounds **C4137a-b** represent another example of poly[2]catenanes based on transition metal templation, introduced in this case by Shimada and Tamaoki[327] using amide coupling protocols.

Other amide-based poly[2]catenanes include (**Figure 4.48**) the compounds **C4138a** and **C4138b** introduced by Leigh,[364–366] as well as the compounds **C4138c-f** introduced by Hagiwara.[346,367] These compounds differ in the polymerization types and co-monomers employed in their synthesis—**C4138a** and **C4138b** are polycarbonates and poly(ethylene terephthalate)s, respectively, obtained by transesterification protocols, while **C4138c-f** are obtained by either Cu^{I}-catalyzed azide-alkyne cycloadditions or Pd-mediated Sonogashira cross coupling reactions. The Sonogashira polymerization is particularly efficient in the case of compound **C4138e**, which was obtained as a gel with a soluble fraction possessing a high molecular weight ($M_N > 2.3 \times 10^5$). Takata[117] has prepared the amide-based poly[2]catenane **C4139**, the synthesis of which is described in **Scheme 2.75** and the accompanying text in **Section 2.3.4.1**.

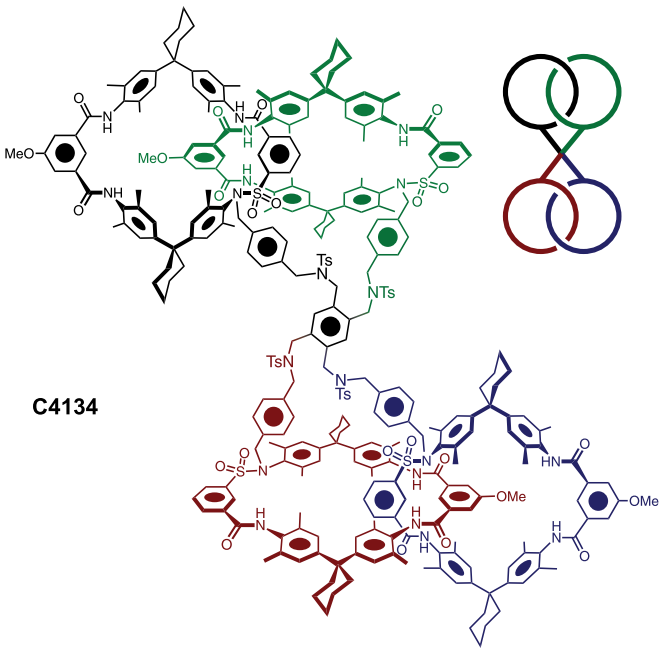


Figure 4.47 Stereoformula of Vögtle's bis(pretzelane).[328]

Not all poly[2]catenanes are based on hydrogen-bonded or transition metal templates. Godt[368] has prepared poly[2]catenanes by reacting the carboxylated terminal groups of her giant 'non-rusty' [2]catenanes obtained by directed synthesis (**Section 2.2**) with α,α´-dibromo-*p*-xylene, resulting in the xylylene polyester **C4140** with an average of 10 mechanically bonded repeating units per polymer chain. Another series of poly[2]catenanes have been introduced[357,358,369] that rely on π-associated donor-acceptor templation. They include (**Figure 4.48**) the polyester **C4141**$^{4n+}$,[357] as well as the poly(bis[2]catenanes) **C4142**$^{9n+}$ and **C4143a/b**$^{8n+}$, the latter two of which are based on metallosupramolecular[358] (Ag^{I}) and polyurethane[357,369] polymerization protocols, respectively.

One-Dimensional Side-Chain Poly[2]catenanes

Side chain poly[2]catenanes have mainly flown under the banner of donor-acceptor template motifs. Examples (**Figure 4.49**) include the polyurethane poly[2]catenane **C4144**$^{4n+}$,[357] the poly(ethylenedioxy)thiophene poly(EDOT)-derived poly[2]catenane **C4145**$^{4n+}$ obtained[370] by electropolymerization of EDOT-functionalized monomers, as well as the poly[2]catenanes[356,371] **C4146**$^{4n+}$ and **C4147**$^{4n+}$ derived from polymethyl methacrylate backbones. All of these compounds possess the 'little blue box' (**Section 2.3.3.7**) as a π-accepting cyclophane engaged in mechanical bonding with π-donating crown ethers, which are either fused directly to the polymer backbone (i.e., **C4144**$^{4n+}$**–C4145**$^{4n+}$)—a geometry which has also been called[357] a 'pendant' poly[2]catenane—or connected to the polymer backbone by a covalently linked (i.e., **C4146**$^{4n+}$**–C4147**$^{4n+}$) side chain.

Two- or Three-Dimensional Side-Chain Poly[2]catenanes

We note that several two- and three-dimensional poly[2]-catenanes have also been prepared[372–375] in the form of coordination polymers or metal-organic frameworks (MOFs). Following the introduction[376,377] of MOFs decorated with crown ethers as porous materials possessing "active domains" that recognize specific guests by virtue of supramolecular interactions, ligands decorated with side-chain donor-acceptor [2]catenanes derived from these crown ether struts and the $CBPQT^{4+}$ cyclophane began[378] to appear. Some of these catenated ligands (**C4148**$^{4+}$**–C4150**$^{4+}$) were

[I] The tetralactam [2]catenane precursors possessed one brominated isophthalamide unit in the constitution of each ring, a situation that leads to a mixture of three possible translational isomers—see **Section 5.1.1**. Polycatenanes **C4135a-d** have all been prepared using only the so-called *in/out* translational isomers as precursors. The *in/out* and *out/out* isomers of **C4135e** were both prepared separately and the *out/out* isomer was found to possess a slightly higher molecular weight (DP ≈ 16–18) than that (DP ≈ 10–13) of the *in/out* isomer.[349]

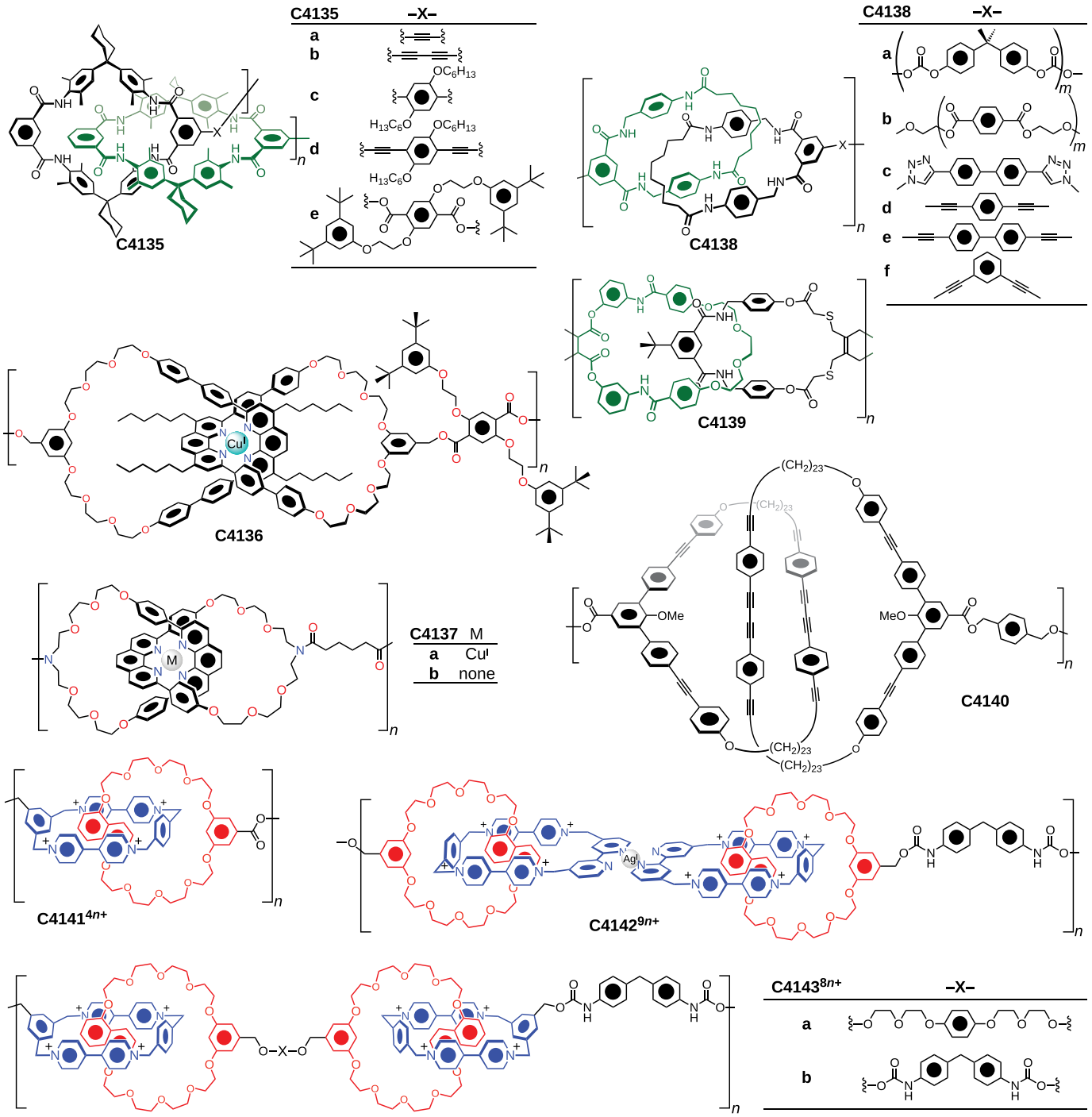


Figure 4.48 Stereoformulas of main-chain poly[2]catenanes and polybis[2]catenanes.[327,360,361,364–366,346,367,117,357,358,368,369]

subsequently implemented[372–374] (**Figure 4.50**) as the struts of MOFs possessing Cu^{II} paddlewheel complexes as the SBUs/nodes of the networks. The coordination polymers **MOF-1011**, **MOF-1030**, and **MOF-1050** are all prepared under solvothermal conditions by heating the bis(carboxylate) catenanes with $Cu(NO_3)_2 \cdot 2.5H_2O$ in mixtures of either DMF or *N*,*N*-diethylformamide (DEF) and aqueous EtOH. The [2]catenane **C4148**$^{4+}$, which possesses a pair of 4-ethynylbenzoate ligands appended to its HQ-based crown ether ring, becomes arranged in layered square-lattice arrays in **MOF-1011**. The [2]catenane struts **C4149**$^{4+}$ and **C4150**$^{4+}$, which possess DNP recognition units for the CBPQT^{4+} ring, are armed with pairs of longer 4-(4-ethynylphenyl)ethynylbenzoate and *para*-terphenylcarboxylate ligand extensions, respectively. While the longest ligand, **C4149**$^{4+}$, leads[373] to the twofold interpenetrated 3D framework **MOF-1030**—see **Figure 1.17** and the accompanying text in **Section 1.2.4**—the intermediate-length **C4150**$^{4+}$ produces the layered 2D gridlike networks of **MOF-1050**. The DNP-based catenanes each possess

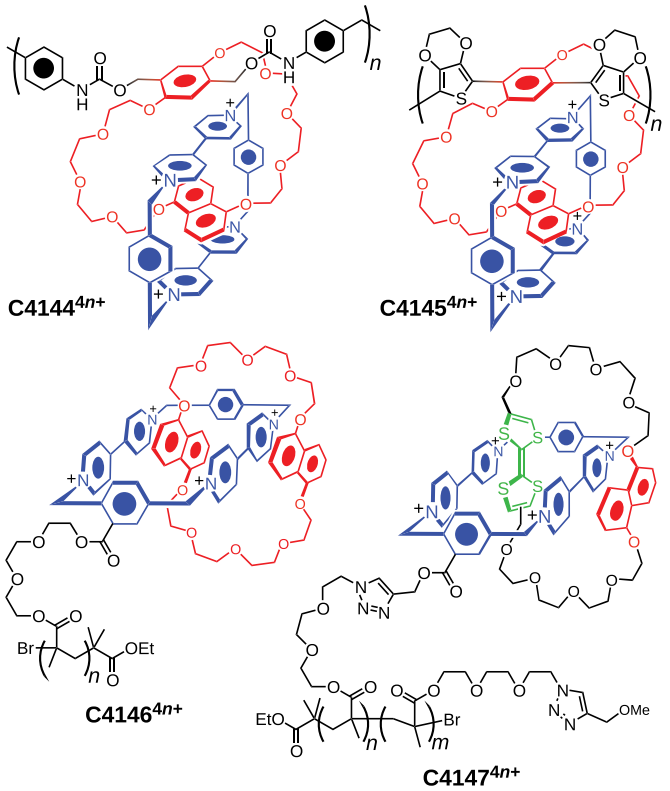


Figure 4.49 Stereoformulas of several donor-acceptor side-chain poly[2]catenanes.[356,357,370,371]

two centers of planar chirality–one associated with the DNP unit and one associated with the central phenylene unit connecting the ligand moieties to the crown ether. Although up to four stereoisomers are possible—namely (*SS*), (*SR*), (*RS*), and (*RR*)—only the *SS* and *RR* stereoisomers are observed in the solid-state structure of **MOF-1050**, where the 2D layers are held together by infinite donor-acceptor stacks comprising regularly alternating *RR* and *SS* stereoisomers.[J] This regular stacking suggests that the non-covalent bonding interactions between these π-donor/π-acceptor catenanes most likely play an important role in the internal organization of the networks during their assembly. This hypothesis is further supported by more recent results[375] involving the incorporation of donor-acceptor [2]catenanes into interpenetrated mixed-ligand 3D MOFs possessing Zn_4O SBUs akin to those underpinning **MOF-5** (see **Figure 4.38a**), where the different ligands incorporate into the framework with "magic number ratios" apparently governed by these noncovalent bonding interactions.

[J] Another coordination framework, **MOF-1051** (not illustrated), possessing a non-degenerate cyclophane containing a diazapyrenium (DAP^{2+}) recognition unit, similarly contains stereoregular donor-acceptor stacks. An additional level of co-conformational selectivity was observed in this case, since only one translational isomer, in which the DAP^{2+} unit is encircled, is observed in the crystal structure.

4.2 Rotaxane Architectures

The nomenclature for rotaxanes originally proposed by Schill[379] has been approved[1] by IUPAC. The name of a rotaxane contains four parts: (i) a bracketed integer prefix denoting the total number of component parts in the rotaxane, (ii) the IUPAC name(s) of the dumbbell species, (iii) the IUPAC name(s) of the macrocyclic species, and (iv) the 'rotaxane' suffix. Vögtle[4] has extended this nomenclature to accommodate rotaxanes with various covalent linkages. While these nomenclatures are sufficient to give any rotaxane a unique and accurate name, they are exceedingly long. We do our best with the vernacular nomenclature that is available, despite several inconsistencies and conflicting naming conventions in the literature. Rotaxane architectures may be subdivided into [*n*]rotaxanes (**Section 4.2.1**), rotaxane dendrimers (**Section 4.2.2**), and other covalently bridged rotaxanes (**Section 4.2.3**).

4.2.1 [*n*]Rotaxanes

In this Section we summarize rotaxane architectures comprising only torus rings and linear dumbbells, beyond the archetypal [2]rotaxanes which are most common. Rotaxanes with more than two component parts may possess one dumbbell and multiple rings (**Section 4.2.1.1**), one ring with multiple dumbbells (**Section 4.2.1.2**), or multiple rings and multiple dumbbells (**Section 4.2.1.3**).

4.2.1.1 Single-Axle Oligo- and Polyrotaxanes

Single-dumbbell oligorotaxanes and polyrotaxanes are among the most prevalent polymer architectures containing mechanical bonds, with >1500 publications relating to these keywords according to a search in SciFinder.[380]

Oligorotaxanes based on transition metal templates

Sauvage[381,382] introduced metallo-oligorotaxanes in 1996 when he employed porphyrin-forming condensation reactions to generate [3]- and [5]rotaxanes from precursors comprising an aldehyde-terminated [3]pseudorotaxane and methylenebis(pyrrole). In the case of the [5]rotaxane (**Figure 4.51**), both the protonated freebase **$Cu_4R404H_6^{4+}$** and the Zn^{II}-metallated **$Cu_4Zn_3R404^{4+}$** were obtained and characterized. More recently, Sauvage[383] synthesized the compound **Cu_4R405^{4+}** and the corresponding demetallated [5]rotaxane **R405**, which also accommodates (**Figure 4.51**) Li^+ and Zn^{II} templates. The rotaxane was synthesized by the typical Cu^I template approach, employing CuAAC click chemistry to connect two metallo-semirotaxanes to the termini of a central metallo[3]pseudorotaxane possessing a bis(bidentate) axle derived from a 4,7-phenanthroline core. Since the central two recognition units are bidentate bpy ligands and the outer two units are tridentate terpy ligands, these sites can also uptake different templates selectively, as in the case of **$Li_2Zn_2R405^{6+}$**, where the middle two templates are Li^+ ions and the outer two templates are Zn^{2+} ions.

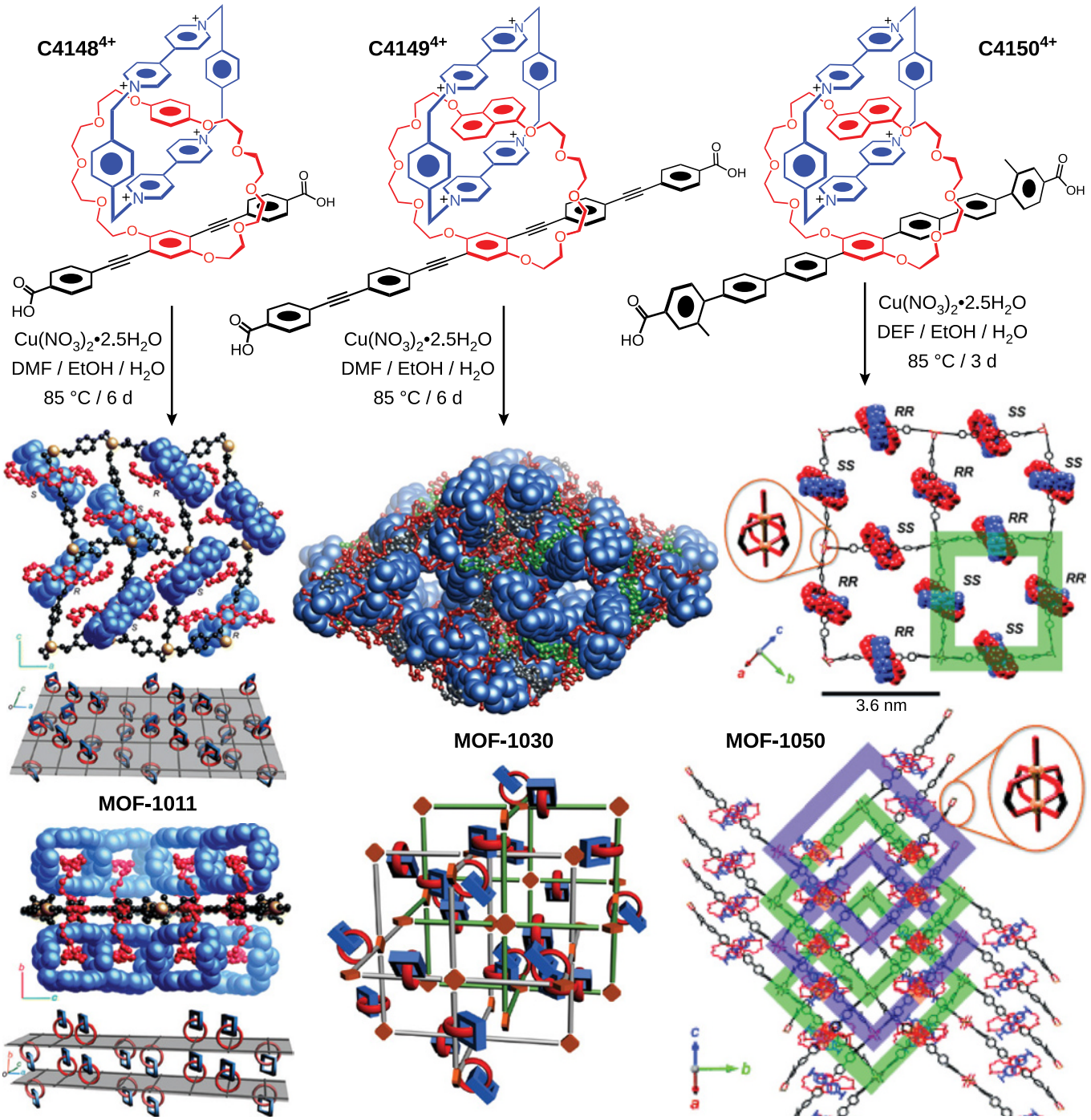


Figure 4.50 Side-chain donor-acceptor [2]catenanes embedded in the extended networks of MOFs possessing Cu^{II} tetracarboxylate paddlewheel coordination complexes as the SBUs.[372–374] **MOF-1011** and **MOF-1050** are layered two-dimensional networks, while **MOF-1030** is a two-fold interpenetrated three-dimensional network. Images reproduced with permission from refs. 372 (copyright 2010 Royal Society of Chemistry), 373 (copyright 2010 Wiley-VCH), and 374 (copyright 2013 Wiley-VCH)

Leigh[384] has described a Pd^{II}-template clipping protocol, by which multiple rings can be locked around a dumbbell containing only a single template over iterative rounds of ring-closing olefin metathesis and template removal. See **Scheme 3.34** in **Section 3.4.1.1**. While [2]-, [3]-, and [4]-rotaxanes were isolated, in principle the number of rings that can be introduced is limited only by the length of the dumbbell.

Oligorotaxanes based on π-donor/π-acceptor templates

Oligorotaxanes based on π-associated donor-acceptor interactions (**Figure 4.52**) were introduced[385] in 1996 in the form of [4]rotaxanes possessing *para*-xylylene bridged BIPY^{2+} trimeric axles, BPP34C10 rings, and stoppers comprising either tetraarylmethane derivatives (**R406a**$^{6+}$) or 3rd-generation benzylic ether dendrimers (**R406b**$^{6+}$). After the advent of CuAAC click chemistry was identified[386,387] as an

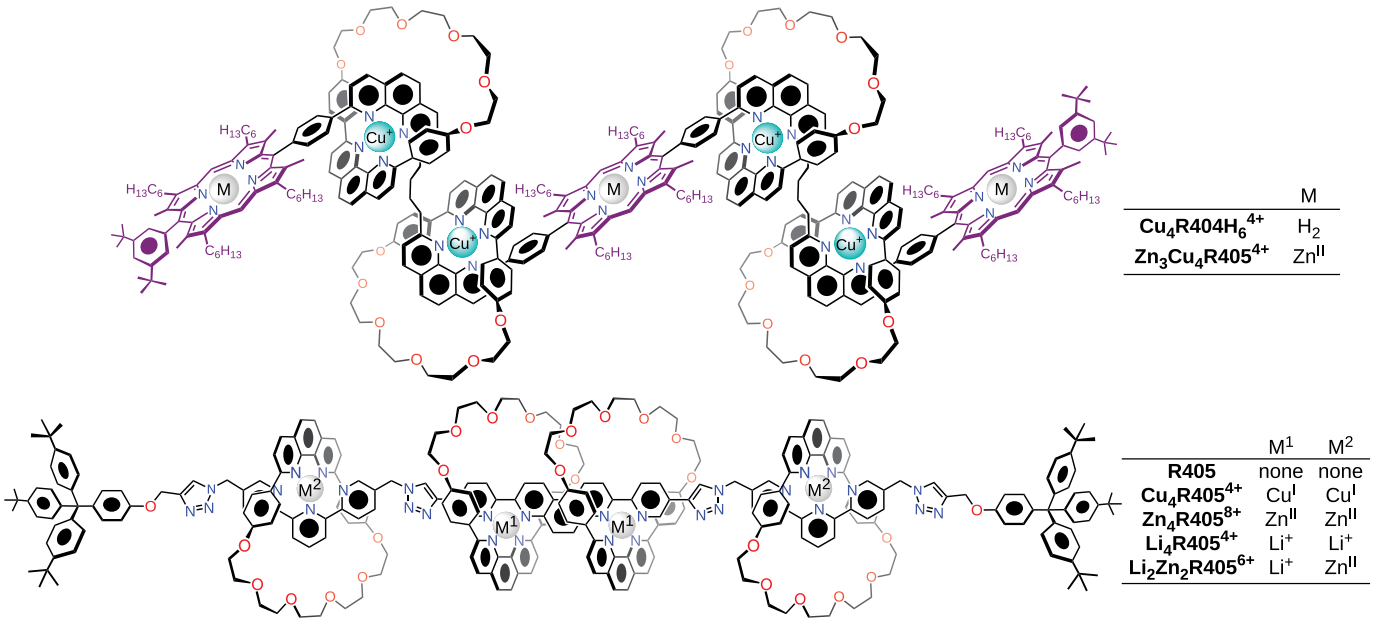


Figure 4.51 Stereoformulas of [5]rotaxanes based on Sauvage's transition metal templates.[381–383]

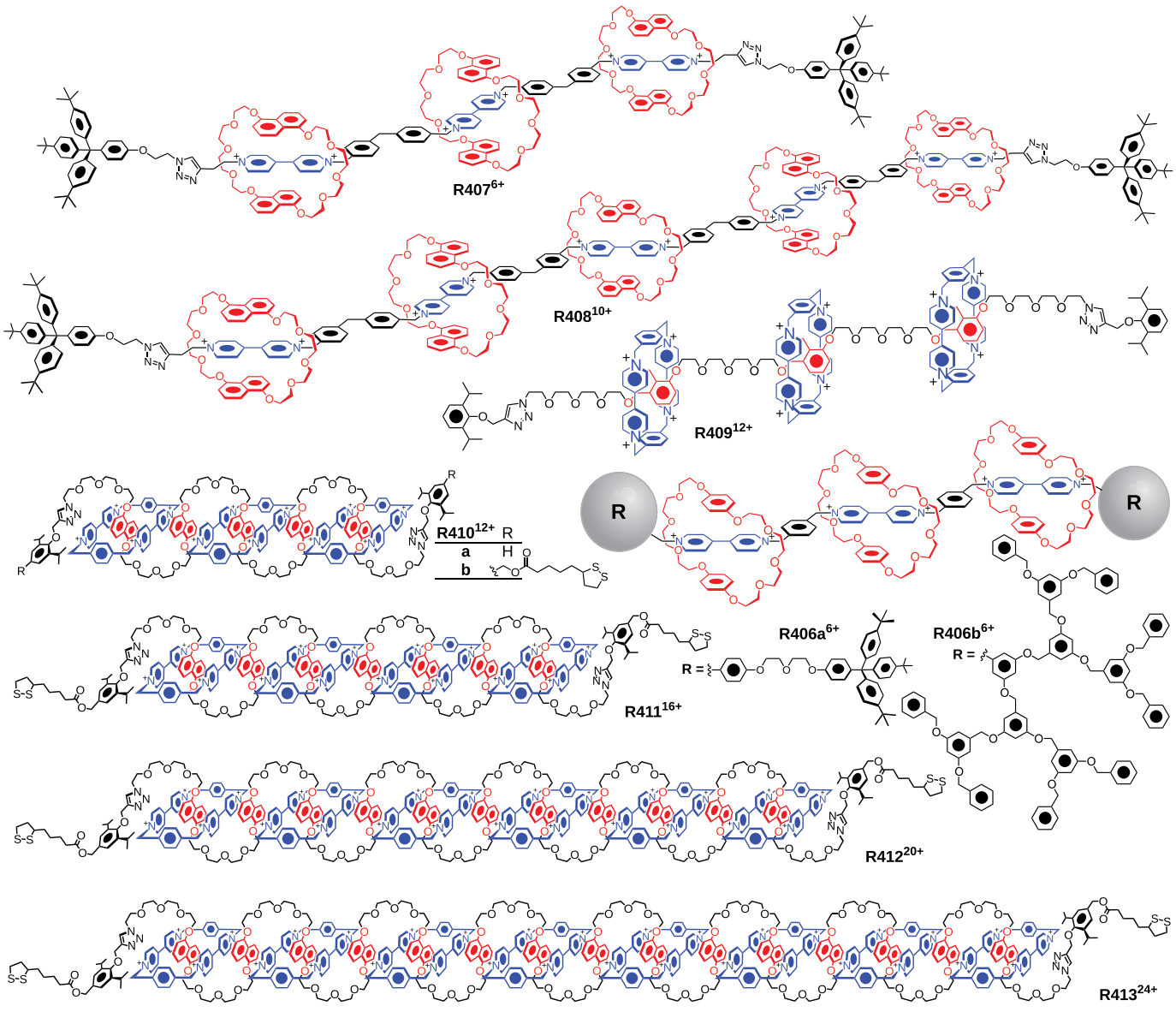


Figure 4.52 Stereoformulas of donor-acceptor oligorotaxanes.[385,388–390]

efficient protocol in the donor-acceptor template synthesis of MIMs, it was employed[388] in the synthesis of the [4]- and [6]rotaxanes **R407^{6+}** and **R408^{10+}**, respectively, from the corresponding pseudorotaxanes based on diphenylmethylene-bridged BIPY^{2+} oligomers encircled by DN38C10 rings.

Donor-acceptor oligorotaxanes (**Figure 4.52**) relying on the molecular recognition of the little blue box, CBPQT^{4+}, have also been investigated,[389–391] particularly in the context of their secondary structures. It transpires that CBPQT^{4+} rings can thread onto polyether-bridged DNP oligomers and polymers in a manner that causes the thread to fold in a serpentine fashion, in order stabilize the assembly by establishing an extended stack of alternating π-donors and π-acceptors. This folding motif, enabled by the mechanical bond, has been observed and characterized both in the solid state[389,392,393] and in solution.[389,390,394] The oligorotaxanes **R410^{12+}–R413^{24+}** constitute a series[390] of these foldamers of varying length. The largest compound, **R413^{24+}**, is a [9]rotaxane with a molecular weight exceeding 15 kDa. Its eight CBPQT^{4+} rings are dispersed among the dumbbell's 15 DNP recognition units such that no two rings occupy adjacent DNP sites, allowing the thread to fold into a conformation that allows unoccupied DNP units to engage in side-on π–π stacking interactions with the BIPY^{2+} units of the CBPQT^{4+} rings. This folding motif repeats itself in the smaller homologues all the way down to a [3]rotaxane possessing two CBPQT^{4+} rings and three DNP units. The [4]rotaxane **R409^{12+}**, by contrast, cannot adopt[389] a folded superstructure because all three of its DNP units are encircled by rings, leaving none available for the alongside stacking interactions that lead to folding. While discrete and monodisperse macromolecules with well-defined secondary (and tertiary) structures are common in Nature on account of the sophisticated machinery that builds proteins, synthetic molecules exhibiting these features remain challenging to produce in the laboratory. These oligorotaxane foldamers suggest that the mechanical bond may be deployed as a tool for instilling well-defined superstructures in macromolecules.

Oligorotaxanes based on hydrogen-bonded templates

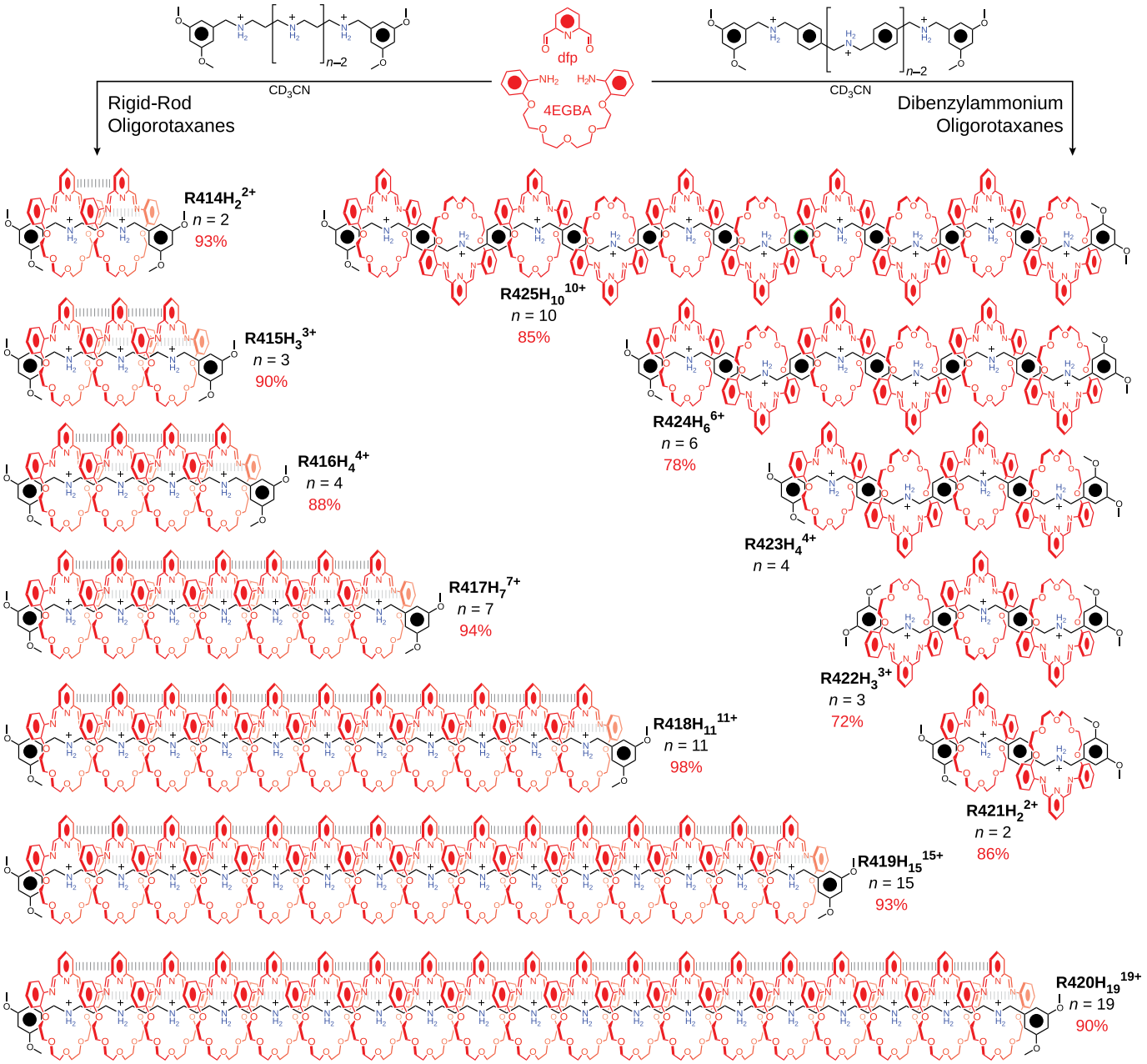
The neutral hydrogen-bonding template motifs (**Sections 2.3.4.1–2.3.4.5**), such as those based on tetralactam macrocycles, seem to have been underemployed as synthons for oligorotaxanes. Vögtle[395] did report one attempt to obtain oligorotaxanes by a step-growth approach. He claimed to have isolated submilligram quantities of [4]- [5]- and [6]rotaxanes, which were characterized only by mass spectrometry. 20 mg of the [4]rotaxane was later obtained[396] in 1.2% yield and fully characterized.

The efficient synthesis[397–399] of mechanomolecules employing the reversible clipping reaction involving imine bond formation and exchange between diformylpyridine (dfp) and tetraethylene glycol bis-*ortho*-aniline (4EGBA) macrocyclic precursors around dialkylammonium axles—see **Section 3.3.1.2**—has provided access (**Scheme 4.23**) to a series of discrete oligorotaxanes in near-quantitative yields. When the oligo(dialkylammonium) templates possess trismethylene linkers between –NH_2^+– recognition units, the imine-based crown ethers of oligorotaxanes **R414H$_2^{2+}$–R420H$_{19}^{19+}$** engage in extended π–π stacking interactions. These *n*-fold stacks of threaded rings, where *n* is the number of –NH_2^+– centers per axle, lead to positive cooperativity[399,400] in the template synthesis of the oligorotaxanes, while rigidifying them into rigid-rod nanostructures, as illustrated (**Figure 4.53**) by their energy-minimized superstructures. The rigid-rod geometry is also evident in the solid-state structure of the [4]rotaxane **R415H$_3^{3+}$**, which is illustrated in **Section 1.2.4**, **Figure 1.16e**. By comparison, the dibenzylammonium oligorotaxanes **R421H$_2^{2+}$–R425H$_{10}^{10+}$** adopt more flexible structures. Their syntheses, while also efficient, exhibit no signs of positive cooperativity. Whereas the dynamic libraries of dibenzylammonium oligorotaxanes require no more than 30 min to reach equilibrium, the equilibration times for the rigid-rod [*n*]rotaxanes rise as *n* increases, reaching as high as 14 h in the case of the [20]rotaxane **R420H$_{19}^{19+}$**. As in the case of the donor-acceptor oligorotaxane foldamers, these systems demonstrate that the mechanical bond can become intimately involved in the stabilization of well-defined macromolecular nanostructures. Recently, this oligorotaxane platform has been adapted as a scaffold for stacking redox-active NDI units in a systematic investigation[401] on how stack size and (co)conformational degrees of freedom influence electron-sharing properties.

Several more examples of dialkylammonium/crown ether oligorotaxanes are illustrated in **Figure 4.54**. Wu[402,403] has employed the dynamic imine-based clipping protocol involving dfp and 4EGBA to prepare the [5]rotaxane **R426H$_4^{4+}$** and the hetero[4]rotaxane **R427H$_4^{4+}$** from identical tetrakis(dialkylammonium) dumbbell templates. The hetero[4]rotaxane **R427H$_4^{4+}$** is obtained[403] by a "threading-followed-by-clipping" protocol in which an oligomethylene-threaded cucurbit[6]uril (CB6) pseudorotaxane becomes stoppered by the clipping of a pair self-assembled crown ethers around the outermost dibenzylammonium recognition units of the axle. Liu and Yin[404] have also relied on the imine-based clipping protocol to assemble the [5]rotaxane **R428H$_4^{4+}$**, which posseses a photoswitchable dithienylethene moiety at the center of its dumbbell. One of the only dialkylammonium/crown ether oligorotaxanes to be obtained under kinetic control was introduced by Takata,[405] who employed his efficient tributylphosphine-catalyzed esterification stoppering protocol—see **Section 2.3.4.6**—in the synthesis of [3]- and [5]rotaxanes, the latter of which (**R429H$_4^{4+}$**) is illustrated in **Figure 4.54**.

Oligorotaxanes based on solvophobic templation

Oligorotaxanes based on the hydrophobic templating forces associated with the molecular recognition of the cyclodextrins (**Section 2.3.1.1**) are illustrated in **Figure 4.55**.



Scheme 4.23 The synthesis of dialkylammonium oligorotaxanes.[397–399] The ring–ring π–π stacking interactions in the rigid-rod oligorotaxanes[398,399] (left-hand side) lead to positive cooperativity[399,400] in their self-assembly, since the more flexible dibenzylammonium oligorotaxanes[397] (right-hand side) are obtained in lower yields by the same protocol.

The [4]rotaxane **R430** and the [6]rotaxane **R431** were synthesized by Fort,[406] employing CuAAC click chemistry, as part of an investigation on carbohydrate protein interactions. These oligorotaxanes and their singly and doubly-threaded homologues were employed to probe the effects of multivalency on the inhibition of agglutination, since the density of their displayed maltose ligands is controlled by the number of mechanically bonded, maltose-decorated cyclodextrin rings. While the inhibition of the binding of agglutinin to asialofetuin is valency-dependent, no synergistic effect was observed with increasing numbers of rings.

Osakada[407,408] has assembled oligorotaxanes from "metallosurfactant" dumbbells, which form aqueous micelles above their critical micelle concentration (CMC) of 0.65 M at 25 °C, yet disassemble in the presence of sufficient amount of α-CD to thread their dynamic $M(en)L_2$ axles by the so-called "magic rod" approach. The [5]rotaxanes **R432a**$^{4+}$ and **R432b**$^{4+}$ comprise (**Figure 4.55**) $Pd(en)^{2+}$ and $Pt(en)^{2+}$ centers, respectively, coordinated by pairs of semi[3]rotaxane ligands derived from *N*-alkylbipyridinium semidumbbells and α-CD rings. Osakada[409] has shown that these [5]rotaxanes can also be deployed as organogelators, which produce metallohydrogels displaying sharp sol-gel transitions.

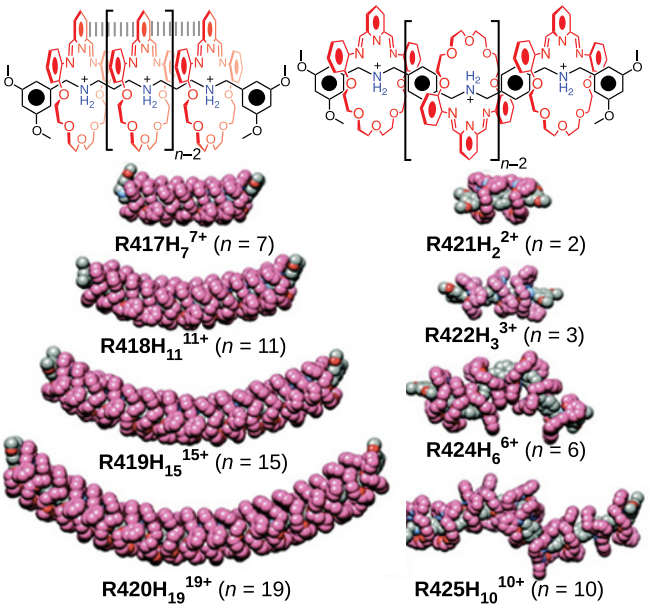


Figure 4.53 Energy-minimized structures of rigid-rod (left-hand side) and dibenzylammonium (right-hand side) oligorotaxanes, reproduced with permission from ref. 399 (copyright 2012 American Chemical Society)

Another class of oligorotaxanes that rely on solvophobic templation have been obtained[410–413] by the cooperative capture[414] approach (**Section 2.3.1.3**) to rotaxane synthesis. Hetero-oligorotaxanes combining the CB6-promoted azide-alkyne cycloaddition (CB6AAC) dumbbell capture protocol (**Section 2.3.1.2**) with the synergistic templating forces of hydrogen-bonded α- or β-cyclodextrins[410] and pillar[5]arenes[411] (PA5) are illustrated in **Schemes 2.28** and **2.29**, respectively, of **Section 2.3.1.3**. The cooperative capture strategy has also been employed to synthesize hetero[4]rotaxanes possessing threaded pillar[6]arene (PA6) cyclophanes (**Scheme 4.24**) and γ-CD (**Figure 4.56**) rings. The hetero[4]rotaxane **R433H$_2^{4+}$** is obtained[412] by a cooperative capture reaction (**Scheme 4.24**) in MeCN from a mixture of PA6, the bimolecular inclusion complex of

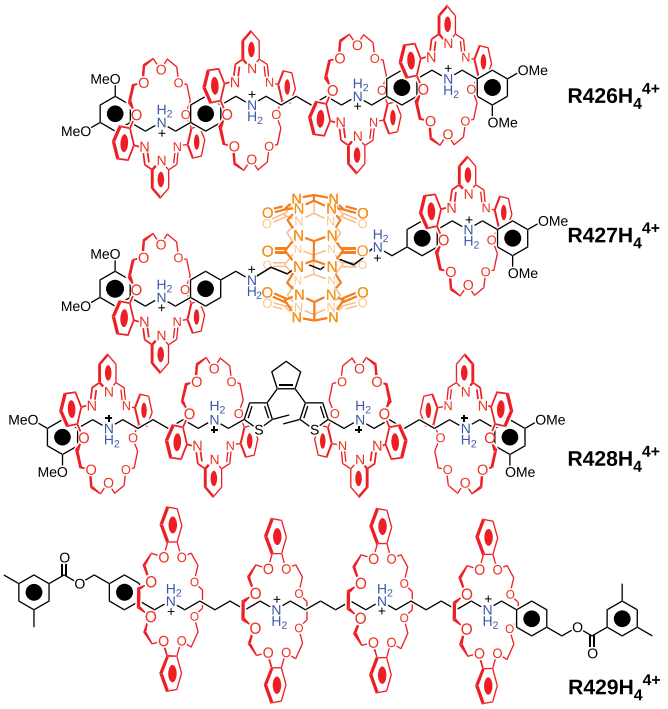


Figure 4.54 Stereoformulas of the [5]rotaxane **R426H$_4^{4+}$** and hetero[4]rotaxane **R427H$_4^{4+}$** self-assembled by Wu,[402,403] the [5]rotaxane **R428H$_4^{4+}$** assembled by Liu and Yin,[404] and the [4]rotaxane **R429H$_4^{4+}$** obtained under kinetic control by Takata.[405]

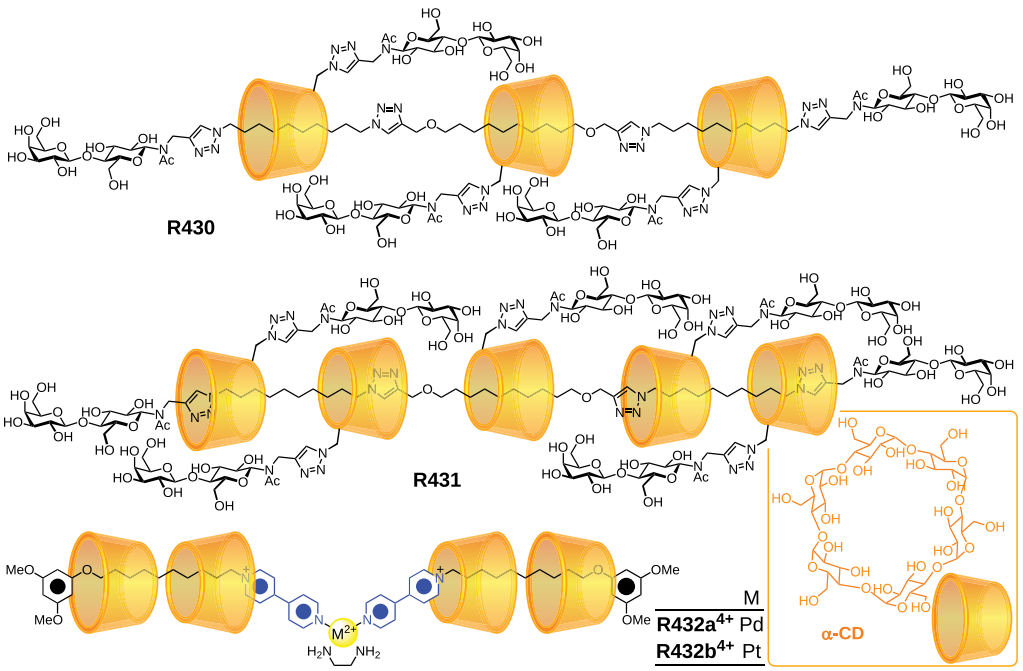
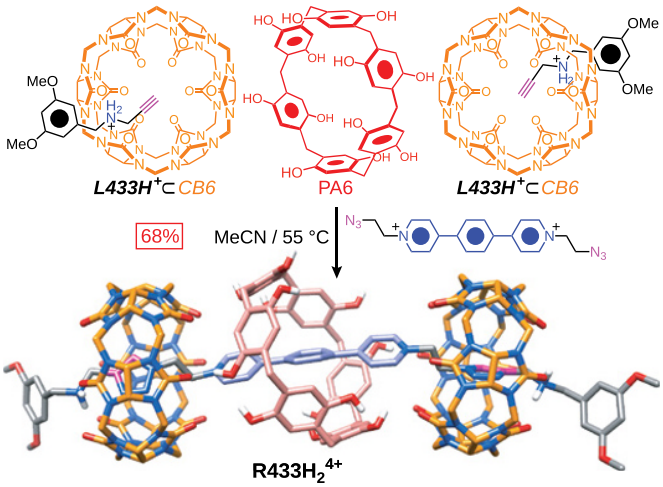


Figure 4.55 Illustrations of oligo-rotaxanes obtained by hydrophobic template syntheses[406–408] under kinetic (**R430–R431**) and thermodynamic (**R432a/b^{4+}**) control. The orientations of the α-CD rings have not been determined.



Scheme 4.24 The cooperative capture synthesis and tubular representation of the solid-state structure of the CB6/PA6 hetero[4]rotaxane **R433H$_2^{4+}$**.[412] C–H protons, solvent molecules, and counterions are omitted for the sake of clarity.

N-(3,5-dimethoxybenzyl)-*N*-propargylammonium (**L433H$^+$**) and CB6, and the extended viologen, 1,4-phenylenebis-4-(*N*-azidoethyl)pyridinium, in 68% yield. In solution, the mobile PA6 ring can exchange between many chiral and achiral geometries by conformational rotations of its HQ subunits, yet it adopts the most energetically favorable conformation with local C_{3V} symmetry in the solid state. Similar hetero[4]rotaxanes were obtained, albeit in lower yields of 38–39%, from PA6-threaded azidoethyl- and azidopropyl-viologen templates.

In the case[413] (**Figure 4.56**) of **R434H$_2^{4+}$**, where cooperative interactions between CB6 and a fluorescent diazoperopyrenium (DAPP^{2+}) fluorophore threaded by γ-CD support a dumbbell capture (**Figure 4.56a**), in which the *N*-azidoethyl groups appended to DAPP^{2+} couple with *N*-(2-pyrenylmethyl)-*N*-propargylammonium by a CB6AAC pathway. The DAPP^{2+} unit of **R434H$_2^{4+}$** is fluorescent (**Figure 4.56b**) in the solid state, since its self-aggregation is prevented by the steric bulk of the threaded cyclodextrins and cucurbiturils. The pyrenylmethyl stoppers are capable of engaging in π-associated donor-acceptor charge-transfer interactions with exposed portions of the DAPP^{2+} core, an event which drives aggregation and leads to red emission as a result of exciplex formation. The sequestration of the pyrenylmethyl stoppers by inclusion within γ-CD restores the green emission of the DAPP^{2+} fluorophore, which emits across a broad range of excitation wavelengths on account of fluorescence resonance energy transfer (FRET) from the pyrenylmethyl stoppers. The aggregation-induced red emission can also be recovered by removal of the γ-CD endcaps with competitive binders, such as 2-adamantylammonium chloride. Conveniently, the

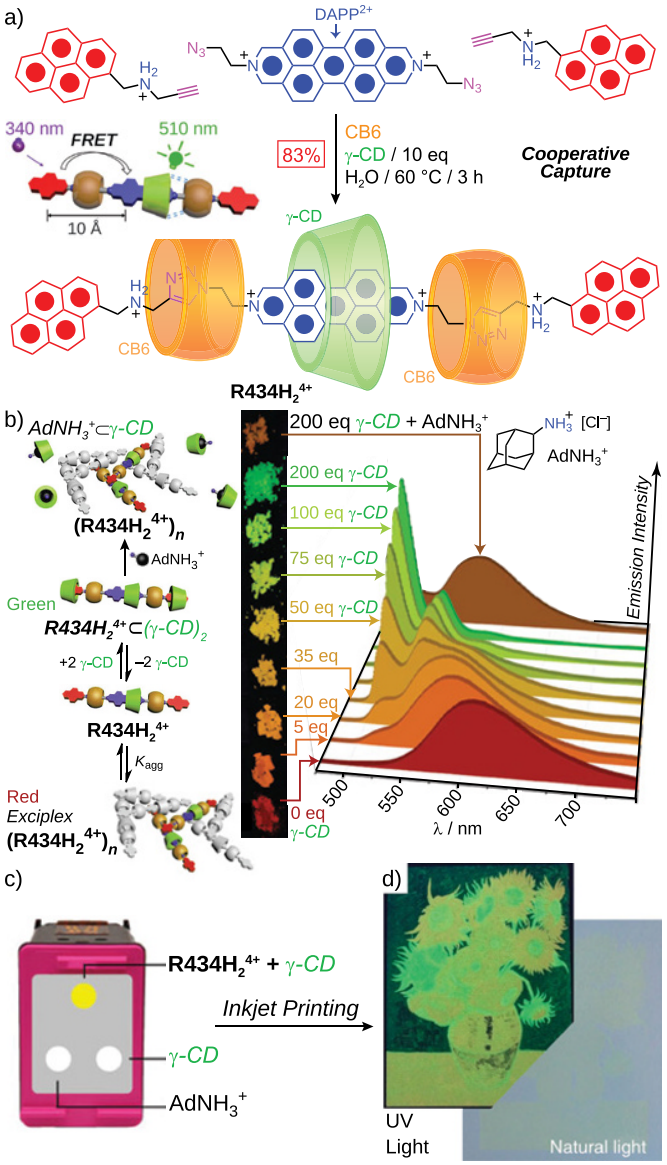


Figure 4.56 A hetero[4]rotaxane with tunable solid-state fluorescence governed by supramolecular equilibria in solution.[413] (a) The synthesis of **R434H$_2^{4+}$** by CB6AAC cooperative capture involving a γ-CD-threaded central DAPP^{2+} fluorophore, which remains fluorescent in the solid-state on account of its insulation by the mechanically bonded rings. (b) The solid-state fluorescence of **R434H$_2^{4+}$** can be tuned from green to red by controlling its aggregation state in solution prior to solvent removal. The formation of red-emitting **(R434H$_2^{4+}$)$_n$** aggregates is driven by exciplex formation between the pyrene stoppers and the DAPP^{2+} fluorophore. The addition of γ-CD favors the green-emitting monomer by insulating the pyrene moieties of the ***R434H$_2^{4+}$*⊂*(γ-CD)$_2$*** complex. The pyrene-bound γ-CD endcaps can be removed by introducing a competitive binder such as AdNH$_3^+$. Aqueous inks of **R434H$_2^{4+}$**, γ-CD, and AdNH$_3^+$ can be (c) loaded into an inkjet printing cartridge and (d) printed onto paper to produce fluorescent images, visible under UV light, the color spectrum of which is highly sensitive to the precise formulations of the inks—a kind of "supramolecular encryption". Images reproduced with permission from ref. 413 under a Creative Commons CC-BY license.

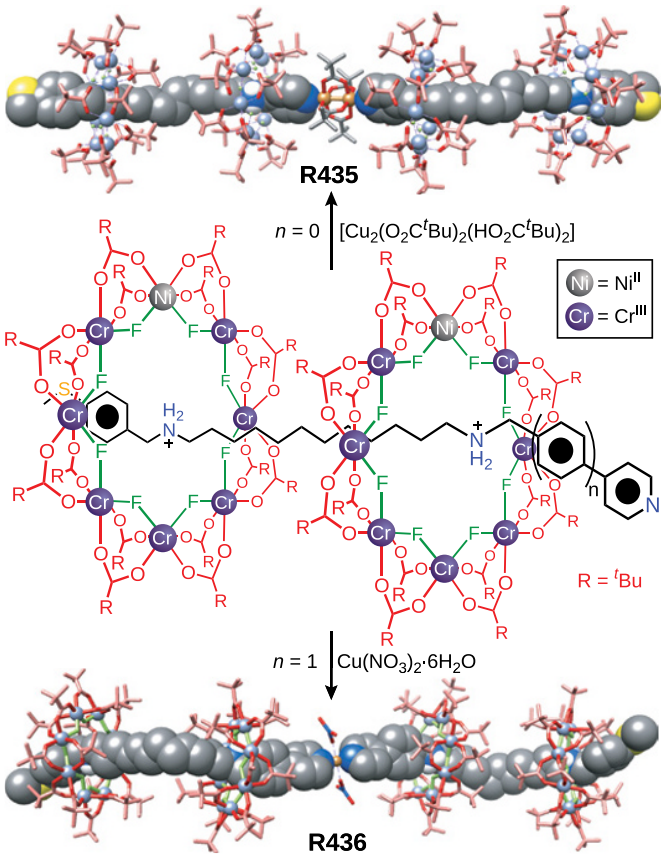
solid-state fluorescence profiles of the rotaxane in its different aggregation states reflect those of the concentrated solutions from which they were obtained. The highly tunable emission spectrum of this oligorotaxane has been applied (**Figure 4.56c**) to the development of fluorescent inks with encrypted security features defined by the complex equilibria underpinning the relationship between the aggregation state of the rotaxane and its emission spectrum. These aqueous inks can be printed on paper and respond rapidly to a wide variety of chemical stimuli, which produce color changes that could be employed as authentication tests. These supramolecularly encoded dynamic color properties would be extremely challenging for counterfeiters to replicate without a complete knowledge of the ink formulations *prior* to printing, owing to the non-linearity of the equations describing the population distributions of red-emitting $\mathbf{(R434H_2^{4+})_n}$ aggregates, green-emitting $\boldsymbol{R434H_2^{4+}} \subset (\gamma\text{-CD})_2$ monomers, and everything in between.

Oligorotaxanes based on ion-pairing interactions

Winpenny[415] has reported the self-assembly of a variety of MIMs based on his ion-pairing templation motif (**Section 2.3.7.1**) involving multicationic dialkylammonium axles threaded by anionic $Cr_7NiF_8(O_2C^tBu)_{16}^-$ inorganic wheels. Among the new architectures are the [5]rotaxanes **R435** and **R436**, the metallosupramolecular self-assembly (**Scheme 4.25**) of which is driven by the dimerization of pyridine-terminated semi[3]rotaxanes around $Cu_2(O_2C^tBu)_4$ paddlewheels and $Cu(NO_3)_2$ centers, respectively. The electrons of these octanuclear heterometallic rings engage in spin–spin interactions, rendering them potentially suitable as qubits for quantum information processing applications.[416] This assembly strategy therefore represents a step toward the development of multi-qubit quantum logic gates. Dendrimers, daisy chains, and poly[3]rotaxanes based on these inorganic-organic hybrids are described in **Sections 4.2.2.3, 4.2.3.2**, and **4.2.3.7**, respectively.

Main-Chain [n]Rotaxane Polymers

A significant portion of the literature on mechanomolecules is devoted to those involving threaded polymers, which can adopt either linear (main-chain) or branched (**Section 4.2.2**) topologies. Since there are approximately 1500 literature references associated with polyrotaxanes and polypseudorotaxanes, according to a keyword search in SciFinder, we are unable to review these compounds comprehensively, and refer the reader to a number of literature resources[116,118,354,417–425] on this topic. In this Section we highlight a number of threaded polymers based on various structural motifs and synthetic protocols. In particular, poly(pseudo)rotaxanes based on the threading of cyclodextrins,[426–428] cucurbiturils,



Scheme 4.25 The self-assembly and solid-state structures of Winpenny's inorganic-organic hybrid [5]rotaxanes,[415] assembled by metallosupramolecular dimerization of pyridine-terminated bis(dialkylammonium) semidumbbells threaded by inorganic $Cr_7NiF_8(O_2C^tBu)_{16}^-$ wheels. C–H protons are omitted for the sake of clarity.

endocyclic chelates, crown ethers,[429] and cyclophanes such as $CBPQT^{4+}$, calix[*n*]arenes, and pillar[*n*]arenes, are well investigated.

Statistically Threaded Polymers

Much of the pioneering research on statistical synthesis of poly(pseudo)rotaxanes (**Figure 4.57**) began in the mid-1980s, when Gibson[418,430,431] began to investigate the interpenetrative polymerization of various polyesters[432–435] polyamides,[432,436–438] and polyurethanes[437,439–444] as well as the polyolefins polyacrylonitrile[445] (PAN), polystyrene[446,447] (PS), poly(methacrylate)[448] (PMA) and poly(methyl methacrylate)[448] (PMMA) in melts with crown ethers. The first crown-threaded polyester was obtained[432] in 1987 by the polymerization of polydecamethylene sebacate (PC10S) from sebacoyl chloride and 1,10-decanediol in a melt with [36]crown-12 (36C12) in 3.4-fold excess. The ratio of threaded rings (*x*) to repeating monomer units (*n*) is a measure (**Table 4.1**) of the threading efficiency (*x*/*n*), which is 0.15 in this case. Other crown-threaded polyesters include those based on poly(tetramethylene sebacate)[433] (PC4S)

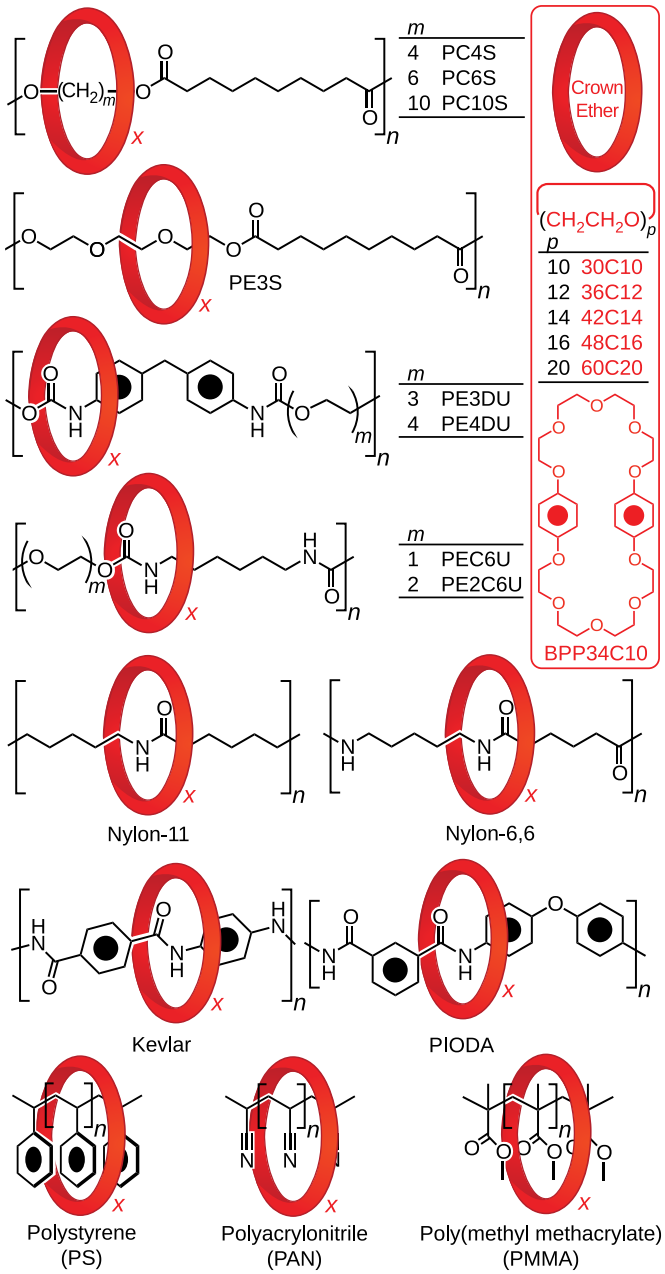


Figure 4.57 Examples of polypseudorotaxanes obtained by the statistical threading of crown ethers during the polymerization of polyesters,[116,432–434] polyurethanes,[437,440,441] polyamides,[432,438] polyaramides,[436,438] and polyolefins.[445–448]

and poly(triethylene glycol sebacate)[433] (PE3S). After detailed investigations on these polymerizations, Gibson concluded[435] that the threading efficiency is a function of ring size and reactant feed ratio, but independent of monomer length and temperature. These conclusions also apply to the self-threading polymerization[440,441] of polyurethanes, such as poly(tri(oxyethylene) diphenylmethylenediurethane)[441] (PE3DU) and poly(tetra(oxyethylene) diphenylmethylenediurethane)[440] (PE4DU), as well as the pseudorotaxanes of poly(ethylene hexamethylenediurethane) (PEC6U) poly(oxydiethylene hexamethylenediurethane) (PE2C6U) introduced by Beckham,[449] since their threading efficiencies also improve with increasing ring size. These results are consistent with Zilkha's model[450] for understanding statistical threading processes—see **Section 2.1**. Crown-threaded polyamides containing nylon[432,437,438] and poly(isophthalic oxydianiline)[436,438] (PIODA) backbones have also been obtained (**Figure 4.58**, **Table 4.1**) by similar protocols.

The mechanical bonds of polypseudorotaxanes lie in a fuzzy grey area—see **Section 3.1.1**—since the outer rings act as supramolecular stoppers for the inner ones. Although they have no covalent stoppers, deslipping of crown ethers from the polyamide backbones is very slow, and ring loss is not significant over repeated cycles of reprecipitation in water, ethyl acetate, and methanol—solvents in which free crown ethers dissolve while polyurethanes crash out. The resistance to deslipping can be explained in part by hydrogen-bonding[442] interactions between the NH donors of the polyurethane backbones and the crown ethers' oxygen atoms. These stabilizing [N–H···O] interactions may also

Table 4.1 Summary of threading efficiencies in the statistical synthesis of crown ether polypseudorotaxanes.

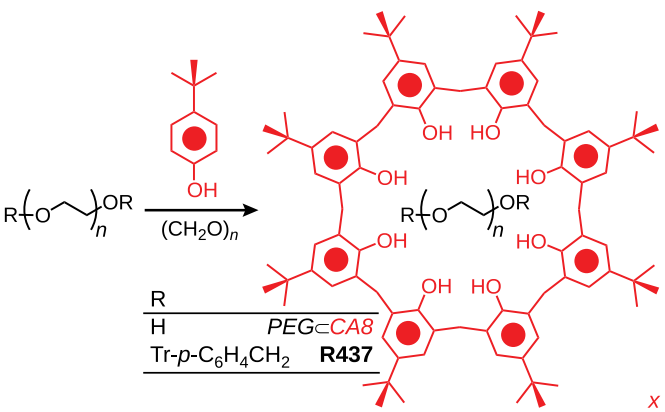
	Polymer	Crown Ether	Feed Ratio[a]	*x*/*n*	Ref.
Polyamides	PC4S	30C10	1.1	0.13	434
	PC4S	42C14	0.8	0.22	434
	PC4S	42C14	1.0	0.33	116
	PC4S	60C20	0.3	0.23	434
	PC4S	60C20	0.5	0.33	434
	PC4S	BPP34C10	1.2	0.03	434
	PC6S	42C14	1.0	0.32	116
	PC10S	36C12	3.4	0.15	432
	PC10S	42C14	1.0	0.31	433
	PC10S	42C14	1.5	0.34	433
	PC10S	42C14	2.0	0.44	433
	PC10S	42C14	4.0	0.46	433
	PE3S	30C10	0.55	0.19	434
	PE3S	60C20	0.55	0.42	434
	PE3S	BPP34C10	0.29	0.04	434
Polyurethanes	PE3DU	36C12	1.5	0.16	441
	PE3DU	42C14	1.5	0.29	441
	PE3DU	48C16	1.5	0.52	441
	PE3DU	60C20	1.5	0.87	441
	PE3DU	60C20	0.8	0.58	441
	PE3DU	60C20	0.6	0.34	441
	PE4DU	36C12	1.5	0.16	440
	PE4DU	42C14	1.5	0.29	437
	PE4DU	60C20	1.1	0.57	440
	PEC6U	30C10	0.5	0.02	449
	PE2C6U	36C12	0.1	0.15	449
Polyamides	Nylon-11	36C12			432
	Kevlar	30C10		0.36	436
	PIODA	30C10		0.07	436
	PIODA	60C20		0.2	436
Polyolefins	PAN	60C20	0.5	0.02	445
	PS	42C14	0.64	0.035	446,447
	PMMA	30C10	1.0	0.0039	448

[a]Feed Ratio = [crown ether] / [polymer].

explain why threading efficiencies are generally higher in the case of the polyurethanes compared to the polyesters. The rings' relative positions and dynamics with respect to the axle can be controlled[443] by disruption of the hydrogen bonds in polar solvents—see **Section 6.8.1**. Although deslipping is more significant in the case of polyester polyrotaxanes, which cannot engage in hydrogen-bonding interactions, the rings still depart the main chain very slowly, indicating that the random coiling of the polymer presents a considerable steric barrier to deslipping. The greater mobility of the chain ends relative to the middle may also drive rings toward the center of the main chain, like a button-on-a-string toy. Of course, dethreading can be prevented by sealing the mechanical bonds with covalent stoppers, either embedded[451–455] in the main chain—see **Section 4.2.3.6** for poly[2]rotaxanes—or capped[434] at the ends of the polymer dumbbells.

An earlier report by Lipatova[456] described the polymerization of polystyrene in the presence of the cyclic urethane, cyclobis(oxydiethylene hexamethyleneurethane) (CE2C6U), to obtain threaded polymers, finding that the number of mechanical bonds in the polymeric products increase in the presence of $ZnCl_2$, most likely on account of a templating effect of the *$ZnCl_2 \subset CE2C6U$* complexes. This conclusion follows from the observation that the molar ratio of threaded rings to polystyrene is 2:3 in the case of *$ZnCl_2 \subset CE2C4U$*, yet only 1:4 in the purely statistical threading-polymerization involving only CE24U.

Yamagishi[457] has obtained statistically threaded polypseudorotaxanes by the polycondensation (**Scheme 4.26**) of *para-tert*-butylphenol and paraformaldehyde in the presence of PEG threads of average molecular weight 1000, 3100, or 10000, yielding calix[8]arene (CA8) pseudorotaxanes *$PEG \subset (CA8)_x$* with threading efficiencies of $x/n = 0.04$, 0.02, and 0.01, respectively. Calix[4]arene (CA4) and calix[6]arene (CA6) are also formed in the reaction, but they are present in very low amounts in the polypseudorotaxanes isolated by chromatography on silica gel.



Scheme 4.26 Yamagishi's synthesis of calix[8]arene poly(pseudo)-rotaxanes by statistical clipping of *p*-^{t}Bu-C_6H_4OH and paraformaldehyde in the presence of PEG.[457]

While deslipping is slow from *$PEG \subset (CA8)_n$*, the CA8 rings can be extracted from the PEG backbones by heating dilute solutions of the threaded polymer in ethylene glycol at 180 °C. If the polycondensation is carried out in the presence of a trityl-functionalized PEG, the rings of the corresponding polyrotaxane **R437** do not escape so readily.

Whereas statistical threading is an inefficient approach to the synthesis of small-molecule [2]rotaxanes, the long molecular lengths of polymers substantially increase the likelihood of threading. The robustness of the statistical approach in a polymer regime is also noteworthy, encompassing all manner of step-growth, free radical, and anionic polymerizations. Not surprisingly, the properties of the polymers change after they become threaded by crown ethers, exhibiting phase transitions at lower temperatures than their parent polymers without mechanical bonds.

Cyclodextrin-Threaded Polymers

Cyclodextrin-based polyrotaxanes[426–428,458,459] represent the largest portion of main-chain polymers with mechanical bonds that have been reported in the literature. The prominent status of CDs in the world of polyrotaxanes can be attributed, not only to their low-cost commercial availability, but also to their promiscuity for recognizing an enormous variety of polymer threads in aqueous solutions, as well as in organic solvents when the hydroxyl groups of the CD rings are appropriately functionalized. As a means of constraint, we focus our attention in this subsection on CD-threaded polymers of particular historical importance, or which appear promising for potential applications on the basis of their novel properties.

Some of the most prevalent cyclodextrin-threaded polymer motifs are summarized in **Figure 4.58**. They include (i) polyethers, such as poly(ethylene glycol)[460] (PEG) and poly(propylene glycol)[461] (PPG) (ii) polyelectrolytes, such as poly(imino-oligomethylenes),[462–466] polyammonium ionenes,[463,464,467] polypyridinium salts,[468–470] and poly(ε-lysine),[471,472] and (iii) hydrophobic polymers, such as siloxanes,[473–477] polyesters,[478–485] polyolefins,[486–491] polyamides,[492–494] and π-conjugated polymers[423,495,496] (*vide infra*).

The seminal papers by Harada[460] and Wenz[462] in 1992, which described the formation of polyrotaxanes templated by the efficient threading of many α-CD rings onto polyethers and polyelectrolytes, respectively, marked the beginning of a period of remarkable growth in research productivity on CD polyrotaxanes. Poly(ethylene glycol)[460] has increasingly high affinity for α-CD as molecular weight increases,[497] while polypropylene glycol[461] and a number of other polyethers[498–501] readily thread the cavities of β- and γ-CD. The pioneering research in this area is summarized in **Section 2.3.1.1**. The *$PEG \subset \alpha$-CD* threading motifs[497,502–506] have remained a staple of polymer mechanostereochemistry on account of their low cost, convenient synthesis, highly tailorable presentation of functional groups, thermally-responsive properties[507–511]—e.g., see **Section 6.9.1.2**—as well as their

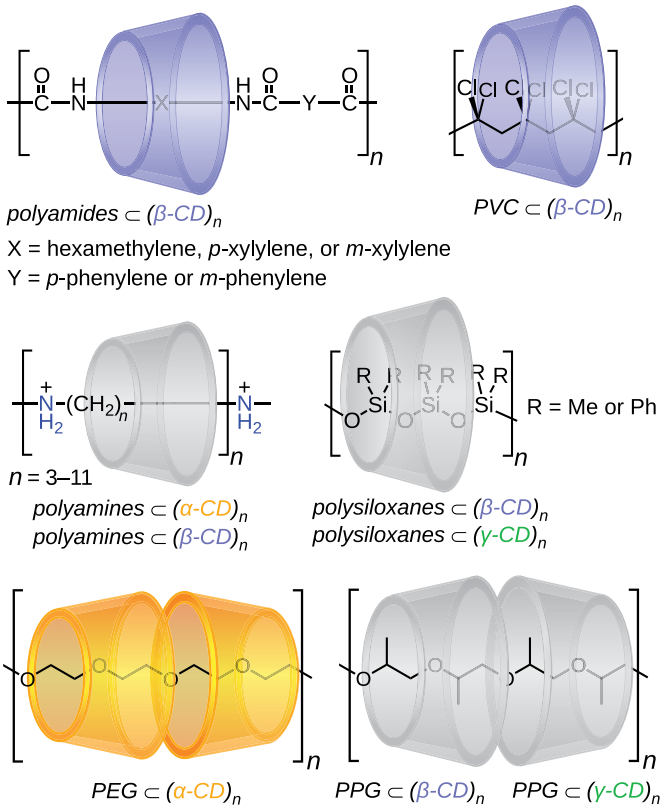


Figure 4.58 Selected seminal examples of cyclodextrin-threaded polymers based on polyamides,[492] poly(vinylidene chloride)[474–476] (PVC), polyamines,[462] polysiloxanes,[473] and polyethers, such as poly(ethylene glycol),[460,486,502] and poly(propylene glycol).[461]

biocompatibility. Consequently, these polyrotaxanes have received a considerable amount of research attention for their potential biomedical applications.[512–517] For example, see **Section 6.15.1.1** for a number of polyether-threaded cyclodextrins that have been employed in controlled-release applications.

The discoveries of cyclodextrin poly(pseudo)rotaxanes based on polyether and polyelectrolyte backbones was predated by a few CD-threaded polymers investigated in the 1970s and 1980s. In 1976, Ogata, Sanui, and Wada[492] obtained threaded polyamides by the reaction of diaminoalkanes with diacid dichlorides in the presence of β-CD. Maciejewski[473–476] also prepared β-CD-threaded polymers in the late 1970s by the aqueous condensation[473] of organosilicon monomers, as well as radical polymerization[474–476] of vinylidene chloride, either in DMF solutions containing β-CD or in the crystalline adducts with β-CD. Methylmethacrylate, acrylonitrile, allyl chloride, and styrene, by contrast, were not found to polymerize through the annulus of β-CD.

The CD rings often thread polymers in a channel-like *head-to-head/tail-to-tail* arrangment, since this orientation establishes the most optimal ring-to-ring hydrogen-bonding interactions. The *head-to-head/tail-to-tail* channel orientation is evident (**Figure 4.59**) in the X-ray crystal structures of α-CD-threaded hexaethylene glycol[518] (6EG) and β-CD-

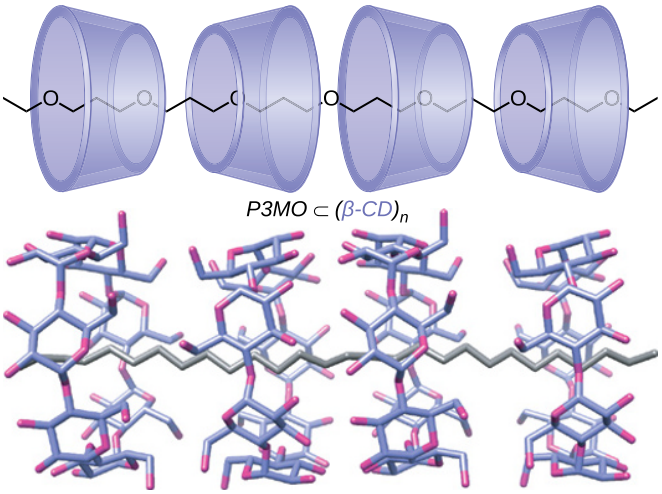


Figure 4.59 The solid-state superstructure[501] of *P3MO ⊂ (β-CD)n* illustrates the *head-to-head/tail-to-tail* threading orientation commonly observed in CD-polythreaded polymers. Hydrogen atoms and solvent molecules are omitted for the sake of clarity.

threaded PEG[519] and poly(trimethylene oxide)[501] (P3MO). See **Section 5.2.1** for a more detailed discussion of orientational isomerism in mechanomolecules. Harada[520] exploited this densely packed and well-ordered threading motif in the PEG-templated synthesis of polymer nanotubes comprising covalently linked α-CD rings. As in the case of the rigid-rod dialkylammonium/crown ether oligorotaxanes (*vide supra*), these ring-to-ring interactions also contribute to the rigidification of the polymer backbone. For example, Liu[521] observed rigid-rod structures in transmission electron microscopy (TEM) images (**Figure 4.60**) of the first CD-threaded

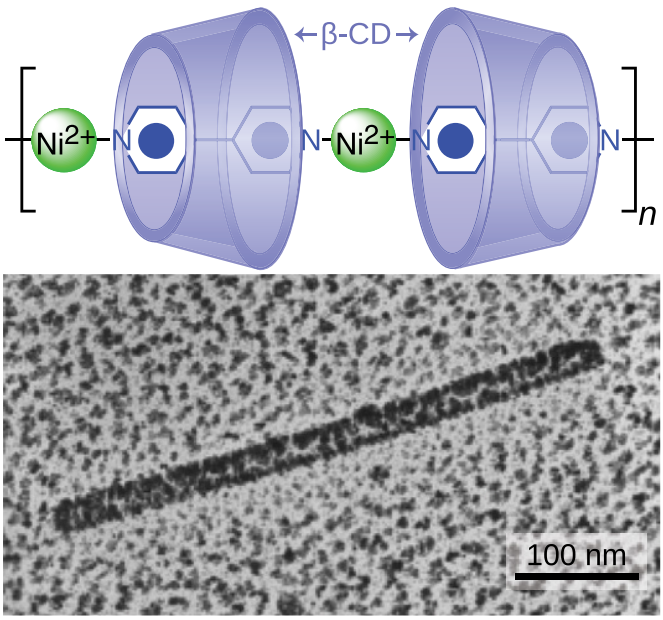
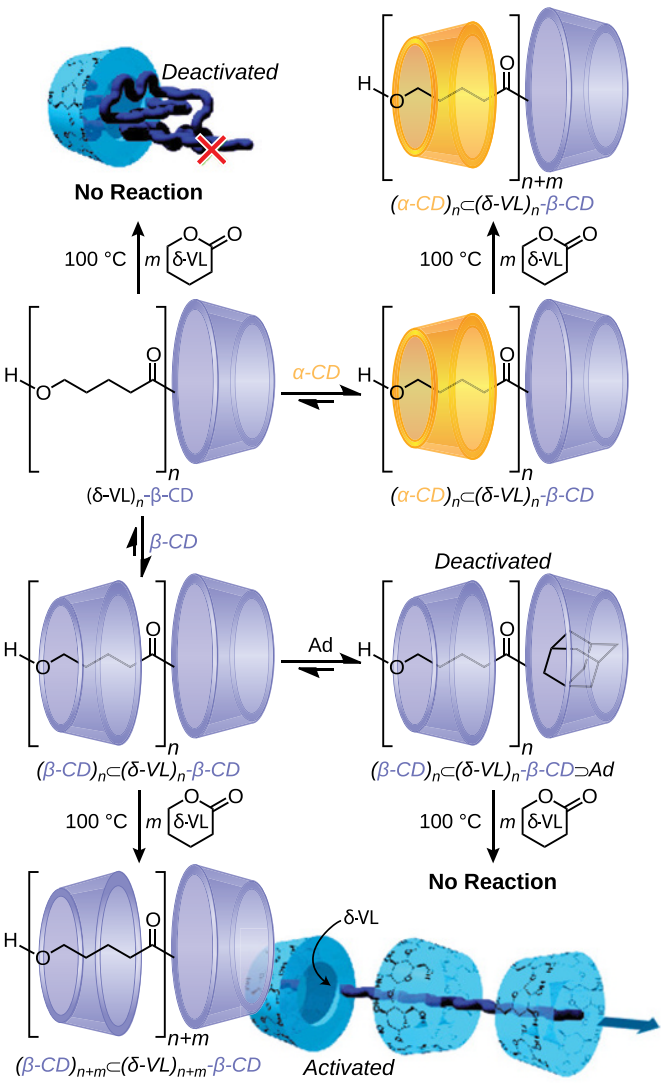


Figure 4.60 A structural representation and TEM image of the β-CD threaded metallosupramolecular polymer introduced by Liu. Data reproduced with permission from ref. 521 (copyright 2003 Wiley-VCH).

polyrotaxanes obtained by metallosupramolecular polymerization, which comprise β-CD-included 4,4´-bipyridine units linked by Ni^{II} centers. Single-molecule microscopy techniques[522] including atomic force microscopy[523,524] (AFM) and scanning tunneling microsopy[525–527] (STM) have also been employed to visualize the rigid-rod superstructures of channel-type polyrotaxanes.

Harada[528] has discovered a unique solvent-free polymerization (**Scheme 4.27**) of δ-valerolactone (δ-VL) driven by polypseudorotaxane formation. The β-CD endcap of the polyvalerolactone, $(\delta\text{-VL})_n$-β-CD, serves as an active site that promotes the insertion of δ-VL monomers into the ester linkage of its secondary face in a bulk melt at 100 °C. The backbone of $(\delta\text{-VL})_n$-β-CD extends by *m* units when it is threaded by α-CD or β-CD rings, where *m* is the number of insertions, yet no polymer extension occurs in the absence of threaded CDs. The crucial role of the threaded CDs in this polymerization is to maintain the catalytic activity of the β-CD endcap by preventing self-threading of the growing polymer chain. In other words, the polymer chain of $(\delta\text{-VL})_n$-β-CD blocks its own active site unless CDs are present to redirect its folding. The extensible axle can also be deactivated upon blocking the β-CD active site by including adamantane (Ad) in its binding pocket. Harada[529] has devised a similar protocol for polymerizing polypseudorotaxanes extending from the β-CD-immobilized surfaces of gold nanoparticles. Recognizing that only one CD ring adjacent to the catalytic endcap is necessary to achieve the chaperone effect, Harada has also designed an artificial molecular clamp[530] comprising a CD dimer that facilitates the same type of extensile polymerization.



Scheme 4.27 Threaded α-CD or β-CD rings act as molecular chaperones[528] that facilitate the β-CD-promoted insertion of δ-valerolactone (δ-VL) monomers into the polymer backbone of $(\delta\text{-VL})_n$-β-CD by directing its main chain away from the active site of the catalytic endcap.

The mechanical bonds of threaded cyclodextrins have been harnessed to enhance the optical, electrical, and luminescent properties of π-conjugated polymers.[423,495,496] The concept of "insulated molecular wires" (IMWs) was introduced by Anderson[531] in 1996 when he reported on the first rotaxanes possessing fully π-conjugated axles—see **Scheme 2.30** in **Section 2.3.1.4**. After the initial synthetic reports on conjugated polyrotaxanes by Anderson,[532,533] Anderson and Cacialli,[534–544] as well as Mróz,[545] have collaborated in investigating the optoelectronic properties of α-CD and β-CD polyrotaxanes with polyelectrolyte backbones derived (**Figure 4.61**) from polycarboxylated poly-*para*-phenylene (PPP),[534,535] polysulfonated poly(*para*-phenylene vinylene)[533] (PPV), poly(*para*-biphenylene vinylene) (PBV),[534–536,538,539,541,543] as well as poly(dicarboxyethylfluorene-*alt*-biphenylene)[534–537,542] (PFBP), poly(fluorene-*alt*-divinylphenylene)[544] (PFVP) and the corresponding methyl esters, Me_2PFBP and Me_2PFVP. These semiconducting polymer backbones can be threaded in aqueous solvents by α-CD or β-CD in aqueous solvents, or by perpropyl-β-cyclodextrin (PP-β-CD) or pertrihexylsilyl-β-cyclodextrin (THS-β-CD) in organic solvents. The mechanical bonds of these polyrotaxanes allow one to exercise control over the intrachain and interchain photophysics,[534,539,546] since the rings suppress intermolecular energy transfer by minimizing π–π stacking and H-aggregation between polymer backbones. The size of the counterions[538,541] and presence of other polymer additives[536] can also influence the optoelectronic properties of these polyrotaxanes in thin films. These parameters can be varied to tune and enhance solid-state luminescence. For example, the organic-soluble green/yellow-emitting polyrotaxanes **PP-β-CD-Me_2PFVP** and **THS-β-CD-Me_2PFBP** can be blended with blue-emitting polymers to generate films exhibiting tunable and white-emitting electroluminescence,[542,544] suggesting that these IMW materials may hold promise for electroluminescent display technologies, LEDs, and so on.

In addition to the conjugated cyclodextrin polyrotaxanes of Anderson and collaborators, a number of groups have investigated β-CD threaded π-conjugated polymers (**Figure 4.62**) as IMWs. Ito and Shimomura[523,525,547] have investigated the insulating effects of β-CD rings threaded

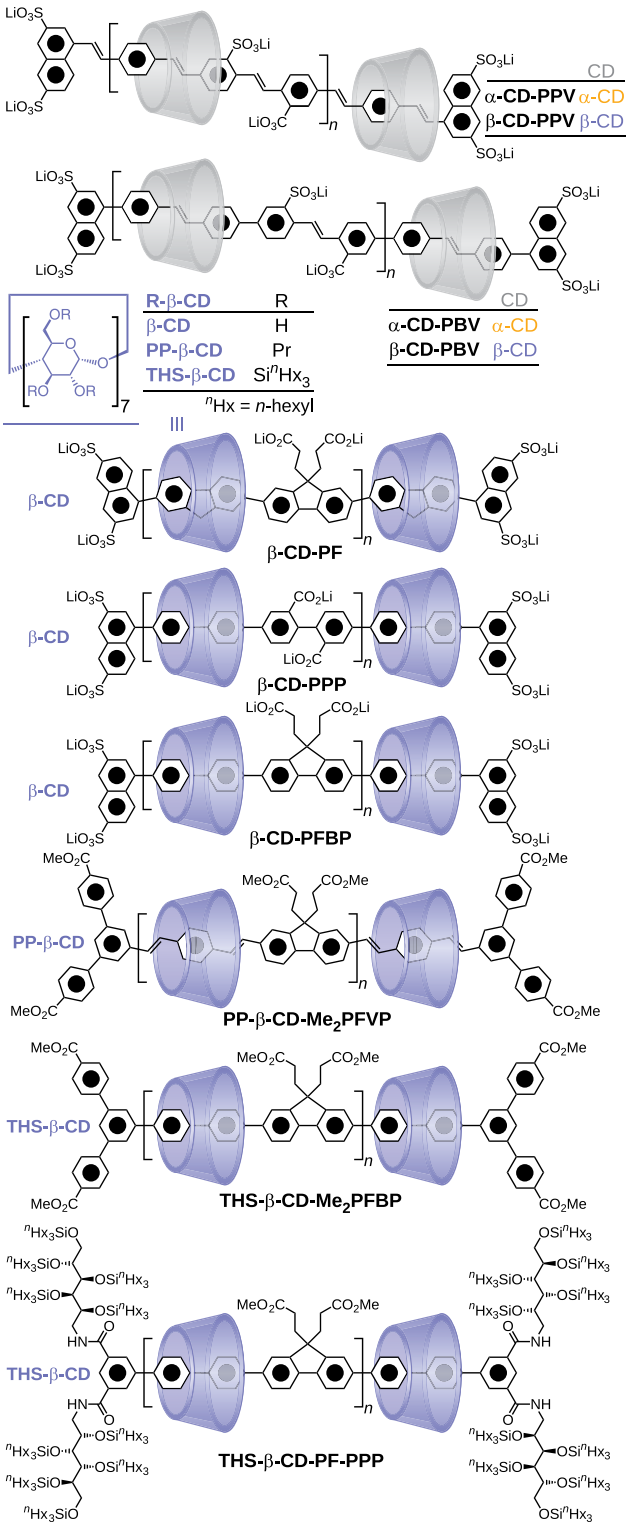


Figure 4.61 Cyclodextrin-threaded π-conjugated polyelectrolytes investigated by Anderson and Cacialli as insulated molecular wires (IMWs).[532–539,541–544]

on polyaniline (PANI) backbones, finding that they confine the backbone to a rigid-rod conformation while preventing it from being chemically oxidized. Farcas[548] has obtained conjugated polyazomethine polyrotaxanes by the imine polycondensation of 1,4-phenylenediamine and 3,6-diformyl-9-butylcarbazole in the presence of β-CD, while Geckeler[549] has done likewise with terephthalaldehyde as the diformylated coupling partner. Liu[527] has also prepared polyazomethine polyrotaxanes from *terephthalaldehyde⊂β-CD* and *ortho-toluidine⊂β-CD* precursors. Hadziioannou[524] has synthesized anthracene-stoppered polythiophene (PT) and polyfluorene (PF) polymers threaded by insulating β-CD rings. Yamaguchi and Yamamoto[550] have also prepared polythiophenes and poly(3-methylthiophene) (P3MT) threads encircled by β-CD. Shinohara[551] has constructed α-CD-threaded poly(phenylene ethynylene)/poly(anthrylene ethynylene) copolymers and observed them directly by single-molecule fluorescence techniques, finding evidence for long-range energy transfer interactions in the corresponding networks of micron-length fibers. Cyclodextrin-threaded single-walled carbon nanotubes[552] (SWNTs) represent another class of IMWs—see **Scheme 2.11** in **Section 2.3.1.1**.

The hydroxyl groups of the cyclodextrins' pyranosyl rings serve as excellent handles for further functionalization. Kidowaki and Ito[553] have appended mesogenic 6-(4′-cyanobiphenyl-4′′-yloxy)hexyl side chains to the α-CD rings of an adamantine-stoppered polyrotaxane with PEG35000, obtaining a novel liquid crystalline material with slide-ring mesogens. Gao[554] has employed PEG/α-CD polyrotaxanes as templates for the growth of platinum

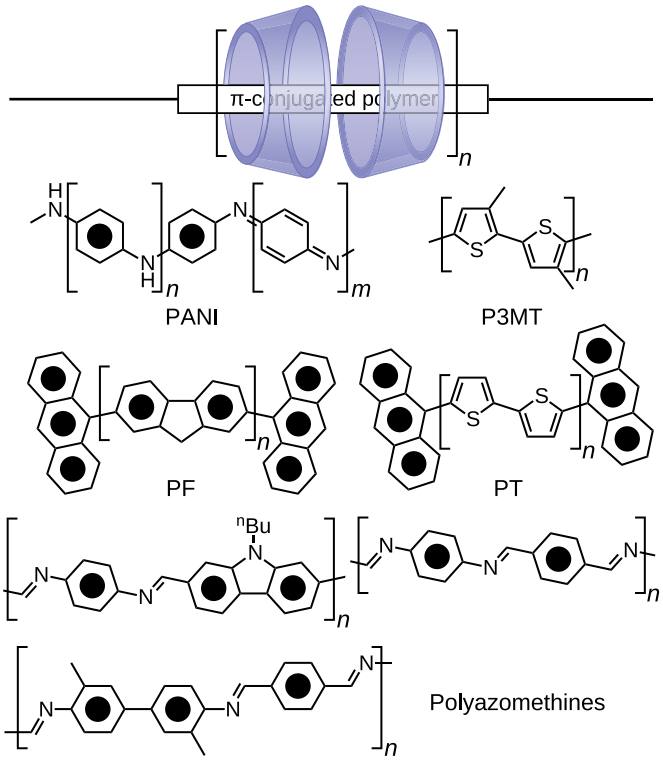


Figure 4.62 More π-conjugated polymer backbones utilized in β-CD-threaded IMWs.

nanowires around their surfaces. Wenz[555] demonstrated that PEG⊂(α-CD)$_n$ polyrotaxanes can serve as scaffolds for brush polymers by employing their CD rings as macroinitiators in the atom transfer radical polymerization (ATRP) of methylmethacrylate, obtaining cylindrical polymer brushes which respond to relatively weak mechanical forces with a rupture in the main chain, releasing the CD-polymer beads into solution. Cacialli, Beljonne, Albinsson, and Anderson[556] have installed triarylamine hole-transport groups as coaxial jackets surrounding the β-CD insulated PFBP polymer core in order to study the photophysics of excitation energy transfer (EET) and photoinduced electron transfer (PET). CD polyrotaxanes may therefore be considered as candidates for multi-chromophore arrays relevant to light harvesting applications.

Cucurbituril-Threaded Polymers

Kim[557–565] has pioneered the use of CB6-threaded ligands in the crystal growth of rotaxanated coordination polymers, including those (**Figure 4.63**) possessing one-dimensional backbones. Ligands employed in the assembly of these coordination polymers include *N*,*N*′-bis-(3-pyridylmethyl)-1,4-butanediammonium (C4N3^{2+}). *N*,*N*′-bis-(4-pyridylmethyl)-1,4-butanediammonium (C4N4^{2+}), and *N*,*N*′-bis(3-pyridylmethyl)-1,5-pentanediammonium (C5N3^{2+}) as their nitrate salts. Some of these ligands were also employed to prepare Kim's metallosupramolecular beaded necklaces—see **Figure 4.15** in **Section 4.1.2.2**. The C4N3^{2+} ligand can be co-crystallized[560] with Ni(NO$_3$)$_2$ or Co(NO$_3$)$_2$ to afford the isostructural 1D coordination polymers, **R438a** and **R438b**, respectively, in which the backbone adopts a zig-zag geometry defined by the *cis*-coordination modes of the threaded ligands conjoined by each octahedral metal center. The same Ni^{II} and Co^{II} reagents afford[560] 1D polyrotaxanes **R439a** and **R439b** with isostructural "square-wave" backbone geometries when combined with the C4N4^{2+} ligand, which instead adopts an axial/*trans*-coordination mode. The remaining open coordination sites of the metal centers are occupied by water molecules. When C4N4^{2+} is co-crystallized[557] with Cu(NO$_3$)$_2$, the corresponding 1D polyrotaxane **R439c** adopts a zig-zag geometry involving the *cis*-coordination of the ligands to two of the basal sites of the square pyramidal Cu(H$_2$O)$_3^{2+}$ joints. A much more linear polyrotaxane coordination polymer **R439d** is obtained[558] from *C4N4*$^{2+}$⊂*CB6* and AgNO$_3$, owing to the linear nature of both the ligand and the ML$_2$ coordination geometry of Ag^{I}. Combining[559] AgNO$_3$ instead with *C5N3*$^{2+}$⊂*CB6*, the corresponding 1D polyrotaxane **R440a** adopts a helical (co)-conformation in the crystal with a pitch of 17.9 Å. Another helical metallosupramolecular polyrotaxane (**R440b**) can be obtained[560] from the same ligand and Cd(NO$_3$)$_2$, yet in this case a much longer helical pitch of ca. 50.5 Å is observed on account of the two different types of Cd^{II} centers, which adopt octahedral and pentagonal bipyramidal geometries involving threaded ligands in *cis*- and *trans*-apical coordination modes, respectively, in alternating fashion along the main-chain backbone. These CB6-threaded ligands have also been employed in the assembly of 2D[558,560,561] and 3D[562] polyrotaxane networks—see **Section 4.2.3.8**.

A number of other groups have recently expanded upon Kim's investigations into this class of polymers. Chen[566,567] has crystallized 1D polyrotaxanes derived from bis(pyridyl) ligands such as *N*,*N*′-bis(3-pyridylmethyl)-1,6-hexanediammonium (C6N3^{2+}), *N*,*N*′-bis(4-pyridylmethyl)-1,6-hexanediammonium (C6N4^{2+}), and *N*,*N*′-bis(3-pyridylmethyl)-*para*-xylylenediammonium (XyN3^{2+}). Xue and Wei[568] and Zhang[569] have employed the C4N3^{2+}, C4N4^{2+}, and C6N3^{2+} ligands in the crystallization of 1D polyrotaxanes threaded by tetramethylated CB6 (Me$_4$CB6) rings. Xue and Liu[570] have also assembled helically chiral 1D polyrotaxanes derived from Me$_4$CB6 and *N*,*N*′-bis(2-pyridylmethyl)-1,6-hexanediaminium (C6N2^{2+}).

Chai and Shi[571] have employed uranyl (UO_2^{2+}) complexes as the coordination centers for CB6-threaded coordination polymers. For example (**Scheme 4.28**), the ligand *N*,*N*′-bis(3-cyanophenyl)butanediammonium (C4CN3^{2+}), which assembles with CB6 into the pseudorotaxane *C4CN3*$^{2+}$⊂*CB6*, crystallizes with UO$_2$(NO$_3$)$_2$ under hydrothermal conditions into the 1D zig-zag polyrotaxane[571] **R441**. The cyano groups of the ligand hydrolyze *in situ* to the corresponding carboxylic acids, which *trans*-coordinate to the basal positions of the pentagonal bipyramidal uranyl centers in both monodentate (η^1) and bidentate (η^2) coordination modes. The open two basal sites are occupied by water molecules, while the apical sites of the U^{VI} center carry the oxo groups of the UO_2^{2+} cation. This polymer represents the first example of an actinide-based coordination polyrotaxane. The same group has assembled CB6-threaded poly[2]rotaxanes[572] and 2D polyrotaxanes[573] by the crystallization of similar ligands with tetranuclear and dinuclear uranyl SBUs, respectively.

A number of all-organic CB6 poly(pseudo)rotaxanes are summarized in **Scheme 4.29** and **Figure 4.64**. Buschmann[574–576] has prepared (**Scheme 4.29**) CB6-threaded polyamides by reacting *1,6-hexanediammonium*⊂*CB6* pseudorotaxanes with various diacid dichlorides, finding that up to 50% of the monomer units retain CB6 beads in the final polypseudorotaxanes. Buschmann[577] has also claimed that the CB6 ring can bind poly(ethylene glycol) chains with stability constants of up to 1500 M^{-1} at 25 °C in 50% aqueous formic acid. Tuncel and Steinke[578] have assembled (**Scheme 4.29**) polypseudorotaxanes by threading CB6 rings onto poly(iminohexamethylene) (PIH) threads. Tuncel[579–581] has also investigated polymers obtained by "catalytic self-threading", which we refer to as the cucurbit[6]uril-promoted azide-alkyne cycloaddition (CB6AAC) dumbbell capture method—see **Section 2.3.1.2**. Although attempts[580,581] to synthesize main-chain [*n*]rotaxane polymers were unsuccessful on account of repulsive interactions between threaded and catalytic CB6 rings, these repulsive interactions could be blocked with stoppers, leading to the successful formation of poly[2]rotaxanes—see **Section 4.2.3.6**.

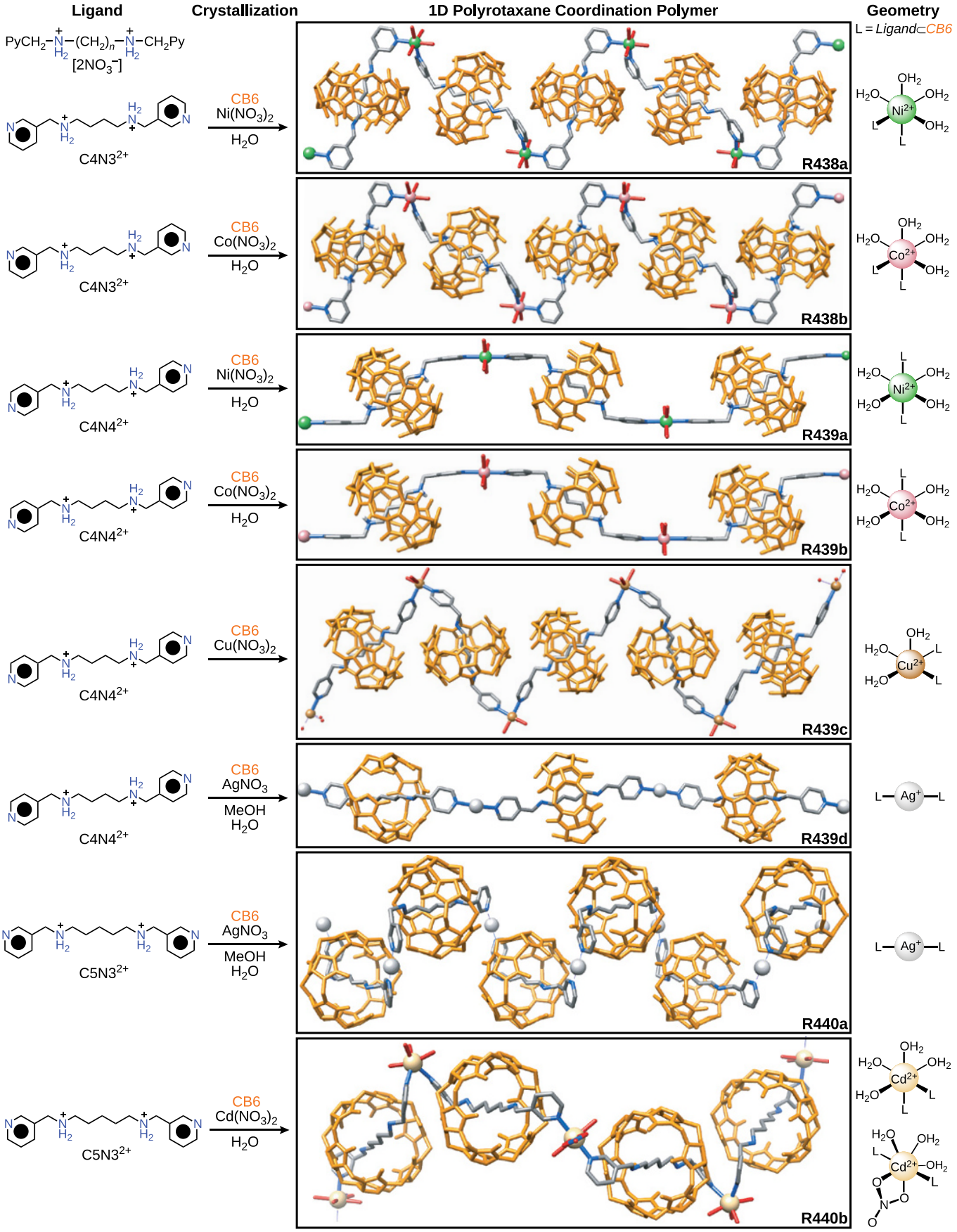
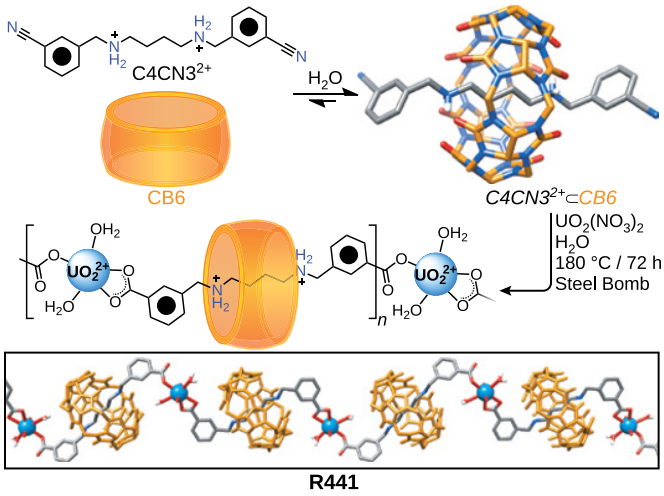


Figure 4.63 Kim's one-dimensional polyrotaxanes comprising CB6-threaded coordination polymers.[557–560] Solvent molecules, hydrogen atoms, and NO_3^- counterions are omitted for the sake of clarity.



Scheme 4.28 The hydrothermal synthesis of the actinide 1D polyrotaxane **R441** based on the CB6-threaded ligand *CB6⊂C4CN3*$^{2+}$ and uranyl complexes.[571] Tubular representations of the solid-state superstructures are illustrated with solvent molecules, hydrogen atoms, and NO_3^- counterions omitted for the sake of clarity.

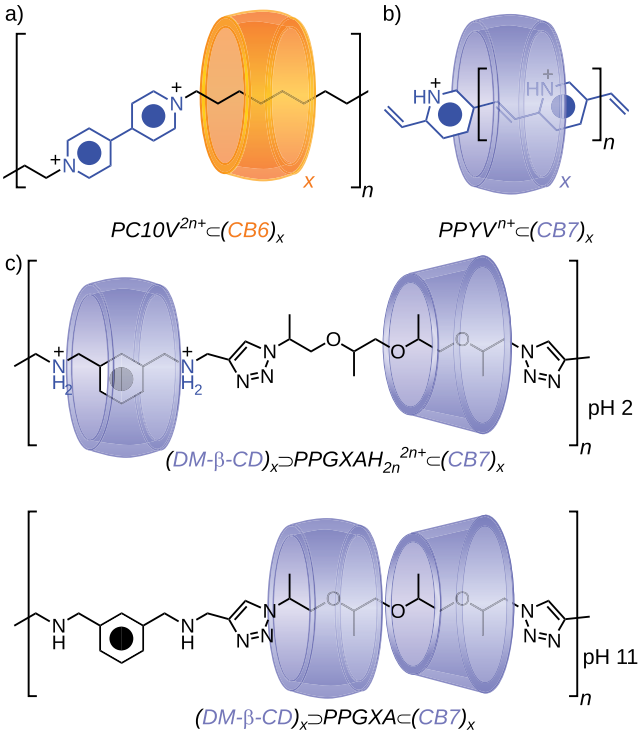
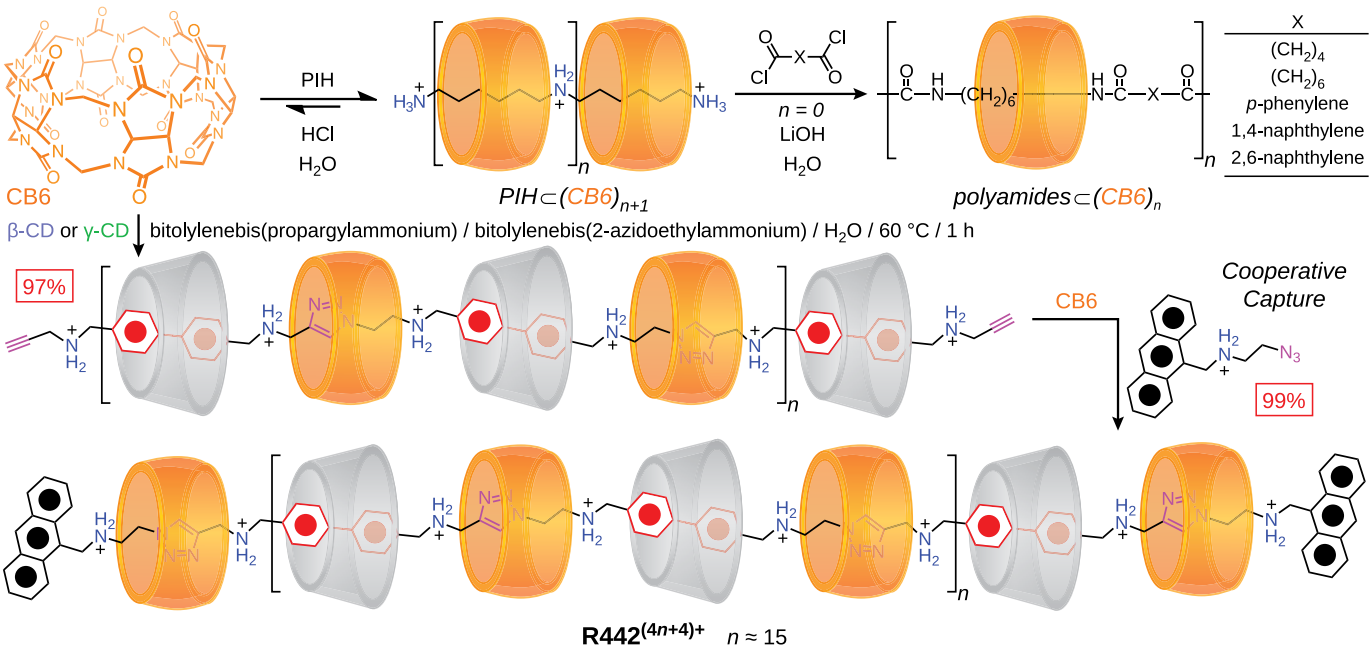


Figure 4.64 Polycationic threads encapsulated by (a) CB6,[582] (b) CB7.[583] and (c) both CB7 and DM-β-CD.[584] Neutralization of the dialkylammonium of the latter polymer at pH 11 leads to a translocation of the CB7 rings with respect to the thread.

On the other hand, main-chain [*n*]rotaxanes have been obtained[410] by a cyclodextrin-assisted, near-quantitative cooperative capture[414] approach—see **Section 2.3.1.3**—providing (**Scheme 4.29**) high molecular weight polymers **R442**$^{(4n+4)+}$, where *n* is the number of repeating units (average ca. 15), corresponding to more than five dozen threaded rings.

Kim[582] has obtained polypseudorotaxanes by allowing CB6 to encapsulate (**Figure 4.64a**) the hydrophobic segments of poly(decamethylene viologen) (PC10V^{2n+}) at ring-to-monomer ratios of 0.1 to 1.0. Evans and Swager[583] have recently reported that CB7 rings can be threaded (**Figure 4.64b**) onto the backbone of a poly(pyridinium



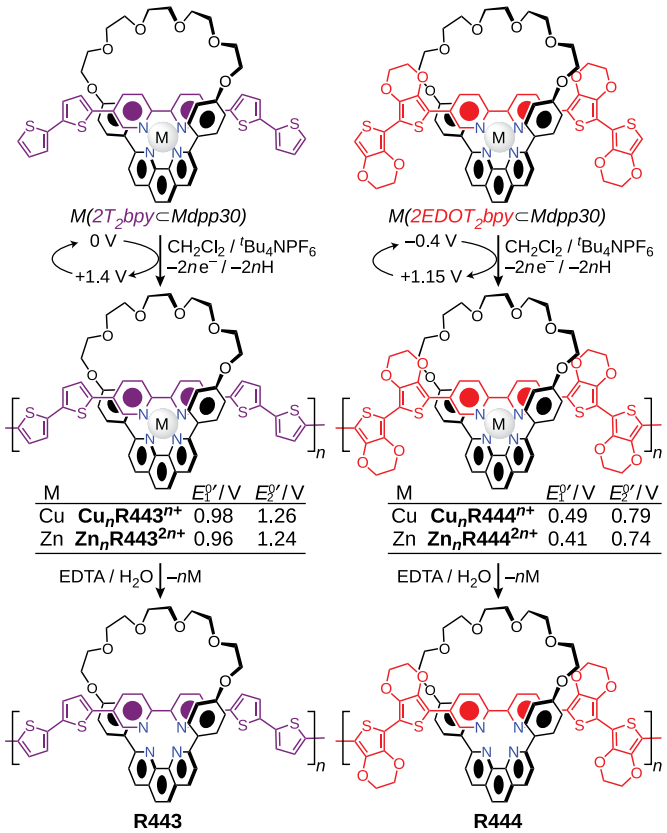
Scheme 4.29 The self-assembly (top) of CB6-threaded polypseudorotaxanes, either by threading[578] of poly(iminohexamethylene) (PIH) or by polymerization[574,575] of $H_3N(CH_2)_6NH_3^{2+}⊂CB6$ pseudorotaxanes to the corresponding inclusion polyamides, as well as the synthesis (bottom) of polyrotaxanes possessing alternating CB6 and cyclodextrin rings by cooperative capture.[410]

vinylene) (PPYV^{n+}) polyelectrolyte in acidic aqueous solutions. In a collaboration between Kim and Yui,[584] CB7 and heptakis(2,6-*O*-dimethyl)-β-cyclodextrin (DM-β-CD) were both threaded (**Figure 4.64c**) onto the polymer PPGXAH$_{2n}^{2n+}$, derived from click-coupled bis(azido)propylene glycol 400 and α,α´-*m*-xylylenebis(propargylamine). While the stability of the polypseudorotaxane, which is enhanced by DM-β-CD, is maintained over a wide pH rnage, the CB7 ring was found to translate between the xylylene and the PPG portions of the polymer axle at low and high pH, respectively. The pH-driven movement of other mechanically interlocked rings is discussed in **Section 6.3**.

Polymers Threaded by Endocyclic Chelates

Swager[585–587] has introduced and investigated a number of π-conjugated polyrotaxanes based on transition metal templation. In 1996, the first conducting polymetallorotaxanes, **Cu$_n$R443^{n+}** and **Zn$_n$R443^{2n+}**, were prepared[585] by the oxidative electropolymerization (**Scheme 4.30**) of pseudorotaxanes derived from Sauvage's macrocyclic ligand Mdpp30, a bidentate 4,4´-bis(bithiophenyl)-2,2´-bipyridine (2T$_2$bpy) axle, and either Cu^{I} or Zn^{II} templates. The polymetallorotaxanes are obtained as thin films by anodic electrochemical deposition[K] on transparent conducting oxide-coated glass while cycling between potentials of 0 and +1.4 V in CH_2Cl_2 with 0.1 M $^tBu_4NPF_6$ supporting electrolyte. Subsequent investigations[586] involved the homologues **Cu$_n$R443^{n+}** and **Zn$_n$R443^{2n+}** based on the ethylenedioxythiophene (EDOT) modified backbone of ligand 2EDOT$_2$bpy, which requires a lower oxidative potential window (–0.4 to +1.15 V) for electropolymerization. Homologous polymetallorotaxanes could not be obtained from bipyridine axles appended with single EDOT groups. The metal templates can be removed reversibly to obtain **R443** and **R443** by washing the films with aqueous solutions of ethylenediamine—a process which is accompanied by significant changes in UV/Vis absorption spectra of the films, which range in color from yellow to red to purple. The films behave as redox conductors, meaning that electrons transfer rapidly between local redox sites. While both Cu^{I}- and Zn^{II}-metallated polyrotaxanes exhibit similar formal first ($E_1^{0\prime}$) and second ($E_2^{0\prime}$) oxidation potentials vs. Ag wire, the much lower resistance (3.2×10^4 Ω) of **Cu$_n$R443^{n+}** films compared to those of **R443** (4.0×10^{10} Ω) and **Zn$_n$R444^{n+}** (7.0×10^9 Ω) indicates that copper is responsible for a 10^6-fold enhancement in conductivity, since its window of electroactivity overlaps with that of the conjugated polymer. The Cu^{I} conductivity enhancement is only 10^2-fold in the case of **Cu$_n$R443^{n+}**, where the main chain's redox potentials lie further away from the Cu^{I}/Cu^{II} redox couple. A number of similarly inspired conducting polymetallorotaxanes derived from bis(bithiophenyl)phenanthroline axles have been investigated by Sauvage[588–592] and his collaborators.[593,594] The ion-sensitive spectroscopic and electrochemical properties of these polyrotaxane films render them viable materials for potential sensing applications.

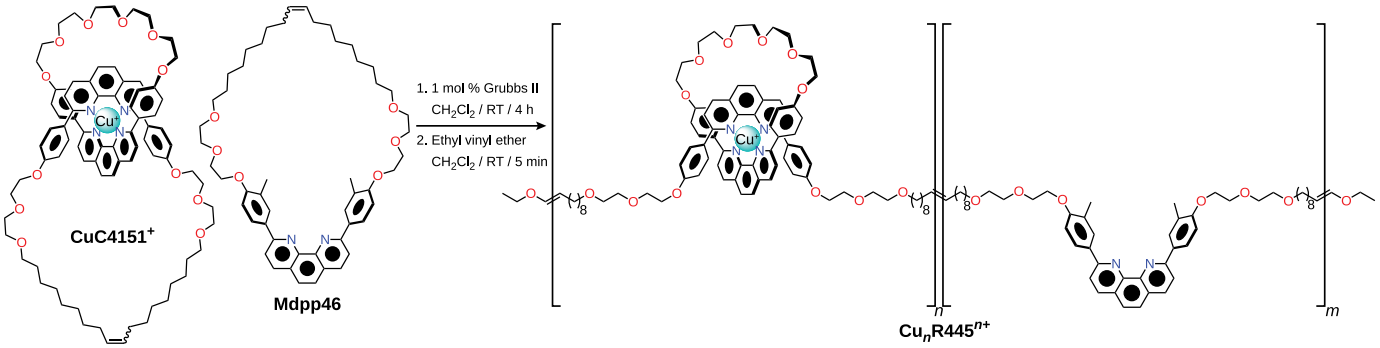
Mayer[595] has conceived of a powerful strategy for controlling (**Table 4.2**) the threading ratios on the backbone of the polymetallopseudorotaxanes **Cu$_n$R445^{n+}**, where *n* is the number of endocyclic chelates encircling the polymer backbone. The strategy involves the Grubbs II-catalyzed ring-opening metathesis (co)polymerization of catenated (**CuC4151$^+$**) and macrocyclic (Mdpp46) monomers based on Sauvage's dpp ligand motif. Analysis of the polymeric products revealed that the percent of backbone ligands encircled by endocyclic chelates closely reflects the feed ratio of the two reactants. It was also possible to calculate the average block size (consecutive rings) as a function of the threading ratios. The rings can also be liberated from the polymer upon removal of the Cu$^+$ templates by demetalation with KCN. Ultimately, this strategy allows one to define precisely the average number of rings on a polymer thread simply by selecting the appropriate feed ratio at the outset of the polymerization.



Scheme 4.30 Swager's syntheses[585,586] of thin-film polymetallorotaxanes by anodic electrochemical deposition, as well as their demetalation to the corresponding polyrotaxanes.

[K] Swager has applied the same type of protocol to the synthises of the side-chain donor-acceptor poly[2]catenane **C4142^{4n+}**—see **Figure 4.49**—as well as a triple-stranded polybis(polyrotaxane), which is described in **Section 4.2.3.4**.

Table 4.2 Mayer's synthesis of polymetallopseudorotaxanes by ring-opening metathesis polymerization, in which the ratio of threaded to unthreaded monomers is controlled by the feed ratio of catenated and macrocyclic reactants.[595]



	Feed Ratio CuC4148$^+$: Mdpp46	Yield %	M_n kDa	DP	PDI	% Sites Threaded	Consecutive Rings
L445	0 : 100	-	32	39	1.5	0	0
Cu_2R445^{2+}	10 : 90	86	22	25	1.4	8.7±5.5	1.1±0.8
Cu_7R445^{7+}	25 : 75	91	28	28	1.7	24.3±4.5	1.3±0.3
$Cu_{19}R445^{19+}$	50 : 50	89	43	38	1.7	49.0±3.1	2.0±0.2
$Cu_{31}R445^{31+}$	75 : 25	87	51	40	1.7	77.0±4.6	4.3±1.1
$Cu_{56}R445^{56+}$	90 : 10	86	83	61	1.6	91.4±5.5	12±8
$Cu_{77}R445^{77+}$	100 : 0	-	110	77	2.0	100	77±2

Crown Ether-Threaded Polymers

Aside from the statistically threaded polyethers introduced by Gibson[418,430,431] (*vide supra*), most of the main-chain [*n*] rotaxanes possessing crown ether rings have relied on [N^+–H···O] hydrogen-bonding interactions involving the –NH_2^+– recognition units of poly(imino-oligomethylene) polymers as a means of templation. A few main-chain [*n*]rotaxane poymers of this type are illustrated in **Figure 4.65**. Grubbs[596] has employed olefin metathesis polymerization of crown-threaded dienes to prepare the polyrotaxanes **R446aH$_n^{n+}$** and **R446bH$_n^{n+}$**. Using ion-mobility mass spectrometry, Scrivens[597] has determined that this polymer remains linear-shaped as its molecular weight increases. The polyrotaxanes **R447H$_n^{n+}$** and **R448H$_n^{n+}$** were prepared in the laboratories of Takata[598] taking polymerization-followed-by-threading and threading-followed-by-polymerization approaches, respectively, to the assembly of their polypseudorotaxane precursors before stoppering them with bulky isocyanates. Recently, Takata[599] has found that the crystallinity of polyesters threaded by only one DB24C8 ring depends not only on the length of the main chain, but also on the mobility of the ring, which can be increased by acylation (**Section 6.7.1**) of a dialkylammonium recognition unit.

The other main class of poly(pseudo)rotaxanes incorporating crown ether rings are based on π-donor/π-acceptor (**Section 2.3.3**) template motifs. Crown ethers containing π-electron rich recognition units, such as the HQ and DNP donors of BPP34C10 and DN38C10, respectively, can recognize π-accepting units of electron-poor polymers, such as polyviologens. Gibson[600,601] investigated (**Figure 4.66**) the self-assembly of BPP34C10 rings and urethane-linked polyviologen ionenes, finding that they can be threaded with near-quantitative efficiencies on account of the strong donor-acceptor templating interactions. The ionic conductivities[602] of these threaded viologens are higher than the parent threads, most likely because they reduce ion-pairing interactions of the viologen recognition units, thus increasing the mobility of the anions. The polypseudorotaxanes can be converted to polyrotaxanes by coupling their reactive isocyanate-functionalized termini with trityl-derived alcohols. When the occupancy of the viologen units of the polymer backbones is not saturated, the BPP34C10 rings can

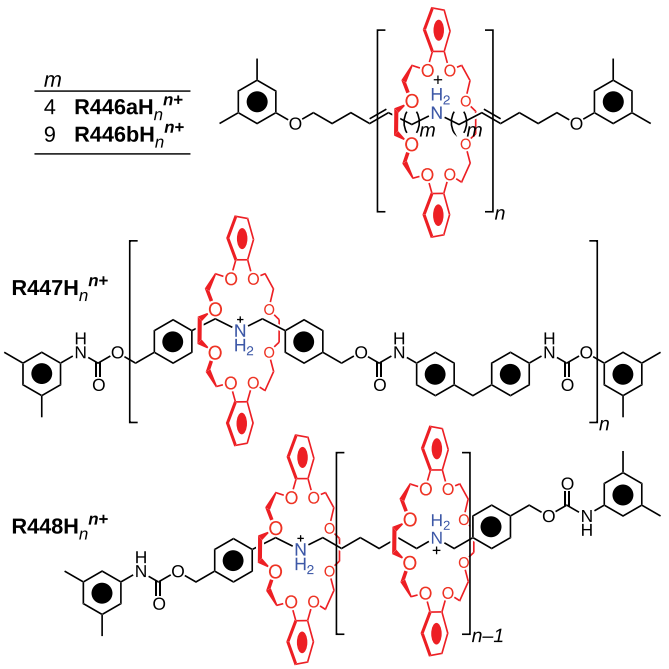


Figure 4.65 Main-chain [*n*]rotaxane poiymers based on *dialkylammonium⊂crown ether* templates.[596,598]

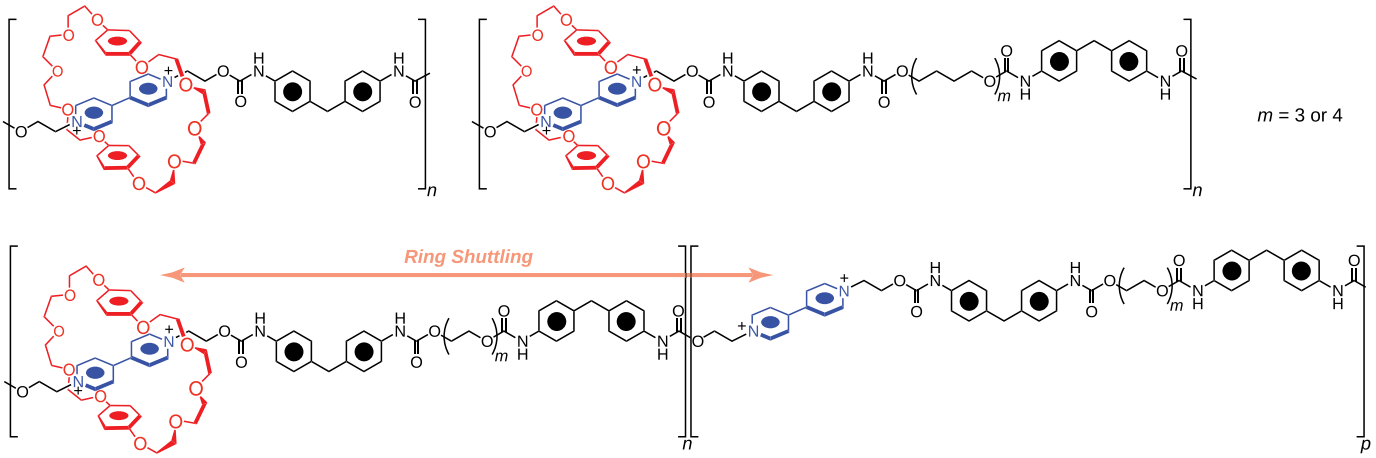


Figure 4.66 Examples of the backbones of BPP34C10-threaded π-donor/π-acceptor polypseudorotaxanes and polyrotaxanes introduced by Gibson.[600–602]

shuttle[601] back and forth between the recognition units. While [2]rotaxane molecular shuttles are well-known—see **Section 5.1.1**—*polymeric* molecular shuttles such as these remain few and far between. A comparison of the shuttling kinetics in monomeric and polymeric homologues of the same molecular shuttle would be a worthy future endeavor for understanding the interplay of macromolecular and mechanostereochemical phenomena.

Cyclophane-Threaded Polymers

The π-donor/π-acceptor recognition system based on the π-accepting tetracationic cyclophane, $CBPQT^{4+}$, has been utilized in the design (**Figure 4.67a**) of a number of mechanically bonded macromolecules. Parsons[603,604] first introduced a multistable polypseudorotaxane derived from a 1:1 mixture of a tetraethylene glycol-based polyether containing alternating HQ and DNP recognition units (PE4HQNP) and $CBPQT^{4+}$, where approximately 60% of the rings are threaded at room temperature in $(CD_3)_2SO$. It was with $PE4HQNP \subset CBPQT^{4+}$ that the concept of "molecular queuing" was first demonstrated—i.e, the rings in the middle of the polymer exchange into solution much more slowly than the rings near the ends of the chain. Hodge[605,606] has assembled a series of D-A polypseudorotaxanes in which $CBPQT^{4+}$ encapsulates polymer backbones based on a number of different polyethers and polyesters. Gibson[607] and Chujo[608] have investigated the threading (not illustrated) of $CBPQT^{4+}$ rings onto polyurethane and poly(dithiafulvene) backbones, respectively.

The threading efficiencies (**Figure 4.67b**) are highly sensitive to the length and constitution of the linkers. Whereas the polyethers plateau at threading efficiencies in the range of 40–70% with an excess of $CBPQT^{4+}$, up to 94% of the π-donors could be occupied by $CBPQT^{4+}$ in the case of the poly(oxalic ester) PE2HQO. Longer linkers exhibit higher threading efficiencies than shorter ones of the same kind. For example, comparing the polyesters based on hydroquinone diacetate (HQA), the proportion of theaded rings in the triethylene glycol bridged PE3HQA is amost 150% greater than that of the diethylene glycol-bridged PE2HQA with two equiv of $CBPQT^{4+}$. In the case (**Figure 4.67c**) of the pseudorotaxane $PE3HQ \subset (CBPQT^{4+})_x$, the four different environments—free, alongside, between, and threaded—of the HQ recognition units were determined across a range of feed ratios. The polymers that reach threading efficiencies near 50% are most likely prone to adopting folded superstructures in which unoccupied recognition units sandwich in between $CBPQT^{4+}$ rings in order to extend the stabilizing donor-acceptor π–π stacking interactions in one dimension. This serpentine folding of the polymer backbone has been observed[393] in the solid-state superstructure (**Figure 4.67d**) of the $PE4NP \subset (CBPQT^{4+})_x$ polypseudorotaxane,[L] Smaller oligorotaxanes have been found to adopt similar secondary structures both in solution[390] and in the solid-state.[389] This type of folding has also been invoked[394] to explain the unusual properties of the polyrotaxanes **[*x*]R449**$^{4x+}$, obtained (**Table 4.3**) by CuAAC stoppering of the corresponding azide-terminated polypseudorotaxanes. Despite their much higher molecular weights (M_n), the polyrotaxanes are apparently smaller than their parent poly(triazole–naphthalene) threads (**PTNP*n*(N$_3$)$_2$**), since they exhibit greater retention volumes by gel permeation chromatography (GPC). This surprising result was further supported by AFM experiments, which showed that the polyrotaxanes are shorter in length than the parent threads when deposited on highly ordered pyrolytic graphite.

[L] The solid-state superstructure of $PE4NP \subset (CBPQT^{4+})_x$ was determined by co-crystallization of $CBPQT^{4+}$ and a pentameric *PE4NP* oligomer. The assembly adopts an infinite chain lattice with crystallographically invisible dislocations in the polymer backbone, which make the chain appear as an infinite polymer rather than a pentamer. A pentameric viologen complexed with DNP38C10 behaves likewise, adopting an inifinite chain lattice superstructure in which the thread "snakes" its way through the rings.

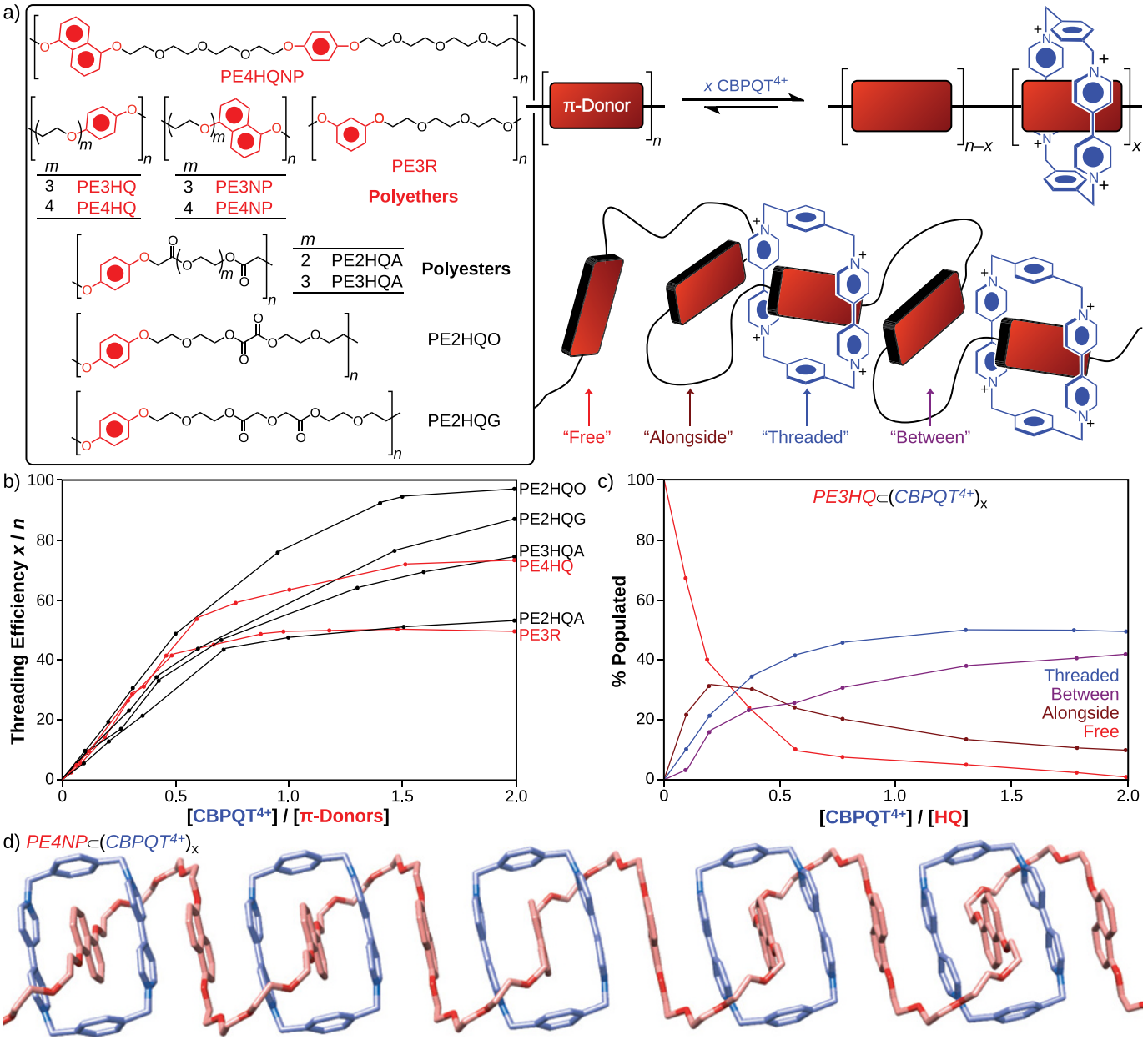


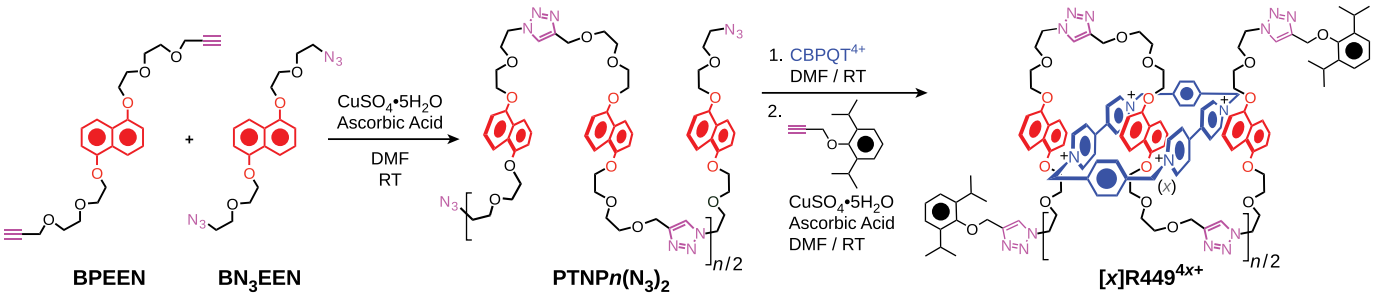
Figure 4.67 The self-assembly and folding of $CBPQT^{4+}$-threaded π-donating polyethers and polyesters.[393,603,605,606] (a) Summary of polymers employed in the assembly of D-A polypseudorotaxanes and a diagram of the different types of environments (threaded, alongside, between, and free) for the π-donors with respect to the rings. (b) Threading efficiencies of various polymers as a function of the $CBPQT^{4+}$ feed ratios.[606] (c) Population ratios of HQ units as a function of the feed ratio.[606] (d) Tubular representation of the solid-state (super)structure of the *PE4NP⊂(CBPQT^{4+})$_x$*, polypseudorotaxane[393] foldamer with hydrogen atoms, PF_6^- counterions, and MeCN solvent molecules omitted for the sake of clarity.

A few polyrotaxanes based on threaded cyclophanes are described elsewhere in this monograph. Ogoshi[609] has prepared polyrotaxanes based on the recognition of pillar[5]-arene for polyviologens—its stereoformula is illustrated in **Figure 1.22** of **Section 1.3.1**. Sessler[610] has orchestrated the self-assembly of 1D polyrotaxanes in which the $TexasBox^{4+}$ cyclophane encapsulates a metallosupramolecular polymer derived from 2,6-naphthalenedicarboxylate and Ag^{I}—a similar polymer sans Ag^{I} is illustrated in **Figure 2.45** of **Section 2.3.3.9**. Pérez[611–614] and co-workers have employed ring-closing olefin metathesis to clip various cyclophanes around SWNTs to afford carbon nanotubes with mechanical bonds—see **Figure 3.31** in **Section 3.4.1.2**.

4.2.1.2 Multi-Axle Rotaxanes/Molecular Sheafs

A number of ternary pseudorotaxanes[133,615–626] possessing two or more[623] axles have appeared in the literature. Rotaxanes possessing two or more axles were not typically associated with a vernacular nickname until recently when

Table 4.3 The average values for the number of repeating DNP units (*n*), $CBPQT^{4+}$ rings (*x*), molecular weight (M_n), polydispersity index (PDI), and retention volumes by gel permeation chromatography for the poly(triazole–naphthalene) polyethers **PTNP*n*(N_3)$_2$** and their corresponding polyrotaxanes, **[*x*]R449^{4x+}**.[394]



BPEEN BN$_3$EEN PTNP*n*(N_3)$_2$ [*x*]R449^{4x+}

Thread	*n*	MW/kDa	PDI	Retention Volume[a]/ml	Rotaxane	*x*[b]	M_n[d]/kDa	Retention Volume[a]/ml
PTNP81(N_3)$_2$	81	32	1.90	24.1	**[72]R449^{288+}**	72	112	25.0
PTNP133(N_3)$_2$	133	53	1.78	23.3	**[98]R449^{392+}**	98	161	24.9
PTNP453(N_3)$_2$	453	181	1.71	22.3	**[262]R449^{1048+}**	262	470	23.3

[a]Retention volumes determined in GPC experiments through two 15-μm columns and one 100-Å column set up in series.
[b]The number (*x*) of threaded rings was determined by integration of the threaded and non-threaded DNP signals observed in the ^{1}H NMR spectra.
[c]Molecular weights estimated based on calculated values for *x*.

Leigh[627] coined the term 'molecular sheafs,' since sheafs are bundles held together by circular bands. The simplest possible molecular sheaf is a [3]rotaxane possessing two dumbbells. While most of the molecular sheafs in the literature have three component parts, a couple of [4]rotaxane molecular sheafs have also been introduced, in which two rings serve as the bands which bundle two dumbbells. It should be possible in principle to prepare even larger polymeric molecular sheafs with many rings, since Harada[628] has already reported on the formation of the first double-axle polypseudorotaxanes. Here we describe a number of molecular sheafs based on various design motifs, which are illustrated in **Figure 4.68**.

Hydrophobic Template Molecular Sheafs

Since γ-CD is the smallest cyclodextrin that tends to form ternary complexes, it is a natural choice for designing molecular sheafs. Anderson[629] introduced the first kinetically stable [3]rotaxane molecular sheaf **R450$^+$**, possessing two different dumbbells derived from stilbene and cyanine dyes, by an iterative approach involving two sequential stoppering protocols by aqueous Suzuki coupling in the presence of γ-CD. Recently, Inouye[630] has prepared the [4]rotaxane molecular sheaf **R451** by stoppering a quaternary complex comprising two dialkynylpyrene axles and two γ-CD rings by an aqueous Heck coupling protocol.

The other prominent class of aqueous receptors are the cucurbiturils. Although CB8 commonly forms[631,632] ternary complexes with π–π stacked aromatic guests, it has not been employed in the synthesis of doubly threaded rotaxanes to our knowledge. However, Isaacs[633] has employed an unusual member of the cucurbituril family, bis-*nor*-*seco*-cucurbit[10]uril, in the synthesis of the double-axle [3]rotaxane **R452H$_4^{4+}$**, possessing a pair of dicationic 1-6-hexanebis-*tert*-butylammonium dumbbells.

Transition Metal Template Molecular Sheafs

Sauvage[634,635] has employed his sterically non-hindering endocyclic ligand motif[636] based on 8,8′-diphenyl-3,3′-biisoquinoline (dpbiq)—see **Section 6.1.2**—in the synthesis of the [3]rotaxane molecular sheafs **M(R453)$^{n+}$**. where M^{n+} is Fe^{2+}, Co^{2+}, or Co^{3+}. The wide profile of the endocyclic dpbiq chelate allows sufficient volume for the through-the-annulus threading of both dumbbells, also derived from dpbiq, which coordinate the templates in an octahedral geometry. The molecular sheafs can be demetallated readily in the case of Co^{II}, but not in the case of Co^{III} or Fe^{II}.

Nitschke[637] has assembled a doubly threaded [3]rotaxane under thermodynamoc control by employing a coordinative imine bonding approach—see **Section 3.3.1.1**. The nine-component self-assembly of the metallosheaf **Pd$_2$R454^{4+}** proceeds quantitatively in MeCN from a mixture of diformylpyridine as the axle precursor, a ^{t}Bu-functionalized *para*-tritylaniline stopper precursor, a large macrocyclic polyether impregnated with two monovalent pyrdine ligands, and $Pd(MeCN)_4BF_4$.

Active Metal Template Molecular Sheafs

Since the active template (**Section 2.4**) protocols for making mechanomolecules are catalytic, the number of rings or dumbbells that are captured by an active metal template are limited only by the size of the ring, provided a sufficient quantity of the substrates is available. This concept was demonstrated by Leigh[627] when he employed a wide-cavity endocyclic terpy ligand in the synthesis of **R455** by an active Ni template protocol involving the sp^3-to-sp^3 homocoupling of haloalkane-based semidumbbells. The mechanism of this type of active-template dumbbell capture is described in **Section 2.4.4.2**. The X-ray crystal structure of **R455** is illustrated in **Figure 1.29c** of **Section 1.3.3**.

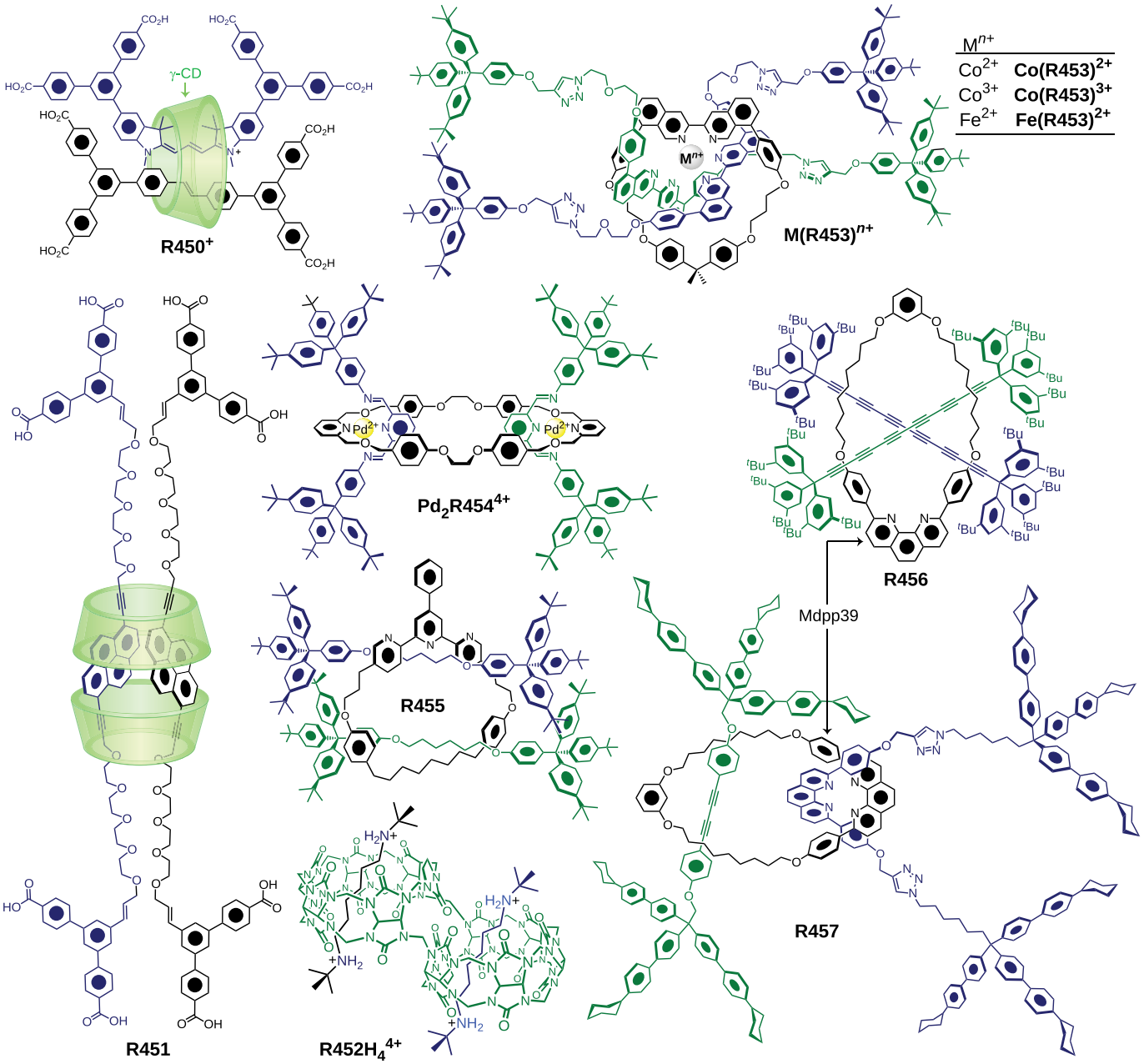


Figure 4.68 Stereoformulas of molecular sheafs.[627,629,630,633–635,637,638,644,645]

Tykwinski and Anderson[638] have recently employed an endocyclic dpp-based ligand, Mdpp39, in the active Cu^{I} template synthesis of the [3]rotaxane molecular sheaf **R456** by a Cadiot-Chodkiewicz cross-coupling of hexayne semi-dumbbells. The corresponding dodecayne axles of the molecular sheaf adopt a criss-crossed geometry within the ring, as determined by X-ray crystallographic analysis of its single crystals. While mechanically bonded rings have been employed to stabilize a number of polyyne compounds,[639–643] polyyne molecular sheafs were previously unprecedented. The bond length alternation is significantly increased in **R456** compared to single-axle homologues, indicating that the π-conjugation of the axles is disturbed by the criss-crossed threading geometry, which enforces very close contact between the central carbon atoms of the oligoyne axles, distorting them from linearity. This mechanically interlocked polyyne is nevertheless stable under ambient conditions.

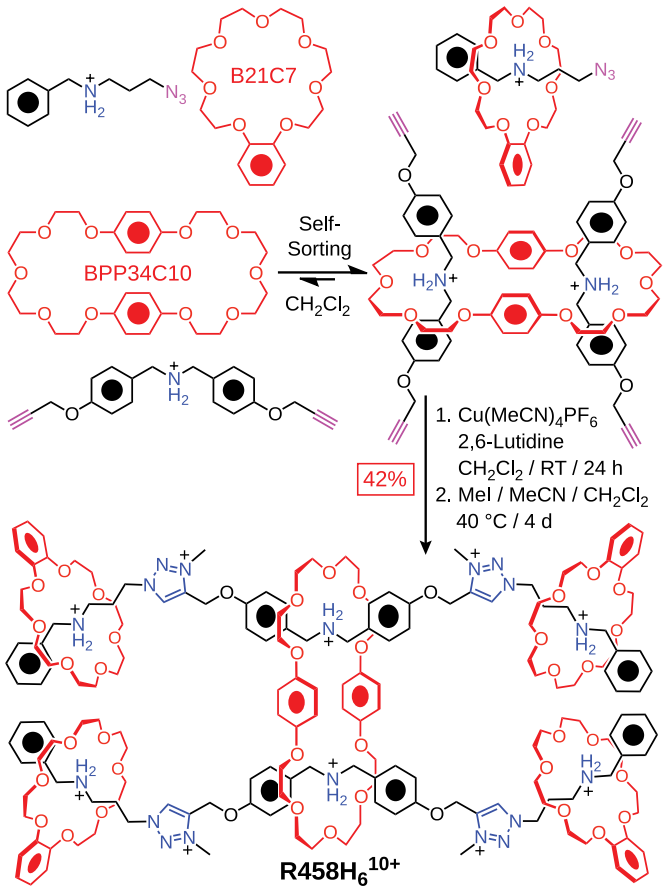
Saito[644,645] has employed the Mdpp39 ring in the synthesis of a number of [3]rotaxane molecular sheafs by a combination of passive and active metal template strategies. One example is compound **R457**, which was synthesized via CuAAC stoppering protocol of the corresponding metallo[2]pseudo[2]rotaxane, a precursor obtained by an Eglinton/Glaser/Hay active template protocol. Active copper templates are reviewed in **Section 2.4.1**.

Inorganic-Organic Hybrid Molecular Sheafs

Leigh and Winpenny[646] employed their ion-paired inorganic-organic hybrid rotaxane motifs (**Section 2.3.7.1**) to introduce a doubly threaded [4]rotaxane molecular sheaf architecture possessing two rings and two dumbbells in 2009. The solid-state structure of this molecular sheaf is illustrated in **Figure 1.29 h** of **Section 1.3.3**.

Hydrogen-bonded Molecular Sheafs

Liu[647] has orchestrated the CuAAC click synthesis (**Scheme 4.31**) of the "twin-axial" hetero[7]rotaxane **R458H$_6^{10+}$**, possessing two dumbbells and five rings, from a total of 11 precursors. The assembly relies on



Scheme 4.31 Synthesis of the twin-axial hetero[7]rotaxane **R458H$_6^{10+}$** by CuAAC coupling of self-sorted *N-benzyl-N-azidopropylammonium⊂B21C7* and *(N,N-di(propargyloxybenzyl) ammonium)$_2$⊂BPP34C10* pseudorotaxanes.[647]

the discriminatory behavior of benzo[21]crown-7 (B21C7), a crown ether which is large enough to encircle dialkylammonium cations, but too small to transgress a phenylene ring. This phenomenon has been exploited, for example, by Schalley[648–651] to obtain sequence-specific (**Section 5.2.2**) multi-threaded assemblies. In the case of **R458H$_6^{10+}$**, the self-sorting of the precursors involves the assembly of a ternary pseudorotaxane made from a pair of *N*,*N*-di(4-propargyloxybenzyl)ammonium axles bundled within BPP34C10, as well as a binary semirotaxane of *N*-benzyl-*N*-azidopropylammonium and B21C7. Four of these azide-terminated semirotaxanes couple with the propargyl groups of the ternary BPP34C10 complex by CuAAC in the presence of $Cu(MeCN)_4PF_6$, and the resulting triazoles are methylated subsequently for purification purposes. Instead of bundling a pair of dumbbells, the central BPP34C10 ring of this molecular sheaf bundles an identical pair of [3]rotaxanes!

4.2.1.3 Multi-Annulated [n]Rotaxanes

Macrobicyclic, macrotricyclic, and higher-order multi-annular receptors can be employed as the rings of rotaxanes, as they can in the case (**Section 4.1.3**) of catenanes. Examples of [2]rotaxanes incorporating multi-annular rings include those based on Rowan's porphyrin basket[99,652–654] (**Scheme 2.60** in **Section 2.3.3.6, Scheme 3.42** in **Section 3.4.2, Scheme 6.38** in **Section 6.3.2, Figure 6.98** in **Section 6.15.3.1**), the macrotricyclic polyethers[655] (**Section 2.3.7**) investigated by Chen[656–661] and Chiu[662–665] (**Figure 2.35** in **Section 2.3.3.7, Figure 2.59b** in **Section 2.3.4.6, Scheme 3.3 in Section 3.1.2, Scheme 6.54** in **Section 6.4.2, Scheme 6.61** in **Section 6.5.1, Schemes 6.92–93** in **Section 6.13.1.4**), and other π-donating cryptands[161–165,666–668] (**Schemes 2.61–63** in **Section 2.3.3.7, Figure 3.25** and **Scheme 3.27** in **Section 3.3.1.2, Figure 3.30 in Section 3.4.1.2**), as well as some calixarene-based ion-binding rotaxanes introduced by Beer[669–672] (**Table 2.34** in **Section 2.3.7.2, Schemes 6.58–59** in **Section 6.4.3**), and the traceless ion template hosts developed by Smith[673–675] (**Scheme 2.110–111** in **Section 2.3.7.3**).

As illustrated by the representative examples in **Figure 4.69**, multi-annulated rotaxane architectures include those involving (i) macrobicyclic hosts with either one or two linear dumbbells, or with a single tripodal dumbbell interpenetrating all of the host's openings, as well as (ii) macrotricyclic hosts threaded by either one or two dumbbells in a number of different possible orientations.

Macrobicyclic [n]Rotaxanes

Examples of three different threading architectures are illustrated (**Figure 4.69**) for macrobicyclic [2]rotaxanes. Huang[666] introduced the triphenylphosphonium-stoppered [2]rotaxane **R459^{4+}** possessing a BMP555C cryptand as the ring—see **Scheme 2.61** in **Section 2.3.3.7**. Liu[676] orchestrated the self-assembly of the [2]rotaxanes **R460a^{3+}–R460b^{3+}** possessing a tripodal axle encased in an imine-clipped macrobicyclic cryptand—see **Figure 3.25** in **Section 3.3.1.2**.

Leigh[677] has employed a macrobicyclic construct possessing a single pyridine ligand in the active metal template (**Section 2.4**) synthesis of [3]rotaxanes possessing two

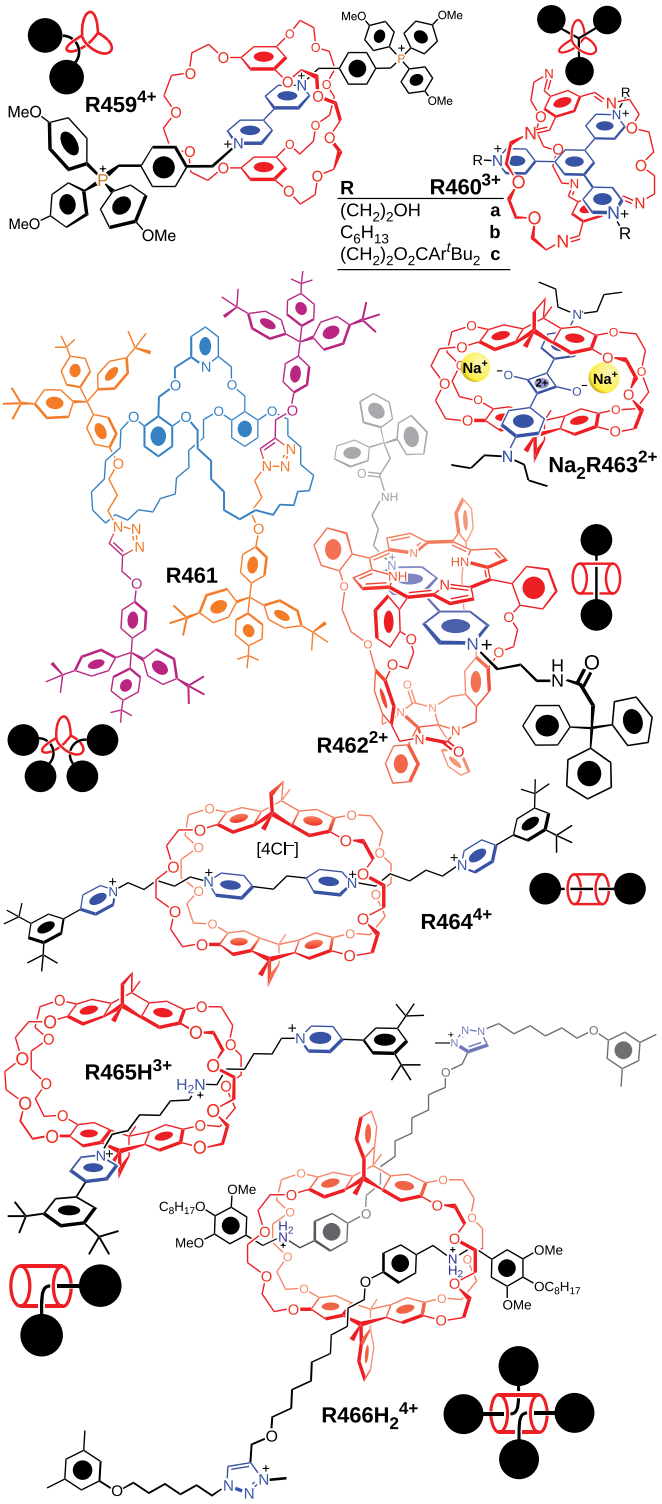


Figure 4.69 Stereoformulas of compounds representing different multi-annular rotaxane architectures.[652,658,662,665,666,676–678]

dumbbells—one passing through each annulus of the macrobicyclic ring. While the two dumbbells of **R461** are identical, a hetero[3]rotaxane possessing differentiated homocoupled (Eglinton-Glaser-Hay) and heterocoupled (CuAAC) dumbbells was also produced.

Macrotricyclic [n]Rotaxanes

A number of examples of macrotricyclic [2]rotaxanes are represented in **Figure 4.69** to illustrate the different orientations that are possible for the dumbbell with respect to the host. Rowan[652] designed the porphyrin basket (PB) [2]rotaxane **R462^{2+}**—see **Scheme 2.60** in **Section 2.3.3.6**. Chiu[662] has employed his DBB$_2$18C6$_2$ and DBB$_2$24C8$_2$ cryptands in synthesis of the [2]rotaxanes **Na$_2$R463^{2+}** and **R464^{4+}** by slippage (**Sections 3.1.5**) and stoppering protocols, respectively. Since the loops of the macrotricycle are not identical, threaded guests often exhibit an orientation bias in a particular direction. Whereas the methylenebis(pyridinium) recognition units thread the smaller DB24C8 side portals of **R464^{4+}**, the squaraine axle of **Na$_2$R463^{2+}** passes through the larger central cavity instead of DBB$_2$18C6$_2$, owing to its smaller portal size and the coordination geometry of the Na$^+$ templates.[678] The viologen dumbbell of **R462^{2+}** also passes through the two larger apertures of the porpyrin basket. More recently, Chiu[665] introduced yet another threading mode for a linear dumbbell with respect to the DBB$_2$24C8$_2$ host, where only one of the DB24C8 portals is threaded in the [2]rotaxane **R465H^{3+}**. The single-portal threading motif is duplicated for two dumbbells in the case of Chen's macrotricyclic [3]rotaxane[658] **R466H$_2$$^{4+}$**. See **Sections 6.5.1** and **6.13.1.4** for discussions of the anion-driven switching behavior of these cage-based rotaxanes.

Clever and Shionoya[679] have reported (**Figure 4.70**) rotaxanes based on self-assembled Pd^{II} and Pt^{II} metallacages. The ring of the [2]rotaxane **R467^{2+}** is a fourfold-symmetric M$_2$L$_4$ cage, which differs from the other macrotricyclics in **Figure 4.69** because all of the annuli are identical in this case. The encapsulation of the doubly sulfonated stilbene recognition unit of the dumbbell is driven by ion-pairing interactions, where the two negatively charged sulfonate groups become

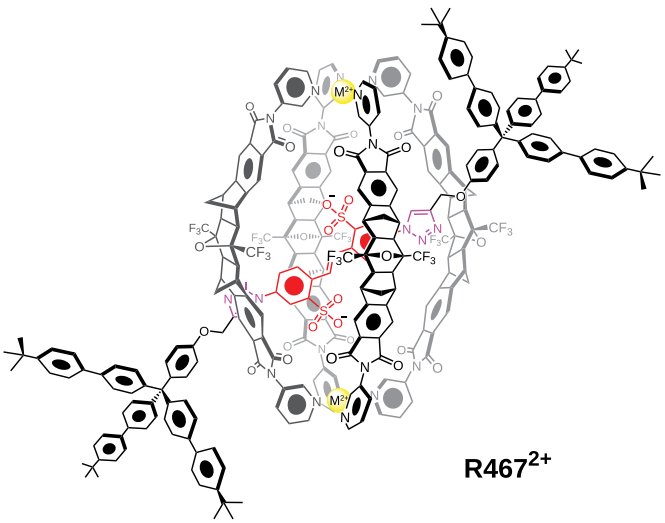


Figure 4.70 The structural formula of a self-assembled [2]rotaxane based on a cationic M$_2$L$_4$ cage and a disulfonated stilbene-based dumbbell.[679]

counterions to the positively charged metals at the vertices of the cage. The coordination-driven self-assembly of **R467**$^{2+}$ is essentially quantitative in CD_3CN at room temperature.

Macrobicyclic Polyrotaxanes

Recently, Davis[680] has developed a macrobicyclic "threading receptor" (**Figure 4.71**) which forms polypseudorotaxanes with polysaccharides. The receptor contains two pyrene units, connected via methylene bridges to three isophthalamide units functionalized with dendrimeric carboxylates for aqueous solubility. On the basis of isothermal titration calorimetry experiments, it was determined that this synthetic lectin binds oligosaccharides with high affinities (up to 19,000 M^{-1}). Molecular models indicate (**Figure 4.71a**) that the interaction is driven by hydrogen-bonding interactions between the hydroxyl groups of the threads and the isophthalamide linkers, as well as [C–H···π] and hydrophobic interactions between the faces of the pyranose and pyrene units. AFM images of threaded cellulose (**Figure 4.71b**) and chitosan (**Figure 4.71c**) provide additional evidence for the threading interactions.

4.2.2 Dendritic Rotaxanes

Dendrimers[681,682] are discrete, monodisperse macromolecules possessing repetitively branched architectures. The synthons for dendrimers, appropriately named dendrons, are branched molecules possessing chemically addressable functional groups, known as focal points. Multiple copies of dendrons converge on a core to produce a dendrimer, which often adopts a three-dimensional spherical geometry as a result of its high symmetry about the core. A dendrimer with *n* generations of branching from its core is characterized by the generation number G*n*. While their capacity to self-assemble and encapsulate guests have made them attractive materials in supramolecular chemistry,[683] dendrimers are also of interest[684,685] in mechanostereochemistry. Research on rotaxane dendrimers is motivated by the possibility of designing materials that combine the advantageous properties of dendrimers with those of mechanical bonds. For example, the switchable mechanical motions of bistable rotaxanes (**Chapter 6**) could influence the dynamics and dimensions of rotaxane dendrimers in controlled uptake and release applications, or perhaps even organocatalysis.

A seminal review[684] by Kimoon Kim identified (**Figure 4.72**) three different classes of rotaxane dendrimers—Type I, Type II, and Type III—which possess mechanical bonds at the core, termini, and branching points, respectively. For Type I and Type II dendrimers, sub-classifications[M] A, B, or C denote that dendrons are linked covalently to the axles, rings, or both, respectively. In the case of Type III, the dendrimer's mechanical bonds

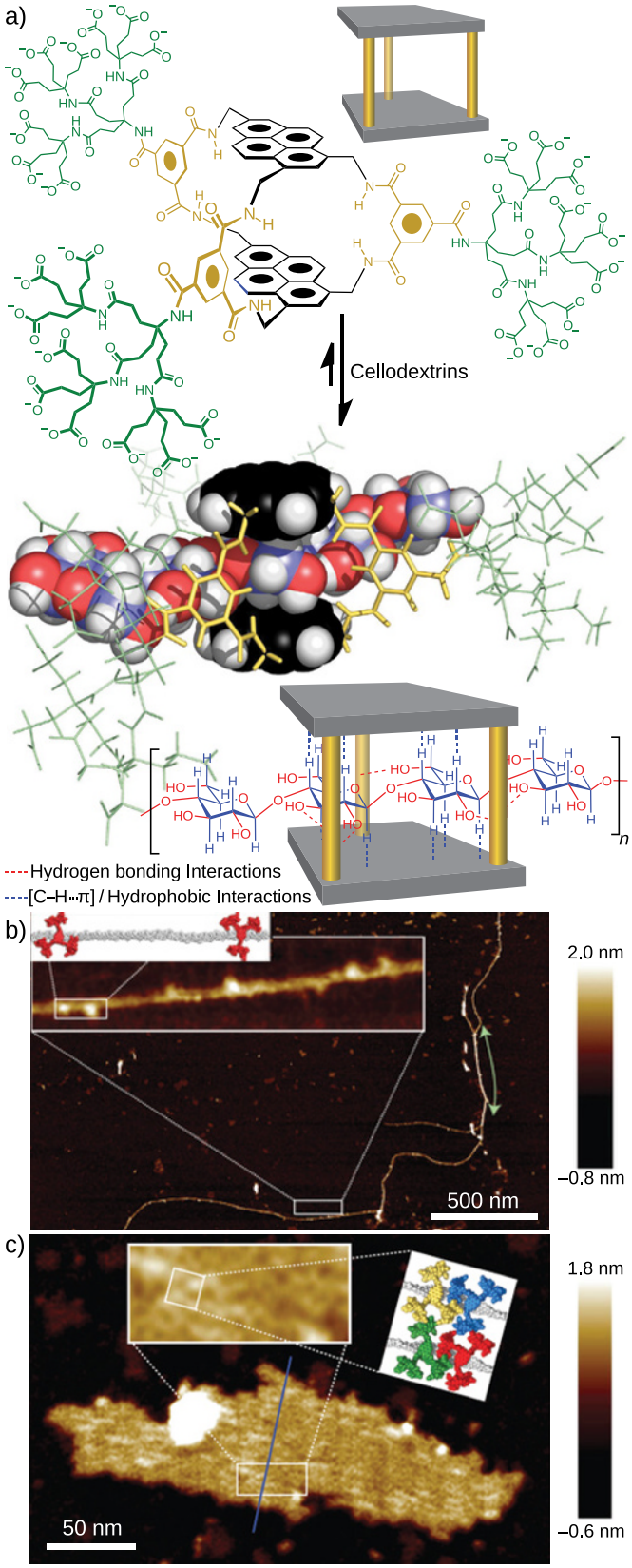


Figure 4.71 Davis' threading receptor for polysaccharides.[680] (a) Stereoformula, graphical representation, and energy-minimized model of the receptor. (b) AFM image of a threaded cellulose. (c) AFM image of threaded chitosan. Adapted with permission from ref. 680 (copyright 2016 Nature Publishing Group)

[M] Although Types IIC and IIIC were not proposed in Kim's seminal review, we suggest that these architectures would be a logical extension of Kim's classification framework.

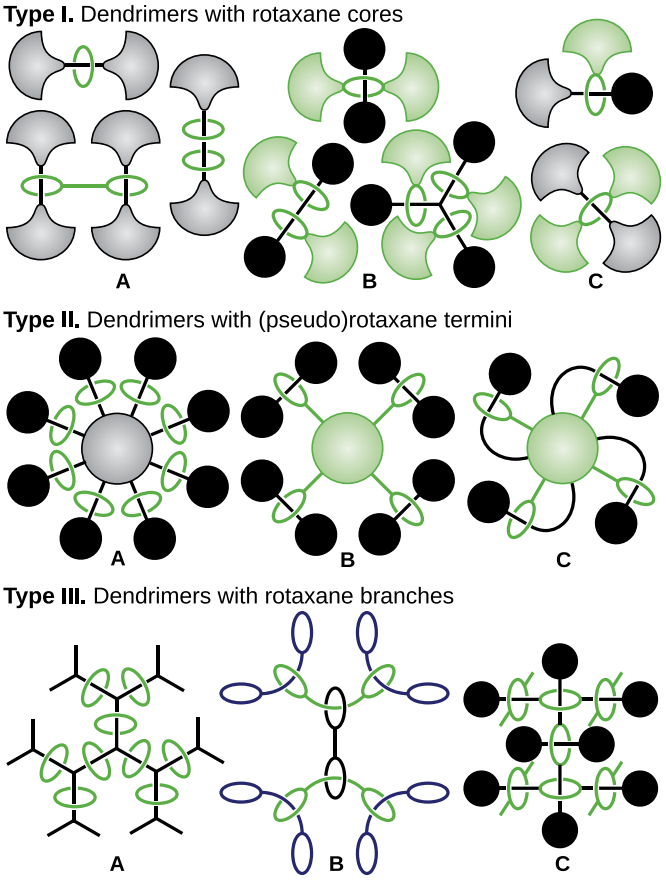


Figure 4.72 Graphical representations of the three types of rotaxane dendrimers.[684] The cores of Type I rotaxane dendrimers possess dendrons attached to their axles (Type IA), rings (Type IB), or both (Type IC). The terminal rotaxanes of Type II are connected to a dendrimeric core by covalent bonds with the axles (Type IIA), rings (Type IIB) or both[κ] (Type IIIC). The mechanical bonds of Type III rotaxane dendrimers can be located either in between branching points (Type IIIA) or they can constitute the branching points (Type IIIB) or both (Type IIIC).

can be located either in between (IIIA) or within (IIIB) the branching points, or both (IIIC). In other words, Type 1 rotaxanes are scaffolds for dendrons, Type II rotaxanes are endcaps for dendrons, and Type III rotaxanes are dendrimers in and of themselves. We note that the lines between these types are not always clear, however, because the categories can overlap, especially in the case of G1 dendrimers. For example, G1 dendrimers of Types IIA and IIIA are one and the same, since the branches and termini are equivalent in this case. Another grey area appears where the rings of Type II or Type III rotaxanes are employed as scaffolds for dendrons, rendering them equally worthy of Type I classification. Alas, despite our best intentions, molecules do not always distribute cleanly into separate conceptual boxes!

The polydisperse, extended relatives of dendrimers are branched and hyperbranched polymers, the threaded versions of which are discussed in **Section 4.2.3.8**. We focus our attention here primarily on rotaxanes, as opposed to pseudorotaxanes, acknowledging that a grey area (**Section 3.1.1**) lies in between these molecules and complexes, respectively.

4.2.2.1 Type I Rotaxane Dendrimers

Type I rotaxane dendrimers are arguably the most synthetically accessible architectures in the family because they can be prepared by simply grafting dendrons onto the dumbbells (Type IA) and rings (Type IB) of simple [2]rotaxanes, or both (Type IC). Rotaxanes with more than two component parts can also be classified as Type I dendrimers, provided they reside at the core of the molecule. Type I rotaxane dendrimers possessing Fréchet-type benzylic ether dendrons—G*n*, G*n*^{t}Bu, and G*n*OMe$_2$, where *n* is the generation number and ^{t}Bu or OMe$_2$ denote functional groups on the outermost branches—are illustrated in **Figure 4.73**.

Type IA

The Type IA rotaxane dendrimer architecture was introduced[385] in the form of G3-stoppered donor-acceptor rotaxanes based on the *BIPY*$^{2+}$⊂*BPP34C10* threading motif, such as the [2]rotaxane **R468**$^{2+}$—its synthesis is summarized in **Scheme 2.51** of **Section 2.3.3.2**—as well as the [3]rotaxane **R469**$^{4+}$. We note that that the G3-stoppered [4]rotaxane **R406b**$^{6+}$—see **Figure 4.52**—is also of Type IA, as are some molecular shuttles (**Section 5.1.1.2**) based on the same motif.

Vögtle[686] has investigated the effect of dendron size on the deslipping kinetics of tetralactam macrocycles departing from the oxymethylene axles of the Type IA [2]rotaxanes **G*n*-R470**, obtained by his anion-template dumbbell capture (**Section 2.3.6.1**) approach. No rotaxane was obtained from the G1-capped axles because the stoppers are too small to stabilize a mechanical bond. While the **G2/G3-R470** rotaxanes are both stable indefinitely at room temperature, the ring of **G2-R470** deslips at 150 °C.

Kim[684] claimed to have prepared dendron-stoppered rotaxanes **G*n*-R471**$^{4+}$ and **G*n*-R472**$^{4+}$ based G*n*OMe$_2$-stoppered hexamethylenebis(viologen) axles threaded by CB6 and CB7 rings, respectively, although the results have not been published.

Loeb[687] has employed the *BPE*$^{2+}$⊂*DB24C8* recognition motif in the template-directed synthesis of the G*n*-stoppered [2]rotaxanes **G*n*-R473**$^{4+}$, as well as a related series of molecular shuttles of Type IC (*vide infra*).

Liu and Yin[688] have constructed the G*n*OMe$_2$-stoppered (*n* = 0–2) [2]rotaxanes **G0-R474H**$^{+}$, **G1-R474H**$^{+}$, and **G2-R474H**$^{+}$ by dialkylammonium template-directed clipping (**Section 3.3.1.2**) followed by reduction of their imine bonds. A dendron-stoppered bis[2]rotaxane **G2-R475H$_2$**$^{2+}$, also based on the *dibenzylammonium*⊂*DB24C8* recognition motif, has been assembled[689] as a Type IA dendrimer with two mechanical bonds.

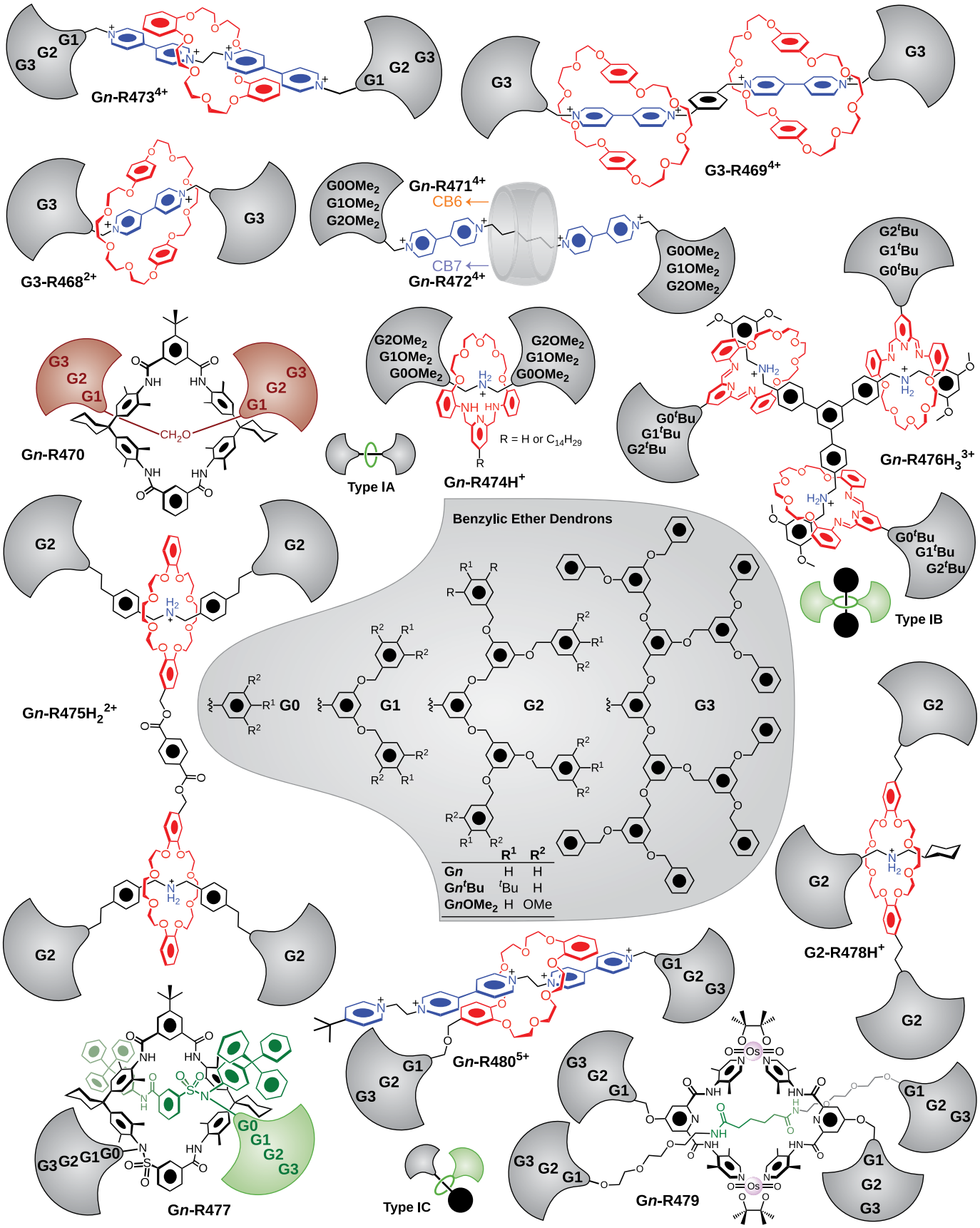


Figure 4.73 Type I rotaxane dendrimers displaying Fréchet-type benzylic ether dendrons.[385,684,686–689,697,698,700–702]

Other types of dendrons have also been incorporated into Type IA rotaxane dendrimers. Oh and Lee[690] have employed CB6AAC dumbbell capture (**Section 2.3.1.2**) to couple polyamidoamine dendrons to the axle of a CB6 [3]rotaxane. Smith[691] has employed his benzylic amide-encircled squaraines as the cores for polyamine and polyguanidinium dendrons. The deep-red fluorescence, water solubility, and excellent chemical stability of these insulated squaraines are ideal features for biological imaging probes. A bistable donor-acceptor [2]rotaxane based on DNP/CBPQT^{4+} and TTF/CBPQT^{4+} interactions has been coupled[692] with cyclohexylbiphenyl-derived mesogenic dendron stoppers, giving rise to a Smectic A liquid crystal (LC) phase that is stable from ambient temperature up to over 100 °C.

Type IB

A number of pseudorotaxanes of Type IB have been introduced, beginning with Diederich's dendron-functionalized cyclophanes, i.e., "dendrophanes",[693–696] which form pseudorotaxanes with hydrophobic guests in aqueous solvents. Rotaxanes of type IB are relatively uncommon, however. One example is that (**Figure 4.73**) of the [4]rotaxane **G*n*-R476H$_3^{3+}$**, obtained[697,698] by imine-based clipping of crown ethers around tripodal tris(dibenzylammonium) templates. See **Scheme 3.26** in **Section 3.3.1.2**. A Type IB pseudo[4]-rotaxane comprising dendron-functionalized DB24C8 rings was described by Gibson.[699] We note that these tripodal mechanomolecules can also be considered as Type IIIA rotaxane dendrimers.

Type IC

Vögtle[700] introduced a Type IC rotaxane dendrimer **G*n*-477** in 2000 by appending (**Figure 4.73**) G1, G2, and G3 benzylic ether dendrons to the sulfonamide moieties in the dumbbell and ring of one of his mechanically planar chiral (**Section 5.2.3.1**) tetralactam [2]rotaxanes.

Driven[701] by a G2-functionalized DB24C8 crown ether's recognition for dialkylammonium cations, the ring passess over a cyclohexyl stopper of a G2 semidumbbell during the self-assembly of the Type IC [2]rotaxane **G2-R478H$^+$**. This type of slippage system is discussed in **Section 3.1.3**.

Jeong[702] has adapted his thermodynamically controlled self-assembly of [2]rotaxanes based on dynamic Os-bridged metallacycles—see **Section 3.2.4.4**—to self-assemble the [2]rotaxane **G*n*-R479**, which displays four dendrons (up to G3) emanating from both hemispheres of its ring as well as its dumbbell.

In addition to the Type IA [2]rotaxanes (*vide supra*) **G*n*-R473^{4+}**, Loeb[687] has constructed a series of bistable molecular shuttles, **G*n*-R480^{5+}**, functionalized asymmetrically with G1–G3 dendrons on both the axle and the ring. The dendron size was found to influence both the thermodynamics and the kinetics of the shuttle. While molecular shuttles are discussed in detail in **Section 5.2.1**, we note that the distribution of translational isomers becomes more biased and the barriers to shuttling increase as the dendrimers increase in size. Another advantageous feature of the appended dendrons is that they dramatically increase the solubility of the polycationic rotaxanes in low-polarity organic solvents, such as benzene and toluene.

4.2.2.2 Type II Rotaxane Dendrimers

Rotaxane dendrimers of Type II contain rotaxanes on the outermost branches of the macromolecule.

Type IIA

Tripodal and tetrapodal [*n*]rotaxanes, which possess branched dumbbell architectures, could be classified either as Type IIA or as Type IIIA rotaxane dendrimers with G1 cores, since the periphery and the branches of the dendrimer are one and the same when $n = 1$. These architectures are therefore discussed in **Section 4.2.2.3**. We are not aware of any Type IIA rotaxane dendrimers with a core G*n* >1, although Kim[684] reviewed a number of host-guest complexes of this type.

Type IIB

As in the case of Types IIA and IIIA, the distinction between Types IIB and IIIB is not clear-cut for G1 dendrimers. Bis-, tris-, and tetrakis[2]rotaxanes comprising covalently bridged rings can be seen as Type IIB dendrimers. A few examples of these architectures are illustrated in **Figure 4.74**. The donor-acceptor bis[2]rotaxane **R481^{8+}** was introduced[355,703] in 1994 by a π-donor/π-acceptor template-directed clipping protocol—see **Section 2.3.3.2**—where both ends of the bis-cyclophane derived from CBPQT^{4+} encircle DNP-based dumbbells. Theremodynamically controlled clipping reactions involving reversible imine exchange[704] (**Section 3.3.1.2**) and coordinative imine bonding[705] (**Section 3.3.1.1**) of macrocyclic polyethers around dialkylammonium templates furnish the bis[2]rotaxanes **R482H$_2^{2+}$** and **Pd$_2$R438H$_2^{2+}$**, respectively. The bis[2]rotaxane **R484H$_2^{2+}$** is obtained[706] by Eglinton-Glaser-Hay homocoupling of [2]rotaxanes with propargylamide-functionalized DB24C8 rings. Qu[707] described a type of bis[2]rotaxane (not illustrated) in which the DB24C8 rings are linked by a photoswitchable overcrowded alkene. Loeb[708] has prepared a G1 rotaxane dendrimer of Type IIB, **R485^{12+}**, by employing his *BPE^{2+}⊂DB24C8* recognition motif in a stoppering protocol involving a tripodal (DB24C8)$_3$ trimer. Vögtle[328] introduced the tetrakis[4]rotaxane **R486** in 1999 based on covalently-bridged trilactam monosulfonamide macrocycles. Not illustrated are Vögtle's examples of bis[2]-rotaxanes[709,710] and tris[2]rotaxanes[710] based on a similar design motif. Supramolecular (pseudorotaxane) dendrimers of Type IIA have also been reported. For example, Gibson[711] has constructed G1 and G3 "crowned dendrimers" comprising poly(propyleneimine) (PPI) dendrimeric cores functionalized with a BMP32C10 corona. The corresponding multi-pseudorotaxanes were assembled by threading the rings with viologen guests.

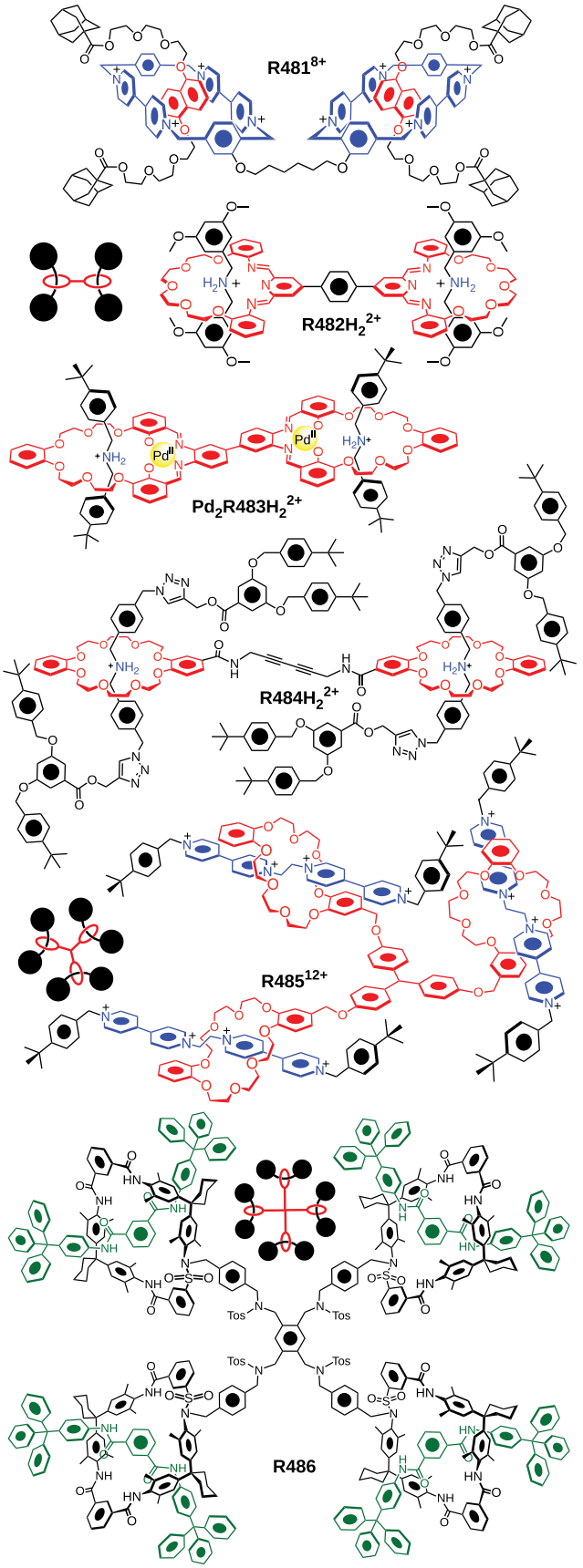
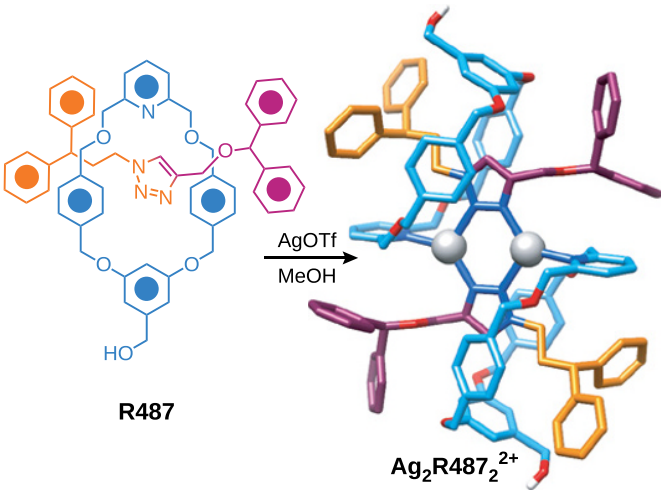


Figure 4.74 Stereoformulas of ring-bridged bis-,[355,703–705] tris-[708], and tetrakis-[328] [2]rotaxanes, which can be considered G1 rotaxane dendrimers of type IIB and/or IIIB.

Type IIC

In the case of Type IIC rotaxane dendrimers (see **Figure 4.72** and footnote **M**), the rings and their threaded axles are both connected to an inner dendritic core. One example (**Scheme 4.32**) of a compound fitting this description is the unusual [1]rotaxane **Ag$_2$R487$_2^{2+}$** introduced by Crowley[712] by dimerization of the triazole-axle [2]rotaxane **R487** with AgOTf. The small, 24-membered macrocycle contains an endotopic pyridine ligand, while the axle contains a triazole unit, on account of the CuAAC active metal template protocol (**Section 2.4.1.1**) used to interlock them. Since the ring is too small to accommodate both the axle and Ag^{I}, the nitrogen donors of the two component parts both cooperate with those of another rotaxane to bond with a pair of central Ag^{I} ions, as observed in the X-ray crystal structure illustrated in **Scheme 4.32**. A similar architecture was obtained[713] from a supramolecular [*c*2]daisy chain (**Section 4.2.3.2**) by a [2+2] cycloaddition of stacked stilbene units within its co-constitution.



Scheme 4.32 Crowley's assembly[712] of a bis[2]rotaxane dimer possessing the architecture of a G1 dendrimer of Type IIIC. Hydrogen atoms, counterions, and solvent molecules are omitted from the portrayed X-ray crystal structure for the sake of clarity.

4.2.2.3 Type III Rotaxane Dendrimers

Type III dendritic rotaxanes are characterized by mechanically bonded branching points instead of covalent ones.

Type IIIA

A number of examples of G1 rotaxane dendrimers of Type IIIA, which are essentially tripodal and tetrapodal [*n*]rotaxanes, are illustrated in **Figure 4.75**. The π-donor/π-acceptor templation motifs (**Section 2.3.3**) have been employed in the slippage synthesis of the BIPY^{2+}/BPP34C10 [4]rotaxane[714,715] **R488^{6+}**, as well as the CuAAC click syntheses of the DNP/CBPQT^{4+} [4]rotaxane[387,716] **R489^{12+}** and the corresponding bistable TTF/DNP [4]rotaxane[717] **R490^{12+}**.

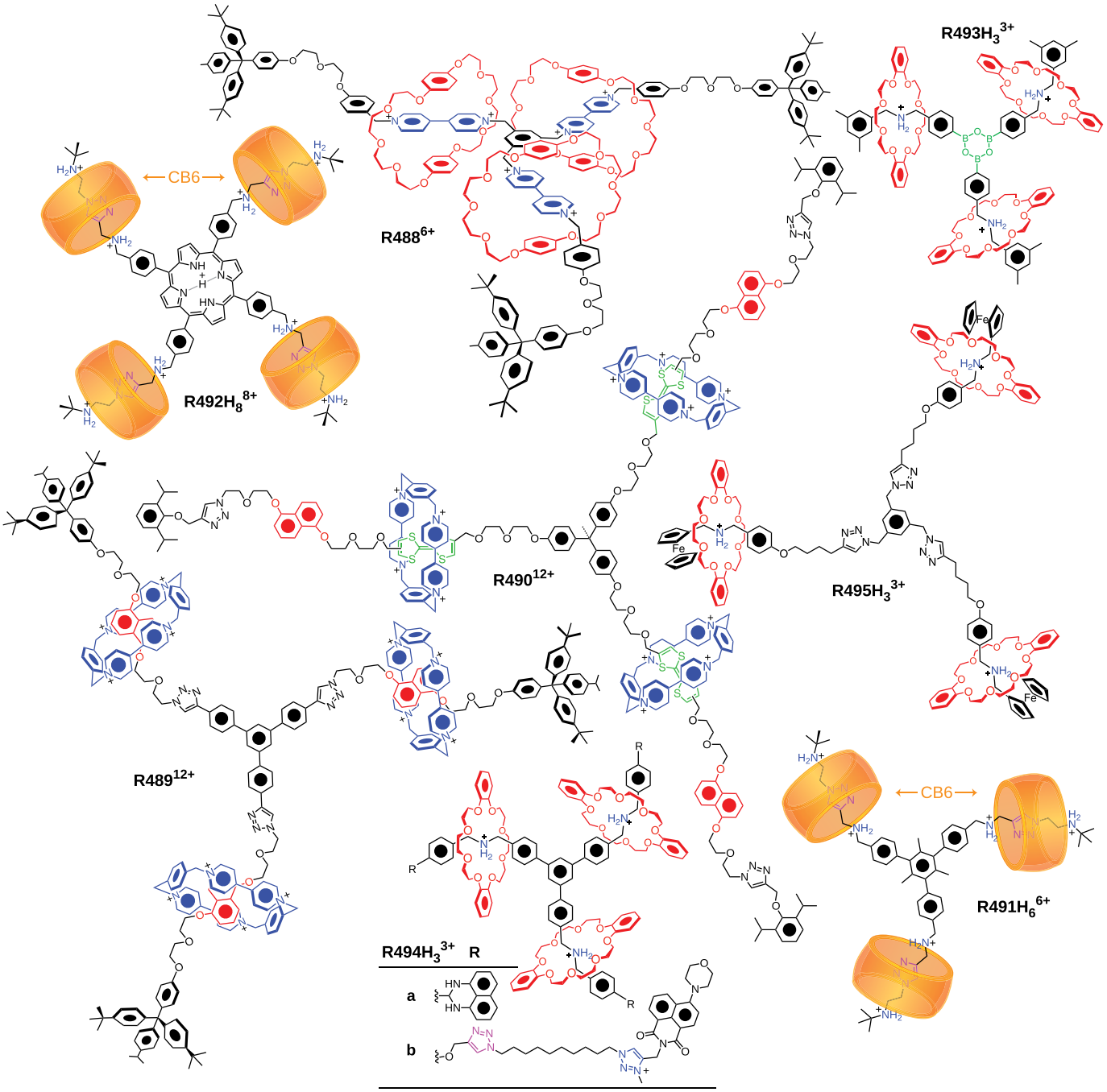


Figure 4.75 Examples of tripodal [4]rotaxanes and tetrapodal [5]rotaxanes, which can be considered G1 rotaxane dendrimers of Type IIA or IIIA.

Steinke and Tuncel[718,719] have obtained branched [4]- and [5]rotaxanes **R491H$_6^{6+}$** and **R492H$_8^{8+}$** by CB6AAC dumbbell capture (**Section 2.3.1.2**) reactions involving (**Figure 4.75**) tripodal and tetrapodal mesitylene and porphyrin precursors, respectively.

The dialkylammonium/crown ether templation motifs have been the most popular platform for building[720,721] (**Figure 4.75**) Type IIIA rotaxanes. We recall from **Section 4.2.2.1** that the tripodal compound **G*n*-R476H$_3^{3+}$** (*n* = 0–2, see **Figure 4.73**) is a Type IIIA core serving as a scaffold for benzylic ether dendrimers of Type IB.[697,698] Kihara and Takata[720] has employed Ru- and Rh-catalyzed hydrosilylation reactions construct [*n*]rotaxanes, one of which is a trimer (not illustrated) obtained by trimerization of three alkyne-terminated *dibenzylammonium*⊂*DB24C8* semirotaxanes around a phenylsilane core. Tokunaga[721] has prepared the branched [4]rotaxane **R493H$_3^{3+}$** by a boroxine-forming condensation (**Section 3.3.3**) of boronic acid-terminated semirotaxanes derived from dibenzylammonium and DB24C8. Chiu[722] has obtained the tripodal [4]rotaxane **R494aH$_3^{3+}$** by a solvent-free protocol—see **Scheme 2.84a** in **Section 2.3.4.6**—which efficiently forms

naphthodihydropyrimidine stoppers from diaminonaphthalene and benzaldehyde precursors during ball milling in the solid state. Qu[723] has obtained a G1 dendrimer **R494bH$_3^{3+}$**, based on the same 1,3,5-triphenylene core, by a CuAAC stoppering protocol with a fluorescent 4-morpholino naphthalene stopper. A porphyrin-cored tetrapodal dendrimer based on this motif has also been described.[724] See **Section 6.13.3**. Osakada[725] has prepared the ferrocene-stoppered tris[2]rotaxane **R495H$_3^{3+}$** by CuAAC click chemistry. Liu, Yoon, and Yin[726] have relied on dialkylammonium template-directed clipping to prepare a branched [4]rotaxane (not illustrated) with a macrocyclic polyether core that recognizes π-accepting guests.

Winpenny[415] has constructed tripodal [4]- and [7]rotaxanes based on the ion-paired inorganic-organic hybrid (**Section 2.3.7.1**) motif. As illustrated by the crystal structure of **R496a** and model of **R496b** in **Figure 4.76**, the dendrimers comprise inorganic $Fe_2Co(O)(O_2C^tBu)_6(H_2O)_3$ cores, ligated by pyridine-terminated dialkylammonium-based axles, which are each threaded by one or two $Cr_7NiF_8(O_2C^tBu)_{16}^-$ heterometallic wheels, respectively. These types of compounds may hold promise for applications in quantum information processing[416]—see the discussion accompanying **Scheme 4.25** in **Section 4.2.1.1**.

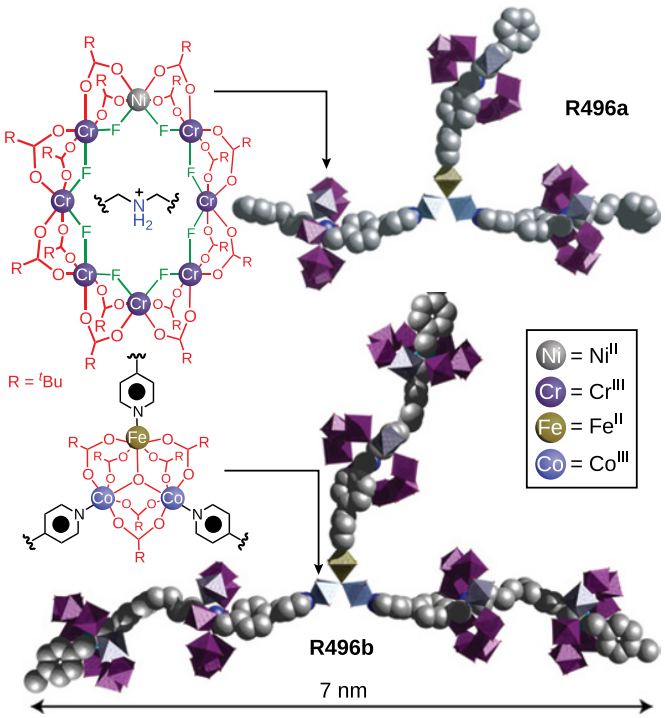
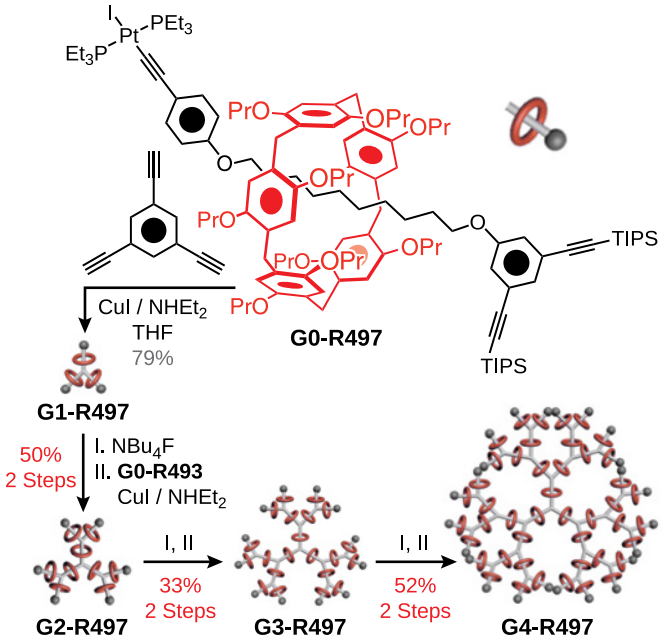


Figure 4.76 The X-ray crystal structure and molecular model of tripodal [4]- and [7]rotaxanes, respectively, obtained by metallo-supramolecular trimerization of ion-paired inorganic-organic hybrid [2]- and [3]semirotaxanes possessing dialkylammonium axles and heterometallic rings.[415] Hydrogen atoms, solvent molecules, and counterions are omitted for the sake of clarity. Models reproduced with permission from ref. 415 under a Creative Commons CC-BY license.



Scheme 4.33 Yang's divergent metallo-assembly of PA5-based rotaxane dendrimers up to the fourth generation.[727]

Arguably the most challenging and exotic dendritic rotaxane architectures yet achieved are the PA5-based rotaxane dendrimers introduced by Yang.[727,728] A divergent step-growth[727] (**Scheme 4.33**) of multi-generation Type IIIA rotaxane dendrimers is driven by the formation of stable organometallic bonds between the differentiated stoppers of the perpropylated PA5-based [2]rotaxane **G0-R497**, which contain donors and acceptors of organometallic bonds on opposite ends of the dumbbell. One stopper is a Pt^{II}-capped acetylide complex and the other stopper is a dendritic triisopropylsilyl (TIPS)-protected 3,5-diethynylbenzene unit. The step-growth dendrimerization begins with the formation of trimer **G1-R497** via the Cu^{I}-catalyzed heterocoupling of three copies of the G0 dendron to a central 1,3,5-triethynylbenzene acceptor by *trans*-coordinated platinum acetylide bonds. After deprotection of the TIPS groups with NBu_4F, the terminal alkynes of the branched stopper become exposed, enabling the production of a second-generation dendrimer **G2-R497** by repeating the Cu^{I}-catalyzed insertion of six G0 donors. These deprotection and insertion steps can be repeated over two more iterations to afford the [22]rotaxane **G3-R497** and the [46]rotaxane **G4-R497**—a discrete, monodisperse molecule with almost 50 mechanical bonds! The high efficiency of the organometallic bond-forming step and the charge neutrality of the stable organometallic products are crucial to the successful synthesis and purification of these remarkable compounds. A comparison of the rotaxane dendrimers with the corresponding non-rotaxane dendrimers by AFM and TEM microscopies suggests that the **G*n*-R497** compounds are rigidified by the mechanically bonded rings, since they have a lower tendency to collapse by self-folding. The terminal alkynes can also serve as handles for further

functionalization, which was demonstrated by the grafting of Fc electrochemical probes to the dendrimer coronas. Employing the type of (organo)metallosupramolecular chemistry originally introduced by Stang,[138,729] Yang[728] has also combined different dendritic rotaxane donors possessing 120° bend angles with 60°, 120°, and 180° acceptors to obtain the metallacyclic multirotaxane architectures illustrated in **Figure 4.77**.

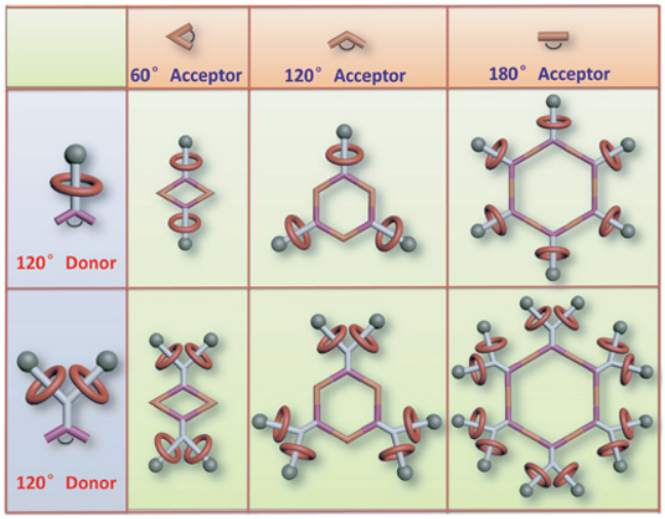


Figure 4.77 Graphical representations of the metallacyclic multirotaxanes obtained by coupling 120° donor [2]- and [3]rotaxanes with bis(platinum) acceptor joints with 60°, 120°, and 180° bend angles. Adapted with permission from ref. 728 (copyright 2015 Wiley-VCH)

Type IIIB

Dendrimers of Type IIIB possess threaded (rotaxane) branching points. As illustrated in **Figure 4.72**, the component parts of these dendrimers comprise ring-terminated dumbbells. Type IIIB rotaxanes of G*n* = 1, such as ring-linked bis- and tris[2]rotaxanes, are discussed in **Section 4.2.2.2**, since Types IIB and IIIB are equivalent as first-generation dendrimers. Here we focus our attention (**Figure 4.78**) on G2 dendrimeric rotaxanes of Type IIIB. Vögtle[730] introduced the second-generation Type IIIB rotaxane dendrimer **G2-R498** in 2001 by employing phenolic [2]rotaxanes as the reactants in a phenolate templated nucleophilic dumbbell capture (**Section 2.3.6.1**) within the annulus of a tetralactam macrocycle.

The remaining examples of Type IIIB dendrimers in **Figure 4.78** are based on dialkylammonium/crown ether templation. Leung[706] has prepared the [4]rotaxane **G2-R499H$_3$$^{3+}$** by CuAAC coupling of propargyl-functionalized [2]rotaxanes to a bis(azido)pseudo[2]rotaxane core. Qu[731] has relied on *dialkylammonium⊂B21C7* and *dibenzylammonium⊂DB24C8* templation to prepare the [4]rotaxane **G2-R4100H$_3$$^{3+}$** by a combination of (i) CuAAC and (ii) esterification stoppering protocols in both convergent (i then ii) and divergent (ii then i) routes, the former being slightly more efficient than the latter.

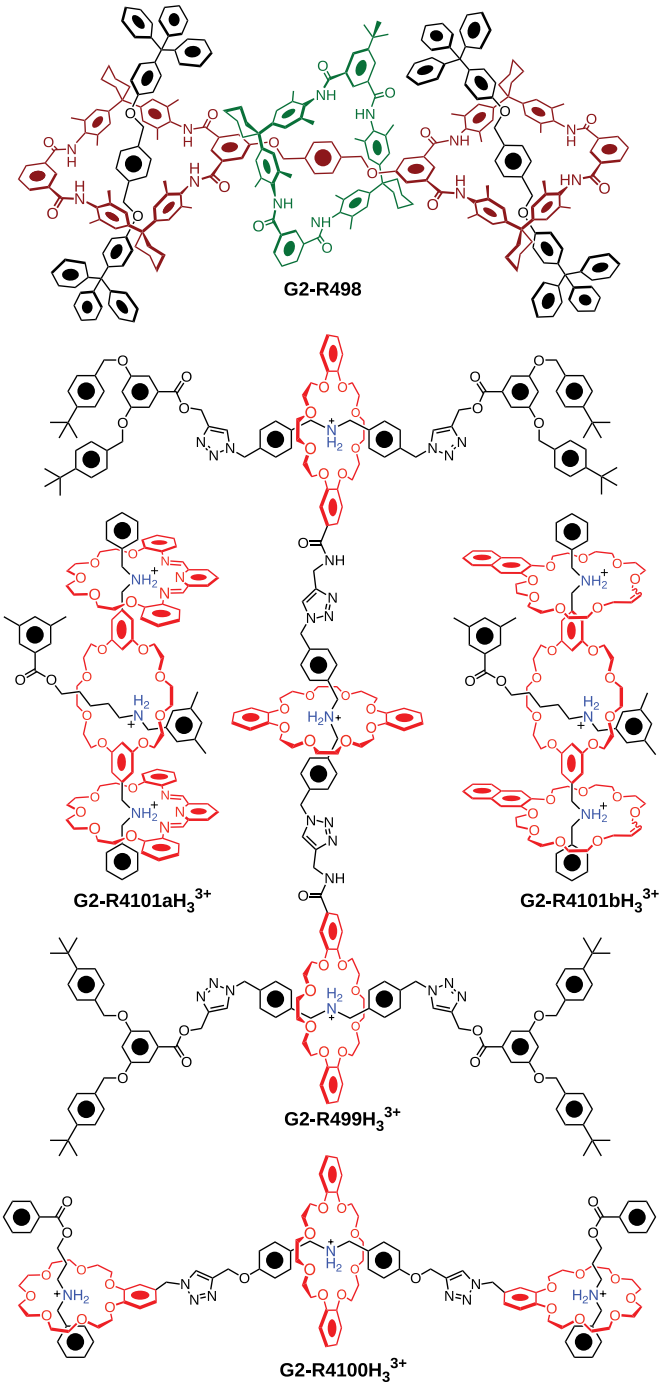


Figure 4.78 Type IIIB and Type IIIC rotaxane dendrimers.[706,726,730,731]

Type IIIC

Liu, Yoon, and Yin[726] have constructed the hetero[*n*]rotaxanes **G2-R4101aH$_3$$^{3+}$** and **G2-R4101bH$_3$$^{3+}$** by a combination of thermodynamically and kinetically controlled approaches. The architectures of these rotaxanes differ from the others because the branches extend from the rings, rather than the axles. We suggest that these novel architectures be classified as Type IIIC dendrimers.

Rotaxane dendrimers appear to be an underdeveloped area of mechanostereochemistry, with only a very limited

number of large, multi-generation compounds known. As mechanically bonded branched macromolecules become more synthetically accessible on the back of the progress summarized here, researchers will be able to focus more of their efforts on how the unusual dynamics and stereochemistry (**Chapter 5**) of mechanomolecules can influence the properties of dendrimers.

4.2.3 Covalently Bridged Rotaxanes

Just as adding covalent bridges between the rings of catenanes gives rise to new topologies (**Section 4.1.4**), the rings and axles of rotaxanes can be connected in various geometries to produce new architectures with mechanical bonds, including [1]rotaxanes (**Section 4.2.3.1**), daisy chains (**Section 4.2.3.2**), Bonnanes (**Section 4.2.3.3**), ladder-like cyclic rotaxanes (**Section 4.2.3.4**), molecular bundles and elevators (**Section 4.2.3.5**), oligo- and poly[2]-rotaxanes (**Section 4.2.3.6**), oligo- and poly[3]rotaxanes (**Section 4.2.3.7**), and extended 2D and 3D polyrotaxane networks (**Section 4.2.3.8**).

4.2.3.1 [1]Rotaxanes

The [1]rotaxane architecture is one in which the mechanical bond is trivialized by (a) covalent bond(s) that connect all of the component parts together. This type of architecture is most commonly realized by linking the ring and axle of a [2]rotaxane, as in the cases of the singly-bridged "molecular ouroboros" (*vide infra*). We note that [1]rotaxanes originating from more than two component parts are also possible, as in the case of the first-generation Type IIC dendrimer[712] $\mathbf{Ag_2R487_2^{2+}}$ illustrated in **Scheme 4.32**, **Section 4.2.2.2**. A case could be made that [1]rotaxanes do not possess mechanical bonds, since—in common with knots—they do not possess distinguishable component parts, yet their residual entanglements constrain intramolecular motion in a manner similar to the mechanical bond of a [2]rotaxane. We note that if two covalent bridges span from the axle to the ring, the axle/ring assembly becomes a self-threaded macrobicycle, an architecture discussed in **Section 4.3.4**.

The Molecular Ouroboros

The *ouroboros* is an ancient symbol of a snake/serpent eating its own tail—its name derives from the Greek roots *ourá* (tail) and *boros* (to eat). This self-devouring serpent has symbolized cyclicality from at least the 14th century B.C.E. in many cultures and contexts, especially those involving re-creation (in common with the phoenix) since it appears to simultaneously consume and rebuild itself. The rotaxane architecture where an axle feeds into the opening of a ring to which it is attached by a single covalent bond has been nicknamed[732] a molecular ouroboros because it resembles the way in which the serpent's body (axle) feeds into its mouth (ring). Engendering translational bistability into [1]rotaxanes allows these molecular ouroboroses to devour and extrude their "tails" under the influence of various energetic stimuli—see **Section 6.13.2**. Here we give an overview of selected examples (**Figure 4.79**) of [1]rotaxanes to showcase the

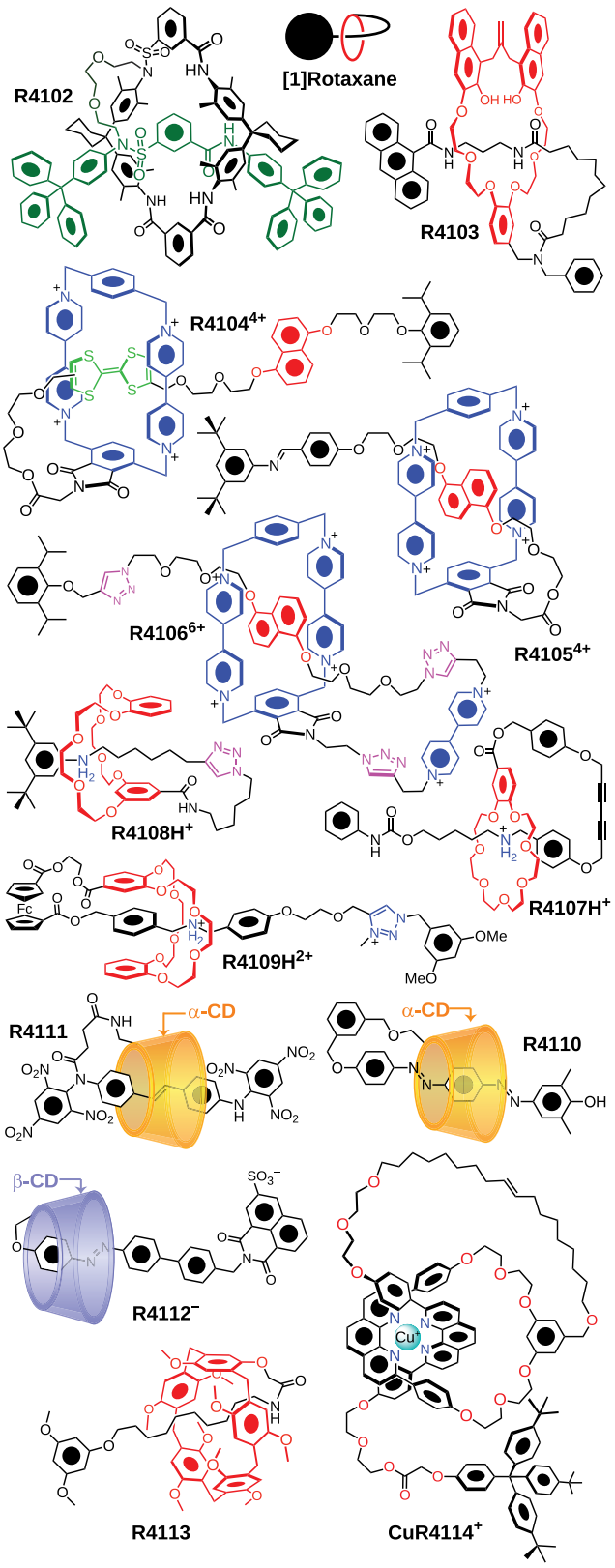


Figure 4.79 Selected examples of [1]rotaxanes.[709,736–738,740–749]

types of design motifs and templation strategies that have been employed in their syntheses.

Vögtle[709] was among the first researchers to begin investigating molecular structures involving the installation[733] of intramolecular covalent bridges between the component parts of rotaxanes. The covalent linking experiments were made possible by redesigning the hydrogen-bonded cyclohexylidene-bisphenylene tetralactam (**Section 2.3.4.1**) macrocycles to possess sulfonamide groups, which are more reactive nucleophiles than the corresponding amides on account of the more acidic SO_2N–H proton, allowing the sulfonamides to react selectively with haloalkanes by S_N2 substitution in the presence of mild bases. The seminal [1]rotaxane was **R4102**, possessing (**Figure 4.79**) a 3EG linker between the ring and axle. The directionality of the ring and axle, attributable to their single sulfonamide groups, endows[329,734,735] the [1]rotaxane with a form of mechanically planar chirality—see **Section 5.2.3.1**.

Hiratani[736] has relied on his covalent-directed dumbbell capture protocol—see **Section 2.2.3**—to obtain (**Figure 4.79**) the [1]rotaxane **R4103** by through-the-annulus aminolysis of a macrobicyclic precursor. The [1]rotaxane binds Li^+, leading to an increase in fluorescence emission from the anthracene stopper, presumably as a result of enhanced energy transfer from the ring's naphthalene groups in the Li^+-bound complex.

The π-donor/π-acceptor motifs have also been employed[732,737–739] (**Figure 4.79**) to template the formation of [1]rotaxanes. The [1]rotaxane **R4104^{4+}** was obtained[737] by a self-templating clipping protocol—see **Table 2.16**, **Section 2.3.3.8**—of the tetracationic cyclophane functionalized with an axle bearing TTF and DNP recognition units. By contrast, the [1]rotaxane **R4105^{4+}** was obtained[738] by a thermodynamically controlled stoppering protocol involving imine exchange (**Section 3.3.1.3**) at the terminus of a self-threaded ring–axle conjugate. **R4106^{6+}** was isolated[739] as the major product among a series of cyclic and acyclic daisy chains in a CuAAC stoppering protocol—**Section 4.2.3.2**.

A number of [1]rotaxanes have been constructed with the assistance of templation by dialkylammonium-threaded crown ethers. Zhao and Yan[740] prepared (**Figure 4.79**) the [1]rotaxane **R4107H$^+$** by Eglinton-Glaser-Hay coupling of a propargyl functionalized B21C7 ring with a threaded dialkylammonium-based semidumbbell displaying a terminal propargyl group. The resulting butadiyne portion of the axle can be converted to a tetramethylene linker by hydrogenation over Pd/C, increasing the mobility of the axle. Coutrot[741,742] has created, by CuAAC click chemistry, [1]rotaxanes such as **R4108H$^+$**, which can be switched by covalent and acid/base stimuli, as discussed in **Section 6.13.2**. Qu[743,744] has investigated the pH-driven translational switching of bistable [1]rotaxanes such as **R4109H^{2+}**, which behave analogously to the other bistable switches comprising DB24C8 rings and dialkylammonium/triazolium axles—see **Section 6.3.3.1**.

Owing to the facile synthesis of monofunctionalized cyclodextrins, these aqueous receptors (**Section 2.3.1.1**) have been frequently employed (**Figure 4.79**) as hosts in the preparation of [1]rotaxanes. Kaneda[745] and Easton[746] independently introduced the first α-CD [1]rotaxanes in 2003. Whereas Kaneda's [1]rotaxane **R4110** was stoppered by azotizing a self-threaded α-CD pseudo[1]rotaxane, Easton's compound **R4111** was prepared by modification of a [2]rotaxane precursor. Tian[747] obtained the [1]rotaxane **R4112$^-$** by employing an aqueous Suzuki coupling protocol to stopper an *azo⊂β-CD* pseudo[1]rotaxane. The photodriven motion of **R4112$^-$** is discussed in **Section 6.13.2**.

Xia and Xue[748] prepared (**Figure 4.79**) the [1]rotaxane **R4113** by coupling an alkylammonium semidumbbell through-the-annulus, guided by ion-pairing and [C–H···π] interactions, with an undecamethoxypillar[5]arene acetate host in the presence of EDC and DMAP.

The [1]rotaxane **CuR4114$^+$**, which Mayer[749] accessed (**Figure 4.79**) by a combination of Cu^I transition metal templation (**Section 2.3.2.1**) and olefin cross metathesis (**Section 3.4.2**), is only a [1]rotaxane in the presence of its Cu^I template, since it disentangles upon template removal, as illustrated in **Section 6.13.2**. This loss of entanglement illustrates that the residual mechanical bond of a [1]rotaxane can be lost by through-the-annulus rotation of the ring–axle linker. Harada[750,751] has also observed this kind of "reeling" motion in cyclodextrin-based (pseudo)[1]rotaxanes.

Bis-, Oligo-, and Poly[1]rotaxanes

Terao[752,753] has developed a family (**Figure 4.80**) of insulated molecular wires (IMWs) comprising oligo- and poly[1]rotaxanes and (oligo/poly)bis[1]rotaxanes derived from permethylated α-CD (PM-α-CD) and π-conjugated polymer backbones. All of these IMWs share the same type of threading motif as the [1]rotaxane[754] **R4115**, where the PM-α-CD ring encircles a phenylacetylene unit to which it is appended by an oxyphenylene linker. This [1]rotaxane design is essentially the subunit of the bis[1]-rotaxanes[755–757] **R4116**, **R4117a**, and **R4117b**, as well as the tetrameric oligo[1]rotaxane[756] **R4118**. A series of poly[1]rotaxanes **(R4119–R4121**) based on these motifs have been prepared to accommodate semiconducting backbones possessing butadiyne[758–760] (**R4119a–d**), *para*-phenylene[759] (**R4120a–b**), and *meta*-phenylene[761] (**R4121a–b**) linkers. Recently, Terao[762] has prepared metallosupramolecular polymers derived from terpyridine-stoppered bis[1]rotaxanes. These compounds exhibit the kinds of enhanced photoluminiescence and charge carrier mobilities that are characteristic of many insulated molecular wires.[423,495,496]

Dendritic Multi[1]rotaxanes

A few multipodal [1]rotaxanes have been prepared, the dendritic architectures of which arise from multiple self-threaded axles connected to a central core. Tian[763] has prepared a bis[1]rotaxane possessing a central Co(salen) linker. Qu[764,765] has investigated the pH-driven radial expansion and contraction motions leading to

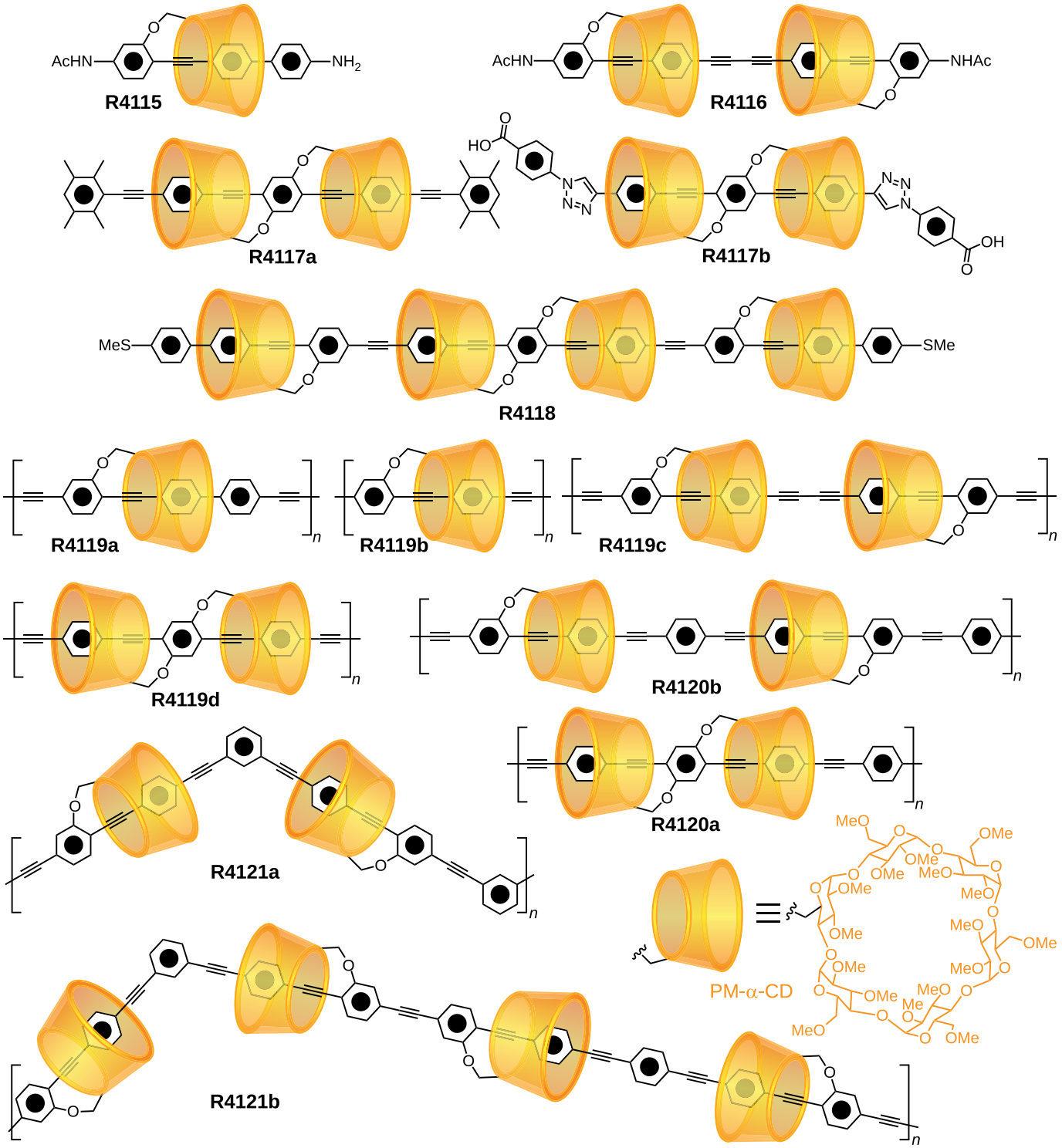


Figure 4.80 Terao's oligo- and poly[1]rotaxanes and polybis[1]rotaxanes are insulated molecular wires based on permethylated α-CD (PM-α-CD) rings and π-conjugated axle polymers. A phenylacetylene recognition unit occupies the PM-α-CD ring of the [1]rotaxane[754] **R4115**, the bis[1]rotaxanes[755–757] **R4116**, **R4117a**, and **R4117b**, and the tetrameric oligo[1]rotaxane[756] **R4118**, as well as poly[1]rotaxanes incorporating these phenylene ethynylene backbones junctioned with butadiyne[758–760] (**R4119a–d**), *para*-phenylene[759] (**R4120a–b**), and *meta*-phenylene[761] (**R4121a–b**) linkers.

changes in the molecular diameter of bis-, tris- and tetrakis[1]rotaxanes—see **Section 6.13.3.2**. Coutrot[766] has employed his pseudorotaxane molecular transporter—a rotaxane-building molecular machine (**Section 6.15.3.3**)—in the synthesis of a tris[1]rotaxane, which could not be accessed by ordinary templation on account of having only very weakly binding triazolium recognition units for the DB24C8-derived rings.

4.2.3.2 Daisy Chains

A daisy chain is a garland created from daisy flowers, in which the stem of one daisy is made to breach a hole located in the stem of another ('stoppered' by the flower's head) to make a continuous chain. In molecular form, daisy chains[767,768] are the cousins of rotaxanes; they are self-complementary rotaxanes with dumbbells appended covalently to rings. They come in cyclic (denoted by an italicized 'c' in brackets) and acyclic (italicized 'a') forms. Thus, a [*cn*]daisy chain is a cyclic daisy chain with *n* mechanically-bonded component parts, and the acyclic counterpart is an [*an*]daisy chain. [*c*2]Daisy chains are the simplest and most commonly made rotaxanes of this architectural family. Many types supramolecular daisy chains,[429,713,767,769–792] which lack stoppers to seal their mechanical bonds, are available to template the formation of rotaxanes of the same name. We can distinguish between molecular daisy chains with and without formal mechanical bonds using a "rotaxane" suffix or a "supramolecular" prefix, respectively.

[cn]Daisy Chains

Seminal examples of cyclic daisy chain rotaxanes belonging to various families of templation motifs are illustrated in **Figure 4.81**. Several claims[793–796] can be made to the first daisy chain rotaxanes—also called Janus[795] or hemaphrodite[797,804] [2]rotaxanes in the case of the [*c*2] architecture—since several groups independently began reporting their investigations on daisy chain rotaxanes at the turn of the millenium in 2000.

The seminal dialkylammonium/crown ether [*c*2]daisy chain **R4122H$_2^{2+}$** was obtained[793] upon dimerization of [2]rotaxanes, possessing aldehyde-functionalized DB24C8 rings and triphenylphosphonium-stoppered dibenzylammonium dumbbells, by Wittig exchange. The unsymmetrical substitution pattern of the ring's benzo units leads to the formation of a pair of enantiomeric stereoisomers and the corresponding *meso*- diastereoisomer. For the sake of simplicity, a similar [2]rotaxane based on the symmetrically substituted benzo-*meta*-phenylene[25]crown-8 (BMP25C8) was also characterized in both solution and, upon reduction of the double bonds,[797] in the solid state by X-ray crystallography—see **Figure 1.29d** and **Figure 1.29f**, respectively, in **Section 1.3.3**. A number of $R_2NH_2^+$/crown [*c*2]daisy chains have been obtained by alternative protocols, including those based on stoppering by nucleophilic substitution[798] and CuAAC click chemistry.[799,800] Chiu[801] has employed his "swelling" approach to rotaxane synthesis—see **Section 2.3.4.6**—to seal the mechanical bond of the [*c*2]daisy chain **R4123H$_2^{2+}$**, which derives (**Figure 4.81**) from paracyclophane-encircled dialkylammonium templates. Cyclic daisy chain dimers have also been obtained by thermodynamically controlled clipping protocols, including ring-closing olefin metathesis[802] (**Section 3.4.1.3**) and the reversible clipping[803] (**Scheme 3.26**, **Section 3.3.1.2**) of imine-containing crown ethers.

Sauvage[796] introduced (**Figure 4.81**) the metallo[*c*2]daisy chain **Cu$_2$R4124^{2+}** by S_N2 stoppering of the corresponding [*c*2] dimer with a terpy-containing semidumbbell. The daisy chain can be contracted, such that the rings encircle the terpy ligand, by template exchange to pentacoordinate Zn^{II}—see **Section 6.13.1.1**.

Cyclodextrins represent (**Figure 4.81**) yet another prominent family of recognition motifs in the world of daisy chains. The first CD-based daisy chain rotaxane **R4125**, which was assembled by Harada[794] using an aqueous S_NAr stoppering protocol of cross-threaded cinnamoyl-α-CD monomers, was found to co-constitute the relatively uncommon [*c*3] architecture. Only days after Harada's seminal report, Kaneda[795] claimed the first synthesis of an α-CD [*c*2]daisy chain (**R4126**) by taking an azo coupling approach to stopper the corresponding supramolecular precursor. Other CD-based daisy chains have also been prepared by Easton,[804,805] Kaneda,[806] Harada,[807,808]

Beer[809] has employed (**Figure 4.81**) one of his [N–H···Cl^-] anion template motifs (**Section 2.3.6.2**) in combination with ring-closing olefin metathesis (**Section 3.4.1.4**) to synthesize the [*c*2]daisy chain **R1427·2Cl**.

The neutral [*c*2]daisy chain **R4128** was constructed (**Figure 4.82**) by Huang[810] from an aminododecyl-modified permethylated PA5 host and an isocyanate-based stopper precursor by way of urea formation. This compound can be operated (**Section 6.13.1.1**) as a solvent-driven molecular switch.

The π-donor/π-acceptor templation motif was relatively late onto the daisy chain rotaxane scene, in spite of being involved in some of the earliest investigations[769] on *supramolecular* daisy chains. Donor-acceptor daisy chain *rotaxanes* were introduced[811] (**Figure 4.81**) in the form of the bistable [*c*2]daisy chain **R4129**, obtained by a typical CuAAC stoppering protocol involving cross-threaded neutral NDI-functionalized π-donating crown ethers. The thermally and electrochemically driven switching of this compound is discussed in **Section 6.13.1.1**.

Winpenny[812] has assembled an inorganic-organic hybrid [*c*2]daisy chain by adapting his templated synthesis of heterometallic anionic rings—see **Section 2.3.7.1**—such that the organic thread, which derives from a pyridine-terminated dialkylammomium cation, acts as both a template and a ligand. The heterometallic rings of the [*c*2]daisy chain **R4130** contain, on average, two Zn^{II} and six Cr^{III} centers per ring, with one of the Zn^{II} centers adopting a pentacoordinate geometry adjacent to the organic thread's attachment point. The second Zn^{II} site cannot be located precisely based on crystallographic measurements, but magnetic and spectroscopic data, which are sensitive to the length of the Cr^{III}_n chains within the ring, indicate that the second Zn^{II} atom is either adcacent to or one atom removed from the first, in a 3:7 ratio, respectively. Both of these isomers are illustrated (**Figure 4.81**) in the stereoformula of **R4130**.

Recently, Qu[813] and Coutrot[814] have independently introduced (**Figure 4.81**) a new [*c*2]daisy hetero[4]rotaxane architecture, in which the axles of a [*c*2]daisy chain are each threaded by an additional ring. Both compounds **R4131H$_2^{2+}$** and **R4132H$_2^{2+}$** are obtained by one-pot CuAAC click chemistry protocols involving self-sorted *dialkylammonium⊂crown* pseudorotaxane precursors.

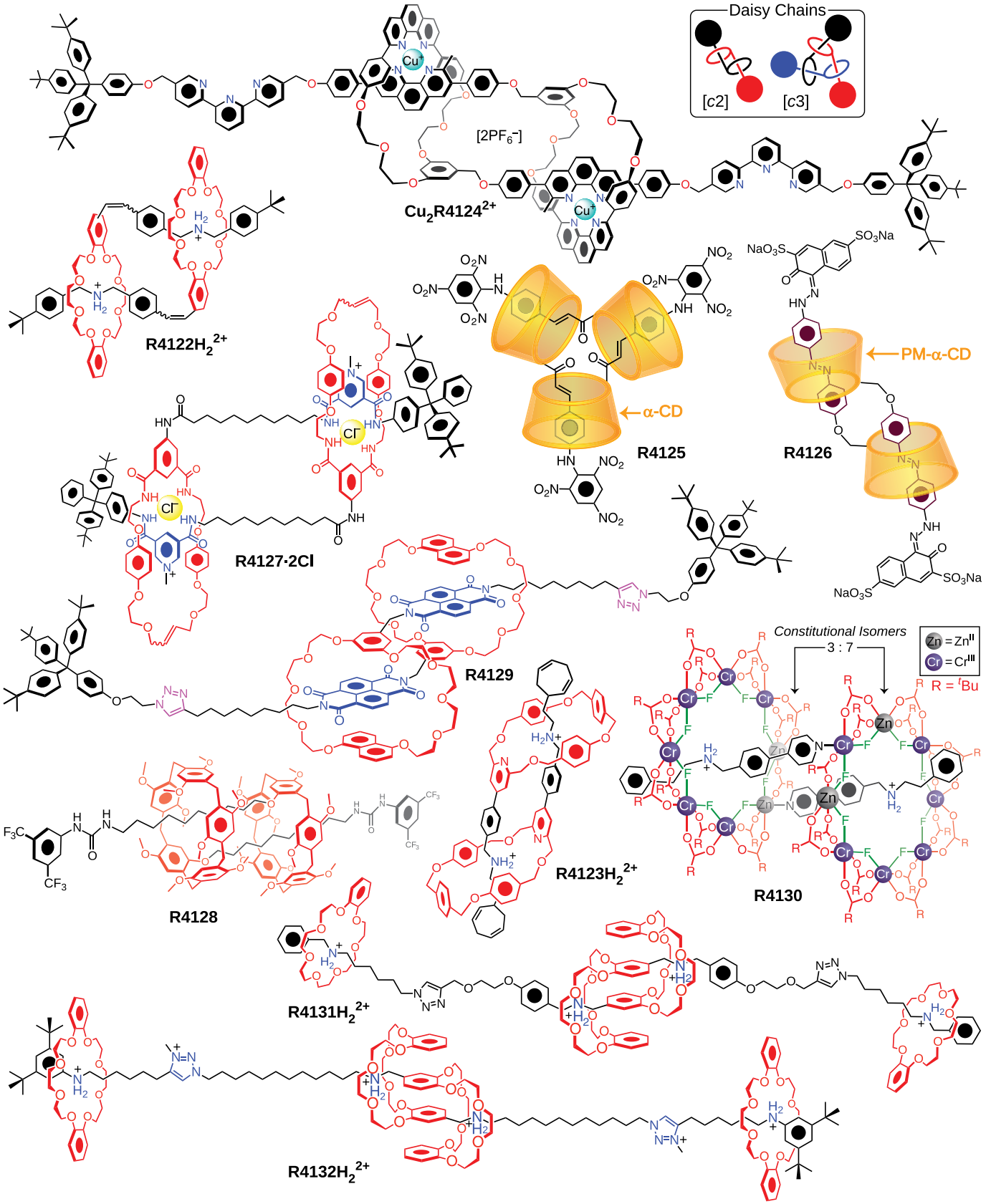


Figure 4.81 Selected examples of cyclic daisy chains.[793–796,801,809–814]

Relying on prior insights from DNA nanotechnology (**Section 2.3.12.1**), Famulok[815] has recently prepared [*c*2]-daisy chain rotaxanes made up of double-stranded DNA. Graphical representations and AFM images of these very large (~100 nm outstretched length) interlocked macromolecules are given in **Figure 4.82**. These daisy chains can be "locked" and "unlocked" from states of high and low co-conformational mobility using strand displacement reactions—see **Section 6.6.2**.

The large-amplitude extensile and contractile motions of [*c*2]daisy chains—see **Section 6.13.1.1**—has generated interest in employing them as artificial muscles.[816–820] Making artificial muscles powered by these molecular machines will require that the daisy chains be integrated into polymer materials in order to scale their nano-motions to the macroscopic level. Towards this end, a number of poly[*c*2]daisy chains have been created by covalent,[802,821–824] supramolecular,[825,826] and metallosupramolecular[827,828] polymerizations. Some of these polymer materials are indeed worthy of the title of artificial muscles—see **Section 6.15.1.2**.

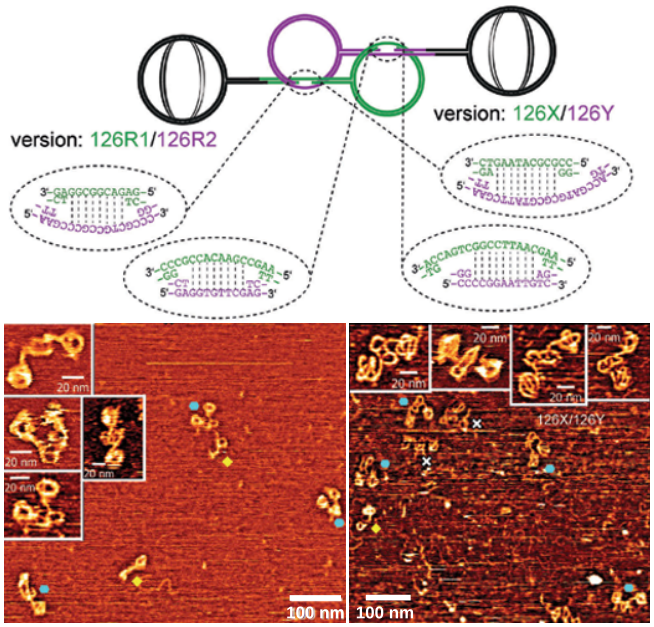
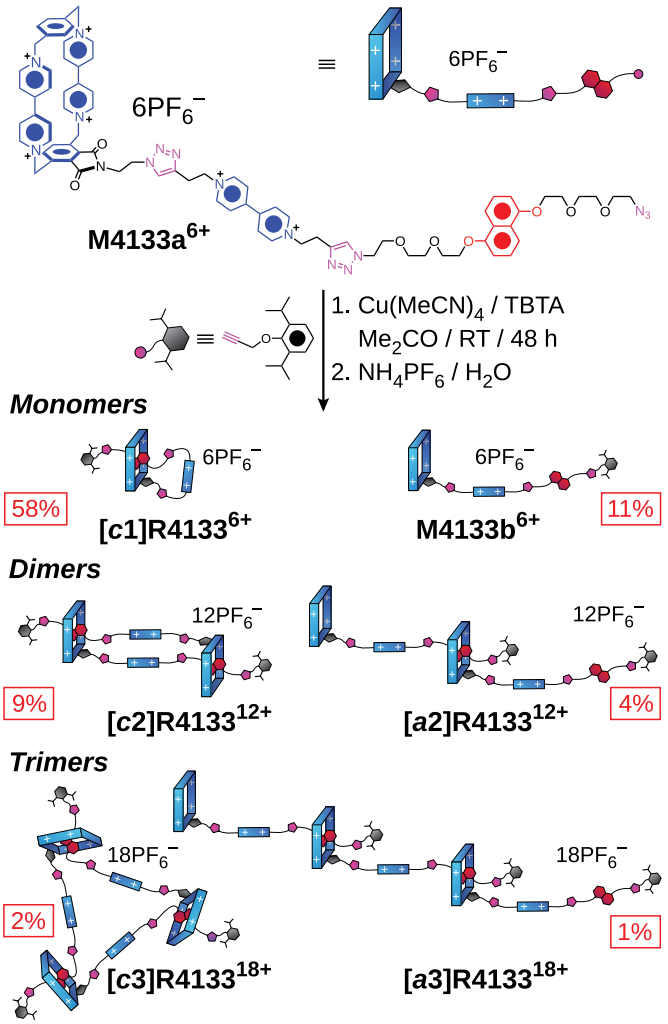


Figure 4.82 Graphical representation and AFM images of Famulok's ssDNA [*c*2]daisy chain rotaxanes.[815]

[an]Daisy Chains

It has proven[739] to be possible to obtain a mixture of cyclic and acyclic daisy chains in a single one-pot reaction. In a CuAAC stoppering protocol (**Scheme 4.34**) based on the DNP/BIPY^{2+}/CBPQT^{4+} monomer **M4133a^{6+}**, the monomeric (**M4133b^{6+}**, **[*c*1]R4133^{6+}**) dimeric (**[*c*2]R4133^{12+}**, **[*a*2]R4133^{12+}**), and trimeric (**[*c*3]R4133^{18+}**, **[*a*3]R4133^{18+}**) products could all be isolated chromatographically by reversed-phase HPLC. These daisy chains are electrochemically extendable, since the axle's BIPY$^{\bullet+}$ radical cation moves within the ring's CBPQT$^{2(\bullet+)}$ diradical dication when reduced electrochemically—see **Section 6.13.1.1**.



Scheme 4.34 One-pot CuAAC "click" synthesis of daisy chain monomers, dimers, and trimers of both cyclic [*cn*] and acyclic [*an*] varieties.[739]

While the distribution of cyclic and acyclic oligomers depends on concentration, the population is highly biased in favor of monomers. Thus, the formation of daisy chain polymers by supramolecular templation necessitates a synthetic strategy that compensates for the entropic driving force to form these kinds of small oligomers.

Although the tendency of self-complementary ring-axle synthons to self-assemble into small cyclic oligomers can interfere with the formation of long, higher-order [*an*]daisy chains, a few accounts of [*an*]daisy chain oligomers and polymers have appeared in the literature. Harada[774] has obtained the low-M_W [*an*]daisy chain polymer **R4134** by stoppering the corresponding supramolecular [*an*]daisy chain assemblies based on 2-cinnamoyl-α-CD. MALDI mass spectrometry revealed (**Figure 4.83**) that oligomers of up to 10 repeating units were isolated.

Huang[829] has circumvented the formation of small cyclic daisy chain oligomers in a "threading-followed-by-polymerization" approach (**Scheme 4.35**), in which the ring–axle bond is formed in the final polymerization step under kinetic control. Relying on Loeb's

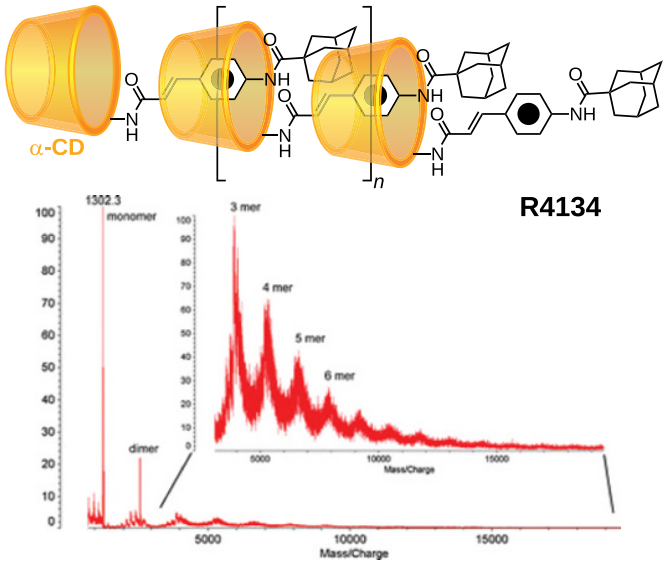
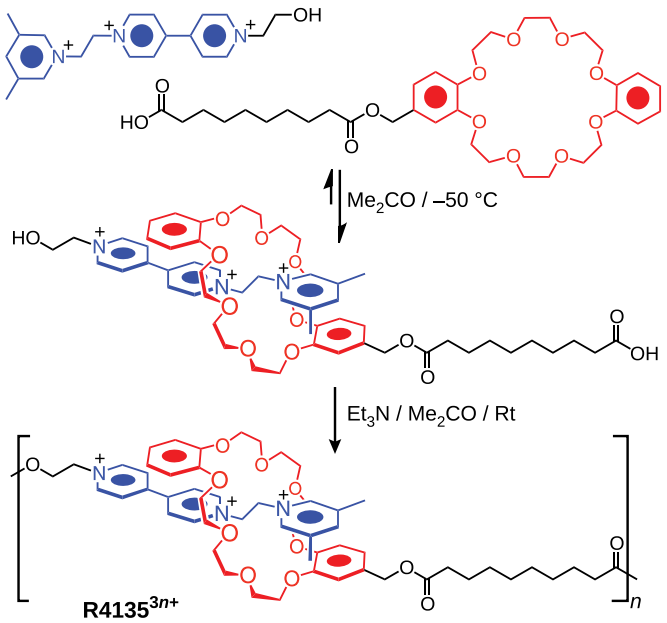


Figure 4.83 MALDI-MS of Harada's [*an*]daisy chain polymer based on adamantane-stoppered 2-cinnamoyl-α-CD.[774]

BPE^{2+}⊂*DB24C8* template motif, a pseudorotaxane is first assembled at low temperature from a sebacoyl chloride-functionalized DB24C8 ring and a hydroxyl-terminated semidumbbell possessing a BPE^{2+} recognition unit. Upon adding NEt_3 as a base and returning to room temperature, the –OH and –COCl groups of the semidumbbell and ring, respectively, are coupled to give the [*an*]daisy chain polyrotaxane **R4135**$^{3n+}$. At a molecular weight of 65 kDa, an average of 45 repeating units are present per polymer chain. An earlier report by Oishi[830] attemped to crosslink the rings and axles of a *dialkylammonium*⊂*DB24C8* semirotaxane by olefin cross metathesis polymerization, yet only oligomers were obtained and their architecture is not well defined on account of the possibility of forming homocoupled macrocycles and dumbbells in the process.



Scheme 4.35 Huang's kinetically controlled synthesis of an [*an*]-daisy chain rotaxane polymer.[829]

The [*an*]daisy chain polymer architecture is only subtly different from a poly[2]rotaxane based on crosslinked rings and dumbbells, in the sense that the daisy chain polymer possesses only one stopper per monomer unit (the ring of an adjacent repeating unit prevents deslipping) instead of two stoppers per monomer. These and other types of poly[2]rotaxanes are discussed in **Section 4.2.3.6**.

4.2.3.3 Ladder Rotaxanes

Having considered architectures based on covalently bridged rings and axles (**Sections 4.2.3.1–4.2.3.2**), we now begin to consider the consequences of introducing covalent bridges between rings (**Sections 4.2.3.3–4.2.3.5**). We focus our attention first on oligo- and polyrotaxane architectures in which multiple bis-macrocyclic component parts thread a pair of dumbbells, forming a mechanically bonded bridge between them. Since polymers possessing covalent bridges of this type are known[831] as ladder polymers, we shall refer to this architecture as that of a "ladder rotaxane".

The simplest possible ladder rotaxane architecture is that (**Figure 4.84**) of the two-rung cyclic [4]rotaxane. This architecture was introduced[704] by the reversible clipping of bis(iminocrown) rings around bis(dialkylammonium) dumbbells, followed by reduction of the imine bonds to give the kinetically stable compound **R4136H**$_4^{4+}$. The imine-based precursor to this compound is illustrated in **Scheme 3.26**, **Section 3.3.1.2**. Wu[402] has employed the same type of clipping protocol to prepare the cyclic [4]rotaxane **R4137H**$_8^{8+}$. The dumbbells of this compound are also component parts (**Figure 4.54**, **Section 4.1.1.1**) of the linear [5]rotaxane[402] **R426H**$_4^{4+}$ and the hetero[4]rotaxane[403] **R427H**$_4^{4+}$ threaded by a central CB6 bead.

Sauvage[832–839] has prepared (**Figure 4.84**) a number of cyclic [4]rotaxanes based on his transition metal template motifs. Two of Sauvage's cyclic metallo[4]rotaxanes possess porphyrinic plates as the bridges between the rings, held either by (i) a rather rigid π-system running between the fused dpp ligands which coordinate the Cu$^+$ templates of the [4]rotaxane[833,834,837] **Cu$_4$R4138**$^{4+}$, or (ii) the relatively flexible polyether loops of the [4]rotaxane[836] **Cu$_4$R4139**$^{4+}$. Remarkably, the solid-state structure of **Cu$_4$R4138**$^{4+}$ has been solved[833] by X-ray crystallography—see **Figure 1.29i** in **Section 1.3.3**. A third cyclic metallo[4]rotaxane,[835,839] **Cu$_4$R4140**$^{4+}$, possesses a rigid design resulting from its short fused pyrazine linkers between the rings. All three of these compounds serve as hosts for appropriately sized guests intercalated between their central plates—e.g., see **Section 6.13.7**. The demetallated [4]rotaxane **R4138** collapses[834] into a compact geometry—see **Section 6.13.6**—in the absence of a transition metal template.

Ladder Polyrotaxanes

Liu[840–842] has constructed (**Figure 4.85**) the ladder poly(pseudo)rotaxanes, *PPG*⊂*(Linker-β-CD$_4$)$_n$*, where the linker is a coordination complex of organoselenium–platinum(IV),[840] bipyridine–copper(II),[841] and biquinoline–

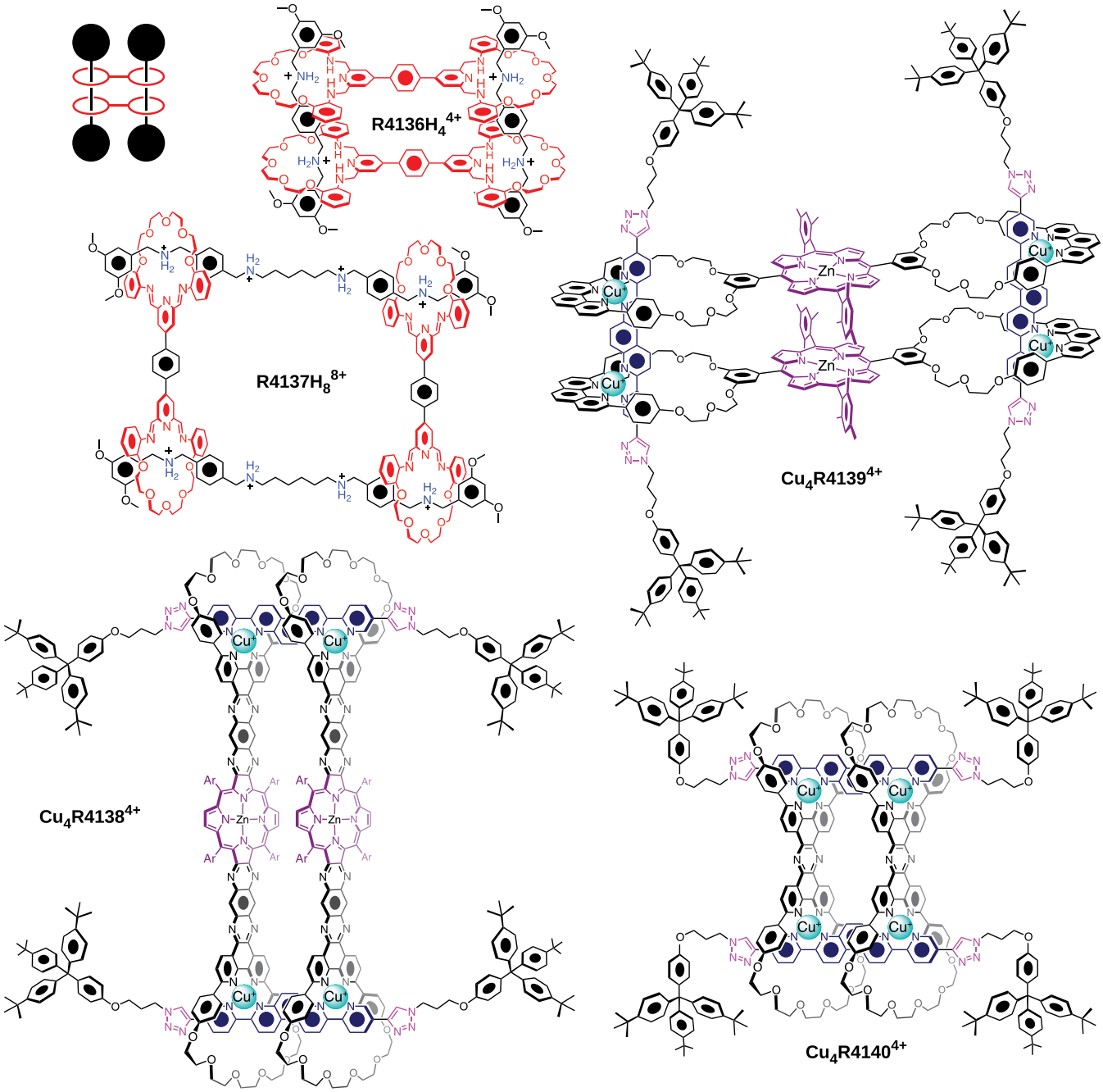


Figure 4.84 Cyclic [4]rotaxanes: two-rung molecular ladders.[402,704,833–836,839]

nickel(II)[842] chelates. The long polymers of uniform width are observable (**Figure 4.85**) by STM and AFM microscopy.

4.2.3.4 Bonnanes/Handcuff Rotaxanes

Another class of ring-bridged MIMs are the "Bonnanes" (**Figure 4.86**), a nickname given by Vögtle[4,396] in homage to the city of Bonn, the former 'bridge capital' of Germany where his group was based. Bonnanes have a robust nomenclature for describing the covalent connections between bridged rings, of the form [*n*]Bonn-*m*(*x*,*y*)ane, where *n* is the combined number of wheels and axles, *m* is the number of covalent bridges, and *x* and *y* are numbers that denote the sequence of the bridged rings along the axle. For example, the most common ring-bridged rotaxane architecture is a [3]Bonn-1(1,2)ane, in which two rings share a single covalent bridge. This particular architecture is also known[843] as a handcuff rotaxane, by analogy with handcuff catenanes—see **Section 4.1.4.2**. Vögtle's inaugural [3]Bonnanes[396] were of this kind, possessing oligomethylene (**R4141a**), oligoether (**R4141b**), and oligoxylene (**R4141c**) bridges. The cyclodirectionality of the trilactam monosulfonamide rings of these Bonnanes enables them to express mechanically planar chirality (**Section 5.2.3.1**), giving rise to a pair of ($R_{mp}R_{mp}$) and ($S_{mp}S_{mp}$) enantiomers and the corresponding *meso* diastereoisomer in each case.

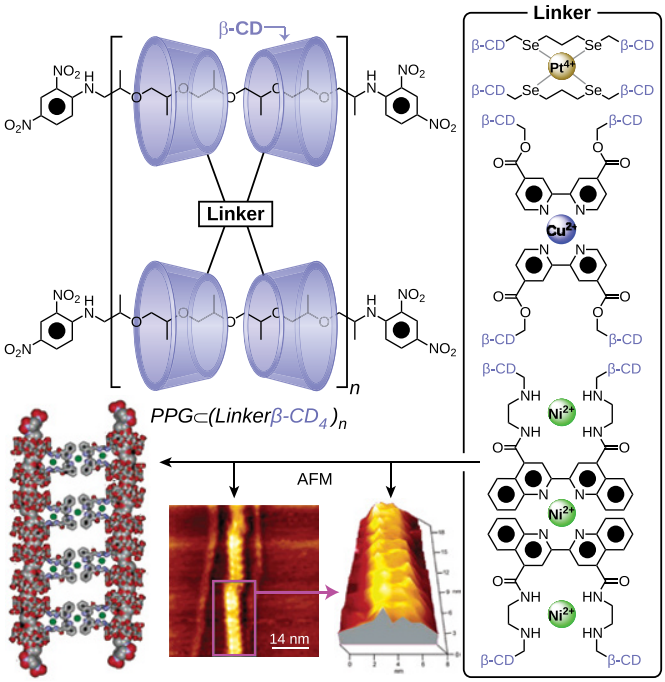


Figure 4.85 Liu's ladder poly(pseudo)rotaxanes based on bridged β-CD rings.[840–842] The model and AFM images of the polymer based on a M_3L_2 Ni^{II} chelate linkers are adapted with permission from ref. 842 (Copyright 2004 American Chemical Society)

The *$R_2NH_2^+$⊂DB24C8* template has been appropriated (**Figure 4.86**) for the syntheses of a number of Bonnanes. Prior to Vögtle's seminal paper[396] on the Bonnane architecture in 2006, a ring-bridged pseudo[3]rotaxane was prepared[844] by olefin cross metathesis of alkyne-functionalized DB24C8 rings encircling bis(dialkylammonium) threads. It was not until 2010, however, that Iwamoto[845,846] finally revisited olefin metathesis in the preparation of the [3]Bonnane **R4142H$_2^{2+}$**—see **Scheme 3.43** in **Section 3.4.2**. In the intervening period, Takata[847] had produced an example of a doubly-bridged [3]Bonnane,[N] or [3]Bonn-2(1,2)ane, **R4143H$_2^{2+}$**. A couple of switchable Bonnanes based on *$R_2NH_2^+$⊂crown* motifs have also been invented: Liu[848] has driven the shuttling of a [3]Bonnane's anthracenebis(B24C8) macrocycle by pH changes—see **Section 6.13.1.3**—and Chen[849] has recently described an unusual kind of "flapping" motion in a [3]Bonnane's pentiptycene-bridged bis(DB24C8) component part—see **Section 6.13.5**.

Gaeta and Neri[843] have employed (**Figure 4.87**) the *dialkylammonium⊂CA6* threading motif (**Section 2.3.9.1**) in order to prepare Bonnanes comprising (**Figure 4.86**) a *meta*-xylylene-bridged OMe_5CA6 bis-macrocycle and a bis-dialkylammonium

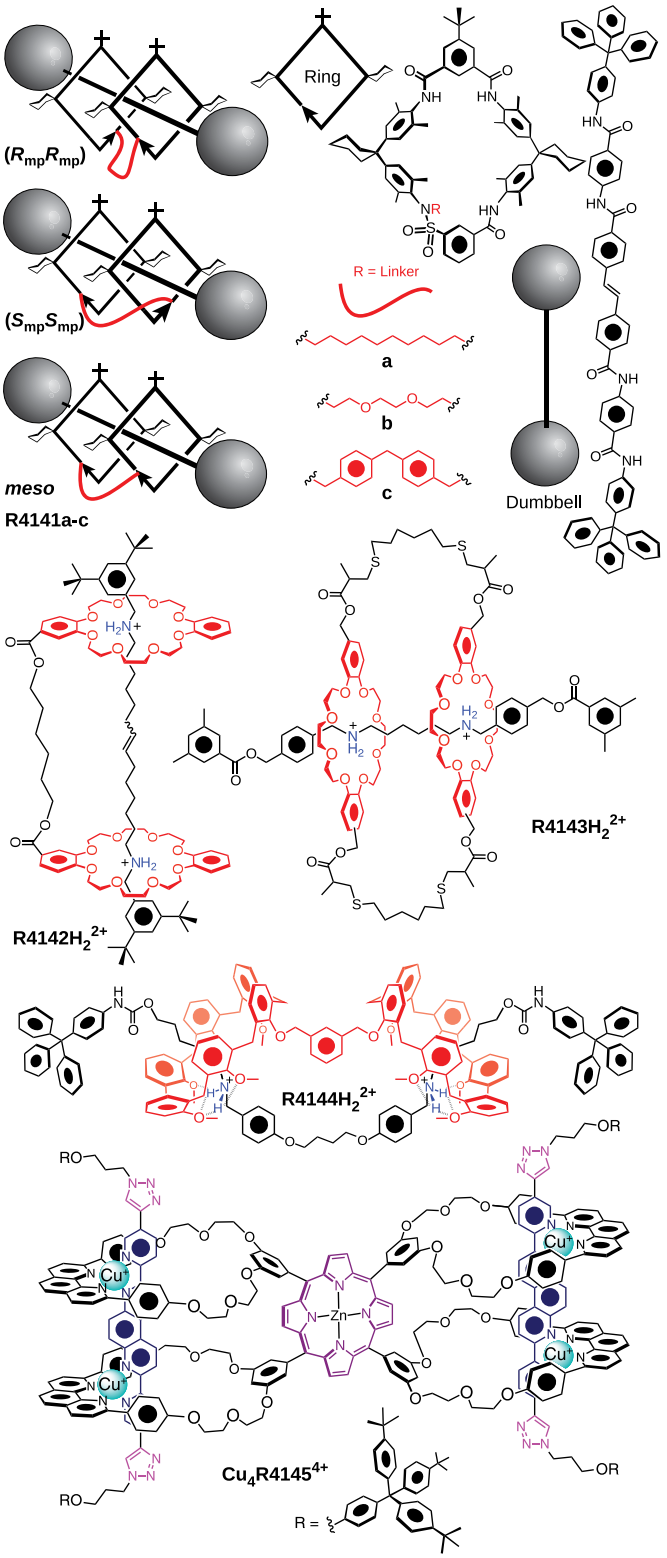


Figure 4.86 Bonnanes.[396,843,845,846,850]

dumbbell by a stoppering approach involving *p*-tritylphenylisocyanate. While multiple orientational isomers (**Section 5.2.1**) are possible, given the asymmetry of the *N*-benzyl-*N*-hexylammonium recognition units and the conical shape of the rings, only the so-called *tail-to-tail* isomer **R4144H$_2^{2+}$** was detected.

[N] We note that the installation of a second covalent bridge between two rings in a Bonnane creates a macrotricyclic species. Therefore, [3]Bonn-2(1,2)anes such as **R4143H$_2^{2+}$** could be equally categorized as macrotricyclic [2]rotaxanes akin to those described in **Section 4.2.1.3**. Likewise, the macrotricyclic and higher-order multicyclic [*n*]rotaxanes could be equally classified as Bonnanes—another case in which mechanomolecular architectures cannot be cleanly subdivided into their respective categories.

Sauvage[850] has constructed a three-component rotaxane that can be characterized as a bis(handcuff) rotaxane or a bis[3]Bonnane. The compound **Cu_4R4145^{4+}** comprises (**Figure 4.86**) a tetramacrocycle based on a central porphyrinic plate, the rings of which thread pairwise onto the same pair of dumbbells as those supporting the ladder-shaped cyclic metallo[4]rotaxanes discussed in **Section 4.2.3.3**.

Poly(Bonnane)s

A few poly(Bonnane)s are illustrated in **Figure 4.87**. Shortly after introducing[460] the *PEG⊂(α-CD)$_n$* threading motif—see **Figure 4.58** in **Section 4.2.1.1**—Harada[520] crosslinked the –OH groups of the CD rings with propylene oxide. The poly(Bonnane) **R4146**, containing a polydisperse distribution of crosslinks between neighboring CD rings, can then be converted into an all-organic polymer nanotube upon hydrolysis of the stoppers with NaOH and extraction of the axle. Liu[851] has described a metallosupramolecular polymerization that affords the polyrotaxane **Cu_nR4147^{2n+}**, which possesses the architecture of a poly([3]-Bonn-1(1,2)ane), owing to its calix[4]arene-based blocking groups within each monomer unit encapsulated by ring-bridged α-CD dimers surrounding the Cu^{II} linkers. Recently, Chen[852] introduced a handcuff polyrotaxane/poly[3]Bonnane of the same architecture (**R4148H$_{2n}^{2n+}$**) by employing a "pseudosuitane" complex based on a triptycene-bridged DB24C8 dimer in a CuAAC click polymerization protocol.

Relying on his Sauvage-inspired polymetallorotaxane motif—see **Scheme 4.30** in **Section 4.2.1.1**—Swager[587] has designed an EDOT-functionalized macrocyclic ligand, Mdpp32EDOT$_2$, the corresponding 2T$_2$bpy-threaded pseudorotaxanes of which electropolymerize (**Scheme 4.36**) to form

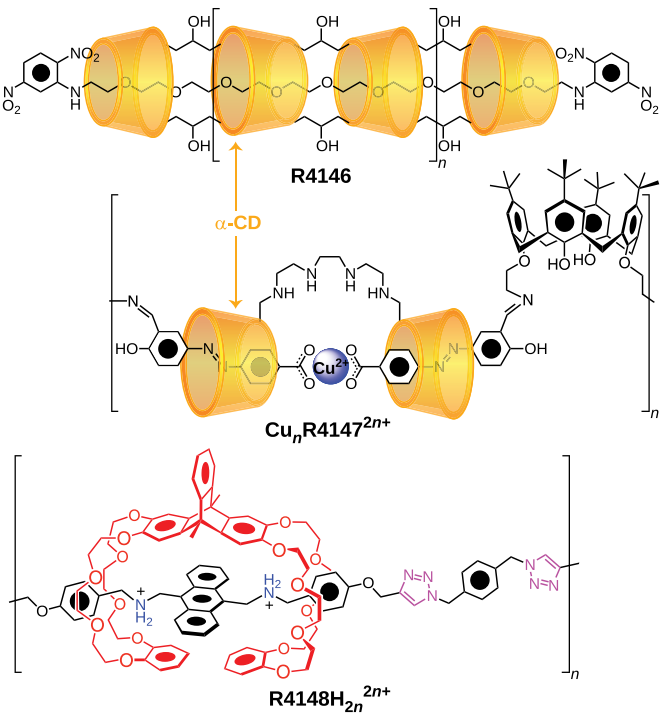
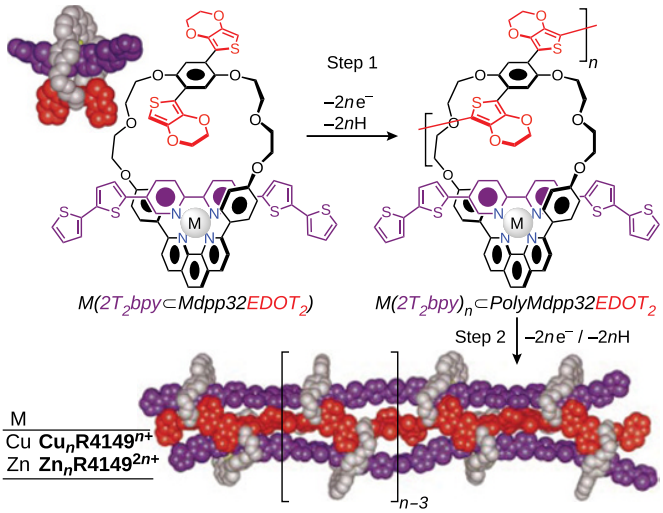


Figure 4.87 Poly(Bonnanes).[460,851,852]



Scheme 4.36 The synthesis by electropolymerization of Swager's bis(polyrotaxane) ladder polymer.[587]

thin films of the triple-stranded ladder polyrotaxanes **Cu_nR4149^{n+}** and **Zn_nR4149^{2n+}**, in which the outer two strands are mechanically bonded to a central one. The polymer is preorganized to form the triple-stranded architecture on account of the EDOT monomers embedded in the loop of the macrocyclic ligand, which is half the length of the 2T$_2$bpy monomers of the axle in the pseudorotaxane *M(2T$_2$bpy⊂Mdpp32EDOT$_2$)*, where M is a Cu^+ or Zn^{2+} ion. The formation of cross-linked (two dimensional) polymers cannot be precluded, on account of the flexibility of polyether loops by which the EDOT monomers are held. The conductivities of these films are much higher (>1 S·cm^{-1}) than those (<10^{-3} S·cm^{-1}) of the polymetallorotaxanes on which they are based. Since the innermost strand of the polymer is a better conductor than the two outermost chains, this material represents another type of insulated molecular wire.

4.2.3.5 n-Fold [2]Rotaxanes: Molecular Bundles

[2]Rotaxanes derived from tripodal, tetrapodal, etc. component parts with *n* interlocked branches (**Figure 4.88**) may be referred to as *n*-fold [2]rotaxanes. These compounds were nicknamed "mechanically interlocked bundles" when they were introduced[853–855] in 2004 from so-called superbundles[856,857] comprising tripodal tris(dibenzylammonium) and tris(crown ether) pairs. While the seminal example[853] (**R4150H$_3^{3+}$**) of this architecture was stoppered by a copper-free azide–alkyne cycloaddition, a similar triply interlocked bundle has been synthesized[858] under thermodynamic control by olefin cross metathesis (**Section 3.4.1.3**) of the rings' olefinic functional groups. When these compounds are designed to express bistability, such that the polycyclic component part can be translocated under the influence of external stimuli with respect to the threaded axles, the switch is known[854,859] as a "molecular elevator" since it resembles a molecular platform moving up and down a rig—see **Section 6.13.1.3**.

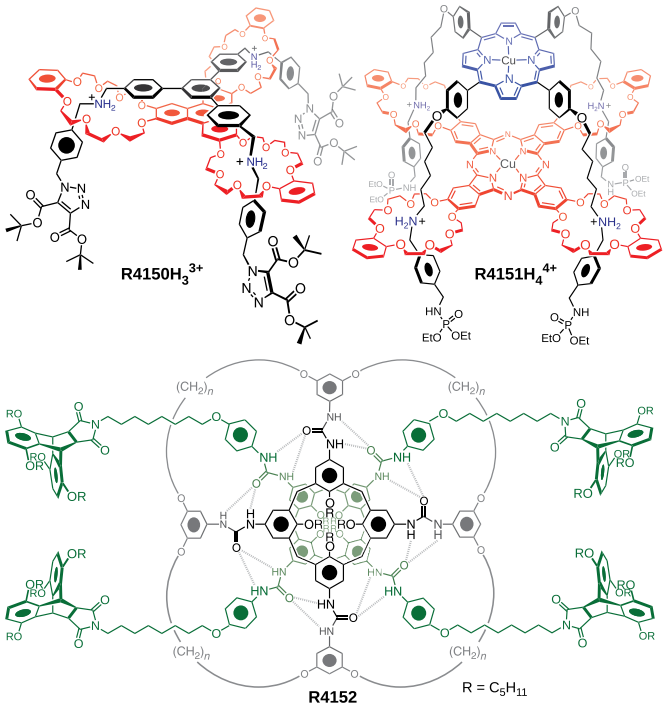


Figure 4.88 Seminal examples of three-fold[853] and four-fold[860,864,865] [2]rotaxane "molecular bundles" based on various hydrogen-bonded template motifs.

In addition to the threefold [2]rotaxanes based on $R_2NH_2^+ \subset$ *crown* templation, a number of fourfold-interlocked [2]rotaxane bundles have been described by Tanaka.[860–863] The tetramacrocycle and the tetradumbbell of the assemblies contain phthalocyanine and porphyrin plates, respectively, creating discrete two-component heterostacks of these metalloheterocycles, constrained within the fourfold rotaxane by the mechanical bond. These compounds exhibit novel host-guest and electronic properties, which can be modulated by pH-triggered (**Section 6.13.1.3**) translational motions. The seminal fourfold [2]rotaxane (**Figure 4.88**) of this family is the compound **R4151H$_4^{4+}$**. In one case,[862] the rings and dumbbells were made to extend from the same platform, providing access to an unusual [3]rotaxane molecular bundle. The solid-state structure of **R4151H$_4^{4+}$** is illustrated in **Figure 1.29d** of **Section 1.3.3**.

The assembly[864,865] of the fourfold [2]rotaxane molecular bundle **R4152** (**Figure 4.88**) based on Böhmer's multiannular tetraureidocalixarene motif is illustrated and discussed in **Scheme 2.83**, **Section 2.3.4.5**. Schalley[866] has recently introduced a hydrogen-bonded threefold [2]rotaxane bundle and employed it as an anion-driven molecular elevator—see **Section 6.13.1.3**.

4.2.3.6 One-Dimensional Oligo- and Poly[2]rotaxanes

We turn away from discrete molecules to focus our attention now on polymeric covalently bridged [2]rotaxanes. As noted in **Section 4.2.1.1**, a number of reviews[116,118,354,417–425] on polyrotaxanes are available in the literature. Poly[2]-rotaxanes can be subdivided into the catogories of main-chain (**Figures 4.89–90**) and side-chain (**Figure 4.91**), and each of these architectures may involve covalent attachments between the rings, dumbbells, or both.

Dumbbell-Linked Main-Chain Poly[2]rotaxanes

One of the earliest cases of a main-chain oligo[2]rotaxane was reported by Zilkha[867] in 1976. During a macrocyclization of a [2]rotaxane to obtain a [2]catenane—see **Scheme 2.3** in **Section 2.1**—oligomers as large a trimer were also observed. A number of other examples of main-chain poly[2]rotaxanes with covalent bridges between the dumbbells are illustrated in **Figure 4.89**. Gibson[451–455] has prepared main-chain poly[2]rotaxanes based on statistically threaded crown ethers by polymerizing polyester and polyurethane precursors in the presence of crown ethers. A more detailed account of Gibson's threaded polymers is given in **Section 4.1.1.1**. The tetraphenylmethane-derived blocking groups within the repeating monomer units of the polyesters **R4153a–e** prevent the rings from deslipping, eliminating the need for a stoppering protocol after polymerization.

Osakada and Yamamoto[868] have obtained the α-CD-threaded poly(alkylenebenzimidazole) poly[2]rotaxane **R4154** by the Ru-catalyzed reaction of 1,12-dodecanediol and 3,3´-diaminobenzidine in the presence of α-CD. Since the benzimidazole groups of the polymer are too small to be included in α-CD, they serve as main-chain stoppers. If the reaction is carried out instead in the presence of β-CD, the resulting threaded product is a main-chain [*n*]pseudorotaxane polymer of the kind discussed in **Section 4.2.1.1**, since the β-CD rings are large enough for deslipping.

Another aqueous polymerization of dumbbell-linked poly[2]rotaxanes has been introduced by Tuncel,[581] employing the CB6AAC dumbbell capture reaction—see **Scheme 2.23** in **Section 2.3.1.2**. Farcas[869] has introduced the CB7-threaded π-conjugated polyrotaxane **R4155**, possessing (**Figure 4.89**) bithiophene/dioctylfluorene backbone, as an insulated molecular wire (IMW). IMWs are also included in the discussions of **Sections 4.2.1.1** and **4.2.3.1**.

Leigh[870] has employed his fumaramide/benzylic amide tetralactam rotaxane motif (**Section 2.3.4.2**) in the synthesis of a number of poly[2]rotaxane architectures. The main-chain poly[2]rotaxane **R4156** is obtained (**Figure 4.89**) by reacting the corresponding [2]rotaxane precursors, possessing protected isocyanate stoppers, with Jeffamine D400, a low-M_w amino-terminated PPG derivative. After heating the rotaxane and bis(amine) comonomers at 175 °C for 1 h, the resulting polymer contains an average of 46 [2]rotaxane units per chain.

Ikeda[871] has prepared a donor-acceptor poly[2]rotaxane **R4157^{4n+}** by electropolymerization of a CBPQT^{4+}-encircled dumbbell derived from EDOT-functionalized quaterthiophene, a polymerization method inspired by the pioneering work of Swager[585–587] and Sauvage[593,594] involving electropolymerized polymetallorotaxanes—e.g., see **Scheme 4.30** in **Sections 4.2.1.1** for a depiction of a typical

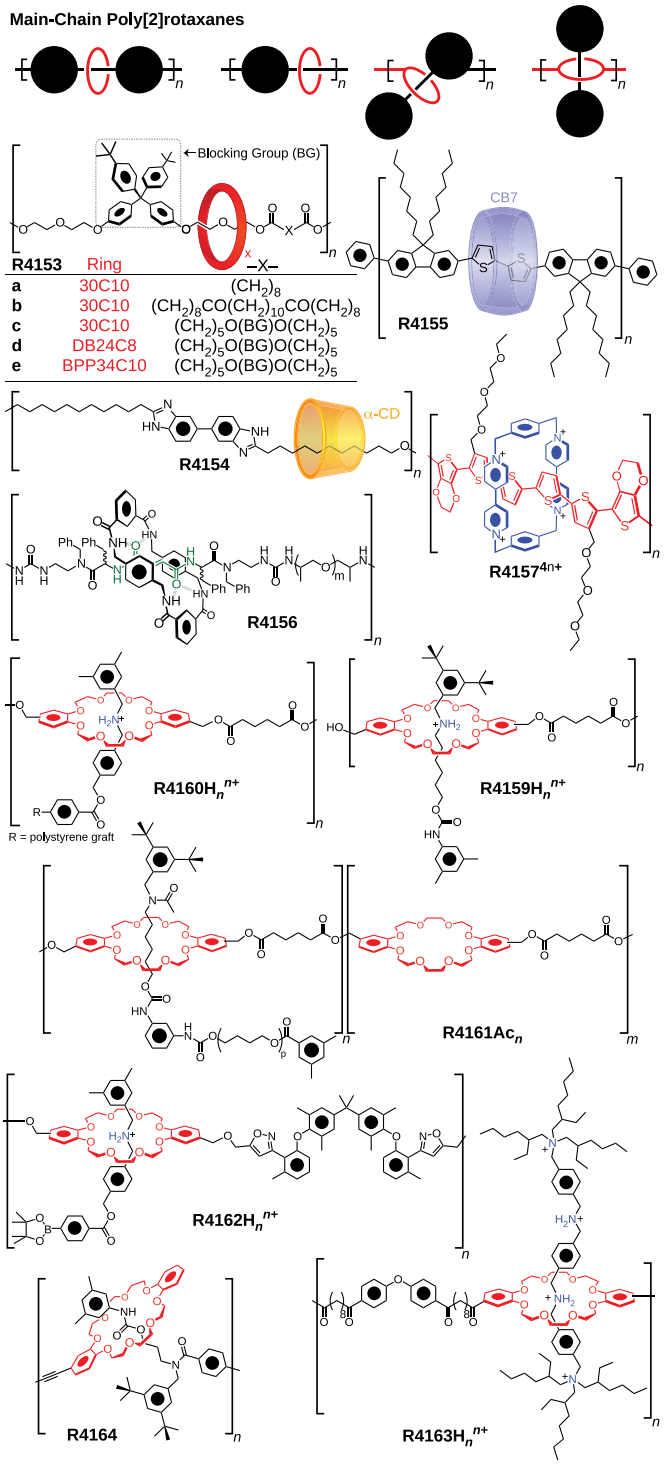


Figure 4.89 Examples of main-chain poly[2]rotaxanes.[451–455,868–871,874–877,879]

electropolymerization protocol based on threaded EDOT monomers. Another poly[2]rotaxane based on CBPQT^{4+} is the inorganic-organic hybrid compound **R4158** whose solid-state structure is illustrated in **Figure 4.90**. Li[872] obtained this poly[2]rotaxane by co-crystallization of copper(I) thiocyanate and CBPQT^{4+}, where the Cu(NCS) salt forms a one-dimensional network passing through the annulus of a string of CBPQT^{4+} rings.

More examples of inorganic-organic hybrid poly[2]rotaxanes have been described by Zang and Wang,[873] in which *ethylenediamine*⊂*CB6* [2]rotaxane repeating units are connected by $[Cd_2Ge_8V_{12}O_{48}]$ polyoxometallate clusters as the stoppers/linkers in the main-chain backbone.

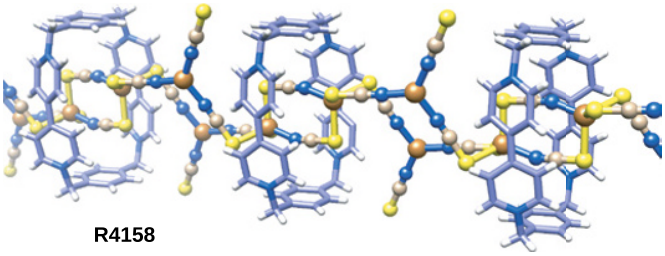


Figure 4.90 The structure of the inorganic-organic hybrid poly[2]rotaxane **R4158**, which comprises organic CBPQT^{4+} rings encircling an inorganic $[Cu_4(SCN)_8]_n$ thread.[872] The CBPQT^{4+} rings (shaded pale blue and white) are represented in tubular form, while the $[Cu_4(SCN)_8]_n$ thread is represented in ball-and-stick form (Cu = orange, N = blue, S = yellow, C = tan).

Ring-Linked Main-Chain Poly[2]rotaxanes

Takata[874–876] has pioneered the development of polyrotaxanes based on poly(DB24C8) backbones. Employing the dialkylammonium/crown ether recognition motif, his group has synthesized the poly[2]rotaxanes (**Figure 4.89**) **R4159H$_n^{n+}$**, **R4160H$_n^{n+}$**, **R4161Ac$_n$**, and **R4162H$_n^{n+}$** by typical threading-followed-by-stoppering protocols—see **Section 2.3.4.6**. In the cases of **R4160H$_n^{n+}$** and **R4161Ac$_n$**, Takata[875,876] has introduced graft polymers on the stoppers of the mechanically linked dumbbells. Polystyrene and poly(THF) have been grafted onto these polymers by stoppering protocols involving the formation of boronate ester and urethane bonds, respectively. It is expected that the high co-conformational mobility of the grafted polymer chains within these ring-linked poly[2]rotaxanes will impart the polymers with unusual mechanical and thermal properties.

Wu and Xu[877] have recently developed a main-chain poly[2]rotaxane **R4163H$_n^{n+}$** as an anion-exchange membrane and demonstrated that the pH- and temperature-controlled shuttling of the mechanically linked dumbbells within each repeating unit accelerates OH^- ion transport in the material.

Heterolinked Poly[2]rotaxanes

Tsivgoulis[878] has discussed a strategy for preparing donor-acceptor ring-to-stopper linked polyrotaxanes by a stepwise procedure involving sequential deprotection and coupling steps, which conjoin the functionalized CBPQT^{4+} rings and dumbbells by esterification.

Takata[879] has polymerized a DB24C8-based [2]rotaxane by Sonogashira coupling of its iodophenyl-functionalized dumbbell and ethynyl-functionalized ring to obtain the poly[2]rotaxane **R4164**—see **Figure 4.89**.

Side-Chain Poly[2]rotaxanes

As their name implies, the mechanical bonds of side-chain poly[2]rotaxanes are not located on the main chain backbone. The first side-chain poly[2]rotaxanes were prepared in the late 1960s by Harrison,[880] who performed repeated statistical threading and stoppering protocols on the surfaces of polymeric peptide resin—see **Section 2.1**. A number of side-chain poly[2]rotaxanes have been built (**Figure 4.91**) on the foundations of supramolecular templation involving hydrogen bonding, hydrophobic forces, π-donor/π-acceptor, and metal coordination. We briefly describe a few examples to illustrate some of the types of architectures, motifs, and polymer backbones that have been investigated to date.

Among the most widely employed backbones in side-chain poly[2]rotaxanes are those of poly(acrylate)s, poly(methacrylate)s and poly(acrylamide)s, since their synthesis by free-radical polymerization is facile, efficient, and tolerant of many functional groups. For example, Takata[881,882] has obtained the polymers **R4165H**$_{(n+m)}^{(n+m)+}$ and **R4166H**$_{(n+m)}^{(n+m)+}$, by polymerization of *dialkylammonium⊂DB24C8* semidumbbells terminated with acrylate (R = H) and methacrylate (R = Me) esters, or by co-polymerization with these monomers and styrene, respectively.

A number of dialkylammonium/crown ether side-chain poly[2]rotaxanes that are not illustrated in **Figure 4.91** are worthy of acknowledgment. Osakada[883] has prepared side-chain poly[2]rotaxanes by clicking ferrocene-capped *dialkylammonium⊂DB24C8* semirotaxanes onto polysiloxanes. Takata[884–887] has introduced a number of π-conjugated polymers in which the pH-controlled co-conformations of side-chain [2]rotaxanes influence the superstructure of the main-chain backbone—see **Section 6.15.1.4**. Ren and Qu[888] have employed CuAAC click chemistry to graft bistable (**Section 6.3.3.1**) dibenzylammonium/crown ether [2]rotaxanes as side-chains of a polymethacrylate backbone. The pH-driven shuttling[888] of the ferrocene-functionalized rings is accompanied by visible fluorescence changes, owing to the distance-dependent energy transfer between the Fc groups and a fluorogenic morpholinonaphthalimide stopper.

Ritter[889–895] has investigated several poly[2]rotaxanes possessing side chains encircled (**Figure 4.91**) by DM-β-CD. For example, the polyacrylamide **R4167** is obtained[895] such that nearly all of its undecamethylene side-chain dumbbells are covered by rings, owing presumably to the high-affinity binding between DM-β-CD and the stoppers derived from cholic acid during free-radical polymerization. Compound **R4168** is Ritter's seminal side-chain poly[2]rotaxane, based[889] on an *undecamethylene⊂DM-β-CD* semidumbbell, which was grafted onto a poly(methacrylamide) backbone by an amide bond-forming nucleophilic attack on a polymeric precursor displaying ethyl ester side chains. Ritter has also relied on nucleophilic DM-β-CD semidumbbells to mount similar side-chains onto backbones based on poly(ether-sulfone)[890,894] poly(ether-ketones)[892] main chains, as well as a side-chain poly(bis[2]rotaxane).[891,893] Osakada's polymer **R4169** contains[896] up to two side-chain [2]rotaxanes per repeating monomer unit, although the

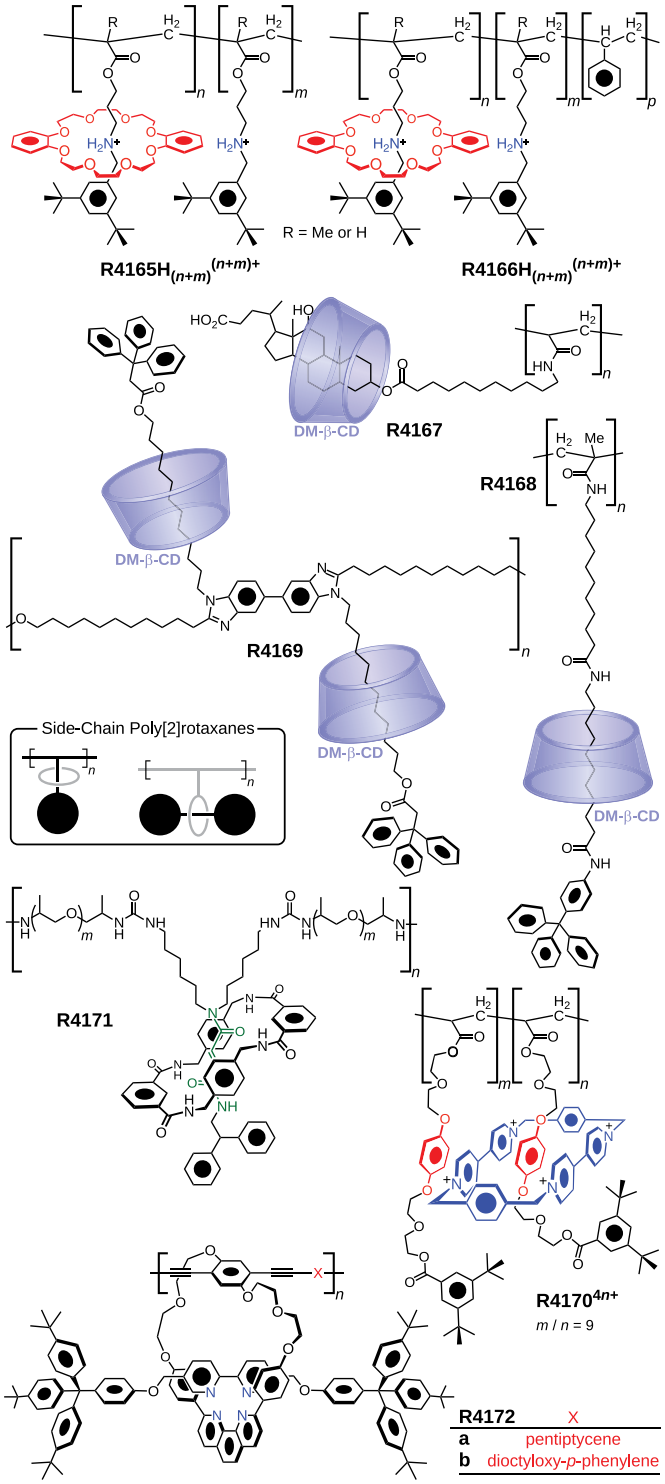


Figure 4.91 Side-chain poly[2]rotaxanes.[870,881,882,889,895–897,900]

bis(benzimidazole) anchor groups in the backbone were not alkylated quantitatively by the corresponding *dodecamethylene⊂TM-β-CD* semidumbbells during its synthesis by S_N2 poly-substitution on the main chain.

Takata[897] prepared the π-donor/π-acceptor poly[2]rotaxane **R4170** by free-radical polymerization of an acrylate-terminated *HQ⊂CBPQT*$^{4+}$ semirotaxane. Only ~10% of the side chains are threaded (**Figure 4.91**) by CBPQT^{4+}

rings, however, owing perhaps to a much faster rate of polymerization of the uncomplexed semidumbbell in equilibrium with the semirotaxane feedstock. More recently, a ring-linked side-chain poly[2]rotaxane based on *DNP*⊂*CBPQT*$^{4+}$ templation was obtained by Cooke,[898] employing CuAAC click chemistry to graft a propargyl-functionalized [2]rotaxane to a side-chain poly(azide).

The side-chain poly[2]rotaxane **R4171** introduced by Leigh[870] has been obtained (**Figure 4.91**) with a degree of polymerization corresponding to 96 rotaxane repeating units per chain in a protocol involving the co-polymerization of Jeffamine D400 and a [2]rotaxane displaying a pair of protected isocyanate groups on one of its stoppers. Lin[899] has introduced a pH-switchable side-chain poly[2]rotaxane based on one of Leigh's square planar Pd^{II} transition metal template motifs—see **Section 2.3.2.4**—which forms different nanosuperstructures upon solvent evaporation depending on the pH.

Exemplifying the ring-linked side-chain poly[2]rotaxane architecture are the compounds **R4172a** and **R4172b**, which were introduced by Swager.[900] The π-conjugated main-chain backbones, possessing (**Figure 4.91**) pentiptycene-ethynylene and dioctyloxy-*para*-phenylene-ethynylene linkers, respectively, enable these mechano-macromolecules to behave as sensory polymers which exhibit fluorescence changes that are highly sensitive to small-molecule analytes, such as phenols and alcohols, which hydrogen bond to the *N*-donors of the rotaxane ligands in the side chain.

4.2.3.7 One-Dimensional Poly[3]rotaxanes

As in the case of poly[2]rotaxanes, poly[3]rotaxanes can adopt a variety of main-chain and side-chain architectures.

Ring-Linked Main-Chain Poly[3]rotaxanes

A number of mechanically bonded macromolecules belonging to the dialkylammonium/crown ether family of MIMs exemplify (**Figure 4.92**) the main-chain poly[3]rotaxane architecture.

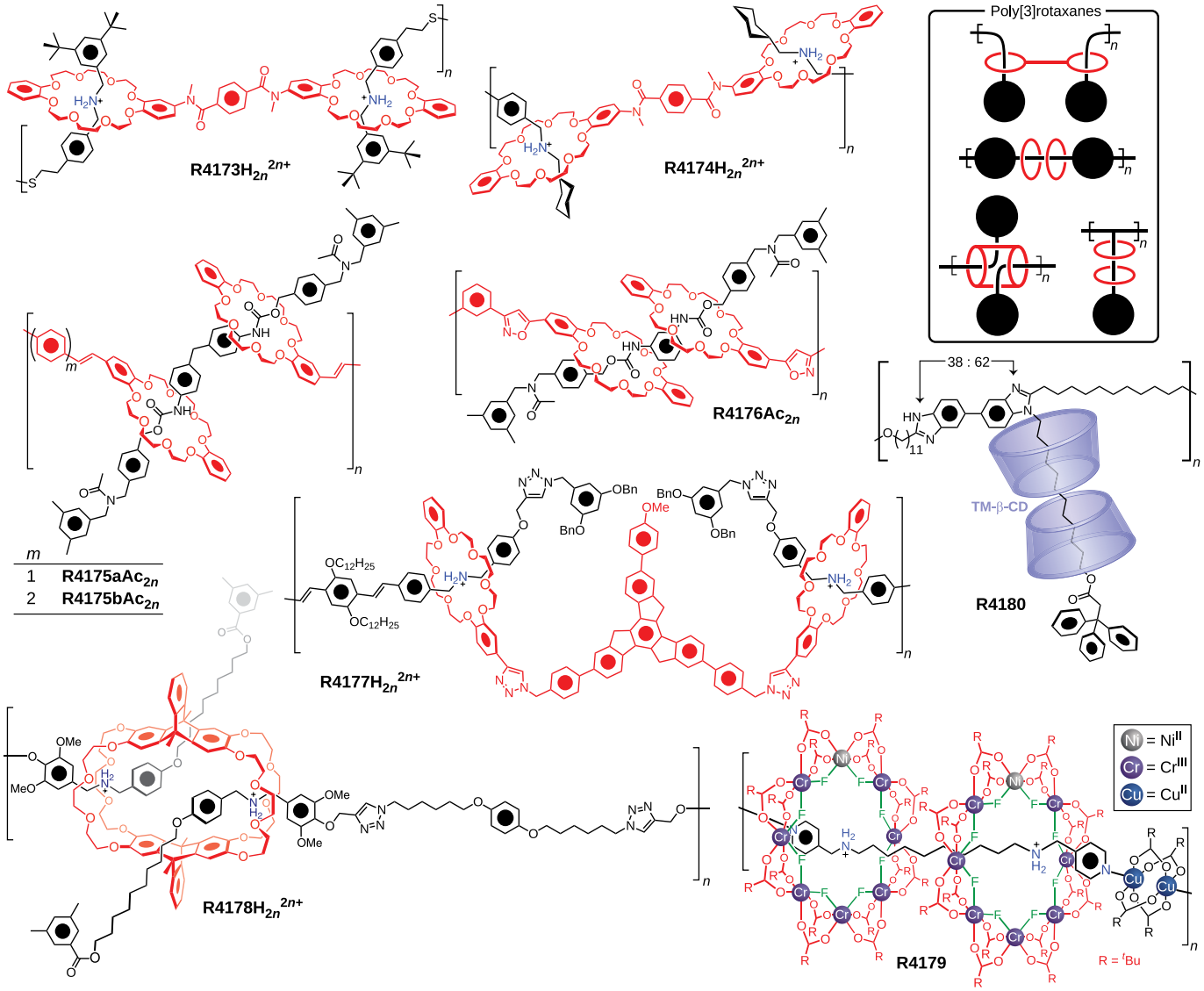


Figure 4.92 Poly[3]rotaxanes.[657,896,901–904,906]

Takata[901–904] has been particularly active in the genesis of poly[3]rotaxanes. He has utilized[901] dynamic thiol exchange processes in the polymerization of a disulfide bond-containing dumbbell and a bis[24]crown-8 handcuff-type macrocycle to yield (**Figure 4.92**) the poly[3]rotaxane **R4173H**$_{2n}^{2n+}$, which exists as a mixture of high molecular weight polymers (M_N = 1.4 kg/mol) and low molecular weight cyclic oligomers. Inspired by the discovery[905] that the cyclohexyl group is a suitable slippage stopper—see **Section 3.1.3**—for the *dialkylammonium⊂DB24C8* recognition motif, Takata[902] has orchestrated the self-assembly of the poly[3]rotaxane **R4174H**$_{2n}^{2n+}$ by "polyslipping". Takata[903] has also prepared the poly[3]rotaxanes **R4175aAc**$_{2n}$ and **R4175bAc**$_{2n}$ by Mizoroki-Heck coupling polymerization of an olefin-terminated [3]rotaxane, as well as the poly[3]rotaxane[904] **R4176** by the efficient isoxazole-forming click polymerization of diynes with nitrile-*N*-oxides.

Takata has been joined in more recent years by other groups in the investigation of poly[3]rotaxanes. Pei[906] has stoppered the co-assemblies of ditopic dialkylammonium axles and crown ethers possessing π-conjugated linkers to obtain two types of main-chain poly[3]rotaxanes, one of which is **R4177H**$_{2n}^{2n+}$. The energy transfer between chromophores provides information about polymer conformation. Huang[907] has shown that it is possible to interconvert a molecule between two states—namely, a [3]rotaxane and a poly[3]rotaxane—by the reversible photodimerization of its anthracene stoppers. This strategy is not unlike the polymerization/macrocyclization of the poly[2]rotaxane **R402**—see **Scheme 4.7** in **Section 4.1.2.2**.

Dumbbell-Linked Poly[3]rotaxanes

An unusual macrotricyclic poly[3]rotaxane architecture (**Figure 4.92**) has been introduced by Chen,[657] employing a ternary bis(propargyl)semirotaxane based on his $T_2$24C8$_2$ receptor to obtain the poly[3]rotaxane **R4178H**$_{2n}^{2n+}$ by a CuAAC click polymerization.

Winpenny[908] has co-crystallized pyridine-terminated [3]rotaxanes based on his ion-paired inorganic-organic hybrid recognition motif (**Section 2.3.7.1**) with bulky Cu^{II} complexes to obtain infinite 1D poly[3]rotaxane coordination polymers. An example (**R4179**) based on $Cu_2(O_2C^tBu)_4$ paddlewheel linkers is illustrated in **Figure 4.92**.

Side-Chain Poly[3]rotaxanes

The side-chain poly[3]rotaxane **R4180** (**Figure 4.92**) was introduced by Osakada[896] as part of his investigations on side-chain poly[2]rotaxanes—see **Section 4.2.3.7**. The *dodecamethylene⊂TM-β-CD* side chain of **R4180** occupies 62% of the benzimidazole anchor points on the backbone, while the remaining 38% of benzimidazole units remain unfunctionalized after grafting the side-chains onto the main chain by nucleophilic substitution in the presence of an excess of TM-β-CD.

4.2.3.8 Extended Polyrotaxane Networks

A number of different strategies have been identified for constructing polyrotaxane networks.[422] Extended polyrotaxane networks[o] include disordered polymers and gels, as well as ordered crystalline coordination polymers or MOFs. We focus our attention first on disordered polymer networks (**Figure 4.93**). Crosslinked polyrotaxane networks can be obtained, for example, by (i) electropolymerization of (pseudo)rotaxane precursors, as demonstrated in 1996 by Sauvage[588] in the case of the polypyrrole polymetallo[2]rotaxane **R4181**, (ii) by statistical interpenetration, as demonstrated by Gibson[909–911] (e.g., **R4182**), or (iii) template-directed polymerization and cross-linking methods, which constitute the remaining examples illustrated in **Figure 4.93**.

Takata[912–917] has made a number of contributions to the area of crosslinked polyrotaxane networks, typically by employing the dialkylammonium/crown pseudorotaxanes as templates for the mechanically interpenetrated crosslinks. For example, the polymers **R4183**$^{(2m+2p)+}$ comprise[912–914] poly(DB24C8) backbones, which are crosslinked by [3]rotaxane linkages based on disulfide- or diphenylmethylurethane linkers. bis(dialkylammonium) used the dialkylammonium-template imine clipping of crown ethers to crosslink a main-chain poly(crown-8) compound, forming a gel in a process which was quantitatively reversible and recyclable.

Employing the same chemistry as that underpinning the main-chain poly[2]rotaxane **R4155** and the side-chain poly[2]rotaxane **R4171**, Leigh[870] synthesized the crosslinked poly[2]rotaxane network **R4184**, a rubber-like material (**Figure 4.93**) which is insoluble in common organic solvents.

As in most polyrotaxane architectures, crosslinked polyrotaxane networks are dominated by the cyclodextrin threading motifs. While much of the attention has been directed at "slide-ring gel" materials of the type introduced by Okumura and Ito[918] (*vide infra*), Takata[915,916] has also investigated cyclodextrin networks crosslinked (**Figure 4.93**) by mechanical bonds. For example, Takata polymerized[916] vinyl polymers in the presence of ring-linked α-CD polymers to obtain bicontinuous networks crosslinked by mechanical bonds. In another case,[915] the polyurethane network **R4185** was obtained by crosslinking the rings of *PEG⊂α-CD* polymers with diphenylmethane diisocyanate. This type of crosslinking was originally demonstrated in the slide-ring gels.

Slide-Ring Gels

A "slide-ring" gel[919–922] (**Figure 4.94**) is a polyrotaxane material originally introduced by Okumura and Ito,[918] comprising long polymer chains, sparsely threaded by mobile rings, which are crosslinked together. Slide-ring gels are commonly

[o] We note that, in spite of classifying threaded macromolecules with extended 2D and 3D architectures as "polyrotaxanes", in actual fact these compounds are topologically rich catenanes, considering the closed loops that form within the networks as a result of crosslinking. They remain in the rotaxane category only because they often derive from rotaxane precursors.

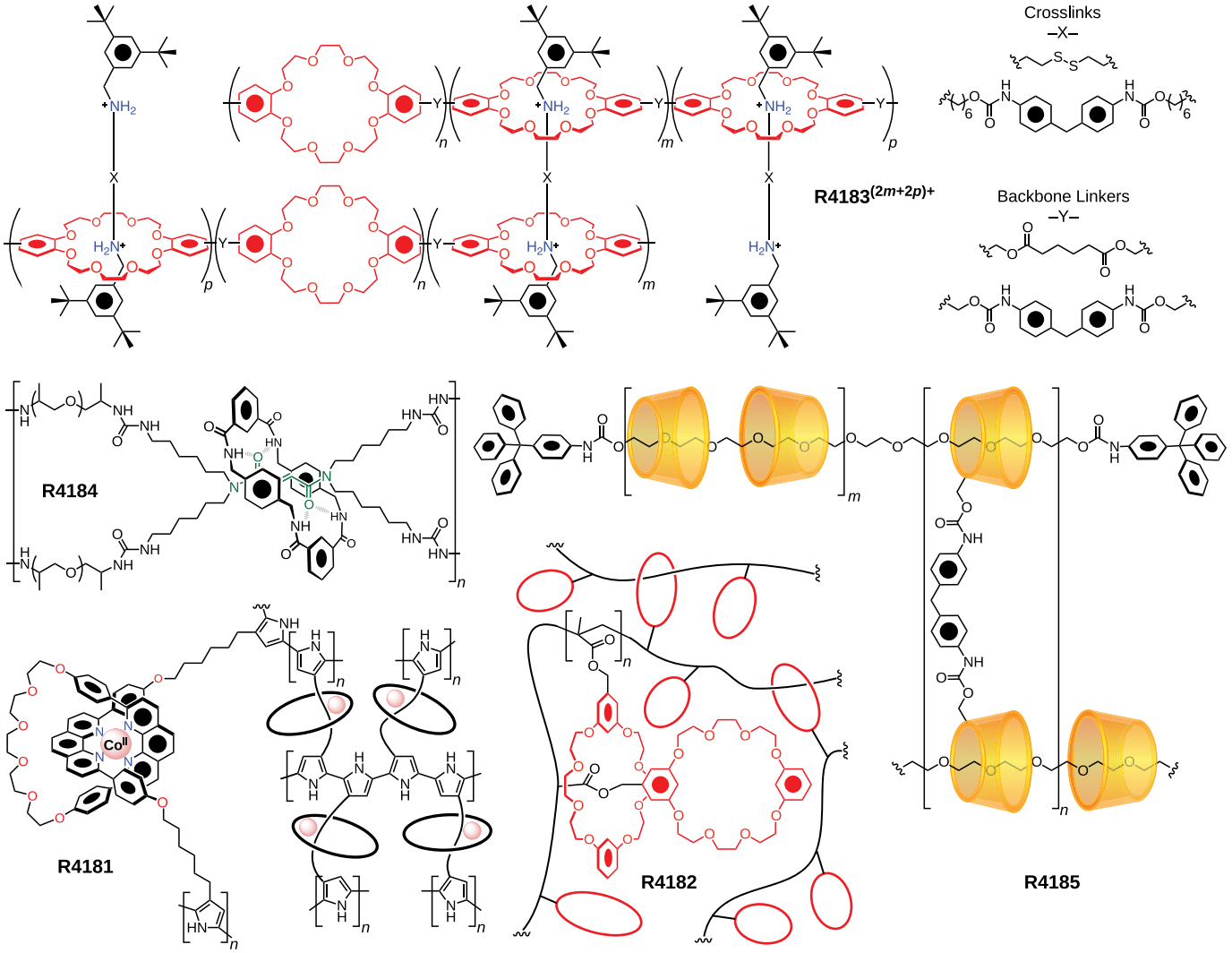


Figure 4.93 Architectures of some crosslinked polyrotaxane networks.[588,870,909–915]

made[506,923–929] from cross-linked cyclodextrins threaded onto polyether chains, although other backbones such as polyisoprene[930] and PDMS[931] have also been incorporated. Slide-ring gels exhibit[932–939] extraordinary viscoelastic and mechanical properties attributable to the "pulley effect"[940–942]—i.e., the high degree of translational freedom available to the mechanically bonded crosslinks, which equalizes the tension throughout the polymer chain. The pulley effect makes slide ring gels both highly stretchable and soft, yet also tough, since tension does not become concentrated in small chain fragments leading to bond cleavage. The seminal slide-ring gel,[918] for example, could be stretched to 24 times its original length.

Although most slide ring gels are based on cyclodextrin chemistry, Ogoshi[943] has prepared a crosslinked polyrotaxane gel based on PA5-threaded poly(tetrahydrofuran) (PTHF).

2D and 3D Rotaxane Coordination Polymers

As illustrated by the polycatenated and interpenetrated coordination networks discussed in **Section 4.1.3.5**, the mechanical bond can be manifested in coordination polymers either by design or by accident. Many network topologies have been identified in MOFs that possess elements of rotaxane-like interpenetration. While we cannot review these materials comprehensively, a number of polyrotaxane network topologies that have been identified by Batten[944] are illustrated in **Figure 4.95**.

A more deliberate strategy for incorporating rotaxanes into 2D and 3D coordination polymers involves the use of rotaxanes as the organic ligands. The first metal-organic rotaxane frameworks[945–947] (MORFs, **Figure 4.96**), as they were later called by Loeb,[945] were introduced by Kim,[558,561,562] alongside his 1D polyrotaxanes described in **Section 4.2.1.1**. The 2D polyrotaxane **R4186** is based on the same *C4N4*$^{2+}$⊂*CB6* ligand employed in the assembly of the molecular necklace **C438H$_6$**$^{12+}$ (**Figure 4.15**, **Section 4.1.2.2**) and the 1D polyrotaxanes **R439a–d** (**Figure 4.63, Section 4.2.1.1**). Each node of the hexagonal **R4186** network (**Figure 4.96a**) comprises a distorted tetrahedron, in which the Ag^+ center is coordinated by three CB6-threaded ligands and a nitrate anion. Kim's

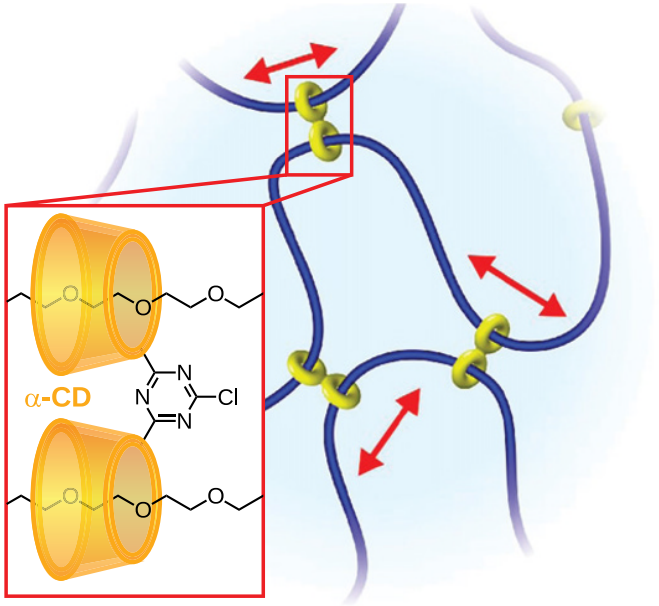


Figure 4.94 Graphical representation of a slide-ring gel, which is characterized by mechanically bonded crosslinks with high translational degrees of freedom. Adapted with permission from ref. 920 (copyright 2010 Elsevier)

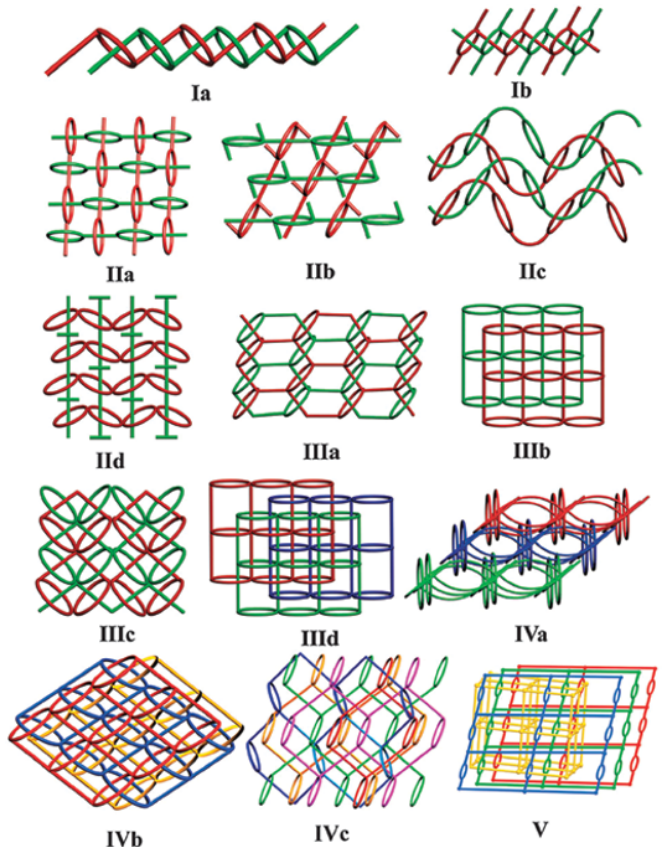


Figure 4.95 Illustrations of polyrotaxane entanglement motifs reviewed by Batten, reprinted with permission from ref. 944 (copyright 2012 Royal Society of Chemistry)

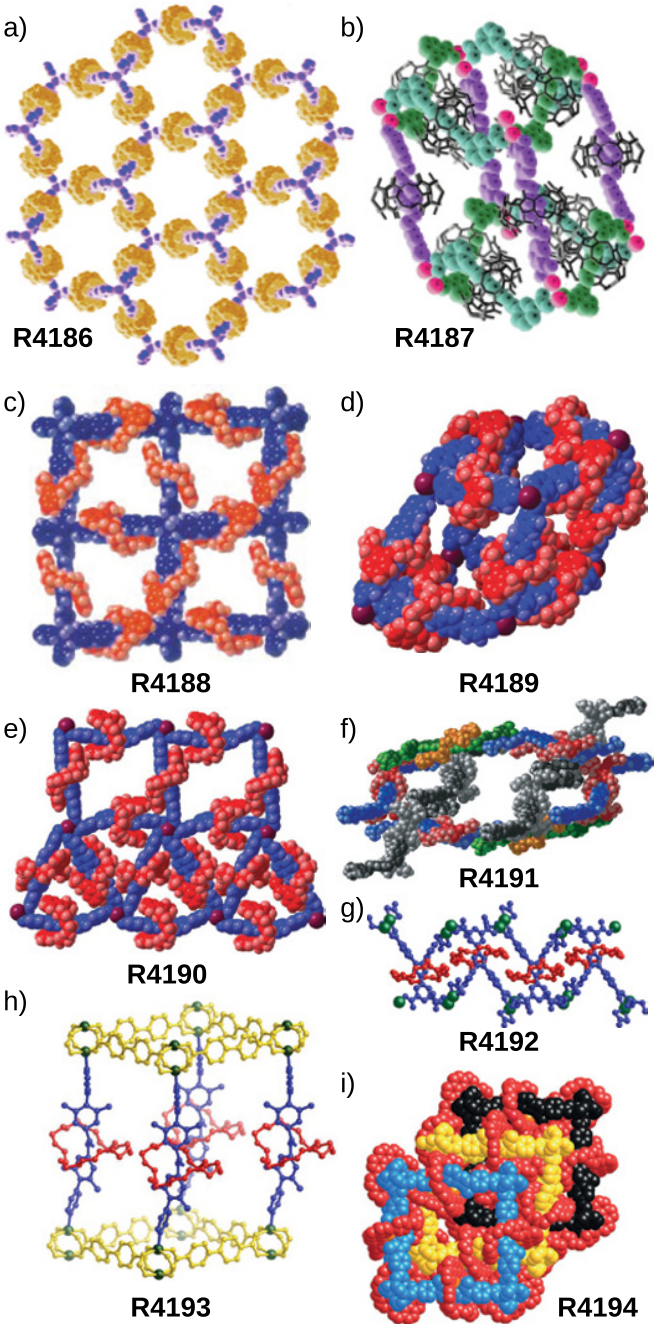


Figure 4.96 Metal-organic rotaxane frameworks (MORFs). The seminal 2D[558] (a) and 3D[562] (b) poly[2]rotaxanes were introduced by Kim. Loeb has obtained the 2D[948,949] (c,e) and 3D[949,954,955,958] (d, f, g, h) MORFs based on hydrogen-bonded crown ether templates. The triply interpenetrated networks of 3D polymetallo[2]rotaxanes[959] (i) have been crystallized in collaboration with Sauvage. The mechanically bonded rings are colored red in (c)–(i). Images reprinted with permission from refs. 558 (copyright 1997 American Chemical Society), 562 (copyright 2000 Wiley-VCH), 948 (copyright 2003 Wiley-VCH), 949 (copyright 2005 Wiley-VCH), 954 (copyright 2013 Wiley-VCH), 958 (copyright 2016 Wiley-VCH), 955 (copyright 2014 American Chemical Society), and 959 (copyright 2012 Wiley-VCH)

seminal 3D MORF is **R4187**, which derives from the *C4CN3*$^{2+}$⊂*CB6* ligand incorporated (**Scheme 4.28, Section 4.2.1.1**) in the uranyl-linked 1D infinite [*n*]rotaxane coordination polymer **R441**. The nodes of the **R4187** network (**Figure 4.96b**) are dimetallic Tb_2 clusters accommodating an approximately octahedral geometry of threaded carboxylate ligands, which are generated *in situ* from the corresponding nitriles during the assembly reaction. Shi[573] has found that the same motif can be used in combination with dinuclear uranyl SBUs to afford a 2D polyrotaxane.

Much of the groundbreaking research on MORFs has been carried out by Loeb.[948–958] His seminal 2D network,[948] **R4188**, comprises a square-grid net (**Figure 4.96c**) of bis(4,4´-bipyridinium)ethane⊂DB24C8 rotaxane linkers connected to the meridonal sites of the $Cd(H_2O)_2^{2+}$ nodes. The bis(*N*-oxide) derivative of the same threaded ligand has been combined[949] with octahedral Sm^{III} nodes in the assembly of the 3D MORF **R4189** (**Figure 4.96d**), as well as the 2D network **R4190** possessing (**Figure 4.96e**) pentacoordinated Yb^{III} nodes. The 3D network **R4191**, which derives[954] (**Figure 4.96f**) from BPE^{2+}/DB24C8 [2]rotaxane ligands armed with Ag^{I}-coordinative thioether bonds in both the rings and dumbbells, adopts an unusual interwoven network of 1D strands that interpenetrate 2D grids. A rotaxane ligand based on triphenylimidazole dumbbell and a 24C6 ring has been employed[958] recently in the construction (**Figure 4.96g**) of the 3D MORF **R4192**, while the same ring encircles[955] a bis(pyridine) axle possessing (**Figure 4.96h**) an aniline recognition unit in **R4193**. Most of these 3D networks provide enough free volume for the ring to move about its mechanical bond with respect to the corresponding axle. The robust dynamics of the mobile interlocked rings within a couple of Loeb's three-dimensional MORFs are described in **Section 5.1.4**. In addition to the many MORFs developed in the laboratories of Loeb, Sauvage's Cu^{I} template rotaxanes have been incorporated[959] (**Figure 4.96i**) into the triply interpenetrated, cubic-grid 3D MORF **R4194**.

In a collaboration involving Wasielewski, Snurr, Hupp, Farha, and our group,[960] [2]rotaxanes based on a trisradical (**Section 2.3.10**) *BIPY*$^{\bullet+}$⊂*CBPQT*$^{2(\bullet+)}$ semidumbbell motif were installed as side-chains within the pores of NU-1000, a zirconium-based MOF, by a process (**Figure 4.97**) known[961] as solvent-assisted ligand incorporation (SALI). In this protocol, hydroxyl ligands lining the wide pores of NU-1000 are displaced by carboxylate anions terminating the semidumbbell.

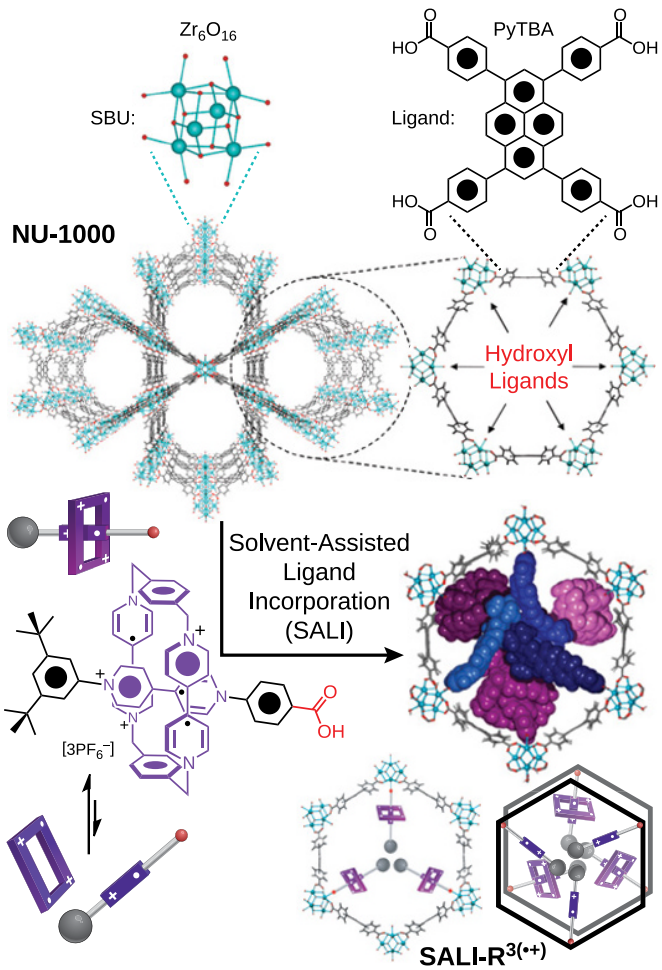


Figure 4.97 Graphical representation of the use of SALI to incorporate electrochemically active [2]rotaxanes within the pores of MOFs.

4.3 Other Architectures with Mechanical Bonds

There are a number of types of mechanically interlocked architectures which do not fit cleanly into either catenane or rotaxane categories, including catenarotaxanes (**Section 4.3.1**), rotamacrocycles (**Section 4.3.2**), ring-in-ring mechanomolecules (**Section 4.3.3**), self-threaded macropolycyclics (**Section 4.3.4**), suitanes (**Section 4.3.5**), foldaxanes (**Section 4.3.6**), and interwoven polymers (**Section 4.3.7**).

4.3.1 Catenarotaxanes

We have already alluded to the history of the catenarotaxane, which has been alternatively called a rotacatenane[3] or catrotaxane.[4] In considering the Latin roots, both names are less than ideal, since the key components in the architecture are a link and an axle; therefore, the IUPAC-recommended[1] catenarotaxane (*catena*/chain+*rota*/wheel+*axis*/axle) is the most descriptive. Catenarotaxanes (**Figure 4.98**) were realized for the first time in 1999, when the donor-acceptor [2]rota[2]catenane **CR401**$^{4+}$ was introduced,[3] taking advantage of the wide cavity of the square shaped "big blue box" receptor (**Section 2.3.3.9**), which accommodates two guests—in this case, the DNP units belonging to the crown ether ring and the dumbbell of the catenarotaxane. A multistable rotacatenane exhibiting bistability with respect to both the rings and the dumbbell has also been described[962]—see **Section 6.13.11**.

A number of other catenarotaxanes are also illustrated in **Figure 4.98**. Li, Jiang, and Wen[963] have constructed the [2]rota[2]catenane **CR402**$^{5+}$, which contains a fused PA5/naphtho[36]crown-10 macrobicyclic core interlocked with $CBPQT^{4+}$ and an imidazolium-based dumbbell. Saito[964,965] has employed active metal template protocols (**Section 2.4**)

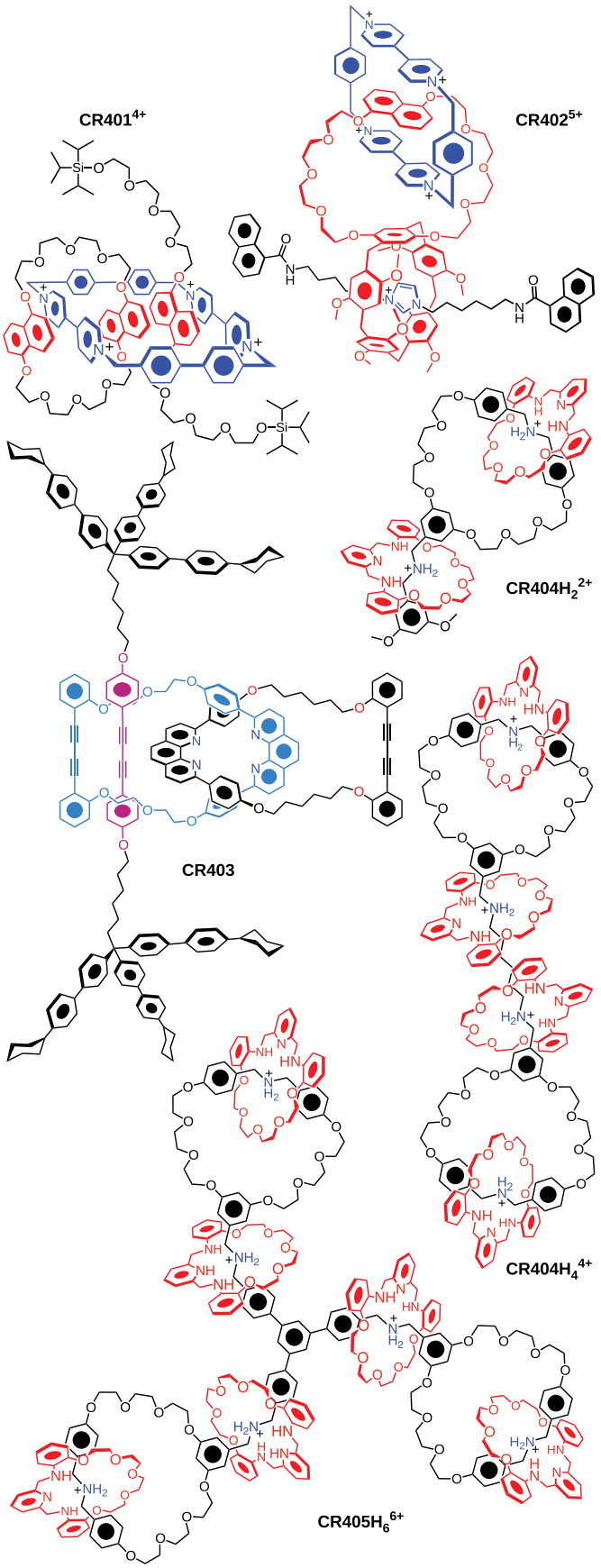
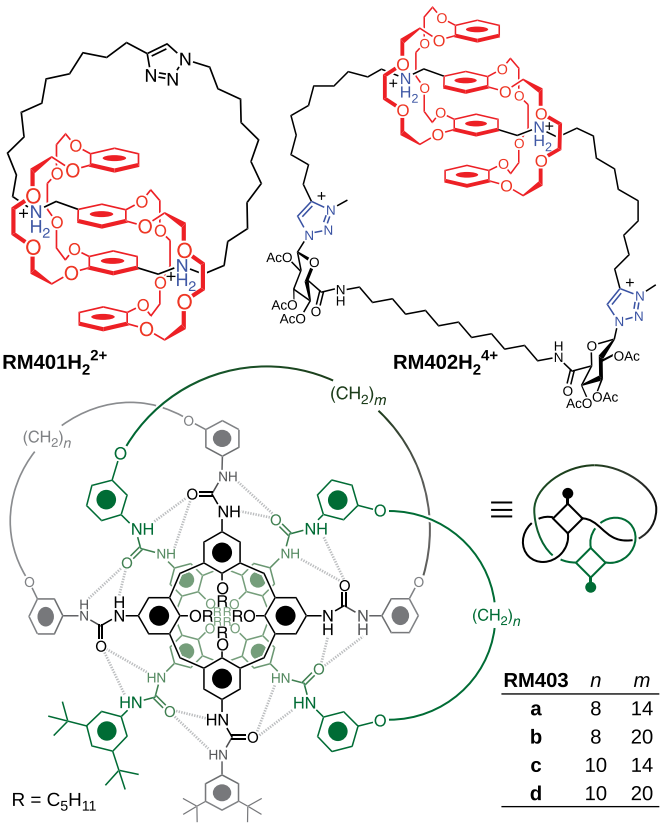


Figure 4.98 Catenarotaxanes.[3,963–966]

in the synthesis of a number of rotacatenanes; **CR403** is one example. The compounds **CR404H$_2^{2+}$**, **CR405H$_4^{4+}$**, and **CR406H$_6^{6+}$** are mono-, bis-, and tris- catenarotaxanes, respectively, which have been introduced by Yin.[966] All three compounds are obtained from covalently linked dialkylammonium-based ring / dumbbell hybrid precursors by thermodynamically controlled clipping (**Section 3.3.1.2**) procedures, followed by reduction of the dynamic imine bonds of the freshly clipped macrocycles.

4.3.2 Rotamacrocycles

If the ends of a daisy chain (**Section 4.2.3.2**) are conjoined to form a closed loop, the resulting topology is neither a catenane nor a rotaxane. The term "rotamacrocycle" was coined by Coutrot[967,968] to describe his so-called double-lasso compounds. **RM401H$_2^{2+}$** and **RM402H$_2^{2+}$** (**Figure 4.99**) belonging to this class of mechanomolecules.



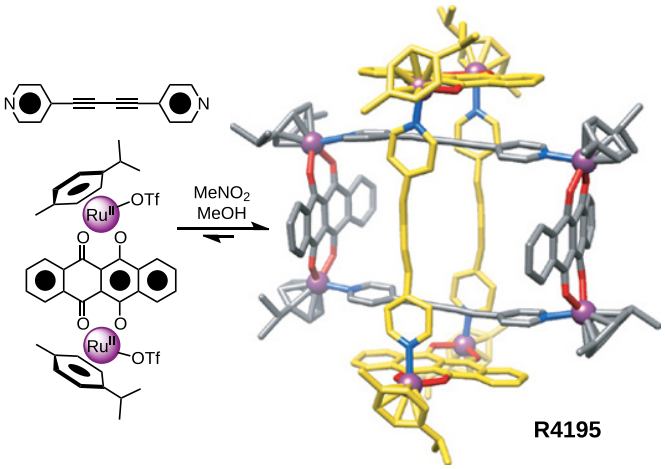
RM403	*n*	*m*
a	8	14
b	8	20
c	10	14
d	10	20

Figure 4.99 Rotamacrocycles.[206,967–969]

This architecture was originally introduced by Böhmer[206,969] using one of his entwined tetraureidocalix[4]arene recognition motifs (**Section 2.3.4.5**), affording compounds **RM403a–RM403d**. Coutrot[967] has also demonstrated that bistable rotamacrocycles can be constricted and dilated under pH control—see **Section 6.13.2**.

4.3.3 Ring-in-Ring Mechanomolecules

Stang[970] has assembled (**Scheme 4.37**) an interlocked metallosupramolecular architecture, **R4195**, comprising two rings that are not catenated. Instead, the two rings



Scheme 4.37 The self-assembly of Stang's ring-in-ring rotaxane.[970] The tubular representation of its solid-state structure is illustrated with hydrogen atoms, counterions, and solvent molecules omitted for the sake of clarity.

adopt a ring-in-ring architecture, in which the ligands carry enough steric bulk to prevent deslipping. The mechanical bonds of these rings are therefore closer to those of a rotaxane than a catenane—i.e., the innermost ring can be considered a macrocyclic dumbbell. Mechanically bonded ring-in-ring motifs have also been observed[971] in one-dimensional coordination polymers. See **Scheme 3.17** in **Section 3.2.4.3** for a [2]catenane assembly based on a similar ligand motif. While many discrete ring-in-ring *complexes* are known,[39–41,43,44,145,972–988] Stang's is the first (and only, to our knowledge) to be locked by a mechanical bond.

4.3.4 Self-Threaded Macropolycyclics

Whereas bridging the axle and ring of a [2]rotaxane results in a [1]rotaxane (**Section 4.2.3.1**), a second bridge between them creates a new macrocycle fused to the first one. This self-threaded macrobicyclic architecture may take the form of a so-called pseudo[1]catenane,[989] or of a so-called Figure-of-Eight,[990–992] depending on if the axle's bridges lead to the same or different locations, respectively, on the ring. Topologically speaking, these compounds are no different than macrobicyclic molecules, although the mechanical bond is capable of preserving their entanglement. Naturally, it is also possible to form self-entanglements in higher order multicyclic compounds such as macrotricycles. Examples of self-threaded macrobicyclic and macrotricyclic compounds are illustrated in **Figure 4.100**.

Self-Threaded Macrobicyclics / Figures-of-Eight

When the thread of a rotaxane-like molecule is anchored to opposite ends of the encircling ring, this architecture (**Figure 4.100a**) is known as a molecular figure-of-eight (Fo8). Vögtle[990] introduced the self-threaded Fo8 **M401**

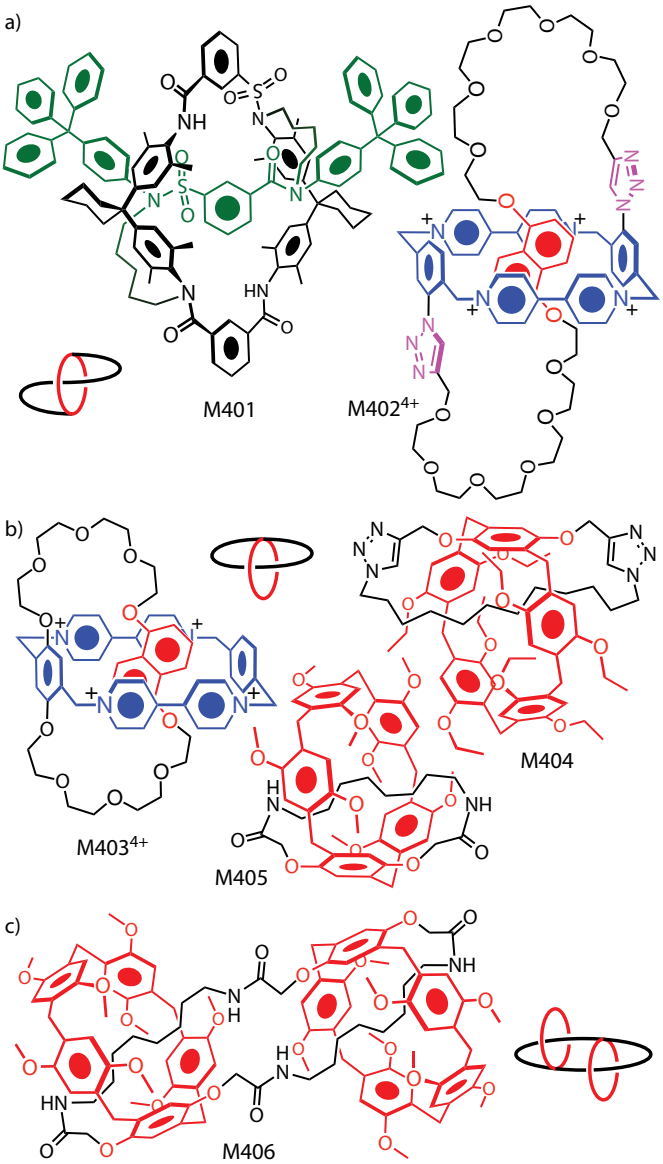


Figure 4.100 Self-threaded macrobicyclic and macrotricyclic compounds. (a) Molecular figures-of-eight (Fo8) based on hydrogen-bonding[990] and π-donor/π-acceptor[991,992] templation. (b) Pseudo[1]catenanes based on self-threaded fused macrobicyclic cyclophanes.[989,993,994] (c) A self-threaded macrotricycle, known also as a self-locked Gemini catenane.[994]

from a [2]rotaxane by installing two pentamethylene linkers, spanning from each end of the axle to each hemisphere of the ring, where each linker runs from a sulfonamide group in one component part to an amide group in the other. Molecular Fo8 compounds (e.g., **M402^{4+}**) have also been prepared[991,992] by using π-donor/π-acceptor templation to "click" the propargylated termini of a threaded DNP-based guest to the phenylene rings of a bis(azido)CBPQT^{4+} derivative. A constitutional isomer of **M402^{4+}** with different relative positions of the triazole linkers was also isolated. The solid-state crystal structure of **M402^{4+}** is illustrated in **Figure 1.29j, Section 1.3.3**.

Pseudo[1]catenanes

When the pseudo[1]catenane architecture (**Figure 4.100b**) was introduced[993] in the form of the donor-acceptor hybrid fused macrobicycle **M403**$^{4+}$, it was dubbed a "molecular chameleon". The DNP unit of the crown ether portion of the macrobicycle, which rests within the cavity of the tetracationic cyclophane, can be displaced by a TTF guest, causing the crown ether to swing out through the annulus to make way for it.

Ogoshi[989] employed the term pseudo[1]catenane to describe his self-threaded pillar[5]arene/cyclophane **M404**, which was obtained (**Figure 4.100b**), by CuAAC macrocyclization of 1,12-diazidododecamethylene with a single bis(propargyl)-functionalized hydroquinol subunit of an otherwise perethylated PA5 host. The guest-triggered swinging of the dodecamethylene portion out of the cavity of the PA5 ring leads to an inversion of planar chirality at the corresponding *para*-phenylene ring that rotates through the annulus.

Self-Threaded Macrotricyclics/Gemini Catenane

Liu[994] recently introduced self-threaded macrotricyclic compounds based on threaded PA5 dimers, naming them "Gemini catenanes". The structure of **M406** constitutes (**Figure 4.100c**) one central ring fused to a pair of PA5 rings, each of which encircles an oligomethylene portion of the central ring. The pseudo[1]catenane **M405** (**Figure 4.100b**) was obtained in the same reaction.

4.3.5 Suitanes

Yet another novel architecture to be forged in the fire of imine chemistry (**Section 3.3.1**) is the class of molecules known as suitanes,[995–997] two-component MIMs in which a molecular 'body' with some number of protruding 'limbs' has its 'torso' encompassed by an all-in-one molecular 'suit'. A bracketed number is placed between 'suit' and 'ane' to describe the number of 'limbs' protruding from the suit, since it is given that all suitanes are made of only two mechanically bonded component parts. Thus, a suit[*n*]ane is an *n*-limbed molecular 'body' enveloped by a molecular suit. Note that suitanes are stable molecules (not supermolecules), yet they cannot be described precisely as rotaxanes since they do not require any stoppers.

In order to possess a formal mechanical bond, the suit[2]ane requires a sterically bulky torso (anthracene in this case) which the suit cannot slip past, while suit[3+]anes do not call for any such special considerations. The first examples of these compounds were a suit[2]ane[995] and a suit[3]ane,[996] both self-assembled around a dialkylammonium-based body with crown ethers that have been bis-functionalized with aldehydes, which connect to a multianiline hub at the torso by means of imine condensation. The solid-state structure of the seminal suit[2]ane is illustrated in **Figure 1.29g** in **Section 1.3.3**.

4.3.6 Foldaxanes

Huc[998–1001] has introduced a new class of supermolecules in which a helical foldamer wraps around an axle/dumbbell in rotaxane-like fashion. The solid-state superstructure of one such "foldaxane" is illustrated in **Figure 1.29a** of **Section 1.3.3**.

4.3.7 Braided and Interwoven Polymer Entanglements

One-dimensional coordination polymers[1002] are also capable of forming many types of entanglements[243] in the solid state. For example, double-helical[1003] and triple-helical[1004] 1D coordination polymers (seminal examples are cited) possess entanglements akin to those of DNA. See **Section 2.3.12.1**. A number of different types of 2D entanglements are also possible in one-dimensional polymers. Warp-and-weave networks comprising criss-crossed meshes of inclined 1D coordination polymers have been described,[1005–1007] as have parallel interwoven networks[1008] resembling the topology of chicken wire. Another type of mechanical bond is that of a braid, which can also be manifested in coordination polymers. For example, Wang[1009,1010] has described the entanglement of one-dimensional coordination polymers upon crystallization to obtain triple-stranded braids. The reader is referred to more comprehensive sources.[243,1002] on entangled coordination polymers for discussions of these materials.

Conclusions and Outlook

A huge array of molecules with mechanical bonds have emerged on the back of the template-directed synthetic techniques introduced in Chapters 2 and 3. An analogy can be drawn with the bonding of carbon in organic chemistry: just as only a few types of covalent bonding (sp, sp^2, sp^3) underpin the whole of diversity of organic molecules, only a few types of mechanical bonding (catenated, threaded, interwoven) underpin the whole diversity of mechanomolecules. Recalling that mechanical bonds exist beyond the realm of molecules (**Section 1.1**), we must take a moment to recognize our parochialism, as the mechanical bond reaches much further still than we have shown in this Chapter. We have neglected, for the most part, entanglements in inorganic crystals and a great many coordination polymers, as well as molecular knots, which do not have mechanically bonded component parts, but nevertheless have entanglements that constrain molecular motions by way of the same types of contact forces as those bounding formal mechanical bonds. Beyond the realm of discrete molecules, researchers have found ways to tie knots and links out of defect lines in chiral nematic liquid crystals,[1011] colloidal composites,[1012] liquid vortices,[1013] and even interfering beams of light.[1014,1015]

New types of bonds give rise to new types of molecules. Indeed, the mechanical bond has enabled the genesis and proliferation of a rapidly growing family of mechanomolecules, with dimensions ranging from small molecules to macroscopic materials. One can envision myriad topologies

and architectures that have not yet been forged into molecular entities. Some of them which have remained elusive, such as the Whitehead link and high molecular weight poly[*n*]catenane chain links, are poised to be made real. There is every reason to believe that the power of the mechanical bond will continue to be wielded in the synthesis of new molecules and materials. The outpouring of molecular diversity that continues to unfold will support the continued development of applications for the mechanical bond in chemistry and beyond, owing to the intimate co-dependent relationship between structure and function.

References

(1) Yerin, A.; Wilks, E. S.; Moss, G. P.; Harada, A. Nomenclature for Rotaxanes and Pseudorotaxanes (IUPAC Recommendations 2008). *Pure Appl. Chem*. **2008**, *80*, 2041–2068.

(2) Vohlídal, J.; Wilks, E. S.; Yerin, A.; Fradet, A.; Hellwich, K.-H.; Hodge, P.; Kahovec, J.; Mormann, W.; Stepto, R.F. T. Terminology and Nomenclature for Macromolecular Rotaxanes and Pseudorotaxanes (IUPAC Recommendations 2012). *Pure Appl. Chem*. **2012**, *84*, 2135–2165.

(3) Amabilino, D. B.; Ashton, P. R.; Bravo, J. A.; Raymo, F. M.; Stoddart, J. F.; White, A. J. P.; Williams, D. J. Molecular Meccano 52. Template-Directed Synthesis of a Rotacatenane. *Eur. J. Org. Chem.* **1999**, 1295–1302.

(4) Safarowsky, O.; Windisch, B.; Mohry, A.; Vögtle, F. Nomenclature for Catenanes, Rotaxanes, Molecular Knots, and Assemblies Derived from These Structural Elements. *J. Prakt. Chem.* **2000**, *342*, 437–444.

(5) Frisch, H. L.; Wasserman, E. Chemical Topology. *J. Am. Chem. Soc*. **1961**, *83*, 3789–3795.

(6) Weisstein, E. W. Prime Link. *Wolfram Mathworld* **2016**.

(7) Alexander, J. W.; Briggs, G. B. On Types of Knotted Curves. *Ann. Math.* **1926**, *28*, 562–586.

(8) Pentecost, C. D.; Chichak, K. S.; Peters, A. J.; Cave, G. W. V.; Cantrill, S. J.; Stoddart, J. F. A Molecular Solomon Link. *Angew. Chem., Int. Ed.* **2007**, *46*, 218–222.

(9) Leigh, D. A.; Pritchard, R. G.; Stephens, A. J. A Star of David Catenane. *Nature Chem.* **2014**, *6*, 978–982.

(10) Wood, C. S.; Ronson, T. K.; Belenguer, A. M.; Holstein, J. J.; Nitschke, J. R. Two-Stage Directed Self-Assembly of a Cyclic [3]Catenane. *Nature Chem.* **2015**, *7*, 354–358.

(11) Nierengarten, J.-F.; Dietrich-Buchecker, C. O.; Sauvage, J.-P. Synthesis of a Doubly Interlocked [2]Catenane. *J. Am. Chem. Soc.* **1994**, *116*, 375–376.

(12) McArdle, C. P.; Vittal, J. J.; Puddephatt, R. J. Molecular Topology: Easy Self-Assembly of an Organometallic Doubly Braided [2]Catenane. *Angew. Chem., Int. Ed*. **2000**, *39*, 3819–3822.

(13) Nierengarten, J.-F.; Buchecker, C. O.; Sauvage, J.-P. Copper(I) Template Synthesis of a Four-Crossing [2]Catenane. *New J. Chem.* **1996**, *20*, 685–693.

(14) Dietrich-Buchecker, C.; Sauvage, J.-P. Lithium Templated Synthesis of Catenanes: Efficient Synthesis of Doubly Interlocked [2]Catenanes. *Chem. Commun.* **1999**, 615–616.

(15) Ibukuro, F.; Fujita, M.; Yamaguchi, K.; Sauvage, J.-P. Quantitative and Spontaneous Formation of a Doubly Interlocking [2]Catenane Using Copper(I) and Palladium(II) as Templating and Assembling Centers. *J. Am. Chem. Soc.* **1999**, *121*, 11014–11015.

(16) Schouwey, C.; Holstein, J. J.; Scopelliti, R.; Zhurov, K. O.; Nagornov, K. O.; Tsybin, Y. O.; Smart, O. S.; Bricogne, G.; Severin, K. Self-Assembly of a Giant Molecular Solomon Link from 30 Subcomponents. *Angew. Chem., Int. Ed*. **2014**, *53*, 11261–11265.

(17) McArdle, C. P.; Jennings, M. C.; Vittal, J. J.; Puddephatt, R. J. Self-Assembly of Rings, Catenanes, and a Doubly Braided Catenane Containing Gold(I): The Hinge-Group Effect in Diacetylide Ligands. *Chem. Eur. J.* **2001**, *7*, 3572–3583.

(18) Chichak, K.; Cantrill, S. J.; Pease, A. R.; Chiu, S.-H.; Cave, G. W. V.; Atwood, J. L.; Stoddart, J. F. Molecular Borromean Rings. *Science* **2004**, *304*, 1308–1312.

(19) Meyer, C. D.; Forgan, R. S.; Chichak, K. S.; Peters, A. J.; Tangchaivang, N.; Cave, G. W. V.; Khan, S. I.; Cantrill, S. J.; Stoddart, J. F. The Dynamic Chemistry of Molecular Borromean Rings and Solomon Knots. *Chem. Eur. J.* **2010**, *16*, 12570–12581.

(20) Prakasam, T.; Lusi, M.; Elhabiri, M.; Platas-Iglesias, C.; Olsen, J.-C.; Asfari, Z.; Cianférani-Sanglier, S.; Debaene, F.; Charbonnière, L. J.; Trabolsi, A. Simultaneous Self-Assembly of a [2]Catenane, a Trefoil Knot, and a Solomon Link From a Simple Pair of Ligands. *Angew. Chem., Int. Ed*. **2013**, *52*, 9956–9960.

(21) Beves, J. E.; Campbell, C. J.; Leigh, D. A.; Pritchard, R. G. Tetrameric Cyclic Double Helicates as a Scaffold for a Molecular Solomon Link. *Angew. Chem., Int. Ed*. **2013**, *52*, 6464–6467.

(22) Beves, J. E.; Danon, J. J.; Leigh, D. A.; Lemonnier, J.-F.; Vitorica-Yrezabal, I. J. A Solomon Link Through an Interwoven Molecular Grid. *Angew. Chem., Int. Ed*. **2015**, *54*, 7555–7559.

(23) Fujita, M.; Tominaga, M.; Hori, A.; Therrien, B. Coordination Assemblies from a Pd(II)-Cornered Square Complex. *Acc. Chem. Res.* **2005**, *38*, 369–378.

(24) Peinador, C.; Blanco, V.; Quintela, J. M. A New Doubly Interlocked [2]Catenane. *J. Am. Chem. Soc.* **2009**, *131*, 920–921.

(25) Frasconi, M.; Kikuchi, T.; Cao, D.; Wu, Y.; Liu, W.-G.; Dyar, S. M.; Barin, G.; Sarjeant, A. A.; Stern, C. L.; Carmieli, R.; Wang, C.; Wasielewski, M. R.; Goddard, W. A., III; Stoddart, J. F. Mechanical Bonds and Topological Effects in Radical Dimer Stabilization. *J. Am. Chem. Soc.* **2014**, *136*, 11011–11026.

(26) Ponnuswamy, N.; Cougnon, F. B. L.; Pantoş, G. D.; Sanders, J. K. M. Homochiral and Meso Figure Eight Knots and a Solomon Link. *J. Am. Chem. Soc.* **2014**, *136*, 8243–8251.

(27) Ciengshin, T.; Sha, R.; Seeman, N. C. Automatic Molecular Weaving Prototyped by Using Single-Stranded DNA. *Angew. Chem., Int. Ed*. **2011**, *50*, 4419–4422.

(28) Sha, R.; Liu, F.; Bruist, M. F.; Seeman, N. C. Parallel Helical Domains in DNA Branched Junctions Containing 5′,5′ and 3′,3′ Linkages. *Biochemistry* **1999**, *38*, 2832–2841.

(29) Ronson, T. K.; Fisher, J.; Harding, L. P.; Rizkallah, P. J.; Warren, J. E.; Hardie, M. J. Stellated Polyhedral Assembly of a Topologically Complicated Pd_4L_4 'Solomon Cube'. *Nature Chem.* **2009**, *1*, 212–216.

(30) Clever, G. H. Molecular Topology: Star-Crossed Self-Assembly. *Nature Chem.* **2014**, *6*, 950–952.

(31) Dietrich-Buchecker, C.; Colasson, B.; Jouvenot, D.; Sauvage, J.-P. Synthesis of Multi-1,10-Phenanthroline Ligands with 1,3-Phenylene Linkers and Their Lithium Complexes. *Chem. Eur. J.* **2005**, *11*, 4374–4386.

(32) Hasenknopf, B.; Lehn, J.-M.; Kneisel, B. O.; Baum, G.; Fenske, D. Self-Assembly of a Circular Double Helicate. *Angew. Chem., Int. Ed. Engl*. **1996**, *35*, 1838–1840.

(33) Hasenknopf, B.; Lehn, J.-M.; Boumediene, N.; Dupont-Gervais, A.; Van Dorsselaer, A.; Kneisel, B.; Fenske, D. Self-Assembly of Tetra-and Hexanuclear Circular Helicates. *J. Am. Chem. Soc.* **1997**, *119*, 10956–10962.

(34) Hasenknopf, B.; Lehn, J.-M.; Boumediene, N.; Leize, E.; Van Dorsselaer, A. Kinetic and Thermodynamic Control in Self-Assembly: Sequential Formation of Linear and Circular Helicates. *Angew. Chem., Int. Ed*. **1998**, *37*, 3265–3268.

(35) Ayme, J.-F.; Beves, J. E.; Leigh, D. A.; McBurney, R. T.; Rissanen, K.; Schultz, D. A Synthetic Molecular Pentafoil Knot. *Nature Chem.* **2012**, *4*, 15–20.

(36) Ayme, J.-F.; Beves, J. E.; Leigh, D. A.; McBurney, R. T.; Rissanen, K.; Schultz, D. Pentameric Circular Iron(II) Double Helicates and a Molecular Pentafoil Knot. *J. Am. Chem. Soc.* **2012**, 9488–9497.

(37) Cantrill, S. J.; Chichak, K. S.; Peters, A. J.; Stoddart, J. F. Nanoscale Borromean Rings. *Acc. Chem. Res*. **2005**, *38*, 1–9.

(38) Hubin, T. J.; Kolchinski, A. G.; Vance, A. L.; Busch, D. H. Template Control of Supramolecular Architecture. *Adv. Supramol. Chem.* **1999**, *5*, 237–357.

(39) Schmittel, M.; Ganz, A.; Fenske, D. Ring-in-Ring Structures from Phenanthroline Macrocycles with Exo- and Endotopic Binding Sites. *Org. Lett.* **2002**, *4*, 2289–2292.

(40) Chiu, S.-H.; Pease, A. R.; Stoddart, J. F.; White, A. J. P.; Williams, D. J. A Ring-in-Ring Complex. *Angew. Chem., Int. Ed*. **2002**, *41*, 270–274.

(41) Loren, J. C.; Yoshizawa, M.; Haldimann, R. F.; Linden, A.; Siegel, J. S. Synthetic Approaches to a Molecular Borromean Link: Two-Ring Threading with Polypyridine Templates. *Angew. Chem., Int. Ed*. **2003**, *42*, 5702–5705.

(42) Forgan, R. S.; Spruell, J. M.; Olsen, J.-C.; Stern, C. L.; Stoddart, J. F. Towards the Stepwise Assembly of Molecular Borromean Rings. A Donor–Acceptor Ring-in-Ring Complex. *J. Mex. Chem. Soc*. **2009**, *53*, 134–138.

(43) Forgan, R. S.; Friedman, D. C.; Stern, C. L.; Bruns, C. J.; Stoddart, J. F. Directed Self-Assembly of a Ring-in-Ring Complex. *Chem. Commun.* **2010**, *46*, 5861–5863.

(44) Forgan, R. S.; Wang, C.; Friedman, D. C.; Spruell, J. M.; Stern, C. L.; Sarjeant, A. A.; Cao, D.; Stoddart, J. F. Donor–Acceptor Ring-in-Ring Complexes. *Chem. Eur. J*. **2012**, *18*, 202–212.

(45) Mao, C.; Sun, W.; Seeman, N. C. Assembly of Borromean Rings From DNA. *Nature* **1997**, *386*, 137–138.

(46) Dolomanov, O. V.; Blake, A. J.; Champness, N. R.; Schroder, M.; Wilson, C. A Novel Synthetic Strategy for Hexanuclear Supramolecular Architectures. *Chem. Commun.* **2003**, 682–683.

(47) Schmittel, M.; He, B.; Fan, J.; Bats, J. W.; Engeser, M.; Schlosser, M.; Deiseroth, H.-J. Cap for Copper(I) Ions! Metallosupramolecular Solid and Solution State Structures on the Basis of the Dynamic Tetrahedral $[Cu(phenAr_2)(Py)_2]^+$ Motif. *Inorg. Chem.* **2009**, *48*, 8192–8200.

(48) Chichak, K. S.; Cantrill, S. J.; Peters, A. J.; Stoddart, J. F. Dynamic Nanoscale Borromean Links. *Chem. Commun.* **2005**, 3391–3393.

(49) Peters, A. J.; Chichak, K. S.; Cantrill, S. J.; Stoddart, J. F. Nanoscale Borromean Links for Real. *Chem. Commun*. **2005**, 3394–3396.

(50) Huang, S.-L.; Lin, Y.-J.; Hor, T. S. A.; Jin, G.-X. Cp*Rh-Based Heterometallic Metallarectangles: Size-Dependent Borromean Link Structures and Catalytic Acyl Transfer. *J. Am. Chem. Soc.* **2013**, *135*, 8125–8128.

(51) Huang, S.-L.; Lin, Y.-J.; Li, Z.-H.; Jin, G.-X. Self-Assembly of Molecular Borromean Rings from Bimetallic Coordination Rectangles. *Angew. Chem., Int. Ed*. **2014**, *53*, 11218–11222.

(52) Thorp-Greenwood, F. L.; Kulak, A. N.; Hardie, M. J. An Infinite Chainmail of M_6L_6 Metallacycles Featuring Multiple Borromean Links. *Nature Chem.* **2015**, *7*, 526–531.

(53) Carlucci, L.; Ciani, G.; Proserpio, D. M. Borromean Links and Other Non-Conventional Links in “Polycatenated” Coordination Polymers: Re-Examination of Some Puzzling Networks Publication. *CrystEngComm* **2003**, *5*, 269–279.

(54) Pan, M.; Su, C.-Y. Coordination Assembly of Borromean Structures. *CrystEngComm* **2014**, *16*, 7847–7859.

(55) Durola, F.; Russo L.; Sauvage, J.-P.; Rissanen, K.; Wenger O. S. Three-Component Entanglements Consisting of Three Crescent-Shaped Bidentate Ligands Coordinated to an Octahedral Metal Centre. *Chem. Eur. J.* **2007**, *13*, 8749–8753.

(56) Lincheneau, C.; Jean-Denis, B.; Gunnlaugsson, T. Self-Assembly Formation of Mechanically Interlocked [2]- and [3]Catenanes Using Lanthanide Ion [Eu(III)] Templation and Ring Closing Metathesis Reactions. *Chem. Commun.* **2014**, *50*, 2857–2860.

(57) Zhu, R.; Lübben, J.; Dittrich, B.; Clever, G. H. Stepwise Halide-Triggered Double and Triple Catenation of Self-Assembled Coordination Cages. *Angew. Chem., Int. Ed*. **2015**, *54*, 2796–2800.

(58) Whitehead, J. H. C. Certain Theorems About Three-Dimensional Manifolds. *Q. J. Math.* **1934**, *5*, 308–320.

(59) Perelman, G. The Entropy Formula for the Ricci Flow and Its Geometric Applications. *ArXive* **2002**, math–0211159v1.

(60) Perelman, G. Ricci Flow with Surgery on Three-Manifolds. *ArXive* **2003**, math–0303109v1.

(61) Perelman, G. Finite Extinction Time for the Solutions to the Ricci Flow on Certain Three-Manifolds. *ArXive* **2003**, math–0307245v1.

(62) Fenlon, E. E. Open Problems in Chemical Topology. *Eur. J. Org. Chem.* **2008**, 5023–5035.

(63) Chambron, J.-C.; Sauvage, J.-P. Topologically Complex Molecules Obtained by Transition Metal Templation: It Is the Presentation That Determines the Synthesis Strategy. *New J. Chem.* **2012**, *37*, 49–57.

(64) Sawada, T.; Yamagami, M.; Ohara, K.; Yamaguchi, K.; Fujita, M. Peptide [4]Catenane by Folding and Assembly. *Angew. Chem., Int. Ed*. **2016**, *128*, 4595–4598.

(65) Sauvage, J.-P.; Weiss, J. Synthesis of Dicopper(I) [3]Catenates: Multiring Interlocked Coordinating Systems. *J. Am. Chem. Soc.* **1985**, *107*, 6108–6110.

(66) Guilhem, J.; Pascard, C.; Sauvage, J.-P.; Weiss, J. Solution Study and Molecular Structure of a [3]-Catenand. Intramolecular Interaction between the Two Peripheral Rings. *J. Am. Chem. Soc*. **1988**, *110*, 8711–8713.

(67) Dietrich-Buchecker, C. O.; Hemmert, C.; Khemiss, A.-K.; Sauvage, J.-P. Synthesis of Dicopper [3]-Catenates and [3]-Catenands by Acetylenic Oxidative Coupling. Preparation and Study of Corresponding Homodimetallic [3]-Catenates [Ag^+, Zn^{2+}, Co^{2+}, and Ni^{2+}]. *J. Am. Chem. Soc*. **1990**, *112*, 8002–8008.

(68) Ashton, P. R.; Brown, C. L.; Chrystal, E. J. T.; Goodnow, T. T.; Kaifer, A. E.; Parry, K. P.; Slawin, A. M. Z.; Spencer, N.; Stoddart, J. F.; Williams, D. J. Self-Assembling [3]Catenanes. *Angew. Chem., Int. Ed. Engl*. **1991**, *30*, 1039–1042.

(69) Amabilino, D. B.; Ashton, P. R.; Reder, A. S.; Spencer, N.; Stoddart, J. F. Olympiadane. *Angew. Chem., Int. Ed. Engl*. **1994**, *33*, 1286–1290.

(70) Amabilino, D. B.; Ashton, P. R.; Brown, C. L.; Córdova, E.; Godinez, L. A.; Goodnow, T. T.; Kaifer, A. E.; Newton, S. P.; Pietraszkiewicz, M.; Philp, D.; Raymo, F. M.; Reder, A. S.; Rutland M. T.; Slawin A. M. Z.; Spencer N.; Stoddart, J. F.; Williams, D. J. Molecular Meccano 2. Self-Assembly of [*n*]Catenanes. *J. Am. Chem. Soc*. **1995**, *117*, 1271–1293.

(71) Armspach, D.; Ashton, P. R.; Ballardini, R.; Balzani, V.; Godi, A.; Moore, C. P.; Prodi, L.; Spencer, N.; Stoddart, J. F.; Tolley, M. S.; Wear, T. J.; Williams, D. J. Catenated Cyclodextrins. *Chem. Eur. J*. **1995**, *1*, 33–55.

(72) Kern, J.-M.; Sauvage, J.-P.; Weidmann, J.-L. Multiring Interlocked Systems *via* Transition Metal-Templated Strategy: The Single-Crystallization Synthesis of [3]-Catenates. *Tetrahedron* **1996**, *52*, 10921–10934.

(73) Amabilino, D. B.; Ashton, P. R.; Boyd, S. E.; Lee, J. Y.; Menzer, S.; Stoddart, J. F.; Williams, D. J. The Five-Stage Self-Assembly of a Branched Heptacatenane. *Angew. Chem., Int. Ed. Engl*. **1997**, *36*, 2070–2072.

(74) Amabilino, D. B.; Ashton, P. R.; Balzani, V.; Boyd, S. E.; Credi, A.; Lee, J. Y.; Menzer, S.; Stoddart, J. F.; Venturi, M.; Williams, D. J. Molecular Meccano 30. Oligocatenanes Made to Order. *J. Am. Chem. Soc*. **1998**, *120*, 4295–4307.

(75) Amabilino, D. B.; Ashton, P. R.; Stoddart, J. F.; White, A. J. P.; Williams, D. J. Molecular Meccano 32. Kinetic and Thermodynamic Effects in the Self-Assembly of [3]Catenanes in the Solution and Solid States. *Chem. Eur. J*. **1998**, *4*, 460–468.

(76) Safarowsky, O.; Vogel, E.; Vögtle, F. Amide-Based [3]Catenanes and [2]Catenanes with Aliphatic Chains. *Eur. J. Org. Chem*. **2000**, 499–505.

(77) Ashton, P. R.; Baldoni, V.; Balzani, V.; Claessens, C. G.; Credi, A.; Hoffmann, H. D. A.; Raymo, F. M.; Stoddart, J. F.; Venturi, M.; White, A. J. P.; Williams, D. J. Molecular Meccano 57. Template-Directed Syntheses, Spectroscopic Properties, and Electrochemical Behavior of [*n*]Catenanes. *Eur. J. Org. Chem.* **2000**, 1121–1130.

(78) Cabezon, B.; Cao, J.; Raymo, F. M.; Stoddart, J. F.; White, A. J. P.; Williams, D. J. Molecular Meccano 59. Self-Complementary [2]Catenanes and Their Related [3]Catenanes. *Chem. Eur. J*. **2000**, *6*, 2262–2273.

(79) Hori, A.; Kumazawa, K.; Kusukawa, T.; Chand, D. K.; Fujita, M.; Sakamoto, S.; Yamaguchi, K. DOSY Study on Dynamic

Catenation: Self-Assembly of a [3]Catenane as a Meta-Stable Compound from Twelve Simple Components. *Chem. Eur. J.* **2001**, *7*, 4142–4149.
(80) Chiu, S.-H.; Elizarov, A. M.; Glink, P. T.; Stoddart, J. F. Translational Isomerism in a [3]Catenane and a [3]Rotaxane. *Org. Lett.* **2002**, *4*, 3561–3564.
(81) Leigh, D. A.; Wong, J. K. Y.; Dehez, F.; Zerbetto, F. Unidirectional Rotation in a Mechanically Interlocked Molecular Rotor. *Nature* **2003**, *424*, 174–179.
(82) Iwamoto, H.; Itoh, K.; Nagamiya, H.; Fukazawa, Y. Convenient Synthesis of [3]Catenane by Olefin Metathesis Dimerizations. *Tetrahedron Lett.* **2003**, *44*, 5773–5776.
(83) Hubbard, A. L.; Davidson, G. J. E.; Patel, R. H.; Wisner, J. A.; Loeb, S. J. Host-Guest Interactions Template: the Synthesis of a [3]Catenane. *Chem. Commun.* **2004**, 138–139.
(84) Blanco, V.; Chas, M.; Abella, D.; Peinador, C.; Quintela, J. M. Molecular Catenation *via* Metal-Directed Self-Assembly and π-Donor/π-Acceptor Interactions: Efficient One-Pot Synthesis, Characterization, and Crystal Structures of [3]Catenanes Based on Pd or Pt Dinuclear Metallocycles. *J. Am. Chem. Soc.* **2007**, *129*, 13978–13986.
(85) Gupta, M.; Kang, S.; Mayer, M. F. A Double Ring-Closing Olefin Metathesis Approach to [3]Catenanes. *Tetrahedron Lett.* **2008**, *49*, 2946–2950.
(86) Blanco, V.; Abella, D.; Pia, E.; Platas-Iglesias, C.; Peinador, C.; Quintela, J. M. Regioselective Catenation-of Dinuclear Palladium and Platinum Metallocycles Promoted by π···π Interactions. *Inorg. Chem.* **2009**, *48*, 4098–4107.
(87) Spruell, J. M.; Coskun, A.; Friedman, D. C.; Forgan, R. S.; Sarjeant, A. A.; Trabolsi, A.; Fahrenbach, A. C.; Barin, G.; Paxton, W. F.; Dey, S. K.; Olson, M. A.; Benitez, D.; Tkatchouk, E.; Colvin, M. T.; Carmielli, R.; Caldwell, S. T.; Rosair, G. M.; Hewage, S. G.; Duclairoir, F.; Seymour, J. L.; Slawin, A. M. Z.; Goddard, W. A., III; Wasielewski, M. R.; Cooke, G.; Stoddart, J. S. Highly Stable Tetrathiafulvalene Radical Dimers in [3]Catenanes. *Nature Chem.* **2010**, *2*, 870–879.
(88) Coskun, A.; Spruell, J. M.; Barin, G.; Fahrenbach, A. C.; Forgan, R. S.; Colvin, M. T.; Carmieli, R.; Benítez, D.; Tkatchouk, E.; Friedman, D. C.; Sarjeant, A. A.; Wasielewski, M. R.; Goddard, W. A., III; Stoddart, J. F. Mechanically Stabilized Tetrathiafulvalene Radical Dimers. *J. Am. Chem. Soc.* **2011**, *133*, 4538–4547.
(89) Forgan, R. S.; Gassensmith, J. J.; Cordes, D. B.; Boyle, M. M.; Hartlieb, K. J.; Friedman, D. C.; Slawin, A. M. Z.; Stoddart, J. F. Self-Assembly of a [2]Pseudorota[3]Catenane in Water. *J. Am. Chem. Soc.* **2012**, *134*, 17007–17010.
(90) Wang, C.; Cao, D.; Fahrenbach, A. C.; Grunder, S.; Dey, S. K.; Sarjeant, A. A.; Stoddart, J. F. The Effects of Conformation on the Noncovalent Bonding Interactions in a Bistable Donor–Acceptor [3]Catenane. *Chem. Commun.* **2012**, *48*, 9245–9247.
(91) Chang, C.-F.; Chuang, C.-J.; Lai, C.-C.; Liu, Y.-H.; Peng, S.-M.; Chiu, S.-H. Using Host-Guest Complexation to Fold a Flexible Linear Organic String: Kinetically Controlled Syntheses of [3]Catenanes and a Five-Membered Molecular Necklace. *Angew. Chem., Int. Ed*. **2012**, *51*, 10094–10098.
(92) Cougnon, F. B. L.; Ponnuswamy, N.; Jenkins, N. A.; Pantoş, G. D.; Sanders, J. K. M. Structural Parameters Governing the Dynamic Combinatorial Synthesis of Catenanes in Water. *J. Am. Chem. Soc.* **2012**, *134*, 19129–19135.
(93) Evans, N. H.; Rahman, H.; Leontiev, A. V.; Greenham, N. D.; Orlowski, G. A.; Zeng, Q.; Jacobs, R. M. J.; Serpell, C. J.; Kilah, N. L.; Davis, J. J.; Beer, P. D. Solution and Surface-Confined Chloride Anion Templated Redox-Active Ferrocene Catenanes. *Chem. Sci.* **2012**, *3*, 1080–1089.
(94) Elbaz, J.; Wang, Z.-G.; Wang, F.; Willner, I. Programmed Dynamic Topologies in DNA Catenanes. *Angew. Chem., Int. Ed*. **2012**, *51*, 2349–2353.
(95) Elbaz, J.; Cecconello, A.; Fan, Z.; Govorov, A. O.; Willner, I. Powering the Programmed Nanostructure and Function of Gold Nanoparticles with Catenated DNA Machines. *Nature Commun*. **2013**, *4*: 2000.
(96) Li, S.; Huang, J.; Cook, T. R.; Pollock, J. B.; Kim, H.; Chi, K.-W.; Stang, P. J. Formation of [3]Catenanes from 10 Precursors *via* Multicomponent Coordination-Driven Self-Assembly of Metallarectangles. *J. Am. Chem. Soc.* **2013**, *135*, 2084–2087.
(97) Iwamoto, H.; Takizawa, W.; Itoh, K.; Hagiwara, T.; Tayama, E.; Hasegawa, E.; Haino, T. Selective Synthesis of [2]- and [3]Catenane Tuned by Ring Size and Concentration. *J. Org. Chem.* **2013**, *78*, 5205–5217.
(98) Wojtecki, R. J.; Wu, Q.; Johnson, J. C.; Ray, D. G.; Korley, L. T. J.; Rowan, S. J. Optimizing the Formation of 2,6-Bis(*N*-alkyl-benzimidazolyl)pyridine-Containing [3]Catenates Through Component Design. *Chem. Sci.* **2013**, *4*, 4440–4448.
(99) Coumans, R. G. E.; Elemans, J. A. A. W.; Rowan, A. E.; Nolte, R. J. M. Interlocked Porphyrin Switches. *Chem. Eur. J*. **2013**, *19*, 7758–7770.
(100) Alemán García, M. Á.; Bampos, N. Synthesis of a Four-Component [3]Catenane Using Three Distinct Noncovalent Interactions. *Org. Biomol. Chem.* **2013**, *11*, 27–30.
(101) Lohmann, F.; Valero, J.; Famulok, M. A Novel Family of Structurally Stable Double Stranded DNA Catenanes. *Chem. Commun.* **2014**, *50*, 6091–6093.
(102) Forgan, R. S.; Blackburn, A. K.; Boyle, M. M.; Schneebeli, S. T.; Stoddart, J. F. The Topological and Chemical Implications of Introducing Oriented Rings to [3]Catenanes. *Supramol. Chem.* **2014**, *26*, 192–201.
(103) Ye, Y.; Wang, S.-P.; Zhu, B.; Cook, T. R.; Wu, J.; Li, S.; Stang, P. J. Self-Assembly of [3]Catenanes and a [4]Molecular Necklace Based on a Cryptand/Paraquat Recognition Motif. *Org. Lett.* **2015**, *17*, 2804–2807.
(104) Iwamoto, H.; Tafuku, S.; Sato, Y.; Takizawa, W.; Katagiri, W.; Tayama, E.; Hasegawa, E.; Fukazawa, Y.; Haino, T. Synthesis of Linear [5]Catenanes *via* Olefin Metathesis Dimerization of Pseudorotaxanes Composed of a [2]Catenane and a Secondary Ammonium Salt. *Chem. Commun.* **2015**, *52*, 319–322.
(105) Wang, K.; Yee, C.-C.; Au-Yeung, H. Y. Facile Syntheses of [3]-, [4]- and [6]Catenanes Templated by Orthogonal Supramolecular Interactions. *Chem. Sci.* **2016**, *7*, 2782–2792.
(106) Schwanke F.; Safarowsky, O.; Heim C.; Silva, G.; Vögtle, F. Amide-Based Oligocatenanes by an Iterative Template Strategy. *Helv. Chim. Acta* **2000**, *83*, 3279–3290.
(107) Weizmann, Y.; Braunschweig, A. B.; Wilner, O. I.; Cheglakov, Z.; Willner, I. A Polycatenated DNA Scaffold for the One-Step Assembly of Hierarchical Nanostructures. *Proc. Natl. Acad. Sci. U.S.A.* **2008**, *105*, 5289–5294.
(108) Lu, C.-H.; Qi, X.-J.; Cecconello, A.; Jester, S.-S.; Famulok, M.; Willner, I. Switchable Reconfiguration of an Interlocked DNA Olympiadane Nanostructure. *Angew. Chem., Int. Ed*. **2014**, *53*, 7499–7503.
(109) Lu, C.-H.; Cecconello, A.; Qi, X.-J.; Wu, N.; Jester, S.-S.; Famulok, M.; Matthies, M.; Schmidt, T.-L.; Willner, I. Switchable Reconfiguration of a Seven-Ring Interlocked DNA Catenane Nanostructure. *Nano Lett.* **2015**, *15*, 7133–7137.
(110) Jin, C.-M.; Lu, H.; Wu, L.-Y.; Huang, J. A New Infinite Inorganic [*n*]Catenane From Silver and Bis(2-methylimidazolyl)methane Ligand. *Chem. Commun.* **2006**, 5039–5041.
(111) Yin, Z.; Zhang, Y.; He, J.; Cheng, J.-P. Hydrogen Bond Assisted Helical Self-Assembly Into [*n*]Catenane. *Chem. Commun.* **2007**, 2599–2601.
(112) Jin, C.-M.; Wu, L.-Y.; Lu, H.; Xu, Y. Two Distinct Supramolecular Motifs from Bis(2-methylimidazo-1-yl) Methane: An Infinite [*n*]Catenane and a Discrete M6 Metal-Organic Framework. *CrysEngComm* **2008**, *8*, 215–218.
(113) Loots, L.; Barbour, L. J. An Infinite Catenane Self-Assembled by π···π Interactions. *Chem. Commun.* **2013**, *49*, 671–673.
(114) Xue, H.; Jiang, F.; Chen, Q.; Yuan, D.; Pang, J.; Lv, G.; Wan, X.; Liang, L.; Hong, M. Conformation Driven in Situ Interlock: From Discrete Metallocycles to Infinite Polycatenanes. *Chem. Commun.* **2015**, *51*, 13706–13709.
(115) Shaffer, T. D.; Tsay, L. M. Pre-Rotaxane Polymers. *J. Polym. Sci. Pol. Chem.* **1991**, *29*, 1213–1215.
(116) Gibson, H. W.; Bheda, M. C.; Engen, P. T. Rotaxanes, Catenanes, Polyrotaxanes, Polycatenanes and Related Materials. *Prog. Polym. Sci.* **1994**, *19*, 843–945.

(117) Watanabe, N.; Ikari, Y.; Kihara, N.; Takata, T. Bridged Polycatenane. *Macromolecules* **2004**, *37*, 6663–6666.

(118) Takata, T.; Kihara, N.; Furusho, Y. Polyrotaxanes and Polycatenanes: Recent Advances in Syntheses and Applications of Polymers Comprising of Interlocked Structures. *Adv. Polym. Sci.* **2004**, *171*, 1–75.

(119) Carella, J. M.; Gotro, J. T.; Graessley, W. W. Thermorheological Effects of Long-Chain Branching in Entangled Polymer Melts. *Macromolecules* **1986**, *19*, 659–667.

(120) Plummer, C. J. G.; Cudré-Mauroux, N.; Kausch, H.-H. Deformation and Entanglement in Semicrystalline Polymers. *Polym. Eng. Sci.* **1994**, *34*, 318–329.

(121) Shaffer, J. S. Effects of Chain Topology on Polymer Dynamics: Bulk Melts. *J. Chem. Phys.* **1994**, *101*, 4205–4210.

(122) Tsui, O. K. C.; Zhang, H. F. Effects of Chain Ends and Chain Entanglement on the Glass Transition Temperature of Polymer Thin Films. *Macromolecules* **2001**, *34*, 9139–9142.

(123) Watanabe, H. Viscoelasticity and Dynamics of Entangled Polymers. *Prog. Polym. Sci.* **1999**, *24*, 1253–1403.

(124) Gil-Ramírez, G.; Leigh, D. A.; Stephens, A. J. Catenanes: Fifty Years of Molecular Links. *Angew. Chem., Int. Ed*. **2015**, *54*, 6110–6150.

(125) Whang, D.; Park, K.-M.; Heo, J.; Ashton, P. R.; Kim, K. Molecular Necklace: Quantitative Self-Assembly of a Cyclic Oligorotaxane from Nine Molecules. *J. Am. Chem. Soc.* **1998**, *120*, 4899–4900.

(126) Bitsch, F.; Dietrich-Buchecker, C. O.; Khemiss, A.-K.; Sauvage, J.-P.; Van Dorsselaer, A. Multiring Interlocked Systems: Structure Elucidation by Electrospray Mass Spectrometry. *J. Am. Chem. Soc.* **1991**, *113*, 4023–4025.

(127) Roh, S.-G.; Park, K.-M.; Park, G.-J.; Sakamoto, S.; Yamaguchi, K.; Kim, K. Synthesis of a Five-Membered Molecular Necklace: A 2 + 2 Approach. *Angew. Chem., Int. Ed*. **1999**, *38*, 638–641.

(128) Chiu, S.-H.; Rowan, S. J.; Cantrill, S. J.; Ridvan, L.; Cantrill, S. J.; Ashton, P. R.; Garrell, R. L.; Stoddart, J. F. Making Molecular-Necklaces from Rotaxanes. *Tetrahedron* **2002**, *58*, 807–814.

(129) Park, K.-M.; Kim, S.-Y.; Heo, J.; Whang, D.; Sakamoto, S.; Yamaguchi, K.; Kim, K. Designed Self-Assembly of Molecular Necklaces. *J. Am. Chem. Soc.* **2002**, *124*, 2140–2147.

(130) Dasgupta, S.; Wu, J. Template-Directed Synthesis of Kinetically and Thermodynamically Stable Molecular Necklace Using Ring Closing Metathesis. *Org. Biomol. Chem.* **2011**, *9*, 3504–3515.

(131) Okada, M.; Harada, A. Poly(polyrotaxane): Photoreactions of 9-Anthracene-Capped Polyrotaxane. *Macromolecules* **2003**, *36*, 9701–9703.

(132) Clark, P. G.; Guidry, E. N.; Chan, W. Y.; Steinmetz, W. E.; Grubbs, R. H. Synthesis of a Molecular Charm Bracelet *via* Click Cyclization and Olefin Metathesis Clipping. *J. Am. Chem. Soc.* **2010**, *132*, 3405–3412.

(133) Ko, Y. H.; Kim, K.; Kang, J.; Chun, H.; Lee, J. W.; Sakamoto, S.; Yamaguchi, K.; Fettinger, J. C.; Kim, K. Designed Self-Assembly of Molecular Necklaces Using Host-Stabilized Charge-Transfer Interactions. *J. Am. Chem. Soc.* **2004**, *126*, 1932–1933.

(134) Li, S.; Huang, J.; Zhou, F.; Cook, T. R.; Yan, X.; Ye, Y.; Zhu, B.; Zheng, B.; Stang, P. J. Self-Assembly of Triangular and Hexagonal Molecular Necklaces. *J. Am. Chem. Soc.* **2014**, *136*, 5908–5911.

(135) Viljoen, E.; Zhu, K.; Loeb, S. J. From Binuclear Complexes to Molecular Necklaces: Incorporating Flexible Ligands into Rotaxanes. *Chem. Eur. J.* **2016**, *22*, 7479–7484.

(136) Loeb, S. J.; Wisner, J. A. 1,2-Bis(4,4′-dipyridinium)ethane: A Versatile Dication for the Formation of [2]Rotaxanes with Dibenzo-24-Crown-8 Ether. *Chem. Commun.* **1998**, 2757–2758.

(137) Yang, H.-B.; Ghosh, K.; Arif, A. M.; Stang, P. J. The Synthesis of New 60° Organometallic Subunits and Self-Assembly of Three-Dimensional M_3L_2 Trigonal-Bipyramidal Cages. *J. Org. Chem.* **2006**, *71*, 9464–9469.

(138) Yang, H.-B.; Ghosh, K.; Northrop, B. H.; Zheng, Y.-R.; Lyndon, M. M.; Muddiman, D. C.; Stang, P. J. A Highly Efficient Approach to the Self-Assembly of Hexagonal Cavity-Cored Tris[2]Pseudorotaxanes From Several Components *via* Multiple Noncovalent Interactions. *J. Am. Chem. Soc.* **2007**, *129*, 14187–14189.

(139) Rowan, S. J.; Cantrill, S. J.; Stoddart, J. F. Triphenylphosphonium-Stoppered [2]Rotaxanes. *Org. Lett.* **1999**, *1*, 129–132.

(140) Langton, M. J.; Matichak, J. D.; Thompson, A. L.; Anderson, H. L. Template-Directed Synthesis of π-Conjugated Porphyrin [2]Rotaxanes and a [4]Catenane Based on a Six-Porphyrin Nanoring. *Chem. Sci.* **2011**, *2*, 1897–1901.

(141) Saito, S.; Takahashi, E.; Nakazono, K. Synthesis of [2]Rotaxanes by the Catalytic Reactions of a Macrocyclic Copper Complex. *Org. Lett.* **2006**, *8*, 5133–5136.

(142) Hoffmann, M.; Kärnbratt, J.; Chang, M.-H.; Herz, L. M.; Albinsson, B.; Anderson, H. L. Enhanced π Conjugation Around a Porphyrin[6] Nanoring. *Angew. Chem., Int. Ed*. **2008**, *47*, 4993–4996.

(143) Hoffmann, M.; Wilson, C. J.; Odell, B.; Anderson, H. L. Template-Directed Synthesis of a π-Conjugated Porphyrin Nanoring. *Angew. Chem., Int. Ed*. **2007**, *46*, 3122–3125.

(144) O'Sullivan, M. C.; Sprafke, J. K.; Kondratuk, D. V.; Rinfray, C.; Claridge, T. D. W.; Saywell, A.; Blunt, M. O.; O'Shea, J. N.; Beton, P. H.; Malfois, M.; Anderson, H. L. Vernier Templating and Synthesis of a 12-Porphyrin Nano-Ring. *Nature* **2012**, *469*, 72–75.

(145) Rousseaux, S. A. L.; Gong, J. Q.; Haver, R.; Odell, B.; Claridge, T. D. W.; Herz, L. M.; Anderson, H. L. Self-Assembly of Russian Doll Concentric Porphyrin Nanorings. *J. Am. Chem. Soc.* **2015**, *137*, 12713–12718.

(146) Neuhaus, P.; Cnossen, A.; Gong, J. Q.; Herz, L. M.; Anderson, H. L. A Molecular Nanotube with Three-Dimensional π-Conjugation. *Angew. Chem., Int. Ed*. **2015**, *127*, 7452–7456.

(147) Pakula, T.; Jeszka, K. Simulation of Single Complex Macromolecules. 1. Structure and Dynamics of Catenanes. *Macromolecules* **1999**, *32*, 6821–6830.

(148) Frisch, H.; Martin, I.; Mark, H. Zur Struktur der Polysiloxene. I. *Monatsh. Chem.* **1953**, *84*, 250–256.

(149) Fyvie, T. J.; Semlyen, J. A.; Mark, J. E. Polymeric Catenanes from Crosslinked Poly(2,6-dimethyl-1,4-phenylene oxide) and Cyclic Poly(dimethylsiloxane). *J. Polym. Sci. Pol. Chem.* **1987**, *25*, 2503–2509.

(150) Huang, W.; Frisch, H. L.; Hua, Y.; Semlyen, J. A. Study of the Properties and Topological Trapping of Cyclic Poly(dimethylsiloxane)in Poly(2,6-dimethyl-1,4-phenylene oxide) Networks. *J. Polym. Sci. Pol. Chem.* **1990**, *28*, 1807–1812.

(151) Patat, F.; Derst, P. Über den thermischen Abbau des Polymeren Phosphornitrilchlorids. *Angew. Chem.* **1959**, *71*, 105–110.

(152) Callahan, D.; Frisch, H. L.; Klempner, D. Polymeric Catenanes. *Polym. Eng. Sci*. **1975**, *15*, 70–72.

(153) Endo, K.; Shiroi, T.; Murata, N.; Kojima, G.; Yamanaka, T. Synthesis and Characterization of Poly(1,2-dithiane). *Macromolecules* **2004**, *37*, 3143–3150.

(154) Endo, K.; Shiroi, T.; Murata, N. Thermal Polymerization of 1,2-Dithiane. *Polym. J.* **2005**, *37*, 512–516.

(155) Endo, K.; Yamanaka, T. Copolymerization of Lipoic Acid with 1,2-Dithiane and Characterization of the Copolymer as an Interlocked Cyclic Polymer. *Macromolecules* **2006**, *39*, 4038–4043.

(156) Yamanaka, T.; Endo, K. Network Formation of Interlocked Copolymer Obtained from Copolymerization of 1,2-Dithiane and Lipoic Acid by Metal Salt. *Polym. J.* **2007**, *39*, 1360–1364.

(157) Ishida, H.; Kisanuki, A.; Endo, K. Ring-Opening Polymerization of Aromatic 6-Membered Cyclic Disulfide and Characterization of the Polymer. *Polym. J.* **2009**, *41*, 110–117.

(158) Rosenthal-Kim, E. Q.; Agapov, R. L.; Puskas, J. E. Visualization of the Architecture of Poly(α-Lipoic Acid) Using Atomic Force Microscopy. *Eur. Polym. J.* **2015**, *65*, 232–237.

(159) Berrocal, J. A.; Pitet, L. M.; Nieuwenhuizen, M. M. L.; Mandolini, L.; Meijer, E. W.; Di Stefano, S. Ring-Opening Metathesis Polymerization of a Diolefinic [2]Catenane–Copper(I) Complex: An Easy Route to Polycatenanes. *Macromolecules* **2015**, *48*, 1358–1363.

(160) IUPAC. Compendium of Chemical Terminology, 2nd Ed. (The "Gold Book"). Compiled by A. D. McNaught and A. Wilkinson.

Blackwell Scientific Publications: Oxford, **1997**. XML Online Corrected Version: http://Goldbook.Iupac.org Created by M. Nic, J. Jirat, B. Kosata; Updates Compiled by A. Jenkins. ISBN 0-9678550-9-8. DOI: 10.1351/Goldbook.

(161) Han, Y.; Jiang, Y.; Chen, C.-F. Cryptand-Based Hosts for Organic Guests. *Tetrahedron* **2015**, *71*, 503–522.

(162) Liu, M.; Li, S.; Zhang, M.; Zhou, Q.; Wang, F.; Hu, M.; Fronczek, F. R.; Li, N.; Huang, F. Three-Dimensional Bis(*m*-phenylene)-32-Crown-10-Based Cryptand/Paraquat Catenanes. *Org. Biomol. Chem.* **2009**, *7*, 1288–1291.

(163) Li, S.; Liu, M.; Zheng, B.; Zhu, K.; Wang, F.; Li, N.; Zhao, X.-L.; Huang, F. Taco Complex Templated Syntheses of a Cryptand/Paraquat [2]Rotaxane and a [2]Catenane by Olefin Metathesis. *Org. Lett.* **2009**, *11*, 3350–3353.

(164) Li, J.; Wei, P.; Wu, X.; Xue, M.; Yan, X.; Zhou, Q. Taco Complex-Templated Dynamic Clipping to Cryptand-Based [2]Rotaxane- and [2]Catenane-Type Mechanically Interlocked Structures. *RSC Adv.* **2013**, *3*, 21289–21293.

(165) Liu, H.; Li, X.-Y.; Zhao, X.-L.; Liu, Y. A.; Li, J.-S.; Jiang, B.; Wen, K. [2]Pseudorotaxanes and [2]Catenanes Constructed by Oxacalixcrowns/Viologen Molecular Recognition Motifs. *Org. Lett*. **2014**, *16*, 5894–5897.

(166) Nielsen, M. B.; Thorup, N.; Becher, J. Synthesis of a Criss-Cross Overlapped Tetrathiafulvalenophane and a Topologically New [2]Catenane. *J. Chem. Soc., Perkin Trans*. *1* **1998**, 1305–1308.

(167) Fujita, M.; Fujita, N.; Ogura, K.; Yamaguchi, K. Spontaneous Assembly of Ten Components into Two Interlocked , Identical Coordination Cages. *Nature* **1999**, *400*, 52–55.

(168) Yamauchi, Y.; Yoshizawa, M.; Fujita, M. Engineering Stacks of Aromatic Rings by the Interpenetration of Self-Assembled Coordination Cages. *J. Am. Chem. Soc.* **2008**, *130*, 5832–5833.

(169) Fukuda, M.; Sekiya, R.; Kuroda, R. A Quadruply Stranded Metallohelicate and Its Spontaneous Dimerization into an Interlocked Metallohelicate. *Angew. Chem., Int. Ed*. **2008**, *47*, 706–710.

(170) Freye, S.; Hey, J.; Torras-Galán, A.; Stalke, D.; Herbst-Irmer, R.; John, M.; Clever, G. H. Allosteric Binding of Halide Anions by a New Dimeric Interpenetrated Coordination Cage. *Angew. Chem., Int. Ed*. **2012**, *51*, 2191–2194.

(171) Frank, M.; Hey, J.; Balcioglu, I.; Chen, Y.-S.; Stalke, D.; Suenobu, T.; Fukuzumi, S.; Frauendorf, H.; Clever, G. H. Assembly and Stepwise Oxidation of Interpenetrated Coordination Cages Based on Phenothiazine. *Angew. Chem., Int. Ed*. **2013**, *52*, 10102–10106.

(172) Black, S. P.; Stefankiewicz, A. R.; Smulders, M. M. J.; Sattler, D.; Schalley, C. A.; Nitschke, J. R.; Sanders, J. K. M. Generation of a Dynamic System of Three-Dimensional Tetrahedral Polycatenanes. *Angew. Chem., Int. Ed*. **2013**, *52*, 5749–5752.

(173) Black, S. P.; Wood, D. M.; Schwarz, F. B.; Ronson, T. K.; Holstein, J. J.; Stefankiewicz, A. R.; Schalley, C. A.; Sanders, J. K. M.; Nitschke, J. R. Catenation and Encapsulation Induce Distinct Reconstitutions Within a Dynamic Library of Mixed-Ligand Zn_4L_6 Cages. *Chem. Sci.* **2016**, *7*, 2614–2620.

(174) Westcott, A.; Fisher, J.; Harding, L. P.; Rizkallah, P.; Hardie, M. J. Self-Assembly of a 3-D Triply Interlocked Chiral [2]Catenane. *J. Am. Chem. Soc.* **2008**, *130*, 2950–2951.

(175) Henkelis, J. J.; Ronson, T. K.; Harding, L. P.; Hardie, M. J. M_3L_2 Metallo-Cryptophanes: [2]Catenane and Simple Cages. *Chem. Commun.* **2011**, *47*, 6560–6562.

(176) Vögtle, F.; Lüer, I.; Balzani, V.; Armaroli, N. Endoreceptors with Convergent Phenanthroline Units: A Molecular Cavity for Six Guest Molecules. *Angew. Chem., Int. Ed. Engl*. **1991**, *30*, 1333–1336.

(177) Hasell, T.; Wu, X.; Jones, J. T. A.; Bacsa, J.; Steiner, A.; Mitra, T.; Trewin, A.; Adams, D. J.; Cooper, A. I. Triply Interlocked Covalent Organic Cages. *Nature Chem.* **2010**, *2*, 750–755.

(178) Zhang, G.; Presly, O.; White, F.; Oppel, I. M.; Mastalerz, M. A Shape-Persistent Quadruply Interlocked Giant Cage Catenane with Two Distinct Pores in the Solid State. *Angew. Chem., Int. Ed*. **2014**, *53*, 5126–5130.

(179) Li, H.; Zhang, H.; Lammer, A. D.; Wang, M.; Li, X.; Lynch, V. M.; Sessler, J. L. Quantitative Self-Assembly of a Purely Organic Three-Dimensional Catenane in Water. *Nature Chem.* **2015**, *7*, 1003–1008.

(180) Li, Z.-T.; Stein, P. C.; Svenstrup, N.; Lund, K. H.; Becher, J. Synthesis of Novel Tetrathiafulvalene-Based [3]Pseudocatenanes by Self-Assembly; Prevention of Trans/Cis Isomerization. *Angew. Chem., Int. Ed. Engl*. **1995**, *34*, 2524–2528.

(181) Li, Z.-T.; Stein, P C; Becher, J.; Jensen, D.; Mørk, P.; Svenstrup, N. Self-Assembling Tetrathiafulvalene-Based Rotaxanes and Catenanes. *Chem. Eur. J*. **1996**, *2*, 624–633.

(182) Li, Z.-T.; Becher, J. Configurationally Selective Self-Assembly of a *cis*-[3]Pseudocatenane Incorporating Three Tetrathiafulvalene Units. *Chem. Commun.* **1996**, 639–640.

(183) Li, Z.-T.; Becher, J. Effects of Fluorine in the Self-Assembly of Tetrathiafulvalene-Based [3]Catenanes-(circum TTF)-A New Approach to Controlling the Regio-and Configurational Selectivity. *Synlett* **1997**, 557–560.

(184) Nielsen, M. B.; Li, Z.-T.; Becher, J. Tetrathiafulvalenophanes and Their Catenanes. *J. Mater. Chem.* **1997**, *7*, 1175–1187.

(185) Frey, J.; Kraus, T.; Heitz, V.; Sauvage, J.-P. A Catenane Consisting of a Large Ring Threaded Through Both Cyclic Units of a Handcuff-Like Compound. *Chem. Commun.* **2005**, 5310–5312.

(186) Frey, J.; Kraus, T.; Heitz, V.; Sauvage, J.-P. Synthesis of a Bis-Macrocycle Containing Two Back-to-Back Rigidly Connected 1,10-Phenanthroline Units as a Central Core and Its Incorporation in a Handcuff-Like Catenane. *Chem. Eur. J.* **2007**, *13*, 7584–7594.

(187) Hartlieb, K. J.; Blackburn, A. K.; Schneebeli, S. T.; Forgan, R. S.; Sarjeant, A. A.; Stern, C. L.; Cao, D.; Stoddart, J. F. Topological Isomerism in a Chiral Handcuff Catenane. *Chem. Sci.* **2014**, *5*, 90–100.

(188) Dietrich-Buchecker, C.; Frommberger, B.; Lüer, I.; Sauvage, J.-P.; Vögtle, F. Multiring Catenanes with a Macrobicyclic Core. *Angew. Chem., Int. Ed. Engl*. **1993**, *32*, 1434–1437.

(189) Dietrich-Buchecker, C. O.; Sauvage, J.-P.; Kitzinger, J. P. Une Nouvelle Famille de Molecules: Les Metallo-Catenanes. *Tetrahedron Lett.* **1983**, *24*, 5095–5098.

(190) Ashton, P. R.; Reder, A. S.; Spencer, N.; Stoddart, J. F. Self-Assembly of a Chiral Bis[2]Catenane. *J. Am. Chem. Soc.* **1993**, *115*, 5286–5287.

(191) Ashton, P. R.; Horn, T.; Menzer, S.; Preece, J. A.; Spencer, N.; Stoddart, J. F.; Williams, D. J. Towards a Molecular Anchor Chain. Synthesis and Catenations of Spiro Crown Ethers. *Synthesis* **1997**, *19*, 480–488.

(192) Liu, M.; Li, S.; Hu, M.; Wang, F.; Huang, F. Selectivity Algorithm for the Formation of Two Cryptand/Paraquat Catenanes. *Org. Lett.* **2010**, *12*, 760–763.

(193) Lankshear, M. D.; Evans, N. H.; Bayly, S. R.; Beer, P. D. Anion-Templated Calix[4]arene-Based Pseudorotaxanes and Catenanes. *Chem. Eur. J.* **2007**, *13*, 3861–3870.

(194) Phipps, D. E.; Beer, P. D. A [2]Catenane Containing an Upper-Rim Functionalized Calix[4]arene for Anion Recognition. *Tetrahedron Lett.* **2009**, *50*, 3454–3457.

(195) Li, Y.; Mullen, K. M.; Claridge, T. D. W.; Costa, P. J.; Félix, V.; Beer, P. D. Sulfate Anion Templated Synthesis of a Triply Interlocked Capsule. *Chem. Commun.* **2009**, 7134–7136.

(196) Nakamura, T.; Kimura, H.; Okuhara, T.; Yamamura, M.; Nabeshima, T. A Hierarchical Self-Assembly System Built Up from Preorganized Tripodal Helical Metal Complexes. *J. Am. Chem. Soc.* **2016**, *138*, 794–797.

(197) Hori, A.; Yamashita, K.-I.; Kusukawa, T.; Akasaka, A.; Biradha, K.; Fujita, M. A Circular Tris[2]Catenane From Molecular "Figure-of-Eight." *Chem. Commun.* **2004**, 1798–1799.

(198) Yamashita, K.-I.; Hori, A.; Fujita, M. Formation of Bis- and Tris[2]Catenanes *via* the Cross-Catenation of Pd(II)- and Pt(II)-Linked Coordination Rings. *Tetrahedron* **2007**, *63*, 8435–8439.

(199) Samanta, D.; Mukherjee, P. S. Sunlight-Induced Covalent Marriage of Two Triply Interlocked Pd_6 Cages and Their Facile

Thermal Separation. *J. Am. Chem. Soc.* **2014**, *136*, 17006–17009.
(200) Walba, D. M.; Zheng, Q. Y.; Schilling, K. Experimental Studies on the Hook and Ladder Approach to Molecular Knots: Synthesis of a Topologically Chiral Cyclized Hook and Ladder. *J. Am. Chem. Soc.* **1992**, *114*, 6259–6260.
(201) Walba, D. M.; Richards, R. M.; Sherwood, S. P.; Haltiwanger, R. C. Strategy for the Synthesis of Cylindrical Macropolycyclic Hosts with Hydrophilic Interior Surfaces: Crown Ether Rings Fused by the Tetrahydroxymethylethylene (THYME) Unit. *J. Am. Chem. Soc.* **1981**, *103*, 6213–6215.
(202) Walba, D. M.; Armstrong, J. D., III; Perry, A. E.; Richards, R. M.; Homan, T. C.; Haltiwanger, R. C. The Thyme Polyethers: An Approach to the Synthesis of a Molecular Knotted Ring. *Tetrahedron* **1986**, *42*, 1883–1894.
(203) Walba, D. M.; Richards, R. M.; Hermsmeier, M.; Haltiwanger, R. C. Conformational Properties of the THYME Polyethers. The Bis-THYME Cylinder: A Three-Dimensional Analog of 18-Crown-6. *J. Am. Chem. Soc*. **1987**, *109*, 7081–7087.
(204) Sekiya, R.; Fukuda, M.; Kuroda, R. Anion-Directed Formation and Degradation of an Interlocked Metallohelicate. *J. Am. Chem. Soc.* **2012**, *134*, 10987–10997.
(205) Vysotsky, M. O.; Bogdan, A.; Wang, L.; Böhmer, V. Template Synthesis of Multi-Macrocycles by Metathesis Reaction. *Chem. Commun.* **2004**, 1268–1269.
(206) Bogdan, A.; Rudzevich, Y.; Vysotsky, M. O.; Böhmer, V. Topologically Novel Multiple Rotaxanes and Catenanes Based on Tetraurea Calix[4]arenes. *Chem. Commun.* **2006**, 2941–2952.
(207) Böhmer, V.; Rudzevich, Y.; Rudzevich, V. Rotaxanes and Catenanes Derived From Tetra-Urea Calix[4]arenes. *Macromol. Symp.* **2010**, *287*, 42–50.
(208) Vysotsky, M. O.; Bolte, M.; Thondorf, I.; Böhmer, V. New Molecular Topologies by Fourfold Metathesis Reactions Within a Hydrogen-Bonded Calix[4]arene Dimer. *Chem. Eur. J.* **2003**, *9*, 3375–3382.
(209) Bogdan, A.; Vysotsky, M. O.; Ikai, T.; Okamoto, Y.; Böhmer, V. Rational Synthesis of Multicyclic Bis[2]Catenanes. *Chem. Eur. J.* **2004**, *10*, 3324–3330.
(210) Molokanova, O.; Bogdan, A.; Vysotsky, M. O.; Bolte, M.; Ikai, T.; Okamoto, Y.; Böhmer, V. Calix[4]arene-Based Bis[2]Catenanes: Synthesis and Chiral Resolution. *Chem. Eur. J.* **2007**, *13*, 6157–6170.
(211) Janke, M.; Rudzevich, Y.; Molokanova, O.; Metzroth, T.; Mey, I.; Diezemann, G.; Marszalek, P. E.; Gauss, J.; Böhmer, V.; Janshoff, A. Mechanically Interlocked Calix[4]arene Dimers Display Reversible Bond Breakage under Force. *Nature Nanotechnol.* **2009**, *4*, 225–229.
(212) Chas, M.; Ballester, P. A Dissymmetric Molecular Capsule with Polar Interior and Two Mechanically Locked Hemispheres. *Chem. Sci.* **2011**, *3*, 186–191.
(213) Henkelis, J. J.; Hardie, M. J. Controlling the Assembly of Cyclotriveratrylene-Derived Coordination Cages. *Chem. Commun.* **2015**, *51*, 11929–11943.
(214) Wang, L.; Vysotsky, M. O.; Bogdan, A.; Bolte, M.; Böhmer, V. Multiple Catenanes Derived from Calix[4]arenes. *Science* **2004**, *304*, 1312–1314.
(215) Molokanova, O.; Podoprygorina, G.; Bolte, M.; Böhmer, V. Multiple Catenanes Based on Tetraloop Derivatives of Calix[4]arenes. *Tetrahedron* **2009**, *65*, 7220–7233.
(216) Zhang, G.; Presly, O.; White, F.; Oppel, I. M.; Mastalerz, M. A Permanent Mesoporous Organic Cage with an Exceptionally High Surface Area. *Angew. Chem., Int. Ed*. **2014**, *53*, 1516–1520.
(217) Batten, S. R.; Robson, R. Interpenetrating Nets: Ordered, Periodic Entanglement. *Angew. Chem., Int. Ed*. **1998**, *37*, 1460–1494.
(218) Sperling, L. H. Interpenetrating Polymer Networks and Related Materials. *J. Polym. Sci. Macromol. Rev.* **1977**, *12*, 141–180.
(219) Frisch, H. L.; Frisch, K. C.; Klempner, D. Advances in Interpenetrating Polymer Networks. *Pure Appl. Chem.* **1981**, *53*, 1557–1566.
(220) Sperling, L. H. *Interpenetrating Polymer Networks and Related Materials*; Plenum Press: New York, **1981**; pp. 1–269.
(221) *Interpenetrating Polymer Networks*; Klempner, D.; Sperling, L. H.; Utracki, L. A., Eds.; American Chemical Society: Washington, DC, **1994**; Vol. *239*.
(222) Gupta, N.; Srivastava, A. K. Interpenetrating Polymer Networks: A Review on Synthesis and Properties. *Polym. Int.* **1994**, *35*, 109–118.
(223) Sperling, L. H.; Mishra, V. The Current Status of Interpenetrating Polvrner Networks. *Polym. Adv. Technol.* **1996**, *7*, 197–208.
(224) Suthar, B.; Xiao, H. X.; Klempner, D.; Frisch, K. C. A Review of Kinetic Studies on the Formation of Interpenetrating Polymer Networks. *Polym. Adv. Technol.* **1996**, *7*, 221–233.
(225) Lipatov, Y. S. Polymer Blends and Interpenetrating Polymer Networks at the Interface with Solids. *Prog. Polym. Sci.* **2002**, *27*, 1721–1801.
(226) Lipatov, Y. S.; Alekseeva, T. T. Phase-Separated Interpenetrating Polymer Networks. *Adv. Polym. Sci.* **2007**, *208*, 1–243.
(227) Huang, M.; Furukawa, H.; Tanaka, Y.; Nakajima, T.; Osada, Y.; Gong, J. P. Importance of Entanglement Between First and Second Components in High-Strength Double Network Gels. *Macromolecules* **2007**, *40*, 6658–6664.
(228) Gong, J. P. Why Are Double Network Hydrogels So Tough? *Soft Matter* **2010**, *6*, 2583–2590.
(229) Haque, M. A.; Kurokawa, T.; Gong, J. P. Super Tough Double Network Hydrogels and Their Application as Biomaterials. *Polymer* **2012**, *53*, 1805–1822.
(230) Dragan, E. S. Design and Applications of Interpenetrating Polymer Network Hydrogels. A Review. *Chem. Eng. J.* **2014**, *243*, 572–590.
(231) Erdodi, G.; Kennedy, J. P. Amphiphilic Conetworks: Definition, Synthesis, Applications. *Prog. Polym. Sci.* **2006**, *31*, 1–18.
(232) Wells, A. F. *Three-Dimensional Nets and Polyhedra*; Wiley: New York, **1977**.
(233) Niggli, P. XII. Die Kristallstruktur Einiger Oxyde I. *Zeitschrift für Kristallographie* **1922**, 253–299.
(234) Neuburger, M. C. Präzisionsmessung der Gitterkonstante von Cuprooxyd Cu_2O. *Zeitschrift für Physik* **1931**, *67*, 845–850.
(235) Kuang, X.; Wu, X.; Yu, R.; Donahue, J. P.; Huang, J.; Lu, C.-Z. Assembly of a Metal-Organic Framework by Sextuple Intercatenation of Discrete Adamantane-Like Cages. *Nature Chem.* **2010**, *2*, 461–465.
(236) Heine, J.; Schmedt auf der Günne, J.; Dehnen, S. Formation of a Strandlike Polycatenane of Icosahedral Cages for Reversible One-Dimensional Encapsulation of Guests. *J. Am. Chem. Soc.* **2011**, *133*, 10018–10021.
(237) Jiang, L.; Ju, P.; Meng, X.-R.; Kuang, X.-J.; Lu, T.-B. Constructions of Two Polycatenanes and One Polypseudo-Rotaxane by Discrete Tetrahedral Cages and Stool-Like Building Units. *Sci. Rep*. **2012**, *2*: 668.
(238) Chen, Q.; Jiang, F.; Yuan, D.; Chen, L.; Lyu, G.; Hong, M. Anion-Driven Self-Assembly: From Discrete Cages to Infinite Polycatenanes Step by Step. *Chem. Commun.* **2013**, *49*, 719–721.
(239) Chen, Q.; Jiang, F.; Yuan, D.; Lyu, G.; Chen, L.; Hong, M. A Controllable and Dynamic Assembly System Based on Discrete Metallocages. *Chem. Sci.* **2014**, *5*, 483–488.
(240) Chen, Q.; Chen, L.; Jiang, F.; Hong, M. Controllable Coordination Self-Assembly Based on Flexible Tripodal Ligands: From Finite Metallocages to Infinite Polycatenanes Step by Step. *Chem. Rec.* **2015**, 15, 711–727.
(241) Chen, L.; Chen, Q.; Wu, M.; Jiang, F.; Hong, M. Controllable Coordination-Driven Self-Assembly: From Discrete Metallocages to Infinite Cage-Based Frameworks. *Acc. Chem. Res.* **2015**, *48*, 201–210.
(242) Batten, S. R. Topology of Interpenetration. *CrystEngComm* **2001**, *3*, 67–72.
(243) Carlucci, L.; Ciani, G.; Proserpio, D. M. Polycatenation, Polythreading and Polyknotting in Coordination Network Chemistry. *Coord. Chem. Rev.* **2003**, *246*, 247–289.
(244) Jiang, H.-L.; Makal, T. A.; Zhou, H.-C. Interpenetration Control in Metal-Organic Frameworks for Functional Applications. *Coord. Chem. Rev.* **2013**, *257*, 2232–2249.

(245) Carlucci, L.; Ciani, G.; Proserpio, D. M.; Mitina, T. G.; Blatov, V. A. Entangled Two-Dimensional Coordination Networks: A General Survey. *Chem. Rev.* **2014**, *114*, 7557–7580.
(246) Li, H.; Eddaoudi, M.; O'Keeffe, M.; Yaghi, O. M. Design and Synthesis of an Exceptionally Stable and Highly Porous Metal-Organic Framework. *Nature* **1999**, *402*, 276–279.
(247) Eddaoudi, M.; Moler, D. B.; Li, H.; Chen, B.; Reineke, T. M.; O'Keeffe, M.; Yaghi, O. M. Modular Chemistry: Secondary Building Units as a Basis for the Design of Highly Porous and Robust Metal−Organic Carboxylate Frameworks. *Acc. Chem. Res.* **2001**, *34*, 319–330.
(248) James, S. L. Metal-Organic Frameworks. *Chem. Soc. Rev*. **2003**, *32*, 276–288.
(249) Yaghi, O. M.; O'Keeffe, M.; Ockwig, N. W.; Chae, H. K.; Eddaoudi, M.; Kim, J. Reticular Synthesis and the Design of New Materials. *Nature* **2003**, *423*, 705–714.
(250) MacGillivray, L. R. *Metal-Organic Frameworks: Design and Application*; Wiley: Hoboken, **2010**.
(251) Cook, T. R.; Zheng, Y.-R.; Stang, P. J. Metal-Organic Frameworks and Self-Assembled Supramolecular Coordination Complexes: Comparing and Contrasting the Design, Synthesis, and Functionality of Metal-Organic Materials. *Chem. Rev.* **2013**, *113*, 734–777.
(252) Janiak, C. Engineering Coordination Polymers Towards Applications. *Dalton Trans.* **2003**, 2781–2804.
(253) Mueller, U.; Schubert, M.; Teich, F.; Puetter, H.; Schierle-Arndt, K.; Pastré, J. Metal-Organic Frameworks—Prospective Industrial Applications. *J. Mater. Chem.* **2006**, *16*, 626–636.
(254) Czaja, A. U.; Trukhan, N.; Müller, U. Industrial Applications of Metal-Organic Frameworks. *Chem. Soc. Rev.* **2009**, *38*, 1284–1293.
(255) Furukawa, H.; Cordova, K. E.; O'Keeffe, M.; Yaghi, O. M. The Chemistry and Applications of Metal-Organic Frameworks. *Science* **2013**, *341*, 123044.
(256) Wang, C.; Liu, D.; Lin, W. Metal-Organic Frameworks as a Tunable Platform for Designing Functional Molecular Materials. *J. Am. Chem. Soc.* **2013**, *135*, 13222–13234.
(257) Rowsell, J. L. C.; Yaghi, O. M. Strategies for Hydrogen Storage in Metal-Organic Frameworks. *Angew. Chem., Int. Ed*. **2005**, *44*, 4670–4679.
(258) Murray, L. J.; Dincă, M.; Long, J. R. Hydrogen Storage in Metal-Organic Frameworks. *Chem. Soc. Rev.* **2009**, *38*, 1294–1314.
(259) Sumida, K.; Rogow, D. L.; Mason, J. A.; McDonald, T. M.; Bloch, E. D.; Herm, Z. R.; Bae, T.-H.; Long, J. R. Carbon Dioxide Capture in Metal-Organic Frameworks. *Chem. Rev.* **2012**, *112*, 724–781.
(260) Suh, M. P.; Park, H. J.; Prasad, T. K.; Lim, D.-W. Hydrogen Storage in Metal-Organic Frameworks. *Chem. Rev.* **2012**, *112*, 782–835.
(261) Li, J.-R.; Kuppler, R. J.; Zhou, H.-C. Selective Gas Adsorption and Separation in Metal-Organic Frameworks. *Chem. Soc. Rev.* **2009**, *38*, 1477–1504.
(262) Li, J.-R.; Sculley, J.; Zhou, H.-C. Metal-Organic Frameworks for Separations. *Chem. Rev.* **2012**, *112*, 869–932.
(263) Farrusseng, D.; Aguado, S.; Pinel, C. Metal-Organic Frameworks: Opportunities for Catalysis. *Angew. Chem., Int. Ed*. **2009**, *48*, 7502–7513.
(264) Lee, J.; Farha, O. K.; Roberts, J.; Scheidt, K. A.; Nguyen, S. T.; Hupp, J. T. Metal-Organic Framework Materials as Catalysts. *Chem. Soc. Rev.* **2009**, *38*, 1450–1459.
(265) Ma, L.; Abney, C.; Lin, W. Enantioselective Catalysis with Homochiral Metal-Organic Frameworks. *Chem. Soc. Rev.* **2009**, *38*, 1248–1256.
(266) Corma, A.; García, H.; Llabrés i Xamena, F. X. Engineering Metal-Organic Frameworks for Heterogeneous Catalysis. *Chem. Rev.* **2010**, *110*, 4606–4655.
(267) Yoon, M.; Srirambalaji, R.; Kim, K. Homochiral Metal-Organic Frameworks for Asymmetric Heterogeneous Catalysis. *Chem. Rev.* **2012**, *112*, 1196–1231.
(268) Zhang, T.; Lin, W. Metal-Organic Frameworks for Artificial Photosynthesis and Photocatalysis. *Chem. Soc. Rev.* **2014**, *43*, 5982–5993.
(269) Kreno, L. E.; Leong, K.; Farha, O. K.; Allendorf, M.; Van Duyne, R. P.; Hupp, J. T. Metal-Organic Framework Materials as Chemical Sensors. *Chem. Rev.* **2012**, *112*, 1105–1125.
(270) Hu, Z.; Deibert, B. J.; Li, J. Luminescent Metal-Organic Frameworks for Chemical Sensing and Explosive Detection. *Chem. Soc. Rev.* **2014**, *43*, 5815–5840.
(271) Allendorf, M. D.; Bauer, C. A.; Bhakta, R. K.; Houk, R. J. T. Luminescent Metal-Organic Frameworks. *Chem. Soc. Rev*. **2009**, *38*, 1330–1352.
(272) Cui, Y.; Yue, Y.; Qian, G.; Chen, B. Luminescent Functional Metal-Organic Frameworks. *Chem. Rev*. **2012**, *112*, 1126–1162.
(273) Kurmoo, M. Magnetic Metal-Organic Frameworks. *Chem. Soc. Rev*. **2009**, *38*, 1353–1379.
(274) Zhang, W.; Xiong, R.-G. Ferroelectric Metal-Organic Frameworks. *Chem. Rev*. **2012**, *112*, 1163–1195.
(275) Wang, C.; Zhang, T.; Lin, W. Rational Synthesis of Noncentrosymmetric Metal-Organic Frameworks for Second-Order Nonlinear Optics. *Chem. Rev.* **2012**, *112*, 1084–1104.
(276) McKinlay, A. C.; Morris, R. E.; Horcajada, P.; Férey, G.; Gref, R.; Couvreur, P.; Serre, C. BioMOFs: Metal-Organic Frameworks for Biological and Medical Applications. *Angew. Chem., Int. Ed*. **2010**, *49*, 6260–6266.
(277) Rocca, Della, J.; Liu, D.; Lin, W. Nanoscale Metal-Organic Frameworks for Biomedical Imaging and Drug Delivery. *Acc. Chem. Res.* **2011**, *44*, 957–968.
(278) Horcajada, P.; Gref, R.; Baati, T.; Allan, P. K.; Maurin, G.; Couvreur, P.; Férey, G.; Morris, R. E.; Serre, C. Metal-Organic Frameworks in Biomedicine. *Chem. Rev*. **2012**, *112*, 1232–1268.
(279) Zhu, Q.-L.; Xu, Q. Metal-Organic Framework Composites. *Chem. Soc. Rev*. **2014**, *43*, 5468–5512.
(280) Tranchemontagne, D. J.; Mendoza-Cortés, J. L.; O'Keeffe, M.; Yaghi, O. M. Secondary Building Units, Nets and Bonding in the Chemistry of Metal-Organic Frameworks. *Chem. Soc. Rev.* **2009**, *38*, 1257–1283.
(281) Tan, J. C.; Cheetham, A. K. Mechanical Properties of Hybrid Inorganic–Organic Framework Materials: Establishing Fundamental Structure–Property Relationships. *Chem. Soc. Rev.* **2011**, *40*, 1059–1080.
(282) O'Keeffe, M.; Peskov, M. A.; Ramsden, S. J.; Yaghi, O. M. The Reticular Chemistry Structure Resource (RCSR) Database of, and Symbols for, Crystal Nets. *Acc. Chem. Res.* **2008**, *41*, 1782–1789.
(283) O'Keeffe, M.; Yaghi, O. M. Deconstructing the Crystal Structures of Metal-Organic Frameworks and Related Materials into Their Underlying Nets. *Chem. Rev.* **2012**, *112*, 675–702.
(284) Mitina, T. G.; Blatov, V. A. Topology of 2-Periodic Coordination Networks: Toward Expert Systems in Crystal Design. *CrysEngComm* **2013**, *13*, 1655–1664.
(285) Zhang, S.-Y.; Zhang, Z.; Zaworotko, M. J. Topology, Chirality and Interpenetration in Coordination Polymers. *Chem. Commun.* **2013**, *49*, 9700–9703.
(286) Li, M.; Li, D.; O'Keeffe, M.; Yaghi, O. M. Topological Analysis of Metal-Organic Frameworks with Polytopic Linkers and/or Multiple Building Units and the Minimal Transitivity Principle. *Chem. Rev.* **2014**, *114*, 1343–1370.
(287) Blatov, V. A.; Shevchenko, A. P.; Proserpio, D. M. Applied Topological Analysis of Crystal Structures with the Program Package ToposPro. *CrysEngComm* **2014**, *14*, 3576–3586.
(288) Yang, G.-P.; Hou, L.; Ma, L.-F.; Wang, Y.-Y. Investigation on the Prime Factors Influencing the Formation of Entangled Metal-Organic Frameworks. *CrystEngComm* **2013**, *15*, 2561–2578.
(289) Hafizovic, J.; Bjørgen, M.; Olsbye, U.; Dietzel, P. D. C.; Bordiga, S.; Prestipino, C.; Lamberti, C.; Lillerud, K. P. The Inconsistency in Adsorption Properties and Powder XRD Data of MOF-5 Is Rationalized by Framework Interpenetration and the Presence of Organic and Inorganic Species in the Nanocavities. *J. Am. Chem. Soc.* **2007**, *129*, 3612–3620.
(290) Bureekaew, S.; Sato, H.; Matsuda, R.; Kubota, Y.; Hirose, R.; Kim, J.; Kato, K.; Takata, M.; Kitagawa, S. Control of

Interpenetration for Tuning Structural Flexibility Influences Sorption Properties. *Angew. Chem., Int. Ed*. **2010**, *49*, 7660–7664.
(291) Zhang, J.-P.; Lin, Y.-Y.; Zhang, W.-X.; Chen, X.-M. Temperature- or Guest-Induced Drastic Single-Crystal-to-Single-Crystal Transformations of a Nanoporous Coordination Polymer. *J. Am. Chem. Soc.* **2005**, *127*, 14162–14163.
(292) Zhang, J.; Wojtas, L.; Larsen, R. W.; Eddaoudi, M.; Zaworotko, M. J. Temperature and Concentration Control Over Interpenetration in a Metal−Organic Material. *J. Am. Chem. Soc.* **2009**, *131*, 17040–17041.
(293) Wang, X.-L.; Qin, C.; Wang, E.-B.; Li, Y.-G.; Su, Z.-M.; Xu, L.; Carlucci, L. Entangled Coordination Networks with Inherent Features of Polycatenation, Polythreading, and Polyknotting. *Angew. Chem., Int. Ed*. **2005**, *44*, 5824–5827.
(294) Shekhah, O.; Wang, H.; Paradinas, M.; Ocal, C.; Schüpbach, B.; Terfort, A.; Zacher, D.; Fischer, R. A.; Wöll, C. Controlling Interpenetration in Metal−Organic Frameworks by Liquid-Phase Epitaxy. *Nature Mater.* **2009**, *8*, 481–484.
(295) Zhang, Z.; Zaworotko, M. J. Template-Directed Synthesis of Metal-Organic Materials. *Chem. Soc. Rev.* **2014**, *43*, 5444–5455.
(296) Wang, X.-L.; Qin, C.; Wang, E.-B.; Su, Z.-M. Metal Nuclearity Modulated Four-, Six-, and Eight-Connected Entangled Frameworks Based on Mono-, Bi-, and Trimetallic Cores as Nodes. *Chem. Eur. J.* **2006**, *12*, 2680–2691.
(297) Wu, C.-D.; Lin, W. Heterogeneous Asymmetric Catalysis with Homochiral Metal-Organic Frameworks: Network-Structure-Dependent Catalytic Activity. *Angew. Chem., Int. Ed*. **2007**, *46*, 1075–1078.
(298) Bury, W.; Fairen-Jimenez, D.; Lalonde, M. B.; Snurr, R. Q.; Farha, O. K.; Hupp, J. T. Control Over Catenation in Pillared Paddlewheel Metal-Organic Framework Materials *via* Solvent-Assisted Linker Exchange. *Chem. Mater.* **2013**, *25*, 739–744.
(299) Farha, O. K.; Malliakas, C. D.; Kanatzidis, M. G.; Hupp, J. T. Control Over Catenation in Metal−Organic Frameworks *via* Rational Design of the Organic Building Block. *J. Am. Chem. Soc.* **2010**, *132*, 950–952.
(300) Lun, D. J.; Waterhouse, G. I. N.; Telfer, S. G. A General Thermolabile Protecting Group Strategy for Organocatalytic Metal−Organic Frameworks. *J. Am. Chem. Soc.* **2011**, *133*, 5806–5809.
(301) Blatov, V. A.; O'Keeffe, M.; Proserpio, D. M. Vertex-, Face-, Point-, Schläfli-, and Delaney-Symbols in Nets, Polyhedra and Tilings: Recommended Terminology. *CrystEngComm* **2010**, *12*, 44–48.
(302) Proserpio, D. M. Topological Crystal Chemistry: Polycatenation Weaves a 3D Web. *Nature Chem.* **2010**, *2*, 435–436.
(303) Carlucci, L.; Ciani, G.; Moret, M.; Proserpio, D. M.; Rizzato, S. Polymeric Layers Catenated by Ribbons of Rings in a Three-Dimensional Self-Assembled Architecture: A Nanoporous Network with Spongelike Behavior. *Angew. Chem., Int. Ed*. **2000**, *39*, 1506–1510.
(304) Konnert, J.; Britton, D. The Crystal Structure of $AgC(CN)_3$. *Inorg. Chem.* **1966**, *5*, 1193–1196.
(305) Kinoshita, Y.; Matsubara, I.; Higuchi, T.; Saito, Y. The Crystal Structure of Bis(adiponitrilo)copper(I)nitrate. *Bull. Chem. Soc. Jpn.* **1959**, *32*, 1221–1226.
(306) Blatov, V. A.; Carlucci, L.; Ciani, G.; Proserpio, D. M. Interpenetrating Metal-Organic and Inorganic 3D Networks: A Computer-Aided Systematic Investigation. Part I. Analysis of the Cambridge Structural Database. *CrystEngComm* **2004**, *6*, 378–395.
(307) Miller, J. S. Interpenetrating Lattices—Materials of the Future. *Adv. Mater.* **2001**, *13*, 525–527.
(308) Chen, B.; Wang, X.; Zhang, Q.; Xi, X.; Cai, J.; Qi, H.; Shi, S.; Wang, J.; Yuan, D.; Fang, M. Synthesis and Characterization of the Interpenetrated MOF-5. *J. Mater. Chem.* **2010**, *20*, 3758–3767.
(309) Kim, H.; Das, S.; Kim, M. G.; Dybtsev, D. N.; Kim, Y.; Kim, K. Synthesis of Phase-Pure Interpenetrated MOF-5 and Its Gas Sorption Properties. *Inorg. Chem.* **2011**, *50*, 3691–3696.
(310) Nugent, P.; Belmabkhout, Y.; Burd, S. D.; Cairns, A. J.; Luebke, R.; Forrest, K.; Pham, T.; Ma, S.; Space, B.; Wojtas, L.; Eddaoudi, M.; Zaworotko, M. J. Porous Materials with Optimal Adsorption Thermodynamics and Kinetics for CO_2 Separation. *Nature* **2013**, *495*, 80–84.
(311) Sun, D.; Ma, S.; Ke, Y.; Collins, D. J.; Zhou, H.-C. An Interweaving MOF with High Hydrogen Uptake. *J. Am. Chem. Soc.* **2006**, *128*, 3896–3897.
(312) Ma, S.; Sun, D.; Ambrogio, M.; Fillinger, J. A.; Parkin, S.; Zhou, H.-C. Framework-Catenation Isomerism in Metal−Organic Frameworks and Its Impact on Hydrogen Uptake. *J. Am. Chem. Soc.* **2007**, *129*, 1858–1859.
(313) Kesanli, B.; Cui, Y.; Smith, M. R.; Bittner, E. W.; Bockrath, B. C.; Lin, W. Highly Interpenetrated Metal-Organic Frameworks for Hydrogen Storage. *Angew. Chem., Int. Ed*. **2005**, *44*, 72–75.
(314) Song, F.; Wang, C.; Falkowski, J. M.; Ma, L.; Lin, W. Isoreticular Chiral Metal−Organic Frameworks for Asymmetric Alkene Epoxidation: Tuning Catalytic Activity by Controlling Framework Catenation and Varying Open Channel Sizes. *J. Am. Chem. Soc.* **2010**, *132*, 15390–15398.
(315) Evans, O. R.; Lin, W. Crystal Engineering of Nonlinear Optical Materials Based on Interpenetrated Diamondoid Coordination Networks. *Chem. Mater.* **2001**, *13*, 2705–2712.
(316) Biradha, K.; Fujita, M. A Springlike 3D-Coordination Network That Shrinks or Swells in a Crystal-to-Crystal Manner Upon Guest Removal or Readsorption. *Angew. Chem., Int. Ed*. **2002**, *41*, 3392–3395.
(317) Kitaura, R.; Seki, K.; Akiyama, G.; Kitagawa, S. Porous Coordination-Polymer Crystals with Gated Channels Specific for Supercritical Gases. *Angew. Chem., Int. Ed*. **2003**, *42*, 428–431.
(318) Thallapally, P. K.; Tian, J.; Radha Kishan, M.; Fernandez, C. A.; Dalgarno, S. J.; McGrail, P. B.; Warren, J. E.; Atwood, J. L. Flexible (Breathing) Interpenetrated Metal−Organic Frameworks for CO_2 Separation Applications. *J. Am. Chem. Soc.* **2008**, *130*, 16842–16843.
(319) Sikdar, N.; Bonakala, S.; Haldar, R.; Balasubramanian, S.; Maji, T. K. Dynamic Entangled Porous Framework for Hydrocarbon (C2-C3) Storage, CO_2 Capture, and Separation. *Chem. Eur. J.* **2016**, *22*, 6059–6070.
(320) Mulfort, K. L.; Farha, O. K.; Malliakas, C. D.; Kanatzidis, M. G.; Hupp, J. T. An Interpenetrated Framework Material with Hysteretic CO_2 Uptake. *Chem. Eur. J.* **2010**, *16*, 276–281.
(321) Jäger, R.; Schmidt, T.; Karbach, D.; Vögtle, F. The First Pretzel-Shaped Molecules - *via* Catenane Precursors. *Synlett* **1996**, 723–725.
(322) Duennwald, T.; Parham, A.-H.; Vögtle, F. Non-Ionic Template Synthesis of Amide-Linked Rotaxanes. Axles with Benzophenone and Cinnamic Acid Units. *Synthesis* **1998**, 339–348.
(323) Yamamoto, C.; Okamoto, Y.; Schmidt, T.; Jaeger, R.; Vögtle, F. Enantiomeric Resolution of Cycloenantiomeric Rotaxane, Topologically Chiral Catenane, and Pretzel-Shaped Molecules: Observation of Pronounced Circular Dichroism. *J. Am. Chem. Soc.* **1997**, *119*, 10547–10548.
(324) Schill, G.; Lüttringhaus, A. Die Gezielte Synthese von Catena-Verbindungen, I. Preparation of Catena Compounds by Directed Synthesis. *Angew. Chem., Int. Ed. Engl*. **1964**, *3*, 546–547.
(325) Schill, G.; Logemann, E.; Vetter, W. Ozonolytic Degradation of a Catenane. *Angew. Chem., Int. Ed. Engl*. **1972**, *11*, 1089–1090.
(326) Lüttringhaus, A.; Isele, G. Synthesis of a Catena Compound by the Semistatistical Principle. *Angew. Chem., Int. Ed. Engl*. **1967**, *6*, 956–957.
(327) Shimada, S.; Ishikawa, K.; Tamaoki, N. Synthesis and Switchable Condensation Reaction of Bifunctional [2]Catenane. *Acta Chem. Scand.* **1998**, *52*, 374–376.
(328) Mohry, A.; Schwierz, H.; Vögtle, F. Supramolecular Assemblies. A Bis(pretzelane) and a Tetrakis(rotaxane). *Synthesis* **1999**, 1753–1758.
(329) Reuter, C.; Mohry, A.; Sobanski, A.; Vögtle, F. [1]Rotaxanes and Pretzelanes: Synthesis, Chirality, and Absolute Configuration. *Chem. Eur. J.* **2000**, *6*, 1674–1682.

(330) Li, Q.; Vogel, E.; Parham, A.-H.; Nieger, M.; Bolte, M.; Fröhlich, R.; Saarenketo, P.; Rissanen, K.; Vögtle, F. Synthesis and X-Ray Structure of Amide-Based Macrocycles, Catenanes and Pretzelane. *Eur. J. Org. Chem.* **2001**, 4041–4049.
(331) Han, M.; Zhang, H.-Y.; Yang, L.-X.; Ding, Z.-J.; Zhuang, R.-J.; Liu, Y. A [2]Catenane and Pretzelane Based on Sn-Porphyrin and Crown Ether. *Eur. J. Org. Chem.* **2011**, 7271–7277.
(332) Liu, Y.; Vignon, S. A.; Zhang, X.; Houk, K. N.; Stoddart, J. F. Conformational Diastereoisomerism in a Chiral Pretzelane. *Chem. Commun.* **2005**, 3927–3929.
(333) Liu, Y.; Vignon, S. A.; Zhang, X.; Bonvallet, P. A.; Khan, S. I.; Houk, K. N.; Stoddart, J. F. Dynamic Chirality in Donor–Acceptor Pretzelanes. *J. Org. Chem.* **2005**, *70*, 9334–9344.
(334) Liu, Y.; Bonvallet, P. A.; Vignon, S. A.; Khan, S. I.; Stoddart, J. F. Donor–Acceptor Pretzelanes and a Cyclic Bis[2]catenane Homologue. *Angew. Chem., Int. Ed*. **2005**, *44*, 3050–3055.
(335) Zhao, Y.-L.; Trabolsi, A.; Stoddart, J. F. A Bistable Pretzelane. *Chem. Commun.* **2009**, 4844–4846.
(336) Ünsal, Ö.; Godt, A. Synthesis of a [2]Catenane with Functionalities and 87-Membered Rings. *Chem. Eur. J.* **1999**, *5*, 1728–1733.
(337) Samorì, P.; Jäckel, F.; Ünsal, Ö.; Godt, A.; Rabe, J. P. Ordered Nanostructures of a [2]Catenane Through Self-Assembly at Surfaces: An STM Study with Sub-Molecular Resolution. *ChemPhysChem* **2001**, *2*, 461–464.
(338) Duda, S.; Godt, A. The Effect of Ring Size on Catenane Synthesis. *Eur. J. Org. Chem.* **2003**, 3412–3420.
(339) Jeschke, G.; Godt, A. Co-Conformational Distribution of Nanosized [2]Catenanes Determined by Pulse EPR Measurements. *ChemPhysChem* **2003**, *4*, 1328–1334.
(340) Godt, A.; Jeschke, G. Separation of Motional Processes in a [2]Catenane by Combining Synthetic, Dual-Frequency EPR and Molecular Modelling Approaches. *Magn. Reson. Chem.* **2005**, *43*, S110–S118.
(341) Evans, N. H.; Serpell, C. J.; Beer, P. D. Chloride Anion Templated Synthesis and Crystal Structure of a Handcuff Catenane. *Angew. Chem., Int. Ed*. **2011**, *50*, 2507–2510.
(342) Zhu, X.-Z.; Chen, C.-F. A Highly Efficient Approach to [4]Pseudocatenanes by Threefold Metathesis Reactions of a Triptycene-Based Tris[2]pseudorotaxane. *J. Am. Chem. Soc.* **2005**, *127*, 13158–13159.
(343) Zhu, X.-Z.; Chen, C.-F. Efficient Synthesis of a Chiral [4]Pseudocatenane and Its Derivatives: A Novel Ship's Wheel-Like Interlocked Structure. *Chem. Eur. J.* **2006**, *12*, 5603–5609.
(344) Jiang, Y.; Zhu, X.-Z.; Chen, C.-F. Multivalency-Directed Magic-Ring [2](3)Catenane by Olefin Metathesis. *Chem. Eur. J.* **2010**, *16*, 14285–14289.
(345) Meng, Z.; Han, Y.; Wang, L.-N.; Xiang, J.-F.; He, S.-G.; Chen, C.-F. Stepwise Motion in a Multivalent [2](3)Catenane. *J. Am. Chem. Soc.* **2015**, *137*, 9739–9745.
(346) Hagiwara, T.; Yamazaki, M.; Suzuki, T.; Sawaguchi, T.; Yano, S. Synthesis of Poly[2]catenane Having Rigid Linkage by 1,3-Dipolar Cycloaddition of Diazido[2]catenane with 4,4′;-Diethynylbiphenyl. *Polymer* **2011**, *52*, 5426–5430.
(347) Hori, A.; Sawada, T.; Yamashita, K.-I.; Fujita, M. Ultramacrocyclization through Reversible Catenation. *Angew. Chem., Int. Ed*. **2005**, *44*, 4896–4899.
(348) Wu, Y.-W.; Tung, S.-T.; Lai, C.-C.; Liu, Y.-H.; Peng, S.-M.; Chiu, S.-H. Cyclic [2]Catenane Dimers, Trimers, and Tetramers. *Angew. Chem., Int. Ed*. **2015**, *127*, 11911–11915.
(349) Muscat, D.; Kohler, W.; Rader, H. J.; Martin, K.; Mullins, S.; Muller, B.; Müllen, K.; Geerts, Y. Synthesis and Characterization of Poly[2]catenanes Containing Rigid Catenane Segments. *Macromolecules* **1999**, *32*, 1737–1745.
(350) Semlyen, J. A.; Wood, B. R.; Hodge, P. Cyclic Polymers: Past, Present and Future. *Polym. Adv. Technol*. **1994**, *5*, 473–478.
(351) Clarkson, G. J.; Leigh, D. A.; Smith, R. A. From Catenanes to Mechanically-Linked Polymers. *Curr. Opin. Solid State Mater. Sci.* **1998**, *3*, 579–584.
(352) Raymo, F. M.; Stoddart, J. F. Interlocked Macromolecules. *Chem. Rev*. **1999**, *99*, 1643–1663.
(353) Niu, Z.; Gibson, H. W. Polycatenanes. *Chem. Rev*. **2009**, *109*, 6024–6046.
(354) Fang, L.; Olson, M. A.; Benítez, D.; Tkatchouk, E.; Goddard, W. A., III; Stoddart, J. F. Mechanically Bonded Macromolecules. *Chem. Soc. Rev*. **2010**, *39*, 17–29.
(355) Ashton, P. R.; Preece, J. A.; Stoddart, J. F.; Tolley, M. S. Template-Directed Syntheses of a Bis[2]catenane and a Bis[2]rotaxane - Towards Self-Assembling Polymers. *Synlett* **1994**, 789–792.
(356) Olson, M. A.; Coskun, A.; Fang, L.; Basuray, A. N.; Stoddart, J. F. Polycatenation under Thermodynamic Control. *Angew. Chem., Int. Ed*. **2010**, *49*, 3151–3156.
(357) Hamers, C.; Raymo, F. M.; Stoddart, J. F. Molecular Meccano 42. Main-Chain and Pendant Poly([2]catenane)s Incorporating Complementary π-Electron-Rich and -Deficient Components. *Eur. J. Org. Chem.* **1998**, 2109–2117.
(358) Hamers, C.; Kocian, O.; Raymo, F. M.; Stoddart, J. F. A Poly(Bis[2]catenane) Containing a Combination of Covalent, Mechanical, and Coordinative Bonds. *Adv. Mater.* **1998**, *10*, 1366–1369.
(359) Geerts, Y.; Muscat, D.; Müllen, K. Synthesis of Oligo[2]-catenanes. *Macromol. Chem. Phys.* **1995**, *196*, 3425–3435.
(360) Weidmann, J.-L.; Kern, J.-M.; Sauvage, J.-P.; Geerts, Y.; Muscat, D.; Müllen, K. Poly[2]Catenanes Containing Alternating Topological and Covalent Bonds. *Chem. Commun.* **1996**, 1243–1244.
(361) Weidmann, J.-L.; Kern, J.-M.; Sauvage, J.-P.; Muscat, D.; Mullins, S.; Köhler, W.; Rosenauer, C.; Räder, H. J.; Martin, K.; Geerts, Y. Poly[2]catenanes and Cyclic Oligo[2]catenanes Containing Alternating Topological and Covalent Bonds: Synthesis and Characterization. *Chem. Eur. J.* **1999**, *5*, 1841–1851.
(362) Moore, J. S.; Stupp, S. I. Room-Temperature Polyesterification. *Macromolecules* **1990**, *23*, 65–70.
(363) Muscat, D.; Witte, A.; Köhler, W.; Müllen, K.; Geerts, Y. Synthesis of a Novel Poly[2]catenane Containing Rigid Catenanes. *Macromol. Rapid Commun.* **1997**, *18*, 233–241.
(364) Fustin, C.-A.; Bailly, C.; Clarkson, G. J.; De Groote, P.; Galow, T. H.; Leigh, D. A.; Robertson, D.; Slawin, A. M. Z.; Wong, J. K. Y. Mechanically Linked Polycarbonate. *J. Am. Chem. Soc.* **2003**, *125*, 2200–2207.
(365) Fustin, C.-A.; Bailly, C.; Clarkson, G. J.; Galow, T. H.; Leigh, D. A. Solution and Solid-State Properties of Mechanically Linked Polycarbonates. *Macromolecules* **2004**, *37*, 66–70.
(366) Fustin, C.-A.; Clarkson, G. J.; Leigh, D. A.; Van Hoof, F.; Jonas, A. M.; Bailly, C. Mechanically Linked Poly(ethylene terephthalate). *Macromolecules* **2004**, *37*, 7884–7892.
(367) Hagiwara, T.; Murano, Y.; Watanabe, Y.; Hoshi, T.; Sawaguchi, T. Catenane Gel: Synthesis of High Molecular Weight Poly[2]catenanes by Sonogashira Coupling Polymerization. *Tetrahedron Lett.* **2012**, *53*, 2805–2808.
(368) Godt, A. Non-Rusty [2]Catenanes with Huge Rings and Their Polymers. *Eur. J. Org. Chem.* **2004**, 1639–1654.
(369) Menzer, S.; White, A. J. P.; Williams, D. J.; Bělohradský, M.; Raymo, F. M.; Hamers, C.; Stoddart, J. F.; Shipway, A. N. Molecular Meccano 25. Self-Assembly of Functionalized [2]Catenanes Bearing a Reactive Functional Group on Either One or Both Macrocyclic Components: From Monomeric [2]Catenanes to Polycatenanes. *Macromolecules* **1998**, *31*, 295–307.
(370) Simone, D. L.; Swager, T. M. A Conducting Poly(cyclophane) and Its Poly([2]catenane). *J. Am. Chem. Soc.* **2000**, *122*, 9300–9301.
(371) Olson, M. A.; Braunschweig, A. B.; Fang, L.; Ikeda, T.; Klajn, R.; Trabolsi, A.; Wesson, P. J.; Benítez, D.; Mirkin, C. A.; Grzybowski, B. A.; Stoddart, J. F. A Bistable Poly[2]catenane Forms Nanosuperstructures. *Angew. Chem., Int. Ed*. **2009**, *48*, 1792–1797.
(372) Li, Q.; Zhang, W.; Miljanić, O. Š.; Knobler, C. B.; Stoddart, J. F.; Yaghi, O. M. A Metal-Organic Framework Replete with Ordered Donor–Acceptor Catenanes. *Chem. Commun.* **2010**, *46*, 380–382.

(373) Li, Q.; Sue, C.-H.; Basu, S.; Shveyd, A. K.; Zhang, W.; Barin, G.; Fang, L.; Sarjeant, A. A.; Stoddart, J. F.; Yaghi, O. M. A Catenated Strut in a Catenated Metal-Organic Framework. *Angew. Chem., Int. Ed*. **2010**, *49*, 6751–6755.

(374) Cao, D.; Juríček, M.; Brown, Z. J.; Sue, A. C. H.; Liu, Z.; Lei, J.; Blackburn, A. K.; Grunder, S.; Sarjeant, A. A.; Coskun, A.; Wang, C.; Farha, O. K.; Hupp, J. T.; Stoddart, J. F. Three-Dimensional Architectures Incorporating Stereoregular Donor–Acceptor Stacks. *Chem. Eur. J.* **2013**, *19*, 8457–8465.

(375) Sue, A. C. H.; Mannige, R. V.; Deng, H.; Cao, D.; Wang, C.; Gándara, F.; Stoddart, J. F.; Whitelam, S.; Yaghi, O. M. Heterogeneity of Functional Groups in a Metal-Organic Framework Displays Magic Number Ratios. *Proc. Natl. Acad. Sci. U.S.A.* **2015**, *112*, 5591–5596.

(376) Li, Q.; Zhang, W.; Miljanić, O. Š.; Sue, C.-H.; Zhao, Y.-L.; Liu, L.; Knobler, C. B.; Stoddart, J. F.; Yaghi, O. M. Docking in Metal-Organic Frameworks. *Science* **2009**, *325*, 855–859.

(377) Valente, C.; Choi, E.; Belowich, M. E.; Doonan, C. J.; Li, Q.; Gasa, T. B.; Botros, Y. Y.; Yaghi, O. M.; Stoddart, J. F. Metal-Organic Frameworks with Designed Chiral Recognition Sites. *Chem. Commun.* **2010**, *46*, 4911–4913.

(378) Zhao, Y.-L.; Liu, L.; Zhang, W.; Sue, C.-H.; Li, Q.; Miljanić, O. Š.; Yaghi, O. M.; Stoddart, J. F. Rigid-Strut-Containing Crown Ethers and [2]Catenanes for Incorporation Into Metal-Organic Frameworks. *Chem. Eur. J.* **2009**, *15*, 13356–13380.

(379) Schill, G. *Catenanes, Rotaxanes, and Knots*; Academic Press: New York, **1971**.

(380) *SciFinder*. Chemical Abstracts Service: Columbus, OH, **2004** (accessed May 23, 2016).

(381) Solladié, N.; Chambron, J.-C.; Dietrich-Buchecker, C.; Sauvage, J.-P. Multicomponent Molecular Systems Incorporating Porphyrins and Copper(I) Complexes: Simultaneous Synthesis of [3]- and [5]Rotaxanes. *Angew. Chem., Int. Ed. Engl*. **1996**, *35*, 906–909.

(382) Solladié, N.; Chambron, J.-C.; Sauvage, J.-P. Porphyrin-Stoppered [3]- and [5]-Rotaxanes. *J. Am. Chem. Soc.* **1999**, *121*, 3684–3692.

(383) Collin, J.-P; Durot, S.; Keller, M.; Sauvage, J.-P.; Trolez, Y.; Cetina, M.; Rissanen, K. Synthesis of [5]Rotaxanes Containing Bi- and Tridentate Coordination Sites in the Axis. *Chem. Eur. J.* **2011**, *17*, 947–957.

(384) Fuller, A.-M. L.; Leigh, D. A.; Lusby, P. J. One Template, Multiple Rings: Controlled Iterative Addition of Macrocycles onto a Single Binding Site Rotaxane Thread. *Angew. Chem., Int. Ed*. **2007**, *46*, 5015–5019.

(385) Amabilino, D. B.; Ashton, P. R.; Balzani, V.; Brown, C. L.; Credi, A.; Fréchet, J. M. J.; Leon, J. W.; Raymo, F. M.; Spencer, N.; Stoddart, J. F.; Venturi, M. Molecular Meccano 13. Self-Assembly of [*n*]Rotaxanes Bearing Dendritic Stoppers. *J. Am. Chem. Soc*. **1996**, *118*, 12012–12020.

(386) Miljanić, O. Š.; Dichtel, W. R.; Mortezaei, S.; Stoddart, J. F. Cyclobis(paraquat-*p*-phenylene)-Based [2]Catenanes Prepared by Kinetically Controlled Reactions Involving Alkynes. *Org. Lett.* **2006**, *8*, 4835–4838.

(387) Dichtel, W. R.; Miljanić, O. Š.; Spruell, J. M.; Heath, J. R.; Stoddart, J. F. Efficient Templated Synthesis of Donor–Acceptor Rotaxanes Using Click Chemistry. *J. Am. Chem. Soc.* **2006**, *128*, 10388–10390.

(388) Gothard, C. M.; Bruns, C. J.; Gothard, N. A.; Grzybowski, B. A.; Stoddart, J. F. Modular Synthesis of Bipyridinium Oligomers and Corresponding Donor–Acceptor Oligorotaxanes with Crown Ethers. *Org. Lett.* **2012**, *14*, 5066–5069.

(389) Basu, S.; Coskun, A.; Friedman, D. C.; Olson, M. A.; Benítez, D.; Tkatchouk, E.; Barin, G.; Yang, J.; Fahrenbach, A. C.; Goddard, W. A., III; Stoddart, J. F. Donor–Acceptor Oligorotaxanes Made to Order. *Chem. Eur. J.* **2011**, *17*, 2107–2119.

(390) Zhu, Z.; Bruns, C. J.; Li, H.; Lei, J.; Ke, C.; Liu, Z.; Shafaie, S.; Colquhoun, H. M.; Stoddart, J. F. Synthesis and Solution-State Dynamics of Donor–Acceptor Oligorotaxane Foldamers. *Chem. Sci.* **2013**, *4*, 1470–1483.

(391) Bruns, C. J.; Stoddart, J. F. Mechanically Interlaced and Interlocked Donor–Acceptor Foldamers. *Adv. Polym. Sci.* **2013**, *261*, 271–294.

(392) Ashton, P. R.; Philp, D.; Spencer, N.; Stoddart, J. F.; Williams, D. J. A Self-Organized Layered Superstructure of Arrayed [2]Pseudorotaxanes. *J. Chem. Soc., Chem. Commun.* **1994**, 181–184.

(393) Zhu, Z.; Li, H.; Liu, Z.; Lei, J.; Zhang, H.; Botros, Y. Y.; Stern, C. L.; Sarjeant, A. A.; Stoddart, J. F.; Colquhoun, H. M. Oligomeric Pseudorotaxanes Adopting Infinite-Chain Lattice Superstructures. *Angew. Chem., Int. Ed*. **2012**, *51*, 7231–7235.

(394) Zhang, W.; Dichtel, W. R.; Stieg, A. Z.; Benítez, D.; Gimzewski, J. K.; Heath, J. R.; Stoddart, J. F. Folding of a Donor–Acceptor Polyrotaxane by Using Noncovalent Bonding Interactions. *Proc. Natl. Acad. Sci. U.S.A.* **2008**, *105*, 6514–6519.

(395) Parham, A.; Schmieder, R.; Vögtle, F. Iterative Synthesis of [*n*]Rotaxanes. *Synlett* **1999**, 1887–1890.

(396) Kishan, M. R.; Parham, A.-H.; Schelhase, F.; Yoneva, A.; Silva, G.; Chen, X.; Okamoto, Y.; Vögtle, F. Bridging Rotaxanes' Wheels – Cyclochiral Bonnanes. *Angew. Chem., Int. Ed*. **2006**, *45*, 7296–7299.

(397) Wu, J.; Leung, K. C.-F.; Stoddart, J. F. Efficient Production of [*n*]Rotaxanes by Using Template-Directed Clipping Reactions. *Proc. Natl. Acad. Sci. U.S.A.* **2007**, *104*, 17266–17271.

(398) Belowich, M. E.; Valente, C.; Stoddart, J. F. Template-Directed Syntheses of Rigid Oligorotaxanes under Thermodynamic Control. *Angew. Chem., Int. Ed*. **2010**, *49*, 7208–7212.

(399) Belowich, M. E.; Valente, C.; Smaldone, R. A.; Friedman, D. C.; Thiel, J.; Cronin, L.; Stoddart, J. F. Positive Cooperativity in the Template-Directed Synthesis of Monodisperse Macromolecules. *J. Am. Chem. Soc.* **2012**, *134*, 5243–5261.

(400) Avestro, A.-J.; Belowich, M. E.; Stoddart, J. F. Cooperative Self-Assembly: Producing Synthetic Polymers with Precise and Concise Primary Structures. *Chem. Soc. Rev.* **2012**, *41*, 5881–5895.

(401) Avestro, A.-J.; Gardner, D. M.; Vermeulen, N. A.; Wilson, E. A.; Schneebeli, S. T.; Whalley, A. C.; Belowich, M. E.; Carmieli, R.; Wasielewski, M. R.; Stoddart, J. F. Gated Electron Sharing Within Dynamic Naphthalene Diimide-Based Oligorotaxanes. *Angew. Chem., Int. Ed*. **2014**, *53*, 4442–4449.

(402) Yin, J.; Dasgupta, S.; Wu, J. Synthesis of [*n*]Rotaxanes by Template-Directed Clipping: The Role of the Dialkylammonium Recognition Sites. *Org. Lett.* **2010**, *12*, 1712–1715.

(403) Yin, J.; Chi, C.; Wu, J. Efficient Synthesis of a Hetero[4]Rotaxane by a "Threading-Stoppering-Followed-by-Clipping" Approach. *Org. Biomol. Chem.* **2010**, *8*, 2594–2599.

(404) Hu, F.; Huang, J.; Cao, M.; Chen, Z.; Yang, Y.-W.; Liu, S. H.; Yin, J. Dithienylethene-Based Rotaxanes: Synthesis, Characterization and Properties. *Org. Biomol. Chem.* **2014**, *12*, 7712–7720.

(405) Watanabe, N.; Yagi, T.; Kihara, N.; Takata, T. Highly Efficient Synthesis of [3]- and [5]Rotaxanes Consisting of Crown Ether and a *sec*-Ammonium Salt. *Chem. Commun.* **2002**, 2720–2721.

(406) Chwalek, M.; Auzély, R.; Fort, S. Synthesis and Biological Evaluation of Multivalent Carbohydrate Ligands Obtained by Click Assembly of Pseudo-Rotaxanes. *Org. Biomol. Chem.* **2009**, *7*, 1680–1689.

(407) Taira, T.; Suzaki, Y.; Osakada, K. [5]Rotaxanes Composed of α-Cyclodextrin and Pd or Pt Complexes with Alkylbipyridinium Ligands. *Chem. Lett*. **2008**, *37*, 182–183.

(408) Taira, T.; Suzaki, Y.; Osakada, K. Pd-II and Pt-III Complexes with Amphiphilic Ligands: Formation of Micelles and [5]Rotaxanes with α-Cyclodextrin in Aqueous Solution. *Chem. Asian J.* **2008**, *3*, 895–902.

(409) Taira, T.; Suzaki, Y.; Osakada, K. Metallohydrogel Formed from Amphiphilic Pd Complex and α-Cyclodextrin: Control of Its Sol-Gel Transition. *Chem. Lett.* **2013**, *42*, 1062–1064.

(410) Ke, C.; Smaldone, R. A.; Kikuchi, T.; Li, H.; Davis, A. P.; Stoddart, J. F. Quantitative Emergence of Hetero[4]Rotaxanes by Template-Directed Click Chemistry. *Angew. Chem., Int. Ed*. **2012**, *52*, 381–387.

(411) Ke, C.; Strutt, N. L.; Li, H.; Hou, X.; Hartlieb, K. J.; McGonigal, P. R.; Ma, Z.; Iehl, J.; Stern, C. L.; Cheng, C.; Zhu, Z.; Vermeulen, N. A.; Meade, T. J.; Botros, Y. Y.; Stoddart, J. F. Pillar[5]arene as a Co-Factor in Templating Rotaxane Formation. *J. Am. Chem. Soc.* **2013**, *135*, 17019–17030.
(412) Hou, X.; Ke, C.; Cheng, C.; Song, N.; Blackburn, A. K.; Sarjeant, A. A.; Botros, Y. Y.; Yang, Y.-W.; Stoddart, J. F. Efficient Syntheses of Pillar[6]arene-Based Hetero[4]-Rotaxanes Using a Cooperative Capture Strategy. *Chem. Commun.* **2014**, *50*, 6196–6199.
(413) Hou, X.; Ke, C.; Bruns, C. J.; McGonigal, P. R.; Pettman, R. B.; Stoddart, J. F. Tunable Solid-State Fluorescent Materials for Supramolecular Encryption. *Nature Commun*. **2015**, *6*: 6884.
(414) Hou, X.; Ke, C.; Stoddart, J. F. Cooperative Capture Synthesis: Yet Another Playground for Copper-Free Click Chemistry. *Chem. Soc. Rev.* **2016**, *45*, 3766–3780.
(415) Fernandez, A.; Ferrando-Soria, J.; Pineda, E. M.; Tuna, F.; Vitorica-Yrezabal, I. J.; Knappke, C.; Ujma, J.; Muryn, C. A.; Timco, G. A.; Barran, P. E.; Ardavan, A.; Winpenny, R. E. P. Making Hybrid [*n*]-Rotaxanes as Supramolecular Arrays of Molecular Electron Spin Qubits. *Nature Commun*. **2016**, *7*: 10240.
(416) Timco, G. A.; Faust, T. B.; Tuna, F.; Winpenny, R. E. P. Linking Heterometallic Rings for Quantum Information Processing and Amusement. *Chem. Soc. Rev.* **2011**, *40*, 3067–3075.
(417) Lipatov, Y. S.; Lipatova, T. E.; Kosyanchuk, L. F. Synthesis and Structure of Macromolecular Topological Compounds. *Adv. Polym. Sci.* **1989**, *88*, 49–76.
(418) Gong, C.; Gibson, H. W. Polyrotaxanes and Related Structures: Synthesis and Properties. *Curr. Opin. Solid State Mater. Sci.* **1997**, *2*, 647–652.
(419) Harada, A. Polyrotaxanes. *Acta Polym.* **1998**, *49*, 3–17.
(420) Panova, I. G.; Topchieva, I. N. Rotaxanes and Polyrotaxanes. Their Synthesis and the Supramolecular Devices Based on Them. *Russian Chem. Rev*. **2001**, *70*, 23–44.
(421) Huang, F.; Gibson, H. W. Polypseudorotaxanes and Polyrotaxanes. *Prog. Polym. Sci*. **2005**, *30*, 982–1018.
(422) Takata, T. Polyrotaxane and Polyrotaxane Network: Supramolecular Architectures Based on the Concept of Dynamic Covalent Bond Chemistry. *Polym. J.* **2006**, *38*, 1–20.
(423) Frampton, M. J.; Anderson, H. L. Insulated Molecular Wires. *Angew. Chem., Int. Ed*. **2007**, *46*, 1028–1064.
(424) Harada, A.; Hashidzume, A.; Yamaguchi, H.; Takashima, Y. Polymeric Rotaxanes. *Chem. Rev*. **2009**, *109*, 5974–6023.
(425) Arunachalam, M.; Gibson, H. W. Recent Developments in Polypseudorotaxanes and Polyrotaxanes. *Prog. Polym. Sci.* **2014**, *39*, 1043–1073.
(426) Wenz, G.; Han, B.-H.; Müller, A. Cyclodextrin Rotaxanes and Polyrotaxanes. *Chem. Rev*. **2006**, *106*, 782–817.
(427) Araki, J.; Ito, K. Recent Advances in the Preparation of Cyclodextrin-Based Polyrotaxanes and Their Applications to Soft Materials. *Soft Matter.* **2007**, *3*, 1456–1473.
(428) Wenz, G. Cyclodextrin Polyrotaxanes Assembled from a Molecular Construction Kit in Aqueous Solution. *J. Polym. Sci. Pol. Chem.* **2009**, *47*, 6333–6341.
(429) Zheng, B.; Wang, F.; Dong, S.; Huang, F. Supramolecular Polymers Constructed by Crown Ether-Based Molecular Recognition. *Chem. Soc. Rev.* **2012**, *41*, 1621–1636.
(430) Gibson, H. W.; Marand, H. Polyrotaxanes: Molecular Composites Derived by Physical Linkage of Cyclic and Linear Species. *Adv. Mater.* **1993**, *5*, 11–21.
(431) Gibson, H. W.; Liu, S. Polyrotaxanes: Past, Present and Future. *Macromol. Symp*. **1996**, *102*, 55–61.
(432) Gibson, H. W.; Engen, P.; Lecavalier, P. Synthesis of Polyrotaxanes. *Polym. Prepr. (Am. Chem. Soc., Div. Polym. Chem.)* **1988**, *29*, 248–249.
(433) Wu, C.; Bheda, M. C.; Lim, C.; Shen, Y. X.; Sze, J. Y.; Gibson, H. W. Synthesis of Polyester Rotaxanes *via* the Statistical Threading Method. *Polym. Commun.* **1991**, *32*, 204–207.
(434) Gibson, H. W.; Liu, S.; Lecavalier, P.; Wu, C.; Shen, Y. X. Synthesis and Preliminary Characterization of Some Polyester Rotaxanes. *J. Am. Chem. Soc.* **1995**, *117*, 852–874.
(435) Gibson, H. W.; Liu, S.; Gong, C.; Ji, Q.; Joseph, E. Studies of the Formation of Poly(ester rotaxane)s from Diacid Chlorides, Diols, and Crown Ethers and Their Properties. *Macromolecules* **1997**, *30*, 3711–3727.
(436) Gibson, H. W.; Wu, C.; Shen, Y. X.; Bheda, M. C.; Sze, J.; Engen, P.; Prasad, A.; Marand, H.; Loveday, D.; Wilkes, G. Control of Processability and Solid State Properties of Polymers Through Rotaxane Formation. *Polym. Prepr. (Am. Chem. Soc., Div. Polym. Chem.)* **1991**, *32*, 593–594.
(437) Gibson, H. W.; Wu, C.; Shen, Y. X.; Bheda, M. C.; Prasad, A.; Marand, H.; Marand, E.; Keith, D. Synthesis, Thermal and Phase Behavior of Polyester, Polyurethane and Polyamide Rotaxanes. *Polym. Prepr. (Am. Chem. Soc., Div. Polym. Chem.)* **1992**, *33*, 235–236.
(438) Lefebvre, H.; Bheda, M. C.; Gibson, H. W. Main Chain Polyamide Rotaxanes from Aliphatic Crown Ethers. *Polymer* **2016**, *90*, 317–330.
(439) Shen, Y. X.; Lim, C.; Gibson, H. W. Synthesis of Polyurethane-Based Polyrotaxanes. *Polym. Prepr. (Am. Chem. Soc., Div. Polym. Chem.)* **1991**, *32*, 166–167.
(440) Shen, Y. X.; Gibson, H. W. Synthesis and Some Properties of Polyrotaxanes Comprised of Polyurethane Backbone and Crown Ethers. *Macromolecules* **1992**, *25*, 2058–2059.
(441) Shen, Y. X.; Xie, D.; Gibson, H. W. Polyrotaxanes Based on Polyurethane Backbones and Crown Ether Cyclics. 1. Synthesis. *J. Am. Chem. Soc*. **1994**, *116*, 537–548.
(442) Marand, E.; Hu, Q.; Gibson, H. W.; Veytsman, B. Spectroscopic Characterization of Hydrogen Bonding in Poly(urethane-rotaxane)s. *Macromolecules* **1996**, *29*, 2555–2562.
(443) Gong, C.; Gibson, H. W. Controlling Microstructure in Polymeric Molecular Shuttles: Solvent-Induced Localization of Macrocycles in Poly(urethane/crown ether) Rotaxanes. *Angew. Chem., Int. Ed. Engl*. **1997**, *36*, 2331–2333.
(444) Gong, C.; Ji, Q.; Subramaniam, C.; Gibson, H. W. Main Chain Polyrotaxanes by Threading Crown Ethers onto a Preformed Polyurethane: Preparation and Properties. *Macromolecules* **1998**, *31*, 1814–1818.
(445) Gibson, H. W.; Engen, P. T. Rotaxanes Based on Polyacrylonitrile. *New J. Chem.* **1993**, *17*, 737–727.
(446) Lee, S.-H.; Engen, P. T.; Gibson, H. W. Blocking Group/Initiators for the Synthesis of Polyrotaxanes *via* Free Radical Polymerizations. *Macromolecules* **1997**, *30*, 337–343.
(447) Gibson, H. W.; Engen, P. T.; Lee, S.-H. Synthesis of Poly[(styrene)-*rotaxa*-(crown ether)]s via Free Radical Polymerization. *Polymer* **1999**, *40*, 1823–1832.
(448) Gibson, H. W.; Bryant, W. S.; Lee, S.-H. Polyrotaxanes by Free-Radical Polymerization of Acrylate and Methacrylate Monomers in the Presence of a Crown Ether. *J. Polym. Sci. Pol. Chem.* **2001**, *39*, 1978–1993.
(449) Nagapudi, K.; Hunt, J.; Shepherd, C.; Baker, J.; Beckham, H. W. Synthesis, Dynamic Mechanical, and Solid-State NMR Spectroscopy of Crown-Ether-Based Linear Aliphatic Polyurethane Rotaxanes. *Macromol. Chem. Phys.* **1999**, *200*, 2541–2550.
(450) Agam, G.; Graiver, D.; Zilkha, A. Studies on the Formation of Topological Isomers by Statistical Methods. *J. Am. Chem. Soc.* **1976**, *98*, 5206–5214.
(451) Gong, C.; Gibson, H. W. Synthesis and Characterization of a Polyester/Crown Ether Rotaxane Derived from a Difunctional Blocking Group. *Macromolecules* **1996**, *29*, 7029–7033.
(452) Gong, C.; Gibson, H. W. Dethreading During the Preparation of Polyrotaxanes. *Macromol. Chem. Phys.* **1997**, *198*, 2321–2332.
(453) Gong, C.; Ji, Q.; Glass, T. E.; Gibson, H. W. A Strategy to Eliminate Dethreading During the Preparation of Poly(ester/crown ether rotaxane)s: Use of Difunctional Blocking Groups. *Macromolecules* **1997**, *30*, 4807–4813.
(454) Gong, C.; Gibson, H. W. Relative Threading Efficiencies of Different Macrocycles: A Competitive Trapping Methodology

Based on Hybrid Polyrotaxanes. *Macromolecules* **1997**, *30*, 8524–8525.
(455) Gong, C.; Glass, T. E.; Gibson, H. W. Poly(urethane/crown ether rotaxane)s with Solvent Switchable Microstructures. *Macromolecules* **1998**, *31*, 308–313.
(456) Lipatova, T. E.; Kosyanchuk, L. F.; Shilov, V. V. Complex Formation Between Cyclic Urethane and Zinc Chloride: Its Effect on Polyrotaxane Synthesis. *J. Macromol. Sci., Chem. A* **1985**, *22*, 361–372.
(457) Yamagishi, T.-A.; Kawahara, A.; Kita, J.; Hoshima, M.; Umehara, A.; Ishida, S.-I.; Nakamoto, Y. *In situ* Polycondensation of *p-tert*-Butylphenol in the Presence of Poly(ethylene glycol)s for Preparation of Polyrotaxanes. *Macromolecules* **2001**, *34*, 6565–6570.
(458) Harada, A. Preparation and Structures of Supramolecules Between Cyclodextrins and Polymers. *Coord. Chem. Rev.* **1996**, *148*, 115–133.
(459) Harada, A. Design and Construction of Supramolecular Architectures Consisting of Cyclodextrins and Polymers. *Adv. Polym. Sci.* **1997**, *133*, 141–191.
(460) Harada, A.; Li, J.; Kamachi, M. The Molecular Necklace: A Rotaxane Containing Many Threaded α-Cyclodextrins. *Nature* **1992**, *356*, 325–327.
(461) Harada, A.; Okada, M.; Li, J.; Kamachi, M. Preparation and Characterization of Inclusion Complexes of Poly(propylene glycol) with Cyclodextrins. *Macromolecules* **1995**, *28*, 8406–8411.
(462) Wenz, G.; Keller, B. Threading Cyclodextrin Rings on Polymer Chains. *Angew. Chem., Int. Ed. Engl*. **1992**, *31*, 197–199.
(463) Wenz, G.; Keller, B. Speed Control for Cyclodextrin Rings on Polymer Chains. *Macromol. Symp.* **1994**, *87*, 11–16.
(464) Herrmann, W.; Keller, B.; Wenz, G. Kinetics and Thermodynamics of the Inclusion of Ionene-6,10 in α-Cyclodextrin in an Aqueous Solution. *Macromolecules* **1997**, *30*, 4966–4972.
(465) Choi, H. S.; Ooya, T.; Lee, S. C.; Sasaki, S.; Kurisawa, M.; Uyama, H.; Yui, N. pH Dependence of Polypseudorotaxane Formation Between Cationic Linear Polyethylenimine and Cyclodextrins. *Angew. Chem., Int. Ed*. **2004**, *37*, 6705–6710.
(466) Wenz, G.; Gruber, C.; Keller, B.; Schilli, C.; Albuzat, T.; Müller, A. Kinetics of Threading α-Cyclodextrin onto Cationic and Zwitterionic Poly(bola-amphiphiles). *Macromolecules* **2006**, *39*, 8021–8026.
(467) Kelch, S.; Caseri, W. R.; Shelden, R. A.; Suter, U. W.; Wenz, G.; Keller, B. Influence of the Ring Size on the Behavior of Polymeric Inclusion Compounds at Mica Surfaces. *Langmuir* **2000**, *16*, 5311–5316.
(468) Harada, A.; Adachi, H.; Kawaguchi, Y.; Okada, M.; Kamachi, M. Complex Formation of Cyclodextrins with Cationic Polymers. *Polym. J.* **1996**, *28*, 159–163.
(469) Meier, L. P.; Heule, M.; Caseri, W. R.; Shelden, R. A.; Suter, U. W.; Wenz, G.; Keller, B. Adsorption of Polymeric Inclusion Compounds on Muscovite Mica. *Angew. Chem., Int. Ed. Engl*. **1996**, *29*, 718–723.
(470) Nelson, A.; Belitsky, J. M.; Vidal, S.; Joiner, C. S.; Baum, L. G.; Stoddart, J. F. A Self-Assembled Multivalent Pseudopolyrotaxane for Binding Galectin-1. *J. Am. Chem. Soc.* **2004**, *126*, 11914–11922.
(471) Huh, K. M.; Ooya, T.; Sasaki, S.; Yui, N. Polymer Inclusion Complex Consisting of Poly(ε-lysine) and α-Cyclodextrin. *Macromolecules* **2001**, *34*, 2402–2404.
(472) Huh, K. M.; Tomita, H.; Ooya, T.; Lee, W. K.; Sasaki, S.; Yui, N. pH Dependence of Inclusion Complexation Between Cationic Poly(ε-lysine) and α-Cyclodextrin. *Macromolecules* **2002**, *35*, 3775–3777.
(473) Maciejewski, M.; Panasiewicz, M.; Jarminska, D. Compounds of β-Cyclodextrin and Organosilicon Oligomers. *J. Macromol. Sci. A* **1978**, *12*, 701–718.
(474) Maciejewski, M. Polymerization and Copolymerization of Some Monomers as Adducts with β-Cyclodextrin. *J. Macromol. Sci. A* **1979**, *13*, 77–85.
(475) Maciejewski, M.; Gwizdowski, A.; Pęczak, P.; Pietrzak, A. Polymer Inclusion Compounds by Polymerization of Monomers in β-Cyclodextrin Matrix in DMF Solution. *J. Macromol. Sci, A* **1979**, *13*, 87–109.
(476) Maciejewski, M.; Durski, Z. On the Structure of β-Cyclodextrin Polymer Adducts. *J. Macromol. Sci. A* **1981**, *16*, 441–450.
(477) Okumura, H.; Okada, M.; Kawaguchi, Y.; Harada, A. Complex Formation Between Poly(dimethylsiloxane) and Cyclodextrins: New Pseudo-Polyrotaxanes Containing Inorganic Polymers. *Macromolecules* **2000**, *33*, 4297–4298.
(478) Harada, A.; Nishiyama, T.; Kawaguchi, Y.; Okada, M.; Kamachi, M. Preparation and Characterization of Inclusion Complexes of Aliphatic Polyesters with Cyclodextrins. *Macromolecules* **1997**, *30*, 7115–7118.
(479) Harada, A.; Kawaguchi, Y.; Nishiyama, T.; Kamachi, M. Complex Formation of Poly(ε-caprolactone) with Cyclodextrin. *Macromol. Rapid Commun.* **1997**, *18*, 535–539.
(480) Weickenmeier, M.; Wenz, G. Threading of Cyclodextrins onto a Polyester of Octanedicarboxylic Acid and Polyethylene Glycol. *Macromol. Rapid Commun.* **1997**, *18*, 1109–1115.
(481) Lei, H.; Allen, E.; Tonelli, A. E. Study of the Inclusion Compounds Formed Between α-Cyclodextrin and High Molecular Weight Poly(ethylene oxide) and Poly (ε-caprolactone). *Polymer* **1998**, *39*, 4857–4865.
(482) Kawaguchi, Y.; Nishiyama, T.; Okada, M.; Kamachi, M.; Harada, A. Complex Formation of Poly(ε-caprolactone) with Cyclodextrins. *Macromolecules* **2000**, *33*, 4472–4477.
(483) Rusa, C. C.; Tonelli, A. E. Polymer/Polymer Inclusion Compounds as a Novel Approach to Obtaining a PLLA/PCL Intimately Compatible Blend. *Macromolecules* **2000**, *33*, 5321–5324.
(484) Shuai, X.; Porbeni, F. E.; Wei, M.; Bullions, T.; Tonelli, A. E. Formation of Inclusion Complexes of Poly(3-hydroxybutyrate)s with Cyclodextrins. 1. Immobilization of Atactic Poly(*R, S*-3-hydroxybutyrate) and Miscibility Enhancement Between Poly(*R,S*-3-hydroxybutyrate) and Poly(ε-caprolactone). *Macromolecules* **2002**, *35*, 3126–3132.
(485) Blin, F.; Przybylski, C.; Bonnet, V.; Clément, M.-J.; Curmi, P. A.; Choppinet, P.; Nakajima, T.; Chéradame, H.; Jarroux, N. Radical Coupling Allows a Fast and Tuned Synthesis of Densely Packed Polyrotaxanes Involving γ-Cyclodextrins and Polydimethylsiloxane. *Macromolecules* **2016**, *49*, 3232–3243.
(486) Harada, A.; Li, J.; Suzuki, S.; Kamachi, M. Complex Formation Between Polyisobutylene and Cyclodextrins: Inversion of Chain-Length Selectivity Between. β-Cyclodextrin and γ-Cyclodextrin. *Macromolecules* **1993**, *26*, 5267–5268.
(487) Li, J.; Harada, A.; Kamachi, M. Formation of Inclusion Complexes of Oligoethylene and Its Derivatives with. α-Cyclodextrin. *Bull. Chem. Soc. Jpn*. **1994**, *67*, 2808–2818.
(488) Harada, A.; Suzuki, S.; Okada, M.; Kamachi, M. Preparation and Characterization of Inclusion Complexes of Polyisobutylene with Cyclodextrins. *Macromolecules* **1996**, *29*, 5611–5614.
(489) Michishita, T.; Okada, M.; Harada, A. Complex Formation of Polybutadiene with Cyclodextrins. *Macromol. Rapid Commun.* **2001**, *22*, 763–767.
(490) Michishita, T.; Takashima, Y.; Harada, A. Complex Formation Between Polyisoprene and Cyclodextrins. *Macromol. Rapid Commun.* **2004**, *25*, 1159–1162.
(491) Rusa, C. C.; Rusa, M.; Gomez, M.; Shin, I. D.; Fox, J. D.; Tonelli, A. E. Nanostructuring High Molecular Weight Isotactic Polyolefins *via* Processing with γ-Cyclodextrin Inclusion Compounds. Formation and Characterization of Polyolefin−γ-Cyclodextrin Inclusion Compounds. *Macromolecules* **2004**, *37*, 7992–7999.
(492) Ogata, N.; Sanui, K.; Wada, J. Novel Synthesis of Inclusion Polyamides. *J. Polym. Sci.: Polym. Lett. Ed.* **1976**, *14*, 459–462.
(493) Huang, L.; Allen, E.; Tonelli, A. E. Inclusion Compounds Formed Between Cyclodextrins and Nylon 6. *Polymer* **1999**, *40*, 3211–3221.

(494) Wei, M.; Davis, W.; Urban, B.; Song, Y.; Porbeni, F. E.; Wang, X.; White, J. L.; Balik, C. M.; Rusa, C. C.; Fox, J.; Tonelli, A. E. Manipulation of Nylon-6 Crystal Structures with Its α-Cyclodextrin Inclusion Complex. *Macromolecules* **2002**, *35*, 8039–8044.
(495) Farcas, A.; Simionescu, C. I. Conjugated Polymers with Rotaxane Architecture. *Rev. Roum. Chim.* **2006**.
(496) Brovelli, S.; Cacialli, F. Optical and Electroluminescent Properties of Conjugated Polyrotaxanes. *Small* **2010**, *6*, 2796–2820.
(497) Harada, A.; Li, J.; Kamachi, M. Preparation and Properties of Inclusion Complexes of Polyethylene Glycol with α-Cyclodextrin. *Macromolecules* **1993**, *26*, 5698–5703.
(498) Harada, A.; Li, J.; Kamachi, M. Complex Formation Between Poly(methyl vinyl ether) and γ-Cyclodextrin. *Chem. Lett.* **1993**, 237–240.
(499) Harada, A.; Okada, M.; Kamachi, M. Complex Formation Between Poly(oxytrimethylene) and Cyclodextrins. *Acta Polym.* **1995**, *46*, 453–457.
(500) Harada, A.; Suzuki, S.; Nakamitsu, T.; Okada, M.; Kamachi, M. Construction of Supramolecules Consisting of Cyclodextrins and Poly(tetrahydrofuran). *Kobunshi Ronbunshu* **1995**, *52*, 594–598.
(501) Kamitori, S.; Matsuzaka, O.; Kondo, S.; Muraoka, S.; Okuyama, K.; Noguchi, K.; Okada, M.; Harada, A. A Novel Pseudo-Polyrotaxane Structure Composed of Cyclodextrins and a Straight-Chain Polymer: Crystal Structures of Inclusion Complexes of β-Cyclodextrin with Poly(trimethylene oxide) and Poly(propylene glycol). *Macromolecules* **2000**, *33*, 1500–1502.
(502) Li, J.; Harada, A.; Kamachi, M. Sol–Gel Transition During Inclusion Complex Formation Between α-Cyclodextrin and High Molecular Weight Poly(ethylene glycol)s in Aqueous Solution. *Polym. J.* **1994**, *26*, 1019–1026.
(503) Harada, A.; Li, J.; Kamachi, M. Formation of Inclusion Complexes of Monodisperse Oligo(ethylene glycol)s with α-Cyclodextrin. *Macromolecules* **1994**, *27*, 4538–4543.
(504) Ceccato, M.; LoNostro, P.; Baglioni, P. α-Cyclodextrin/ Polyethylene Glycolpolyrotaxane: A Study of the Threading Process. *Langmuir* **1997**, *13*, 2436–2439.
(505) Zhao, T.; Beckham, H. W. Direct Synthesis of Cyclodextrin-Rotaxanated Poly(ethylene glycol)s and Their Self-Diffusion Behavior in Dilute Solution. *Macromolecules* **2003**, *36*, 9859–9865.
(506) Araki, J.; Zhao, C.; Ito, K. Efficient Production of Polyrotaxanes from α-Cyclodextrin and Poly(ethylene glycol). *Macromolecules* **2005**, *38*, 7524–7527.
(507) Fujita, H.; Ooya, T.; Kurisawa, M.; Mori, H.; Terano, M.; Yui, N. Thermally Switchable Polyrotaxane as a Model of Stimuli-Responsive Supramolecules for Nano-Scale Devices. *Macromol. Rapid Commun.* **1996**, *17*, 509–515.
(508) Fujita, H.; Ooya, T.; Yui, N. Thermally Induced Localization of Cyclodextrins in a Polyrotaxane Consisting of β-Cyclodextrins and Poly(ethylene glycol)−Poly(propylene glycol) Triblock Copolymer. *Macromolecules* **1999**, *32*, 2534–2541.
(509) Ikeda, T.; Watabe, N.; Ooya, T.; Yui, N. Study on the Solution Properties of Thermo-Responsive Polyrotaxanes with Different Numbers of Cyclic Molecules. *Macromol. Chem. Phys.* **2001**, *202*, 1338–1344.
(510) Karino, T.; Okumura, Y.; Zhao, C.; Kidowaki, M.; Kataoka, T.; Ito, K.; Shibayama, M. Sol−Gel Transition of Hydrophobically Modified Polyrotaxane. *Macromolecules* **2006**, *39*, 9435–9440.
(511) Kidowaki, M.; Zhao, C.; Kataoka, T.; Ito, K. Thermoreversible Sol−Gel Transition of an Aqueous Solution of Polyrotaxane Composed of Highly Methylated α-Cyclodextrin and Polyethylene Glycol. *Chem. Commun.* **2006**, 4102–4103.
(512) Yui, N.; Ooya, T. Molecular Mobility of Interlocked Structures Exploiting New Functions of Advanced Biomaterials. *Chem. Eur. J.* **2006**, *12*, 6730–6737.
(513) Loethen, S.; Kim, J.-M.; Thompson, D. H. Biomedical Applications of Cyclodextrin Based Polyrotaxanes. *Polymer Rev.* **2007**, *47*, 383–418.
(514) Yui, N.; Katoono, R.; Yamashita, A. Functional Cyclodextrin Polyrotaxanes for Drug Delivery. *Adv. Polym. Sci.* **2009**, *222*, 55–77.
(515) Li, J. J.; Zhao, F.; Li, J. Polyrotaxanes for Applications in Life Science and Biotechnology. *Appl. Microbiol. Biotechnol.* **2011**, *90*, 427–443.
(516) Higashi, T.; Motoyama, K.; Arima, H. Cyclodextrin-Based Polyrotaxanes and Polypseudorotaxanes as Drug Delivery Carriers. *J. Drug. Del. Sci. Tech.* **2013**, *23*, 523–529.
(517) Tamura, A.; Yui, N. Threaded Macromolecules as a Versatile Framework for Biomaterials. *Chem. Commun.* **2014**, *50*, 13433–13446.
(518) Harada, A.; Li, J.; Kamachi, M.; Kitagawa, Y.; Katsube, Y. Structures of Polyrotaxane Models. *Carbohyd. Res*. **1998**, *305*, 127–129.
(519) Udachin, K. A.; Wilson, L. D.; Ripmeester, J. A. Solid Polyrotaxanes of Polyethylene Glycol and Cyclodextrins: The Single Crystal X-Ray Structure of PEG-β-Cyclodextrin. *J. Am. Chem. Soc.* **2000**, *122*, 12375–12376.
(520) Harada, A.; Li, J.; Kamachi, M. Synthesis of a Tubular Polymer from Threaded Cyclodextrins. *Nature* **1993**, *364*, 516–518.
(521) Liu, Y.; Zhao, Y.-L.; Zhang, H.-Y.; Song, H.-B. Polymeric Rotaxane Constructed from the Inclusion Complex of β-Cyclodextrin and 4,4′-Dipyridine by Coordination with Nickel(II) Ions. *Angew. Chem., Int. Ed*. **2003**, *42*, 3260–3263.
(522) He, Y.; Fu, P.; Shen, X.; Gao, H. Cyclodextrin-Based Aggregates and Characterization by Microscopy. *Micron* **2008**, *39*, 495–516.
(523) Shimomura, T.; Akai, T.; Abe, T.; Ito, K. Atomic Force Microscopy Observation of Insulated Molecular Wire Formed by Conducting Polymer and Molecular Nanotube. *J. Chem. Phys.* **2002**, *116*, 1753–1756.
(524) van den Boogaard, M.; Bonnet, G.; van't Hof, P.; Wang, Y.; Brochon, C.; van Hutten, P.; Lapp, A.; Hadziioannou, G. Synthesis of Insulated Single-Chain Semiconducting Polymers Based on Polythiophene, Polyfluorene, and β-Cyclodextrin. *Chem. Mater.* **2004**, *16*, 4383–4385.
(525) Yoshida, K.-I.; Shimomura, T.; Ito, K.; Hayakawa, R. Inclusion Complex Formation of Cyclodextrin and Polyaniline. *Langmuir* **1999**, *15*, 910–913.
(526) Shigekawa, H.; Miyake, K.; Sumaoka, J.; Harada, A.; Komiyama, M. The Molecular Abacus: STM Manipulation of Cyclodextrin Necklace. *J. Am. Chem. Soc.* **2000**, *122*, 5411–5412.
(527) Liu, Y.; Zhao, Y.-L.; Zhang, H.-Y.; Li, X.-Y.; Liang, P.; Zhang, X.-Z.; Xu, J.-J. Supramolecular Polypseudorotaxane with Conjugated Polyazomethine Prepared Directly from Two Inclusion Complexes of β-Cyclodextrin with Tolidine and Phthaldehyde. *Macromolecules* **2004**, *37*, 6362–6369.
(528) Osaki, M.; Takashima, Y.; Yamaguchi, H.; Harada, A. An Artificial Molecular Chaperone: Poly-Pseudo-Rotaxane with an Extensible Axle. *J. Am. Chem. Soc.* **2007**, *129*, 14452–14457.
(529) Osaki, M.; Takashima, Y.; Yamaguchi, H.; Harada, A. Nanospheres with Polymerization Ability Coated by Polyrotaxane. *J. Org. Chem.* **2009**, *74*, 1858–1863.
(530) Takashima, Y.; Osaki, M.; Ishimaru, Y.; Yamaguchi, H.; Harada, A. Artificial Molecular Clamp: A Novel Device for Synthetic Polymerases. *Angew. Chem., Int. Ed*. **2011**, *50*, 7524–7528.
(531) Anderson, S.; Anderson, H. L. Synthesis of a Water-Soluble Conjugated [3]Rotaxane. *Angew. Chem., Int. Ed. Engl*. **1996**, *35*, 1956–1959.
(532) Taylor, P. N.; O'Connell, M. J.; McNeill, L. A.; Hall, M. J.; Aplin, R. T.; Anderson, H. L. Insulated Molecular Wires: Synthesis of Conjugated Polyrotaxanes by Suzuki Coupling in Water. *Angew. Chem., Int. Ed*. **2000**, *39*, 3456–3460.

(533) Terao, J.; Tang, A.; Michels, J. J.; Krivokapic, A.; Anderson, H. L. Synthesis of Poly(*para*-phenylenevinylene) Rotaxanes by Aqueous Suzuki Coupling. *Chem. Commun.* **2004**, 56–57.
(534) Cacialli, F.; Wilson, J. S.; Michels, J. J.; Daniel, C.; Silva, C.; Friend, R. H.; Severin, N.; Samorì, P.; Rabe, J. P.; O'Connell, M. J.; Taylor, P. N.; Anderson, H. L. Cyclodextrin-Threaded Conjugated Polyrotaxanes as Insulated Molecular Wires with Reduced Interstrand Interactions. *Nature Mater.* **2002**, *1*, 160–164.
(535) Michels, J. J.; O'Connell, M. J.; Taylor, P. N.; Wilson, J. S.; Cacialli, F.; Anderson, H. L. Synthesis of Conjugated Polyrotaxanes. *Chem. Eur. J.* **2003**, *9*, 6167–6176.
(536) Sardone, L.; Williams, C. C.; Anderson, H. L.; Marletta, G.; Cacialli, F.; Samorì, P. Phase Segregation in Thin Films of Conjugated Polyrotaxane– Poly(ethylene oxide) Blends: A Scanning Force Microscopy Study. *Adv. Funct. Mater.* **2007**, *17*, 927–932.
(537) Frampton, M. J.; Sforazzini, G.; Brovelli, S.; Latini, G.; Townsend, E.; Williams, C. C.; Charas, A.; Zalewski, L.; Kaka, N. S.; Sirish, M.; Parrott, L. J.; Wilson, J. S.; Cacialli, F.; Anderson, H. L. Synthesis and Optoelectronic Properties of Nonpolar Polyrotaxane Insulated Molecular Wires with High Solubility in Organic Solvents. *Adv. Funct. Mater.* **2008**, *18*, 3367–3376.
(538) Latini, G.; Parrott, L.-J.; Brovelli, S.; Frampton, M. J.; Anderson, H. L.; Cacialli, F. Cyclodextrin-Threaded Conjugated Polyrotaxanes for Organic Electronics: The Influence of the Counter Cations. *Adv. Funct. Mater.* **2008**, *18*, 2419–2427.
(539) Brovelli, S.; Latini, G.; Frampton, M. J.; McDonnell, S. O.; Oddy, F. E.; Fenwick, O.; Anderson, H. L.; Cacialli, F. Tuning Intrachain Versus Interchain Photophysics *via* Control of the Threading Ratio of Conjugated Polyrotaxanes. *Nano Lett.* **2008**, *8*, 4546–4551.
(540) Petrozza, A.; Brovelli, S.; Michels, J. J.; Anderson, H. L.; Friend, R. H.; Silva, C.; Cacialli, F. Control of Rapid Formation of Interchain Excited States in Sugar-Threaded Supramolecular Wires. *Adv. Mater.* **2008**, *20*, 3218–3223.
(541) Latini, G.; Winroth, G.; Brovelli, S.; McDonnell, S. O.; Anderson, H. L.; Mativetsky, J. M.; Samorì, P.; Cacialli, F. Enhanced Luminescence Properties of Highly Threaded Conjugated Polyelectrolytes with Potassium Counter-Ions upon Blending with Poly(ethylene oxide). *J. Appl. Phys.* **2010**, *107*, 124509.
(542) Brovelli, S.; Meinardi, F.; Winroth, G.; Fenwick, O.; Sforazzini, G.; Frampton, M. J.; Zalewski, L.; Levitt, J. A.; Marinello, F.; Schiavuta, P.; Suhling, K.; Anderson, H. L.; Cacialli, F. White Electroluminescence by Supramolecular Control of Energy Transfer in Blends of Organic-Soluble Encapsulated Polyfluorenes. *Adv. Funct. Mater.* **2010**, *20*, 272–280.
(543) Di Stasio, F.; Korniychuk, P.; Brovelli, S.; Uznanski, P.; McDonnell, S. O.; Winroth, G.; Anderson, H. L.; Tracz, A.; Cacialli, F. Highly Polarized Emission from Oriented Films Incorporating Water-Soluble Conjugated Polymers in a Polyvinyl Alcohol Matrix. *Adv. Mater.* **2011**, *23*, 1855–1859.
(544) Brovelli, S.; Sforazzini, G.; Serri, M.; Winroth, G.; Suzuki, K.; Meinardi, F.; Anderson, H. L.; Cacialli, F. Emission Color Trajectory and White Electroluminescence Through Supramolecular Control of Energy Transfer and Exciplex Formation in Binary Blends of Conjugated Polyrotaxanes. *Adv. Funct. Mater.* **2012**, *22*, 4284–4291.
(545) Mróz, M. M.; Sforazzini, G.; Zhong, Y.; Wong, K. S.; Anderson, H. L.; Lanzani, G.; Cabanillas-Gonzalez, J. Amplified Spontaneous Emission in Conjugated Polyrotaxanes Under Quasi-cw Pumping. *Adv. Mater.* **2013**, *25*, 4347–4351.
(546) Mróz, M. M.; Lanzani, G.; Virgili, T.; Mc Donnell, S. O.; Frampton, M. J.; Anderson, H. L. Photoinduced on-Chain Charge-Separation and Ultrafast Recombination in a Sugar-Coated Insulated Molecular Wire. *Phys. Rev. B* **2009**, *80*, 045111–045118.
(547) Shimomura, T.; Yoshida, K.-I.; Ito, K.; Hayakawa, R. Insulation Effect of an Inclusion Complex Formed by Polyaniline and β-Cyclodextrin in Solution. *Polym. Adv. Technol.* **2000**, *11*, 837–839.
(548) Farcas, A.; Grigoras, M. Synthesis and Characterization of a Fully Aromatic Polyazomethine with Rotaxane Architecture. *Polym. Int.* **2003**, *52*, 1315–1320.
(549) Nepal, D.; Samal, S.; Geckeler, K. E. The First Fullerene-Terminated Soluble Poly(azomethine) Rotaxane. *Macromolecules* **2003**, *36*, 3800–3802.
(550) Yamaguchi, I.; Kashiwagi, K.; Yamamoto, T. β-Cyclodextrin Pseudopolyrotaxanes with π-Conjugated Polymer Axles. *Macromol. Rapid Commun.* **2004**, *25*, 1163–1166.
(551) Shinohara, K.-I.; Suzuki, T.; Kitami, T.; Yamaguchi, S. Simultaneous Imaging of the Structure and Fluorescence of a Supramolecular Nanostructure Formed by the Coupling of π-Conjugated Polymer Chains in the Intermolecular Interaction. *J. Polym. Sci. Pol. Chem.* **2006**, *44*, 801–809.
(552) Dodziuk, H.; Ejchart, A.; Anczewski, W.; Ueda, H.; Krinichnaya, E.; Dolgonos, G.; Kutner, W. Water Solubilization, Determination of the Number of Different Types of Single-Wall Carbon Nanotubes and Their Partial Separation with Respect to Diameters by Complexation with η-Cyclodextrin. *Chem. Commun.* **2003**, 986–987.
(553) Kidowaki, M.; Nakajima, T.; Araki, J.; Inomata, A.; Ishibashi, H.; Ito, K. Novel Liquid Crystalline Polyrotaxane with Movable Mesogenic Side Chains. *Macromolecules* **2007**, *40*, 6859–6862.
(554) Wu, J.; He, H.; Gao, C. β-Cyclodextrin-Capped Polyrotaxanes: One-Pot Facile Synthesis *via* Click Chemistry and Use as Templates for Platinum Nanowires. *Macromolecules* **2010**, *43*, 2252–2260.
(555) Teuchert, C.; Michel, C.; Hausen, F.; Park, D.-Y.; Beckham, H. W.; Wenz, G. Cylindrical Polymer Brushes by Atom Transfer Radical Polymerization from Cyclodextrin–PEG Polyrotaxanes: Synthesis and Mechanical Stability. *Macromolecules* **2013**, *46*, 2–7.
(556) Sforazzini, G.; Kahnt, A.; Wykes, M.; Sprafke, J. K.; Brovelli, S.; Montarnal, D.; Meinardi, F.; Cacialli, F.; Beljonne, D.; Albinsson, B.; Anderson, H. L. Synthesis and Photophysics of Coaxial Threaded Molecular Wires: Polyrotaxanes with Triarylamine Jackets. *J. Phys. Chem. C* **2014**, *118*, 4553–4566.
(557) Whang, D.; Jeon, Y. M.; Heo, J.; Kim, K. Self-Assembly of a Polyrotaxane Containing a Cyclic "Bead" in Every Structural Unit in the Solid State: Cucurbituril Molecules Threaded on a One-Dimensional Coordination Polymer. *J. Am. Chem. Soc.* **1996**, *118*, 11333–11334.
(558) Whang, D.; Kim, K. Polycatenated Two-Dimensional Polyrotaxane Net. *J. Am. Chem. Soc.* **1997**, *119*, 451–452.
(559) Whang, D.; Heo, J.; Kim, C.-A.; Kim, K. Helical Polyrotaxane: Cucurbituril "Beads" Threaded onto a Helical One-Dimensional Coordination Polymer. *Chem. Commun.* **1997**, 2361–2362.
(560) Park, K.-M.; Whang, D.; Lee, E.; Heo, J.; Kim, K. Transition Metal Ion Directed Supramolecular Assembly of One- and Two-Dimensional Polyrotaxanes Incorporating Cucurbituril. *Chem. Eur. J.* **2002**, *8*, 498–508.
(561) Lee, E.; Kim, J.; Heo, J.; Whang, D.; Kim, K. A Two-Dimensional Polyrotaxane with Large Cavities and Channels: A Novel Approach to Metal-Organic Open-Frameworks by Using Supramolecular Building Blocks. *Angew. Chem., Int. Ed.* **2001**, *40*, 399–402.
(562) Lee, E.; Heo, J.; Kim, K. A Three-Dimensional Polyrotaxane Network. *Angew. Chem., Int. Ed.* **2000**, *39*, 2699–2701.
(563) Kim, K. Mechanically Interlocked Molecules Incorporating Cucurbituril and Their Supramolecular Assemblies. *Chem. Soc. Rev.* **2002**, *31*, 96–107.
(564) Park, K.-M.; Roh, S.-G.; Lee, E.; Kim, J.; Kim, H.-J.; Lee, J. W.; Kim, K. Construction of a Square-Wave-Shaped One-Dimensional Polyrotaxane Using a Preorganized

L-Shaped Pseudorotaxane. *Supramol. Chem.* **2002**, *14*, 153–158.
(565) Park, K. M.; Lee, E.; Roh, S. G.; Kim, J.; Kim, K. A Double-Chained Polyrotaxane: Cucurbituril 'Beads' Threaded onto a Double-Chained One-Dimensional Coordination Polymer. *Bull. Kor. Chem. Soc.* **2004**, *25*, 1711–1713.
(566) Wang, Z.-B.; Zhu, H.-F.; Zhao, M.; Li, Y.-Z.; Okamura, T.-A.; Sun, W.-Y.; Chen, H.-L.; Ueyama, N. Silver(I) Ion Assisted Assembly of One-Dimensional Polyrotaxanes Incorporating Cucurbit[6]uril. *Cryst. Growth Des.* **2006**, *6*, 1420–1427.
(567) Wang, Z.-B.; Zhao, M.; Li, Y.-Z.; Chen, H.-L. Metal Ion-Assisted Assembly of One-Dimensional Polyrotaxanes Incorporating Cucurbit[6]uril. *Supramol. Chem.* **2008**, *20*, 689–696.
(568) Zeng, J.-P.; Zhang, S.-M.; Zhang, Y.-Q.; Tao, Z.; Zhu, Q.-J.; Xue, S.-F.; Wei, G. Use of Silver(I) and Copper(II) Ions to Assist the Self-Assembly of Polyrotaxanes Incorporating Symmetrical α, α′, δ, δ′-Tetramethyl-Cucurbit[6]uril. *Cryst. Growth Des.* **2010**, *10*, 4509–4515.
(569) Wei, X.; Zeng, J.-P.; Cong, H.; Zhang, Y.-Q.; Tao, Z.; Zhu, Q.-J.; Xue, S.-F. Synthesis of Supramolecular Polyrotaxanes Assemblies Incorporating Symmetrical α, α′, δ, δ′-Tetramethyl-Cucurbit[6]uril Moieties Using Polychloride Zinc(II) and Cadium(II) Anions. *Supramol. Chem.* **2014**, *26*, 692–697.
(570) Zeng, J.-P.; Cong, H.; Chen, K.; Xue, S.-F.; Zhang, Y.-Q.; Zhu, Q.-J.; Liu, J.-X.; Tao, Z. A Novel Strategy to Assemble Achiral Ligands to Chiral Helical Polyrotaxane Structures. *Inorg. Chem.* **2011**, *50*, 6521–6525.
(571) Mei, L.; Wu, Q.-Y.; Liu, C.-M.; Zhao, Y.-L.; Chai, Z.-F.; Shi, W.-Q. The First Case of an Actinide Polyrotaxane Incorporating Cucurbituril: A Unique "Dragon-Like" Twist Induced by a Specific Coordination Pattern of Uranium. *Chem. Commun.* **2014**, *50*, 3612–3614.
(572) Mei, L.; Wang, L.; Liu, C.-M.; Zhao, Y.-L.; Chai, Z.-F.; Shi, W.-Q. Tetranuclear Uranyl Polyrotaxanes: Preferred Selectivity Toward Uranyl Tetramer for Stabilizing a Flexible Polyrotaxane Chain Exhibiting Weakened Supramolecular Inclusion. *Chem. Eur. J.* **2015**, *21*, 10226–10235.
(573) Mei, L.; Wang, L.; Yuan, L.-Y.; An, S.-W.; Zhao, Y.-L.; Chai, Z.-F.; Burns, P. C.; Shi, W.-Q. Supramolecular Inclusion-Based Molecular Integral Rigidity: A Feasible Strategy for Controlling the Structural Connectivity of Uranyl Polyrotaxane Networks. *Chem. Commun.* **2015**, *51*, 11990–11993.
(574) Meschke, C.; Buschmann, H.-J.; Schollmeyer, E. Synthesis of Mono-, Oligo- and Polyamide-Cucurbituril Rotaxanes. *Macromol. Rapid Comm.* **1998**, *19*, 59–63.
(575) Meschke, C.; Buschmann, H.-J.; Schollmeyer, E. Polyrotaxanes and Pseudopolyrotaxanes of Polyamides and Cucurbituril. *Polymer* **1999**, *40*, 945–949.
(576) Buschmann, H.-J. From Small Cucurbituril Complexes to Large Ordered Networks. *Isr. J. Chem.* **2011**, *51*, 533–536.
(577) Buschmann, H.-J.; Jansen, K.; Schollmeyer, E. Cucurbituril and α- and β-Cyclodextrins as Ligands for the Complexation of Nonionic Surfactants and Polyethyleneglycols in Aqueous Solutions. *J. Incl. Phenom. Macrocycl. Chem.* **2000**, *37*, 231–236.
(578) Tuncel, D.; Steinke, J. H. G. Mainchain Pseudopolyrotaxanes *via* Post-Threading with Cucurbituril. *Chem. Commun.* **2001**, 253–254.
(579) Tuncel, D.; Steinke, J. H. G. Catalytically Self-Threading Polyrotaxanes. *Chem. Commun.* **1999**, 1509–1510.
(580) Tuncel, D.; Steinke, J. H. G. Catalytic Self-Threading: A New Route for the Synthesis of Polyrotaxanes. *Macromolecules* **2004**, *37*, 288–302.
(581) Tuncel, D.; Ünal, Ö.; Artar, M. Supramolecular Assemblies Constructed by Cucurbituril-Catalyzed Click Reaction. *Isr. J. Chem.* **2011**, *51*, 525–532.
(582) Choi, S.; Lee, J. W.; Ko, Y. H.; Kim, K. Pseudopolyrotaxanes Made to Order: Cucurbituril Threaded on Polyviologen. *Macromolecules* **2002**, *35*, 3526–3531.
(583) Willis-Fox, N.; Belger, C.; Fennell, J. F., Jr.; Evans, R. C.; Swager, T. M. Threading the Needle: Fluorescent Poly-Pseudo-Rotaxanes for Size-Exclusion Sensing. *Chem. Mater.* **2016**, *28*, 2685–2691.
(584) Ooya, T.; Inoue, D.; Choi, H. S.; Kobayashi, Y.; Loethen, S.; Thompson, D. H.; Ko, Y. H.; Kim, K.; Yui, N. pH-Responsive Movement of Cucurbit[7]uril in a Diblock Polypseudorotaxane Containing Dimethyl β-Cyclodextrin and Cucurbit[7]uril. *Org. Lett.* **2006**, *8*, 3159–3162.
(585) Zhu, S. S.; Carroll, P.; Swager, T. M. Conducting Polymetallorotaxanes: A Supramolecular Approach to Transition Metal Ion Sensors. *J. Am. Chem. Soc.* **1996**, *118*, 8713–8714.
(586) Zhu, S. S.; Swager, T. M. Conducting Polymetallorotaxanes: Metal Ion Mediated Enhancements in Conductivity and Charge Localization. *J. Am. Chem. Soc.* **1997**, *119*, 12568–12577.
(587) Buey, J.; Swager, T. M. Three-Strand Conducting Ladder Polymers: Two-Step Electropolymerization of Metallorotaxanes. *Angew. Chem., Int. Ed*. **2000**, *39*, 608–612.
(588) Kern, J.-M.; Sauvage, J.-P.; Bidan, G.; Billon, M.; Divisia-Blohorn, B. Electroactive Films with a Polyrotaxane Organic Backbone. *Adv. Mater.* **1996**, *8*, 580–582.
(589) Bidan, G.; Billon, M.; Divisia-Blohorn, B.; Kern, J.-M.; Raehm, L.; Sauvage, J.-P. Electrode-Deposited Films of Polyrotaxanes: Electrochemically Induced Gliding Motion. *New J. Chem.* **1998**, *22*, 1139–1141.
(590) Vidal, P.-L.; Divisia-Blohorn, B.; Bidan, G.; Kern, J.-M.; Sauvage, J.-P.; Hazemann, J.-L. Conjugated Polyrotaxanes Incorporating Mono- or Divalent Copper Complexes. *Inorg. Chem.* **1999**, *38*, 4203–4210.
(591) Vidai, P. L.; Divisia-Blohom, B.; Billon, M.; Bidan, G.; Kern, J. M.; Sauvage, J.-P. Conjugated Polyrotaxanes Containing Coordinating Units. *Synth. Met.* **1999**, *102*, 1478–1479.
(592) Sauvage, J.-P.; Kern, J.-M.; Bidan, G.; Divisia-Blohorn, B.; Vidal, P.-L. Conjugated Polyrotaxanes: Improvement of the Polymer Properties by Using Sterically Hindered Coordinating Units. *New J. Chem.* **2002**, *26*, 1287–1290.
(593) Divisia-Blohorn, B.; Genoud, F.; Borel, C.; Bidan, G.; Kern, J.-M.; Sauvage, J.-P. Conjugated Polymetallorotaxanes: *In-Situ* ESR and Conductivity Investigations of Metal-Backbone Interactions. *J. Phys. Chem. B* **2003**, *107*, 5126–5132.
(594) Kieffer, J.; Divisia-Blohorn, B.; Bidan, G.; Schaffner-Hamann, C.; Kern, J.-M.; Sauvage, J.-P. Polymétallorotaxanes Conjugués Contenant des Unités Pentacoordinantes. *Compt. Rend. Chim.* **2007**, *10*, 1234–1242.
(595) Kang, S.; Cetin, M. M.; Jiang, R.; Clevenger, E. S.; Mayer, M. F. Synthesis of Metalated Pseudorotaxane Polymers with Full Control Over the Average Linear Density of Threaded Macrocycles. *J. Am. Chem. Soc.* **2014**, *136*, 12588–12591.
(596) Momčilović, N.; Clark, P. G.; Boydston, A. J.; Grubbs, R. H. One-Pot Synthesis of Polyrotaxanes *via* Acyclic Diene Metathesis Polymerization of Supramolecular Monomers. *J. Am. Chem. Soc.* **2011**, *33*, 19087–19089.
(597) Scarff, C. A.; Snelling, J. R.; Knust, M. M.; Wilkins, C. L.; Scrivens, J. H. New Structural Insights into Mechanically Interlocked Polymers Revealed by Ion Mobility Mass Spectrometry. *J. Am. Chem. Soc.* **2012**, *134*, 9193–9198.
(598) Nakazono, K.; Ishino, T.; Takashima, T.; Saeki, D.; Natsui, D.; Kihara, N.; Takata, T. Directed One-Pot Syntheses of Crown Ether Wheel-Containing Main Chain-Type Polyrotaxanes with Controlled Rotaxanation Ratios. *Chem. Commun.* **2014**, *50*, 15341–15344.
(599) Chen, Z.; Aoki, D.; Uchida, S.; Marubayashi, H.; Nojima, S.; Takata, T. Effect of Component Mobility on the Properties of Macromolecular [2]Rotaxanes. *Angew. Chem., Int. Ed*. **2016**, *55*, 2778–2781.
(600) Loveday, D.; Wilkes, G. L.; Bheda, M. C.; Shen, Y. X.; Gibson, H. W. Structure-Property Relationships in Segmented

Polyviologen Ionene Rotaxanes. *J. Macromol. Sci. A* **1995**, *32*, 1–27.
(601) Gibson, H. W.; Shen, Y. X.; Bheda, M. C.; Gong, C. Polymeric Molecular Shuttles: Polypseudorotaxanes & Polyrotaxanes Based on Viologen(paraquat) Urethane Backbones & Bis(*p*-phenylene)-34-Crown-10. *Polymer* **2014**, *55*, 3202–3211.
(602) Lee, M.; Choi, U. H.; Colby, R. H.; Gibson, H. W. Ion Conduction in a Semicrystalline Polyviologen and Its Polyether Mixtures. *Macromol. Chem. Phys.* **2014**, *216*, 344–349.
(603) Mason, P. E.; Parsons, I. W.; Tolley, M. S. The First Demonstration of Molecular Queuing in Pseudo[*n*]-Polyrotaxanes: A Novel Variant of Supramolecular Motion. *Angew. Chem., Int. Ed. Engl*. **1996**, *35*, 2238–2241.
(604) Mason, P. E.; Parsons, I. W.; Tolley, M. S. Dynamic Behaviour of a Pseudo[*n*]polyrotaxane Containing a Bipyridyl-Based Cyclophane: Spectroscopic Observations. *Polymer* **1998**, *39*, 3981–3991.
(605) Owen, G. J.; Hodge, P. Synthesis of Some New Polypseudorotaxanes. *Chem. Commun.* **1997**, 11–12.
(606) Hodge, P.; Monvisade, P.; Owen, G. J.; Heatley, F.; Pang, Y. ^{1}H NMR Spectroscopic Studies of the Structures of a Series of Pseudopolyrotaxanes Formed by "Threading". *New J. Chem.* **2000**, *24*, 703–709.
(607) Mason, P. E.; Bryant, W. S.; Gibson, H. W. Threading/Dethreading Exchange Rates as Structural Probes in Polypseudorotaxanes. *Macromolecules* **1999**, *32*, 1559–1569.
(608) Naka, K.; Uemura, T.; Chujo, Y. Self-Complexation of a Poly-Conjugated Donor Molecule with a Cyclic Acceptor. *Bull. Chem. Soc. Jpn.* **2002**, *75*, 2053–2057.
(609) Ogoshi, T.; Nishida, Y.; Yamagishi, T.-A.; Nakamoto, Y. High Yield Synthesis of Polyrotaxane Constructed From Pillar[5]arene and Viologen Polymer and Stabilization of Its Radical Cation. *Macromolecules* **2010**, *43*, 7068–7072.
(610) Gong, H.-Y.; Rambo, B. M.; Karnas, E.; Lynch, V. M.; Keller, K. M.; Sessler, J. L. Environmentally Responsive Threading, Dethreading, and Fixation of Anion-Induced Pseudorotaxanes. *J. Am. Chem. Soc.* **2011**, *133*, 1526–1533.
(611) de Juan, A.; Mar Bernal, M.; Pérez, E. M. Optimization and Insights into the Mechanism of Formation of Mechanically Interlocked Derivatives of Single-Walled Carbon Nanotubes. *ChemPlusChem* **2015**, *80*, 1153–1157.
(612) de Juan, A.; Pouillon, Y.; Ruiz-González, L.; Torres-Pardo, A.; Casado, S.; Martín, N.; Rubio, Á.; Pérez, E. M. Mechanically Interlocked Single-Wall Carbon Nanotubes. *Angew. Chem., Int. Ed*. **2014**, *53*, 5394–5400.
(613) López-Moreno, A.; Pérez, E. M. Pyrene-Based Mechanically Interlocked SWNTs. *Chem. Commun* **2015**, *51*, 5421–5424.
(614) Martínez-Periñán, E.; de Juan, A.; Pouillon, Y.; Schierl, C.; Strauss, V.; Martín, N.; Rubio, Á.; Guldi, D. M.; Lorenzo, E.; Pérez, E. M. The Mechanical Bond on Carbon Nanotubes: Diameter-Selective Functionalization and Effects on Physical Properties. *Nanoscale* **2016**, *8*, 9254–9264.
(615) Ueno, A.; Takahashi, K.; Osa, T. One Host-Two Guests Complexation Between γ-Cyclodextrin and Sodium α-Naphthylacetate as Shown by Excimer Fluorescence. *J. Chem. Soc., Chem. Commun.* **1980**, 921–922.
(616) Tamaki, T. Reversible Photodimerization of Water-Soluble Anthracenes Included in γ-Cyclodextrin. *Chem. Lett.* **1984**, 53–56.
(617) Hamai, S. Exciplex Formation Between Perylene and *N,N*-Dimethylaniline in a Ternary Inclusion Compound with γ-Cyclodextrin in H_2O-Ethanol (7:3) Mixture. *Bull. Chem. Soc. Jpn.* **1991**, *64*, 431–438.
(618) Ashton, P. R.; Chrystal, E. J. T.; Glink, P. T.; Menzer, S.; Schiavo, C.; Stoddart, J. F.; Tasker, P. A.; Williams, D. J. Doubly Encircled and Double-Stranded Pseudorotaxanes. *Angew. Chem., Int. Ed. Engl.* **1995**, *34*, 1869–1871.
(619) Asakawa, M.; Ashton, P. R.; Menzer, S.; Raymo, F. M.; Stoddart, J. F.; White, A. J. P.; Williams, D. J. Molecular Meccano 8. Cyclobis(paraquat-4,4'-biphenylene) - An Organic Molecular Square. *Chem. Eur. J.* **1996**, *2*, 877–893.
(620) Herrmann, W.; Wehrle, S.; Wenz, G. Supramolecular Control of the Photochemistry of Stilbenes by Cyclodextrins. *Chem. Commun.* **1997**, 1709–1710.
(621) Ashton, P. R.; Collins, A. N.; Fyfe, M. C. T.; Menzer, S.; Stoddart, J. F.; Williams, D. J. Supramolecular Weaving. *Angew. Chem., Int. Ed. Engl.* **1997**, *36*, 735–739.
(622) Ashton, P. R.; Collins, A. N.; Fyfe, M. C. T.; Glink, P. T.; Menzer, S.; Stoddart, J. F.; Williams, D. J. An Interwoven Supramolecular Cage. *Angew. Chem., Int. Ed. Engl.* **1997**, *36*, 59–62.
(623) Fyfe, M. C. T.; Glink, P. T.; Menzer, S.; Stoddart, J. F.; White, A. J. P.; Williams, D. J. Anion-Assisted Self-Assembly. *Angew. Chem., Int. Ed. Engl.* **1997**, *36*, 2068–2070.
(624) Ashton, P. R.; Fyfe, M. C. T.; Martínez-Díaz, M.-V.; Menzer, S.; Schiavo, C.; Stoddart, J. F.; White, A. J. P.; Williams, D. J. Molecular Meccano 39. Doubly Docked Pseudorotaxanes. *Chem. Eur. J.* **1998**, *4*, 1523–1534.
(625) Kim, J.; Jung, I.-S.; Kim, S.-Y.; Lee, E.; Kang, J.-K.; Sakamoto, S.; Yamaguchi, K.; Kim, K. New Cucurbituril Homologues: Syntheses, Isolation, Characterization, and X-Ray Crystal Structures of Cucurbit[*n*]uril (*n* = 5, 7, and 8). *J. Am. Chem. Soc.* **2000**, *122*, 540–541.
(626) Ko, Y. H.; Kim, E.; Hwang, I.; Kim, K. Supramolecular Assemblies Built with Host-Stabilized Charge-Transfer Interactions. *Chem. Commun.* **2007**, 1305–1315.
(627) Cheng, H. M.; Leigh, D. A.; Maffei, F.; McGonigal, P. R.; Slawin, A. M. Z.; Wu, J. En Route to a Molecular Sheaf: Active Metal Template Synthesis of a [3]Rotaxane with Two Axles Threaded Through One Ring. *J. Am. Chem. Soc.* **2011**, *133*, 12298–12303.
(628) Harada, A.; Li, J.; Kamachi, M. Double-Stranded Inclusion Complexes of Cyclodextrin Threaded on Poly(ethylene glycol). *Nature* **1994**, *370*, 126–128.
(629) Klotz, E. J. F.; Claridge, T. D. W.; Anderson, H. L. Homo- and Hetero-[3]Rotaxanes with Two π-Systems Clasped in a Single Macrocycle. *J. Am. Chem. Soc.* **2006**, *128*, 15374–15375.
(630) Inouye, M.; Hayashi, K.; Yonenaga, Y.; Itou, T.; Fujimoto, K.; Uchida, T.-A.; Iwamura, M.; Nozaki, K. A Doubly Alkynylpyrene-Threaded [4]Rotaxane That Exhibits Strong Circularly Polarized Luminescence from the Spatially Restricted Excimer. *Angew. Chem., Int. Ed.* **2014**, *53*, 14392–14396.
(631) Kim, H.-J.; Heo, J.; Jeon, W. S.; Lee, E.; Kim, J.; Sakamoto, S.; Yamaguchi, K.; Kim, K. Selective Inclusion of a Hetero-Guest Pair in a Molecular Host: Formation of Stable Charge-Transfer Complexes in Cucurbit. *Angew. Chem., Int. Ed.* **2001**, *40*, 1526–1529.
(632) Sindelar, V.; Cejas, M. A.; Raymo, F. M.; Chen, W.; Parker, S. E.; Kaifer, A. E. Supramolecular Assembly of 2,7-Dimethyldiazapyrenium and Cucurbit[8]uril: A New Fluorescent Host for Detection of Catechol and Dopamine. *Chem. Eur. J.* **2005**, *11*, 7054–7059.
(633) Wittenberg, J. B.; Costales, M. G.; Zavalij, P. Y.; Isaacs, L. A Clipped [3]Rotaxane Derived From Bis-*nor-seco*-Cucurbit[10]uril. *Chem. Commun.* **2011**, *47*, 9420–9422.
(634) Prikhod'ko, A.; Durola, F.; Sauvage, J.-P. Iron(II)-Templated Synthesis of [3]Rotaxanes by Passing Two Threads Through the Same Ring. *J. Am. Chem. Soc.* **2008**, *130*, 448–449.
(635) Prikhod'ko, A.; Sauvage, J.-P. Passing Two Strings Through the Same Ring Using an Octahedral Metal Center as Template: A New Synthesis of [3]Rotaxanes. *J. Am. Chem. Soc.* **2009**, *131*, 6794–6807.
(636) Durola, F.; Sauvage, J.-P.; Wenger, O. S. Sterically Non-Hindering Endocyclic Ligands of the Bi-Isoquinoline Family. *Chem. Commun.* **2006**, 171–173.
(637) Browne, C.; Ronson, T. K.; Nitschke, J. R. Palladium-Templated Subcomponent Self-Assembly of Macrocycles, Catenanes, and Rotaxanes. *Angew. Chem., Int. Ed.* **2014**, *53*, 10701–10705.

(638) Movsisyan, L. D.; Franz, M.; Hampel, F.; Thompson, A. L.; Tykwinski, R. R.; Anderson, H. L. Polyyne Rotaxanes: Stabilization by Encapsulation. *J. Am. Chem. Soc.* **2016**, *138*, 1366–1376.

(639) Weisbach, N.; Baranová, Z.; Gauthier, S.; Reibenspies, J. H.; Gladysz, J. A. A New Type of Insulated Molecular Wire: A Rotaxane Derived from a Metal-Capped Conjugated Tetrayne. *Chem. Commun.* **2012**, *48*, 7562–7564.

(640) Movsisyan, L. D.; Kondratuk, D. V.; Franz, M.; Thompson, A. L.; Tykwinski, R. R.; Anderson, H. L. Synthesis of Polyyne Rotaxanes. *Org. Lett.* **2012**, *14*, 3424–3426.

(641) Sahnoune, H.; Baranová, Z.; Bhuvanesh, N.; Gladysz, J. A.; Halet, J.-F. A Metal-Capped Conjugated Polyyne Threaded Through a Phenanthroline-Based Macrocycle. Probing Beyond the Mechanical Bond to Interactions in Interlocked Molecular Architectures. *Organometallics* **2013**, *32*, 6360–6367.

(642) Baranová, Z.; Amini, H.; Bhuvanesh, N.; Gladysz, J. A. Rotaxanes Derived from Dimetallic Polyynediyl Complexes: Extended Axles and Expanded Macrocycles. *Organometallics* **2014**, *33*, 6746–6749.

(643) Schrettl, S.; Contal, E.; Hoheisel, T. N.; Fritzsche, M.; Balog, S.; Szilluweit, R.; Frauenrath, H. Facile Synthesis of Oligoyne Amphiphiles and Their Rotaxanes. *Chem. Sci.* **2014**, *6*, 564–574.

(644) Yamashita, Y.; Mutoh, Y.; Yamasaki, R.; Kasama, T.; Saito, S. Synthesis of [3]Rotaxanes That Utilize the Catalytic Activity of a Macrocyclic Phenanthroline-Cu Complex: Remarkable Effect of the Length of the Axle Precursor. *Chem. Eur. J.* **2015**, *21*, 2139–2145.

(645) Hayashi, R.; Mutoh, Y.; Kasama, T.; Saito, S. Synthesis of [3]Rotaxanes by the Combination of Copper-Mediated Coupling Reaction and Metal-Template Approach. *J. Org. Chem.* **2015**, *80*, 7536–7546.

(646) Lee, C.-F.; Leigh, D. A.; Pritchard, R. G.; Schultz, D.; Teat, S. J.; Timco, G. A.; Winpenny, R. E. P. Hybrid Organic-Inorganic Rotaxanes and Molecular Shuttles. *Nature* **2009**, *458*, 314–318.

(647) Zhang, Z.-J.; Zhang, H.-Y.; Wang, H.; Liu, Y. A Twin-Axial Hetero[7]rotaxane. *Angew. Chem., Int. Ed.* **2011**, *50*, 10834–10838.

(648) Jiang, W.; Winkler, H. D. F.; Schalley, C. A. Integrative Self-Sorting: Construction of a Cascade-Stoppered Hetero[3]rotaxane. *J. Am. Chem. Soc.* **2008**, *130*, 13852–13853.

(649) Jiang, W.; Schalley, C. A. Integrative Self-Sorting Is a Programming Language for High Level Self-Assembly. *Proc. Natl. Acad. Sci. U.S.A.* **2009**, *106*, 10425–10429.

(650) Jiang, W.; Sattler, D.; Rissanen, K.; Schalley, C. A. [4]Pseudorotaxanes with Remarkable Self-Sorting Selectivities. *Org. Lett.* **2011**, *13*, 4502–4505.

(651) Jiang, W.; Nowosinski, K.; Löw, N. L.; Dzyuba, E. V.; Klautzsch, F.; Schäfer, A.; Huuskonen, J.; Rissanen, K.; Schalley, C. A. Chelate Cooperativity and Spacer Length Effects on the Assembly Thermodynamics and Kinetics of Divalent Pseudorotaxanes. *J. Am. Chem. Soc.* **2012**, *134*, 1860–1868.

(652) Rowan, A. E.; Aarts, P. P. M.; Koutstaal, K. W. M. Novel Porphyrin–Viologen Rotaxanes. *Chem. Commun.* **1998**, 611–612.

(653) Thordarson, P.; Bijsterveld, E. J. A.; Rowan, A. E.; Nolte, R. J. M. Epoxidation of Polybutadiene by a Topologically Linked Catalyst. *Nature* **2003**, *424*, 915–918.

(654) Coumans, R. G. E.; Elemans, J. A. A. W.; Thordarson, P.; Nolte, R. J. M.; Rowan, A. E. Synthesis of Porphyrin-Containing [3]Rotaxanes by Olefin Metathesis. *Angew. Chem., Int. Ed.* **2003**, *42*, 650–654.

(655) Chen, C.-F. Novel Triptycene-Derived Hosts: Synthesis and Their Applications in Supramolecular Chemistry. *Chem. Commun.* **2011**, *47*, 1674–1688.

(656) Han, T.; Chen, C.-F. Efficient Potassium-Ion-Templated Synthesis and Controlled Destruction of [2]Rotaxanes Based on Cascade Complexes. *J. Org. Chem.* **2008**, *73*, 7735–7742.

(657) Jiang, Y.; Guo, J.-B.; Chen, C.-F. A Bifunctionalized [3]Rotaxane and Its Incorporation into a Mechanically Interlocked Polymer. *Chem. Commun.* **2010**, *46*, 5536–5538.

(658) Jiang, Y.; Guo, J.-B.; Chen, C.-F. A New [3]Rotaxane Molecular Machine Based on a Dibenzylammonium Ion and a Triazolium Station. *Org. Lett.* **2010**, *12*, 4248–4251.

(659) Gu, Y.-K.; Han, Y.; Chen, C.-F. Guest-Dependent Complexation of Triptycene-Derived Macrotricyclic Host Containing One Anthracene Moiety with Paraquat Derivatives: Construction of [2]Rotaxanes. *Supramol. Chem.* **2014**, *27*, 357–363.

(660) Meng, Z.; Chen, C.-F. Highly Efficient Synthesis of a Tristable Molecular Shuttle and Its Controlled Motion under Chemical Stimuli. *Org. Biomol. Chem.* **2014**, *12*, 6937–6943.

(661) Meng, Z.; Xiang, J.-F.; Chen, C.-F. Tristable [*n*]Rotaxanes: From Molecular Shuttle to Molecular Cable Car. *Chem. Sci.* **2014**, *5*, 1520–1525.

(662) Lin, C.-F.; Lai, C.-C.; Liu, Y.-H.; Peng, S.-M.; Chiu, S.-H. Use of Anions to Allow Translational Isomerism of a [2]Rotaxane. *Chem. Eur. J.* **2007**, *13*, 4350–4355.

(663) Chuang, C.-J.; Li, W.-S.; Lai, C.-C.; Liu, Y.-H.; Peng, S.-M.; Chao, I.; Chiu, S.-H. A Molecular Cage-Based [2]Rotaxane That Behaves as a Molecular Muscle. *Org. Lett.* **2009**, *11*, 385–388.

(664) Hsueh, S.-Y.; Lai, C.-C.; Chiu, S.-H. Squaraine-Based [2]Rotaxanes That Function as Visibly Active Molecular Switches. *Chem. Eur. J.* **2010**, *16*, 2997–3000.

(665) Chuang, C.-J.; Lai, C.-C.; Liu, Y.-H.; Peng, S.-M.; Chiu, S.-H. A Two-Stage Molecular Retractable Cable Featuring Push-Button and Rotary Two-Way Switching Modes. *Chem. Eur. J.* **2012**, *18*, 16698–16707.

(666) Li, S.; Liu, M.; Zhang, J.; Zheng, B.; Zhang, C.; Wen, X.; Li, N.; Huang, F. High-Yield Preparation of [2]Rotaxanes Based on the Bis(*m*-phenylene)-32-Crown-10-Based Cryptand/Paraquat Derivative Recognition Motif. *Org. Biomol. Chem.* **2008**, *6*, 2103–2107.

(667) Klivansky, L. M.; Koshkakaryan, G.; Cao, D.; Liu, Y. Linear π-Acceptor-Templated Dynamic Clipping to Macrobicycles and [2]Rotaxanes. *Angew. Chem., Int. Ed.* **2009**, *48*, 4185–4189.

(668) Wu, X.; Xue, M.; Li, J.; Yan, X.; Zhou, Q. Two Protocols for the Preparation of [2]Rotaxanes Based on the Dibenzo-24-Crown-8-Based Cryptand/Paraquat Recognition Motif. *Tetrahedron Lett.* **2013**, *54*, 6640–6643.

(669) McConnell, A. J.; Serpell, C. J.; Thompson, A. L.; Allan, D. R.; Beer, P. D. Calix[4]arene-Based Rotaxane Host Systems for Anion Recognition. *Chem. Eur. J.* **2010**, *16*, 1256–1264.

(670) Leontiev, A. V.; Jemmett, C. A.; Beer, P. D. Anion Recognition and Cation-Induced Molecular Motion in a Heteroditopic [2]Rotaxane. *Chem. Eur. J.* **2010**, *17*, 816–825.

(671) Hancock, L. M.; Beer, P. D. Sodium and Barium Cation-Templated Synthesis and Cation-Induced Molecular Pirouetting of a Pyridine *N*-Oxide Containing [2]Rotaxane. *Chem. Commun.* **2011**, *47*, 6012–6014.

(672) Knighton, R. C.; Beer, P. D. Axle Component Separated Ion-Pair Recognition by a Neutral Heteroditopic [2]Rotaxane. *Chem. Commun.* **2014**, *50*, 1540–1542.

(673) Shukla, R.; Deetz, M. J.; Smith, B. D. [2]Rotaxane with a Cation-Binding Wheel. *Chem. Commun.* **2000**, 2397–2398.

(674) Deetz, M.; Shukla, R.; Smith, B. D. Recognition-Directed Assembly of Salt-Binding [2]Rotaxanes. *Tetrahedron* **2002**, *58*, 799–805.

(675) Mahoney, J. M.; Shukla, R.; Marshall, R. A.; Beatty, A. M.; Zajicek, J.; Smith, B. D. Templated Conversion of a Crown Ether-Containing Macrobicycle Into [2]Rotaxanes. *J. Org. Chem.* **2002**, *67*, 1436–1440.

(676) Pun, A.; Hanifi, D. A.; Kiel, G.; O'Brien, E.; Liu, Y. Facile Route to an All-Organic, Triply Threaded, Interlocked Structure by Templated Dynamic Clipping. *Angew. Chem., Int. Ed.* **2012**, *51*, 13119–13122.

(677) Goldup, S. M.; Leigh, D. A.; McGonigal, P. R.; Ronaldson, V. E.; Slawin, A. M. Z. Two Axles Threaded Using a Single Template Site: Active Metal Template Macrobicyclic [3]Rotaxanes. *J. Am. Chem. Soc.* **2010**, *132*, 315–320.
(678) Hsueh, S.-Y.; Lai, C.-C.; Liu, Y.-H.; Wang, Y.; Peng, S.-M.; Chiu, S.-H. Protecting a Squaraine Near-IR Dye Through Its Incorporation in a Slippage-Derived [2]Rotaxane. *Org. Lett.* **2007**, *9*, 4523–4526.
(679) Clever, G. H.; Shionoya, M. A pH Switchable Pseudorotaxane Based on a Metal Cage and a Bis-Anionic Thread. *Chem. Eur. J.* **2010**, *16*, 11792–11796.
(680) Mooibroek, T. J.; Casas-Solvas, J. M.; Harniman, R. L.; Renney, C. M.; Carter, T. S.; Crump, M. P.; Davis, A. P. A Threading Receptor for Polysaccharides. *Nature Chem.* **2016**, *8*, 69–74.
(681) Fréchet, J. M. Functional Polymers and Dendrimers: Reactivity, Molecular Architecture, and Interfacial Energy. *Science* **1994**, *263*, 1710–1715.
(682) Bosman, A. W.; Janssen, H. M.; Meijer, E. W. About Dendrimers: Structure, Physical Properties, and Applications. *Chem. Rev.* **1999**, *99*, 1665–1688.
(683) Zeng, F.; Zimmerman, S. C. Dendrimers in Supramolecular Chemistry: From Molecular Recognition to Self-Assembly. *Chem. Rev.* **1997**, *97*, 1681–1712.
(684) Lee, J. W.; Kim, K. Rotaxane Dendrimers. *Top. Curr. Chem* **2003**, *228*, 111–140.
(685) Leung, K. C.-F.; Lau, K.-N. Self-Assembly and Thermodynamic Synthesis of Rotaxane Dendrimers and Related Structures. *Polym. Chem.* **2010**, *1*, 988–1000.
(686) Hubner, G.; Nachtsheim, G.; Li, Q. Y.; Seel, C.; Vögtle, F. The Spatial Demand of Dendrimers: Deslipping of Rotaxanes. *Angew. Chem., Int. Ed.* **2000**, *39*, 1269–1272.
(687) Tramontozzi, D. A.; Suhan, N. D.; Eichhorn, S. H.; Loeb, S. J. The Effect of Incorporating Fréchet Dendrons Into Rotaxanes and Molecular Shuttles Containing the 1,2-Bis(pyridinium) ethane⊂[24]Crown-8 Templating Motif. *Chem. Eur. J.* **2010**, *16*, 4466–4476.
(688) Liu, G.; Li, Z.; Wu, D.; Xue, W.; Li, T.; Sheng, H. L.; Yin, J. Dendritic [2]Rotaxanes: Synthesis, Characterization, and Properties. *J. Org. Chem.* **2014**, *79*, 643–652.
(689) Elizarov, A.; Chiu, S.-H.; Glink, P. T.; Stoddart, J. F. Dendrimer with Rotaxane-Like Mechanical Branching. *Org. Lett.* **2002**, *4*, 679–682.
(690) Han, S.-C.; Yoon, J.-H.; Oh, J.-H.; Lee, J. W. Synthesis of [3]-Rotaxane Dendrimers by Host-mediated Click Chemistry. *Bull. Kor. Chem. Soc.* **2011**, *32*, 3809–3812.
(691) Xiao, S.; Fu, N.; Peckham, K.; Smith, B. D. Efficient Synthesis of Fluorescent Squaraine Rotaxane Dendrimers. *Org. Lett.* **2010**, *12*, 140–143.
(692) Aprahamian, I.; Yasuda, T.; Ikeda, T.; Saha, S.; Dichtel, W. R.; Isoda, K.; Kato, T.; Stoddart, J. F. A Liquid-Crystalline Bistable [2]Rotaxane. *Angew. Chem., Int. Ed.* **2007**, *46*, 4675–4679.
(693) Mattei, S.; Seiler, P.; Diederich, F.; Gramlich, V. Dendrophanes: Water-Soluble Dendritic Receptors. Preliminary Communication. *Helv. Chim. Acta* **1995**, *78*, 1904–1912.
(694) Wallimann, P.; Seiler, P.; Diederich, F. Dendrophanes: Novel Steroid-Recognizing Dendritic Receptors. Preliminary Communication. *Helv. Chim. Acta* **1996**, *79*, 779–788.
(695) Wallimann, P.; Mattei, S.; Seiler, P.; Diederich, F. New Cyclophanes as Initiator Cores for the Construction of Dendritic Receptors: Host-Guest Complexation in Aqueous Solutions and Structures of Solid-State Inclusion Compounds. *Helv. Chim. Acta* **1997**, *80*, 2368–2390.
(696) Kenda, B.; Diederich, F. Supramolecular Aggregates of Dendritic Cyclophanes (Dendrophanes) Threaded on Molecular Rods with Steroid Termini. *Angew. Chem., Int. Ed.* **1998**, *37*, 3154–3158.
(697) Leung, K. C.-F.; Aricó, F.; Cantrill, S. J.; Stoddart, J. F. Template-Directed Dynamic Synthesis of Mechanically Interlocked Dendrimers. *J. Am. Chem. Soc.* **2005**, *127*, 5808–5810.
(698) Leung, K. C.-F.; Aricó, F.; Cantrill, S. J.; Stoddart, J. F. Dynamic Mechanically Interlocked Dendrimers: Amplification in Dendritic Dynamic Combinatorial Libraries. *Macromolecules* **2007**, *40*, 3951–3959.
(699) Gibson, H. W.; Yamaguchi, N.; Hamilton, L.; Jones, J. W. Cooperative Self-Assembly of Dendrimers *via* Pseudorotaxane Formation from a Homotritopic Guest Molecule and Complementary Monotopic Host Dendrons. *J. Am. Chem. Soc.* **2002**, *124*, 4653–4665.
(700) Reuter, C.; Pawlitzki, G.; Wörsdörfer, U.; Plevoets, M.; Mohry, A.; Kubota, T.; Okamoto, Y.; Vögtle, F. Chiral Dendrophanes, Dendro[2]Rotaxanes, and Dendro[2]Catenanes: Synthesis and Chiroptical Phenomena. *Eur. J. Org. Chem.* **2000**, 3059–3067.
(701) Elizarov, A.; Chang, T.; Chiu, S.-H.; Stoddart, J. F. Self-Assembly of Dendrimers by Slippage. *Org. Lett.* **2002**, *4*, 3565–3568.
(702) Jeong, K.-S.; Park, E.-J. Self-Assembly of Interlocked Supramolecular Dendrimers. *J. Org. Chem.* **2004**, *69*, 2618–2621.
(703) Ashton, P. R.; Huff, J.; Menzer, S.; Parsons, I. W.; Preece, J. A.; Stoddart, J. F.; Tolley, M. S.; White, A. J. P.; Williams, D. J. Molecular Meccano 5. Bis[2]catenanes and a Bis[2]rotaxane: Model Compounds for Polymers with Mechanically Interlocked Components. *Chem. Eur. J.* **1996**, *2*, 31–44.
(704) Aricó, F.; Chang, T.; Cantrill, S. J.; Cantrill, S. J.; Khan, S. I.; Stoddart, J. F. Template-Directed Synthesis of Multiply Mechanically Interlocked Molecules under Thermodynamic Control. *Chem. Eur. J.* **2005**, *11*, 4655–4666.
(705) Narita, M.; Yoon, I.; Aoyagi, M.; Goto, M.; Shimizu, T.; Asakawa, M. Transition Metal(II)–Salen and –Salophen Macrocyclic Complexes for Rotaxane Formation: Syntheses and Crystal Structures. *Eur. J. Inorg. Chem.* **2007**, 4229–4237.
(706) Ho, W. K. W.; Lee, S.-F.; Wong, C.-H.; Zhu, X.-M.; Kwan, C.-S.; Chak, C.-P.; Mendes, P. M.; Cheng, C. H. K.; Leung, K. C.-F. Type III-B Rotaxane Dendrimers. *Chem. Commun* **2013**, *49*, 10781–10783.
(707) Zhou, W.; Guo, Y.-J.; Qu, D.-H. Photodriven Clamlike Motion in a [3]Rotaxane with Two [2]Rotaxane Arms Bridged by an Overcrowded Alkene Switch. *J. Org. Chem.* **2013**, *78*, 590–596.
(708) Loeb, S. J.; Tramontozzi, D. A. Branched [*n*]Rotaxanes (n = 2–4) from Multiple Dibenzo-24-Crown-8 Ether Wheels and 1,2-Bis(4,4′-dipyridinium)ethane Axles. *Org. Biomol. Chem.* **2005**, *3*, 1393–1401.
(709) Jäger, R.; Händel, M.; Harren, J.; Rissanen, K.; Vögtle, F. Chemistry with Rotaxanes: Intra- and Intermolecularly Covalently Linked Rotaxanes. *Liebigs Ann.* **1996**, 1201–1207.
(710) Dünnwald, T.; Jäger, R.; Vögtle, F. Chemistry with Rotaxanes. II. Synthesis of Rotaxane Assemblies. *Chem. Eur. J.* **1997**, *3*, 2043–2051.
(711) Jones, J. W.; Bryant, W. S.; Bosman, A. W.; Janssen, R. A. J.; Meijer, E. W.; Gibson, H. W. Crowned Dendrimers: pH-Responsive Pseudorotaxane Formation. *J. Org. Chem.* **2003**, *68*, 2385–2389.
(712) Noor, A.; Lo, W. K. C.; Moratti, S. C.; Crowley, J. D. CuAAC “Click” Active-Template Synthesis of Functionalised [2]Rotaxanes Using Small Exo-Substituted Macrocycles: How Small Is Too Small? *Chem. Commun.* **2014**, *50*, 7044–7047.
(713) Amirsakis, D. G.; Elizarov, A. M.; Garcia-Garibay, M. A.; Glink, P. T.; Stoddart, J. F.; White, A. J. P.; Williams, D. J. Diastereospecific Photochemical Dimerization of a Stilbene-Containing Daisy Chain Monomer in Solution as Well as in the Solid State. *Angew. Chem., Int. Ed.* **2003**, *42*, 1126–1132.
(714) Amabilino, D. B.; Ashton, P. R.; Bělohradský, M.; Raymo, F. M.; Stoddart, J. F. The Self-Assembly of Branched [*n*]Rotaxanes: The First Step Towards Dendritic Rotaxanes. *J. Chem. Soc., Chem. Commun.* **1995**, 751–754.

(715) Amabilino, D. B.; Asakawa, M.; Ashton, P. R.; Ballardini, R.; Balzani, V.; Bělohradský, M.; Credi, A.; Higuchi, M.; Raymo, F. M.; Shimizu, T.; Stoddart, J. F.; Venturi, M.; Yase, K. Molecular Meccano 36. Aggregation of Self-Assembling Branched [*n*]Rotaxanes. *New J. Chem.* **1998**, *22*, 959–972.
(716) Spruell, J. M.; Dichtel, W. R.; Heath, J. R.; Stoddart, J. F. A One-Pot Synthesis of Constitutionally Unsymmetrical Rotaxanes Using Sequential Cu^{I}-Catalyzed Azide-Alkyne Cycloadditions. *Chem. Eur. J.* **2008**, *14*, 4168–4177.
(717) Aprahamian, I.; Olsen, J.-C.; Trabolsi, A.; Stoddart, J. F. Tetrathiafulvalene Radical Cation Dimerization in a Bistable Tripodal [4]Rotaxane. *Chem. Eur. J.* **2008**, *14*, 3889–3895.
(718) Tuncel, D.; Steinke, J. H. G. The Synthesis of [2], [3] and [4]Rotaxanes and Semirotaxanes. *Chem. Commun.* **2002**, 496–497.
(719) Tuncel, D.; Cindir, N.; Koldemir, Ü. [5]Rotaxane and [5]Pseudorotaxane Based on Cucurbit[6]uril and Anchored to a Meso-Tetraphenyl Porphyrin. *J. Incl. Phenom. Macrocycl. Chem* **2006**, *55*, 373–380.
(720) Sasabe, H.; Kihara, N.; Mizuno, K.; Ogawa, A.; Takata, T. Efficient Synthesis of [2]- and Higher Order Rotaxanes *via* the Transition Metal-Catalyzed Hydrosilylation of Alkyne. *Tetrahedron Lett.* **2005**, *46*, 3851–3853.
(721) Tokunaga, Y.; Ito, T.; Sugawara, H.; Nakata, R. Dynamic Covalent Chemistry of a Boronylammonium Ion and a Crown Ether: Formation of a C_3-Symmetric [4]Rotaxane. *Tetrahedron Lett.* **2008**, *49*, 3449–3452.
(722) Hsueh, S.-Y.; Cheng, K.-W.; Lai, C.-C.; Chiu, S.-H. Efficient Solvent-Free Syntheses of [2]- and [4]Rotaxanes. *Angew. Chem., Int. Ed.* **2008**, *47*, 4436–4439.
(723) Zhang, J.-N.; Li, H.; Zhou, W.; Yu, S.-L.; Qu, D.-H.; Tian, H. Fluorescence Modulation in Tribranched Switchable [4]Rotaxanes. *Chem. Eur. J.* **2013**, *19*, 17192–17200.
(724) Zhang, H.; Liu, Q.; Li, J.; Qu, D.-H. A Novel Star-Shaped Zinc Porphyrin Cored [5]Rotaxane. *Org. Lett.* **2013**, *15*, 338–341.
(725) Yu, G.; Suzaki, Y.; Osakada, K. Ferrocene-Containing [1]-, [2]-, [3]- and [4]Rotaxanes Synthesized from a Common Precursor. *RSC Adv.* **2016**, *6*, 41369–41375.
(726) Li, Z.; Liu, G.; Xue, W.; Wu, D.; Yang, Y.-W.; Wu, J.; Liu, S. H.; Yoon, J.; Yin, J. Construction of Hetero[*n*]rotaxanes by Use of Polyfunctional Rotaxane Frameworks. *J. Org. Chem.* **2013**, *78*, 11560–11570.
(727) Wang, W.; Chen, L.-J.; Wang, X.-Q.; Sun, B.; Li, X.; Zhang, Y.; Shi, J.; Yu, Y.; Zhang, L.; Liu, M.; Yang, H. B. Organometallic Rotaxane Dendrimers with Fourth-Generation Mechanically Interlocked Branches. *Proc. Natl. Acad. Sci. U.S.A.* **2015**, *112*, 5597–5601.
(728) Wang, W.; Sun, B.; Wang, X.-Q.; Ren, Y.-Y.; Chen, L.-J.; Ma, J.; Zhang, Y.; Li, X.; Yu, Y.; Tan, H.; Yang, H. B. Discrete Stimuli-Responsive Multirotaxanes with Supramolecular Cores Constructed Through a Modular Approach. *Chem. Eur. J.* **2015**, *21*, 6286–6294.
(729) Seidel, S. R.; Stang, P. J. High-Symmetry Coordination Cages *via* Self-Assembly. *Acc. Chem. Res.* **2002**, *35*, 972–983.
(730) Osswald, F.; Vogel, E.; Safarowsky, O.; Schwanke, F.; Vögtle, F. Rotaxane Assemblies with Dendritic Architecture. *Adv. Synth. Catal.* **2001**, *343*, 303–309.
(731) Luo, Q.-F.; Zhu, L.; Rao, S.-J.; Li, H.; Miao, Q.; Qu, D.-H. Two Stepwise Synthetic Routes Toward a Hetero[4]rotaxane. *J. Org. Chem.* **2015**, *80*, 4704–4709.
(732) Nygaard, S.; Liu, Y.; Stein, P C; Flood, A. H.; Jeppesen, J. O. Using Molecular Force to Overcome Steric Barriers in a Springlike Molecular Ouroboros. *Adv. Funct. Mater.* **2007**, *17*, 751–762.
(733) Vögtle, F.; Safarowsky, O.; Heim, C.; Affeld, A.; Braun, O.; Mohry, A. Catenanes, Rotaxanes and Pretzelanes-Template Synthesis and Chirality. *Pure Appl. Chem.* **1999**, *71*, 247–251.
(734) Reuter, C.; Seel, C.; Nieger, M.; Vögtle, F. Chiral [1]Rotaxanes: X-Ray Structures and Chiroptical Properties. *Helv. Chim. Acta* **2000**, *83*, 630–640.
(735) Lukin, O.; Godt, A.; Vögtle, F. Residual Topological Isomerism of Intertwined Molecules. *Chem. Eur. J.* **2004**, *10*, 1878–1883.
(736) Hiratani, K.; Kaneyama, M.; Nagawa, Y.; Koyama, E.; Kanesato, M. Synthesis of [1]Rotaxane *via* Covalent Bond Formation and Its Unique Fluorescent Response by Energy Transfer in the Presence of Lithium Ion. *J. Am. Chem. Soc.* **2004**, *126*, 13568–13569.
(737) Liu, Y.; Saha, S.; Vignon, S. A.; Flood, A. H.; Stoddart, J. F. Template-Directed Syntheses of Configurable and Reconfigurable Molecular Switches. *Synthesis* **2005**, 3437–3445.
(738) Liu, Y.; Flood, A. H.; Moskowitz, R. M.; Stoddart, J. F. Versatile Self-Complexing Compounds Based on Covalently Linked Donor–Acceptor Cyclophanes. *Chem. Eur. J.* **2005**, *11*, 369–385.
(739) Bruns, C. J.; Frasconi, M.; Iehl, J.; Hartlieb, K. J.; Schneebeli, S. T.; Cheng, C.; Stupp, S. I.; Stoddart, J. F. Redox Switchable Daisy Chain Rotaxanes Driven by Radical–Radical Interactions. *J. Am. Chem. Soc.* **2014**, *136*, 4714–4723.
(740) Zhou, Q.; Wei, P.; Zhang, Y.; Yu, Y.; Yan, X. Benzo-21-Crown-7-Based [1]Rotaxanes: Syntheses, X-Ray Crystal Structures, and Dynamic Characteristics. *Org. Lett.* **2013**, *15*, 5350–5353.
(741) Clavel, C.; Romuald, C.; Brabet, E.; Coutrot, F. A pH-Sensitive Lasso-Based Rotaxane Molecular Switch. *Chem. Eur. J.* **2013**, *19*, 2982–2989.
(742) Clavel, C.; Fournel-Marotte, K.; Coutrot, F. A pH-Sensitive Peptide-Containing Lasso Molecular Switch. *Molecules* **2013**, *18*, 11553–11575.
(743) Li, H.; Zhang, H.; Zhang, Q.; Zhang, Q.-W.; Qu, D.-H. A Switchable Ferrocene-Based [1]Rotaxane with an Electrochemical Signal Output. *Org. Lett.* **2012**, *14*, 5900–5903.
(744) Li, H.; Zhang, J.-N.; Zhou, W.; Zhang, H.; Zhang, Q.; Qu, D.-H.; Tian, H. Dual-Mode Operation of a Bistable [1]Rotaxane with a Fluorescence Signal. *Org. Lett.* **2013**, *15*, 3070–3073.
(745) Fukuhara, G.; Fujimoto, T.; Kaneda, T. Synthesis and Characterization of the First Pair of an Unlocked and a Locked Self-Inclusion Complex From a Permethylated α-Cyclodextrin Derivative. *Chem. Lett.* **2003**, *32*, 536–537.
(746) Onagi, H.; Blake, C. J.; Easton, C. J.; Lincoln, S. F. Installation of a Ratchet Tooth and Pawl to Restrict Rotation in a Cyclodextrin Rotaxane. *Chem. Eur. J.* **2003**, *9*, 5978–5988.
(747) Ma, X.; Qu, D.; Ji, F.; Wang, Q.; Zhu, L.; Xu, Y.; Tian, H. A Light-Driven [1]Rotaxane *via* Self-Complementary and Suzuki-Coupling Capping. *Chem. Commun.* **2007**, 1409–1411.
(748) Xia, B.; Xue, M. Design and Efficient Synthesis of a Pillar[5]arene-Based [1]Rotaxane. *Chem. Commun.* **2014**, *50*, 1021–1023.
(749) Xue, Z.; Mayer, M. F. Actuator Prototype: Capture and Release of a Self-Entangled [1]Rotaxane. *J. Am. Chem. Soc.* **2010**, *132*, 3274–3276.
(750) Inoue, Y.; Miyauchi, M.; Nakajima, H.; Takashima, Y.; Yamaguchi, H.; Harada, A. Self-Threading of a Poly(ethylene glycol) Chain in a Cyclodextrin-Ring: Control of the Exchange Dynamics by Chain Length. *J. Am. Chem. Soc.* **2006**, *128*, 8994–8995.
(751) Yamauchi, K.; Miyawaki, A.; Takashima, Y.; Yamaguchi, H.; Harada, A. A Molecular Reel: Shuttling of a Rotor by Tumbling of a Macrocycle. *J. Org. Chem.* **2010**, *75*, 1040–1046.
(752) Terao, J. Permethylated Cyclodextrin-Based Insulated Molecular Wires. *Polym. Chem.* **2011**, *2*, 2444–2452.
(753) Terao, J. π-Conjugated Molecules Covered by Permethylated Cyclodextrins. *Chem. Rec.* **2011**, *11*, 269–283.

(754) Tsuda, S.; Terao, J.; Kambe, N. Synthesis of an Organic-Soluble π-Conjugated [1]Rotaxane. *Chem. Lett.* **2009**, *38*, 76–77.
(755) Tsuda, S.; Terao, J.; Tsurui, K.; Kambe, N. Synthesis of a Linked [1]–[1] Rotaxane. *Chem. Lett.* **2009**, *38*, 190–191.
(756) Tsuda, S.; Terao, J.; Tanaka, Y.; Maekawa, T.; Kambe, N. Synthesis of Linked Symmetrical [3] and [5]Rotaxanes Having an Oligomeric Phenylene Ethynylene (OPE) Core Skeleton as a π-Conjugated Guest *via* Double Intramolecular Self-Inclusion. *Tetrahedron Lett.* **2009**, *50*, 1146–1150.
(757) Terao, J.; Ikai, K.; Kambe, N.; Seki, S.; Saeki, A.; Ohkoshi, K.; Fujihara, T.; Tsuji, Y. Synthesis of a Head-to-Tail-Type Cyclodextrin-Based Insulated Molecular Wire. *Chem. Commun.* **2011**, *47*, 6816–6818.
(758) Terao, J.; Tsuda, S.; Tanaka, Y.; Okoshi, K.; Fujihara, T.; Tsuji, Y.; Kambe, N. Synthesis of Organic-Soluble Conjugated Polyrotaxanes by Polymerization of Linked Rotaxanes. *J. Am. Chem. Soc.* **2009**, *131*, 16004–16005.
(759) Terao, J.; Tanaka, Y.; Tsuda, S.; Kambe, N.; Taniguchi, M.; Kawai, T.; Saeki, A.; Seki, S. Insulated Molecular Wire with Highly Conductive π-Conjugated Polymer Core. *J. Am. Chem. Soc.* **2009**, *131*, 18046–18047.
(760) Terao, J.; Tsuda, S.; Tsurui, K.; Kambe, N. Synthesis of Highly Insulated Molecular Wires by Polymerization of Organic-Soluble Symmetrical Linked Inclusion Complex Monomers. *Macromol. Symp.* **2010**, *297*, 54–60.
(761) Terao, J.; Wadahama, A.; Matono, A.; Tada, T.; Watanabe, S.; Seki, S.; Fujihara, T.; Tsuji, Y. Design Principle for Increasing Charge Mobility of π-Conjugated Polymers Using Regularly Localized Molecular Orbitals. *Nature Commun.* **2013**, *4*: 1691.
(762) Terao, J.; Hosomi, T.; Masai, H.; Matsuda, W.; Seki, S.; Fujihara, T.; Tsuji, Y. Synthesis and Redox Response of Insulated Molecular Wire Elongated through Iron–Terpyridine Coordination Bonds. *Chem. Lett.* **2014**, *43*, 1289–1291.
(763) Gao, C.; Ma, X.; Zhang, Q.; Wang, Q.; Qu, D.; Tian, H. A Light-Powered Stretch–Contraction Supramolecular System Based on Cobalt Coordinated [1]Rotaxane. *Org. Biomol. Chem.* **2011**, *9*, 1126–1132.
(764) Li, H.; Li, X.; Cao, Z.-Q.; Qu, D.-H.; Ågren, H.; Tian, H. A Switchable Bis-Branched [1]Rotaxane Featuring Dual-Mode Molecular Motions and Tunable Molecular Aggregation. *ACS Appl. Mater. Interfaces* **2014**, *6*, 18921–18929.
(765) Li, H.; Li, X.; Ågren, H.; Qu, D.-H. Two Switchable Star-Shaped [1](*n*)Rotaxanes with Different Multibranched Cores. *Org. Lett.* **2014**, *16*, 4940–4943.
(766) Waelès, P.; Clavel, C.; Fournel-Marotte, K.; Coutrot, F. Synthesis of Triazolium-Based Mono- and Tris-Branched [1]Rotaxanes Using a Molecular Transporter of Dibenzo-24-Crown-8. *Chem. Sci.* **2015**, *6*, 4828–4836.
(767) Ashton, P. R.; Baxter, I.; Cantrill, S. J.; Fyfe, M. C. T.; Glink, P. T.; Stoddart, J. F.; White, A. J. P.; Williams, D. J. Supramolecular Daisy Chains. *Angew. Chem., Int. Ed.* **1998**, *37*, 1294–1297.
(768) Rotzler, J.; Mayor, M. Molecular Daisy Chains. *Chem. Soc. Rev.* **2013**, *42*, 44–62.
(769) Ashton, P. R.; Parsons, I. W.; Raymo, F. M.; Stoddart, J. F.; White, A. J. P.; Williams, D. J.; Wolf, R. Self-Assembling Supramolecular Daisy Chains. *Angew. Chem., Int. Ed.* **1998**, *37*, 1913–1916.
(770) Cantrill, S. J.; Youn, G. J.; Williams, D. J.; Stoddart, J. F. Molecular Meccano 64. Supramolecular Daisy Chains. *J. Org. Chem.* **2001**, *66*, 6857–6872.
(771) Fujimoto, T.; Nakamura, A.; Inoue, Y.; Sakata, Y.; Kaneda, T. Photoswitching of the Association of a Permethylated α-Cyclodextrin-Azobenzene Dyad Forming a Janus [2] Pseudorotaxane. *Tetrahedron Lett.* **2001**, *42*, 7987–7989.
(772) Miyauchi, M.; Harada, A. A Helical Supramolecular Polymer Formed by Host–Guest Interactions. *Chem. Lett.* **2005**, *34*, 104–105.
(773) Miyauchi, M.; Hoshino, T.; Yamaguchi, H.; Kamitori, S.; Harada, A. A [2]Rotaxane Capped by a Cyclodextrin and a Guest: Formation of Supramolecular [2]Rotaxane Polymer. *J. Am. Chem. Soc.* **2005**, *127*, 2034–2035.
(774) Miyawaki, A.; Miyauchi, M.; Takashima, Y.; Yamaguchi, H.; Harada, A. Formation of Supramolecular Isomers; Poly[2]Rotaxane and Supramolecular Assembly. *Chem. Commun.* **2008**, 456–458.
(775) Yamauchi, K.; Takashima, Y.; Hashidzume, A.; Yamaguchi, H.; Harada, A. Switching Between Supramolecular Dimer and Nonthreaded Supramolecular Self-Assembly of Stilbene Amide-α-Cyclodextrin by Photoirradiation. *J. Am. Chem. Soc.* **2008**, *130*, 5024–5025.
(776) Wang, F.; Han, C.; He, C.; Zhou, Q.; Zhang, J.; Wang, C.; Li, N.; Huang, F. Self-Sorting Organization of Two Heteroditopic Monomers to Supramolecular Alternating Copolymers. *J. Am. Chem. Soc.* **2008**, *130*, 11254–11255.
(777) Liu, Y.; Yang, Z.-X.; Chen, Y. Syntheses and Self-Assembly Behaviors of the Azobenzenyl Modified β-Cyclodextrins Isomers. *J. Org. Chem.* **2008**, *73*, 5298–5304.
(778) Gibson, H. W.; Yamaguchi, N.; Niu, Z.; Jones, J. W.; Slebodnick, C.; Rheingold, A. L.; Zakharov, L. N. Self-Assembly of Daisy Chain Oligomers from Heteroditopic Molecules Containing Secondary Ammonium Ion and Crown Ether Moieties. *J. Polym. Sci. Pol. Chem.* **2010**, *48*, 975–985.
(779) Zhang, Z.; Luo, Y.; Chen, J.; Dong, S.; Yu, Y.; Ma, Z.; Huang, F. Formation of Linear Supramolecular Polymers That Is Driven by C–H···π Interactions in Solution and in the Solid State. *Angew. Chem., Int. Ed.* **2011**, *50*, 1397–1401.
(780) Zhang, Z.; Yu, G.; Han, C.; Liu, J.; Ding, X.; Yu, Y.; Huang, F. Formation of a Cyclic Dimer Containing Two Mirror Image Monomers in the Solid State Controlled by van der Waals Forces. *Org. Lett.* **2011**, *13*, 4818–4821.
(781) Voignier, J.; Frey, J.; Kraus, T.; Budesinsky, M.; Cvačka, J.; Heitz, V.; Sauvage, J.-P. Transition-Metal-Complexed Cyclic [3]- and [4]Pseudorotaxanes Containing Rigid Ring-and-Filament Conjugates: Synthesis and Solution Studies. *Chem. Eur. J.* **2011**, *17*, 5404–5414.
(782) Yan, X.; Xu, D.; Chi, X.; Chen, J.; Dong, S.; Ding, X.; Yu, Y.; Huang, F. A Multiresponsive, Shape-Persistent, and Elastic Supramolecular Polymer Network Gel Constructed by Orthogonal Self-Assembly. *Adv. Mater.* **2012**, *24*, 362–369.
(783) Cao, L.; Isaacs, L. Daisy Chain Assembly Formed From a Cucurbit[6]uril Derivative. *Org. Lett.* **2012**, *14*, 3072–3075.
(784) Cao, D.; Wang, C.; Giesener, M. A.; Liu, Z.; Stoddart, J. F. A Rigid Donor–Acceptor Daisy Chain Dimer. *Chem. Commun.* **2012**, *48*, 6791–6793.
(785) Vinciguerra, B.; Cao, L.; Cannon, J. R.; Zavalij, P. Y.; Fenselau, C.; Isaacs, L. Synthesis and Self-Assembly Processes of Monofunctionalized Cucurbit[7]uril. *J. Am. Chem. Soc.* **2012**, *134*, 13133–13140.
(786) Strutt, N. L.; Zhang, H.; Giesener, M. A.; Lei, J.; Stoddart, J. F. A Self-Complexing and Self-Assembling Pillar[5]arene. *Chem. Commun.* **2012**, *48*, 1647–1649.
(787) Zheng, B.; Zhang, M.; Dong, S.; Liu, J.; Huang, F. A Benzo-21-Crown-7/Secondary Ammonium Salt [*c*2]Daisy Chain. *Org. Lett.* **2012**, *14*, 306–309.
(788) Rotzler, J.; Drayss, S.; Hampe, O.; Häussinger, D.; Mayor, M. Molecular Daisy Chains: Synthesis and Aggregation Studies of an Amphiphilic Molecular Rod. *Chem. Eur. J.* **2013**, *19*, 2089–2101.
(789) Wang, X.; Han, K.; Li, J.; Jia, X.; Li, C. Pillar[5]arene–Neutral Guest Recognition Based Supramolecular Alternating Copolymer Containing [*c*2]Daisy Chain and Bis-pillar[5]arene Units. *Polym. Chem.* **2013**, *4*, 3998–4003.
(790) Wang, K.; Wang, C.-Y.; Zhang, Y.; Zhang, S. X.-A.; Yang, B.; Yang, Y.-W. Ditopic Pillar[5]arene-Based Fluorescence Enhancement Material Mediated by [*c*2]Daisy Chain Formation. *Chem. Commun.* **2014**, *50*, 9458–9461.

(791) Ni, M.; Hu, X.-Y.; Jiang, J.; Wang, L. The Self-Complexation of Mono-Urea-Functionalized Pillar[5]arenes with Abnormal Urea Behaviors. *Chem. Commun.* **2014**, *50*, 1317–1319.

(792) Wang, Y.; Xu, J.-F.; Chen, Y.-Z.; Niu, L.-Y.; Wu, L.-Z.; Tung, C.-H.; Yang, Q.-Z. Photoresponsive Supramolecular Self-Assembly of Monofunctionalized Pillar[5]arene Based on Stiff Stilbene. *Chem. Commun.* **2014**, *50*, 7001–7003.

(793) Rowan, S. J.; Cantrill, S. J.; Stoddart, J. F.; White, A. J. P.; Williams, D. J. Toward Daisy Chain Polymers: "Wittig Exchange" of Stoppers in [2]Rotaxane Monomers. *Org. Lett.* **2000**, *2*, 759–762.

(794) Hoshino, T.; Miyauchi, M.; Kawaguchi, Y.; Yamaguchi, H.; Harada, A. Daisy Chain Necklace: Tri[2]rotaxane Containing Cyclodextrins. *J. Am. Chem. Soc.* **2000**, *122*, 9876–9877.

(795) Fujimoto, T.; Sakata, Y.; Kaneda, T. The First Janus [2]Rotaxane. *Chem. Commun.* **2000**, 2143–2144.

(796) Jiménez, M. C.; Dietrich-Buchecker, C.; Sauvage, J.-P. Towards Synthetic Molecular Muscles: Contraction and Stretching of a Linear Rotaxane Dimer. *Angew. Chem., Int. Ed.* **2000**, *39*, 3284–3287.

(797) Chiu, S.-H.; Rowan, S. J.; Cantrill, S. J.; Stoddart, J. F.; White, A. J. P.; Williams, D. J. An Hermaphroditic [*c*2]Daisy Chain. *Chem. Commun.* **2002**, 2948–2949.

(798) Wu, J.; Leung, K. C.-F.; Benítez, D.; Han, J.-Y.; Cantrill, S. J.; Fang, L.; Stoddart, J. F. An Acid-Base-Controllable [*c*2]Daisy Chain. *Angew. Chem., Int. Ed.* **2008**, *47*, 7470–7474.

(799) Coutrot, F.; Romuald, C.; Busseron, E. A New pH-Switchable Dimannosyl[*c*2]daisy Chain Molecular Machine. *Org. Lett.* **2008**, *10*, 3741–3744.

(800) Romuald, C.; Busseron, E.; Coutrot, F. Very Contracted to Extended *co*-Conformations with or without Oscillations in Two- and Three-Station [*c*2]Daisy Chains. *J. Org. Chem.* **2010**, *75*, 6516–6531.

(801) Ueng, S.-H.; Hsueh, S.-Y.; Lai, C.-C.; Liu, Y.-H.; Peng, S.-M.; Chiu, S.-H. Capturing a [*c*2]Daisy Chain Using the Threading-Followed-by-Swelling Approach. *Chem. Commun.* **2008**, 817–819.

(802) Clark, P. G.; Day, M. W.; Grubbs, R. H. Switching and Extension of a [*c*2]Daisy-Chain Dimer Polymer. *J. Am. Chem. Soc.* **2009**, *131*, 13631–13633.

(803) Bozdemir, O. A.; Barin, G.; Belowich, M. E.; Basuray, A. N.; Beuerle, F.; Stoddart, J. F. Dynamic Covalent Templated-Synthesis of [*c*2]Daisy Chains. *Chem. Commun.* **2012**, *48*, 10401–10403.

(804) Onagi, H.; Easton, C. J.; Lincoln, S. F. An Hermaphrodite [2]Rotaxane: Preparation and Analysis of Structure. *Org. Lett.* **2001**, *3*, 1041–1044.

(805) Dawson, R. E.; Lincoln, S. F.; Easton, C. J. The Foundation of a Light Driven Molecular Muscle Based on Stilbene and α-Cyclodextrin. *Chem. Commun.* **2008**, 3980–3982.

(806) Tsuda, S.; Aso, Y.; Kaneda, T. Linear Oligomers Composed of a Photochromically Contractible and Extendable Janus [2]Rotaxane. *Chem. Commun.* **2006**, 3072–3074.

(807) Tsukagoshi, S.; Miyawaki, A.; Takashima, Y.; Yamaguchi, H.; Harada, A. Contraction of Supramolecular Double-Threaded Dimer Formed by α-Cyclodextrin with a Long Alkyl Chain. *Org. Lett.* **2007**, *9*, 1053–1055.

(808) Li, S.; Taura, D.; Hashidzume, A.; Harada, A. Light-Switchable Janus [2]Rotaxanes Based on α-Cyclodextrin Derivatives Bearing Two Recognition Sites Linked with Oligo(ethylene glycol). *Chem. Asian J.* **2010**, *5*, 2281–2289.

(809) Evans, N. H.; Beer, P. D. A Janus [2]Rotaxane Synthesized by Using an Anion-Templated Clipping Methodology. *Chem. Eur. J.* **2011**, *17*, 10542–10546.

(810) Zhang, Z.; Han, C.; Yu, G.; Huang, F. A Solvent-Driven Molecular Spring. *Chem. Sci* **2012**, *3*, 3026–3031.

(811) Bruns, C. J.; Li, J.; Frasconi, M.; Schneebeli, S. T.; Iehl, J.; Jacquot de Rouville, H.-P.; Stupp, S. I.; Voth, G. A.; Stoddart, J. F. An Electrochemically and Thermally Switchable Donor-Acceptor [*c*2]Daisy Chain Rotaxane. *Angew. Chem., Int. Ed.* **2014**, *53*, 1953–1958.

(812) Fernandez, A.; Pineda, E. M.; Ferrando-Soria, J.; McInnes, E. J. L.; Timco, G. A.; Winpenny, R. E. P. A Hybrid Organic-Inorganic Molecular Daisy Chain. *Chem. Commun.* **2015**, *51*, 11126–11129.

(813) Fu, X.; Zhang, Q.; Rao, S.-J.; Qu, D.-H.; Tian, H. One-Pot Synthesis of a [*c*2]Daisy-Chain-Containing Hetero[4]rotaxane via a Self-Sorting Strategy. *Chem. Sci.* **2016**, *7*, 1696–1701.

(814) Waelès, P.; Riss-Yaw, B.; Coutrot, F. Synthesis of a pH-Sensitive Hetero[4]rotaxane Molecular Machine that Combines [*c*2]Daisy and [2]Rotaxane Arrangements. *Chem. Eur. J.* **2016**, *22*, 6837–6845.

(815) Weigandt, J.; Chung, C.-L.; Jester, S.-S.; Famulok, M. Daisy Chain Rotaxanes Made from Interlocked DNA Nanostructures. *Angew. Chem., Int. Ed* **2016**, *55*, 5512–5516.

(816) Collin, J.-P.; Dietrich-Buchecker, C.; Gaviña, P.; Jimenez-Molero, M. C.; Sauvage, J.-P. Shuttles and Muscles: Linear Molecular Machines Based on Transition Metals. *Acc. Chem. Res.* **2001**, *34*, 477–487.

(817) Jimenez-Molero, M. C.; Dietrich-Buchecker, C.; Sauvage, J.-P. Towards Artificial Muscles at the Nanometric Level. *Chem. Commun.* **2003**, 1613–1616.

(818) Bruns, C. J.; Stoddart, J. F. Molecular Machines Muscle Up. *Nature Nanotechnol* **2013**, *8*, 9–10.

(819) Bruns, C. J.; Stoddart, J. F. Rotaxane-Based Molecular Muscles. *Acc. Chem. Res.* **2014**, *47*, 2186–2199.

(820) Niess, F.; Duplan, V.; Sauvage, J.-P. Molecular Muscles: From Species in Solution to Materials and Devices. *Chem. Lett.* **2014**, *43*, 964–974.

(821) Guidry, E. N.; Li, J.; Stoddart, J. F.; Grubbs, R. H. Bifunctional [*c*2]Daisy-Chains and Their Incorporation Into Mechanically Interlocked Polymers. *J. Am. Chem. Soc.* **2007**, *129*, 8944–8945.

(822) Fang, L.; Hmadeh, M.; Wu, J.; Olson, M. A.; Spruell, J. M.; Trabolsi, A.; Yang, Y.-W.; Elhabiri, M.; Albrecht-Gary, A.-M.; Stoddart, J. F. Acid-Base Actuation of [*c*2]Daisy Chains. *J. Am. Chem. Soc.* **2009**, *131*, 7126–7134.

(823) Hmadeh, M.; Fang, L.; Trabolsi, A.; Elhabiri, M.; Albrecht-Gary, A.-M.; Stoddart, J. F. On the Thermodynamic and Kinetic Investigations of a [*c*2]Daisy Chain Polymer. *J. Mater. Chem.* **2010**, *20*, 3422–3430.

(824) Iwaso, K.; Takashima, Y.; Harada, A. Fast Response Dry-Type Supramolecular Artificial Muscles with [*c*2]Daisy Chains. *Nature Chem.* **2016**, *8*, 625–632.

(825) Wolf, A.; Moulin, E.; Cid, J.-J.; Goujon, A.; Du, G.; Busseron, E.; Fuks, G.; Giuseppone, N. pH and Light-Controlled Self-Assembly of Bistable [*c*2]Daisy Chain Rotaxanes. *Chem. Commun.* **2015**, *51*, 4212–4215.

(826) Goujon, A.; Du, G.; Moulin, E.; Fuks, G.; Maaloum, M.; Buhler, E.; Giuseppone, N. Hierarchical Self-Assembly of Supramolecular Muscle-Like Fibers. *Angew. Chem., Int. Ed.* **2016**, *55*, 703–707.

(827) Du, G.; Moulin, E.; Jouault, N.; Buhler, E.; Giuseppone, N. Muscle-Like Supramolecular Polymers: Integrated Motion from Thousands of Molecular Machines. *Angew. Chem., Int. Ed.* **2012**, *51*, 12504–12508.

(828) Gao, L.; Zhang, Z.; Zheng, B.; Huang, F. Construction of Muscle-Like Metallo-Supramolecular Polymers from a Pillar[5]arene-Based [*c*2]Daisy Chain. *Polym. Chem.* **2014**, *5*, 5734–5739.

(829) Zhang, M.; Li, S.; Dong, S.; Chen, J.; Zheng, B.; Huang, F. Preparation of a Daisy Chain *via* Threading-Followed-by-Polymerization. *Macromolecules* **2011**, *44*, 9629–9634.

(830) Yamabuki, K.; Isobe, Y.; Onimura, K.; Oishi, T. Dual Polyrotaxane: One-Pot Synthesis of Topological Polymer by Using Metathesis Reaction. *Chem. Lett.* **2007**, *36*, 1196–1197.

(831) Scherf, U. Ladder-Type Materials. *J. Mater. Chem* **1999**, *9*, 1853–1864.

(832) Collin, J.-P.; Frey, J.; Heitz, V.; Sakellariou, E.; Sauvage, J.-P.; Tock, C. Copper(I)-Induced Threading of Two Bis-macrocycles on Two Rods: A Cyclic [4]Rotaxane. *New J. Chem.* **2006**, *30*, 1386–1389.

(833) Collin, J.-P.; Durola, F.; Frey, J.; Heitz, V.; Reviriego, F.; Sauvage, J.-P.; Trolez, Y.; Rissanen, K. Templated Synthesis of Cyclic [4]Rotaxanes Consisting of Two Stiff Rods Threaded through Two Bis-macrocycles with a Large and Rigid Central Plate as Spacer. *J. Am. Chem. Soc.* **2010**, *132*, 6840–6850.

(834) Durola, F.; Heitz, V.; Reviriego, F.; Sauvage, J.-P.; Trolez, Y. A Cyclic [4]Rotaxane that Behaves as a Switchable Molecular Receptor: Formation of a Rigid Scaffold from a Collapsed Structure by Complexation with Copper(I) Ions. *Angew. Chem., Int. Ed.* **2010**, *49*, 10172–10175.

(835) Sauvage, J.-P.; Trolez, Y.; Canevet, D.; Sallé, M. Intercalation of Tetrathiafulvalene Between the Two Plates of a Copper(I)-Complexed [4]Rotaxane. *Eur. J. Org. Chem.* **2011**, 2413–2416.

(836) Roche, C.; Sour, A.; Sauvage, J.-P. A Flexible Copper(I)-Complexed [4]Rotaxane Containing Two Face-to-Face Porphyrinic Plates that Behaves as a Distensible Receptor. *Chem. Eur. J.* **2012**, *18*, 8366–8376.

(837) Ventura, B.; Flamigni, L.; Collin, J.-P.; Durola, F.; Heitz, V.; Reviriego, F.; Sauvage, J.-P.; Trolez, Y. NIR Emission of Cyclic [4]Rotaxanes Containing π-Extended Porphyrin Chromophores. *Phys. Chem. Chem. Phys.* **2012**, *14*, 10589–10594.

(838) Durola, F.; Heitz, V.; Reviriego, F.; Roche, C.; Sauvage, J.-P.; Sour, A.; Trolez, Y. Cyclic [4]Rotaxanes Containing Two Parallel Porphyrinic Plates: Toward Switchable Molecular Receptors and Compressors. *Acc. Chem. Res.* **2014**, *47*, 633–645.

(839) Heitz, V.; Sauvage, J.-P.; Trolez, Y. Cu(I)/Zn^{2+} Exchange Has No Geometrical Effect in a Cyclic [4]Rotaxane Whereas It Induces Rearrangement in a Simpler [3]Rotaxane. *Inorg. Chim. Acta* **2014**, *417*, 186–191.

(840) Liu, Y.; You, C.-C.; Zhang, H.-Y.; Kang, S.-Z.; Zhu, C.-F.; Wang, C. Bis(molecular tube)s: Supramolecular Assembly of Complexes of Organoselenium-Bridged β-Cyclodextrins with Platinum(IV). *Nano Lett.* **2001**, *1*, 613–616.

(841) Liu, Y.; Li, L.; Zhang, H.-Y.; Zhao, Y.-L.; Wu, X. Bis(pseudopolyrotaxane)s Possessing Copper(II) Ions Formed by Different Polymer Chains and Bis(β-cyclodextrin)s Bridged with a 2,2′-Bipyridine-4,4′-Dicarboxy Tether. *Macromolecules* **2002**, *35*, 9934–9938.

(842) Liu, Y.; Song, Y.; Wang, H.; Zhang, H.-Y.; Li, X.-Q. Bis(polypseudorotaxane)s Formed by Multiple Metallo-Bridged β-Cyclodextrins and the Thermodynamic Origin of Their Molecular Aggregation. *Macromolecules* **2004**, *37*, 6370–6375.

(843) Ciao, R.; Talotta, C.; Gaeta, C.; Margarucci, L.; Casapullo, A.; Neri, P. An Oriented Handcuff Rotaxane. *Org. Lett.* **2013**, *15*, 5694–5697.

(844) Cantrill, S. J.; Grubbs, R. H.; Lanari, D.; Leung, K. C.-F.; Nelson, A.; Poulin-Kerstien, K. G.; Smidt, S. P.; Stoddart, J. F.; Tirrell, D. A. Template-Directed Olefin Cross Metathesis. *Org. Lett.* **2005**, *7*, 4213–4216.

(845) Iwamoto, H.; Yawata, Y.; Fukazawa, Y.; Haino, T. Tether-Assisted Synthesis of [3]Rotaxane by Olefin Metathesis. *Chem. Lett.* **2010**, *39*, 24–25.

(846) Iwamoto, H.; Yawata, Y.; Fukazawa, Y.; Haino, T. Highly Efficient Synthesis of [3]Rotaxane Assisted by Preorganisation of Pseudorotaxane Using Bis(crown ether)s. *Supramol. Chem.* **2010**, *22*, 815–826.

(847) Sato, T.; Takata, T. Rotaxane Axle as an Effective Scaffold: Synthesis of Functionalized [3]Rotaxane and Connection of the Wheel Components Arranged on the Axle. *Tetrahedron Lett.* **2007**, *48*, 2797–2801.

(848) Zhang, Z.-J.; Han, M.; Zhang, H.-Y.; Liu, Y. A Double-Leg Donor-Acceptor Molecular Elevator: New Insight into Controlling the Distance of Two Platforms. *Org. Lett.* **2013**, *15*, 1698–1701.

(849) Ma, Y.-X.; Meng, Z.; Chen, C.-F. A Novel Pentiptycene Bis(crown ether)-Based [2](2)Rotaxane Whose Two DB24C8 Rings Act as Flapping Wings of a Butterfly. *Org. Lett.* **2014**, *16*, 1860–1863.

(850) Roche, C.; Sauvage, J.-P.; Sour, A.; Strutt, N. L. A [3]Rotaxane Composed of a Zinc Porphyrin Tetra-Substituted with Coordinating Macrocycles and of Two Short Rigid Axles. *New J. Chem.* **2011**, *35*, 2820–2825.

(851) Liu, Y.; Wang, H.; Zhang, H.-Y.; Liang, P. A Metallo-Capped Polyrotaxane Containing Calix[4]arenes and Cyclodextrins and Its Highly Selective Binding for Ca^{2+}. *Chem. Commun.* **2004**, 2266–2267.

(852) Zeng, F.; Meng, Z.; Han, Y.; Chen, C.-F. Formation of a "Pseudosuitane"-type Complex Between a Triptycene-Derived Bis(crown ether) Host and 1,1′-(Anthracene-9,10-diyl) bis(*N*-benzylmethanaminium): A New Method for the Synthesis of Linear Polyrotaxanes. *Chem. Commun.* **2014**, *50*, 7611–7613.

(853) Badjić, J. D.; Balzani, V.; Credi, A.; Lowe, J. N.; Silvi, S.; Stoddart, J. F. A Mechanically Interlocked Bundle. *Chem. Eur. J.* **2004**, *10*, 1926–1935.

(854) Badjić, J. D.; Balzani, V.; Credi, A.; Silvi, S.; Stoddart, J. F. A Molecular Elevator. *Science* **2004**, *303*, 1845–1849.

(855) Badjić, J. D.; Cantrill, S. J.; Grubbs, R. H.; Guidry, E. N.; Orenes, R.; Stoddart, J. F. The Exclusivity of Multivalency in Dynamic Covalent Processes. *Angew. Chem., Int. Ed.* **2004**, *43*, 3273–3278.

(856) Balzani, V.; Clemente-León, M.; Credi, A.; Lowe, J. N.; Badjić, J. D.; Stoddart, J. F.; Williams, D. J. Controlling Multivalent Interactions in Triply-Threaded Two-Component Superbundles. *Chem. Eur. J.* **2003**, *9*, 5348–5360.

(857) Badjić, J. D.; Cantrill, S. J.; Stoddart, J. F. Can Multivalency Be Expressed Kinetically? The Answer is Yes. *J. Am. Chem. Soc.* **2004**, *126*, 2288–2289.

(858) Hou, H.; Leung, K. C.-F.; Nelson, A.; Stoddart, J. F.; Grubbs, R. H. Template-Directed One-Step Synthesis of Cyclic Trimers by ADMET. *J. Am. Chem. Soc.* **2006**, *128*, 15358–15359.

(859) Badjić, J. D.; Ronconi, C. M.; Stoddart, J. F.; Ashton, P. R.; Balzani, V.; Silvi, S.; Credi, A. Operating Molecular Elevators. *J. Am. Chem. Soc.* **2006**, *128*, 1489–1499.

(860) Yamada, Y.; Okamoto, M.; Furukawa, K.; Kato, T.; Tanaka, K. Switchable Intermolecular Communication in a Four-Fold Rotaxane. *Angew. Chem., Int. Ed.* **2012**, *51*, 709–713.

(861) Yamada, Y.; Mihara, N.; Tanaka, K. Synthesis of a Hetero-Dinuclear Metal Complex in a Porphyrin/Phthalocyanine Four-Fold Rotaxane. *Dalton Trans.* **2013**, *42*, 15873–15876.

(862) Yamada, Y.; Okada, M.-A.; Tanaka, K. Repetitive Stepwise Rotaxane Formation Toward Programmable Molecular Arrays. *Chem. Commun.* **2013**, *49*, 11053–11055.

(863) Yamada, Y.; Mihara, N.; Shibano, S.; Sugimoto, K.; Tanaka, K. Triply Stacked Heterogeneous Array of Porphyrins and Phthalocyanine Through Stepwise Formation of a Fourfold Rotaxane and an Ionic Complex. *J. Am. Chem. Soc.* **2013**, *135*, 11505–11508.

(864) Gaeta, C.; Vysotsky, M. O.; Bogdan, A.; Böhmer, V. Fourfold [2]Rotaxanes Based on Calix[4]arenes. *J. Am. Chem. Soc.* **2005**, *127*, 13136–13137.

(865) Molokanova, O.; Vysotsky, M. O.; Cao, Y.; Thondorf, I.; Böhmer, V. Fourfold [2]Rotaxanes of Calix[4]arenes by Ring Closure. *Angew. Chem., Int. Ed.* **2006**, *45*, 8051–8055.

(866) Kaufmann, L.; Traulsen, N. L.; Springer, A.; Schröder, H. V.; Mäkelä, T.; Rissanen, K.; Schalley, C. A. Evaluation of Multivalency as an Organization Principle for the Efficient Synthesis of Doubly and Triply Threaded Amide Rotaxanes. *Org. Chem. Front.* **2014**, *1*, 521–531.

(867) Agam, G.; Zilkha, A. Synthesis of a Catenane by a Statistical Double-Stage Method. *J. Am. Chem. Soc.* **1976**, *98*, 5214–5216.

(868) Yamaguchi, I.; Osakada, K.; Yamamoto, T. Polyrotaxane Containing a Blocking Group in Every Structural Unit of the Polymer Chain. Direct Synthesis of Poly(alkylenebenzimidazole) Rotaxane from Ru Complex-Catalyzed Reaction of 1,12-Dodecanediol and 3,3′-Diaminobenzidine in the Presence of Cyclodextrin. *J. Am. Chem. Soc.* **1996**, *118*, 1811–1812.

(869) Farcas, A.; Aubert, P.-H.; Mohanty, J.; Lazar, A. I.; Cantin, S.; Nau, W. M. Molecular Wire Formation from Poly[2,7-(9,9-dioctylfluorene)-*alt*-(5,5′-bithiophene/cucurbit[7]uril)] Polyrotaxane Copolymer. *Eur. Polym. J.* **2015**, *62*, 124–129.

(870) Kidd, T. J.; Loontjens, T. J. A.; Leigh, D. A.; Wong, J. K. Y. Rotaxane Building Blocks Bearing Blocked Isocyanate Stoppers: Polyrotaxanes through Post-Assembly Chain Extension. *Angew. Chem., Int. Ed.* **2003**, *42*, 3379–3383.

(871) Ikeda, T.; Higuchi, M.; Kurth, D. G. From Thiophene [2]Rotaxane to Polythiophene Polyrotaxane. *J. Am. Chem. Soc.* **2009**, *131*, 9158–9159.

(872) Yu, L.; Li, M.; Zhou, X.-P.; Li, D. Hybrid Inorganic–Organic Polyrotaxane, Pseudorotaxane, and Sandwich. *Inorg. Chem.* **2013**, *52*, 10232–10234.

(873) Wei, M.-J.; Zang, H.-Y.; Zhou, E.-L.; Shao, K.-Z.; Song, B.-Q.; Wang, X.-L.; Su, Z.-M. Coordination and Supramolecular Assembly of $\{Cd_2Ge_8V_{12}O_{48}\}$ Building Block and Cucurbit[6]uril to Form Rotaxane-Shaped Hybrids. *Dalton Trans.* **2016**, *45*, 4989–4992.

(874) Takata, T.; Kohsaka, Y.; Konishi, G.-I. Main Chain-Type Polyrotaxane with Controlled Ratio of Rotaxanated Units. *Chem. Lett.* **2007**, *36*, 292–293.

(875) Kohsaka, Y.; Koyama, Y.; Takata, T. Graft Polyrotaxanes: a New Class of Graft Copolymers with Mobile Graft Chains. *Angew. Chem., Int. Ed* **2011**, *50*, 10417–10420.

(876) Koyama, Y.; Suzuki, Y.; Asakawa, T.; Kihara, N.; Nakazono, K.; Takata, T. Polymer Architectures Assisted by Dynamic Covalent Bonds: Synthesis and Properties of Boronate-Functionalized Polyrotaxane and Graft Polyrotaxane. *Polymer* **2011**, 1–8.

(877) Ge, X.; He, Y.; Guiver, M. D.; Wu, L.; Ran, J.; Yang, Z.; Xu, T. Alkaline Anion-Exchange Membranes Containing Mobile Ion Shuttles. *Adv. Mater.* **2016**, *28*, 3467–3472.

(878) Werts, M. P. L.; Van Den Boogaard, M.; Hadziioannou, G.; Tsivgoulis, G. M. Towards Mechanically Linked Polyrotaxanes by Sequential Deprotection–Coupling Steps of Bifunctional Rotaxanes. *Chem. Commun.* **1999**, 623–624.

(879) Sasabe, H.; Inomoto, N.; Kihara, N.; Suzuki, Y.; Ogawa, A.; Takata, T. Synthesis of Poly[2]rotaxane by Sonogashira Polycondensation. *J. Polym. Sci. Pol. Chem.* **2007**, *45*, 4154–4160.

(880) Harrison, I. T.; Harrison, S. The Synthesis of a Stable Complex of a Macrocycle and a Threaded Chain. *J. Am. Chem. Soc.* **1967**, *89*, 5723–5724.

(881) Takata, T.; Kawasaki, H.; Asai, S.; Kihara, N.; Furusho, Y. Radically Polymerizable Pseudorotaxane Monomers: Versatile Building Units for Side Chain Polyrotaxane Synthesis. *Chem. Lett.* **1999**, 111–112.

(882) Takata, T.; Kawasaki, H.; Kihara, N.; Furusho, Y. Synthesis of Side-Chain Polyrotaxane by Radical Polymerizations of Pseudorotaxane Monomers Consisting of Crown Ether Wheel and Acrylate Axle Bearing Bulky End-Cap and Ammonium Group. *Macromolecules* **2001**, *34*, 5449–5456.

(883) Yu, G.; Suzaki, Y.; Abe, T.; Osakada, K. Introduction of Ferrocene-Containing [2]Rotaxanes onto Siloxane, Silsesquioxane and Polysiloxanes *via* Click Chemistry. *Dalton Trans.* **2013**, *42*, 1476–1482.

(884) Ishiwari, F.; Nakazono, K.; Koyama, Y.; Takata, T. Rational Control of a Polyacetylene Helix by a Pendant Rotaxane Switch. *Chem. Commun.* **2011**, *47*, 11739–11741.

(885) Ishiwari, F.; Fukasawa, K.-I.; Sato, T.; Nakazono, K.; Koyama, Y.; Takata, T. A Rational Design for the Directed Helicity Change of Polyacetylene Using Dynamic Rotaxane Mobility by Means of Through-Space Chirality Transfer. *Chem. Eur. J.* **2011**, *17*, 12067–12075.

(886) Suzuki, S.; Ishiwari, F.; Nakazono, K.; Takata, T. Reversible Helix–Random Coil Transition of Poly(*m*-Phenylenediethynylene) by a Rotaxane Switch. *Chem. Commun.* **2012**, *48*, 6478–6480.

(887) Zhu, N.; Nakazono, K.; Takata, T. Reversible Polyphenylacetylene Helix Conversion Driven by a Thermoresponsive Rotaxane Switch in the Solid State. *Chem. Commun.* **2016**, *52*, 3647–3649.

(888) Cao, Z.-Q.; Luan, Z.-L.; Zhang, Q.; Gu, R.-R.; Ren, J.; Qu, D.-H. An Acid/Base Responsive Side-Chain Polyrotaxane System with a Fluorescent Signal. *Polym. Chem.* **2016**, 1866–1870.

(889) Born, M.; Ritter, H. Comb-like Rotaxane Polymers Containing Non-Covalently Bound Cyclodextrins in the Side Chains. *Makromol. Chem., Rapid Commun.* **1991**, *12*, 471–476.

(890) Born, M.; Koch, T.; Ritter, H. Side-Chain Polyrotaxanes .2. Functionalized Polysulfone with Noncovalently Anchored Cyclodextrins in the Side-Chains. *Acta Polym.* **1994**, *45*, 68–72.

(891) Born, M.; Ritter, H. Side-Chain Polyrotaxanes with a Tandem Structure Based on Cyclodextrins and a Polymethacrylate Main Chain. *Angew. Chem., Int. Ed.* **1995**, *34*, 309–311.

(892) Born, M.; Koch, T.; Ritter, H. Side-Chain Polyrotaxanes .3. Synthesis, Characterization and Enzymatically Catalyzed Degradation of Noncovalently Anchored Cyclodextrins in the Side-Chains of Poly(ether-ether-ketone)s. *Macromol. Chem. Phys.* **1995**, *196*, 1761–1767.

(893) Born, M.; Ritter, H. Pseudo-Polymer Analogous Reactions: Methylation of Alcohol Groups of Non-Covalently Anchored 2,6-Dimethyl-Beta-Cyclodextrin Components Located in Branched Side Chains of a Poly(tandem-rotaxane). *Adv. Mater* **1996**, *8*, 149–151.

(894) Born, M.; Ritter, H. Topologically Unique Side-Chain Polyrotaxanes Based on Triacetyl-Beta-Cyclodextrin and a Poly(ether sulfone) Main Chain. *Macromol. Rapid Commun.* **1996**, *17*, 197–202.

(895) Noll, O.; Ritter, H. Synthesis of New Side-Chain Polyrotaxanes *via* Free Radical Polymerization of a Water-Soluble Semi-Rotaxane Monomer Consisting of 2,6-Dimethyl-β-Cyclodextrin and 3-*O*-(11-Acryloylaminoundecanoyl)cholic Acid. *Macromol. Chem. Phys.* **1998**, *199*, 791–794.

(896) Yamaguchi, I.; Osakada, K.; Yamamoto, T. Introduction of a Long Alkyl Side Chain to Poly(benzimidazole)s. *N*-Alkylation of the Imidazole Ring and Synthesis of Novel Side Chain Polyrotaxanes. *Macromolecules* **1997**, *30*, 4288–4294.

(897) Takata, T.; Hasegawa, T.; Kihara, N.; Furusho, Y. Synthesis of Side-Chain Polyrotaxane via Radical Polymerizations of Vinylic Pseudorotaxane Monomers Having Paraquat-Type Macrocycle as a Wheel Component. *Polymer* **2004**, *36*, 927–932.

(898) Bria, M.; Bigot, J.; Cooke, G.; Lyskawa, J.; Rabani, G.; Rotello, V. M.; Woisel, P. Synthesis of a Polypseudorotaxane, Polyrotaxane, and Polycatenane Using “Click” Chemistry. *Tetrahedron* **2009**, *65*, 400–407.

(899) Raju, M. V. R.; Raghunath, P.; Lin, M.-C.; Lin, H.-C. An Acid–Base Controllable Hierarchical Nanostructure from a NIR-Absorbing Conjugated Polyrotaxane-Based Optical Molecular Switch. *Macromolecules* **2013**, *46*, 6731–6743.

(900) Kwan, P. H.; MacLachlan, M. J.; Swager, T. M. Rotaxanated Conjugated Sensory Polymers. *J. Am. Chem. Soc.* **2004**, *126*, 8638–8639.

(901) Oku, T.; Furusho, Y.; Takata, T. First Poly[3]rotaxane Synthesized through the Noncovalent Step-Growth Polymerization of a Homoditopic Dumbbell Compound and a Macrocycle with a Reversible Thiol-Disulfide Interchange Reaction. *J. Polym. Sci. Pol. Chem.* **2003**, *41*, 119–123.

(902) Sohgawa, Y.-H.; Fujimori, H.; Shoji, J.; Furusho, Y.; Kihara, N.; Takata, T. Polyslipping: A New Approach to Polyrotaxane-Like Assemblies. *Chem. Lett.* **2001**, 774–775.

(903) Sato, T.; Takata, T. Synthesis and Characterization of Poly[3]rotaxane Through the Mizoroki-Heck Coupling Polymerization of Divinyl-Functionalized [3]Rotaxane. *Polymer* **2009**, *41*, 470–476.

(904) Lee, J.-J.; White, A. G.; Baumes, J. M.; Smith, B. D. Microwave-Assisted Slipping Synthesis of Fluorescent Squaraine Rotaxane Probe for Bacterial Imaging. *Chem. Commun.* **2010**, *46*, 1068–1069.

(905) Ashton, P. R.; Baxter, I.; Fyfe, M. C. T.; Raymo, F. M.; Spencer, N.; Stoddart, J. F.; White, A. J. P.; Williams, D. J. Rotaxane or Pseudorotaxane? That Is the Question! *J. Am. Chem. Soc.* **1998**, *120*, 2297–2307.

(906) Han, J.-M.; Zhang, Y.-H.; Wang, X.-Y.; Liu, C.-J.; Wang, J.-Y.; Pei, J. Main-Chain Linear Polyrotaxanes: Synthesis, Characterization, and Conformational Modulation. *Chem. Eur. J.* **2012**, *19*, 1502–1510.

(907) Wei, P.; Yan, X.; Huang, F. Reversible Formation of a Poly[3]rotaxane Based on Photo Dimerization of an Anthracene-Capped [3]Rotaxane. *Chem. Commun.* **2014**, *50*, 14105–14108.
(908) Whitehead, G. F. S.; Cross, B.; Carthy, L.; Milway, V. A.; Rath, H.; Fernandez, A.; Heath, S. L.; Muryn, C. A.; Pritchard, R. G.; Teat, S. J.; Timco, G. A.; Winpenny, R. E. P. Rings and Threads as Linkers in Metal-Organic Frameworks and Poly-Rotaxanes. *Chem. Commun.* **2013**, *49*, 7195–7197.
(909) Gibson, H. W.; Nagvekar, D. S.; Powell, J.; Gong, C.; Bryant, W. S. Polyrotaxanes by *In Situ* Self Threading During Polymerization of Functional Macrocycles. Part 2: Poly(ester crown ether)s. *Tetrahedron* **1997**, *53*, 15197–15207.
(910) Gong, C.; Gibson, H. W. Self-Threading-Based Approach for Branched and/or Cross-Linked Poly(methacrylate rotaxane)s. *J. Am. Chem. Soc.* **1997**, *119*, 5862–5866.
(911) Gibson, H. W.; Nagvekar, D. S.; Yamaguchi, N.; Bhattacharjee, S.; Wang, H.; Vergne, M. J.; Hercules, D. M. Polyamide Pseudorotaxanes, Rotaxanes, and Catenanes Based on Bis(5-carboxy-1,3-phenylene)-(3 *x* + 2)-Crown-*x* Ethers. *Macromolecules* **2004**, *37*, 7514–7529.
(912) Oku, T.; Furusho, Y.; Takata, T. A Concept for Recyclable Cross-Linked Polymers: Topologically Networked Polyrotaxane Capable of Undergoing Reversible Assembly and Disassembly. *Angew. Chem., Int. Ed.* **2004**, *43*, 966–969.
(913) Bilig, T.; Oku, T.; Furusho, Y.; Koyama, Y.; Asai, S.; Takata, T. Polyrotaxane Networks Formed *via* Rotaxanation Utilizing Dynamic Covalent Chemistry of Disulfide. *Macromolecules* **2008**, *41*, 8496–8503.
(914) Kohsaka, Y.; Konishi, G.-I.; Takata, T. Synthesis of a Main Chain-Type Polyrotaxane Consisting of Poly(crown ether) and *sec*-Ammonium Salt Axle and its Application to Polyrotaxane Network. *Polymer* **2007**, *39*, 861–873.
(915) Kihara, N.; Hinoue, K.; Takata, T. Solid-State End-Capping of Pseudopolyrotaxane Possessing Hydroxy-Terminated Axle to Polyrotaxane and Its Application to the Synthesis of a Functionalized Polyrotaxane Capable of Yielding a Polyrotaxane Network. *Macromolecules* **2005**, *38*, 223–226.
(916) Arai, T.; Jang, K.; Koyama, Y.; Asai, S.; Takata, T. Versatile Supramolecular Cross-Linker: A Rotaxane Cross-Linker That Directly Endows Vinyl Polymers with Movable Cross-Links. *Chem. Eur. J.* **2013**, *19*, 5917–5923.
(917) Ogawa, M.; Kawasaki, A.; Koyama, Y.; Takata, T. Synthesis and Properties of a Polyrotaxane Network Prepared From a Pd-Templated Bis-Macrocycle as a Topological Cross-Linker. *Polymer* **2011**, *43*, 909–915.
(918) Okumura, Y.; Ito, K. The Polyrotaxane Gel: A Topological Gel by Figure-of-Eight Cross-links. *Adv. Mater.* **2001**, *13*, 485–487.
(919) Ito, K. Novel Cross-Linking Concept of Polymer Network: Synthesis, Structure, and Properties of Slide-Ring Gels with Freely Movable Junctions. *Polymer* **2007**, *39*, 489–499.
(920) Mayumi, K.; Ito, K. Structure and Dynamics of Polyrotaxane and Slide-Ring Materials. *Polymer* **2010**, *51*, 959–967.
(921) Kato, K.; Ito, K. Polymer Networks Characterized by Slidable Crosslinks and the Asynchronous Dynamics of Interlocked Components. *React. Funct. Polym.* **2013**, *73*, 405–412.
(922) Noda, Y.; Hayashi, Y.; Ito, K. From Topological Gels to Slide-Ring Materials. *J. Appl. Polym. Sci.* **2014**, *131*: 40509.
(923) Fleury, G.; Schlatter, G.; Brochon, C.; Hadziioannou, G. From High Molecular Weight Precursor Polyrotaxanes to Supramolecular Sliding Networks. The “Sliding Gels.” *Polymer* **2005**, *46*, 8494–8501.
(924) Sakai, T.; Murayama, H.; Nagano, S.; Takeoka, Y.; Kidowaki, M.; Ito, K.; Seki, T. Photoresponsive Slide-Ring Gel. *Adv. Mater* **2007**, *19*, 2023–2025.
(925) Murayama, H.; Imran, A. B.; Nagano, S.; Seki, T.; Kidowaki, M.; Ito, K.; Takeoka, Y. Chromic Slide-Ring Gel Based on Reflection from Photonic Bandgap. *Macromolecules* **2008**, *41*, 1808–1814.
(926) Araki, J. Polyrotaxane Derivatives. II. Preparation and Characterization of Ionic Polyrotaxanes and Ionic Slide-Ring Gels. *J. Polym. Sci. Pol. Chem* **2011**, *49*, 2199–2209.
(927) Murakami, T.; Schmidt, B. V. K. J.; Brown, H. R.; Hawker, C. J. One-Pot “Click” Fabrication of Slide-Ring Gels. *Macromolecules* **2015**, *48*, 7774–7781.
(928) Kato, K.; Okabe, Y.; Okazumi, Y.; Ito, K. A Significant Impact of Host-Guest Stoichiometry on the Extensibility of Polyrotaxane Gels. *Chem. Commun.* **2015**, *51*, 16180–16183.
(929) Araki, J.; Sainou, N. Amino Acid-Derivatized Slide-Ring Gels: Chemical Crosslinking of Polyrotaxane Conjugates with Different Amino Acid Pendant Groups. *Polymer* **2015**, *74*, 133–143.
(930) Kali, G.; Eisenbarth, H.; Wenz, G. One Pot Synthesis of a Polyisoprene Polyrotaxane and Conversion to a Slide-Ring Gel. *Macromol. Rapid Commun.* **2015**, *37*, 67–72.
(931) Kato, K.; Inoue, K.; Kidowaki, M.; Ito, K. Organic−Inorganic Hybrid Slide-Ring Gels: Polyrotaxanes Consisting of Poly(dimethylsiloxane) and γ-Cyclodextrin and Subsequent Topological Cross-Linking. *Macromolecules* **2009**, *42*, 7129–7136.
(932) Karino, T.; Okumura, Y.; Zhao, C.; Kataoka, T.; Ito, K.; Shibayama, M. SANS Studies on Deformation Mechanism of Slide-Ring Gel. *Macromolecules* **2005**, *38*, 6161–6167.
(933) Fleury, G.; Schlatter, G.; Brochon, C.; Hadziioannou, G. Unveiling the Sliding Motion in Topological Networks: Influence of the Swelling Solvent on the Relaxation Dynamics. *Adv. Mater.* **2006**, *18*, 2847–2851.
(934) Murata, N.; Konda, A.; Urayama, K.; Takigawa, T.; Kidowaki, M.; Ito, K. Anomaly in Stretching-Induced Swelling of Slide-Ring Gels with Movable Cross-Links. *Macromolecules* **2009**, *42*, 8485–8491.
(935) Mayumi, K.; Tezuka, M.; Bando, A.; Ito, K. Mechanics of Slide-Ring Gels: Novel Entropic Elasticity of a Topological Network Formed by Ring and String. *Soft Matter* **2012**, *8*, 8179–8183.
(936) Katsuno, C.; Konda, A.; Urayama, K.; Takigawa, T.; Kidowaki, M.; Ito, K. Pressure-Responsive Polymer Membranes of Slide-Ring Gels with Movable Cross-links. *Adv. Mater.* **2013**, *25*, 4636–4640.
(937) Kato, K.; Yasuda, T.; Ito, K. Viscoelastic Properties of Slide-Ring Gels Reflecting Sliding Dynamics of Partial Chains and Entropy of Ring Components. *Macromolecules* **2013**, *46*, 310–316.
(938) Bin Imran, A.; Esaki, K.; Gotoh, H.; Seki, T.; Ito, K.; Sakai, Y.; Takeoka, Y. Extremely Stretchable Thermosensitive Hydrogels by Introducing Slide-Ring Polyrotaxane Cross-Linkers and Ionic Groups into the Polymer Network. *Nature Commun.* **2014**, *5*: 5124.
(939) Zhou, H.; Wang, Y.; Zheng, Z.; Ding, X.; Peng, Y. Periodic Auto-Active Gels with Topologically “Polyrotaxane-Interlocked” Structures. *Chem. Commun.* **2014**, *50*, 6372–6374.
(940) Karino, T.; Shibayama, M.; Okumura, Y.; Ito, K. SANS Study on Pulley Effect of Slide-Ring Gel. *Phys. B Condens. Matter.* **2006**, *385–386*, 807–809.
(941) Fleury, G.; Schlatter, G.; Brochon, C.; Travelet, C.; Lapp, A.; Lindner, P.; Hadziioannou, G. Topological Polymer Networks with Sliding Cross-Link Points: The “Sliding Gels.” Relationship Between Their Molecular Structure and the Viscoelastic as Well as the Swelling Properties. *Macromolecules* **2007**, *40*, 535–543.
(942) Kato, K.; Karube, K.; Nakamura, N.; Ito, K. The Effect of Ring Size on the Mechanical Relaxation Dynamics of Polyrotaxane Gels. *Polym. Chem.* **2015**, *6*, 2241–2248.
(943) Ogoshi, T.; Aoki, T.; Ueda, S.; Tamura, Y.; Yamagishi, T.-A. Pillar[5]arene-Based Nonionic Polyrotaxanes and a Topological Gel Prepared From Cyclic Host Liquids. *Chem. Commun.* **2014**, *50*, 6607–6609.
(944) Yang, J.; Ma, J.-F.; Batten, S. R. Polyrotaxane Metal-Organic Frameworks (PMOFs). *Chem. Commun.* **2012**, *48*, 7899–7912.
(945) Loeb, S. J. Metal-Organic Rotaxane Frameworks; MORFs. *Chem. Commun.* **2005**, 1511–1518.
(946) Loeb, S. J. Rotaxanes as Ligands: From Molecules to Materials. *Chem. Soc. Rev.* **2007**, *36*, 226–235.
(947) Zhu, K.; Loeb, S. J. Organizing Mechanically Interlocked Molecules to Function Inside Metal-Organic Frameworks. *Top. Curr. Chem.* **2014**, *354*, 213–251.

(948) Davidson, G. J. E.; Loeb, S. J. Channels and Cavities Lined with Interlocked Components: Metal-Based Polyrotaxanes That Utilize Pyridinium Axles and Crown Ether Wheels as Ligands. *Angew. Chem., Int. Ed.* **2003**, *42*, 74–77.
(949) Hoffart, D. J.; Loeb, S. J. Metal-Organic Rotaxane Frameworks: Three-Dimensional Polyrotaxanes from Lanthanide-Ion Nodes, Pyridinium *N*-Oxide Axles, and Crown-Ether Wheels. *Angew. Chem., Int. Ed.* **2005**, *117*, 923–926.
(950) Mercer, D. J.; Vukotic, V. N.; Loeb, S. J. Linking [2]Rotaxane Wheels to Create a New Type of Metal Organic Rotaxane Framework. *Chem. Commun.* **2010**, *47*, 896–898.
(951) Vukotic, V. N.; Loeb, S. J. One-, Two- and Three-Periodic Metal-Organic Rotaxane Frameworks (MORFs): Linking Cationic Transition-Metal Nodes with an Anionic Rotaxane Ligand. *Chem. Eur. J.* **2010**, *16*, 13630–13637.
(952) Mercer, D. J.; Yacoub, J.; Zhu, K.; Loeb, S. K.; Loeb, S. J. [2]Pseudorotaxanes, [2]Rotaxanes and Metal-Organic Rotaxane Frameworks Containing Tetra-Substituted Dibenzo[24]Crown-8 Wheels. *Org. Biomol. Chem.* **2012**, *10*, 6094–6104.
(953) Vukotic, V. N.; Harris, K. J.; Zhu, K.; Schurko, R. W.; Loeb, S. J. Metal-Organic Frameworks with Dynamic Interlocked Components. *Nature Chem.* **2012**, *4*, 456–460.
(954) Frank, N. C.; Mercer, D. J.; Loeb, S. J. An Interwoven Metal-Organic Framework Combining Mechanically Interlocked Linkers and Interpenetrated Networks. *Chem. Eur. J.* **2013**, *19*, 14076–14080.
(955) Zhu, K.; Vukotic, V. N.; O'Keefe, C. A.; Schurko, R. W.; Loeb, S. J. Metal-Organic Frameworks with Mechanically Interlocked Pillars: Controlling Ring Dynamics in the Solid-State *via* a Reversible Phase Change. *J. Am. Chem. Soc.* **2014**, *136*, 7403–7409.
(956) Zhu, K.; O'Keefe, C. A.; Vukotic, V. N.; Schurko, R. W.; Loeb, S. J. A Molecular Shuttle That Operates Inside a Metal-Organic Framework. *Nature Chem.* **2015**, *7*, 514–519.
(957) Vukotic, V. N.; O'Keefe, C. A.; Zhu, K.; Harris, K. J.; To, C.; Schurko, R. W.; Loeb, S. J. Mechanically Interlocked Linkers Inside Metal-Organic Frameworks: Effect of Ring Size on Rotational Dynamics. *J. Am. Chem. Soc.* **2015**, *137*, 9643–9651.
(958) Farahani, N.; Zhu, K.; O'Keefe, C. A.; Schurko, R. W.; Loeb, S. J. Thermally Driven Dynamics of a Rotaxane Wheel About an Imidazolium Axle Inside a Metal-Organic Framework. *ChemPlusChem* **2016**, *81*, 1–7.
(959) Coskun, A.; Hmadeh, M.; Barin, G.; Gándara, F.; Li, Q.; Choi, E.; Strutt, N. L.; Cordes, D. B.; Slawin, A. M. Z.; Stoddart, J. F.; Sauvage, J.-P.; Yaghi, O. M. Metal-Organic Frameworks Incorporating Copper-Complexed Rotaxanes. *Angew. Chem., Int. Ed.* **2012**, *51*, 2160–2163.
(960) McGonigal, P. R.; Deria, P.; Hod, I.; Moghadam, P. Z.; Avestro, A.-J.; Horwitz, N. E.; Gibbs-Hall, I. C.; Blackburn, A. K.; Chen, D.; Botros, Y. Y.; Wasielewski, M. R.; Snurr, R. Q.; Hupp, J. T.; Farha, O. K.; Stoddart, J. F. Electrochemically Addressable Trisradical Rotaxanes Organized Within a Metal-Organic Framework. *Proc. Natl. Acad. Sci. U.S.A.* **2015**, *112*, 11161–11168.
(961) Deria, P.; Mondloch, J. E.; Tylianakis, E.; Ghosh, P.; Bury, W.; Snurr, R. Q.; Hupp, J. T.; Farha, O. K. Perfluoroalkane Functionalization of NU-1000 via Solvent-Assisted Ligand Incorporation: Synthesis and CO_2 Adsorption Studies. *J. Am. Chem. Soc.* **2013**, *135*, 16801–16804.
(962) Barin, G.; Coskun, A.; Friedman, D. C.; Olson, M. A.; Colvin, M. T.; Carmielli, R.; Dey, S. K.; Bozdemir, O. A.; Wasielewski, M. R.; Stoddart, J. F. A Multistate Switchable [3]Rotacatenane. *Chem. Eur. J.* **2011**, *17*, 213–222.
(963) Hu, W.-B.; Hu, W.-J.; Zhao, X.-L.; Liu, Y. A.; Li, J.-S.; Jiang, B.; Wen, K. A [2]Rota[2]catenane, Constructed from a Pillar[5]arene-Crown Ether Fused Double-Cavity Macrocycle: Synthesis and Structural Characterization. *Chem. Commun.* **2015**, *51*, 13882–13885.
(964) Hayashi, R.; Wakatsuki, K.; Yamasaki, R.; Mutoh, Y.; Kasama, T.; Saito, S. Synthesis of Rotacatenanes by the Combination of Cu-Mediated Threading Reaction and the Template Method: The Dual Role of One Ligand. *Chem. Commun.* **2014**, *50*, 204–206.
(965) Hayashi, R.; Slavík, P.; Mutoh, Y.; Kasama, T.; Saito, S. Sequence-Selective Synthesis of Rotacatenane Isomers. *J. Org. Chem.* **2016**, *81*, 1175–1184.
(966) Xue, W.; Li, Z.; Liu, G.; Chen, X.; Li, T.; Liu, S. H.; Yin, J. Construction of Rotacatenanes Using Rotaxane and Catenane Frameworks. *Org. Biomol. Chem.* **2014**, *12*, 4862–4871.
(967) Romuald, C.; Ardá, A.; Clavel, C.; Jiménez-Barbero, J.; Coutrot, F. Tightening or Loosening a pH-Sensitive Double-Lasso Molecular Machine Readily Synthesized from an Ends-Activated [*c*2]Daisy Chain. *Chem. Sci.* **2012**, *3*, 1851–1857.
(968) Romuald, C.; Cazals, G.; Enjalbal, C.; Coutrot, F. Straightforward Synthesis of a Double-Lasso Macrocycle from a Nonsymmetrical [*c*2]Daisy Chain. *Org. Lett.* **2013**, *15*, 184–187.
(969) Bogdan, A.; Bolte, M.; Böhmer, V. Molecules with New Topologies Derived from Hydrogen-Bonded Dimers of Tetraurea Calix[4]arenes. *Chem. Eur. J.* **2008**, *14*, 8514–8520.
(970) Vajpayee, V.; Song, Y. H.; Cook, T. R.; Kim, H.; Lee, Y.; Stang, P. J.; Chi, K.-W. A Unique Non-Catenane Interlocked Self-Assembled Supramolecular Architecture and Its Photophysical Properties. *J. Am. Chem. Soc.* **2011**, *133*, 19646–19649.
(971) Ju, H.; Clegg, J. K.; Park, K.-M.; Lindoy, L. F.; Lee, S. S. Formation of a Dicopper Platform Based Polyrotaxane Whose "String" and "Bead" Are Constructed from the Same Components. *J. Am. Chem. Soc.* **2015**, *137*, 9535–9538.
(972) Vögtle, F.; Müller, W. M. Complexes of γ-Cyclodextrin with Crown Ethers, Cryptands, Coronates, and Cryptates. *Angew. Chem., Int. Ed. Engl.* **1979**, *18*, 623–624.
(973) Kamitori, S.; Hirotsu, K.; Higuchi, T. Crystal and Molecular Structure of the γ-Cyclodextrin–12-Crown-4 1 : 1 Inclusion Complex. *J. Chem. Soc., Chem. Commun.* **1986**, 690–691.
(974) Kamitori, S.; Hirotsu, K.; Higuchi, T. Crystal and Molecular Structures of Double Macrocyclic Inclusion Complexes Composed of Cyclodextrins, Crown Ethers, and Cations. *J. Am. Chem. Soc.* **1987**, *109*, 2409–2414.
(975) Kamitori, S.; Hirotsu, K.; Higuchi, T. Crystal and Molecular Structure of Double Macrocyclic Inclusion Complexes, γ-Cycl odextrin·12-Crown-4·NaCl, a Model for the Transport of Ions Through Membranes. *Bull. Chem. Soc. Jpn.* **1988**, *61*, 3825–3830.
(976) Gafni, A.; Cohen, Y. Complexes of Macrocycles with γ-Cyclodextrin as Deduced from NMR Diffusion Measurements. *J. Org. Chem.* **1997**, *62*, 120–125.
(977) Kim, S.-Y.; Jung, I.-S.; Lee, E.; Kim, J.; Sakamoto, S.; Yamaguchi, K.; Kim, K. Macrocycles within Macrocycles: Cyclen, Cyclam, and Their Transition Metal Complexes Encapsulated in Cucurbit[8]uril. *Angew. Chem., Int. Ed.* **2001**, *40*, 2119–2121.
(978) Day, A. I.; Blanch, R. J.; Arnold, A. P.; Lorenzo, S.; Lewis, G. R.; Dance, I. A Cucurbituril-Based Gyroscane: A New Supramolecular Form. *Angew. Chem., Int. Ed.* **2002**, *41*, 275–277.
(979) Lim, C. W.; Sakamoto, S.; Yamaguchi, K.; Hong, J.-I. Versatile Formation of [2]Catenane and [2]Pseudorotaxane Structures; Threading and Noncovalent Stoppering by a Self-Assembled Macrocycle. *Org. Lett.* **2004**, *6*, 1079–1082.
(980) Kawase, T.; Tanaka, K.; Shiono, N.; Seirai, Y.; Oda, M. Onion-Type Complexation Based on Carbon Nanorings and a Buckminsterfullerene. *Angew. Chem., Int. Ed.* **2004**, *43*, 1722–1724.
(981) Iwanaga, T.; Nakamoto, R.; Yasutake, M.; Takemura, H.; Sako, K.; Shinmyozu, T. Cyclophanes Within Cyclophanes: The Synthesis of a Pyromellitic Diimide-Based Macrocycle as a Structural Unit in a Molecular Tube and Its Inclusion Phenomena. *Angew. Chem., Int. Ed.* **2006**, *45*, 3643–3647.

(982) Liu, Y. Self-Assembled Ring-in-Ring Complexes from Metal–Ligand Coordination Macrocycles and β-Cyclodextrin. *Tetrahedron Lett.* **2007**, *48*, 3871–3874.

(983) Kawase, T.; Nishiyama, Y.; Nakamura, T.; Ebi, T.; Matsumoto, K.; Kurata, H.; Oda, M. Cyclic [5]Paraphenyleneacetylene: Synthesis, Properties, and Formation of a Ring-in-Ring Complex Showing a Considerably Large Association Constant and Entropy Effect. *Angew. Chem., Int. Ed.* **2007**, *46*, 1086–1088.

(984) Juríček, M.; Barnes, J. C.; Dale, E. J.; Liu, W.-G.; Strutt, N. L.; Bruns, C. J.; Vermeulen, N. A.; Ghooray, K. C.; Sarjeant, A. A.; Stern, C. L.; Botros, Y. Y.; Goddard, W. A., III; Stoddart, J. F. Ex^{2}Box: Interdependent Modes of Binding in a Two-Nanometer-Long Synthetic Receptor. *J. Am. Chem. Soc.* **2013**, *135*, 12736–12746.

(985) Sun, J.; Frasconi, M.; Liu, Z.; Barnes, J. C.; Wang, Y.; Chen, D.; Stern, C. L.; Stoddart, J. F. Formation of Ring-in-Ring Complexes Between Crown Ethers and Rigid TVBox^{8+}. *Chem. Commun.* **2015**, *51*, 1432–1435.

(986) Danjo, H.; Hashimoto, Y.; Kidena, Y.; Nogamine, A.; Katagiri, K.; Kawahata, M.; Miyazawa, T.; Yamaguchi, K. Nestable Tetrakis(spiroborate) Nanocycles. *Org. Lett.* **2015**, *17*, 2154–2157.

(987) Klosterman, J. K.; Veliks, J.; Frantz, D. K.; Yasui, Y.; Loepfe, M.; Zysman-Colman, E.; Linden, A.; Siegel, J. S. Conformations of Large Macrocycles and Ring-in-Ring Complexes. *Org. Chem. Front.* **2016**, *3*, 661–666.

(988) Veliks, J.; Seifert, H. M.; Frantz, D. K.; Klosterman, J. K.; Tseng, J.-C.; Linden, A.; Siegel, J. S. Towards the Molecular Borromean Link with Three Unequal Rings: Double-Threaded Ruthenium(II) Ring-in-Ring Complexes. *Org. Chem. Front.* **2016**, *3*, 667–672.

(989) Ogoshi, T.; Akutsu, T.; Yamafuji, D.; Aoki, T.; Yamagishi, T.-A. Solvent- and Achiral-Guest-Triggered Chiral Inversion in a Planar Chiral Pseudo[1]Catenane. *Angew. Chem., Int. Ed.* **2013**, *52*, 8111–8115.

(990) Reuter, C.; Wienand, W.; Schmuck, C.; Vögtle, F. A Self-Threaded "Molecular 8." *Chem. Eur. J.* **2001**, *7*, 1728–1733.

(991) Boyle, M. M.; Forgan, R. S.; Friedman, D. C.; Gassensmith, J. J.; Smaldone, R. A.; Stoddart, J. F.; Sauvage, J.-P. Donor–Acceptor Molecular Figures-of-Eight. *Chem. Commun.* **2011**, *47*, 11870–11872.

(992) Boyle, M. M.; Gassensmith, J. J.; Whalley, A. C.; Forgan, R. S.; Smaldone, R. A.; Hartlieb, K. J.; Blackburn, A. K.; Sauvage, J.-P.; Stoddart, J. F. Stereochemistry of Molecular Figures-of-Eight. *Chem. Eur. J.* **2012**, *18*, 10312–10323.

(993) Wolf, R.; Asakawa, M.; Ashton, P. R.; Gómez-López, M.; Hamers, C.; Menzer, S.; Parsons, I. W.; Spencer, N.; Stoddart, J. F.; Tolley, M. S.; Williams, D. J. A Molecular Chameleon: Chromophoric Sensing by a Self-Complexing Molecular Assembly. *Angew. Chem., Int. Ed.* **1998**, *37*, 975–979.

(994) Li, S.-H.; Zhang, H.-Y.; Xu, X.; Liu, Y. Mechanically Selflocked Chiral Gemini-Catenanes. *Nature Commun.* **2015**, *6*: 7590.

(995) Williams, A. R.; Northrop, B. H.; Chang, T.; Stoddart, J. F.; White, A. J. P.; Williams, D. J. Suitanes. *Angew. Chem., Int. Ed.* **2006**, *45*, 6665–6669.

(996) Northrop, B. H.; Aricó, F.; Tangchiavang, N.; Badjić, J. D.; Stoddart, J. F. Template-Directed Synthesis of Mechanically Interlocked Molecular Bundles Using Dynamic Covalent Chemistry. *Org. Lett.* **2006**, *8*, 3899–3902.

(997) Northrop, B. H.; Spruell, J. M.; Stoddart, J. F. Efficient Routes to Novel Molecular Architectures: Template-Directed Synthesis of Mechanically Interlocked Structures. *Chim. Oggi* **2007**, *25*, 4–7.

(998) Gan, Q.; Ferrand, Y.; Bao, C.; Kauffmann, B.; Grelard, A.; Jiang, H.; Huc, I. Helix-Rod Host-Guest Complexes with Shuttling Rates Much Faster Than Disassembly. *Science* **2011**, *331*, 1172–1175.

(999) Ferrand, Y.; Gan, Q.; Kauffmann, B.; Jiang, H.; Huc, I. Template-Induced Screw Motions Within an Aromatic Amide Foldamer Double Helix. *Angew. Chem., Int. Ed.* **2011**, *50*, 7572–7575.

(1000) Gan, Q.; Ferrand, Y.; Chandramouli, N.; Kauffmann, B.; Aube, C.; Dubreuil, D.; Huc, I. Identification of a Foldaxane Kinetic Byproduct during Guest-Induced Single to Double Helix Conversion. *J. Am. Chem. Soc.* **2012**, *134*, 15656–15659.

(1001) Denisov, S. A.; Gan, Q.; Wang, X.; Scarpantonio, L.; Ferrand, Y.; Kauffmann, B.; Jonusauskas, G.; Huc, I.; McClenaghan, N. D. Electronic Energy Transfer Modulation in a Dynamic Foldaxane: Proof-of-Principle of a Lifetime-Based Conformation Probe. *Angew. Chem., Int. Ed.* **2016**, *55*, 1328–1333.

(1002) Leong, W. L.; Vittal, J. J. One-Dimensional Coordination Polymers: Complexity and Diversity in Structures, Properties, and Applications. *Chem. Rev.* **2011**, *111*, 688–764.

(1003) Dance, I. G.; Fitzpatrick, L. J.; Rae, A. D.; Scudder, M. L. The Intertwined Double-(-AgSR-).*Infin*.-Strand Chain Structure of Crystalline (3-Methylpentane-3-thiolato) Silver, in Relation to $(AgSr)_8$ Molecules in Solution. *Inorg. Chem.* **1983**, *22*, 3785–3788.

(1004) Sailaja, S.; Rajasekharan, M. V. One-Dimensional Coordination Polymers of Silver(I) with Aminomethylpyridines. Example of a Triple Helical Infinite Chain. *Inorg. Chem.* **2000**, *39*, 4586–4590.

(1005) Van Calcar, P. M.; Olmstead, M. M.; Balch, A. L. Construction of a Knitted Crystalline Polymer Through the Use of Gold(I)–Gold(I) Interactions. *J. Chem. Soc., Chem. Commun.* **1995**, 1773–1774.

(1006) Carlucci, L.; Ciani, G.; Gramaccioli, A.; Proserpio, D. M.; Rizzato, S. Crystal Engineering of Coordination Polymers and Architectures Using the $[Cu(2,2'\text{-bipy})]^{2+}$ Molecular Corner as Building Block (bipy = 2,2′-bipyridyl). *CrystEngComm* **2000**, *2*, 154–163.

(1007) Ino, I.; Zhong, J. C.; Munakata, M.; Kuroda-Sowa, T.; Maekawa, M.; Suenaga, Y.; Kitamori, Y. 2-D Interwoven and 3-D 5-Fold Interpenetrating Silver(I) Complexes of 1-(Isocyanidomethyl)-1*H*-benzotriazole and 1,3-Bis(dicyanomethylidene)Indan. *Inorg. Chem.* **2000**, *39*, 4273–4279.

(1008) Axtell, E. A.; Liao, J.-H.; Kanatzidis, M. G. Flux Synthesis of LiAuS and NaAuS: "Chicken-Wire-Like" Layer Formation by Interweaving of $(AuS)_n^{n-}$ Threads. Comparison with α-HgS and AAuS (A = K, Rb). *Inorg. Chem.* **1998**, *37*, 5583–5587.

(1009) Luan, X.-J.; Wang, Y.-Y.; Li, D.-S.; Liu, P.; Hu, H.-M.; Shi, Q.-Z.; Peng, S.-M. Self-Assembly of an Interlaced Triple-Stranded Molecular Braid with an Unprecedented Topology through Hydrogen-Bonding Interactions. *Angew. Chem., Int. Ed.* **2005**, *44*, 3864–3867.

(1010) Luan, X.-J.; Cai, X.-H.; Wang, Y.-Y.; Li, D.-S.; Wang, C.-J.; Liu, P.; Hu, H.-M.; Shi, Q.-Z.; Peng, S.-M. An Investigation of the Self-Assembly of Neutral, Interlaced, Triple-Stranded Molecular Braids. *Chem. Eur. J.* **2006**, *12*, 6281–6289.

(1011) Tkalec, U.; Ravnik, M.; Čopar, S.; Žumer, S.; Muševič, I. Reconfigurable Knots and Links in Chiral Nematic Colloids. *Science* **2011**, *333*, 62–65.

(1012) Martinez, A.; Ravnik, M.; Lucero, B.; Visvanathan, R.; Žumer, S.; Smalyukh, I. I. Mutually Tangled Colloidal Knots and Induced Defect Loops in Nematic Fields. *Nature Mater.* **2014**, *13*, 258–263.

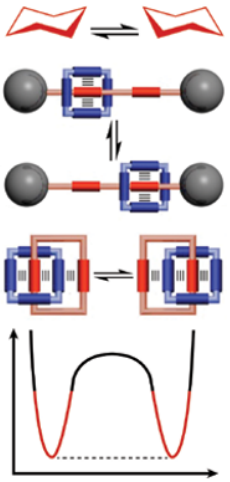
(1013) Kleckner, D., Irvine, W. T. M. Creation and Dynamics of Knotted Vortices. *Nature Phys.* **2013**, *9*, 253–258.

(1014) Irvine, W. T. M.; Bouwmeester, D. Linked and Knotted Beams of Light. *Nature Phys.* **2008**, *4*, 716–720.

(1015) Dennis, M. R.; King, R. P.; Jack, B.; O'Holleran, K.; Padgett, M. J. Isolated Optical Vortex Knots. *Nature Phys.* **2010**, *6*, 118–121.

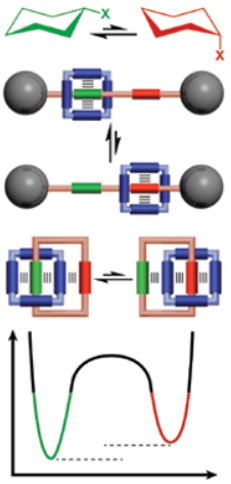
Chapter 5 The Stereochemistry of the Mechanical Bond

Conspectus



In his monograph entitled “An Introduction to Stereochemistry” published in 1965, Kurt Mislow comments that “*Stereochemistry is an old science (Louis Pasteur was its first practitioner) and terminology has not kept pace with the development of substantive matter.*” In his treatment of this evolutionary science emphasizing the fundamentals of structural stereochemistry, new terminology and images were introduced quite freely. Half a century later a similar situation prevails. With the advent of the mechanical bond, there is a present and prescient need to invent precise language to describe the rapidly emerging aspects of mechanostereochemistry.

The conceptual basis for mechanostereochemistry—both static and dynamic—can be appreciated most readily by drawing analogies with the stereochemistry of compounds whose molecules possess only covalent bonds—for example, cyclohexane and its (monosubstituted) derivatives. Since compounds such as catenanes and rotaxanes contain mechanically interlocked entities, it is convenient to call these entities *component parts*. Thus, if stereoisomers are isomers possessing identical constitutions which differ in the arrangement of their atoms in space, then *mechanostereoisomers* are simply isomers that possess identical mechanically interlocked component parts but which differ in the arrangement of these parts in space. In common with the existence of static and dynamic stereoisomerism in covalent chemistry, we can contemplate both *static* and *dynamic mechanostereoismerism*, which recognizes the three-dimensional nature of the mechanical bond. As more often is the case than not in chemistry, the boundaries between static and dynamic mechanostereochemistry are not at all clearly defined. There are dynamic processes where interconversion occurs between different ‘static’ mechanostereoisomers and there are potentially ‘dynamic’ mechanostereoisomers that are prevented from undergoing isomerization by insurmountable energy barriers.



Whereas molecular structure can be defined at the level of a molecule’s constitution, configuration and conformation, when considering mechanomolecules, multiple molecular entities encompass the structural domain. They can be easily understood and explained by adding the prefix ‘co-’ to denote *co-constitution*, *co-configuration* and *co-conformation*. While co-constitution and co-configuration describe the constitution and chirality, respectively, of a mechanomolecule, co-conformation describes the relative positions of the component parts affording spatial distinction between mechanostereoisomers, which can be interconverted by intramolecular movements involving *translation*, *pirouetting*, *circumrotation* and/or *rocking* under the jurisdiction of the mechanical bond. These intramolecular movements are generally characterized by very much larger amplitudes than are feasible in the realm of conformational change as it is expressed in covalent chemistry: for example, a substituent X located on the chair conformation of a cyclohexane ring undergoing interconversion between an equatorial and an axial orientation. It is these relatively large amplitude motions between the component parts in non-degenerate bistable catenanes and, in particular, rotaxanes, which can be switched and actuated chemically, electrochemically and photochemically, that provide a fruitful platform for the furtherance of *molecular nanotechnology*.

The realm of static mechanostereochemistry is bristling with opportunities for stereochemically astute and enquiring minds. Molecules containing mechanical bonds and entanglements open up a veritable Pandora’s box for stereoisomerism as it relates to differences in (i) *sequences* and (ii) *orientations* of component parts in mechanically interlocked molecules, as well as (iii) the infinite possibilities for *chirality* to be expressed mechanically in *planar*, *axial*, *helical* and *topological* contexts. The fact that, for example, catenanes, knots, and extended networks occupy an exclusive domain between chemical topology and mechanostereochemistry has given rise to the discipline of *topological stereochemistry* from which mechanically interlocked molecules such as rotaxanes are excluded. *Topological stereoisomers* are molecules that are both *homeomorphic* and *non-isotopic*. When chirality is introduced into topological stereochemistry it transpires that molecules can display either *enantiomerism* or *diastereoisomerism* in both an *unconditional* and *conditional* sense. For example, while a doubly interlocked [2]catenane (Solomon knot) and a trefoil knot are *unconditionally chiral*, molecular Borromean rings and Hopf link [2]catenanes are *conditionally chiral* when their rings are constitutionally cyclodirectional.

Chemical topology and mechanostereochemistry can be regarded as *emergent stereochemical concepts* arising from a combination of the topological and Euclidean stereochemistry of covalently bonded component parts that share mechanical bonds. These emergent concepts constitute one of the most intellectually challenging and unprecedented lines of fundamental research in contemporary stereochemistry.

The Nature of the Mechanical Bond: From Molecules to Machines, First Edition. Carson J. Bruns and J. Fraser Stoddart.
© 2017 John Wiley & Sons, Inc. Published 2017 by John Wiley & Sons, Inc.

Introduction 472
5.1 Dynamic Mechanostereoisomerism 473
5.1.1 Translation and Circumrotation 474
5.1.1.1 Non-Degenerate Translational Isomers 476
5.1.1.2 Degenerate Translational Isomers 487
5.1.2 Pirouetting 502
5.1.2.1 Within-the-Annulus Pirouetting 503
5.1.2.2 Through-the-Annulus Pirouetting 508
5.1.2.3 Super-Rotation 512
5.1.3 Rocking 512
5.1.4 Robust Dynamics 513
5.2 Static Mechanostereoisomerism 515
5.2.1 Orientational Mechanostereoisomers 515
5.2.2 Sequence Mechanostereoisomers 520
5.2.3 Mechanically Chiral Mechanostereoisomers 522
5.2.3.1 Mechanically Planar Chirality 523
5.2.3.2 Mechanically Axial Chirality 526
5.2.3.3 Mechanical Helicity 528
5.2.4 Topological Stereoisomerism 531
5.2.4.1 Topological Enantiomers 533
5.2.4.2 Conditional Topological Isomers 539
Concluding Remarks 540
References 541

Introduction

Much of the static and dynamic stereochemistry of molecules with mechanical bonds can be understood by drawing analogies with the stereochemistry of molecules possessing only covalent bonds[1]—a tactic we will adopt as we introduce the different Sections of this Chapter. We will employ the term 'mechanostereoisomer' to describe isomers arising from the stereochemistry associated with mechanical bonds, since the term 'stereoisomer' is reserved for isomerism associated with covalent and coordinate bonds. Stereoisomers are molecules with identical molecular formulas and constitutions (sequences) of atoms, yet different three-dimensional arrangements of these atoms in space. By analogy, mechanostereoisomers are molecules comprising mechanically bonded component parts with identical constitutions, yet different three-dimensional orientations of these component parts in space.

Stereoisomerism[2]—Isomerism arising from differences in the spatial arrangement of atoms without any differences in connectivity or bond multiplicity between the isomers.

Mechanostereoisomerism—Isomerism arising from differences in the spatial arrangement of the component parts in a mechanomolecule without any differences in the constitution of the component parts.

Stereoisomers[2]—Isomers that possess identical constitutions, but which differ in the arrangement of their atoms in space.

Mechanostereoisomers—Isomers that possess identical mechanically interlocked component parts, but which differ in the arrangement of their component parts in space.

Mechanostereoisomerism should not be conflated with topological isomerism, since mechanostereoisomers share identical topologies, whereas topological isomers do not—see **Section 5.2.4**. Some mechanostereoisomers can be interconverted by the unique types of mechanical motion enabled by mechanical bonds, while other types of mechanostereoisomers arise from differences in the orientation, sequence, and chirality of the component parts. Thus, it is convenient to classify types of mechanostereoisomerism into dynamic (**Section 5.1**) and static (**Section 5.2**) categories. In general, dynamic mechanostereoisomers can be interconverted by intramolecular mechanical motion, while static mechanostereoisomers do not typically interconvert unless a mechanical bond is broken and re-formed.

Dynamic mechanostereoisomers—Isomers that can be converted by dynamic processes constrained by mechanical bonds.

Static mechanostereoisomers—Isomers arising from differences in the relative orientations, sequences, or mechanical/topological chirality of component parts engaged in mechanical bonding.

In reality, the line between static and dynamic mechanostereoisomers is blurred, as one can find examples of

dynamic processes that interconvert different 'static' mechanostereoisomers, as well as examples of 'dynamic' mechanostereoisomers that do not isomerize on account of insurmountable activation barriers.

The structures of molecules can be summarized by the 'three C's': constitution, configuration, and conformation. Since mechanomolecules like catenanes and rotaxanes have more than one component part, each possessing its own constitution, configuration, and conformation, the 'three C's' of mechanomolecules may be written with the prefix 'co-', denoting the involvement of multiple molecular entities. Co-constitution, co-configuration, and co-conformation may thus be understood in relation to their analogues lacking mechanical bonds. For example:

Constitution[2]—The description of the identity and connectivity (and corresponding bond multiplicities) of the atoms in a molecular entity (omitting any distinction arising from their spatial arrangement).

Co-Constitution—The sum of the constitutions of the component parts engaged in mechanical bonding.

Co-conformation and co-configuration are defined in **Sections 5.1** and **5.2.3**, respectively. In addition to this Chapter, several reviews[3–5] on the stereochemical and dynamical consequences of mechanical bonding in molecules are available in the literature.

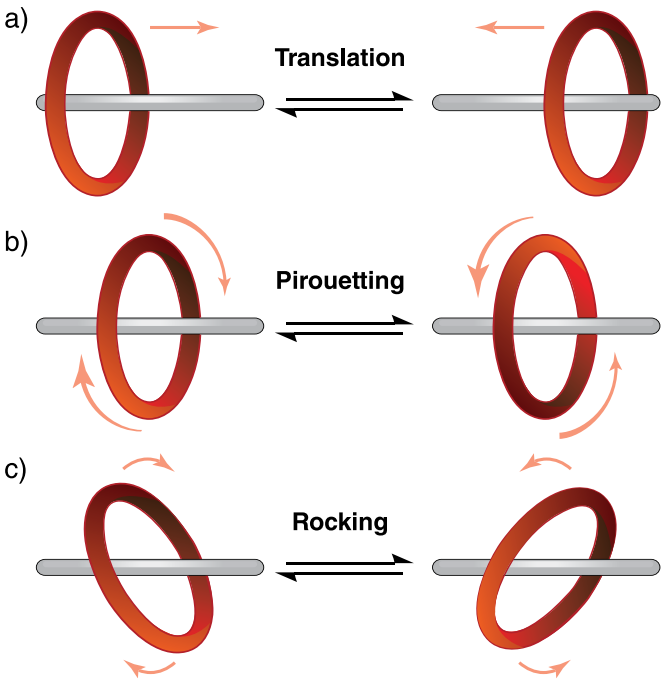


Figure 5.1 Dynamic processes available to a ring encircling an axle constrained by the mechanical bond, as in catenanes and rotaxanes. (a) *Translation* along the axle. (b) *Pirouetting* about the axle. (c) *Rocking* orthogonally to the axle. The axle is fixed in this frame of reference—note that the axle can execute the same motions with respect to a fixed ring.

5.1 Dynamic Mechanostereoisomerism

Molecules never stop moving. An incessant flux of thermal energy leads to atomistic 'jigglings and wigglings'—as described by Feynman[6]—as a result of stretching, bending, and rotation of molecular bonds while tumbling and traversing through space, especially in the liquid and gaseous states. Mechanical bonds add an extra dimension to the types of motion that can be expressed by molecules. Whereas the component parts of a mechanically interlocked molecule (MIM) are all subject individually to the typical stretching, bending, and rotation of their covalent bonds, they are also subject to the dynamics of motion constrained by the mechanical bond, giving rise to completely new types of isomerism.

Stereoisomers that interconvert by rotations about single or partial double bonds are known[2] as conformational isomers, conformers, or rotamers. Correspondingly, supramolecular and mechanically bonded isomers that interconvert as a result of the dynamics of noncovalent and mechanical bonds in supermolecules and MIMs, respectively, are known[7,8] as co-conformational isomers or co-conformers. At the most general level, a molecular ring encircling an 'axle' belonging to either the ring of a catenane or the dumbbell of a rotaxane can interconvert between co-conformations by any of three kinds of processes: (i) translation (**Figure 5.1a**, **Section 5.1.1**) of the ring along the axle, (ii) rotation (**Figure 5.1b**, **Section 5.2.2**) of a ring with respect to the axle which it encircles, a process known as pirouetting, and (iii) rocking (**Figure 5.1c**, **Section 5.1.3**), a process in which the ring and axle swivel about orthogonal axes, the range of which is limited by their steric interactions. In the case of catenanes, where all component parts are rings, the distinction between translation and pirouetting is a subtle one—see **Section 5.1.2**. The term 'circumrotation' has also been introduced[9] to describe the revolutions of a catenane's rings. In a [2]catenane, for example, the circumrotatory translation of one ring is tantamount to the pirouetting of the other ring—i.e., if ring A is pirouetting, then ring B is circumrotating, and vice versa. In general, the terms 'translation' or 'circumrotation' may be employed to describe the motion of a small ring with respect to a larger one. Thus, although we have reviewed circumrotational motions in catenanes in this Chapter primarily under the banner of pirouetting (**Section 5.1.2**), it would be equally appropriate to discuss them in the context of translation (**Section 5.1.1**).

Conformation[2]—The spatial arrangement of the atoms affording distinction between stereoisomers which can be interconverted by rotations about single or partial double bonds.

Co-conformation—The spatial arrangement of the component parts affording distinction between mechanostereoisomers which can be interconverted by translation, pirouetting, or rocking motions constrained by the mechanical bond.

Translation—An intramolecular motion constrained by the mechanical bond involving the movement of a component part from one position to another, relative to a component part with which it is mechanically interlocked.

Pirouetting—An intramolecular motion constrained by the mechanical bond involving the rotation of a ring about an axis.

Rocking—An intramolecular motion constrained by the mechanical bond involving the swiveling of one component part orthogonally to that of another component part.

Circumrotation—An intramolecular motion in catenanes involving the rotation of a ring such that its atoms pass through the annulus of another ring.

We note that the motions of component parts are relative in most cases. It is convenient conceptually to fix one component as a point of reference—e.g., a rotor and a stator—although there is no difference, at least in solution, between a ring translating along an axle versus an axle translating through a ring, or a ring rotating about an axle versus an axle rotating within a ring. The fixed point of reference is less arbitrary at interfaces and in the solid state, where it is possible to anchor components to solid supports, leading[10] to 'robust dynamics' (**Section 5.1.4**) characterized by precisely defined motion and higher resistance to degradation.

In molecules with mechanical bonds, conformational changes—i.e., bond torsions—happening at the molecular level are superimposed on the co-conformational changes (translation, pirouetting, rocking, etc.) at the mechanomolecular level. We concern ourselves here primarily with the latter kind of dynamics. We also note that MIMs prepared by the statistical, directed, or active template methods rarely exhibit strong intramolecular interactions between component parts, giving rise often to mechanostereoisomerism and solution-state dynamics that are not well defined. By contrast, many mechanomolecules obtained by template-directed synthesis possess local intramolecular interactions that 'live on' from the corresponding templates, a feature which typically biases the distribution of mechanostereoisomers to favor a limited number of co-conformations. Our discussion is therefore restricted mainly to templated molecules, whose isomerism and dynamics are more easily characterized employing the tenets and rigor of physical chemistry. While our understanding of molecular dynamics constrained by mechanical bonds has relied extensively on the transition-state theory[11] (TST) of chemical reactivity—see **Section 5.1.1**—we note that this theory is merely an approximation. It may also be appropriate in some cases to turn to reaction-rate theories[12] such as the celebrated one introduced by Kramers[13] in 1940.

The dynamics of mechanomolecules, in particular the large-amplitude mechanical motions that can be expressed by translation, are important to the design of molecular switches and other machines (**Chapter 6**) and can also have far-reaching effects on the mechanical properties of bulk materials, especially in the context of polymers—see **Sections 4.1.2.1, 4.1.4.5, 4.2.1.1**, and **4.2.3.6–4.2.3.8**.

5.1.1 Translation and Circumrotation

The mechanical bond constrains the translational motion of a ring to an approximately one-dimensional pathway defined by the axle of a rotaxane, while the corresponding pathway in a catenane is two-dimensional because it is circular. The translational isomers (**Figure 5.2**) of rotaxanes and catenanes are therefore interconverted by translation of the rings along these mechanically constrained pathways. These mechanostereoisomers may also be referred[14] to as circumrotational isomers in the case of catenanes. An analogy can be drawn with the dynamic stereoisomerism of molecules associated with rotation around covalent bonds – namely, torsional isomers or rotamers.

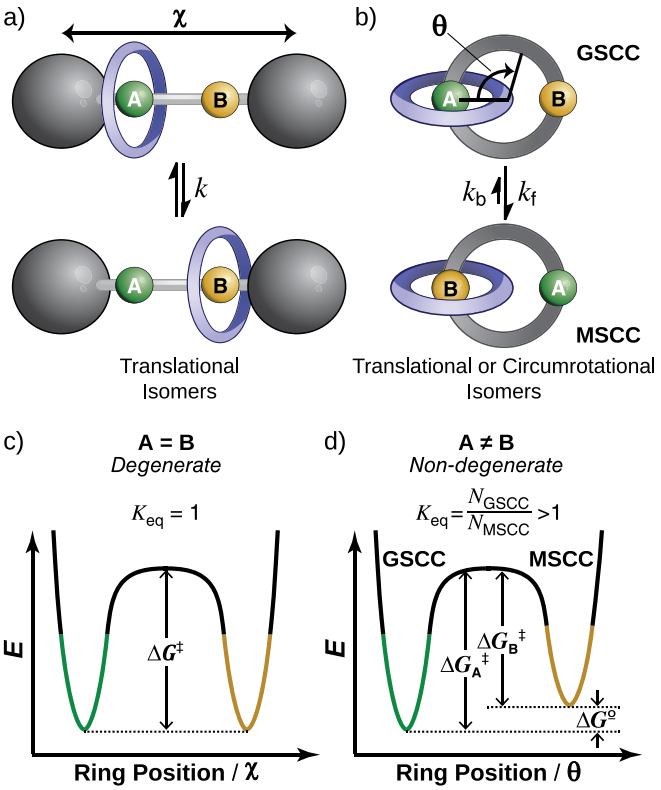


Figure 5.2 Graphical representations of the translational isomers of (a) a bistable [2]rotaxane and (b) a bistable [2]catenane, as well as energy landscapes illustrating (c) degenerate and (d) non-degenerate bistability. Interconversion between translational isomers is associated with the movement of a ring between two recognition units, labeled A and B, representing free energy minima. At equilibrium, the population of the translational isomers are equal ($K_{eq} = 1$) in degenerate (A = B) systems, while non-degenerate (A ≠ B) population distributions ($K_{eq} > 1$) are determined by the difference in free energy, ΔG°, between the two minima—the ground state co-conformation (GSCC) and the metastable state co-conformation (MSCC). The rate (k) of interconversion between translational isomers is determined by the difference in free energy, $\Delta G^{\ddagger}$, between these stable co-conformations and a transition state in which the ring resides in between the recognition units A and B.

Torsional stereoisomers[2]—Stereoisomers that can be converted (actually or conceptually) by torsion about a bond axis.

Translational isomers—Mechanostereoisomers that can be converted (actually or conceptually) by translation of mechanically bonded component parts.

In conformational analysis,[15] an energy barrier is associated with the bond torsions that interconvert the stable and/or metastable conformations of a molecule. Likewise, one can assess the thermodynamics and kinetics of conversion between the co-conformations of a MIM—an activity we can refer to as co-conformational analysis. An important concept in co-conformational analysis is that of bistability. A molecule is said to be bistable if it exists in two stable states at equilibrium. Bistability manifests itself in rotaxanes (**Figure 5.2a**) and catenanes (**Figure 5.2b**) as a situation in which a ring can translocate between two recognition units (A and B), which are either degenerate (A = B) or non-degenerate (A ≠ B). In this Section, we present examples of bistable MIMs expressing non-degenerate (**Section 5.1.1.1**) and degenerate (**Section 5.1.1.2**) translational isomerism in solution, along with information on the thermodynamics and kinetics of the co-conformational isomerizations, when possible.

In the generalized free energy profiles of degenerate (**Figure 5.2c**) and non-degenerate (**Figure 5.2d**) MIMs, the energy barrier to translational isomerization is equal to the difference in free energies ($\Delta G^{\ddagger}$) between local minima, representing stable or metastable co-conformations, and local saddle points representing transition states.[A] In the case of non-degenerate MIMs (**Figure 5.2d**), an additional energy term ($\Delta G°$) describes the difference in free energy between the globally most stable mechanostereoisomer, known[16,17] as the ground state co-conformation (GSCC), and the locally stable mechanostereoisomer known[16,17] as the metastable state co-conformation (MSCC), according to Equation 5.1.

$$\Delta G^{\circ} = \Delta G_{MSCC} - \Delta G_{GSCC} \tag{5.1}$$

$\Delta G°$ is related to the dimensionless co-conformational equilibrium constant K_{eq}, which is defined by the ratio of co-conformers in the GSCC to those in the MSCC (N_{GSCC}/N_{MSCC}), according to Equation 5.2, where R is the Universal Gas Constant and T is the absolute temperature –

$$K_{eq} = \frac{N_{GSCC}}{N_{MSCC}} = e^{-\Delta G^{\circ}/RT} \tag{5.2}$$

In practice, K_{eq} and $\Delta G°$ are determined by measuring the GSCC:MSCC ratio in an equilibrated sample of the bistable compound using spectroscopic, electrochemical, or calorimetric techniques. Note that the influence of enthalpy ΔH and entropy ΔS on ΔG and K_{eq} can be deduced from the Gibbs-Helmholtz Equation 5.3 and the van't Hoff Equation 5.4 respectively –

$$\Delta G = \Delta H - T\Delta S \tag{5.3}$$

$$\ln K_{eq} = -\frac{\Delta H}{RT} + \frac{\Delta S}{R} \tag{5.4}$$

Equations 5.1–5.4 define the thermodynamic parameters on the potential energy surface of a MIM. The kinetics of translation, on the other hand, are determined by the transition state energy, $\Delta G^{\ddagger}$, corresponding to the free energy of activation for isomerization between the GSCC and MSCC. The rate constant k for this process is defined by the Eyring Equation 5.5 –

$$k = \frac{k_B T}{h} e^{-\Delta G^{\ddagger}/RT} \tag{5.5}$$

where h is the Planck constant and k_B is the Boltzmann constant. If the rate k is known, rearrangement—see Equation 5.6—of the Eyring Equation provides a value for $\Delta G^{\ddagger}$:

$$\Delta G^{\ddagger} = -RT \ln\left(\frac{hk}{k_B T}\right) \tag{5.6}$$

The free energy terms in Equations 5.1–5.6 are illustrated conceptually on the potential energy surface diagrams of degenerate and non-degenerate bistable MIMs in **Figure 5.2c–d**, while the entries in **Table 5.1** demonstrate the relationship between the GSCC:MSCC ratio in the

Table 5.1 Exemplifying the relationship between the ground state distribution, expressed as a GSCC:MSCC ratio, and K_{eq} and $\Delta G°$ values.

GSCC : MSCC	K_{eq} / M^{-1}	$\Delta G°$ / kcal·mol^{-1}
1:1	1	0
2:1	2	0.4
10:1	10	1.4
100:1	100	2.7
1000:1	1000	4.1
10000:1	10000	5.5

[A] The free energy diagrams in **Figure 5.2**, which are based in TST, are more simplistic than those of most real systems. A more realistic model would take into account the intermediate species corresponding to local minima on the linker in between recognition units. The shuttling process in most bistable catenanes and rotaxanes is most likely multistep, such that (i) the ring overcomes a relatively large energetic barrier in order to escape from one recognition site (station A), allowing the ring to (ii) sample various high-lying local minima on the linker by a random walk before (iii) overcoming a low energy barrier as it moves to encircle a second recognition site (station B). The steady state approximation, which assumes that intermediates are consumed as quickly as they are generated, is typically invoked in order to treat the system as one that possesses a single rate-determining step as suggested by **Figure 5.2**, an assumption which is valid and appropriate in most cases.

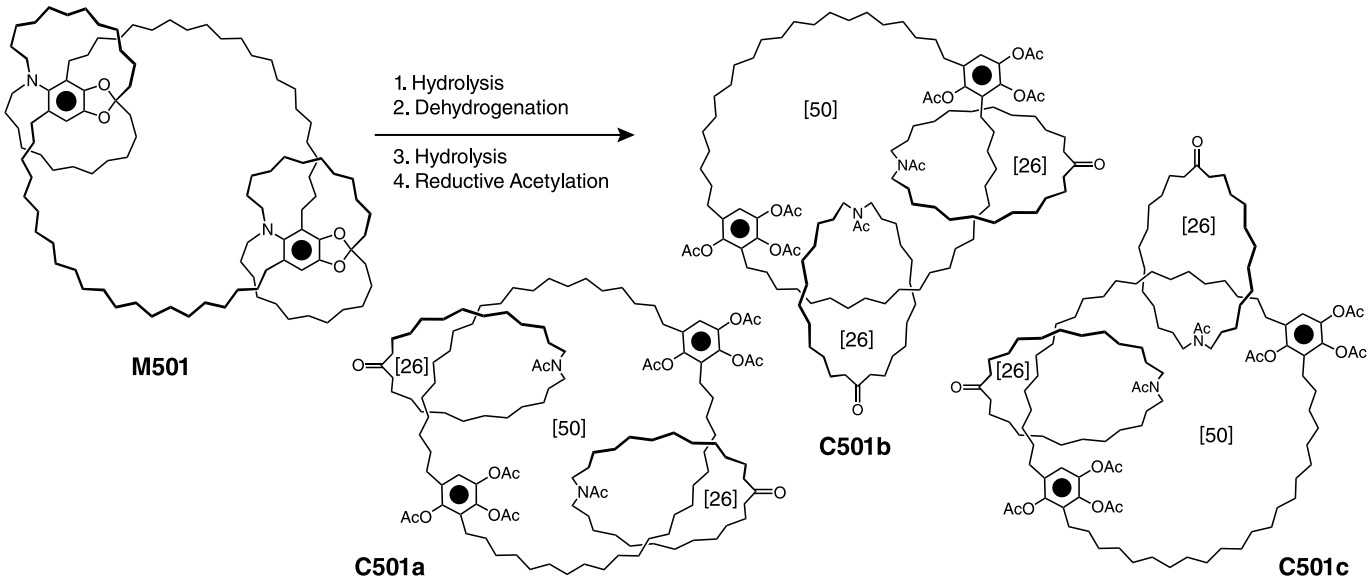
ground state, the equilibrium constant K_{eq}, and $\Delta G°$, at room temperature. See **Figure 3.2** in **Section 3.1** for a plot depicting how the timescale of a reaction depends on the activation barrier $\Delta G^{‡}$.

5.1.1.1 Non-Degenerate Translational Isomers

The concept of translational isomerism was originally introduced and demonstrated (**Scheme 5.1**) by Schill,[18,19] who observed a mixture of mechanostereoisomers upon cleavage of the covalent templates of the macrocyclic precursor **M501** during his directed synthesis of the [3]catenane **C501**. The translational isomer **C501a** was separated chromatographically from a mixture of **C501b** and **C501c** and characterized unambiguously by ^{1}H NMR spectroscopy. The central ring of the [3]catenane, which comprises two multi-substituted aromatic rings, each bridged by two C_{22} oligomethylene chains, is sufficiently bulky in the vicinity of these aromatic rings to prevent the interconversion of translational isomers, even at 80 °C in a biphasic mixture of benzene and 30% aqueous NaOH. **C501b** and **C501c** appear similar because they both involve the two smaller rings encircling a single C_{22} chain, yet they too are non-degenerate translational isomers on account of the larger ring's lack of rotational symmetry, which distinguishes the chemical environments of each C_{22} chain. Although Schill's translational isomers do not interconvert on account of the steric bulk of the aromatic units, it would be possible in principle to convert them, given a sufficient influx of energy, by allowing one of the rings to transgress one of these bulky hurdles.

Following in the footsteps of Schill's translationally isomeric [3]catenanes, a number of [2]catenanes derived from supramolecular templates have been prepared as a mixture of non-interconverting translational isomers. Vögtle[20] described a series of [2]catenanes (**C502**) based on tetralactam macrocycles with non-equivalent functional groups appended to the isophthalamide recognition units, which can exist (**Figure 5.3**) as the so-called *out/out* isomer **C502a**, the *in/in* isomer **C502b**, and the *in/out* or *out/in* isomer **C502c**, and according to the different possible locations of the bulkiest (in this case, methoxyl) functional groups. The *in/in*, *in/out*, and *out/in* (the latter two being degenerate) isomers are obtained in lower yields (1.4 and 17%, respectively) than that (23%) of the *out/out* isomer, although it is not clear if this difference in populations, in which bulkier R groups are less likely to occupy the inner cavities of the [2]catenane, arises from thermodynamic or kinetic effects. Leigh[21–23] has employed protecting groups as chemically responsive elements for switching MIMs between regimes of interconvertible and non-interconvertible translational isomers in various ratchet mechanisms based on mechanically interlocked hydrogen-bonding motifs—see **Section 6.15.2**.

In cases of non-degenerately bistable MIMs with sufficiently low activation barriers to reach equilibrium, the populations of translational isomers are governed by the free energy difference, $\Delta G°$, between the stable (GSCC) and metastable (MSCC) co-conformations. The question arises as to whether data on the relative strengths of the underlying binding interactions could be used[24,25] as predictors in a "thermodynamic forecast" of the ground state distribution. Thermodynamic forecasting thus entails predicting the relative stabilities of the GSCC and MSCC in the free energy profile of a bistable MIM by assuming that $\Delta G°$ is equal, or at least proportional to, the difference in the free energies of association, ΔG_a, for pseudorotaxanes comprising the same recognition units and rings as the bistable MIM in question. Predictions of this sort would be very useful in the design of artificial molecular machines such as



Scheme 5.1 Schill's seminal synthesis[19] of three translational isomers of the [3]catenane **C501**, of which one (**C501a**) could be separated chromatographically from a mixture of the other two translational isomers **C501b-c**. The number of atoms in each ring are denoted in square brackets.

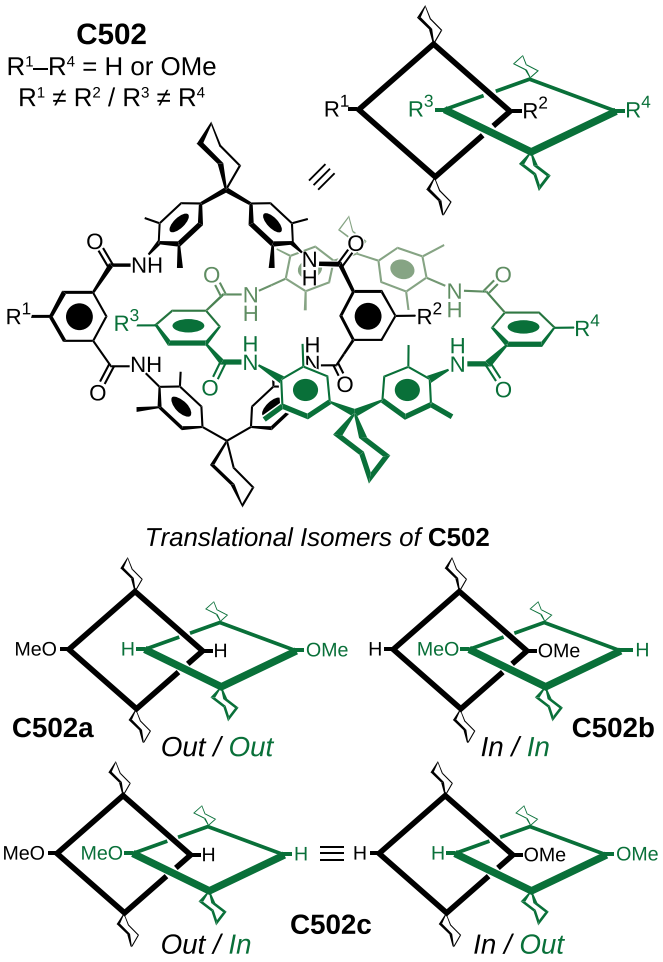


Figure 5.3 Non-interconverting translational isomers[20] of Vögtle's tetralactam-based [2]catenane **C502**.

switches and motors (**Chapter 6**), for example, if they were indeed reliable. In other words, a thermodynamic forecast would require that ΔG_{GSCC} and ΔG_{MSCC} could be approximated accurately by $\Delta\Delta G_a$, as defined by Equation 5.7

$$\Delta\Delta G_a = \Delta G_{a,A} - \Delta G_{a,B} \qquad (5.7)$$

where A and B are the two different guests acting as model compounds for the recognition units of the corresponding bistable MIM. The parameter ΔG_a is often determined by the association constant, K_a, of the model pseudorotaxane host-guest complex (*Guest⊂Host*), as defined by Equation 5.8 –

$$K_a = \frac{[Guest \subset Host]}{[Guest][Host]} = e^{-\Delta G_a / RT} \qquad (5.8)$$

Figure 5.4 compares the free energy profiles of a bistable rotaxane (**Figure 5.4a**) with a pair of pseudorotaxanes (**Figure 5.4b**) comprising the same ring and recognition units, labeled A and B. The key, and potentially dubious, assumption in this kind of thermodynamic forecast is that $\Delta\Delta G_a$ is indeed proportional to $\Delta G°$. Our case study (*vide infra*) on donor-acceptor MIMs suggests that this assumption is often true in bistable rotaxanes, but not so true in bistable catenanes, mainly because the enforced 'alongside' interactions in catenanes can change their thermodynamic landscape.

Case Study on Non-Degenerately Bistable Donor-Acceptor MIMs

Much of the early research on the thermodynamics[25,26] and kinetics[26,27] of dynamic translational isomers was investigated in the context of π-associated donor-acceptor (D-A) MIMs. Therefore, we will undertake a case study of translational isomerism in bistable and multistable D-A MIMs in order to introduce the various parameters that can influence the populations of different co-conformations. The translational isomerism of D-A catenanes and rotaxanes has been investigated and summarized in several publications[28–48] belonging to a 67-part 'Molecular Meccano' series purveyed in various journals throughout the 1990s and early 2000s. Although we are unable to summarize these investigations in a fully comprehensive manner, we have selected several of them as illustrative examples for a case

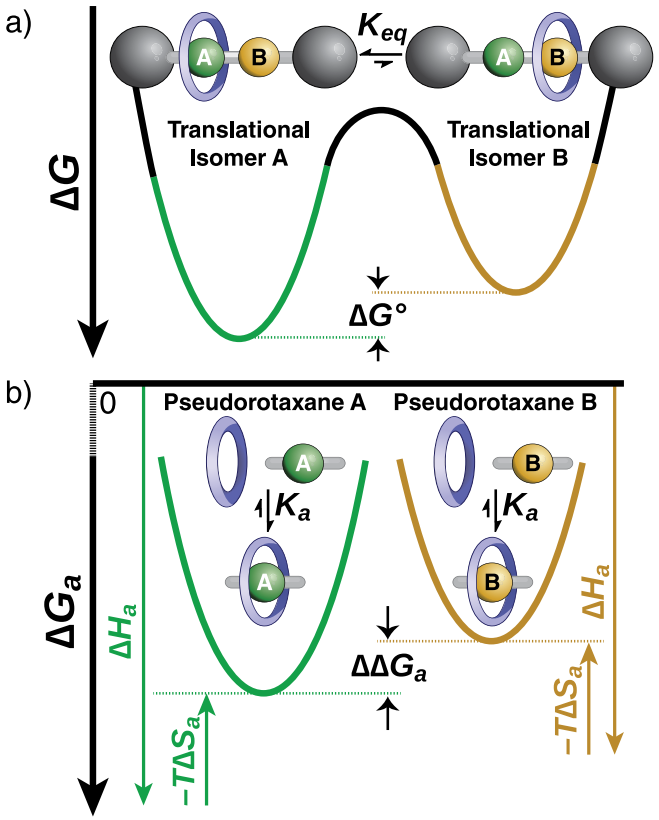


Figure 5.4 Free energy profiles of (a) a bistable [2]rotaxane and (b) model pseudorotaxanes comprising the same ring and recognition units A and B. The difference in free energy of association, $\Delta\Delta G_a$, between pseudorotaxanes A and B, as dictated by each of their association constants, K_a, can be used as a 'thermodynamic forecast' for the free energy difference, $\Delta G°$, between the rotaxane translational isomers A and B, which is governed by the equilibrium constant K_{eq}.

study, which demonstrates how the sterics and electronics of covalent, noncovalent, and mechanical bonds can influence mechanostereoisomerism in solution and in the solid state. Specifically, we will look at how the thermodynamics and kinetics of translational isomerism are influenced by structural parameters such as (i) recognition units, (ii) linkers, (iii) ring sizes, (iv) topology / architecture, and (v) constitution of a MIM. All cationic compounds were investigated as their PF_6^- salts in solution unless noted otherwise. See **Tables 2.12–2.14** in **Section 2.3.3.8** for K_a values recorded for the π-donors and π-acceptors in this case study.

The Influence of the Recognition Units

The relative strengths of the noncovalent bonding interactions, which 'live on' in MIMs derived from supramolecular templates, are suspected to be among the most important factors for understanding how the different co-conformations are populated. The non-degenerate bistable [2]catenanes illustrated in **Figure 5.5** are shown as their prevalent translational isomers—i.e., the GSCC—in order to demonstrate how different π-donating and π-accepting recognition units can affect the equilibrium constants (K_{eq}) governing the ground state distribution of translational isomers.

Whereas the $CBPQT^{4+}$ ring of the bistable [2]catenane **C503**$^{4+}$ encircles[39,49] the HQ recognition unit by more than a twofold margin (7:3 **C503**$^{4+}_{HQ}$:**C503**$^{4+}_{DNP}$) in CD_3COCD_3, the analogous tetracationic cyclophane comprising 1,2-bis(4-pyridinium)ethene[31] ($BIPYE^{2+}$) π-acceptors populates the **C504**$^{4+}_{DNP}$ and **C504**$^{4+}_{HQ}$ translational isomers[B] equally (K_{eq} = 1) in CD_3COCD_3. Both of these catenanes are sensitive to solvent polarity—**C503**$^{4+}_{HQ}$ is the GSCC in relatively low-polarity organic solvents such as Me_2CO and MeCN, yet **C503**$^{4+}_{DNP}$ becomes the dominant translational isomer in higher polarity solvents such as Me_2SO.[C] Moreover, the 1:1 GSCC:MSCC ratio in CD_3COCD_3 rises to >50:1 in favor of **C504**$^{4+}_{DNP}$ in CD_3CN.[C] Recognition units assuming the 'alongside' role in $CBPQT^{4+}$-based catenanes with high co-conformational selectivity in the company of HQ include the naphthalene-2,6-dimethylyl[42] (DMNP) and tetrafluorohydroquinone[37,50] (F_4HQ) units of the bistable [2]catenanes **C505**$^{4+}_{HQ}$ and **C506**$^{4+}_{HQ}$, respectively. The 1,5-dithianaphthalene (DTNP) unit representing the isomer **C507**$^{4+}_{DTNP}$ dominates[34] the ground state distribution (K_{eq} = 1.5) at 30 °C, yet the **C507**$^{4+}_{DNP}$ translational isomer is favored by the same ratio at –30 °C.[D] When DNP competes with the 1,4-dimercaptobenzene (DMB) recognition unit, however, only the **C508**$^{4+}_{DNP}$ translational isomer can be detected in solution.[34] Catenanes with non-degenerate π-acceptors—namely, $BIPY^{2+}$,[51] $BIPYE^{2+}$,[31,52] and 2,7-diazapyrenium[44] (DAP^{2+})—also exhibit[31,44,51] biased distributions of translational isomers. Regardless of whether the

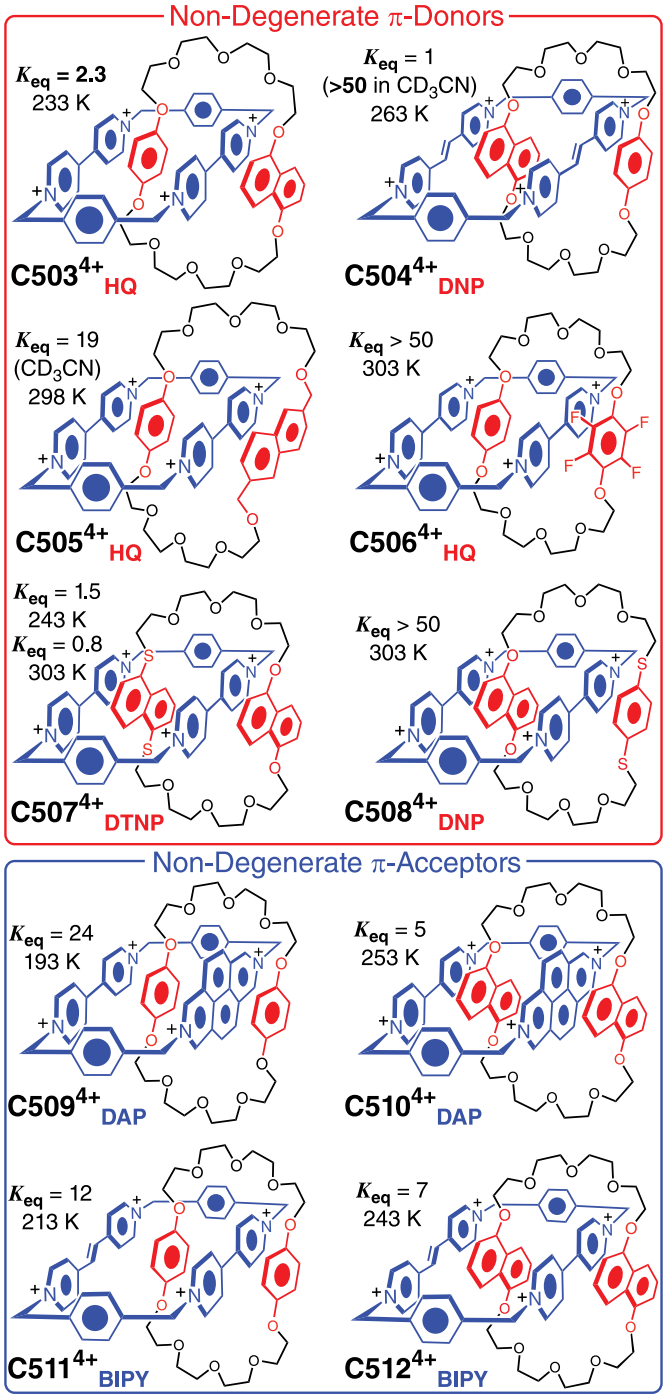
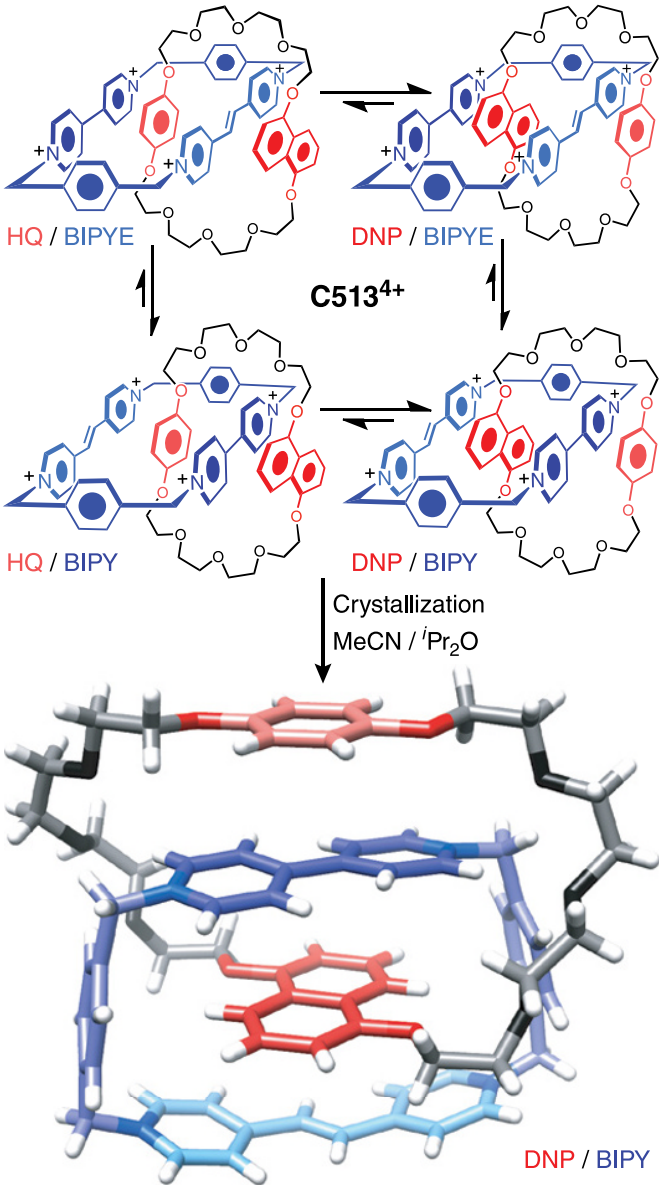


Figure 5.5 Examples of how different recognition units can influence translational isomerism. Stereoformulas of the dominant translational isomers, or ground state co-conformations (GSCCs), of non-degenerate bistable D-A [2]catenanes and their corresponding equilibrium constants (K_{eq}) are given at various temperatures in CD_3COCD_3 except where noted. Non-degenerate recognition units encircled in the GSCC are denoted in subscripts. See refs. 31, 37, 42, 44, 49, 51, 53.

[B] Subscripts denote a non-degenerate recognition unit representing the encircled site in a particular translational isomer of a MIM.
[C] Translational isomers with population distributions that are highly sensitive to solvent polarity are useful for the design of solvent-driven artificial molecular switches—see **Section 6.6**.
[D] Translational isomers with population distributions that are highly sensitive to temperature are useful for the design of thermally driven artificial molecular switches—see **Section 6.8.2**.

π-donors of the crown ether are HQ or DNP units, the encirclement of π-acceptors is prioritized according to the trend DAP^{2+}>BIPY^{2+}>BIPYE^{2+}, as demonstrated by the GSCCs of the bistable [2]catenanes **C509**$^{4+}_{DAP}$,[44] **C510**$^{4+}_{DAP}$,[44] **C511**$^{4+}_{BIPY}$,[31,52,53] and **C512**$^{4+}_{BIPY}$.[31,53]

Although the majority of MIMs in the literature are either monostable or bistable, MIMs with even more metastable mechanostereoisomers can be designed (**Scheme 5.2**) by introducing more recognition units. For example,[54] the D-A



Scheme 5.2 Although up to four translational isomers are available to the tetrastable [2]catenane **C513**$^{4+}$, the compound crystallizes exclusively, and exists predominantly in solution, as the isomer in which 1,5-dioxynaphthalene (DNP) and 4,4′-bipyridinium (BIPY^{2+}) units represent the encircled π-donors and π-acceptors, while hydroquinone (HQ) and bis(pyridinium)ethene (BIPYE^{2+}) represent the corresponding alongside recognition units, respectively.[54] A tubular representation of the solid-state structure of **C513**$^{4+}$ is shown with solvent molecules and PF_6^- counterions omitted for the sake of clarity.

[2]catenane **C513**$^{4+}$ possesses four different recognition units—HQ and DNP π-donors, BIPY^{2+} and BIPYE^{2+} π-acceptors—leading to a tetrastable free energy profile. The GSCC of this [2]catenane is the translational isomer in which DNP and BIPY^{2+} units occupy the 'inside' positions at the core of the catenane, while HQ and BIPYE^{2+} units occupy the 'alongside' positions at the periphery. At room temperature in CD_3COCD_3, the BIPY^{2+} and BIPYE^{2+} units exchange sites rapidly on the ^{1}H NMR timescale and the ratio of DNP- to HQ-encircled translational isomers is 88:12. At –40 °C, when the translation/circumrotation of both rings is frozen out on the ^{1}H NMR timescale, only two isomers, DNP/BIPY^{2+} and HQ/BIPY^{2+}, are detected in a 95:5 ratio. In other words, although **C513**$^{4+}$ is tetrastable, it exhibits a high co-conformational selectivity for only two of the four mechanostereoismers. Crystallization (**Scheme 5.2**) of the [2]catenane by slow vapor diffusion of $^{i}Pr_2O$ in MeCN affords only the DNP/BIPY^{2+} isomer (the GSCC) in the solid state.

Tetrathiafulvalene (TTF) has been an important π-donor for the design of D-A MIMs with controllable translational isomerism. Recalling from **Table 2.14** in **Section 2.3.3.8** that many TTF derivatives have been characterized as guests for CBPQT·4PF$_6$, we have a large 'meccano set' of building blocks for constructing bistable D-A MIMs with highly tunable thermodynamics[25] and kinetics.[27] The ground state distributions in MeCN of a number of CBPQT^{4+}-based rotaxanes and catenanes comprising various TTF derivatives accompanying either HQ or DNP π-donors are summarized in **Figure 5.6**. Since the *TTF⊂CBPQT*$^{4+}$ charge transfer interactions typically produce green-colored (λ_{max} ≥ 800 nm) solutions, in contrast with the red-colored (λ_{max} ≈ 400–600 nm) solutions arising from dioxyarenes and CBPQT^{4+}, it will be convenient to distinguish the translational isomers of MIMs based on these recognition elements as '*green*' or '*red*' isomers, respectively. The high variability in populations of *red* and *green* isomers in the examples illustrated in **Figure 5.6** show that the balance of co-conformations can be modulated over a wide range simply by changing the substituents on TTF. We will return to these MIMs throughout our case study on the influence of different parameters on the thermodynamics and kinetics of non-degenerate translational isomers.

TTF derivatives are most commonly installed as the chief recognition units encircled in the GSCCs of bistable D-A MIMs on account of their low-lying and reversibly accessible redox states, which renders them excellent switches—see **Section 6.1.1.1**. The distribution of translational isomers at equilibrium, as governed by K_{eq}, is an important aspect of artificial molecular switches that rely on mechanical bonds because the most highly biased populations of translational isomers are able to express the most 'clean' or 'high fidelity' switching—terms employed when the vast majority of a molecular population undergoes the same controlled translational isomerization event. One of the tightest binding guests for CBPQT^{4+}, with up to 7.7 kcal·mol^{-1} of

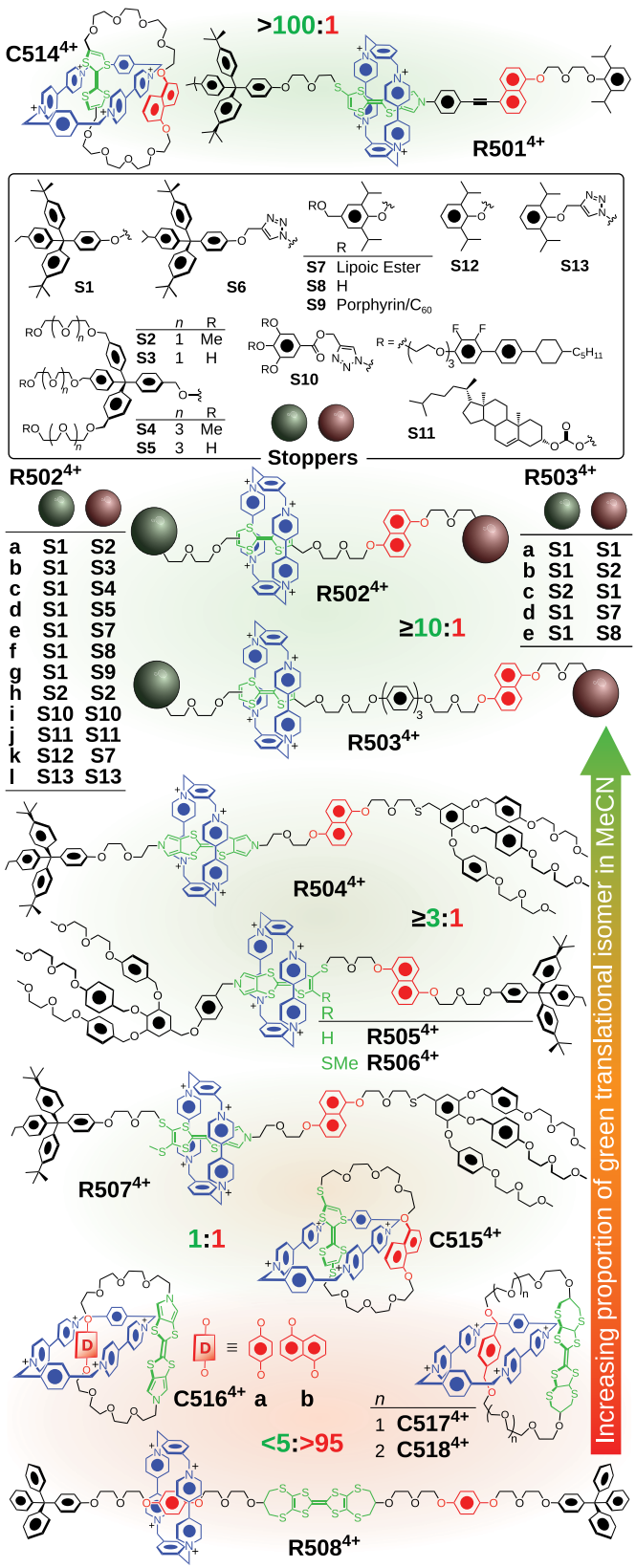


Figure 5.6 Stereoformulas of the GSCCs of bistable MIMs incorporating tetrathiafulvalene (TTF) derivatives. See refs. 17, 55, 58, 71–90, 100–103, 106, 118, 121, 123, 124, 126. Noted in green/red text are approximate ratios of *green*:*red* translational isomers in MeCN near room temperature.

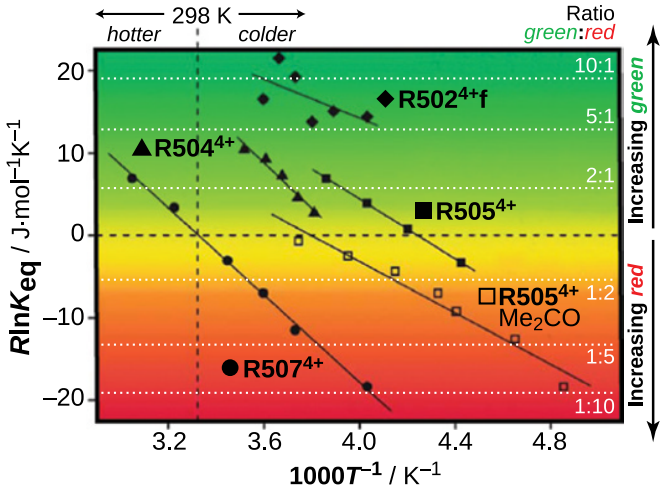


Figure 5.7 Van't Hoff plots of several bistable [2]rotaxanes, revealing how the population distributions change with temperature and solvent. Background colors reflect the GSCC:MSCC (*green*:*red*) ratios, which are also denoted in dashed white lines. Data was recorded in MeCN except where noted. Adapted with permission from ref. 26 (copyright 2005 Springer).

free energy, ΔG_a, of association[55] (K_a = 380,000 M^{-1}) at room temperature is the polyether-functionalized TTF-dimethanol unit,[56] first introduced[57] as the π-donor representing the GSCC of the bistable [2]catenane **C514⁴⁺**. The *green* isomer of **C514⁴⁺** is populated[58] almost exclusively (K_{eq} = 510) in MeCN. Other catenanes[16,24,59–70] and rotaxanes[17,55,58,71–99] possessing the TTF-dimethanol and DNP recognition units, of which there have been many, also exhibit highly biased population distributions. The *green*:*red* ratios in CBPQT⁴⁺ derived TTF/DNP [2]rotaxanes are estimated to be 10:1 *green*:*red* or greater in most cases, either by analysis[55,58,77] of electrochemical data or simply because the *red* isomers are not detected in CD_3CN or CD_3COCD_3 by ^1H NMR spectroscopy. **R502⁴⁺** and **R503⁴⁺** represent a number of TTF/DNP/CBPQT⁴⁺ rotaxanes that have been prepared with different stoppers—namely, **R502⁴⁺a**,[55,71,72] **R502⁴⁺b-d**,[73] **R502⁴⁺e**,[72,74–76] **R502⁴⁺f**,[17,77,78] **R502⁴⁺g**,[79] **R502⁴⁺h**,[80] **R502⁴⁺i**,[81,82] **R502⁴⁺j**,[83] **R502⁴⁺k**,[84] **R502⁴⁺l**,[58] **R503⁴⁺a**,[85,86] **R503⁴⁺b**,[86–88] **R503⁴⁺c**,[86–88] **R503⁴⁺d**,[89] and **R503⁴⁺e**.[78,90]

A drawback of the TTF-dimethanol unit, however, is that it exists as a pair of *cis* and *trans* isomers, both of which are typically present in a MIM, with the *trans* isomer usually occurring as the major species. The *cis*/*trans* isomers can complicate spectroscopic data interpretation,[E] since a bistable MIM based on TTF-dimethanol can exist as four isomers: *green*/*trans*, *green*/*cis*, *red*/*trans*, and *red*/*cis*. Pyrrolotetrathiafulvalene (PTTF) and bispyrrolotetrathiafulvalene (BPTTF) are attractive alternatives to TTF-dimethanol because PTTF and BPTTF cannot exist as *cis* and *trans* isomers. A comparison (**Figure 5.7**) of the van't Hoff plots[26] of several bistable [2]rotaxanes employing TTF, PTTF

[E] Although torsion around the TTF-diol C=C bond is slow on the NMR timescale, it is fast on the laboratory timescale.

thioether (PTTFS), and BPTTF recognition units reveals that the bistable rotaxanes based on PTTFS and BPTTF vary considerably in their relative populations across different solvents and temperatures. The distribution of translational isomers of the [2]rotaxane **R502^{4+}f** based on TTF-dimethanol is, by contrast, less sensitive to temperature changes. The BPTTF recognition unit of the bistable [2]rotaxane[100] **R504^{4+}** and the PTTFS-derived units of the bistable [2]rotaxanes[77,101–103] **R505^{4+}–R507^{4+}**, bind the CBPQT^{4+} ring with affinities (10^3–10^4 M^{-1}, see **Table 2.14i–l** in **Section 2.3.3.8**) comparable to DNP, and consequently exhibit (**Figure 5.6–5.7**) only marginal disparities between the populations of *green* and *red* translational isomers, respectively. The incongruity between populations of **R506^{4+}** (~4:1 green:red) and **R507^{4+}** (~1:1 green:red) under the same conditions, with their identical thiomethylated PTTFS (PTTFS-SMe) recognition sites, serves to remind us that all parts of a MIM might have an influence on the stability of a translational isomer. A probable explanation for this particular case is that the acidic C–H protons of the CBPQT^{4+} ring of the *green* isomer **R506$^{4+}_{PTTFS\text{-}SMe}$** are stabilized by the oxygen atoms of the polyether loops in the adjacent hydrophilic stopper, whereas the hydrophilic stopper is too distant to stabilize the CBPQT^{4+} ring of **R507$^{4+}_{PTTFS=SMe}$** in an effective manner.

A TTF bis(thioether) unit (STTFS), the preparation[104–106] of which is arguably more facile than that[56,107,108] of TTF-dimethanol, has also been characterized as a guest for CBPQT^{4+} (see **Table 2.14d** in **Section 2.3.3.8**) and incorporated into a number of bistable catenanes[106,109–111] and rotaxanes.[112–115] Since the polyether-appended STTFS and DNP units both bind CBPQT^{4+} with similar affinities, their corresponding catenanes and rotaxanes do not often exhibit high co-conformational selectivities. The STTFS/DNP/CBPQT^{4+} [2]catenane[106] **C515^{4+}**, which exists (**Figure 5.8**) in solution as a 1:1 mixture of *green* and *red* translational

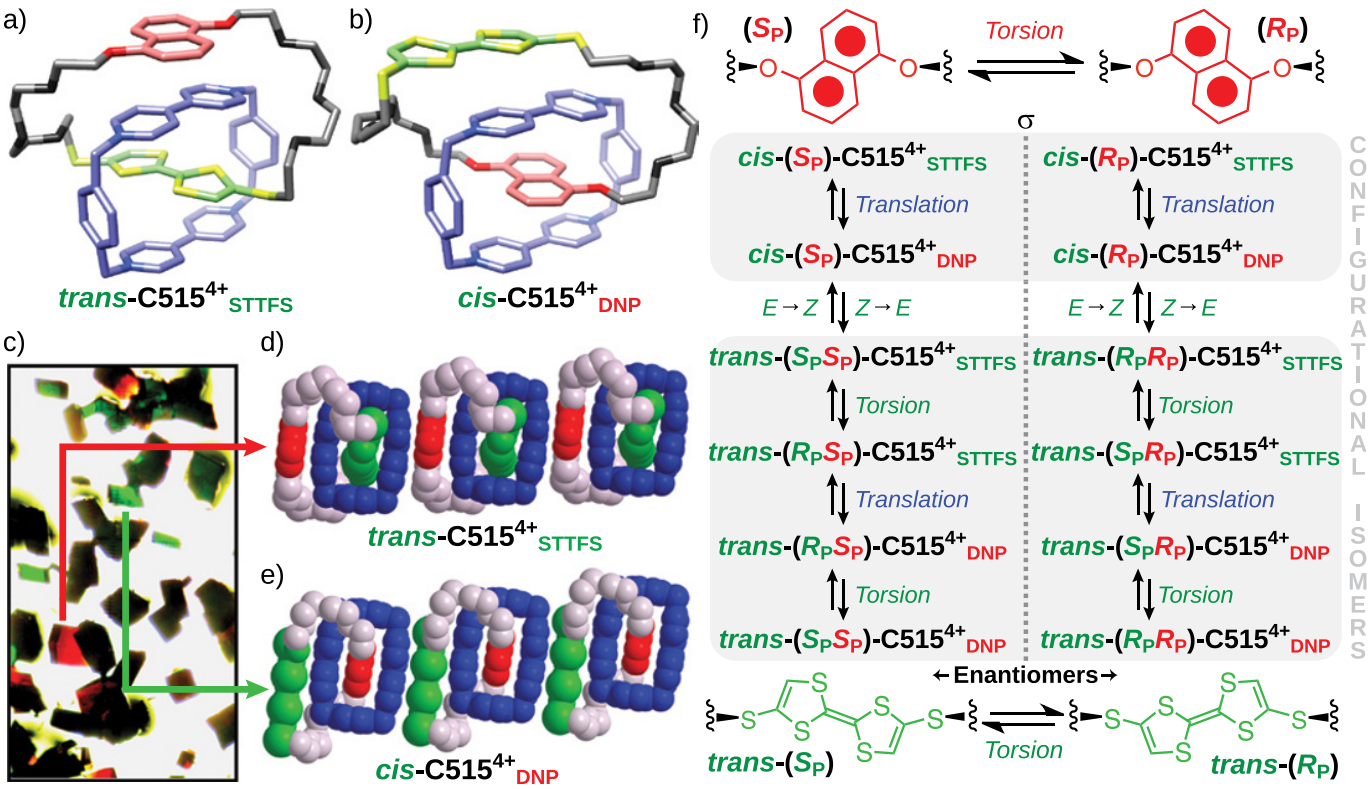


Figure 5.8 Mechanostereoisomerism[106] of the bistable [2]catenane **C515^{4+}**. Tubular representations of the solid-state structures of (a) ***trans*-C515$^{4+}_{STTFS}$**·4PF$_6$ and (b) **cis-C515$^{4+}_{DNP}$**·4PF$_6$ illustrate the *green* and *red* translational isomers associated with the inclusion of a crown ether's STTFS and DNP recognition units, respectively, within the cavity of a CBPQT^{4+} ring, as well as the configurational isomerism associated with the *trans* and *cis* isomers of the STTFS unit. (c) A photograph of the conglomerate of ***trans*-C515$^{4+}_{STTFS}$** (red crystals) and ***cis*-C515$^{4+}_{DNP}$** (green crystals) obtained by crystallization of an equilibrated sample of the catenane. Space-filling representations of the solid-state superstructures of (d) ***trans*-C515$^{4+}_{STTFS}$** and (e) ***cis*-C515$^{4+}_{DNP}$** reveal the continuous D-A π–π stacking of recognition units in neighboring catenanes. The "alongside" charge-transfer interactions in this stack explain why crystals of the *green* isomer appear red and crystals of the *red* isomer appear green. X-ray crystal structures are shown with hydrogen atoms, solvent molecules, and counterions omitted for the sake of clarity. (f) Taking into account the planar chirality of the DNP and *trans*-STTFS units, the [2]catenane **C515^{4+}** equilibrates in solution between six pairs of enantiomers as a result of (i) translation/circumrotation of the rings, which interconvert the **C515$^{4+}_{STTFS}$** and **C515$^{4+}_{DNP}$** translational isomers, (ii) *E*/*Z* isomerizations, which interconvert the *cis*- and *trans*- configurations of the STTFS recognition unit, and (iii) conformational bond torsions that invert the planes of chirality in the DNP and *trans*-STTFS units, which differentiate the corresponding (R_p) and (S_p) enantiomers and diastereoisomers of the catenane.

isomers, has been crystallized as a conglomerate in which both translational isomers are represented. Although the STTFS unit also equilibrates between *cis* and *trans* configurations in solution, only the ***trans*-C515$^{4+}_{STTFS}$** (**Figure 5.8a**) and ***cis*-C515$^{4+}_{DNP}$** (**Figure 5.8b**) mechanostereoisomers are observed in the crystalline conglomerate. The green-colored crystals of ***cis*-C515$^{4+}_{DNP}$** and the red-colored crystals of ***trans*-C515$^{4+}_{STTFS}$** assume (**Figure 5.8c**) opposite colors in the solid state than the corresponding solutions on account of crystal packing effects (**Figure 5.8d–e**) that enhance the side-on charge-transfer interactions between neighboring catenanes in the crystal lattice. The local C_2 symmetry of the DNP and *trans*-STTFS units imparts them with planes of chirality in the setting of the [2]catenane, leading to a situation (**Figure 5.8f**) in which the [2]catenane can equilibrate between 12 species. The four isomers of ***cis*-C515^{4+}** comprise two pairs of enantiomeric translational isomers, each of which invert rapidly on the ^{1}H NMR timescale between the (R_P) and (S_P) configurations associated with the conformational bond torsions of the DNP unit, while the number of isomers double to eight in the case of ***trans*-C515^{4+}** on account of the plane of chirality in the *trans*-STTFS unit, which also inverts rapidly between (R_P) and (S_P) configurations. The [2]catenane **C515^{4+}** thus exemplifies the marked increase in (mechano)stereochemical complexity that can arise when variability in both conformational and co-conformational isomerism are superimposed on the same molecule. A similar level of dynamic complexity has been observed in π-donor/π-acceptor pretzelanes.[63,116,117]

One of the earliest TTF derivatives to be investigated[53,118] as a recognition unit for the CBPQT^{4+} ring was (**Figure 5.6**) the bis(2-oxy-1,3-propylenedithio)tetrathiafulvalene (BPDTTF) unit appearing[32,118,119] as the alongside π-donor in the [2]catenanes[119] **C517$^{4+}_{Xy}$** and **C518$^{4+}_{Xy}$**, as well as the [2]rotaxane[32,118] **R508$^{4+}_{HQ}$**. The *red* translational isomers are populated to a much higher extent (>95%) than the *green* isomers. This observation does not agree with the thermodynamic forecast, since a BPDTTF polyether exhibits[119] (**Table 2.14o** in **Section 2.3.3.8**) a relatively high affinity ($K_a \approx 10^4$ M^{-1}) for CBPQT^{4+} which is greater than that[120] ($K_a \approx 10^3$ M^{-1}, **Table 2.12** in **Section 2.3.3.8**) of an analogous HQ polyether. This deviation from the thermodynamic forecast is not uncommon (*vide infra*) in catenanes on account of their topologically and sterically enforced 'alongside' interactions, yet it is unusual to see such a dramatic deviation from expectations in D-A bistable rotaxanes.

The Influence of Linkers

The nature of the linkers—i.e., the moieties in between recognition units—can have a profound effect on the ratio of translational isomers in a bistable mechanomolecule, as well as the kinetics of isomerization. A comparison (**Figure 5.9**) of three bistable [2]rotaxanes, comprising the CBPQT^{4+} ring and dumbbells incorporating PTTF and naphthalene derivatives as recognition units, reveals how the potential energy surface in Me_2CO is modulated by the presence of a rigid phenylethynylene linker versus a flexible polyether one. A retrospective analysis[25] of published[121] cyclic voltammetry (CV) data on the functionally rigid bistable [2]rotaxane **R501^{4+}**, which possesses PTTFS-SMe and DNP recognition units for the CBPQT^{4+} ring, determined a high K_{eq} value in of 350, which is much more unbalanced than that ($K_{eq} \approx 1$) of the flexible PTTFS-SMe/DNP rotaxane **R507^{4+}** containing (**Figure 5.6**) a polyether linker. The enhanced selectivity for **R501$^{4+}_{PTTFS-SMe}$** (the *green* isomer) most likely arises from (i) the rigid spacer's capacity to decrease the contributions to co-conformational stability coming from hydrogen-bonding interactions involving polyether sidearms and BIPY^{2+} protons, which are approximately equal for both recognition units, while consequently (ii) increasing the importance of contributions from D-A π-stacking interactions, which are stronger in the case of PTTFS-SMe than DNP. Even the length of the polyether linker can influence the co-conformational equilibrium, an influence attributable (*vide infra*) in part to the size or diameter of a mechanomolecule's component parts.

The kinetics of translation governed by $\Delta G^{\neq}$ are influenced primarily by (i) the binding strengths of the recognition units and (ii) the steric properties of the linker. The $\Delta G^{\neq}$ values for three bistable [2]rotaxanes based on tetrathiafulvalene, naphthalene, and CBPQT^{4+} recognition elements are also compared in **Figure 5.9**. The rigid [2]rotaxane **R501^{4+}** is characterized[121] by a relatively low activation barrier, which is attributable to the rigid phenylenethynylene linker that connects its PTTFS-SMe and naphthalene (NP) recognition units. Variable-temperature NMR experiments on a degenerate analogue of **R501^{4+}** have shown[122] that the barrier to shuttling over this ~1 nm distance is only 9.6 kcal·mol^{-1} in CD_3COCD_3, which is much lower than that ($\Delta G^{\neq}$ = 15 kcal·mol^{-1}) for the [2]rotaxane **R505^{4+}** possessing similar recognition elements connected by a diethylene glycol linker. This enormous difference in activation energies can be attributed to (i) the relatively lower CBPQT^{4+}-binding affinities of the recognition units of **R501^{4+}**, as well its (ii) relatively unimpeded pathway in between recognition sites, involving less steric barriers and local minima in between the GSCC and MSCC (beyond the simple rate-determining step approximation of TST) on account of fewer noncovalent bonding interactions engaging the CBPQT^{4+} ring. One of the most disruptive manipulations of the $\Delta G^{\ddagger}$ barrier by TTF substituents arises[101–103] from the thiomethyl group of the PTTFS-SMe unit when it is located in between the recognition sites of a bistable MIM. A comparison between the $\Delta G^{\neq}$ values for the bistable [2]rotaxanes **R505^{4+}** and **R506^{4+}**, which are otherwise identical, reveals that the thiomethyl group raises the activation energy to translation by an additional ~9 kcal·mol^{-1}. Thus, it is possible to tune the kinetics of translation in D-A rotaxanes over a very wide range, from transition state energies of ~10 kcal·mol^{-1} in the case of the functionally rigid **R501^{4+}** up to ~24 kcal·mol^{-1} in the case of the flexible **R506^{4+}** equipped with the thiomethyl 'speedbump'.

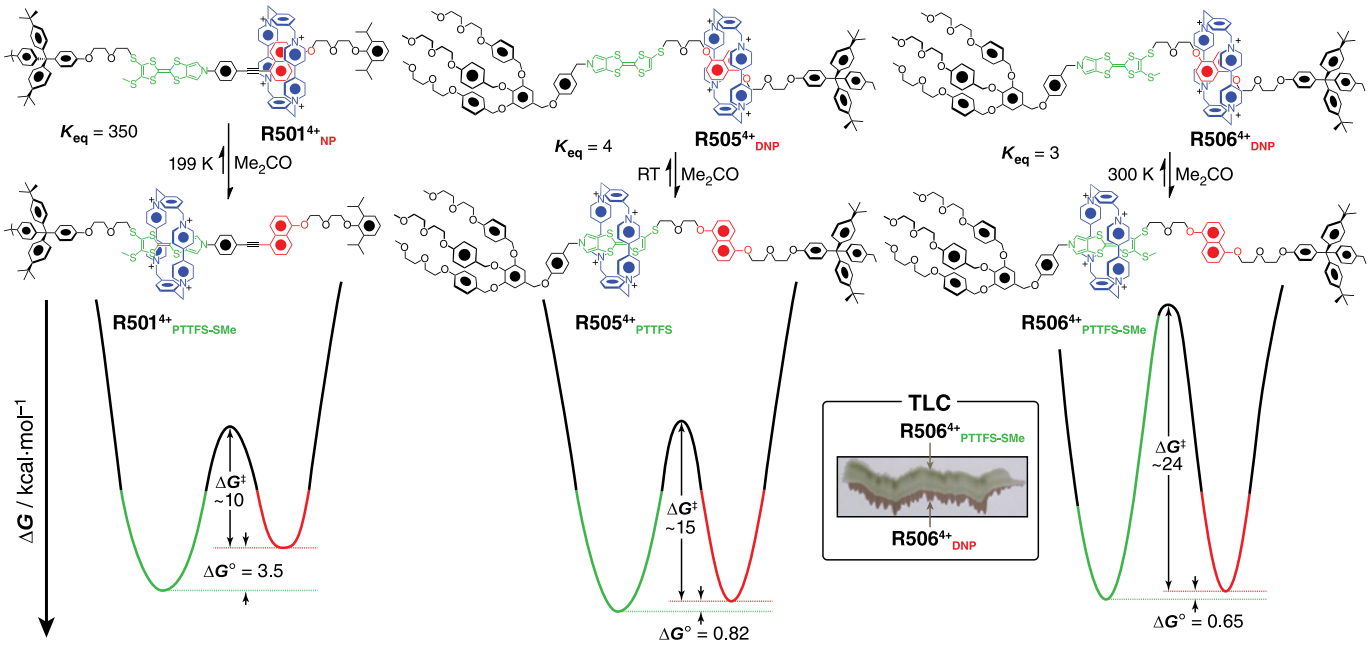


Figure 5.9 Comparing the free energy profiles, illustrated to scale, describing the thermodynamics ($\Delta G°$) and kinetics ($\Delta G^{‡}$) in Me_2CO of bistable [2]rotaxanes comprising the π-accepting $CBPQT^{4+}$ ring and dumbbells possessing π-donors derived from PTTFS and naphthalene units with different linkers and steric blocking groups. See refs. 25, 101, 103, 121. The functionally rigid bistable [2]rotaxane[121] **R501⁴⁺** exhibits[25] the most biased population distribution (highest $\Delta G°$) and the fastest kinetics (lowest $\Delta G^{‡}$) owing to its phenylethynylene linker, which reduces steric and electronic contributions to the ring's local binding interactions relative to the polyether linker in between the recognition units of **R505⁴⁺** and **R506⁴⁺**. The polyether linker stabilizes both *green* and *red* translational isomers of **R505⁴⁺** and **R506⁴⁺**, which nearly equalizes their stabilities ($\Delta G° < 1$) while raising the activation barriers ($\Delta G^{‡}$) to 15 and 24 kcal·mol^{-1}, respectively.[101,103] The inset image of a TLC plate demonstrates that the *green* and *red* translational isomers of **R506⁴⁺** can be separated[101] chromatographically owing to the slow kinetics of isomerization afforded the thiomethyl 'speedbump' appended to its PTTFS-SMe unit, which is responsible for the corresponding high value of $\Delta G^{‡}$.

The steric obstruction introduced by the speedbump of the latter compound is sufficiently high to slow the shuttling kinetics ($k = 2 \times 10^{-5}$ s^{-1}) enough to isolate (**Figure 5.9** inset) the red and green translational isomers by preparative thin layer chromatography (TLC) at 0 °C. See **Section 5.1.1.2** for further discussion on the role of linker sterics and electronics in tuning $\Delta G^{\neq}$ values. Linker effects are also important for tuning the kinetics of translation for the establishment of flash memory in crossbar molecular memory devices—see **Sections 1.3.6, 6.14.1.1**, and **6.15.1.3**.

The Influence of Ring Size

Ring size factors into conformational and co-conformational degrees of freedom in a MIM because smaller rings are more confined by the mechanical bond. The equilibrium between translational isomers can therefore be influenced by ring size or dumbbell proportions. Investigations[123,124] involving tetramethylated BPTTF (Me_4BPTTF) recognition units revealed (**Figure 5.10**) that the ring size of the macrocyclic polyether plays a critical role in determining the *green:red* ratio (K_{eq}) in the bistable D-A [2]catenanes **C519⁴⁺–C521⁴⁺**. Whereas the *green* translational isomer is the major co-conformer of the bistable [2]catenane **C519⁴⁺** possessing diethylene glycol (2EG) linkers, the *green* mechanostereoisomers represent ≤10% of the room-temperature population in the catenanes **C520⁴⁺** and **C521⁴⁺** possessing triethylene gycol (3EG) and tetraethylene glycol (4EG) linkers, respectively, in CD_3SOCD_3. Once again, hydrogen-bonding interactions between the oxygen atoms of the polyether loops and the protons of the tetracation's $BIPY^{2+}$ units are among the most important contributions to the relative stabilization of these two translational isomers. In the case of the 3EG-based **C520⁴⁺**, the MSCC and GSCC are equally populated at 120 °C.

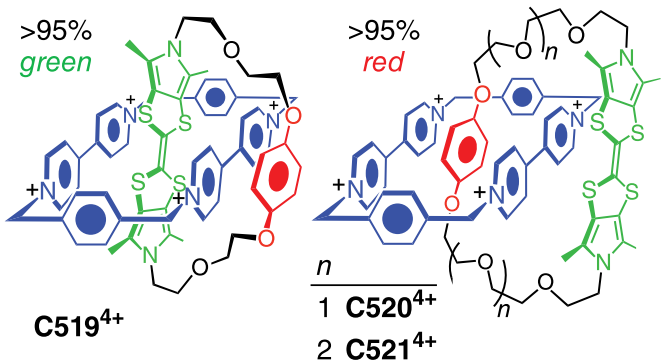


Figure 5.10 An example of how differences in ring size can lead to different translational isomers. Whereas the *green* isomer of **C519⁴⁺** is populated almost exclusively when the crown's Me_4BPTTF and HQ recognition units for the $CBPQT^{4+}$ ring are connected by 2EG linkers, the *red* isomers are populated almost exclusively in **C520⁴⁺** and **C521⁴⁺**, which posess 3EG and 4EG linkers, respectively.[123,124]

The Influence of Topology / Architecture

The topology (for catenanes) or architecture (for rotaxanes) of a bistable mechanomolecule can have a dramatic influence on its translational isomerism. It transpires that thermodynamic forecasting of the ΔG° values in rotaxanes on the basis of the $\Delta\Delta G_a$ values of corresponding pseudorotaxane model systems is often straightforward and reliable, at least qualitatively, if not semi-quantitatively. Bistable catenanes, however, deviate more often than not from the predictions of this type of forecast, since their topologies limit the conformational freedom of the linkers and their unoccupied recognition units are mechanically enforced into 'alongside' interactions which do not necessarily exist in most (pseudo)rotaxanes. For example, although DNP polyethers exhibit much higher affinities (K_a ~ 10^5 M^{-1}) for $CBPQT^{4+}$ rings than do analogous HQ polyethers (K_a ~10^3 M^{-1}, see **Table 2.12** in **Section 2.3.3.8**) in MeCN, the dominant translational isomer (**Figure 5.5**) of the HQ/DNP/$CBPQT^{4+}$ [2]catenane is $\mathbf{C503^{4+}_{HQ}}$ rather than $\mathbf{C503^{4+}_{DNP}}$ in MeCN. The DTNP unit representing the GSCC of $\mathbf{C507^{4+}_{DTNP}}$ at 30 °C (**Figure 5.5**) is another example of a site which is preferentially encircled[34] in a catenane despite having weaker affinity (see **Table 2.13** in **Section 2.3.3.8**) for $CBPQT^{4+}$ than its alongside DNP counterpart.

Figures 5.11–5.12 compares the free energy profiles of pseudorotaxane model systems[28,42,125] with the corresponding bistable D-A [2]rotaxanes and [2]catenanes comprising $CBPQT^{4+}$ rings interlocked with dumbbells or rings,

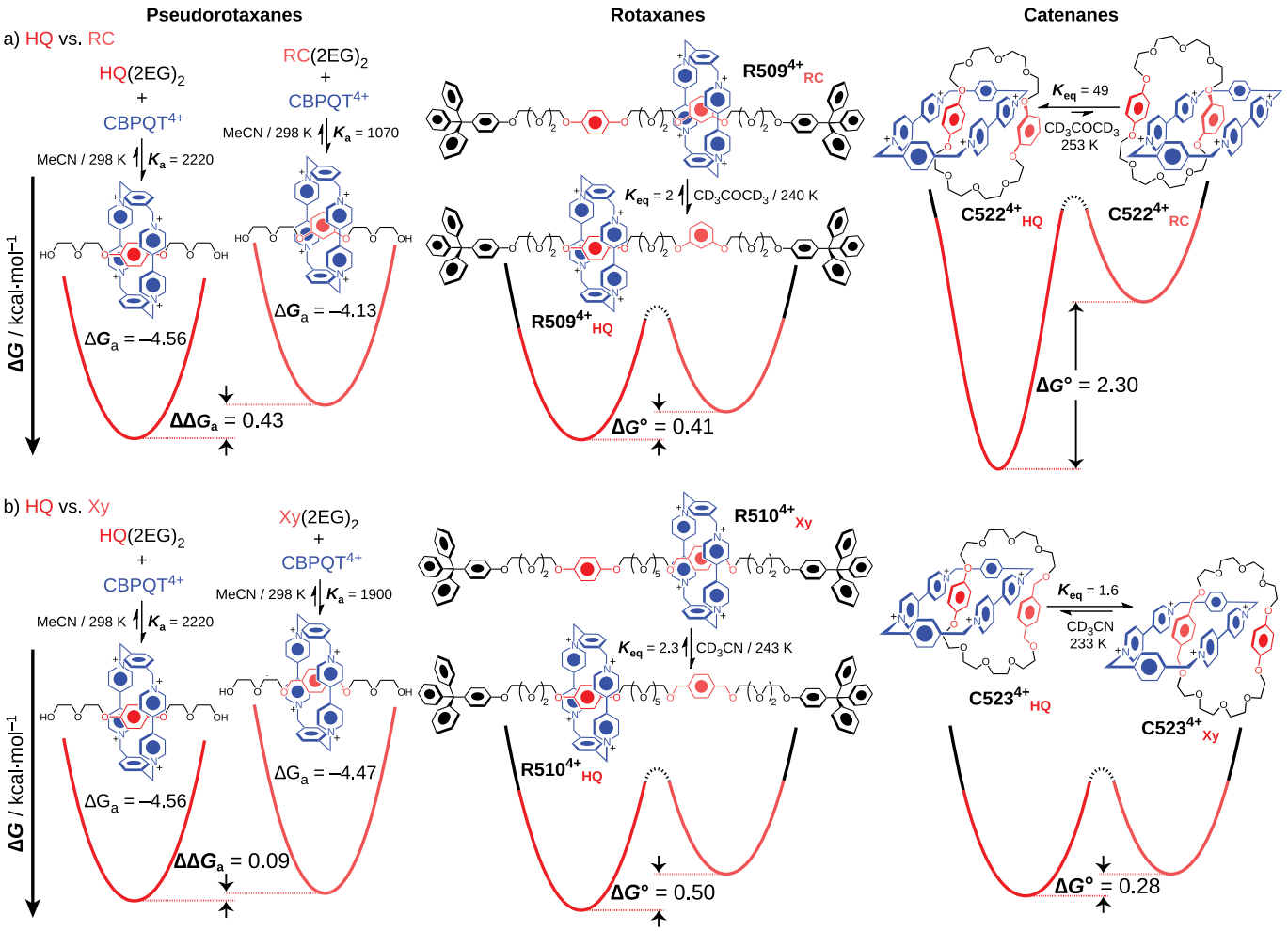


Figure 5.11 Examples of how differences in the architecture of a mechanical bond can influence the free energy profiles of non-degenerate bistable rotaxanes and catenanes employing HQ as the primary recognition unit. See refs. 30, 32, 33, 42, 125. (a) Comparison of the free energy profiles of the bistable [2]rotaxane[33] $\mathbf{R509^{4+}}$ and the bistable [2]catenane[125] $\mathbf{C522^{4+}}$, in which the $CBPQT^{4+}$ ring translates between hydroquinone (HQ) and resorcinol (RC) recognition units, as well as the corresponding pseudorotaxane[28,125] model systems. The distribution of translational isomers defined by ΔG° reflects the thermodynamic forecast ($\Delta\Delta G_a$) based on the pseudorotaxanes in the case of the rotaxane, but not the catenane. (b) Comparison of the bistable [2]rotaxane[32] $\mathbf{R510^{4+}}$ and the bistable [2]catenane[42] $\mathbf{C523^{4+}}$, in which the $CBPQT^{4+}$ ring translates between HQ and *para*-xylene (Xy) recognition units, as well as the corresponding pseudorotaxane[28,42] model systems. In this case, the thermodynamic forecast of ΔG° based on $\Delta\Delta G_a$ is qualitatively predictive of both the rotaxane and catenane populations. In the potential energy surface diagrams, the troughs corresponding to $\Delta\Delta G_a$ and ΔG° are illustrated to scale, whereas the peaks corresponding to $\Delta G^{\ddagger}$ are not illustrated to scale.

respectively, possessing identical π-donating recognition units. A dramatic difference has been observed between the co-conformational selectivity (**Figure 5.11a**) of the bistable [2]rotaxane[33] **R509**$^{4+}$ and the bistable [2]catenane[30,125] **C522**$^{4+}$, each possessing HQ and resorcinol (RC) recognition units. Whereas the ratio of the HQ- and RC-encircled translational isomers (**R509**$^{4+}_{HQ}$ and **R509**$^{4+}_{RC}$, respectively) is only 2:1 (K_{eq} = 2) in the case of the rotaxane, the **C522**$^{4+}_{HQ}$:**C522**$^{4+}_{RC}$ ratio is 98:2 (K_{eq} = 49), reflecting a much more biased population distribution in the case of the catenane. This dramatic difference in the ground state distributions of homologous rotaxanes and catenanes most likely arises from the 'alongside' interactions which are enforced by the topological link of the catenane, yet not by the mechanical bond of the rotaxane. These mechanically enforced 'alongside' interactions do not always cause a dramatic increase in co-conformational selectivity, however, since the case (**Figure 5.11b**) of HQ versus Xy reveals that the bistable [2]catenane **C523**$^{4+}_{HQ}$ is populated[42] to a lesser, yet similar extent (K_{eq} = 1.6) as the bistable [2]rotaxane **R510**$^{4+}_{HQ}$ (K_{eq} = 2.3) is populated[32] at low temperatures in CD_3CN. The ground-state distribution[42] of **C523**$^{4+}$ is more biased (K_{eq} = 7.3) in favor of the HQ-encircled isomer in CD_3COCD_3. Thus, the

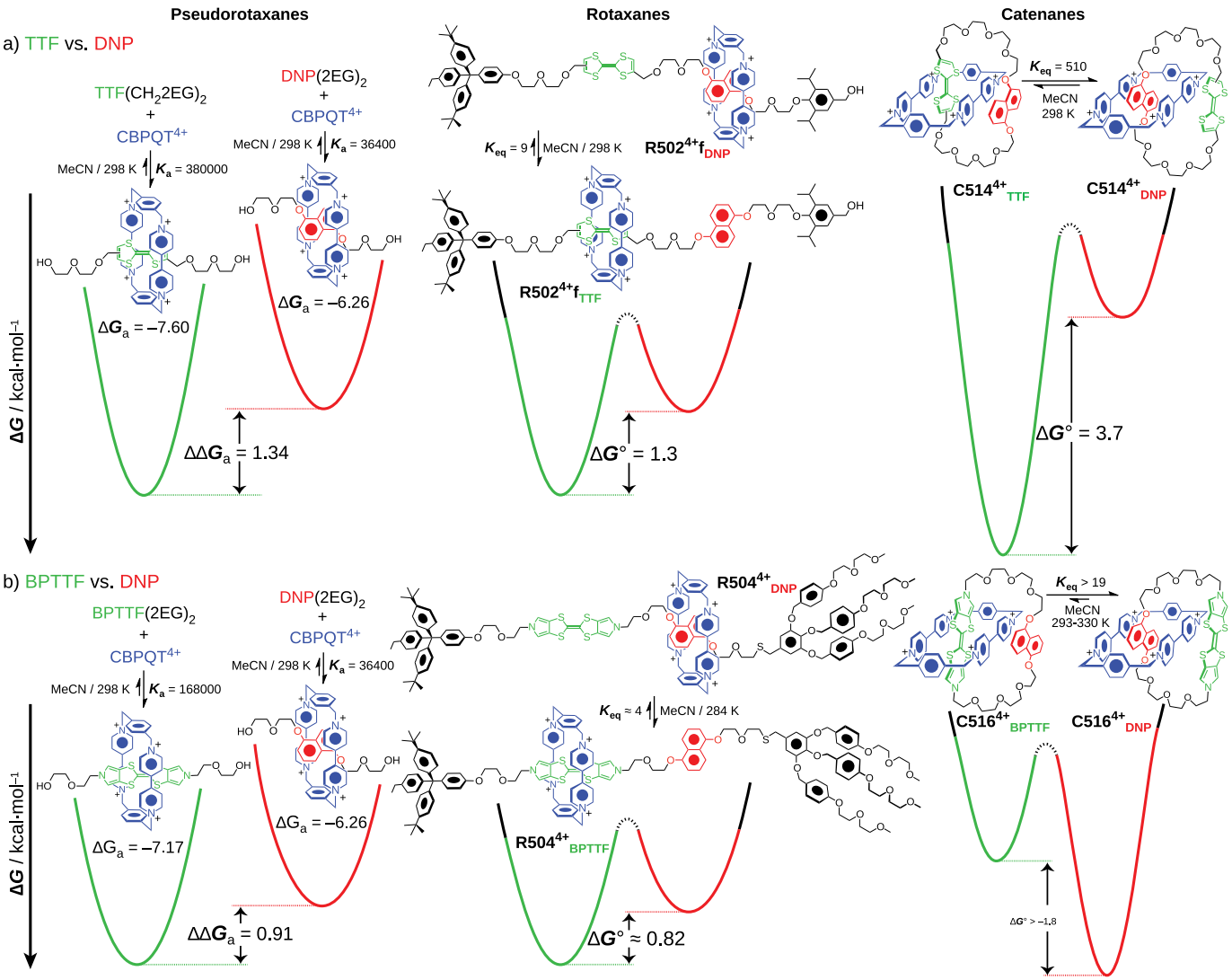


Figure 5.12 Examples of how differences in the architecture of a mechanical bond can influence the free energy profiles of non-degenerate bistable rotaxanes and catenanes employing TTF derivatives as the primary recognition units. (a) Comparison of the bistable [2]rotaxane[17,77] **R502**$^{4+}$**f** and the bistable [2]catenane[57,58] **C514**$^{4+}$, in which the CBPQT^{4+} ring translates between TTF and DNP recognition units, as well as the corresponding pseudorotaxane[55] model systems. The thermodynamic forecast of $\Delta G°$ based on $\Delta\Delta G_a$ is predictive of the rotaxane, yet not of the catenane population distributions. (b) Comparison of the free energy profiles of the bistable [2]rotaxane[55,100] **R504**$^{4+}$ and the bistable [2]catenane[126] **C516**$^{4+}$, in which the CBPQT^{4+} ring translates between BPTTF and DNP recognition units, as well as the corresponding pseudorotaxane[55] model systems. Once again, the quantity $\Delta\Delta G_a$ is reflected in the $\Delta G°$ value for the rotaxane and not the catenane. In the potential energy surface diagrams, the troughs corresponding to $\Delta\Delta G_a$ and $\Delta G°$ are illustrated to scale, whereas the peaks corresponding to $\Delta G^{\ddagger}$ are not illustrated to scale.

thermodynamic forecasts are reasonably predictive of the population distributions except in the case of **C522**$^{4+}$—see the **Figure 5.11** caption. These results indicate that the distribution of translational isomers is influenced by topology and architecture, yet not in an easily generalizable or predictable manner when dealing with catenanes.

Another case (**Figure 5.12**) of great disparity between the distribution of translational isomers in analogous catenanes and rotaxanes is that of the CBPQT^{4+}-based bistable MIMs with DNP recognition units accompanying either TTF[17,57,58,77] (**Figure 5.12a**) or BPTTF[55,100,126] (**Figure 5.12b**) π-donors in their interlocked component parts. In both cases, the $\Delta\Delta G_a$ values of model pseudorotaxanes provide[55] remarkably accurate thermodynamic forecasts for the distributions of the corresponding bistable rotaxanes[17,55,77,100] **R502**$^{4+}$**f** and **R504**$^{4+}$ in MeCN. On the other hand, the analogous bistable [2]catenanes[57,58,126] **C514**$^{4+}$ and **C516**$^{4+}$, respectively, deviate substantially from the same forecast. Whereas **C514**$^{4+}$ is remarkably biased[58] ($K_{eq} \approx 500$) toward the *green* isomer **C514**$^{4+}_{TTF}$, the [2]catenane **C516**$^{4+}$ is remarkably biased[126] ($K_{eq} > 19$, an estimate reflecting a conservative detection limit in ^{1}H NMR spectroscopy) in favor of the red isomer **C516**$^{4+}_{DNP}$. Neither of the corresponding $\Delta G°$ values exceeding 3.7 and –1.7 kcal·mol^{-1}, respectively, equate with the corresponding $\Delta\Delta G_a$ values (1.34 and 0.91 kcal·mol^{-1}) for the pseudorotaxanes. In the particularly unusual case of **C516**$^{4+}_{DNP}$, hydrogen bonding is most likely one of the overriding incentives for the weaker π-donor to represent the major translational isomer, since the BPTTF unit can still engage in alongside D-A π-stacking with the CBPQT^{4+} ring. Additionallly, the extended nature of the BPTTF unit probably also restricts the polyether loops from attaining their optimal hydrogen bond lengths, whereas the HQ and DNP units are short enough to allow their nearest polyether oxygen atoms to participate in hydrogen-bonding interactions with acidic α protons of the BIPY^{2+} units when encircled by the CBPQT^{4+} ring.

The Influence of Constitution

It transpires that even constitutional isomers with only subtle differences in atom and bond connectivity can exhibit dramatically different mechanostereoisomerism. Several comparisons (**Figure 5.13**) of mechanically bonded constitutional isomers reveal how differences in constitution can lead to differences in the co-conformation of a mechanomolecule.

Several cases[35,42] of bistable [2]catenanes employing dioxynaphthalene constitutional isomers as recognition units reveal (**Figure 5.13a–b**) that the populations of translational isomers are highly sensitive to the positions of alkoxy substitution around the naphthalene core. The CBPQT^{4+} rings of the bistable [2]catenane **C524**$^{4+}$ encircle the DNP unit (81%) over the Xy unit (19%) at 193 K in CD_3COCD_3 (**Figure 5.13a**), whereas Xy represents the favored translational isomer (>95%) when DNP is replaced by the 1,6-dioxynaphthalene (16NP), 2,6-dioxynaphthalene (26NP), and 2,7-dioxynaphthalene (27NP) units of **C525**$^{4+}$**a-c**, respectively, under the same conditions. When both π-donor units of CBPQT^{4+}-based bistable [2]catenanes constitute[35] dioxynaphthalene isomers (**Figure 5.13b**), DNP outcompetes 16NP, 26NP, or 27NP

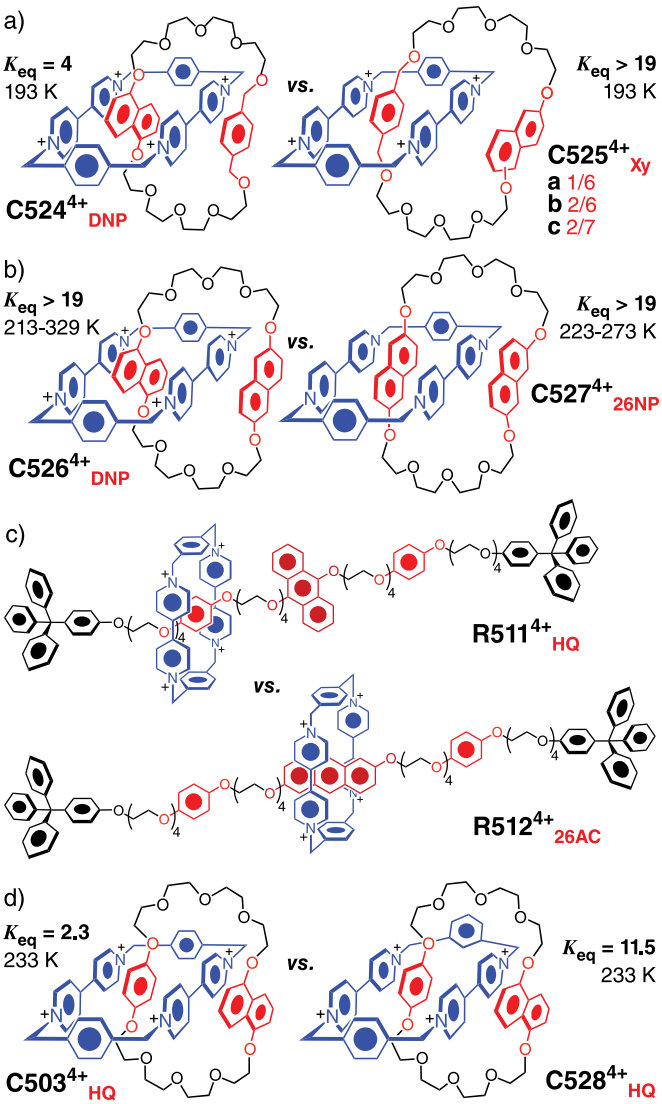


Figure 5.13 Pairs of MIMs existing as both constitutional and translational isomers in CD_3COCD_3. (a) The DNP unit outcompetes the Xy unit for the cavity of CBPQT^{4+} in **C524**$^{4+}_{DNP}$, yet Xy outcompetes 1,6-, 2,6-, or 2,7-dioxynaphthalene π-donors (16NP, 26NP, and 27NP, respectively) in catenanes **C525a-c**$^{4+}$.[42] (b) A 26NP recognition unit falls to DNP for ring occupancy in **C526**$^{4+}_{DNP}$, yet wins out over 27NP in **C527**$^{4+}_{26NP}$.[35] (c) Whereas 9,10-dioxyanthracene acts as a bulky barrier forbidding the translation of a CBPQT^{4+} ring between HQ recognition units in the [2]rotaxane **R511**$^{4+}_{HQ}$, 2,6-dialkoxyanthracene (26AC) outcompetes HQ for the CBPQT^{4+} ring in **R512**$^{4+}_{26AC}$.[45] (d) Replacing one *para*-phenylene for a *meta*-phenylene linker in the CBPQT^{4+} ring of **C503**$^{4+}_{HQ}$ leads to a more biased distribution in favor of **C528**$^{4+}_{HQ}$.[30]

to the extent that the metastable co-conformations are not detected (K_{eq} > 19) in solution by ^{1}H NMR spectroscopy, as observed in the case of **C526$^{4+}_{DNP}$**. This bias probably reflects the order-of-magnitude greater binding affinity of a DNP polyether versus a 16NP polyether—see **Table 2.13** in **Section 2.3.3.8**. When DNP is eliminated from the picture, however, the other dioxynaphthalene derivatives have a chance to occupy the cavity of CBPQT^{4+}, as in **C527^{4+}** which selects 26NP over 27NP for occupancy of the ring by a >95% margin. This observation is more surprising, since the corresponding model pseudorotaxanes have very similar stabilities, with a 27NP polyether showing a slightly higher affinity (K_a = 221) for CBPQT^{4+} than that (K_a = 177 M^{-1}) of the corresponding 26NP polyether—another case in which thermodynamic forecasting cannot be applied to the assessment of catenane bistability.

Since the different dioxynaphthalene constitutional isomers are associated with remarkable differences in the population of translational isomers, it comes as no surprise that dioxyanthracene derivatives (**Figure 5.13c**) can behave[45] likewise. In the [2]rotaxane **R511$^{4+}_{HQ}$**, the central 9,10-dioxyanthracene unit is essentially a stopper, which the CBPQT^{4+} ring cannot transgress in order to reach the second degenerate HQ unit. In stark contrast to this situation, the constitutional isomer 2,6-dioxyanthracene (26AC) in **R512^{4+}** serves as an excellent π-donating recognition unit, claiming nearly all of the population of CBPQT^{4+} rings to itself in order to engage in π-associated D-A charge transfer interactions.

Constitutional isomers of the tetracationic cyclophane can also generate[30] different ground state distributions, as demonstrated by comparing (**Figure 5.13d**) the effects of the *para*-phenylene linker of **C503$^{4+}_{HQ}$** against the *meta*-phenylene linker of **C528$^{4+}_{HQ}$**. Although HQ represents the dominant translational isomer in both cases, the catenane **C528^{4+}** possessing a *meta*-phenylene linker is much more biased toward this isomer (K_{eq} = 11.5) than is the *para*-phenylene derived catenane **C503^{4+}** (K_{eq} = 2.3) at 233 K in CD_3COCD_3. We note that these constitutional isomers influence the size of the tetracationic ring, which undoubtedly influences the distance between the ring's recognition units, and so consequently modulates the D-A π–π stacking and charge-transfer interactions.

The ground-state distributions of most of the bistable mechanomolecules from our case study on non-degenerate translational isomerism are summarized in **Tables 5.2–5.3**. These data have revealed that the distribution of translational isomers in D-A MIMs and the kinetics of their interconversion are sensitive to the sterics and electronics of (i) the recognition units, as well as (ii) the linkers and/or stoppers, (iii) the topology/architecture of the mechanical bond, and even (iv) constitutional isomerism. Here is a brief summary of the insights revealed by this case study on dynamic non-degenerate D-A MIMs:

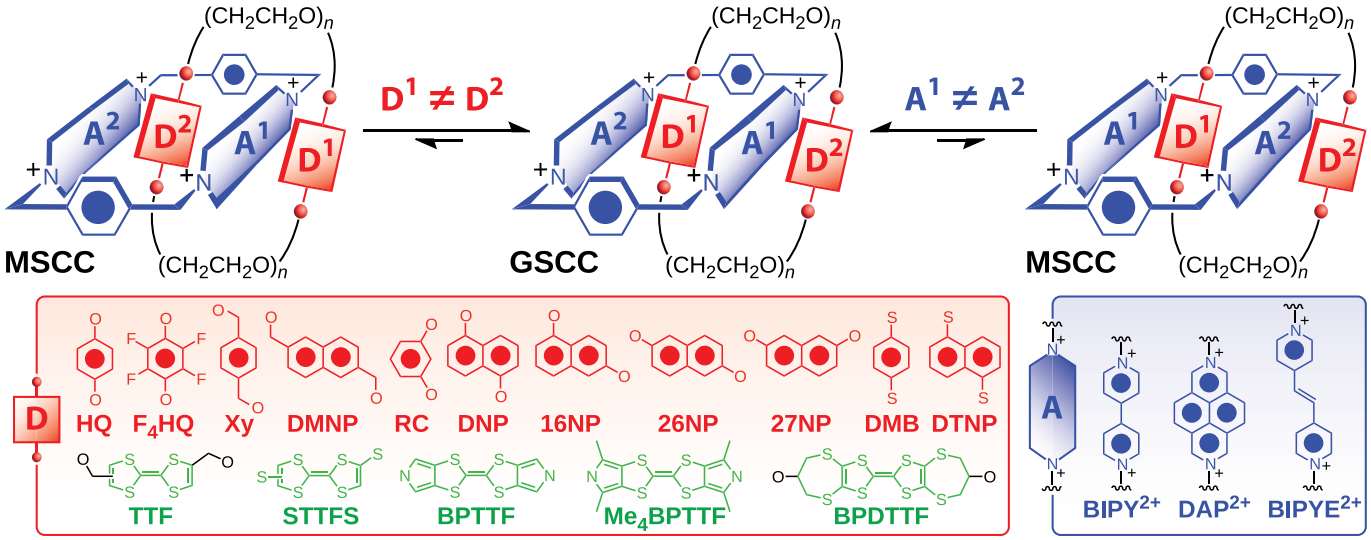
- Modulating the strength of noncovalent bonding interactions between recognition units and rings is an effective way to tune the distribution of translational isomers. Larger differences in free energies of binding correspond to more highly biased populations.
- The distribution of translational isomers in rotaxanes often reflects the thermodynamic stabilities of pseudorotaxanes comprising the same rings and recognition units, whereas the distribution is much less predictable for catenanes as a result of 'alongside' interactions constrained by the topology of a link.
- All parts of a MIM can influence the population of translational isomers, even stoppers and linkers located at a distance from the ring's binding sites.
- Differences in architecture can correspond to large differences in the populations of translational isomers, even for MIMs comprising identical recognition units.
- Even subtle constitutional changes, which inevitably influence the steric and electronic landscape, can alter the thermodynamics and kinetics of translation in MIMs, sometimes quite dramatically.

Non-degenerate translational isomerization processes involving activation barriers that are low enough so as to be overcome in solution are central to the operation of artificial molecular switches, machines, and motors with mechanical bonds. In these cases, the population of translational isomers can typically be influenced by changing one or more experimentally controlled parameters—e.g., redox state, pH, solvent polarity, temperature, pressure, exposure to light, or the presence of other additives in solution such as cations, anions, small molecules, or polymers. These systems, inclusive of many design motifs beyond π-associated donor-acceptor MIMs, are the main topic for discussion in **Chapter 6**. As summarized in the following Section, the kinetics of translation can often be tuned over a range of timescales by modulating various structural parameters, allowing them to be adjusted to suit the requirements of different devices and applications.

5.1.1.2 Degenerate Translational Isomers

In this Section we will focus on translational isomerism in degenerately bistable rotaxanes and catenanes with sufficiently low barriers to allow exchange processes to take place. Degenerate systems are simpler to consider than non-degenerate ones because $\Delta G°$ is zero in the former case. It is convenient to investigate $\Delta G^{‡}$ in degenerate mechanomolecules because its value is identical in the 'forward' and 'backward' translational directions. Degenerately bistable rotaxanes and catenanes can therefore serve as model compounds for researchers interested in understanding how different structural and experimental parameters influence the kinetics of translation in bistable MIMs. The three most significant factors influencing the kinetics of translation are (i) the strength of the local noncovalent bonding interactions, which can be conceptualized as the

Table 5.2 Summary of the ground-state distributions of translational isomers in donor-acceptor [2]catenanes comprising tetracationic cyclophanes possessing two π-acceptors (A1 and A2), and crown ethers possessing two π-donors (D1 and D2) bridged by oligo(ethylene glycol) linkers with *n* repeating units.



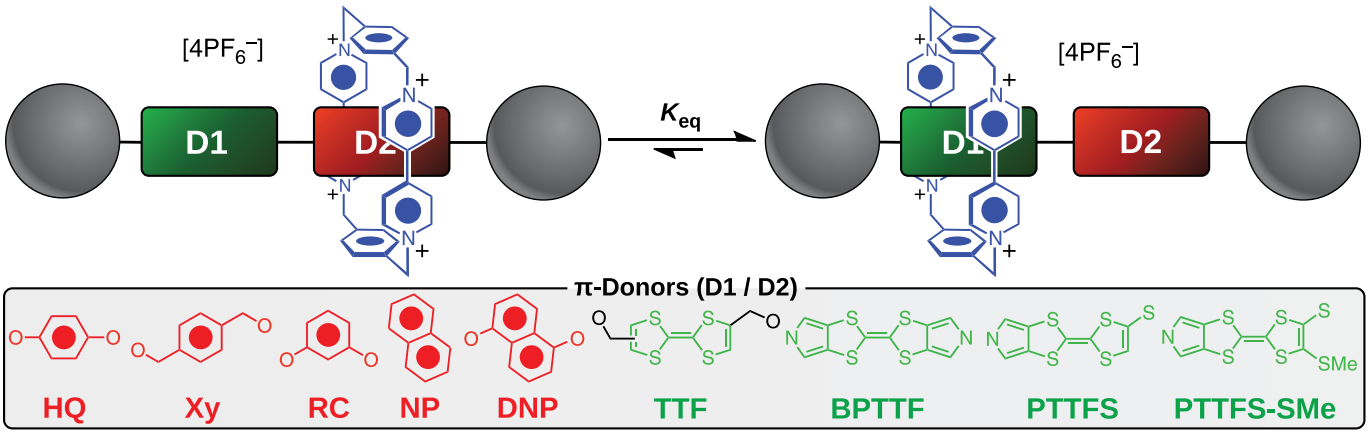
	GSCC / *Inside*		MSCC / *Alongside*				T[a]	$\Delta G°$			
	A1	D1	A2	D2	*n*	Solvent	K	K_{eq}[b]	kcal·mol^{-1}	Method[c]	Ref.
C503^{4+}	$BIPY^{2+}$	HQ	$BIPY^{2+}$	DNP	4	CD_3COCD_3	RT	2.3	0.5	NMR	49
C503^{4+}	$BIPY^{2+}$	HQ	$BIPY^{2+}$	DNP	4	CD_3SOCD_3	RT	0.5	0.4	NMR	49
C504^{4+}	$BIPYE^{2+}$	DNP	$BIPYE^{2+}$	HQ	4	CD_3COCD_3	263	1	0	NMR	31
C504^{4+}	$BIPYE^{2+}$	DNP	$BIPYE^{2+}$	HQ	4	CD_3CN	233	>50	>1.8	NMR	31
C505^{4+}	$BIPY^{2+}$	HQ	$BIPY^{2+}$	DMNP	4	CD_3CN	298	19	1.7	NMR	42
C505^{4+}	$BIPY^{2+}$	HQ	$BIPY^{2+}$	DMNP	4	CD_3SOCD_3	298	>19	>1.7	NMR	42
C506^{4+}	$BIPY^{2+}$	HQ	$BIPY^{2+}$	F_4HQ	4	CD_3COCD_3	303	>50	>2.3	NMR	37
C507^{4+}	$BIPY^{2+}$	DTNP	$BIPY^{2+}$	DNP	4	CD_3CN	243	1.5	0.2	NMR	34
C507^{4+}	$BIPY^{2+}$	DTNP	$BIPY^{2+}$	DNP	4	CD_3CN	303	0.8	0.1	NMR	34
C508^{4+}	$BIPY^{2+}$	DNP	$BIPY^{2+}$	DMB	4	CD_3COCD_3	303	>50	>1.8	NMR	34
C509^{4+}	DAP^{2+}	HQ	$BIPY^{2+}$	HQ	4	CD_3COCD_3	193	24	1.2	NMR	44
C510^{4+}	DAP^{2+}	DNP	$BIPY^{2+}$	DNP	4	CD_3COCD_3	253	5	0.8	NMR	44
C511^{4+}	$BIPY^{2+}$	HQ	$BIPE^{2+}$	HQ	4	CD_3COCD_3	213	12	1.1	NMR	31
C512^{4+}	$BIPY^{2+}$	DNP	$BIPE^{2+}$	DNP	4	CD_3COCD_3	243	7	0.9	NMR	31
C513^{4+}	$BIPY^{2+}$	DNP	$BIPYE^{2+}$	HQ	4	CD_3COCD_3	233	19	1.7	NMR	54
C513^{4+}	$BIPY^{2+}$	DNP	$BIPYE^{2+}$	HQ	4	CD_3COCD_3	313	7	0.9	NMR	54
C514^{4+}	$BIPY^{2+}$	TTF	$BIPY^{2+}$	DNP	4	MeCN	298	510	3.7	CV Eq	58
C515^{4+}	$BIPY^{2+}$	STTFS	$BIPY^{2+}$	DNP	4	MeCN	298	1	0	CV	110
C516a^{4+}	$BIPY^{2+}$	HQ	$BIPY^{2+}$	BPTTF	4	CD_3CN or CD_3SOCD_3	RT	>19	>1.7	NMR, CV	126
C516b^{4+}	$BIPY^{2+}$	DNP	$BIPY^{2+}$	BPTTF	4	CD_3CN or CD_3SOCD_3	RT	>19	>1.7	NMR, CV	126
C517^{4+}	$BIPY^{2+}$	Xy	$BIPY^{2+}$	BPDTTF	3	CD_3COCD_3	298	>19	>1.7	NMR, CV	119
C518^{4+}	$BIPY^{2+}$	Xy	$BIPY^{2+}$	BPDTTF	4	CD_3COCD_3	298	>19	>1.7	NMR, CV	119
C519^{4+}	$BIPY^{2+}$	Me_4BPTTF	$BIPY^{2+}$	HQ	2	CD_3SOCD_3	RT	>19	>1.7	NMR	123
C520^{4+}	$BIPY^{2+}$	HQ	$BIPY^{2+}$	Me_4BPTTF	3	CD_3SOCD_3	RT	10	1.4	NMR	123
C520^{4+}	$BIPY^{2+}$	HQ	$BIPY^{2+}$	Me_4BPTTF	3	CD_3SOCD_3	393	1	0	NMR	123
C521^{4+}	$BIPY^{2+}$	HQ	$BIPY^{2+}$	Me_4BPTTF	4	CD_3SOCD_3	RT	20	1.8	NMR	123
C522^{4+}	$BIPY^{2+}$	HQ	$BIPY^{2+}$	RC	4	CD_3COCD_3	253-273	49	2.1	NMR	30/125
C523^{4+}	$BIPY^{2+}$	HQ	$BIPY^{2+}$	Xy	4	CD_3COCD_3	233	7.3	0.3	NMR	42
C523^{4+}	$BIPY^{2+}$	HQ	$BIPY^{2+}$	Xy	4	CD_3CN	233	1.6	0.3	NMR	42
C524^{4+}	$BIPY^{2+}$	DNP	$BIPY^{2+}$	Xy	4	CD_3COCD_3	193	4.3	0.6	NMR	42
C524^{4+}	$BIPY^{2+}$	DNP	$BIPY^{2+}$	Xy	4	CD_3COCD_3	282	1.5	0.2	NMR	42
C524^{4+}	$BIPY^{2+}$	DNP	$BIPY^{2+}$	Xy	4	CD_3CN	228	2.7	0.4	NMR	42
C524^{4+}	$BIPY^{2+}$	DNP	$BIPY^{2+}$	Xy	4	CD_3CN	281	1.2	0.1	NMR	42
C525a^{4+}	$BIPY^{2+}$	Xy	$BIPY^{2+}$	16NP	4	CD_3COCD_3	267	>19	>1.6	NMR	42
C525b^{4+}	$BIPY^{2+}$	Xy	$BIPY^{2+}$	26NP	4	CD_3CN	343	>19	>2.0	NMR	42
C525c^{4+}	$BIPY^{2+}$	Xy	$BIPY^{2+}$	27NP	4	CD_3CN	313	>19	>1.8	NMR	42
C526^{4+}	$BIPY^{2+}$	DNP	$BIPY^{2+}$	26NP	4	CD_3COCD_3 or CD_3CN	213-329	>19	>1.9	NMR	35
C527^{4+}	$BIPY^{2+}$	26NP	$BIPY^{2+}$	27NP	4	CD_3COCD_3	223-273	>19	>1.6	NMR	35

[a] T = temperature. RT = room temperature.

[b] In cases where only one translational isomer has been detected by ^{1}H NMR spectroscopy, we assume a conservative detection limit, that the MSCC represents <5% of the ground-state distribution (K_{eq} > 19) unless a different lower limit has been stated explicitly.

[c] Methods. NMR: Population ratios were estimated by integration of the signals corresponding to the GSCC and MSCC in a slow exchange regime on the ^{1}H NMR timescale. CV: Population ratios were estimated by signal integration in the cyclic voltammograms. CV Eq: Population ratios were estimated by applying the Nernst equation to CV data—see refs. 25 and 58.

Table 5.3 Summary of the ground-state distributions of translational isomers in donor-acceptor [2]rotaxanes based on a CBPQT^{4+} ring and a dumbbell possessing two π-donors, D1 and D2.



	D2	D2	Solvent	*T* / K	K_{eq}	ΔG° / kcal·mol^{-1}	Method[b]	Ref.
R501^{4+}	PTTFS	NP	Me_2CO	199	350	2.3	CV Eq	121, 25
R502f^{4+}	TTF	DNP	MeCN	298	9	1.3	CV	55
R502l^{4+}	TTF	DNP	MeCN	298	15	1.6	CV Eq	58
R504^{4+}	BPTTF	DNP	CD_3CN	295	3	0.6	NMR	55
R505^{4+}	PTTFS	DNP	CD_3COCD_3	206	0.11	0.9	NMR	103
R505^{4+}	PTTFS	DNP	CD_3COCD_3	231	0.43	0.4	NMR	103
R505^{4+}	PTTFS	DNP	CD_3COCD_3	267	0.92	0.04	NMR	103
R505^{4+}	PTTFS	DNP	CD_3COCD_3	RT	4	0.8	NMR	103
R505^{4+}	PTTFS	DNP	CD_3CN	226	0.67	0.2	NMR	103
R505^{4+}	PTTFS	DNP	CD_3CN	259	2.3	0.4	NMR	103
R506^{4+}	PTTFS-SMe	DNP	CD_3COCD_3	298	1	0	NMR	102
R506^{4+}	PTTFS-SMe	DNP	CD_3CN	298	3	0.6	NMR	102
R506^{4+}	PTTFS-SMe	DNP	MeCN	298	4	0.8	DPV	102
R506^{4+}	PTTFS-SMe	DNP	CD_3SOCD_3	298	1	0	NMR	101
R506^{4+}	PTTFS-SMe	DNP	CD_3SOCD_3	425	9	1.9	NMR	101
R507^{4+}	PTTFS-SMe	DNP	CD_3COCD_3	245	≥0.05[a]	≥1.5[a]	NMR	102
R507^{4+}	PTTFS-SMe	DNP	CD_3COCD_3	300	0.33	0.6	NMR	102
R507^{4+}	PTTFS-SMe	DNP	MeCN	298	0.67	0.2	DPV	102
R507^{4+}	PTTFS-SMe	DNP	CD_3CN	RT	1	0	NMR	102
R507^{4+}	PTTFS-SMe	DNP	CD_3CN	350	8	1.4	NMR	102
R507^{4+}	PTTFS-SMe	DNP	CD_3SOCD_3	300	2	0.4	NMR	102
R509^{4+}	HQ	RC	CD_3COCD_3	240	2	0.3	NMR	33
R510^{4+}	HQ	Xy	CD_3CN	243	2.3	0.4	NMR	32

[a]Estimates based on the observation of ^{1}H NMR signals attributable to a minor translational isomer, combined with an assumed detection limit of ≤5% by ^{1}H NMR spectroscopy. [b]Methods. NMR: Population ratios were estimated by integration of the signals corresponding to the GSCC and MSCC in a slow exchange regime on the ^{1}H NMR timescale. CV: Population ratios were estimated by signal integration in the cyclic voltammograms. CV Eq: Population ratios were estimated by applying the Nernst equation to CV data—see refs. 25 and 58. DPV: Population ratios were estimated by signal integration in the differential pulse voltammograms.

depth of the wells on the potential energy surface of a mechanomolecule, (ii) the sterics and electronics of the linkers situated in between the ring's two docking sites, and (iii) the physical environment, which encapsulates parameters such as temperature, solvent polarity, viscosity, etc. These parameters can be modulated to tune the rate constants over many orders of magnitude. The ability to control kinetics at this level is crucial to the design of molecular switches, machines, and motors (**Chapter 6**) that fulfill the requirements of a given application. For example, whereas bistable MIMs acting as the switching elements in molecular electronic memory devices[127] ought to have sufficiently high activation barriers (≥~22 kcal·mol) so as not to isomerize spontaneously, 'molecular muscles'[128] should respond ideally very quickly to an energetic stimulus and therefore possess much lower activation barriers.

As a practical matter, the shuttling rates in degenerate bistable MIMs are often determined by dynamic NMR spectroscopic techniques (**Figure 5.14**), such as spin polarization transfer by selective inversion recovery[129] (SPT-SIR), two-dimensional exchange-correlated spectroscopy[130,131] (2D EXSY), and line shape analysis.[132,133] Each method has its own advantages and limitations. The SPT-SIR method entails the selective irradiation at the frequency of a nuclear

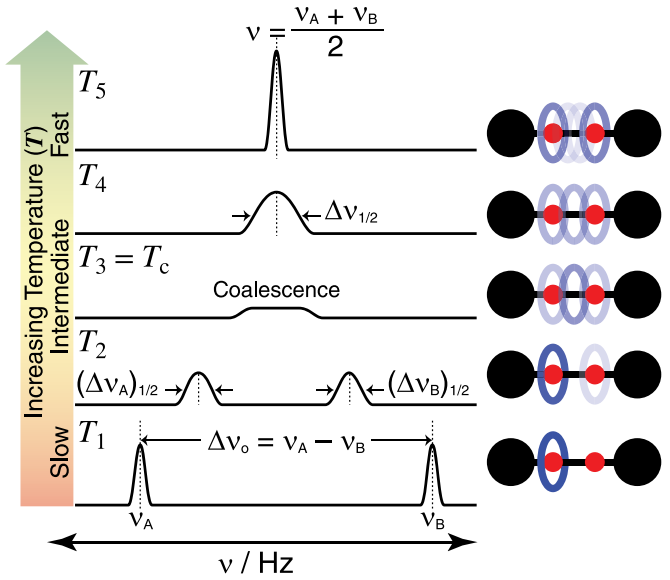


Figure 5.14 Generalized conceptual example of NMR line shape analysis of the resonance signals of two nuclei undergoing degenerate site exchange via ring translation in a VT NMR spectrum of a degenerately bistable [2]rotaxane molecular shuttle, with relevant terms applicable to Equations 5.9–5.13 defined.

resonance, followed by an observation of the resulting perturbance to a resonance with which it is exchanging in dynamic equilibrium. The limitations of SPT-SIR are that the system must be in slow exchange on the NMR timescale, and that it becomes increasingly difficult with decreasing separation between the chemical shifts of interest. 2D EXSY relies on similar principles and carries with it the same limitations. Line shape analysis is possible even when resonances are in fast exchange on the NMR timescale, yet it is more error prone and requires that spectra be recorded over a range of temperatures. We note that these methods are applicable to estimating the kinetics, not only of translation, but also to other co-conformational exchange processes such as pirouetting (**Section 5.1.2**) and rocking (**Section 5.1.3**), as well as the superimposed conformational exchange processes involving covalent bond torsions. Since line shape analysis has been the most commonly employed method for measuring the kinetics of mechanostereochemical exchange, we will offer a more detailed explanation of this method. Line shape analysis hinges on the fact that the NMR spectrum is a function of the rate of exchange, k, as well as the difference in the resonance frequencies, $\Delta\nu$, of the two nuclei—call them A and B—undergoing site exchange, according to Equation 5.9 –

$$\Delta\nu = \nu_A - \nu_B \tag{5.9}$$

where ν_A and ν_B are the resonance frequencies of nuclei A and B, respectively. For energy barriers[F] in the range of ca. 3–20 kcal·mol^{-1}, the line shape of the NMR spectrum is given[134] by the function $g(\nu)$ (Equation 5.10)

$$g(\nu) = \frac{C\tau(\nu_A - \nu_B)^2}{\left(\frac{\nu_A}{2} - \frac{\nu_B}{2} - \nu\right)^2 + 4\pi^2\tau^2(\nu_A - \nu)^2(\nu_B - \nu)^2} \tag{5.10}$$

where $g(\nu)$ is the intensity at frequency ν, C is a normalization constant, and $\tau = k/2$. The rate constant k can be estimated by approximations that are applied in different exchange rate regimes. Two atomic nuclei exchanging chemically equivalent sites by an intramolecular process can do so on a timescale that is either fast, slow, or approximately equal (intermediate) to the NMR timescale. When the rate of exchange is very slow, k may be estimated by Equation 5.11 –

$$k = \frac{\pi}{\sqrt{2}}\sqrt{\Delta\nu_o^2 - \Delta\nu_e^2} \tag{5.11}$$

where $\Delta\nu_o$ and $\Delta\nu_o$ represent the differences in resonance frequencies when k is as close to zero as possible—i.e., at the lowest possible temperature—and at the temperature of the experimental observation, respectively. The two signals (not coupled[G] to each other) corresponding to nuclei A and B in the NMR spectrum merge into a single, flat-topped signal at the coalescence temperature, T_c, where the rate of exchange is given[134] by Equation 5.12.

$$k_C = \frac{\pi\Delta\nu_o}{\sqrt{2}} \tag{5.12}$$

Equation 5.12 reveals why it is particularly simple to estimate k_c, and from it, the transition state energy, $\Delta G^{\ddagger}$, at T_c. Finally, when site exchange is fast on the NMR timescale, the rate constant can be estimated by Equation 5.13 –

$$k = \frac{\pi\Delta\nu_o^2}{2(\Delta\nu_e)_{1/2} - 2(\Delta\nu_o)_{1/2}} \tag{5.13}$$

where $(\Delta\nu_e)_{1/2}$ represents the full width at half maximum (FWHM) of the merged, yet not fully collapsed, signal in the observed spectrum, and $(\Delta\nu_o)_{1/2}$ is the limit of the FWHM, i.e., the narrowest signal that is experimentally obtainable. If k is measured at only one temperature, often T_c using Equation 5.12, then $\Delta G_c^{\ddagger}$ may be estimated using Equation 5.6. If k is measured across a range of temperatures, however, then the transition state enthalpy $\Delta H^{\ddagger}$ and entropy $\Delta S^{\ddagger}$ may also be obtained from the slope and the intercept, respectively, in a graph of $\ln(k/T)$ vs. T^{-1}, the Eyring plot. The above approximations have been employed to assess the kinetics, not only of translation (**Section 5.1.1**), but also of pirouetting (**Section 5.1.2**) and rocking

[F] Energy barriers that are too high for line shape analysis can still be measured by SPT-SIR experiments. See refs. 129 and 131

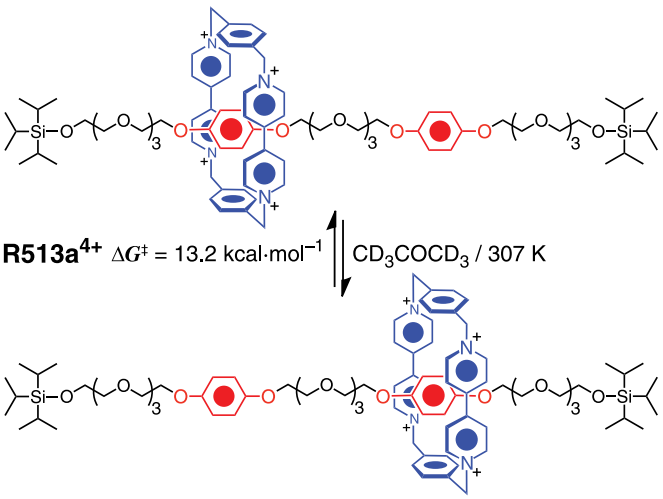
[G] For a coupled AB system with a coupling constant J_{AB}, the rate k_c is given by $\pi[\Delta\nu_o^2+6J_{AB}^2]^{1/2}/\sqrt{2}$.

(**Section 5.1.3**) motions that can be detected on the basis of variable temperature (VT) ^{1}H NMR spectra.

Donor-Acceptor Molecular Shuttles

Bistable rotaxanes are also known[135] as molecular shuttles[H] because the ring 'shuttles' between two recognition units, typically by a diffusive Brownian process of random walk, which relies on thermal noise to supply the energy required to translate the ring between sites over a course of random movements constrained by the mechanical bond. The original donor-acceptor molecular shuttle[135] **R513a^{4+}** involved a CBPQT^{4+} ring shuttling (**Scheme 5.3**) between two HQ recognition units separated by an oligoether linker. The transition state energy, $\Delta G^{\ddagger}$, defining the energy barrier to shuttling in CD_3COCD_3 was determined by VT ^{1}H NMR spectroscopy to be approximately 13.2 kcal·mol^{-1}, which corresponds to a rate of about 1300 s^{-1} at 298 K. An analogous molecular shuttle with porphyrin stoppers shuttles[136] at a slightly slower rate governed by a higher $\Delta G^{\ddagger}$ value of 13.6 kcal·mol^{-1}. The modest increase in activation free energy in the latter case may arise from 'alongside' interactions between the porphyrinic stoppers and the CBPQT^{4+} ring, adding stability to the ground state co-conformation. Benniston and Harriman[137] have prepared analogous molecular shuttles with ferrocene and anthracene derived stoppers.

The effects conferred by different recognition units and linkers on the $\Delta G^{\ddagger}$ values of degenerate bistable D-A rotaxanes can be probed by comparing the various molecular shuttles, **R513^{4+}–R520**, represented in **Table 5.4**, see refs. 32, 44, 135, 136, 138–143. Recalling that the three most important factors influencing the shuttling rates are (i) the strength of the interactions between recognition units, (ii) the steric and electronic effects of the linkers, and (iii) the physical environment, we begin to see how the interplay between these three domains accelerate or decelerate the kinetics of exchange by translational motion.



Scheme 5.3 The original donor-acceptor molecular shuttle, in which a rotaxane's CBPQT^{4+} ring (blue) translocates between two HQ recognition units (red) in acetone.[135]

The Influence of the Recognition Units

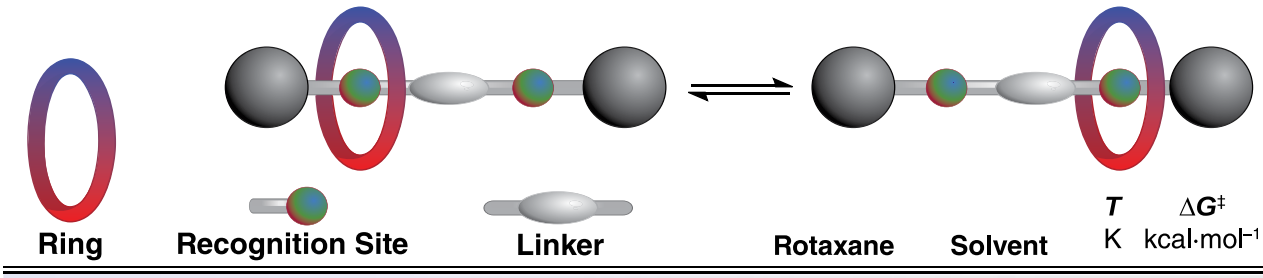
We have described in **Section 5.1.1.1** how local noncovalent bonding interactions affect the population distributions of translational isomers, as governed by $\Delta G°$. These interactions also influence kinetics, since lower-lying potential energy wells correspond to higher $\Delta G^{\ddagger}$ values. For example, compare (**Table 5.4**) the molecular shuttles[135,136,144] **R513a^{4+}**, **R514a^{4+}**, and **R515^{4+}**, which are similar in their constitutions except for the sites of the dumbbells' recognition units. The $\Delta G^{\ddagger}$ values increase from approximately 13 to 15 to 17 kcal·mol^{-1} as these units are swapped from HQ to DNP to TTF, owing to their increasingly more stable π-associated D-A charge transfer interactions with the CBPQT^{4+} ring in the ground state. In the case[143] of comparing charge-neutral D-A rotaxanes **R520a** and **R520b**, the π-donating crown ether 1,5-dinaphtho[38]crown-10 (DN38C10) shuttles between naphthalene diimide (NDI) π-acceptors with a much higher barrier (~14 kcal·mol^{-1}) than it does between more weakly stabilizing pyromellitic diimide (PMDI) units (~11 kcal·mol^{-1}) in CD_2Cl_2.

Changing recognition units in the ring of a molecular shuttle is an equally viable strategy for controlling the rate constants. For example, swapping out the CBPQT^{4+} ring for the cyclobis(2,7-diazapyrenium-*para*-phenylene) (CBDAP^{4+}) ring, with its wider π-accepting surface area, raises the $\Delta G^{\ddagger}$ value (**Table 5.4**) of the HQ-based shuttle[44] **R518^{4+}** all the way up to >18 kcal·mol^{-1}. In general, shuttling these tetracationic cyclophanes appears to be a higher energy process than that of the crown ether counterparts (all else being equal), most likely on account of the tetracationic rings' relatively smaller, more rigid apertures, as well as their tendency to bind guests with higher affinities than the crown ethers. For example, whereas translation of a CBPQT^{4+} ring between two HQ units over the polyether linker of **R513a^{4+}** requires >13 kcal·mol^{-1} of energy in , shuttling[145,146] of the HQ-based ring bis-*para*-phenylene[34]crown-10 (BPP34C10) between two BIPY^{2+} units over the *para*-xylyl linker of **R519a^{4+}** requires only 9.9 kcal·mol^{-1} of energy in acetone. The latter kind of shuttle has been adapted by Otera,[147] who demonstrated the concept of degenerate bistable rotaxanes as 'intermittent' molecular shuttles which can be turned on and off by dimerizing a 2,2′bipyridine linker around a Cu^{I} center.

The homophilic supramolecular templation motif[98] driven by radical-pairing interactions (**Section 2.3.10**) between viologen radical cations has provided access to an unusual class[140] of molecular shuttles (**R517a^{6+}–R517h^{6+}**) possessing no recognition units for the CBPQT^{4+} ring and highly tunable activation barriers. The CBPQT^{4+} ring preferentially encircles one or other of the oligomethylene chains connecting the stoppers to a central BIPY^{2+} unit as an

[H] Although the term 'molecular shuttle' was originally intended to describe degenerately bistable rotaxanes, the term has been adopted in the literature in scenarios that include non-degenerate bistable and multistable rotaxanes as well.

Table 5.4 Summary of the activation barriers ($\Delta G^{\ddagger}$) and shuttling rate constants (k) for various degenerately bistable D-A molecular shuttles.



Ring	Recognition Site	Linker		Rotaxane	Solvent	T K	$\Delta G^{\ddagger}$ kcal·mol^{-1}	k s^{-1}	Ref
CBPQT^{4+}				**R513a**$^{4+}$	CD_3COCD_3	307	13.2	2360	135
					CD_3COCD_3	263	13.6	25	136
				R513b^{4+}	$(CD_3)_2NCHO$	278	13.9	71	32
					CD_3SOCD_3	338	16.8	98	
					CD_3CN	265	12.7	169	
					CD_3COCD_3	274	13.1	187	
				R514a^{4+}	CD_3COCD_3	247	15.2	0.2	144
					CD_3COCD_3	293	15.4	20	
				R514b^{4+}	CD_3COCD_3	236	14.8	0.1	144
					CD_3COCD_3	293	15.1	33	
				R514c^{4+}	CD_3COCD_3	248	15.3	0.2	144
					CD_3COCD_3	293	15.5	19	
				R514d^{4+}	CD_3COCD_3	296	15.5	22	138
				R514e^{4+}	CD_3CN	322	15.6	22	139
				R514f^{4+}	CD_3CN	350	>18	<40	139
				R514g^{6+}	H_2O[a]	343[a]	>17[a]	<50[a]	149
				R515^{4+}	CD_3COCD_3	293	17.5	0.53	144
				R516a^{4+}	CD_3COCD_3	208	10.3	131	122
				R516b^{4+}	CD_3COCD_3	208	10.0	119	122
	$-(CH_2)_n-$		n = 3	**R517a**$^{6+}$	CD_3COCD_3	238-251	11.4	-	140
			n = 4	**R517b**$^{6+}$		256-267	12.3	-	
			n = 5	**R517c**$^{6+}$		256-258	12.7	-	
			n = 6	**R517d**$^{6+}$		266-271	13.7	-	
			n = 7	**R517e**$^{6+}$		287-303	14.6	-	
			n = 8	**R517f**$^{6+}$		300-321	15.4	-	
			n = 9	**R517g**$^{6+}$		295-29	15.8	-	
			$n \geq 10$	**R517h**$^{6+}$		330	>16	-	
CBDAP^{4+}				**R518**$^{4+}$	CD_3CN	350	18.1	30	44
BPP34C10				**R519a**$^{4+}$	CD_3COCD_3	215	9.9	338	141
			Me	**R519b**$^{4+}$	CD_3CN	240	11.5	157	142
			Et	**R519c**$^{4+}$		238	12.1	38	
			R = Ph	**R519d**$^{4+}$		283	14.9	20	
			i-Pr	**R519e**$^{4+}$		283	14.5	38	
			t-Bu	**R519f**$^{4+}$		353	>17.2	<65	
DN38C10				**R520a**	CD_2Cl_2	226	11.4	45	143
					CD_2Cl_2	294	10.9	50k	
				R520b	CD_2Cl_2	266	14.1	16	143
					CD_2Cl_2	294	14.0	250	

Cationic rotaxanes were investigated as their PF_6^- salts except where noted. [a]The rotaxane was converted to its chloride salt in order to impart water solubility.

electrostatic speedbump. Since the $CBPQT^{4+}$ ring exhibits[140,148] essentially no affinity for the oligomethylene chains while being repelled electrostatically by the dumbbell's $BIPY^{2+}$ unit, these rotaxanes possess very high-lying potential energy surfaces—so high that a $BIPY^{\bullet+}$ radical cation becomes an increasingly favorable dumbbell species as these chains are shortened. Longer oligomethylene chains allow the $CBPQT^{4+}$ ring to position itself at a further distance from the $BIPY^{2+}$ unit, corresponding to a lower free energy relative to that of rotaxanes possessing shorter linkers. The translational activation barriers (**Table 5.4**) thus depend heavily on the number of carbon atoms in these hydrocarbon landing sites, ranging from 11.4 kcal·mol^{-1} in the case of a propylene chain to >16 kcal·mol^{-1} in the case of a decamethylene chain. Since the repulsive Coulombic interactions between the $CBPQT^{4+}$ ring and $BIPY^{2+}$ speedbump are constant across all of the rotaxanes in the series, the tunability of the free energy barriers can be attributed entirely to ground state effects—the ground state energies are lowered as the oligomethylene chains are lengthened because they allow the ring to occupy space at a greater distance from the dumbbell's $BIPY^{2+}$ unit.

The Influence of Linkers

The entries in **Table 5.4** also afford us an opportunity to compare how linkers affect the kinetics of translation. The $BIPY^{2+}$ linker in the abovementioned $-(CH_2)_n-\subset CBPQT^{4+}$ molecular shuttles clearly presents an electrostatic barrier to the shuttling process. The $BIPY^{2+}$ unit has also been investigated[149] as an electrostatic speedbump in $CBPQT^{4+}$ molecular shuttles possessing DNP recognition units. In the case of **R514g^{6+}**, the ring shuttles slowly on the ^{1}H NMR timescale even at 343 K, corresponding to a $\Delta G^{\ddagger}$ value of >17 kcal·mol^{-1}.

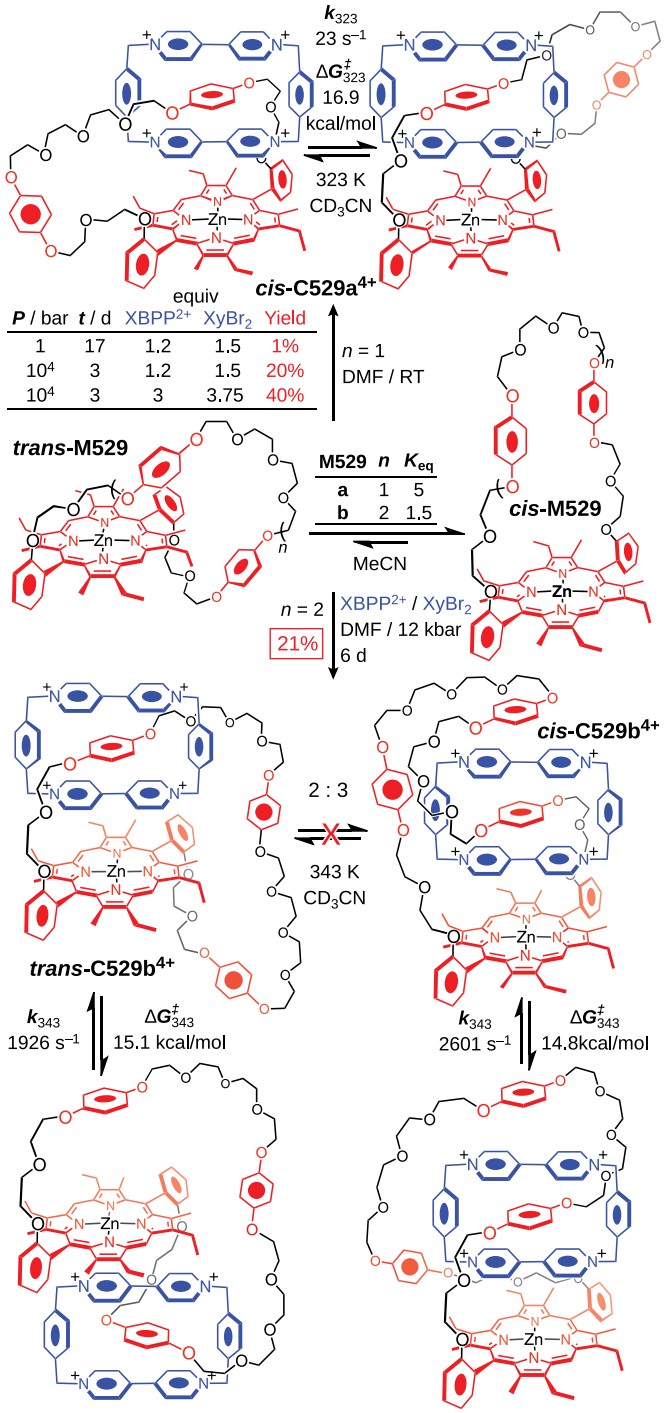
The effects of linker sterics on shuttling rates can be appreciated by comparing (**Table 5.4**) the bistable [2]rotaxanes **R519b^{4+}–R519f^{4+}**, in which a bis-*para*-phenylene[34]crown-10 (BPP34C10) ring shuttles back and forth over meta-xylylene linkers functionalized with a systematically varied series of increasingly bulky groups.[141,142] Not surprisingly, growth in the linker's steric bulk correlates well with increases in the corresponding $\Delta G^{\ddagger}$ values. The barriers range from 11.5 (R = Me) to >17.2 (R = ^{t}Bu) kcal·mol^{-1} in CD_3CN.

The Influence of the Physical Environment

The role of the physical environment on the kinetics of translation in donor-acceptor MIMs has been investigated in much greater depth with non-degenerate systems. These examples are discussed in **Sections 5.1.1.1** and **Section 6.14.1**. In general, the influence of factors such as temperature, solvent polarity, and viscosity follow expectations—shuttling rates increase with temperature, as predicted by the Eyring Equation 5.5, as well as with increasing solvent polarity, in most cases. One exception to this trend is the case[32] (**Table 5.4**) of the [2]rotaxane **R513b^{4+}**, in which a $CBPQT^{4+}$ ring translates between two HQ recognition units over a linker containing a BPDTTF unit, which is itself a recognition site. The solvent's ability to accelerate translational motion in this molecular shuttle proceeds as $CD_3CN>CD_3COCD_3>$ NMP>DMF. In other words, the solvents that most effectively destabilize the $HQ\subset CBPQT^{4+}$ interactions are, counterintuitively, giving rise to higher $\Delta G^{\ddagger}$ values. A likely explanation for this observation is that the BPDTTF linker recruits the ring to itself more effectively in these solvents. This hypothesis is consistent with results[102,103] from non-degenerate bistable shuttles, in which the $CBPQT^{4+}$ ring's relative affinity for TTF derivatives is enhanced in more polar solvents. Viscosity may provide an alternative or complementary explanation, since the more polar solvents in this case are also significantly more viscous than the less polar ones.

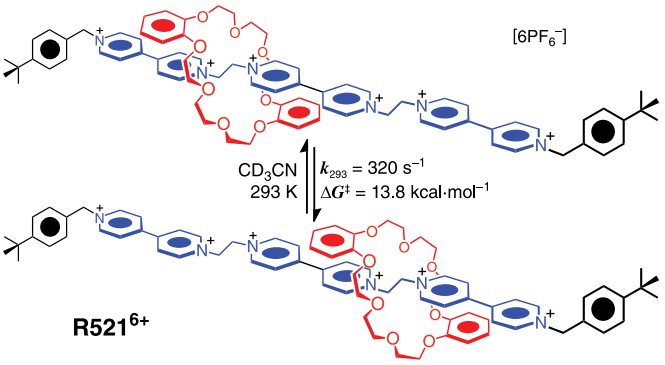
Table 5.4 is not a comprehensive list of degenerate donor-acceptor molecular shuttles. For example, Zhou[150] has examined $CBPQT^{4+}$ shuttling between HQ sites in hybrid [3]rotaxanes possessing a benzylic amide ring, while Abraham[151] has investigated $CBPQT^{4+}$ molecular shuttles with acridane and acridinium stoppers which are *nearly* degenerate. Several more examples of D-A molecular shuttles are featured in **Schemes 5.4–5.6**.

Gunter[152,153] has described a number of D-A [2]catenanes (**Scheme 5.4**) in which a $CBPQT^{4+}$ ring encircles a macrocyclic strapped porphyrin (**Section 2.3.3.6**) possessing multiple HQ recognition units. The parent porphyrinic macrocycles **M529a** and **M529b**, possessing two and three polyether-bridged HQ units, respectively, were converted to the corresponding [2]catenanes **C529a^{4+}** and **C529b^{4+}** by high-pressure clipping protocols that are typical for $CBPQT^{4+}$-based catenanes—see **Section 2.3.3.2**. Whereas the macrocycles **M529a-b** equilibrate in MeCN between *cis*- and *trans*- atropisomers, the corresponding [2]catenanes do not isomerize, indicating that the $CBPQT^{4+}$ ring raises the torsional barrier for the porphyrin-appended aryl rings responsible for atropisomerization. In the case of the smaller [2]catenane **C529a^{4+}**, only the *cis* isomer is generated—molecular models indicate that the *trans* isomer would be severely strained in the presence of a catenated $CBPQT^{4+}$ ring. By contrast, the *trans*- and *cis*- isomers of **C529b^{4+}** are generated in a 2:3 ratio, which reflects the equilibrium ratio (K_{eq} = 1.5) of ***trans/cis*-M529b**. In both cases, the prevailing co-conformations in solution, as detected by ^{1}H NMR spectroscopic techniques, involve side-on interactions between the $CBPQT^{4+}$ rings and the porphyrin units, with the porphyrin-adjacent HQ units occupying the $CBPQT^{4+}$ cavity. The translational motions that allow the two degenerate states in each of these catenanes to interconvert are approximately two orders of magnitude slower in the case of the double-HQ [2]catenane **C529a^{4+}** (23 s^{-1} at a T_C = 323 K) than in either the *cis*- or *trans*- isomers (1926–2601 s^{-1} at T_C = 343 K) of the triple-HQ [2]catenane **C529b^{4+}**. The difference in shuttling rates is most likely attributable to the difference in the alonside π–π interactions, which are better enforced by the [2]catenane with a smaller ring size. Gunter[152] also isolated [3]catenanes derived from **M529b**, finding that the presence of a second $CBPQT^{4+}$ disrupts the alongside porphyrin–$BIPY^{2+}$ interactions.



Scheme 5.4 The synthesis of Gunter's porphyrin-strapped [2]catenanes, which possess either two (**C529a**$^{4+}$) or three (**C529b**$^{4+}$) HQ recognition units for an interlocked $CBPQT^{4+}$ ring, and the translational motions that lead to exchange of degenerate HQ units within the $CBPQT^{4+}$ ring's cavity.[152]

Loeb[154] has constructed and characterized (**Scheme 5.5**) the degenerate [2]rotaxane molecular shuttle **R521**$^{6+}$, which relies on the hydrogen-bonded and donor-acceptor recognition motif involving bis(pyridinium)ethane (BPE^{2+}) units encircled by the crown ether dibenzo[24]crown-8 (DB24C8), as introduced in **Section 2.3.3.3**. Loeb[154] found



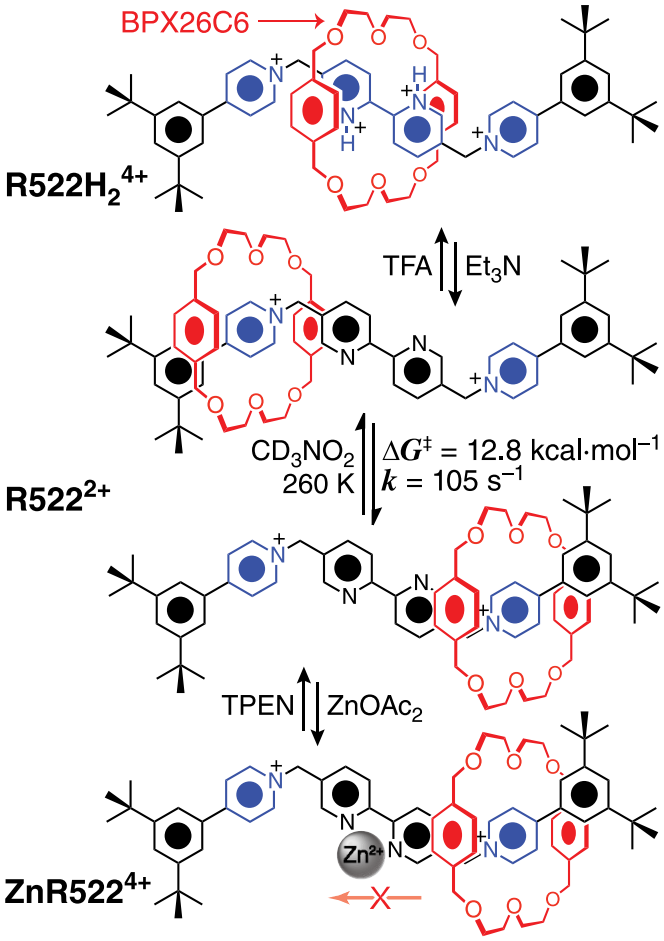
Scheme 5.5 Loeb's molecular shuttle based on the BPE^{2+}⊂*DB24C8* recognition motif.[154]

that the DB24C8 ring of **R521**$^{6+}$ moves back and forth between the dumbbell's BPE^{2+} sites at a rate of about 320 times per second at 20 °C, corresponding to an activation barrier of 13.8 kcal·mol^{-1} in CD_3CN. The Windsor group[154,155] has also prepared similar bistable rotaxanes possessing unsymmetrical dumbbell constitutions, which are therefore non-degenerate. Indeed, the distributions of translational isomers are not 1:1 in these unsymmetrical bistable rotaxanes in spite of the fact that the submolecular recognition units are identical, reminding us that peripheral groups and stoppers can still influence the thermodynamic and kinetic parameters of a molecular shuttle.

Chiu[156] has prepared and investigated the bistable [2]rotaxane **R522**$^{2+}$, in which a bis-*para*-xylyl[26]crown-6 (BPX26C6) wheel shuttles (**Scheme 5.6**) between pyridinium recognition units over a 2,2′-bipyridine (bpy) linker—a design which is conceptually akin to the aforementioned metal-sensitive D-A molecular shuttle first described by Otera,[147] yet based on a different recognition motif—see **Section 2.3.3.4**. In this case, the ring must overcome an energy barrier of 12.8 kcal·mol^{-1} in order to exchange between degenerate sites in CD_3NO_2, allowing it to oscillate with a frequency of ~105 Hz at the ^{1}H NMR coalescence temperature of 260 K. The movement of the ring can be frozen on the ^{1}H NMR timescale even at 298 K when Zn^{2+} is added in solution as a blocking ion, which becomes coordinated by the bpy linker in **ZnR522**$^{4+}$. Alternatively, the ring can be 'parked' on the linker itself by protonating it under acidic conditions, affording **R522H$_2$**$^{4+}$. The position and movement of the ring can thus be controlled with a high degree of specificity by introducing *in situ* the appropriate chemical reagents.

Hydrogen-bonded Molecular Shuttles

Leigh[157] has prepared and investigated the properties of a number of molecular shuttles (**Figure 5.15a**) based on the benzylic amide tetralactam rings encircling peptide recognition units. The bistable [2]rotaxanes **R523a-f** are identical, except that they possess different linkers in between the glycylglycine recognition units of the dumbbells. A comparison of the octamethylene and hexadecamethylene linkers of **R523a** and **R523b**, respectively, reveals that shuttling rates



Scheme 5.6 Shuttling of the BPX26C6 ring between the two pyridinium units of **R522**$^{2+}$ can be stopped by modifying the central 2,2´-bipyridine linker, either by protonation with acid, which 'parks' the ring around the corresponding bipyridinium dication, or by introducing Zn^{2+} as a blocking cation, which forbids the ring from exchanging sites.[156]

are influenced by the distance that the ring must traverse between its binding sites, since the ring of **R523b** requires 1.2 kcal·mol^{-1} more energy to exchange sites than does that of **R523a**. Curiously, the rotaxane **R523c** possessing a thioether linker shuttles at the same rate ($\Delta G^{\ddagger}$ = 10.9 kcal·mol^{-1}) as the derivatives **R523d-e**, which are accessed by oxidation of the linker to the corresponding sulfoxide or sulfone, respectively. Leigh has also found[157] that small amounts of CD_3OD can increase the shuttling rates dramatically. For example, the rate of shuttling in **R523c** doubles from 8 s^{-1} to 16 s^{-1} at 203 K with only 0.1% CD_3OD in CD_2Cl_2, and reaches 2300 s^{-1} at 5% CD_3OD,[l] corresponding to a rate constant of >10^6 s^{-1} at room temperature. Shuttling can also be halted (**Figure 5.15b**) completely by introducing a bulky tosyl group in the linker and restarted again by its removal using chemical reagents that protect and deprotect the thioether site in **R523c** and **R523f**, respectively. In addition, Leigh[158] described a simple double-minimum potential quantum mechanical model of the shuttles **R523a-c**, which agrees well with experimental observations on the kinetics of shuttling. Counter to intuition, the model predicts that the ring spends the majority of its time at the center of the linker when the thermal energy slightly exceeds that of the transition state $\Delta G^{\ddagger}$, whereas it occupies primarily the recognition units when the thermal energy is significantly above or below that of the transition state.

Albert Brouwer[159] at the University of Amsterdam has also prepared a number of benzylic amide molecular shuttles. Among them, the benzylic amide ring of the [2]rotaxane **R524** must traverse (**Scheme 5.7**) a long –$C_{26}H_{52}$– oligomethylene chain as it translates between glycyl-NDI recognition units. This process was found to occur with a barrier of ca. 11.8 kcal·mol^{-1} in $CDCl_3$, while the enthalpy and entropy of the transition state were estimated to be $\Delta H^{\ddagger}$ = 10 kcal·mol^{-1} and $\Delta S^{\ddagger}$ = –6.5 cal·mol^{-1}K^{-1}, respectively. Homologues with shorter oligomethylene and rigid phenylene-ethynylene linkers were also prepared. It was established that shorter and more rigid linkers accelerate the shuttling rates, although the activation barriers were not quantified in these cases, in part because of solubility issues at low temperature. Berná[160] has demonstrated an ability to control the rate of benzylic amide ring shuttling in

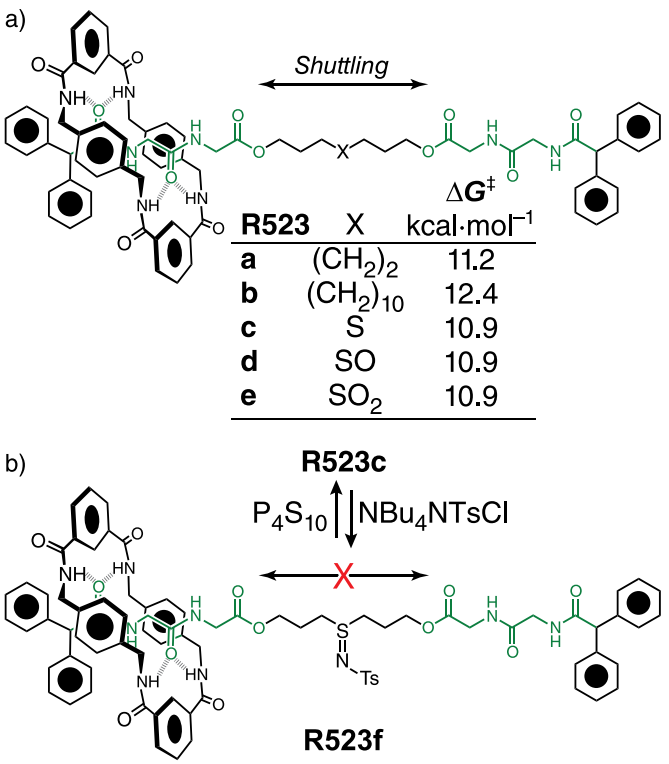
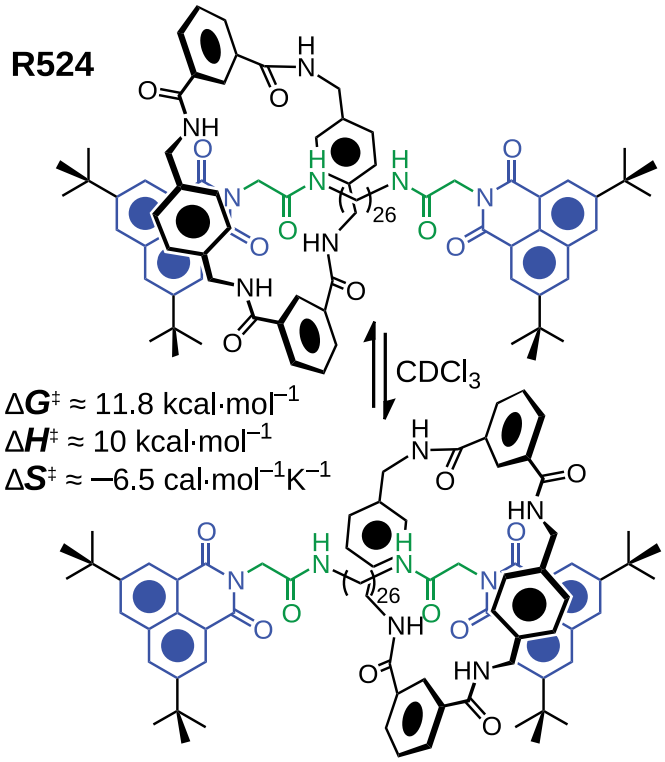


Figure 5.15 Peptide-based molecular shuttles with benzylic amide rings.[157] (a) Structural formulas and activation barriers for the degenerate bistable [2]rotaxanes **R523a-e** in $CDCl_3$. (b) Shuttling can be stopped and restarted by protecting and deprotecting the thioether of **R523c** and **R523f**, respectively.

[l] The co-conformations of these molecular shuttles are not well defined in solvents exceeding 5% MeOH, while the polarophobic linker itself is the encircled site in high polarity solvents such as Me_2SO and DMF—see **Section 6.8.1**.

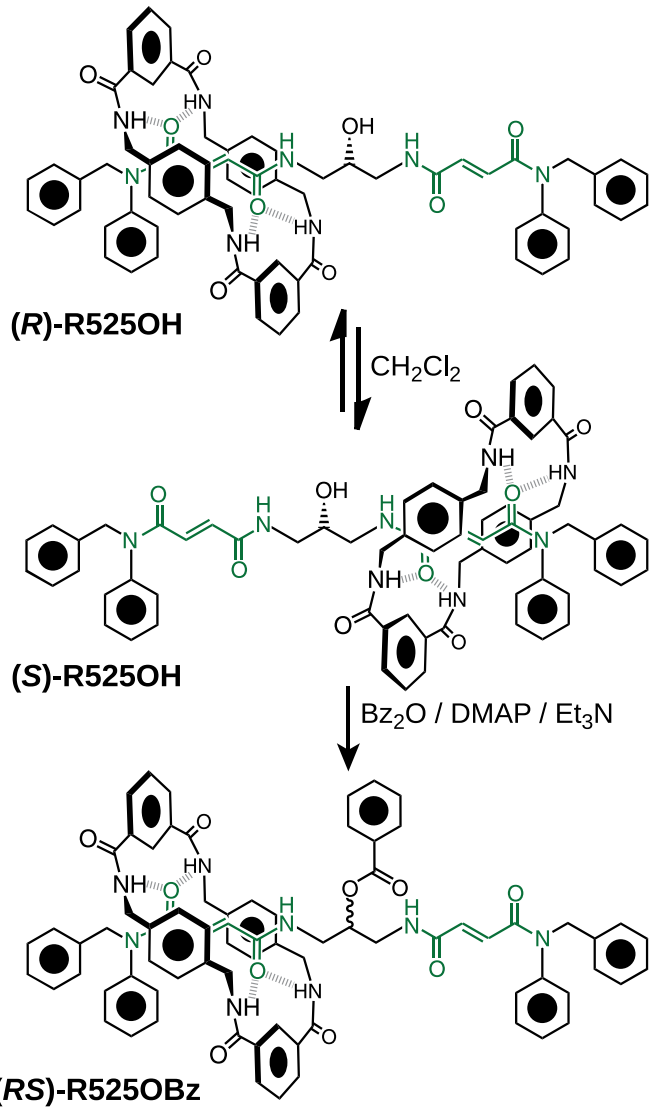


Scheme 5.7 Brouwer's molecular shuttle in which a benzylic amide ring translates between glycylNDI recognition units over a long oligomethylene linker.[159]

degenerate molecular shuttles by using redox stimuli to switch the recognition sites between azo- and hydrazodicarboxamide species. A non-degenerate homologue of these shuttles is discussed in **Section 6.7.5**.

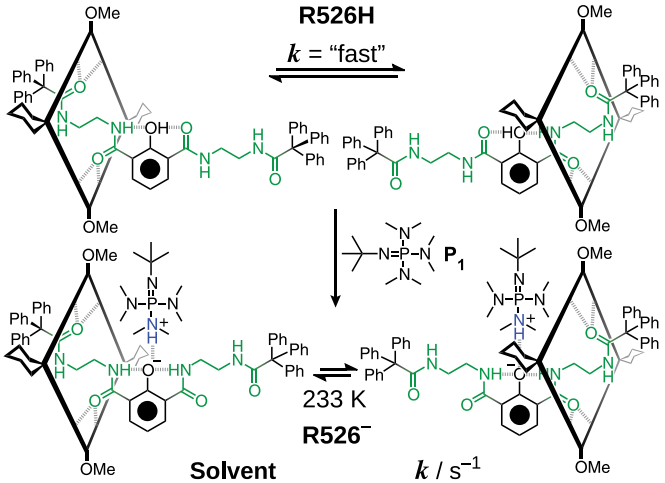
Leigh[23] has demonstrated how the dynamics of translation (**Scheme 5.8**) can lead to the rapid inversion of absolute configuration in the degenerately bistable molecular shuttle **R525OH**, thus constituting a form of "dynamic chirality".[4,48] The dumbbell component of this [2]rotaxane possesses two fumaramide recognition units and a short oligomethylene linker functionalized with a hydroxyl group on its central prochiral carbon atom. Formation of the [2]rotaxane **R525OH** results in this prochiral center being transformed into a stereogenic center whose absolute configuration is inverted as the benzylic amide ring passes between the fumaramide units in **(*R*)-525OH** and **(*S*)-R525OH**. Thus, the absolute configuration of a stereogenic center in a degenerate [2]rotaxane, derived from a prochiral center in its dumbbell precursor, is determined by the location of a mechanical bond! This dynamic inversion of chirality may be shut down by functionalizing the hydroxyl group with a sufficiently bulky barrier—esterification with benzoic anhydride affords **(*RS*)-R525OBz** as a racemate. See **Section 6.12.2.3** for a discussion of how the dynamic chirality of **R525OH** may be used in combination with a chiral organocatalyst during esterification in order to produce an 'information ratchet' that biases the distribution of (*R*) and (*S*) enantiomers of **R525OBz**. Other kinds of chirality resulting from mechanical bonds are discussed throughout **Section 5.2**.

Schalley, Lützen, and Gschwind[161] have described the unintentional discovery of shuttling in the tetralactam-derived [2]rotaxane **R526H** based on Schalley's phenolate anion-binding motif[162]—see **Section 2.3.6.2**. The tetralactam ring's shuttling rate is sensitive to the protonation state of the central phenolic linker. Deprotonation of **R526H** with Schwesinger's P_1 base[163] affords the anionic rotaxane P_1H·**R526**. Although rate constants were not reported[J] for **R526H**, the shuttling rate constants for **R526**$^-$ in several



Scheme 5.8 Dynamic chirality in Leigh's degenerate molecular shuttle **R525OH** possessing[23] a stereogenic center. **R525OH** undergoes inversion of configuration at its stereogenic center as the ring shuttles between sites, a process which can be halted by conversion to the benzoic aster **R525OBz**. The corresponding (*R*) and (*S*) enantiomers of **R525OBz** cannot undergo inversion on account of the much higher kinetic barrier to translation.

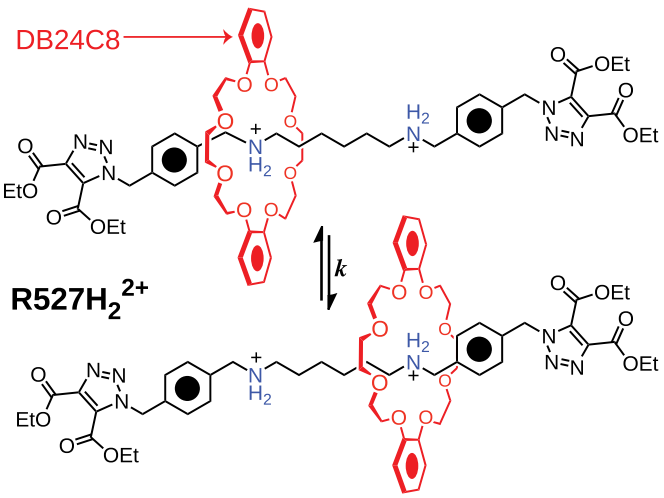
[J] The solvent systems available to probe shuttling in **R526H** are limited by its low solubility. It was reported, however, that shuttling rates in **R526**$^-$ and **R526H** both plateau at ~0.1 s^{-1} in mixtures of CD_2Cl_2 and $(CD_3)_2NCDO$.



Solvent	k / s^{-1}
CD_2Cl_2	0.051
10% CD_3SOCD_3	0.070
20% CD_3SOCD_3	0.104
40% CD_3SOCD_3	0.105
$(CD_3)_2CDO$	0.109
20% CD_3SOCD_3	0.091
40% CD_3SOCD_3	0.088

Scheme 5.9 A tetralactam ring, which is 'cartoonized' in the scheme, shuttles between two ethylenediamide recognition units in the bistable [2]rotaxane **R526H**. Shuttling can be slowed down by deprotonation of the phenolic linker with P_1 base.[161] The association of the corresponding P_1H^+ cation with the phenolate anion of **R526**$^-$ inhibits shuttling more effectively in less polar solvent systems.

Table 5.5 Comparison of K_a values for $Bn_2NH_2^+ \subset DB24C8$ pseudorotaxanes with $\Delta G^‡$ and k values for the molecular shuttle **R527H$_2^{2+}$** based on the same recognition motif.[164]



Solvent	K_a / M^{-1} $Bn_2NH_2^+ \subset DB24C8$	T K	k s^{-1}	$\Delta G^‡$ kcal·mol^{-1}
$(CD_3)_2NCDO$	~0	217	108	10.5
CD_3COCD_3	360	275	106	13.5
CD_3CN	420	286	182	13.8
CD_3NO_2	22000	303	155	14.7
$C_2D_2Cl_4$	>25000	353	62	17.9

solvent systems are listed in **Scheme 5.9**. It was argued that the P_1H^+ cation acts as a 'brake' because it associates with the phenolate anion of the rotaxane's central linker, and thus interferes with the ring's translational motion. The rate of shuttling in **R526**$^-$ is thus faster in more polar solvents (i.e, DMF, Me_2SO) which solvate the P_1H^+ cation more effectively than does CD_2Cl_2.

When molecular shuttles based on the *dialkylammonium ⊂crown* ether molecular recognition motif (**Section 2.3.4.6**) were introduced,[164] a clear relationship between the thermodynamic stabilities of the local noncovalent bonding interactions and the shuttling rates was established by comparing (**Table 5.5**) the association constants of model pseudorotaxanes comprising dibenzylammonium ($Bn_2NH_2^+$) and dibenzo[24]crown-8 (DB24C8) with the shuttling rates (k) and transition state energies ($\Delta G^‡$) of the bistable [2]rotaxane **R527H$_2^{2+}$** in different solvents. The stability of the $R_2NH_2^+ \subset DB24C8$ interaction can be tuned over a very wide range by changing solvents, since the strength of these interactions is highly sensitive to the solvent's electron-donating ability. The K_a values of the model pseudorotaxanes rise from 0 to >25000 M^{-1} as the solvent is changed from dimethylformamide (most polar) to tetrachloroethane (least polar), while the transition state energies cover a correspondingly wide range of values, from 10.5 to 17.9 kcal·mol^{-1}. Replacing the hexamethylene linker of **R527H$_2^{2+}$** with a bulkier *para*-xylyl linker results in a high $\Delta G^‡$ value of 21.3 kcal·mol^{-1} in $(CD_3)_2SO$.

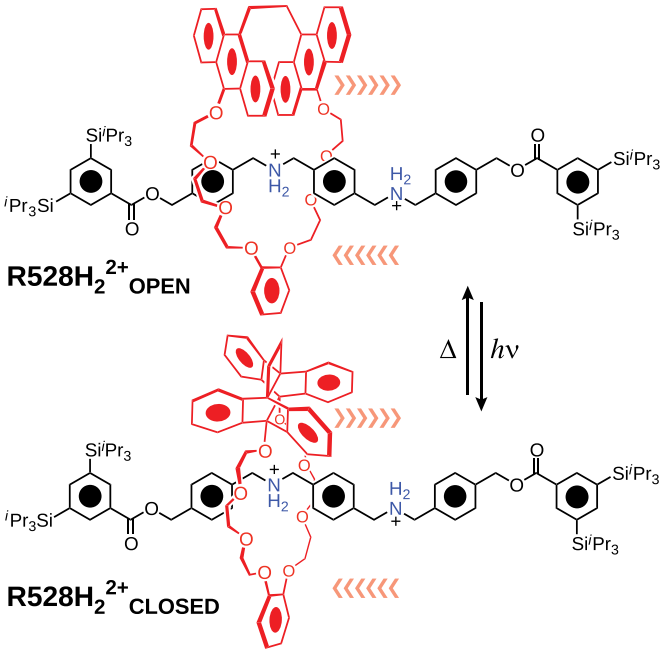
Hirose[165] devised a strategy to 'brake' shuttling motions reversibly in the bistable dialkylammonium-based [2]rotaxane **R528H$_2^{2+}$** by imparting it with a ring that can be constricted and dilated using radiant and thermal stimuli, respectively. The open-form crown ether ring possesses a dianthrylethane[166] moiety, which is photodimerized quantitatively to the corresponding closed-form by cycloaddition at 0 °C under UV irradiation. Thermal reversion occurs[166] within 10 min at 303 K, and within 148 min at 283 K. Since the open-form ring is larger than the closed-form ring, the rate of shuttling (**Table 5.6**) in **R528H$_2^{2+}$$_{OPEN}$** is much faster than that of **R528H$_2^{2+}$$_{CLOSED}$** in deuterated PhMe and THF, to the extent that a coalescence temperature is not observed in the latter form. Hirose's strategy is an elegant way to control shuttling rates, since it is fast, efficient, and generates no waste products.

Aqueous Molecular Shuttles

Harada[167] has reported on the nearly degenerate[K] molecular shuttle **R529^{6+}**, in which an α-cyclodextrin (α-CD) ring translates (**Scheme 5.10**) between two hydrophobic dodecamethylene chains, which are each flanked by hydrophilic

[K] Owing to the constitutional asymmetry of the α-CD ring along the axis passing through its cavity, the bistable [2]rotaxane **R529^{6+}** is not truly degenerate. In fact, the two translational isomers are orientational isomers—see **Section 5.2.1**—which just happen to be equally populated.

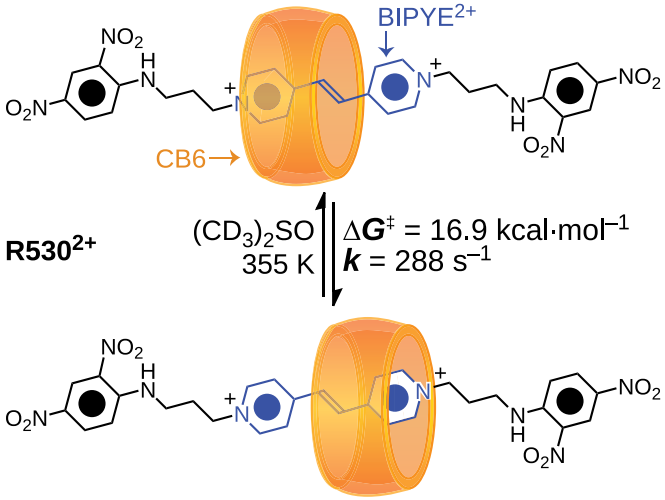
Table 5.6 Parameters describing shuttling in a bistable dialkylammonium/crown ether [2]rotaxane with a reversible brake function driven by anthracene photodimerization and thermal reversion.[165]



	Solvent	T_c K	k s^{-1}	$\Delta H^{\ddagger}$ kcal·mol^{-1}	$\Delta S^{\ddagger}$ cal·mol^{-1}K^{-1}
R528H$_2^{2+}$	$C_6D_5CD_3$	266	860	37	–65
OPEN	THF-d_8	243	4500	36	–65
R528H$_2^{2+}$	$C_6D_5CD_3$	>303	<19	-	-
CLOSED	THF-d_8	>323	<86	-	-

BIPY^{2+} units. The energy of the transition state is high, with a coalescence temperature of 130 °C and a barrier of 20 kcal·mol^{-1} in CD_3SOCD_3, corresponding to a rate of less than one oscillation per minute at room temperature. Although a coalescence temperature is not reached in D_2O, shuttling appears to be slower, most likely because of an expectedly higher stability of the *dodecamethylene⊂α-CD* interactions in H_2O on account of the hydrophobic effect. Cai[168] has investigated **R529^{6+}** computationally using molecular dynamics simulations on microsecond timescales in H_2O and Me_2SO. The simulations agree well with experiment, since the authors found that shuttling is allowed in Me_2SO, yet forbidden in H_2O where the energetic cost of shuttling is too high on account of the water molecules' more favorable interactions with the BIPY^{2+} units and less favorable interactions with the dodecamethylene chains.

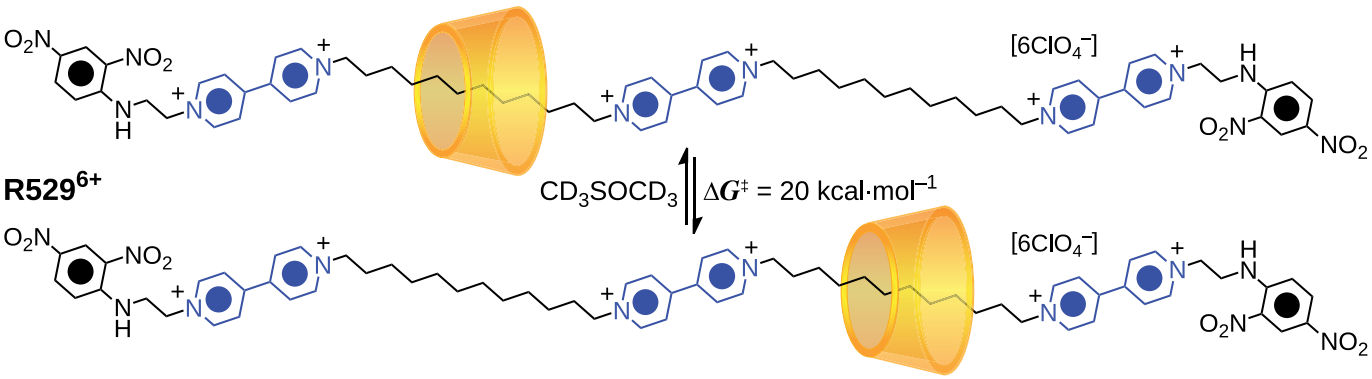
Cucurbit[*n*]urils (CB*n*) represent another suitable motif (**Section 2.3.1.2**) for designing molecular shuttles. Sindelar[169] has prepared the molecular shuttle **R530^{2+}**, in which a CB6 ring passes (**Scheme 5.11**) back and forth between the two poles of a BIPYE^{2+} recognition unit. Using VT ^{1}H NMR spectroscopy, a shuttling rate of 288 s^{-1} was estimated at the coalescence temperature of 355 K in CD_3SOCD_3, corresponding to an energy barrier of 16.9 kcal·mol^{-1}.



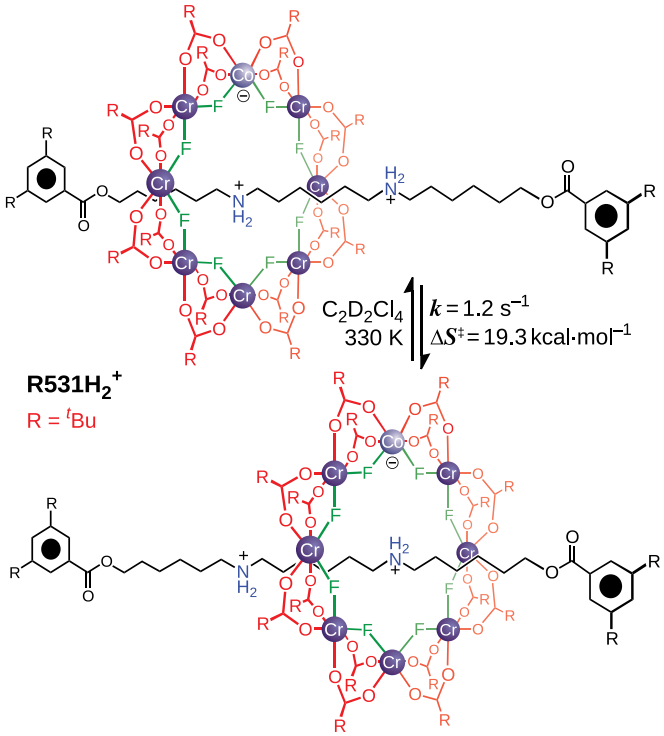
Scheme 5.11 A CB6 molecular shuttle.[169]

Inorganic-Organic Hybrid Molecular Shuttles

One of the inorganic-organic hybrid rotaxanes (**Section 2.3.7.1**) introduced by Leigh and Winpenny[170,171] is the molecular shuttle **R531H$_2^+$**, in which the ring is an inorganic mixed-valence $Cr^{II}_7Co^{III}$ anionic cluster exchanging (**Scheme 5.12**) between two dialkylammonium recognition



Scheme 5.10 Harada's molecular shuttle derived from α-CD and BIPY^{2+}-flanked dodecamethylene chains.[167]



Scheme 5.12 An inorganic-organic hybrid [2]rotaxane molecular shuttle.[170].

sites in the dumbbell. Shuttling is a high-energy process, since a coalescence temperature is not reached in the VT ^{1}H NMR spectrum in $C_2D_2Cl_4$ even at 360 K. Two-dimensional exchange spectroscopy revealed a rate constant of 1.2 Hz at 330 K, corresponding to a $\Delta G^{\ddagger}$ value of 19.3 kcal·mol^{-1}. This high activation barrier can be attributed to ion-pairing interactions and the network of [N$^+$–H···F] hydrogen bonds that must be broken completely in order for the ring cluster to translocate to the other dialkylammonium site.

Molecular Shuttles Based on Directed Synthesis

A number of degenerate molecular shuttles (**R532a–R532dH$_2^{2+}$**) prepared by Kawai's reversible covalent template protocol[172] are illustrated in **Figure 5.16**. Although the transition state energies and shuttling rates were not quantified in most cases, the coalescence temperatures provide a qualitative basis of comparison. The influence of structural parameters, including (i) the ring having endotopic aniline versus anilinium groups, (ii) the dumbbell having dithiolane versus aldehyde hurdles appended to the central linker, and (iii) the presence of *para*-xylylene versus triethylene glycol (3EG) units as landing sites for the ring. The influence of endotopic aniline groups versus anilinium ones can be probed by comparing **R532a** with **R532aH$_2^{2+}$** or **R533b** with **R533bH$_2^{2+}$**. It transpires that the uncharged

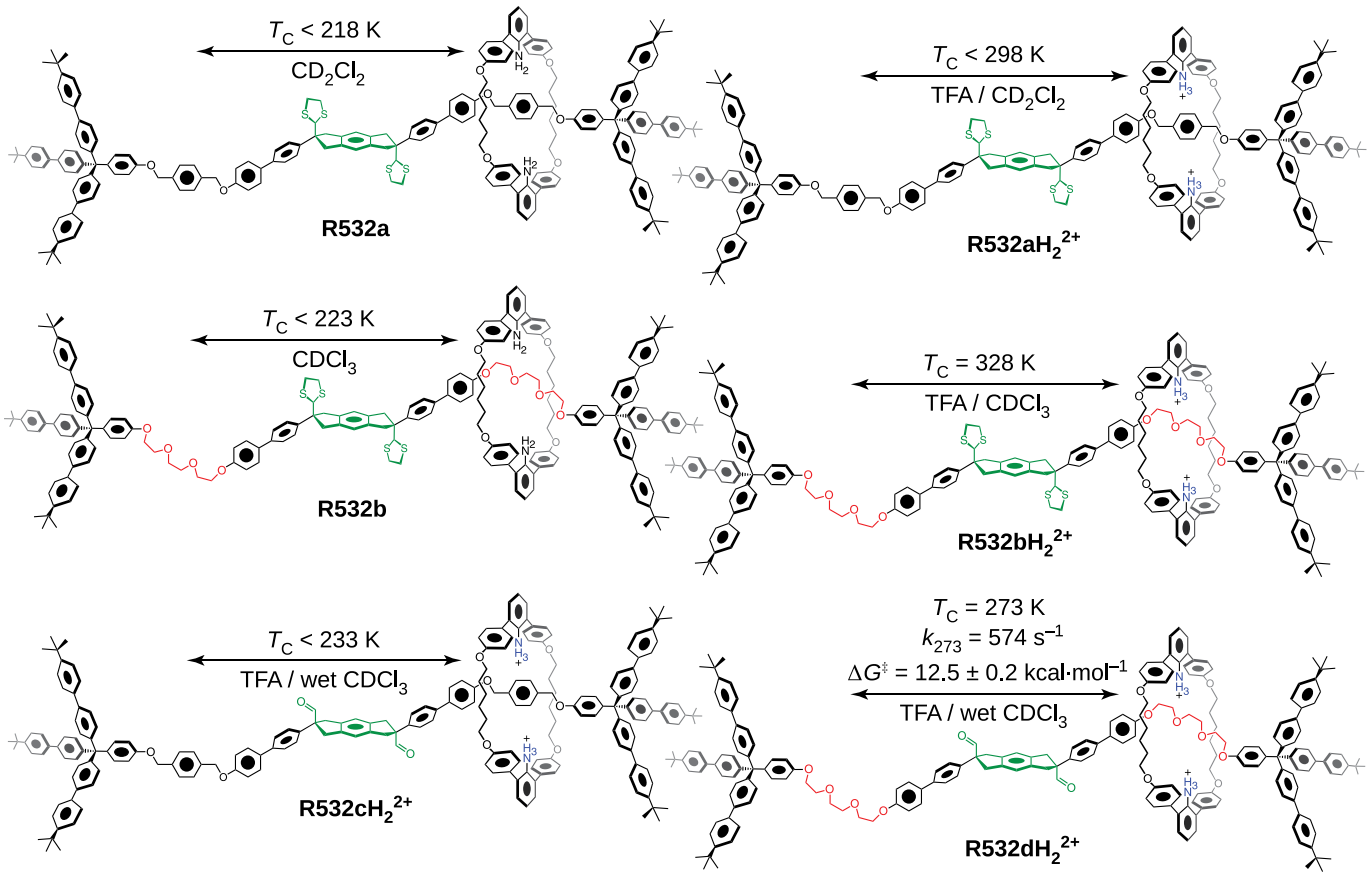


Figure 5.16 A collection of degenerate molecular shuttles from the Kawai group.[172] Shuttles on the left-hand side exhibit relatively fast shuttling dynamics relative to the shuttles on the right-hand side, as a result of differences between the endotopic functional groups, as well as the dumbbells linkers and recognition units.

aniline-based rings shuttle more quickly than the corresponding cationic anilinium-based rings, most likely because the latter are bulkier when ion-paired with their trifluoroacetate counterions and because they engage in stronger noncovalent bonding interactions with the recognition units. The influence of *para*-xylylene versus 3EG recognition units is revealed by comparing **R532a** with **R532b**, **R532aH$_2^{2+}$** with **R532bH$_2^{2+}$**, and **R533cH$_2^{2+}$** with **R533dH$_2^{2+}$**. Shuttling is slower in the presence of the 3EG linker, owing to its ability to engage in [N–H···O] hydrogen bonding with the ring. Finally, the consequences of protecting the central linker's formyl groups as dithiolanes slows down the rate of shuttling—as revealed by comparing **R532aH$_2^{2+}$** with **R532cH$_2^{2+}$** or **R532bH$_2^{2+}$** with **R532dH$_2^{2+}$**—which is expected since the dithiolanes are bulkier than the aldehydes.

Molecular Shuttles Based on Active Templates

Leigh's CuAAC active template protocol (**Section 2.4.1.1**) has been applied[173] to the preparation of the molecular shuttle **R533**, which possesses (**Figure 5.17**) two triazole recognition units that can participate in the coordination of transition metal ions, together with the interlocked macrocyclic ligand Mpy29-O. In the absence of a transition metal, the ring of **R533** freely samples the entire length of the axle, yet it becomes confined primarily to one of the two triazole units when a Cu^{I} or Pd^{II} center is introduced. In the presence of Cu^{I}, the ring of the shuttle **Cu(R533)PF$_6$** oscillates rapidly between the two triazole stations, carrying the Cu^{I} center with it. In 9:1 CD_3CN/CD_2Cl_2, the shuttling is so rapid that a slow exchange regime could not be accessed even at low temperatures in order to quantify the shuttling rates by line shape analysis of the VT ^{1}H NMR spectra. The Pd^{II} chelate **Pd(R533)Cl$_2$** is kinetically stable by

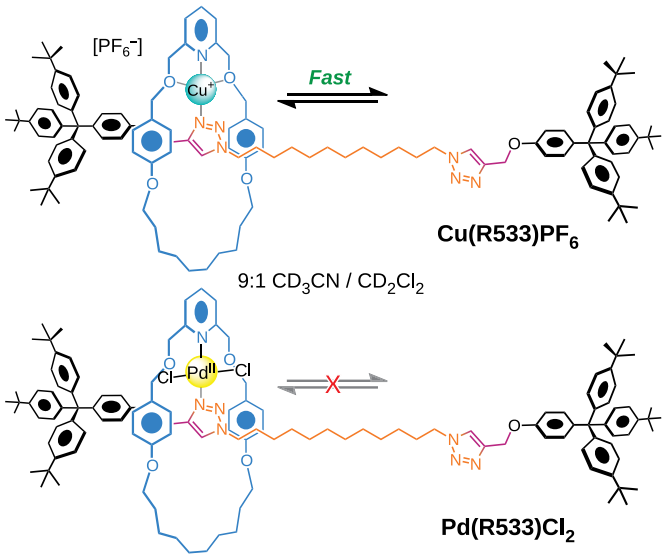
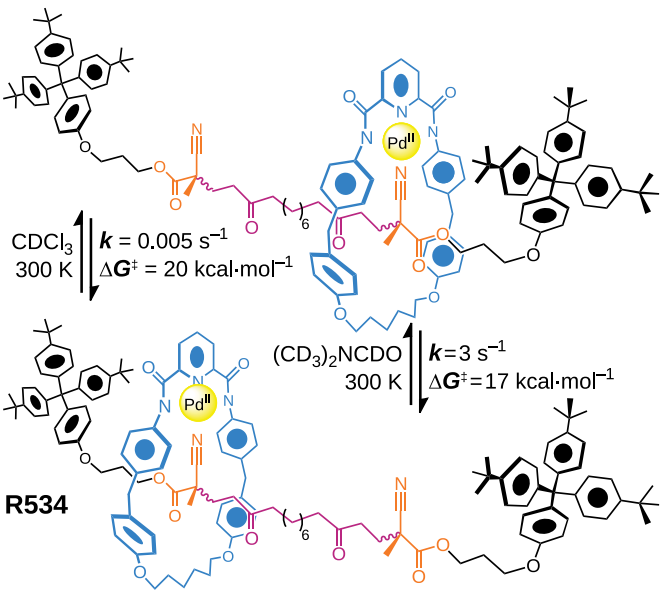


Figure 5.17 Stereoformulas of the Cu^{I} and Pd^{II} chelates of Leigh's bis(triazole) [2]rotaxane **R533**. The ring shuttles[173] rapidly between triazole sites in the presence of Cu^{I}, but not in the presence of Pd^{II}.

comparison, since the macrocyclic chelate does not migrate back and forth between the axle's triazole units on the timescale of a ^{1}H NMR experiment even near the boiling point of CD_3CN at 343 K.

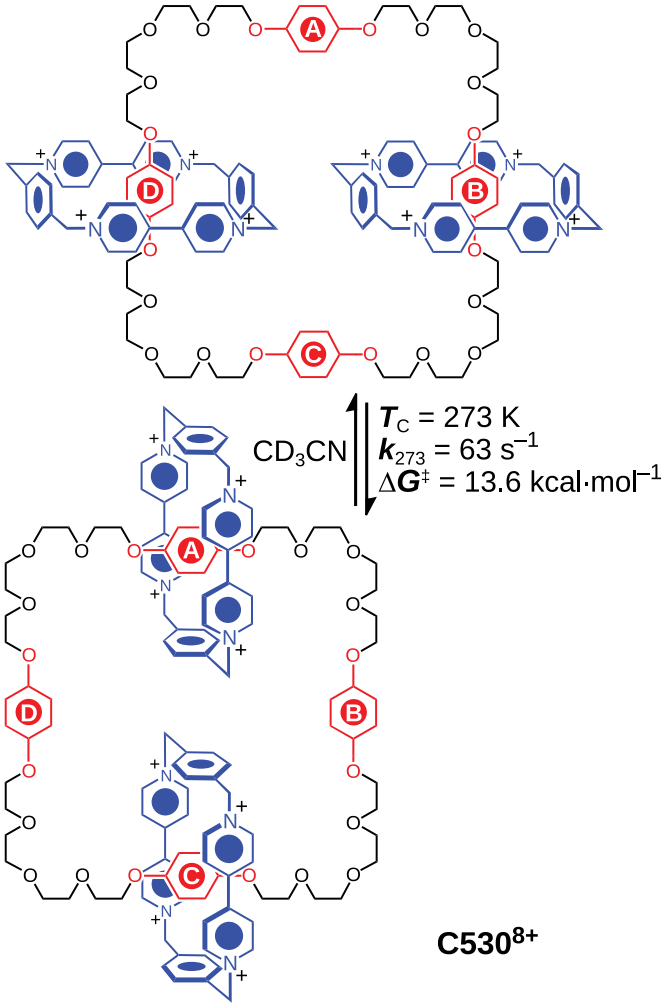
Leigh[174] has relied on active metal template synthesis to generate the [2]rotaxane **R534**, which houses an endocyclic Pd^{II} chelate shuttling (**Scheme 5.13**) between two nitrile recognition units competing for the open coordination site around its Pd^{II} metal center. The shuttle does not reach a coalescence temperature in its VT ^{1}H NMR spectrum in $CDCl_3$, while T_c = 390 K in $(CD_3)_2NCDO$. The exchange rate in $CDCl_3$ at 300 K increases 200-fold, from 0.005 to 1 s^{-1}, when 1 equiv of pyridine is introduced as a competitor with the dumbbell's nitrile groups in coordinating the Pd^{II} center of the ring, while a 600-fold increase (3 s^{-1}) is observed when shuttling occurs in $(CD_3)_2NCDO$. The rate of shuttling can thus be tuned over nearly four orders of magnitude.



Scheme 5.13 A degenerate molecular shuttle comprising a tridentate Pd^{II} endocyclic chelate as the ring and a pair of nitrile ligands as the dumbbell's recognition units.[174]

Molecular Trains

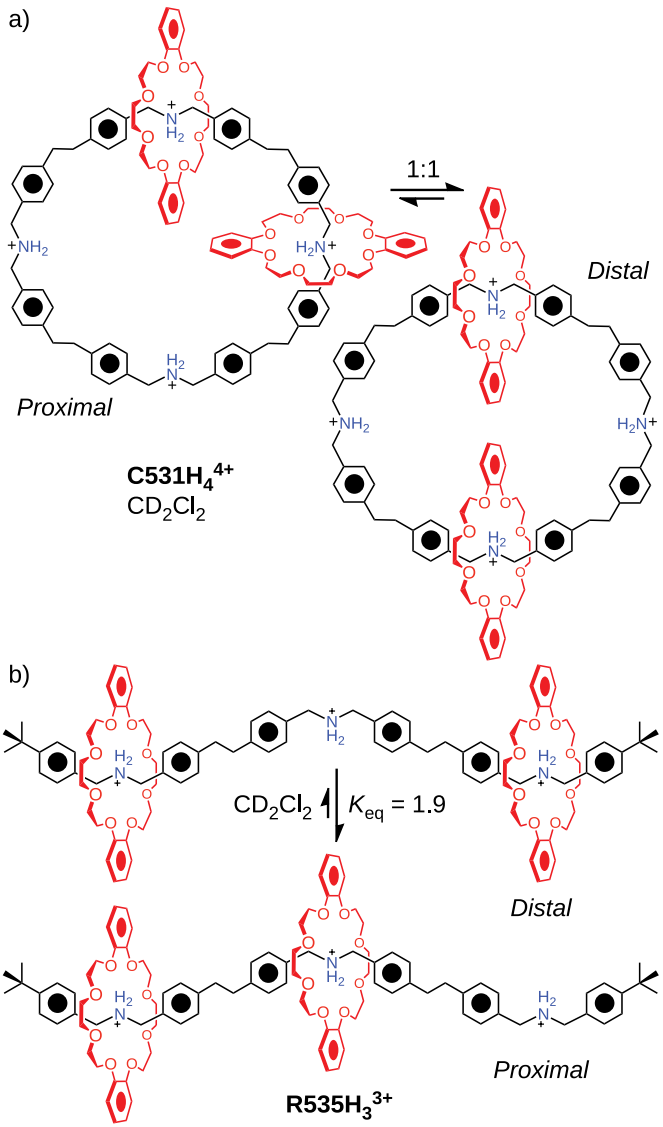
In the same spirit as the 'molecular shuttle' nickname, degenerate bistable and multistable catenanes have been called 'molecular trains', since they comprise mobile rings circumnavigating a molecular "track".[175] [2]Catenane molecular trains with three[29,176] or four[29,175] HQ recognition units have been described. A unique type of co-conformational selectivity (**Scheme 5.14**) has been observed[175] in the case of the multistable [3]catenane **C530^{8+}**, where two CBPQT^{4+} rings run around a track possessing four HQ recognition units, since no spectroscopic evidence has been found for the *proximal* translational isomer in which two adjacent HQ units are encircled by rings. If we label each of the degenerate HQ units in the molecular track as A, B, C, and D, the only translational isomer observed in solution is the *distal*



Scheme 5.14 A "molecular train" in which two CBPQT^{4+} rings undergo translation between degenerate HQ recognition units.[175] Translational isomers involving rings occupying adjacent HQ sites—i.e., A/B, B/C, or C/D—were not observed by ^{1}H NMR spectroscopy.

one, in which the CBPQT^{4+} rings encircle A and C, which is degenerate with the rings encircling B and D. We interpret this result as suggesting that the motion of the rings is "correlated", in the sense that the translation of one ring leads to the translation of the other ring as a consequence of ring-to-ring Coulombic repulsions, although the motion itself is most likely not be happening simultaneously in both rings. **C530**$^{8+}$ exhibits lower T_c (273 K) and $\Delta G^{\ddagger}$ (13.6 kcal·mol^{-1}) values than does the analogous degenerate [2]catenane (T_c = 286.5 K, $\Delta G^{\ddagger}$ = 14.1 kcal·mol^{-1}) containing only one CBPQT^{4+} ring shuttling between four HQ recognition units, indicating that the ring-to-ring Coulombic repulsion destabilizes the GSCC of **C530**$^{8+}$. Molecular trains comprising the inverted recognition system, i.e., crown ethers circling the track of a large octacationic cyclophane, have also been described.[43] ^{1}H NMR spectroscopy indicates that the activation barriers to translation in these molecular trains are relatively low, since time averaged signals are observed even at low temperatures.

Molecular trains based on the hydrogen-bonded dialkylammonium / crown ether motif (**Section 2.3.4.6**) have also been described.[177] In the case (**Scheme 5.15a**) of the [3]catenane **C531H$_4$**$^{4+}$, the two DB24C8 rings have the option of encircling any of four dibenzylammonium recognition units. Since the *proximal* isomer is twice as likely as the *distal* isomer, statistically speaking, the observed 1:1 population of both isomers in CD_2Cl_2 indicates a slight preference for the *distal* isomer. Since the DB24C8 rings are neutral in this case, the population bias is most likely attributable to steric rather than electrostatic repulsion in the *proximal* isomer.

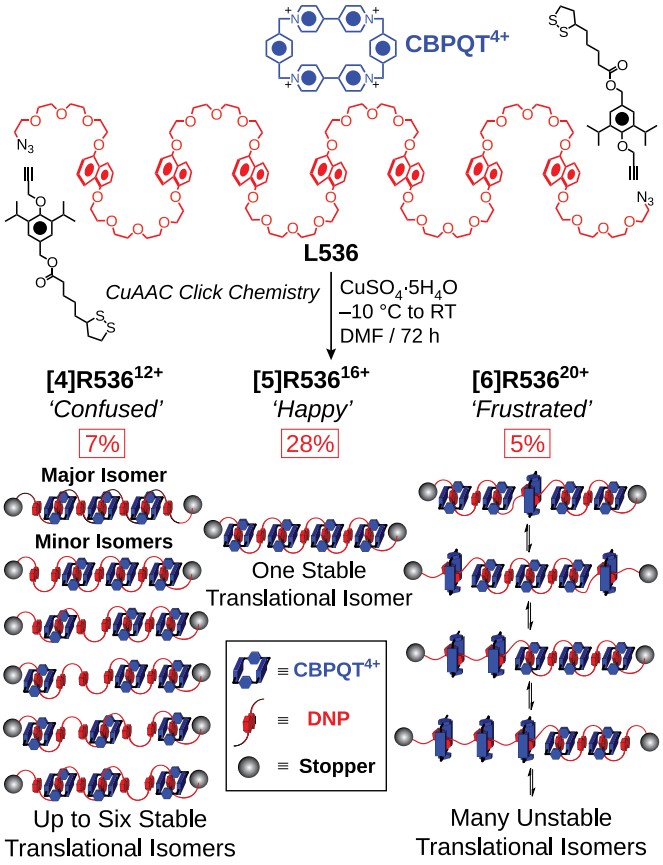


Scheme 5.15 The translational isomers of dibenzylammonium-based mechanomolecules possessing two DB24C8 rings.[177] (a) The [3]catenane **C531H$_4$**$^{4+}$ exists as a 1:1 mixture of the *proximal* and *distal* translational isomers, indicating a preference for the *distal* isomer, since a statistical mixture would be 2:1 *proximal*:*distal*. (b) The *proximal* translational isomer is the dominant species in the case of the [3]rotaxane **R535H$_3$**$^{3+}$.

Translational Isomerism of Oligorotaxanes

A close relative of the dibenzylammonium/crown [3]catenane **C531H$_4^{4+}$** is the [3]rotaxane **R535H$_3^{3+}$**, which possesses[177] three dibenzylammonium recognition sites for its two DB24C8 rings. Again, the *proximal* isomer is expected to be twice as populated (K_{eq} = 2) as the *distal* isomer in a purely statistical mixture, yet the population distribution (**Scheme 5.15b**) favors slightly the *distal* isomer, as indicated by an observed K_{eq} of only 1.9 at 298 K in both CD_2Cl_2 and CD_3SOCD_3. A van't Hoff analysis revealed that the *proximal* isomer is more enthalpically stable, while the *distal* isomer is more entropically stable.

The CBPQT^{4+} molecular trains avoid occupying adjacent degenerate recognition sites on the "track", when possible. A similar principle governs[178,179] the translational isomerism of donor-acceptor oligorotaxanes based on DNP recognition units and CBPQT^{4+} rings. For example, the synthesis (**Scheme 5.16**) of oligorotaxanes based on the heptameric DNP diazide **L536** using Cu^{I}-catalyzed azide-alkyne cycloaddition (CuAAC) click chemistry leads to a mixture of rotaxanes (**[4]R536^{12+}**–**[6]R536^{20+}**) possessing different DNP:CBPQT^{4+} ratios. Each of these three oligorotaxanes exhibit remarkably different translational isomerism and dynamics as indicated by ^{1}H NMR spectroscopy. In the case of the [4]rotaxane **[4]R536^{12+}**, up to six translational isomers are possible in which the CBPQT^{4+} rings do not occupy adjacent DNP sites. These multiple isomers give rise to highly complicated ^{1}H NMR spectra in the slow exchange regime at low temperatures. The [5]rotaxane **[5]R536^{16+}**, by contrast, gives rise to a relatively simple ^{1}H NMR spectrum because it overwhelmingly adopts a single translational isomer in solution, since only one translational isomer allows all four of its CBPQT^{4+} rings to be separated by unoccupied DNP units. Finally, neighboring CBPQT^{4+} rings cannot be avoided in **[6]R536^{20+}**, leading to line broadening in the ^{1}H NMR spectrum as a result of its equilibration between several relatively unstable translational isomers. The oligorotaxanes **[4]R536^{12+}**, **[5]R536^{16+}**, and **[6]R536^{20+}** have been described illustratively as "confused", "happy", and "frustrated", respectively, in relation to their adherence to the electrostatically driven selection rule—see the **Scheme 5.16** caption and **Section 4.2.1.1** for more details on these oligorotaxane foldamers.



Scheme 5.16 The CuAAC click synthesis[178] of donor-acceptor oligorotaxanes based on CBPQT^{4+} and a polyether-bridged DNP heptamer (**L536**) leads to a mixture of rotaxanes expressing different kinds of translational isomerism, depending on the DNP:CBPQT^{4+} ratio. An empirically determined selection rule dictates that the most stable translational isomers are those in which no two CBPQT^{4+} rings encircle adjacent DNP sites. The translational isomerism can be described, by anthropomorphic metaphor, according to their 'moods'. The [4]rotaxane **[4]R536^{12+}** seems 'confused' because it can adopt multiple stable translational isomers that satisfy the selection rule, whereas the [6]rotaxane **[6]R536^{20+}** seems 'frustrated' because it cannot adopt any co-conformation satisfying the selection rule. Only the [5]rotaxane **[5]R536^{16+}** is 'happy' because only one of its translational isomers satisfies the selection rule. The fact that this rotaxane is obtained in the highest yields reflects an enhanced thermodynamic stability arising from its well-defined folded superstructure held together by continuous D-A π–π stacking and hydrogen-bonding interactions.

5.1.2 Pirouetting

While the terms 'rotation' and 'torsion' are employed[122] to describe motions leading to the conformational isomerism of rotamers, the term 'pirouetting' has been used[180–183]—alongside that of circumrotation[9,30,184–186] in the case of catenanes—to describe the relative rotational motions of mechanically interlocked component parts. When these terms were introduced[9,30,180] in the context of donor-acceptor [2]catenanes, a distinction was made[30] initially between circumrotation and pirouetting, such that circumrotation described the motions leading to site exchange of the crown ether's π-donor units, whereas pirouetting described the motions leading to site exchange of a tetracationic cyclophane's π-acceptor units. Since the term 'pirouetting' has been applied[160,180–183,187–193] more widely to all kinds of MIMs, it has become our word of choice for describing how rings revolve around mechanical bonds. Pirouetting (**Figure 5.18**) may describe either (i) the spinning of an axle within a ring, (ii) the spinning of a ring about an axle, or (iii) a ring and axle revolving, not with respect to one another, but together as a single 'subcomplex'. We refer to these three types of mechano-rotational motions as (i) within-the-annulus pirouetting (**Section 5.1.2.1**), (ii) around-the-axle pirouetting, and (iii) super-rotation[178,194,195] (**Section 5.1.2.3**),

respectively. In the case of rotaxanes diffusing freely in solution, around-the-axle pirouetting is indistinguishable from within-the-annulus pirouetting. In the case of catenanes, however, around-the-axle pirouetting is equivalent to through-the-annulus (**Section 5.1.2.2**) pirouetting.

We wish to reiterate the differences between pirouetting processes in rotaxanes and catenanes. Within-the-annulus and around-the-axle pirouetting motions cannot be distinguished in most rotaxanes, where these motions are relative and depend only upon which component part is fixed in the frame of reference. In solution, both types of motion are one and the same. Rotaxanes possessing immobilized component parts within a crystal or at an interface, however, would not suffer from the same problem. For example, see **Section 5.1.4** for a discussion of how 'robust dynamics'[10] can be realized in solid-state rotaxanes, where around-the-axle pirouetting of the rings can be distinguished from within-the-annulus pirouetting of the axles as a result of their incorporation into an extended network. Catenanes, on the other hand, can exhibit local within-the-annulus pirouetting motions that are different, even in solution, from around-the-axle rotary motions, the latter of which cause one ring to pass through the annulus of the other ring. Local within-the-annulus pirouetting in catenanes is essentially a conformational rotation of covalent bonds (torsions), that occur with respect to a mechanically interlocked ring. Through-the-annulus / around-the-axle pirouetting in catenanes is tantamount to translation or circumrotation—i.e., one ring's through-the-annulus pirouetting is another ring's circumrotation. Again, the assignment of translation / circumrotation to one ring and pirouetting to the other ring depends entirely on the frame of reference, which is arbitrary in the solution state. Super-rotation, in which a ring-and-axle pirouette as a unified 'subcomplex', operate likewise in both catenanes and rotaxanes.

Pirouetting motions tend to require lower energy barriers than translational motions because they can often occur without breaking all of the local noncovalent bonding interactions between component parts. Consequently, pirouetting is not always easy to detect and measure because it can happen over relatively fast timescales. It is not uncommon to observe resonances in ^{1}H NMR spectroscopy representing time-averaged chemical shifts as a result of rapid pirouetting processes. For example, all attempts[188,196] to quantify circumrotational and pirouetting motions in the seminal catenated cyclodextrins—see **Scheme 2.20** in **Section 2.3.1.1**—have been unsuccessful. Apparently, the methylated ß-CD rings pirouette and translate relative to their mechanically interlocked biphenyl polyether rings very rapidly on the ^{1}H NMR timescale, even at temperatures below 213 K in CD_2Cl_2. Indeed, available data on pirouetting rates are confined mostly to bistable and multistable MIMs simply because they provide the spectroscopic handles that allow for quantification. Thousands of monostable catenanes and rotaxanes that have been reported remain uncharacterized in this regard, either because the measurements were not attempted or because of experimental limitations. We have tried to offer several illustrative examples in **Section 5.1.2.1–5.1.2.2**, but they do not represent a fully comprehensive survey of the literature.

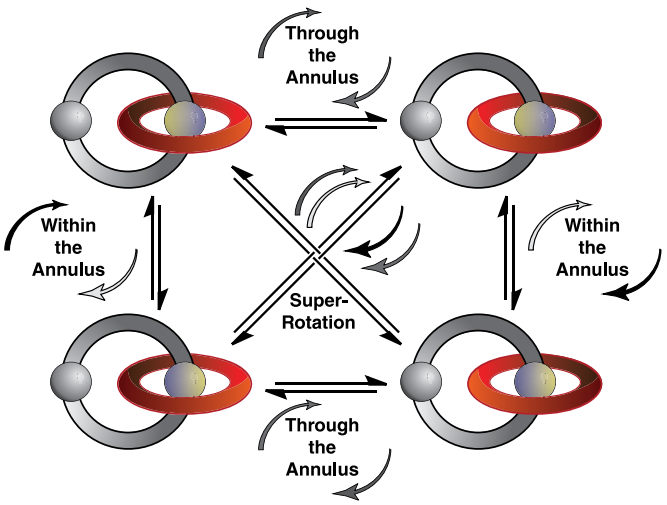


Figure 5.18 Graphical representation of the pirouetting processes in a [2]catenane.

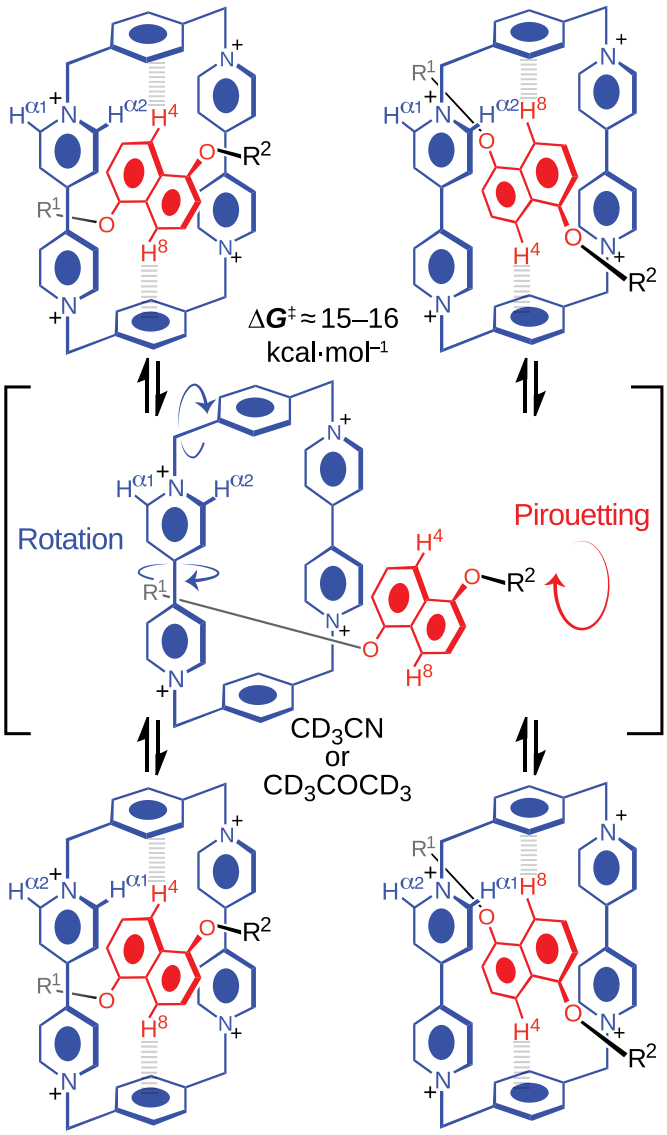
5.1.2.1 Within-the-Annulus Pirouetting

Within-the-annulus pirouetting may refer to either (i) the rotation of an entire axle (for pseudorotaxanes) or dumbbell (for rotaxanes) with respect to an encircling ring, or (ii) a local conformational rotation of a segment of an axle, dumbbell, or ring occuring with respect to an interlocked ring. The reader is reminded that 'within-the-annulus' pirouetting is no different than 'around-the-axle' pirouetting in the case of rotaxanes diffusing freely in solution, where the rotational motions of component parts are only considered relative to one another. In the case of catenanes, however, local conformational rotations within-the-annulus are not identical to around-the-axle rotations, which are also known as through-the-annulus pirouetting (**Section 5.1.2.2**), since they cause the atoms of one ring to pass through the cavity of another ring.

Pirouetting in Donor-Acceptor Mechanomolecules

This concept may be understood by considering the example (**Scheme 5.17**) of a DNP unit pirouetting within-the-annulus of a $CBPQT^{4+}$ ring. Solid-state structures[197] and ^{1}H NMR spectroscopy[L] reveal that the DNP unit orients itself preferentially such that its protons at the 4/8 positions point directly into the center of the tetracationic

[L] The pirouetting of DNP within-the-annulus can be detected by ^{1}H NMR spectroscopy because the DNP unit's local C_2 symmetry is imposed on the $BIPY^{2+}$ π-acceptors of the otherwise D_{2h}-symmetric $CBPQT^{4+}$ host—a situation which leads to signal separation for the α and β protons of $CBPQT^{4+}$ in the slow exchange regime. It is the coalescence of these signals that enables the indirect estimation of $\Delta G^{\ddagger}$ by line shape analysis.

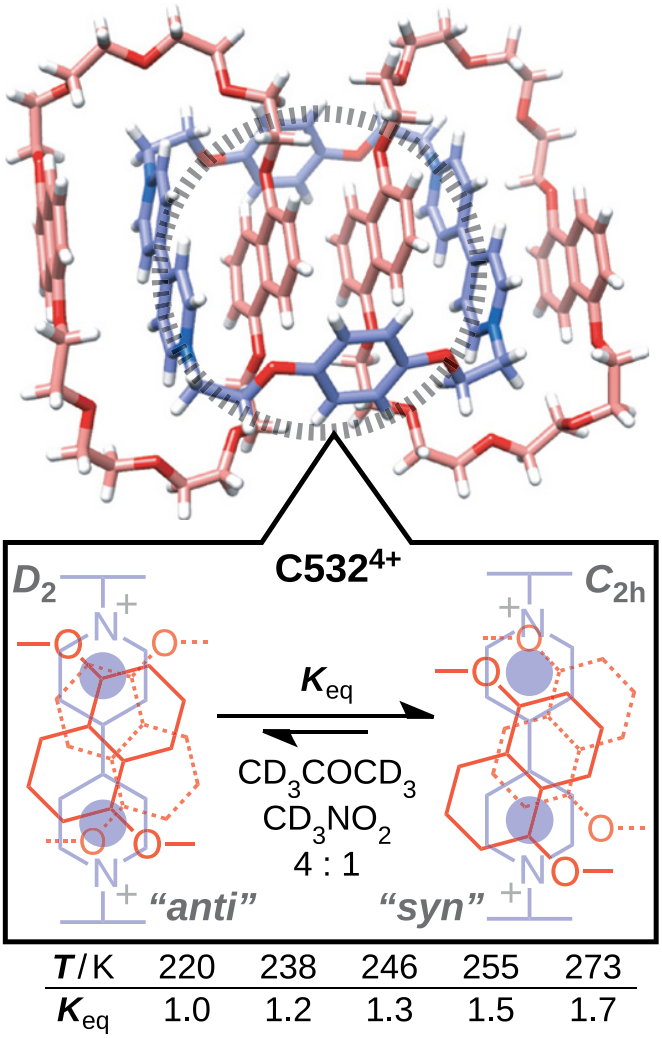


Scheme 5.17 An illustration depicting how within-the-annulus pirouetting of a DNP unit with respect to a CBPQT^{4+} ring leads to site exchange of the 4/8-naphthalene protons. In reality, pirouetting most likely occurs only when the DNP unit has been ejected from the host cavity, a process which also allows the CBPQT^{4+} ring's pyridinium and phenylene units to rotate about the axes that connect them to the methylene cornerpieces. Since the within-the-annulus pirouetting of DNP is a degenerate process, the corresponding energy barrier cannot be measured directly by ^{1}H NMR spectroscopic line shape analysis. The barriers to rotation of the pyridinium and phenylene units, which are most likely in the same range as DNP pirouetting, can be measured by line shape analysis because the symmetry of the CBPQT^{4+} ring is reduced by the local C_2 symmetry imposed on it by the DNP unit, which differentiates protons α1 and α2, for example. The energies associated with these processes (~15–16 kcal·mol^{-1} in CD_3COCD_3 or CD_3CN) are remarkably well conserved across a range of interlocked structures. See refs. 34, 35, 41, 197, 200-202.

cyclophane's *para*-phenylene rings in order to establish stabilizing [C–H···π] interactions. The protons at positions 4 and 8 within the DNP unit exchange between degenerate sites, most likely by exiting the host's cavity where it has the necessary degrees of freedom to execute this pirouetting motion before re-inserting back into the binding pocket. The energies associated with DNP pirouetting are typically inferred by measuring the rotational barriers of the CBPQT^{4+} ring's pyridinium and/or phenylene units, since they become free to rotate only when the DNP unit has been ejected. Regardless of whether this within-the-annulus process results from the rotation of entire component parts or from local conformational rotations, the DNP units pirouette against remarkably similar barriers ($\Delta G^{\ddagger}_c \approx 15$–16 kcal·mol^{-1} at the coalescence temperature T_c) in CD_3CN or CD_3COCD_3 across a range of different architectures, including pseudorotaxanes[198] ($\Delta G^{\ddagger}_{303}$ = 15.4 kcal·mol^{-1} / CD_3CN), [2]rotaxanes[199] ($\Delta G^{\ddagger}_{320}$ = 15.0–15.8 kcal·mol^{-1} / CD_3CN), degenerately bistable [2]catenanes[35,197] ($\Delta G^{\ddagger}_{325}$ = 15.8 kcal·mol^{-1} / CD_3COCD_3[197] or CD_3CN[35]), non-degenerately bistable [2]catenanes[34,35] ($\Delta G^{\ddagger}_{350}$ = 15.4–16.7 kcal·mol^{-1} / CD_3CN), oligocatenanes[41] ($\Delta G^{\ddagger}$ = 14.5–16.0 kcal·mol^{-1} / CD_3CN), main-chain poly[2]catenanes[200] ($\Delta G^{\ddagger}_{344}$ = 16.0–16.2 kcal·mol^{-1} / CD_3CN), handcuff [2]catenanes[201] ($\Delta G^{\ddagger}_{298+} \approx 16$ kcal·mol^{-1} / CD_3SOCD_3), and daisy chains[202] ($\Delta G^{\ddagger}_{323}$ = 14.8–15.3 kcal·mol^{-1} / CD_3CN). If the symmetry of the CBPQT^{4+} ring is reduced—e.g., by functionalization of one of the phenylene rings, as in the case of [1]rotaxanes,[202] daisy chains,[202] and molecular figures-of-eight,[203]—then pirouetting becomes a non-degenerate process, which can give rise to unequal populations of the corresponding co-conformers.

Surprisingly, the energy barrier for DNP pirouetting is relatively unaffected ($\Delta G^{\ddagger}_{322}$ = 15.2 kcal·mol^{-1} / CD_3CN) in catenanes employing[44] the tetracationic cyclophane CBDAP^{4+}, which binds DNP derivatives more tightly than does CBPQT^{4+}. The barrier to pirouetting can be lowered substantially, however, if the cavity of the cyclophane is widened. For example, the transition state associated with the pirouetting of DNP is lowered by ~2 kcal·mol ($\Delta G^{\ddagger}_{273}$ = 13.1–13.3 kcal·mol^{-1}) in the cases of a [2]catenane and a rotacatenane based on the 'molecular square' cyclobis(paraquat-4,4′-biphenylene) (CBPQB^{4+}, see **[2]C241a^{4+}** in **Scheme 2.65**, **Section 2.3.3.9**) in CD_3COCD_3.[204] A [3]catenane comprising an even larger tetracationic cyclophane exhibits[46] a pirouetting barrier of only 10.2 kcal·mol at its coalescence temperature of 213 K in CD_3COCD_3. Within-the-annulus pirouetting of a smaller resorcinol (1,3-dioxybenzene) recognition unit encircled by the CBPQT^{4+} ring of a [2]catenane based on bis-*meta*-phenylene[32]crown-10 (BMP32C10) has been found[30] to occur with a $\Delta G^{\ddagger}$ value of 12 kcal·mol^{-1} at a coalescence temperature of 240 K in CD_3COCD_3. This result, coupled with that of the CBDAP^{4+} [2]catenanes, suggests that sterics may play a more dominant role than electronics in determining the pirouetting rates of these D-A systems. This hypothesis is further supported by the fact that pirouetting rates are much faster (lower $\Delta G^{\ddagger}$ values) within the larger and more flexible π-donating crown ethers, since coalescence temperatures associated with within-the-annulus pirouetting are not typically reached even at the low temperature limits of the ^{1}H NMR experiments.[205]

A novel type of mechanostereoisomerism (**Figure 5.19**) has been observed[36] in the [3]catenane **C532**$^{4+}$ based on a large tetracationic cyclophane reminiscent of the "big blue box" (**Section 2.3.3.9**), in which a pair of encircled DNP units interconvert between parallel ("*syn*") and anti-parallel ("*anti*") orientations as a result of their within-the-annulus pirouetting motions. Here again we have a case where pirouetting motions arising from conformational rotations (torsions) give rise to differences in co-conformation at the level of the mechanomolecule. The *syn*:*anti* ratio increases from 1:1 to almost 2:1 over the temperature range 220–273K in 4:1 CD_3COCD_3:CD_3NO_2. Like the within-the-annulus pirouetting of DNP units encircled by CBPQT^{4+} rings, these pirouetting motions occur with a free energy barrier of 15–16 kcal·mol^{-1} over this temperature range.



T/K	220	238	246	255	273
K_{eq}	1.0	1.2	1.3	1.5	1.7

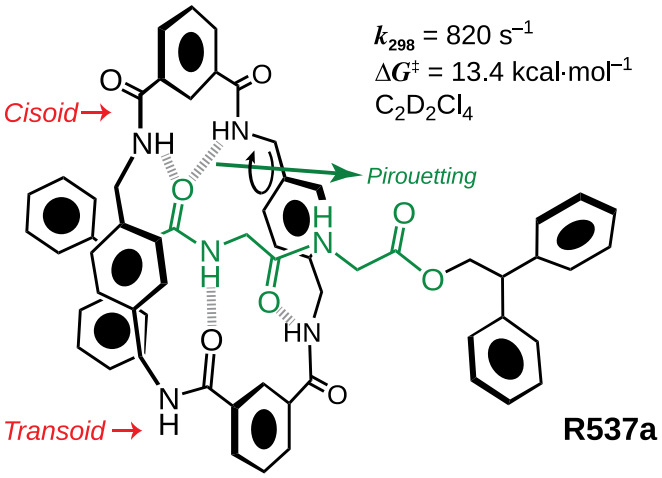
Figure 5.19 A tubular representation of the solid-state structure of the D-A [3]catenane **C532**$^{4+}$, and an accompanying graphical representation illustrating how within-the-annulus pirouetting of the DNP units interconverts the "*syn*" and "*anti*" mechanostereoisomers, which are populated to different extents over a range of temperatures.[36] PF_6^- counterions and solvent molecules are omitted for the sake of clarity.

In the case of the neutral [2]rotaxanes **R520a** and **R520b** comprising (**Table 5.4**) DN38C10 and either PMDI or NDI recognition units, respectively, the local C_2 symmetry of the DNP units is imposed on the π-acceptor units below the coalescence temperature, reducing their time averaged symmetry. A $\Delta G^{\ddagger}$ value of only 11.5 kcal·mol^{-1} was estimated[143] at 239 K in CD_2Cl_2 for this pirouetting process in both PMDI- and NDI-based rotaxanes, a value much lower than those observed in tetracationic molecules shuttles, corresponding to much faster pirouetting rates exceeding 50,000 s^{-1} at room temperature.

Pirouetting in Hydrogen-bonded Mechanomolecules

The rates of pirouetting (**Figure 5.18**) of glycylglycine (GlyGly) dipeptide axles encircled by Leigh's benzylic amide rings in the [2]rotaxanes **R537a** and **R537b** have been estimated[206] in low-polarity halogenated solvents by ^{1}H NMR spectroscopic methods. It can be appreciated in view of the stereoformulas of the GSCCs illustrated in **Figure 5.20** that the rotaxanes adopt different hydrogen-bonding motifs, depending on whether the benzylic amide rings are constituted by isophthalamide or pyridine-2,6-dicarboxamide hydrogen bond donors. See **Scheme 2.74** in **Section 2.3.4.2** for an X-ray crystal structure of **R537b**. These different hydrogen-bonding motifs have major consequences for the pirouetting rates. The more robust hydrogen bond network of **R537b** is fortified by its pyridine units, which reinforce their appended amide donors into a *transoid* conformation. The two endotopic NH donors of the *transoid* conformation bind the carbonyl groups of the GlyGly axle much more strongly than does a *cisoid* conformation. Indeed, one of the isophthalamide units of **R537a** adopts a *cisoid* conformation, such that its endotopic carbonyl group can engage in hydrogen bonding with one of the axle's glycine NH donors. As a consequence, the rate of pirouetting at 298 K is much faster (820 s^{-1}) in **R537a** than it is in the case of **R537b** (100 s^{-1}), corresponding to a difference in transition state energies ($\Delta G^{\ddagger}$) of ~1.3 kcal·mol^{-1}. The pyridine-based benzylic amide ring of **R537b** also protects the dipeptide axle from hydrogen bonding with much more polar CD_3SOCD_3 solvent molecules, more than does the isophthalamide-based ring of rotaxane **R537a**, since the former remains mostly locked in position while the latter moves freely along the dumbbell backbone.

Berná[207] has shown that the pirouetting rates in a series (**Figure 5.21**) of succinamide-based [2]rotaxanes, **R538a-e**, can be modulated substantially by introducing noncovalent bonding interactions—namely, [C–H···π] contacts—between the stoppers and the ring. Whereas the diagnostic ^{1}H NMR signals of the benzyl-stoppered [2]rotaxanes **R538d-e** coalesce below room temperature ($\Delta G^{\ddagger} \leq 12.5$ kcal·mol^{-1}), the cyclohexyl-stoppered homologues **R538a-c** require heating to reach their coalescence temperatures, and they exhibit significantly higher pirouetting barriers of ≥14 kcal·mol^{-1} in halogenated solvents. This large difference (≥1.7 kcal·mol^{-1}) in dynamic rate constants, attributable to



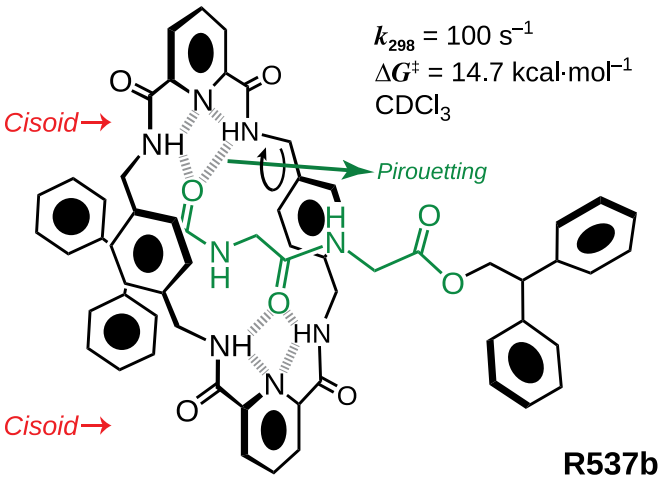
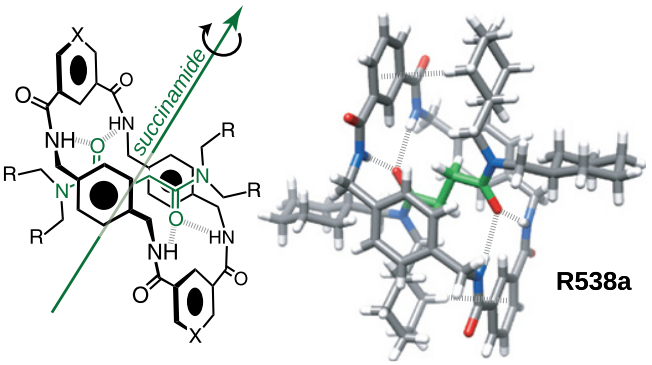


Figure 5.20 Stereoformulas and pirouetting rates of dipeptide-based benzylic amide rotaxanes.[206] Pirouetting is slower when the macrocyclic hydrogen bond donors are constituted by pyridine-2,6-dicarboxamide (**R537b**) than in the case of isophthalamide (**R537a**), since the cisoid conformation of these donors, which form much stronger hydrogen bonds with the carbonyl units of the axles, is reinforced by the hydrogen bond accepting pyridyl units of **R537b**.

the difference in stoppers, vastly exceeds the differences (0.2–0.7 kcal·mol^{-1}) between rotaxanes possessing isophthalamide (**R538a**, **R538d**) versus 3,5-dicarboxamidopyridine (**R538c**, **R538e**) units in the constitution of the ring. The cyclohexyl-stoppered [2]rotaxanes' elevated barriers may be attributed to [C–H···π] interactions, which are evident in the solid-state structure (**Figure 5.21**) of **R538a**, extending from the axial protons of the cyclohexyl groups to the π-surfaces of ring's isophthalic subunits.

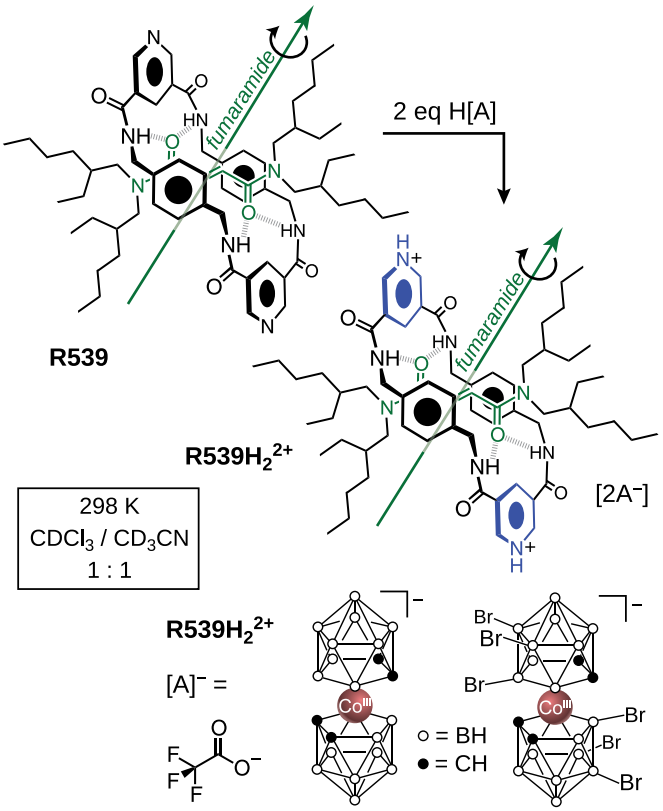
Farras and Teixidor[192] have investigated pH and counterion effects on the pirouetting (**Figure 5.22**) of fumaramide-based benzylic amide rotaxanes. The neutral, bis(2-ethylhexyl)-stoppered [2]rotaxane **R539** can be converted to the dicationic **R539H$_2^{2+}$** by protonation of the ring's exotopic pyridyl groups. Three different acids were employed in the protonation step, leading to **R539H$_2^{2+}$** salts of trifluoroacetate (TFA$^-$), as well as the cobaltabisdicarbollides [3,3′-Co(1,2-$C_2H_{11}B_9)_2$]$^-$ and [8,8′-9,9′-12,12′-Br_6-3,3′-Co(1,2-$C_2H_8B_9)_2$]$^-$. The room-temperature rate constants and free energies for pirouetting were estimated by the 2D-EXSY technique—see the introduction to **Section 5.1.1.2**—instead of line shape analysis. In all cases, protonation of the macrocycle leads to a dramatic enhancement in pirouetting rates within **R539H$_2^{2+}$**, by approximately two orders of magnitude (10^{-1}→10^{1} s^{-1}) compared to that of the neutral **R539**. The different salts of **R539H$_2^{2+}$** also exhibit different pirouetting rates, with the largest, most diffuse anions furnishing the largest rate enhancements. The anion effect is much more subtle, however, since the rate enhancement is approximately only twofold in this case, yet it can be rationalized by the expectation that tighter ion pairs will pirouette more slowly on account of the larger solvent shells they must carry as they revolve. A related zwitterionic [2]rotaxane has also been prepared[192] with covalently-linked cobaltabisdicarbollide stoppers.

The pirouetting rates in several of Leigh's benzylic amide [2]rotaxanes (**Figure 5.23a**) can be controlled under the intervention of external stimuli. The fumaramide[208] [2]rotaxanes (***E*)-R540a-c** can be photoisomerized (**Figure 5.23a**) under irradiation with 254 nm light, resulting in a remarkable increase[209] in the pirouetting rates of the corresponding maleamide [2]rotaxanes **(*Z*)-R540a-c**. For example, the



R538	X	R	Solvent	T_c K	k_c s^{-1}	$\Delta G^{\ddagger}$ kcal·mol^{-1}
a	CH	Cy	CD_2Cl_2	333	1536	14.7
b	$CCO_2{}^tBu$	Cy	CD_2Cl_2	323	1492	14.3
c	N	Cy	CD_2Cl_2	318	1459	14.0
d	CH	Ph	$C_2D_2Cl_4$	286	1692	12.5
e	N	Ph	$C_2D_2Cl_4$	281	1707	12.3

Figure 5.21 Stopper-controlled pirouetting in succinamide-based benzylic amide rotaxanes.[207] The cyclohexylmethyl-stoppered [2]rotaxanes **R538a–c** pirouette against a much higher free energy barrier (>14 kcal·mol^{-1}) than the homologous benzyl-stoppered [2]rotaxanes **R538d-e**. The tubular representation of the solid-state structure of **R538a** reveals the the presence of stabilizing [C–H···π] contacts between the ring's isophthalamide units and the dumbbell's cyclohexyl stoppers, an interaction most likely responsible for the elevated pirouetting barrier.



	R539	$[TFA]^-$	$[Co(C_2H_{11}B_9)_2]^-$	$[Co(C_2H_8B_9Br_3)_2]^-$
k	0.21	19.75	40.33	45.59
$\Delta G^{\ddagger}$	18.37	15.67	15.25	15.17

Figure 5.22 pH- and anion-controlled pirouetting in succinamide-based benzylic amide rotaxanes.[192] Rate constants (*k*) and free energy barriers ($\Delta G^{\ddagger}$) are given in units of s^{-1} and $kcal \cdot mol^{-1}$, respectively.

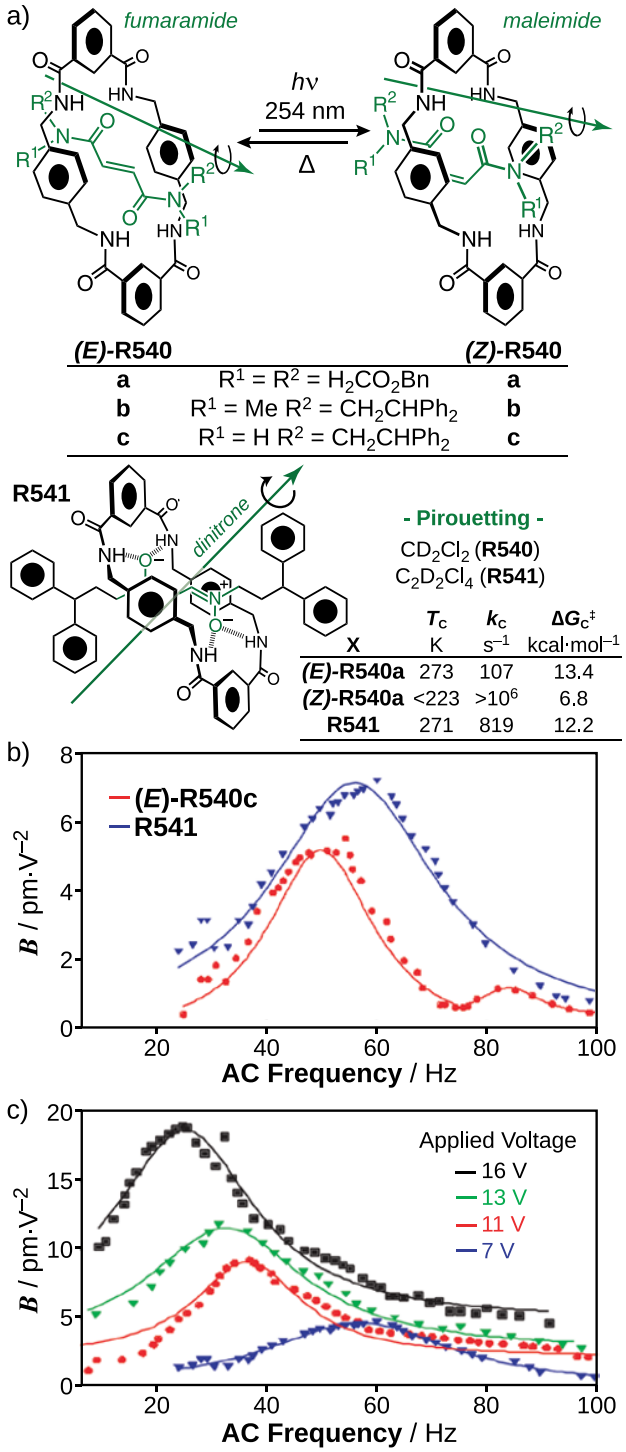


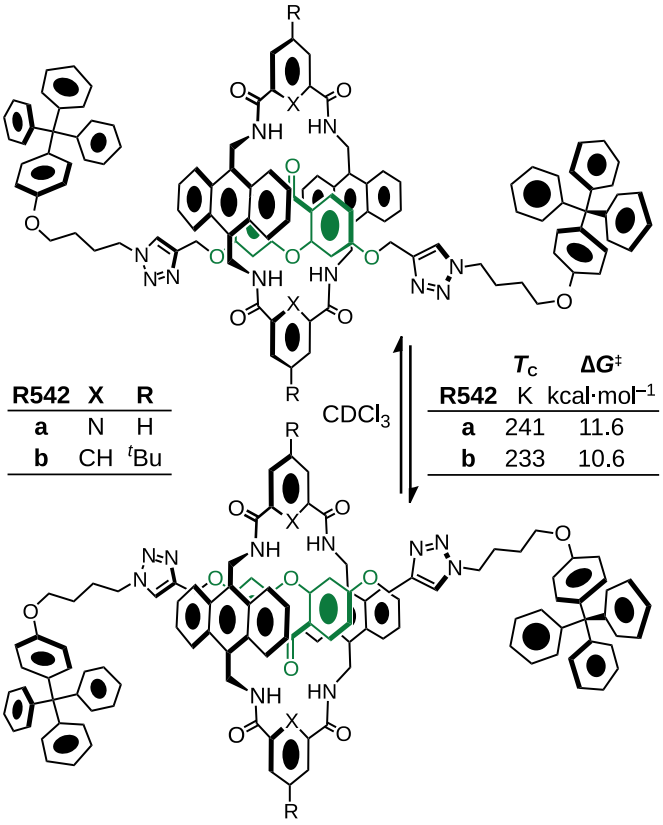
Figure 5.23 Controling pirouetting in benzylic amide [2]rotaxanes.[210] (a) Stereoformulas and pirouetting rates of the photoswitchable fumaramide/maleamide, [2]rotaxanes **(*E*)-R540a-c** and **(*Z*)-R540a-c**, as well as the dinitrone [2]rotaxane **R541**. (b) Plot of the observed[210] Kerr constant of **(*E*)-R540c** (red) and **R541** (blue) at 296 K in dioxane as a function of the frequency of an AC electric field at a strength of 0.35 $V \cdot \mu m^{-1}$. (c) Kerr constant measurements of **(*E*)-R540c** at different applied voltage reveal that the frequency at which the Kerr effect is maximized, and therefore rate of pirouetting, increases with increasing field strength. Data reproduced with permission from ref. 210 (copyright 2000 Nature Publishing Group)

maleamide [2]rotaxane **(*Z*)-R540a** pirouettes (>10^6 s^{-1} at 223 K) more than six orders of magnitude faster than does **(*E*)-R540a** (~1 s^{-1} at 223 K) in CD_2Cl_2 as a result of the disruption of intercomponent hydrogen-bonding interactions caused upon *trans*→*cis* isomerization.

Leigh[210] has also claimed that the rates of pirouetting in the benzylic amide [2]rotaxane **(*E*)-R540c** and the dinitrone[211] [2]rotaxane **R541** can be influenced by an alternating current (AC) electric field, introduced at an applied voltage of 7 V across a 20 μm gap between electrodes, corresponding to a field strength of 0.35 $V \cdot \mu m^{-1}$. The experiments (**Figure 5.23b–c**) in support of this claim involve monitoring the optical properties of the [2]rotaxanes in dioxane while scanning a range of AC field strengths and frequencies. The optical property of interest in this case is a form of birefringence known as the electro-optic Kerr effect, or the quadratic electro-optic effect, which describes the quadratic dependence of the refractive index in an applied electric field. The Kerr constant, *B*, which is given in units of $m \cdot V^{-2}$, quantifies the variance in the refraction index as a function of the electric field

strength and the wavelength of light. Pirouetting frequencies, which were determined experimentally by ^{1}H NMR spectroscopy, as well as computationally by MD simulations, occur on a similar timescale—within an order of magnitude—as the observed (**Figure 5.23b**) Kerr effects in solutions of **(*Z*)-R540c** and **R541**. It is believed that the Kerr constant is maximized when the frequency of the AC field matches the frequency of pirouetting. The pirouetting rates are slightly different in rotaxanes **(*Z*)-R540** and **R541**, owing most likely to differences in the strengths of the hydrogen bonds between the rings' isophthalamide donors and the axles' hydrogen bond acceptors undergoing site exchange. Correspondingly, the frequency of maximum birefringence is slightly different when comparing the two rotaxanes. The hypothesis that the enhanced Kerr effect is caused[M] by pirouetting is supported by (i) control experiments, which show that solutions of non-interlocked rings and dumbbells do not produce the same effect, as well as (ii) the observation that the maximum enhancements in the Kerr effect occur at frequencies that increase with temperature, which is consistent with the fact that pirouetting is a thermally activated process. The frequency of maximum birefringence changes (**Figure 5.23c**) as the strength the AC field is varied, indicating perhaps that the pirouetting rates can be monitored and controlled with the Kerr constant and the voltage, respectively.

Smith[212] has investigated the pirouetting (**Scheme 5.18**) of a xanthone axle within the annulus of anthrylic amide tetralactam rings comprising the [2]rotaxanes **R542a** and **R542b**, which differ only in the nature of the *meta*-diamide recognition units in the macrocycle. Owing to the constitutional asymmetry of the xanthone unit across the plane aligned with the axle and orthogonal to its faces, the exchange process that occurs by means of a 180° within-the-annulus rotation can be observed directly by VT ^{1}H NMR spectroscopy. In an alternative frame of reference, this process can also be interpreted as an around-the-axle pirouette of the ring. The free energy barrier is higher in the case of the [2]rotaxane **R542a** ($\Delta G^{\ddagger}$ = 11.6 kcal·mol^{-1}) based on the ring incorporating 2,6-dicarboxamidopyridine units, as compared to the isophthalamide-based [2]rotaxane **R542b** ($\Delta G^{\ddagger}$ = 10.6 kcal·mol^{-1}) at low temperatures in $CDCl_3$. Since it is believed that "macrocycle breathing" facilitates the pirouetting process, the higher barrier in the case of **R542a** is rationalized by the ring's more robust internal hydrogen bond network, which contracts the ring relative to its isophthalamide-based counterpart. This rationale is consistent with similar investigations (**Figure 5.20**) on the benzylic amide [2]rotaxanes **R537a-b**.



Scheme 5.18 The pirouetting of a xanthone axle within-the-annulus of a mechanically interlocked anthrylic amide ring.[212]

Schalley[161] found that the barrier to pirouetting in the degenerately bistable [2]rotaxane molecular shuttle (see **Scheme 5.9** in **Section 5.1.1.2**) **R526H** is 12.9 kcal·mol^{-1} at a coalescence temperature of 278 K in CD_2Cl_2, a value which happens to be equal to the transition state energy for shuttling the translational (shuttling) process.

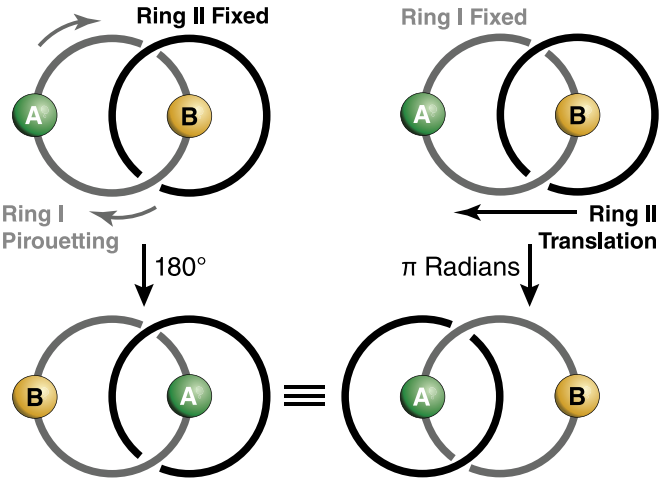
Pirouetting in Inorganic-Organic Hybrids

Pirouetting is estimated[170] to cost less than 9 kcal·mol^{-1} in the case of the inorganic-organic hybrid [2]rotaxane **R531H$_2^+$**—see **Scheme 5.12** in **Section 5.1.1.2**—since the bifurcated [N$^+$–H···F] hydrogen bonds between component parts do not need to be fully broken while the axle and ring rotate with respect to one another, in contrast with the much more energetically demanding translational process.

5.1.2.2 Through-the-Annulus Pirouetting

Through-the-annulus pirouetting involves one ring rotating such that its atoms pass through the cavity of another mechanically interlocked ring, and is therefore only possible in catenanes and their derivatives. The distinction between through-the-annulus pirouetting and translational / circumrotational motion (**Section 5.1.1**) in catenanes is only a matter of semantics, since it depends on one's frame of reference. The graphical representations of a bistable [2]catenane in **Scheme 5.19** illustrate how through-the-annulus pirouetting of one ring (Ring I) in one frame of

[M] A second, smaller peak in the Kerr effect measurements has been observed (**Figure 5.23b**) at ~80 Hz in the case of **(*Z*)-R540c**. Leigh proposed that this frequency may correspond to a rocking motion of the kind described in **Section 5.1.3**. A physical explanation for the link between these mechanical motions and the Kerr effect has not been offered.

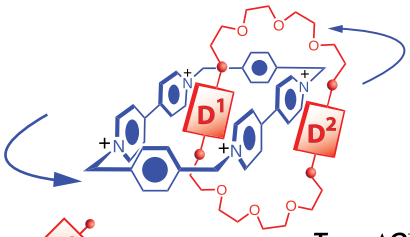


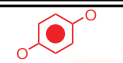
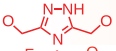
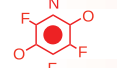
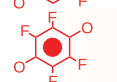
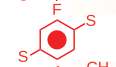
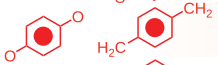
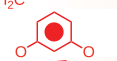
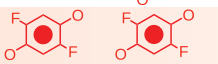
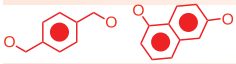
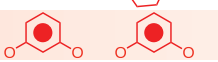
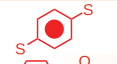
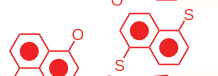
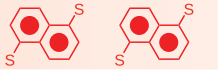
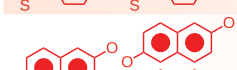
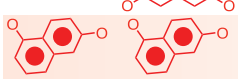
Scheme 5.19 A graphical schematic demonstrating the relationship between through-the-annulus pirouetting and translational processes in a [2]catenane. A through-the-annulus pirouetting motion of Ring I by 180° is equivalent to the translational motion of Ring II by π radians, since both processes lead to the exchange of recognition units A and B between the inside and alongside positions of the [2]catenane. The translational motion of one ring can thus be understood as a pirouetting of the other ring, and vice versa, depending on which ring is fixed in the frame of reference.

reference is identical to translation of another ring (Ring II) in a different frame of reference. This Section is therefore equally eligible to fall under the heading of 'translation' as it is 'pirouetting'. Effectively, the many different arbitrary vantage points one can assume while describing mechanical motion in freely diffusing catenanes renders it acceptable to describe this through-the-annulus dynamic process as being translation, circumrotation, or pirouetting.

The pirouetting of $CBPQT^{4+}$ rings through-the-annulus of π-donating crown ethers has been observed in many donor-acceptor [2]catenanes—see refs. 30, 34, 35, 37, 40, 42, 180, 197, 213. **Table 5.7** lists the energy barriers ($\Delta G^{\ddagger}$) and corresponding rates (k) for these pirouetting motions in D-A [2]catenanes (**C533a^{4+}–C533y^{4+}**) possessing two π-donating recognition units (D1 and D2) in CD_3COCD_3 or CD_3CN solution, as probed by VT ^{1}H NMR spectroscopy. In order to execute this motion, the 'inside' and 'alongside' $BIPY^{2+}$ recognition units of the $CBPQT^{4+}$ ring must forsake some of their D-A π–π stacking interactions, minimally with the alongside donor D2, before transposing their relative positions via a 180° rotation of the tetracationic cyclophane with respect to the axis of D1. This pirouetting motion can also be understood as a translation / circumrotation of the π-donating crown ether from one $BIPY^{2+}$ unit to the other, as in a degenerate molecular train. The $\Delta G^{\ddagger}$ values, which span a wide range from <9 to >13 kcal·mol^{-1}, are influenced by the sterics and electronics of both the inside (D1) and the alongside (D2) recognition units. In general, recognition units with relatively low affinities for the $CBPQT^{4+}$ ring (see **Tables 2.12–2.14** in **Section 2.3.3.8**) or relatively small steric bulk give rise to faster pirouetting rates. For example, the introduction of fluorine substituents on the aromatic HQ units is known[37]

Table 5.7 Values of $\Delta G^{\ddagger}$ and k at various temperatures for the pirouetting of $CBPQT^{4+}$ rings through the annulus of π-donating crown ethers in D-A [2]catenanes.

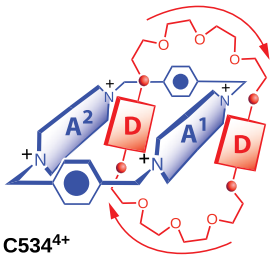


	C533^{4+}	Solvent	T K	$\Delta G^{\ddagger}$ kcal·mol^{-1}	k s^{-1}	Ref
	a	CD_3COCD_3	250	12.0	165	180
	b	CD_3COCD_3	210	10.0	161	213
	c	CD_3COCD_3	247	12.2	84	37
	d	CD_3COCD_3	235	11.4	117	37
	e	CD_3COCD_3	223	10.8	127	34
	f	CD_3COCD_3	205	9.2	650	42
	g	CD_3COCD_3	228	11.1	105	30
	h	CD_3COCD_3	239	11.2	260	35
	i	CD_3COCD_3	243	11.4	315	35
	j	CD_3COCD_3	254	11.9	299	35
	k	CD_3COCD_3	267	12.8	169	40
	l	CD_3COCD_3	240	11.6	149	37
	m	CD_3COCD_3	267	13.4	60	42
	n	CD_3COCD_3	240	12.0	60	30
	o	CD_3COCD_3	213	10.3	111	34
	p	CD_3COCD_3	257	12.7	75	197
	q	CD_3COCD_3	253	11.8	355	34
	r	CD_3COCD_3	227	11.1	104	35
	s	CD_3COCD_3	242	11.7	149	35
	t	CD_3COCD_3	245	11.5	351	35
	u	CD_3COCD_3	221	10.1	440	34
	v	CD_3CN	226	11.4	49	35
	w	CD_3COCD_3	237	11.0	351	35
	x	CD_3CN	208	9.8	201	35
	y	CD_3COCD_3	182	8.9	89	35

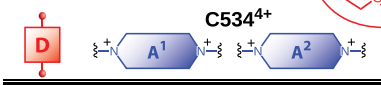
to reduce the strength of the $F_nHQ{\subset}CBPQT^{4+}$ interactions—correspondingly, the $\Delta G^{\ddagger}$ values for pirouetting decrease as more aromatic fluorine substituents are added to the HQ recognition units of D-A [2]catenanes, as in the [2]catenanes **C533c**$^{4+}$, **C533d**$^{4+}$, and **C533l**$^{4+}$. Likewise, $\Delta G^{\ddagger}$ values[35] are slightly lower when the D2 units are 16NP (**C533h**$^{4+}$, **C533r**$^{4+}$, **C533x**$^{4+}$), 26NP (**C533i**$^{4+}$, **C533s**$^{4+}$, **C533v**$^{4+}$, **C533w**$^{4+}$), or 27NP (**C533j**$^{4+}$, **C533t**$^{4+}$, **C533w**$^{4+}$, **C533y**$^{4+}$) than in cases involving the tighter-binding DNP unit, such as in **C533p**$^{4+}$. Other low-affinity π-donor units such as 1,2,4-triazole[213] (**C533b**$^{4+}$), or thioether-appended[34] benzene (**C533e**$^{4+}$, **C533o**$^{4+}$) and naphthalene (**C533q**$^{4+}$, **C533u**$^{4+}$) units also tend to increase pirouetting rates relative to high-affinity donors such as HQ and DNP. Conversely, if the alongside unit D2 is very strong π-donor, as in the case[40] of anthracene (**C533k**$^{4+}$), the activation energies are raised and the corresponding pirouetting rates are lowered. Similarly, the porphryinic $CBPQT^{4+}$ [2]catenanes introduced by Gunter[153,182]—see **Figure 2.32** in **Section 2.3.3.6**—pirouettes against a barrier reaching as high as 15.7 kcal·mol^{-1}. There are, of course, some exceptions whereby catenanes do not behave according to expectations. For example, the highest $\Delta G^{\ddagger}$ value (13.4 kcal·mol^{-1}) observed among the [2]catenanes summarized in **Table 5.7** belongs[42] to the [2]catenane **C533m**$^{4+}$ comprising two relatively low-affinity donor units, namely, *p*-xylylene and 16NP.

The other type of through-the-annulus pirouetting motions that take place in D-A [2]catenanes, such as compounds[N] **C534a**$^{4+}$**–C534u**$^{4+}$, involves site exchange of the two π-donating units of a crown ether. **Table 5.8** tabulates the free energy barriers ($\Delta G^{\ddagger}$) and corresponding rates (k) for the pirouetting of crown ethers possessing two degenerate π-donor units (D) about the axis of an encircled π-accepting unit, A1, contained within an interlocked tetracationic cyclophane possessing an alongside π-acceptor, A2. This through-the annulus pirouetting process requires that all of the D-A π–π stacking interactions between component parts be ruptured and re-formed in order to allow a 180° rotation of the crown ether. This pirouetting motion can also be understood as a translation / circumrotation of the tetracationic cyclophane between the two degenerate donor units, as in a degenerate molecular train. Unsurprisingly, the trends observed for $CBPQT^{4+}$ pirouetting (**Table 5.7**) are mirrored (**Table 5.8**) by the π-donating crown ethers in the sense that increasing steric and electronic interactions between recognition units tends to increase the $\Delta G^{\ddagger}$ values and thus slow down the kinetics of pirouetting. The catenanes with the lowest activation barriers to pirouetting are those with the weakest alongside recognition units, such as extended viologens (**C534b**$^{4+}$, **C534g**$^{4+}$, **C534l**$^{4+}$, **C534q**$^{4+}$),[31] as well as azopyridinium and hydrazopyridinium[47] (**C534a**$^{4+}$)

Table 5.8 Values of $\Delta G^{\ddagger}$ and k at various temperatures for the pirouetting of π-donating crown ethers through the annulus of π-accepting tetracationic cyclophanes in D-A [2]catenanes.



$C534^{4+}$



		Solvent	T K	ΔG‡ kcal/mol	k s^{-1}	Ref
	a	CD_3COCD_3	280	12.3	1440	47
	b	CD_3CN	300	13.1	1848	30
	c	CD_3CN	354	15.6	1505	180
		CD_3COCD_3	313	15.7	60	28
	d	CD_3COCD_3	293	15.4	21	48
	e	CD_3CN	355	18.5	40	44
	f	CD_3CN	369	20.8	3	44
	g	CD_3COCD_3	285	12.5	1360	31
	h	CD_3COCD_3	279	12.4	1190	37
	i	CD_3COCD_3	283	12.2	2200	34
	j	CD_3COCD_3	233	11.9	180	42
	k	CD_3COCD_3	304	13.6	1015	30
	l	CD_3CN	345	16.8	169	31
		CD_3SOCD_3	345	16.4	287	31
	m	CD_3CN	359	17.2	240	197
	n	CD_3COCD_3	293	16.6	2.6	48
	o	CD_3CN	355	19.1	10	44
	p	CD_3SOCD_3	388	23.7	0.4	77
	q	CD_3COCD_3	301	15.1	71	31
	r	CD_3COCD_3	313	15.4	118	34
	s	CD_3CN	278	13.5	147	35
	t	CD_3CN	305	14.4	331	35
	u	CD_3COCD_3	302	13.9	593	35

π-acceptors. Conversely, the activation barrier to through-the-annulus pirouetting is raised in the [2]catenanes **C534f**$^{4+}$ and **C534p**$^{4+}$ possessing the stronger DAP^{2+} π-acceptor, the latter having the highest recorded value at 23.7 kcal·mol^{-1}. The methylated π-acceptor, 3,3′-dimethyl-4,4′-bipyridinium, also known as bipicolinium[48] ($BPIC^{2+}$), is a weaker π-acceptor than $BIPY^{2+}$, yet the steric bulk of $BPIC^{2+}$ raises the circumrotational activation barrier to a similar level as that of its unmethylated $BIPY^{2+}$ counterpart, comparing the [2]catenanes **C534c**$^{4+}$ and **C534d**$^{4+}$ or **C534m**$^{4+}$ and **C534n**$^{4+}$. Thus, unsurprisingly, the thermodynamics and

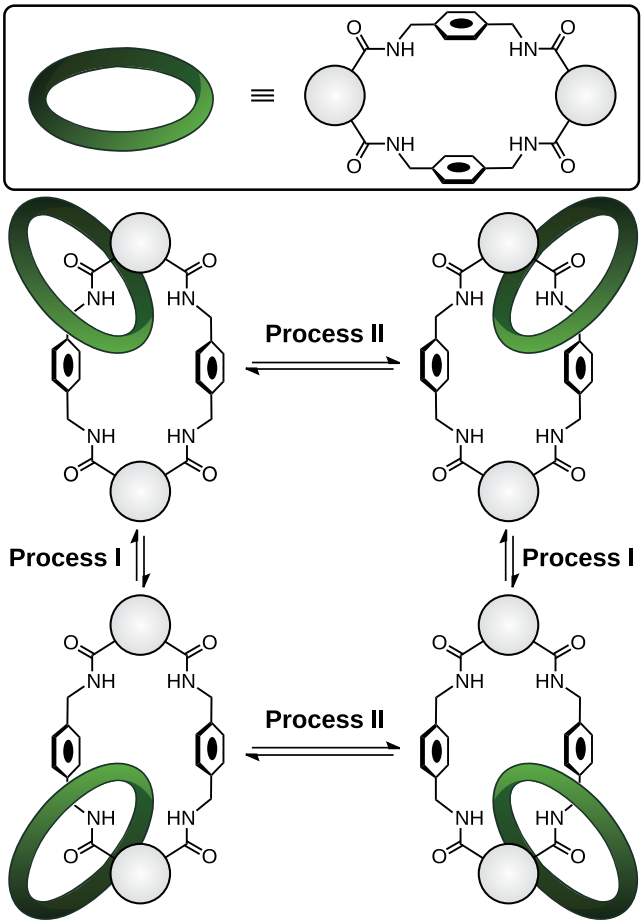
[N] We note that several of the [2]catenanes in **Table 5.7** are duplicated in **Table 5.8**. **C533a**$^{4+}$ = **C534c**$^{4+}$, **C533l**$^{4+}$ = **C534h**$^{4+}$, **C533p**$^{4+}$ = **C534m**$^{4+}$, **C533n**$^{4+}$ = **C534k**$^{4+}$, **C533u**$^{4+}$ = **C534r**$^{4+}$, **C533v**$^{4+}$ = **C534t**$^{4+}$, **C533y**$^{4+}$ = **C534u**$^{4+}$.

kinetics of mechanical motion in MIMs is defined by an interplay of electronic and steric factors arising chiefly from the noncovalent bonding interactions—in this case, π-associated D-A stacking and hydrogen bonding—and the bulkiness of the recognition units, respectively.

Sanders[214] has recently characterized in detail the pirouetting motions in several of his aqueous π-donor/π-acceptor [2]catenanes—see **Figure 3.36** in **Section 3.5.1.2**. In the cases of D-A-D-A stacked hetero[2]catenanes comprising naphthalene-derived π-donating rings and NDI-derived π-accepting rings, through-the-annulus pirouetting of the NDI units occurs with a free energy barrier ($\Delta G^{\ddagger}$) of approximately 17–18 kcal·mol^{-1} at 298 K in H_2O, corresponding to only a few revolutions per second. The pirouetting rates are governed mainly by (i) the extent to which the hydrophobic surfaces become exposed to solvent throughout the motion, (ii) the size of the catenated rings, and (iii) the stacking arrangement of π-donors and π-acceptors.

Another class of compounds with well characterized[185,215,216] pirouetting motions (**Table 5.9**) are the catenated benzylic amide rings honed up to perfection in the Leigh laboratories. A full pirouetting cycle can be understood as a combination of two translational processes—labeled as Process I and Process II accompanying the scheme in **Table 5.9**—in which one of the benzylic amide rings passes over the xylylene or the dicarboxamide units, respectively, of the corresponding concatenated ring. The constitution of the dicarboxamide subunit is critical to the dynamics of these molecules. Both processes I and II are relatively fast in the case (**C535a**) of isophthalamide[o] units. In sharp contrast, Process I (translation over xylylene) is remarkably slow in the case (**C535b**) of pyridine-2,6-dicarboxamide, especially in $C_2D_2Cl_4$ where the high $\Delta G^{\ddagger}$ value of 20.5 kcal·mol^{-1} corresponds to a pirouetting rate of only 0.003 revolutions per second. A homo[2]catenane (**C535c**) of rings comprising thiophene-2,5-dicarboxamide units is the fastest circumrotator in the series, reaching rates as high as 9600 s^{-1} in $C_2D_2Cl_4$ and 28000 in CD_3SOCD_3 at 298 K. This wide range of rates has been attributed mostly to the differences in the strength and connectivity of the intramolecular hydrogen bonding networks, especially the tendency of pyridine-2,6-dicarboxamides to adopt *cisoid* conformations which enhance binding to carbonyl units, as discussed in the case of the glygly rotaxane (**R537b**, **Figure 5.20**) in **Section 5.1.2.1**. MD simulations[216] have offered an even more detailed description of the mechanism of circumrotation as a stepwise process involving the making and breaking of intramolecular hydrogen bonds. The other major class of tetralactam [2]catenanes based on cyclohexylidenebisphenylene linkers, as introduced (**Section 2.3.4.1**) by

Table 5.9 The energy barriers ($\Delta G^{\ddagger}$) of translational processes I and II, which combine to complete a full circumrotational cycle in the benzylic amide catenanes **C535a–c**, as well as the rates of pirouetting (k) defined by the rate-limiting process at 298 K in various solvents.[215]



	Solvent	Process	$\Delta G^{\ddagger}$ / kcal·mol^{-1}	k / s^{-1}
	$C_2D_2Cl_4$	I	12.3	72
	$C_2D_2Cl_4$	II	14.5	
	CD_3OD	I	↓[a]	16000
C535a	CD_3OD	II	11.3	
	$C_2D_2Cl_4$	I	20.5	0.003
	$C_2D_2Cl_4$	II	11.3	
	CD_3SOCD_3	I	17.9	0.2
C535b	CD_3SOCD_3	II	↓[a]	
	$C_2D_2Cl_4$	I	11.6	9600
	$C_2D_2Cl_4$	II	↓[a]	
	CD_3SOCD_3	I	11.0	28000
C535c	CD_3SOCD_3	II	↓[a]	

[a]The downward arrow indicates that $\Delta G^{\ddagger}$ is too low to measure.

[o] Functionalization of the isophthalamide units of benzylic amide catenanes at the 3, 4, or 5 positions with an organic functional group, R ≠ H, prevents the rings from undergoing a complete 360° pirouetting cycle.

Hunter[217] and Vögtle,[218] do not pirouette through-the-annulus on account of their bulky cyclohexylidene-bisphenylene linkers.

5.1.2.3 Super-Rotation

Super-rotation is a term that has been proposed[178,194] to describe pirouetting motions executed by a 'subcomplex' rather than by a single component part. Thus, a local *host⊂guest* subcomplex must be 'frozen' on the timescale of a pirouetting motion for this motion to be considered super-rotation. The two examples in **Figure 5.24** illustrate how a 180° super-rotation of a *DNP⊂CBPQT*$^{4+}$ subcomplex influences the co-conformation of the [3]catenane[194] **C536**$^{8+}$ (**Figure 5.24a**) and the oligorotaxane foldamer[178,179,219] **[5]R536**$^{16+}$ (**Figure 5.24b**)—see also **Scheme 5.16** and the corresponding discussion in **Section 5.1.1.2**. As in the case of within-the-annulus pirouetting, super-rotation may involve conformational rotations in one component part that lead to differences in the co-conformation of the mechanomolecule as a whole. The extent to which super-rotation occurs, as opposed to a combination of within-the-annulus and around-the-axle pirouetting motions, depends on the rates associated with each of these processes. The rates of within-the-annulus and super-rotation pirouetting motions are inversely proportional, such that the rate of super-rotation increases as the rate of within-the-annulus pirouetting decreases, and vice versa.

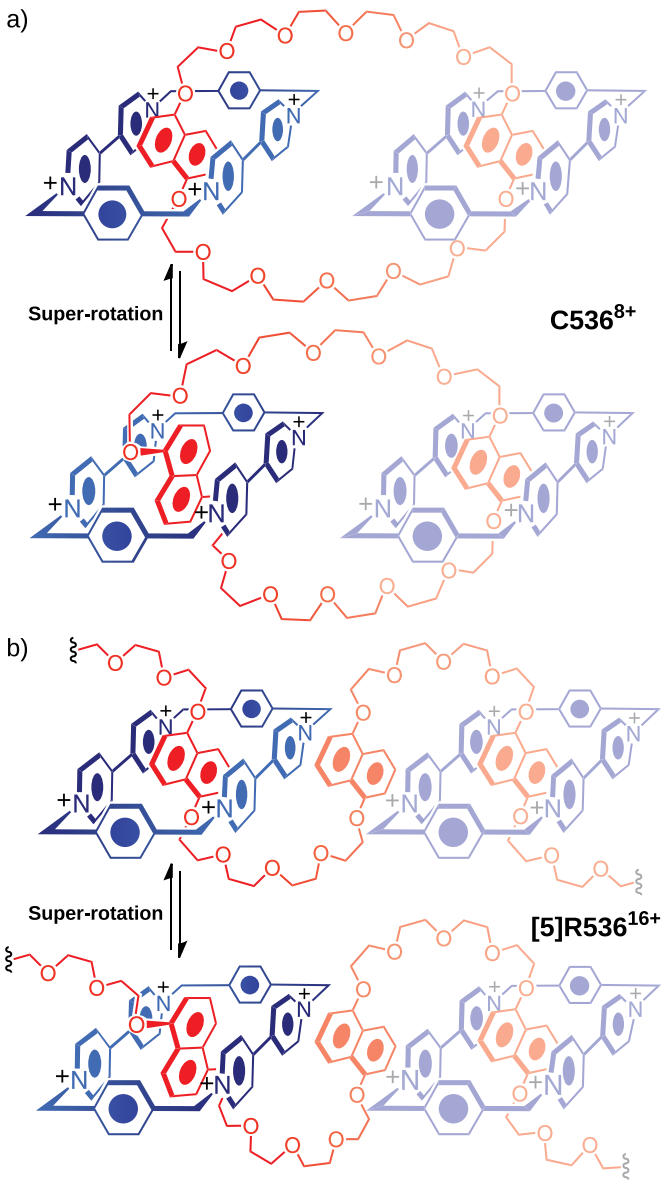


Figure 5.24 Stereoformulas illustrating super-rotation processes in (a) donor-acceptor [3]catenane[194] and (b) donor-acceptor oligorotaxane foldamers.[178] In both cases, the local *DNP⊂CBPQT*$^{4+}$ subcomplex rotates as a single unit.

Subcomplex—A local host-guest interaction within a larger supermolecule or mechanomolecule.

Super-rotation—An intramolecular motion involving the pirouetting of a ring-and-axle subcomplex.

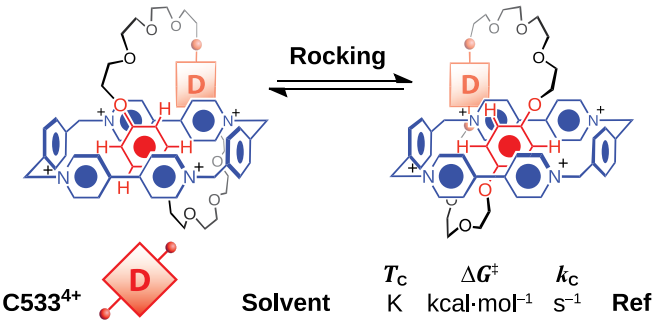
5.1.3 Rocking

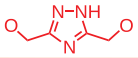
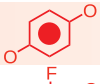
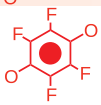
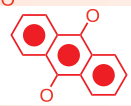
'Rocking' is a process whereby two component parts of a MIM rotate about intersecting axes, such that they cannot complete a full rotation as they come into steric contact. Rocking is seldom analyzed by quantitative methods because it is not usually associated with stable or metastable co-conformations, but rather with Brownian motion. One motif in which degenerate co-conformers can be interconverted by rocking motions are MIMs based on *HQ⊂CBPQT*$^{4+}$ inclusion (sub)complexes. Since the *HQ⊂CBPQT*$^{4+}$ interaction is stabilized by [C–H···π] contacts extending from the HQ protons to the π surfaces of the ring's *para*-phenylene linkers, these assemblies can adopt two degenerate co-conformations, as illustrated in **Table 5.10**.[34,35,37,40,213,220] The catenanes comprise a number of members of the series (**C533a**$^{4+}$**–C533y**$^{4+}$) exhibiting through-the-annulus pirouetting—see **Table 5.7** in **Section 5.1.2.2**. The date in **Table 5.10** reveal that the nature of the alongside recognition unit influences the rocking rates in a manner similar to pirouetting motions. The transition state energies are much lower, however, on the order of 9–10 kcal·mol^{-1}. In addition to these catenanes, the rate of HQ/CBPQT^{4+} rocking in Gunter's strapped porphyrin [2]catenane[152] **C529a**$^{4+}$ (see **Scheme 5.4** in **Section 5.1.1**) is estimated to be 85 s^{-1} at a coalescence temperature of –65 °C in $(CD_3)_2CO$, corresponding to a free energy barrier of 10.5 kcal·mol^{-1}. This barrier is relatively high, especially in consideration of the large size of the polyether macrocycle, suggesting that the alongside BIPY^{2+}–porphyrin interaction is a relatively strong one.

Another case of rocking has been observed in neutral D-A systems. Sanders[221] has found that rocking (**Scheme 5.20**) in pseudorotaxanes comprising *N*,*N*′-dihexylnaphthalenediimide (Hx_2NDI) and DN38C10 occurs at a rate of 7 s^{-1} in $CDCl_3$:CD_3OD (98:2 v/v) at 220 K, corresponding to a $\Delta G^{\ddagger}$ value of <12 kcal·mol^{-1}.

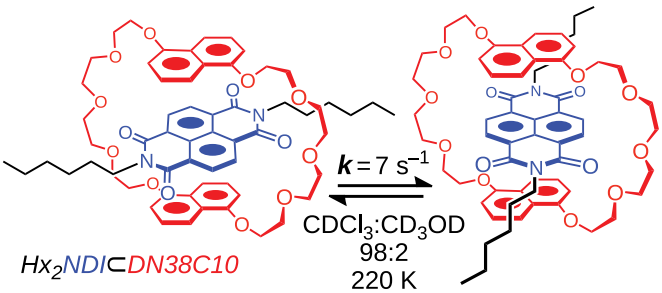
Dynamic rocking motions may be linked to a form of static mechanostereoisomerism we refer to as mechanical

Table 5.10 The energy barriers ($\Delta G^{\ddagger}$) and rate constants (k) for the rocking of HQ units within the $CBPQT^{4+}$ rings of bistable D-A [2]catenanes.



$C533^{4+}$		Solvent	T_c K	$\Delta G^{\ddagger}$ kcal·mol^{-1}	k_c s^{-1}	Ref
a		CD_3COCD_3	218	9.0	3832	213
b		CD_3COCD_3	215	9.0	3100	220
d		CD_3COCD_3	207	9.6	311	37
e		CD_3COCD_3	228	9.6	3037	34
i		CD_3COCD_3	203	8.5	3047	35
j		CD_3COCD_3	245	10.6	3038	35
l		CD_3COCD_3	225	9.5	2897	40
$C529a^{4+}$ porphyrin		CD_3COCD_3	208	10.5	85	152

helicity. Some mechanomolecules exhibiting helical chirality may invert their co-configurations as a result of rocking—see **Figures 5.32–5.33** and the corresponding discussion in **Section 5.2.3.3**. These systems exemplify the idea that the boundaries between static and dynamic mechanostereoisomerism are not always clear.



Scheme 5.20 Rocking in a neutral D-A pseudo[2]rotaxane.[221]

5.1.4 Robust Dynamics

The term 'robust dynamics' was coined[10] in 2010 to describe "*constructs where the repeated dynamics of one entity does not effect the integrity of any others linked to it.*" In the context of extended reticular structures such as metal-organic frameworks (MOFs) or coordination polymers, robust dynamics implies a situation in which the molecular linkers are capable of expressing dynamic motions—an opportunity afforded by the mechanical bond, for example—without compromising the topology or stability of the network. Furthermore, the integration of dynamic MIMs within the rigid lattice of these three-dimensional frameworks will minimize their random motions while increasing their order and coherence, which will most likely improve their stability and performance in any intended application. In short, it has been proposed that coupling the dynamics of MIMs with the rigidity of MOFs will produce materials that are rigid and robust, yet dynamic, hence the namesake of robust dynamics. We note that robust dynamics are also possible without mechanical bonds, such as in the crystalline molecular rotors or 'amphidynamic crystals' developed by Garcia-Garibay,[222] or the surface-mounted dipolar molecular rotors that have been investigated by Michl,[223] for example.

Loeb[224] has pioneered the synthesis of materials that embody the vision of robust dynamics for the mechanical bond. In 2012 he introduced a MOF (**UWDM-1**) in which crown ether rings undergo independent rotary motion (**Figure 5.25**) about the axles of the rigid struts that constitute the framework. The crystal structure (**Figure 5.25a**) of **UWDM-1** reveals a network of rotaxane struts in which each dumbbell is integrated through four Cu^{II} paddlewheel clusters. The unusual topology of the network resembles a lattice of polyhedra with narrow hexagonally shaped parallel channels running continuously throughout the extended structure. The network provides sufficient void space for the crown ether rings encircling the rigid, fixed axles to move independently. This material represents a rare case in which within-the-annulus pirouetting (**Section 5.1.2.1**) of an axle can be distinguished from around-the-axle pirouetting of a ring. The dynamics of the rings as a function of temperature were probed by VT solid-state ^{2}H NMR spectroscopy (SSNMR), enabled by the deuterated protons installed during the synthesis (**Figure 5.25a**) of the [2]rotaxane **R543H$^+$**, the precursor to **UWDM-1**. A comparison of the VT ^{2}H SSNMR spectra of activated **UWDM-1** (**Figure 5.25b**) with simulated spectra (**Figure 5.25c**) accounting for a model of the ring's dynamics (**Figure 5.25d**) reveals that the back-and-forth rocking of the deuterium atoms, which occurs in the crystal above 250 K, is accompanied at even higher temperatures (>324 K) by the pirouetting of the entire ring about the stationary axle of the framework. These observations proved that robust dynamics is indeed possible to realize in crystalline materials.

Loeb[225] has recently extended the concept of robust dynamics to translational motion with the introduction of **UWDM-4**, a MOF incorporating (**Figure 5.26**) a degenerate molecular shuttle within the rigid struts of the network. The rotaxane **R544**, which is the precursor ligand of the MOF, comprises two triphenylenedicarboxylic acid struts conjoined by rigid bridge in which a [24]crown-8 (24C8) ring shuttles back and forth between two fused

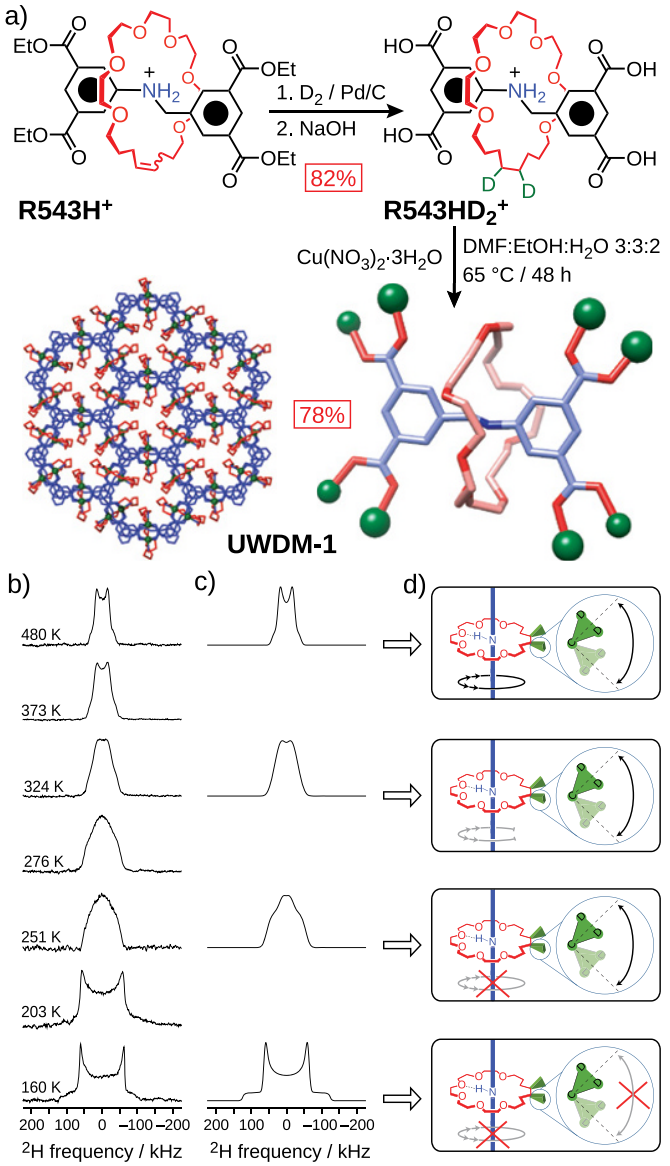


Figure 5.25 Robust pirouetting dynamics in a metal-organic rotaxane framework (MORF). (a) Synthesis of **UWDM-1**, a MOF with crown ethers encircling the struts. Tubular representations of the solid-state structure are portrayed with protons and solvent molecules omitted for the sake of clarity. (b) Solid-state VT ^{2}H NMR data of the crown ether's ^{2}D signal. (c) Simulated ^{2}H NMR data accounting for the dynamics illustrated in (d), showing that the rings rotate above temperatures of 324 K, with full revolutions taking place faster than the ^{2}H NMR timescale at 480 K. Adapted with permission from ref. 224 (copyright 2012 Nature Publishing Group)

imidazole recognition units. See **Scheme 2.56** in **Section 2.3.3.3** and the accompanying text for more details on the synthesis of this type of rotaxane. In the neutral compound **R544**, the lack of cationic groups allows the ring to shuttle rapidly (>10^{7} s^{-1} at 298 K in PhMe) between the hydrogen bond donating imidazole groups. A drop of HBF_4 is added to the reaction mixture before MOF crystals are grown from **R544** and $Zn(BF_4)_2{\cdot}6H_2O$ at 85 °C in 1:1:2 DMF:Me_2SO:EtOH, affording **UWDM-4**·HBF_4. In the MOF obtained by this method, the struts contain one imidazole unit and one imidazolium unit encircled by the crown ether. The **UWDM-4**·HBF_4 material contains 47% void space—much higher than the 11% void space calculated in the case of **UWDM-1**—with large channels for the inclusion of solvent molecules. Shuttling is not expected to occur in these non-degenerate rotaxane struts, however, because imidazolium derivatives bind 24C8 with orders-of-magnitude higher affinities than do the

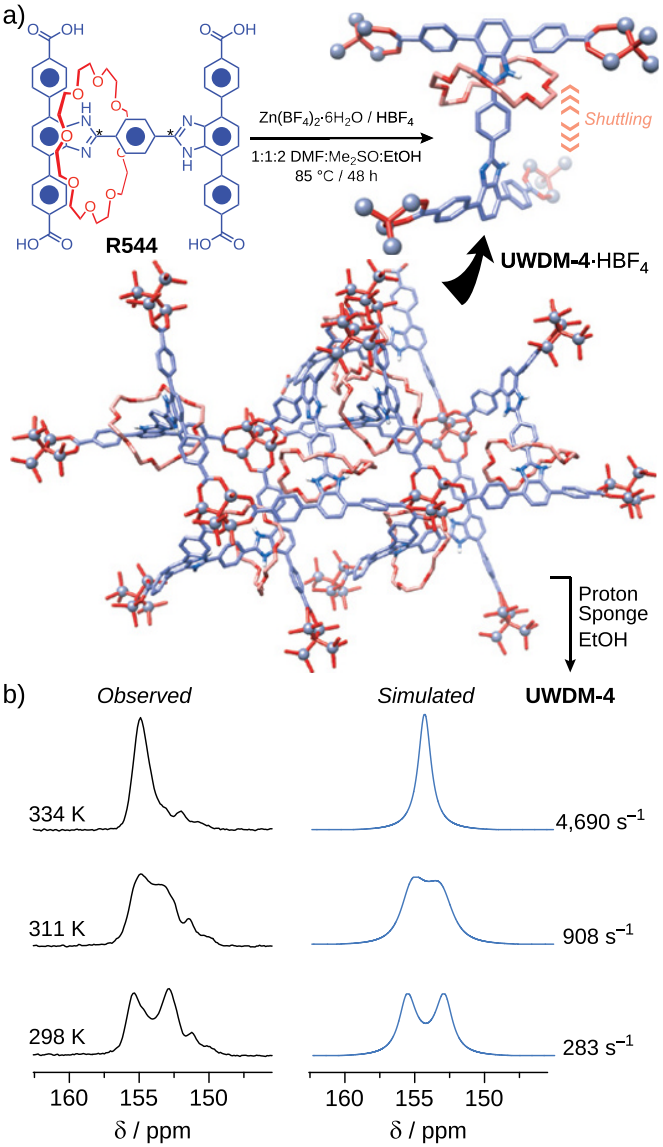


Figure 5.26 A MOF imbued with degenerate molecular shuttles that operate in the solid state.[225] (a) The synthesis of **UWDM-4**·HBF_4 from the [2]rotaxane molecular shuttle **R544**, with tubular representations of sections of the extended solid-state structure, omitting solvent molecules, protons, and counterions for the sake of clarity. (b) Experimental and simulated VT ^{13}C SSNMR data for the neutralized MOF **UWDM-4**, which reveals signal coalescence attributable to increasing shuttling rates at elevated temperatures. These signals arise from the ^{13}C-enriched atoms labeled with asterisks in the steroformula of **R544**. Data reproduced with permission from ref. 225 (Copyright 2015 Nature Publishing Group)

corresponding imidazole derivatives. The degeneracy of the shuttle is recuperated in the crystal by deprotonating the imidazolium unit with *N*,*N*,*N*′,*N*′-tetramethylnaphthalene-1,8-diamine (proton sponge) to afford **UWDM-4**. Two of the imidazole carbon atoms of the struts (labeled with asterisks in the stereoformula in **Figure 5.26a**) were enriched to 50% ^{13}C in order to facilitate an investigation (**Figure 5.26b**) of ring shuttling in the solid state using ^{13}C SSNMR techniques. The ring shuttles back and forth at a rate of approximately 283 Hz at 298 K in the crystal.

Since Loeb has demonstrated that it is possible to construct porous materials in which molecular pirouetting and translational (shuttling) motions operate in periodic and well-defined void spaces, the field is now poised to generate even more sophisticated materials exhibiting robust dynamics that are coherent, correlated, stimulus-responsive, point-addressable, etc., in the course of time.

5.2 Static Mechanostereoisomerism

In the previous Section, we described how mechanostereoisomers are interconverted by the relative dynamic motions of component parts. In this Section, we are going to discuss mechanostereoisomers that exist independently of these mechanical motions. Although it remains possible, in some cases, to convert between different types of these mechanostereoisomers dynamically, we refer to them as 'static' because their isomerism is described by the gross spatial arrangements of component parts in the ground state. We have identified four types of isomerism (**Figure 5.27**) that are unique to molecules possessing mechanical bonds and entanglements—namely, orientational (**Section 5.2.1**), sequence (**Section 5.2.2**), and chiral mechanostereoisomers (**Section 5.2.3**), the latter of which can be further differentiated into mechanically planar (**Section 5.2.3.1**), axial (**Section 5.2.3.2**), and helical (**Section 5.2.3.3**) chirality, as well as topological isomers (**Section 5.2.4**) differentiated by chiral (**Section 5.2.4.1**) or conditional (**Section 5.2.4.2**) features.

5.2.1 Orientational Mechanostereoisomers

Orientational mechanostereoisomerism arises in MIMs with rings that lack mirror symmetry commensurate with the plane of their cavity. Conical hosts such as cyclodextrins (**Section 2.3.1.1**) and calix[*n*]arenes (**Section 2.3.9.1**) are inherently desymmetrized with respect to this plane, as are pillar[*n*]arenes (**Section 2.3.9.2**), which also happen to possess *n* elements of planar chirality. Pillar[*n*]arenes[226] and other hosts may also be desymmetrized through synthetic modification. When another component part is engaged in a mechanical bond with this kind of desymmetrized ring, it can give rise to orientational mechanostereoisomerism if the interlocking component part also lacks mirror symmetry across the plane of the ring's cavity.

Orientational mechanostereoisomers—Mechanostereoisomers arising from differences in the relative orientations of component parts that lack mirror symmetry across the plane of a mechanically bonded ring's cavity

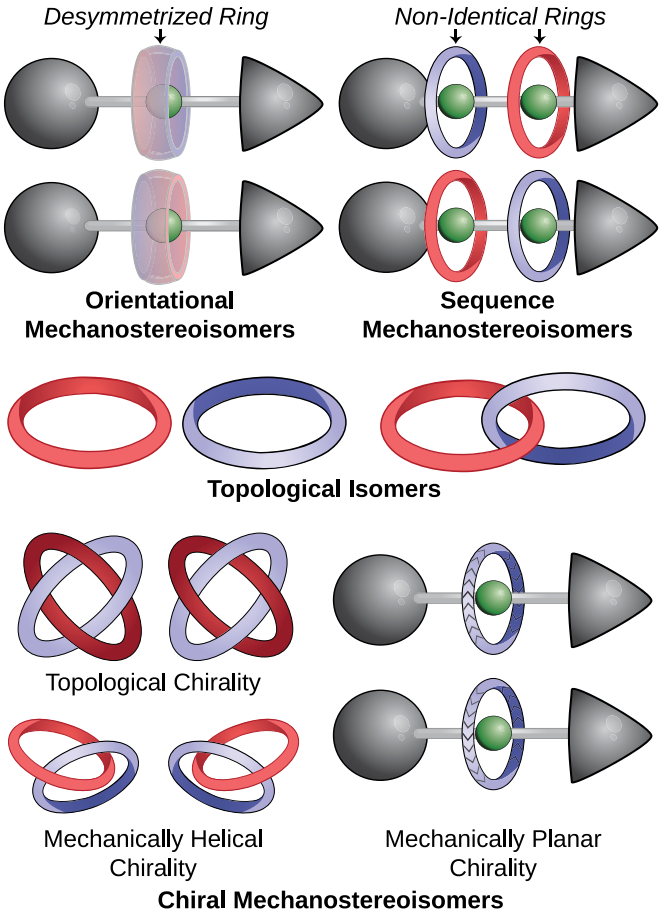


Figure 5.27 Graphical representations of different types of static mechanostereoisomers.

In other words, the conditions for orientational isomerism call for an 'oriented' component part to be interlocked with a desymmetrized ring. In the case of orientationally isomeric [2]rotaxanes, for example, the ring and dumbbell must both possess constitutional asymmetry in order to avoid having a mirror plane orthogonal to the axle through the plane of the ring's cavity. The conceptual equivalent in the case of [2]catenanes also leads to the differentiation of isomers. In many cases, catenated orientational isomers also fall under the umbrella of topological isomerism and topological chirality—see **Section 5.2.4**.

[2]Rotaxane Orientational Isomers

The concept of orientational mechanostereoisomers began to emerge when Kaifer[227,228] synthesized rotaxanes comprising αCD rings encircling constitutionally asymmetric zwitterionic dumbbells. See **Scheme 2.13** and the accompanying discussion in **Section 2.3.1.1** for a description of these orientational isomers. CD (pseudo)rotaxanes with unsymmetrical dumbbells are often prepared as a mixture of orientational isomers.[229–236] In some cases, it has been possible to prepare (**Figure 5.28**) αCD-based

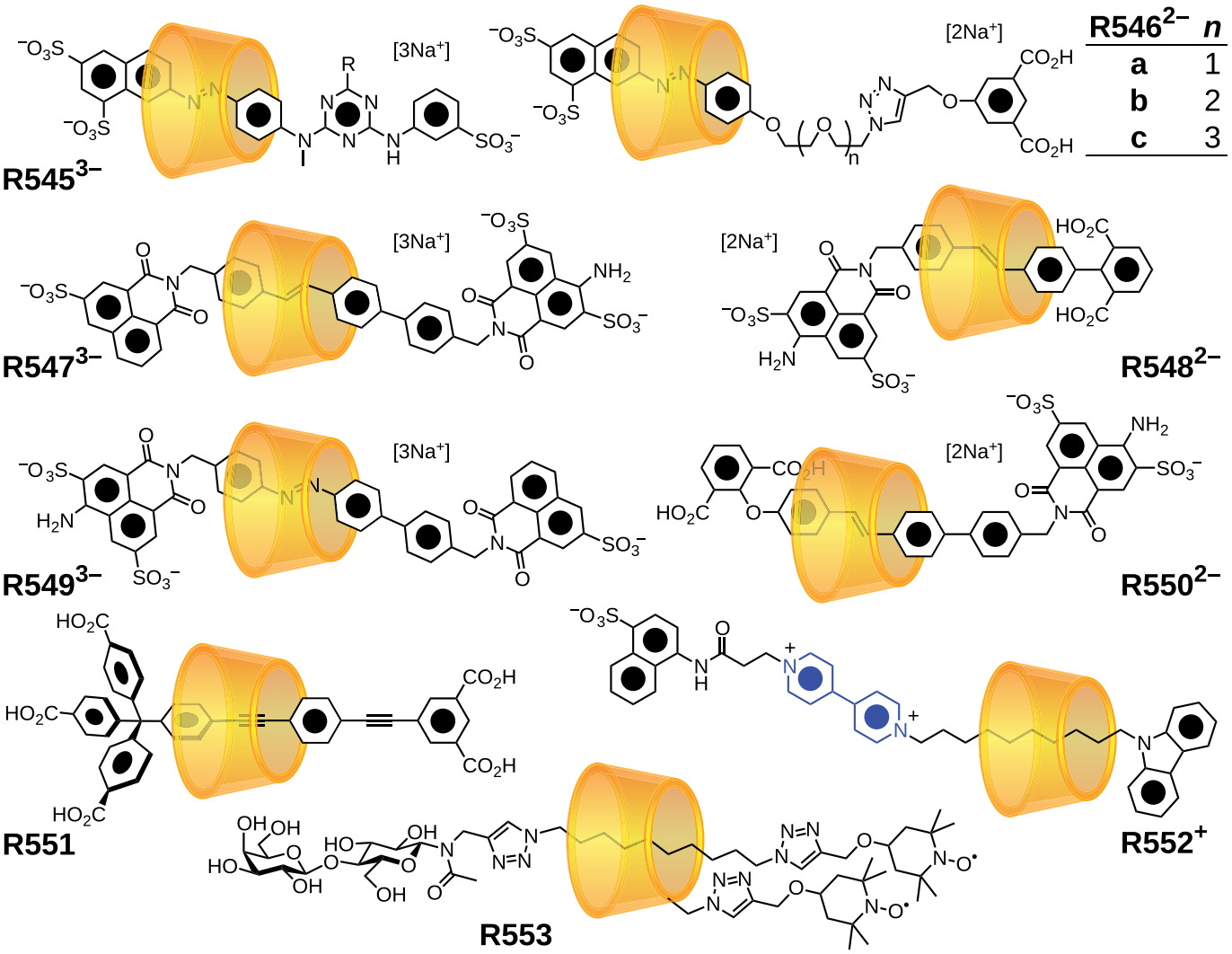


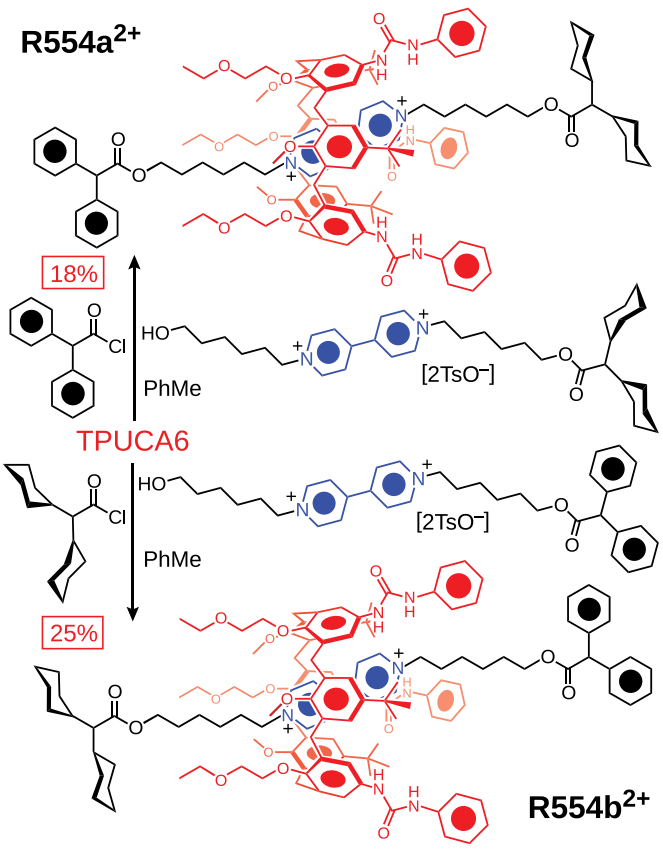
Figure 5.28 Structural formulas of several αCD rotaxanes obtained as pure orientational mechanostereoisomers. See refs. 237, 240–243, 248, 249. The orientational isomers with oppositely facing αCD cones were not observed in most cases.

[2]rotaxanes as orientationally pure mechanostereoisomers. Anderson[237] has discovered that an azo dye of naphthalene-1,3-disulfonate is threaded by a permethylated αCD ring exclusively such that its wider 2,3-rim faces the sulfonated napthalene stopper in the [2]rotaxane **R545**$^{3-}$. Zhao[238–240] has prepared similar *azo⊂αCD* [2]rotaxanes **R546a-c**$^{2-}$ that are also obtained solely as one of two possible orientational isomers. Tian[241–243] has described the synthesis of a number of αCD rotaxanes (**R547**$^{3-}$, **R548**$^{2-}$, **R549**$^{3-}$, **R550**$^{2-}$), which have all been obtained as pure orientational mechanostereoisomers from Suzuki stoppering reactions. The solid-phase synthesis[244] of the [2]rotaxane **R551** affords predominantly the orientational isomer in which the secondary rim of αCD faces a carboxylated trityl stopper preferentially over one derived from isophthalic acid. Matsuo[245] and Park[246,247] have independently found that both αCD and ßCD encircle alkylviologen guests such that their secondary faces (2,3-rim) are oriented toward the dication, a feature which has been exploited in the synthesis[248] of the [2]rotaxane **R552**$^{+}$ as a single mechanostereoisomer. More recently, Mezzina and Lucarini[249] have employed electron spin resonance (ESR) spectroscopy to support the claim that a single orientational mechanostereoisomer is obtained in the click synthesis of the lactose-stoppered [2]rotaxane **R553** possessing TEMPO radicals as spin-labels on each component part.

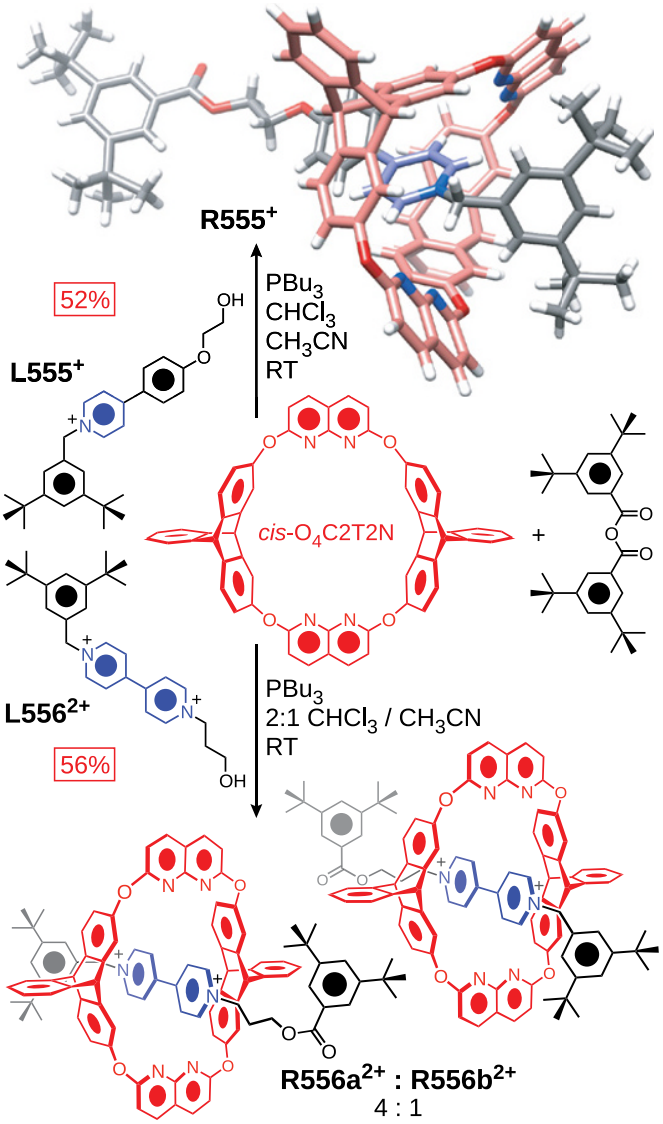
Another group of hosts which are predisposed to generating orientational isomers are the calix[*n*]arenes—see **Section 2.3.9.1**. Arduini[250] has synthesized (**Scheme 5.21**) a pair of [2]rotaxane orientational isomers, **R554a**$^{2+}$ and **R554b**$^{2+}$, which comprise the triphenylureacalix[6]arene-derived host TPUCA6 and BIPY^{2+}-derived dumbbells with differentiated endcaps consisting of either diphenylmethane or dicyclohexylmethane stoppers. In PhMe, the rotaxanes can be prepared and isolated as their OTs^{-} salts in a selective manner, depending on the nature of the semi-dumbbell and stopper precursors. The selectivity arises from the fact that when the semidumbbell threads[251] the cavity of the TPUCA6 host, it approaches exclusively from the wider urea-decorated rim in apolar solvents. This

'unidirectional' threading process may arise from (i) kinetic effects associated with the improved accessibility of the wider rim of the host, (ii) kinetic effects associated with the desolvation of the BIPY·2OTs ion pairs assisted by the urea appendages, (iii) thermodynamic effects associated with the hydrogen bond donating urea appendages, which interact favorably with the terminal alcohol of the semidumbbell, as well as with its counterions, or some combination thereof. By contrast, the same precursors that lead exclusively to **R554^{2+}a** in PhMe lead to an equimolar mixture of the **R554^{2+}a** and **R554^{2+}b** orientational isomers in MeCN, revealing that solvent polarity is an important factor in the selection of these orientational mechanostereoisomers.

Chen[252] has employed his tetraoxacalix[2]triptycene[2]-naphthyridine[253,254] (O_4C2T2N) host—see **Section 2.3.9.1**—in the synthesis (**Scheme 5.22**) of [2]rotaxane orientational isomers possessing pyridinium-based dumbbells. The stoppering protocol involves the esterification of equally sized, 3,5-*tert*-butylbenzyl-stoppered semidumbbells, **L555^{+}** and **L556^{2+}**, derived from monopyridinium and bipyridinium recognition units, respectively. As these semidumbbell precursors thread the annulus of O_4C2T2N, they may approach through either of two rims, which are differentiated on account of the 1,3-substitution pattern of its triptycene units. We shall refer to these rims as 'N-rim' and the 'T-rim', corresponding to the naphthyridine (N) and triptycene (T) functional groups located at each rim's surface.



Scheme 5.21 Arduini's selective syntheses of calix[6]arene-based [2]rotaxanes as pure orientational isomers.[250]



Scheme 5.22 Chen's synthesis of [2]rotaxane orientational isomers based on *cis*-O_4C2T2N hosts and pyridinium derived guests.[252] Whereas the stoppering reaction involving the monopyridinium precursor **L555^{+}** is selective for only one orientational isomer of **R555^{+}**, the bipyridinium-derived precursor **L556^{2+}** yields a 4:1 mixture of orientational isomers **R556a^{2+}** and **R556b^{2+}** under the same reaction conditions. The tubular representation of the X-ray crystal structure of **R555^{+}** is illustrated with PF_6^- counterions and solvent molecules omitted for the sake of clarity.

The monopyridinium [2]rotaxane **R555^{+}** is obtained selectively as a single orientational isomer, in which the T-rim faces the ester stopper, suggesting the semidumbbell precursor approached through the N-rim. Under the same conditions, two orientational isomers, **R556a^{2+}** and **R556b^{2+}**, are obtained in a 4:1 ratio from the bipyridinium semidumbbell, with the T-rim of the dominant isomer now facing the benzyl stopper, having therefore approached through the T-rim. These opposite threading scenarios are rationalized by experiments and DFT calculations in support of the argument that a competition exists between electrostatic

interactions, which favor the formation of **R556a**$^{2+}$, and steric interactions, which favor the formation of **R556b**$^{2+}$. In the case of **L555**$^{+}$, with its more electron-rich phenolic subunit, electrostatic and steric effects cooperatively favor the mechanostereoselective formation of **R555**$^{+}$, as opposed to its other orientational isomer.

The pillar[*n*]arenes (PA*n*)—see **Section 2.3.9.2**—are another type of host lacking mirror symmetry across the plane of their cavities, enabling the emergence of orientational isomerism in PA*n*-based MIMs. For example, Ogoshi[255–257] has investigated several rotaxanes (**Figure 5.29**) based on PA5, including the [2]rotaxanes **(*R*$_{mp}$)-R557**$^{+}$ and **(*S*$_{mp}$)-R557**$^{+}$, where the Et10PA5 rings possess five planes of chirality associated with each of their aryl rings. In the absence of a mechanically interlocked dumbbell, the PA5 rings can atropisomerize between the planar chiral ($R_PR_PR_PR_PR_P$) and ($S_PS_PS_PS_PS_P$) forms via concerted through-the-annulus conformational torsions of the aryl rings. When a PA5 ring encircles the dumbbell of a rotaxane, however, this atropisomerization is forbidden, which allows for the expression of orientational isomers if the dumbbell is not constitutionally symmetrical. One could make the argument that these rotaxanes also qualify as mechanically planar mechanostereoisomers—see **Section 5.2.3.1**.

[3]Rotaxane Orientational Isomers

More orientational isomers become possible as more desymmetrized rings are added. For example, the rings of the [3]rotaxanes **(*RR*)-R558**$^{2+}$ and **(*SS*)-R558**$^{2+}$, illustrated in **Figure 5.29**, possess only the R_P or S_P descriptors, respectively, while the [3]rotaxane ***meso*-R558**$^{2+}$ possesses a combination of all-S_P and all-R_P PA5 rings. Ogoshi[256] separated all three of these co-configurations by chiral HPLC and characterized them by circular dichroism, confirming the chirality of the **(*RR*)-R558**$^{2+}$ and **(*SS*)-R558**$^{2+}$ enantiomers, as well as the achirality of ***meso*-R558**$^{2+}$.

We recall from **Figure 2.76** in **Section 2.3.9.1** that Neri and Gaeta[258–263] have constructed a number of MIMs based on hexamethoxycalix[6]arene (OMe_6CA6) exhibiting orientationally mechanostereoselective threading arrangements. The [3]rotaxanes, for example, can exist as so-called *head-to-head*, *tail-to-tail*, or *head-to-tail* orientational isomers, depending on the relative orientations of the conical OMe_6CA6 rings. A unique feature of these orientational isomers is their ability to interconvert[260] by cone-to-cone inversion of the OMe_6CA6 rings upon deprotonation of the ammonium centers serving as recognition units. Flood's cyclochiral bowl-shaped cyanostar macrocycles also give rise to [3]rotaxane orientational isomers[264]—see **Section 2.3.6.4**.

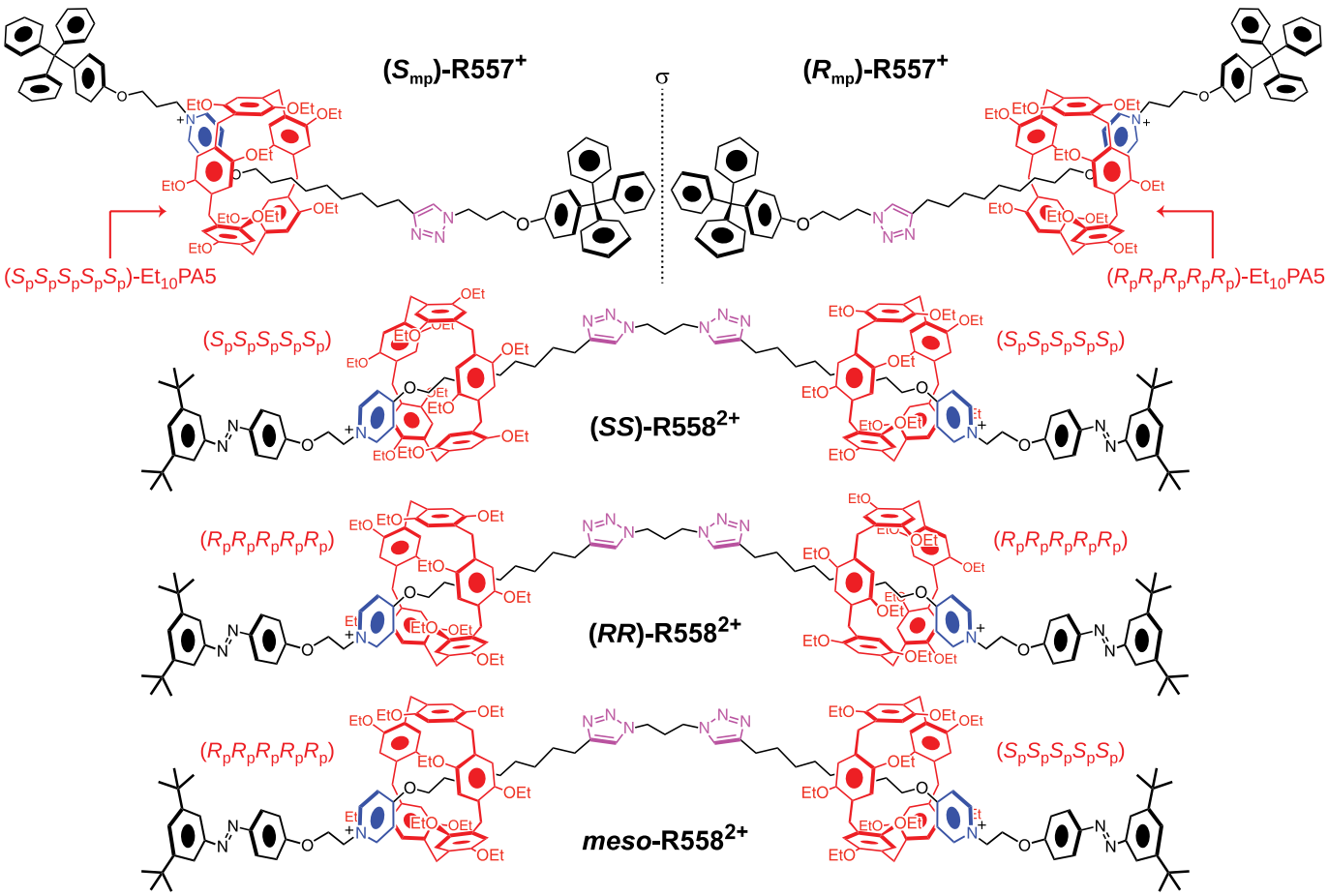
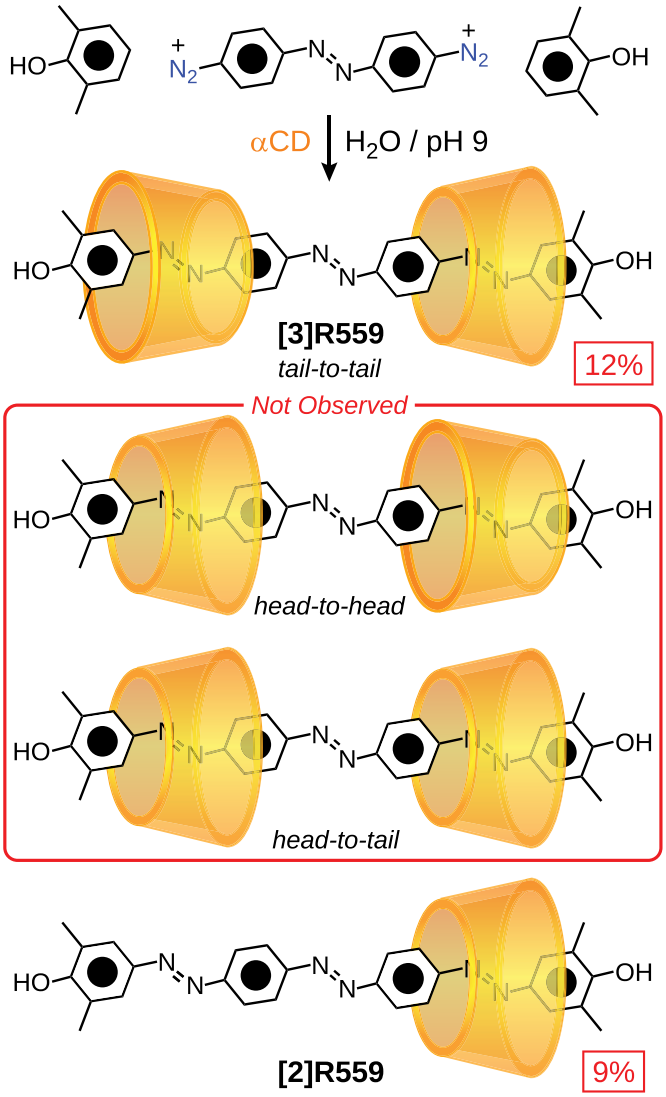


Figure 5.29 Stereoformulas of Ogoshi's [2]rotaxane and [3]rotaxane orientational isomers possessing planar chiral PA5 rings. The isomers possessing only ($S_PS_PS_PS_PS_P$)-Et_{10}PA5 and ($R_PR_PR_PR_PR_P$)-Et_{10}PA5 rings are obtained diastereoselectively. [256]



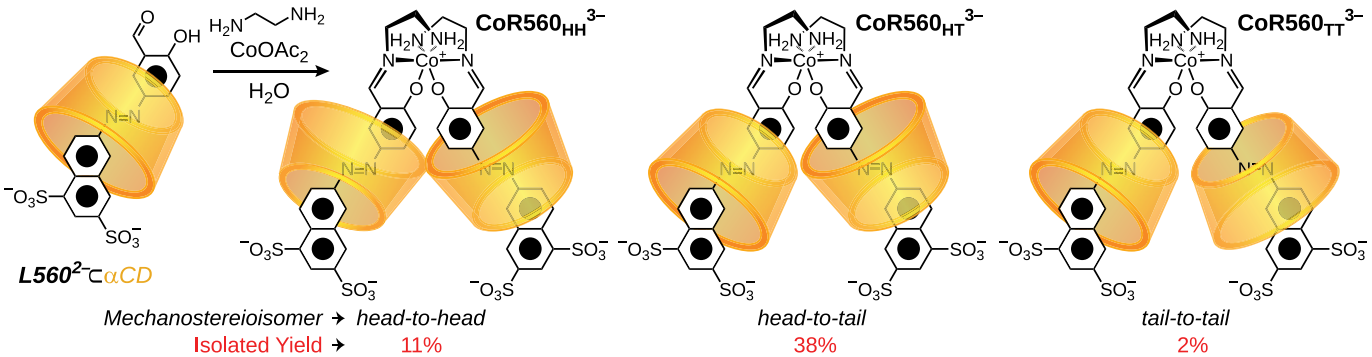
Scheme 5.23 Anderson's mechanostereoselective synthesis[265] of the *azo⊂αCD* [3]rotaxane **[3]R559**, which is obtained solely as the *Tail-to-Tail* orientational mechanostereoisomer among three possibilities.

An early example of orientational isomerism in [3]rotaxanes was described by Anderson,[265] whose synthesis (**Scheme 5.23**) of compound **[3]R559** from azo dye precursors and αCD happens to be mechanostereoselective in the sense that only one of three possible orientational isomers is obtained, along with the corresponding [2]rotaxane **[2]R559**, in yields of 12 and 9%, respectively. The [3]rotaxane **[3]R559** is obtained solely as the *tail-to-tail* isomer, in which the narrower primary faces (6-rims) of the cyclodextrin rings face inward toward one another with respect to the azo dumbbell, while the *head-to-head* and *tail-to-tail* isomers were not observed. A *head-to-tail* orientational isomer of an *oligophenylene(ethynylene)⊂(αCD)*$_2$ [3]rotaxane has been obtained[244] by Anderson's solid-phase synthetic protocol, while Tian[266] has also isolated a CD-based [3]rotaxane as a pure orientational mechanostereoisomer. In one case[267] of an aqueous αCD [3]rotaxane synthesis (**Scheme 5.24**) driven by metal-ligand assembly of the salicylaldehyde-functionalized pseudorotaxane ***L560***$^{2-}$*⊂αCD* with ethylene diamine and Co(OAc)$_2$, Anderson[267] was able to isolate all three orientational isomers—*head-to-head* **CoR560**$_{HH}^{3-}$ (11%), *head-to-tail* **CoR560**$_{HT}^{3-}$ (38%), and *tail-to-tail* **CoR560**$_{TT}^{3-}$ (2%)—by preparative anion exchange chromatography. The metal complex of **CoR560**$^{3-}$ is stabilized by the *in situ* oxidation of the Co^{II} template to Co^{III}, which locks the complex kinetically and prevents the isomers from undergoing exchange processes in solution. The corresponding Zn^{II} templated [3]rotaxane, by contrast, is kinetically labile.

Other Orientational Isomers

Orientational mechanostereoisomerism is also possible beyond the realm of [2]- and [3]rotaxanes. The seminal cyclodextrin [3]catenanes were isolated[196] as a 1:1 mixture of the two possible orientational isomers—see **Scheme 2.20** in **Section 2.3.1.1**. It is believed[268,269] that polyrotaxanes based on PEG and αCD also assemble with high mechanostereoselectivity into an arrangement with a repeating *head-to-head* / *tail-to-tail* orientational pattern. Other oligo- and polyrotaxanes—**see Section 4.2.1.1**—possessing desymmetrized rings, such as those based on pillar[*n*]arenes most likely exist as statistical mixtures of orientational isomers.

What are the research frontiers for orientational mechanostereoisomers? Recently, Hou, Meng, and Li[270] have shown that desymmetrized pillar[5]arene rings with rims differentiated by methoxy and pentoxy groups are threaded mechanostereoselectively—(see **Section 6.15.2.2**) by constitutionally asymmetric guests, rendering them suitable for the synthesis



Scheme 5.24 Anderson's chelation-driven synthesis[267] and isolation of all three orientational isomers of the azo/αCD [3]rotaxane **R558**$^{3-}$.

of analogous rotaxanes as single orientational isomers. These results indicate that a cone-shaped ring is not a prerequisite for orientational selectivity. We note that Ghadiri's biomolecular transmembrane rotaxanes (**Figure 2.84** in **Section 2.3.12.2**) are also assembled[271] exclusively as one orientational isomer. Although chirality is not a prerequisite for orientational isomerism, we speculate that the homochirality inherent to many biomolecules may render orientationally selective syntheses of mechanical bonds more likely in these systems. The foundations have been laid as well for another type of orientational isomerism arising from the different orientations that linear guests can adopt with respect to heterotopic macrobicyclic[272,273] or macrotricyclic[274] hosts.[275] The ability to control orientational mechanostereoisomerism may also be related to an ability to control directional motion in appropriately bistable or multistable systems—see **Section 6.15.2**.

5.2.2 Sequence Mechanostereoisomers

Sequence-defined polymers are a hallmark of biomolecules, such as DNA, RNA, and proteins. Only four nucleobases in various sequences encode the information that governs the structure and function of an entire organism. If two such molecules share identical molecular formulas, yet different sequences, they express a kind of constitutional isomerism. On the other hand, if two MIMs with identical molecular formulas possess component parts that are arranged in different sequences, their isomerism is not constitutional because the sequences are maintained by mechanical bonds rather than by covalent ones. Leigh[276] has suggested the term "sequence isomerism" to describe this kind of mechanostereoisomerism in MIMs. In his seminal publication[276] on this topic, he describes the minimum requirements (**Figure 5.30**) for sequence isomerism to be expressed in various multi-ring mechanically interlocked architectures. Rotaxanes and catenanes require at least three components in order to display sequence isomerism. [3]Rotaxanes[P] require a constitutionally asymmetric dumbbell and two non-equivalent rings, whereas larger [*n*]rotaxanes ($n \geq 4$) can express sequence isomerism even if they have symmetrical dumbbells, provided at least two of the rings are not identical. Any linear [*n*]catenane ($n \geq 3$) also requires only two non-equivalent rings. Symmetry considerations render the requirements more stringent for [*n*]catenanes of the 'molecular necklace' variety ($n \geq 4$). Sequence isomers of a [4]molecular necklace cannot have any identical rings and the central one must possess a kind of cyclodirectionality. Larger [*n*]molecular necklaces ($n \geq 5$), however, require no more than two differentiated peripheral rings, nor are there any symmetry requirements for the central ring. It may also be possible to uncover forms of sequence mechanostereoisomerism in other mechanically interlocked architectures (**Chapter 4**) such as dendritic rotaxanes and rotacatenanes, for example.

[P] Another possible situation that would be able to display sequence isomerism would be a [3]rotaxane comprising one constitutionally asymmetric ring and two non-equivalent dumbbells that are unable to exchange sites between their respective hemispheres of the host's cavity.

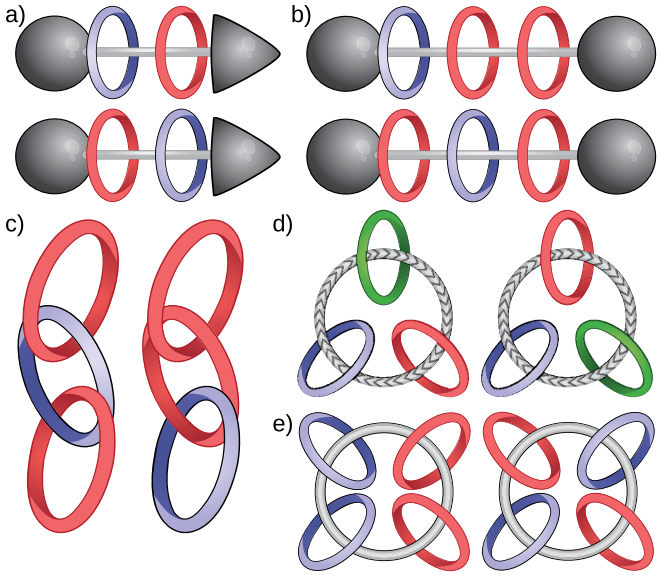
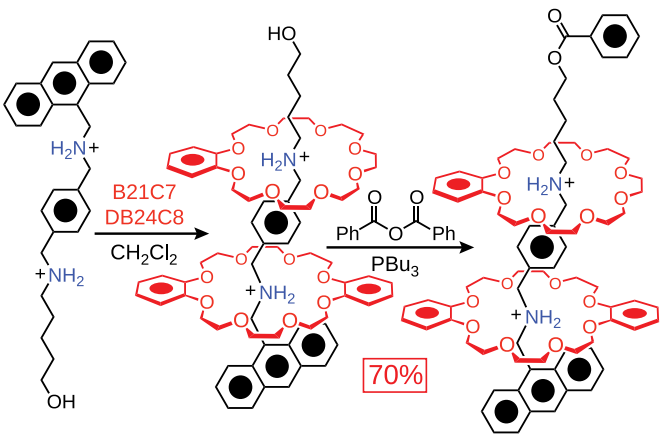


Figure 5.30 Graphical representations illustrating the minimum requirements for the expression of sequence isomerism in various multi-ring architectures.[276] (a) A [3]rotaxane with two non-equivalent rings (red and blue) must encircle an unsymmetrical dumbbell. (b) A symmetrical dumbbell is compatible with sequence isomerism in [*n*≥4]rotaxanes possessing at least two differentiated rings. (c) A linear [*n*]catenane chain ($n \geq 3$) requires no more than two non-equivalent rings. (d) A [4]catenane molecular necklace cannot exhibit sequence isomerism unless all three peripheral rings are differentiated with respect to a cyclodirectional central ring. e) [*n*] Molecular necklaces ($n \geq 5$) require no more than two different kinds of rings encircling a central ring.

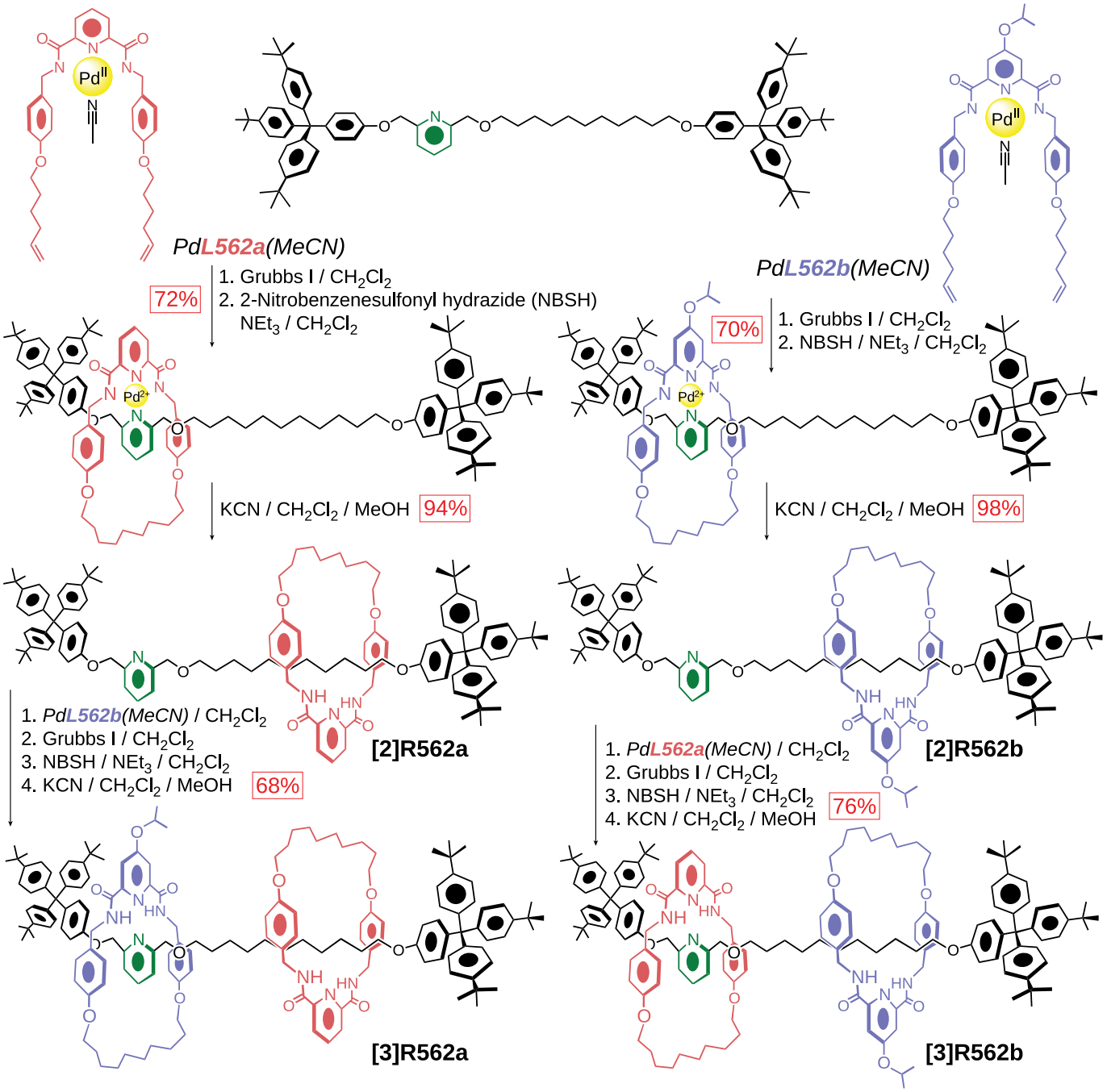
Although [3]rotaxanes possessing two non-equivalent rings—i.e., hetero[3]rotaxanes—have been reported[277–280] from as early as 1995, hetero[3]rotaxanes endowed with the possibility of expressing sequence isomerism by virtue of unsymmetrical dumbbells were not described until Schalley[281] began investigating the synthesis of rotaxanes from self-sorted[281–283] templates in 2008. Schalley's protocol (**Scheme 5.25**) relies on the



Scheme 5.25 Schalley's synthesis of the hetero[3]rotaxane **R561H$_2^{2+}$** as a single sequence isomer by integrative self-sorting.[281]

difference in cavity sizes between benzo[21]crown-7 (B21C7) and dibenzo[24]crown-8 (DB24C8). Whereas DB24C8 can easily slip over a *para*-phenylene unit, a phenyl group is bulky enough to act[284] as a stopper for B21C7. Thus, the semidumbbell **L561H$_2$$^{2+}$** was designed to possess two cationic dialkylammonium recognition sites separated by a *para*-xylylene linker, such that only the DB24C8 ring can access the –NH$_2$$^+$– center adjacent to the stopper. Consequently, the semidumbbell and the rings assemble in solution into a self-sorting hetero[3]-pseudorotaxane as a single complex, which is converted to the so-called 'cascade-stoppered' hetero[3]rotaxane **R561H$_2$$^{2+}$** by acylative end-capping of the terminal alcohol with benzoic anhydride.

When Leigh[276] introduced the concept of sequence isomerism in 2010, he synthesized (**Scheme 5.26**) a pair of the [3]rotaxane sequence isomers (**[3]R562a-b**) as a demonstration, employing a single-template olefin metathesis protocol similar to the one[285] described in **Section 3.4.1.1**. The [3]rotaxanes are prepared separately and the sequences are defined by the order of addition of the reactant macrocyclic precursors comprising olefin-terminated 2,6-dicarboxamidopyridine Pd^{II} chelates. These precursors, ***PdL562a****(MeCN)* and ***PdL562b****(MeCN)*, are differentiated



Scheme 5.26 Leigh's synthesis[276] of the [3]rotaxane sequence mechanostereoisomers **[3]R560a** and **[3]R560b**.

only by the functional group (R = H of O^{i}Pr, respectively) appended to their isophthalamide units. A pyridine recognition unit embedded in an asymmetric dumbbell displaces the MeCN ligand of these chelates before the Grubbs I catalyst is introduced as a clipping reagent, and the resulting mechanically interlocked macrocycles are subsequently hydrogenated to afford the [2]rotaxanes **[2]R562a** and **[2]R562b**. The Pd^{II} template is removed and the process is repeated once again with another precursor to afford the [3]rotaxanes **[3]R562a** and **[3]R562b** in 46 and 52% total yield over seven steps starting from ***PdL562a****(MeCN)* and ***PdL562b****(MeCN)*, respectively. The sequences of these rotaxanes are maintained mechanically because the rings are not large enough to pass each other while encircling the dumbbell.

Sequence isomerism in mechanically bonded architectures other than [3]rotaxanes is largely unexplored territory. Although there are plenty examples of hetero[3]catenanes (see refs. 29, 41, 43, 46, 66, 69, 177, 194, 196, 286-306), linear hetero[*n*≥4]catenanes (see refs. 29, 41, 43, 291, 293, 294), and hetero[*n*≥4]rotaxanes[307–309] in the literature, they have always been isolated as single sequence isomers. Radial [*n*]catenane molecular necklaces[303,310–319] have also remained elusive as sequence isomers because they have always possessed identical peripheral rings. In other words, exercising sequence control over most multicomponent MIMs beyond [3]rotaxanes remains a standing challenge in mechanostereochemistry.

Sequence isomerism can also be expressed in supramolecular systems such as pseudorotaxanes. Gaeta, Schalley, and Neri[262] have recently assembled pseudo[3]rotaxanes based on combinations of OMe_6CA6 and *p-tert*-butyl-functionalized OMe_6CA6 rings that self-sort with an asymmetric thread into a single heteroternary complex. Among the possible products (**Figure 5.31**) are four sets of four orientational isomers, eight of which are heteroternary complexes belonging to either of two possible sequence isomers.

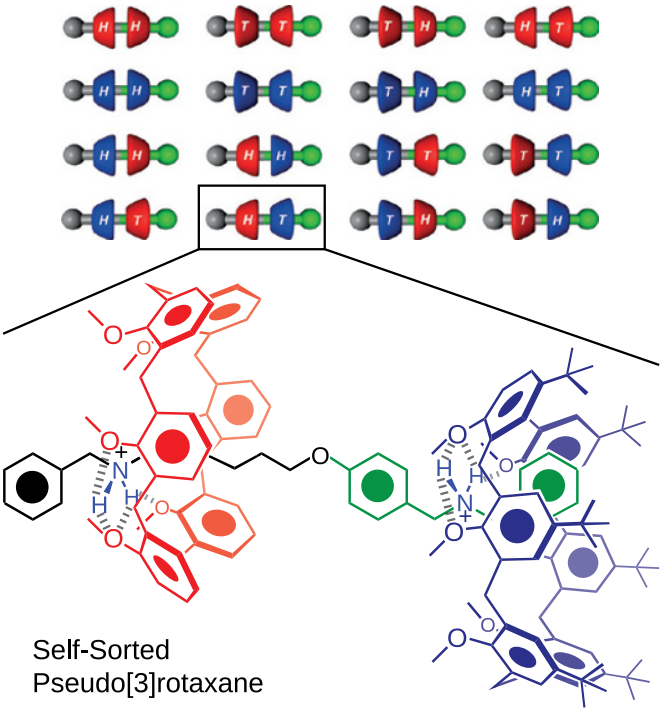


Figure 5.31 Stereoformula of a heteroternary pseudo[3]-rotaxane that self-assembles as a single complex in a head-to-tail orientation with high sequence selectivity among the 16 possible ternary assemblies.[262] Cartoon representations of the 16 possible pseudo[3]rotaxanes are reproduced with permission from ref. 262 (copyright 2013 Wiley).

5.2.3 Mechanically Chiral Mechanostereoisomers

Louis Pasteur's discovery[320] of the optical activity of certain organic compounds, i.e., their ability to rotate linearly polarized light, his inference of their basis in molecular asymmetry, and his isolation of the (*R*) and (*S*) enantiomers of tartaric acid in 1848, marked the birth of stereochemistry. These properties arising from molecular chirality were explained by Le Bel[321] and van't Hoff[322] as a consequence of the tetrahedral arrangement of inequivalent functional groups surrounding a carbon atom. Lord Kelvin[323] coined[324,325] the term *chirality* in 1893, defining it as a property of an object "*if its image in a plane mirror, ideally realized, cannot be brought to coincide with itself,*" i.e., an object possessing a non-superimposable mirror image. Every chemistry student learns about the chirality of tetrahedral centers possessing four nonequivalent substituents. Beyond the chirality of stereogenic centers, other forms of chirality in covalently bonded molecules include (i) planar chirality, which involves the spatial arrangement of out-of-plane groups with respect to a plane of chirality. (ii) axial chirality, in which four groups are arranged in pairs about an axis of chirality, and (iii) helical chirality, which is associated with the helicity of molecules possessing chiral propeller or screw-like geometries.

Two competing schools of thought surround the subcategorization of chirality. One side recognizes that the different stereochemical labels for chirality are somewhat superficial, since symmetry may be considered a global property of a molecular system, yet the other side recognizes them as useful insofar as they illuminate the different structural features—e.g., centers, planes, axes, etc.—that give rise to chirality in molecules, and provide chemists with much-needed stereodescriptors—e.g., *R* and *S*, *M* and *P*, Δ and Λ, *re* and *si*, etc.– for defining absolute stereochemistry. Citing a handful of examples, many MIMs possessing elements of covalent chirality about centers,[23,326–339] planes,[9,256,340–343] and axes[48,344–354] have been reported, as well as MIMs possessing elements of helical chirality within their component parts.[355–360] Takata[361,362] has even observed the transfer of chirality through the mechanical bond, from the axially chiral units in the rings of rotaxane side-chains to the helicity of a polyacetylene backbone. A non-classical form of chirality associated with the curvature of concave molecules, known[363–365] as inherent chirality, has also appeared[264] in the component parts of a MIM—see **Figure 2.67a** in **Section 2.3.6.4**, as well as **Table 5.11** and **Figure 5.34** in **Section 5.2.3.1**.

It is also possible for non-classical forms of chirality to be expressed as a direct result of the spatial arrangements

of component parts entangled in mechanical bonds. The types of chirality available to molecules with mechanical bonds include mechanically planar chirality (**Section 5.2.3.1**), mechanically axial chirality (**Section 5.2.3.2**), and mechanically helical chirality (**Section 5.2.3.3**), as well as topological chirality, which is discussed in **Section 5.2.4.1**. Since covalent chirality is beyond the scope of this book, we confine our discussion only to these mechanical and topological forms of chirality in MIMs. In the tradition[7] of employing the prefix 'co-' as a means of distinguishing covalent stereochemistry from supramolecular and mechanostereochemistry, as in the case (**Section 5.1**) of conformation versus co-conformation, we propose the term 'co-configuration' to be employed for describing the absolute (mechano)stereochemistry surrounding a mechanical bond.

Configuration[2]—The spatial arrangement of atoms in a molecular entity that distinguishes stereoisomers, the isomerism between which is not attributable to conformation differences. Absolute configuration is the stereochemical description of a chiral molecular entity, while relative configuration is the stereochemical description of a stereogenic center with respect to another stereogenic center in the same molecule.

Co-Configuration—The spatial arrangement of component parts engaged in mechanical bonding that give rise to mechanostereoisomerism, which is not attributable to co-conformation differences, but rather to differences in the expression of chirality.

5.2.3.1 Mechanically Planar Chirality

The mechanical bond allows molecules to exhibit chirality even if none of the component parts exhibit chirality in and of themselves. For example, the combination of a constitutionally asymmetric dumbbell and an oriented[Q] ring can give rise to a pair of enantiomeric [2]rotaxanes, owing to the two different orientations that the ring and dumbbell can adopt with respect to each other. When both component parts possess these directional atom sequences in their constitution, their mirror images are non-superimposable. Borrowing from the vernacular of Prelog,[366] Schill[367] has referred to these types of MIMs as cyclochiral. Vögtle[368–372] has adopted the same vocabulary in discussing 'cycloenantiomers' and 'cyclodiastereomers' of rotaxanes. This language may be misleading, however, since cycloenantiomers are, strictly speaking, cyclic molecules constituting[373] a rotationally directional sequence of atoms and multiple sites of asymmetry. After Takata[374] described the chirality of sequence-directional rotaxanes as a form of planar chirality, Goldup[375] proposed the term 'mechanically planar' in order to distinguish planar chirality associated with a mechanical bond from more classical forms of planar chirality. In Goldup's notation, the right-handed and left-handed co-configurations of mechanically planar rotaxanes are written as (R_{mp}) and (S_{mp}), respectively, with the subscript 'mp' denoting mechanically planar chirality. Taking the example (**Figure 5.32**) of a mechanically planar [2]rotaxane, assignment of absolute co-configuration involves prioritizing the atoms in the constitution of the ring and dumbbell according to the Cahn-Ingold-Prelog[324] convention in order to establish an arrow of directionality within each component part, from the highest-priority atom to the highest-priority point of difference among its ligands that belong to the sequence of atoms constituting the component part. The (R_{mp}) co-configuration is assigned to rotaxanes in which the arrow of the ring is disposed in a clockwise direction when viewed down the arrow of the dumbbell, while the (S_{mp}) co-configuration is assigned to the corresponding enantiomer in which the ring is disposed in an anticlockwise direction.

Planar chirality[2]—Term used by some authorities to refer to stereoisomerism resulting from the arrangement of out-of-plane groups with respect to a plane. The configuration of molecular entities possessing planar chirality is specified by the stereodescriptors R_P and S_P (or *P* and *M*).

Mechanically planar chirality[375]—Mechanostereoisomerism resulting from the different relative orientations of (a) rotationally unsymmetrical ring(s) and axle(s) with two non-equivalent ends.

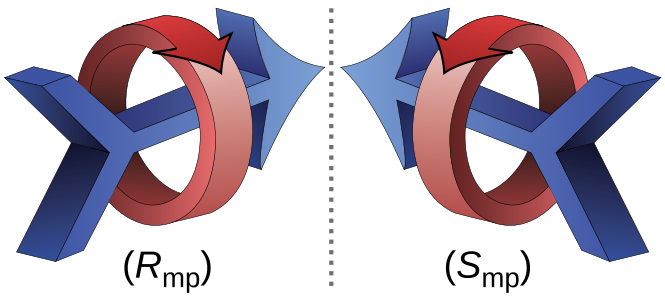


Figure 5.32 Assigning the absolute co-configuration of the enantiomers of mechanically planar[375] [2]rotaxanes. The arrowhead in each unsymmetrical component part represents the direction from the highest priority atom to the adjacent highest priority point of difference, according to the Cahn-Ingold-Prelog[324] sequence rules. The ring of right-handed (R_{mp}) enantiomers exhibits a clockwise directionality with respect to the dumbbell, while that of the (S_{mp}) enantiomer exhibits anticlockwise directionality.

[Q] An oriented ring has sufficiently reduced symmetry to cause the expression of some form of (mechano)stereoisomerism. In the context of orientational isomers (**Section 5.2.1**), the ring must lack mirror symmetry across the plane of its cavity. In the context of mechanically planar isomers, as well as topological isomers (**Section 5.2.4**), an oriented ring possesses a kind of rotational asymmetry, lacking mirror symmetry across any plane perpendicular to that of the cavity.

Mechanically Planar [2]Rotaxanes

Although Schill[367] described the possibility of "cycloenantiomeric" rotaxanes as early as 1971, they were not prepared synthetically until 1996, when Vögtle[368,369] introduced sulfonamide groups into his lactam-based hosts and employed them to make mechanical bonds. The [2]rotaxane **R563** incorporates (**Figure 5.33**) single sulfonamide units into each of its component parts, such that a pair of mechanically planar enantiomers are generated during its synthesis by a standard clipping protocol. Vögtle[369] also separated the two enantiomers **(R_{mp})-R563** and **(S_{mp})-R563** using chiral stationary phase high-performance liquid chromatography (chiral HPLC), and applied the same chiral separations methodology to [1]rotaxanes,[372] [2]catenanes,[369] and pretzelanes[369] possessing similar forms of chirality associated with their mechanical bonds—see also **Section 5.2.4.1**. The enantiomers eluted from the chiral stationary phase with baseline separation. Although the absolute co-configurations were not assigned, the chirality of each pure enantiomer was verified by analysis of their circular dichroism and optical rotation properties. Although Vögtle[328] has also prepared mechanically planar chiral [2]rotaxanes as diastereoisomers by virtue of their chiral tetrabenzoyl-β-D-glucopyranosyl stoppers, their separation into enantiopure mechanostereoisomers was not reported.

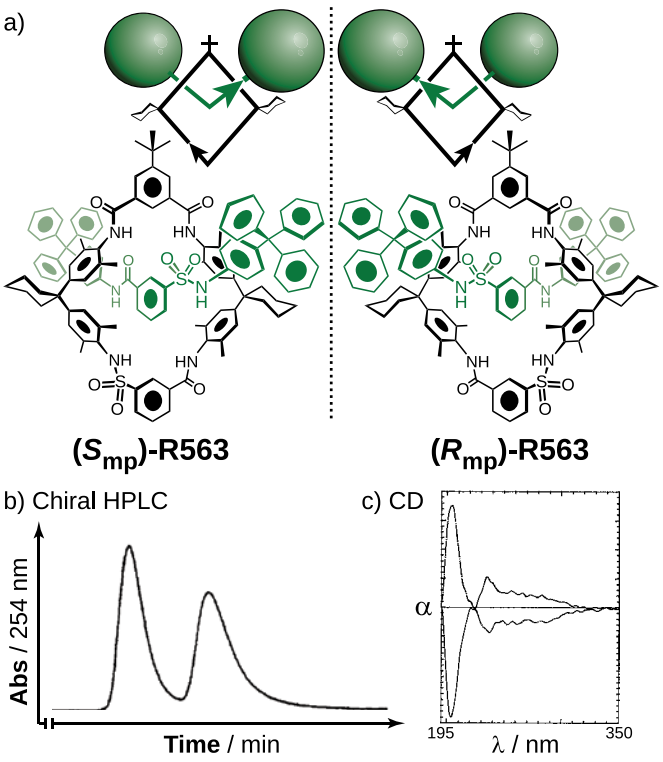


Figure 5.33 Vögtle's mechanically planar [2]rotaxane **R563**.[369] (a) Stereoformula of **R563**, which exists as a pair of (S_{mp}) and (R_{mp}) enantiomers on account of the mechanical bond between a linearly and rotationally unsymmetrical dumbbell and ring, respectively. (b) HPLC chromatogram of the racemate of **R563** on a chiral stationary phase, leading to resolution of the two enantiomers. (c) Circular dichroism (CD) spectra of each purified enantiomer, revealing mirror-image optical rotation. Data reproduced with permission from ref. 369 (copyright 1997 American Chemical Society)

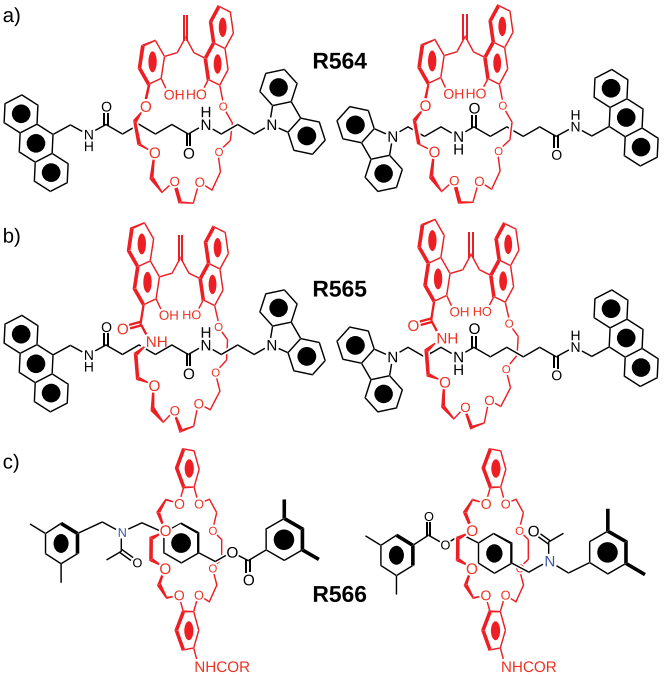
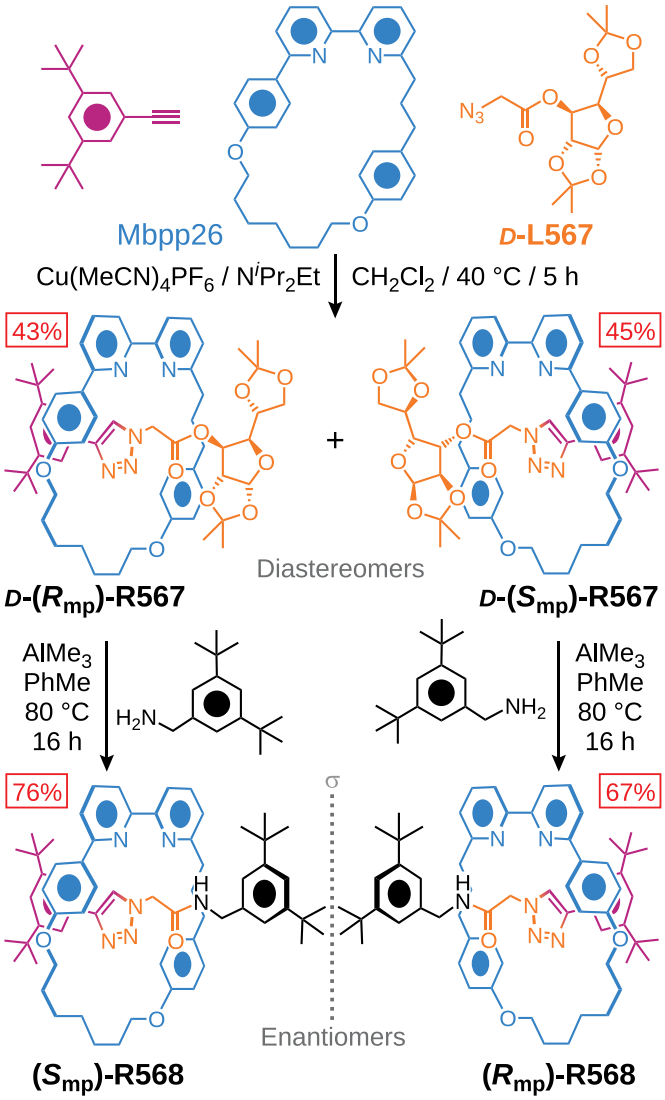


Figure 5.34 Stereoformulas of mechanically planar [2]rotaxanes based on rotationally unsymmetrical crown ethers, which exist as pairs of (S_{mp}) and (R_{mp}) enantiomers. (a) **R564**.[376] (b) **R565**.[377] (c) **R566**.[374] All of these compounds were prepared as racemates and resolved by chiral HPLC.

Several mechanically planar rotaxanes (**Figure 5.34**) based on rotationally unsymmetrical crown ethers and directional dumbbells have also been reported.[374,376,377] The [2]rotaxanes **R564** and **R565**, which were introduced by Hiratani[376,377] using a covalent-directed capture protocol (**Section 2.2.2**), were prepared (**Figure 5.34a–b**) as racemates. The racemate has been separated in each case into the corresponding mechanically planar enantiomers by chiral HPLC. **R565** has been shown[377] to 'sense' the chirality of amino acids, since one of its enantiomers interacts selectively with L-phenylalaninol. Takata[374] has prepared (**Figure 5.34c**) the racemate of the [2]rotaxane **R566** by *dialkylammonium⊂crown* template-directed synthesis (**Section 2.3.4.6**), and resolved the mechanically planar enantiomers by chiral HPLC. A similar kind of mechanically planar isomerism is expressed[378–381] in a number of [*c*2] daisy chains based on crown ethers and dialkylammonium cations.

Recently, Goldup[375] has devised a method for producing mechanically planar [2]rotaxanes in high enantiopurity without the use of chiral HPLC separation techniques. His approach (**Scheme 5.27**) combines active copper template synthesis (**Section 2.4.1**) with the use of a chiral auxiliary—namely, the stopper precursor **D-L567**—with the cyclodirectional ligand Mbpp26 in order to produce a 1:1 mixture of the diastereoisomeric [2]rotaxanes **D-(R_{mp})-R567** and **D-(S_{mp})-R567**, which are separable by conventional normal



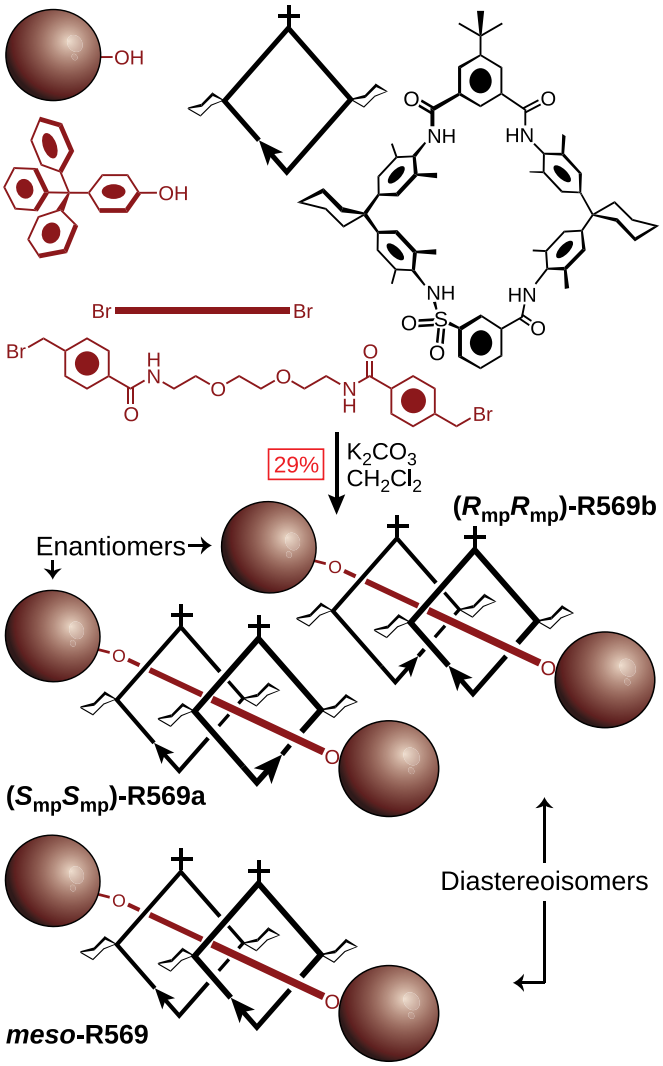
Scheme 5.27 Goldup's efficient synthesis[375] of the mechanically planar [2]rotaxanes **(*R*$_{mp}$)-R568** and **(*S*$_{mp}$)-R568** in high enantiopurity by a novel route involving displacement of a chiral auxiliary stopper derived from **D-L567** in the diastereomeric precursors **D-(*R*$_{mp}$)-R567** and **D-(*S*$_{mp}$)-R567**, which are separable by ordinary chromatography techniques following their capture by the rotationally unsymmetrical macrocyclic ligand Mbpp26 during active metal template synthesis. The absolute co-configurations of each compound were assigned based on single-crystal X-ray structures of both diastereoisomers of **R567**.

phase chromatography. These diastereoisomers were obtained as single crystals and characterized in the solid state by X-ray crystallography in order to assign their absolute co-configurations unambiguously. The chiral auxiliaries were substituted subsequently by an achiral 3,5-di-*tert*-butylbenzylamine stopper in order to obtain the corresponding mechanically planar enantiomers **(*S*$_{mp}$)-R568** and **(*R*$_{mp}$)-R568**, respectively, as pure compounds after another round of normal phase chromatography. The stopper exchange reverses the directionality of the dumbbell according to Cahn-Ingold-Prelog[324] sequence rules, which explains why the (*S*$_{mp}$) enantiomer of **R568** is derived from the (*D*,*R*$_{mp}$) diastereoisomer of **R567**, while the (*R*$_{mp}$) enantiomer is derived from the (*D*,*S*$_{mp}$) diastereoisomer. The optical purities (>99% ee) of **(*S*$_{mp}$)-R568** and **(*R*$_{mp}$)-R568** were verified by analytical chiral HPLC and circular dichroism. This chiral auxiliary strategy for synthesis and purification of mechanically planar mechanomolecules is promising,[382] not only because it should render other types of mechanically planar rotaxanes more accessible, but also because it will support the possibility of scale-up and potential applications involving chiral sensing, asymmetric catalysis, and building molecular machines see **Section 6.15**.

Several of the [2]rotaxanes we introduced in the context of orientational mechanostereoisomerism (**Section 5.2.1**) also possess mechanically planar chirality. For example, cyclodextrin-based [2]rotaxane orientational isomers express mechanically planar chirality on account of the cyclodirectional polarity of their glucopyranose linkages. Thus, the CD-based [2]rotaxanes **R545^{3-}–R553** in **Figure 5.28**, **Section 5.2.1** may all be counted among those expressing mechanically planar chirality. One could argue that pillar[*n*]arene orientational isomers, such as the [2]- and [3]rotaxanes **R557^{+}** and **R558^{2+}** described in **Figure 5.29**, **Section 5.2.1**, also exhibit mechanically planar chirality, since an arrow of cyclodirectionality may be assigned to the PA5 rings, disposed in the direction of the skew lines that can be used to assign their configurations. Since the PA5 rings are already chiral in and of themselves, however, the mechanically planar designation does not offer any extra information about the chirality of these compounds.

Mechanically Planar [3]Rotaxanes

In 1999, Vögtle[370] prepared (**Scheme 5.28**) the [3]rotaxane **R569** by threading two rotationally unsymmetrical lactam/sulfonamide rings onto a symmetrical dumbbell using the anion-templated nucleophilic capture method summarized in **Section 2.3.6.1**. The presence of two rings on the dumbbell enables the expression of mechanically planar chirality involving a pair of enantiomers, as well as a corresponding *meso*-isomer, which is not chiral. The two chiral enantiomers **R569a** and **R569b** were resolved and separated from ***meso*-R569** by chiral HPLC. Although the absolute co-configurations were not assigned, the (+) and (–) enantiomers were found to rotate polarized light, confirming their chirality and enantiopurity. The isomer ***meso*-R569**, by contrast, is not optically active. In 2006, the sulfonamide groups of these rotaxanes were conjoined[383] with covalent linkers in order to prepare so-called 'bonnanes' (**Section 4.2.3.4**) which also exhibit cyclochirality. More recently, Flood[264] reported on the synthesis of a [3]rotaxane derived from the inherently chiral cyanostar macrocycle (**Section 2.3.6.4**), which is also obtained as a mixture of orientational isomers / mechanically planar enantiomers and the corresponding *meso* diastereoisomer.



Scheme 5.28 Vögtle's nucleophilic capture synthesis of the [3]rotaxane **R569** from a rotationally unsymmetrical wheel and symmetrical dumbbell precursors results in the formation of two enantiomers, as well as the corresponding *meso* diastereomer, in a statistical 1:1:2 ratio.[370]

5.2.3.2 Mechanically Axial Chirality

As it is defined[2] in the IUPAC Gold Book, axial chirality refers to a situation when two pairs of functional groups are disposed in a non-planar arrangement relative to an axis passing through each pair. Following Goldup's lead on the use of the prefix, 'mechanically', as a means of distinguishing planar chirality associated with mechanical bonds from that of covalent ones, we propose to describe MIMs possessing axial chirality about a mechanical bond as having 'mechanically axial chirality'. The mechanical bond can act as a source of mechanically axial chirality when the 'mechanostereogenic' pairs of chemically inequivalent substituents belong to

Axial chirality[2]—Stereoisomerism resulting from the non-planar arrangement of four groups in pairs about a chirality axis. It is exemplified by allenes abC=C=Ccd (or abC=C=Cab) and by the atropisomerism of *ortho*-substituted biphenyls

Mechanically axial chirality—Mechanostereoisomerism resulting from the non-planar arrangement of four groups in pairs about an axis of chirality that passes through a mechanical bond, as a result of the pairs belonging to different component parts of a mechanomolecule

Mechanostereogenic—Four or more atoms or substituents of a mechanomolecule are *mechanostereogenic* if their non-planar arrangement in space is a topological and/or Euclidean consequence of the presence of a mechanical bond.

The absolute co-configuration of axially chiral catenanes may be assigned (**Figure 5.35b**) in a manner analogous to the assignment (**Figure 5.35a**) of configuration in axially chiral allenes, for example. First, each of the four substituents terminating the axis of chirality—call them a, b, c, and d—are ranked according to the Cahn-Ingold-Prelog[324] priority rules in a pairwise manner. The adjacent substituents ab and cd are ranked such that a>b and c>d. When viewed down the axis of chirality, the sequence a→b→c→d appears to follow a clockwise path in the case of an (*R*) enantiomer, while it follows an anticlockwise path in the case of an (*S*) enantiomer. The chirality is defined precisely by the direction of b→c, since a and b are coplanar, as are substituents c and d. Since the subscript 'a' is employed to denote axial chirality in the stereochemical labels (R_a) and (S_a), the mechanically axial chirality of catenanes may be denoted by 'ma' subscripts, furnishing the labels (R_{ma}) and (S_{ma}). These suggestions are consistent with the precedent established by Goldup[375] regarding mechanically planar chirality—see **Section 5.2.3.1**.

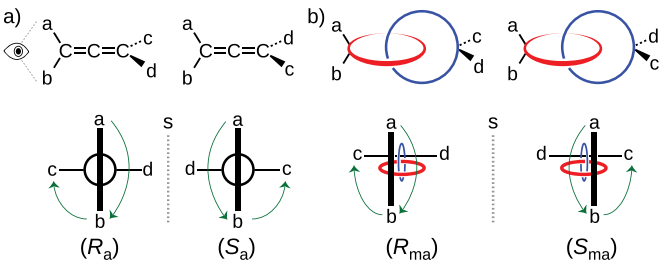


Figure 5.35 A comparison between a) the assignment of configuration in allenes exhibiting axial chirality, versus b) the assignment of co-configuration in [2]catenanes exhibiting mechanically axial chirality. When viewed down the axis of chirality, which passes through covalent bonds in the case of allenes or a mechanical bond in the case of catenanes, the 'near' and 'far' substituents are ranked in pairs (a>b, c>d) according to Cahn-Ingold-Prelog[324] priority rules. From this down-the-axis view, the stereochemical labels (*R*) and (*S*) are assigned to molecules in which the sequence (a→b→c→d) of substituents are disposed in a clockwise or anticlockwise manner, respectively, while the subscripts 'a' or 'ma' denote axial or mechanically axial chirality, respectively,

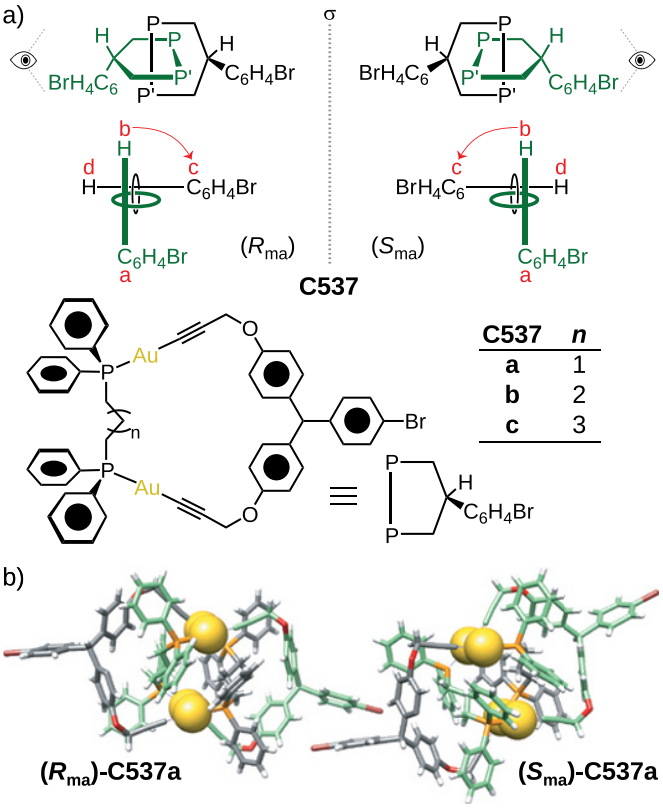


Figure 5.36 The mechanically axial chirality of Puddephatt's aurophilic [2]catenanes[384] possessing *p*-bromophenyl "hinge groups". (a) The structural formula of the organometallic Au^{I} metallacycle and graphical representations of the corresponding homo[2]catenanes **C537a-c** reveal how absolute co-configuration is assigned to the pairs of enantiomers, which result from the two possible arrangements of thr hinge groups with respect to an axis of chirality passing through the mechanical bond. (b) Tubular representation of the solid-state (super)structure of **C537a**, which crystallizes as the racemate of (R_{ma}) and (S_{ma}) enantiomers.

Credit must be attributed to Puddephatt[384] for introducing mechanically axial chirality in the form (**Figure 5.36**) of the organometallic homo[2]catenanes **C537a-c**, in which each of the digold(I) acetylide metallacycles are functionalized with *p*-bromophenylmethylene "hinge groups" that protrude outward orthogonally to the plane of their ring's cavity. When the metallacycles become interpenetrated, the corresponding catenanes can adopt either of two enantiomeric co-configurations (**Figure 5.36a**) defined by the relative arrangement of these hinge groups with respect to an axis of chirality passing through the mechanical bond. Although the rings are constitutionally symmetrical, they are both desymmetrized by the presence of these one-sided *p*-bromophenyl hinge groups, such that they also meet the criteria for conditional topological chirality (**Section 5.2.4.1**), which arises from in-plane substituent differences rather than out-of-plane ones. For example, the two phosphorus centers of the phosphine ligands, which are equivalent in the non-interlocked Au^{I} metallacycles, are not equivalent in the catenanes, as reflected by the P and P´ labels in the graphical representations. Indeed, the non-equivalence of these atoms was confirmed by ^{31}P NMR spectroscopy. The mechanically axial chirality of these catenanes can also be observed (**Figure 5.36b**) in the solid-state (super)structure, obtained by X-ray crystallography, of **C537a**, which crystallizes as the racemate of (R_{ma}) and (S_{ma}) enantiomers. We have assigned (**Figure 5.36b**) the absolute co-configuration of each enantiomer in the crystal. To our knowledge, attempts to resolve the (R_{ma}) and (S_{ma}) enantiomers on chiral stationary phases and characterize the optical rotation dispersions of mechanomolecules expressing mechanically axial chirality have not been reported.

Marinetti[333] has described a Cu^{I} metallo[2]catenane, **CuC538^{+}**, which also exemplifies (**Figure 5.37**) the concept of mechanically axial chirality. **Cu538^{+}** is a homo[2]catenate, the rings of which comprise dpp ligands and a polyether loop possessing two stereogenic (*S*) carbon centers and a prochiral phenyl phosphine oxide group. The presence of the prochiral centers in each ring causes **CuC538^{+}** and its demetallated counterpart **C538** to exist in pairs of (R_{ma})-(*SSSS*) and (S_{ma})-(*SSSS*) diastereoisomers. The assignment of absolute co-configuration of the metallo-catenane is illustrated in **Figure 5.37**. The (R_{ma}) and (S_{ma}) mechanostereoisomers of the demetallated species **C538** were separated by preparative RP-HPLC, suggesting that the introduction of covalent stereogenic centers is a convenient strategy for enabling the separation of mechanostereoisomers possessing unconventional forms of chirality, without the need for chiral stationary phases.

We note that Fujita's seminal ultramacrocyclic bis[2]catenane[385]—illustrated in **Figure 4.42** in **Section 4.1.4.4**—also possesses pairs of prochiral centers appended to each of the rings of the catenated moieties, which most likely generates enantiomeric and diastereoisomeric mixtures of mechanostereoisomers displaying mechanically axial chirality.

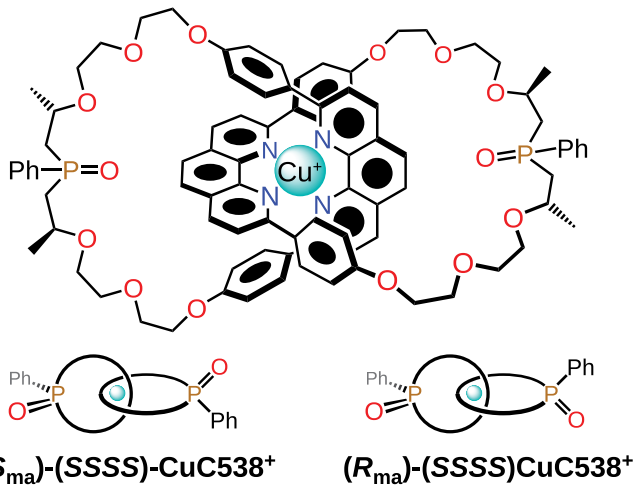


Figure 5.37 Stereoformula of Marinetti's metallo[2]catenane **CuC538^{+}**, which exists as a pair of diastereomers owing to the presence of four stereogenic (*S*) carbon centers, combined with the mechanically axial chirality of the link afforded by the prochiral phosphine groups within each ring.[333]

5.2.3.3 Mechanical Helicity

We will refer to molecules possessing helicity about a mechanical bond as having *mechanical helicity*. Since helicity is already broadly defined to encompass all molecular entities exhibiting helically chiral geometries, the prefix 'mechanical' is, admittedly, extraneous—however, the descriptor may be useful insofar as it attributes the helicity of a molecule to a mechanical bond. In our view, any molecule exhibiting helical chirality may earn the 'mechanical' prefix if the mechanical bond is involved, causally and/or structurally, in the emergence of helicity.

Helicity[2]—The chirality of a helical, propeller, or screw-shaped molecular entity

Mechanical Helicity—Helicity arising from the causal or structural influence of a mechanical bond.

Sauvage[386] noticed in 1987 that a Cu^{I} homo[2]catenate **CuC539**$^{+}$ comprising sterically crowded 27-membered dpp-based endocyclic chelates exhibits (**Figure 5.38**) mechanically helical chirality, owing to the helicity of the ligands surrounding the Cu^{I} center. The chirality of the catenate was inferred by the observation of diastereotopically induced signal separation in the ^{1}H NMR spectrum upon addition of a chiral shift reagent. Whereas Sauvage's original homo[2]catenate[387] (**Section 2.3.2.1**) comprising 30-membered rings inverts helicities rapidly (ΔG_c = 7.7 kcal·mol^{-1}) on the ^{1}H NMR timescale above temperatures of –95 °C, the smaller 27-membered rings of **CuC539**$^{+}$ undergo helical inversion slowly (ΔG_{433} > 25 kcal·mol^{-1}) on the ^{1}H NMR timescale even above 160 °C, owing to the highly crowded environment provided by the ligands around the Cu^{I} center, enforced by the steric constraints of the relatively small interlocked rings. The situation for the helical $Cu(dpp)_2^{+}$ center of the [2]catenate **CuC539**$^{+}$ is reminiscent of atropisomersm, since steric strain hinders the torsions that would lead to helix inversion. We feel that 'mechanical helicity' is an appropriate descriptor for this compound's chirality because the steric barrier that prevents dynamic helical inversion is a direct consequence of mechanical bonding.

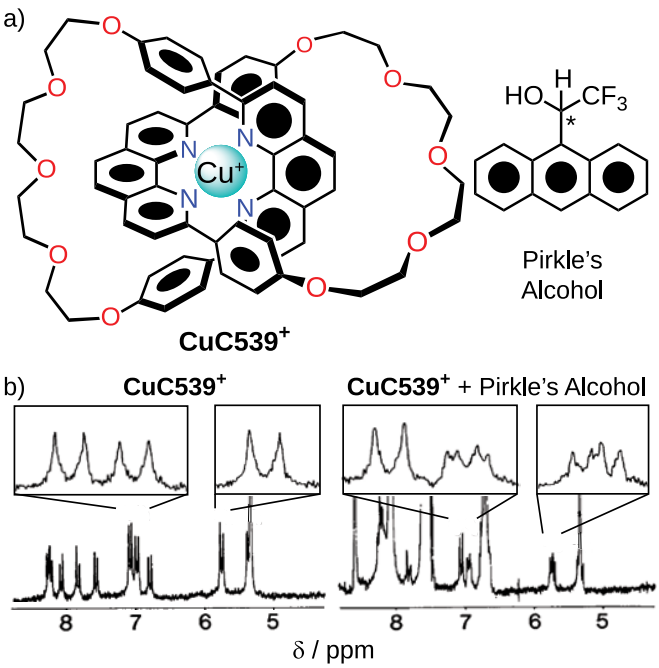


Figure 5.38 Sauvage's mechanically helical [2]catenate.[386] (a) Stereoformulas of **CuC539**$^{+}$ and the chiral shift agent, Pirkle's alcohol. (b) Partial ^{1}H NMR spectrum (200 MHz, CD_2Cl_2) of **CuC539**$^{+}$ before and after the addition of Pirkle's alcohol, revealing a splitting of signals attributable to the helicity of the ligands around the Cu^{I} center. Data reproduced with permission from ref. 386 (copyright 1987 Elsevier).

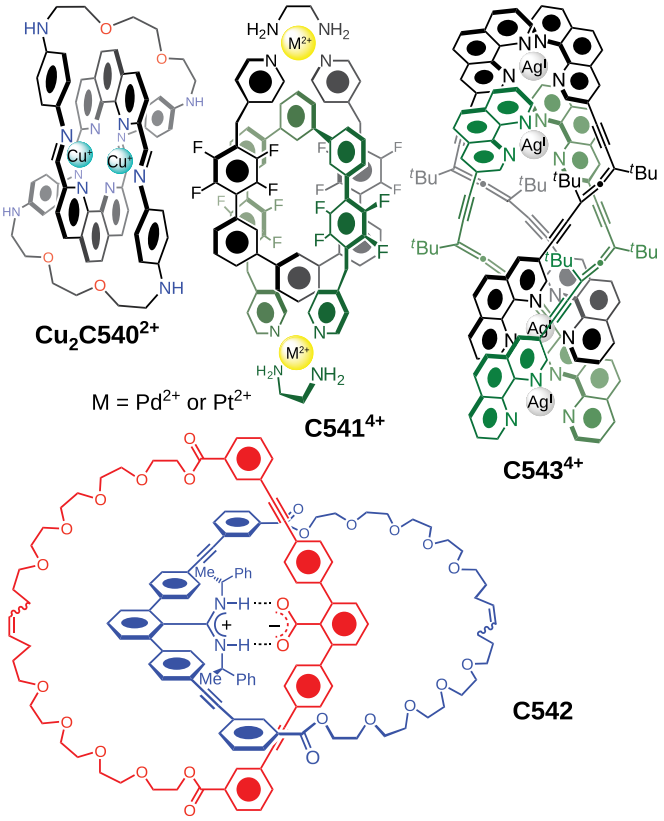


Figure 5.39 Examples of [2]catenanes possessing elements of mechanically helical chirality which 'live on' from the corresponding entwined templates. The mechanical bonds of the [2]catenate[388] **Cu_2C540**$^{2+}$ and the Ag^{I}-bridged [2]catenane[391] **C543**$^{4+}$ originate from metallo-helicate templates, while **C541**$^{4+}$[389] and **C542**[337] possess helicity arising from entwined templates possessing oligophenylene moieties, the helical stacking of which is driven by hydrophobic and ion-pairing interactions, respectively.

Since helical assemblies are often employed as templates in the synthesis of mechanical bonds via the 'entwining' approach—see **Section 2.3.2.1**—MIMs possessing elements of helical chirality around their mechanical bonds are not uncommon. A few examples of MIMs in which the helicity 'lives on' from the corresponding entwined helical templates are illustrated in **Figure 5.39**. Even though the mechanical bond's contribution to the helicity of these compounds is not always essential, it is at least causally and/or structurally involved,

according to our definition of mechanical helicity. The examples include Nitschke's [2]catenate[388] **Cu_2C540^{2+}** self-assembled from dinuclear Cu^{I} helicates (**Section 3.4.1**), Fujita's self-assembled metallosupramolecular [2]catenane[389] **$C541^{4+}$** possessing oligo(*m*-phenylene) double helices (**Section 3.3.1.1**), and the ion-paired amidinium-carboxylate helical template (**Section 2.3.7.1**) underpinning the assembly of the [2]catenane **C542** introduced by Furusho and Yashima.[337] Beer's anion-binding catenated strapped porphyrins[390] described in **Section 2.3.6.2**, **Figure 2.62**, also exhibit helicity that is evident in their solid-state structures. Diederich's recently introduced[391] homochiral [2]catenanes and bis[2]-catenanes derived from alleno-acetylenic helicates—e.g., **$C543^{4+}$**—represent a very robust form of mechanical helicity, which is maintained by 'narcissistic self-sorting' of Ag^{I}-cornered metallacycles—see **Section 3.2.2.2**. We note also that MIMs derived from linear double helicates, such as Sauvage's Solomon Link—see **Section 5.2.4.1**—as well as circular double helicates, including the Pentafoil Knot,[392,393] (**Figure 1.25, Section 1.3.2**) Solomon Link[394] (**Section 4.1.1.1**), and Star of David[395] (**Section 4.1.1.2**) catenanes introduced by Leigh, also retain the helicity of their templates, as do the triply interlocked cages (**Scheme 4.19, Section 4.1.3.3**) held together by helical coordination complexes introduced by Hardie.[396]

Although we have categorized mechanical helicity as a static form of mechanostereoisomerism, it remains possible to invert mechanical helicity by dynamic processes. For example, the oligophenylene double helix underpinning the mechanical bond of the metallosupramolecular [2]catenane **$C541^{4+}$** may be inverted by a flipping motion that transposes the aromatic units engaged in π-stacking interactions. Dynamic mechanical helicity can also arise in MIMs that are not derived from helical templates. Recognizing[397] that the rocking process (**Section 5.1.3**) operating within the original donor-acceptor [2]catenane **$C533a^{4+}$**—see **Table 5.7**—inverts its co-configuration (**Figure 5.40a**) dynamically between (*M*) and (*P*) mechanical helicities (**Figure 5.40b**), this phenomenon can be detected (**Figure 5.40c–d**) by ^{1}H NMR spectroscopy with the judicious use of chiral shift reagents. The (*S*) entantiomer of *tert*-butyl-1-(naphthen-1-yl)ethylcarbamate, (*S*)-^{t}BuNPEC, which associates with the catenane via an alongside D-A π–π stacking interactions involving the exposed $BIPY^{2+}$ unit of the $CBPQT^{4+}$ ring, induces a diastereotopic signal separation in the ^{1}H-decoupled ^{1}H NMR spectrum (**Figure 5.40c**) of **$C533a^{4+}$** in the slow exchange regime at 197 K in CD_3COCD_3. The (*S*) enantiomer of the Lacour-type[398] chiral phosphate anion **(*S*)-3^{-}**, which associates electrostatically with the catenane, induces a change in the population of (*M*) and (*P*) helicities, since the HQ signals in the slow exchange regime are observed (**Figure 5.40d**) in a 1:2 ratio in this case. In addition to blurring the lines between static and dynamic mechanostereochemistry, the dynamic mechanical helicity of these MIMs may create opportunities for novel function—for example, perhaps a future generation of catalytic molecular switches will be

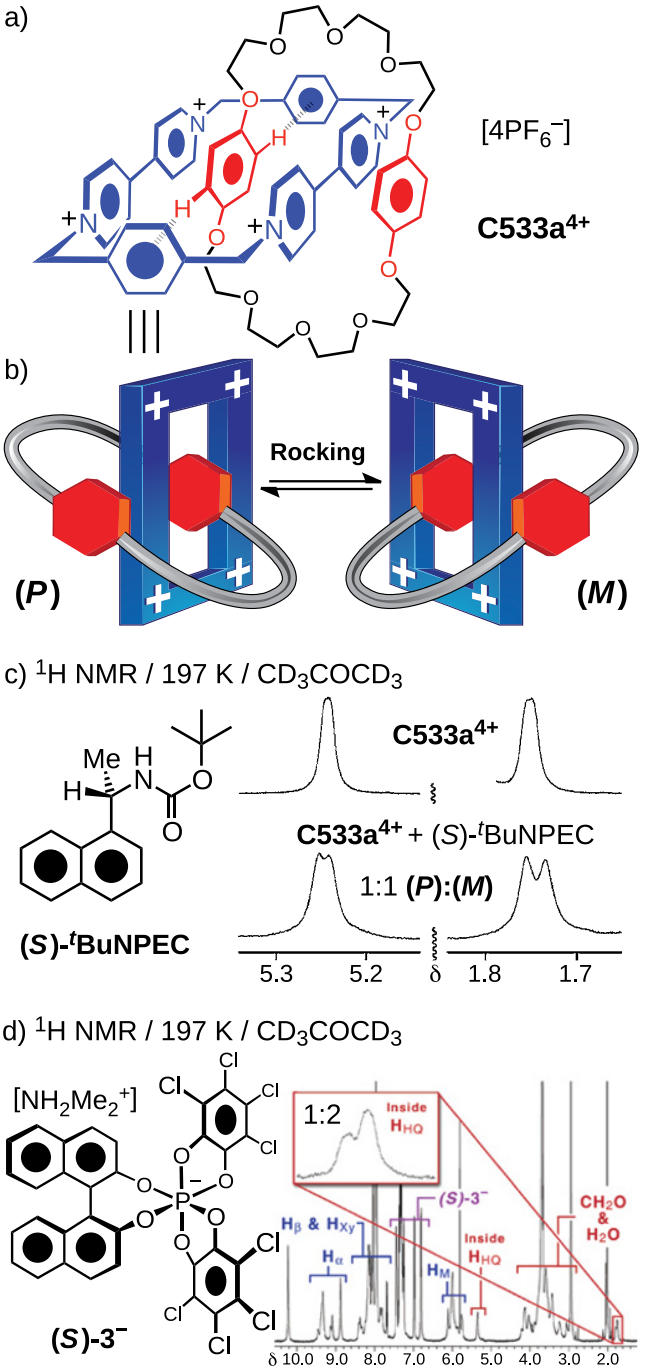
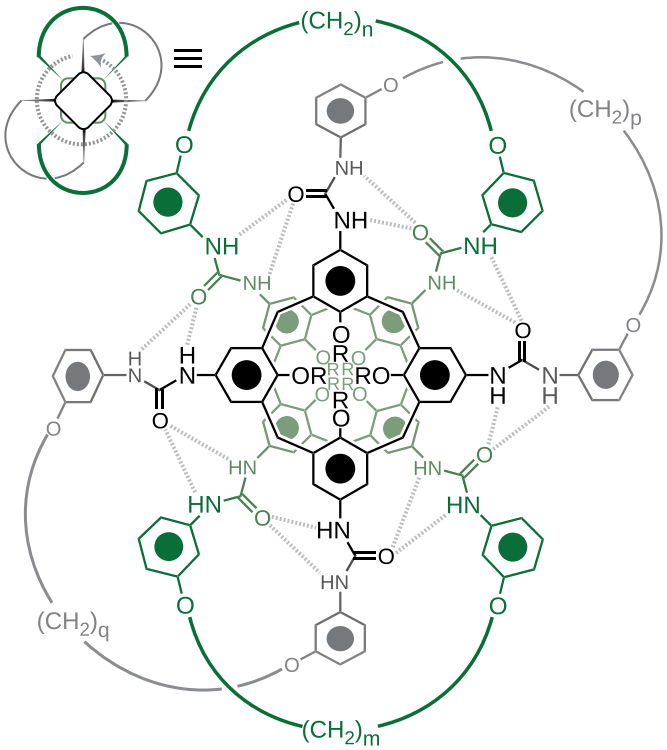


Figure 5.40 The mechanically helical (dynamic) chirality[397] of the original D-A [2]catenane[180] **$C533a^{4+}$**. (a) Stereoformula of **$C533a^{4+}$**, showing the [C–H···π] interactions responsible for tilting the interlocked rings away from orthogonality. (b) Conversion between (*P*) and (*M*) mechanical helicities by rocking (**Section 5.1.3**). (c) Partial ^{1}H NMR spectra (CD_3COCD_3, 197 K) of **$C533a^{4+}$**, showing the ^{1}H-decoupled HQ resonance signals before and after the addition of the chiral shift reagent (S)-^{t}BuNPEC, revealing a 1:1 mixture of mechanically helical isomers in solution. (d) The ^{1}H NMR spectrum (CD_3COCD_3, 197 K) of **$C533a^{4+}$** as a salt of the chiral anion **(*S*)-3^{-}**, revealing a 1:2 mixture of helicities. Data reproduced with permission from ref. 397 (copyright 2004 American Chemical Society)

able to invert their mechanically helical chirality, and thereby their configurational selectivity, in a controllable manner.

Böhmer[399,400] has applied the recognition motif (**Section 2.3.4.5**) based on dimeric tetraureidocalix[4]-arene capsules to the synthesis of mechanically helical cyclic bis[2]catenanes using an olefin metathesis clipping protocol followed by hydrogenation of the double bonds—**(Section 3.4.1.3)**. The Mainz group synthesized no fewer than 14 cyclic bis[2]catenanes (**C544a-n**, **Table 5.11**) with systematic modifications to (i) the functional groups (R = CH_3, *n*-C_5H_{11}, or *n*-$C_{10}H_{21}$) appended to the central calix[4]arene units, as well as to (ii) the loop sizes defined by the four oligomethylene linkers (*n*, *m*, *p*, *q* = 8, 10, 14, or 20) bridging their intercalated phenylurea appendages. The symmetry properties of these bis[2]-catenanes depends (**Figure 5.41**) on the distribution of different loop sizes. The homobis[2]catenanes **C544a-j** all possess four identical loops, which allows them to exist as a pair of enantiomers, the helicity of which are determined with respect to the direction of the (kinetically stable) hydrogen bond network of the capsules' urea-lined seams.[R] Although compounds **C544k-l** possess non-identical loops, they are also homocatenanes, which are interlocked in an orientationally selective manner, such that the small and large loops always intersect. Although

Table 5.11 Structural formulas of a series of Böhmer's bis[2]-catenanes derived from interpenetrated tetraureidocalix[4]arene dimeric capsules.[399,400]



	R	*n*	*m*	*p*	*q*
C544a	CH_3	8	8	8	8
C544b	CH_3	10	10	10	10
C544c	CH_3	14	14	14	14
C544d	CH_3	20	20	20	20
C544e	*n*-C_5H_{11}	8	8	8	8
C544f	*n*-C_5H_{11}	10	10	10	10
C544g	*n*-C_5H_{11}	14	14	14	14
C544h	*n*-C_5H_{11}	20	20	20	20
C544i	*n*-$C_{10}H_{21}$	10	10	10	10
C544j	*n*-$C_{10}H_{21}$	14	14	14	14
C544k	*n*-C_5H_{11}	8	14	14	8
C544l	*n*-C_5H_{11}	8	20	20	8
C544m	*n*-C_5H_{11}	8	8	14	14
C544n	*n*-C_5H_{11}	8	8	20	20

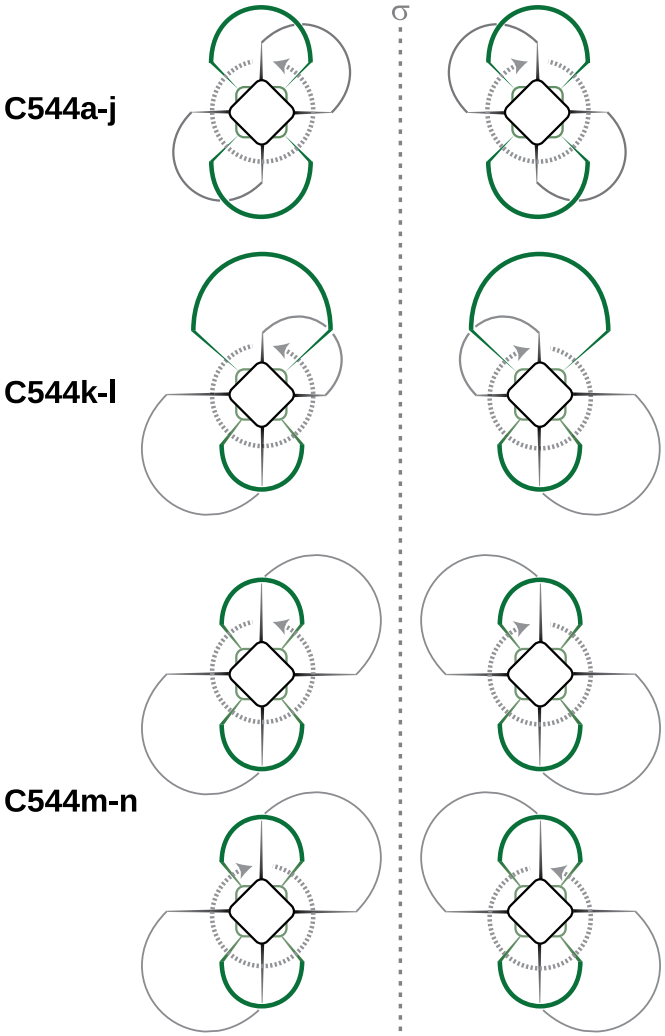


Figure 5.41 The mechanically helical enantiomers of Böhmer's bis[2]catenanes[400] **C544a-n**—see **Table 5.11**. Dashed arrows indicate the directionality of the hydrogen bond network, which is kinetically stable, comprising the seams of urea appendages.

[R] One compound, **C544f**, was obtained as single crystals suitable for structural determination by X-ray crystallography. Curiously, the seam of hydrogen-bonded urea groups belonging to the dimeric calix[4]arene capsule, which templates the catenane's formation, is broken such that the calix subunits are not associated in the solid-state, resulting in a completely different co-conformation than the one detected in solution.

the symmetry (C_1) of **C544k-l** is reduced compared to that (C_2) of **C544a-j**, the catenanes also exist as a pair of enantiomers. The heterobis[2]catenanes **C544m-n** are the only compounds exhibiting diastereotopic mechanical helicity, since the helicity of the non-identical component parts are not coupled with the rotationally directional seam of hydrogen bonds. Chiral resolution was achieved for many of the catenanes by chiral HPLC, although it was not possible to rationalize the separation properties on chiral stationary phases on the basis of the systematically modified structural parameters R, *n*, *m*, *p*, and *q*. In general, however, the homobis[2]catenanes were easier to separate than the heterobis[2]catenanes, with separation factors[S] (α) ranging from ~1 in the worst case scenarios (e.g., **C544k,m**) to >2 in the best case scenarios (e.g., **C544f,j**). Ballester[401] has prepared a similar macrotricyclic heterobis[2]catenane—see **Figure 4.29** in **Section 4.1.3.2**—which probably possesses the same kind of mechanical helicity as **C544m-n**. The special kind of chirality exhibited by these systems might also be appropriately classified under the banner of inherent chirality,[363–365] a term associated with the configurations of cyclodirectional bowl-shaped compounds.

Another potential source of helicity resulting from mechanical bonding may arise in oligorotaxanes. We imagine that it will be possible to stack rings along an axle such that the relative orientations of their appended functional groups constitute a helical arrangement, not unlike the helical stacking of base pairs in DNA. Indeed, there is some evidence,[402,403] based on molecular models and crystal structures, to suggest that this kind of mechanical helicity is possible in certain oligorotaxanes constructed from oligo(dialkylammonium) cations and crown ethers. Sevick[404] has modeled the dynamics of a rotaxane structures possessing three rings with appended substituents that interact through repulsive forces and she has observed the appearance of helical states under some conditions.

5.2.4 Topological Stereoisomerism

The seminal 1961 paper by Frisch and Wasserman[405] on "chemical topology" marked the birth of a new subfield in chemistry. Mathematical topology considers the geometric properties and spatial relationships of objects that are unchanged throughout continuous deformation, while chemical topology applies these considerations to molecular constitutions. Continuous deformation is an operation that allows an edge or surface to compress, stretch, or bend, without breaking, intersecting with, or passing through another edge or surface, and thus stands in contrast with Euclidean ideas of geometry, which fall under the umbrella of stereochemistry in the molecular world. Walba[406] proposed the term topological stereochemistry in 1985 to describe molecular entities, such as catenanes, knots, and Möbius ladders, that stand at the interface of chemical topology and stereochemistry. Topological stereochemistry has been discussed magnificently by pioneers such as Frisch and Wasserman,[405] Prelog,[407] Schill,[367] Sokolov,[408] Walba,[406,409] Sauvage,[410] Mislow,[411] and Hunter.[412] More recent reviews[413–416] on chemical topology are also available in the literature.

Topological stereochemistry is rooted in the existence of molecules whose isomerism arises solely from differences in the topology of their constitution, regardless of differences in Euclidean forms of stereoisomerism such as conformation. Quintessential examples of topological isomers include different types of knots (**Figure 5.42a**), which are understood in mathematical topology as embeddings of a circle (closed loops), as well as links (**Figure 5.42b**), which comprise two or more entangled, non-intersecting knots, in three-dimensional space. Chemical topology and stereochemistry both rely on molecular graph theory—analysis of representations of molecules as vertices (nodes) connected by edges (lines)—in order to understand differences in structure and properties. Whereas the Euclidean geometry (i.e., topography) employed in stereochemistry considers only rigid mappings of a molecular graph, topological analysis of a molecular graph tolerates continuous deformation

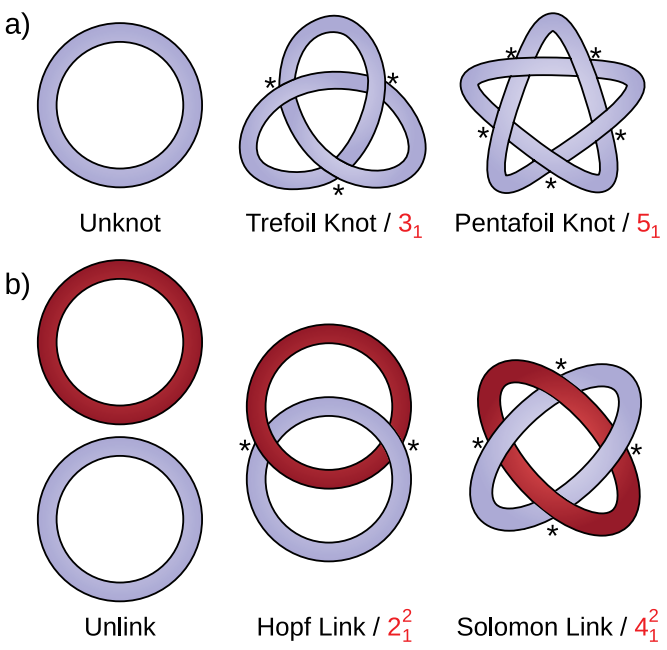


Figure 5.42 Simplified molecular graphs exemplifying the concept of topological isomerism in knots and links. (a) The unknot, trefoil knot, and pentafoil knot are topological isomers with of 0, 3, and 5 crossings, respectively, in the two-dimensional projections of their graphs. (b) The unlink, Hopf link, and Solomon link are topological isomers with 0, 2, and 4 crossings, respectively, in the two-dimensional projections of their graphs. Crossings are labeled with asterisks. The Alexander-Briggs notation for the non-trivial knots and links are listed in red.

[S] The separation factor α is defined as k_2/k_1, where k_1 and k_2 are the retention factors for the two analytes of interest. The rentention factor *k* is the ratio of time an analyte spends in the stationary phase versus the mobile phase.

by any function that does not allow edges and vertices to break, cross, or merge. For conceptual purposes, it is convenient to imagine that Euclidean graphs are made of glass, whereas topological graphs are made of infinitely flexible and stretchable rubber, for example. The various shapes that a graph can assume throughout continuous deformation are known as *presentations*.

The vertices of a graph may be differentiated with different 'colors', which can be understood in chemical terms as different atoms—e.g., carbon versus nitrogen. Therefore, the stereoformulas of molecules are essentially molecular graphs, where atoms represent vertices and (covalent) bonds represent edges. Whereas most stereoisomers—those associated with stereogenic centers, axes, and planes—are distinguished by some form of Euclidean rigidity, topological isomers are distinguished only by differences in the topology of the graph. Although all graphs possess a topology, non-trivial topologies are typically associated with *non-planar* graphs.[417] A graph is said to be planar if it can be drawn in a plane—i.e., projected into two-dimensional space—without any of the edges crossing.[T] A non-planar graph therefore has one or more crossings in a plane. Generally speaking, the graphs of Euclidean stereoisomers are planar, while those of topological stereoisomers are non-planar. The fact that it is impossible to draw a catenane in two dimensions without crossings, yet possible to draw a (deformed) rotaxane without crossings, explains why rotaxanes are considered topologically trivial species in spite of having mechanical bonds.

Two important concepts in topology are homeomorphism and isotopism. Two graphs are *homeomorphic* if they possess identical connectivity, regardless of the dimensionality of the space in which they are mapped. On the other hand, two graphs are *isotopic* if they cannot be differentiated on the basis of their topology in a given space. For example, the knots in **Figure 5.42a** are all homeomorphic, since all knots are embeddings of a circle, which means that they could be converted through continuous deformation into a circle in a higher-dimensional space. Yet the unknot, trefoil knot, and pentafoil knot are not *isotopic* because they cannot be interconverted through continuous deformation in three-dimensional space. Topological stereoisomers are therefore defined[406] as those molecules that are homeomorphic and non-isotopic. The graphs of topological stereoisomers can be distinguished from other types of isomers as follows:

Constitutional Isomers: non-homeomorphic, non-isotopic
Topological Isomers: homeomorphic, non-isotopic
(Euclidean) Stereoisomers: homeomorphic, isotopic

[T] Kuratowski[417] proved that all non-planar graphs must contain subgraphs of either (i) the complete graph on five vertices, known as K_5, which comprises five vertices all mutually connected by edges, or (ii) the complete bipartite graph, known as $K_{3,3}$, which comprises six vertices, three of which are linked to each of the other three.

Readers are reminded that chemical topology and mechanostereochemistry occupy overlapping but separate domains of chemistry, since many molecules with mechanical bonds such as rotaxanes lie mostly outside the realm of topology, while many topologically rich molecules, including knots,[418] extended networks,[419] ravels,[420,421] Möbius ladders,[422,423] and molecular analogues of the K_5[424–426] and $K_{3,3}$[427] Kuratowski graphs[T] do not possess mechanical bonds. Much in the realm of chemical topology is therefore beyond the scope of this book. See **Figure 2.1** and accompanying discussion in the introduction to **Chapter 2**. Molecular topology is also discussed in **Section 1.3.2** and **Section 4.1**.

One of the ways in which different knot and link topologies are determined and characterized is by the minimum number of crossings in the two-dimensional projections of their three-dimensional graphs. The unknot, trefoil knot, and pentafoil knot, for example, possess 0, 3, and 5 crossings (**Figure 5.42a**) in their projections, while the unlink, Hopf link, and Solomon link, possess 0, 2, and 4 crossings (**Figure 5.42b**), respectively. Alexander-Briggs notation characterizes knots and links by these crossing numbers, with subscripts (assigned arbitrarily) that distinguish different topologies of equal crossing number, and superscripts (in the case of links) denoting the number of entangled knots. Topological isomers can therefore be understood also as molecules possessing identical constitutions, yet different crossings in their non-planar molecular graphs.

Although topological isomers of DNA (**Section 1.1.1**) are well-known in biochemistry, where they are referred to as topoisomers,[428] the isolation of topological isomers is relatively uncommon in synthetic chemistry. Walba's synthetic prisms and Möbius ladders[422,423] derived from the so-called THYME polyethers[429] are noteworthy exceptions—see **Section 2.2.3**—despite the fact that these examples remain outside the realm of the mechanical bond. Although the literature is now replete with molecules expressing beautiful and challenging mechanically bonded topological structures (**Section 4.1**), pairs or collections of topological isomers are rarely isolated and compared. Lüttringhaus[430] was among the first investigators to compare the physical properties of the unlink and the Hopf link in molecular form—see **Scheme 2.6** and the accompanying discussion in **Section 2.2.1**. The component parts of the unlink are often generated as unwanted byproducts of clipping reactions in the formation of catenanes, although they are rarely recombined as a physical mixture for comparison with the corresponding Hopf links. Moreover, one could argue[423] that the unlink is not an isomer of the Hopf link (or any other link) because the unlink comprises two separate molecules, whereas catenanes are considered as single molecules. The same argument does not apply to knots because the unknot is also a single molecule, yet knots do not possess mechanical bonds *per se* because they lack distinguishable component parts.

One of the most impressive demonstrations of topological isomerism in the molecular world was achieved by Sanders,[431] who isolated (**Figure 5.43**) the topological

isomers **K545a**$^{8-}$ (trefoil knot), **K545b**$^{8-}$ (figure eight knot), **C545**$^{8-}$ (Solomon link), and **M545**$^{8-}$ (the unknot) from a dynamic combinatorial library of the L-cysteine-terminated bis(NDI) monomer **(*RR*)-L545**$^{2-}$ under oxidative aqueous conditions that promote the formation of disulfide bonds. Each of these compounds are tetramers possessing identical molecular formulas, yet their topological differences lead to different physical properties, including their retention times on a stationary phase during chromatography. The RP-HPLC chromatogram in **Figure 5.43** visualizes the approximate yield of each tetramer in the library on the basis of their integrated signals, revealing the Solomon link **C545**$^{8-}$ (60%) and the figure eight knot **K545b**$^{8-}$ (18%) to be the major products. The formation of the various entangled topological isomers is driven by the hydrophobic effect, where the most stable products are those that most effectively protect the hydrophobic NDI surfaces from the aqueous environment. Space-filling molecular models suggest that tetramers with more than four crossings are not possible on account of steric constraints.

Mechanically bonded topological stereoisomers are more commonly limited to those arising from differences in topological chirality (**Section 5.2.4.1**) or conditional (**Section 5.2.4.2**) circumstances, rather than to differences in crossing number.

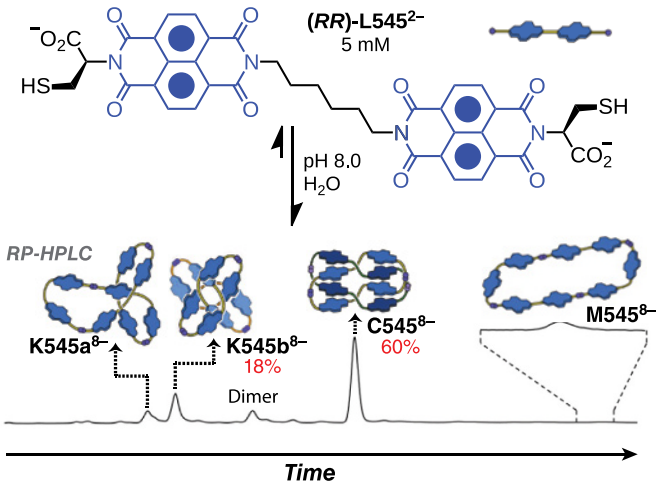


Figure 5.43 RP-HPLC chromatogram of the topological isomers of disulfide-bridged bis(NDI) tetramers that form as the main products in an aqueous dynamic combinatorial library. Adapted with permission from ref. 431 (copyright 2014 American Chemical Society).

5.2.4.1 Topological Enantiomers

Walba[406] conjectured that at least one of the following elements are required for the expression of topological chirality: (i) a link containing oriented rings (oriented link), (ii) a chiral link, (iii) a chiral knot, or (iv) a chiral non-planar molecular graph. An oriented link (**Figure 5.44a**) is the conceptual homologue of a mechanically planar rotaxane

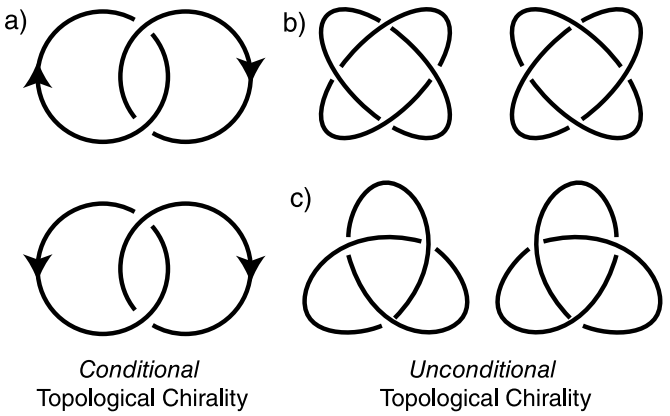


Figure 5.44 Simplified molecular graphs of topological enantiomers. (a) A Hopf link with two oriented rings exhibits conditional topological chirality. (b) Solomon links and (c) trefoil knots possess unconditional topological chirality, requiring no oriented loops.

(**Section 5.2.3.1**), which can be understood as a link in which directions are assigned to each of the component parts—often represented as arrowheads in a molecular graph—on the basis of a non-symmetrical sequence of atoms in their constitution. A chiral link is any link topology that cannot be continuously deformed into its own mirror image. The doubly interlocked topology of the Solomon link (**Figure 5.44b**), for example, imparts a chirality arising from the four crossing points not unlike mechanically helical chirality. The same can be said of trefoil knots (**Figure 5.44c**). Chiral non-planar graphs encompass various other types of non-trivial molecular topologies. It is possible to distinguish between *conditional* and *unconditional* forms of topological chirality, since certain topologies—e.g., Hopf links—are chiral only on the condition that the rings contain oriented sequences, while many (but not all) topologies with more than two crossings in their non-planar graphs, such as Solomon links and trefoil knots, are unconditionally chiral—i.e., they do not require an oriented sequence within their constitution in order to possess a non-superimposable mirror image.

The determination of topological chirality in knots and links can be made empirically or using polynomials. Mislow[411] has summarized both of these approaches comprehensively. Of all the prime links[u] with fewer than eight crossings (**Section 1.3.2**, **Figure 1.23**), only 2^2_1 (Hopf link), 6^2_2, and 6^3_2 (Borromean rings) are achiral. The vast majority of prime links are therefore topologically chiral, unconditionally. Since the Hopf link is the most synthetically accessible prime link, however, much of the pioneering research on topologically chiral molecules was carried out on conditionally chiral catenanes possessing oriented rings.

[u] A prime link is a link that cannot be represented as a sum of other links—see **Section 4.1.1**.

Conditional Topological Chirality

For molecular topologies that are not chiral in three-dimensional space, such as the 2^2_1 Hopf link or the 6^3_2 Borromean[v] rings,[334,432–438] topological chirality may be expressed on the condition that the rings are oriented by a directional sequence of atoms. The absolute co-configuration of an oriented Hopf link may be assigned in the same manner as mechanically planar (**Section 5.2.3.1**) rotaxanes. In the direction of the arrow pointing from the highest priority atom to its highest priority neighbor, according to Cahn-Ingold-Prelog[324] sequence rules, the interlocked rings of (*R*)-enantiomers are disposed in a clockwise manner, while the rings of (*S*)-enantiomers are disposed in an anticlockwise manner.

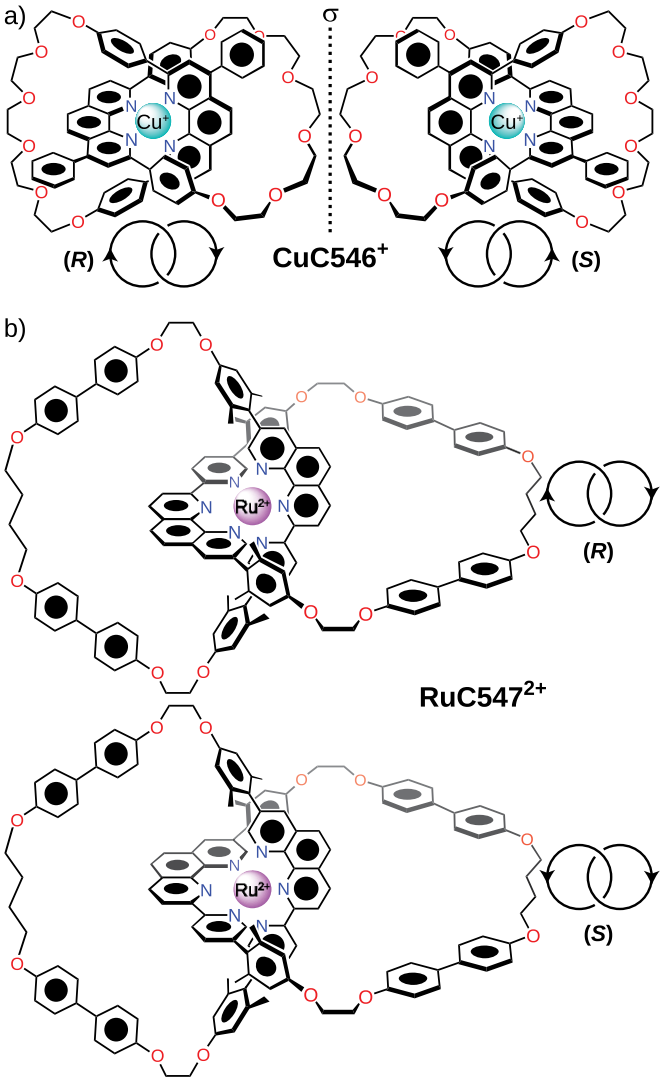


Figure 5.45 Stereoformulas of the the enantiomers of (conditionally) topologically chiral [2]catenates. (a) Sauvage's original topologically chiral Cu^{I} [2]catenate, the oriented rings of which are based on asymmetric tpp ligating moieties.[439,440] (b) One of Siegel's topologically chiral Ru^{II} [2]catenates, the oriented rings of which are based on asymmetric pphen ligating moieties.[442]

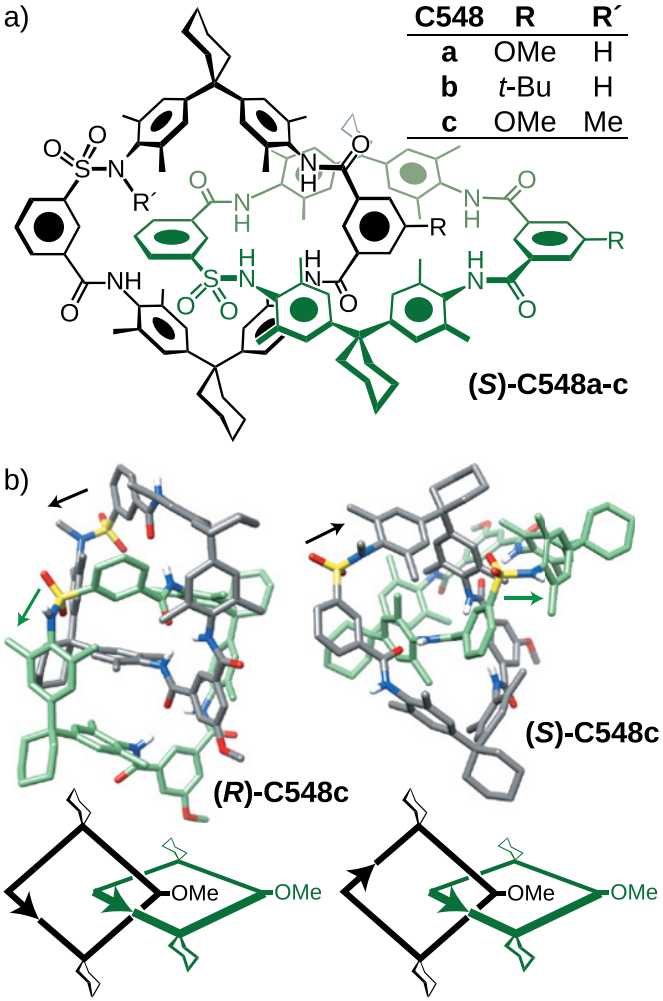


Figure 5.46 The conditional topological chirality of Vogtle's [2]catenanes derived from trilactam monosulfonamide rings.[369,443,444] (a) Stereoformulas of the [2]catenanes **C548a-c** as the (*S*)-enantiomers. (b) Tubular and graphical representatios of the X-ray crystal structure[444] of the hetero[2]catenane **C548c** as the racemate of both (*R*) and (*S*) co-configurations. Solven molecules and CH protons are omitted for the sake of clarity.

Sauvage[439,440] reported in 1988 the first synthesis of a topologically chiral [2]catenate **CuC546**$^{+}$, which he made by interlocking (**Figure 5.45a**) rings derived from dissymmetric 2,4,9-triphenyl-1,10-phenanthroline (tpp) ligating moieties instead of the usual 2,9-diphenyl,1,10-phenanthroline (dpp) ligand system. In 1993, a collaboration with Okamoto[441] allowed the topological enantiomers to be resolved by chiral HPLC, employing amylose tris(3,5-dimethylphenylcarbamate) on silica gel as the stationary phase. Siegel[442] has employed a similar strategy to generate topologically chiral [2]catenates based on Ru^{II} octahedral templates (**Section 2.3.2.3**), one of which is the [2]catenate **RuC547**$^{2+}$

[v] Although examples possessing stereogenic centers are known,[334] molecular Borromean rings exhibiting conditional topological chirality have not been reported in the literature, to our knowledge, except for those based on DNA, the backbone of which is oriented by virtue of the polarity of phosphodiester bonds.

possessing (**Figure 5.45b**) 2-(2-pyridyl)-1,10-phenanthroline (pphen) ligands as the source of asymmetry.

Vögtle[369,443,444] has prepared the oriented [2]catenanes **C548a-c** (**Figure 5.46a**) by installing a single sulfonamide unit as one of the hydrogen-bonding groups in each of the rings. Whereas **C548a** and **C548b** are topologically chiral homo[2]-catenanes, **C548c** is a topologically chiral hetero[2]catenane, since only one of its rings possesses a methylated sulfonamide unit. The enantiomers of **C548b** and **C548c** have been resolved[369,444] by chiral HPLC, and a crystal structure (**Figure 5.46b**) has been obtained[444] in the case of **C548c**. Both the (*R*) and (*S*) conditional topological enantiomers are present in the crystal. The [2]catenane **C548c** was also dimerized (**Scheme 5.29**) with 1,2-bis(2-iodoethoxy)ethane to afford the bis[2]catenane **C549**, which forms as a mixture of the **(*RR*)-C549** and **(*SS*)-C540** enantiomers, as well as the achiral conditional topological diastereoisomer ***meso*-C549**.

A noteworthy example of a [2]catenane exhibiting conditional topological chirality is that of Sanders' homo[2]-catenane **C550**, which emerges[445] from a dynamic combinatorial library of functionalized dipeptides in the presence of an acetylcholine template. The (*R*) enantiomer of **C550** is illustrated in **Figure 5.47**. The directional sequence of each ring's

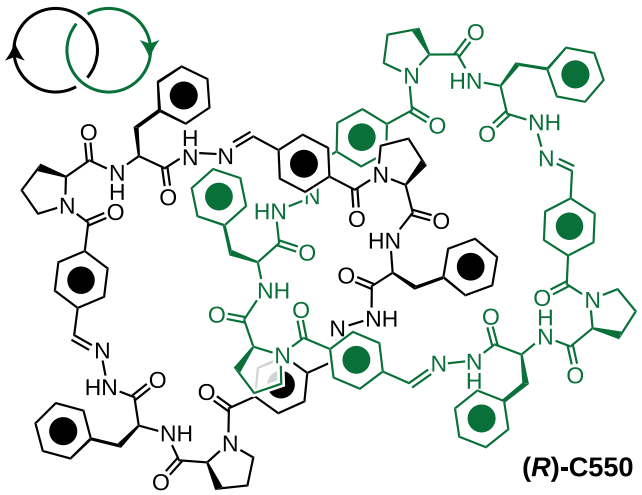
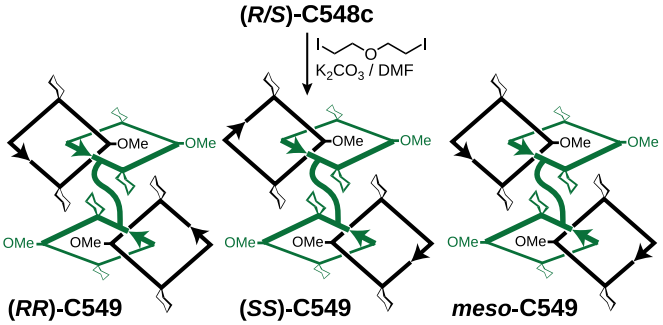


Figure 5.47 Structural formula of one of the enantiomers obtained from a dynamic combinatorial library of benzaldehyde- and hydrazide-functionalized proline-phenylalanine dipaptides, which is amplified by an acetylcholine template.[445]

constitution is defined by the polarity of the peptide bonds. See **Scheme 1.2** and the corresponding discussion in **Section 1.3.5** for a discussion of this catenane's synthesis.

Ogoshi[343] has synthesized a [2]catenane, **C551**$^+$, which exhibits (**Figure 5.48**) conditional topological chirality. A unique aspect of this particular case is that the orientation of the perethylated PA5 ring (Et_{10}PA5) is defined, not by a directional sequence of atoms, but rather by the planar chirality of its five aromatic subunits. The synthesis of **C551**$^+$ by olefin ring closing metathesis—see **Section 3.4.1.2**—is diastereoselective for the ($S_PS_PS_PS_PS_P$)-Et_{10}PA5 and ($R_PR_PR_PR_PR_P$)-Et_{10}PA5 enantiomers, which represent only



Scheme 5.29 Vögtle's covalent dimerization[444] of the racemate of **C548c** affords a mixture of the topologically chiral bis[2]-catenane enantiomers **(*RR*)-C549** and **(*SS*)-C549**, as well as the corresponding achiral diastereomer ***meso*-C549**.

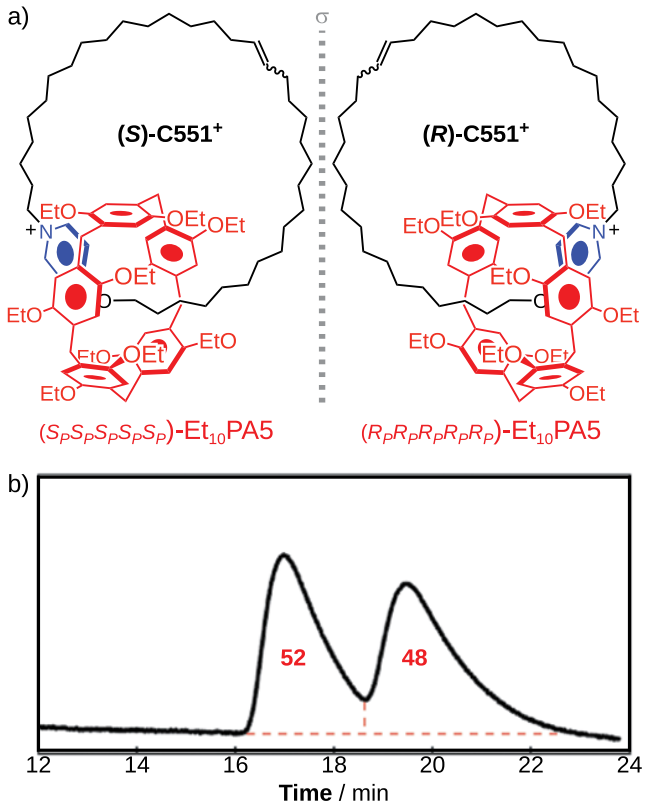


Figure 5.48 Ogoshi's topologically chiral PA5 [2]catenane.[343] (a) The [2]catenane **C551**$^+$ exhibits conditional topological chirality, where co-configuration is determined by the relative orientations of a pyridinium macroring interlocked with Et_{10}PA5. The orientation of Et_{10}PA5 is determined by the arrangement of its five planar chiral subunits. The synthesis is diastereoselective for the ($S_PS_PS_PS_PS_P$) and the ($R_PR_PR_PR_PR_P$) PA5 configurations, among eight possible diastereoisomers, in **(S)-C551**$^+$ and **(*R*)-C551**$^+$, respectively. (b) A chiral HPLC chromatogram demonstrating resolution of the topological enantiomers of **C551**$^+$ eluting in hexane/EtOAc/TFA (94.9:5:0.1 on a Daicel Chiralpack IA chiral stationary phase. Data in b) reprinted with permission from ref. 343 (copyright 2014 Royal Society of Chemistry)

two of the eight possible diastereoisomers of this macrocycle. The orientations of these rings relative to the arrow of directionality in the pyridinium macroring defines the absolute co-configurations (**Figure 5.48a**) of **(S)-C551**$^+$ and

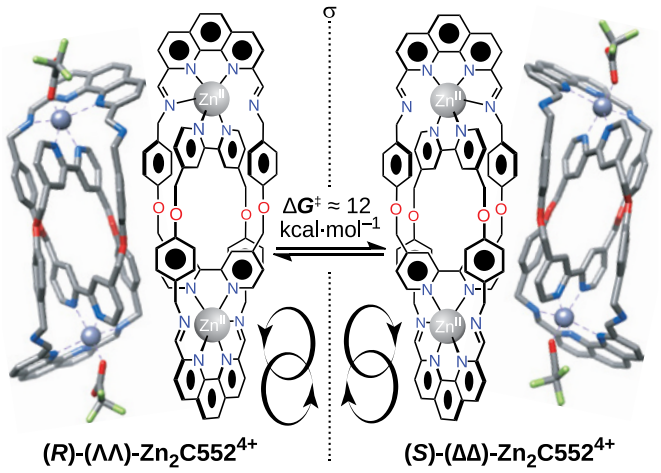


Figure 5.49 Stereoformulas and tubular representations of the solid-state stuctures of two enantiomers of the homo[2]catenane **Zn_2C552^{4+}**, which inverts its conditional topological chirality upon dynamic rearrangement of its coordination bonds.[446] The rings' orientations arise from the tridentate chelation of Zn^{II} ions within a tetradentate phenanthrolinebis(imine) pocket, a coordination complex that oscillates between (Δ) and (Λ) configurations by decoordinating and recoordinating either of the two equatorial imine groups.

(*R*)-C551$^+$. The chirality of these compounds has been confirmed (**Figure 5.48b**) by chiral HPLC, which separates the (*S*) and (*R*) enantiomers on a chiral stationary phase.

Recently, Charbonnière and Trabolsi,[446] have introduced a bimetallic [2]catenate, **Zn_2C552^{4+}**, in which conditional topological chirality inverts (**Figure 5.49**) as a result of the dynamic intramolecular translocation of a transition metal center. Although the rings of **Zn_2C552^{4+}** are not oriented in and of themselves, an orientational direction is introduced by the tridentate coordination of a Zn^{II} ion to the tetradentate phenanthrolinebis(imine) cleft of each macrocycle. The presence of two stereogenic transition metal coordination centers in **Zn_2C552^{4+}** allows for up to six possible isomers comprising three diastereoisomeric pairs of topological enantiomers: (*S*)-(ΔΔ) / (*R*)-(ΔΔ), (*S*)-(ΔΛ) / (*R*)-(ΔΛ), and (*S*)-(ΛΛ) / (*R*)-(ΛΛ), yet only **(*S*)-(ΔΔ)-Zn_2C552^{4+}** and **(*R*)-(ΛΛ)-Zn_2C552^{4+}** were observed in the solid-state superstructure (**Figure 5.49**) obtained upon crystallization. In solution, the Zn^{II} centers invert between Δ and Λ configurations with a free energy barrier ($\Delta G^{\ddagger}$) of ~12 kcal·mol^{-1}, most likely by a two-step process involving (i) decoordination of one imine–Zn^{II} bond to form a five-coordinate intermediate, followed by (ii) re-coordination to the Zn^{II} center by the other imine group. This process is responsible for the ~12 kcal·mol^{-1} enthalpic penalty which dominates the free energy barrier to inversion. We note that the helix inversion of either coordination complex (Δ / Λ), which happens at a rate of nearly 1000 times per second at 283 K, leads to a concomitant inversion in topological chirality (*R*/*S*) because this inversion reverses the cyclodirectionality of the ring. Thus, the dynamic chirality of **Zn_2C552^{4+}** is the inverse of the scenario we described in the case (**Section 5.1.1.2**, **Scheme 5.8**) of Leigh's [2]rotaxane molecular shuttle **R525OH**, in which a stereogenic center undergoes inversion of configuration as a result of the dynamic translational of a ring—here, topological chirality inverts as a result of dynamic bond rearrangement. In other words, **R525OH** demonstrates the link between covalent stereochemistry and the dynamics of mechanical bonds, while **Zn_2C552^{4+}** demonstrates the link between mechanostereochemistry and dynamics of covalent (coordinative) bonds.

Unconditional Topological Chirality

The original strategy for preparing knots and higher order links was the one introduced by Sauvage involving double-stranded helicates as templates, where the number of crossovers in the double helix determines (**Figure 5.50**) the number of crossings, *n*, in the resulting topology upon ring closure. Helices with an odd number of crossings lead to knots, such as the trefoil (*n* = 3) and the pentafoil (*n* = 5) knots, while even-numbered crossings lead to links, such as the Solomon link (*n* = 4) and the Star of David link (*n* = 6). The oriented skew lines convention has been identified[406] as an appropriate method of assigning the (co-)configuration of unconditionally chiral knots and links. An equally viable approach deforms the knot or link such that its crossing points are localized in a double-helical arrangement akin to Sauvage's original template designs, and assigns chirality to the knot or link on the basis of its helicity. The right hand rule[447] can also be employed at this stage to make the assignments. We showcase in this Section a

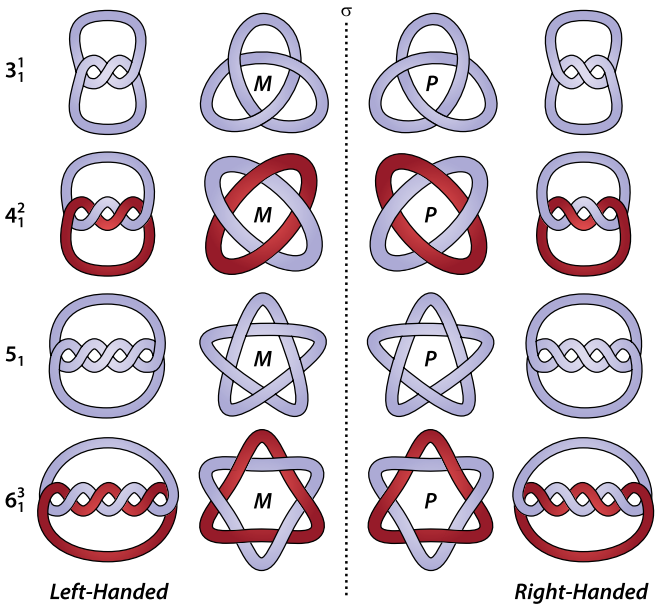


Figure 5.50 Simplified graphs of knots and links possessing unconditional topological chirality. Both the *P* and *M* enantiomers of the trefoil knot (3_1), Solomon Link (4^2_1), pentafoil knot (5_1), and Star of David link (6^2_1) are illustrated on either side of the central mirror plane, σ. The helical portrayals in the outermost columns assist in the determination of handedness.

number of multiply interlocked links that are unconditionally chiral on account of their topologies.

Although molecular knots[418] lack mechanical bonds, their importance in topological chirality is noteworthy, having influenced the topological stereochemistry of links as well. Trefoil knots are unconditionally chiral, since any trefoil knot possesses a non-superimposable mirror image. The first synthetic trefoil knot was synthesized by Sauvage[448] using transition metal templation (**Section 2.3.2**), and the knot's chirality was proven definitively upon characterization[449] by X-ray crystallography, which revealed that the compound undergoes spontaneous resolution upon crystallization, since a conglomerate of enantiopure left-handed and right-handed crystals was obtained. Resolution[450,451] of Sauvage's dicopper(I) trefoil knot was also achieved by recrystallization of the corresponding diastereoisomeric triflate salts of 1,1´-binaphthyl-2,2´-diyl phosphate, allowing his Strasbourg team to assign[451] absolute configuration and characterize[452] the optical rotation properties of the topologically enantiomeric knots. Vögtle[453–461] has also synthesized a number of trefoil knots, or 'knotanes' by his nomenclature,[453,462] using a hydrogen bond templation (**Section 2.3.4**) strategy. Although these oligoamide trefoil knots crystallize as the racemates, several of the knotted compounds have been resolved by chiral HPLC in collaboration with Okamoto and Grimme,[454] allowing for characterization of the chiroptical properties and the assignment of absolute configuration to each enantiomer. Although molecular knots are at the fringes of mechanostereochemistry, we wish to point out that many more examples of synthetic trefoil knots have emerged in the literature, including more examples based on transition metals[463,464] and hydrogen bonds,[465] as well as π-donor/π-acceptor templation,[466] covalent templates,[467] solvophobic/homophilic interactions in dynamic combinatorial libraries,[468] alkali metal templates,[469] lanthanide templates,[470] DNA,[471] and active metal templates,[472] X-ray crystal structures of the seminal trefoil and pentafoil knots are represented in **Figure 1.25**, **Section 1.3.2**.

Among the handful of synthetic molecular Solomon links (**Section 4.1.1.1**) that have been reported[431,473–486] in the literature, several have been obtained as single crystals suitable for X-ray crystallography. The solid-state structures of the [2]catenanes **C553**, $\mathbf{Cu_2Zn_2C554^{8+}}$, $\mathbf{C555^{8+}}$, $\mathbf{Fe_4C556^{8+}}$, $\mathbf{Cu_6C557^{30+}}$, and $\mathbf{Zn_4C558^{8+}}$ are illustrated in **Figure 5.51**. Although only the (*M*)-enantiomers are represented in **Figure 5.51**, all of these compounds crystallize as the racemate of (*M*) and (*P*) topological enantiomers. In the case of the Solomon link $\mathbf{C545^{8-}}$ assembled by Sanders[431] from a dynamic combinatorial library (**Figure 5.43**), although the presence of stereogenic centers in the rings opens up the possibility of generating diastereoisomers, MS, NMR, and CD data suggest that these homochiral monomers direct the formation of only one of the two possible topologically chiral enantiomers, yet the absolute co-configuration (*M*/*P*) was not assigned unambiguously.

Although Sauvage[487] successfully prepared double-stranded helicates with five and six metal centers corresponding to five and six crossings, which would generate a pentafoil knot and a Star of David link, respectively, attempts to isolate these links upon cyclization were unsuccessful. Recently, Leigh[395] succeeded in synthesizing the first molecular Star of David catenane by crosslinking the ligands of a hexameric Fe^{II} circular helicate template using olefin metathesis. The stereoformula and the X-ray crystal structure of the (*P*) enantiomer of this topologically chiral catenane are illustrated in **Section 1.3.2**, **Figures 1.24** and **1.27**, respectively. The assembly reaction is depicted in **Scheme 4.1** of **Section 4.1.1.2**. Although only the right-handed enantiomers are illustrated in each case, the compound is isolated as the racemate of both (*M*) and (*P*) enantiomers.

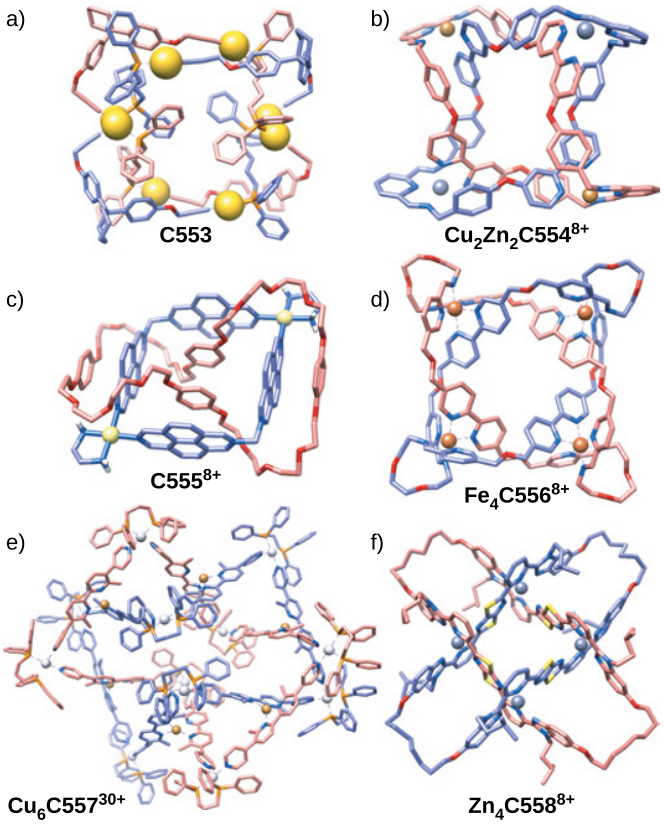


Figure 5.51 Tubular representations of the solid-state structures of molecular Solomon links with metallic backbones (left column) and metallic templates (right column). (a) Puddephatt's organometallic Au^{I} acetylide Solomon link **C553**.[478] (b) The Solomon link $\mathbf{Cu_2Zn_2C554^{8+}}$ self-assembles from *endo*-bidentate bipyridyl and *exo*-tridentate diiminopyridine ligands in the presence of a 1:1 mixture of Zn^{II} and Cu^{II} templates.[480] (c) Peinador and Quintela's π-donor/π-acceptor Solomon link $\mathbf{C555^{8+}}$.[484] (d) A Solomon link $\mathbf{Fe_4C556^{8+}}$ assembled[483] in one pot from a tetrameric Fe^{II} circular helicate using reversible coordinative imine bonds. (e) Severin's giant metallo-organic Solomon link $\mathbf{Cu_6C557^{30+}}$, in which two Pd_6L_{12} metallacycles are doubly wrapped around six Cu^{I} templates.[477] (f) Leigh's molecular Solomon link $\mathbf{Zn_4C558^{8+}}$ assembled from an interwoven metallosupramolecular grid as a template.[486] All of these compounds crystallize as racemates of (*M*) and (*P*) topological chiralities, yet only the *M* co-configurations are portrayed. Hydrogen atoms, solvent molecules, and counterions are omitted for the sake of clarity.

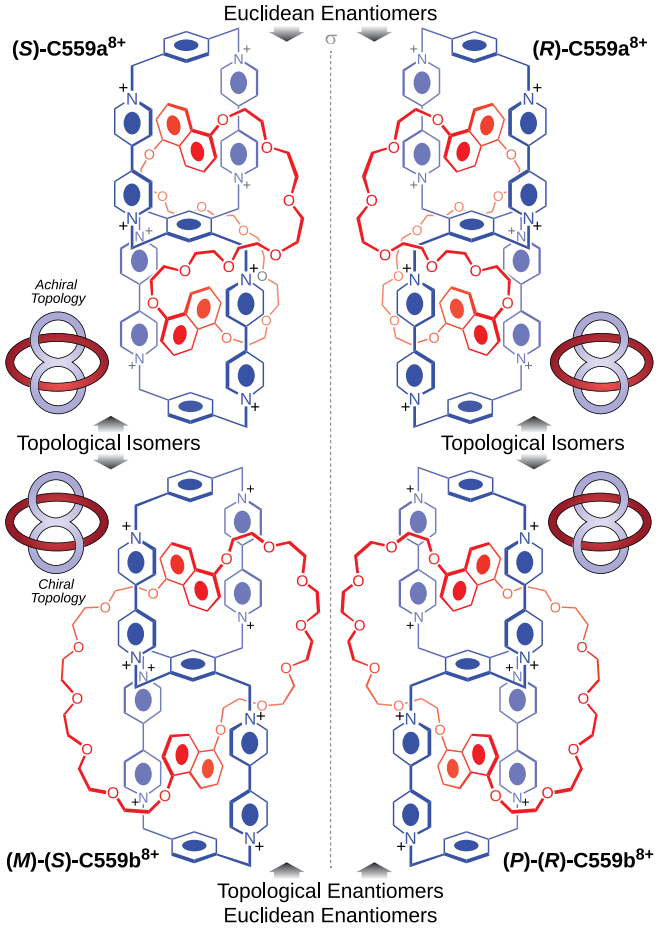


Figure 5.52 The topological isomerism and topological chirality of the donor-acceptor handcuff [2]catenanes **C559a**$^{8+}$ and **C559b**$^{8+}$,[201] which are superimposed on the elements of (Euclidean) planar chirality arising from the centermost aryl ring of the octacationic bis(cyclophane). Ignoring the Euclidean chirality, the topology of the **C559a**$^{8+}$ handcuff catenane is achiral, whereas the topology of **C559b**$^{8+}$ is unconditionally chiral. Therefore, **C559b**$^{8+}$ exists as a pair of topological enantiomers, while the enantiomers of **C559a**$^{8+}$ are only Euclidean in nature.

Prime links (**Section 4.1.1**) and knots are not the only molecules that can express topological chirality. For example, a π-associated donor-acceptor handcuff [2]catenane based on a planar chiral bis-CBPQT^{4+} host has been isolated[201] as a mixture of the topological isomers **C559a**$^{8+}$ and **C559b**$^{8+}$, only one of which (**C559b**$^{8+}$) exists (**Figure 5.52**) as a pair of topological enantiomers, since the other (**C558a**$^{8+}$) possesses an achiral topology. The topologies of **C559a**$^{8+}$ and **C559b**$^{8+}$ cannot be interconverted—the only difference between them is the manner in which the polyether loops of the central dinaphtho[50]crown-14 (DN50C14) ring wrap around the octacationic bis-cyclophane. The simplified molecular graphs accompanying the stereoformulas of these mechanostereoisomers in **Figure 5.52** reveal that the chiral topology of **C559b**$^{8+}$ is reminiscent of a Solomon link—indeed, this topology would be the result of conjoining one of the rings of a Solomon link at its center through the annulus of the other ring. By contrast, the *topology* of **C559a**$^{8+}$ has a superimposable mirror image as a result of the σ plane passing through its central ring, although this σ plane is not present in the Euclidean sense because of the planar chirality of the bis-cyclophane.[w] The major isomer observed in solution and in the solid-state upon isolation of the handcuff catenane after a clipping protocol is **C559a**$^{8+}$, although **C559b**$^{8+}$ can be detected nevertheless by ^{1}H NMR spectroscopy. Overall, the mixture of the **C559a**$^{8+}$ and **C559b**$^{8+}$ topological isomers consists of four species—the two Euclidean enantiomers of **(*S*)-C559a**$^{8+}$ and **(*R*)-C559a**$^{8+}$, and the two topological/Euclidean enantiomers **(*M*)-(*S*)-C559b**$^{8+}$ and **(*P*)-(*R*)-C559b**$^{8+}$.

Residual Topological Chirality

Although the topology of a catenane is trivialized by the installation of covalent bridges between component parts, the chirality of these molecules can be maintained from their topologically chiral precursors. Vögtle[488] has described this situation as *residual topological chirality*. Thus, when covalently bridged MIMs are made from topologically chiral precursors—either conditionally or unconditionally—the resulting molecules possess the residual topology of those precursors. Vögtle's sulfonamide-bridged hydrogen-bonded pretzelanes[488] (**Figure 5.53**) serve as an archetypal example of molecules possessing residual topological chirality, while other types of covalently bridged catenanes—see **Section 4.1.4**—have the potential to express chirality in a similar manner.

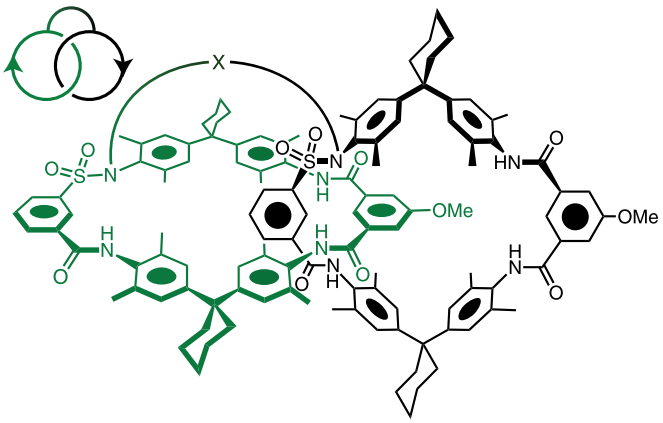


Figure 5.53 Vögte's pretzelanes exhibit residual topological chirality,[488] since their rings retain the cyclodirectionality of their topologically chiral [2]catenane that would result from breaking the linker –X– connecting them. See **Section 4.1.4.1**.

[w] The original publication[201] on the handcuff [2]catenane misassigns the absolute configuration associated with the plane of chirality and overlooks the topological chirality of the minor mechanostereoisomer.

5.2.4.2 Conditional Topological Isomers

Conditional topological isomers are not to the same as conditional topological enantiomers. Whereas conditional topological chirality depends on oriented rings to induce a non-superimposable mirror image, conditional topological isomerism involves assigning constraints to component parts that differentiate the topologies of otherwise *achiral* mechanomolecules.

Conditional Topological Isomers of [3]Catenanes

Although the Hopf link [2]catenane becomes chiral if both rings are oriented, a pair of oriented rings intersecting the central ring of a linear [3]catenane represents an achiral topology. In spite of their amphichirality, the peripheral rings' two relative orientations (**Figure 5.54a**) nevertheless differentiate a pair of *conditional* topological isomers,[195] named as such because their isomerism is possible only on the *condition* that the outer rings are oriented. One example (**Figure 5.54b**) of a pair of conditional topological isomers is that of the [3]catenanes **C560a**$^{4+}$ and **C560b**$^{4+}$, which comprises a pair of cyclodirectional derivatives of BPP34C10 (oriented by the presence of a single ester bond) mechanically interlocked[489] with a central cyclobis(paraquat-4,4´-biphenylene) (CBPQB^{4+}) ring. These isomers are isolated in admixture, presumably in equal ratios, following a typical clipping protocol akin to those summarized in **Section 2.3.3.9**. Attempts to separate the isomers chromatographically were unsuccessful. More recently, the donor-acceptor [3]catenane **C561**$^{8+}$, comprising cyclodirectional azide-functionalized CBPQT^{4+} rings interlocked around a central DN50C14 crown ether, was obtained[195] as single crystals. Structure resolution by X-Ray diffraction reveal (**Figure 5.54c**) that the crystals contain only one of the two conditional topological isomers which presumably coexist in solution. The seminal cyclodextrin [3]catenanes,[188,196] described in **Section 2.3.1.1**, represent another example of conditional topological isomers, since their peripheral CD rings are oriented by the polarities of their glycosidic bonds.

In general, the introduction of oriented rings into catenanes adds considerable complexity to the interpretation of their ^{1}H NMR spectra in solution, owing to their low symmetries. At 253 K, where dynamic within-the-annulus and through-the-annulus pirouetting motions are slow on the ^{1}H NMR timescale, the ^{1}H NMR spectrum of **C561**$^{8+}$ is intractably complicated. Although it is expected that **C561**$^{8+}$ and its conditional topological isomer are both present in solution, separate signals corresponding to these isomers could not be observed in the fast exchange regime at elevated temperatures where pirouetting is fast on the ^{1}H NMR timescale. These sorts of analytical difficulties will most likely appear more frequently as increasingly complex topologies continue to emerge.

Topological Rubber Gloves

There are examples[490–493] of molecules known as 'topological rubber gloves', which are defined as objects that are topologically achiral, yet rigidly chiral in every possible presentation. In other words, a topological rubber glove is chiral on the condition that it is considered in a frozen presentation. Chambron and Mislow's seminal example[492] of a topological rubber glove in the form (**Figure 5.55**) of

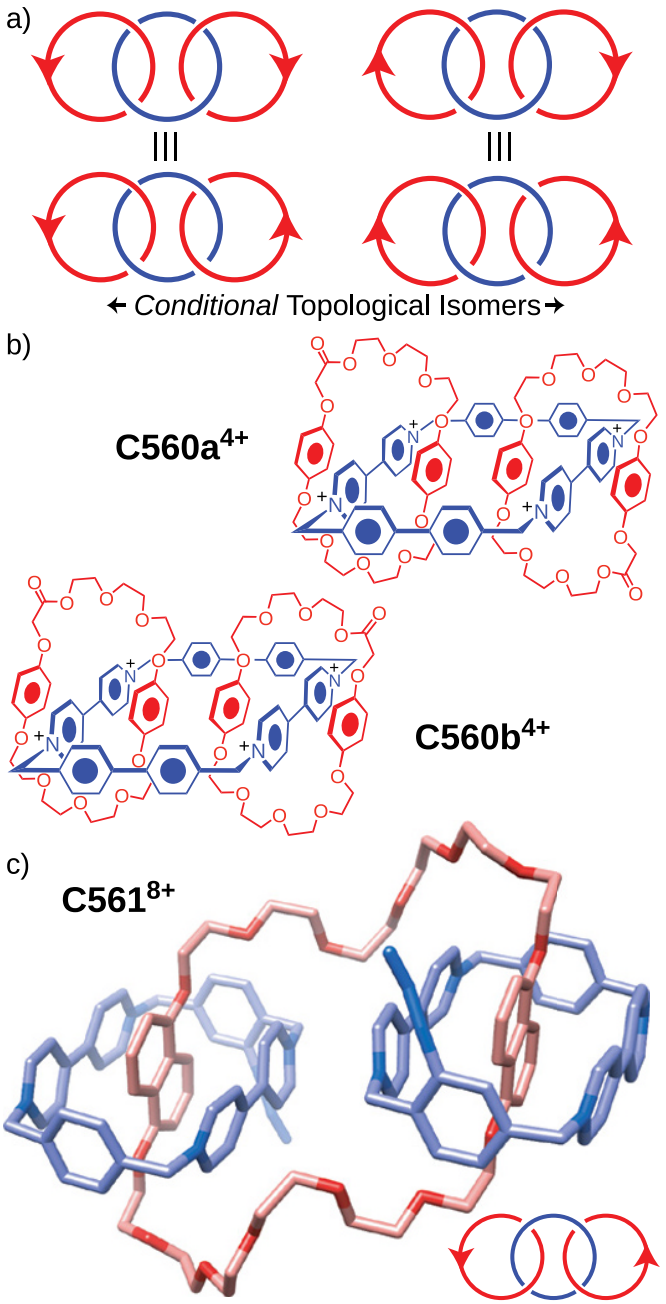


Figure 5.54 Conditional topological chirality. (a) The graph of a three-link chain possessing two oriented peripheral rings is topologically achiral, yet two conditional topological isomers are possible depending on the relative orientations of the rings. (b) Stereoformulas of the conditional topological isomers, **C560a**$^{4+}$ and **C560b**$^{4+}$, comprising a tetracationic cyclophane interlocked with two cyclodirectional crown ethers. (c) The donor-acceptor [3]catenane **C561**$^{8+}$, which possesses two oriented azide-functionalized CBPQT^{4+} rings, crystallizes apparently as only one of the two possible conditional topological isomers.[195] A tubular representation of the solid-state structure is illustrated with hydrogen atoms and PF_6^- counterions omitted for the sake of clarity.

a molecular link is the [2]catenand **C562**, which was obtained by demetalation of the corresponding Cu^{I} [2]catenate. Only one of the rings—the one based on *p*-tolyl-1,10-phenanthroline—is oriented. The other ring containing a DNP unit, which is not oriented, can attain a conformation with C_2 symmetry, yet this symmetry is destroyed upon catenation with the oriented ring, since the σ plane within each ring cannot become coplanar in the catenated state. The mirror-image presentations (**Figure 5.55**) of **C562** are asymmetric, yet they can be converted by rotating the DNP unit 180° about its central C–C bond. These rotations occur rapidly on the ^{1}H NMR timescale, leading to a time-averaged C_2 symmetry, in spite of the fact that no individual conformation or presentation of **C562** can belong to this point group!

Concluding Remarks

A very rich array of isomerism is possible as a direct consequence of the mechanical bond, allowing mechanomolecules to express completely new types of structure and motion that have never been observed before. In many cases, the isomers resulting from mechanical bonds—i.e., mechanostereoisomers—are illuminated by analogies and comparisons involving the stereoisomerism associated with covalent bonds. Words such as co-constitution, co-conformation, and co-configuration are employed in mechanostereochemistry to describe concepts in mechanical bonding that are reminiscent of their counterparts in the stereochemistry of covalent bonds. Co-constitution and co-configuration describe the constitution and chirality, respectively, of a mechanomolecule, while co-conformation describes the relative positions of its components parts.

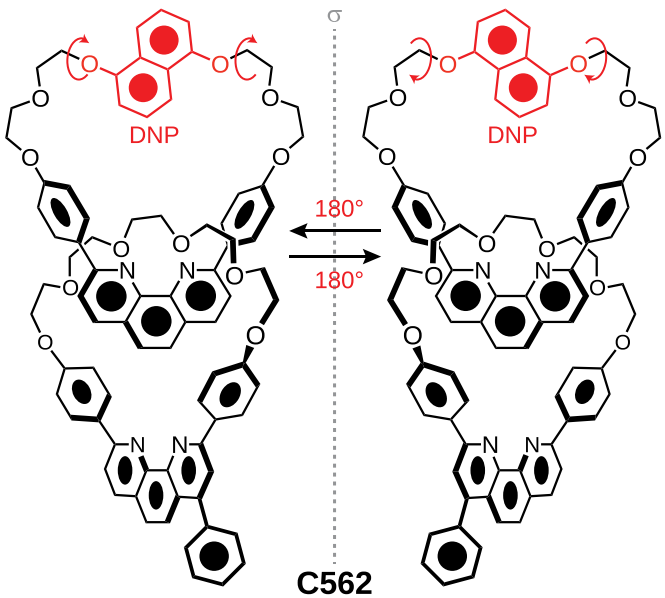


Figure 5.55 The [2]catenane **C562** is a topological rubber glove because it is topologically achiral, yet rigidly chiral in every presentation.[492] In spite of the achiral topology, the Euclidean chirality of the link is a consequence of the mechanical bond, since it is responsible for the loss of the non-oriented ring's C_2 axis of symmetry upon catenation by the oriented link. The chiral presentations related by a mirror plane can be deformed into one another by a 180° rotation of the DNP unit about its central C–C bond.

Readers are reminded that, although mechanostereoisomerism may be subdivided into dynamic (**Section 5.1**) and static (**Section 5.2**) forms, the line between them is blurred by cases where dynamic mechanostereoisomers are rendered static, as well as by cases where static mechanostereoisomers interconvert dynamically. Exemplifying the former scenario, we have reviewed many dynamic mechanostereoisomers that interconvert between different co-conformations by intramolecular translation (**Section 5.1.1**), yet there are also cases of translational isomers—e.g., Schill's [3]catenanes[19] **C501a-c**, Vögtle's [2]catenanes[20] **C502a-c**, molecular shuttles **ZnR522**$^{4+}$,[156] **R523f**,[157] and **R525OBz**,[23] as well as several of the ratchets[21–23,494,495] described in **Section 6.15.2**—which are rendered static by high kinetic barriers to translation. Conversely, static mechanostereoisomers arising from differences in orientation (**Section 5.2.1**), ring sequence (**Section 5.2.2**), mechanical chirality (**Section 5.2.3**) or topology (**Section 5.2.4**) can sometimes be interconverted by dynamic processes—e.g., the inversion of mechanical helicity (**Section 5.2.3.3**) by dynamic rocking (**Section 5.2.3**) processes,[389,397] the inversion of mechanically planar chirality by bowl-to-bowl inversion[264] of cyanostar macrocycles (**Section 2.3.6.4**) and calixarenes[260] (**Section 2.3.9.1**), and the inversion[446] of conditional topological chirality (**Section 5.2.4.1**) as a result of the dynamic rearrangement of coordinative bonds in **Zn$_2$C552**$^{4+}$. The dynamics associated with mechanical bonds can also influence stereochemical configuration, as demonstrated[23] by the dynamic inversion of a prochiral center in the degenerate molecular shuttle **R525OH**, for example. Thus, the (mechano)stereochemistry of mechanomolecules may be understood as the emergent structural properties arising from a combination of the Euclidean and topological stereochemistry of covalently bonded molecular entities (component parts) that share mechanical bonds.

The mechanical bonds that constrain translation (**Section 5.1.1**), pirouetting (**Section 5.1.2**), and rocking (**Section 5.1.3**) in mechanomolecules allow them to express intramolecular motions with much greater amplitudes than most intramolecular motions constrained by covalent bonds, such as conformational torsions and (*E*/*Z*) isomerization. These large-amplitude motions set the stage for the design of sophisticated aritificial molecular machines, such as switches and motors (**Chapter 6**), which represent one of the most contemporary frontiers in molecular nanotechnology. The promise of robust dynamics (**Section 5.1.2.4**) in solid-state materials and at interfaces may support the development of novel functions for these mechanically bonded systems. On the other hand, static mechanostereoisomerism arising from differences in the orientations (**Section 5.2.1**), sequences (**Section 5.2.2**), mechanical chirality (**Section 5.2.3**), and topology (**Section 5.2.4**) of MIMs provides a virtual playground of

intellectually stimulating activity for chemists to contemplate. There remains a bounty of open problems and challenges that are poised to be tackled by synthetic and theoretical chemists alike. For example, it is particularly striking, from a theoretical perspective, that little can be done at this stage to predict the relative ground-state energies of the translational isomers (**Section 5.1.1.1**) of bistable and multistable catenanes. On the experimental side, there remain many challenges associated with, not only discovering new forms of isomerism and chirality, but also understanding how they affect structure-property relationships. Many of these concepts, such as sequence isomerism and mechanically planar/helical/axial chiralities, are still very new, representing the cutting edge of contemporary research in (mechano)stereochemistry.

References

(1) Eliel, E. L. *Stereochemistry of Carbon Compounds*; McGraw-Hill Book Company: New York, **1962**.

(2) IUPAC. *Compendium of Chemical Terminology*, 2nd Ed. (the “Gold Book”). Compiled by A. D. McNaught and A. Wilkinson. Blackwell Scientific Publications, Oxford (**1997**). XML on-Line Corrected Version: http://Goldbook.Iupac.org Created by M. Nic, J. Jirat, B. Kosata; Updates Compiled by A. Jenkins. ISBN 0-9678550-9-8. DOI: 10.1351/Goldbook.

(3) Vignon, S. A.; Stoddart, J. F. Exploring Dynamics and Stereochemistry in Mechanically-Interlocked Compounds. *Collect. Czech. Chem. Commun*. **2005**, *70*, 1493–1576.

(4) Leigh, D. A.; Pérez, E. M. Dynamic Chirality: Molecular Shuttles and Motors. *Top. Curr. Chem*. **2006**, *265*, 185–208.

(5) Neal, E. A.; Goldup, S. M. Chemical Consequences of Mechanical Bonding in Catenanes and Rotaxanes: Isomerism, Modification, Catalysis and Molecular Machines for Synthesis. *Chem. Commun*. **2014**, *50*, 5128–5142.

(6) Feynman, R. P.; Leighton, R. B.; Sands, M. *The Feynman Lectures on Physics*. Basic Books: New York, **1963**.

(7) Fyfe, M. C. T.; Glink, P. T.; Menzer, S.; Stoddart, J. F.; White, A. J. P.; Williams, D. J. Anion-Assisted Self-Assembly. *Angew. Chem., Int. Ed. Engl.* **1997**, *36*, 2068–2070.

(8) Fyfe, M. C. T.; Stoddart, J. F. Synthetic Supramolecular Chemistry. *Acc. Chem. Res.* **1997**, *30*, 393–401.

(9) Ashton, P. R.; Reder, A. S.; Spencer, N.; Stoddart, J. F. Self-Assembly of a Chiral Bis[2]catenane. *J. Am. Chem. Soc*. **1993**, *115*, 5286–5287.

(10) Deng, H.; Olson, M. A.; Stoddart, J. F.; Yaghi, O. M. Robust Dynamics. *Nature Chem*. **2010**, *2*, 439–443.

(11) Truhlar, D. G.; Garrett, B. C.; Klippenstein, S. J. Current Status of Transition-State Theory. *J. Phys. Chem*. **1996**, *100*, 12771–12800.

(12) Hänggi, P.; Talkner, P.; Borkovec, M. Reaction-Rate Theory: Fifty Years After Kramers. *Rev. Mod. Phys*. **1990**, *62*, 251–341.

(13) Kramers, H. A. Brownian Motion in a Field of Force and the Diffusion Model of Chemical Reactions. *Physica* **1940**, *7*, 284–304.

(14) Coskun, A.; Spruell, J. M.; Barin, G.; Dichtel, W. R.; Flood, A. H.; Botros, Y. Y.; Stoddart, J. F. High Hopes: Can Molecular Electronics Realise Its Potential? *Chem. Soc. Rev*. **2012**, *41*, 4827–4859.

(15) Eliel, E. L.; Allinger, N. L.; Angyal, S. J.; Morrison, G. A. *Conformational Analysis*; John Wiley & Sons: New York, **1965**.

(16) Collier, C. P.; Mattersteig, G.; Wong, E. W.; Luo, Y.; Beverly, K.; Sampaio, J.; Raymo, F. M.; Stoddart, J. F.; Heath, J. R. A [2]Catenane-Based Solid State Electronically Reconfigurable Switch. *Science* **2000**, *289*, 1172–1175.

(17) Steuerman, D. W.; Tseng, H.-R.; Peters, A. J.; Flood, A. H.; Jeppesen, J. O.; Nielsen, K. A.; Stoddart, J. F.; Heath, J. R. Molecular-Mechanical Switch-Based Solid-State Electrochromic Devices. *Angew. Chem., Int. Ed.* **2004**, *43*, 6486–6491.

(18) Schill, G.; Doerjer, G.; Logemann, E.; Vetter, W. Reduktive Spaltung von 2,2-Dialkyl-1,3-benzodioxol-Derivaten mit Diisobutylaluminiumhydrid. Synthese eines [2]-Catenans mit einem 22-Gliedrigen Makroheterocyclus. *Chem. Ber.* **1980**, *113*, 3697–3705.

(19) Schill, G.; Rissler, K.; Fritz, H.; Vetter, W. Synthesis, Isolation, and Identification of Translationally Isomeric [3] Catenanes. *Angew. Chem., Int. Ed. Engl.* **1981**, *20*, 187–189.

(20) Ottens-Hildebrandt, S.; Meier, S.; Schmidt, W.; Vögtle, F. Isomeric Catenanes of Lactam Type and Their Formation Mechanism. *Angew. Chem., Int. Ed. Engl.* **1994**, *33*, 1767–1770.

(21) Hernandez, J. V.; Kay, E. R.; Leigh, D. A. A Reversible Synthetic Rotary Molecular Motor. *Science* **2004**, *306*, 1532–1537.

(22) Chatterjee, M. N.; Kay, E. R.; Leigh, D. A. Beyond Switches: Ratcheting a Particle Energetically Uphill with a Compartmentalized Molecular Machine. *J. Am. Chem. Soc*. **2006**, *128*, 4058–4073.

(23) Alvarez-Pérez, M.; Goldup, S. M.; Leigh, D. A.; Slawin, A. M. Z. A Chemically-Driven Molecular Information Ratchet. *J. Am. Chem. Soc*. **2008**, *130*, 1836–1838.

(24) Olson, M. A.; Braunschweig, A. B.; Ikeda, T.; Fang, L.; Trabolsi, A.; Slawin, A. M. Z.; Khan, S. I.; Stoddart, J. F. Thermodynamic Forecasting of Mechanically Interlocked Switches. *Org. Biomol. Chem*. **2009**, *7*, 4391–4405.

(25) Fahrenbach, A. C.; Bruns, C. J.; Cao, D.; Stoddart, J. F. Ground-State Thermodynamics of Bistable Redox-Active Donor–Acceptor Mechanically Interlocked Molecules. *Acc. Chem. Res*. **2012**, *45*, 1581–1592.

(26) Moonen, N. N. P.; Flood, A. H.; Fernández, J. M.; Stoddart, J. F. Towards a Rational Design of Molecular Switches and Sensors From Their Basic Building Blocks. *Top. Curr. Chem*. **2005**, *262*, 99–132.

(27) Fahrenbach, A. C.; Bruns, C. J.; Li, H.; Trabolsi, A.; Coskun, A.; Stoddart, J. F. Ground-State Kinetics of Bistable Redox-Active Donor–Acceptor Mechanically Interlocked Molecules. *Acc. Chem. Res*. **2014**, *47*, 482–493.

(28) Anelli, P.-L.; Ashton, P. R.; Ballardini, R.; Balzani, V.; Delgado, M.; Gandolfi, M. T.; Goodnow, T. T.; Kaifer, A. E.; Philp, D.; Pietraszkiewicz, M.; Prodi, L.; Reddington, M. V.; Slawin. A. M. Z.; Spencer, N.; Stoddart, J. F.; Vicent, C.; Williams, D. J. Molecular Meccano 1. [2]Rotaxanes and a [2]Catenane Made to Order. *J. Am. Chem. Soc.* **1992**, *114*, 193–218.

(29) Amabilino, D. B.; Ashton, P. R.; Brown, C. L.; Córdova, E.; Godinez, L. A.; Goodnow, T. T.; Kaifer, A. E.; Newton, S. P.; Pietraszkiewicz, M.; Philp, D.; Raymo, f. M.; Reder, A. S.; Rutland, M. T.; Slawin, A. M. Z.; Spencer, N.; Stoddart, J. F.; Williams, D. J. Molecular Meccano 2. Self-Assembly of [*n*]-Catenanes. *J. Am. Chem. Soc.* **1995**, *117*, 1271–1293.

(30) Amabilino, D. B.; Anelli, P.-L.; Ashton, P. R.; Brown, G. R.; Córdova, E.; Godínez, L. A.; Hayes, W.; Kaifer, A. E.; Philp, D.; Slawin, A. M. Z.; Spencer, N.; Stoddart, J. F.; Tolley, M. S.; Williams, D. J. Molecular Meccano 3. Constitutional and Translational Isomerism in [2]Catenanes and [*n*]-Pseudorotaxanes. *J. Am. Chem. Soc.* **1995**, *117*, 11142–11170.

(31) Ashton, P. R.; Ballardini, R.; Balzani, V.; Credi, A.; Gandolfi, M. T.; Menzer, S.; Pérez-García, L.; Prodi, L.; Stoddart, J. F.; Venturi, M.; White, A. J. P.; Williams, D. J. Molecular Meccano 4. The Self-Assembly of [2]Catenanes Incorporating Photoactive and Electroactive π-Extended Systems. *J. Am. Chem. Soc.* **1995**, *117*, 11171–11197.

(32) Anelli, P.-L.; Asakawa, M.; Ashton, P. R.; Bissell, R. A.; Clavier, G.; Górski, R.; Kaifer, A. E.; Langford, S. J.; Mattersteig, G.; Menzer, S.; Philp, D.; Slawin, A. M. Z.; Spencer, N.; Stoddart, J. F.; Tolley, M. S.; Williams, D. J. Molecular Meccano 10. Toward Controllable Molecular Shuttles. *Chem. Eur. J.* **1997**, *3*, 1113–1135.

(33) Amabilino, D. B.; Ashton, P. R.; Boyd, S. E.; Gómez-López, M.; Hayes, W.; Stoddart, J. F. Molecular Meccano 17. Translational Isomerism in Some Two- and Three-Station [2]Rotaxanes. *J. Org. Chem.* **1997**, *62*, 3062–3075.
(34) Asakawa, M.; Ashton, P. R.; Dehaen, W.; L'abbé, G.; Menzer, S.; Nouwen, J.; Raymo, F. M.; Stoddart, J. F.; Tolley, M. S.; Toppet, S.; White, A. J. P.; Williams, D. J. Molecular Meccano 19. Self-Assembly of Novel [2]Catenanes and [2]Pseudorotaxanes Incorporating Thiacrown Ethers or Their Acyclic Analogs. *Chem. Eur. J.* **1997**, *3*, 772–787.
(35) Asakawa, M.; Ashton, P. R.; Boyd, S. E.; Brown, C. L.; Gillard, R. E.; Kocian, O.; Raymo, F. M.; Stoddart, J. F.; Tolley, M. S.; White, A. J. P.; Williams, D. J. Molecular Meccano 11. Recognition of Bipyridinium-Based Derivatives by Hydroquinone- and/or Dioxynaphthalene-Based Macrocyclic Polyethers: From Inclusion Complexes to the Self-Assembly of [2]Catenanes. *J. Org. Chem.* **1997**, *62*, 26–37.
(36) Ashton, P. R.; Boyd, S. E.; Boyd, S. E.; Claessens, C. G.; Gillard, R. E.; Menzer, S.; Stoddart, J. F.; Tolley, M. S.; White, A. J. P.; Williams, D. J. Molecular Meccano 20. A Novel Type of Isomerism in [3]Catenanes. *Chem. Eur. J.* **1997**, *3*, 788–798.
(37) Ballardini, R.; Balzani, V.; Credi, A.; Brown, C. L.; Gillard, R. E.; Montalti, M.; Philp, D.; Stoddart, J. F.; Venturi, M.; White, A. J. P.; Williams, B. J.; Williams, D. J. Molecular Meccano 22. Controlling Catenations, Properties and Relative Ring-Component Movements in Catenanes with Aromatic Fluorine Substituents. *J. Am. Chem. Soc.* **1997**, *119*, 12503–12513.
(38) Gillard, R. E.; Raymo, F. M.; Stoddart, J. F. Molecular Meccano 26. Controlling Self-Assembly. *Chem. Eur. J.* **1997**, *3*, 1933–1940.
(39) Raymo, F. M.; Houk, K. N.; Stoddart, J. F. Molecular Meccano 28. Origins of Selectivity in Molecular and Supramolecular Entities: Solvent and Electrostatic Control of the Translational Isomerism in [2]Catenanes. *J. Org. Chem.* **1998**, *63*, 6523–6528.
(40) Ballardini, R.; Balzani, V.; Credi, A.; Gandolfi, M. T.; Marquis, D.; Pérez-García, L.; Stoddart, J. F. Molecular Meccano 29. The Synthesis and Spectroscopic Properties of a [2]Catenane Incorporating an Anthracene Chromophoric Unit. *Eur. J. Org. Chem.* **1998**, 81–89.
(41) Amabilino, D. B.; Ashton, P. R.; Balzani, V.; Boyd, S. E.; Credi, A.; Lee, J. Y.; Menzer, S.; Stoddart, J. F.; Venturi, M.; Williams, D. J. Molecular Meccano 30. Oligocatenanes Made to Order. *J. Am. Chem. Soc.* **1998**, *120*, 4295–4307.
(42) Ballardini, R.; Balzani, V.; Gandolfi, M. T.; Gillard, R. E.; Stoddart, J. F.; Tabellini, E. Molecular Meccano 31. The Synthesis and Spectroscopic Properties of Macrocyclic Polyethers Containing Two Different Aromatic Moieties and Their [2]Catenanes Incorporating Cyclobis(paraquat-*p*-phenylene). *Chem. Eur. J.* **1998**, *4*, 449–459.
(43) Amabilino, D. B.; Ashton, P. R.; Stoddart, J. F.; White, A. J. P.; Williams, D. J. Molecular Meccano 32. Kinetic and Thermodynamic Effects in the Self-Assembly of [3]Catenanes in the Solution and Solid States. *Chem. Eur. J.* **1998**, *4*, 460–468.
(44) Ashton, P. R.; Boyd, S. E.; Brindle, A.; Langford, S. J.; Menzer, S.; Pérez-García, L.; Preece, J. A.; Raymo, F. M.; Spencer, N.; Stoddart, J. F.; White, A. J. P.; Williams, D. J. Molecular Meccano 50. Diazapyrenium-Containing Catenanes and Rotaxanes. *New J. Chem.* **1999**, *23*, 587–602.
(45) Ballardini, R.; Balzani, V.; Dehaen, W.; Dell'Erba, A. E.; Raymo, F. M.; Stoddart, J. F.; Venturi, M. Molecular Meccano 56. Anthracene-Containing [2]Rotaxanes: Synthesis, Spectroscopic, and Electrochemical Properties. *Eur. J. Org. Chem.* **2000**, 591–602.
(46) Cabezon, B.; Cao, J.; Raymo, F. M.; Stoddart, J. F.; White, A. J. P.; Williams, D. J. Molecular Meccano 59. Self-Complementary [2]Catenanes and Their Related [3]Catenanes. *Chem. Eur. J.* **2000**, *6*, 2262–2273.
(47) Ashton, P. R.; Brown, C. L.; Cao, J.; Lee, J.-Y.; Newton, S. P.; White, A. J. P.; Raymo, F. M.; Stoddart, J. F.; Williams, D. J. Molecular Meccano 62. Azopyridinium-Containing [2]Pseudorotaxanes and Hydrazopyridinium-Containing [2]Catenanes. *Eur. J. Org. Chem.* **2001**, 957–965.
(48) Tseng, H.-R.; Vignon, S. A.; Celestre, P. C.; Stoddart, J. F.; White, A. J. P.; Williams, D. J. Molecular Meccano 66. Dynamic Chirality: Keen Selection in the Face of Stereochemical Diversity in Mechanically Bonded Compounds. *Chem. Eur. J.* **2003**, *9*, 543–556.
(49) Ashton, P. R.; Blower, M. A.; Philp, D.; Spencer, N.; Stoddart, J. F.; Tolley, M. S.; Ballardini, R.; Ciano, M.; Balzani, V.; Gandolfi, M. T.; Prodi, L; McLean, C. H. The Control of Translational Isomerism in Catenated Structures. *New J. Chem*. **1993**, *17*, 689–695.
(50) Gillard, R. E.; Stoddart, J. F.; White, A. J. P.; Williams, B. J.; Williams, D. J. A Novel Fluorine-Containing [2]Catenane. *J. Org. Chem*. **1996**, *61*, 4504–4505.
(51) Claessens, C. G.; Stoddart, J. F. π–π Interactions in Self-Assembly. *J. Phys. Org. Chem.* **1997**, *10*, 254–272.
(52) Ashton, P. R.; Ballardini, R.; Balzani, V.; Gandolfi, M. T.; Marquis, D. J.-F.; Pérez-García, L.; Prodi, L.; Stoddart, J. F.; Venturi, M. The Self Assembly of Controllable [2]Catenanes. *J. Chem. Soc., Chem. Commun.* **1994**, 177–180.
(53) Amabilino, D. B.; Ashton, P. R.; Pérez-García, L.; Stoddart, J. F. Kinetic Selection in the Template-Directed Self-Assembly of [2]Catenanes. *Angew. Chem., Int. Ed. Engl.* **1995**, *34*, 2378–2380.
(54) Ashton, P. R.; Pérez-García, L.; Stoddart, J. F.; White, A. J. P.; Williams, D. J. Controlling Translational Isomerism in [2]Catenanes. *Angew. Chem., Int. Ed. Engl.* **1995**, *34*, 571–574.
(55) Choi, J. W.; Flood, A. H.; Steuerman, D. W.; Nygaard, S.; Braunschweig, A. B.; Moonen, N. N. P.; Laursen, B. W.; Luo, Y.; DeIonno, E.; Peters, A. J.; Jeppesen, J. O.; Xu, K.; Stoddart, J. F.; Heath, J. R. Ground-State Equilibrium Thermodynamics and Switching Kinetics of Bistable [2]Rotaxanes Switched in Solution, Polymer Gels, and Molecular Electronic Devices. *Chem. Eur. J*. **2006**, *12*, 261–279.
(56) Asakawa, M.; Ashton, P. R.; Balzani, V.; Credi, A.; Mattersteig, G.; Matthews, O. A.; Montalti, M.; Spencer, N.; Stoddart, J. F.; Venturi, M. Electrochemically Induced Molecular Motions in Pseudorotaxanes: A Case of Dual-Mode (Oxidative and Reductive) Dethreading. *Chem. Eur. J*. **1997**, *3*, 1992–1996.
(57) Asakawa, M.; Ashton, P. R.; Balzani, V.; Credi, A.; Hamers, C.; Mattersteig, G.; Montalti, M.; Shipway, A. N.; Spencer, N.; Stoddart, J. F.; Tolley, M. S.; Venturi, M.; White, A. J. P.; Williams, D. J. A Chemically and Electrochemically Switchable [2]Catenane Incorporating a Tetrathiafulvalene Unit. *Angew. Chem., Int. Ed.* **1998**, *37*, 333–337.
(58) Fahrenbach, A. C.; Barnes, J. C.; Li, H.; Benítez, D.; Basuray, A. N.; Fang, L.; Sue, C.-H.; Barin, G.; Dey, S. K.; Goddard, W. A. III; Stoddart, J. F. Measurement of the Ground-State Distributions in Bistable Mechanically Interlocked Molecules Using Slow Scan Rate Cyclic Voltammetry. *Proc. Natl. Acad. Sci. U.S.A.* **2011**, *108*, 20416–20421.
(59) Balzani, V.; Credi, A.; Mattersteig, G.; Matthews, O. A.; Raymo, F. M.; Stoddart, J. F.; Venturi, M.; White, A. J. P.; Williams, D. J. Molecular Meccano 54. Switching of Pseudorotaxanes and Catenanes Incorporating a Tetrathiafulvalene Unit by Redox and Chemical Inputs. *J. Org. Chem.* **2000**, *65*, 1924–1936.
(60) Diehl, M. R.; Steuerman, D. W.; Tseng, H.-R.; Vignon, S. A.; Star, A.; Celestre, P. C.; Stoddart, J. F.; Heath, J. R. Single-Walled Carbon Nanotube Based Molecular Switch Tunnel Junctions. *ChemPhysChem* **2003**, *4*, 1335–1339.
(61) Deng, W.-Q.; Flood, A. H.; Stoddart, J. F.; Goddard, W. A. III. An Electrochemical Color-Switchable RGB Dye: Tristable [2]Catenane. *J. Am. Chem. Soc*. **2005**, *127*, 15994–15995.
(62) Ikeda, T.; Saha, S.; Aprahamian, I.; Leung, K. C.-F.; Williams, A.; Deng, W.-Q.; Flood, A. H.; Goddard, W. A. III; Stoddart, J. F. Toward Electrochemically Controllable Tristable Three-Station [2]Catenanes. *Chem. Asian J*. **2007**, *2*, 76–93.
(63) Zhao, Y.-L.; Trabolsi, A.; Stoddart, J. F. A Bistable Pretzelane. *Chem. Commun.* **2009**, 4844–4846.

(64) Olson, M. A.; Braunschweig, A. B.; Fang, L.; Ikeda, T.; Klajn, R.; Trabolsi, A.; Wesson, P. J.; Benítez, D.; Benítez, D.; Mirkin, C. A.; Grzybowski, B. A.; Stoddart, J. F. A Bistable Poly[2]-catenane Forms Nanosuperstructures. *Angew. Chem., Int. Ed.* **2009**, *48*, 1792–1797.
(65) Klajn, R.; Fang, L.; Coskun, A.; Olson, M. A.; Wesson, P. J.; Stoddart, J. F.; Grzybowski, B. A. Metal Nanoparticles Functionalized with Molecular and Supramolecular Switches. *J. Am. Chem. Soc*. **2009**, *131*, 4233–4235.
(66) Spruell, J. M.; Coskun, A.; Friedman, D. C.; Forgan, R. S.; Sarjeant, A. A.; Trabolsi, A.; Fahrenbach, A. C.; Barin, G.; Paxton, W. F.; Dey, S. K.; Olson, M. A.; Benítez, D.; Tkatchouk, E.; Colvin, M. T.; Carmielli, R.; Caldwell, S. T.; Rosair, G. M.; Hewage, S. G.; Duclairoir, F.; Seymour, J. L.; Slawin, A. M. Z. Goddard, W. A. III; Wasielewski, M. R.; Cooke, G.; Stoddart, J. F. Highly Stable Tetrathiafulvalene Radical Dimers in [3]Catenanes. *Nature Chem*. **2010**, *2*, 870–879.
(67) Barin, G.; Coskun, A.; Friedman, D. C.; Olson, M. A.; Colvin, M. T.; Carmielli, R.; Dey, S. K.; Bozdemir, O. A.; Wasielewski, M. R.; Stoddart, J. F. A Multistate Switchable [3]Rotacatenane. *Chem. Eur. J*. **2011**, *17*, 213–222.
(68) Coskun, A.; Spruell, J. M.; Barin, G.; Fahrenbach, A. C.; Forgan, R. S.; Colvin, M. T.; Carmieli, R.; Benítez, D.; Tkatchouk, E.; Friedman, D. C.; Sarjeant, A. A.; Wasielewski, M. R. Goddard, W. A. III; Stoddart, J. F. Mechanically Stabilized Tetrathiafulvalene Radical Dimers. *J. Am. Chem. Soc*. **2011**, *133*, 4538–4547.
(69) Wang, C.; Cao, D.; Fahrenbach, A. C.; Grunder, S.; Dey, S. K.; Sarjeant, A. A.; Stoddart, J. F. The Effects of Conformation on the Noncovalent Bonding Interactions in a Bistable Donor–Acceptor [3]Catenane. *Chem. Commun*. **2012**, *48*, 9245–9247.
(70) Barin, G.; Frasconi, M.; Dyar, S. M.; Iehl, J.; Buyukcakir, O.; Sarjeant, A. A.; Carmieli, R.; Coskun, A.; Wasielewski, M. R.; Stoddart, J. F. Redox-Controlled Selective Docking in a [2]Catenane Host. *J. Am. Chem. Soc*. **2013**, *135*, 2466–2469.
(71) Luo, Y.; Collier, C. P.; Jeppesen, J. O.; Nielsen, K. A.; DeIonno, E.; Ho, G.; Perkins, J.; Tseng, H.-R.; Yamamoto, T.; Stoddart, J. F.; Heath, J. R. Two-Dimensional Molecular Electronics Circuits. *ChemPhysChem* **2002**, *3*, 519–525.
(72) Jang, S. S.; Jang, Y. H.; Kim, Y.-H.; Goddard, W. A. III; Flood, A. H.; Laursen, B. W.; Tseng, H.-R.; Stoddart, J. F.; Jeppesen, J. O.; Choi, J. W.; Steuerman, D. W.; DeIonno, E.; Heath, J. R. Structures and Properties of Self-Assembled Monolayers of Bistable [2]Rotaxanes on Au(111) Surfaces From Molecular Dynamics Simulations Validated with Experiment. *J. Am. Chem. Soc*. **2005**, *127*, 1563–1575.
(73) Lee, I. C.; Frank, C. W.; Yamamoto, T.; Tseng, H.-R.; Flood, A. H.; Stoddart, J. F.; Jeppesen, J. O. Langmuir and Langmuir-Blodgett Films of Amphiphilic Bistable Rotaxanes. *Langmuir* **2004**, *20*, 5809–5828.
(74) Yu, H.; Luo, Y.; Beverly, K.; Stoddart, J. F.; Tseng, H.-R.; Heath, J. R. The Molecule-Electrode Interface in Single-Molecule Transistors. *Angew. Chem., Int. Ed.* **2003**, *42*, 5706–5711.
(75) Tseng, H.-R.; Wu, D.; Fang, N. X.; Zhang, X.; Stoddart, J. F. The Metastability of an Electrochemically Controlled Nanoscale Machine on Gold Surfaces. *ChemPhysChem* **2004**, *5*, 111–116.
(76) Zheng, Y. B.; Yang, Y.-W.; Jensen, L.; Fang, L.; Juluri, B. K.; Flood, A. H.; Weiss, P. S.; Stoddart, J. F.; Huang, T. J. Active Molecular Plasmonics: Controlling Plasmon Resonances with Molecular Switches. *Nano Lett*. **2009**, *9*, 819–825.
(77) Flood, A. H.; Peters, A. J.; Vignon, S. A.; Steuerman, D. W.; Tseng, H.-R.; Kang, S.; Heath, J. R.; Stoddart, J. F. The Role of Physical Environment on Molecular Electromechanical Switching. *Chem. Eur. J*. **2004**, *10*, 6558–6564.
(78) Nguyen, T. D.; Liu, Y.; Saha, S.; Leung, K. C.-F.; Stoddart, J. F.; Zink, J. I. Design and Optimization of Molecular Nanovalves Based on Redox-Switchable Bistable Rotaxanes. *J. Am. Chem. Soc*. **2007**, *129*, 626–634.
(79) Saha, S.; Flood, A. H.; Stoddart, J. F.; Impellizzeri, S.; Silvi, S.; Venturi, M.; Credi, A. A Redox-Driven Multicomponent Molecular Shuttle. *J. Am. Chem. Soc*. **2007**, *129*, 12159–12171.
(80) Aprahamian, I.; Dichtel, W. R.; Ikeda, T.; Heath, J. R.; Stoddart, J. F. A Clicked Bistable [2]Rotaxane. *Org. Lett*. **2007**, *9*, 1287–1290.
(81) Aprahamian, I.; Yasuda, T.; Ikeda, T.; Saha, S.; Dichtel, W. R.; Isoda, K.; Kato, T.; Stoddart, J. F. A Liquid-Crystalline Bistable [2]Rotaxane. *Angew. Chem., Int. Ed.* **2007**, *46*, 4675–4679.
(82) Yasuda, T.; Tanabe, K.; Tsuji, T.; Cotí, K. K.; Aprahamian, I.; Stoddart, J. F.; Kato, T. A Redox-Switchable [2]Rotaxane in a Liquid-Crystalline State. *Chem. Commun*. **2010**, *46*, 1224–1226.
(83) Zhao, Y.-L.; Aprahamian, I.; Trabolsi, A.; Erina, N.; Stoddart, J. F. Organogel Formation by a Cholesterol-Stoppered Bistable [2]Rotaxane and Its Dumbbell Precursor. *J. Am. Chem. Soc*. **2008**, *130*, 6348–6350.
(84) Coskun, A.; Wesson, P. J.; Klajn, R.; Trabolsi, A.; Fang, L.; Olson, M. A.; Dey, S. K.; Grzybowski, B. A.; Stoddart, J. F. Molecular-Mechanical Switching at the Nanoparticle-Solvent Interface: Practice and Theory. *J. Am. Chem. Soc*. **2010**, *132*, 4310–4320.
(85) Tseng, H.-R.; Vignon, S. A.; Stoddart, J. F. Toward Chemically Controlled Nanoscale Molecular Machinery. *Angew. Chem., Int. Ed.* **2003**, *42*, 1491–1495.
(86) Tseng, H.-R.; Vignon, S. A.; Celestre, P. C.; Perkins, J.; Jeppesen, J. O.; Di Fabio, A.; Ballardini, R.; Gandolfi, M. T.; Venturi, M.; Balzani, V.; Stoddart, J. F. Redox-Controllable Amphiphilic [2]Rotaxanes. *Chem. Eur. J*. **2004**, *10*, 155–172.
(87) Huang, T. J.; Tseng, H.-R.; Sha, L.; Lu, W.; Brough, B.; Flood, A. H.; Yu, B.-D.; Celestre, P. C.; Chang, J. P.; Stoddart, J. F.; Ho, C.-M. Mechanical Shuttling of Linear Motor-Molecules in Condensed Phases on Solid Substrates. *Nano Lett*. **2004**, *4*, 2065–2071.
(88) Nørgaard, K.; Laursen, B. W.; Nygaard, S.; Kjaer, K.; Tseng, H.-R.; Flood, A. H.; Stoddart, J. F.; Bjørnholm, T. Structural Evidence of Mechanical Shuttling in Condensed Monolayers of Bistable Rotaxane Molecules. *Angew. Chem., Int. Ed.* **2005**, *44*, 7035–7039.
(89) Ye, T.; Kumar, A. S.; Saha, S.; Takami, T.; Huang, T. J.; Stoddart, J. F.; Weiss, P. S. Changing Stations in Single Bistable Rotaxane Molecules under Electrochemical Control. *ACS Nano* **2010**, *4*, 3697–3701.
(90) Nguyen, T. D.; Tseng, H.-R.; Celestre, P. C.; Flood, A. H.; Liu, Y.; Stoddart, J. F.; Zink, J. I. A Reversible Molecular Valve. *Proc. Natl. Acad. Sci. U.S.A*. **2005**, *102*, 10029–10034.
(91) Huang, T. J.; Brough, B.; Ho, C.-M.; Liu, Y.; Flood, A. H.; Bonvallet, P. A.; Tseng, H.-R.; Stoddart, J. F.; Baller, M.; Magonov, S. A Nanomechanical Device Based on Linear Molecular Motors. *Appl. Phys. Lett*. **2004**, *85*, 5391–5393.
(92) Liu, Y.; Flood, A. H.; Bonvallet, P. A.; Vignon, S. A.; Northrop, B. H.; Tseng, H.-R.; Jeppesen, J. O.; Huang, T. J.; Brough, B.; Baller, M.; Magonov, S.; Solares, S. D.; Goddard, W. A. III; Ho, C.-M.; Stoddart, J. F. Linear Artificial Molecular Muscles. *J. Am. Chem. Soc*. **2005**, *127*, 9745–9759.
(93) Brough, B.; Northrop, B. H.; Schmidt, J. J.; Tseng, H.-R.; Houk, K. N.; Stoddart, J. F.; Ho, C.-M. Evaluation of Synthetic Linear Motor-Molecule Actuation Energetics. *Proc. Natl. Acad. Sci. U.S.A*. **2006**, *103*, 8583–8588.
(94) Flood, A. H.; Wong, E. W.; Stoddart, J. F. Models of Charge Transport and Transfer in Molecular Switch Tunnel Junctions of Bistable Catenanes and Rotaxanes. *Chem. Phys*. **2006**, *324*, 280–290.
(95) Aprahamian, I.; Olsen, J.-C.; Trabolsi, A.; Stoddart, J. F. Tetrathiafulvalene Radical Cation Dimerization in a Bistable Tripodal [4]Rotaxane. *Chem. Eur. J*. **2008**, *14*, 3889–3895.
(96) Juluri, B. K.; Kumar, A. S.; Liu, Y.; Ye, T.; Yang, Y.-W.; Flood, A. H.; Fang, L.; Stoddart, J. F.; Weiss, P. S.; Huang, T. J. A Mechanical Actuator Driven Electrochemically by Artificial Molecular Muscles. *ACS Nano* **2009**, *3*, 291–300.
(97) Trabolsi, A.; Fahrenbach, A. C.; Dey, S. K.; Share, A. I.; Friedman, D. C.; Basu, S.; Gasa, T. B.; Khashab, N. M.; Saha, S.; Aprahamian, I.; Khatib, H. A.; Flood, A. H.; Stoddart, J. F. A Tristable [2]Pseudo[2]Rotaxane. *Chem. Commun*. **2010**, *46*, 871–873.

(98) Trabolsi, A.; Khashab, N.; Fahrenbach, A. C.; Friedman, D. C.; Colvin, M. T.; Cotí, K. K.; Benítez, D.; Tkatchouk, E.; Olsen, J.-C.; Belowich, M. E.; Carmielli, R.; Khatib, H. A.; Goddard, W. A. III; Wasielewski, M. R.; Stoddart, J. F. Radically Enhanced Molecular Recognition. *Nature Chem.* **2010**, *2*, 42–49.

(99) Avellini, T.; Li, H.; Coskun, A.; Barin, G.; Trabolsi, A.; Basuray, A. N.; Dey, S. K.; Credi, A.; Silvi, S.; Stoddart, J. F.; Venturi, M. Photoinduced Memory Effect in a Redox Controllable Bistable Mechanical Molecular Switch. *Angew. Chem., Int. Ed.* **2012**, *51*, 1611–1615.

(100) Laursen, B. W.; Nygaard, S.; Jeppesen, J. O.; Stoddart, J. F. Counterion-Induced Translational Isomerism in a Bistable [2]Rotaxane. *Org. Lett*. **2004**, *6*, 4167–4170.

(101) Jeppesen, J. O.; Perkins, J.; Becher, J.; Stoddart, J. F. Slow Shuttling in an Amphiphilic Bistable [2]Rotaxane Incorporating a Tetrathiafulvalene Unit. *Angew. Chem., Int. Ed.* **2001**, *40*, 1216–1221.

(102) Jeppesen, J. O.; Nielsen, K. A.; Perkins, J.; Vignon, S. A.; Di Fabio, A.; Ballardini, R.; Gandolfi, M. T.; Venturi, M.; Balzani, V.; Becher, J.; Stoddart, J. F. Amphiphilic Bistable Rotaxanes. *Chem. Eur. J.* **2003**, *9*, 2982–3007.

(103) Jeppesen, J. O.; Nygaard, S.; Vignon, S. A.; Stoddart, J. F. Honing Up a Genre of Amphiphilic Bistable [2]Rotaxanes for Device Settings. *Eur. J. Org. Chem.* **2005**, *196–220*.

(104) Jia, C.; Zhang, D.; Xu, W.; Zhu, D. A New Approach to 4-Alkylthio-1,3-dithiole-2-thione: An Unusual Reaction of a Zinc Complex of 1,3-Dithole-2-thione-4,5-dithiolate. *Org. Lett*. **2001**, *3*, 1941–1944.

(105) Guo, X.; Zhang, D.; Zhang, H.; Fan, Q.; Xu, W.; Ai, X.; Fan, L.; Zhu, D. Donor–Acceptor–Donor Triads Incorporating Tetrathiafulvalene and Perylene Diimide Units: Synthesis, Electrochemical and Spectroscopic Studies. *Tetrahedron* **2003**, *59*, 4843–4850.

(106) Wang, C.; Olson, M. A.; Fang, L.; Benítez, D.; Tkatchouk, E.; Basu, S.; Basuray, A. N.; Zhang, D.; Zhu, D.; Goddard, W. A. III; Stoddart, J. F. Isolation by Crystallization of Translational Isomers of a Bistable Donor-Acceptor [2]Catenane. *Proc. Natl. Acad. Sci. U.S.A*. **2010**, *107*, 13991–13996.

(107) Pittman, C. U., Jr; Narita, M.; Liang, Y. F. Preparation and Reactions of Bifunctionalized Tetrathiafulvalenes. *J. Org. Chem*. **1976**, *41*, 2855–2860.

(108) Nozdryn, T.; Clemenceau, D.; Cousseau, J.; Morisson, V.; Gorgues, A.; Orduna, J.; Uriel, S.; Garin, J. Selective Reduction of the Ester Group in the 1,3-Dithiol-2-(thi)one and Tetrathiafulvalene Series. Access to the Related Phosphonium Salts and Their Wittig Reactions. *Synth. Met*. **1993**, *56*, 1768–1771.

(109) Fang, L.; Wang, C.; Fahrenbach, A. C.; Trabolsi, A.; Botros, Y. Y.; Stoddart, J. F. Dual Stimulus Switching of a [2]Catenane in Water. *Angew. Chem., Int. Ed.* **2011**, *50*, 1805–1809.

(110) Wang, C.; Cao, D.; Fahrenbach, A. C.; Fang, L.; Olson, M. A.; Friedman, D. C.; Basu, S.; Dey, S. K.; Botros, Y. Y.; Stoddart, J. F. Solvent-Dependent Ground-State Distributions in a Donor-Acceptor Redox-Active Bistable [2]Catenane. *J. Phys. Org. Chem*. **2012**, *25*, 544–552.

(111) Wang, C.; Dyar, S. M.; Cao, D.; Fahrenbach, A. C.; Horwitz, N.; Colvin, M. T.; Carmieli, R.; Stern, C. L.; Dey, S. K.; Wasielewski, M. R.; Stoddart, J. F. Tetrathiafulvalene Hetero Radical Cation Dimerization in a Redox-Active [2]Catenane. *J. Am. Chem. Soc*. **2012**, *134*, 19136–19145.

(112) Feng, M.; Guo, X.; Lin, X.; He, X.; Ji, W.; Du, S.; Zhang, D.; Zhu, D.; Gao, H. Stable, Reproducible Nanorecording on Rotaxane Thin Films. *J. Am. Chem. Soc*. **2005**, *127*, 15338–15339.

(113) Feng, M.; Gao, L.; Deng, Z.; Ji, W.; Guo, X.; Du, S.; Shi, D.; Zhang, D.; Zhu, D.; Gao, H. Reversible, Erasable, and Rewritable Nanorecording on an H2 Rotaxane Thin Film. *J. Am. Chem. Soc*. **2007**, *129*, 2204–2205.

(114) Guo, X.; Zhou, Y.; Feng, M.; Xu, Y.; Zhang, D.; Gao, H.; Fan, Q.; Zhu, D. Tetrathiafulvalene-, 1,5-Dioxynaphthalene-, and Cyclobis(paraquat-*p*-phenylene)-Based [2]Rotaxanes with Cyclohexyl and Alkyl Chains as Spacers: Synthesis, Langmuir–Blodgett Films, and Electrical Bistability. *Adv. Funct. Mater*. **2007**, *17*, 763–769.

(115) Feng, M.; Gao, L.; Du, S. X.; Deng, Z. T.; Cheng, Z. H.; Ji, W.; Zhang, D.; Guo, X. F.; Lin, X.; Chi, L. F.; Fuchs, H.; Gao, H. Observation of Structural and Conductance Transition of Rotaxane Molecules at a Submolecular Scale. *Adv. Funct. Mater*. **2007**, *17*, 770–776.

(116) Liu, Y.; Vignon, S. A.; Zhang, X.; Houk, K. N.; Stoddart, J. F. Conformational Diastereoisomerism in a Chiral Pretzelane. *Chem. Commun*. **2005**, *3927–3929*.

(117) Liu, Y.; Vignon, S. A.; Zhang, X.; Bonvallet, P. A.; Khan, S. I.; Houk, K. N.; Stoddart, J. F. Dynamic Chirality in Donor-Acceptor Pretzelanes. *J. Org. Chem*. **2005**, *70*, 9334–9344.

(118) Ashton, P. R.; Bissell, R. A.; Spencer, N.; Stoddart, J. F.; Tolley, M. S. Towards Controllable Molecular Shuttles. 3. *Synlett* **1992**, 923–926.

(119) Asakawa, M.; Ashton, P. R.; Balzani, V.; Boyd, S. E.; Credi, A.; Mattersteig, G.; Menzer, S.; Montalti, M.; Raymo, F. M.; Ruffilli, C.; Stoddart, J. F. Venturi, M.; Williams, D. J. Molecular Meccano 49. Pseudorotaxanes and Catenanes Containing a Redox-Active Unit Derived From Tetrathiafulvalene. *Eur. J. Org. Chem.* **1999**, 985–994.

(120) Castro, R.; Nixon, K. R.; Evanseck, J. D.; Kaifer, A. E. Effects of Side Arm Length and Structure of *para*-Substituted Phenyl Derivatives on Their Binding to the Host Cyclobis(paraquat-*p*-phenylene). *J. Org. Chem*. **1996**, *61*, 7298–7303.

(121) Nygaard, S.; Leung, K. C.-F.; Aprahamian, I.; Ikeda, T.; Saha, S.; Laursen, B. W.; Kim, S.-Y.; Hansen, S. W.; Stein, P. C.; Flood, A. H.; Stoddart, J. F.; Jeppesen, J. O. Functionally Rigid Bistable [2]Rotaxanes. *J. Am. Chem. Soc*. **2007**, *129*, 960–970.

(122) Yoon, I.; Benítez, D.; Zhao, Y.-L.; Miljanić, O. Š.; Kim, S.-Y.; Tkatchouk, E.; Leung, K. C.-F.; Khan, S. I.; Goddard, W. A. III; Stoddart, J. F. Functionally Rigid and Degenerate Molecular Shuttles. *Chem. Eur. J*. **2009**, *15*, 1115–1122.

(123) Lau, J.; Nielsen, M. B.; Thorup, N.; Cava, M. P.; Becher, J.; Bis(pyrrolo)tetrathiafulvalene—An Efficient π-Donor in Supramolecular Chemistry. *Eur. J. Org. Chem*. **1999**, 3335–3341.

(124) Ballardini, R.; Balzani, V.; Di Fabio, A.; Gandolfi, M. T.; Becher, J.; Lau, J.; Nielsen, M. B.; Stoddart, J. F. Macrocycles, Pseudorotaxanes and Catenanes Containing a Pyrrolo-Tetrathiafulvalene Unit: Absorption Spectra, Luminescence Properties and Redox Behavior. *New J. Chem*. **2001**, *25*, 293–298.

(125) Amabilino, D. B.; Ashton, P. R.; Brown, G. R.; Hayes, W.; Stoddart, J. F.; Williams, D. J.; Tolley, M. S. Self-Assembled [2]Catenanes Exhibiting Highly Selective Translational Isomerism. *J. Chem. Soc., Chem. Commun.* **1994**, 2479–2482.

(126) Tomcsi, M. R.; Stoddart, J. F. Bispyrrolotetrathiafulvalene-Containing [2]Catenanes. *J. Org. Chem*. **2007**, *72*, 9335–9338.

(127) Green, J. E.; Choi, J. W.; Boukai, A.; Bunimovich, Y.; Johnston-Halperin, E.; DeIonno, E.; Luo, Y.; Sheriff, B. A.; Xu, K.; Shin, Y. S.; Tseng, H.-R.; Stoddart, J. F.; Heath, J. R. A 160-Kilobit Molecular Electronic Memory Patterned at 10^{11} Bits Per Square Centimetre. *Nature* **2007**, *445*, 414–417.

(128) Bruns, C. J.; Stoddart, J. F. Rotaxane-Based Molecular Muscles. *Acc. Chem. Res.* **2014**, *47*, 2186–2199.

(129) Dahlquist, F. W.; Longmer, K. J.; Vernet, Du, R. B. Direct Observation of Chemical Exchange by a Selective Pulse NMR Technique. *J. Magn. Res*. **1975**, *17*, 406–410.

(130) Jeener, J.; Meier, B. H.; Bachmann, P.; Ernst, R. R. Investigation of Exchange Processes by Two-Dimensional NMR Spectroscopy. *J. Chem. Phys*. **1979**, *71*, 4546–4553.

(131) Perrin, C. L.; Dwyer, T. J. Application of Two-Dimensional NMR to Kinetics of Chemical Exchange. *Chem. Rev*. **1990**, *90*, 935–967.

(132) Gutowski, H. S.; Saika, A. J. Dissociation, Chemical Exchange, and the Proton Magnetic Resonance in Some Aqueous Electrolytes. *J. Chem. Phys*. **1953**, *21*, 1688–1694.
(133) Bovey, F. A. *Nuclear Magnetic Resonance Spectroscopy*; Academic Press: New York, **1969**.
(134) Sutherland, I. O. The Investigation of the Kinetics of Conformational Changes by Nuclear Magnetic Resonance Spectroscopy. *Annu. Rep. NMR Spectroscopy* **1971**, *4*, 71–235.
(135) Anelli, P.-L.; Spencer, N.; Stoddart, J. F. A Molecular Shuttle. *J. Am. Chem. Soc*. **1991**, *113*, 5131–5133.
(136) Ashton, P. R.; Johnston, M. R.; Stoddart, J. F.; Tolley, M. S.; Wheeler, J. The Template-Directed Synthesis of Porphyrin-Stoppered [2]Rotaxanes. *J. Chem. Soc., Chem. Commun.* **1992**, 1128–1131.
(137) Benniston, A. C.; Harriman, A.; Lynch, D. E. Photoactive [2]Rotaxanes: Structure and Photophysical Properties of Anthracene-and Ferrocene-Stoppered [2]Rotaxanes. *J. Am. Chem. Soc*. **1995**, *117*, 5275–5291.
(138) Braunschweig, A. B.; Dichtel, W. R.; Miljanić, O. Š.; Olson, M. A.; Spruell, J. M.; Khan, S. I.; Heath, J. R.; Stoddart, J. F. Modular Synthesis and Dynamics of a Variety of Donor-Acceptor Interlocked Compounds Prepared by Click Chemistry. *Chem. Asian J*. **2007**, *2*, 634–647.
(139) Coskun, A.; Friedman, D. C.; Li, H.; Patel, K.; Khatib, H. A.; Stoddart, J. F. A Light-Gated STOP-GO Molecular Shuttle. *J. Am. Chem. Soc*. **2009**, *131*, 2493–2495.
(140) Li, H.; Zhu, Z.; Fahrenbach, A. C.; Savoie, B. M.; Ke, C.; Barnes, J. C.; Lei, J.; Zhao, Y.-L.; Lilley, L. M.; Marks, T. J.; Ratner, M. A.; Stoddart, J. F. Mechanical Bond-Induced Radical Stabilization. *J. Am. Chem. Soc*. **2013**, *135*, 456–467.
(141) Ashton, P. R.; Philp, D.; Spencer, N.; Stoddart, J. F. A New Design Strategy for the Self-Assembly of Molecular Shuttles. *J. Chem. Soc., Chem. Commun.* **1992**, 1124–1128.
(142) Bělohradský, M.; Elizarov, A. M.; Stoddart, J. F. Speed-Controlled Molecular Shuttles. *Collect. Czech. Chem. Commun*. **2002**, *67*, 1719–1728.
(143) Iijima, T.; Vignon, S. A.; Tseng, H.-R.; Jarrosson, T.; Sanders, J. K. M.; Marchioni, F.; Venturi, M.; Apostoli, E.; Balzani, V.; Stoddart, J. F. Controllable Donor-Acceptor Neutral [2]Rotaxanes. *Chem. Eur. J*. **2004**, *10*, 6375–6392.
(144) Kang, S.; Vignon, S. A.; Tseng, H.-R.; Stoddart, J. F. Molecular Shuttles Based on Tetrathiafulvalene Units and 1,5-Dioxynaphthalene Ring Systems. *Chem. Eur. J*. **2004**, *10*, 2555–2564.
(145) Ashton, P. R.; Bělohradský, M.; Philp, D.; Spencer, N.; Stoddart, J. F. The Self Assembly of [2]- and [3]Rotaxanes by Slippage. *J. Chem. Soc., Chem. Commun.* **1993**, 1274–1277.
(146) Ashton, P. R.; Bělohradský, M.; Philp, D.; Stoddart, J. F. Slippage—An Alternative Method for Assembling [2]Rotaxanes. *J. Chem. Soc., Chem. Commun*. **1993**, 1269–1274.
(147) Jiang, L.; Okano, J.; Orita, A.; Otera, J. Intermittent Molecular Shuttle as a Binary Switch. *Angew. Chem., Int. Ed.* **2004**, *43*, 2121–2124.
(148) Cheng, C.; McGonigal, P. R.; Liu, W.-G.; Li, H.; Vermeulen, N. A.; Ke, C.; Frasconi, M.; Stern, C. L.; Goddard, W. A. III; Stoddart, J. F. Energetically Demanding Transport in a Supramolecular Assembly. *J. Am. Chem. Soc*. **2014**, *136*, 14702–14705.
(149) Hmadeh, M.; Fahrenbach, A. C.; Basu, S.; Trabolsi, A.; Benítez, D.; Li, H.; Albrecht-Gary, A.-M.; Elhabiri, M.; Stoddart, J. F. Electrostatic Barriers in Rotaxanes and Pseudorotaxanes. *Chem. Eur. J*. **2011**, *17*, 6076–6087.
(150) Zhao, X.; Jiang, X.-K.; Shi, M.; Yu, Y.-H.; Xia, W.; Li, Z.-T. Self-Assembly of Novel [3]- and [2]Rotaxanes with Two Different Ring Components: Donor−Acceptor and Hydrogen Bonding Interactions and Molecular-Shuttling Behavior. *J. Org. Chem*. **2001**, *66*, 7035–7043.
(151) Vetter, A.; Abraham, W. Controlling Ring Translation of Rotaxanes. *Org. Biomol. Chem*. **2010**, *8*, 4666–4681.
(152) Gunter, M. J.; Farquhar, S. M.; Jeynes, T. P. Translational Isomerism and Dynamics in Multi-Hydroquinone Derived Porphyrin [2]- and [3]-Catenanes. *Org. Biomol. Chem*. **2003**, *1*, 4097–4112.
(153) Gunter, M. J. Superstructured Porphyrins as Effectors in Dynamic Supramolecular Assemblies: Receptors, Rotaxanes and Catenanes. *Eur. J. Org. Chem*. **2004**, 1655–1673.
(154) Loeb, S. J.; Wisner, J. A. [2]Rotaxane Molecular Shuttles Employing 1,2-Bis(pyridinium)ethane Binding Sites and Dibenzo-24-Crown-8 Ethers. *Chem. Commun.* **2000**, 1939–1940.
(155) Tramontozzi, D. A.; Suhan, N. D.; Eichhorn, S. H.; Loeb, S. J. The Effect of Incorporating Fréchet Dendrons Into Rotaxanes and Molecular Shuttles Containing the 1,2-Bis(pyridinium) ethane⊂[24]Crown-8 Templating Motif. *Chem. Eur. J*. **2010**, *16*, 4466–4476.
(156) Chen, N.-C.; Lai, C.-C.; Liu, Y.-H.; Peng, S.-M.; Chiu, S.-H. Parking and Restarting a Molecular Shuttle in Situ. *Chem. Eur. J*. **2008**, *14*, 2904–2908.
(157) Lane, A. S.; Leigh, D. A.; Murphy, A. Peptide-Based Molecular Shuttles. *J. Am. Chem. Soc*. **1997**, *119*, 11092–11093.
(158) Leigh, D. A.; Troisi, A.; Zerbetto, F. Reducing Molecular Shuttling to a Single Dimension. *Angew. Chem., Int. Ed.* **2000**, *39*, 350–353.
(159) Günbaş, D. D.; Brouwer, A. M. Degenerate Molecular Shuttles with Flexible and Rigid Spacers. *J. Org. Chem*. **2012**, *77*, 5724–5735.
(160) Berná, J.; Alajarín, M.; Marín-Rodríguez, C.; Franco-Pujante, C. Redox Divergent Conversion of a [2]Rotaxane Into Two Distinct Degenerate Partners with Different Shuttling Dynamics. *Chem. Sci*. **2012**, *3*, 2314–2320.
(161) Ghosh, P.; Federwisch, G.; Kogej, M.; Schalley, C. A.; Haase, D.; Saak, W.; Lützen, A.; Gschwind, R. M. Controlling the Rate of Shuttling Motions in [2]Rotaxanes by Electrostatic Interactions: A Cation as Solvent-Tunable Brake. *Org. Biomol. Chem*. **2005**, *3*, 2691–2700.
(162) Ghosh, P.; Mermagen, O.; Schalley, C. A. Novel Template Effect for the Preparation of [2]Rotaxanes with Functionalised Centre Pieces. *Chem. Commun.* **2002**, 2628–2629.
(163) Schwesinger, R.; Schlemper, H. Peralkylated Polyaminophosphazenes—Extremely Strong, Neutral Nitrogen Bases. *Angew. Chem., Int. Ed. Engl.* **1987**, *26*, 1167–1169.
(164) Cao, J.; Fyfe, M. C. T.; Stoddart, J. F.; Cousins, G. R. L.; Glink, P. T. Molecular Meccano 55. Molecular Shuttles by the Protecting Group Approach. *J. Org. Chem.* **2000**, *65*, 1937–1946.
(165) Hirose, K.; Shiba, Y.; Ishibashi, K.; Doi, Y.; Tobe, Y. A Shuttling Molecular Machine with Reversible Brake Function. *Chem. Eur. J*. **2008**, *14*, 3427–3433.
(166) Hirose, K.; Shiba, Y.; Ishibashi, K.; Doi, Y.; Tobe, Y. An Anthracene-Based Photochromic Macrocycle as a Key Ring Component to Switch a Frequency of Threading Motion. *Chem. Eur. J*. **2008**, *14*, 981–986.
(167) Kawaguchi, Y.; Harada, A. A Cyclodextrin-Based Molecular Shuttle Containing Energetically Favored and Disfavored Portions in Its Dumbbell Component. *Org. Lett*. **2000**, *2*, 1353–1356.
(168) Liu, P.; Chipot, C.; Shao, X.; Cai, W. Solvent-Controlled Shuttling in a Molecular Switch. *J. Phys. Chem. C* **2012**, *116*, 4471–4476.
(169) Kolman, V.; Khan, M. S. A.; Babinský, M.; Marek, R.; Sindelar, V. Supramolecular Shuttle Based on Inclusion Complex Between Cucurbit[6]uril and Bispyridinium Ethylene. *Org. Lett*. **2011**, *13*, 6148–6151.
(170) Lee, C.-F.; Leigh, D. A.; Pritchard, R. G.; Schultz, D.; Teat, S. J.; Timco, G. A.; Winpenny, R. E. P. Hybrid Organic-Inorganic Rotaxanes and Molecular Shuttles. *Nature* **2009**, *458*, 314–318.
(171) Ballesteros, B.; Faust, T. B.; Lee, C.-F.; Leigh, D. A.; Muryn, C. A.; Pritchard, R. G.; Schultz, D.; Teat, S. J.; Timco, G. A.;

Winpenny, R. E. P. Synthesis, Structure, and Dynamic Properties of Hybrid Organic-Inorganic Rotaxanes. *J. Am. Chem. Soc.* **2010**, *132*, 15435–15444.
(172) Umehara, T.; Kawai, H.; Fujiwara, K.; Suzuki, T. Entropy- and Hydrolytic-Driven Positional Switching of Macrocycle Between Imine- and Hydrogen-Bonding Stations in Rotaxane-Based Molecular Shuttles. *J. Am. Chem. Soc.* **2008**, *130*, 13981–13988.
(173) Aucagne, V.; Berná, J.; Crowley, J. D.; Goldup, S. M.; Hänni, K. D.; Leigh, D. A.; Lusby, P.; Ronaldson, V. E.; Slawin, A. M. Z.; Viterisi, A.; Walker, B. A. Catalytic "Active-Metal" Template Synthesis of [2]Rotaxanes, [3]Rotaxanes, and Molecular Shuttles, and Some Observations on the Mechanism of the Cu(I)-Catalyzed Azide-Alkyne 1,3-Cycloaddition. *J. Am. Chem. Soc.* **2007**, *129*, 11950–11963.
(174) Goldup, S. M.; Leigh, D. A.; Lusby, P. J.; McBurney, R. T.; Slawin, A. M. Z. Active Template Synthesis of Rotaxanes and Molecular Shuttles with Switchable Dynamics by Four-Component Pd^{II}-Promoted Michael Additions. *Angew. Chem., Int. Ed.* **2008**, *47*, 3381–3384.
(175) Ashton, P. R.; Brown, C. L.; Chrystal, E. J. T.; Parry, K. P.; Pietraszkiewicz, M.; Spencer, N.; Stoddart, J. F. Molecular Trains: Self Association and Dynamic Properties of Two New Catenanes. *Angew. Chem., Int. Ed. Engl.* **1991**, *30*, 1042–1045.
(176) Amabilino, D. B.; Ashton, P. R.; Stoddart, J. F.; Menzer, S.; Williams, D. J. The Solid-State Self-Organization of a Self-Assembled [2]Catenane. *J. Chem. Soc., Chem. Commun.* **1994**, 2475–2478.
(177) Chiu, S.-H.; Elizarov, A. M.; Glink, P. T.; Stoddart, J. F. Translational Isomerism in a [3]Catenane and a [3]Rotaxane. *Org. Lett*. **2002**, *4*, 3561–3564.
(178) Zhu, Z.; Bruns, C. J.; Li, H.; Lei, J.; Ke, C.; Liu, Z.; Shafaie, S.; Colquhoun, H. M.; Stoddart, J. F. Synthesis and Solution-State Dynamics of Donor–Acceptor Oligorotaxane Foldamers. *Chem. Sci*. **2013**, *4*, 1470–1483.
(179) Bruns, C. J.; Stoddart, J. F. Mechanically Interlaced and Interlocked Donor–Acceptor Foldamers. *Adv. Polym. Sci.* **2013**, *261*, 271–294.
(180) Ashton, P. R.; Goodnow, T. T.; Kaifer, A. E.; Reddington, M. V.; Slawin, A. M. Z.; Spencer, N.; Stoddart, J. F.; Vicent, C.; Williams, D. J. A [2]Catenane Made to Order. *Angew. Chem., Int. Ed. Engl.* **1989**, *28*, 1396–1399.
(181) Livoreil, A.; Dietrich-Buchecker, C. O.; Sauvage, J.-P. Electrochemically Triggered Swinging of a [2]-Catenate. *J. Am. Chem. Soc.* **1994**, *116*, 9399–9400.
(182) Gunter, M. J.; Hockless, D. C. R.; Johnston, M. R.; Skelton, B. W.; White, A. H. Self-Assembling Porphyrin [2]Catenanes. *J. Am. Chem. Soc.* **1994**, *116*, 4810–4823.
(183) Johnston, A. G.; Leigh, D. A.; Murphy, A.; Smart, J. P.; Deegan, M. D. The Synthesis and Solubilization of Amide Macrocycles via Rotaxane Formation. *J. Am. Chem. Soc.* **1996**, *118*, 10662–10663.
(184) Ottens-Hildebrandt, S.; Nieger, M.; Rissanen, K.; Rouvinen, J.; Meier, S.; Harder, G.; Vögtle, F. Amide-Based Furano-Catenanes: Regioselective Template Synthesis and Crystal Structure. *J. Chem. Soc., Chem. Commun.* **1995**, 777–778.
(185) Johnston, A. G.; Leigh, D. A.; Nezhat, L.; Smart, J. P.; Deegan, M. D. Structurally Diverse and Dynamically Versatile Benzylic Amide [2]Catenanes Assembled Directly From Commercially Available Precursors. *Angew. Chem., Int. Ed. Engl.* **1995**, *34*, 1212–1216.
(186) Hamilton, D. G.; Davies, J. E.; Prodi, L.; Sanders, J. K. M. Synthesis, Structure and Photophysics of Neutral Pi-Associated [2]Catenanes. *Chem. Eur. J.* **1998**, *4*, 608–620.
(187) Ashton, P. R.; Philp, D.; Spencer, N.; Stoddart, J. F. The Self-Assembly of [*n*]Pseudorotaxanes. *J. Chem. Soc., Chem. Commun.* **1991**, 1677–1679.
(188) Armspach, D.; Ashton, P. R.; Moore, C. P.; Spencer, N.; Stoddart, J. F.; Wear, T. J.; Williams, D. J. Self-Assembly of Catenanes with Cyclodextrin Units. *Angew. Chem., Int. Ed. Engl.* **1993**, *32*, 854–858.
(189) Arunkumar, E.; Forbes, C. C.; Noll, B. C.; Smith, B. D. Squaraine-Derived Rotaxanes: Sterically Protected Fluorescent Near-IR Dyes. *J. Am. Chem. Soc.* **2005**, *127*, 3288–3289.
(190) Cao, D.; Amelia, M.; Klivansky, L. M.; Koshkakaryan, G.; Khan, S. I.; Semeraro, M.; Silvi, S.; Venturi, M.; Credi, A.; Liu, Y. Probing Donor−Acceptor Interactions and Co-Conformational Changes in Redox Active Desymmetrized [2]Catenanes. *J. Am. Chem. Soc.* **2010**, *132*, 1110–1122.
(191) Hancock, L. M.; Beer, P. D. Sodium and Barium Cation-Templated Synthesis and Cation-Induced Molecular Pirouetting of a Pyridine N-Oxide Containing [2]Rotaxane. *Chem. Commun.* **2011**, *47*, 6012–6014.
(192) Farràs, P.; Escudero-Adán, E. C.; Viñas, C.; Teixidor, F. Controlling the Pirouetting Motion in Rotaxanes by Counterion Exchange. *Inorg. Chem.* **2014**, *53*, 8654–8661.
(193) Ramakrishnam Raju, M. V.; Lin, H.-C. Self-Assembly of Tetraphenylethene-Based [2]Catenane Driven by Acid–Base-Controllable Molecular Switching and Its Enabled Aggregation-Induced Emission. *Org. Lett.* **2014**, *16*, 5564–5567.
(194) Forgan, R. S.; Gassensmith, J. J.; Cordes, D. B.; Boyle, M. M.; Hartlieb, K. J.; Friedman, D. C.; Slawin, A. M. Z.; Stoddart, J. F. Self-Assembly of a [2]Pseudorota[3]Catenane in Water. *J. Am. Chem. Soc.* **2012**, *134*, 17007–17010.
(195) Forgan, R. S.; Blackburn, A. K.; Boyle, M. M.; Schneebeli, S. T.; Stoddart, J. F. The Topological and Chemical Implications of Introducing Oriented Rings to [3]Catenanes. *Supramol. Chem.* **2014**, *26*, 192–201.
(196) Armspach, D.; Ashton, P. R.; Ballardini, R.; Balzani, V.; Godi, A.; Moore, C. P.; Prodi, L.; Spencer, N.; Stoddart, J. F.; Tolley, M. S.; Wear, T. J.; Williams, D. J. Catenated Cyclodextrins. *Chem. Eur. J.* **1995**, *1*, 33–55.
(197) Ashton, P. R.; Brown, C. L.; Chrystal, E. J. T.; Goodnow, T. T.; Kaifer, A. E.; Parry, K. P.; Philp, D.; Slawin, A. M. Z.; Spencer, N.; Stoddart, J. F.; Williams, D. J. The Self-Assembly of a Highly Ordered [2]Catenane. *J. Chem. Soc., Chem. Commun.* **1991**, 634–639.
(198) Ashton, P. R.; Philp, D.; Spencer, N.; Stoddart, J. F.; Williams, D. J. A Self-Organized Layered Superstructure of Arrayed [2]Pseudorotaxanes. *J. Chem. Soc., Chem. Commun.* **1994**, 181–184.
(199) Bravo, J.; Bravo, J. A.; Stoddart, J. F.; Raymo, F. M.; White, A. J. P.; Williams, D. J. Molecular Meccano 45. High Yielding Template-Directed Syntheses of [2]Rotaxanes. *Eur. J. Org. Chem.* **1998**, 2565–2571.
(200) Hamers, C.; Raymo, F. M.; Stoddart, J. F. Molecular Meccano 42. Main-Chain and Pendant Poly([2]catenane)s Incorporating Complementary π-Electron-Rich and -Deficient Components. *Eur. J. Org. Chem.* **1998**, 2109–2117.
(201) Hartlieb, K. J.; Blackburn, A. K.; Schneebeli, S. T.; Forgan, R. S.; Sarjeant, A. A.; Stern, C. L.; Cao, D.; Stoddart, J. F. Topological Isomerism in a Chiral Handcuff Catenane. *Chem. Sci*. **2014**, *5*, 90–100.
(202) Bruns, C. J.; Frasconi, M.; Iehl, J.; Hartlieb, K. J.; Schneebeli, S. T.; Cheng, C.; Stupp, S. I.; Stoddart, J. F. Redox Switchable Daisy Chain Rotaxanes Driven by Radical–Radical Interactions. *J. Am. Chem. Soc.* **2014**, *136*, 4714–4723.
(203) Boyle, M. M.; Gassensmith, J. J.; Whalley, A. C.; Forgan, R. S.; Smaldone, R. A.; Hartlieb, K. J.; Blackburn, A. K.; Sauvage, J.-P.; Stoddart, J. F. Stereochemistry of Molecular Figures-of-Eight. *Chem. Eur. J.* **2012**, *18*, 10312–10323.
(204) Amabilino, D. B.; Ashton, P. R.; Bravo, J. A.; Raymo, F. M.; Stoddart, J. F.; White, A. J. P.; Williams, D. J. Molecular Meccano 52. Template-Directed Synthesis of a Rotacatenane. *Eur. J. Org. Chem.* **1999**, 1295–1302.
(205) Ashton, P. R.; Ballardini, R.; Balzani, V.; Bělohradský, M.; Gandolfi, M. T.; Philp, D.; Prodi, L.; Raymo, F. M.; Reddington, M. V.; Spencer, N.; Stoddart, J. F.; Venturi, M.; Williams, D. J. Molecular Meccano 9. Self-Assembly, Spectroscopic, and

Electrochemical Properties of [*n*]Rotaxanes. *J. Am. Chem. Soc.* **1996**, *118*, 4931–4951.
(206) Leigh, D. A.; Murphy, A.; Smart, J. P.; Slawin, A. M. Z. Glycylglycine Rotaxanes—The Hydrogen Bond Directed Assembly of Synthetic Peptide Rotaxanes. *Angew. Chem., Int. Ed. Engl.* **1997**, *36*, 728–732.
(207) Berná, J.; Alajarín, M.; Martínez-Espín, J. S.; Buriol, L.; Martins, M. A. P.; Orenes, R.-A. Dampened Circumrotation by CH···π Interactions in Hydrogen Bonded [2]Rotaxanes. *Chem. Commun*. **2012**, *48*, 5677–5679.
(208) Gatti, F. G.; Leigh, D. A.; Nepogodiev, S. A.; Slawin, A. M. Z.; Teat, S. J.; Wong, J. K. Y. Stiff, and Sticky in the Right Places: The Dramatic Influence of Preorganizing Guest Binding Sites on the Hydrogen Bond-Directed Assembly of Rotaxanes. *J. Am. Chem. Soc.* **2001**, *123*, 5983–5989.
(209) Gatti, F. G.; León, S.; Wong, J. K.; Bottari, G.; Altieri, A.; Morales, M. A. F.; Teat, S. J.; Frochot, C.; Leigh, D. A.; Brouwer, A. M. Photoisomerization of a Rotaxane Hydrogen Bonding Template: Light-Induced Acceleration of a Large Amplitude Rotational Motion. *Proc. Natl. Acad. Sci. U.S.A.* **2003**, *100*, 10–14.
(210) Bermudez, V.; Capron, N.; Gase, T.; Gatti, F. G.; Kajzar, F.; Leigh, D. A.; Zerbetto, F.; Zhang, S. Influencing Intramolecular Motion with an Alternating Electric Field. *Nature* **2000**, *406*, 608–611.
(211) D'Souza, D. M.; Leigh, D. A.; Mottier, L.; Mullen, K. M.; Paolucci, F.; Teat, S. J.; Zhang, S. Nitrone [2]Rotaxanes: Simultaneous Chemical Protection and Electrochemical Activation of a Functional Group. *J. Am. Chem. Soc.* **2010**, *132*, 9465–9470.
(212) Murgu, I.; Baumes, J. M.; Eberhard, J.; Gassensmith, J. J.; Arunkumar, E.; Smith, B. D. Macrocycle Breathing in [2]Rotaxanes with Tetralactam Macrocycles. *J. Org. Chem.* **2011**, *76*, 688–691.
(213) Alcalde, E.; Pérez-García, L.; Ramos, S.; Stoddart, J. F.; White, A. J. P.; Williams, D. J. Nondegenerate π-Donor/π-Acceptor [2]Catenanes Containing Proton-Ionizable 1*H*-1,2,4-Triazole Subunits: Synthesis and Spontaneous Resolution. *Chem. Eur. J.* **2007**, *13*, 3964–3979.
(214) Cougnon, F. B. L.; Ponnuswamy, N.; Pantoş, G. D.; Sanders, J. K. M. Molecular Motion of Donor–Acceptor Catenanes in Water. *Org. Biomol. Chem.* **2015**, *13*, 2927–2930.
(215) Leigh, D. A.; Murphy, A.; Smart, J. P.; Deleuze, M. S.; Zerbetto, F. Controlling the Frequency of Macrocyclic Ring Rotation in Benzylic Amide [2]Catenanes. *J. Am. Chem. Soc.* **1998**, *120*, 6458–6467.
(216) Deleuze, M.; Leigh, D. A.; Zerbetto, F. How Do Benzylic Amide [2]Catenane Rings Rotate? *J. Am. Chem. Soc.* **1999**, *121*, 2364–2379.
(217) Hunter, C. A. Synthesis and Structure Elucidation of a New [2]Catenane. *J. Am. Chem. Soc.* **1992**, *114*, 5303–5311.
(218) Vögtle, F.; Meier, S.; Hoss, R. One-Step Synthesis of a Fourfold Functionalized Catenane. *Angew. Chem., Int. Ed. Engl.* **1992**, *31*, 1619–1622.
(219) Basu, S.; Coskun, A.; Friedman, D. C.; Olson, M. A.; Benítez, D.; Tkatchouk, E.; Barin, G.; Yang, J.; Fahrenbach, A. C.; Goddard, W. A. III; Stoddart, J. F. Donor–Acceptor Oligorotaxanes Made to Order. *Chem. Eur. J.* **2011**, *17*, 2107–2119.
(220) Ashton, P. R.; Preece, J. A.; Stoddart, J. F.; Tolley, M. S.; White, A. J. P.; Williams, D. J. The Self-Assembly and Dynamic Properties of Thiophene-Containing [2]Catenanes. *Synthesis* **1994**, 1344–1352.
(221) Pascu, S. I.; Naumann, C.; Kaiser, G.; Bond, A. D.; Sanders, J. K. M.; Jarrosson, T. Structures and Solution Dynamics of Pseudorotaxanes Mediated by Alkali-Metal Cations. *Dalton Trans.* **2007**, 3874–3884.
(222) Khuong, T.-A. V.; Nuñez, J. E.; Godinez, C. E.; Garcia-Garibay, M. A. Crystalline Molecular Machines: A Quest Toward Solid-State Dynamics and Function. *Acc. Chem. Res.* **2006**, *39*, 413–422.
(223) Zhao, K.; Dron, P. I.; Kaleta, J.; Rogers, C. T.; Michl, J. Arrays of Dipolar Molecular Rotors in Tris(*O*-phenylenedioxy)-cyclotriphosphazene. *Top. Curr. Chem.* **2014**, *354*, 163–211.
(224) Vukotic, V. N.; Harris, K. J.; Zhu, K.; Schurko, R. W.; Loeb, S. J. Metal–Organic Frameworks with Dynamic Interlocked Components. *Nature Chem.* **2012**, *4*, 456–460.
(225) Zhu, K.; O'Keefe, C. A.; Vukotic, V. N.; Schurko, R. W.; Loeb, S. J. A Molecular Shuttle That Operates Inside a Metal–Organic Framework. *Nature Chem.* **2015**, *7*, 514–519.
(226) Strutt, N. L.; Zhang, H.; Schneebeli, S. T.; Stoddart, J. F. Functionalizing Pillar[*n*]arenes. *Acc. Chem. Res.* **2014**, *47*, 2631–2642.
(227) Isnin, R.; Kaifer, A. E. Novel Class of Asymmetric Zwitterionic Rotaxanes Based on α-Cyclodextrin. *J. Am. Chem. Soc.* **1991**, *113*, 8188–8190.
(228) Isnin, R.; Kaifer, A. E. A New Approach to Cyclodextrin-Based Rotaxanes. *Pure Appl. Chem.* **1993**, *65*, 495–498.
(229) Buston, J. E. H.; Young, J. R.; Anderson, H. L. Rotaxane-Encapsulated Cyanine Dyes: Enhanced Fluorescence Efficiency and Photostability. *Chem. Commun.* **2000**, 905–906.
(230) Buston, J. E. H.; Anderson, H. L.; Marken, F. Enhanced Chemical Reversibility of Redox Processes in Cyanine Dye Rotaxanes. *Chem. Commun.* **2001**, 1046–1047.
(231) Saudan, C.; Dunand, F. A.; Abou-Hamdan, A.; Bugnon, P.; Lye, P. G.; Lincoln, S. F.; Merbach, A. E. A Model for Sequential Threading of α-Cyclodextrin Onto a Guest: A Complete Thermodynamic and Kinetic Study in Water. *J. Am. Chem. Soc.* **2001**, *123*, 10290–10298.
(232) Park, J. W.; Song, H. J. Isomeric [2]Rotaxanes and Unidirectional [2]Pseudorotaxane Composed of α-Cyclodextrin and Aliphatic Chain-Linked Carbazole-Viologen Compounds. *Org. Lett.* **2004**, *6*, 4869–4872.
(233) Baer, A. J.; Macartney, D. H. Orientational Isomers of α-Cyclodextrin [2]Semi-Rotaxanes with Asymmetric Dicationic Threads. *Org. Biomol. Chem.* **2005**, *3*, 1448–1453.
(234) Oshikiri, T.; Takashima, Y.; Yamaguchi, H.; Harada, A. Kinetic Control of Threading of Cyclodextrins Onto Axle Molecules. *J. Am. Chem. Soc.* **2005**, *127*, 12186–12187.
(235) Baer, A. J.; Macartney, D. H. Orientational Isomers of Cyclodextrin Semirotaxanes and Rotaxanes with Organic and Transition Metal Complex Stoppers. *Supramol. Chem.* **2007**, *19*, 537–546.
(236) Yamauchi, K.; Miyawaki, A.; Takashima, Y.; Yamaguchi, H.; Harada, A. A Molecular Reel: Shuttling of a Rotor by Tumbling of a Macrocycle. *J. Org. Chem.* **2010**, *75*, 1040–1046.
(237) Craig, M. R.; Hutchings, M. G.; Claridge, T. D. W.; Anderson, H. L. Rotaxane-Encapsulation Enhances the Stability of an Azo Dye, in Solution and When Bonded to Cellulose. *Angew. Chem., Int. Ed.* **2001**, *40*, 1071–1074.
(238) Yan, H.; Teh, C.; Sreejith, S.; Zhu, L.; Kwok, A.; Fang, W.; Ma, X.; Nguyen, K. T.; Korzh, V.; Zhao, Y. Functional Mesoporous Silica Nanoparticles for Photothermal-Controlled Drug Delivery in Vivo. *Angew. Chem., Int. Ed.* **2012**, *51*, 8373–8377.
(239) Yan, H.; Zhu, L.; Li, X.; Kwok, A.; Pan, X.; Zhao, Y. A Photoswitchable [2]Rotaxane Array on Graphene Oxide. *Asian J. Org. Chem.* **2012**, *1*, 314–318.
(240) Yan, H.; Zhu, L.; Li, X.; Kwok, A.; Li, X.; Ågren, H.; Zhao, Y. Photothermal-Responsive [2]Rotaxanes. *RSC Adv.* **2013**, *3*: 2341.
(241) Wang, Q.-C.; Qu, D.-H.; Ren, J.; Chen, K.; Tian, H. A Lockable Light-Driven Molecular Shuttle with a Fluorescent Signal. *Angew. Chem., Int. Ed.* **2004**, *43*, 2661–2665.
(242) Qu, D.-H.; Wang, Q.-C.; Ren, J.; Tian, H. A Light-Driven Rotaxane Molecular Shuttle with Dual Fluorescence Addresses. *Org. Lett.* **2004**, *6*, 2085–2088.
(243) Wang, Q.-C.; Ma, X.; Qu, D.-H.; Tian, H. Unidirectional Threading Synthesis of Isomer-Free [2]Rotaxanes. *Chem. Eur. J.* **2006**, *12*, 1088–1096.
(244) Daniell, H. W.; Klotz, E. J. F.; Odell, B.; Claridge, T. D. W.; Anderson, H. L. Solid-Phase Synthesis of

Oligo(Phenylene Ethynylene) Rotaxanes. *Angew. Chem., Int. Ed.* **2007**, *46*, 6845–6848.
(245) Yonemura, H.; Nojiri, T.; Matsuo, T. Stereoselective Formation of a 2: 1 Molecular Complex Between α-Cyclodextrin and Carbazole-Viologen Linked Compound with a Long Alkyl Chain as the Spacer. *Chem. Lett.* **1994**, 2097–2100.
(246) Park, J. W.; Song, H. E.; Lee, S. Y. Face Selectivity of Inclusion Complexation of Viologens with β-Cyclodextrin and 6-*O*-(2-Sulfonato-6-naphthyl)-β-Cyclodextrin. *J. Phys. Chem. B* **2002**, *106*, 7186–7192.
(247) Park, J. W.; Song, H. J.; Cho, Y. J.; Park, K. K. Thermodynamics and Kinetics of Formation of Orientationally Isomeric [2]Pseudorotaxanes Between α-Cyclodextrin and Aliphatic Chain-Linked Aromatic Donor-Viologen Acceptor Compounds. *J. Phys. Chem. C* **2007**, *111*, 18605–18614.
(248) Park, J. W.; Song, H. J.; Chang, H.-J. Unidirectional α-Cyclodextrin-Based [2]Rotaxanes Bearing Viologen Unit on Axle. *Tetrahedron Lett.* **2006**, *47*, 3831–3834.
(249) Casati, C.; Franchi, P.; Pievo, R.; Mezzina, E.; Lucarini, M. Unraveling Unidirectional Threading of α-Cyclodextrin in a [2]Rotaxane Through Spin Labeling Approach. *J. Am. Chem. Soc.* **2012**, *134*, 19108–19117.
(250) Arduini, A.; Ciesa, F.; Fragassi, M.; Pochini, A.; Secchi, A. Selective Synthesis of Two Constitutionally Isomeric Oriented Calix[6]arene-Based Rotaxanes. *Angew. Chem., Int. Ed.* **2005**, *44*, 278–281.
(251) Arduini, A.; Calzavacca, F.; Pochini, A.; Secchi, A. Unidirectional Threading of Triphenylureidocalix[6] arene-Based Wheels: Oriented Pseudorotaxane Synthesis. *Chem. Eur. J.* **2003**, *9*, 793–799.
(252) Wang, H.-X.; Meng, Z.; Xiang, J.-F.; Xia, Y.-X.; Sun, Y.; Hu, S.-Z.; Chen, H.; Yao, J.; Chen, C.-F. Guest-Dependent Directional Complexation Based on Triptycene Derived Oxacalixarene: Formation of Oriented Rotaxanes. *Chem. Sci.* **2016**, *7*, 469–474.
(253) Hu, S.-Z.; Chen, C.-F. Triptycene-Derived Oxacalixarene with Expanded Cavity: Synthesis, Structure and Its Complexation with Fullerenes C_{60} and C_{70}. *Chem. Commun.* **2010**, *46*, 4199–4201.
(254) Hu, S.-Z.; Chen, C.-F. Triptycene-Derived Oxacalixarenes as New Wheels for the Synthesis of [2]Rotaxanes: Acid-Base- and Metal-Ion-Switchable Complexation Processes. *Chem. Eur. J.* **2011**, *17*, 5424–5431.
(255) Ogoshi, T.; Yamafuji, D.; Aoki, T.; Yamagishi, T.-A. Thermally Responsive Shuttling Behavior of a Pillar[6]Arene-Based [2]Rotaxane. *Chem. Commun.* **2012**, *48*, 6842–6844.
(256) Ogoshi, T.; Yamafuji, D.; Aoki, T.; Kitajima, K.; Yamagishi, T.-A.; Hayashi, Y.; Kawauchi, S. High-Yield Diastereoselective Synthesis of Planar Chiral [2]- and [3]Rotaxanes Constructed From Per-Ethylated Pillar[5]arene and Pyridinium Derivatives. *Chem. Eur. J.* **2012**, *18*, 7493–7500.
(257) Ogoshi, T.; Yamafuji, D.; Yamagishi, T.-A.; Brouwer, A. M. Förster Resonance Energy Transfer by Formation of a Mechanically Interlocked [2]Rotaxane. *Chem. Commun.* **2013**, *49*, 5468–5470.
(258) Talotta, C.; Gaeta, C.; Pierro, T.; Neri, P. Sequence Stereoisomerism in Calixarene-Based Pseudo[3]Rotaxanes. *Org. Lett.* **2011**, *13*, 2098–2101.
(259) Pierro, T.; Gaeta, C.; Talotta, C.; Casapullo, A.; Neri, P. Fixed or Invertible Calixarene-Based Directional Shuttles. *Org. Lett.* **2011**, *13*, 2650–2653.
(260) Talotta, C.; Gaeta, C.; Neri, P. Stereoprogrammed Direct Synthesis of Calixarene-Based [3]Rotaxanes. *Org. Lett.* **2012**, *14*, 3104–3107.
(261) Gaeta, C.; Talotta, C.; Mirra, S.; Margarucci, L.; Casapullo, A.; Neri, P. Catenation of Calixarene Annulus. *Org. Lett.* **2013**, *15*, 116–119.
(262) Talotta, C.; Gaeta, C.; Qi, Z.; Schalley, C. A.; Neri, P. Pseudorotaxanes with Self-Sorted Sequence and Stereochemical Orientation. *Angew. Chem., Int. Ed.* **2013**, *52*, 7437–7441.
(263) Gaeta, C.; Talotta, C.; Neri, P. Pseudorotaxane Orientational Stereoisomerism Driven by π-Electron Density. *Chem. Commun.* **2014**, *50*, 9917–9920.
(264) Lee, S.; Chen, C.-H.; Flood, A. H. A Pentagonal Cyanostar Macrocycle with Cyanostilbene CH Donors Binds Anions and Forms Dialkylphosphate [3]Rotaxanes. *Nature Chem.* **2013**, *5*, 704–710.
(265) Craig, M. R.; Claridge, T. D. W.; Anderson, H. L.; Hutchings, M. G. Synthesis of a Cyclodextrin Azo Dye [3]Rotaxane as a Single Isomer. *Chem. Commun.* **1999**, 1537–1538.
(266) Qu, D.-H.; Wang, Q.-C.; Ma, X.; Tian, H. A [3]Rotaxane with Three Stable States That Responds to Multiple-Inputs and Displays Dual Fluorescence Addresses. *Chem. Eur. J.* **2005**, *11*, 5929–5937.
(267) Cheetham, A. G.; Claridge, T. D. W.; Anderson, H. L. Metal-Driven Ligand Assembly in the Synthesis of Cyclodextrin [2] and [3]Rotaxanes. *Org. Biomol. Chem.* **2007**, *5*, 457–462.
(268) Harada, A.; Li, J.; Kamachi, M. The Molecular Necklace: A Rotaxane Containing Many Threaded α-Cyclodextrins. *Nature* **1992**, *356*, 325–327.
(269) Liu, P.; Chipot, C.; Shao, X.; Cai, W. How Do α-Cyclodextrins Self-Organize on a Polymer Chain? *J. Phys. Chem. C* **2012**, *116*, 17913–17918.
(270) Shu, X.; Chen, W.; Hou, D.; Meng, Q.; Zheng, R.; Li, C. Novel Binding Regioselectivity in the Interpenetration of a Non-Symmetric Axle Into a Non-Symmetric Pillar[5]arene Wheel. *Chem. Commun.* **2014**, *50*, 4820–4823.
(271) Sánchez-Quesada, J.; Saghatelian, A.; Cheley, S.; Bayley, H.; Ghadiri, M. R. Single DNA Rotaxanes of a Transmembrane Pore Protein. *Angew. Chem., Int. Ed.* **2004**, *43*, 3063–3067.
(272) Zhang, J.; Huang, F.; Li, N.; Wang, H.; Gibson, H. W.; Gantzel, P.; Rheingold, A. L. Paraquat Substituent Effect on Complexation with a Dibenzo-24-Crown-8-Based Cryptand. *J. Org. Chem.* **2007**, *72*, 8935–8938.
(273) Saha, S.; Santra, S.; Ghosh, P. [2]Pseudorotaxane Composed of Heteroditopic Macrobicycle and Pyridine *N*-Oxide Based Axle: Recognition Site Dependent Axle Orientation. *Org. Lett.* **2015**, *17*, 1854–1857.
(274) Gu, Y.-K.; Han, Y.; Chen, C.-F. Guest-Dependent Complexation of Triptycene-Derived Macrotricyclic Host Containing One Anthracene Moiety with Paraquat Derivatives: Construction of [2]Rotaxanes. *Supramol. Chem.* **2014**, *27*, 357–363.
(275) Han, Y.; Jiang, Y.; Chen, C.-F. Cryptand-Based Hosts for Organic Guests. *Tetrahedron* **2015**, *71*, 503–522.
(276) Fuller, A.-M. L.; Leigh, D. A.; Lusby, P. J. Sequence Isomerism in [3]Rotaxanes. *J. Am. Chem. Soc.* **2010**, *132*, 4954–4959.
(277) Amabilino, D. B.; Ashton, P. R.; Bělohradský, M.; Raymo, F. M.; Stoddart, J. F. The Controlled Self-Assembly of a [3]Rotaxane Incorporating Three Constitutionally Different Components. *J. Chem. Soc., Chem. Commun.* **1995**, 747–750.
(278) Asakawa, M.; Ashton, P. R.; Ballardini, R.; Balzani, V.; Bělohradský, M.; Gandolfi, M. T.; Kocian, O.; Prodi, L.; Raymo, F. M.; Stoddart, J. F.; Venturi, M. Molecular Meccano 12. The Slipping Approach to Self-Assembling [*n*]Rotaxanes. *J. Am. Chem. Soc.* **1997**, *119*, 302–310.
(279) Chen, L.; Zhao, X.; Chen, Y.; Zhao, C.-X.; Jiang, X.-K.; Li, Z.-T. Self-Assembly of Novel [3]- and [2]Rotaxanes Based on Donor−Acceptor and Hydrogen-Bonding Interactions. Intensified Inter-Ring Repulsion Interaction and Shuttling Behavior. *J. Org. Chem.* **2003**, *68*, 2704–2712.
(280) Wilson, E. A.; Vermeulen, N. A.; McGonigal, P. R.; Avestro, A.-J.; Sarjeant, A. A.; Stern, C. L.; Stoddart, J. F. Formation of a Hetero[3]rotaxane by a Dynamic Component-Swapping Strategy. *Chem. Commun.* **2014**, *50*, 9665–9668.
(281) Jiang, W.; Winkler, H. D. F.; Schalley, C. A. Integrative Self-Sorting: Construction of a Cascade-Stoppered Hetero[3]-rotaxane. *J. Am. Chem. Soc.* **2008**, *130*, 13852–13853.
(282) Jiang, W.; Schalley, C. A. Integrative Self-Sorting Is a Programming Language for High Level Self-Assembly. *Proc. Natl. Acad. Sci. U.S.A.* **2009**, *106*, 10425–10429.

(283) Jiang, W.; Sattler, D.; Rissanen, K.; Schalley, C. A. [4]Pseudorotaxanes with Remarkable Self-Sorting Selectivities. *Org. Lett.* **2011**, *13*, 4502–4505.
(284) Zhang, C.; Li, S.; Zhang, J.; Zhu, K.; Li, N.; Huang, F. Benzo-21-Crown-7/Secondary Dialkylammonium Salt [2]Pseudorotaxane- and [2]Rotaxane-Type Threaded Structures. *Org. Lett.* **2007**, *9*, 5553–5556.
(285) Fuller, A.-M. L.; Leigh, D. A.; Lusby, P. J. One Template, Multiple Rings: Controlled Iterative Addition of Macrocycles Onto a Single Binding Site Rotaxane Thread. *Angew. Chem., Int. Ed.* **2007**, *46*, 5015–5019.
(286) Sauvage, J.-P.; Weiss, J. Synthesis of Dicopper(I) [3]Catenates: Multiring Interlocked Coordinating Systems. *J. Am. Chem. Soc.* **1985**, *107*, 6108–6110.
(287) Dietrich-Buchecker, C. O.; Guilhem, J.; Khemiss, A.-K.; Kintzinger, J.-P.; Pascard, C.; Sauvage, J.-P. Molecular Structure of a [3]Catenate: Folding of the Linked System by Interaction Between Two Copper Complex Subunits. *Angew. Chem., Int. Ed. Engl.* **1987**, *26*, 661–663.
(288) Guilhem, J.; Pascard, C.; Sauvage, J.-P.; Weiss, J. Solution Study and Molecular Structure of a [3]Catenand. Intramolecular Interaction Between the Two Peripheral Rings. *J. Am. Chem. Soc.* **1988**, *110*, 8711–8713.
(289) Dietrich-Buchecker, C. O.; Hemmert, C.; Khemiss, A.-K.; Sauvage, J.-P. Synthesis of Dicopper [3]Catenates and [3]Catenands by Acetylenic Oxidative Coupling. Preparation and Study of Corresponding Homodimetallic [3]Catenates Ag^{+}, Zn^{2+}, Co^{2+}, and Ni^{2+}. *J. Am. Chem. Soc.* **1990**, *112*, 8002–8008.
(290) Ashton, P. R.; Brown, C. L.; Chrystal, E. J. T.; Goodnow, T. T.; Kaifer, A. E.; Parry, K. P.; Slawin, A. M. Z.; Spencer, N.; Stoddart, J. F.; Williams, D. J. Self-Assembling [3]Catenanes. *Angew. Chem., Int. Ed. Engl.* **1991**, *30*, 1039–1042.
(291) Amabilino, D. B.; Ashton, P. R.; Reder, A. S.; Spencer, N.; Stoddart, J. F. Olympiadane. *Angew. Chem., Int. Ed. Engl.* **1994**, *33*, 1286–1290.
(292) Kern, J.-M.; Sauvage, J.-P.; Weidmann, J.-L. Multiring Interlocked Systems via Transition Metal-Templated Strategy: The Single-Crystallization Synthesis of [3]-Catenates. *Tetrahedron* **1996**, *52*, 10921–10934.
(293) Amabilino, D. B.; Ashton, P. R.; Boyd, S. E.; Lee, J. Y.; Menzer, S.; Stoddart, J. F.; Williams, D. J. The Five-Stage Self-Assembly of a Branched Heptacatenane. *Angew. Chem., Int. Ed. Engl.* **1997**, *36*, 2070–2072.
(294) Ashton, P. R.; Baldoni, V.; Balzani, V.; Claessens, C. G.; Credi, A.; Hoffmann, H. D. A.; Raymo, F. M.; Stoddart, J. F.; Venturi, M.; White, A. J. P.; Williams, D. J. Molecular Meccano 57. Template-Directed Syntheses, Spectroscopic Properties, and Electrochemical Behavior of [*n*]Catenanes. *Eur. J. Org. Chem.* **2000**, 1121–1130.
(295) Safarowsky, O.; Vogel, E.; Vögtle, F. Amide-Based [3]Catenanes and [2]Catenanes with Aliphatic Chains. *Eur. J. Org. Chem.* **2000**, 499–505.
(296) Hori, A.; Kumazawa, K.; Kusukawa, T.; Chand, D. K.; Fujita, M.; Sakamoto, S.; Yamaguchi, K. DOSY Study on Dynamic Catenation: Self-Assembly of a [3]Catenane as a Meta-Stable Compound From Twelve Simple Components. *Chem. Eur. J.* **2001**, *7*, 4142–4149.
(297) Leigh, D. A.; Wong, J. K. Y.; Dehez, F.; Zerbetto, F. Unidirectional Rotation in a Mechanically Interlocked Molecular Rotor. *Nature* **2003**, *424*, 174–179.
(298) Iwamoto, H.; Itoh, K.; Nagamiya, H.; Fukazawa, Y. Convenient Synthesis of [3]Catenane by Olefin Metathesis Dimerizations. *Tetrahedron Lett.* **2003**, *44*, 5773–5776.
(299) Hubbard, A. L.; Davidson, G. J. E.; Patel, R. H.; Wisner, J. A.; Loeb, S. J. Host-Guest Interactions Template: The Synthesis of a [3]Catenane. *Chem. Commun.* **2004**, 138–139.
(300) Blanco, V.; Chas, M.; Abella, D.; Peinador, C.; Quintela, J. M. Molecular Catenation via Metal-Directed Self-Assembly and π-Donor/π-Acceptor Interactions: Efficient One-Pot Synthesis, Characterization, and Crystal Structures of [3]Catenanes Based on Pd or Pt Dinuclear Metallocycles. *J. Am. Chem. Soc.* **2007**, *129*, 13978–13986.
(301) Gupta, M.; Kang, S.; Mayer, M. F. A Double Ring-Closing Olefin Metathesis Approach to [3]Catenanes. *Tetrahedron Lett.* **2008**, *49*, 2946–2950.
(302) Blanco, V.; Abella, D.; Pia, E.; Platas-Iglesias, C.; Peinador, C.; Quintela, J. M. Regioselective Catenation of Dinuclear Palladium and Platinum Metallocycles Promoted by π···π Interactions. *Inorg. Chem.* **2009**, *48*, 4098–4107.
(303) Chang, C.-F.; Chuang, C.-J.; Lai, C.-C.; Liu, Y.-H.; Peng, S.-M.; Chiu, S.-H. Using Host-Guest Complexation to Fold a Flexible Linear Organic String: Kinetically Controlled Syntheses of [3]Catenanes and a Five-Membered Molecular Necklace. *Angew. Chem., Int. Ed.* **2012**, *51*, 10094–10098.
(304) Cougnon, F. B. L.; Ponnuswamy, N.; Jenkins, N. A.; Pantoş, G. D.; Sanders, J. K. M. Structural Parameters Governing the Dynamic Combinatorial Synthesis of Catenanes in Water. *J. Am. Chem. Soc.* **2012**, *134*, 19129–19135.
(305) Li, S.; Huang, J.; Cook, T. R.; Pollock, J. B.; Kim, H.; Chi, K.-W.; Stang, P. J. Formation of [3]Catenanes From 10 Precursors via Multicomponent Coordination-Driven Self-Assembly of Metallarectangles. *J. Am. Chem. Soc.* **2013**, *135*, 2084–2087.
(306) Iwamoto, H.; Takizawa, W.; Itoh, K.; Hagiwara, T.; Tayama, E.; Hasegawa, E.; Haino, T. Selective Synthesis of [2]- and [3]Catenane Tuned by Ring Size and Concentration. *J. Org. Chem.* **2013**, *78*, 5205–5217.
(307) Ke, C.; Smaldone, R. A.; Kikuchi, T.; Li, H.; Davis, A. P.; Stoddart, J. F. Quantitative Emergence of Hetero[4]rotaxanes by Template-Directed Click Chemistry. *Angew. Chem., Int. Ed.* **2012**, *52*, 381–387.
(308) Ke, C.; Strutt, N. L.; Li, H.; Hou, X.; Hartlieb, K. J.; McGonigal, P. R.; Ma, Z.; Iehl, J.; Stern, C. L.; Cheng, C.; Zhu, Z.; Vermeulen, N. A.; Meade, T. J.; Botros, Y. Y.; Stoddart, J. F. Pillar[5]arene as a Co-Factor in Templating Rotaxane Formation. *J. Am. Chem. Soc.* **2013**, *135*, 17019–17030.
(309) Hou, X.; Ke, C.; Cheng, C.; Song, N.; Blackburn, A. K.; Sarjeant, A. A.; Botros, Y. Y.; Yang, Y.-W.; Stoddart, J. F. Efficient Syntheses of Pillar[6]arene-Based Hetero[4]-rotaxanes Using a Cooperative Capture Strategy. *Chem. Commun.* **2014**, *50*, 6196–6199.
(310) Whang, D.; Park, K.-M.; Heo, J.; Ashton, P. R.; Kim, K. Molecular Necklace: Quantitative Self-Assembly of a Cyclic Oligorotaxane From Nine Molecules. *J. Am. Chem. Soc.* **1998**, *120*, 4899–4900.
(311) Roh, S.-G.; Park, K.-M.; Park, G.-J.; Sakamoto, S.; Yamaguchi, K.; Kim, K. Synthesis of a Five-Membered Molecular Necklace: A 2+2 Approach. *Angew. Chem., Int. Ed.* **1999**, *38*, 638–641.
(312) Park, K.-M.; Kim, S.-Y.; Heo, J.; Whang, D.; Sakamoto, S.; Yamaguchi, K.; Kim, K. Designed Self-Assembly of Molecular Necklaces. *J. Am. Chem. Soc.* **2002**, *124*, 2140–2147.
(313) Chiu, S.-H.; Rowan, S. J.; Cantrill, S. J.; Ridvan, L.; Cantrill, S. J.; Ashton, P. R.; Garrell, R. L.; Stoddart, J. F. Making Molecular-Necklaces From Rotaxanes. *Tetrahedron* **2002**, *58*, 807–814.
(314) Ko, Y. H.; Kim, K.; Kang, J.; Chun, H.; Lee, J. W.; Sakamoto, S.; Yamaguchi, K.; Fettinger, J. C.; Kim, K. Designed Self-Assembly of Molecular Necklaces Using Host-Stabilized Charge-Transfer Interactions. *J. Am. Chem. Soc.* **2004**, *126*, 1932–1933.
(315) Clark, P. G.; Guidry, E. N.; Chan, W. Y.; Steinmetz, W. E.; Grubbs, R. H. Synthesis of a Molecular Charm Bracelet via Click Cyclization and Olefin Metathesis Clipping. *J. Am. Chem. Soc.* **2010**, *132*, 3405–3412.
(316) Langton, M. J.; Matichak, J. D.; Thompson, A. L.; Anderson, H. L. Template-Directed Synthesis of π-Conjugated Porphyrin [2]Rotaxanes and a [4]Catenane Based on a Six-Porphyrin Nanoring. *Chem. Sci.* **2011**, *2*, 1897–1901.
(317) Dasgupta, S.; Wu, J. Template-Directed Synthesis of Kinetically and Thermodynamically Stable Molecular Necklace

Using Ring Closing Metathesis. *Org. Biomol. Chem.* **2011**, *9*, 3504–3515.
(318) Coumans, R. G. E.; Elemans, J. A. A. W.; Rowan, A. E.; Nolte, R. J. M. Interlocked Porphyrin Switches. *Chem. Eur. J.* **2013**, *19*, 7758–7770.
(319) Li, S.; Huang, J.; Zhou, F.; Cook, T. R.; Yan, X.; Ye, Y.; Zhu, B.; Zheng, B.; Stang, P. J. Self-Assembly of Triangular and Hexagonal Molecular Necklaces. *J. Am. Chem. Soc.* **2014**, *136*, 5908–5911.
(320) Pasteur, L. *Researches on the Molecular Asymmetry of Natural Organic Products*; Alembic Club Reprints: Edinburgh, **1860**; Vol. *14* (1905), pp. 1–46.
(321) Le Bel, J. A. Sur les Relations qui Existent Entre les Formules Atomiques des Corps Organiques, et le Pouvoir Rotatoire de Leurs Dissolutions. *Bull Chim. Soc. Fr.* **1874**, *22*, 337–347.
(322) van't Hoff, J. H. Sur les Formules de Structure dans L'espace. *Arch. Néerl. Sci. Ex. Nat.* **1875**, *9*, 445–454.
(323) Kelvin, L. The Molecular Tactics of a Crystal. *J. Oxford Univ. Junior Scientific Club* **1894**, *18*, 3–57.
(324) Cahn, R. S.; Ingold, C.; Prelog, V. Specification of Molecular Chirality. *Angew. Chem., Int. Ed. Engl.* **1966**, *5*, 385–415.
(325) Bentley, R. From Optical Activity in Quartz to Chiral Drugs: Molecular Handedness in Biology and Medicine. *Perspectives in Biology and Medicine* **1995**, *38*, 188–229.
(326) Ashton, P. R.; Iriepa, I.; Reddington, M. V.; Spencer, N.; Slawin, A. M. Z.; Stoddart, J. F.; Williams, D. J. An Optically-Active [2]Catenane Made to Order. *Tetrahedron Lett.* **1994**, *35*, 4835–4838.
(327) Archut, A.; Müller, W. M.; Baumann, S.; Habel, M.; Vögtle, F. Rotaxanes with Chiral Stoppers and Complexation of Cations by Podand Axleswith Sugar Terminal Groups. *Liebigs Ann./ Recueil* **1997**, 495–499.
(328) Schmidt, T.; Schmieder, R.; Mueller, W.; Kiupel, B.; Vögtle, F. Chiral Amide Rotaxanes with Glucose Stoppers. Synthesis, Chiroptical Properties and Wheel-Axle Interactions. *Eur. J. Org. Chem.* **1998**, 2003–2007.
(329) Kauffmann, C.; Vögtle, F.; Weinman, S.; Abramson, S.; Fuchs, B. Rotaxanes with Chiral Stoppers and Photoresponsive Central Unit. *Synthesis* **1999**, 849–853.
(330) Coutrot, F.; Leigh, D. A.; Murphy, A.; Wong, J. K. Y.; Zerbetto, F. From Reactants to Products via Simple Hydrogen-Bonding Networks: Information Transmission in Chemical Reactions. *Proc. Natl. Acad. Sci. U.S.A.* **2002**, *99*, 4967–4971.
(331) Asakawa, M.; Fanti, M.; Leigh, D. A.; Shimizu, T.; Slawin, A. M. Z.; Wong, J. K. Y.; Zerbetto, F.; Zhang, S. Switching "On" and "Off" the Expression of Chirality in Peptide Rotaxanes. *J. Am. Chem. Soc.* **2002**, *124*, 2939–2950.
(332) Bottari, G.; Leigh, D. A.; Pérez, E. M. Chiroptical Switching in a Bistable Molecular Shuttle. *J. Am. Chem. Soc.* **2003**, *125*, 13360–13361.
(333) Theil, A.; Mauve, C.; Adeline, M.-T.; Marinetti, A.; Sauvage, J.-P. Phosphorus-Containing [2]Catenanes as an Example of Interlocking Chiral Structures. *Angew. Chem., Int. Ed.* **2006**, *45*, 2104–2107.
(334) Pentecost, C. D.; Peters, A. J.; Chichak, K. S.; Cave, G. W. V.; Cantrill, S. J.; Stoddart, J. F. Chiral Borromeates. *Angew. Chem., Int. Ed.* **2006**, *45*, 4099–4104.
(335) Chui, S. S.-Y.; Chen, R.; Che, C.-M. A Chiral [2]Catenane Precursor of the Antiarthritic Gold(I) Drug Auranofin. *Angew. Chem., Int. Ed.* **2006**, *45*, 1621–1624.
(336) Hirose, K.; Nakamura, Y.; Tobe, Y. Remarkable Effects of Chirality on Deslipping Reactions of Diastereomeric Rotaxanes and Relevant Mechanism Involving Pre-Equilibrium. *Org. Lett.* **2009**, *11*, 145–147.
(337) Nakatani, Y.; Furusho, Y.; Yashima, E. Amidinium Carboxylate Salt Bridges as a Recognition Motif for Mechanically Interlocked Molecules: Synthesis of an Optically Active [2]Catenane and Control of Its Structure. *Angew. Chem., Int. Ed.* **2010**, *49*, 5463–5467.
(338) Ko, J.-L.; Ueng, S.-H.; Chiu, C.-W.; Lai, C.-C.; Liu, Y.-H.; Peng, S.-M.; Chiu, S.-H. Using a Threading-Followed-by-Swelling Approach to Synthesize [2]Rotaxanes. *Chem. Eur. J.* **2010**, *16*, 6950–6960.
(339) Shinoda, S.; Maeda, T.; Miyake, H.; Tsukube, H. Dynamically Capped Rotaxanes: Metal Coordination vs. Acid–Base Pairing in the Chiral End-Capping. *Supramol. Chem.* **2011**, *23*, 244–248.
(340) Ashton, P. R.; Boyd, S. E.; Menzer, S.; Pasini, D.; Raymo, F. M.; Spencer, N.; Stoddart, J. F.; White, A. J. P.; Williams, D. J.; Wyatt, P. G. Molecular Meccano 23. Self-Assembling Cyclophanes and Catenanes Possessing Elements of Planar Chirality. *Chem. Eur. J.* **1998**, *4*, 299–310.
(341) Okada, Y.; Miao, Z.; Akiba, M.; Nishimura, J. Synthesis and Characterization of Chiral Catenanes Based on Rigid Calix[4]arene. *Tetrahedron Lett.* **2006**, *47*, 2699–2702.
(342) Zhao, Y.-L.; Liu, L.; Zhang, W.; Sue, C.-H.; Li, Q.; Miljanić, O. Š.; Yaghi, O. M.; Stoddart, J. F. Rigid-Strut-Containing Crown Ethers and [2]Catenanes for Incorporation Into Metal-Organic Frameworks. *Chem. Eur. J.* **2009**, *15*, 13356–13380.
(343) Kitajima, K.; Ogoshi, T.; Yamagishi, T.-A. Diastereoselective Synthesis of a [2]Catenane From a Pillar[5]arene and a Pyridinium Derivative. *Chem. Commun.* **2014**, *50*, 2925–2927.
(344) Asakawa, M.; Ashton, P. R.; Boyd, S. E.; Brown, C. L.; Menzer, S.; Pasini, D.; Stoddart, J. F.; Tolley, M. S.; White, A. J. P.; Wyatt, P. G. Molecular Meccano 16. Axially Chiral Catenanes and π-Electron-Deficient Receptors. *Chem. Eur. J.* **1997**, *3*, 463–481.
(345) Ashton, P. R.; Heiss, A. M.; Pasini, D.; Raymo, F. M.; Shipway, A. N.; Stoddart, J. F.; Spencer, N. Molecular Meccano 51. Diastereoselective Self-Assembly of [2]Catenanes. *Eur. J. Org. Chem.* **1999**, 995–1004.
(346) Cantrill, S. J.; Fyfe, M. C. T.; Heiss, A. M.; White, A. J. P.; Williams, D. J.; Stoddart, J. F. Rotaxane Construction with a Binaphthol-Derived Crown Ether. *Chem. Commun.* **1999**, 1251–1252.
(347) Tachibana, Y.; Kihara, N.; Ohga, Y.; Takata, T. Rotaxanes Functionalized by Chirality. Novel Rotaxanes Consisting of Binaphthol-Based Chiral Crown Ether. *Chem. Lett.* **2000**, 806–807.
(348) Koizumi, M.; Dietrich-Buchecker, C.; Sauvage, J.-P. A [2]Catenane Containing 1,1'-Binaphthyl Units and 1,10-Phenanthroline Fragments: Synthesis and Intermolecular Energy Transfer Processes. *Eur. J. Org. Chem.* **2004**, 770–775.
(349) Burchell, T. J.; Eisler, D. J.; Puddephatt, R. J. A Chiral [2]Catenane Self-Assembled From *meso*-Macrocycles of Palladium(II). *Dalton Trans.* **2005**, 268–272.
(350) Zhu, X.-Z.; Chen, C.-F. Efficient Synthesis of a Chiral [4]Pseudocatenane and Its Derivatives: A Novel Ship's Wheel-Like Interlocked Structure. *Chem. Eur. J.* **2006**, *12*, 5603–5609.
(351) Kang, S.; Aprahamian, I.; Stoddart, J. F. Pirouetting in Chiral [2] Catenanes. *Isr. J. Chem.* **2007**, *47*, 253–262.
(352) Tachibana, Y.; Kihara, N.; Takata, T. Asymmetric Benzoin Condensation Catalyzed by Chiral Rotaxanes Tethering a Thiazolium Salt Moiety via the Cooperation of the Component: Can Rotaxane Be an Effective Reaction Field? *J. Am. Chem. Soc.* **2004**, *126*, 3438–3439.
(353) Tachibana, Y.; Kihara, N.; Nakazono, K.; Takata, T. Thiazolium-Tethering Rotaxane-Catalyzed Asymmetric Benzoin Condensation: Unique Asymmetric Field Constructed by the Cooperation of Rotaxane Components. *Phosphorus, Sulfur Silicon Relat. Elem.* **2010**, *185*, 1182–1205.
(354) Yang, W.; Li, Y.; Zhang, J.; Chen, N.; Chen, S.; Liu, H.; Li, Y. A Controllable Chiral Molecular Machine: Movement on Molecular Level. *Small* **2012**, *8*, 2602–2607.
(355) Whang, D.; Kim, K. Helical Polyrotaxane: Cucurbituril "Beads" Threaded Onto a Helical One-Dimensional Coordination Polymer. *Chem. Commun.* **1997**, 2361–2362.
(356) Try, A. C.; Harding, M. M.; Hamilton, D. G.; Sanders, J. K. M. Reversible Five-Component Assembly of a [2]Catenane From

a Chiral Metallomacrocycle and a Dinaphtho-Crown Ether. *Chem. Commun.* **1998**, 723–724.
(357) Moretto, A.; Menegazzo, I.; Crisma, M.; Shotton, E. J.; Nowell, H.; Mammi, S.; Toniolo, C. A Rigid Helical Peptide Axle for a [2]Rotaxane Molecular Machine. *Angew. Chem., Int. Ed.* **2009**, *48*, 8986–8989.
(358) Gan, Q.; Ferrand, Y.; Bao, C.; Kauffmann, B.; Grelard, A.; Jiang, H.; Huc, I. Helix-Rod Host-Guest Complexes with Shuttling Rates Much Faster Than Disassembly. *Science* **2011**, *331*, 1172–1175.
(359) Suzuki, S.; Ishiwari, F.; Nakazono, K.; Takata, T. Reversible Helix–Random Coil Transition of Poly(*m*-phenylenediethynylene) by a Rotaxane Switch. *Chem. Commun.* **2012**, *48*, 6478–6480.
(360) Aboshyan-Sorgho, L.; Cantuel, M.; Bernardinelli, G.; Piguet, C. Looking for the Origin of the Switch Between Coordination-Captured Helicates and Catenates. *Dalton Trans.* **2012**, *41*, 7218–7226.
(361) Ishiwari, F.; Fukasawa, K.-I.; Sato, T.; Nakazono, K.; Koyama, Y.; Takata, T. A Rational Design for the Directed Helicity Change of Polyacetylene Using Dynamic Rotaxane Mobility by Means of Through-Space Chirality Transfer. *Chem. Eur. J.* **2011**, *17*, 12067–12075.
(362) Ishiwari, F.; Nakazono, K.; Koyama, Y.; Takata, T. Rational Control of a Polyacetylene Helix by a Pendant Rotaxane Switch. *Chem. Commun.* **2011**, *47*, 11739–11741.
(363) Böhmer, V.; Kraft, D.; Tabatabai, M. Inherently Chiral Calixarenes. *J. Incl. Phenom. Macrocycl. Chem.* **1994**, *19*, 17–39.
(364) Dalla Cort, A.; Mandolini, L.; Pasquini, C.; Schiaffino, L. “Inherent Chirality” and Curvature. *New J. Chem.* **2004**, *28*, 1198–1199.
(365) Szumna, A. Inherently Chiral Concave Molecules—From Synthesis to Applications. *Chem. Soc. Rev.* **2010**, *39*, 4274–4285.
(366) Prelog, V.; Gerlach, H. Cycloenantiomerie und Cyclodiastereomerie. 1. Mitteilung. *Helv. Chim. Acta* **1964**, *47*, 2288–2294.
(367) Schill, G. *Catenanes, Rotaxanes, and Knots*; Academic Press: New York, **1971**.
(368) Jäger, R.; Händel, M.; Harren, J.; Rissanen, K.; Vögtle, F. Chemistry with Rotaxanes: Intra- and Intermolecularly Covalently Linked Rotaxanes. *Liebigs Ann.* **1996**, 1201–1207.
(369) Yamamoto, C.; Okamoto, Y.; Schmidt, T.; Vögtle, F. Enantiomeric Resolution of Cycloenantiomeric Rotaxane, Topologically Chiral Catenane, and Pretzel-Shaped Molecules: Observation of Pronounced Circular Dichroism. *J. Am. Chem. Soc.* **1997**, *119*, 10547–10548.
(370) Schmieder, R.; Hubner, G.; Seel, C.; Vögtle, F. The First Cyclodiasteromeric [3]Rotaxane. *Angew. Chem., Int. Ed.* **1999**, *38*, 3528–3530.
(371) Reuter, C.; Schmieder, R.; Vögtle, F. From Rotaxanes to Knots. Templating, Hydrogen Bond Patterns, and Cyclochirality. *Pure Appl. Chem.* **2000**, *72*, 2233–2241.
(372) Reuter, C.; Seel, C.; Nieger, M.; Vögtle, F. Chiral [1]Rotaxanes: X-Ray Structures and Chiroptical Properties. *Helv. Chim. Acta* **2000**, *83*, 630–640.
(373) Eliel, E. L.; Wilen, S. H.; Mander, L. N. *Stereochemistry of Organic Compounds*; John Wiley & Sons: New York, **1994**.
(374) Makita, Y.; Kihara, N.; Nakakoji, N.; Takata, T.; Inagaki, S.; Yamamoto, C.; Okamoto, Y. Catalytic Asymmetric Synthesis and Optical Resolution of Planar Chiral Rotaxane. *Chem. Lett.* **2007**, *36*, 162–163.
(375) Bordoli, R. J.; Goldup, S. M. An Efficient Approach to Mechanically Planar Chiral Rotaxanes. *J. Am. Chem. Soc.* **2014**, *136*, 4817–4820.
(376) Kameta, N.; Hiratani, K.; Nagawa, Y. A Novel Synthesis of Chiral Rotaxanes via Covalent Bond Formation. *Chem. Commun.* **2004**, 466–467.
(377) Kameta, N.; Nagawa, Y.; Karikomi, M.; Hiratani, K. Chiral Sensing for Amino Acid Derivative Based on a [2]Rotaxane Composed of an Asymmetric Rotor and an Asymmetric Axle. *Chem. Commun.* **2006**, 3714–3716.
(378) Wu, J.; Leung, K. C.-F.; Benítez, D.; Han, J.-Y.; Cantrill, S. J.; Fang, L.; Stoddart, J. F. An Acid-Base-Controllable [*c*2]Daisy Chain. *Angew. Chem., Int. Ed.* **2008**, *47*, 7470–7474.
(379) Coutrot, F.; Romuald, C.; Busseron, E. A New pH-Switchable Dimannosyl[*c*2]Daisy Chain Molecular Machine. *Org. Lett.* **2008**, *10*, 3741–3744.
(380) Clark, P. G.; Day, M. W.; Grubbs, R. H. Switching and Extension of a [*c*2]Daisy-Chain Dimer Polymer. *J. Am. Chem. Soc.* **2009**, *131*, 13631–13633.
(381) Fang, L.; Hmadeh, M.; Wu, J.; Olson, M. A.; Spruell, J. M.; Trabolsi, A.; Yang, Y.-W.; Elhabiri, M.; Albrecht-Gary, A.-M.; Stoddart, J. F. Acid-Base Actuation of [*c*2]Daisy Chains. *J. Am. Chem. Soc.* **2009**, *131*, 7126–7134.
(382) Moulin, E.; Giuseppone, N. A Move in the Right Direction. *Nature Nanotechnol.* **2014**, *9*, 331–332.
(383) Kishan, M. R.; Parham, A.-H.; Schelhase, F.; Yoneva, A.; Silva, G.; Chen, X.; Okamoto, Y.; Vögtle, F. Bridging Rotaxanes’ Wheels-Cyclochiral Bonnanes. *Angew. Chem., Int. Ed.* **2006**, *45*, 7296–7299.
(384) McArdle, C. P.; Van, S.; Jennings, M. C.; Puddephatt, R. J. Gold(I) Macrocycles and Topologically Chiral [2]Catenanes. *J. Am. Chem. Soc.* **2002**, *124*, 3959–3965.
(385) Hori, A.; Sawada, T.; Yamashita, K.-I.; Fujita, M. Ultramacrocyclization Through Reversible Catenation. *Angew. Chem., Int. Ed.* **2005**, *44*, 4896–4899.
(386) Dietrich-Buchecker, C. O.; Edel, A.; Kintzinger, J.-P.; Sauvage, J.-P. Syntheses and Study of a Chiral Catenate of Two Interlocked 27-Membered Rings Coordinated to Copper. *Tetrahedron* **1987**, *43*, 333–344.
(387) Dietrich-Buchecker, C. O.; Sauvage, J.-P. Une Nouvelle Famille de Molecules: les Metallo-Catenanes. *Tetrahedron Lett.* **1983**, *24*, 5095–5098.
(388) Hutin, M.; Schalley, C. A.; Bernardinelli, G.; Nitschke, J. R. Helicate, Macrocycle, or Catenate: Dynamic Topological Control Over Subcomponent Self-Assembly. *Chem. Eur. J.* **2006**, *12*, 4069–4076.
(389) Hori, A.; Akasaka, A.; Biradha, K.; Sakamoto, S.; Yamaguchi, K.; Fujita, M. Chirality Induction Through the Reversible Catenation of Coordination Rings. *Angew. Chem., Int. Ed.* **2002**, *41*, 3269–3272.
(390) Brown, A.; Langton, M. J.; Kilah, N. L.; Thompson, A. L.; Beer, P. D. Chloride-Anion-Templated Synthesis of a Strapped-Porphyrin-Containing Catenane Host System. *Chem. Eur. J.* **2015**, *21*, 17664–17675.
(391) Gidron, O.; Jirásek, M.; Trapp, N.; Ebert, M.-O.; Zhang, X.; Diederich, F. Homochiral [2]Catenane and Bis[2]Catenane From Alleno-Acetylenic Helicates—A Highly Selective Narcissistic Self-Sorting Process. *J. Am. Chem. Soc.* **2015**, *137*, 12502–12505.
(392) Ayme, J.-F.; Beves, J. E.; Leigh, D. A.; McBurney, R. T.; Rissanen, K.; Schultz, D. A Synthetic Molecular Pentafoil Knot. *Nature Chem.* **2012**, *4*, 15–20.
(393) Ayme, J.-F.; Beves, J. E.; Leigh, D. A.; McBurney, R. T.; Rissanen, K.; Schultz, D. Pentameric Circular Iron(II) Double Helicates and a Molecular Pentafoil Knot. *J. Am. Chem. Soc.* **2012**, 9488–9497.
(394) Ayme, J.-F.; Beves, J. E.; Campbell, C. J.; Leigh, D. A. The Self-Sorting Behavior of Circular Helicates and Molecular Knots and Links. *Angew. Chem., Int. Ed.* **2014**, *53*, 7823–7827.
(395) Leigh, D. A.; Pritchard, R. G.; Stephens, A. J. A Star of David Catenane. *Nature Chem.* **2014**, *6*, 978–982.
(396) Westcott, A.; Fisher, J.; Harding, L. P.; Rizkallah, P.; Hardie, M. J. Self-Assembly of a 3-D Triply Interlocked Chiral [2]Catenane. *J. Am. Chem. Soc.* **2008**, *130*, 2950–2951.
(397) Vignon, S. A.; Wong, J.; Tseng, H.-R.; Stoddart, J. F. Helical Chirality in Donor-Acceptor Catenanes. *Org. Lett.* **2004**, *6*, 1095–1098.

(398) Lacour, J.; Ginglinger, C.; Grivet, C.; Bernardinelli, G. Synthesis and Resolution of the Configurationally Stable Tris(tetrachlorobenzenediolato)phosphate(V) Ion. *Angew. Chem., Int. Ed. Engl.* **1997**, *36*, 608–610.

(399) Bogdan, A.; Vysotsky, M. O.; Ikai, T.; Okamoto, Y.; Böhmer, V.; Rational Synthesis of Multicyclic Bis[2]Catenanes. *Chem. Eur. J.* **2004**, *10*, 3324–3330.

(400) Molokanova, O.; Bogdan, A.; Vysotsky, M. O.; Bolte, M.; Ikai, T.; Okamoto, Y.; Böhmer, V. Calix[4]arene-Based Bis[2]-catenanes: Synthesis and Chiral Resolution. *Chem. Eur. J.* **2007**, *13*, 6157–6170.

(401) Chas, M.; Ballester, P. A Dissymmetric Molecular Capsule with Polar Interior and Two Mechanically Locked Hemispheres. *Chem. Sci.* **2011**, *3*, 186–191.

(402) Belowich, M. E.; Valente, C.; Smaldone, R. A.; Friedman, D. C.; Thiel, J.; Cronin, L.; Stoddart, J. F. Positive Cooperativity in the Template-Directed Synthesis of Monodisperse Macromolecules. *J. Am. Chem. Soc.* **2012**, *134*, 5243–5261.

(403) Avestro, A.-J.; Gardner, D. M.; Vermeulen, N. A.; Wilson, E. A.; Schneebeli, S. T.; Whalley, A. C.; Belowich, M. E.; Carmieli, R.; Wasielewski, M. R.; Stoddart, J. F. Gated Electron Sharing Within Dynamic Naphthalene Diimide-Based Oligorotaxanes. *Angew. Chem., Int. Ed.* **2014**, *53*, 4442–4449.

(404) Sevick, E. M.; Williams, D. R. M. Conformational Isomers of Linear Rotaxanes. *J. Chem. Phys.* **2014**, *141*, 114904.

(405) Frisch, H. L.; Wasserman, E. Chemical Topology. *J. Am. Chem. Soc.* **1961**, *83*, 3789–3795.

(406) Walba, D. M. Topological Stereochemistry. *Tetrahedron* **1985**, *41*, 3161–3212.

(407) Prelog, V. Problems in Chemical Topology. *Chem. Brit.* **1968**, *4*, 382–387.

(408) Sokolov, V. I. Topological Ideas in Stereochemistry. *Russian Chem. Rev.* **1973**, *42*, 452–463.

(409) Walba, D. M. A Topological Hierarchy of Molecular Chirality and Other Tidbits in Topological Stereochemistry. In *New Developments in Molecular Chirality*; Mezey, P. G., Ed.; Kluwer Academic Publishers: Boston, **1991**; Vol. *5*, pp. 119–129.

(410) Chambron, J.-C.; Dietrich-Buchecker, C.; Sauvage, J.-P. From Classical Chirality to Topologically Chiral Catenands and Knots. *Top. Curr. Chem.* **1993**, *165*, 131–162.

(411) Liang, C.; Mislow, K. Topological Chirality and Achirality of Links. *J. Math. Chem.* **1995**, *18*, 1–24.

(412) Breault, G. A.; Hunter, C. A.; Mayers, P. C. Supramolecular Topology. *Tetrahedron* **1999**, *55*, 5265–5293.

(413) Siegel, J. S. Chemical Topology and Interlocking Molecules. *Science* **2004**, *304*, 1256–1258.

(414) Fenlon, E. E. Open Problems in Chemical Topology. *Eur. J. Org. Chem.* **2008**, 5023–5035.

(415) Amabilino, D. B.; Pérez-García, L. Topology in Molecules Inspired, Seen and Represented. *Chem. Soc. Rev.* **2009**, *38*, 1562–1571.

(416) Forgan, R. S.; Sauvage, J.-P.; Stoddart, J. F. Chemical Topology: Complex Molecular Knots, Links, and Entanglements. *Chem. Rev.* **2011**, *111*, 5434–5464.

(417) Kuratowski, K. Sur le Problème des Courbes Gauches en Topologie. *Fund. Math.* **1930**, *15*, 271–283.

(418) Dietrich-Buchecker, C.; Colasson, B. X.; Sauvage, J.-P. Molecular Knots. *Top. Curr. Chem.* **2005**, *249*, 261–283.

(419) O'Keeffe, M.; Eddaoudi, M.; Li, H.; Reineke, T.; Yaghi, O. M. Frameworks for Extended Solids: Geometrical Design Principles. *J. Solid State Chem.* **2000**, *152*, 3–20.

(420) Castle, T.; Evans, M. E.; Hyde, S. T. Ravels: Knot-Free but Not Free. Novel Entanglements of Graphs in 3-Space. *New J. Chem.* **2008**, *32*, 1484–1492.

(421) Li, F.; Clegg, J. K.; Lindoy, L. F.; Macquart, R. B.; Meehan, G. V. Metallosupramolecular Self-Assembly of a Universal 3-Ravel. *Nature Commun.* **2011**, *2*: 205.

(422) Walba, D. M.; Richards, R. M.; Haltiwanger, R. C. Total Synthesis of the First Molecular Möbius Strip. *J. Am. Chem. Soc.* **1982**, *104*, 3219–3221.

(423) Walba, D. M.; Homan, T. C.; Richards, R. M.; Haltiwanger, R. C. Synthesis and Cutting "In Half" of a Molecular Möbius Strip. *New J. Chem.* **1993**, *17*, 661–681.

(424) Simmons, H. E.; Maggio, J. E. Synthesis of the First Topologically Non-Planar Molecule. *Tetrahedron Lett.* **1981**, *22*, 287–290.

(425) Paquette, L. A.; Vazeux, M. Threefold Transannular Epoxide Cyclization. Synthesis of a Heterocyclic C_{17}-Hexaquinane. *Tetrahedron Lett.* **1981**, *22*, 291–294.

(426) Kuck, D.; Schuster, A. Centrohexaindan, the First Hydrocarbon with Topologically Non-Planar Molecular Structure. *Angew. Chem., Int. Ed. Engl.* **1988**, *27*, 1192–1194.

(427) Chen, C. T.; Gantzel, P.; Siegel, J. S. Baldridge, K. K.; English, R. B.; Ho, D. M. Synthesis and Structure of the Nanodimensional Multicyclophane "Kuratowski Cyclophane," an Achiral Molecule with Nonplanar $K_{3,3}$ Topology. *Angew. Chem., Int. Ed. Engl.* **1995**, *34*, 2657–2660.

(428) Wang, J. C. Cellular Roles of DNA Topoisomerases: a Molecular Perspective. *Nat. Rev. Mol. Cell. Biol.* **2002**, *3*, 430–440.

(429) Walba, D. M.; Armstrong, J. D., III; Richards, R. M.; Homan, T. C.; Haltiwanger, R. C. The THYME Polyethers: An Approach to the Synthesis of a Molecular Knotted Ring. *Tetrahedron* **1986**, *42*, 1883–1894.

(430) Lüttringhaus, A.; Isele, G. Synthesis of a Catena Compound by the Semistatistical Principle. *Angew. Chem., Int. Ed. Engl.* **1967**, *6*, 956–957.

(431) Ponnuswamy, N.; Cougnon, F. B. L.; Pantoş, G. D.; Sanders, J. K. M. Homochiral and *meso* Figure Eight Knots and a Solomon Link. *J. Am. Chem. Soc.* **2014**, *136*, 8243–8251.

(432) Mao, C.; Sun, W.; Seeman, N. C. Assembly of Borromean Rings From DNA. *Nature* **1997**, *386*, 137–138.

(433) Dolomanov, O. V.; Blake, A. J.; Champness, N. R.; Schroder, M.; Wilson, C. A Novel Synthetic Strategy for Hexanuclear Supramolecular Architectures. *Chem. Commun.* **2003**, 682–683.

(434) Chichak, K. S.; Cantrill, S. J.; Pease, A. R.; Chiu, S.-H.; Cave, G. W. V.; Atwood, J. L.; Stoddart, J. F. Molecular Borromean Rings. *Science* **2004**, *304*, 1308–1312.

(435) Peters, A. J.; Chichak, K. S.; Cantrill, S. J.; Cantrill, S. J.; Stoddart, J. F. Nanoscale Borromean Links for Real. *Chem. Commun.* **2005**, *3394–3396*.

(436) Cantrill, S. J.; Chichak, K. S.; Peters, A. J.; Stoddart, J. F. Nanoscale Borromean Rings. *Acc. Chem. Res.* **2005**, *38*, 1–9.

(437) Huang, S.-L.; Lin, Y.-J.; Hor, T. S. A.; Jin, G.-X. Cp*Rh-Based Heterometallic Metallarectangles: Size-Dependent Borromean Link Structures and Catalytic Acyl Transfer. *J. Am. Chem. Soc.* **2013**, *135*, 8125–8128.

(438) Huang, S.-L.; Lin, Y.-J.; Li, Z.-H.; Jin, G.-X. Self-Assembly of Molecular Borromean Rings From Bimetallic Coordination Rectangles. *Angew. Chem., Int. Ed.* **2014**, *53*, 11218–11222.

(439) Mitchell, D. K.; Sauvage, J.-P. A Topologically Chiral [2]Catenand. *Angew. Chem., Int. Ed. Engl.* **1988**,*27*, 930–931.

(440) Chambron, J.-C.; Mitchell, D. K.; Sauvage, J.-P. Synthesis, Characterization, and a Proton NMR Study of Topologically Chiral Copper(I) [2]-Catenates and Achiral Analogs. *J. Am. Chem. Soc.* **1992**, *114*, 4625–4631.

(441) Kaida, Y.; Okamoto, Y.; Chambron, J.-C.; Mitchell, D.; Sauvage, J.-P. The Separation of Optically Active Copper(I) Catenates. *Tetrahedron Lett.* **1993**, *34*, 1019–1022.

(442) Loren, J. C.; Gantzel, P.; Linden, A.; Siegel, J. S. Synthesis of Achiral and Racemic Catenanes Based on Terpyridine and a Directionalized Terpyridine Mimic, Pyridyl-Phenanthroline. *Org. Biomol. Chem.* **2005**, *3*, 3105–3116.

(443) Ottens-Hildebrandt, S.; Schmidt, T.; Harren, J.; Vögtle, F. Sulfonamide-Based Catenanes—Regioselective Template Synthesis. *Liebigs Ann.* **1995**, 1855–1860.

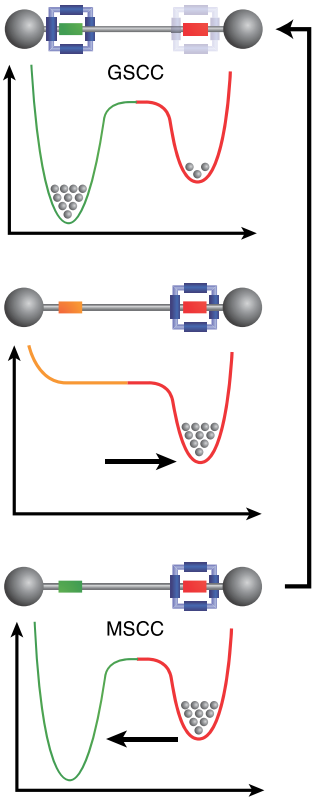
(444) Mohry, A.; Vögtle, F.; Nieger, M.; Hupfer, H. Regioselective Template Synthesis, X-Ray Structure, and Chiroptical Properties of a Topologically Chiral Sulfonamide Catenane. *Chirality* **2000**, *12*, 76–83.

(445) Lam, R. T. S.; Belenguer, A.; Roberts, S. L.; Naumann, C.; Jarrosson, T.; Otto, S.; Sanders, J. K. M. Amplification of Acetylcholine-Binding Catenanes From Dynamic Combinatorial Libraries. *Science* **2005**, *308*, 667–669.
(446) Prakasam, T.; Lusi, M.; Nauha, E.; Olsen, J.-C.; Sy, M.; Platas-Iglesias, C.; Charbonnière, L. J.; Trabolsi, A. Dynamic Stereoisomerization in Inherently Chiral Bimetallic [2]Catenanes. *Chem. Commun.* **2015**, *51*, 5840–5843.
(447) Barta, N. S.; Stille, J. R. Grasping the Concepts of Stereochemistry. *J. Chem. Ed.* **2005**, *71*, 20–23.
(448) Dietrich-Buchecker, C. O.; Sauvage, J.-P. A Synthetic Molecular Trefoil Knot. *Angew. Chem., Int. Ed. Engl.* **1989**, *28*, 189–192.
(449) Dietrich-Buchecker, C. O.; Guilhem, J.; Pascard, C.; Sauvage, J.-P. Structure of a Synthetic Trefoil Knot Coordinated to Two Copper(I) Centers. *Angew. Chem., Int. Ed. Engl.* **1990**, *29*, 1154–1156.
(450) Rapenne, G.; Dietrich-Buchecker, C.; Sauvage, J.-P. Resolution of a Molecular Trefoil Knot. *J. Am. Chem. Soc.* **1996**, *118*, 10932–10933.
(451) Dietrich-Buchecker, C.; Rapenne, G.; Sauvage, J.-P.; De Cian, A.; Fischer, J. A Dicopper(I) Trefoil Knot with *m*-Phenylene Bridges Between the Ligand Subunits: Synthesis, Resolution, and Absolute Configuration. *Chem. Eur. J.* **1999**, *5*, 1432–1439.
(452) Meskers, S.; Dekkers, H.; Rapenne, G.; Sauvage, J.-P. Chiroptical Properties of an Optically Pure Dicopper(I) Trefoil Knot and Its Enantioselectivity in Luminescence Quenching Reactions. *Chem. Eur. J.* **2000**, *6*, 2129–2134.
(453) Safarowsky, O.; Nieger, M.; Fröhlich, R.; Vögtle, F. A Molecular Knot with Twelve Amide Groups: One-Step Synthesis, Crystal Structure, Chirality. *Angew. Chem., Int. Ed.* **2000**, *39*, 1616–1618.
(454) Vögtle, F.; Hünten, A.; Vogel, E.; Buschbeck, S.; Safarowsky, O.; Recker, J.; Parham, A.-H.; Knott, M.; Müller, W. M.; Müller, U.; Okamoto, Y.; Kubota, T.; Lindner, W.; Francotte, E.; Grimme, S. Novel Amide-Based Molecular Knots: Complete Enantiomeric Separation, Chiroptical Properties, and Absolute Configuration. *Angew. Chem., Int. Ed.* **2001**, *40*, 2468–2471.
(455) Recker, J.; Müller, W. M.; Müller, U.; Kubota, T.; Okamoto, Y.; Nieger, M.; Vögtle, F. Dendronized Molecular Knots: Selective Synthesis of Various Generations, Enantiomer Separation, Circular Dichroism. *Chem. Eur. J.* **2002**, *8*, 4434–4442.
(456) Lukin, O.; Recker, J.; Böhmer, A.; Müller, W. M.; Kubota, T.; Okamoto, Y.; Nieger, M.; Fröhlich, R.; Vögtle, F. A Topologically Chiral Molecular Dumbbell. *Angew. Chem., Int. Ed.* **2003**, *42*, 442–445.
(457) Lukin, O.; Kubota, T.; Okamoto, Y.; Schelhase, F.; Schelhase, F.; Yoneva, A.; Müller, W. M.; Müller, U.; Vögtle, F. Knotaxanes-Rotaxanes with Knots as Stoppers. *Angew. Chem., Int. Ed.* **2003**, *42*, 4542–4545.
(458) Lukin, O.; Kubota, T.; Okamoto, Y.; Vögtle, F. Topologically Chiral Covalent Assemblies of Molecular Knots with Linear, Branched, and Cyclic Architectures. *Chem. Eur. J.* **2004**, *10*, 2804–2810.
(459) Lukin, O.; Vögtle, F. Knotting and Threading of Molecules: Chemistry and Chirality of Molecular Knots and Their Assemblies. *Angew. Chem., Int. Ed.* **2005**, *44*, 1456–1477.
(460) Passaniti, P.; Ceroni, P.; Balzani, V.; Lukin, O.; Yoneva, A.; Vögtle, F. Amide-Based Molecular Knots as Platforms for Fluorescent Switches. *Chem. Eur. J.* **2006**, *12*, 5685–5690.
(461) Brueggemann, J.; Bitter, S.; Mueller, S.; Mueller, W.; Maier, N.; Lindner, W.; Vögtle, F. Spontaneous Knotting - From Oligoamide Threads to Trefoil Knots. *Angew. Chem., Int. Ed.* **2007**, *46*, 254–259.
(462) Safarowsky, O.; Windisch, B.; Mohry, A.; Vögtle, F. Nomenclature for Catenanes, Rotaxanes, Molecular Knots, and Assemblies Derived From These Structural Elements. *J. Prakt. Chem.* **2000**, *342*, 437–444.
(463) Rapenne, G.; Dietrich-Buchecker, C.; Sauvage, J.-P. Copper(I)- or Iron(II)-Templated Synthesis of Molecular Knots Containing Two Tetrahedral or Octahedral Coordination Sites. *J. Am. Chem. Soc.* **1999**, *121*, 994–1001.
(464) Guo, J.; Mayers, P. C.; Breault, G. A.; Hunter, C. A. Synthesis of a Molecular Trefoil Knot by Folding and Closing on an Octahedral Coordination Template. *Nature Chem.* **2010**, *2*, 218–222.
(465) Feigel, M.; Ladberg, R.; Engels, S.; Herbst-Irmer, R.; Fröhlich, R. A Trefoil Knot Made of Amino Acids and Steroids. *Angew. Chem., Int. Ed.* **2006**, *45*, 5698–5702.
(466) Ashton, P. R.; Matthews, O. A.; Menzer, S.; Raymo, F. M.; Spencer, N.; Stoddart, J. F.; Williams, D. J. Molecular Meccano 27. A Template-Directed Synthesis of a Molecular Trefoil Knot. *Liebigs Ann./Recueil* **1997**, 2485–2494.
(467) Arias, K. I.; Zysman-Colman, E.; Loren, J. C.; Linden, A.; Siegel, J. S. Synthesis of a D_3-Symmetric "Trefoil" Knotted Cyclophane. *Chem. Commun.* **2011**, *47*, 9588–9590.
(468) Ponnuswamy, N.; Cougnon, F. B. L.; Clough, J. M.; Pantoş, G. D.; Sanders, J. K. M. Discovery of an Organic Trefoil Knot. *Science* **2012**, *338*, 783–785.
(469) Dietrich-Buchecker, C.; Geum Hwang, N.; Sauvage, J.-P. A Trefoil Knot Coordinated to Two Lithium Ions: Synthesis and Structure. *New J. Chem.* **1999**, *23*, 911–914.
(470) Ayme, J.-F.; Gil-Ramírez, G.; Leigh, D. A.; Lemonnier, J.-F.; Markevicius, A.; Muryn, C. A.; Zhang, G. Lanthanide Template Synthesis of a Molecular Trefoil Knot. *J. Am. Chem. Soc.* **2014**, *136*, 13142–13145.
(471) Mueller, J. E.; Du, S. M.; Seeman, N. C. Design and Synthesis of a Knot From Single-Stranded DNA. *J. Am. Chem. Soc.* **1991**, *113*, 6306–6308.
(472) Barran, P. E.; Cole, H. L.; Goldup, S. M.; Leigh, D. A.; McGonigal, P. R.; Symes, M. D.; Wu, J.; Zengerle, M. Active-Metal Template Synthesis of a Molecular Trefoil Knot. *Angew. Chem., Int. Ed.* **2011**, *50*, 12280–12284.
(473) Nierengarten, J.-F.; Dietrich-Buchecker, C. O.; Sauvage, J.-P. Synthesis of a Doubly Interlocked [2]-Catenane. *J. Am. Chem. Soc.* **1994**, *116*, 375–376.
(474) Nierengarten, J.-F.; Buchecker, C. O.; Sauvage, J.-P. Copper(I) Template Synthesis of a Four-Crossing [2]Catenane. *New J. Chem.* **1996**, *20*, 685–693.
(475) Dietrich-Buchecker, C.; Sauvage, J.-P. Lithium Templated Synthesis of Catenanes: Efficient Synthesis of Doubly Interlocked [2]-Catenanes. *Chem. Commun.* **1999**, 615–616.
(476) Ibukuro, F.; Fujita, M.; Yamaguchi, K.; Sauvage, J.-P. Quantitative and Spontaneous Formation of a Doubly Interlocking [2]Catenane Using Copper(I) and Palladium(II) as Templating and Assembling Centers. *J. Am. Chem. Soc.* **1999**, *121*, 11014–11015.
(477) Schouwey, C.; Holstein, J. J.; Scopelliti, R.; Zhurov, K. O.; Nagornov, K. O.; Tsybin, Y. O.; Smart, O. S.; Bricogne, G.; Severin, K. Self-Assembly of a Giant Molecular Solomon Link From 30 Subcomponents. *Angew. Chem., Int. Ed.* **2014**, *53*, 11261–11265.
(478) McArdle, C. P.; Vittal, J. J.; Puddephatt, R. J. Molecular Topology: Easy Self-Assembly of an Organometallic Doubly Braided [2]Catenane. *Angew. Chem., Int. Ed.* **2000**, *39*, 3819–3822.
(479) McArdle, C. P.; Jennings, M. C.; Vittal, J. J.; Puddephatt, R. J. Self-Assembly of Rings, Catenanes, and a Doubly Braided Catenane Containing Gold(I): The Hinge-Group Effect in Diacetylide Ligands. *Chem. Eur. J.* **2001**, *7*, 3572–3583.
(480) Pentecost, C. D.; Chichak, K. S.; Peters, A. J.; Cave, G. W. V.; Cantrill, S. J.; Stoddart, J. F. A Molecular Solomon Link. *Angew. Chem., Int. Ed.* **2007**, *46*, 218–222.
(481) Meyer, C. D.; Forgan, R. S.; Chichak, K. S.; Peters, A. J.; Tangchaivang, N.; Cave, G. W. V.; Khan, S. I.; Cantrill, S. J.; Stoddart, J. F. The Dynamic Chemistry of Molecular Borromean Rings and Solomon Knots. *Chem. Eur. J.* **2010**, *16*, 12570–12581.
(482) Prakasam, T.; Lusi, M.; Elhabiri, M.; Platas-Iglesias, C.; Olsen, J.-C.; Asfari, Z.; Cianférani-Sanglier, S.; Debaene, F.; Charbonnière, L. J.; Trabolsi, A. Simultaneous Self-Assembly

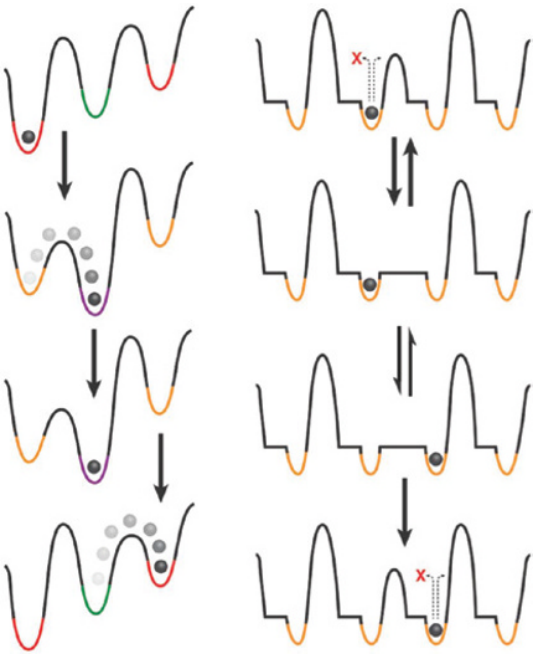
of a [2]Catenane, a Trefoil Knot, and a Solomon Link From a Simple Pair of Ligands. *Angew. Chem., Int. Ed.* **2013**, *52*, 9956–9960.
(483) Beves, J. E.; Campbell, C. J.; Leigh, D. A.; Pritchard, R. G. Tetrameric Cyclic Double Helicates as a Scaffold for a Molecular Solomon Link. *Angew. Chem., Int. Ed.* **2013**, *52*, 6464–6467.
(484) Peinador, C.; Blanco, V.; Quintela, J. M. A New Doubly Interlocked [2]Catenane. *J. Am. Chem. Soc.* **2009**, *131*, 920–921.
(485) Frasconi, M.; Kikuchi, T.; Cao, D.; Wu, Y.; Liu, W.-G.; Dyar, S. M.; Barin, G.; Sarjeant, A. A.; Stern, C. L.; Carmieli, R.; Wang, C.; Wasielewski, M. R.; Goddard, W. A. III; Stoddart, J. F. Mechanical Bonds and Topological Effects in Radical Dimer Stabilization. *J. Am. Chem. Soc.* **2014**, *136*, 11011–11026.
(486) Beves, J. E.; Danon, J. J.; Leigh, D. A.; Lemonnier, J.-F.; Vitorica-Yrezabal, I. J. A Solomon Link Through an Interwoven Molecular Grid. *Angew. Chem., Int. Ed.* **2015**, *54*, 7555–7559.
(487) Dietrich-Buchecker, C.; Colasson, B.; Jouvenot, D.; Sauvage, J.-P. Synthesis of Multi-1,10-Phenanthroline Ligands with 1,3-Phenylene Linkers and Their Lithium Complexes. *Chem. Eur. J.* **2005**, *11*, 4374–4386.
(488) Lukin, O.; Godt, A.; Vögtle, F. Residual Topological Isomerism of Intertwined Molecules. *Chem. Eur. J.* **2004**, *10*, 1878–1883.
(489) Asakawa, M.; Ashton, P. R.; Menzer, S.; Raymo, F. M.; Stoddart, J. F.; White, A. J. P.; Williams, D. J. Molecular Meccano 8. Cyclobis(paraquat-4,4'-biphenylene) - An Organic Molecular Square. *Chem. Eur. J.* **1996**, *2*, 877–893.
(490) Du, S. M.; Seeman, N. C. Synthesis of a DNA Knot Containing Both Positive and Negative Nodes. *J. Am. Chem. Soc.* **1992**, *114*, 9652–9655.
(491) Flapan, E.; Seeman, N. C. A Topological Rubber Glove Obtained From a Synthetic Single-Stranded DNA Molecule. *J. Chem. Soc., Chem. Commun.* **1995**, 2249–2250.
(492) Chambron, J.-C.; Sauvage, J.-P.; Mislow, K. A Chemically Achiral Molecule with No Rigidly Achiral Presentations. *J. Am. Chem. Soc.* **1997**, *119*, 9558–9559.
(493) Chambron, J.-C.; Sauvage, J.-P.; Mislow, K.; De Cian, A.; Fischer, J. A [2]Catenane and a [2]Rotaxane as Prototypes of Topological and Euclidean Molecular "Rubber Gloves." *Chem. Eur. J.* **2001**, *7*, 4085–4096.
(494) Carlone, A.; Goldup, S. M.; Lebrasseur, N.; Leigh, D. A.; Wilson, A. A Three-Compartment Chemically-Driven Molecular Information Ratchet. *J. Am. Chem. Soc.* **2012**, *134*, 8321–8323.
(495) Cheng, C.; McGonigal, P. R.; Schneebeli, S. T.; Li, H.; Vermeulen, N. A.; Ke, C.; Stoddart, J. F. An Artificial Molecular Pump. *Nature Nanotechnol.* **2015**, *10*, 547–553.

Chapter 6 Molecular Switches and Machines with Mechanical Bonds

Conspectus



Mechanically interlocked molecules (MIMs) which contain two or more different recognition sites in the shape of noncovalent bonds between their component parts provide the perfect prototypes for the design and synthesis of molecular switches and machines. In some of the best known examples, namely bistable catenanes and rotaxanes, it is convenient to identify a ground state co-conformation (GSCC) and a higher energy metastable state co-conformation (MSCC) where the GSCC:MSCC ratio at room temperature in solution is ideally for most purposes in the range of at least 10:1. Many different ways can then be sought to perturb temporarily this equilibrium by applying, usually to the recognition site associated with the GSCC, stimuli which are routinely provided (i) physically by (a) light – including photoinduced electron transfer (PET) processes, (b) heat (e.g., noncovalent bond interactions which stabilize the GSCC of a polyrotaxane, for example, and are enthalpically favorable at low temperatures whereas increased ring mobility becomes entropically favorable with rising temperatures), (c) pressure, (d) solvent polarity, etc., (ii) chemically by (a) using acid/base (pH changes), often in order to influence hydrogen bonding, (b) employing reductants and oxidants to change redox states which control donor-acceptor and radical-radical interactions, (c) altering coordination numbers and geometries between ligands and transition metal ions, (d) probing competitive recognition processes triggered by cations, anions and small molecules, including allosteric effects, (e) promoting photoisomerizations (e.g., between *cis* and *trans* configurations of double bonds) and photoreactions, etc., and (iii) electrochemically by controlling interactions all the way from electrostatic and hydrogen bonding to π–π stacking and hydrophobic bonding in aqueous solutions. Different classes of mechanically interlocked molecular switches operate at very different speeds, e.g., donor-acceptor based switches are a lot slower than benzylic amide based ones, for example, while different ligands associated with transition metal cations control kinetics that span several orders of magnitude. In addition, molecular switches based on bistable MIMs continue to perform in condensed phases with very similar thermodynamic characteristics, although their performance is invariably dampened considerably when it comes to their rate of relaxation from the MSCC back to the GSCC.



While artificial molecular switches based on bistable MIMs have been well-explored and have found applications in the fabrication of nanoelectromechanical systems capable of storing memory and momentum, as well as in executing logic and truth statements, artificial molecular machines which perform work on their surroundings are few and far between. Aside from their performing work, designing and developing machines requires that they circumvent microscopic reversibility (the principle that the mechanism of a reversible process in the forward direction is exactly the reverse of that in the backward direction) either by means of non-reciprocating cycles where the forward and backward pathways are different, and/or by a motion constrained by a mechanical bond that is biased in a particular direction—call it mechanostereoselective motion. Molecular machines employ ratchet mechanisms: in an information ratchet, the position of a microscopic entity is employed to pump a system away from equilibrium: in an energy ratchet, the biased movement of an energy form is attained by raising and lowering energy minima and maxima asymmetrically. Making the transition from switches to machines is challenging at both the level of conceptualization and in the realization of the concepts. It requires the coupling of mechanical motions in settings where symmetry is broken or the scaling of mechanical motion at the molecular level with those on the nano-, micro- and macroscopic scales in order to produce chemo-, electro- and photomechanical devices and functional materials that exhibit responsive behavior over multiple length scales. The challenge of creating these highly integrated systems in which operating molecular machines are interfaced with complex networks that are programmed to fulfill particular tasks is one that promises to be transformative in more ways than one. The mechanical bond is poised to play a major role in this potpourri of systems chemistry without borders.

The Nature of the Mechanical Bond: From Molecules to Machines, First Edition. Carson J. Bruns and J. Fraser Stoddart.
© 2017 John Wiley & Sons, Inc. Published 2017 by John Wiley & Sons, Inc.

Introduction **558**
6.1 Redox-Driven Switches **560**
6.1.1 Redox-Switchable Donor-Acceptor (D-A) MIMs 560
6.1.1.1 Oxidative D-A Redox Switching *560*
6.1.1.2 Reductive D-A Redox Switching *563*
6.1.2 Redox Switching of Metallo-Mechanomolecules 566
6.1.3 Redox Switching of Hydrogen-Bonded MIMs 572
6.1.4 Aqueous Redox Switching 573
6.2 Photo-Driven Switches **574**
6.2.1 Switching Driven by Photoinduced Electron Transfer 574
6.2.1.1 Switching in Charge-Separated States *575*
6.2.1.2 Photosensitized Switching *575*
6.2.2 Switching Driven by Photoisomerization 577
6.2.2.1 Mechanically Bonded Azobenzene Switches 577
6.2.2.2 Mechanically Bonded Stilbene Switches 578
6.2.2.3 Mechanically Bonded Fumaramide Switches 579
6.2.2.4 Mechanically Bonded Spiropyran Switches 579
6.2.3 Switching in a Dissociative Excited State 580
6.2.4 Switching Driven by Photochemical Reactions 580
6.3 Acid/Base-Driven Switches **581**
6.3.1 pH Switching Driven by Hydrophobic Effects 581
6.3.2 pH Switching Driven by Electrostatic Repulsion 583
6.3.3 pH Switching Driven by Hydrogen Bonding 584
6.3.3.1 pH-Controlled Dialkylammonium/Crown MIMs 584
6.3.3.2 pH-Controlled Benzylic Amide MIMs 587
6.3.4 pH Switching Driven by Metal Chelation 588
6.4 Cation-Triggered Switches **591**
6.4.1 Switching with Transition Metal Cations 591
6.4.1.1 Switches Driven by Adding or Removing Coordinative Bonds 591
6.4.1.2 Changing Templates with Different Coordination Geometries 593
6.4.1.3 Allosteric Control 594
6.4.1.4 Switches Driven by Cation-Induced Electronic Changes 594
6.4.2 Switching with Alkali Metal Cations 594
6.4.3 Switching with Alkaline Earth Metal Cations 597
6.5 Anion-Triggered Switches **598**
6.5.1 Switches Driven by Anion Solvation Effects 598
6.5.2 Switching Through Second-Sphere Interactions 600
6.5.3 Switches Driven by Anion Binding 600
6.5.3.1 Switching with Inorganic Anions 600
6.5.3.2 Switching with Organic Anions 603
6.6 Switches Driven by Molecular Recognition **604**
6.6.1 Switches Driven by Neutral Small Molecules 604
6.6.2 Switches Driven by DNA Strand Displacement 606
6.7 Switches Driven by Covalent Reactions **607**
6.7.1 Switches Driven by Acylations of Amines 607
6.7.2 Switches Driven by Reactions of Pyridines 609
6.7.2.1 Benzylation/Debenzylation 609
6.7.2.2 Pyridine N*-Oxides* 609
6.7.3 Switches Driven by Protection of Aldehydes 610
6.7.4 Switches Driven by Diels-Alder Reactions 610
6.7.5 Switches Driven by (De)Hydrogenation 610
6.7.6 Switches Driven by the Mitsunobu Reaction 610
6.8 Solvent-Driven Switches **611**
6.8.1 Switching Driven by Hydrogen Bond Disruption 612
6.8.2 Switching Driven by Solvation Effects 615

6.9 Thermally Driven Switches 616
6.9.1 Switching Driven by Entropic Effects 616
6.9.1.1 Thermally Switched Donor-Acceptor MIMs 617
6.9.1.2 Cyclodextrin Polyrotaxane Thermal Switches 617
6.9.1.3 Thermally Switched Benzylic Amide Rotaxanes 619
6.9.1.4 Thermally Switched Pillararene Rotaxanes 620
6.9.1.5 Thermal Switches Driven by Imine Hydrolysis 621
6.9.2 Switching Driven by Thermal Decomposition 621
6.10 Pressure-Driven Switches 622
6.11 Switches Driven by Electric Fields 623
6.12 Switches Driven by Mechanical Force 624
6.13 Beyond Translation and Circumrotation 627
6.13.1 Expansion and Contraction: Molecular Muscles with Mechanical Bonds 627
6.13.1.1 Antiparallel Sliding in [c2]Daisy Chains 628
6.13.1.2 Pressing Motions in Palindromic Rotaxanes 635
6.13.1.3 Pressing Motions in Molecular Elevators 635
6.13.1.4 Telescoping Motions in Cage Rotaxanes 638
6.13.1.5 Metrics of Rotaxane-Based Molecular Muscles 639
6.13.2 Ultramacrocyclic Constriction/Dilation 639
6.13.3 Motions of Branched Rotaxanes 643
6.13.3.1 Radial Translation 644
6.13.3.2 Radial Expansion/Contraction 645
6.13.4 The Gemini Co-Conformation 645
6.13.5 Rotaxane Flapping 646
6.13.6 Collapsing Mechanomolecules 647
6.13.7 Mechanically Constrained Inflation/Deflation 647
6.13.8 Folding/Unfolding in Mechanomolecules 647
6.13.9 Stepwise Motion in Pseudocatenanes 649
6.13.10 Molecular Pulleys 649
6.13.11 Multicomponent Pirouetting and Translation 649
6.13.12 Molecular Conveyor Belts 652
6.14 Condensed-Phase Switching 652
6.14.1 Condensed-Phase Redox Switches 652
6.14.1.1 Redox Switching in Langmuir-Blodgett Films 653
6.14.1.2 Redox Switching in Surface Monolayers 660
6.14.1.3 Redox Switching in High Viscosity Fluids 663
6.14.1.4 Single-Molecule Redox Switching 664
6.14.2 Condensed-Phase Photoswitches 666
6.14.2.1 Photoswitching in Surface Monolayers 666
6.14.2.2 Photoswitching in High Viscosity Fluids 667
6.14.3 Condensed-Phase Chemical Switches 667
6.14.3.1 Condensed-Phase Acid/Base Switching 667
6.14.3.2 Condensed-Phase Ion Switching 668
6.14.3.3 Condensed-Phase Solvent Switching 668
6.15 Mechanomolecular Motors and Machines 669
6.15.1 Systems-Coupled Functional Switches 670
6.15.1.1 Rotaxanes in Controlled Release Applications 670
6.15.1.2 Artificial Muscles 684
6.15.1.3 Molecular Computation & Information Storage 686
6.15.1.4 Switches Influencing Molecular Organization 689
6.15.1.5 Switches Regulating Catalysis 692
6.15.2 Brownian Ratchets with Mechanical Bonds 694
6.15.2.1 Thermodynamics of a Brownian Motor 694
6.15.2.2 Mechanostereoselective Motion 697

6.15.2.3 Mechanically Interlocked Energy Ratchets 701
6.15.2.4 Mechanically Interlocked Information Ratchets 704
6.15.3 Mechanically Bonded Molecular Assemblers 706
6.15.3.1 Mechanically Constrained Processive Catalysis 706
6.15.3.2 Mechanically Constrained Peptide Synthesis 707
6.15.3.3 Rotaxane-Building Molecular Machines 707
Conclusions and Outlook **708**
References **709**

Introduction

Machines are tools that historically have used a power supply and moving parts to convert energy from one form into another and accomplish some task in the process. By comparison, molecules are also constantly moving, driven by the kinetic energy of their surrounding molecules—which we detect as temperature—that bump into and jostle with each other in a random manner known as Brownian motion. These random "wiggles and jiggles" seem to preclude machine-like precision and function, and yet Nature has managed to tame and incorporate them into systems that express awe-inspiring locomotion and even intentionality. Nature teaches us that it is possible to design molecules that respond, when stimulated by external inputs, with specific and well-defined directed movements, in spite of the chaos of Brownian motion. Mechanomolecules are intrinsically equipped with this potential because the mechanical bond allows components to move along certain pathways while restricting motion along other pathways.

When dealing with the specific ways in which the component parts of a mechanomolecule can move, we have employed[1] the term 'co-conformation' to describe the different mechanical arrangements—i.e., (mechano) stereoisomers—that they can adopt. See **Section 5.1**. In contrast, 'conformation' is used[2] to describe the specific three-dimensional arrangement of atoms in molecules as a result of torsions around single and partial double bonds. While ordinary molecules invert and interconvert between conformational isomers through these torsional movements around covalent bonds, the range of motions (translational, circumrotational, etc.) that dictate movement in molecules with mechanical bonds is a whole lot richer—see **Chapter 5**. Since directly detecting specific molecular motions is highly non-trivial on account of Brownian motion, researchers in this field infer that these motions have taken place by detecting different co-conformational isomers (or 'co-conformers') with conventional analytical techniques—spectroscopy, electrochemistry, microscopy, etc.—before and after the application of an appropriate stimulus. In the context of the machine analogy, the stimulus is equivalent to the power supply that drives motion. At the heart of this Chapter is the library of stimuli that have been employed so far to incite switching events around mechanical bonds.

An important concept in molecular switching is that of bistability. A molecule is said to be bistable if there are two (co-)conformations that represent energetic minima, as opposed to only one. In a bistable mechanically interlocked molecule (MIM), the global energetic minimum is often referred to as the ground state co-conformation (GSCC), and any higher-energy minimum, a metastable state co-conformation (MSCC). The equations describing the thermodynamics and kinetics of bistable mechanostereoisomers are described in **Section 5.1.1**. Relevant terms such as the difference in free energies of translational isomers, $\Delta G°$, and the free energy of activation for translation, $\Delta G^{‡}$, are defined on the potential energy surface (**Figure 6.1**) of a bistable [2]rotaxane. Controlled co-conformational switching typically relies on the application of an external stimulus which acts to change the magnitude of $\Delta G°$ by raising or lowering the stability of one or more translational isomers, which often modulates $\Delta G^{‡}$ as a consequence. A conceptual example of this strategy in action is illustrated in **Figure 6.2**. The stimulus is applied in order to 'turn off' the noncovalent bonding interactions stabilizing the GSCC of a bistable rotaxane, which populates the secondary binding site as a consequence. When the stimulus is reversed, the MSCC represents the dominant isomer for some period of time until the system relaxes back to the GSCC.

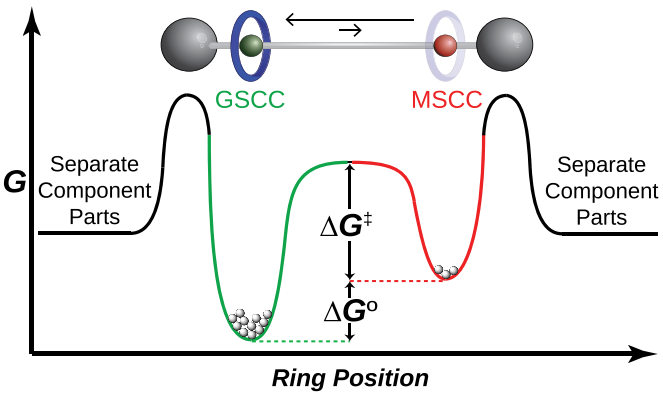


Figure 6.1 Potential energy surface diagram of a bistable [2]rotaxane, with the difference in free energy ($\Delta G°$) between translational isomers and the activation barrier ($\Delta G^{‡}$) for translational isomerization from a metastable state co-conformation (MSCC) to the ground state co-conformation (GSCC).

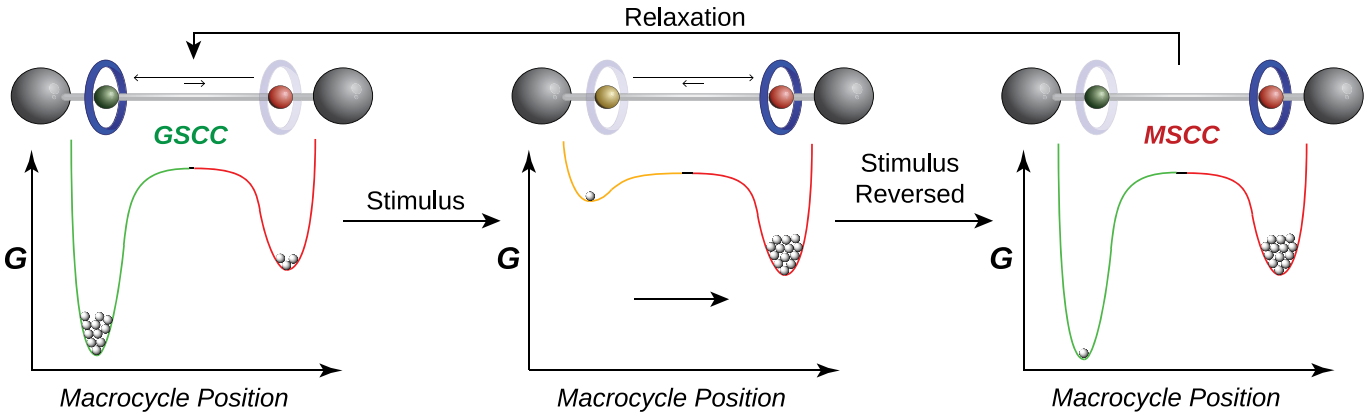


Figure 6.2 Universal mechanism of switching in MIMs, exemplified by the potential energy surface diagram of a bistable [2]rotaxane.

The general working mechanism for controlling motion in molecules with mechanical bonds is independent of the stimulus that is used—in all cases, some form of energy input is converted into a net mechanical output on the molecular scale. We begin this Chapter, however, with a cautionary note on semantics. A few words about our words…

(i) When describing bistable species existing in equilibrium, such as the various co-conformations of a catenane or rotaxane, it is (strictly speaking) incorrect to use "all-or-nothing" language. For example, it is more correct to say "*the equilibrium distribution is heavily biased in favor of the co-conformer in which the ring encircles recognition site X*" than it is to say "*the ring encircles recognition site X*." In many cases, however, the equilibrium is so heavily biased toward a single co-conformation that the use of such language is acceptable in our view. Thus, any usage of "all-or-nothing" language in this context can be interpreted as a shorthand notation for equilibria (see **Table 5.1** in **Section 5.1.1**) that are biased, i.e., non-degenerate.

(ii) Ring translation or circumrotation caused by external stimuli—events which change the energy landscapes of molecules with mechanical bonds—are most often accomplished by processes of biased Brownian motion. Again, we will occasionally employ technically imprecise language as a shorthand notation for systems in this regime. For example, a rotaxane ring which "shuttles" does not make a direct or deliberate move—it relies on thermal fluctuations to fall into a new energy well, typically approaching it by a random walk as the system re-equilibrates.

(iii) In the case of molecular "switches," "machines," "motors," etc, we wish to be more deliberate with our choice of words. A genuine molecular machine is not as simple as a molecular switch. A molecular switch simply changes (co-)conformations in response stimuli. Machines and motors, however, do mechanical work. They move a system uphill on an energy landscape. Accomplishing work in the molecular world is far from trivial—it remains a challenging contemporary pursuit in chemistry. The mechanical bond is likely to play a critical role in molecular machines that convert heat, light, electricity, etc. into mechanical energy in the form of motion. See **Section 6.15** for a discussion on molecular machines. We ourselves, in common with many others, have been guilty of brandishing an exaggerated rhetoric that likens bistable MIMs to machines and motors. The time has come,[3,4] however, for chemists to begin following rules, as they do in physics[5] and biology,[6] for what constitutes a machine or a motor in light of a more rigorous understanding of work at the molecular scale. What we and others have called "machines" are, more often than not, merely switches. Without coupling these "mechanomolecular" movements to something in the environment on which they can do work, no net effect can be detected that is distinguishable from Brownian motion. The switches we discuss herein, nonetheless, most likely represent the key forerunners to authentic molecular machines of the future for the simple reason that the mechanical bond is an arbiter of large-amplitude molecular mechanical motion.

We note that there have also been many examples (see **Chapter 5**) of mechanomolecules in which the dynamics—e.g., shuttling rates of rings between two recognition sites in rotaxanes and catenanes, rates of ring circumrotation, etc.—can be influenced and controlled by external stimuli. In some cases, this phenomenon is trivial, such as the rate-enhancing effect of temperature on dynamic processes. In other cases, these dynamics can be controlled by unusual stimuli such as an alternating electric field[7] or a light source.[8] Although these compounds are also 'switchable' in a sense, the switches in this Chapter are primarily thermodynamic in nature. The topic of mechanically interlocked molecular switches (**Section 6.1–6.14**), often referred to as machines, has been reviewed in the literature—see refs. 9–20—while a summary of the literature on artificial molecular machines, more specifically, is given in **Section 6.15**.

6.1 Redox-Driven Switches

The use of redox stimuli for switching between co-conformers has been an important milestone in mechanostereochemistry, not only because electrochemical switching was among the first to be developed, but also because it minimizes waste. Moreover, by analogy with electronic switches and machines in the macroscopic world, the idea of using an electrical stimulus to control submolecular motion precisely has inspired our imaginations and desire to innovate in molecular electronics and nanotechnology more generally. It is easier to conceive of a molecular electronic device (MED) that runs on electrical input as opposed to chemical input—pH changes, for example—for intuitively practical reasons, and indeed much progress has already been made toward developing nanoscale solid-state platforms toward this end—see **Section 6.14**. Furthermore, a wide range of recognition motifs has been adapted for electrochemical switching, including π-associated donor-acceptor MIMs (**Section 6.1.1**), transition metal-complexed MIMs (**Section 6.1.2**), hydrogen-bonded MIMs (**Section 6.1.3**), and MIMs based on the hydrophobic effect (**Section 6.1.4**). Reviews on electrochemically driven switches and machines are available in the literature.[11,14,21–34]

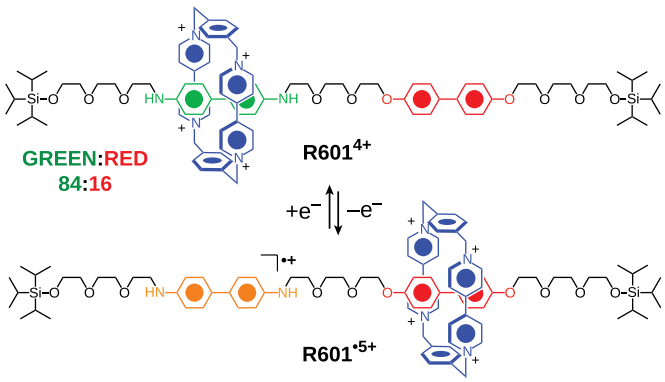
6.1.1 Redox-Switchable Donor-Acceptor (D-A) MIMs

π-Associated donor-acceptor MIMs are highly amenable to redox-driven switching because the π-conjugated recognition sites embedded within the ring and dumbbell components are often redox-active. The transfer of electrons in and out of these redox-active units introduces major changes in their electronic structures, which influences the strength of various noncovalent bonding interactions, and in turn, leads to mechanical motion. This strategy has been realized under oxidative (**Section 6.1.1.1**) as well as reductive (**Section 6.1.1.2**) control.

6.1.1.1 Oxidative D-A Redox Switching

In making its debut among electromechanical switches, the original π-donor/π-acceptor mechanomolecule to undergo[35] redox-controlled shuttling (**Scheme 6.1**) was the bistable [2]rotaxane **R601^{4+}**, which comprises the tetracationic cyclophane, cyclobis(paraquat-*p*-phenylene) (CBPQT^{4+}) interlocked with a dumbbell possessing a redox-active benzidine recognition site and a biphenol unit. The translational isomer in which the CBPQT^{4+} ring encircles the benzidine unit represents the GSCC (84% of the molecular population), while the weaker-binding[36] (by one order of magnitude) biphenol recognition site is occupied (16%) in the MSCC. Introducing a positive charge onto the benzidine unit by electrochemical oxidation generates the radical pentacation **R601$^{\bullet 5+}$** in which a repulsive interaction between the benzidine radical cation and the CBPQT^{4+} ring causes the ring to shuttle almost quantitatively to the biphenol recognition site. Positive charges can also be introduced by protonation of the benzidine unit—see **Section 6.3.2**. After the registration of this landmark in 1994, a lot of effort has been devoted to improving the properties of related electrochemical switches, e.g., by (i) tuning the thermodynamic landscape of bistable MIMs to control the ground state distributions of co-conformers, (ii) altering the kinetics of mechanical switching, and (iii) assessing their robustness over many switching cycles. Many of the efforts to impart bistable donor-acceptor MIMs with high-fidelity redox-driven switching properties in solution by systematic investigation of structure-property relationships are discussed in **Sections 5.1.1.1–5.1.1.2**.

Following the first partial success[35] and a few initial unsuccessful attempts[37–39] to create controllable molecular switches with highly selective population distributions, more donor-acceptor motifs were uncovered,[40–50] some of which possess[44–47] electrochemically switchable properties that are even more favorable than those displayed in the first example illustrated in **Scheme 6.1**. Among the most important of these developments was the incorporation[51] of an easily and reversibly oxidized ($E_{1/2}$ = 320 mV vs. SCE) compound known as tetrathiafulvalene[52,53] (TTF) which exhibits a high association constant[42] (K_a ~10^4 M^{-1}) when it forms a 1:1 inclusion complex with CBPQT·4PF_6 at room temperature in MeCN solution. MIMs prepared from this building block as a recognition unit are often paired with relatively redox-inactive ($E_{1/2}$ > 1 V vs. SCE) donor sites that bind the CBPQT^{4+} ring much more weakly—such as HQ (K_a ~10^1 M^{-1} in MeCN)[54] or 1,5-dioxynaphthalene (DNP) (K_a ~10^3 M^{-1} in MeCN)[54] units—which become encircled by the CBPQT^{4+} ring in the MSCC. The electrochemical switching mechanism of the first TTF-based bistable [2]catenane[44] **C601^{4+}** is shown in **Figure 6.3a**. In its GSCC, the TTF unit is encircled by the CBPQT^{4+} ring. Two one-electron oxidations of the TTF unit gives the hexacationic **C601^{6+}** species in which the TTF^{2+} dication has been expelled from the ring as a result of Coulombic repulsion. Reduction of TTF^{2+} back to TTF populates the MSCC of **C601^{4+}** before the GSCC is recovered. Dozens of investigations (*vide infra*) have followed on the back of this bistable catenane's excellent switching fidelity, i.e., a large K_{eq} and fully reversible behavior. Here, we will only summarize the most important insights gained from these investigations.



Scheme 6.1 The first bistable donor-acceptor molecular shuttle[35] driven by redox stimuli, **R601^{4+}**.

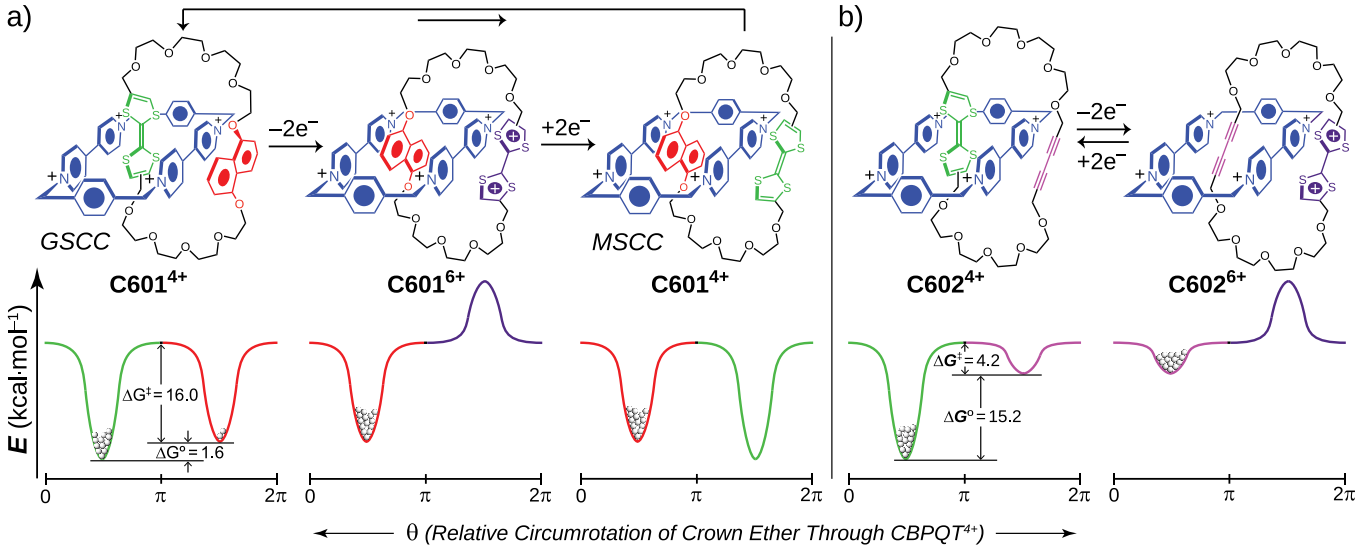


Figure 6.3 Comparison between the bistable [2]catenane[44] **C601^{4+}** and the 'push-button' [2]catenane[57] **C602^{4+}**. (a) Electrochemical oxidation of **C601^{4+}** to **C601^{6+}** and subsequent reversal of the redox stimulus populates the MSCC of **C601^{4+}**, which is stable enough to live for some time before relaxing back to the GSCC. (b) The MSCC is all but inaccessible in **C602^{4+}** because its miniscule stabilization energy allows the GSCC to be recovered almost instantaneously after the reduction of **C602^{6+}**.

The superior binding affinity (see **Table 2.14** in **Section 2.3.3.8**) of the CBPQT^{4+} ring for a TTF-polyether unit is reflected in the high co-conformational selectivity of the corresponding bistable switches. The value of K_{eq} depends on $\Delta G°$, which is influenced mainly by the binding strengths of the recognition units and the topology/architecture of the mechanomolecule—see **Section 5.1.1.1**. In general, the GSCC:MSCC ratio exceeds 10:1 ($K_{eq} \geq 10$) under ambient conditions, which tends to leave no detectable spectroscopic evidence of a minor translational isomer in the ground state. A method[55] employing slow scan rate cyclic voltammetry (CV) to evaluate these highly lopsided distributions of TTF-based MIM co-conformers has revealed (**Figure 6.4**) that K_{eq} is an order of magnitude greater in the bistable [2]catenane **C601^{4+}** ($K_{eq} \approx 500$) than in a closely related bistable [2]rotaxane[56] **R602^{4+}** ($K_{eq} = 10 \pm 2$), given the same primary recognition sites. The larger K_{eq} for this [2]catenane can be rationalized by invoking stabilizing 'alongside' donor-acceptor interactions from the DNP unit, a situation which is dictated by the catenane's topology, whereas the DNP unit in the bistable [2]rotaxane is not mechanically constrained to do likewise.

In terms of creating switches with highly selective population distributions, another important insight was the realization that fully switchable molecules with improved fidelity can be created from essentially monostable MIMs, since a [2]catenane with a single recognition site would consequently exist as only one translational isomer in the ground state for all intents and purposes. As a proof of principle, a CBPQT^{4+}-based [2]catenane **C602^{4+}** was prepared[57] in which the macrocyclic polyether incorporates one TTF recognition site along with a butadiyne unit exhibiting virtually no recognition (**Figure 6.3b**) for the CBPQT^{4+} ring. In this catenane, the GSCC:MSCC distribution ($K_{eq} = 6800 \pm 300$) is remarkably one-sided,[55] since the binding affinity of TTF for CBPQT^{4+} exceeds that of butadiyne by 15 kcal·mol^{-1}, compared with a mere 1.6 kcal·mol^{-1} difference between the TTF and DNP recognition sites in the already highly biased distribution exhibited by the classical bistable [2]catenane[44] **C601^{4+}**. The activation barrier for circumrotation in these catenanes can be measured by populating the MSCC and recording the MSCC → GSCC relaxation time. The MSCC can be populated by oxidizing the TTF units, thus generating TTF$^{\bullet+}$ radical cations or TTF^{2+} dications which repel the CBPQT^{4+} ring by Coulombic forces, followed by reduction back to the neutral TTF unit upon reversal of the electrochemical stimulus. Since the MSCC of **C601^{4+}** is stabilized by the *DNP⊂CBPQT*$^{4+}$ interactions under ambient conditions, a significant energy barrier must be overcome to restore the GSCC, and the corresponding MSCC → GSCC transition is relatively slow. By contrast, the GSCC is recovered very rapidly upon reduction of the oxidized catenane **C602^{6+}** back to **C602^{4+}** because the *butadiyne⊂CBPQT*$^{4+}$ interaction in the MSCC is negligible. Since there is essentially no intermediate between the 'on' and 'off' states of **C602^{4+}**, the term "push-button" has been suggested[57] to describe this kind of molecular switch. A side-by-side comparison between the two switching modes is presented in **Figure 6.3**. The large K_{eq} value for the push-button catenane, which resides primarily in its large $\Delta G°$ value, is reflected in **Figure 6.4**.

The translational isomerism of non-degenerate bistable D-A catenanes and rotaxanes based on TTF recognition units is discussed in detail in **Section 5.1.1.1**. The majority of these MIMs—namely, those in which TTF is encircled in the GSCC—can be switched under oxidative control by a mechanism analogous to that described for the

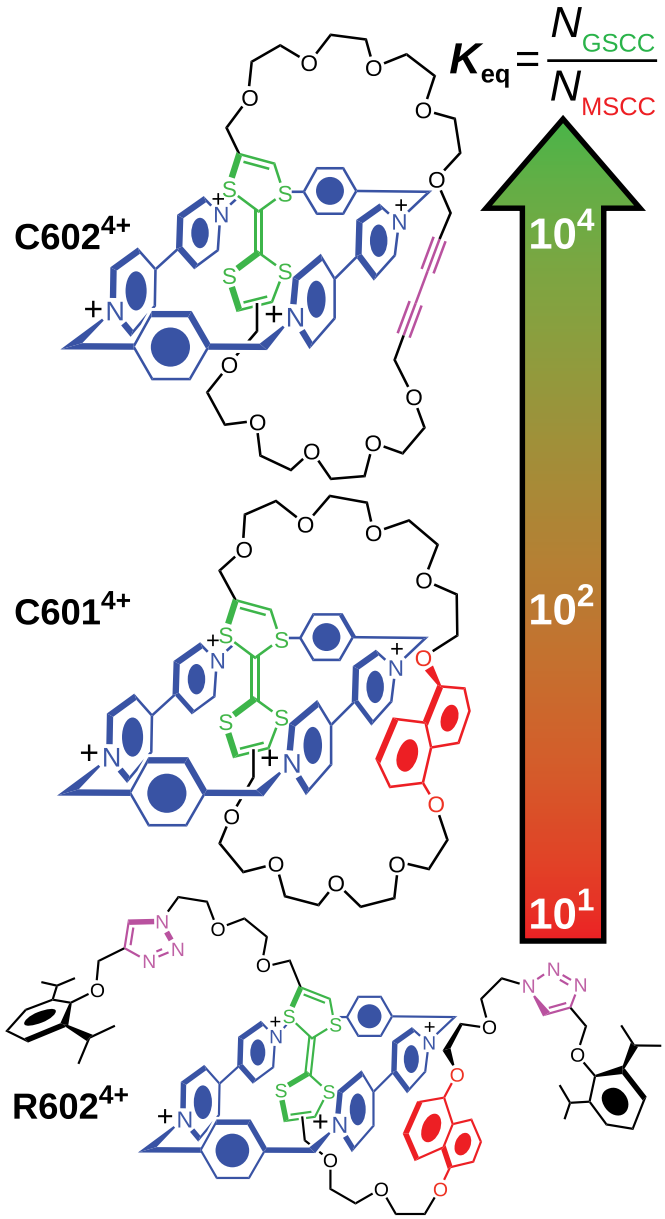
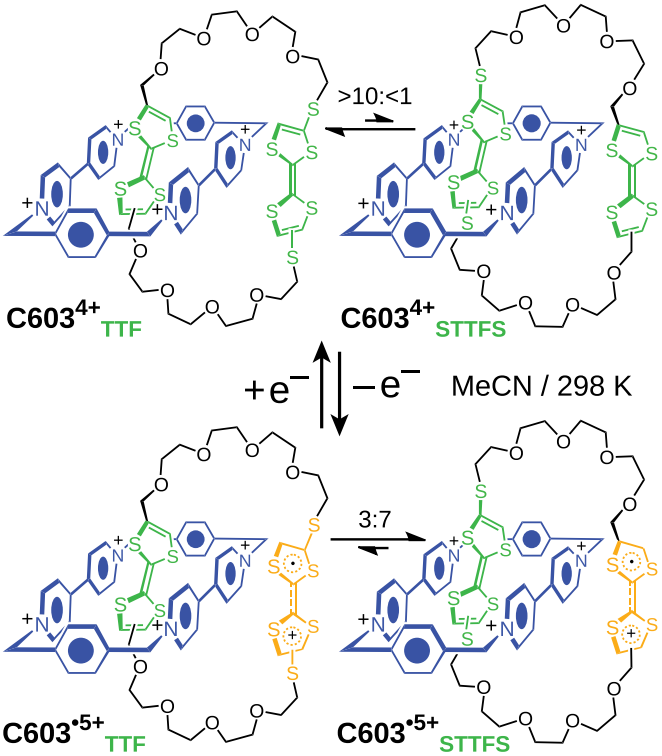


Figure 6.4 Structural differences in bistable MIMs correspond to dramatic differences in the ground state distributions of co-conformational isomers.[44,55,57]

[2]catenane **C601^{4+}**. In almost all of these cases, it has been verified electrochemically that the TTF unit can indeed be oxidized reversibly, marking out TTF as a reliable handle for redox control in switchable MIMs. Moreover, because of their excellent fidelity, TTF-based switches have become close to indispensible,[58] supporting a wide range of experiments that have relied on their switching behavior in solution,[44,56,59–82] in condensed phases and at interfaces[25,83–100] (**Section 6.14.1**), and in electronic circuits.[101–105] Aside from our own interests, other researchers have also made and investigated the properties of TTF-based MIMs: they include Becher,[106–112] Zhang and Zhu,[113] Gao,[114] Flood and Jeppesen,[82,115,116] and Liu and Li.[117]

In all of the oxidation-driven D-A mechanoswitches, the TTF recognition unit is accompanied by a secondary recognition unit with a much higher oxidation potential lying outside the electrochemical operating window of the switch. In contrast, the bistable D-A [2]catenane[118] **C603^{4+}** possesses (**Scheme 6.2**) two redox-active TTF derivatives as π-donating recognition units for the CBPQT^{4+} ring. An ordinary TTF recognition unit is encircled in the GSCC, while a TTF bis(thioether) (STTFS) occupies the cavity of CBPQT^{4+} in the MSCC. In the ground state, the population distribution favors the **C603$^{4+}_{TTF}$** translational isomer over **C603$^{4+}_{STTFS}$** by a ratio exceeding 10:1 in MeCN. Upon application of a ~500 mV potential vs. Ag/AgCl or introduction of one equiv of $Fe(ClO_4)_3$ as an oxidizing agent, a one-electron reduction generates the radical pentacation **C603$^{\bullet 5+}$**, in which the radical is partitioned between the TTF and STTFS units in a 3:7 ratio, with the corresponding STTFS$^{\bullet+}$ and TTF$^{\bullet+}$ radical cations occupying the 'alongside' positions of the **C603$^{\bullet 5+}_{STTFS}$** and **C603$^{\bullet 5+}_{TTF}$** translational isomers, respectively. In other words, the CBPQT^{4+} ring translates from TTF to STTFS in >60% of the population upon re-establishing equilibrium after the one-electron oxidation event. Further oxidation occurs as a three-electron process whereby both TTF and STTFS units are converted to the corresponding dications at the same potential.

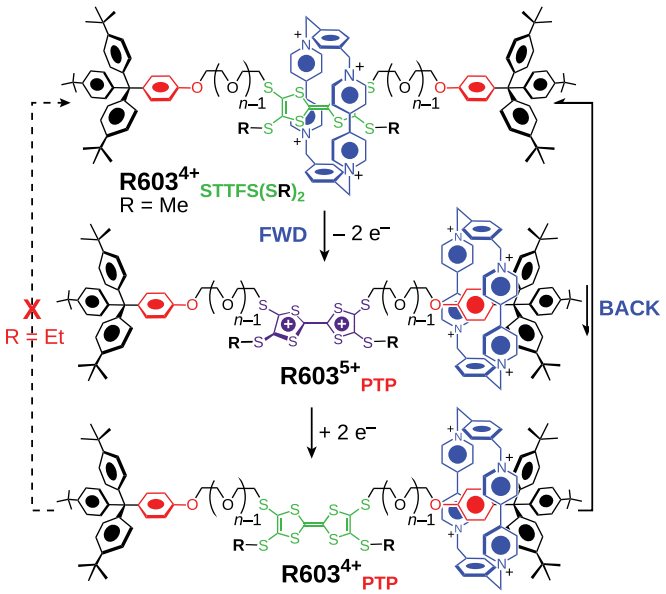


Scheme 6.2 The one-electron oxidation of a bistable [2]catenane possessing two redox-active recognition units (TTF and STTFS) with similar oxidation potentials leads to an equilibrium in which the ratio of TTF$^{\bullet+}$ and STTFS$^{\bullet+}$ radical cations, and thus the ratio of translational isomers, shifts from >10:<1 before oxidation to 3:7 after oxidation In MeCN at 298 K.[118]

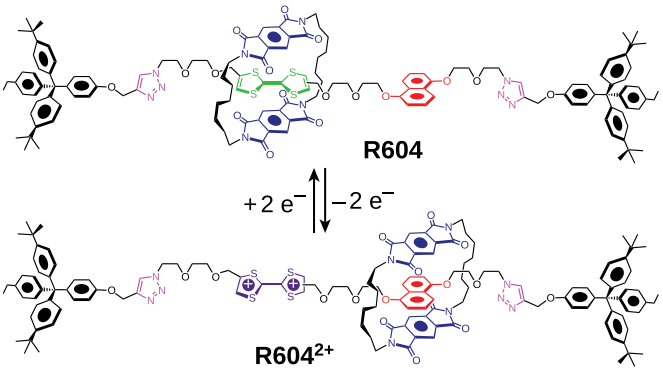
The role of linker length in the electrochemically switchable CBPQT^{4+} [2]rotaxanes **R603^{4+}a-d** was recently determined (**Table 6.1**) in a Flood-Jeppesen collaboration.[82] The dumbbell of these [2]rotaxanes comprise a central STTFS(SMe)$_2$ unit, the SMe groups of which act[60,61,66,119,120] as steric "speedbumps" that slow down the transgression of CBPQT^{4+}—see **Section 5.1.1.1**—connected via oligo(ethylene glycol) linkers (*n*EG, where *n* = 2, 3, 4, or 8) directly to the stoppers derived from *para*-tritylphenol (PTP). In the absence of another recognition unit, the CBPQT^{4+} ring associates with either of the stoppers' oxyphenylene sites upon oxidation of the STTFS(SMe)$_2$ unit. Analysis of variable scan-rate and variable temperature cyclic voltammetry (CV) data revealed (**Table 6.1**) that (i) the rates of forward escape upon oxidation (**R603$^{4+}_{STTFS}$** → **R603$^{5+}_{PTP}$**) outpace the backward process (**R603$^{4+}_{PTP}$** → **R603$^{4+}_{STTFS}$**) upon reversal of the redox stimulus, and (ii) the longer linkers accelerate the forward escapes driven by electrostatic repulsion between TTF^{+} and CBPQT^{4+}, while slowing down the backward translations associated with the recovery of the GSCC. This faster forward, slower backward effect may be rationalized by the increased stability of the MSCC as the linkers are lengthened as a result of their more favorable [C–H···O] interactions with the CBPQT^{4+} protons, as well as the presence of folded states promoting alongside STTFS–CBPQT^{4+} interactions that transpire only in the case of the longer dumbbells and not with the shorter ones. If the SMe speedbumps are replaced by SEt groups, the forward escape is an irreversible process because the GSCC cannot be recovered on account of an insurmountable activation barrier to backward translation. Most of the parameters that influence ring translation in π-donor/π-acceptor mechanomolecules are discussed in the case study in **Section 5.1.1.1**.

Although tetracationic cyclophanes have been the most propitiously used rings in redox-switchable donor-acceptor MIMs, neutral π-electron deficient hosts can serve in the same capacity. For example, a cyclophane based on pyromellitic diimide (PMDI) has been employed[47] to prepare a neutral rotaxane **R604** that can be induced to shuttle (**Scheme 6.3**) under oxidative control. Although the electrochemical generation of the TTF^{2+} dication in **R604^{2+}** does not generate the same repulsive Coulombic forces as those present in analogous MIMs based on CBPQT^{4+}, the ring's affinity for TTF is still lost, causing it to shuttle over to the alternative DNP recognition site by a process of random walk in Me_2CO or CH_2Cl_2 solution.

Table 6.1 The kinetics and activation parameters for the oxidation-induced forward (FWD) and reduction-induced backward (BACK) translation of a CBPQT^{4+} ring in the [2]rotaxanes **R603a^{4+}–R603d^{4+}** possessing different *n*EG oligoether linkers.[82]



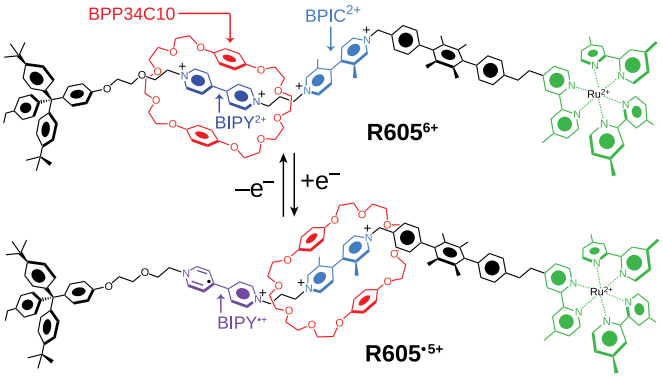
R603^{4+}		*n*	k_{293} s^{-1}	$t_{1/2}$ ms	Δ*G* kcal·mol^{-1}	Δ*H* kcal·mol^{-1}	Δ*S* cal·K^{-1}mol^{-1}
F	**a**	2	11.5	60	15.7	14.5	–4.1
W	**b**	3	20	35	15.4	13.8	–5.5
D	**c**	4	32.5	21	15.2	14.5	–2.3
	d	8	>100	<7	>14.5		
B	**a**	2	0.50	1.4	17.6	6.9	–37
A	**b**	3	0.10	6.9	18.5	12	–20
C	**c**	4	0.04	17.3	19.0	17	–6.6
K	**d**	8	<0.01	>69	>19.8		



Scheme 6.3 Redox actuation of a neutral TTF-based donor-acceptor bistable rotaxane.[47]

6.1.1.2 Reductive D-A Redox Switching

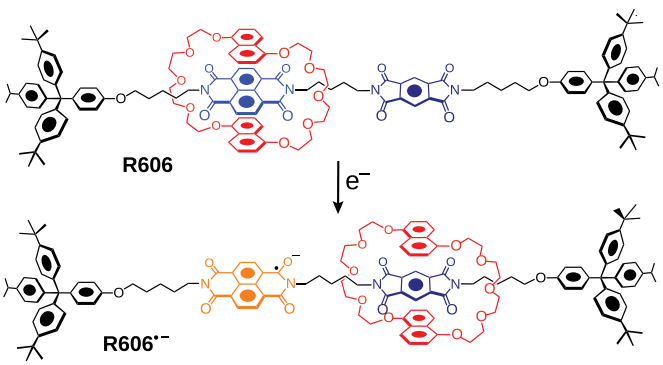
While TTF represents the most common handle for oxidative switching in donor-acceptor MIMs, there are several electron-deficient recognition units that can be switched under reductive control, most notably 4,4´-bipyridinium (BIPY^{2+}) units, since their two one-electron reductions are reversible at low potentials ($E_{1/2}$ ≈ –350 and –750 mV vs. SCE) and they are well-known to form donor-acceptor pseudorotaxanes—see **Sections 2.3.3.2–2.3.3.5**—with π-electron rich crown ethers. The reduction potentials and binding affinities of bipyridinium salts can also be adjusted with substituents. The bistable [2]rotaxane[45] **R605^{6+}** has two nondegenerate bipyridinium recognition sites (**Scheme 6.4**) which both undergo two reversible one-electron reduction processes at significantly different potentials. Steric hindrance



Scheme 6.4 A redox-switchable [2]rotaxane **R605**$^{6+}$ employing[45] nondegenerate bipyridinium recognition sites.

imposed by the methyl groups in the 3,3′-dimethyl-4,4′-bipyridinium (bipicolinium, $BPIC^{2+}$) unit endows it with a more negative reduction potential and weaker binding with bis(*para*-phenylene)[34]crown-10 (BPP34C10) compared to that of the $BIPY^{2+}$ recognition site. The BPP34C10 ring resides primarily (K_{eq} = 23) on $BIPY^{2+}$ until the first reversible one-electron reduction, which generates a $BIPY^{\bullet+}$ radical cation in **R605**$^{\bullet5+}$, induces it to move to the $BPIC^{2+}$ recognition site. One-electron oxidation of the $BIPY^{\bullet+}$ unit returns **R605**$^{6+}$ to its GSCC in which BPP34C10 encircles the $BIPY^{2+}$ unit. Although this rotaxane was primarily designed to be switched photochemically by virtue of its photosensitizing stopper—see **Section 6.2.1.2**—the crown ether/$BIPY^{2+}$/$BPIC^{2+}$ system proved to be yet another well-behaved bistable redox switch. An analogue, in which the $BIPY^{2+}$ and $BPIC^{2+}$ units have been transposed, was also found[121] to exhibit identical electrochemical, but not photochemical, switching behavior, ignoring the direction in which the ring shuttles. BPP34C10 rings encircling viologen recognition units can also be circumrotated under reductive control in donor-acceptor [2]- and [3]catenanes possessing dialkylammonium recognition units as the secondary binding sites.[122]

Completely neutral bistable rotaxanes are attainable by substituting electron-deficient diimides for bipyridinium units in the crown-ether based MIMs. A well-behaved rotaxane switch[46] **R606**, based on neutral π-associated donor-acceptor interactions, can also be switched (**Scheme 6.5**)



Scheme 6.5 A redox-switchable bistable [2]rotaxane[46] based on the recognition of DN38C10 for aromatic diimides.

electrochemically. The 1,5-dinaphtho[38]crown-10 (DN38C10) ring has a higher affinity for a naphthalene diimide (NDI) recognition site than for a PMDI unit, since NDI is a stronger π-acceptor. Although the population of translational isomers in the PMDI-complexed MSCC is below the ^{1}H NMR spectroscopic detection limit, a K_{eq} value of 33 has been estimated[30] retrospectively from the cyclic voltammetry data. One-electron reduction of the NDI unit to $NDI^{\bullet-}$ causes the DN38C10 ring to shuttle to the PMDI recognition site in **R606**$^{\bullet-}$: the reduction wave in the cyclic voltammogram, however, is not fully reversible. An essentially monostable rotaxane utilizing the same DN38C10 and NDI recognition units has recently been demonstrated[123] to behave as a 'push-button' molecular switch.

Several more examples[49,50,124] of reductively controlled switches rely upon a combination of $BIPY^{2+}$ and diimides for the construction of bistable switches. In the case of the bistable catenane **C604**$^{2+}$ (**Figure 6.5a**) and the bistable rotaxane **R607**$^{2+}$ (**Figure 6.5b**), both of which possess NDI and $BIPY^{2+}$ recognition units for a DN38C10 ring, the ground-state distributions in both compounds suffer from having relatively unbiased population ratios (6:4) between their two translational isomers. While a redox-induced change in the distribution of **C604**$^{2+}$ could not be detected electrochemically, presumably on account of an excessively high circumrotational barrier exceeding 28 kcal · mol^{-1},[49] the rotaxane **R607**$^{2(\bullet-)}$ generated[50] by four successive one-electron reductions ($NDI \rightarrow NDI^{2-}$, $BIPY^{2+} \rightarrow BIPY$) is translationally biased in favor of the fully reduced neutral BIPY unit, in DMF—a solvent in which the activation barrier to shuttling is relatively low. The DN38C10 ring of **R607**$^{2(\bullet-)}$ most likely prefers the BIPY unit on account of repulsive forces involving the negatively charged NDI^{2-} dianion.

Liu[124,125] has approached the $BIPY^{2+}$/diimide hybrids with a design much closer to the "blue box" family (**Section 2.3.3.8**) of catenanes—e.g., **C601**$^{4+}$**–C603**$^{4+}$—by simply substituting one of the bipyridinium units of $CBPQT^{4+}$ ring with an appropriate diimide. Of the resulting bistable, electrochemically switchable (**Scheme 6.6**) [2]catenanes **C605a**$^{2+}$**–C605f**$^{2+}$, the one (**C605a**$^{2+}$) with the weakest-interacting BPP34C10 ring, expresses the highest integrity as a bistable switch under reductive control. **C605a**$^{2+}$ is the only bistable catenane in the series for which electrochemical evidence suggested that the MSCC can be accessed selectively after two one-electron reductions of $BIPY^{2+}$ to $BIPY^0$. In every other case (**C605b**$^{2+}$**–C605f**$^{2+}$), the second reduction of $BIPY^{\bullet+}$ to $BIPY^0$ is accompanied by the first reduction of accompanying neutral π-acceptor ($PMDI \rightarrow PMDI^{\bullet-}$ or $NDI \rightarrow NDI^{\bullet-}$), followed by a distribution in which the ring exhibits no preference for either recognition site.

The relatively recent discovery[76] of a new recognition motif mediated by radical-pairing interactions (**Section 2.3.10**) between bipyridinium radical cations has led to yet another class of reductively electroswitchable MIMs. On account

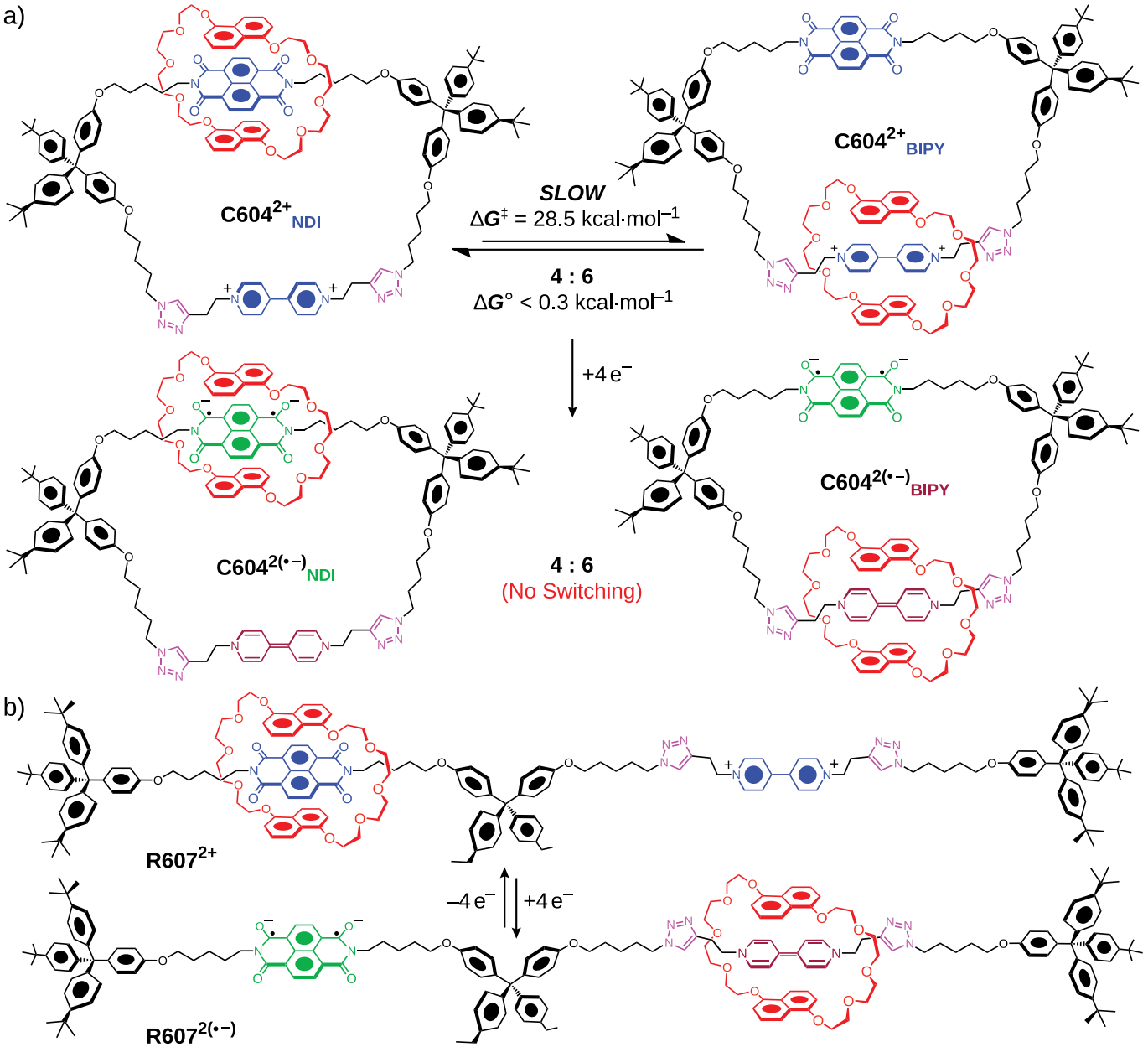
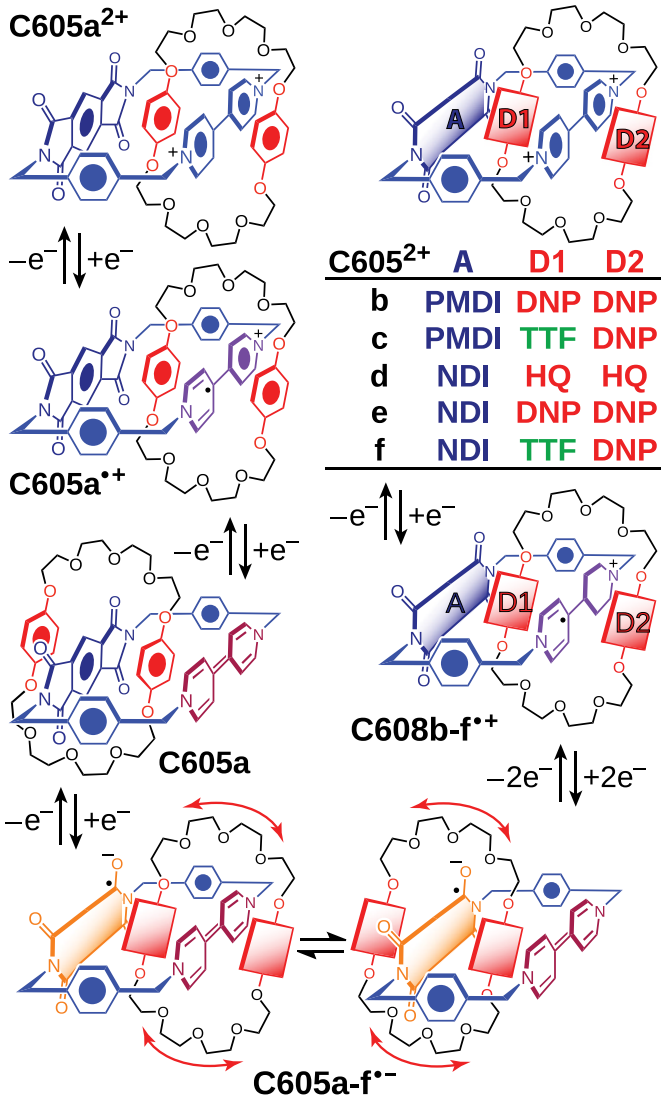


Figure 6.5 A bistable [2]catenane[49] (a) and a bistable [2]rotaxane[50] (b) based on the DN38C10 ring and NDI/BIPY^{2+} recognition units, both of which exhibit relatively unbiased (6:4) populations of NDI- and BIPY^{2+}-encircled translational isomers, respectively, exhibit different switching behaviors under reductive conditions.

of their positive charges, a repulsive electrostatic interaction exists between the CBPQT^{4+} ring and BIPY^{2+} units. A strongly associated ($K_a \approx 5.0 \times 10^4$ M^{-1}, determined[126] by isothermal titration calorimetry in MeCN) [2]pseudorotaxane *BIPY*$^{\bullet+}$⊂*CBPQT*$^{2(\bullet+)}$ is formed between these two 'molecular enemies', however, when they are reduced to their radical cations, CBPQT$^{2(\bullet+)}$ and BIPY$^{\bullet+}$, representing yet another way to achieve near-perfect on/off switching. Indeed, radical-pairing interactions have ushered in an unprecedented and efficient switching mechanism in bistable MIMs by allowing access to a so-called radical state co-conformation (RSCC). Highly efficient switching in these types of systems has been demonstrated in bistable [2]rotaxanes[76,127,128] tristable [2]rotaxanes,[76] as well as electrochemically bistable [2]catenanes,[128–130] daisy chains[131] and [3]rotaxanes.[132] The latter two switches are discussed in **Sections 6.13.1.1** and **6.13.8**, respectively. The electrochemically bistable [2]rotaxane[76] **R608**$^{6+}$ can be actuated (**Scheme 6.7**) under reductive control in order to translocate a CBPQT^{4+} ring from a DNP unit in the GSCC to a BIPY$^{\bullet+}$ unit in the RSCC of trisradical tricationic **R608**$^{3(\bullet+)}$.

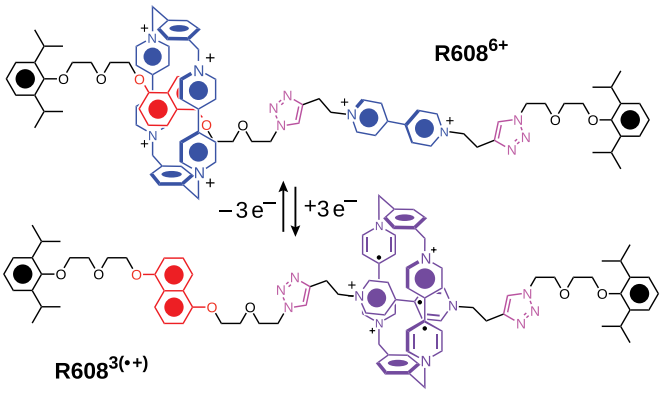
The ability to switch donor-acceptor mechanomolecules under both oxidative and reductive control



C605²⁺	A	D1	D2
b	PMDI	DNP	DNP
c	PMDI	TTF	DNP
d	NDI	HQ	HQ
e	NDI	DNP	DNP
f	NDI	TTF	DNP

Scheme 6.6 The switching mechanism of [2]catenanes with desymmetrized BIPY^{2+} cyclophanes incorporating neutral NDI or PMDI units.[124] Among the six homologues **C605a^{2+}–C605f^{2+}**, only **C605a^{2+}** exhibits site-specific switching from BIPY^{2+} to PMDI after two one-electron reduction steps to generate a neutral BIPY unit. The remaining analogues **C605b^{2+}–C605f^{2+}** have no site specificity when BIPY is fully reduced because the reduction of BIPY$^{\bullet+}$ coincides with the reduction of PMDI or NDI to the corresponding radical anions PMDI$^{\bullet-}$ or NDI$^{\bullet-}$. The radical anionic state of all six catenanes **C605a$^{\bullet-}$–C605f$^{\bullet-}$** are ill-defined co-conformations in which the rings rotate freely with minimal site recognition.

enables the design of high-fidelity tristable switches. The three-state [2]rotaxane **R609^{6+}** has been prepared based on this kind of control.[76] As illustrated in **Scheme 6.8**, the CBPQT^{4+} ring resides primarily around a TTF recognition unit in the ground state, but it can be induced to shuttle, either to a DNP unit in **R609^{8+}** under oxidative conditions, or to a BIPY$^{\bullet+}$ unit in **R609$^{3(\bullet+)}$** under reductive conditions.

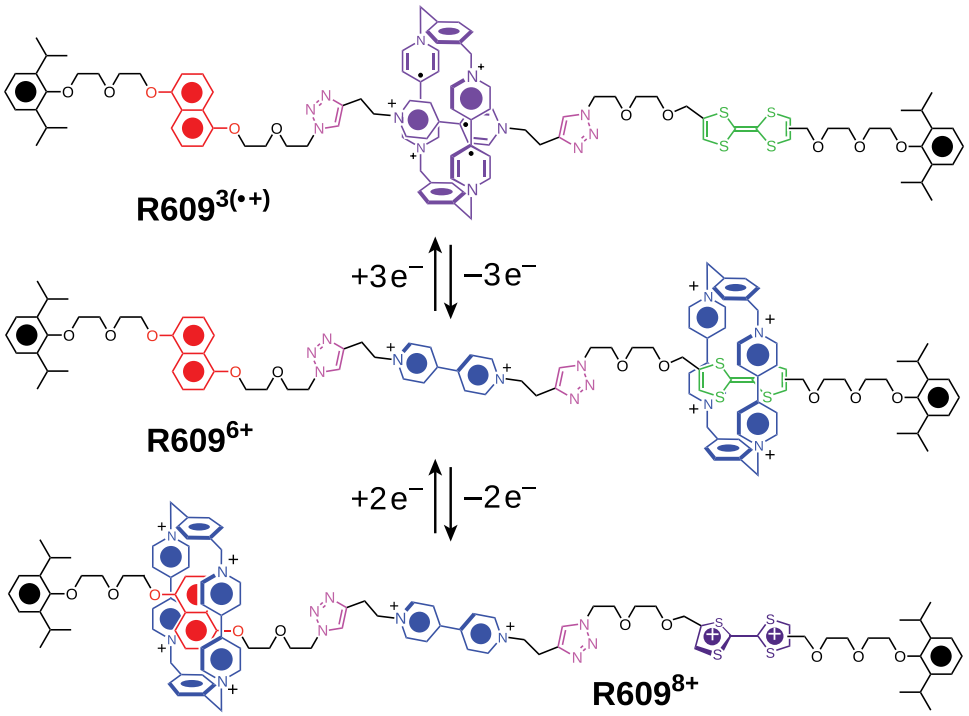


Scheme 6.7 An electrochemically bistable [2]rotaxane[76] **R608^{6+}** in which the radical state co-conformation (RSCC) **R608$^{3(\bullet+)}$** is accessed under reductive conditions.

6.1.2 Redox Switching of Metallo-Mechanomolecules

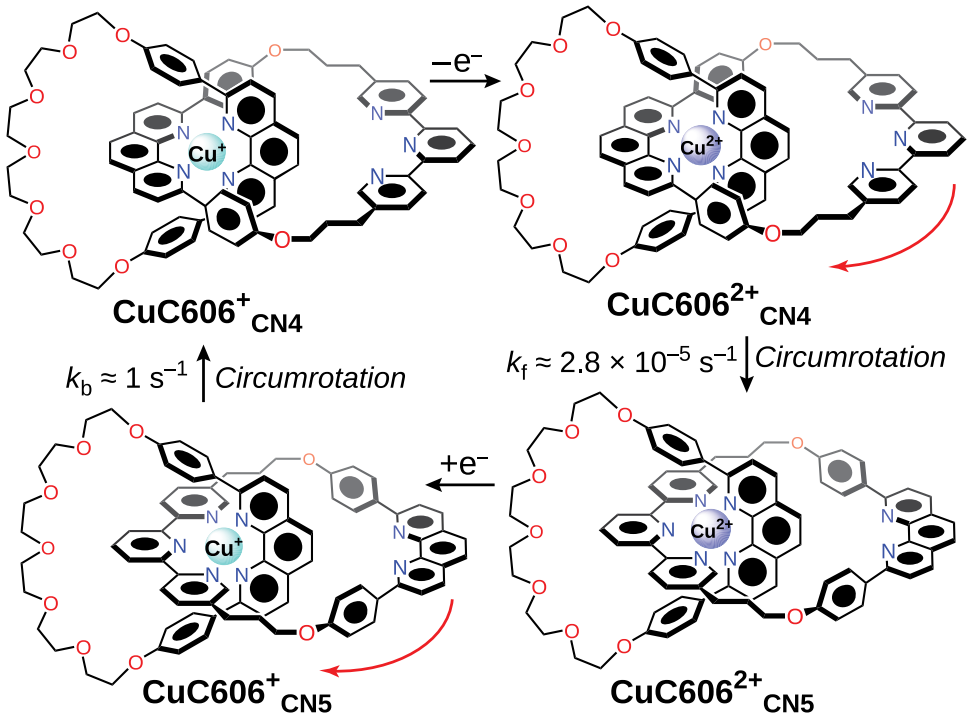
At about the same time as the advent of switchable donor-acceptor MIMs, the Sauvage group in Strasbourg was engaging in similar experiments motivated by the design of transition metal-based molecular machine prototypes. Redox chemistry is only one of a host of stimuli that have been employed to actuate molecular switches and machines that rely on transition metals—see refs. 22, 133–142. The key principle behind electrochemical switches of this ilk is that doing redox chemistry on the transition metal template can change its coordination geometry. Cu^{I}, for example, tends to form tetrahedral four-coordinate complexes, whereas Cu^{II} prefers five- and six-coordinate geometries. The operation of the first redox-switchable MIM described by Sauvage[143] is shown in **Scheme 6.9**. He ingeniously designed the Cu^{I} [2]catenate **CuC606$^{+}_{CN4}$** to have a ring containing both 2,9-diphenyl-1,10-phenanthroline (dpp) and terpyridine (terpy) ligands. The subscripted term CN4 in denotes the coordination number (CN) of the metal ion. Mechanical switching in this catenate is induced electrochemically by invoking Lehn's principle of maximum site occupancy[144] at the Cu center. A one-electron oxidation of the Cu^{I} ion generates **CuC606$^{2+}_{CN4}$** as an unstable intermediate—the unfavorable 4-coordinate geometry around Cu^{II} causes the rings to circumrotate such that the terpy ligand can take part in the more stable 5-coordinate complex of **CuC606$^{2+}_{CN5}$**. Reducing the copper dication back to the monocationic state generates the corresponding **CuC606$^{+}_{CN5}$** intermediate en route to the original state of **CuC606$^{+}_{CN4}$**.

Let us make a few general statements that are applicable to all of Sauvage's Cu-complexed MIMs. Firstly, we note that the oxidation or reduction of copper ions can be regarded, for all intents and purposes, as instantaneous compared to the mechanical motions that ensue as a result: it follows that mechanical motions are not limited by electron transfer rates. Another very general phenomenon associated with this class of switches is a directional dependence on kinetics—rearrangement from CN 4 to CN 5 is always slower than the reverse situation because ligand



Scheme 6.8 A tristable [2]rotaxane[76] that possesses donor-acceptor and radical-pairing recognition motifs to obtain three distinct translational isomers under ambient (**R609**$^{6+}$), reductive (**R609**$^{3(\bullet+)}$), and oxidative (**R609**$^{8+}$) conditions.

exchange reactions are easier around Cu^{I} than those around Cu^{II}. In other words, it is more costly to rearrange the unstable 4-coordinate Cu^{II} intermediates than the transient 5-coordinate Cu^{I} species. For example, the forward process (CN4 → CN5) that generates **CuC606**$^{2+}_{CN5}$ proceeds[143] with a first order rate constant ($k_f \approx 2.8 \times 10^{-5}\ s^{-1}$) that is five orders of magnitude slower than the corresponding backward process ($k_b \approx 1\ s^{-1}$) that regenerates **CuC606**$^{+}_{CN4}$ at 298 K in MeCN. Finally, we note that the Strasbourg group has, for the most part, compared cyclic voltammograms at different scan rates to estimate rate constants, employing an approach that often provides upper or lower limits on the rates rather than precise numbers. With these provisos, we will continue highlighting the discoveries that have emanated from Sauvage's laboratory during the past 20 or so years.



Scheme 6.9 Sauvage's first electromechanical molecular switch.[143] The bracketed number in the compound descriptors denote the coordination number of the metal center.

Sauvage[22,140,145] has demonstrated that the same mechanism of switching between different coordination geometries of Cu^{I} and Cu^{II} can be used to control both pirouetting[145–147] (**Figure 6.6**) and translation (**Figure 6.7**) in metallo[2]rotaxanes. In the case of the [2]rotaxane **CuR610$^{+}_{CN4}$**, for example, the ring component is identical to that of the electrochemically bistable catenane **CuC606$^{+}_{CN4}$**, with endohedral bidentate dpp and tridentate terpy ligands. Thus, upon electrochemical oxidation of the Cu^{I} ion, the ring circumrotates (**Figure 6.6**) around the axle (or the axle pirouettes within the ring) to adopt a pentacoordinate geometry in **CuR610$^{2+}_{CN5}$**. The Strasbourg team has also performed some physical chemistry on a family of homologues (**Figure 6.6**) belonging to this class of pirouetting rotaxanes. The effects of structural modifications on the pirouetting kinetics of these rotaxanes clearly implicate the sterics around copper as an important factor. Rotaxanes **CuR610^{+}–CuR612^{+}** demonstrate progressively faster pirouetting rates as the steric constraints around the Cu^{I}/Cu^{II} couple are reduced. The dpp ligand of the dumbbell in **CuR610^{+}** is the most sterically crowded, leading to the slowest redox-driven pirouetting rates. The 2,2´-bipyridine (bpy) ligand with distant stoppers connected by flexible polyether linkers in the dumbbell of **CuR612^{+}** is the least crowded scenario, leading to the fastest rates of ligand rearrangement. Overall, these simple dumbbell modifications can lead to rate discrepancies spanning almost four orders of magnitude (0.007–12 s^{-1}) in the $Cu^{I} \rightarrow Cu^{II}$ direction and two orders of magnitude (17–1200 s^{-1}) in the $Cu^{II} \rightarrow Cu^{I}$ direction. **CuR612^{+}** has been implemented[148] as a set-reset machine which is capable of information storage—see **Section 6.15.1.3**.

Naturally, ring translation can also be achieved in Sauvage's rotaxanes by installing a combination of bidentate and tridentate ligands in the dumbbell. By synthesizing a rotaxane with phenanthroline (phen) and terpy ligands in the dumbbell component, the mechanically interlocked 30-membered macrocyclic diphenylphenanthroline (Mdpp30) ligand can be translocated between these two sites (**Figure 6.7**) through electrochemical manipulation of a copper template's redox state.[149] Accordingly, the macrocyclic chelate encircles the phen ligand in **CuR613$^{+}_{CN4}$**, yet the ring translates (**Figure 6.7a**) over a tetramethylene linker to engage the terpy ligand in **CuR613$^{2+}_{CN5}$**, where it adopts a pentacoordinate geometry. A first order rate constant of $k_f = 1.5 \times 10^{-4}$ s^{-1} was estimated for the forward translational isomerization (Cu^{II}, CN4 → CN5), while the rate, k_b, of the backward translation (Cu^{I}, CN5 → CN4) is less than 10^{-2} s^{-1}, corresponding to half-lives of approximately 1.3 h and >69 s, respectively. The metallo[2]rotaxane[150] **CuR614^{+}**, possessing a *para*-phenylene linker between the axel's binding sites, shuttles (**Figure 6.7b**) at comparably sluggish rates. In the metallo[2]rotaxane **CuR615^{+}**, which lacks a linker in between the phen and terpy chelating units, Gaviña and Tatay[151] observed (**Figure 6.7c**) faster kinetics for the redox-driven shuttling of the Mdpp30 ring. The forward rate, k_f, is 2 s^{-1} in MeCN and falls to 0.6 s^{-1} in 9:1 CH_2Cl_2/MeCN, the rate enhancement being attributable to this rotaxane's shorter pathway to ligand rearrangment.

Another way to decrease steric crowding around the copper ion—and consequently increase the rates of mechanical motion—is to increase the size and/or flexibility of the ring's cavity near the chelating site. A breakthrough on this front came with the introduction[29,152–154] of the

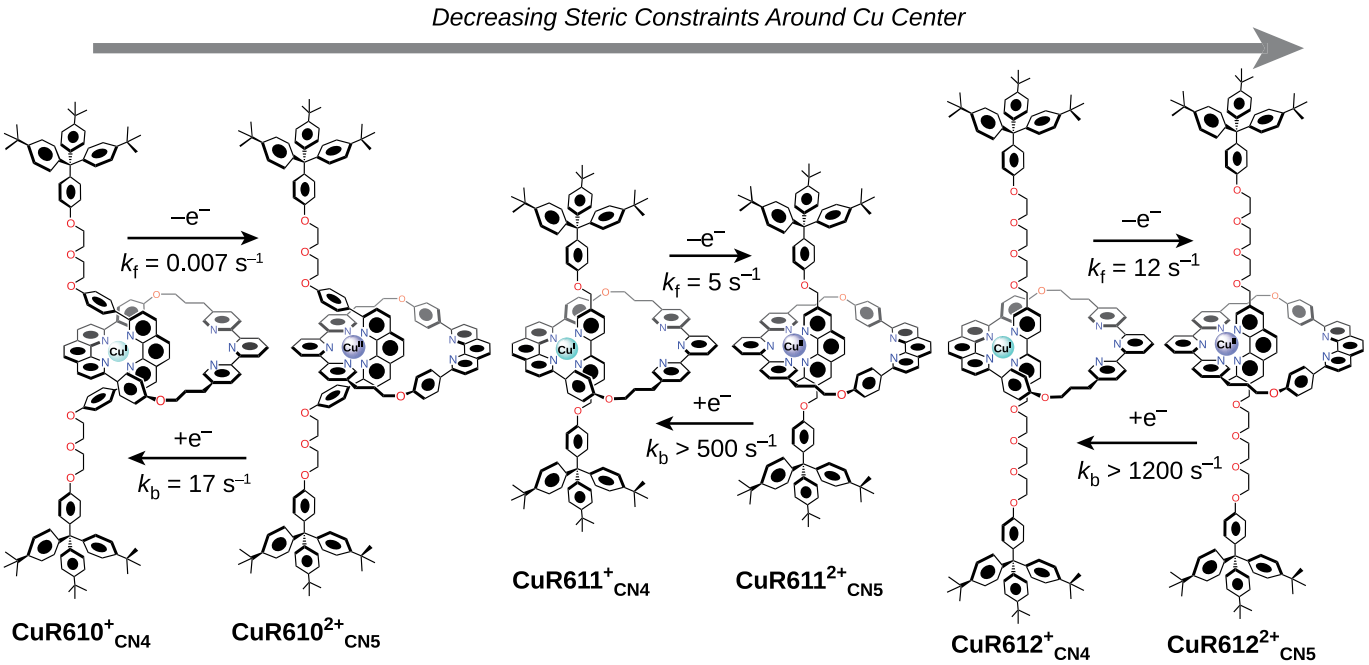


Figure 6.6 A series of electrochemically switchable pirouetting rotaxanes[145–147] with progressively larger rate constants associated with rearrangement, an observation which corresponds to decreasing steric crowding around the copper centers.

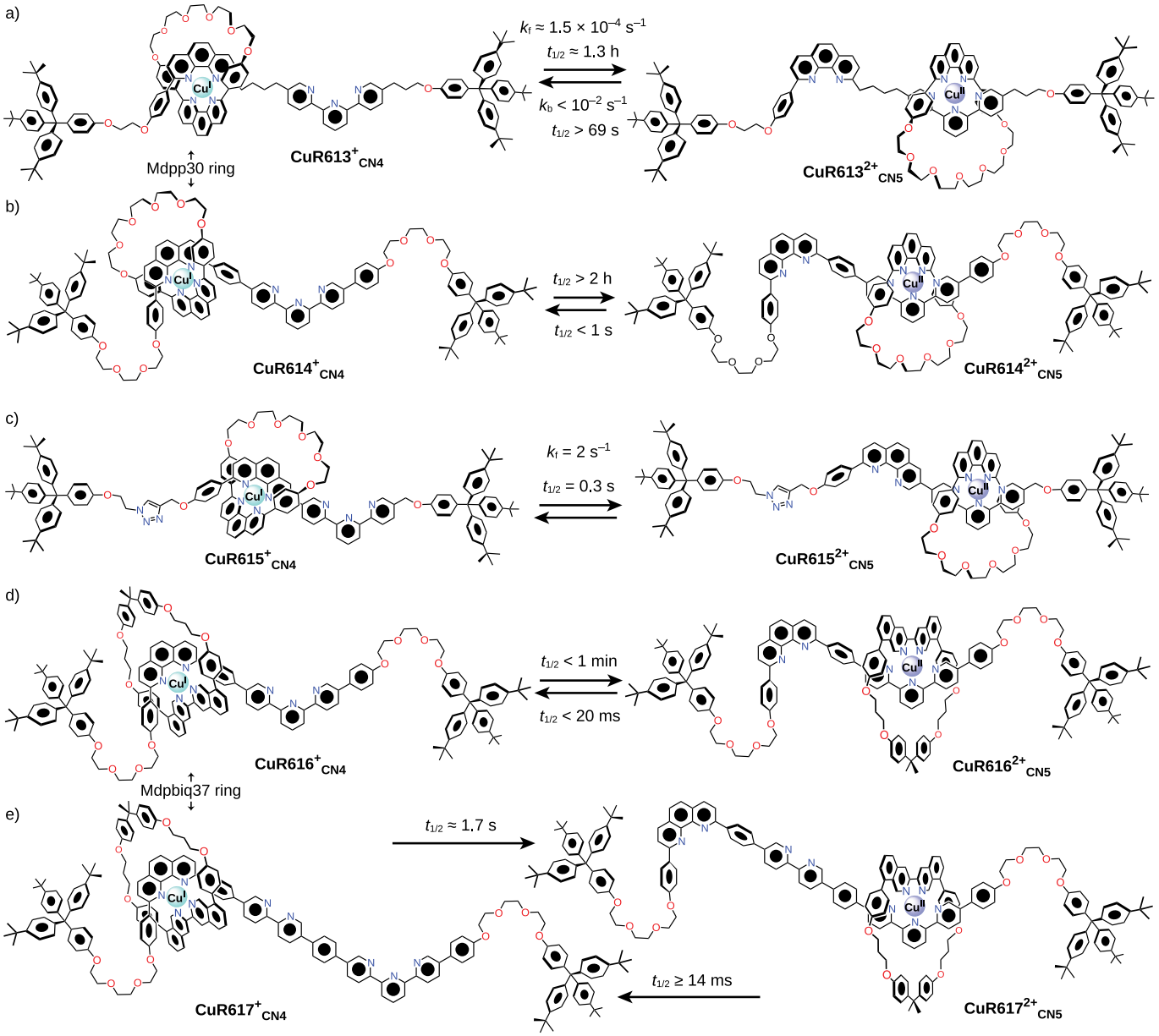


Figure 6.7 Comparison of electrochemically-induced ring translation in some metallo[2]rotaxanes. (a) Following a one-electron oxidation of the metal template from Cu^{II} to Cu^{II}, **CuR613$^{+}_{CN4}$** switches to **CuR613$^{2+}_{CN5}$** by translocating the Mdpp30 ring forward and backward between a tridentate terpy ligand and a bidentate phen ligand, repectively, in order to satisfy the metal center's ligand field. (b) An identical ligand system is found in **CuR614^{+}/CuR614$^{2+}_{CN5'}$** where the phen and terpy units are connected in this case by a rigid *para*-phenylene linker.[150,155] (c) The forward rate of translational isomerization is faster when the linker between the phen and terpy ligands is eliminated completely, as in the case[151] of **CuR615$^{+}_{CN4}$ → CuR615$^{2+}_{CN5}$**. (d) The larger macrocyclic ligand Mdpbiq37 increases the rate of shuttling during the redox-controlled interconversion of **CuR616$^{+}_{CN4}$** and **CuR616$^{2+}_{CN5}$** relative to the homologue based on the more confining Mdpp30 macrocycle.[150,155] (e) Shuttling rates are further accelerated[153] by installing a bidentate bpy ligand as the linker in between the dpp and terpy binding sites of **CuR617$^{+}_{CN4}$** and **CuR617$^{2+}_{CN5}$**.

37-membered endocyclic biisoquinoline ligand Mdpbiq37, replacing the more sterically hindered counterpart, Mdpp30. The 8,8′-diphenyl-3,3′-biisoquinoline (dpbiq) chelating moeity in Mdpbiq37 leaves a much more open space (**Figure 6.8**) for coordination for copper, with a separation distance (11 Å) between phenyl rings that is almost 50% larger than that (7 Å) of Mdpp30. Mdpbiq37 has been incorporated[150,155] (**Figure 6.7d–e**) into electrochemically bistable rotaxane switches, namely **CuR616$^{+}_{CN4}$/CuR616$^{2+}_{CN5}$** and **CuR617$^{+}_{CN4}$/CuR617$^{2+}_{CN5}$**. A comparison of the Mdpp30 and Mdpbiq37 switches possessing identical dumbbell constitutions in **Figures 6.7b** and **6.7d**, respectively, confirms that reducing the steric demands of the ring's cavity leads to faster rates of translation by a few orders of magnitude.

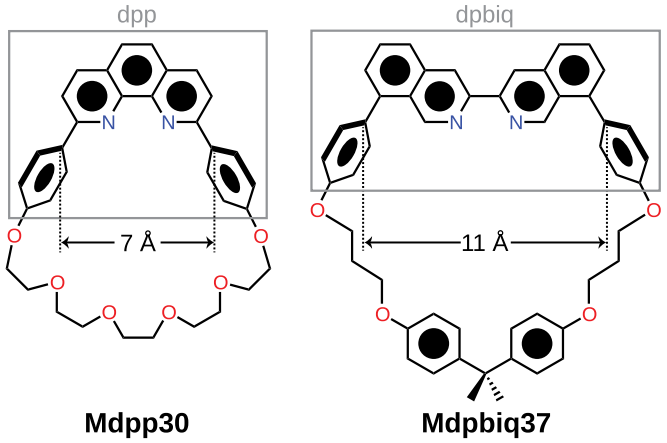


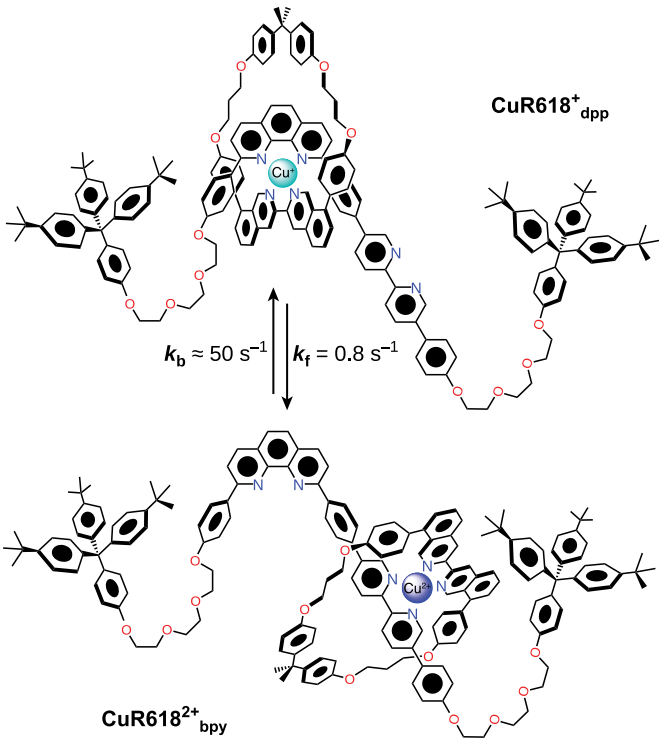
Figure 6.8 Sauvage's endocyclic chelates[150,155] based on 2,9-diphenyl-1,10-phenanthroline (dpp) and 8,8′-diphenyl-3,3′-biisoquinoline (dpbiq) ligands (boxed in grey). The dpbiq-based macrocycle **Mbpdiq37** has almost 50% more space between the phenylene units compared with **Mdpp30** (7 Å and 11 Å, respectively), creating a more open coordination site for metal ions.

Both rotaxanes shuttle relatively quickly from CN 5 to CN 4—with half-lives below 1 s and 20 ms, respectively—and much slower in going from CN 4 to CN 5 with half-lives from >2 h to <1 min. Shuttling rates are fastest (**Figure 6.7e**) in Sauvage's [2]rotaxane[153] **CuR617$^{+/2+}$**, which possesses a bidentate bpy ligand as the linker in between the dpp and terpy moieties. First order rate constants of 0.4 s^{-1} and 50 s^{-1} were estimated for the forward ($Cu^{I} \rightarrow Cu^{II}$) and backward ($Cu^{II} \rightarrow Cu^{I}$) process, corresponding to half-lives of approximately 1.7 s and 14 ms, respectively. The relatively fast shuttling rates in this system are most likely attributable to the ability of the bpy linker to participate in lower-energy intermediates during translational isomerization.

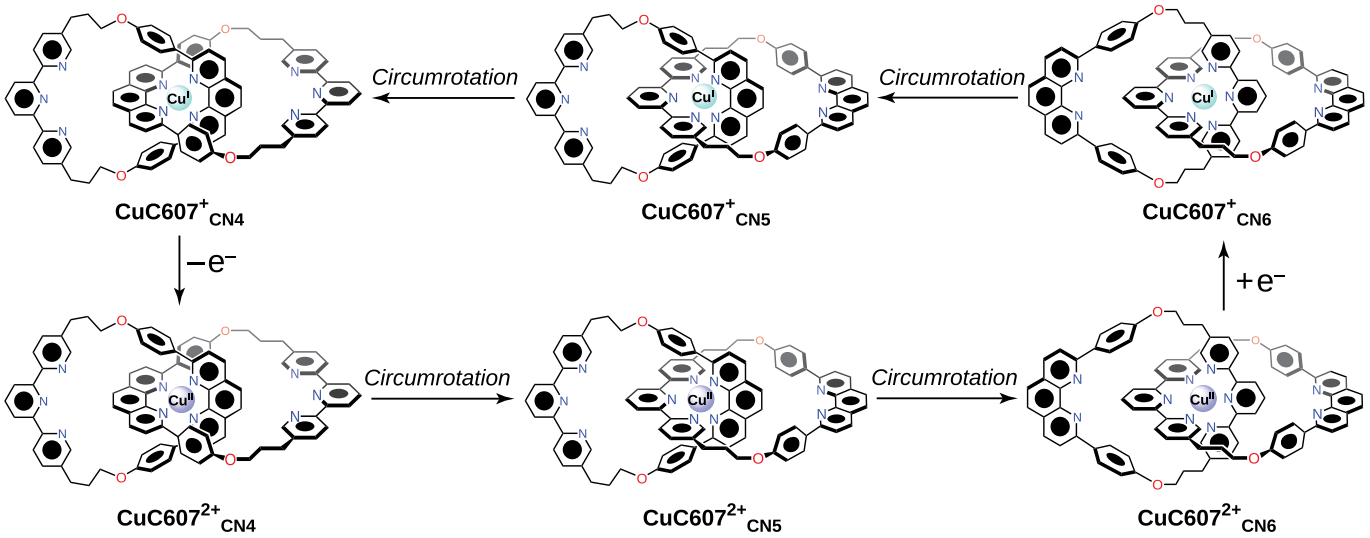
While the structural homologues in **Figures 6.6** and **6.7** demonstrate that the kinetics of mechanical motion can be widely tuned through molecular design, the Strasbourg team has also tuned these parameters by changing the physical environment—particularly solvents and counterions—of the switches. For example, water was found[156] to slow down the kinetics of circumrotation in **CuC606^{+}** because a single water molecule stabilizes the intermediate species by forming a ***Cu(H$_2$O)C606$^{2+}_{CN4}$*** complex. Hard counterions have the opposite effect, especially in low-polarity solvents. Cl^- ions reduce reaction times from hours to minutes in CH_2Cl_2 because the Cu–Cl bond weakens the Cu–N bonds. The Cl^- ions also stabilize the coordinatively unsaturated intermediate states during rearrangement, dramatically lowering the corresponding activation barrier.

Another design from the Strasbourg group[157] is a class (**Scheme 6.10**) of switchable Cu-complexed shuttles in which both ligands are bidentate. By replacing the terpy ligand of the dumbbell with bpy as the second ligand for Cu^{II}, CN is 4 in all translational isomers. The ground state distributions of **CuR618^{+}** and **CuR618^{2+}** are therefore governed by steric effects in this case, rather than by coordination geometry. Whereas Cu^{I} is better stabilized by the more sterically hindered dpp ligand in **CuR618$^{+}_{dpp}$**, the unfavorable tetrahedral geometry around Cu^{II} dictates that it is better stabilized by the least sterically crowded configuration available at the bpy ligand in **CuR618$^{2+}_{bpy}$**. With rate constants of $k_f = 0.8\ s^{-1}$ on the oxidation stroke and $k_b \approx 50\ s^{-1}$ on the reduction stroke, the switching kinetics of **CuR618$^{+/2+}$** are comparable to those of its predecessor, **CuR616$^{+/2+}$**.

Extending the principles of their transition metal-complexed MIMs in a different direction, Sauvage[158] prepared a [2]catenate in which the double-chelate phen/terpy macrocycle comprises each of the two interlocked rings. With both doubly- and triply-ligating ligands in each component, **CuC607^{+}** and **Cu607^{2+}** could potentially access CN 4, CN 5, or CN 6 geometries, for a total of six possible states (**Scheme 6.11**) during redox switching. While **CuC607$^{+}_{CN4}$** and **CuC607$^{2+}_{CN6}$** represent the most stable circumrotational isomers in the Cu^{I} and Cu^{II} redox states, respectively, the transient 5-coordinate species could still be detected and characterized spectroscopically and electrochemically.



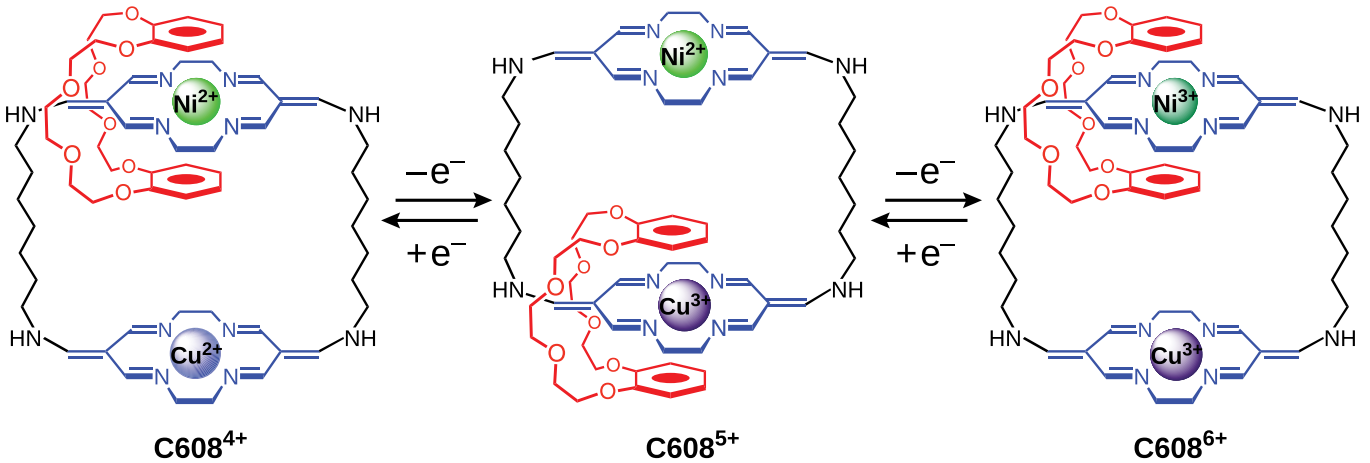
Scheme 6.10 An electrochemically bistable [2]rotaxane[157] with CN = 4 in both translational isomers, such that the ground state distributions in each oxidation state are governed by steric effects rather than by CN. The more sterically protected site stabilizes Cu^{I}, whereas the less hindered one stabilizes Cu^{II}.



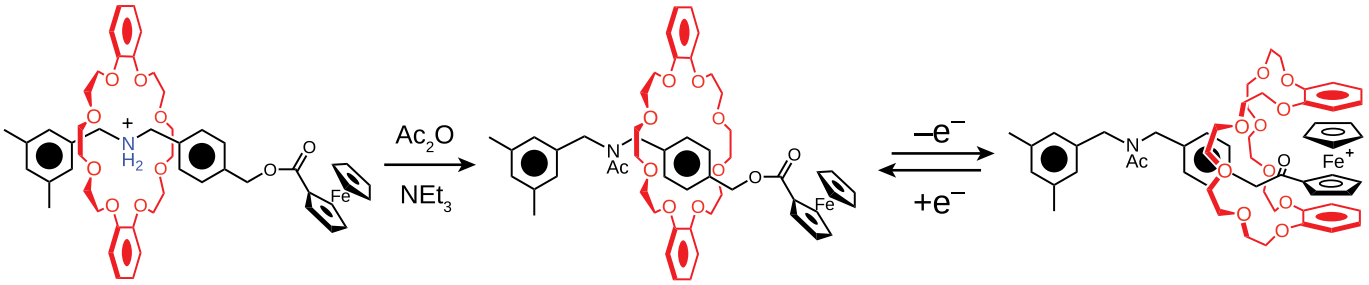
Scheme 6.11 An electrochemically bistable [2]catenate which passes through six states in a full switching cycle.[158]

More than 20 years' worth of research in Strasbourg and elsewhere on redox-active metallo-catenanes and rotaxanes has showcased the versatility of Cu-complexes in the design of molecular switches. By linking together in various different constellations a relatively simple library of subcomponents—copper(I/II), along with phen, dpp, bpy, terpy, and dpbiq ligands—Sauvage has explored an impressive diversity of motions while exercising remarkable control over kinetics which span several orders of magnitude, while employing several different kinds of experimental and structural handles to tailor them at will.

Although they are more rare outside of Strasbourg, one can find more examples in the literature of mechanomolecular switches driven by the redox chemistry of transition metals. The bistable [2]catenane **C608**$^{4+}$, which employs heterodinuclear tetraazamacrocyclic chelates as recognition sites for a dibenzo[24]crown-8 (DB24C8) ring, has been prepared and actuated (**Scheme 6.12**) by Korybut-Daszkiewicz.[159] The crown ether preferentially encircles the Ni^{II} tetraazamacrocyclic over its Cu^{II} counterpart in **C608**$^{4+}$. Oxidation of Cu^{I} to Cu^{III} causes the DB24C8 ring to shuttle to the Cu^{III} site in **C608**$^{5+}$. The ring then travels the same path in reverse after Ni^{II} is oxidized to Ni^{III}, landing back on the Ni^{III} chelate in **C608**$^{6+}$. Normal-pulse voltammetry in MeCN was performed in a regime in which two distinguishable waves were observed for the oxidation of Ni^{II}—one corresponding to each of the catenane's translational isomers—and a rate constant $k = 5.3\,s^{-1}$ for the shuttling event was calculated by estimating the distribution based on the ratio of oxidation waves at various pulse rates.



Scheme 6.12 Electrochemically controlled shuttling in a heterodinuclear [2]catenane. A DB24C8 ring shuttles between Ni and Cu complexes depending on the oxidation state of the metal. When both metals have the same oxidation state (**C608**$^{4+}$ and **C608**$^{6+}$), the DB24C8 ring interacts preferentially with the Ni site, yet it favors the more cationic Cu^{III} complex in the mixed-valence **C608**$^{5+}$ species.[159]

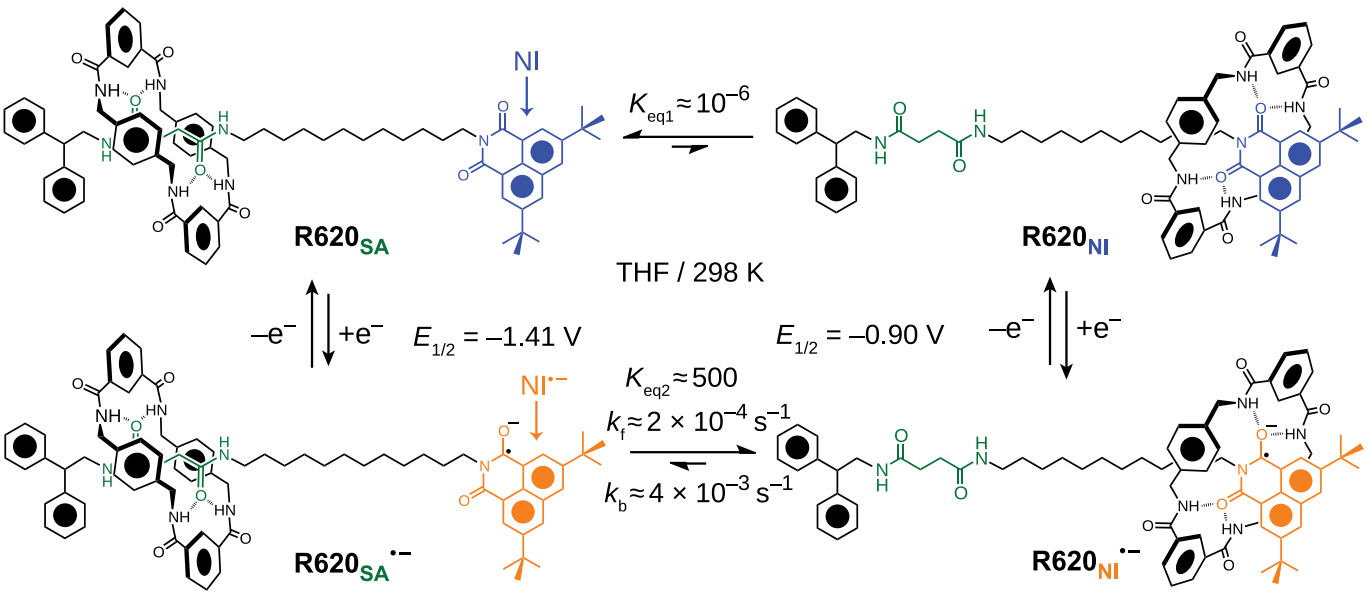


Scheme 6.13 An electrochemically switchable [2]rotaxane **R619Ac** derived from the dialkylammonium-binding rotaxane **R619H**$^+$, in which removal of all the hydrogen bonds by deactivation of the –NH_2^+– site with Ac_2O allows a much weaker interaction between the DB24C8 ring and the ferrocene (Fc) stopper to define the switching motion on redox actuation of the Fc/Fc$^+$ couple.[160]

6.1.3 Redox Switching of Hydrogen-Bonded MIMs

Takata[160] has shown that the dialkylammonium-based DB24C8 rotaxanes can be adapted for redox-switchability on removing the hydrogen bonds from the system by acylating the nitrogen atom and installing a redox-active ferrocene (Fc) stopper in the dumbbell. The –NH_2^+– recognition site in the Fc-stoppered rotaxane **R619H**$^+$ can be deactivated (**Scheme 6.13**) on acetylation to yield **R619Ac**, a species in which the DB24C8 ring encircles preferentially the innermost benzenoid nucleus, at least according to ^{1}H NMR spectroscopy, on account of the lack of any significant noncovalent bonding interations between the components of the molecule. When Fc is oxidized to Fc$^+$ to generate **R619Ac**$^+$, an 80 mV shift in the redox potential of Fc/Fc$^+$ indicates that the ring moves closer to the stopper in order to stabilize the Fc$^+$ cation. Deactivating the –NH_2^+– center is crucial to the successful operation of this shuttle, since the DB24C8···Fc$^+$ interaction is too weak to induce shuttling in **R619H**$^+$ or even be detected between the non-interlocked DB24C8 ring and the Fc$^+$ stopper. This research represents an example of how mechanical bonds can be used to stabilize very weak interactions—see **Section 7.1.1.5**—and how they can even be harnessed in the construction of molecular switches.

The benzylic amide rotaxanes and catenanes developed by Leigh[161–163] have been designed[164–168] for electrochemical switching through the use of naphthalene imides and diimides as the redox-active recognition sites. **R620** was Leigh's first iteration[164,165] (**Scheme 6.14**), where a 1,8-naphthalimide (NI) unit serves as both a secondary recognition site and as a stopper. The benzylic amide ring encircles preferentially the succinamide (SA) unit in the ground state because NI is a poor hydrogen bond acceptor. One-electron reduction of NI generates the NI$^{\bullet-}$ radical anion, which is a better hydrogen bond acceptor than SA, causing the ring to favor encircling this site in



Scheme 6.14 A square scheme depicting the mechanism of a benzylic amide electromechanical switch **R620** designed by Leigh.[165] Reduction of the naphthalimide (NI) stopper improves its ability to accept hydrogen bonds, causing the benzylic amide ring to shuttle from the succinamide (SA) recognition site to the NI$^{\bullet-}$ radical anion with excellent distributional bias of translational isomers in each redox state.

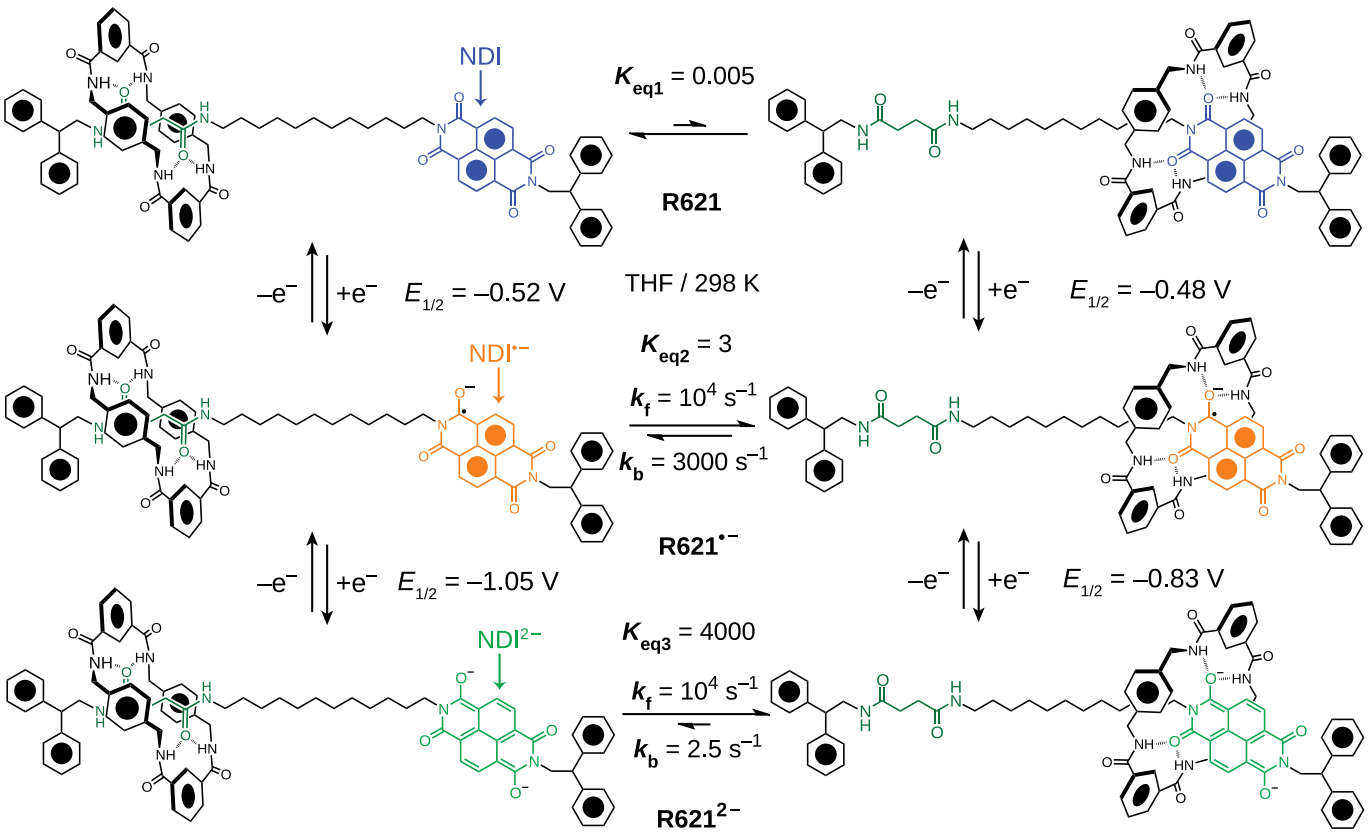
R620$^{\bullet-}$. This system exhibits excellent co-conformational integrity, with the co-conformer **R620**$_{SA}$ and the opposing co-conformer **R620**$_{NI}^{\bullet-}$ being populated almost exclusively in their respective redox states at 298 K in THF. A more recent investigation[168] found that the shuttling rate is reduced when PMDI is employed instead as the redox-active recognition site, suggesting that both the succinamide and the aromatic imide recognition sites are involved in the indermediate species responsible for the rate-determining step during translation.

One disadvantage of **R620** is the large potential of –1.41 V required to reduce NI to NI$^{\bullet-}$, preventing it from being operable on surfaces. Leigh[167] has overcome this challenge by replacing NI with a naphthalene diimide (NDI) subunit which has a lower first reduction potential of –0.68 V, and can also undergo a second reduction to the dianion NDI$^{2(\bullet-)}$, giving access (**Scheme 6.15**) to six species related to **R621**—two co-conformers with distinct population distributions for each of the three NDI redox states. The two extrema **R621** and **R621**$^{2-}$ were highly resolved, with the dominant isomer in each redox state being present in 200- and 4000-fold excess, respectively. The intermediary monoanion **R621**$^{\bullet-}$ accommodates a 1:2 distribution of succinamide:NDI isomers. A closely related [2]rotaxane[169,170] has been actuated in a surface monolayer—see **Section 6.14.1.2**.

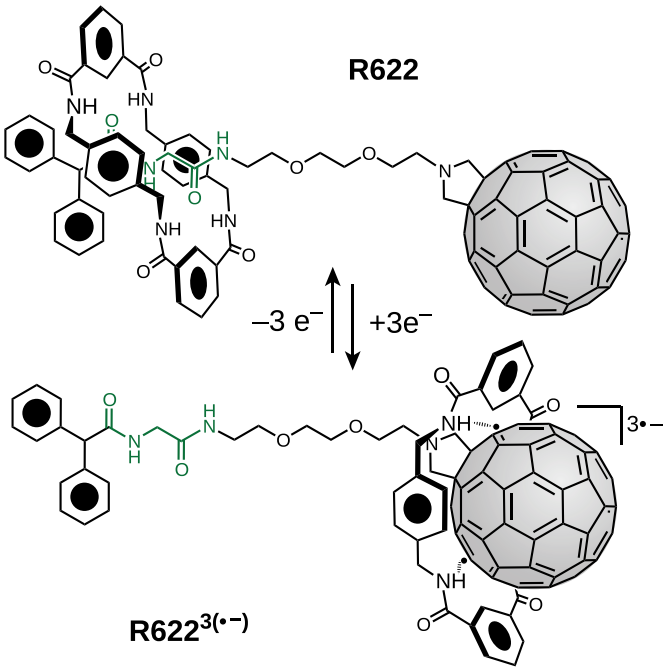
Electrochemically-switchable shuttles of the benzylic amide variety have also been reported by Mateo-Alonso,[171] who employed buckminsterfullerene (C_{60}) to serve as both a stopper and a recognition site in a design that is conceptually similar to Leigh's redox-switchable rotaxanes. In the bistable rotaxane **R622**, the benzylic amide ring encircles (**Scheme 6.16**) a glycylglycine recognition site preferentially, with a distribution constant $K_{eq} = 100$ in THF, while a three-electron reduction of C_{60} shifts the distribution in favor of the anionic C_{60} stopper of **R622**$^{3(\bullet-)}$ in an 8:1 ratio.

6.1.4 Aqueous Redox Switching

A couple of examples of redox-switchable rotaxanes that are operable in water by virtue of solvophobic templation motifs have been reported.[79,172,173] Kaifer[172] has demonstrated redox-driven switching (**Scheme 6.17**) in a [2]pseudorotaxane based on a cucurbit[7]uril (CB7) ring and a guest **L601**$^{2+}$ with redox-active ferrocene recognition sites. The ring prefers to reside over one of the hydrophobic ferrocenes at the guest termini in compound ***L601***$^{2+}\subset$*CB7*, but shuttles inward to the hexamethylene bis-ammonium chain at the guest's center when the ferrocene units are oxidized to the more hydrophilic ferrocenium (Fc^+) cations, affording ***L601***$^{4+}\subset$*CB7*.

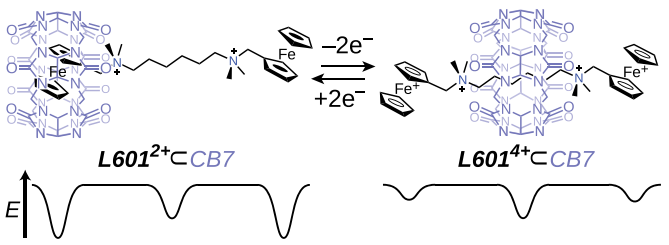


Scheme 6.15 The mechanism of electrochemically controlled shuttling in **R621**. By employing an NDI unit as a redox-active recognition site, Leigh[167,168] lowered the first reduction potential while raising the number of accessible redox states for switches. **R621** can access six different states, with highly biased populations arising in both the neutral **R621** and dianionic **R621**$^{2-}$ species.

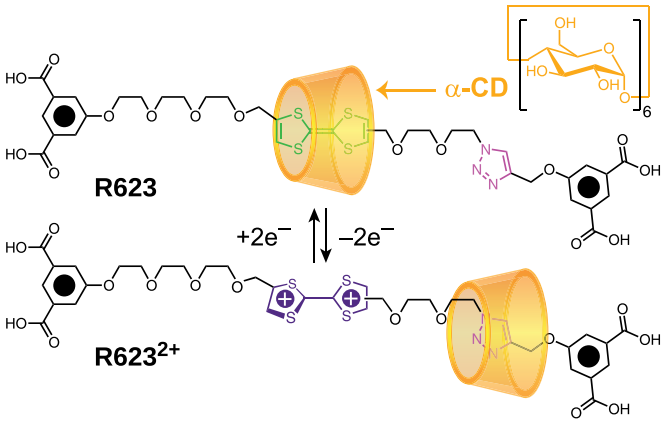


Scheme 6.16 C_{60} Acts as both stopper and recognition site in Mateo-Alonso's[171] electrochemically switchable [2]rotaxane **R622**. A three-electron reduction process causes the benzylic amide ring to shuttle from a glycylglycine recognition site to stabilize the triply anionic C_{60} stopper.

Redox-induced changes in hydrophilicity also underpin[173] the actuation (**Scheme 6.18**) of the bistable [2]rotaxane **R623**. The preferred recognition site for this rotaxane's α-cyclodextrin (α-CD) ring is a redox-active TTF unit, while a triazole unit serves as a secondary recognition site. When the TTF unit is oxidized by chemical or electrochemical means to either the $TTF^{\bullet+}$ radical cation or the TTF^{2+} dication, the ring becomes associated with the triazole unit in **R623²⁺**. The mechanism of this switching motif has been investigated computationally,[174] confirming that solvent-associated hydrophobic and hydrophilic interactions are the main driving forces for redox-induced shuttling. The oxidation of TTF has also been employed as one of two handles for the actuation[79] of a "dual-stimulus" switchable donor-acceptor [2]catenane that operates in water. The second stimulus that can be employed to switch this [2]catenane is the introduction of small-molecule amines, which form charge-transfer adducts between one of the π-accepting recognition units of the cyclophane. This switching motif is featured in the discussion in **Section 6.6.1** covering mechanomolecular switches driven by small-molecule recognition.



Scheme 6.17 Kaifer's[172] CB7-based electrochemically switchable [2]pseudorotaxane. Although the ferrocene units are the favored binding site for CB7 in ***L601***$^{2+}$$\subset$*CB7*, their hydrophilicity can be increased by electrochemical oxidation to ferrocenium (Fc^{+}) ions, causing the rings to favor the central hydrophobic hexamethylene chain in ***L601***$^{4+}$$\subset$*CB7*.



Scheme 6.18 The [2]rotaxane **R623**, comprising an α-CD ring and a dumbbell with a redox-active TTF unit, works as a redox switch in water.[173] Oxidation of TTF to TTF^{2+} increases its hydrophilicity, causing the α-CD ring to relocate onto the triazole unit in **R623²⁺**.

6.2 Photo-Driven Switches

The sun provides us with our most abundant and renewable energy source: light. Light is an excellent power source[175] for molecular machines because it can be introduced with excellent spatial and temporal precision (even in closed systems), over a highly wavelength-tunable range of energies, while generating little to no byproducts. Photoswitchable mechanomolecules have been featured in many literature reviews.[21,176–191] In this Section, photo-driven switches with mechanical bonds are organized according to the different strategies that have been implemented to transduce radiant energy into directed mechanical motion.

6.2.1 Switching Driven by Photoinduced Electron Transfer

Electron transfer (ET) reactions that are fueled by radiant energy (light) are broadly classified under the heading of photoinduced electron transfer (PET). Since electron transfer is, by definition, a redox reaction, many of the electrochemically switchable MIMs discussed in the previous Section can also be actuated photochemically, in principle, by coupling the energy of a light source with PET mechanisms of redox chemistry. PET can be employed to power[192,193] molecular switches and machines, either in short-lived charge-separated states (**Section 6.2.1.1**) or by photosensitization (**Section 6.2.1.2**).

6.2.1.1 Switching in Charge-Separated States

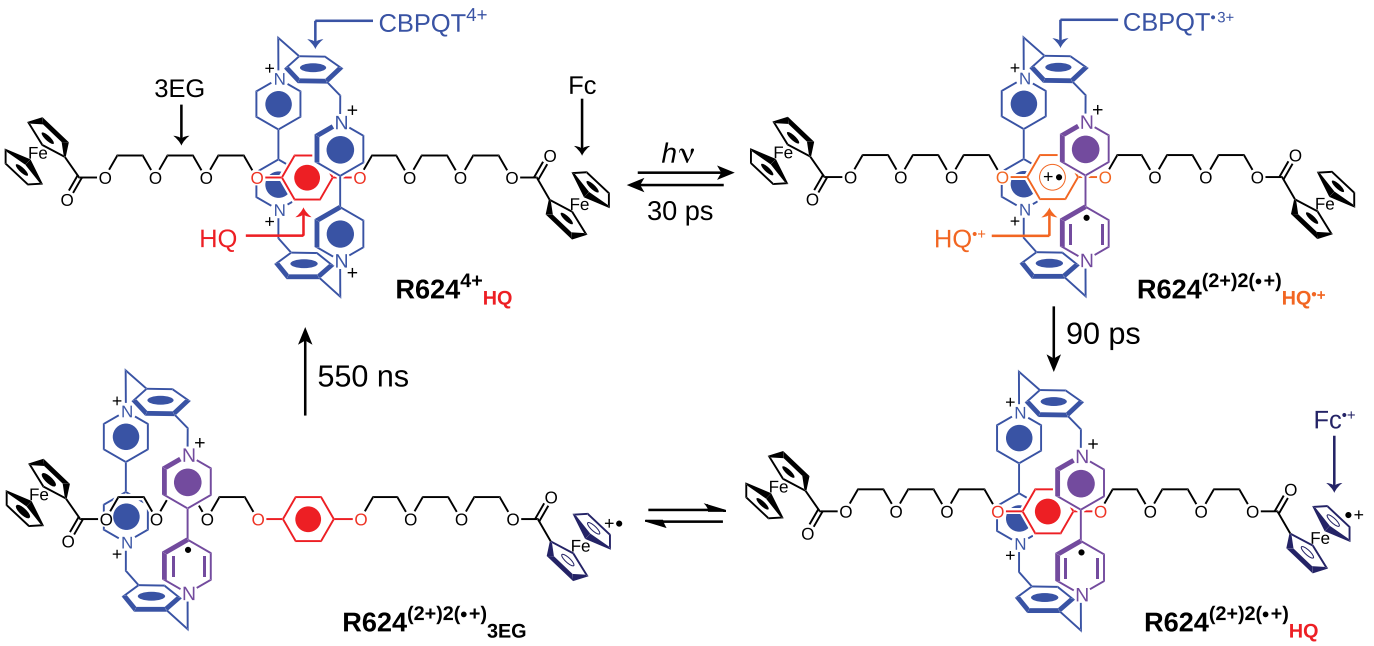
One of the earliest examples (**Scheme 6.19**) of a light-induced molecular switch was an adaptation of donor-acceptor rotaxanes based on a $CBPQT^{4+}$ ring and a HQ recognition site. By employing redox-active Fc groups as stoppers in the rotaxane **R624^{4+}**, Benniston and Harriman[194] demonstrated by transient absorption spectroscopy that laser excitation of the charge transfer complex between the ring and dumbbell components promotes the formation of a radical ion-pair, generating the reduced cyclophane $CBPQT^{\bullet 3+}$ and the oxidized hydroquinone π-radical cation $HQ^{\bullet +}$. With a large thermodynamic driving force for $HQ^{\bullet +}$ to oxidize the Fc stoppers ($\Delta G° = -0.68$ eV), an electron is transferred rapidly (90 ps) from $HQ^{\bullet +}$ to Fc, generating $Fc^{\bullet +}$. This electron transfer proceeds with ~25% efficiency, since the ET reaction competes with the faster (30 ps) charge recombination process. The more spatially charge-separated state **R624$^{(2+)2(\bullet +)}$** lives for over 500 ns, which is potentially enough time for the $CBPQT^{\bullet 3+}$ ring to diffuse away from HQ.

6.2.1.2 Photosensitized Switching

While the short-lived switching of **R624^{4+}** was an important step towards light-controlled mechanical switches, an obvious next step was to develop systems in which the lifetime of each co-conformation could be controlled by experimental inputs instead of the dynamics of recombination in charge-separated states. The answer to this challenge was lurking in the supramolecular literature as early as 1993, when Balzani[195] demonstrated that the $CBPQT^{4+}$ ring can be permanently reduced by a photosensitizer (9-anthracenecarboxylic acid) in the presence of a sacrificial reductant—in this case, triethanolamine (TEOA)—which regenerates the ground state of the photosensitizer and thus prevents back electron transfer (BET). Photo-driven switches that rely on a photosensitizer and a sacrificial electron donor have been designed using donor-acceptor, transition metal, radical–radical, and hydrogen-bonded templates.

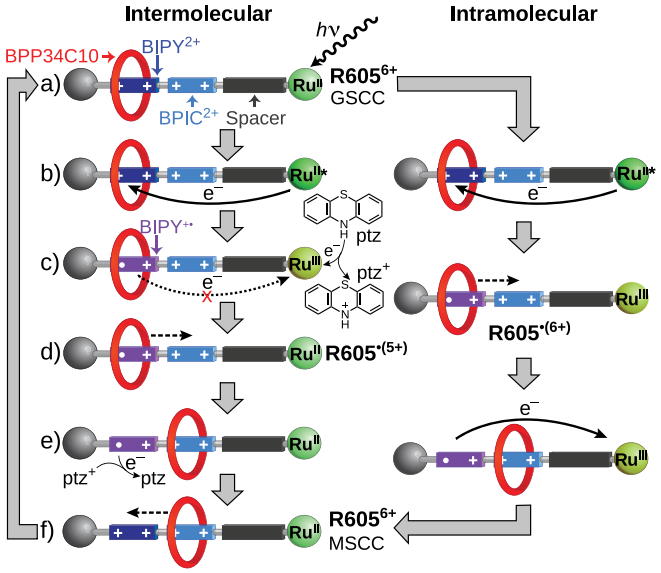
Photosensitization of Donor-Acceptor Switches

Although PET had been exploited to control threading/dethreading in a number of donor-acceptor pseudorotaxane complexes,[43,196–199] it was not implemented in systems with formal mechanical bonds until the bistable rotaxane **R605^{6+}** was introduced[45] in 2000—see **Scheme 6.4** in **Section 6.1.1**. An evolution of this protocol was reported[200] in 2006, when **R605^{6+}** was found to function autonomously. **Scheme 6.20** summarizes the mechanism of an autonomous molecular shuttle fueled by light, which proceeds as follows: (a) visible light ($\lambda = 532$ nm) absorbed by the Ru^{II} stopper generates the long-lived, highly reducing metal-to-ligand charge-transfer (MLCT) excited state, Ru^{II*}, (b) PET from Ru^{II*} to the $BIPY^{2+}$ recognition site generates a $BIPY^{\bullet +}$ radical cation, (c) an electron relay, such as phenothiazine (ptz), reduces the photo-oxidized Ru^{III} center back to Ru^{II}, generating ptz^{+} and the radical cation **R605$^{\bullet 5+}$**, preventing BET, (d) the BPP34C10 ring, given enough time to diffuse, relocates to the $BPIC^{2+}$ unit as a result of its lower affinity for $BIPY^{\bullet +}$, (e) ptz^{+} is reduced by $BIPY^{\bullet +}$, affording the MSCC of **R605^{6+}** before ultimately (f) reverting back to the GSCC, which completes the cycle. This autonomous, molecular photoactuator was found to operate with a quantum efficiency of up to 12%, it can be driven at 1 kHz, and it is stable for at least 10^3



Scheme 6.19 The generation of a radical ion pair by photoexcitation of the Fc-stoppered $CBPQT^{4+}$/HQ [2]rotaxane **R624^{4+}** causes[194] electron transfer from HQ to Fc. The relatively long-lived (500 ns) charge-separated state may allow time for the reduced $CBPQT^{\bullet 3+}$ ring to dissociate temporarily from HQ before charge recombination takes place.

cycles. In the absence of ptz as an electron relay, the macrocycle still shuttles (**Scheme 6.20**, right-hand side) autonomously, albeit with lower efficiency (2%) owing to its higher rate of BET. The intramolecular mechanism is attractive nevertheless, since it is concentration independent—thus, in principle, these shuttles may be operated autonomously even at the single-molecule level.



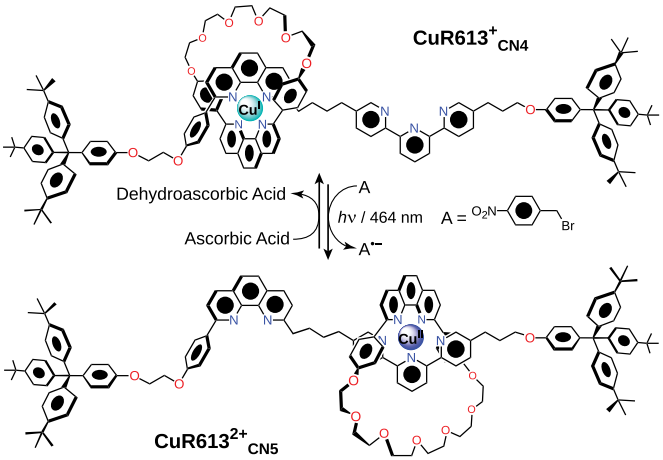
Scheme 6.20 Autonomous shuttling mechanism[200] of the photoswitchable [2]rotaxane **R605**$^{6+}$. For its structural formula, see **Scheme 6.4** (a) Irradiation at 532 nm generates the MLCT excited state in the Ru^{II} stopper. (b) PET from the Ru^{II}* stopper to the BIPY^{2+} unit generates the BIPY$^{\bullet+}$ radical cation. (c) ptz reduces Ru^{III} back to Ru^{II}, preventing back electron transfer from occurring. (d) The BPP34C10 ring diffuses from the BIPY$^{\bullet+}$ to the BPIC^{2+} unit. (e) The BIPY$^{\bullet+}$ radical cation reduces ptz^{+} back to ptz. (f) Diffusion of the ring regenerates the GSCC of **R605**$^{6+}$.

Photosensitization of Switches with Metal Templates

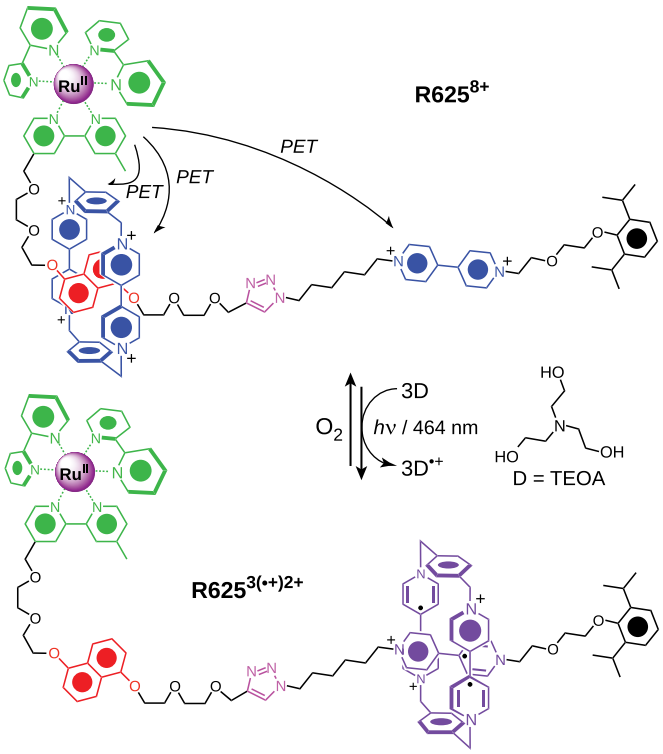
Sauvage's transition-metal MIMs are also amenable to PET-based photoswitching.[149] One way to achieve photoswitching (**Scheme 6.21**) in these systems is by PET from the MLCT excited states of their native coordination centers. In the rotaxane **CuR613**$^{+}_{CN4}$, for example, the tetrahedral Cu^{I} center can be photo-oxidized to Cu^{II} in the presence of *p*-nitrobenzyl bromide as an electron acceptor (A), generating the pentacoordinate rotaxane **CuR613**$^{2+}_{CN5}$ after translation of the ring from the bidentate phen site to the tridentate terpy site.[149] Although it has not often been implemented, this strategy for photoswitching could be applied in principle to most of Sauvage's redox-driven switches—see **Section 6.1.2**.

Photosensitization of Radical–Radical Interactions

The recently introduced[76] generation of switches that utilize π-associated radical–radical interactions for molecular recognition have also been equipped[127] for photoswitchability (**Scheme 6.22**) using a photosensitizer. The



Scheme 6.21 Sauvage's redox-switchable copper-complexed metallo[2]rotaxanes can be actuated[149] with light. In this example, the Cu^{I} center of **CuR613**$^{+}_{CN4}$ is photo-oxidized to Cu^{II} using *p*-nitrobenzyl bromide as a sacrificial electron acceptor (A → A$^{\bullet-}$), causing the expected translation of the Mdpp30 ring to generate **CuR613**$^{2+}_{CN5}$. The Cu^{II} ion is converted back to Cu^{I} with a reductant such as ascorbic acid.

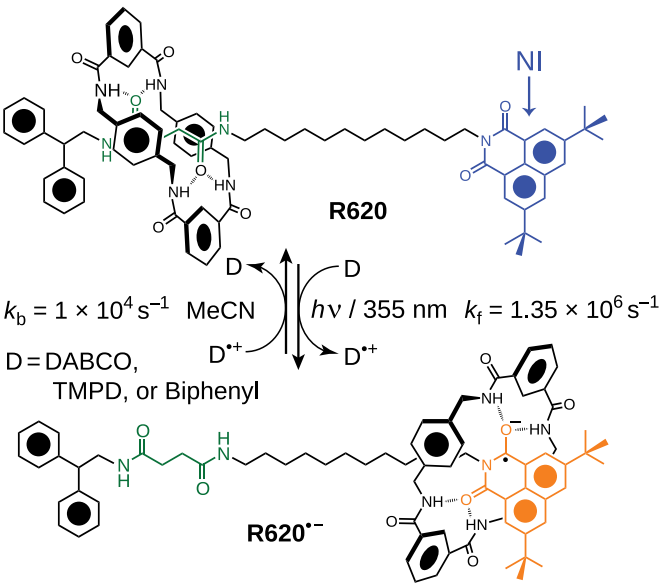


Scheme 6.22 A photoswitchable [2]rotaxane based on a π-associated radical-pairing mechanism.[127] When all three BIPY^{2+} units within the rotaxane are reduced to the corresponding radical cations by PET during photoirradiation of the Ru^{II} stopper in the presence of TEOA as a sacrificial electron donor (D → D$^{\bullet+}$), the ring is no longer stabilized by donor-acceptor interactions with the DNP unit and so shuttles to the BIPY$^{\bullet+}$ radical cation to participate in π-associated radical–radical interactions.

photosensitizing Ru^{II} stopper of the [2]rotaxane **R625**$^{8+}$ can deliver electrons to the $BIPY^{2+}$ units of the ring and dumbbell by PET processes. A sacrificial electron donor such as TEOA is essential in this process because three electrons are required to produce a stable $BIPY^{\bullet+} \subset CBPQT^{2(\bullet+)}$ tris-radical complex, while PET from Ru^{II}* is only a one-electron process. The Ru^{II} photosensitizer is therefore regenerated at least three times by TEOA to complete the switching event, yielding **R625**$^{3(\bullet+)2+}$. Exposing the compound to O_2 in ambient air oxidizes the radicals and returns the rotaxane to its ground state. Recently, a [2]catenanae bearing the same recognition units and a photosensitizing Ru^{II} complex appended to the $CBPQT^{4+}$ ring has been described, the photo-driven circumrotation of which operates according to a similar mechanism.[201]

Photosensitization of Benzylic Amide Switches

The electrochemically switchable benzylic amide MIMs championed by Leigh[164,166,202,203] can also be designed to respond (**Scheme 6.23**) to photochemical stimuli.[204,205] The most well-studied of these MIMs is the bistable [2]rotaxane[164] **R620.** A SA recognition site is encircled predominantly by the benzylic amide ring of **R620**$_{SA}$ in the ground state, while a NI unit serves as a redox/photoactive secondary recognition site. Although the $NI^{\bullet-}$ radical anion can be generated electrochemically—see **Scheme 6.14** in **Section 6.1.3**—it can also be generated photochemically with a 355 nm laser pulse in the presence of an electron donor (D), such as 1,4-diazabicyclo[2.2.2]octane (DABCO), tetramethylphenylenediamine (TMPD), or biphenyl. The laser pulse generates the triplet excited state ^{3}NI* as a result of intersystem crossing from the singlet ^{1}NI*. BET is therefore spin-forbidden (slow), allowing sufficient time for D to reduce the triplet and generate the $D^{\bullet+}$ and $NI^{\bullet-}$ radical ion pairs. Although NI is a poor hydrogen bond acceptor, $NI^{\bullet-}$ is a good hydrogen bond acceptor. Thus, photoreduction of NI causes the ring to shuttle, by random walk,[202] from the succinamide recognition site to the $NI^{\bullet-}$ radical anion as a result of the stronger hydrogen-bonding interactions in the case of the latter. The quantum yield of this process is ~20%. Charge recombination of $D^{\bullet+}$ and $NI^{\bullet-}$ regenerates the ground state with no byproducts.



Scheme 6.23 R620 can be photoreduced with a 355 nm laser pulse in the presence of an electron donor D to control the shuttling of a benzylic amide ring between a succinamide recognition site in the ground state and a $NI^{\bullet-}$ radical anion after excitation. Charge recombination between $D^{\bullet+}$ and $NI^{\bullet-}$ reinstates the ground state on a fast (~100 ms) timescale.[164]

The rates of mechanical shuttling in **R620** are remarkably high. The rate (k_f) of the forward process (**R620** → **R620**$^{\bullet-}$) is on the order of $10^6\ s^{-1}$, while the rate (k_b) of the backward shuttling (**R620**$^{\bullet-}$ → **R620**) is on the order of $10^4\ s^{-1}$. These rates mean that the switch can be cycled up to 10^4 times per second, corresponding to a power output of up to ~10^{-15} W per molecule. This rotaxane's shuttling rates[206] in more viscous environments are summarized in **Section 6.14.2.2**. Leigh[207] has recently found that water "lubricates" the shuttling process in his hydrogen bonded molecular shuttles, increasing shuttling rates by more than threefold in 5% v/v D_2O in MeCN. The rate enhancements most likely result from water's ability to form miniature hydrogen bonding networks locally around the molecular switches' mobile component parts.

6.2.2 Switching Driven by Photoisomerization

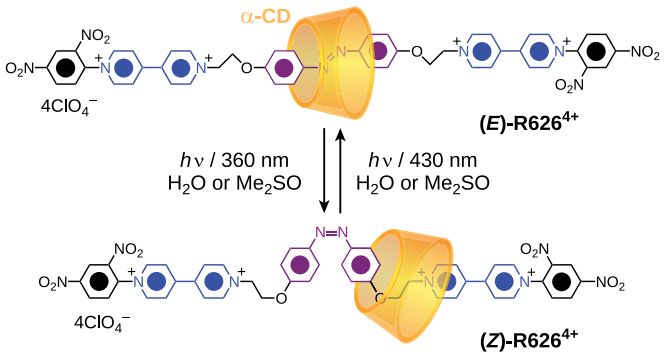
The photoswitchable MIMs discussed in the previous Section use light to initiate redox processes that drive switching, and are thus an extension of the electrochemical switches discussed in **Section 6.1.1**. A fundamentally different strategy for switching molecules with light is to use photoisomerizations that change the local steric and/or electronic environment in order to drive mechanical motion. The most popular components in these types of switches have been azobenzene (**Section 6.2.2.1**), stilbene (**Section 6.2.2.2**), and fumaramide (FA) units (**Section 6.2.2.3**), which undergo *cis-trans* (*E*/*Z*) photoisomerization about a central double bond, while spiropyran (**Section 6.2.2.4**) is another photoisomerizable unit that can be employed to drive shuttling. Azobenzene and stilbene derivatives form pseudorotaxanes with several types of hosts, including cyclodextrins,[208,209] cucurbiturils,[210,211] pillararenes,[212,213] and the $CBPQT^{4+}$ ring,[214,215] usually binding with much greater affinity as the *trans* isomers than as the *cis* isomers. MIMs that have exploited the photoswitchable binding properties of azobenzene and stilbene have been based primarily on cyclodextrins, while fumaramide and spiropyran have been primarily in the design of photoswitchable benzylic amide MIMs.

6.2.2.1 Mechanically Bonded Azobenzene Switches

The first example of a rotaxane in which the shuttling of the ring component was controlled by photoisomerization was reported by Nakashima,[216,217] who designed α-CD-based rotaxanes comprising photoactive azobenzene units

with dinitrobenzene-capped viologen units as stoppers, which function (**Scheme 6.24**) in both water and Me_2SO. The α-CD ring, which encircles the *trans*-azobenzene unit in **(*E*)-R626^{4+}**, moves toward one of the stoppers with a rate constant $k = 2.3 \times 10^{-4}$ s^{-1} at 30 °C when irradiated with UV light (360 nm) in order to avoid the more sterically demanding azobenzene unit in **(*Z*)-R626^{4+}**, which is populated in a ratio of up to 74%. The process is completely reversible—the (*E*)-isomer is regenerated using visible (430 nm) light and the rotaxane can be cycled several times without performance degradation.

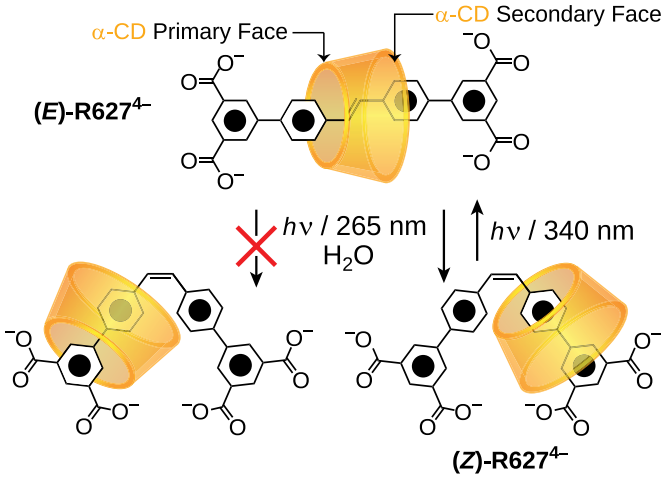
Other CD-based rotaxanes that utilize azobenzene photoisomerization to induce ring translocation have been reported by the groups of Harada,[218,219] Easton,[220] Zhao,[221–223] Tian,[224–228] Tsolomitis.[229] and Winnik.[230] Stang[231] has described a photoreversible [3]catenane in which a pair of β-CD rings interlock with and escape from a central metallacycle bridged by dynamic Pd–N bonds as a result of the photocontrolled *trans* and *cis* isomerism, respectively, of its azobenzene recognition units. See **Section 6.13.1.1** for examples of photoswitchable daisy chain rotaxanes based on azobenzene.



Scheme 6.24 Nakashima[216,217] introduced the concept of using photoisomerization to displace the ring of a rotaxane with **(*E*/*Z*)-R626^{4+}**. The α-CD ring, which encircles the (*E*)-isomer of the dumbbell's central azobenzene unit, moves preferentially toward one of the viologen units at the periphery after photoisomerization to the (*Z*)-isomer.

6.2.2.2 Mechanically Bonded Stilbene Switches

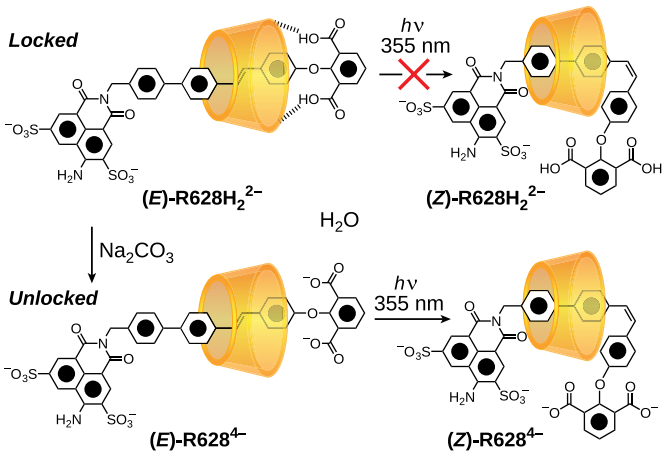
Anderson[232] has exploited the asymmetric, conical shape of cyclodextrin and the photoinduced *cis-trans* isomerization of stilbene to translate (**Scheme 6.25**) a ring 'unidirectionally' (or mechanostereoselectively—see **Section 6.15.2.2**) along a symmetrical dumbbell. Rotaxane **(*E*)-R627^{4-}** comprises an α-CD ring encircling a photoactive *trans*-stilbene unit in the dumbbell, which is stoppered by isophthalate end-groups. The photoisomerization of stilbene occurs with a quantum yield of 0.06. In the photostationary state, the *cis* isomer, **(*Z*)-R627^{4-}**, in which the secondary face of α-CD interacts with the stopper, is populated exclusively. This conclusion was drawn from ^{1}H NMR nuclear Overhauser effect (NOE) data, since through-space interactions between the cyclodextrin's internal protons were observed on



Scheme 6.25 The α-CD ring of rotaxane **R627^{4-}** experiences mechanostereoselective translation[232] when the stilbene unit undergoes (*E*) → (*Z*) photoisomerization as a result of the asymmetrical conical shape of the α-CD ring.

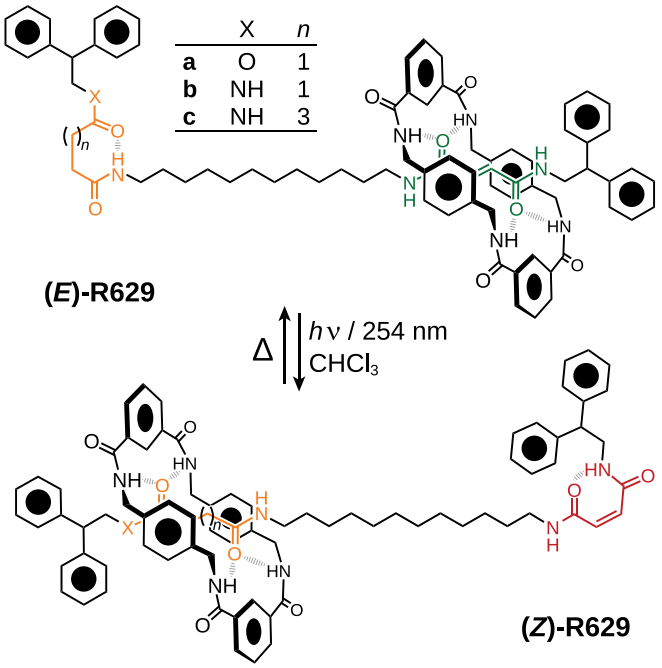
only one side of the dumbbell. While this selective shuttling must be attributed to the facial asymmetry of α-CD, it remains unclear why only one of two possible orientational isomers is populated.

Tian[233] has reported a photoswitchable rotaxane **(*E*)-R628^{2-}** which utilizes a similar stilbene/α-CD motif to Anderson's **R627^{4-}**, but adds on a locking mechanism (**Scheme 6.26**) based on hydrogen bonds. Although its dumbbell does not have palindromic symmetry, **R628^{2-}** is obtained as only one of two possible orientational isomers—see **Section 5.2.1**—in which the secondary face of α-CD is nearest to the isophthalic acid stopper. The primary face is positioned beside a biphenyl unit connected to a 4-amino-3,6-disulfonic-1,8-naphthalimide stopper. The lower pK_a of the sulfonic acid sites, with respect to the



Scheme 6.26 The isophthalic acid stopper in Tian's[233] photoswitchable rotaxane **R628H$_2^{2-}$** acts as a 'molecular lock', since (*E*) → (*Z*) photoisomerization of the α-CD-encircled stilbene unit is forbidden at neutral pH when it is protonated (**R628H$_2^{2-}$**) and allowed after it becomes ionized at high pH (**R628^{4-}**).

carboxylic acids of the isophthalic stopper, allows the latter to be protonated and deprotonated without affecting the charge of the sulfonates, thus maintaining water solubility and enabling the locking mechanism. At neutral pH, no photoisomerization is observed in **(*E*)-R628**$^{2-}$ even after 1 h of irradiation at 335 nm. **(*Z*)-R628**$^{2-}$ cannot be accessed because strong hydrogen bonds between the secondary face of α-CD and the isophthalic acid stopper prevent dissociation. At pH 10.5, however, the isophthalate stopper is deprotonated to give the tetraanionic **R628**$^{4-}$ and the hydrogen-bonded "lock" is opened. With (*E*/*Z*) photoisomerization now being allowed, the ring shuttles toward the naphthalene-based stopper and onto the biphenyl unit under irradiation, and the (*Z*)-isomer **(*Z*)-R628**$^{4-}$ represents 63% of the population in the photostationary state. The population of **(*Z*)-R628**$^{4-}$ is accompanied by a proportional enhancement in the compound's fluorescence signal intensity, providing a convenient output signal for observing the switching event. Rotaxanes of this type have evolved into switches that are capable of performing logic operations—see refs. 189, 224, 233–235 and **Section 6.15.1.3**. Cyclodextrin rotaxanes driven by the photoisomerization of stilbene have also been described by Easton,[220,236] including one of the daisy chains described in **Section 6.13.1.1**.



Scheme 6.27 A fumaramide unit acts as the primary binding site for a the benzylic amide ring in **(*E*)-R629a–c**, but its conversion to maleamide as a result of (*E*) → (*Z*) photoisomerization causes the ring to prefer a saturated secondary recognition site in **(*Z*)-R629a–c**.[238]

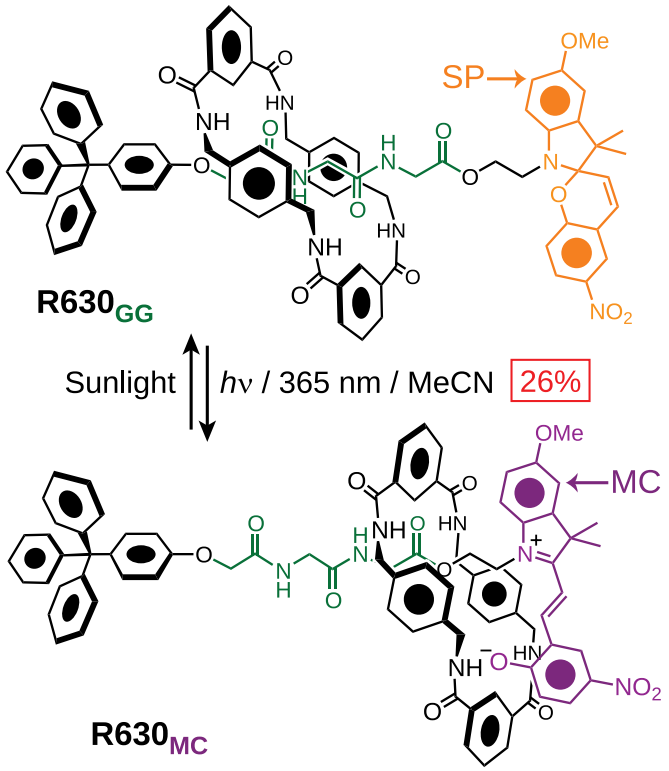
6.2.2.3 Mechanically Bonded Fumaramide Switches

While the α-CD-based rotaxanes have been fruitful photochemical switches in the hands of talented researchers, Leigh has also generated a number of impressive photoswitchable MIMs based on benzylic amide rings. The workhorse of this research[237] has been the fumaramide (FA) unit. Fumaramide contains a *trans*-olefin at its core, which can be photoisomerized with 254 nm light to give a *cis*-olefin unit known as maleamide (MA). Fumaramide was first introduced[238] in the photoswitchable (**Scheme 6.27**) rotaxanes **R629a-c** in 2003. The occupancy of the FA recognition site by the ring is >95%—the detection limit of ^{1}H NMR spectroscopy—in the ground state of **(*E*)-R629** even at room temperature, despite the similarity of the hydrogen-bonding motifs between the two recognition sites. This positional selectivity is particularly striking for **R629b**, since its two recognition sites differ only in the saturation of their two central carbon atoms. Although the population of (*Z*)-isomers reaches only 40-50% in the photostationary state, the positional discrimination of the ring in **(*Z*)-R629** is likewise highly biased, populating the secondary binding site with >95% selectivity in **(*Z*)-R629a-b** and 85% selectivity in **(*Z*)-R629c**. This pronounced positional discrimination is influenced by the ability of each recognition site to hydrogen bond in an intramolecular fashion, as depicted in **Scheme 6.27**, when the ring is absent.

Leigh has elaborated the fumaramide-based photoswitchable MIMs to demonstrate a number of important concepts. For example, a chiroptical switch has been prepared[239] in which the secondary recognition site for the benzylic amide ring is a chiral peptide sequence. A strong induced circular dichroism response is observed only under the application of a radiant stimulus, which generates the maleamide isomer of the primary recognition site and causes the ring to encircle the chiral peptide. In another case,[240] by making a few modifications to the design of **R629**—i.e., the installation of pyridinium groups in the benzylic amide ring and a fluorescent anthracene stopper on the dumbbell—a light-responsive fluorescent switch with an ON/OFF ratio of 85:1 has been generated. An ingenious adaptation[241] of this system has been adsorbed on surfaces that can move droplets under irradiation by virtue of their ability to change the surface energy with their mechanical motion—see **Figure 1.35** in **Section 1.3.6**, as well as the discussion in **Section 6.14.2.1**. Li[242] has also constructed a bistable [2]rotaxane based on the fumaramide/benzylic amide motif in which the ring's photodriven motion influences the energy transfer and fluorescence properties of the compound. The isomerizable fumaramide unit has also been a critical component of the MIMs that appear in a number of landmark articles[240,243–246] from the Leigh group that deal with molecular ratchets, motors, and machines—see **Section 6.15**.

6.2.2.4 Mechanically Bonded Spiropyran Switches

A unique use of photoisomerization which does *not* rely on steric effects to initiate mechanical motion has been used by Li[247] to control (**Scheme 6.28**) a rotaxane shuttle.



Scheme 6.28 The photoactive stopper in the rotaxane **R630** takes the form[247] of either a neutral spiropyran (SP) isomer or, under UV irradiation, a zwitterionic merocyanine (MC) isomer. The benzylic amide ring encircles predominantly the glycylglycine recognition site when the stopper is in the SP form, but prefers to be close to the stopper in order to stabilize the anionic site in the MC isomer.

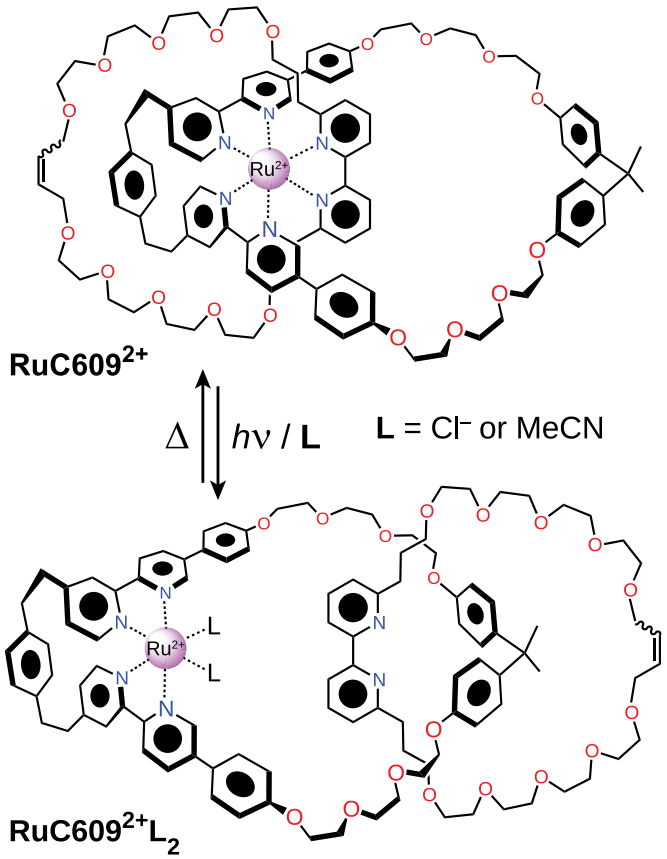
In the rotaxane **R630**, the hydrogen-bonded benzylic amide ring popularized by Leigh encircles a dumbbell with a glycylglycine dipeptide recognition unit and a spiropyran (SP) stopper. SP can be photoisomerized to the zwitterionic version known as merocyanine (MC) with UV light, and returned back to the charge-neutral SP unit with visible light. While the ring prefers the dipeptide recognition site in **R630$_{GG}$**, it shuttles away from this site in order to interact with the MC stopper after photoisomerization to **R630$_{MC}$**. Although the MC isomer represents only 26% of the molecular population in the photostationary state, the movement of the ring to the stopper is essentially quantitative within this minority species.

6.2.3 Switching in a Dissociative Excited State

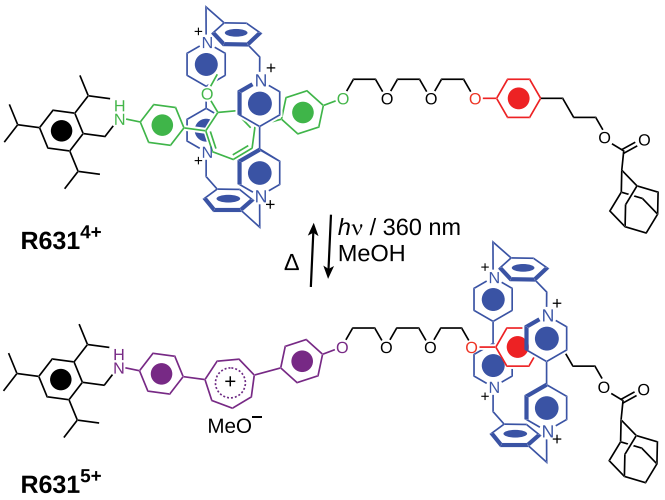
Sauvage[248–252] and Collin[248–251,253] devised a unique strategy for photoswitching mechanomolecules based on Ru^{II} transition metal templates by a photoexpulsion process[254] in which the formation of a dissociative ligand-field excited state induces mechanical motion. Upon irradiation of the photoactive Ru^{II} center of the [2]catenate[252] **RuC609^{2+}** with light ($\lambda > 300$ nm), the absorption maximum of the solution changes from red ($\lambda_{max} = 458$ nm) to purple ($\lambda_{max} = 561$ nm) as a result of the circumrotation (**Scheme 6.29**) of the smaller bidentate ring, which opens up two coordination sites to generate **RuC609^{2+}L$_2$**, where L (Cl$^-$ or MeCN) is a replacement ligand on Ru^{II}. This switching event is estimated to occur with >95% efficiency and is thermally reversible. The Strasbourg group has prepared homologous [2]rotaxanes—see compound **RuR234^{2+}** in **Section 2.3.2.3**—which switch according to a similar mechanism.[249,250]

6.2.4 Switching Driven by Photochemical Reactions

The final type of photochemical switching paradigm was pioneered by Abraham,[255–259] who has used photochemical heterolysis to control mechanical actuation in rotaxanes of the donor-acceptor variety. The first demonstration[255,256] of this concept took the form of rotaxane **R631OMe^{4+}**, the components of which are a CBPQT^{4+} ring and a dumbbell comprised of a photoreactive triarylcycloheptatriene unit and an inert, weakly-binding phenolic ring as the secondary recognition site. Irradiation at 360 nm causes (**Scheme 6.30**) a photoheterolysis reaction to take place, cleaving the OMe group and aromatizing the heptatriene ring. Since the photogenerated tropylium ion is cationic, the CBPQT^{4+} ring is repelled from it by electrostatic forces and so shuttles to the

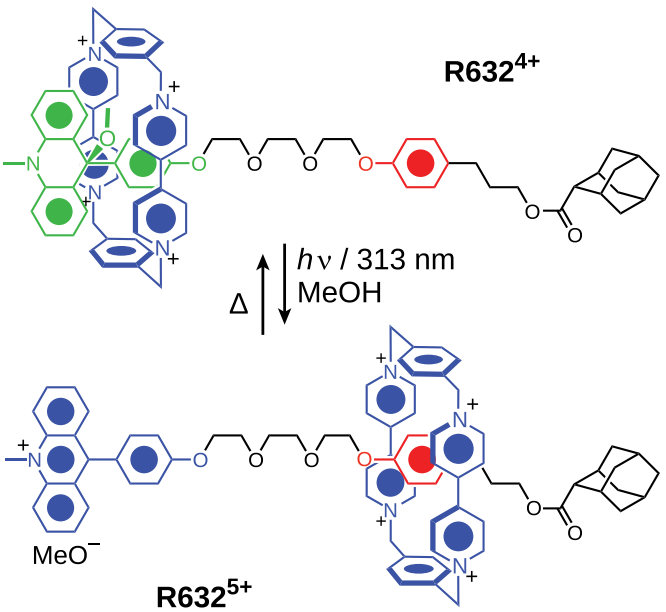


Scheme 6.29 Sauvage's[252] photoswitchable [2]catenane **C609^{2+}**, in which circumrotation is initiated by photoexcitation of the Ru^{II} center, which causes the bidentate ring to dissociate and be replaced by either Cl$^-$ or MeCN ligands.



Scheme 6.30 A ring-aromatizing photoheterolysis[255,256] which generates a tropylium methoxide ion pair from a methoxy-substituted cycloheptatriene unit, causes the CBPQT^{4+} ring to shuttle from its favored recognition site on the triene in **R631OMe^{4+}** to the recognition site in **R631^{5+}** as a result of electrostatic repulsion.

phenolic ring at the other end of the dumbbellin **R631^{5+}**. The photoheterolysis is thermally reversible and can be cycled repeatedly. Compound **R632OMe^{4+}** represents a second generation[257–259] of rotaxanes which operate (**Scheme 6.31**) under exactly the same regime. In this case, the photoheterolyzable unit is an acridane moiety, which also serves as a stopper on account of its steric bulk. Although the acridane unit is encircled preferentially (80%) by the ring under normal conditions, photoheterolysis under 360 nm light generates the cationic acridinium species and so causes the



Scheme 6.31 An acridane unit serves[257–259] as both a recognition site and as a stopper in **R632^{4+}**. Reversible photoheterolysis to the acridinium cation induces the movement of the CBPQT^{4+} ring to the phenolic recognition site.

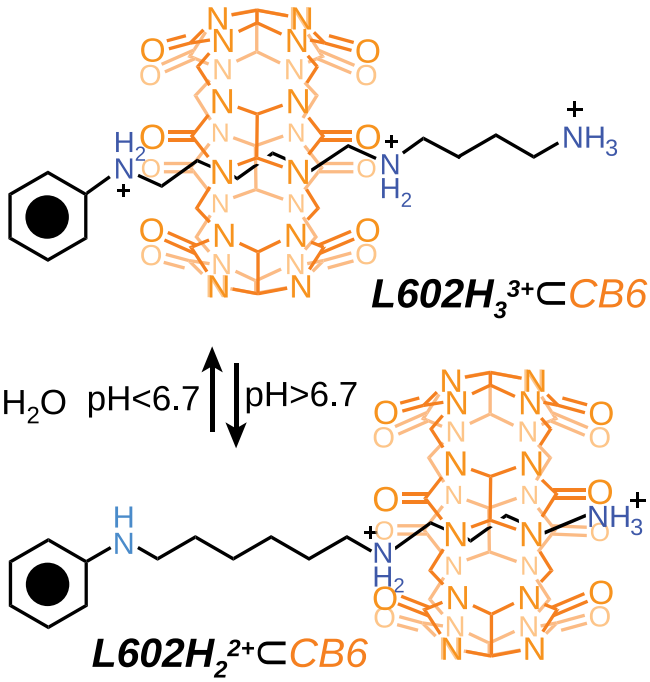
CBPQT^{4+} ring to relocate to the phenolic unit in **R632^{5+}**. This clever use of photochemistry to drive mechanical motion deserves more consideration in the future.

6.3 Acid/Base-Driven Switches

Controlling co-conformational (translational) isomerism using acid-base chemistry as a stimulus typically involves the addition or removal of protons at one or more sites in a molecule, leading to changes in local hydrogen-bonding and/or electrostatic interactions and ultimately results in mechanical movement. This strategy has been realized in many types of MIMs and related systems, including those that rely primarily on hydrophobic interactions (**Section 6.3.1**), π-associated donor-acceptor interactions (**Section 6.3.2**), hydrogen-bonding interactions (**Section 6.3.3**), and coordination bonds (**Section 6.3.4**).

6.3.1 pH Switching Driven by Hydrophobic Effects

Mock[260] was the pioneer who demonstrated in 1990 that pH could be used to control (**Scheme 6.32**) the position of

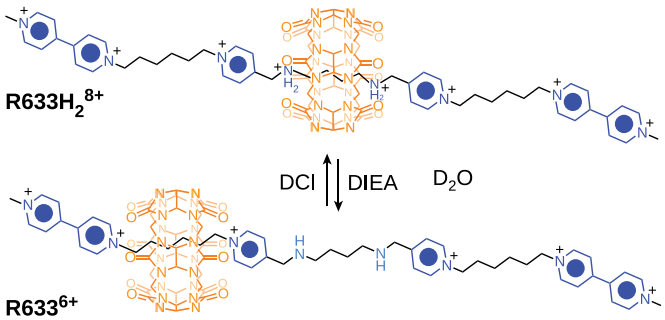


Scheme 6.32 Mock's pH-switchable pseudorotaxane.[260] A CB6 ring encircles the anilinium-terminated hexamethylene chain of the **L602H$_3^{3+}$** guest at low pH. Above pH 6.7, selective deprotonation of the anilinium ion causes the CB6 ring to encircle the adjacent butane-1,4-diammonium site of **L602H$_2^{2+}$**.

a ring along an axle. The cucurbit[6]uril (CB6)-based pseudorotaxane ***L602H$_3^{3+}$⊂CB6*** has a guest with three different ammonium groups—butane-1,4-diammonium dications on one end of the thread and an adjacent hexamethylene chain terminated by an anilinium cation on the other end. The –C_4H_8– and –C_6H_{12}– recognition sites thus share a

central $-NH_2^+-$ ion at the center of the dumbbell, but are terminated by cationic endgroups with different pK_a values. The key to this design lies in the lower pK_a of anilinium ions with respect to alkylammonium ions, as well as the fact that the butane-1,4-diammonium dication binds CB6 more weakly (~$10^5\,M^{-1}$) than does hexane-1,6-diammonium (~$10^6\,M^{-1}$) in water. Thus, when all three of the amines of the **L602H$_3^{3+}$** guest are protonated at low pH, the CB6 ring encircles the hexamethylene chain. When the anilinium unit becomes selectively deprotonated around pH 6.7, however, the CB6 ring encircles the tetramethylene chain of **L602H$_2^{2+}$** instead, where it can remain surrounded on both of its portals by ammonium ions.

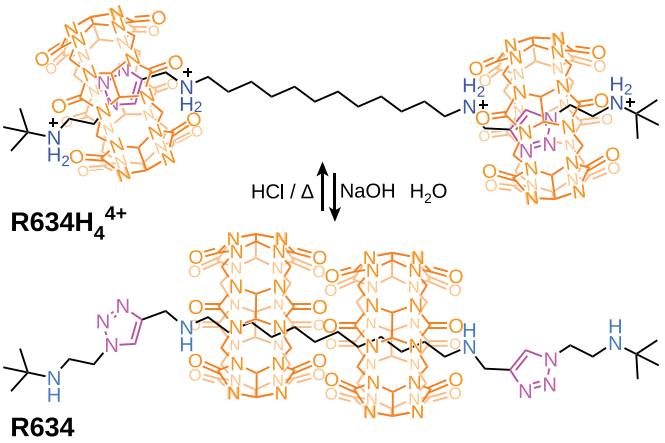
It was not until about a decade later that more examples of cucurbituril acid-base actuation motifs, reminiscent of Mock's pH-switchable pseudorotaxane, began to appear. Kimoon Kim[261,262] was among the next generation of pioneers who have developed MIMs and molecular switches based on cucurbituril, yet it should be added that examples[263,264] of pH-switchable rotaxanes of this variety are still few and far between. Kim's first entry[263] into this area simply involved replacing the anilinium unit of **L602H$_3^{3+}$** with a fluorenyl unit as a fluorescence signaling domain, since it can report the position of the CB6 ring in the form of fluorescence emission. Shortly thereafter, pH-switching was demonstrated[264] in a new molecular design involving a CB6 rotaxane with electrostatic BIPY^{2+} stoppers. The acid-base actuation between **R633H$_2^{8+}$** and **R633^{6+}** is depicted in **Scheme 6.33**.



Scheme 6.33 The CB6 ring in Kim's[264] electrostatically stoppered pH-switchable [2]rotaxane moves from the central butanediammonium site of **R633H$_2^{8+}$** to one of the peripheral bis(pyridinium) hexane units in **R633^{6+}**, which is generated by raising the pH with diisopropylethylamine (DIEA). The CB6 ring can be returned to the central unit by restoring a low pH with acid in D_2O.

Although hexamethylene diamines bind CB6 more strongly than tetramethylene diamines, the CB6 ring of **R633H$_2^{8+}$** still favors the central tetramethylene chain over the peripheral hexamethylene chain because it can participate in stronger hydrogen-bonding interactions with the ammonium groups of the former. The CB6 ring moves to one of the pyridinium-flanked hexamethylene chains, however, when the ammonium groups are deprotonated in **R633^{6+}**.

Although a few other CB6-based pseudorotaxane switches have subsequently appeared,[265–267] the only



Scheme 6.34 Tuncel's pH-switchable palindromic [3]rotaxane.[269,270] Although the CB6 rings reside near the dumbbell's termini in the tetracationic **R634H$_4^{4+}$**, both rings move to the central hydrocarbon chain of **R634** upon neutralization of the dialkylammonium centers with NaOH. This process can be reversed with hydrochloric acid, while recognizing that a substantial activation barrier demands the application of heat to achieve shuttling on a reasonable timescale.

CB-based rotaxanes to exhibit pH-controlled mechanical shuttling, to our knowledge, are those reported by Tuncel.[268–270] In one example (**Scheme 6.34**) of her work, the [3]rotaxane[269,270] **R634H$_4^{4+}$** carries two CB[6] rings, each encircling triazole-bis(ammonium) units near the termini of the ^{t}Bu-stoppered symmetrical dumbbell. When the ammonium groups are neutralized with aqueous NaOH, the rings of **R634** relocate (**Scheme 6.34**) to the more hydrophobic dodecamethylene spacer at the dumbbell's core. A substantial activation barrier accompanies the reverse process (**R634** → **R634H$_4^{4+}$**), since the rings return very slowly to the triazole units after the amines have been reprotonated with HCl. By assessing the rate of repopulation using ^{1}H NMR spectroscopy, an activation barrier for this process was determined to be 23.9 kcal · mol^{-1} at room temperature. A tetrapodal [5]rotaxane[268] based on a similar actuation motif is described in **Section 6.13.3.1**.

Yui[271–273] has described polyrotaxanes in which pH controls (**Figure 6.9**) the localization of derivatized α-CD rings

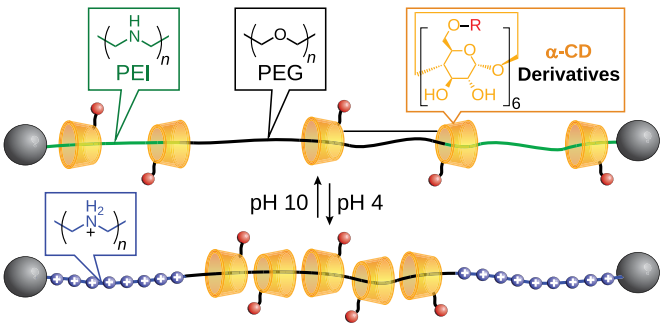


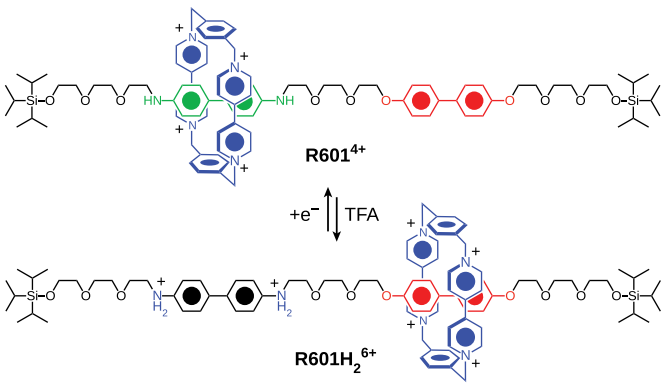
Figure 6.9 Graphical representation of polyrotaxanes in which the pH-controlled protonation and deprotonation of PEI blocks controls the localization of α-CD derivatives on the axle.

onto different sections of a block copolymer axle comprising poly(ethylene imine) (PEI) and poly(ethylene glycol) (PEG). At high pH, the rings translate freely along the entire length of a dumbbell's PEI-*block*-PEG-*block*-PEI axle, whereas the rings are localized to the PEG block at low pH when the PEI blocks are rendered cationic by protonation of the amines. More recently, Brochon and Hadziioannou[274] have extended this pH switching concept to pH switchable cross-linked sliding gel networks based on α-CD.

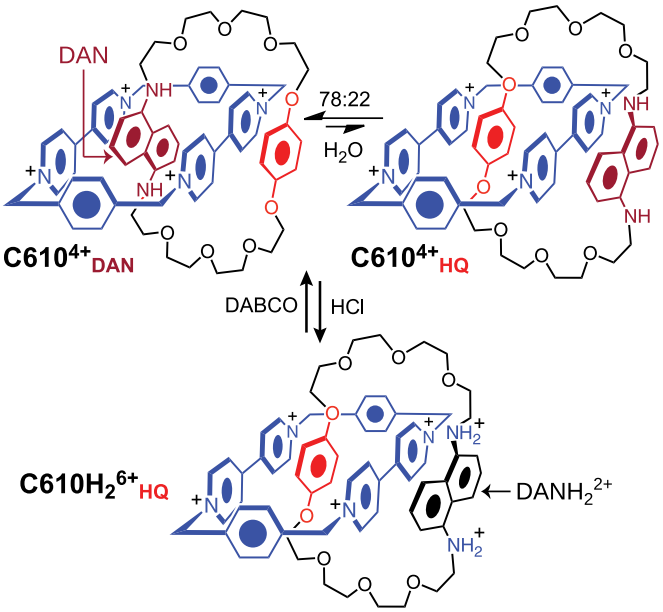
6.3.2 pH Switching Driven by Electrostatic Repulsion

pH-Controlled shuttling (**Scheme 6.35**) in donor-acceptor MIMs was introduced[35] concurrently (**Section 6.1.1**) with the first electrochemically switchable rotaxane **R601**$^{4+}$. Whereas the benzidine radical cation of **R601**$^{\bullet 5+}$ generates a repulsive Coulombic force that pushes the CBPQT^{4+} ring over to the alternative HQ unit under redox control, the doubly-charged benzidinium ion of **R601H$_2$**$^{6+}$, which is generated by protonation of the nitrogen atoms with trifluoroacetic acid (TFA), creates a similar repulsive interaction that drives translational isomerization. **R601**$^{4+}$ is therefore switchable by both redox and pH stimuli.

Although acid-base switchable MIMs were realized at an early stage, pH has been exercised as a stimulus for donor-acceptor MIMs much less often than redox chemistry. Most of the switches that fall into this category have appeared relatively recently. One such example[275] is the donor-acceptor [2]catenane **C610**$^{4+}$, which operates (**Scheme 6.36**) in water by virtue of the hydrophilicity of the CBPQT^{4+} cyclophane as its chloride salt. Two co-conformational isomers, **C610**$^{4+}_{DAN}$ and **C610**$^{4+}_{HQ}$, exist at equilibrium ($K_{eq} \approx 4$) in water, in which the CBPQT^{4+} ring encircles diaminonaphthalene (DAN) and HQ recognition units, respectively. Protonation of the amino groups in the DAN unit at low pH results in the formation of **C610H$_2$**$^{6+}_{HQ}$ as a single isomer, where the HQ unit is encircled exclusively as a result of Coulombic repulsion between DANH$_2^{2+}$ and the CBPQT^{4+} ring. The 78:22 distribution of DAN and HQ isomers in **C610**$^{4+}$ can be restored by returning to higher pH using DABCO as base, an actuation process which can be cycled



Scheme 6.35 The first pH-switchable rotaxane[35] based on π-associated donor-acceptor interactions.

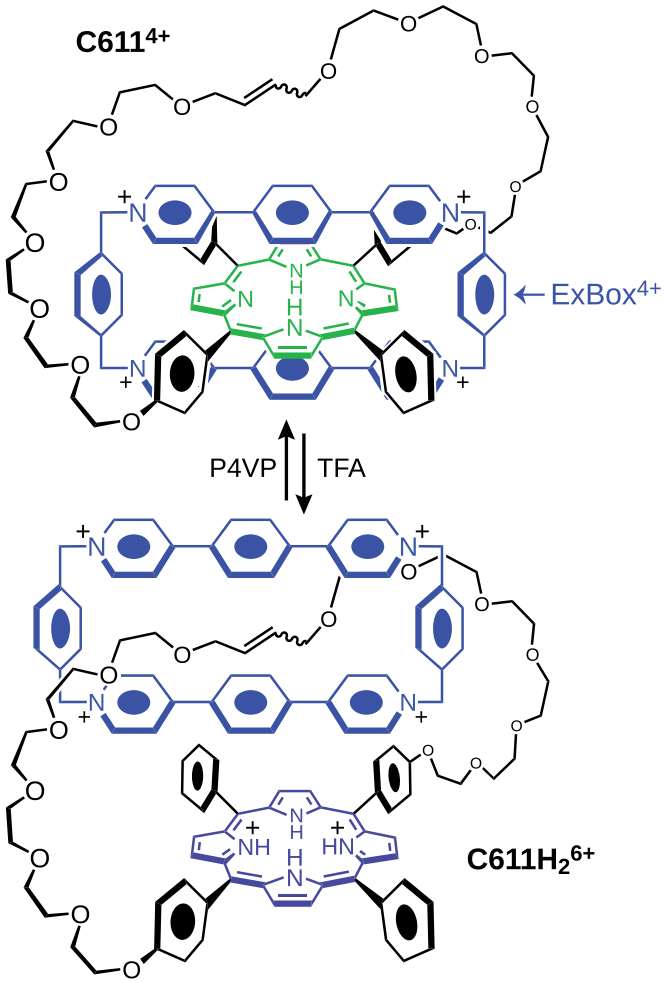


Scheme 6.36 A donor-acceptor [2]catenane which is actuated with acid/base in water.[275] The DAN and HQ units of a crown ether ring (red) compete for the cavity of the CBPQT^{4+} ring in **C610**$^{4+}$. At low pH, only HQ resides in the CBPQT^{4+} ring's cavity in **C610H$_2$**$^{6+}$ on account of repulsive Coulombic interactions introduced by deprotonation of the nitrogen atoms in DAN.

at least five times with high reproducibility. All three of the catenanes were isolated and characterized by single-crystal X-ray structural analysis. Interestingly, **C610**$^{4+}_{DAN}$ and **C610**$^{4+}_{HQ}$ co-crystallize in a 32:68 ratio, respectively, which deviates heavily from their equilibrium distribution in solution.

A π-donor/π-acceptor [2]catenane has been created[276] based on the ExBox^{4+} series[277–279] of extended tetracationic cyclophanes. The acid-base actuation (**Scheme 6.37**) of **C611**$^{4+}$ relies on the protonation and deprotonation, respectively, of a porphyrin unit, which serves as the only recognition site for the ExBox^{4+} ring. Thus, the porphyrin unit is held within the cavity of ExBox^{4+}, stabilized by π-associated donor-acceptor interactions, until enough TFA is added to protonate two of its pyrrole units, at which point the crown ether circumrotates to minimize the repulsive interactions between positive charges. The porphyrin is returned to the ExBox^{4+} cavity by deprotonation with a cross-linked poly-4-vinylpyridine (P4VP) polymer as the base. This catenane is considered to be a "push-button" switch—see **Section 6.1.1**—since the olefin-polyether chain that displaces the porphyrin in **C611H$_2$**$^{6+}$ has essentially no association, to all intents and purposes, with the cyclophane. The ExBox^{4+} ring of **C611**$^{4+}$ can also be reduced electrochemically, affording a freely spinning catenane with no well-defined co-conformation.

Prior to the ExBox^{4+} pH switch, Rowan and Nolte[280] have reported a series of acid-base switchable [2]catenanes and [2]rotaxanes based on the viologen/porphyrin basket motif—see **Section 2.3.3.6**—which are also driven by repulsive electrostatic interactions involving the protonated porphyrin



Scheme 6.37 A pH-switchable ExBox^{4+} push-button [2]catenane[276] **C611**$^{4+}$. Ring circumrotation is caused by pH-triggered double protonation of the crown ether's porphyrin unit to generate **C611H$_2^{6+}$**.

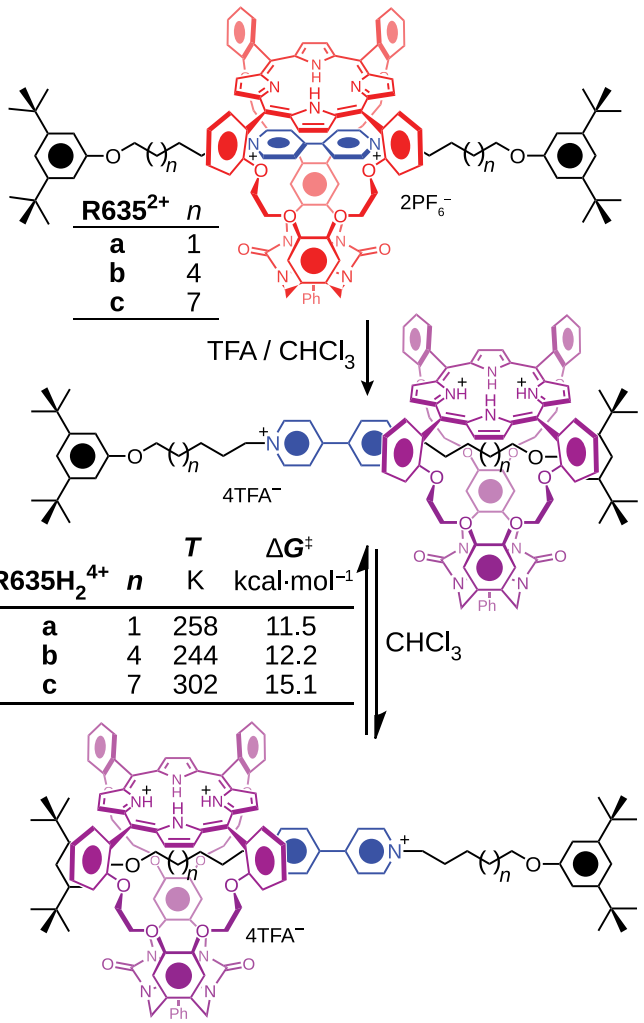
center. The pH-controlled shuttling (**Scheme 6.38**) of the [2]rotaxanes **R635a**$^{2+}$**–R635c**$^{2+}$ involves displacing the porphyrin basket from an ensconced viologen unit by protonation of the porphyrinic pyrroles with TFA. The protonated [2]rotaxanes **R635H$_2$a**$^{4+}$**–R635H$_2$c**$^{4+}$ behave as molecular shuttles, in which the dicationic porphyrin basket shuttles back and forth over the viologen unit between the oligomethylene linkers of the dumbbell, with an activation barrier that depends on the length of the linker. The activation barriers range from 11.5 kcal · mol^{-1} (at 258 K) with a relatively short linker (**R635H$_2$a**$^{4+}$) to 15.1 kcal · mol^{-1} (at 302 K) for a relatively long linker (**R635H$_2$c**$^{4+}$) in $CHCl_3$. A [2]catenane based on the same chemistry expresses similar switching behavior and activation barriers.[280]

6.3.3 pH Switching Driven by Hydrogen Bonding

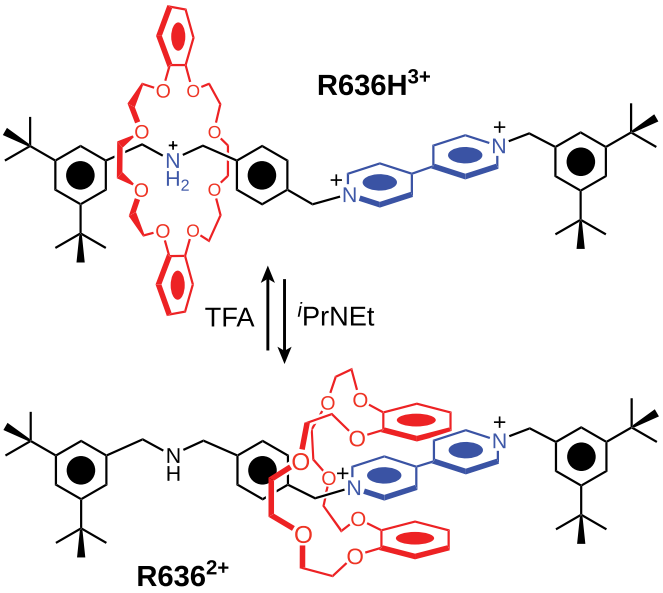
The most popular systems for making pH-switchable MIMs are based on hydrogen-bonding interactions, especially between dialkylammonium ions and crown ethers (**6.2.3.1**) and benzylic amide MIMs (**6.3.3.2**).

6.3.3.1 pH-Controlled Dialkylammonium/Crown MIMs

Acid/base-driven shuttling (**Scheme 6.39**) in dialkylammonium/crown ether rotaxanes was introduced[281] in 1997 in the form of the bistable [2]rotaxane **R636H**$^{3+}$. The dumbbell of **R636H**$^{3+}$ has two cationic binding sites for its DB24C8 ring—a dialkylammonium (–NH_2^+–) center and a BIPY^{2+} unit. The important feature of this co-constitution is that the –NH_2^+– binding site is ionizable, whereas the secondary BIPY^{2+} site is permanently charged. Thus, the DB24C8 ring encircles –NH_2^+– almost exclusively in **R636H**$^{3+}$, whereas conversion to the corresponding amine **R636**$^{2+}$ with base causes the ring to shuttle to the BIPY^{2+} unit. The reagents used for deprotonating the –NH_2^+– center are typically either tertiary amines or phosphazene bases. Rotaxane **R636H**$^{3+}$ can be easily regenerated by simply re-protonating the amine with TFA in MeCN.



Scheme 6.38 A porphyrin glycoluril cage, which encircles a viologen recognition site in rotaxane **R635**$^{2+}$, can be doubly protonated with TFA in $CHCl_3$ to generate **R635H$_2$**$^{4+}$. Electrostatic repulsion between the charged cage and the BIPY^{2+} unit causes the cage to travel between the two ends of the dumbbell, with an activation barrier that increases as the chain lengths become longer between the viologen units and the stoppers.[280]

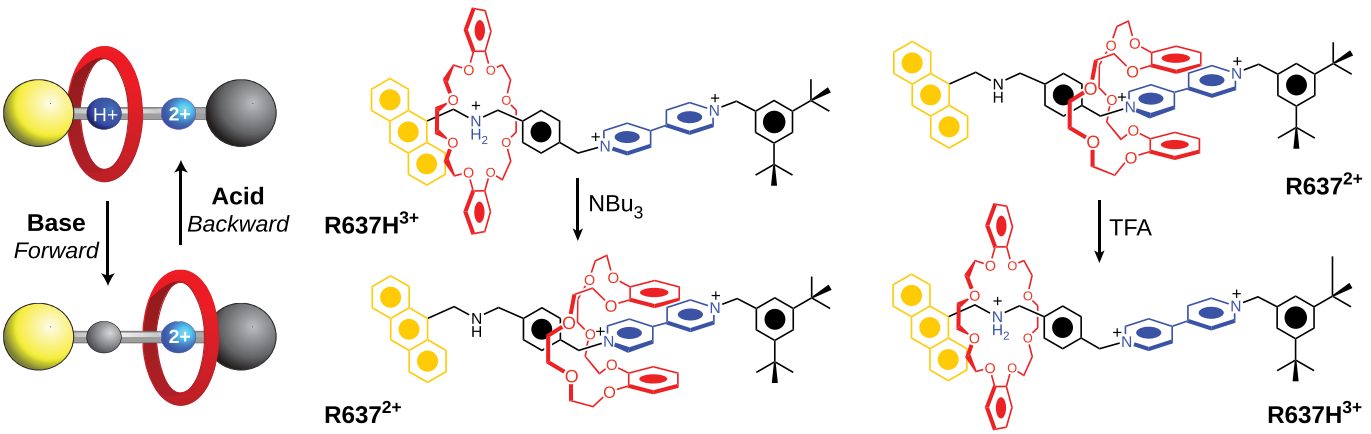


Scheme 6.39 The first pH-controlled molecular shuttle based on a dialkylammonium/crown ether motif.[281] A DB24C8 ring encircles the $-NH_2^+-$ center almost exclusively in **R636H^{3+}** under acidic conditions. Deprotonation of the $-NH_2^+-$ center under basic conditions generates **R636^{2+}** in which the DB24C8 ring encircles the permanently charged BIPY^{2+} unit instead.

The mechanism behind the operation of **R636H^{3+}**, in which a crown ether translates between $-NH_2^+-$ and BIPY^{2+} recognition units in acidic and basic conditions, respectively, has been exercised in a number of mechanically interlocked molecular switches.[48,281–290] The stopper adjacent to the $-NH_2^+-$ center has been replaced[48] with the anthracene fluorophore of compound **R637H^{3+}** for the simple reason that its absorption, luminescence, and redox properties can be used to monitor the state of the system. This modification made it possible to obtain[282] detailed kinetic information using stopped-flow absorption spectroscopy. **Table 6.2** summarizes the forward (k_f) and backward (k_b) rate constants and activation parameters for the shuttling of the DB24C10 ring to and from the BIPY^{2+} unit, respectively, following deprotonation and reprotonation of the dialkylammonium/amine site. The results show that (i) the backward shuttling (BIPY^{2+} to $-NH_2^+-$) is faster than the forward shuttling ($-NH_2^+-$ to BIPY^{2+}), and (ii) counterions have a small but non-negligible effect on the shuttling rates, since the addition of 100 molar equiv of hexafluorophosphate/tosylate salts results in only a slight decrease/increase in the forward rates, respectively.

An expansion of this class of pH-switchable rotaxanes (**Figure 6.10**) has been accomplished—with the combined efforts of several research groups—by iterative

Table 6.2 Rate constants (k) and activation parameters (E_a, $\Delta G^{\ddagger}$, $\Delta H^{\ddagger}$, $\Delta S^{\ddagger}$) for the forward and backward shuttling of the DB24C10 ring in **R637H^{3+}/R637^{2+}** in MeCN solution at 293 K.[282]



	Forward	Backward
k (s^{-1})	0.72±0.05	40±3
E_a (kcal·mol^{-1})[a]	6.5±1.0	10±1.0
$\Delta G^{\ddagger}$ (kcal·mol^{-1})[b]	17.3	15.0
$\Delta H^{\ddagger}$ (kcal·mol^{-1})[b]	5.90	9.48
$\Delta S^{\ddagger}$ (cal·mol^{-1}·K^{-1})[b]	–38.8	–18.8
k (s^{-1}), 100 eq PF_6^-	0.62±0.05	15±1
k (s^{-1}), 100 eq TsO^-	1.4±0.1	30±2

[a]Calculated from an Arrhenius plot over the temperature range 277–303 K.
[b]Calculated from an Eyring plot over the temperature range 277–303 K (estimated error <10%).

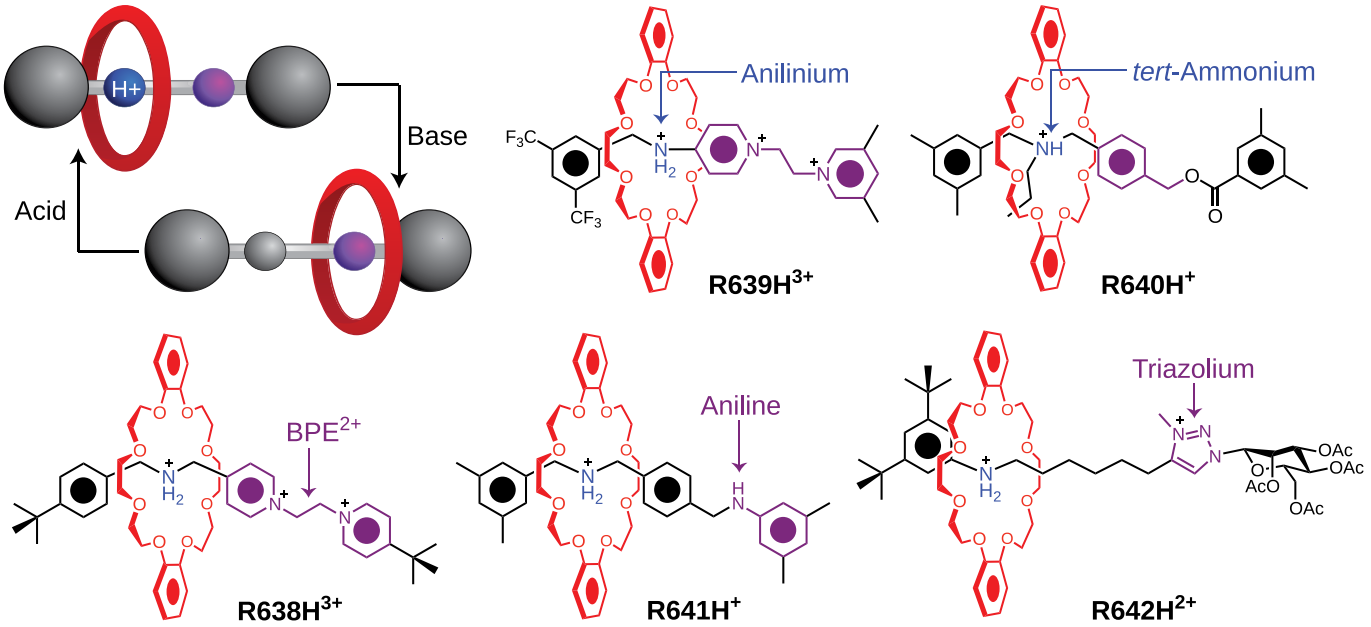
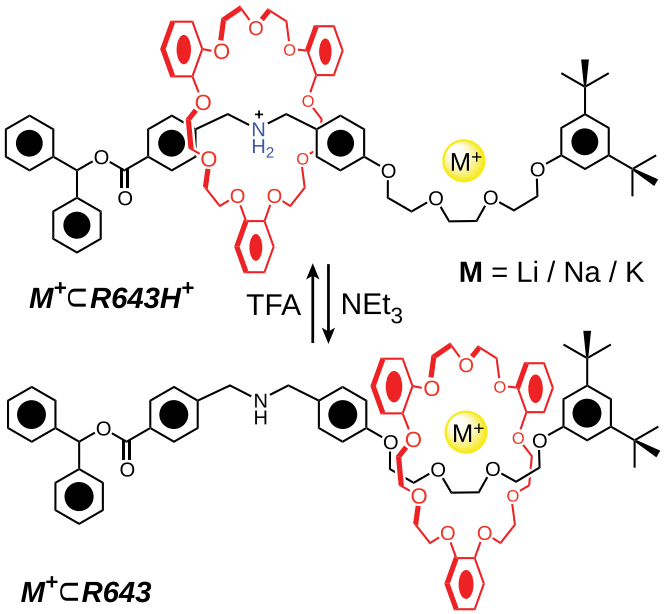


Figure 6.10 Evolution of pH-switchable molecular shuttles based on DB24C8. The bistable rotaxanes **R638H^{3+}–R642H^{2+}** all operate by a mechanism in which an –NH_2^+– group (blue) serves as the primary recognition site for DB24C8. Deprotonation causes the ring to shuttle to a charged or neutral second binding site (purple) under alkaline conditions. Top row: modifications to the –NH_2^+– (blue) recognition site.[294] Bottom row: modifications to the second (purple) recognition site.[291,296,299]

modifications to the components of the system without disrupting the fundamental operating mechanism. The pH-switchable [2]rotaxane[291] **R638H^{3+}**, for example, utilizes the 1,2-bis(pyridinium)ethane (BPE^{2+}) units that have been introduced by Loeb[292,293] in place of $BIPY^{2+}$ as the second recognition site for DB24C8. Loeb[294] has also designed and synthesized pH-controllable shuttles where the –NH_2^+– site is an anilinium ion rather than dibenzylammonium one, as in the case of the bistable rotaxane **R639H^{3+}**. Takata[295] has found that a tertiary ammonium (–NRH^+–) group can also serve as the pH-switchable recognition site in the [2]rotaxane **R640H$^+$**. Deprotonation of **R640H$^+$** to generate the neutral compound **R640** causes the DB24C8 ring to shuttle away from the tertiary amine and encircle a benzyloxy unit. Tokunaga[296] has combined the dibenzylammonium and aniline units into a single dumbbell in the [2]rotaxane **R641H$^+$**. Taking advantage of the difference in pK_a values between secondary amines and anilines, this rotaxane can access three states—the ring preferentially encircles the dibenzylammonium site under acidic conditions (**R641H$_2^{2+}$** or **R641H$^+$**), but prefers to encompass the aniline unit in the corresponding neutral rotaxane **R641** under basic conditions. A similar approach that relies on pK_a discrepancies between different amines has also been reported by Leigh.[297] The most popular modification in these systems, however, has been the use of a triazolium ion as the second recognition site for the crown ether. This triazolium motif,[298] which was first incorporated into the rotaxane **R642H^{2+}** by Coutrot,[299] is synthetically elegant because the triazolium ion can be generated efficiently by the regioselective methylation of the triazole formed during a Cu^I-catalyzed azide-alkyne cycloaddition (CuAAC) 'click' stoppering reaction. The triazolium recognition site has been featured in a number of Coutrot's pH-switchable MIMs,[298–308] and has also been adopted to generate multi-state and multicomponent mechanomolecules by several other researchers, including Liu,[309,310] Chen,[311–313] Li,[314–316] Qu,[317–324] Tian,[323] Álvarez,[325] Lützen,[326] and Lin.[327]

Other descendents of these pH-switchable rotaxanes based on ionizable amines have incorporated[328–335] modified crown ethers, such as those containing pyridines and amines,[330] isophthalimides,[331] or chiral binaphthyl units[332–334] into their operation. Tokunaga[328] has described the rotaxane **R643H$^+$**, in which a tribenzo[27]crown-9 (TB27C9) ring encircles the –NH_2^+– center in place of the conventional DB24C8 ring. A simple tri(ethylene glycol) (3EG) chain acts as the secondary recognition site in this rotaxane. In the presence of alkali metal cations, the TB27C9 ring shuttles (**Scheme 6.40**) under basic conditions from the amine to the 3EG segment of the dumbbell in order to stabilize M^+—where M is Li, Na, or K—generating the species ***M$^+$⊂R643***.

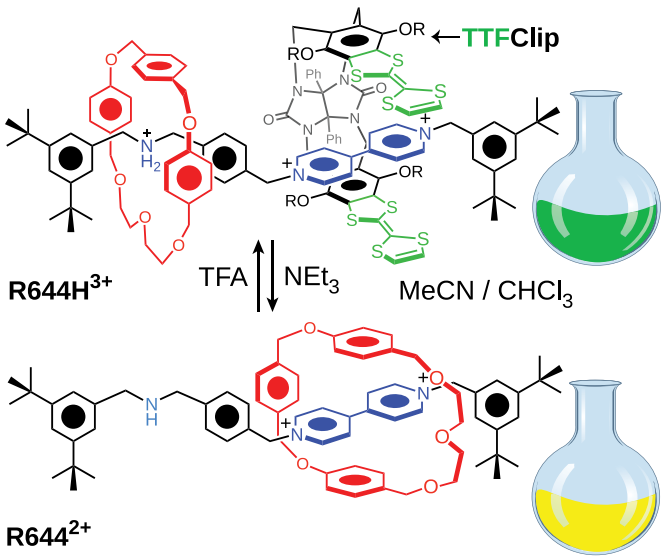
Chiu[329] has replaced the DB24C8 ring with a benzylic crown/cyclophane hybrid ring PO292PC—see **Section 2.3.3.5**—to afford **R644H^{3+}**. An innovation on the acid/base actuation (**Scheme 6.41**) of this switch is the presence of a tweezer- or pincer-type compound based on tetrathiafulvalene—call it **TTFclip**—which recognizes the $BIPY^{2+}$ unit with an association constant of 4100 ± 400 M^{-1} in 5:1 $MeCN:CHCl_3$. **TTFclip** provides a way to detect the macrocycle's position with the naked eye, since the green-colored ***BIPY^{2+}⊂TTFclip*** charge-transfer complex forms in solution only when the ring encircles the secondary dialkylammonium center of **R644H^{3+}**. In the deprotonated rotaxane **R644^{2+}**, the ring migrates to the $BIPY^{2+}$ unit and displaces the clip, producing a yellow-colored solution.



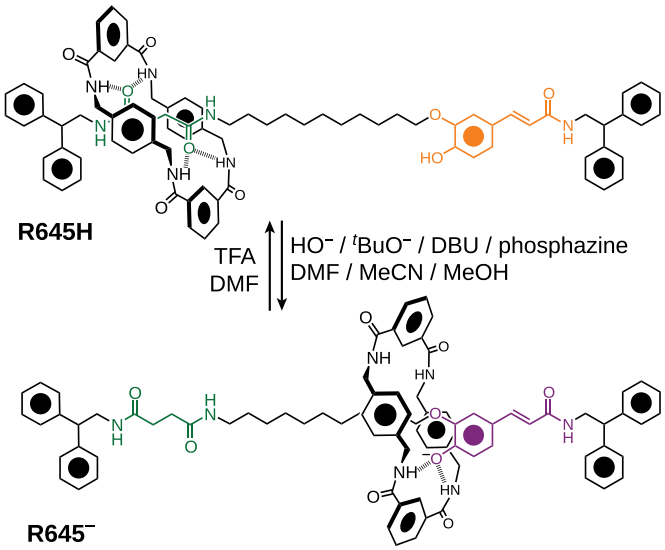
Scheme 6.40 An alkali metal cation (M^+) that is weakly associated with a tri(ethylene)glycol chain serves[328] as the second binding site in rotaxane **R643**$^+$, when deprotonation of the dialkylammonium center causes the TB27C9 ring to shuttle there in order to increase the stabilization of M^+ in **R643**.

6.3.3.2 pH-Controlled Benzylic Amide MIMs

Although crown ethers have been perhaps the most widely utilized components in pH-switchable molecular shuttles, several other recognition motifs have also been effectively adapted for this purpose. The Leigh group in particular has designed a number of pH-switchable molecular shuttles and rotors based on their benzylic amide molecular recognition motifs. Their first entry[336] into this area involved the rotaxane **R645H**, which employs (**Scheme 6.42**) anion recognition rather than cation recognition to drive pH-triggered shuttling. This compound's pH-addressable recognition site is a coumaric amide chromophore, with a phenolic group that can be deprotonated by a variety of bases to afford an oxyanion. The benzylic amide ring, which encircles a succinamide recognition site preferentially in the neutral state, shuttles away under basic conditions to participate in strong hydrogen-bonding interactions with the corresponding phenolic oxyanion of **R645**$^-$. Although these types of rotaxanes undergo switching typically in low-polarity solvents, this anion-induced shuttling only works in more polar solvents such as DMF, MeOH, and MeCN, and is insensitive to the nature of the counterions. One equivalent of TFA reprotonates the phenolic group and returns the ring to the succinamide location. It is worth noting that the coumaric amide chromophore is significantly stabilized, by nearly 3 pK_a units, in the rotaxane versus its counterpart in solution,[337] although its (*E*)→(*Z*) photoconversion efficiencies are relatively lower.[338]

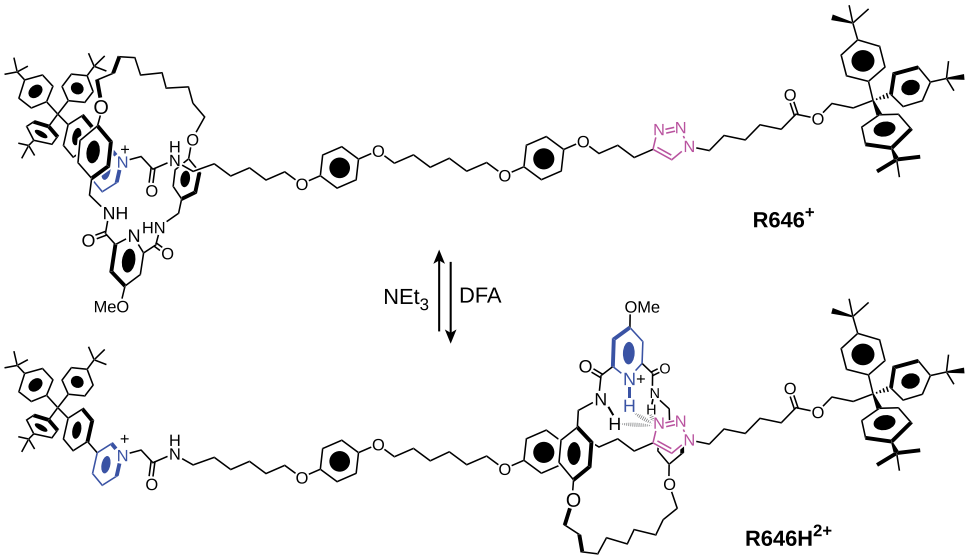


Scheme 6.41 **TTFClip** forms a pincer-type complex with $BIPY^{2+}$, allowing a readout of ring position in **R644H**$^{3+}$/**R644**$^{2+}$ that is visible to the naked eye, owing to the green-colored TTF–$BIPY^{2+}$ charge-transfer complex which forms only under acidic conditions when the ring encircles the $-NH_2^+-$ center.[329]



Scheme 6.42 The first acid/base switchable rotaxane shuttle based on Leigh's cyclic lactams relies[336] on anion recognition. Deprotonation of a phenolic site in **R645H** causes the ring to leave its succinamide recognition site in the neutral species in favor of the oxyanion of **R645**$^-$ in polar solvents.

Lüning[339] has recently reported a pH-switchable molecular shuttle with a long axle that operates (**Scheme 6.43**) by protonation/deprotonation of the ring. The benzylic amide ring of **R646**$^+$, which possesses a pyridyl group in between its hydrogen-bonded amide units, resides at one end of the dumbbell where it can participate in hydrogen bonds and donor-acceptor interactions with amide and pyridinium units adjacent to the stopper. When the ring's pyridyl group is protonated with difluoroacetic acid (DFA), the ring in **R646H**$^{2+}$ is driven away by (i) electrostatic repulsion and (ii) an increased propensity to interact with the HQ and



Scheme 6.43 Protonation of the pyridyl group in the ring of rotaxane **R646**$^{+}$ causes[339] the ring to move away from a bipyridinium recognition site and interact with a triazole unit at the other end of the dumbbell in **R646H**$^{2+}$.

triazole units at the other end of the dumbbell. Lüning[340] has also described a similar molecular shuttle possessing a fluorinated ring.

6.3.4 pH Switching Driven by Metal Chelation

Another one of Leigh's examples[341] of pH-induced mechanical motion (**Figure 6.11**) involves the benzylic amide catenane **C612**, which comprises two pyridyl rings—one with amide groups and the other without—and a Pd^{II} coordination center. The mechanism of circumrotational motion in this catenane depends upon protonation and deprotonation events that exchange the ligands of the central Pd^{II} complex. When the amide groups are deprotonated with a strong base, both rings participate in the square planar coordination complex of **PdC612**. After protonation of the amide groups with HCl, one of the rings is displaced by chloride and MeCN ligands, generating **Pd(C612H$_2$)(MeCN)Cl$_2$**. Both species were characterized by single-crystal X-ray diffraction, and their solid-state structures unambiguously reveal (**Figure 6.11**) that ring circumrotation has taken place.

Leigh[342] has also created a pH-switchable rotaxane **R647** based on the same Pd-complexed benzylic amide macrocycle. This switch design (**Scheme 6.44**) takes advantage of the differences in basicity between pyridine (py) and dimethylaminopyridine (DMAP) recognition sites. Since DMAP is a stronger base, it coordinates preferentially to the open site of the triply-coordinated Pd^{II} ion ensconced in the macrocycle in **R647$_{DMAP}$**. Since the N–H bond is stronger than the N–Pd bond, however, the addition of an equivalent of *p*-toluenesulfonic acid (TsOH) protonates the DMAP unit selectively, causing the ring to migrate to the weaker PY recognition site. The translational isomer **R647H$^{+}_{py}$** dominates the population distribution (11:89) over **R647H$^{+}_{DMAP}$** (not illustrated) under acidic conditions at 383 K in DMF, while **R647$_{DMAP}$** is the dominant species (86:14) under neutral conditions. A second generation of this molecular switch was designed subsequently, which improved[343]

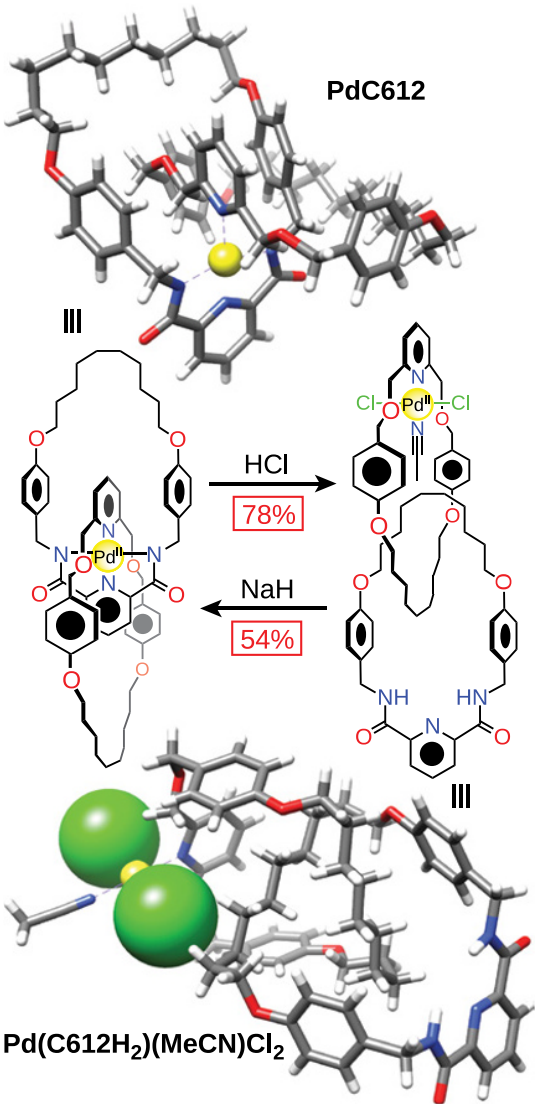
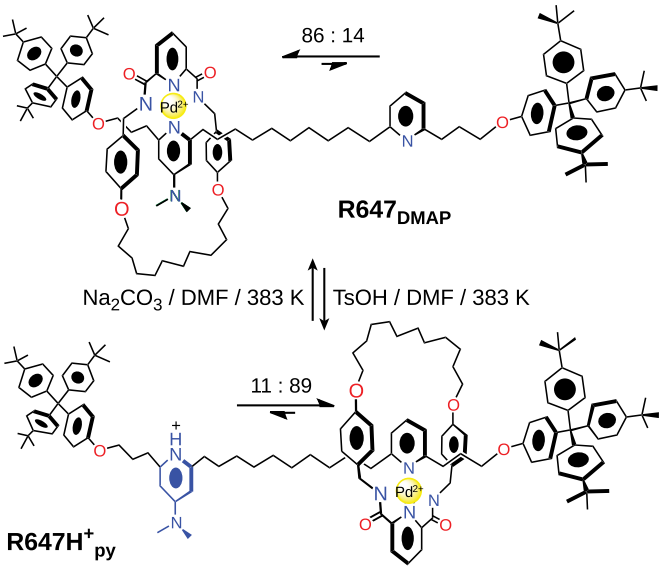


Figure 6.11 The solid-state structures and structural formulas of the metallo[2]catenanes **PdC612** and **Pd(C612H$_2$)(MeCN)Cl$_2$**, which can be interconverted with acid and base.[341]



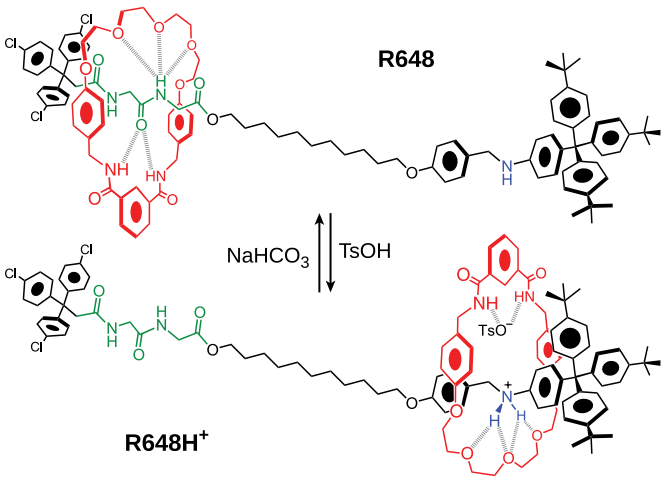
Scheme 6.44 The acid-induced switching of rotaxane **R647$_{DMAP}$** relies[342] on subtle differences between its DMAP and pyridine recognition sites. Since DMAP is a stronger base, it has a stronger affinity for the open coordination site in the Pd^{II}-based metallacycle ring component, yet the DMAP unit is also protonated preferentially in acidic conditions for the same reason, causing the ring to move to the pyridine site in **R647H$^+_{py}$**.

these ratios to 32:1 and 12:1, respectively, at lower temperature (323 K) by enlarging the co-constitution of the molecule in both of its component parts.

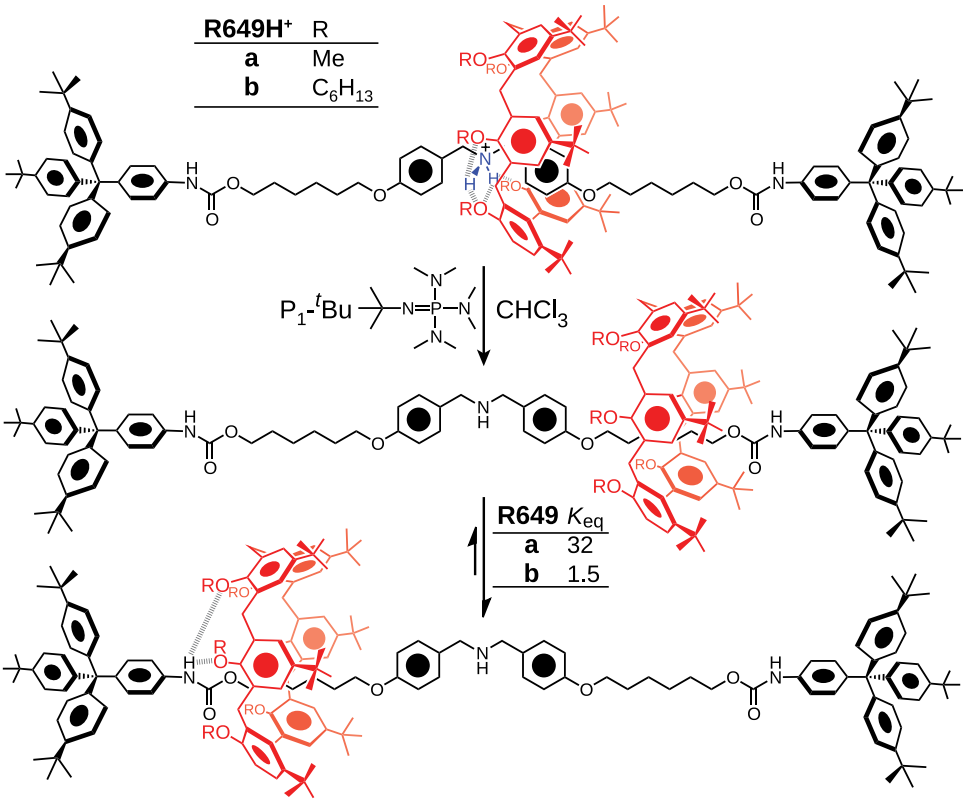
By replacing one half of a benzylic amide macrocycle with a polyether loop, Leigh[344] has demonstrated a pH-controllable shuttle (**Scheme 6.45**) with dual-mode binding properties. The ring encircles a glycylglycine (GlyGly) recognition site predominantly in the neutral form of **R648**, stabilized by hydrogen-bonding interactions between the amide groups of the ring and axle. Protonation of an aniline group at the other end of the dumbbell with TsOH generates **R648H$^+$**. The ring favors the anilinium recognition site in **R648H$^+$** as a result of more favorable hydrogen bonding between the anilinium ion and the polyether region of the macrocycle, while the ring's amide groups form hydrogen bonds with the tosylate counterion. This amide-anion interaction is not essential to the function of this switch, however, since the ring remains on the anilinium recognition site, even in the presence of non-coordinating BF_4^- counterions. This switch works with high positional discrimination, since the alternative co-conformers are not detected by ^{1}H NMR spectroscopy. Several molecular shuttles based on this hybrid polyether/amide macrocycle, which operate using the same principles, have also been developed by Li.[331,345,346]

An Italian team led by Gaeta and Neri[347] has brought pH-switchable calixarene-based rotaxanes into the fold with a design (**Scheme 6.46**) involving a calix[6]arene (CA6) derivative encircling a dibenzylammonium recognition unit in the [2]rotaxanes **R649aH$^+$** and **R649bH$^+$**, which differ only in their methoxyl and *n*-hexyloxyl groups, respectively, appended to the narrow rim of CA6. Although the constitution of the dumbbell is identical on both sides of the central $-NH_2^+-$ center (palindromic symmetry), the assymetric cone-shaped geometry of CA6 leads to a pair of orientational isomers when it escapes from the dibenzylammonium recognition unit. Upon deprotonation of the ammonium group with P$_1$*t*Bu base, the biased Brownian motion of the ring results in an unequal population distribution in the corresponding [2]rotaxanes **R649a-b**. The equilibrium distribution of the orientational isomers of **R649a** is much more biased (K_{eq} = 32) than that (K_{eq} = 1.5) of **R649b**, which may be related to each ring's ability to engage in stabilizing hydrogen-bonding interactions with the urethane linkages of the stoppers. Furthermore, only the methoxy-functionalized CA6 ring of **R649a** can undergo a cone-to-cone inversion via through-the-annulus passage of its OMe groups, with an activation barrier of 14.8 kcal·mol^{-1}, while the hexyloxyl groups of the CA6 ring in **R649b** are too bulky to allow this inversion to occur. Symmetrical [3]rotaxanes based on an analogous motif have also been prepared[348] by the same group.

It is clear to us that pH-switchable molecular shuttles and rotors are overwhelmingly driven by cation recognition. One of the rare exceptions to accompany Leigh's rotaxane **R645H/R645$^-$** in the use of anion recognition (**Scheme 6.47**) is Beer's[349] [2]catenane **C613H$^+$**. This catenane has a phenolic, electron rich isophthalamide ring (shaded red) and a pyridinium-based electron poor isophthalamide ring (shaded blue). When the phenolic hydroxyl group is protonated in **C613H$^+$**, the pyridinium unit of the blue ring resides between the two electron-rich HQ units of the red ring, stabilized by donor-acceptor interactions and hydrogen bonds



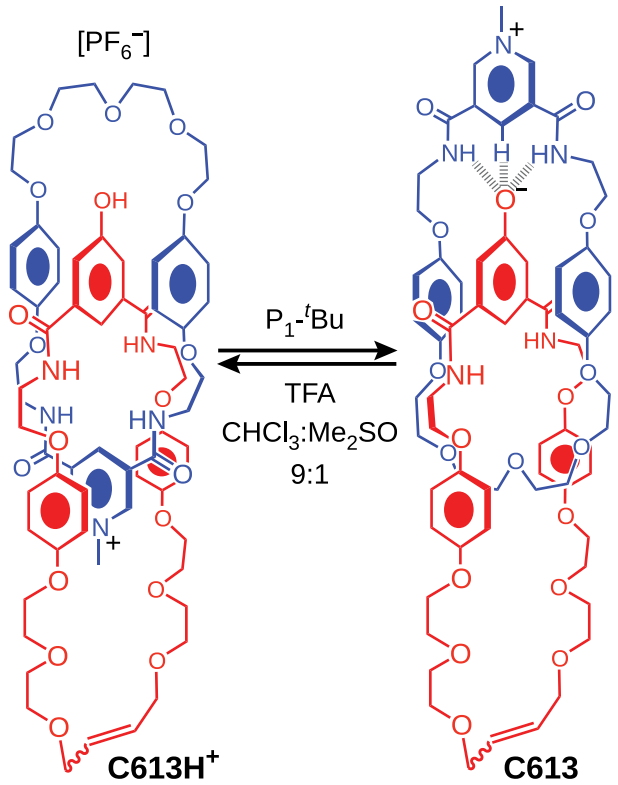
Scheme 6.45 The dual-mode rotaxane shuttle **R648** represents a hybridization of the crown ether-based rotaxanes and benzylic amide rotaxanes.[344] The benzylic amide units underpin the ring's recognition for a GlyGly peptide recognition site in the neutral species. Under acidic conditions, however, the ring of **R648H$^+$** preferentially encircles an $-NH_2^+-$ recognition site, aided and abetted by strong hydrogen-bonding interactions involving the ring's crown polyether loops.



Scheme 6.46 The pH-controlled protonation/deprotonation of a secondary dialkylamine induces[347] actuation in a family of calix[6]arene-based rotaxanes. Under acidic conditions, the ring of **R649H**$^+$ encircles an $-NH_2^+-$ center, whereas the ring shuttles along the full length of the dumbbell in the neutral compound **R649**. If the narrow rim of the ring is functionalized with methoxy groups, the ring can undergo a cone-to-cone inversion, which facilitates its recognition for a urethane site near the stopper. Bulky hexyloxy groups on the calixarene's narrow rim prevent this inversion and reduce co-conformational selectivity in **R649**.

from the adjacent glycol chains. Deprotonation of the phenolic site with a phosphazine base generates the charge-balanced [2]catenane **C613**, in which the rings have circumrotated such that the amide groups and acidic phenylene proton of the blue ring can stabilize the corresponding oxyanion. The process can be reversed with the addition of TFA in order to reprotonate the phenol. The counterion in **C613**$^+$ plays an important role in this system—whereas the switching mechanism operates as-described with PF_6^- counterions, Cl^- counterions become coordinated inside the catenane's cavity and 'lock' the rings in place, preventing circumrotation.

The examples highlighted in this Section show that modifying a MIM with as little as a single proton can lead to dramatic molecular rearrangement constrained by the mechanical bond, making simple acid/base chemistry a powerful means of controlling switching processes on the nanoscale. Although acids and bases have a special standing as chemical additives to induce mechanical motion, they do not stand alone. Many other chemical entitites can be used to control molecular shuttles and rotors, including cations (**Section 6.4**), anions (**Section 6.5**), and organic molecules (**Section 6.6**), as well as chemical reagents (**Section 6.7**) that promote covalent modification, and solvents (**Section 6.8**). Note also that the redox-active MIMs discussed in **Section 6.1** can also be switched with chemical oxidants and reductants, but these redox switches will not be discussed again here since their basic operating mechanisms are otherwise identical.



Scheme 6.47 An acid-base switchable [2]catenane that uses anion recognition to induce[349] circumrotation. Deprotonation of the phenol in **C613H**$^+$ causes the rings to rotate such that the corresponding oxyanion of **C613** can be stabilized by hydrogen bonds from an electron-deficient pyridinium bis(amide) unit in a process that can be reversed with the addition of acid.

6.4 Cation-Triggered Switches

The interactions between cations and one or more chelating sites in a MIM serve as yet another basis for switching. Indeed, appropriately designed systems have been employed by chemists to demonstrate this concept with a wide range of cations, including transition metals (**Section 6.4.1**) alkali metals (**Section 6.4.2**), and alkaline earth metals (**Section 6.4.3**).

6.4.1 Switching with Transition Metal Cations

By judiciously incorporating ligands into the constitution of a mechanomolecule, it is possible to utilize the coordination of transition metal cations to induce co-conformational changes. The simplest actuation method involves metalation and demetalation (**Section 6.4.1.1**), where one or more metal-ligand complexes define different relative positions of component parts in the metalated and non-metalated species. An equally viable protocol (**Section 6.4.1.2**) is to exchange metal templates in order to cause a change in coordination geometry that leads to a mechanical rearrangement of interlocked components. An interesting strategy, which Nature has mastered in the context of protein function, is to design allosterically controlled switches, in which metal-ligand complexation in a certain location influences the environment at a different location, such that mechanical motion is initiated remotely—see **Section 6.4.1.3**. Since the making and breaking of coordinative bonds also influences electronics, transition metal cation-induced electronic changes can also be exploited (**Section 6.4.1.4**) in mechanical switches.

6.4.1.1 Switches Driven by Adding or Removing Coordinative Bonds

It was Sauvage[350] who pioneered switching processes in catenates by demonstrating how metalation and demetalation can be used to induce (**Figure 6.12**) mechanical changes in virtually all of the metallo-catenanes and rotaxanes

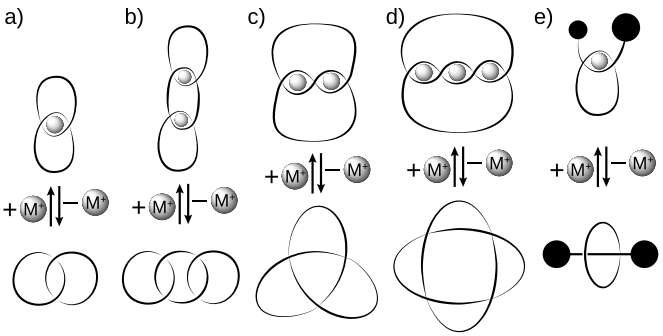


Figure 6.12 The addition and removal of a metal template, M^+, causes mechanical rearrangements in a variety of MIMs prepared[356–359] by Sauvage including (a) [2]catenanes, (b) [3]catenanes, (c) trefoil knots, (d) doubly-interlocked [2]catenanes or Solomon Knots, and (e) [2]rotaxanes.

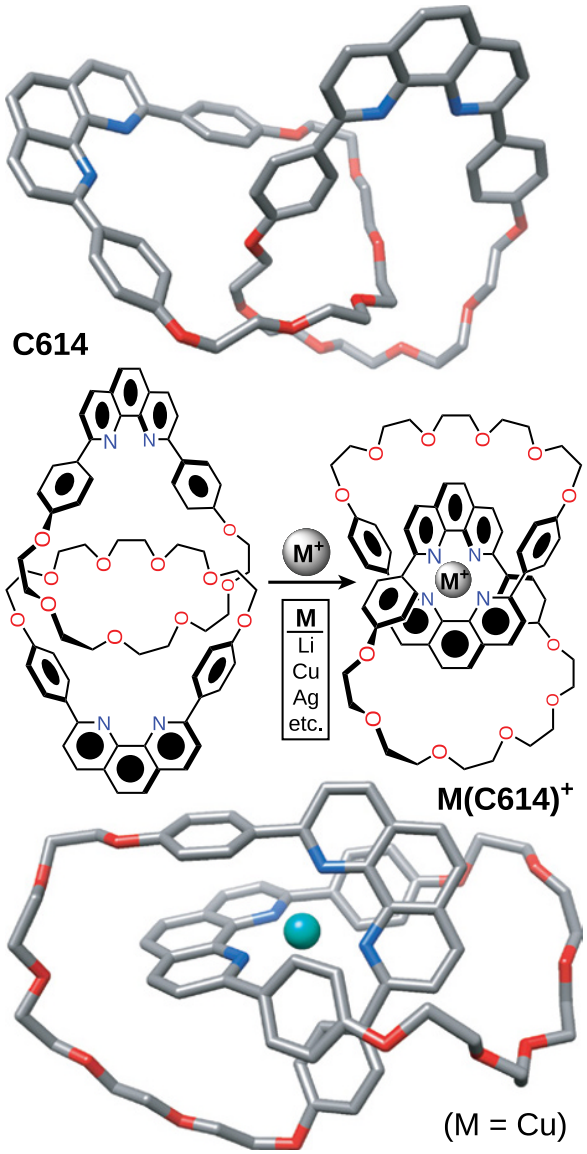
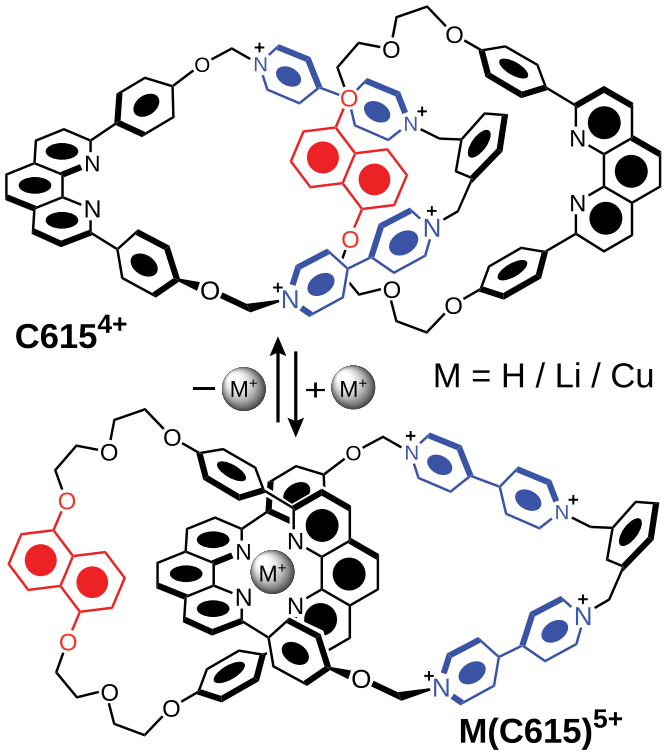


Figure 6.13 Structural formulas and solid-state structures[355] of Sauvage's original [2]catenane **C614**. Without a metal, the ligand is referred to as a *catenand*, whereas it becomes a *catenate* when it has sequestered a metal cation.

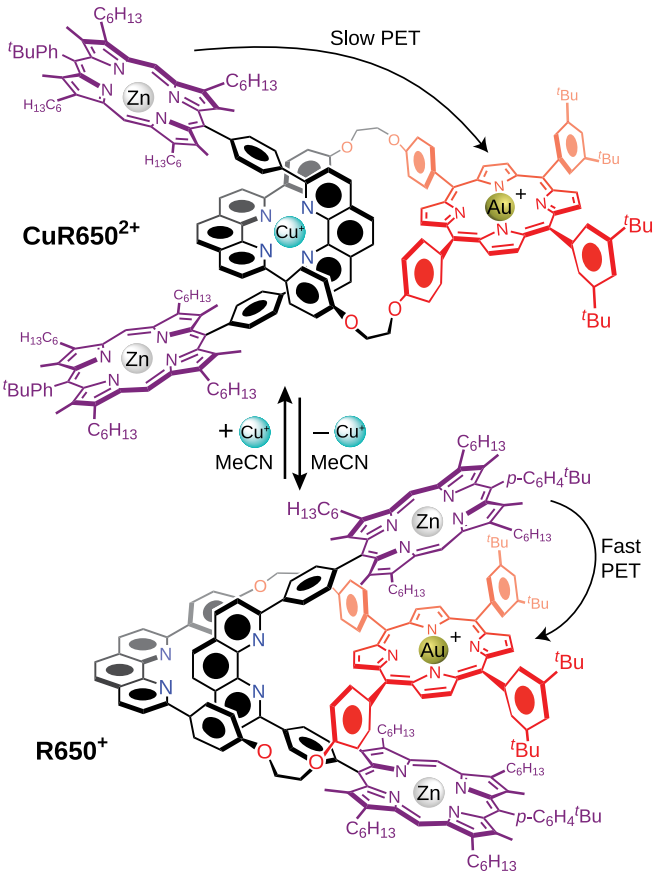
that have emerged over the years from the Strasbourg group. Sauvage's first example[350] (**Figure 6.13**) of this principle came in 1984 when he introduced the terms 'catenand' and 'catenate' to describe, respectively, the non-metalated and metalated catenane topological ligands, borrowing as he did from the lexicon of the Nobel prize-winning cryptate/cryptand chemistry pioneered[351–353] in the late 1960's by himself and his PhD supervisor, Jean-Marie Lehn. The catenand **C614** can thus coordinate a variety of metal cations M^+—where M = Li. Ag, Cu, etc.—in a binding event that locks the phenanthroline units together at the core of the structure **M(C614)$^+$**. Introducing a positive charge on one of the phenanthroline nitrogen atoms with a proton ($M = H^+$) at low pH induces the same kind of geometrical

changes as metal cations.[354] **Figure 6.13** depicts the structural formulas and the X-ray crystal structures[355] of both the catenand and the Cu^{I} catenate. The solid-state structure reveals that the rings circumrotate to accommodate the cationic template. Not surprisingly, Sauvage rapidly expanded this switching strategy (**Figure 6.12a**) to a string of new interlocked architectures, including [3]catenanes[356] (**Figure 6.12b**), trefoil knots[357] (**Figure 6.12c**), Solomon knots[358] (**Figure 6.12d**), and rotaxanes[359] (**Figure 6.12e**). Demetalation is often carried out by extracting with an excess of a competing ligand, most commonly the CN^{-} ion of KCN. A less toxic method involving aqueous NH_4OH as a demetalating agent has been reported by Megiatto and Schuster.[360]

In some cases, demetalation gives rise to a new geometry that is still well-defined on account of weaker noncovalent bonding interactions. One such example (**Scheme 6.48**) was identified[361] in 1996, where the [2]catenand **C615**$^{4+}$ and the corresponding [2]catenates **M(C615)**$^{5+}$ represent a hybridization of the transition metal (**Section 2.3.2**) and π-donor/π-acceptor (**Section 2.3.3**) template motifs. Each ring of the [2]catenate has a phenanthroline ligand, but one ring is closed with a π-donating DNP-polyether, while the closure of the other ring comprises a *meta*-phenylene-bis(bipyridinium) moiety reminiscent of the "blue box" π-accepting cyclophanes. In the presence of a cationic template M^{+} (M = Li/Cu), the phenanthroline ligands of **M(C615)**$^{5+}$ stabilize the metal ion at the center of the structure. The rings of the demetallated **C615**$^{4+}$ circumrotate in the absence of a cationic template in order to engage in much weaker π-associated donor-acceptor charge transfer and hydrogen-bonding interactions between the DNP and $BIPY^{2+}$ recognition units. We note that the same switching action can be controlled with acid/base chemistry using a protonated pyridinium cation as the template. While the general mechanism behind this switching scheme is identical to that of Sauvage's original catenand **C614**, the additional donor-acceptor interactions in **C615**$^{4+}$ engender a more well-defined geometry in the demetallated species.



Scheme 6.48 A transition metal/donor-acceptor hybrid [2]catenane.[361] The weak donor-acceptor charge transfer and hydrogen-bonding interactions between the DNP and $BIPY^{2+}$ units in **C615**$^{4+}$ are displaced through circumrotation by stronger ion-ligand interactions when an appropriate cation M^{+} is added to generate the catenate **M(C615)**$^{5+}$.

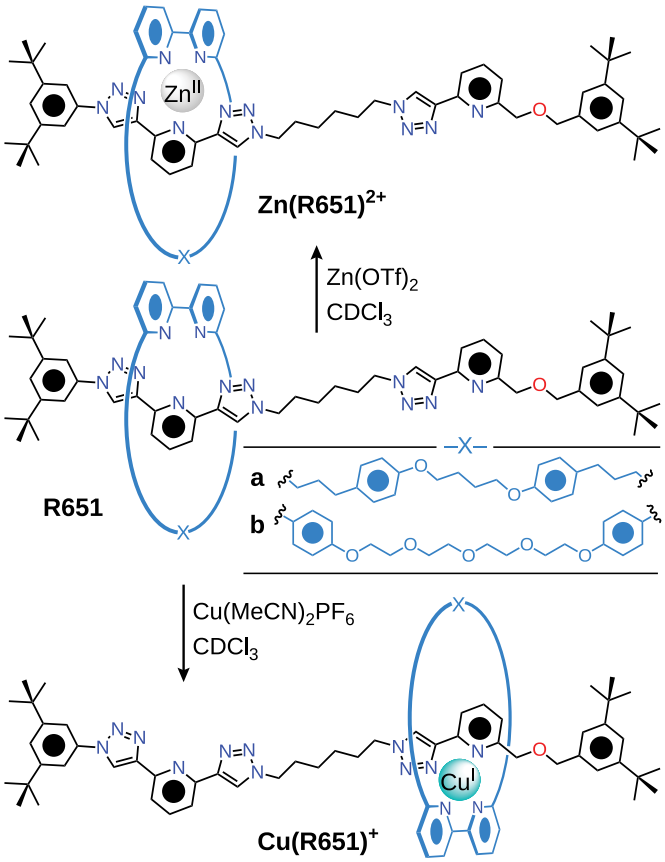


Scheme 6.49 The Au^{III} metalloporphyrin (red) appended to a dpp-based ring undergoes circumrotation with respect to the two Zn^{II} metalloporphyrin stoppers of a dumbbell as Cu^{I} ions are removed or added in Sauvage's metallorotaxane **CuR650**$^{2+}$/**R650**$^{+}$.[362] PET from the Zn^{II} metalloporphyrin to the Au^{III} metalloporphyrin is much faster in the porphyrin-stacked co-conformation of **R650**$^{+}$ than in **CuR650**$^{2+}$.

An example (**Scheme 6.49**) of a cation-switchable metallorotaxane based on Sauvage's ligand motif is that[362] of **R650**$^{+}$/**CuR650**$^{2+}$. The Au^{III} metalloporphyrin appended to the ring component can accept electrons in a PET process from the Zn^{II} metalloporphyrin stoppers of the corresponding dumbbell. In the presence of a Cu^{I} template, the locked co-conformation of the **CuR650**$^{2+}$ catenate fixes the distance between the Au^{III} and Zn^{II} centers, where a measurable rate ($k = 5 \times 10^{9}\ s^{-1}$) of PET has been

recorded. In the absence of the Cu^{I} template, the Au^{III} metalloporphyrin of the catenand **R650**$^{+}$ is able to circumrotate in order to position itself at a much closer distance, sandwiched as it is in between the Zn^{II} centers. The rate of PET in this porphyrin-stacked co-conformation is too fast to measure, i.e., it falls below the 20 ps timescale. This photoactive rotaxane demonstrates that ring-stopper interactions can be utilized to control switching and electron transfer processes on the molecular scale. Sauvage[363–365] has described a number of porphyrinic metallorotaxanes incorporating similar design motifs.

Goldup[366] recently investigated a pair of [2]rotaxanes, **R651a** and **R651b**, prepared by an active metal template CuAAC protocol (**Section 2.4.1.1**), in which the position of a macrocyclic 2,2´-bipyridine ligand can be set (**Scheme 6.50**)



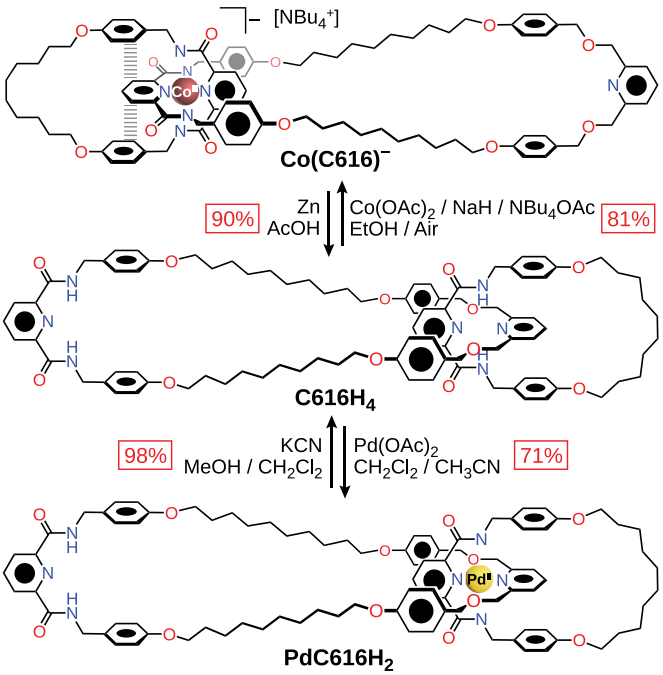
Scheme 6.50 The ring of Goldup's [2]catenane **R651** can be positioned[366] around the axle's tridentate or bidentate ligands by introducing Zn^{II} or Cu^{I} templates, respectively.

with respect to the dumbbell by the introduction of either Zn^{II} or Cu^{I} templates. The axle's chelation site in **Zn(R651)**$^{2+}$ is a tridentate bis(triazolo)pyridine ligand in a pentacoordinate geometry, while **Cu(R651)**$^{+}$ adopts a tetrahedral coordination geometry surrounding the axles alternative mono(triazolo) pyridine unit. In principle, this rotaxane could be actuated by Cu^{I}/Zn^{II} template exchange (**Section 6.4.1.2**) with the assistance of an efficient demetalation procedure.

6.4.1.2 Changing Templates with Different Coordination Geometries

Another way to switch Sauvage's class of MIMs is to install multiple ligand motifs into a single molecule, such that the exchange of one metal cation for a different metal cation calls for a rearrangement of mechanical bonds in order to accommodate a new coordination geometry. This strategy is similar conceptually to transition metal-based MIMs driven by electrochemical or photochemical redox changes. Instead of changing the redox state of the transition metal, the transition metal itself is exchanged. Sauvage[367] introduced this idea in a seminal paper in 2000 on 'molecular muscles' which have subsequently come to be known[43,368] more commonly as 'daisy chain' rotaxanes. Metal exchange has also been utilized[369] to generate a 'flapping' motion in a [3]rotaxane. See **Sections 6.13.1.1** and **6.13.5**, respectively, for details on these switches. Although this strategy has appeared only in a few cases, it can be applied, in principle, to almost any of Sauvage's redox-driven metallo-switches—see **Section 6.1.3**.

Leigh[370] has designed the [2]catenane **C616H$_4$** from dicarboxamidopyridine and pyridine templates such that its metalation (**Scheme 6.51**) with either Co^{III} or Pd^{II} templates affords the [2]catenates **Co(C616)**$^{-}$ and **PdC616H$_2$**, respectively, which assume different geometries as a result of their different coordination numbers. The smaller macrocyclic Pd^{II} chelate surrounds the larger ring's monodentate pyridine moiety in the square planar **PdC616H$_2$**, whereas both dicarboxamidopyridine ligands in the coconsitution of **Co(C616)**$^{-}$ engage its octahedral Co^{III}

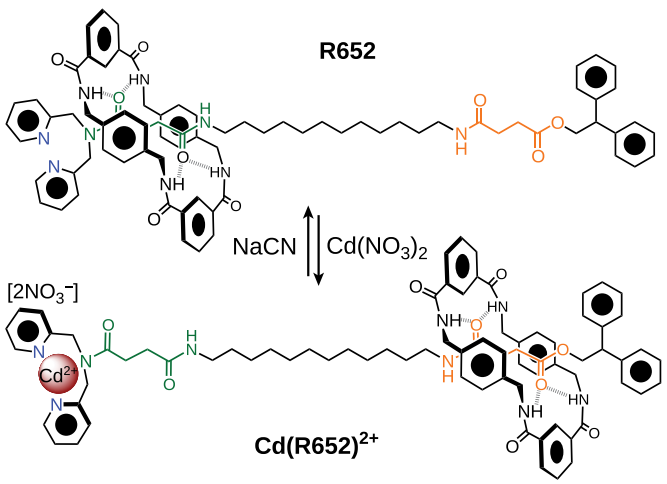


Scheme 6.51 The half-circumrotation of catenated benyzlic amide rings can be controlled by exchanging Co^{III} and Pd^{II} templates.[370]

center. Template exchange, which can be accomplished by demetalation and remetalation reactions in good to high yields, thus induces one ring's translation by π radians, corresponding to a 180° pirouetting motion in the other ring.

6.4.1.3 Allosteric Control

Allosterism[371] is a phenomenon commonly observed in proteins, where the active site is regulated by the binding of an 'effector' molecule at a different site. In 2006, Leigh[372] designed a [2]rotaxane with a chelating stopper that offers allosteric control (**Scheme 6.52**) over the ring position. In **R652**, the allosteric chelate is a tridentate stopper appended directly to a succinamide unit that serves as the primary recognition site for the ring component. Over 95% of the molecular population encircles this site in the absence of an effector. The effector in this [2]rotaxane is $Cd(NO_3)_2$, which competes with the benzylic amide ring for the same three-dimensional space surrounding the allosteric site. Thus, the triple-coordination of Cd^{2+} to the nitrogen atoms of the stopper causes the ring of **CdR652^{2+}** to encircle a weaker succinic amide ester recognition site at the other end of the dumbbell. Since the metal coordination is a quantitative reaction, the corresponding ring translation is likewise essentially quantitative. The Cd^{2+} ion can be stripped away with 5 equiv NaCN, reinstating the original position of the ring in **R652**. A rotaxane with a similar design to **R652** was reported[373] in the same year, in which the chelating stopper was positioned slightly further away from the succinamide recognition site. The ring is also displaced by the complexation of Cd^{II} or Cu^{II} ions in this case, but only after one of the –NH– protons of the succinamide unit has been deprotonated, allowing the corresponding nitrogen atom to coordinate with the metal.



Scheme 6.52 An allosterically regulated molecular shuttle.[372] The benzylic amide ring is more strongly associated with the ligand-appended succinamide recognition unit in **R652**, until a Cd^{2+} 'effector' molecule that competes for the same space displaces it, forcing the ring to move over to the more weakly-associated succinic amide ester recognition site in **Cd(R652)$^{2+}$**.

Although allosterically regulated molecular shuttles such as **R652** are rare, there is reason to believe that many other bistable MIMs could be adapted to function likewise. For example, allosteric effects have regulated the reactivity of an endoperoxide cycloreversion reaction in one of Smith's squaraine-based rotaxanes,[374] while their influence on complexation properties have also been found in the porphyrin-glycoluril hosts championed (**Section 2.3.3.6**) by Nolte and Rowan,[375,376] who have demonstrated that axial coordination of a ligand to the metalated porphyrin on the exterior of its cavity affects the association strengths of viologen guests within the cavity.

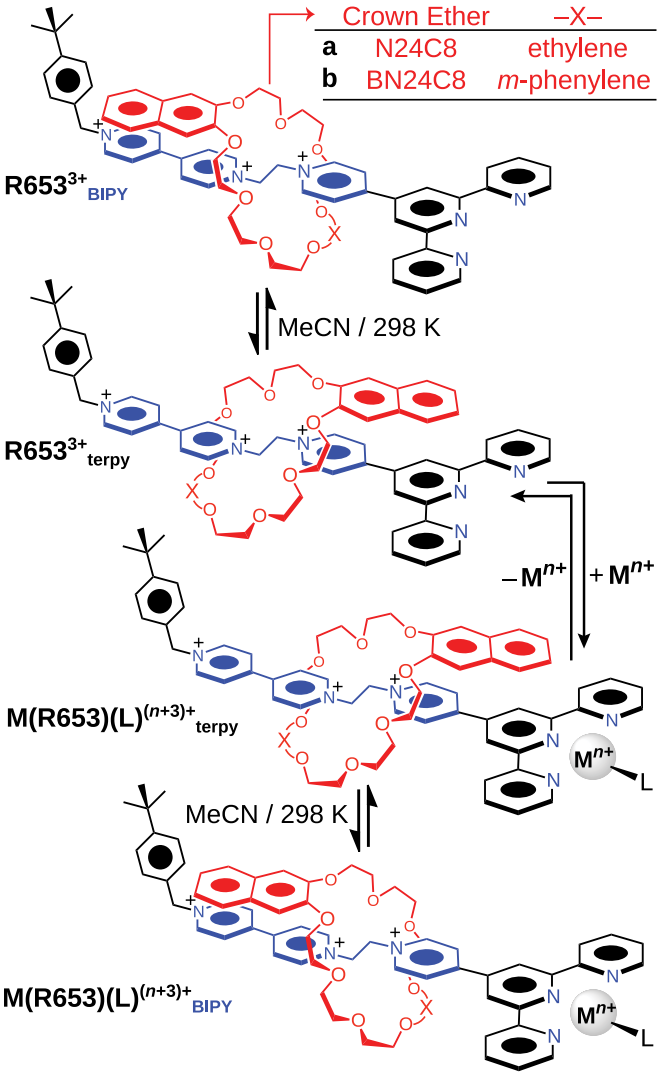
6.4.1.4 Switches Driven by Cation-Induced Electronic Changes

Loeb[377] has investigated the metal-dependent co-conformational isomerism (**Table 6.3**) of mechanically interlocked "flip switches" based on his *BPE*$^{2+}$⊂*crown* recognition motif. The rotaxanes **R653a^{3+}** and **R653b^{3+}** possess naphtho[24]-crown-8 (N24C8) and benzonaphtho[24]crown-8 (BN24C8) rings, respectively, each encircling a constitutionally asymmetric dumbbell containing $BIPY^{2+}$ and terpy recognition units. The flip switches operate by modulating the sterics and electronics of the terpy ligand with transition metal complexes, which influences the relative affinities of the electron-rich naphtho unit engaging in π-associated D-A interactions with the two recognition units. The naphtho units of N24C8 and BN24C8 interact preferentially with $BIPY^{2+}$ in the absence of a transition metal or when the template is $Ru(terpy)^{2+}$, since the dumbbell's terpy recognition unit is sterically overcrowded in **Ru(R653)(terpy)$^{5+}$** and a relatively poor π-acceptor in **R653^{3+}**. On the contrary, the introduction of PtMe or $Ag(MeCN)^{+}$ complexes causes the naphtho groups to interact preferentially with the terpy unit in **Pt(R653)(Me)$^{4+}$** and **Ag(R653)(MeCN)$^{4+}$**, owing to a decrease in π-electron density and increase in π-surface area of the terpy unit afforded by their square planar metal centers. These flip switches respond similarly, regardless of whether they derive from homologues **a** (N24C8) or **b** (BN24C8), albeit with slight differences in their population distributions. The most biased populations of each co-conformer are manifested in **Pt(R653a)(Me)$^{4+}$** (88% terpy isomer) and **Ru(R653b)(terpy)$^{5+}$** (62% $BIPY^{2+}$ isomer) at 298 K in MeCN. At least in the case of **Ag(R653b)(MeCN)$^{4+}$**, Loeb has reversed the flip switch by introducing NBu_4Cl in solution in order to restore the initial state of **R653b^{3+}** by precipitation of the Ag^{I} template as AgCl.

6.4.2 Switching with Alkali Metal Cations

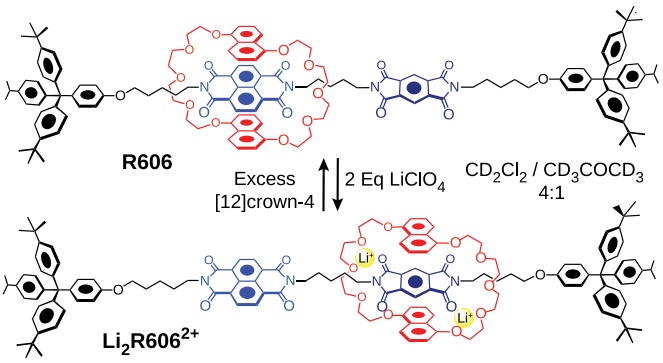
Although the alkali metals (**Section 2.3.8.1**) have received less attention from chemists conducting research on mechanical bonds than have transition metals, they are no less capable of inducing mechanical motion through competitive binding in appropriately designed systems.

Table 6.3 Loab's [2]rotaxane flip switches.[377] A crown ether's naphtho group stacks predominantly with either a $BIPY^{2+}$ recognition unit or a terpy ligand, depending on the latter's coordination mode.



M(R653)(L)$^{(m+3)+}$	M^{n+}	L	Crown Ether	Ratio BIPY:terpy
R653a^{3+}	–	–	N24C8	59:41
Pt(R653a)(Me)$^{4+}$	Pt^{2+}	Me^-	N24C8	12:88
Ru(R653a)(terpy)$^{5+}$	Ru^{2+}	terpy	N24C8	59:41
R653b^{3+}	-	-	BN24C8	61:39
Pt(R653b)(Me)$^{4+}$	Pt^{2+}	Me^-	BN24C8	26:74
Ru(R653b)(terpy)$^{5+}$	Ru^{2+}	terpy	BN24C8	62:38
Ag(R653b)(MeCN)$^{4+}$	Ag^+	MeCN	BN24C8	38:62

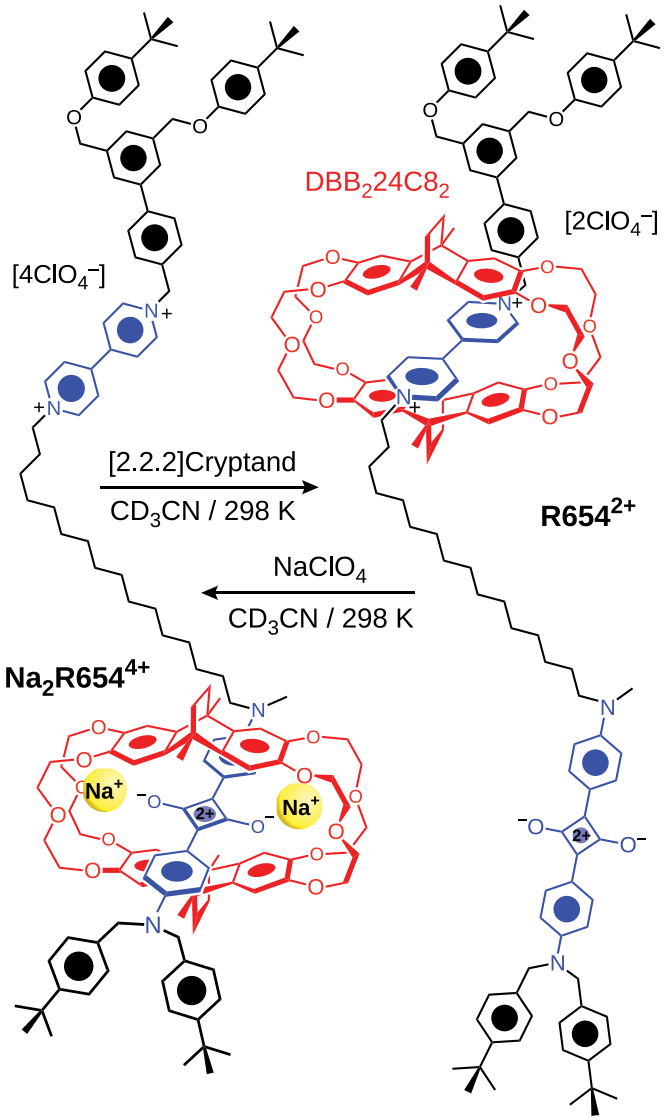
The design[378] of a Li^+-driven (**Scheme 6.53**) bistable donor-acceptor [2]rotaxane **R606**—first introduced[46] as a redox-driven (**Section 6.1.1**, **Scheme 6.5**) switch—relies on Sanders' discovery[379] that the affinity of PMDI for the π-electron-rich crown ether DN38C10 is enhanced by Li^+ ions. Ordinarily, the DN38C10 host has a higher affinity for NDI than for PMDI, but PMDI outcompetes NDI when two equivalents of Li^+ ions are present, on account of their co-assembly with PMDI in the crown's polyether chains. Thus, the DN38C10 ring encircles the NDI unit in **R606**, but encircles the PMDI unit in **Li_2R606^{2+}**. The process is reversed by removal of the Li^+ ions with [12]crown-4 or by extraction with water, returning the DN38C10 ring to the NDI recognition site.



Scheme 6.53 Two Li^+ ions induce the DN38C10 ring to move away from its preferred NDI recognition site (blue) because they become more stabilized[378] when the ring encircles the PMDI unit (dark blue) in rotaxane **R606**.

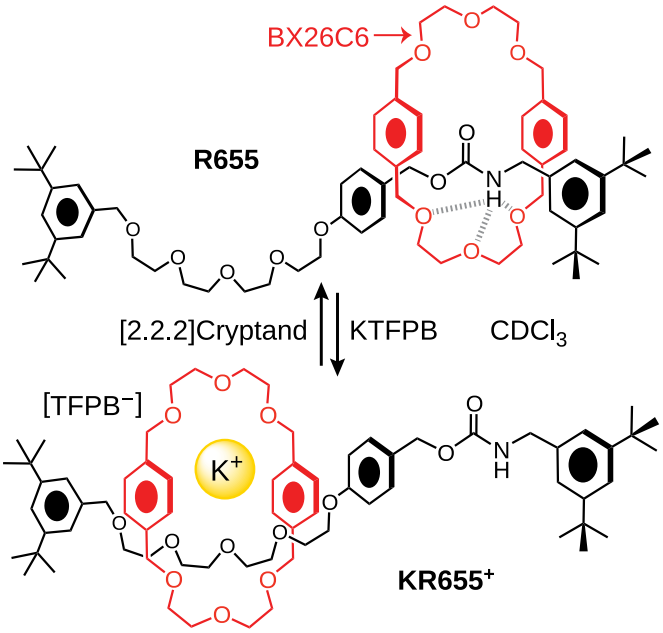
A similar mode of actuation has been investigated by Chiu[380] in rotaxanes comprising $DBB_2$24C8_2 macrotricyclic crown ethers (**Section 2.3.3.5**), which encircle dumbbells possessing recognition units derived from squaraine and pyridinium. In one example (**Scheme 6.54**), the ring of the [2]rotaxane **R654^{2+}** encircles a bipyridinium recognition unit, stabilized most likely by [C–H···O] hydrogen bonding and D-A π–π stacking interactions. The addition of $NaClO_4$ in MeCN at 298 K causes the component parts to translate such that the $DBB_2$24C8_2 host and the squaraine units cooperatively interact with a pair of Na^+ templates in **Na_2R654^{4+}**, stabilized in this case by [C–O···Na^+] interactions. The switch can be reset by removal of the Na^+ ions using [2.2.2] cryptand as a competitive binder. Chen[381,382] has also employed macrotricyclic hosts in order to prepare tristable molecular switches, where the position of the ring at any of three recognition sites—namely, anthraquinone, triazolium, and PMDI—can be controlled by the presence (or absence) of different alkali metal salts that engage in similar carbonyl- and polyether-stabilized alkali metal complexes.

Chiu[383] has also employed simple ion-dipole interactions between the oxygen atoms of polyether loops and K^+ to drive (**Scheme 6.55**) the translation of a bis-*p*-xylyl[26]-crown-6 (BX26C6) ring in the [2]rotaxane **R655**. The ring of **R655** engages in hydrogen-bonding interactions with the dumbbell's carbamate site in the absence of alkali metal cations, yet it moves to a tetraethylene glycol (4EG) site in order to cooperate in the stabilization of a K^+ cation upon introducting potassium tetrakis(3,5-trifluoromethylphenyl) borate (TFPB) in $CDCl_3$ solution. The shuttling process is reversed by the addition of [2.2.2.]cryptand as a competitive binding agent for the K^+ ion.



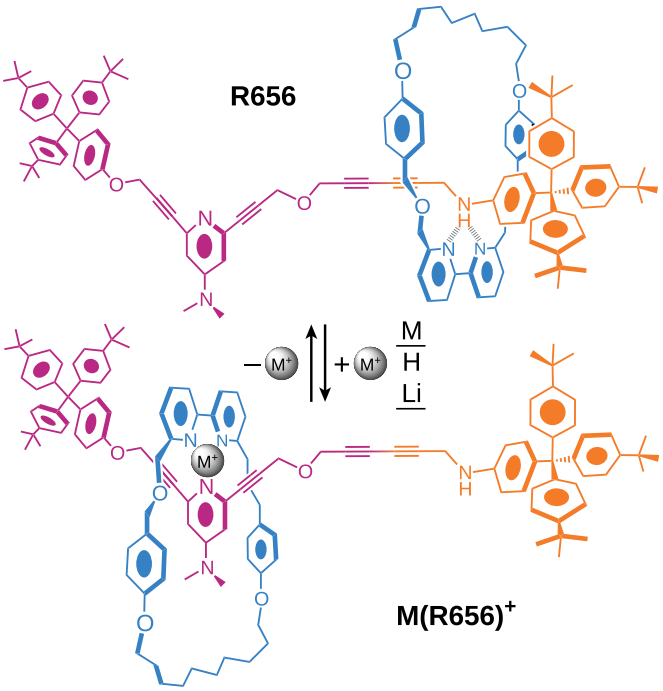
Scheme 6.54 Sodium-triggered translation of a macrotricyclic polyether host in Chiu's squaraine [2]rotaxane.[380]

The ability of active metal template synthesis (**Section 2.4**) to create MIMs in which the interactions between component parts are minimal has opened up new possibilities for designing switches governed by very weak interactions. Rotaxane **R656**, a cation-driven switch developed by Leigh,[384] operates (**Scheme 6.56**) on interactions that are too weak for templating mechanical bonds. **R656** can be isolated without a metal template by virtue of active template synthesis. In this state, the ring resides near an aniline-linked stopper, supported by weak hydrogen-bonding interactions between the ring's bipyridine unit and the –NH– group. The introduction of a cationic site M$^+$—where M is a Li atom or a proton—in the rotaxane **M(R656)$^+$** causes the ring to occupy the DMAP recognition site predominantly, since the DMAP and bipyridine units can both participate in ion stabilization. The Li$^+$ template can be removed by extraction with water to reinstate the original co-conformation of **R656**.

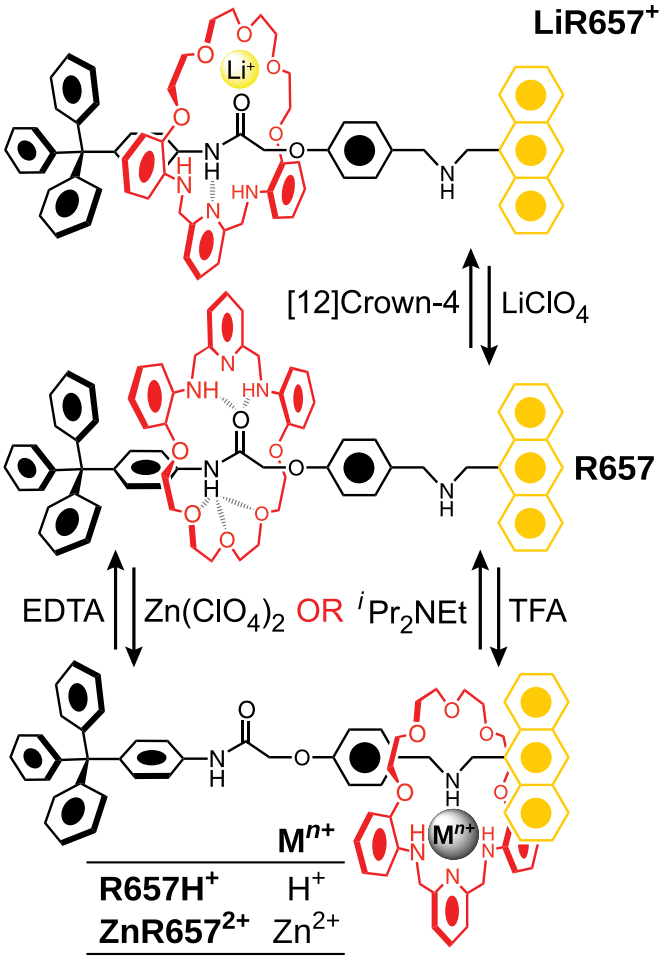


Scheme 6.55 The BX26C6 ring of Chiu's [2]rotaxane **R655** migrates away from its hydrogen bonded carbamate station to encircle a 4EG loop upon the introduction of KTFPB salt in order to cooperatively chelate the K$^+$ ion in **KR655$^+$**.[383]

Li[330] has designed and synthesized a novel fluorescent rotaxane switch with multiple levels of chemical addressability (**Scheme 6.57**), including pH, in addition to transition metal and alkali metal cations. The structure of **R657** com-



Scheme 6.56 The active template synthesis of rotaxane **R656** creates[384] a situation in which the ring has very little affinity for any potential recognition site on the dumbbell. Hydrogen bonds place the ring predominantly around the stopper's aniline (blue) unit until a cationic charge is introduced, either through protonation or coordination of a Li$^+$ ion at the DMAP recognition site (green) in **M(R656)$^+$**.

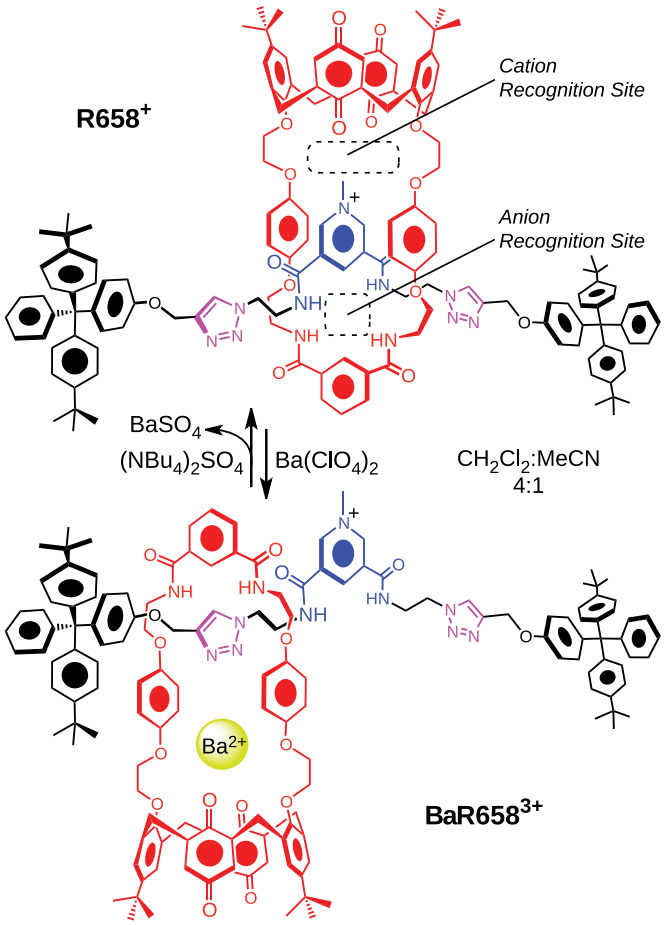


Scheme 6.57 The [2]rotaxane **R657** adopts[330] different co-conformations in response to chemical stimuli, including Li^+ (**LiR657**$^+$), Zn^{II} (**ZnR657**$^{2+}$), or acid (**R657H**$^+$).

prises a crown-like ring and a dumbbell with a dialkylamine recognition site adjacent to a fluorescent anthracene stopper and an amide recognition site adjacent to a trityl stopper. The key to the function of this rotaxane lies in the ring, which is prepared by reduction of imine bonds following an efficient thermodynamically controlled clipping reaction—see **Section 3.4.2**. The ring can coordinate both alkali and transition metal cations by virtue of its 2,6-pyridinedimethanamine unit, which also allows it to donate and accept—along with the polyether loops—hydrogen bonds. The native co-conformation of **R657** is one in which the ring encircles the amide group, stabilized by a number of hydrogen-bonding interactions. As an acid/base controlled switch, the ring binds the dialkylammonium site upon acid-induced protonation to generate **R657H**$^+$, in a manner analogous to the pH-controlled [2]rotaxane **R637H**$^{3+}$ (**Section 6.3.3.1**, **Table 6.2**). **R657** also exhibits two different cation-triggered responses. The addition of Zn^{II} ions to a solution of **R657** in dichloroethane induces ring translation, such that the amine groups in the dumbbell and ring can both participate with the pyridine unit in coordinative bonding to the Zn^{II} ion in **ZnR657**$^{2+}$. On the other hand, Li^+ ions cause the ring of **R657** to circumrotate in order to allow its polyether loops to form a binding pocket for the Li^+ cations together with the carbonyl group in the dumbbell of **LiR657**$^+$. The anthracene fluorophore serves to report the co-conformational state of the rotaxane, since its fluorescence signal at 370 nm excitation is different for each species—emission is increasingly quenched according to the trend **R657H**$^+$ > **R657** > **LiR657**$^+$ > **ZnR657**$^{2+}$.

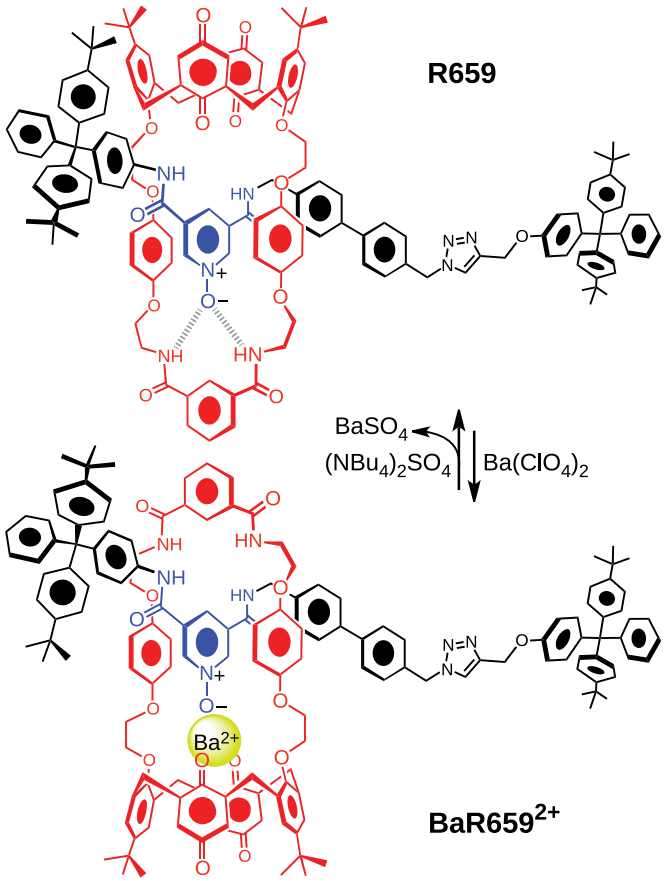
6.4.3 Switching with Alkaline Earth Metal Cations

The example of alkaline earth metal cation-triggered shuttling presented in **Scheme 6.58** comes courtesy of Beer,[385] whose [2]rotaxane **R658**$^+$ possesses distinct binding pockets for both cations and anions. This rotaxane was synthesized by stoppering a pseudorotaxane comprising a calix[4]diquinone (C4DQ)/isophthalamide macrocycle and a bis(amide)-pyridinium thread using using click chemistry, leaving triazole groups in between the pyridinium



Scheme 6.58 Barium-triggered shuttling[385] in a rotaxane (**R658**$^+$) which binds both cationic and anionic guests. The large Ba^{2+} ion displaces a pyridinium recognition site (blue) when it binds the calix[4]diquinone wheel (red) of **BaR658**$^{3+}$, causing the corresponding ring to encircle the alternative triazole recognition site. Monovalent cations and anions do not trigger this co-conformational switching at all.

recognition site and the tetraphenyl stoppers. The amide groups of the ring and dumbbell cooperate in the binding of anions, especially halides, whereas the hydroquinone groups of the C4DQ unit can bind cations via ion-dipole interactions. Anions (e.g., Cl^-, Br^-, $H_2PO_4^-$, AcO^-) and monovalent cations (e.g., Na^+, K^+, NH_4^+) bind these respective sites with reasonable affinities ($K_a = 10^2$–$10^3\,M^{-1}$) in 4:1 CH_2Cl_2/MeCN without affecting the position of the ring. The large, divalent Ba^{2+} cation, however, displaces the pyridinium unit from the cavity of the ring as it resides preferentially in the calixarene pocket of **BaR658^{3+}**. The rearrangement is most likely driven by electrostatic repulsion, which leads to repositioning of the ring around one of the triazole units near the dumbbell terminus. Although the Ba^{2+} guest is attracted into the cavity of the ring by several orders of magnitude moreso than its monovalent counterparts ($K_a > 10^6\,M^{-1}$), it is easily stripped away to restore **R658$^+$** upon the addition of $(NBu_4)_2SO_4$, which precipitates $BaSO_4$ as a byproduct. This rotaxane constitutes a rare use of heavy group II elements in a mechanostereochemical context. The binding of a Ba^{2+} dication int the C4DQ pocket of this ring has also been exploited in **R659** to induce pirouetting (**Scheme 6.59**) in both a [2]rotaxane (**R659**),[386] as well as in a [2]catenane.[387]



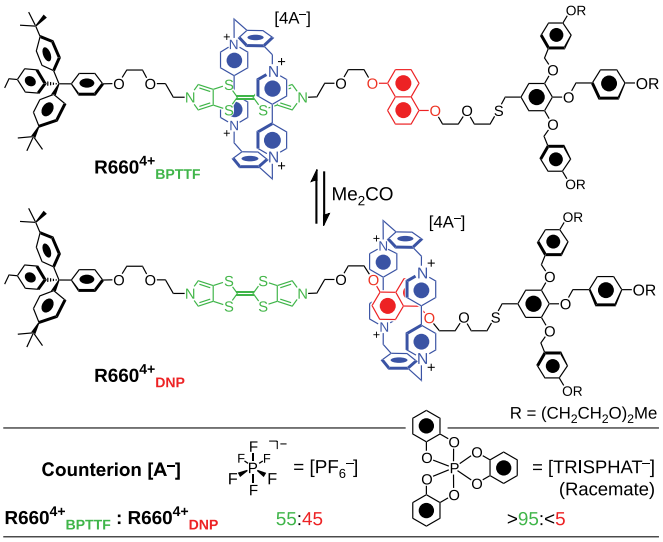
Scheme 6.59 Barium-triggered pirouetting[386] of a calix[4]-diquinone ring with respect to the pyridine *N*-oxide axle of the [2]rotaxane **R659**. The same pirouetting motion can also be induced by Na^+ ions.

6.5 Anion-Triggered Switches

Anions have been employed to drive circumrotational and translational movement in MIMs by mechanisms that involve anion solvation effects (**Section 6.5.1**), second-sphere interations (**Section 6.5.2**), and competitive anion binding (**Section 6.5.3**).

6.5.1 Switches Driven by Anion Solvation Effects

The different solvation effects of hard and soft anions have been exploited in order to control translational isomerism in a variety of mechanically interlocked switches. For example, the counterions of the tetracationic cyclophane CBPQT^{4+} can influence[388] (**Scheme 6.60**) the co-conformational isom-



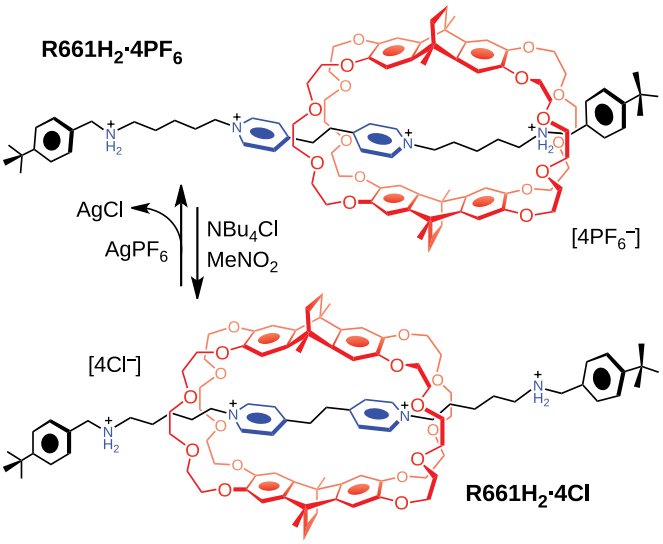
Scheme 6.60 The counteranions play a significant role[388] in the distribution of co-conformational isomers of **R660^{4+}**.

erism of the π-donor/π-acceptor bistable [2]rotaxane **R660^{4+}**. Whereas the DNP and BPTTF recognition sites are almost equally populated in the "red" and "green" translational isomers, respectively, of **R660**·4PF_6, whereas the equilibrium distribution greatly favors (>95%) the green translational isomer **R660$_{BPTTF}$**·4TRISPHAT in Me_2CO solution. Lacour's $TRISPHAT^-$ anion[389] is tris(tetrachlorobenzenediolato)phosphate(V), which is a larger and more diffuse redox-stable counterion than hexafluorophosphate. The large differences between equilibrium distributions of the red and green translational isomers of each salt can be attributed to differences in the (i) electronics and (ii) sterics of the counteranions: (i) the weaker ion-pairing interactions of $TRISPHAT^-$ render CBPQT·4TRISPHAT a stronger π-electron acceptor than CBPQT·4PF_6, thus enhancing its relative affinity for the more electron-rich BPTTF recognition site, and (ii) the bulkier $TRISPHAT^-$ ions compete for more of the space that the DNP polyether loops require to effectively stabilize the red **R660$^{4+}_{DNP}$** translational isomer with [C–H···O] hydrogen-bonding interactions with the acidic α protons of the bipyridinium rings in CBPQT^{4+}. Although

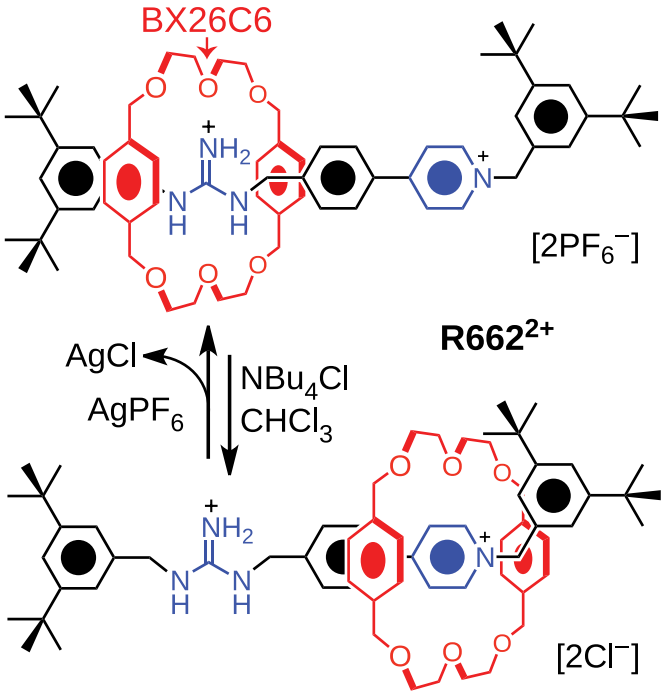
counterion effects are often ignored in these systems, **R660**$^{4+}$ demonstrates that they can have a profound effect on the translational isomerism of charged mechanomolecules.

Counterion exchange has also proven to be a useful strategy for switching bistable rotaxanes that utilize a triptycene-based bis[24]crown-8 cagelike host (see **Section 2.3.4.2**), a type of structure which was developed independently circa 2006 by Chiu.[390,391] and Chen.[392,393] This kind of multicyclic building block has allowed both of their groups to synthesize novel mechanomolecules.[311,394–397] See **Chapter 4**. Chiu[398] discovered that mechanical switches involving dialkylammonium-containing dumbbells that penetrate both crowns of the cage, which were originally designed for pH actuation, respond better to anion exchange than they do to acids and bases. For example, **R661H$_2$**$^{4+}$ adopts (**Scheme 6.61**) one of two different co-conformations depending on the counterions, an effect caused by different ion-pairing strengths. In the rotaxane **R661H$_2$**·4PF$_6$, 80% of the molecules exist as the asymmetrical co-conformer in $MeNO_2$, where one crown of the cage encircles a dialkylammonium center near the end of the dumbbell and the other crown encircles a central pyridinium recognition site. Since halogens form much stronger ion-pairs with dialkylammonium ions, the exchange of PF_6^- counterions for Cl^- ions with NBu_4Cl causes the cage to adopt exclusively the symmetrical co-conformation (**R661H$_2$**·4Cl) in which the cage embraces both pyridinium units located near the center of the dumbbell. The tetrachloride **R661H$_2$**·4Cl can be converted back to **R661H$_2$**·4PF$_6$ with $AgPF_6$, which precipitates the insoluble AgCl salt as a byproduct.

Although it is completely different in its constitution, Chiu's rotaxane **R662**$^{2+}$ can also be actuated (**Scheme 6.62**) using



Scheme 6.61 Chiu's cage-based [2]rotaxane **R661H$_2$**$^{4+}$ can be actuated[398] by counterion exchange. As the PF_6^- salt, the polyether cage interacts with one of the dialkylammonium recognition sites. Halide exchange causes the cage to avoid the $-NH_2^+-$ centers because they participate in stronger ion-pairing interactions with the Cl^- ions.

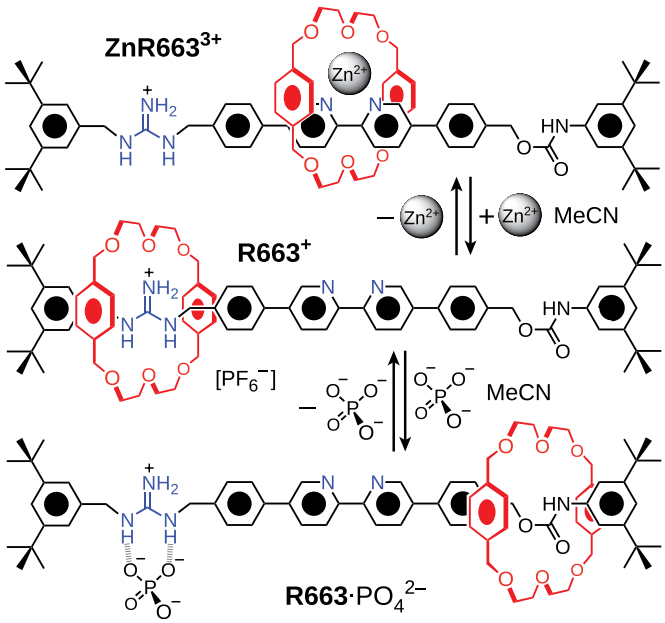


Scheme 6.62 In the anion-switchable [2]rotaxane **R662**$^{2+}$, the BX26C6 ring encircles a guanidinum recognition site as a PF_6^- salt, but occupies a pyridinium recognition site as a Cl^- salt on account of stronger guanidinium-chloride ion-pairing interactions in the latter case.[399]

the ion-pairing effects.[399] The BX26C6 ring encircles the guanidinium ion preferentially instead of the pyridinium recognition site in the dumbbell as the PF_6^- salt **R662**·2PF$_6$ in $CHCl_3$ and $MeNO_2$. Thus, the [N–H···O] hydrogen bonding between the guanidinium ion and the crown ether outcompete the [C–H···O] hydrogen bonds and π-associated donor-acceptor interactions between the crown ether and pyridinium unit in low-polarity solvents. Note, however, that the opposite situation is true in more polar solvents—see **Section 6.6**. Upon the addition of NBu_4Cl, the BX26C6 ring is displaced by a tighter-binding Cl^- ion in **R662**·2Cl and migrates to surround the pyridinium unit as a result. Removal of the Cl^- ions by precipitation of AgCl with $AgPF_6$ restores the original co-conformation to **R662**·2PF$_6$. Br^- and OAc^- ions elicit the same response as the Cl^- ion.

An evolutionary descendent[400] of **R662**$^{2+}$ is the tristable rotaxane **R663**$^+$, which uses both cationic and anionic stimuli (**Scheme 6.63**) for controlling the position of the BX26C6 ring. At the outset, hydrogen-bonding interactions position the ring predominantly around a guanidinium ion in **R663**·PF$_6$. The absence of a second cationic site allows this switch to operate with some fidelity—the precise equilibrium distributions have not been estimated—in MeCN, a solvent of unusually high polarity for neutral hydrogen-bonded switches. Chiu uses phosphate anions instead of halides to drive the ring away from guanidinium in this case: the strong electrostatic pairing and hydrogen bonding between the phosphate and guanidinium ions displaces the ring in **R663**$^+$·PO_4^{3-}, forcing it to occupy a low-affinity urethane

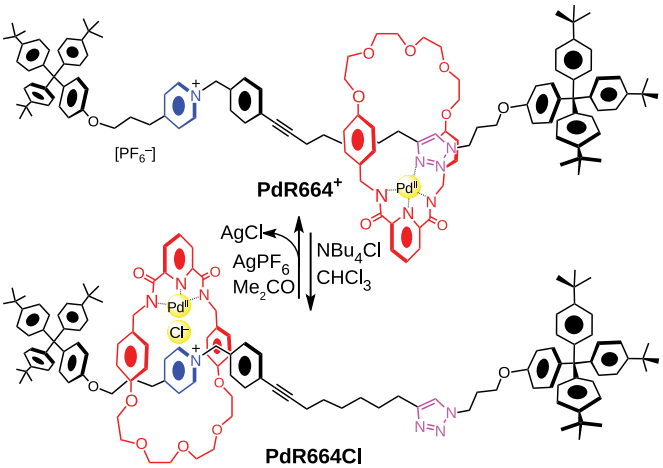
recognition site at the other end of the dumbbell for lack of a better site. The ring moves to the bipyridine ligand at the center of the dumbbell, however, when it assumes a cationic charge. This charge can be introduced by protonating the nitrogen atoms with acid—see **Section 6.3** for pH-triggered shuttles—or by coordination of transition metal cations—see **Section 6.4.1** for transition metal-triggered shuttles. Thus, the addition of $Zn(ClO_4)_2$ causes the ring to migrate to the center of the axle in **ZnR663**$^{3+}$. This Zn^{2+} template can be stripped away with a tighter-binding *N*,*N*,*N*′,*N*′-tetrakis-(2-pyridylmethyl)ethylenediamine ligand. Conceptually similar multi-stable [2]rotaxanes made from different combinations of components that can be actuated by a combination of stimuli, including competitive anion binding, have been reported by Wang.[401–403]



Scheme 6.63 A three-station [2]rotaxane **R663**$^{+}$ which responds to both cationic and anionic stimuli.[400]

6.5.2 Switching Through Second-Sphere Interactions

Although second-sphere coordination, in which hosts and receptors interact with the ligands of metal complexes, has long been recognized as a valuable interaction for the construction of novel supramolecular motifs,[404–407] it was not exploited to template the formation of mechanical bonds until Wisner[408–411] began introducing a series of second-sphere mechanomolecules in 2005—see **Section 3.3.1**. In 2008, when Leigh[412] discovered serendipitously the ion-pairing behavior of the rotaxane **PdR664**$^{+}$, second-sphere interactions finally entered the realm of molecular switches. The Edinburgh (now Manchester) group found that the endotopic Pd^{II} ion within the ring of **PdR664**$^{+}$ can be positioned (**Scheme 6.64**) at one of two sites on the dumbbell component with high fidelity (>98% co-conformational



Scheme 6.64 A switchable [2]rotaxane driven by second-sphere ion-pairing interactions.[412] The axle's triazole unit coordinates the Pd^{II} center of the charge-neutral ring in **PdR664**·PF_6, whereas the anionic PdCl-based ring of **PdR664Cl** binds to the pyridinium recognition site.

selectivity in each state) by modulating the coordinative Pd–Cl bond with ion-pairing effects. When it is not housing a Cl^- ion, the ring is charge-neutral and the open coordination site on the Pd^{II} center in **PdR664**$^{+}$ is occupied by the dumbbell's triazole group. When the triazole unit is displaced by a Cl^- ion, however, the ring in **PdR664Cl** becomes anionic, and thus forms a tight ion pair with the cationic pyridinium recognition site at the other end of the dumbbell, where it is stabilized by [C–H···O] and [C–H···Cl] hydrogen bonds. The Cl^- ion can be removed by precipitation with $AgPF_6$, generating AgCl as a byproduct.

6.5.3 Switches Driven by Anion Binding

By analogy with cation-driven (**Section 6.4**) mechanomolecular switches, which rearrange in response to different cationic templates, anion-template switches should also be capable being driven template exchange. Indeed, mechanically bonded molecular switches can be actuated by the competitive binding of either inorganic (**Section 6.5.1.1**) or organic (**Section 6.5.1.2**) anions.

6.5.3.1 Switching with Inorganic Anions

Just as Sauvage's catenands and catenates can be actuated between states of relatively well- and poorly- defined co-conformations by template addition and removal, respectively, one can add or remove anionic templates to influence the co-conformations of anion-binding catenanes. The homo[2]catenanes illustrated in **Figure 6.14** serve as illustrative examples of this kind of switch design. Sessler[413] has prepared a benzylic amide catenane **C617** derived (**Figure 6.14a**) from bipyrrole—see **Section 2.3.6.1**—while Li and Li[414] have prepared the catenated macrocyclic bis(triazolo)indolocarbazoles **C618**, and solved the catenane's structure (**Figure 6.14b**) in the solid state by single-crystal X-ray diffraction. Both of these [2]catenanes

adopt co-conformations dominated by internal hydrogen-bonding interactions until a chloride template is introduced in solution, at which point the rings rearrange (**Figure 6.14c**) such that their bipyrrole or indolocarboazole recognition units, respectively, can stabilize the Cl^- anions in a centralized binding pocket.

Much of the work on the anion-templated formation of mechanical bonds has been carried out by Beer[415–418] at Oxford. A succession of reports from the Beer group reveal that the dynamics of their anion-templated MIMs are strongly influenced by the specific anion in question, especially for halide ions such as chloride and bromide. In some cases,[349,419] the sequestration of a halide ion 'locks' the components and thus considerably restricts their dynamics. Computer simulations[420,421] of these compounds' molecular dynamics, however, indicate that the overall geometries are usually influenced only subtly by the exchange or removal of anions. Exceptions to this tendency have nevertheless emerged. In the first[422] (**Scheme 6.65**) of two such examples, the rotaxane **R665Cl**$^+$ has been shown to sequester chloride at its center by virtue of hydrogen bonds from the isophthalamide macrocycle and the acidic protons of a bis(imidazolium) recognition site. When **R665** $\cdot 2PF_6$ is free of any halide templates, the isophthalamide groups on the

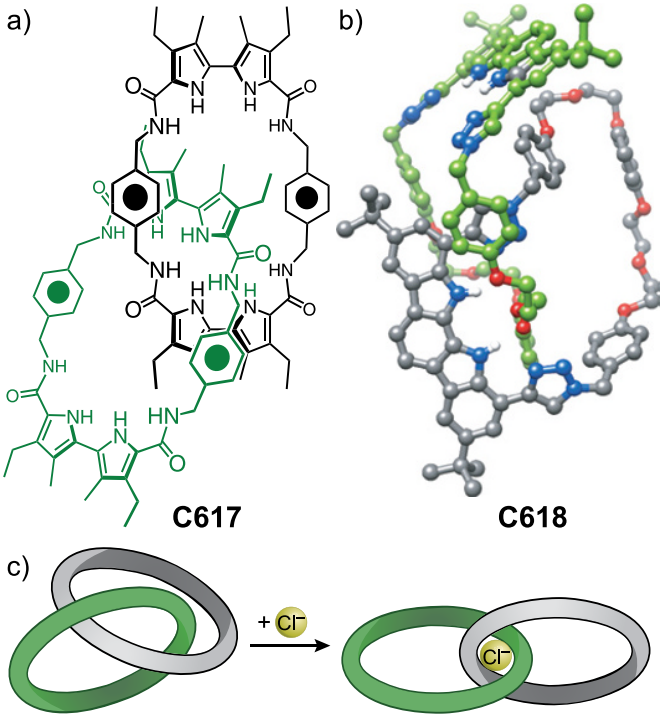
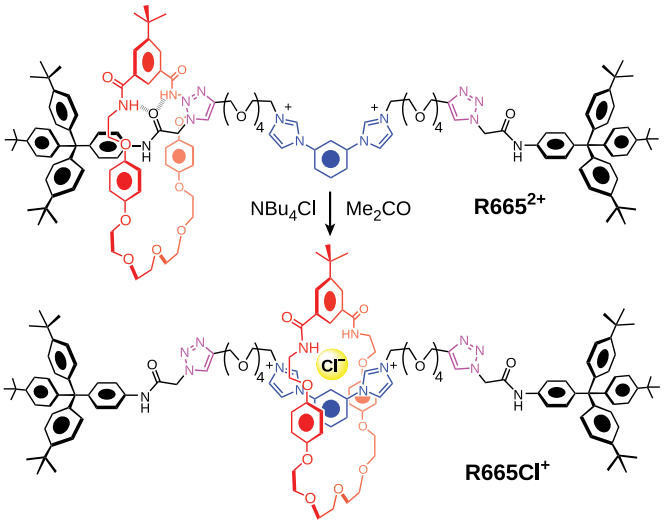


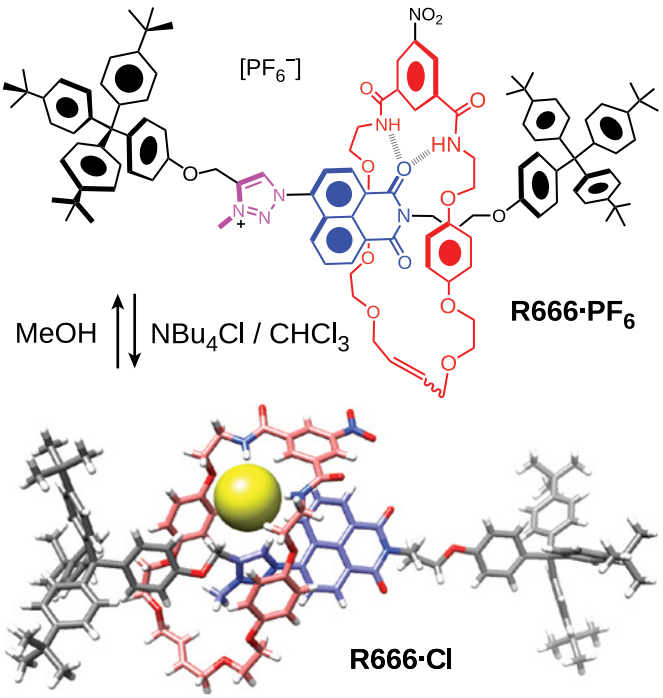
Figure 6.14 Examples of anion-driven motion in chloride-binding [2]catenanes. (a) Stereoformula of Sessler's catenated benzylic amides containing bipyrrole recognition units. (b) Ball-and-stick representation of Li and Li's acridane-based homo[2]catenane, with CH protons omitted for the sake of clarity. (c) Graphical representation of the chloride-triggered process that locks the catenated rings in a co-conformation that allows their recognition units to surround the Cl^- center.



Scheme 6.65 Beer's chloride-switchable [2]rotaxane.[422] Although hydrogen-bonding interactions place the isophthalamide-based ring preferentially around one of the amide-triazole linkers near the dumbbell's stoppers in **R665**$^{2+}$, a chloride ion induces the ring to move to the central bis(imidazolium) recognition site where it is stabilized by the acidic protons of each component part in **R665Cl**$^+$.

ring bond noncovalently with one of the amide linkages that connect the stoppers to the dumbbell.

The other anion switchable shuttle which we have chosen to highlight (**Scheme 6.66**) from the Beer collection[423] is **R666**$^+$. The ring in this rotaxane has the standard design one associates with the Beer laboratory, incorporating an isophthalamide unit—made more electron deficient with a nitro functional group—and HQ units adjacent to the ring's



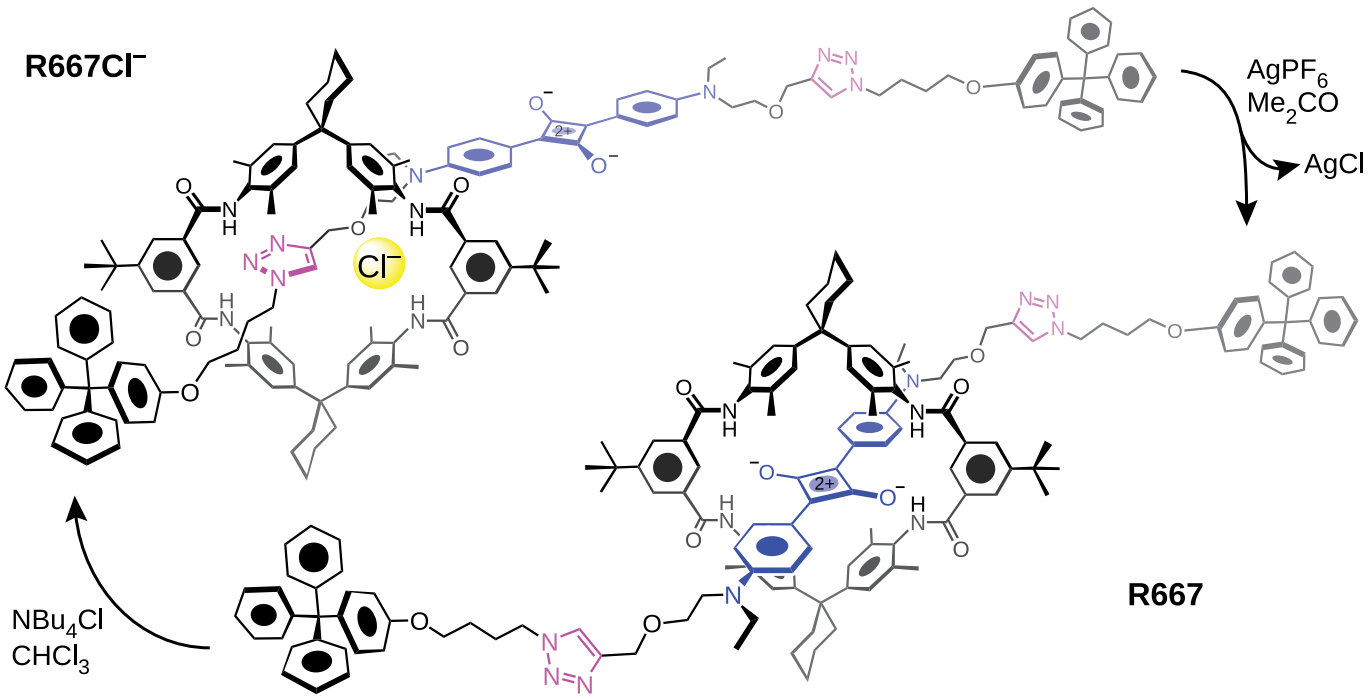
Scheme 6.66 The anion-driven switching and solid-state structure[423] of the chloride-switchable [2]rotaxane **R666** $\cdot$ **Cl**.

olefinic ether loop. The two recognition sites on the dumbbell are the electron-deficient naphthalimide and triazolium units. The ring encircles the naphthalamide recognition site predominantly when the triazolium counterion is hexafluorophosphate—as in **R666**·PF_6—stabilized by π-donor···π-acceptor interactions and hydrogen bonds between isophthalamide and the imide's carbonyl groups. Exchanging the counterion to **R666Cl** causes the ring to prefer occupying the triazolium site, however, because the ring and triazolium create a binding pocket for the Cl^- anion. This binding pocket involves hydrogen bonds between the protons of the isophthalamide and triazolium units with the coordinated Cl^- anion. **R666Cl** has been characterized in the solid state by X-ray crystallography, a rare feat[123,424] for rotaxanes with such bulky stoppers. The ring can be returned to the naphthalamide site of **R666**·PF_6 by removing the halide template with the addition of a competitive protic solvent such as MeOH.

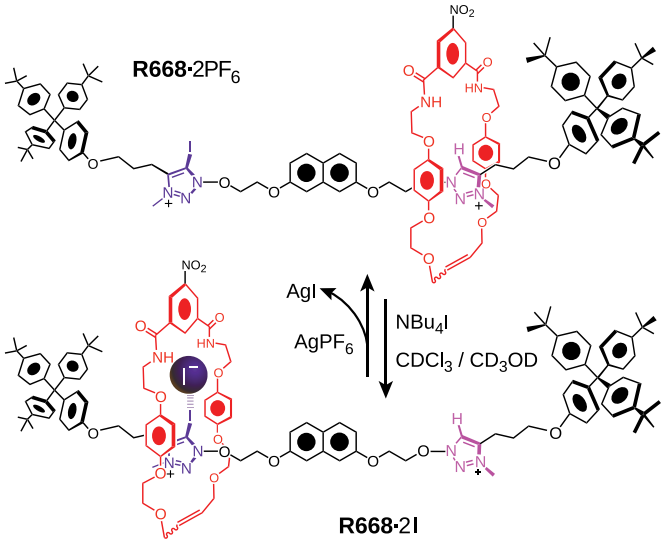
Smith[425] discovered that the position of a tetralactam ring in one of his squaraine rotaxanes **R667** can be controlled (**Scheme 6.67**) through competitive binding of Cl^- ions. The tetralactam ring encircles the squaraine unit predominantly in **R667** so as to stabilize its negatively charged carbonyl groups with hydrogen bonds. When a soluble chloride salt (NBu_4Cl) is added in $CHCl_3$ solution, the Cl^- ions outcompete the squaraine unit for those hydrogen bonds. Thus, the ring of the complex **R667Cl**$^-$ is located at either end of the dumbbell, where the Cl^- ion can accept an additional hydrogen bond from the activated C–H moiety of a triazole unit. The ring can be returned to the squaraine unit at the center of the dumbbell by precipitating the Cl^- ion as AgCl upon the addition of $AgPF_6$. Since the fluorescence emission of the squaraine unit is quenched by the ring, this rotaxane can be used as an optical chloride sensor. Recently, Smith[426] has relied on similar principles in developing another chloride-sensing rotaxane based on a benzylic amide ring and a dihydroxyl-substituted squaraine dye, giving a ratiometric response to Cl^- ions at deep-red wavelengths.

Beer[427] has recently brought halogen-bonding anion recognition into the fold of switchable molecular shuttles. The design of his bistable [2]rotaxane **R668**$^{2+}$ involves the same 4-nitroisophthalamide-based ring as the chloride-switchable predecessor **R668**$^+$, interlocked with a two-station dumbbell possessing triazolium and iodotriazolium recognition units. As a switchable shuttle, this bistable [2]rotaxane is driven (**Scheme 6.68**) by iodide ions. Whereas the ring spends nearly 100% of its time around the triazolium unit of the **R668**·$2PF_6$, the addition of up to 4 equiv of NBu_4I as a source of iodide redistributes the ring population to favor (54%) the iodotriazolium unit of **R668**·2I. A halogen bond between the iodine atom of the iodotriazolium unit and an iodide counterion are responsible for stabilizing this species. The shuttling process can be reversed by restoring **R668**$^{2+}$ to the PF_6^- salt by adding $AgPF_6$, causing Ag^I to precipitate as an isoluble byproduct. The response to iodide is selective—the addition of chloride ions, for example, locks the ring more tightly around the triazolium unit.

A [2]rotaxane which that switches as a result of competitive anion binding in a tetralactam ring and a triazole-based dumbbell has been described by Schalley,[428] while



Scheme 6.67 A chloride-switchable squaraine-based molecular shuttle.[425] The competitive binding of chloride anions between the acidic protons of a triazole unit and a tetralactam macrocycle displaces the preferred squaraine recognition site of **R667**.

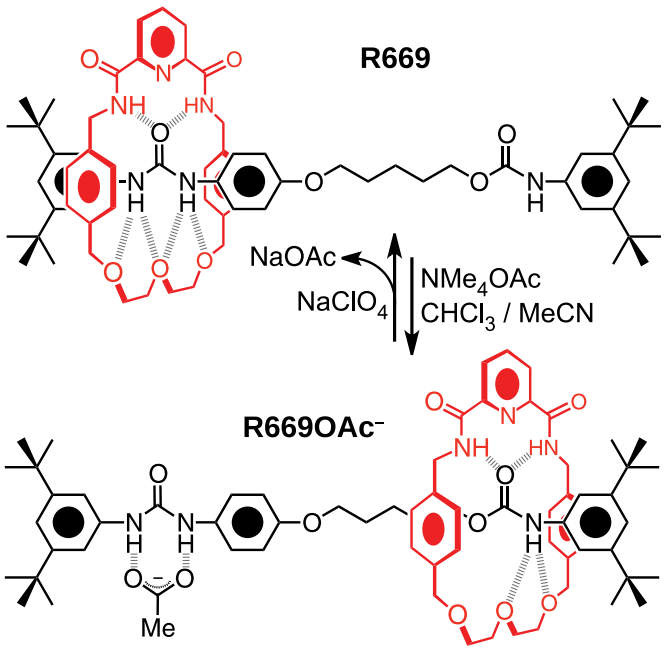


Scheme 6.68 Ring shuttling in Beer's bistable [2]rotaxane **R668**$^{2+}$ is driven by halogen-bonding anion recognition.[427]

a molecular elevator based on this design is described in **Section 6.13.1.3**.

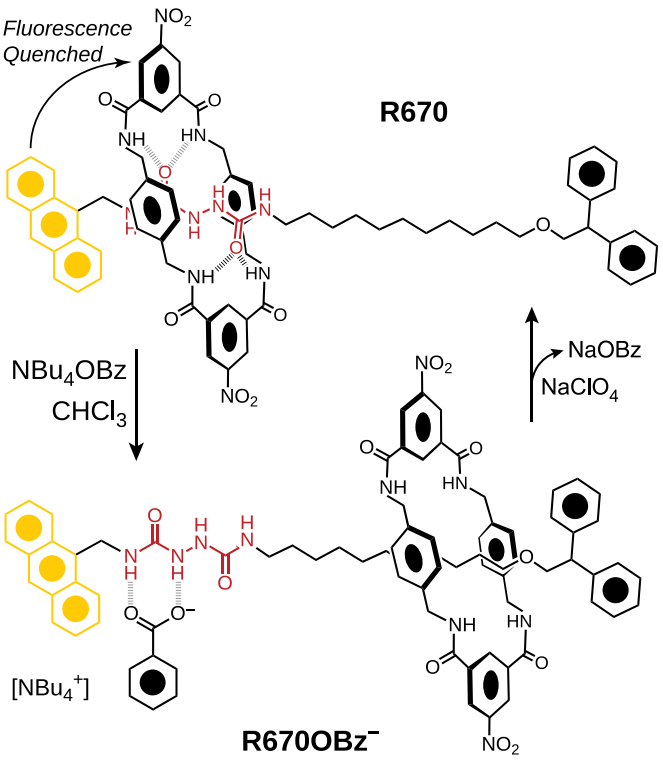
6.5.3.2 Switching with Organic Anions

Chiu[429] has shown that competitive binding of acetate anions to a urea recognition site can induce translation (**Scheme 6.69**) of a benzylic amide crown ether in the [2]rotaxane **R669**. Since the ring is capable of both accepting and donating hydrogen bonds by virtue of its 2,6-pyridinediamide units, it binds to urea derivatives with reasonably high K_a values of 10^2–$10^4\,M^{-1}$ in organic solvents. The dumbbell of **R669** has a diphenylurea recognition site and a weaker-binding carbamate group as the secondary binding site. Thus, the ring encircles the diphenylurea unit predominantly in a 1:1 mixture of $CDCl_3$ and MeCN, but migrates to the carbamate site when NBu_4OAc is added to the solution, since the OAc^- anion competes effectively for hydrogen bonding with the urea's –NH– groups by virtue of its strong hydrogen bond accepting character and its complementary Y-shaped geometry. The acetate ions can be removed by precipitation of NaOAc with the addition of $NaClO_4$, returning the ring to the urea binding site.



Scheme 6.69 The competitive binding of acetate ions with the urea unit in the rotaxane **R669** drives[429] its ring to associate with a lower-affinity carbamate site.

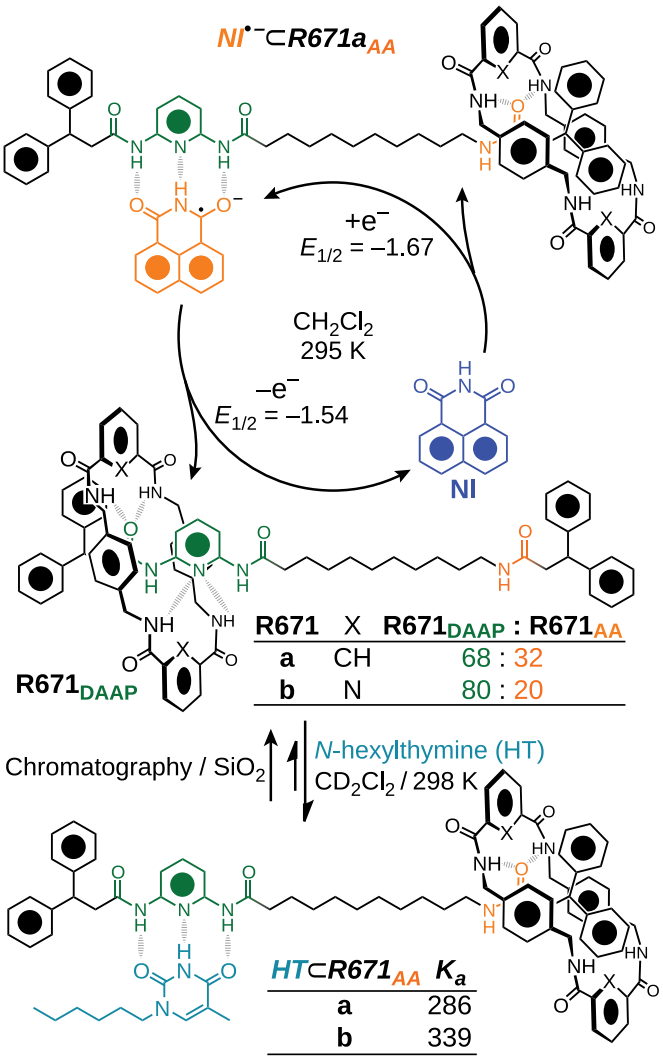
Berná[430] has investigated (**Scheme 6.70**) the anion-dirven actuation of the [2]rotaxane **R670**, which contains a single



Scheme 6.70 The translation of a benzylic amide ring in Berná's [2]rotaxane **R670** is driven by the competitive binding and precipitation of a benzoate anion.[430]

hydrazodicarboxamide recognition site for its benzylic amide ring. In the presence of 3 equiv NBu_4OBz, the ring of **R670** is displaced by the benzoate anion, which binds the hydrazodicarboxamide unit with a log$K$ of 4.5, or approximately $32{,}000\,M^{-1}$. The presence of an anthrylic atopper adjacent to the recognition site engenders this switch with a fluorescence readout, since emission from anthracene is quenched much more effectively by the 4-nitro-isophthalamide units of the ring when it encircles the hydrazodicarboxamide recognition unit, as opposed to the undecamethylene linker of **R670OBz**$^-$. The switch can be reset by precipitation of the benzoate competitor as NaOBz with the addition of $NaClO_4$ as a source of Na^+. The switch can also be reset by an oxidative covalent modifcation (**Section 6.7**) of the hydrazodicarboxamide unit to azodicarboxamide, a recognition unit which binds the ring with much greater affinity.

Berná[431,432] has designed the bistable [2]rotaxanes **R671a** and **R671b** to respond (**Scheme 6.71**) to competitive binding interactions involving both anionic and neutral small molecules. While both rotaxanes possess identical dumbbells containing di(acylamino)pyridine (DAAP) and acetamide (AA) recognition units, the benzylic amide rings of **R671a** and **R671b** contain isophthalamide and dicaboxamidopyridine recognition units, respectively. The translation (**Scheme 6.71**) of the benzylic isophthalamide ring can be controlled[431] electrochemically by the competitive binding of a radical anion. While the majority (68%) of the population exists as the translational isomer $\mathbf{R671a}_{\mathbf{DAAP}}$ in the presence of naphthalimide (NI, $K_a = 74\ M^{-1}$), the electrochemically reduced radical anion $NI^{\bullet-}$ outcompetes the benzylic amide ring for the DAAP site, populating the acetamide-encircled translational isomer in the complex $\boldsymbol{NI^{\bullet-}\subset R671a_{AA}}$ ($K_a = 13000\ M^{-1}$) at 295 K in CH_2Cl_2. The half-wave reduction potential ($E_{1/2}$) of the NI unit is less negative when complexed with **R671a** ($E_{1/2} = -1.54$ V) than is the free NI unit ($E_{1/2} = -1.67$ V), on account of the DAAP unit's ability to stabilize the $NI^{\bullet-}$ radical anion with hydrogen-bonding interactions that are much stronger than those of the charge-neutral NI. The shuttling motions driven by the competitive binding of neutral molecules to these [2]rotaxanes are described in **Section 6.6.1**.



Scheme 6.71 The reversible redox properties of a naphthalene imide and its radical anion drive[431] the shuttling of a benzylic amide ring, owing to competitive binding interactions between the radical anion and the dumbbell's di(acylamino)pyridine recognition unit.

Although anion sensing and binding is a rich field of supramolecular chemistry with a rapidly growing library of recognition motifs,[433–442] most of this research effort has not yet been adapted for the making of mechanical bonds, leaving new research directions in the area of anion-driven molecular switches and machines wide open for investigation in the future.

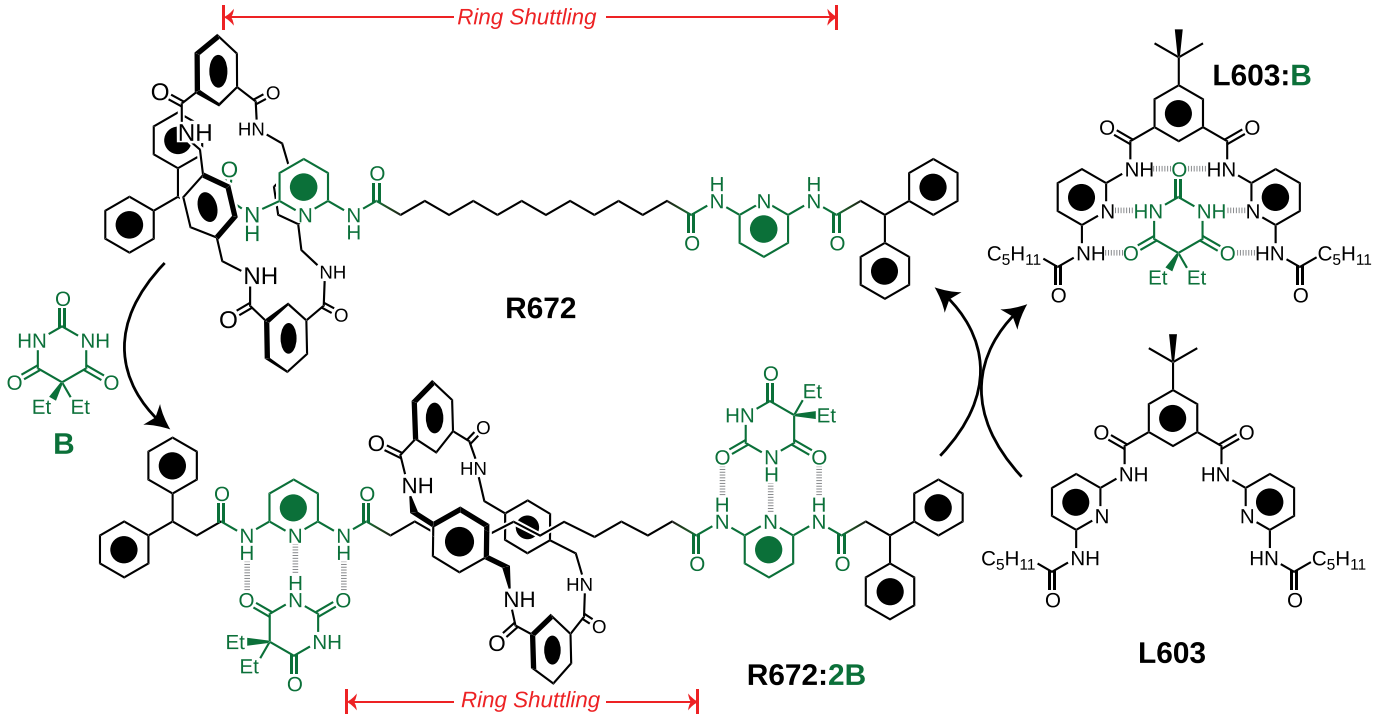
6.6 Switches Driven by Molecular Recognition

When competitive binding is utilized as the stimulus for a mechanically interlocked molecular switch, it is typically driven by cations (**Section 6.4**) or anions (**Section 6.5**). In this Section, we discuss competitive binding interactions that lead to mechanical switching motions as a result of molecular recognition, either of neutral small molecules (**Section 6.6.1**) or single stranded DNA (**Section 6.6.2**).

6.6.1 Switches Driven by Neutral Small Molecules

As described by **Scheme 6.71** and the corresponding discussion in **Section 6.5.3.2**, the benzylic isophthalamide and dicarboxamidopyridine macrocycles of Berná's [2]rotaxanes **R671a** and **R671b**, respectively, can be displaced[431,432] by competitive binding interactions involving the dumbbell's primary recognition site, DAAP. The hydrogen bond donors (D) and acceptors (A) of this di(acylamino)pyridine recognition unit constitute a DAD sequence, which is complementary to ADA molecules, including not only $NI^{\bullet-}$ and NI, but other neutral molecules such as barbital (B) and *N*-hexylthymine (T). In the absense of a competitive binder, occupation of the DAAP recognition site by the benzylic isophthalamide ring is 68% in **R671a**, while the dicarboxamidopyridine-based ring encircles the DAAP unit in ~80% of the population of **R671b**. In both cases, the benzylic amide rings are displaced by the competivive binding ($K_a = 286$–$339\ M^{-1}$) of *N*-hexylthymine at 298 K in CD_2Cl_2. The original states, in which the benzylic amide rings encircle the DAAP units, can be recovered either by the introduction of a competitive binder for thymine, or by normal-phase chromatographic separation of thymine on silca gel.

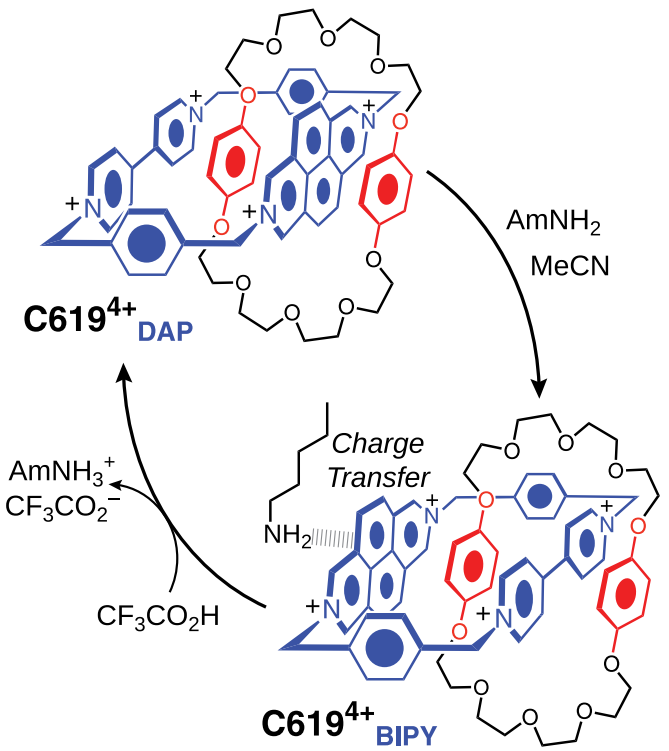
Berná's seminal example[443] of ring displacement driven by the competitive binding (**Scheme 6.72**) of neutral molecules was that of the degenerately bistable [2]rotaxane **R672**, in which the benzylic isophthalamide macrocycle spends most of its time (96%) occupying either of the dumbbell's DAAP recognition units in CD_2Cl_2. Although the affinity of the triple-hydrogen-bond DAD-ADA complexes based on



Scheme 6.72 The competitive binding of neutral barbital (**B**) molecules at the diacylaminopyridine recognition sites of rotaxane **R672**, which is promoted by a triple hydrogen bonded DAD-ADA motif, restricts the translation amplitude of a benzylic amide ring in the dumbbell of **R672:2B**.[443] The barbital competitors can be sequestered by a stronger receptor **L603**.

these compounds is reduced in CD_2Cl_2 from 178 to 108 M^{-1} for barbital, and from 405 to 156 M^{-1} for *N*-hexylthymine, the introduction of either one of these competitors into the solution displaces the benzylic amide ring. The case of barbital as a competitive binder is illustrated in **Scheme 6.72**. ^{1}H NMR Spectroscopic investigations reveal that the ring shuttles between each of the two recognition sites in the absence of barbital, whereas ring motion is restricted primarily to the dumbbell's central dodecamethylene chain when barbital is added in excess to generate the ternary complex **R672:2B**. These restrictions can be lifted by the introduction of the bis-diacylaminopyridine host **L603**, which competes more effectively for barbital. In summary, a neutral small-molecule can be used as a switching stimulus by virtue of competitive binding interactions. The ability to constrain molecular motion through competitive binding in this manner has been compared to the role of cofactors in regulating enzyme activity in biology.

The [n···π] charge-transfer interactions between 2,7-diazopyrenium (DAP^{2+}) dications and various aliphatic amines have been utilized[444] in the chemically-driven switching (**Scheme 6.73**) of the bistable [2]catenane[445] **C619^{4+}**. Whereas the BPP34C10 ring of this [2]catenane encircles the DAP^{2+} recognition unit over the $BIPY^{2+}$ unit in a 96:4 ratio at –80 °C in $(CD_3)_2CO$, the formation of a stable charge-transfer adduct that competes for the π-surface of the DAP^{2+} dication renders the $BIPY^{2+}$-encircled co-conformer **C619$^{4+}_{BIPY}$** the major species in a solution containing *n*-amylamine. The GSCC of **C619$^{4+}_{DAP}$**

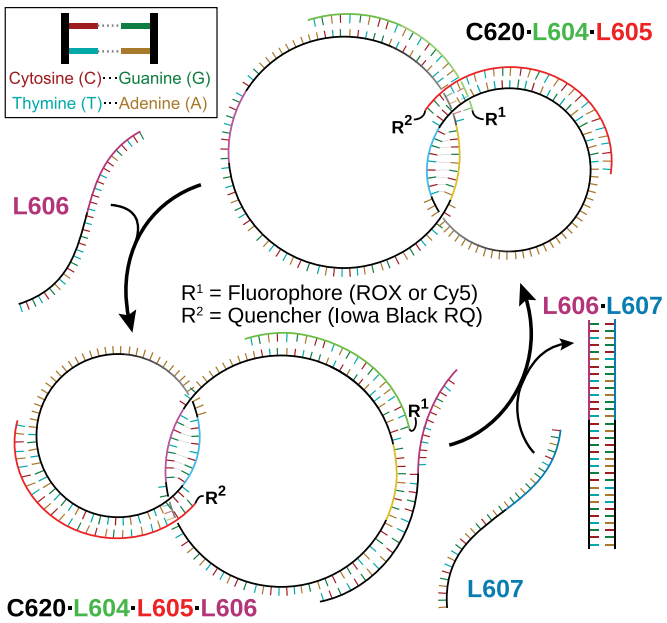


Scheme 6.73 The circumrotation of a tetracationic cyclophane in the [2]catenane **C619^{4+}** is driven[444] by the formation of a competitive binding CT complex between amylamine and its DAP^{2+} recognition unit, an interaction which can be reversed by protonation of the amine with TFA.

can be restored quantitatively if the charge-transfer (CT) complex is interrupted by protonation of the amine with TFA. A dual-mode donor-acceptor [2]catenane has also been been conceived,[79] in which the amine···DAP^{2+} interaction controls the circumrotation of a tetracationic cyclophane, while the oxidation and reduction (**Section 6.1.1.1**) of a TTF unit controls the pirouetting of the corresponding crown ether.

6.6.2 Switches Driven by DNA Strand Displacement

DNA strand displacement[446] is a reaction in which the hybridization of two DNA strands with partial or full complementarity displaces one or more duplexed strands. Willner[447] has pioneered the application of strand displacement for powering motions in mechanomolecules comprising interlocked DNA strands—see **Section 2.3.12.1**. A relatively simple case scenario[448] of this mechanism of action is depicted in **Scheme 6.74**. The [2]catenane **C620** comprises two circular single-stranded DNA (ssDNA) macrorings of 89 and 69 nucleotides. The large ring contains two domains that recognize a sequence (shaded blue) of 9 base pairs (bp) within the small ring—one domain (yellow) hybridizes completely with this sequence, while a second domain (magenta) forms a weaker duplex as a result of having two nucleobase mismatches. The large and small rings also contain sequences that recognize the complementary ssDNA strands, **L604** and **L605**, armed with a fluorophore (ROX or Cy5) and a quencher (Iowa Black RQ), respectively, placed such that the distance-dependent quenching of the fluorophore by FRET reports the relative positions of the rings. This catenated switch assembly, **C620·L604·L605**, can be induced to circumrotate by the introduction of the 32-bp ssDNA strand **L606**, which displaces the smaller ring to its weaker recognition site by hybridizing 18 of its nucleobases, six of which compete for the same 9-bp binding sequence, with the larger ring in **C620·L604·L605·L606**. The remaining 12-bp unduplexed sequence serves as a "toehold" that facilitates the removal of **L606** by the addition of a complementary 32-bp ssDNA **L607**, which outcompetes the catenane for hybrization with **L606**. A noticeable change in the fluorescence output was observed as the switch was actuated multiple times by this strand displacement scheme, owing to the concomitant repositioning of the FRET pairs. The strand displacement strategy for actuating DNA mechanomolecules has been expanded to more sophisticated DNA topologies and architectures, including DNA/nanoparticle hybrid rotaxanes[449] and catenanes,[450] three-state [2]catenane rotors,[451,452] [3]catenanes,[448] [5]catenanes,[453] and branched [7]catenanes.[454]



Scheme 6.74 Circumrotation driven by strand displacement in Willner's seminal reconfigurable DNA [2]catenane **C620**.[448]

Recently, Cockroft[455] has adapted DNA/protein rotaxanes of the kind originally described by Ghadiri[456] in order to create the "autonomously reciprocating transmembrane nanoactuator" **R673**, in which a streptavidin-stoppered DNA-PEG-Biotin dumbbell translates autonomously (**Figure 6.15a**) back and forth through an α-hemolysin (α-HL) transmembrane nanopore using the enzymatic degradation of DNA as fuel. The single-molecule construction of this type of DNA/protein hybrid rotaxane is described in **Section 2.3.12.2**. The 3´ end of the DNA axle extending into the "*cis*" compartment of the transmembrane device hybridizes with the primer **L608** in order to stopper the rotaxane's axle, preventing it from passing through the α-HL nanopore under the force of electroosmostic flow supplied by an electric field, which drives the axle toward the opposing "*trans*" compartment. In the presence of $V_2O_7^-$ and Mg^{2+} ions, the stepwise degradation of the primer by enzyme-catalyzed pyrovanadolysis with exonuclease III results in a sawtooth pattern (**Figure 6.15b**) in the transmembrane ion current, indicative of the stepwise motion of the axle through the pore. The ion current decreases as each nucleobase is severed because the nanopore becomes increasingly blocked as the PEG segment is extruded into the *trans* compartment and DNA enters the cavity, hindering the passage of ions through the channel. The 3´-end of the axle, which overhangs from the primer-hybridized stopper, is protected from nucleobase cleavage because it is not a substrate for DNA polymerase. The strand displacement reaction that ratchets the axle back to its original position against the direction of electroosmostic flow becomes increasingly likely as the primer degrades, since the loss of each base exposes a larger toehold to initiate the reset process. Under the conditions of the experiment, strand displacement by the full-length primer occurs on average after seven bases have been cleaved, but the enzymatic and strand displacement reactions are not tightly coupled, resulting in a probabilistic distribution for the timing of forward and

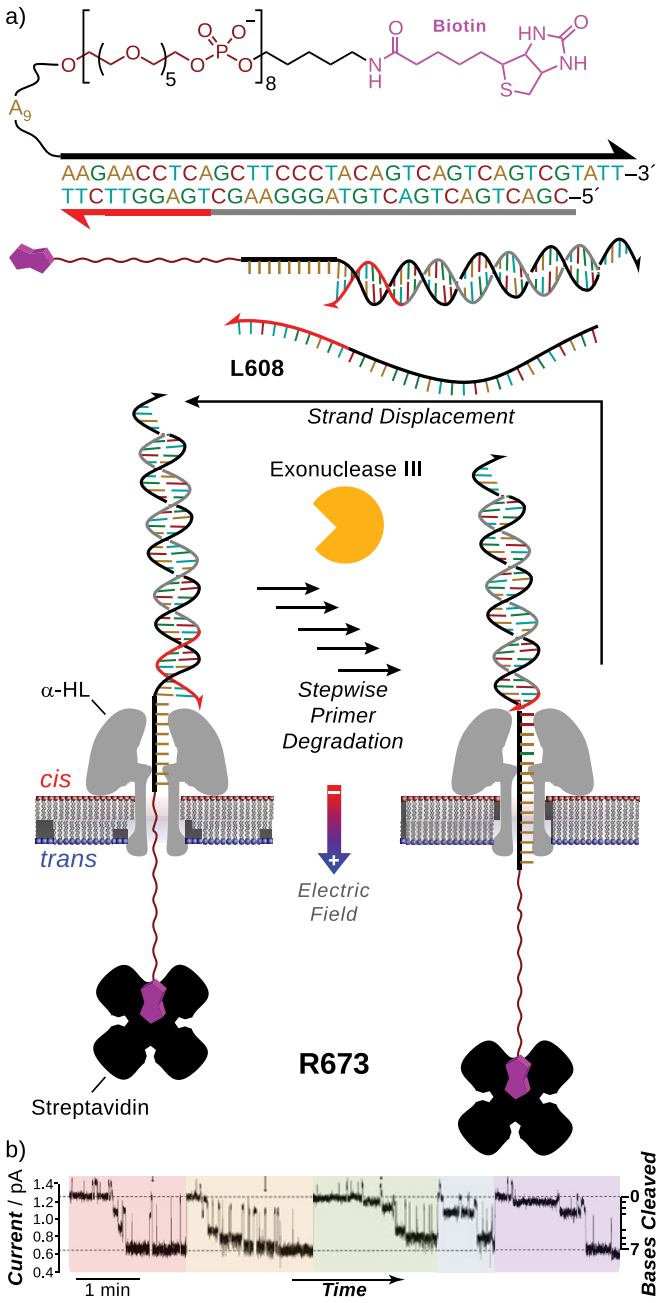


Figure 6.15 Cockroft's autonomously reciprocating transmembrane nanoactuator.[455] (a) Graphical representations of the co-constitution and autonomous actuation of the single transmembrane DNA/protein hybrid [2]rotaxane **R673**. Strand displacement reactions involving primer **L608** drive the rotaxane away from the direction of electroosmotic flow, while enzymatic degradation of the primer allows the axle to pass through the stopper as bases are pyrovanadolyzed in a stepwise manner. (b) Real-time ion current trace for a single transmembrane nanoactuator, which executes five cycles (shaded different colors) of degradation and strand displacement. Spikes in current that are not attributable to the strand displacement reaction correspond to enzyme binding events, while losses in current correspond to pyrovanadolysis events that shorten the length of the primer, allowing primer degradation to be monitored precisely with base-by-base resolution.

backward strokes. Thus, the autonomously cycling reaction powered by strand degradation and strand displacement, which consumes primer **L608** as fuel, is coupled with the back-and-forth motion of the axle with respect to nanopore that confines it at the membraneous interface.

6.7 Switches Driven by Covalent Reactions

The switches reviewed in this Section involve mechanical motions that are induced by reactions that make or break covalent bonds, which do not fall into the categories of pH-controlled protonation/deprotonation or metal-ligand bonds. They include the acylation of amines (**Section 6.7.1**), aldehyde protection (**Section 6.7.2**), substitution of pyridines (**Section 6.7.3**), Diels-Alder reactions (**Section 6.7.4**), hydrogenation/dehydrogenation (**Section 6.7.5**), and the Mitsunobu reaction (**Section 6.7.6**). Covalent bond-forming reactions have also been utilized in the design of a number of molecular machines that operate by ratchet mechanisms—see **Section 6.15.2**.

6.7.1 Switches Driven by Acylations of Amines

The foundations for controlling molecular shuttles with covalent chemical reactions were laid[457] with the advent of the so-called protecting group approach to molecular shuttles. In its debut, this approach involved the removal of a *tert*-butoxycarbonyl (Boc) protecting group from a [2]rotaxane to render two degenerate $–NH_2^+–$ recognition sites, between which a crown ether ring can shuttle—see **Section 5.1.1.2**, **Table 5.5**. In contrast with this covalent bond-breaking procedure, the examples illustrated in **Figure 6.16** utilize covalent bond-forming reactions to introduce steric and electronic interactions that displace crown ether rings from their dialkylammonium recognition sites.

Takata[458] has developed efficient reactions for modifying the dibenzylammonium site of the [2]rotaxanes in order to induce the directional shuttling of a DB24C8 ring. His first approach (**Figure 6.16a**) involved *N*-acylation, in which the reaction between **R674H**$^+$ and an appropriate electrophile (ROR or RCl) under basic conditions yields one of the compounds **R674Ra–i**. The steric bulk of the R group and corresponding loss of NH_2^+ hydrogen bond donors causes the ring to encircle the central phenylene unit of the dumbbell. The same outcome was achieved[295] subsequently using *N*-alkylation (**Figure 6.16b**) reactions, in which reductive amination of aldehydes with **R675H**$^+$ in the presence of an excess (15 eq) of sodium tri(acyloxy)borohydride yields the tertiary amine-based rotaxanes **R675Rj-o**. In some cases, such as **R675Ro**, the corresponding borohydride is not active enough to produce aldehyde intermediates *in situ*: in these cases, the reaction can be promoted by the addition of an excess of an appropriate aldehyde.

Tokunaga[459] has investigated a similar collection of [2]rotaxanes **R676Ha-f**$^+$, in which selective Boc-protection

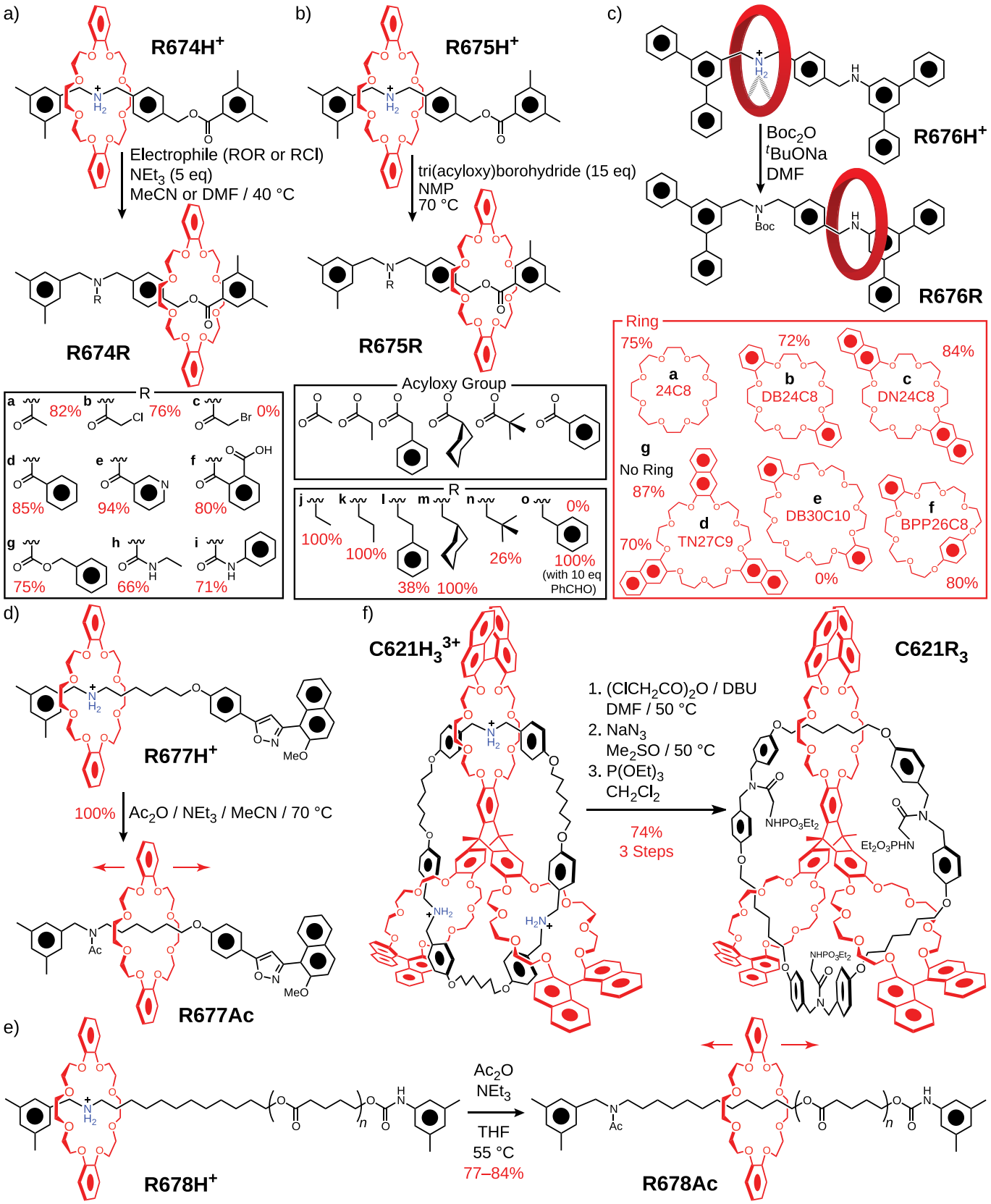


Figure 6.16 Ring motion driven by the acylation of dialkylammonium/crown mechanomolecules.[459,461,462] (a) Shuttling[458] of the DB24C8 ring in the [2]rotaxane **R674H**$^+$ is driven by *N*-acylation. (b) **R675H**$^+$ can also be switched[295] by *N*-alkylation. (c) A variety of crown ethers are induced[459] to shuttle by Boc-protection of the dumbbell in rotaxanes **R676H**$^+$**a-f**. *N*-Acylation of (d) **R677H**$^+$ and (e) **R678H**$^+$ increases[461] ring mobility, as well as polymer crystallinity in the latter case. (f) A three-step installation of bulky phosphoramidate stoppers on the dibenzylammonium groups induces[462] relative rotary motion of the 'ship's wheel' [2]catenane **C621H$_3$**$^{3+}$.

of the dibenzylammonium group is accomplished (**Figure 6.16c**) with a variety of different rotaxanes containing crown ethers, causing the macrocyclic polyethers to encircle an aniline recognition site in the corresponding [2]rotaxanes **R676Ra-f**.

Takata[460] has utilized *N*-acylation (**Figure 6.16d**) to modulate the fluorescence of the DB24C8-based [2]rotaxane **R677H$^+$/R677Ac** possessing an emissive boron enaminoketonate stopper. More recently, Takata[461] described macromolecular [2]rotaxanes possessing polyester axles, **R678H$^+$/R678Ac**, in which the increased DB24C8 ring mobility caused by *N*-acylation (**Figure 6.16e**) of the dialkylammonium recognition unit induces a change in the crystallinity of the polymer at a critical chain length, as determined by differential scanning calorimetry. This result suggests that even subtle mechanical motions in mechanomolecules can be amplified in macromolecular settings to change their bulk physical and mechanical properties.

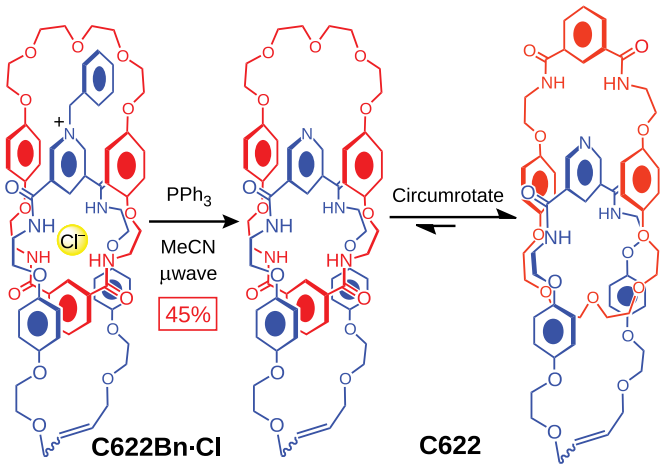
Zhu and Chen[462] have applied (**Figure 6.16f**) the protecting group approach to control submolecular motion in the unusual [2]catenane 'ship's wheel' architecture of **C621H$_3^{3+}$**. This catenane expresses relative rotary motion as a result of protecting its dibenzylammonium units with the bulky diethyl phosphoramidate stopper groups of **C621R$_3$**.

6.7.2 Switches Driven by Reactions of Pyridines

The nucleophilicity of pyridine derivatives renders them amenable to facile modification. Molecular switches with mechanical bonds have relied on benzylation (**Section 6.7.4.1**) and oxidation (**Section 6.7.4.2**) to drive shuttling processes.

6.7.2.1 Benzylation/Debenzylation

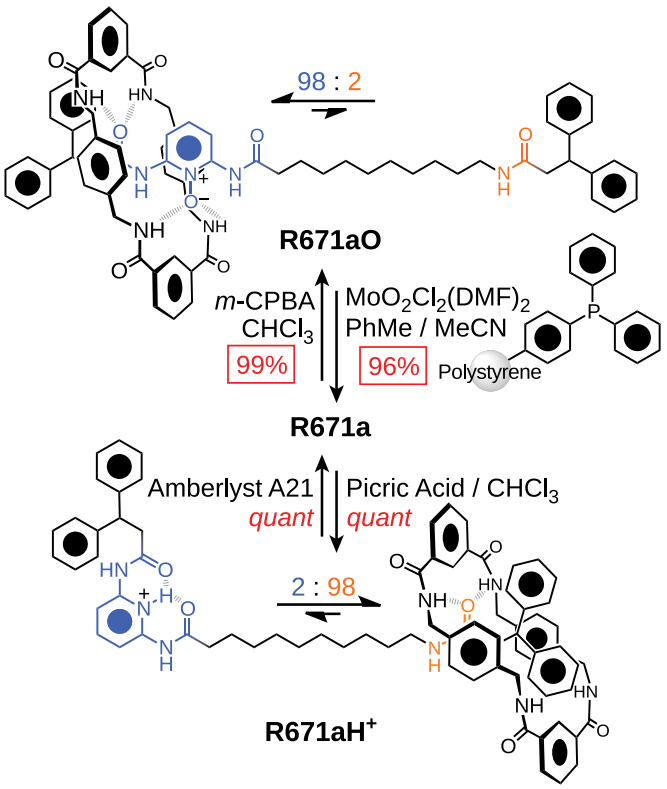
An example (**Scheme 6.75**) of a switch that is driven by covalent chemistry is the chloride-binding [2]catenane **C622Bn·Cl** described by Beer.[419] Debenzylation of this catenane affords the neutral catenane **C622**. The rings of **C622** can rotate rapidly in solution, but ^{1}H NMR spectroscopic evidence suggests that the co-conformer in which the rings undergo circumrotation by 180° with respect to the co-conformation of **C622Bn·Cl** is the dominant isomer in $CHCl_3$.



Scheme 6.75 Debenzylation of the [2]catenane **C622Bn·Cl** affords[419] a neutral [2]catenane **C622** in which the dominant co-conformation is one in which the rings are circumrotated by 180°.

6.7.2.2 Pyridine N-Oxides

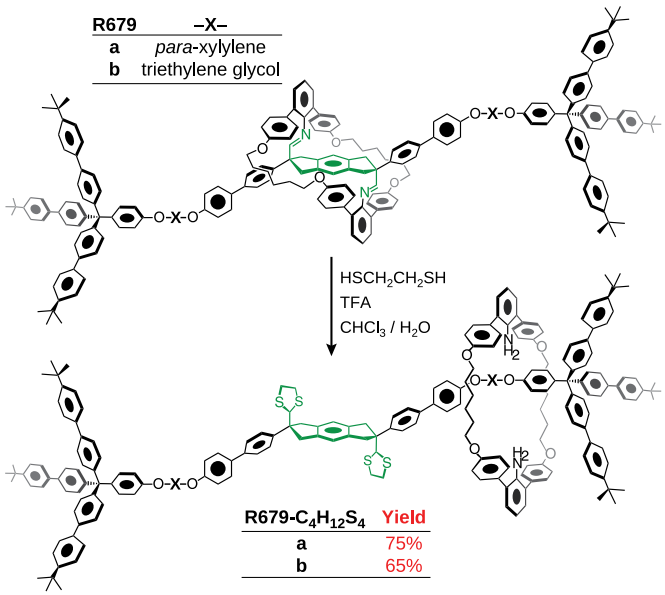
The [2]rotaxane **R671a**, which can be driven by competitive binding as described in **Scheme 6.71**, can also be induced to switch by covalent modification (**Scheme 6.76**) of the di(acylamino)pyridine recognition unit. Berná[431] has found that the benzylic amide ring predominantly encircles the acetamide group in **R671aH$^+$** on account of the self-fulfilling hydrogen-bonding interactions within the diacylaminopyridinium unit, whereas the ring encircles the diacylaminopyridine *N*-oxide unit of **R671aO**. These compounds are accessed by protonation or oxidation, respectively, of the pyridine subunit of **R671a** with picric acid or *m*-CPBA. The original state of **R671a** can be restored by deprotonation of **R671aH$^+$** with Amberlyst® A-21 resin or by reduction of **R671aO** with $MoO_2Cl_2(DMF)_2$/diphenylphosphino-polystyrene. All of these reactions that control the position of the ring with high fidelity ($K_{eq} \approx 50$ in each state) can be performed in near-quantitative (≥96%) yields.



Scheme 6.76 A bistable switch driven by the oxidation or protonation of a di(acylamino)pyridine recognition site in the [2]rotaxane **R671a** to the corresponding pyridine *N*-oxide **R671aO** or pyridinium **R671aH$^+$**, respectively.

6.7.3 Switches Driven by Protection of Aldehydes

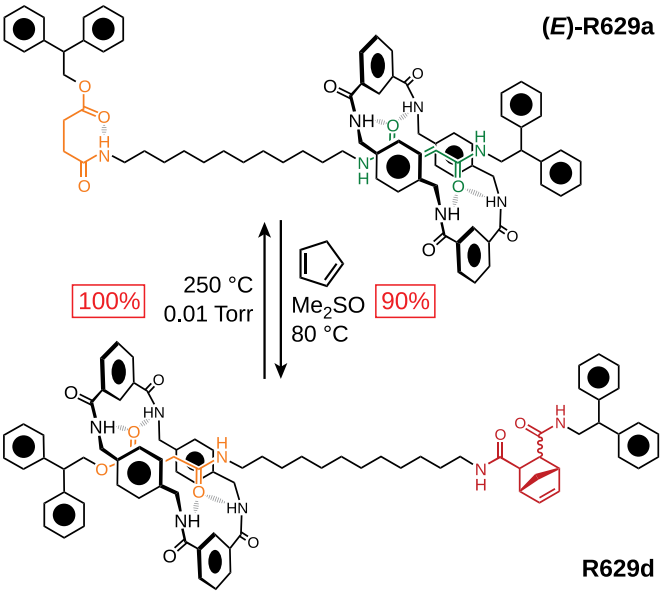
Kawai[463,464] has creatively exploited the reversible covalent chemistry of aldehydes and imines to direct mechanical switching processes (**Scheme 6.77**) in the rotaxanes **R679a** and **R679b**. The ring component of these rotaxanes possesses two endotopic amines with the capacity to condense with the formyl groups at the axial positions of the dumbbell's central hydrindacene unit. The modulation of this covalent imine bridge with chemical reagents serves as a basis for mechanical switching. Two different strategies for using chemical reactions to sever the imine bridge have been investigated—one of them (**Scheme 6.77**) involves the condensation of 1,2-ethanedithiol with the hydrindacene's aldehyde groups in order to block imine condensation from occurring with the macrocyclic diamine. Thus, dithioacetylization affords the [2]rotaxanes **R679a-$C_4H_{12}S_4$** and **R679b-$C_4H_{12}S_4$**, in which the ring is mobilized and left free to shuttle along the length of the dumbbell—see **Section 5.1.2.2**. The second strategy for switching these compounds involves a thermally sensitive hydrolysis of the imine bond in acidic media—see **Section 6.9.1.5**.



Scheme 6.77 Liberating the rings of imine-bridged rotaxanes with covalent exchange reactions.[463,464] Dithioacetylization of the aldehyde groups appended to the central hydrindacene unit of pre-rotaxanes **R679a** and **R679b** allows the macrocylic diamine freedom to shuttle in the corresponding [2]rotaxanes **R679-$C_4H_{12}S_4$**.

6.7.4 Switches Driven by Diels-Alder Reactions

Rotaxanes based on benzylic amide rings have also been fashioned for covalent-bond driven switching. The photoswitchable [2]rotaxane **(*E*)-R629a**—see **Scheme 6.27** in **Section 6.2.2.2**—has been coupled[465] with Diels-Alder chemistry in order to induce the ring's translation (**Scheme 6.78**) away from its preferred fumaramide



Scheme 6.78 The formation of a Diels-Alder adduct between cyclopentadiene and fumaramide drives[465] the ring from the fumaramide site in (***E*)-R629a** to a succinic amide ester in **R629d**.

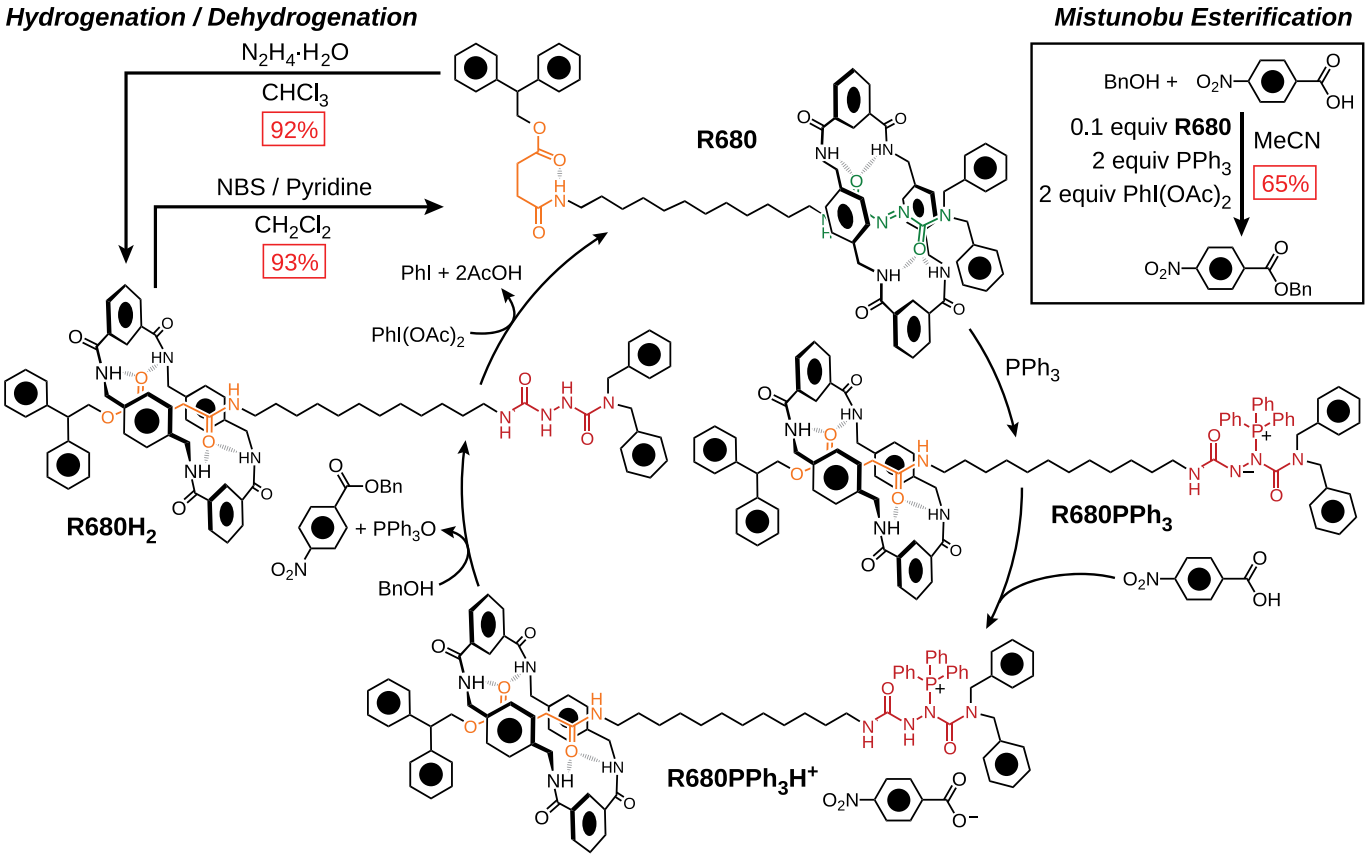
recognition site. The formation of a Diels-Alder adduct between fumaramide and cyclopentadiene generates the rotaxane **R629d** in 90% yield, where the ring avoids the steric bulk of the adduct by encircling the succinic amide ester recognition site.

6.7.5 Switches Driven by (De)Hydrogenation

Berná[466] described a covalent-driven shuttling process in the [2]rotaxane **R680** possessing a co-constitution similar to (***E*)-R629a**, except that its primary recognition site comprises an azodicarboxamide ($R_2NCON{=}NCONR_2$) unit instead of fumaramide. The position of the ring in **R680** can be controlled (**Scheme 6.79**) by hydrogenation and dehydrogenation of the azodicarboxamide unit with N_2H_4 and *N*-bromosuccinimide (NBS)/pyridine, respectively. The benzylic amide ring has a lower affinity for this recognition site upon hydrogenation to the hydrazodicarboxamide of **R680H_2**, causing it to encircle the succinic amide ester instead. The reaction-driven shuttling motions are highly efficient in both the forward and backward directions.

6.7.6 Switches Driven by the Mitsunobu Reaction

Berná[466] has described an alternative strategy for driving a switch based on the covalent reactivity of the azodicarboxamide unit in the bistable [2]rotaxane **R680** involving its organocatalysis (**Scheme 6.79**) in an ester-forming Mitsunobu reaction. The 4-nitrobenzoic acid and benzyl alcohol substrates are coupled with 65% efficiency in the presence of 0.1 molar equiv of **R680** and 2 equiv each of PPh_3 and $PhI(OAc)_2$. Mechanistically, it is proposed that the ring shuttles to the succinic



Scheme 6.79 Berná's bistable molecular switch driven by the covalent reactivity of azodicarboxamide.[466] Left hand side: a benzylic isophthalamide macrocycle translates to the succinic amide unit of **R680H$_2$** upon hydrogenation of the azodicarboxamide recognition site of **R680** with triazine, a process which can be reversed by dehydrogenation with NBS. Right hand side: it is proposed that the ring shuttles back and forth between recognition sites autonomously while consuming PPh_3 and $PhI(OAc)_2$ as fuel when **R680** is employed as an organocatalyst in the Mitsunobu esterification of 4-nitrobenzoic acid with benzyl alcohol, owing to the role of the azodicarboxamide unit in the transformation, where the bulky PPh_3 group displaces the ring in the betaine intermediate **R680PPh$_3$** and the corresponding **R680PPh$_3$H$^+$**···4-nitrobenzoate ion pair.

amide ester in order to avoid the bulky triphenylphosphine group of the betaine intermediate **R680PPh$_3$** and the corresponding azophosphonium **R680PPh$_3$H$^+$**, yet returns to the azodicarboxamide site of **R680** by an *in situ* oxidative dehydrogenation of the hydrazodicarboxamide **R680H$_2$** product with $PhI(OAc)_2$. This mechanism is consistent with the fact that a [2]rotaxane lacking a second recognition site for the ring to occupy converts the same substrates in much lower yield (16%), most likely as a result of its inability to translate the ring away from the catlytically active site of the betaine and azophosphonium intermediates. Thus, the switch **R680** oscillates autonomously during the Mitsunobu reaction, consuming triphenylphosphine and bis(acetoxy)iodobenzene as fuel while producing triphenylphosphine oxide, iodobenzene, and acetic acid as waste.

6.8 Solvent-Driven Switches

Since a molecule's local environment in solution is defined largely by the surrounding solvent molecules, solvent polarity is one of the most universal handles for controlling the co-conformational isomerism of mechanomolecules in liquids. The interactions between solvent molecules and the solvent-accessible sites on a MIM represent a major component of the energy landscape in solution, a realization which is not at all surprising, considering that (i) intramolecular interactions between interlocked components and (ii) intermolecular interactions between solvent and solute molecules are both governed by relatively weak noncovalent bonds such as ion-dipole, dipole-dipole, induced dipole-dipole, and dispersion forces. In polar solvents, a mechanomolecule is expected to minimize its energy by adopting co-conformations that expose its most polar functional groups to the solvent. Conversely, in low polarity solvents, exposing the most lipophilic groups to the solvent will be more favorable. Highlighted in this Section are a handful of illustrative examples of how changing solvent can drive motion in bistable mechanomolecules as a result of hydrogen bond disruption (**Section 6.8.1**) and other solvation effects (**Section 6.8.2**).

6.8.1 Switching Driven by Hydrogen Bond Disruption

Several of the earliest examples of solvent-driven switches (**Figure 6.17**) rely on the solvent's ability to disrupt hydrogen-bonding interactions. These rotaxanes are characterized by well-defined co-conformations in low polarity solutions and ill-defined (rapidly exchanging) co-conformations in high polarity solutions. In the peptide-based [2]rotaxane[467] **R681**, for example, the benzylic amide ring spends most of its time around the two glycylglycine recognition sites as it shuttles back and forth between them in $CHCl_3$, but has no preference for any particular site in Me_2SO. The same effect was found[468] in rotaxane **R682**, which contains a similar recognition motif. It appears that the solvent-dependent behavior of the rotaxane **R683**, which was reported recently by Raju and Lin,[469] remains in question to some extent because of conflicting accounts of its dominant co-conformation in Me_2SO, whether originating from experimental[469] and computational[470] investigations. The benzylic amide ring of **R683** tends to encircle a hydrogen bond accepting pyridine unit in $CHCl_3$, while the ring most likely samples many isoenergetic co-conformations in Me_2SO. In Gibson's[471] polyrotaxane **R684**, the [30]-crown-10 (30C10) ring encircles the polymer thread's urethane groups predominantly in $CDCl_3$, whereas in Me_2SO the rings freely traverse the region of the polymer backbone that span in between its tetraphenyl blocking groups.

Leigh[472] also recognized the potential of solvent-induced switching at a very early stage. He described the effect of solvent polarity on the co-conformations (**Scheme 6.80**) of the benzylic amide [2]catenane **C623**. The two identical rings of **C623** have some amphiphilic character, since they each possess a polar isophthalamide unit and a greasy octamethylene chain. In Me_2SO, the isophthalamide units live on the outskirts of the catenane, where they can expose themselves to the polar solvent molecules. In $CHCl_3$, however, they hide within the internal surfaces of the catenane and allow the octamethylene chains to occupy more of the exterior space.

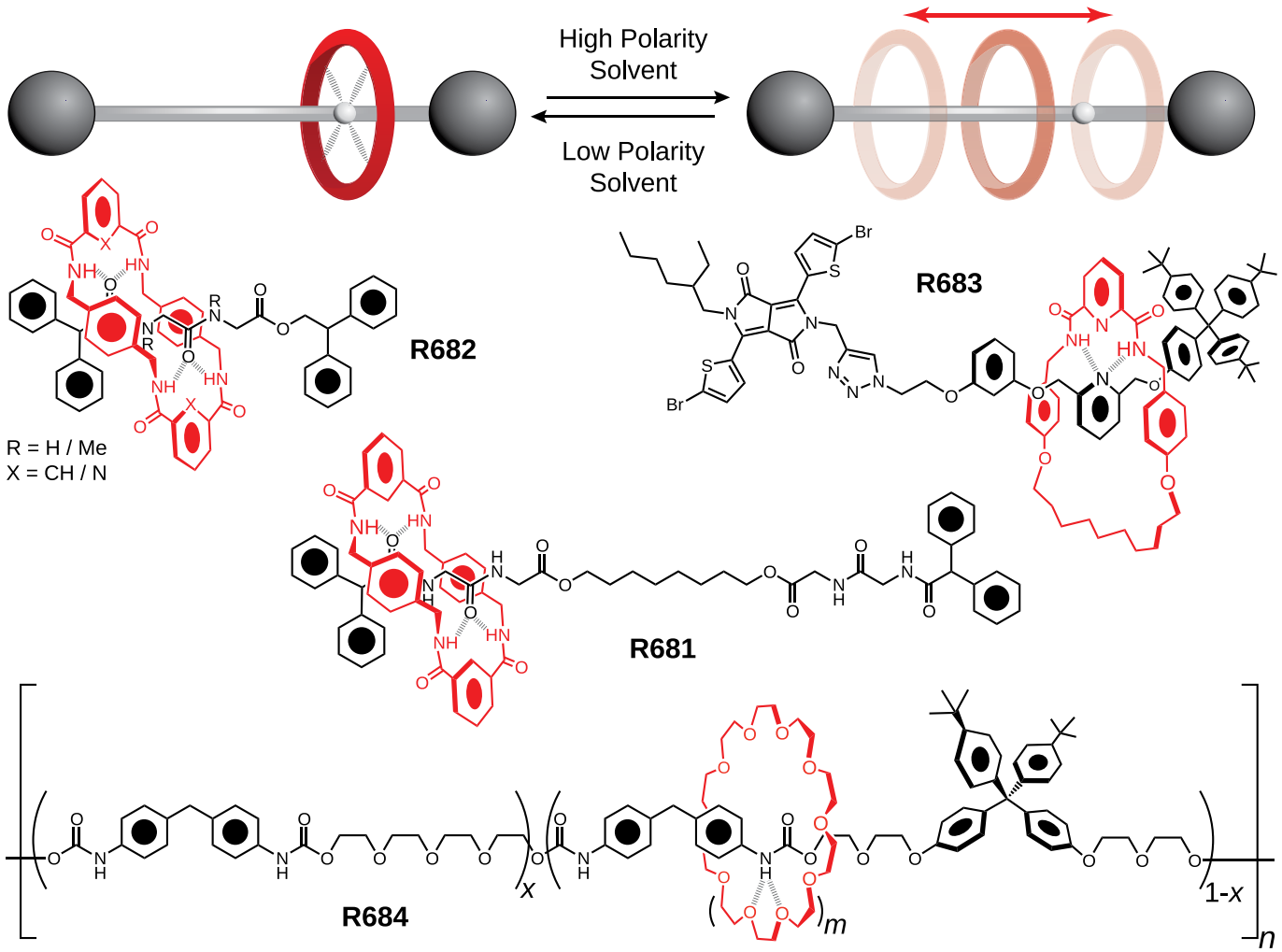
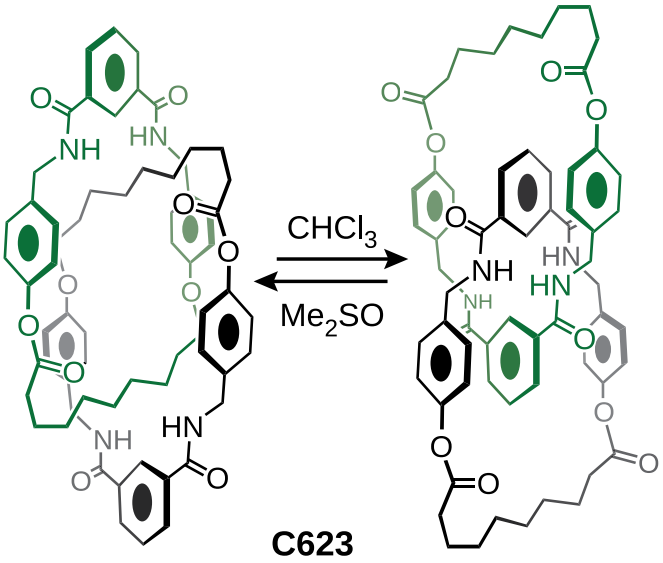


Figure 6.17 Some early examples[467–469,471] of solvent-driven switches that rely on hydrogen-bonding interactions to adopt well-defined co-conformations in low polarity solvents (e.g., $CHCl_3$) and poorly defined co-conformations with rapid ring movement in high polarity solvent (e.g. Me_2SO).

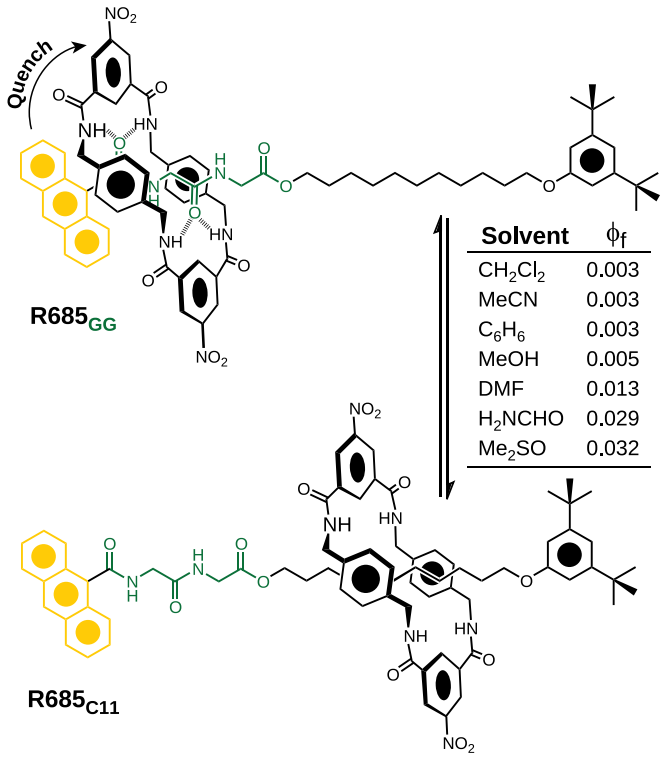


Scheme 6.80 The co-conformational changes expressed by the amphiphilic catenane **C623** in high polarity (Me_2SO) and low polarity ($CHCl_3$) solutions.[472]

Leigh[473–475] has also prepared rotaxanes with amphiphilic threads, which express co-conformations that can be differentiated in low- and high-polarity solvents. One[475] among these examples (**Scheme 6.81**) is the rotaxane **R685**, which possesses an anthranyl stopper that effectively reports the position of the ring with its fluorescence signal. The benzylic amide ring of **R685** resides around the glycylglycine (GG) peptide recognition site in low polarity solvents like CH_2Cl_2, but migrates to a solvophobic undecamethylene (C_{11}) hydrocarbon chain in high polarity solvents like Me_2SO. Since the electron-accepting nitro groups appended to the ring's isophthaloyl units quench the anthracene-based stopper's fluorescence, the quantum yield (φ_f) of the rotaxane depends on the distance between the ring and the fluorophore. Consequently, solutions of **R685** become increasingly fluorescent as solvent polarity increases, A poly(methyl methacrylate)-derivative (**polyR685**) containing the same rotaxane motif (~10% w/w) has been deposited[475] from CH_2Cl_2 onto glass surfaces and actuated in the condensed phase—see **Section 6.14.3.3**—and the corresponding surface patterns are capable of performing logic (**Section 6.15.1.4**) operations.

Several solvent-switchable fullerene-stoppered rotaxanes based on benzylic amides have also been described,[473,476–481] many of which originate from the lab of Mateo-Alonso[476–481] A few examples are shown in **Figure 6.18**. The first solvent-switchable fullerene-stoppered [2]rotaxane[473] **R686**, which incorporates the same motif as the anthracene stoppered **R685**, operates (**Figure 6.18a**) analogously, where the solvent polarity defines the extent to which the ring encircles a hydrogen-bonded recognition site or a solvophobic chain. In rotaxane **R687**, which is based[476] on a succinamide recognition site instead of a peptide, the ring shuttles (**Figure 6.18b**) quite unexpectedly in the reverse direction. The ring resides primarily near the C_{60} stopper instead of the hydrocarbon chain in a hydrogen bond disrupting Me_2SO solution. We note that the electrochemically bistable [2]rotaxane **R622**—see **Scheme 6.16** in **Section 6.1.4**—is influenced (**Figure 6.18c**) in a similar fashion by solvent polarity.[480] The ability to control the distance between a C_{60} stopper and a mobile ring component in rotaxanes such as these has implications for directing phenomena such as electron transfer reactions[477] and nonlinear optical properties[478] through submolecular mechanical motion.

More solvent-switchable benzylic amide rotaxanes have been identified and investigated. Leigh[468] has described how solvent polarity influences the populations and dynamics of two interconverting rotamers in the dumbbell of a benzylic amide rotaxane with a sarcosine recognition site. In another case, the solvent polarity was used[474] in combination with the cleavage of some appropriate bonds to template the formation of a [2]rotaxane in



Scheme 6.81 A solvent-switchable molecular shuttle[475] with a fluorophoric stopper. The translational isomers $\mathbf{R685_{GG}}$ and $\mathbf{R685_{C11}}$, in which the benzylic amide ring encircles glycylglycine (GG) and undecamethylene (C_{11}) moieties, respectively, can be populated differently in various solvents. Since the electron accepting ring of **R685** quenches the fluorescence of the anthrylic stopper in a distance-dependent manner, the fluorescence quantum yields (ϕ_f) reflect the population distribution. The higher ϕ_f values in more polar solvents indicate an increasing population of $\mathbf{R685_{C11}}$, since these solvents disrupt intercomponent hydrogen-bonding interactions at the GG site and promote solvophobic interactions at the C_{11} site.

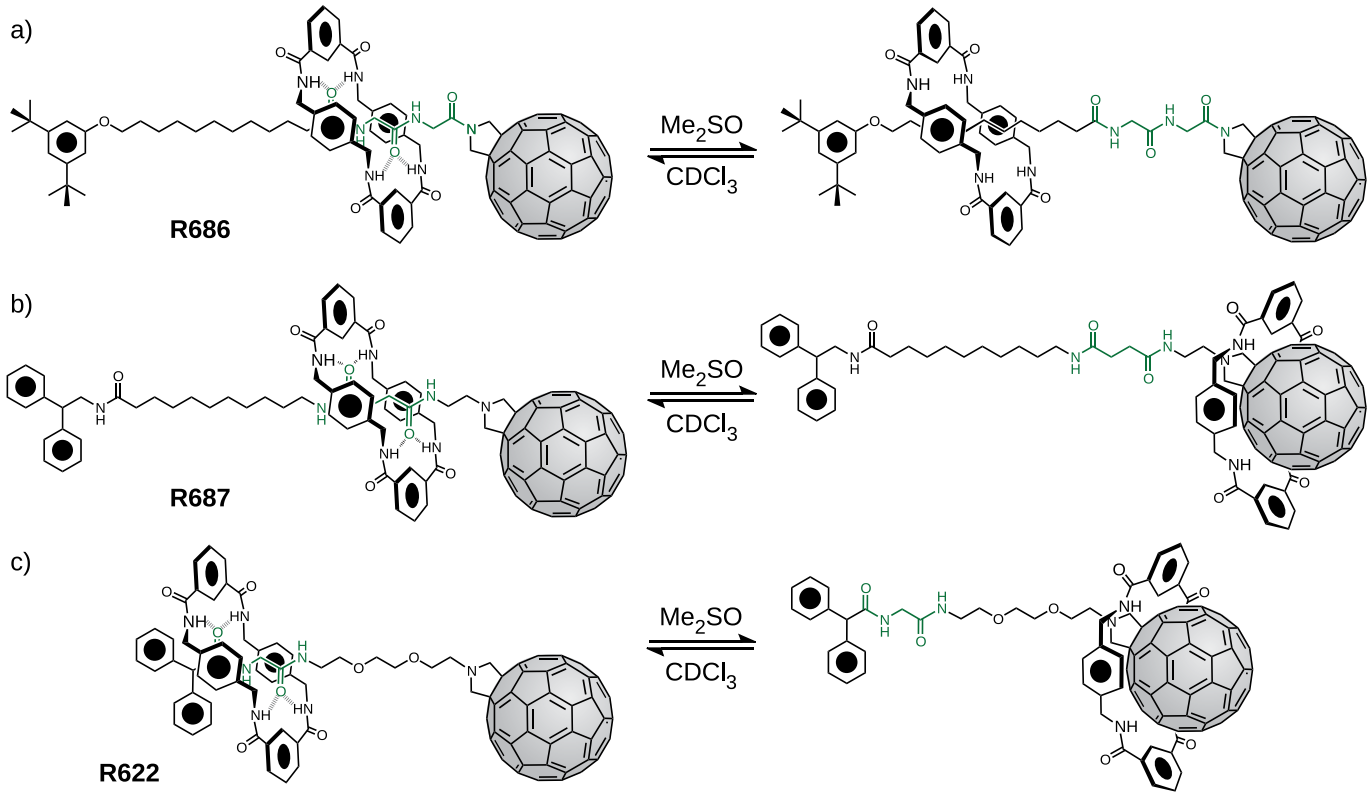
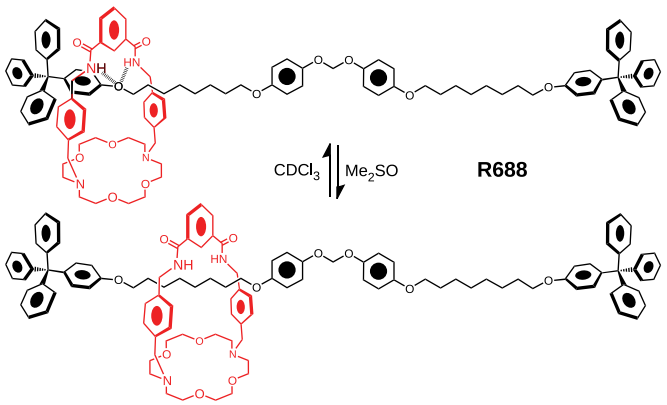


Figure 6.18 Controlling the co-conformations of fullerene-stoppered rotaxanes with solvent polarity.[473,476,480] (a) The first fullerene-stoppered benzylic amide shuttle **R686**.[473] (b) Rotaxane **R687** acts as a reverse shuttle,[476] wherein the benzylic amide ring moves toward the fullerene stopper in polar media instead of toward the solvophobic hydrocarbon chain. (c) The electrochemically switchable rotaxane **R622** (see **Scheme 6.16**) is also solvent switchable.[480]

which the benzylic amide ring encircles a dumbbell with no major recognition sites. More recently, the solvent-controlled luminescence response of a pyrene-stoppered rotaxane based on similar design principles has been reported.[481] A solvent-switchable bistable [2]rotaxane switch comprising a benzylic amide ring and a dumbbell with maleamide and glycylglycine recognition sites has been described by Moretto.[482] The ring's preference for these two recognition sites, which are separated by a rigid, hexameric helical peptide sequence of aminoisobutyric acid (Aib_6), can be controlled by heating at 50–55 °C in various solvents. The ring occupies the maleamide site with 95% selectivity in $CDCl_3$ or $Cl_2DCCDCl_2$, whereas it occupies the glycylglycine station with 90% selectivity in CD_3CN. This solvent sensitivity has been attributed to the participation of the glycylclycine recognition site in the intramolecular self-assembly of the Aib_6 helix, an interaction which competes effectively with the binding of the ring in $CDCl_3$ or tetrachloroethane, but not in CD_3CN. Other bistable [2]rotaxanes (e.g., **(*EIZ*)-R647**) incorporating the maleamide recognition unit are employed more often as photoswitches—see **Sections 6.2.2.3** and **6.15.2.3**.

The position of a macrobicyclic ring in the [2]rotaxane **R688** investigated by Smith[483] responds (**Scheme 6.82**) to solvent changes in a manner reminiscent of the C_{60}-stoppered rotaxanes **R685–R687**. In this case, the ring spends most of its time around either of the two phenolic groups contiguous with the dumbbell's trityl stoppers in $CDCl_3$, whereas it predominantly encircles either one of the octamethylene chains in Me_2SO.



Scheme 6.82 The macrobicyclic isophthalamide ring of **R688** is more likely to be found[483] near phenolic groups in $CDCl_3$ and near an octamethylene chain in Me_2SO.

6.8.2 Switching Driven by Solvation Effects

It was recognized[39] at an early stage in the development of charged π-donor/π-acceptor MIMs that their co-conformational isomerism is highly sensitive to solvent polarity. The first non-degenerate [2]catenane in which the relationship between solvent polarity and translational isomerism was examined[484] in detail is **C624**$^{4+}$, which is illustrated in **Figure 6.19** as both of its translational isomers—one (**C624**$_{DNP}^{4+}$) in which the CBPQT^{4+} ring encircles a dioxynaphthalene (DNP) unit and the other (**C624**$_{HQ}^{4+}$) in which the CBPQT^{4+} ring encircles a HQ unit. Since DNP-based guests bind CBPQT^{4+} more strongly than HQ guests, it was anticipated that **C624**$_{DNP}^{4+}$ would dominate the molecular population in solution. Unexpectedly, however, **C624**$_{HQ}^{4+}$ was found to be the dominant species in Me_2CO by a factor of about 7:3 at room temperature and below. The most likely explanation for this surprising observation is that the larger π-surface of the DNP unit can more effectively insulate the exterior surface of the tetracationic cyclophane from unfavorable cation-solvent interactions in relatively low polarity solvents. In solvents of higher polarity, therefore, the less costly ion-solvation effects produce the opposite result. This explanation of the system has been confirmed computationally by Houk.[485] The plot in **Figure 6.19** demonstrates a clear relationship between the dielectric constant of the solvent and the population of translational isomers, where the included DNP:HQ ratio spans from 25:75 in the least polar solvent system (1:4 $CDCl_3$:$(CD_3)_2CO$) to approximately 70:30 in the most polar $(CD_3)_2SO$ solution. Interestingly, the same trend does not hold[41] in an analogous catenane based on extended viologens, namely (*E*)-1,2-bis-(4,4´-pyridyl)ethane.

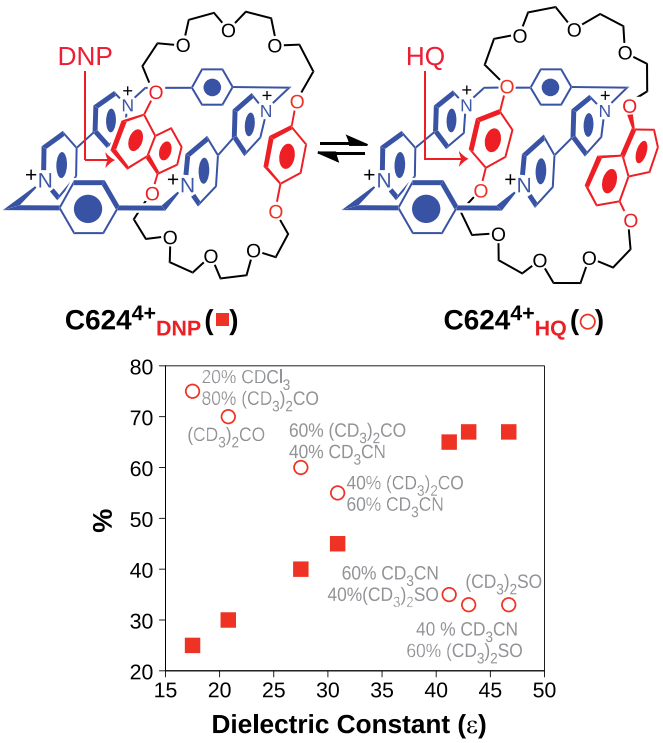


Figure 6.19 The effect[484] of solvent polarity, plotted as the dielectric constant, on the distribution of the two co-conformational isomers of the bistable donor-acceptor [2]catenane **C624**$^{4+}$ at room temperature.

More donor-acceptor mechanomolecules (**R689**$^{4+}$–**R691b**$^{4+}$, **C625**$^{4+}$) possessing TTF-derived recognition units that exhibit solvent-dependent distributions of translational isomers are illustrated in **Figure 6.20**. Several rotaxanes[60,61,66,388] based on DNP and pyrollo-TTF derivatives, including **R660**$^{4+}$ from **Section 6.5.1**, tend to populate the "red" DNP-encircled translational isomer in relatively low polarity solvents such as Me_2CO, while the TTF-derived sites of the "green" isomers become more occupied in higher polarity solvents such as Me_2SO. In the case[61] of **R691b**$^{4+}$, for example, the red:green ratio is 3:1 in Me_2CO, 1:1 in MeCN, and 1:2 in Me_2SO. The population of the red and green translational isomers of **R689**$^{4+}$ exhibits[42] a similar trend in solvent dependency, ranging from a red:green ratio of >99:<1 in CD_3COCD_3 to 67:33 in CD_3SOCD_3. In the donor-acceptor [2]catenane **C625**$^{4+}$, the red:green distribution is 1:1 in MeCN and 1:7 in a binary mixture of MeCN and H_2O (1:1 v/v) near room temperature, a phenomenon governed[486] by entropic rather

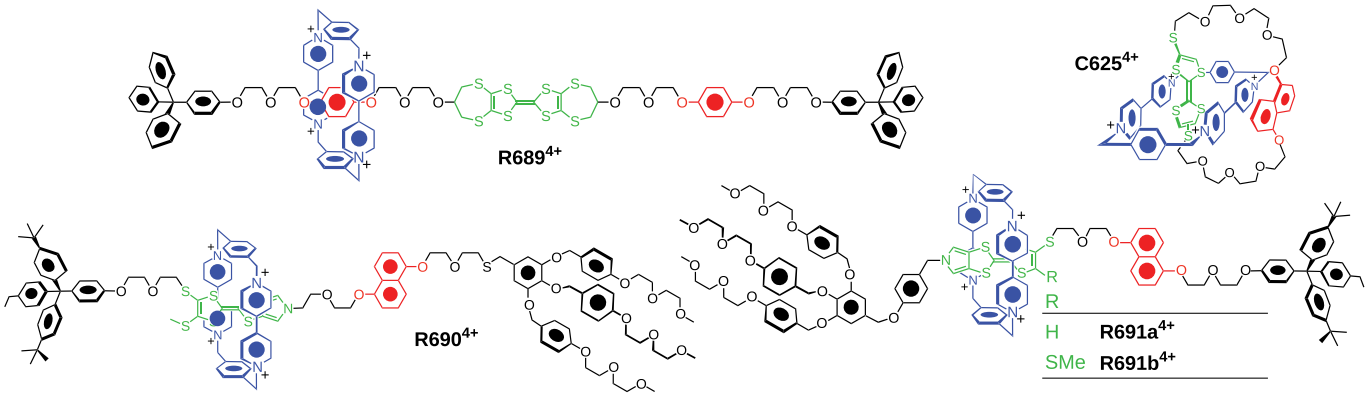


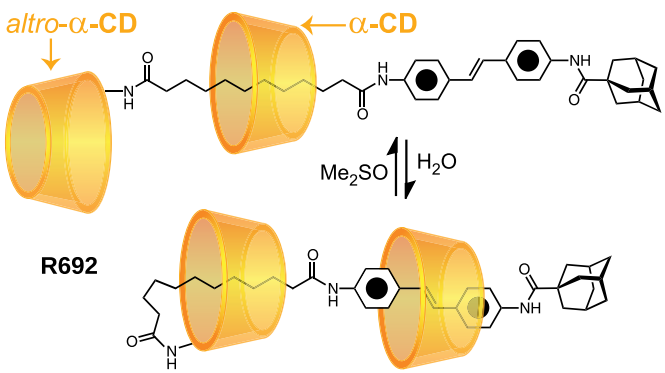
Figure 6.20 Stereoformulas of D-A mechanomolecules that exhibit solvent-sensitive ground-state distributions of "red" and "green" translational isomers.

than enthalpic considerations. We note that all of these switches can also be actuated electrochemically under oxidative control according to the principles described in **Section 6.1.1.1**.

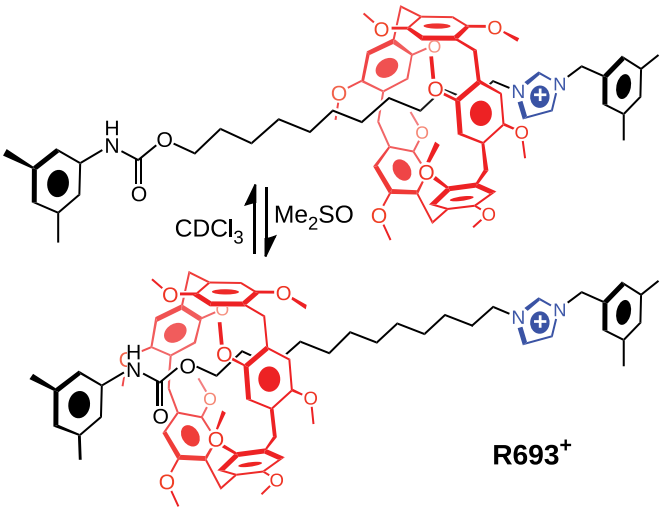
Harada[487] has described a novel mode of solvent switching (**Scheme 6.83**) for the CD-stoppered [2]rotaxane **R692**. The dumbbell of this rotaxane has two suitable sites for the interlocked α-CD ring to encircle: (i) a decamethylene chain and (ii) a stilbene unit. An amide bond connects the decamethylene chain to an *altro*-α-CD stopper (*altro*-α-CD has one D-altropyranosyl unit and five D-glucopyranosyl units). In Me_2SO, the α-CD ring encircles the decamethylene chain predominantly. In water, however, the *altro*-α-CD stopper 'reels' in on the hydrocarbon chain to form a pseudo[1]rotaxane type of complex, while the α-CD ring occupies the stilbene unit.

Molecular switches that are driven by anion solvation effects (**Section 6.5.3**) are expected to respond also to solvent changes, on account of the central role of solvent–anion interactions in these systems. The macrotricyclic ring of the [2]rotaxane **R661H$_2$**·4PF$_6$—see **Scheme 6.61** in **Section 6.5.1**—translates[398] from the dialkylammonium recognition site in $MeNO_2$ to the central ethane-1,2-bis(pyridinium) site in Me_2SO. Chiu's rotaxane **R662^{2+}** (see **Scheme 6.62**) is also solvent switchable,[399] since its BX26C6 ring encircles a guanidinium unit in low-polarity solvents and a pyridinium unit in high-polarity solvents. These effects are explained in large part by the ability of more polar solvents to disrupt the [N–H···O] hydrogen bonds that stabilize co-conformations involving recognition sites such as dialkylammonium and guanidinium ions.

Huang[488] has described solvent-induced switching (**Scheme 6.84**) between different co-conformations of the pillar[5]arene-based rotaxane **R693$^+$**. In $CHCl_3$, the pillar[5]arene ring resides around the methylene units adjacent to an imidazolium recognition site, yet the ring is driven toward the other end of the dumbbell's dodecamethylene chain, residing closer to the carbamate-linked stopper in Me_2SO. This behavior can be attributed to a number of solvent-dependent interactions, including (i) the increased solvation



Scheme 6.83 In Harada's [2]rotaxane **R692**, the position of the α-CD ring on the dumbbell is influenced[487] by the 'reeling' of an *altro*-α-CD stopper onto the decamethylene chain in H_2O, which does not take place in Me_2SO.



Scheme 6.84 The solvent-switchable pillar[6]arene [2]rotaxane **R693$^+$**.[488]

of the imidazolium bromide ion pair in Me_2SO, (ii) the solvophobic nature of the dodecamethylene chain, and (iii) the ability of Me_2SO to disrupt the [C–H···O] interactions between the rim of pillar[5]arene and imidazolium unit. See **Section 6.13.1.1** for a solvent-driven "molecular muscle" based on a similar molecular design.[489]

6.9 Thermally Driven Switches

Temperature can be employed as a handle for controlling the co-conformation of mechanomolecules by mechnisms attributable to entropic effects (**Section 6.9.1**), as well as thermal decomposition (**Section 6.9.2**).

6.9.1 Switching Driven by Entropic Effects

Mechanomolecules that rearrange co-conformations in response to temperature changes are inherently driven entropically, since entropy is tied to temperature in the Gibbs free energy equation, which determines the Δ*G* value defining the ground state distribution. Thus, co-conformational isomerism can be controlled with temperature when enthalpic (Δ*H*) and entropic (*T*Δ*S*) contributions to the free energy landscape are in competition—i.e., when they are both of the same sign, either positive or negative. This scenario is not at all uncommon, since the noncovalent bonding interactions that typically stabilize a particular co-conformation in the GSCC are enthalpically favorable, whereas the increased ring mobility afforded by forsaking the GSCC is entropically favorable. Interactions between mechanomolecules and the solvent molecules (see **Section 6.8**) can, however, outweigh these factors when switching in solution. This Section highlights thermally driven switches in which the competition between enthalpy and entropy arises from donor-acceptor (**Section 6.9.1.1**), hydrophobic (**Section 6.9.1.2**), or hydrogen-bonding (**Section 6.9.1.3**) interactions, pillararenes (**Section 6.9.1.4**), and covalent bonds (**Section 6.9.1.5**).

6.9.1.1 Thermally Switched Donor-Acceptor MIMs

Donor-acceptor mechanomolecules have been known to exhibit thermal switching (**Figure 6.21**) capabilities since at least 1993, when it was noticed[484] that the translational isomers of the [2]catenane **C624**$^{4+}$, comprising a CBPQT^{4+} ring interlocked with *para*-phenylene-1,5-naphtho[36]crown-10 exhibits (**Figure 6.21a**) a subtle difference (5%) in the population of circumrotational isomers at –40 °C and room temperature in CD_3COCD_3. In 1995, a tetrastable D-A [2]catenane[490]—see **Scheme 5.2** in **Section 5.1.1**—was also found to exhibit different populations of translational isomers at low and high temperatures. Subsequently, a number of non-degenerate bistable [2]catenanes derived from CBPQT^{4+} and π-donating crown ethers with temperature-sensitive distributions of translational isomers began to emerge.[491,492] The bistable [2]catenanes **C626**$^{4+}$**–C628**$^{4+}$, whose crown ethers incorporate 1,5-dithianaphthalene (DTNP) or *p*-xylene (Xy) π-donor units along with the more commonly employed HQ and DNP recognition units in their constitution, exist as mixtures of translational isomers in CD_3CN. In the most dramatic case (**Figure 6.21c**), the translational isomer **C627**$^{4+}_{HQ}$ dominates the distribution (7:3 ratio) at 243 K, whereas the ratio is reversed (3:7 in favor of **C627**$^{4+}_{DTNP}$) upon heating to 303 K. **C626**$^{4+}_{DNP}$/**C626**$^{4+}_{DTNP}$ and **C628**$^{4+}_{DNP}$/**C628**$^{4+}_{Xy}$ behave analogously, albeit with smaller changes in the distribution of isomers at the high and low temperature extremes. Temperature sensitive ground-state distributions were also noticed[60,61,66] in the bistable rotaxanes **R690–R691b**$^{4+}$—see **Figure 6.20** in **Section 6.8.2**—where the ratio of green:red isomers (GSCC:MSCC) rises from 1:1 at room temperature to ≥8:1 at high temperature, as well as in a bistable [2]catenane[106] based on a tetramethylated BPTTF (Me_4BPTTF) unit, where the GSCC:MSCC ratio is 10:1 at room temperature and 1:1 at 120 °C—see **Tables 5.2–5.3** in **Section 5.1.1**.

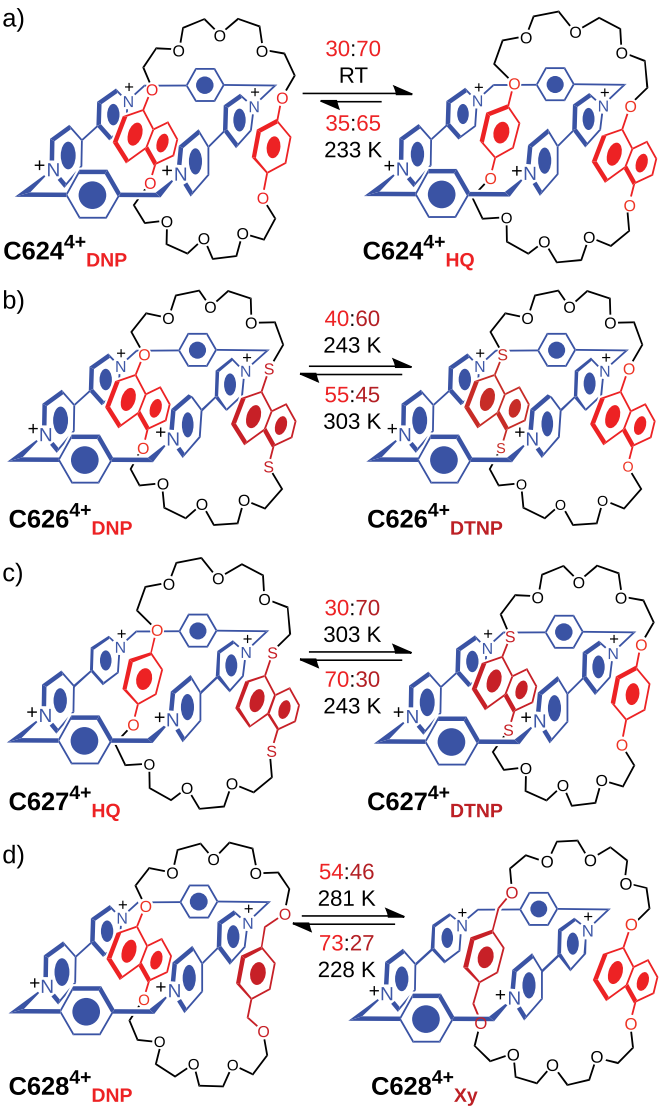


Figure 6.21 Bistable [2]catenanes with temperature sensitive distributions of translational isomers in CD_3COCD_3 (a) or CD_3CN (b–d).[484,491,492]

6.9.1.2 Cyclodextrin Polyrotaxane Thermal Switches

Cyclodextrin-based polyrotaxanes were among the earliest mechanically interlocked compounds to be recognized for their capacity to be switched by thermal stimuli. This idea was pioneered by Yui,[493–495] who developed the first thermally responsive (**Figure 6.22**) polyrotaxanes. The polyrotaxane **R694**$^{4-}$ comprises[493] a triblock copolymer thread with two terminal poly(ethylene glycol) (PEG) blocks and a central poly(propylene glycol) (PPG) block, which is encircled by ~20 β-cyclodextrin (β-CD) rings and stoppered by anionic 2-naphthylamine-6,8-disulfonic acid endgroups. The polyrotaxane is essentially insoluble in water at room temperature and below, but becomes soluble reversibly as the aqueous solution is heated up to 80 °C. Since β-CD is known to associate with PPG and not with PEG (see **Chapter 2.3.1.1**), it was postulated that the β-CD rings become localized and aggregated (**Figure 6.22a**) on the PPG block (stabilized by enthalpically favorable ring–ring hydrogen-bonding interactions) at low temperatures, whereas the rings become mobilized (an entropically favorable phenomenon) along the entire length of the triblock copolymer at elevated temperatures. A control polypseudorotaxane identical to **R694**$^{4-}$ except that it lacks stoppers is also soluble at elevated temperatures, but does not precipitate from solution, as the rotaxane does, upon cooling back down to room temperature.

The polyrotaxane **R695**$^{2-}$ is modified ever so slightly compared with **R694**$^{4-}$—it has fluorescein stoppers linked to the triblock copolymer by thiourea groups and fewer (~7) β-CD rings. In spite of these seemingly minor differences, the thermally responsive properties (**Figure 6.22b**) of **R695**$^{2-}$ are completely different.[494,495] First of all, the compound could not be dissolved in water or phosphate buffered saline (PBS). Thus, the investigations on **R695**$^{2-}$

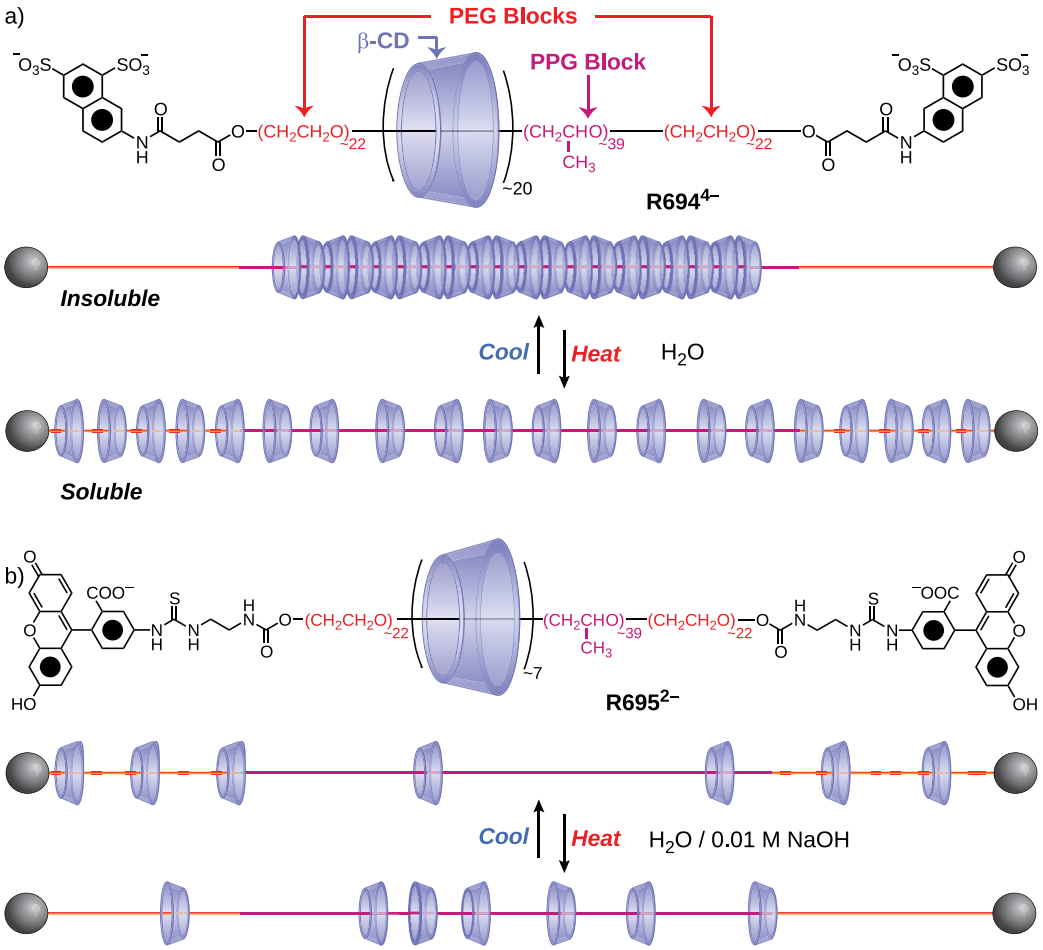
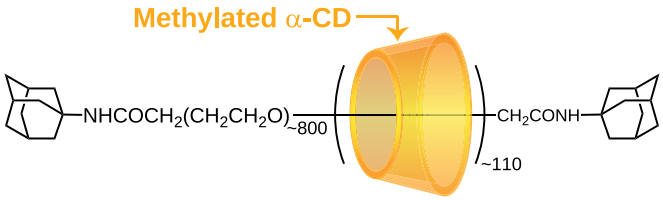


Figure 6.22 Temperature-dependent ring localization in polyrotaxanes based on β-cyclodextrin (β-CD) rings and PEG-PPG-PEG triblock copolymer dumbbells.[493–495] (a) Heating and cooling of **R694⁴⁻** in water results in a reversible precipitation and dissolution of the compound, a result which is thought to be caused by the aggregation and mobilization, respectively, of the β-CD rings. (b) The fluorescein-stoppered anologue **R695²⁻** has fewer rings and is insoluble in neat water. In alkaline aqueous solutions, the ionized β-CD rings do not aggregate or cause precipitation. In this case, heating causes the rings to become increasingly localized on the central PPG block.

were carried out in 0.01 M NaOH, in which up to half of the hydroxyl groups of β-CD are ionized in order to enhance solubility. Thermal cycling does not lead to reversible precipitation and dissolution under these conditions. Rather, it was found, primarily by means of high-field ^{1}H NMR spectroscopy, that the β-CD rings are localized increasingly on the central PPG block at higher temperatures. It was calculated[494] from signal integration that an average of 1.3 β-CD rings occupy the PPG segment at 10 °C, whereas ~5.2 rings encircle PPG at 50 °C. A subsequent follow-up study[495] described similar results for analogous polyrotaxanes with ~4 or ~10 β-CD rings. Note that the rings do not aggregate at any temperature—as they are belived to do in **R694⁴⁻**—on account of electrostatic repulsion between their ionized hydroxyl groups. This behavior, in which heating **R695²⁻** causes the rings to move toward PPG, is exactly the opposite to that which was proposed for **R694⁴⁻**. The explanation is most likely related to an enhancement in hydrophobic interactions between the cavity of β-CD and the methylene chains of PPG at higher temperatures.

Ito[496,497] has investigated (**Figure 6.23**) the thermally responsive polyrotaxanes **R696a–c**, which are based on PEG35000 dumbbells possessing approximately 110 methylated α-CD rings, corresponding to 28% coverage of the PEG chains. These polyrotaxanes form gels in 2 wt. % aqueous solutions when they are heated above their lower critical solution temperature (LCST). LCST behavior is an aggregation process based on the entropically driven liberation of structured solvent molecules, which is frequently found in water-soluble polymers with hydrophobic groups such as methylcellulose and poly(*N*-isopropylacrylamide).[498] Unique to the **R696** polymers is the fact that LCST behavior is governed by the mechanical bond, i.e., the localization and mobility of the methylated α-CD rings. A sol-gel transition is observed only when the hydroxyl groups of the α-CD rings carry a sufficient amount of methoxyl groups. The temperature at which gelation occurs depends on the α-CD methylation ratio (87, 74, or 52%), where more highly methylated polymers exhibit lower LCSTs. Calorimetry, rheology, and X-ray diffraction data all support the claim that gelation is driven by the formation of microcrystalline aggregates of the methylated α-CD rings acting as crosslinks. These microcrystalline domains assemble because the entropic penalty associated with the structured water molecules surrounding the rings' methoxyl groups becomes greater at elevated temperatures, leading to microphase separation (hydrophobic collapse) and the release of these high-energy water molecules above the LCST.



R696	α-CD Methylation Ratio	LCST / °C
a	87%	22
b	74%	53
c	52%	none

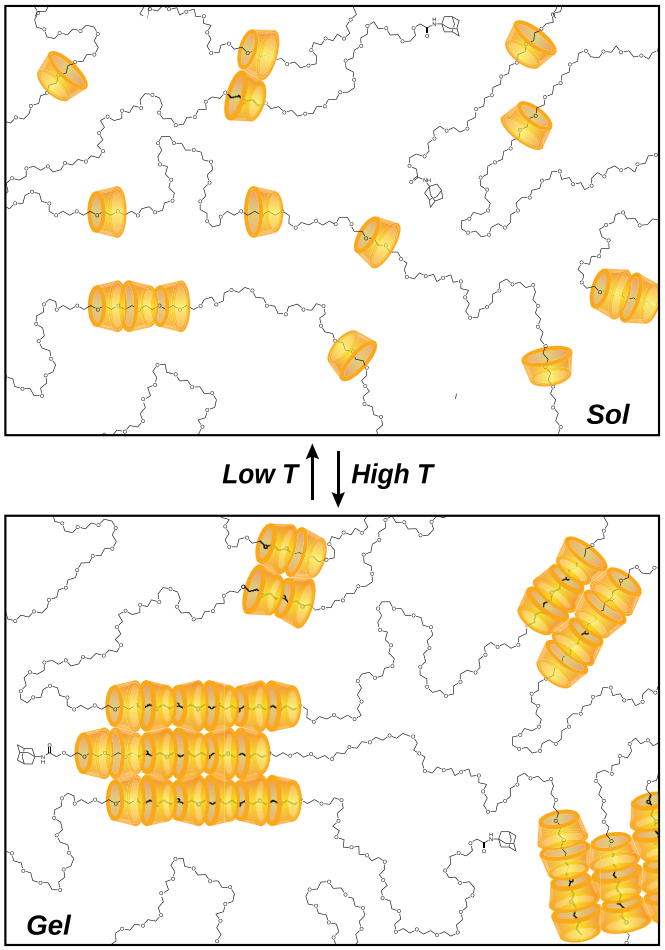
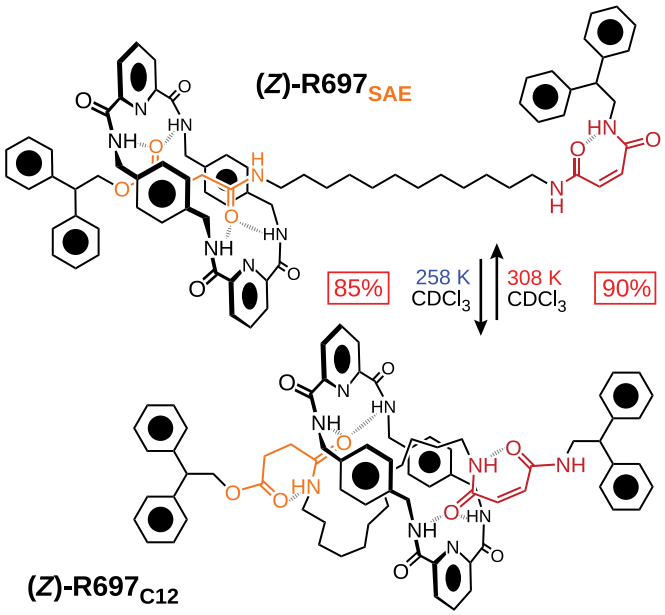


Figure 6.23 Polyrotaxanes **R696a-c**, which comprise methylated α-CD rings and polyether dumbbells, undergo[496,497] thermally driven sol-gel transitions in 2 wt % aqueous solutions. The lower critical solution temperature (LCST) is sensitive to the methylation ratio on the α-CD rings, where more methoxyl groups correspond to lower LCSTs, and gelation does not occur if the ratio is too low. Gelation is caused by the entropy-driven formation of microcrystalline α-CD aggregates as noncovalent cross-links at elevated temperatures.

6.9.1.3 Thermally Switched Benzylic Amide Rotaxanes

Leigh[499] has also reported on the entropy-driven switching (**Scheme 6.85**) of the tristable molecular shuttle (***Z*)-R697**. The structure of **(*Z*)-R697** is very similar to that of the photochemically and covalently switchable [2]rotaxane **(*Z*)-R629a**—see **Scheme 6.27** in **Section 6.2.2.2**—except that it possess a benzylic dicarboxamidopyridine ring instead of a benzylic isophthamide. The rotaxane is indeed photoswitchable and the ring encircles the fumaramide recognition site preferentially as the (*E*)-isomer. When the (*Z*)-isomer (maleamide) is populated (54% in the photostationary state) by irradiation with 254 nm light, an equilibrium between two co-conformations emerges. These co-conformations are (i) the expected one **(*Z*)-R697$_{SAE}$** in which the ring encircles the succinic amide ester (SAE) recognition site, and (ii) an unusual third translational isomer **(*Z*)-R697$_{C12}$**, in which the ring spans the central dodecamethylene chain to participate in hydrogen-bonding interactions with both of the dumbbell's recognition sites. This behavior is exclusive to **(*Z*)-R697** and is not observed in the (*E*)-isomer or even in analogues with shorter spacers or slightly different constitutions, such as the **(*Z*)-R629a** predecessor. The enthalpic and entropic competition in this rotaxane involves amide–amide hydrogen-bonding interactions between the ring and the maleamide unit—which are enthalpically more favorable (~2 kcal·mol^{-1}) than with the succinic ester—pitted against the entropically unfavorable compression of the dodecamethylene spacer required to allow the ring to engage the amides in both recognition sites. The rotational freedom of the C_{12} linker must be considerably restricted in **(*Z*)-R697$_{C12}$**, which is why this co-conformation is relatively less stable at higher temperatures.

Brouwer[500] has investigated the temperature-dependent co-conformational isomerism (**Figure 6.24**) of the



Scheme 6.85 Entropy-driven translation of the pyridyl-based benzylic amide ring of the bistable rotaxane **(*Z*)-R697** in $CHCl_3$.[499] The ring spends most of its time around the succinic amide ester recognition site in **(*Z*)-R697$_{SAE}$** above room temperature, yet it predominantly spans a dodecamethylene spacer while hydrogen bonding with two recognition sites in **(*Z*)-R697$_{C12}$** at low temperatures.

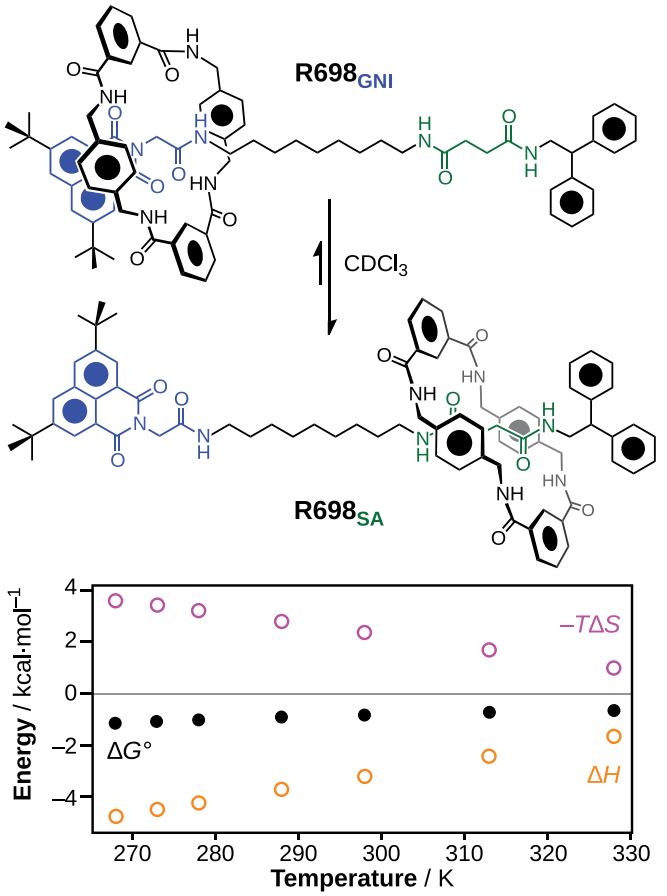


Figure 6.24 The temperature-dependent free energy parameters for the non-degenerately bistable [2]rotaxane **R698**.[500]

non-degenerately bistable [2]rotaxane **R698**, which possesses *N*-glycylnaphthalimide (GNI) and succinamide (SA) recognition units for a benzylic isophthalamide ring. The ground-state co-conformation in $CDCl_3$ is $\mathbf{R698_{SA}}$, representing almost 90% of the population distribution at 268 K. The difference in Gibbs free energy, $\Delta G°$, between the translational isomers decreases from –1.1 to –0.7 kcal · mol as the temperature is raised to 328 K, corresponding to an increase in the ratio of the metastable-state co-conformation $\mathbf{R698_{GNI}}$, which reaches as high as ~25% of the distribution. Although the modest changes in $\Delta G°$ as a function of temperature allows only 15% of the molecular population to be manipulated in this temperature window, despite the fact that the changes in the enthalpic ($\Delta H°$) and entropic ($-T\Delta S°$) contributions to free energy vary dramatically as a function of temperature, The van't Hoff plot for this system is distinctly non-linear, an observation attributable to a non-negligible change in heat capacity, which was calculated to be $\Delta C_p = 52\ \text{cal} \cdot \text{mol}^{-1} \cdot \text{K}^{-1}$.

6.9.1.4 Thermally Switched Pillararene Rotaxanes

The first pillar[6]arene-based rotaxane $\mathbf{R699^+}$, which was reported by Ogoshi,[501] was found to exhibit (**Figure 6.25**) thermally controlled shuttling behavior. The two binding sites on the dumbbell for the perethylated pillar[6]arene ring are located on either side of a pyridinium unit—one is a trimethylene chain adjacent to one of the stoppers, and the other is a nonamethylene chain at the center of the dumbbell. The electron-rich rims of the pillar[6]arene ring are able to interact with the cationic pyridinium unit from each of these sites. The two co-conformers $\mathbf{R699^+_{C3}}$ and $\mathbf{R699^+_{C9}}$ were observed in a 57:43 ratio at –50 °C in $CDCl_3$, in which the dominant species is the one with the pillar[6]arene encircling the trimethylene chain. This ratio is gradually reversed (**Figure 6.25**), as the temperature approaches –25 °C. A van't Hoff analysis of this data allowed for quantification of the ethalpic ($\Delta H = -2.4 \pm 0.1\ \text{kcal} \cdot \text{mol}^{-1}$) and entropic ($\Delta S = -10.4 \pm 0.1\ \text{cal} \cdot \text{mol}^{-1} \cdot \text{K}^{-1}$) contributions to the free energy associated with this shuttling process.

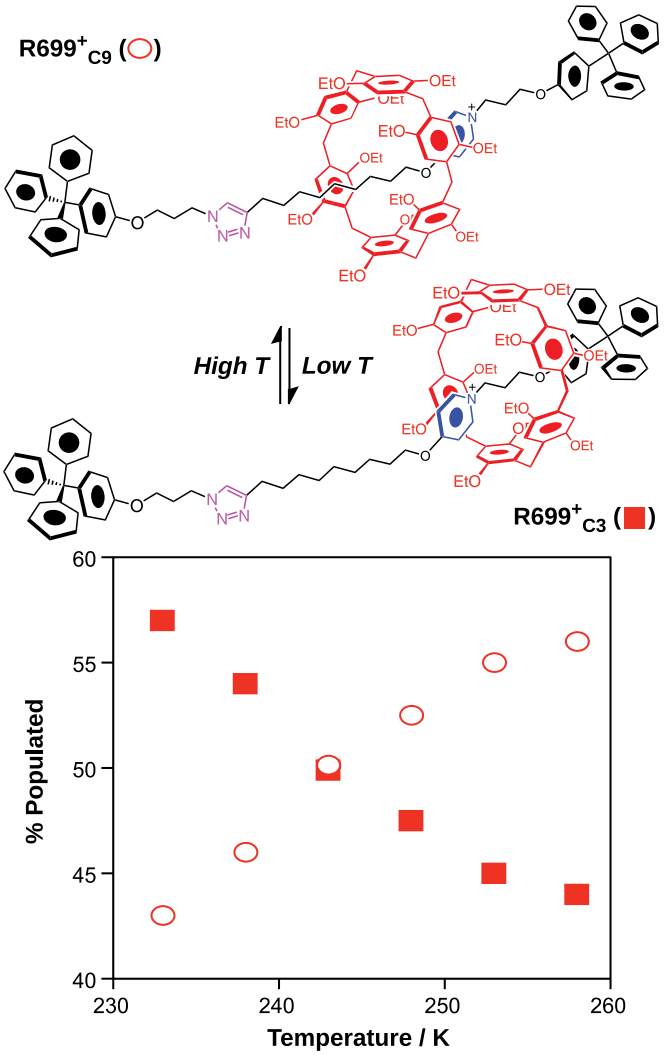


Figure 6.25 The pillar[6]arene-based rotaxane $\mathbf{R699^+}$ equilibrates[501] between two co-conformations in which the ring encircles either a trimethylene or a nonamethylene chain located nearby a pyridinium unit. Nonamethylene encapsulation is favored at higher (248 K) temperatures and trimethylene co-conformer dominates at low (223 K) temperatures.

Thus the system is dominated by the enthalpic term at lower temperatures ($\Delta G = -0.12\,\text{kcal}\cdot\text{mol}^{-1}$ at –50 °C) and by the entropic term at higher temperatures ($\Delta G = +0.15\,\text{kcal}\cdot\text{mol}^{-1}$ at –25 °C). The larger cavity of the pillar[6]arene ring (~7.5 Å) with respect to pillar[5]arene (~5 Å) is important in enabling this thermally-controlled switching, since a per-ethylated pillar[5]arene ring remains encircled around the nonamethylene chain and does not shuttle on an identical dumbbell.

6.9.1.5 Thermal Switches Driven by Imine Hydrolysis

The entropically-driven switching[464] of the imine-bridged rotaxanes **R679a** and **R679b**—see **Scheme 6.77** in the **Section 6.7.3**—is summarized in **Figure 6.26**. Although the distribution of the fixed-ring rotaxanes (**R679a** and **R679b**) and post-hydrolysis mobile-ring rotaxanes (**R679aO$_2$H$_6^{2+}$** and **R679bO$_2$H$_6^{2+}$**) are sensitive to temperature in both cases, the positional discrimination at high and low temperatures is much better in the latter case. Hydrolysis of the imine bonds of **R679a** is less complete in wet acidic $CHCl_3$, since the parent diimine populates up to 81% of the molecular distribution at the relatively high temperature of 313 K, but also remains the dominant species (42%) at a low temperature of 243 K. On the contrary, **R679b** represents >95% of the population at 373 K and <5% of the population at 273 K. These differences can be explained on the basis of a thermodynamic analysis. It was verified that hydrolysis of the imine bonds of **R679a** is enthalpically favored ($\Delta H = -6.0 \pm 0.4\,\text{kcal}\cdot\text{mol}^{-1}$) and entropically disfavored ($\Delta S = -26 \pm 1.4\,\text{cal}\cdot\text{mol}^{-1}\cdot\text{K}^{-1}$). Thus, the entropic penalty for the addition of two H_2O molecules outweighs the entropic reward from mobilizing the ring upon imine hydrolysis. The more biased temperature-dependent equilibrium distribution in the case of **R679b** can therefore be attributed to hydrogen bonding between the protonated macrocyclic diamine of **R679bO$_2$H$_6^{2+}$** and the dumbbell's polyether loops. Since these hydrogen bonds are enthalpically favorable, they stabilize the hydrolytic species more efficiently at low temperatures, where the entropic penalties are less severe. Indeed, the enthalpic contribution to free energy in a polyether-bearing relative of **R679b** was found to be much larger ($\Delta H = -16.7 \pm 0.7\,\text{kcal}\cdot\text{mol}^{-1}$) than that ($\Delta H = -6.0 \pm 0.4\,\text{kcal}\cdot\text{mol}^{-1}$) of **R679a**.

6.9.2 Switching Driven by Thermal Decomposition

A research program led by Takata[502] has employed a reaction associated with thermal decomposition to drive the shuttling (**Scheme 6.86**) of the DB24C8 ring in rotaxane **R6100H$^+$**. The key design feature of this strategy is the use of a trichloroacetate counterion. When a solid-state sample of **R6100H**$\cdot Cl_3CCO_2$ is heated above 70 °C, decarboxylation of $Cl_3CCO_2^-$ extracts a proton from the dibenzylammonium group of the rotaxane's dumbbell and generates the neutral [2]rotaxane **R6100** along with CO_2 and $CHCl_3$ as products. ^{1}H NMR spectroscopy confirms that the ring migrates away from the nitrogen atom when samples heated above the decarboxylation temperature are dissolved the in $CDCl_3$. **R6100H**$\cdot Cl_3CCO_2$ is regenerated by the addition of trichloroacetic acid.

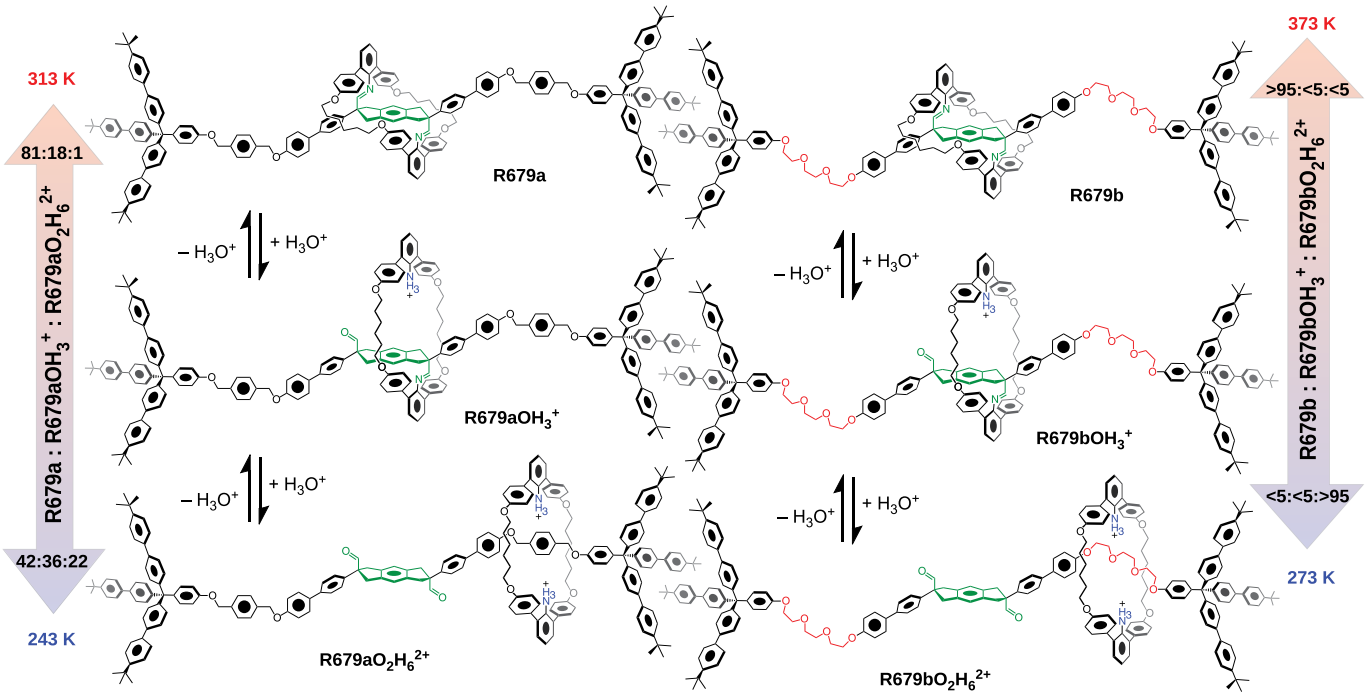
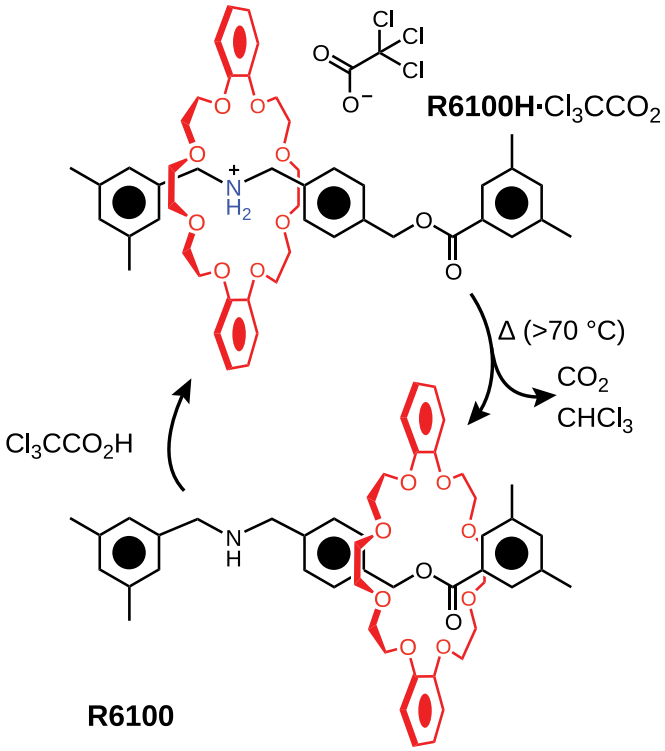


Figure 6.26 The temperature dependence of the equilibrium distribution[464] of imine-bridged rotaxanes **R679a** and **R679b** and corresponding partially hydrolyzed (**R679aOH$_3^+$**, **R679bOH$_3^+$**) and fully hydrolyzed (**R679aO$_2$H$_6^{2+}$**, **R679bO$_2$H$_6^{2+}$**) products in the presence of TFA (<1% v/v) in wet $CDCl_3$.



Scheme 6.86 The thermal decomposition of a trichloroacetate counteranion drives[502] the shuttling of the DB24C8 ring in **R6100H**$^+$ by extracting a proton to give **R6100**, CO_2, and $CHCl_3$ as products.

The thermal decomposition temperature is higher in a *N*-methylated analogue of **R6100H**$^+$ (100 °C) and especially in the bare dumbbell (158 °C) with no interlocked ring, revealing that the crown ether of the rotaxane architecture facilitates the thermal decomposition of the Cl_3CCOO^- anion. Recently, Takata[503] has exploited this thermally driven shuttling process in the side chains of poly[2]rotaxanes in order to change the color and helical pitch of solid-state polyphenylacetylene materials reversibly—see **Section 6.15.1.4**.

6.10 Pressure-Driven Switches

There is only one example, to our knowledge, in which the effect of pressure on the distribution of co-conformational isomers in MIMs has been described. The pressure-controlled (**Figure 6.27**) bistable [2]rotaxane **R6101**$^{4+}$ was introduced recently by Jeppesen.[504] Contrary to most bistable rotaxanes based on HQ and TTF-derived recognition units—see **Sections 5.1.1.1** and **6.1.1.1**—the thermodynamically most stable co-conformation of **R6101**$^{4+}$ is the "red" isomer, **R6101**$^{4+}_{HQ}$. This GSCC is unexpected because the MPTTF unit—the ring's site of occupation in the "green" isomer **R6101**$^{4+}_{MPTTFS\text{-}SMe}$—is a stronger π-electron donor than HQ. The higher stability of the red translational isomer has been attributed to the steric bulk of the *tert*-butylbenzene stopper adjacent to the MPTTF unit, which prevents the ring from assuming an optimal geometry at this site. The thiomethyl 'speedbump' of the MPTTF unit presents a considerable activation barrier, which prevents the ring from shuttling quickly on the laboratory timescale. This slow shuttling enables the observation of different red:grene ratios following the clipping synthesis of **R6101**$^{4+}$ at different pressures. It is clear that the green isomer is increasingly favored at higher pressures. Since the green isomer is the kinetic product and not the thermodynamic one, this pressure sensitivity can be explained by the kinetics of the synthetic protocol, where the rate of clipping a $CBPQT^{4+}$ ring around MPTTF has a steeper dependence on pressure than that of HQ. It is too early to comment on the potential scope of pressure-driven switching, but this initial example of pressure sensitivity presents a promising new avenue of research.

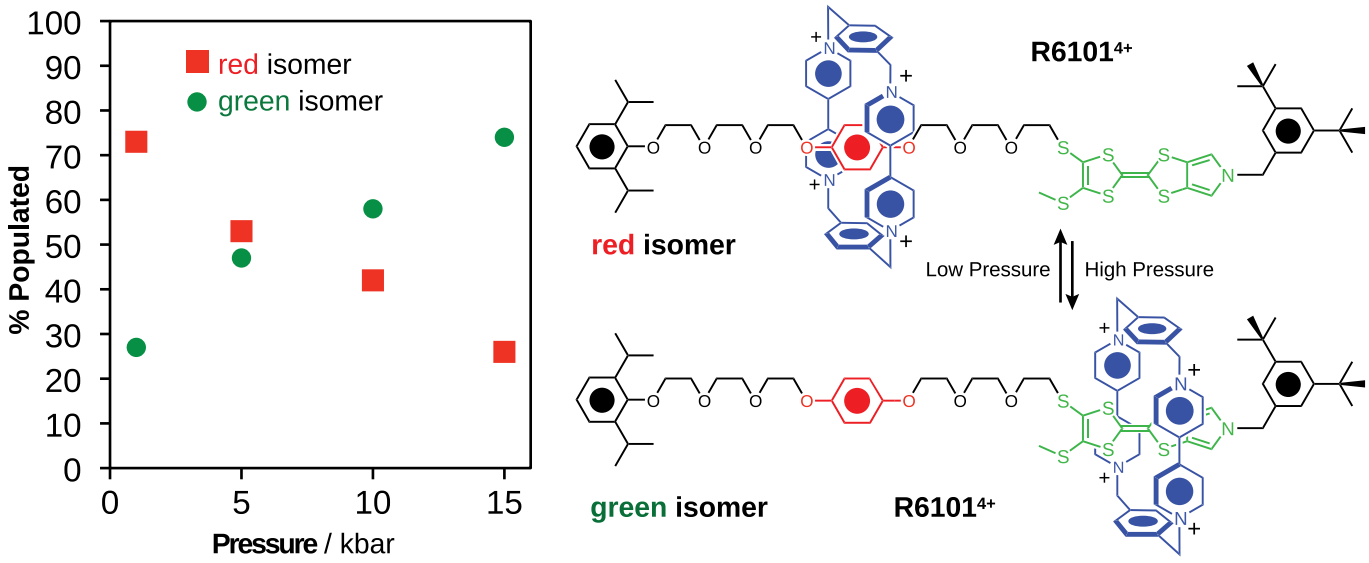


Figure 6.27 The ratio of red (GSCC) and green (MSCC) co-conformers of **R6101**$^{4+}$ is sensitive to pressure.[504]

6.11 Switches Driven by Electric Fields

The seminal work of Ghadiri[456] on the development of the transmembrane rotaxane **R6102** comprising DNA axles and protein nanopore rings—see **Section 2.3.12.2**—produced devices in which the position of the axle with respect to the protein nanopore embedded in a lipid membrane can be controlled by an external electric field, as depicted in **Figure 6.28**. Applying an electric field in this system generates an electroosmotic force that acts on the DNA polyelectrolyte axle, driving it toward the source of positive potential. A mechanical bond sealed by *biotin⊂streptavidin* and DNA hairpin stoppers confines the axle to the hemolysin (α-HL) nanopore, preventing the polyelectrolyte from escaping into either the "cis" or "trans" compartments separated by the lipid bilayer membrane. Conveniently, the transmembrane ion current stabilizes at significantly different levels depending on whether the lumen of α-HL is occupied by DNA or PEG, since DNA blocks the passage of ions more effectively

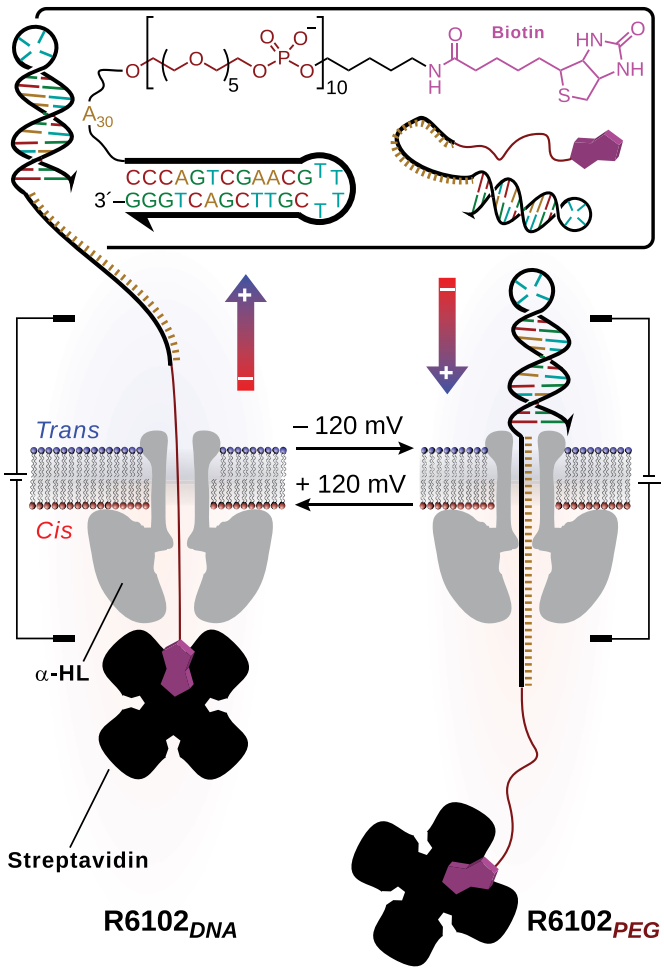


Figure 6.28 Diagram of the design of Ghadiri's single transmembrane rotaxane and its actuation in an electric field.[456] The DNA/PEG axle translates through the α-HL protein nanopore following the direction of electroosmotic flow (indicated by red/blue arrows) until one of bulky stoppers comprising either *biotin⊂streptavidin* or self-duplexed DNA hairpin domain.

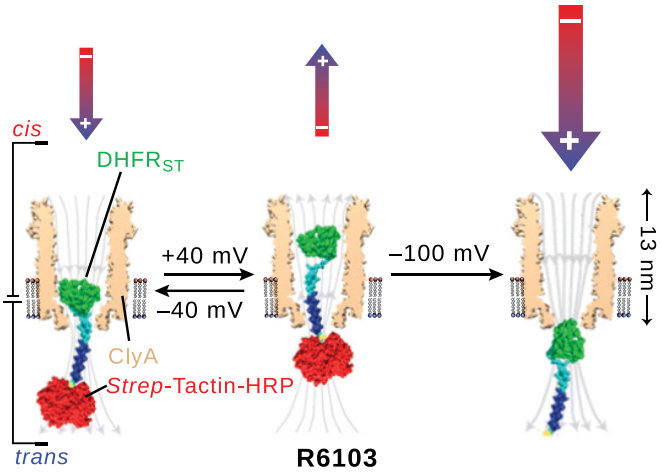


Figure 6.29 Maglia's all-protein transmembrane [2]rotaxane based on a ClyA nanopore.[507] The dumbbell comprises the $DHFR_{ST}$ protein (green) with its C-terminus extended by a polypeptide thread (blue) terminated by a *Strep*-Tag sequence (yellow), which binds an engineered *Strep*-Tactin-HRP (red) stopper protein when the $DHFR_{ST}$ fusion protein protrudes into the *trans* compartment. At applied potentials of < ±40 mV, the direction of the electric field controls the electroosmostic forces acting on the dumbbell, allowing it to be translated back and forth with respect to the ClyA nanopore. At higher potential (–100 mV) the rotaxane is dismantled by the extrusion of DHFR into the *trans* compartment. Illustrations adapted with permission from ref. 507 (copyright 2015 American Chemical Society).

than does PEG. This kind of rotaxane system has been adapted[505,506] into devices that can sense DNA polymerase activity. We also recall from **Section 6.6.2** that this platform has enabled the design[455] of "an autonomously reciprocating nanoactuator".

Maglia[507] has expanded upon the concept of transmembrane rotaxane devices by introducing the all-protein rotaxane **R6103**, comprising (**Figure 6.29**) a Cytolysin A (ClyA) protein nanopore threaded by a polypeptide axle, which is stoppered covalently in the *cis* compartment by a genetically modified dihydrofolate reductase ($DHFR_{ST}$), and noncovalently in the *trans* compartment by the engineered strepdavidin *Strep*-Tactin-HRP, courtesy of a *Strep*-Tag peptide binding sequence terminating the $DHFR_{ST}$ fusion protein. In this case, the dumbbell escapes from the rotaxane by deslipping into the *trans* compartment at sufficiently high applied negative potential (–100 mV), yet the dumbbell remains interlocked with the ClyA nanopore indefinitely at applied potentials lower than ±40 mV. As in the case of DNA, reversing the direction of the electric field reverses the direction of electroosmotic flow and therefore also reverses the translational movement of the dumbbell. The existence of a threshold potential for deslipping, which is attributable to the relationship between the magnitude of the electric field and the dwell time of the protein in the lumen of ClyA, allows one to exercise remarkable control over the traffic of proteins across the membrane.

6.12 Switches Driven by Mechanical Force

The advent of atomic-resolution microscopies has allowed mechanostereochemists to not only image MIMs, but also to study their dynamics at the single molecule level. The tip of a scanning tunneling microscope (STM) can deliver a mechanical force to a single molecule adsorbed on a surface, while the cantilever of an atomic force microscope (AFM) can be employed to stretch or pull on surface-anchored molecules.

Shigekawa and Komiyama[508] were among the first researchers to demonstrate (**Figure 6.30**) that mechanical force could be used to reposition the ring of a rotaxane. The probe of a STM was used to supply a mechanical force to an α-CD ring, causing it to translatie along the polyether backbone comprising the axle of Harada's seminal polyrotaxane[509]—see **Section 2.3.1.1**. The images reproduced in **Figure 6.30** portray the position of the α-CD ring before and after a tip sweeping movement. The ring is moved diagonally along the surface in the same direction of the tip sweep, while the movement of other nearby rings is not observed. This movement is reversible—a tip sweep in the reverse direction returns the ring to its former position. It is noteworthy that stable images of these α-CD polyrotaxanes can be obtained at room temperature in air, since STM imaging is often performed at very low pressures and temperatures,

Leigh,[510] utilized a similar tip-sweeping movement in an AFM to perturb mechanically (**Figure 6.31**) benzylic amide

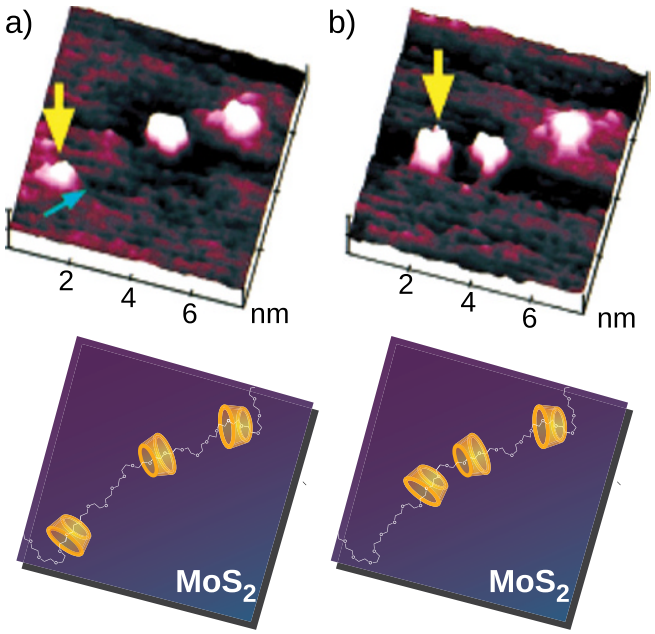


Figure 6.30 An STM tip uses supplies the mechanical force required to displace an α-CD ring on an α-CD/PEG polyrotaxane adsorbed on MoS_2.[508] (a) STM Image and graphical representation of the polymer before switching. The yellow arrow denotes the target α-CD ring and the blue arrow denotes the direction of the tip's movement as it acts on the ring. (b) STM Image and graphical representation of the polyrotaxane after tip-driven translation of the ring. STM images reproduced with permission from ref. 508 (copyright 2000 American Chemical Society)

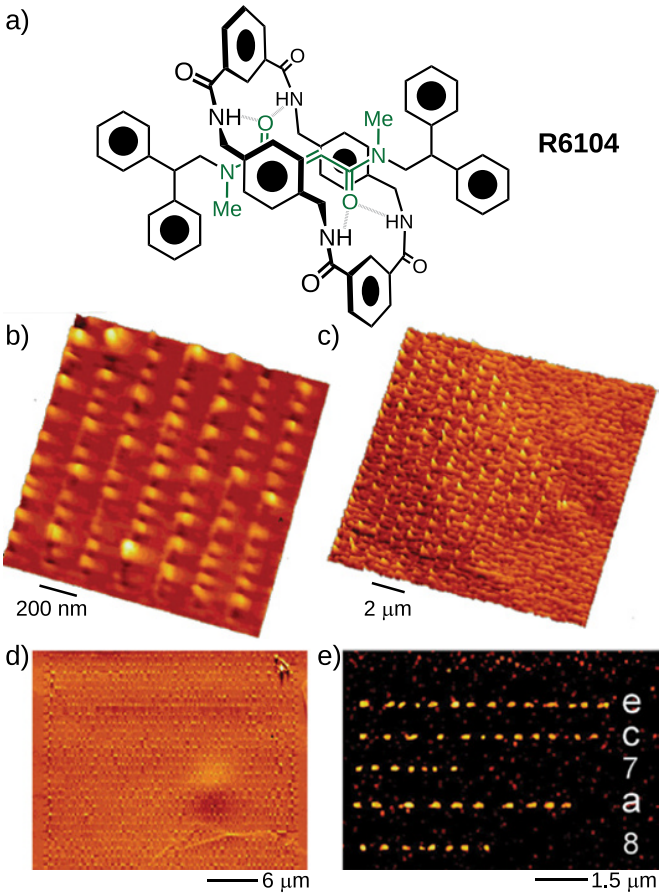


Figure 6.31 Writing features in thin films of benzylic amide [2]rotaxanes with the mechanical force of an AFM tip.[510] (a) Stereoformula of the [2]rotaxane **R6104**. (b)–(d) AFM micrographs at difference size scales, showing the raised features that arise from parallel lines of tip-sweeping motions in films of **R6104** drop-cast on HOPG. (e) Surface patterns can be written for the purposes of information storage, as exemplified by a hexidecimal code for "e c 7 a 8" in the area of only a few square micrometers. Data reprinted with permission from ref. 510 (Copyright 2003 AAAS).

rotaxanes, such as the fumaramide [2]rotaxane **R6104**, embedded in neat thin films deposited on either highly ordered pyrolytic graphic (HOPG) or mica. Above a threshold loading force of 2 nN, the movement of the AFM tip in a straight line results in the appearance (**Figure 6.31b–d**) of a series of dots of uniform height, diameter, and pitch. The dot size and spacing is controlled by the thickness of the film. Molecular models suggest that the raised features in the films arise when the tip supplies enough mechanical energy to induce the circumrotation of the benzylic amide rings between two nearly degenerate states, leading to a local recrystallization event. The same raised features are not observed in control compounds that lack a mechanical bond. Strings of bits, such as the hexadecimal sequence "e c 7 a 8", can be written (**Figure 6.31e**) in the film at an information storage density of up to 100 $Gbit \cdot in^{-2}$. See **Section 6.15.1.3** for a discussion on information storage by molecular machines.

AFM techniques have been called upon to carry out mechanically driven single-molecule switching experiments. For example, an AFM cantiliever has been employed[92] to move (**Figure 6.32**) the ring of a bistable donor-acceptor [2]rotaxane into energetically unfavorable co-conformations and measure the forces associated with these actions. The rotaxane **R6105^{4+}** comprises an SiO_2-immobilized dumbbell possessing DNP and TTF recognition units, threaded by a CBPQT^{4+} ring functionalized with a dithiolane tether that can be anchored to a gold-coated AFM cantilever by forming strong bidentate gold-thiolate bonds. Following covalent immobilization of **R6105^{4+}** or its chemically oxidized counterpart **R6105^{6+}** on the SiO_2 surface, individual rotaxane molecules are approached by the gold-coated AFM tip in a "fishing" experiment, which "grabs" (when successful) the disulfide tether of the CBPQT^{4+} ring. The force required for the ring to transgress the stopper in these rotaxanes depends on (i) the energy required to remove the ring from its energetic minimum near a recognition site, and (ii) the energy required to overcome the steric barrier associated with forcing the stopper through the ring's cavity. These are the two primary barriers that prevent deslipping in **R6105^{4+}**. In the case of the TTF-oxidized **R6105^{6+}**, an additional barrier involving (iii) repulsive Coulombic forces that build up as the tetracationic cyclophane passes over the dicationic TTF^{2+} unit from its stabilized position around the DNP unit. Whereas an average of 66 pN of force is required to separate the ring and dumbbell in **R6105^{4+}**, an average of 145 pN is required to dissociate the ring in **R6105^{6+}**, indicating that the repulsive electrostatic interactions between CBPQT^{4+} and TTF^{2+} could generate up to 79 pN of force.

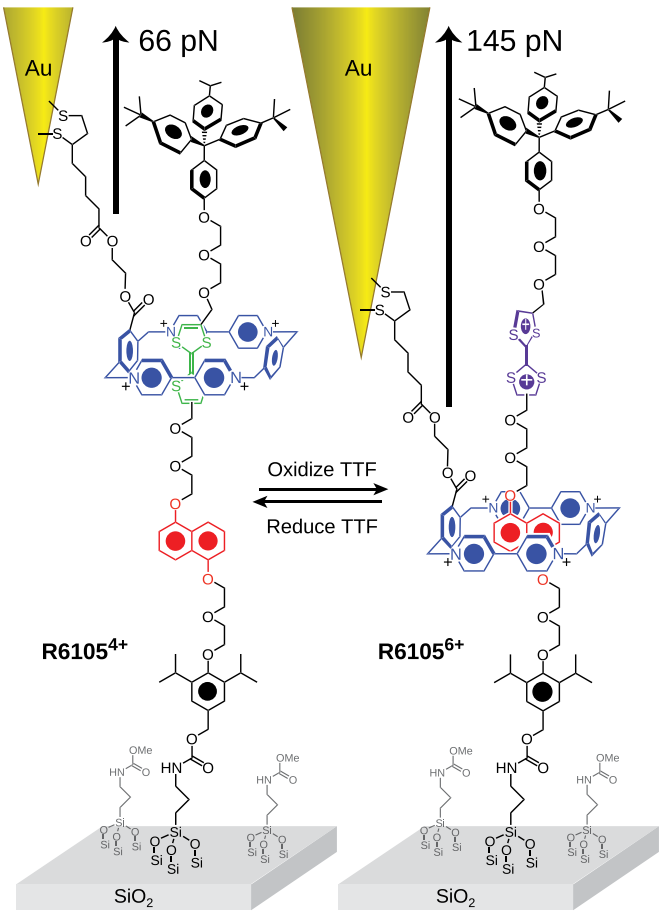


Figure 6.32 An AFM pulling experiment[92] on an immobilized bistable donor-acceptor rotaxane in both the TTF-neutral state (**R6105^{4+}**) and TTF-oxidized state (**R6105^{6+}**). Repulsive Coulombic forces between the CBPQT^{4+} ring and the TTF^{2+} dication **R6105^{6+}** require the application of more force (145 pN) to pass the ring over the dumbbell's stopper than the force (66 pN) required to do likewise in **R6105^{4+}**, indicating that the redox actuation of this rotaxane can generate up to 79 pN of force per cycle.

Böhmer and Janshoff[511] have described the effects of stretching (**Figure 6.33**) a surface-immobilized calix[4]arene dimer-based catenane oligomer (**C629$_n$**) using an AFM. The **C629** monomer is equipped with two decamethylene tethers appended to the calix wheels, which carry a carboxylic acid (*C*-terminus) and a primary amine (*N*-terminus). This chemical functionalization allows the catenanes to be oligomerized via amide bond formation, while also enabling their immobilization at SAM/Au surfaces between a substrate and an AFM tip, respectively. The *C*-terminus is adsorbed electrostatically onto a cationic SAM on a gold substrate, while the *N*-terminus is attached covalently to a SAM on an AFM tip by coupling efficiently with a succinimidyl ester. The thermodynamically stable co-conformation of these multicatenanes involves eight interdigitated arms at the center of a tetraurea-calix[4]arene dimer participating in a circular network of 16 hydrogen bonds. The force-induced rupture of these hydrogen bonds is uniquely reversible in this experimental setup by virtue of the mechanical bond, which holds the two strained calixarene rings at a certain critical distance beyond which they cannot be further dissociated without breaking covalent bonds. It was found that the network of 16 hydrogen bonds is ruptured in a concerted fashion when a force of 40–60 pN (3–4 pN per hydrogen bond) is applied. Furthermore, each dimer is ruptured in succession—tension in the oligomer is built up and released in steps, corresponding to a sawtooth pattern in the force-extension curves output by the instrument. Combining molecular dynamics simulations with these force-extension profiles also revealed a stable intermediate species for **C629** in between the hydrogen bond-ruptured state and the conformationally locked state under a high external load. As expected, the hydrogen bonds are re-formed as the tip is lowered and strain is released. The observed rupture and rejoining forces depend on the rate at which force is applied, but they converge on equal values at sufficiently low, near-equilibrium loading rates.

Mechanical force investigations have also been applied (**Figure 6.34**) to benzylic amide MIMs by Leigh and Duweiz.[512] In their experimental setup, a PEG chain attached to the benzylic amide ring of the surface-immobilized

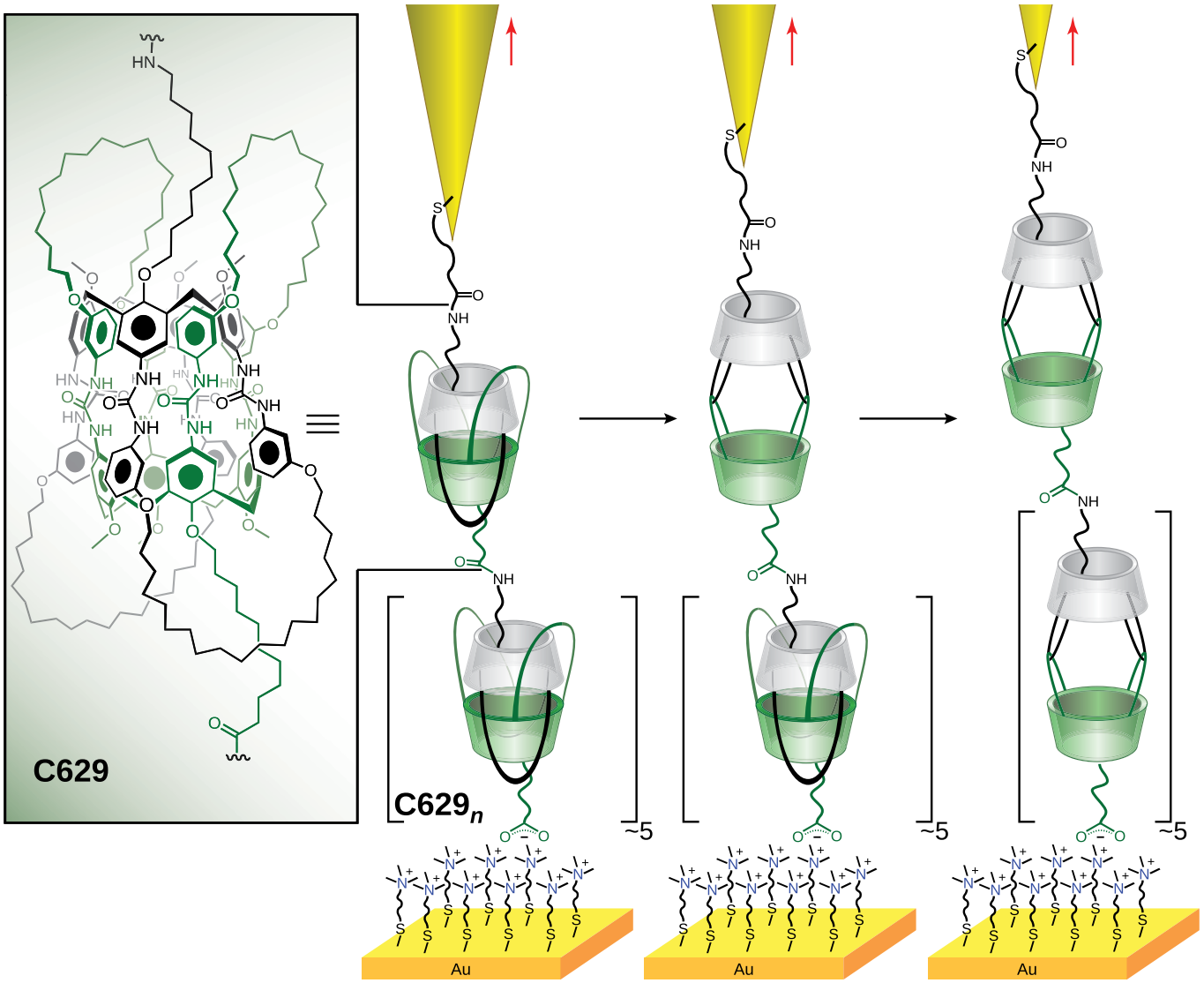


Figure 6.33 An AFM pulling experiment[511] conducted on oligomers of Bohmer's calix[4]arene-derived multi[2]catenanes (**C629**$_n$), which are adsorbed electrostatically at one terminus to a cationic SAM on gold and covalently bound at the other terminus to a SAM on a gold-coated AFM tip.

rotaxane **R6106** is physisorbed onto a Si_3N_4 AFM tip. After being pulled away from the primary fumaramide recognition site—a process requiring ~45 pN of force in trichloroethane and ~27 pN of force in DMF—the ring can travel by biased Brownian motion back toward the fumaramide unit against an applied external load of up to 30 pN, corresponding to ~6 kcal·mol^{-1} of mechanical work. The same research duo also subsequently carried out an investigation[513] involving the mechanical stretching of a PEG chain with a single benzylic amide catenane at its center. It was found that the catenane's ring mobility, as controlled by solvent polarity or chemical derivitization, could be detected at the single-molecule level in the form of different polymer countour lengths, as determined by an appropriate model of the force-extension profile.

On an aminopropylsilylated silicon surface, Lindsay[514] has constructed [2]rotaxanes comprising (i) a β-CD ring functionalized with a PEG linker that reaches to an AFM tip and (ii) an anchored dumbbell possessing an adamantyl recognition unit, conjugated to a DNA strand stoppered by a Texas Red dye. When the ring's PEG chain is pulled (**Figure 6.35**) away from the surface by the tip of an AFM cantilever, the ring can be forced to slide along the DNA backbone until it reaches the bulky stopper, at which point further extension results in the breaking of covalent bonds. Although the ring's passage over different nucleobases cannot be distinguished in the force-extension profiles, one can nevertheless detect and probe the mechanics of DNA secondary structures in this "tape reader" geometry. In the case (**Figure 6.35a**) of the [2]rotaxane **R6107**$^{82-}$, the β-CD ring traverses two DNA hairpins, *H1* and *H2*, comprising four and seven base pairs, respectively. The force (**Figure 6.35b**) required to transgress *H2* is greater than that of *H1*. In this geometry, the DNA hairpins unfold against a force

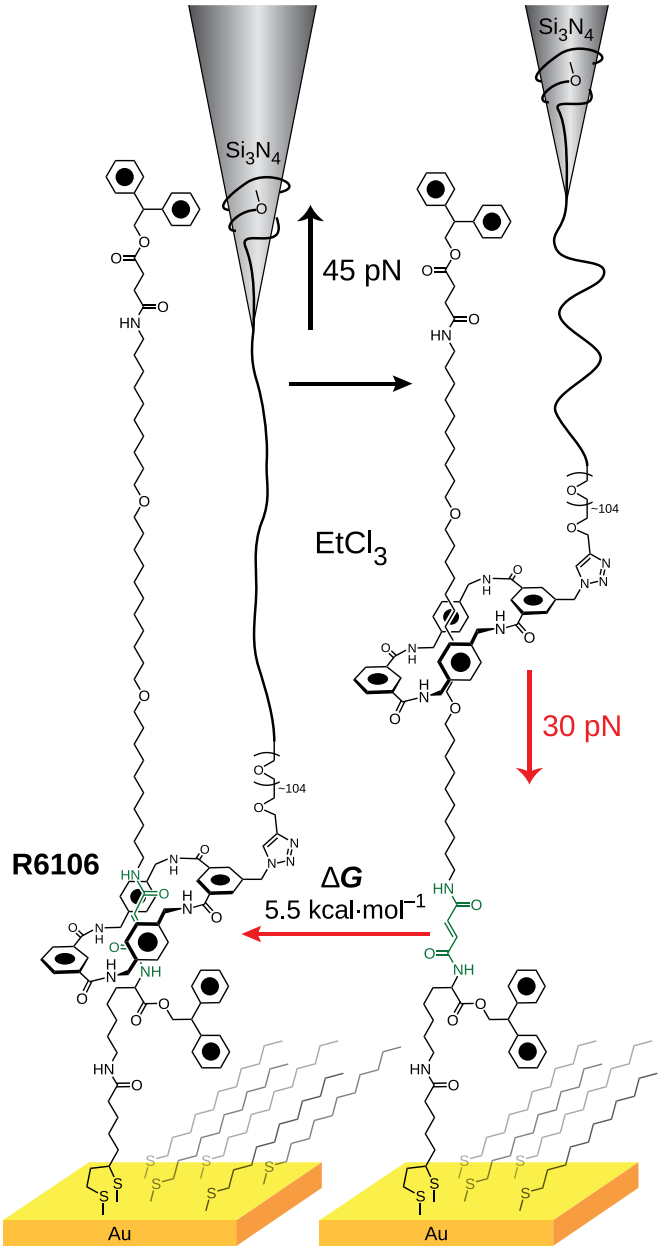


Figure 6.34 The bistable [2]rotaxane[512] **R6106** has its dumbbell anchored to a gold surface by dint of strong thiol-gold bonds and its benzylic amide ring anchored to an AFM tip by physisorption of a polyether chain. A mean force (black arrows) of 45 pN is required to break the hydrogen bonds that stabilize the rotaxane in the GSCC. When the tension in the polyether tether is relaxed, the biased Brownian motion of the benzylic amide ring can generate (red arrows) up to 30 pN of force against the external load supplied by the AFM cantilever.

that is approximately 40 times greater than that required to unfold the same hairpins by pulling directly on the ends of the DNA strand. It is envisioned that similarly inspired molecular apertures encircling DNA might one day serve as reading heads for next-generation DNA sequencing technologies.

In summary, the research reviewed in this Section reveals, not only that microscopes can supply a mechanical force to induce co-conformational changes at the single-molecule level, but also that molecular switches can generate forces on the order of 20–80 pN under an external load. These forces are at least equivalent to or even in excess of the forces (5–60 pN) generated by biological molecular machines,[515] which bodes well for pursuit of genuine artificial molecular machinery—see **Section 6.15**.

6.13 Beyond Translation and Circumrotation

In **Sections 6.1–6.12**, we have focused on translation and pirouetting motions, mostly in [2]rotaxanes and [2]catenanes, as driven by various stimuli. We turn our attention now to alternative kinds of motion constrained by the mechanical bond and induced by these stimuli in more sophisticated molecular topologies and architectures. Through judicious design of their component parts, mechanomolecules can be made to express muscle-like extensile and contractile motions (**Section 6.13.1**) in a variety of architectures, constriction and dilation (**Section 6.13.2**) of an aperture, radial motions (**Section 6.13.3**) emanating from a central core, twisting into an unusual "Gemini" coconformation (**Section 6.13.4**), flapping (**Section 6.13.5**), collapsing (**Section 6.13.6**), inflation/deflation (**Section 6.13.7**), folding/unfolding (**Section 6.13.8**), as well as stepwise (**Section 6.13.9**), pulley-like (**Section 6.13.10**), multi-directional (**Section 6.13.11**), and conveyer belt-like (**Section 6.13.12**) motions in multiply interlocked and multicomponent mechanomolecules.

6.13.1 Expansion and Contraction: Molecular Muscles with Mechanical Bonds

Muscle is characterized at both microscopic and macroscopic scales by its ability to change the distance between two points at the expense of chemical energy in order to produce force and motion. This essential trait is enabled by an exquisite hierarchical organization of molecular machines and filaments—billions of them moving in concert, bringing their nanoscale motions to bear on the macroscopic world. The construction of artificial muscles that mimic this function is a flourishing field of contemporary research. Since rotaxanes also possess movable filamentous components, they are inherently well-suited to mimic muscle function.[516,517] This Section is dedicated mostly to a variety (**Figure 6.36**) of rotaxane-based artificial muscle architectures. We focus here on a number of rotaxane architectures of greater complexity than simple [2]rotaxanes and their corresponding extensile and contractile motions. Efforts towards scaling these motions beyond low Reynolds number are outlined in **Section 6.15.1.2**.

The basic repeating unit of a muscle cell is the sarcomere. Three of the most important components of the sarcomere are the thick myosin filaments, thin actin filaments, and the Z-discs, which are colored in red, blue, and black, respectively, in the graphical representation of a sarcomere in **Figure 6.36a**. The contraction of a sarcomere is caused by antiparallel sliding motions between the actin and myosin filaments, which bring the Z-discs to which they are

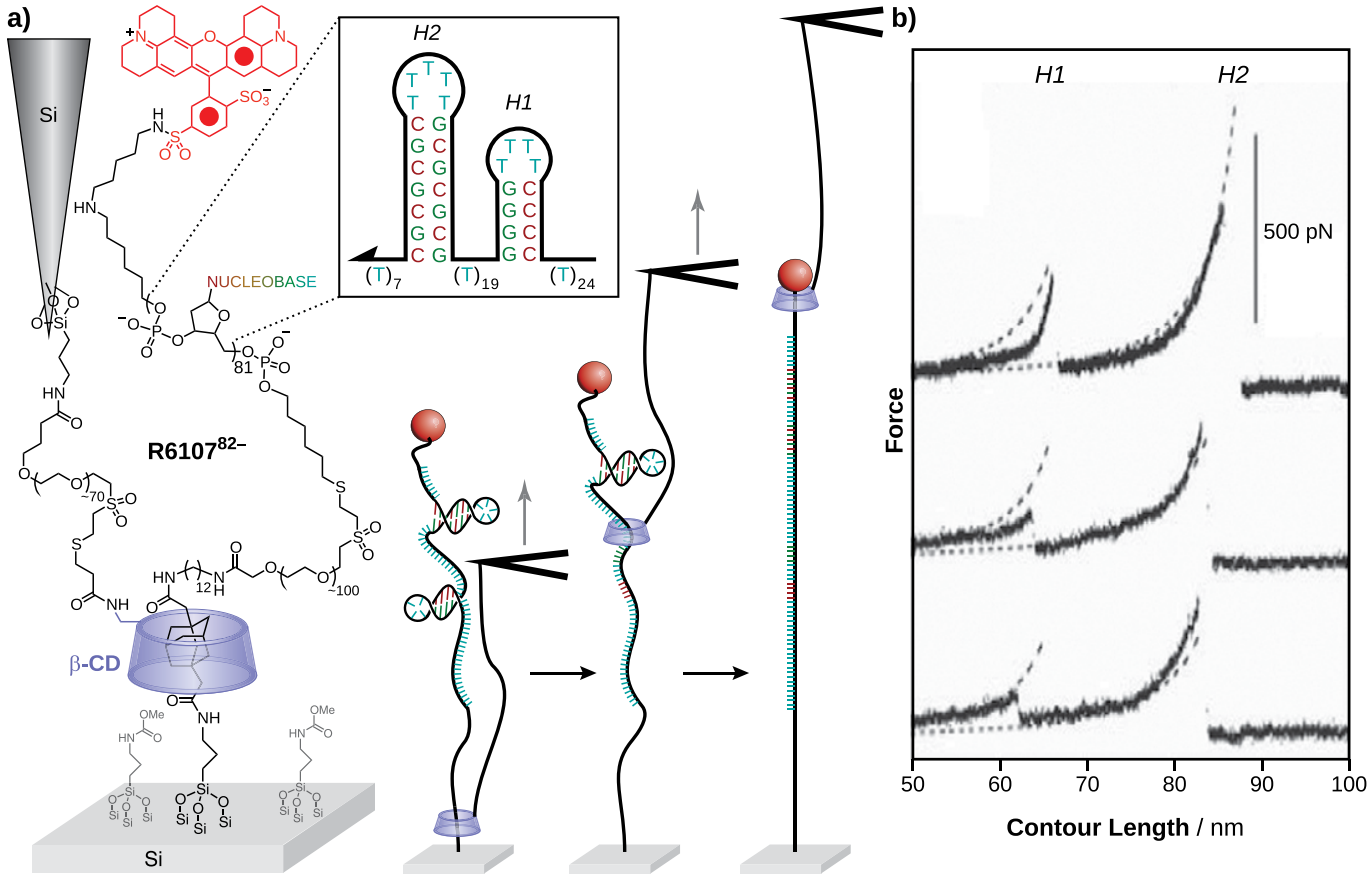


Figure 6.35 Lindsay's "tape reader" [2]rotaxane.[514] (a) Diagram of the pulling experiment in which a β-CD ring, attached covalently to an AFM cantilever by a polymer linker, is translated over the entire length of a surface-immobilied PEG/DNA dumbbell over two hairpin structures, *H1* and *H2*, in the [2]rotaxane **R6107**$^{82-}$. (b) The ring's passage over DNA hairpins *H1* and *H2* can be detected and differentiated in the force-extension profiles of three single-molecule pulling experiments.

connected closer together. This antiparallel sliding is initiated by a Ca^{2+}-triggered exposure of myosin binding sites on the actin filaments. Motor proteins that decorate the myosin fibers bind to these sites as they hydrolyze ATP to fuel a mechanical bending motion that exerts a force on the actin filaments, which moves them a few nanometers before the cycle is repeated. A number of "molecular muscles" (**Figure 6.36b–e**) can be defined[516] by substituting the myosin, actin, and Z-disc components conceptually for the mechanically interlocked components of a rotaxane. These architectures (see **Chapter 4**) include daisy chains (**Section 6.13.1.1**), ordinary and multicomponent rotaxanes (**Section 6.13.1.2**), molecular elevators (**Section 6.13.1.3**), and cage rotaxanes (**Section 6.13.1.4**). The graphical representations of these architectures are color-coded in red, blue, and black in **Figure 6.36** according to the roles they assume—myosin, actin, and Z-disc, respectively—in mimicking the sarcomere.

Rotaxane-based molecular muscles express different kinds of contractile motion (**Figure 6.36f-h**) depending on their architectures. Bistable [*c*2]daisy chains, for example, are arguably the closest mimics because their dumbbells are able to express antiparallel sliding motions (**Figure 6.36f**) with respect to one another when actuated. Molecular elevators and other rotaxanes—even ordinary [2]rotaxanes if the components acting as Z-discs are appropriately designated—can be switched to achieve a 'pressing' motion (**Figure 6.36g**) involving a compression of the Z-discs, which bears some resemblance to that of a machine press. Finally, cage-based rotaxanes are capable of compressing one or more dumbbells within the cage, affording telescoping motions (**Figure 6.36h**) that smack of objects with concentric tubular parts such as hydraulics and extendable antennae. The present summary of these compounds is in many ways an adaptation and expansion of our recent review[516] on rotaxane-based molecular muscles.

6.13.1.1 Antiparallel Sliding in [c2]Daisy Chains

Bistable daisy chains (**Figure 6.36b**) have been the primary focal point for rotaxane-based molecular muscles, having been investigated in this context since they were introduced (**Scheme 6.87**) by Sauvage[367] in 2000. In particular, [*c*2]daisy chains have been pursued for their ability to express antiparallel sliding motions (**Figure 6.36f**) that closely mimic those of the sarcomere.

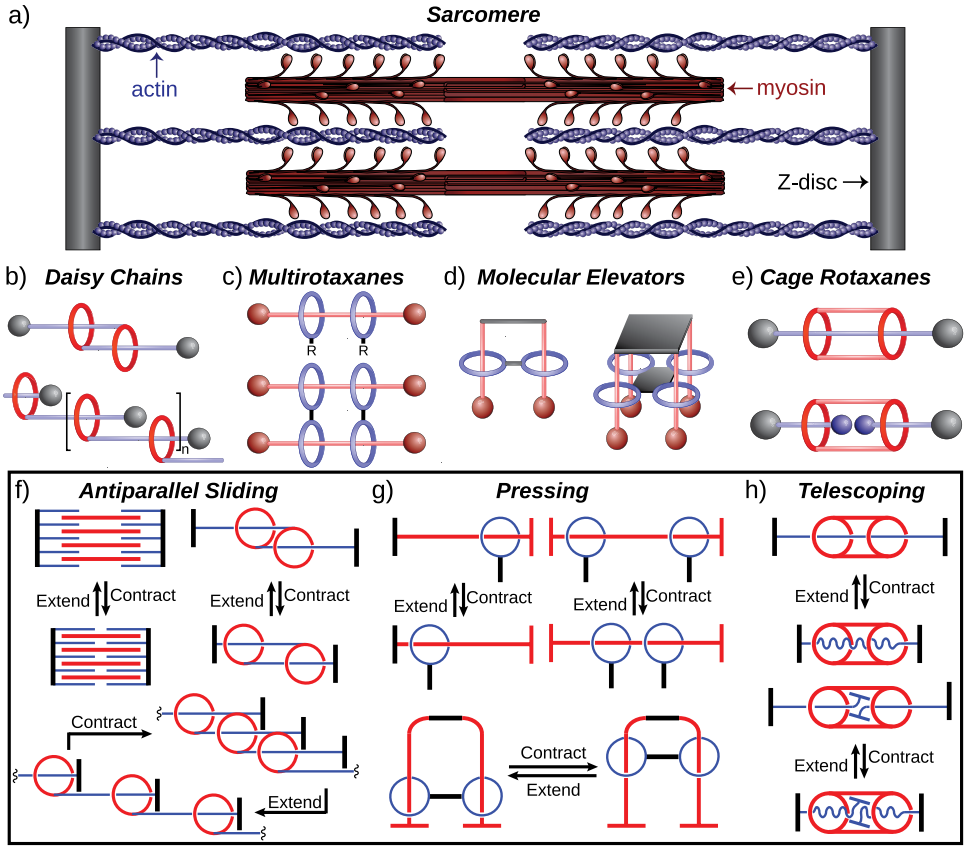
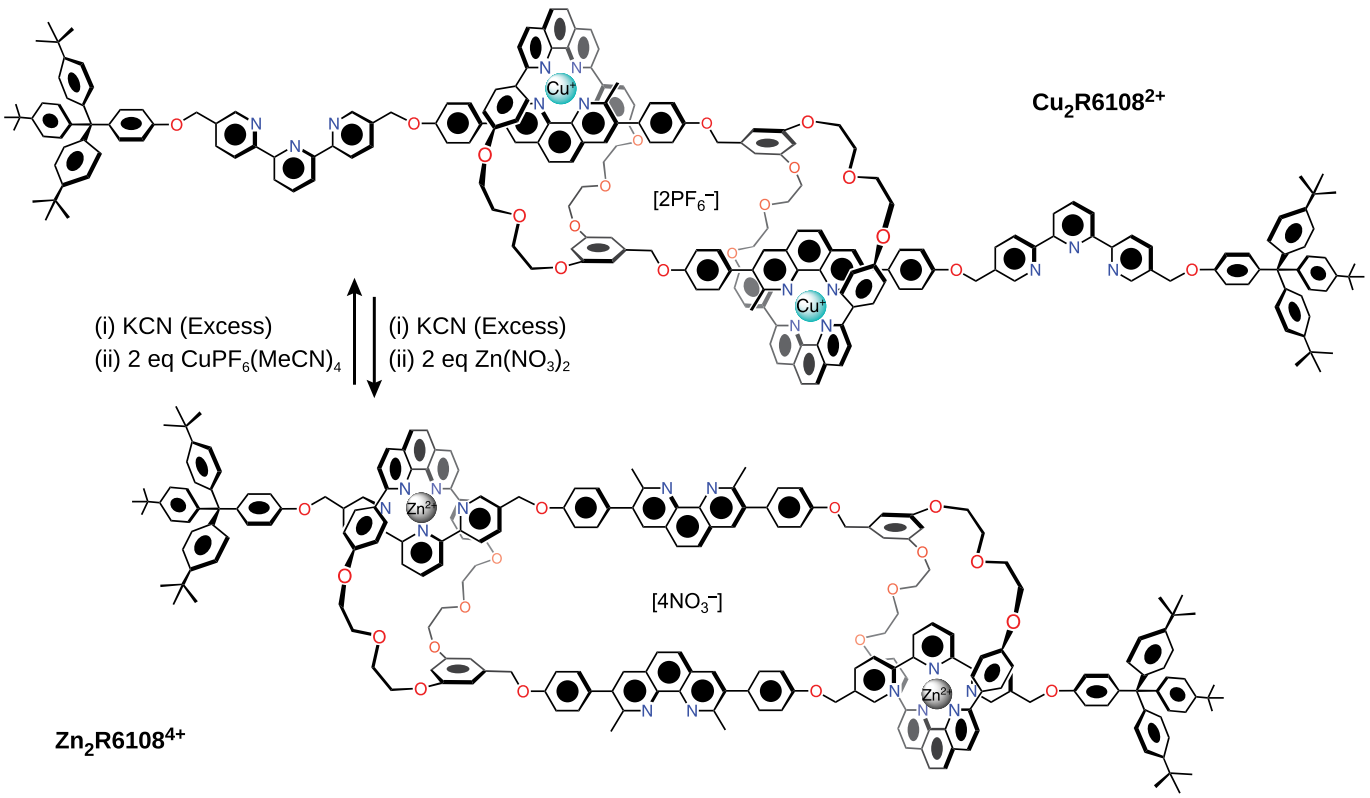


Figure 6.36 Summary of the architectures and motions of natural and rotaxane-based artificial muscles.[516] (a) Simplified representation of the sarcomere. (b)–(d) Illustrations of the various rotaxane-based 'molecular muscle' architectures. (f)–(h) The extensile and contractile motions of the sarcomere and rotaxanes are compared. The components that assume the roles of the sarcomere's actin filaments, myosin filaments, and Z-discs are colored in blue, red, and black, respectively.



Scheme 6.87 Sauvage's metal-complexed [*c*2]daisy chain operates[367] by template exchange. The rings' endotopic phenanthroline ligands pair with the dumbbell's phenanthroline ligands when Cu^{I} serves as the templating ion to give an extended geometry for **Cu_2R6108^{2+}**. The ring ligands pair with the dumbbell's terpyridine units when the templates are exchanged for Zn^{II} to afford a contracted geometry in **Zn_2R6108^{4+}**.

The idea of mimicking the sarcomere with a switchable rotaxane was pioneered by Sauvage,[367,518] who noted that the cross-threaded architecture of the rotaxane dimer **Cu_2R6108^{2+}** is suited for contractile motion by means of antiparallel sliding among its two interlocked component parts. Thus, an extended state is adopted when Cu^{I} is used as a template (**Scheme 6.87**) as a result of the tetrahedral geometry of two phenanthroline ligands—one in each dumbbell and ring component. Conversely, exchanging the Cu^{I} template for Zn^{II} results in a contracted state, in which the rings ligate Zn^{II} with the terpyridine ligands adjacent to the stoppers of **Zn_2R6108^{4+}**, where they participate in a pyramidal coordination geometry.

The next class of bistable [*c*2]daisy chains to come on the scene were pH-switchable (**Figure 6.37**) compounds[286,300] based on crown ethers and dialkylammonium ions, namely **R6109H$_2^{6+}$** and **R6110H$_2^{4+}$**. These switches operate in a manner analogous to those described in **Section 6.3.3.1**, where the pH-controlled protonation and deprotonation of the dialkylammonium recognition site is propogated into ring movement. Acid/base actuation of these switches results in antiparallel sliding and extension/contraction in molecular length. These two rotaxanes differ in their secondary recognition sites, which are constituted by bipyridinium units[286] in **R6109H$_2^{6+}$** and triazolium units[300] in **R6110H$_2^{4+}$**.

A tristable analogue[301] of [*c*2]daisy chain **R6110H$_2^{4+}$** is Coutrot's molecular muscle **R6111H$_2^{6+}$**, which can be actuated (**Figure 6.38**) by a variety of stimuli, including covalent modification, pH, solvent, and temperature. When the dialkylmmonium recognition site is deactivated (**Figure 6.38a**) with either base (**R6111^{4+}**) or Boc-protection (**R6111Boc$_2^{4+}$**) the rings are faced with a choice between occupying a pyridinium (PY^+) amide unit or a triazolium (TZ^+) unit. The rings in the base-treated compound **R6111^{4+}** oscillate between these two sites as the compound decomposes relatively quickly. On the other hand, the **R6111Boc$_2^{4+}{}_{PY}$** and **R6111Boc$_2^{4+}{}_{TZ}$** isomers are stable, and their populations are sensitive to both solvent (**Figure 6.38b**) and temperature (**Figure 6.38c**). In low polarity solvents, the rings tend to encircle the pyridinium unit, whereas they opt for encircling the triazolium unit in high polarity solvents. In CH_2Cl_2—and probably other solvents as well—**R6111Boc$_2^{4+}{}_{PY}$** becomes more favored as the temperature is lowered. A tristable [2]rotaxane, in which a DB24C8 ring translates between the same array of recognition units in the axle, has also been reported by Coutrot.[302]

Huang's pillar[5]arene-based [*c*2]daisy chain **R6112** exhibits[489] a kind of analogue switching (**Scheme 6.88**) in which the solvent polarity represents the dial. The average position of the pillar[5]arene rings as the daisy chain oscillates in solution is influenced by the solvent polarity, where the rings spend more time near urea groups (**R6112$_U$**) in a low polarity $CDCl_3$ solution, and more time at the center of a solvophobic decamethylene chain (**R6112$_{C10}$**) in a polar $(CD_3)_2SO$ solution. The time-averaged position of the ring in

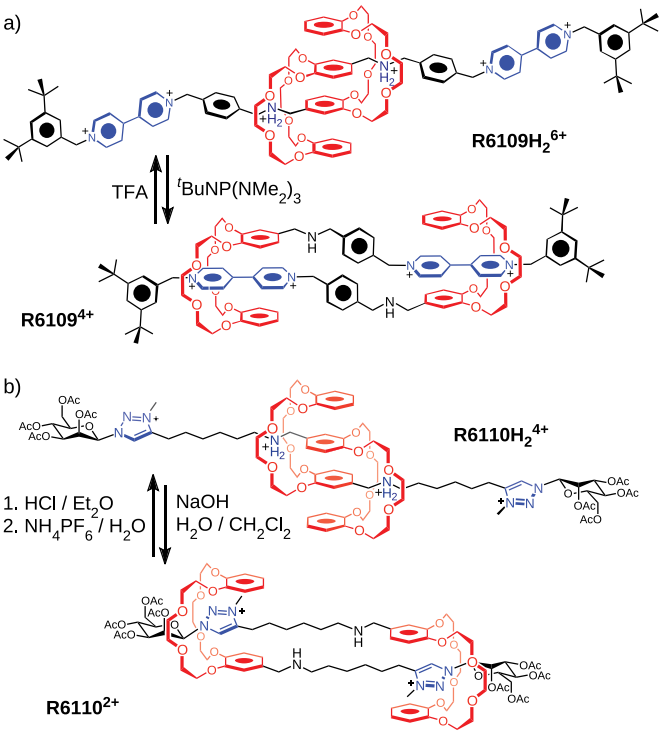
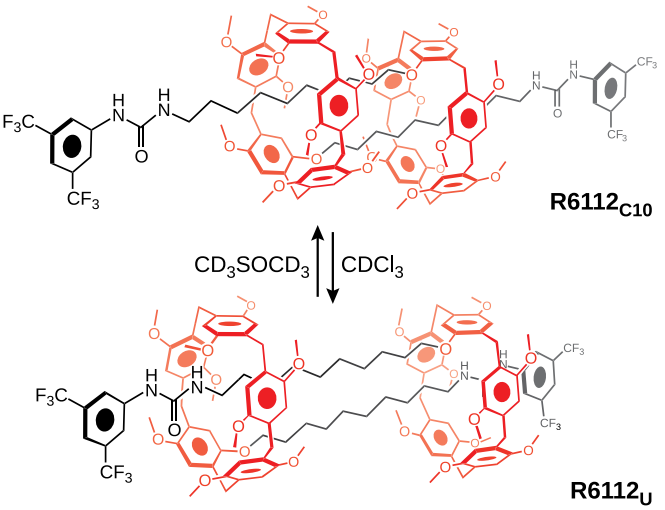


Figure 6.37 pH-Switchable [*c*2]daisy chains.[286,300] (a) **R6109H$_2^{6+}$** is held in an extended geometry involving crown ether–dialkylammonium interactions. Base-triggered deprotonation of the dialkylammonium centers leads to a contracted co-conformation in **R6109^{4+}** in which the rings move to encircle bipyridinium units.[286] (b) **R6110H$_2^{4+}$** and **R6110^{2+}** are actuated analogously, except that the rings encircle triazolium units in the contracted state.[300]

binary solvent mixtures thereof represents an intermediate in between these two extremes.

Harada[519] introduced solvent switchable (**Scheme 6.89**) daisy chains when his group reported on properties of the α-CD rotaxane **R6113**. The α-CD rings encircle cinnamamide



Scheme 6.88 Solvent switching between two co-conformations in Huang's pillar[5]arene [*c*2]daisy chain **R6112**.[489]

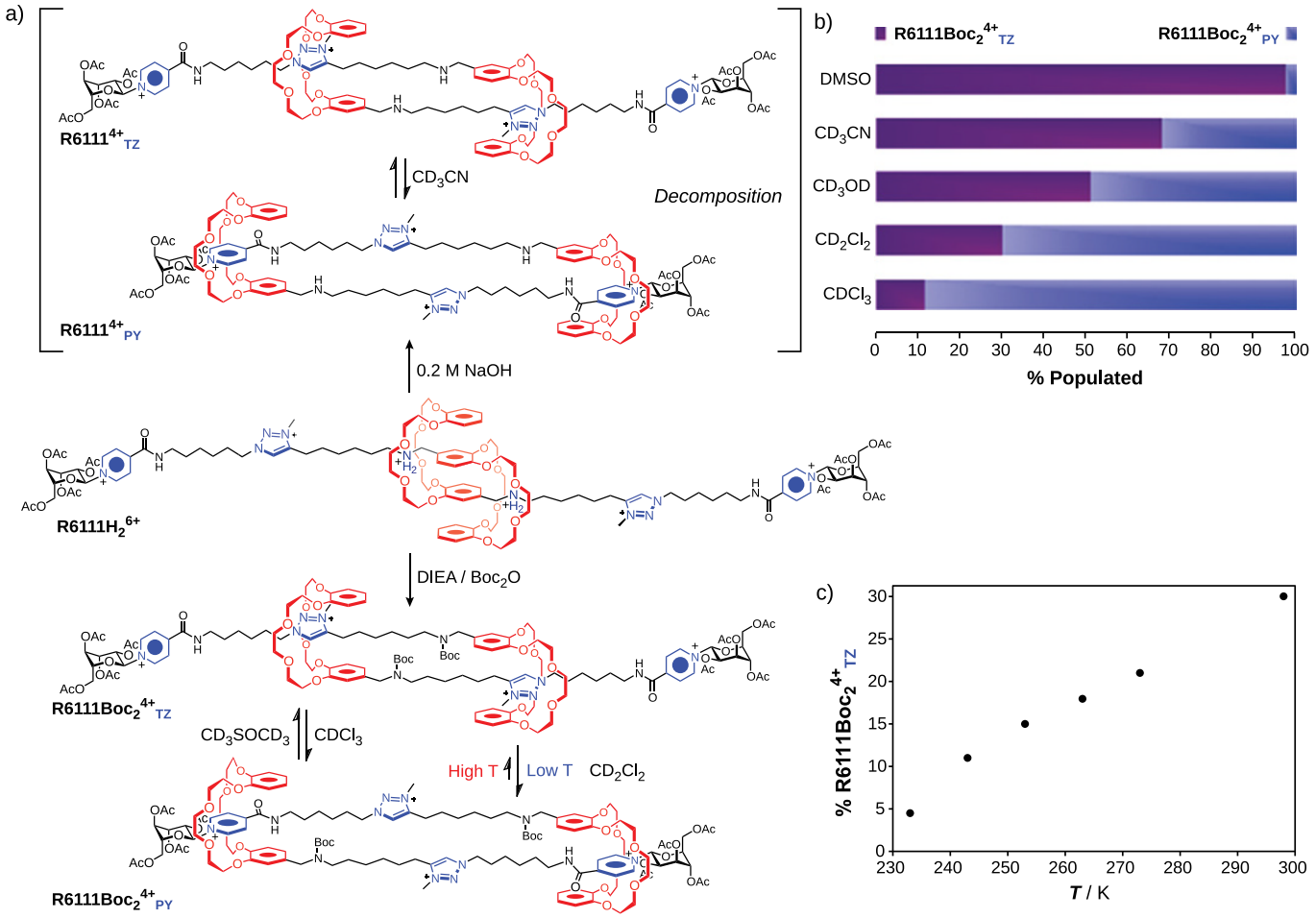
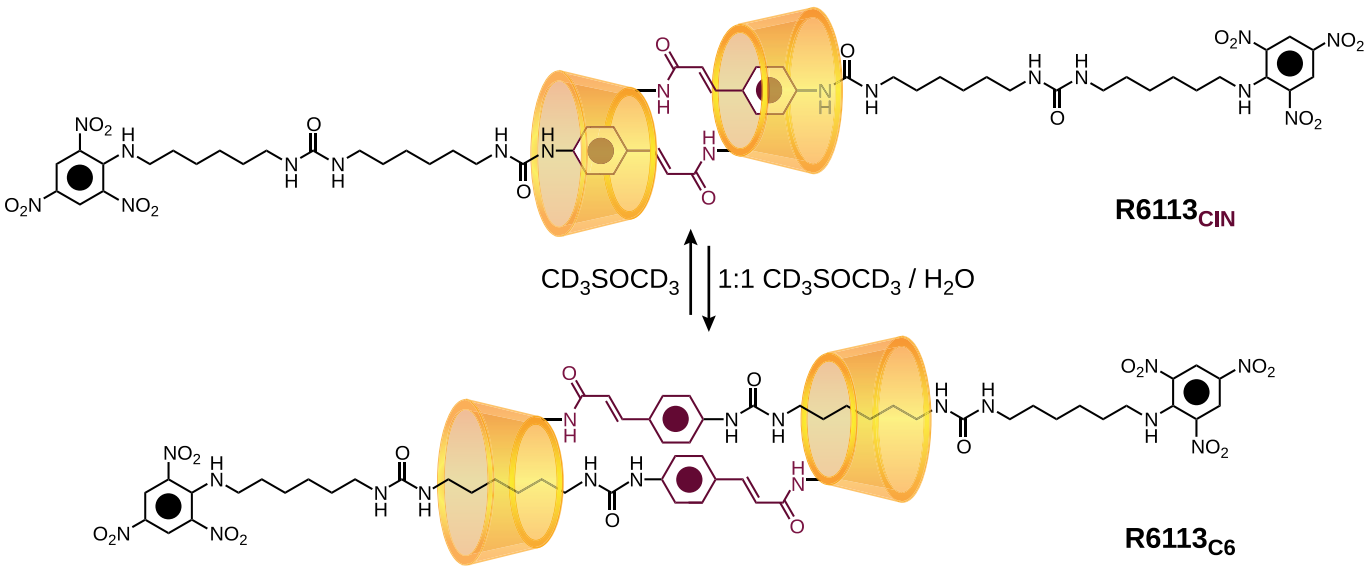


Figure 6.38 Coutrot's multi-addressable tristable [*c*2]daisy chain.[301] (a) The fully extended co-conformation of **R6111H$_2^{6+}$** can be transformed to a more contracted geometry, either by base-triggered deprotonation (**R6111^{4+}**) or by Boc-protection (**R6111Boc$_2^{4+}$**). (b) The two stable co-conformations of the Boc-protected daisy chain, **R611Boc$_2^{4+}{}_{TZ}$** (half-contracted) and **R611Boc$_2^{4+}{}_{PY}$** (fully contracted), are populated in a solvent-sensitive manner, where the half-contracted isomer is favored in more polar solvents (e.g., Me$_2$SO) and the fully contracted isomer is favored in less polar solvents (e.g., CDCl$_3$). (c) In CD$_2$Cl$_2$, the population of the minor, half-contracted co-conformer **R611Boc$_2^{4+}{}_{TZ}$** is even further diminished with decreasing temperature.



Scheme 6.89 Harada's solvent-switchable α-CD [*c*2]daisy chain **R6113**.[519]

(CIN) recognition sites in $(CD_3)_2SO$, but move outward to a more hydrophobic hexamethylene (C6) chain when H_2O is introduced in a 1:1 ratio. Thus, it is possible to influence the ratio of translational isomers **R6113$_{CIN}$** and **R6113$_{C6}$** by the addition or removal of water from the solvent.

With the exception of **R6113**, most of the bistable cyclodextrin-based daisy chains have been photoswitchable compounds. Three examples are illustrated in **Figure 6.39**. Kaneda[520,521] introduced this class of compounds in the form of **(*EE*)-R6114**. While the *trans*-azobenzene units of this compound are encapsulated by permethylated α-CD (PM-α-CD) rings, they are extruded from the CD cavities upon photoisomerization to **(*ZZ*)-R6114**, affording a net contraction in molecular length. The photoconversion under 366 nm is unfortunately not very efficient, since the (*EZ*)- and (*ZZ*)-isomers represent only 20 and 5% of the population, respectively, in the photostationary state. Easton's [*c*2]daisy chain **(*EE*)-R6115** uses stilbene as the photoactive unit. Owing to their high stability, the (*EE*)-, (*EZ*)-, and (*ZZ*)-isomers of **R6115** (2:2:1 in the photostationary state under 350 nm irradiation) could be isolated chromatographically and characterized as pure compounds. Harada[219] incorporated relatively long PEG chains between the azobenzene and hexamethylene recognition sites of the [*c*2]daisy chain **R6116**. The azobenzene units are converted from (*E*)- to (*Z*)-isomers with 40% efficiency in H_2O and 85% efficiency in MeOH with 365 nm irradiation. The kinetics of photoisomerization are essentially identical in **R6116** and an analogue incorporating a shorter PEG spacer, exhibiting a pseudo-first order rate constant $k_{E\rightarrow Z} = 5 \times 10^{-3}$ s^{-1} in each case, indicating that the rate of isomerization is insensitive to the linker length.

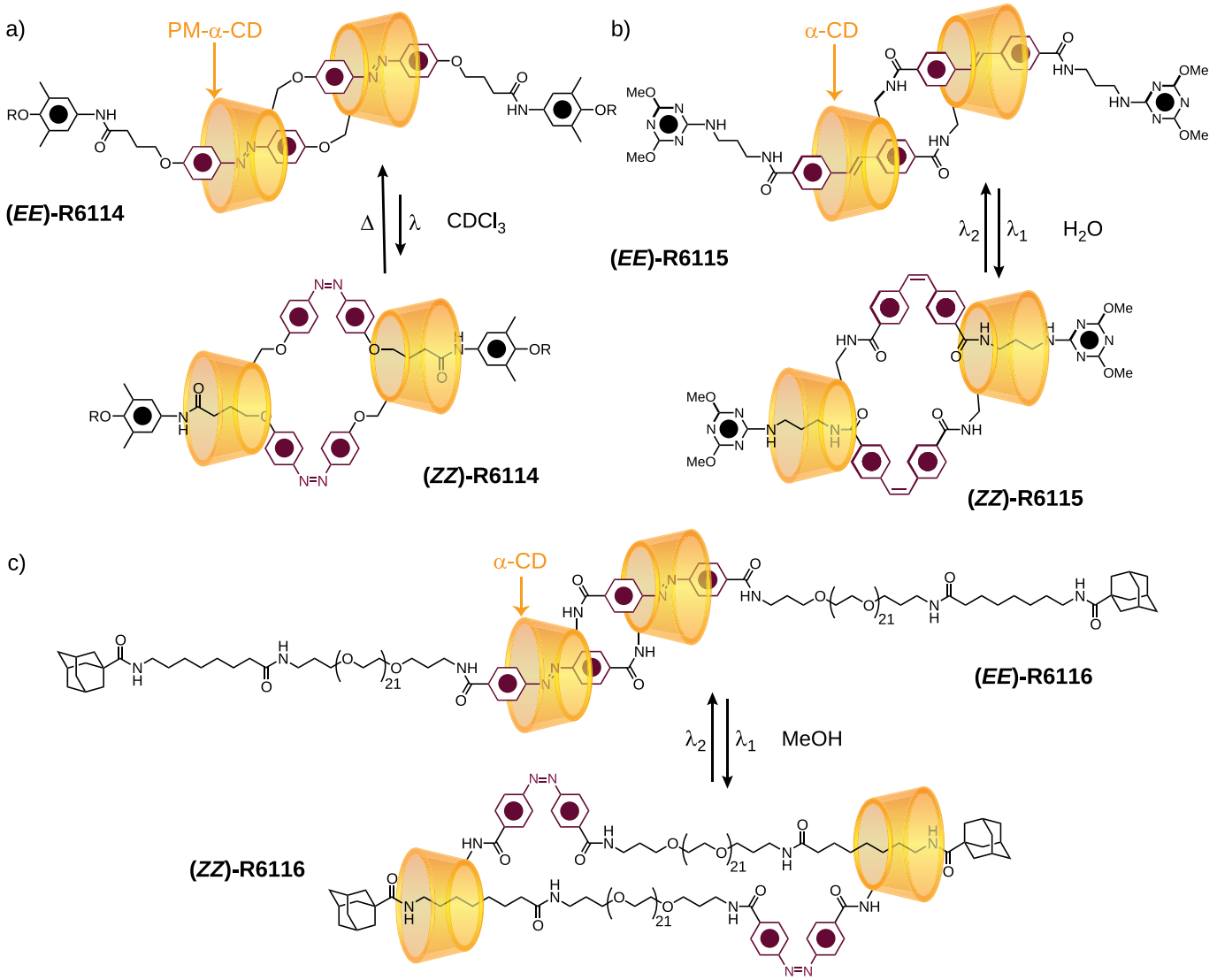


Figure 6.39 Photoswitchable cyclodextrin-based [*c*2]daisy chains involving the extrusion of azobenzene or stilbene guests upon photoinduced $E \rightarrow Z$ isomerization. (a) Photothermal switching[521] of Kaneda's permethylated α-CD daisy chain **(*EE*)-R6114**/**(*ZZ*)-R6114**. (b) Photoswitching[236] of Easton's α-CD/stilbene daisy chain **(*EE*)-R6115**/**(*ZZ*)-R6115**. (c) Photoswitching[219] of Harada's [*c*2]daisy chain polymer **(*EE*)-R6116**/**(*ZZ*)-R6116**.

Recently, π-associated donor-acceptor recognition motifs have also been employed[131,522] to construct daisy chains. Compound **R6117** is based on recognition between naphthalene diimide (NDI) and π-electron rich crown ethers.[522] This daisy chain contracts (**Figure 6.40a**) in response to an electrochemical stimulus, since the loss of the crown ethers' recognition for $NDI^{2(\bullet-)}$ radical anions causes the rings to encircle predominantly the triazole recognition sites in $\mathbf{R6117^{4-}}$. This daisy chain also behaves unexpectedly as a temperature-controlled (**Figure 6.40b**) switch. ^{1}H NMR Spectroscopic evidence and molecular dynamics simulations reveal that the MSCC $\mathbf{R6117_{tz}}$ becomes increasingly populated at lower temperatures in $CDCl_3$, where the value of K_{eq} is reduced from >10 above room temperature to nearly 1 at –45 °C. Thus, almost 50% of the GSCC ($\mathbf{R6117_{NDI}}$) undergoes translational motion as the temperature is lowered, while the vast majority of the same population succumbs to translation under electrochemical control.

The [*c*2]daisy chain[131] illustrated in **Scheme 6.90** is based on the $CBPQT^{4+}$ ring and its ability to recognize π-donors in its native state as well as π-radicals under reducing conditions. Daisy chain $\mathbf{R6118^{12+}}$ is not bistable in the ground state because the only recognition site with any affinity for the ring is the DNP unit. When $\mathbf{R6118^{12+}}$ is reduced electrochemically to the hexaradical hexacation $\mathbf{R6118^{6(\bullet+)}}$, however, the molecule extends to allow both of its $CBPQT^{2(\bullet+)}$ rings to encircle the corresponding $BIPY^{\bullet+}$ radical cations of the dumbbell in the radical-state co-conformation, stabilized in this case by radical–radical spin-pairing interactions.

Thousands to millions of sarcomeres are lined up in linear arrays (myofibrils) and bundled in tubular cells (myocytes). This hierarchical organization scales the synchronized extensile and contractile motions of sarcomeres all the way up from nanometers to centimeters. The polymeric nature of muscle tissue motivates the design poly[*c*2]daisy chains. Achieving macroscopic motion from polyrotaxane-based artificial muscles will require the efficient and relatively large-scale preparation of high molecular weight polymers. Synthesizing high molecular weight poly[*c*2]daisy chains has been challenging, however, to realize in practice. Kaneda's attempt[521] to polymerize **(*EE*)-R6114** at its terminal amide groups with *p*-xylyl linkers, for example, afforded a mere pentamer as the heaviest product.

Most of the poly[*c*2]daisy chains (**Table 6.4**) that have been reported to date involve pH-controlled switching motifs based on crown ethers and dialkylammonium ions. Attempts[287,523] to polymerize a derivative of $\mathbf{R6109H_2^{6+}}$ using click chemistry gave polymer ($\mathbf{R6119H_{2n}^{6n+}}$), which has only 11 repeating units on average. Its relatively small size notwithstanding, it was verified upon base-triggered generation of $\mathbf{R6119^{4n+}}$ that a concerted contractile motion is indeed achievable along a polymer backbone. Remarkably, the rate of this contraction, as well as the rate

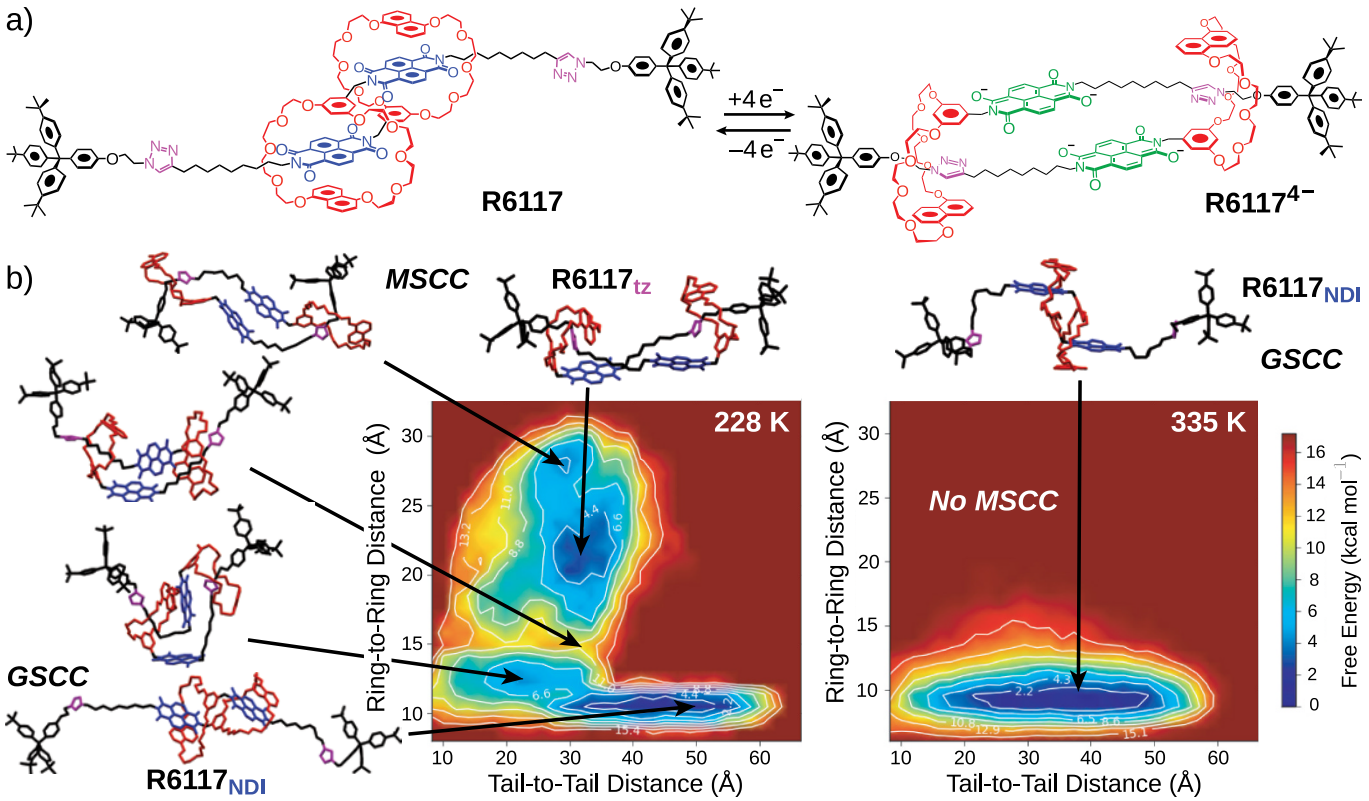
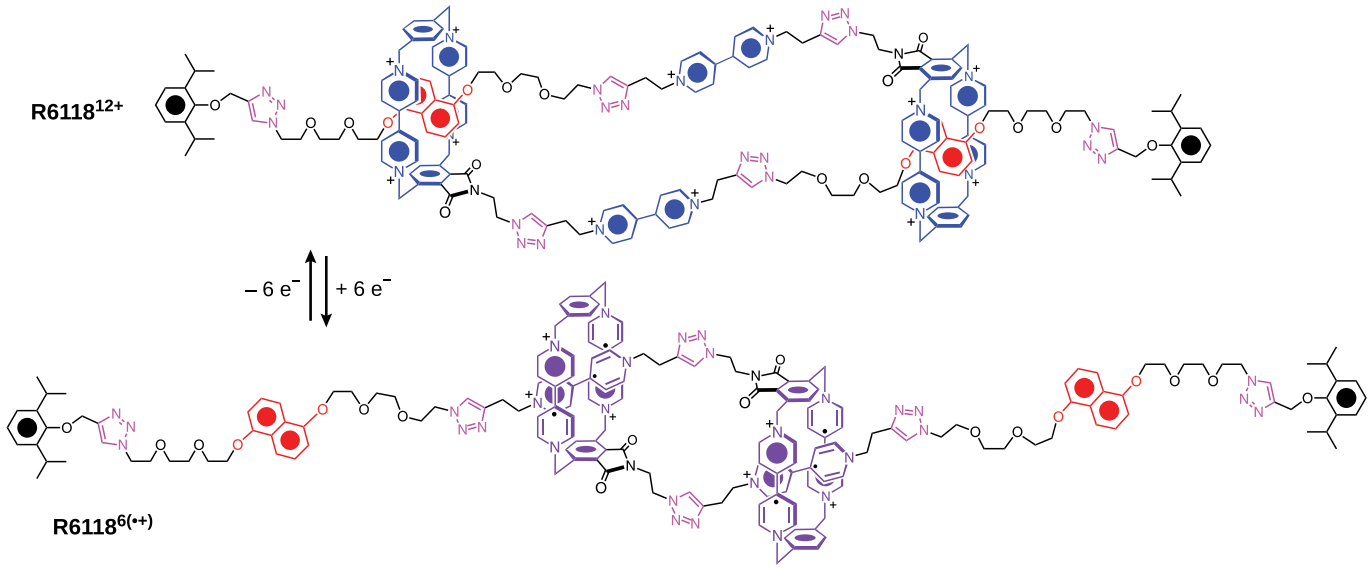


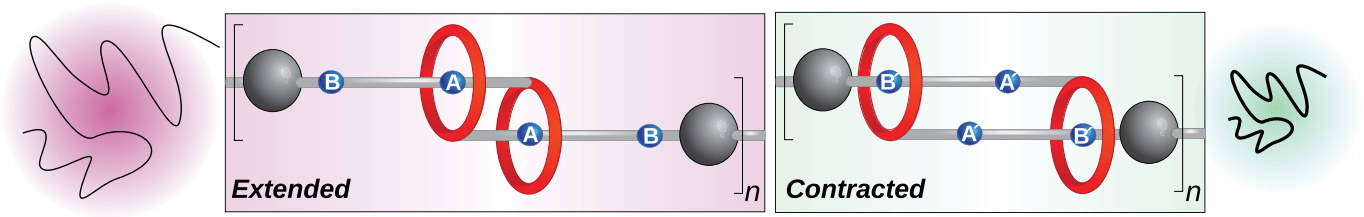
Figure 6.40 The electrochemically and thermally switchable donor-acceptor [*c*2]daisy chain **R6117**.[522] (a) Redox actuation of **R6117** involved reducing the NDI units to the NDI^{2-} dianions of $\mathbf{R6117^{4-}}$, which diminishes their affinity for the crown ethers and leads to the contracted geometry in which the rings encircle triazole units. (b) Free energy profiles obtained by MD simulations indicate that the contracted geometry of $\mathbf{R6117_{tz}}$ is the MSCC at low temperatures (228 K), whereas only the GSCC, $\mathbf{R6117_{NDI}}$, is not stable at elevated temperatures (335 K) in chloroform.



Scheme 6.90 The [*c*2]daisy chain[131] **R6118**$^{12+}$ is not bistable in the ground state because it possesses only one recognition unit (DNP) per CBPQT^{4+}-derived ring. Under reducing conditions, however, **R6118**$^{6(\bullet+)}$ becomes bistable and favors an extended co-conformation involving spin-pairing interactions between viologen radical cations (BIPY$^{\bullet+}$) in the ring and dumbbell components.

of acid-triggered extension (**R6119**$^{4n+}$ → **R6119H**$_{2n}$$^{6n+}$), is faster in the case of the polymer than in the corresponding monomer. In another click polymerization of a [*c*2]daisy chains, Grubbs[524] obtained **R6120H**$_{2n}$$^{2n+}$, which possesses ~22 repeating units. The covalent actuation of this polymer is achieved by acylation of the –NH_2^+– centers to generate **R6120Ac**$_{2n}$. Finally, Buhler and Giuseppone[525] solved the low molecular weight problem by taking a metallosupramolecular approach in the polymerization of the poly[*c*2]daisy chains **Fe**$_n$**R6121H**$_{2n}$$^{6n+}$ and **Fe**$_n$**R6121**$^{4n+}$. The repeating units of these polymers are based[300] directly (**Figure 6.37**) on Coutrot's daisy chain **R6110H**$_2$$^{4+}$/**R6110**$^{2+}$, with the only

Table 6.4 Summary of switchable dialkylammonium-based crown ether poly[*c*2]daisy chains.



Extended Polymer	DP *n*	Linker	Contracted Polymer	Ref
R6119H$_{2n}$$^{6n+}$	11		**R6119**$^{4n+}$	287 523
R6120Ac$_{2n}$	22		**R6120H**$_{2n}$$^{2n+}$	524
Fe$_n$**R6121H**$_{2n}$$^{6n+}$	3000		**Fe**$_n$**R6121**$^{4n+}$	525

modification being the use of terpy ligands as stoppers. The long metallosupramolecular polymers (~3000 repeating units) are formed spontaneously upon the addition of Fe^{II} in solution, owing to the dimerization of terpy ligands around the Fe^{II} ions. X-Ray scattering experiments revealed a 6.5 micron difference in the contour lengths of $\mathbf{Fe_nR6121H_{2n}^{6n+}}$ (15.9 μm) and $\mathbf{Fe_nR6121^{4n+}}$ (9.4 μm), providing unequivocal proof[525,526] that poly[*c*2]daisy chains can amplify the tiny motions of rotaxane-based molecular muscles over several orders of magnitude. More recently, Giuseppone[527,528] has shown that [*c*2]daisy chains of this type can be functionalized with alternative stoppering groups that yield other kinds of supramolecular polymers, and that the contractile actuation of their monomers influences the morphologies of the corresponding aggregates—see **Section 6.15.1.4**. A hydrogen-bonded [*c*2]daisy chain supramolecular polymer has also been investigated by Qu.[529]

Famulok[530] has recently reported on a new class of macromolecular [*c*2]daisy chains comprising DNA nanostructure motifs akin to those described in **Section 2.3.12.1**. These [*c*2]daisy chains can be switched between rigid and flexible states under the command of strand displacement (**Section 6.6.2**) reactions that add or remove DNA bridges which connect and disconnect the two component parts.

6.13.1.2 Pressing Motions in Palindromic Rotaxanes

A variety of rotaxane architectures can be designed to express "pressing" motions (**Figure 6.36g**) by appropriately designating the conceptual Z-disc substituents. Pressing is arguably the most generalizable type of muscle-like switching, since essentially any bistable rotaxane could be adapted, in principle, as a molecular press. It is important to note, however, that at least one of the rings of a rotaxane must be derivatized in order to garner any muscle-like function, since the stopper-to-stopper distance is essentially fixed in any case of a pressing motion. Even simple [2]rotaxanes can act as molecular presses if they are functionalized asymmetrically. Take the AFM pulling experiment on the [2]rotaxane **R6106** by Leigh and Duwez[512] as an example—see **Figure 6.34** in **Section 6.12**. Let the surface-anchored stopper of **R6106** represent Z-disc *A*, and let the tip-anchored ring represent Z-disc *B*. The biased Brownian motion of Z-disc *B* toward Z-disc *A* represents a contractile motion, and indeed exerts a force that can be detected by AFM sensors. Pressing motions are thus characterized by the ability of one or more mobile rings to change the distance between two points of interest.

In this Section, we focus our attention on pressing motions in palindromic rotaxanes. A palindrome is a symmetrical sequence that reads identically in forward and reverse directions. Examples of palindromic words include *racecar* and *detartrated*. The rotaxanes in this Section are considered palindromes because they possess planes of symmetry through the midpoints of their dumbbells, such that each half of the rotaxane mirrors the other. Thus, a bistable palindromic [3]rotaxane can express mirror-image translational motions across its mirror plane. Several palindromic [3]rotaxanes,[316,325,531–533] including the CB6 [3]rotaxane $\mathbf{R634H_4^{4+}}$ described by Tuncel[269,270]—see **Scheme 6.34** in **Section 6.3.1**—exhibit these types of symmetrical pressing motions.

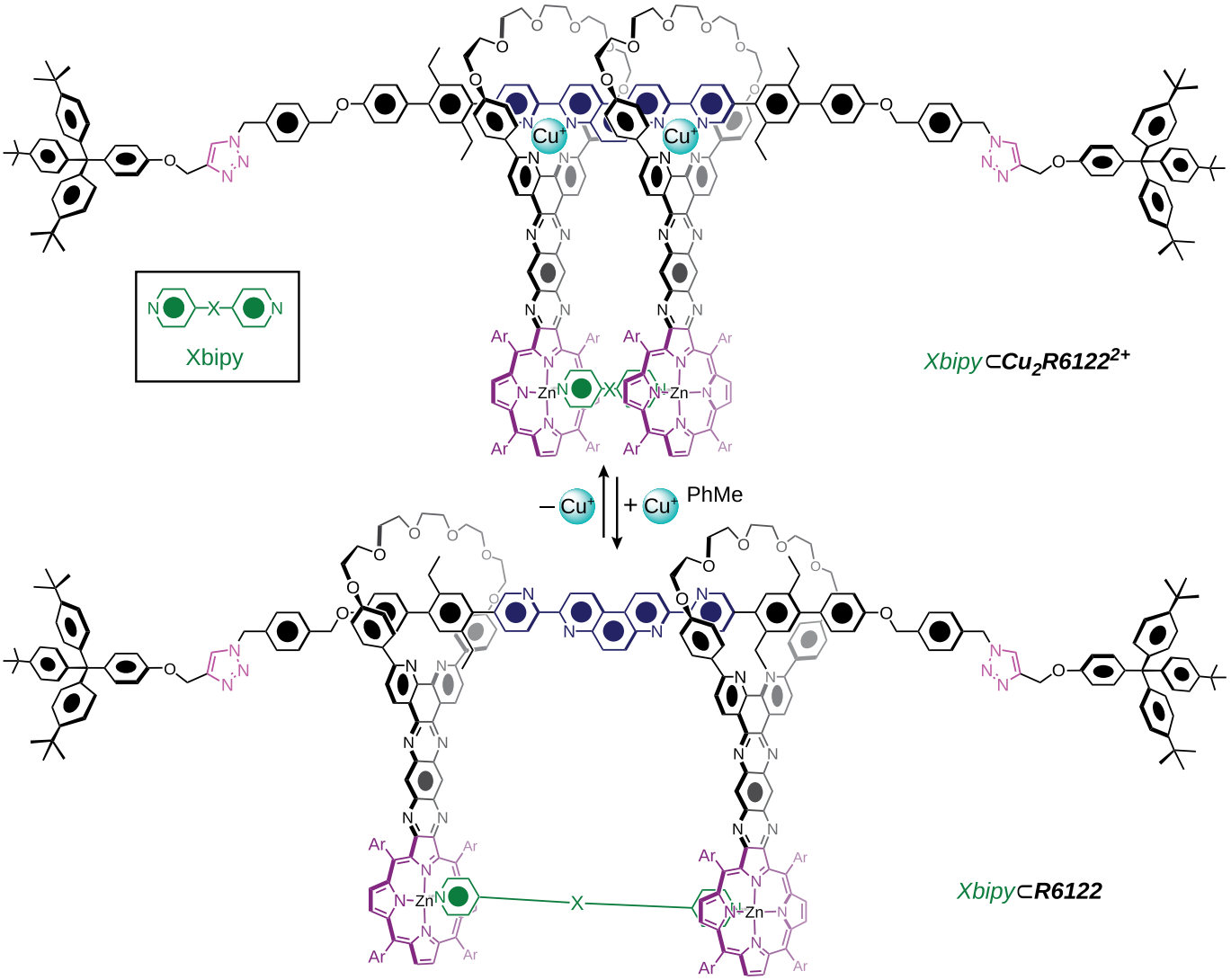
Sauvage[534,535] has employed the ion-driven pressing motions (**Figure 6.41**) of the palindromic [3]rotaxane $\mathbf{R6122/Cu_2R6122^{2+}}$ to create an adjustable receptor for various ditopic bis-pyridyl (Xbipy) guests. When Cu^{I} ions lock the compound $\mathbf{Cu_2R6122^{2+}}$ into a relatively rigid geometry, the porphyrinic plates appended to each of the two rings represent a better receptor for shorter guests such as 4,4′-bipyridine. On the other hand, in the absence of a Cu^{I} template, the more freely moving rings of **R6122** accommodate longer guests such as 1,10-bis(pyridyl)decane ($C_{10}H_{20}$bipy) more efficiently.

An example of a pH-switchable molecular press (**Scheme 6.91**) is given[309] by Liu's palindromic [3]rotaxane $\mathbf{R6123H_2^{4+}}$. Appended to each of the DB24C8 rings are electron-donating pyrenebutyric ester moieties, which are capable of forming π-associated charge-transfer complexes with the dumbbell's central NDI unit. When the crown ethers encircle the dialkylammonium ions of $\mathbf{R6123H_2^{4+}}$, the pyrenebutyric ester groups cannot adopt an appropriate geometry to interact with the NDI unit. When the rings are located around the triazole units in $\mathbf{R6123^{2+}}$, however, the outstretched pyrenes engage more easily in π-donor/π-acceptor interactions with the NDI unit. It has been demonstrated, therefore, that the pressing motions of rotaxane-based molecular muscles can be utilized to control energy transfer processes. This switchable quenching concept has also been demonstrated in several bistable [2]rotaxane-based switches. See refs. 240, 242, 319, 330, 346, 475, 479, 481, 536–538.

Palindromic [3]rotaxanes have been recognized for their potential to be utilized as artificial muscles. For example, devices[91,95,539] that rely on the actuation of redox-switchable palindromic [3]rotaxanes to bend the surfaces of microcantilevers are discussed in **Section 6.15.1.2**. Qu[540] has investigated the properties of a palindromic bis[1]rotaxane related to its pH-controlled expansion and contraction, which are discussed in more detail in **Section 6.15.1.4**.

6.13.1.3 Pressing Motions in Molecular Elevators

"Molecular elevators" are a class of rotaxanes, the component parts of which express pressing motions by the movement of a multivalent "platform" of rings interlocked with a multivalent thread/stopper "rig". Although these architectures should be generalizable to almost any of the recognition and switching motifs described in the previous sections, so far they have been confined

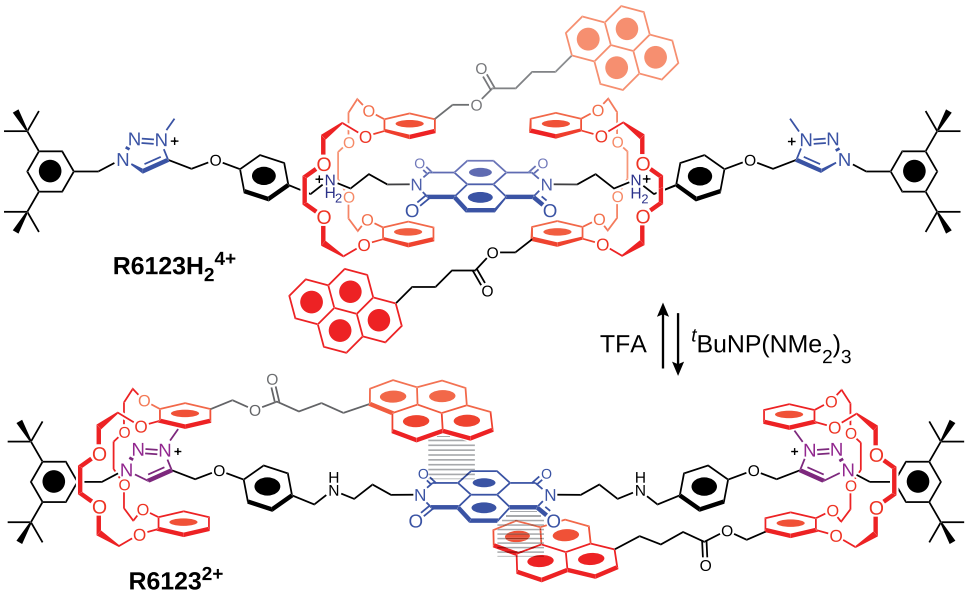


Xbipy	–X–	Xbipy Length / nm	Xbipy⊂Cu$_2$R6122^{2+} K_a / ×10^6 M^{-1})	Xbipy⊂R6122 K_a / ×10^6 M^{-1}
bipy	None	0.82	1.0	6.3
C_6H_4bipy	–*p*-C_6H_4–	1.23	10	32
$(C_6H_4)_2$bipy	–$(C_6H_4)_2$–	1.65	10	10
$C_{10}H_{20}$BIPY	–$C_{10}H_{20}$–	1.80	32	6.3

Figure 6.41 The pressing motions of Sauvage's [3]rotaxane **Cu$_2$R6122^{2+}/R6122** influences the affinity of ditopic guests of various lengths as they coordinate the axial positions of the rings' porphyrinic plates.[534,535]

mostly to examples (**Figure 6.42**) of acid/base-triggered switches.[284,285,310,541] All three of these molecular elevators rely on a similar actuation strategy involving protonation and deprotonation of the rig's dialkylammonium ions with trifluoroacetic acid and a phosphazene base, respectively, which modulates their affinity for the crown ethers of the platform components.

Molecular elevators were introduced[284,285] in the form of the triply interlocked rotaxane **R6124H$_3^{9+}$** in which three crown ethers fused trigonally to an aromatic core constitute the platform and the trifurcated 'rig' component possesses dialkylammonium (–NH$_2^+$–) and BIPY^{2+} recognition sites. The rings of the platform occupy (**Figure 6.42a**) the –NH$_2^+$– centers in **R6124H$_3^{9+}$**, whereas they encircle the BIPY^{2+} sites in **R6124^{6+}**. The rings are able to translate between the sites in a stepwise manner, rather than by a concerted motion of the entire platform, owing to the conformational flexibility of the rig. It has been estimated from a thermodynamic analysis[284] that the base-triggered mechanical stroke could generate up to 200 pN of force.



Scheme 6.91 Liu's[309] palindromic [3]rotaxane **R6123H$_2$**$^{4+}$/**R6123**$^{2+}$ utilizes pH-controlled pressing motions to control the charge transfer interaction between pyrene and NDI chromophores.

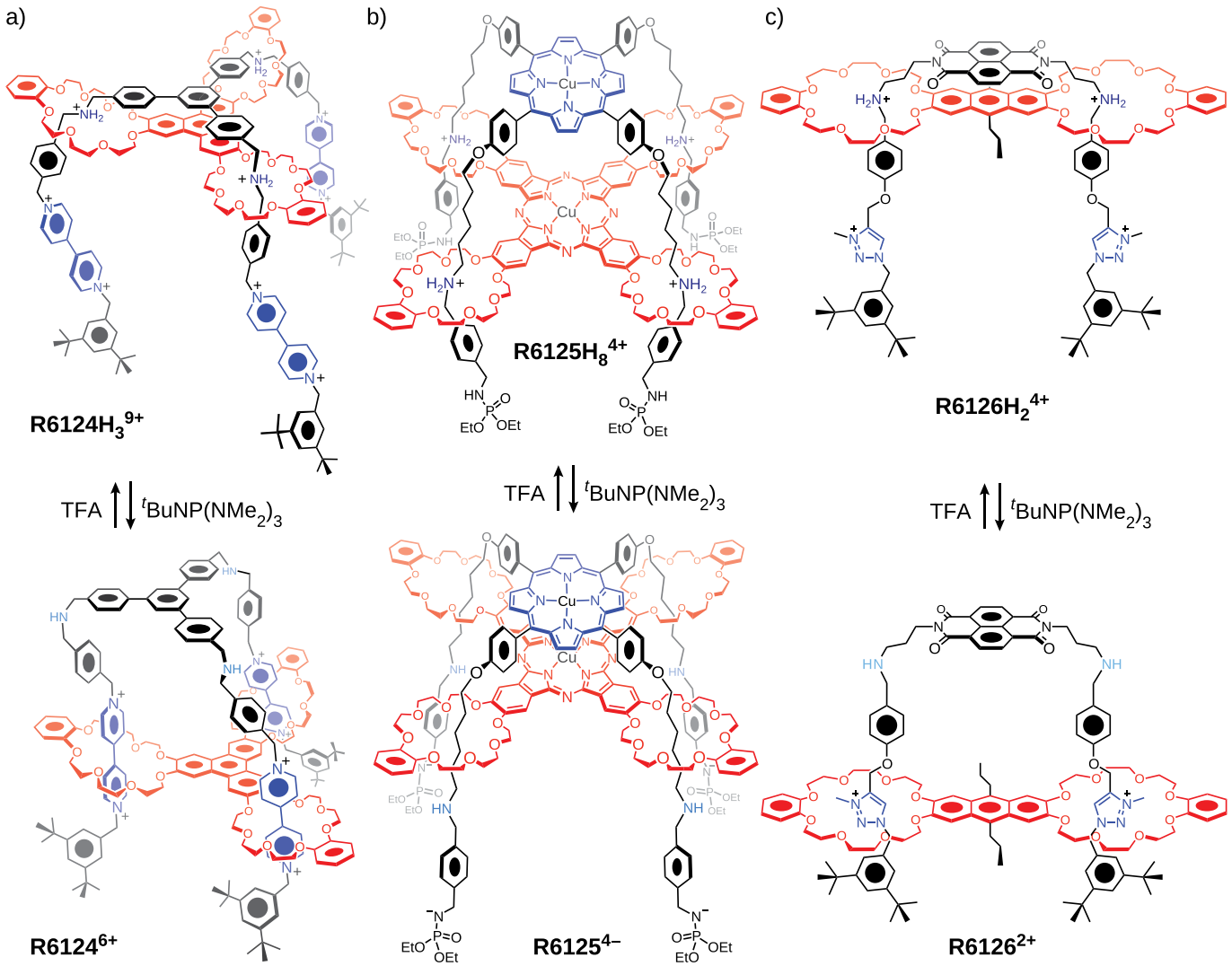


Figure 6.42 pH-Switchable molecular elevators involving crown ether–dialkylammonium recognition. (a) Acid/base actuation of a tripodal molecular elevator **R6124H$_3$**$^{9+}$/**R6124**$^{6+}$.[284,285] (b) Acid/base actuation[541] of a tetrapodal molecular elevator **R6125H$_8$**$^{4+}$/**R6125**$^{4-}$. (c) Acid/base actuation[310] of a bipodal molecular elevator **R6126H$_2$**$^{4+}$/**R6126**$^{2+}$.

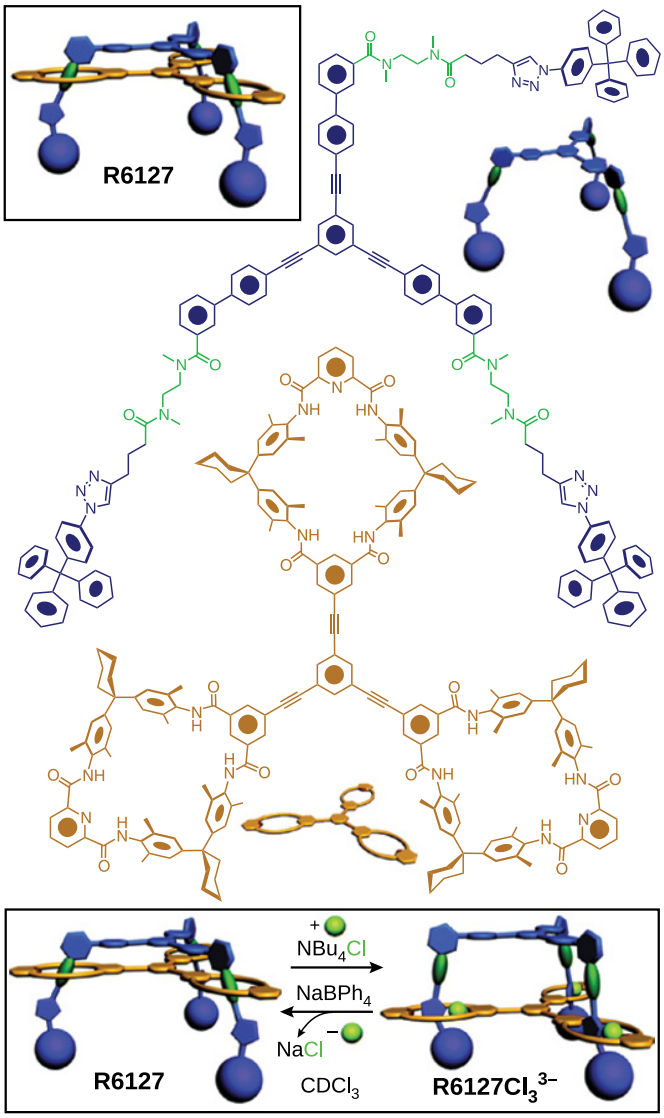


Figure 6.43 The platform of Schalley's hydrogen-bonded molecular elevator is lowered and raised by the addition and removal, respectively, of Cl^- ions as a result of competitive anion-binding interactions involving the rig's triazole units.[543]

Tanaka's quadruply-interlocked molecular elevator **R6125H$_8^{4+}$** relies[541] on a different kind of recognition chemistry (**Figure 6.42b**) to control platform movement upon deprotonation of the rig's dialkylammonium ions and phosphoramidate stoppers to generate **R6125^{4-}**. In fact, the dialkylammonium centers act as the only real recognition sites for the crown ether rings. It is the stacking and spin-exchange interactions between Cu^{II} phthalocyanine unit of the tetra-macrocyclic platform and the Cu^{II} porphyrin center of the tetrapodal rig that define the contracted state of **R6125^{4-}**, rather than ring-dumbbell interactions. This expectation was confirmed by electron paramagnetic resonance (EPR) spectroscopy, which revealed that the phthalocyanine and porphyrin platforms establish electronic communication only in **R6125^{4-}** and not in **R6125H$_8^{4+}$**.

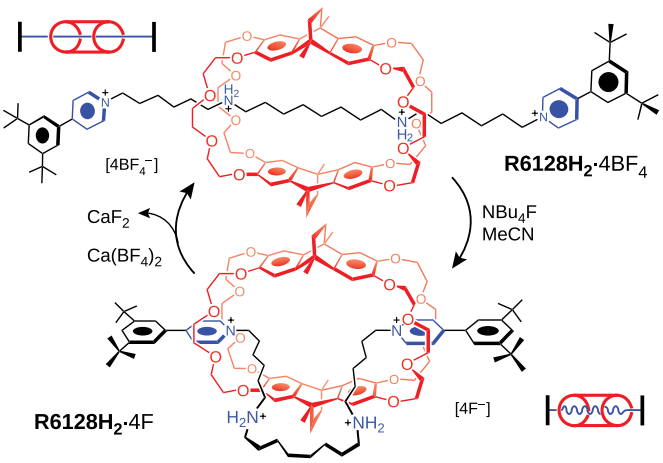
pH-Controlled movement also influences[310] the interaction between NDI and anthracene chromophores in the rig and platform components, respectively, during the actuation (**Figure 6.42c**) of Liu's bipodal molecular elevator **R6126H$_2^{4+}$/R6126^{2+}**. This result has been confirmed by ^{1}H NMR spectroscopy and computer simulations, although changes in the NDI–anthracene charge transfer absorption band could not be observed because the phosphazene base forms a CT complex with the NDI unit. A similar pH-switchable bipodal molecular elevator possessing a ferrocene "platform" has been reported by Qu.[542]

Schalley[543] has recently introduced the anion-switchable (**Figure 6.43**) molecular elevator **R6127**, in which a trivalent platform based on tetralactam macrocycles translates between the tripodal rig's diamide and triazole recognition units in the absense and presence, respectively, of Cl^- ions introduced as tetrabutylammonium salts in $CDCl_3$. The Cl^- ions, which bind the elevator at the triazole sites to generate **R6127Cl$_3^{3-}$**, can be removed by the addition of $NaBPh_4$, which causes NaCl to precipitate. It was determined spectroscopically that the three sides of the elevator do not assume identical geometries, since the Cl^- ions bind the 2,6-dicarboxamidopyridine units of "outer hemisphere" of the tetralactam rings, while the third ring binds chloride in its isophthalamide-derived "inner hemisphere". Mass spectroscopic evidence suggests, albeit inconclusively, that the anion-induced translation might be a concerted process, since signal for the 3:1 anion:elevator complex dominates over the 2:1 and 1:1 signals even in the presence of substoichiometric amounts of Cl^-.

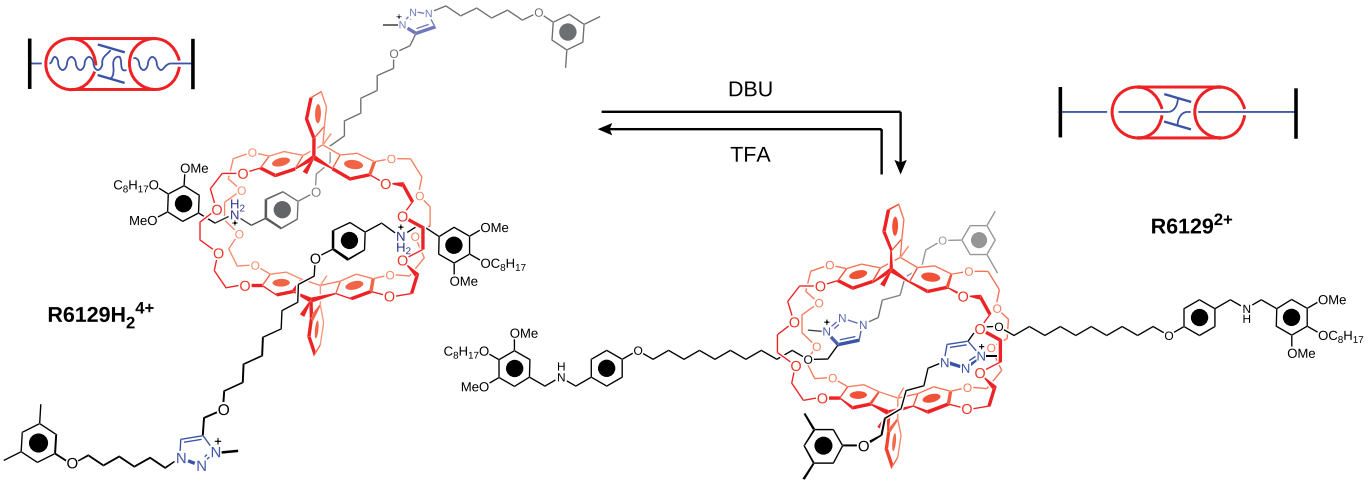
The volume of the cavity that exists in between the center of the rig and the platform of a molecular elevator is expanded and contracted considerably throughout the actuation of molecular elevators. It has to be said, however, that this feature has not yet been exploited to carry out muscle-like functions—e.g., the compression or extension of a contained guest.

6.13.1.4 Telescoping Motions in Cage Rotaxanes

Anion-driven switching (**Scheme 6.92**) in the cage-based [2]rotaxane **R6128H$_2^{4+}$** is caused[544] by ion solvation effects in common with the rotaxane **R661H$_2^{4+}$**—see



Scheme 6.92 The telescoping motion of a cage [2]rotaxane **R6128^{4+}** is accomplished by ion exchange.[544]



Scheme 6.93 The acid/base actuation of the cage-based [3]rotaxane **R6129H$_2^{4+}$**/**R6129^{2+}** leads to extension and contraction along orthogonal axes with respect to the cage.[311]

Scheme 6.61 in **Section 6.5.1**. The compression of the dumbbell in **R6128H$_2^{4+}$** is accomplished by exchanging the counterions from either PF_6^- or BF_4^- to F^-. It transpires that F^- is the only counterion that pairs strongly enough with the dialkylammonium centers in **R6128H$_2^{4+}$** to induce a dumbbell-compressing switching event, which resembles a telescoping motion. Thus **R6128H$_2$**·4BF_4 adopts a co-conformation in which the dumbbell is fully extended in MeCN, such that both crowns can stabilize the central dialkylammonium ions, whereas it compresses significantly in **R6128**·4F to accommodate bipyridinium-crown interations. A convenient protocol for converting back to the PF_6^- salt involves precipitation of an insoluble CaF_2 byproduct from MeCN solution upon addition of $Ca(BF_4)_2$.

Chen's cage-based [3]rotaxane[311] utilizes a nearly identical cage component with two dumbbells—one passing through each of its two crown ethers. Although the acid/base actuation (**Scheme 6.93**) of **R6129H$_2^{4+}$** works in a fashion analogous to that of ordinary [2]rotaxanes based on the same dialkylammonium/crown ether recognition motif (**Section 6.3.3.1**), the resulting motions are unique. As the acid- or base-triggered protonation/deprotonation events are propogated into the translation of the dumbbells with respect to the cage, the molecular length extends along one axis, while contracting simultaneously along a perpindicular axis. This kind of inversely related two-dimensional muscle-like actuation would appear to be unique, at least for now, to the cage [3]rotaxane architecture.

6.13.1.5 Metrics of Rotaxane-Based Molecular Muscles

Quantitative estimates[516] of the contraction distances for the rotaxane-based molecular muscles discussed in **Sections 6.12.1.1–6.12.1.4** are listed in **Table 6.5**. Most estimates are based on computer models, although some of the values have been measured experimentally in the form of hydrodynamic radius (R_H), radius of gyration (R_G), or contour length (L). The poly[*c*2]daisy chains, especially the very long metallosupramolecular polymer **Fe$_n$R6121H$_{2n}^{6n+}$**, make it clear that polymers can indeed scale up the collective motions of molecular switches with mechanical bonds.

6.13.2 Ultramacrocyclic Constriction/Dilation

A sphincter is a general type of anatomical muscle with a circular geometry, which can constrict or dilate in order to close or open, respectively, a cavity or channel. The human body has over 50 types of sphincters, which range from relatively large sizes—e.g., the pupillary sphincter of the eye's iris—to microscopically small—e.g., precapillary sphincters involved in blood circulation. Now it is possible to create nanoscale mimics of these muscle structures in the form of mechanically interlocked ultramacrocycles. The main type of architecture in which this kind of muscle-like switching has been realized is known by several different names, including [1]rotaxane,[545] molecular ouroboros[A],[116] lasso rotaxane,[303,546] and [*c*1]daisy chain.[131] These terms will be used interchangeably here.

One of the earliest cases[547] of a switchable (**Scheme 6.94**) bistable molecular ouroboros is that of compound

[A] The term 'ouroboros', from the Greek roots *ourá* (tail) and *boros* (to eat), refers to the ancient alchemical symbol of a tail-eating serpent, which also allegedly appeared to Kekulé in the (highly skepticized) dream that led him to the correct structure of benzene. These structures have been called 'ouroboros' because their self-complexation resembles that of the self-devouring serpent.

Table 6.5 Estimated metrics of contractile/extensile motions in rotaxane-based molecular muscles[516]

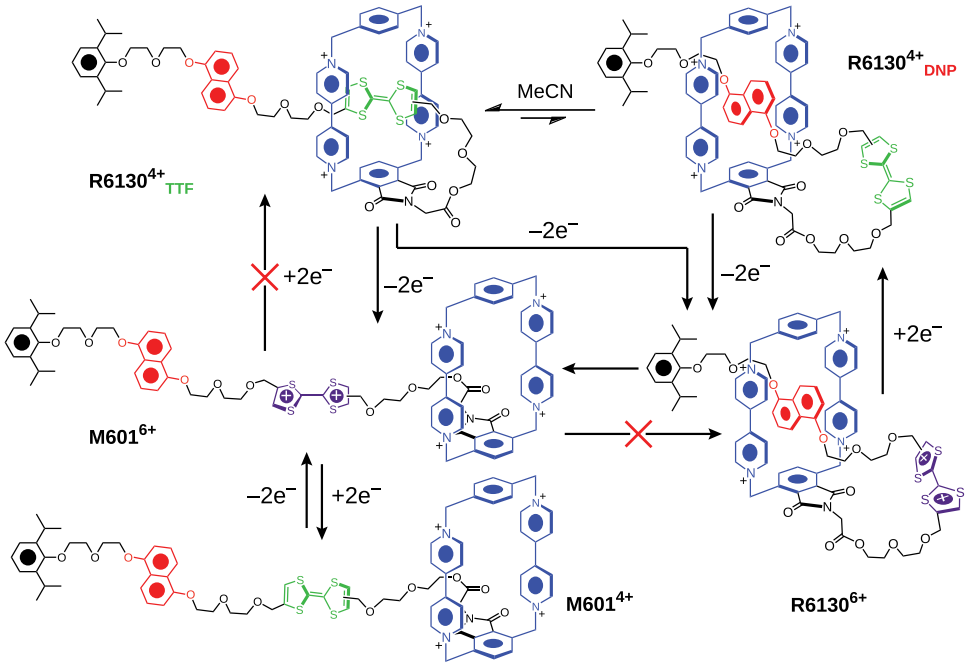
Extended State	Extended Length nm	Contracted State	Contracted Length nm	Contraction Distance nm	Contraction Ratio[a] %	Stimulus	Ref
Cu_2**R6108**$^{2+}$	8.3	Zn_2**R6108**$^{4+}$	6.5	1.8	22	Cations	367
R6109H$_2^{6+}$	3.1	**R6109**$^{4+}$	2.2	0.9	29	pH	286
R6110H$_2^{4+}$	4.2	**R6110**$^{2+}$	3.0	1.2	29	pH	300
R6111H$_2^{6+}$	6.4	**R6111**$^{4+}_{TZ}$/**R6111**$^{4+}_{PY}$	4.4–5.4	1–2	31	pH	301
R6111H$_2^{6+}$	6.4	**R6111Boc**$_2^{4+}_{PY}$	4.4	2.0	45	*N*-Acylation	301
R6111Boc$_2^{4+}_{TZ}$	5.4	**R6111Boc**$_2^{4+}_{PY}$	4.4	1.0	19	Solvent	301
R6112$_{C10}$	3.7	**R6112**$_U$	3.1	0.6	16	Solvent	489
R6113$_{CIN}$	–	**R6113**$_{C6}$	–	0.7	–	Solvent	519
(*EE*)-6114	3.0	**(*ZZ*)-6114**	2.3	0.7	23	*hν*	521
(*EE*)-6115	3.0	**(*ZZ*)-6115**	2.3	0.7	23	*hν*	236
(*EE*)-6116	8.8[b]	**(*ZZ*)-6116**	7.2[b]	1.6	18	*hν*	219
R6117	5.2	**R6117**$^{4(\bullet-)}$	3.4	1.8	35	Redox	522
R6117$_{NDI}$	5.2	**R6117**$_{TZ}$	3.4	1.8	35	Temp	522
R6118$^{6(\bullet+)}$	10.1	**R6118**$^{12+}$	6.7	3.4	34	Redox	131
R6119H$_{2n}^{6n+}$	5.1[c]	**R6119**$^{4n+}$	–	–	–	pH	287, 523
R6120Ac$_{2n}$	42.8[c]	**R6120H**$_{2n}^{2n+}$	29.6[c]	13.2	31	*N*-Acylation	524
Fe_n**R6121H**$_{2n}^{6n+}$	15900[d]	Fe_n**R6121**$^{4n+}$	9400[d]	6500	41	pH	525
C_{10}*BIPY*⊂***R6122***	**1.8**	*BIPY*⊂***Cu*$_2$*R6122***$^{2+}$	0.8	1.0	56	Cations	534, 535
R6123^{2+}	3.1	**R6123H**$_2^{4+}$	1.6	1.5	48	pH	309
R6124^{6+}	1.1	**R6124H**$_3^{9+}$	0.4	0.7	64	pH	284, 285
R6125H$_8^{4+}$	0.9	**R6125**$^{4-}$	0.4	0.5	56	pH	541
R6126^{2+}	1.2	**R6126H**$_2^{4+}$	0.4	0.8	67	pH	310
R6128 · 4PF_6	4.0	**R6128** · 4F	2.5	1.5	38	Anions	544
R6129^{2+}	7.7	**R6129H**$_2^{4+}$	3.2	4.5	58	pH	311

[a]Contraction Ratio = (contraction distance/extended length) = 1 – (contracted length/extended length).
[b]Reported value is twice the measured R_H, corresponding to a hydrodynamic diameter.
[c]Reported value is twice the radius of gyration R_g.
[d]Countour length.

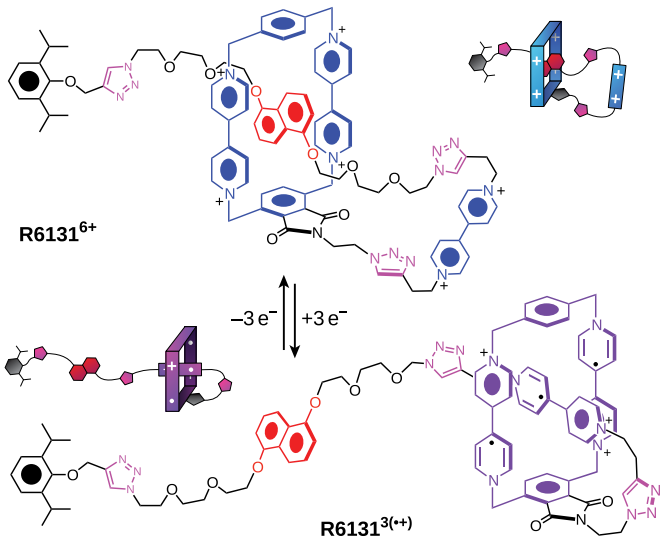
R6130^{4+}. An equilibrium exists in which several metastable co-conformations exchange in the ground state, leading to an intractably complicated ^{1}H NMR spectrum. The intricate isomerism of **R6130**$^{4+}$ arises from the fact that the TTF-encircled and DNP-encircled co-conformations each exist as a distribution of isomers unto themselves, since the TTF unit comprises both *cis*- and *trans*- isomers and the DNP unit can adopt either of two geometries—see **Section 5.1.2.1**—as a consequence of its characteristic pirouetting motions with respect to the CBPQT^{4+} ring. The spectrum simplifies considerably upon chemical oxidation of the TTF units, owing to their expulsion from the CBPQT^{4+} rings. If compound **R6130**$^{6+}$ is held in this oxidized state for a prolonged (12 h) period of time, approximately 40% of the population is converted to the dethreaded species **M601**$^{6+}$, which becomes the tetracation **M601**$^{4+}$ upon reduction. This dethreading process is irreversible and only takes place in the TTF-oxidized state, since (i) **R6130**$^{4+}$ is not converted to **M601**$^{4+}$ without a redox cycle and (ii) neither **M601**$^{6+}$ nor **M601**$^{4+}$ are converted back to their threaded **R6130**$^{4+/6+}$ states. A related monostable ouroboros based on MPTTF was also found[116] to dethread during a redox cycle. These TTF-based [1]rotaxanes are unique examples of how the electrostatic and mechanical forces generated by MIMs during a switching cycle can be used to overcome steric barriers that are otherwise insurmountable.

A relative of the donor-acceptor molecular ouroboros is the [*c*1]daisy chain **R6131**$^{6+}$, which is actuated (**Scheme 6.95**) using radical chemistry. The [*c*1]daisy chain is isolated[131] as the major product of a one-pot click reaction alongside of the [*c*2]daisy chain **R6118**$^{12+}$—see **Scheme 6.90** in **Section 6.13.1.1**—as well as a few other cyclic and acyclic daisy chains. See **Scheme 4.34** in **Section 4.2.3.2** The [*c*1]daisy chain **R6131**$^{6+}$ operates in the same manner as its [c2]daisy chain homologue. It is monostable in the ground state, adopting a dilated co-conformation in which the CBPQT^{4+} ring encircles the DNP unit. Upon reduction to the trisradical trication **R6131**$^{3(\bullet+)}$, the ultramacrocyclic cavity undergoes considerable constriction in order to allow for *BIPY*$^{\bullet+}$⊂*CBPQT*$^{2(\bullet+)}$ radical–radical interactions to take place. In contrast with the TTF-based predecessor **R6130**$^{4+}$, no evidence for dethreading was found during the electrochemical switching cycle.

An example (**Scheme 6.96**) of a pH-switchable lasso[317,318] based on dialkylammonium and crown ether recognition is Qu's [1]rotaxane **R6132H**$^{2+}$. A Fc unit appended to the ring acts as a hinge, which is also capable of quenching the fluorescence of the NI stopper by means of a PET mechanism. In the protonated state, when the



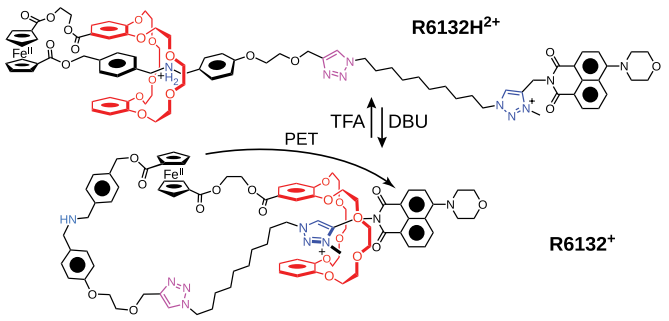
Scheme 6.94 Over coming steric barriers with molecular force in the partially irreversible switching of a bistable donor-acceptor [1]rotaxane.[547] Oxidation of the TTF unit of the green isomer of **R6130**$^{4+}$ gives a mixture of the dethreaded compound **M601**$^{6+}$ and the oxidized counterpart of the RED isomer, **R6130**$^{6+}$. Although switching between **R6131**$^{4+}$ and **R6130**$^{6+}$ is a reversible process, the appearance of **M601**$^{6+}$ from either **R6130**$^{4+}$ or **R6130**$^{6+}$ is irreversible, since re-oxidation of **M601**$^{6+}$ leads only to **M601**$^{4+}$.



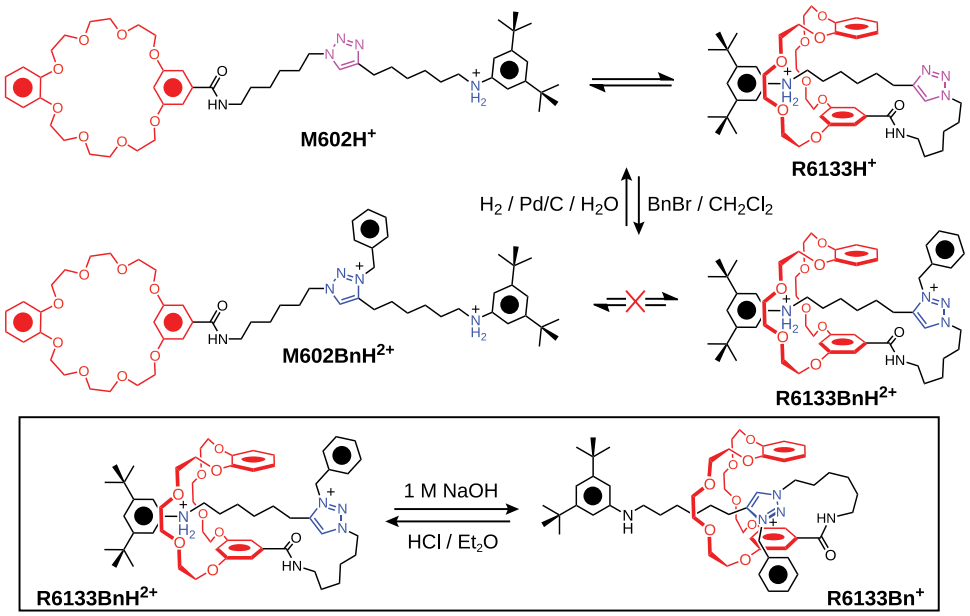
Scheme 6.95 The electrochemically driven constriction and dilation of the [*c*1]daisy chains **R6131**$^{6+}$ and **R6131**$^{3(\bullet+)}$, respectively, is governed by donor-acceptor interactions in the former and radical-pairing interactions in the latter.[131]

ring encircles the dialkylammonium ion, the Fc unit is located much too far away (~3.6 nm) from the NI stopper to quench fluorescence efficiently. Upon deprotonation, the movement of the **R6132**$^{+}$ ring to the triazolium recognition site carries the Fc group in close enough proximity (~1.3 nm) to cause an 80% decrease in fluorescence intensity and lifetime. Oxidizing the Fc unit to Fc^{+}, which cancels its ability to partake in PET with the NI stopper, can turn off the fluorescence switching without affecting the pH-induced mechanical movement. More recently, Qu[540] has described a bis[1]rotaxane that aggregates in a pH-controlled manner that is causally linked to its translational motion—see **Section 6.15.1.4**.

Acid/base switching (**Scheme 6.97**) in [1]rotaxanes based on dialkylammonium ions and crown ethers has also been demonstrated[304,305] in Coutrot's lassos **R6133BnH**$^{2+}$ and **R6133Bn**$^{+}$. A benzometaphenylene[25]crown-8 (BMP25C8) ring which is employed in this case is convenient for ^{1}H NMR spectroscopic investigations on account of its higher symmetry in comparison with derivatized DB[24]C8 rings. A benzyl group appended to the triazolium recognition site is important in this architecture because it introduces a steric barrier that prevents **R6133BnH**$^{2+}$ from converting to the unentangled



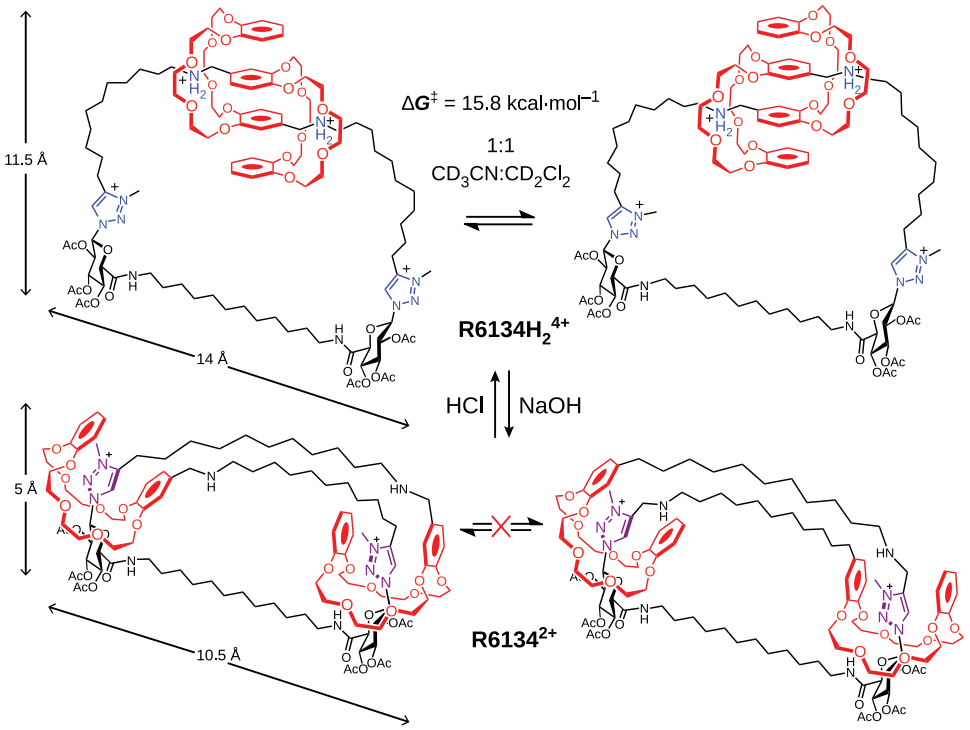
Scheme 6.96 Qu's[318] acid/base switchable, ferrocene-hinged bistable [1]rotaxane is fluorescent in one state (**R6132H**$^{2+}$) and quenched in the other (**R6132**$^{+}$) state as a result of its ability to modulate the distance between a ferrocene donor as a quencher and NI acceptor as a fluorophore.



Scheme 6.97 Coutrot's[304] molecular lasso can be actuated by pH stimuli (**R6133BnH⁺**/**R6133Bn⁺**) as well as by benzylation/debenzylation of the triazole unit (**R6133H⁺**/**R6133BnH²⁺**).

M602BnH²⁺ homologue. Deprotonation of the anilinium stopper of **R6133BnH²⁺** shifts the ring to the benzyl triazolium recognition site of **R6133Bn⁺**, leading to a constriction of the self-entangled loop. The debenzylated versions **R6133H⁺** and **M602H⁺**, on the other hand, equilibrate in solution simply through bond rotations near the ring-dumbbell connection. The former might therefore be classified more appropriately as a pseudo[1]rotaxane.[548] The exchange between **R6133H⁺** and **M602H⁺** is slow on the ^{1}H NMR timescale, with a solvent-dependent ratio in which the self-entangled **R6133H⁺** is more favored in lower polarity solvents. In an analogue of **R6133BnH²⁺**, which carries a tripeptide sequence in between the ring and the $-NH_2^+-$ recognition unit, the pH-responsive tightening and loosening of the lasso structure influences the conformation of the peptide.[305]

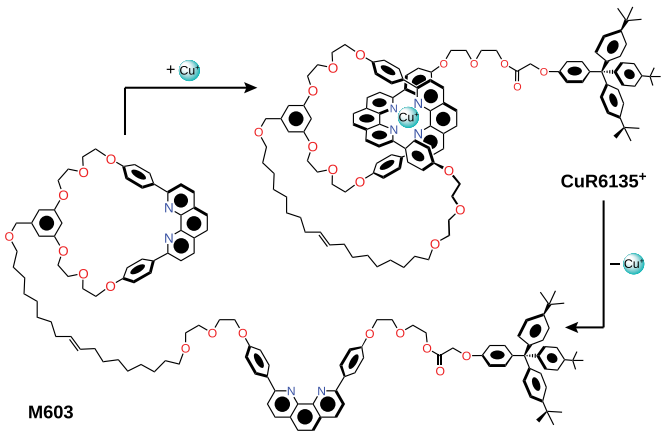
Coutrot[303] has also described the constriction and dilation (**Scheme 6.98**) of a "double lasso" macrocyclic



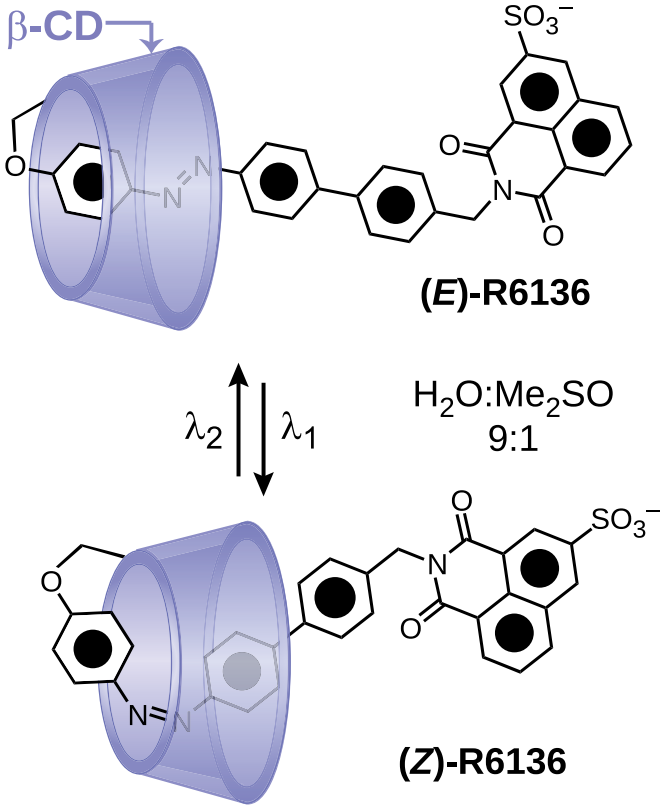
Scheme 6.98 Coutrot's double-lasso molecular switch.[303] The ultramacrocyclic cavity of **R6134H₂⁴⁺**/**R6134²⁺** constricts and dilates according to the conventional protocol of bistable rotaxanes based on crown ethers and dialkylammonium ions. The cavity size also influences rate of inversion in helical chirality by means of through-the-annulus ring rotations, i.e., superrotation.

rotaxane **R6134H$_2^{4+}$**, which is a derivative of the [*c*2]daisy chain **R6110H$_2^{4+}$**—see **Figure 6.37b** in **Section 6.13.1.1**. The structure of **R6134H$_2^{4+}$** does not fit well into the category of rotaxanes because it has been cyclized as a result of its two mannosyl stoppers being connected with a 1,12-diaminododecane linker. The pH switchability of **R6134H$_2^{4+}$** is analogous to its daisy chain precursor **R6110H$_2^{4+}$** and other pH switches—see **Section 6.3.3.1**—except that its motions and dimensions are different on account of its cyclic structure. The double lasso expresses a type of helical co-conformation as a result of having a section of overlapping threads in its ultramacrocyclic loop. Helix inversion proceeds by a through-the-annulus superrotation (**Section 5.1.2.3**) of the crown ethers—the corresponding isomers have been described as rotamers since they are essentially interconverted by bond rotation. When the double lasso is relatively 'loose' in **R6134H$_2^{4+}$**, the rotamers exchange on the ^{1}H NMR timescale in CD_3CN and CD_2Cl_2. The activation barrier for this process was found to be 15.8 kcal · mol^{-1} in ~1:1 CD_3CN/CD_2Cl_2. Helix inversion is much more inhibited by the 'tight' co-conformation of **R6134^{2+}**, proceeding too slowly for an activation barrier to be measured by dynamic NMR spectroscopy.

Mayer[549] has demonstrated (**Scheme 6.99**) a reversible 'capture and release' switching of a Sauvage-type [1]rotaxane. The coordination of two phen ligands around Cu^{I}—one each from the ring and dumbbell portions of the molecule—leads to the self-entangled structure of **CuR6135$^+$**. The non-interlocked structure of **M603** is realized in the absence of a metal template. These two forms can be interconverted efficiently upon the addition and removal of the Cu^{I} template with $Cu(MeCN)_4PF_6$ and KCN, respectively. The [1]rotaxane **CuR6135$^+$** is obtained from **M603** in 94% yield at a concentration of 100 mM, and 80% yield at a concentration of 1 mM. Since the stopper is too bulky to pass through the ring—a slippage-like mechanism (**Section 3.1**)—the mechanism of interconversion between self-threaded and non-interlocked species must involve a through-the-annulus, turnstile-like motion of the tethered thread.



Scheme 6.99 Mayer's 'capture and release' strategy for interconverting between a self-entangled (**CuR6135$^+$**) and non-interlocked (**M603**) molecular switch.[549]



Scheme 6.100 Tian's photoswitchable [1]rotaxane (***E*/*Z*)-R6136**.[226,550,551]

Tian[226,550,551] has developed a series of photoswitchable [1]rotaxanes and a bis[1]rotaxanes[227] based on β-CD and azobenzene. The light-driven switching (**Scheme 6.100**) of the [1]rotaxane **(*E*/*Z*)-R6136** involves the *cis-trans* isomerization of an azobenzene unit, causing the dumbbell to rearrange within the β-CD cavity. This rearrangement leads to a subtle contraction and also changes the angle of the transition dipole moment with respect to the β-CD ring, leading to substantial changes in the induced circular dichroism (ICD) spectrum. The ICD spectra of **(*E*/*Z*)-R6136** are rather complex—molecular dynamics simulations revealed[551] that four pairs of enantiomers exist and that they and diastereoisomers interconvert through various bond rotatations, most notably those in between the NI stopper and the biphenyl unit. The [1]rotaxane **(*Z*)-R6136** is populated to ~50% in the photostationary state, which is reached in 15 min under 365 nm irradiation, and switching is reproducible over more than five cycles.

6.13.3 Motions of Branched Rotaxanes

Dendritic rotaxanes (**Section 4.2**) can undergo more sophisticated motions, such as radial translation (**Section 6.13.3.1**) and expansion (**Section 6.13.3.2**), by virtue of having multiple rings that can move along multiple pathways.

6.13.3.1 Radial Translation

The rings of [*n*]rotaxanes (*n* > 3) possessing branched or dendritc architectures—see **Section 4.2.2**—can translate radially from a central core in a manner similar to the pressing motions involving palindromic [3]rotaxanes, as described in **Section 6.13.1.2**.

Three tripodal [4]rotaxanes that rely on crown ether/dialkylammonium recognition motifs to control the acid/base driven radial translation of the rings are illustrated in **Figure 6.44**. Qu[322] has investigated the switching and redox properties of **R6137H$_3^{6+}$**, the ferrocene-functionalized DB24C8 rings of which translate radially outward to encircle *N*-methyltriazolium units upon base-triggered deprotonation of each axle's dibenzylammonium cation. By contrast, deprotonation of the dendritic [4]rotaxanes

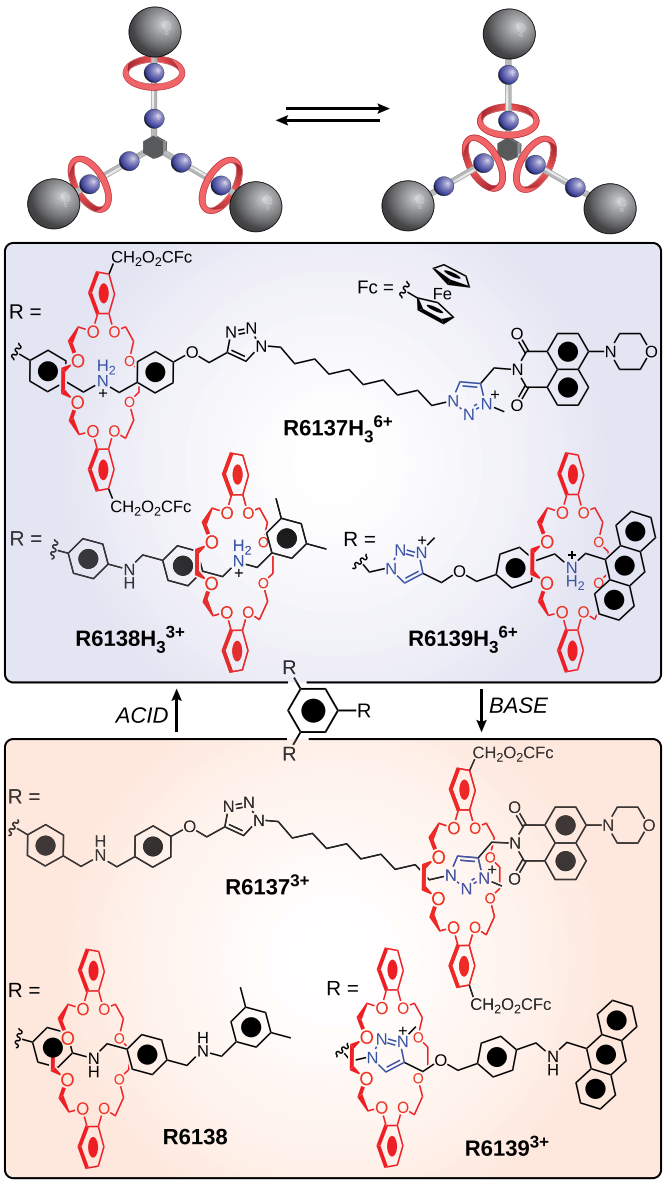


Figure 6.44 Radial translation in a few pH-switchable tripodal [4]rotaxanes.[322,325,552]

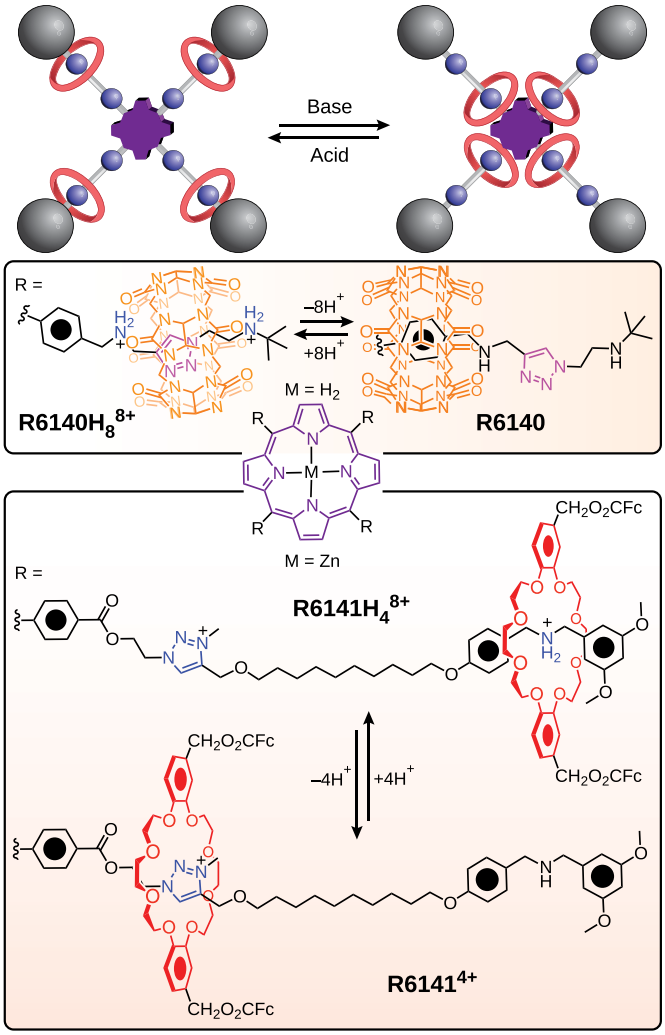


Figure 6.45 Radial translation in pH-switchable tetrapodal [5]rotaxanes.[268,320]

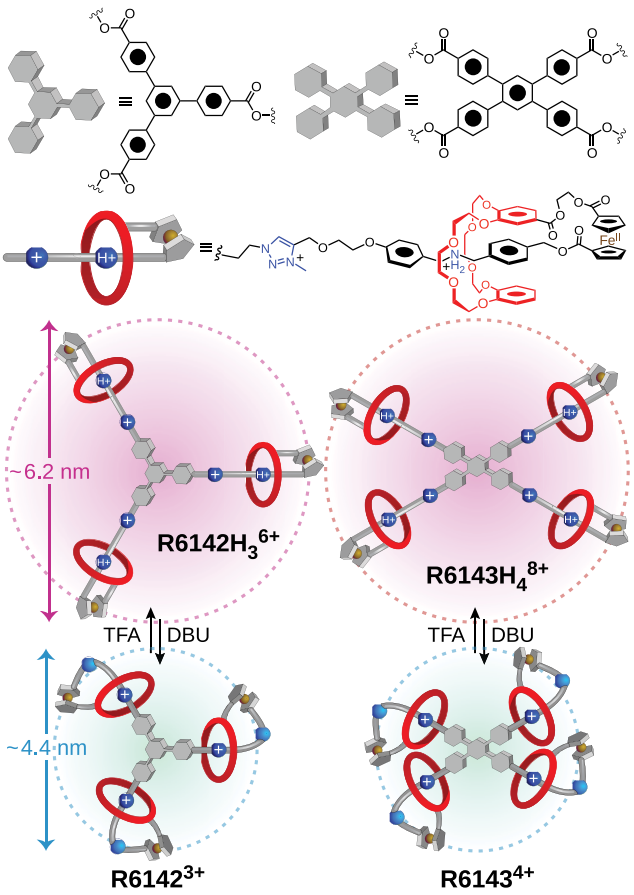
R6138H$_3^{3+}$ and **R6139H$_3^{6+}$**, introduced by Tokunaga/Hisada[552] and Álvarez[325], respectively, causes their DB24C8 rings to translate radially inward in order to encircle the aniline and triazolium moieties of **R6138** and **R6139^{3+}**. Compound **R6139^{3+}/R6139H$_3^{6+}$** has also been investigated in the context of switchable organocatalysts—see **Section 6.15.1.5**. The acid/base actuation of mechanomolecules based on these motifs are discussed in **Section 6.3.3.1**.

A couple of tetrapodal [5]rotaxanes have also been designed (**Figure 6.45**) to exhibit radial translation driven by pH changes emanating from a porphyrinic core. Tuncel[268] has employed the CB6-promoted azide-alkyne cycloaddition to obtain the [5]rotaxane **R6140H$_8^{8+}$**, in which the CB6 rings translate inward to protect the triphenylene core's hydrophobic aryl units from aqueous solvent in the neutral **R6140** under alkaline conditions. In the case of the branched [5]rotaxane **R6141H$_4^{8+}$** introduced by Qu,[320] pH actuation allows the ferrocene-functionalized DB24C8 rings to translate between dibenzylammoniun

and *N*-methyltriazolium recognition sites, in a manner analogous to the tripodal [4]rotaxanes possessing triazolium units.

6.13.3.2 Radial Expansion/Contraction

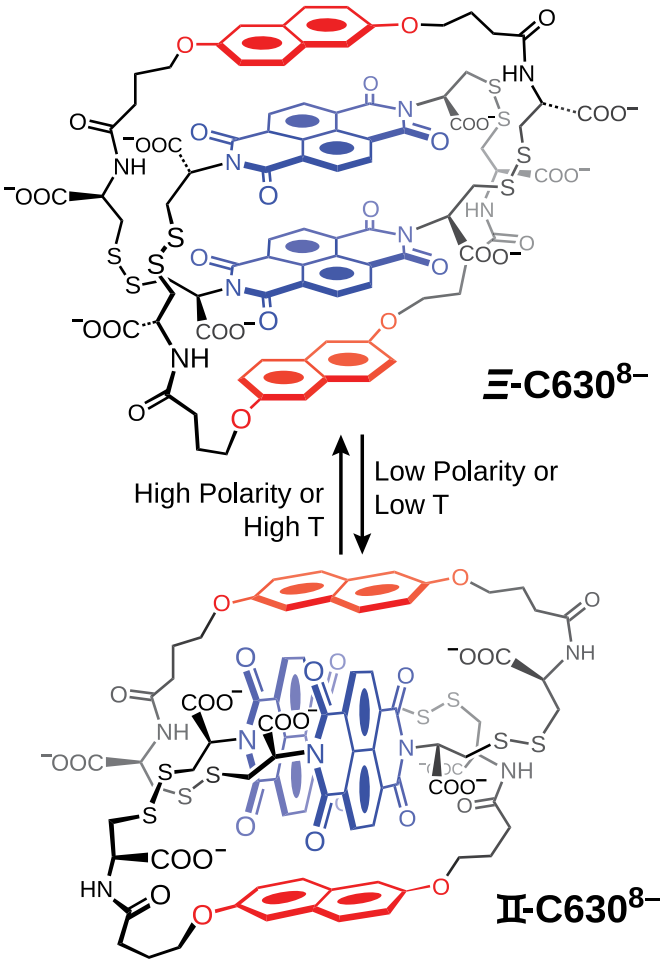
Qu[553] has recently adapted his ferrocene-linked [1]rotaxanes into a class of switches which expand and contract (**Scheme 6.101**) radially in response to pH changes by virtue of their branched architectures. The tris[1]rotaxane **R6142H$_3^{6+}$** and the tetrakis[1]rotaxane **R6143H$_4^{8+}$** possess lasso-like arms extending from central triphenylene or tetraphenylene cores in tripodal and tetrapodal geometries, respectively. These compounds respond to acid/base stimuli in analogous fashion to Qu's earlier [1]rotaxane **R6132H^{2+}**—see **Scheme 6.96** in **Section 6.13.2**. The DB24C8-derived rings, which encircle the dibenzylammonium recognition units in **R6142H$_3^{6+}$** and **R6143H$_4^{8+}$** at low pH, are induced to shuttle to the permanently charged triazolium recognition sites upon neutralization of the –NH$_2^+$– centers at higher pH. Employing molecular dynamics simulations, molecular radii were estimated based on the average distance between the Fe^{II} centers of the peripheral ferrocene units and the centerpoints of the branched cores. Both the tripodal and tetrapodal switches extend to a diameter of ~6.6 nm when protonated, and contract down to ~4.4 nm when deprotonated.



Scheme 6.101 pH-Triggered radial expansion and contraction in the discotic tris- and tetrakis[1]rotaxanes **R6142H$_3^{6+}$** and **R6143H$_4^{8+}$**, respectively.[553]

6.13.4 The Gemini Co-Conformation

Sanders[554] has described a unique kind of co-conformational switching (**Scheme 6.102**) in the self-assembled donor-acceptor [2]catenane **C630^{8-}**. This catenane was found to exist as two co-conformations in D_2O. The expected co-conformation was **Ξ-C630^{8-}**, in which the NDI and DNP units engage in hydrophobic and π–π stacking interactions, with the larger, more hydrophobic NDI

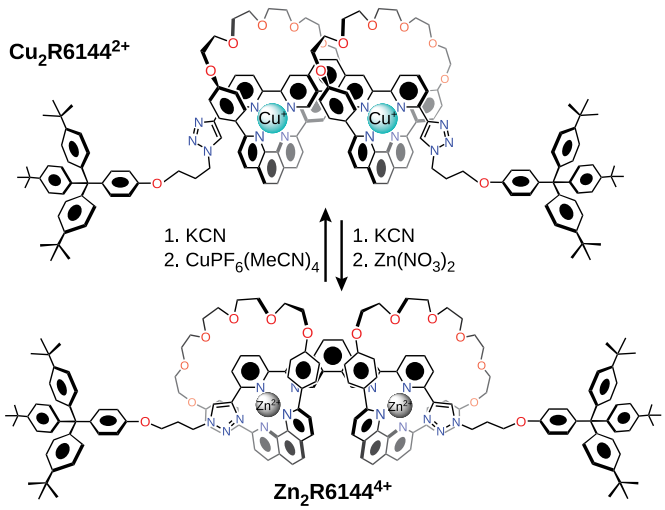


Scheme 6.102 The self-assembled donor-acceptor [2]catenane **C630^{8-}** exhibits an unusual type of co-conformational switching in response to either solvent polarity or temperature changes.[554] The expected co-conformation (**Ξ-C630^{8-}**) involving stacked NDI-DNP charge transfer interactions is displaced by an unexpected co-conformation (**Π-C630^{8-}**) in which an NDI dimer is sandwiched between two DNP units at the bay positions.

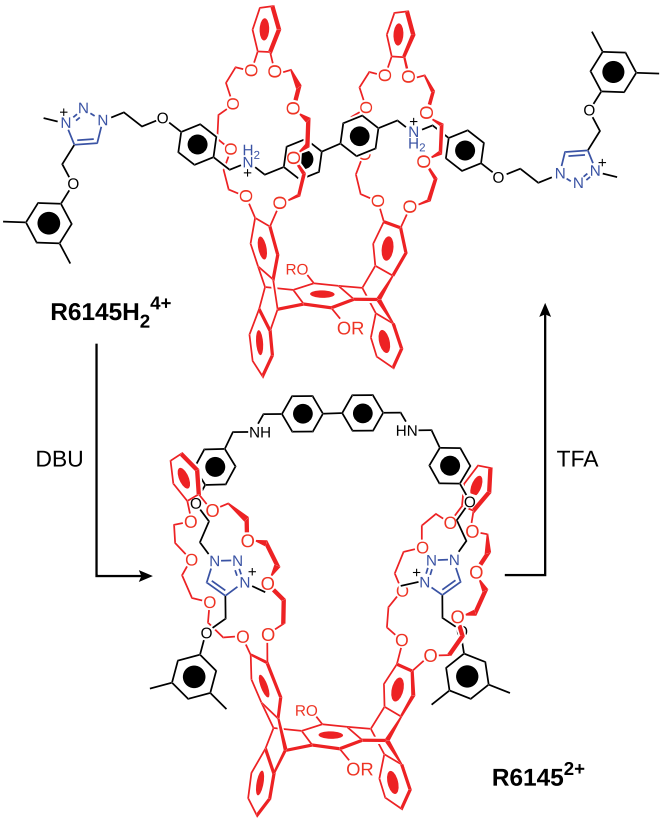
units at the catenane's center. When the temperature is lowered to near-freezing or the solvent is made less polar by the addition of CD_3COCD_3, a second set of ^1H NMR signals assignable to **Ⅱ-C630**$^{8-}$ becomes increasingly evident. This co-conformer is characterized by an arrangement resembling the astrological Gemini sign Ⅱ, in which a sandwiched NDI face-to-face homodimer is formed as a result of its bay protons partaking in [C–H $\cdots$ π] interactions with the DNP units. We opted to use the Greek character Xi (**Ξ**) to symbolize the face-to-face π-stacked co-conformer because its three parallel lines resemble this type of donor-acceptor stacking. Solvent polarity is a particularly effective control element, since the Ⅱ co-conformer is populated all but exclusively above 40% v/v CD_3COCD_3 in D_2O and the **Ξ** co-conformer is the sole species in 0.5 M $NaNO_3$. From variable temperature studies, a ΔH value of –4.1 kcal $\cdot$ mol^{-1} and a ΔS value of –15.5 cal $\cdot$ mol^{-1} $\cdot$ K^{-1} has been measured for the equilibrium between **Ξ-C630**$^{8-}$ and **Ⅱ-C630**$^{8-}$. A delicate interplay of forces is most likely behind this unique type of bistability involving 90° sandwiched rotation, since an analogue with slightly shorter linkers does not adopt the Ⅱ co-conformation.

6.13.5 Rotaxane Flapping

Sauvage[555] has described several types of novel motions in transition metal-based rotaxanes by means of template exchange. One novel type of rotaxane-based motion (**Scheme 6.103**) to be defined by Sauvage[369] is that of a 'flapping' [3]rotaxane. The two dpp-based rings of **Cu_2R6144**$^{2+}$ participate in tetrahedral complexes (CN 4) wherein each of the two bidentate pyridyl ligands are



Scheme 6.103 Switching between the four-coordinate geometry of Cu^{I} and the five-coordinate geometry of Zn^{II} causes the rings of [3]rotaxanes **Cu_2R6144**$^{2+}$ and **Zn_2R6144**$^{4+}$ to tilt back and forth like flapping wings as they are interconverted by template exchange.[369]



Scheme 6.104 pH-Driven "wing flapping" motions of a pentiptycene-linked dimer of DB24C8 rings interlocked with a palindromic dumbbell.[312]

fused to the center of the dumbbell. Two triazole rings—one appended to each end of these recognition sites—are not involved in metal-ligand interactions in this species. When the Cu^{II} templates of **Cu_2R6144**$^{2+}$ are exchanged for the Zn^{II} templates of **Zn_2R6144**$^{4+}$, however, the triazoles become active ligands and afford a pentacoordinate geometry which causes the rings to tilt in opposite directions by ~30°. The same outcome can be achieved electrochemically using the Cu^{I}/Cu^{II} redox couple, where Cu^{I} adopts the four-coordinate geometry in which the triazole unit is not involved and Cu^{II} adopts the five-coordinate geometry in which the triazole ligand participates in metal-ligand interactions. The mirrored tilting motions that take place in the rings as a result of going from CN 4 to CN 5 and back has been likened to the flapping of a bird's wings.

Chen[312] has investigated flapping motions (**Scheme 6.104**) in the pH-switchable [2]rotaxane **R6145H$_2$**$^{4+}$, the architecture of which is similar to a bipodal molecular elevator, yet the curvature of its pentiptycene platform positions the two crown ethers out-of-plane. The acid/base driven actuation between **R6145H$_2$**$^{4+}$ and its deprotonated homologue **R6145**$^{2+}$ resultls in a "wing-flapping" motion as the pentiptycene-linked DB24C8 crown ethers move between the dialkylammonium and triazolium recognition units, respectively, of the palindromic dumbbell.

6.13.6 Collapsing Mechanomolecules

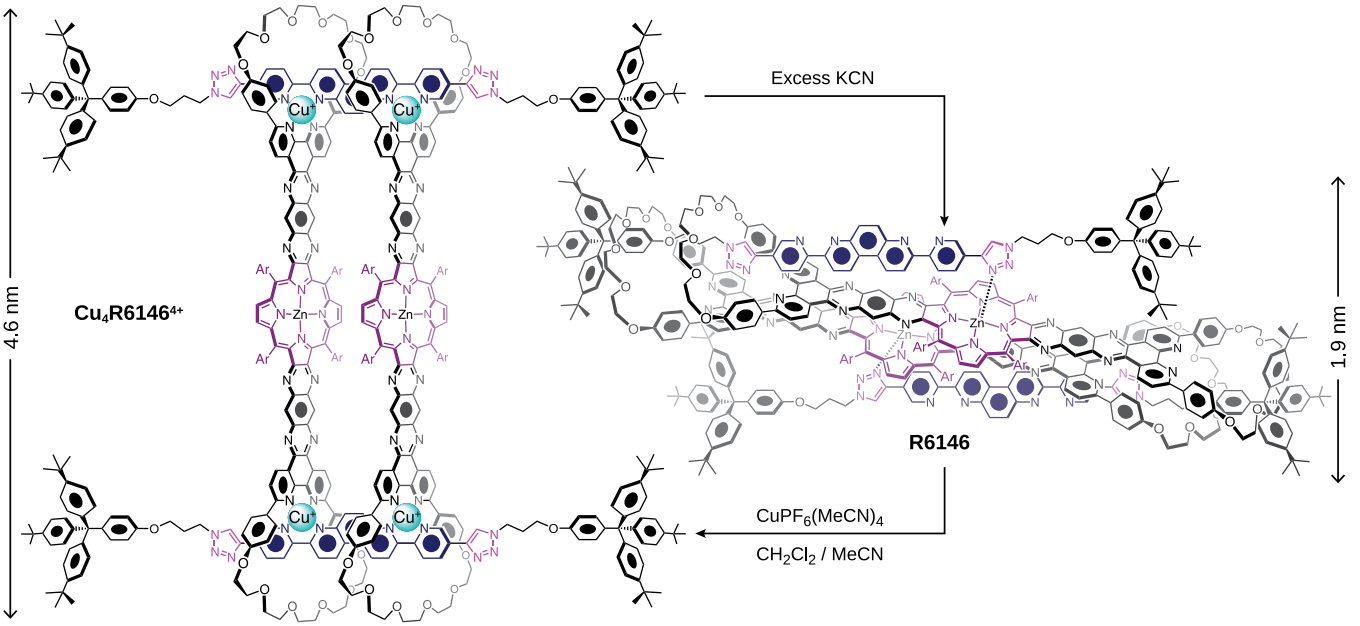
Sauvage[556] has observed a large-amplitude collapsing motion (**Scheme 6.105**) driven by the metalation and demetalation of the cyclic [4]rotaxane **R6146**, which comprises two rigid bis(triazolylbipyridine) dumbbells and two porphyrin-based phenanthroline-containing bis-macrocycles. The [4]rotaxane **Cu_4R6146^{4+}** adopts a rigid square-shaped geometry held together at its corners by tetrahedral coordination complexes. When the Cu^{I} ions are stripped away with KCN, the structure of the resulting [4]rotaxane **R6146** collapses in order to allow one triazole group from each dumbbell to engage in axial coordination with the zinc porphyrin centers in the bis-macrocycles. The molecular diameter in one dimension has been estimated to shrink from 4.6 to 1.9 nm as a result of this internal collapse of the molecule.

6.13.7 Mechanically Constrained Inflation/Deflation

Yet another novel type of mechanical switching, which has been described by Sauvage,[557] is the 'inflation' and 'deflation' (**Figure 6.46**) of the cyclic [4]rotaxane **Cu_4R6147^{4+}** through guest exchange. The cyclic [4]rotaxane **Cu_4R6147^{4+}** is similar to the collapsible [4]rotaxane **Cu_4R6146^{4+}**, since it possesses the same architecture and dumbbell components. The porphyrinic bis-macrocycles in **Cu_4R6147^{4+}** differ from it predecessor, however, by the fact that the rings' dpp ligands are held at the periphery by flexible polyether loops in the latter case. This feature allows the structure to 'breathe' through the oscillating motions of the two zinc porphyrins. When ditopic guests are ligated to the axial sites of each porphyrin center, the porphyrin-to-porphyrin distance becomes fixed at a length defined by the guest. These distances can range from 0.26 to 1.6 nm when the guests are DABCO and Ph_2BIPY, respectively. The association constants are approximately 1.3×10^8 (DABCO), 1.6×10^6 (BIPY), 1.3×10^6 (PhBIPY), and $4.0 \times 10^5\ M^{-1}$ (Ph_2BIPY) at 294 K in PhMe, revealing that the host-guest interaction weakens with increasing guest length.

6.13.8 Folding/Unfolding in Mechanomolecules

Woźny[558] has described a degenerate [2]rotaxane based on the same tetraazamacrocyclic Ni^{II} recognition unit employed in the heterodinuclear metallacyclic [2]catenane **C608^{4+}**—see **Scheme 6.12** in **Section 6.1.2**. The [2]rotaxane **R6148^{4+}** undergoes a unique kind of unfolding motion (**Scheme 6.106**) upon electrochemical oxidation. In the ground state, the DB24C8 ring of **R6148^{4+}** shuttles back and forth along the tetramethylene chain which links the two Ni^{II} chelate units, which serve dual roles as recognition sites and stoppers, with an activation barrier of $\Delta G^{\ddagger} = 9.7\ kcal \cdot mol^{-1}$. The time-averaged solution-state structure of the shuttle is believed to be a folded co-conformation involving one of the Ni^{II} cyclams engaging in alongside π-stacking interactions with the ring's benzo units. The mechanically bound DB24C8 ring influences the oxidation potentials of both Ni^{II} centers. The electron donating power of the ring lowers the oxidation potential of the Ni^{II} center which it encircles, while the alongside Ni^{II} center becomes harder to oxidize by 0.14 V while it remains engaged with the π-stack. This subtle influence on the redox landscape of the rotaxane allows for the non-degenerate mixed-valence rotaxane **R6148^{5+}** to be accessed within this 0.14 V potential window at fast scan rates. The increased charge of the Ni^{III} center in **R6148^{5+}** causes the alongside Ni^{II} cyclam to swing away on account of Coulombic repulsion, corresponding to an unfolding motion with respect to



Scheme 6.105 Sauvage's cyclic [4]rotaxane expands (**Cu_4R6146^{4+}**) and collapses (**R6146**) upon metalation and demetalation, respectively.[556]

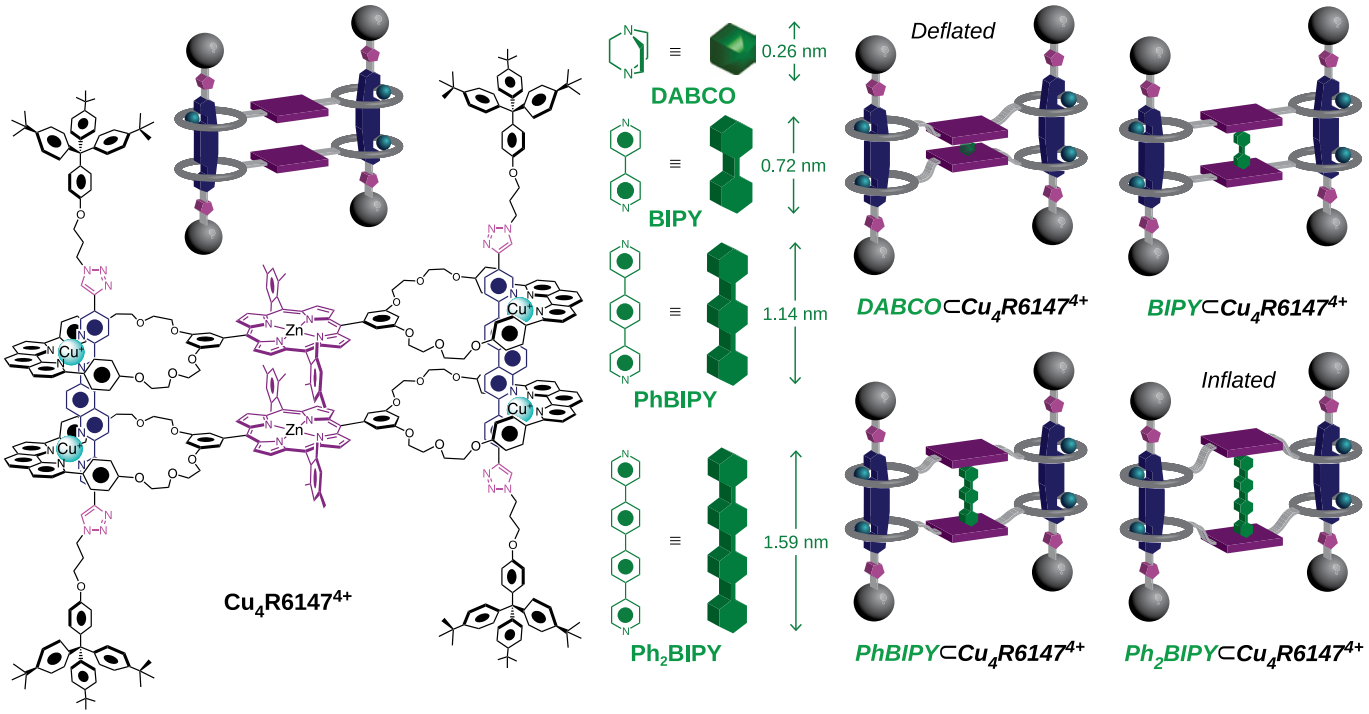
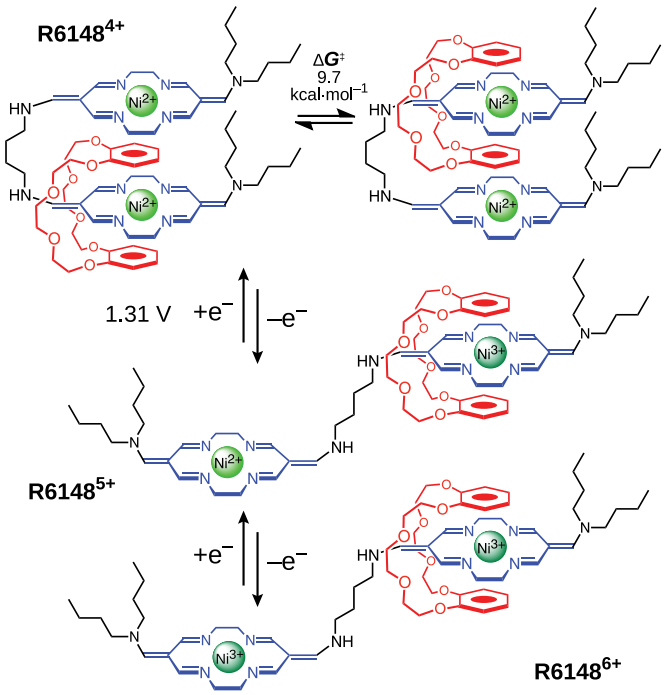


Figure 6.46 The central cavity of the flexible cyclic [4]rotaxane **Cu_4R6147^{4+}** can be inflated or deflated to a distance defined by the length of a ditopic guest, which bridges the two porphyrin centers by means of axial coordination.[557]



Scheme 6.106 The folded [2]rotaxane molecular shuttle **R6148^{4+}** unfolds on account of electrostatic repulsion after one of its two degenerate tetraazamacrocyclic Ni^{II} recognition units becomes oxidized, affording the non-degenerate [2]rotaxane **R6148^{5+}** as a transient species before accessing the unfolded degenerate [2]rotaxane **R6148^{6+}**.[558]

the rotaxane's dumbbell. The ring is expected to spend the majority of its time near the Ni^{III} center in **R6148^{5+}** because it is a stronger acceptor of π-electrons than Ni^{II}. The degenerate [2]rotaxane **R6148^{6+}** is always generated during electrochemical scans, however, because the reduction potential of the Ni^{II} center is lowered as soon as the molecule unfolds in this manner. Woźny has therefore demonstrated that even degenerate molecular shuttles can behave as electromechanical switches. An analogous non-degenerate molecular shuttle in which one of tetraazamacrocyclic recognition sites houses a Cu^{II} center has been described recently.[559]

Lin[327] has prepared a BODIPY-stoppered [2]rotaxane possessing two triazolium units which are not encircled by the crown ether ring in the ground state. This [2]rotaxane exhibits an observable change in its fluorescence response as it binds the $H_2PO_4^-$ anion. ^{1}H NMR spectroscopy and molecular models suggest that the axle adopts a compact folded structure in the presence of $H_2PO_4^-$ in order to allow both of its peripheral triazolium units to engage in stabilizing interactions with the anion. The outcome is that the rotaxane folds and unfolds in the presence and absence, respectively, of $H_2PO_4^-$ anions, although the mechanical bond is not essential to the folding mechanism in this case. The donor-acceptor oligorotaxane foldamers[560–562] described in **Sections 4.2.1.1** and **5.1.1.2** most likely fold and unfold to variable degrees as a function of temperature, solvent polarity, mechanical

force, etc, although these properties have not yet been examined in detail.

The templation motif based on viologen radical–radical interactions—see **Section 2.3.10**—has been utilized[132] in the construction of oligorotaxanes that exhibit novel folding/unfolding motions (**Scheme 6.107**) under reductive control. In the case of **R6149^{18+}**, the two CBPQT^{4+} rings encircle hexamethylene linkers terminating the xylylene-bridged pentaviologen axle of the dumbbell. Although the ring positions are dominated in this redox state by repulsive Coulombic interactions, the viologen radical cations re-assemble under reductive conditions into a ninefold stack of π-radicals, in which the rings are driven to intercalate with a serpentine-like conformation of the oligoviologen axle by establishing favorable radical-pairing interactions in **R6149$^{9(\bullet+)}$**. This reversible, redox-driven folding leads to dramatic changes in molecular length that render these compounds suitable candidates for a new class of "molecular muscles"—see **Section 6.13.1**.

6.13.9 Stepwise Motion in Pseudocatenanes

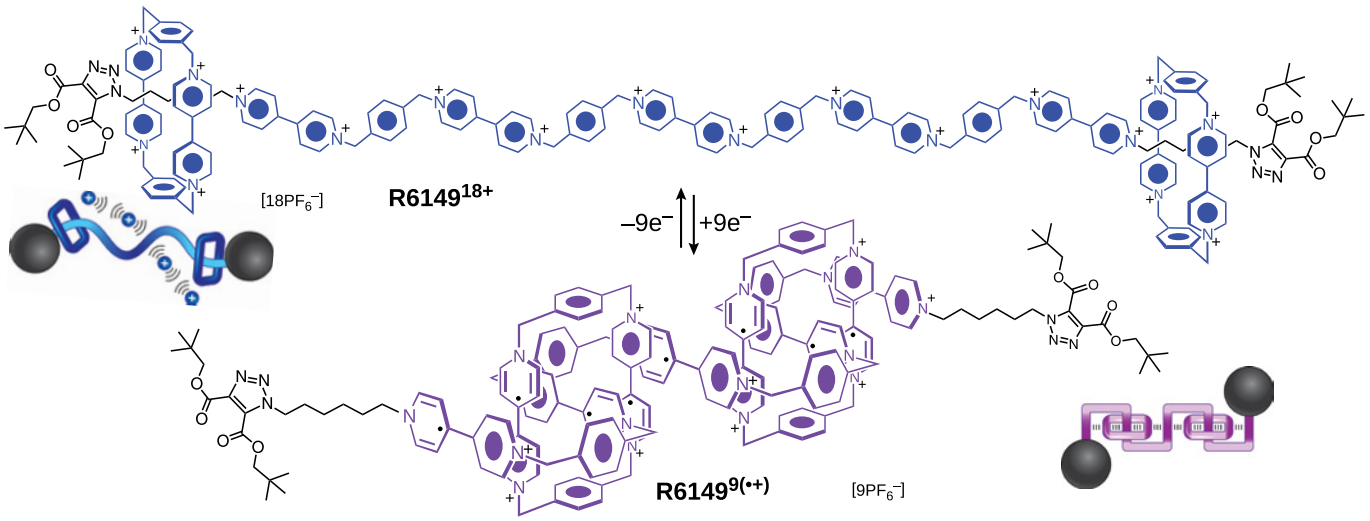
Chen[313] has shown that the pH-controlled translation of the three crown ether subunits of the [4]pseudocatenane **C631H$_3^{6+}$** can be actuated in a stepwise manner, resulting in a unique set (**Figure 6.47**) of different co-conformations and corresponding mechanical motions. Treatment of this [4]pseudocatenane with 1,8-diazabicyclo[5.4.0]undec-7-ene (DBU) leads to the deprotonation of the dibenzylammonium recognition units and consequent translation of the crown ether subunits to the *N*-methyltriazolium sites in a stepwise manner (**Figure 6.47a**), owing to the different dissocation equilibria for each proton, corresponding to pKa values that rise from 9.78 to 11.33 with each step. Thus, the four protonation states of the [4]pseudocatenane co-exist in different ratios as DBU is added in solution, where **C631H$_2^{5+}$** and **C631H^{4+}** are intermediate states that can be detected (**Figure 6.47b**) and characterized in between the fully protonated **C631H$_3^{6+}$**, in which all of the dibenzylammonium units are encircled, and **C631^{3+}**, in which all of the triazolium units are encircled by crown ethers.

6.13.10 Molecular Pulleys

Chen[563] has recently described a triply interlocked [2]rotaxane (**R6150H$_3^{6+}$**) based on a triptycene-derived tris(crown ether) whose acid/base actuation (**Scheme 6.108**) causes the axle of the dumbbell to translate in a rotatory manner reminiscent of a pulley. The axle possesses three dibenzylammonium recognition units interspersed with three *N*-methyltriazolium recognition units. While the –NH$_2^+$– centers occupy each of the triptycene-linked DB24C8 rings of the host in **R6150H$_3^{6+}$**, deprotonation of these sites with DBU generates the [2]rotaxane **R6150^{3+}**, in which the triazolium units occupy the rings' cavities. The three mechanical bonds that confine the axle to the periphery of the central triptycene unit cause the axle to bend in a semicircle as it translates by biased Brownian motion in response to pH stimuli, mimicking the unique blend of linear and rotational motion that is characteristic of pulleys.

6.13.11 Multicomponent Pirouetting and Translation

When a single ring interlocks two or more component parts, those parts become constrained to a very small spatial region, increasing their local concentration. The mechanical bond in this scenerio may be considered as a



Scheme 6.107 The electrochemically induced folding of the oligoviologen [3]rotaxane **R6149^{18+}** is driven by intercalative radical-pairing interactions between the BIPY$^{\bullet+}$ radical cations of the rings and the axle of **R6149$^{9(\bullet+)}$** under reductive conditions.[132]

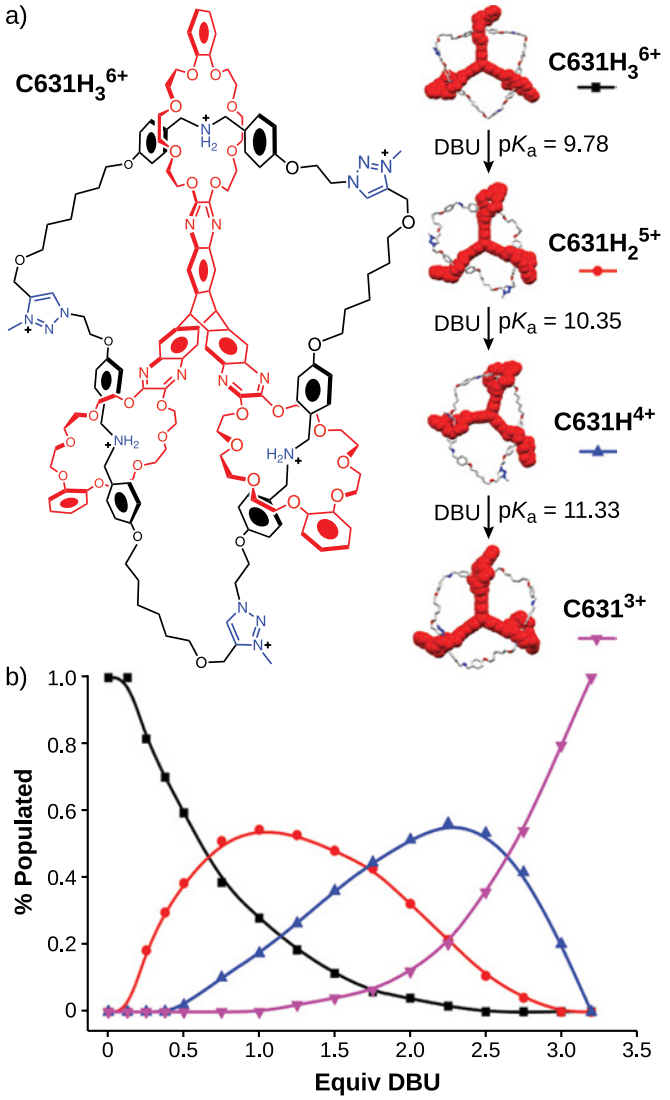
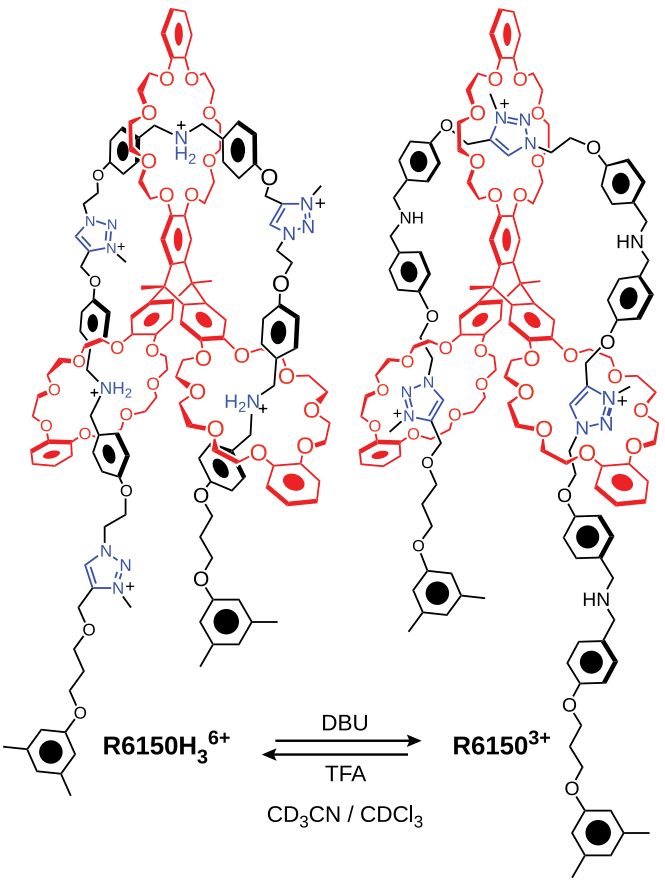


Figure 6.47 Base-triggered stepwise motion in a [4]pseudocatenane.[313] (a) The stereoformula of **C631H$_3$$^{6+}$** is illustrated alongside the energy-minimized co-conformations of the pseudocatenanes **C631H$_3$$^{6+}$–C631^{3+}**, accessed by stepwise deprotonation of the three dibenzylammonium recognition units. (b) The relative populations of the [4]pseudocatenane in each of its protonation states are given as a function of the amount of added base. Data and simulated structures adapted with permission from ref. 313 (copyright 2015 American Chemical Society)

type of molecular flask,[564] since it "contains" the component parts within a topologically limited space. In some cases, the overall co-conformation of the mechanomolecule may involve only very weak associative interactions. Indeed, a number of investigations have demonstrated that the mechanical bond is capable of stabilizing weak[474,565] and even repulsive[566,567] noncovalent interactions. Among these weak interactions are the radical–radical and mixed-valence dimers of tetrathiafulvalene in its three reversibly accessible redox states: (i) the neutral TTF, (ii) the TTF$^{\bullet+}$ radical cation, and (iii) the TTF^{2+} dication. In a few multicomponent donor-acceptor mechanoswitches, the co-conformations associated with certain redox states become dominated by the feeble forces between these TTF dimers.[77,78,568]

The donor-acceptor mechanomolecules illustrated in **Figure 6.48** are all co-constituted by multiple TTF-polyether component parts interlocked mechanically with the "molecular square" cyclobis(paraquat-4,4´-biphenylene) (CBPQB^{4+}). TTF dimers have been stabilized by the mechanical bonds of the push-button [3]catenane[77] **C632^{4+}**, as well as the multistable [3]catenane[78] **C633^{4+}** and [3]rotacatenane[568] **C634^{4+}**. In spite of their similarities, these three catenanes display different behaviors with respect to TTF dimerization, corresponding to the expression of different redox-triggered motions. The mono-oxidized species—namely, **C632$^{\bullet5+}$**, **C633$^{\bullet5+}$**, and **C634$^{\bullet5+}$**—all retain the mixed-valence dimer $(TTF_2)^{\bullet+}$ within the cavity of CBPQB^{4+}, but their behaviors differ after a second one-electron oxidation to the corresponding hexacationic species. In the case of the TTF-DNP MIMs **C633^{6+}** and **C634^{4+}**, the DNP recognition units compete with $(TTF^{\bullet+})_2$ for the interior of the cyclophane's cavity, such that only about half of the population includes the radical dimer within CBPQB^{4+}—60% for **C633^{6+}** and 50% for **C634^{4+}**. On the other hand, $(TTF^{\bullet+})_2$ occupies the cyclophane's cavity all but completely in the push-button catenane **C632^{6+}** since the butadiyne units have virtually no affinity for the cavity of CBPQB^{4+}. Thus, the TTF-DNP MIMs



Scheme 6.108 The acid/base actuation of Chen's triply interlocked [2]rotaxane molecular pulley.[563]

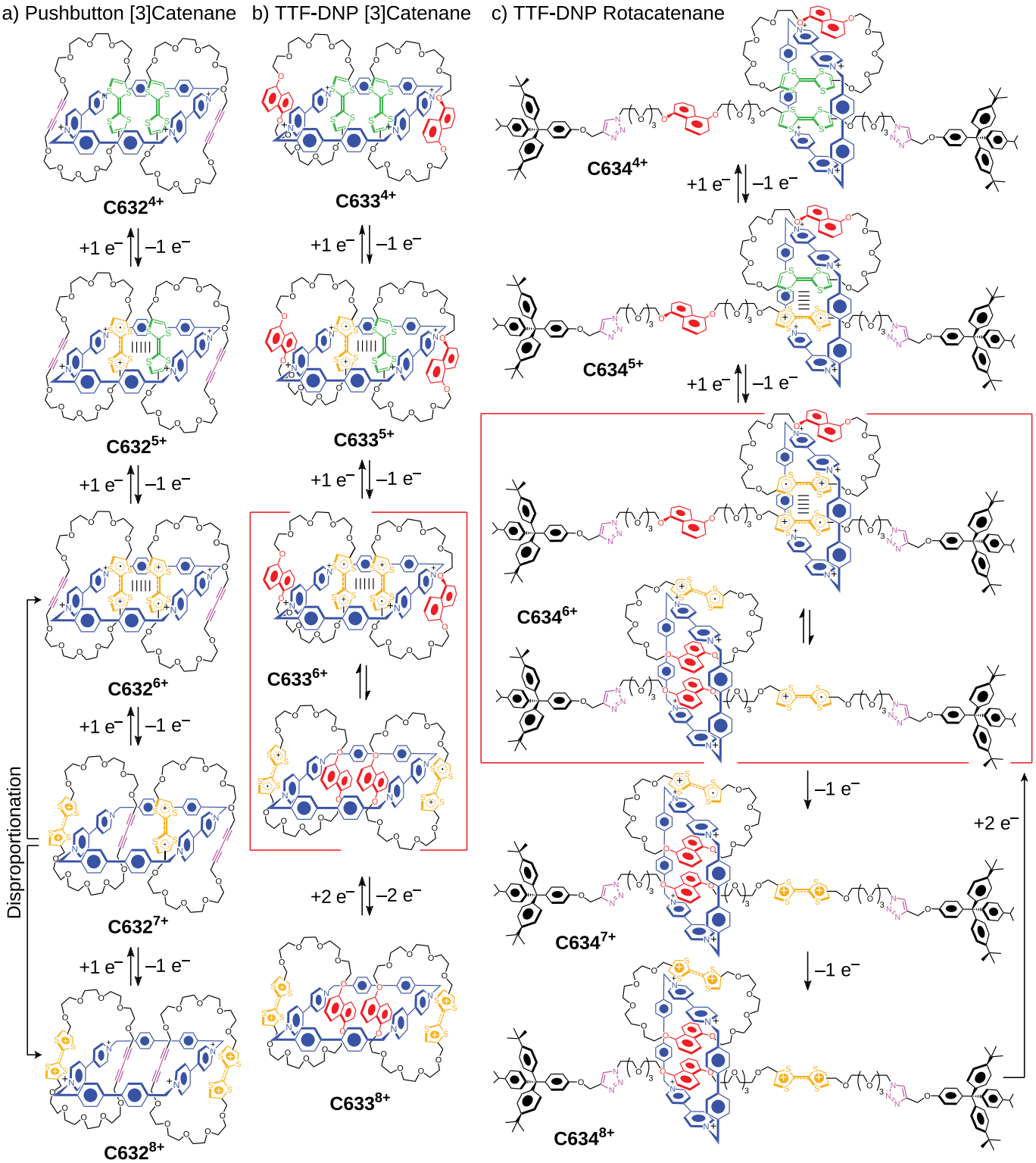


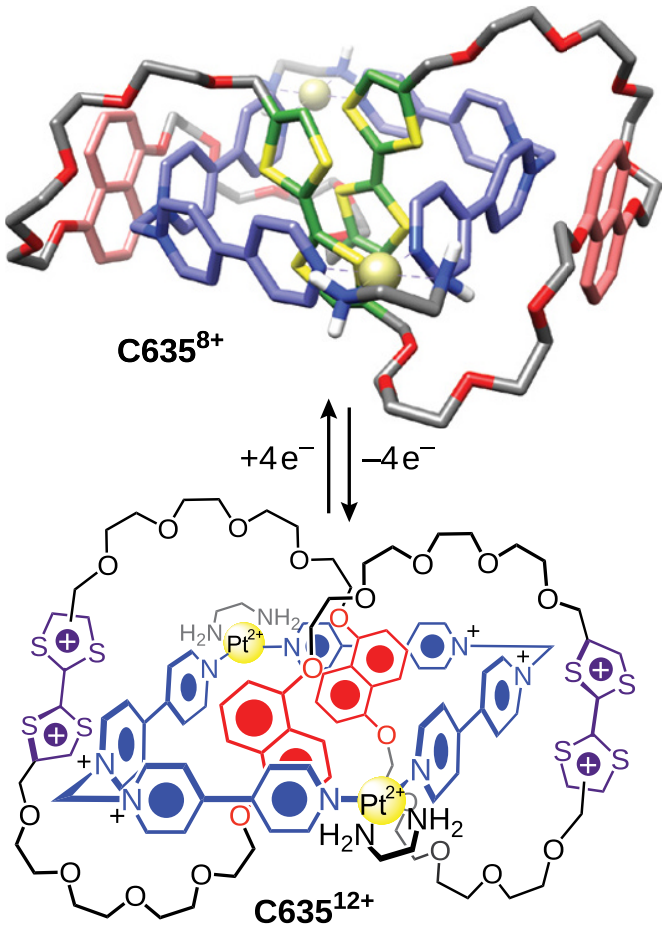
Figure 6.48 Mechanisms of circumrotation and TTF radical dimerization in several three-component MIMs: (a) a push-button [3]catenane,[77] (b) a TTF-DNP [3]catenane,[78] and (c) a TTF-DNP rotacatenane.[568]

and push-button catenane follow slightly different mechanisms thereafter. In the case of **C633**$^{6+}$ and **C634**$^{6+}$, two-electron oxidations to give **C633**$^{8+}$ and **C634**$^{8+}$ are observed, since there is a significant amount of 'alongside' TTF$^{\bullet+}$ radical in the hexacationic equilibrium distribution. However, a **C632**$^{7+}$ species is generated in the case of the push-button [3]catenane before disproportionating quickly to the more stable **C632**$^{6+}$ and **C632**$^{8+}$ species. In all three MIMs, the TTF units reside outside of CBPQB^{4+} after fully oxidizing them to the dicationic state. The proposed mechanisms

illustrated in **Figure 6.48** are supported by experimental evidence from NMR and EPR spectroscopies, cyclic voltammetry, spectroelectrochemistry, X-ray crystallography, and high-level density functional theory (DFT) calculations.

6.13.12 Molecular Conveyor Belts

The bistable donor-acceptor Solomon Link **C635^{8+}** has been actuated[569] under oxidative control to produce a reptation (**Scheme 6.109**) resembling that of a conveyor belt. The link is constituted by a crown ether possessing pairs of TTF and DNP π-donating recognition units, doubly interlocked with an octacationic, dinuclear Pt^{II} metallacycle lined with pyridinium-based π-acceptors. Whereas both TTF units occupy the cavity of the metallacycle in **C635^{8+}**, the DNP units traject into this pocket in the quadruply oxidized **C635^{12+}**. It is noteworthy that the $(TTF_2)^{\bullet+}$ radical cation and the $(TTF^{\bullet+})_2$ radical cation dimer are stabilized by this kind of topological link, as is the case in the CBPQB^{4+}-based catenanes **C632^{4+}–C634^{4+}**. In contrast with the other catenanes, however, the $(TTF)_2^{\bullet+}$ dimer occurs only fleetingly in the Solomon Link.



Scheme 6.109 The crown ether of the Solomon Link **C635^{8+}** responds to chemical or electrochemical oxidation of its TTF recognition units with a topologically constrained motion[569] resembling that of a conveyor belt, as opposed to pirouetting or translation, with respect to the doubly interlocked octacationic metallacycle. A tubular representation of the X-ray crystal structure of the link in its GSCC is illustrated with hydrogen atoms, counterions, and solvent molecules omitted for the sake of clarity.

6.14 Condensed-Phase Switching

The single-molecule experiments described in **Section 6.12** and many of the molecular machines that will be described in **Section 6.15** involve molecular motion in condensed phases and at interfaces, motivating the pursuit of a more fundamental understanding of how these phases influence the thermodynamics and kinetics of switching. In this Section we describe investigations on switchable mechanomolecules in a number of condensed-phase settings and interfaces. The actuation of molecules with mechanical bonds in condensed phases has also been discussed in several reviews[31,570–576] in the literature.

6.14.1 Condensed-Phase Redox Switches

The nature of physical environment can influence[63,83] dramatically the kinetics of switching—an important consideration that is especially pertinent to the design of devices that rely on bistable or multistable molecules as nanoscale components. Although redox-switchable mechanomolecules are mechanistically well suited for applications, for example, in molecular electronic devices (MEDs), they must first of all be characterized and understood in the condensed phases that are representative of those settings. When taken into condensed-phase environments, electrochemically switchable bistable MIMs exhibit both similarities and differences when compared with their solution-phase counterparts. Often there are enough similarities to justify solution-phase switching as an efficient way to screen molecules for desired condensed-phase switching properties, such as co-conformational selectivity. In any condensed-phase application, it must be verified that switching remains accessible, reproducible, and kinetically appropriate for the application in mind. Since the oxidatively controlled switches based on TTF have driven most of the research[31] in this area, this Section will be dedicated to bistable MIMs based on the familiar TTF/CBPQT^{4+} combination for the most part. It stands to reason that the trends and insights uncovered here might also apply to other families of bistable MIMs in condensed phases.[572]

If mechanomolecular switches are to find a role in MEDs, then they must be (i) operable in condensed phases at nanometer length scales, (ii) able to withstand an enormous number of switching cycles without showing any signs of degradation, in addition to having (iii) high cycling speeds, (iv) intrinsically strong signals, and (v) reproducible responses to electrochemical interrogation with (vi) minimal defects. It has been definitively proven (vide infra) that (i) is realistic and achievable, but attributes (ii)–(vi) still remain challenging to achieve for MEDs such as random access memory or integrated circuits. Still more challenges facing molecular electronics are associated with implementing an appropriate architecture with which to operate

the molecular switches.[58] Of course, many other applications for molecular switches of this ilk may also arise from a deeper fundamental understanding of condensed-phase switching. Summarized in this Section are investigations that have been conducted on redox-switchable donor-acceptor MIMs at interfaces and in more restrictive physical environs than bulk solution, including Langmuir-Blodgett films (**Section 6.1.2.1**), self-assembled monolayers (**Section 6.1.2.2**), and viscous polymer matrices (**Section 6.1.2.3**), which are relevant settings for the development of nanoelectronic devices for memory and computing applications. The topic of switching electrochemically bistable MIMs at interfaces and in devices has been covered in several literature reviews.[31,58,577]

6.14.1.1 Redox Switching in Langmuir-Blodgett Films

A Langmuir-Blodgett[578] (LB) film is a monolayer or multilayer of organic molecules, deposited from solution, usually aqueous, onto an immersed solid substrate. LB Films are typically made with amphiphilic molecules on account of their ability to form monolayers at the air-water interface below their critical micelle concentrations. Irving Langmuir described[579] in 1917 the monolayered nature of oily molecules at the liquid-air interface (known today as Langmuir monolayers) and how they are related to monolayers on solids. Langmuir also developed[580] a technique circa 1919 for transferring the monolayers onto glass slides by slowly withdrawing the slide from solution. In 1934, Langmuir's former student Katherine Blodgett discovered[581] that multilayers could be built up on glass by sequentially withdrawing and re-immersing the substrate, with each passage through the Langmuir monolayer adding a new layer onto the glass-supported film. LB films have been utilized[582,583] extensively to deposit molecules on surfaces with excellent uniformity and precise control over thickness and density. Mechanomolecules are no exception!

The technique (**Figure 6.49**) for making LB films involves an apparatus known as a LB trough (**Figure 6.49a**), which is used to compress a surface monolayer on top of an aqueous subphase, while using a Wilhelmy plate tensiometer to measure the surface pressure, π. The π–*A* isotherm

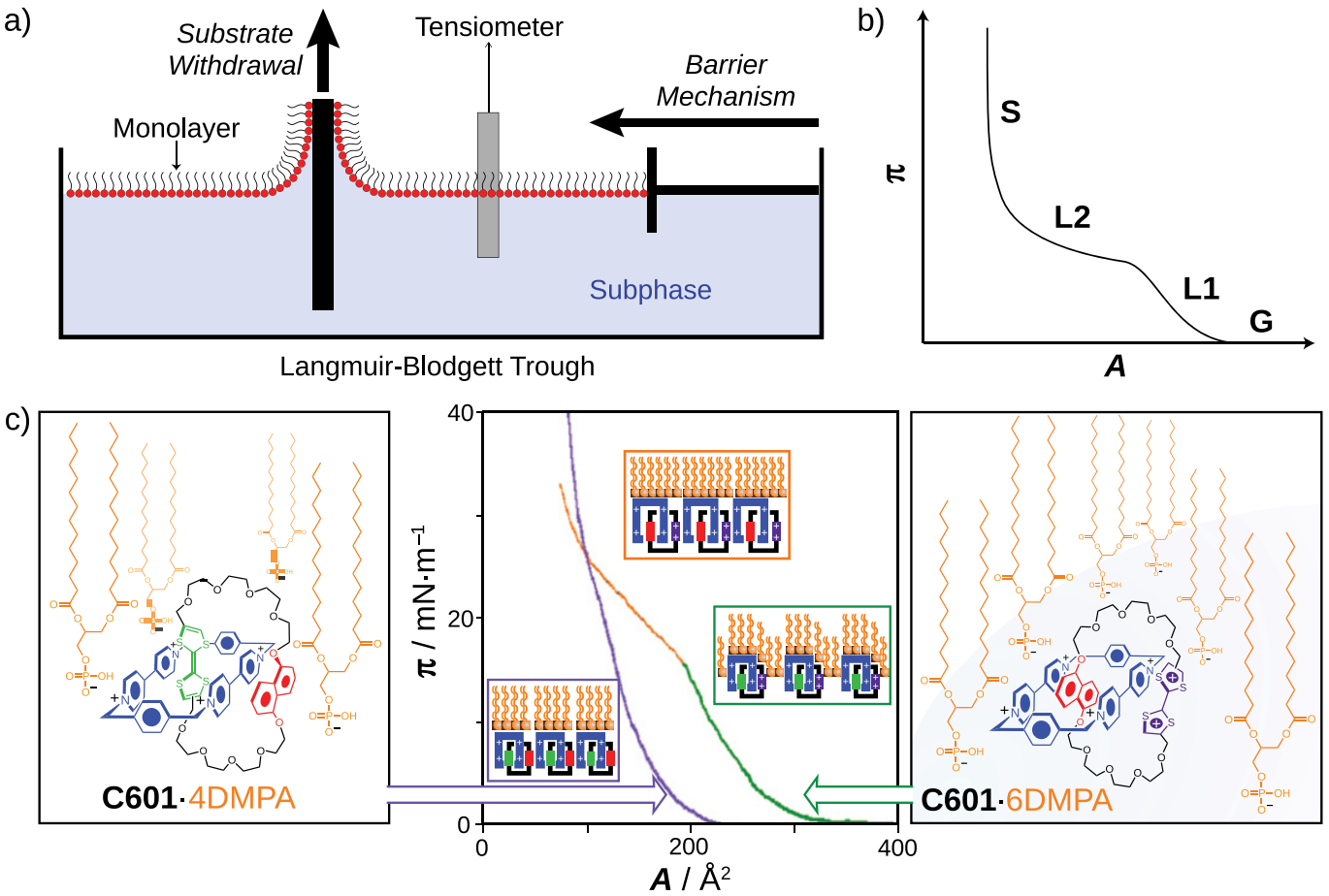


Figure 6.49 The Langmuir-Blodgett (LB) technique.[578] (a) Diagram of a LB trough, showing how a movable barrier at the liquid-air interface can be used to compress a Langmuir monolayer while changes in surface pressure (π) are monitored with a tensiometer. The monolayer can be transferred to a substrate by withdrawing it from the subphase. (b) A sample π–*A* isotherm, showing the regions that characterize gaseous (G), expanded and condensed liquid (L1 and L2, respectively), and solid (S) monolayer phases. (c) π–*A* isotherms of Langmuir monolayers[586] of the $DMPA^-$ salts of $\mathbf{C601^{4+}}$ and the TTF-oxidized counterpart $\mathbf{C601^{6+}}$.

(**Figure 6.49b**), which records surface pressure against molecular area, *A*, is an important tool for characterizing the properties of a Langmuir monolayer. A monolayer can pass through several different phases as it is compressed, which can be identified in different regions of the π–*A* isotherm. Commonly identifiable phases include gaseous (G), expanded liquid (L1), condensed liquid (L2), and solid (S), corresponding to increasingly higher packing densities. The use of the LB technique for depositing charged donor-acceptor MIMs was worked out as early as 1993 by our group in collaboration with Helmut Ringsdorf.[584–586] In order to render the $CBPQT^{4+}$ ring and mechanically interlocked derivatives thereof sufficiently amphiphilic for forming stable monolayers, the hexafluorophosphate (PF_6^-) counterions can be exchanged for dimyristoylphosphatidyl ($DMPA^-$) phospholipids. Whereas π–*A* isotherms of the PF_6^- salts have low reproducibility and indicate structural collapse even at low surface pressures, the corresponding $DMPA^-$ salts form stable monolayers. The π–*A* isotherms (**Figure 6.49c**) of the bistable [2]catenane **C601**$^{4+}$ and the corresponding TTF-oxidized catenane **C601**$^{6+}$ as $DMPA^-$ salts show that **C601**$^{4+}$ packs with a density of ~1.2 nm^2 per catenane, whereas **C601**$^{6+}$ forms two stable phases with packing densities of 1.5 nm^2 above 25 $mN \cdot m^{-1}$ and 2.7 nm^2 below 20 $mN \cdot m^{-1}$ of pressure. Since the cross-sectional area of eight closely packed alkyl chains of four $DMPA^-$ counterions is approximately equal in size to those of the catenanes in the denser phases (1.2–1.5 nm^2 per catenane), these monolayers most likely comprise a layer of closely packed catenanes involved in π–π stacking interactions, situated underneath a layer of closely packed $DMPA^-$ counterions.

LB Films of Redox-Driven Switches in Molecular Switch Tunnel Junctions (MSTJs)

LB Monolayers have been the workhorse for constructing tiny electrodes bridged by monolayers of MIM-based switches. This Section covers mechanically interlocked switches that have been studied in a crossbar (or crosspoint) architecture (**Figure 6.50**) involving a two-dimensional tiled array of molecular switch tunnel junctions (MSTJs). MSTJs are called as such because the mechanism for current flow is the resonant tunneling of electrons through the electronic states of the electrode-bridging molecules. This body of work, beginning around 1998, was a collaborative venture with Jim Heath, given his truly remarkable expertise in fabricating devices, and our extensive collection of bistable donor-acceptor MIMs.

In the crossbar architecture, a monolayer of molecules is sandwiched between a bottom electrode and a top electrode oriented orthogonally to the bottom one. Each crossing point, or junction, represents an individually addressable, solid-state, two-terminal electrochemical cell. The area of a MSTJ is defined by the width of the electrodes, which can be fabricated, for example, using bottom-up approaches[587] or lithographic techniques.[588] A typical MSTJ fabrication process[102] is summarized in **Figure 6.50a**. Typically, polysilicon wires are photolithographically

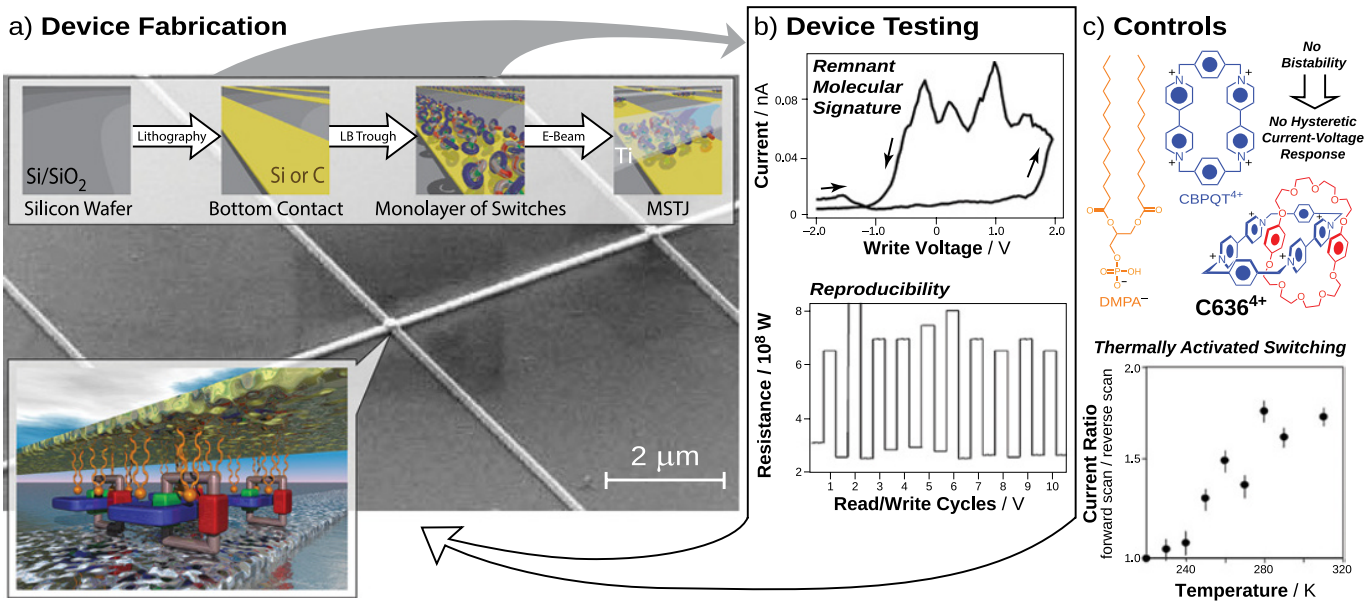


Figure 6.50 Summary of MSTJ crossbar devices.[58] (a) Device fabrication involves the transfer of a LB film of molecular switches onto patterned polysilicon bottom electrodes, followed by evaporation of Ti/Al top electrodes. (b) Successful devices have a hysteretic current–voltage (*I*–*V*) curve known as a remnant molecular signature and can be cycled reproducibly without signal decay. These data are shown for MSTJs based on **C601**·4DMPA. (c) Control experiments verify that mechanical switching is responsible for the remnant molecular signature, since non-switchable species such as $DMPA^-$, $CBPQT^{4+}$, and the degenerate [2]catenane **C636**$^{4+}$ do not exhibit hysteretic *I*–*V* curves. The loss of signal at low temperatures shows that switching is an activated process, which is consistent with the switching mechanism of bistable MIMs.

patterned on a silicon wafer prior to deposition of a monolayer of molecular switches using the LB technique. Then a thin layer of Ti and a thicker layer of Al are evaporated through a shadow mask using electron-beam lithography to form the top electrodes. The importance of the molecule-electrode contacts in these devices is paramount.[103] SiO_2-passivated Si is typically employed as the bottom electrode material, because hysteretic electrochemical switching signatures characteristic of molecular bistability, which are known as remnant molecular signatures, have not been observed on metal electrodes[103,589–591] such as Au and Pt. Carbon is also suitable as a bottom electrode material, since MSTJs fabricated with single-walled carbon nanotubes (SWNTs) exhibit a remnant molecular signature.[592] Concerning the top electrode, it is important to avoid damaging the switching components of the molecules during the metal deposition process. Furthermore, it is believed, with some evidence from IR spectroscopy,[593] that the success of the device fabrication also relies to some extent on an 'annealing' event, in which Ti–C bonds are formed between the hydrophobic parts of the molecular switches and the top electrodes during electron-beam lithography.

The main advantages[594] of the crossbar architecture are that (i) its simplicity makes it relatively easy and cost-effective to implement, (ii) it is scalable to the 'nano' size regime, (iii) it has the versatility to be configured for multiple purposes such as memory or logic, and (iv) it is defect tolerant since individual defective junctions can be identified and ignored. It also circumvents the need for high-speed switching to some extent, since up to 50% of the junctions may be actuated simultaneously, in principle. These advantages are particularly important for chemically assembled devices because they are prone to defects as a result of finite reaction yields. The main disadvantages of the MSTJ platform are associated with the two-terminal device architecture, since it is not possible to tile three-terminal devices, such as field effect transistors (FETs), in two dimensions while still being able to address an embedded device without also addressing surrounding devices. Having only two terminals to address each device introduces the following constraints: (i) the devices cannot demonstrate signal gain (amplification of a signal's intensity), (ii) voltage (*V*) characteristics must be very well-defined, since three tasks (opening, closing, reading) must be performed using only two terminals, meaning each task is done at a different voltage instead of at different electrodes, and (iii) the Fermi levels of the electrodes must be appropriately aligned with the redox states of the molecular switches to allow current to flow through the junctions. Points (i)–(iii) mean that the molecules must be carefully designed to have (i) intrinsically strong signal responses—current (*I*) or resistance (*R*), for example—(ii) a hysteretic *I*–*V* curve, a property which is not trivial for most molecules, and (iii) appropriate molecular orbital energy levels, respectively.

Bistable donor-acceptor MIMs are well suited for meeting the challenges posed by two-terminal crosspoint devices because the mechanical motions of their component parts can create the hysteretic *I*–*V* curves (**Figure 6.50b**) required for voltage-dependent reading/writing processes. Both in solution and in the MSTJs, the voltage required to switch a redox-operated bistable MIM is the sum of its ionization energy and an activation barrier. In solution, the most effective way to maintain a high population of rings around the weaker-binding recognition site (associated with the MSCC) is to maintain the ionized state, such that no driving force exists to reinstate the GSCC. In a MSTJ, however, the molecule cannot remain ionized because junctions that hold charge are capacitors and not conductors. The stability of the MSCC and activation barrier must therefore be carefully tuned such that the switch can be actuated in the device between two charge-neutral states in which ionization is just a temporary impetus for a mechanical transition to the MSCC. This extra requirement of charge-neutral switching is the major difference between mechanically interlocked electrochemical molecular switches in solution and those in MSTJs, and presents a formidable challenge from the perspective of the molecular blueprints. How does one design a molecule that can be switched[595] electrochemically between two states with different *I*–*V* characteristics, with no changes in net charge?[B]

The first landmark[101] in the MSTJ platform involved (i) the successful incorporation (**Figure 6.51a**) of the donor-acceptor rotaxane **R6151**$^{4+}$ into a crossbar architecture using the same technique summarized in **Figures 6.49–50**, (ii) the electrochemical actuation of the corresponding MSTJs, and (iii) the demonstration that the MSTJs could be configured into logic gates. The molecular switching behavior in this system was irreversible, however, for once a switch had been 'opened' it could not be 'closed' again. The MSTJs gave unexpectedly high separations between high and low current levels in the open and closed states (**Figure 6.51b–c**), rendering them relatively insensitive to defects associated with noise. Consequently, these singly configurable MSTJs could be fabricated into AND and OR logic gates with good signal to noise ratios of 15:1 and 30:1, respectively.

The next step forward was to make a reconfigurable platform[102] in order to make the junctions arbitrarily rewritable. We reasoned that electrochemically switchable, bistable molecules such as the bistable catenane **C601**$^{4+}$ with $DMPA^-$ counterions would be suitable candidates. A monolayer of **C601**·4DMPA at a density of one molecule per 125 Å^2 was transferred onto a substrate with 7 μm-wide amorphous Si bottom electrodes, and 10 μm-wide Ti/Al electrodes were installed on top, producing devices

[B] On the basis of first principles DFT calculations, Subramanian[595] has suggested that the applied bias at the cathode of a MSJT device can alter the energetic landscape of a bistable [2]rotaxane sufficiently to drive the ring from the GSCC to the MSCC without chemical oxidation ever taking place, although it is not yet clear the extent to which this mechanism is involved in the experiments summarized in this Section.

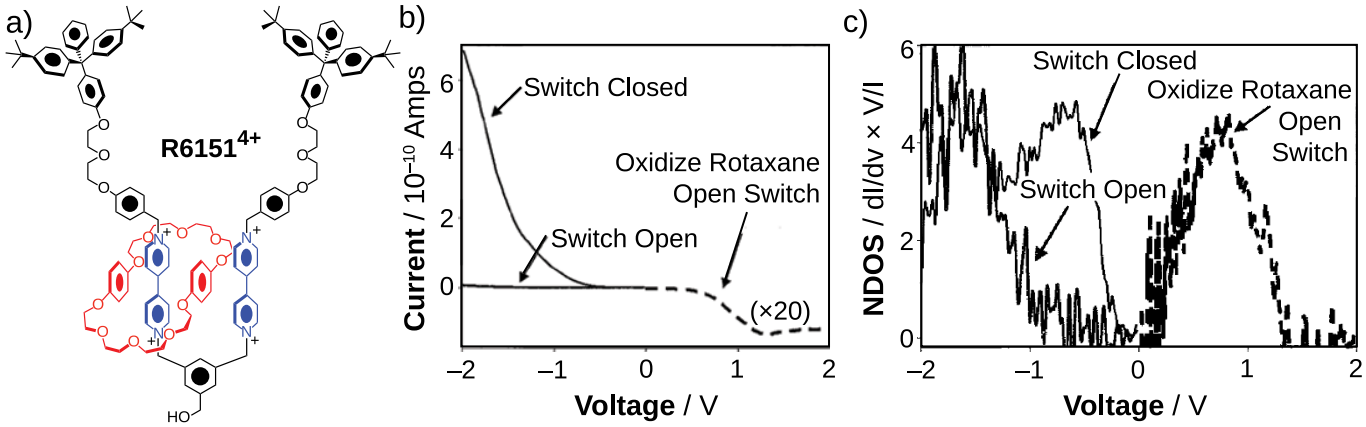


Figure 6.51 The earliest MSTJ platform from the Heath laboratory.[101] (a) Structural formula of the rotaxane **R6151^{4+}** incorporated into the junctions as LB monolayers. (b) Current-Voltage response of the MSTJs before and after irreversibly opening the switches under oxidative bias. Junctions are interrogated at negative bias where the difference in response between open and closed switches is largest. (c) A plot of the normalized density of states (NDOS) vs. Voltage shows that oxidation of **R6151^{4+}** at around +0.7 V changes the molecules, quenching resonant tunneling and causing the NDOS to fall to zero.

containing ca. 50–60 million catenanes per junction. The MSTJs are 'open' when the bistable catenanes are in the GSCC and 'closed' when they are in their MSCC, which is accessed by applying a –2.0 V pulse, before returning to near-zero bias. Application of a +2 V potential restores the GSCC. The junctions are read at –100 mV and the resistance between their closed and open states differs by a factor of at least two (potentially suitable for memory but not for logic applications), although the ~20 pA currents through the junctions in the closed-switch state are admittedly low. The molecular remnant signatures and cycling data for this system are shown in **Figure 6.50b**. The devices could be cycled hundreds of times over two months under ambient conditions without a noticeable drop in performance.

The proposed mechanism for these MSTJs, which also holds for all bistable donor-acceptor MIMs that were introduced into MSTJs subsequently, asserts that the electrochemically induced mechanical movement of the interlocked components is responsible for the hysteretic *I*–*V* behavior, where the MSCC (the 'switch closed' or 'ON' state) is a better conductor because it has a higher density of states for the resonant tunneling of electrons. This mechanism is well-supported by control experiments (**Figure 6.50c**) involving non-switchable compounds such as DMPA^{-}, CBPQT^{4+}, and the degenerate [2]catenane **C636^{4+}**, which exhibit *I*–*V* hysteresis magnitudes that are less than 1% of those for the bistable catenane **C601^{4+}** and decay quickly (attributable to residual capacitance) over time. Bistability is therefore an important factor in creating reconfigurable solid-state switches by the MSTJ method. Another important control is a plot of the on/off current ratio (read at –100 mV) against temperature (**Figure 6.50c**), in which the loss of signal at low temperatures indicates that switching is an activated process, in good agreement with the proposed mechanism.

What developed[31] subsequently over the course of almost a decade was a feedback loop in which MSTJ-based experimental results guided the synthesis of iteratively better and better bistable molecular switches, concurrently with the continual miniaturization of MSTJ feature sizes, as summarized in **Figure 6.52**. It was hypothesized that the low current in the bistable [2]catenane MSTJs could be attributed to the long, insulating phospholipid counterions occupying the bulk of the inter-electrode gap, and that a linear MIM with more evenly distributed redox-active sites, such as a pseudorotaxane or rotaxane, might be even better at demonstrating resonant tunneling currents. This new generation of switches began[85] with the bistable amphiphilic [2]pseudorotaxane ***L609*** ⊂ *CBPQT*$^{4+}$. Indeed, MSTJs constructed from ***L609*** ⊂ *CBPQT*$^{4+}$ had far better currents (100 nA at +100 V) but ill-defined read voltages (poor resolution between open and closed states at negative bias), which was explained, with evidence from microscopy, by so-called 'domain switching.' Domain switching is characterized by large domains of molecules driven by nucleation statistics, i.e., not acting as individuals. The domain switching may have arisen either (i) from the supramolecular nature of the complex in which the ring is free to dissociate, or, more generally, (ii) by an excessively small molecular cross-sectional area. A hydrophilic stopper was therefore developed[85] and tested in the amphiphilic monostable [2]rotaxane **R6152^{4+}**. The monostable rotaxane **R6152^{4+}** resolved simultaneously the domain switching problem and confirmed that bistability is crucial, since it had negligible hysteresis in the *I*–*V* curve near zero bias and withstood only a few read/write cycles before failure.

The combination of insights provided by ***L609*** ⊂ *CBPQT*$^{4+}$ and **R6152^{4+}** ultimately led to the development (**Figure 6.52**) of the amphiphilic [2]rotaxanes[104] **R690^{4+}** and **R6153^{4+}**, with (i) wide-footprint (1.4 nm^2) hydrophilic stoppers to prevent domain switching, (ii) a long axis to span the entire inter-electrode gap for enhanced currents, and (iii) bistability to ensure a well-defined hysteretic *I*–*V* response. These more highly optimized molecular designs were accompanied by

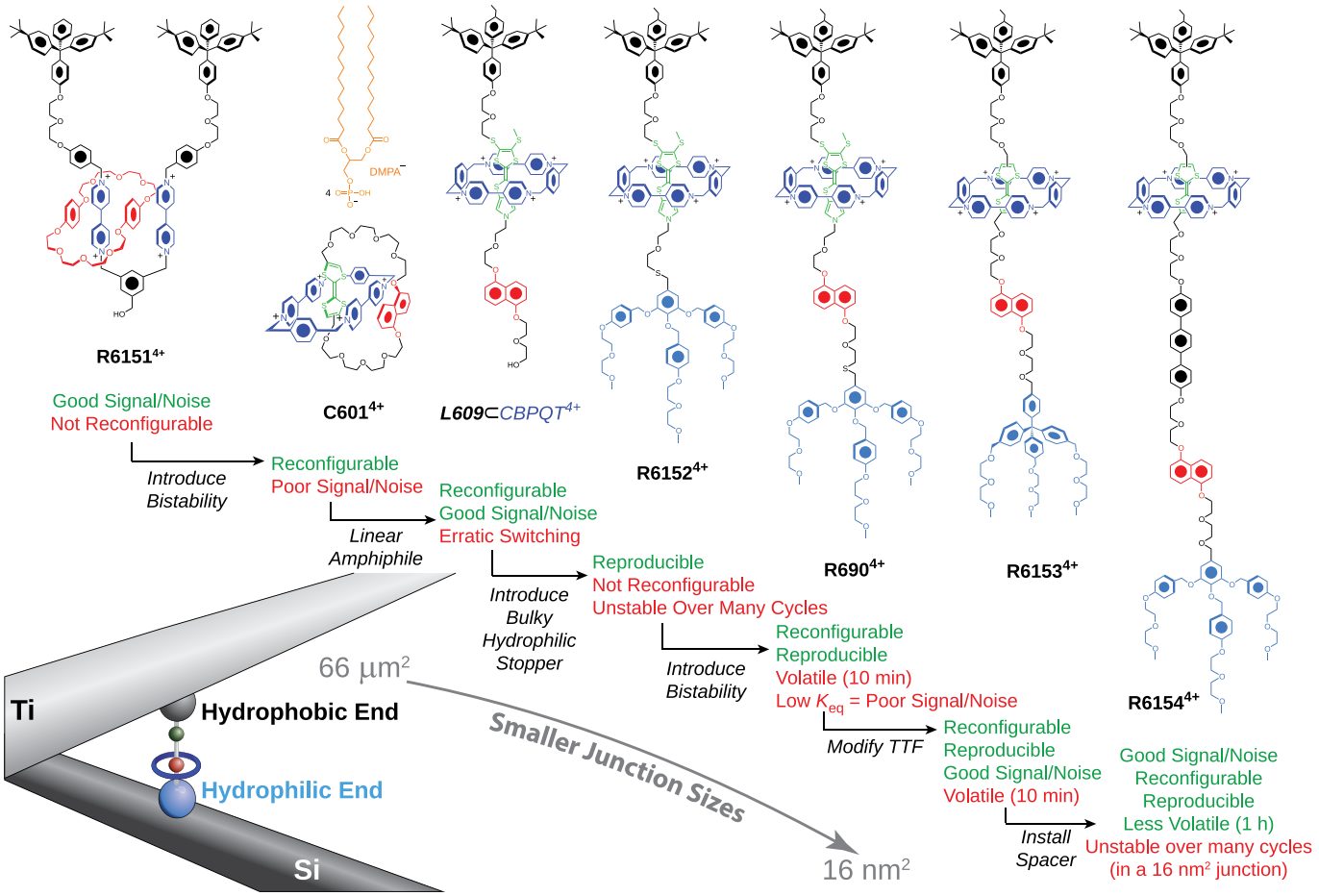


Figure 6.52 The evolution of molecular switches for MSTJs.[101–105]

a revitalized fabrication protocol that delivered a dramatic scale-down of the electrode junctions, from previous cross-sectional areas on the order of tens of square microns to as small as tens of square nanometers. Remarkably, the device signatures were essentially invariant when scaling down to the nanometer size regime, although current levels suffered (reducing from 1 nA in large devices to 50 pA in small ones), as did the working device yield (from 80–100% in micron-scale junctions to 15–25% in nanoscale junctions). The signal was nevertheless well defined and stable over many cycles, and the longevity of the switch-closed or ON state (MSCC) lasted 10–15 minutes before it relaxed back to the switch-open or OFF state (GSCC), which was stable over an arbitrary amount of time. Furthermore, it was demonstrated that the more robust larger junctions were point-addressable and configurable for both two-dimensional memory and logic circuits. While **R690**$^{4+}$ and **R6153**$^{4+}$ exhibited similar behaviors, **R6153**$^{4+}$ had a higher switching amplitude, an observation which speculation might attribute to its more biased population distribution (K_{eq} = 10) in the ground state or its more stable (to oxidation) stopper lacking any phenolic moieties.

A decade's worth of research on electrochemically switchable mechanomolecules in MSTJs culminated (**Figure 6.52**) in 2007 when Heath[105] prepared a 160-kbit memory device patterned at a density of 10^{11} bits·cm^{-2}—see **Figure 1.36** and the corresponding discussion in **Section 1.3.6**. The molecular switch[62] in this device was the bistable rotaxane **R6154**$^{4+}$, in which an improvement on **R6153**$^{4+}$ was achieved by incorporating a rigid triphenyl spacer between the recognition sites. This spacer delivers a four-fold increase in the half-life of the MSCC up to about an hour. As for the crossbar architecture, the top and bottom electrodes were each scaled all the way down to 16 nm width for the device, corresponding to only approximately 100 rotaxane molecules per junction. Again only ~25% of the junctions had sufficient on/off ratios for configuration into the memory circuit. Unfortunately, the bits typically survived no more than 10 cycles before failure, possibly as a result of the enhanced susceptibility of the tiny 16 nm^2 junctions to molecular damage, since only a few molecules represent a significant fraction of the total number of switches per MSTJ on this size scale.

Here are some bullet points summarizing the main lessons gained from a decade's worth of experiments switching bistable MIMs in a MSTJ platform:

- Amphiphilic MIMs can be sandwiched between two electrodes in a crossbar architecture by transfer of a LB monolayer onto the bottom electrode and subsequent

vapor-phase deposition of the top electrode to produce a two-dimensional array of point-addressable MSTJs.

- Molecules in the LB monolayer must be packed in sufficient density to avoid nonspecific damage from vapor deposition of the top electrode and corresponding poor switching characteristics.[593]
- Current flows through MSTJs by resonant tunneling of electrons through the electronic states of the molecules, which calls for switches with a high density of states aligned with the Fermi levels of the electrodes and redox-active sites that are evenly distributed throughout the gap.
- Bistability in the molecular switches is crucial to obtaining large-amplitude hysteresis near zero-bias in the current–voltage curve, which is a necessary feature for computing with a two-terminal device such as those afforded by the crossbar architecture.
- For switches based on $CBPQT^{4+}$ rings and DNP and TTF-derived recognition units, the more highly conductive state (ON) is the MSCC, in which the $CBPQT^{4+}$ ring encircles the DNP unit.
- The non-ionized MSCC in a bistable MIM can be accessed by applying an ionizing voltage in the MSTJ and then returning to near-zero bias, allowing for overall charge-neutral mechanical switching.
- The kinetics of relaxation from the MSCC back to the GSCC can be slowed down by maximizing packing density in the monolayer, as well as by installing a barrier in between the two recognition sites.
- Large-area molecular domains in the MSTJs result in poor device characteristics, which can be avoided by implementing a wide molecular footprint in the form of a bulky hydrophilic stopper.
- Working device yield, robustness over many cycles, and current amplitude decrease as the cross-sectional area of the junctions is scaled down, but operable memory circuits can still be prepared from MSTJs with very small (16 nm^2) cross-sections.

Our current understanding of the mechanism behind the electrochemical operation of these bistable donor-acceptor mechanomolecules in MSTJs has been corroborated by other groups, although it was questioned[596] and disputed[597,598] for a period of time. From a theoretical standpoint, the Goddard group[599,600] has obtained support for the mechanism by using DFT[599,600] to calculate the electronic structure of the GSCC and MSCC. Their calculations predict[600] a 40–60-fold difference in conductivities between the GSCC and MSCC, which is in good agreement with the 10–100 fold differences observed experimentally. This behavior is rationalized (**Figure 6.53**) by the distribution of the frontier molecular orbitals, where substantially more delocalized HOMOs and LUMOs in the MSCC facilitate resonant tunneling. The LUMO is delocalized over both the TTF and *DNP⊂CBPQT*$^{4+}$ portions of the MSCC, whereas it is highly localized on TTF in the GSCC. More experimental evidence described below also lends further

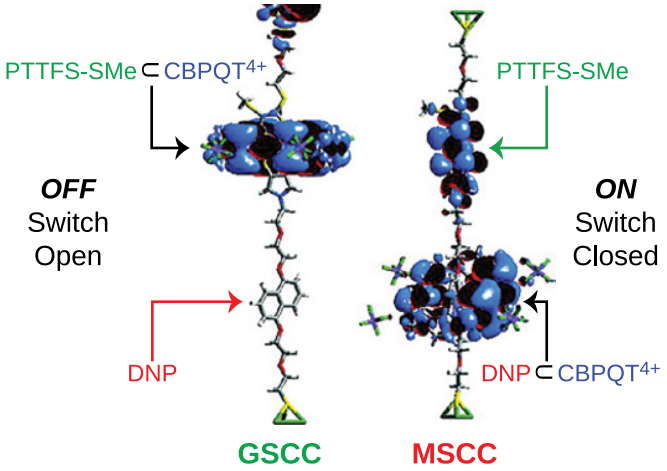


Figure 6.53 The calculated LUMOs of the translational isomers of a bistable rotaxane modeled with a $CBPQT^{4+}$ ring encircling an axle possessing PTTFS-SMe and DNP recognition units, which are encircled in the GSCC (left) and MSCC (right), respectively.[600] The more widely distributed orbital in the MSCC accounts for its higher conductivity for resonant tunneling electrons.

support to this mechanistic understanding of conductance switching in thin films of bistable donor-acceptor MIMs.

Other LB Films of Redox-Driven MIMs

One challenge associated with switching in condensed phases is identifying appropriate analytical techniques for characterization, since many of the most useful techniques for solution-state characterization—e.g., NMR and absorption spectroscopies—are not transferrable to molecularly thin films. A technique that is capable of analyzing stimulus-induced translational movement quantitatively at this scale is X-ray photoelectron spectroscopy (XPS). Since the photoemission intensity of an element depends on its depth within the film, XPS can be used to track the vertical movement of mechanically interlocked components in the film. Ho and Huang[86] have demonstrated that this kind of ring-tracking is possible in the case of the bistable [2]rotaxane **R6154**$^{4+}$. Since the $CBPQT^{4+}$ ring is the only component with nitrogen atoms, any changes in intensity of the nitrogen photoemission spectrum in the different redox states of TTF can be attributed to ring movement. Indeed, exposing a LB monolayer of **R6154**$^{4+}$ to a chemical oxidizing agent induces a drop in the nitrogen photoemission intensity, since the TTF^{2+} cation forces the $CBPQT^{4+}$ ring toward the DNP unit, which is located deeper within the film. Based on this signal attenuation, the distance of the ring translation was calculated to be 1.9 nm. An additional method that shows promise[601] in this area, surface enhanced Raman scattering (SERS), is still widely unexplored in the context of electromechanical switches.

Another X-ray-based method that has provided direct structural evidence for redox-driven mechanical motion in molecularly thin films of **R691a**$^{4+}$/**R691a**$^{6+}$ is synchrotron X-ray reflectometry (XR). Bjørnholm[88] characterized Langmuir monolayers of these bistable rotaxanes at the

air-water interface by XR and observed differences in the film's electron density profiles that are attributable to the molecular motion of the CBPQT^{4+} ring. These results also offered a glimpse (**Figure 6.54**) of how the amphiphilic bistable rotaxanes pack in the Langmuir monolayers. The tilt angle of the rotaxanes is highest when the area per molecule (and, therefore, surface pressure) is lowest. This picture of molecular packing has also been observed in molecular dynamics simulations of Langmuir monolayers of the bistable rotaxane modeled by Goddard.[602]

Several researchers at the Chinese Academy of Sciences in Beijing led by Gao[113,114,603,604] have investigated (**Figure 6.55**) the electrochemical switching properties of their own versions of bistable donor-acceptor rotaxanes based on dialkylthio-TTF (STTFS), DNP, and CBPQT^{4+} with dendritic stoppers in condensed phases. The centerpieces of these investigations are the bistable rotaxanes **R6155a^{4+}** and **R6155b^{4+}**, which differ only in the pentamethylene and 1,4-cyclohexylene spacers, respectively, located in between their STTFS and DNP units. The dumbbells of these rotaxanes lack polyether loops which enhance the stabilities of the *DNP*⊂*CBPQT*$^{4+}$ and *TTF*⊂*CBPQT*$^{4+}$ interactions by way of hydrogen bonding. These missing pieces lower the synthetic yields for obtaining the rotaxanes, but they do not compromise the rotaxanes' amenability to redox switching.[113] Although these rotaxanes are not amphiphilic in a conventional sense (the most hydrophilic moiety is probably the CBPQT^{4+} ring, which has very low water solubility as the PF_6^- salt) they could be deposited nevertheless on surfaces using the LB technique when mixed with chloroform to assist in the formation of a monolayer on water. It was first of all confirmed that these bistable rotaxanes could be switched in LB multilayers when the authors prepared[603] two-terminal devices from 70-nm thick LB multilayers of **R6155a^{4+}** on conductive substrates. These devices showed a sharp and sudden (~60 ns) transition from low conductivity to high conductivity at a potential of 1.4 V in the *I*–*V* curve. The low conductivity state can be recovered in a reverse voltage scan. Although these devices act like a single MSTJ of large dimensions, it is noteworthy that the high-conductivity state can live for at least 12 hours in this setting.

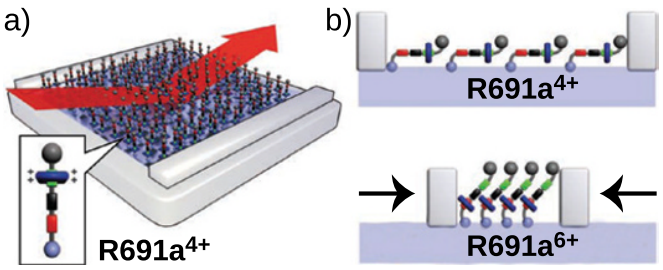


Figure 6.54 Probing LB monolayers of **R691a^{4+}** by X-ray reflectometry.[88] (a) Diagram of the reflection of an X-ray beam through an LB monolayer of **R691a^{4+}** in a LB trough. (b) Graphical representation of the changes in tilt angle in different oxidation states and at different surface pressures.

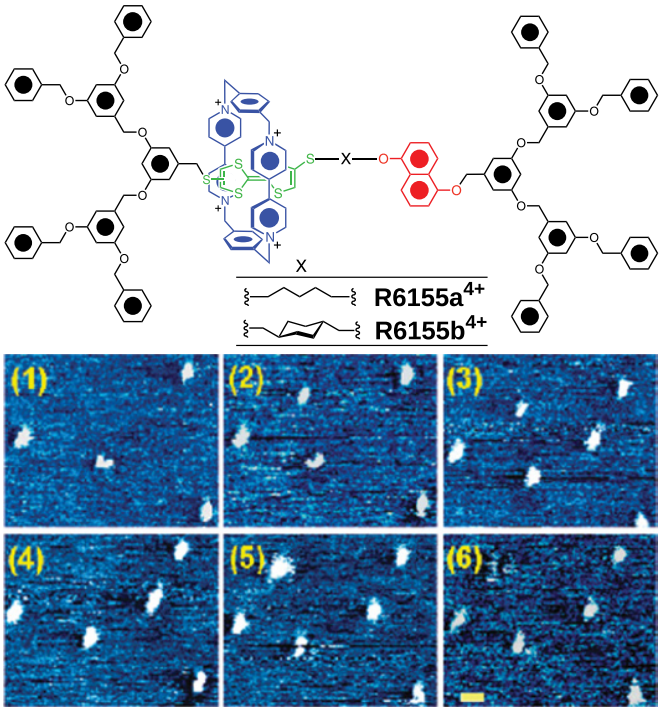


Figure 6.55 Nanorecording on LB films of the bistable [2]rotaxanes **R6155a^{4+}** and **R6155b^{4+}** through a STM tip.[603,604] Frames (1)–(6) are conducting AFM images of dots written as bright spots of enhanced conductivity on a ~70 nm LB multilayer film of **R6155b^{4+}** on a HOPG substrate with a 5 ms positive voltage pulse of 2 V, enabled by electrochemically-induced translational isomerization, which populates the MSCC. Frames (1)–(3) follow a sequential writing of new dots (1 → 2, 2 → 3), while frames (3)–(6) follow the erasing (3 → 4), re-writing (4 → 5), and re-erasing (5 → 6) of a single dot. Frames reproduced with permission from ref. 603 (copyright 2005 American Chemical Society)

The Beijing team has used scanning tunneling microscopy (STM) for nanorecording[603,604] and conductance switching[113] on similar LB multilayers of these bistable rotaxanes at very small length scales. A 20-nm thick LB multilayer of **R6155b^{4+}** on highly ordered pyrolytic graphite (HOPG) serves[603,604] as the medium for nanorecording. Dots 3 nm in size were written (**Figure 6.55**) on the film by the application of a positive voltage pulse of 2 V for 5 ms with an STM tip. The same dot-recording behavior is not observed at negative voltage pulses or on bare HOPG substrates. These films also showed remarkable stability, since dots are still readable and nanorecording is still possible after two months under ambient conditions. The dots can be observed directly by AFM in conductance mode, but are not visible in the topographic map, indicating that they written by means of a change in electronic states. In the initial study,[603] the dots of **R6155a^{4+}** could not be erased with a negative pulse and subsequently rewritten. On replacing **R6155a^{4+}** with the bistable [2]rotaxane **R6155b^{4+}** in the LB multilayer, a subsequent investigation revealed[604] that the nanorecording on otherwise identical films becomes erasable and rewritable. It has been suggested[604] that the more rigid cyclohexylene spacer present in **R6155b^{4+}** more effectively isolates

each switch from neighboring switchable rotaxanes in the environment of the LB multilayer, thus lowering the barrier to reset the GSCC. The same investigation also revealed that the Raman spectra of the films change before and after switching, an observation which supports the hypothesis that conductance changes are caused by translation of the $CBPQT^{4+}$ ring upon oxidation of the TTF unit.

6.14.1.2 Redox Switching in Surface Monolayers

Another environment pertinent to the study of physical constraints[63] on electromechanical switching is that of a self-assembled monolayer[605] (SAM). SAMs are characterized by ordered domains of molecules that form spontaneously by adsorption on surfaces, which is often, but not necessarily, assisted by functional groups—e.g., thiols, silanes, phosphonates—with a strong affinity for the substrate. These molecules anchor to the surface as a single layer, or monolayer. SAMs are typically stronger than LB monolayers because the head groups in the former can be adsorbed very strongly onto the surface by spontaneous interactions such as thiolate-gold bonds[606] (~25 kcal · mol^{-1}) or even the covalent Si–O–R bonds[607] (>100 kcal · mol^{-1}) formed between trichlorosilane and free hydroxyl groups on silica.

Self-Assembled Monolayers (SAMs) on Gold

An investigation by Willner[608,609] on surface-attached $CBPQT^{4+}$-based rotaxanes revealed that the environment above a monolayer can affect the switching kinetics within a SAM. The [2]rotaxane **R6156^{4+}** was assembled (**Figure 6.56**) on gold monolayers, employing imine chemistry at a density of 0.5 molecules · nm^{-2} as estimated by quartz-crystal microbalance (QCM) measurements. The π-electron rich phenylenediimine site is the preferred recognition site for the $CBPQT^{4+}$ ring to encircle in the ground state. When $CBPQT^{4+}$ is reduced electrochemically to $CBPQT^{2(\bullet+)}$, its diminished affinity for the binding site as well as its electrostatic attraction to the negatively charged electrode causes the ring to move closer to the surface. Oxidation back to the tetracationic state restores the original co-conformation. Both of these shuttling processes have been investigated in detail by double potential step chronoamperometry (DPSC). In the DPSC experiments, a reductive potential step is oscillated between values of –0.33 V (>99% $CBPQT^{4+}$) and –0.53 V (>99% $CBPQT^{2(\bullet+)}$), while a kinetic analysis of the current transients generates values for the rate of electron transfer k_{et}, which is known[610] to depend on the distance of the redox-active site from the electrode. Thus, the rate of electron transfer is slower ($k_{et1} = 80\ s^{-1}$) from the electrode to $CBPQT^{4+}$ than back-electron transfer ($k_{et2} = 1100\ s^{-1}$) from the closer-residing $CBPQT^{2(\bullet+)}$ species. For appropriately scaled delays between steps, a biexponential transient reveals the presence of two populations—one for each translational isomer of the rotaxane—and the time-dependent changes in the population distribution can be used to estimate first-order rate constants for ring translation. In 0.1 M phosphate buffer at 25 °C, the rate constant for movement of the ring toward the electrode ($k_{toward} = 318\ s^{-1}$) is faster than the rate constant for the ring moving away from the electrode ($k_{away} = 8.6\ s^{-1}$), a situation which is attributable to the directional attractive electrostatic force acting on the positively charged ring by the negatively charged electrode. With respect to the physical environment, the authors investigated[609] the temperature and 'friction' dependence of these rate constants, and found that, while both processes are dependent on friction—i.e., viscosity, as modulated by a glycerol additive in the medium—only k_{away} is temperature dependent and k_{toward} is not. The unidirectional temperature dependence is consistent with the hypothesis that attractive electrostatic interactions between the $CBPQT^{4+}$ ring and electrode influence the kinetic and thermodynamic landscape, since it implies that 'away' is thermally activated and 'toward' is a completely downhill process. This concept is summarized by the potential energy curves in **Figure 6.56**, while the temperature and viscosity-dependent rate constants are compiled in **Table 6.6**.

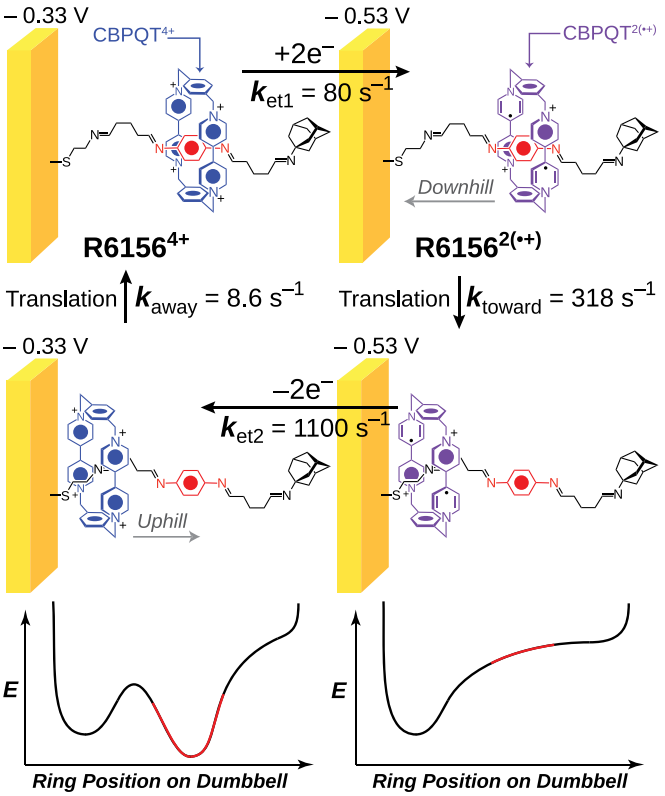


Figure 6.56 The working mechanism of a gold-anchored $CBPQT^{4+}$-based molecular switch **R6156^{4+}** developed in the Willner group.[608,609] Double potential step chronoamperometry allows the elucidation of electron transfer and shuttling rates in all four steps of a switching cycle. Two-electron reduction of $CBPQT^{4+}$ to $CBPQT^{2(\bullet+)}$ removes recognition for the phenylenediimine site (colored red) and causes the cyclophane to translate toward the electrode as a result of attractive electrostatic interactions. Since electron tranfer rates are distance-dependent, this reduction is slower ($k_{et1} = 80\ s^{-1}$) than oxidation back ($k_{et2} = 1100\ s^{-1}$) to $CBPQT^{4+}$. The directional nature of the electrostatic attraction between the negatively charged electrode and the tetracationic cyclophane dictates that motion toward the electrode is *downhill* ($k_{toward} = 318\ s^{-1}$), while the return path ($k_{away} = 8.6\ s^{-1}$) is *uphill* and thermally activated, as illustrated by the reaction coordinate diagrams.

Table 6.6 First-order rate constants k_{away} and k_{toward} (s^{-1}) for the shuttling of $CBPQT^{4+}/CBPQT^{2(\bullet+)}$ in **R6156**$^{4+}$ in gold monolayers in 0.1 M phosphate buffer at various temperatures and viscosities tuned by glycerol concentration.[609]

% Glycerol	k_{toward} 25 °C[a]	k_{away} 5 °C	k_{away} 25 °C	k_{away} 55 °C
0	318.2	6.57	8.62	20.43
1	296.0	5.95	8.02	18.75
2	207.2	3.87	5.63	14.13
5	162.8	2.44	4.45	7.34
10	55.5	1.54	1.86	3.40

[a]Rate constants k_{toward} were found to be temperature-independent.

Another proof for the existence of the MSCC in monolayers of bistable rotaxanes akin to those employed in MSTJs has been accomplished[87] in SAMs of the disulfide-tethered bistable [2]rotaxane **R6157**$^{4+}$. The thermodynamic parameters of switching were determined for this system using variable scan-rate and variable temperature cyclic voltammetry. The MSCC, **R6157**$^{4+}_{DNP}$, is populated (**Figure 6.57**) by the oxidation of the GSCC, **R6157**$^{4+}_{TTF}$, followed by reduction of the oxidized compound **R6157**$^{6+}_{DNP}$ which forms rapidly as the ring's translational motion is driven by Coulombic repulsion from the TTF^{2+} dication. At sufficiently high scan rates, an enhanced signal corresponding to the oxidation of the MSCC is observed in the second scan (**Figure 6.57**) before the GSCC has been fully recovered. The SAMs of **R6157**$^{4+}$ were packed at approximately 0.25 molecules/nm^2, corresponding to a 4 nm^2 footprint, which is significantly less dense than the 1.4 nm^2 footprint of **R6153**$^{4+}$ possessing the same ring-and-axle portion of the switch in the setting of the MSTJ crossbar devices. This lower packing density might explain why the activation barrier for GSCC recovery (See **Table 6.7** in **Section 6.14.1.3**) from the MSCC is significantly lower (18 kcal · mol^{-1}) in SAMs of **R6157**$^{4+}$ than it is in MSTJs (22 kcal · mol^{-1}) of **R6153**$^{4+}$. The SAM of **R6157**$^{4+}$ is also similar to the LB monolayers of **R6153**$^{4+}$ in terms of stability, with the added advantage that no loss in signal is observed over 100 CV cycles and multiple days in 0.05 M $LiClO_4$ MeCN solution.

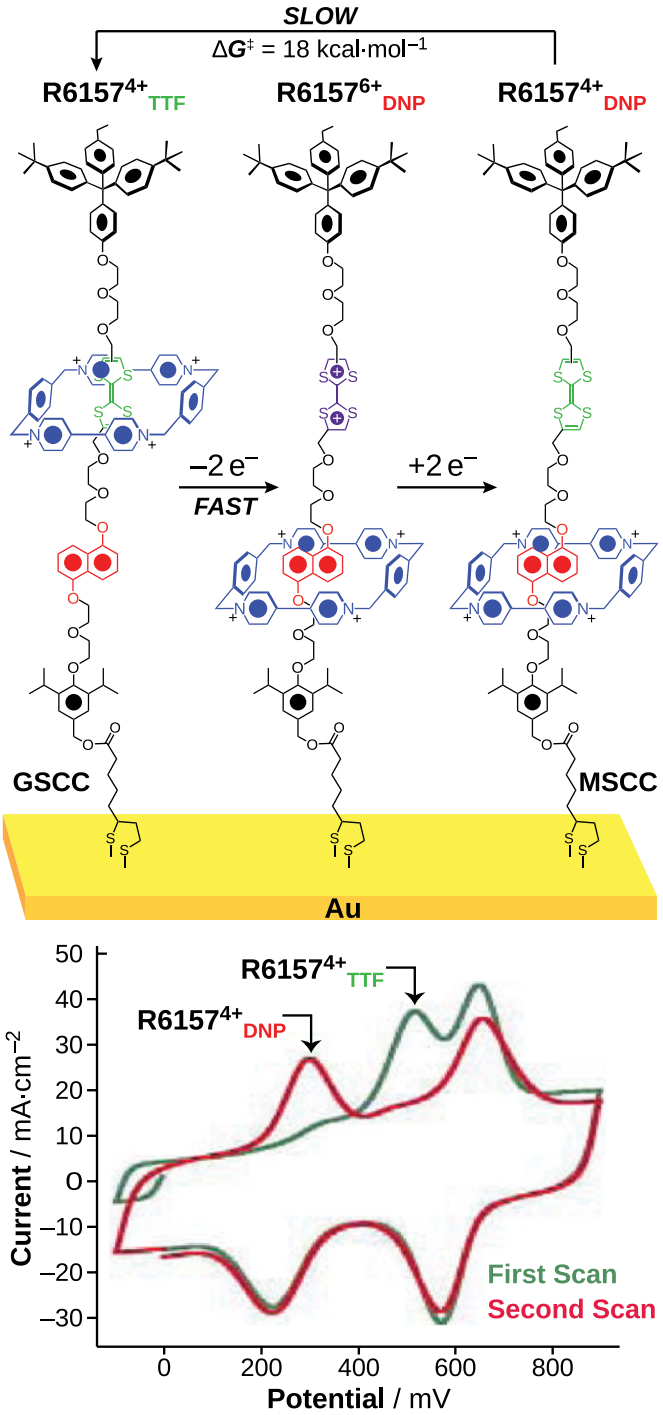


Figure 6.57 Traces of the first (green) and second (red) scan in the cyclic voltammogram (300 mV · s^{-1}, MeCN, 50 mM $LiClO_4$, 288 K) of the redox-switchable, bistable [2]rotaxane **R6157**$^{4+}$ immobilized on a gold surface.[87] The signal corresponding to the oxidation of the MSCC is enhanced in the second scan as a result of the slow recovery of the GSCC after the first scan. CV data reprinted with permission from ref. 87 (copyright 2004 Wiley-VCH)

SAMs on Nanoparticles

SAMs of bistable mechanical switches have also been actuated on the surfaces (**Figure 6.58**) of various nanoparticles, including Au, Pt, Pd, and TiO_2 nanoparticles,[611,612] as well as gold nanodiscs.[94] The gold nanoparticle platform coated with molecular switches **C637**$^{4+}$ and **R6158**$^{4+}$ has proven[96,612] to be a versatile method for probing the effect of physical environment on switching behavior, since the diameter of the nanoparticles—and thereby the curvature of the surface—as well as the surface coverage can be tuned precisely. The general trend observed for **R6158**$^{4+}$ is that the MSCC → GSCC recovery time scales with the diameter of the nanoparticle—faster recovery at larger diameters—with correspondingly higher activation barriers $\Delta G^{\ddagger}$ at smaller diameters. Surprisingly, the percent coverage of switches on the

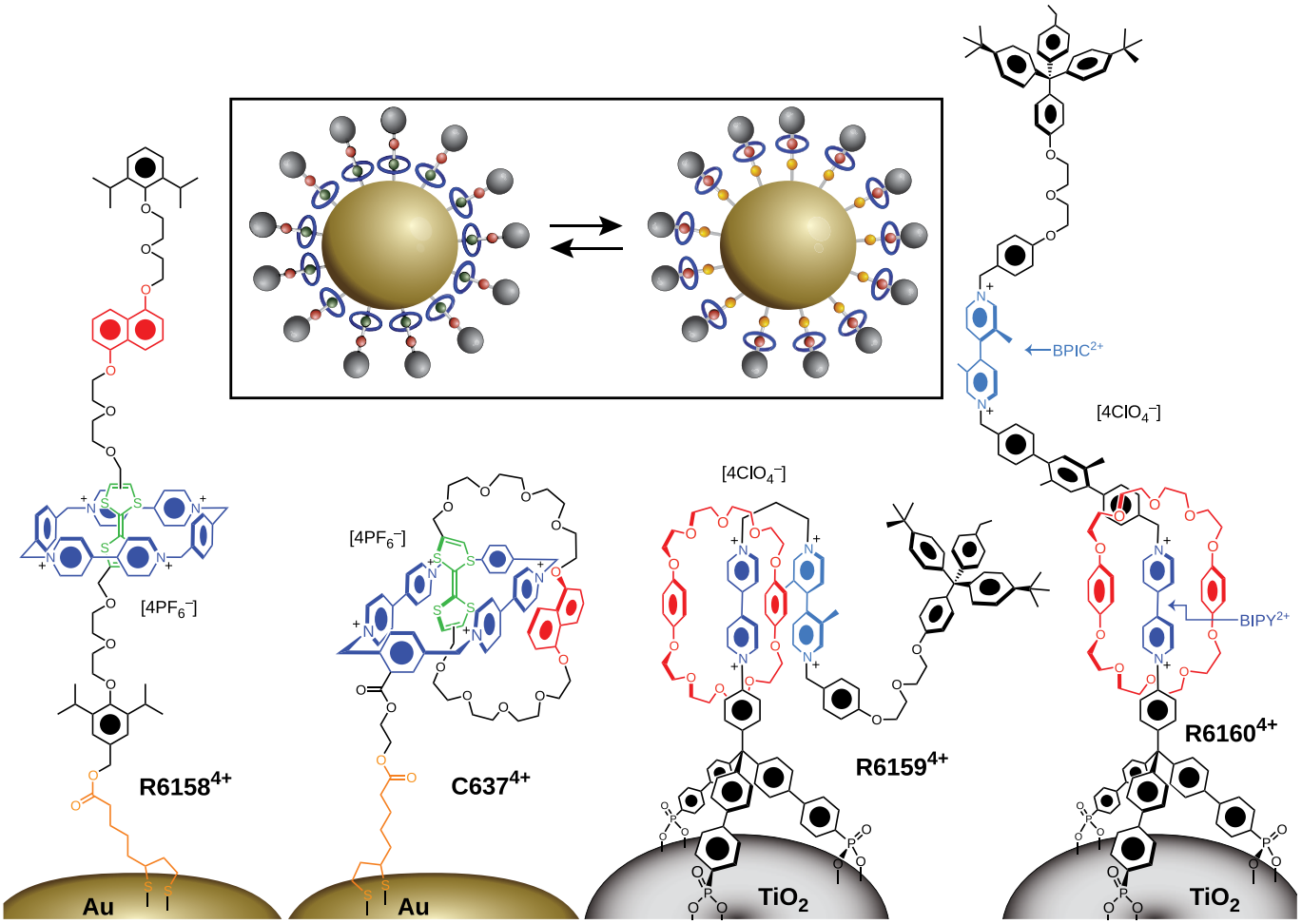


Figure 6.58 Bistable donor-acceptor switches that have been actuated at the surface of various nanoparticles.[96,611–613]

nanoparticle has a relatively insignificant effect on the kinetics, at least for coverage fractions $c \leq 0.50$. With $\Delta G^{\ddagger}$ values ranging from 14–16 kcal·mol^{-1}, however, the switches on these spherical nanoparticles are no less restricted by the environment than their freely diffusing counterparts in solution—see **Table 6.7** in **Section 6.14.1.3**. One might point to the many degrees of freedom allowed by either the reduced surface coverage or the highly curved surfaces of the nanoparticles to explain the low activation barriers in these particular SAMs.

Monolayers on TiO_2

Fitzmaurice[611,613] has reported on a different class of nanoparticles with bistable rotaxanes immobilized (**Figure 6.58**) at the surface—namely, TiO_2 nanoparticles and the molecular switches **R6159**$^{4+}$ and **R6160**$^{4+}$ based on crown ether/BIPY^{2+} recognition motifs akin to those of **R605**$^{6+}$—see **Scheme 6.4** in **Section 6.1.1**. The switchability of **R6159**$^{4+}$ has been verified electrochemically. The transfer of electrons from the conduction band of the TiO_2 nanoparticles leads to the stepwise reduction of the bipyridinium subunits, causing the crown ether to translate along the dumbbell. In contrast with **R605**$^{6+}$, however, the ring only translocates after the second reduction of BIPY^{2+} (BIPY^{2+} → BIPY$^{\bullet+}$ → BIPY) has taken place. Surprisingly, the crown ether never shuttles on the analogous bistable rotaxane **R6160**$^{4+}$, which differs only in its rigid spacer separating the BIPY^{2+} (blue) and BPIC^{2+} (purple) units, despite prior studies[614] showing that the ring shuttles after the first BIPY^{2+} reduction in solution. These differences in behavior have been attributed to a number of factors that change with the flexibility of the spacer that bridges the BIPY^{2+} and BPIC^{2+} units—the flexible bridge in **R6159**$^{4+}$ allows the dumbbell to fold onto itself, such that BIPY^{2+} and BPIC^{2+} are roughly equidistant to the TiO_2 surface, whereas the rigid spacer in **R6160**$^{4+}$ may disrupt folding. Thus, the more rigid dumbbell traverses the largest gradient of potential in the electric double-layer that extends outward from the nanoparticle, which raises the activation barrier to shuttling. Overall, these SAM-nanoparticle results indicate that solution-state switching mechanisms are not always translatable to condensed phases as they have been in the case of the MIM-based molecular switches embedded in MSTJs.

Graphitic Monolayers

The photo-driven [2]rotaxanes that rely on radical–radical interactions in the so-called radical-state co-conformation[c] (RSCC)—see **Section 6.1**—have been actuated[615] (**Figure 6.59**) on graphene surfaces in interface-engineered devices. Monolayers of redox-bistable [2]rotaxanes were deposited (**Figure 6.59a**) non-covalently on high-quality graphene-coated Si/SiO_2 surfaces in between Au source and drain electrodes in a microfluidic device. The co-constitution of the rotaxane is very similar to that (**Scheme 6.22** in **Section 6.2.1.2**) of the [2]rotaxane **R625**$^{6+}$, except that it possesses a longer linker and a pyrenebutyric acid appendage that recognizes and binds the graphene surface. By delivering TEOA as a sacrificial electron donor to the interface through an irradiated microfluidic channel, the rotaxanes immobilized in these devices are converted into the corresponding trisradical trications in which the $BIPY^{\bullet+} \subset CBPQT^{2(\bullet+)}$ interaction defines the RSCC. The population of the RSCC changes the conductance of the underlying graphene sheet as a result of differences in the local electric field and electronic structure near the graphene surface. The source-drain current (I_D) exhibits (**Figure 6.59b**) reversible changes in amplitude (~12%) as the rotaxane monolayer is actuated between the GSCC and RSCC. Photoreduction of dumbbell-only controls in the same device architecture exhibit conductance changes of <3%, suggesting that the translational motions of mechanically bonded rings play an important role in the device operation. Both the forward and backward processes occur with rate constants of approximately 8×10^{-3} s^{-1}. The two conductance states of the GSCC and RSCC are stable for prolonged periods of time under oxidative and reductive conditions, respectively. These devices have also been employed in logic operations—see **Section 6.15.1.4**—which utilize TEOA and light as inputs and I_D values as outputs.

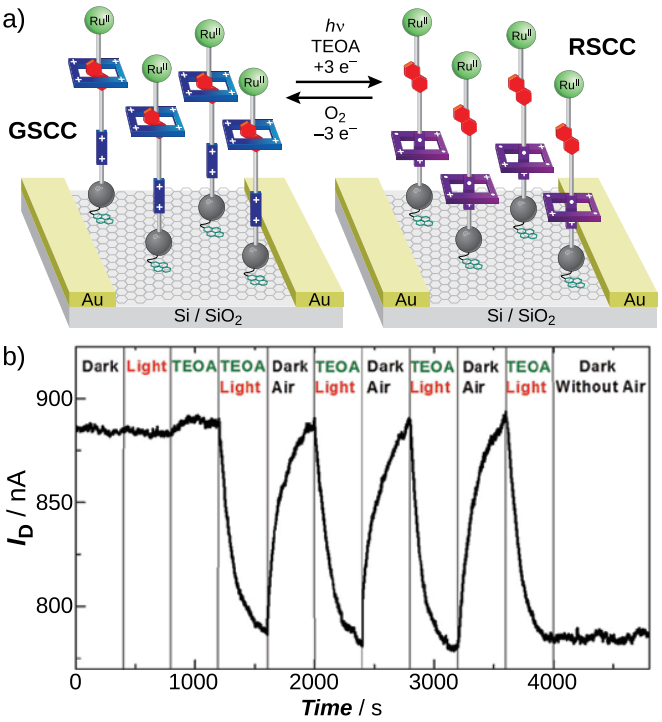


Figure 6.59 Photosensitized switching of redox-bistable [2]rotaxanes in graphitic monolayer devices.[615] (a) Graphical representation of the light-driven actuation of [2]rotaxanes adsorbed on high-quality graphene sheets in between Au source and drain electrodes on a Si/SiO_2 substrate. (b) A plot of the source-drain current (I_D) versus time under various conditions shows a reversible ~12% decrease in current when the RSCC is populated under illumination in the presence of TEOA, and that this state is stable in the dark when isolated from air. The GSCC is recovered by exposure to atmospheric O_2 in the dark. Data reproduced with permission from ref. 615 (copyright 2013 Wiley).

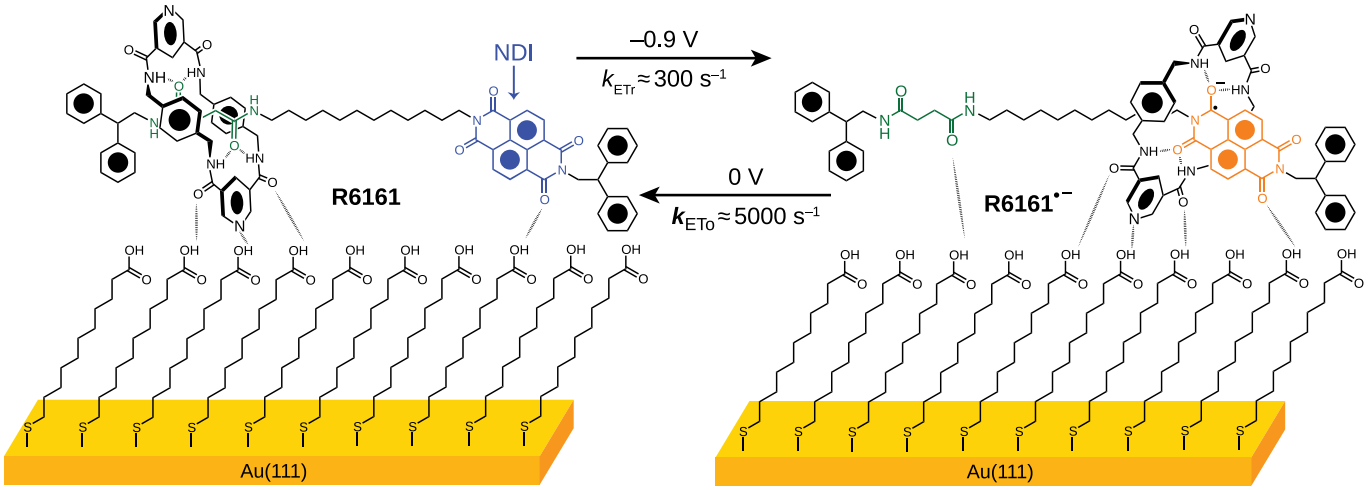
Phsyisorbed Monolayers

Leigh[169,170] has investigated the condensed-phase redox switching properties of the hydrogen-bonded [2]rotaxane **R6161**, which incorporates 3,5-dicarboxamidopyridine recognition units in its benzylic amide ring. The pyridyl moieties enhance the hydrogen bond accepting capabilities of **R6161**, assisting in its deposition on a mercaptoundecanoic acid Au(111) SAM by means of hydrogen-bonding interactions. The relatively low first reduction potential of NDI allowed electrochemical actuation (**Scheme 6.110**) between **R6161** and **R6161**$^{\bullet-}$ on the surface without compromising the SAM. The electron transfer rates to NDI were slow, as expected on account of the presence of long insulating alkanethiol chains. A difference in electron transfer rates between the reduction step ($k_{ETr} \approx 300\ s^{-1}$ as determined by DPSC) and the re-oxidation step ($k_{ETo} \approx 5000\ s^{-1}$ for $^2/_3$ of the population of **R6161**$^{\bullet-}$ in which the ring encircles NDI) provide strong evidence that the **R6161** switches can be actuated on the SAM and also that its distribution is similar to that of **R6161** in solution. Remarkably, the ring shuttling events appear to keep pace with the electron transfer, with the switches reaching their equilibrium distributions within the timescale of the redox steps.

6.14.1.3 Redox Switching in High Viscosity Fluids

The results we have evaluated so far not only fuel the hopes and expectations that molecular switches might be put to good use in technology, but also raise questions about which properties of the switches are conserved when they are transitioned from their well-studied solvated phases into new condensed-phase environments. One important consideration in condensed phases is the increasing contribution of "friction", i.e., resistive forces against motion, which are manifest as fluid viscosity.

[c] Although "co-conformation" is typically employed when comparing the geometries of isomeric compounds, we note that the radical-state co-conformation is not isomeric with the ground-state co-conformation on account of their different redox states.



Scheme 6.110 Electrochemical actuation of **R6161** on a mercaptoundecanoic acid SAM.[170]

It stands to reason, therefore, that a high viscosity liquid phase could be an appropriate setting for mapping how the thermodynamic landscape changes as molecular switches are brought into condensed phases. To this end, investigations[63,83] on several donor-acceptor mechanomolecules have been carried out in a viscous polymethylmethacrylate (PMMA) polymer gel matrix comprising 70:7:20:3 (w:w:w:w) MeCN/PMMA/propylene carbonate/$LiClO_4$. While this polymer matrix can be viewed as a solvent, its viscosity exceeds that of typical organic solvents (MeCN, for example) by approximately four orders of magnitude, and therefore represents an intermediate between solution and solid-state environments.

Intuitively, one would expect the kinetics of switching to slow down with increasing viscosity, and indeed this is the case. The body of work[616–618] on unimolecular reaction rates suggests that the rate of recovery of the GSCC after populating the MSCC should be reduced by two or three orders of magnitude in the polymer matrix relative to that observed for solution-phase switches. **Table 6.7** summarizes the effect of the physical environment on the switching kinetics of a handful of electrochemically switchable bistable catenanes and rotaxanes. It is immediately clear that the polymer matrix—in common with other condensed phases—slows down the recovery of the GSCC from the MSCC, although the rates are only reduced by about one order of magnitude relative to those associated with solution-state switching. In rotaxane **R6162**$^{4+}$, for example, the polymer matrix slows the rate of GSCC recovery from 8 to 0.3 s^{-1}, corresponding to about a 2 kcal · mol^{-1} difference in activation energy.[63] The MSTJ switches, on the other hand, appear to relax at a rate that is at least another order of magnitude slower than those in a polymer matrix, as observed[83] in the cases of **R660**$^{4+}$ and **R6153**$^{4+}$, with their rate constants on the order of 10^{-4} s^{-1}.

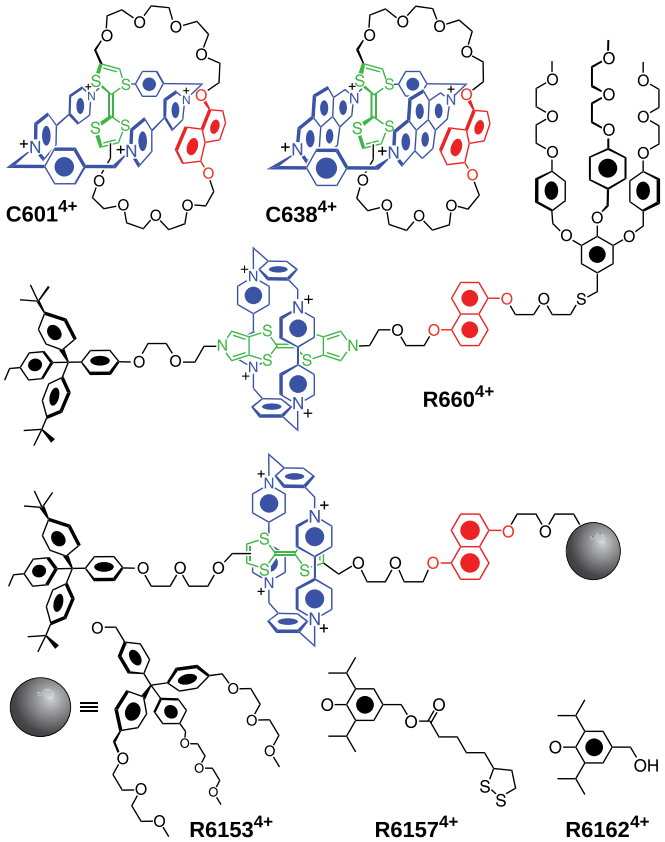
It is important to note that the strength of the noncovalent bonding interactions and steric constraints inherent to the switches also play a crucial role in the thermodynamics[30] and kinetics[33] of switching. Comparing **C638**$^{4+}$ with **C601**$^{4+}$, for example, it is evident that the viscous polymer environment has a much more dramatic effect on the "stickier" and more sterically encumbered catenane **C638**$^{4+}$ than **C601**$^{4+}$, on account of the use of diazopyrenium (DAP^{2+}) π-accepting recognition units instead of $BIPY^{2+}$ ones in the tetracationic cyclophane of the former. With the exception of **C601**$^{4+}$, the condensed phase environments appear to raise the activation barrier $\Delta G_{298}^{\ddagger}$ by ~2 kcal · mol^{-1} or more, which has a dramatic impact on the kinetics governing the recovery of the ground state distribution.

6.14.1.4 Single-Molecule Redox Switching

On the single-molecule size scale, STM is a tool that covers every need at once. It can be used both to deliver an electrical or mechanical stimulus and to detect the result subsequently. STM has been employed to drive[619] a variety of molecular machines, including those based on mechanical bonds. Indeed, electrochemical STM has led to the direct *in situ* observation[97,114] of electrochemically induced ring translation in bistable rotaxanes.

Gao[114] has performed a series of STM experiments (**Figure 6.60**) at 77 K on isolated molecules of rotaxane **R6155b**$^{4+}$, the stereoformula of which is illustrated in **Figure 6.52**, **Section 6.14.1.1**. Current-Voltage (*I*–*V*) curves (**Figure 6.60b**) were recorded by employing an STM tip as an electrode for probing the conductance switching of an isolated molecule of **R6155b**$^{4+}$ physisorbed on top of a CH_2Cl_2 SAM on gold. The physisorbed bistable rotaxanes can adopt a variety of (co)conformations atop a CH_2Cl_2 SAM, since their images (**Figure 6.60a**) as visualized by STM come in at least 25 varieties. Only about two-thirds of the **R6155b**$^{4+}$ molecules that were probed exhibited conductance switching. It is not yet clear exactly to what extent the different (co)conformations affect the probability of successful switching. Among the molecules that do switch their conductivity under the applied bias of the STM tip, it is clear that electron tunneling occurs through the entire molecule, since nearly identical *I*–*V* responses are observed (**Figure 6.60b**)

Table 6.7 The activation barriers ($\Delta G^{\ddagger}$), rate constants (k), and half-lives (t) for the MSCC → GSCC recovery in various tetracationic donor-acceptor MIMs as their PF_6^- salts at 298 K, following electrochemically-driven population of the MSCC in different physical environments.[63,83,87]



		MSCC → GSCC			
MIM	**Environment**[a]	$\Delta G^{\ddagger}$ kcal·mol^{-1}	k s^{-1}	τ s	**Ref**
C601^{4+}	Solution	16.7	4.1	0.24	63
C601^{4+}	Gel	17.0	1.6	0.6	63
C638^{4+}	Solution	19.2	0.057	17.5	63
C638^{4+}	Gel	21.0	0.0013	800	63
R660^{4+}	Solution	17.69	0.69	1.26	83
R660^{4+}	Gel	19.15	0.059	10.2	83
R660^{4+}	MSTJ	21.7	.00084	624	83
R6153^{4+}	MSTJ	22.21	.00031	3250	83
R6162^{4+}	Solution	16.2	8.11	0.123	63
R6162^{4+}	Gel	18.1	0.286	3.5	63
R6157^{4+}	SAM	18.0	0.39	2.56	87

[a]Physical environments: Solution = 100 mM NBu_4PF_6 in MeCN. Gel = MeCN, polymethylmethacrylate, propylene carbonate, $LiClO_4$ (70:7:20:3 w:w:w:w). SAM = self-assembled monolayer, 0.25 molecules/nm^2, 50 mM $LiClO_4$ in MeCN. MSTJ = molecular switch tunnel junction, bottom electrode n-type polySi (5 μm width), top electrode Ti/Al (10 μm width).

when scanning at different points on the molecule. Importantly, this work also suggests that conductance switching is caused by the translation of the CBPQT^{4+} ring between its two recognition sites, since changes in conductance are typically accompanied by reproducible changes in molecular shape as visualized by STM.

Another single-molecule investigation (**Figure 6.61**) carried out by our group in a collaboration with Paul Weiss[97] at UCLA involved rotaxanes that were tethered (**Figure 6.61a**) directly onto a gold surface. The dumbbell of the bistable [2]rotaxane **R6163^{4+}** was equipped with disulfide groups on its stoppers for attachment to an Au(111) surface via thiolate-gold bonds. In the STM images (**Figure 6.61b–e**) the CBPQT^{4+} rings appeared as protrusions. By applying an electrode potential of +530 mV during the scan—sufficient to oxidize TTF—significant displacements of the CBPQT^{4+} protrusions were observed. These displacements were reversed when the scanning potential was reduced to +120 mV in order to reinstate the neutral state of TTF, suggesting the return of the rings to the TTF sites. No CBPQT^{4+} ring displacements were observed at +120 mV when the initial +530 mV potential was omitted, lending

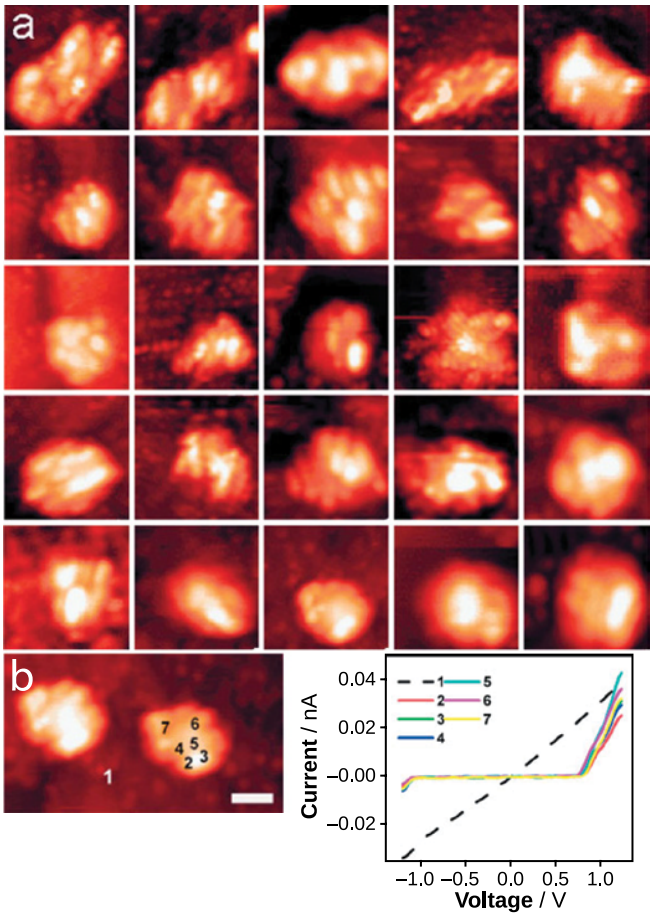


Figure 6.60 Single-molecule studies on rotaxane **R6155b^{4+}**.[114] (a) STM images of 25 (co)conformations of **R6155b^{4+}** physisorbed on a CH_2Cl_2 SAM on gold. (b) Scanning tunneling spectroscopy (current–voltage curves), comparing the response of the bare substrate (line 1) with scans of the rotaxane probed at different sites on the molecule (lines 2–7). The accompanying image shows the location of each scan (scale bar: 2 nm). Reprinted with permission from ref. 114, copyright 2007 Wiley-VCH.

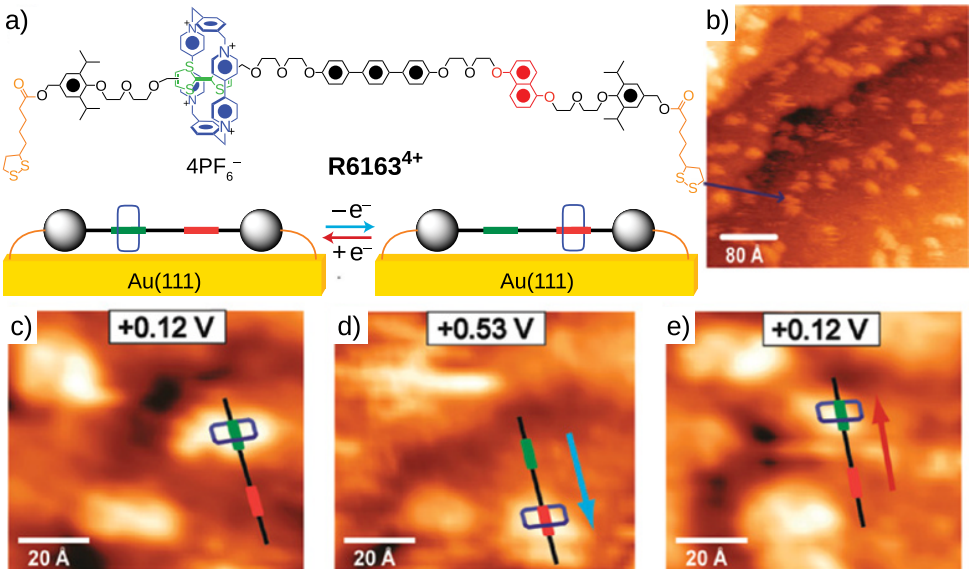


Figure 6.61 Switching individual bistable rotaxanes with an STM tip.[97] (a) Structure of a bistable [2]rotaxane **R6163**$^{4+}$ anchored to an Au(111) surface. (b) Protrusions in the STM image are assigned to the (blue) CBPQT^{4+} rings. (c) An individual rotaxane molecule is shown as the ring encircles the green TTF recognition station. (d) When a bias of +530 mV is applied through the STM tip, TTF is oxidized to its radical cation (TTF$^{+\cdot}$) and the CBPQT^{4+} ring migrates in the direction of the blue arrow. (e) On returning TTF to neutrality, the CBPQT^{4+} ring migrates to the TTF site, moving in the direction of the red arrow. Images in (b)–(d) reprinted from ref [97], Copyright 2010 American Chemical Society.

support to the same general switching mechanism observed in solution and other condensed phases. Although a range of displacements was observed, a mean displacement of 2.0 nm was determined by statistical anaylsis. This value is in remarkably good agreement with the XPS measurements[86] on the nearly isostructural [2]rotaxane **R6154**$^{4+}$, but lower than the 3.5 nm displacement that would be expected in a situation where the dumbbell is fully extended. These experiments corroborate intuition, pointing to the idea that this class of bistable rotaxanes tends to adopt folded, rather than linear and extended, (co-)conformations.

6.14.2 Condensed-Phase Photoswitches

A few of the photoswitchable motifs described in **Section 6.2** have been actuated in condensed-phase environments, including surface monolayers (**Section 6.14.2.1**) and high viscosity fluids (**Section 6.14.2.2**).

6.14.2.1 Photoswitching in Surface Monolayers

Willner[620] has investigated the photoswitchable rotaxane **R6164** based on azobenzene and a Fc-functionalized α-CD ring on the surface of a gold electrode and its effect on electron transfer (ET) rates. ET from Fc to the Au electrode was determined by chronoamperometry to proceed (**Figure 6.62**) at approximately one-fifth the rate in **(*Z*)-R6164** compared with that in **(*E*)-R6164**. Thus, it has been shown that the predictable, light-controlled mechanical movements in this class of rotaxanes can be used to tune the distance of the ring from a surface.

Zhao[621] has constructed azobenzene/α-CD [3]catenanes by immobilizing both ends of the corresponding dithiolane-terminated, Pd^{II}-bridged [3]pseudorotaxane precursors onto the surfaces of AuNPs—see **Section 3.11**. Although it was verified spectroscopically that the azobenzene units

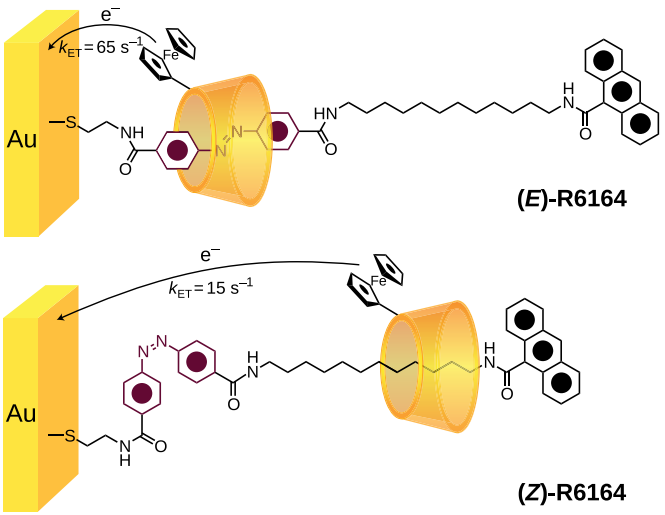


Figure 6.62 The photochemical actuation[620] of an azobenzene unit in rotaxane **(*E*/*Z*)-R6164** controls the distance between the redox-active ferrocene unit of the α-CD ring and the Au electrode to which the dumbbell is attached by means of a thiolate linkage. This distance dependence is detected in the form of different electron transfer rates (k_{ET}) for the (*E*) and (*Z*) isomers in the monolayer.

undergo (*E*)/(*Z*) photoisomerization under UV irradiation, the direction of ring movement and the extent to which the different isomers are populated in the photostationary state have not been characterized in detail. Two possible co-conformations of **(*EE*)-C639**$^{4+}$ and **(*ZZ*)-C639**$^{4+}$ are illustrated in **Figure 6.63**.

We note that Leigh[241] has also actuated photoswitchable [2]rotaxanes physisorbed on surfaces and exploited the resulting changes in the solvophobicity of the surface to drive the transport of a macroscopic droplet with light. See **Figure 1.36** and the corresponding discussion in **Section 1.3.6**.

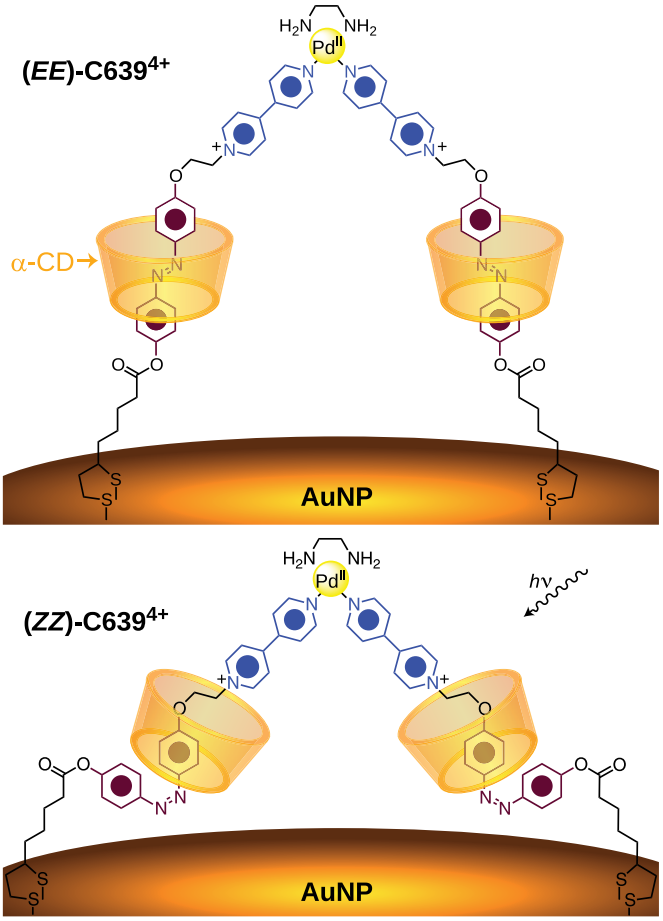


Figure 6.63 Illustrations of two possible co-conformations of the self-assembled [3]catenane **C639**$^{4+}$ adsorbed on AuNPs as the (*EE*) and (*ZZ*) isomers.[621]

6.14.2.2 *Photoswitching in High Viscosity Fluids*

Since a predictable logarithmic relationship exists between the concentration of poly(methylacrylonitrile) (PMAN) and viscosity, Leigh and Brouwer[206] have investigated (**Table 6.8**) the relationship between viscosity and the photosensitized shuttling rates in the benzylic amide [2]rotaxane **R620** in PMAN–MeCN and PMAN–PrCN solutions. The photocontrolled ring shuttling in **R620** is described in **Scheme 6.23**, **Section 6.2.1.2**. The forward shuttling rates remain remarkably fast over a viscosity range spanning seven orders of magnitude, reaching only as low as ~$10^4\,s^{-1}$ in the most viscous (1250 Pa·s) solutions. Even the slowest among these rates are many orders of magnitude faster than the π-donor/π-acceptor switches described in **Table 6.7** (**Section 6.14.1.3**), even in low viscosity solutions.

6.14.3 Condensed-Phase Chemical Switches

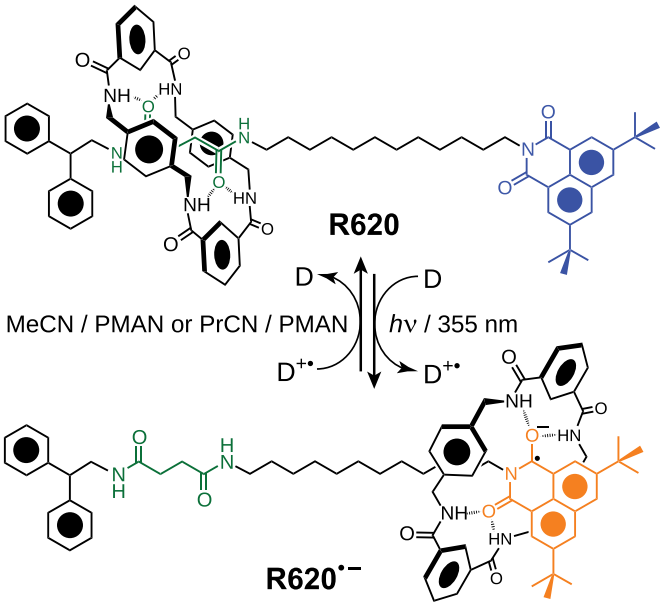
Aside from redox and photoswitches, mechanomolecules have been actuated in condensed phases by other chemical stimuli, including acids and bases (**Section 6.14.3.1**), ions (**Section 6.14.3.2**), and solvent (**Section 6.14.3.3**).

6.14.3.1 *Condensed-Phase Acid/Base Switching*

The acid/base switchable [2]rotaxane[48,282] **R637**$^{2+}$/**R637H**$^{3+}$—see **Table 6.2** in **Section 6.3.3.1**—can be organized in LB monolayers and multilayers, where the rotaxanes can still be switched by exposure[283] to HCl and NH_3 vapor.

Qu[622] has immobilized bistable dialkylammonium/crown ether molecular shuttles on the surfaces of SiO_2 nanoparticles using click chemistry and demonstrated that their acid- and base-triggered ring translations are accompanied by visible changes (**Figure 6.64**) in the fluorescence output (λ_{em} = 521 nm) of a 4-morpholinonaphthalimide stopper, owing to the distance-dependent quenching effect of Fc groups appended to the DB24C8 ring. The acid/base switching of compounds **R6165**$^{+}$ and **R6165H**$^{2+}$ with TFA and DBU, respectively, operates analogously to other rotaxane switches possessing dialkylammonium and *N*-methyltriazolium recognition sites for DB24C8—see

Table 6.8 The effect[206] of viscosity and solvent on the shuttling rates of **R620**: rate constants of photoinduced shuttling in solutions of poly(methylacrylonitrile) (PMAN) in MeCN and PrCN.



Solvent	% PMAN	MW PMAN	Viscosity (η) Pa·s	k_f/s^{-1}
MeCN	0	-	0.00064	1.3×10^6
	5	50	.0018	9.0×10^5
	5	460	.065	7.2×10^5
	15	50	.014	7.2×10^5
	15	460	0.5	3.8×10^5
	33	50	0.59	3.4×10^5
	33	460	1250	$<1\times10^4$
PrCN	0	-	0.00089	2.9×10^5
	5	50	.0032	1.5×10^5
	15	50	.032	8.3×10^4
	33	50	2.4	2.0×10^4

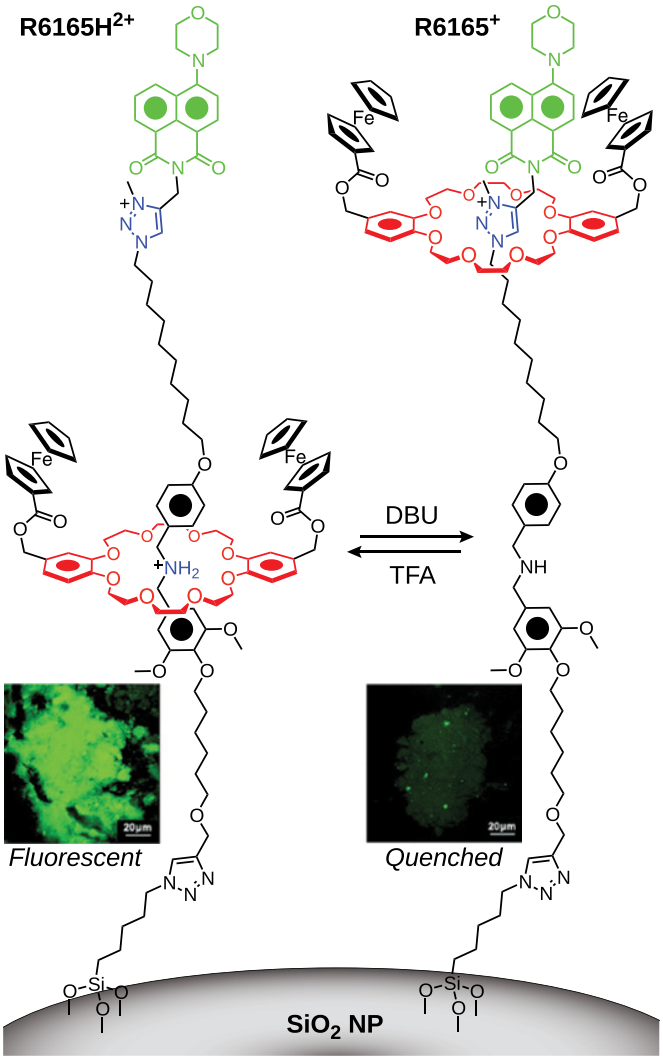


Figure 6.64 The acid/base actuation of Qu's pH-bistable [2]rotaxane **R6165H²⁺/R6165⁺** immobilized on SiO_2 nanoparticles results in substantial changes in the fluorescence of the material (see inset photographs at 20 μm scale), owing to the distance-dependent quenching of the fluorescent naphthalimide stopper by the ferrocene-functionalized DB24C8 rings. Inset photographs of the nanoparticles reprinted with permission from ref. 622 (copyright 2015 Royal Society of Chemistry)

Section 6.3.3.1. The fact that this fluorescence quenching at the SiO_2 interface behaves comparably to that of the same rotaxane in solution confirms that the pH-driven switches can be actuated in condensed phases.

Recently, Camposeo, Credi, and Pisignano[623] have shown that the condensed-phase actuation of pH-switchable dialkylammonium/crown ether [2]pseudorotaxanes influences the internal structure and mechanical properties of a nanofibrous polymer matrix in which they are embedded—see **Section 6.15.1.5** for more examples of switches that influence mechanical properties by means of molecular reorganization.

6.14.3.2 Condensed-Phase Ion Switching

Lin and Kern[624] have found that Sauvage's [2]catenand **C614**—see **Figure 6.11** in **Section 6.4.1.1** for a stereoformula—can be converted (**Figure 6.65**) to the [2]catenate **CuC614⁺** while adsorbed on a Ag(111) surface under ultra high vacuum (UHV) conditions. STM Micrographs (**Figure 6.65a**) of **C614**, as deposited in UHV by organic molecular beam epitaxy, indicate that the [2]catenands form linear chains of dimers, stabilized most likely by π–π stacking interactions among the phenanthroline units. After the *in situ* addition of Cu atoms by electron-beam evaporation, the STM images reveal (**Figure 6.65b**) isolated molecules, which can be attributed to the corresponding [2]catenate according to X-ray photoelectron spectroscopy (XPS) measurements that provide evidence for the N–Cu bonds of **CuC614**. The structural change induced by Cu^{I} complexation in this condensed phase is consistent with the dissolution of the chain aggregates of **C614** dimers observed by microscopy, suggesting that it is possible to actuate metallomechanomolecules even in UHV on surfaces.

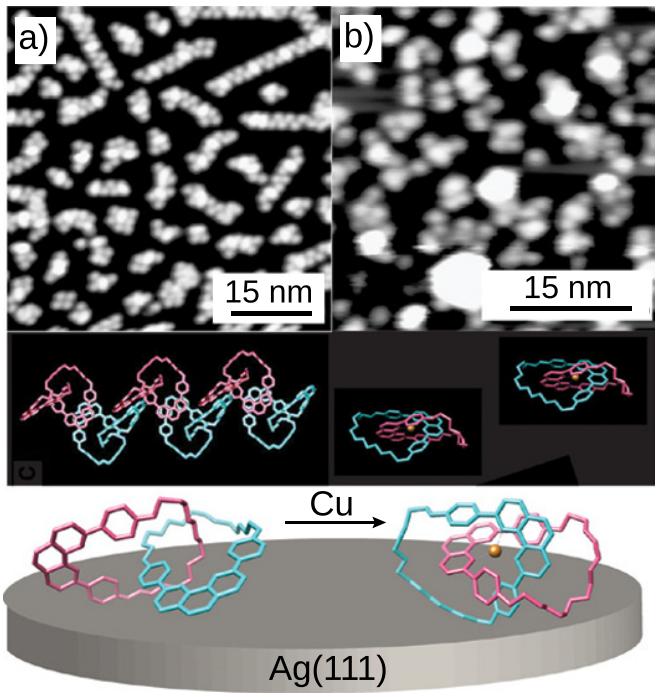


Figure 6.65 Condensed-phase, cation-triggered actuation of metallo-catenanes. A monolayer of (a) the [2]catenand **C614** adsorbed on Ag(111) as linear chains of π–π-stacked dimers can be switched to (b) the [2]catenate **CuC614⁺** as isolated molecules by the *in situ* introduction of Cu by electron-beam evaporation. STM Images reproduced with permission from ref. 624 (copyright 2007 American Chemical Society).

6.14.3.3 Condensed-Phase Solvent Switching

Leigh[475] has investigated the condensed-phase solvent switching properties of the poly(methyl methacrylate)-based poly[2]rotaxane, the side-chain of which shares its

constitution with the [2]rotaxane **R685** in **Scheme 6.81**, **Section 6.8.1**. The polymer **R6166** has been deposited from CH_2Cl_2 onto glass surfaces and actuated by exposing the film to Me_2SO solvent vapors. Since the fluorescence of the rotaxane is "turned on" only where the rotaxanes have undergone translational isomerization as a result of exposure to Me_2SO, fluorescent patterns can be written (**Figure 6.66**) through a vapor mask. Some of these surface patterns are capable of performing logic operations—see **Section 6.15.1.4**.

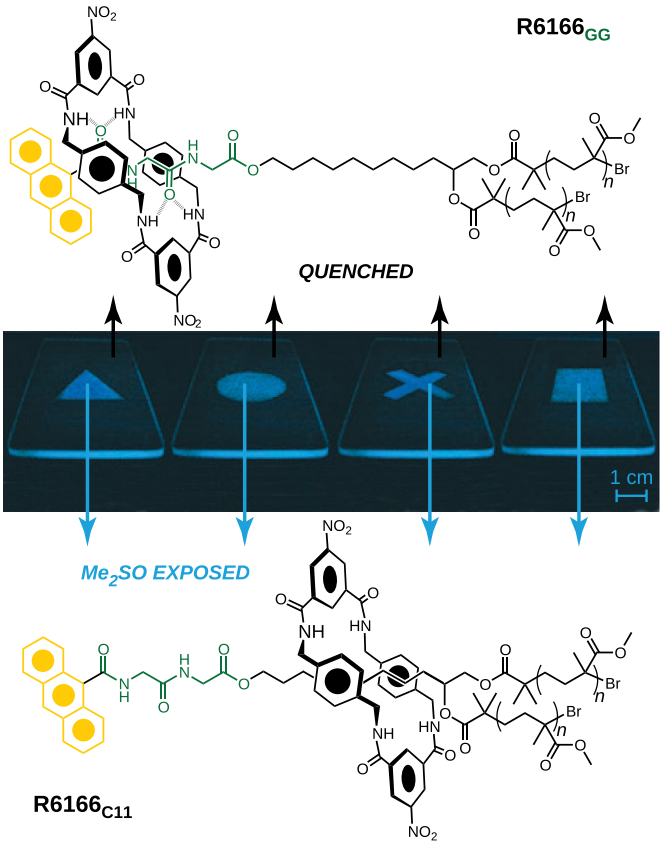


Figure 6.66 Patterned exposure of Me_2SO vapors to thin films of the side-chain poly[2]rotaxane **R6166$_{GG}$** on glass induces translational isomerization to **R6166$_{C11}$** in the solvent-switchable side chains, resulting in an enhancement in fluorescence emission on account of the movement of the fluorescence-quenching ring away from the fluorophoric stopper.[475]

Concluding Remarks

Taken as a whole, the body of research on bistable donor-accceptor MIMs in condensed phases provides convincing evidence that electromechanical switching is achievable in high-friction environments. Moreover, it appears that the same generic switching mechanism—see **Figure 6.2** in the Introduction to this Chapter—is conserved across the various liquid and condensed phases, where the physical environment simply modifies the thermodynamics and more so the kinetics of these processes, especially the relaxation of the MSCC back to the GSCC after an electrochemical stimulus has been applied. There are still more condensed-phase environments on the horizon for these compounds. Recently, bistable [2]rotaxanes have been organized[69] and actuated[98] in liquid crystalline phases. The kinetics and thermodynamics of their switching, however, have yet to be investigated. Another promising arena is that involving metal-organic frameworks, where the dynamics of degenerately bistable mechanomolecules have been investigated[625,626] and non-degenerately bistable switches have been incorporated,[627] but not yet actuated, in these porous molecular crystals. The discoveries collected and lessons learned in this Section will serve as the backdrop for these and other future investigations on molecular switches for many promising potential applications for molecular machinery—see **Section 6.15**.

6.15 Mechanomolecular Motors and Machines

In the previous Sections we have enumerated many mechanically interlocked switches associated with the various recognition motifs and stimuli that have been used to actuate them. Although these switches are remarkable in their own right, it needs to be appreciated that they are not machines in spite of their ability to convert a source of energy into mechanical motion on the molecular scale. Unless that mechanical energy is used to drive a non-spontaneous event, it will simply be lost to the environment as wasted heat. On account of thermal noise, extracting work from machines is not as straightforward in the Brownian world as it is in the macroscopic one. The difference between forces at microscopic and macroscopic length scales is made apparent by Stokes' discovery[628] of the relationship (Equation 6.1) between inertial forces to viscous forces. This ratio of inertial to viscous forces is a dimensionless value known as the Reynolds Number (*Re*), named after Osborne Reynolds[629] who popularized it among others[630]:

$$Re \approx a \cdot n \cdot r \cdot h^{-1} \qquad (6.1)$$

where *a* describes the size of the object on which the inertial and viscous forces act, *n* is its velocity, *r* is fluid density, and *h* is fluid viscosity. Since *h* is the denominator in this relationship, it is clear that viscous forces dominate when the Reynold's number is small ($Re << 1$). Inertia does not matter at low Reynolds number—the motion of objects are determined by the forces exerted on them moment-to-moment rather than by their past trajectories. As Purcell[631] pointed out in his celebrated 1977 lecture on 'Life at Low Reynolds Number', the nano- and microscopic world of biological molecular motors and machines is characterized by this regime. Astumian and Hänggi[5] have put this concept eloquently into perspective:

> *"Consider that the chemical power available to a typical molecular motor, which consumes around 100–1000 molecules of adenosine triphosphate (ATP) per second, is 10^{-16} to 10^{-17} W. In comparison, a molecular*

motor moving through water exchanges about 4×10^{-21} J (the thermal energy kT at room temperature) with its environment in a thermal relaxation time of 10^{-13} s. Thus, a thermal noise power of about 10^{-8} W continually washes back and forth over the molecule. That power, which, according to the second law of thermodynamics cannot be harnessed to perform work, is 8–9 orders of magnitude greater than the power available to drive directed motion. For molecules, moving in a straight line would seem to be as difficult as walking in a hurricane is for us. Nonetheless, molecular motors are able to move, and with almost deterministic precision."

The principle of microscopic reversibility[632] holds that thermal noise fluctuations are always of a symmetrical nature at equilibrium and therefore cannot be utilized to exact work. Energy must be consumed in order to drive molecular machines away from equilibrium, at which point any biased Brownian motions undergone before the system re-equilibrates can be harnessed for work. Chemists engaged in building artificial molecular machines (AMMs) are inspired by the "tricks" that Nature has evolved for the operation of biological molecular machines,[633–640] which rely on the randomness of thermal noise fluctuations to drive their directed motions. In the Brownian world, machines must rely on barriers that prevent backward motion, rather than external forces that push forward motion. Consider the diffrences between macroscopic and molecular machines.

Macroscopic Machines	Molecular Machines
Motions dominated by inertia and gravity	Motions dominated by thermal noise
Motions driven by the application of external forces	Motions driven by the modulation of energy wells and barriers
Far from mechanical equilibrium	Far from thermodynamic equilibrium
Described by classical mechanics	Described by statistical mechanics

In this Section, we focus our attention on AMMs with mechanical bonds.[4,208,641,642] We note, however, that important contributions to the broader field of molecular machines[3,16,571,643–667] have featured many kinds of non-interlocked molecules, such as molecular rotors,[668,669] including those based on sterically crowded alkenes,[670–672] triptycenes,[673,674] (*o*-phenylenedioxy)cyclotriphosphazines,[675] ferrocenes[676,677] and other cyclopentadienyl complexes,[678–680] surface-adsorbed nanocars,[681,682] as well as switches and machines based on azobenzenes,[683–685] stilbenes,[686] diarylethenes,[687,688] hydrazones,[689–691] spiropyrans,[692–694] reversible covalent bonds,[695,696] amphidynamic crystals,[697–700] coordination compounds,[701,702] peptides,[703] and DNA.[704–706]

At the risk of being tautological we stress that the fundamental feature of a molecular machine is that it must be capable of doing work, i.e., to accomplish a non-spontaneous task as energy is transferred from one system to another. We advocate that it is inappropriate to refer to a molecule as a 'machine' or a 'motor' unless this requirement is met. Several strategies can be identified for making synthetic molecules, including those with mechanical bonds, behave as AMMs: (i) coupling and integrating molecular switches with systems (**Section 6.15.1**) that allow them to perform a functional task (mechanical work), (ii) realizing any of the various "ratchet" mechanisms (**Section 6.15.2**) that allow molecular machines to move a system energetically uphill (thermodynamic work), (iii) molecular machines or "assemblers" (**Section 6.15.3**) that consume energy in order to build other molecules (chemical work).

6.15.1 Systems-Coupled Functional Switches

By coupling the mechanical actuation of a mechanically bonded molecular switch with other systems, such as a molecule or a material, it is possible to accomplish a task or perform a function. This concept of systems-coupled switches acting as machines has been realized in the genesis of nanovalves and other rotaxanes that mediate the controlled release (**Section 6.15.1.1**) of dyes, therapeutics, and diagnostic agents, as well as artificial muscle materials (**Section 6.15.1.2**) that bend in response to stimuli, devices that employ mechanomolecular switches in computation and information storage (**Section 6.15.1.3**), and switches that regulate the self-assembly (**Section 6.15.1.4**) of other molecules.

6.15.1.1 Rotaxanes in Controlled Release Applications

One of the most widely investigated potential applications for rotaxanes involves utilizing their stimulus responsiveness in the controlled release of therapeutic and diagnostic agents. These strategies often involve either (i) rotaxane "nanovalves" that regulate the passage of molecules in and out of mesoporous materials, or (ii) rotaxane delivery vehicles that release chemical agents when they are stimulated or degraded by biologically relevant processes.

Rotaxane Nanovalves

The use of mesoporous silica materials[707,708] for the controlled release of molecular cargoes, especially for the purpose of drug delivery,[709–711] has been a rapidly developing technology since the turn of the millennium. In order to be effective as a drug delivery system, mesoporous silica must be modified such that it retains cargo in storage and circulation, yet releases its payload upon reaching its target. One of the most effective strategies (**Figure 6.67**) for controlling release of cargo from mesoporous silica nanoparticles[712–715] (MSNPs) involves decorating their pores with molecular switches that open and close the apertures of the pores by virtue of their controllable mechanical motions. Several reviews[715–722] on these "mechanized" silica

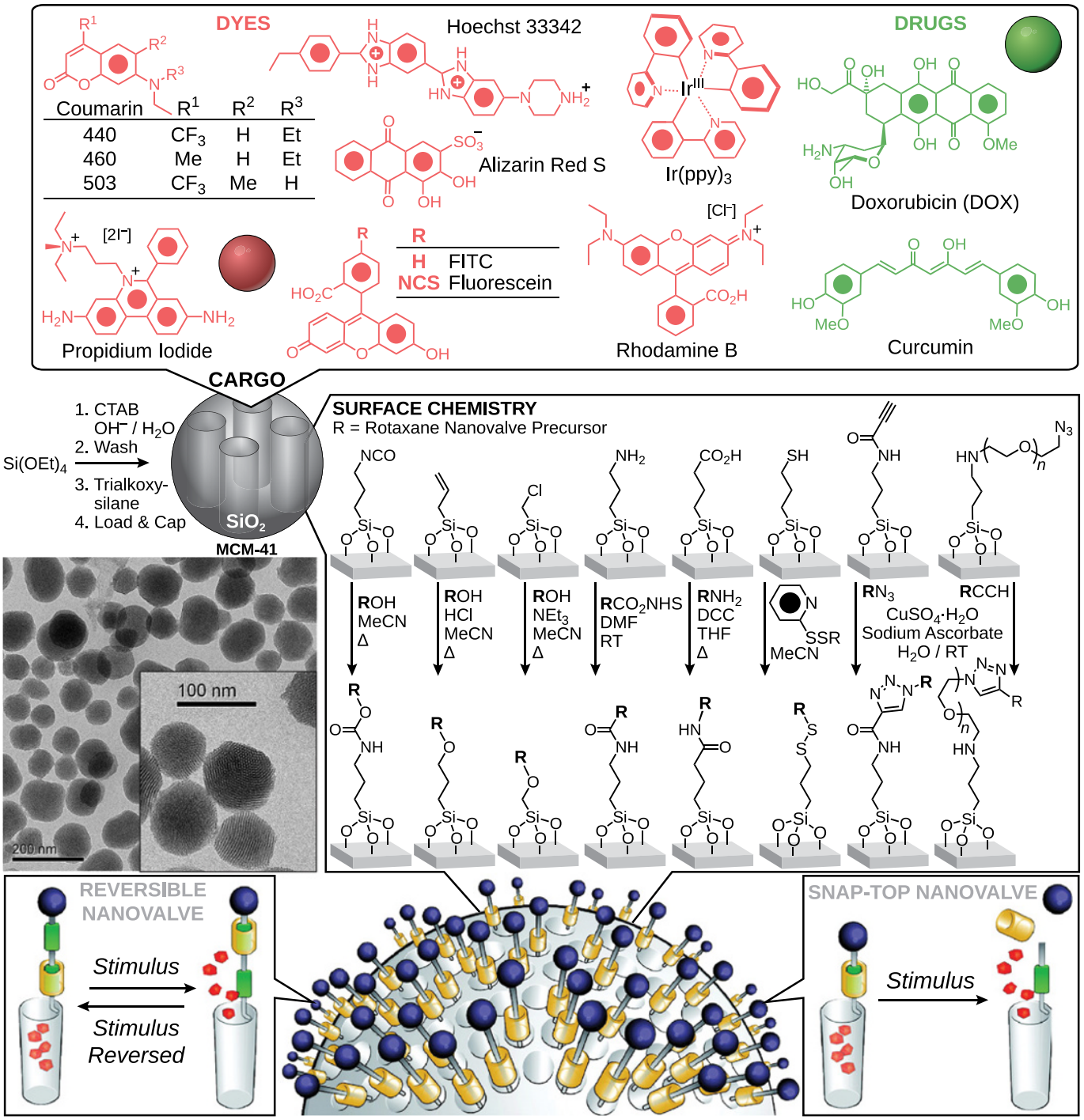


Figure 6.67 An overview of mechanized mesoporous silica nanoparticles (MSNPs) possessing rotaxane nanovalves. The inset TEM image visualizes a typical size distribution of MCM-41, MSNPs of ~2-nm pore width commonly employed as nanocarriers in nanovalve research. The MCM-41 MSNPs can be functionalized with organosilanes possessing reactive groups and loaded with cargo, such as dyes and drugs, before being capped with rotaxane nanovalve precursors by a variety of reactions—e.g., nucleophilic additions and substitutions, peptide coupling, disulfide exchange, and CuAAC click chemistry—at the SiO_2 interface in either aqueous or organic suspensions. The graphical representations (bottom) of mechanized MSNPs illustrate two approaches to controlled cargo release that rely on the mechanical bonds of rotaxanes: (i) reversible nanovalves, which open and close the mesopore apertures by reversible ring-translation motions, and (ii) snap-top nanovalves, which remain closed until they open irreversibly as a result of stimulus-induced bond cleavage.

nanoparticles are available in the literature. In this Section, we focus specifically on mechanically bonded nanovalves,[89,93,221,723–732] which can be further subdivided into reversible switches[89,93,221,723–725] and irreversible "snap-tops".[726–732] The majority of these nanovalves have been mounted on MCM-41 (**Figure 6.67**), an easily functionalized type of MSNP of 100–200 nm diameter with hexagonally arrayed ~2 nm pores templated by cetyl trimethylammonium bromide (CTAB) surfactants, which can be extracted and replaced by nanoscale cargo, such as dyes and drugs. The nanovalves can be localized on SiO_2 within the pores of MCM-41 or only on their exterior surfaces, depending on whether the organosilane functional groups are introduced before or after pore evacuation. When operated successfully, reversible and snap-top nanovalves are considered genuine artificial molecular machines because they consume energy as they undergo mechanical changes that allow them to perform a specific functional task.

Redox-Switchable Reversible Nanovalves

Reversible rotaxane nanovalves were introduced[89,93] in the form (**Figure 6.68**) of the SiO_2-mounted donor-acceptor [2]rotaxane **R6167^{4+}** and its oxidized counterpart **R6167^{6+}**, the ring-and-axle portions of which are identical to the MSTJ switch **R6154^{4+}** (**Section 6.14.1.1**). MCM-41 MSNPs were charged with various dye molecules, including $Ir(ppy)_3$ (ppy = 2-phenylpyridine), coumarin 440 and 460, and rhodamine B. Care must be taken in the surface-mounting step to establish a tight seal and avoid premature release of the cargo, since the smaller coumarin dyes leak from the mechanized MSNPs when the rotaxane linkers are too long.[93] When the sterics of the nanovalves and dyes are appropriately matched, the nanocarriers remain sealed until the nanovalves are opened. For example, a release profile reveals (**Figure 6.68**) that an $Ir(ppy)_3$ dye escapes very slowly from these mechanized MSNPs when the nanovalve is closed (**R6167^{6+}**) under oxidative conditions in the presence of $Fe(ClO_4)_3 \cdot 6H_2O$, yet a rapid increase in emission is observed upon the addition of ascorbic acid, owing to the loss of fluorescence quenching associated with the dye's escape from the MSNP nanopores in the gate-open (**R6167^{4+}**) state. The central terphenylene spacer separating the recognition units of **R6167$^{4+/6+}$** proved to be unnecessary in this case, since a similar bistable donor-acceptor [2]rotaxane lacking this spacer was also effective as a nanovalve. In principle, the dye/drug delivery systems employing reversible nanovalves can be reloaded with cargo in the gate-open state, re-sealed in the gate-closed state, and re-used over and over. Indeed, one batch of these mechanized MSNPs was reloaded with rhodamine B and shown to exhibit the same controlled release profile on the second cycle.

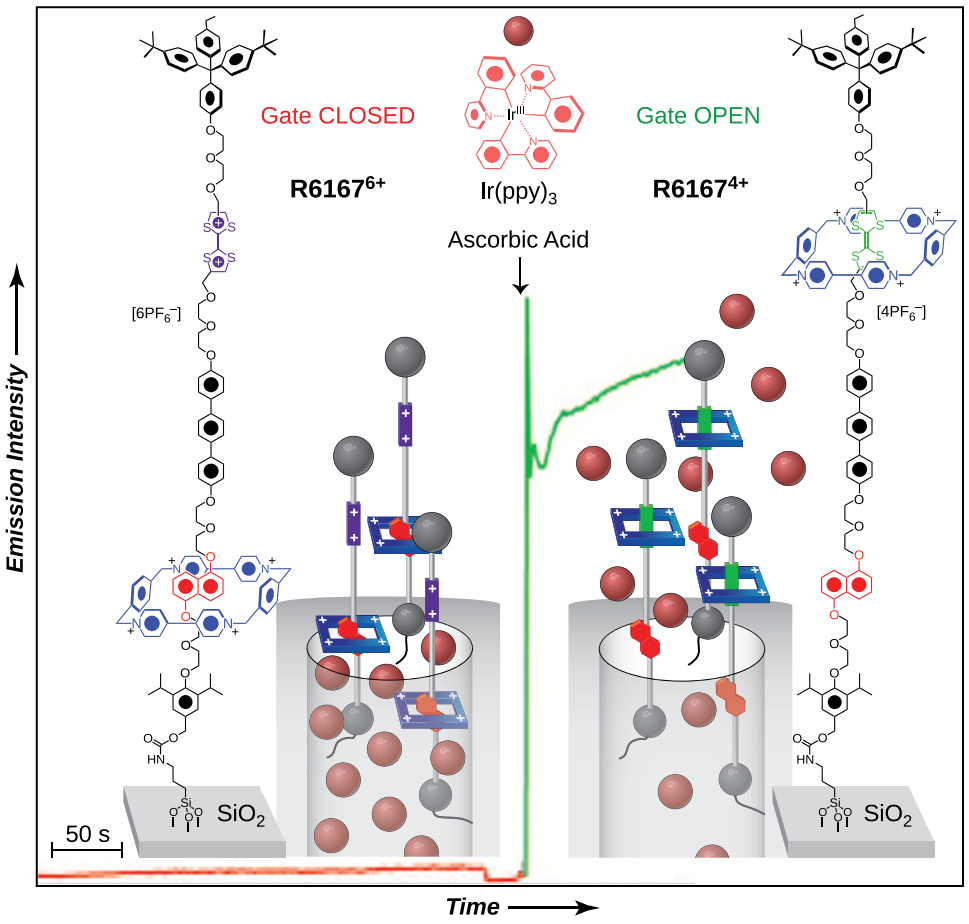


Figure 6.68 Time-resolved release profile of the first mechanized mesoporous silica nanoparticles (MSNPs) employing bistable rotaxanes as reversible nanovalves.[89] In the gate-closed state (red trace), where the oxidized [2]rotaxane **R6167^{6+}** seals the apertures of the MSNPs, the enclosed $Ir(ppy)_3$ cargo is quenched, resulting in low fluorescence emission intensity. When ascorbic acid is added in solution to reduce the nanovalves to the gate-open **R6167^{4+}** (green trace), the movement of the CBPQT^{4+} rings from DNP to TTF recognition units opens up the pore apertures and allows the $Ir(ppy)_3$ cargo to escape, resulting in a sharp increase in fluorescence emission.

Photo-Switchable Reversible Nanovalves

Zhao[221] has utilized (**Figure 6.69**) the thermally and photochemically controlled *cis*-to-*trans* isomerization of an azo dye within the axle of the α-CD [2]rotaxane **R6168**$^{2-}$ as a trigger for MSNP nanovalves. The nanovalves open (**Figure 6.69a**) when the *cis*-azobenzene unit of **(*Z*)-R6168**$^{2-}$ isomerizes under visible irradiation or thermal heating to the corresponding isomer **(*E*)-R6168**$^{2-}$, owing to the translation of the α-CD ring from a triazole unit near the SiO_2 surface in the former to the *trans*-azobenzene unit of the latter. Although photo and thermal stimuli are both effective triggers for opening the nanopores, the release (**Figure 6.69b**) of curcumin dye from these mechanized nanoparticles in aqueous solution (4:1 H_2O/EtOH) is more significant and efficient when heating from 5 to 37 °C than when irradiating with visible light (λ_{ex} = 420 nm) at 5 °C. Since this nanovalve system shows promise for (photo) thermal therapy, a zebrafish embryo model was employed to demonstrate[221] the triggered release of curcumin *in vivo*. The transparency of the zebrafish bodies allows their brains to be visualized (**Figure 6.69c**), such that release of curcumin can be monitored by the decline in curcumin fluorescence as it is metabolized upon release from the MSNPs. The antioxidant properties of cucurmin also render it suitable for treating heart failure, and indeed the stimulated release of cucurmin in this model system improved the cardiac output of zebrafish embryos that had been manipulated to experience heart failure. By immobilizing the same [2]rotaxanes on the surfaces of Au-nanorod–mesoporous silica core-shell hybrid particles, Zhao[723] was able to reconfigure the nanovalves to respond to NIR light, an appealing stimulus on account of its relatively deep tissue penetration. Mechanistically, the isomerization of the azo dye is driven in this case by local heating caused by the plasmonic excitation of the Au nanorods. Using another zebrafish embryo model, the NIR-triggered release of doxorubicin was demonstrated *in vivo*.

Zink[724] has also reported a reversible nanovalve based on the translation of α-CD driven by azobenzene isomerization. The "open" and "closed" states of the [2]rotaxane nanovalve **R6169** run contrary to **R6168**$^{2-}$, since the gate-closed state is the *trans*-azobenzene isomer **(*E*)-R6169**, and the gate-open state is the *cis*- isomer **(*Z*)-R6169**. The α-CD ring encircles the azobenzene unit close to the SiO_2 surface in **(*E*)-R6169**, whereas it associates with an adamantyl stopper far from the surface in **(*Z*)-R6169**. The release profile in **Figure 6.70** demonstrates that fluorescent propidium iodide cargo molecules are liberated from the MCM-41 MSNPs armed with these nanovalves only after the stimulus is applied—namely, irradiation with 403 nm light. **R6169** is a suitable nanovalve in this setting for relatively bulky cargoes (see **Figure 6.67**) such as propidium iodide and Hoechst 33342, while a similar rotaxane lacking a linker in between the azo and adamantyl units serves as an effective nanovalve for smaller cargoes (see **Figure 6.67**) such as Alizarin Red S. Both nanocarrier platforms can be recycled by reloading them with cargo with no observable loss in performance in controlled release on the second cycle. The two photoswitchable nanovalve designs put forward by Zhao (**R6168**$^{2-}$) and Zink (**R6169**) are complementary in their operation, since they are opened and

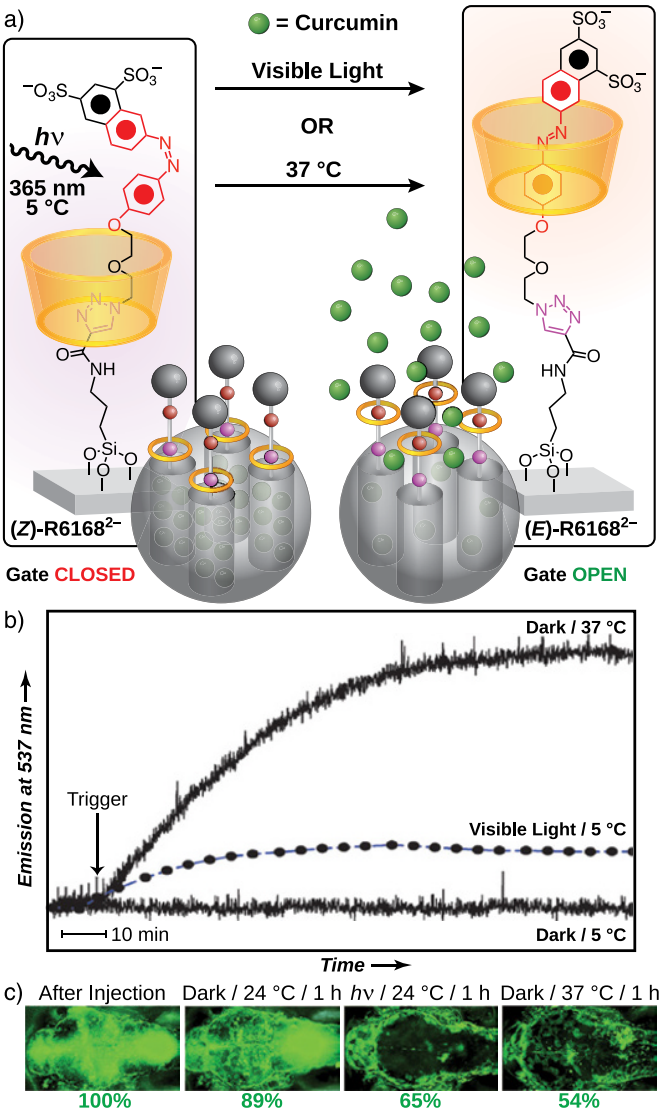


Figure 6.69 Zhao's light- and heat-triggered nanovalves,[221,723] driven by the photothermal isomerization of α-CD encircled azobenzenes. (a) Stereoformulas and graphical representations illustrating how the closed nanovalve **(*Z*)-R6168**$^{2-}$ is converted to the open nanovalve **(*E*)-R6168**$^{2-}$ by visible illumination or thermal heating, allowing cucurmin to release from the SiO_2 nanopores to which they are anchored. (b) Curcumin release profiles in response to visible light illumination at 5 °C, as well as heating at 37 °C, compared to a control at 5 °C in the dark. (c) Fluorescence images and relative intensities of emission (%) in zebrafish brains injected with the curcumin-loaded MSNPs gated with **(Z)-R6168**$^{2-}$ reveal that the release of curcumin is more efficient *in vivo* when photo or thermal stimuli (right-hand side) are applied to open the nanovalves, compared to controls (left-hand side) in the dark. Losses in fluorescence intensity are indicative of drug release because these losses are attributable to the metabolic breakdown of curcumin, which most likely occurs only when curcumin is liberated from the nanopores. Data reproduced with permission from ref. 221 (copyright 2012 Wiley)

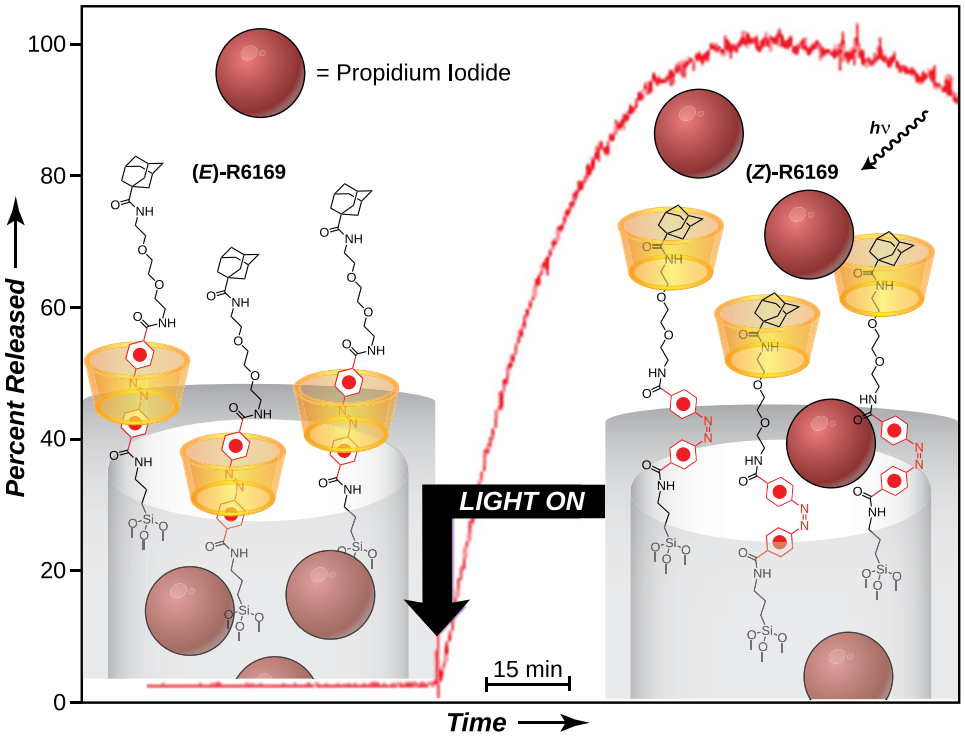


Figure 6.70 Time-resolved release profile of mechanized MSNPs decorated with photoswitchable reversible nanovalves.[724] In the gate-closed state, the α-CD rings encircle the *trans*-azobenzene unit of **(*E*)-R6169**. Illumination of the sample with UV light (λ = 403 nm) populates the gate-open photostationary state, in which propidium iodide cargo is released from the MSNP as a result of the translocation of the ring to an adamantyl stopper in **(*Z*)-R6169**. Data reproduced with permission from ref. 724 (copyright 2014 American Chemical Society)

closed by opposing stimuli and control the relase of a wide range of nanoscale cargoes.

Recently, Berná[725] has contributed the first rotaxane nanovalves based on the benzylic amide recognition motif to the field of mechanized MSNPs. The operation (**Figure 6.71**) of these controlled-release nanocarriers relies on the photostimulated actuation of the MSNP-mounted [2]rotaxane **R6170**. Whereas the benzylic isophthalamide ring encircles a fumaramide recognition unit near the stopper of the nanovalve in the GSCC of **(*E*)-R6170**, the ring encircles a glycylglycine unit near the SiO_2 surface after the photoactive fumaramide unit has been isomerized to the maleamide unit of **(*Z*)-R6170** under UV irradiation at 254 nm wavelength. This gate-closed state can be reset to the gate-open state by restoring the fumaramide recognition unit under irradiation at λ = 365 nm. The release profiles (**Figure 6.71**) of these mechanized MSNPs loaded with rhodamine B reveal that the "closed" nanovalves **(*Z*)-R6170** act as successful gatekeepers in both CH_2Cl_2 and H_2O, since leakage is not observed for at least 10 min before the light is turned on to "open" them. The cargo release is more significant and rapid in CH_2Cl_2 on account of the higher positional discrimination of the ring in this solvent, since the hydrophobic oligomethylene linker of the axle acts as another recognition unit in H_2O. Nevertheless, the slow-release profile of **(*E*/*Z*)-R6170** in H_2O is desirable for potential delivery applications involving highly potent and/or short half-life drugs.

Enzyme-Triggered Snap-Top Nanovalves

Snap-top nanovalves (**Figure 6.72**) are rotaxanes that undergo bond cleavage in order to release cargo from the nanopores of mechanized MSNPs. The snap-tops are typically designed in such a way that the cleavage event is mediated by a biological signal, such as enzymes and other biomolecules overexpressed in cancer cells, which are relevant to drug delivery applications. The seminal work[726] on this particular type of molecular machinery involved the cleavage of an adamantyl ester stopper from the α-CD rotaxane **R6171** by an esterase. The design and release profile for this system are summarized in **Figure 1.37** and the accompanying discussion in **Section 1.3.6**. More recently, He[727] has designed the α-CD snap-top nanovalve **R6172** possessing a tumor-targeting $GFLGR_7RGDS$ peptide stopper, the GFLG sequence of which is hydrolyzed by cathepsin B, an enzyme overexpressed in the lysozomes of tumor cells. The corresponding nanocarriers have been found to selectively target and enter tumor cells, courtesy of the RGDS peptide sequence that targets integrin receptors overexpressed in tumor cell membranes and the highly cationic R_7 sequence that facilitates membrane penetration. Approximately 80% of doxorubicin loaded within the mechanized MSNPs is released within the cells, presumably as a result of enzymatic digestion of the GFLG peptide, leading to a high rate of cell death in an *in vitro* assay.

Redox-Triggered Snap-Top Nanovalves

The redox-responsive snap-top nanovalves **R6173–R6176** summarized in **Figure 6.72** all rely on biomolecular thiols to cleave disulfide bonds in the cargo-liberating step. In the context of drug delivery, it is envisioned that disulfide-linked snap-top nanocarriers will release cargo selectively in the cytosol of living cells, where high concentrations (10 mM) of glutathione (GSH) maintain reducing conditions. Redox responsive snap-tops were introduced[728] in the form

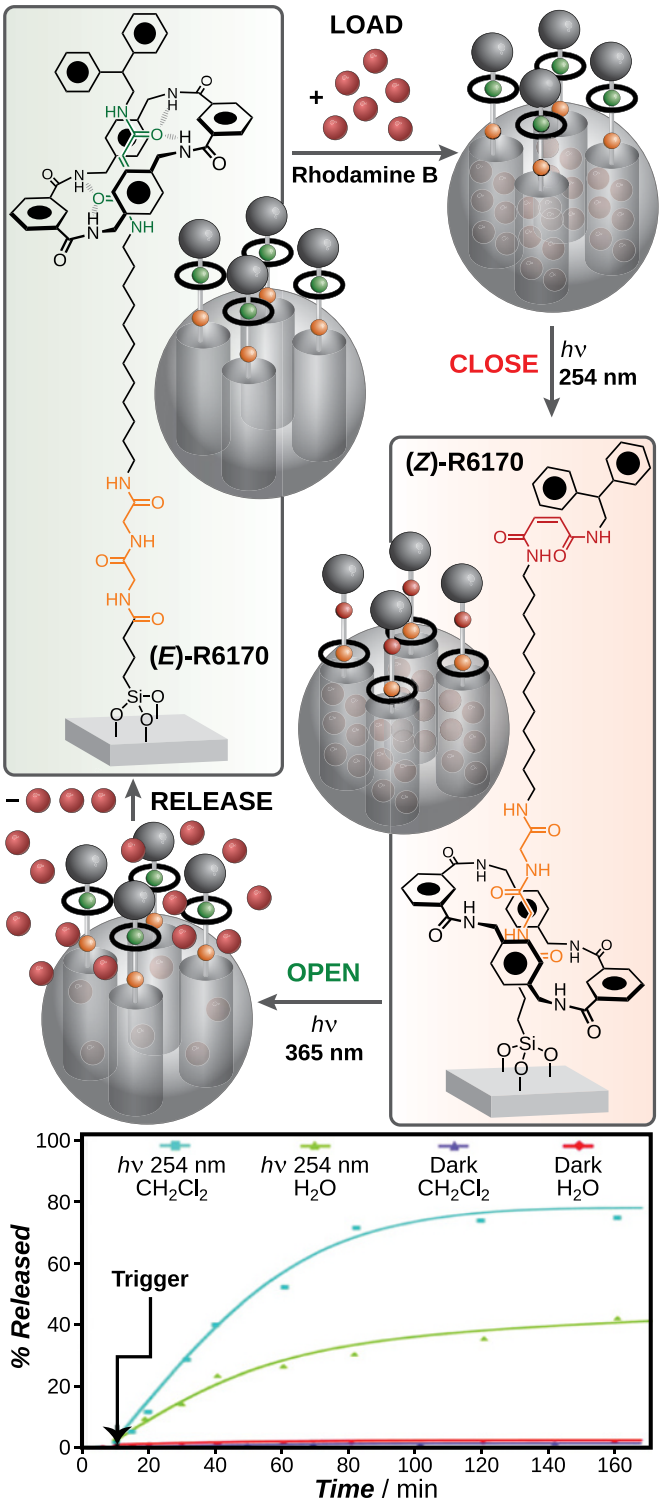


Figure 6.71 Graphical representations and release profiles in CH_2Cl_2 and H_2O for Berná's mechanized MSNPs mounted with photoswitchable bistable [2]rotaxane nanovalves based on benzylic amide recognition motifs. Data reproduced with permission from ref. 725 (copyright 2015 Royal Society of Chemistry)

of the MSNP-mounted [2]rotaxanes **R6173a** and **R6173b**, which comprise a short triazole-containing stalk terminated by a disulfide-linked adamantyl stopper and encircled by α-CD and CB6 rings, respectively. It was demonstrated in this proof-of-concept that the introduction of thiols such as 2-mercaptoethanol (ME) and dithiothreitol (DTT) to aqueous solutions above a bed of either of the snap-top nanocarriers leads to the release of fluorescent rhodamine B cargo from the MSNPs into the solution, with no observable leakage prior to the application of the stimulus. The release occurs gradually over the course of ~2 hours when ME is added to nanocarriers mechanized with **R6173a** snap-tops, whereas most of the cargo releases relatively suddenly (minutes) from **R6173b** snap-tops exposed to DTT.

The remaining disulfide snap-tops in **Figure 6.72** have been tested in biological settings. Cai and Zhao[729] have mounted the α-CD rotaxane **R6174** possessing folate groups as tumor-targeting stoppers on hollow MSNPs (HMSNPs). The team demonstrated that that the corresponding mechanized nanocarriers exhibit enhanced tumor targeting *in vitro*, where they selectively induce the apoptosis and death of tumor cells, and also that the doxorubicin-loaded nanocarriers mitigate (**Figure 6.73**) tumor growth with minimal side effects in an *in vivo* mouse model. More recently, a folate-stoppered disulfide snap-top nanovalve **R6175** employing a macrocyclic Pd^{II} chelate as the ring was described by Wu.[730] When loaded with fluorescein and doxorubicin, these mechanized MSNPs were found to enter and induce apoptosis in cancer cells, presumably as a result of the release of doxorubicin in the cytosol as a result of disulfide bond cleavage near the base of the nanovalve stalk. In an *in vitro* model, the viabilities of HeLa cancer cells were much lower when treated with these doxorubicin-loaded mechanized MSNPs, compared to either the empty MSNPs or free doxorubicin. A similar snap-top rotaxane has been utilized by Cai[731] in the delivery of doxorubicin from "yolk–shell" mechanized MSNPs to tumor cells. Kros[732] has also relied on the reductive cleavage of disulfide bonds by either dithiothreitol (DTT) or GSH to stimulate the controlled release of fluorescein from snap-top nanocarriers gated with the α-CD rotaxane **R6176**. The snap-top nanovalves are stoppered in this case by a 12-amino-acid peptide sequence, CGRRRQRRKKRG, a domain of the HIV-1 virus that facilitates translocation of exogenous molecules across cell membranes. Indeed, the MSNPs decorated with these peptidic snap tops are efficiently internalized *in vivo* by HeLa cells.

Pseudorotaxane Nanovalves

In addition to the nanovalves possessing formal mechanical bonds, many nanovalves based on surface-anchored host-guest complexes have also been invented, based on motifs including the little blue box,[733,734] crown ethers,[735–738] cucurbiturils,[737,739–752] cyclodextrins,[737,741,753–774] pillararenes,[775–777] calixarenes,[776,778–780] and metallo-organic chelates,[781] which respond to stimuli such as pH changes,[735–737,739,740,742,743,745,749–754,756–764,766–768,770,772,775,778] reduction/oxidation,[741,762,773,777,782] small molecules,[745,746,768,775–778] enzymes[746,765,778,782,783] cations,[777] anions,[781] UV/Visible/NIR light,[733,734,743,747,748,755,767,769,770] ultrasound,[738] heat,[748] as well as local heating caused by

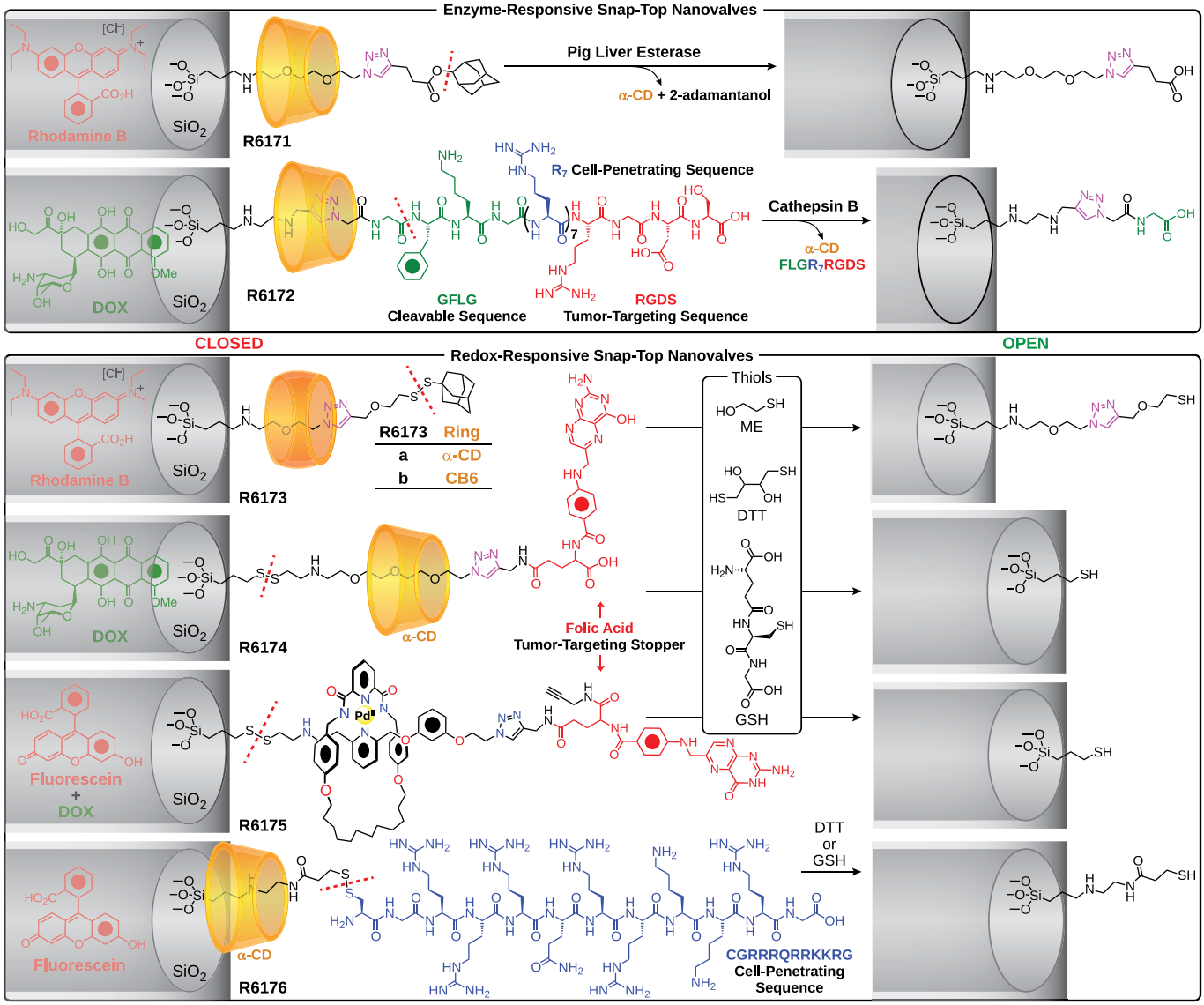


Figure 6.72 Snap-top nanovalves on mesoporous silica.[726–730,732] Molecular cargoes (left hand side), such as dyes and drugs, are released from the nanopores in response to enzymatic bond cleavage (top) or reductive cleavage (bottom) of disulfide bonds.

oscillating magnetic fields,[744] or plasmonic excitation with NIR light.[774,779] The remarkable variety of nanovalves and handles for controlling them, coupled with this Section's success stories on controlled cargo release, and especially drug delivery *in vitro* and *in vivo*, suggest that nanomachines with mechanical bonds could become important technologies in biomedical applications.

Controlled-Release Rotaxanes

Instead of employing rotaxanes as stimulus-responsive gates to nanocarriers, an alternative strategy for controlled release involves employing the rotaxane itself as the delivery vehicle for therapeutic and/or diagnostic agents. This strategy often involves an irreversible reaction (**Figure 6.74**) that destroys the rotaxane in the process of releasing a molecule of interest from its co-constitution. The applications of rotaxanes in biological contexts such as these have also been considered in a few recent literature reviews.[784–786]

Controlled-Release Polyrotaxanes

One of the early pioneers to employ rotaxanes in controlled release applications was Yui,[787–789] who began this work at the Japan Advanced Institute for Science and Technology (JAIST) and continued at the Tokyo Medical and Dental University. Yui's design[790,791] (**Tables 6.9–6.10**) for controlled-release molecules involves PEG⊂(α-CD)$_n$ polyrotaxanes capped with peptidic stoppers—especially benzyl-protected phenylalanine[790–799] or tyrosine[800–810] residues. These biodegradable stoppers may be hydrolyzed by enzymes such as papain,[790] amidopeptidase M,[801,802] α-chymotrypsin,[795] and other proteases, or they may be connected to the axle by other types of biodegradable linkers, such as disulfide bonds[807,808] (cleaved by glutathione) or β-thiopropionate bonds[809] (cleaved at low pH levels, such as those within the lysosome). The conjugation of ligands to the polyrotaxane framework introduces opportunities for (i) site- or cell-specific targeting driven by

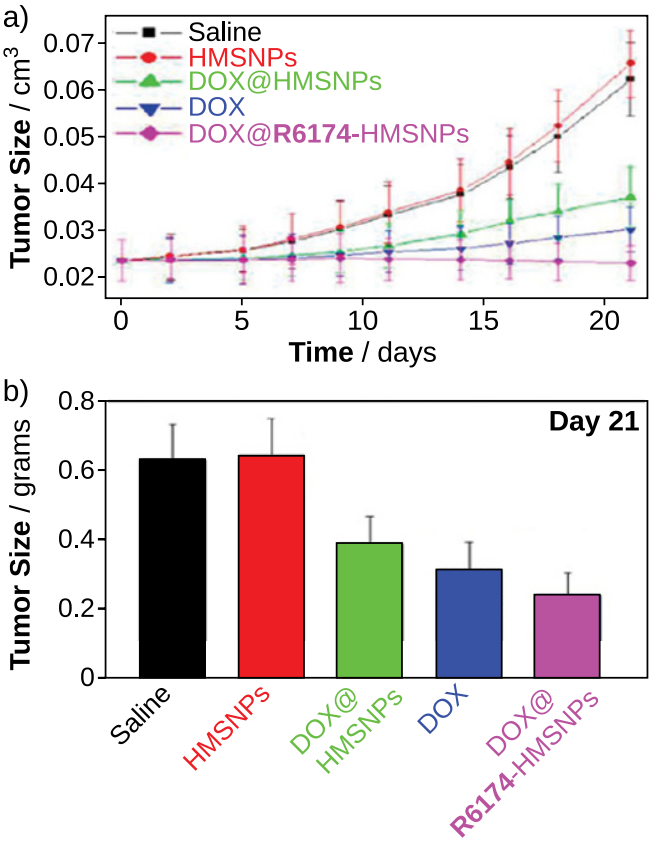


Figure 6.73 Tumor size data in an *in vivo* mouse model for testing snap-top mechanized MSNPs in cancer treatment.[729] (a) A time-resolved plot comparing the average tumor sizes in mice injected with HeLa tumor cells after treatment with saline, hollow mesoporous silica nanoparticles (HMSNPs), doxorubicin-loaded HMSNPs (DOX@HMSNPs), doxorubicin (DOX), and DOX-loaded HMSNPs mechanized with **R6174** snap-top nanovalves.[729] (b) A bar graph comparing the average weight of the dissected tumor after 21 days of treatment. Data reproduced with permission from ref. 729 (copyright 2013 American Chemical Society)

multivalent ligand–receptor interactions, and (ii) controlled-release delivery of chemical agents driven by the degradation of biocleavable linkers in any of the polyrotaxane component parts. Owing to their promise in a number of biomedical applications, the Tokyo group has produced a large family of cyclodextrin/PEG polyrotaxanes possessing various ligands and drugs conjugated to the α-CD rings.

Multivalent Binding and Controlled-Release Inhibition

A number of investigations have shown that the enhanced ligand mobility along the polyrotaxane backbone, which is attributable to the rings' translational freedom enabled by the mechanical bond, enhances their ability to participate in multivalent binding interactions (e.g., with cell membrane receptors), which bodes well for inhibition (**Table 6.9**) and targeting purposes. Polyrotaxanes **R6177a-b** with hydroxypropyl ether (HPE)-functionalized α-CD rings were found to interact[792] with the lipid membranes of rat skin cells and enhance[793] penetration of indomethicin through rat skin, suggesting potential opportunities for transdermal drug delivery. The same polyrotaxanes were also found[794] to inhibit Ca^{2+} release associated with thrombin-induced platelet activation for potential applications in blood-contacting devices. The anionic polyrotaxanes **R6178a-f**, which are threaded by carboxyethylester-functionalized α-CD rings, also bind Ca^{2+} ions, enabling the inhibition[799,800] of Ca^{2+}-dependent trypsin enzymes. The mechanical bonds of maltose-decorated polyrotaxanes **R6179a-l** enhance[803,804] multivalent interactions between maltose and concanavalin A proteins, owing possibly to an increase[805,806] in structured water molecules surrounding the ring-mobilized maltose groups, allowing them to inhibit hemagglutination, the clumping of red blood cells. Multivalent binding interactions of dipeptide (Val-Lys)-decorated polyrotaxanes **R6180a-d** inhibit[796] the PEPT1 protein responsible for intestinal cell uptake of di- and tripeptides generated during digestion, an effect which may be useful in dietary restriction treatments. The biotin-deocrated polyrotaxanes **R6181a-c** have also been investigated[797,798] as multivalency-assisted targeting molecules for the sodium-dependent multivitamin transporter proteins of intestinal cells. Polycationic polyrotaxanes **R6182a-d** possessing α-CD rings displaying *N*,*N*-dimethylaminoethyl (DMAE) groups have been found[811] to act

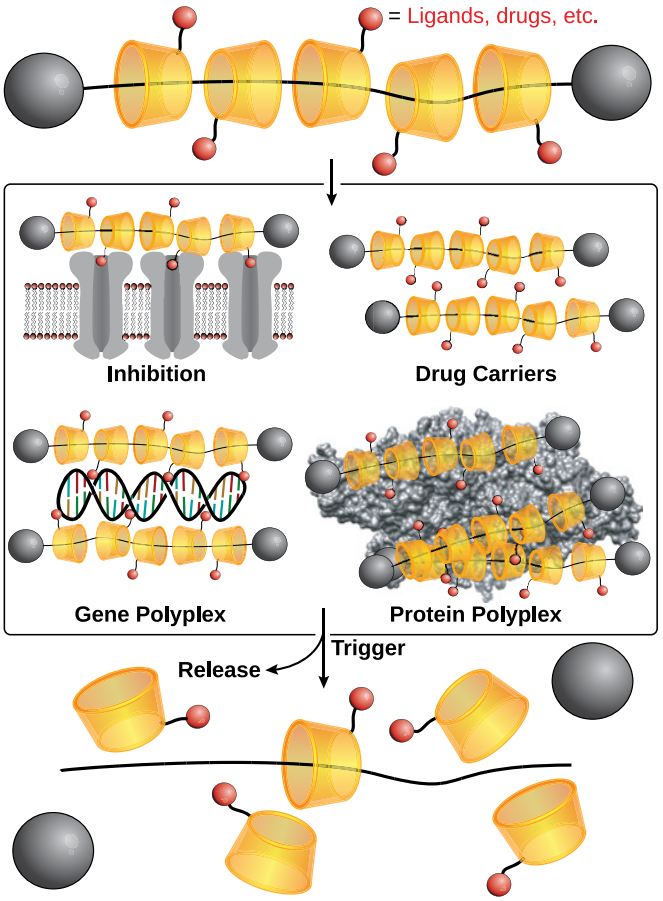
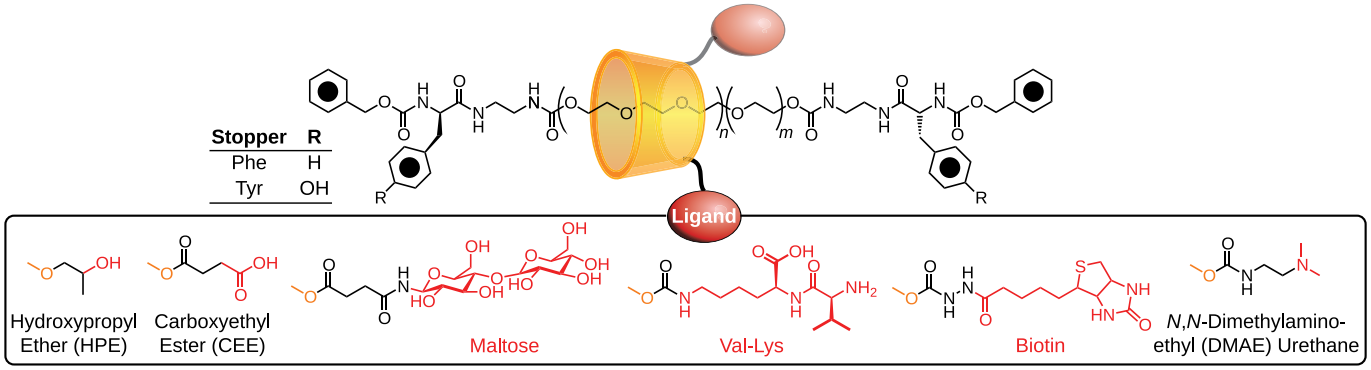


Figure 6.74 A generalized graphical representation of controlled-release rotaxanes, which can be employed in stimulus-responsive inhibition applications, as well as in the delivery of drugs, genes, proteins, etc.

Table 6.9 Summary of Yui's polyrotaxane inhibitors possessing biocleavable peptidic stoppers.



	Stopper	No. of Rings	M_n PEG	Ligand	Average No. of Ligands per Ring	Total Ligands per Molecule	Inhibition	Ref
R6177a	Phe	11	2000	HPE	8	88	Platelet activation by Ca^{2+} release	794
R6177b	Phe	23	4000	HPE	8	184		
R6178a	Phe	22	4000	CEE	1.5	33		
R6178b	Phe	22	4000	CEE	3.1	68		799
R6178c	Phe	22	4000	CEE	6.0	132	Ca^{2+}-mediated protein digestion by trypsin	
R6178d	Tyr	11	2000	CEE	6.0	66		
R6178e	Tyr	16	2000	CEE	6.0	96		800
R6178f	Tyr	22	2000	CEE	6.0	132		
R6179a	Tyr	50	20000	Maltose	0.8	40		
R6179b	Tyr	50	20000	Maltose	1.2	60		
R6179c	Tyr	50	20000	Maltose	2.8	140		
R6179d	Tyr	50	20000	Maltose	4.6	230		
R6179e	Tyr	85	20000	Maltose	0.5	44		
R6179f	Tyr	85	20000	Maltose	0.7	58	Concanavalin A induced hemagglutination	803
R6179g	Tyr	85	20000	Maltose	1.4	122		
R6179h	Tyr	85	20000	Maltose	2.9	244		
R6179i	Tyr	120	20000	Maltose	0.3	42		
R6179j	Tyr	120	20000	Maltose	0.5	64		
R6179k	Tyr	120	20000	Maltose	1.0	117		
R6179l	Tyr	120	20000	Maltose	2.0	240		
R6180a	Phe	22	4000	Val-Lys	0.05	1		
R6180b	Phe	16	4000	Val-Lys	0.1	2	Peptide transport protein PEPT1	796
R6180c	Phe	9	4000	Val-Lys	1.2	11		
R6180d	Phe	21	4000	Val-Lys	2.2	46		
R6181a	Phe	20	4000	Biotin	5.2	104	Sodium-dependent multivitamin transporter proteins	
R6181b	Phe	22	4000	Biotin	5.1	113		797
R6181c	Phe	22	4000	Biotin	8.5	188		
R6182a	Tyr	16	4000	DMAE	3.8	61	Cellular uptake of L-carnitine mediated by organocation transporter protein OCTN2	
R6182b	Tyr	15	20000	DMAE	4.7	75		811
R6182c	Tyr	50	20000	DMAE	4.7	240		
R6182d	Tyr	120	20000	DMAE	4.0	480		

as non-cytotoxic inhibitors of cellular cation transport processes. In all cases, multivalent interactions enabled by the ring-mobilized ligands leads to binding interactions that are greater than the sum of the individual ligands. In general, polyrotaxanes displaying a higher total number of ligands exhibit stronger multivalent binding interactions. In principle, the stimulus-controlled degradation of inhibitory polyrotaxanes could offer new modes of temporal and spatial control over the localization of therapeutics in the body.

Protein Delivery

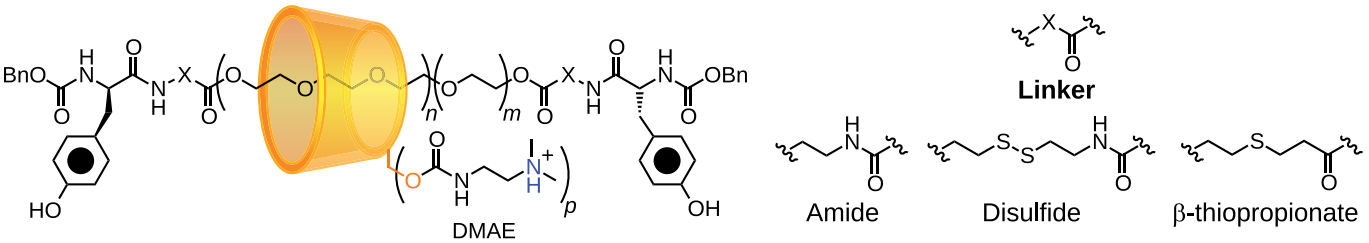
Yui has also employed polyelectrolytes comprising PEG-threaded α-CD rings functionalized with cationic DMAE groups—see polyrotaxanes **R6182–R6184** in **Table 6.10**—in the cellular delivery of genes[807,809,812–817] (*vide infra*) and proteins.[808,810] In the case of protein delivery, the polycations **R6182e-k** and **R6183a**, which are degraded by enzymatic hydrolysis and reductive disulfide bond cleavage, respectively, associate electrostatically

with the negatively charged enzyme β-galactosidase (β-gal) to form nanoparticulate polyplexes. The intracellular uptake and sustained activity of the β-gal enzyme *in vitro* was found[810] to be higher in the polyrotaxane-β-gal polyplexes than in comparable polyplexes of poly[2-(*N*,*N*-dimethylaminoethyl)methacrylate]. Surprisingly, however, the efficiency of uptake and post-delivery enzymatic activity showed little dependence on the density of DMAE groups displayed by these polyrotaxanes. Importantly, the investigations[808] of the disulfide-linked polyrotaxane **R6183a** verified that the release of the α-CD rings from the dumbbell, achieved in this case by the reductive cleavage of disulfide bonds in the presence of glutathione, are necessary for the recovery of enzymatic activity.

Gene Delivery

Yui's recent efforts have focused on employing biocleavable polyrotaxanes as non-viral gene delivery vectors.[807,809,812–817] In general, this research involves the use of α-CD rings functionalized with cationic DMAE groups, as in the polyrotaxanes summarized in **Table 6.10**, which allows them to associate strongly with the anionic backbones of DNA[807,812–816] or RNA[809,815,817] molecules by forming polyplexes stabilized by multivalent ion-pairing and electrostatic interactions. The efficiency of uptake and release in these nanoparticulate constructs can be tuned by adjusting the density of DMAE ligands displayed by the polyrotaxanes, since the binding interactions with genetic materials increase as more DMAE groups are introduced, yet the triggered release is more efficient for lower numbers of DMAE

Table 6.10 Summary of Yui's mechanically bonded polycations possessing biocleavable peptidic stoppers.



	Linker (–X–)	α-CD Rings (*n*)	M_n PEG	DMAE Groups per Ring (*p*)	Total No. of DMAE Groups	Trigger	Delivery	Ref
R6182e	Amide	25	9810	1.6	41	Hydrolysis by Proteases	β-Galactosidase	808 810
R6182f	Amide	25	9810	3.8	96			
R6182g	Amide	25	9810	6.0	150			
R6182h	Amide	56	9810	0.9	52			
R6182i	Amide	56	9810	1.7	97			
R6182j	Amide	56	9810	2.7	149			
R6182k	Amide	46	9810	5.7	264			
R6182l	Amide	16	4000	0.9	14	Hydrolysis by Proteases	pDNA	814
R6182m	Amide	16	4000	1.8	29			
R6182n	Amide	16	4000	3.8	61			
R6182o	Amide	16	4000	6.0	96			
R6182p	Amide	29	4000	1.0	29			
R6182q	Amide	29	4000	2.4	71			
R6182r	Amide	29	4000	3.3	97			
R6182s	Amide	29	4000	5.7	164			
R6183a	Disulfide	52	9810	5.8	301	Reductive Cleavage by Glutathione	β-Galactosidase	808
R6183b	Disulfide	18	4000	0.8	14		pDNA	807 814
R6183c	Disulfide	18	4000	1.6	29			
R6183d	Disulfide	18	4000	4.2	76			
R6183e	Disulfide	18	4000	5.5	99			
R6183f	Disulfide	29	4000	1.2	35			
R6183g	Disulfide	29	4000	1.8	52			
R6183h	Disulfide	29	4000	3.8	110			
R6183i	Disulfide	29	4000	6	180			
R6184a	β-thiopropionate	22	4550	1.0	21	Hydrolysis at Low pH	siRNA	809
R6184b	β-thiopropionate	22	4550	2.1	47			
R6184c	β-thiopropionate	22	4550	3.3	72			
R6184d	β-thiopropionate	29	4550	3.0	87			

groups.[814] Gene delivery to the cell nucleus is also more effective when the polyrotaxane-DNA nanoparticles are encapsulated[807,816] within lipid nanocarriers. Polyrotaxanes derived from DMAE-functionalized α-CD rings lacking controlled-release stoppers have also been successfully employed in siRNA delivery by Thompson,[818] calling into question the importance of a stimulus-controlled release mechanism in these polyplexed delivery vehicles—a topic which requires further investigation.

One of the main challenges associated gene delivery is the avoidance of the lysosome, an intracellular organelle comprising an acidic compartment packed with nuclease enzymes that degrade foreign DNA entering the cell through the clathrin-mediated endocytosis pathway. Pan and Feng[819] have found that pDNA polyplexes of the α-CD polyrotaxanes **R6185** functionalized with highly cationic dendritic polyamidoamide (PAMAM) moieties bypass (**Figure 6.75**) the lysosome by entering HEK293A cells through an alternative, cavaolae-mediated endocytotic pathway. Since the neutral-pH caveosome is a much less damaging endosome for genetic material, **R6185** exhibits a higher gene delivery efficiency compared to similarly charged PEI-DNA polyplexes, which enter primarily through the clathrin-mediated (lysosomal) pathway. Another important factor that is not often considered in preclinical trials of gene delivery polyplexes is their dilution stability, since many of these constructs are likely to dissociate as they are diluted in the bloodstream. In the case of the **R6185**-pDNA polyplexes maintain their stability even at very high dilution ratios and deliver genes successfully to the nuclei of a number of different cell lines.

In addition to these examples, Li[820–822] and Chen[823] have both constructed polyrotaxanes for gene delivery possessing highly cationic polyethyleneimine (PEI)-grafted cyclodextrin rings. These polyrotaxanes also exhibit higher gene transfection efficiencies than covalently bonded PEI polymers. Chen[823] demonstrated that folate stoppered polyrotaxanes of this type exhibit an enhanced antitumor effect in nude mice relative to a comparable PEI-DNA polyplex. Taking a departure from the PEG backbones of the polyrotaxane axles, Wenz[824] has constructed polyrotaxanes comprising hexactionic α-CD derivatives threaded onto ionene-11 polycationic backbones, and tested the corresponding DNA polyplexes (200 nm diameter particles) for gene delivery *in vitro*, finding that they too outperform PEI-DNA polyplexes in gene transfection. Taken together, these investigations suggest that the controlled release of genes mediated by the mechanical bond holds a lot of promise in gene delivery applications.

Drug Delivery

By conjugating drugs directly to the primary faces of the cyclodextrin rings via biodegradable linkages, the polyrotaxane framework can improve drug efficacy as a result of (i) enhanced aqueous solubility of the drug, (ii) trafficking the drug to targeted sites, (iii) controlled release of the drug, or any combination thereof. Several drug delivery vehicles comprising cyclodextrin polyrotaxanes are summarized in

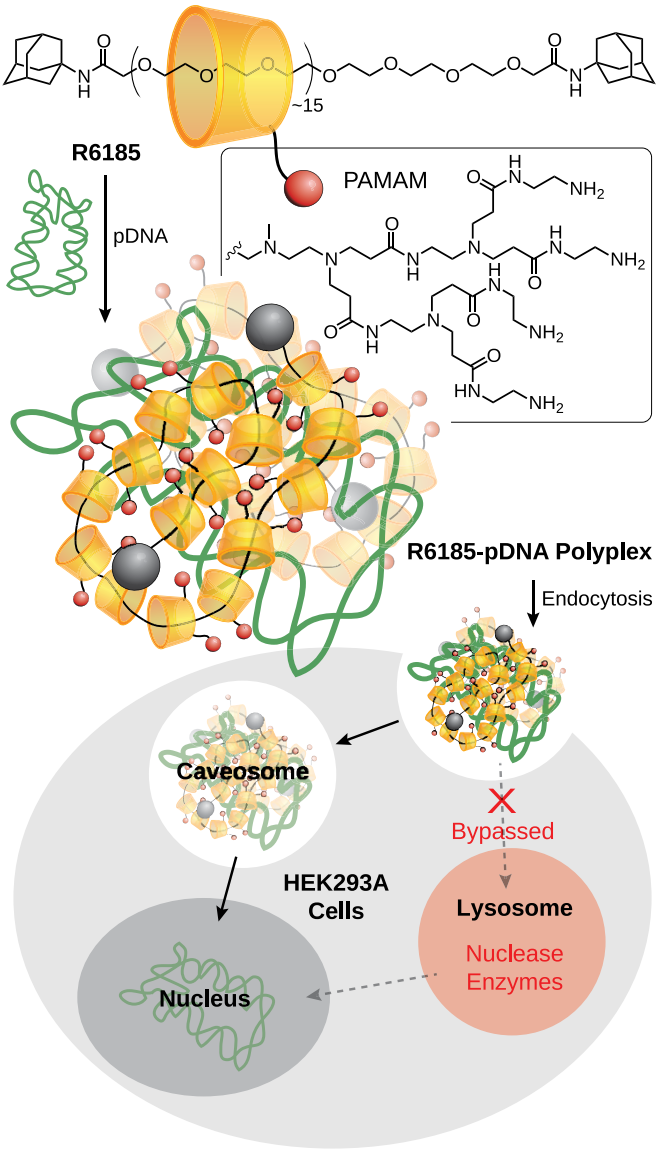


Figure 6.75 Graphical representation of gene delivery via caveolae-mediated endocytosis[819] of a polyplex comprising plasmid DNA (pDNA) and the polycationic dendrimer-grafted polyrotaxane **R6185**. The efficiency of gene delivery to the nucleus is enhanced relative to polyplexes introduced by the more commonly observed clathrin-mediated endocytosis, since the lysosome is bypassed in the caveolae-mediated pathway.

Table 6.11. Yui[795] has demonstrated the controlled release of theophylline-modified α-CD rings from the polyether dumbbell of **R6186a-b** upon exposure to the hydrolytic enzyme, papain. Yang[825] has prepared the polypeptide-stoppered polyrotaxane **R6187** possessing doxorubicin-conjugated α-CD rings. These polymers, which exhibit a sustained release of the drug over four days in phosphate-buffered saline (PBS) at pH 7.4, are taken up by A2780 human ovarian cancer cells *in vitro*, confirming their promise as drug delivery vehicles. The hydrolysis of biodegradable bonds in the polyrotaxane **R6188**, derived from polypropylene glycol (PPG) and β-CD, has been exploited by Yang[826] to deliver scutellarin, an antiproliferative and

cytotoxic drug, to human colon cancer cell lines *in vitro*, where the antiproliferative activity of the polyrotaxane was found to be higher than that of ordinary scutellarin. Wu and Jiang[827] have conjugated paclitaxel to the rings of the *PPG⊂β-CD* polyrotaxane **R6189** and demonstrated that these constructs show superior antitumor efficacy relative to Taxol *in vivo* using nude mice as model organisms. Yang and Zhao[828] have designed the polyrotaxanes **R6190** possessing folate-stoppered PPG dumbbells to deliver β-CD-conjugated artesunate, a cytotoxic drug, to human colon cancer cell lines.

In addition to the therapeutic promise of the drug-modified polyrotaxanes in **Table 6.11**, Thompson[829,830] has found that polyrotaxanes containing 2-hydroxypropyl-β-cyclodextrin (HP-β-CD) show promise as therapeutic drugs for the treatmant of Niemann-Pick Type C disease, a lysosomal storage disorder characterized by the neurological and organismal disfunction caused by the accumulation of unesterified cholesterol in cell lysosomes. The HP-β-CD polyrotaxane constructs mobilize abnormally stored cholesterol in an *in vitro* model, most likely as a result of encapsulation within the HP-β-CD rings released from the polymers.

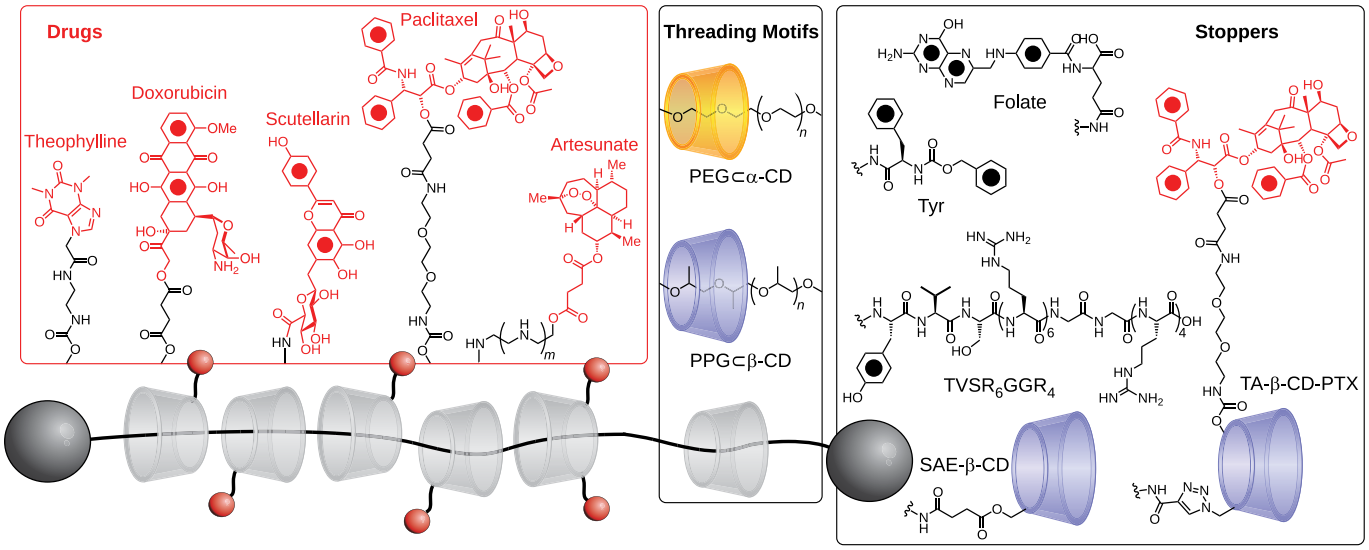
An alternative strategy for employing polyrotaxanes as drug delivery vehicles involves the encapsulation of drugs in polyrotaxane aggregates, such as micellar nanoparticles,[831–837] hydrogels,[838] multilayers,[839] and capsules.[840,841] Drugs may be released from these assemblies, either by dilution—e.g., in the bloodstream—or by embedding them with biocleavable bonds akin to those described above.

Controlled-Release [2]Rotaxanes

Polyrotaxanes are not the only platform for transporting cargo into cells. A number of examples of [2]rotaxane delivery agents have been described by Smithrud,[842–845] who discovered that dialkylammonium [2]rotaxanes possessing DB24C8 derivatized with cationic peptides can host amino acids, dipeptides, and fluorophores in aqueous solutions and facilitate their transport[842,844,846] into cells. The mechanical bond is essential to the fiunction of these so-called host-[2]rotaxanes, since the translational motion of the ring has been implicated in both the enhanced binding[845] of guests and in their transport[844,846] across cell membranes. Smithrud has also found that similar [2]rotaxanes possessing benzo[18]crown-6 stoppers bind[847] metal cations, and that these rotaxane ionophores can be utilized[848] as cytotoxic agents that cause apoptotic cell death by transporting Ca^{2+} and perhaps Mg^{2+} ions into cells, with IC_{50} values as low as 0.5 μM. Continuing this work, Zhu, Pang, and Bao[849] have found that pyrene- and Rhodamine B-stoppered [2]rotaxanes can also host and transport doxorubicin to tumor cells. Kimura and Ono[850] have found that a [2]rotaxane compound comprising the bis-3,5-dimethylbenzoic ester of diethanolamine (dumbbell) and DB24C8 (ring) is cytotoxic by itself, since it induces apoptosis efficiently in leukemia cells.

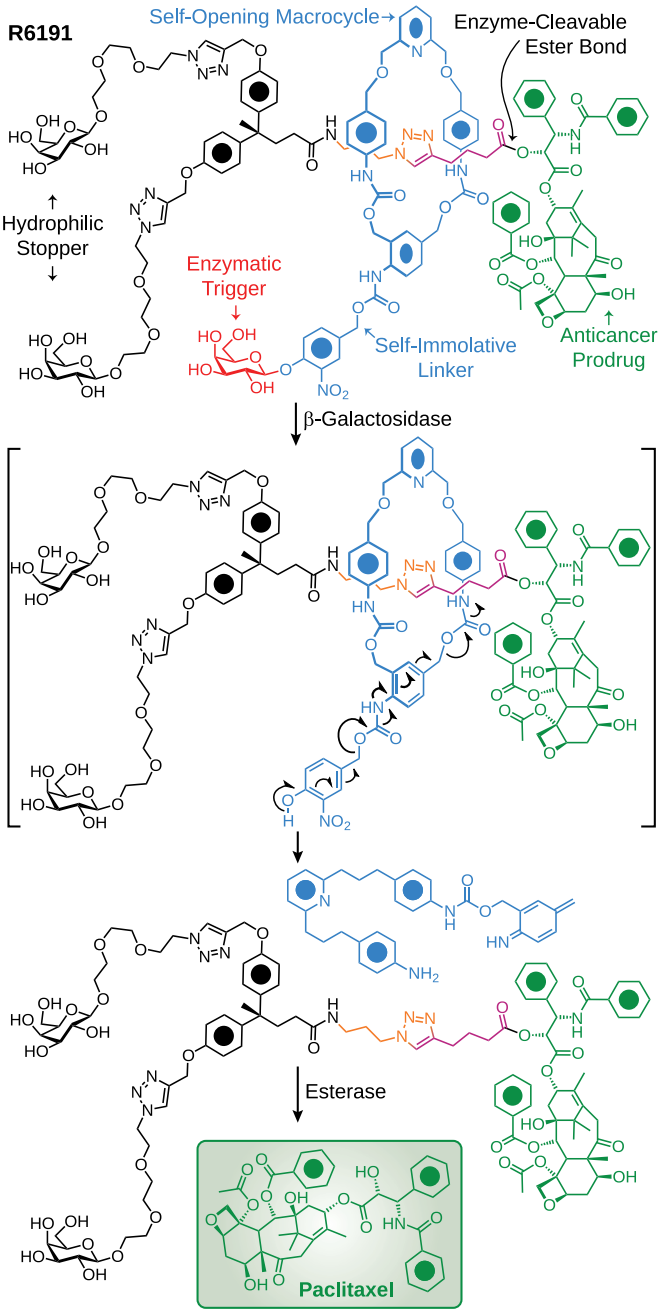
Following a couple of proof-of-concept demonstrations by Leigh,[851,852] which showed that a rotaxane possessing a self-immolative linker can release a peptide in response to

Table 6.11 Summary of drug-conjugated polyrotaxanes.



	Threading Motif	No. of Rings	Stopper	Drug	Average No. of Drugs per Ring	Total No. of Immobilized Drugs	Trigger	Ref
R6186a	*PEG⊂α-CD*	2–4	Tyr	Theophylline	0.5	1–2	Hydrolysis	795
R6186b	*PEG⊂α-CD*	13–14	Tyr	Theophylline	0.5	6–7		
R6187	*PEG⊂α-CD*	30	$TVSR_6GGR_4$	Doxorubicin	0.4	12	Hydrolysis	825
R6188	*PPG⊂β-CD*	11	SAE-β-CD	Scutellarin	0.7	8	Hydrolysis	826
R6189	*PPG⊂β-CD*	11	TA-β-CD-PTX	Paclitaxel	0.7	8	Hydrolysis	827
R6190	*PPG⊂β-CD*	8–9	Folate	Artesunate	0.6	5–6	Hydrolysis	828

an enzymatic trigger, Papot[853] designed "a mechanically interlocked molecular system programmed for the delivery of an anticancer drug." The [2]rotaxane **R6191**, prepared by an active template CuAAC protocol (**Section 2.4.1.1**), possesses a number of moieties within its co-constitution that enable it to release (**Scheme 6.111**) paclitaxel, a potent anticancer drug, selectively inside of tumor cells. The ring of **R6191** prevents the ester-linked paclitaxel stopper from premature hydrolysis by protecting it from esterases in blood plasma, but its galactosylated self-immolative linker undergoes a series of 1,6-elimination reactions that ultimately open up the ring upon activation by β-galactosidase, an intracellular enzyme (not present in the bloodstream) overexpressed in cancer cells. After this enzyme-triggered, self-immolative unmasking step, the ester bond becomes accessible to intracellular esterases, which release paclitaxel by hydrolytic degradation of the dumbbell. Although biological evaluation of **R6191** as an anticancer agent revealed that it is ~4–5 times less toxic than ordinary paclitaxel on KB, H661, and MDA-MB-231 cancer cell lines, the rotaxane does exhibit higher selectivity for KB cells overexpressing β-galactosidase compared to KB cells that were manipulated to prevent the overexpression of this enzymatic trigger. The mechanical bond is therefore essential to the selectivity of this enzymatically responsive prodrug.



Scheme 6.111 The mechanism of degradation in a rotaxane designed to deliver an anticancer drug to cells.[853] An ester bond is protected from hydrolysis until intracellular β-galactosidase enzymes trigger the self-immolating linker to open the macrocycle, allowing esterases to access the ester bond and liberate the paclitaxel stopper from the dumbbell.

Delivery of Diagnostics

The application of rotaxanes as diagnostic agents, such as fluorescent and chemiluminescent probes for near-infrared imaging of cells and tissues, was originally recognized by Smith,[854–862] who has designed a series of squaraine-based benzylic amide rotaxanes (**Section 2.3.4.2**) with excellent photostabilities enabled[863,864] by the mechanical bond, albeit without any well-defined controlled-release properties. Although these mechanomolecular probes typically embed themselves in lipid membranes, in principle they may be redesigned into switchable or controlled-release probes by incorporating biocleavable bonds of the noncovalent or covalent varieties, respectively, into their co-consitutions, in accordance with the other systems we have surveyed in this Section.

Wemmer, Pines, and Francis[865,866] have described a family of CB6 [2]rotaxanes, in which a chemical or biochemical event triggers the release (**Figure 6.76**) of a CB6 ring, which serves as a contrast agent for the sensitive detection of analytes by ^{129}Xe magnetic resonance techniques. ^{129}Xe magnetic resonance imaging (MRI) is a technology that detects xenon, a non-toxic gas that partitions throughout many of the body's tissues, instead of the ^{1}H atoms (detected by conventional MRI) of water. The main potential advantage of ^{129}Xe MRI is sensitivity, since (i) ^{129}Xe can be hyperpolarized, a process which dramatically improves its NMR/MRI signal by biasing the populations of nuclear spins, and (ii) the ^{129}Xe background signal is very weak because of xenon's low abundance in the body, leading to higher signal-to-noise (S/N) ratios. ^{129}Xe MRI contrast agents are often screened by a technique[867] known as hyperpolarized chemical exchange saturation transfer (hyperCEST) NMR spectroscopy, which further improves S/N ratios by invoking the saturation transfer of hyperpolarized ^{129}Xe atoms in dynamic chemical exchange between the bulk solvent and the contrast agent. Dmochowski's recent discovery[868] that CB6 binds Xe with reasonably high affinity (490 M^{-1}) in PBS to produce contrast by ^{129}Xe hyperCEST has enabled the Berkeley team[865,866] to design cleavable CB6 rotaxanes (**Figure 6.76a**) as controlled-release

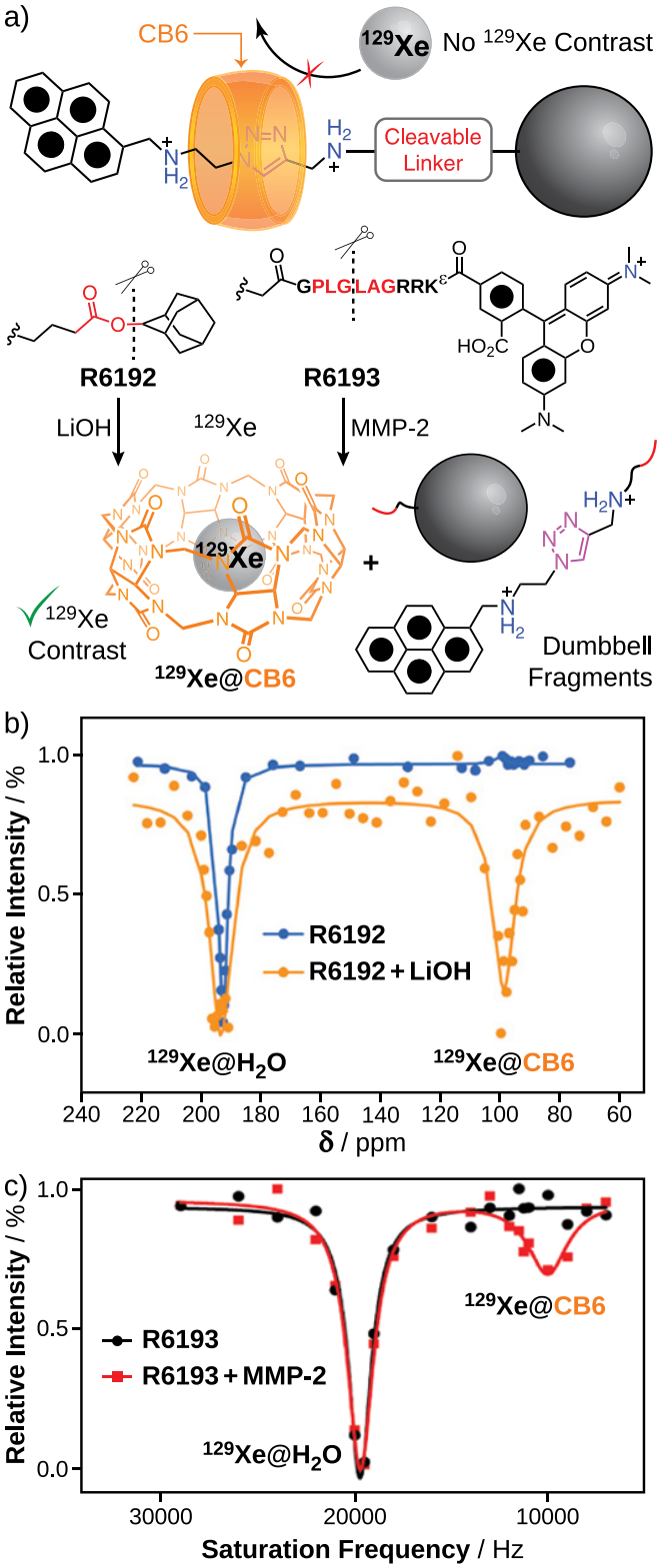


Figure 6.76 Controlled-release CB6 rotaxanes for ^{129}Xe magnetic resonance detection and imaging. (a) The cleavage of stoppers in rotaxanes **R6192** and **R6193** upon treatment with LiOH and MMP-2 enzymes, respectively, releases CB6 as a host for xenon. The ^{129}Xe@CB6 complex generates a detectable signal in the ^{129}Xe hyperCEST NMR spectra of (b) base-treated **R6192** and (c) enzyme-treated **R6193**. Data reproduced with permission from refs. 865 and 866.

contrast agents. The CB6 ring of the [2]rotaxane **R6192** encircles a triazole-based bis(dialkylammonium) dumbbell possessing pyrene and adamantyl ester stoppers encapsulated in β-CD for aqueous solubility. No observable hyperCEST signal at the resonance frequency of ^{129}Xe@CB6 is produced (**Figure 6.76b**) until the adamantyl ester stopper has been cleaved by LiOH. This proof-of-concept demonstrating that contrast can be "turned on" by a chemical signal led to the development[866] of a number of related polypeptide-stoppered rotaxanes, such as **R6193**, which suppresses (**Figure 6.76c**) the ^{129}Xe@CB6 hyperCEST signal until CB6 is released from its co-constitution upon cleavage of the polypeptide stopper by matrix metalloprotease 2, an enzyme overexpressed in cancer cells. These "contrast-upon-activation" rotaxanes hold promise for targeted delivery of contrast agents for early detection and disease imaging by ^{129}Xe MRI.

Huang[869] has investigated (**Figure 6.77**) the "theranostic" (therapeutic + diagnostic) [2]rotaxane **R6194DOX$_2^{2+}$**, which releases DOX in cells while reporting the location of release in the form of a fluorescent signal. The rotaxane comprises (**Figure 6.77a**) (i) a pair of DOX prodrug moieties, conjugated by acid-labile imine bonds to (ii) a PA5 ring encircling (iii) a dumbbell possessing (iv) triphenylphosphonium and (v) fluorogenic tetraphenylethene (TPE) stoppers, which serve as targeting and imaging probes, respectively. Since the absorption maximum (500 nm) of DOX overlaps with the emission range (450–700 nm) of the TPE stopper, the rotaxane's emission is quenched with high efficiency (up to 81%) as a result of energy transfer from TPE to DOX, until DOX is released from its co-constitution by hydrolysis (**Figure 6.77a**) of the imine bonds to give **R6194O$_2^{2+}$**. The theranostic compound **R6194DOX$_2^{2+}$** was formulated into nanoparticles by precipitation in water and introduced to HeLa (cancerous) and HEK293 (healthy) cells *in vitro*. The confocal laser scanning microscopy (CLSM) images in **Figure 6.77b** show that the rotaxane localizes primarily in mitochondrial membranes. HeLa cells exhibit an increase in both DOX and **R6194O$_2^{2+}$** emission intensities, comparing the 2 h and 8 h timepoints after treatment with **R6194DOX$_2^{2+}$**, owing presumably to the release of DOX over this 6 h period. Emission is much lower after 8 h in HEK293 cells treated likewise. The rotaxane's higher activity in cancer cells is rationalized by their more negative membrane potentials, which are targeted by the Ph_3P^+ stopper. It was also verified that other drugs possessing amines, including temozolomide, cyterabine hydrochloride, and gemcitabine, could be condensed onto the benzaldehyde units in the PA5 ring of **R6194O$_2^{2+}$**, and that the antiproliferative activity of the corresponding rotaxanes is retained in all cases.

In summary, the mechanical bond has proven to be a very useful tool for designing molecular machines that control the release of therapeutic and/or diagnostic chemical agents, either from assemblies such as mesoporous silica nanoparticles and micellar nanoparticles, or from their own co-constitutions by biochemical degradation.

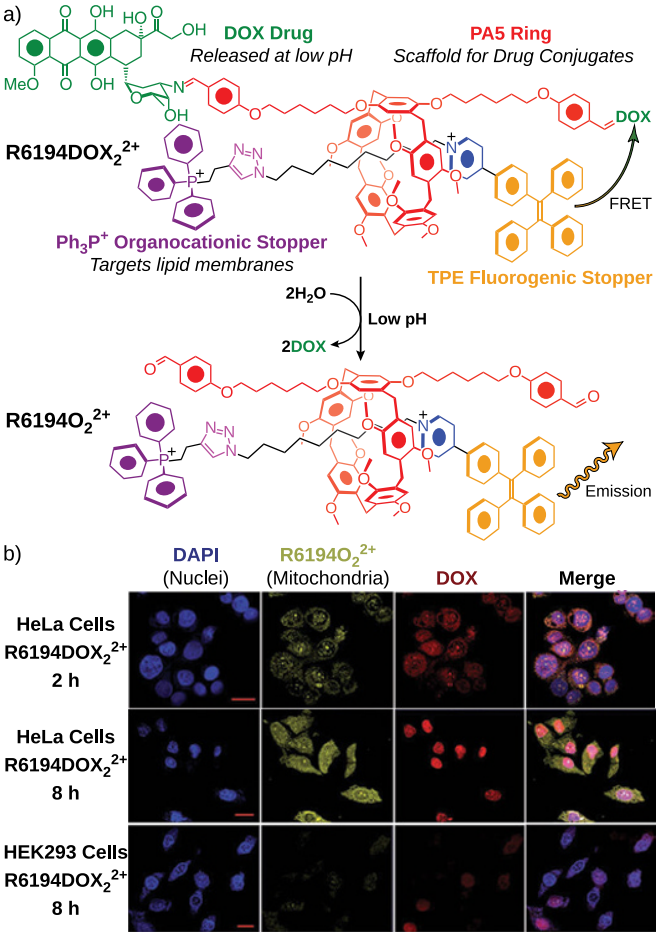


Figure 6.77 A theranostic [2]rotaxane that targets cancer cells and reports the pH-triggered release of cytotoxic DOX drugs from its co-constitution in the form of a fluorescence enhancement from its TPE stopper.[869] (a) A scheme depicting the release of DOX from the self-quenching [2]rotaxane **R6194DOX$_2^{2+}$** by imine hydrolysis to afford the fluorescent [2]rotaxane **R6194O$_2^{2+}$**. (b) CLSM images of HeLa and HEK293 cells stained with DAPI (a nuclear stain) and **R6194DOX$_2^{2+}$**. An increase in emission in the **R6194O$_2^{2+}$** and DOX channels after 6 h incubation with the theranostic indicates the gradual release of DOX in the HeLa cancer cells, whereas the normal HEK293 cells exhibit much lower fluorescence in these channels under the same conditions. Data reproduced with permission from ref. 869 (copyright 2016 Royal Society of Chemistry)

6.15.1.2 Artificial Muscles

In this Section we outline strategies by which large ensembles of molecular machines operating synchronously can produce net motions at meso- and macroscopic length scales, where work can be accomplished according to the principles of classical mechanics. Reflecting on the many types of muscle-like molecular actuation summarized in **Section 6.13.1**, it is apparent that the mechanical bond can be harnessed to program a remarkable variety of relative intercomponent motions, which can be controlled by a wide range of external stimuli. The challenge now is to integrate these and other switches into hierarchical systems where they can be utilized as machines in the true sense of the word. A biomimetic approach to this challenge involves the arrangement of many molecular switches/machines into large ordered structures and superstructures akin to muscle tissue. The key to this strategy is the fact that thermal noise is inversely proportional to the square of the number of molecules *N* involved in a system—for sufficiently large values of *N*, thermal noise is negligible and an integrated system will eventually obey the laws of classical mechanics, in which inertial forces become dominant and supplant viscous forces. This rule underpins the pursuit of artificial muscles, broadly defined here as any material characterized by ensembles of molecular switches operating in synchrony such that their mechanical motions are scaled up beyond the nano size regime.

Applying the Alexander model[870] of polymer brushes to these molecular switches provides[667] a framework (**Figure 6.78**) for engineering artificial muscles. A polymer brush is understood in this model as a polymer chain with one end anchored to a surface at a grafting density s, which is the quotient of the surface area (*A*) and the number (*n*) of polymer chains. Consider (**Figure 6.78a**) a bundle of *n* polymers which possess an average of *N* molecular muscle monomers serving as the repeating units. The 'molecular muscle' repeating unit has an average length *l* in its

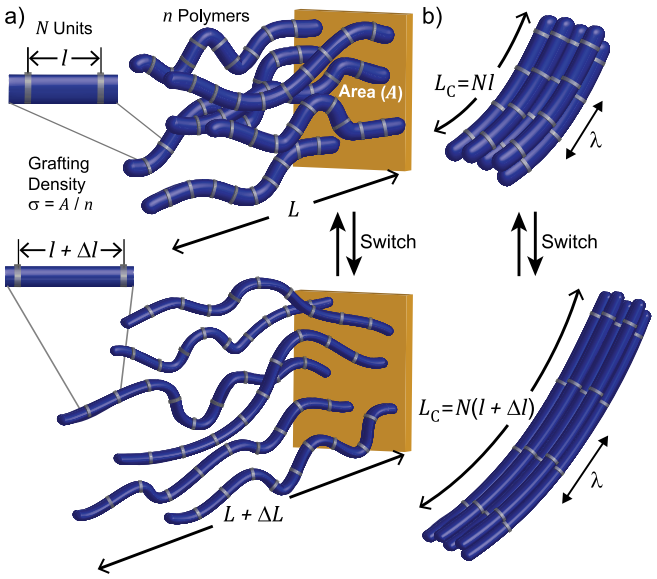


Figure 6.78 Definitions relating to the theoretical treatment of artificial muscle polymers based on repeating units of muscle-like molecular switches. (a) Application of a polymer brush model to the extension and contraction of an artificial muscle polymer bundle. The bundle's change in length is given by ΔL, which depends on the length (l), change in length (Δl), and the number (N) of repeating units, the grafting density (σ) which depends on the number (n) of polymer chains and the area (A) of the grafting surface, as well as on the excluded volume (ω) of the polymer, according to Equation 6.3. (b) In a bundle of highly aligned and densely packed polymers of persistence length l, the contour length (L_C) is determined by N, l, and Δl.

equilibrium state and a length ($l+\Delta l$) when it is switched. The length L of the bundle is given[667] by equation 6.2:

$$L = l^{2/3} N (\omega\sigma)^{1/3} \qquad (6.2)$$

where w is the excluded volume parameter—the volume of one polymer chain that is inaccessible to other molecules—and σ is the grafting density (A/n). The length ($L+\Delta L$) of the bundle—when the muscle unit is switched—is likewise given[870] by Equation 6.3:

$$(L + \Delta L) = (l + \Delta l)^{2/3} N (\omega\sigma)^{1/3} \qquad (6.3)$$

These equations show that the extent to which the polymer bundle extends or contracts (ΔL) depends, not only on the contraction length Δl of the repeat units (see **Table 6.5 in Section 6.13.1.5**), but also on the number, density, and volume of the polymer chains. In order, therefore, to maximize ΔL, artificial muscle polymers should have high degrees of polymerization, volumes, and be as densely bundled as possible. Since work scales with displacement, more work can be accomplished in systems with greater values of ΔL. The free energy ΔG of the integrated system, which can be used to estimate the work that can be extracted from the polymer brush as it is switched, is approximated[667] by Equation 6.4:

$$\Delta W = \Delta G \simeq nN \left(\frac{\sigma\omega}{l}\right)^{2/3} \left(\frac{\Delta l}{l + \Delta l}\right)^{2} k_B T \qquad (6.4)$$

This equation reveals that work depends on the same terms as do ($L+\Delta L$), in addition to the number n of polymer chains in the bundle and the magnitude of thermal energy given by $k_B T$. It follows that the work output by this kind of artificial muscle polymer can be optimized by lining up the molecular switching units as straight as possible along the axis of their extension and contraction, at the highest densities that are allowed while still being able to actuate the switches with an external stimulus. The same principles hold in a polymer bundle that is not grafted to a surface (**Figure 6.78b**). In a polymer bundle, the contour length (L_C) is the product of N and l, and the persistence length (λ) scales with $El/k_B T$, where E is the Young's modulus and I is the moment of inertia, which is proportional to n.

Surface-Bending Rotaxanes

Palindromic [3]rotaxanes (**Section 6.13.1.2**) were recognized for their potential to be utilized as artificial muscles (**Figure 6.79**) with the introduction[91,95,539] of the donor-acceptor rotaxane **R6195**$^{8+}$. The two CBPQT^{4+} rings of this molecular muscle, which encircle the outermost TTF recognition sites, are anchored to one side of a gold-coated microcantilever in a monolayer of ~8 billion molecules through gold-thiolate bonds. Both chemical[91,539] and electrochemical[95] oxidation of TTF to TTF^{2+} induces the movement of the CBPQT^{4+} rings toward the innermost naphthalene

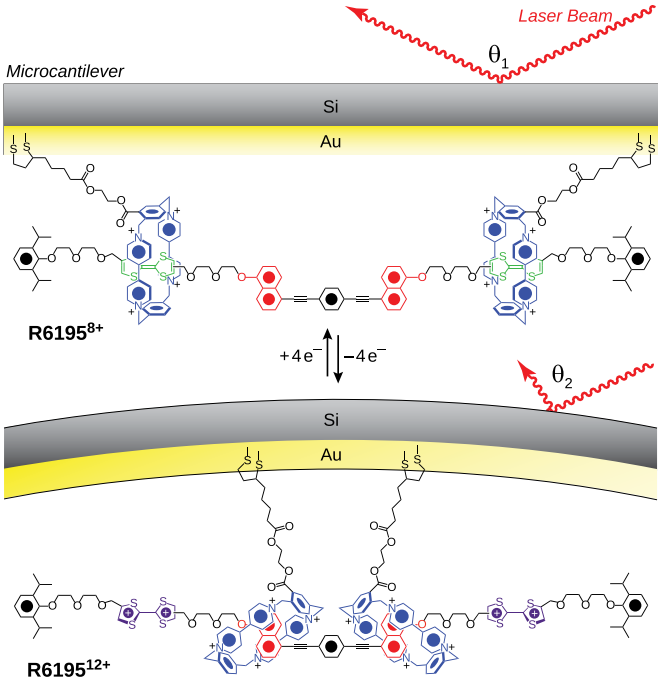


Figure 6.79 A monolayer of bistable donor-acceptor molecular muscles.[91,95,539] A SAM of the palindromic [3]rotaxane **R6195**$^{8+}$ is deposited on a gold-coated Si microcantilever by means of gold-thiolate anchors appended to the two CBPQT^{4+} rings. The inward motions of the rings from the TTF^{2+} dications to the DNP units upon chemical[91,539] or electrochemical[95] oxidation exerts a contractile force on the microcantilever that causes it to bend, a movement which can be detected as a change in the angle (θ_1/θ_2) at which a laser beam is reflected from the surface.

units and so causes the surface to bend, a motion which can be detected by changes in the angle (θ) of deflection of a laser beam focused on the cantilever. See **Figure 1.34** and the corresponding discussion in **Section 1.3.6**.

Actuation of Macroscopic Gels with Mechanical Bonds

Harada[871] has recently investigated the macroscopic actuation (**Figure 6.80**) of hydrogels and xerogels comprising polyether star polymers, crosslinked by the photoswitchable azobenzene/α-CD [*c*2]daisy chain **R6196**. The contraction of these gels is driven by irradiation with UV light, owing to the local molecular contractions (**Figure 6.80a**) that occur as a result of the *trans*-to-*cis* isomerization of the daisy chains **(*EE*)-R6196**. Both the hydrogels and the xerogels bend (**Figure 6.80b**) toward a UV light source. Since the surface of the gel facing the lamp absorbs the most light, one side of the gel becomes more populated with crosslinking daisy chains in contracted states such as **(*ZZ*)-R6196**. The corresponding xerogel, prepared by lyophilization of the hydrogel, responds remarkably quickly (seconds) to UV irradiation, compared to the timescale (hours) required to bend the hydrogel over similar distances. The bending of the hydrogel is reversed thermally in the dark or in visible light. Although the bending of the xerogel is not reversible, a bend in one direction can be counteracted by irradiation on the opposite side of the gel,

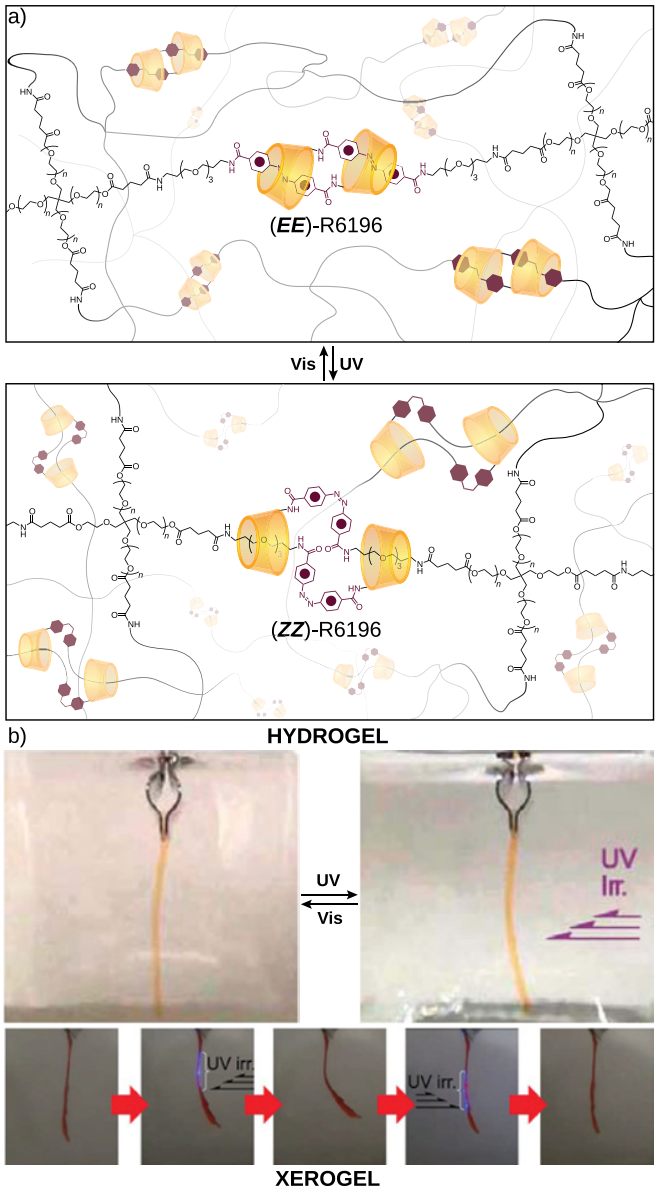


Figure 6.80 Harada's artificial muscle polymers comprising the crosslinked azobenzene/α-CD [*c*2]daisy chains **R6196**.[871] (a) Graphical representations of the hydrogels and xerogels at the molecular scale while photoswitching the *trans/cis*-azobenzene units of the daisy chain monomers **(*EE*)-R6196** and **(*ZZ*)-R6196**, respectively. (b) Photographs depicting the bending of hydrogels and xerogels of crosslinked **R6196** (~1 mm thickness) in response to irradiation with UV light. Photographs reproduced with permission from ref. 871 (copyright 2016 Nature Publishing Group)

leading to a bend in the opposite direction. A control xerogel crosslinked covalently by azobenzene units does not respond to light at all, suggesting that it is the mechanically bonded architecture of the [*c*2]daisy chain that enables actuation in the dry state. The results of this investigation are important for molecular machines, not only because of the remarkably fast performance of the xerogel, but also because they demonstrate for the first time that mechanomolecules may serve the actuating elements of macroscopic smart materials such as artificial muscle.

6.15.1.3 Molecular Computation & Information Storage

Although most computers rely on Si-based transistors as switching elements to store and process information, there is a growing interest in employing molecules as next-generation switching elements, since (i) their much smaller profiles could lead to further miniaturization of computation and storage media, and (ii) they may be compatible with environments that are not ideal for semiconductors, such as cells and tissues. Ratner's revolutionary 1974 proposal[872] on "molecular rectifiers" introduced the world to the idea of molecular devices. The field[873] of molecular logic-based computation was born in 1988, when Aviram[874] proposed that spiro-linked oligothiophene dimers could be employed as voltage-gated electronic switches for memory and computing devices. While Aviram's seminal proposal laid the foundation for electronic-based switches, including the molecular devices based on MSTJs (**Section 6.14.1.1**), an important 1993 paper by A.P. de Silva,[875] describing an AND logic gate based on ion-sensitive fluorescent signaling, marked the beginning of a paradigm shift that led to a much wider view of molecular logic—one that embraces not only molecular electronics, but all sorts of other inputs and outputs, such as the absorption and emission of light, as well as interactions with other forms of energy or chemical probes.

In contrast with the semiconductor computing paradigm, where differently connected copies of a single parent structure lead to different types of logic gates, the molecular computing paradigm relies on structural differences to achieve new logic functions. The molecule and the device are one and the same. Thus, the key to molecular logic lies in defining the appropriate inputs and outputs that meet the requirements of a particular logic gate, which is typically based on Boolean algebra. George Boole's algebraic system, which reduces all values to either TRUE or FALSE, is represented by a binary number system of 1 and 0, respectively. A logic gate is a device that produces a single output, the value of which depends on that of one or more inputs. A number of basic logic gates are illustrated in **Figure 6.81**. Each gate is accompanied by a truth table, which summarizes the relationship between the inputs (IN_1, IN_2, etc.) and outputs (OUT) of the device.

Countless molecules are capable of performing Boolean logic operations, especially optically active compounds such as indicators and sensors. For example, "off→on" chemical sensors are YES, gates, while "on→off" sensors are NOT gates. Mechanically interlocked switches are a natural platform for molecular logic-based computation[876] because—as **Sections 6.1–6.12** confirm—they respond in a variety of ways to a remarkable number of input stumuli. Mechanomolecules based on cyclodextrin,[189,224,233–235,318] π-donor/π-acceptor,[100,122] hydrogen-bonded templates,[190,527,877,878] and DNA[879,880] templates have been investigated deliberately as logic operators, although virtually all of the molecular switches in this Chapter could be described by a logic gate upon assignment of appropriate inputs and outputs. One example (**Figure 6.82**) of a mechanomolecular logic gate is the donor-acceptor [2]catenane **C640^{4+}**, which

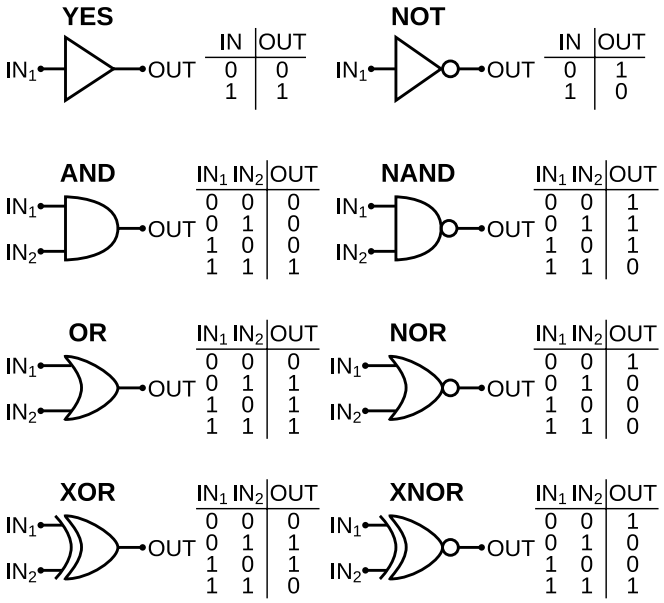


Figure 6.81 Symbols and truth tables for some basic logic gates.

undergoes dual-mode switching driven by pH and redox inputs.[122] If the BPP34C10 ring's relative position, which can be read by spectroscopic and electrochemical means, is considered to be the output, then this [2]catenane represents an AND logic gate. The ring encircles a dibenzylammonium unit (OUT = 1) only in environments that are both

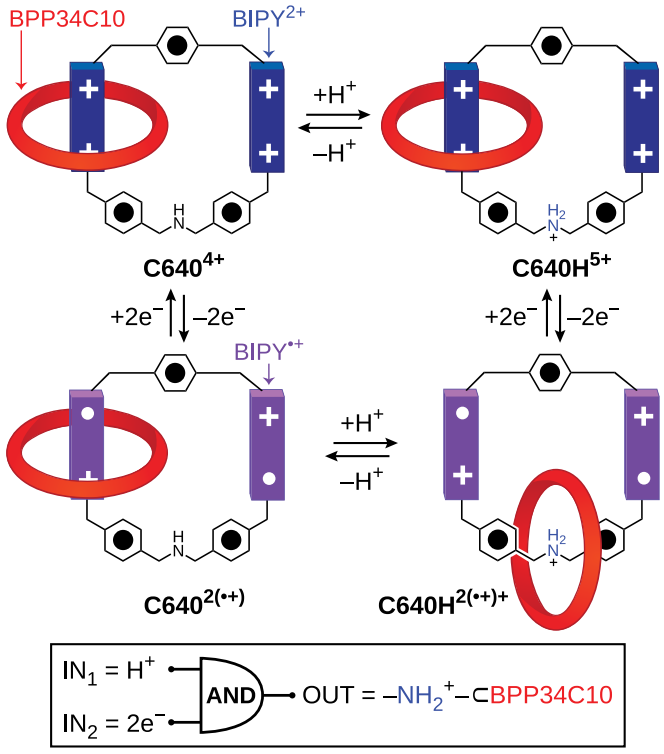
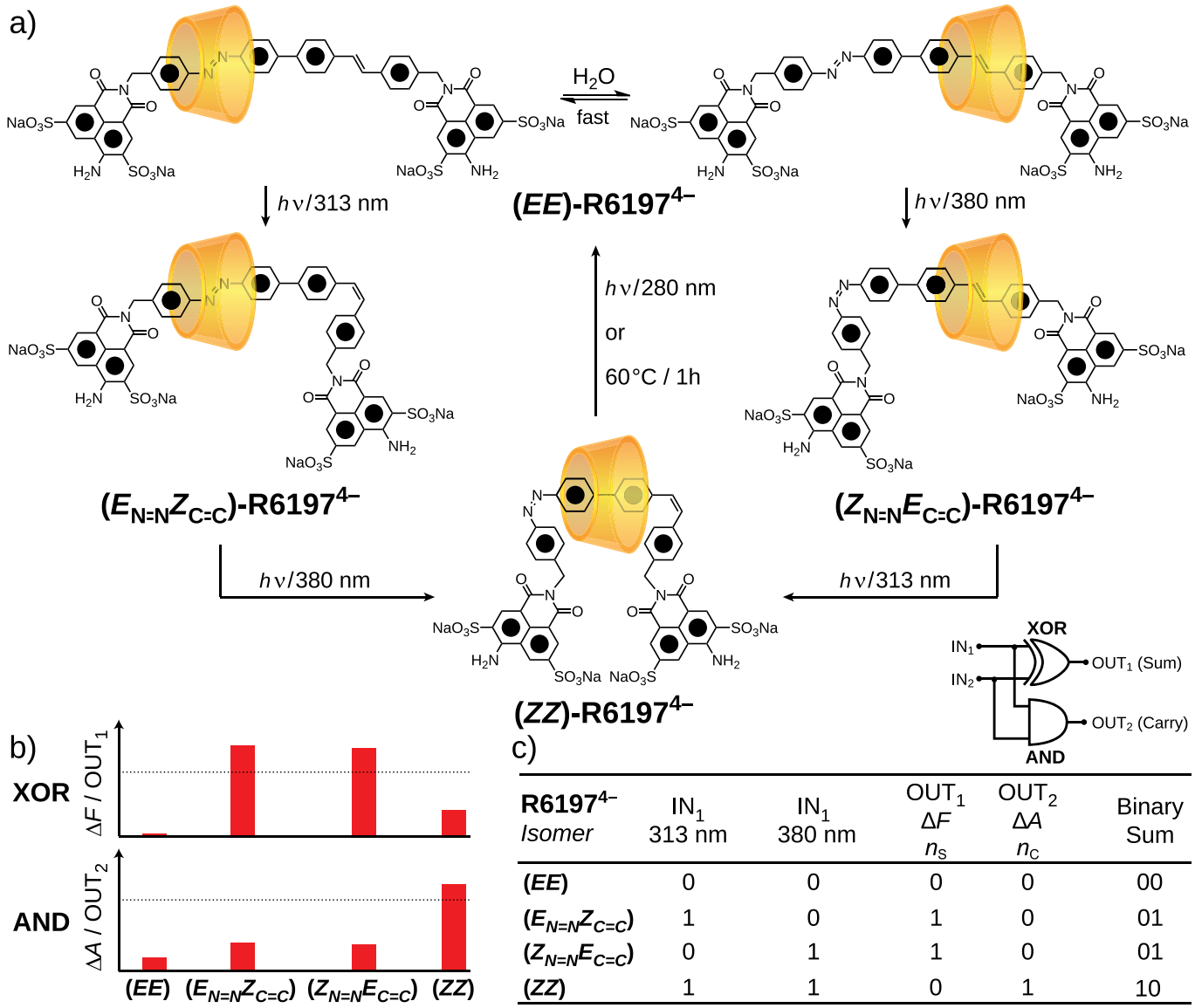


Figure 6.82 The dual-mode switchable [2]catenane **C640^{4+}** exhibits AND logic, since the ring encircles the dialkylammonium unit (OUT = 1) if and only if the catenane has been treated with both acidic ($IN_1 = 1$) and reductive ($IN_2 = 1$) stimuli.[122]

acidic ($IN_1 = 1$) and reducing ($IN_2 = 1$), as in the case of the protonated diradical dication **C640H$^{2(•+)+}$**, but not when either stimulus is missing, as in the cases of **C640H^{5+}** and **C640$^{2(•+)}$**, which represent inputs 01 and 10, respectively.

Although many molecules possess an intrinsic capacity for basic Boolean logic, it remains challenging to integrate multiple molecular logic gates into circuits that can perform more complex tasks. Tian[234] has described a [2]rotaxane whose combination of optical inputs and outputs constitute the necessary conditions for a more sophisticated gate known as a half-adder, which combines (**Figure 6.83**) XOR and AND logic gates. The α-CD ring of the naphthalimide disulfonate-stoppered [2]rotaxane **R6197^{4-}** shuttles (**Figure 6.83a**) between stilbene and azobenzene recognition units in water. Since the photostationary state of stilbene and azobenzene are accessed at different excitation wavelengths, two independent inputs—namely, irradiation at 313 nm (IN_1) and 380 nm (IN_2)—are employed to populate different *cis* and *trans* isomers as a result of $E \rightarrow Z$ photoisomerization. IN_1 preferentially converts the stilbene unit, populating the **($E_{N=N}Z_{C=C}$)-R6197^{4-}** isomer, where α-CD encircles the azobenzene unit. IN_2 preferentially isomerizes the azobenzene unit, populating the **($Z_{N=N}E_{C=C}$)-R6197^{4-}** isomer, in which stilbene is encircled. Double-excitation at both of these wavelengths generates **(*ZZ*)-R6197^{4-}**, where the α-CD ring is forced to surround the biphenyl unit that constitutes the innermost half of each photoactive station on the dumbbell. The reverse process, $(Z) \rightarrow (E)$ photoisomerization, can be achieved in all cases, either by the application of heat (60 °C for 1 h) or light (280 nm for stilbene and 450 nm for azobenzene) to repopulate the ground state, **(*EE*)-R6197^{4-}**. Thus, the two input signals can be used to switch between four unique isomers. The desired isomer represents close to 60% of the molecular population in each of the photostationary states. Significant differences were observed when comparing the absorption and emission spectra of each species. By judicious assignment (**Figure 6.83b**) of these spectral features as output parameters, **R6197^{4-}** was made to perform binary logic operations. The XOR gate's output signal (OUT_1) is the parameter ΔF, defined as the percent change in fluorescence intensity between the photostationary state and the prior state at the emission signal of interest ($\lambda_{max} = 395$ or 520 nm, depending on the input signal). ΔF functions as an XOR output because its value is relatively low when $IN_1 = IN_2$ and high when $IN_1 \neq IN_2$. The second output signal (OUT_2) is defined as ΔA, the ratio of the differences in absorbance of two absorption bands at 270 and 350 nm with respect to an isosbestic point at 301 nm ($\Delta A = |A_{350} - A_{270}|/A_{301}$). ΔA represents AND logic because its value is large (0.73) only in **(*ZZ*)-R6197^{4-}**, when both IN_1 and IN_2 are true. **Figure 6.83c** contains a diagram and truth table for the half adder. The XOR gate (OUT_1) represents the sum digit (n_S) and the AND gate (OUT_2) represents the carry digit (n_C), allowing the half adder to compute the binary sum of its inputs.

Materials beyond the small molecule are also capable of molecular logic. Leigh[475] has demonstrated that his thin



R6197^{4-} *Isomer*	IN_1 313 nm	IN_1 380 nm	OUT_1 ΔF n_S	OUT_2 ΔA n_C	Binary Sum
(*EE*)	0	0	0	0	00
($E_{N=N}Z_{C=C}$)	1	0	1	0	01
($Z_{N=N}E_{C=C}$)	0	1	1	0	01
(*ZZ*)	1	1	0	1	10

Figure 6.83 A [2]rotaxane half-adder.[234] (a) An α-CD ring shuttles rapidly between stilbene and azobenzene units in the dumbbell of ***EE*-R6197^{4-}**. Three additional co-conformations can be accessed by irradiation of stilbene (313 nm) and azobenzene (380 nm). The $E_{N=N}Z_{C=C}$ and $Z_{N=N}E_{C=C}$ isomers are populated in the photostationary states of stilbene and azobenzene, respectively, while the *ZZ* isomer is populated if both units are stimulated. (b) Bar graphs showing the relative magnitude of Δ*F* and Δ*A*—parameters derived from fluorescence and absorption spectra, respectively—in each of the four isomers of **R6197^{4-}**. The parameters Δ*F* and Δ*A* represent XOR and AND logic gates, respectively, at an appropriate detection limit (dashed line). (c) A diagram and truth table for the half-adder, demonstrating how setting Δ*F* as the sum digit (n_s) and ΔA as the carry digit (n_c) performs the function of a binary half-adder.

films of the side-chain poly[2]rotaxane **R6166$_{GG}$**—see **Figure 6.66** in **Section 6.14.3.3**—serve as INHIBIT gates, where IN_1 and IN_2 are defined as exposure to Me_2SO vapor and TFA vapor, respectively, and OUT is defined as quenched fluorescence from the anthracene stopper. According to this logic operator, fluorescence is quenched (OUT = 1) only when $IN_1 = 0$ and $IN_2 = 1$. Fluorescence is not quenched when $IN_1 = IN_2 = 1$ because the quenching effect of TFA is counteracted by Me_2SO vapor, since Me_2SO causes the benzylic 3,5-dicarboxamidopyridinium ring to translate away from the fluorogenic anthracene stopper whose fluorescence is quenched when the ring is nearby.

Logic gates based on mechanized MSNPs—see **Section 6.15.1.1**—have also been described. For example, Zink[743] has developed pseudorotaxane-mechanized MSNPs (**Section 6.15.1.1**) exhibiting dual-controlled nanoparticles exhibiting AND logic when considering cargo release as output 1, since the cargo is released only when both stimuli—namely, irradiation at λ = 448 nm and deprotonation with NaOH (input 11)—are applied. Cargo is not released (OUT = 0) when neither stimulus is applied (input 00), or when only light (input 10) or pH (input 01) are applied. Other dual-controlled mechanized MSNPs[745,751,765,767,768,777,782] that release cargo (output 1) in response to either or both of two

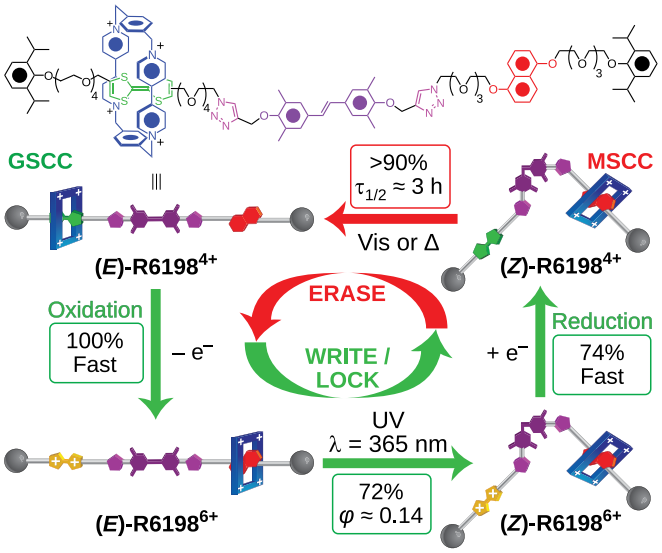


Figure 6.84 Summary of the operation[100] of a redox-switchable donor-acceptor [2]rotaxane possessing an azobenzene gate that introduces a memory effect on the translational isomerism under UV irradiation.

input stimuli (01, 10, or 11) constitute OR logic operators. We note that molecular switch tunnel junctions in crossbar arrays can also serve[101,104,881] as elements for configurable logic gates—see **Section 6.14.1.1**.

Information Storage

Several strategies have been identified for employing mechanically interlocked molecular switches as information storing elements. One strategy involves physically writing information, as arrays of dots, for example, when [2]rotaxanes are deposited on substrates as thin films. This approach was introduced by Leigh,[510] who relied on the mechanical force of an AFM tip to write lines of regularly spaced dots in thin films of benzylic amide [2]rotaxanes—see **Figure 6.31** in **Section 6.12**. Gao[113,114,603,604] has also written dots in thin films of redox-active [2]rotaxanes by applying electrochemical energy to the rotaxanes through an STM tip—see **Figure 6.55** in **Section 6.14.1.1**. Another information storage strategy[105] involves the organization of bistable mechanomolecules in a crossbar array of molecular switch tunnel junctions, where each junction in the array represents a bit that can be written and erased by redox stimuli. The molecular memory device based on the [2]rotaxane **R6154**$^{4+}$—see **Figure 6.52** in **Section 6.13.1.1**—is depicted in **Figure 1.36** of **Section 1.3.6**.

Yet another approach to molecular information storage involves encoding information within a molecular structure, such as a co-conformation in the case of MIMs. For example, a photoactive azobenzene unit in between the TTF and DNP recognition units of the bistable [2]rotaxane **(*E*)-R6198**$^{4+}$ enables this switch to serve[100] as a memory element. The memory effect (**Figure 6.84**) occurs when "data"—a change in the ring's position with respect to the axle—is "written" on the rotaxane by the oxidation of its TTF unit to the TTF^{2+} dication of **(*E*)-R6198**$^{6+}$, and subsequently "stored" by the *trans*-to-*cis* isomerization of the azobenzene unit, generating the species **(*Z*)-R6198**$^{6+}$ under UV irradiation. When **(*Z*)-R6198**$^{6+}$ is reduced to **(*Z*)-R6198**$^{4+}$, the steric barrier of the *cis*-azobenzene unit acts as a gate,[882] which prevents the CBPQT^{4+} ring from returning to its preferred TTF site from the DNP unit. Thus, the introduction of this photoswitchable gate allows the rotaxane to "remember" the position of its ring under irradiation with light. The data are stored for several hours in the dark at room temperature before the GSCC of **(*E*)-R6198**$^{4+}$ is recovered by thermal *cis*-to-*trans* isomerization of the azobenzene gate.

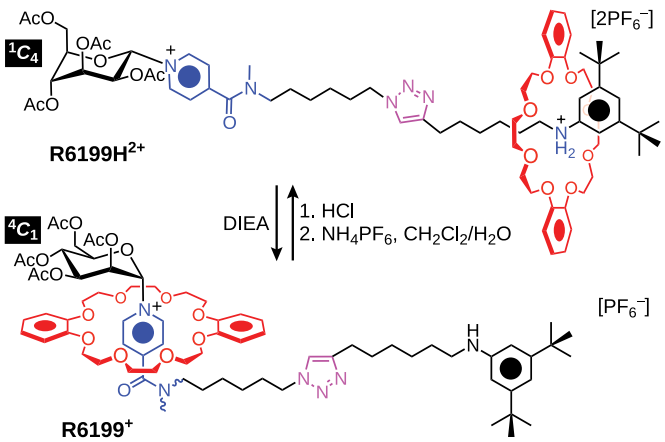
Another mechanomolecule with molecular memory capabilities is Sauvage's electrochemically-driven pirouetting [2]rotaxane **CuR612**$^+_{CN4}$—see **Section 6.1.2**—which has been implemented[148] as a finite-state set–reset machine. This molecular machine can store a bit of information, where 0 and 1 are encoded by the two stable states—**CuR612**$^+_{CN4}$ and **CuR612**$^{2+}_{CN5}$, respectively—of the rotaxane. States 1 and 0 can be written by a set potential and reset potential, respectively, while they are detected by the observation of anodic (oxidation) and cathodic (reduction) peaks in the voltammetric scans.

6.15.1.4 Switches Influencing Molecular Organization

A number of switches have utilized the constraints of mechanical bonds in order to do work on other molecules. Here we describe a few representative examples of how switchable MIMs, when coupled to other molecules and materials, can channel the energy they dissipate into a function involving the (re)organization of matter at the molecular level.

Controlling Conformation

Coutrot[883] has investigated the mannopyranosyl-stoppered [2]rotaxane **R6199H**$^{2+}$, in which the pH-driven motion (**Scheme 6.112**) of the DB24C8 ring with respect to the axle influences the chair conformation of the pyranose ring.



Scheme 6.112 A molecular machine that controls the chair conformation of a pyranose ring.[883]

A phenomenon known as the reverse anomeric effect defines the chair's conformation in the protonated state of **R6199H$^+$**, where the cationic charge of the pyridinium unit located at the anomeric position of the glucopyranosyl ring renders the equatorial position the most favorable one for the aglycone, although the many of the other substituents on the glucopyranosyl ring must adopt the unfavorable axial orientations as a consequence. Whereas the DB24C8 ring encircles an alkylanilinium recognition unit in **R6199H^{2+}**, the base-induced translation of the ring to the 4-(methylcarbamoyl)pyridinium recognition site of **R6199$^+$** leads to a chair flip ($^1C_4 \rightarrow {}^4C_1$), owing to the ring's influence on the local environment of the mannopyranosyl ring. The methylated carbamoyl group of the pyridinium-based recognition unit is crucial to the observation of the chair-to-chair flip, since a switch possessing an amide linkage at the same site does not display the same pH-triggered switching of glucidic conformation.

Controlling Helicity

Takata[332–334] has found that a mechanically bonded crown-8 ring possessing a planar chiral (*R*)-binaphtho unit in its constitution can be translated along the side-chain of a polymer backbone in a manner that controls (**Figure 6.85**) its helicity. The poly[2]rotaxanes **(*R*)-6200aH^{n+}** and **(*R*)-6200bH^{n+}** comprise polyacetylene[332,333] and poly(*m*-phenylenediethynylene)[334] backbones, each appended with nearly isostructural *tert*-ammonium side chains encircled by the planar chiral crown-8 ring. In this state, polymer **(*R*)-6200aH^{n+}** is a racemic helix and **(*R*)-6200bH^{n+}** is a random coil. Deprotonation of the tertiary nitrogen center with an excess of DBU causes the ring to encircle an ester linkage near the main-chain backbone of the polymers **(*R*)-6200a** and **(*R*)-6200b**. From this proximal position, the chirality of the binaphtho units are apparently transferred to the polymer backbone, resolving each polymer into a one-handed helix, as detected by circular dichroism. Rings possessing (*S*)-binaphtho units transfer their chirality to a polymer helix of the opposite hand.[333] The switch is reversible, since the work accomplished by adding DBU can be undone by protonating the amines with TFA. The protonated polymers are also capable of undergoing solvent-driven switching. The polyacetylene helix of **(*R*)-6200aH^{n+}** is racemic in $CHCl_3$ and THF, yet one-handed in Me_2CO and Me_2SO, owing again to the relatively distal and proximal positions of the ring with repect to the backbone in these solvents. The hydrophobic poly(*m*-phenylenediethynylene) backbone of **(*R*)-6200bH^{n+}** collapses into a one-handed helix in polar MeCN, yet remains a random coil in $CHCl_3$, so its pH actuation is carried out in a 1:1 mixture of these two solvents. Thus, the side-chain [2]rotaxanes of these polymers act as tiny machines whose multi-modal (pH and solvent) actuation directly controls the superstructure of the helix.

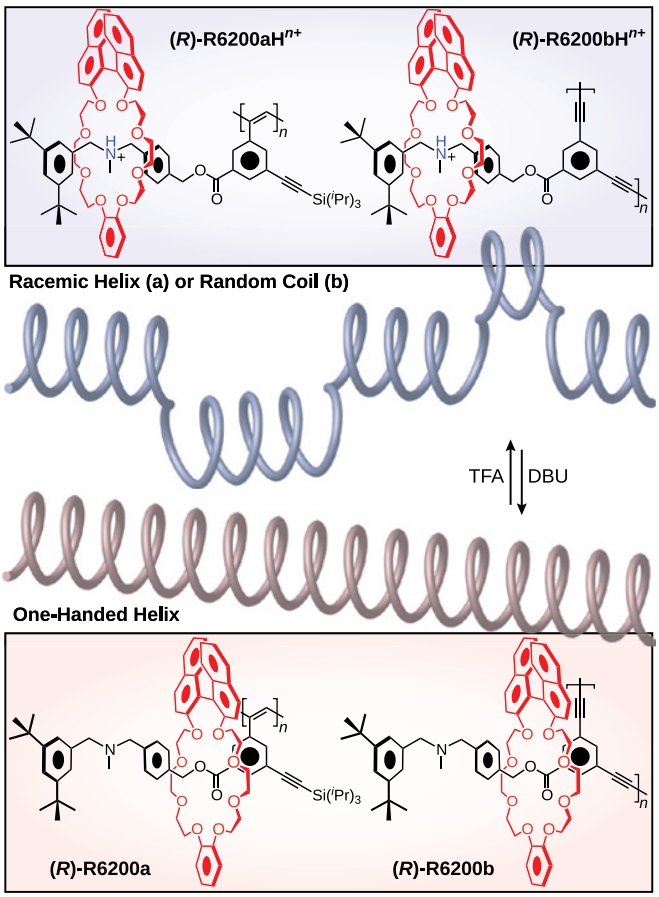


Figure 6.85 The pH-controlled actuation of the side-chain molecular machines regulates the helicity of the main-chain backbones in Takata's poly[2]rotaxanes.[332–334]

Recently, Takata[503] has found that the helical pitch of a polyacetylene backbone can be controlled (**Figure 6.86**) by the actuation of an achiral side-chain [2]rotaxane in the poly[2]rotaxane **R6201H^{n+}**, which is converted to the neutral **R6201** in the solid state by thermal decomposition (**Section 6.9.2**) of its trichloroacetate counterions at 100 °C. The changes in helical pitch can be observed by the naked eye, since they are accompanied by substantial changes in the absorption of polyacetylene, which changes from red to yellow as the pitch of the helix increases. The work done on the helix by thermal decomposition can be reversed by reprotonating the tertiary amine centers of the side chains while dipping the thin film in a mixture of trichloroacetic acid and hexane.

Controlling Aggregation

If a mechanomolecular switch can be coupled to a moiety that drives its aggregation in a manner that is sensitive to the relative position of the ring, it becomes possible to employ it as a molecular machine that regulates macroscopically observable properties of a material.

Li[884] has described a solvent-switchable [2]rotaxane **R6202** possessing a stopper derived from tetracyanobutadiene (TCBD), which drives the formation (**Figure 6.87**) of different nanostructural morphologies depending on the position of the ring. The benzylic isophthalamide ring encircles (**Figure 6.87a**) the axle's glycine (**R6202$_G$**) portion in $CHCl_3$ and a decamethylene (**R6202$_{C10}$**) linker in Me_2SO on account of hydrogen

bonding and solvophobic effects, respectively, in these solvent systems. The variable position of the ring influences the morphology of the nanosuperstructures that form in different solvents. Bundled nanofibers self-assemble (**Figure 6.87b**) when hexane is introduced to a $CHCl_3$ solution of **R6202$_G$**, while hollow spherical nanoparticles emerge (**Figure 6.87c**) if MeOH is added instead. These assembies are attributed to the aggregation of TCBD units into fibrous and bilayered superstructures. On the contrary, the nearby rings interfere with the aggregation of TCBD in **R6202$_{C10}$**, leading to the formation (**Figure 6.87d**) of wormlike nanoparticles in Me_2SO. When the dumbbell is not interlocked with the ring, it forms completely different aggregates when exposed to the same conditions, confirming that the solvent-driven translation of the ring influences the morphology of the aggregates.

Qu[540] has investigated the pH-controlled actuation and aggregation (**Figure 6.88**) of a palindromic bis[1]rotaxane comprising a fluorescent, self-aggregating perylenediimide (PDI) unit flanked by a pair of ferrocene-hinged [1]rotaxanes, which closely resemble compound **R6132H^{2+}** from **Section 6.13.2**, **Scheme 6.96** in terms of structure and operation. According to energy-minimized models (**Figure 6.88a**), the pH-controlled gliding of the crown-8 rings between ammonium (**R6203H$_2^{4+}$**) and triazolium (**R6203^{2+}**) units gives rise to molecular lengths that differ by more than 1.7 nm. In the extended state of **R6203H$_2^{4+}$**, the π–π stacking of PDI units drives the formation of spherical aggregates

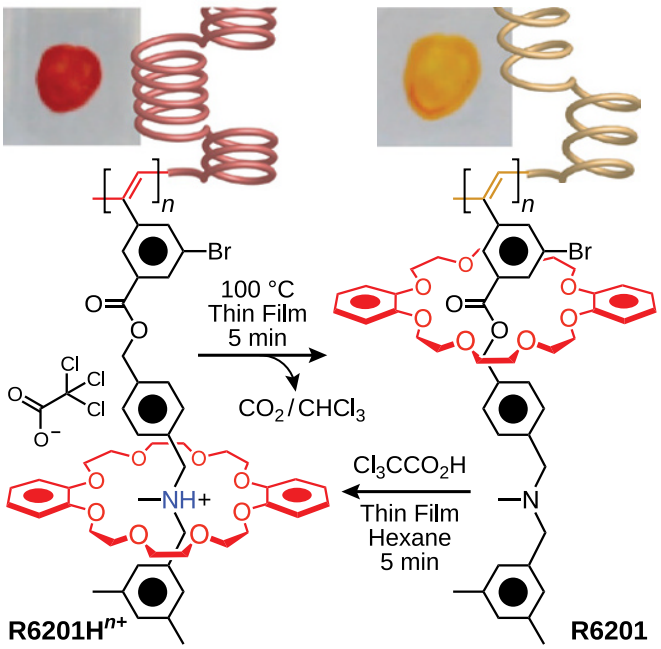


Figure 6.86 The helical pitch of a polyacetylene helix is switched by the actuation of its side chain [2]rotaxane, which is driven by deprotonative thermal decomposition of trichloroacetate in the solid state. Inset photographs show the different colors of thin films in each state, associated with pitch changes in the racemic polymer helix, reproduced with permission from ref. 503 (copyright 2016 Royal Society of Chemistry)

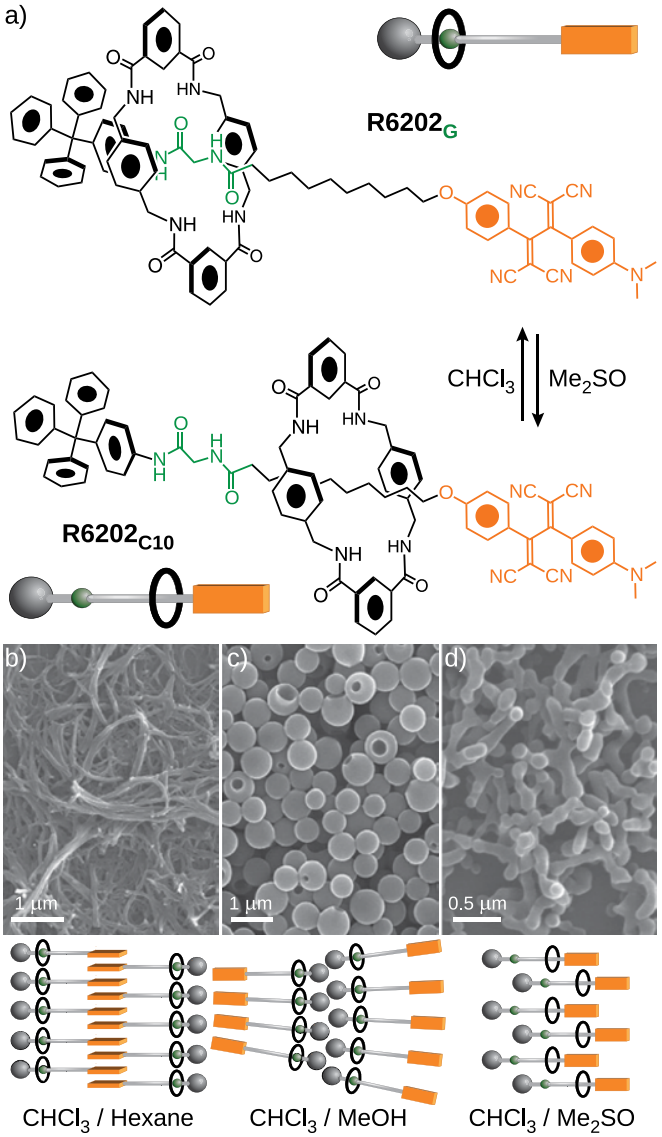


Figure 6.87 A solvent switchable rotaxane molecular machine that regulates the aggregation of its TCBD stopper.[884] (a) Steroformulas **R6202$_G$** and **R6202$_{C10}$**, the dominant translational isomers in $CHCl_3$ and Me_2SO, respectively. SEM Images and graphical representations of proposed superstructures of the rotaxanes are pictured for aggregates that self-assemble in (b) $CHCl_3$/hexane, (c) $CHCl_3$/MeOH, and (d) Me_2SO. SEM images reproduced with permission from ref. 884 (copyright 2009 Wiley)

(**Figure 6.88b**) in 1:1 Me_2CO/MeCy. Upon the addition of Zn^{2+}, the intramolecular crosslinking of triazole groups drives these assemblies to form (**Figure 6.88c**) larger, more crystalline aggregates. If DBU is added instead to access the contracted state of **R6203^{2+}**, the local steric crowding around the PDI unit interferes with its self-aggregation, resulting in more amorphous nanomorphologies (**Figure 6.88d**) in the corresponding aggregates. Since the fluorescence of the PDI unit is quenched in a distance-dependent manner by the ring-appended ferrocence units, the position of the ring is reported by the intensity of fluorescence emission from the sample.

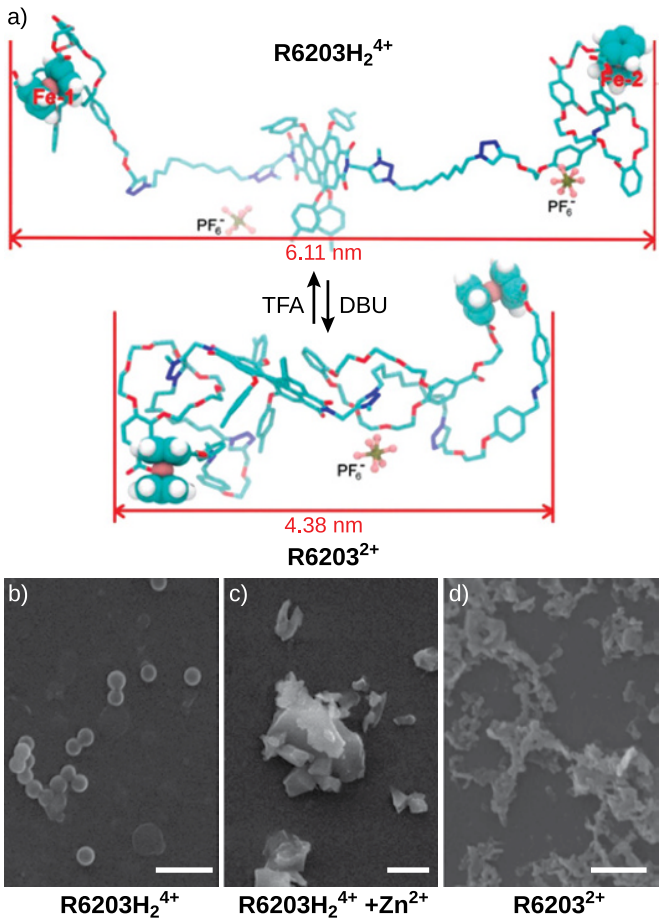


Figure 6.88 pH- and ion-controlled aggregation of a switchable bis[1]rotaxane.[540] (a) MD snapshots of **R6203H$_2$$^{4+}$** (extended state) and **R6203^{2+}** (contracted state), which differ not only in length, but in steric crowding around the central PDI unit. SEM images of the aggregates arising from Me_2CO/MeCy (1:1 $^{v}/_{v}$) solutions of (b) **R6203H$_2$$^{4+}$**, (c) **R6203H$_2$$^{4+}$** with 2 equiv $Zn(ClO_4)_2 \cdot 6H_2O$, and (d) **R6203^{2+}** in the presence of 2.5 equiv DBU. All scale bars are 2 µm. Images reprinted with permission from ref. 540 (copyright 2014 American Chemical Society)

Camposeo, Credi, and Pisignano[623] have embedded [2]pseudorotaxane switches in electrospun PMMA nanofiber matrices and demonstrated that their pH-controlled actuation, not only remains operable in the nanofibers, but also influences their mechanical properties. In aligned arrays of the electrospun nanofibers, the base-triggered dethreading of the ring leads to an enhancement in stiffness, whereas control fibers embedding only the axle component part do not respond likewise to deprotonation.

Giuseppone[527,528] has recently shown that the muscle-like actuation of [*c*2]daisy chains—see **Section 6.13.1.1**—can be exploited in modulating the self-assembly of supramolecular polymers derived thereof. For example (**Figure 6.89**), the extended [*c*2]daisy chain[528] **R6204H$_2$$^{4+}$** and the corresponding contracted state **R6204^{2+}** were designed with 2,6-diacetylaminopyridine stoppers, which display D-A-D hydrogen-bonding motifs that are complimentary to the A-D-A patterns of the bis(uracil) compound **L610**. In 4:1 $CHCl_3$:MeCN, equimolar mixtures of these co-monomers produce mesoscale aggregates at concentrations greater than 4 mM. The supramolecular polymer **R6204H$_2$$^{4+}$: L610** forms multimicron-length fibers comprising 10–20 nm-wide bundles of smaller fibers approximately 3 nm in diameter, while the contracted state of **R6204^{2+} : L610** forms discrete nanoparticles, 200–400 nm in diameter, which are also composed of bundled 3-nm fibers. These nanostructures were characterized by SEM and AFM microscopy, as well as by static light scattering and small-angle neutron scattering experiments. It was also confirmed that these mesostructures can be interconverted (**Figure 6.89**) *in situ*, since the base-triggered contraction and acid-triggered extension of the aggregated daisy chains are accompanied by transitions from fibrous to discrete, and discrete to fibrous morphologies, respectively.

Controlling Mechanical Properties

Yui[885] has employed one of his controlled-release (**Section 6.15.1.1**) α-CD polyrotaxanes as photo-cleavable cross-linkers in photocurable resin plastics. In visible light, the α-CD rings of the polyrotaxanes reinforce the strength of the resin by serving as crosslinks in its poly(hydroxyethyl methacrylate) network. Upon exposure to 254 nm UV light, however, the polyrotaxane stoppers are cleaved and the rings are released from the dumbbell under mechanical stress, resulting in a 60% reduction in the ultimate tensile strength of the plastic. We anticipate that in the future, molecular machines will be employed more often as crossinks that regulate the properties of dynamic and responsive solid-state materials.

6.15.1.5 Switches Regulating Catalysis

Artificial switchable catalysts[886,887] may be considered molecular machines that perform chemical work by expending energy in order to regulate the progress of a reaction. Among the rotaxane catalysts[888] that have been investigated, a few of them have relied on the stimulus-triggered translation of a ring to control the access of substrates to an active site,[325,889–892] beginning with the [2]rotaxane **R6205H^{3+}** introduced by Leigh[889] in 2012. The switch does not differ substantially from the pH-driven dialkylammonium/triazolium/crown ether switches described in **Section 6.3.3.1**—the key innovation here lies not in structure but in function. The secondary amine that becomes exposed (**Figure 6.90a**) in **R6205^{2+}** as a result of the ring's translation to one of the triazolium units upon deprotonation of the ammonium center can be utilized (**Figure 6.90b–g**) for catalysis. **R6205^{2+}** was found[890] to be particularly effective in catalyzing various Michael additions (**Figure 6.90b–e**), as well as the chlorination (**Figure 6.90f**) of aldehydes with *N*-chlorosuccinimide and a Diels-Alder reaction (**Figure 6.90g**). The reactions that proceed through iminium catalysis (**b–d**, **g**) are more efficient than those proceeding through enamine catalysis (**e**, **f**) in CH_2Cl_2. It was also demonstrated that conditions (**b**) and (**e**) could be employed

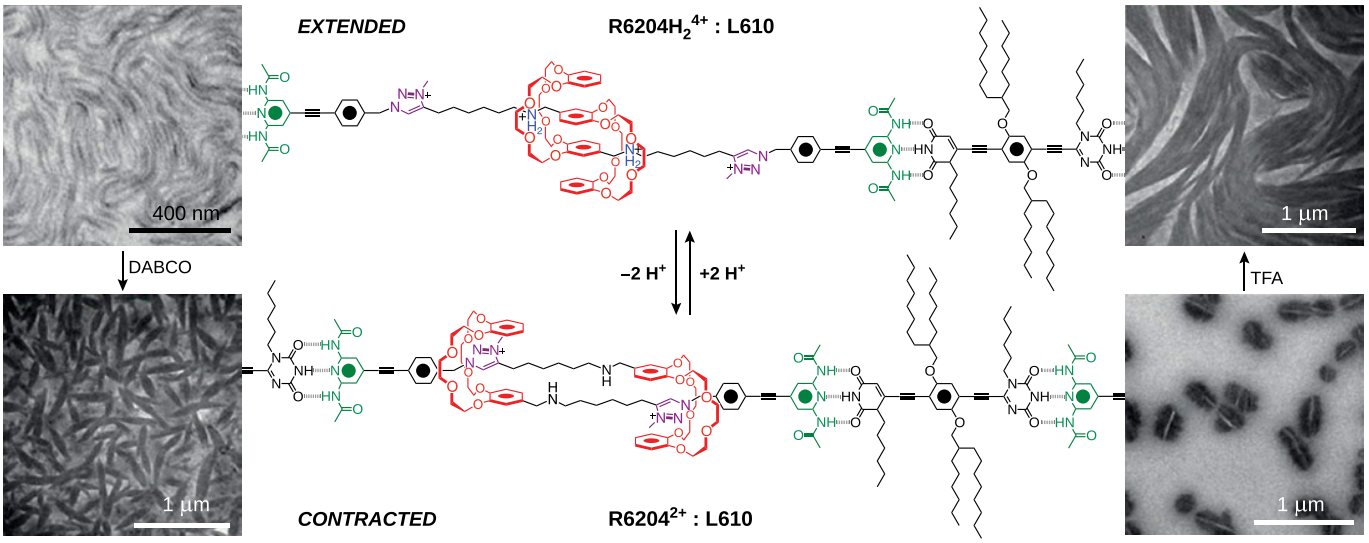
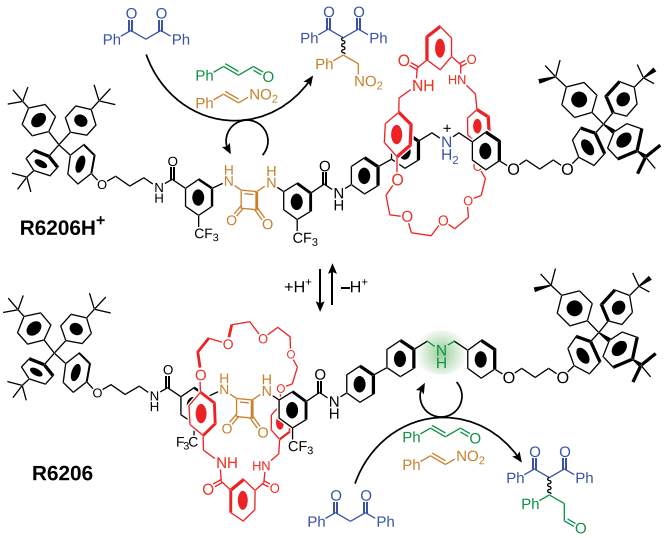


Figure 6.89 The morphological changes in Giuseppone's supramolecular muscle polymers accompanying the pH-controlled actuation of their [c2]daisy chain co-monomers.[528] SEM Images show the *in situ* aggregate morphologies before and after the base-triggered contraction (left hand side) and acid-triggered extension (right hand side) of **R6204H$_2^{4+}$: L610** and **R6204^{2+} : L610**, respectively, in 4:1 $CHCl_3$: MeCN.

in a tandem reaction on *trans*-cinnamaldehyde in 50% yield. While none of the reactions proceed when **R6205H^{3+}** is introduced as the catalyst, the catalyst can be activated *in situ* with base to initiate catalysis by **R6205^{2+}**. A rotaxane based on the same recognition motif has also been equipped with a stereocenter adjacent to its amine active site and utilized in asymmetric organocatalysis, promoting a Michael addition similar to that in **Figure 6.90d** in up to 70% yield and 86% enantiomeric excess.[891]

More sophisticated organocatalytic rotaxanes have emerged. For example, Álvarez[325] has compared the catalytic activity of multicomponent rotaxanes possessing one, two, or three catalytic dibenzylamine units, finding that the rates and yields of rotaxane-catalyzed Michael additions are enhanced significantly by the presence of multiple catalytic centers. Leigh[892] has designed a bistable [2]rotaxane possessing two different organocatalytic recognition sites. As illustrated in **Scheme 6.113**, the acid/base-triggered switching between states **R6206H$^+$** and **R6206** moves the isophthalic crown ether between dibenzylamine and squaramide active sites, respectively, exposing the non-encircled site for catalysis. While the amine site of **R6206** promotes the Michael addition of activated methylene-1,3-dicarbonyl compounds to α,β-unsaturated aldehydes by iminium catalysis, the squaramide unit of **R6206H$^+$** promotes a similar Michael addition of *trans*-β-nitrostyrene by hydrogen bond catalysis. In a proof of concept, the rotaxane was introduced to a pool of 1,3-diphenylpropane-1,3-dione, crotonaldehyde, and *trans*-β-nitrostyrene. The state of the rotaxane determines the outcome of the reaction, since **R6206H$^+$** converts the crotonaldehyde and **R6206** converts the nitrostyrene.

Since cellular enzymes carry out catalysis in a highly parallel manner, their activities are often regulated by their interactions with small molecules and other proteins that serve as triggers or establish feedback loops in order to maintain precise spatial and temporal control of the cell's reaction network. Artificial switchable catalysts such as the rotaxanes described in this Section may one day offer researchers a similar level of control over reaction sequences and transformations in chemical processes and networks.



Scheme 6.113 A dual-catalytic switchable rotaxane, which converts different reactants from the same pool depending on its state.[892]

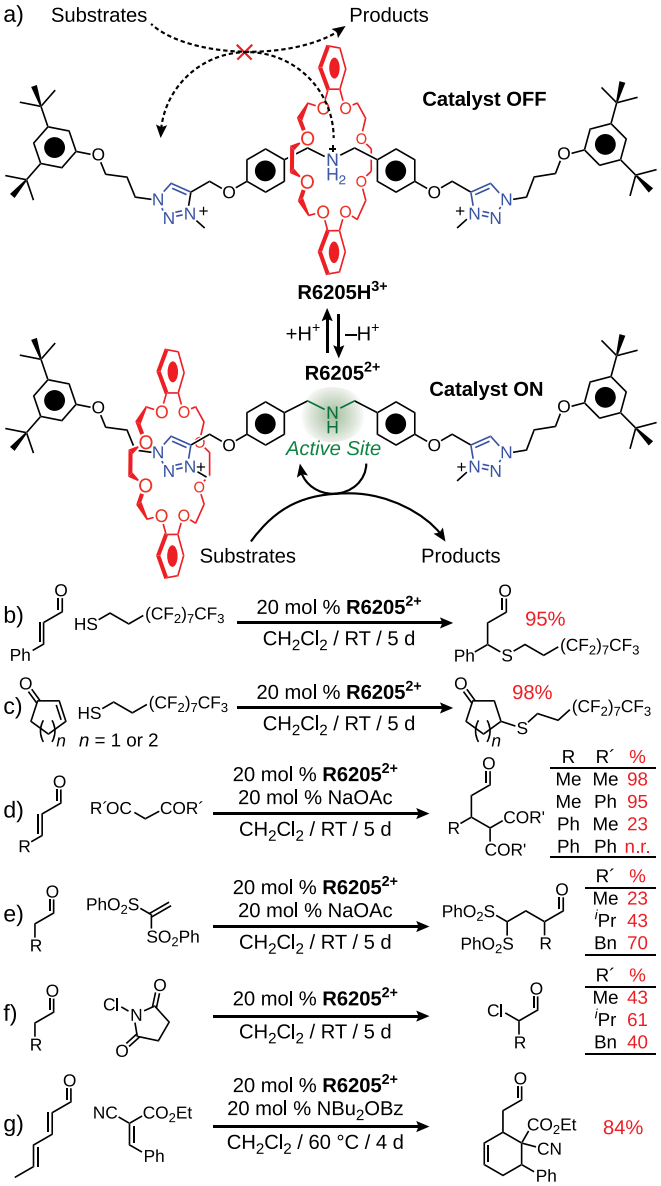


Figure 6.90 Leigh's switchable rotaxane organocatalyst.[889,890] (a) The rotaxane is converted between a catalytically inactive state, **R6205H^{3+}**, and a catalytically active state, **R6205^{2+}**, by protonation and deprotonation, respectively, of its dibenzylammonium center with acid and base. The scope of reactions catalyzed by **R6205^{2+}** include Michael additions of (b) thiols to *trans*-cinnamaldehyde, (c) thiols to cyclic α,β-unsaturated ketones, (d) activated methylene compounds to α,β-unsaturated aldehydes, (e) aldehydes to vinyl sulfones, as well as (f) α-chlorination of aldehydes and (f) a Diels-Alder reaction between a 2,4-dienal and a cyanoacetate dienophile. None of the reactions in (b)–(g) proceed when **R6205H^{3+}** is employed as the organocatalyst.

6.15.2 Brownian Ratchets with Mechanical Bonds

In this Section, we outline how the thermal energy of stochastic processes can be harnessed in molecules with mechanical bonds to perform thermodynamic work as a result of periodic switching in an asymmetric medium. The actuation of these molecules induces biased Brownian motion that would be extraordinarily unlikely under equilibrium conditions. The difference between a ratchet and a switch is that a ratchet follows a different pathway on its return to equilibrium than the one it followed upon perturbation by a stimulus in the first place. The thermodynamics of these molecules are explained in **Section 6.15.1.1**. We describe the biased Brownian movement of mechanomolecules as being "mechanostereoselective" when motions associated with mechanostereoisomerization, such as translation and pirouetting, are involved. Mechanostereoselectivity is illustrated in the context of pseudorotaxane threading and dethreading in **Section 6.15.1.2**, while mechanomolecules that obey ratchet mechisms are described in **Sections 6.15.1.3–6.15.1.4**.

6.15.2.1 Thermodynamics of a Brownian Motor

Molecular machines in nature employ a variety of strategies to accomplish work against the turbulence of thermal noise. At the most general level, these strategies are known[893] as ratchet mechanisms, which are named for a thought experiment first proposed by von Smoluchowski[894] in 1912 and popularized by Feynman[895] in 1962. The thought experiment demonstrates that useful work cannot be extracted from fluctuations at thermal equilibrium. The Feynman-Smoluchowski ratchet (**Figure 6.91a**) is a setup involving two compartments. The first compartment is held at temperature T_1 and houses the ratchet—a microscopic gear possessing an asymmetric sawtooth pattern and a corresponding pawl, which is intended to allow the gear to rotate in only one direction. The gear is connected by an axle to a paddle wheel within the second compartment held at temperature T_2. The paddle wheel is small enough to be rotated at the urge of a single gas molecule collision. Although the random collisions of gas molecules will turn the paddle wheel in either direction with equal probability, the one-way ratchet and pawl would rectify rotation into a single direction, in apparent violation of the second law. Feynman proved that, in fact, no unidirectional rotation takes place when both compartments are held at equal temperatures ($T_1 = T_2$) since the pawl and the paddle wheel are both equally subject to Brownian motion. If the temperatures of the two compartments, however, are not equal ($T_1 \neq T_2$) the device will exihibit a net unidirectional rotation without violating the second law as a result of unequal kinetic forces acting on the paddle wheel and the ratchet/pawl. The unidirectional rotation of the axle could perform work, for example, by winding up a string against a load. Thus, extracting work from stochastic systems requires (i) the incorporation of one or more symmetry breaking elements, and (ii) that the system be driven away from thermal equilibrium.

The intellectual predecessor of the Feynman-Smulochowski ratchet is Maxwell's demon. James Clerk Maxwell[896] was one of the first scientists to propose a thought experiment dealing with the apparent violation of the second law of thermodynamics. He imagined a two-compartment box of gas with a door that is controlled

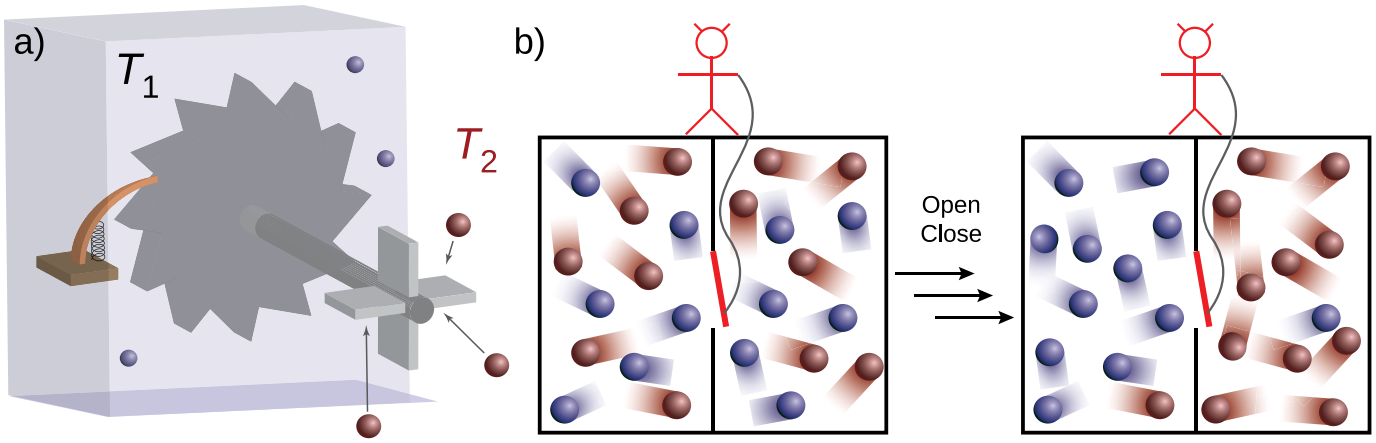


Figure 6.91 Historical thought experiments on the second law of thermodynamics. (a) In a Feynman-Smulochowski ratchet, a ratchet-and-pawl in compartment 1 is connected by an axle to a paddlewheel in compartment 2. The device rotates randomly when $T_1 = T_2$, but produces a net directional rotation when $T_1 \neq T_2$. (b) Maxwell's demon battles entropy as it uses information to sort hot and cold gas particles by timing appropriately the opening and closing of a trap door in between two compartments.

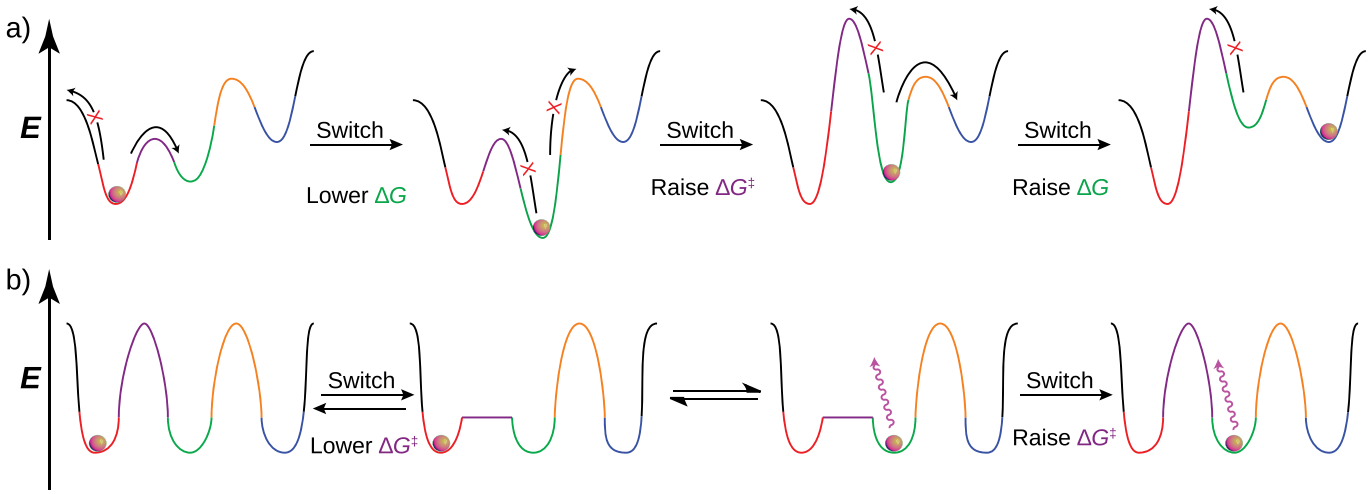


Figure 6.92 Energy diagrams of ratchet mechanisms for the directional transport of a ball representing a population of molecular states. (a) An example of an energy ratchet. First, the green well (ΔG) is lowered by a switching event, causing the ball to move from the red well to the green one as the system re-equilibrates. Then, the purple hill ($\Delta G^{\ddagger}$) and the green well (ΔG) are raised, causing the ball to roll over into the blue well, since a large kinetic barrier ($\Delta G^{\ddagger}$) prevents the ball from returning to the lowest-energy red well. (b) An example of an information ratchet. The activation barrier ($\Delta G^{\ddagger}$) between the red and green wells acts as a gate. When the gate is opened, the system populates both wells as it equilibrates. If the system is designed to report its position – symbolized by a wavy magenta arrow – only in the green well, for example, this information can be used to close the gate at an appropriate moment so as to trap the system in the green well. A similar process could then be repeated at the orange gate in order to access the blue well.

(**Figure 6.91b**) by a "demon" who opens the door only for particles approaching it with a faster-than-average kinetic energy. Maxwell's sorting demon[D] would thus create a temperature difference between the two compartments, reducing the entropy of the system. Szilard[897] pointed out that a real-life Maxwellian demon would have to expend energy to observe the particle and open the door, increasing its own entropy by more than that of the compartment, such that the second law is not violated.

[D] A Maxwellian demon could also sort compartments by pressure.

The manifestations of non-law-violating versions of Feynman's ratchet and Maxwell's demon have been interpreted (**Figure 6.92**) for molecular systems. Feynman's ratchet is an example of an energy ratchet (**Section 6.15.2.3**), which, as its name suggests, expends energy to perform thermodynamic work. A molecular energy ratchet is characterized by the non-equilibrium modulation of a thermodynamic landscape in order to achieve directed transport—i.e., biased movement of an energy form such as mechanical motion, current, etc.—often by raising and lowering (**Figure 6.92a**) local energy minima and maxima asymmetrically. Maxwell's demon, on the other hand,

exemplifies an information ratchet (**Section 6.15.2.4**), where information about the position of a microscopic entity is utilized to pump a system away from equilibrium. It relies on a time-resolved knowledge of the system in order to raise and lower gates at appropriate moments to achieve directional transport. The distinction between these two types of ratchets is somewhat superficial, however, since the storage and access of information is associated with enthalpic and entropic costs. The second law is not violated in either case because the energy required actuate the thermodynamic landscape is greater than the exergy—i.e., available energy—that has been ratcheted into the system.

Molecules that implement ratchet mechanisms are known[898,899] as Brownian motors. Natural and artificial examples[667] of how Brownian motors are exploited include (i) energy storage, (ii) facilitating chemical transformations, (iii) transporting nanoscale cargos, and (iv) assembling and manipulating nanostructures. Regardless of the application, doing work at this scale requires that the constraints of microscopic reversibility be circumvented. Microscopic reversibility is defined[632] as the principle that the mechanism of a reversible reaction in the forward direction is exactly the reverse of that in the backward direction.[E] This principle is an important consideration[655] in any situation involving a molecular switch/machine that is coupled (**Figure 6.93**) with another system. Any work absorbed or dissipated on the forward stroke will be cancelled out (**Figure 6.93a**) by the exact opposite process as the path is retraced in the backward stroke.

Microscopic reversibility can be circumvented by designing a system to undergo a non-reciprocating cycle—a description meaning that the forward and backward pathways are different. The conceptual illustration in **Figure 6.93b** demonstrates how the coupling and decoupling of a molecular machine's substrate in an appropriate sequence constitutes a non-reciprocating cycle. An integrated system coupled to the Brownian motor might take the form of a molecular spring that stores energy as it is drawn away from its thermodynamically most stable conformation, or a catalyst[900] that is switched between different states. The non-reciprocating cycle of a Brownian motor involves (i) the 'power stroke' of the machine, which is fuelled by an energy source and (ii) the machine acting on the substrate spring or catalyst during this power stroke, followed by (iii) a decoupling of the machine and substrate, which allows the spring or catalyst to perform work on the environment, before (iv) the two components are re-coupled in their initial states and the cycle is ready to be repeated. This type of non-reciprocating cycle is also known as a stochastic pump.[901] Li[289] and Credi[290] have described rotaxane-based "molecular transporters" closely related to **R636H^{3+}** (**Scheme 6.39**, **Section 6.3.3.1**) that complete non-reciprocating cycles by the "catch and release" molecular cargo before and after a pH-controlled shuttling event, although the energy dissipated by these systems have not yet been harnessed for a functional purpose.

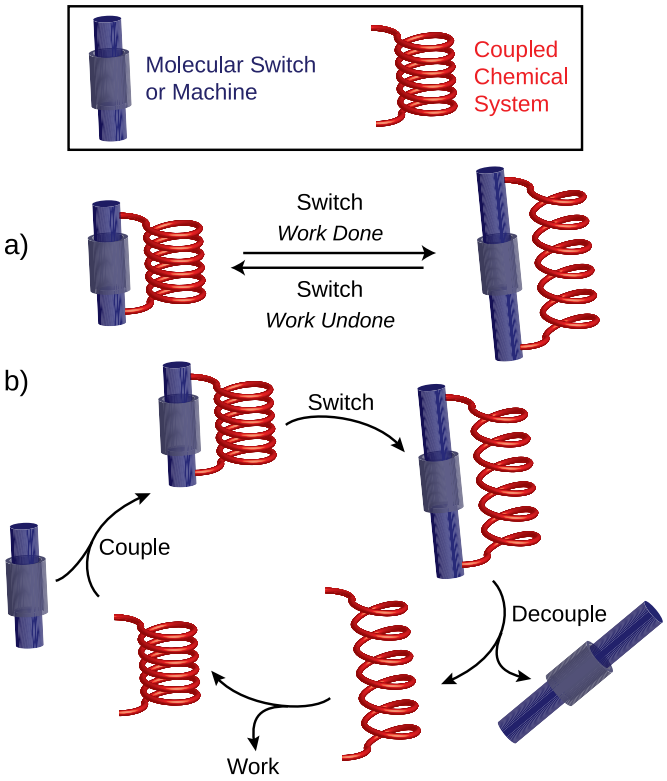


Figure 6.93 Overcoming the principle of microscopic reversibility. (a) A molecular switch cannot perform work even if it is coupled with another system—e.g., a spring or catalyst—unless (b) a stochastic pumping (or non-reciprocating) cycle involving periodic fluctuations—e.g., coupling/decoupling of a spring, or chirality switching of a catalyst—is tapped as the symmetry breaking element.

The molecular versions of second-law-abiding energy ratchets (**Section 6.15.2.3**) and information ratchets (**Section 6.15.2.4**) have sometimes enlisted the help of the mechanical bond to achieve directed transport at the molecular level. Directed transport in these systems is characterized by motions that exhibit a net bias along one pathway over another alternative pathway—e.g., clockwise versus counterclockwise rotation or directionally biased translation of a ring. We find the term 'unidirectional' misleading because, in a Brownian regime, more than one pathway can often be taken—one of them is simply the most probable route. We therefore refer[33,128] to this kind of net-biased directional transport in MIMs as mechanostereoselective motion.

The frame of reference is an important consideration when describing the relative motions of component parts in molecular machines. Imagine a car driving north on a highway. An observer from the east will see the car's wheels rotating clockwise, while an observer from the west will see the wheels rotating anticlockwise. The car continues north,

[E] The principle of microscopic reversibility does not apply to reactions initiated by photochemical excitation.

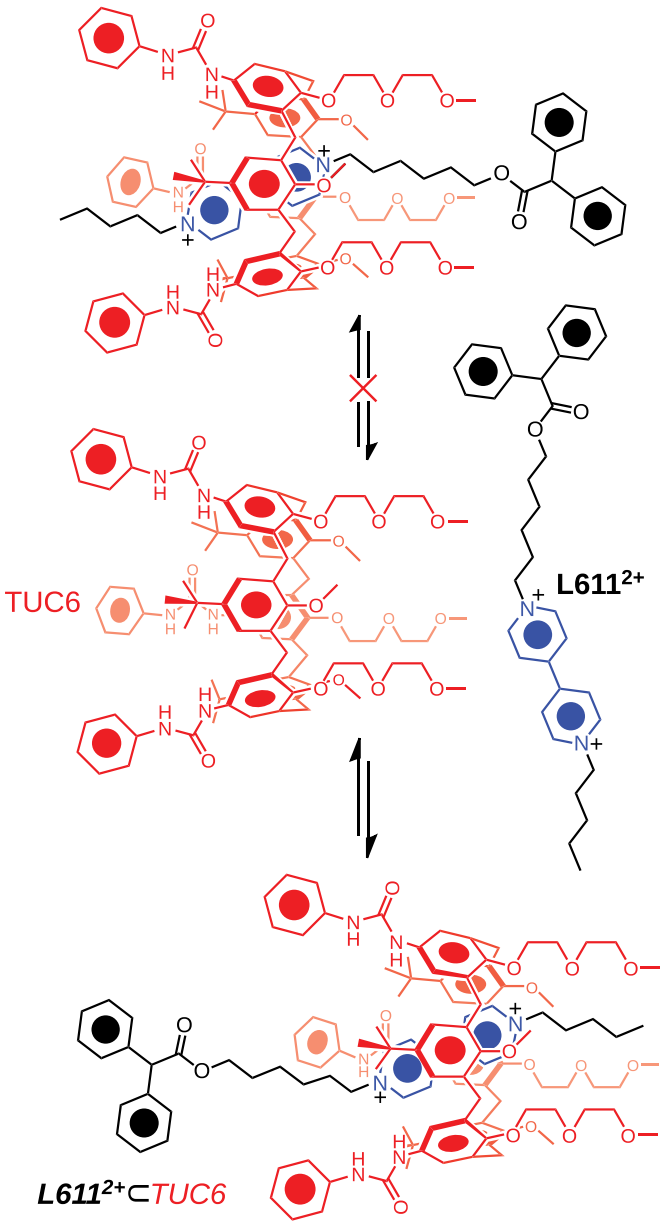
however, doing work on its passengers, because the wheels' rotations are unidirectional in any frame of reference that is fixed with respect to the car. The relative mechanical motions taking place in a molecular machine in solution can be understood in a similar manner. If the laboratory or the flask is taken as the frame of reference, molecular motions change directions incessantly and randomly. In a frame of reference that is fixed with respect to an individual molecule, however, it makes sense to describe the net mechanical motions of a molecular machine as directed, biased, unidirectional, mechanostereoselective, etc. If the motions of many molecules are aligned with respect to an outside frame of reference, the system may be appropriate for scale-up materials such as artificial muscles (**Section 6.15.1.2**).

In principle, any of the switches reviewed in this Chapter could be re-designed as artificial molecular machines, since their biased Brownian motions in response to being pushed away from equilibrium by external stimuli need only be interfaced with an appropriate strategy for breaking microscopic reversibility to do work. We summarize here the work of those that have taken the first step—i.e., non-reciprocating cycles and mechanostereoselectivity—on what is surely a long road that lies ahead.

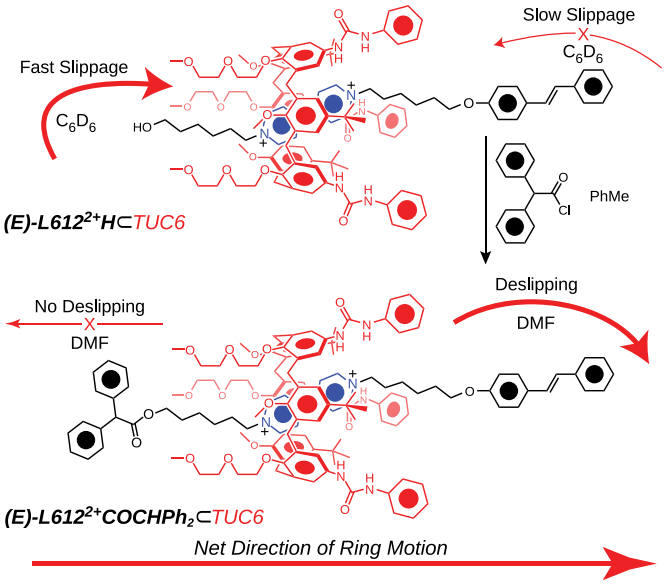
6.15.2.2 Mechanostereoselective Motion

Mechanostereoselectivity is defined[33,128] as a motion constrained by the mechanical bond that happens faster along one path than another. A more general term encompassing everything beyond mechanomolecules is biased Brownian motion. The foundations for mechanostereoselective motion have been laid in a number of pseudorotaxane-based systems that express asymmetric threading/dethreading schemes. An asymmetric threading event with respect to the 'axle' component is trivial to accomplish, since any pseudorotaxane involving a semidumbbell with one stopper will penetrate the cavity of the ring only by means of its unfettered terminus. Asymmetric threading with respect to the ring component is only slightly more challenging, requiring a constitutionally asymmetric ring with two non-identical rims. One of the earliest examples[232] of this principle is that of Anderson's α-CD-based [2]rotaxane **(*E*)-R627**$^{4-}$, in which the one-way transport of the α-CD ring—see **Scheme 6.25** in **Section 6.2.2.1**—is induced by a light-driven isomerization. Several pseudorotaxanes and rotaxanes with asymmetric axles and CD rings have been found[902–912] to exist in distributions that are highly biased in favor of only one of the two possible orientational isomers associated with the direction of CD threading, indicating that directionally biased motion is not uncommon in CD-based systems. Surprisingly, however, CD-based ratchets have not progressed beyond the types of photoinduced mechanostereoselective translation introduced in Anderson's seminal work. One of the main focuses of interest in the context of designing pseudorotaxane-based molecular ratchets is to achieve mechanostereoselectivity in a threading/dethreading cycle, such that the ring approaches the axle at one end and exits the axle from the other end. In accordance with the principles we have outlined in the previous Section, the design of a mechanostereoselective threading/dethreading cycle requires, minimally, (i) an element of asymmetry in at least one of the components, i.e., the ring or the axle, and (ii) a means of pushing the system away from equilibrium, typically by introducing one of the stimuli for switching described earlier on in this Chapter.

A pseudorotaxane system, which exhibits (**Scheme 6.114**) mechanostereoselective threading of a BIPY^{2+}-based half-dumbbell **L611**$^{2+}$ with respect to an asymmetric



Scheme 6.114 Mechanostereoselective threading of a BIPY^{2+} half-dumbbell **L611**$^{2+}$ in the conical tetraureidocalix[6]arene host TUC6.[913]



Scheme 6.115 The dual use of covalent stoppering and solvent exchange causes the TUC6 ring to enter a $BIPY^{2+}$-based axle on the opposite end from which it departs.[917]

triphenylureido-calix[6]arene (*TUC6*) host, has been developed by Arduini.[913] The conical shape of the *TUC6* host differentiates the size and functionality of its two rims. ^1H NMR Spectroscopic analysis of the pseudorotaxane ***L611***$^{2+}$$\subset$*TUC6* in C_6D_6 reveals that the **L611**$^{2+}$ guest approaches the cavity of the *TUC6* host only from the wider triphenylureido rim. Explanations for this mechanostereoselective threading include the assumption that the steric barrier imposed by the oligoethers appended to *TUC6* obstruct entry from the narrow rim, as well as the observation[914] that the $BIPY^{2+}$ dication forms a tight ion-pair with its tosylate counterions in low polarity solvents, an interaction left more intact when entering the cavity from the wider rim. The same type of one-way threading can be achieved[915] when the $BIPY^{2+}$ recognition unit is substituted with two alkyl chains of different lengths, whereupon the ring is kinetically more disposed to thread onto shorter chains. It was also demonstrated[916] that various $BIPY^{2+}$-based [2]rotaxanes can be prepared from *TUC6*, which could, in principle, lead to mechanostereoselective translational motion in molecular switches derived therefrom.

The *TUC6*/$BIPY^{2+}$ system has been adapted[917] into a design (**Scheme 6.115**) in which the combined use of covalent modification and solvent exchange results in the *TUC6* ring following a one-way path with respect to the axle during a threading/dethreading cycle. When the *TUC6* wheel and the ***(E)-L612H***$^{2+}$ axle components are mixed in C_6D_6, the ring passes over the hydroxyl-terminated end of the ***(E)-L612H***$^{2+}$ axle, with the axle penetrating the wheel preferentially through its wider rim. In agreement with the system portrayed in **Scheme 6.114**, the observation of only one orientational isomer indicates that threading does not occur over the bulkier stilbene pseudo-stopper. The pseudorotaxane ***(E)-L612H***$^{2+}$$\subset$*TUC6* is then trapped kinetically by stoppering the terminal primary hydroxyl group with diphenylacetyl chloride to afford ***(E)-L612COCHPh***$_2^{2+}$$\subset$*TUC6*. The dethreading process of this pseudorotaxane is promoted in a high-polarity DMF solution, which disrupts the stabilizing hydrogen-bonding, charge transfer, and ion-pairing interactions. Since the diphenyl stopper is too bulky for the *TUC6* ring to pass over it, the ring departs from the axle over the stilbene unit on the opposite end from which it entered. The rate of deslipping can be modulated by photoisomerization of the stilbene unit, since the ring departs more quickly ($k_{off} = 5.9 \times 10^{-3}$ s^{-1}) over the (*E*)-stilbene unit of ***(E)-L612COCHPh***$_2^{2+}$ than it does ($k_{off} = 2.3 \times 10^{-5}$ s^{-1}) over the (*Z*)-stilbene unit of ***(Z)-L612COCHPh***$_2^{2+}$. This cycle could be repeated, in principle, by hydrolyzing the diphenyl stopper's ester bond.

Harada[918] has observed a face-selective translational process involving the passage of a rotaxane's threaded α-CD ring over a 2-methylpyridinium hurdle. If we arbitrarily assign forward and backward directions to the ring's passage, where the forward direction is congruent with the net dipole of the pyridinium subunit, then the ring passes over the hurdle much faster in the forward direction (**Figure 6.94**) when the secondary face leads the way (k_2) as opposed to the primary face (k_1) at 70 °C in D_2O. The ratio of the forward rates (k_2/k_1) differ by a factor of 34. In the backward direction (not shown), the ring passes over the hurdle faster when it is led by the primary face, and the rates differ by a factor of 17. This kind of kinetically controlled face-selective translation renders this motif eligible for the design of "unidirectional" catenanes and motors.

Venturi and Credi[919] have described the directionally controlled transit (**Scheme 6.116**) of a DB24C8 ring over the azobenzene- and cyclopentyl-stoppered dialkylammonium axle ***(E/Z)-L613H***$^+$. In the ground state, the DB24C8 ring passes over the *trans*-azobenzene stopper of ***(E)-L613H***$^+$ at a much faster rate ($k_{on} = 22\ L \cdot mol^{-1}s^{-1}$) than is the case for the cyclopentyl stopper, which is on the order of

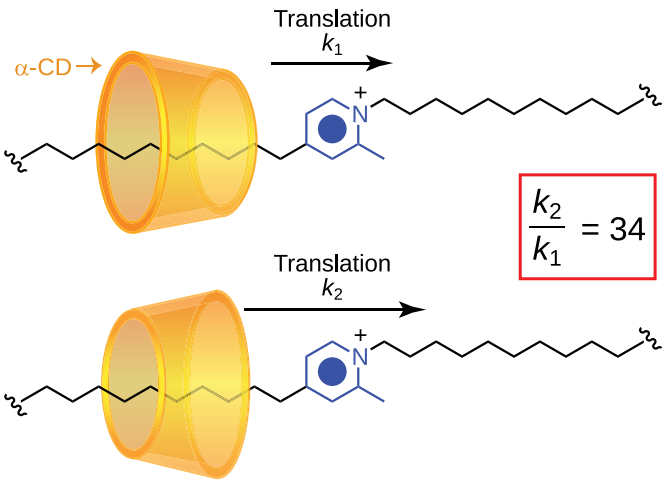
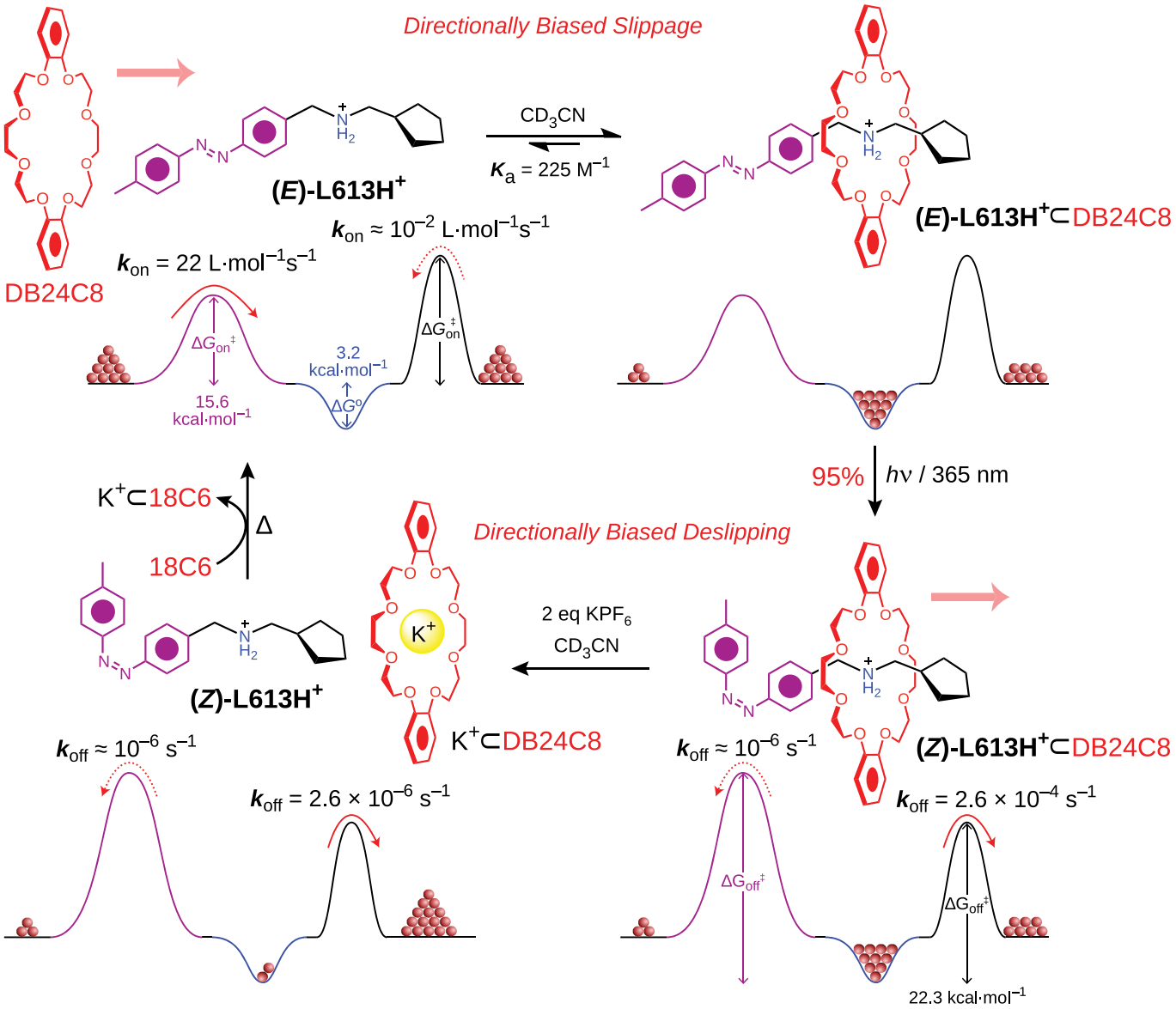


Figure 6.94 Face-selective translation of an α-CD ring over a 2-methylpyridinium hurdle.[918]



Scheme 6.116 Directionally biased transit of a DB24C8 ring along an azobenzene- and cyclopentyl-stoppered dialkylammonium axle (***E/Z*)-L613H**$^+$.[919] The system relies on light as a stimulus to modulate the activation barriers for slippage and deslipping process, while using the addition and removal of K^+ ions to control the threading and dethreading processes.

10^{-2} L · mol^{-1}s^{-1}, based on experiments performed on a control complex with two cyclopentyl pseudo-stoppers. When the *trans*-azobenzene unit of corresponding pseudorotaxane ***(E)-L613H***$^+$⊂*DB24C8* is photoisomerized under 365 nm irradiation with a quantum efficiency of 95% in the photostationary state, the activation barrier for the ring to pass over the *cis*-azobenzene unit is raised considerably. Thus, a directionally biased deslipping process is observed upon K^+-triggered decomplexation of the DB24C8 ring from ***(Z)-L613H***$^+$⊂*DB24C8*, since the rate of deslipping (k_{off} = 2.6 10^{-4} s^{-1}) is faster over the cyclopentyl unit than it is over the *cis*-azobenzene unit, which is on the order of ~10^{-6} s^{-1}, based on experiments performed on a control complex with two *cis*-azobenzene pseudo-stoppers. A net directional bias of the ring's motion with respect to the axle is generated by this protocol, since the DB24C8 ring dethreads from the opposite end onto which it threaded initially. The system can be reset by extracting the K^+ ions with [18]crown-6 (18C6) and allowing the thermal relaxation of the *cis*-azobenzene unit back to the *trans* isomer to take place, a process which occurs with a half-life of 8 days at room temperature. Measured values for $\Delta G^{\ddagger}$ and $\Delta G°$ are denoted for the steps of this switching cycle in **Scheme 6.116**.

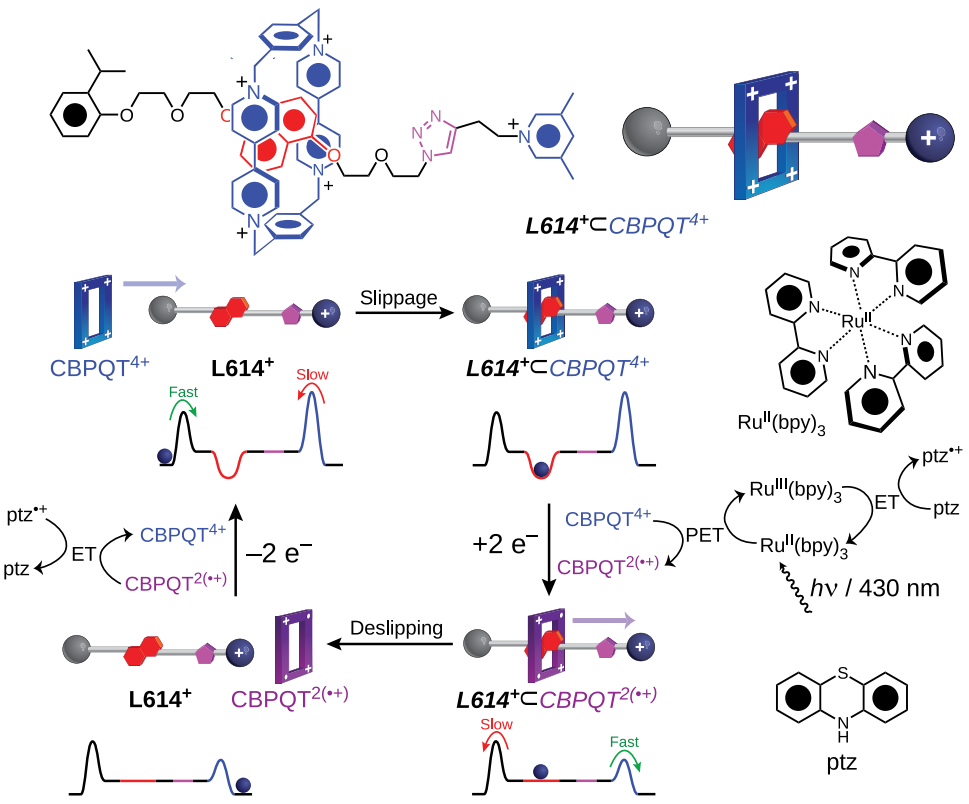
Building on these results, Credi[920] has found that **L613H**$^+$ passes mechanostereoselectively through dinaphtho[24]-crown-8 (DN24C8) in a cycle that repeats itself autonomously in the photostationary state. Mechanistically, the net one-way transit is governed by energy landscapes very similar to those illustrated in **Scheme 6.116**. The autonomous mode is enabled by the facts that (i) **(*E*)-L613H**$^+$ binds

DN24C8 more tightly than does **(*Z*)-L613H$^+$**, and (ii) the isomerization of azobenzene is not subject to microscopic reversibility because it is a photochemical reaction. Thus, the slippage process happens with higher probability over the *trans*-azobenzene unit of **(*E*)-L613H$^+$**, while deslipping occurs with higher probability over the cyclopentane unit of **(*Z*)-L613H$^+$** as the compound oscillates between *cis* and *trans* configurations in the photostationary state. Numeric simulations indicate that the cycling rate is 1.7×10^{-10} M·s^{-1} in CH_2Cl_2 at 20 °C at an efficiency of 430 photons per cycle. The practical appeal[921] of this system as a molecular machine relates to its unsophisticated molecular pieces, as well as its clean operation based on an efficient and reversible photoisomerization reaction with relatively high resistance to fatigue. It is anticipated that these types of molecular ratchets could be utilized as photodriven pumps[922] that transport molecular cargo across membranes, for example.

Kihara[923–925] has also reported a few mechanostereoselective motions in dialkylammonium/crown ether rotaxanes, where the ring's motion is induced by *N*-acylation, in common with the switches described in **Section 6.7.1**.

Recently, a pseudorotaxane based on the π-associated donor-acceptor recognition motif of CBPQT^{4+} has been designed[926] to exhibit mechanostereoselective transit (**Scheme 6.117**) fueled by redox stimuli. The pseudo-stoppered DNP-based dumbbell **L614$^+$** carries a neutral 'hurdle' at one terminus and a charged blocking group at the other terminus. Most of the CBPQT^{4+} rings encircling **L614$^+$** are induced to dethread upon reduction to CBPQT$^{2(\bullet+)}$ as a result of the lower affinity of CBPQT$^{2(\bullet+)}$ for DNP guests. Whereas the reduced CBPQT$^{2(\bullet+)}$ diradical dication is more disposed to slip over the charged 3,5-dimethylpyridinium hurdle, the tetracationic CBPQT^{4+} ring requires less energy to slip over the neutral *ortho*-isopropylphenyl impediment. Thus a two-electron reduction/oxidation cycle leads to a net mechanostereoselective motion, in which the ring of ***L614$^+$*** $\subset$ ***CBPQT^{4+}*** threads over the neutral impediment, and the ring of ***L614$^+$*** $\subset$ ***CBPQT$^{2(\bullet+)}$*** dethreads over the charged hurdle. The redox stimulus to drive this process can be introduced chemically, electrochemically, or photochemically. The cycle has been designed to run autonomously under irradiation with 430 nm light by using a $Ru(bpy)_3Cl_2$ photosensitizer in combination with the ptz/ptz$^{\bullet+}$ redox couple as an electron relay. The electron transfer scheme in this system operates in a similar manner to that (**Scheme 6.20** in **Section 6.2.1**) of the autonomously shuttling rotaxane **R605^{6+}**. The reduction of CBPQT^{4+} to CBPQT$^{2(\bullet+)}$ is accomplished by PET from the photoexcited Ru^{II}* center. The resulting Ru^{III} species is reduced back to Ru^{II} by ptz, giving the ptz$^{\bullet+}$ radical cation as a product. The cycle is completed when the CBPQT$^{2(\bullet+)}$ ring transfers its electrons to ptz$^{\bullet+}$, which resets the system and leaves it ready for another cycle.

Directionally biased threading has also been observed[927] recently in constitutionally asymmetric pillar[5]arene-based hosts with asymmetrically substituted tetramethylene axles. Since a number of methods for functionalizing pillararenes have been mastered[928] recently, these systems are also



Scheme 6.117 Redox-driven, directionally-biased translation[926] of a CBPQT^{4+} ring with respect to the DNP-based dumbbell **L614$^+$**, which possesses neutral and charged pseudo-stoppers. In a solution containing a Ru^{II} photosensitizer and a phenothiazine (ptz) electron relay, the redox cycle proceeds autonomously under 430 nm irradiation.

poised to be fashioned into mechanostereoselective switches and machines.

Pseudorotaxanes in which the ring enters and exits on opposite ends of the thread realize a non-reciprocating switching cycle, but do not perform work because the ring is returned to the solution from whence it came. The ratchets described in **Sections 6.15.2.3** and **6.15.2.4** possess mechanical bonds, which prevent the rings from escaping back into solution.

6.15.2.3 Mechanically Interlocked Energy Ratchets

Mechanostereoselective motion in rotaxanes and catenanes is typically associated with directionally biased, or 'unidirectional', translation of a ring in the former case, and ring circumrotation in the latter case. As already outlined in **Section 6.15.2.1**, this type of behavior becomes possible when the principles of microscopic reversibility and symmetry are broken by a chemical system operating away from equilibrium. There are two different ways to conceptualize the 'machine' in terms of molecular ratchets with mechanical bonds. If one considers the rotaxane or catenane holistically, then it must be coupled and decoupled (see **Figure 6.93**) with a system of interest in order to perform work. An alternative framework for thinking about these systems is to treat one component as the machine and the other component(s) as the substrate. If the dumbbell of a switchable rotaxane, for example, is treated as the machine, then it can perform work on the corresponding ring. A challenge arises, however, when targeting motor-like function in rotaxanes: resetting the ring to its former position in order to perform a new cycle undoes any work that was performed, since the ring must return to its starting position along the same path it followed previously. A catenane, on the other hand, can return a ring to its initial position along a different path from whence it came, thereby performing net work on the ring. Iterative cycles of mechanostereoselective switching in catenanes can therefore be considered a form of work, whereas mechanostereoselective switching in rotaxanes can only embody work if the ring never returns to its starting place. All the same, designing and understanding mechanostereoselective motion in both types of architectures is expected to shed light, not only on how biological molecular machines operate, but also on how to mimic their remarkable functions.

We will rely partially on the vocabulary employed by Leigh[3,245] to discuss MIM-based molecular ratchets. Some important terms are defined below –

Balance: Balance is the thermodynamically preferred distribution of molecular states in a system, reflecting the population of the thermodynamic landscape at thermal equilibrium. Balance breaking can therefore be understood as a process that changes the thermodynamic landscape and typically causes the system to re-equilibrate unless it is forbidden sterically and/or electronically to do so.

Ratcheting: We define ratcheting as a process that moves a substrate from a state of lower energy to higher energy, in which the substrate cannot return to the lower energy state on account of a high kinetic barrier for the reverse process.

Linking: In the context of a Brownian ratchet mechanism, linking is a process that lowers an activation barrier such that a substrate can exchange between different thermodynamic wells. Unlinking, therefore, is the raising of kinetic barriers in order to trap the substrate in a certain state.

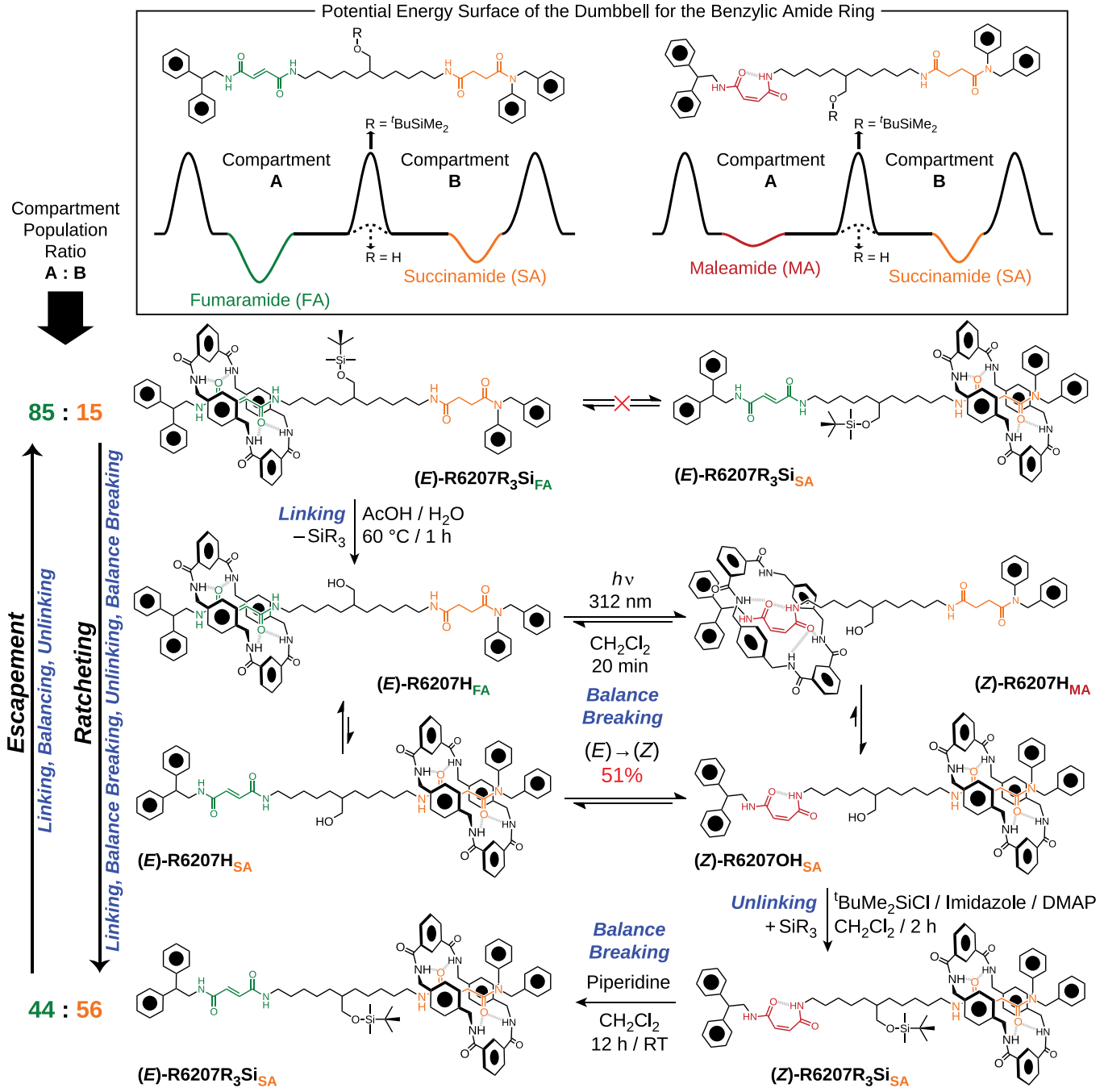
Escapement: Escapement is the release of a ratcheted substrate, which is caused by lowering the kinetic barrier associated with the ratcheting step (linking) and allows a system to approach equilibrium once again.

Taking all these terms into consideration, a molecular machine can ratchet a substrate energetically uphill by executing an interleaving sequence of balance breaking and linking/unlinking steps. Work can then be done, either by coupling an escapement step with another system on which it can act, or by implementing the ratcheting mechanism in a non-reciprocating cycle.

Ratcheting in Compartmentalized Rotaxanes

Brownian ratchets rely on compartmentalization. For example, two compartments with different temperatures represent the basis of the historical thought experiments in **Figure 6.91**. On the thermodynamic landscape of a molecular ratchet (**Figure 6.92**), compartments are represented by thermodynamic wells surrounded by kinetic barriers. Leigh's simple two-compartment bistable [2]rotaxane **(*E*)-R6207R$_3$Si** energy ratchet exemplifies[245] (**Scheme 6.118**) the underlying principles of compartmentalization. Two recognition sites are available for the benzylic amide ring of **(*E*)-R6207R$_3$Si**—the primary recognition site (Compartment A) is a fumaramide (FA) unit, while the secondary recognition site (Compartment B) is a succinamide (SA) unit. The fumaramide unit can undergo (*E*) → (*Z*) isomerization to maleamide (FA) under UV irradiation. A thermodynamically balanced ratio of 85:15 characterizes the ground-state distribution of the **(*E*)-R6207R$_3$Si$_{FA}$** and **(*E*)-R6207R$_3$Si$_{SA}$** isomers, respectively. A siloxyl protecting group located at the center of the dumbbell serves as a chemically addressable steric gate, which prevents the ring from exchanging between compartments. **Scheme 6.118** illustrates how executing a series of compartment linking and unlinking steps, i.e., protection and deprotection, can be used as a means of ratcheting the ring of **(*E*)-R6207R$_3$Si** energetically uphill, using light as an energy source for balance-breaking.

Linking compartments A and B involves acidic deprotection of the siloxyl group in order to lower the kinetic barrier for the ring to exchange sites, affording the corresponding 85:15 distribution of **(*E*)-R6207H$_{FA}$** and **(*E*)-R6207H$_{SA}$**. The first balance-breaking step involves the (*E*) → (*Z*) photo-isomerization of fumaramide to maleamide, a process which proceeds with 51% efficiency under 312 nm irradiation. Since the SA unit is a more



Scheme 6.118 The dumbbell of Leigh's two-compartment rotaxane can ratchet a benzylic amide ring energetically uphill.[245] The fumaramide (FA) and succinamide (SA) recognition units, which represent compartments A and B, respectively, are separated by a siloxyl protecting group which prevents the ring from exchanging between compartments. A ratio of 85:15 represents the thermodynamically balanced distribution of **(*E*)-R6207R$_3$Si$_{FA}$** and **(*E*)-R6207R$_3$Si$_{SA}$** translational isomers. This 85:15 distribution can be ratcheted uphill to a ratio of 44:56 by performing a sequence of compartment linking (deprotection), balance-breaking (*cis*/*trans* isomerization), and compartment unlinking (re-protection) steps. Returning the excess of ratcheted rings in Compartment B to Compartment A upon deprotection restores thermodynamic balance is an energy-releasing process known as escapement.

favorable binding site for the ring than the MA unit, the distribution of the four possible isomers of **(*E*/*Z*)-R6207H** is biased in favor of **(*Z*)-R6207H$_{SA}$**. When the compartments are unlinked by re-protecting the primary hydroxyl group with ^{t}BuMe$_2$SiCl, the population of rings in each compartment of **(*E*/*Z*)-R6207R$_3$Si** has changed, reflecting that of the photostationary state of **(*E*/*Z*)-R6207H**. Allowing the MA unit to relax back to FA in a final, balance breaking (*Z*) → (*E*) thermal isomerization affords a situation in which **(*E*)-R6207R$_3$Si$_{SA}$** isomer claims the majority (56%)

of the distribution, completing the ratcheting sequence.[F] If the siloxyl gate is once again lifted to allow exchange between compartments, the population will restore thermodynamic balance by returning to the 85:15 ratio, a process defined[245] by Leigh as 'escapement'. Escapement releases the energy stored by the ratchet and could be used, in principle, to carry out some other form of work.

We note that the rotaxane-building molecular pump[929] described in **Section 6.15.2.3** is also an energy ratchet.

Mechanostereoselective Circumrotation in Catenanes

Prior to reporting his two-compartment rotaxane ratchet, Leigh[244] had described the energy ratcheting (**Figure 6.95**) of the compartmentalized bistable [2]catenane **(*E*)-C641**, which uses a similar set of principles and design motifs. The structure (**Figure 6.95a**) of the catenane comprises a large ring with two recognition units (FA and SA) between which are two independently addressable protecting groups (SiR_3 and trityl) that serve as gates. The benzylic amide ring of **(*E*)-C641** can be circumrotated mechanostereoselectively in either a 'clockwise' or 'anticlockwise' direction, with respect to an arbitrary fixed point of reference in the larger ring, by switching between (*E*)- and (*Z*)-isomers while opening and closing—i.e., deprotecting and protecting—each of the gates in an appropriate sequence. From the point of reference illustrated in **Figure 6.95**, the ring follows a clockwise path (**Figure 6.95b**) if the siloxyl group of **(*E*)-C641$_{FA}$** is deprotected before the balance-breaking (*E*)→(*Z*) photoisomerization step, avoiding the sterically hindering trityl group as it populates **(*Z*)-C641$_{SA}$** en route to **(*E*)-C641$_{SA}$**. Conversely, the ring follows an anticlockwise pathway when the trityl group is deprotected before the photoisomerization step. The same feature is built into the escapement step, where the ring's multi-step pathway of relaxation from **(*E*)-C641$_{SA}$** back to **(*E*)-C641$_{FA}$** depends on which one of the two sterically hindering groups is removed (by deprotection) and restored (by re-protection) in the process. The identity of each intermediate species throughout the switching cycle has been confirmed by ^{1}H NMR spectroscopy. Since the mechanostereoselective circumrotation of the benzylic amide ring in this catenane can be cycled repeatedly in either direction at the will of the experimentalist, the larger ring which acts on it can be considered a reversible rotary motor.

Directionally biased circumrotational motion in catenanes was first introduced (**Figure 6.96**) by Leigh[243] in 2003 in the form of the multistable [3]catenane **C642**. The structure (**Figure 6.96a**) of **(*EE*)-C642** comprises two benzylic amide rings encircling a larger ring possessing four recognition units, two of which are photoswitchable fumaramide derivatives. One of the fumaramide units (orange) is attached to a benzophenone group, a photosensitizer which allows selective isomerization[237] under 350 nm irradiation. An *N*,*N*′-dimethylfumaramide unit (red) serves as the second photoswitchable recognition site. More weakly associating succinic amide ester (pink) and amide (purple) units are available for the rings to encircle when the fumaramide recognition units, i.e. (*E*)-isomers, are converted to maleamide units, i.e. (*Z*)-isomers. Overall, the recognition units are ranked in the following order in terms of their affinity for the benzylic amide rings: fumaramide > dimethylfumaramide > succinic amide ester > amide > maleamide > dimethylmaleamide.

Mechanostereoselectivity in **C642** is enabled by each of the benzylic amide rings acting as a kinetic barrier, which obstructs the other ring from moving towards it, thus biasing

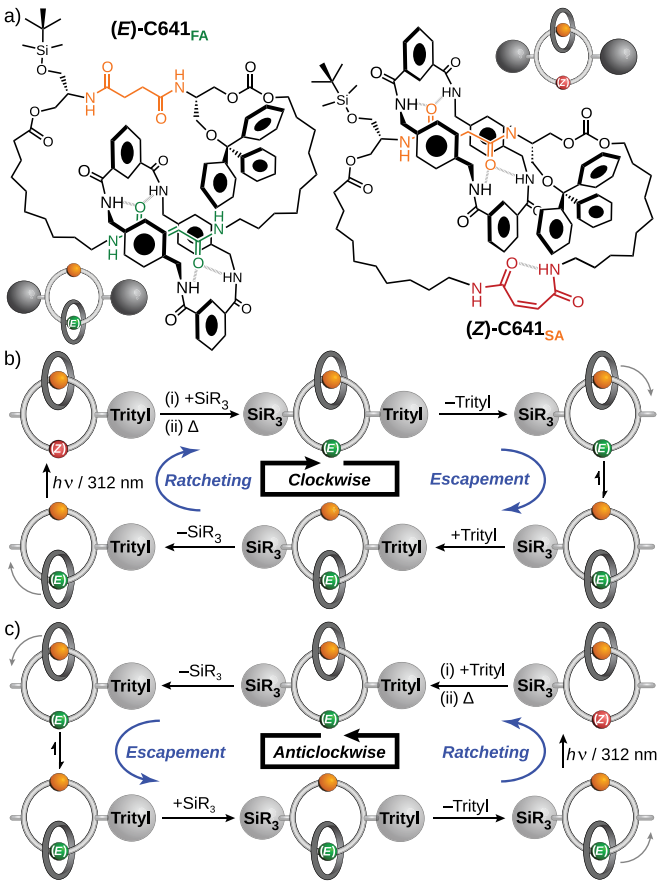


Figure 6.95 Mechanostereoselective circumrotation in Leigh's two-compartment ratcheting [2]catenane.[244] Two SiR_3 and trityl protecting groups serve as independently addressable gates between the two compartments. The benzylic amide ring can be circumrotated in a clockwise or anticlockwise direction, with respect to a fixed reference point in the larger ring, depending on the sequence of linking/unlinking (protection/deprotection) and balance-breaking (photoisomerization) processes. (a) Structural formulas of **(*E*)-C641$_{FA}$** and **(*Z*)-C641$_{SA}$** are illustrated for the purposes of identifying the graphical representations of their component parts and portions. (b) Sequence of steps for inducing clockwise circumrotation. (c) Sequence of steps for inducing anticlockwise rotation.

[F] Note that the same ratcheting effect could be also achieved by performing the balance-breaking step prior to the linking and unlinking steps, provided the photo-isomerization of fumaramide is possible in *fum*-**(*E*)-R6207R$_3$Si$_{FA}$**.

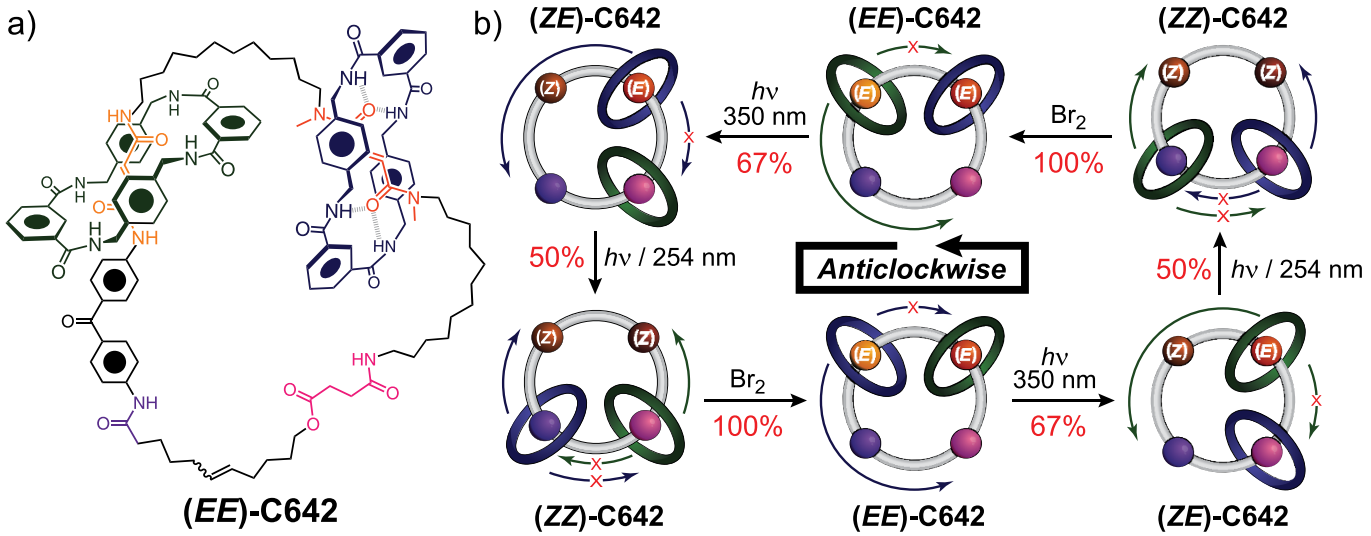


Figure 6.96 Kinetically-controlled mechanostereoselective circumrotation in Leigh's [3]catenane **C642**.[243] (a) Structural formula of **(*EE*)-C642**. (b) Graphical diagram of a six-step cycle which results in a full anticlockwise rotation, with respect to the fixed reference point as drawn, of the benzylic amide rings.

motion in a particular direction. These kinetic barriers imposed by the rings in **C642** are the conceptual equivalents of the steric barriers imposed by protecting groups in **C641**. A full switching cycle (**Figure 6.96b**) involves three reactions in the following sequence: (1) **(*EE*)-C642** → **(*ZE*)-C642**: Selective photoisomerization (67% in the photostationary state) of the fumaramide unit with 350 nm light in CH_2Cl_2. (2) **(*ZE*)-C642** → **(*ZZ*)-C642**: Selective photoisomerization (50% in the photostationary state) of the dimethylfumaramide unit with 254 nm light in CH_2Cl_2. (3) **(*ZZ*)-C642** → **(*EE*)-C642**: Thermal relaxation of the (*Z*)-isomers back to (*E*)-isomers, which proceeds quantitatively with catalytic Br_2 in CH_2Cl_2 at –78 °C, or at 100 °C in $C_2H_2Cl_4$. After one cycle of steps (1)–(3), the fraction of the population which have undergone all three isomerization steps, (*EE*) → (*ZE*) → (*ZZ*) → (*EE*), have transposed the positions of the two benzylic amide rings, which are colored green and blue in **Figure 6.96** for the sake of clarity. Steps (1)–(3) must therefore be repeated to complete a full rotation of the rings and reset the initial state of **(*EE*)-C642** after a non-reciprocating cycle. This sequence of reactions leads to a net anticlockwise rotation of the rings, with respect to a fixed reference point as illustrated in **Figure 6.96**, because the clockwise rotation of one ring in steps (1) and (2) is impeded by the presence of the other ring. In common with all Brownian ratchets, this 'follow-the-leader' process is not immune to mistakes. Rotation in the reverse direction can and does happen. It simply happens with less frequency. The activation barriers for translation of the benzylic amide rings ranges from <8 to 11.3 kcal · mol^{-1}, while the barrier for circumrotation of the larger ring is >23 kcal · mol^{-1} at 298 K in $CDCl_3$. Although the catenane does not possess three-dimensional chirality, it is chiral in the two-dimensional plane of the large ring, and follows a chiral sequence of binding events—the green ring, for example, visits the recognition sites in the sequence [yellow/pink/red/purple/yellow] which does not read the same in the reverse direction.

6.15.2.4 Mechanically Interlocked Information Ratchets

An information ratchet is a variation on the energy ratchet in which information about the position of the substrate is essential to the ratcheting process. The first example (**Figure 6.97**) of a molecular information ratchet was the two-compartment rotaxane **R6208H$_2^{2+}$** described by Leigh.[930] The [24]crown-8 ring of **R6208H$_2^{2+}$** is substituted with a benzophenone (PhCOPh) photosensitizer. The two compartments of rotaxane **R6208H$_2^{2+}$** contain dialkylammonium-based recognition units located in proximal (prox) and distal (dist) positions with respect to a photoactive α-methylstilbene gate. In CD_3OD at 298 K, the distribution of ***prox*-R6208H$_2^{2+}$** to ***dist*-R6208H$_2^{2+}$** isomers is 65:35, respectively. Upon irradiation with 350 nm light, the (*E*):(*Z*) ratio of the α-methylstilbene gate reaches 41:59, while the *prox:dist* translational isomer ratio remains at 65:35. In the presence of 5 equiv of a benzil (PhCOCOPh) photosensitizer, however, the (*E*):(*Z*) ratio rises to 80:20 and the *prox:dist* ratio falls to 45:55. A control experiment with an analogous rotaxane lacking the benzophenone photosensitizer does not pump rings likewise from the more energetically favorable *prox* center to the less favorable *dist* recognition site under the same conditions.

The key to the operation (**Figure 6.97**) of the information ratchet **R6208H$_2^{2+}$** is the distance dependence of energy transfer. (*E*) → (*Z*) Photoisomerization of the α-methylstilbene unit occurs primarily by energy transfer from the triplet excited states of the photosensitizers. Since the *dist* unit is separated from the α-methylstilbene gate by a long hydrocarbon chain, energy transfer from the excited state of benzophenone takes place only when the ring encircles the *prox* unit. The position of the ring is the information, therefore,

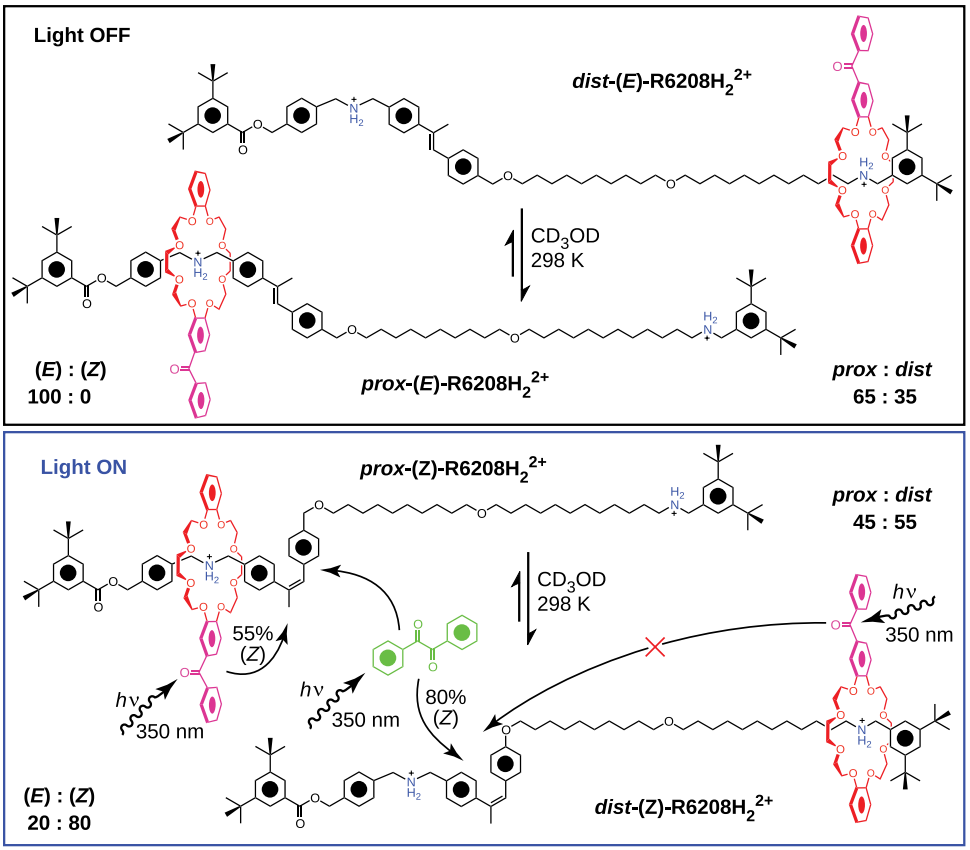
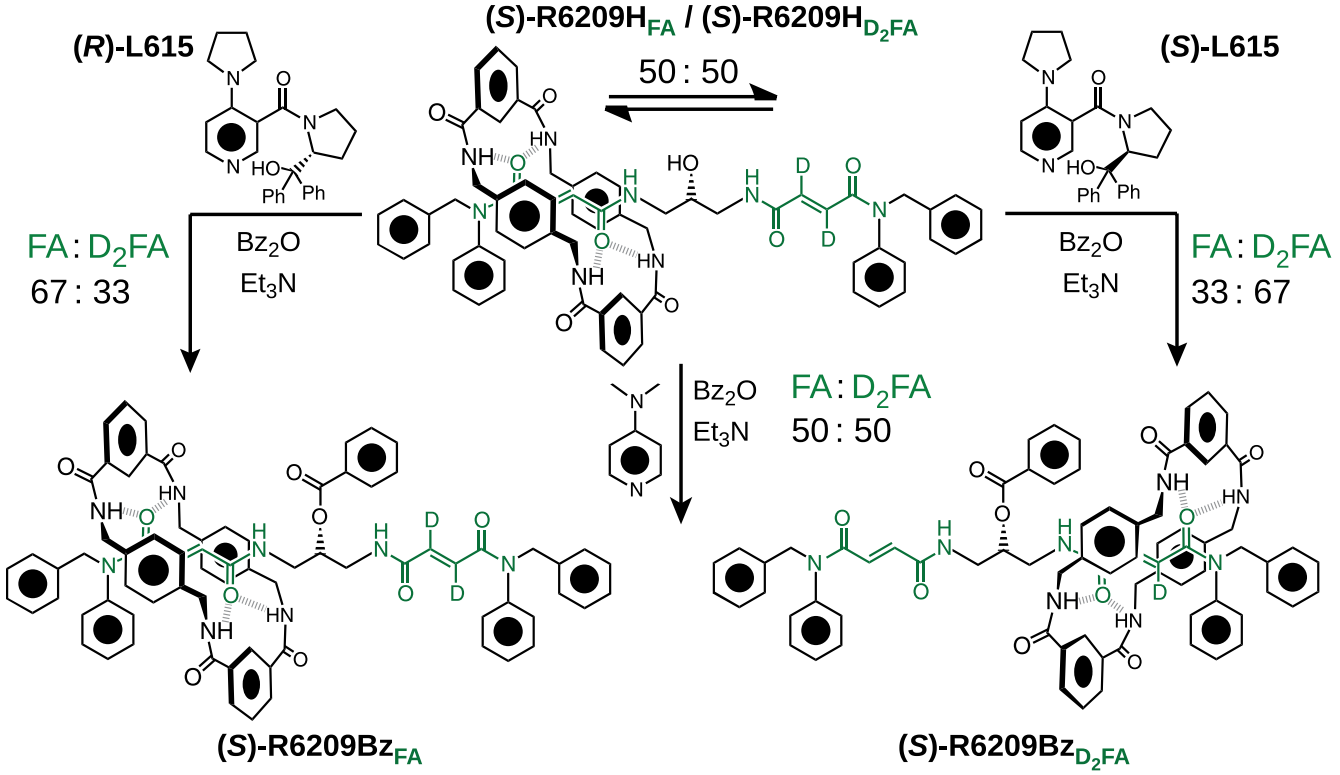


Figure 6.97 Leigh's light-fueled[930] molecular information ratchet. The thermodynamically balanced distribution (light off) of the benzophenone-functionalized ring among the proximal (*prox*) and distal (*dist*) recognition sites is 65:35, respectively. An α-methylstilbene unit, which is photoisomerized by energy transfer from the excited state of a photosensitizer, acts as a gate that prevents the ring from exchanging compartments as the (*Z*)-isomer. The gate is predominantly closed (80%) under 350 nm irradiation (light on) in the presence of benzil. The ring's benzophenone unit produces a lower (*E*):(*Z*) ratio (45:55) than benzil in the photostationary state, yet it can only transfer energy to the stilbene gate from the *prox* position. Energy transfer is therefore the line of communication which 'reports' the position of the ring to the gate which opens automatically when the ring is proximal, and closes automatically when the ring is distal, biasing kinetically the distribution in the photostationary state without affecting the local binding energies.

which is essentially 'reported' to the α-methylstilbene gate by means of energy transfer. Benzil is a more effective photosensitizer for an α-methylstilbene control compound, producing an 18:82 (*E*):(*Z*) ratio in the photostationary state, whereas benzophenone produces a 45:55 ratio. Thus, under 350 nm irradiation In the presence of benzil, the α-methylstilbene gate of **R6208H$_2^{2+}$** is mostly in the 'closed' state (80%) as the (*Z*)-isomer. Since the (*E*):(*Z*) ratio is lower in the photostationary state when the α-methylstilbene gate engages in energy transfer with benzophenone, the gate will have a tendency to open only when the ring occupies the *prox* recognition site. In other words, the gate opens automatically for the ring when it encircles the more favorable *prox* recognition site, and closes automatically when the ring randomly diffuses far enough toward the *dist* recognition site to turn off the energy transfer of benzophenone. The change in the populations of the ***prox*-R6208H$_2^{2+}$** and ***dist*-R6208H$_2^{2+}$** isomers under irradiation is caused by this built-in kinetically biased gate action, without affecting the binding energies of the recognition sites.

Another kind of information ratchet (**Scheme 6.119**) invented by Leigh[931] relies on chiral information. The two-compartment rotaxane **(*S*)-R6209H** is nearly degenerate, with two recognition sites—FA and deuterofumaramide (D2FA)—which are identical except that one of them is deuterated with ^{1}H NMR spectroscopy in mind. A hydroxyl group, which serves as a handle for the covalent-driven attachment and removal of a sterically hindering group, is located on a short chain at the dumbbell's center in order to establish a chiral environment around the OH group in combination with the ring's occupancy on either of the two recognition sites. The ring shuttles rapidly on the ^{1}H NMR timescale in 1:1 $CDCl_3$:CD_3OD with equal preference for both recognition sites. Benzoylation of the hydroxyl group unlinks the compartments by preventing the ring from exchanging sites. Promoting this benzoylation reaction withan achiral DMAP catalyst results in a 50:50 distribution of the **(*S*)-R6209Bz$_{FA}$** and **(*S*)-R6209Bz$_{D2FA}$** products. The chiral catalysts **(*S*)-L615** and **(*R*)-L615**, on the other hand, discriminate between the two rapidly exchanging translational isomers of **(*S*)-R6209H**. The distribution of **(*S*)-R6209Bz$_{FA}$** and **(*S*)-R6209Bz$_{D2FA}$** are biased to 33:67 and 67:33 when the protection is catalyzed by **(*S*)-L615** and **(*R*)-L615**, respectively. This enthalpically neutral and entropically uphill event is made possible by the spatial asymmetry of the rotaxane and catalyst. There is no thermodynamic driving force for this process to take place—instead, an energetically less favorable state is trapped kinetically because the rate of protecting one translational isomer is greater than that of protecting the opposite translational isomer for a given chiral catalyst.

In principle, any molecular shuttle in which the ring enhances asymmetry around a reactive center can be ratcheted using a similar strategy based on chiral reagents or catalysts. This concept has been demonstrated in both a non-degenerate two-compartment rotaxane[931] as well as an achiral three-compartment rotaxane.[932] In the latter case, the chiral DMAP-based catalysts can ratchet the ring more



Scheme 6.119 A chiral, chemically-driven information ratchet.[931] The benzylic amide ring of **(*S*)-R6209H** establishes a different chiral environment around the central hydroxyl group, depending on whether it encircles the deuterated or non-deuterated fumaramide recognition site. Although the ring of **(*S*)-R6209H** occupies each recognition site with equal preference, employing a chiral DMAP-based catalyst during a benzoylation of the OH group leads to a biased distribution of the two translational isomers of **(*S*)-R6209Bz**, where the major product (67%) depends on the handedness of the catalyst.

than once, such that it ends up residing predominantly at one end of the dumbbell depending on the handedness of the catalyst.

6.15.3 Mechanically Bonded Molecular Assemblers

The work accomplished by the molecular machines described in this Section is chemical in nature, since they rely on the mechanical bond, in combination with various reagents and energy sources, to make chemicals, including polymers (**Section 6.15.3.1**), peptide sequences (**Section 6.15.3.2**), and rotaxanes (**Section 6.15.3.3**).

6.15.3.1 Mechanically Constrained Processive Catalysis

The synthesis and degradation of DNA, which is essential to sustaining all known life, is mediated by enzymes, many of which "clamp" their domains around the DNA helix—see **Figure 1.5b** in **Section 1.1.1**. The mechanical bonds of these toroidal proteins underpin their enzymatic function, since they reinforce local interactions with the DNA substrates while turning them over in a processive[G] manner. Inspired by this concept, Rowan and Nolte[933–940] have been designing rotaxane architectures based on porphyrinic hosts—see **Section 2.3.3.6**—which are intended to mimic nature's capacity for processive catalysis. Their original design[933] (**Figure 6.98a**) involved threading a long polybutadiene axle through the annulus of a Mn^{III}-metallated porphyrin basket. Owing to the presence of a bulky 4-*tert*-butylpyridine ligand at the outward-facing axial coordination site of the metalloporphyrin, the photocatalytic epoxidation of the olefin units occurs only within the cavity of the basket. Confined by the mechanical bond, the ring slides along the polymer backbone until all of the double bonds have been epoxidized. Among the insights gleaned from a number of mechanistic investigations[935–940] was that the ring epoxidizes double bonds randomly while gliding along the polymer chain, since the rate of ring translocation is much faster at 750 picometers per second than the rate of epoxidation at only one picometer per second. It is anticipated[940] that strings of adjacent olefins will be turned over in sequence if the rate of epoxidation meets or exceeds that of translation.

Takata[941] has utilized a metallo-rotaxane motif in mechanically bonded processive catalysis, where the ring's endotopic Pd^{II} centers promote the formation (**Figure 6.98b**) of oxazolidines from allyl or propargyl urethane groups embedded in threaded oligomers. The Pd-catalyzed

[G] Processive catalysis differs from conventional catalysis. Whereas a processive catalyst promotes multiple transformations on the same substrate, conventional catalysts convert substrates randomly, molecule by molecule.

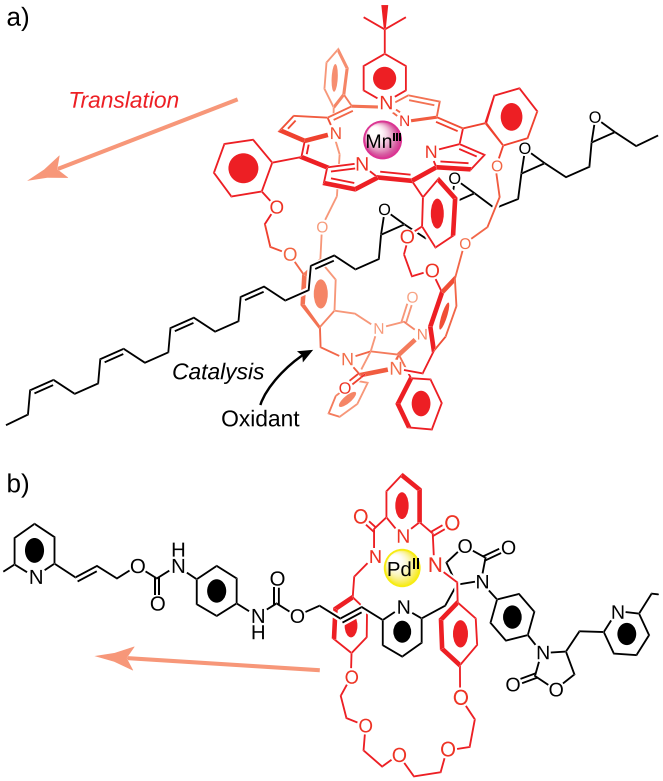


Figure 6.98 Mechanically bonded processive catalysis. (a) An idealized representation of processive epoxidation of polybutadiene by Rowan and Nolte's Mn^{III}-porphyrin basket.[933] (b) An idealized representation of processive Pd-catalyzed rearrangement of Takata's allyl urethanes.[941]

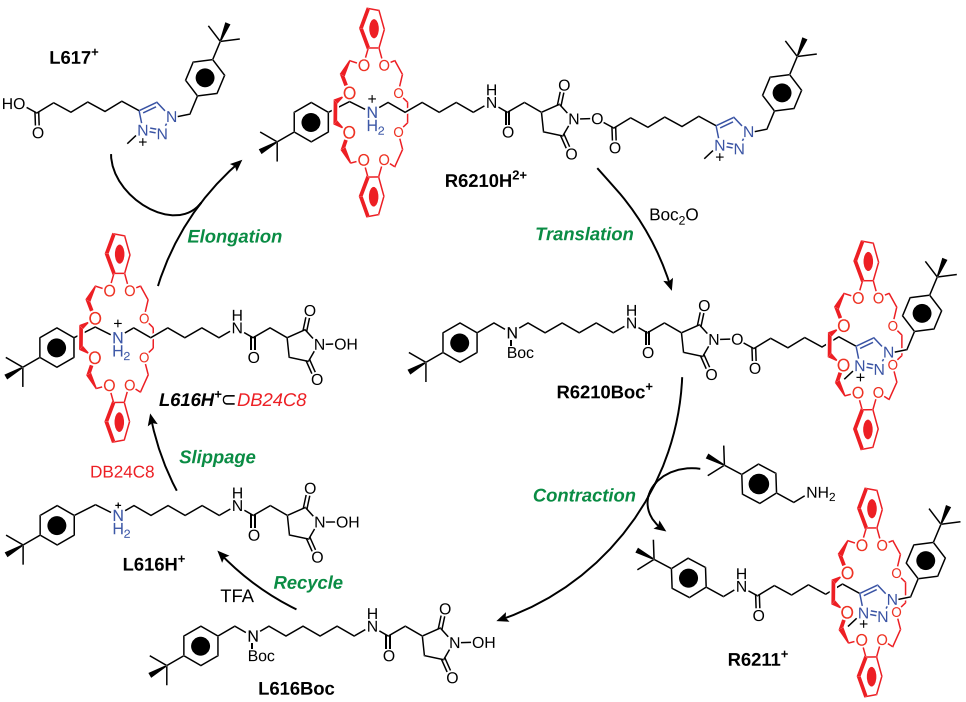
rearrangement is much more efficient (near-quantitative) in the case of the allyl urethane axle, compared to that (68%) of propargyl urethanes. Control experiments showed that no oxazolidines are generated from the same component parts when the metallo-organic ring is not encircling the axle, underlining the importance of the mechanical bond in achieving processivity.

6.15.3.2 Mechanically Constrained Peptide Synthesis

Leigh[942,943] has described a rotaxane-based molecular machine that has been celebrated for its ability to construct a polypeptide in a sequence-specific manner—a task carried out by a remarkable machine known as the ribosome in the biological world. Native chemical ligation of peptidic monomers immobilized on the axle of the rotaxane are transferred to the ring in a sequence-specific manner as a consequence of the constraints imposed on the ring's motion by the mechanical bond, then the ring is released automatically from the axle when the sequence is complete. See **Scheme 1.5** and the corresponding discussion in **Section 1.3.6** for a more detailed account of this machine's operation.

6.15.3.3 Rotaxane-Building Molecular Machines

Coutrot[307] has designed a recyclable molecular transporter, **L616H**$^+$, which builds (**Scheme 6.120**) copies of a [2]rotaxane that is energetically challenging to make. The transporter functions as follows: (i) *slippage* of a DB24C8 ring over an *N*-hydroxysuccinimide (NHS) endgroup generates the dialkylammonium pseudorotaxane ***L616H***$^+\subset$*DB24C8*, (ii) *elongation* of the pseudorotaxane into the [2]rotaxane **R6210H**$^{2+}$ by coupling the carboxylate-terminated triazolium semidumbbell **L617**$^+$ to the NHS unit, (iii) *translation* of the ring to the triazolium unit driven by *N*-acylation, affording **R6210Boc**$^+$, (iv) *contraction*, driven by displacement of the NHS ester linkage with a 4-*tert*-butylbenzylamine stopper precursor, affording the [2]rotaxane **R6211**$^+$ and the Boc-protected transporter **L616Boc**, which is finally (v) *recycled* back to **L616H**$^+$ by treatment



Scheme 6.120 Coutrot's ***L616H***$^+\subset$*DB24C8* pseudorotaxane is a molecular machine that transports a ring onto a weakly binding triazolium dumbbell when supplied with the appropriate sequence of stimuli, building the [2]rotaxane **R6211**$^+$ in the process.[307]

with TFA. Although the triazolium group has often served[298] as a second binding site for DB24C8 in bistable MIMs, the *triazolium⊂DB24C8* interaction is too weak to effectively template the formation of the corresponding mechanomolecules—triazolium guests, such as the semidumbbell compound **L617**$^{+}$, bind DB24C8 with only extremely low affinities. More recently, the same molecular transporter has been employed in the synthesis of challenging mono- and tris[1]rotaxanes possessing only triazolium recognition units.[308] An earlier benzylic amide ring transporter driven by a combination of solvent changes and covalent reactions was described for making "impossible" rotaxanes by Leigh.[474]

Building on the idea[944] of molecular energy ratchets—see **Section 6.15.2.3**—a molecular machine that pumps (**Figure 6.99**) CBPQT^{4+} rings energetically uphill onto a dumbbell has been conceived.[929] The dumbbell **L618**$^{3+}$ is constituted by the same dimethylpyridinium and isopropylphenol pseudo-stoppers as **L614**$^{+}$ in **Scheme 6.117**. Slippage of a CBPQT$^{2(\bullet+)}$ ring over the **L618**$^{+(\bullet+)}$ radical dication under reductive conditions generates the corresponding pseudorotaxane. Oxidation of this threaded species back to the ground state generates the pseudorotaxane ***L618***$^{3+}$$\subset$*CBPQT*$^{4+}$, where the ring resides in between the BIPY^{2+} and isopropylphenol units. In this state, the steric barrier of the isopropylphenol hurdle is lower than the electrostatic barriers imposed by the BIPY^{2+} and dimethylpyridinium units. Given enough thermal energy ($\Delta G^{\ddagger} = 23\,\text{kcal}\cdot\text{mol}^{-1}$), the ring translates to the dumbbell's oligomethylene chain and becomes kinetically trapped there, leading to the [2]rotaxane **R6212**$^{7+}$. A mechanical bond has been sealed at this stage, since no deslipping occurs at room temperature in MeCN even in the case of the trisradical **R6212**$^{3(\bullet+)+}$. The same flashing energy ratchet cycle can then be repeated a second time, ultimately affording the [3]rotaxane **R6213**$^{11+}$. The first and second rings are captured with efficiencies of 95 and 85%, respectively. This minimalistic molecular pump thus performs work by taking two steps uphill on the thermodynamic landscape, driving the rings from solution toward a higher local concentration where they surround an oligomethylene chain that offers them no significant stabilizing interactions.

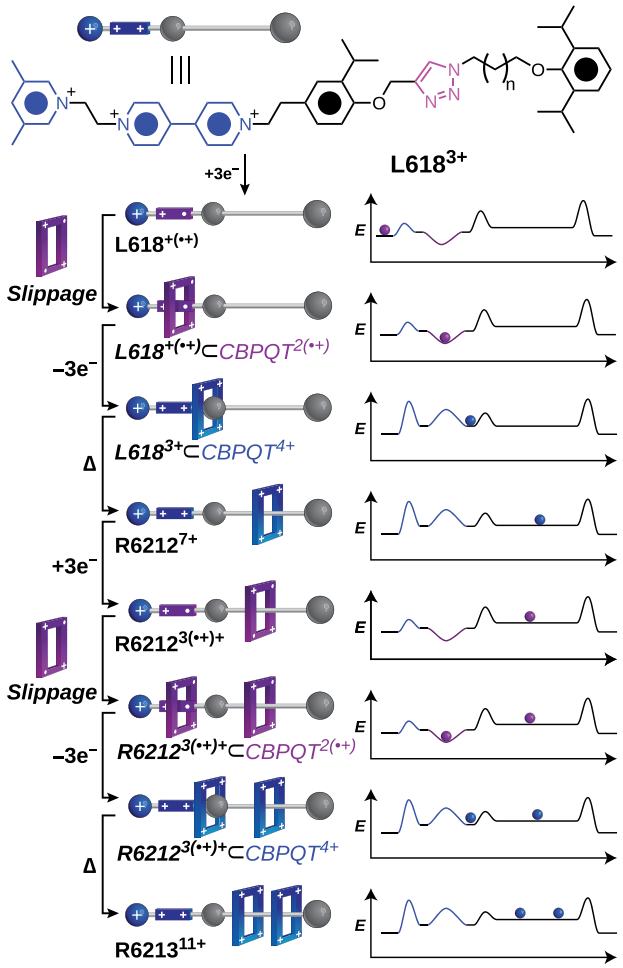


Figure 6.99 A redox-driven molecular pump that threads CBPQT^{4+} rings onto an oligomethylene chain,[929] driving them away from equilibrium toward a higher local concentration.

Conclusions and Outlook

The hundreds of examples touched upon in this Chapter leave us in no doubt that the mechanical bond offers a remarkably versatile platform for designing and making molecular switches and machines. Up to now, >90% of the research efforts have been directed towards producing switches. Artificial molecular switches (AMSs) incorporating mechanical bonds are now highly developed. Many of them can be made in high yields in only a few steps. They have been fashioned and tailored to respond to a dozen different kinds of stimuli—redox, light, pH, cations, anions, neutral competitors, covalent modifications, solvents, temperature, pressure, electric fields, and mechanical force—with each type of stimulus having its own diverse set of design motifs and strategies. The majority of these switches express high positional integrity, in which the ring's ability to discriminate between a variety of recognition sites in another ring or dumbbell component part is highly prejudiced as it is actuated between different states. In solution, the kinetics of switching span a remarkable range of timescales, from sub-microseconds to many hours. The response times are governed by numerous factors, including (i) the temperature, (ii) solvent polarity, and (iii) viscosity, as well as (iv) the types of local noncovalent bonds and their interaction strengths, and (v) the types of stimuli used to induce switching. Several representative classes of mechanically interlocked switches have also been introduced into condensed phases, such as (i) viscous polymer matrices, (ii) monolayers and multilayers at interfaces and surfaces, and (iii) tunnel junctions. These switches are not only operable in these high-friction environments, but also obey, for the most part, the same rules and general mechanisms as those observed in solution. Since AMSs can be screened more rapidly in solution for desired properties before being

introduced into condensed phases with a reasonably high degree of confidence and predictability, this feature bodes well for their further development leading to applications.

In contrast with AMSs, the appearance of genuine artificial molecular machines (AMMs) are not only recent, but also fairly rudimentary in nature. While considerable inroads have been made on coupling switches with other systems for functional purposes, only a handful of examples have been developed in which microscopic reversibility is circumvented by means of non-reciprocating cycles and/or mechanostereoselective motions. Among this handful, work is only done, at best, on the ring of a catenane or rotaxane. Using these AMMs to perform work on different kinds of coupled chemical systems and generalizing them for a variety of applications remains a future prospect for the time being. Fortunately, mechanically interlocked AMMs stand on the strong foundation of AMSs. The limited number of examples of molecular muscles, ratchets, pumps, etc., are based directly on molecular systems that began as relatively simple AMSs. The transition from a molecular switch to a machine is, in many cases, merely a matter of coupling or scaling mechanical motions, either in settings of broken symmetry or in macroscopic materials. Many of the design motifs involved in molecular switches can and should be expected to evolve into genuine AMMs in the hands of the current and next generation of researchers.

Looking forward, it would appear that the time has come to divert much more of our intellectual and technical resources toward the more challenging task of learning how to design, synthesize, and study AMMs. Equally important will be the task of creating integrated systems in which the activity of AMMs are coupled in networks of increasingly higher complexity. If we are to expect MIMs to carry out functions of high sophistication and usefulness, then we must learn how to persuade AMMs with mechanical bonds to work with each other and with many other types of molecules, as naturally occuring molecular machines do in biology. The concentration of proteins in a cell are almost as high as they are in the solid (crystalline) state. In this highly crowded environment, a vast number of biomolecular machines still manage to participate in a dazzling array and complex network of processes with many interconnections, cascade reactions, and mutual dependencies. Nature is telling us that complexity is the path toward goal-directed, self-sustaining, self-replicating, non-equilibrium, energy-dissipating—i.e., life-like—function at the molecular scale. With the advent and development of molecular switches and machines employing mechanical bonds, our foot is lodged firmly in the door.

References

(1) Fyfe, M. C. T.; Glink, P. T.; Menzer, S.; Stoddart, J. F.; White, A. J. P.; Williams, D. J. Anion-Assisted Self-Assembly. *Angew. Chem., Int. Ed. Engl*. **1997**, *36*, 2068–2070.

(2) Cross, L. C.; Klyne, W. IUPAC Rules for the Nomenclature of Organic Chemistry. *Pure Appl. Chem.* **1976**, *45*, 11–30.

(3) Kay, E. R.; Leigh, D. A.; Zerbetto, F. Synthetic Molecular Motors and Mechanical Machines. *Angew. Chem., Int. Ed*. **2007**, *46*, 72–191.

(4) Kay, E. R.; Leigh, D. A. Beyond Switches: Rotaxane- and Catenane-Based Synthetic Molecular Motors. *Pure Appl. Chem.* **2008**, *80*, 17–29.

(5) Astumian, R. D.; Hänggi, P. Brownian Motors. Phys. Today **2002**, *55*, 33–39.

(6) Alberts, B. The Cell as a Collection of Protein Machines: Preparing the Next Generation of Molecular Biologists. *Cell* **1998**, *92*, 291–294.

(7) Bermudez, V.; Capron, N.; Gase, T.; Gatti, F. G.; Kajzar, F.; Leigh, D. A.; Zerbetto, F.; Zhang, S. Influencing Intramolecular Motion with an Alternating Electric Field. *Nature* **2000**, *406*, 608–611.

(8) Hirose, K. Molecular Brake Systems Controlled by Light and Heat. *J. Incl. Phenom. Macrocycl. Chem.* **2010**, *68*, 1–24.

(9) Stoddart, J. F. Whither and Thither Molecular Machines. *Chem. Aust.* **1992**, *59*, 576–577.

(10) Gómez-López, M.; Preece, J. A.; Stoddart, J. F. The Art and Science of Self-Assembling Molecular Machines. *Nanotechnology* **1996**, *7*, 183–192.

(11) Balzani, V.; Gómez-López, M.; Stoddart, J. F. *Molecular Machines. Acc. Chem. Res.* **1998**, *31*, 405–414.

(12) Chambron, J.-C.; Sauvage, J.-P. Functional Rotaxanes: From Controlled Molecular Motions to Electron Transfer Between Chemically Nonconnected Chromophores. *Chem. Eur. J.* **1998**, *4*, 1362–1366.

(13) Balzani, V.; Credi, A.; Raymo, F. M.; Stoddart, J. F. Artificial Molecular Machines. *Angew. Chem., Int. Ed*. **2000**, *39*, 3348–3391.

(14) Liu, J.; Gómez-Kaifer, M.; Kaifer, A. E. Switchable Molecular Devices: From Rotaxanes to Nanoparticles. *Struct. Bond.* **2001**, *99*, 141–162.

(15) Flood, A. H.; Ramirez, R. J. A.; Deng, W.-Q.; Muller, R. P.; Goddard, W. A., III; Stoddart, J. F. Meccano on the Nanoscale—A Blueprint for Making Some of the World's Tiniest Machines. *Aust. J. Chem.* **2004**, *57*, 301–322.

(16) Balzani, V.; Credi, A.; Ferrer, B.; Silvi, S.; Venturi, M. Artificial Molecular Motors and Machines: Design Principles and Prototype Systems. *Top. Curr. Chem.* **2005**, *262*, 1–27.

(17) Credi, A. Artificial Nanomachines Based on Interlocked Molecules. *J. Phys.: Condens. Matter* **2006**, *18*, S1779–S1795.

(18) Balzani, V.; Credi, A.; Silvi, S.; Venturi, M. Artificial Nanomachines Based on Interlocked Molecular Species: Recent Advances. *Chem. Soc. Rev.* **2006**, *35*, 1135–1149.

(19) Feringa, B. L.; Browne, W. R. *Molecular Switches*; Wiley-VCH: Weinheim, **2011**.

(20) Yang, W.; Li, Y.; Liu, H.; Chi, L.; Li, Y. Design and Assembly of Rotaxane-Based Molecular Switches and Machines. *Small* **2012**, *8*, 504–516.

(21) Benniston, A. C. Photo- and Redox-Active [2]Rotaxanes and [2]Catenanes. *Chem. Soc. Rev.* **1996**, *25*, 427–435.

(22) Sauvage, J.-P. Transition Metal-Containing Rotaxanes and Catenanes in Motion: Toward Molecular Machines and Motors. *Acc. Chem. Res.* **1998**, *31*, 611–619.

(23) Collin, J.-P.; Dietrich-Buchecker, C.; Gaviña, P.; Jimenez-Molero, M. C.; Sauvage, J.-P. Shuttles and Muscles: Linear Molecular Machines Based on Transition Metals. *Acc. Chem. Res.* **2001**, *34*, 477–487.

(24) Moonen, N. N. P.; Flood, A. H.; Fernández, J. M.; Stoddart, J. F. Towards a Rational Design of Molecular Switches and Sensors From Their Basic Building Blocks. *Top. Curr. Chem.* **2005**, *262*, 99–132.

(25) Flood, A. H.; Wong, E. W.; Stoddart, J. F. Models of Charge Transport and Transfer in Molecular Switch Tunnel Junctions of Bistable Catenanes and Rotaxanes. *Chem. Phys.* **2006**, *324*, 280–290.

(26) Nijhuis, C. A.; Ravoo, B. J.; Huskens, J.; Reinhoudt, D. N. Electrochemically Controlled Supramolecular Systems. *Coord. Chem. Rev.* **2007**, *251*, 1761–1780.

(27) Suzaki, Y.; Taira, T.; Osakada, K.; Horie, M. Rotaxanes and Pseudorotaxanes with Fe-, Pd- and Pt-Containing Axles. Molecular Motion in the Solid State and Aggregation in Solution. *Dalton Trans.* **2008**, *4823–4833*.

(28) Collin, J.-P.; Sauvage, J.-P. Caténanes et Rotaxanes Électroactifs: Prototypes de Machines Moléculaires. *L'actualité Chimique* **2009**, *327–328*, 114–119.

(29) Durola, F.; Sauvage, J.-P.; Wenger, O. S. The Magic Effect of Endocyclic but Non-Sterically Hindering Biisoquinoline Chelates: From Fast-Moving Molecular Shuttles to [3]Rotaxanes. *Coord. Chem. Rev.* **2010**, *254*, 1748–1759.

(30) Fahrenbach, A. C.; Bruns, C. J.; Cao, D.; Stoddart, J. F. Ground-State Thermodynamics of Bistable Redox-Active Donor–Acceptor Mechanically Interlocked Molecules. *Acc. Chem. Res.* **2012**, *45*, 1581–1592.

(31) Coskun, A.; Spruell, J. M.; Barin, G.; Dichtel, W. R.; Flood, A. H.; Botros, Y. Y.; Stoddart, J. F. High Hopes: Can Molecular Electronics Realise Its Potential? *Chem. Soc. Rev.* **2012**, *41*, 4827–4859.

(32) Venturi, M.; Credi, A. Electroactive [2]catenanes. *Electrochim. Acta* **2014**, *140*, 467–475.

(33) Fahrenbach, A. C.; Bruns, C. J.; Li, H.; Trabolsi, A.; Coskun, A.; Stoddart, J. F. Ground-State Kinetics of Bistable Redox-Active Donor–Acceptor Mechanically Interlocked Molecules. *Acc. Chem. Res.* **2014**, *47*, 482–493.

(34) Le Poul, N.; Colasson, B. Electrochemically and Chemically Induced Redox Processes in Molecular Machines. *ChemElectroChem* **2015**, *2*, 475–496.

(35) Bissell, R. A.; Córdova, E.; Kaifer, A. E.; Stoddart, J. F. A Chemically and Electrochemically Switchable Molecular Shuttle. *Nature* **1994**, *369*, 133–137.

(36) Córdova, E.; Bissell, R. A.; Spencer, N.; Ashton, P. R.; Stoddart, J. F.; Kaifer, A. E.; Novel Rotaxanes Based on the Inclusion Complexation of Biphenyl Guests by Cyclobis(paraquat-*p*-phenylene). *J. Org. Chem.* **1993**, *58*, 6550–6552.

(37) Ashton, P. R.; Bissell, R. A.; Spencer, N.; Stoddart, J. F.; Tolley, M. S. Towards Controllable Molecular Shuttles. 1. *Synlett* **1992**, 914–918.

(38) Ashton, P. R.; Bissell, R. A.; Górski, R.; Philp, D.; Spencer, N.; Stoddart, J. F.; Tolley, M. S. Towards Controllable Molecular Shuttles. 2. *Synlett* **1992**, 919–922.

(39) Ashton, P. R.; Bissell, R. A.; Spencer, N.; Stoddart, J. F.; Tolley, M. S. Towards Controllable Molecular Shuttles. 3. *Synlett* **1992**, 923–926.

(40) Ashton, P. R.; Ballardini, R.; Balzani, V.; Gandolfi, M. T.; Marquis, D. J.-F.; Pérez-García, L.; Prodi, L.; Stoddart, J. F.; Venturi, M. The Self Assembly of Controllable [2]Catenanes. *J. Chem. Soc., Chem. Commun*. **1994**, 177–180.

(41) Ashton, P. R.; Ballardini, R.; Balzani, V.; Credi, A.; Gandolfi, M. T.; Menzer, S.; Pérez-García, L.; Prodi, L.; Stoddart, J. F.; Venturi, M.; White, A. J. P.; Williams, D. J.; Molecular Meccano 4. The Self-Assembly of [2]Catenanes Incorporating Photoactive and Electroactive π-Extended Systems. *J. Am. Chem. Soc*. **1995**, *117*, 11171–11197.

(42) Anelli, P.-L.; Asakawa, M.; Ashton, P. R.; Bissell, R. A.; Clavier, G.; Górski, R.; Kaifer, A. E.; Langford, S. J.; Mattersteig, G.; Menzer, S.; Philp, D.; Slawin, A. M. Z.; Spencer, N.; Stoddart, J. F.; Tolley, M. S.; Williams, D. J. Molecular Meccano 10. Toward Controllable Molecular Shuttles. *Chem. Eur. J.* **1997**, *3*, 1113–1135.

(43) Ashton, P. R.; Ballardini, R.; Balzani, V.; Boyd, S. E.; Credi, A.; Gandolfi, M. T.; Gómez-López, M.; Iqbal, S.; Philp, D.; Preece, J. A.; Prodi, L.; Ricketts, H. G.; Stoddart, J. F.; Tolley, M. S.; Venturi, M.; White, A. J. P.; William, D. J. Molecular Meccano 14. Simple Mechanical Molecular and Supramolecular Machines: Photochemical and Electrochemical Control of Switching Processes. *Chem. Eur. J.* **1997**, *3*, 152–170.

(44) Asakawa, M.; Ashton, P. R.; Balzani, V.; Credi, A.; Hamers, C.; Mattersteig, G.; Montalti, M.; Shipway, A. N.; Spencer, N.; Stoddart, J. F.; Tolley, M. S.; Venturi, M.; White, A. J. P.; Williams, D. J. A Chemically and Electrochemically Switchable [2]Catenane Incorporating a Tetrathiafulvalene Unit. *Angew. Chem., Int. Ed.* **1998**, *37*, 333–337.

(45) Ashton, P. R.; Ballardini, R.; Balzani, V.; Credi, A.; Dress, K. R.; Ishow, E.; Kleverlaan, C. J.; Kocian, O.; Preece, J. A.; Spencer, N.; Stoddart, J. F.; Venturi, M.; Wenger, S. Molecular Meccano 61. A Photochemically Driven Molecular-Level Abacus. *Chem. Eur. J.* **2000**, *6*, 3558–3574.

(46) Iijima, T.; Vignon, S. A.; Tseng, H.-R.; Jarrosson, T.; Sanders, J. K. M.; Marchioni, F.; Venturi, M.; Apostoli, E.; Balzani, V.; Stoddart, J. F. Controllable Donor-Acceptor Neutral [2]Rotaxanes. *Chem. Eur. J.* **2004**, *10*, 6375–6392.

(47) Olsen, J.-C.; Fahrenbach, A. C.; Trabolsi, A.; Friedman, D. C.; Dey, S. K.; Gothard, C. M.; Shveyd, A. K.; Gasa, T. B.; Spruell, J. M.; Olson, M. A.; Wang, C.; Jacquot de Rouville, H.-P.; Botros, Y. Y.; Stoddart, J. F. A Neutral Redox-Switchable [2]Rotaxane. *Org. Lett*. **2011**, *9*, 7126–7133.

(48) Ashton, P. R.; Ballardini, R.; Balzani, V.; Baxter, I.; Credi, A.; Fyfe, M. C. T.; Gandolfi, M. T.; Gómez-López, M.; Martínez-Díaz, M.-V.; Piersanti, A.; Spencer, N.; Stoddart, J. F.; Venturi, M.; White, A. J. P.; Williams, D. J. Molecular Meccano 46. Acid-Base Controllable Molecular Shuttles. *J. Am. Chem. Soc*. **1998**, *120*, 11932–11942.

(49) Coskun, A.; Saha, S.; Aprahamian, I.; Stoddart, J. F. A Reverse Donor-Acceptor Bistable [2]Catenane. *Org. Lett.* **2008**, *10*, 3187–3190.

(50) Dey, S. K.; Coskun, A.; Fahrenbach, A. C.; Barin, G.; Basuray, A. N.; Trabolsi, A.; Botros, Y. Y.; Stoddart, J. F. A Redox-Active Reverse Donor–Acceptor Bistable [2]Rotaxane. *Chem. Sci.* **2011**, *2*, 1046–1053.

(51) Philp, D.; Slawin, A. M. Z.; Spencer, N.; Stoddart, J. F.; Williams, D. J. The Complexation of Tetrathiafulvalene by Cyclobis(paraquat-*p*-phenylene). *J. Chem. Soc., Chem. Commun*. **1991**, 1584–1586.

(52) Segura, J. L.; Martín, N. New Concepts in Tetrathiafulvalene Chemistry. *Angew. Chem., Int. Ed*. **2001**, *40*, 1372–1409.

(53) Canevet, D.; Sallé, M.; Zhang, G.; Zhang, D.; Zhu, D. Tetrathiafulvalene (TTF) Derivatives: Key Building-Blocks for Switchable Processes. *Chem. Commun.* **2009**, *2245–2269*.

(54) Castro, R.; Nixon, K. R.; Evanseck, J. D.; Kaifer, A. E. Effects of Side Arm Length and Structure of Para-Substituted Phenyl Derivatives on Their Binding to the Host Cyclobis(paraquat-*p*-phenylene). *J. Org. Chem.* **1996**, *61*, 7298–7303.

(55) Fahrenbach, A. C.; Barnes, J. C.; Li, H.; Benítez, D.; Basuray, A. N.; Fang, L.; Sue, C.-H.; Barin, G.; Dey, S. K.; Goddard, W. A., III; Stoddart, J. F. Measurement of the Ground-State Distributions in Bistable Mechanically Interlocked Molecules Using Slow Scan Rate Cyclic Voltammetry. *Proc. Natl. Acad. Sci. U.S.A.* **2011**, *108*, 20416–20421.

(56) Aprahamian, I.; Dichtel, W. R.; Ikeda, T.; Heath, J. R.; Stoddart, J. F. A Clicked Bistable [2]Rotaxane. *Org. Lett.* **2007**, *9*, 1287–1290.

(57) Spruell, J. M.; Paxton, W. F.; Olsen, J.-C.; Benítez, D.; Tkatchouk, E.; Stern, C. L.; Trabolsi, A.; Friedman, D. C.; Goddard, W. A., III; Stoddart, J. F. A Push-Button Molecular Switch. *J. Am. Chem. Soc.* **2009**, *131*, 11571–11580.

(58) Pease, A. R.; Jeppesen, J. O.; Stoddart, J. F.; Luo, Y.; Collier, C. P.; Heath, J. R. Switching Devices Based on Interlocked Molecules. *Acc. Chem. Res.* **2001**, *34*, 433–444.

(59) Balzani, V.; Credi, A.; Mattersteig, G.; Matthews, O. A.; Raymo, F. M.; Stoddart, J. F.; Venturi, M.; White, A. J. P.; Williams, D. J. Molecular Meccano 54. Switching of Pseudorotaxanes and Catenanes Incorporating a Tetrathiafulvalene Unit by Redox and Chemical Inputs. *J. Org. Chem*. **2000**, *65*, 1924–1936.

(60) Jeppesen, J. O.; Perkins, J.; Becher, J.; Stoddart, J. F. Slow Shuttling in an Amphiphilic Bistable [2]Rotaxane Incorporating a Tetrathiafulvalene Unit. *Angew. Chem., Int. Ed*. **2001**, *40*, 1216–1221.

(61) Jeppesen, J. O.; Nielsen, K. A.; Perkins, J.; Vignon, S. A.; Fabio, A. D.; Ballardini, R.; Gandolfi, M. T.; Venturi, M.; Balzani, V.; Becher, J.; Stoddart, J. F. Amphiphilic Bistable Rotaxanes. *Chem. Eur. J.* **2003**, *9*, 2982–3007.

(62) Tseng, H.-R.; Vignon, S. A.; Stoddart, J. F. Toward Chemically Controlled Nanoscale Molecular Machinery. *Angew. Chem., Int. Ed*. **2003**, *42*, 1491–1495.
(63) Flood, A. H.; Peters, A. J.; Vignon, S. A.; Steuerman, D. W.; Tseng, H.-R.; Kang, S.; Heath, J. R.; Stoddart, J. F. The Role of Physical Environment on Molecular Electromechanical Switching. *Chem. Eur. J.* **2004**, *10*, 6558–6564.
(64) Tseng, H.-R.; Vignon, S. A.; Celestre, P. C.; Perkins, J.; Jeppesen, J. O.; Fabio, A. D.; Ballardini, R.; Gandolfi, M. T.; Venturi, M.; Balzani, V.; Stoddart, J. F. Redox-Controllable Amphiphilic [2]Rotaxanes. *Chem. Eur. J.* **2004**, *10*, 155–172.
(65) Deng, W.-Q.; Flood, A. H.; Stoddart, J. F.; Goddard, W. A., III. An Electrochemical Color-Switchable RGB Dye: Tristable [2]Catenane. *J. Am. Chem. Soc.* **2005**, *127*, 15994–15995.
(66) Jeppesen, J. O.; Nygaard, S.; Vignon, S. A.; Stoddart, J. F. Honing Up a Genre of Amphiphilic Bistable [2]Rotaxanes for Device Settings. *Eur. J. Org. Chem.* **2005**, *196–220*.
(67) Ikeda, T.; Saha, S.; Aprahamian, I.; Leung, K. C.-F.; Williams, A.; Deng, W.-Q.; Flood, A. H.; Goddard, W. A., III; Stoddart, J. F. Toward Electrochemically Controllable Tristable Three-Station [2]Catenanes. *Chem. Asian J*. **2007**, *2*, 76–93.
(68) Saha, S.; Flood, A. H.; Stoddart, J. F.; Impellizzeri, S.; Silvi, S.; Venturi, M.; Credi, A. A Redox-Driven Multicomponent Molecular Shuttle. *J. Am. Chem. Soc.* **2007**, *129*, 12159–12171.
(69) Aprahamian, I.; Yasuda, T.; Ikeda, T.; Saha, S.; Dichtel, W. R.; Isoda, K.; Kato, T.; Stoddart, J. F. A Liquid-Crystalline Bistable [2]Rotaxane. *Angew. Chem., Int. Ed*. **2007**, *46*, 4675–4679.
(70) Aprahamian, I.; Olsen, J.-C.; Trabolsi, A.; Stoddart, J. F. Tetrathiafulvalene Radical Cation Dimerization in a Bistable Tripodal [4]Rotaxane. *Chem. Eur. J.* **2008**, *14*, 3889–3895.
(71) Zhao, Y.-L.; Aprahamian, I.; Trabolsi, A.; Erina, N.; Stoddart, J. F. Organogel Formation by a Cholesterol-Stoppered Bistable [2]Rotaxane and Its Dumbbell Precursor. *J. Am. Chem. Soc.* **2008**, *130*, 6348–6350.
(72) Zhao, Y.-L.; Trabolsi, A.; Stoddart, J. F. A Bistable Pretzelane. *Chem. Commun.* **2009**, 4844–4846.
(73) Olson, M. A.; Braunschweig, A. B.; Fang, L.; Ikeda, T.; Klajn, R.; Trabolsi, A.; Wesson, P. J.; Benítez, D.; Mirkin, C. A.; Grzybowski, B. A.; Stoddart, J. F. A Bistable Poly[2]catenane Forms Nanosuperstructures. *Angew. Chem., Int. Ed*. **2009**, *48*, 1792–1797.
(74) Olson, M. A.; Braunschweig, A. B.; Ikeda, T.; Fang, L.; Trabolsi, A.; Slawin, A. M. Z.; Khan, S. I.; Stoddart, J. F. Thermodynamic Forecasting of Mechanically Interlocked Switches. *Org. Lett.* **2009**, *7*, 4391–4405.
(75) Trabolsi, A.; Fahrenbach, A. C.; Dey, S. K.; Share, A. I.; Friedman, D. C.; Basu, S.; Gasa, T. B.; Khashab, N. M.; Saha, S.; Aprahamian, I.; Katib, H. A.; Flood, A. H.; Stoddart, J. F. A Tristable [2]Pseudo[2]rotaxane. *Chem. Commun.* **2010**, *46*, 871–873.
(76) Trabolsi, A.; Khashab, N.; Fahrenbach, A. C.; Friedman, D. C.; Colvin, M. T.; Cotí, K. K.; Benítez, D.; Tkatchouk, E.; Olsen, J.-C.; Belowich, M. E.; Carmielli, R.; Khatib, H. A.; Goddard, W. A., III; Wasielewski, M. R.; Stoddart, J. F. Radically Enhanced Molecular Recognition. *Nature Chem.* **2010**, *2*, 42–49.
(77) Spruell, J. M.; Coskun, A.; Friedman, D. C.; Forgan, R. S.; Sarjeant, A. A.; Trabolsi, A.; Fahrenbach, A. C.; Barin, G.; Paxton, W. F.; Dey, S. K.; Olson, M. A.; Benítez, D.; Tkatchouk, E.; Colvin, M. T.; Carmielli, R.; Caldwell, S. T.; Rosair, G. M.; Hewage, S. G.; Duclairoir, F.; Seymour, J. L.; Slawin, A. M. Z.; Goddard, W. A., III; Wasielewski, M. R.; Cooke, G.; Stoddart, J. F. Highly Stable Tetrathiafulvalene Radical Dimers in [3]Catenanes. *Nature Chem.* **2010**, *2*, 870–879.
(78) Coskun, A.; Spruell, J. M.; Barin, G.; Fahrenbach, A. C.; Forgan, R. S.; Colvin, M. T.; Carmieli, R.; Benítez, D.; Tkatchouk, E.; Friedman, D. C.; Sarjeant, A. A.; Wasielewski, M. R.; Goddard, W. A., III; Stoddart, J. F. Mechanically Stabilized Tetrathiafulvalene Radical Dimers. *J. Am. Chem. Soc.* **2011**, *133*, 4538–4547.
(79) Fang, L.; Wang, C.; Fahrenbach, A. C.; Trabolsi, A.; Botros, Y. Y.; Stoddart, J. F. Dual Stimulus Switching of a [2]Catenane in Water. *Angew. Chem., Int. Ed*. **2011**, *50*, 1805–1809.
(80) Zhang, K.-D.; Zhao, X.; Wang, G.-T.; Liu, Y.; Zhang, Y.; Lu, H.-J.; Jiang, X.-K.; Li, Z.-T. Foldamer-Tuned Switching Kinetics and Metastability of [2]Rotaxanes. *Angew. Chem., Int. Ed*. **2011**, *50*, 9866–9870.
(81) Wang, C.; Cao, D.; Fahrenbach, A. C.; Grunder, S.; Dey, S. K.; Sarjeant, A. A.; Stoddart, J. F. The Effects of Conformation on the Noncovalent Bonding Interactions in a Bistable Donor–Acceptor [3]Catenane. *Chem. Commun.* **2012**, *48*, 9245–9247.
(82) Andersen, S. S.; Share, A. I.; Poulsen, B. L. C.; Kørner, M.; Duedal, T.; Benson, C. R.; Hansen, S. W.; Jeppesen, J. O.; Flood, A. H. Mechanistic Evaluation of Motion in Redox-Driven Rotaxanes Reveals Longer Linkers Hasten Forward Escapes and Hinder Backward Translations. *J. Am. Chem. Soc.* **2014**, *136*, 6373–6384.
(83) Choi, J. W.; Flood, A. H.; Steuerman, D. W.; Nygaard, S.; Braunschweig, A. B.; Moonen, N. N. P.; Laursen, B. W.; Luo, Y.; DeIonno, E.; Peters, A. J.; Jeppesen, J. O.; Xu, K.; Stoddart, J. F.; Heath, J. R. Ground-State Equilibrium Thermodynamics and Switching Kinetics of Bistable [2]Rotaxanes Switched in Solution, Polymer Gels, and Molecular Electronic Devices. *Chem. Eur. J.* **2006**, *12*, 261–279.
(84) Asakawa, M.; Higuchi, M.; Mattersteig, G.; Nakamura, T.; Pease, A. R.; Raymo, F. M.; Shimizu, T.; Stoddart, J. F. Current/Voltage Characteristics of Monolayers of Redox-Switchable [2]Catenanes on Gold. *Adv. Mater.* **2000**, *12*, 1099–1102.
(85) Collier, C. P.; Jeppesen, J. O.; Luo, Y.; Perkins, J.; Wong, E. W.; Heath, J. R.; Stoddart, J. F. Molecular-Based Electronically Switchable Tunnel Junction Devices. *J. Am. Chem. Soc.* **2001**, *123*, 12632–12641.
(86) Huang, T. J.; Tseng, H.-R.; Sha, L.; Lu, W.; Brough, B.; Flood, A. H.; Yu, B.-D.; Celestre, P. C.; Chang, J. P.; Stoddart, J. F.; Ho, C.-M. Mechanical Shuttling of Linear Motor-Molecules in Condensed Phases on Solid Substrates. *Nano Lett.* **2004**, *4*, 2065–2071.
(87) Tseng, H.-R.; Wu, D.; Fang, N. X.; Zhang, X.; Stoddart, J. F. The Metastability of an Electrochemically Controlled Nanoscale Machine on Gold Surfaces. *ChemPhysChem* **2004**, *5*, 111–116.
(88) Nørgaard, K.; Laursen, B. W.; Nygaard, S.; Kjaer, K.; Tseng, H.-R.; Flood, A. H.; Stoddart, J. F.; Bjørnholm, T. Structural Evidence of Mechanical Shuttling in Condensed Monolayers of Bistable Rotaxane Molecules. *Angew. Chem., Int. Ed*. **2005**, *44*, 7035–7039.
(89) Nguyen, T. D.; Tseng, H.-R.; Celestre, P. C.; Flood, A. H.; Liu, Y.; Stoddart, J. F.; Zink, J. I. A Reversible Molecular Valve. *Proc. Natl. Acad. Sci. U.S.A.* **2005**, *102*, 10029–10034.
(90) Jang, S. S.; Jang, Y. H.; Kim, Y.-H.; Goddard, W. A., III; Flood, A. H.; Laursen, B. W.; Tseng, H.-R.; Stoddart, J. F.; Jeppesen, J. O.; Choi, J. W.; Steuerman, D. W.; Delonno, E.; Heath, J. R. Structures and Properties of Self-Assembled Monolayers of Bistable [2]Rotaxanes on Au(111) Surfaces From Molecular Dynamics Simulations Validated with Experiment. *J. Am. Chem. Soc.* **2005**, *127*, 1563–1575.
(91) Liu, Y.; Flood, A. H.; Bonvallet, P. A.; Vignon, S. A.; Northrop, B. H.; Tseng, H.-R.; Jeppesen, J. O.; Huang, T. J.; Brough, B.; Baller, M.; Solares, S. D.; Goddard, W. A., III; Ho, C.-M.; Stoddart, J. F. Linear Artificial Molecular Muscles. *J. Am. Chem. Soc.* **2005**, *127*, 9745–9759.
(92) Brough, B.; Northrop, B. H.; Schmidt, J. J.; Tseng, H.-R.; Houk, K. N.; Stoddart, J. F.; Ho, C.-M. Evaluation of Synthetic Linear Motor-Molecule Actuation Energetics. *Proc. Natl. Acad. Sci. U.S.A.* **2006**, *103*, 8583–8588.
(93) Nguyen, T. D.; Liu, Y.; Saha, S.; Leung, K. C.-F.; Stoddart, J. F.; Zink, J. I. Design and Optimization of Molecular Nanovalves Based on Redox-Switchable Bistable Rotaxanes. *J. Am. Chem. Soc.* **2007**, *129*, 626–634.
(94) Zheng, Y. B.; Yang, Y.-W.; Jensen, L.; Fang, L.; Juluri, B. K.; Flood, A. H.; Weiss, P. S.; Stoddart, J. F.; Huang, T. J. Active

Molecular Plasmonics: Controlling Plasmon Resonances with Molecular Switches. *Nano Lett.* **2009**, *9*, 819–825.
(95) Juluri, B. K.; Kumar, A. S.; Liu, Y.; Ye, T.; Yang, Y.-W.; Flood, A. H.; Fang, L.; Stoddart, J. F.; Weiss, P. S.; Huang, T. J. A Mechanical Actuator Driven Electrochemically by Artificial Molecular Muscles. *ACS Nano* **2009**, *3*, 291–300.
(96) Coskun, A.; Wesson, P. J.; Klajn, R.; Trabolsi, A.; Fang, L.; Olson, M. A.; Dey, S. K.; Grzybowski, B. A.; Stoddart, J. F. Molecular-Mechanical Switching at the Nanoparticle-Solvent Interface: Practice and Theory. *J. Am. Chem. Soc.* **2010**, *132*, 4310–4320.
(97) Ye, T.; Kumar, A. S.; Saha, S.; Takami, T.; Huang, T. J.; Stoddart, J. F.; Weiss, P. S. Changing Stations in Single Bistable Rotaxane Molecules Under Electrochemical Control. *ACS Nano* **2010**, *4*, 3697–3701.
(98) Yasuda, T.; Tanabe, K.; Tsuji, T.; Cotí, K. K.; Aprahamian, I.; Stoddart, J. F.; Kato, T. A Redox-Switchable [2]Rotaxane in a Liquid-Crystalline State. *Chem. Commun.* **2010**, *46*, 1224–1226.
(99) Zhang, W.; DeIonno, E.; Dichtel, W. R.; Fang, L.; Trabolsi, A.; Olsen, J.-C.; Benítez, D.; Heath, J. R.; Stoddart, J. F. A Solid-State Switch Containing an Electrochemically Switchable Bistable Poly[*n*]rotaxane. *J. Mater. Chem.* **2011**, *21*, 1487–1495.
(100) Avellini, T.; Li, H.; Coskun, A.; Barin, G.; Trabolsi, A.; Basuray, A. N.; Dey, S. K.; Credi, A.; Silvi, S.; Stoddart, J. F.; Venturi, M. Photoinduced Memory Effect in a Redox Controllable Bistable Mechanical Molecular Switch. *Angew. Chem., Int. Ed*. **2012**, *51*, 1611–1615.
(101) Collier, C. P.; Wong, E. W.; Belohradský, M.; Raymo, F. M.; Stoddart, J. F.; Kuekes, P. J.; Williams, R. S.; Heath, J. R. Electronically Configurable Molecular-Based Logic Gates. *Science* **1999**, *285*, 391–394.
(102) Collier, C. P.; Mattersteig, G.; Wong, E. W.; Luo, Y.; Beverly, K.; Sampaio, J.; Raymo, F. M.; Stoddart, J. F.; Heath, J. R. A [2]Catenane-Based Solid State Electronically Reconfigurable Switch. *Science* **2000**, *289*, 1172–1175.
(103) Yu, H.; Luo, Y.; Beverly, K.; Stoddart, J. F.; Tseng, H.-R.; Heath, J. R. The Molecule-Electrode Interface in Single-Molecule Transistors. *Angew. Chem., Int. Ed*. **2003**, *42*, 5706–5711.
(104) Luo, Y.; Collier, C. P.; Jeppesen, J. O.; Nielsen, K. A.; DeIonno, E.; Ho, G.; Perkins, J.; Tseng, H.-R.; Yamamoto, T.; Stoddart, J. F.; Heath, J. R. Two-Dimensional Molecular Electronics Circuits. *ChemPhysChem* **2002**, *3*, 519–525.
(105) Green, J. E.; Choi, J. W.; Boukai, A.; Bunimovich, Y.; Johnston-Halperin, E.; DeIonno, E.; Luo, Y.; Sheriff, B. A.; Xu, K.; Shin, Y. S.; Tseng, H,-R.; Stoddart, J. F.; Heath, J. R. A 160-Kilobit Molecular Electronic Memory Patterned at 10^{11} Bits Per Square Centimetre. *Nature* **2007**, *445*, 414–417.
(106) Lau, J.; Nielsen, M. B.; Thorup, N.; Cava, M. P.; Becher, J. Bis(pyrrolo)tetrathiafulvalene – An Efficient π-Donor in Supramolecular Chemistry. *Eur. J. Org. Chem.* **1999**, *3335–3341*.
(107) Li, Z.-T.; Stein, P. C.; Svenstrup, N.; Lund, K. H.; Becher, J. Synthesis of Novel Tetrathiafulvalene-Based [3]Pseudocatenanes by Self-Assembly; Prevention of *trans/cis* Isomerization. *Angew. Chem., Int. Ed. Engl*. **1995**, *34*, 2524–2528.
(108) Li, Z.-T.; Stein, P. C.; Becher, J.; Jensen, D.; Mørk, P.; Svenstrup, N. Self-Assembling Tetrathiafulvalene-Based Rotaxanes and Catenanes. *Chem. Eur. J.* **1996**, *2*, 624–633.
(109) Li, Z.-T.; Becher, J. Configurationally Selective Self-Assembly of a *cis*-[3]Pseudocatenane Incorporating Three Tetrathiafulvalene Units. *Chem. Commun.* **1996**, 639–640.
(110) Li, Z.-T.; Becher, J. Effects of Fluorine in the Self-Assembly of Tetrathiafulvalene-Based [3]Catenanes-(circum TTF) – A New Approach to Controlling the Regio-and Configurational Selectiviy. *Synlett* **1997**, 557–560.
(111) Nielsen, M. B.; Thorup, N.; Becher, J. Synthesis of a Criss-Cross Overlapped Tetrathiafulvalenophane and a Topologically New [2]Catenane. *J. Chem. Soc., Perkin Trans. 1* **1998**, 1305–1308.
(112) Damgaard, D.; Nielsen, M. B.; Lau, J.; Jensen, K. B.; Zubarev, R.; Levillain, E.; Becher, J. Synthesis of Linear Oligo-TTFs and Their [2]Rotaxanes with Cyclobis(paraquat-*p*-phenylene). *J. Mater. Chem.* **2000**, *10*, 2249–2258.
(113) Guo, X.; Zhou, Y.; Feng, M.; Xu, Y.; Zhang, D.; Gao, H.; Fan, Q.; Zhu, D. Tetrathiafulvalene-, 1,5-Dioxynaphthalene-, and Cyclobis(paraquat-*p*-phenylene)-Based [2]Rotaxanes with Cyclohexyl and Alkyl Chains as Spacers: Synthesis, Langmuir–Blodgett Films, and Electrical Bistability. *Adv. Funct. Mater.* **2007**, *17*, 763–769.
(114) Feng, M.; Gao, L.; Du, S. X.; Deng, Z. T.; Cheng, Z. H.; Ji, W.; Zhang, D. Q.; Guo, X. F.; Lin, X.; Chi, L. F.; Zhu, D. B.; Fuchs, H.; Gao, H.-J. Observation of Structural and Conductance Transition of Rotaxane Molecules at a Submolecular Scale. *Adv. Funct. Mater.* **2007**, *17*, 770–776.
(115) Nygaard, S.; Hansen, S. W.; Huffman, J. C.; Jensen, F.; Flood, A. H.; Jeppesen, J. O. Two Classes of Alongside Charge-Transfer Interactions Defined in One [2]Catenane. *J. Am. Chem. Soc.* **2007**, *129*, 7354–7363.
(116) Nygaard, S.; Liu, Y.; Stein, P C; Flood, A. H.; Jeppesen, J. O. Using Molecular Force to Overcome Steric Barriers in a Springlike Molecular Ouroboros. *Adv. Funct. Mater*. **2007**, *17*, 751–762.
(117) Zhang, K.-D.; Zhao, X.; Wang, G.-T.; Liu, Y.; Zhang, Y.; Lu, H.-J.; Jiang, X.-K.; Li, Z.-T. Foldamers in Pseudo[2]rotaxanes and [2]Rotaxanes: Tuning the Switching Kinetics and Metastability. *Tetrahedron* **2012**, *68*, 4517–4527.
(118) Wang, C.; Dyar, S. M.; Cao, D.; Fahrenbach, A. C.; Horwitz, N.; Colvin, M. T.; Carmieli, R.; Stern, C. L.; Dey, S. K.; Wasielewski, M. R.; Stoddart, J. F. Tetrathiafulvalene Hetero Radical Cation Dimerization in a Redox-Active [2]Catenane. *J. Am. Chem. Soc.* **2012**, *134*, 19136–19145.
(119) Jeppesen, J. O.; Becher, J.; Stoddart, J. F. Poised on the Brink Between a Bistable Complex and a Compound. *Org. Lett.* **2002**, *4*, 557–560.
(120) Jeppesen, J. O.; Vignon, S. A.; Stoddart, J. F. In the Twilight Zone Between [2]Pseudorotaxanes and [2]Rotaxanes. *Chem. Eur. J.* **2003**, *9*, 4611–4625.
(121) Balzani, V.; Clemente-León, M.; Credi, A.; Semeraro, M.; Venturi, M.; Tseng, H.-R.; Wenger, S.; Saha, S.; Stoddart, J. F. A Comparison of Shuttling Mechanisms in Two Constitutionally Isomeric Bistable Rotaxane-Based Sunlight-Powered Nanomotors. *Aust. J. Chem.* **2006**, *59*, 193–206.
(122) Ashton, P. R.; Baldoni, V.; Balzani, V.; Credi, A.; Hoffmann, H. D. A.; Martínez-Díaz, M.-V.; Raymo, F. M.; Stoddart, J. F.; Venturi, M. Molecular Meccano 63. Dual-Mode "Co-Conformational" Switching in Catenanes Incorporating Bipyridinium and Dialkylammonium Recognition Sites. *Chem. Eur. J.* **2001**, *7*, 3482–3493.
(123) Jacquot de Rouville, H.-P.; Iehl, J.; Bruns, C. J.; McGrier, P. L.; Frasconi, M.; Sarjeant, A. A.; Stoddart, J. F. A Neutral Naphthalene Diimide [2]Rotaxane. *Org. Lett*. **2012**, *14*, 5188–5191.
(124) Cao, D.; Amelia, M.; Klivansky, L. M.; Koshkakaryan, G.; Khan, S. I.; Semeraro, M.; Silvi, S.; Venturi, M.; Credi, A.; Liu, Y. Probing Donor−Acceptor Interactions and Co-Conformational Changes in Redox Active Desymmetrized [2]Catenanes. *J. Am. Chem. Soc.* **2010**, *132*, 1110–1122.
(125) Liu, Y.; Klivansky, L. M.; Khan, S. I.; Zhang, X. Templated Synthesis of Desymmetrized [2]Catenanes with Excellent Translational Selectivity. *Org. Lett.* **2007**, *9*, 2577–2580.
(126) Fahrenbach, A. C.; Barnes, J. C.; Lanfranchi, D. A.; Li, H.; Coskun, A.; Gassensmith, J. J.; Liu, Z.; Benítez, D.; Trabolsi, A.; Goddard, W. A., III; Elhabiri, M.; Stoddart, J. F. Solution-Phase Mechanistic Study and Solid-State Structure of a Tris(bipyridinium radical cation) Inclusion Complex. *J. Am. Chem. Soc.* **2012**, *134*, 3061–3072.

(127) Li, H.; Fahrenbach, A. C.; Coskun, A.; Zhu, Z.; Barin, G.; Zhao, Y.-L.; Botros, Y. Y.; Sauvage, J.-P.; Stoddart, J. F. A Light-Stimulated Molecular Switch Driven by Radical–Radical Interactions in Water. *Angew. Chem., Int. Ed*. **2011**, *50*, 6782–6788.
(128) Fahrenbach, A. C.; Zhu, Z.; Cao, D.; Liu, W.-G.; Li, H.; Dey, S. K.; Basu, S.; Trabolsi, A.; Botros, Y. Y.; Goddard, W. A., III; Stoddart, J. F. Radically Enhanced Molecular Switches. *J. Am. Chem. Soc.* **2012**, *134*, 16275–16288.
(129) Zhu, Z.; Fahrenbach, A. C.; Li, H.; Barnes, J. C.; Liu, Z.; Dyar, S. M.; Zhang, H.; Lei, J.; Carmieli, R.; Sarjeant, A. A.; Stern, C. L.; Wasielewski, M. R.; Stoddart, J. F. Controlling Switching in Bistable [2]Catenanes by Combining Donor–Acceptor and Radical–Radical Interactions. *J. Am. Chem. Soc.* **2012**, *134*, 11709–11720.
(130) Gibbs-Hall, I. C.; Vermeulen, N. A.; Dale, E. J.; Henkelis, J. J.; Blackburn, A. K.; Barnes, J. C.; Stoddart, J. F. Catenation Through a Combination of Radical Templation and Ring-Closing Metathesis. *J. Am. Chem. Soc.* **2015**, *137*, 15640–15643.
(131) Bruns, C. J.; Frasconi, M.; Iehl, J.; Hartlieb, K. J.; Schneebeli, S. T.; Cheng, C.; Stupp, S. I.; Stoddart, J. F. Redox Switchable Daisy Chain Rotaxanes Driven by Radical–Radical Interactions. *J. Am. Chem. Soc.* **2014**, *136*, 4714–4723.
(132) Wang, Y.; Frasconi, M.; Liu, W.-G.; Sun, J.; Wu, Y.; Nassar, M. S.; Botros, Y. Y.; Goddard, W. A., III; Wasielewski, M. R.; Stoddart, J. F. Oligorotaxane Radicals Under Orders. *ACS Cent. Sci.* **2016**, *2*, 89–98.
(133) Raehm, L.; Sauvage, J.-P. Molecular Machines and Motors Based on Transition Metal-Containing Catenanes and Rotaxanes. *Struct. Bond.* **2001**, *99*, 55–78.
(134) Colasson, B. X.; Dietrich-Buchecker, C.; Jimenez-Molero, M. C.; Sauvage, J.-P. Towards Molecular Machines and Motors Based on Transition Metal Complexes. *J. Phys. Org. Chem.* **2002**, *15*, 476–483.
(135) Dietrich-Buchecker, C.; Jimenez-Molero, M. C.; Sartor, V.; Sauvage, J.-P. Rotaxanes and Catenanes as Prototypes of Molecular Machines and Motors. *Pure Appl. Chem.* **2003**, *75*, 1383–1393.
(136) Sauvage, J.-P. Transition Metal-Complexed Catenanes and Rotaxanes as Molecular Machine Prototypes. *Chem. Commun.* **2005**, 1507–1510.
(137) Collin, J.-P.; Heitz, V.; Bonnet, S.; Sauvage, J.-P. Transition Metal-Complexed Catenanes and Rotaxanes in Motion: Towards Molecular Machines. *Inorg. Chem.* **2005**, *8*, 1063–1074.
(138) Bonnet, S.; Collin, J.-P.; Koizumi, M.; Mobian, P.; Sauvage, J.-P. Transition-Metal-Complexed Molecular Machine Prototypes. *Adv. Mater*. **2006**, *18*, 1239–1250.
(139) Champin, B.; Mobian, P.; Sauvage, J.-P. Transition Metal Complexes as Molecular Machine Prototypes. *Chem. Soc. Rev.* **2007**, *36*, 358–366.
(140) Durot, S.; Reviriego, F.; Sauvage, J.-P. Copper-Complexed Catenanes and Rotaxanes in Motion: 15 Years of Molecular Machines. *Dalton Trans.* **2010**, *39*, 10557–10570.
(141) Sauvage, J.-P.; Collin, J.-P.; Durot, S.; Frey, J.; Heitz, V.; Sour, A.; Tock, C. From Chemical Topology to Molecular Machines. *Compt. Rend. Chim.* **2010**, *13*, 315–328.
(142) Durot, S.; Heitz, V.; Sour, A.; Sauvage, J.-P. Transition-Metal-Complexed Catenanes and Rotaxanes: From Dynamic Systems to Functional Molecular Machines. *Top. Curr. Chem.* **2014**, *354*, 35–70.
(143) Livoreil, A.; Dietrich-Buchecker, C. O.; Sauvage, J.-P. Electrochemically Triggered Swinging of a [2]-Catenate. *J. Am. Chem. Soc.* **1994**, *116*, 9399–9400.
(144) Lehn, J.-M. *Supramolecular Chemistry: Concepts and Perspectives*; Wiley-VCH: Weinheim, **1995**.
(145) Weber, N.; Hamann, C.; Kern, J.-M.; Sauvage, J.-P. Synthesis of a Copper [3]Rotaxane Able to Function as an Electrochemically Driven Oscillatory Machine in Solution, and to Form SAMs on a Metal Surface. *Inorg. Chem.* **2003**, *42*, 6780–6792.
(146) Raehm, L.; Kern, J.-M.; Sauvage, J.-P. A Transition Metal Containing Rotaxane in Motion: Electrochemically Induced Pirouetting of the Ring on the Threaded Dumbbell. *Chem. Eur. J.* **1999**, *5*, 3310–3317.
(147) Kern, J.-M.; Raehm, L.; Sauvage, J.-P.; Divisia-Blohorn, B.; Vidal, P.-L. Controlled Molecular Motions in Copper-Complexed Rotaxanes: An XAS Study. *Inorg. Chem.* **2000**, *39*, 1555–1560.
(148) Periyasamy, G.; Collin, J.-P.; Sauvage, J.-P.; Levine, R. D.; Remacle, F. Electrochemically Driven Sequential Machines: An Implementation of Copper Rotaxanes. *Chem. Eur. J.* **2009**, *15*, 1310–1313.
(149) Armaroli, N.; Balzani, V.; Collin, J.-P.; Gaviña, P.; Sauvage, J.-P.; Ventura, B. Rotaxanes Incorporating Two Different Coordinating Units in Their Thread: Synthesis and Electrochemically and Photochemically Induced Molecular Motions. *J. Am. Chem. Soc.* **1999**, *121*, 4397–4408.
(150) Durola, F.; Sauvage, J.-P. Fast Electrochemically Induced Translation of the Ring in a Copper-Complexed [2]Rotaxane: the Biisoquinoline Effect. *Angew. Chem., Int. Ed*. **2007**, *46*, 3537–3540.
(151) Coronado, E.; Gaviña, P.; Ponce, J.; Tatay, S. Fast Redox-Triggered Shuttling Motions in a Copper Rotaxane Based on a Phenanthroline–Terpyridine Conjugate. *Org. Lett.* **2014**, *12*, 7572–7580.
(152) Durola, F.; Sauvage, J.-P.; Wenger, O.-S. Sterically Non-Hindering Endocyclic Ligands of the Bi-isoquinoline Family. *Chem. Commun.* **2006**, 171–173.
(153) Collin, J.-P.; Durola, F.; Lux, J.; Sauvage, J.-P. A Rapidly Shuttling Copper-Complexed [2]Rotaxane with Three Different Chelating Groups in Its Axis. *Angew*. *Chem., Int. Ed*. **2009**, *48*, 8532–8535.
(154) Durola, F.; Lux, J.; Sauvage, J.-P.; Wenger, O. S. Bigger, Better, Faster: Molecular Shuttles with Sterically Non-Hindering Biisoquinoline Chelates. *Supramol. Chem.* **2011**, *23*, 42–52.
(155) Durola, F.; Lux, J.; Sauvage, J.-P. A Fast-Moving Copper-Based Molecular Shuttle: Synthesis and Dynamic Properties. *Chem. Eur. J.* **2009**, *15*, 4124–4134.
(156) Livoreil, A.; Sauvage, J.-P.; Armaroli, N.; Balzani, V.; Flamigni, L.; Ventura, B. Electrochemically and Photochemically Driven Ring Motions in a Disymmetrical Copper [2]-Catenate. *J. Am. Chem. Soc.* **1997**, *119*, 12114–12124.
(157) Collin, J.-P.; Durola, F.; Lux, J.; Sauvage, J.-P. A Copper-Based Shuttling [2]Rotaxane with Two Bidentate Chelates in the Axis: Steric Control of the Motion. *New J. Chem.* **2010**, *34*, 34–43.
(158) Cárdenas, D. J.; Livoreil, A.; Sauvage, J.-P. Redox Control of the Ring-Gliding Motion in a Cu-Complexed Catenane: A Process Involving Three Distinct Geometries. *J. Am. Chem. Soc.* **1996**, *118*, 11980–11981.
(159) Korybut-Daszkiewicz, B.; Więckowska, A.; Bilewicz, R.; Domagała, S.; Woźniak, K. An Electrochemically Controlled Molecular Shuttle. *Angew. Chem., Int. Ed*. **2004**, *43*, 1668–1672.
(160) Kihara, N.; Hashimoto, M.; Takata, T. Redox Behavior of Ferrocene-Containing Rotaxane: Transposition of the Rotaxane Wheel by Redox Reaction of a Ferrocene Moiety Tethered at the End of the Axle. *Org. Lett.* **2004**, *6*, 1693–1696.
(161) Johnston, A. G.; Leigh, D. A.; Pritchard, R. J.; Deegan, M. D. Facile Synthesis and Solid-State Structure of a Benzylic Amide [2]Catenane. *Angew. Chem., Int. Ed. Engl*. **1995**, *34*, 1209–1212.
(162) Johnston, A. G.; Leigh, D. A.; Nezhat, L.; Smart, J. P.; Deegan, M. D. Structurally Diverse and Dynamically Versatile Benzylic Amide [2]Catenanes Assembled Directly From Commercially Available Precursors. *Angew. Chem., Int. Ed. Engl*. **1995**, *34*, 1212–1216.
(163) Kay, E. R.; Leigh, D. A. Hydrogen Bond-Assembled Synthetic Molecular Motors and Machines. *Top. Curr. Chem.* **2005**, *262*, 133–177.

(164) Brouwer, A. M.; Frochot, C.; Gatti, F. G.; Leigh, D. A.; Mottier, L.; Paolucci, F.; Roffia, S.; Wurpel, G. W. H. Photoinduction of Fast, Reversible Translational Motion in a Hydrogen-Bonded Molecular Shuttle. *Science* **2001**, *291*, 2124–2128.
(165) Altieri, A.; Gatti, F. G.; Kay, E. R.; Leigh, D. A.; Martel, D.; Paolucci, F.; Slawin, A. M. Z.; Wong, J. K. Y. Electrochemically Switchable Hydrogen-Bonded Molecular Shuttles. *J. Am. Chem. Soc.* **2003**, *125*, 8644–8654.
(166) Jagesar, D. C.; Hartl, F.; Buma, W. J.; Brouwer, A. M. Infrared Study of Intercomponent Interactions in a Switchable Hydrogen-Bonded Rotaxane. *Chem. Eur. J.* **2008**, *14*, 1935–1946.
(167) Fioravanti, G.; Haraszkiewicz, N.; Kay, E. R.; Mendoza, S. M.; Bruno, C.; Marcaccio, M.; Wiering, P. G.; Paolucci, F.; Rudolf, P.; Brouwer, A. M.; Leigh, D. A. Three State Redox-Active Molecular Shuttle That Switches in Solution and on a Surface. *J. Am. Chem. Soc.* **2008**, *130*, 2593–2601.
(168) Baggerman, J.; Haraszkiewicz, N.; Wiering, P. G.; Fioravanti, G.; Marcaccio, M.; Paolucci, F.; Kay, E. R.; Leigh, D. A.; Brouwer, A. M. Induction of Motion in a Synthetic Molecular Machine: Effect of Tuning the Driving Force. *Chem. Eur. J.* **2013**, *19*, 5566–5577.
(169) Cecchet, F.; Pilling, M.; Hevesi, L.; Schergna, S.; Wong, J. K. Y.; Clarkson, G. J.; Leigh, D. A.; Rudolf, P. Grafting of Benzylic Amide Macrocycles Onto Acid-Terminated Self-Assembled Monolayers Studied by XPS, RAIRS, and Contact Angle Measurements. *J. Phys. Chem. B* **2003**, *107*, 10863–10872.
(170) Cecchet, F.; Rudolf, P.; Rapino, S.; Margotti, M.; Paolucci, F.; Baggerman, J.; Brouwer, A. M.; Kay, E. R.; Wong, J. K. Y.; Leigh, D. A. Structural, Electrochemical, and Photophysical Properties of a Molecular Shuttle Attached to an Acid-Terminated Self-Assembled Monolayer. *J. Phys. Chem. B* **2004**, *108*, 15192–15199.
(171) Mateo-Alonso, A.; Fioravanti, G.; Marcaccio, M.; Paolucci, F.; Rahman, G. M. A.; Ehli, C.; Guldi, D. M.; Prato, M. An Electrochemically Driven Molecular Shuttle Controlled and Monitored by C_{60}. *Chem. Commun.* **2007**, 1945–1947.
(172) Sobransingh, D.; Kaifer, A. E. Electrochemically Switchable Cucurbit[7]uril-Based Pseudorotaxanes. *Org. Lett.* **2006**, *8*, 3247–3250.
(173) Zhao, Y.-L.; Dichtel, W. R.; Trabolsi, A.; Saha, S.; Aprahamian, I.; Stoddart, J. F. A Redox-Switchable α-Cyclodextrin-Based [2]Rotaxane. *J. Am. Chem. Soc.* **2008**, *130*, 11294–11296.
(174) Zhang, Q.; Tu, Y.; Tian, H.; Zhao, Y.-L.; Stoddart, J. F.; Ågren, H. Working Mechanism for a Redox Switchable Molecular Machine Based on Cyclodextrin: A Free Energy Profile Approach. *J. Phys. Chem. B* **2010**, *114*, 6561–6566.
(175) Ballardini, R.; Balzani, V.; Credi, A.; Gandolfi, M. T.; Venturi, M. Artificial Molecular-Level Machines: Which Energy to Make Them Work? *Acc. Chem. Res.* **2001**, *34*, 445–455.
(176) Balzani, V.; Credi, A.; Venturi, M. Light-Powered Molecular-Scale Machines. *Pure Appl. Chem.* **2003**, *75*, 541–547.
(177) Kay, E. R.; Leigh, D. A. Photochemistry: Lighting Up Nanomachines. *Nature* **2006**, *440*, 286–287.
(178) Baranoff, E.; Barigelletti, F.; Bonnet, S.; Collin, J.-P.; Flamigni, L.; Mobian, P.; Sauvage, J.-P. From Photoinduced Charge Separation to Light-Driven Molecular Machines. *Struct. Bond.* **2007**, *123*, 41–78.
(179) Saha, S.; Stoddart, J. F. Photo-Driven Molecular Devices. *Chem. Soc. Rev*. **2007**, *36*, 77–92.
(180) Amelia, M.; Semeraro, M.; Silvi, S.; Credi, A. Artificial Molecular Machines Powered by Light. *Chimia* **2008**, *62*, 204–209.
(181) Credi, A.; Venturi, M. Molecular Machines Operated by Light. *Cent. Eur. J. Chem.* **2008**, *6*, 325–339.
(182) Balzani, V.; Bergamini, G.; Ceroni, P. From the Photochemistry of Coordination Compounds to Light-Powered Nanoscale Devices and Machines. *Coord. Chem. Rev.* **2008**, *252*, 2456–2469.
(183) Semeraro, M.; Silvi, S.; Credi, A. Artificial Molecular Machines Driven by Light. *Front Biosci* **2008**, *13*, 1036–1049.
(184) Balzani, V.; Credi, A.; Venturi, M. Light Powered Molecular Machines. *Chem. Soc. Rev.* **2009**, *38*, 1542–1550.
(185) Credi, A.; Venturi, M.; Balzani, V. Light on Molecular Machines. *ChemPhysChem* **2010**, *11*, 3398–3403.
(186) Ma, X.; Tian, H. Bright Functional Rotaxanes. *Chem. Soc. Rev*. **2010**, *39*, 70–80.
(187) Zheng, Y. B.; Hao, Q.; Yang, Y.-W.; Kiraly, B.; Chiang, I.-K.; Huang, T. J. Light-Driven Artificial Molecular Machines. *J. Nanophoton*. **2010**, *4*, 042501.
(188) Silvi, S.; Venturi, M.; Credi, A. Light Operated Molecular Machines. *Chem. Commun.* **2011**, *47*, 2483–2489.
(189) Qu, D.-H.; Tian, H. Future Applications of Photo-Driven Molecular Machines. *Curr. Phys. Chem.* **2011**, *1*, 261–274.
(190) Avellini, T.; Baroncini, M.; Ragazzon, G.; Silvi, S.; Venturi, M.; Credi, A. Photochemically Controlled Molecular Machines with Sequential Logic Operation. *Isr. J. Chem.* **2014**, *54*, 553–567.
(191) Credi, A.; Silvi, S.; Venturi, M. Light-Operated Machines Based on Threaded Molecular Structures. *Top. Curr. Chem.* **2014**, *354*, 1–34.
(192) Ballardini, R.; Balzani, V.; Credi, A.; Gandolfi, M. T.; Venturi, M. Molecular-Level Artificial Machines Based on Photoinduced Electron-Transfer Processes. *Struct. Bond.* **2001**, *99*, 163–188.
(193) Credi, A.; Ferrer, B. Rotaxane-Based Molecular Machines Operated by Photoinduced Electron Transfer. *Pure Appl. Chem.* **2005**, *77*, 1051–1057.
(194) Benniston, A. C.; Harriman, A. A Light-Induced Molecular Shuttle Based on a [2] Rotaxane-Derived Triad. *Angew. Chem., Int. Ed. Engl*. **1993**, *32*, 1459–1461.
(195) Ballardini, R.; Balzani, V.; Gandolfi, M. T.; Prodi, L.; Venturi, M.; Philp, D.; Ricketts, H. G.; Stoddart, J. F. A Photochemically Driven Molecular Machine. *Angew. Chem., Int. Ed. Engl*. **1993**, *32*, 1301–1303.
(196) Ballardini, R.; Balzani, V.; Credi, A.; Gandolfi, M. T.; Langford, S. J.; Menzer, S.; Prodi, L.; Stoddart, J. F.; Venturi, M.; Williams, D. J. Simple Molecular Machines: Chemically Driven Unthreading and Rethreading of a [2]Pseudorotaxane. *Angew. Chem., Int. Ed. Engl*. **1996**, *35*, 978–981.
(197) Credi, A.; Montalti, M.; Balzani, V.; Langford, S. J.; Raymo, F. M.; Stoddart, J. F. Simple Molecular-Level Machines. Interchange Between Different Threads in Pseudorotaxanes. *New J. Chem*. **1998**, *22*, 1061–1065.
(198) Ashton, P. R.; Balzani, V.; Kocian, O.; Prodi, L.; Spencer, N.; Stoddart, J. F. A Light-Fueled "Piston Cylinder" Molecular-Level Machine. *J. Am. Chem. Soc.* **1998**, *120*, 11190–11191.
(199) Ballardini, R.; Balzani, V.; Clemente-León, M.; Credi, A.; Gandolfi, M. T.; Ishow, E.; Perkins, J.; Stoddart, J. F.; Tseng, H.-R.; Wenger, S. Photoinduced Electron Transfer in a Triad That Can Be Assembled/Disassembled by Two Different External Inputs. Toward Molecular-Level Electrical Extension Cables. *J. Am. Chem. Soc.* **2002**, *124*, 12786–12795.
(200) Balzani, V.; Clemente-León, M.; Credi, A.; Ferrer, B.; Venturi, M.; Flood, A. H.; Stoddart, J. F. Autonomous Artificial Nanomotor Powered by Sunlight. *Proc. Natl. Acad. Sci. U.S.A.* **2006**, *103*, 1178–1183.
(201) Sun, J.; Wu, Y.; Liu, Z.; Cao, D.; Wang, Y.; Cheng, C.; Chen, D.; Wasielewski, M. R.; Stoddart, J. F. Visible Light-Driven Artificial Molecular Switch Actuated by Radical–Radical and Donor–Acceptor Interactions. *J. Phys. Chem. A* **2015**, *119*, 6317–6325.
(202) Panman, M. R.; Bodis, P.; Shaw, D. J.; Bakker, B. H.; Newton, A. C.; Kay, E. R.; Brouwer, A. M.; Buma, W. J.; Leigh, D. A.; Woutersen, S. Operation Mechanism of a Molecular Machine Revealed Using Time-Resolved Vibrational Spectroscopy. *Science* **2010**, *328*, 1255–1258.
(203) Panman, M. R.; Bodis, P.; Shaw, D. J.; Bakker, B. H.; Newton, A. C.; Kay, E. R.; Leigh, D. A.; Buma, W. J.; Brouwer, A. M.; Woutersen, S. Time-Resolved Vibrational Spectroscopy of a Molecular Shuttle. *Phys. Chem. Chem. Phys.* **2012**, *14*, 1865–1875.
(204) Sauvage, J.-P. A Light-Driven Linear Motor at the Molecular Level. *Science* **2001**, *291*, 2105–2106.
(205) Brouwer, A. M.; Fazio, S. M.; Frochot, C.; Gatti, F. G.; Leigh, D. A.; Wong, J. K. Y.; Wurpel, G. W. H. Photoinduced

Dynamics in Hydrogen-Bonded Rotaxanes. *Pure Appl. Chem.* **2003**, *75*, 1055–1060.
(206) Jagesar, D. C.; Fazio, S. M.; Taybi, J.; Eiser, E.; Gatti, F. G.; Leigh, D. A.; Brouwer, A. M. Photoinduced Shuttling Dynamics of Rotaxanes in Viscous Polymer Solutions. *Adv. Funct. Mater.* **2009**, *19*, 3440–3449.
(207) Panman, M. R.; Bakker, B. H.; den Uyl, D.; Kay, E. R.; Leigh, D. A.; Buma, W. J.; Brouwer, A. M.; Geenevasen, J. A. J.; Woutersen, S. Water Lubricates Hydrogen-Bonded molecular Machines. *Nature Chem.* **2013**, *5*, 929–934.
(208) Harada, A. Cyclodextrin-Based Molecular Machines. *Acc. Chem. Res*. **2001**, *34*, 456–464.
(209) Harada, A.; Takashima, Y. Macromolecular Recognition and Macroscopic Interactions by Cyclodextrins. *Chem. Rec.* **2013**, *13*, 420–431.
(210) del Barrio, J.; Horton, P. N.; Lairez, D.; Lloyd, G. O.; Toprakcioglu, C.; Scherman, O. A. Photocontrol Over Cucurbit[8]uril Complexes: Stoichiometry and Supramolecular Polymers. *J. Am. Chem. Soc.* **2013**, *135*, 11760–11763.
(211) Taylor, R. W.; Coulston, R. J.; Biedermann, F.; Mahajan, S.; Baumberg, J. J.; Scherman, O. A. In Situ SERS Monitoring of Photochemistry Within a Nanojunction Reactor. *Nano Lett.* **2013**, *13*, 5985–5990.
(212) Yu, G.; Han, C.; Zhang, Z.; Chen, J.; Yan, X.; Zheng, B.; Liu, S.; Huang, F. Pillar[6]arene-Based Photoresponsive Host–Guest Complexation. *J. Am. Chem. Soc.* **2012**, *134*, 8711–8717.
(213) Ogoshi, T.; Kida, K.; Yamagishi, T.-A. Photoreversible Switching of the Lower Critical Solution Temperature in a Photoresponsive Host–Guest System of Pillar[6]arene with Triethylene Oxide Substituents and an Azobenzene Derivative. *J. Am. Chem. Soc.* **2012**, *134*, 20146–20150.
(214) Asakawa, M.; Ashton, P. R.; Balzani, V.; Brown, C. L.; Credi, A.; Matthews, O. A.; Newton, S. P.; Raymo, F. M.; Shipway, A. N.; Spencer, N.; Quick, A.; Stoddart, J. F.; White, A. J. P.; Williams, D. J. Molecular Meccano 44. Photoactive Azobenzene-Containing Supramolecular Complexes and Related Interlocked Molecular Compounds. *Chem. Eur. J*. **1999**, *5*, 860–875.
(215) Balzani, V.; Credi, A.; Marchioni, F.; Stoddart, J. F. Artificial Molecular-Level Machines. Dethreading-Rethreading of a Pseudorotaxane Powered Exclusively by Light Energy. *Chem. Commun.* **2001**, 1860–1861.
(216) Murakami, H.; Kawabuchi, A.; Kotoo, K.; Kunitake, M.; Nakashima, N. A Light-Driven Molecular Shuttle Based on a Rotaxane. *J. Am. Chem. Soc.* **1997**, *119*, 7605–7606.
(217) Murakami, H.; Kawabuchi, A.; Matsumoto, R.; Ido, T.; Nakashima, N. A Multi-Mode-Driven Molecular Shuttle: Photochemically and Thermally Reactive Azobenzene Rotaxanes. *J. Am. Chem. Soc.* **2005**, *127*, 15891–15899.
(218) Hu, J.; Hashidzume, A.; Harada, A. Photoregulated Switching of the Recognition Site of α-Cyclodextrin in a Side Chain Polyrotaxane Bearing Two Recognition Sites Linked with Oligo(ethylene glycol). *Macromol. Chem. Phys.* **2011**, *212*, 1032–1038.
(219) Li, S.; Taura, D.; Hashidzume, A.; Harada, A. Light-Switchable Janus [2]Rotaxanes Based on α-Cyclodextrin Derivatives Bearing Two Recognition Sites Linked with Oligo(ethylene glycol). *Chem. Asian J.* **2010**, *5*, 2281–2289.
(220) Dawson, R. E.; Maniam, S.; Lincoln, S. F.; Easton, C. J. Synthesis of α-Cyclodextrin [2]-Rotaxanes Using Chlorotriazine Capping Reagents. *Org. Biomol. Chem.* **2008**, *6*, 1814–1821.
(221) Yan, H.; Teh, C.; Sreejith, S.; Zhu, L.; Kwok, A.; Fang, W.; Ma, X.; Nguyen, K. T.; Korzh, V.; Zhao, Y. Functional Mesoporous Silica Nanoparticles for Photothermal-Controlled Drug Delivery In Vivo. *Angew. Chem., Int. Ed*. **2012**, *51*, 8373–8377.
(222) Yan, H.; Zhu, L.; Li, X.; Kwok, A.; Pan, X.; Zhao, Y. A Photoswitchable [2]Rotaxane Array on Graphene Oxide. *Asian J. Org. Chem.* **2012**, *1*, 314–318.
(223) Yan, H.; Zhu, L.; Li, X.; Kwok, A.; Li, X.; Ågren, H.; Zhao, Y. Photothermal-Responsive [2]Rotaxanes. *RSC Adv.* **2013**, *3*, 2341–2350.
(224) Qu, D.-H.; Wang, Q.-C.; Ren, J.; Tian, H. A Light-Driven Rotaxane Molecular Shuttle with Dual Fluorescence Addresses. *Org. Lett.* **2004**, *6*, 2085–2088.
(225) Qu, D.-H.; Wang, Q.-C.; Ma, X.; Tian, H. A [3]Rotaxane with Three Stable States That Responds to Multiple-Inputs and Displays Dual Fluorescence Addresses. *Chem. Eur. J.* **2005**, *11*, 5929–5937.
(226) Ma, X.; Qu, D.; Ji, F.; Wang, Q.; Zhu, L.; Xu, Y.; Tian, H. A Light-Driven [1]Rotaxane via Self-Complementary and Suzuki-Coupling Capping. *Chem. Commun.* **2007**, 1409–1411.
(227) Gao, C.; Ma, X.; Zhang, Q.; Wang, Q.; Qu, D.; Tian, H. A Light-Powered Stretch–Contraction Supramolecular System Based on Cobalt Coordinated [1]Rotaxane. *Org. Lett.* **2011**, *9*, 1126–1132.
(228) Zhu, L.; Lu, M.; Qu, D.; Wang, Q.; Tian, H. Coordination-Assembly for Quantitative Construction of Bis-Branched Molecular Shuttles. *Org. Lett.* **2011**, *9*, 4226–4233.
(229) Deligkiozi, I.; Papadakis, R.; Tsolomitis, A. Synthesis, Characterization and Photoswitchability of a New [2]Rotaxane of α-Cyclodextrin with a Diazobenzene Containing π-Conjugated Molecular Dumbbell. *Supramol. Chem.* **2012**, *24*, 333–343.
(230) Qiu, X.-P.; Korchagina, E. V.; Rolland, J.; Winnik, F. M. Synthesis of a Poly(*N*-isopropylacrylamide) Charm Bracelet Decorated with a Photomobile α-Cyclodextrin Charm. *Polym. Chem.* **2014**, *5*, 3656–3665.
(231) Zhang, D.; Nie, Y.; Saha, M. L.; He, Z.; Jiang, L.; Zhou, Z.; Stang, P. J. Photoreversible [2] Catenane via the Host–Guest Interactions Between a Palladium Metallacycle and β-Cyclodextrin. *Inorg. Chem.* **2015**, *54*, 11807–11812.
(232) Stanier, C. A.; Alderman, S. J.; Claridge, T. D. W.; Anderson, H. L. Unidirectional Photoinduced Shuttling in a Rotaxane with a Symmetric Stilbene Dumbbell. *Angew. Chem., Int. Ed*. **2002**, *41*, 1769–1772.
(233) Wang, Q.-C.; Qu, D.-H.; Ren, J.; Chen, K.; Tian, H. A Lockable Light-Driven Molecular Shuttle with a Fluorescent Signal. *Angew. Chem., Int. Ed*. **2004**, *43*, 2661–2665.
(234) Qu, D.-H.; Wang, Q.-C.; Tian, H. A Half Adder Based on a Photochemically Driven [2]Rotaxane. *Angew. Chem., Int. Ed*. **2005**, *44*, 5296–5299.
(235) Qu, D.-H.; Ji, F.-Y.; Wang, Q.-C.; Tian, H. A Double INHIBIT Logic Gate Employing Configuration and Fluorescence Changes. *Adv. Mater.* **2006**, *18*, 2035–2038.
(236) Dawson, R. E.; Lincoln, S. F.; Easton, C. J. The Foundation of a Light Driven Molecular Muscle Based on Stilbene and α-Cyclodextrin. *Chem. Commun.* **2008**, 3980–3982.
(237) Gatti, F. G.; León, S.; Wong, J. K. Y.; Bottari, G.; Altieri, A.; Morales, M. A. F.; Teat, S. J.; Frochot, C.; Leigh, D. A.; Brouwer, A. M.; Zerbetto, F. Photoisomerization of a Rotaxane Hydrogen Bonding Template: Light-Induced Acceleration of a Large Amplitude Rotational Motion. *Proc. Natl. Acad. Sci. U.S.A.* **2003**, *100*, 10–14.
(238) Altieri, A.; Bottari, G.; Dehez, F.; Leigh, D. A.; Wong, J. K. Y.; Zerbetto, F. Remarkable Positional Discrimination in Bistable Light- and Heat-Switchable Hydrogen-Bonded Molecular Shuttles. *Angew. Chem., Int. Ed*. **2003**, *42*, 2296–2300.
(239) Bottari, G.; Leigh, D. A.; Pérez, E. M. Chiroptical Switching in a Bistable Molecular Shuttle. *J. Am. Chem. Soc.* **2003**, *125*, 13360–13361.
(240) Pérez, E. M.; Dryden, D. T. F.; Leigh, D. A.; Teobaldi, G.; Zerbetto, F. A Generic Basis for Some Simple Light-Operated Mechanical Molecular Machines. *J. Am. Chem. Soc.* **2004**, *126*, 12210–12211.
(241) Berná, J.; Leigh, D. A.; Lubomska, M.; Mendoza, S. M.; Pérez, E. M.; Rudolf, P.; Teobaldi, G.; Zerbetto, F. Macroscopic Transport by Synthetic Molecular Machines. *Nature Mater.* **2005**, *4*, 704–710.
(242) Li, Y.; Li, H.; Li, Y.; Liu, H.; Wang, S.; He, X.; Wang, N.; Zhu, D. Energy Transfer Switching in a Bistable Molecular Machine. *Org. Lett.* **2005**, *7*, 4835–4838.

(243) Leigh, D. A.; Wong, J. K. Y.; Dehez, F.; Zerbetto, F. Unidirectional Rotation in a Mechanically Interlocked Molecular Rotor. *Nature* **2003**, *424*, 174–179.

(244) Hernández, J. V.; Kay, E. R.; Leigh, D. A. A Reversible Synthetic Rotary Molecular Motor. *Science* **2004**, *306*, 1532–1537.

(245) Chatterjee, M. N.; Kay, E. R.; Leigh, D. A. Beyond Switches: Ratcheting a Particle Energetically Uphill with a Compartmentalized Molecular Machine. *J. Am. Chem. Soc.* **2006**, *128*, 4058–4073.

(246) Altoè, P.; Haraszkiewicz, N.; Gatti, F. G.; Wiering, P. G.; Frochot, C.; Brouwer, A. M.; Balkowski, G.; Shaw, D.; Woutersen, S.; Buma, W. J.; Zerbetto, F.; Orlandi, G.; Leigh, D. A.; Garavelli, M. Multistate Photo-Induced Relaxation and Photoisomerization Ability of Fumaramide Threads: A Computational and Experimental Study. *J. Am. Chem. Soc.* **2009**, *131*, 104–117.

(247) Zhou, W.; Chen, D.; Li, J.; Xu, J.; Lv, J.; Liu, H.; Li, Y. Photoisomerization of Spiropyran for Driving a Molecular Shuttle. *Org. Lett.* **2007**, *9*, 3929–3932.

(248) Laemmel, A.-C.; Collin, J.-P.; Sauvage, J.-P.; Accorsi, G.; Armaroli, N. Macrocyclic Complexes of $[Ru(N\text{-}N)_2]^{2+}$ Units [N-N = 1,10 Phenanthroline or 4-(*p*-Anisyl)-1,10-Phenanthroline]: Synthesis and Photochemical Expulsion Studies. *Eur. J. Inorg. Chem.* **2003**, 467–474.

(249) Pomerane, D.; Jouvenot, D.; Chambron, J.-C.; Collin, J.-P.; Heitz, V.; Sauvage, J.-P. Templated Synthesis of a Rotaxane with a $[Ru(Diimine)_3]^{2+}$ Core. *Chem. Eur. J.* **2003**, *9*, 4247–4254.

(250) Collin, J.-P.; Jouvenot, D.; Koizumi, M.; Sauvage, J.-P. A Ruthenium(II)-Complexed Rotaxane Whose Ring Incorporates a 6,6′-Diphenyl-2,2′-Bipyridine: Synthesis and Light-Driven Motions. *Eur. J. Inorg. Chem.* **2005**, 1850–1855.

(251) Collin, J.-P.; Sauvage, J.-P. Transition Metal-Complexed Catenanes and Rotaxanes as Light-Driven Molecular Machines Prototypes. *Chem. Lett.* **2005**, *34*, 742–747.

(252) Mobian, P.; Kern, J.-M.; Sauvage, J.-P. Light-Driven Machine Prototypes Based on Dissociative Excited States: Photoinduced Decoordination and Thermal Recoordination of a Ring in a Ruthenium(II)-Containing [2]Catenane. *Angew. Chem., Int. Ed*. **2004**, *43*, 2392–2395.

(253) Bonnet, S.; Collin, J.-P. Ruthenium-Based Light-Driven Molecular Machine Prototypes: Synthesis and Properties. *Chem. Soc. Rev.* **2008**, *37*, 1207–1217.

(254) Schofield, E. R.; Collin, J.-P.; Gruber, N.; Sauvage, J.-P. Photochemical and Thermal Ligand Exchange in a Ruthenium(II) Complex Based on a Scorpionate Terpyridine Ligand. *Chem. Commun.* **2003**, 188–189.

(255) Abraham, W.; Grubert, L.; Grummt, U.-W.; Buck, K. A Photoswitchable Rotaxane with a Folded Molecular Thread. *Chem. Eur. J.* **2004**, *10*, 3562–3568.

(256) Schmidt-Schäffer, S.; Grubert, L.; Grummt, U.-W.; Buck, K.; Abraham, W. A Photoswitchable Rotaxane with an Unfolded Molecular Thread. *Eur. J. Org. Chem*. **2006**, 378–398.

(257) Abraham, W.; Buck, K.; Orda-Zgadzaj, M.; Schmidt-Schäffer, S.; Grummt, U.-W. Novel Photoswitchable Rotaxanes. *Chem. Commun.* **2007**, 3094–3096.

(258) Abraham, W.; Wlosnewski, A.; Buck, K.; Jacob, S. Photoswitchable Rotaxanes Using the Photolysis of Alkoxyacridanes. *Org. Lett.* **2009**, *7*, 142–154.

(259) Vetter, A.; Abraham, W. Controlling Ring Translation of Rotaxanes. *Org. Lett.* **2010**, *8*, 4666–4681.

(260) Mock, W. L.; Pierpont, J. A Cucurbituril-Based Molecular Switch. *J. Chem. Soc., Chem. Commun.* **1990**, 1509–1511.

(261) Kim, K. Mechanically Interlocked Molecules Incorporating Cucurbituril and Their Supramolecular Assemblies. *Chem. Soc. Rev.* **2002**, *31*, 96–107.

(262) Lee, J. W.; Samal, S.; Selvapalam, N.; Kim, H.-J.; Kim, K. Cucurbituril Homologues and Derivatives: New Opportunities in Supramolecular Chemistry. *Acc. Chem. Res.* **2003**, *36*, 621–630.

(263) Jun, S. I.; Lee, J. W.; Sakamoto, S.; Yamaguchi, K.; Kim, K. Rotaxane-Based Molecular Switch with Fluorescence Signaling. *Tetrahedron Lett.* **2000**, *41*, 471–475.

(264) Lee, J. W.; Kim, K.; Kim, K. A Kinetically Controlled Molecular Switch Based on Bistable [2]Rotaxane. *Chem. Commun.* **2001**, 1042–1043.

(265) Chakrabarti, S.; Mukhopadhyay, P.; Lin, S.; Isaacs, L. Reconfigurable Four-Component Molecular Switch Based on pH-Controlled Guest Swapping. *Org. Lett.* **2007**, *9*, 2349–2352.

(266) Kolman, V.; Kulhanek, P.; Sindelar, V. Inclusion of Carboxyl Function Inside of Cucurbiturils and Its Use in Molecular Switches. *Chem. Asian J.* **2010**, *5*, 2386–2392.

(267) Gao, C.; Silvi, S.; Ma, X.; Tian, H.; Credi, A.; Venturi, M. Chiral Supramolecular Switches Based on (*R*)-Binaphthalene-Bipyridinium Guests and Cucurbituril Hosts. *Chem. Eur. J.* **2012**, *18*, 16911–16921.

(268) Tuncel, D.; Cindir, N.; Koldemir, Ü. [5]Rotaxane and [5]Pseudorotaxane Based on Cucurbit[6]uril and Anchored to a Meso-Tetraphenyl Porphyrin. *J. Incl. Phenom. Macrocycl. Chem*. **2006**, *55*, 373–380.

(269) Tuncel, D.; Özsar, Ö.; Tiftik, H. B.; Salih, B. Molecular Switch Based on a Cucurbit[6]uril Containing Bistable [3]Rotaxane. *Chem. Commun.* **2007**, 1369–1371.

(270) Tuncel, D.; Katterle, M. pH-Triggered Dethreading-Rethreading and Switching of Cucurbit[6]uril on Bistable [3]Pseudorotaxanes and [3]Rotaxanes. *Chem. Eur. J.* **2008**, *14*, 4110–4116.

(271) Choi, H. S.; Lee, S. C.; Yamamoto, K.; Yui, N. Block-Selective Movement of α-Cyclodextrins in Polyrotaxanes of PEI-*b*-PEG-*b*-PEI Copolymer. *Macromolecules* **2005**, *38*, 9878–9881.

(272) Choi, H. S.; Ooya, T.; Yui, N. One-Pot Synthesis of a Polyrotaxane via Selective Threading of a PEI-*b*-PEG-*b*-PEI Copolymer. *Macromol. Biosci.* **2006**, *6*, 420–424.

(273) Choi, H. S.; Hirasawa, A.; Ooya, T.; Kajihara, D.; Hohsaka, T.; Yui, N. pH-Sensitive Locomotion of Cyclodextrins in a Block-Selective Mobile Polyrotaxane. *ChemPhysChem* **2006**, *7*, 1671–1673.

(274) Karaky, K.; Brochon, C.; Schlatter, G.; Hadziioannou, G. pH-Switchable Supramolecular “Sliding” Gels Based on Polyrotaxanes of Polyethyleneimine-*block*-Poly(ethylene Oxide)-*block*-Polyethyleneimine Block Copolymer and α-Cyclodextrin: Synthesis and Swelling Behaviour. *Soft Matter* **2008**, *4*, 1165–1168.

(275) Grunder, S.; McGrier, P. L.; Whalley, A. C.; Boyle, M. M.; Stern, C.; Stoddart, J. F. A Water-Soluble pH-Triggered Molecular Switch. *J. Am. Chem. Soc.* **2013**, *135*, 17691–17694.

(276) Juríček, M.; Barnes, J. C.; Strutt, N. L.; Vermeulen, N. A.; Ghooray, K. C.; Dale, E. J.; McGonigal, P. R.; Blackburn, A. K.; Avestro, A.-J.; Stoddart, J. F. An ExBox [2]Catenane. *Chem. Sci.* **2014**, *5*, 2724–2731.

(277) Barnes, J. C.; Juríček, M.; Strutt, N. L.; Frasconi, M.; Sampath, S.; Giesener, M. A.; McGrier, P. L.; Bruns, C. J.; Stern, C. L.; Sarjeant, A. A.; Stoddart, J. F. ExBox: A Polycyclic Aromatic Hydrocarbon Scavenger. *J. Am. Chem. Soc.* **2013**, *135*, 183–192.

(278) Barnes, J. C.; Juríček, M.; Vermeulen, N. A.; Dale, E. J.; Stoddart, J. F. Synthesis of Ex^{n}Box Cyclophanes. *J. Org. Chem.* **2013**, *78*, 11962–11969.

(279) Dale, E. J.; Vermeulen, N. A.; Juríček, M.; Barnes, J. C.; Young, R. M.; Wasielewski, M. R.; Stoddart, J. F. Supramolecular Explorations: Exhibiting the Extent of Extended Cationic Cyclophanes. *Acc. Chem. Res.* **2016**, *49*, 262–273.

(280) Coumans, R. G. E.; Elemans, J. A. A. W.; Rowan, A. E.; Nolte, R. J. M. Interlocked Porphyrin Switches. *Chem. Eur. J.* **2013**, *19*, 7758–7770.

(281) Martínez-Díaz, M.-V.; Spencer, N.; Stoddart, J. F. The Self-Assembly of a Switchable [2]Rotaxane. *Angew. Chem., Int. Ed. Engl*. **1997**, *36*, 1904–1907.

(282) Garaudée, S.; Silvi, S.; Venturi, M.; Credi, A.; Flood, A. H.; Stoddart, J. F. Shuttling Dynamics in an Acid-Base-Switchable [2]Rotaxane. *ChemPhysChem* **2005**, *6*, 2145–2152.
(283) Clemente-León, M.; Credi, A.; Martínez-Díaz, M.-V.; Mingotaud, C.; Stoddart, J. F. Towards Organization of Molecular Machines at Interfaces: Langmuir Films and Langmuir-Blodgett Multilayers of an Acid-Base Switchable Rotaxane. *Adv. Mater.* **2006**, *18*, 1291–1296.
(284) Badjić, J. D.; Balzani, V.; Credi, A.; Silvi, S.; Stoddart, J. F. A Molecular Elevator. *Science* **2004**, *303*, 1845–1849.
(285) Badjić, J. D.; Ronconi, C. M.; Stoddart, J. F.; Balzani, V.; Silvi, S.; Credi, A. Operating Molecular Elevators. *J. Am. Chem. Soc.* **2006**, *128*, 1489–1499.
(286) Wu, J.; Leung, K. C.-F.; Benítez, D.; Han, J.-Y.; Cantrill, S. J.; Fang, L.; Stoddart, J. F. An Acid-Base-Controllable [*c*2]Daisy Chain. *Angew. Chem., Int. Ed.* **2008**, *47*, 7470–7474.
(287) Fang, L.; Hmadeh, M.; Wu, J.; Olson, M. A.; Spruell, J. M.; Trabolsi, A.; Yang, Y.-W.; Elhabiri, M.; Albrecht-Gary, A.-M.; Stoddart, J. F. Acid-Base Actuation of [*c*2]Daisy Chains. *J. Am. Chem. Soc.* **2009**, *131*, 7126–7134.
(288) Bleve, V.; Schäfer, C.; Franchi, P.; Silvi, S.; Mezzina, E.; Credi, A.; Lucarini, M. Reversible Mechanical Switching of Magnetic Interactions in a Molecular Shuttle. *ChemistryOpen* **2015**, *4*, 18–21.
(289) Li, J.; Li, Y.; Guo, Y.; Xu, J.; Lv, J.; Li, Y.; Liu, H.; Wang, S.; Zhu, D. A Novel Supramolecular System: Combination of Two Switchable Processes in a [2]Rotaxane. *Chem. Asian J.* **2008**, *3*, 2091–2096.
(290) Schäfer, C.; Ragazzon, G.; Colasson, B.; La Rosa, M.; Silvi, S.; Credi, A. An Artificial Molecular Transporter. *ChemistryOpen* **2016**, *5*, 120–124.
(291) Elizarov, A. M.; Chiu, S.-H.; Stoddart, J. F. An Acid-Base Switchable [2]Rotaxane. *J. Org. Chem.* **2002**, *67*, 9175–9181.
(292) Loeb, S. J.; Wisner, J. A. 1,2-Bis(4,4′-dipyridinium)ethane: A Versatile Dication for the Formation of [2]Rotaxanes with Dibenzo-24-Crown-8 Ether. *Chem. Commun.* **1998**, 2757–2758.
(293) Loeb, S. J.; Wisner, J. A. A New Motif for the Self-Assembly of [2]Pseudorotaxanes; 1, 2-Bis(pyridinium)ethane Axles and [24]Crown-8 Ether Wheels. *Angew. Chem., Int. Ed.* **1998**, *37*, 2838–2840.
(294) Vella, S. J.; Tiburcio, J.; Loeb, S. J. Optically Sensed, Molecular Shuttles Driven by Acid–Base Chemistry. *Chem. Commun.* **2007**, 4752–4754.
(295) Suzuki, S.; Nakazono, K.; Takata, T. Selective Transformation of a Crown Ether/*sec*-Ammonium Salt-Type Rotaxane to *N*-Alkylated Rotaxanes. *Org. Lett.* **2010**, *12*, 712–715.
(296) Tokunaga, Y.; Kawabata, M.; Matsubara, N. Three-State Molecular Shuttles Operated Using Acid/Base Stimuli with Distinct Outputs. *Org. Lett.* **2011**, *9*, 4948–4953.
(297) Leigh, D. A.; Thomson, A. R. An Ammonium/Bis-Ammonium Switchable Molecular Shuttle. *Tetrahedron* **2008**, *64*, 8411–8416.
(298) Coutrot, F. A Focus on Triazolium as a Multipurpose Molecular Station for pH-Sensitive Interlocked Crown-Ether-Based Molecular Machines. *ChemistryOpen* **2015**, *4*, 556–576.
(299) Coutrot, F.; Busseron, E. A New Glycorotaxane Molecular Machine Based on an Anilinium and a Triazolium Station. *Chem. Eur. J.* **2008**, *14*, 4784–4787.
(300) Coutrot, F.; Romuald, C.; Busseron, E. A New pH-Switchable Dimannosyl[*c*2]Daisy Chain Molecular Machine. *Org. Lett.* **2008**, *10*, 3741–3744.
(301) Romuald, C.; Busseron, E.; Coutrot, F. Very Contracted to Extended *co*-Conformations with or Without Oscillations in Two- and Three-Station [*c*2]Daisy Chains. *J. Org. Chem.* **2010**, *75*, 6516–6531.
(302) Busseron, E.; Romuald, C.; Coutrot, F. Bistable or Oscillating State Depending on Station and Temperature in Three-Station Glycorotaxane Molecular Machines. *Chem. Eur. J.* **2010**, *16*, 10062–10073.
(303) Romuald, C.; Ardá, A.; Clavel, C.; Jiménez-Barbero, J.; Coutrot, F. Tightening or Loosening a pH-Sensitive Double-Lasso Molecular Machine Readily Synthesized From an Ends-Activated [*c*2]Daisy Chain. *Chem. Sci.* **2012**, *3*, 1851–1857.
(304) Clavel, C.; Romuald, C.; Brabet, E.; Coutrot, F. A pH-Sensitive Lasso-Based Rotaxane Molecular Switch. *Chem. Eur. J.* **2013**, *19*, 2982–2989.
(305) Clavel, C.; Fournel-Marotte, K.; Coutrot, F. A pH-Sensitive Peptide-Containing Lasso Molecular Switch. *Molecules* **2013**, *18*, 11553–11575.
(306) Busseron, E.; Coutrot, F. *N*-Benzyltriazolium as Both Molecular Station and Barrier in [2]Rotaxane Molecular Machines. *J. Org. Chem.* **2013**, *78*, 4099–4106.
(307) Chao, S.; Romuald, C.; Fournel-Marotte, K.; Clavel, C.; Coutrot, F. A Strategy Utilizing a Recyclable Macrocycle Transporter for the Efficient Synthesis of a Triazolium-Based [2]Rotaxane. *Angew. Chem., Int. Ed.* **2014**, *53*, 6914–6919.
(308) Waelès, P.; Clavel, C.; Fournel-Marotte, K.; Coutrot, F. Synthesis of Triazolium-Based Mono- and Tris-Branched [1]Rotaxanes Using a Molecular Transporter of Dibenzo-24-Crown-8. *Chem. Sci.* **2015**, *6*, 4828–4836.
(309) Jiang, Q.; Zhang, H.-Y.; Han, M.; Ding, Z.-J.; Liu, Y. pH-Controlled Intramolecular Charge-Transfer Behavior in Bistable [3]Rotaxane. *Org. Lett.* **2010**, *12*, 1728–1731.
(310) Zhang, Z.-J.; Han, M.; Zhang, H.-Y.; Liu, Y. A Double-Leg Donor-Acceptor Molecular Elevator: New Insight into Controlling the Distance of Two Platforms. *Org. Lett.* **2013**, *15*, 1698–1701.
(311) Jiang, Y.; Guo, J.-B.; Chen, C.-F. A New [3]Rotaxane Molecular Machine Based on a Dibenzylammonium Ion and a Triazolium Station. *Org. Lett.* **2010**, *12*, 4248–4251.
(312) Ma, Y.-X.; Meng, Z.; Chen, C.-F. A Novel Pentiptycene Bis(crown ether)-Based [2](2)Rotaxane Whose Two DB24C8 Rings Act as Flapping Wings of a Butterfly. *Org. Lett.* **2014**, *16*, 1860–1863.
(313) Meng, Z.; Han, Y.; Wang, L.-N.; Xiang, J.-F.; He, S.-G.; Chen, C.-F. Stepwise Motion in a Multivalent [2](3)Catenane. *J. Am. Chem. Soc.* **2015**, *137*, 9739–9745.
(314) Yang, W.; Li, Y.; Zhang, J.; Chen, N.; Chen, S.; Liu, H.; Li, Y. Directed Synthesis of [2]Catenanes Incorporating Naphthalenediimide and Crown Ethers by Associated Interactions of Templates. *J. Org. Chem.* **2011**, *76*, 7750–7756.
(315) Yang, W.; Li, Y.; Zhang, J.; Yu, Y.; Liu, T.; Liu, H.; Li, Y. Synthesis of a [2]Rotaxane Operated in Basic Environment. *Org. Lett.* **2011**, *9*, 6022–6026.
(316) Yang, W.; Li, Y.; Zhang, J.; Chen, N.; Chen, S.; Liu, H.; Li, Y. A Controllable Chiral Molecular Machine: Movement on Molecular Level. *Small* **2012**, *8*, 2602–2607.
(317) Li, H.; Zhang, H.; Zhang, Q.; Zhang, Q.-W.; Qu, D.-H. A Switchable Ferrocene-Based [1]Rotaxane with an Electrochemical Signal Output. *Org. Lett.* **2012**, *14*, 5900–5903.
(318) Li, H.; Zhang, J.-N.; Zhou, W.; Zhang, H.; Zhang, Q.; Qu, D.-H.; Tian, H. Dual-Mode Operation of a Bistable [1]Rotaxane with a Fluorescence Signal. *Org. Lett.* **2013**, *15*, 3070–3073.
(319) Zhang, H.; Hu, J.; Qu, D.-H. Dual-Mode Control of PET Process in a Ferrocene-Functionalized [2]Rotaxane with High-Contrast Fluorescence Output. *Org. Lett.* **2012**, *14*, 2334–2337.
(320) Zhang, H.; Liu, Q.; Li, J.; Qu, D.-H. A Novel Star-Shaped Zinc Porphyrin Cored [5]Rotaxane. *Org. Lett.* **2013**, *15*, 338–341.
(321) Zhou, W.; Zhang, H.; Li, H.; Zhang, Y.; Wang, Q.-C.; Qu, D.-H. A Bis-Spiropyran-Containing Multi-State [2]Rotaxane with Fluorescence Output. *Tetrahedron* **2013**, *69*, 5319–5325.
(322) Zhang, J.-N.; Li, H.; Zhou, W.; Yu, S.-L.; Qu, D.-H.; Tian, H. Fluorescence Modulation in Tribranched Switchable [4]Rotaxanes. *Chem. Eur. J.* **2013**, *19*, 17192–17200.
(323) Zhang, H.; Zhou, B.; Li, H.; Qu, D.-H.; Tian, H. A Ferrocene-Functionalized [2]Rotaxane with Two Fluorophores as Stoppers. *J. Org. Chem.* **2013**, *78*, 2091–2098.

(324) Cao, Z.-Q.; Luan, Z.-L.; Zhang, Q.; Gu, R.-R.; Ren, J.; Qu, D.-H. An Acid/Base Responsive Side-Chain Polyrotaxane System with a Fluorescent Signal. *Polym. Chem.* **2016**, *7*, 1–5.
(325) Álvarez, C. M.; Barbero, H.; Miguel, D. Multivalent Molecular Shuttles - Effect of Increasing the Number of Centers in Switchable Catalysts. *Eur. J. Org. Chem.* **2015**, 6631–6640.
(326) Berg, M.; Nozinovic, S.; Engeser, M.; Lützen, A. A Cholesterol Containing pH-Sensitive Bistable [2]Rotaxane. *Eur. J. Org. Chem.* **2015**, 5966–5978.
(327) Arumugaperumal, R.; Srinivasadesikan, V.; Raju, M. V. R.; Lin, M.-C.; Shukla, T.; Singh, R.; Lin, H.-C. Acid/Base and $H_2PO_4^-$ Controllable High-Contrast Optical Molecular Switches with a Novel BODIPY Functionalized [2]Rotaxane. *ACS Appl. Mater. Interfaces* **2015**, *7*, 26491–26503.
(328) Tokunaga, Y.; Nakamura, T.; Yoshioka, M.; Shimomura, Y. A Molecular Switch Based on Acid and Base Promoted, Cation Governed Binding in a Crown Ether Threaded Rotaxane. *Tetrahedron Lett.* **2006**, *47*, 5901–5904.
(329) Cheng, K.-W.; Lai, C.-C.; Chiang, P.-T.; Chiu, S.-H. Reading the Operation of an Acid/Base-Controllable Molecular Switch by Naked Eye. *Chem. Commun.* **2006**, 2854–2856.
(330) Zhou, W.; Li, J.; He, X.; Li, C.; Lv, J.; Li, Y.; Wang, S.; Liu, H.; Zhu, D. A Molecular Shuttle for Driving a Multilevel Fluorescence Switch. *Chem. Eur. J.* **2008**, *14*, 754–763.
(331) Zheng, H.; Zhou, W.; Lv, J.; Yin, X.; Li, Y.; Liu, H.; Li, Y. A Dual-Response [2]Rotaxane Based on a 1,2,3-Triazole Ring as a Novel Recognition Station. *Chem. Eur. J.* **2009**, *15*, 13253–13262.
(332) Ishiwari, F.; Nakazono, K.; Koyama, Y.; Takata, T. Rational Control of a Polyacetylene Helix by a Pendant Rotaxane Switch. *Chem. Commun.* **2011**, *47*, 11739–11741.
(333) Ishiwari, F.; Fukasawa, K.-I.; Sato, T.; Nakazono, K.; Koyama, Y.; Takata, T. A Rational Design for the Directed Helicity Change of Polyacetylene Using Dynamic Rotaxane Mobility by Means of Through-Space Chirality Transfer. *Chem. Eur. J.* **2011**, *17*, 12067–12075.
(334) Suzuki, S.; Ishiwari, F.; Nakazono, K.; Takata, T. Reversible Helix–Random Coil Transition of Poly(*m*-phenylenediethynylene) by a Rotaxane Switch. *Chem. Commun.* **2012**, *48*, 6478–6480.
(335) Zhou, W.; Wu, Y.; Zhai, B.-Q.; Wang, Q.-C.; Qu, D.-H. An Anthracene-Containing Bistable [2] Rotaxane Featuring Color and Fluorescence Changes. *RSC Adv.* **2014**, *4*, 5148–5151.
(336) Keaveney, C. M.; Leigh, D. A. Shuttling Through Anion Recognition. *Angew. Chem., Int. Ed*. **2004**, *43*, 1222–1224.
(337) Berná, J.; Brouwer, A. M.; Fazio, S. M.; Haraszkiewicz, N.; Leigh, D. A.; Lennon, C. M. A Rotaxane Mimic of the Photoactive Yellow Protein Chromophore Environment: Effects of Hydrogen Bonding and Mechanical Interlocking on a Coumaric Amide Derivative. *Chem. Commun.* **2007**, 1910–1912.
(338) Brouwer, A. M.; Fazio, S. M.; Haraszkiewicz, N.; Leigh, D. A.; Lennon, C. M. Coumaric Amide Rotaxanes: Effects of Hydrogen Bonding and Mechanical Interlocking on the Photochemistry and Photophysics. *Photochem. Photobiol. Sci.* **2007**, *6*, 480–486.
(339) Hesseler, B.; Zindler, M.; Herges, R.; Lüning, U. A Shuttle for the Transport of Protons Based on a [2]Rotaxane. *Eur. J. Org. Chem.* **2014**, 3885–3901.
(340) Beyer, O.; Hesseler, B.; Lüning, U. A Convenient Access to a [2]Rotaxane Proton Shuttle by Using a Fluorous Ponytail. *Synthesis* **2015**, *47*, 2485–2495.
(341) Leigh, D. A.; Lusby, P. J.; Slawin, A. M. Z.; Walker, D. B. Half-Rotation in a [2]Catenane via Interconvertible Pd(II) Coordination Modes. *Chem. Commun.* **2005**, 4919–4921.
(342) Crowley, J. D.; Leigh, D. A.; Lusby, P. J.; Mcburney, R. T.; Perret-Aebi, L.-E.; Petzold, C.; Slawin, A. M. Z.; Symes, M. D. A Switchable Palladium-Complexed Molecular Shuttle and Its Metastable Positional Isomers. *J. Am. Chem. Soc.* **2007**, *129*, 15085–15090.
(343) Leigh, D. A.; Lusby, P. J.; McBurney, R. T.; Symes, M. D. Improved Dynamics and Positional Bias with a Second Generation Palladium(II)-Complexed Molecular Shuttle. *Chem. Commun.* **2010**, *46*, 2382–2384.
(344) Leigh, D. A.; Thomson, A. R. Switchable Dual Binding Mode Molecular Shuttle. *Org. Lett.* **2006**, *8*, 5377–5379.
(345) Zhou, W.; Xu, J.; Zheng, H.; Liu, H.; Li, Y.; Zhu, D. Charge Transfer Chromophore-Stopped [2]Rotaxane Through [2+2] Cycloaddition. *J. Org. Chem.* **2008**, *73*, 7702–7709.
(346) Zhao, Y.; Li, Y.; Lai, S.-W.; Yang, J.; Liu, C.; Liu, H.; Che, C.-M.; Li, Y. Construction of a Functional [2]Rotaxane with Multilevel Fluorescence Responses. *Org. Biomol. Chem.* **2011**, *9*, 7500–7503.
(347) Pierro, T.; Gaeta, C.; Talotta, C.; Casapullo, A.; Neri, P. Fixed or Invertible Calixarene-Based Directional Shuttles. *Org. Lett.* **2011**, *13*, 2650–2653.
(348) Talotta, C.; Gaeta, C.; Neri, P. Stereoprogrammed Direct Synthesis of Calixarene-Based [3]Rotaxanes. *Org. Lett.* **2012**, *14*, 3104–3107.
(349) Ng, K.-Y.; Félix, V.; Santos, S. M.; Rees, N. H.; Beer, P. D. Anion Induced and Inhibited Circumrotation of a [2]Catenane. *Chem. Commun.* **2008**, 1281–1283.
(350) Dietrich-Buchecker, C. O.; Sauvage, J.-P.; Kern, J.-M. Templated Synthesis of Interlocked Macrocyclic Ligands: The Catenands. *J. Am. Chem. Soc.* **1984**, *106*, 3043–3045.
(351) Dietrich, B.; Lehn, J.-M.; Sauvage, J.-P. Diaza-Polyoxa-Macrocycles et Macrobicycles. *Tetrahedron Lett*. **1969**, *10*, 2885–2888.
(352) Dietrich, B.; Lehn, J.-M.; Sauvage, J.-P. Les Cryptates. *Tetrahedron Lett*. **1969**, *10*, 2889–2892.
(353) Lehn, J.-M.; Sauvage, J.-P. Cryptates. XVI.[2]-Cryptates. Stability and Selectivity of Alkali and Alkaline-Earth Macrobicyclic Complexes. *J. Am. Chem. Soc*. **1975**, *97*, 6700–6707.
(354) Cesario, M.; Dietrich, C. O.; Edel, A.; Guilhem, J.; Kintzinger, J.-P.; Pascard, C.; Sauvage, J.-P. Topological Enhancement of Basicity: Molecular Structure and Solution Study of a Monoprotonated Catenand. *J. Am. Chem. Soc.* **1986**, *108*, 6250–6254.
(355) Cesario, M.; Dietrich-Buchecker, C. O.; Guilhem, J.; Pascard, C.; Sauvage, J.-P. Molecular Structure of a Catenand and Its Copper(I) Catenate: Complete Rearrangement of the Interlocked Macrocyclic Ligands by Complexation. *J. Chem. Soc., Chem. Commun.* **1985**, 244–247.
(356) Sauvage, J.-P.; Weiss, J. Synthesis of Dicopper(I) [3]Catenates: Multiring Interlocked Coordinating Systems. *J. Am. Chem. Soc.* **1985**, *107*, 6108–6110.
(357) Dietrich-Buchecker, C. O.; Sauvage, J.-P. A Synthetic Molecular Trefoil Knot. *Angew. Chem., Int. Ed. Engl*. **1989**, *28*, 189–192.
(358) Nierengarten, J.-F.; Dietrich-Buchecker, C. O.; Sauvage, J.-P. Synthesis of a Doubly Interlocked [2]-Catenane. *J. Am. Chem. Soc.* **1994**, *116*, 375–376.
(359) Chambron, J.-C.; Harriman, A.; Heitz, V.; Sauvage, J.-P. Effect of the Spacer Moiety on the Rates of Electron Transfer within Bis-Porphyrin-Stoppered Rotaxanes. *J. Am. Chem. Soc.* **1993**, *115*, 7419–7425.
(360) Megiatto, J. D., Jr.; Schuster, D. I. Alternative Demetalation Method for Cu(I)-Phenanthroline-Based Catenanes and Rotaxanes. *Org. Lett.* **2011**, *13*, 1808–1811.
(361) Amabilino, D. B.; Dietrich-Buchecker, C. O.; Livoreil, A.; Pérez-García, L.; Sauvage, J.-P.; Stoddart, J. F. A Switchable Hybrid [2]-Catenane Based on Transition Metal Complexation and π-Electron Donor-Acceptor Interactions. *J. Am. Chem. Soc.* **1996**, *118*, 3905–3913.
(362) Linke, M.; Chambron, J.-C.; Heitz, V.; Sauvage, J.-P.; Encinas, S.; Barigelletti, F.; Flamigni, L. Multiporphyrinic Rotaxanes: Control of Intramolecular Electron Transfer Rate by Steering the Mutual Arrangement of the Chromophores. *J. Am. Chem. Soc.* **2000**, *122*, 11834–11844.
(363) Linke, M.; Chambron, J.-C.; Heitz, V.; Sauvage, J.-P.; Semetey, V. Complete Rearrangement of a Multi-Porphyrinic

Rotaxane by Metalation-Demetalation of the Central Coordination Site. *Chem. Commun.* **1998**, 2469–2470.
(364) Andersson, M.; Linke, M.; Chambron, J.-C.; Davidsson, J.; Heitz, V.; Sauvage, J.-P.; Hammarström, L. Porphyrin-Containing [2]-Rotaxanes: Metal Coordination Enhanced Superexchange Electron Transfer Between Noncovalently Linked Chromophores. *J. Am. Chem. Soc.* **2000**, *122*, 3526–3527.
(365) Andersson, M.; Linke, M.; Chambron, J.-C.; Davidsson, J.; Heitz, V.; Hammarström, L.; Sauvage, J.-P. Long-Range Electron Transfer in Porphyrin-Containing [2]-Rotaxanes: Tuning the Rate by Metal Cation Coordination. *J. Am. Chem. Soc.* **2002**, *124*, 4347–4362.
(366) Lewis, J. E. M.; Bordoli, R. J.; Denis, M.; Fletcher, C. J.; Galli, M.; Neal, E. A.; Rochette, E. M.; Goldup, S. M. High Yielding Synthesis of 2,2′-Bipyridine Macrocycles, Versatile Intermediates in the Synthesis of Rotaxanes. *Chem. Sci.* **2016**, *7*, 3154–3161.
(367) Jiménez, M. C.; Dietrich-Buchecker, C.; Sauvage, J.-P. Towards Synthetic Molecular Muscles: Contraction and Stretching of a Linear Rotaxane Dimer. *Angew. Chem., Int. Ed.* **2000**, *39*, 3284–3287.
(368) Rotzler, J.; Mayor, M. Molecular Daisy Chains. *Chem. Soc. Rev.* **2013**, *42*, 44–62.
(369) Joosten, A.; Trolez, Y.; Collin, J.-P.; Heitz, V.; Sauvage, J.-P. Copper(I)-Assembled [3]Rotaxane Whose Two Rings Act as Flapping Wings. *J. Am. Chem. Soc.* **2012**, *134*, 1802–1809.
(370) Leigh, D. A.; Lusby, P. J.; Slawin, A. M. Z.; Walker, D. B. Half-Rotation in a Kinetically Locked [2]Catenane Induced by Transition Metal Ion Substitution. *Chem. Commun.* **2012**, *48*, 5826–5828.
(371) Changeux, J. P.; Edelstein, S. J. Allosteric Mechanisms of Signal Transduction. *Science* **2005**, *308*, 1424–1428.
(372) Marlin, D. S.; Cabrera, D. G.; Leigh, D. A.; Slawin, A. M. Z. An Allosterically Regulated Molecular Shuttle. *Angew. Chem., Int. Ed.* **2006**, *45*, 1385–1390.
(373) Marlin, D. S.; Cabrera, D. G.; Leigh, D. A.; Slawin, A. M. Z. Complexation-Induced Translational Isomerism: Shuttling Through Stepwise Competitive Binding. *Angew. Chem., Int. Ed.* **2006**, *45*, 77–83.
(374) Baumes, J. M.; Murgu, I.; Connell, R. D.; Culligan, W. J.; Oliver, A. G.; Smith, B. D. Allosteric Regulation of a Reactive Squaraine Rotaxane Endoperoxide. *Supramol. Chem.* **2011**, *24*, 14–22.
(375) Thomassen, P. J.; Foekema, J.; i Lluch, R. J.; Thordarson, P.; Elemans, J. A. A. W.; Nolte, R. J. M.; Rowan, A. E. Self-Assembly Studies of Allosteric Photosynthetic Antenna Model Systems. *New J. Chem.* **2006**, *30*, 148–155.
(376) Veling, N.; Thomassen, P. J.; Thordarson, P.; Elemans, J. A. A. W.; Nolte, R. J. M.; Rowan, A. E. Construction of Supramolecular Multi-Component Assemblies by Using Allosteric Interactions. *Tetrahedron* **2008**, *64*, 8535–8542.
(377) Davidson, G. J. E.; Sharma, S.; Loeb, S. J. A [2]Rotaxane Flip Switch Driven by Coordination Geometry. *Angew. Chem., Int. Ed.* **2010**, *49*, 4938–4942.
(378) Vignon, S. A.; Jarrosson, T.; Iijima, T.; Tseng, H.-R.; Sanders, J. K. M.; Stoddart, J. F. Switchable Neutral Bistable Rotaxanes. *J. Am. Chem. Soc.* **2004**, *126*, 9884–9885.
(379) Kaiser, G.; Jarrosson, T.; Otto, S.; Ng, Y.-F.; Bond, A. D.; Sanders, J. K. M. Lithium-Templated Synthesis of a Donor-Acceptor Pseudorotaxane and Catenane. *Angew. Chem., Int. Ed.* **2004**, *43*, 1959–1962.
(380) Hsueh, S.-Y.; Lai, C.-C.; Chiu, S.-H. Squaraine-Based [2]Rotaxanes That Function as Visibly Active Molecular Switches. *Chem. Eur. J.* **2010**, *16*, 2997–3000.
(381) Meng, Z.; Chen, C.-F. Highly Efficient Synthesis of a Tristable Molecular Shuttle and Its Controlled Motion Under Chemical Stimuli. *Org. Biomol. Chem.* **2014**, *12*, 6937–6943.
(382) Meng, Z.; Xiang, J.-F.; Chen, C.-F. Tristable [*n*]Rotaxanes: From Molecular Shuttle to Molecular Cable Car. *Chem. Sci.* **2014**, *5*, 1520–1525.
(383) Wu, K.-D.; Lin, Y.-H.; Lai, C.-C.; Chiu, S.-H. Na^+ Ion Templated Threading of Oligo(ethylene glycol) Chains Through BPX26C6 Allows Synthesis of [2]Rotaxanes Under Solvent-Free Conditions. *Org. Lett.* **2014**, *16*, 1068–1071.
(384) Berná, J.; Goldup, S. M.; Lee, A.-L.; Leigh, D. A.; Symes, M. D.; Teobaldi, G.; Zerbetto, F. Cadiot-Chodkiewicz Active Template Synthesis of Rotaxanes and Switchable Molecular Shuttles with Weak Intercomponent Interactions. *Angew. Chem., Int. Ed.* **2008**, *47*, 4392–4396.
(385) Leontiev, A. V.; Jemmett, C. A.; Beer, P. D. Anion Recognition and Cation-Induced Molecular Motion in a Heteroditopic [2]Rotaxane. *Chem. Eur. J.* **2010**, *17*, 816–825.
(386) Hancock, L. M.; Beer, P. D. Sodium and Barium Cation-Templated Synthesis and Cation-Induced Molecular Pirouetting of a Pyridine *N*-Oxide Containing [2]Rotaxane. *Chem. Commun.* **2011**, *47*, 6012–6014.
(387) Leontiev, A. V.; Serpell, C. J.; White, N. G.; Beer, P. D. Cation-Induced Molecular Motion of Spring-Like [2]Catenanes. *Chem. Sci.* **2011**, *2*, 922–927.
(388) Laursen, B. W.; Nygaard, S.; Jeppesen, J. O.; Stoddart, J. F. Counterion-Induced Translational Isomerism in a Bistable [2]Rotaxane. *Org. Lett.* **2004**, *6*, 4167–4170.
(389) Lacour, J.; Goujon-Ginglinger, C.; Grivet, C.; Bernardinelli, G. Synthesis and Resolution of the Configurationally Stable Tris(tetrachlorobenzenediolato)phosphate(V) Ion. *Angew. Chem., Int. Ed. Engl.* **1997**, *36*, 608–610.
(390) Lin, C.-F.; Liu, Y.-H.; Lai, C.-C.; Peng, S.-M.; Chiu, S.-H. An Extremely Stable Host–Guest Complex That Functions as a Fluorescence Probe for Calcium Ions. *Chem. Eur. J.* **2006**, *12*, 4594–4599.
(391) Lin, C.-F.; Liu, Y.-H.; Lai, C.-C.; Peng, S.-M.; Chiu, S.-H. Precise Facial Control in Threading Guests Into a Molecular Cage and the Formation of a Turtlelike Supramolecular Complex. *Angew. Chem., Int. Ed.* **2006**, *45*, 3176–3181.
(392) Zong, Q.-S.; Chen, C.-F. Novel Triptycene-Based Cylindrical Macrotricyclic Host: Synthesis and Complexation with Paraquat Derivatives. *Org. Lett.* **2006**, *8*, 211–214.
(393) Zong, Q.-S.; Zhang, C.; Chen, C.-F. Self-Assembly of Triptycene-Based Cylindrical Macrotricyclic Host with Dibenzylammonium Ions: Construction of Dendritic [3]Pseudorotaxanes. *Org. Lett.* **2006**, *8*, 1859–1862.
(394) Han, T.; Chen, C.-F. Efficient Potassium-Ion-Templated Synthesis and Controlled Destruction of [2]Rotaxanes Based on Cascade Complexes. *J. Org. Chem.* **2008**, *73*, 7735–7742.
(395) Jiang, Y.; Guo, J.-B.; Chen, C.-F. A Bifunctionalized [3]Rotaxane and Its Incorporation Into a Mechanically Interlocked Polymer. *Chem. Commun.* **2010**, *46*, 5536–5538.
(396) Chang, C.-F.; Chuang, C.-J.; Lai, C.-C.; Liu, Y.-H.; Peng, S.-M.; Chiu, S.-H. Using Host-Guest Complexation to Fold a Flexible Linear Organic String: Kinetically Controlled Syntheses of [3]Catenanes and a Five-Membered Molecular Necklace. *Angew. Chem., Int. Ed.* **2012**, *51*, 10094–10098.
(397) Chuang, C.-J.; Lai, C.-C.; Liu, Y.-H.; Peng, S.-M.; Chiu, S.-H. A Two-Stage Molecular Retractable Cable Featuring Push-Button and Rotary Two-Way Switching Modes. *Chem. Eur. J.* **2012**, *18*, 16698–16707.
(398) Lin, C.-F.; Lai, C.-C.; Liu, Y.-H.; Peng, S.-M.; Chiu, S.-H. Use of Anions to Allow Translational Isomerism of a [2]Rotaxane. *Chem. Eur. J.* **2007**, *13*, 4350–4355.
(399) Lin, T.-C.; Lai, C.-C.; Chiu, S.-H. A Guanidinium Ion-Based Anion- and Solvent Polarity-Controllable Molecular Switch. *Org. Lett.* **2009**, *11*, 613–616.
(400) You, Y.-C.; Tzeng, M.-C.; Lai, C.-C.; Chiu, S.-H. Using Oppositely Charged Ions to Operate a Three-Station [2]Rotaxane in Two Different Switching Modes. *Org. Lett.* **2012**, *14*, 1046–1049.
(401) Liu, L.; Liu, Y.; Liu, P.; Wu, J.; Guan, Y.; Hu, X.; Lin, C.; Yang, Y.; Sun, X.; Ma, J.; Wang, L. Phosphine Oxide Functional Group Based Three-Station Molecular Shuttle. *Chem. Sci.* **2013**, *4*, 1701–1706.
(402) Liu, P.; Li, W.; Liu, L.; Wang, L.; Ma, J. Theoretical Study on Conformation Dynamics of Three-Station Molecular Shuttle in Different Environments and Its Influence on NMR Chemical

Shifts and Binding Interactions. *J. Phys. Chem. A* **2014**, *118*, 9032–9044.
(403) Cheng, M.; Liu, L.; Cao, Y.; Jiang, J.; Wang, L. A Phosphine Oxide Functional Group Based [2]Rotaxane That Operates as a Multistable Molecular Shuttle. *ChemPhysChem* **2016**, *17*, 1835–1839.
(404) Colquhoun, H. M.; Stoddart, J. F.; Williams, D. J. Second Sphere Coordination—A Novel Role for Molecular Receptors. *Angew. Chem., Int. Ed. Engl*. **1986**, *25*, 487–507.
(405) Raymo, F. M.; Stoddart, J. F. Second-Sphere Coordination. *Chem. Ber*. **1996**, *129*, 981–990.
(406) Mercer, D. J.; Loeb, S. J. Metal-Based Anion Receptors: An Application of Second-Sphere Coordination. *Chem. Soc. Rev.* **2010**, *39*, 3612–3620.
(407) Liu, Z.; Schneebeli, S. T.; Stoddart, J. F. Second-Sphere Coordination Revisited. *Chimia* **2014**, *68*, 315–320.
(408) Blight, B. A.; Van Noortwyk, K. A.; Wisner, J. A.; Jennings, M. C. [2]Pseudorotaxanes Through Second-Sphere Coordination. *Angew. Chem., Int. Ed*. **2005**, *44*, 1499–1504.
(409) Blight, B. A.; Wisner, J. A.; Jennings, M. C. Synthesis of a [2]Rotaxane Through First- and Second-Sphere Coordination. *Chem. Commun.* **2006**, 4593–4595.
(410) Blight, B. A.; Wei, X.; Wisner, J. A.; Jennings, M. C. [2]Pseudorotaxane and [2]Rotaxane Molecular Shuttles: Self-Assembly Through Second-Sphere Coordination of Thiocyanate Ligands. *Inorg. Chem*. **2007**, *46*, 8445–8447.
(411) Blight, B. A.; Wisner, J. A.; Jennings, M. C. Reversible Formation of a [2]Catenane Through First- and Second-Sphere Coordination. *Angew. Chem., Int. Ed*. **2007**, *46*, 2835–2838.
(412) Barrell, M. J.; Leigh, D. A.; Lusby, P. J.; Slawin, A. M. Z. An Ion-Pair Template for Rotaxane Formation and Its Exploitation in an Orthogonal Interaction Anion-Switchable Molecular Shuttle. *Angew. Chem., Int. Ed*. **2008**, *47*, 8036–8039.
(413) Andrievsky, A.; Ahuis, F.; Sessler, J. L.; Vögtle, F.; Gudat, D.; Moini, M. Bipyrrole-Based [2]Catenane: A New Type of Anion Receptor. *J. Am. Chem. Soc.* **1998**, *120*, 9712–9713.
(414) Zhao, Y.; Li, Y.; Li, Y.; Zheng, H.; Yin, X.; Liu, H. Construction of an Interpenetrated Structure of Macrocycles. *Chem. Commun.* **2010**, *46*, 5698–5700.
(415) Vickers, M. S.; Beer, P. D. Anion Templated Assembly of Mechanically Interlocked Structures. *Chem. Soc. Rev.* **2007**, *36*, 211–225.
(416) Lankshear, M. D.; Beer, P. D. Interweaving Anion Templation. *Acc. Chem. Res.* **2007**, *40*, 657–668.
(417) Caballero, A.; Zapata, F.; Beer, P. D. Interlocked Host Molecules for Anion Recognition and Sensing. *Coord. Chem. Rev.* **2013**, *257*, 2434–2455.
(418) Spence, G. T.; Beer, P. D. Expanding the Scope of the Anion Templated Synthesis of Interlocked Structures. *Acc. Chem. Res.* **2013**, *46*, 571–586.
(419) Evans, N. H.; Serpell, C. J.; Beer, P. D. A [2]Catenane Displaying Pirouetting Motion Triggered by Debenzylation and Locked by Chloride Anion Recognition. *Chem. Eur. J.* **2011**, *17*, 7734–7738.
(420) Brown, A.; Mullen, K. M.; Ryu, J.; Chmielewski, M. J.; Santos, S. M.; Felix, V.; Thompson, A. L.; Warren, J. E.; Pascu, S. I.; Beer, P. D. Interlocked Host Anion Recognition by an Indolocarbazole-Containing [2]Rotaxane. *J. Am. Chem. Soc.* **2009**, *131*, 4937–4952.
(421) Evans, N. H.; Allinson, E. S. H.; Lankshear, M. D.; Ng, K.-Y.; Cowley, A. R.; Serpell, C. J.; Santos, S. M.; Costa, P. J.; Félix, V.; Beer, P. D. Anion Templated Assembly of [2]Catenanes Capable of Chloride Anion Recognition in Aqueous Solvent Media. *RSC Adv.* **2011**, *1*, 995–1003.
(422) Serpell, C. J.; Chall, R.; Thompson, A. L.; Beer, P. D. Chloride Anion Triggered Motion in a Bis-Imidazolium Rotaxane. *Dalton Trans.* **2011**, *40*, 12052–12055.
(423) Spence, G. T.; Pitak, M. B.; Beer, P. D. Anion-Induced Shuttling of a Naphthalimide Triazolium Rotaxane. *Chem. Eur. J.* **2012**, *18*, 7100–7108.
(424) Zhao, Y.-L.; Shveyd, A. K.; Stoddart, J. F. Solid-State Structures and Superstructures of Two Charged Donor-Acceptor Rotaxanes. *Tetrahedron Lett.* **2011**, *52*, 2044–2047.
(425) Gassensmith, J. J.; Matthys, S.; Lee, J.-J.; Wojcik, A.; Kamat, P. V.; Smith, B. D. Squaraine Rotaxane as a Reversible Optical Chloride Sensor. *Chem. Eur. J.* **2010**, *16*, 2916–2921.
(426) Collins, C. G.; Peck, E. M.; Kramer, P. J.; Smith, B. D. Squaraine Rotaxane Shuttle as a Ratiometric Deep-Red Optical Chloride Sensor. *Chem. Sci.* **2013**, *4*, 2557–2563.
(427) Caballero, A.; Swan, L.; Zapata, F.; Beer, P. D. Iodide-Induced Shuttling of a Halogen- and Hydrogen-Bonding Two-Station Rotaxane. *Angew. Chem., Int. Ed*. **2014**, *53*, 11854–11858.
(428) Dzyuba, E. V.; Kaufmann, L.; Löw, N. L.; Meyer, A. K.; Winkler, H. D. F.; Rissanen, K.; Schalley, C. A. CH···O Hydrogen Bonds in “Clicked” Diketopiperazine-Based Amide Rotaxanes. *Org. Lett.* **2011**, *13*, 4838–4841.
(429) Huang, Y.-L.; Hung, W.-C.; Lai, C.-C.; Liu, Y.-H.; Peng, S.-M.; Chiu, S.-H. Using Acetate Anions to Induce Translational Isomerization in a Neutral Urea-Based Molecular Switch. *Angew. Chem., Int. Ed*. **2007**, *46*, 6629–6633.
(430) Berná, J.; Franco-Pujante, C.; Alajarín, M. Competitive Binding for Triggering a Fluorescence Response in a Hydrazodicarboxamide-Based [2]Rotaxane. *Org. Biomol. Chem.* **2014**, *12*, 474–478.
(431) Martinez-Cuezva, A.; Pastor, A.; Cioncoloni, G.; Orenes, R.-A.; Alajarín, M.; Symes, M. D.; Berná, J. Versatile Control of the Submolecular Motion of Di(acylamino)pyridine-Based [2]Rotaxanes. *Chem. Sci.* **2015**, *6*, 3087–3094.
(432) Martinez-Cuezva, A.; Carro-Guillen, F.; Pastor, A.; Marin-Luna, M.; Orenes, R.-A.; Alajarín, M.; Berná, J. Co-Conformational Exchange Triggered by Molecular Recognition in a Di(acylamino)pyridine-Based Molecular Shuttle Containing Two Pyridine Rings at the Macrocycle. *ChemPhysChem* **2016**, *17*, 1920–1926.
(433) Martínez-Máñez, R.; Sancenón, F. Fluorogenic and Chromogenic Chemosensors and Reagents for Anions. *Chem. Rev.* **2003**, *103*, 4419–4476.
(434) Sessler, J. L.; Camiolo, S.; Gale, P. A. Pyrrolic and Polypyrrolic Anion Binding Agents. *Coord. Chem. Rev.* **2003**, *240*, 17–55.
(435) Llinares, J. M.; Powell, D.; Bowman-James, K. Ammonium Based Anion Receptors. *Coord. Chem. Rev.* **2003**, *240*, 57–75.
(436) Yoon, J.; Kim, S. K.; Singh, N. J.; Kim, K. S. Imidazolium Receptors for the Recognition of Anions. *Chem. Soc. Rev.* **2006**, *35*, 355–360.
(437) Gale, P. A. Structural and Molecular Recognition Studies with Acyclic Anion Receptors. *Acc. Chem. Res.* **2006**, *39*, 465–475.
(438) Dydio, P.; Lichosyt, D.; Jurczak, J. Amide- and Urea-Functionalized Pyrroles and Benzopyrroles as Synthetic, Neutral Anion Receptors. *Chem. Soc. Rev.* **2011**, *40*, 2971–2985.
(439) Custelcean, R. Dynamic Chemistry of Anion Recognition. *Top. Curr. Chem.* **2011**, *322*, 193–216.
(440) Rambo, B. M.; Gong, H.-Y.; Oh, M.; Sessler, J. L. The “Texas-Sized” Molecular Box: A Versatile Building Block for the Construction of Anion-Directed Mechanically Interlocked Structures. *Acc. Chem. Res.* **2012**, *45*, 1390–1401.
(441) Fabbrizzi, L.; Poggi, A. Anion Recognition by Coordinative Interactions: Metal–Amine Complexes as Receptors. *Chem. Soc. Rev.* **2013**, *42*, 1681–1699.
(442) Chifotides, H. T.; Dunbar, K. R. Anion−π Interactions in Supramolecular Architectures. *Acc. Chem. Res.* **2013**, *46*, 894–906.
(443) Martinez-Cuezva, A.; Berná, J.; Orenes, R.-A.; Pastor, A.; Alajarín, M. Small-Molecule Recognition for Controlling Molecular Motion in Hydrogen-Bond-Assembled Rotaxanes. *Angew. Chem., Int. Ed*. **2014**, *53*, 6762–6767.
(444) Balzani, V.; Credi, A.; Langford, S. J.; Raymo, F. M.; Stoddart, J. F.; Venturi, M. Constructing Molecular Machinery:

A Chemically-Switchable [2]Catenane. *J. Am. Chem. Soc.* **2000**, *122*, 3542–3543.
(445) Ashton, P. R.; Boyd, S. E.; Brindle, A.; Langford, S. J.; Menzer, S.; Pérez-García, L.; Preece, J. A.; Raymo, F. M.; Spencer, N.; Stoddart, J. F.; White, A. J. P.; Williams, D. J. Molecular Meccano 50. Diazapyrenium-Containing Catenanes and Rotaxanes. *New J. Chem.* **1999**, *23*, 587–602.
(446) Zhang, D. Y.; Seelig, G. Dynamic DNA Nanotechnology Using Strand-Displacement Reactions. *Nature Chem.* **2011**, *3*, 103–113.
(447) Liu, X.; Lu, C.-H.; Willner, I. Switchable Reconfiguration of Nucleic Acid Nanostructures by Stimuli-Responsive DNA Machines. *Acc. Chem. Res.* **2014**, *47*, 1673–1680.
(448) Elbaz, J.; Wang, Z.-G.; Wang, F.; Willner, I. Programmed Dynamic Topologies in DNA Catenanes. *Angew. Chem., Int. Ed*. **2012**, *51*, 2349–2353.
(449) Cecconello, A.; Lu, C.-H.; Elbaz, J.; Willner, I. Au Nanoparticle/DNA Rotaxane Hybrid Nanostructures Exhibiting Switchable Fluorescence Properties. *Nano Lett.* **2013**, *13*, 6275–6280.
(450) Elbaz, J.; Cecconello, A.; Fan, Z.; Govorov, A. O.; Willner, I. Powering the Programmed Nanostructure and Function of Gold Nanoparticles with Catenated DNA Machines. *Nature Commun*. **2013**, *4*: 2000.
(451) Lu, C.-H.; Cecconello, A.; Elbaz, J.; Credi, A.; Willner, I. A Three-Station DNA Catenane Rotary Motor with Controlled Directionality. *Nano Lett.* **2013**, *13*, 2303–2308.
(452) Qi, X.-J.; Lu, C.-H.; Cecconello, A.; Yang, H.-H.; Willner, I. A Two-Ring Interlocked DNA Catenane Rotor Undergoing Switchable Transitions Across Three States. *Chem. Commun.* **2014**, *50*, 4717–4720.
(453) Lu, C.-H.; Qi, X.-J.; Cecconello, A.; Jester, S.-S.; Famulok, M.; Willner, I. Switchable Reconfiguration of an Interlocked DNA Olympiadane Nanostructure. *Angew. Chem., Int. Ed*. **2014**, *53*, 7499–7503.
(454) Lu, C.-H.; Cecconello, A.; Qi, X.-J.; Wu, N.; Jester, S.-S.; Famulok, M.; Matthies, M.; Schmidt, T.-L.; Willner, I. Switchable Reconfiguration of a Seven-Ring Interlocked DNA Catenane Nanostructure. *Nano Lett.* **2015**, *15*, 7133–7137.
(455) Watson, M. A.; Cockroft, S. L. An Autonomously Reciprocating Transmembrane Nanoactuator. *Angew. Chem., Int. Ed*. **2016**, *55*, 1345–1349.
(456) Sánchez-Quesada, J.; Saghatelian, A.; Cheley, S.; Bayley, H.; Ghadiri, M. R. Single DNA Rotaxanes of a Transmembrane Pore Protein. *Angew. Chem., Int. Ed*. **2004**, *43*, 3063–3067.
(457) Cao, J.; Fyfe, M. C. T.; Stoddart, J. F.; Cousins, G. R. L.; Glink, P. T. Molecular Meccano 55. Molecular Shuttles by the Protecting Group Approach. *J. Org. Chem*. **2000**, *65*, 1937–1946.
(458) Tachibana, Y.; Kawasaki, H.; Kihara, N.; Takata, T. Sequential *O*- and *N*-Acylation Protocol for High-Yield Preparation and Modification of Rotaxanes: Synthesis, Functionalization, Structure, and Intercomponent Interaction of Rotaxanes. *J. Org. Chem.* **2006**, *71*, 5093–5104.
(459) Tokunaga, Y.; Iwamoto, T.; Nakashima, S.; Shoji, E.; Nakata, R. Electrochemical Properties of 3,5-Diphenylaniline Units Encapsulated Within a Crown Ether. Effects of the Macrocycle's Aromatic Functionality and Ring Size. *Tetrahedron Lett*. **2011**, *52*, 240–243.
(460) Koyama, Y.; Matsumura, T.; Yui, T.; Ishitani, O.; Takata, T. Fluorescence Control of Boron Enaminoketonate Using a Rotaxane Shuttle. *Org. Lett.* **2013**, *15*, 4686–4689.
(461) Chen, Z.; Aoki, D.; Uchida, S.; Marubayashi, H.; Nojima, S.; Takata, T. Effect of Component Mobility on the Properties of Macromolecular [2]Rotaxanes. *Angew. Chem., Int. Ed*. **2016**, *55*, 2778–2781.
(462) Zhu, X.-Z.; Chen, C.-F. Efficient Synthesis of a Chiral [4]Pseudocatenane and Its Derivatives: A Novel Ship's Wheel-Like Interlocked Structure. *Chem. Eur. J.* **2006**, *12*, 5603–5609.
(463) Kawai, H.; Umehara, T.; Fujiwara, K.; Tsuji, T.; Suzuki, T. Dynamic Covalently Bonded Rotaxanes Cross-Linked by Imine Bonds Between the Axle and Ring: Inverse Temperature Dependence of Subunit Mobility. *Angew. Chem., Int. Ed*. **2006**, *45*, 4281–4286.
(464) Umehara, T.; Kawai, H.; Fujiwara, K.; Suzuki, T. Entropy- and Hydrolytic-Driven Positional Switching of Macrocycle Between Imine- and Hydrogen-Bonding Stations in Rotaxane-Based Molecular Shuttles. *J. Am. Chem. Soc.* **2008**, *130*, 13981–13988.
(465) Leigh, D. A.; Pérez, E. M. Shuttling Through Reversible Covalent Chemistry. *Chem. Commun.* **2004**, 2262–2263.
(466) Berná, J.; Alajarín, M.; Orenes, R.-A. Azodicarboxamides as Template Binding Motifs for the Building of Hydrogen-Bonded Molecular Shuttles. *J. Am. Chem. Soc.* **2010**, *132*, 10741–10747.
(467) Lane, A. S.; Leigh, D. A.; Murphy, A. Peptide-Based Molecular Shuttles. *J. Am. Chem. Soc.* **1997**, *119*, 11092–11093.
(468) Clegg, W.; Gimenez-Saiz, C.; Leigh, D. A.; Murphy, A.; Slawin, A. M. Z.; Teat, S. J. "Smart" Rotaxanes: Shape Memory and Control in Tertiary Amide Peptido[2]rotaxanes. *J. Am. Chem. Soc.* **1999**, *121*, 4124–4129.
(469) Raju, M. V. R.; Lin, H.-C. A Novel Diketopyrrolopyrrole (DPP)-Based [2]Rotaxane for Highly Selective Optical Sensing of Fluoride. *Org. Lett.* **2013**, *15*, 1274–1277.
(470) Jena, N. K.; Murugan, N. A. Solvent-Dependent Conformational States of a [2]Rotaxane-Based Molecular Machine: A Molecular Dynamics Perspective. *J. Phys. Chem. C* **2013**, *117*, 25059–25068.
(471) Gong, C.; Gibson, H. W. Controlling Microstructure in Polymeric Molecular Shuttles: Solvent-Induced Localization of Macrocycles in Poly(urethane/crown ether) Rotaxanes. *Angew. Chem., Int. Ed. Engl*. **1997**, *36*, 2331–2333.
(472) Leigh, D. A.; Moody, K.; Smart, J. P.; Watson, K. J.; Slawin, A. M. Z. Catenane Chameleons: Environment-Sensitive Translational Isomerism in Amphiphilic Benzylic Amide [2]Catenanes. *Angew. Chem., Int. Ed. Engl*. **1996**, *35*, 306–310.
(473) Da Ros, T.; Guldi, D. M.; Morales, A. F.; Leigh, D. A.; Prato, M.; Turco, R. Hydrogen Bond-Assembled Fullerene Molecular Shuttle. *Org. Lett.* **2003**, *5*, 689–691.
(474) Hannam, J. S.; Lacy, S. M.; Leigh, D. A.; Saiz, C. G.; Slawin, A. M. Z.; Stitchell, S. G. Controlled Submolecular Translational Motion in Synthesis: A Mechanically Interlocking Auxiliary. *Angew. Chem., Int. Ed*. **2004**, *43*, 3260–3264.
(475) Leigh, D. A.; Morales, M. A. F.; Pérez, E. M.; Wong, J. K. Y.; Saiz, C. G.; Slawin, A. M. Z.; Carmichael, A. J.; Haddleton, D. M.; Brouwer, A. M.; Buma, W. J.; Wurpel, G. W. H.; León, S.; Zerbetto, F. Patterning Through Controlled Submolecular Motion: Rotaxane-Based Switches and Logic Gates That Function in Solution and Polymer Films. *Angew. Chem., Int. Ed*. **2005**, *44*, 3062–3067.
(476) Mateo-Alonso, A.; Fioravanti, G.; Marcaccio, M.; Paolucci, F.; Jagesar, D. C.; Brouwer, A. M.; Prato, M. Reverse Shuttling in a Fullerene-Stoppered Rotaxane. *Org. Lett.* **2006**, *8*, 5173–5176.
(477) Mateo-Alonso, A.; Ehli, C.; Rahman, G. M. A.; Guldi, D. M.; Fioravanti, G.; Marcaccio, M.; Paolucci, F.; Prato, M. Tuning Electron Transfer Through Translational Motion in Molecular Shuttles. *Angew. Chem., Int. Ed.* **2007**, *46*, 3521–3525.
(478) Mateo-Alonso, A.; Iliopoulos, K.; Couris, S.; Prato, M. Efficient Modulation of the Third Order Nonlinear Optical Properties of Fullerene Derivatives. *J. Am. Chem. Soc.* **2008**, *130*, 1534–1535.
(479) Mateo-Alonso, A. Mechanically Interlocked Molecular Architectures Functionalised with Fullerenes. *Chem. Commun.* **2010**, *46*, 9089–9099.
(480) Scarel, F.; Valenti, G.; Gaikwad, S.; Marcaccio, M.; Paolucci, F.; Mateo-Alonso, A. A Molecular Shuttle Driven by Fullerene Radical-Anion Recognition. *Chem. Eur. J.* **2012**, *18*, 14063–14068.

(481) Mateo-Alonso, A.; Ehli, C.; Guldi, D. M.; Prato, M. A Three-Level Luminescent Response in a Pyrene/Ferrocene Rotaxane. *Org. Lett.* **2013**, *15*, 84–87.
(482) Moretto, A.; Menegazzo, I.; Crisma, M.; Shotton, E. J.; Nowell, H.; Mammi, S.; Toniolo, C. A Rigid Helical Peptide Axle for a [2]Rotaxane Molecular Machine. *Angew. Chem., Int. Ed*. **2009**, *48*, 8986–8989.
(483) Mahoney, J. M.; Shukla, R.; Marshall, R. A.; Beatty, A. M.; Zajicek, J.; Smith, B. D. Templated Conversion of a Crown Ether-Containing Macrobicycle Into [2]Rotaxanes. *J. Org. Chem.* **2002**, *67*, 1436–1440.
(484) Ashton, P. R.; Blower, M.; Philp, D.; Spencer, N.; Stoddart, J. F.; Tolley, M. S.; Ballardini, R.; Ciano, M.; Balzani, V.; Gandolfi, M. T.; Prodi, L.; McLean, C. H. The Control of Translational Isomerism in Catenated Structures. *New J. Chem.* **1993**, *17*, 689–695.
(485) Raymo, F. M.; Houk, K. N.; Stoddart, J. F. Molecular Meccano 28. Origins of Selectivity in Molecular and Supramolecular Entities: Solvent and Electrostatic Control of the Translational Isomerism in [2]Catenanes. *J. Org. Chem*. **1998**, *63*, 6523–6528.
(486) Wang, C.; Cao, D.; Fahrenbach, A. C.; Fang, L.; Olson, M. A.; Friedman, D. C.; Basu, S.; Dey, S. K.; Botros, Y. Y.; Stoddart, J. F. Solvent-Dependent Ground-State Distributions in a Donor-Acceptor Redox-Active Bistable [2]Catenane. *J. Phys. Org. Chem.* **2012**, *25*, 544–552.
(487) Yamauchi, K.; Miyawaki, A.; Takashima, Y.; Yamaguchi, H.; Harada, A. A Molecular Reel: Shuttling of a Rotor by Tumbling of a Macrocycle. *J. Org. Chem.* **2010**, *75*, 1040–1046.
(488) Dong, S.; Yuan, J.; Huang, F. A Pillar[5]arene/Imidazolium [2]Rotaxane: Solvent- and Thermo-Driven Molecular Motions and Supramolecular Gel Formation. *Chem. Sci.* **2013**, *5*, 247–252.
(489) Zhang, Z.; Han, C.; Yu, G.; Huang, F. A Solvent-Driven Molecular Spring. *Chem. Sci*. **2012**, *3*, 3026–3031.
(490) Ashton, P. R.; Pérez-García, L.; Stoddart, J. F.; White, A. J. P.; Williams, D. J. Controlling Translational Isomerism in [2]Catenanes. *Angew. Chem., Int. Ed. Engl*. **1995**, *34*, 571–574.
(491) Asakawa, M.; Ashton, P. R.; Dehaen, W.; L'abbé, G.; Menzer, S.; Nouwen, J.; Raymo, F. M.; Stoddart, J. F.; Tolley, M. S.; Toppet, S.; White, A. J. P.; Williams, D. J. Molecular Meccano 19. Self-Assembly of Novel [2]Catenanes and [2]Pseudorotaxanes Incorporating Thiacrown Ethers or Their Acyclic Analogs. *Chem. Eur. J*. **1997**, *3*, 772–787.
(492) Ballardini, R.; Balzani, V.; Gandolfi, M. T.; Gillard, R. E.; Stoddart, J. F.; Tabellini, E. Molecular Meccano 31. The Synthesis and Spectroscopic Properties of Macrocyclic Polyethers Containing Two Different Aromatic Moieties and Their [2]Catenanes Incorporating Cyclobis(paraquat-*p*-phenylene). *Chem. Eur. J*. **1998**, *4*, 449–459.
(493) Fujita, H.; Ooya, T.; Kurisawa, M.; Mori, H.; Terano, M.; Yui, N. Thermally Switchable Polyrotaxane as a Model of Stimuli-Responsive Supramolecules for Nano-Scale Devices. *Macromol. Rapid Comm.* **1996**, *17*, 509–515.
(494) Fujita, H.; Ooya, T.; Yui, N. Thermally Induced Localization of Cyclodextrins in a Polyrotaxane Consisting of β-Cyclodextrins and Poly(ethylene glycol)−Poly(propylene glycol) Triblock Copolymer. *Macromolecules* **1999**, *32*, 2534–2541.
(495) Ikeda, T.; Watabe, N.; Ooya, T.; Yui, N. Study on the Solution Properties of Thermo-Responsive Polyrotaxanes with Different Numbers of Cyclic Molecules. *Macromol. Chem. Phys.* **2001**, *202*, 1338–1344.
(496) Kidowaki, M.; Zhao, C.; Kataoka, T.; Ito, K. Thermoreversible Sol-Gel Transition of an Aqueous Solution of Polyrotaxane Composed of Highly Methylated α-Cyclodextrin and Polyethylene Glycol. *Chem. Commun.* **2006**, 4102–4103.
(497) Kataoka, T.; Kidowaki, M.; Zhao, C.; Minamikawa, H.; Shimizu, T.; Ito, K. Local and Network Structure of Thermoreversible Polyrotaxane Hydrogels Based on Poly(ethylene glycol) and Methylated α-Cyclodextrins. *J. Phys. Chem. B* **2006**, *110*, 24377–24383.
(498) Pelton, R. Temperature-Sensitive Aqueous Microgels. *Adv. Coll. Interface Sci.* **2000**, *85*, 1–33.
(499) Bottari, G.; Dehez, F.; Leigh, D. A.; Nash, P. J.; Pérez, E. M.; Wong, J. K. Y.; Zerbetto, F. Entropy-Driven Translational Isomerism: A Tristable Molecular Shuttle. *Angew. Chem., Int. Ed*. **2003**, *42*, 5886–5889.
(500) Günbaş, D. D.; Zalewski, L.; Brouwer, A. M. Energy Landscape of a Hydrogen-Bonded Non-Degenerate Molecular Shuttle. *Chem. Commun.* **2010**, *46*, 2061–2063.
(501) Ogoshi, T.; Yamafuji, D.; Aoki, T.; Yamagishi, T.-A. Thermally Responsive Shuttling Behavior of a Pillar[6]arene-Based [2]Rotaxane. *Chem. Commun.* **2012**, *48*, 6842–6844.
(502) Abe, Y.; Okamura, H.; Nakazono, K.; Koyama, Y.; Uchida, S.; Takata, T. Thermoresponsive Shuttling of Rotaxane Containing Trichloroacetate Ion. *Org. Lett.* **2012**, *14*, 4122–4125.
(503) Zhu, N.; Nakazono, K.; Takata, T. Reversible Polyphenylacetylene Helix Conversion Driven by a Thermoresponsive Rotaxane Switch in the Solid State. *Chem. Commun.* **2016**, *52*, 3647–3649.
(504) Sørensen, A.; Andersen, S. S.; Flood, A. H.; Jeppesen, J. O. Pressure Effects in the Synthesis of Isomeric Rotaxanes. *Chem. Commun.* **2013**, *49*, 5936–5938.
(505) Cockroft, S. L.; Chu, J.; Amorin, M.; Ghadiri, M. R. A Single-Molecule Nanopore Device Detects DNA Polymerase Activity with Single-Nucleotide Resolution. *J. Am. Chem. Soc.* **2008**, *130*, 818–820.
(506) Chu, J.; González-López, M.; Cockroft, S. L.; Amorin, M.; Ghadiri, M. R. Real-Time Monitoring of DNA Polymerase Function and Stepwise Single-Nucleotide DNA Strand Translocation Through a Protein Nanopore. *Angew. Chem., Int. Ed*. **2010**, *49*, 10106–10109.
(507) Biesemans, A.; Soskine, M.; Maglia, G. A Protein Rotaxane Controls the Translocation of Proteins Across a ClyA Nanopore. *Nano Lett.* **2015**, *15*, 6076–6081.
(508) Shigekawa, H.; Miyake, K.; Sumaoka, J.; Harada, A.; Komiyama, M. The Molecular Abacus: STM Manipulation of Cyclodextrin Necklace. *J. Am. Chem. Soc.* **2000**, *122*, 5411–5412.
(509) Harada, A.; Li, J.; Kamachi, M. The Molecular Necklace: A Rotaxane Containing Many Threaded α-Cyclodextrins. *Nature* **1992**, *356*, 325–327.
(510) Cavallini, M.; Biscarini, F.; León, S.; Zerbetto, F.; Bottari, G.; Leigh, D. A. Chemistry: Information Storage Using Supramolecular Surface Patterns. *Science* **2003**, *299*, 531.
(511) Janke, M.; Rudzevich, Y.; Molokanova, O.; Metzroth, T.; Mey, I.; Diezemann, G.; Marszalek, P. E.; Gauss, J.; Böhmer, V.; Janshoff, A. Mechanically Interlocked Calix[4]arene Dimers Display Reversible Bond Breakage Under Force. *Nature Nanotechnol.* **2009**, *4*, 225–229.
(512) Lussis, P.; Svaldo-Lanero, T.; Bertocco, A.; Fustin, C.-A.; Leigh, D. A.; Duwez, A.-S. A Single Synthetic Small Molecule That Generates Force Against a Load. *Nature Nanotechnol.* **2011**, *6*, 553–557.
(513) Van Quaethem, A.; Lussis, P.; Leigh, D. A.; Duwez, A.-S.; Fustin, C.-A. Probing the Mobility of Catenane Rings in Single Molecules. *Chem. Sci.* **2014**, *5*, 1449–1452.
(514) Ashcroft, B. A.; Spadola, Q.; Qamar, S.; Zhang, P.; Kada, G.; Bension, R.; Lindsay, S. An AFM/Rotaxane Molecular Reading Head for Sequence-Dependent DNA Structures. *Small* **2008**, *4*, 1468–1475.
(515) Bustamante, C.; Chemla, Y. R.; Forde, N. R.; Izhaky, D. Mechanical Processes in Biochemistry. *Annu. Rev. Biochem.* **2004**, *73*, 705–748.
(516) Bruns, C. J.; Stoddart, J. F. Rotaxane-Based Molecular Muscles. *Acc. Chem. Res*. **2014**, *47*, 2186–2199.
(517) Niess, F.; Duplan, V.; Sauvage, J.-P. Molecular Muscles: From Species in Solution to Materials and Devices. *Chem. Lett.* **2014**, *43*, 964–974.

(518) Jimenez-Molero, M. C.; Dietrich-Buchecker, C.; Sauvage, J.-P. Towards Artificial Muscles at the Nanometric Level. *Chem. Commun.* **2003**, 1613–1616.
(519) Tsukagoshi, S.; Miyawaki, A.; Takashima, Y.; Yamaguchi, H.; Harada, A. Contraction of Supramolecular Double-Threaded Dimer Formed by α-Cyclodextrin with a Long Alkyl Chain. *Org. Lett.* **2007**, *9*, 1053–1055.
(520) Fujimoto, T.; Sakata, Y.; Kaneda, T. The First Janus [2]Rotaxane. *Chem. Commun.* **2000**, 2143–2144.
(521) Tsuda, S.; Aso, Y.; Kaneda, T. Linear Oligomers Composed of a Photochromically Contractible and Extendable Janus [2]Rotaxane. *Chem. Commun.* **2006**, 3072–3074.
(522) Bruns, C. J.; Li, J.; Frasconi, M.; Schneebeli, S. T.; Iehl, J.; Jacquot de Rouville, H.-P.; Stupp, S. I.; Voth, G. A.; Stoddart, J. F. An Electrochemically and Thermally Switchable Donor-Acceptor [*c*2]Daisy Chain Rotaxane. *Angew. Chem., Int. Ed*. **2014**, *53*, 1953–1958.
(523) Hmadeh, M.; Fang, L.; Trabolsi, A.; Elhabiri, M.; Albrecht-Gary, A.-M.; Stoddart, J. F. On the Thermodynamic and Kinetic Investigations of a [*c*2]Daisy Chain Polymer. *J. Mater. Chem.* **2010**, *20*, 3422–3430.
(524) Clark, P. G.; Day, M. W.; Grubbs, R. H. Switching and Extension of a [*c*2]Daisy-Chain Dimer Polymer. *J. Am. Chem. Soc.* **2009**, *131*, 13631–13633.
(525) Du, G.; Moulin, E.; Jouault, N.; Buhler, E.; Giuseppone, N. Muscle-Like Supramolecular Polymers: Integrated Motion From Thousands of Molecular Machines. *Angew. Chem., Int. Ed*. **2012**, *51*, 12504–12508.
(526) Bruns, C. J.; Stoddart, J. F. Molecular Machines Muscle Up. *Nature Nanotechnol*. **2013**, *8*, 9–10.
(527) Wolf, A.; Moulin, E.; Cid, J.-J.; Goujon, A.; Du, G.; Busseron, E.; Fuks, G.; Giuseppone, N. pH and Light-Controlled Self-Assembly of Bistable [*c*2]Daisy Chain Rotaxanes. *Chem. Commun.* **2015**, *51*, 4212–4215.
(528) Goujon, A.; Du, G.; Moulin, E.; Fuks, G.; Maaloum, M.; Buhler, E.; Giuseppone, N. Hierarchical Self-Assembly of Supramolecular Muscle-Like Fibers. *Angew. Chem., Int. Ed*. **2015**, *55*, 703–707.
(529) Fu, X.; Gu, R.-R.; Zhang, Q.; Rao, S.-J.; Zheng, X.-L.; Qu, D.-H.; Tian, H. Phototriggered Supramolecular Polymerization of a [*c*2]Daisy Chain Rotaxane. *Polym. Chem*. **2016**, *7*, 2166–2170.
(530) Weigandt, J.; Chung, C.-L.; Jester, S.-S.; Famulok, M. Daisy Chain Rotaxanes Made From Interlocked DNA Nanostructures. *Angew. Chem., Int. Ed.* **2016**, *55*, 5512–5516.
(531) Tokunaga, Y.; Ikezaki, S.; Kimura, M.; Hisada, K.; Kawasaki, T. Five-State Molecular Switching of a [3]Rotaxane in Response to Weak and Strong Acid and Base Stimuli. *Chem. Commun.* **2013**, *49*, 11749–11751.
(532) Witus, L. S.; Hartlieb, K. J.; Wang, Y.; Prokofjevs, A.; Frasconi, M.; Barnes, J. C.; Dale, E. J.; Fahrenbach, A. C.; Stoddart, J. F. Relative Contractile Motion of the Rings in a Switchable Palindromic [3]Rotaxane in Aqueous Solution Driven by Radical-Pairing Interactions. *Org. Biomol. Chem.* **2014**, *12*, 6089–6093.
(533) Brouwer, A. M.; Jagesar, D. C.; Wiering, P. G.; Kay, E. R.; Leigh, D. A. Successive Translocation of the Rings in a [3]Rotaxane. *ChemPhysChem* **2016**, *17*, *49*, 1902–1912.
(534) Frey, J.; Tock, C.; Collin, J.-P.; Heitz, V.; Sauvage, J.-P. A [3]Rotaxane with Two Porphyrinic Plates Acting as an Adaptable Receptor. *J. Am. Chem. Soc.* **2008**, *130*, 4592–4593.
(535) Collin, J.-P.; Frey, J.; Heitz, V.; Sauvage, J.-P.; Tock, C.; Allouche, L. Adjustable Receptor Based on a [3]Rotaxane Whose Two Threaded Rings Are Rigidly Attached to Two Porphyrinic Plates: Synthesis and Complexation Studies. *J. Am. Chem. Soc.* **2009**, *131*, 5609–5620.
(536) Onagi, H.; Rebek, J., Jr. Fluorescence Resonance Energy Transfer Across a Mechanical Bond of a Rotaxane. *Chem. Commun.* **2005**, 4604–4606.
(537) Zhou, W.; Zhang, S.; Li, G.; Zhao, Y.; Shi, Z.; Liu, H.; Li, Y. Fluorescent Alteration on a Bistable Molecular Shuttle. *ChemPhysChem* **2009**, *10*, 2066–2072.
(538) Han, X.; Cao, M.; Xu, Z.; Wu, D.; Chen, Z.; Wu, A.; Liu, S. H.; Yin, J. Aggregation-Induced Emission Behavior of a pH-Controlled Molecular Shuttle Based on a Tetraphenylethene Moiety. *Org. Biomol. Chem.* **2015**, *13*, 9767–9774.
(539) Huang, T. J.; Brough, B.; Ho, C.-M.; Liu, Y.; Flood, A. H.; Bonvallet, P. A.; Tseng, H.-R.; Stoddart, J. F.; Baller, M.; Magonov, S. A Nanomechanical Device Based on Linear Molecular Motors. *Appl. Phys. Lett.* **2004**, *85*, 5391–5393.
(540) Li, H.; Li, X.; Cao, Z.-Q.; Qu, D.-H.; Ågren, H.; Tian, H. A Switchable Bis-Branched [1]Rotaxane Featuring Dual-Mode Molecular Motions and Tunable Molecular Aggregation. *ACS Appl. Mater. Interfaces* **2014**, *6*, 18921–18929.
(541) Yamada, Y.; Okamoto, M.; Furukawa, K.; Kato, T.; Tanaka, K. Switchable Intermolecular Communication in a Four-Fold Rotaxane. *Angew. Chem., Int. Ed*. **2012**, *51*, 709–713.
(542) Li, H.; Li, X.; Wu, Y.; Ågren, H.; Qu, D.-H. A Musclelike [2](2)Rotaxane: Synthesis, Performance, and Molecular Dynamics Simulations. *J. Org. Chem.* **2014**, *79*, 6996–7004.
(543) Kaufmann, L.; Traulsen, N. L.; Springer, A.; Schröder, H. V.; Mäkelä, T.; Rissanen, K.; Schalley, C. A. Evaluation of Multivalency as an Organization Principle for the Efficient Synthesis of Doubly and Triply Threaded Amide Rotaxanes. *Org. Chem. Front.* **2014**, *1*, 521–531.
(544) Chuang, C.-J.; Li, W.-S.; Lai, C.-C.; Liu, Y.-H.; Peng, S.-M.; Chao, I.; Chiu, S.-H. A Molecular Cage-Based [2]Rotaxane That Behaves as a Molecular Muscle. *Org. Lett.* **2009**, *11*, 385–388.
(545) Reuter, C.; Mohry, A.; Sobanski, A.; Vögtle, F. [1]Rotaxanes and Pretzelanes: Synthesis, Chirality, and Absolute Configuration. *Chem. Eur. J*. **2000**, *6*, 1674–1682.
(546) Romuald, C.; Cazals, G.; Enjalbal, C.; Coutrot, F. Straightforward Synthesis of a Double-Lasso Macrocycle From a Nonsymmetrical [*c*2]Daisy Chain. *Org. Lett.* **2013**, *15*, 184–187.
(547) Liu, Y.; Saha, S.; Vignon, S. A.; Flood, A. H.; Stoddart, J. F. Template-Directed Syntheses of Configurable and Reconfigurable Molecular Switches. *Synthesis* **2005**, 3437–3445.
(548) Miyawaki, A.; Kuad, P.; Takashima, Y.; Yamaguchi, H.; Harada, A. Molecular Puzzle Ring: Pseudo[1]rotaxane From a Flexible Cyclodextrin Derivative. *J. Am. Chem. Soc.* **2008**, *130*, 17062–17069.
(549) Xue, Z.; Mayer, M. F. Actuator Prototype: Capture and Release of a Self-Entangled [1]Rotaxane. *J. Am. Chem. Soc.* **2010**, *132*, 3274–3276.
(550) Ma, X.; Wang, Q.; Tian, H. Disparate Orientation of [1]Rotaxanes. *Tetrahedron Lett.* **2007**, *48*, 7112–7116.
(551) Di Motta, S.; Avellini, T.; Silvi, S.; Venturi, M.; Ma, X.; Tian, H.; Credi, A.; Negri, F. Photophysical Properties and Conformational Effects on the Circular Dichroism of an Azobenzene-Cyclodextrin [1]Rotaxane and Its Molecular Components. *Chem. Eur. J.* **2013**, *19*, 3131–3138.
(552) Tokunaga, Y.; Kimura, M.; Ueda, M.; Miyagawa, S.; Kawasaki, T.; Hisada, K. Base-Acid-Induced Translational Isomerism in a Branched [4]Rotaxane. *Tetrahedron Lett.* **2016**, *57*, 1120–1123.
(553) Li, H.; Li, X.; Ågren, H.; Qu, D.-H. Two Switchable Star-Shaped [1](*n*)Rotaxanes with Different Multibranched Cores. *Org. Lett.* **2014**, *16*, 4940–4943.
(554) Au-Yeung, H. Y.; Pantoş, G. D.; Sanders, J. K. M. A Water Soluble Donor-Acceptor [2]Catenane That Can Switch Between a Coplanar and a Gemini-Sign Conformation. *Angew. Chem., Int. Ed*. **2010**, *49*, 5331–5334.
(555) Durola, F.; Heitz, V.; Reviriego, F.; Roche, C.; Sauvage, J.-P.; Sour, A.; Trolez, Y. Cyclic [4]Rotaxanes Containing Two Parallel Porphyrinic Plates: Toward Switchable Molecular

Receptors and Compressors. *Acc. Chem. Res.* **2014**, *47*, 633–645.
(556) Collin, J.-P.; Durola, F.; Heitz, V.; Reviriego, F.; Sauvage, J.-P.; Trolez, Y. A Cyclic [4]Rotaxane That Behaves as a Switchable Molecular Receptor: Formation of a Rigid Scaffold From a Collapsed Structure by Complexation with Copper(I) Ions. *Angew. Chem., Int. Ed*. **2010**, *49*, 10172–10175.
(557) Roche, C.; Sour, A.; Sauvage, J.-P. A Flexible Copper(I)-Complexed [4]Rotaxane Containing Two Face-to-Face Porphyrinic Plates That Behaves as a Distensible Receptor. *Chem. Eur. J.* **2012**, *18*, 8366–8376.
(558) Woźny, M.; Pawłowska, J.; Osior, A.; Świder, P.; Bilewicz, R.; Korybut-Daszkiewicz, B. An Electrochemically Switchable Foldamer – A Surprising Feature of a Rotaxane with Equivalent Stations. *Chem. Sci.* **2014**, *5*, 2836–2842.
(559) Woźny, M.; Pawtowska, J.; Tomczyk, K. M.; Bilewicz, R.; Korybut-Daszkiewicz, B. Potential-Controlled Rotaxane Molecular Shuttles Based on Electron-Deficient Macrocyclic Complexes. *Chem. Commun.* **2014**, *50*, 13718–13721.
(560) Basu, S.; Coskun, A.; Friedman, D. C.; Olson, M. A.; Benítez, D.; Tkatchouk, E.; Barin, G.; Yang, J.; Fahrenbach, A. C.; Goddard, W. A., III; Stoddart, J. F. Donor-Acceptor Oligorotaxanes Made to Order. *Chem. Eur. J.* **2011**, *17*, 2107–2119.
(561) Zhu, Z.; Bruns, C. J.; Li, H.; Lei, J.; Ke, C.; Liu, Z.; Shafaie, S.; Colquhoun, H. M.; Stoddart, J. F. Synthesis and Solution-State Dynamics of Donor–Acceptor Oligorotaxane Foldamers. *Chem. Sci.* **2013**, *4*, 1470–1483.
(562) Bruns, C. J.; Stoddart, J. F. Mechanically Interlaced and Interlocked Donor–Acceptor Foldamers. *Adv. Polym. Sci.* **2013**, *261*, 271–294.
(563) Meng, Z.; Chen, C.-F. A Molecular Pulley Based on a Triply Interlocked [2]Rotaxane. *Chem. Commun.* **2015**, *51*, 8241–8244.
(564) Yoshizawa, M.; Klosterman, J. K.; Fujita, M. Functional Molecular Flasks: New Properties and Reactions Within Discrete, Self-Assembled Hosts. *Angew. Chem., Int. Ed*. **2009**, *48*, 3418–3438.
(565) Leigh, D. A.; Lusby, P. J.; Slawin, A. M. Z.; Walker, D. B. Rare and Diverse Binding Modes Introduced Through Mechanical Bonding. *Angew. Chem., Int. Ed*. **2005**, *44*, 4557–4564.
(566) Barnes, J. C.; Fahrenbach, A. C.; Cao, D.; Dyar, S. M.; Frasconi, M.; Giesener, M. A.; Benítez, D.; Tkatchouk, E.; Chernyashevskyy, O.; Shin, W. H.; Li, H.; Sampath, S.; Stern, C. L.; Sarjeant, A. A.; Hartlieb, K. J.; Liu, Z.; Carmieli, R.; Botros, Y. Y.; Choi, J. W.; Slawin, A. M. Z.; Ketterson, J. B.; Wasielewski, M. R.; Goddard, W. A., III; Stoddart, J. F. A Radically Configurable Six-State Compound. *Science* **2013**, *339*, 429–433.
(567) Li, H.; Zhu, Z.; Fahrenbach, A. C.; Savoie, B. M.; Ke, C.; Barnes, J. C.; Lei, J.; Zhao, Y.-L.; Lilley, L. M.; Marks, T. J.; Ratner, M. A.; Stoddart, J. F. Mechanical Bond-Induced Radical Stabilization. *J. Am. Chem. Soc.* **2013**, *135*, 456–467.
(568) Barin, G.; Coskun, A.; Friedman, D. C.; Olson, M. A.; Colvin, M. T.; Carmielli, R.; Dey, S. K.; Bozdemir, O. A.; Wasielewski, M. R.; Stoddart, J. F. A Multistate Switchable [3]Rotacatenane. *Chem. Eur. J.* **2011**, *17*, 213–222.
(569) Frasconi, M.; Kikuchi, T.; Cao, D.; Wu, Y.; Liu, W.-G.; Dyar, S. M.; Barin, G.; Sarjeant, A. A.; Stern, C. L.; Carmieli, R.; Wang, C.; Wasielewski, M. R.; Goddard, W. A., III; Stoddart, J. F. Mechanical Bonds and Topological Effects in Radical Dimer Stabilization. *J. Am. Chem. Soc.* **2014**, *136*, 11011–11026.
(570) Shipway, A. N.; Willner, I. Electronically Transduced Molecular Mechanical and Information Functions on Surfaces. *Acc. Chem. Res.* **2001**, *34*, 421–432.
(571) Balzani, V.; Credi, A.; Venturi, M. Molecular Machines Working on Surfaces and at Interfaces. *ChemPhysChem* **2008**, *9*, 202–220.
(572) Coronado, E.; Gaviña, P.; Tatay, S. Catenanes and Threaded Systems: From Solution to Surfaces. *Chem. Soc. Rev.* **2009**, *38*, 1674–1689.
(573) Davis, J. J.; Orlowski, G. A.; Rahman, H.; Beer, P. D. Mechanically Interlocked and Switchable Molecules at Surfaces. *Chem. Commun.* **2010**, *46*, 54–63.
(574) Lanari, D.; Bonollo, S.; Vaccaro, L. [2]Catenanes on Surfaces as Candidates for Nanoelectronic Devices. *Curr. Org. Synth*. **2012**, *9*, 188–198.
(575) Yang, Y.-W.; Sun, Y.-L.; Song, N. Switchable Host–Guest Systems on Surfaces. *Acc. Chem. Res.* **2014**, *47*, 1950–1960.
(576) Zhang, Q.; Qu, D.-H. Artificial Molecular Machine Immobilized Surface: A New Platform to Construct Functional Materials. *ChemPhysChem* **2016**, *17*, 1759–1768.
(577) Braunschweig, A. B.; Northrop, B. H.; Stoddart, J. F. Structural Control at the Organic–Solid Interface. *J. Mater. Chem.* **2006**, *16*, 32–44.
(578) Blodgett, K. B.; Langmuir, I. Built-Up Films of Barium Stearate and Their Optical Properties. *Phys. Rev.* **1937**, *51*, 964–982.
(579) Langmuir, I. The Constitution and Fundamental Properties of Solids and Liquids. II. Liquids. 1. *J. Am. Chem. Soc*. **1917**, *39*, 1848–1906.
(580) Langmuir, I. The Mechanism of the Surface Phenomena of Flotation. *Trans. Faraday Soc.* **1920**, *15*, 62–74.
(581) Blodgett, K. B. Monomolecular Films of Fatty Acids on Glass. *J. Am. Chem. Soc.* **1934**, *56*, 495–495.
(582) Roberts, G. G. *Langmuir-Blodgett Films*; Plenum Press: New York, **1990**.
(583) Zasadzinski, J. A.; Viswanathan, R.; Madsen, L.; Garnaes, J.; Schwartz, D. K. Langmuir-Blodgett Films. *Science* **1994**, *263*, 1726–1733.
(584) Ahuja, R. C.; Caruso, P.-L.; Möbius, D.; Wildburg, G.; Ringsdorf, H.; Philp, D.; Stoddart, J. F.; Preece, J. A. Molecular Organization via Ionic Interactions at Interfaces. 1. Monolayers and LB Films of Cyclic Bisbipyridinium Tetracations and Dimyristoylphosphatidic Acid. *Langmuir* **1993**, *9*, 1534–1544.
(585) Ahuja, R. C.; Caruso, P.-L.; Möbius, D.; Philp, D.; Preece, J. A.; Ringsdorf, H.; Stoddart, J. F.; Wildburg, G. Langmuir Films and Langmuir-Blodgett Multilayers Incorporating Mechanically-Threaded Molecules-Pseudorotaxanes. *Thin Solid Films* **1996**, *284–285*, 671–677.
(586) Brown, C. L.; Jonas, U.; Preece, J. A.; Ringsdorf, H.; Seitz, M.; Stoddart, J. F. Introduction of [2]Catenanes Into Langmuir Films and Langmuir-Blodgett Multilayers. A Possible Strategy for Molecular Information Storage Materials. *Langmuir* **2000**, *16*, 1924–1930.
(587) Lu, W.; Lieber, C. M. Nanoelectronics From the Bottom Up. *Nature Mater.* **2007**, *6*, 841–850.
(588) Gates, B. D.; Xu, Q.; Stewart, M.; Ryan, D.; Willson, C. G.; Whitesides, G. M. New Approaches to Nanofabrication: Molding, Printing, and Other Techniques. *Chem. Rev.* **2005**, *105*, 1171–1196.
(589) Stewart, D. R.; Ohlberg, D. A. A.; Beck, P. A.; Chen, Y.; Williams, R. S.; Jeppesen, J. O.; Nielsen, K. A.; Stoddart, J. F. Molecule-Independent Electrical Switching in Pt/Organic Monolayer/Ti Devices. *Nano Lett.* **2004**, *4*, 133–136.
(590) Chen, Y.; Ohlberg, D. A. A.; Li, X.; Stewart, D. R.; Williams, R. S.; Jeppesen, J. O.; Nielsen, K. A.; Stoddart, J. F.; Olynick, D. L.; Anderson, E. Nanoscale Molecular-Switch Devices Fabricated by Imprint Lithography. *Appl. Phys. Lett.* **2003**, *82*, 1610–1612.
(591) Chen, Y.; Jung, G.-Y.; Ohlberg, D. A. A.; Li, X.; Stewart, D. R.; Jeppesen, J. O.; Nielsen, K. A.; Stoddart, J. F.; Williams, R. S. Nanoscale Molecular-Switch Crossbar Circuits. *Nanotechnology* **2003**, *14*, 462–468.
(592) Diehl, M. R.; Steuerman, D. W.; Tseng, H.-R.; Vignon, S. A.; Star, A.; Celestre, P. C.; Stoddart, J. F.; Heath, J. R. Single-Walled Carbon Nanotube Based Molecular Switch Tunnel Junctions. *ChemPhysChem* **2003**, *4*, 1335–1339.
(593) DeIonno, E.; Tseng, H.-R.; Harvey, D. D.; Stoddart, J. F.; Heath, J. R. Infrared Spectroscopic Characterization of [2]Rotaxane Molecular Switch Tunnel Junction Devices. *J. Phys. Chem. B* **2006**, *110*, 7609–7612.

(594) Heath, J. R.; Kuekes, P. J.; Snider, G. S.; Williams, R. S. A Defect-Tolerant Computer Architecture: Opportunities for Nanotechnology. *Science* **1998**, *280*, 1716–1721.
(595) Phoa, K.; Neaton, J. B.; Subramanian, V. First-Principles Studies of the Dynamics of [2]Rotaxane Molecular Switches. *Nano Lett.* **2009**, *9*, 3225–3229.
(596) Service, R. F. Molecular Electronics. Next-Generation Technology Hits an Early Midlife Crisis. *Science*, **2003**, *302*, 556–559.
(597) Heath, J. R.; Stoddart, J. F.; Williams, R. S.; Chandross, E. A.; Weiss, P. S.; Service, R. More on Molecular Electronics. *Science* **2004**, *303*, 1136–1137.
(598) Flood, A. H.; Stoddart, J. F.; Steuerman, D. W.; Heath, J. R. Whence Molecular Electronics? *Science* **2004**, *306*, 2055–2056.
(599) Jang, Y. H.; Hwang, S.; Kim, Y.-H.; Jang, S. S.; Goddard, W. A., III. Density Functional Theory Studies of the [2]Rotaxane Component of the Stoddart−Heath Molecular Switch. *J. Am. Chem. Soc.* **2004**, *126*, 12636–12645.
(600) Deng, W.-Q.; Muller, R. P.; Goddard, W. A., III. Mechanism of the Stoddart-Heath Bistable Rotaxane Molecular Switch. *J. Am. Chem. Soc.* **2004**, *126*, 13562–13563.
(601) Paxton, W. F.; Kleinman, S. L.; Basuray, A. N.; Stoddart, J. F.; Van Duyne, R. P. Surface-Enhanced Raman Spectroelectrochemistry of TTF-Modified Self-Assembled Monolayers. *J. Phys. Chem. Lett.* **2011**, *2*, 1145–1149.
(602) Jang, S. S.; Jang, Y. H.; Kim, Y.-H.; Goddard, W. A., III; Choi, J. W.; Heath, J. R.; Laursen, B. W.; Flood, A. H.; Stoddart, J. F.; Nørgaard, K.; Bjørnholem, T. Molecular Dynamics Simulation of Amphiphilic Bistable [2]Rotaxane Langmuir Monolayers at the Air/Water Interface. *J. Am. Chem. Soc.* **2005**, *127*, 14804–14816.
(603) Feng, M.; Guo, X.; Lin, X.; He, X.; Ji, W.; Du, S.; Zhang, D.; Zhu, D.; Gao, H. Stable, Reproducible Nanorecording on Rotaxane Thin Films. *J. Am. Chem. Soc.* **2005**, *127*, 15338–15339.
(604) Feng, M.; Gao, L.; Deng, Z.; Ji, W.; Guo, X.; Du, S.; Shi, D.; Zhang, D.; Zhu, D.; Gao, H. Reversible, Erasable, and Rewritable Nanorecording on an H2 Rotaxane Thin Film. *J. Am. Chem. Soc.* **2007**, *129*, 2204–2205.
(605) Schreiber, F. Structure and Growth of Self-Assembling Monolayers. *Prog. Surf. Sci.* **2000**, *65*, 151–257.
(606) Love, J. C.; Estroff, L. A.; Kriebel, J. K.; Nuzzo, R. G.; Whitesides, G. M. Self-Assembled Monolayers of Thiolates on Metals as a Form of Nanotechnology. *Chem. Rev.* **2005**, *105*, 1103–1170.
(607) Onclin, S.; Ravoo, B. J.; Reinhoudt, D. N. Engineering Silicon Oxide Surfaces Using Self-Assembled Monolayers. *Angew. Chem., Int. Ed.* **2005**, *44*, 6282–6304.
(608) Katz, E.; Lioubashevsky, O.; Willner, I. Electromechanics of a Redox-Active Rotaxane in a Monolayer Assembly on an Electrode. *J. Am. Chem. Soc.* **2004**, *126*, 15520–15532.
(609) Katz, E.; Baron, R.; Willner, I.; Richke, N.; Levine, R. D. Temperature-Dependent and Friction-Controlled Electrochemically Induced Shuttling Along Molecular Strings Associated with Electrodes. *ChemPhysChem* **2005**, *6*, 2179–2189.
(610) Katz, E.; Willner, I. Kinetic Separation of Amperometric Responses of Composite Redox-Active Monolayers Assembled Onto Au Electrodes: Implications to the Monolayers' Structure and Composition. *Langmuir* **1997**, *13*, 3364–3373.
(611) Long, B.; Nikitin, K.; Fitzmaurice, D. Assembly of an Electronically Switchable Rotaxane on the Surface of a Titanium Dioxide Nanoparticle. *J. Am. Chem. Soc.* **2003**, *125*, 15490–15498.
(612) Klajn, R.; Fang, L.; Coskun, A.; Olson, M. A.; Wesson, P. J.; Stoddart, J. F.; Grzybowski, B. A. Metal Nanoparticles Functionalized with Molecular and Supramolecular Switches. *J. Am. Chem. Soc.* **2009**, *131*, 4233–4235.
(613) Lestini, E.; Nikitin, K.; Stolarczyk, J. K.; Fitzmaurice, D. Electron Transfer and Switching in Rigid [2]Rotaxanes Adsorbed on TiO_2 Nanoparticles. *ChemPhysChem* **2012**, *13*, 797–810.
(614) Nikitin, K.; Lestini, E.; Stolarczyk, J. K.; Müller-Bunz, H.; Fitzmaurice, D. Quantitative Conformational Study of Redox-Active [2]Rotaxanes, Part 2: Switching in Flexible and Rigid Bistable [2]Rotaxanes. *Chem. Eur. J.* **2008**, *14*, 1117–1128.
(615) Jia, C.; Li, H.; Jiang, J.; Wang, J.; Chen, H.; Cao, D.; Stoddart, J. F.; Guo, X. Interface-Engineered Bistable [2]Rotaxane-Graphene Hybrids with Logic Capabilities. *Adv. Mater.* **2013**, *25*, 6752–6759.
(616) Kramers, H. A. Brownian Motion in a Field of Force and the Diffusion Model of Chemical Reactions. *Physica* **1940**, *7*, 284–304.
(617) Grote, R. F.; Hynes, J. T. The Stable States Picture of Chemical Reactions. II. Rate Constants for Condensed and Gas Phase Reaction Models. *J. Chem. Phys*. **1980**, *73*, 2715–2732.
(618) Sumi, H.; Marcus, R. A. Dynamical Effects in Electron Transfer Reactions. *J. Chem. Phys.* **1986**, *84*, 4894–4914.
(619) Moresco, F. Driving Molecular Machines Using the Tip of a Scanning Tunneling Microscope. In *Single Molecular Machines and Motors*; Joachim, C.; Rapenne, G., Eds.; Springer International Publishing: Cham, **2015**; pp. 165–186.
(620) Willner, I.; Pardo-Yissar, V.; Katz, E.; Ranjit, K. T. A Photoactivated "Molecular Train" for Optoelectronic Applications: Light-Stimulated Translocation of a β-Cyclodextrin Receptor Within a Stoppered Azobenzene-Alkyl Chain Supramolecular Monolayer Assembly on a Au-Electrode. *J. Electroanal. Chem.* **2001**, *497*, 172–177.
(621) Zhu, L.; Yan, H.; Nguyen, K. T.; Tian, H.; Zhao, Y. Sequential Self-Assembly for Construction of Pt(II)-Bridged [3]Rotaxanes on Gold Nanoparticles. *Chem. Commun.* **2012**, *48*, 4290–4292.
(622) Cao, Z.-Q.; Miao, Q.; Zhang, Q.; Li, H.; Qu, D.-H.; Tian, H. A Fluorescent Bistable [2]Rotaxane Molecular Switch on SiO_2 Nanoparticles. *Chem. Commun.* **2015**, *51*, 4973–4976.
(623) Fasano, V.; Baroncini, M.; Moffa, M.; Iandolo, D.; Camposeo, A.; Credi, A.; Pisignano, D. Organic Nanofibers Embedding Stimuli-Responsive Threaded Molecular Components. *J. Am. Chem. Soc.* **2014**, *136*, 14245–14254.
(624) Payer, D.; Rauschenbach, S.; Malinowski, N.; Konuma, M.; Virojanadara, C.; Starke, U.; Dietrich-Buchecker, C.; Collin, J.-P.; Sauvage, J.-P.; Lin, N.; Kern, K. Toward Mechanical Switching of Surface-Adsorbed [2]Catenane by in Situ Copper Complexation. *J. Am. Chem. Soc.* **2007**, *129*, 15662–15667.
(625) Vukotic, V. N.; Harris, K. J.; Zhu, K.; Schurko, R. W.; Loeb, S. J. Metal–Organic Frameworks with Dynamic Interlocked Components. *Nature Chem.* **2012**, *4*, 456–460.
(626) Zhu, K.; O'Keefe, C. A.; Vukotic, V. N.; Schurko, R. W.; Loeb, S. J. A Molecular Shuttle That Operates Inside a Metal–Organic Framework. *Nature Chem.* **2015**, *7*, 514–519.
(627) Cao, D.; Juríček, M.; Brown, Z. J.; Sue, A. C.-H.; Liu, Z.; Lei, J.; Blackburn, A. K.; Grunder, S.; Sarjeant, A. A.; Coskun, A.; Wang, C.; Farha, O. K.; Hupp, J. T.; Stoddart, J. F. Three-Dimensional Architectures Incorporating Stereoregular Donor-Acceptor Stacks. *Chem. Eur. J.* **2013**, *19*, 8457–8465.
(628) Stokes, G. G. On the Effect of the Internal Friction of Fluids on the Motion of Pendulums. *Camb. Phil. Soc. Trans.* **1851**, *9*, 8–106.
(629) Reynolds, O. An Experimental Investigation of the Circumstances Which Determine Whether the Motion of Water Shall Be Direct or Sinuous, and of the Law of Resistance in Parallel Channels. *Phil. Trans. R. Soc. Lond.* **1883**, *174*, 935–982.
(630) Rott, N. Note on the History of the Reynolds Number. *Annu. Rev. Fluid Mech.* **1990**, *22*, 1–12.
(631) Purcell, E. M. Life at Low Reynolds Number. *Am. J. Phys.* **1977**, *45*, 3–11.
(632) Müller, P. Glossary of Terms Used in Physical Organic Chemistry (IUPAC Recommendations 1994). *Pure Appl. Chem*. **1994**, *66*, 1077–1184.

(633) Urry, D. W. Molecular Machines: How Motion and Other Functions of Living Organisms Can Result From Reversible Chemical Changes. *Angew. Chem., Int. Ed. Engl*. **1993**, *32*, 819–841.
(634) Piccolino, M. Biological Machines: From Mills to Molecules. *Nat. Rev. Mol. Cell Biol.* **2000**, *1*, 149–152.
(635) Bustamante, C.; Keller, D.; Oster, G. The Physics of Molecular Motors. *Acc. Chem. Res.* **2001**, *34*, 412–420.
(636) *Molecular Motors*; Schliwa, M., Ed.; Wiley-VCH Verlag GmbH & Co.: Weinheim, **2003**.
(637) van den Heuvel, M. G. L.; Dekker, C. Motor Proteins at Work for Nanotechnology. *Science* **2007**, *317*, 333–336.
(638) Huang, T. J.; Juluri, B. K. Biological and Biomimetic Molecular Machines. *Nanomedicine* **2008**, *3*, 107–124.
(639) Bell, T. W.; Cline, J. I. Molecular Machines: Natural and Artificial Molecular Motors. In *Chemical Evolution II: From the Origins of Life to Modern Society*; Zaikowski, L.; Friedrich, J. M.; Seidel, S. R., Eds.; American Chemical Society: Washington DC, **2009**; Vol. *1025*, pp. 233–248.
(640) Karagiannis, P.; Ishii, Y.; Yanagida, T. Molecular Machines Like Myosin Use Randomness to Behave Predictably. *Chem. Rev.* **2014**, *114*, 3318–3334.
(641) Li, D.; Paxton, W. F.; Baughman, R. H.; Huang, T. J.; Stoddart, J. F.; Weiss, P. S. Molecular, Supramolecular, and Macromolecular Motors and Artificial Muscles. *MRS Bull.* **2009**, *34*, 671–681.
(642) Hashidzume, A.; Yamaguchi, H.; Harada, A. Cyclodextrin-Based Molecular Machines. *Top. Curr. Chem*. **2014**, *354*, 71–110.
(643) Schneider, T. D. Sequence Logos, Machine/Channel Capacity, Maxwell's Demon, and Molecular Computers: A Review of the Theory of Molecular Machines. *Nanotechnology* **1994**, *5*, 1–18.
(644) Asfari, Z.; Vicens, J. Molecular Machines. *J. Incl. Phenom. Macrocycl. Chem.* **2000**, *36*, 101–115.
(645) Stoddart, J. F. Molecular Machines. *Acc. Chem. Res*. **2001**, *34*, 410–411.
(646) Rapenne, G. Synthesis of Technomimetic Molecules: Towards Rotation Control in Single-Molecular Machines and Motors. *Org. Lett.* **2005**, *3*, 1165–1169.
(647) Kinbara, K.; Aida, T. Toward Intelligent Molecular Machines: Directed Motions of Biological and Artificial Molecules and Assemblies. *Chem. Rev.* **2005**, *105*, 1377–1400.
(648) Browne, W. R.; Feringa, B. L. Making Molecular Machines Work. *Nature Nanotechnol*. **2006**, *1*, 25–35.
(649) Feringa, B. L. The Art of Building Small: From Molecular Switches to Molecular Motors. *J. Org. Chem.* **2007**, *72*, 6635–6652.
(650) Garcia-Garibay, M. A. Molecular Machines: Nanoscale Gadgets. *Nature Mater.*, **2008**, *7*, 431–432.
(651) Balzani, V.; Venturi, M.; Credi, A. *Molecular Devices and Machines: a Journey Into the Nanoworld*; 2nd ed.; Wiley-VCH: Weinheim, **2008**.
(652) Konstas, K.; Langford, S. J.; Latter, M. J. Advances Towards Synthetic Machines at the Molecular and Nanoscale Level. *Int. J. Mol. Sci.* **2010**, *11*, 2453–2472.
(653) Ball, P. Welcome to the Machine. *Chem. World-UK* **2010**, *7*, Issue 1, pp. 56–60.
(654) *From Non-Covalent Assemblies to Molecular Machines*; Sauvage, J.-P.; Gaspard, P., Eds.; Wiley-VCH: Weinheim, **2011**.
(655) Astumian, R. D. Microscopic Reversibility as the Organizing Principle of Molecular Machines. *Nature Nanotechnol.* **2012**, *7*, 684–688.
(656) Ishihara, S.; Wakayama, Y.; Hiroshiba, N.; Hill, J. P.; Ariga, K. Novel Concepts for Organic Syntheses Based on Interfaces and Molecular Machines. *Curr. Org. Synth.* **2012**, *9*, 428–438.
(657) *Single Molecular Machines and Motors*; Joachim, C.; Rapenne, G., Eds.; Springer: Cham, **2014**.
(658) Astumian, R. D. Enhanced Diffusion, Chemotaxis, and Pumping by Active Enzymes: Progress Toward an Organizing Principle of Molecular Machines. *ACS Nano* **2014**, *8*, 11917–11924.
(659) Abendroth, J. M.; Bushuyev, O. S.; Weiss, P. S.; Barrett, C. J. Controlling Motion at the Nanoscale: Rise of the Molecular Machines. *ACS Nano* **2015**, *9*, 7746–7768.
(660) Cheng, C.; McGonigal, P. R.; Stoddart, J. F.; Astumian, R. D. Design and Synthesis of Nonequilibrium Systems. *ACS Nano* **2015**, *9*, 8672–8688.
(661) Kay, E. R.; Leigh, D. A. Rise of the Molecular Machines. *Angew. Chem., Int. Ed*. **2015**, *54*, 10080–10088.
(662) Erbas-Cakmak, S.; Leigh, D. A.; McTernan, C. T.; Nussbaumer, A. L. Artificial Molecular Machines. *Chem. Rev.* **2015**, *115*, 10081–10206.
(663) Peplow, M. March of the Machines. *Nature* **2015**, *525*, 18–21.
(664) Richards, V. Molecular Machines. *Chemistry World* **2016**, http:—www.rsc.org–chemistryworld–2016–02–molecular–machines–rotaxanes–macrocycles–nano–walkers.
(665) Cheng, C.; Stoddart, J. F. Wholly Synthetic Molecular Machines. *ChemPhysChem* **2016**, *17*, 1–15.
(666) Watson, M. A.; Cockroft, S. L. Man-Made Molecular Machines: Membrane Bound. *Chem. Soc. Rev*. **2016**, *45*, DOI:10.1039–C5CS00874C.
(667) Coskun, A.; Banaszak, M.; Astumian, R. D.; Stoddart, J. F.; Grzybowski, B. A. Great Expectations: Can Artificial Molecular Machines Deliver on Their Promise? *Chem. Soc. Rev.* **2012**, *41*, 19–30.
(668) Kottas, G. S.; Clarke, L. I.; Horinek, D.; Michl, J. Artificial Molecular Rotors. *Chem. Rev*. **2005**, *105*, 1281–1376.
(669) Rapenne, G.; Joachim, C. Single Rotating Molecule-Machines: Nanovehicles and Molecular Motors. *Top. Curr. Chem.* **2014**, *354*, 253–277.
(670) Koumura, N.; Zijlstra, R. W. J.; van Delden, R. A.; Harada, N.; Feringa, B. L. Light-Driven Monodirectional Molecular Rotor. *Nature* **1999**, *401*, 152–155.
(671) Feringa, B. L. In Control of Motion: From Molecular Switches to Molecular Motors. *Acc. Chem. Res.* **2001**, *34*, 504–513.
(672) Cnossen, A.; Browne, W. R.; Feringa, B. L. Unidirectional Light-Driven Molecular Motors Based on Overcrowded Alkenes. *Top. Curr. Chem.* **2014**, *354*, 139–162.
(673) Kelly, T. R.; De Silva, H.; Silva, R. A. Unidirectional Rotary Motion in a Molecular System. *Nature* **1999**, *401*, 150–152.
(674) Kelly, T. R. Progress Toward a Rationally Designed Molecular Motor. *Acc. Chem. Res.* **2001**, *34*, 514–522.
(675) Zhao, K.; Dron, P. I.; Kaleta, J.; Rogers, C. T.; Michl, J. Arrays of Dipolar Molecular Rotors in Tris(*o*-phenylenedioxy) cyclotriphosphazene. *Top. Curr. Chem.* **2014**, *354*, 163–211.
(676) Kinbara, K.; Muraoka, T.; Aida, T. Chiral Ferrocenes as Novel Rotary Modules for Molecular Machines. *Org. Biomol. Chem.* **2008**, *6*, 1871–1876.
(677) Scottwell, S. Ø; Crowley, J. D. Ferrocene-Containing Non-Interlocked Molecular Machines. *Chem. Commun*. **2016**, *52*, 2451–2464.
(678) Jacquot de Rouville, H.-P.; Vives, G.; Rapenne, G. A Family of Electron-Triggered Molecular Motors Based on Aromatic Building Blocks. *Pure Appl. Chem*. **2008**, *80*, 659–667.
(679) Vives, G.; Jacquot de Rouville, H.-P.; Carella, A.; Launay, J.-P.; Rapenne, G. Prototypes of Molecular Motors Based on Star-Shaped Organometallic Ruthenium Complexes. *Chem. Soc. Rev*. **2009**, *38*, 1551–1561.
(680) Stefak, R.; Sirven, A. M.; Fukumoto, S.; Nakagawa, H.; Rapenne, G. Desymmetrization on Both Ligands of Pentaphenylcyclopentadienylhydrotris(Indazolyl) Borate Ruthenium(II) Complexes: Prototypes of Organometallic Molecular Gears and Motors. *Coord. Chem. Rev.* **2015**, *287*, 79–88.
(681) Vives, G.; Tour, J. M. Synthesis of Single-Molecule Nanocars. *Acc. Chem. Res.* **2009**, *42*, 473–487.
(682) Joachim, C.; Rapenne, G. Molecule Concept Nanocars: Chassis, Wheels, and Motors? *ACS Nano* **2013**, *7*, 11–14.
(683) Kumar, G. S.; Neckers, D. C. Photochemistry of Azobenzene-Containing Polymers. *Chem. Rev*. **1989**, *89*, 1915–1925.

(684) Bandara, H. M. D.; Burdette, S. C. Photoisomerization in Different Classes of Azobenzene. *Chem. Soc. Rev.* **2012**, *41*, 1809–1825.
(685) Kundu, P. K.; Klajn, R. Watching Single Molecules Move in Response to Light. *ACS Nano* **2014**, *8*, 11913–11916.
(686) Waldeck, D. H. Photoisomerization Dynamics of Stilbenes. *Chem. Rev*. **1991**, *91*, 415–436.
(687) Irie, M. Diarylethenes for Memories and Switches. *Chem. Rev.* **2000**, *100*, 1685–1716.
(688) Irie, M.; Fukaminato, T.; Matsuda, K.; Kobatake, S. Photochromism of Diarylethene Molecules and Crystals: Memories, Switches, and Actuators. *Chem. Rev.* **2014**, *114*, 12174–12277.
(689) Su, X.; Aprahamian, I. Hydrazone-Based Switches, Metallo-Assemblies and Sensors. *Chem. Soc. Rev.* **2014**, *43*, 1963–1981.
(690) Aprahamian, I. Molecular Machines: Molecules Bearing Robotic Arms. *Nature Chem.* **2015**, *8*, 97–99.
(691) Kassem, S.; Lee, A. T. L.; Leigh, D. A.; Markevicius, A.; Solà, J. Pick-Up, Transport and Release of a Molecular Cargo Using a Small-Molecule Robotic Arm. *Nature Chem.* **2015**, *8*, 138–143.
(692) Berkovic, G.; Krongauz, V.; Weiss, V. Spiropyrans and Spirooxazines for Memories and Switches. *Chem. Rev.* **2000**, *100*, 1741–1754.
(693) Minkin, V. I. Photo-, Thermo-, Solvato-, and Electrochromic Spiroheterocyclic Compounds. *Chem. Rev.* **2004**, *104*, 2751–2776.
(694) Klajn, R. Spiropyran-Based Dynamic Materials. *Chem. Soc. Rev.* **2014**, *43*, 148–184.
(695) Stadler, A.-M.; Ramírez, J. Synthetic Molecular Machines and Polymer/Monomer Size Switches That Operate Through Dynamic and Non-Dynamic Covalent Changes. *Top. Curr. Chem.* **2011**, *322*, 261–289.
(696) Leigh, D. A.; Lewandowska, U.; Lewandowski, B.; Wilson, M. R. Synthetic Molecular Walkers. *Top. Curr. Chem*. **2014**, *354*, 111–138.
(697) Garcia-Garibay, M. A. Crystalline Molecular Machines: Encoding Supramolecular Dynamics Into Molecular Structure. *Proc. Natl. Acad. Sci. U.S.A.* **2005**, *102*, 10771–10776.
(698) Karlen, S. D.; Garcia-Garibay, M. A. Amphidynamic Crystals: Structural Blueprints for Molecular Machines. *Top. Curr. Chem.* **2005**, *262*, 179–227.
(699) Khuong, T.-A. V.; Nuñez, J. E.; Godinez, C. E.; Garcia-Garibay, M. A. Crystalline Molecular Machines: A Quest Toward Solid-State Dynamics and Function. *Acc. Chem. Res.* **2006**, *39*, 413–422.
(700) Vogelsberg, C. S.; Garcia-Garibay, M. A. Crystalline Molecular Machines: Function, Phase Order, Dimensionality, and Composition. *Chem. Soc. Rev.* **2012**, *41*, 1892–1910.
(701) Amendola, V.; Fabbrizzi, L.; Mangano, C.; Pallavicini, P. Molecular Machines Based on Metal Ion Translocation. *Acc. Chem. Res.* **2001**, *34*, 488–493.
(702) Shinkai, S.; Ikeda, M.; Sugasaki, A.; Takeuchi, M. Positive Allosteric Systems Designed on Dynamic Supramolecular Scaffolds: Toward Switching and Amplification of Guest Affinity and Selectivity. *Acc. Chem. Res.* **2001**, *34*, 494–503.
(703) Urry, D. W. Five Axioms for the Functional Design of Peptide-Based Polymers as Molecular Machines and Materials: Principle for Macromolecular Assemblies. *Biopolymers* **1998**, *47*, 167–178.
(704) Liu, H.; Liu, D. DNA Nanomachines and Their Functional Evolution. *Chem. Commun.* **2009**, 2625–2636.
(705) Wang, F.; Willner, B.; Willner, I. DNA-Based Machines. *Top. Curr. Chem*. **2014**, *354*, 279–338.
(706) Castro, C. E.; Su, H.-J.; Marras, A. E.; Zhou, L.; Johnson, J. Mechanical Design of DNA Nanostructures. *Nanoscale* **2015**, *7*, 5913–5921.
(707) Hoffmann, F.; Cornelius, M.; Morell, J.; Fröba, M. Silica-Based Mesoporous Organic–Inorganic Hybrid Materials. *Angew. Chem., Int. Ed*. **2006**, *45*, 3216–3251.
(708) Klichko, Y.; Liong, M.; Choi, E.; Angelos, S.; Nel, A. E.; Stoddart, J. F.; Tamanoi, F.; Zink, J. I. Mesostructured Silica for Optical Functionality, Nanomachines, and Drug Delivery. *J. Am. Ceram. Soc.* **2009**, *92*, S2–S10.
(709) Vallet-Regí, M.; Balas, F.; Arcos, D. Mesoporous Materials for Drug Delivery. *Angew. Chem., Int. Ed*. **2007**, *46*, 7548–7558.
(710) He, Q.; Shi, J. Mesoporous Silica Nanoparticle Based Nano Drug Delivery Systems: Synthesis, Controlled Drug Release and Delivery, Pharmacokinetics and Biocompatibility. *J. Mater. Chem*. **2011**, *21*, 5845–5855.
(711) Yang, P.; Gai, S.; Lin, J. Functionalized Mesoporous Silica Materials for Controlled Drug Delivery. *Chem. Soc. Rev.* **2012**, *41*, 3679–3698.
(712) Slowing, I. I.; Trewyn, B. G.; Giri, S.; Lin, V. S.-Y. Mesoporous Silica Nanoparticles for Drug Delivery and Biosensing Applications. *Adv. Funct. Mater.* **2007**, *17*, 1225–1236.
(713) Liong, M.; Angelos, S.; Choi, E.; Patel, K.; Stoddart, J. F.; Zink, J. I. Mesostructured Multifunctional Nanoparticles for Imaging and Drug Delivery. *J. Mater. Chem.* **2009**, *19*, 6251–6257.
(714) Tang, F.; Li, L.; Chen, D. Mesoporous Silica Nanoparticles: Synthesis, Biocompatibility and Drug Delivery. *Adv. Mater*. **2012**, *24*, 1504–1534.
(715) Li, Z.; Barnes, J. C.; Bosoy, A.; Stoddart, J. F.; Zink, J. I. Mesoporous Silica Nanoparticles in Biomedical Applications. *Chem. Soc. Rev.* **2012**, *41*, 2590–2605.
(716) Saha, S.; Leung, K. C.-F.; Nguyen, T. D.; Stoddart, J. F.; Zink, J. I. Nanovalves. *Adv. Funct. Mater*. **2007**, *17*, 685–693.
(717) Angelos, S.; Johansson, E.; Stoddart, J. F.; Zink, J. I. Mesostructured Silica Supports for Functional Materials and Molecular Machines. *Adv. Funct. Mater.* **2007**, *17*, 2261–2271.
(718) Angelos, S.; Liong, M.; Choi, E.; Zink, J. I. Mesoporous Silicate Materials as Substrates for Molecular Machines and Drug Delivery. *Chem. Eng. J.* **2008**, *137*, 4–13.
(719) Cotí, K. K.; Belowich, M. E.; Liong, M.; Ambrogio, M. W.; Lau, Y. A.; Khatib, H. A.; Zink, J. I.; Khashab, N. M.; Stoddart, J. F. Mechanised Nanoparticles for Drug Delivery. *Nanoscale* **2009**, *1*, 16–39.
(720) Boyle, M. M.; Smaldone, R. A.; Whalley, A. C.; Ambrogio, M. W.; Botros, Y. Y.; Stoddart, J. F. Mechanised Materials. *Chem. Sci*. **2011**, *2*, 204–210.
(721) Yang, Y.-W. Towards Biocompatible Nanovalves Based on Mesoporous Silica Nanoparticles. *Med. Chem. Commun.* **2011**, *2*, 1033–1049.
(722) Ambrogio, M. W.; Thomas, C. R.; Zhao, Y.-L.; Zink, J. I.; Stoddart, J. F. Mechanized Silica Nanoparticles: A New Frontier in Theranostic Nanomedicine. *Acc. Chem. Res.* **2011**, *44*, 903–913.
(723) Li, M.; Yan, H.; Teh, C.; Korzh, V.; Zhao, Y. NIR-Triggered Drug Release From Switchable Rotaxane-Functionalized Silica-Covered Au Nanorods. *Chem. Commun.* **2014**, *50*, 9745–9748.
(724) Tarn, D.; Ferris, D. P.; Barnes, J. C.; Ambrogio, M. W.; Stoddart, J. F.; Zink, J. I. A Reversible Light-Operated Nanovalve on Mesoporous Silica Nanoparticles. *Nanoscale* **2014**, *6*, 3335–3343.
(725) Martinez-Cuezva, A.; Valero-Moya, S.; Alajarin, M.; Berna, J. Light-Responsive Peptide [2]Rotaxanes as Gatekeepers of Mechanised Nanocontainers. *Chem. Commun.* **2015**, *51*, 14501–14504.
(726) Patel, K.; Angelos, S.; Dichtel, W. R.; Coskun, A.; Yang, Y.-W.; Zink, J. I.; Stoddart, J. F. Enzyme-Responsive Snap-Top Covered Silica Nanocontainers. *J. Am. Chem. Soc.* **2008**, *130*, 2382–2383.
(727) Cheng, Y.-J.; Luo, G.-F.; Zhu, J.-Y.; Xu, X.-D.; Zeng, X.; Cheng, D.-B.; Li, Y.-M.; Wu, Y.; Zhang, X.-Z.; Zhuo, R.-X.; He, F. Enzyme-Induced and Tumor-Targeted Drug Delivery System Based on Multifunctional Mesoporous Silica Nanoparticles. *ACS Appl. Mater. Interfaces* **2015**, *7*, 9078–9087.

(728) Ambrogio, M. W.; Pecorelli, T. A.; Patel, K.; Khashab, N. M.; Trabolsi, A.; Khatib, H. A.; Botros, Y. Y.; Zink, J. I.; Stoddart, J. F. Snap-Top Nanocarriers. *Org. Lett*. **2010**, *12*, 3304–3307.
(729) Luo, Z.; Ding, X.; Hu, Y.; Wu, S.; Xiang, Y.; Zeng, Y.; Zhang, B.; Yan, H.; Zhang, H.; Zhu, L.; Liu J.; Li, J.; Cai, K.; Zhao, Y. Engineering a Hollow Nanocontainer Platform with Multifunctional Molecular Machines for Tumor-Targeted Therapy *in Vitro* and *in Vivo*. *ACS Nano* **2013**, *7*, 10271–10284.
(730) Gayam, S. R.; Wu, S.-P. Redox Responsive Pd(II) Templated Rotaxane Nanovalve Capped Mesoporous Silica Nanoparticles: A Folic Acid Mediated Biocompatible Cancer-Targeted Drug Delivery System. *J. Mater. Chem. B* **2014**, *2*, 7009–7016.
(731) Dai, L.; Zhang, Q.; Gu, H.; Cai, K. Facile Synthesis of Yolk-Shell Silica Nanoparticles for Targeted Tumor Therapy. *J. Mat. Chem. B* **2015**, *3*, 8303–8313.
(732) Porta, F.; Lamers, G. E. M.; Zink, J. I.; Kros, A. Peptide Modified Mesoporous Silica Nanocontainers. *Phys. Chem. Chem. Phys.* **2011**, *13*, 9982–9985.
(733) Hernandez, R.; Tseng, H.-R.; Wong, J. W.; Stoddart, J. F.; Zink, J. I. An Operational Supramolecular Nanovalve. *J. Am. Chem. Soc.* **2004**, *126*, 3370–3371.
(734) Nguyen, T. D.; Leung, K. C.-F.; Liong, M.; Liu, Y.; Stoddart, J. F.; Zink, J. I. Versatile Supramolecular Nanovalves Reconfigured for Light Activation. *Adv. Funct. Mater.* **2007**, *17*, 2101–2110.
(735) Nguyen, T. D.; Leung, K. C.-F.; Liong, M.; Pentecost, C. D.; Stoddart, J. F.; Zink, J. I. Construction of a pH-Driven Supramolecular Nanovalve. *Org. Lett.* **2006**, *8*, 3363–3366.
(736) Leung, K. C.-F.; Nguyen, T. D.; Stoddart, J. F.; Zink, J. I. Supramolecular Nanovalves Controlled by Proton Abstraction and Competitive Binding. *Chem. Mater.* **2006**, *18*, 5919–5928.
(737) Guo, W.; Wang, J.; Lee, S.-J.; Dong, F.; Park, S. S.; Ha, C.-S. A General pH-Responsive Supramolecular Nanovalve Based on Mesoporous Organosilica Hollow Nanospheres. *Chem. Eur. J.* **2010**, *16*, 8641–8646.
(738) Lee, S.-F.; Zhu, X.-M.; Wang, Y.-X. J.; Xuan, S.-H.; You, Q.; Chan, W.-H.; Wong, C.-H.; Wang, F.; Yu, J. C.; Cheng, C. H. K.; Leung, K. C.-F. Ultrasound, pH, and Magnetically Responsive Crown-Ether-Coated Core/Shell Nanoparticles as Drug Encapsulation and Release Systems. *ACS Appl. Mater. Interfaces* **2013**, *5*, 1566–1574.
(739) Angelos, S.; Yang, Y.-W.; Patel, K.; Stoddart, J. F.; Zink, J. I. pH-Responsive Supramolecular Nanovalves Based on Cucurbit[6]uril Pseudorotaxanes. *Angew. Chem., Int. Ed*. **2008**, *47*, 2222–2226.
(740) Khashab, N. M.; Belowich, M. E.; Trabolsi, A.; Friedman, D. C.; Valente, C.; Lau, Y.; Khatib, H. A.; Zink, J. I.; Stoddart, J. F. pH-Responsive Mechanised Nanoparticles Gated by Semirotaxanes. *Chem. Commun.* **2009**, 5371–5373.
(741) Khashab, N. M.; Trabolsi, A.; Lau, Y. A.; Ambrogio, M. W.; Friedman, D. C.; Khatib, H. A.; Zink, J. I.; Stoddart, J. F. Redox- and pH-Controlled Mechanized Nanoparticles. *Eur. J. Org. Chem.* **2009**, 1669–1673.
(742) Angelos, S.; Khashab, N. M.; Yang, Y.-W.; Trabolsi, A.; Khatib, H. A.; Stoddart, J. F.; Zink, J. I. pH Clock-Operated Mechanized Nanoparticles. *J. Am. Chem. Soc.* **2009**, *131*, 12912–12914.
(743) Angelos, S.; Yang, Y.-W.; Khashab, N. M.; Stoddart, J. F.; Zink, J. I. Dual-Controlled Nanoparticles Exhibiting and Logic. *J. Am. Chem. Soc.* **2009**, *131*, 11344–11346.
(744) Thomas, C. R.; Ferris, D. P.; Lee, J.-H.; Choi, E.; Cho, M. H.; Kim, E. S.; Stoddart, J. F.; Shin, J.-S.; Cheon, J.; Zink, J. I. Noninvasive Remote-Controlled Release of Drug Molecules in Vitro Using Magnetic Actuation of Mechanized Nanoparticles. *J. Am. Chem. Soc.* **2010**, *132*, 10623–10625.
(745) Liu, J.; Du, X. pH- and Competitor-Driven Nanovalves of Cucurbit[7]uril Pseudorotaxanes Based on Mesoporous Silica Supports for Controlled Release. *J. Mater. Chem.* **2010**, *20*, 3642–3649.
(746) Liu, J.; Du, X.; Zhang, X. Enzyme-Inspired Controlled Release of Cucurbit[7]uril Nanovalves by Using Magnetic Mesoporous Silica. *Chem. Eur. J.* **2011**, *17*, 810–815.
(747) Sun, Y.-L.; Yang, B.-J.; Zhang, S. X.-A.; Yang, Y.-W. Cucurbit[7]uril Pseudorotaxane-Based Photoresponsive Supramolecular Nanovalve. *Chem. Eur. J.* **2012**, *18*, 9212–9216.
(748) Croissant, J.; Zink, J. I. Nanovalve-Controlled Cargo Release Activated by Plasmonic Heating. *J. Am. Chem. Soc.* **2012**, *134*, 7628–7631.
(749) Chen, T.; Fu, J. J. pH-Responsive Nanovalves Based on Hollow Mesoporous Silica Spheres for Controlled Release of Corrosion Inhibitor. *Nanotechnology* **2012**, *23*, 235605.
(750) Chen, T.; Yang, N. W.; Fu, J. J. Controlled Release of Cargo Molecules From Hollow Mesoporous Silica Nanoparticles Based on Acid and Base Dual-Responsive Cucurbit[7]uril Pseudorotaxanes. *Chem. Commun.* **2013**, *49*, 6555–6557.
(751) Fu, J. J.; Chen, T.; Wang, M. D.; Yang, N. W.; Li, S. N.; Wang, Y.; Liu, X. D. Acid and Alkaline Dual Stimuli-Responsive Mechanized Hollow Mesoporous Silica Nanoparticles as Smart Nanocontainers for Intelligent Anticorrosion Coatings. *ACS Nano* **2013**, *7*, 11397–11408.
(752) Wang, M. D.; Chen, T.; Ding, C. D.; Fu, J. J. Mechanized Silica Nanoparticles Based on Reversible Bistable [2]Pseudorotaxanes as Supramolecular Nanovalves for Multistage pH-Controlled Release. *Chem. Commun.* **2014**, *50*, 5068–5071.
(753) Park, C.; Oh, K.; Lee, S. C.; Kim, C. Controlled Release of Guest Molecules From Mesoporous Silica Particles Based on a pH-Responsive Polypseudorotaxane Motif. *Angew. Chem., Int. Ed*. **2007**, *46*, 1455–1457.
(754) Du, L.; Liao, S.; Khatib, H. A.; Stoddart, J. F.; Zink, J. I. Controlled-Access Hollow Mechanized Silica Nanocontainers. *J. Am. Chem. Soc.* **2009**, *131*, 15136–15142.
(755) Ferris, D. P.; Zhao, Y.-L.; Khashab, N. M.; Khatib, H. A.; Stoddart, J. F.; Zink, J. I. Light-Operated Mechanized Nanoparticles. *J. Am. Chem. Soc.* **2009**, *131*, 1686–1688.
(756) Meng, H.; Xue, M.; Xia, T.; Zhao, Y.-L.; Tamanoi, F.; Stoddart, J. F.; Zink, J. I.; Nel, A. E. Autonomous in Vitro Anticancer Drug Release From Mesoporous Silica Nanoparticles by pH-Sensitive Nanovalves. *J. Am. Chem. Soc.* **2010**, *132*, 12690–12697.
(757) Zhao, Y.-L.; Li, Z.; Kabehie, S.; Botros, Y. Y.; Stoddart, J. F.; Zink, J. I. pH-Operated Nanopistons on the Surfaces of Mesoporous Silica Nanoparticles. *J. Am. Chem. Soc.* **2010**, *132*, 13016–13025.
(758) Li, Z.; Nyalosaso, J. L.; Hwang, A. A.; Ferris, D. P.; Yang, S.; Derrien, G.; Charnay, C.; Durand, J.-O.; Zink, J. I. Measurement of Uptake and Release Capacities of Mesoporous Silica Nanoparticles Enabled by Nanovalve Gates. *J. Phys. Chem. C* **2011**, *115*, 19496–19506.
(759) Gao, Y.; Ma, R.; An, Y.; Shi, L. Nanogated Vessel Based on Polypseudorotaxane-Capped Mesoporous Silica via a Highly Acid-Labile Benzoic-Imine Linker. *J. Control. Release* **2011**, *152*, e81–e82.
(760) Du, L.; Song, H.; Liao, S. A Biocompatible Drug Delivery Nanovalve System on the Surface of Mesoporous Nanoparticles. *Microporous Mesoporous Mater*. **2012**, *147*, 200–204.
(761) Xue, M.; Cao, D.; Stoddart, J. F.; Zink, J. I. Size-Selective pH-Operated Megagates on Mesoporous Silica Materials. *Nanoscale* **2012**, *4*, 7569–7574.
(762) Wang, C.; Li, Z.; Cao, D.; Zhao, Y.-L.; Gaines, J. W.; Bozdemir, O. A.; Ambrogio, M. W.; Frasconi, M.; Botros, Y. Y.; Zink, J. I.; Stoddart, J. F. Stimulated Release of Size-Selected Cargos in Succession From Mesoporous Silica Nanoparticles. *Angew. Chem., Int. Ed*. **2012**, *51*, 5460–5465.
(763) Clemens, D. L.; Lee, B.-Y.; Xue, M.; Thomas, C. R.; Meng, H.; Ferris, D.; Nel, A. E.; Zink, J. I.; Horwitz, M. A. Targeted

Intracellular Delivery of Antituberculosis Drugs to *Mycobacterium tuberculosis*-Infected Macrophages via Functionalized Mesoporous Silica Nanoparticles. *Antimicrob. Agents Chemother.* **2012**, *56*, 2535–2545.
(764) Dong, J.; Xue, M.; Zink, J. I. Functioning of Nanovalves on Polymer Coated Mesoporous Silica Nanoparticles. *Nanoscale* **2013**, *5*, 10300–10306.
(765) Díez, P.; Sánchez, A.; Gamella, M.; Martínez-Ruíz, P.; Aznar, E.; de la Torre, C.; Murguía, J. R.; Martínez-Máñez, R.; Villalonga, R.; Pingarrón, J. M. Toward the Design of Smart Delivery Systems Controlled by Integrated Enzyme-Based Biocomputing Ensembles. *J. Am. Chem. Soc.* **2014**, *136*, 9116–9123.
(766) Hwang, A. A.; Lu, J.; Tamanoi, F.; Zink, J. I. Functional Nanovalves on Protein-Coated Nanoparticles for in Vitro and in Vivo Controlled Drug Delivery. *Small* **2014**, *11*, 319–328.
(767) Guardado-Alvarez, T. M.; Russell, M. M.; Zink, J. I. Nanovalve Activation by Surface-Attached Photoacids. *Chem. Commun.* **2014**, *50*, 8388–8390.
(768) Li, Q.-L.; Wang, L.; Qiu, X.-L.; Sun, Y.-L.; Wang, P.-X.; Liu, Y.; Li, F.; Qi, A.-D.; Gao, H.; Yang, Y.-W. Stimuli-Responsive Biocompatible Nanovalves Based on β-Cyclodextrin Modified Poly(glycidyl methacrylate). *Polym. Chem.* **2014**, *5*, 3389–3395.
(769) Croissant, J.; Chaix, A.; Mongin, O.; Wang, M.; Clément, S.; Raehm, L.; Durand, J.-O.; Hugues, V.; Blanchard-Desce, M.; Maynadier, M.; Gallud, A.; Gary-Bobo, M.; Garcia, M.; Lu, J.; Tamanoi, F.; Ferris, D. P.; Tarn, D.; Zink, J. I. Two-Photon-Triggered Drug Delivery via Fluorescent Nanovalves. *Small* **2014**, *10*, 1752–1755.
(770) Wang, W.; Wen, Y.; Xu, L.; Du, H.; Zhou, Y.; Zhang, X. A Selective Release System Based on Dual-Drug-Loaded Mesoporous Silica for Nanoparticle-Assisted Combination Therapy. *Chem. Eur. J.* **2014**, *20*, 7796–7802.
(771) Zhou, S.; Sha, H.; Ke, X.; Liu, B.; Wang, X.; Du, X. Combination Drug Release of Smart Cyclodextrin-Gated Mesoporous Silica Nanovehicles. *Chem. Commun.* **2015**, *51*, 7203–7206.
(772) Li, Z.; Clemens, D. L.; Lee, B.-Y.; Dillon, B. J.; Horwitz, M. A.; Zink, J. I. Mesoporous Silica Nanoparticles with pH-Sensitive Nanovalves for Delivery of Moxifloxacin Provide Improved Treatment of Lethal Pneumonic Tularemia. *ACS Nano* **2015**, *9*, 10778–10789.
(773) Wang, T.; Sun, G.; Wang, M.; Zhou, B.; Fu, J. Voltage/pH-Driven Mechanized Silica Nanoparticles for the Multimodal Controlled Release of Drugs. *ACS Appl. Mater. Interfaces* **2015**, *7*, 21295–21304.
(774) Cui, L.; Zhang, F.; Wang, Q.; Lin, H.; Yang, C.; Zhang, T.; Tong, R.; An, N.; Qu, F. NIR Light Responsive Core-Shell Nanocontainers for Drug Delivery. *J. Mat. Chem. B* **2015**, *3*, 7046–7054.
(775) Sun, Y.-L.; Yang, Y.-W.; Chen, D.-X.; Wang, G.; Zhou, Y.; Wang, C.-Y.; Stoddart, J. F. Mechanized Silica Nanoparticles Based on Pillar[5]arenes for on-Command Cargo Release. *Small* **2013**, *9*, 3224–3229.
(776) Zhou, Y.; Tan, L.-L.; Li, Q.-L.; Qiu, X.-L.; Qi, A.-D.; Tao, Y.; Yang, Y.-W. Acetylcholine-Triggered Cargo Release From Supramolecular Nanovalves Based on Different Macrocyclic Receptors. *Chem. Eur. J.* **2014**, *20*, 2998–3004.
(777) Huang, X.; Du, X. Pillar[6]arene-Valved Mesoporous Silica Nanovehicles for Multiresponsive Controlled Release. *ACS Appl. Mater. Interfaces* **2014**, *6*, 20430–20436.
(778) Sun, Y.-L.; Zhou, Y.; Li, Q.-L.; Yang, Y.-W. Enzyme-Responsive Supramolecular Nanovalves Crafted by Mesoporous Silica Nanoparticles and Choline-Sulfonatocalix[4]arene [2]Pseudorotaxanes for Controlled Cargo Release. *Chem. Commun.* **2013**, *49*, 9033–9035.
(779) Li, H.; Tan, L.-L.; Jia, P.; Li, Q.-L.; Sun, Y.-L.; Zhang, J.; Ning, Y.-Q.; Yu, J.; Yang, Y.-W. Near-Infrared Light-Responsive Supramolecular Nanovalve Based on Mesoporous Silica-Coated Gold Nanorods. *Chem. Sci.* **2014**, *5*, 2804–2808.
(780) Zhou, Y.; Li, H.; Yang, Y.-W. Controlled Drug Delivery Systems Based on Calixarenes. *Chin. Chem. Lett.* **2015**, *26*, 825–828.
(781) Raju, M. V. R.; Lin, H.-C. A Cyanide-Responsive Supramolecular Nanovalve Based on Pd(II)-Templated Pseudo-Rotaxane. *J. Mater. Chem. A* **2015**, *3*, 6414–6422.
(782) Xiao, Y.; Wang, T.; Cao, Y.; Wang, X.; Zhang, Y.; Liu, Y.; Huo, Q. Enzyme and Voltage Stimuli-Responsive Controlled Release System Based on β-Cyclodextrin-Capped Mesoporous Silica Nanoparticles. *Dalton Trans.* **2015**, *44*, 4355–4361.
(783) Schlossbauer, A.; Kecht, J.; Bein, T. Biotin-Avidin as a Protease-Responsive Cap System for Controlled Guest Release From Colloidal Mesoporous Silica. *Angew. Chem., Int. Ed*. **2009**, *48*, 3092–3095.
(784) Higashi, T.; Motoyama, K.; Arima, H. Cyclodextrin-Based Polyrotaxanes and Polypseudorotaxanes as Drug Delivery Carriers. *J. Drug. Del. Sci. Tech.* **2013**, *23*, 523–529.
(785) Ornelas-Megiatto, C.; Becher, T. B.; Megiatto, J. D. Interlocked Systems in Nanomedicine. *Curr. Top. Med. Chem.* **2015**, *15*, 1236–1256.
(786) Pairault, N.; Barat, R.; Tranoy-Opalinski, I.; Renoux, B.; Thomas, M.; Papot, S. Rotaxane-Based Architectures for Biological Applications. *Compt. Rend. Chim.* **2016**, *19*, 103–112.
(787) Yui, N.; Ooya, T. Molecular Mobility of Interlocked Structures Exploiting New Functions of Advanced Biomaterials. *Chem. Eur. J.* **2006**, *12*, 6730–6737.
(788) Yui, N.; Katoono, R.; Yamashita, A. Functional Cyclodextrin Polyrotaxanes for Drug Delivery. *Adv. Polym. Sci.* **2009**, *222*, 55–77.
(789) Tamura, A.; Yui, N. Threaded Macromolecules as a Versatile Framework for Biomaterials. *Chem. Commun.* **2014**, *50*, 13433–13446.
(790) Ooya, T.; Mori, H.; Terano, M.; Yui, N. Synthesis of a Biodegradable Polymeric Supramolecular Assembly for Drug Delivery. *Macromol. Rapid Comm.* **1995**, *16*, 259–263.
(791) Ooya, T.; Yui, N. Synthesis and Characterization of Biodegradable Polyrotaxane as a Novel Supramolecular-Structured Drug Carrier. *J. Biomater. Sci. Polym. Ed.* **1997**, *8*, 437–455.
(792) Kamimura, W.; Ooya, T.; Yui, N. Interaction of Supramolecular Assembly with Hairless Rat Stratum Corneum. *J. Control. Release* **1997**, *44*, 295–299.
(793) Ooya, T.; Sugawara, H.; Yui, N. Interaction of Supramolecular-Structured Polyrotaxanes with Hairless Rat Stratum Corneum and Its Effect on Indomethacin Permeation. *Drug Delivery Systems* **1997**, *12*, 89–94.
(794) Yui, N.; Ooya, T.; Kumeno, T. Effect of Biodegradable Polyrotaxanes on Platelet Activation. *Bioconjugate Chem.* **1998**, *9*, 118–125.
(795) Ooya, T.; Yui, N. Synthesis of Theophylline-Polyrotaxane Conjugates and Their Drug Release via Supramolecular Dissociation. *J. Control. Release* **1999**, *58*, 251–269.
(796) Yui, N.; Ooya, T.; Kawashima, T.; Saito, Y.; Tamai, I.; Sai, Y.; Tsuji, A. Inhibitory Effect of Supramolecular Polyrotaxane−Dipeptide Conjugates on Digested Peptide Uptake via Intestinal Human Peptide Transporter. *Bioconjugate Chem.* **2002**, *13*, 582–587.
(797) Ooya, T.; Kawashima, T.; Yui, N. Synthesis of Polyrotaxane-Biotin Conjugates and Surface Plasmon Resonance Analysis of Streptavidin Recognition. *Biotechnol. Bioprocess Eng.* **2001**, *6*, 293–300.
(798) Ooya, T.; Yui, N. Multivalent Interactions Between Biotin-Polyrotaxane Conjugates and Streptavidin as a Model of New Targeting for Transporters. *J. Control. Release* **2002**, *80*, 219–228.
(799) Ooya, T.; Eguchi, M.; Ozaki, A.; Yui, N. Carboxyethylester-Polyrotaxanes as a New Calcium Chelating Polymer: Synthesis, Calcium Binding and Mechanism of Trypsin Inhibition. *Int. J. Pharm.* **2002**, *242*, 47–54.

(800) Eguchi, M.; Ooya, T.; Yui, N. Controlling the Mechanism of Trypsin Inhibition by the Numbers of α-Cyclodextrins and Carboxyl Groups in Carboxyethylester-Polyrotaxanes. *J. Control. Release* **2004**, *96*, 301–307.
(801) Ooya, T.; Arizono, K.; Yui, N. Synthesis and Characterization of an Oligopeptide-Terminated Polyrotaxane as a Drug Carrier. *Polym. Adv. Technol.* **2000**, *11*, 642–651.
(802) Ooya, T.; Eguchi, M.; Yui, N. Enhanced Accessibility of Peptide Substrate Toward Membrane-Bound Metalloexopeptidase by Supramolecular Structure of Polyrotaxane. *Biomacromolecules* **2001**, *2*, 200–203.
(803) Ooya, T.; Eguchi, M.; Yui, N. Supramolecular Design for Multivalent Interaction: Maltose Mobility Along Polyrotaxane Enhanced Binding with Concanavalin A. *J. Am. Chem. Soc.* **2003**, *125*, 13016–13017.
(804) Ooya, T.; Utsunomiya, H.; Eguchi, M.; Yui, N. Rapid Binding of Concanavalin a and Maltose−Polyrotaxane Conjugates Due to Mobile Motion of α-Cyclodextrins Threaded Onto a Poly(ethylene glycol). *Bioconjugate Chem.* **2005**, *16*, 62–69.
(805) Hirose, H.; Sano, H.; Mizutani, G.; Eguchi, M.; Ooya, T.; Yui, N. Effect of the Mobility of Ligands in Polyrotaxanes on Order Structure of Water Clusters. *Langmuir* **2004**, *20*, 2852–2854.
(806) Hirose, H.; Sano, H.; Mizutani, G.; Eguchi, M.; Ooya, T.; Yui, N. Providing Natural Water Structure Surrounding Highly Mobile Maltose Groups Conjugated with Polyrotaxanes. *Polym J* **2006**, *38*, 1093–1097.
(807) Yamada, Y.; Nomura, T.; Harashima, H.; Yamashita, A.; Katoono, R.; Yui, N. Intranuclear DNA Release Is a Determinant of Transfection Activity for a Non-Viral Vector: Biocleavable Polyrotaxane as a Supramolecularly Dissociative Condenser for Efficient Intranuclear DNA Release. *Biol. Pharm. Bull.* **2010**, *33*, 1218–1222.
(808) Tamura, A.; Ikeda, G.; Seo, J.-H.; Tsuchiya, K.; Yajima, H.; Sasaki, Y.; Akiyoshi, K.; Yui, N. Molecular Logistics Using Cytocleavable Polyrotaxanes for the Reactivation of Enzymes Delivered in Living Cells. *Sci. Rep.* **2013**, *3*: 2252.
(809) Tamura, A.; Yui, N. A Supramolecular Endosomal Escape Approach for Enhancing Gene Silencing of siRNA Using Acid-Degradable Cationic Polyrotaxanes. *J. Mater. Chem. B* **2013**, *1*, 3535–3544.
(810) Tamura, A.; Ikeda, G.; Nishida, K.; Yui, N. Cationic Polyrotaxanes as a Feasible Framework for the Intracellular Delivery and Sustainable Activity of Anionic Enzymes: a Comparison Study with Methacrylate-Based Polycations. *Macromol. Biosci.* **2015**, *15*, 1134–1145.
(811) Utsunomiya, H.; Katoono, R.; Yui, N.; Sugiura, T.; Kubo, Y.; Kato, Y.; Tsuji, A. Cationic Polyrotaxanes Effectively Inhibit Uptake via Carnitine/Organic Cationic Transporters Without Cytotoxicity. *Macromol. Biosci.* **2008**, *8*, 665–669.
(812) Ooya, T.; Choi, H. S.; Yamashita, A.; Yui, N.; Sugaya, Y.; Kano, A.; Maruyama, A.; Akita, H.; Ito, R.; Kogure, K.; Harashima, H. Biocleavable Polyrotaxane−Plasmid DNA Polyplex for Enhanced Gene Delivery. *J. Am. Chem. Soc.* **2006**, *128*, 3852–3853.
(813) Yamashita, A.; Yui, N.; Ooya, T.; Kano, A.; Maruyama, A.; Akita, H.; Kogure, K.; Harashima, H. Synthesis of a Biocleavable Polyrotaxane-Plasmid DNA (pDNA) Polyplex and Its Use for the Rapid Nonviral Delivery of pDNA to Cell Nuclei. *Nature Protoc.* **2006**, *1*, 2861–2869.
(814) Yamashita, A.; Kanda, D.; Katoono, R.; Yui, N.; Ooya, T.; Maruyama, A.; Akita, H.; Kogure, K.; Harashima, H. Supramolecular Control of Polyplex Dissociation and Cell Transfection: Efficacy of Amino Groups and Threading Cyclodextrins in Biocleavable Polyrotaxanes. *J. Control. Release* **2008**, *131*, 137–144.
(815) Yamada, Y.; Hashida, M.; Nomura, T.; Harashima, H.; Yamasaki, Y.; Kataoka, K.; Yamashita, A.; Katoono, R.; Yui, N. Different Mechanisms for Nanoparticle Formation Between pDNA and siRNA Using Polyrotaxane as the Polycation. *ChemPhysChem* **2012**, *13*, 1161–1165.
(816) Yamada, Y.; Nomura, T.; Harashima, H.; Yamashita, A.; Yui, N. Post-Nuclear Gene Delivery Events for Transgene Expression by Biocleavable Polyrotaxanes. *Biomaterials* **2012**, *33*, 3952–3958.
(817) Tamura, A.; Yui, N. Cellular Internalization and Gene Silencing of siRNA Polyplexes by Cytocleavable Cationic Polyrotaxanes with Tailored Rigid Backbones. *Biomaterials* **2013**, *34*, 2480–2491.
(818) Kulkarni, A.; DeFrees, K.; Schuldt, R. A.; Hyun, S.-H.; Wright, K. J.; Yerneni, C. K.; VerHeul, R.; Thompson, D. H. Cationic α-Cyclodextrin:Poly(ethylene glycol) Polyrotaxanes for siRNA Delivery. *Mol. Pharmaceutics* **2013**, *10*, 1299–1305.
(819) Huang, H.; Cao, D.; Qin, L.; Tian, S.; Liang, Y.; Pan, S.; Feng, M. Dilution-Stable PAMAM G1-Grafted Polyrotaxane Supermolecules Deliver Gene Into Cells Through a Caveolae-Dependent Pathway. *Mol. Pharmaceutics* **2014**, *11*, 2323–2333.
(820) Li, J.; Yang, C.; Li, H.; Wang, X.; Goh, S. H.; Ding, J. L.; Wang, D. Y.; Leong, K. W. Cationic Supramolecules Composed of Multiple Oligoethylenimine-Grafted β-Cyclodextrins Threaded on a Polymer Chain for Efficient Gene Delivery. *Adv. Mater.* **2006**, *18*, 2969–2974.
(821) Yang, C.; Wang, X.; Li, H.; Tan, E.; Lim, C. T.; Li, J. Cationic Polyrotaxanes as Gene Carriers: Physicochemical Properties and Real-Time Observation of DNA Complexation, and Gene Transfection in Cancer Cells. *J. Phys. Chem. B* **2009**, *113*, 7903–7911.
(822) Yang, C.; Li, H.; Wang, X.; Li, J. Cationic Supramolecules Consisting of Oligoethylenimine- Grafted α-Cyclodextrins Threaded on Poly(ethylene oxide) for Gene Delivery. *J. Biomed. Mater. Res. A* **2009**, *89A*, 13–23.
(823) Zhou, Y.; Wang, H.; Wang, C.; Li, Y.; Lu, W.; Chen, S.; Luo, J.; Jiang, Y.; Chen, J. Receptor-Mediated, Tumor-Targeted Gene Delivery Using Folate-Terminated Polyrotaxanes. *Mol. Pharmaceutics* **2012**, *9*, 1067–1076.
(824) Albuzat, T.; Keil, M.; Ellis, J.; Alexander, C.; Wenz, G. Transfection of Luciferase DNA Into Various Cells by Cationic Cyclodextrin Polyrotaxanes Derived From Ionene-11. *J. Mater. Chem.* **2012**, *22*, 8558–8565.
(825) Moon, C.; Kwon, Y. M.; Lee, W. K.; Park, Y. J.; Yang, V. C. *In Vitro* Assessment of a Novel Polyrotaxane-Based Drug Delivery System Integrated with a Cell-Penetrating Peptide. *J. Control. Release* **2007**, *124*, 43–50.
(826) Jiang, R.-J.; Yang, B.; Liu, Z.-K.; Zhao, Y.-L.; Liao, X.-L.; Yang, J.; Gao, C.-Z.; Wang, F.; Han, B.. A Novel Polyrotaxane-Based Delivery System for Scutellarin: Preparation, Characterization, and in Vitro Evaluation. *Carbohyd. Res.* **2013**, *380*, 149–155.
(827) Yu, S.; Zhang, Y.; Wang, X.; Zhen, X.; Zhang, Z.; Wu, W.; Jiang, X. Synthesis of Paclitaxel-Conjugated β-Cyclodextrin Polyrotaxane and Its Antitumor Activity. *Angew. Chem., Int. Ed*. **2013**, *52*, 7272–7277.
(828) Gong, X.-S.; Jiang, R.-J.; Liao, X.-L.; Xie, H.-D.; Ma, X.; Gao, C.-Z.; Yang, B.; Zhao, Y.-L. Synthesis, Characterization and in Vitro Evaluation of a Series of Novel Polyrotaxane-Based Delivery System for Artesunate. *Carbohyd. Res.* **2015**, *412*, 7–14.
(829) Mondjinou, Y. A.; McCauliff, L. A.; Kulkarni, A.; Paul, L.; Hyun, S.-H.; Zhang, Z.; Wu, Z.; Wirth, M.; Storch, J.; Thompson, D. H. Synthesis of 2-Hydroxypropyl-β-Cyclodextrin/Pluronic-Based Polyrotaxanes via Heterogeneous Reaction as Potential Niemann-Pick Type C Therapeutics. *Biomacromolecules* **2013**, *14*, 4189–4197.
(830) Mondjinou, Y. A.; Hyun, S.-H.; Xiong, M.; Collins, C. J.; Thong, P. L.; Thompson, D. H. Impact of Mixed β-Cyclodextrin Ratios on Pluronic Rotaxanation Efficiency and Product Solubility. *ACS Appl. Mater. Interfaces* **2015**, *7*, 23831–23836.
(831) Zhang, X.; Zhu, X.; Ke, F.; Ye, L.; Chen, E.-Q.; Zhang, A.-Y.; Feng, Z.-G. Preparation and Self-Assembly of Amphiphilic Triblock Copolymers with Polyrotaxane as a Middle Block and

Their Application as Carrier for the Controlled Release of Amphotericin B. *Polymer* **2009**, *50*, 4343–4351.
(832) Adeli, M.; Sarabi, R. S.; Yadollahi Farsi, R.; Mahmoudi, M.; Kalantari, M. Polyrotaxane/Gold Nanoparticle Hybrid Nanomaterials as Anticancer Drug Delivery Systems. *J. Mater. Chem.* **2011**, *21*, 18686–18695.
(833) He, B.; Liu, R.; Lai, Y.; He, B.; Li, Y.; Wang, G.; Chang, S.; Gu, Z. Supramolecular Nanoparticles Generated by the Self-Assembly of Polyrotaxanes for Antitumor Drug Delivery. *Int. J. Nanomedicine* **2012**, *7*, 5249–5258.
(834) Jiang, L.; Gao, Z.-M.; Ye, L.; Zhang, A.-Y.; Feng, Z.-G. A pH-Sensitive Nano Drug Delivery System of Doxorubicin-Conjugated Amphiphilic Polyrotaxane-Based Block Copolymers. *Biomater. Sci.* **2013**, *1*, 1282–1291.
(835) Jiang, L.; Gao, Z.-M.; Ye, L.; Zhang, A.-Y.; Feng, Z.-G. A Tumor-Targeting Nano Doxorubicin Delivery System Built From Amphiphilic Polyrotaxane-Based Block Copolymers. *Polymer* **2013**, *54*, 5188–5198.
(836) Ye, L.; Liu, X.; Ito, K.; Feng, Z. The Preparation of an Azo-Substituted Polyrotaxane End-Capped with PNIPPAAm and Its Dual Stimuli-Responsive Behavior for Drug Delivery Applications. *J. Mat. Chem. B* **2014**, *2*, 5746–5757.
(837) Tardy, B. L.; Dam, H. H.; Kamphuis, M. M. J.; Richardson, J. J.; Caruso, F. Self-Assembled Stimuli-Responsive Polyrotaxane Core–Shell Particles. *Biomacromolecules* **2014**, *15*, 53–59.
(838) Pradal, C.; Grøndahl, L.; Cooper-White, J. J. Hydrolytically Degradable Polyrotaxane Hydrogels for Drug and Cell Delivery Applications. *Biomacromolecules* **2015**, *16*, 389–403.
(839) Dam, H. H.; Caruso, F. Construction and Degradation of Polyrotaxane Multilayers. *Adv. Mater.* **2011**, *23*, 3026–3029.
(840) Dam, H. H.; Caruso, F. Modular Click Assembly of Degradable Capsules Using Polyrotaxanes. *ACS Nano* **2012**, *6*, 4686–4693.
(841) Dam, H. H.; Caruso, F. Formation and Degradation of Layer-by-Layer-Assembled Polyelectrolyte Polyrotaxane Capsules. *Langmuir* **2013**, *29*, 7203–7208.
(842) Dvornikovs, V.; House, B. E.; Kaetzel, M.; Dedman, J. R.; Smithrud, D. B. Host–[2]Rotaxanes as Cellular Transport Agents. *J. Am. Chem. Soc.* **2003**, *125*, 8290–8301.
(843) Smukste, I.; Smithrud, D. B. Structure−Function Relationship of Amino Acid−[2]Rotaxanes. *J. Org. Chem.* **2003**, *68*, 2547–2558.
(844) Bao, X.; Isaacsohn, I.; Drew, A. F.; Smithrud, D. B. Determining the Intracellular Transport Mechanism of a Cleft−[2]Rotaxane. *J. Am. Chem. Soc.* **2006**, *128*, 12229–12238.
(845) Zhu, J.; Smithrud, D. B. Host-Rotaxanes Model Proteins That Promote Ligand Association Through a Favorable Change in Configurational Entropy. *Org. Biomol. Chem.* **2007**, *5*, 2992–2299.
(846) Wang, X.; Bao, X.; McFarland-Mancini, M.; Isaacsohn, I.; Drew, A. F.; Smithrud, D. B. Investigation of the Intracellular Delivery of Fluoresceinated Peptides by a Host-[2]Rotaxane. *J. Am. Chem. Soc.* **2007**, *129*, 7284–7293.
(847) Wang, X.; Zhu, J.; Smithrud, D. B. Synthesis and Investigation of Host-[2]Rotaxanes That Bind Metal Cations. *J. Org. Chem.* **2010**, *75*, 3358–3370.
(848) Smithrud, D. B.; Wang, X.; Tarapore, P.; Ho, S.-M. Crown Ether Host-Rotaxanes as Cytotoxic Agents. *ACS Med. Chem. Lett.* **2013**, *4*, 27–31.
(849) Shi, J.; Xu, Y.; Wang, X.; Zhang, L.; Zhu, J.; Pang, T.; Bao, X. Synthesis and Evaluation of a Novel Rhodamine B Pyrene [2]Rotaxane as an Intracellular Delivery Agent for Doxorubicin. *Org. Biomol. Chem.* **2015**, *13*, 7517–7529.
(850) Kimura, M.; Makio, K.; Hara, K.; Hiruma, W.; Fujita, Y.; Takata, T.; Nishio, K.; Ono, N. A Supramolecular Substance, [2]Rotaxane, Induces Apoptosis in Human Molt-3 Acute Lymphoblastic Leukemia Cells. *Drug Res.* **2015**, *65*, 614–616.
(851) Fernandes, A.; Viterisi, A.; Coutrot, F.; Potok, S.; Leigh, D. A.; Aucagne, V.; Papot, S. Rotaxane-Based Propeptides: Protection and Enzymatic Release of a Bioactive Pentapeptide. *Angew. Chem., Int. Ed*. **2009**, *48*, 6443–6447.
(852) Fernandes, A.; Viterisi, A.; Aucagne, V.; Leigh, D. A.; Papot, S. Second Generation Specific-Enzyme-Activated Rotaxane Propeptides. *Chem. Commun.* **2012**, *48*, 2083–2085.
(853) Barat, R.; Legigan, T.; Tranoy-Opalinski, I.; Renoux, B.; Peraudeau, E.; Clarhaut, J.; Poinot, P.; Fernandes, A. E.; Aucagne, V.; Leigh, D. A.; Papot, S. A Mechanically Interlocked Molecular System Programmed for the Delivery of an Anticancer Drug. *Chem. Sci.* **2015**, *6*, 2608–2613.
(854) Johnson, J. R.; Fu, N.; Arunkumar, E.; Leevy, W. M.; Gammon, S. T.; Piwnica-Worms, D.; Smith, B. D. Squaraine Rotaxanes: Superior Substitutes for Cy-5 in Molecular Probes for Near-Infrared Fluorescence Cell Imaging. *Angew. Chem., Int. Ed*. **2007**, *46*, 5528–5531.
(855) Gassensmith, J. J.; Baumes, J. M.; Smith, B. D. Discovery and Early Development of Squaraine Rotaxanes. *Chem. Commun.* **2009**, 6329–6338.
(856) Baumes, J. M.; Gassensmith, J. J.; Giblin, J.; Lee, J.-J.; White, A. G.; Culligan, W. J.; Leevy, W. M.; Kuno, M.; Smith, B. D. Storable, Thermally Activated, Near-Infrared Chemiluminescent Dyes and Dye-Stained Microparticles for Optical Imaging. *Nature Chem.* **2010**, *2*, 1025–1030.
(857) Lee, J.-J.; White, A. G.; Baumes, J. M.; Smith, B. D. Microwave-Assisted Slipping Synthesis of Fluorescent Squaraine Rotaxane Probe for Bacterial Imaging. *Chem. Commun.* **2010**, *46*, 1068–1069.
(858) Lee, J.-J.; Gonçalves, A.; Smith, B. A.; Palumbo, R.; White, A. G.; Smith, B. D. Singlet Oxygen Release and Cell Toxicity of a Chemiluminescent Squaraine Rotaxane Dye: Implications for Molecular Imaging. *Aust. J. Chem.* **2011**, *64*, 604–610.
(859) Cole, E. L.; Arunkumar, E.; Xiao, S.; Smith, B. A.; Smith, B. D. Water-Soluble, Deep-Red Fluorescent Squaraine Rotaxanes. *Org. Biomol. Chem.* **2012**, *10*, 5769–5773.
(860) Smith, B. A.; Xie, B.-W.; van Beek, E. R.; Que, I.; Blankevoort, V.; Xiao, S.; Cole, E. L.; Hoehn, M.; Kaijzel, E. L.; Löwik, C. W. G. M.; Smith, B. D. Multicolor Fluorescence Imaging of Traumatic Brain Injury in a Cryolesion Mouse Model. *ACS Chem. Neurosci.* **2012**, *3*, 530–537.
(861) Lee, J.-J.; White, A. G.; Rice, D. R.; Smith, B. D. *In Vivo* Imaging Using Polymeric Nanoparticles Stained with Near-Infrared Chemiluminescent and Fluorescent Squaraine Catenane Endoperoxide. *Chem. Commun.* **2013**, *49*, 3016–3018.
(862) Guha, S.; Shaw, G. K.; Mitcham, T. M.; Bouchard, R. R.; Smith, B. D. Croconaine Rotaxane for Acid Activated Photothermal Heating and Ratiometric Photoacoustic Imaging of Acidic pH. *Chem. Commun.* **2016**, *52*, 120–123.
(863) Arunkumar, E.; Forbes, C. C.; Noll, B. C.; Smith, B. D. Squaraine-Derived Rotaxanes: Sterically Protected Fluorescent Near-IR Dyes. *J. Am. Chem. Soc.* **2005**, *127*, 3288–3289.
(864) Arunkumar, E.; Forbes, C. C.; Smith, B. D. Improving the Properties of Organic Dyes by Molecular Encapsulation. *Eur. J. Org. Chem.* **2005**, 4051–4059.
(865) Finbloom, J. A.; Slack, C. C.; Bruns, C. J.; Jeong, K.; Wemmer, D. E.; Pines, A.; Francis, M. B. Rotaxane-Mediated Suppression and Activation of Cucurbit[6]uril for Molecular Detection by ^{129}Xe hyperCEST NMR. *Chem. Commun.* **2016**, *52*, 3119–3122.
(866) Slack, C. C.; Finbloom, J. A.; Jeong, K.; Bruns, C. J.; Wemmer, D. E.; Pines, A.; Francis, M. B. Rotaxane Probes for Protease Detection by ^{129}Xe hyperCEST NMR. *Submitted* **2016**.
(867) Schröder, L.; Lowery, T. J.; Hilty, C.; Wemmer, D. E.; Pines, A. Molecular Imaging Using a Targeted Magnetic Resonance Hyperpolarized Biosensor. *Science* **2006**, *314*, 446–449.
(868) Wang, Y.; Dmochowski, I. J. Cucurbit[6]uril Is an Ultrasensitive ^{129}Xe NMR Contrast Agent. *Chem. Commun.* **2015**, *51*, 8982–8985.

(869) Yu, G.; Wu, D.; Li, Y.; Zhang, Z.; Shao, L.; Zhou, J.; Hu, Q.; Tang, G.; Huang, F. A Pillar[5]arene-Based [2]Rotaxane Lights Up Mitochondria. *Chem. Sci.* **2016**, *7*, 3017–3024
(870) Alexander, S. Adsorption of Chain Molecules with a Polar Head a Scaling Description. *J. Phys. France* **1977**, *38*, 983–987.
(871) Iwaso, K.; Takashima, Y.; Harada, A. Fast Response Dry-Type Supramolecular Artificial Muscles with [*c*2]Daisy Chains. *Nature Chem*. **2016**, *8*, 625–632
(872) Aviram, A.; Ratner, M. A. Molecular Rectifiers. *Chem. Phys. Lett*. **1974**, *29*, 277–283.
(873) de Silva, A. P. *Molecular Logic-Based Computation*; Royal Society of Chemistry: Cambridge, **2012**.
(874) Aviram, A. Molecules for Memory, Logic, and Amplification. *J. Am. Chem. Soc.* **1988**, *110*, 5687–5692.
(875) de Silva, A. P.; Gunaratne, N. H. Q.; McCoy, C. P. A Molecular Photoionic and Gate Based on Fluorescent Signalling. *Nature* **1993**, *364*, 42–44.
(876) Pease, A. R.; Stoddart, J. F. Computing at the Molecular Level. *Struct. Bond.* **2001**, *99*, 189–236.
(877) Credi, A.; Balzani, V.; Langford, S. J.; Stoddart, J. F. Logic Operations at the Molecular Level. An XOR Gate Based on a Molecular Machine. *J. Am. Chem. Soc.* **1997**, *119*, 2679–2681.
(878) Wong, W.-Y.; Leung, K. C.-F.; Stoddart, J. F. Self-Assembly, Stability Quantification, Controlled Molecular Switching, and Sensing Properties of an Anthracene-Containing Dynamic [2]Rotaxane. *Org. Biomol. Chem.* **2010**, *8*, 2332–2343.
(879) Lohmann, F.; Weigandt, J.; Valero, J.; Famulok, M. Logic Gating by Macrocycle Displacement Using a Double-Stranded DNA [3]Rotaxane Shuttle. *Angew. Chem., Int. Ed*. **2014**, *53*, 10372–10376.
(880) Li, T.; Lohmann, F.; Famulok, M. Interlocked DNA Nanostructures Controlled by a Reversible Logic Circuit. *Nature Commun*. **2014**, *5*: 5940.
(881) Heath, J. R. Wires, Switches, and Wiring. A Route Toward a Chemically Assembled Electronic Nanocomputer. *Pure Appl. Chem*. **2000**, *72*, 11–20.
(882) Coskun, A.; Friedman, D. C.; Li, H.; Patel, K.; Khatib, H. A.; Stoddart, J. F. A Light-Gated STOP-GO Molecular Shuttle. *J. Am. Chem. Soc.* **2009**, *131*, 2493–2495.
(883) Coutrot, F.; Busseron, E. Controlling the Chair Conformation of a Mannopyranose in a Large-Amplitude [2]Rotaxane Molecular Machine. *Chem. Eur. J.* **2009**, *15*, 5186–5190.
(884) Zhou, W.; Xu, J.; Zheng, H.; Yin, X.; Zuo, Z.; Liu, H.; Li, Y. Distinct Nanostructures From a Molecular Shuttle: Effects of Shuttling Movement on Nanostructural Morphologies. *Adv. Funct. Mater.* **2009**, *19*, 141–149.
(885) Seo, J.-H.; Fushimi, M.; Matsui, N.; Takagaki, T.; Tagami, J.; Yui, N. UV-Cleavable Polyrotaxane Cross-Linker for Modulating Mechanical Strength of Photocurable Resin Plastics. *ACS Macro Lett.* **2015**, *4*, 1154–1157.
(886) Blanco, V.; Leigh, D. A.; Marcos, V. Artificial Switchable Catalysts. *Chem. Soc. Rev*. **2015**, *44*, 5341–5370.
(887) Pan, T.; Liu, J. Catalysts Encapsulated in Molecular Machines. *ChemPhysChem* **2016**, *17*, 1752–1758.
(888) Leigh, D. A.; Marcos, V.; Wilson, M. R. Rotaxane Catalysts. *ACS Catal*. **2014**, *4*, 4490–4497.
(889) Blanco, V.; Carlone, A.; Hänni, K. D.; Leigh, D. A.; Lewandowski, B. A Rotaxane-Based Switchable Organocatalyst. *Angew. Chem., Int. Ed*. **2012**, *51*, 5166–5169.
(890) Blanco, V.; Leigh, D. A.; Lewandowska, U.; Lewandowski, B.; Marcos, V. Exploring the Activation Modes of a Rotaxane-Based Switchable Organocatalyst. *J. Am. Chem. Soc.* **2014**, *136*, 15775–15780.
(891) Blanco, V.; Leigh, D. A.; Marcos, V.; Morales-Serna, J. A.; Nussbaumer, A. L. A Switchable [2]Rotaxane Asymmetric Organocatalyst That Utilizes an Acyclic Chiral Secondary Amine. *J. Am. Chem. Soc.* **2014**, *136*, 4905–4908.
(892) Beswick, J.; Blanco, V.; De Bo, G.; Leigh, D. A.; Lewandowska, U.; Lewandowski, B.; Mishiro, K. Selecting Reactions and Reactants Using a Switchable Rotaxane Organocatalyst with Two Different Active Sites. *Chem. Sci.* **2015**, *6*, 140–143.
(893) Reimann, P. Brownian Motors: Noisy Transport Far From Equilibrium. *Phys. Rep.* **2002**, *361*, 57–265.
(894) von Smoluchowski, M. Experimentell Nachweisbare, Der Üblichen Thermodynamik Widersprechende Molekular Phänomene. *Phys. Zeitschrift*, **1912**, *XIII*, 1069–1080.
(895) Feynman, R. P.; Leighton, R. B.; Sands, M. *The Feynman Lectures on Physics*; 2013 ed.; Basic Books: New York, 1963.
(896) Maxwell, J. C. *Theory of Heat*; Dover Publications, **1871**.
(897) Szilard, L. On the Decrease of Entropy in a Thermodynamic System by the Intervention of Intelligent Beings. *Zeitschrift für Physik* **1929**, *53*, 840–856.
(898) Reimann, P.; Bartussek, R.; Häussler, R.; Hanggi, P. Brownian Motors Driven by Temperature Oscillations. *Phys. Lett. A* **1996**, *215*, 26–31.
(899) Astumian, R. D. Thermodynamics and Kinetics of a Brownian Motor. *Science* **1997**, *276*, 917–922.
(900) Astumian, R. D.; Robertson, B. Imposed Oscillations of Kinetic Barriers Can Cause an Enzyme to Drive a Chemical Reaction Away From Equilibrium. *J. Am. Chem. Soc.* **1993**, *115*, 11063–11068.
(901) Astumian, R. D. Stochastic Conformational Pumping: A Mechanism for Free-Energy Transduction by Molecules. *Annu. Rev. Biophys.* **2011**, *40*, 289–313.
(902) Abou-Hamdan, A.; Bugnon, P.; Saudan, C.; Lye, P. G.; Merbach, A. E. High-Pressure Studies as a Novel Approach in Determining Inclusion Mechanisms: Thermodynamics and Kinetics of the Host−Guest Interactions for α-Cyclodextrin Complexes. *J. Am. Chem. Soc.* **2000**, *122*, 592–602.
(903) Buston, J. E. H.; Young, J. R.; Anderson, H. L. Rotaxane-Encapsulated Cyanine Dyes: Enhanced Fluorescence Efficiency and Photostability. *Chem. Commun.* **2000**, *905–906*.
(904) Craig, M. R.; Hutchings, M. G.; Claridge, T. D. W.; Anderson, H. L. Rotaxane-Encapsulation Enhances the Stability of an Azo Dye, in Solution and When Bonded to Cellulose. *Angew. Chem., Int. Ed*. **2001**, *40*, 1071–1074.
(905) Park, J. W.; Song, H. J. Isomeric [2]Rotaxanes and Unidirectional [2]Pseudorotaxane Composed of α-Cyclodextrin and Aliphatic Chain-Linked Carbazole-Viologen Compounds. *Org. Lett.* **2004**, *6*, 4869–4872.
(906) Oshikiri, T.; Takashima, Y.; Yamaguchi, H.; Harada, A. Kinetic Control of Threading of Cyclodextrins Onto Axle Molecules. *J. Am. Chem. Soc.* **2005**, *127*, 12186–12187.
(907) Wang, Q.-C.; Ma, X.; Qu, D.-H.; Tian, H. Unidirectional Threading Synthesis of Isomer-Free [2]Rotaxanes. *Chem. Eur. J.* **2006**, *12*, 1088–1096.
(908) Yamaguchi, H.; Oshikiri, T.; Harada, A. Rotaxanes with Unidirectional Cyclodextrin Array. *J. Phys. Condens. Matter* **2006**, *18*, S1809–S1816.
(909) Tomatsu, I.; Hashidzume, A.; Harada, A. Cyclodextrin-Based Side-Chain Polyrotaxane with Unidirectional Inclusion in Aqueous Media. *Angew. Chem., Int. Ed*. **2006**, *45*, 4605–4608.
(910) Park, J. W.; Song, H. J.; Chang, H.-J. Unidirectional α-Cyclodextrin-Based [2]Rotaxanes Bearing Viologen Unit on Axle. *Tetrahedron Lett.* **2006**, *47*, 3831–3834.
(911) Cheetham, A. G.; Hutchings, M. G.; Claridge, T. D. W.; Anderson, H. L. Enzymatic Synthesis and Photoswitchable Enzymatic Cleavage of a Peptide-Linked Rotaxane. *Angew. Chem., Int. Ed*. **2006**, *45*, 1596–1599.
(912) Casati, C.; Franchi, P.; Pievo, R.; Mezzina, E.; Lucarini, M. Unraveling Unidirectional Threading of α-Cyclodextrin in a [2]Rotaxane Through Spin Labeling Approach. *J. Am. Chem. Soc.* **2012**, *134*, 19108–19117.
(913) Arduini, A.; Calzavacca, F.; Pochini, A.; Secchi, A. Unidirectional Threading of Triphenylureidocalix[6]arene-Based Wheels: Oriented Pseudorotaxane Synthesis. *Chem. Eur. J.* **2003**, *9*, 793–799.

(914) Credi, A.; Dumas, S.; Silvi, S.; Venturi, M.; Arduini, A.; Pochini, A.; Secchi, A. Viologen-Calix[6]arene Pseudorotaxanes. Ion-Pair Recognition and Threading/Dethreading Molecular Motions. *J. Org. Chem*. **2004**, *69*, 5881–5887.
(915) Arduini, A.; Bussolati, R.; Credi, A.; Secchi, A.; Silvi, S.; Semeraro, M.; Venturi, M. Toward Directionally Controlled Molecular Motions and Kinetic Intra- and Intermolecular Self-Sorting: Threading Processes of Nonsymmetric Wheel and Axle Components. *J. Am. Chem. Soc.* **2013**, *135*, 9924–9930.
(916) Arduini, A.; Bussolati, R.; Credi, A.; Pochini, A.; Secchi, A.; Silvi, S.; Venturi, M. Rotaxanes with a Calix[6]arene Wheel and Axles of Different Length. Synthesis, Characterization, and Photophysical and Electrochemical Properties. *Tetrahedron* **2008**, *64*, 8279–8286.
(917) Arduini, A.; Bussolati, R.; Credi, A.; Monaco, S.; Secchi, A.; Silvi, S.; Venturi, M. Solvent- and Light-Controlled Unidirectional Transit of a Nonsymmetric Molecular Axle Through a Nonsymmetric Molecular Wheel. *Chem. Eur. J.* **2012**, *18*, 16203–16213.
(918) Oshikiri, T.; Yamaguchi, H.; Takashima, Y.; Harada, A. Face Selective Translation of a Cyclodextrin Ring Along an Axle. *Chem. Commun*. **2009**, 5515–5517.
(919) Baroncini, M.; Silvi, S.; Venturi, M.; Credi, A. Photoactivated Directionally Controlled Transit of a Non-Symmetric Molecular Axle Through a Macrocycle. *Angew. Chem., Int. Ed*. **2012**, *51*, 4223–4226.
(920) Ragazzon, G.; Baroncini, M.; Silvi, S.; Venturi, M.; Credi, A. Light-Powered Autonomous and Directional Molecular Motion of a Dissipative Self-Assembling System. *Nature Nanotechnol.* **2015**, *10*, 70–75.
(921) Sevick, E. Nanomachines: A Light-Driven Molecular Pump. *Nature Nanotechnol.* **2015**, *10*, 18–19.
(922) Ragazzon, G.; Baroncini, M.; Silvi, S.; Venturi, M.; Credi, A. Light-Powered, Artificial Molecular Pumps: A Minimalistic Approach. *Beilstein J. Nanotechnol.* **2015**, *6*, 2096–2104.
(923) Nishiyama, J.; Makita, Y.; Kihara, N.; Takata, T. Acylative Uni-Directional Transport on Level Periodic Potential Surface Using a Rotaxane Platform with a Isopropylidene Separator. *Chem. Lett.* **2015**, *44*, 1428–1430.
(924) Nishiyama, J.; Makita, Y.; Kihara, N. Rapid and Efficient Acylative Active Transport on a Rotaxane. *Chem. Asian J.* **2015**, *4*, 1056–1064.
(925) Nishiyama, J.; Makita, Y.; Kihara, N. The Cyclopentyl Group, as a Small but Bulky Terminal Group, Allows Rapid and Efficient Active Transport. *Org. Lett.* **2015**, *17*, 138–141.
(926) Li, H.; Cheng, C.; McGonigal, P. R.; Fahrenbach, A. C.; Frasconi, M.; Liu, W.-G.; Zhu, Z.; Zhao, Y.; Ke, C.; Lei, J.; Young, R. M.; Dyar, S. M.; Co, D. T.; Yang, Y.-W.; Botros, Y. Y.; Goddard, W. A., III.; Wasielewski, M. R.; Astumian, R. D.; Stoddart, J. F. Relative Unidirectional Translation in an Artificial Molecular Assembly Fueled by Light. *J. Am. Chem. Soc.* **2013**, *135*, 18609–18620.
(927) Shu, X.; Chen, W.; Hou, D.; Meng, Q.; Zheng, R.; Li, C. Novel Binding Regioselectivity in the Interpenetration of a Non-Symmetric Axle Into a Non-Symmetric Pillar[5]arene Wheel. *Chem. Commun.* **2014**, *50*, 4820–4823.
(928) Strutt, N. L.; Zhang, H.; Schneebeli, S. T.; Stoddart, J. F. Functionalizing Pillar[*n*]arenes. *Acc. Chem. Res.* **2014**, *47*, 2631–2642.
(929) Cheng, C.; McGonigal, P. R.; Schneebeli, S. T.; Li, H.; Vermeulen, N. A.; Ke, C.; Stoddart, J. F. An Artificial Molecular Pump. *Nature Nanotechnol*. **2015**, *10*, 547–553.
(930) Serreli, V.; Lee, C.-F.; Kay, E. R.; Leigh, D. A. A Molecular Information Ratchet. *Nature* **2007**, *445*, 523–527.
(931) Alvarez-Pérez, M.; Goldup, S. M.; Leigh, D. A.; Slawin, A. M. Z. A Chemically-Driven Molecular Information Ratchet. *J. Am. Chem. Soc.* **2008**, *130*, 1836–1838.
(932) Carlone, A.; Goldup, S. M.; Lebrasseur, N.; Leigh, D. A.; Wilson, A. A Three-Compartment Chemically-Driven Molecular Information Ratchet. *J. Am. Chem. Soc.* **2012**, *134*, 8321–8323.
(933) Thordarson, P.; Bijsterveld, E. J. A.; Rowan, A. E.; Nolte, R. J. M. Epoxidation of Polybutadiene by a Topologically Linked Catalyst. *Nature* **2003**, *424*, 915–918.
(934) Thordarson, P.; Nolte, R. J. M.; Rowan, A. E. Mimicking the Motion of Life: Catalytically Active Rotaxanes as Processive Enzyme Mimics. *Aust. J. Chem.* **2004**, *57*, 323–327.
(935) Coumans, R. G. E.; Elemans, J. A. A. W.; Nolte, R. J. M.; Rowan, A. E. Processive Enzyme Mimic: Kinetics and Thermodynamics of the Threading and Sliding Process. *Proc. Natl. Acad. Sci. U.S.A.* **2006**, *103*, 19647–19651.
(936) Ramos, P. H.; Coumans, R. G. E.; Deutman, A. B. C.; Smits, J. M. M.; de Gelder, R.; Elemans, J. A. A. W.; Nolte, R. J. M.; Rowan, A. E. Processive Rotaxane Systems. Studies on the Mechanism and Control of the Threading Process. *J. Am. Chem. Soc*. **2007**, *129*, 5699–5702.
(937) Elemans, J. A. A. W.; Bijsterveld, E. J. A.; Rowan, A. E.; Nolte, R. J. M. Manganese Porphyrin Hosts as Epoxidation Catalysts – Activity and Stability Control by Axial Ligand Effects. *Eur. J. Org. Chem.* **2007**, 751–757.
(938) Deutman, A. B. C.; Monnereau, C.; Elemans, J. A. A. W.; Ercolani, G.; Nolte, R. J. M.; Rowan, A. E. Mechanism of Threading a Polymer Through a Macrocyclic Ring. *Science* **2008**, *322*, 1668–1671.
(939) Monnereau, C.; Ramos, P. H.; Deutman, A. B. C.; Elemans, J. A. A. W.; Nolte, R. J. M.; Rowan, A. E. Porphyrin Macrocyclic Catalysts for the Processive Oxidation of Polymer Substrates. *J. Am. Chem. Soc.* **2010**, *132*, 1529–1531.
(940) Deutman, A. B. C.; Cantekin, S.; Elemans, J. A. A. W.; Rowan, A. E.; Nolte, R. J. M. Designing Processive Catalytic Systems. Threading Polymers Through a Flexible Macrocycle Ring. *J. Am. Chem. Soc.* **2014**, *136*, 9165–9172.
(941) Miyagawa, N.; Watanabe, M.; Matsuyama, T.; Koyama, Y.; Moriuchi, T.; Hirao, T.; Furusho, Y.; Takata, T. Successive Catalytic Reactions Specific to Pd-Based Rotaxane Complexes as a Result of Wheel Translation Along the Axle. *Chem. Commun.* **2010**, *46*, 1920–1922.
(942) Lewandowski, B.; De Bo, G.; Ward, J. W.; Papmeyer, M.; Kuschel, S.; Aldegunde, M. J.; Gramlich, P. M. E.; Heckmann, D.; Goldup, S. M.; D'Souza, D. M.; Fernandes, A. E.; Leigh, D. A. Sequence-Specific Peptide Synthesis by an Artificial Small-Molecule Machine. *Science* **2013**, *339*, 189–193.
(943) De Bo, G.; Kuschel, S.; Leigh, D. A.; Lewandowski, B.; Papmeyer, M.; Ward, J. W. Efficient Assembly of Threaded Molecular Machines for Sequence-Specific Synthesis. *J. Am. Chem. Soc.* **2014**, *136*, 5811–5814.
(944) Goldup, S. Artificial Molecular Machines: Two Steps Uphill. *Nature Nanotechnol.* **2015**, *10*, 488–489.

Appendix A: Glossary of Terminology

Active Template[1] – A chemical species acting simultaneously as a template and a catalyst

Alexander-Briggs[2] **Notation** – A means of characterizing knots and links by crossing number, with subscripts (assigned arbitrarily) that distinguish different topologies of equal crossing number, and superscripts (in the case of links) denoting the number of entangled knots

Allostery[3] – A phenomenon whereby the conformation of an enzyme or other protein is altered by complexation, at a site other than the substrate-binding site, with a small molecule, referred to as an effector, which results in either increased or decreased activity by the enzyme. Artificial systems displaying similar behavior are also classified as allosteric.

Annulus – A ring-shaped structure, object, or region

Architecture – A generic term for describing the structure of a molecule

Artificial Molecular Switch (AMS) – A molecule in which the interconversion between two or more (co)conformational states can be controlled by external stimuli

Axial Chirality[3] – Chirality arising from the nonplanar arrangement of four groups about an axis called a chiral axis: it is exemplified by allenes abC = C = Cab and by the atropisomerism of *ortho*-tetrasubstituted biphenyls.

Axle – The portion of an acyclic component part in a mechanomolecule that passes through the annulus of a ring. Synonymous terms include *rod* and *thread*.

Balance[4] – The thermodynamically preferred distribution of molecular states in a system

Balance Breaking[4] – A process that moves a system away from thermodynamic equilibrium

Binding – The act of forming a complex stabilized by noncovalent bonding interactions

Bistability – A (mechano)molecule is said to be bistable if there are two (co-)conformations that represent energy minima as opposed to only one. The two (co-)conformations are said to be *degenerate* if they are indistinguishable, and *non-degenerate* if they are different.

Bonnane[5,6] – A rotaxane containing one or more covalent bridges between rings

Borromean Rings – A three-ring Brunnian link. In Alexander-Briggs notation, it is the 6^3_2 link

Brownian Motion – The random motion of particles suspended in a liquid or a gas resulting from their collisions with other particles

Brownian Ratchet – A thought experiment, first proposed by Smoluchowski[7] and revisited/popularized by Feynman[8], involving a microscopic ratchet-and-pawl which seemingly violates the second law of thermodynamics. A synonymous term is a Feynman–Smoluchowski ratchet.

Brunnian Links – Topological links interlocked in such a manner that breaking any of the component knots unlinks all of the remaining knots

Catenation – The act of forming a catenane

Catenand[9] – A molecule containing topologically linked macrocyclic ligands

Catenand Effect[10] – A phenomenon of enhanced stability in metals coordinated by catenands

Catenane – A molecule containing two or more topologically linked macrocyclic component parts

Catenarotaxane – A mechanomolecule possessing both links and dumbbells as component parts—i.e., a catenane / rotaxane hybrid molecule. Synonyms include *rotacatenane*[11] and *catrotaxane*.[5]

Catenate[10] – A transition metal complex containing topologically linked macrocyclic ligands

Chemical Bond[3,12] – Forces acting between two atoms or groups of atoms that lead to the formation of a stable independent molecular entity

Chemical Topology[13] – The properties of a molecule that are independent of any spatial arrangements and bond distortions that can be performed without allowing covalent bonds to break or pass through one another

Chirality[3] – The geometric property of a rigid object being non-superimposable on its mirror image; such an object has no symmetry elements of the second kind (mirror plane, center of inversion, rotation-reflection axis).

Circumrotation – Translation of one ring with respect to another ring in a catenane

Clipping – A synthetic protocol which proceeds by macrocyclization of a ring around a template (e.g., a ring or dumbbell) in order to form a mechanical bond

Co-Configuration – The spatial arrangement of component parts engaged in mechanical bonding that give rise to

The Nature of the Mechanical Bond: From Molecules to Machines, First Edition. Carson J. Bruns and J. Fraser Stoddart.
© 2017 John Wiley & Sons, Inc. Published 2017 by John Wiley & Sons, Inc.

mechanostereoisomerism, which is not attributable to co-conformational differences, but rather to differences in the expression of chirality.

Co-Conformation – The spatial arrangement of the component parts affording distinction between mechanostereoisomers which can be interconverted by translation, pirouetting, or rocking motions constrained by the mechanical bond

Co-Constitution – The sum of the constitutions of the component parts in a MIM engaged in mechanical bonding

Complex[3] – A molecular entity formed by loose association involving two or more component molecular entities. The bonding between the components is normally weaker than that of a covalent bond.

Component Part – A molecular entity engaged in mechanical bonding with another molecular entity in a mechanomolecule

Composite Links – A link comprising combinations of other links. The simplest example is that of a linear four-crossing [3]catenane.

Conditional Topological Chirality – The chirality of an entity that is conditional on its graph having directionally oriented sequences of elements

Conditional Topological Isomers – Isomerism which involves assigning constraints to component parts that differentiate the topologies of otherwise achiral mechanomolecules

Configuration[3] – The spatial arrangement of atoms in a molecule that distinguishes stereoisomers, the isomerism between which is not due to conformation differences

Conformation[3] – The spatial arrangement of the atoms in a molecule affording distinction between stereoisomers which can be interconverted by rotations about formally single bonds

Constitution[3] – The description of the identity and connectivity (and corresponding bond multiplicities) of the atoms in a molecule omitting any distinction arising from their spatial arrangement

Continuous Deformation – Any function that transforms a topological space—e.g., stretching, bending—without allowing edges or surfaces to break, intersect, or merge. Such a function is known as a *homeomorphism* in mathematical topology.

Cooperative Capture[14] – A synthetic strategy that relies on cooperative templating interactions between multiple macrocycles to promote a ring capture or dumbbell capture reaction, such as the cucurbit[6]uril-promoted azide-alkyne cycloaddition (CB6AAC), leading to the formation of mechanical bonds

Coordination[3] **–** The formation of a covalent bond, the two shared electrons of which have come from only one of the two parts of the molecular entity linked by it, as in the reaction of a Lewis acid and a Lewis base to form a Lewis adduct

Coordination Number[3] – The number of atoms directly linked to a specified atom

Covalent Capture – The introduction of covalent bonds in the kinetic stabilization of noncovalent bonding interactions

Crossing – A point in a graph where lines / edges intersect

Crossing Number – The minimal number of topological crossings in a graph

Crown[3] – A molecular entity comprising a monocyclic ligand assembly that contains three or more binding sites held together by covalent bonds and capable of binding a guest in a central (or nearly central) position. The best known members of this group are macrocyclic polyethers, containing several repeating units $–CR_2CR_2O–$ (where R is most commonly H), and known as crown ethers.

Cryptand[3] – A molecular entity comprising a cyclic or polycyclic assembly of binding sites that contains three or more binding sites held together by covalent bonds, and which defines a molecular cavity in such a way as to bind (and thus 'hide' in the cavity) another molecular entity, the guest (a cation, an anion or a neutral species), more strongly than do the separate parts of the assembly (at the same total concentration of binding sites). The adduct thus formed is called a *cryptate*. The term is usually restricted to bicyclic or oligocyclic molecular entities.

Cucurbit[*n*]uril (CB*n*) – A molecule belonging to a family[15–17] of macrocycles comprising a number *n* of repeating methylene-bridged glycoluril units in a torus

Cyclodextrins – Naturally occurring macrocyclic oligosaccharides composed commonly of six (α-CD), seven (β-CD) and eight (γ-CD) α-1,4-linked D-glucopyranosyl residues

Cyclophanes – Compounds having (i) mancude-ring systems (i.e., rings possessing the maximal number of non-cumulative double bonds), or assemblies of mancude-ring systems, and (ii) atoms and/or saturated or unsaturated chains as alternate components of a large ring

Daisy Chain – A rotaxane comprising a number *n* of covalently bridged ring–axle component parts, the mechanical bonds of which give rise to cyclic ([*cn*]daisy chains) or acyclic ([*an*]daisy chains) oligomer/polymer architectures

Dendrimer[18] – A monodisperse macromolecule with a regular and highly branched three-dimensional architecture

Deslipping – A process whereby a ring escapes the axle/dumbbel of a rotaxane by transgressing a stopper. A synonym is *dethreading*.

Directed Synthesis – An approach to the synthesis of mechanical bonds and entanglements that is characterized by the preorganization of reactants around a covalent template that can be cleaved subsequently to afford the product

Dumbbell – A component part of a rotaxane consisting of an axle and stoppers

Dumbbell Capture – A synthetic protocol where two semi-dumbbells are coupled within the cavity of a reaction-promoting ring to form a rotaxane

Dynamic Combinatorial Library[19] **(DCL)** – A thermodynamically controlled mixture of interconverting chemical species that can respond to various stimuli

Dynamic Covalent Chemistry[20] **(DCC)** – Combinatorial chemistry under thermodynamic control

Dynamic Mechanostereoisomers – Isomers that can be converted by dynamic processes associated with mechanical bonds such as translation, pirouetting, circumrotation, and rocking

Emergence[21] – A process whereby larger entities, patterns, and regularities arise through interactions among smaller or simpler entities that themselves do not exhibit such properties

Energy Ratchet – A molecular machine that achieves directed transport / biased Brownian motion by a ratcheting mechanism that involves the raising and lowering of thermodynamic wells

Escapement[4] – The release of a ratcheted substrate from its kinetically trapped state of relatively high energy, which allows the system to approach thermodynamic equilibrium

Foldaxanes[22] – A class of rotaxanes in which the ring is involved in at least one noncovalent bond and adopts a closed-ring structure through a reversible folding process

Graphical Representations – Cartoons or illustrations that aid in the visualization of molecules

Ground State Co-Conformation (GSCC) – A co-conformation representing the global energy minimum on the thermodynamic landscape of a supermolecule or mechanomolecule

Halogen Bonding[23] – A net attraction between an electrophilic region associated with a halogen atom in a molecular entity and a nucleophilic region in another, or the same, molecular entity

Helicity[3] – The chirality of a twisted object, such as a helix, propeller or screw. It is right-handed (*P*) if the sense of the twist is clockwise as one progresses along the axis of the helix, propeller or screw away from the observer, and left-handed (*M*) if the corresponding sense of the twist is counterclockwise.

Hetero[*n*]catenane – A catenane of *n* constitutionally non-identical component parts

Homophilic Interactions – Associative stabilizing interactions between identical or like molecules

Homo[*n*]catenane – A catenane of *n* constitutionally identical component parts

Hydrogen Bond[24] – An attractive interaction between a hydrogen atom from a molecule or molecular fragment X–H in which X is more electronegative than H, and an atom or group of atoms in the same or different molecule, in which there is evidence of noncovalent bond formation

Hydrophobic Interaction[3] – The association of non-polar groups or molecules in an aqueous environment which arises from the tendency of water to exclude non-polar molecules. Analogous intermolecular interactions in non-aqueous media are called *solvophobic* interactions.

Information Ratchet – A molecular machine that achieves directed transport / biased Brownian motion by a ratcheting mechanism that involves the appropriately timed raising and lowering of kinetic barriers

Ion Pair[3] – A pair of oppositely charged ions held together by Coulombic attraction without formation of a covalent bond

Isomer – One of several species (or molecular entities) that have the same atomic composition (molecular formula) but different line formulas or stereochemical formulas and hence different physical and/or chemical properties

Isotopism – Two graphs are isotopic if they cannot be differentiated on the basis of their topology in a given space.

Knot – In mathematics, a knot is an embedding of a circle in three-dimensional space—i.e., a closed loop.

Ladder Rotaxane – Any rotaxane in which multiple bis-macrocyclic component parts form mechanically bonded bridges between a pair of parallel dumbbells

Langmuir-Blodgett (LB) Film – Monolayers or multilayers of a molecular compound deposited on the surface of a liquid, which can be transferred to a solid surface by immersing (and emersing) a substrate into the liquid

Link – In mathematics, a link is a collection of topologically entangled knots that do not intersect.

Linker – A moiety that links two portions of a (mechano) molecule

Linking[4] – In the context of a ratcheting mechanism, linking is a process that lowers an activation barrier such that a substrate can exchange between different thermodynamic wells. Unlinking, therefore, is the raising of kinetic barriers in order to trap the substrate in a certain state.

Macrocyclic – Of, relating to, or denoting a macrocycle

Macrocycle – A cyclic molecule, the annulus of which constitutes[25] 12 or more atoms note that the IUPAC definition is too restrictive to accommodate the term as it is used in the literature.[26]

Macromolecule[3] – A molecule of high relative molecular mass, the structure of which essentially comprises multiple repetition units derived, actually or conceptually, from molecules of low relative molecular mass

Maximum Site Occupancy[27] – The principle whereby the most thermodynamically stable state of a coordination complex is one in which the highest possible number of available binding sites are occupied on both the ligand and the metal

Maxwell's Demon[28] **–** A thought experiment created by James Clerk Maxwell suggesting how the Second Law of Thermodynamics could hypothetically be violated by a being that sorts gas particles into two compartments by opening and closing a gate between the compartments with appropriate timing informed by the being's knowledge of the particles' trajectories

Mechanical Bond – An entanglement in space between two or more molecular entities (component parts) such that they cannot be separated without breaking or distorting chemical bonds between atoms

Mechanical Helicity – Helicity arising from the causal or structural influence of a mechanical bond—i.e., the chirality of a helical, propeller, or screw-shaped mechanomolecule

Mechanical Chirality – A non-classical form of chirality resulting from the spatial arrangements of component parts connected by mechanical bonds

Mechanically Axial Chirality – Mechanostereoisomerism resulting from the non-planar arrangement of four groups in pairs about an axis of chirality that passes through a mechanical bond, as a result of the pairs belonging to different component parts of a mechanomolecule

Mechanically Interlocked Molecules (MIMs) – Molecules containing mechanical or topological entanglements

Mechanically Planar Chirality[29] – Chirality resulting from the different relative orientations of (a) rotationally unsymmetrical ring(s) and a constitutionally unsymmetrical axle(s)/dumbbell(s)

Mechanomolecule – A molecule possessing one or more mechanical bonds

Mechanomolecular – Of, relating to, or denoting a mechanomolecule

Mechanostereochemistry[30] – The stereochemistry of molecules with mechanical bonds

Mechanostereogenic – Four or more atoms or substituents in a mechanomolecule are mechanostereogenic if their non-planar arrangement in space is a topological and/or Euclidean consequence of the presence of a mechanical bond.

Mechanostereoisomerism – Isomerism due to differences in the spatial arrangement of component parts of a mechanomolecule without regard to any differences in the constitutions of the component parts

Mechanostereoisomers – Isomers that possess identical mechanically interlocked component parts, but which differ in the arrangement of their component parts in space

Mechanostereoselectivity[31] – A motion constrained by a mechanical bond that happens faster along one path than along another

Metallo- – A prefix denoting the presence of one or more transition metal ions

Metal-Organic Frameworks[32] **(MOFs)** – Robust, crystalline coordination polymers comprising networks of organic ligands coordinated to metal or metal-cluster secondary building units (SBUs), which often exhibit high porosities on account of their rigid reticular architectures

Metastable State Co-Conformation (MSCC) – A co-conformation representing a local energy minimum on the thermodynamic landscape of a supermolecule or mechanomolecule

Metathesis[3] – A bimolecular process formally involving the exchange of a bond (or bonds) between similar interacting chemical species so that the bonding affiliations in the products are identical (or closely similar) to those in the reactants

Microscopic Reversibility[3] – The principle that, in a reversible reaction, the mechanism in one direction is exactly the reverse of the mechanism in the opposite direction. The principle does not apply to processes that are photochemically initiated.

Möbius Strip – A chiral closed band with only one surface and one edge

Molecular Graph[3] – A graph with differently labelled (colored) vertices which represent different kinds of atoms and differently labeled (colored) edges related to different types of bonds

Molecular Machine – A molecule that consumes energy in order to perform a task

Molecular Muscle – A molecular switch or machine designed to control the distance between two points

Molecular Shuttle – A rotaxane in which a ring translates back and forth between two or more recognition units

Molecular Switch Tunnel Junction (MSTJ) – A device comprising two electrodes separated by a monolayer of molecules through which electrons may tunnel in the presence an applied potential field

Monolayer – A single, closely packed layer of atoms or molecules

Nanovalve – A surface-mounted (pseudo)rotaxane that regulates the release of cargo from a material (typically, mesoporous silica) by responding to stimuli in a manner that modulates the effective aperture size of nearby nanopores. Nanovalves may be classified as "snap-top" if their response involves irreversible bond cleavage, or "reversible" if the response involves reversible translational isomerization.

Non-Planar Graph – A graph that cannot be projected onto a plane without one or more crossings

Orientational Mechanostereoisomers – Mechanostereoisomerism arising from differences in the relative orientations of component parts that lack mirror symmetry across the plane of a mechanically bonded ring's cavity

Pentafoil Knot – A five-crossing prime knot. In Alexander-Briggs notation, it is the 5_1 knot.

Perspective Formula[3] – A type of projection which portrays the geometrical features of a molecule as a view from an appropriate direction

Pirouetting – An intramolecular motion constrained by a mechanical bond involving the rotation of one component about the axis of another component

Planar Chirality[3] – Chirality resulting from the arrangement of out-of-plane groups with respect to a reference plane / chirality plane. The configuration of molecules possessing planar chirality is specified by the stereodescriptors (R_p) and (S_p) or (*P*) and (*M*).

Planar Graph – A graph that can be drawn in a plane without any of the edges crossing

Polymer[3] – A macromolecule containing multiple repeating units derived, actually or conceptually, from molecules of low relative molecular mass

Portion – A moiety within one of a mechanomolecule's component parts, such as a linker or a stopper

Pressing – A motion constrained by a mechanical bond that shortens the distance between two relatively planar moieties or "plates"

Pretzelane – A [2]pseudocatenane in which the mechanical bond associated with a Hopf link is trivialized by a covalent connection between the rings

Prime Link – A link that cannot be represented as a knot sum of other links

Processive Catalysis[33] – A catalyst is processive if it remains attached to a polymer substrate in order to perform multiple rounds of catalysis before dissociating.

Pseudocatenane – Catenanes containing covalent bridges between rings

Pseudorotaxane[34] – A complex resembling a rotaxane without stoppers, leaving the ring(s) free to dissociate from the axle—i.e., its component parts are held together chiefly by noncovalent bonds rather than by mechanical bonds

Radical Pair[3] – Two radicals in close proximity in solution, stabilized by the correlation of their unpaired electron spins

Ratcheting – A process that moves a substrate from a state of lower energy to higher energy, in which the substrate cannot return to the lower energy state on account of a high kinetic barrier for the reverse process

Recognition Unit – A moiety that acts as a stable or metastable binding site for a ring

Residual Topological Isomerism[35] – The isomerism of a topologically trivial molecule (e.g., a pretzelane) which derives from a topologically non-trivial molecule (e.g., a catenane)

Reynolds Number[36] – A dimensionless quantity describing the ratio of inertial forces to viscous forces under given flow conditions

Ring – A macrocyclic component part in a mechanomolecule or supermolecule. Synonyms include *annulus*, *macrocycle*, and *wheel*.

Ring Capture – The trapping of a ring within another by virtue of one ring's ability to promote a coupling reaction within its cavity, thus forming a catenane

Robust Dynamics[37] – A property of materials that are intrinsically robust and rigid, yet dynamic, where the repeated local dynamics of one entity does not affect the integrity of any others linked to it

Rocking – An intramolecular motion constrained by a mechanical bond involving the rotation of one component orthogonally with respect to the rotational axis of another component

Rotamacrocycle[38] – An ultramacrocycle containing rotaxane-like threaded elements

Rotaxanation – The act of forming a rotaxane

Rotaxane[26] – A molecule comprising at least one macrocyclic component part, i.e., ring(s), with at least one linear component part, i.e., axle(s), threaded through the ring(s) and terminated by bulky end-groups (stoppers) large enough to prevent dethreading of the dumbbell(s) resulting from the existence/formation of chemical (covalent and/or coordinative) bonds between the stoppers and the axle(s)

Semidumbbell – A molecular entity comprising an axle and one stopper—i.e., a half-dumbbell

Semirotaxane[39] – A pseudorotaxane possessing one or more semidumbbells

Sequence (Mechanostereo)isomers[40] – Two MIMs with identical molecular formulas possessing component parts that are arranged in different sequences

Shrinking[41] – An approach to rotaxane synthesis in which a pseudorotaxane is converted into a rotaxane by a reaction that decreases the effective size of a ring's aperture

Slippage[42] – A process whereby a ring becomes mechanically interlocked with a dumbbell to form a rotaxane by passing over a size-complementary stopper

Static Mechanostereoisomers – Isomers arising from differences in the relative orientations, sequences, or mechanical / topological chirality of component parts engaged in mechanical bonding

Solomon Knot – A four-crossing two-component prime link, also known[43] as a *Solomon Link*. In Alexander-Briggs notation, it is the 4^2_1 link.

Star of David Link[44] – A six-crossing two-component prime link. In the Alexander-Briggs notation, it is the 6^2_1 link.

Statistical Synthesis – An approach to the synthesis of MIMs that relies solely on the low statistical probability of cyclic and acyclic molecules occasionally becoming entangled in solution by random/events chance

Stereochemistry[45] – The study of the relative spatial arrangements of atoms that form the structures of molecules and their manipulation

Stereoformula[3] – A three-dimensional view of a molecule either as such or in a projection

Stereogenic Element – A focus of stereoisomerism (stereogenic center, axis or plane) in a molecule such that interchange of two ligands attached to an atom in such a molecule (e.g., a and b on a tetrahedral atom Cabcd or in an alkene abC=Cab or in an allene abC=C=Cab) leads to a stereoisomer

Stereoisomerism[3] – Isomerism due to differences in the spatial arrangement of atoms without any differences in connectivity or bond multiplicity between the isomers

Stereoisomers[3] – Isomers that possess identical constitutions, but which differ in the arrangement of their atoms in space

Stopper – A bulky group in the dumbbell of a rotaxane that prevents the ring from deslipping. Synonymous terms include *endcap* and *blocking group*.

Stoppering – A synthetic protocol for making rotaxanes involving the attachment of bulky stoppers to both ends of the axle of a pseudorotaxane in order to prevent the ring from deslipping. Synonymous terms include *capping* and *end-capping*.

Subcomplex – A local host-guest interaction within a larger supermolecule or mechanomolecule

Suit[*n*]ane[46] – A two-component mechanomolecule consisting of a molecular body with *n* branches, the core or "torso" of which is surrounded by a close-fitting all-in-one molecular cage or "suit". A nearly synonymous term is *carceplex*. In contrast with suitanes, however, carceplex encapsulants do not necessarily protrude from the cage.

Supermolecule – A supramolecular complex

Super-rotation[47,48] – An intramolecular motion involving the pirouetting of a ring-and-axle subcomplex with respect to another site in the molecule

Supramolecular Chemistry[3,27] – A field of chemistry related to species of greater complexity than molecules, that are held together and organized by means of intermolecular interactions. The objects of supramolecular chemistry are supermolecules and other polymolecular entities that result from the spontaneous association of a large number of components into a specific phase (membranes, vesicles, micelles, solid state structures, etc.)

Swelling[49] – An approach to rotaxane synthesis in which a pseudorotaxane is converted to a rotaxane by a rearrangement that increases the steric bulk of the axle's endgroups

Switching – The act of actuating an artificial molecular switch

Technomorph[50] – A graphical representation that establishes a symbolic link between a molecule's structure and a macroscopic object

Telescoping – A motion constrained by the mechanical bond in which one or more of a rotaxane's dumbbells extend outward from a cage-like host

Template[51] – A chemical template organizes an assembly of atoms, with respect to one or more geometric loci, in order to achieve a particular linking of atoms.

Template-Directed Synthesis – Any approach to synthesis involving the use of one or more templates

Thermodynamic Forecasting[52] – Predicting all or part of the potential energy surface, also called the free energy profile or 'thermodynamic landscape', of a bistable or multistable (mechano)molecule on the basis of the stabilities of structurally related model compounds

Threading – Passing through an annulus in the manner of a thread

Topological Chirality – The topological property of an object that cannot be transformed into its own mirror image through any process of continuous deformation.

Topological Stereoisomers – Isomers arising from differences in molecular topology without any differences in constitution

Topological Rubber Glove – An object that is topologically achiral, yet rigidly chiral in every possible presentation—i.e., a fundamentally chiral object that can be deformed into its own mirror image

Topological Stereochemistry[53] – The stereochemistry of topological stereoisomers

Topological Stereoisomers – Molecules that are homeomorphic and non-isotopic—i.e., molecules that possess identical connectivity but different topology

Topology – The mathematical study of the properties of space that remain invariant throughout any process of continuous deformation

Torsional Stereoisomers – Stereoisomers that can be converted by torsion about a bond axis. A synonymous term is *conformational stereoisomers*.

Translation – An intramolecular motion constrained by a mechanical bond involving the linear movement of one component part with respect to another component part

Translational Isomers – Mechanostereoisomers that can be converted (actually or conceptually) by translation of mechanically bonded component parts

Trefoil Knot – A three-crossing prime knot. In Alexander-Briggs notation, it is the 3_1 knot.

Ultramacrocycle – A macrocyclic molecule containing smaller macrocycles within its (co-)constitution

Unconditional Topological Chirality – The chirality of an entity possessing a topology that is intrinsically non-superimposable on its mirror image

Unknot – An embedding of a circle with no crossings

Whitehead Link – A five-crossing link of two knots. In the Alexander-Briggs notation, it is the 5^2_1 link.

π-Donor – A molecular entity or moiety that can donate π-electron density to another molecular entity or moiety

π-Acceptor – A molecular entity or moiety that can accept π-electron density from another molecular entity or moiety

π–π Stacking – Any associative face-to-face interactions between aromatic molecular entities

Appendix A References

(1) Aucagne, V.; Berná, J.; Crowley, J. D.; Goldup, S. M.; Hänni, K. D.; Leigh, D. A.; Lusby, P. J.; Ronaldson, V. E.; Slawin, A. M. Z.; Viterisi, A.; Walker, D. B. Catalytic "Active-Metal" Template Synthesis of [2]Rotaxanes, [3]Rotaxanes, and Molecular Shuttles, and Some Observations on the Mechanism of the Cu(I)-Catalyzed Azide-Alkyne 1,3-Cycloaddition. *J. Am. Chem. Soc.* **2007**, *129*, 11950–11963.

(2) Alexander, J. W.; Briggs, G. B. On Types of Knotted Curves. *Ann. Math.* **1926**, *28*, 562–586.

(3) IUPAC. Compendium of Chemical Terminology, 2nd ed. (the "Gold Book"). Compiled by A. D. McNaught and A. Wilkinson. Blackwell Scientific Publications, Oxford (1997). XML On-line Corrected Version: http://goldbook.iupac.org (2006-) created by M. Nic, J. Jirat, B. Kosata; updates compiled by A. Jenkins.

(4) Chatterjee, M. N.; Kay, E. R.; Leigh, D. A. Beyond Switches: Ratcheting a Particle Energetically Uphill with a Compartmentalized Molecular Machine. *J. Am. Chem. Soc.* **2006**, *128*, 4058–4073.

(5) Safarowsky, O.; Windisch, B.; Mohry, A.; Vögtle, F. Nomenclature for Catenanes, Rotaxanes, Molecular Knots, and Assemblies Derived From These Structural Elements. *J. Prakt. Chem.* **2000**, *342*, 437–444.

(6) Kishan, M. R.; Parham, A.-H.; Schelhase, F.; Yoneva, A.; Silva, G.; Chen, X.; Okamoto, Y.; Vögtle, F. Bridging Rotaxanes' Wheels—Cyclochiral Bonnanes. *Angew. Chem., Int. Ed*. **2006**, *45*, 7296–7299.

(7) von Smoluchowski, M. Experimentell Nachweisbare, der Üblichen Thermodynamik Widersprechende Molekularphänomene. **1912**, *XIII*, 1069–1080.

(8) Feynman, R. P.; Leighton, R. B.; Sands, M. *The Feynman Lectures on Physics*; 2013 ed.; Basic Books: New York, 1963.

(9) Dietrich-Buchecker, C. O.; Sauvage, J.-P.; Kern, J.-M. Templated Synthesis of Interlocked Macrocyclic Ligands: The Catenands. *J. Am. Chem. Soc.* **1984**, *106*, 3043–3045.

(10) Albrecht-Gary, A.-M.; Saad, Z.; Dietrich-Buchecker, C. O.; Sauvage, J.-P. Interlocked Macrocyclic Ligands: A Kinetic Catenand Effect in Copper(I) Complexes. *J. Am. Chem. Soc.* **1985**, *107*, 3205–3209.

(11) Amabilino, D. B.; Ashton, P. R.; Bravo, J. A.; Raymo, F. M.; Stoddart, J. F.; White, A. J. P.; Williams, D. J. Molecular Meccano 52. Template-Directed Synthesis of a Rotacatenane. *Eur. J. Org. Chem.* **1999**, 1295–1302.

(12) Pauling, L. *The Nature of the Chemical Bond*; Cornell University Press: Ithaca, 1939.

(13) Frisch, H. L.; Wasserman, E. Chemical Topology. *J. Am. Chem. Soc*. **1961**, *83*, 3789–3795.

(14) Hou, X.; Ke, C.; Stoddart, J. F. Cooperative Capture Synthesis: Yet Another Playground for Copper-Free Click Chemistry. *Chem. Soc. Rev.* **2016**, *45*, 3766–3780.

(15) Freeman, W. A.; Mock, W. L.; Shih, N. Y. Cucurbituril. *J. Am. Chem. Soc*. **1981**, *103*, 7367–7368.

(16) Kim, J.; Jung, I.-S.; Kim, S.-Y.; Lee, E.; Kang, J.-K.; Sakamoto, S.; Yamaguchi, K.; Kim, K. New Cucurbituril Homologues: Syntheses, Isolation, Characterization, and X-Ray Crystal Structures of Cucurbit[*n*]uril (*n* = 5, 7, and 8). *J. Am. Chem. Soc.* **2000**, *122*, 540–541.

(17) Lagona, J.; Mukhopadhyay, P.; Chakrabarti, S.; Isaacs, L. The Cucurbit[*n*]uril Family. *Angew. Chem., Int. Ed*. **2005**, *44*, 4844–4870.

(18) Bosman, A. W.; Janssen, H. M.; Meijer, E. W. About Dendrimers: Structure, Physical Properties, and Applications. *Chem. Rev.* **1999**, *99*, 1665–1688.

(19) Cougnon, F. B. L.; Sanders, J. K. M. Evolution of Dynamic Combinatorial Chemistry. *Acc. Chem. Res.* **2012**, *45*, 2211–2221.

(20) Corbett, P. T.; Leclaire, J.; Vial, L.; West, K. R.; Wietor, J.-L.; Sanders, J. K. M.; Otto, S. Dynamic Combinatorial Chemistry. *Chem. Rev.* **2006**, *106*, 3652–3711.

(21) Emergence. *Wikipedia*. http://en.wikipedia.org (accessed 26 June 2016)

(22) Ferrand, Y.; Gan, Q.; Kauffmann, B.; Jiang, H.; Huc, I. Template-Induced Screw Motions Within an Aromatic Amide Foldamer Double Helix. *Angew. Chem., Int. Ed*. **2011**, *50*, 7572–7575.

(23) Desiraju, G. R.; Ho, P. S.; Kloo, L.; Legon, A. C.; Marquardt, R.; Metrangolo, P.; Politzer, P.; Resnati, G.; Rissanen, K. Definition of the Halogen Bond (IUPAC Recommendations 2013). *Pure Appl. Chem*. **2013**, *85*, 1711–1713.

(24) Arunan, E.; Desiraju, G. R.; Klein, R. A.; Sadlej, J.; Scheiner, S.; Alkorta, I.; Clary, D. C.; Crabtree, R. H.; Dannenberg, J. J.; Hobza, P.; Kjaergaard, H. G.; Legon, A. C.; Mennucci, B.; Nesbitt, D. J. Defining the Hydrogen Bond: An Account (IUPAC Technical Report). *Pure Appl. Chem.* **2011**, *83*, 1619–1636.

(25) Parker, S. P. Macrocycle. *McGraw-Hill Science Technology Dictionary*; McGraw-Hill: **2002**. ISBN: 978-0070423138.

(26) Yerin, A.; Wilks, E. S.; Moss, G. P.; Harada, A. Nomenclature for Rotaxanes and Pseudorotaxanes (IUPAC Recommendations 2008). *Pure Appl. Chem*. **2008**, *80*, 2041–2068.

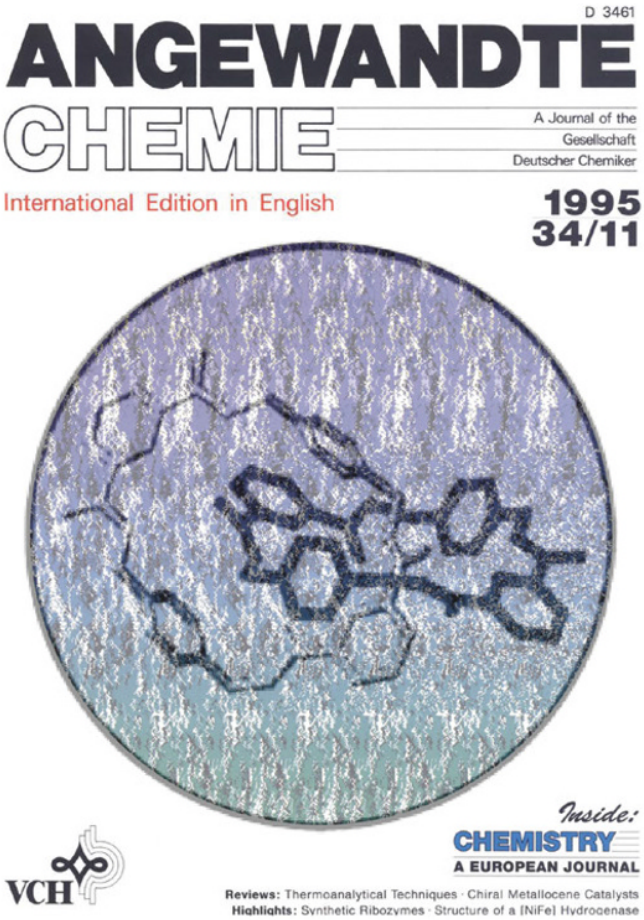
(27) Lehn, J.-M. *Supramolecular Chemistry: Concepts and Perspectives*; Wiley-VCH: Weinheim, 1995.
(28) Maxwell, J. C. *Theory of Heat*; Dover Publications, 1871.
(29) Bordoli, R. J.; Goldup, S. M. An Efficient Approach to Mechanically Planar Chiral Rotaxanes. *J. Am. Chem. Soc.* **2014**, *136*, 4817–4820.
(30) Olson, M. A.; Botros, Y. Y.; Stoddart, J. F. Mechanostereochemistry. *Pure Appl. Chem.* **2010**, *82*, 1569–1574.
(31) Fahrenbach, A. C.; Bruns, C. J.; Li, H.; Trabolsi, A.; Coskun, A.; Stoddart, J. F. Ground-State Kinetics of Bistable Redox-Active Donor–Acceptor Mechanically Interlocked Molecules. *Acc. Chem. Res.* **2014**, *47*, 482–493.
(32) Li, H.; Eddaoudi, M.; O'Keeffe, M.; Yaghi, O. M. Design and Synthesis of an Exceptionally Stable and Highly Porous Metal-Organic Framework. *Nature* **1999**, *402*, 276–279.
(33) Thordarson, P.; Bijsterveld, E. J. A.; Rowan, A. E.; Nolte, R. J. M. Epoxidation of Polybutadiene by a Topologically Linked Catalyst. *Nature* **2003**, *424*, 915–918.
(34) Ashton, P. R.; Philp, D.; Spencer, N.; Stoddart, J. F. The Self-Assembly of [*n*]Pseudorotaxanes. *J. Chem. Soc., Chem. Commun.* **1991**, 1677–1679.
(35) Lukin, O.; Godt, A.; Vögtle, F. Residual Topological Isomerism of Intertwined Molecules. *Chem. Eur. J.* **2004**, *10*, 1878–1883.
(36) Reynolds, O. An Experimental Investigation of the Circumstances Which Determine Whether the Motion of Water Shall Be Direct or Sinuous, and of the Law of Resistance in Parallel Channels. *Phil. Trans. Royal Soc.* **1883**, *174*, 935–982.
(37) Deng, H.; Olson, M. A.; Stoddart, J. F.; Yaghi, O. M. Robust Dynamics. *Nature Chem.* **2010**, *2*, 439–443.
(38) Romuald, C.; Ardá, A.; Clavel, C.; Jiménez-Barbero, J.; Coutrot, F. Tightening or Loosening a pH-Sensitive Double-Lasso Molecular Machine Readily Synthesized From an Ends-Activated [*c*2]Daisy Chain. *Chem. Sci.* **2012**, *3*, 1851–1857.
(39) Clifford, T.; Abushamleh, A.; Busch, D. H. Factors Affecting the Threading of Axle Molecules Through Macrocycles: Binding Constants for Semirotaxane Formation. *Proc. Natl. Acad. Sci. U.S.A.* **2002**, *99*, 4830–4836.
(40) Fuller, A.-M. L.; Leigh, D. A.; Lusby, P. J. Sequence Isomerism in [3]Rotaxanes. *J. Am. Chem. Soc.* **2010**, *132*, 4954–4959.
(41) Yoon, I.; Narita, M.; Shimizu, T.; Asakawa, M. Threading-Followed-by-Shrinking Protocol for the Synthesis of a [2]Rotaxane Incorporating a Pd(II)-Salophen Moiety. *J. Am. Chem. Soc.* **2004**, *126*, 16740–16741.
(42) Ashton, P. R.; Bělohradský, M.; Philp, D.; Stoddart, J. F. Slippage – An Alternative Method for Assembling [2]Rotaxanes. *J. Chem. Soc., Chem. Commun.* **1993**, 1269–1274.
(43) Pentecost, C. D.; Chichak, K. S.; Peters, A. J.; Cave, G. W. V.; Cantrill, S. J.; Stoddart, J. F. A Molecular Solomon Link. *Angew. Chem., Int. Ed.* **2007**, *46*, 218–222.
(44) Leigh, D. A.; Pritchard, R. G.; Stephens, A. J. A Star of David Catenane. *Nature Chem.* **2014**, *6*, 978–982.
(45) Eliel, E. L. *Stereochemistry of Carbon Compounds*; McGraw-Hill Book Company: New York, 1962.
(46) Williams, A. R.; Northrop, B. H.; Chang, T.; Stoddart, J. F.; White, A. J. P.; Williams, D. J. Suitanes. *Angew. Chem., Int. Ed.* **2006**, *45*, 6665–6669.
(47) Forgan, R. S.; Gassensmith, J. J.; Cordes, D. B.; Boyle, M. M.; Hartlieb, K. J.; Friedman, D. C.; Slawin, A. M. Z.; Stoddart, J. F. Self-Assembly of a [2]Pseudorota[3]catenane in Water. *J. Am. Chem. Soc.* **2012**, *134*, 17007–17010.
(48) Zhu, Z.; Bruns, C. J.; Li, H.; Lei, J.; Ke, C.; Liu, Z.; Shafaie, S.; Colquhoun, H. M.; Stoddart, J. F. Synthesis and Solution-State Dynamics of Donor–Acceptor Oligorotaxane Foldamers. *Chem. Sci.* **2013**, *4*, 1470–1483.
(49) Chiu, C.-W.; Lai, C.-C.; Chiu, S.-H. "Threading-Followed-by-Swelling": A New Protocol for Rotaxane Synthesis. *J. Am. Chem. Soc.* **2007**, *129*, 3500–3501.
(50) Schummer, J. Gestalt Switch in Molecular Image Perception: The Aesthetic Origin of Molecular Nanotechnology in Supramolecular Chemistry. *Found. Chem.* **2006**, *8*, 53–72.
(51) Busch, D. H. Structural Definition of Chemical Templates and the Prediction of New and Unusual Materials. *J. Incl. Phenom. Macrocycl. Chem.* **1992**, *12*, 389–395.
(52) Olson, M. A.; Braunschweig, A. B.; Ikeda, T.; Fang, L.; Trabolsi, A.; Slawin, A. M. Z.; Khan, S. I.; Stoddart, J. F. Thermodynamic Forecasting of Mechanically Interlocked Switches. *Org. Biomol. Chem.* **2009**, *7*, 4391–4405.
(53) Walba, D. M. Topological Stereochemistry. *Tetrahedron* **1985**, *41*, 3161–3212.

Appendix B: Cover Art Gallery

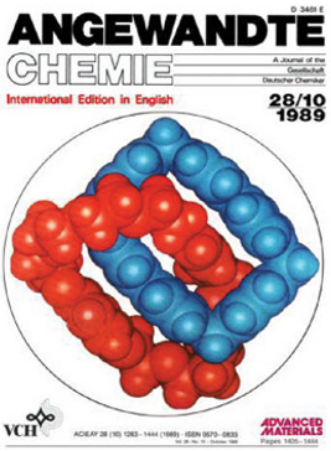
The images in the following gallery of journal cover art portraying mechanically interlocked structures have been reprinted with permission from the publishers. Page 742: *Nature Phys*,[1] *Nature Mater*,[2] *Nature Struct Molec Biol*,[3] *Nature Chem*,[4–7] copyright Nature Publishing Group. Page 743: *Angew Chem,*[8–24] copyright Wiley. Page 744: *Chem Commun*,[25–41] copyright Royal Society of Chemistry. Page 745: *Chem Eur J*,[42–54], copyright Wiley. Page 746: *Acc Chem Res*,[55–57] *Chem Rev*,[58] *J Am Chem Soc*,[59] *J Phys Chem A*,[60] *J Phys Chem B*,[61] *Macromolecules*,[62,63] *J Chem Ed*,[64] *Langmuir*,[65] *Crystal Growth Des*,[66] *J Org Chem*,[67,68] copyright American Chemical Society. Pages 747–748: *Chem Soc Rev*,[69–74] *Nanoscale*,[75] *Chem Sci*,[76,77] *Soft Matter*,[78,79] *Polymer Chem*,[80,81] *Phys Chem Chem Phys*,[82] *J Mater Chem*,[83] *Dalton Trans*,[84–87] *Org Biomol Chem*,[88–94], *New J Chem*,[95–98] copyright Royal Society of Chemistry. Page 749 (other titles): *Molecular Catenanes, Rotaxanes, and Knots*,[99] *Functional Organic Materials*,[100] *From Non-Covalent Assemblies to Molecular Machines*,[101] *Molecular Devices and Machines: A Journey Into the Nanoworld*,[102] *Supramolecular Polymer Chemistry*,[103] copyright Wiley-VCH. *Adv Mater,*[104] *Adv Funct Mater*,[105] *Chem Asian J*,[106] *Eur J Org Chem*,[107] *Eur J Inorg Chem*,[108] *ChemPlusChem*, [109] *ChemPhysChem*,[110] *Macromol Chem Phys*,[111,112] *Macromol Rapid Comm*,[113] copyright Wiley. *Chem Biol*,[114] copyright Elsevier. *PNAS*,[115] copyright National Academy of Sciences. *Nucleic Acids Res*,[116] copyright Oxford University Press. *Polym J*,[117] copyright Nature Publishing Group. *Aust J Chem*,[118] copyright CSIRO Publishing.



© 2017 John Wiley & Sons, Inc. Published 2017 by John Wiley & Sons, Inc.


D 3461
ANGEWANDTE
CHEMIE
A Journal of the Gesellschaft Deutscher Chemiker
International Edition in English
1995
34/11
Inside:
CHEMISTRY
A EUROPEAN JOURNAL
Reviews: Thermoanalytical Techniques · Chiral Metallocene Catalysts
Highlights: Synthetic Ribozymes · Structure of a [NiFe] Hydrogenase
VCH


ANGEWANDTE
CHEMIE
International Edition in English
28/ 2
1989
VCH
ADVANCED

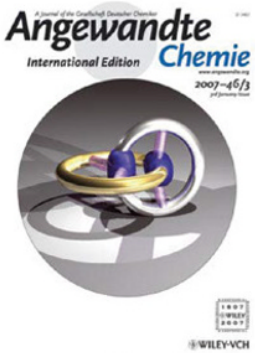

ANGEWANDTE
CHEMIE
International Edition in English
28/10
1989
VCH
ADVANCED MATERIALS

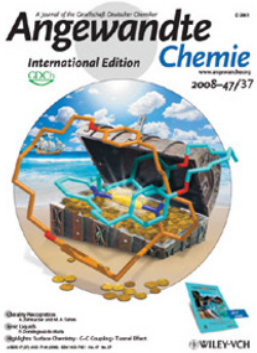

ANGEWANDTE
CHEMIE
28/ 7
1989

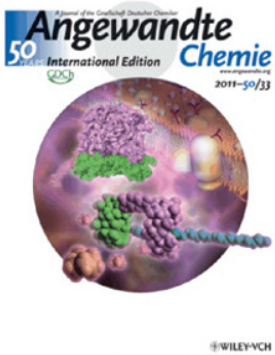

Angewandte
International Edition
Chemie


Angewandte
International Edition
Chemie
WILEY-VCH


Angewandte
International Edition
Chemie
WILEY-VCH

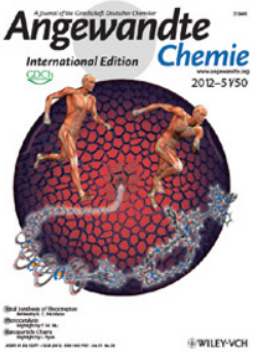

Angewandte
International Edition
Chemie
2007–46/3
WILEY-VCH


Angewandte
International Edition
Chemie
2008–47/37
WILEY-VCH

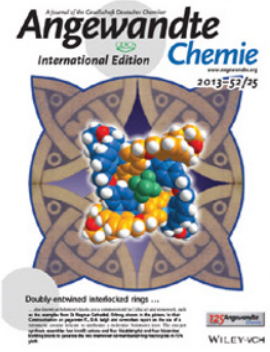

Angewandte
50 Years
International Edition
Chemie
2011–50/33
WILEY-VCH


Angewandte
50 Years
International Edition
Chemie
2011–50/51
WILEY-VCH

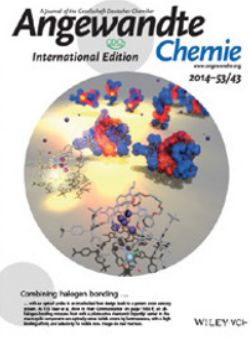

Angewandte
International Edition
Chemie
2012–51/10
WILEY-VCH

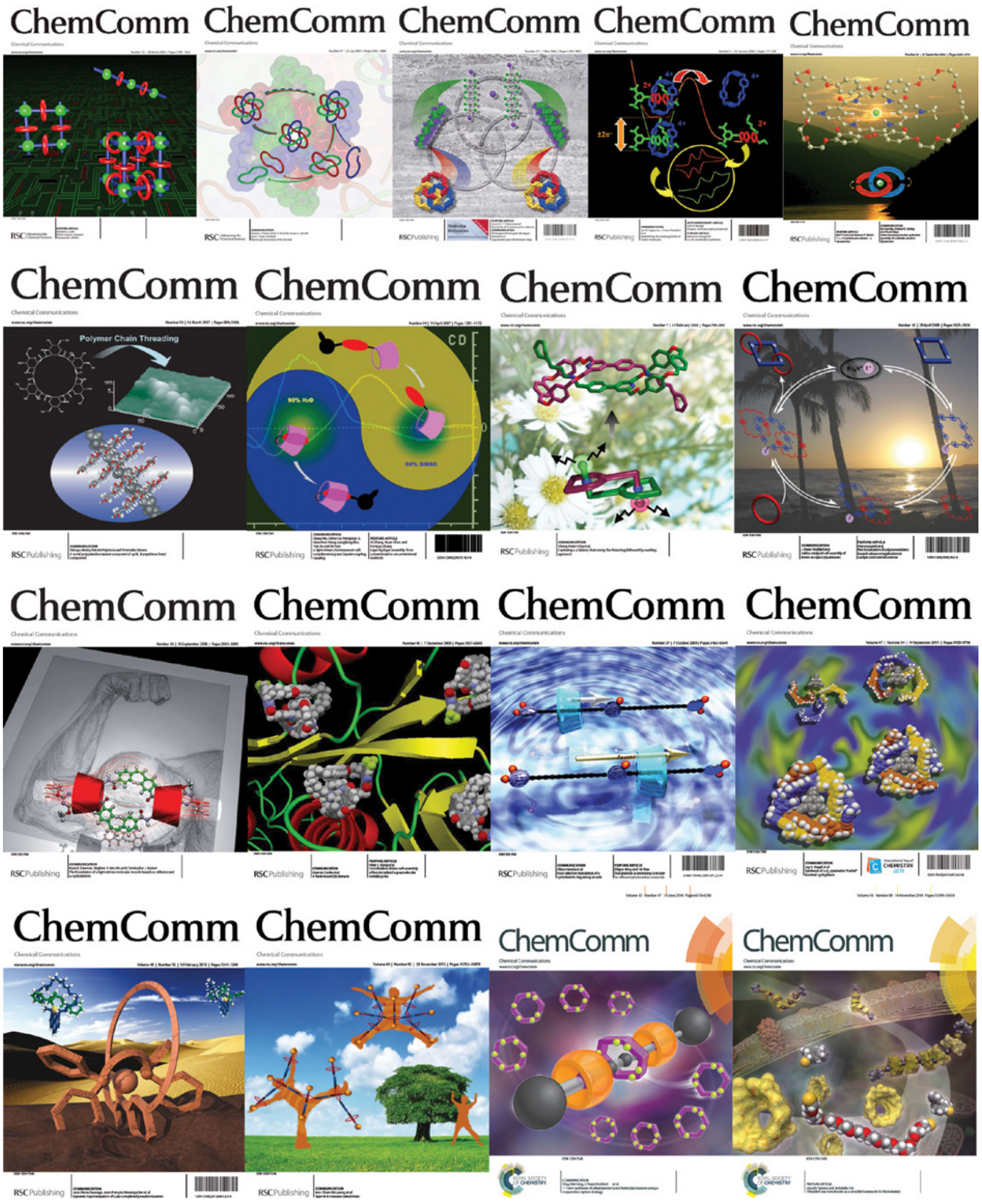

Angewandte
International Edition
Chemie
2012–5150
WILEY-VCH


Angewandte
International Edition
Chemie
2013–52/3
WILEY-VCH


Angewandte
International Edition
Chemie
2013–52/25
Doubly-entwined interlocked rings ...
WILEY-VCH


Angewandte
International Edition
Chemie
2013–52/38
WILEY-VCH


Angewandte
International Edition
Chemie
2014–53/43
WILEY-VCH


ChemComm
Chemical Communications
RSC Publishing
Polymer Chain Threading
CD
90% H2O
90% DMSO


CHEMISTRY
A EUROPEAN JOURNAL
9/2
2003
CHEMISTRY
A EUROPEAN JOURNAL
12/1
2006
Catenanes
Rotaxanes
CHEMISTRY
A EUROPEAN JOURNAL
18/44
2012
WILEY-VCH
www.chemeurj.org
CHEMISTRY
A EUROPEAN JOURNAL
14/11
2008
CHEMISTRY
A EUROPEAN JOURNAL
15/21
2009
CHEMISTRY
A EUROPEAN JOURNAL
16/13
2010
CHEMISTRY
A EUROPEAN JOURNAL
16/39
2010
CHEMISTRY
A EUROPEAN JOURNAL
17/1
2011
CHEMISTRY
A EUROPEAN JOURNAL
17/3
2011
CHEMISTRY
A EUROPEAN JOURNAL
17/14
2011
Symmetrical
Unsymmetrical
CHEMISTRY
A EUROPEAN JOURNAL
17/49
2011
Pseudorotaxane
Axle Substitution
CHEMISTRY
A EUROPEAN JOURNAL
19/9
2013
WANTED!
CHEMISTRY
A European Journal
2015-21/26

Appendix B


Special Issue on Molecular Machines
ACCOUNTS of CHEMICAL RESEARCH
ACCOUNTS of CHEMICAL RESEARCH
ACCOUNTS of CHEMICAL RESEARCH
p 5434
CHEMICAL REVIEWS
JACS
JOURNAL OF THE AMERICAN CHEMICAL SOCIETY
THE JOURNAL OF PHYSICAL CHEMISTRY A
THE JOURNAL OF PHYSICAL CHEMISTRY B
Macromolecules
Macromolecules
Cyclodextrin polyrotaxane
Polyrotaxane brush by ATRP
Burst to cyclodextrin stars
Chemical Education
Langmuir
The ACS Journal of Surfaces and Colloids
Rational Adjustment of Multicolor Emissions by Cucurbiturils-Based Host–Guest Chemistry and Photochemistry
CRYSTAL GROWTH & DESIGN
JOC The Journal of Organic Chemistry
JOC The Journal of Organic Chemistry
PUBLISHED BY THE AMERICAN CHEMICAL SOCIETY
ACS Publications


Chem Soc Rev
Chemical Society Reviews
Themed issue: Dedicated to Professor Jean-Pierre Sauvage
RSC Publishing
Chem Soc Rev
Chemical Society Reviews
RSC Publishing
Chem Soc Rev
Chemical Society Reviews
RSC Publishing
Chem Soc Rev
Chemical Society Reviews
RSC Publishing
Chem Soc Rev
Chemical Society Reviews
Themed issue: Alfred Werner Nobel Prize 100 year celebration
RSC Publishing
Chem Soc Rev
Chemical Society Reviews
RSC Publishing
Chem Soc Rev
Chemical Society Reviews
Themed issue: Supramolecular polymers
RSC Publishing
Nanoscale
NCNST
RSC Publishing
Chemical Science
RSC Publishing
Chemical Science
Soft Matter
RSC Publishing
Soft Matter
Polymer Chemistry
RSC Publishing
Polymer Chemistry
PCCP
Physical Chemistry Chemical Physics
Journal of Materials Chemistry
Themed issue: Inorganic nanoparticles for biological sensing, imaging, and therapeutics
RSC Publishing


Dalton Transactions
An international journal of inorganic chemistry
Dalton Transactions
An international journal of inorganic chemistry
Dalton Transactions
An international journal of inorganic chemistry
Dalton Transactions
An international journal of inorganic chemistry
RSC Publishing
Organic & Biomolecular Chemistry
Organic & Biomolecular Chemistry
Organic & Biomolecular Chemistry
Organic & Biomolecular Chemistry
Organic & Biomolecular Chemistry
Organic & Biomolecular Chemistry
Organic & Biomolecular Chemistry
NJC
New Journal of Chemistry
An international journal of the chemical sciences
NJC
New Journal of Chemistry
An international journal of the chemical sciences
NJC
New Journal of Chemistry
An international journal of the chemical sciences
NJC
New Journal of Chemistry
A journal for new directions in chemistry
RSC Publishing
CNRS


WILEY-VCH
Molecular Catenanes, Rotaxanes and Knots
A Journey Through the World of Molecular Topology
J.-P. Sauvage, C. Dietrich-Buchecker (Eds.)
Edited by Thomas J. J. Müller and Uwe H. F. Bunz
Functional Organic Materials
Syntheses, Strategies and Applications
Volume 1
Edited by Jean-Pierre Sauvage and Pierre Gaspard
From Non-Covalent Assemblies to Molecular Machines
V. Balzani, M. Venturi, A. Credi
Molecular Devices and Machines
A Journey into the Nanoworld
Edited by Akira Harada
Supramolecular Polymer Chemistry
ADVANCED MATERIALS
www.advmat.de
ADVANCED FUNCTIONAL MATERIALS
Chemistry & Biology
A sliding clamp on duplex DNA
PNAS
Electron transfer in a molecular shuttle
CHEMISTRY
AN ASIAN JOURNAL
EurJOC
European Journal of Organic Chemistry
EurJIC
European Journal of Inorganic Chemistry
CHEMPLUSCHEM
CENTERING ON CHEMISTRY
3/2012
CHEMPHYSCHEM
Write
Read
6/2002
Macromolecular Rapid Communications
11/2009
Macromolecular Chemistry and Physics
10/2011
Macromolecular Chemistry and Physics
20/2009
Nucleic Acids Research
NAR ONELINE
Polymer Journal
AUSTRALIAN JOURNAL OF CHEMISTRY

Appendix B References

(1) Kleckner, D. Irvine, W. T. M. Creation and Dynamics of Knotted Vortices. *Nature Phys.* **2013**, *9*, 253–258.

(2) Martinez, A.; Ravnik, M.; Lucero, B.; Visvanathan, R.; Žumer, S.; Smalyukh, I. I. Mutually Tangled Colloidal Knots and Induced Defect Loops in Nematic Fields. *Nature Mater.* **2014**, *13*, 258–263.

(3) Mears, J. A.; Lackner, L. L.; Fang, S.; Ingerman, E.; Nunnari, J.; Hinshaw, J. E. Conformational Changes in Dnm1 Support a Contractile Mechanism for Mitochondrial Fission. *Nature Struct. Mol. Biol.* **2011**, *18*, 20–26.

(4) Baumes, J. M.; Gassensmith, J. J.; Giblin, J.; Lee, J.-J.; White, A. G.; Culligan, W. J.; Leevy, W. M.; Kuno, M.; Smith, B. D. Storable, Thermally Activated, Near-Infrared Chemiluminescent Dyes and Dye-Stainedmicroparticles for Optical Imaging. *Nature Chem.* **2010**, *2*, 1025–1030.

(5) Ayme, J.-F.; Beves, J. E.; Leigh, D. A.; McBurney, R. T.; Rissanen, K.; Schultz, D. A Synthetic Molecular Pentafoil Knot. *Nature Chem.* **2012**, *4*, 15–20.

(6) Vukotic, V. N.; Harris, K. J.; Zhu, K.; Schurko, R. W.; Loeb, S. J. Metal–Organic Frameworks with Dynamic Interlocked Components. *Nature Chem.* **2012**, *4*, 456–460.

(7) Langton, M. J.; Robinson, S. W.; Marques, I.; Félix, V. T.; Beer, P. D. Halogen Bonding in Water Results in Enhanced Anion Recognition in Acyclic and Rotaxane Hosts. *Nature Chem.* **2014**, *6*, 1039–1043.

(8) Dietrich-Buchecker, C. O.; Guilhem, J.; Khemiss, A.-K.; Kintzinger, J.-P.; Pascard, C.; Sauvage, J.-P. Molecular Structure of a [3]-Catenate: Curling up of the Interlocked System by Interaction Between Two Copper Complex Subunits. *Angew. Chem., Int. Ed. Engl.* **1987**, *26*, 661–663.

(9) Dietrich-Buchecker, C. O.; Sauvage, J.-P. A Synthetic Molecular Trefoil Knot. *Angew. Chem., Int. Ed. Engl.* **1989**, *28*, 189–192.

(10) Ashton, P. R.; Goodnow, T. T.; Kaifer, A. E.; Reddington, M. V.; Slawin, A. M. Z.; Spencer, N.; Stoddart, J. F.; Vicent, C.; Williams, D. J. A [2]Catenane Made to Order. *Angew. Chem., Int. Ed. Engl.* **1989**, *28*, 1396–1399.

(11) Johnston, A. G.; Leigh, D. A.; Pritchard, R. J.; Deegan, M. D. Facile Synthesis and Solid-State Structure of a Benzylic Amide [2]Catenane. *Angew. Chem., Int. Ed. Engl.* **1995**, *34*, 1209–1212.

(12) Sánchez-Quesada, J.; Saghatelian, A.; Cheley, S.; Bayley, H.; Ghadiri, M. R. Single DNA Rotaxanes of a Transmembrane Pore Protein. *Angew. Chem., Int. Ed.* **2004**, *43*, 3063–3067.

(13) Leigh, D. A.; Morales, M. A. F.; Pérez, E. M.; Wong, J. K. Y.; Saiz, C. G.; Slawin, A. M. Z.; Carmichael, A. J.; Haddleton, D. M.; Brouwer, A. M.; Buma, W. J.; Wurpel, G. W. H.; León, S.; Zerbetto, F. Patterning Through Controlled Submolecular Motion: Rotaxane-Based Switches and Logic Gates That Function in Solution and Polymer Films. *Angew. Chem., Int. Ed.* **2005**, *44*, 3062–3067.

(14) Lukin, O.; Vögtle, F. Knotting and Threading of Molecules: Chemistry and Chirality of Molecular Knots and Their Assemblies. *Angew. Chem., Int. Ed.* **2005**, *44*, 1456–1477.

(15) Bäuerle, P.; Ammann, M.; Wilde, M.; Götz, G.; Mena- Osteritz, E.; Rang, A.; Schalley, C. A. Oligothiophene- Based Catenanes: Synthesis and Electronic Properties of a Novel Conjugated Topological Structure. *Angew. Chem., Int. Ed.* **2007**, *46*, 363–368.

(16) Goldup, S. M.; Leigh, D. A.; Lusby, P. J.; McBurney, R. T.; Slawin, A. M. Z. Gold(I)-Template Catenane and Rotaxane Synthesis. *Angew. Chem., Int. Ed.* **2008**, *47*, 6999–7003.

(17) Barran, P. E.; Cole, H. L.; Goldup, S. M.; Leigh, D. A.; McGonigal, P. R.; Symes, M. D.; Wu, J.; Zengerle, M. Active-Metal Template Synthesis of a Molecular Trefoil Knot. *Angew. Chem., Int. Ed.* **2011**, *50*, 12280–12284.

(18) Elbaz, J.; Wang, Z.-G.; Wang, F.; Willner, I. Programmed Dynamic Topologies in DNA Catenanes. *Angew. Chem., Int. Ed.* **2012**, *51*, 2349–2353.

(19) Beves, J. E.; Campbell, C. J.; Leigh, D. A.; Pritchard, R. G. Tetrameric Cyclic Double Helicates as a Scaffold for a Molecular Solomon Link. *Angew. Chem., Int. Ed.* **2013**, *52*, 6464–6467.

(20) Prakasam, T.; Lusi, M.; Elhabiri, M.; Platas-Iglesias, C.; Olsen, J.-C.; Asfari, Z.; Cianférani-Sanglier, S.; Debaene, F.; Charbonnière, L. J.; Trabolsi, A. Simultaneous Self-Assembly of a [2]Catenane, a Trefoil Knot, and a Solomon Link From a Simple Pair of Ligands. *Angew. Chem., Int. Ed.* **2013**, *52*, 9956–9960.

(21) Mullaney, B. R.; Thompson, A. L.; Beer, P. D. An All-Halogen Bonding Rotaxane for Selective Sensing of Halides in Aqueous Media. *Angew. Chem., Int. Ed.* **2014**, *53*, 11458–11462.

(22) Takashima, Y.; Osaki, M.; Ishimaru, Y.; Yamaguchi, H.; Harada, A. Artificial Molecular Clamp: A Novel Device for Synthetic Polymerases. *Angew. Chem., Int. Ed.* **2011**, *50*, 7524–7528.

(23) Du, G.; Moulin, E.; Jouault, N.; Buhler, E.; Giuseppone, N. Muscle-Like Supramolecular Polymers: Integrated Motion From Thousands of Molecular Machines. *Angew. Chem., Int. Ed.* **2012**, *51*, 12504–12508.

(24) Caputo, C. B.; Zhu, K.; Vukotic, V. N.; Loeb, S. J.; Stephan, D. W. Heterolytic Activation of H_2 Using a Mechanically Interlocked Molecule as a Frustrated Lewis Base. *Angew. Chem., Int. Ed.* **2013**, *52*, 960–963.

(25) Loeb, S. J. Metal–Organic Rotaxane Frameworks; MORFs. *Chem. Commun.* **2005**, 1511–1518.

(26) Peters, A. J.; Chichak, K. S.; Cantrill, S. J.; Stoddart, J. F. Nanoscale Borromean Links for Real. *Chem. Commun.* **2005**, 3394–3396.

(27) Liantonio, R.; Metrangolo, P.; Meyer, F.; Pilati, T.; Navarrini, W.; Resnati, G. Metric Engineering of Supramolecular Borromean Rings. *Chem. Commun.* **2006**, 1819–1821.

(28) Nygaard, S.; Laursen, B.; Flood, A. H.; Hansen, C.; Jeppesen, J. O.; Stoddart, J. F. Quantifying the Working Stroke of Tetrathiafulvalene-Based Electrochemically-Driven Linear Motor-Molecules. *Chem. Commun.* **2006**, 144–146.

(29) Ng, K.-Y.; Cowley, A. R.; Beer, P. D. Anion Templated Double Cyclization Assembly of a Chloride Selective [2]Catenane. *Chem. Commun.* **2006**, 3676–3678.

(30) Hirata, T.; Fujimura, F.; Kimura, S. A Novel Polypseudorotaxane Composed of Cyclic Beta-Peptide as Bead Component. *Chem. Commun.* **2007**, 1023–1025.

(31) Ma, X.; Qu, D.; Ji, F.; Wang, Q.; Zhu, L.; Xu, Y.; Tian, H. A Light-Driven [1]Rotaxane *via* Self-Complementary and Suzuki-Coupling Capping. *Chem. Commun.* **2007**, 1409–1411.

(32) Ueng, S.-H.; Hsueh, S.-Y.; Lai, C.-C.; Liu, Y.-H.; Peng, S.-M.; Chiu, S.-H. Capturing a [*c*2]Daisy Chain Using the Threading-Followed-by-Swelling Approach. *Chem. Commun.* **2008**, 817–819.

(33) Patel, K.; Miljanić, O. Š.; Stoddart, J. F. Iodide-Catalysed Self-Assembly of Donor-Acceptor [3]Catenanes. *Chem. Commun.* **2008**, 1853–1855.

(34) Dawson, R. E.; Lincoln, S. F.; Easton, C. J. The Foundation of a Light Driven Molecular Muscle Based on Stilbene and α-Cyclodextrin. *Chem. Commun.* **2008**, 3980–3982.

(35) Caldwell, S. T.; Cooke, G.; Fitzpatrick, B.; Long, D.-L.; Rabani, G.; Rotello, V. M. A Flavin-Based [2]Catenane. *Chem. Commun.* **2008**, 5912–5914.

(36) Oshikiri, T.; Yamaguchi, H.; Takashima, Y.; Harada, A. Face Selective Translation of a Cyclodextrin Ring Along an Axle. *Chem. Commun.* **2009**, 5515–5517.

(37) Arias, K. I.; Zysman-Colman, E.; Loren, J. C.; Linden, A.; Siegel, J. S. Synthesis of a D_3-Symmetric "Trefoil" Knotted Cyclophane. *Chem. Commun.* **2011**, *47*, 9588–9590.

(38) Mohankumar, M.; Holler, M.; Schmitt, M.; Sauvage, J.-P.; Nierengarten, J.-F. Dynamic Topomerization of Cu(I)-Complexed Pseudorotaxanes. *Chem. Commun.* **2013**, *49*, 1261–1263.

(39) Ho, W. K. W.; Lee, S.-F.; Wong, C.-H.; Zhu, X.-M.; Kwan, C.-S.; Chak, C.-P.; Mendes, P. M.; Cheng, C. H. K.; Leung, K. C.-F.

Type III-B Rotaxane Dendrimers. *Chem. Commun.* **2013**, *49*, 10781–10783.
(40) Hou, X.; Ke, C.; Cheng, C.; Song, N.; Blackburn, A. K.; Sarjeant, A. A.; Botros, Y. Y.; Yang, Y.-W.; Stoddart, J. F. Efficient Syntheses of Pillar[6]arene-Based Hetero[4]rotaxanes Using a Cooperative Capture Strategy. *Chem. Commun.* **2014**, *50*, 6196–6199.
(41) Tamura, A.; Yui, N. Threaded Macromolecules as a Versatile Framework for Biomaterials. *Chem. Commun.* **2014**, *50*, 13433–13446.
(42) Tseng, H.-R.; Vignon, S. A.; Celestre, P. C.; Stoddart, J. F.; White, A. J. P.; Williams, D. J. Molecular Meccano 66. Dynamic Chirality: Keen Selection in the Face of Stereochemical Diversity in Mechanically Bonded Compounds. *Chem. Eur. J.* **2003**, *9*, 543–556.
(43) Choi, J. W.; Flood, A. H.; Steuerman, D. W.; Nygaard, S.; Braunschweig, A. B.; Moonen, N. N. P.; Laursen, B. W.; Luo, Y.; DeIonno, E.; Peters, A. J.; Jeppesen, J. O.; Xu, K.; Stoddart, J. F.; Heath, J. R. Ground-State Equilibrium Thermodynamics and Switching Kinetics of Bistable [2]Rotaxanes Switched in Solution, Polymer Gels, and Molecular Electronic Devices. *Chem. Eur. J.* **2006**, *12*, 261–279.
(44) Hirose, K.; Shiba, Y.; Ishibashi, K.; Doi, Y.; Tobe, Y. A Shuttling Molecular Machine with Reversible Brake Function. *Chem. Eur. J.* **2008**, *14*, 3427–3433.
(45) Coutrot, F.; Busseron, E. Controlling the Chair Conformation of a Mannopyranose in a Large-Amplitude [2]Rotaxane Molecular Machine. *Chem. Eur. J.* **2009**, *15*, 5186–5190.
(46) Zalewski, L.; Wykes, M.; Brovelli, S.; Bonini, M.; Breiner, T.; Kastler, M.; Dötz, F.; Beljonne, D.; Anderson, H. L.; Cacialli, F.; Samorì, P. A Conjugated Thiophene-Based Rotaxane: Synthesis, Spectroscopy, and Modeling. *Chem. Eur. J.* **2010**, *16*, 3933–3941.
(47) Clever, G. H.; Shionoya, M. A pH Switchable Pseudorotaxane Based on a Metal Cage and a Bis-Anionic Thread. *Chem. Eur. J.* **2010**, *16*, 11792–11796.
(48) Barin, G.; Coskun, A.; Friedman, D. C.; Olson, M. A.; Colvin, M. T.; Carmielli, R.; Dey, S. K.; Bozdemir, O. A.; Wasielewski, M. R.; Stoddart, J. F. A Multistate Switchable [3]Rotacatenane. *Chem. Eur. J.* **2011**, *17*, 213–222.
(49) Liu, J.; Du, X.; Zhang, X. Enzyme-Inspired Controlled Release of Cucurbit[7]uril Nanovalves by Using Magnetic Mesoporous Silica. *Chem. Eur. J.* **2011**, *17*, 810–815.
(50) Menuel, S.; Azaroual, N.; Landy, D.; Six, N.; Hapiot, F.; Monflier, E. Unusual Inversion Phenomenon of β- Cyclodextrin Dimers in Water. *Chem. Eur. J.* **2011**, *17*, 3949–3955.
(51) Saha, S.; Ravikumar, I.; Ghosh, P. A Fluorophoric-Axle- Based, Nonfluorescent, Metallo Anti-[3]Pseudorotaxane: Recovery of Fluorescence by Means of an Axle Substitution Reaction. *Chem. Eur. J.* **2011**, *17*, 13712–13719.
(52) Scarel, F.; Valenti, G.; Gaikwad, S.; Marcaccio, M.; Paolucci, F.; Mateo-Alonso, A. A Molecular Shuttle Driven by Fullerene Radical-Anion Recognition. *Chem. Eur. J.* **2012**, *18*, 14063–14068.
(53) Clavel, C.; Romuald, C.; Brabet, E.; Coutrot, F. A pH- Sensitive Lasso-Based Rotaxane Molecular Switch. *Chem. Eur. J.* **2013**, *19*, 2982–2989.
(54) Martí-Centelles, V.; Beer, P. D.Nitrate Anion Recognition in Organic-Aqueous Solvent Mixtures by a Bis(triazolium)acridine-Containing [2]Rotaxane. *Chem. Eur. J.* **2015**, *21*, 9397–9404.
(55) Pease, A. R.; Jeppesen, J. O.; Stoddart, J. F.; Luo, Y.; Collier, C. P.; Heath, J. R. Switching Devices Based on Interlocked Molecules. *Acc. Chem. Res.* **2001**, *34*, 433–444.
(56) Evans, O. R.; Lin, W. Crystal Engineering of NLO Materials Based on Metal–Organic Coordination Networks. *Acc. Chem. Res.* **2002**, *35*, 511–522.
(57) Cantrill, S. J.; Chichak, K. S.; Peters, A. J.; Stoddart, J. F. Nanoscale Borromean Rings. *Acc. Chem. Res.* **2005**, *38*, 1–9.
(58) Forgan, R. S.; Sauvage, J.-P.; Stoddart, J. F. Chemical Topology: Complex Molecular Knots, Links, and Entanglements. *Chem. Rev.* **2011**, *111*, 5434–5464.
(59) Barnes, J. C.; Juríček, M.; Strutt, N. L.; Frasconi, M.; Sampath, S.; Giesener, M. A.; McGrier, P. L.; Bruns, C. J.; Stern, C. L.; Sarjeant, A. A.; Stoddart, J. F. ExBox: a Polycyclic Aromatic Hydrocarbon Scavenger. *J. Am. Chem. Soc.* **2013**, *135*, 183–192.
(60) Sandanayaka, A. S. D.; Sasabe, H.; Araki, Y.; Kihara, N.; Furusho, Y.; Takata, T.; Ito, O. Axle Length Effect on Photoinduced Electron Transfer in Triad Rotaxane with Porphyrin, [60]Fullerene, and Triphenylamine. *J. Phys. Chem. A* **2010**, *114*, 5242–5250.
(61) Ceccarelli, M.; Mercuri, F.; Passerone, D.; Parrinello, M. The Microscopic Switching Mechanism of a [2]Catenane. *J. Phys. Chem. B* **2005**, *109*, 17094–17099.
(62) Lee, Y.-G.; Koyama, Y.; Yonekawa, M.; Takata, T. Synthesis of Main-Chain-Type Polyrotaxanes by New Click Polymerization Using Homoditopic Nitrile *N*-Oxides *via* Rotaxanation–Polymerization Protocol. *Macromolecules* **2010**, *43*, 4070–4080.
(63) Teuchert, C.; Michel, C.; Hausen, F.; Park, D.-Y.; Beckham, H. W.; Wenz, G. Cylindrical Polymer Brushes by Atom Transfer Radical Polymerization From Cyclodextrin–PEG Polyrotaxanes: Synthesis and Mechanical Stability. *Macromolecules* **2013**, *46*, 2–7.
(64) Pentecost, C. D.; Tangchaivang, N.; Cantrill, S. J.; Chichak, K. S.; Peters, A. J.; Stoddart, J. F. Making Molecular Borromean Rings – A Gram-Scale Synthetic Procedure for the Undergraduate Organic Lab. *J. Chem. Ed.* **2007**, *84*, 855–859.
(65) Yang, H.; Liu, Y.; Liu, K.; Yang, L.; Wang, Z.; Zhang, X. Rational Adjustment of Multicolor Emissions by Cucurbiturils-Based Host–Guest Chemistry and Photochemistry. *Langmuir* **2013**, *29*, 12909–12914.
(66) Jin, J.-C.; Wang, Y.-Y.; Liu, P.; Liu, R.-T.; Ren, C.; Shi, Q.-Z. An Unusual Independent 1D Metal–Organic Nanotube with Mesohelical Structure and 1D → 2D Interdigitation. *Crystal Growth Des.* **2010**, *10*, 2029–2032.
(67) Balzani, V.; Credi, A.; Mattersteig, G.; Matthews, O. A.; Raymo, F. M.; Stoddart, J. F.; Venturi, M.; White, A. J. P.; Williams, D. J. Molecular Meccano 54. Switching of Pseudorotaxanes and Catenanes Incorporating a Tetrathiafulvalene Unit by Redox and Chemical Inputs. *J. Org. Chem.* **2000**, *65*, 1924–1936.
(68) Schuster, D. I. Reflections on a Fifty-Year Career in Organic Photochemistry: A Personal Perspective. *J. Org. Chem.* **2013**, *78*, 6811–6841.
(69) Meyer, C. D.; Joiner, C. S.; Stoddart, J. F. Template- Directed Synthesis Employing Reversible Imine Bond Formation. *Chem. Soc. Rev.* **2007**, *36*, 1705–1723.
(70) Stoddart, J. F. The Master of Chemical Topology. *Chem. Soc. Rev.* **2009**, *38*, 1521–1529.
(71) Fang, L.; Olson, M. A.; Benítez, D.; Tkatchouk, E.; Goddard, W. A., III; Stoddart, J. F. Mechanically Bonded Macromolecules. *Chem. Soc. Rev.* **2010**, *39*, 17–29.
(72) Coskun, A.; Spruell, J. M.; Barin, G.; Dichtel, W. R.; Flood, A. H.; Botros, Y. Y.; Stoddart, J. F. High Hopes: Can Molecular Electronics Realise Its Potential? *Chem. Soc. Rev.* **2012**, *41*, 4827–4859.
(73) Avestro, A.-J.; Belowich, M. E.; Stoddart, J. F. Cooperative Self-Assembly: Producing Synthetic Polymers with Precise and Concise Primary Structures. *Chem. Soc. Rev.* **2012**, *41*, 5881.
(74) Ayme, J.-F.; Beves, J. E.; Campbell, C. J.; Leigh, D. A. Template Synthesis of Molecular Knots. *Chem. Soc. Rev.* **2013**, *42*, 1700–1712.
(75) de Juan, A.; Pérez, E. M. Getting Tubed: Mechanical Bond in Endohedral Derivatives of Carbon Nanotubes? *Nanoscale* **2013**, *5*, 7141–7148.
(76) Langton, M. J.; Matichak, J. D.; Thompson, A. L.; Anderson, H. L. Template-Directed Synthesis of π- Conjugated Porphyrin [2]Rotaxanes and a [4]Catenane Based on a Six-Porphyrin Nanoring. *Chem. Sci.* **2011**, *2*, 1897–1901.
(77) Chen, Q.; Jiang, F.; Yuan, D.; Lyu, G.; Chen, L.; Hong, M. A Controllable and Dynamic Assembly System Based on Discrete Metallocages. *Chem. Sci.* **2014**, *5*, 483–488.

(78) Tong, X.; Zhang, X.; Ye, L.; Zhang, A.-Y.; Feng, Z.-G. Synthesis and Characterization of Block Copolymers Comprising a Polyrotaxane Middle Block Flanked by Two Brush-Like PCL Blocks. *Soft Matter* **2009**, *5*, 1848–1855.

(79) Renner, C. B.; Doyle, P. S. Stretching Self-Entangled DNA Molecules in Elongational Fields. *Soft Matter* **2015**, *11*, 3105–3114.

(80) Leung, K. C.-F.; Lau, K.-N. Self-Assembly and Thermodynamic Synthesis of Rotaxane Dendrimers and Related Structures. *Polym. Chem.* **2010**, *1*, 988–1000.

(81) Li, S.; Weng, G.-H.; Lin, W.; Sun, Z.-B.; Zhou, M.; Zhu, B.; Ye, Y.; Wu, J. An Acid/Base Switchable and Reversibly Cross-Linkable Polyrotaxane. *Polym. Chem.* **2014**, *5*, 3994–4001.

(82) Panman, M. R.; Bodis, P.; Shaw, D. J.; Bakker, B. H.; Newton, A. C.; Kay, E. R.; Leigh, D. A.; Buma, W. J.; Brouwer, A. M.; Woutersen, S. Time-Resolved Vibrational Spectroscopy of a Molecular Shuttle. *Phys. Chem. Chem. Phys.* **2012**, *14*, 1865–1875.

(83) Liong, M.; Angelos, S.; Choi, E.; Patel, K.; Stoddart, J. F.; Zink, J. I. Mesostructured Multifunctional Nanoparticles for Imaging and Drug Delivery. *J. Mater. Chem.* **2009**, *19*, 6251–6257.

(84) Suzaki, Y.; Taira, T.; Osakada, K. Irreversible and Reversible Formation of a [2]Rotaxane Containing Platinum(II) Complex with an *N*-Alkyl Bipyridinium Ligand as the Axis Component. *Dalton Trans.* **2006**, 5345–5351.

(85) Suzaki, Y.; Osakada, K. Ferrocene-Containing [2]- and [3]Rotaxanes. Preparation *via* an End-Capping Cross-Metathesis Reaction and Electrochemical Properties. *Dalton Trans.* **2007**, 2376–2383.

(86) Suzaki, Y.; Taira, T.; Osakada, K.; Horie, M. Rotaxanes and Pseudorotaxanes with Fe-, Pd- and Pt-Containing Axles. Molecular Motion in the Solid State and Aggregation in Solution. *Dalton Trans.* **2008**, 4823–4833.

(87) Alvariño, C.; Terenzi, A.; Blanco, V.; García, M. D.; Peinador, C.; Quintela, J. M. [2]Catenanes and Inclusion Complexes Derived From Self-Assembled Rectangular Pd^{II} and Pt^{II} Metallocycles. *Dalton Trans*. **2012**, *41*, 11992–11998.

(88) Georges, N.; Loeb, S. J.; Tiburcio, J.; Wisner, J. A. [2]Rotaxanes Containing Pyridinium-Phosphonium Axles and 24-Crown-8 Ether Wheels. *Org. Biomol. Chem.* **2004**, *2*, 2751–2756.

(89) Ghosh, P.; Federwisch, G.; Kogej, M.; Schalley, C. A.; Haase, D.; Saak, W.; Lützen, A.; Gschwind, R. M. Controlling the Rate of Shuttling Motions in [2]Rotaxanes by Electrostatic Interactions: A Cation as Solvent-Tunable Brake. *Org. Biomol. Chem.* **2005**, *3*, 2691–2700.

(90) Cheetham, A. G.; Claridge, T. D. W.; Anderson, H. L. Metal-Driven Ligand Assembly in the Synthesis of Cyclodextrin [2] and [3]Rotaxanes. *Org. Biomol. Chem.* **2007**, *5*, 457–462.

(91) Mullen, K. M.; Johnstone, K. D.; Webb, M.; Bampos, N.; Sanders, J. K. M.; Gunter, M. J. Monitoring the Thermodynamically-Controlled Formation of Diimide-Based Resin-Attached Rotaxanes by Gel-Phase HR MAS ^{1}H NMR Spectroscopy. *Org. Biomol. Chem.* **2008**, *6*, 278–286.

(92) Olson, M. A.; Braunschweig, A. B.; Ikeda, T.; Fang, L.; Trabolsi, A.; Slawin, A. M. Z.; Khan, S. I.; Stoddart, J. F. Thermodynamic Forecasting of Mechanically Interlocked Switches. *Org. Biomol. Chem.* **2009**, *7*, 4391–4405.

(93) Chhun, C.; Richard-Daniel, J.; Kempf, J.; Schmitzer, A. R. Transport of Macrocyclic Compounds Across Phospholipid Bilayers by Umbrella-Rotaxane s. *Org. Biomol. Chem.* **2013**,*11*, 6023–6028.

(94) Li, Z.; Hu, F.; Liu, G.; Xue, W.; Chen, X.; Shen, J.; Yin, J. Photo-Responsive [2]Catenanes: Synthesis and Properties. *Org. Biomol. Chem.* **2014**, *12*, 7702–7711.

(95) Castle, T.; Evans, M. E.; Hyde, S. T. Ravels: Knot-Free but Not Free. Novel Entanglements of Graphs in 3-Space. *New J. Chem*. **2008**, *32*, 1484–1492.

(96) Yamashita, K.-I.; Sato, K.-I.; Kawano, M.; Fujita, M. Photoinduced Self-Assembly of Pt(II)-Linked Rings and Cages *via* the Photolabilization of a Pt(II)-Pyridine Bond. *New J. Chem.* **2009**, *33*, 264–270.

(97) Collin, J.-P.; Durola, F.; Lux, J.; Sauvage, J.-P. A Copper- Based Shuttling [2]Rotaxane with Two Bidentate Chelates in the Axis: Steric Control of the Motion. *New J. Chem.* **2010**, *34*, 34–43.

(98) Raymont, V.; Wilson, H.; Pfrunder, M.; McMurtrie, J. C.; Mullen, K. M. New Approaches to the Synthesis of Strapped Porphyrin Containing Bipyridinium [2]Rotaxanes. *New J. Chem.* **2013**, *37*, 893–900.

(99) *Molecular Catenanes, Rotaxanes, and Knots*; Dietrich-Buchecker, C. O.; Sauvage, J.-P., Eds.; Wiley-VCH: Weinheim, 1999.

(100) *Functional Organic Materials: Syntheses, Strategies, and Applications*; Müller, T. J. J.; Bunz, U. H. F., Eds.; Wiley-VCH: Weinheim, 2007.

(101) *From Non-Covalent Assemblies to Molecular Machines*; Sauvage, J.-P.; Gaspard, P., Eds.; Wiley-VCH: Weinheim, 2011.

(102) Balzani, V.; Venturi, M.; Credi, A. *Molecular Devices and Machines: A Journey Into the Nanoworld*; Wiley-VCH: Weinheim, 2003.

(103) *Supramolecular Polymer Chemistry*; Harada, A., Ed.; Wiley-VCH: Weinheim, 2012.

(104) Dam, H. H.; Caruso, F. Construction and Degradation of Polyrotaxane Multilayers. *Adv. Mater.* **2011**, *23*, 3026–3029.

(105) Saha, S.; Leung, K. C.-F.; Nguyen, T. D.; Stoddart, J. F.; Zink, J. I. *Nanovalves. Adv. Funct. Mater.* **2007**, *17*, 685– 693.

(106) Zhao, Y.-L.; Benítez, D.; Yoon, I.; Stoddart, J. F. Inclusion Behavior of β-Cyclodextrin with Bipyridine Molecules: Factors Governing Host-Guest Inclusion Geometries. *Chem. Asian J.* **2009**, *4*, 446–456.

(107) Sauvage, J.-P.; Trolez, Y.; Canevet, D.; Sallé, M. Intercalation of Tetrathiafulvalene Between the Two Plates of a Copper(I)-Complexed [4]Rotaxane. *Eur. J. Org. Chem.* **2011**, 2413–2416.

(108) Saha, S.; Santra, S.; Ghosh, P. Cu^{II}-Templated Threading of a Bis-Amide-Tris-Amine Macrocycle by Substituted 2,2′(-Bipyridyl Derivatives Assisted by Strong π–π Stacking and Second-Sphere H-Bonding Interactions. *Eur. J. Inorg. Chem.* **2014**, 2029–2037.

(109) Barin, G.; Coskun, A.; Fouda, M. M. G.; Stoddart, J. F. Mechanically Interlocked Molecules Assembled by π–π Recognition. *ChemPlusChem* **2012**, *77*, 159–185.

(110) Luo, Y.; Collier, C. P.; Jeppesen, J. O.; Nielsen, K. A.; DeIonno, E.; Ho, G.; Perkins, J.; Tseng, H.-R.; Yamamoto, T.; Stoddart, J. F.; Heath, J. R. Two-Dimensional Molecular Electronics Circuits. *ChemPhysChem* **2002**, *3*, 519–525.

(111) Wu, J.; Gao, C. Click Chemistry Approach to Rhodamine B- Capped Polyrotaxanes and Their Unique Fluorescence Properties. *Macromol. Chem. Phys.* **2009**, *210*, 1697–1708.

(112) Hu, J.; Hashidzume, A.; Harada, A. Photoregulated Switching of the Recognition Site of α-Cyclodextrin in a Side Chain Polyrotaxane Bearing Two Recognition Sites Linked with Oligo(ethylene glycol). *Macromol. Chem. Phys.* **2011**, *212*, 1032–1038.

(113) Fan, M.-M.; Yu, Z.-J.; Luo, H.-Y.; Zhang, S.; Li, B.-J. Supramolecular Network Based on the Self-Assembly of γ-Cyclodextrin with Poly(ethylene glycol) and Its Shape Memory Effect. *Macromol. Rapid Comm.* **2009**, *30*, 897–903.

(114) Ryan, K.; Kool, E. T. Triplex-Directed Self-Assembly of an Artificial Sliding Clamp on Duplex DNA. *Chem. Biol.* **1998**, *5*, 59–67.

(115) Barnes, J. C.; Fahrenbach, A. C.; Dyar, S. M.; Frasconi, M.; Giesener, M. A.; Zhu, Z.; Liu, Z.; Hartlieb, K. J.; Carmieli, R.; Wasielewski, M. R.; Stoddart, J. F. Mechanically Induced Intramolecular Electron Transfer in a Mixed- Valence Molecular Shuttle. *Proc. Natl. Acad. Sci. U.S.A.* **2012**, *109*, 11546–11551.

(116) Bucka, A.; Stasiak, A. Construction and Electrophoretic Migration of Single-Stranded DNA Knots and Catenanes. *Nucleic Acids Res.* **2002**, *30*, e24.

(117) Suzuki, S.; Matsuura, K.; Nakazono, K.; Takata, T. Effect of a Side Chain Rotaxane Structure on the Helix-Folding of Poly(*m*-phenylene diethynylene). *Polym. J.* **2014**, *46*, 355–365.

(118) Thordarson, P.; Nolte, R. J. M.; Rowan, A. E. Mimicking the Motion of Life: Catalytically Active Rotaxanes as Processive Enzyme Mimics. *Aust. J. Chem.* **2004**, *57*, 323–327.

Index

absolute configuration 26
absolute stereochemistry 52
acids 555, 576, 579, 581–92, 597–602, 609–11, 621, 630, 634, 636, 637–9, 641, 644–6, 649, 650, 663, 664, 667, 668, 680, 683, 687, 690, 692–4, 701
activation barriers 12, 23, 25
acylations 521, 572, 607–9, 634, 640, 700, 707
additions, conjugate 169
Alexander-Briggs notation 21, 61–2, 352, 354, 356
allosteric 555, 591, 594
amides 169
aminations, reductive 170
amphichirality 69
amphidynamic crystals 43
amphiphilicity 74
anions 555, 564, 566, 572–4, 577, 579, 580, 587, 589, 590, 597–604, 616, 617, 622, 633, 638, 640, 648, 675, 677, 679, 708
  binding of 74, 174, 273
  polyoxometallate 380
  recognition of 174
annulenes 72, 200
ansa compounds 66
Arbuzov-type dealkylation 170
architectures 14–17
arenes, macrocyclic 199
association constants 27, 105, 107
asymmetry, sources of 65
atomic force microscopy 403
atropisomerism 56, 58
atropisomerization 23, 48
Auranofin antiarthritic drug 293
autocatalysis 150
autocatalytic cycles 151
axes, stereogenic 62
azobenzene-coated silica 332
azobenzenes 108, 289, 577, 578, 632, 643, 666, 670, 673, 674, 685–9, 698–700

bacteriophages 7
ball-milling 170
barbiturates 155
base-pairing, Watson-Crick 357
bases 555, 581–90, 592, 597, 599, 630, 631, 633, 636–42, 644–7, 649, 650, 667, 668, 690–4
beauty in chemistry 5
benzimidazolium derivatives 115
benzylic amides 154
  rings 23, 35, 41
  tetralactam rings 24
  see also macrocycles
BET (Brunauer-Emmett-Teller) 575–7
bicycles 353
big blue box, also called $CBPQB^{4+}$ 35, 132, 208, 290, 650–2
binding sites 25
binding, competitive 555, 592, 594, 595, 597–606, 609, 614, 616, 638, 650, 708
Bingel reaction 111
biomedical materials 382
bis[2]catenanes 387–9
bisloop derivatives 377
bisrotaxanes 420, 425
bistable 555, 558–66, 568–75, 577, 579, 584, 586, 594, 595, 598, 599, 602–5, 609–17, 619–22, 625, 627, 628, 630–5, 639–42, 646, 648, 650–9, 661–9, 672, 675, 685, 689, 693, 701–3, 708
bonds
  coordinate 4
  coordination 581
  covalent 3
  dative 4
  dynamic coordinative 295, 302
  electrostatic 3, 190
  gold thiolate 330
  imine 26, 68, 128, 303, 305, 310, 332, 358
  kinetically labile 26
  kinetically stable coordinative 94
  labile metal-ligand 286
  metallic 3
  reversible 89, 330, 333
  topological 3, 209, 352
  see also halogen bonding, hydrogen bonding
Bonnanes 22, 55, 141, 324, 424, 431–3
boronic acid condensations 313
boronic esters 26, 303, 312–13, 379
boroxines 303, 312
Borromean links 359
Borromean rings 8–10, 18, 21, 24, 27, 29, 63–4, 212, 214, 229, 300, 303, 305, 352, 354, 358
braids 353
bridges, covalent 425
Brownian motion 21, 30, 558, 559, 589, 626, 627, 635, 649, 669, 670, 694–7, 701, 704
Brunnian links 21, 356
Brunnian topology, *see* topology
buckminsterfullerene 6

Cadiot-Chodkiewicz reactions 219, 223
Cahn-Ingold-Prelog sequence rules 53, 56
calixarenes 46, 48, 60, 177, 200, 203–4, 399, 589–90, 597–8, 625–6, 697–8
calixpyrroles 200
Cambridge Structural Database 382
capture
  anion-templated 175
  covalently-directed 54, 69
  dumbbell 60, 176, 219, 221
cartoons 6, 11, 15, 17
cascade stoppered heterorotaxanes 51
catalysts 7
  Grubbs I 314
  Grubbs II 314, 319
  Hoveyda-Grubbs II 314, 319
  ruthenium-alkylidene 314
  transition metal 218, 226
catalytic hydrogenolysis 67
catechols 108
catenands 12–13, 316
catenane synthesis 125, 307
catenane synthesis, by disulfide exchange 325
catenane synthesis, semistatistical method of 67
catenane synthesis, template-directed 79
catenanes 3, 90, 130, 153
  all-hydrocarbon 26
  anion-binding 322
  barium 302
  benzylic amide 15, 144, 149
  benzylic imine 98
  bis-macrobicyclo[2]- 375
  bistable 7, 10–11, 13, 16, 34
  branched 23
  co-conformation of 42
  covalently bridged 352, 386
  directed synthesis of 68
  DNA-based 211, 215, 369
  donor-acceptor 9, 18, 29, 41, 108, 119–20, 289, 307, 318, 326, 328, 375
  doubly interlocked 293
  gold 210
  macrobicyclic 370
  metal-templated 89
  metallo- 68, 229
  metathesis-mediated cycloalkane 313
  multi-annular 369–70, 374
  porphyrin-based 298
  surface-mounted 331
  tetralactam 140
  topologically chiral 67
  topologies of 351–2
  with macrobicyclic cores 371
  see also handcuff catenanes and rotaxanes
[2]catenanes 168, 197, 199
  benzylic amide 145, 180
  bimetallic 66
  chloride-templated 183
  copper homo[2]- 58
  cyclic oligo[2]- 389
  desymmetrized 132
  donor-acceptor 128, 392
  furano-tetralactam 141
  hybrid DNA-oligopeptide 215
  ladder polymerization of 363
  mechanically helical 58
  metallosupramolecular 59
  mixed-metal 296
  naphthalenediimide-based 110
  neutral anion-binding 181
  neutral π-associated donor-acceptor 110

The Nature of the Mechanical Bond: From Molecules to Machines, First Edition. Carson J. Bruns and J. Fraser Stoddart.
© 2017 John Wiley & Sons, Inc. Published 2017 by John Wiley & Sons, Inc.

[2]catenanes (*cont'd*)
non-rusty 68, 390
oriented 65
pH-switchable 134
post-synthetic modification of 66–7
pyrromethimide-based 110
side-chain, donor-acceptor 393
solvent-induced switchability of 145
sulfate-binding 184
tetralactam-based 141, 290
three-dimensional 374
topologically chiral 64
trianglamine 81
[3]catenanes 122, 132
conditional topological isomers of 69
cyclic 305, 315, 374
mixture of two orientational isomers 80
[4]catenanes 360–1, 368
[6]catenanes
branched 368
[7]catenane, tetrahedral, self-assembly of 376
[7]catenanes
branched 369
[n]catenanes
branched 361, 363
chain polymers 363
donor-acceptor branched 368
infinite chains of 363
linear 361–2, 369
polydispersed branched 369
radical 361, 364
catenarotaxanes 353, 441–2
catenates 12, 14, 293, 298
[2]catenates 94–6
[3]catenates 92, 316
benzylic amine 99
organometallic 99
catenation 65, 90, 99
crystallization-induced 210
nodes 384
cations 555, 560–6, 571–6, 580–4, 586–600, 604–6, 615, 620, 625, 626, 633, 634, 640, 644, 649–52, 658, 661–6, 668, 674, 675, 677–81, 685, 687, 689, 690l, 698, 700, 708
catrotaxanes 441
chainmail 7–8, 211, 358, 368
chains 64
channel, ionic conductance of 218
chelates, macrocyclic 100–101
chemical aesthetics 6
chemical sensing 382
chiral auxiliaries 54–5
chiral shift reagents 58–9
chirality 52, 54, 61
axial 56
axis of 52
conditional topological 57, 64, 66, 69
cyclo- 55
dynamic 26, 66
helical 52, 191, 287
induced 286
inherent 52, 61
mechanically axial 56–7, 71
mechanically helical 45, 53, 58, 60
mechanically planar 45, 53, 56, 70–71, 221, 425
non-classical forms of 53
planar 11–12, 68, 392
planes of 48
residual toplogical 68
ring sequence mechanical 70
topological 45, 53, 63, 67–8, 72, 80
transfer of 52
unconditional 63, 66–7
Christian iconography 8
circular dichroism 48, 54, 387
circumrotation 3–4, 32, 41, 315
citations, distribution of 36
click chemistry, copper-free 82, 168, 181
click synthesis 27, 32, 91–3, 113, 122, 128, 130–31, 142, 153, 156, 180, 184, 189, 193, 198–9, 205, 215, 219, 393, 420, 425, 427, 429
clipping reactions 54, 60–61, 108–10, 128, 132, 147, 153, 171, 178, 307, 366
anion-templated 177
dynamic 306–7
iterative metal-ligand 315
macrobicyclic 307
reversible 427
thermodynamically controlled 306, 442
with imine exchange 305–6, 308
yields 110
co-configurations 53, 55–6, 64, 70
absolute 55–7, 64–5, 67
enantiomeric 57
inversion of 43
co-conformational switching 327
co-conformations 3–4, 7, 9, 23, 25, 35, 53, 60, 68, 70, 106, 124, 132, 144, 558–62, 565, 566, 573–5, 581–3, 589–601, 605, 609, 611–17, 619–22, 625, 627, 630–4, 639, 640, 643, 645–50, 652, 660, 663, 666, 667, 688, 689
ground-state (GSCC) 4–5, 8, 21, 555, 558–65, 575, 576, 605, 616, 617, 622, 627, 633, 652, 655–65, 669, 674, 689
meta-stable (MSCC) 4–5, 16, 42, 558,
processes affecting 20
co-constitutions 3, 70, 285, 295
coalescence temperature 20, 28–30, 34–5, 38
colloidal composites 444
combinatorial library, dynamic 28, 63, 65, 67, 211, 271
complexes 560, 564, 566, 570, 571, 575–7, 586–8, 591, 594, 595, 600, 602, 604–6, 616, 627, 629, 635, 638, 643, 646, 647, 656, 668, 670, 675, 683, 699, 709
charge transfer 103
dialkylammonium-crown ether 173
face-to-face 157
homoleptic 93
host-guest 106, 133, 157, 166
kinetically labile 292
ring-in-ring 166, 443
complexity 28, 555, 627, 689, 709
component parts 2–4, 22, 33, 40, 45, 50, 52–3, 56, 61–2, 69–70, 430, 444
component-swapping processes 307
composite links 352
composite materials 382
cone-to-cone inversion 48, 203
conetworks, amphiphilic 379
configuration 53
absolute 67
inversion of 66
conformation 3
conformational analysis 5
constitution 3, 16, 161
cooperative capture 85–7, 397, 407
cooperativity 194, 395
coordination 285, 569, 591, 594–6, 600, 643, 647, 648, 670
coordination center 576, 588
coordination complexes
helical 59
octahedral 303
coordination networks 382–3
coordination number 89, 555, 566, 567, 593
coordination polymers 43
mechanically entangled 386
one-dimensional 443
rotaxane 439
three-dimensional 383
coordination sites 570, 580, 589, 600, 706
Cope rearrangement 171
copolymers, catenated 65
Coulombic attractions 103
Coulombic repulsions 23, 31, 208
counterfeiters 399
counterion exchange 169
covalent fixation approach 146
covalent organic cages (COFs) 211, 377
cross-catalytic cycles 151
cross-catenated structures 287
cross-turn coupling 215
crossbar molecular memory devices 13
crown ethers 40, 107–9, 159–60, 399, 597, 612, 614
1,5-dioxynaphtho[38]crown-10 104
[20]crown-6 162
[21]crown-7 162, 171
[22]crown-7 162
[24]crown-8 115
aza[12]crown-4 276
bis-para-phenylene[34]crown-10 104, 108
bis-para-xylyl[26]crown-6 117
BMP25C8 641
BN24C8 594, 595
BPP34C10 564, 575, 576, 605, 655–7, 662, 687
BX26C6 595, 596, 599, 600
DB24C8 571, 572, 584–6, 607–9, 621, 622, 630, 631, 634, 635–8, 641, 642, 644–50, 667, 668, 689–94, 698, 699, 704, 705, 707, 708
DBB224C82 595, 596, 599, 638
dibenzo- 63–4, 157
dipyrido[24]crown-8 163
DN24C8 699, 700
DN38C10 564–6, 595
N24C8 594, 595
PO292PC 586, 587
T224C82 639
TB27C9 586, 587
tetrabenzo[24]crown-8 163
tris-para-phenylene[34]crown-10 21
cryptands 121–2
catenated 373
macrobicyclic 372
macrocyclic 124
macrocyclic polyether 120
multi-annulated 370
nomenclature of 90
cryptates 90
crystal structures 14–16, 211
cubane 6
cucurbiturils 28, 74, 81, 208, 284, 332, 399, 412
CB6 581, 582, 635, 644, 682, 683
CB7 573, 574
electrostatic potential map of 81
host-guest complexes of 82

cyanostar macrocycles 48, 55, 189–90
cyclic [3]catenanes 354, 359
  co-conformation of 359
  self-assembly of 360
  synthesis of 359
cyclic[4]catenanes 354
cyclization, metal-directed 101
cycloadditions 157, 168
cyclobis(diazapyrenium-*p*-phenylene) 21
cyclobis(paraquat-4,4'-biphenylene) (CBPQB^{4+}), *see* big blue box
cyclobis(paraquat-*p*-phenylene) (CBPQT^{4+}), *see* little blue box
cyclodextrin rotaxanes 75, 77
cyclodextrins 27, 45, 49, 74, 81, 207, 283, 289, 300, 395, 399, 577
  catenane 49
  catenated 33, 49, 81
  daisy chain 427
  inclusion complexes 75, 79
  maltose-decorated 396
  polyrotaxane 77–8
  α-CD 574, 577–9, 582, 616, 618, 619, 624, 631, 632, 666, 667, 673–81, 685, 686–8, 692, 698
  β-CD 617, 618, 626–8, 643, 681, 683
  γ-CD
cyclodiastereoisomers 53
cyclodirectionality 69
cycloenantiomers 53
cyclophanes 74, 131, 399
  ionic 87
  nomenclature 87
  octacationic 31, 68
  tetracationic 16, 18, 21, 34, 39–40, 35, 104, 110, 125, 132, 425
cyclotriveratrylene 200

daisy chains 22, 25, 27, 32, 34, 130, 306, 319, 352, 424, 427
  [*an*]daisy chains 429–30
  [*cn*]daisy chains 427
  cyclic 428
  metallo- 427
  rotaxanated 427
dendrimers
  rotaxane 353
  third generation 112
  Type I, with rotaxane cores 417–18
  Type II, with rotaxane-like termini 417, 419
  Type III, with rotaxane branches 417, 420
deslipping 60, 163, 277–9, 281–3
dialkylammonium ions 564, 572, 582, 584–7, 590, 597, 599, 607–9, 616, 630, 633–42, 644, 646, 667, 668, 681, 683, 687, 692, 698–700, 704, 705, 707
  crown ethers as hosts for 27, 31, 166
  oligorotaxanes 396
  rotaxanes with 171
  secondary 158, 160, 165, 167
  substitutents, effects of 163
diastereoisomers 55, 65
Diels-Alder reactions 28, 171, 607, 610, 692, 694
diformylpyridine 304–5
dimerization, covalent 65
dimethyldiazapyrenium ions 105
1,5-dioxynaphthalene (DNP) 126, 560–6, 576, 592, 598, 615, 617, 625, 633, 634, 640, 645, 646, 650–2, 658, 659, 661, 672, 685, 689, 700
diquat 104, 122
dispersion forces 4
disulfide exchange 324, 331
disulfide linkages 26, 111, 217, 325
DNA 604, 606, 607, 623, 626–8, 635, 670, 679, 680, 686, 706
  B-DNA strands 357
  catenanes 212, 217
  circular 214
  double helix 212
  hybrid 217
  macrocyclic 606
  minicircles 214
  nanotechnology 211
  origami 215–16
  polyhedra 213
  rings, catenated 215
  rotaxanes 217
  sequencing 218
  technology 429
  topology, triple crossover 213
  triple helices 211
  Z-DNA strands 357
dodecahedrane 6
domains, tetramerization of 217
π-donating derivatives 107
donor number 329
donor-acceptor motifs 555, 560, 561, 563–7, 574–6, 580, 581, 583, 587, 589, 592, 595, 599, 606, 615–17, 625, 633, 640, 641, 645–8, 650–665, 672, 685–7, 689, 700
donor-acceptor stacks 41, 392
dumbbell capture 61, 83–4, 405
  covalent-directed 425
  nucleophilic 423
  active-template 412
dumbbells
  constitutionally asymmetric 50, 52–4, 70, 76
  constitutionally symmetric 50, 56
  dibenzylammonium 277–9
  ion-paired 320
  macrocyclic 443
  metallosurfactant 396
  π-conjugated 87
dynamic covalent chemistry (DCC) 271
dynamic exchange 310

effect
  catenand 95, 181
  cryptand 137
  cryptate preorganization 121
  hydrophobic 28, 63, 74, 134, 327
  Kerr 37–8
  kinetic 47
  macrobicyclic 121, 137
  stereoelectronic 140
  thermodynamic 47
Eglinton-Glaser-Hay, *see* homocoupling
electrochemistry 555, 558–74, 577, 583, 593, 604, 613–16, 633, 634, 641, 646–9, 652–64, 669, 685, 687, 689, 700
electronics 560, 562, 577, 591, 594, 598, 607, 638, 652–4, 658, 659, 663, 686, 701
electropolymerization, oxidative 408
emergence 28, 35
enantiomers
  conditional topological 65
  Euclidean 68
  mechanically planar 54–5
  topological 63–4, 66–8
encrypted security features 399
energy 558, 559, 561, 570, 574, 579, 611, 616, 618, 620, 621, 624, 625, 627, 633, 635, 650, 655, 660, 664, 669, 670, 672, 683, 685, 686, 689, 691, 692, 694–6, 699–706, 708, 709
energy states, high lying 210
energy storage technologies 210
entanglements, mechanical 71, 379
enthalpy 4
entwining strategy 300
enzymatic ligation 215
enzymes 7–8
equilibria 309, 555, 559, 562, 583, 589, 598, 599, 619, 621, 625, 640, 646, 651, 663, 670, 685, 694–7, 701, 708, 709
equilibrium constants 8
equilibrium, co-conformational 12
esters 169
Euclidean geometrical forms 61–2
ExBox^{4+} 131, 134–6, 316, 583–4
ExCage^{6+}, *see* molecular cages
extended solid-state structures 44
extrinsic graph theory 73
Eyring equation 5, 272
Eyring plot 20

ferroelectric materials 103, 382
ferromagnetic materials 103
figure-of-eight motif 22, 63, 73, 97, 214, 327
Finkelstein reaction 329
flash memory 13
fluorenones 108
fluorescent inks 399
foldamers 24–5, 130, 278, 395
foldaxanes 353, 444
forces
  dispersion 134
  hydrophobic 8, 39
  repulsive electrostatic 208
frameworks
  diamond-like 379
  interpenetrated 391
free energies of association 6
free energy 558, 616, 620, 621, 633
free radicals, *see* radicals
free-energy barriers 40
fluorescence resonance energy transfer (FRET) 398
fumaramide 577, 579, 610, 619, 624, 626, 627, 674, 675, 701–6
fuzzy logic 273
fuzzy sets 273

G-quadruplexes 211–12, 215
gas storage 382
Gemini catenanes 443–4
gene replication 8
geometry 555, 566, 568, 570, 589, 591–3, 603, 622, 626, 629–31, 633, 635, 639, 646, 647
  coordination 102, 566, 568, 570, 591, 593, 630
  tetrahedral 96
  trigonal bipyramidal 96
  see also Euclidean geometrical forms
glycols 108
glycosylation 170

glycylglycine (GlyGly, GG) 573, 574, 580, 589, 612–14, 674, 690, 691
gold electrodes 331
Goldberg amidations 28
graphical representations 6, 14, 16–18, 26, 32, 38, 45, 57, 62, 74
Grignard reagents, mechanically interlocked 302
grinding 170
growth factors 217
growth inhibitors 217
GSCC, *see* co-conformations, ground-state
guests
  constitutionally asymmetric 49
  halide ion-pair 177
  nanodroplets of 380

halogen bonding 3, 173–5, 185–8, 190, 321
handcuff catenanes and rotaxanes 22–4, 27, 68, 315, 322, 352–3, 372, 386, 431
heat 555, 559, 582, 614, 617–21, 669, 673, 675, 687
Heck cross couplings 28, 226
helicates 66, 285, 304, 356
helices, double 211
hetero[n]catenanes 52, 61, 64, 89, 375–7
hetero[n]catenates 97–8
hetero[n]rotaxanes 85, 307, 395, 398, 423
heteroarenes, macrocyclic 199
heteropseudorotaxanes 51
Holliday junctions 212
homo[n]catenanes 60, 65–6, 97, 209, 286–8, 290, 301–2, 312, 318, 321, 326, 354, 373
homo[n]rotaxanes 307
homochirality 50
homocoupling 27, 91
  alkyne 227
  Eglinton-Glaser-Hay 68, 91–2, 97, 111, 128, 130, 219, 222–4, 413, 419, 425
  palladium-catalyzed 226
hook-and-ladder approach 376
hooplanes 63
Hopf links 21, 61–2, 64, 352, 354, 386
hosts
  anion-binding 177
  benzylic amide 143
  cryptand-based 370
  heterotopic macropolycyclic 50
  macrotricyclic 124
  porphyrinic π-donating 119
  strapped porphyrin 119
  tetralactam-based 139–40
  triptycene-based 122, 143
  π-acceptor 104
  π-donor 104
Hunter-Sanders model 103
hybrid structures 119, 192
hydrazones 303, 310
hydrogels, double network 379
hydrogen bonding 3–4, 17, 30–31, 35, 41, 74, 99, 114, 138, 156, 158, 162–3, 180, 182–4, 187, 190, 194, 201, 273, 366, 373, 395, 555, 560, 572, 575, 577–82, 584, 587, 589, 590, 592, 595–605, 607, 609, 611–13, 616, 617, 619, 621, 625, 627, 635, 638, 652, 659, 663, 686, 690, 692, 693, 698
  in [C—H···F] 166
  in [C—H···N] 166, 205
  in [C—H···O] 105–6, 114, 126, 129, 132, 138, 164, 176–9, 186, 190, 192, 195, 204
  in [N^+—H···O] 164, 173, 409
  in [N—H···anion] 176
  in [N—H···O] 195
hydrophobicity 555, 560, 573, 574, 581, 616, 618, 632, 644, 645, 655, 674, 690
hydroquinones 110

imidazolium derivatives 115
imines, chemistry of 271, 303, 307, 309–10
inclusion complexes 83, 208
integrated systems 39
interactions
  [C—H···π] 126, 138, 165–6, 195, 205, 210
  [N^+—H···π] 165–6
  alongside 23, 59, 130
  anion binding 189, 194, 321
  anion-π 186
  aurophilic 210
  cation-π 165, 204
  charge transfer 21, 73, 103, 126, 135–6, 138, 190, 201, 204
  cooperative 398
  dipole-dipole 4, 74
  donor-acceptor 102, 115, 138, 204, 273, 373
  edge-to-face 186, 195
  electrostatic 555, 563, 565, 580, 581–4, 587, 598, 599, 618, 625, 626, 640, 648, 660, 678, 679, 708
  homophilic 74, 210
  host-guest 204
  hydrogen bonding 16, 37
  hydrophobic 58, 67, 273, 326, 373
  intramolecular 2, 4, 41
  ion-dipole 74, 178, 198, 309
  ion-pairing 4, 29, 58, 74, 138, 161, 191, 399
  multivalent 384
  noncovalent bonding 4, 12, 17–18, 61, 73, 90, 186, 285, 392, 555, 558, 560, 572, 592, 601, 611, 616, 619, 650, 664, 682, 708
  second-sphere 192
  solvophobic 74, 294
  van der Waals 62, 210–11
  π–π stacking 103, 108, 131–2, 117, 138, 166–7, 176, 178–9, 186, 190, 192, 204, 210–11
inversion, helical dynamic 58
ionic lattice 4
isomerism 2, 8, 14, 50–51, 68–9
  co-conformational 12
  constitutional 17
  sequence 52
isomerization 673
  cis-trans 578, 643, 673, 685
  photo- 555, 577, 578–80, 632, 666, 673, 674, 687, 697–701, 703–5
  thermal 673, 702
  translational 558, 583, 669
isomers 558, 573, 579, 580, 583, 594, 609, 617, 622, 630, 631, 640, 643, 666, 673, 687, 688, 704, 705
  (E)/(Z)-mechanostereo- 558, 578–9, 589, 619, 632, 666–7, 685, 688, 694, 697–8, 701–5
  circumrotational 570, 617
  cis/trans- 577, 578, 640, 673, 685, 689, 699, 702
  co-conformational 558, 562, 581, 583, 594, 598, 611, 615, 616, 619, 622
  conditional topological 69
  conformational 558
  constitutional 16, 225
    non-homeomorphic 62
    non-isotopic 62
  diastereo- 643
  orientational 47–8, 55, 76, 80, 204
  stereo- 558
  topological 45, 59, 61–3, 73, 100–101
  translational 4–7, 9, 11–13, 16–19, 30–32, 70–71, 307, 558, 560–2, 564–5, 567–73, 581, 588, 598–9, 604, 613, 615, 617, 619–20, 622, 632, 641, 658–60, 663, 689, 691, 702, 704–6
isothermal titration calorimetry 135
IUPAC Gold Book 56

K_a values 8, 27, 161, 163
Kerr constant 37
kinetics 555, 558, 560, 563, 566, 568, 570, 571, 585, 622, 632, 652, 658, 660, 662, 664, 669, 694, 695, 698, 701–5, 708
knots 141
  cystine 217
  graphs of 66
  non-intersecting 61
  nonameric trefoil 327
  pentafoil 22, 27, 59, 61–2, 67, 303, 305
  topologically enantiomeric 67
  trefoil 21–2, 27, 61–3, 65–7, 71–2, 315
  unconditionally chiral 66

ladder polymers and rotaxanes 430, 432
Langmuir surface area 384
Langmuir-Blodgett 653–60
lanthanides 199
lectins, synthetic 154
ligand exchange 221
ligands, photodissociation of 300
light 559, 574–81, 619, 643, 663, 666, 673–6, 685–9, 692, 697, 699–701, 704, 705, 708
line formulas 16
line-shape analysis 34
linearly polarized light 52
links
  composite
  compound 361
  topological 15, 379
lipoic acid 332
liquid crystals, chiral nematic 444
liquid vortices 444
little blue box, also called $CBPQT^{4+}$ 14, 21, 23, 31–2, 34, 69, 125, 127, 131, 372, 560–3, 565–7, 575–7, 580, 581, 583, 598, 615, 617, 622, 625, 633, 634, 640, 641, 649, 652–66, 672, 685, 689, 700, 708
logic 555, 579, 613, 655–7, 663, 669, 686–9
logic gates, multi-qubit quantum 399
luminescent materials 382

machines 11, 558–60, 566, 568, 574, 579, 597, 624, 627, 628, 652, 664, 669–707

macrobicycles
  catenated 370–1
  cryptands 184
  heterocatenated 370
  homocatenated 373–4
  self-threaded 443
macrocycles 65
  benzylic amide 555, 572–4, 577, 579, 580, 584, 586–9, 594, 600–605, 609–14, 619, 620, 624–7, 663, 667, 674, 675, 682, 688–90, 701–6, 708
  macrotricyclic 376
macrocyclic ligands 571, 580, 588, 589, 591–4, 596, 600, 629, 635, 636, 643, 647, 648, 682, 706, 707
  Mdpbiq37 569, 570
  Mdpp30 568–70, 576, 591, 646, 668
  porphyrin basket 583, 584, 594, 706, 707
macrocyclic polyethers 13, 104, 111, 122, 124, 166–7, 195, 370
macrocyclic polymers 94
macrocyclic precursors 67
macromolecules 555
macropentacycles, catenated 380
macropolycycles, self-threaded 443
macroscopic 555, 560, 627, 633, 666, 669, 670, 684, 685, 690, 709
macrotricyclics 376
magic rings and rods 285, 318, 323
magnetic materials 382
maximum birefringence, frequency of 38
maximum site occupancy principle 88, 303
meccano sets 9, 107, 130–31, 170, 157–8, 196
mechanical helicity 58–9, 61, 70, 294, 373
mechanical motion 2, 39
mechanically bonded architectures 52, 130
mechanically interlocked macrocycles 52
mechanized mesoporous nanoparticles 33
mechanochemistry 170
mechanomolecules 3–4, 17–19, 31, 35, 42–3, 56–7, 61–2, 69–70, 88, 93, 96, 104, 111, 120–21, 130, 201, 308, 351, 399, 412
  anion-binding 187
  anion-templated 321
  bistable 12, 14
  carbohydrate-containing 154
  co-constitution of 351
  coordination polymer 444
  dialkylammonium-crown ether 320
  halide-templated, halogen bonding 185
  hydrogen bonding in 318
  mercury 297
  metal-templated 315
  pirouetting in 35
  ring-in-ring 442
  self-assembled 298, 332
  stereochemistry of 424
  surface-mounted 330
  tripodal 419
  vernacular of 351
  zinc 297
mechanostereochemistry 4, 11, 17, 19, 22, 28, 30, 36, 52–3, 60, 66–7, 71, 73, 100, 102–3, 125, 138–9, 141, 157, 167, 173, 198, 200, 204, 210, 285, 333, 351–2
mechanostereochemoselective motion 318
mechanostereogenic 56
mechanostereoisomerism 2, 8, 11, 16, 35, 42–3, 49, 59, 162
mechanostereoisomers 2, 5, 13, 48, 68, 70, 98
  dynamic 2, 70
  mechanically chiral 52
  orientational 45–7
  sequence 45, 51
mechanostereoselective formation 48, 555, 578, 694, 697–701, 703, 709
Menschutkin reaction 109, 112
Merrifield resin 62
meso-isomers 55
mesoporous silica nanoparticles (MSNPs) 33, 670–7, 688
metal-organic frameworks (MOFs) 16, 43, 108, 320, 382, 384, 393, 439–40
metallacages 288, 377, 380–1
metallacycles 57, 208, 289
metallo-assembly, divergent 422
metallo-supramolecular architectures 285
metallo-supramolecular assemblies 300
metallo-supramolecular trimerization 422
metallogrids 297
metathesis
  cross-coupling 169, 324
  olefin 26, 91, 95, 111, 113, 128, 157, 271, 303, 308, 313, 319, 323, 325, 387, 425
  polymerization 95, 369
  ring-closing 97, 99, 174, 192, 313–15, 318, 354, 367, 387, 393, 427
  ring-opening 313
  ring-opening ring-closing 314
methyl viologen 104, 105, 108, 118, 121, 124
Michael additions 28, 111, 113, 226, 324, 330
microbalance 660
microcantilever 635, 685
microcrystallinity 618, 619
microfluidic 663
microscopic 555, 627, 639, 657, 669, 692, 694, 696
microscopic reversibility 555, 670, 696, 697, 700, 701, 709
microscopy 558, 624, 627, 657, 659, 668, 683, 692
milling 170
mitochondria 8
Mitsunobu reaction 607, 610, 611
Mizoroki-Heck coupling 438
Möbius forms 12, 60–62, 71–3, 217
molecular biology 8
molecular bundles 27, 424, 433–4
molecular cages 373, 379
  blue cage 137
  catenated 380–1
  ExCage^{6+} 137
  interlocked 288, 377
  macrobicyclic 373
  metallosupramolecular 373
  tetrahedral 380–1
  three-dimensional 379
molecular chainmail 213
molecular chameleon 444
molecular clamps 403
molecular electronic devices 19, 33
molecular elevators 22, 24, 424, 433
molecular entanglements 72
molecular graphs 61–2
molecular knots 3, 12, 67, 444
molecular ladders 431
molecular lassos 22
molecular locking mechanism 330
molecular machines 30, 39, 97, 203, 426
  artificial 13, 34–5, 70, 333
molecular meccano 7, 107
molecular motors 43
molecular muscles 19, 32, 593, 616, 627–40, 649, 670, 684–6, 692, 693, 697, 709
molecular Möbius strips 72
molecular nanotechnology 6, 18
molecular necklaces 22–4, 27, 50, 52, 85, 223, 289, 323, 352, 364–7, 369, 405
molecular ouroboros 70, 424
molecular ratchets 30
molecular recognition 31, 61–2, 184
molecular sheafs 24, 228, 352–3, 411–14
molecular shuttles 18, 23–4, 26–7, 203, 221, 226, 410
  based on active templates 30
  based on directed synthesis 29
  benzylic amide 25
  bistable 130, 185
  degenerate 26, 30, 43–4, 70
  donor-acceptor 21–2
  hydrogen bonding in 24
  switching in 124, 161
molecular squares 133, 354
molecular switches 4, 9, 13, 30–31, 39, 70, 188, 203, 333
  catalytic 59
  cation-driven 198
  tunnel junctions 33
molecular trains 3–31, 39–40
molecular transporter 426
molecular trefoil knot 221
monolayers 332, 573, 653–63, 665–8, 685, 708
motifs 120
  anion-binding 174
  DNA double crossover 213
  polyrotaxane 386, 440
  Roman handshake 138
  π-donor/π-acceptor 104, 120, 425
motor molecules 30, 559
MSCC, *see* co-conformations, meta-stable
multi[n]catenanes 157, 379
multi[n]rotaxanes 423, 425
multiple-threaded assemblies 414

nanoactuators 606, 607, 623
nanocages 379
nanocarriers 671–6, 680
nanocars 670
nanodiscs 661
nanoelectromechanical 555
nanoelectronic 653
nanofibers 668, 691, 692
nanometers 628, 633, 652, 657
nanomorphology 691
nanoparticles 606, 661, 662, 667, 668, 670–7, 679–81, 683, 688, 691, 692
nanopores 606, 607, 623, 672–6
nanorecording 659
nanorings 200
nanorods 673
nanoscale 555, 560, 590, 627, 639, 652, 655, 657, 669, 672–6, 684, 696
nanostructures 635, 690–2, 696
nanotechnology 560
nanotubes 79, 316, 319, 655
nanovalves 670–7

naphthalene diimide (NDI) 564–6, 595, 633, 637, 638, 645, 646
narcissistic self-sorting 294
native proteins 217
nature 558, 559, 591, 670, 694, 706, 709
nets
  coordination 382
  entangled coordination 382
  polymer 379
  three-connected 383
  two-dimensional 382
networks
  bicontinuous interpenetrated 384
  catenated 16
  cation binding 215
  coordination 379, 384–5
  cyclodextrin 438
  extended 62, 393
  gridlike 391
  hydrogen bonded 35, 60
  interpenetrated 16, 353, 379, 383
  parallel interwoven 444
  polycatenated 353, 382–2
  polymer 379
  topologically entangled 353, 379, 382
  topologies of 439
  two-dimensional 380
  warp-and-weave 444
NMR line-shape analysis 20
nomenclature
  carbohydrate 351
  cyclophane 119
  IUPAC 351
  vernacular 352, 392
non-degenerate 559, 561, 563, 615, 617, 620, 647, 648, 669, 705
non-equilibrium systems 28, 39
non-linear optical materials 382, 384
nucleic acids 8
nucleophilic substitution 76, 108, 324, 327
nylon 196

oligocatenanes 34, 305, 368, 387
oligomethylene chains 23
oligorotaxanes 25, 32, 61, 130, 307, 353, 424–6
  dibenzylammonium 395, 397
  donor-acceptor 394–5
  foldamer, donor-acceptor 42
  linear 306
  template synthesis of 395
  translational isomerism of 32
oligothiophenes 93, 200
Olympiadanes 15, 24, 352, 361, 363, 387
optical purity 55
organocatalysis 74, 218
oxacalixcrowns 124
oxidants 555, 590

para-benzoquinone 139
paracyclophanes 87, 165, 200
paraquat, *see* methyl viologen
Pauling principle 83
pentacycles 353
pentafoil knots, *see* knots
peptides
  [4]catenane metallo- 360
  benzylic amide rotaxane 36
  cyclic 154–5
perspective stereoformulas 14, 18
PET, *see* photoinduced electron transfer
photocyclization 156
photodimerization 79
photoinduced electron transfer (PET) 91, 555, 574–7, 592, 593, 640, 641, 700
photoluminescence excitation intensity mapping 317
physical environment 23
pillararenes 45, 48, 86, 200, 204, 207, 399
  PA5 616, 621, 630, 684
  PA6 620
pimers 207
pirouetting 3–4, 32, 40, 70
  around-the-annulus 42
  around-the-axle 32–3, 38
  in donor-acceptor mechanomolecules 33
  pH- and anion-controlled 37
  rates of 35–6, 38, 40–41
  through-the-annulus 33, 38–9, 41, 69
  within-the-annulus 33–5, 42–3, 69
planar chirality, see chirality
platonic solids 6, 26
poly(ethylene)glycol 401
polyamides 400
polyaramides 400
polycatenanes 34, 363, 379–82
  poly[2]catenanes 148, 388–92
  polybis[2]catenanes 391
polycyclic aromatic hydrocarbons (PAHs) 134–6, 210
polydispersity indices 94
polyelectrolytes 79, 404
polyesters 400
polymerization 68, 313, 399, 438
polymers
  backbones, conjugated 404
  catenated 64, 94
  coordination 406
  crown ether threaded 409
  cucurbituril-threaded 405
  cyclodextrin-threaded 401–2
  entanglements in 444
  metallosupramolecular 402
  polyurethane-based 276
  sequence defined 50
  statistically threaded 399
  threaded by endocylic chelates 408
  see also polyrotaxanes 409
polymetallorotaxanes 408–9
polyolefins 400
polyoxometallates 379
polypeptides 196
polypseudorotaxanes 64, 77–8, 154, 399–401, 407, 410
polyrotaxanes 70, 79, 83–4, 86, 367, 411, 439, 441, 555, 582, 612, 617–19, 624, 633, 676–81, 692
  conjugated cyclodextrin 403
  cucurbituril-promoted capture polymerization of 84
  donor-acceptor 410
  entanglement in 440
  macrobicyclic 416
  main chain 409, 434, 437, 399
  networks of 438–9
  poly[1]rotaxanes 425–6
  poly[2]rotaxanes 401, 424, 434–8
  poly[3]rotaxanes 438
  polybis[1]rotaxanes 426
  single-axle 392
  π-conjugated 408
polyurethanes 400
polyviologens 409, 411
porphyrin baskets 119, 324
porphyrin nanorings 367
porphyrinic ExBox 134
porphyrinic oligorotaxanes 91
porphyrins, macrocyclic strapped 23
positive cooperativity 189
precatenanes 67–8
pressure 129, 555, 622, 624, 653, 654, 659, 695, 708
pretzelanes 22–4, 54, 141, 353, 385–6, 390
prime links 21, 352–3, 361, 369
prochiral centers 26, 57, 70
prokaryotes 8
proteinaceous lasso 217
proteins
  catenated structures in 217
  folding of 312
  knotted structures in 217
  nanopores in 218
protocols
  active metal template 441
  clipping and stoppering 108, 122, 131, 147, 153, 156, 169, 171, 177, 179–80, 193, 206, 295, 415
  dumbbell capture 225
  shrinking and swelling 172–3
pseudocatenanes 22, 352–3, 363, 386–7, 395
  pseudo[1]catenanes 443–4
  pseudo[2]rotaxanes 166
  pseudo[3]catenanes 372
  ship's wheel 24
pseudoknots, topological 217
pseudolinks, topological 217
pseudorotaxanes 4, 7, 14–15, 23, 27, 33–4, 60, 75, 84, 87, 98, 104–7, 112–16, 124–5, 127, 132, 137, 140, 144, 153, 157–60, 162, 174, 176, 178, 182, 198–9, 201–2, 204, 271–3, 275, 277, 280–1, 290, 305, 325
  [3]pseudorotaxanes 118
  benzylic amide-based 143
  donor-acceptor 112, 130, 196
  Hammett correlation for 164
  K_a values for 164
  macrotricyclic host-based 123
  metallo- 90–91, 95–6, 100
  methyl viologen 120–21
  polyether-based 63
  polyurethane-based 64
  self-assembly of 143, 188–9, 195, 202, 205–6
  statistically threaded 65
  ternary 414
  tetralactam-based 281
pseudosuitanes 433
publications, distribution of 37
pulley effect 439
pyromellitic diimide (PMDI) 563, 564, 566, 573, 595
pyrrolotetrathiafulvalene 10, 126

radicals 207, 209, 555, 560–2, 564–7, 572, 574–7, 583, 604, 633, 634, 640, 641, 649–52, 663, 666, 687, 700, 708
  as dimers 133
  organic 209
  pairing of 21

random walk 559, 563, 577
ratchets 555, 579, 606, 607, 670, 694–706, 708, 709
ravels 23
reactions
  dynamic nucleophilic 26, 271
  kinetically controlled 61–2
  mechanochemical 170
  reversible nucleophilic 324
  S_N2 169
  solid-state 170
  thermodynamically controlled 95, 143
  thiol-yne 171
  transition metal catalyzed 169
receptors
  anion-binding 182, 372
  bis-2,6-diamidopyridine 155
  for 1,2-bis(pyridinium)ethane 114
  halogen bonding 186, 188
  heteroditopic 182, 193
  neutral mechanically interlocked 181
  porphyrinic basket-shaped 119–20
recognition motifs 24, 27, 32, 73
recognition processes, halogen bonding 173
recognition units 9, 17, 25, 30–31, 44, 47, 52
  alongside 39
  dialkylammonium 409
  dibenzylammonium 31
  dioxynaphthalene 110
  hydrogen bond accepting 147
  imidazolium 117
  influence of translational isomers 21
  squaraine 285
recognition
  anion 191
  ion-pair 193
  nitrate anion 189
reductant 555, 575, 576, 590
reductions 564–8, 573, 575–7, 583, 590, 604, 605, 633, 660, 672, 689, 700
regioselectivity 169
resolution 67
resorcinarenes 200
Reynolds number 35
ring size, effects of 161
ring-in-ring assemblies 3
rings
  benzylic amide 153
  capture of 60
  concatenated 217
  paradromic 71
  shuttling of 45
  triazole 109
rocking 3–4
Roman handshake, *see* motifs
rotacatenanes 3, 24–5, 34, 50, 307, 352, 441–2
rotamacrocycles, bistable 442
rotation 3
rotaxanations 130, 196, 315
rotaxanes 3, 62, 76, 90, 129–30, 162, 178, 189, 310, 325–6
  anion-templated, slippage of 284
  architecture of 351
  barbiturate-containing 156
  benzylic amide 36–8, 146–51, 283, 323
  biomolecular transmembrane 50
  bistable 7, 10–11, 15, 20–21, 24, 27, 323
  branched dendritic 352
  bundled, triply interpenetrated 307
  cage-based 415
  capture of, nucleophilic 175, 194
  chromophoric 77
  covalent-directed capture 71
  covalently bridged 353, 392, 424
  cross-metathesis of 323
  cucurbituril 83, 85
  cucurbituril-promoted capture of 84
  cyclic ladder-like 424
  cyclobis(paraquat-*p*-phenylene) 128
  daisy chain 322, 429
  degenerate 24
  dendrimeric 50, 392, 416, 419, 423
  diazoperopyrenium 112
  disulfide bridged 331
  donor-acceptor 120, 275–6, 331
  fumaramide 36
  helix-rod 25
  heteroleptic 99
  inorganic-organic hybrid 192
  macrotricyclic 415
  mechanically planar 55
  metal-templated 93
  metallo- 98–9, 229
  multi-annular 353, 414–15
  multi-axle 411
  natural hydrogen bonding 281
  neutral 35
  nomenclature of 392
  orientational isomers 45, 48
  palindromic bistable 32
  photoswitchable 32
  polymer, *see also* polyrotaxanes
  ring-in-ring 25, 300, 443
  self-assembled porphyrin 298
  self-replicating 150–51
  squaraine 152, 154
  stoppered 290
  surface-anchored 183, 331
  tetralactam-based 142–3, 183, 285
  thermodynamically controlled assembly of 306
  thiosquaraines 154
  transmembrane 218
  triply interlocked 319
  with π-conjugated dumbbells 88
[1]rotaxanes 141, 424–6
[2]rotaxanes 118, 197, 202, 206–7, 154
  anion-binding 179
  bistable, pH-switchable 143
  chloride-binding 178
  click synthesis of 190
  cyclodextrin-stoppered 187
  directed synthesis of 70
  donor-acceptor 118, 129, 131
  glycosidic 170
  glycylglycine 146
  hemaphrodite 427
  Janus 427
  lanthanide-appended 180
  macrobicylic 414
  metal-templated 91
  neutral 96
  nitride-lanthanide 199
  noncovalent protein 217
  peptido- 146
  photoactive 180
  polymerically covalently bridged 434
  porphyrin basket 415
  ring-bridged, tris 420
  semistatistical strategy for 67
  tetrakis, ring-bridged 420
  zwitterionic 75, 116
[3]rotaxanes 54–5, 122, 412
[4]rotaxanes 421–2, 430–1
[5]rotaxanes 394, 399, 421
[7]rotaxanes, tripodal 422

salt bridges 191
scanning tunneling microscopy (STM) 68, 403
Schiff bases 303
Schotten-Baumann reaction 80
second-sphere coordination 290, 292, 600
secondary building units 16
secondary structure 11, 92, 129, 312, 395
selectivity 560, 561, 564, 578, 579, 581, 582, 586, 588, 590, 600, 602, 607, 614, 652, 674, 675, 682, 696–9, 704
  co-conformational 15, 30
self-aggregation 210
self-assembled monolayers (SAMs) 26, 330
self-assembly 108
  biomolecular 74
  coordination-driven 295, 366
  crystallization-induced 211
  electrostatic 145–6
  metallosupramolecular 271
  sulfate-directed 183
  with donor-acceptor units 310
semidumbbells 283
semirotaxanes 112, 118, 169, 332, 421, 430, 436
sensors 322
sensory polymers 437
separations 382
shrinking 61, 304–5
shuttling 23, 25, 29
silylation 170
single-molecule microscopy 403
site exchange 20
slide-ring gels 438–40
slippage 26, 60, 75, 85, 271–4, 279, 281, 283–5, 328–9, 333, 415
  hydrophobic interaction influenced 283
  in hydrogen-bonding rotaxanes 277–8
  ion-sensitive 277–8
  stopper 280
  use in synthesis 276
small molecules 555, 574, 604, 605, 672, 675, 687, 693
Solomon cubes 356
Solomon knots 9–10, 15, 29, 293
Solomon links 21, 24, 59, 61–3, 66–8, 288, 305, 315, 327, 352, 354–6
solvent polarity 159, 555, 570, 587, 599, 611–16, 626, 630, 642, 645, 646, 648, 698, 708
solvent-assisted ligand incorporation (SALI) 441
Sonogashira reactions 219, 233
space-filling models and representations 15–16, 22, 63, 74
spectroscopy 558, 572, 575, 579, 582, 585, 589, 618, 621, 638, 643, 655, 658, 665, 668, 682, 703, 705
spiropyrans 577, 579, 580, 670
squaraines 142, 150, 152–4, 285, 318
square planar geometry 100, 305
staple strands 216
Star of David catenanes 21, 24, 27, 356

Star of David links 67, 229, 354, 356
stationary phases, chiral 61
Staudinger ligation 170
stereochemistry, covalent 66
stereoformulas 14, 16, 22, 26
stereogenic centers 57, 62
stereogenic planes 62
stereoisomerism 2, 55–6
stereoselectivity 169
stilbene 577–9, 616, 632, 670, 687, 688, 698, 704, 705
stimulus / stimuli 555, 558–61, 566, 574, 577, 579, 581, 583, 597, 599, 600, 604, 605, 617, 627, 630, 633, 640, 642, 645, 649, 658, 664, 667, 669–80, 684, 685, 687–9, 692, 694, 697, 699, 700, 707, 708
stopper exchange 149
stoppering protocols 60–61
  S_N2-mediated 112
  template-directed 130
  thermodynamically controlled 63
stoppers 279, 321
  boronic ester based 313
  dioxaborate 313
  electrostatic 75
  imine-linked 309
  porphyrin 300
  trityl 64
subcomplexes 42
succinimides 572, 573, 577, 587, 594, 610, 611, 613, 619, 620, 701–3
suitanes 3, 7, 22, 307, 352–3, 444
sulfones, macrocyclic polyether 172
super-rotation 32–3, 42
superbundles 319
supermolecules 3–4
superstructures, solid-state 57, 105
supramolecular forms 4, 11, 18
supramolecular encryption 398
surrogate 169
swelling 61
switches 555–668
symmetry 555, 566, 578, 589, 599, 635, 641, 670, 694, 696, 697, 701, 709
synthesis
  active copper template 90, 222
  active metal template 54, 89, 221, 223, 316
  active nickel template 228
  active palladium template 227
  active template 27, 30, 92, 218–26, 330
  anion-directed 175
  chloride-templated 179–80, 322
  clipping 178
  cooperative capture 398
  covalent templated 66
  covalent-directed 70
  directed 67, 69, 229
  Goldberg active template 224
  hydrothermal 407
  magic ring 319
  magic rod 325
  mechanostereoselective 49
  nitrate-templated 184, 188
  nucleophilic capture 56
  oxidative Heck active template 226
  radical templated 209
  sodium-ion templated 197
  solvent-free 198
  statistical 61–4, 229, 329
  template-directed 4, 11, 13, 26, 62, 73, 104, 136, 147, 170, 173, 198, 229–30, 285, 361, 395, 444
  Ullmann-type active template 222

taco complexes 316
tartaric acid 52
technomorphic representations 18, 33, 35
technomorphism 18
technomorphs 14, 18
temperature 558–60, 563, 579, 582, 585, 589, 615–22, 624, 630, 631, 633, 645, 646, 648, 654, 656, 660, 661, 670, 689, 694, 695, 699, 701, 708
templates 4, 20, 26, 66, 148, 425
  acetylcholine 65, 311
  active copper 219
  active metal 67, 367
  active nickel 227
  active palladium 226
  active zinc 225
  alkali metal 195
  alkaline earth metal 198
  ammonium-crown ether 157
  anion-binding 174, 230
  anionic 184, 193, 320
  aromatic 65
  benzimidazole 117
  biomolecular 211
  brominated 174
  bundles in 24
  calixarenes as 156
  cation-binding 199
  cationic 195, 199
  covalent 65, 67–9, 72
  crown ether 110, 128
  cyclobis(paraquat-*p*-phenylene) 128
  cyclophanes 230
  dalkylammonium 306
  donor-acceptor 39, 88, 92, 184, 229, 366, 390
  fluorinated anionic 184
  halide 176, 179
  halogen bonding 174, 230
  helical 363
  homophilic 210, 230
  hydrogen bonding 39, 139, 147, 229, 362
  hydrophobic 229
  integrated ion-pair 191
  iodinated 174
  ion-pairing 230, 191, 321
  linear 101
  macrocyclic arene 200
  metal 92, 305
  metal coordination 13
  metal-ligand 73
  metallo-helicate 58
  metallo-organic 229
  neutral 395
  octahedral 64, 98
  organic cationic 192
  organic oxyanion 182
  pseudorotaxane 314, 320
  pyridinium-based 307
  radical pair 207, 230
  self-sorted 50
  solvophobic 229
  square planar 99
  tetrahedral 89, 96
  tetralactam 182
  tetraureido-calixarene 318
  thiosquaraine 153
  traceless ion-pair 194
  transition metal 39, 88–9, 392, 394, 430
  transition metal ion-pair 192
  trigonal bipyramidal 95
  viologen 86, 124
  π-donating motif 104
templation 130, 211
  donor-acceptor 67, 102
  fold-directed 217
  hydrogen bonding 436
  hydrophilic 395
  hydrophobic 436
  metal coordination 436
  solvophobic 395, 397
  transition metal 67, 408, 425
  π-donor/π-acceptor 427, 436
TEMPO radicals 46
tether-assisted approach 324
tetracycles 353
tetrahedral geometry 90
tetralactams 363, 602, 638
  anthrylic 153
  catenanes based on 7
  hydrogen bonding 301
  macrocyclic 6, 175, 183
  rings in 27
  rotaxanes derived from 26
  triptycene 142
tetrathiafulvalenes (TTFs) 9–10, 103, 126, 207, 354, 560–3, 566, 567, 574, 586, 587, 598, 606, 615, 617, 622, 625, 640, 641, 650–4, 657–61, 665, 666, 672, 685, 689
Texas-sized box 137–8, 295
thermodynamic control
thermodynamic forecasting 6–7, 14
thermodynamics 555, 558–60, 575, 597, 621, 622, 636, 652, 660, 661, 664, 669, 670, 694, 695
thiols 26, 169
threading 47, 64
threading-followed-by-shrinking 172
threading-followed-by-swelling 171
topography 19, 61, 212
topological protection methodology 212
topological rubber gloves 69–70, 376
topological stereoisomers 61–2, 67
topology 14–19, 43, 59, 62, 71–3, 377, 379
  achiral 69
  Brunnian 357, 359
  chemical 3, 12, 59–62, 72, 352
  knotted 212
  mathematical 22, 61
  network 382
  non-trivial 62
  prime link 354
  self-interlocked 356
torsional stereoisomers 5
transition metals, square planar 100
transition state theory 4–5
translation 3–4, 70
  kinetics of 23
translational motion 45
transmembrane potential 218
trianglamines, *see* [2]catenanes
trianglimines 80
tricycles 353

tropylium cations 122
tubular representations 66–7
Turing machine 35
TVBox^{8+} 136

Ulmann couplings 27
ultramacrocycles 639, 640, 642, 643
unidirectional motion 30
units
  1,2-bis(pyridinium)ethane 103
  1,5-diaminonaphthalene 103
  1,5-dioxynaphthalene 103
  4,4'-biphenol 103
  benzidine 103
  bis(pyrrolo)tetrathiafulvalene 103, 109
  deoxynaphthalene 16
  diazaperopyrenium 103
  diazopyrenium 106
  dioxynaphthalene 107
  hydroquinone 103, 109
  perylene diimide 103
  pyromellitic diimide 103
  pyrrolotetrathiafulvalene 103
  tetrathiafulvalene 103
universal 3-ravel 300
unknots 21, 61–3, 71
unlink 61
unlock-lock strategy 325
ureas 169
urethanes 169

van 't Hoff analysis 32
van 't Hoff plots 10
van der Waals interactions 4
Venn diagram 230
viologens 103–4
  extended 40
viral capsids 213
viscosity 23

wheel, rotationally unsymmetrical 54, 56
Whitehead link 354, 360, 445
Williamson ether synthesis 98, 370
word art images 37
work 555, 559, 626, 669, 670, 684, 685, 689, 690, 692, 694–7, 701, 703, 706, 708, 709

WILEY END USER LICENSE AGREEMENT

Go to www.wiley.com/go/eula to access Wiley's ebook EULA.